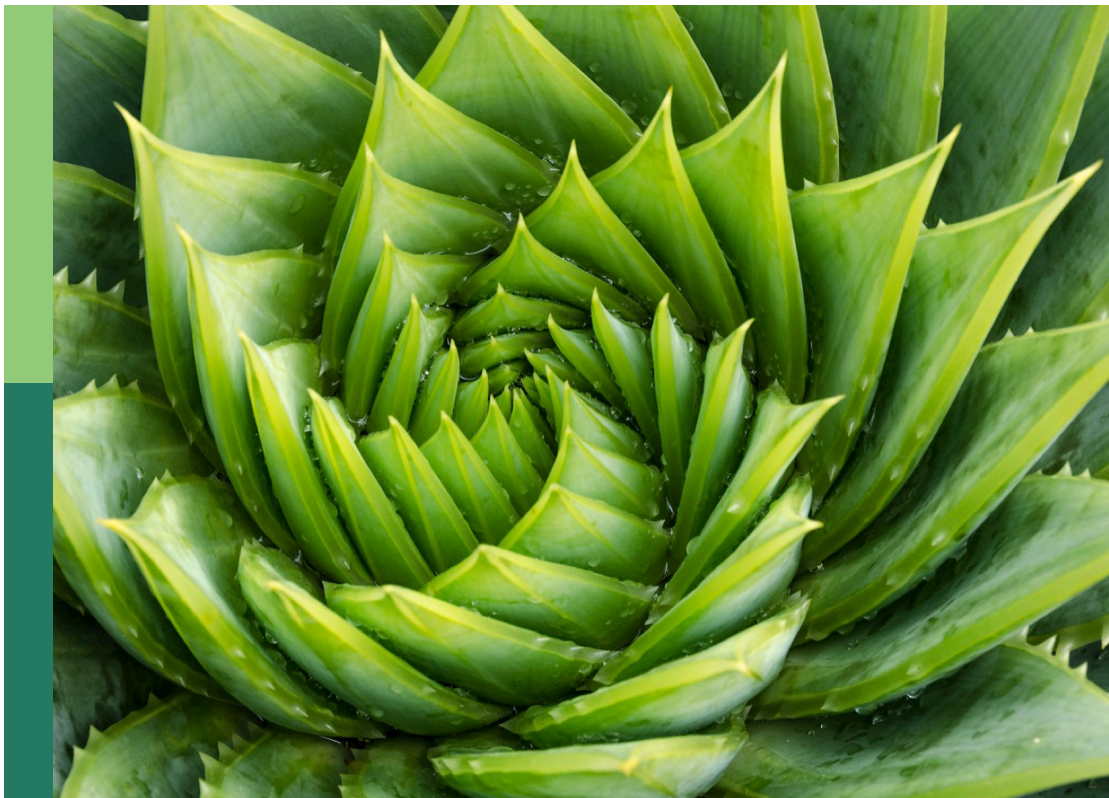
frontiers | Research Topics

Abiotic stress adaptation and tolerance mechanisms in crop plants, 2nd edition

Edited by
Jiban Shrestha, Ji-Hong Liu, Bhaskar Gupta and Mirza Hasanuzzaman

Published in
Frontiers in Plant Science



FRONTIERS EBOOK COPYRIGHT STATEMENT

The copyright in the text of individual articles in this ebook is the property of their respective authors or their respective institutions or funders. The copyright in graphics and images within each article may be subject to copyright of other parties. In both cases this is subject to a license granted to Frontiers.

The compilation of articles constituting this ebook is the property of Frontiers.

Each article within this ebook, and the ebook itself, are published under the most recent version of the Creative Commons CC-BY licence. The version current at the date of publication of this ebook is CC-BY 4.0. If the CC-BY licence is updated, the licence granted by Frontiers is automatically updated to the new version.

When exercising any right under the CC-BY licence, Frontiers must be attributed as the original publisher of the article or ebook, as applicable.

Authors have the responsibility of ensuring that any graphics or other materials which are the property of others may be included in the CC-BY licence, but this should be checked before relying on the CC-BY licence to reproduce those materials. Any copyright notices relating to those materials must be complied with.

Copyright and source acknowledgement notices may not be removed and must be displayed in any copy, derivative work or partial copy which includes the elements in question.

All copyright, and all rights therein, are protected by national and international copyright laws. The above represents a summary only. For further information please read Frontiers' Conditions for Website Use and Copyright Statement, and the applicable CC-BY licence.

ISSN 1664-8714
ISBN 978-2-8325-5092-2
DOI 10.3389/978-2-8325-5092-2

About Frontiers

Frontiers is more than just an open access publisher of scholarly articles: it is a pioneering approach to the world of academia, radically improving the way scholarly research is managed. The grand vision of Frontiers is a world where all people have an equal opportunity to seek, share and generate knowledge. Frontiers provides immediate and permanent online open access to all its publications, but this alone is not enough to realize our grand goals.

Frontiers journal series

The Frontiers journal series is a multi-tier and interdisciplinary set of open-access, online journals, promising a paradigm shift from the current review, selection and dissemination processes in academic publishing. All Frontiers journals are driven by researchers for researchers; therefore, they constitute a service to the scholarly community. At the same time, the *Frontiers journal series* operates on a revolutionary invention, the tiered publishing system, initially addressing specific communities of scholars, and gradually climbing up to broader public understanding, thus serving the interests of the lay society, too.

Dedication to quality

Each Frontiers article is a landmark of the highest quality, thanks to genuinely collaborative interactions between authors and review editors, who include some of the world's best academicians. Research must be certified by peers before entering a stream of knowledge that may eventually reach the public - and shape society; therefore, Frontiers only applies the most rigorous and unbiased reviews. Frontiers revolutionizes research publishing by freely delivering the most outstanding research, evaluated with no bias from both the academic and social point of view. By applying the most advanced information technologies, Frontiers is catapulting scholarly publishing into a new generation.

What are Frontiers Research Topics?

Frontiers Research Topics are very popular trademarks of the *Frontiers journals series*: they are collections of at least ten articles, all centered on a particular subject. With their unique mix of varied contributions from Original Research to Review Articles, Frontiers Research Topics unify the most influential researchers, the latest key findings and historical advances in a hot research area.

Find out more on how to host your own Frontiers Research Topic or contribute to one as an author by contacting the Frontiers editorial office: frontiersin.org/about/contact

Abiotic stress adaptation and tolerance mechanisms in crop plants, 2nd edition

Topic editors

Jiban Shrestha — Nepal Agricultural Research Council, Nepal
Ji-Hong Liu — Huazhong Agricultural University, China
Bhaskar Gupta — Government General Degree College, Singur, India
Mirza Hasanuzzaman — Sher-e-Bangla Agricultural University, Bangladesh

Citation

Shrestha, J., Liu, J.-H., Gupta, B., Hasanuzzaman, M., eds. (2023). *Abiotic stress adaptation and tolerance mechanisms in crop plants, 2nd edition*. Lausanne: Frontiers Media SA. doi: 10.3389/978-2-8325-5092-2

Publisher's note: This is a 2nd edition due to an article retraction.

Table of contents

07 Editorial: Abiotic stress adaptation and tolerance mechanisms in crop plants
Bhaskar Gupta and Jiban Shrestha

13 Purple stem *Brassica napus* exhibits higher photosynthetic efficiency, antioxidant potential and anthocyanin biosynthesis related genes expression against drought stress
Weiqi Chen, Yilin Miao, Ahsan Ayyaz, Fakhir Hannan, Qian Huang, Zaid Ulhassan, Yingying Zhou, Faisal Islam, Zheyuan Hong, Muhammad Ahsan Farooq and Weijun Zhou

29 Identification of *TaBADH-A1* allele for improving drought resistance and salt tolerance in wheat (*Triticum aestivum* L.)
Ming Yu, Yang Yu, Sihai Guo, Mingfei Zhang, Nan Li, Shuangxing Zhang, Hongwei Zhou, Fan Wei, Tianqi Song, Jie Cheng, Qiru Fan, Caiyin Shi, Wenhan Feng, Yukun Wang, Jishan Xiang and Xiaoke Zhang

41 Proline-mediated regulation on jasmonate signals repressed anthocyanin accumulation through the MYB-bHLH-WDR complex in rice under chromium exposure
Qing Zhang, Yu-Xi Feng, Peng Tian, Yu-Juan Lin and Xiao-Zhang Yu

53 The role of silicon in regulating physiological and biochemical mechanisms of contrasting bread wheat cultivars under terminal drought and heat stress environments
Waseem Ashfaq, Sigfredo Fuentes, Graham Brodie and Dorin Gupta

71 Transcriptomic and metabolomic reveals silicon enhances adaptation of rice under dry cultivation by improving flavonoid biosynthesis, osmoregulation, and photosynthesis
Hao Jiang, Ze Song, Qing-Wang Su, Zhi-Heng Wei, Wan-Chun Li, Zi-Xian Jiang, Ping Tian, Zhen-Hui Wang, Xue Yang, Mei-Ying Yang, Xiao-Shuang Wei and Zhi-Hai Wu

89 Genome-Wide Identification and Functional Analysis of Polyamine Oxidase Genes in Maize Reveal Essential Roles in Abiotic Stress Tolerance
Yan Xi, Wenjing Hu, Yue Zhou, Xiang Liu and Yexiong Qian

108 Exogenous silicon alleviates the adverse effects of cinnamic acid-induced autotoxicity stress on cucumber seedling growth
Jian Lyu, Ning Jin, Xin Meng, Li Jin, Shuya Wang, Xuemei Xiao, Zeci Liu, Zhongqi Tang and Jihua Yu

121 Systemic regulation of soybean nodulation and nitrogen fixation by nitrogen via isoflavones
Xiaochen Lyu, Chunyan Sun, Tao Lin, Xuelai Wang, Sha Li, Shuhong Zhao, Zhenping Gong, Ziwei Wei, Chao Yan and Chunmei Ma

133 Genome-wide analysis of HSP20 gene family and expression patterns under heat stress in cucumber (*Cucumis sativus* L.)
Junjun Huang, Zhaoxin Hai, Ruoyi Wang, Yuanyuan Yu, Xin Chen, Weihong Liang and Huahua Wang

147 Characterization of NAC transcription factor NtNAC028 as a regulator of leaf senescence and stress responses
Lichao Wen, Tao Liu, Zhichao Deng, Zenglin Zhang, Qi Wang, Weifeng Wang, Wei Li and Yongfeng Guo

161 CRISPR/Cas9 mediated gene-editing of *GmHdz4* transcription factor enhances drought tolerance in soybean (*Glycine max* [L.] Merr.)
Xuanbo Zhong, Wei Hong, Yue Shu, Jianfei Li, Lulu Liu, Xiaoyang Chen, Faisal Islam, Weijun Zhou and Guixiang Tang

176 Physiological and transcriptome analyses reveal the photosynthetic response to drought stress in drought-sensitive (Fengjiao) and drought-tolerant (Hanjiao) *Zanthoxylum bungeanum* cultivars
Haichao Hu, Beibei He, Lei Ma, Xin Chen, Peilin Han, Yingli Luo, Yonghong Liu, Xitong Fei and Anzhi Wei

193 Rice protein phosphatase 1 regulatory subunits OsINH2 and OsINH3 participate actively in growth and adaptive responses under abscisic acid
Sawaira Jadoon, Qianqian Qin, Weiqiang Shi, Yan Longfeng and Suiwen Hou

211 Combined transcriptome and metabolome reveal glutathione metabolism plays a critical role in resistance to salinity in rice landraces HD961
Shan Yang, Mengshuang Liu, Na Chu, Guanxiu Chen, Panpan Wang, Junjie Mo, Haifeng Guo, Jianghuan Xu and Hongkai Zhou

228 Abscisic acid: Metabolism, transport, crosstalk with other plant growth regulators, and its role in heavy metal stress mitigation
Sandeep Kumar, Sajad Hussain Shah, Yerramilli Vimala, Hanuman Singh Jatav, Parvaiz Ahmad, Yinglong Chen and Kadambot H. M. Siddique

243 Transcriptome data reveal gene clusters and key genes in pepper response to heat shock
Bingqian Tang, Xiumin Li, Xinhao Zhang, Qinbiao Yin, LingLing Xie, Xuexiao Zou, Feng Liu and Xiongze Dai

258 Integration of mRNA and microRNA analysis reveals the molecular mechanisms underlying drought stress tolerance in maize (*Zea mays* L.)
Peng Jiao, Ruiqi Ma, Chunlai Wang, Nannan Chen, Siyan Liu, Jing Qu, Shuyan Guan and Yiyong Ma

275 Comparative physiological, transcriptomic, and WGCNA analyses reveal the key genes and regulatory pathways associated with drought tolerance in Tartary buckwheat
Heng-Ling Meng, Pei-Yuan Sun, Jia-Rui Wang, Xiao-Qian Sun, Chuan-Zhi Zheng, Ting Fan, Qing-Fu Chen and Hong-You Li

297 Genetic variation for effects of drought stress on yield formation traits among commercial soybean [*Glycine max* (L.) Merr.] cultivars adapted to Ontario, Canada
Michael Gebretsadik Gebre, Istvan Rajcan and Hugh James Earl

312 Genomics and transcriptomics to protect rice (*Oryza sativa*. L.) from abiotic stressors: -pathways to achieving zero hunger
Mushtaq Ahmad

338 The end-use quality of wheat can be enhanced by optimal water management without incurring yield loss
Kun Sheng, Lina Xu, Mingxia Wang, Heng Lei and Aiwang Duan

355 Cotton straw biochar and compound *Bacillus* biofertilizer reduce Cd stress on cotton root growth by regulating root exudates and antioxidant enzymes system
Yongqi Zhu, Xin Lv, Tiansheng Li, Mingtao Zhong, Jianghui Song, Haijiang Wang and Jing Cui

370 Shading decreases lodging resistance of wheat under different planting densities by altering lignin monomer composition of stems
Yongli Luo, Yonglan Chang, Chunhui Li, Yuanyuan Wang, Haixing Cui, Min Jin, Zhenlin Wang and Yong Li

386 Integrating transcriptomic and metabolomic analysis in roots of wild soybean seedlings in response to low-phosphorus stress
Mingxia Li, Ji Zhou, Xianyu Lang, Defu Han, Yongjun Hu, Yinan Ding, Guangye Wang, Jixun Guo and Lianxuan Shi

404 Brassinolide improves the tolerance of *Malus hupehensis* to alkaline stress
Zhijuan Sun, Yawen Zou, Cheng Xie, Lei Han, Xiaodong Zheng, Yike Tian, Changqing Ma, Xiaoli Liu and Caihong Wang

418 Regulation of salt tolerance in the roots of *Zea mays* by L-histidine through transcriptome analysis
Hongfei Ji, Guoping Yang, Xiu Zhang, Qiumei Zhong, Yuxi Qi, Kaihua Wu and Tingting Shen

435 Spermidine exogenous application mollifies reproductive stage heat stress ramifications in rice
Sourabh Karwa, Jyoti Taunk, Sadhana Maurya, Adhip Das, G. K. Krishna, Sunder Singh Arya, Awadhesh Kumar, Sudhir Kumar, Pramod Kumar, Viswanathan Chinnusamy and Madan Pal

452 Impacts of drought and elevated temperature on the seeds of malting barley
Manuela Nagel, Erwann Arc, Loïc Rajjou, Gwendal Cueff, Marlene Bailly, Gilles Clément, Inmaculada Sanchez-Vicente, Christophe Bailly, Charlotte E. Seal, Thomas Roach, Hardy Rolletschek, Oscar Lorenzo, Andreas Börner and Ilse Kranner

466 Physio-biochemical and molecular stress regulators and their crosstalk for low-temperature stress responses in fruit crops: A review
Amit Kumar Goswami, Naveen Kumar Maurya, Suneha Goswami, Kirti Bardhan, Sanjay Kumar Singh, Jai Prakash, Satyabrata Pradhan, Amarjeet Kumar, Viswanathan Chinnusamy, Prabhat Kumar, Radha Mohan Sharma, Stuti Sharma, Deepak Singh Bisht and Chavlesh Kumar

484 Seasonal decline in leaf photosynthesis in perennial switchgrass explained by sink limitations and water deficit
Mauricio Tejera-Nieves, Michael Abraha, Jiquan Chen, Stephen K. Hamilton, G. Philip Robertson and Berkley James Walker

497 Transcriptomic and metabolic regulatory network characterization of drought responses in tobacco
Zhengrong Hu, Zexue He, Yangyang Li, Qing Wang, Pengfei Yi, Jiashuo Yang, Chenkai Yang, Gennadii Borovskii, Xuejiao Cheng, Risheng Hu and Wenli Zhang

513 Integrating linkage mapping and comparative transcriptome analysis for discovering candidate genes associated with salt tolerance in rice
Leiyue Geng, Wei Zhang, Tuo Zou, Qi Du, Xiaoding Ma, Di Cui, Bing Han, Qixing Zhang and Longzhi Han

529 The persistent impact of drought stress on the resilience of summer maize
Lanshu Jing, Baisha Weng, Denghua Yan, Shanjun Zhang, Wuxia Bi and Siying Yan

543 Targeted and untargeted metabolomics reveals deep analysis of drought stress responses in needles and roots of *Pinus taeda* seedlings
Chu Wu, Yun Wang and Honggang Sun

570 Metabolic imprint induced by seed halo-priming promotes a differential physiological performance in two contrasting quinoa ecotypes
Leonardo Cifuentes, Máximo González, Katherine Pinto-Irish, Rodrigo Álvarez, Teodoro Coba de la Peña, Enrique Ostria-Gallardo, Nicolás Franck, Susana Fischer, Gabriel Barros, Catalina Castro, José Ortiz, Carolina Sanhueza, Néstor Fernández Del-Saz, Luisa Bascunan-Godoy and Patricio A. Castro

585 Effects of high night temperature on soybean yield and compositions
Lin Yang, Wenwen Song, Cailong Xu, Enoch Sapey, Dong Jiang and Cunxiang Wu

598 MicroRNA162 regulates stomatal conductance in response to low night temperature stress *via* abscisic acid signaling pathway in tomato
Yangyang Li, Yang Liu, Zhenhua Gao, Feng Wang, Tao Xu, Mingfang Qi, Yufeng Liu and Tianlai Li

frontiers | Frontiers in Plant Science

TYPE Editorial
PUBLISHED 22 September 2023
DOI 10.3389/fpls.2023.1278895

Check for updates

OPEN ACCESS

EDITED AND REVIEWED BY
Luisa M. Sandalio,
Spanish National Research Council (CSIC), Spain

*CORRESPONDENCE
Bhaskar Gupta
bhaskarzoology@gmail.com;
bhaskar.zoology@singurgovtcollege.org

RECEIVED 17 August 2023
ACCEPTED 12 September 2023
PUBLISHED 22 September 2023

CITATION
Gupta B and Shrestha J (2023) Editorial: Abiotic stress adaptation and tolerance mechanisms in crop plants.
Front. Plant Sci. 14:1278895.
doi: 10.3389/fpls.2023.1278895

COPYRIGHT
© 2023 Gupta and Shrestha. This is an open-access article distributed under the terms of the Creative Commons Attribution License (CC BY). The use, distribution or reproduction in other forums is permitted, provided the original author(s) and the copyright owner(s) are credited and that the original publication in this journal is cited, in accordance with accepted academic practice. No use, distribution or reproduction is permitted which does not comply with these terms.

Editorial: Abiotic stress adaptation and tolerance mechanisms in crop plants

Bhaskar Gupta[1]* and Jiban Shrestha[2]

[1]Department of Zoology, Government General Degree College, Singur, West Bengal, India, [2]Nepal Agricultural Research Council, National Plant Breeding and Genetics Research Centre, Khumaltar, Lalitpur, Nepal

KEYWORDS

abiotic stress, drought, omics, polyamine, stress adaptation

The Editorial on the Research Topic
Abiotic stress adaptation and tolerance mechanisms in crop plants

A major challenge for world agriculture involves the production of 60% more food crop to feed 9.3 billion people worldwide by 2050 (UN, 2012). In recent years, the escalating threat of climate change and its associated environmental stresses (osmotic stress, drought, UV-B radiation, mineral nutrient deficiency, pH variation, metal toxicity and extreme temperatures like heat waves and cold waves have significantly impacted the growth, survival, longevity, reproduction, and global productivity of crop plants (Redondo-Gómez, 2013). Abiotic stress involves modulations in various physiological and metabolic processes, depending on the severity and duration of the stress, and eventually inhibits crop production. To adapt to these hostile environmental cues, plants have developed various physiological and biochemical mechanisms, which include, but are not limited to; (1) ion homeostasis and compartmentalization; (2) ion transport and uptake; (3) biosynthesis of osmoprotectants and compatible solutes' (4) activation of antioxidant enzyme and synthesis of antioxidant compounds; (5) synthesis of polyamines; (6) generation of nitric oxide (NO); (7) hormone modulation; and (8) expression of stress regulatory genes (Ghosh and Xu, 2014; Gupta and Huang, 2014; Saha et al., 2015; Hasanuzzaman, 2020; Zhang et al., 2022). These adaptive responses help plants survive and recover from stress, while non-adaptive responses result in damage or dysfunction (Zhang et al., 2022).

The Research Topic titled "*Abiotic stress adaptation and tolerance mechanisms in crop plants*," explores cutting-edge research on mechanisms that allow crop plants adapt to and tolerate abiotic stresses. This editorial aims to provide an overview and critical analysis of the book's contents, which include 35 original research articles and 3 review articles, highlighting the key insights and advancements made in this field. The book explores key topics such as molecular responses, genetic aspects, physiological adjustments, biochemical signals and agronomic strategies that enable crops to cope with adverse environmental conditions.

1 Transcriptomics, genomics and metabolomics: unveiling pathways and plant stress responses

Transcriptomics and genomics are two fields of study that use different methods and data to understand the molecular biology of plants. Rice (*Oryza sativa* L.) is a major food crop for almost half of the world population. In this Research Topic, Ahmad demonstrated that the identification of numerous important QTL genes, promoter elements, transcription factors and miRNAs involved in rice response to abiotic stress was made possible by a spectrum of genomic and transcriptomic techniques. In fact, multiple "omics" approaches have emerged as successful technologies for plant systems over the last few decades (Yang et al., 2021).

The study by Li et al. focused on analyzing the roots of two different wild soybean seedling ecotypes to understand how they adapt to low-phosphorus (P) stress. The study found that one of the ecotypes, barren-tolerant wild soybean (GS2), enhanced soil P uptake through mechanisms such as increasing root length, promoting the synthesis and secretion of lignin and organic acids, and upregulating certain genes [inorganic phosphate transporter (PHT1-2 and PHT1-3), acid phosphatase (ACP1), and purple acid phosphatase] related to phosphate transport and phosphatase activity. This helped maintain stable P content in plants, and thus better adaptation to low-P stress. Additionally, GS2 showed increased activities of pectin esterase and phospholipase C to reuse structural P, generated sulfoquinovosyl diacylglycerol to maintain biofilm structure stability, and enhanced the synthesis of antioxidants like anthocyanins to reduce oxidative damage due to P deficiency. The study identified specific transcription factors (HSFA6b and MYB61) as key regulators in the resistance of barren-tolerant wild soybeans to low-P stress. Overall, this research offers insights into plant adaptation to different P levels and provides quantitative parameters for resource evaluation.

The comparative transcriptome analysis of drought-tolerant and drought-sensitive genotypes of 'tartary buckwheat', under field soil drought stress, was performed by Meng et al., utilizing the weighted gene co-expression network analysis (WGCNA) data mining tools (Langfelder and Horvath, 2008), which revealed key genes and metabolomic pathways involved in tartary buckwheat drought tolerance. Furthermore, Ji et al., through detailed transcriptome analysis, demonstrated the regulation of salt tolerance in the roots of *Zea mays* by L-histidine, one of the standard amino acids in proteins and critical for plant growth and development. Hu et al. did a comprehensive transcriptomic and metabolic regulatory network characterization of drought responses in tobacco, which could pave the way for engineering manipulation for breeding new tobacco varieties with enhanced drought tolerance. The strategy of integrating linkage mapping and comparative transcriptome analysis has been deployed by Geng et al. to discover candidate genes associated with salt tolerance in rice. Wu et al. measured changes in metabolite levels in the roots and needles of pine (*Pinus taeda*) seedlings under long-term drought stress, and identified major metabolic pathways in pine seedlings related to drought stress. This work lays the foundation for understanding the metabolic mechanisms of drought tolerance in coniferous species.

Priming is a strategy to change the performance of seeds to cope with stress. Halopriming applied to seeds triggers plant stress memory, preventing the deleterious impact of abiotic stresses such as drought and salinity (Pagano et al., 2023). In a study on two contrasting Chilean quinoa ecotypes (*Chenopodium quinoa*), Cifuentes et al. showed that metabolic imprint induced by seed halo-priming promotes a differential physiological performance in two contrasting quinoa ecotypes.

Drought and salt stress are serious threats to crop productivity worldwide and identification of genetic, biochemical, and molecular cues for increasing plant adaptation is of paramount significance. Chen et al. demonstrated that purple stem *Brassica napus* plants, in comparison to green stem ones, exhibits higher photosynthetic efficiency, antioxidant potential and anthocyanin biosynthesis - related gene expression against drought stress. Based on their findings, it can be concluded that green stem genotypes are more sensitive to drought stress than their purple stem counterparts. Furthermore, this research article also provides practical guidance for plant biologists who are developing stress-tolerant crops by using anthocyanin biosynthesis or regulatory genes. Betaine aldehyde dehydrogenase (BADH) is a key enzyme in the synthesis of the osmotic regulator betaine in wheat. Overexpression of *TaBADH* (*T. aestivum* L.) in *Arabidopsis* was found to enhance betaine accumulation and salt tolerance (Sun et al., 2019). Yu et al. cloned a region of the *TaBADH-A1* promoter and genomic DNA that included the introns and exons, from four Chinese wheat cultivars. The authors have found seven haplotypes of the *TaBADH-A1* gene in wheat, the seven haplotypes were divided with 254 bp indel into two alleles. The expression level of *BADH-A1b* was shown to be significantly higher than that of *BADH-A1a* under drought and salt stress. *BADHA1b* increased the betaine content of wheat and further enhanced its drought resistance and salt tolerance. *BADH-A1b*, on the contrary, had no effect on the agronomic traits of wheat grown under normal conditions. This study provides evidence indicating that *BADH-A1b* could be an excellent candidate allele for breeding to improve the drought resistance and salt tolerance of wheat. The study of Jiao et al. describes the miRNA–mRNA analysis and molecular mechanisms involved in drought response in the maize root system. Moreover, four metabolic pathways, namely, "plant hormone signal transduction", "phenylpropane biosynthesis", "glutathione metabolism", and "starch and sucrose metabolism", were predicted to have important roles in the response of the maize root system to drought. Jing et al. conducted field experiments to quantitatively describe the persistent effects of drought on summer maize growth indexes and yield. Furthermore, Jing et al. constructed the comprehensive resilience assessment method based on the growth indexes and quantitatively analyzed the resilience under different drought degrees and durations. Gebre et al. showed that currently cultivated commercial soybean [*Glycine max* (L.) Merr.] cultivars grown in Canada (Ontario) differ significantly in their response to drought stress in terms of their growth, yield and yield components (pod number, seeds per pod, single-seed weight). Lignin is a complex phenolic compound, which is an important component of the plant cell wall. The effects of low-light stress on lignin metabolism, and

lignin monomer composition, as well as their relationships with lodging resistance, have been explored by Luo et al.

2 Addressing other abiotic stressors

Heavy metal stress causes devastating losses in crop productivity and affects ecology and human health worldwide. Plants try to overcome and adapt to heavy metal toxicity to survive because it adversely affects plant growth, development, reproduction, physiological-biochemical processes, and crop productivity by disturbing cellular ionic balance, metabolic balance, cell membrane integrity, and protein and enzyme activities. The role of ABA in plant abiotic stress signaling and adaptation is well established. Kumar et al. have done an exhaustive review of ABA metabolism, transport, crosstalk with other plant growth regulators, and its role in heavy metal stress mitigation. Toxic metal-induced overaccumulation of anthocyanin in plants can oxidize proteins and break DNA. Here, a study by Zhang et al. presents the latest evidence to update the positive role of exogenous proline in regulating jasmonate signals and activating the MYB-bHLH-WDR complex to repress anthocyanin accumulation in rice plants under Cr(VI) stress. Additionally, Zhu et al. demonstrated that cotton straw biochar and compound *Bacillus* biofertilizer reduce Cd stress on cotton root growth by regulating the antioxidant enzyme system, the pathways of ABC transporters and phenylalanine metabolism and root exudates. The effect of Zn-lysine and biochar (alone and in combination) on the growth and physiology of wheat (*Triticum aestivum* L.) to alleviate salinity stress has been studied comprehensively by Aibdin et al. Their results indicate that Zn-lysine and biochar alone and in combination enhanced the biomass of wheat, improved the antioxidant activity in leaves and assisted the nutrient uptake by wheat plants under salt stress.

The implication of silicon in regulating physiological and biochemical mechanisms of contrasting bread wheat cultivars under terminal drought and heat stress environments has been studied by Ashfaq et al. Their research shows that silicon treatment has the potential to mitigate the detrimental effects of individual and combined stress of drought stress, heat stress, and drought-heat stress at an early grain-filling stage in susceptible and tolerant wheat cultivars in a controlled environment. Another study on silicon, using transcriptomic and metabolomic data reveal that silicon enhances the adaptation of rice under dry cultivation by improving flavonoid biosynthesis, osmoregulation, and photosynthesis (Jiang et al.). The authors claimed that the establishment of the system for increasing the yield of rice under dry cultivation provides theoretical and technical support, thereby promoting the rapid development of rice in Northeast China, and ensure national food security. Autotoxicity is a key factor that leads to obstacles in continuous cropping systems, which refers to the phenomenon where the successive planting of the same crop on the same land leads to a decline in crop yield and quality (Xiao et al., 2019). Lyu et al. show that exogenous silicon alleviates the adverse effects of cinnamic acid-induced autotoxicity stress on cucumber seedling growth. Brassinosteroid hormones multitask to smoothly regulate a wide array of vital physiological and biochemical processes in plants, and have been found to play a significant role is diverse plant abiotic stresses, including salt and alkali stress (Chaudhuri et al., 2022). Sun et al. elaborated on the information available on the main mechanisms underlying plant tolerance to abiotic stress by further analyzing the mechanism of exogenous analog brassinolide in improving the alkaline tolerance of apple plants (*Malus hupehensis*).

The evaluation of irrigation water efficiency plays an important role in the efficient use of agricultural water resources and the sustainable development of agriculture (Dong et al., 2020). Notably, regulated deficit irrigation, a water-saving irrigation method widely adopted in China, can be employed to reduce water consumption without causing a significant wheat yield loss (Sheng et al.). Tejera-Nieves et al. discussed the underlying mechanism and revealed that the seasonal decline in leaf photosynthesis in perennial switchgrass (*Panicum virgatum* L.) can be explained by sink limitations and water deficits.

3 Polyamines: growth regulators and stress responders

Polyamines are critical players in growth, developmental processes and stress responses in plants (Gupta et al., 2013; Gupta et al., 2016; Sengupta et al., 2016; Chen et al., 2019). Here, whole genome-wide screening of polyamine oxidase *(PAO)* genes in maize was done by Xi et al. and nine *ZmPAO* genes were identified in this study, named as *ZmPAO1-9*. Extensive functional analysis of these *PAO* genes established their essential roles in abiotic stress tolerance (heat, drought, and salinity stress). The symbiotic relationship between soybean (*Glycine max* L.) and rhizobium to form root nodules, which can fix nitrogen from the air for their own growth, is well established (Mulder et al., 2005). Lyu et al., in their research article, have proposed the systemic regulation of soybean (*Glycine max* L.) nodulation and nitrogen fixation by nitrogen via isoflavones. Heat shock proteins (HSPs) are evolutionarily conserved, ancient intracellular molecular chaperones that widely exist in almost all organisms (Dattilo et al., 2015). When organisms are subjected to environmental stresses, HSPs have been shown to improve the adaptation of organisms to stress by stabilizing the cell structure, transporting, and folding auxiliary proteins and maintaining cell function (Gupta and Huang, 2014; Yadav et al., 2021). Huang et al. have done genome-wide analysis of HSP20 gene family in cucumber (*Cucumis sativus* L.) and studied their expression patterns under heat stress. These findings are expected to provide a reference for revealing the role of HSP family members in cucumber development regulation and stress response and serve as molecular resources for further cultivating new varieties that are resistant to high temperatures. The NAC (NAM, ATAF1/2, and CUC2) transcription factor family is one of the largest families of transcription factors in plants. NAC transcription factors are named after no apical meristem (NAM) proteins found in *Petunia* hybrids, *Arabidopsis* transcription activation factor (ATAF1/2) proteins, and cup-shaped cotyledon (CUC2) proteins of *A. thaliana* (Jiang et al., 2021). Wen et al. in their study found that a tobacco *NAC* gene (*NtNAC028)* was rapidly upregulated in response to high salinity,

dehydration, and abscisic acid (ABA) stresses, suggesting a vital role of this gene in abiotic stress response. *NtNAC028* loss-of-function tobacco plants generated *via* CRISPR-Cas9 showed delayed leaf senescence and increased tolerance to drought and salt stresses. Further mutation and overexpression analysis revealed that *NtNAC028* might act as a vital regulator for plant stress response likely by mediating ROS scavenging ability. The study by Karwa et al. analyzed the impact of heat stress on rice growth and yield metrics and demonstrated the ameliorating effect of exogenous spermidine application in inducing heat stress tolerance in rice at the reproductive stage.

4 Harnessing molecular tools for stress adaptation

The ground-breaking gene editing tool, CRISPR/Cas9 (clustered regularly interspaced short palindromic repeats/CRISPR-associated protein 9), has opened new and exciting avenues for the analysis of gene function. While the original methodology dealt with targeted gene disruption, recent technological research advancements have yielded a wide spectrum of tools to modify genes and gene expression in various ways (Horodecka and Düchler, 2021). Here, Zhong et al. have utilized the CRISPR/Cas9 mediated gene-editing tool to identify and comprehensively analyze the drought tolerance potential of Soybean *(G. max [L.] Merr.) GmHdz4* transcription factor gene. Hu et al. investigated the influence of drought stress on photosynthetic parameters, stomatal status, and chlorophyll content of two different cultivars of an economically and medicinally important plant species, *Zanthoxylum bungeanum*, with contrasting drought tolerance phenotype. The role of rice protein phosphatase 1 regulatory subunits in growth and abscisic acid (ABA) mediated abiotic stress signaling was extensively studied by Jadoon et al. They have established that rice OsINH2 and OsINH3, the homologs of *Arabidopsis* INH2 and INH3 respectively, actively participate in the reproductive growth of rice, regulate ABA-mediated inhibition of seed germination, and contribute to ROS homeostasis. Recently, the research article by Cimini et al. (2022) has highlighted the multifactorial regulation of glutathione metabolism behind salt tolerance in rice.

An integrative analysis of transcriptome and metabolome explored (Yang et al.) the relationship between differentially expressed genes (DEGs) and significantly regulated metabolites (SRMs) under salt stress in two rice cultivars [HD961 (salt-tolerant) and 9311 (salt-sensitive)]. The HD961 cultivar showed enriched glutathione metabolism pathways, with specific SRMs and DEGs. Correlations were found between certain genes [16 genes (12 up-regulated genes and four down-regulated genes)] and metabolites (GSH, dehydroascorbic acid, L-cysteine) involved in glutathione metabolism, highlighting their potential roles in GSH synthesis under salt stress.

5 Temperature extremes and their implications for plant growth and productivity

Global warming, unpredictable weather patterns, and extreme temperatures have become more frequent, harnessing ever-increasing environmental stress challenges for plants. Such stress disrupts the normal growth and development of plants and is a major threat for food safety and security (Jagadish et al., 2021). Understanding the primary molecular and physiological mechanisms that drive the adaptation of crop plants to various abiotic stresses is crucial to bridge the knowledge gap in this area. Yang et al. evaluated the effect of high night temperature on the yield and seed compositions of soybean during seed filling stage and analyzed the dynamic changes in photosynthetic physiological characteristics, dry matter accumulation and non-structural carbohydrates linked to stress tolerance triggered by high night temperature. Yang et al. have argued that in the context of global warming, breeding soybean varieties with low respiration and high energy efficiency is one of the most important ways to effectively address the world food crisis. Goswami et al., in their review article, delved into recent insights of physio-biochemical and molecular stress regulators and their crosstalk for low- temperature stress responses in fruit crops. The regulatory function of non-coding small RNAs, especially miRNAs, in tomato plants has been comprehensively explored by Li et al. miRNAs are endogenous non-coding small RNAs that participate in plant development, organ formation, signal transduction, and stress response (Cai et al., 2009). Li et al. constructed small RNA libraries from wild-type tomato plants and ABA-deficient mutant plants under normal growth and low- night temperature stress conditions. They demonstrated that miRNA162 regulates stomatal conductance through regulation of the abscisic acid (ABA) signaling pathway in tomato. To study the genome-wide gene expression under heat, Tang et al. performed a time-course (0.5 to 24 h) transcriptome analysis in the leaf and root of 40-day-old pepper plants under control and 40 °C. Comparative transcriptome analysis between the heat-treated and control plants identified differentially expressed genes, which showed the largest degree of change at 24 h. Interestingly, their work revealed that more differentially expressed genes were identified in the root than in the leaf. Additionally, Tang et al. analyzed the gene expression of 25 heat shock factor genes (HSFs) in pepper after heat stress, identified five of these HSFs that responded to heat stress, and characterized the role of these genes in heat-tolerant and heat-susceptible pepper lines. These findings are expected to improve the knowledge and understanding of the genome-wide heat stress response in pepper plants. High seed quality is a key to agricultural production, which is increasingly affected by climate change. Nagel et al. studied the effects of drought and elevated temperature on key seed quality traits of two malting barley (*Hordeum sativum* L.) genotypes during seed production and demonstrated that drought, but not elevated temperature, affected the metabolism of amino acids, organic acids, osmolytes and nitrogen assimilation in the malting barley seeds.

6 Conclusion and future directions

The abiotic stress adaptation and tolerance mechanisms in crop plants have become significant issues in the pursuit of global food security and sustainable agricultural practices. The Research Topic "*Abiotic Stress Adaptation and Tolerance Mechanisms in Crop Plants*" has provided a comprehensive exploration of the intricate interplay between plants and their environment, shedding light on the diverse strategies that crops employ to withstand and mitigate the detrimental effects of abiotic stresses.

In conclusion, the comprehensive exploration of abiotic stress adaptation and tolerance mechanisms in crop plants has provided valuable insights into the various strategies to cope with adverse environmental conditions. The growing challenges posed by climate change and its associated stressors demand innovative approaches to enhance crop productivity and ensure global food security. This specialty edition presents a thorough investigation into various aspects of abiotic stress response, including molecular, genetic, physiological, and metabolic processes. Through studies on transcriptomics, genomics, and metabolomics, researchers have unveiled intricate pathways and genes associated with stress tolerance. The integration of advanced techniques such as CRISPR/Cas9 gene editing has enabled targeted manipulation of stress-responsive genes, shedding light on their roles in conferring tolerance. The versatile role of polyamines as critical growth regulators in ameliorating plant abiotic stress is highlighted here. The interplay between different genes, metabolites, and pathways underscores the complexity of stress adaptation mechanisms. Moreover, studies on temperature extremes emphasize the urgency of addressing the impacts of global warming on plant growth and productivity. The research articles and reviews published in this Research Topic not only enhance our understanding of how plants respond to various stressors but also offer potential avenues for crop improvement through genetic engineering, breeding, and management practices. As the agricultural landscape evolves in the face of changing climates, these insights will guide future research and innovations aimed at developing resilient crop varieties that can thrive in adverse conditions and contribute to sustainable global food production.

6.1 Key insights and contributions

Throughout the Research Topic, the intricate mechanisms underlying the adaptation and tolerance of crop plants to abiotic stresses have been meticulously dissected. From the molecular and physiological responses at the cellular level to the broader implications for crop productivity and resilience, the authors have skillfully presented a holistic view of the subject. Some of the key insights that have emerged from this exploration include.

6.1.1 Molecular signaling networks

This Research Topic emphasizes the pivotal role of intricate molecular signaling networks in orchestrating a plant's response to abiotic stresses. Through a detailed analysis of stress-responsive genes, transcription factors, and signaling pathways, readers have gained a deeper understanding of how plants perceive and transmit stress signals, ultimately influencing their adaptive strategies.

6.1.2 Metabolic and physiological adjustments

The Research Topic has highlighted the remarkable metabolic and physiological adjustments that plants undergo to counteract the adverse effects of abiotic stresses. From osmotic regulation to antioxidative defense mechanisms, these insights underscore the remarkable plasticity of crop plants and their capacity to reconfigure their internal systems in the face of challenges.

6.1.3 Genetic variation and breeding

The exploration of genetic diversity and breeding strategies has illuminated the potential for developing stress-tolerant crop varieties. By identifying key genetic determinants and employing advanced breeding techniques, researchers and practitioners are poised to harness the power of natural variation to create resilient and high-yielding crop cultivars.

6.1.4 Emerging technologies

The Research Topic has provided a glimpse into the future with its discussion of cutting-edge technologies such as genome editing, RNA interference, and omics approaches. These emerging tools offer unprecedented opportunities to engineer stress-tolerant crops with enhanced precision and efficiency.

6.2 Future directions

As we stand at the crossroads of scientific discovery and agricultural innovation, several advances may improve the study of abiotic stress adaptation and tolerance mechanisms in crop plants.

6.2.1 Integrating multi-omics approaches

The integration of genomics, transcriptomics, proteomics, and metabolomics holds the potential to unravel the intricacies of plant stress responses with unparalleled depth. Future research should strive to integrate multi-omics data to provide a holistic view of stress adaptation mechanisms.

6.2.2 Synthetic biology and engineering

The field of synthetic biology offers a unique opportunity to engineer plants with tailored stress tolerance traits. By designing and assembling novel biological components, researchers can create crops that exhibit enhanced resilience while minimizing undesirable side effects.

6.2.3 Climate-adaptive crop management

With the increasing unpredictability of climatic conditions, innovative crop management strategies are needed. Future research should focus on developing site-specific, climate-adaptive approaches that optimize crop performance under diverse stress scenarios.

6.2.4 Global collaboration for knowledge sharing

The challenges posed by abiotic stresses are not confined to a single region. Establishing global networks for knowledge sharing, data exchange, and collaborative research will facilitate the rapid dissemination of insights and solutions globally.

6.2.5 Ethical and regulatory considerations

As we venture into the realm of genetic engineering and synthetic biology, ethical and regulatory frameworks must be established to ensure responsible innovation and the sustainable deployment of stress-tolerant crop varieties.

In conclusion, the research presented in this Research Topic has provided a profound understanding of the strategies employed by plants to thrive in challenging environments. By collectively embracing the research avenues and future directions mentioned earlier, we can work towards a sustainable and resilient agricultural future that ensures global food security.

Author contributions

BG: Writing – review & editing, Methodology, Conceptualization, Writing – original draft. JS: Writing – review & editing.

Acknowledgments

Financial assistance from W.B. State DST (Govt. of West Bengal - G.O. No. 167 (Sanc)/ST/P/S&T/1G-12/2011 date 06.05.2013) and DBT (RGYI) (Govt. of India) are gratefully acknowledged.

Conflict of interest

The authors declare that the research was conducted in the absence of any commercial or financial relationships that could be construed as a potential conflict of interest.

Publisher's note

All claims expressed in this article are solely those of the authors and do not necessarily represent those of their affiliated organizations, or those of the publisher, the editors and the reviewers. Any product that may be evaluated in this article, or claim that may be made by its manufacturer, is not guaranteed or endorsed by the publisher.

References

Cai, Y., Yu, X., Hu, S., and Yu, J. (2009). A brief review on the mechanisms of miRNA regulation. *Genom. Proteomics Bioinform.* 7, 147–154. doi: 10.1016/S1672-0229(08)60044-3

Chaudhuri, A., Halder, K., Abdin, M. Z., Majee, M., and Datta, A. (2022). Abiotic stress tolerance in plants: brassinosteroids navigate competently. *Int. J. Mol. Sci.* 23, 14577. doi: 10.3390/ijms232314577

Chen, D., Shao, Q., Yin, L., Younis, A., and Zheng, B. (2019). Polyamine function in plants: metabolism, regulation on development, and roles in abiotic stress responses. *Front. Plant Sci.* 9. doi: 10.3389/fpls.2018.01945

Cimini, S., Locato, V., Giacinti, V., Molinari, M., and De Gara, L. (2022). A multifactorial regulation of glutathione metabolism behind salt tolerance in rice. *Antioxid. (Basel)* 11 (6), 1114. doi: 10.3390/antiox11061114

Dattilo, S., Mancuso, C., Koverech, G., Di Mauro, P., Ontario, M. L., Petralia, C. C., et al. (2015). Heat shock proteins and hormesis in the diagnosis and treatment of neurodegenerative diseases. *Immun. Ageing* 12, 20. doi: 10.1186/s12979-015-0046-8

Dong, L., Lihui, Z., Heng, L., Qiang, F., Mo, L., Faiz, M. A., et al. (2020). Optimization of irrigation water use efficiency evaluation indicators based on DPSIR-ISD model. *Water Supply* 20 (1), 83–94. doi: 10.2166/ws.2019.135

Ghosh, D., and Xu, J. (2014). Abiotic stress responses in plant roots: a proteomics perspective. *Front. Plant Sci.* 5. doi: 10.3389/fpls.2014.00006

Gupta, K., Dey, A., and Gupta, B. (2013). Plant polyamines in abiotic stress responses. *Acta Physiol. Plant* 35, 2015–2036. doi: 10.1007/s11738-013-1239-4

Gupta, B., and Huang, B. (2014). Mechanism of salinity tolerance in plants: physiological, biochemical, and molecular characterization. *Int. J. Genomics* 2014, 701596. doi: 10.1155/2014/701596

Gupta, K., Sengupta, A., Chakraborty, M., and Gupta, B. (2016). Hydrogen peroxide and polyamines act as double edged swords in plant abiotic stress responses. *Front. Plant Sci.* 7. doi: 10.3389/fpls.2016.01343

Hasanuzzaman, M. (2020). *Plant Ecophysiology and Adaptation under Climate Change: Mechanisms and Perspectives II: Mechanisms of Adaptation and Stress Amelioration* (Singapore: Springer Nature).

Horodecka, K., and Düchler, M. (2021). CRISPR/Cas9: principle, applications, and delivery through extracellular vesicles. *Int. J. Mol. Sci.* 22 (11), 6072. doi: 10.3390/ijms22116072

Jagadish, S. V. K., Way, D. A., and Sharkey, T. D. (2021). Plant heat stress: concepts directing future research. *Plant Cell Environ.* 44, 1992–2005. doi: 10.1111/pce.14050

Jiang, L., Sun, Q., Wang, Y., Chang, P., Kong, H., Luo, C., et al. (2021). Genome-wide identification and characterization of NAC genes in Brassica juncea var. *Tumida PeerJ.* 9, e11212. doi: 10.7717/peerj.11212

Langfelder, P., and Horvath, S. (2008). WGCNA: an r package for weighted correlation network analysis. *BMC Bioinf.* 9, 559. doi: 10.1186/1471-2105-9-559

Mulder, L., Hogg, B., Bersoult, A., and Cullimore, J. V. (2005). Integration of signalling pathways in the establishment of the legume-rhizobia symbiosis. *Physiol. Plant* 123, 207–218. doi: 10.1111/j.1399-3054.2005.00448.x

Pagano, A., Macovei, A., and Balestrazzi, A. (2023). Molecular dynamics of seed priming at the crossroads between basic and applied research. *Plant Cell Rep.* 42 (4), 657–688. doi: 10.1007/s00299-023-02988-w

Redondo-Gómez, S. (2013). "Abiotic and biotic stress tolerance in plants," in *Molecular Stress Physiology of Plants*. Eds. G. R. Rout and A. B. Das (New Delhi: Springer India), 1–20.

Saha, J., Brauer, E. K., Sengupta, A., Popescu, S. C., Gupta, K., and Gupta, B. (2015). Polyamines as redox homeostasis regulators during salt stress in plants. *Front. Environ. Sci.* 3. doi: 10.3389/fenvs.2015.00021

Sengupta, A., Chakraborty, M., Saha, J., Gupta, B., and Gupta, K. (2016). "Polyamines: osmoprotectants in plant abiotic stress adaptation," in *Osmolytes and Plants Acclimation to Changing Environment: Emerging Omics Technologies*. Eds. N. Iqbal, R. Nazar and N. A. Khan (New Delhi: Springer), 97–127.

Sun, Y. L., Liu, X., Fu, L. S., Qin, P., Li, T., Ma, X. F., et al. (2019). Overexpression of TaBADH increases the salt tolerance in Arabidopsis. *Can. J. Plant Sci.* 99, 546–555. doi: 10.1139/cjps-2018-0190

UN (2012). *Feeding the World Sustainably* (New York, NY: United Nations Chronicle). Available at: https://www.un.org/en/chronicle/article/feeding-world-sustainably.

Xiao, X., Cheng, Z., Lv, J., Xie, J., Ma, N., and Yu, J. (2019). A green garlic (Allium sativum L.) based intercropping system reduces the strain of continuous monocropping in cucumber (*Cucumis sativus* L.) by adjusting the micro-ecological environment of soil. *Peer J.* 7, e7267. doi: 10.7717/peerj.7267

Yadav, R., Juneja, S., and Kumar, S. (2021). Cross priming with drought improves heat-tolerance in chickpea (Cicer arietinum L.) by stimulating small heat shock proteins and antioxidative defense. *Environ. Sustain.* 4, 171–182. doi: 10.1007/s42398-020-00156-4

Yang, Y., Saand, M. A., Huang, L., Abdelaal, W. B., Zhang, J., Wu, Y., et al. (2021). Applications of multi-omics technologies for crop improvement. *Front. Plant Sci.* 12. doi: 10.3389/fpls.2021.563953

Zhang, H., Zhu, J., Gong, Z., and Zhu, JK. (2022). Abiotic stress responses in plants. *Nat. Rev. Genet.* 23, 104–119. doi: 10.1038/s41576-021-00413-0

frontiers | Frontiers in Plant Science

TYPE Original Research
PUBLISHED 28 July 2022
DOI 10.3389/fpls.2022.936696

Check for updates

OPEN ACCESS

EDITED BY
Jiban Shrestha,
Nepal Agricultural Research Council, Nepal

REVIEWED BY
Juan B. Arellano,
Spanish National Research Council (CSIC), Spain
Manish Kumar Patel,
Agricultural Research Organization (ARO), Israel

*CORRESPONDENCE
Weijun Zhou
wjzhou@zju.edu.cn
Muhammad Ahsan Farooq
ahsanfarooq143@yahoo.com

SPECIALTY SECTION
This article was submitted to Plant Abiotic Stress, a section of the journal Frontiers in Plant Science

RECEIVED 05 May 2022
ACCEPTED 04 July 2022
PUBLISHED 28 July 2022

CITATION
Chen W, Miao Y, Ayyaz A, Hannan F, Huang Q, Ulhassan Z, Zhou Y, Islam F, Hong Z, Farooq MA and Zhou W (2022) Purple stem *Brassica napus* exhibits higher photosynthetic efficiency, antioxidant potential and anthocyanin biosynthesis related genes expression against drought stress.
Front. Plant Sci. 13:936696.
doi: 10.3389/fpls.2022.936696

COPYRIGHT
© 2022 Chen, Miao, Ayyaz, Hannan, Huang, Ulhassan, Zhou, Islam, Hong, Farooq and Zhou. This is an open-access article distributed under the terms of the Creative Commons Attribution License (CC BY). The use, distribution or reproduction in other forums is permitted, provided the original author(s) and the copyright owner(s) are credited and that the original publication in this journal is cited, in accordance with accepted academic practice. No use, distribution or reproduction is permitted which does not comply with these terms.

Purple stem *Brassica napus* exhibits higher photosynthetic efficiency, antioxidant potential and anthocyanin biosynthesis related genes expression against drought stress

Weiqi Chen[1], Yilin Miao[2], Ahsan Ayyaz[1], Fakhir Hannan[1], Qian Huang[1], Zaid Ulhassan[3], Yingying Zhou[1], Faisal Islam[3], Zheyuan Hong[3], Muhammad Ahsan Farooq[3]* and Weijun Zhou[1]*

[1]Institute of Crop Science, Ministry of Agriculture and Rural Affairs Key Laboratory of Spectroscopy Sensing, Zhejiang University, Hangzhou, China, [2]Agricultural Technology and Water Conservancy Service Center, Jiaxing, China, [3]Institute of Crop Science, Zhejiang Key Laboratory of Crop Germplasm, Zhejiang University, Hangzhou, China

Purple-stem *Brassica napus* (*B. napus*) is a phenotype with unique color because of its high anthocyanins content. Anthocyanins are naturally occurring plant pigments that have antioxidants activity and play important role in plant defense against abiotic and biotic stresses. In the present study, drought induced effects on plants were investigated in hydroponically grown seedlings of green stem (GS) and purple stem (PS) genotypes of *B. napus*. The results of this study showed that the major function of anthocyanins accumulation during drought was to enhance the antioxidant capability and stress tolerance in *B. napus* plants. Our results showed that drought significantly inhibited the plant growth in terms of decreased biomass accumulation in both genotypes, although marked decline was observed in GS genotype. The reduction in photosynthetic attributes was more noticeable in the GS genotype, whereas the PS genotype showed better performance under drought stress. Under stressful conditions, both the genotype showed excessive accumulation of reactive oxygen species (ROS) and malondialdehyde (MDA), as well as higher levels of antioxidant enzymes activities. Under drought conditions, the GS genotype showed apparent damages on chloroplast deformation like in thylakoid membrane and grana structural distortion and fewer starch grains and bigger plastoglobuli. Moreover, during drought stress, the PS genotype exhibited maximum expression levels of anthocyanins biosynthesis genes and antioxidant enzymes accompanied by higher stress tolerance relative to GS genotype. Based on these findings, it can be concluded that GS genotype found more sensitive to drought stress than the PS genotype. Furthermore this research paper also provides practical guidance for plant biologists who are developing stress-tolerant crops by using anthocyanin biosynthesis or regulatory genes.

KEYWORDS

antioxidant enzyme activities, drought, photosynthesis, gas exchange, microscopic study, purple and green stem oilseed rape, reactive oxygen species

Introduction

Abiotic stresses are the global challenges that have a significant impact on plant growth and yield attributes (Ahanger et al., 2019). Drought stress has been identified as one of the most severe abiotic stress in the last 40 years than any other natural hazard (Ahanger et al., 2018). Drought is a complex natural phenomenon with varying intensities, durations, regional extents, and consequences. Water deficiency inhibits the cell division, leaf surface, stems growth, cause root cell proliferation, increases reactive oxygen species (ROS) levels and impairs plant growth features (Farooq et al., 2016). Drought is predicted to become more frequent and last longer as a result of global climate change, which may leads to the death of drought-vulnerable plants and have a detrimental impact on global food security (Grieco et al., 2020).

Crop plant exhibits a different range of sensitivity to water stress (Ahanger et al., 2017; Begum et al., 2020). Drought stress damage may affect the opening and closing of plant stomata, osmotic homeostasis, antioxidant system, hormone signal transduction, light protection and metabolic pathway (Shi et al., 2018). Due to the reduction of stomatal closure and CO_2 diffusion, drought stress reduces the photosynthetic capacity of leaves, lead to ions imbalance, seriously affect the growth and development of plants and reduce crop yield (Ayyaz et al., 2021). Under environmental stressful conditions, photorespiration pathways, photosynthetic machinery and mitochondrial respiration primarily generate the ROS in plant cell. Excess ROS production results in oxidative stress, which disrupts plant cellular metabolism including photosynthetic efficiency, mineral transport and assimilation (Ahmad et al., 2019). To scavenge ROS production, plants activate their antioxidants defense system in the form of enzyme activities such as superoxide dismutase (SOD), peroxidase (POD), catalase (CAT), ascorbate peroxidase (APX), and glutathione reductase (GR) (Khadka et al., 2020). Furthermore, accumulation of secondary metabolites (such as anthocyanins, phenylpropanoids, and terpenoids) boosts antioxidant capabilities and lowers the oxidative stress (He et al., 2017; Ahanger et al., 2019).

Anthocyanins are naturally occurring compounds that are synthesized through biosynthesis of flavonoids. They are responsible for plant pigmentation and grant special colors (including blue, purple and red) to different plant tissues. Anthocyanins are mostly produced in vegetative tissues in response to environmental stress conditions such as low temperatures, pathogens attacks, nutritional deficiency, and heavy metals (He et al., 2020). There are evidences that anthocyanins may protect photosynthetic tissues from photo-inhibition by absorbing blue-green light and therefore limiting the amount of light reaching the chloroplasts (Feild et al., 2001; Neill and Gould, 2003; Hughes et al., 2005; Merzlyak et al., 2008). Flavonoids, like as anthocyanins, are potent antioxidants, raising the possibility that they might scavenge the excess ROS generated during photosynthesis, especially under photoinhibition conditions. Anthocyanins are often present in vacuoles near ROS generation sites (Hatier and Gould, 2008). ROS such as H_2O_2 may move rapidly across membranes, various cell compartments, and vacuoles during abiotic stress (Yamasaki et al., 1997; Mittler et al., 2004). Given their antioxidant characteristics, anthocyanins protect the plants against growth retardation and cell death by lowering oxidative stress by scavenging abiotic stress-induced ROS, allowing plants to respond to abiotic stress (Petrussa et al., 2013; Naing et al., 2017; Ai et al., 2018; Wang et al., 2018).

Numerous attempts have been made to increase the anthocyanin in plant tissues (Schwinn et al., 2014). For example, PAP1 gene (*AtPAP1*) is known as the main component of anthocyanin biosynthesis in *Arabidopsis*. The expression of *AtPAP1* genes in tobacco plants resulted in red and purple pigmentations (He et al., 2020). Similarly, transgenic *Brassica napus* plants showed a 50-fold increase in pigmentation including cyanidin and pelargonidin and 5-fold increment in quercetin and sinapic acid (Li et al., 2010). *Brassica napus* is an herbaceous agricultural crop considered as a major cash crop due to its numerous commercial applications such as vegetable oil, animal fodder and biodiesel. In addition, only edible vegetable oil of *B. napus* contributes for about 12% of the global market (Channaoui et al., 2017). Although the green stem color in mustard is related to chlorophyll deposition and purple pigmentation is mostly associated with anthocyanin accumulation. In this study, the new purple stem mustard genotype gives an excellent opportunity to explore the mechanisms of anthocyanins function under drought stress in comparison to green stem mustard genotype. Therefore, we imposed water deficits and evaluated the effect of plant water status on (1) total anthocyanin content, (2) chlorophyll contents and photosystem II efficiency, (3) ROS accumulation and antioxidants mechanism, and (4) the transcriptional regulation of various defense and anthocyanin biosynthesis genes.

Materials and methods

Experimental design and growth conditions

Canola (*B. napus*) seeds were obtained from the College of Agriculture and Biotechnology, Zhejiang University, Hangzhou, China. The two genotypes are isolated from segregating populations of the same inbred line and are phenotypically stable after multiple generations of inbreeds. Seeds of these two genotypes were surface sterilized using 0.01% NaClO solution for 15 min followed by vigorous washing with distilled water. The seeds were incubated in darkness for 2 days and placed in growth chamber under control

conditions with 16-h photoperiod, the temperature of 24/16°C (day/night) in 300 mM m^{-2} s^{-1} intensity, and 60%–70% relative humidity. After 1 week of seed germination, the seedlings were shifted into one-liter plastic pots filled with half-strength Hoagland nutrient solution (pH 5.8), which contained the following macronutrients: 10 mM NO_3, 1 mM PO_4, 6 mM K, 5 mM Ca, 2 mM Mg, and 2 mM SO_4 and the following micronutrients: 50 μM Fe-EDTA, 230 μM H_3BO_3, 3.5 μM Zn, 1.85 μM MoO_4, 1.6 μM Cu, and 0.7 μM Mn (Dun et al., 2016) for acclimation. Followed by full strength nutrient solution after 1 week of culture. At the third leaf stage, the plants were exposed to drought stress with 10% PEG-6000 solution for 4 days and 8 days. After 8 days of treatment, full strength nutrient solution was used to rewater for 3 days. Each treatment has four pots and each pot has five plants. After treatment, samples were kept in liquid nitrogen and stored at –80°C for further analysis.

Morphological parameters

After 1 week of drought stress treatments, plants were separated into roots and shoots for biomass measurement. Plants were kept in an oven at 85°C until the seedlings become stable for dry weight determination (Momoh and Zhou, 2001).

Determination of chlorophyll and gas exchange parameters

The chlorophyll contents were measured by grinding the fresh mature leaf (0.2 g) in 80% acetone at normal room temperature. The mixture was centrifuged at 12,000 rpm for 20 min, and the supernatant was collected for absorbance by spectrophotometer (Hitachi F-4600) according to Arnon (1949).

The photosynthesis rate, stomatal conductance, and transpiration rate of fully matured leaves were evaluated between 9:00 to 11:00 h using a portable photosynthesis system (LI-COR LI-6400XT). Photosynthetic rate (Pn), stomatal conductance (Gs), intercellular CO_2 concentration (Ci), and transpiration rate (Tr) were determined on the top most fully expanded leaf. The fully expanded leaves were kept in a chamber at 1,000 μmol m^{-2} s^{-1} photon flux density, irradiance 100 w m^{-2} (400–700 nm) with a flow rate at 500 μmol s^{-1} with leaf temperature 28°C. The ambient CO_2 concentration was kept at 380 μmol CO_2 mol^{-1} air by keeping the vapor pressure deficit at 2.0 kPa.

Leaf relative water content (RWC) and electrolyte leakage analysis

The relative water content (RWC) of all the treatments was measured by randomly selecting the mature *Brassica* leaves and fresh weight (FW) was measured. The leaf turgid weight (TW) was measured after dipping the leaves in distilled water for 8 h. Later on, leaves were oven-dried at 70°C for 24 h and then dry weight (DW) was measured (Farooq et al., 2013). The RWC content was calculated by the following formula.

$$RWC = [(FW - DW) / (TW - DW)] \times 100.$$

Electrolytic leakage was measured by taking fresh leaf discs (1 disc =3 cm × 1 cm) after washing properly. Each leaf disc was added in falcon tube containing deionized water (4 ml). Tubes were shaken for 30 min and EC1 was measured on EC meter. Then, EC2 was measured after boiling the sample for 30 min (Dionisio-Sese and Tobita, 1998).

$$\text{Membrane stability index} = (EC1 / EC2) \times 100.$$

Chlorophyll fluorescence measurement

A handheld Fluorometer FP-110 (Photon System Instruments, Drasow, Czech Republic) was used to evaluate the photosystem II (PSII) efficiency. Before measurements, samples were put in dark-adaptation for 20 min. PSII fluorescence parameters include the maximum QY (Fv/Fm) of PSII, measured by the following formula Fv = (Fm – Fo). Leaf absorbance for PSI at 830 and 870 nm was balanced first. A weak red light was used to measure Fo and then a saturated pulse of 8,000 μmol $m^{-2}s^{-1}$ with 0.8 s width was applied to measure Fm and maximum QY (Fv/Fm) of PSII photochemistry. Various intensities of red actinic light was used which increased stepwise from 0, 11, 18, 27, 58, 100, 131, 221, 344, 536, and830 in 20 s intervals over 5 min. The non-photochemical dissipation of absorbed light energy (NPQ) was measured by the following equation NPQ = [(Fm–Fm′) / (Fm′)]. The gradients of photosynthetic active radiation (PAR) were kept as 0, 100, 200, 300, 400, and 600 μmol m^{-2} s^{-1}, respectively (Bilger and Björkman, 1991; Javed et al., 2022).

Histochemical analyses

The deposition of superoxide (O_2^-) and hydrogen peroxide (H_2O_2) were visualized by staining the plant leaves with nitro blue tetrazolium (NBT) and 3, 3-diaminobenzidine (DAB). The leaves were kept in dark for 24 h, and ROS accumulation can be visualized in the form of dark and brown spots on leaf surface (Romero-Puertas et al., 2004).

Membrane lipid peroxidation and reactive oxygen species (ROS) analysis

Malondialdehyde (MDA) is produced by lipid peroxidation and determined by TBA (thiobarbituric acid) reaction (Hong et al., 2010). Leaf tissues (0.5 g) were homogenized with 0.1% TCA (W/V) solution in pre-cooled pistil and mortar. The mixture was centrifuged at 12,000 × *g* for 15 min, and the extract was collected in separate tubes. The reaction solution containing 0.5 ml supernatant, 0.5 ml of 5% TBA and 20% TCA solution incubated in a water bath at 95°C temperature. The reaction stopped by

shifting the reaction solution in an ice bath. The absorbance was measured at 532 and 600 nm using spectrophotometer (Hitachi F-4600).

The H_2O_2 contents were observed according to the methodology of Chen et al. (2010). Leaf tissues (0.5 g) homogenized with 5 ml of 0.1% TCA (W/V) solution in pre-cooled pistil and mortar. The mixture was centrifuged and extract was collected in separate tubes. The reaction solution contained 0.5 ml enzyme extract, 0.5 ml of 50-mM PBS and 1 ml of 1 M potassium iodide (KI) solution. The reaction stopped by shifting the reaction solution in an ice bath. The absorbance was measured at 390 nm using spectrophotometer (Hitachi F-4600).

Biochemical assay of antioxidant enzymes, total soluble sugars, and free proline analysis

Leaf samples (0.5 g) were ground in chilled pistil and mortar with 50-mM PBS and centrifuged at 12,000 rpm for 25 min. The extract shifted into another tube for further analysis. SOD assay was determined by following the methodology of Zhang et al. (2008), which depends on SOD capability of NBT inhibition rate of photochemical reduction. The reaction solution comprises of 50-mM PBS, 2-μM riboflavin, 13-mM methionine, 75-μM NBT, 0.1-mM EDTA, and 100-μl enzyme extract making a total volume of 3 ml. The control solution was kept in dark used as blank. One unit activity of SOD is the amount of enzyme required for the inhibition of 50% NBT reduction and measured at 560 nm. CAT activity was assessed by following the methodology of Aebi (1984). POD efficiency was measured following the Chance and Maehly (1955). The reaction solution consists of 50-mM sodium phosphate buffer, 1% guaiacol, 0.4% H_2O_2 and 100-μl enzyme extract. The oxidation of guaiacol was assessed at 470 nm. The H_2O_2 dependent oxidation rate of ascorbic acid (AsA) was used to measure APX activity, as suggested by Farooq et al. (2016). Glutathione reductase (GR) activity was calculated by the oxidation of NADPH at 340 nm (extinction coefficient 6.2 mM cm^{-1}) for 1 min (Islam et al., 2016). Total soluble sugar content was assayed by following the methodology of Fong et al. (1953) and free proline by Bates et al. (1973).

Ultra-structural observation by transmission electron microscopy

Ultrastructural observations were performed according to Islam et al. (2016). Leaf fragments without veins (about 1 mm^2) were fixed in glutaraldehyde overnight and then washed three times with PBS. The samples were post fixed in OsO_4 for 1 h and washed again three times with PBS. After that, the samples were dehydrated in a graded series of ethanol for 15–20 min each and then in absolute acetone for 20 min. After dehydration, the samples were embedded in Spurr's resin overnight. The specimens were heating at 70°C for 9 h, the ultra-thin sections (80 nm) were cut and mounted on copper grids for the transmission electron microscope (TEM 1230EX, JEOL, Japan) at 60.0 kV.

Quantitative real-time PCR (RT-qPCR) assay

RT-qPCR assays was followed the method used by Ali et al. (2018), Total RNA was extracted from 100 mg of leaf and root tissues using Trizol (manual) method. Prime script™ RT reagent with genome DNA (gDNA) eraser kit (Takara Co. Ltd., Japan) was used to remove genomic DNA and cDNA synthesis. The synthesized cDNA from different treatment was assayed for quantitative real-time (qRT-PCR) in the iCycleriQTM Real-time detection system (Bio-Rad, Hercules, CA, United States) by using CYBR Premix Ex Taq II (Takara Co. Ltd., Japan).

Statistical analysis

Data obtained from the current study was the mean (± SE) of at least three replicates. Duncan's Multiple Range Test was performed to test the significance of data and the least significant difference (LSD) was calculated at $p < 0.0001$ by using the Graph Pad Prism7.

Results

Purple sem (PS) maintained higher biomass, relative water content (RWC) and total soluble sugar than green stem (GS) under drought stress

Drought stress significantly reduced the plant growth attributes such as shoot and root biomass (fresh and dry weights) and RWC of both PS and GS *B. napus* genotypes compared to control plants (Figures 1A–D). Drought stress reduced ($p < 0.0001$) the shoot fresh biomass of PS genotype by 42% and 78% and GS genotype by 68% and 85% at the 4th and 8th days of PEG treatments respectively, as compared to relative controls (Figure 1A). Similarly, under PEG stress, shoot dry biomass of PS and GS genotypes reduced ($p < 0.0001$) by 39% and 54% at the 4th day, and 48% and 67% at the 8th day, respectively as compared to control plants (Figure 1B). Likewise, root fresh of PS genotype and GS genotype decreased ($p < 0.0001$) by 24% and 41% at the 4th day, and 37% and 57% at the 8th day, respectively, under PEG stress. While, PEG stress reduced root dry biomass by 31% and 46% at the 4th day, and 37% and 61% at the 8th day, respectively compared to control plants (Figures 1C,D). In comparison to controls, the PS genotype showed the greatest increase in shoot

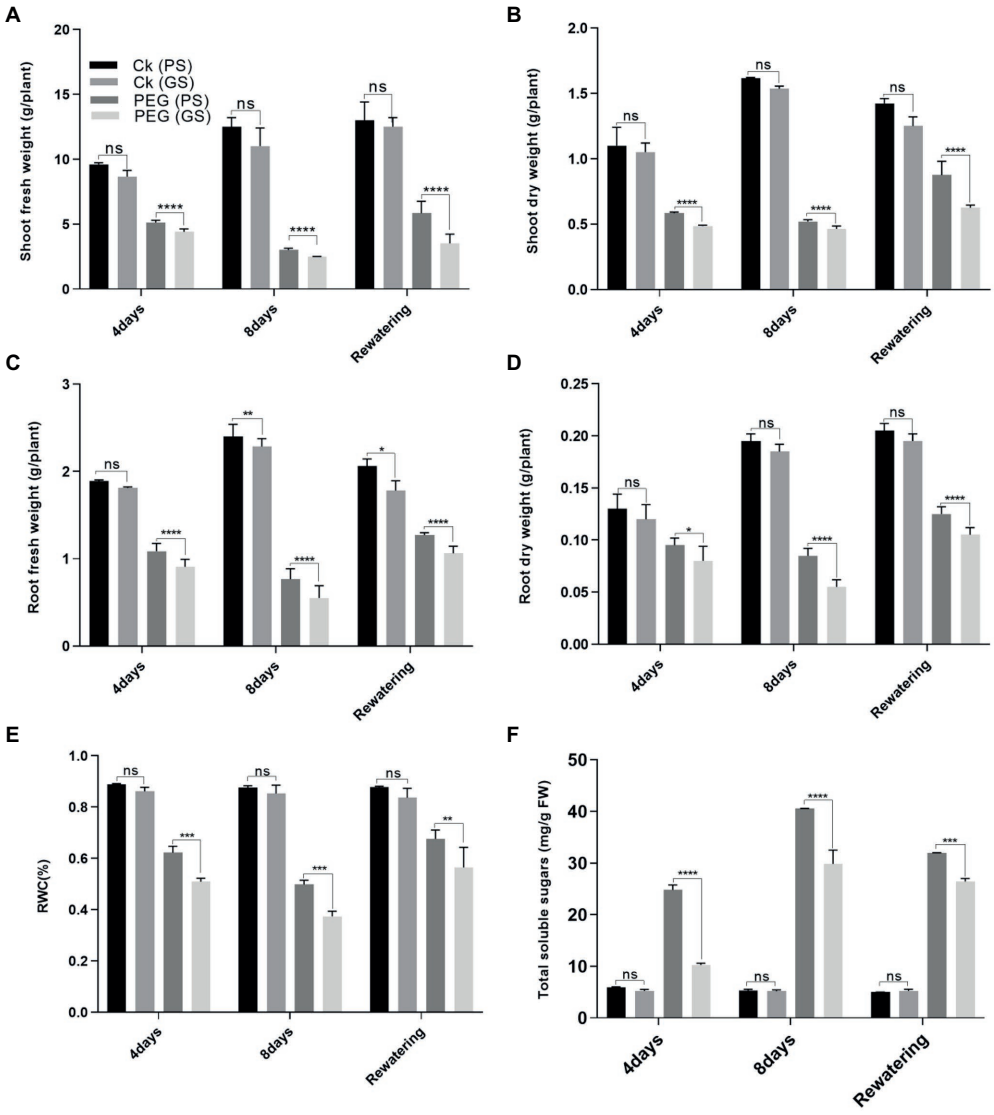


FIGURE 1
Purple and green stem *Brassica napus* plants growth and morphology under drought (10% PEG-6000), **(A)** shoot fresh weight, **(B)** shoot dry weight, **(C)** root fresh weight, **(D)** root dry weight, **(E)** relative water content (RWC), and **(F)** total soluble sugars, respectively. Different symbols represent significance level as *p=0.05, **p=0.01, ***p=0.001, ****p=0.0001. ns, non-significance.

fresh biomass by 47% and dry biomass 33% after the re-watering period (Figures 1A–D).

Drought stress reduced ($p < 0.0001$) the RWC content of PS and GS genotypes by 31% and 44%, and 40% and 55%, respectively, after the 4th and 8th days of PEG treatments, as compared to control plants (Figure 1E). Re-watering resulted in in a 10% increase in RWC content of PS genotype when compared to controls. According to our results, the PS genotype was more drought tolerance than the GS genotype, as evidenced by the minimum reduction in fresh and dry biomass and RWC content. Similarly, a considerable increase in TSS content due to PEG enhanced drought tolerance in PS genotype (3- and 7.9-fold change) than GS genotype (1.05-, and 1.4-fold) after 4 and 8 days respectively, as compared to control plants (Figure 1F).

Purple stem (PS) seedlings accumulated higher chlorophyll contents and photosynthetic efficiency than green stem (GS)

Drought stress reduced chlorophyll production and photosynthetic parameters significantly ($p < 0.0001$) as compared to control. The drought-induced reductions in chlorophyll a of PS and GS genotypes by 18% and 24% at 4th and 31% and 46% at 8th days, respectively, and chlorophyll b by 15% and 19%, and 46% and 62% at 4th and 8th days, respectively, after PEG treatments. While, the carotenoids content of PS and GS genotypes after 4th and 8th days decreased by 15% and 20%, and 26% and 53%, respectively, under PEG treatments (Figures 2A–C). Re-watering

on the other hand, resulted in a very slow recovery values for chlorophyll and carotenoids in both genotypes. Anthocyanins accumulation increased in stem, by 31%, in PS genotype after 4th days and 46% after 8th days of PEG treatments (Figure 2D). In GS genotype, the accumulation of anthocyanins was about 13% after 4th days and 18% after 8th days of PEG treatments. However, following re-watering, the PS genotype showed the maximum increase (86%) in anthocyanin among PEG treated plants. Similarly, the decline in Pn rate of PS genotype was about 67% and 80%, and GS genotype was 75% and 86% after 4th and 8th days of PEG treatment respectively, as compared to control plants (Figure 3A). When compared to controls, Gs rate reduced by 26, and 37% in the PS genotype and 36% and 44% in the GS genotype after 4th and 8th days of PEG treatments, respectively (Figure 3B). Relative to control plants, after 4th and 8th days, of PEG treatments, net Ci rate declined by 14% and 23%, and 36% and 39% in PS and GS genotypes respectively, compared to control plants (Figure 3C). Similarly when compared to control plants, Tr rate decreased by 26% and 37% in the PS genotype and 36% and 44% in the GS genotype after 4th and 8th days of PEG treatments, respectively (Figure 3D). Nevertheless, PS seedlings maintained higher photosynthetic pigments and net photosynthetic rate than GS genotype with minimum reduction with and without drought stress compared to controls.

Maximum quantum yield (QY) of photosystem II (PSII) efficacy of purple stem (PS) seedlings under drought stress relative to green stem (GS)

There is a negative correlation between chlorophyll fluorescence and photosynthetic efficiency. The light energy absorbed by the photosystem can go in different directions: heat dissipation, photochemistry, and fluorescence emission. Measuring the emission of fluorescence light can estimate the proportion of energy flowing to photochemistry. Drought stress remarkably reduced the PSII performance in both *B. napus* genotypes. In the chlorophyll a fluorescence transient, the momentary maximum fluorescence intensity represents the subsequent kinetic bottlenecks of the electron transport chain and depicts the redox state of limitations of plastoquinone (Q_B). Transients chlorophyll fluorescence of dark adopted leaves under control and drought stress plants disclosed normal light curve (LC1) kinetics in PS that of GS, indicating the better transport of electrons in electron transport chain and redox state of Q_B. According to our findings regarding the light response curve, in both the genotypes under normal or drought stress, an increase in the electron transport rate through PSII and an increase in non-photochemical quenching are positively correlated with a decrease in PSII efficiency caused by an increase in light intensity (0–800 mol $m^{-2} s^{-1}$; Figures 4A,B). Chlorophyll fluorescence relative values (time based $0–4 \times 10^8$ µmol m^{-2} s^{-1}) suggested an evident decrease in GS seedlings under drought stress. After 7 days of drought stress, the maximum recovery of PSII activity was observed in PS genotype as compared to GS genotype in re-watering compared to control. Drought stress significantly reduced the quantum yield (QY) of PSII in both *B. napus* genotypes, although this reduction was more apparent in GS than PS relatives to controls (Figures 4C,D). Rapid light curve responsive curve (LC1) analysis disclosed the changes in electron transport ETR (II) and heat dissipation in terms of non-photochemical quenching (NPQ) of both *B. napus* genotypes with and without drought stress. ETR (II) governs the relative electron transport rate (ETR) over PSII, which was declined in both *B. napus* genotypes, ultimately limiting the PSII efficiency. The decrease in ETR (II) was more obvious in GS genotype relative to PS genotype (Figures 4E,F). Under drought stress, NPQ was increased in both PS and GS genotypes, while maximum upsurge was observed in PS genotype than GS genotype (Figures 4G,F). These findings suggested that drought tolerant PS genotypes exhibit greater PSII quantum yield, ETR (II) efficacy and higher photochemical protective mechanisms than drought sensitive GS genotype under drought stress compared to controls.

Green stem (GS) plants exhibit higher ROS accumulation along with electrolyte leakage (EL) under drought stress

Drought stress remarkably enhanced H_2O_2 accumulation, resulting in the lipid peroxidation as MDA and EL in plant cell. PEG treatments on the 4th and 8th days increased H_2O_2 and MDA contents by 58% and 94% in PS genotype and 86% and 137% in GS genotype, respectively, as compared to their respective control plants (Figures 5A,B). Similarly the EL of GS genotype was about 76% and 137% at 4th and 8th days under PEG stimulated drought as compared with the PS genotype (34% and 68%; Figure 5C). Furthermore, histochemical analyses with DAB and NBT staining were used to verify the accumulation of ROS (H_2O_2 and O_2^-). The leaves of both *B. napus* genotypes were stained with and without drought stress conditions (Figures 6A–H). Relative to controls, drought stressed plants displayed brown (H_2O_2; Figures 6A–H) and blue (O_2^-; Figures 5I–L) staining spots on leaf surface. Under drought stress, DAB and NBT staining revealed that the leaves of the GS genotype exhibits high ROS production and were stained to the deepest extent compare to the PS genotype. While, the least intensity of colored staining of PS genotype suggests that these plants have remarkable efficacy to alleviate the excessive generation and accumulation of ROS under stressful conditions relative to controls.

Drought tolerant genotype possess higher activities of antioxidant enzymes and proline content under drought stress

The antioxidant enzymes activity (SOD, POD, CAT, APX, and GR) and proline content varied significantly among both

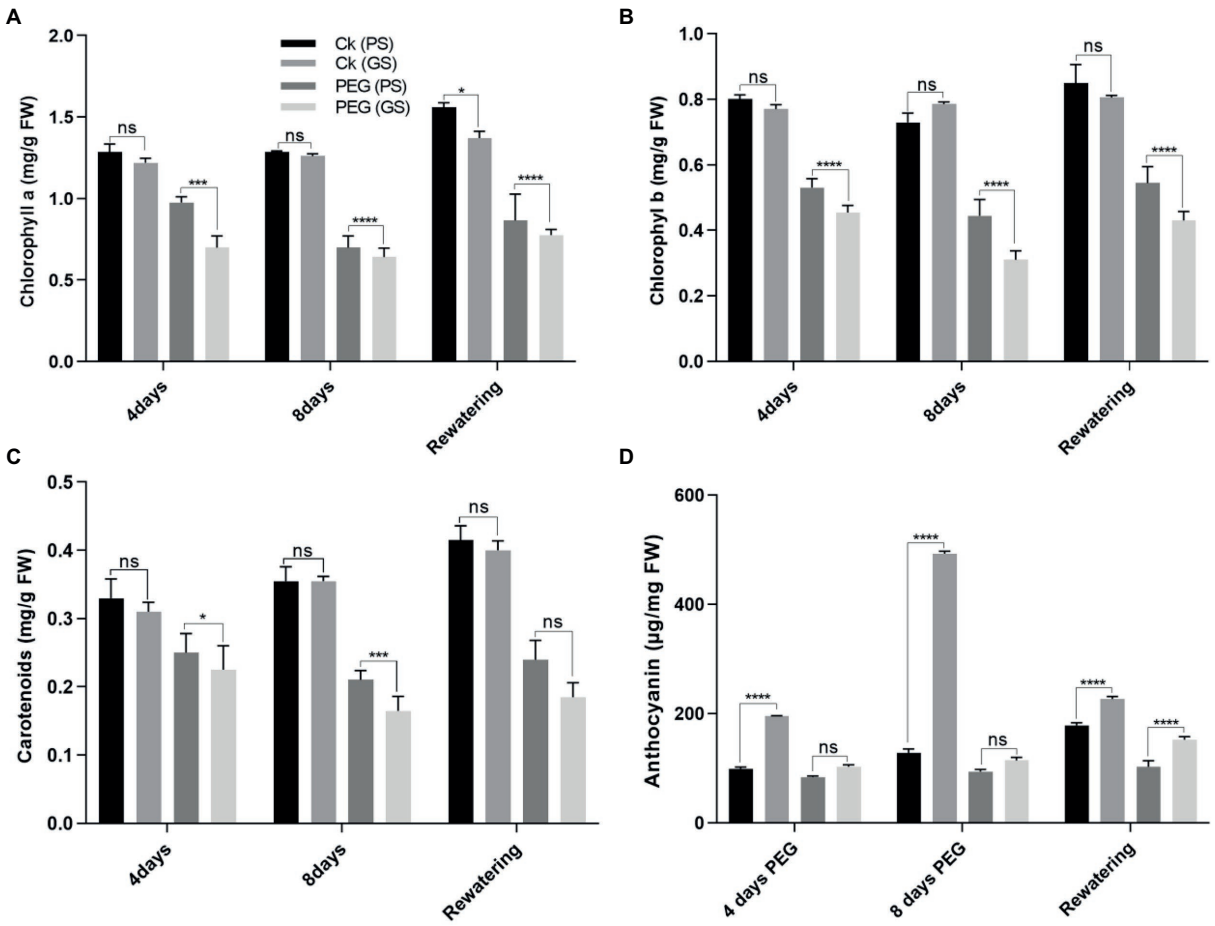


FIGURE 2
Purple and green stem *Brassica napus* plants under drought (10% PEG-6000), **(A)** chlorophyll a, **(B)** chlorophyll b, **(C)** carotenoids, and **(D)** anthocyanins, respectively. Different symbols represents significance level as *p=0.05, **p=0.01, ***p=0.001, ****p=0.0001. ns, non-significance.

B. napus genotypes. Under drought stress, antioxidants activities were considerably increased with higher SOD and POD in PS genotype (96% and 146%) and (68% and 105%) than GS genotype (38% and 58%) and (48% and 89%) as compared to controls plants after the 4th and 8th days of treatments, respectively (Figures 7A,B). Likewise, CAT activity increased by 80% and 195% in the PS genotype and 37% and 66% in the GS genotype after 4th and 8th days, respectively of PEG treatments (Figure 7C). The activities of APX, GR and proline content under drought stress enhanced in PS genotype after at 4th and 8th days (40%, 108%, and 73% and 68%, 147%, and 120%) than of GS genotype (23%, 73%, and 56% and 52%, 88%, and 69%) as compared to control plants, respectively (Figures 7D–F). This indicated that the PS genotype had higher drought tolerance as noticed by the increased antioxidants enzymes activity than GS genotype with and without drought stress.

TEM reveals differential sub-cellular modifications in *Brassica napus* genotypes under drought stress

When drought tolerant and sensitive genotypes were compared to controls chloroplast ultra-structures revealed considerable differences in their tissues (Figures 8A–D). Under control conditions, mesophyll cells of the PS genotype showed well-differentiated chloroplasts, mature grana, multiple thylakoid membranes, less plastoglobuli and well-developed stroma lamellae (Figure 8A). The chloroplasts of both the genotypes PS and GS were significantly impacted by drought stress treatment, and chloroplast deformation was obvious. Under drought stress, the chloroplast had fewer disorganized grana and thylakoid membrane with wide intrathylakoid spaces, and small plastoglobuli and decreased number of starch grain as compared to control plants (Figure 8B). Drought stress resulted in visible

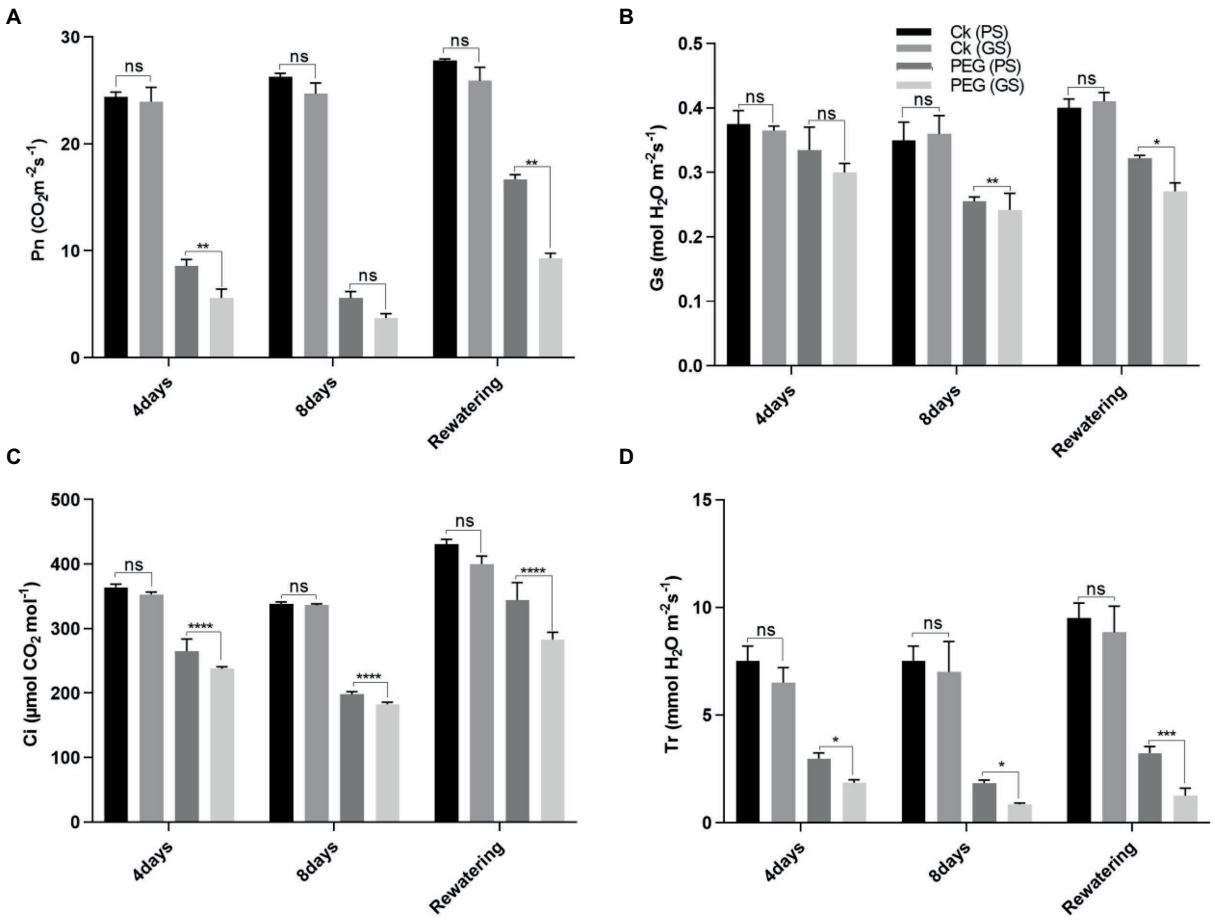


FIGURE 3
Purple and green stem *Brassica napus* plants under drought (10% PEG-6000), **(A)** net photosynthesis (Pn), **(B)** stomatal conductance (Gs), **(C)** corban dioxide intake (CI), and **(D)** transpiration rate, respectively. Different symbols represents significance level as *p=0.05, **p=0.01, ***p=0.001, ****p=0.0001. ns, non-significance.

damage to mesophyll cells of rapeseed plants, although impact was more clear in GS genotype than PS, indicating the higher susceptibility of plants under stressful conditions (Figures 8C,D).

Drought tolerant genotype showed higher biosynthesis and antioxidant enzymes related gene expression

To explain relative transcript levels of particular genes, qRT-PCR was performed to explain the processes of an expression model for biosynthesis, transcription factors and antioxidant enzyme related genes. Under control and in stressful conditions, the anthocyanin biosynthesis genes including (*CHS*, *CHI*, *F3'H*, *DFR*, *ANS*, and *UGT79B1*) of *B. napus* were differently expressed (Figure 9A). Under drought stress, anthocyanin biosynthesis related genes were significantly expressed as noticed by *CHS* (3.51- and 0.51-fold), *CHI* (2.15- and 0.27-fold), *F3'H* (2.07- and 0.71-fold), *DFR* (1.93- and 1.03-fold), biosynthesis genes *ANS* (2.88- and 1.02-fold), and *UGT79B1* (1.67- and 0.74-fold) were significantly expressed in PS and GS genotypes, respectively relative to controls (Figure 9A). Under drought stress antioxidants enzymes related gene expression level including *BnSOD*, *BnPOD*, *BnCAT*, and *BnAPX* considerably upregulated with a maximum increment of 3.4-, 0.79-, 0.56-, and 2.4-fold and 2.13-, 0.4-, 0.78-, and 1.05-fold in PS and GS genotypes, respectively, compared to controls (Figure 9B). However, the PS genotype exhibited higher expression levels of anthocyanin biosynthesis and antioxidant enzymes related genes relative to GS genotype with and without drought stress, respectively (Figures 9A,B).

Discussion

Water shortage has a negative impact on agricultural plant development and yield. In the present study, two *B. napus* genotypes (PS and GS) showed considerable genetic variation against drought stress. Based on growth and physio-biochemical attributes, purple stem genotype is considered as drought tolerant

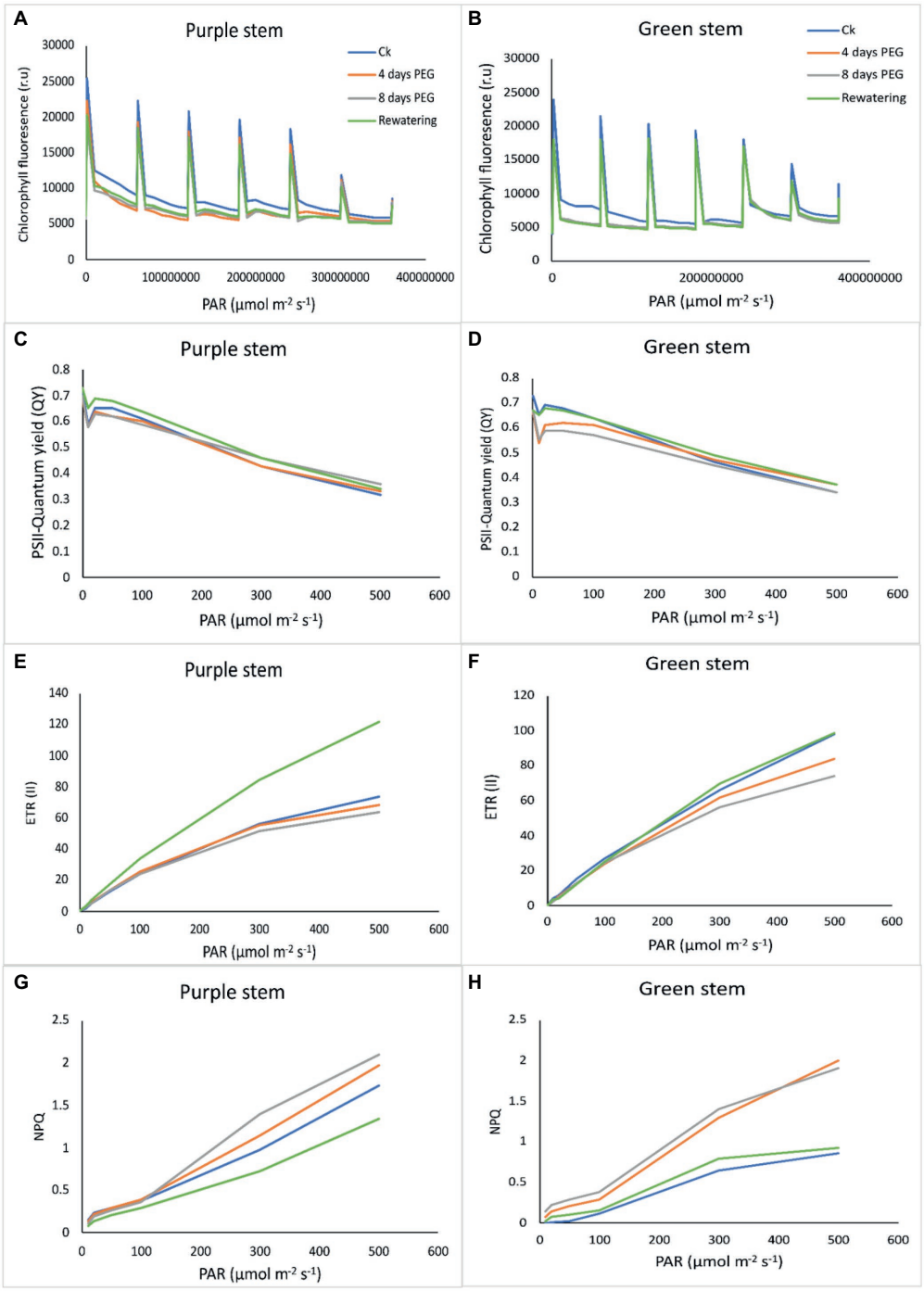


FIGURE 4
Purple and green stem *Brassica napus* plants under drought (10% PEG-6000), **(A,B)** chlorophyll fluorescence (r.u), **(C,D)** PSII quantum yield (QY), **(E,F)** electron transport rate (ETR II), and **(G,H)** non-photochemical uenching (NPQ), respectively.

and green stem genotype as drought sensitive. Such genetic variability in drought tolerance in *B. napus* genotypes may be due to the differences in physiological and biochemical responses in stressful conditions (Ayyaz et al., 2021). Plant fresh and dry biomass represents growth characteristics and is considered as a key indicator of drought stress assessment. According to our results, drought stress also significantly reduced the plant growth attributes (plant fresh and dry biomass along with RWC) of both *B. napus* genotypes (Figures 1A–F). The reduction was more obvious in drought sensitive GS genotype relative to drought tolerant PS genotype as observed in previous studies on *B. napus*, *Brassica rapa*, and *B. campestris* (Cha et al., 2020; Chen et al., 2020;

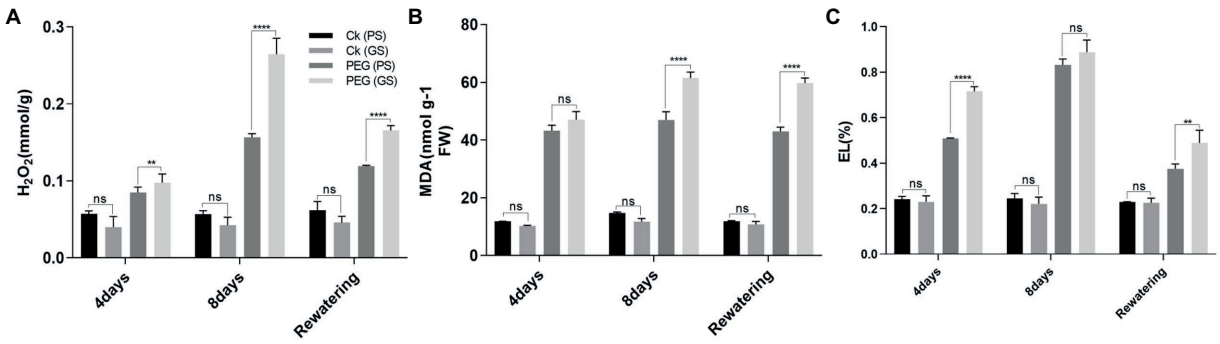


FIGURE 5
Purple and green stem *Brassica napus* plants under drought (10% PEG-6000), **(A)** hydrogen peroxide (H_2O_2), **(B)** malonaldehyde (MDA), and **(C)** membrane stability index: elelectrolyte leakage (EL), respectively. Different symbols represents significance level as *p=0.05, **p=0.01, ***p=0.001, ****p=0.0001. ns, non-significance.

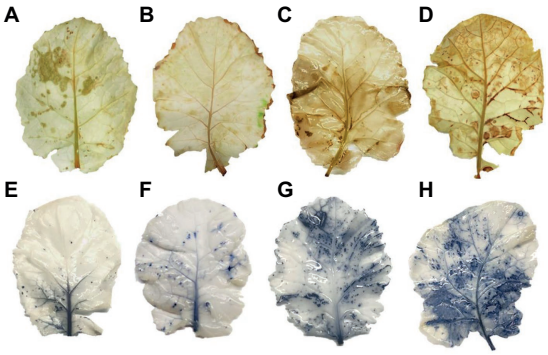


FIGURE 6
Purple and green stem *Brassica napus* plants growth and morphology under drought (10% PEG-6000) on, respectively. DAB staining **(A)** PS (Ck), **(B)** GS (Ck), **(C)** PS (PEG), **(D)** GS (PEG) and NBT staining, **(E)** PS (Ck), **(F)** GS (Ck), **(G)** PS (PEG), and **(H)** GS (PEG), respectively.

Grieco et al., 2020; Khanzada et al., 2020; Shawon et al., 2020). Drought stress mediated plant growth reduction is mainly associated with the loss of cell turgor pressure, affected the cell wall biosynthesis and reduced the cell division or cell expansion (Pakdel et al., 2020). These results are quite similar to several studies suggesting that drought stress severely affects the plant growth and RWC in *B. napus*, *B. carinata*, and *Brassica oleracea*, respectively (Dai et al., 2020; He et al., 2020; Samanta et al., 2020). Some previous reports also evaluated the effect of anthocyanin accumulation in wild-type (WT) plants and anthocyanin-enriched transgenic plants that indicated a positive correlation between anthocyanin accumulation and water loss prevention, as well as drought stress tolerance (Nakabayashi et al., 2014; Li et al., 2017a; Naing et al., 2017).

Drought stress reduced the chlorophyll contents and photosynthetic rate along with PSII performance (Khanzada et al., 2020). Plants photosynthetic efficiency is majorly associated with the number of photosynthetic tissues, photosynthetic pigment, CO_2 influx through stomata, its fixation efficacy and the solar energy conversion efficiency into biochemical energy (Pan et al., 2018; Dąbrowski et al., 2019; Javed et al., 2022). A considerable reduction in photosynthetic pigments and photosynthetic efficacy by drought stress was observed in both *B. napus* genotypes (Figures 2A–D). This might occur due to the enhanced pigments degradation as observed earlier in *B. napus* (Dai et al., 2020). Additionally, the enhanced activity of chlorophyllase enzyme or distortion in thylakoid membrane (Shen et al., 2020) may also involve in inhibiting the photosynthetic efficacy. The anthocyanin rich plants compared with plants lacking anthocyanins may also have the ability to decrease stomatal conductance, which preserves water homeostasis by delaying water loss and wilting during drought stress (Kaku et al., 1992; Choinski and Johnson, 1993).

Reduced photosynthetic performance may also affect the photosystem (PSII) efficiency, which plays significant roles in photosynthetic response against drought stress (Lawlor and Tezara, 2009). Drought stress decreased the quantum yield (QY) of PSII, which is considered a potential indicator of photo-inhibitory damages of PSII (Golding and Johnson, 2003; Kaldenhoff et al., 2007; Lawlor and Tezara, 2009; Bano et al., 2021). Drought stress causes a rapid disassembly of light harvesting complex (LHCII) of PSII. It was observed that short-term and long-term exposure of drought stress makes PSII dimers unstable in *Arabidopsis* seedlings (Chen et al., 2016). This suggests that the assembly of LHCII-PSII super complexes prevents the PSII from photo-damages under drought stress (Chen et al., 2016). The results of our study showed that the QY value of both genotypes leaves was decreased at drought exposure. Comparatively greater reduction in QY values were observed in GS. Zhang et al. (2018) also reported that QY values of the green *Mikania micrantha* were significantly decreased as compared to red *M. micrantha* under low temperature stress. They verified that the accumulation of anthocyanins can improve the plant tolerance under stressful conditions. Similar type of results was also observed in our study where the purple stem *B. napus* plants showed improved performance of photosystem efficiency under drought stress.

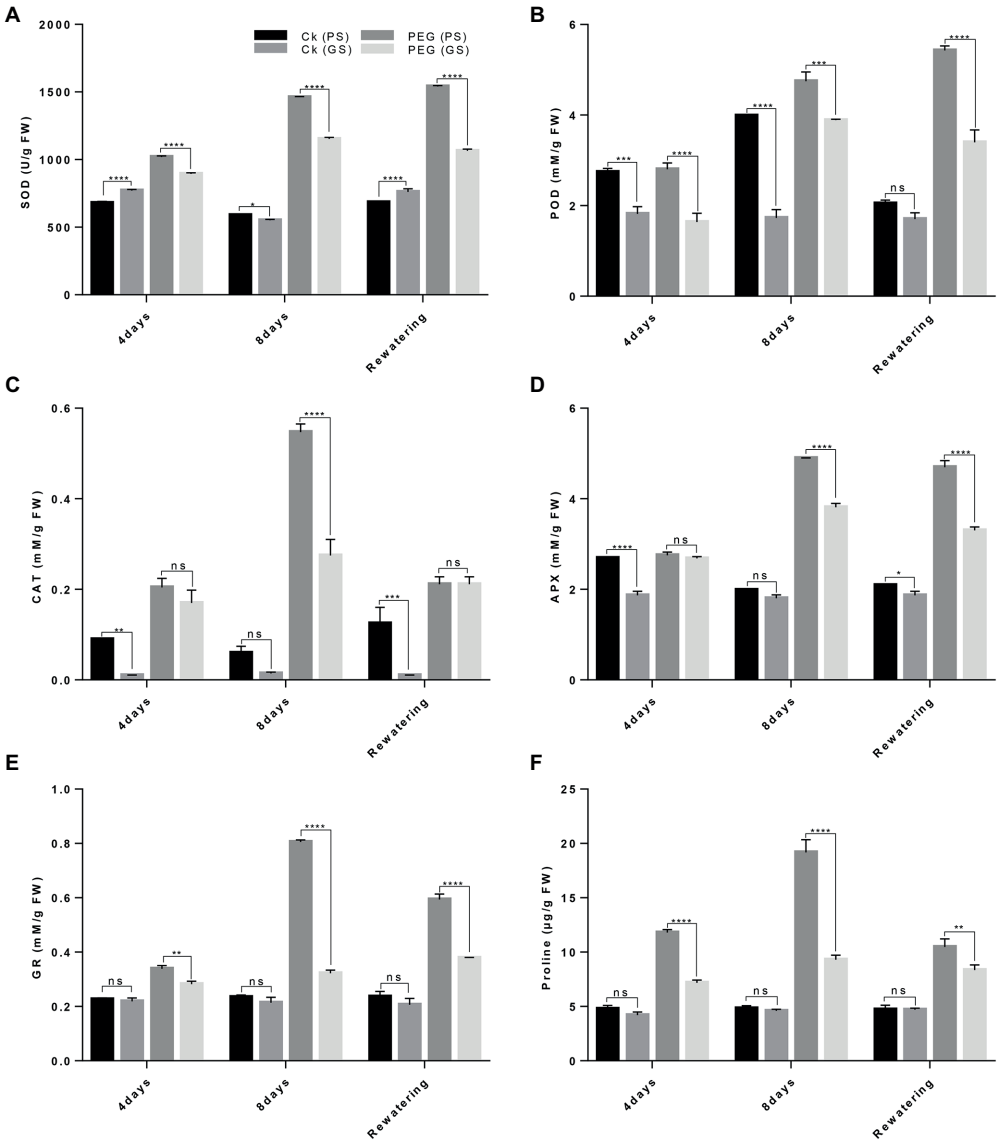


FIGURE 7
Purple and green stem *Brassica napus* plants under drought (10% PEG-6000), **(A)** superoxide dismutase (SOD), **(B)** peroxidase (POD), **(C)** catalase (CAT), **(D)** ascorbate peroxidase (APX), **(E)** glutathione reductase (GR), and **(F)** proline content of purple and green stem, respectively. Different symbols represents significance level as *p=0.05, **p=0.01, ***p=0.001, ****p=0.0001. ns, non-significance.

The rapid light curve responses revealed that drought stress showed a maximum reduction of PSII efficiency with an increase of light intensity from 0 to 800 μmol m^{-2} s^{-1}, which is positively correlates with an increase in electron transport rate (ETRII) and non-photochemical quenching of PSII with and without drought stress in both *B. napus* genotypes (Figures 4E,F). Drought stress induced reduction of ETRII and enhanced NPQ in both the *B. napus* genotypes suggested a considerable accumulation of maximum electrons at PSII acceptor sites that causes an increase in non-photochemical quenching (NPQ; Figures 4G,H). Overall, the reduction in PSII efficiency and ETRII can occur due to reduced size of antenna complex and degradation of LHCII complex proteins. Earlier study also revealed that drought stress severely damaged the LHCII proteins but increased the PsbS proteins (A xanthophyll cycle activating protein of PSII) in *Arabidopsis* seedlings (Chen et al., 2016). Hence, drought tolerant colorful *B. napus* genotype possess higher QY of PSII, ETRII, and NPQ which suggests the maximum photosynthetic performance than green stem seedlings with and without drought stress. Recent studies also showed higher degree of photoinhibition (*Fv/Fm*) in green leaves as compared to the red leaves (Javed et al., 2022).

Drought stress notably increased ROS generation, as measured by MDA, H_2O_2, and EL and cause impairments in structural and functional components such as total soluble proteins, lipids and DNA (Zhou and Leul, 1998; Ahmad et al., 2020; Biswas et al., 2020; Rogers, 2020). In the present study,

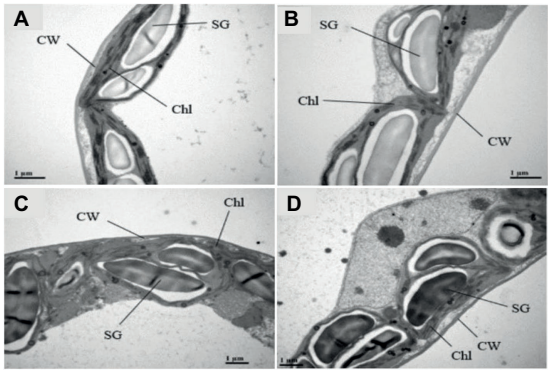


FIGURE 8
Purple and green stem *Brassica napus* plants under drought (10% PEG-6000), ultrastructure of organelles in mesophyll cells of purple and green stem *B. napus* seedlings under drought and control conditions Chl (Chloroplast), Thy (Thylakoids), CW (Cell wall), SG (Starch grains) of **(A)** PS (Ck), **(B)** PS (PEG), **(C)** GS (Ck), and **(D)** GS (PEG), respectively.

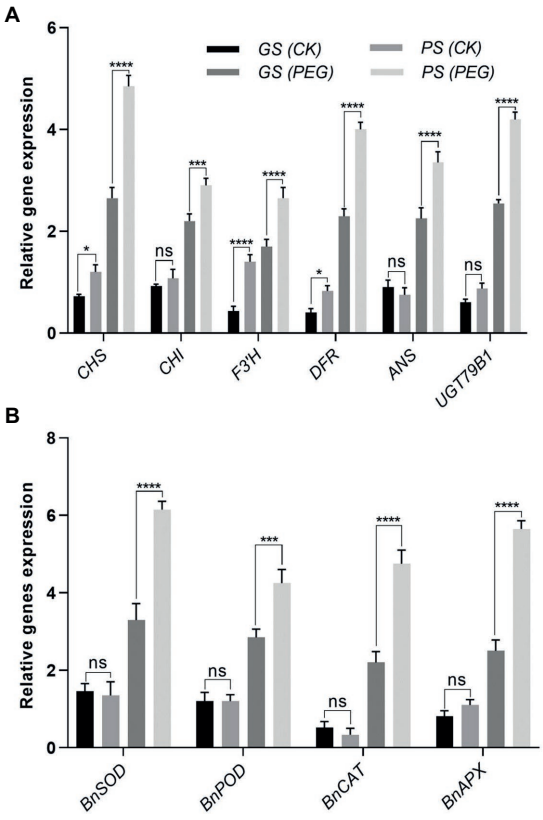


FIGURE 9
Purple and green stem *Brassica napus* plants under drought (10% PEG-6000). **(A)** Relative expression of anthocyanin biosynthesis genes including *CHS*, *CHI*, *F3'H*, *DFR*, *ANS*, and *UGT79B1*. **(B)** Relative expression of antioxidants enzymes related genes such as *BnSOD*, *BnPOD*, *BnCAT*, and *BnAPX*, respectively. Different symbols represents significance level as **p*=0.05, ***p*=0.01, ****p*=0.001, *****p*=0.0001. ns, non-significance.

drought sensitive (GS) genotype exhibited higher H_2O_2, MDA and EL levels than drought tolerant (PS) genotype against drought stress relative to controls (Figures 5A,B). Several studies provide ample evidences for ROS-induced cellular damage ultra-structural changes and cell death caused by drought stress (Chowardhara et al., 2020; Ray et al., 2020). Our results revealed that drought facilitated membrane lipid peroxidation and electrolyte leakage were declined in drought tolerant *B. napus* genotype (Figures 5B,C). Earlier outcomes also noticed ROS-scavenging, reduction in lipid peroxidation and enhancement in antioxidants enzyme activities in *B. napus*, *Lycopersicon esculentum*, and *Prosopis juliflora* (Mir et al., 2021). This indicates that drought tolerant genotype had strong and efficient antioxidative defense system, which imparts ROS-scavenging process under drought stress. The induction of anthocyanins coupled with increased antioxidant activity may have occurred due to drought-stress-induced ROS signaling, followed by the transcription of anthocyanin-related genes. Nakabayashi et al. (2014) also demonstrated drought-induced anthocyanins accumulation in *Arabidopsis via* transcriptomic and metabolomics analysis. The identified drought-induced anthocyanins were directly associated with oxidative and drought stress tolerance. This may be due to the fact that anthocyanins mainly accumulate in vacuoles close to ROS production sites such as chloroplasts and peroxisomes. Anthocyanins likely scavenge the drought stress-induced ROS that enter the vacuoles, thereby inhibiting chain reactions to avoid excessive ROS accumulation and ensure water homeostasis for plant growth and drought stress tolerance. This association between anthocyanin and drought tolerance was reported in Tobacco (Cirillo et al., 2021) and red and green pretty purple peppers (Bahler et al., 1991). Moreover it is also observed that PS genotype trigger the accumulation of proline and total soluble protein more under drought stress. Mbarki et al. (2018) also reported that the colored wheat genotypes having higher anthocyanin content and proline content under salt stress. It was estimated that high contents of proline and anthocyanin support an active protective response to abiotic stress (Chutipaijit et al., 2011; Sperdouli and Moustakas, 2012).

Plants exposed to environmental stress experienced a disruption in cellular homeostasis, impairing the functioning of cellular components such as chloroplast and cell membranes (Asada, 2006). Ultrastructural analysis revealed that drought exposed plants have enlarged and vesiculated thylakoid membranes of chloroplasts compared to controls. Several researchers also observed ROS-induced chloroplast damage, which was similar to our findings (Sofo et al., 2005; Atkin and Macherel, 2009). Chloroplasts are considered as basic site of ROS generation and severely affected under oxidative stress. ROS scavenging and elimination are promptly required in their site of production before they move to protect the target molecules in thylakoid membrane and stroma of chloroplast (Zhang et al., 2015; Złotek et al., 2015). TEM results suggested that drought stress caused severe damages to structural and functional abnormalities of photosynthetic components under drought stress

(Figures 8A–D). While, colorful *B. napus* PS genotype maintained better structural and functional cell integrity compared to green stem GS under same level of drought stress. Similarly, under temperature stress (both heat and chilling), plants synthesize more phenolic compounds such as anthocyanins, flavonoids, and phenolic acids, which ultimately protect the plant cells (Ancillotti et al., 2015; Złotek et al., 2015; Martinez et al., 2016). Anthocyanin application has recently been shown to enhance the ultrastructure of rice seedling under stressful condition. Visualization of leaf cells surface sprayed with anthocyanin showed alleviation of cell shrinkage, mitochondrion and chloroplast damage, and an increase in amounts of endoplasmic reticulum and vesicles (He et al., 2017). Flavonoids biosynthesis occurs by the conversion of 4-coumaroyl CoA to chalcone and naringenin to di-hydro flavonol. Previous studies suggested that *CHS* is considered as the initial rate-limiting enzyme of the flavonoids biosynthesis pathway (Earley et al., 2006; Hichri et al., 2011). Later on, the dihydroflavonol 4-reductase (*DFR*) transfers the dihydroflavonols molecules into colorless leucoanthocyanidins, which are converted into the colored anthocyanidins by anthocyanidin synthase (*ANS*; Falcone Ferreyra et al., 2012). Anthocyanidins after their synthesis glycosylated by UDP-glucose anthocyanidin glucosyltransferase (*UGT79B1*) to form anthocyanins, which further, stabilize through either methylation or acylation (Bhalla and Singh, 2008). The anthocyanins biosynthesis gene expression (*CHS*, *CHI*, *F3'H*, *DFR*, *ANS*, and *UGT79B1*) of purple and green stem plants were significantly enhanced under drought stress when compared with relative controls (Figure 9A). These results were in correspondence with previous studies suggesting that higher anthocyanins accumulation may occurs due to the higher abundance of biosynthesis-related genes (*CHS*, *CHI*, *F3'H*, and *DFR*; Petroni and Tonelli, 2011; Zhang et al., 2014; Gharibi et al., 2019). A significantly enhanced expression of *ANS* and *UGT79B1* genes were noticed under drought stress conditions (Figure 9A), suggesting maximum anthocyanin stability and biosynthesis as compared to control. These transcript levels trigger the promoters of flavonoids metabolic pathways (Kim et al., 2017; Li et al., 2017b; Sun et al., 2017; Naing et al., 2018). The expression of *CHS*, *CHI*, *F3'H*, *DFR*, *ANS*, and *UGT79B1* genes were upregulated in PS than GS with and without drought stress (Figure 9A). This reflects the positive effect on the anthocyanin biosynthesis, which may help plant to cope with various environmental stresses. Overexpression of anthocyanin biosynthesis genes or regulatory TFs in several plant species leads to a higher production of anthoycanins. The anthocyanins scavenge ROS and maintain osmotic balance, thereby increasing abiotic stress tolerance (Wang et al., 2016, 2018; Naing et al., 2017; Ali et al., 2018).

Relative to controls, genes related to antioxidants enzymes such as *BnSOD*, *BnPOD*, and *BnCAT* and *BnAPX* were significantly enhanced with and without drought stress in the PS genotype (Figure 9B). SOD, POD, and CAT encoding genes expression was upregulated along with their enzyme activities in *B. juncea* against high temperature and drought stress (Evaristo de Deus et al., 2015; Saha et al., 2016; Xia et al., 2016; Verma et al., 2021). Naing et al. (2018) also found stress-induced upregulation of antioxidant-related genes (CAT, SOD, and POX) was positively linked with the presence of anthocyanins content (Naing et al., 2018). Drought and salinity stress tolerance in transgenic plants has also been documented due to increased antioxidant and proline activities, which boost water uptake and photosynthesis rate for plant development (Kim et al., 2017; Wang et al., 2016). Similarly, the altered expression of C-repeat binding factor 1 (CBF1) in response to cold stress was observed in the studies of Nakabayashi et al. (2014) and Naing et al. (2018), in which it regulates expression of the two glycosyltransferases genes (UGT79B2 and UGT79B3) involved in modifying anthocyanin metabolic pathways to enhance the abiotic stress tolerance (Nakabayashi et al., 2014). In summary, antioxidants were thoughts to be potentially upregulated in our study as a result of transcriptional and post-transcriptional changes.

Conclusion

The difference revealed in the current study between purple and green stem *B. napus* shows that both genotypes have different capability to deal with drought stress. Drought severely affected the plant growth attributes, although GS genotype proving to be more sensitive genotype. When exposed to the same level of drought, the colorful PS genotype maintained greater structural and functional cell integrity as compared to green stem GS. The accumulation of anthocyanins in PS genotype under drought stress resulted in improved proline and total soluble sugar contents. Under drought stress, PS plants with increased antioxidant activities reflected the improved ability to reduce excessive ROS generation in cellular organelles. The electron microscopic study indicated that ultrastructural damages in leaf mesophyll cells were more prominent in the GS genotype as compared to the PS genotype under drought stress. Further information is needed on the physiological and metabolic responses observed in color drought-tolerant or resistant species, in order to functionally characterize genes involved in adaptation processes.

Data availability statement

The original contributions presented in the study are included in the article, further inquiries can be directed to the corresponding authors.

Author contributions

WC and WZ conceptualized and supervised the work. WC, YM, and AA performed experiments. FH, QH, and ZU helped in analyzing physiological parameters. MF, YZ, and FI provided technical and helpful discussions. AA, ZH, MF, and WZ wrote and edited the manuscript. All authors contributed to the article and approved the submitted version.

Funding

This work was supported by the Science and Technology Department of Zhejiang Province (2021C02064-2), Collaborative Innovation Center for Modern Crop Production co-sponsored by Province and Ministry (CIC-MCP), and the Agriculture and Rural Affairs Department of Zhejiang Province (2021XTTGLY0202).

Acknowledgments

We thank Rui Sun and Weizhen Hu from Agricultural Experiment Station of Zhejiang University for their assistance.

Conflict of interest

The authors declare that the research was conducted in the absence of any commercial or financial relationships that could be construed as a potential conflict of interest.

Publisher's note

All claims expressed in this article are solely those of the authors and do not necessarily represent those of their affiliated organizations, or those of the publisher, the editors and the reviewers. Any product that may be evaluated in this article, or claim that may be made by its manufacturer, is not guaranteed or endorsed by the publisher.

References

Aebi, H. (1984). Catalase in vitro. *Methods Enzymol.* 105, 121–126.

Ahanger, M. A., Alyemeni, M. N., Wijaya, L., Alamri, S. A., Alam, P., Ashraf, M., et al. (2018). Potential of exogenously sourced kinetin in protecting *Solanum lycopersicum* from NaCl-induced oxidative stress through up-regulation of the antioxidant system, ascorbate-glutathione cycle and glyoxalase system. *PLoS One* 13:e0202175.

Ahanger, M. A., Qin, C., Begum, N., Maodong, Q., Dong, X. X., El-Esawi, M., et al. (2019). Nitrogen availability prevents oxidative effects of salinity on wheat growth and photosynthesis by up-regulating the antioxidants and osmolytes metabolism, and secondary metabolite accumulation. *BMC Plant Biol.* 19, 1–12.

Ahanger, M. A., Tomar, N. S., Tittal, M., Argal, S., and Agarwal, R. (2017). Plant growth under water/salt stress: ROS production; antioxidants and significance of added potassium under such conditions. *Physiol. Mol. Biol. Plants* 23, 731–744.

Ahmad, P., Ahanger, M. A., Alam, P., Alyemeni, M. N., Wijaya, L., Ali, S., et al. (2019). Silicon (Si) supplementation alleviates NaCl toxicity in mung bean [*Vigna radiata* (L.) Wilczek] through the modifications of physio-biochemical attributes and key antioxidant enzymes. *J. Plant Growth Regul.* 38, 70–82.

Ahmad, P., Alyemeni, M. N., Al-Huqail, A. A., Alqahtani, M. A., Wijaya, L., Ashraf, M., et al. (2020). Zinc oxide nanoparticles application alleviates arsenic (As) toxicity in soybean plants by restricting the uptake of as and modulating key biochemical attributes, antioxidant enzymes, ascorbate-glutathione cycle and glyoxalase system. *Plan. Theory* 9:825

Ai, T. N., Naing, A. H., Yun, B.-W., Lim, S. H., and Kim, C. K. (2018). Overexpression of RSMYB1 enhances anthocyanin accumulation and heavy metal stress tolerance in transgenic Petunia. *Front. Plant Sci.* 9:1388. doi: 10.3389/fpls.2018.01388

Ali, S., Gill, R. A., Ulhassan, Z., Najeeb, U., Kanwar, M. K., Abid, M., et al. (2018). Insights on the responses of *Brassica napus* cultivars against the cobalt-stress as revealed by carbon assimilation, anatomical changes and secondary metabolites. *Environ. Exp. Bot.* 156, 183–196.

Ancillotti, C., Bogani, P., Biricolti, S., Calistri, E., Checchini, L., Ciofi, L., et al. (2015). Changes in polyphenol and sugar concentrations in wild type and genetically modified *Nicotiana langsdorffii* Weinmann in response to water and heat stress. *Plant Physiol. Biochem.* 97, 52–61. doi: 10.1016/j.plaphy.2015.09.012

Arnon, D. I. (1949). Copper enzymes in isolated chloroplasts. Polyphenoloxidase in *Beta vulgaris*. *Plant Physiol.* 24:1.

Asada, K. (2006). Production and scavenging of reactive oxygen species in chloroplasts and their functions. *Plant Physiol.* 141, 391–396.

Atkin, O. K., and Macherel, D. (2009). The crucial role of plant mitochondria in orchestrating drought tolerance. *Ann. Bot.* 103, 581–597.

Ayyaz, A., Miao, Y., Hannan, F., Islam, F., Zhang, K., Xu, J., et al. (2021). Drought tolerance in *Brassica napus* is accompanied with enhanced antioxidative protection, photosynthetic and hormonal regulation at seedling stage. *Physiol. Plant.* 172, 1133–1148.

Bahler, B., Steffen, K., and Orzolek, M. (1991). Morphological and biochemical comparison of a purple-leafed and a green-leafed pepper cultivar. *HortScience* 26:736

Bano, H., Athar, H. U. R., Zafar, Z. U., Kalaji, H. M., and Ashraf, M. (2021). Linking changes in chlorophyll a fluorescence with drought stress susceptibility in mung bean [*Vigna radiata* (L.) Wilczek]. *Physiol. Plant.* 172, 1244–1254.

Bates, L. S., Waldren, R. P., and Teare, I. (1973). Rapid determination of free proline for water-stress studies. *Plant Soil* 39, 205–207.

Begum, N., Ahanger, M. A., and Zhang, L. (2020). AMF inoculation and phosphorus supplementation alleviates drought induced growth and photosynthetic decline in *Nicotiana tabacum* by up-regulating antioxidant metabolism and osmolyte accumulation. *Environ. Exp. Bot.* 176:104088.

Bhalla, P. L., and Singh, M. B. (2008). Agrobacterium-mediated transformation of *Brassica napus* and *Brassica oleracea*. *Nat. Protoc.* 3, 181–189.

Bilger, W., and Björkman, O. (1991). Temperature dependence of violaxanthin de-epoxidation and non-photochemical fluorescence quenching in intact leaves of *Gossypium hirsutum* L. and *Malva parviflora* L. *Planta* 184, 226–234.

Biswas, K., Adhikari, S., Tarafdar, A., Kumar, R., Saha, S., and Ghosh, P. (2020). "Reactive oxygen species and antioxidant defence systems in plants: role and crosstalk under biotic stress," in *Sustainable Agriculture in the Era of Climate Change* (New York: Springer), 265–292.

Cha, Y. R., Kim, S., Lee, J. H., and Shim, I.-S. (2020). Enhanced drought tolerance in Chinese cabbage (*Brassica campestris* L.) seedlings upon pretreatment with exogenous salicylic acid. *Hortic. Sci. Technol.* 38, 9–20.

Chance, B., and Maehly, A. (1955). Assay of catalases and peroxidases. *Methods Enzymol.* 2, 764–775.

Channaoui, S., El Kahkahi, R., Charafi, J., Mazouz, H., El Fechtali, M., and Nabloussi, A. (2017). Germination and seedling growth of a set of rapeseed (*Brassica napus*) varieties under drought stress conditions. *Int. J. Environ. Agric. Biotech.* 2:238696.

Chen, Y. E., Liu, W. J., Su, Y. Q., Cui, J. M., Zhang, Z. W., Yuan, M., et al. (2016). Different response of photosystem II to short and long-term drought stress in *Arabidopsis thaliana*. *Physiol. Plant.* 158, 225–235.

Chen, L., Xu, B., Liu, L., Luo, Y., Yin, J., Zhou, H., et al. (2010). Hydrogen peroxide inhibits mTOR signaling by activation of AMPKα leading to apoptosis of neuronal cells. *Lab. Investig.* 90, 762–773.

Chen, X., Zhao, P., Ouyang, L., Zhu, L., Ni, G., and Schäfer, K. V. (2020). Whole-plant water hydraulic integrity to predict drought-induced Eucalyptus urophylla mortality under drought stress. *For. Ecol. Manag.* 468:118179.

Choinski, J. Jr., and Johnson, J. (1993). Changes in photosynthesis and water status of developing leaves of *Brachystegia spiciformis* Benth. *Tree Physiol.* 13, 17–27.

Chowardhara, B., Borgohain, P., Saha, B., Awasthi, J. P., and Panda, S. K. (2020). Differential oxidative stress responses in *Brassica juncea* (L.) Czern and Coss cultivars induced by cadmium at germination and early seedling stage. *Acta Physiol. Plant.* 42, 1–12.

Chutipaijit, S., Chaum, S., and Sompornpailin, K. (2011). High contents of proline and anthocyanin increase protective response to salinity in *Oryza sativa* L. spp. indica. *Aust. J. Crop. Sci.* 5, 1191–1198.

Cirillo, V., D'Amelia, V., Esposito, M., Amitrano, C., Carillo, P., Carputo, D., et al. (2021). Anthocyanins are key regulators of drought stress tolerance in tobacco. *Biology* 10:139.

Dąbrowski, P., Baczewska-Dąbrowska, A. H., Kalaji, H. M., Goltsev, V., Paunov, M., Rapacz, M., et al. (2019). Exploration of chlorophyll a fluorescence and plant gas exchange parameters as indicators of drought tolerance in perennial ryegrass. *Sensors* 19:2736.

Dai, L., Li, J., Harmens, H., Zheng, X., and Zhang, C. (2020). Melatonin enhances drought resistance by regulating leaf stomatal behaviour, root growth and catalase activity in two contrasting rapeseed (*Brassica napus* L.) genotypes. *Plant Physiol. Biochem.* 149, 86–95.

Dionisio-Sese, M. L., and Tobita, S. (1998). Antioxidant responses of rice seedlings to salinity stress. *Plant Sci.* 135, 1–9.

Dun, X., Tao, Z., Wang, J., et al. (2016). Comparative transcriptome analysis of primary roots of *Brassica napus* seedlings with extremely different primary root lengths using RNA sequencing. *Front. Plant Sci.* 7:1238. doi: 10.3389/fpls.2016.01238

Earley, K. W., Haag, J. R., Pontes, O., Opper, K., Juehne, T., Song, K., et al. (2006). Gateway-compatible vectors for plant functional genomics and proteomics. *Plant J.* 45, 616–629.

Evaristo de Deus, K., Lanna, A. C., Abreu, F. R. M., Dias Silveira, R. D., Jacinto Pereira, W., Brondani, C., et al. (2015). Molecular and biochemical characterization of superoxide dismutase (SOD) in upland rice under drought. *Aust. J. Crop. Sci.* 9:53643644.

Falcone Ferreyra, M. L., Rius, S., and Casati, P. (2012). Flavonoids: biosynthesis, biological functions, and biotechnological applications. *Front. Plant Sci.* 3:222. doi: 10.3389/fpls.2012.00222

Farooq, M. A., Ali, S., Hameed, A., Ishaque, W., Mahmood, K., and Iqbal, Z. (2013). Alleviation of cadmium toxicity by silicon is related to elevated photosynthesis, antioxidant enzymes; suppressed cadmium uptake and oxidative stress in cotton. *Ecotoxicol. Environ. Saf.* 96, 242–249.

Farooq, M. A., Gill, R. A., Ali, B., Wang, J., Islam, F., Ali, S., et al. (2016). Subcellular distribution, modulation of antioxidant and stress-related genes response to arsenic in *Brassica napus* L. *Ecotoxicology* 25, 350–366.

Feild, T. S., Lee, D. W., and Holbrook, N. M. (2001). Why leaves turn red in autumn. The role of anthocyanins in senescing leaves of red-osier dogwood. *Plant Physiol.* 127, 566–574.

Fong, J., Schaffer, F. L., and Kirk, P. L. (1953). The ultramicrodetermination of glycogen in liver. A comparison of the anthrone and reducing-sugar methods. *Arch. Biochem. Biophys.* 45, 319–326.

Gharibi, S., Tabatabaei, B. E. S., Saeidi, G., Talebi, M., and Matkowski, A. (2019). The effect of drought stress on polyphenolic compounds and expression of flavonoid biosynthesis related genes in *Achillea pachycephala* Rech.F. *Phytochemistry* 162, 90–98.

Golding, A. J., and Johnson, G. N. (2003). Down-regulation of linear and activation of cyclic electron transport during drought. *Planta* 218, 107–114.

Grieco, M., Roustan, V., Dermendjiev, G., Rantala, S., Jain, A., Leonardelli, M., et al. (2020). Adjustment of photosynthetic activity to drought and fluctuating light in wheat. *Plant Cell Environ.* 43, 1484–1500.

Hatier, J. H. B., and Gould, K. S. (2008). "Anthocyanin function in vegetative organs," in *Anthocyanins*. New York, NY: Springer, 1–9.

He, X., Li, Y., Lawson, D., and Xie, D. Y. (2017). Metabolic engineering of anthocyanins in dark tobacco varieties. *Physiol. Plant.* 159, 2–12.

He, F., Thiele, B., Santhiraraja-Abresch, S., Watt, M., Kraska, T., Ulbrich, A., et al. (2020). Effects of root temperature on the plant growth and food quality of Chinese broccoli (*Brassica oleracea var. alboglabra* bailey). *Agronomy* 10:702.

Hichri, I., Barrieu, F., Bogs, J., Kappel, C., Delrot, S., and Lauvergeat, V. (2011). Recent advances in the transcriptional regulation of the flavonoid biosynthetic pathway. *J. Exp. Bot.* 62, 2465–2483.

Hong, T. B., Rahumatullah, A., Yogarajah, T., Ahmad, M., and Yin, K. B. (2010). Potential effects of chrysin on MDA-MB-231 cells. *Int. J. Mol. Sci.* 11, 1057–1069.

Hughes, N., Neufeld, H., and Burkey, K. (2005). Functional role of anthocyanins in high-light winter leaves of the evergreen herb *Galax urceolata*. *New Phytol.* 168, 575–587.

Islam, F., Ali, B., Wang, J., Farooq, M. A., Gill, R. A., Ali, S., et al. (2016). Combined herbicide and saline stress differentially modulates hormonal regulation and antioxidant defense system in *Oryza sativa* cultivars. *Plant Physiol. Biochem.* 107, 82–95.

Javed, M., Ashraf, M., Iqbal, M., Farooq, M. A., Zafar, Z. U., and Athar, H.-u.-R. (2022). Chlorophyll fluorescence, ion uptake, and osmoregulation are potential indicators for detecting ecotypic variation in salt tolerance of *Panicum antidotale* Retz. *Arid Land Res. Manage.* 36, 84–108.

Kaku, S., Iwaya-Inoue, M., and Toki, K. (1992). Anthocyanin influence on water proton NMR relaxation times and water contents in leaves of evergreen woody plants during the winter. *Plant Cell Physiol.* 33, 131–137.

Kaldenhoff, R., Bertl, A., Otto, B., Moshelion, M., and Uehlein, N. (2007). Characterization of plant aquaporins. *Methods Enzymol.* 428, 505–531.

Khadka, K., Earl, H. J., Raizada, M. N., and Navabi, A. (2020). A physio-morphological trait-based approach for breeding drought tolerant wheat. *Front. Plant Sci.* 11:715. doi: 10.3389/fpls.2018.01739

Khanzada, H., Wassan, G. M., He, H., Mason, A. S., Keerio, A. A., Khanzada, S., et al. (2020). Differentially evolved drought stress indices determine the genetic variation of *Brassica napus* at seedling traits by genome-wide association mapping. *J. Adv. Res.* 24, 447–461.

Kim, J., Lee, W. J., Vu, T. T., Jeong, C. Y., Hong, S.-W., and Lee, H. (2017). High accumulation of anthocyanins via the ectopic expression of AtDFR confers significant salt stress tolerance in *Brassica napus* L. *Plant Cell Rep.* 36, 1215–1224.

Lawlor, D. W., and Tezara, W. (2009). Causes of decreased photosynthetic rate and metabolic capacity in water-deficient leaf cells: a critical evaluation of mechanisms and integration of processes. *Ann. Bot.* 103, 561–579.

Li, X., Gao, M.-J., Pan, H.-Y., Cui, D.-J., and Gruber, M. Y. (2010). Purple canola: Arabidopsis PAP1 increases antioxidants and phenolics in *Brassica napus* leaves. *J. Agric. Food Chem.* 58, 1639–1645.

Li, P., Li, Y. J., Zhang, F. J., Zhang, G. Z., Jiang, X. Y., Yu, H. M., et al. (2017a). The Arabidopsis UDP-glycosyltransferases UGT79B2 and UGT79B3, contribute to cold, salt and drought stress tolerance via modulating anthocyanin accumulation. *Plant J.* 89, 85–103.

Li, Q., Yu, H.-M., Meng, X.-F., Lin, J.-S., Li, Y.-J., and Hou, B.-K. (2017b). Ectopic expression of glycosyltransferase UGT76E11 increases flavonoid accumulation and enhances abiotic stress tolerance in Arabidopsis. *Plant Biol.* 20, 10–19. doi: 10.1111/plb.12627

Martinez, V., Mestre, T. C., Rubio, F., Girones-Vilaplana, A., Moreno, D. A., Mittler, R., et al. (2016). Accumulation of flavonols over hydroxycinnamic acids favors oxidative damage protection under abiotic stress. *Front. Plant Sci.* 7:838. doi: 10.3389/fpls.2016.00838

Mbarki, S., Sytar, O., Cerda, A., Zivcak, M., Rastogi, A., He, X., et al. (2018). "Strategies to mitigate the salt stress effects on photosynthetic apparatus and productivity of crop plants," in *Salinity Responses and Tolerance in Plants. Vol. 1.* Cham: Springer, 85–136.

Merzlyak, M. N., Chivkunova, O. B., Solovchenko, A. E., and Naqvi, K. R. (2008). Light absorption by anthocyanins in juvenile, stressed, and senescing leaves. *J. Exp. Bot.* 59, 3903–3911.

Mir, R. A., Argal, S., Ahanger, M. A., Tomar, N. S., and Agarwal, R. (2021). Variation in phenolic compounds, antioxidant activity and Osmotica of different cultivars of *Tagetes erecta* L. at different growth stages and effect of its leachates on germination and growth of wheat (*Triticum aestivum* L.). *J. Plant Growth Regul.* 41, 907–921.

Mittler, R., Vanderauwera, S., Gollery, M., and Van Breusegem, F. (2004). Reactive oxygen gene network of plants. *Trends Plant Sci.* 9, 490–498.

Momoh, E., and Zhou, W. (2001). Growth and yield responses to plant density and stage of transplanting in winter oilseed rape (*Brassica napus* L.). *J. Agron. Crop Sci.* 186, 253–259.

Naing, A. H., Park, K. I., Ai, T. N., Chung, M. Y., Han, J. S., Kang, Y.-W., et al. (2017). Overexpression of snapdragon Delila (DEL) gene in tobacco enhances anthocyanin accumulation and abiotic stress tolerance. *BMC Plant Biol.* 17:65. doi: 10.1186/s12870-017-1015-5

Naing, A. H., Park, D. Y., Park, K. I., and Kim, C. K. (2018). Differential expression of anthocyanin structural genes and transcription factors determines coloration patterns in gerbera flowers. 3. *Biotech* 8, 1–12.

Nakabayashi, R., Yonekura-Sakakibara, K., Urano, K., Suzuki, M., Yamada, Y., Nishizawa, T., et al. (2014). Enhancement of oxidative and drought tolerance in Arabidopsis by overaccumulation of antioxidant flavonoids. *Plant J.* 77, 367–379.

Neill, S. O., and Gould, K. S. (2003). Anthocyanins in leaves: light attenuators or antioxidants? *Funct. Plant Biol.* 30, 865–873.

Pakdel, H., Hassani, S. B., Ghotbi-Ravandi, A. A., and Bernard, F. (2020). Contrasting the expression pattern change of polyamine oxidase genes and photosynthetic efficiency of maize (*Zea mays* L.) genotypes under drought stress. *J. Biosci. (Bangalore)* 45, 1–12.

Pan, C., Ahammed, G. J., Li, X., and Shi, K. (2018). Elevated CO_2 improves photosynthesis under high temperature by attenuating the functional limitations to energy fluxes, electron transport and redox homeostasis in tomato leaves. *Front. Plant Sci.* 9:1739. doi: 10.3389/fpls.2018.01739

Petroni, K., and Tonelli, C. (2011). Recent advances on the regulation of anthocyanin synthesis in reproductive organs. *Plant Sci.* 181, 219–229.

Petrussa, E., Braidot, E., Zancani, M., Peresson, C., Bertolini, A., Patui, S., et al. (2013). Plant flavonoids—biosynthesis, transport and involvement in stress responses. *Int. J. Mol. Sci.* 14, 14950–14973. doi: 10.3390/ijms140714950

Ray, R. L., Ampim, P. A., and Gao, M. (2020). "Crop protection under drought stress," in *Crop Protection under Changing Climate* (New York: Springer), 145–170.

Rogers, L. K. (2020). Cellular targets of oxidative stress. *Current Opinion in Toxicology* 20, 48–54.

Romero-Puertas, M., Rodríguez-Serrano, M., Corpas, F., Gomez, M.d., Del Rio, L., and Sandalio, L. (2004). Cadmium-induced subcellular accumulation of O2·− and H_2O_2 in pea leaves. *Plant Cell Environ.* 27, 1122–1134.

Saha, B., Mishra, S., Awasthi, J. P., Sahoo, L., and Panda, S. K. (2016). Enhanced drought and salinity tolerance in transgenic mustard [*Brassica juncea* (L.) Czern & Coss.] overexpressing Arabidopsis group 4 late embryogenesis abundant gene (AtLEA4-1). *Environ. Exp. Bot.* 128, 99–111.

Samanta, S., Singh, A., and Roychoudhury, A. (2020). "Involvement of sulfur in the regulation of abiotic stress tolerance in plants," in *Protective Chemical Agents in the Amelioration of plant abiotic Stress: Biochemical and Molecular Perspectives*. eds. A. Roychoudhury and D. K. Tripathi (Hoboken, NJ: John Wiley & Sons Ltd.), 437–466.

Schwinn, K. E., Boase, M. R., Bradley, J. M., Lewis, D. H., Deroles, S. C., Martin, C. R., et al. (2014). MYB and bHLH transcription factor transgenes increase anthocyanin pigmentation in petunia and lisianthus plants, and the petunia phenotypes are strongly enhanced under field conditions. *Front. Plant Sci.* 5:603. doi: 10.3389/fpls.2014.00603

Shawon, R. A., Kang, B. S., Lee, S. G., Kim, S. K., Lee, H. J., Katrich, E., et al. (2020). Influence of drought stress on bioactive compounds, antioxidant enzymes and glucosinolate contents of Chinese cabbage (*Brassica rapa*). *Food Chem.* 308:125657.

Shen, J., Guo, M.-J., Wang, Y.-G., Yuan, X.-Y., Wen, Y.-Y., Song, X.-E., et al. (2020). Humic acid improves the physiological and photosynthetic characteristics of millet seedlings under drought stress. *Plant Signal. Behav.* 15:1774212.

Shi, G. Q., Fu, J. Y., Rong, L. J., Zhang, P. Y., Guo, C. J., and Xiao, K. (2018). TaMIR1119, a miRNA family member of wheat (*Triticum aestivum*), is essential in the regulation of plant drought tolerance. *J. Integr. Agric.* 17, 5–14.

Sofo, A., Tuzio, A. C., Dichio, B., and Xiloyannis, C. (2005). Influence of water deficit and rewatering on the components of the ascorbate–glutathione cycle in four interspecific Prunus hybrids. *Plant Sci.* 169, 403–412.

Sperdouli, I., and Moustakas, M. (2012). Interaction of proline, sugars, and anthocyanins during photosynthetic acclimation of *Arabidopsis thaliana* to drought stress. *J. Plant Physiol.* 169, 577–585. doi: 10.1016/j.jplph.2011.12.015

Sun, M., Feng, X.-X., Gao, J.-J., Peng, R.-H., Yao, Q.-H., and Wang, L.-J. (2017). VvMYBA6 in the promotion of anthocyanin biosynthesis and salt tolerance in transgenic *Arabidopsis*. *Plant Biotechnol. Rep.* 11, 299–314.

Verma, D., Upadhyay, S. K., and Singh, K. (2021). Characterization of APX and APX-R gene family in *Brassica juncea* and *B. rapa* for tolerance against abiotic stresses. *Plant Cell Rep.* 41, 571–592.

Wang, F., Ren, G., Li, F., Qi, S., Xu, Y., Wang, B., et al. (2018). A chalcone synthase gene AECHS from *Abelmoschus esculentus* regulates flavonoid accumulation and abiotic stress tolerance in transgenic arabidopsis. *Acta Physiol. Plant.* 40:97. doi: 10.1007/s11738-018-2680-1

Wang, F., Zhu, H., Kong, W., Peng, R., Liu, Q., and Yao, Q. (2016). The antirrhinum AmDEL gene enhances flavonoids accumulation and salt and drought tolerance in transgenic arabidopsis. *Planta* 244, 59–73. doi: 10.1007/s00425-016-2489-3

Xia, L., Yang, L., Sun, N., Li, J., Fang, Y., and Wang, Y. (2016). Physiological and antioxidant enzyme gene expression analysis reveals the improved tolerance to drought stress of the somatic hybrid offspring of *Brassica napus* and *Sinapis alba* at vegetative stage. *Acta Physiol. Plant.* 38, 1–10.

Yamasaki, H., Sakihama, Y., and Ikehara, N. (1997). Flavonoid-peroxidase reaction as a detoxification mechanism of plant cells against H_2O_2. *Plant Physiol.* 115, 1405–1412.

Zhang, Y., Butelli, E., and Martin, C. (2014). Engineering anthocyanin biosynthesis in plants. *Curr. Opin. Plant Biol.* 19, 81–90.

Zhang, H., Guo, C., Li, C., and Xiao, K. (2008). Cloning, characterization and expression analysis of two superoxide dismutase (SOD) genes in wheat (*Triticum aestivum* L.). *Front. Agric. China* 2, 141–149.

Zhang, C., Shi, S., Wang, B., and Zhao, J. (2018). Physiological and biochemical changes in different drought-tolerant alfalfa (*Medicago sativa* L.) varieties under PEG-induced drought stress. *Acta Physiol. Plant.* 40, 1–15.

Zhang, F.-J., Zhang, K.-K., Du, C.-Z., Li, J., Xing, Y.-X., Yang, L.-T., et al. (2015). Effect of drought stress on anatomical structure and chloroplast ultrastructure in leaves of sugarcane. *Sugar Tech* 17, 41–48.

Zhou, W., and Leul, M. (1998). Uniconazole-induced alleviation of freezing injury in relation to changes in hormonal balance, enzyme activities and lipid peroxidation in winter rape. *Plant Growth Regul.* 26, 41–47.

Zlatev, Z., Lidon, F., Ramalho, J., and Yordanov, I. (2006). Comparison of resistance to drought of three bean cultivars. *Biol. Plant.* 50, 389–394.

Złotek, U., Szymanowska, U., Baraniak, B., and Karaś, M. (2015). Antioxidant activity of polyphenols of adzuki bean (vigna angularis) germinated in abiotic stress conditions. *Acta Sci. Pol. Technol. Aliment.* 14, 55–63. doi: 10.17306/j.afs.2015.1.6

frontiers | Frontiers in Plant Science

TYPE Original Research
PUBLISHED 01 August 2022
DOI 10.3389/fpls.2022.942359

Check for updates

OPEN ACCESS

EDITED BY
Bhaskar Gupta,
Government General Degree College,
Singur, India

REVIEWED BY
Jesus Alfredo Rosas Rodríguez,
University of Sonora, Mexico
Cinzia Montemurro,
University of Bari Aldo Moro, Italy

*CORRESPONDENCE
Jishan Xiang
xiangjsh@126.com
Xiaoke Zhang
zhangxiaoke66@126.com

SPECIALTY SECTION
This article was submitted to
Plant Abiotic Stress,
a section of the journal
Frontiers in Plant Science

RECEIVED 12 May 2022
ACCEPTED 13 July 2022
PUBLISHED 01 August 2022

CITATION
Yu M, Yu Y, Guo S, Zhang M, Li N, Zhang S, Zhou H, Wei F, Song T, Cheng J, Fan Q, Shi C, Feng W, Wang Y, Xiang J and Zhang X (2022) Identification of *TaBADH-A1* allele for improving drought resistance and salt tolerance in wheat (*Triticum aestivum* L.).
Front. Plant Sci. 13:942359.
doi: 10.3389/fpls.2022.942359

COPYRIGHT
© 2022 Yu, Yu, Guo, Zhang, Li, Zhang, Zhou, Wei, Song, Cheng, Fan, Shi, Feng, Wang, Xiang and Zhang. This is an open-access article distributed under the terms of the Creative Commons Attribution License (CC BY). The use, distribution or reproduction in other forums is permitted, provided the original author(s) and the copyright owner(s) are credited and that the original publication in this journal is cited, in accordance with accepted academic practice. No use, distribution or reproduction is permitted which does not comply with these terms.

Identification of *TaBADH-A1* allele for improving drought resistance and salt tolerance in wheat (*Triticum aestivum* L.)

Ming Yu[1], Yang Yu[1], Sihai Guo[1], Mingfei Zhang[2], Nan Li[2], Shuangxing Zhang[1], Hongwei Zhou[1], Fan Wei[1], Tianqi Song[1], Jie Cheng[1], Qiru Fan[1], Caiyin Shi[1], Wenhan Feng[1], Yukun Wang[1], Jishan Xiang[2]* and Xiaoke Zhang[1]*

[1]College of Agronomy, Northwest A&F University, Xianyang, China, [2]Academy of Agricultural Sciences, Key Laboratory of Agro-Ecological Protection & Exploitation and Utilization of Animal and Plant Resources in Eastern Inner Mongolia, Chifeng University, Chifeng, China

Drought and salt stress can strongly affect the growth and development of wheat. Wheat adapts to drought and salt stress through osmotic regulation. Betaine aldehyde dehydrogenase (BADH) is a key enzyme in the synthesis of betaine, an osmotic regulator. We cloned a region of the *TaBADH-A1* promoter and genomic DNA that included the introns and exons, from four Chinese wheat cultivars. Following the analysis of *TaBADH-A1* genomic DNA and promoter sequence polymorphisms of 4 cloned and 15 cultivars from the database, 7 haplotypes of *TaBADH-A1* gene were identified. We divided the 7 haplotypes with a 254bp insertion or deletion (indel) into two main alleles, *BADH-A1a* and *BADH-A1b*. Meanwhile, a molecular marker was developed based on the 254bp indel of the third intron of *TaBADH-A1* gene. Expression levels of *BADH-A1b* were found to be significantly higher than those of *BADH-A1a* under drought and salt stress conditions. Betaine accumulation was significantly higher in wheat containing *BADH-A1b* compared to *BADH-A1a* under drought and salt stress. We also identified that the average relative germination and survival rates of wheat with the *BADH-A1b* allele were significantly higher than wheat with the *BADH-A1a* allele. The results reveal that wheat containing *BADH-A1b* has stronger drought and salt tolerance than wheat with *BADH-A1a*. Meanwhile, the geographic distribution and frequency of the *TaBADH-A1* locus alleles indicate that *BADH-A1a* has been preferred in Chinese wheat breeding programs, while *BADH-A1b*, associated with favorable stress tolerance, has been neglected. The results of this study provide evidence for an excellent candidate allele for marker-assisted selection of new wheat cultivars with increased salt tolerance and drought resistance.

KEYWORDS

wheat, drought, salt, *TaBADH-A1*, allele

Introduction

It is well known that wheat is one of the most important and widely cultivated cereals, supporting the daily caloric and protein requirements of 60% of the world's population (Tadesse et al., 2017). Drought has become a serious environmental problem due to global climate change, and a reduction of water by up to 40% causes a reduction in wheat yield of up to 21% (Younis et al., 2020). At the same time, salinization is also an important factor in reduced crop productivity. Salt issues affect about 20% of the total global land area and almost 40% of irrigated lands; this phenomenon shows an increasing trend, and 50% of total cultivated land worldwide is projected to be salinized by 2050 (Urbanavičiūtė et al., 2021). Among all abiotic stresses, stress due to drought and salt is the main challenge for plant growth and development, causing great damage to food production worldwide (Ma et al., 2020). Therefore, improving the drought and salt tolerance is an urgent problem to be solved in wheat breeding. One effective way to improve drought and salt resistance in wheat is to explore and utilize excellent alleles of genes related to drought resistance and salt tolerance.

Both drought and salt stress trigger osmotic regulation in plants, which is the main component of the physiological mechanism determining the drought resistance and salt tolerance of plants (Khoshro et al., 2013; Zhu, 2016). Under drought and salt stress, there is an increased accumulation of substances involved in osmotic regulation, such as betaine, proline, soluble sugar, and inorganic ions, which decreases the osmotic potential and increases the osmotic pressure of cells, resulting in buffering of the redox potential and the maintenance of protein structure, and photosynthetic organs are protected from stress damage (Gadallah, 1999; Mäkelä et al., 2000; Cha-Um and Kirdmanee, 2010; Wang et al., 2018). Betaine, an important osmotic regulatory substance, also has multiple functions in reducing cell osmotic potential and increasing cell osmotic pressure to protect plants from abiotic stress (Zhang et al., 2020). Betaine aldehyde dehydrogenase (BADH) is an important enzyme that catalyzes the final step of betaine production (Fujiwara et al., 2008). The *BADH* gene was first cloned in *Spinacia oleracea* (Weretilnyk and Hanson, 1990) and has, to date been isolated in a large number of plants, such as *Sesuvium portulacastrum*, *Amaranthus hypochondriacus* L., *Arabidopsis thaliana*, and *Triticum aestivum* L. (Legaria et al., 1998; Missihoun et al., 2011; Yang et al., 2015; Sun et al., 2019). Previous studies have shown that *BADH* overexpression in plants can increase their tolerance to various abiotic stresses (Fan et al., 2012; Yang et al., 2015; Sun et al., 2019). For example, overexpression of *SoBADH* (*S. oleracea*) in transgenic sweet potato improved tolerance to salt and oxidative stress and low temperature by increasing betaine accumulation (Fan et al., 2012). Overexpression of *SpBADH* (*S. portulacastrum*) in *Arabidopsis* resulted in higher betaine content and increased tolerance to drought/osmotic stress (Yang et al., 2015). Overexpression of *TaBADH* (*T. aestivum* L.) in *Arabidopsis* was found to enhance betaine accumulation and salt tolerance (Sun et al., 2019). The betaine content and *TaBADH* expression level of different wheat cultivars were found to be significantly different under abiotic stresses such as drought and salt (Jing et al., 1999; Zhao et al., 2001; Li et al., 2005). We speculate that there may be differences in the transcriptional regulatory sequences of the *TaBADH* that lead to the differing betaine contents of the various wheat cultivars.

In the process of evolution, domestication, and breeding, wheat has undergone two doublings, *via* crossing, in reaching its present polyploid form. Since the A genome is the basic genome of wheat evolution, it plays a central role in the evolution of polyploid wheat, contributing to its rich genetic diversity. In this study, we analyzed the *TaBADH-A1* gene sequence polymorphisms in 19 wheat cultivars, evaluated the drought resistance and salt tolerance of *TaBADH-A1* locus alleles, and explored the molecular and physiological mechanisms, and this information was used in the development of a functional molecular marker, 6 AM. We also explored the correlation between *TaBADH-A1* locus alleles and agronomic traits, the distribution of alleles in Chinese wheat zones, and the occurrence frequency of *TaBADH-A1* locus alleles in wheat breeding years. As a result of our study, we present an excellent candidate allele for the molecular breeding of wheat with improved drought and salt tolerance.

Materials and methods

Plant materials

Four Chinese wheat cultivars (Taishan 1, Zhongmai 9, Bima 4, and Lantian 23) with different levels of adaptability were selected for cloning *TaBADH-A1*. Taishan 1 has the excellent characteristic of strong resistance to stress; Zhongmai 9 withstood the rare occurrence of freezing damage in 1993–1994 and exhibits strong resistance to abiotic stresses; Bima 4 is one of the backbone parents of wheat in China with a large cultivation area, and it is planted in regions with sufficient water and fertilizer; and Lantian 23 is a high-yielding cultivar adapted to abundant water and fertile conditions. A set of nulli-tetrasomic lines of Chinese Spring (N6AT6B, N6BT6D, and N6DT6A) was used as PCR template, agarose gel electrophoresis results as a reference for the chromosome localization of primers. A total of 121 wheat cultivars (lines; population 1) in different ecological regions covering 10 wheat-producing areas in China were selected for the identification of drought resistance at the germination stage to evaluate the drought resistance of different alleles. Using Chinese Spring and Yanfu 188 as parents, a population of F_6 recombinant inbred lines (population 2) was constructed to verify the drought and salt resistance of *TaBADH-A1* locus different alleles. Similarly, another population of F_6 recombinant inbred lines (population 3) was created using Chinese Spring and Ning 9940; two F_6 populations were obtained using the single-seed descent approach. The relationship between *TaBADH-A1* locus alleles and agronomic traits was validated in both populations. A wheat mini-core collection (population 4, 262 cultivars (lines; landraces), provided by Chenyang Hao at the Chinese Academy of Agricultural Sciences), which is characterized by wide geographic distribution,

was used for geographic distribution analysis of the *TaBADH-A1* locus alleles. In addition, 121 cultivars (lines; population 1) also were selected to analyze the geographic distribution and frequency of *TaBADH-A1* locus alleles in breeding years.

DNA extraction, *TaBADH-A1* gene cloning, and sequence analysis

Genomic DNA of the 4 wheat cultivars (Taishan1, Bima 4, Zhongmai 9, and Lantian 23) and 4 populations was extracted using the CTAB method (Stein et al., 2010). *TaBADH-A1*-specific primers were designed (Supplementary Table S1) according to the assembled *TaBADH-A1* sequences (*TraesCS6A02G371100*) using Oligo 7.0 software. Subsequently, a region of the promoter and genomic DNA sequence that includes the introns and exons of *TaBADH-A1* was cloned from each of the 4 cultivars. The PCR system details are as follows: 50 µl reactions contained 2 µl each of forward and reverse primers (10 µM) and 2 µl DNA (300 ng·µL^{-1}), 25 µl of 2 × Phanta Max Buffer, 1 µl dNTP Mix, 1 µl Phanta Max Super-Fidelity DNA Polymerase, and 17 µl ddH_2O. The PCR program comprised a cycle of 95°C for 3 min followed by 34 cycles of 95°C for 15 s, 62°C for 15 s, and 72°C for 8 min, followed by 95°C for 15 s, 62°C for 15 s, and 72°C for 8 min, and finally 72°C for 5 min (Phanta Max Super-Fidelity DNA Polymerase, Vazyme).

Sequences for the *TaBADH-A1* promoter and genomic region including introns and exon of 15 wheat cultivars (ArinaLrFor, Cadenza, Claire, Jagger, Julius, Lancer, Paragon, SY Mattis, Robigus, Weebill, Stanley, Landmark, Norin 61, Mace, and Chinese Spring) were downloaded from the Ensembl Plants database[1]. The *TaBADH-A1* gene sequence polymorphisms were analyzed in Taishan 1, Bima 4, Zhongmai 9, Lantian 23, and the 15 wheat cultivars. To analyze the *TaBADH-A1* sequences of genomic (include intron and exon) and promoter regions, the Giri[2] and PlantCare[3] databases were used for the prediction of transposons and *cis*-acting elements. DNAMAN 9.0 software was used for sequence alignment.

Development of a molecular marker

After analyzing the *TaBADH-A1* gene sequence polymorphism in Taishan 1, Bima 4, Zhongmai 9, Lantian 23, and 15 wheat cultivars based on sequences from the database, the molecular marker 6 AM was developed based on the insertion/deletion (indel) of 254 bp in the third intron region. Primers for the molecular marker 6 AM were designed as 5′-CGCAAG TCAATGGGCTGTGTAT-3′ and 5′-CAAGACAGGAGGGGAA TGGGAAAT-3′. The PCR system components were as follows: 10 µl of 2× Rapid Taq Master Mix, 7 µl ddH_2O, 1 µl 6 AM-F (10 µM), 1 µl 6 AM-R (10 µM), and1 µL DNA (300 ng·µL^{-1}; Rapid Taq Master Mix, Vazyme). The PCR program for 6 AM comprised a cycle at 95°C for 3 min, 95°C for 15 s, 62°C for 15 s, and 72°C for 15 s, followed by 34 additional cycles of 95°C for 15 s, 62°C for 15 s, and 72°C for 15 s, and finally 72°C for 5 min. The PCR products were separated on 2% agarose gel. The primer pairs were located by PCR amplification using the nulli-tetrasomic lines of Chinese Spring as a template. The validity of the 6 AM primers was verified using PCR-based amplified fragment length polymorphism. Genotyping was performed in population 1, 2, 3, and 4 using the 6 AM molecular marker to characterize the function of alleles.

RNA extraction and qRT-PCR analysis

The 5 randomly selected recombination inbred lines (population 2), Yanfu 188, and Bima 4 with the *BADH-A1a* allele and the 5 randomly selected lines of population 2, Taishan 1, and Chinese Spring with the *BADH-A1b* allele were planted in half-strength Hoagland nutrient solution in a light incubator at 22°C under controlled conditions (60% relative humidity, 16/8 h light/dark cycle). At 4-leaf stage seedlings, Yanfu 188, Bima 4, Taishan 1, and Chinese Spring leaf samples were collected at untreated 0, 1, 6, 12, and 24 h. Subsequently, all wheat at 4-leaf stage seedlings were treated with half-strength Hoagland nutrient solution containing 200 mM NaCl or 20% PEG 6000. Leaf samples were collected at treated 0, 1, 6, 12, and 24 h. All samples were immediately stored at −80°C for further RNA extraction.

Total RNA was extracted using TRIzol (Qingke, Beijing), and cDNA was then synthesized using EasyScript One-Step gDNA Removal and cDNA Synthesis SuperMix (TransGen Biotech, Beijing). Quantitative real-time PCR (qRT-PCR) was performed using Perfect Start™ Green qPCR Supermix (TransGen Biotech, Beijing). *TaActin* was used as an internal reference gene for wheat. All qRT-PCR analyses were conducted in this study based on 3 technical replicates and 3 biological replicates. Relative gene expression levels were calculated using the $2^{-\Delta\Delta Ct}$ method (Ma et al., 2020).

Betaine content determination

The materials used for expression analysis, Ning 9940 with *BADH-A1a* allele and Longfumai 18 with *BADH-A1b* allele, were grown and treated in the same way as above (RNA extraction and qRT-PCR analysis section). Leaf samples were collected from Longfumai 18, Taishan 1, Chinese Spring, Bima 4, Yanfu 188, and Ning 9940 to determine betaine content after plants had undergone stress treatments for 0, 1, 6, 12, 24, and 48 h with half-strength Hoagland nutrient solution containing 200 mM NaCl or 20% PEG 6000. Similarly, population 2 leaf samples were collected after stress treatment for 48 h with half-strength Hoagland nutrient solution

1 https://plants.ensembl.org/index.html
2 https://www.rosaceae.org/
3 https://bioinformatics.psb.ugent.be/webtools/plantcare/html/

containing 200 mM NaCl or 20% PEG 6000. All the samples were dried, each 0.2 g dry weight sample was thoroughly mixed with 1 mL of 80% methanol at 60°C for 30 min and centrifuged at 10,000 rpm for 15 min, and the supernatant from the sample that had absorbed methanol was completely volatilized to a constant volume of 1 ml as the sample solution. Betaine solutions at 0.1, 0.2, 0.3, 0.4, 0.5, 0.6, 0.7, 0.8, 0.9, and 1.0 $mg{\cdot}L^{-1}$ were prepared as standard solutions, with ddH_2O as the blank or negative control. Then, 0.1 mL each of sample solution, standard solution, and ddH_2O was thoroughly and separately mixed with 1 ml of saturated Reinecke salt solution (pH = 1) and incubated at 4°C for 2 h, centrifuged at 8000 rpm for 15 min, then the supernatant was removed and mixed with ether, followed by centrifuging at 8000 rpm for 15 min, and the supernatant from this step was then mixed with 70% acetone. The absorbance of this mixture was then measured at 525 nm. A standard curve was drawn using the absorbance values of the standard solutions. The experimental method and the formula for calculation of betaine content were used as indicated in the instructions of the Solarbio betaine content detection kit (BC3130). Three biological and technical replicates were analyzed for each condition.

Identification of drought resistance and salt tolerance in wheat

The drought resistance of 121 cultivars (lines; population 1) at the germination stage was characterized. A total of 100 seeds were placed into a $12 \times 12 \times 5\ cm^3$ germinating box, and single-layer filter paper was used as the sprout bed. Then, 12 mL of 20% PEG 6000 was added to the treatment group and 12 mL of ddH_2O was added to the control group. A further 100 seeds were used as replicates, and the experiments for the treatment and control groups were repeated 4 times each. The standard for wheat seed germination was defined as the point at which the length of the wheat radicle was equal to the length of the seed and the length of the germ reached half the length of the seed. The number of germinated seeds was investigated, and the relative germination rate of seeds was calculated after 168 h of culture at 20°C in the dark as a ratio of the germination rate of the treatment group divided by that of the control group.

Five lines with *BADH-A1a* and five lines with *BADH-A1b* from the recombination inbred lines (population 2) were planted in pots with nutritive soil (matrix of soil: vermiculite = 3:1) in a light incubator. The flowerpot dimensions were $10 \times 10\ cm^2$ at the top, $7.5 \times 7.5\ cm^2$ at the bottom, and 7.5 cm high, and each pot was filled with 165 g of nutritious soil and planted with 4 wheat seedlings. Drought and salinity stress treatments were imposed at the 4-leaf stage. Under drought treatment, wheat plants were deprived of water for 15 days and then re-watered for 5 days. Under salt stress treatment, wheat plants were irrigated with H_2O solution containing 700 mM NaCl for 25 days. The ultimate number of surviving plants and survival rates were determined. Each experiment (with each line including 36 wheat plants) was repeated 3 times.

Field management and investigation of agronomic traits

In 2020, a total of 194 lines from population 2 and 182 lines from population 3 were planted in Yangling (34°16' N, 108°4′ E; Shaanxi Province, China). Each line was planted in one 0.5 m row, with about 20–30 plants in each row, spaced 25 cm apart in each row. Compound (20% nitrogen, 18% phosphorus, 5% potassium; 300 kg/ha) and nitrogen (46% nitrogen; 300 kg/ha) fertilizers were applied to the wheat before planting. The field was irrigated in December 2020. Data on agronomic traits, including grain number per spike (GN), effective spikelet number per spike (ESN), thousand kernel weight (TKW), flag leaf area per plant (FLA), spike length (SL), length of last internode (LLI), and plant height (PH), were collected from populations 2 and 3. Three plants from each strain were randomly selected to measure GN, ESN, FLA, SL, LLI, and PH. The average values of the measurements were taken as the value for each agronomic trait. Spikelets containing grains were defined as effective spikelets. FLA was calculated as 0.7 × leaf length × leaf width. SL, LLI, and PH were measured from the bottom to the top of the spike, from the last internode to the bottom of the spike, and from ground level to the tip of the spike, respectively.

Association analysis

Genotyping of populations (1, 2, 3, and 4) was performed using the molecular marker 6 AM. Recombinant inbred lines (populations 2 and 3) were used to analyze the correlations between alleles and agronomic traits. The wheat mini-core collection (population 4) and 121 cultivars (lines) (population 1) were used to analyze the geographic distribution of different alleles, and the frequency of different alleles in wheat releasing years was analyzed using population 1.

Statistical analysis

The statistically significant differences in *TaBADH-A1* expression level, betaine content, and phenotype between *BADH-A1a* and *BADH-A1b* were evaluated in SPSS 20 software.

Results

Sequence polymorphism and molecular marker development of *TaBADH-A1* in wheat

A single pair of *TaBADH-A1*-specific primers were designed (Supplementary Table S1) to clone the region of promoter and genomic DNA containing introns and exons of *TaBADH-A1* from the wheat cultivars Taishan 1, Bima 4, Zhongmai 9, and Lantian

23. Based on comparisons with the coding sequence (*TraesCS6A02G371100*), the sequence of *TaBADH-A1* was found to consist of 15 exons and 14 introns (Figure 1). The length of promoter and genomic DNA that includes introns and exons of *TaBADH-A1* in Taishan 1, Bima 4, Zhongmai 9, and Lantian 23 was 7,675, 7,919, 7,919, and 7,919 bp, respectively. The *TaBADH-A1* gene sequence polymorphisms were analyzed in the 4 cloned cultivars and 15 cultivars from the database; we found 42 single nucleotide polymorphisms (SNPs) and four 1 bp and two 2 bp indels in the promoter region of *TaBADH-A1* (Supplementary Table S2), and 28 SNPs, a 254 bp, two 1 bp, and a 2 bp indels in the genomic DNA. The *TaBADH-A1* gene variations were grouped into 7 haplotypes (Supplementary Table S2). Haplotypes 3–7 had 2 additional ABREs, 1 additional I-box, 1 additional O_2-site, 1 additional G-box, 1 additional STRE, 1 additional TCA-element, 1 additional W-box, 1 additional AT-TATA-box, and 1 less TGA element than haplotypes 1 and 2 in their promoter region. In the third intron region, the 254 bp fragment of insert, which was a DNA miniature inverted-repeat transposable element (MITE), contained 1 Box-4, 1 MRX, 2 W-box, 2 CAAT-box, and 11 TATA-box elements. The SNPs in exons do not lead to amino acid mutations. As DNA MITE can have a greater impact on gene function, we divided the 7 haplotypes with 254 bp indel fragments into 2 main alleles, *BADH-A1a* and *BADH-A1b* (Figure 1; Supplementary Table S2).

Subsequently, specific primers were designed according to sequences at both ends of the 254 bp indel of the *TaBADH-A1* third intron (Supplementary Table S1). DNA of Chinese Spring, N6AT6B, N6BT6D, and N6DT6A and ddH_2O was used as templates for PCR using molecular marker primers. The PCR products using N6AT6B DNA and ddH_2O as a template did not contain the target gene, while the other PCR products all contained the target gene (Supplementary Figure S1). The 6 AM marker primers amplify a region located in wheat chromosome 6A. Genotyping of all populations using a molecular marker showed the presence of amplified fragment length polymorphisms in PCR products, indicating the effectiveness of 6 AM as a molecular marker (Supplementary Figure S2). The amplified fragments of 6 AM were 828 and 574 bp, which correspond to *BADH-A1a* and *BADH-A1b*, respectively (Supplementary Figure S2). The functional molecular marker 6 AM was developed based on the 254 bp indel in *TaBADH-A1* (Supplementary Table S1).

Expression analysis of *TaBADH-A1* locus two alleles in wheat under drought and salt stress

DNA MITE insertion in the third intron might affect gene expression (Dumesic et al., 2013; Kim Guisbert and Sontheimer, 2013). At the 4-leaf stage, Yanfu 188 and Bima 4 with *BADH-A1a* and Taishan 1 and Chinese Spring with *BADH-A1b* were selected to investigate the expression of the two alleles. Under normal conditions, the expression pattern of *TaBADH-A1* gene in the 4 cultivars was consistent, which showed no change in expression level at 0, 1, 6, 12, and 24 h (Supplementary Figure S3). Subsequently, the expression level of the *TaBADH-A1* gene at 0 h of treated can be representative of the expression level of 1, 6, 12, and 24 h of untreated. Under stress treatment for 0 h, the expression level of *BADH-A1b* gene was higher than that of *BADH-A1a*. The expression pattern of *TaBADH-A1* gene in the 4 cultivars was consistent, first increasing and then decreasing with the extension of the drought and salt stress time (Figures 2A,B). Notably, we found that expression levels of *BADH-A1b* were all significantly higher than those of *BADH-A1a* before and after stress (Figures 2A,B). Considering the differences in the genetic background among wheat cultivars, the population of F_6 recombinant inbred lines (population 2) were constructed using Chinese Spring and Yanfu 188 as parents to further verify the above result. Lines 1–5 of population 2 with *BADH-A1a* and lines 6–10 of population 2 with *BADH-A1b* were selected for further study. Under drought and salt stress, the expression of *TaBADH-A1* gene was found to first increase and then decrease (Figures 2C,D). Meanwhile, expression levels of *BADH-A1b* were significantly higher than those of *BADH-A1a* before and after stress treatment

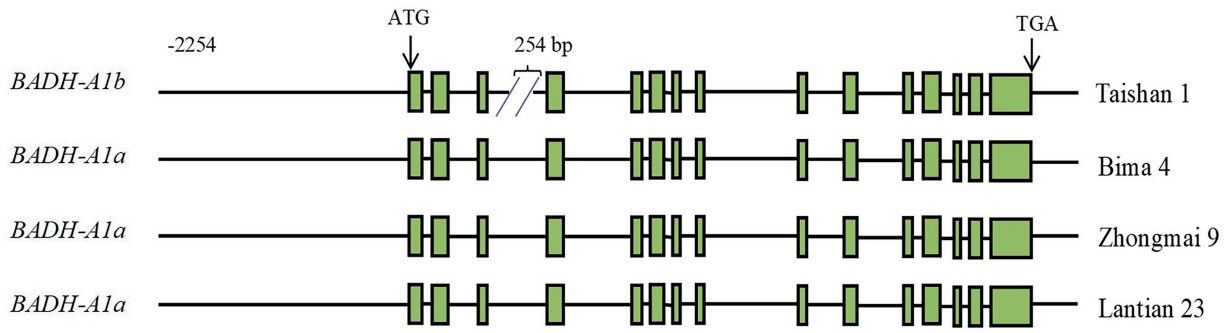


FIGURE 1
Schematic diagram of *TaBADH-A1* gene structure. ATG start codon is designated as position 1bp. Green rectangles are exons; black line before ATG is promoter region; black lines after ATG and before TGA are intron regions; black line after TGA is 3′ untranslated region.

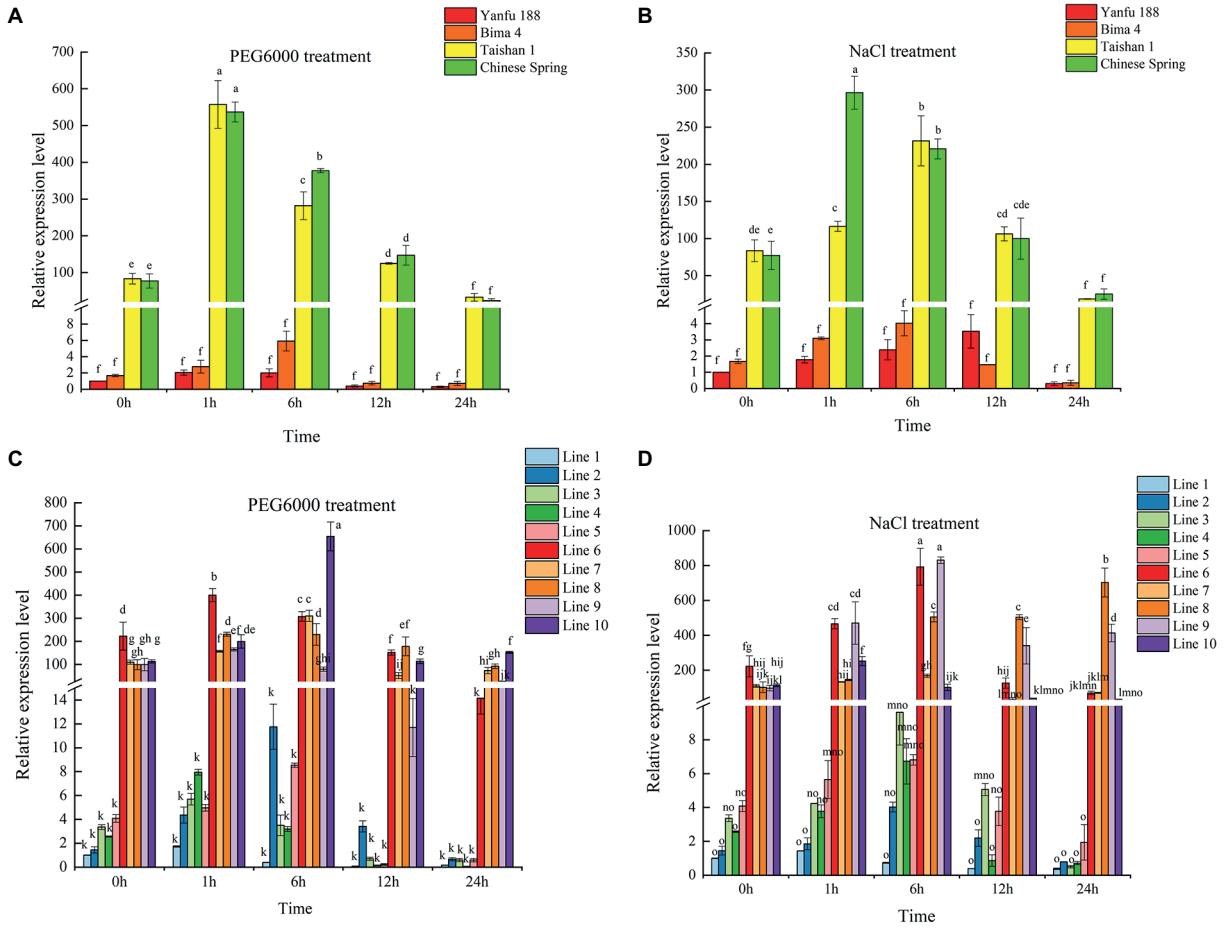


FIGURE 2
Expression patterns of *TaBADH-A1* locus alleles in salt (200mM NaCl) and drought (20% PEG 6000). Wheat was subjected to drought and salt stress at 4-leaf stage; leaves were used as samples for RNA extraction. **(A,B)** *TaBADH-A1* expression of Yanfu 188 under control treatment was used as standard. Yanfu 188 and Bima 4 containing *BADH-A1a*; Taishan 1 and Chinese Spring containing *BADH-A1b*. **(C,D)** *TaBADH-A1* expression of line 1 under control treatment was used as standard; lines 1–5 containing *BADH-A1a*; lines 6–10 containing *BADH-A1b*. The $2^{-\Delta\Delta CT}$ method was used to calculate relative gene expression. Statistically significant differences are indicated with different letters (LSD, $p<0.05$).

(Figures 2C,D). Therefore, the deletion of DNA MITE can enhance *TaBADH-A1* gene expression.

Analysis of betaine content in wheat containing different alleles under drought and salt stress

Through genotyping of the 6 AM molecular marker, wheat cultivars with *BADH-A1b* (Longfumai 18, Taishan 1, Chinese Spring) and wheat cultivars with *BADH-A1a* (Bima 4, Yanfu 188, Ning 9940) were selected to identify betaine content under drought and salt stress at the 4-leaf stage. Under drought stress, we found that the betaine content in leaves of wheat cultivars containing *BADH-A1b* decreased slightly at 1 h and then increased gradually, while the content in cultivars containing *BADH-A1a* decreased slightly at 1 h, then increased and peaked at 12 h, and then began to decline (Figure 3A). Under salt stress, betaine content in the leaves of wheat cultivars containing *BADH-A1a* and *BADH-A1b* decreased slightly at 1 h, increased and peaked at 6 h, and then began to decline. However, the betaine content of wheat cultivars containing *BADH-A1b* increased again at 48 h (Figure 3B). It is noteworthy that the betaine content in leaves of wheat cultivars containing *BADH-A1b* was always higher compared to cultivars containing *BADH-A1a* regardless of drought or salt stress, and the largest difference was at 48 h of stress. This might be due to the fact that the expression level of *BADH-A1b* gene was always higher than that of *BADH-A1a*. Furthermore, we used recombinant inbred lines (population 2) to identify the betaine content of lines containing different alleles after 48 h of drought and salt stress. Under drought stress 48 h, the betaine content of lines 6–10, containing *BADH-A1b*, was 24, 23, 23, 25, and 24 μmol·g^{-1} (dry weight, DW), respectively, and the betaine content of lines 1–5, containing *BADH-A1a*, was 17, 16, 16, 16, and 16 μmol·g^{-1} (DW), respectively (Figure 3C). Under salt stress 48 h, the betaine content of lines 6–10 was 23, 22, 24, 25, and 23 μmol·g^{-1} (DW), respectively,

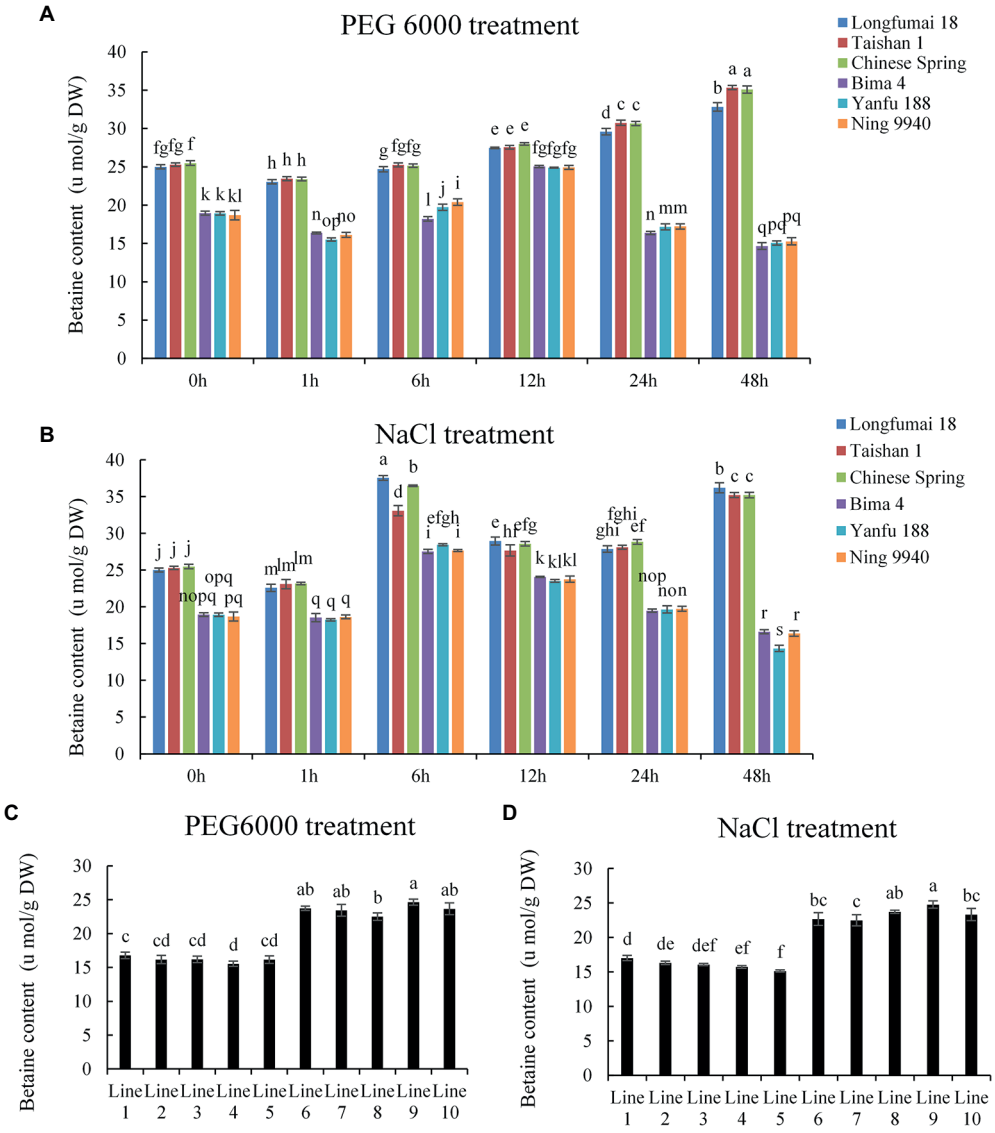


FIGURE 3
Betaine content of wheat containing different alleles under drought (20% PEG 6000) and salt stress (200mM NaCl) at 4-leaf stage. DW, dry weight. **(A,B)** Bima 4, Yanfu 188, and Ning 9940 contain *BADH-A1a*; Longfumai 18, Taishan 1, and Chinese Spring containing *BADH-A1b*. **(C,D)** Betaine content of wheat under stress for 48h; lines 1–5 containing *BADH-A1a*; lines 6–10 containing *BADH-A1b*. Statistically significant differences are indicated with different letters (LSD, $p<0.05$).

and the content of lines 1–5 was 17, 16, 16, 16, and 15 μmol·g^{-1} (DW), respectively (Figure 3D). Therefore, wheat containing *BADH-A1b* had significantly higher betaine content than wheat with *BADH-A1a* under drought and salt stress.

Analysis of drought and salt resistance of wheat with different alleles

We identified the relative germination rate of 121 cultivars (lines; population 1). The average relative germination rate of wheat containing *BADH-A1a* was 51.2%, while that of *BADH-A1b* was 67.3% (Table 1). The wheat cultivars (lines) containing *BADH-A1b* had a significantly higher average relative germination rate than those with *BADH-A1a*, which shows that *BADH-A1b* can increase the drought resistance of wheat during the germination period.

The recombinant inbred lines (population 2) containing different alleles were treated with drought and salt in the 4-leaf stage. Under drought stress, the effects on lines 6–10, containing *BADH-A1b*, were relatively more mild (grew well with green leaves) than lines 1–5, containing *BADH-A1a* (Figure 4A). After 5 days of recovery water treatment, the survival rates of lines 6–10 were 49.3, 61.7, 52.3, 59.0, and 51.0%, respectively, while the survival rates of lines 1–5 were 38.7, 37.7, 36.7, 35.7, and 32.0%, respectively (Figure 4A). The results indicate that *BADH-A1b*

could significantly increase the drought resistance of wheat at the 4-leaf stage. After 25 days of salt stress, leaves of lines 1–5, containing *BADH-A1a*, were more withered than those of lines 6–10, with *BADH-A1b*; the survival rates of lines 1–5 were 56.0, 71.3, 59.0, 66.7, and 72.0%, respectively, while the survival rates of lines 6–10 were 91.7, 85.0, 89.7, 86.7, and 88.0%, respectively (Figure 4B). The results show that *BADH-A1b* can significantly increase the salt tolerance of wheat at the 4-leaf stage.

Association of *TaBADH-A1* locus alleles with agronomic traits

The recombinant inbred line populations (2 and 3) were genotyped according to PCR amplified fragment length polymorphisms using the 6 AM molecular marker. Subsequently, relationships between *TaBADH-A1* locus alleles and agronomic traits were analyzed, including grain number per spike (GN), effective spikelet number per spike (ESN), thousand kernel weight (TKW), flag leaf area per plant (FLA), spike length (SL), length of the last internode (LLI), and plant height (PH). We found no significant differences in GN, ESN, TKW, FLA, SL, LLI, and PH between plants carrying either *BADH-A1a* or *BADH-A1b* (Supplementary Table S3).

Geographic distribution of *BADH-A1a* and *BADH-A1b* in Chinese zones

The wheat production area in China is divided into 10 major agro-ecological production zones based on cropping season, variety type, and ecological conditions (Li et al., 2016). The mini-core collection and 121 cultivars (lines; populations 1 and 4) covering all 10 zones were used to evaluate the geographic distribution of *TaBADH-A1* locus alleles. Overall, *BADH-A1a* and *BADH-A1b* were distributed in all zones (Figure 5A). *BADH-A1a* was present in 59% of the mini-core collection (population 4), while *BADH-A1b* was present in 41% (Figure 5A). However, not all wheat zones had more plants with *BADH-A1a* than *BADH-A1b* in population 4, only the Northeastern Spring Wheat Zone, Southern Autumn-Sown Spring Wheat Zone, Qinghai-Tibetan Plateau Spring–Winter Wheat Zone, Southwestern Autumn-Sown Spring Wheat Zone, Middle and Lower Yangtze Valley Autumn-Sown Spring Wheat Zone, and more overseas introduction plants had *BADH-A1a* than *BADH-A1b*. In population 1, *BADH-A1a* accounted for the vast majority at 90%. The coverage of *BADH-A1b* was only slightly higher than *BADH-A1a* in the Northern Winter Wheat Zone, Northeastern Spring Wheat Zone, and Xinjiang Winter–Spring Wheat Zone (Figure 5B). The results show a weak selection of the favorable allele, *BADH-A1b*, in all zones.

TABLE 1 Relative germination rate of *TaBADH-A1* locus alleles in 121 cultivars (lines).

Alleles	Cultivar (lines) number	Relative germination rate (%)	
		Average	Range
BADH-A1a	109	51.2b	91.8–15.5
BADH-A1b	12	67.3a	92.8–45.3
Total	121	52.8	15.5–92.8

Significant differences are indicated with different letters in average relative germination rate (LSD, $p < 0.05$).

Frequency of *TaBADH-A1* locus alleles in wheat breeding history

To assess *TaBADH-A1* locus allele frequency in different breeding years, the 121 cultivars (lines) were divided into 6 subgroups according to whether their release dates were in the 1950s, 1960s, 1970s, 1980s, or 1990s, or post-2000. *BADH-A1a* was present in 90% of the 121 cultivars (lines) and all 6 subgroups (Table 2). *BADH-A1b*, which first appeared in the 1980s and reached its peak in the post-2000s, accounted for only 10%, which indicates the allele *BADH-A1b* was selected by breeders to resist progressively deteriorating climatic conditions.

Discussion

Analysis of the mechanism of allele *BADH-A1b* in improving drought and salt tolerance in wheat

Osmotic adjustment is the main component of the physiological machinery of drought and salt tolerance in wheat (Khoshro et al., 2013). Betaine, a small, nontoxic organic metabolite, functions as an osmotic regulator under drought and salt stress (Yang et al., 2015). Betaine aldehyde dehydrogenase (BADH) is an important enzyme that catalyzes the last step of betaine synthesis (Fujiwara et al., 2008). In this study, the *TaBADH-A1* gene, which encodes BADH, was cloned in Taishan 1, Bima 4, Zhongmai 9, and Lantian 23. Based on sequence polymorphism analysis, we found 7 haplotypes of the *TaBADH-A1* gene in the 4 cloned wheat cultivars and 15 wheat cultivars from the database. We divided the seven haplotypes with 254 bp indel fragments into two main alleles, *BADH-A1a* and *BADH-A1b*, and the molecular marker 6 AM was developed based on these fragments.

First, the 254 bp fragment inserted into the third intron of *BADH-A1a* contains a TATA-box and W-box. A TATA-box is the core promoter element that initiates gene transcription and participates in the formation of the transcription initiation complex (Bernard et al., 2010). The WRKY transcription factors can bind to W-box, while most of the WRKY transcription factors of known function are negative regulators, with only a few of those

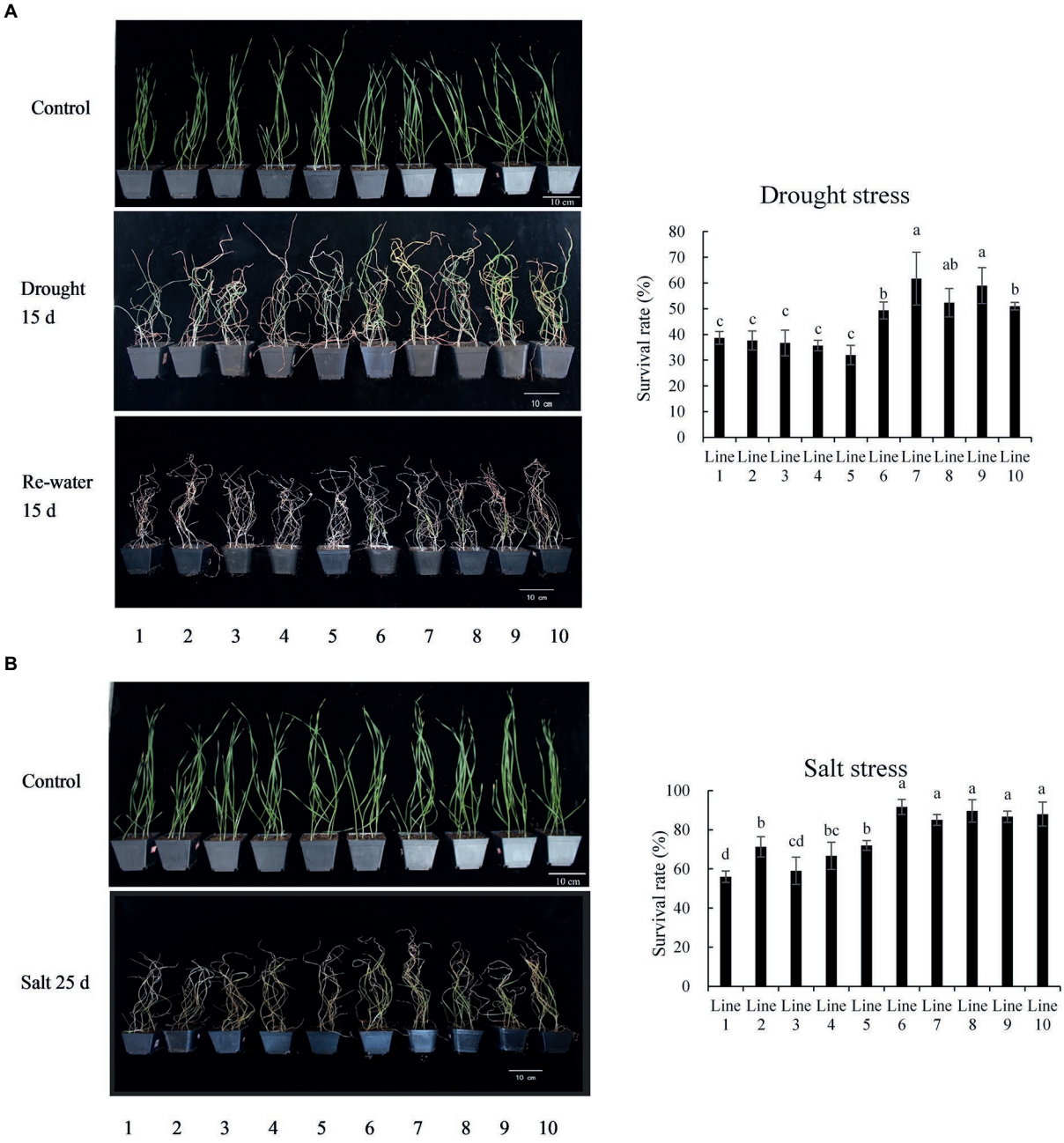


FIGURE 4
Phenotype analysis of recombinant inbred lines of *TaBADH-A1* locus alleles under drought and salt stress. Lines 1–5 containing *BADH-A1a*; lines 6–10 containing *BADH-A1b*. **(A)** Survival rates calculated after withholding water for 15 days and water recovery for 5 days. **(B)** Survival rates were calculated under salt solution (700 mM NaCl) irrigation for 25 days. Statistically significant differences are indicated with different letters (LSD, $p<0.05$).

characterized as having a positive regulatory role (Jiang et al., 2017). The WRKY transcription factors may recruit other proteins to bind to the W-box of the fragment inserted into the third intron of *BADH-A1a* to jointly inhibit *BADH-A1a* expression. Introns were previously considered useless gene sequences, but they have since been shown to regulate gene expression. For example, the adaptor protein MINI ZINC FINGER 2 binds to the *WUSCHEL* (*WUS*) intron and recruits KNUCKLES, TOPLESS, and HISTONE DEACETYLASE 19 to form a transcriptional repressor complex that represses *WUS* expression in *A. thaliana* (Bollier et al., 2018).

Second, pre-mRNAs containing transposons are subject to inefficient splicing (Dumesic et al., 2013). The introns that contain transposons exhibited a greater dwell time on spliceosomes, and pre-mRNAs in the stalled spliceosomes became substrates for the synthesis of siRNAs used to dampen

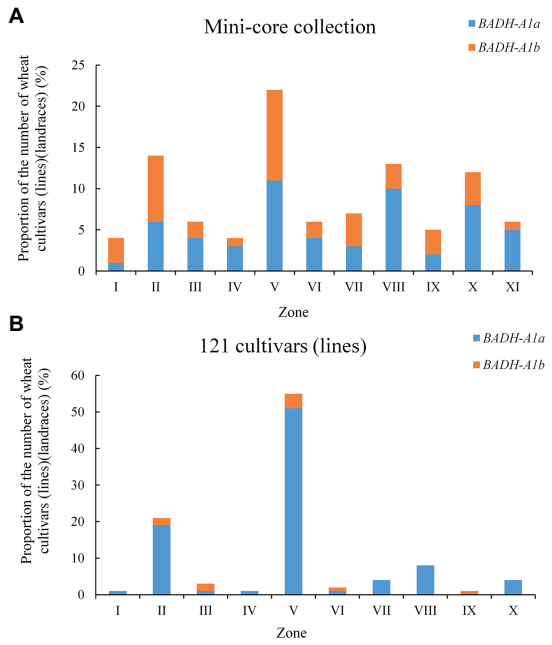


FIGURE 5
Geographic distribution of *BADH-A1a* and *BADH-A1b* in Chinese wheat production zones. **(A)** In mini-core collection population; **(B)** In 121 cultivars (lines) population. I, Northern Spring Wheat Zone; II, Northern Winter Wheat Zone; III, Northeastern Spring Wheat Zone; IV, Southern Autumn-Sown Spring Wheat Zone; V, Yellow and Huai River Valley Facultative Wheat Zone; VI, Qinghai-Tibetan Plateau Spring–Winter Wheat Zone; VII, Northwestern Spring Wheat Zone; VIII, Southwestern Autumn-Sown Spring Wheat Zone; IX, Xinjiang Winter–Spring Wheat Zone; X, Middle and Lower Yangtze Valley Autumn-Sown Spring Wheat Zone; XI, Overseas introduction.

TABLE 2 *TaBADH-A1* locus allele frequency in population 1 wheat breeding years (%).

Years	*BADH-A1a*	*BADH-A1b*	Total
1950s	2	0	2
1960s	3	0	3
1970s	3	0	3
1980s	9	3	12
1990s	20	2	21
Post-2000s	52	5	57
Total	90	10	100

expression of the corresponding gene (Kim Guisbert and Sontheimer, 2013). The 254 bp fragment inserted into the third intron of *BADH-A1a* contain DNA miniature inverted-repeat transposable elements, which might reduce splicing efficiency and thus suppress *BADH-A1a* expression. The above two processes may be responsible for the higher expression level of *BADH-A1b* than *BADH-A1a* before and after stress.

BADH-A1b was always found to be expressed at a high level, which results in increased betaine content. After 48 h of stress, leaves of wheat containing *BADH-A1a* had decreased betaine content, while leaves of wheat containing *BADH-A1b* maintained a higher betaine content. We also identified that the average relative germination and survival rates of wheat with *BADH-A1b* allele under drought and salt stress were significantly higher compared to wheat with *BADH-A1a* allele. *BADH-A1b* which can increase the content of betaine may decrease the osmotic potential and increase the osmotic pressure of cells for over a longer period of stress time more markedly than *BADH-A1a*, further enhancing the drought resistance and salt tolerance of wheat (Table 1 and Figure 4). Meanwhile, in wheat growing under normal water supply, *BADH-A1b* had no effect on the agronomic traits, which indicated excellent growth performance (Supplementary Table S3). However, *BADH-A1b* may confer improvements measurable in some agronomic traits in wheat subject to drought and salt conditions, though further research is required to determine whether this is the case.

Distribution of *TaBADH-A1* locus alleles in Chinese wheat

In Chinese wheat, the mini-core collection (population 4) accounts for 70% of the genetic representation. The two alleles of *TaBADH-A1* locus were almost equally represented in the wheat mini-core collection (population 4; Figure 5A). The genetic resources of the two alleles were present in all wheat regions of China. This might be due to the fact that wheat zones have not been dry for many years. Wheat breeding in China has experienced three stages since the 1950s: disease resistance and stable yield, dwarfing and high yield, and high yield and excellent quality (He et al., 2011). Therefore, improving the adaptability of wheat has been neglected. This has resulted in an extremely uneven distribution of the two studied alleles in 121 cultivars (lines; population 1): *BADH-A1a* accounts for 90% while *BADH-A1b* accounts for only 10% (Figure 5B). Improving wheat stress resistance and paying attention to water saving have been proposed since the 1980s (He et al., 2018). This purpose might well explain the absence of *BADH-A1b* prior to the 1980s (Table 2). Since 2011, research efforts focusing on the lasting resistance of wheat have increased, considering such aspects as drought resistance, heat resistance, and adaptability to other factors (He et al., 2011). Therefore, the favorable allele *BADH-A1b* should be continuously selected for wheat growth under future unpredictable climate deterioration.

In summary, we found seven haplotypes of the *TaBADH-A1* gene in wheat, the seven haplotypes divided with 254 bp indel into two alleles. The expression level of *BADH-A1b* was significantly higher than that of *BADH-A1a* under drought and salt stress. *BADH-A1b* can increase the betaine content of wheat and further enhance its drought resistance and salt tolerance. *BADH-A1b* had no effect on the agronomic traits of wheat grown under normal conditions. Notably, the favorable allele *BADH-A1b* has been neglected in the

selection, but it should be continuously selected in the face of future climate deterioration. Our study provides evidence indicating that *BADH-A1b* is an excellent candidate allele for breeding to improve the drought resistance and salt tolerance of wheat.

Data availability statement

The original contributions presented in the study are included in the article/Supplementary Material, further inquiries can be directed to the corresponding authors.

Author contributions

XZ and JX conceived and designed the experiments. MY and YY performed the experiments, analyzed the data, and wrote the manuscript. YY, MZ, SG, NL, FW, SZ, and HZ revised the manuscript. All authors contributed to the article and approved the submitted version.

Funding

This study was funded by the National Natural Science Foundation of China (32171992, 31671693 and 31260324), Key Research and Development Project of Shaanxi Province (2019ZDLNY04-05), Central Guidance on Local Science and Technology Development Fund of Mongolia Autonomous Region (ZY20200089), Program for Young Talents of Science and Technology in Universities of Inner Mongolia Autonomous Region (NJYT-19-A25), and Research Program of Science and Technology at Universities of Inner Mongolia Autonomous Region (NJZZ22132).

Acknowledgments

We thank funding for our support and teacher Haochen Yang, for providing the mini-core collection.

Conflict of interest

The authors declare that the research was conducted in the absence of any commercial or financial relationships that could be construed as a potential conflict of interest.

Publisher's note

All claims expressed in this article are solely those of the authors and do not necessarily represent those of their affiliated organizations, or those of the publisher, the editors and the reviewers. Any product that may be evaluated in this article, or claim that may be made by its manufacturer, is not guaranteed or endorsed by the publisher.

Supplementary material

The Supplementary Material for this article can be found online at: https://www.frontiersin.org/articles/10.3389/fpls.2022.942359/full#supplementary-material

References

Bernard, V., Brunaud, V., and Lecharny, A. (2010). TC-motifs at the TATA-box expected position in plant genes: a novel class of motifs involved in the transcription regulation. *BMC Genomics* 11:166. doi: 10.1186/1471-2164-11-166

Bollier, N., Sicard, A., Leblond, J., Latrasse, D., Gonzalez, N., and Gévaudant, F. (2018). At-mini zinc finger 2 and sl-inhibitor of meristem activity, a conserved missing link in the regulation of floral meristem termination in Arabidopsis and tomato. *Plant Cell* 30, 83–100. doi: 10.1105/tpc.17.00653

Cha-Um, S., and Kirdmanee, C. (2010). Effect of glycinebetaine on proline, water use, and photosynthetic efficiencies, and growth of rice seedlings under salt stress. *Turk. J. Agric. For.* 34, 517–527. doi: 10.3906/tar-0906-34

Dumesic, P. A., Natarajan, P., Chen, C., Drinnenberg, I. A., Schiller, B. J., and Thompson, J. (2013). Stalled spliceosomes are a signal for RNAi-mediated genome defense. *Cell* 152, 957–968. doi: 10.1016/j.cell.2013.01.046

Fan, W. J., Zhang, M., Zhang, H. X., and Zhang, P. (2012). Improved tolerance to various abiotic stresses in transgenic sweet potato (*Ipomoea batatas*) expressing spinach betaine aldehyde dehydrogenase. *PLoS One* 7:e37344. doi: 10.1371/journal.pone.0037344

Fujiwara, T., Hori, K., Ozaki, K., Yokota, Y., Mitsuya, S., Ichiyanagi, T., et al. (2008). Enzymatic characterization of peroxisomal and cytosolic betaine aldehyde dehydrogenases in barley. *Physiol. Plant.* 134, 22–30. doi: 10.1111/j.1399-3054.2008.01122.x

Gadallah, M. A. A. (1999). Effects of proline and glycinebetaine on Viciafaba responses to salt stress. *Biol. Plant.* 42, 249–257. doi: 10.1023/A:1002164719609

He, Z. H., Xia, X. C., Chen, X. M., and Zhuang, Q. S. (2011). Progress of wheat breeding in China and the future perspective. *Acta Agron. Sin.* 37, 202–215. doi: 10.3724/SP.J.1006.2011.00202

He, Z. H., Zhuang, Q. S., Cheng, S. H., Yu, Z. W., Zhao, Z. D., and Liu, X. (2018). Wheat production and technology improvement in China. *J. Agric.* 8, 99–106. doi: 10.11923/j.issn.2095-4050.cjas2018-1-107

Jiang, J., Ma, S., Ye, N., Jiang, M., Cao, J., and Zhang, J. (2017). WRKY transcription factors in plant responses to stresses. *J. Integr. Plant Biol.* 59, 86–101. doi: 10.1111/jipb.12513

Jing, R. L., Chang, X. P., Hu, H. R., and Dong, Y. C. (1999). A relationship between betaine metabolism and drought resistance of winter wheat seedling under changed watering. *Acta Agron. Sin.* 25, 494–498.

Khoshro, H. H., Taleei, A., Bihamta, M. R., Shahbazi, M., and Abbasi, A. (2013). Expression analysis of the genes involved in osmotic adjustment in bread wheat (*Triticum aestivum* L.) cultivars under terminal drought stress conditions. *J. Crop Sci. Biotechol.* 16, 173–181. doi: 10.1007/s12892-013-0040-7

Kim Guisbert, K. S., and Sontheimer, E. J. (2013). Quit stalling or you'll be silenced. *Cell* 152, 938–939. doi: 10.1016/j.cell.2013.02.025

Legaria, J., Rajsbaum, R., Muñoz-Clares, R. A., Villegas-Sepúlveda, N., Simpson, J., and Iturriaga, G. (1998). Molecular characterization of two genes encoding betaine aldehyde dehydrogenase from amaranth. Expression in leaves under short-term exposure to osmotic stress or abscisic acid. *Gene* 218, 69–76. doi: 10.1016/s0378-1119(98)00381-3

Li, B., Li, Q. R., Mao, X. G., Li, A., Wang, J. Y., Chang, X. P., et al. (2016). Two novel AP2/EREBP transcription factor genes *TaPARG* gave pleiotropic functions on plant architecture and yield-related traits in common wheat. *Front. Plant Sci.* 7:1191. doi: 10.3389/fpls.2016.01191

Li, Y. H., Wang, W., Yang, X. H., and Zou, Q. (2005). Expression of *BADH* and betaine content in wheat cultivars with different drought resistance under drought stress. *Acta Agron. Sin.* 31, 425–430.

Ma, X. J., Fu, J. D., Tang, Y. M., Yu, T. F., Yin, Z. G., Chen, J., et al. (2020). *GmNFYA13* improves salt and drought tolerance in transgenic soybean plants. *Front. Plant Sci.* 11:587244. doi: 10.3389/fpls.2020.587244

Mäkelä, P., Karkkainen, J., and Somersalo, S. (2000). Effect of glycinebetaine on chloroplast ultrastructure, chlorophyll and protein content, and RuBPCO activities in tomato grown under drought or salinity. *Biol. Plant.* 43, 471–475. doi: 10.1023/A:1026712426180

Missihoun, T. D., Schmitz, J., Klug, R., Kirch, H. H., and Bartels, D. (2011). Betaine aldehyde dehydrogenase genes from Arabidopsis with different sub-cellular localization affect stress responses. *Planta* 233, 369–382. doi: 10.1007/s00425-010-1297-4

Stein, N., Herren, G., and Keller, B. (2010). A new DNA extraction method for high-throughput marker analysis in a large-genome species such as *Triticum aestivum*. *Plant Breed.* 120, 354–356. doi: 10.1046/j.1439-0523.2001.00615.x

Sun, Y. L., Liu, X., Fu, L. S., Qin, P., Li, T., Ma, X. F., et al. (2019). Overexpression of *TaBADH*increases the salt tolerance in Arabidopsis. *Can. J. Plant Sci.* 99, 546–555. doi: 10.1139/cjps-2018-0190

Tadesse, W., Halila, H., Jamal, M., El-hanafi, S., Assefa, S., Oweis, T., et al. (2017). Role of sustainable wheat production to ensure food security in the CWANA region. *J. Exp. Biol. Agricult. Sci.* 5, 15–32. doi: 10.18006/2017.5(Spl-1-SAFSAW)

Urbanavičiūtė, I., Bonfiglioli, L., and Pagnotta, M. A. (2021). One hundred candidate genes and their roles in drought and salt tolerance in wheat. *Int. J. Mol. Sci.* 22:6378. doi: 10.3390/ijms22126378

Wang, X. L., Zhang, X. X., Chen, J., Wang, X., Cai, J., Zhou, Q., et al. (2018). Parental drought-priming enhances tolerance to post-anthesis drought in offspring of wheat. *Front. Plant Sci.* 9:261. doi: 10.3389/fpls.2018.00261

Weretilnyk, E. A., and Hanson, A. D. (1990). Molecular cloning of a plant betaine-aldehyde dehydrogenase, an enzyme implicated in adaptation to salinity and drought. *Proc. Natl. Acad. Sci. U. S. A.* 87, 2745–2749. doi: 10.1073/pnas.87.7.2745

Yang, C. L., Zhou, Y., Fan, J., Fu, Y. H., Shen, L. B., Yao, Y., et al. (2015). *SpBADH* of the halophyte *Sesuvium portulacastrum* strongly confers drought tolerance through ROS scavenging in transgenic Arabidopsis. *Plant Physiol. Biochem.* 96, 377–387. doi: 10.1016/j.plaphy.2015.08.010

Younis, A., Ramzan, F., Ramzan, Y., Zulfiqar, F., Ahsan, M., and Lim, K. B. (2020). Molecular markers improve abiotic stress tolerance in crops: a review. *Plan. Theory* 9:1374. doi: 10.3390/plants9101374

Zhang, T. P., Li, Z. M., Li, D. X., Li, C. Y., Wei, D. D., Li, S. F., et al. (2020). Comparative effects of glycinebetaine on the thermotolerance in coda- and *BADH*-transgenic tomato plants under high temperature stress. *Plant Cell Rep.* 39, 1525–1538. doi: 10.1007/s00299-020-02581-5

Zhao, S. Q., Lin, C., Yang, X. H., and Wei-Hua, W. U. (2001). Relationship between drought resistance and betaine aldehyde dehydrogenase in the shoots of different genotypic wheat and sorghum. *Acta Bot. Sin.* 43, 108–110.

Zhu, J. K. (2016). Abiotic stress signaling and responses in plants. *Cell* 167, 313–324. doi: 10.1016/j.cell.2016.08.029

frontiers | Frontiers in Plant Science

TYPE Original Research
PUBLISHED 02 August 2022
DOI 10.3389/fpls.2022.953398

Check for updates

OPEN ACCESS

EDITED BY
Mirza Hasanuzzaman,
Sher-e-Bangla Agricultural University,
Bangladesh

REVIEWED BY
Tajammul Husain,
University of Allahabad, India
Susete Martins-Dias,
Universidade de Lisboa, Portugal
Stefan Trapp,
Technical University of Denmark Kongens Lyngby, Denmark
Geetika Sirhindi,
Punjabi University, India

*CORRESPONDENCE
Xiao-Zhang Yu
xzyu@glut.edu.cn

†These authors have contributed equally to this work

SPECIALTY SECTION
This article was submitted to Plant Abiotic Stress, a section of the journal Frontiers in Plant Science

RECEIVED 26 May 2022
ACCEPTED 04 July 2022
PUBLISHED 02 August 2022

CITATION
Zhang Q, Feng Y-X, Tian P, Lin Y-J and Yu X-Z (2022) Proline-mediated regulation on jasmonate signals repressed anthocyanin accumulation through the MYB-bHLH-WDR complex in rice under chromium exposure.
Front. Plant Sci. 13:953398.
doi: 10.3389/fpls.2022.953398

COPYRIGHT
© 2022 Zhang, Feng, Tian, Lin and Yu. This is an open-access article distributed under the terms of the Creative Commons Attribution License (CC BY). The use, distribution or reproduction in other forums is permitted, provided the original author(s) and the copyright owner(s) are credited and that the original publication in this journal is cited, in accordance with accepted academic practice. No use, distribution or reproduction is permitted which does not comply with these terms.

Proline-mediated regulation on jasmonate signals repressed anthocyanin accumulation through the MYB-bHLH-WDR complex in rice under chromium exposure

Qing Zhang†, Yu-Xi Feng†, Peng Tian, Yu-Juan Lin and Xiao-Zhang Yu*

College of Environmental Science and Engineering, Guilin University of Technology, Guilin, China

Toxic metal-induced overaccumulation of anthocyanin (ATH) in plants can oxidize proteins and break DNA. Herein, the role of exogenous proline (Pro) on the repression of ATH accumulation in rice seedlings during hexavalent chromium [Cr(VI)] exposure was studied. Results indicated that exogenous Pro-mediated regulation of jasmonate signals activated the MYB-bHLH-WDR complex to repress ATH accumulation in rice tissues under Cr(VI) stress. Biochemical and transcript analysis indicated that exogenous Pro promoted the synthesis of jasmonic acid (JA) and its molecularly active metabolite jasmonic acid isoleucine (JA-Ile) in rice tissues under Cr(VI) stress. Increment in the endogenous level of jasmonates positively triggered the expression of genes responsible for the JA signaling pathway and activated the MYB-bHLH-WDR complex, eventually repressing the glycosylation of anthocyanidin to form ATH in rice tissues. In conclusion, exogenous proline-mediated regulation on jasmonate signals was tissue-specific under Cr(VI) stress and a more positive effect was detected in shoots rather than roots.

KEYWORDS

rice, chromium, proline, jasmonic acid, anthocyanin

Introduction

The occurrence of chromium (Cr) contamination in the agricultural system has attained pivotal concern worldwide (Shahid et al., 2017). Rice is the most important staple food in Asia (Awotide et al., 2016). Numerous researches reported that soil Cr contamination results in a remarkable decrease in the yield and quality of rice (Ma et al., 2016; Infante et al., 2021; Xiao et al., 2021). One of the most frequently detected modes of Cr(VI) phytotoxicity is to stimulate over-production of reactive oxygen species (ROS) in plant tissues that destroy the plant's internal defense system and cause oxidative damage,

whereas irreversible modification of proteins, lipid peroxidation, and DNA lesion is detectable, and eventually retards plant growth and even causes cell death (Gomes et al., 2017; Fan et al., 2020; Nie et al., 2021; Zhang et al., 2021).

Mostly, alteration of secondary metabolism is one of the most important survival strategies of plants in response to the imposition of toxic metals (Shitan, 2016), in which plants can use phenylalanine by assimilating this precursor directly into secondary metabolism *via* the phenylpropanoid pathway (Lin et al., 2019). Among other intermediates, anthocyanin (ATH) is the most conspicuous in the family of flavonoids with dual roles *in vivo* during plant growth and development (Ling et al., 2021), most likely depending on its content and subcellular distribution in plant cells. ATH accumulated in vacuole can protect chloroplasts against photo-oxidation and UV irradiation damage (Collin et al., 2008; Park et al., 2011). While excessive accumulation of ATH in cytosol has cytotoxic/genotoxic effects (Zhao et al., 2008), it weakens the yield and quality of crop plants (Ling et al., 2021).

Jasmonates are spontaneously occurring signaling molecules in plants. Among other active metabolites, jasmonic acid (JA) is a vital hormone in plants that serves as a regulatory agent to mediate multiple physiological processes and also functions as a defense signaling molecule to cope with Cr(VI) stress (Michael et al., 2015; Kamran et al., 2021). Numerous studies reported the importance of JA in the regulation of ATH accumulation in plants under various abiotic conditions (Kondo et al., 2021). Additionally, JA-mediated regulation of various transcription factors (TFs) corresponding to different abiotic stresses in plants has been experimentally clarified (Ruan et al., 2019). Other studies suggested that the MYB-bHLH-WDR complex has an important regulatory role to reduce ATH accumulation in plants (Broun, 2005; Qi et al., 2011). Therefore, concerted attempts are needed to clarify the bridge of the MYB-bHLH-WDR complex involved in the interaction between the jasmonate signals and ATH accumulation in plants under Cr(VI) exposure.

Recently, the application of exogenous amino acids has become one of the most effective methods to regulate plant growth and development under environmental abuse. For example, Kan et al. (2017) reported that exogenous glutamate can rapidly induce the expression of genes involved in the metabolism and defense responses in rice plants. Sadak et al. (2012) observed that exogenous arginine can enhance the photosynthesis system and regulate the physiological performance of sunflowers under salt stress. It is intriguing to notice that the function of proline (Pro) in plants is manifold compared with other amino acids, such as osmolyte balancer, free radical scavenger, and macromolecules stabilizer (Zhang et al., 2015, 2021). Previous studies suggested that exogenous Pro positively regulated the enzyme activities of the ascorbate-glutathione cycle in tobacco under salt stress, and minimized the negative effect (Hoque et al., 2007). A decrease in soluble sugar was detected in *Arabidopsis* in response to drought stress in presence of exogenous Pro by lifting the efficiency of the photosystem II system (Moustakas et al., 2011). Exogenous Pro reduced MDA content and root cell viability in Cr(VI)-treated rice seedlings and decreased lipid peroxidation (Yu et al., 2017). Also, crosstalk between Pro and plant hormone (e.g., JA, gibberellins, abscisic acid, cytokinins, and ethylene) in plants under stress conditions has been documented (Alvarez et al., 2022). However, little is known about the Pro-mediated regulation of ATH accumulation through the JA signaling pathway and MYB-bHLH-WDR complex in rice seedlings under Cr(VI) exposure.

Herein, we hypothesized that exogenous Pro-mediated regulation of jasmonate signals initiates the MYB-bHLH-WDR complex to repress ATH accumulation in rice plants in response to Cr(VI) stress. To clarify this hypothesis, the following studies were carried out: (1) to determine the content of 12-oxo-phytodienoic acid (OPDA), JA, jasmonic acid isoleucine (JA-Ile), and ATH in rice plants under Cr(VI) stress, with or without application of exogenous Pro; (2) to quantify the transcript level of JA synthesis, JA signaling pathway, MYB-bHLH-WDR complex, and anthocyanidin synthesis related genes in rice plants under Cr(VI) stress, with or without application of exogenous Pro; (3) to construct the Pro-mediated regulation network involved in jasmonate signals, MYB-bHLH-WDR complex, and anthocyanidin synthesis in rice plants under Cr(VI) stress.

Materials and methods

Plant cultivation and chemical preparation

The seeds of rice (*Oryza sativa* L. XZX 45) were obtained from the Hunan Academy of Agricultural Sciences, which were prepared as described in our previous work (Zhang et al., 2021). In brief, rice seeds were soaked for 12 h before cultivation, then placed in clean river sand inside plastic cups, and deployed in an artificial climate chamber to maintain stable running conditions (light: 20,000 lux, temperature: 25°C ± 0.5°C and humidity: 60% ± 2%). The modified 8692 nutrient solution was prepared as per the protocol (Feng et al., 2019). After 16-day pre-growth, seedlings were collected and cleaned with distilled water for the subsequent tests.

Two different treatments were conducted: (1) Cr(VI) treatment: 16-days old seedlings were grown in nutrient solution containing 0, 2.0, 8.0, and 16.0 mg Cr/L for 2-days exposure; (2) "Pro + Cr(VI)" treatment: 16-days old seedlings were first pretreated in Pro solution (1 mM) after soaking for 12 h (Yang et al., 2021), and then transferred into the nutrient solution containing 0, 2.0, 8.0, and 16.0 mg Cr/L for 2-days exposure. Three different effective concentrations of Cr(VI; i.e., EC_{20}, EC_{50}, and EC_{75}) were used based on the inhibition rate with 20%, 50%, and 75% of relative growth rate during 2-days exposure (Zhang et al., 2021). The pH of solution was approximately 6.7 to 6.9

during the entire period of exposure. To lessen water loss and repress the growth of algae, each flask was wrapped with aluminum foil. Four independent replicates were deployed in each experiment, and 10 seedlings of similar size were taken for each replicate (Zhang et al., 2021). The grade of all chemicals used was analytical purity (AR).

Measurement of jasmonates

After exposing to Cr(VI) solution, the rice tissues were collected and ground with liquid nitrogen with internal standards. The powdery tissue samples were used for the extraction, purification, and analysis of jasmonates. Quantification of jasmonates, including 12-oxo-phytodienoic acid (OPDA), jasmonic acid (JA), and jasmonic acid isoleucine (JA-Ile) was determined by ultra-performance liquid chromatography–tandem mass spectrometry (UPLC-MS/MS). The procedures for extraction, purification, and analysis were described by Shao et al. (2019; Supporting Information M1). Three biological replicates were prepared for each sample.

Quantification of anthocyanin (ATH)

After freezing with liquid nitrogen, rice tissues were ground and immersed in 5 ml of hydrochloric acid methanol solution (15% hydrochloric acid, 95% methanol = 15:85, v/v), and isolated from light at room temperature (~25°C) for 4 h. After centrifuging at 3,500 g for 5 min at 4°C, the supernatants were collected for ATH measurement by a spectrophotometric method against hydrochloric acid methanol solution as a reference (Ling et al., 2021). Calculation of ATH content in plant tissues was based on the following equation:

$$C_{ATH}\left(nmol/g\right) = \frac{\left[\left(OD_{530}-OD_{620}\right)-0.1\times\left(OD_{650}-OD_{620}\right)\right]}{\varepsilon}\times\frac{V}{M}\times 10^{6} \quad (1)$$

Where *OD* is the absorbance at 530, 620, and 650 nm, respectively, ε is the molar extinction coefficient of ATH (4.62×10^{6}), *V* is the total extract volume (ml), and *M* is the weight of fresh samples (g).

RNA extraction

Total RNA was extracted from rice tissues of the Cr-treated and non-treated seedlings by using an Ultrapure RNA Kit (CWBio, Taizhou, China). DNase I (CWBio, Taizhou, China) was used to clear away genomic DNA contamination in RNA extract. After that, an RNeasy MinElute Cleanup Kit (Qiagen, Hilden, Germany) was selected to purify the total RNA. Four biological replicates were prepared for each sample.

Gene identification and RT-qPCR analysis

Thirty-eight genes responsible for JA synthesis (Module 1, 16 genes), JA signaling pathway (Module 2, 8 genes), MYB-bHLH-WDR complex (Module 3, 11 genes), and anthocyanidin synthesis (Module 4, 3 genes), respectively, were identified from three rice databases (RGAP, CRTC, and RAP-DB) and assayed for RT-qPCR tests after Cr(VI) exposure. All gene primer sequences are listed in Supplementary Table S1.

RT-qPCR cycling conditions were set up as follows: (1) denaturation at 95°C for 10 s; (2) annealing at 58°C for 30 s; and (3) extension at 72°C for 32 s. This cycle was repeated 40 times. The RT-qPCR analysis was performed by the 7,500 Fast RT-qPCR system (Applied Biosystems) and SYBR green chemistry. The house-keeping gene was *OsGAPDH* (glyceraldehyde-3-phosphate dehydrogenase, LOC_Os08g03290.1; Yang et al., 2021). The relative expression of each targeted gene was calculated by the standard $2^{-\Delta\Delta CT}$ method (Schmittgen and Livak, 2008).

Estimation of gene expression variation factors

The gene expression variation factors (*GEVFs*) were used to estimate the effect of exogenous Pro on the expression of genes in rice plants after Cr(VI) exposure, based on the following equation (Zhang et al., 2022):

$$GEVFs = \frac{FC_{(Pro+Cr)}-FC_{(Cr)}}{FC_{(Cr)}}\times 100\% \quad (2)$$

Wherein $FC_{(Pro+Cr)}$ refers to the gene expression from the "Pro + Cr(VI)" treatments; $FC_{(Cr)}$ refers to the gene expression from the Cr(VI) treatments. The threshold values of *GEVFs* are deployed as >25% (promoting genes) or <−25% (repressing genes). Noted that the "promoting genes" under different ECs of Cr(VI) were discussed in this study.

Data analysis

The experimental results were given as mean ± SD. The significant difference between the treatments and control was studied by Tukey multiple comparison test at $p < 0.05$. The asterisk (*) represents the significant difference between Cr treatments and "Pro + Cr(VI)" treatments. The letter indicates the significant difference between the treated seedlings and the control. Exogenous Pro-mediated gene expression of Modules 1 to 3 in rice seedlings at 0 mg Cr/L treatment (i.e., Control) is shown in Supplementary Figure S1. The Search Tool for the Retrieval of Interacting Genes (STRING)

program was used to analyze and visualize the gene interaction network.

Results

The content of jasmonates in rice seedlings

The content of OPDA (ng/g FW) linearly decreased in rice roots with increasing Cr(VI) concentrations ($p < 0.05$), while the content of OPDA showed an inverted "U" curve in rice shoots, with the highest content (487.90 ± 13.59 ng/g FW) at 8.0 mg Cr/L. Exogenous Pro significantly ($p < 0.05$) increased the content of OPDA in rice roots compared to the control, while the content of OPDA generally decreased in rice shoots, with the lowest content (380.45 ± 11.65 ng/g FW) at 2.0 mg Cr/L (Figures 1A,B).

The content of JA remarkably ($p < 0.05$) reduced in root tissues under Cr(VI) stress compared to the control, ranging from 7.82 ± 0.12 to 2.56 ± 0.17 ng/g FW, while a similar decreasing trend was observed in rice shoots. The content of JA significantly ($p < 0.05$) decreased in rice roots from 9.49 ± 0.29 to 2.81 ± 0.11 ng/g FW under "Pro + Cr(VI)" treatments compared to the control. Interestingly, the content of JA significantly ($p < 0.05$) increased in rice shoots at 16.0 mg Cr/L with 19.03 ± 0.66 ng/g FW (Figures 1C,D).

The content of JA-Ile increased very little in rice roots under Cr(VI) stress, ranging from 0.70 ± 0.01 to 0.73 ± 0.01 ng/g FW. Similarly, the content of JA-Ile increased from 1.98 ± 0.07 to 3.93 ± 0.24 ng/g FW in rice shoots under Cr(VI) stress. Under the "Pro + Cr(VI)" treatment, the content of JA-Ile first increased and then decreased in rice roots, with the highest value of 0.82 ± 0.01 ng/g FW at 8.0 mg Cr/L. The content of JA-Ile significantly ($p < 0.05$) increased in rice shoots at 16.0 mg Cr/L with 3.93 ± 0.24 ng/g FW (Figures 1E,F).

It is noticed that the content of OPDA, JA, and JA-Ile in both rice roots and shoots from "Pro + Cr(VI)" treatments was generally higher than that from Cr(VI) treatments, suggesting a positive regulatory role of exogenous Pro on the synthesis of jasmonates-related compounds in rice seedlings under Cr(VI) exposure.

The content of ATH in rice seedlings

The content of ATH (nmol/g FW) slightly increased in rice roots with enhancing Cr(VI) concentrations, while the content of ATH remarkably ($p < 0.05$) increased in rice shoots with enhancing Cr(VI) concentrations. A similar accumulation pattern of ATH in both rice tissues was observed in the "Pro + Cr(VI)" treatments with increasing Cr(VI) concentration (Figures 1G,H). However, the content of ATH in rice shoots from "Pro + Cr(VI)" treatments was lower ($p < 0.05$) than that from Cr(VI) treatments. This result suggested that exogenous Pro effectively reduced ATH accumulation in rice shoots under Cr(VI) stress.

Expression of genes responsible for jasmonate signals in rice seedlings

Gene expression at EC_{20} of Cr(VI)

In roots of rice seedlings, expression of JA synthesis-related genes, that is, *OsLOX1.1*, *OsLOX2.2*, *OsAOS1*, *OsAOS4*, *OsAOC*, *OsOPR7*, *OsOPR8*, *OsJMT2*, and *OsJMT3*, from the "Pro + Cr(VI)" treatments were significantly ($p < 0.05$) higher than that of Cr(VI) treatments. Also, expression of genes related to the JA signaling pathway, that is, *OsJAR2*, *OsCOI1*, *OsJAZ12*, and *OsJAZ28*, under "Pro + Cr(VI)" treatments were significantly upregulated ($p < 0.05$), compared with Cr(VI) treatments (Figure 2A).

In shoots of rice seedlings, Pro-mediated upregulation ($p < 0.05$) of JA synthesis-related genes, that is, *OsLOX2.2*, *OsAOS4*, *OsAOC*, *OsOPR7*, *OsOPR8*, and *OsJMT1* was detected, compared with Cr(VI) treatments. Higher expression of genes related to the JA signaling pathway, that is, *OsJAR1*, *OsJAR2*, *OsCOI1*, *OsCOI2*, *OsJAZ1*, *OsJAZ5*, and *OsJAZ28* from the "Pro + Cr(VI)" treatments was also detected ($p < 0.05$), compared with Cr(VI) treatments (Figure 2B).

Gene expression at EC_{50} of Cr(VI)

In root tissues, JA synthesis-related genes, that is, *OsLOX1.1* and *OsOPR7* under "Pro + Cr(VI)" treatments were significantly ($p < 0.05$) upregulated, compared with Cr(VI) treatments. Higher expression of genes activated in the JA signaling pathway, that is, *OsJAR2*, *OsCOI1*, and *OsJAZ12*, under "Pro + Cr(VI)" treatments was observed ($p < 0.05$), compared with Cr(VI) treatments (Figure 2A).

In shoot tissues, JA synthesis-related genes, that is, *OsLOX1.1* and *OsOPR7*, under "Pro + Cr(VI)" treatments were significantly ($p < 0.05$) upregulated, compared with Cr(VI) treatments. Higher expression of genes involved in the JA signaling pathway, that is, *OsCOI2*, *OsJAZ5*, and *OsJAZ28*, under "Pro + Cr(VI)" treatments was determined ($p < 0.05$), compared with Cr(VI) treatments (Figure 2B).

Genes expression at EC_{75} of Cr(VI)

In root tissues, JA synthesis-related genes, that is, *OsLOX1.1*, *OsLOX2.2*, *OsAOS1*, *OsAOS4*, *OsAOC*, *OsOPR7*, *OsJMT2*, and *OsJMT3*, under "Pro + Cr(VI)" treatments were significantly ($p < 0.05$) upregulated, compared with Cr(VI) treatments. Higher expression of genes related to the JA signaling pathway, that is, *OsJAR2* under "Pro + Cr(VI)" treatments were noticed ($p < 0.05$), compared with Cr(VI) treatments (Figure 2A).

In shoot tissues, JA synthesis-related genes, that is, *OsLOX1.1*, *OsLOX2.2*, *OsAOS1*, *OsOPR7*, *OsOPR8*, *OsJMT1*, and *OsJMT3*, under "Pro + Cr(VI)" treatments were significantly ($p < 0.05$)

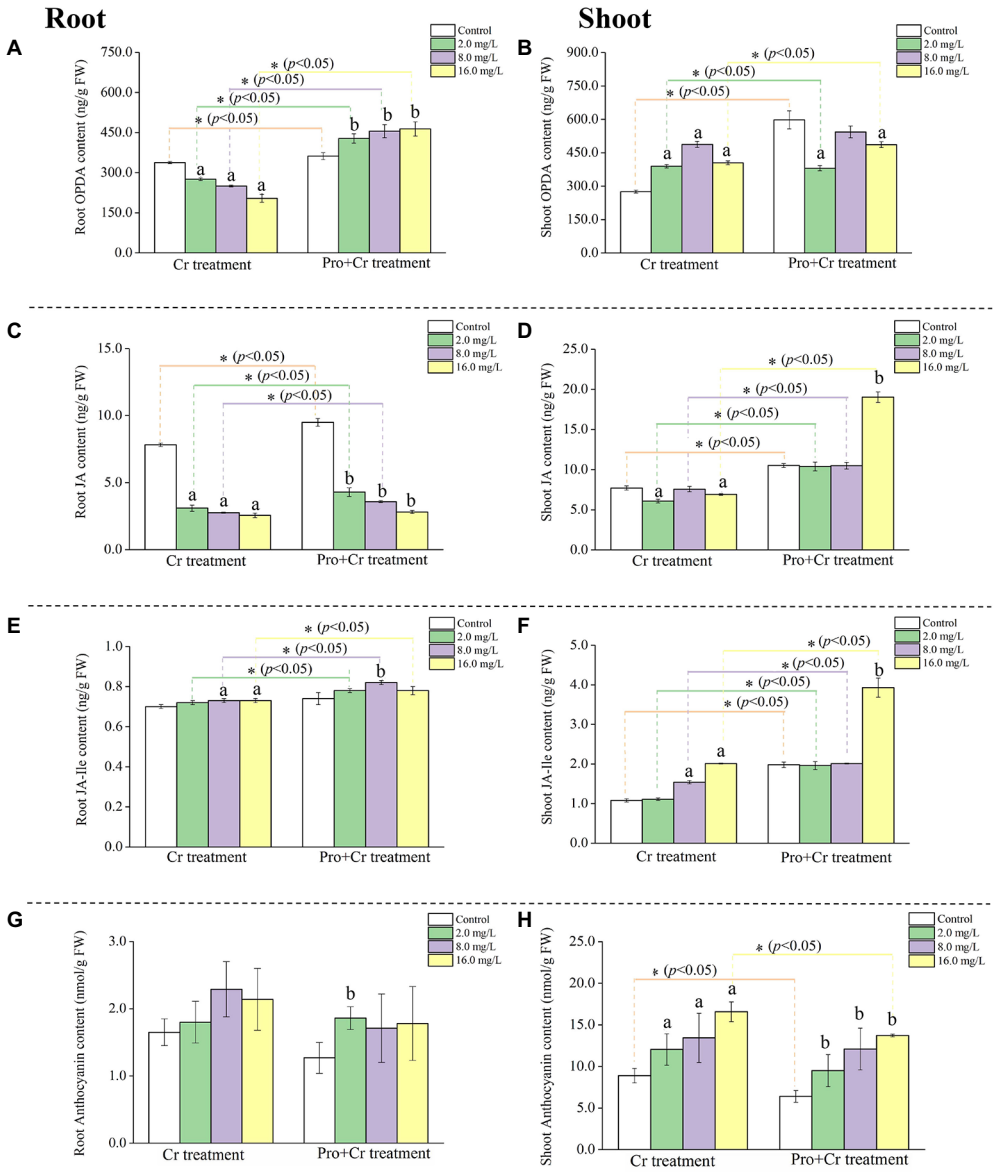


FIGURE 1
The content of jasmonates and ATH in rice tissues under Cr(VI) stress in the presence or absence of Pro. The content of OPDA in rice roots **(A)** and shoots **(B)**; The content of JA in rice roots **(C)** and shoots **(D)**; The content of JA-Ile in rice roots **(E)** and shoots **(F)**; The content of ATH in rice roots **(G)** and shoot **(H)**. The asterisk (*) refers to the significant difference between Cr(VI) treatments and Pro + Cr(VI) treatments. The letter refers to the significant difference between the treated seedlings and the control.

upregulated, compared with Cr(VI) treatments. Higher expression of genes involved in the JA signaling pathways, that is, *OsJAR2*, *OsCOI2*, *OsJAZ5*, and *OsJAZ28*, under "Pro + Cr(VI)" treatments were detected ($p < 0.05$), compared with Cr(VI) treatments (Figure 2B).

These results suggested that the expression of jasmonate signals-related genes in rice seedlings is tissue-specific and highly dependent on the Cr(VI) concentrations. Application of exogenous Pro can mediate the response of jasmonate signals-related genes in rice seedlings under Cr(VI) stress, which further affects the expression of downstream genes.

Expression of genes activated in the MYB-bHLH-WDR complex in rice seedlings

Gene expression at EC_{20} of Cr(VI)

In rice roots, relatively higher expression of *OsbHLH6*, *OsbHLH008*, *OsbHLH010*, *OsbHLH014*, *OsMYB55*, and *OsC1-Myb* was detected from "Pro + Cr(VI)" treatments than that from Cr(VI) treatments ($p < 0.05$), while in rice shoots, relatively higher expression of *OsbHLH6*, *OsbHLH010*, *OsbHLH165*, *OsMYB55*, *OsC1-Myb*, and *OsTTG1* was observed from "Pro + Cr(VI)"

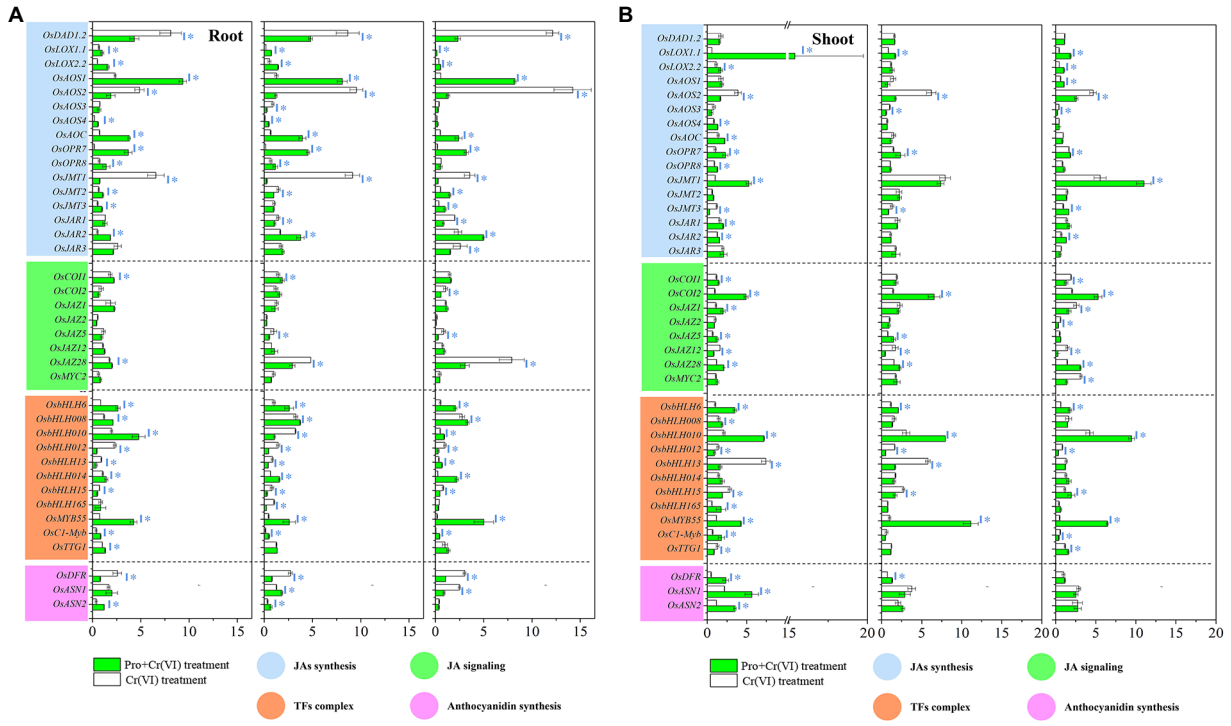


FIGURE 2
The relative expression of JA synthesis, JA signaling, MYB-bHLH-WDR complex, and anthocyanidin synthesis-related genes in rice seedlings under Cr(VI) stress in the presence or absence of Pro. **(A)** The expression of these genes in rice roots under Cr(VI) stress in the presence or absence of Pro. **(B)** The expression of these genes in rice shoots under Cr stress in the presence or absence of Pro. The relative expression level of control is 1. The asterisk (*) refers to the significant difference between Cr(VI) treatments and Pro + Cr(VI) treatments.

treatments than that from Cr(VI) treatments ($p < 0.05$; Figures 2A,B).

Gene expression at EC_{50} of Cr(VI)

In rice roots, significantly higher expression of *OsbHLH6*, *OsbHLH008*, *OsbHLH014*, *OsMYB55*, and *OsC1-Myb* was detected from "Pro + Cr(VI)" treatments than that from Cr(VI) treatments ($p < 0.05$), while in rice shoots, significantly higher expression of *OsbHLH6*, *OsbHLH010*, and *OsMYB55* was observed from "Pro + Cr(VI)" treatments than that from Cr(VI) treatments ($p < 0.05$; Figures 2A,B).

Gene expression at EC_{75} of Cr(VI)

In rice roots, relatively higher expression of *OsbHLH6*, *OsbHLH008*, *OsbHLH010*, *OsbHLH13*, *OsbHLH014*, *OsMYB55*, and *OsC1-Myb* was detected from "Pro + Cr(VI)" treatments than that from Cr(VI) treatments ($p < 0.05$), while in rice shoots, relatively higher expression of *OsbHLH6*, *OsbHLH010*, *OsbHLH15*, *OsMYB55*, and *OsMYB55* was observed from "Pro + Cr(VI)" treatments than that from Cr(VI) treatments ($p < 0.05$; Figures 2A,B).

These results indicated that the expression of MYB-bHLH-WDR complex-related genes in rice tissues is highly dependent on the EC concentrations of Cr(VI). Exogenous Pro can positively regulate the expression of genes functioning in the MYB-bHLH-WDR complex in rice plants under Cr(VI) stress and affects anthocyanidin synthesis.

Expression of genes responsible for anthocyanidin synthesis in rice seedlings

Gene expression at EC_{20} of Cr(VI)

In rice roots, *OsASN1* and *OsASN2* under "Pro + Cr(VI)" treatments were significantly ($p < 0.05$) upregulated, compared with Cr(VI) treatments, while in rice shoots, higher expression of *OsDFR*, *OsASN1*, and *OsASN2* under "Pro + Cr(VI)" treatments was observed ($p < 0.05$), rather than Cr(VI) treatments (Figures 2A,B).

Gene expression at EC_{50} of Cr(VI)

In rice roots, higher expression of *OsASN1* and *OsASN2* under "Pro + Cr(VI)" treatments was detected ($p < 0.05$), rather than Cr(VI) treatments, while in rice shoots, higher expression of *OsDFR* and *OsASN2* under "Pro + Cr(VI)" treatments was detected ($p < 0.05$), rather than Cr(VI) treatments (Figures 2A,B).

Gene expression at EC_{75} of Cr(VI)

No significant difference was observed in the expression of genes responsible for anthocyanidin synthesis in both rice tissues

at all treatments (Figures 2A,B). These results suggested that the regulatory effects of exogenous Pro in rice seedlings were weak under EC_{75} of Cr(VI).

The gene expression variation factors at different ECs of Cr(VI)

Influence of exogenous Pro on the expression of genes responsible for JA synthesis (Module 1), JA signaling pathway (Module 2), MYB-bHLH-WDR complex (Module 3), and anthocyanidin synthesis (Module 4) at different ECs of Cr(VI) was estimated by the *GEVFs* (Figure 3), and the detailed information was shown in Supplementary Table S2. Venn diagram showed that *OsLOX1.1, OsLOX2.2, OsAOS1, OsAOS4, OsAOC, OsOPR7,* and *OsJAR2* (Module 1) and *OsbHLH6, OsbHLH014, OsMYB55,* and *OsC1-Myb,* (Module 3) are the common "promoting genes" detected at three ECs of Cr(VI) in rice roots (Figure 3A), suggesting that exogenous Pro had a stronger impact on the JA synthesis and the MYB-bHLH-WDR complex than others in rice seedlings at three treatment concentrations of Cr(VI). Additionally, we noticed that the number of "promoting genes" in both rice tissues decreased with the increasing Cr(VI) concentrations, indicating the higher Cr(VI) concentration the less regulation effect of exogenous Pro. Herein, five "promoting genes" with the highest *GEVF* values in rice tissues at different ECs of Cr(VI) were listed. In the root part, genes *OsMYB55* (Module 3), *OsAOC* (Module 1), *OsAOS1* (Module 1), *OsJAR2* (Module 1), and *OsLOX2.2* (Module 1) showed higher *GEVFs* values at EC_{20} of Cr(VI); *OsAOS1* (Module 1), *OsAOC* (Module 1), *OsMYB55* (Module 3), *OsAOS4* (Module 1), and *OsLOX1.1* (Module 1) displayed the higher *GEVFs* values at EC_{50} of Cr(VI); *OsbHLH014* (Module 3), *OsC1-Myb* (Module 3), *OsLOX1.1* (Module 1), *OsAOC* (Module 1), and *OsbHLH6* (Module 3) presented higher *GEVFs* values at EC_{75} of Cr(VI).

In rice shoots, Venn diagram showed that *OsLOX1.1* (Module 1), *OsJAZ28*, *OsJAZ5*, and *OsCOI2* (Module 2), and *OsbHLH6*, *OsbHLH014*, *OsJAZ28*, and *OsMYB55* (Module 3) are the common "promoting genes" detected at three ECs of Cr(VI; Figure 3B). Also, *OsJMT1* (Module 1), *OsCOI2* (Module 2), *OsDFR* (Module 4), *OsMYB55* (Module 3), and *OsLOX1.1* (Module 1) showed the higher *GEVFs* values at EC_{20} of Cr(VI); *OsCOI2* (Module 2), *OsbHLH010* (Module 3), *OsLOX1.1* (Module 1), *OsMYB55* (Module 2), and *OsJAZ5* (Module 2) displayed the higher *GEVFs* values at EC_{50} of Cr(VI); *OsLOX1.1* (Module 1), *OsbHLH6* (Module 3), *OsCOI2* (Module 2), *OsLOX2.2* (Module 2), and *OsbHLH010* (Module 3) presented higher *GEVFs* values at EC_{75} of Cr(VI).

Gene interaction and regulation network in rice plants

The interaction network of genes selected in this study is shown in Figure 4A. Based on the analysis of the interaction network, genes of *OsAOS1, OsAOC, OsJAZ5, OsAOS2, OsAOS3, OsAOS4, OsCOI1, OsJAR3, OsCOI2, OsLOX1.1, OsJAZ1, OsJAR1, OsDFR, OsJAR3, OsJAR1,* and *OsJAR2* had higher combined scores (>0.9), suggesting higher interactive capacities. In addition, heatmap presentation of Pro-mediated response of genes activated in Modules 1 to 4 in rice tissues in response to Cr(VI) exposure was mapped (Figures 4B,C), suggesting that exogenous Pro-mediated regulation was tissue-specific and a more positive effect was detected in shoots than roots under Cr(VI) exposure.

Discussion

Plant growth and development are highly coordinated with species and levels of hormones in their cells. Fluctuation and imbalance of phytohormone levels in plant tissues are crucial to integrating with signaling modulation and stress responses (Sytar et al., 2019). A previous study indicated that Cr exposure evoked a series of complex hormone responses in plants and disturbed the physiological and molecular processes (Asad et al., 2018). Being a plant nutritional regulator, Pro is considered to be a useful "alleviator" that curtails the adverse impact induced by Cr pollution on rice plants (Gomes et al., 2017; Yang et al., 2021). In this study, we focused on the effects of exogenous Pro on the resistance and tolerance of rice plants to different ECs of Cr(VI), judged by the repression of ATH accumulation through regulating jasmonate signals and the MYB-bHLH-WDR complex. Therefore, the possible regulation mechanisms of exogenous Pro on these biochemical and molecular processes in rice under Cr(VI) stress is discussed accordingly.

Exogenous proline mediates jasmonate signals in rice under Cr(VI) stress

Synthesis of JA in plants occurs in the plastid, peroxisome, and cytoplasm (Raza et al., 2021). Various stresses can activate phospholipases in the plastid membrane and promote the conversion of linolenic acid (a precursor for JA synthesis) into OPDA in the presence of enzymes LOX, AOS, and AOC (Ruan et al., 2019). After that, JA is synthesized from OPDA by the OPR and three cycles of β-oxidation (Ruan et al., 2019). Results from the current study demonstrated that Cr(VI) exposure at three EC concentrations significantly increased the content of JA in rice shoots. Also, JA synthesis-related genes (i.e., *OsDAD1.2*, *OsAOS2*, *OsAOC,* and *OsOPR7*) showed upregulation in rice shoots under different ECs of Cr(VI) exposure. These results indicated that JA synthesis in rice plants is positive in response to Cr(VI) stress. A recent study suggested that Cd exposure significantly regulated the expression of JA synthesis-related genes in *A. thaliana*, with an increase in endogenous JA levels in root parts (Lei et al., 2020). Also, previous studies reported that exogenous JA can alleviate the detrimental effects of toxic metals (e.g., Ni, Cu, and Pb) on plants by regulating antioxidants (Sirhindi et al., 2016), increasing

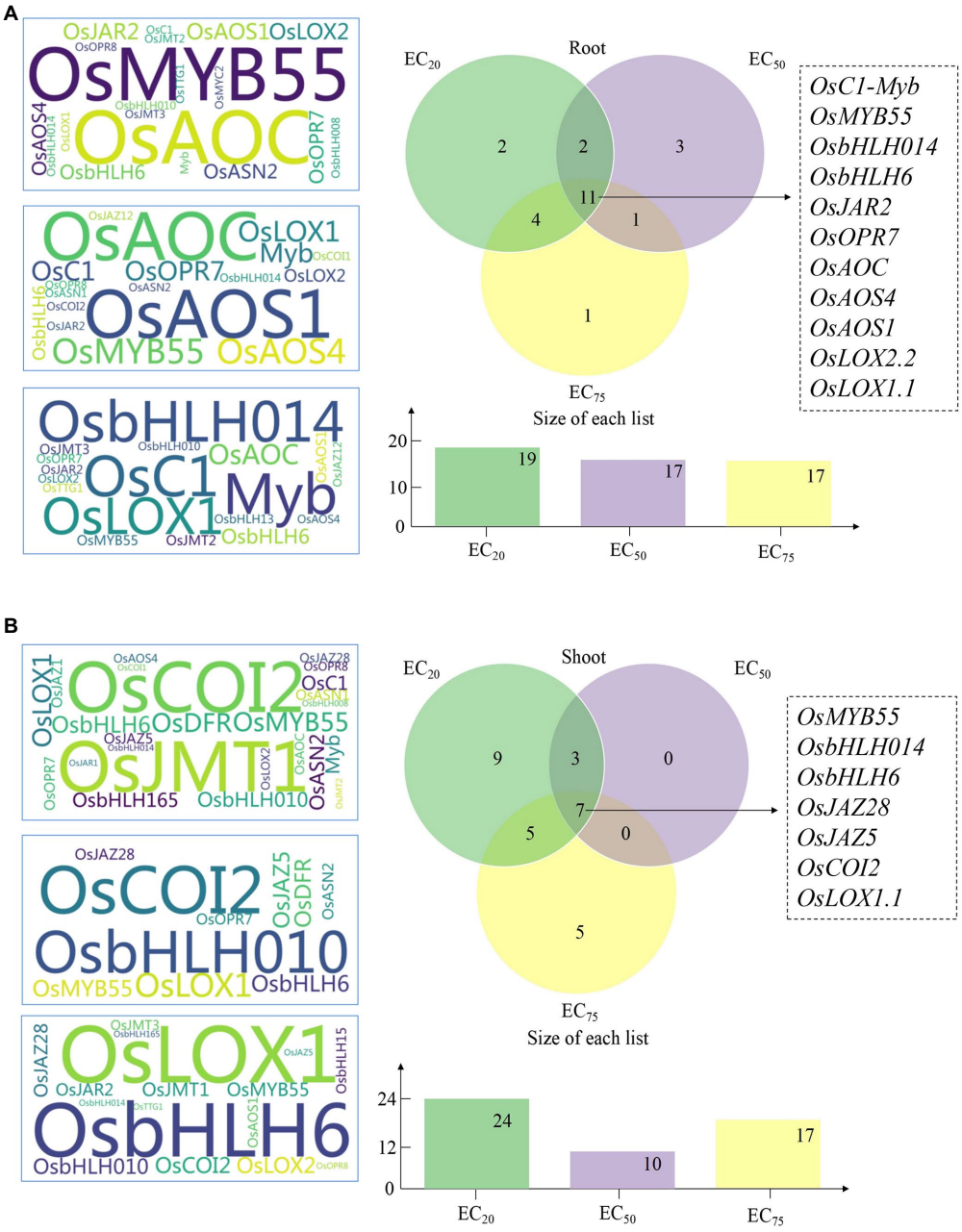


FIGURE 3
The genetic expression variation factors (*GEVFs*) between Cr(VI) treatments and Pro + Cr treatments in rice seedlings. **(A)** Left: the *GEVFs* of "promoting genes" in root tissues at three ECs of Cr(VI; *the larger size of gene symbol indicates a higher value of *GEVFs*); Right: the Venn diagram of these "promoting genes" at three ECs of Cr(VI). **(B)** Left: the *GEVFs* of "promoting genes" in shoot tissues at three ECs of Cr(VI; *the larger size of gene symbol indicates a higher value of *GEVFs*); Right: the Venn diagram of these "promoting genes" at three ECs of Cr(VI).

chlorophyll content (Dai et al., 2020), and inducing synthesis of secondary metabolites (e.g., total phenols, polyphenols, and flavonoids; Bali et al., 2019).

In the cytoplasm, JA can conjugate with isoleucine (Ile) to form JA-Ile, while it is also converted into JA-Me through JA carboxylmethyl transferase (Ali and Baek, 2020). Both compounds initiate the JA signaling pathway. In this study, we noticed that the content of JA-Ile in rice shoots increased with enhancing Cr(VI) concentrations, and upregulation of JA-Ile synthesis-related genes (i.e., *OsJAR1*, *OsJAR2*, and *OsJAR3*) was detected in rice shoots at three ECs of Cr(VI) exposure. In addition, genes involved in JA-Me synthesis (i.e., *OsJMT1* and *OsJMT2*) were positively activated in shoot tissues at EC_{50} and EC_{75} of Cr(VI) exposure. These results suggested that Cr(VI) exposure at EC_{50} and EC_{75} stimulated the synthesis of JA-Ile and JA-Me in rice shoots, while JA-Ile synthesis at EC_{20} of Cr(VI)

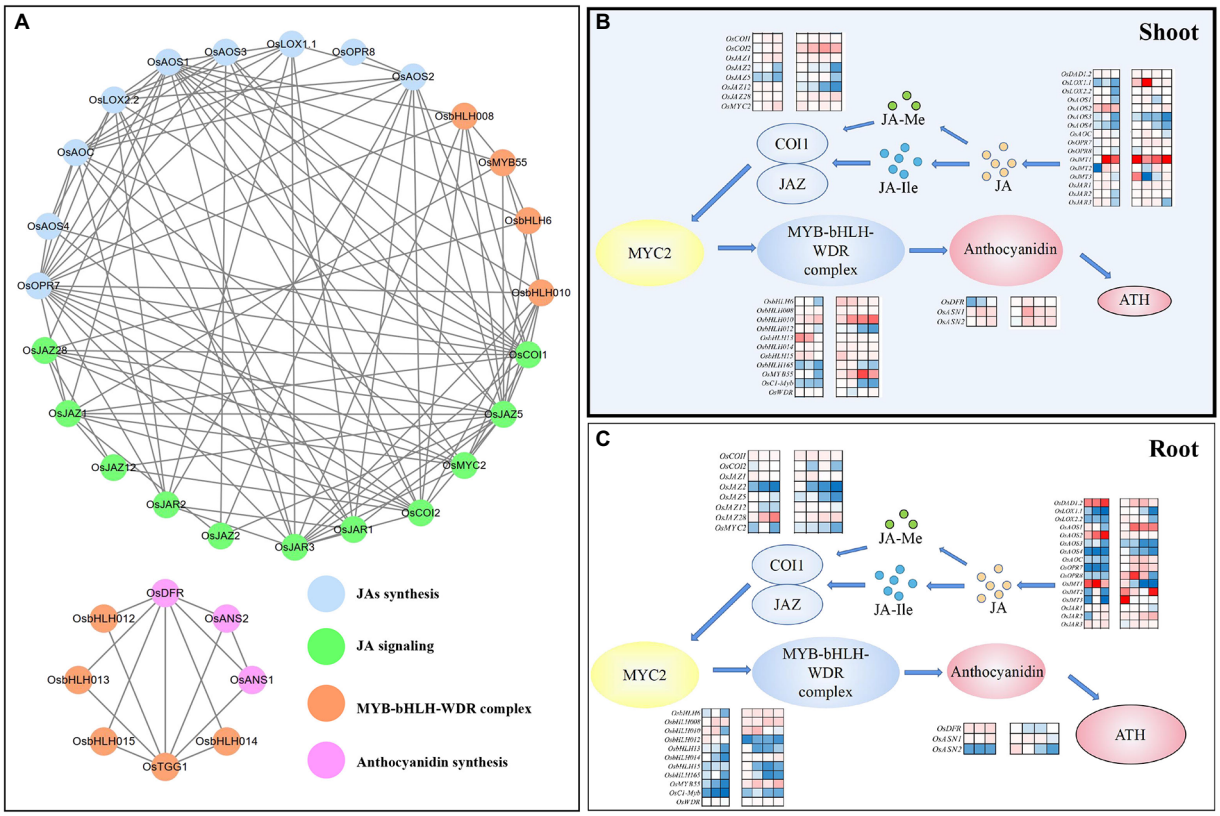


FIGURE 4
The schematic representation of the Pro-mediated regulation network of JA synthesis, JA signaling, MYB-bHLH-WDR complex, and anthocyanidin synthesis in rice seedlings under Cr stress. **(A)** The genetic interaction network in rice seedlings; **(B)** Heatmap presentation of Pro-mediated regulation of JA synthesis, JA signaling, MYB-bHLH-WDR complex, and anthocyanidin synthesis in rice shoots under Cr stress; **(C)** Heatmap presentation of Pro-mediated regulation of JA synthesis, JA signaling, MYB-bHLH-WDR complex, and anthocyanidin synthesis in rice roots under Cr stress.

exposure was more sensitive than JA-Me synthesis. It is known that JA-Ile as a bioactive compound in plant cells is always kept at a very low level under normal conditions (Fonseca et al., 2009), in which genes responsible for the JA signaling pathway remained in the inactivated state (Ali and Baek, 2020). When plants suffered unfavorable conditions, the trade-off between epimerization of JA into JA-Ile and accumulation of JA-Ile became a mandatory routine in the cytoplasm of aerial parts, afterwards, JA signaling pathway was activated by JA-Ile accumulated (Truman et al., 2007; Li et al., 2017). Herein, the expression of JA signaling pathway-related genes (i.e., *OsCOI1, OsCOI2, OsJAZ1, OsJAZ12, OsJAZ28*) was significantly upregulated in rice shoots after Cr(VI) exposure, suggesting that JA-Ile can positively bind with the COI and JAZ proteins and activated their capacity of signal transduction (Wasternack and Hause, 2013; Wasternack and Song, 2017; Raza et al., 2021). In addition, a significant increase in the expression of *OsMYC2* was observed in rice shoots after Cr(VI) exposure. It is known that *OsMYC2* is highly involved in the JA signaling pathway in rice through binding to the JAZ and COI proteins, thereby stimulating the expression of downstream JA response genes (Thines et al., 2007).

Proline functioning in plants as an osmoprotectant, ROS scavenger, and membrane stabilizer has been studied extensively (Hoque et al., 2007; Moustakas et al., 2011; Yu et al., 2017; Zhang et al., 2021). Herein, exogenous Pro-mediated regulation on JAs synthesis and signaling pathway was first documented in rice plants under Cr(VI) stress. Endogenous level of JA and JA-Ile in rice shoots under "Pro + Cr(VI)" treatments was higher than that of Cr(VI) treatments, suggesting that exogenous Pro promoted the synthesis of JA and JA-Ile in rice plants under Cr(VI) stress. PCR analysis also showed a positive role of exogenous Pro on the expression of JA synthesis and signaling pathway-related genes in shoots of rice seedlings at different ECs of Cr(VI; Figure 4B). Calculation of *GEVFs* indicated that exogenous Pro-mediated regulation was tissue-specific. A stronger regulation impact of exogenous Pro on the JA synthesis was observed in roots, while both JA synthesis and signal pathway in shoots were regulated by exogenous Pro applied. Additionally, Venn diagram showed that *OsLOX1.1* (Module 1) was the common promoting gene regulating JA synthesis in both rice tissues in response to Cr(VI) stress. An indirect link between Pro and plant hormone was observed in plants during Cr stress (Alvarez et al., 2022),

wherein Pro regulates the level of other signaling molecules (e.g., ROS, H_2S, and NO; Verbruggen and Hermans, 2008), thereby affecting the response pattern of JA and JA-Ile content in plants.

Exogenous proline activates the MYB-BHLH-WDR complex in rice under Cr(VI) stress

A previous study indicated that the MYB-bHLH-WDR complex in plants is a valve between the JA signal pathway and the downstream JA response genes in responses to various stresses (Qi et al., 2011). In this current study, more genes activated in MYB-bHLH-WDR complex were upregulated in "Pro + Cr(VI)" treatments than Cr(VI) treatments, and higher expression of genes was observed in "Pro + Cr(VI)" treatments than Cr(VI) treatments (Figure 4B). Additionally, calculation of *GEVFs* indicated that *OsbHLH6, OsbHLH014,* and *OsMYB55* are the common promoting genes in both rice tissues regulating the MYB-bHLH-WDR complex under Cr(VI) stress. We also noticed that the regulation role of exogenous Pro on the MYB-bHLH-WDR complex in rice shoots was highly dependent on Cr(VI) concentrations, in which expression of *OsMYB55*, *OsbHLH010* and *OsMYB55*, and *OsbHLH6* and *OsbHLH010* was highly activated by exogenous Pro at EC_{20}, EC_{50}, and EC_{75} of Cr(VI), respectively. These results indicated different regulation strategies of the MYB-bHLH-WDR complex mediated by exogenous Pro in rice plants under Cr(VI) stress.

Exogenous proline inhibits ATH accumulation in rice under Cr(VI) stress

It is known that anthocyanidin can possess great potential for alleviating photooxidation as a shelter to protect the damaging impact of excess light absorbed on chloroplasts (Zhang et al., 2002; Zhang and Becker, 2015), and serves as a ROS scavenger to diminish oxidative burst in plants (Luo et al., 2016). Anthocyanin is a byproduct formed by the glycosidic bond between anthocyanidin and sugars (Ling et al., 2021), which is frequently detected in plants under unfavorable conditions (Ling et al., 2021). Herein, although expression of anthocyanidin synthesis-related genes (*OsDFR, OsASN1,* and *OsASN2*) in rice shoots was upregulated at all treatments, the glycosylation of anthocyanidin into ATH in rice plants was also detected. More accumulation of ATH was observed in rice plants with enhancing Cr(VI) concentrations, suggesting that Cr(VI) exposure can simulate the glycosylation of anthocyanidin and enhance the accumulation of ATH in plants. However, a reduction in the endogenous level of ATH in Cr(VI)-treated rice seedlings was observed due to the application of exogenous Pro, suggesting that exogenous Pro can effectively repress the glycosylation of anthocyanidin and decrease ATH accumulation in rice plants under Cr(VI) stress.

Environmental implications

Chromium pollution from industrial processes seriously influences the safety of the ecosystem. In some cases, a higher level of Cr can enter the agricultural systems and threaten the yield, quality, and food safety of crops. Recently, plant-derived growth regulators (PDGRs) have been used to minimize the adverse effects imposed by heavy metals, due to their availability (Yang et al., 2021). Compared with other chemical reagents used, PDGRs not only improve the resistance capacity of plants against heavy metal stresses but also alter the distribution pattern of heavy metals in plant tissues (Hao et al., 2012). Due to their different chemical properties and occurrence in plant cells, the regulatory mechanisms of PDGRs in alleviating phytotoxicity caused by heavy metals is different. For instance, exogenous H_2S can manage Cr(VI) toxicity in wheat, rice, and bean through the ethylene signaling, sulfur assimilation, and ascorbate-glutathione cycle (Husain et al., 2020, 2021, 2022; Singh et al., 2022a,b). Also, exogenous amino acids (e.g., Pro, gamma-aminobutyric acid, and glutamate) can minimize heavy metal toxicity in rice, tomato, and brinjal (Jiang et al., 2020; Suhel et al., 2022; Zhang et al., 2022) by mediating the transcription factors and the antioxidant systems. Additionally, exogenous plant hormones (e.g., JA, auxin, kinetin, and melatonin) can regulate metal uptake, photosynthetic pigments, and antioxidant systems to enhance stress resistance (López et al., 2007; Wang et al., 2015; Dai et al., 2020; Hodžić et al., 2021). In this study, we displayed the effects of exogenous Pro on ATH accumulation through regulating Jasmonate signals and MYB-bHLH-WDR complex and protecting rice plants from Cr(VI) stress.

Conclusion

This study presents the latest evidence to update the positive role of exogenous Pro on regulating jasmonate signals and activating the MYB-bHLH-WDR complex to repress ATH accumulation in rice plants under Cr(VI) stress. New findings include: (1) exogenous Pro promotes an endogenous level of JA and JA-Ile in rice tissues under Cr(VI) stress; (2) increment in the level of jasmonates triggers the expression of genes activated in the JA signaling pathway; (3) the activation of MYB-bHLH-WDR complex inhibits the glycosylation of anthocyanidin in rice tissue and decreases ATH accumulation in rice plants; (4) exogenous Pro-mediated regulation on jasmonate signals was tissue-specific under Cr(VI) stress and a more positive effect was detected in rice shoots rather than roots.

Data availability statement

The original contributions presented in the study are included in the article/Supplementary material, further inquiries can be directed to the corresponding author.

Author contributions

X-ZY: conceptualization, methodology, supervision, writing-reviewing and editing, and funding acquisition. QZ: investigation. Y-XF: writing-original draft preparation and visualization. PT: investigation, data analysis, visualization, and software. Y-JL: data analysis, visualization, and software. All authors contributed to the article and approved the submitted version.

Funding

This work was financially supported by the Natural Science Foundation of Guangxi (no. 2018GXNSFDA281024).

Conflict of interest

The authors declare that the research was conducted in the absence of any commercial or financial relationships that could be construed as a potential conflict of interest.

Publisher's note

All claims expressed in this article are solely those of the authors and do not necessarily represent those of their affiliated organizations, or those of the publisher, the editors and the reviewers. Any product that may be evaluated in this article, or claim that may be made by its manufacturer, is not guaranteed or endorsed by the publisher.

Supplementary material

The Supplementary material for this article can be found online at: https://www.frontiersin.org/articles/10.3389/fpls.2022.953398/full#supplementary-material

References

Ali, M. S., and Baek, K. H. (2020). Jasmonic acid signaling pathway in response to abiotic stresses in plants. *Int. J. Mol. Sci.* 21:621. doi: 10.3390/ijms21020621

Alvarez, M. E., Savouré, A., and Szabados, L. (2022). Proline metabolism as regulatory hub. *Trends Plant Sci.* 27, 39–55. doi: 10.1016/j.tplants.2021.07.009

Asad, S. A., Masood, R., Ahmad, R., and Umer, M. (2018). Differential uptake of cadmium and chromium in *Brassica oleraceae* in response to application of plant growth promoting rhizobacteria. *Int. J. Agric. Biol.* 20, 1613–1622. doi: 10.17957/IJAB/15.0682

Awotide, B. A., Karimov, A. A., and Diagne, A. (2016). Agricultural technology adoption, commercialization and smallholder rice farmers' welfare in rural Nigeria. *Agric. Food Econ.* 4:3. doi: 10.1186/s40100-016-0047-8

Bali, S., Jamwal, V. L., Kohli, S. K., Kaur, P., Tejpal, R., Bhalla, V., et al. (2019). Jasmonic acid application triggers detoxification of lead (Pb) toxicity in tomato through the modifications of secondary metabolites and gene expression. *Chemosphere* 235, 734–748. doi: 10.1016/j.chemosphere.2019.06.188

Broun, P. (2005). Transcriptional control of flavonoid biosynthesis: a complex network of conserved regulators involved in multiple aspects of differentiation in Arabidopsis. *Curr. Opin. Plant Biol.* 8, 272–279. doi: 10.1016/j.pbi.2005.03.006

Collin, V. C., Eymery, F., Genty, B., Rey, P., and Havaux, M. (2008). Vitamin E is essential for the tolerance of *Arabidopsis thaliana* to metal-induced oxidative stress. *Plant Cell Environ.* 31, 244–257. PMID: 17996014. doi: 10.1111/j.1365-3040.2007.01755.x

Dai, H., Wei, S., Pogrzeba, M., Rusinowski, S., Krzyżak, J., and Jia, G. (2020). Exogenous jasmonic acid decreased cu accumulation by alfalfa and improved its photosynthetic pigments and antioxidant system. *Ecotox. Environ. Safe.* 190:110176. doi: 10.1016/j.ecoenv.2020.110176

Fan, W. J., Feng, Y. X., Li, Y. H., Lin, Y. J., and Yu, X. Z. (2020). Unraveling genes promoting ROS metabolism in subcellular organelles of *Oryza sativa* in response to trivalent and hexavalent chromium. *Sci. Total Environ.* 744:140951. doi: 10.1016/j.scitotenv.2020.140951

Feng, Y. X., Yu, X. Z., Mo, C. H., and Lu, C. J. (2019). Regulation network of sucrose metabolism in response to trivalent and hexavalent chromium in *Oryza sativa*. *J. Agric. Food Chem.* 67, 9738–9748. doi: 10.1021/acs.jafc.9b01720

Fonseca, S., Chini, A., Hamberg, M., Adie, B., Porzel, A., Kramell, R., et al. (2009). (+)-7-iso-Jasmonoyl-L-isoleucine is the endogenous bioactive jasmonate. *Nat. Chem. Biol.* 5, 344–350. doi: 10.1038/nchembio.161

Gomes, M. A. D. C., Hauser-Davis, R. A., Suzuki, M. S., and Vitória, A. P. (2017). Plant chromium uptake and transport, physiological effects and recent advances in molecular investigations. *Ecotox. Environ. Safe.* 140, 55–64. doi: 10.1016/j.ecoenv.2017.01.042

Hao, H. Z., Shen, Y. H., Zhong, R. G., Fu, Z. Y., Liu, C. W., and Zhong, X. B. (2012). The effect of plant growth regulator for phytoremediation. *Adv. Mat. Res.* 573−574, 1086–1089.

Hodžić, E., Galijašević, S., Balaban, M., Rekanović, S., Makić, H., Kukavica, B., et al. (2021). The protective role of melatonin under heavy metal-induced stress in *Melissa Officinalis* L. *Turkish J. Chem.* 45, 737–748. doi: 10.3906/kim-2012-7

Hoque, M. A., Banu, M. N. A., Okuma, E., Amako, K., Nakamura, Y., Shimoishi, Y., et al. (2007). Exogenous proline and glycinebetaine increase NaCl-induced ascorbate–glutathione cycle enzyme activities, and proline improves salt tolerance more than glycinebetaine in tobacco bright Yellow-2 suspension-cultured cells. *J. Plant Physiol.* 164, 1457–1468. doi: 10.1016/j.jplph.2006.10.004

Husain, T., Fatima, A., Suhel, M., Singh, S., Sharma, A., Prasad, S. M., et al. (2020). A brief appraisal of ethylene signaling under abiotic stress in plants. *Plant Signal. Be.* 15:1782051. doi: 10.1080/15592324.2020.1782051

Husain, T., Suhel, M., Prasad, S. M., and Singh, V. P. (2021). Ethylene needs endogenous hydrogen sulfide for alleviating hexavalent chromium stress in *Vigna mungo* L. and *Vigna radiata* L. *Environ. Pollut.* 290:117968. doi: 10.1016/j.envpol.2021.117968

Husain, T., Suhel, M., Prasad, S. M., and Singh, V. P. (2022). Ethylene and hydrogen sulphide are essential for mitigating hexavalent chromium stress in two pulse crops. *Plant Biol.* 24, 652–659. doi: 10.1111/plb.13324

Infante, E. F., Dulfo, C. P., Dicen, G. P., Hseu, Z. Y., and Navarrete, I. A. (2021). Bioaccumulation and human health risk assessment of chromium and nickel in paddy rice grown in serpentine soils. *Environ. Sci. Pollut. Res.* 28, 17146–17157. doi: 10.1007/s11356-020-12176-y

Jiang, M., Jiang, J., Li, S., Li, M., Tan, Y., Song, S., et al. (2020). Glutamate alleviates cadmium toxicity in rice via suppressing cadmium uptake and translocation. *J. Hazard. Mater.* 384:121319. doi: 10.1016/j.jhazmat.2019.121319

Kamran, M., Wang, D., Alhaithloul, H. A. S., Alghanem, S. M., Aftab, T., Xie, K., et al. (2021). Jasmonic acid-mediated enhanced regulation of oxidative, glyoxalase defense system and reduced chromium uptake contributes to alleviation of chromium (VI) toxicity in choysum (*Brassica parachinensis* L.). *Ecotox. Environ. Safe.* 208:111758. doi: 10.1016/j.ecoenv.2020.111758

Kan, C. C., Chung, T. Y., Wu, H. Y., Juo, Y. A., and Hsieh, M. H. (2017). Exogenous glutamate rapidly induces the expression of genes involved in metabolism and defense responses in rice roots. *BMC Genomics* 18:186. doi: 10.1186/s12864-017-3588-7

Kondo, S., Tomiyama, H., Opio, P., Komiya, R., Saito, T., Okawa, K., et al. (2021). L-isoleucine (Ile) promotes anthocyanin accumulation in apples. *J. Plant Growth Regul.* 40, 541–549. doi: 10.1007/s00344-020-10117-0

Lei, G. J., Sun, L., Sun, Y., Zhu, X. F., Li, G. X., and Zheng, S. J. (2020). Jasmonic acid alleviates cadmium toxicity in Arabidopsis *via* suppression of cadmium uptake and translocation. *J. Integr. Plant Biol.* 62, 218–227. doi: 10.1111/jipb.12801

Li, Y. Z., Qin, L., Zhao, J. J., Muhammad, T., Cao, H. H., Li, H. L., et al. (2017). SlMAPK3 enhances tolerance to tomato yellow leaf curl virus (TYLCV) by regulating salicylic acid and jasmonic acid signaling in tomato (*Solanum lycopersicum*). *PLoS One* 12:e0172466. doi: 10.1371/journal.pone.0172466

Lin, Y. J., Yu, X. Z., and Zhang, Q. (2019). Transcriptome analysis of *Oryza sativa* in responses to different concentrations of thiocyanate. *Environ. Sci. Pollut. Res.* 26, 11696–11709. doi: 10.1007/s11356-019-04544-0

Ling, Q. L., Feng, Y. X., Lu, C. J., Lin, Y. J., and Yu, X. Z. (2021). Genetic variation and gene expression of anthocyanin synthesis and transport related enzymes in *Oryza sativa* against thiocyanate. *Plant Physiol. Biochem.* 160, 18–26. doi: 10.1016/j.plaphy.2021.01.005

López, M. L., Peralta-Videa, J. R., Parsons, J. G., Benitez, T., and Gardea-Torresdey, J. L. (2007). Gibberellic acid, kinetin, and the mixture indole-3-acetic acid-kinetin assisted with EDTA-induced lead hyperaccumnulation in alfalfa plants. *Environ. Sci. Technol.* 41, 8165–8170. doi: 10.1021/es0714080

Luo, P., Shen, Y. X., Jin, S. X., Huang, S. S., Cheng, X., Wang, Z., et al. (2016). Overexpression of *Rosa rugosa* anthocyanidin reductase enhances tobacco tolerance to abiotic stress through increased ROS scavenging and modulation of ABA signaling. *Plant Sci.* 245, 35–49. doi: 10.1016/j.plantsci.2016.01.007

Ma, J., Lv, C., Xu, M., Chen, G., Lv, C., and Gao, Z. (2016). Photosynthesis performance, antioxidant enzymes, and ultrastructural analyses of rice seedlings under chromium stress. *Environ. Sci. Pollut. Res.* 23, 1768–1778. doi: 10.1007/s11356-015-5439-x

Michael, R., Rohit, D., Mohamed, H., Berta, M., Ajay, K., and Peter, N. (2015). Exploring jasmonates in the hormonal network of drought and salinity responses. *Front. Plant Sci.* 6:1077. doi: 10.3389/fpls.2015.01077

Moustakas, M., Sperdouli, I., Kouna, T., Antonopoulou, C.-I., and Therios, I. (2011). Exogenous proline induces soluble sugar accumulation and alleviates drought stress effects on photosystem II functioning of *Arabidopsis thaliana* leaves. *Plant Growth Regul.* 65, 315–325. doi: 10.1007/s10725-011-9604-z

Nie, G., Liao, Z., Zhong, M., Zhou, J., and Zhang, X. (2021). Microrna-mediated responses to chromium stress provide insight into tolerance characteristics of *miscanthus sinensis*. *Front. Plant Sci.* 12:666117. doi: 10.3389/fpls.2021.666117

Park, N. I., Xu, H., Li, X., Jang, I. H., Park, S., Ahn, G. H., et al. (2011). Anthocyanin accumulation and expression of anthocyanin biosynthetic genes in radish (*Raphanus sativus*). *J. Agric. Food Chem.* 59, 6034–6039. doi: 10.1021/jf200824c

Qi, T., Song, S., Ren, Q., Wu, D., Huang, H., Chen, Y., et al. (2011). The Jasmonate-ZIM-domain proteins interact with the WD-repeat/bHLH/MYB complexes to regulate Jasmonate-mediated anthocyanin accumulation and trichome initiation in *Arabidopsis thaliana*. *Plant Cell* 23, 1795–1814. doi: 10.1105/tpc.111.083261

Raza, A., Charagh, S., Zahid, Z., Mubarik, M. S., Javed, R., Siddiqui, M. H., et al. (2021). Jasmonic acid: a key frontier in conferring abiotic stress tolerance in plants. *Plant Cell Rep.* 40, 1513–1541. doi: 10.1007/s00299-020-02614-z

Ruan, J., Zhou, Y., Zhou, M., Yan, J., Khurshid, M., Weng, W., et al. (2019). Jasmonic acid signaling pathway in plants. *Int. J. Mol. Sci.* 20:2479. doi: 10.3390/ijms20102479

Sadak, M. S., El-Monem, A., El-Bassiouny, H., and Badr, N. M. (2012). Physiological response of sunflower (*helianthus annuus* l.) to exogenous arginine and putrescine treatments under salinity stress. *J. Appl. Sci. Res.* 8, 4943–4957.

Schmittgen, T., and Livak, K. (2008). Analyzing real-time PCR data by the comparative CT method. *Nat. Protoc.* 3, 1101–1108. doi: 10.1038/nprot.2008.73

Shahid, M., Shamshad, S., Rafiq, M., Khalid, S., Bibi, I., Niazi, N. K., et al. (2017). Chromium speciation, bioavailability, uptake, toxicity and detoxification in soil-plant system: a review. *Chemosphere* 178, 513–533. doi: 10.1016/j.chemosphere.2017.03.074

Shao, Y., Zhou, H. Z., Wu, Y. R., Zhang, H., Lin, J., Jiang, X. Y., et al. (2019). OsSPL3, an SBP-domain protein, regulates crown root development in rice. *Plant Cell* 31, 1257–1275. doi: 10.1105/tpc.19.00038

Shitan, N. (2016). Secondary metabolites in plants: transport and self-tolerance mechanisms. *Biosci. Biotech. Bioch.* 80, 1283–1293. doi: 10.1080/09168451.2016.1151344

Singh, S. K., Husain, T., Suhel, M., Prasad, S. M., and Singh, V. P. (2022a). Hydrogen sulphide ameliorates hexavalent chromium toxicity in two cereal crops: role of antioxidant enzymes and proline metabolism. *Plant Biol.* 24, 636–641. doi: 10.1111/plb.13413

Singh, S. K., Suhel, M., Husain, T., Prasad, S. M., and Singh, V. P. (2022b). Hydrogen sulfide manages hexavalent chromium toxicity in wheat and rice seedlings: the role of sulfur assimilation and ascorbate-glutathione cycle. *Environ. Pollut.* 307:119509. doi: 10.1016/j.envpol.2022.119509

Sirhindi, G., Mir, M. A., Abd Allah, E. F., Ahmad, P., and Gucel, S. (2016). Jasmonic acid modulates the physio-biochemical attributes, antioxidant enzyme activity, and gene expression in *glycine max* under nickel toxicity. *Front. Plant Sci.* 7:591. doi: 10.3389/fpls.2016.00591

Suhel, M., Husain, T., Prasad, S. M., and Singh, V. P. (2022). GABA requires nitric oxide for alleviating arsenate stress in tomato and brinjal seedlings. *J. Plant Growth Regul.*, 1–14. doi: 10.1007/s00344-022-10576-7

Sytar, O., Kumari, P., Yadav, S., Brestic, M., and Rastogi, A. (2019). Phytohormone priming: regulator for heavy metal stress in plants. *J. Plant Growth Regul.* 38, 739–752. doi: 10.1007/s00344-018-9886-8

Thines, B., Katsir, L., Melotto, M., Niu, Y., Mandaokar, A., Liu, G., et al. (2007). JAZ repressor proteins are targets of the SCFCOI1 complex during jasmonate signalling. *Nature* 448, 661–665. doi: 10.1038/nature05960

Truman, W., Bennett, M. H., Kubigsteltig, I., Turnbull, C., and Grant, M. (2007). Arabidopsis systemic immunity uses conserved defense signaling pathways and is mediated by jasmonates. *Proc. Natl. Acad. Sci. U. S. A.* 104, 1075–1080. doi: 10.1073/pnas.0605423104

Verbruggen, N., and Hermans, C. (2008). Proline accumulation in plants: a review. *Amino Acids* 35, 753–759. doi: 10.1007/s00726-008-0061-6

Wang, R., Wang, J., Zhao, L., Yang, S., and Song, Y. (2015). Impact of heavy metal stresses on the growth and auxin homeostasis of Arabidopsis seedlings. *Biometals* 28, 123–132. doi: 10.1007/s10534-014-9808-6

Wasternack, C., and Hause, B. (2013). Jasmonates: biosynthesis, perception, signal transduction and action in plant stress response, growth and development. *Ann. Bot.* 111, 1021–1058. doi: 10.1093/aob/mct067

Wasternack, C., and Song, S. (2017). Jasmonates: biosynthesis, metabolism, and signaling by proteins activating and repressing transcription. *J. Exp. Bot.* 68, 1303–1321. doi: 10.1093/jxb/erw443

Xiao, W., Ye, X., Zhu, Z., Zhang, Q., Zhao, S., Chen, G., et al. (2021). Combined effects of rice straw-derived biochar and water management on transformation of chromium and its uptake by rice in contaminated soils. *Ecotoxicol. Environ. Saf.* 208:111506. doi: 10.1016/j.ecoenv.2020.111506

Yang, L., Feng, Y. X., Lin, Y. J., and Yu, X. Z. (2021). Comparative effects of sodium hydrosulfide and proline on functional repair in rice chloroplast through the D1 protein and thioredoxin system under simulated thiocyanate pollution. *Chemosphere* 284:131389. doi: 10.1016/j.chemosphere.2021.131389

Yu, X. Z., Lin, Y. J., Fan, W. J., and Lu, M. R. (2017). The role of exogenous proline in amelioration of lipid peroxidation in rice seedlings exposed to Cr(VI). *Int. Biodeter. Biodegr.* 123, 106–112. doi: 10.1016/j.ibiod.2017.06.010

Zhang, L., and Becker, D. F. (2015). Connecting proline metabolism and signaling pathways in plant senescence. *Front. Plant Sci.* 6:552. doi: 10.3389/fpls.2015.00552

Zhang, W., Curtin, C., Kikuchi, M., and Franco, C. (2002). Integration of jasmonic acid and light irradiation for enhancement of anthocyanin biosynthesis in *Vitis vinifera* suspension cultures. *Plant Sci.* 162, 459–468. doi: 10.1016/S0168-9452(01)00586-6

Zhang, Q., Feng, Y. X., Lin, Y. J., and Yu, X. Z. (2021). Indigenous proline is a two-dimensional safety-relief valve in balancing specific amino acids in rice under hexavalent chromium stress. *J. Agric. Food Chem.* 69, 11185–11195. doi: 10.1021/acs.jafc.1c02575

Zhang, Q., Feng, Y. X., Lin, Y. J., and Yu, X. Z. (2022). Mathematical quantification of interactive complexity of transcription factors involved in proline-mediated regulative strategies in *Oryza sativa* under chromium stress. *Plant Physiol. Biochem.* 182, 36–44. doi: 10.1016/j.plaphy.2022.04.005

Zhang, J., Han, Z. Y., Tian, J., Zhang, X., Song, T. T., and Yao, Y. C. (2015). The expression level of anthocyanidin synthase determines the anthocyanin content of crabapple (Malus sp.) petals. *Acta Physiol. Plant.* 37:109. doi: 10.1007/s11738-015-1857-0

Zhao, C. L., Zhang, L. M., and Liu, F. C. (2008). Existent states of anthocyanins in vacuole and their coloration effects in higher plants. *Guihaia.* 28, 395–401.

frontiers | Frontiers in Plant Science

TYPE Original Research
PUBLISHED 03 August 2022
DOI 10.3389/fpls.2022.955490

Check for updates

OPEN ACCESS

EDITED BY
Mirza Hasanuzzaman,
Sher-e-Bangla Agricultural University, Bangladesh

REVIEWED BY
Myeong-Cheoul Cho,
Allium Vegetable Research Institute, South Korea
Boon Chin Tan,
University of Malaya, Malaysia

*CORRESPONDENCE
Dorin Gupta
dorin.gupta@unimelb.edu.au
Waseem Ashfaq
washfaq@student.unimelb.edu.au

SPECIALTY SECTION
This article was submitted to Plant Abiotic Stress, a section of the journal Frontiers in Plant Science

RECEIVED 28 May 2022
ACCEPTED 04 July 2022
PUBLISHED 03 August 2022

CITATION
Ashfaq W, Fuentes S, Brodie G and Gupta D (2022) The role of silicon in regulating physiological and biochemical mechanisms of contrasting bread wheat cultivars under terminal drought and heat stress environments.
Front. Plant Sci. 13:955490.
doi: 10.3389/fpls.2022.955490

COPYRIGHT
© 2022 Ashfaq, Fuentes, Brodie and Gupta. This is an open-access article distributed under the terms of the Creative Commons Attribution License (CC BY). The use, distribution or reproduction in other forums is permitted, provided the original author(s) and the copyright owner(s) are credited and that the original publication in this journal is cited, in accordance with accepted academic practice. No use, distribution or reproduction is permitted which does not comply with these terms.

The role of silicon in regulating physiological and biochemical mechanisms of contrasting bread wheat cultivars under terminal drought and heat stress environments

Waseem Ashfaq*, Sigfredo Fuentes, Graham Brodie and Dorin Gupta*

School of Agriculture and Food, Faculty of Veterinary and Agricultural Sciences, The University of Melbourne, Parkville, VIC, Australia

The individual and cumulative effects of drought stress (DS) and heat stress (HS) are the primary cause of grain yield (GY) reduction in a rainfed agricultural system. Crop failures due to DS and HS are predicted to increase in the coming years due to increasingly severe weather events. Plant available silicon (Si, H_4SiO_4) has been widely reported for its beneficial effects on plant development, productivity, and attenuating physiological and biochemical impairments caused by various abiotic stresses. The current study investigated the impact of pre-sowing Si treatment on six contrasting wheat cultivars (four drought and heat stress-tolerant and two drought and heat stress-susceptible) under individual and combined effects of drought and heat stress at an early grain-filling stage. DS, HS, and drought-heat combined stress (DHS) significantly ($p < 0.05$) altered morpho-physiological and biochemical attributes in susceptible and tolerant wheat cultivars. However, results showed that Si treatment significantly improved various stress-affected morpho-physiological and biochemical traits, including GY (>40%) and yield components. Si treatment significantly ($p < 0.001$) increased the reactive oxygen species (ROS) scavenging antioxidant activities at the cellular level, which is linked with higher abiotic stress tolerance in wheat. With Si treatment, osmolytes concentration increased significantly by >50% in tolerant and susceptible wheat cultivars. Similarly, computational water stress indices (canopy temperature, crop water stress index, and canopy temperature depression) also improved with Si treatment under DS, HS, and DHS in susceptible and tolerant wheat cultivars. The study concludes that Si treatment has the potential to mitigate the detrimental effects of individual and combined stress of DS, HS, and DHS at an early grain-filling

stage in susceptible and tolerant wheat cultivars in a controlled environment. These findings also provide a foundation for future research to investigate Si-induced tolerance mechanisms in susceptible and tolerant wheat cultivars at the molecular level.

KEYWORDS

***Triticum aestivum*, silicon, oxidative stress, stress alleviation, stress adaptation, abiotic stress, antioxidants**

Introduction

Bread wheat is an important staple food crop in most parts of the world. With a total grain production of around 760 million tons in 2020 (FAOSTAT, 2020), wheat grain provides ~20% of the total vegetal calories and proteins for nearly 4.5 billion people worldwide (Shiferaw et al., 2013). However, global wheat productivity faces challenges due to climatic adversities, which are becoming more acute in most of the world's established agricultural regions, raising concerns for future food security (FAO, 2019). In a rainfed cropping system, temperature and water availability play a critical role in determining optimum crop growth and productivity (Rezaei et al., 2015; Tricker et al., 2018).

Abiotic stress factors, such as drought and heat are the primary cause of grain yield (GY) reduction worldwide, and the frequency of their concomitant effects has increased in the semi-arid wheat belts of the world (Fahad et al., 2017). Due to the expected rise in global temperature (Buis, 2019; NOAA, 2020; IPCC, 2022) and change in the precipitation patterns of dryland agriculture (Rojas et al., 2019), the individual and combined effects of drought and heat stresses would disrupt morphological, biochemical, and physiological processes more than any other environmental stresses (Zandalinas et al., 2018; Sattar et al., 2020). Drought and heat stress-induced altered/affected processes during grain filling includes a reduction in photosynthesis, various oxidative damages to cell organelles (mitochondria, chloroplast), earlier senescence, shortening of the plant life cycle, and significant losses in the grain yield (Barnabás et al., 2008; Rezaei et al., 2015; Tricker et al., 2018). The exposure of plants to drought stress (DS) and heat stress (HS) disturbs the reactive oxygen species (ROS) quenching ability of different antioxidants, leading to excessive production of several ROS. As a result of this overproduction, ROS intracellular levels rapidly increase and negatively affect various cellular metabolic processes (Sharma et al., 2012; Alzahrani et al., 2018). Plants with increased antioxidants, either in constitutive or induced forms, have demonstrated maximum tolerance against oxidative stress damages to cells and organelles. Higher antioxidants level also supports the accumulation of various osmolytes, such as amino acids, soluble sugars, proline, and different organic acids (Biju et al., 2017).

Plant responses to combined drought and heat stress (DHS) are very complicated, and the intensity of one stress might alter responses for the other. Combined stress has significantly higher detrimental and negative impacts on plant phenology and physiology. The combined effects of DHS resulted in suppressing various physiological processes, i.e., net photosynthetic rate and higher canopy temperature (T_c), which causes disproportionate plant development and productivity compared to individual stress effects (Barnabás et al., 2008; Prasad et al., 2008; Zandalinas et al., 2018; Sattar et al., 2020). Various antioxidants and osmolytes induced a tolerance response in the plants against individual stresses; however, the functioning of these response mechanisms was altered significantly under combined stress. Higher yield penalties have been linked with an extended period of heatwaves over 32°C, coinciding with DS during anthesis and grain-filling stages (Perdomo et al., 2015; Tricker et al., 2018).

Silicon (Si) is the second most ubiquitous element (31%) in the geosphere after oxygen (49%), and it exists mainly in the form of silicates (Luyckx et al., 2017). Although Si has not been recognized as an essential plant element, the benefits of Si application in improving the development and yield of many plant species are well-documented (Cooke and Leishman, 2016; Debona et al., 2017; Luyckx et al., 2017). Plant roots can uptake Si in uncharged mono silicic acid form (H_4SiO_4) *via* aquaporin channels (NIPs: Nodulin26-like intrinsic proteins) when the pH of the growth medium is below 9. The NIPs, which belong to the major intrinsic proteins, form highly selective transport channels to facilitate the passive transport of moisture and uncharged molecules (Grégoire et al., 2012; Deshmukh et al., 2013), including silicic acid (Ma et al., 2006). Mono silicic acid is a weak acid in an aqueous solution, mainly accumulated in cell walls and plant tissues. However, Si concentration in plants varies significantly from 0.1 to 10% of the total shoot dry weight (DW) (Hodson et al., 2005).

Several research studies showed that plants with a high Si ratio in the roots and shoots are less prone to abiotic stresses (Debona et al., 2017; Etesami and Jeong, 2018). The Si accumulation in plants can alleviate the harmful effects of various abiotic stresses by targeting oxidative stress reduction through enzymatic regulations (Biju et al., 2017), enhanced antioxidant activities (Biju et al., 2017; Etesami and Jeong, 2018),

modification of gas exchange apparatus (Cooke and Leishman, 2016; Debona et al., 2017), various osmotic adjustments, improved nutrient uptake, and regulation of different osmolytes (Rizwan et al., 2015; Cooke and Leishman, 2016; Etesami and Jeong, 2018). A meta-analysis of 145 research studies concluded that Si application significantly improved DW, chlorophyll biosynthesis, net assimilation rate, and antioxidants activity in several plant species grown under various abiotic stresses (Cooke and Leishman, 2016). Si application also proves to have beneficial effects in maintaining plant water status (Etesami and Jeong, 2018), computational water stress indices (Ashfaq et al. unpublished data), GY, and yield-related components under abiotic stresses (Cooke and Leishman, 2016).

Although the response of the wheat crop to individual DS and HS has been quite comprehensively investigated in recent years, the combined effects of these stresses on wheat morphology and physiology have received limited attention (Mahrookashani et al., 2017; Urban et al., 2018). The ability of Si to enhance drought tolerance by regulating the physiological and biochemical mechanisms is known in many crops, including monocots (rice, wheat) and dicots (lentils, soybean) (Debona et al., 2017). First, the Si role against the combined effects of drought and heat in wheat has not been studied to date (Frew et al., 2018). Second, complex mechanisms and their interactions in Si-mediated tolerance against the individual and the combined effects of DS and HS in wheat need to be addressed at the physiological and biochemical levels at critical growth stages to estimate the impact on GY correctly. The study aimed to investigate the Si-mediated tolerance in wheat against individual and combined effects of terminal DS and HS at physiological and biochemical levels in a controlled environment.

Materials and methods

Plant materials

Six contrasting wheat cultivars, RAC875, Excalibur, ECH957, RAC622, Kukri, and CM59443, were used as experimental materials. RAC875 and Excalibur have shown relatively stable yield performance under the drought and heat-adapted environment of South Australia (SA). At the same time, Kukri, a hard wheat cultivar, suffers significant GY losses under moderate to low rainfall environments of SA (Fleury et al., 2010). RAC875, Excalibur, and Kukri show similar phenology (3–5 days heading time difference) under optimum growing conditions and possess RHt2 semi-dwarfing genes. These South Australian wheat cultivars were also comprehensively characterized and physiologically investigated by Izanloo et al. (2008). Similarly, cultivars, i.e., ECH957 and RAC622, showed relatively stable morpho-physiological performance and GY in controlled environment DS and HS experiments. Conversely, CM59443 endures significantly lower yield performance in similar DS- and HS-controlled environment experiments (Ashfaq et al., unpublished data).

Experimental design and establishment

To determine the role of Si in response to terminal DS, HS, and DHS on contrasting wheat cultivars, an experiment was conducted in a controlled greenhouse at Dookie Campus, the University of Melbourne (−36.384 S, 145.707 E) from July to November in 2019. A factorial experimental arrangement in a complete randomized design was used with three replications. Before sowing, 4 mM of Si solution was prepared using distilled water (dH_2O) at pH 7.0 (Deshmukh et al., 2013) and applied at two levels, i.e., $Si_0 = 0$ mM and $Si_1 = 4$ mM (Alzahrani et al., 2018). Respective Si solutions were thoroughly mixed in the individual respective treatment pot growth medium (standard potting mix, pH ~ 6.0) using a spray bottle.

Five uniformly selected seeds were sown in each polypropylene square-shape perforated nursery pot (466 cm^3 volume), containing the same mass (2 kg) of the oven-dried standard potting mix. Polylining was applied to the bottom of the pots to prevent Si from leaching. Appropriate fertilization (ICL Peters Excel CalMag grower water-soluble fertilizer) was applied before sowing, followed by three doses at tillering, jointing, and booting stage to ensure recommended nutrition supply for optimum plant growth.

To estimate pot field capacity, two perforated pots filled with 2 kg of the oven-dried potting mix were overflowed with tap water and allowed to drain for 12 h. When the water stopped dripping, the potting mix from both pots was weighed separately for their saturated weight and oven-dried (70°C for 36 h) for their DW. The percent moisture contents of the potting mix were measured using Equation 1 as described by Topp et al. (2008).

$$\text{Soil water content } (\%) = \frac{[\text{potting mix saturated weight (g)} - \text{potting mix dry weight (g)}}{\text{potting mix dry weight(g)}]} \times 100 \quad (1)$$

The day- and night-time temperatures in a glasshouse were maintained at 24 ± 1 and 18 ± 1°C (13/11), respectively, to replicate the average Australian wheat belt growing environment for optimum plant growth. All pots were watered up to full-field capacity daily until the Zadok's scale growth stage 75 (10 days after complete anthesis of the main tiller) (Zadok stage 75: Zadoks et al., 1974).

Plants were monitored individually to determine when their main tiller reached 10 days after complete anthesis (Zadok stage 75: Zadoks et al., 1974; Telfer et al., 2015); as in the Mediterranean environments, the wheat yield is determined mainly by the main stem contribution. At this stage, single extreme events, such as DS, HS, and a combination of both,

DHS were imposed on the designated pots of the experiment. For DS treatment, drought with 38 ± 3% field capacity was imposed on the DS, and DHS selected pots for 14 days. Before DS treatment, irrigation was gradually reduced for 5–7 days for acclimation to attain 38 ± 3% field capacity. Pots were weighed daily to measure the mass of moisture loss through evapotranspiration. Based on moisture loss, pots were watered accordingly to maintain the required field capacity. The effects of Si and DS on the tolerant and susceptible wheat cultivars were monitored by destructive (estimation of relative water content; RWC) and non-destructive sampling (measure of chlorophyll fluorescence and flag leaf senescence with Mini-Palm-II and portable SPAD-502, respectively).

For HS treatment, designated pots of HS and DHS group were shifted to separate plant growth chambers (Conviron, PGR15) 1 week before HS treatment to acclimatize with the PGR15 growing environment. Plant growth chambers were programed at 24 ± 1°C and 18 ± 1°C (13/11 h) for light and dark periods to support circadian clock genes expressions (Izanloo et al., 2008). The PGR15 was equipped with high-pressure sodium lamps for red, blue, and far-red light spectrum composition and high-power discharge metal halide. Light intensity was adjusted to 500–550 μ mol/m²/s at the top of the plant canopy to supplement natural radiation (Watson et al., 2018). The RH of PGR15 was set according to the glasshouse. Both HS and DHS group plants were subjected to high-temperature acclimation for 3 days with day/night temperatures of 36/22°C for 8 and 12 h, respectively, to mimic the hot day events which are common in the SA wheat belt (Spiertz et al., 2006; Telfer et al., 2015). Before and after 8 h of HS of 36°C, growth chambers were programed in a cyclic pattern of 28 and 32°C for 1 h each for a gradual increase and decrease in temperature. The RH was set at 45–50% during HS. In the DHS group, DS with 38 ± 3% field capacity was also maintained along with HS for the combined stress treatment. At the same time, irrigation was applied to the HS group to remove any confounding effect of drought. After 14 days of DS, normal irrigation was resumed in the DS and DHS groups. After the HS treatment, pots were shifted back to the glasshouse for the remaining growth cycle. During the imposed period of DS, HS, and DHS, water was normally applied to control (C) pots with full-field capacity. During the experiment, the pots were shuffled manually inside the glasshouse after every 2 weeks to avoid pseudo replications and border effects.

Plant sampling

On the last day of DS, HS, and DHS, the sampled leaves were taken from each replicate and stored at −80°C for the assay of enzymatic antioxidants, total soluble sugars (TSS), fructose contents (FCs), free amino acid (AA), and proline concentration.

Chlorophyll content, chlorophyll fluorescence, and relative water content measurements

Except for RWC, measurements were made non-destructively using flag leaves from each replicate on the last day of the stress treatments. The chlorophyll content of flag leaves was estimated using a SPAD-502 Plus (Konica Minolta, Japan). Chlorophyll content (SPAD value) was measured in intact expanded flag leaves at different leaf positions. A rapid, non-invasive chlorophyll fluorescence assessment was done using a portable red LED modulation fluorescence system (Mini-Palm-II with leaf clip holder, Heinz Walz, Germany). Chlorophyll fluorescence was determined (means of five measurements) 1 day before the end of the stress treatments. Minimal chlorophyll fluorescence (F_o) for 30 min of dark-adapted leaves was measured by using a pulse of low-intensity light (>0.1 $\mu molm^{-2}\ s^{-1}$). After that, maximal chlorophyll fluorescence (F_m) was recorded by applying a pulse of saturated white light (>3,000 $\mu molm^{-2}\ s^{-1}$) for 1 s in the disks of the same leaves. The quantum yield (F_v/F_m) of PSII for dark-adapted leaves was estimated as described by Carvalho and Amâncio (2002).

$$Fv/Fm = \frac{(F_m - F_o)}{F_m} \quad (2)$$

Where F_o corresponds to the minimal fluorescence level, F_m is the maximum possible level of fluorescence, and F_v is the variable fluorescence under stress.

The RWC was estimated by following the standard method described by Barrs and Weatherley (1962). Two samples (8–10 cm long) were taken from a mid-section of developed leaves. Fresh weight (FW) was determined instantly after excision, followed by placing in falcon tubes containing 10 ml of water (H_2O) for 12 h in a standard room environment. Following hydration, the samples were taken out from the H_2O, gently dried with tissue, and weighed immediately for turgid weight (TW). Then, the samples were oven-dried at 70°C for 72 h to determine their DW. The RWC was calculated using Equation 3 as below.

$$RWC\ (\%) = [(FW - DW)\ /\ (TW - DW)]\ \times\ 100 \quad (3)$$

Computational water stress indices through infrared thermography

On the last day of DS, HS, and DHS, infrared thermal imaging (IRTI) of each replicate was taken by using a high-performance handheld thermal imaging camera (T-series, Model 1050sc, with true HD 1,024 × 768 pixels resolution) (FLIR Systems AB, Täby Sweden) (FLIR, 2015). The thermal sensitivity (NETD) of the 1050sc camera was <20 mK at 30°C

with a 0.47 milliradians spatial resolution (IFOV). The object temperature measurement range was between −40 and 150°C. Each pixel of the image holds thermal reading in units of °C. All IRTI were taken from a constant distance of 2 m to view the plant at a 30° angle from the horizontal direction. All thermal images were taken in standard room conditions to avoid plant canopy and leaf temperature acclimatization with the surrounding environment and minimize pixel temperature variations. Each thermal image was then converted to .dat files. Data were extracted using MATLAB code scripted in MATLAB R2017b (Math works Inc. Natick, Massachusetts, USA) through the image analysis toolbox (Figure 1). While analyzing the images for canopy temperature (T_c), canopy temperature depression (CTD), and crop water stress index (CWSI), the background temperature effects were subtracted by setting the minimal and maximal thermal pixels within the canopy in the thermal histogram. The CWSI was calculated by following the protocols established by Fuentes et al. (2012).

$$\text{CWSI} = \frac{(\text{Tc}-\text{Tw})}{(\text{Td}-\text{Tw})} \quad (4)$$

Where T_c is the canopy temperature of each replicate, T_w and T_d are the corresponding temperature (°C) of the control and stressed plants, respectively.

While CTD was calculated by subtracting the T_c from the mean environmental temperature (T_a), it is positive when T_c is lower than the surrounding environment.

$$\text{CTD} = \text{Ta} - \text{Tc} \quad (5)$$

Determination of TSS and FC

The TSS and FC were determined spectrophotometrically at 620 and 420 nm, respectively, by following the protocol proposed by Dubois et al. (1951). Frozen leaf samples (0.2 gm) were taken and homogenized with TissueLyser II (Qiagen, Germany) in 4 ml of 80% (v/v) ethanol (C_2H_5OH). The extract was centrifuged at 4,000 rpm for 20 min, and the supernatant was pooled in a flask by repeating the procedure thrice. The total volume of the flask with 80% ethanol was maintained at 10 ml. The TSS and FC were determined using the anthrone reagent and H_2SO_4, respectively, followed by incubation at 95°C for 15 min. Absorbance readings were recorded using a single beam UV scanning spectrophotometer (Halo RB-10, Dynamica Scientific Ltd.). The concentration of TSS and FC was calculated from the standard curve and expressed as mg g^{-1} of FW.

Determination of proline and free AA

The free level of proline and AA were determined spectrophotometrically at 520 and 570 nm, respectively, by following the method of Bates et al. (1973). Frozen leaf samples (0.2 gm) were homogenized with TissueLyser-II (Qiagen, Germany) in 5 ml of 3% aqueous sulfosalicylic acid (SA) solution, followed by centrifugation at 4,000 rpm for 15 min. An aliquot of 2 ml was reacted with a 4 ml solution (2 ml each) of glacial acetic acid and acid ninhydrin in a 20 ml glass tube at 100°C. After 1 h, the reaction was terminated in an ice bath. After that, 4 ml of toluene was added to the reaction mixture (RM) and mixed vigorously with a glass tube stirrer for 30 s. After 1 h, when toluene was aspirated, absorbance was recorded using a single beam UV spectrophotometer (Halo RB-10, Dynamica Scientific Ltd.). The blank was prepared by adding toluene in place of sample extract. The standard curves for proline and amino acids were prepared by dissolving different concentrations (10–50 μg/ml) of proline and leucine in 3% of SA, respectively. Proline extracts and AA concentrations were estimated from the standard curve and calculated on an FW basis.

$$\mu\text{mol proline/g FW sample} = \frac{[(\mu\text{g proline/ml}\times\text{toluene (ml)})/115.5\ \mu\text{g}/\mu\text{mol}]}{[(\text{g sample})/5]} \quad (6)$$

Assays for antioxidant enzymatic activities

The peroxidase (POX) activity was estimated by measuring the mmol guaiacol ($C_7H_8O_2$) mg^{-1} protein min^{-1}. Enzyme extract (200 μl) was added to an RM containing 2 ml of 0.1M Sodium phosphate buffer (Na-PB) (pH 6.8), 50 μml of 10 mM H_2O_2, and 0.95 ml of 20 mM guaiacol. POX activity was assayed spectrophotometrically at 470 nm by measuring the change in the absorption for 3 min due to an increase in the oxidation of $C_7H_8O_2$ in the presence of H_2O_2 (Chance and Maehly, 1955). For ascorbate peroxidase (APX) activity estimation, enzyme extract (250 μl) was added to an RM of 0.05 M of Na-PB (pH 7.2), 30% H_2O_2 (v/v), and 0.5 mM ascorbic acid (ASC). Ascorbate peroxidase activity was estimated in mmol ascorbate mg^{-1} protein min^{-1} by quantifying the ASC oxidation with a reduction in absorbance for 2 min difference at 290 nm (Chen and Asada, 1989). Superoxide dismutase (SOD) activity was assayed spectrophotometrically at 560 nm by following Dhindsa et al. (1981). The enzyme extract (300 μl) was added into an RM of 0.3 ml of 130 μM of methionine, 1.5 ml of 50 mM of Na-PB (pH 7.8), 0.3 ml of 100 μM of methylene diamine tetraacetic acid, 0.3 ml of 20 μM riboflavin, 0.3 ml of 750 μM of nitro-blue tetrazolium (NBT), and 100 μl of dH_2O. A 20-watt fluorescent lamp then illuminated on the reaction tubes for 20 min. The reaction was terminated by incubating tubes in dark conditions by covering them with aluminum foil. One unit of SOD (mg^{-1} protein min^{-1}) is equal to the enzyme amount involved in 50% inhibition of the NBT reduction compared to the control. The catalase (CAT) activity was assayed by adding 250 μl of enzyme

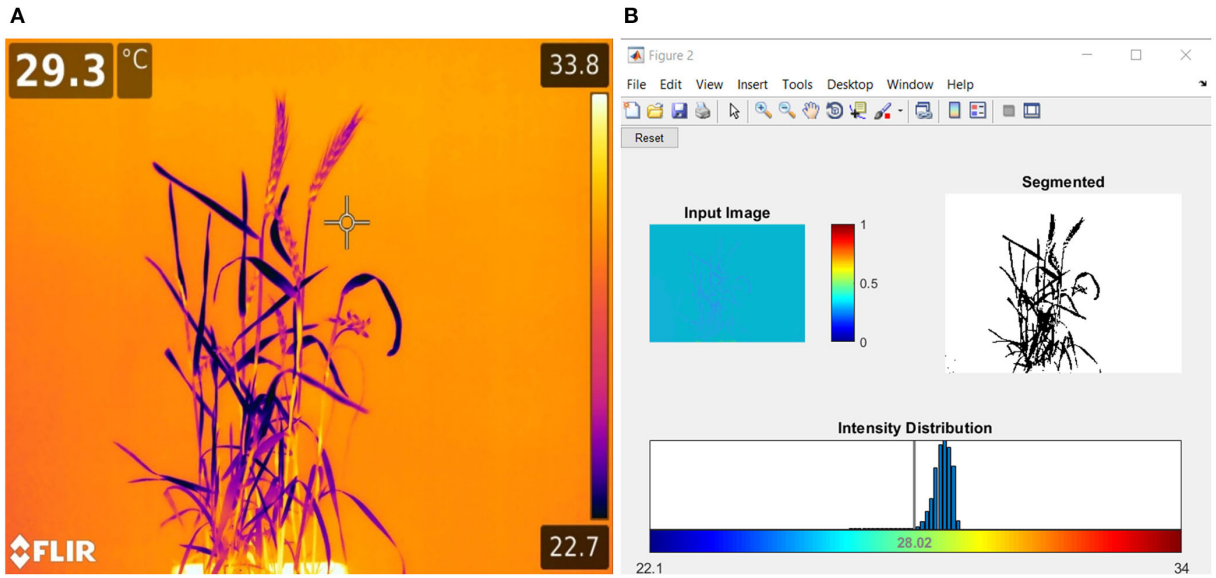


FIGURE 1
(A) Sample thermal image and **(B)** image analysis graphic user interphase (GUI) used for crop water stress index (CWSI), canopy temperature (T_c), and canopy temperature depression (CTD) calculations of plants through a customized code written in MATLAB (Fuentes et al., 2012).

extract to the RM having 1.5 ml of 50 mM of Na-PB (pH 7.8), 300 µl of 0.1 M H_2O_2, and 1 mL of dH_2O. The change in the absorbance in 2 min at 240 nm was recorded as a measure of CAT activity (Chance and Maehly, 1955).

Determination of grain yield and yield components

At maturity, all five plants from each pot were cut at the surface level and weighed to record above-ground biomass. Grain yield (GY; gm pot^{-1}) was measured as the weight of harvested grains from all five plants within each replicate. Thousand grains weight (TGW, gm), grain number per spike (GNS), three spikes grains weight (GWS, gm), and the number of spikelets per spike (NSPS) (three spikes average) were also determined. Harvest index (HI) was recorded as GY divided by the total above-ground dry matter (Yue et al., 2006).

$$\text{HI}\ (\%) = \frac{\text{Grain yield}}{\text{Total above ground biomass}} \times 100 \qquad (7)$$

Statistical analysis

Statistical significance of the variation of the trait with repeated measures was tested by factorial analysis of variance (ANOVA) for treatment effects ($p < 0.05$) by keeping Si and stress treatments as fixed factors within the cultivars. A least significant difference (LSD) and pairwise comparison test were used for comparing treatment means, standard error (SE) of the means, and their interaction effect calculated through "agricolae" package of R statistical software (Mendiburu, 2020; R Core Team, 2020). Thermal image data were derived using MATLAB code scripted in MATLAB R2017b (Mathworks, 2017) through Images Analysis Toolbox for T_c, CTD, and CWSI (Fuentes et al., 2012) and analyzed through R software. The "ggplot2" package was used for plotting and data visualization (Wickham, 2016).

Results

Effect of Si on chlorophyll fluorescence, chlorophyll content, and RWC

Overall, Si treatment recovered the efficiency of PSII with a difference in the extent and ability of a cultivar under experimental stress treatments. The quantum yield of the flag leaves of the cultivars showed a net drop with the onset of the stress treatments. However, Si treatment significantly ($p < 0.001$) enhanced the F_v/F_m under DS, HS, and DHS. Under DSSi, a maximum increase, compared to susceptible cultivars (Kukri, 12.8%; CM59443, 7.9%), was observed in RAC622 (14.3%) and Excalibur (14.1%). Interestingly, the percent increase under HSSi was almost the same across the tolerant and susceptible cultivars (6.5%). However, under DHSSi, a maximum increase was observed in the susceptible cultivar, Kukri (14.8%), followed by tolerant

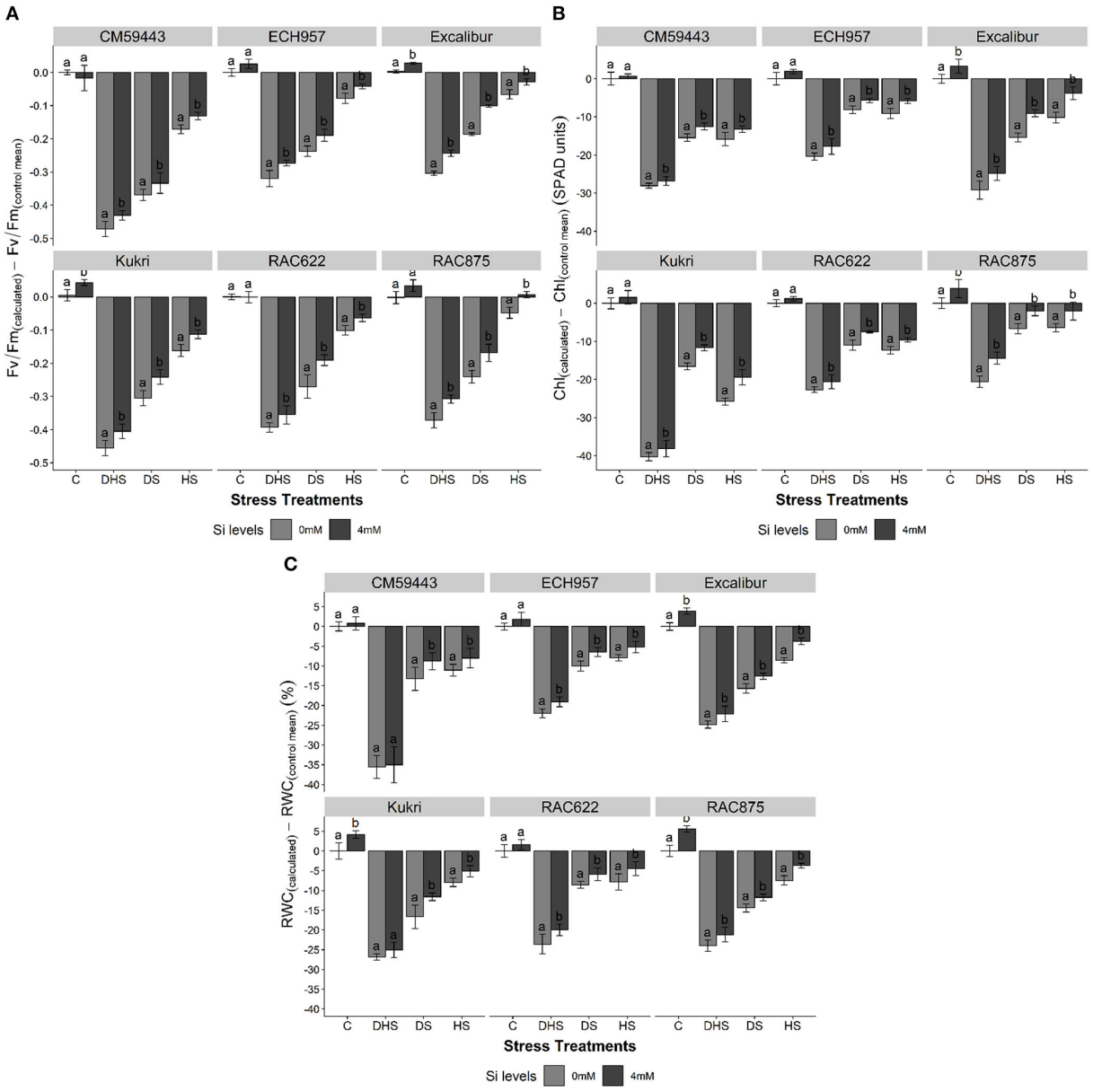


FIGURE 2
(A–C) Effect of silicon on **(A)** chlorophyll fluorescence (F_v/F_m), **(B)** chlorophyll content (SPAD unit), and **(C)** relative water content (RWC) (%) of six contrasting wheat cultivars under terminal drought stress (DS), heat stress (HS), and drought-heat combined stress (DHS) in a controlled glasshouse condition. F_v/F_m is a mean of $n = 9$, SPAD value is a mean of $n = 27$. Mean values are presented with ± standard error (SE); SE represents error bars. Different letters indicate significant differences within the cultivars at $p < 0.05$.

cultivars (RAC875, 14.3; Excalibur, 12.4%; ECH957, 9.6%, and RAC622, 8.8%) (Figure 2A).

A declining behavior in chlorophyll content (SPAD readings) was observed throughout the stress treatment. Under C, all cultivars, except RAC875 and Excalibur, showed a non-significant increase with Si treatment. Compared with C, the highest decrease in the chlorophyll content was observed under DHS, followed by HS and DS across the cultivars. However, Si treatment significantly ($p < 0.001$) increased the chlorophyll content across the cultivars regardless of the stress treatments. With Si treatment, the highest chlorophyll content percent increase was observed in Kukri (DSSi, 11.1%; HSSi, 18.3%, and DHSSi, 10.8%) followed by RAC875 (DSSi, 7.8%; HSSi, 7.2%, and DHSSi, 13.4%) and Excalibur (DSSi, 11.6%; HSSi, 10.7%, and DHSSi, 10.4%) (Figure 2B).

Under C, the RWC among studied cultivars ranged between 80.5 and 86.9%. However, RWC progressively declined under DS, HS, and DHS compared to C (Figure 2C). The decreasing trend was more evident among susceptible cultivars (CM59443, 79.1% and Kukri, 47.0%) compared to the tolerant cultivars (Excalibur, 40.0%; RAC622, 39.3%; RAC875, 38.6%; ECH957, 36.2%). The Si treatment significantly improved RWC under HS compared to C treatment, followed by DS and DHS and the results were more pronounced in susceptible cultivars compared to tolerant cultivars. Under DS, Kukri and CM59443 had 7.5 and 6.6% increase in RWC, respectively, than ECH957 (4.9%), Excalibur (4.3%), RAC875 (3.7%), and RAC622 (3.6%). Similarly, under HS, the maximum percent increase was observed in Excalibur (6.2%), followed by RAC875 (4.8%) and RAC622 (4.5%). However, under DHSSi, only tolerant cultivars showed a significant increase in RWC (RAC622, 6.0%; ECH957, 4.8%; RAC875, 4.5% and Excalibur, 4.4%), and susceptible showed a non-significant increase in RWC.

Effect of Si on computational water stress indices

The IRTI analysis outputs (T_c, CTD, CWSI) are shown in Figures 3A–C. Cultivars exhibited significant differences ($p < 0.001$) for T_c with Si under all stress treatments. In a studied panel, the values of T_c under C ranged from 20.28 to 22.11°C. Under DHS, higher T_c values were recorded in susceptible cultivars (CM59443, 29.0°C and Kukri, 28.5°C), followed by RAC875 and Excalibur (28.1°C). Under DS and HS, T_c values of susceptible cultivars ranged from 22.4 to 23.0°C and 26.9–27.2°C, respectively, compared with 22.2–22.9°C and 26.3–26.8°C among tolerant cultivars, respectively. However, a significant reduction in T_c was observed with Si treatment under all stress treatments. On average, under all stress treatments, Excalibur performed better with Si (4.4% reduction in T_c), followed by RAC875 (4.3% reduction in T_c) and Kukri (3.3% reduction in T_c). Except for CM59443 under DHS, both susceptible cultivars significantly reduced T_c across the stress treatments after Si treatment (Figure 3A).

Similarly, all cultivars showed lower CTD values under DS, HS, and DHS. However, Si treatment showed a positive effect in improving the CTD across the stress treatments (Figure 3B). The positive CTD values were observed under C and DS, whereas HS and DHS showed negative CTD values across the cultivars. Under HS, the tolerant cultivars exhibited almost the same CTD levels (∼-3.5°C) compared with ∼-4.0°C in the susceptible cultivars. However, a significant improvement ($p < 0.001$) in CTD was observed with Si treatment under DS, HS, and DHS across the cultivars. The maximum increase with Si treatment under DSSi was observed in RAC875 (62.3%), followed by 39.5% under HSSi in Excalibur and 16.0% under DHSSi in RAC622. A similar increasing trend was observed in susceptible cultivars, except for a non-significant increase in CM59443 under DHSSi.

A significant effect ($p < 0.001$) of Si was observed among stress treatments and their respective control in improving CWSI (Figure 3C). The highest CWSI values were observed under DHS and ranged between 0.83 and 0.89, respectively, followed by 0.65–0.77 and 0.42–0.56 under DS and HS, respectively. However, results showed that Si treatment significantly normalized the CWSI across the stress treatments. Under HSSi, the maximum reduction among tolerant cultivars was observed in RAC875 (16.0%), followed by ECH957 (14.8%), Excalibur (11.7%), and RAC622 (10.2%). The susceptible cultivars, Kukri and CM59443, also showed a significant decrease under HSSi in CWSI by 14.1 and 11.8%, respectively. Similarly, under DSSi, the same decreasing trend in CWSI was observed for all tolerant and susceptible cultivars. Among tolerant cultivars, the maximum reduction in CWSI was observed in RAC875 (12.1%) compared with the susceptible cultivar Kukri (9.0%). Under DHSSi, Excalibur, among the tolerant cultivars, and Kukri, among the susceptible cultivars, performed better with an overall decrease of 7.9% and 7.0%, respectively.

Effect of Si on osmolytes accumulation

In the studied cultivars (Excalibur, RAC875, ECH957, RAC622, CM59443, and Kukri), Si treatment significantly ($p \leq 0.05$) increased the concentrations of all estimated osmolytes in response to stress treatments (DS, HS, and DHS) except for the proline (Figures 4A–D). For TSS and FC, a considerable variation was observed across the cultivars under all stress treatments. Without Si treatment, the concentration of TSS was reduced by 11.9–22.9 % under DS, 18.9–37.4% under HS, and 50.4–78.6% under DHS compared to their respective controls (Figure 4A). Results indicated that Si treatment positively enhanced TSS concentration ($p < 0.01$). Under HSSi, the TSS concentration of tolerant cultivars increased significantly and ranged from 17.9 to 22.5%, compared with a 19.3 and 7.8% increase in Kukri and CM59443, respectively. Under DSSi, CM59443 had the highest increase (23.1%) in TSS compared with ECH957, which exhibited a maximum increase (20.5%) in TSS among the tolerant cultivars. Under DHSSi, RAC875 had the maximum increase in TSS (16.1%), followed by Excalibur (7.4%). Among the susceptible cultivars, the TSS of Kukri increases significantly (6.7%) under DHSSi. However, no significant effect of Si treatment on the TSS concentration was observed on RAC622, ECH957 (tolerant cultivars), and CM59443 (susceptible cultivar) under DHSSi.

The FC of all the cultivars increased with Si treatment under DS, HS, and DHS ($p < 0.01$). Under HSSi, the FC, compared with the non-treated controls, was markedly higher in the susceptible (CM59443, 36.6% and Kukri, 24.8%) and the tolerant

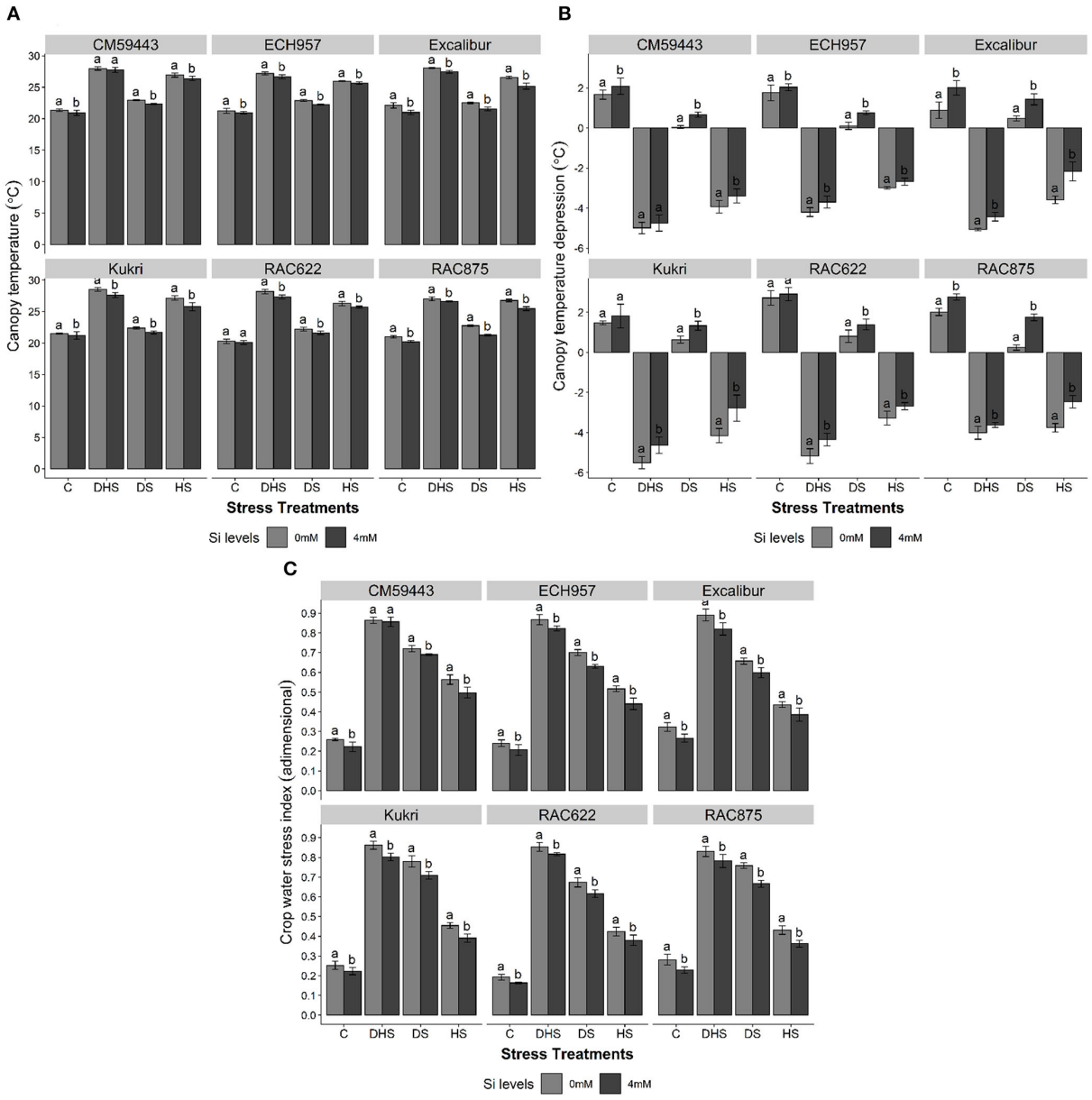


FIGURE 3
Effect of silicon on **(A)** plant's canopy temperature (°C), **(B)** canopy temperature depression (°C), and **(C)** crop water stress index (adimensional) of six contrasting wheat cultivars under terminal drought, heat and drought-heat combined stress in controlled glasshouse conditions. Mean values are presented with ± SE, represented with error bars. Different letters indicate statistical significance within each cultivar at $p < 0.05$.

cultivars (RAC875, 16.1%; RAC622, 19.2%; Excalibur, 17.9% and ECH957, 10.3%) (Figure 4B). Results showed that CM59443 had the maximum FC increase under DSSi followed by Kukri (24.8%), RAC622 (22.0%), RAC875 (18.2%), Excalibur (12.8%), and ECH957 (11.4%). Under HSSi, RAC875 and Kukri had similar FC (63.2 ± 3.0 and 64.6 ± 3.0 mg g^{-1} FW, respectively) compared with the 32% lower concentration in Excalibur (48.1 ± 1.9 mg g^{-1} FW). Under DHSSi, no significant effect of Si was observed in CM59443 and ECH957. The maximum increase under DSSi was observed in Excalibur (45.8%), followed by Kukri (39.7%), RAC622 (19.7%) and RAC875 (9.5%). This result showed that Si positively enhanced FC under DS, followed by HS and DHS.

Exposure to DS, HS, and DHS induced proline accumulation to a maximum level across the cultivars. The maximum proline concentration was observed under DHS across the cultivars. Under DS, proline concentration was found to be higher in the tolerant cultivars (86.0 ± 2.5 and 66.9 ± 2.2 μmol g^{-1} FW in

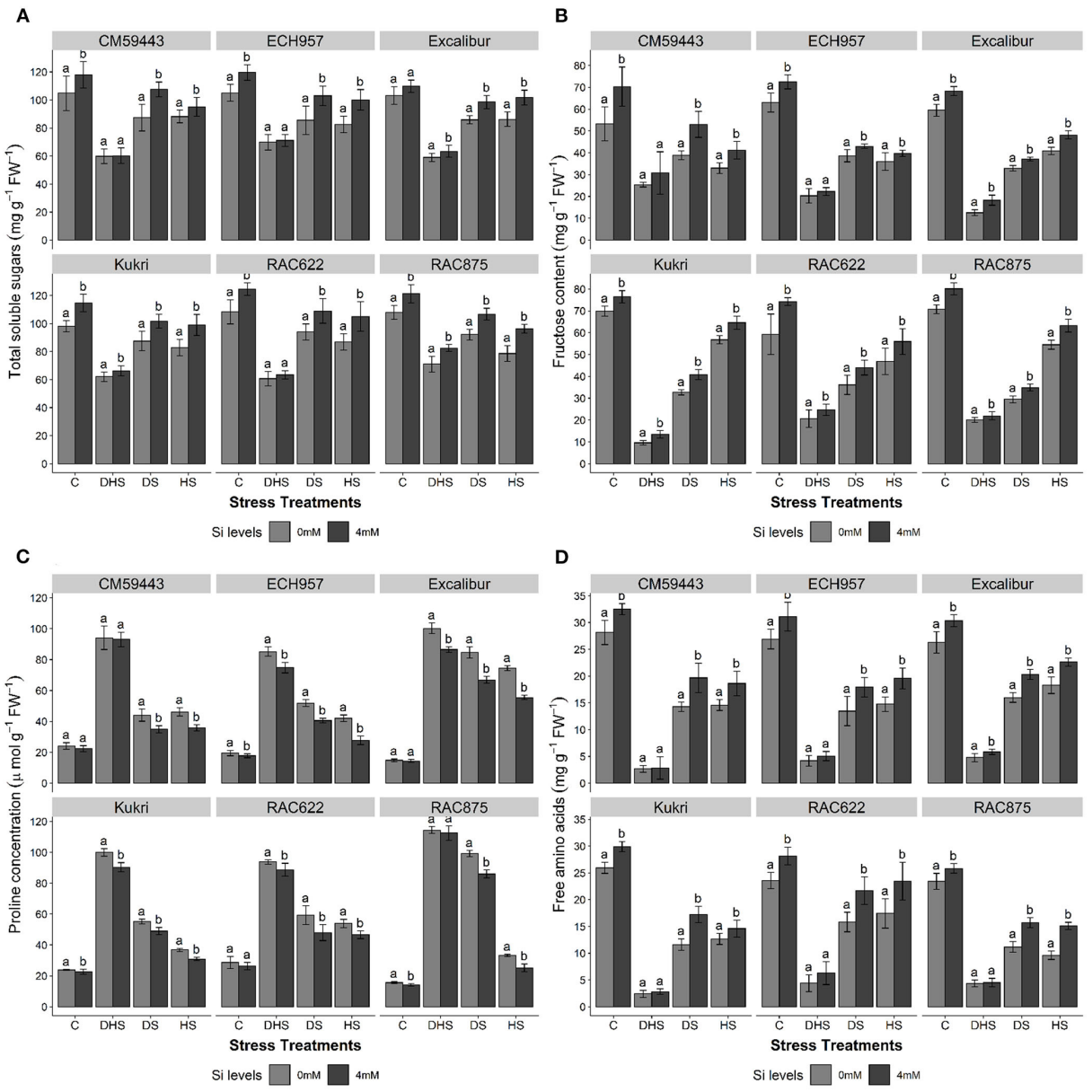


FIGURE 4
(A–D) Effect of silicon on **(A)** total soluble sugars (TSS) (mg g^{-1}FW), **(B)** fructose content (FC) (mg g^{-1}FW), **(C)** proline concentration (µmol g^{-1}FW), and **(D)** free amino acids (AA) (mg g^{-1}FW) of six contrasting wheat cultivars under terminal DS, HS, and DHS in a controlled glasshouse conditions. Mean values are presented with ± SE, represented with error bars. Different letters denote statistical significance within each cultivar at $p < 0.05$.

RAC875 and Excalibur, respectively) when compared with the susceptible cultivars (49.0 ± 2.4 and 44.0 ± 3.9 µmol g^{-1} FW in Kukri and CM59443, respectively). However, Si treatment significantly reduced proline concentration across the cultivars ($p < 0.001$). Excalibur showed reduced proline concentration of 25.4, 21.0, and 13.8% under HS, DS, and DHS, respectively, followed by ECH957 under HS, DS, and DHS (34.0, 21.8, and 12.1% respectively). Among the susceptible cultivars, decreased proline concentrations of 16.0, 11.2, and 9.6% were observed in Kukri under HS, DHS, and DS, respectively, compared with their respective controls (Figure 3C). Cultivars RAC875 and CM59443 did not show any significant effect of Si treatment on proline concentration under DHS.

A significant increase ($p < 0.001$) in AA concentration was also observed with Si treatment across the cultivars (Figure 4D). Compared with the tolerant cultivars, a maximum decrease was observed in Kukri and CM59443 after the DH and HS. Under DSSi, the maximum increase in AA

TABLE 1 Activity of enzymatic antioxidants of six contrasting wheat cultivars under drought stress (DS), heat stress (HS), and drought-heatcombined stress (DHS) in controlled glasshouse conditions.

	Traits	Treatment	C		DS		HS		DHS	
		Cultivars	-Si	+Si	-Si	+Si	-Si	+Si	-Si	+Si
Enzymatic antioxidants	POX	RAC875	3.3 ± 0.8a	4.2 ± 0.5a	6.3 ± 0.6a	8.2 ± 05b	8.3 ± 0.6a	9.8 ± 1.0b	10.7 ± 1.1a	11.1 ± 1.1a
		Kukri	2.4 ± 0.2a	3.2 ± 0.4b	6.1 ± 1.16a	8.0 ± 0.2b	8.5 ± 0.4a	9.9 ± 0.7b	10.9 ± 0.4a	11.5 ± 1.2a
		Excalibur	2.2 ± 0.5a	2.9 ± 0.3b	6.0 ± 0.5a	7.8 ± 0.7b	7.7 ± 0.7a	9.4 ± 0.5b	10.2 ± 0.7a	11.0 ± 1.1b
		ECH957	4.1 ± 0.3a	4.6 ± 0.4a	6.7 ± 0.4a	7.8 ± 0.1b	6.9 ± 0.2a	8.0 ± 0.2b	10.1 ± 0.3a	11.0 ± 0.6b
		RAC622	4.4 ± 0.7a	5.1 ± 0.7a	7.3 ± 0.5a	8.7 ± 0.7b	8.7 ± 0.3a	10.3 ± 0.5b	11.4 ± 0.6a	12.0 ± 0.7a
		CM59443	4.0 ± 0.6a	4.6 ± 0.3a	6.8 ± 0.5a	7.9 ± 0.6b	8.6 ± 0.3a	9.4 ± 0.6b	11.6 ± 0.3a	11.9 ± 0.6a
	CAT	RAC875	5.5 ± 0.9a	6.9 ± 0.7b	17.4 ± 1.3a	22.3 ± 2.7b	15.0 ± 2.1a	20.6 ± 1.3b	32.4 ± 3.5a	36.7 ± 1.6b
		Kukri	8.2 ± 1.3a	9.3 ± 0.7a	18.1 ± 1.8a	25.3 ± 1.9b	17.1 ± 1.6a	21.5 ± 1.5b	34.7 ± 1.5a	39.9 ± 2.8b
		Excalibur	9.4 ± 0.6a	12.0 ± 1.0b	21.5 ± 0.1a	26.8 ± 2.1b	18.8 ± 1.1a	24.4 ± 1.5b	34.9 ± 1.4a	38.5 ± 2.1b
		ECH957	8.4 ± 1.1a	9.7 ± 1.8b	18.7 ± 0.1a	21.2 ± 0.9b	20.3 ± 1.4a	21.5 ± 1.1b	28.6 ± 1.3a	31.7 ± 2.4b
		RAC622	10.2 ± 1.1a	10.5 ± 1.8a	21.1 ± 0.9a	22.8 ± 0.9b	21.6 ± 1.4a	23.9 ± 1.2b	30.5 ± 1.9a	33.0 ± 2.5b
		CM59443	10.4 ± 0.7a	11.4 ± 0.4b	23.3 ± 1.4a	25.2 ± 1.4b	19.7 ± 1.0a	21.1 ± 0.1b	32.4 ± 2.1a	33.2 ± 1.2a
	APX	RAC875	12.9 ± 2.2a	15.7 ± 1.4b	45.2 ± 2.1a	51.9 ± 5.0b	53.3 ± 1.3a	59.5 ± 3.1b	65.7 ± 3.0a	71.9 ± 1.7b
		Kukri	7.1 ± 1.4a	8.6 ± 2.2a	39.0 ± 4.2a	44.8 ± 3.1b	48.1 ± 1.7a	51.4 ± 2.5b	57.6 ± 1.3a	59.5 ± 1.7b
		Excalibur	11.9 ± 2.7a	14.3 ± 0.8a	45.7 ± 3.0a	49.0 ± 2.4b	48.1 ± 0.5a	52.4 ± 1.3b	59.0 ± 1.7a	61.9 ± 2.1b
		ECH957	11.9 ± 0.5a	12.9 ± 0.8a	44.8 ± 1.7a	46.7 ± 1.3b	42.4 ± 1.3a	45.2 ± 0.5b	51.9 ± 1.3a	55.2 ± 1.3b
		RAC622	21.4 ± 0.8a	22.9 ± 0.8a	39.5 ± 1.7a	41.9 ± 1.0b	43.3 ± 1.7a	52.4 ± 1.3b	50.5 ± 1.7a	52.9 ± 0.8b
		CM59443	17.1 ± 0.8a	19.5 ± 1.3b	41.9 ± 1.7a	45.2 ± 0.8b	45.7 ± 0.8a	48.6 ± 0.8b	57.1 ± 0.8a	59.0 ± 2.1a

POX, Peroxidase; CAT, catalase; APX, ascorbate peroxidase. Each value represents the mean ± SE. Alphabets denote statistical significance at $p < 0.05$ within cultivars and treatment effect.

compared with respective control was observed in Kukri (48.3%), followed by RAC875 (40.5%) and CM59443 (37.7%). For HSSi, the tolerant cultivars performed better with Si treatment with a higher increase in AA than the susceptible cultivars. The RAC875 induced a significant increase of 57.0% in AA under HSSi, followed by 32.6% in RAC622. The Si-induced increase in AA was also recorded in CM59443 and Kukri by 27.5 and 15.1%, respectively. However, except for Excalibur, AA did not change significantly with Si treatment under DHS.

Effects of Si on the antioxidant enzymes activities

The activities of enzymatic antioxidants, i.e., POX, CAT, and APX, were considerably increased under DS, HS, and DHS compared with the respective controls. However, results showed that Si treatment effectively further enhanced the activities of these antioxidants under all stress treatments (Table 1).

Silicon treatment significantly enhanced the POX activity under all stress treatments ($p < 0.01$). Under DSSi, compared to the DS (no Si), the POX activity was significantly elevated across all the cultivars by 15.4–30.3%. The maximum Si-induced increase in the POX activity under DSSi was observed in Kukri (30.3%), followed by RAC875 (30.2%), compared to CM59443 with the least increase in POX activity with Si (15.4%). Whereas, under HSSi, the increased percentage ranged from 9.3 to 22.1% among the cultivars. Under HSSi, the maximum increase in the POX was observed in Excalibur (22.1%), followed by RAC622 (19.1%). Kukri and CM59443, susceptible cultivars, had a 16.5 and 9.3% increase in Si-induced POX activity under HSSi. Under DHSSi, ECH957 and Excalibur exhibited the most significant increase in the POX activity (8.9 and 7.8%, respectively) compared with Kukri and CM59443 with the slightest increase in POX activity (5.5 and 2.2%, respectively).

Similarly, Si treatment exerted a significant ($p < 0.01$) positive effect in enhancing the CAT activity across the cultivars. With Si treatment under DS (DSSi), the CAT activity was significanlty enhanced by 28.5, 24.7, 13.6, and 8.2% in RAC875, Excalibur, ECH957, and RAC622 (tolerant cultivars), respectively, compared with a 39.8% increase in Kukri and an 8.3% in CM59443 (susceptible cultivars). Under HSSi, the CAT activity was also accelerated by 36.9, 29.9, 10.3, and 6.0% in RAC875, Excalibur, RAC622, and ECH957 (tolerant cultivars), respectively, compared with a 25.9% increase in Kukri and a 7.2% increase in CM59443 (susceptible cultivars).

Although, compared with DSSi and HSSi, the CAT activity was highest under DHSSi, but the increased percentage with Si treatment was minimum across the tolerant cultivars (RAC875 = 13.4%, Excalibur = 10.6%, ECH957 = 8.9%, RAC622 = 8.2%), compared to susceptible cultivar, Kukri (15.2%) (Table 1).

For APX, a significant ($p < 0.001$) increase with Si was observed across all the cultivars under DS, HS, and DHS treatments. Under DSSi, the increase in APX activity ranged between 4.3 and 14.7% across the cultivars and the highest increase was observed in RAC875 (14.7%) and Kukri (14.6%). Similarly, under HSSi, the increase in the APX activity ranged between 6.3 and 20.9%, and the highest APX activity was observed in RAC622 (20.9%), followed by RAC875 (11.6%). The APX activity under HSSi was significantly enhanced in susceptible cultivars as well, and it was 6.3% and 6.9% in CM59443 and Kukri, respectively. Under DHSSi, the highest APX activity was recorded in RAC875 (9.4%), followed by ECH957 (6.4%) as compared with a 3.3% increase in each of the susceptible cultivars (Kukri and CM59443) (Table 1).

GY and yield components

Under C, all cultivars performed their best yield potential and were found to have comparable GY (Figure 5). In contrast, experimental stress treatments resulted in a significant reduction in GY among the cultivars. Up to 66 % GY reduction was observed under DHS across all the cultivars and the lowest yield was recorded in CM59443 (5.9 ± 0.2 gm pot^{-1}). The reduction in GY under HS was the highest in Kukri (58.8%), followed by RAC875 (39.1%) and Excalibur (38.8%) compared with the C. Similarly, DS treatment resulted in significant GY losses in the susceptible cultivars CM59443 and Kukri, and they yielded 56 and 10.1% less GY than the average GY of tolerant cultivars. However, the Si treatment compared with controls resulted in significantly ($p < 0.001$) higher GY across the cultivars under all the stress treatments. Cultivars RAC875 and Excalibur produced 3 folds (∼30%) extra GYunder DSSi than Kukri and CM59443 (∼10%). Under HSSi, the GY was improved by 12.2% when averaged across the cultivars. When compared among cultivars, Kukri yielded 20.2% more grains than the untreated C and 16.6% extra grains than RAC875 under HSSi. Under DHSSi, a maximum increase was observed in RAC875 (16.5%), followed by RAC622 (9.7%) and Kukri (8.11%). Overall, the tolerant cultivars produced a higher GY (40.7%) than susceptible cultivars (31.9%) under all stress treatments with Si effects.

Different stress treatments significantly reduced the GY of wheat cultivars and hence the HI (Figure 5). The reduction in the HI of the cultivars under DS, HS, and DHS ranged between 6.9 and 25.9%, 8.3–31.1%, and 13.4–28.4 %, respectively, compared with the C treatment. With Si treatment, a significant increase in the HI was observed across all the stress treatments. Excalibur had the highest HI increase (18.4%) under DSSi and CM59443 had the highest growth in HI (23.6%) under HSSi compared with the C treatment. On average, susceptible cultivars produced 16.4% more HI with Si treatment across the stress treatments than the tolerant cultivars.

Like GY, TGW reduced significantly with DS, HS, and DHS. A significant increase ($p < 0.01$) in TGW was observed with Si across the stress treatments. Silicon treatment induced a 2.6–9.3% increase in TGW under DS, 1.4–7.3% increase under HS, and 4.4–13.8% increase under DHS when averaged across the cultivars. The highest averaged Si-induced increase in TGW across the stress treatments was observed in Excalibur (8.6%), followed by Kukri (6.9%) and CM59443 (4.9%). When compared within DSSi, Kukri increased TGW twice (9.4%) as compared with RAC875 (4.1%) and Excalibur (4.8%) and almost four times when compared with ECH957 (2.6%). Similarly, under HSSi, Excalibur had the highest increase (7.3%) in TGW among the tolerant cultivars, compared with Kukri with 4.5% increase among the susceptible cultivars. Similarly, Excalibur obtained the maximum TGW (13.8%), followed by CM59443 (8.1%) under DHSSi.

For grains per spike, stress treatment caused a significant decrease across all the cultivars. The highest average GNS decrease across the cultivars was observed in DHS (17.3%), followed by DS (9.7%) and HS (5.9%). Results showed that Si treatment significantly ($p < 0.05$) increased the GNS under DS, HS, and DHS across the cultivars. Excalibur, CM59443, and Kukri had increased GNS with almost the same number (4.5%) compared with a 2-fold increase in RAC875 (8.8%) under DS. For HSSi, RAC875 and RAC622 had increased GNS by 3.5 %. However, the no-significant effect of Si on the GNS was observed under DHSSi across the cultivars.

Similarly, GWS was severely impacted by stress treatments across the cultivars. Compared with C, the GWS was severely reduced by up to 80, 41.8, and 44.3% under DHS, DS, and HS, respectively. Results showed that Si treatment significantly increased the GWS by up to 5.0–13.8% in DS, 2.4–7.8% in HS, and 5.0–13.7% in DHS. Overall, the maximum Si-induced increase in GWS was observed in Excalibur (10.4%), followed by the susceptible cultivars, Kukri (9.8%) and CM59443 (7.2%).

Discussion

RWC, chlorophyll fluorescence, and chlorophyll contents

The RWC is an important physiological attribute for assessing cell and tissue dehydration during DS and HS. Higher RWC is a result of higher osmotic regulations and confers normal metabolic activity and other adaptations by plants (Erice et al., 2010). In the current study, severe RWC reduction was observed under DHS, followed by DS and HS across the studied cultivars, suggesting that combined stress is more detrimental

10.3389/fpls.2022.955490

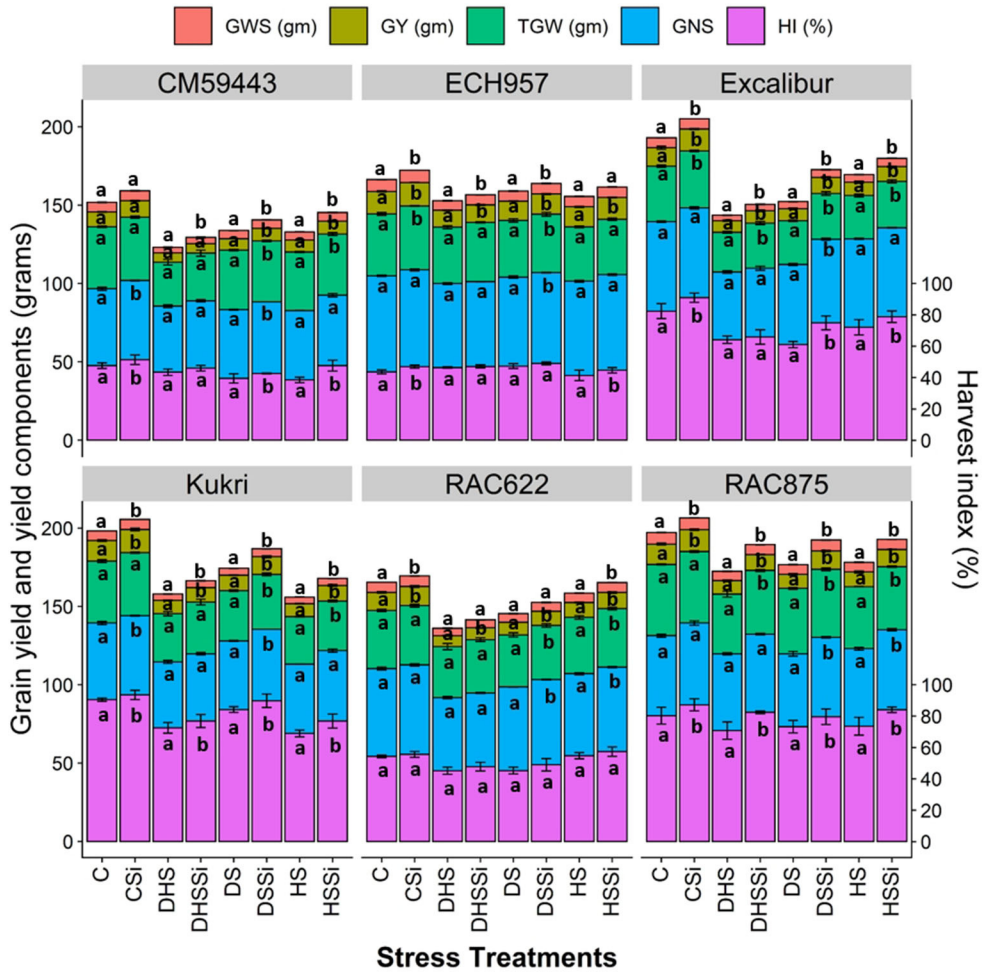


FIGURE 5
Effect of silicon on the mean values of grain yield (GY) and yield components of six contrasting wheat cultivars under DS, HS, and DHS in a controlled glasshouse condition. Each value represents the mean ± SE, represented with error bars. Different letters indicate significant differences within the cultivars at $p < 0.05$. Abbreviations are grain weight per spike (GWS, grams; presented as GWS × 10^0.5), grain yield per pot (GY, grams), 1,000 grains weight (TGW, grams), number of grains per spike (GNS), and harvest index (HI, %).

for plants irrespective of their tolerance level. Our study reported that Si treatment helped maintain leaf osmotic potential (except in susceptible cultivars under DHS) and RWC at a higher level due to the net accumulation of various solutes in the symplast (Figures 4A–D). However, Alzahrani et al. (2018) suggested that Si treatment lowered the ion leakage and improved the cell membrane integrity under stressful environments. To ensure maximum productivity under DS and HS, wheat cultivars with higher RWC might have maintained protoplast hydration for long (Biju et al., 2018; Sattar et al., 2020). Higher RWC also links with higher photosynthetic activity, stomatal conductance, and leaf transpiration, leading to sustained plant growth and GY.

Cultivars with higher chlorophyll fluorescence (F_v/F_m) and chlorophyll contents (SPAD value), after stress treatments have been shown to stay green for extended periods (Murchie and Lawson, 2013). In this study, Kukri (a susceptible cultivar) senesced earlier due to stress-induced pale green leaves and lower chlorophyll contents than RAC875 and Excalibur, which maintained dark green leaves. The result showed that the pre-sowing treatment of Si alleviated the inhibition of photosynthetic apparatus caused by DS, HS, and DHS through improved photochemical efficiency of the PSII photosystem. The Si treatment decreased the oxidative stress during terminal DS and HS and was accompanied by higher F_v/F_m (Figure 2A) (Izanloo et al., 2008). In contrast, high leaf senescence and leaf abscission are significantly accelerated under DHS (Wang et al., 2011). Although Si treatment helped alleviate F_v/F_m level under DHS but to a non-significant level, it shows DHS that affects plants, leading to reduced and/or ceasing of photosynthesis due

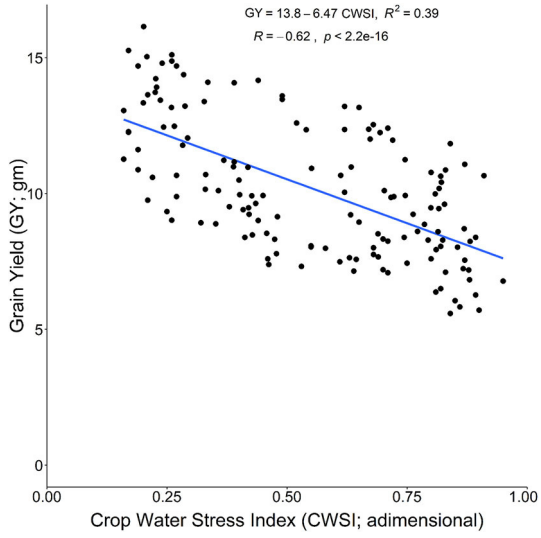


FIGURE 6
Relationship between GY across the cultivars as the dependent variable with crop water stress index as an independent variable under DS, HS, and DHS conditions.

to the early onset of senescence, which leads to yield losses in grain crops.

Computational water stress indices

In the current study, thermal imaging analysis has successfully been used as an integrative approach to accurately estimate T_c, CTD, and CWSI under DS, HS, and DHS. Previously, T_c has been used by many researchers as a reliable measure of the overall plant water status and an important selection criterion for the DS environment (Fuentes et al., 2012; Costa et al., 2013; Biju et al., 2018). In a well-watered condition, water normally transpires through open stomata to maintain T_c below T_a. However, results showed that DS, HS, and DHS directly affected the T_c of all the cultivars, resulting in increased transpiration and later higher T_c, especially in susceptible wheat cultivars. Similar or higher T_c, compared with T_a under stressful conditions (DS, HS, and DHS), is due to the closing of stomata as a preventive measure to maintain leaf turgor pressure. Results showed that Si treatment led to a significant reduction ($p < 0.01$, up to 4.4%) in T_c across the cultivars under all stress treatments. These findings confirm that added Si helps plants maintain adequate water status by keeping low T_c compared to T_a for optimum photosynthetic activity under DS, HS, and combined DHS. Under DHS, Kukri exhibited a significantly lowered T_c with Si treatment, which showed that Si has the potential to alleviate the effects of combined DHS and HS even in susceptible wheat cultivars (Figure 3A).

Canopy temperature depression has been categorized as an important trait for the overall plant water stress status and is directly correlated with the transpirational status of the crops. It is the key plant attribute for comparing/assessing genotypic response to environmental stresses, i.e., DS or HS (Balota et al., 2007), and positively correlated with GY under stressful environments. The current study showed that CTD decreased with the severity of the stress, and the maximum severity was observed in susceptible cultivars under DHS (Figure 3B), which is understandable as combined stress adds to the degree of complexity compared to individual stresses. The differences observed in CTD values for the tolerant and susceptible cultivars are possibly due to canopy development differences due to their different genetic constitutions among cultivars and cultivars × environment (G × E) interaction in a controlled environment. The Si treatment improved the CTD by maintaining cell turgor through osmotic adjustments in the plant cells. Our results suggest that individual and combined DHS during the early grain-filling stage can be critical for employing CTD in explaining the GY variation and its related components with and without Si treatment. The grain-filling stage is more vulnerable to DS and HS, mainly affecting grains per spike and thousand-grain weight. However, cooler T_c and higher CTD could improve the photosynthesis during grain filling and, consequently, final GY under stressful environmental conditions.

The CWSI is an important indicator for plant water status based on T_c. The CWSI fluctuated with the various stress treatments of DS, HS, and DHS, and previously, it was successfully used to quantify the plant water status under DS (Biju et al., 2018). The CWSI showed a significant increase in the current study under DS, HS, and DHS irrespective of the tolerant and susceptible cultivars. However, the Si treatment positively reduced the CWSI across the stress treatments (Figure 3C). Compared to the tolerant cultivars, susceptible cultivars also showed a significant decrease in CWSI with Si treatment under DS, HS, and DHS. The reduction in CWSI might be linked with Si-induced improved osmotic adjustments, and increased plasma membrane aquaporins function for higher root water uptake under abiotic stress environments (Shi et al., 2016). Also, CWSI has a strong negative correlation with the GY under DS and HS. Results showed that GY increased significantly with the decrease in CWSI of the tolerant and susceptible wheat cultivars. The relationship between GY (as a dependent variable) and CWSI (as an independent variable) is presented in Figure 6. It indicates GY declined with increasing CWSI ($R^2 = 0.39$). This result agrees with the previous findings in wheat (Alghory and Yazar, 2019). It also shows a direct linear relationship between T_c, which means CWSI increases with the increase in T_c.

Osmolytes

The most common stress tolerance mechanisms in plants against DS, HS, and DHS are the excessive production of various osmolytes (TSS, FCs, proline, and free AA), the first adaptive mechanism in response to adverse environmental conditions. The synthesis of these compatible solutes is widely recognized as essential for plant adaptation in cellular dehydration and stabilizes various enzymatic antioxidants to contribute to abiotic stress tolerance (Biju et al., 2017; Sattar et al., 2020).

In the current study, DS, HS, and DHS induced a significant adverse effect on producing different osmolytes/solutes in the tolerant and susceptible cultivars. Various osmotic adjustments under DS and HS are innate behavior of plants that help them maintain water balance across the cells by synthesizing various osmolytes. The current study results showed that Si treatment significantly increased the TSS and FCs in tolerant and susceptible wheat cultivars under DS, HS, and to some extent in DHS (Figures 4A,B). Added Si under DS and HS might enhance the anabolism of organic solutes to maintain cell turgor and protect the cell structures and functions from dehydrative damage (Pei et al., 2010; Alzahrani et al., 2018). Also, Si-induced increase in cell water resulted in minimum cellular dehydration (Pei et al., 2010) and, therefore, less oxidative stress due to low ROS levels, which directly enhanced the tolerance levels of susceptible and tolerant wheat cultivars under DS, HS, and to some extent in DHS. Additionally, Si-induced accumulation of higher organic solutes might be available for quick breakdown at the end of stress (DS, HS, and DHS) as a source of energy to repair damaged cells and tissues. From the current study results, it can be concluded that Si-induced higher accumulation of various osmolytes might also be linked with increased activity of different antioxidants for the scavenging of overproduced ROS to enhance HS and DS tolerance in the susceptible wheat cultivars, as well as the tolerant cultivars. Therefore, based on the results, we suggest that the synergistic association of various organic solutes with antioxidants enhances DS and HS tolerance in bread wheat (Abid et al., 2018).

In the present study, under DS, HS, and DHS, both tolerant and susceptible cultivars had increased biosynthesis and accumulation of proline. Under stressful conditions, increased proline concentration is linked with stress tolerance and helps maintain the osmotic potential for alleviating stress effects across the cultivars. Added Si led to a significant adjustment to proline biosynthesis both in the tolerant and the susceptible wheat cultivars, particularly under DS and HS, which might show that stress relief responses due to alleviation of various cellular damages, including oxidative burst and peroxidative damage to the cell membrane (Figure 4C). Consistent with the results presented here, several other studies have also reported that Si application reduces the proline accumulation on multiple crops like wheat (Pei et al., 2010), rice (Mauad et al., 2016), lentil (Biju et al., 2017), and sorghum (Yin et al., 2013). Results showed that Si might have a definite controlling effect on proline biosynthesis, as reported by Vivet et al. (2000). The Si-induced breakdown of proline due to the controlling effect may support the generation of ATP to repair stress-induced damages in the cytosol for substantial cytoplasmic osmotic adjustments of treated wheat cultivars (Ashraf and Foolad, 2007). Accumulation of higher proline concentration under stressful conditions has been correlated in tolerant cultivars more than in susceptible cultivars, as reported by Ashraf and Foolad (2007) but results from the current study showed that this relationship might not be universal. For example, proline accumulation under HS was higher in Kukri than in the tolerant cultivar, RAC875. Similarly, CM59443 accumulated more proline than ECH957 under DHS (Figure 4C).

Free AA concentrations increased across the tolerant and susceptible wheat cultivars with Si treatment under DS and HS (Figure 4D). Results showed that DHS significantly impacted the free AA concentration, and no significant increase in AA was observed with Si treatment across the wheat cultivars (except Excalibur). The percent increase in free AA in tolerant and susceptible wheat cultivars might be associated with the enhanced production of various antioxidants in response to DS and HS. The ROS scavenging minimizes AA oxidation, which could help maintain the integrity of protein structure under DS and HS as reported by Ashraf and Foolad (2007). Previously, Cvikrová et al. (2013) reported that enhanced free AA concentration partially converted to proline to relieve DS and HS effects. Si-induced increase in free AA and TSS helps plants to make structural and biochemical adjustments to cope with stress environments (Sallam et al., 2019).

Antioxidant enzymes

With normal cellular metabolisms, plants continuously produce various ROS. The exposure of plants to individual and combined DS and HS during their life cycle disturbs the quenching activity of different antioxidants, especially in susceptible cultivars, leading to excessive production of several ROS (Alzahrani et al., 2018). Plants with higher antioxidant levels, both in constitutive or induced form, have demonstrated maximum tolerance against oxidative stress damages to cells and organelles.

In the current study, APX, POX, and CAT activities were triggered with the onset of DS, HS, and DHS. However, the increase in the activities of these antioxidants was higher with Si treatment than with control across the cultivars (Table 1). Si-induced increased APX activity across the cultivars (tolerant and susceptible) suggests Si treatment might dismutase O_2^- to H_2O_2 in the mitochondria, chloroplast, and cytoplasm to prevent cellular damage under DS, HS, and DHS. Accumulation of H_2O_2 that results from APX canalization reaction is further detoxified by the POX-mediated ascorbate-glutathione

cycle. Silicon-induced higher CAT activity eliminates H_2O_2 by breaking it down into oxygen and water molecules. Other research findings have also shown that higher POX activity is correlated with increased stress tolerance to various oxidative stresses (Alzahrani et al., 2018; Etesami and Jeong, 2018). DS- and HS-induced OH^-, coupled with H_2O_2 can react with macromolecules without discrimination, facilitating cellular damage across the cultivars. The results showed that Si-induced integrating activities of APX, CAT, and POX under DS, HS, and DHS could inhibit or reduce OH^- formation among the tolerant and susceptible wheat cultivars; similar results have been reported by Pei et al. (2010) and Biju et al. (2017). The increased APX, POX, and CAT activities with Si treatment prevented the studied wheat cultivars from cellular damage with improved tolerance to DS, HS, and DHS.

GY and yield components

Abiotic stresses, particularly combined DHS, have detrimental impacts on GY and yield-related components (Reynolds et al., 2005). Genotypic efficiency for stress tolerance is usually quantified by GY and its related components under a stressful environment and mainly depends on the degree and severity of the stress treatment. In the current experiment, genotypes × environmental interaction was highly variable, showing that all cultivars responded differently to control and stress treatments (DS, HS, and DHS). A significant difference was observed among tolerant and susceptible cultivars in their response to DS, HS, and DHS. The differential sensitivity of the cultivars for various yield components, such as HI, thousand grains weight, GNS, and grain weight per spike to DS, HS, and DHS was indicative of their varied response (Figure 5). With added Si, while encountering stress, susceptible cultivars also performed better and produced higher GY and yield components (TGW and GWS). Compared to the control treatment, this recovery might be due to enhanced photosynthetic assimilates linked with Si-induced higher photosynthesis and soluble carbohydrates under DS and HS (Figure 4A).

Conclusion

Terminal DS and HS frequently occur in most of the wheat belt, which reduces grain weight, grain number, and ultimately, final GY. The current study results suggested that Si inclusion as a nutritional element is beneficial under normal and adverse environmental conditions. Si treatment has maintained various physiological and biochemical attributes by regulating the leaf water potential under DS, HS, and DHS both in the tolerant and susceptible wheat cultivars. In addition, our findings also validated that tolerance to DS and HS in susceptible and tolerant wheat cultivars with pre-sowing Si treatment was linked with the enhanced antioxidant defense activities and alleviation of oxidative stress damages. Results showed that Si-induced higher percent improvement in morpho-physiological and biochemical traits was observed under DS, compared with HS and DHS. Overall, RAC875 among the tolerant cultivars and Kukri among the susceptible cultivars performed better with Si treatment across the stress treatments. However, a better understanding of individual and combined stress and the response of different cultivars with and without Si under field conditions will assist in validating controlled study results.

Data availability statement

The raw data supporting the conclusions of this article will be made available by the authors, without undue reservation.

Author contributions

Conceptualization and writing—review and editing: WA, DG, SF, and GB. Methodology: WA and DG. Supervision and funding acquisition: DG. Investigation, data curation, statistical analysis, and writing—original draft preparation: WA. Resources and equipment: DG, SF, and GB. Software: WA and SF. All authors have read and approved the final version of the manuscript.

Acknowledgments

The authors are grateful to the Faculty of Veterinary and Agricultural Sciences, the University of Melbourne for the Melbourne Research Scholarship given to WA for PhD research and funding support to conduct this research work. The authors would also like to thank Dr Ravneet Kaur Jhajj (lab manager, Dookie Campus) and Dr Muhammad Kaleem (visiting research fellow at that time) for their help, and support during the biochemical analysis.

Conflict of interest

The authors declare that the research was conducted in the absence of any commercial or financial relationships that could be construed as a potential conflict of interest.

Publisher's note

All claims expressed in this article are solely those of the authors and do not necessarily represent those of their affiliated organizations, or those of the publisher, the editors and the reviewers. Any product that may be evaluated in this article, or claim that may be made by its manufacturer, is not guaranteed or endorsed by the publisher.

References

Abid, M., Ali, S., Qi, L. K., Zahoor, R., Tian, Z., Jiang, D., et al. (2018). Physiological and biochemical changes during drought and recovery periods at tillering and jointing stages in wheat (*Triticum aestivum* L.). *Sci. Rep.* 8, 1–15. doi: 10.1038/s41598-018-21441-7

Alghory, A., and Yazar, A. (2019). Evaluation of crop water stress index and leaf water potential for deficit irrigation management of sprinkler-irrigated wheat. *Irrig. Sci.* 37, 61–77. doi: 10.1007/s00271-018-0603-y

Alzahrani, Y., Kuşvuran, A., Alharby, H. F., Kuşvuran, S., and Rady, M. M. (2018). The defensive role of silicon in wheat against stress conditions induced by drought, salinity or cadmium. *Ecotoxicol. Environ. Saf.* 154, 187–196. doi: 10.1016/j.ecoenv.2018.02.057

Ashraf, M., and Foolad, M. R. (2007). Roles of glycine betaine and proline in improving plant abiotic stress resistance. *Environ. Exp. Bot.* 59, 206–216. doi: 10.1016/j.envexpbot.2005.12.006

Balota, M., Payne, W. A., Evett, S. R., and Lazar, M. D. (2007). Canopy temperature depression sampling to assess grain yield and genotypic differentiation in winter wheat. *Crop Sci.* 47, 1518–1529. doi: 10.2135/cropsci2006.06.0383

Barnabás, B., Jäger, K., and Fehér, A. (2008). The effect of drought and heat stress on reproductive processes in cereals. *Plant Cell Environ.* 31, 11–38. doi: 10.1111/j.1365-3040.2007.01727.x

Barrs, H., and Weatherley, P. (1962). A re-examination of the relative turgidity technique for estimating water deficits in leaves. *Aust. J. Biol. Sci.* 15, 413–428. doi: 10.1071/BI9620413

Bates, L. S., Waldren, R. P., and Teare, I. D. (1973). Rapid determination of free proline for water-stress studies. *Plant Soil* 39, 205–207. doi: 10.1007/BF00018060

Biju, S., Fuentes, S., and Gupta, D. (2017). Silicon improves seed germination and alleviates drought stress in lentil crops by regulating osmolytes, hydrolytic enzymes and antioxidant defense system. *Plant Physiol. Biochem.* 119, 250–264. doi: 10.1016/j.plaphy.2017.09.001

Biju, S., Fuentes, S., and Gupta, D. (2018). The use of infrared thermal imaging as a non-destructive screening tool for identifying drought-tolerant lentil genotypes. *Plant Physiol. Biochem.* 127, 11–24. doi: 10.1016/j.plaphy.2018.03.005

Buis, A. (2019). *A Degree Of Concern: Why Global Temperatures Matter–Climate Change: Vital Signs Of The Planet. Climate Change*. Nasa. Gov. Available online at: https://climate.nasa.gov/news/2865/a-degree-of-concern-why-global-temperatures-matter/ (accessed September 19, 2019).

Carvalho, L. C., and Amâncio, S. (2002). Antioxidant defence system in plantlets transferred from *in vitro* to *ex vitro*: effects of increasing light intensity and CO2 concentration. *Plant Sci.* 162, 33–40. doi: 10.1016/S0168-9452(01)00524-6

Chance, B., and Maehly, A. (1955). [136] Assay of catalases and peroxidases. *Methods Enzymol.* 2, 764–775. doi: 10.1016/S0076-6879(55)02300-8

Chen, G. X., and Asada, K. (1989). Ascorbate peroxidase in tea leaves: occurrence of two isozymes and the differences in their enzymatic and molecular properties. *Plant Cell Physiol.* 30, 987–998.

Cooke, J., and Leishman, M. R. (2016). Consistent alleviation of abiotic stress with silicon addition: a meta-analysis. *Funct. Ecol.* 30, 1340–1357. doi: 10.1111/1365-2435.12713

Costa, J. M., Grant, O. M., and Chaves, M. M. (2013). Thermography to explore plant–environment interactions. *J. Exp. Bot.* 64, 3937–3949. doi: 10.1093/jxb/ert029

Cvikrová, M., Gemperlová, L., Martincová, O., and Vanková, R. (2013). Effect of drought and combined drought and heat stress on polyamine metabolism in proline-over-producing tobacco plants. *Plant Physiol. Biochem.* 73, 7–15. doi: 10.1016/j.plaphy.2013.08.005

Debona, D., Rodrigues, F. A., and Datnoff, L. E. (2017). Silicon's role in abiotic and biotic plant stresses. *Annu. Rev. Phytopathol.* 55, 85–107. doi: 10.1146/annurev-phyto-080516-035312

Deshmukh, R. K., Vivancos, J., Guérin, V., Sonah, H., Labbé, C., Belzile, F., et al. (2013). Identification and functional characterization of silicon transporters in soybean using comparative genomics of major intrinsic proteins in Arabidopsis and rice. *Plant Mol. Biol.* 83, 303–315. doi: 10.1007/s11103-013-0087-3

Dhindsa, R. S., Plumb-Dhindsa, P., and Thorpe, T. A. (1981). Leaf senescence: correlated with increased levels of membrane permeability and lipid peroxidation, and decreased levels of superoxide dismutase and catalase. *J. Exp. Bot.* 32, 93–101. doi: 10.1093/jxb/32.1.93

Dubois, M., Gilles, K., Hamilton, J. K., Rebers, P. A., and Smith, F. (1951). A colorimetric method for the determination of sugars. *Nature* 168, 167. doi: 10.1038/168167a0

Erice, G., Louahlia, S., Irigoyen, J. J., Sanchez-Diaz, M., and Avice, J.-C. (2010). Biomass partitioning, morphology and water status of four alfalfa genotypes submitted to progressive drought and subsequent recovery. *J. Plant Physiol.* 167, 114–120. doi: 10.1016/j.jplph.2009.07.016

Etesami, H., and Jeong, B. R. (2018). Silicon (Si): review and future prospects on the action mechanisms in alleviating biotic and abiotic stresses in plants. *Ecotoxicol. Environ. Saf.* 147, 881–896. doi: 10.1016/j.ecoenv.2017.09.063

Fahad, S., Bajwa, A. A., Nazir, U., Anjum, S. A., Farooq, A., Zohaib, A., et al. (2017). Crop production under drought and heat stress: plant responses and management options. *Front. Plant Sci.* 8, 1147. doi: 10.3389/fpls.2017.01147

FAO (2019). *Agriculture and Climate Change – Challenges and Opportunities at the Global and Local Level – Collaboration on Climate-Smart Agriculture*. Rome, 52. Licence: CC BY-NC-SA 3.0 IGO.

FAOSTAT (2020). *Crops and Livestock Products*. Food and Agriculture Organization of the United Nations. Available online at: https://www.fao.org/faostat/en/#data/QCL/visualize (accessed January 10, 2022).

Fleury, D., Jefferies, S., Kuchel, H., and Langridge, P. (2010). Genetic and genomic tools to improve drought tolerance in wheat. *J. Exp. Bot.* 61, 3211–3222. doi: 10.1093/jxb/erq152

FLIR (2015). *FLIR T1050sc: HD thermal imaging for RandD applications. HD performance in a portable handheld infrared camera*. FLIR Systems, Inc. Available online at: http://www.flirmedia.com/MMC/THG/Brochures/RND_050/RND_050_APAC.pdf (accessed June 05, 2019).

Frew, A., Weston, L. A., Reynolds, O. L., and Gurr, G. M. (2018). The role of silicon in plant biology: a paradigm shift in research approach. *Ann. Bot.* 121, 1265–1273. doi: 10.1093/aob/mcy009

Fuentes, S., De Bei, R., Pech, J., and Tyerman, S. (2012). Computational water stress indices obtained from thermal image analysis of grapevine canopies. *Irrig. Sci.* 30, 523–536. doi: 10.1007/s00271-012-0375-8

Grégoire, C., Rémus-Borel, W., Vivancos, J., Labbé, C., Belzile, F., and Bélanger, R. R. (2012). Discovery of a multigene family of aquaporin silicon transporters in the primitive plant *Equisetum arvense*. *Plant J.* 72, 320–330. doi: 10.1111/j.1365-313X.2012.05082.x

Hodson, M., White, P., Mead, A., and Broadley, M. (2005). Phylogenetic variation in the silicon composition of plants. *Ann. Bot.* 96, 1027–1046. doi: 10.1093/aob/mci255

IPCC (2022). *Climate Change 2022: Impacts, Adaptation and Vulnerability*. Working Group II Contribution to the IPCC Sixth Assessment Report. IPCC Six Assessment Report ed.

Izanloo, A., Condon, A. G., Langridge, P., Tester, M., and Schnurbusch, T. (2008). Different mechanisms of adaptation to cyclic water stress in two South Australian bread wheat cultivars. *J. Exp. Bot.* 59, 3327–3346. doi: 10.1093/jxb/ern199

Luyckx, M., Hausman, J.-F., Lutts, S., and Guerriero, G. (2017). Silicon and plants: current knowledge and technological perspectives. *Front. Plant Sci.* 8, 411. doi: 10.3389/fpls.2017.00411

Ma, J. F., Tamai, K., Yamaji, N., Mitani, N., Konishi, S., Katsuhara, M., et al. (2006). A silicon transporter in rice. *Nature* 440, 688–691. doi: 10.1038/nature04590

Mahrookashani, A., Siebert, S., Hüging, H., and Ewert, F. (2017). Independent and combined effects of high temperature and drought stress around anthesis on wheat. *Journal of Agronomy and Crop Science* 203, 453–463. doi: 10.1111/jac.12218

Mathworks, M. (2017). *MATLAB and Statistics Toolbox Release*. Natick, MA: The MathWorks. Inc.

Mauad, M., Crusciol, C. A. C., Nascente, A. S., G.rassi, Filho, H., and Lima, G. P. P. (2016). Effects of silicon and drought stress on biochemical characteristics of leaves of upland rice cultivars. *Rev. Ciência Agron.* 47, 532–539. doi: 10.5935/1806-6690.20160064

Mendiburu, F. D. (2020). *Agricolae: Statistical Procedures for Agricultural Research*. R package version 1.3-1. Available online at: https://CRAN.R-project.org/package=agricolae.

Murchie, E. H., and Lawson, T. J. J. O. E. B. (2013). Chlorophyll fluorescence analysis: a guide to good practice and understanding some new applications. *J. Exp. Bot.* 64, 3983–3998. doi: 10.1093/jxb/ert208

NOAA (2020). *State of the Climate: Global Climate Report for July 2020. National Centers for Environmental Information, published online August 2020.* Available online at: https://www.ncei.noaa.gov/access/monitoring/monthly-report/global/202008 (accessed December 15, 2021).

Pei, Z., Ming, D., Liu, D., Wan, G., Geng, X., Gong, H., et al. (2010). Silicon improves the tolerance to water-deficit stress induced by polyethylene glycol in wheat (*Triticum aestivum* L.) seedlings. *J. Plant Growth Regul.* 29, 106–115. doi: 10.1007/s00344-009-9120-9

Perdomo, J. A., Conesa, M. À., Medrano, H., Ribas-Carbó, M., and Galmés, J. (2015). Effects of long-term individual and combined water and temperature stress on the growth of rice, wheat and maize: relationship with morphological and physiological acclimation. *Physiol. Plant.* 155, 149–165. doi: 10.1111/ppl.12303

Prasad, P. V. V., Staggenborg, S. A., and Ristic, Z. (2008). Impacts of drought and/or heat stress on physiological, developmental, growth, and yield processes of crop plants. *Response Crops Limited Water* 1, 301–321. doi: 10.2134/advagricsystmodel1.c11

R Core Team (2020). *R: A Language and Environment for Statistical Computing.* R Foundation for Statistical Computing, Vienna, Austria. Available online at: https://www.R-project.org/.

Reynolds, M., Mujeeb-Kazi, A., and Sawkins, M. (2005). Prospects for utilising plant-adaptive mechanisms to improve wheat and other crops in drought-and salinity-prone environments. *Ann. Appl. Biol.* 146, 239–259. doi: 10.1111/j.1744-7348.2005.040058.x

Rezaei, E. E., Webber, H., Gaiser, T., Naab, J., and Ewert, F. (2015). Heat stress in cereals: mechanisms and modelling. *Eur. J. Agron.* 64, 98–113. doi: 10.1016/j.eja.2014.10.003

Rizwan, M., Ali, S., Ibrahim, M., Farid, M., Adrees, M., Bharwana, S. A., et al. (2015). Mechanisms of silicon-mediated alleviation of drought and salt stress in plants: a review. *Environ. Sci. Pollut. Res.* 22, 15416–15431. doi: 10.1007/s11356-015-5305-x

Rojas, M., Lambert, F., Ramirez-Villegas, J., and Challinor, A. J. (2019). Emergence of robust precipitation changes across crop production areas in the 21st century. *Proc. Nat. Acad. Sci. U. S. A.* 116, 6673–6678. doi: 10.1073/pnas.1811463116

Sallam, A., Alqudah, A. M., Dawood, M. F., Baenziger, P. S., and Börner, A. (2019). Drought stress tolerance in wheat and barley: advances in physiology, breeding and genetics research. *Int. J. Mol. Sci.* 20, 3137. doi: 10.3390/ijms20133137

Sattar, A., Sher, A., Ijaz, M., Ul-Allah, S., Rizwan, M. S., Hussain, M., et al. (2020). Terminal drought and heat stress alter physiological and biochemical attributes in flag leaf of bread wheat. *PLoS ONE* 15, e0232974. doi: 10.1371/journal.pone.0232974

Sharma, P., Jha, A. B., Dubey, R. S., and Pessarakli, M. (2012). Reactive oxygen species, oxidative damage, and antioxidative defense mechanism in plants under stressful conditions. *J. Bot.* (2012) 2012, 217037. doi: 10.1155/2012/217037

Shi, Y., Zhang, Y., Han, W., Feng, R., Hu, Y., Guo, J., et al. (2016). Silicon enhances water stress tolerance by improving root hydraulic conductance in *Solanum lycopersicum* L. *Front. Plant Sci.* 7, 196. doi: 10.3389/fpls.2016.00196

Shiferaw, B., Smale, M., Braun, H. J., Duveiller, E., Reynolds, M., and Muricho, G. J. F. S. (2013). Crops that feed the world 10. Past successes and future challenges to the role played by wheat in global food security. *Food Security* 5, 291–317. doi: 10.1007/s12571-013-0263-y

Spiertz, J., Hamer, R., Xu, H., Primo-Martin, C., Don, C., and Van Der Putten, P. (2006). Heat stress in wheat (*Triticum aestivum* L.): effects on grain growth and quality traits. *Eur. J. Agron.* 25, 89–95. doi: 10.1016/j.eja.2006.04.012

Telfer, P., Edwards, J., Bennett, D., and Kuchel, H. (2015). *Heat Stress Tolerance Of Wheat.* GRDC. Available online at: https://grdc.com.au/resources-and-publications/grdc-update-papers/tab-content/grdc-update-papers/2015/02/heat-stress-tolerance-of-wheat (accessed October 14, 2018).

Topp, G. C., Parkin, G., Ferré, T. P., Carter, M., and Gregorich, E. (2008). "Soil water content," in *Soil Sampling and Methods of Analysis* (Boca Raton, FL: Taylor & Francis Group, CRC Press), 939–962.

Tricker, P. J., Elhabti, A., Schmidt, J., and Fleury, D. (2018). The physiological and genetic basis of combined drought and heat tolerance in wheat. *J. Exp. Bot.* 69, 3195–3210. doi: 10.1093/jxb/ery081

Urban, O., Hlaváčová, M., Klem, K., Novotná, K., Rapantová, B., Smutná, P., et al. (2018). Combined effects of drought and high temperature on photosynthetic characteristics in four winter wheat genotypes. *Field Crops Res.* 223, 137–149. doi: 10.1016/j.fcr.2018.02.029

Vivet, B., Cavelier, F., and Martinez, J. (2000). Synthesis of silaproline, a new proline surrogate. *Eur. J. Organic Chem.* 2000, 807–811. doi: 10.1002/(SICI)1099-0690(200003)2000:5andlt;807::AID-EJOC807andgt;3.0.CO;2-E

Wang, X., Cai, J., Jiang, D., Liu, F., Dai, T., and Cao, W. (2011). Pre-anthesis high-temperature acclimation alleviates damage to the flag leaf caused by post-anthesis heat stress in wheat. *J. Plant Physiol.* 168, 585–593. doi: 10.1016/j.jplph.2010.09.016

Watson, A., Ghosh, S., Williams, M. J., Cuddy, W. S., Simmonds, J., Rey, M.-D., et al. (2018). Speed breeding is a powerful tool to accelerate crop research and breeding. *Nat. Plants* 4, 23–29. doi: 10.1038/s41477-017-0083-8

Wickham, H. (2016). *ggplot2: Elegant Graphics for Data Analysis*. New York, NY: Springer-Verlag. doi: 10.1007/978-3-319-24277-4_9

Yin, L., Wang, S., Li, J., Tanaka, K., and Oka, M. (2013). Application of silicon improves salt tolerance through ameliorating osmotic and ionic stresses in the seedling of Sorghum bicolor. *Acta Physiol. Plantarum* 35, 3099–3107. doi: 10.1007/s11738-013-1343-5

Yue, B., Xue, W., Xiong, L., Yu, X., Luo, L., Cui, K., et al. (2006). Genetic basis of drought resistance at reproductive stage in rice: separation of drought tolerance from drought avoidance. *Genetics* 172, 1213–1228. doi: 10.1534/genetics.105.045062

Zadoks, J. C., Chang, T. T., and Konzak, C. F. (1974). A decimal code for the growth stages of cereals. *Weed Res.* 14, 415–421. doi: 10.1111/j.1365-3180.1974.tb01084.x

Zandalinas, S. I., Mittler, R., Balfagón, D., Arbona, V., and Gómez-Cadenas, A. (2018). Plant adaptations to the combination of drought and high temperatures. *Physiol. Plant.* 162, 2–12. doi: 10.1111/ppl.12540

frontiers | Frontiers in Plant Science

TYPE Original Research
PUBLISHED 04 August 2022
DOI 10.3389/fpls.2022.967537

Check for updates

OPEN ACCESS

EDITED BY
Bhaskar Gupta,
Government General Degree College, Singur, India

REVIEWED BY
Yanlun Ju,
Northwest A&F University, China
Yingnan Wang,
Northeast Forestry University, China

*CORRESPONDENCE
Xiao-Shuang Wei
weixiaoshuang@jlau.edu.cn
Zhi-Hai Wu
wuzhihai@jlau.edu.cn

SPECIALTY SECTION
This article was submitted to Plant Abiotic Stress, a section of the journal Frontiers in Plant Science

RECEIVED 13 June 2022
ACCEPTED 07 July 2022
PUBLISHED 04 August 2022

CITATION
Jiang H, Song Z, Su Q-W, Wei Z-H, Li W-C, Jiang Z-X, Tian P, Wang Z-H, Yang X, Yang M-Y, Wei X-S and Wu Z-H (2022) Transcriptomic and metabolomic reveals silicon enhances adaptation of rice under dry cultivation by improving flavonoid biosynthesis, osmoregulation, and photosynthesis.
Front. Plant Sci. 13:967537.
doi: 10.3389/fpls.2022.967537

COPYRIGHT
© 2022 Jiang, Song, Su, Wei, Li, Jiang, Tian, Wang, Yang, Yang, Wei and Wu. This is an open-access article distributed under the terms of the Creative Commons Attribution License (CC BY). The use, distribution or reproduction in other forums is permitted, provided the original author(s) and the copyright owner(s) are credited and that the original publication in this journal is cited, in accordance with accepted academic practice. No use, distribution or reproduction is permitted which does not comply with these terms.

Transcriptomic and metabolomic reveals silicon enhances adaptation of rice under dry cultivation by improving flavonoid biosynthesis, osmoregulation, and photosynthesis

Hao Jiang[1], Ze Song[1], Qing-Wang Su[1], Zhi-Heng Wei[1], Wan-Chun Li[1], Zi-Xian Jiang[1], Ping Tian[1], Zhen-Hui Wang[1], Xue Yang[2], Mei-Ying Yang[2], Xiao-Shuang Wei[1]* and Zhi-Hai Wu[1,3]*

[1]College of Agronomy, Jilin Agricultural University, Changchun, China, [2]College of Life Sciences, Jilin Agricultural University, Changchun, China, [3]National Crop Variety Approval and Characteristic Identification Station, Jilin Agricultural University, Changchun, China

Dry cultivation is a new rice crop mode used to alleviate water shortage and develop water-saving agriculture. There is obvious genetic difference compared with drought-tolerant rice. Silicon (Si) plays an important role in plant adaptation to adverse environmental conditions and can significantly improve the drought tolerance and yield of rice. However, the regulatory mechanism via which Si provides plant tolerance or adaptation under dry cultivation is not well understood. The present study investigated the changes in plant growth, photosynthetic gas exchange, and oxidative stress of the rice cultivar "Suijing 18" under dry cultivation. Si improved photosynthetic performance and antioxidant enzyme activity and subsequently reduced lipid peroxidation of rice seedlings, promoted LAI and promoted leaf growth under dry cultivation. Further, transcriptomics combined with quasi-targeted metabolomics detected 1416 and 520 differentially expressed genes (DEGs), 38 and 41 differentially accumulated metabolites (DAMs) in the rice leaves and roots, respectively. Among them, 13 DEGs were involved in flavonoid biosynthesis, promoting the accumulation of flavonoids, anthocyanins, and flavonols in the roots and leaves of rice under dry cultivation. Meanwhile, 14 DEGs were involved in photosynthesis, promoting photosystem I and photosystem II responses, increasing the abundance of metabolites in leaves. On the other hand, 24 DAMs were identified involved in osmoregulatory processes, significantly increasing amino acids and carbohydrates and their derivatives in roots. These results provide new insight into the role of Si in alleviating to adverse environmental, Si enhanced the accumulation

of flavonoids and osmoregulatory metabolites, thereby alleviating drought effect on the roots. On the other hand, improving dehydration resistance of leaves, guaranteeing normal photosynthesis and downward transport of organic matter. In conclusion, Si promoted the coordinated action between the above-ground and below-ground plant parts, improved the root/shoot ratio (R/S) of rice and increased the sugar content and enhancing rice adaptability under dry cultivation conditions. The establishment of the system for increasing the yield of rice under dry cultivation provides theoretical and technical support thereby promoting the rapid development of rice in Northeast China, and ensuring national food security.

KEYWORDS

rice, dry cultivation, transcriptomic, quasi-targeted metabolomics, photosynthesis, osmoregulatory, flavonoid metabolism

Introduction

The increasing environmental stress and irrigation water scarcity had been posing serious threats to global rice production (Garg et al., 2003). The International Food Policy Research Institute (IFPRI) study predicted a 15% decrease in irrigated rice yields by 2050 in developing countries due to climate change. Therefore, there is an urgent need to balance the contradiction between food demand and ecological security. Rice under dry cultivation is a mode wherein rice is directly sown under dryland preparation without nursery and transplantation. Here, the whole reproductive period of rice relies on natural precipitation. Moreover, adequate water is resupplied only during critical growth periods or drought. Rice under dry cultivation has been carried out and is rapidly developing worldwide to develop water-saving agriculture and a light and simplified production measure (Jiang et al., 2021). The development of rice under dry cultivation mode can alleviate the water shortage crisis, reduce greenhouse gas emissions and reduce agricultural surface pollution (Adekoya et al., 2014; Weller et al., 2016). However, there is significant genetic (Xia et al., 2014) and epigenetic difference (Luo, 2010; Xia et al., 2016) compared to rice in terms of drought tolerance. Therefore, it is important to explore the mechanisms of plant response to environmental stresses under the dry crop model to improve the adaptability and application of rice.

It is important that crops maintain their normal metabolic processes for long during drought stress (Hu and Xiong, 2014). Maintaining photosynthetic capacity under drought conditions is an important feature of drought-resistant crops (Ma X. et al., 2016). Mumtaz et al. (2020) showed that drought inhibits rice growth by reducing photosynthetic capacity, reducing grain yield and quality. Photosynthetic capacity lowers during drought due to reduced available CO_2 by stomatal closure or reactive oxygen species (ROS)-induced photooxidative damage under dehydration (Chaves et al., 2009; Saibo et al., 2009). However, many drought-tolerant mechanisms, such as regulation of osmotic pressure through osmolytes, protective metabolites, proteins, and ROS scavenging systems, maintain normal photosynthesis under dehydrated conditions, leading to relatively high biomass accumulation and yield (Valliyodan and Nguyen, 2006). At the cellular level, drought signaling promotes stress-protectant metabolites such as proline and trehalose, triggers the antioxidant system to maintain redox homeostasis, and deploys peroxidase enzymes to prevent acute cellular damage and membrane integrity. Various other factors such as the extent of water stress and the plant organ sensing the stress also trigger specific signaling responses, including, but not limited to, abscisic acid, brassinosteroid, and ethylene phytohormone pathways (Gupta et al., 2020). Plant metabolic responses under drought stress are currently attracting more attention because many metabolites are thought to play a central role in stress tolerance. Moreover, metabolites are better targets for improving drought tolerance than the individual genes as they are generated by the interaction of various genes and pathways, which lead to systemic effects in response to stress (Guo et al., 2018). Ma X. et al. (2016) found that 4-hydroxycinnamic acid and ferulic acid were significantly correlated with drought tolerance in two rice cultivars, and the DEGs involved in the pathways of these metabolites were proposed as good candidate genes to improve drought-tolerance (Ma X. et al., 2016). Meanwhile, Siriwach et al. (2020) examined the metabolic pathways of Arabidopsis thaliana during stress response based on silicon analysis and identified the responses and metabolites related to drought adaptation (Siriwach et al., 2020).

Silicon is the second most abundant element in soil, which exists in almost all plants. It is beneficial to plant growth, especially under biotic and abiotic stress conditions (Huang and Ma, 2020; Ranjan et al., 2021; Huang et al., 2022; Thorne et al., 2022). Studies have shown that Si application improves growth under drought, heavy metals, and salinity in

rice, barley, tomato, cucumber, and other crops (Ma, 2004; Ma and Yamaji, 2006; Liang et al., 2007; Zhu and Gong, 2013; Luyckx et al., 2017; Réthoré et al., 2020). Yin et al. (2016) showed that Si upregulated several key phytohormone synthetic genes under salt stress, which also identified the phytohormone involved in Si-induced salt tolerance in sorghum and provided evidence for the role of Si in mediating salt tolerance (Yin et al., 2016). Si also increased root water uptake, regulated phytohormone levels, and increased antioxidant defenses in cucumber under salt stress (Zhu et al., 2019). Recently, Coskun et al. (2019) summarized the roles of Si in higher plants and proposed the "apoplastic obstruction hypothesis" based on molecular and phenotypic data. This model argues for a fundamental role of Si as an extracellular prophylactic agent against biotic and abiotic stresses (as opposed to an active cellular agent), with important cascading effects on plant form and function (Coskun et al., 2019). Several studies have shown that Si induces differential gene expression in response to biotic and abiotic stresses. Chain et al. (2009) analyzed the effect of Si on the transcriptomic changes in wheat under powdery mildew stress and found that Si supply nearly reversed the gene expressions under pathogen attack (Chain et al., 2009). Holz et al. (2015) identified 1136 DEGs induced by supplemental sodium silicate in *in vitro*-generated cucumber clone (Holz et al., 2015). Rasoolizadeh et al. (2018) observed that Silicon protects soybean plants against *Phytophthora sojae*, with the addition of Si, the plant transcriptome remains unaffected under pathogen stress, the expression of effector-coding genes by the pathogen is reduced (Rasoolizadeh et al., 2018). Yoo et al. (2019) compared rice plants treated with *Paenibacillus yonginensis* DCY84T (DCY84T) and Si with untreated rice using RNA-seq, under Si treatment, 576 genes were upregulated and 394 genes were downregulated, and the treatment improved initial seedling growth and enhanced resistance to environmental stresses (Yoo et al., 2019). However, under abiotic stresses, Haddad et al. (2019) studied the transcriptomics of *Brassica napus* roots in response to Si supply and found differential expression of genes involved in plant hormone metabolism and stress response (Haddad et al., 2019). Meanwhile, Zhu et al. (2019) sequenced the transcriptome of control and salt-stressed cucumber leaves in the presence and absence of Si addition. They reported changes in the expression of 1469 genes in response to Si treatment, these genes were mainly involved in hormone and signal transduction and stress and defense responses. Under salt stress, Si treatment shifted the transcriptome of stressed cucumber back to that of the control (Zhu et al., 2019).

Drought and its relationship with silicon have been well studied. For example, in some plants such as sugarcane (*Saccharum officinarum* L.), wheat (*Triticum aestivum* L.) under drought stress, silicon increases ascorbate peroxidase activity, total soluble sugars content, relative water content (Mavrič Čermelj et al., 2021). In some studies, on rice (*Oryza sativa* L.) was found in Si induced different responses regarding to proline accumulation which could be beneficial for drought exposed plants (Mauad et al., 2016). Si might also trigger the transcription of genes that are related to antioxidant defense, photosynthesis, osmotic adjustment, lignin, and suberin metabolism (Zhu and Gong, 2013). However, the effects of silicon on rice under dry cultivation has not yet been studied in detail. Typically, the yield and quality of rice under dry cultivation can be affected due to the changes in cultivation patterns. Our preliminary analysis showed that the optimal silicon application rate suitable for high yield in Jilin Province ranged from 30 to 47.68 kg·ha^{-1}, resulting in 38–47% yield increase in rice under dry cultivation (Su et al., 2022). The present study analyzed the transcriptome and metabolome of rice treated with Si under dry cultivation. Further, a correlation analysis combined with morphological and physiological trait analysis was performed to identify the specific metabolites, genes, metabolic pathways, and their interactions. The study thus comprehensively evaluates the regulatory role and mechanism of Si under dry cultivation, reveals the molecular mechanism of Si to enhance the adaptability of dry farming rice, and lay the foundation for the sustainable development of the dry cultivation model.

Materials and methods

Experiment setup and materials

The experiment was conducted at the National Crop Variety Approval and Characterization Station at the Jilin Agricultural University of Changchun City, Jilin Province (125°39 E and 44°46 N). The soil of this region has an organic matter content of 18.7 g·kg^{-1}, alkaline dissolved nitrogen of 117.02 mg·kg^{-1}, available phosphorus of 41.11 mg·kg^{-1}, available potassium of 245.16 mg·kg^{-1}, available silicon of 113.46 mg·kg^{-1}, and pH of 6.2.

The high-yielding rice cultivar "Suijing 18" (China Rice Data Center, No. 2014021)[1] was used as the test material in this study. Preliminary analysis revealed that "Suijing 18" is a high-quality drought-resistant cultivar suitable for dry farming in the central region of Jilin Province.

The experiment was conducted in pots with rice grown under four treatments of flooding cultivation (W), flooding cultivation with Si treatment (WS), dry cultivation (D), and dry cultivation with Si treatment (DS); Sow five holes in each pot and eight seeds in each hole. The environment of the test is greenhouse, and the temperature is maintained at 25 ± 1°C, the humidity is 80%, and the light/dark cycle of 12 h/12 h is carried out during the whole growth process. Triplicates were maintained per treatment. Biori Russian mineral silica

1 https://www.ricedata.cn/variety/varis/614593.htm

with an effective silica content of ≥72% was applied as a base fertilizer at 45 kg·ha^{-1}. Calcium superphosphate (P_2O_5; 12%) at the rate of 75 kg·ha^{-1} and potassium chloride (K_2O; 60%) at the rate of 75 kg·ha^{-1} were applied as a one-time substrate, and urea (pure N; 46%) at the rate of 160 kg·ha^{-1} was applied three times as basal fertilizer, tiller fertilizer, and spike fertilizer (5:3:2). The indexes involved in the experiment were measured by collecting samples 45 days after sowing.

Evaluation of physiological indexes

Root system index

The root samples were collected, and the root volume was measured following the drainage method (Gong et al., 2014), The length of the longest root and the number of roots per hole were measured. Three repetitions per treatment were used for the measurements, and the average value was calculated.

Leaf photosynthetic parameter

The Li-6400XT photosynthesizer (LI-6400, LI-COR, Inc., Lincoln, NE, United States) was used to measure the photosynthetic parameters with a built-in fixed light source and a light quantum density setting of 1200 μmol·m^{-2}·s^{-1}. Five representative plants per treatment were selected for the analysis. The photosynthetic rate was measured between 9:00 and 11:30 in the morning on a clear and windless day, with three replicates per treatment. The mean values were calculated (Wu et al., 2022).

Superoxide anion, hydrogen peroxide, and malondialdehyde content

The superoxide anion (O_2^-) production was determined by the method described by Sadeghi et al. (2020). The concentration of hydrogen peroxide (H_2O_2) was determined according to Brennan's method (Brennan and Frenkel, 1977). Malondialdehyde (MDA) content in the first unfolded leaf at the upper part of the plant was determined following the thiobarbituric acid method (Zheng et al., 2020). Each experiment was independently repeated thrice.

Antioxidant enzyme activity

About 0.2 g of seedling stage frozen plant tissue was homogenized in 5 mL of extraction buffer (100 mmol/L phosphate buffer, pH 7.00). The homogenate was centrifuged at 10,000 × *g* at 4°C for 10 min, and the supernatant was used to determine SOD, CAT, and POD activities. The SOD activity was determined following the nitrogen blue tetrazolium method, POD activity following the guaiacol method, and the CAT activity following the ultraviolet absorption method (Ling et al., 2020), replicated three times measurement, and the mean values were calculated.

Leaf area index

Five plants of uniform growth were selected for each treatment, and the total leaf area of all the leaves of a plant was determined using a leaf area meter (CID-203, produced by CID company, WA, United States). The measurements were repeated three times, and the average value was calculated. The leaf area per square meter (leaf area index; LAI) was calculated based on the number of plants per square meter.

Leaf relative water content and electrical conductivity

Water retention in the leaves was determined following the method by Clarke (Clarke and Mccaig, 1982). Fresh leaves were collected from each treatment, rinsed with deionized water, and wiped with blotting paper; then, the fresh weight (a) was recorded. The sample was immersed in 28°C distilled water for 24 h, and the turgid weight (b) was determined. The sample was then dried at 85°C for 24 h, and the dry weight (c) was recorded. The water retention rate of the isolated leaves was calculated as follows (b−c/a−c) × 100%

Electrical conductivity was measured based on the method by Sairam and Srivastava (2002). Use portable conductivity meter (DDBJ-305, produced by Shanghai Precision Scientific Instruments Co., Ltd., Shanghai, China). Approximately 0.5 g of leaf tissue was collected, washed, placed into three centrifuge tubes containing 10 mL of ultra-pure water and maintained in a shaking incubator (25°C, 150 rpm) for 2 h. The initial conductivity (E1) was measured, and the conductivity (E0) of the blank control deionized water was also measured, then, the sample was boiled in water for 30 min and cooled the room temperature, then, measuring the electrical conductivity (E2).

Root/shoot ratio

The root and shoot samples were dried in an oven at 105°C for 30 min and drying at 85°C to constant weight, then weighed to determine the root shoot ratio. Each treatment was repeated three times, and the average value was calculated.

Sugar content

According to the method by Ma et al. (2021), 0.02 g fresh weight of plant tissues were boiled with 800 μL of 80% ethanol in an 80°C water bath for 30 min. The resulting extract was collected to measure the soluble sugar, sucrose, and fructose content using the sulfuric acid anthrone colorimetric method with slight modifications (Ma et al., 2021).

RNA-seq

The transcriptomes of rice under dry cultivation with and without Si treatment were generated through the high throughput RNA sequencing. Leaves and roots of fully expanded were collected 45 days after sowing, each sample was frozen in liquid nitrogen with three biological replicates. Total RNA was extracted from samples using TRIzol reagent. RNA integrity

was assessed using the RNA Nano 6000 Assay Kit of the Bioanalyzer 2100 system (Agilent Technologies Inc., Santa Clara, CA, United States). The cDNA library was sequenced on the Illumina sequencing was performed at the Beijing Novogene Bioinformatics Technology Co., Ltd. (Beijing, China).[2] Index of the reference genome was built using Hisat2 v2.0.5 and paired-end clean reads were aligned to the reference genome using Hisat2 v2.0.5. featureCounts v1.5.0-p3 was used to count the reads numbers mapped to each gene. And then FPKM of each gene was calculated based on the length of the gene and reads count mapped to this gene (For DESeq2 with biological replicates). Differential expression analysis of two conditions/groups (two biological replicates per condition) was performed using the DESeq2 R package (1.20.0). Gene Ontology (GO) and Kyoto Encyclopedia of Genes and Genomes (KEGG) tools were used to analyze the DEGs.

Quasi-targeted metabolomics

The above-mentioned samples were also used for the metabolome analysis. LC-MS/MS analyses were performed using an ExionLC^{TM} AD system (SCIEX) coupled with a QTRAP® 6500+ mass spectrometer (SCIEX) in Novogene Co., Ltd. (Beijing, China). The detection of the experimental samples using MRM (Multiple Reaction Monitoring) were based on novogene in-house database, Following their standard procedures extraction metabolites, These metabolites were annotated using the KEGG database,[3] HMDB database,[4] and Lipidmaps database.[5] Principal component analysis (PCA) and (orthogonal) partial least-squares discriminant analysis [(O)PLS-DA] were carried out to visualize the metabolic alterations among the experimental groups after mean centering and unit variance scaling. The variable importance in the projection (VIP) was used to rank the overall contribution of each variable to the (O)PLS-DA model; variables with VIP $>$ 1.0 were considered relevant for group discrimination. The metabolites with both multivariate and univariate statistical significance (VIP $>$ 1.0 and $p < 0.05$) were considered as differentially accumulated metabolites (DAMs). Principal component analysis was conducted to visualize the impact of Si on the dry farming rice metabolome.

Co-expression network analysis of the metabolome and transcriptome

The Metware Cloud website[6] was used to assess the correlation between metabolome and transcriptome. Firstly, log2 conversion was performed on the data uniformly before analysis. For the joint analysis between metabolome and transcriptome, the Pearson Correlation Coefficient (PCC) and the corresponding *P*-value were used for screening, and the screening criteria were set at PCC $>$ 0.8.

Reverse transcription and gene quantitative real-time PCR analysis

Leaf or root samples were collected during the seeding stage, immediately frozen in liquid nitrogen and stored at −80°C for future use. RNA was extracted using TRIZOL RNA extraction reagent following the manufacturer's procedure. The first-strand cDNA was reverse transcribed from 1 μg of the total RNA using the PrimeScript^{TM} RT reagent Kit (TaKaRa, RR047A, supplied by TAKARA in Japan). The quantitative real-time PCR (qRT-PCR) was carried out on a Light Cycler 480 Real-Time PCR System (Roche, Germany). Specific primers for each candidate gene were designed using Primer 5 software (Premier Inc., Canada). The qRT-PCR reactions were conducted with three technical replications in a 20 μL reaction volume using the TB Green Premix Ex Taq II (TaKaRa, RR820A) (SYBR Green). The relative gene expression was calculated using the $2^{-\Delta\Delta Ct}$ method (Livak and Schmittgen, 2001).

Statistical analysis

All experiments were conducted in triplicate ($n = 3$). One-way analysis of variance (ANOVA) and statistical analysis was performed to determine statistically significant differences between the control and other treatments using SPSS 20.0 software (SPSS Inc., Chicago, IL, United States); differences were considered statistically significant at $P < 0.05$. Data are presented as the mean ± standard deviation (SD) of three replicates.

Results

Influence of Si on the physiological response of rice under dry cultivation

First, plant phenotype were investigated to examine the effect of Si on the growth of dry farming rice. In this study, plant growth actually increased significantly after Si treatment under both dry and flooded cultivation conditions. The length in the Si-treated rice was significantly longer than that no Si-treated rice (**Figure 1A**). Si also has a certain effect on the physiological characters of rice under dry cultivation, as shown in **Figure 1B**, the relative water retention rate of the leaves in the Si-treated rice was higher than in other treatments. Thus, Si treatment maintained the water-holding capacity of the isolated leaves under dry cultivation. In addition, an indicator of plant lipid peroxidation, MDA can adversely affect membrane integrity under oxidative stress. Relative electrical

2 http://www.novogene.com
3 http://www.genome.jp/kegg/
4 http://www.hmdb.ca/
5 http://www.lipidmaps.org/
6 https://cloud.metware.cn/#/tools/tool-form?toolId=70

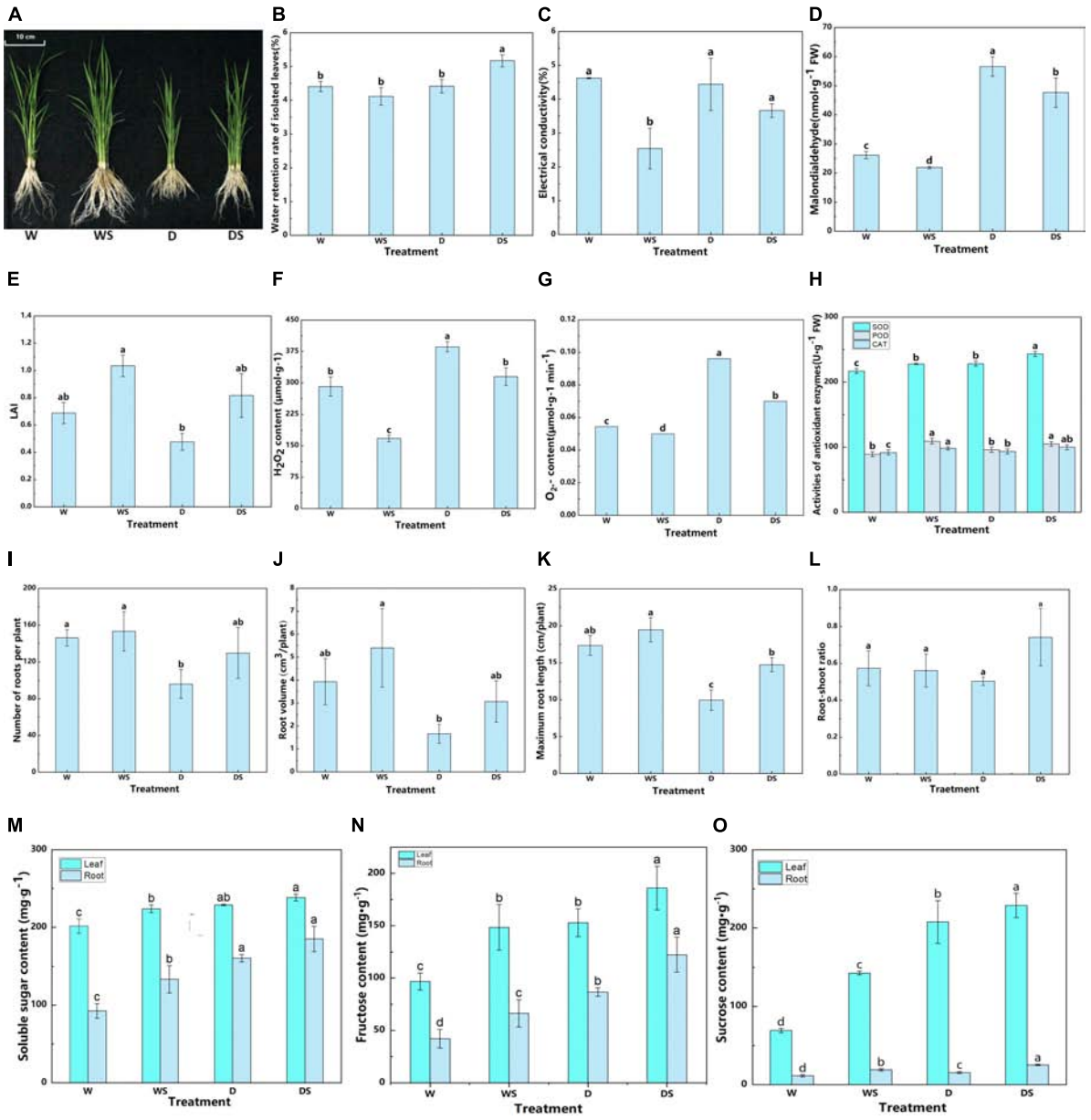


FIGURE 1
Effect of silicon application on rice under two cultivation conditions. Phenotypes of rice with and without Si under flooding and dry cultivation conditions **(A)**; Relative water retention rate **(B)**, electrical conductivity **(C)**, malondialdehyde (MDA) content **(D)**, leaf area index **(E)**, H_2O_2 content **(F)**, O_2^- content **(G)**, and antioxidant enzyme activity **(H)**, root number **(I)**, root volume **(J)**, root length **(K)**, root to shoot ratio **(L)**, soluble sugar content **(M)**, fructose content **(N)**, and sucrose content **(O)** of rice. The panels **(H,M–O)**, different lowercase letters indicate unified indicators significant differences between different treatments. Each experiment was repeated three times. Data represented are the means ± SD of three biological replicates. Different lowercase letters indicate significant differences ($P < 0.05$). W: Rice under flooding cultivation, WS: Rice under flooding cultivation with Si treatment, D: Rice under dry cultivation, DS: Rice under dry cultivation with Si treatment.

conductivity is another important index used to evaluate membrane integrity and instability under oxidative stress. Si treatment significantly reduced the MDA content and electrical conductivity compared to those without Si application, both under flooding and dry cultivation (Figures 1C,D). Meanwhile, LAI of rice decreased by 30.81% after dry cultivation, and Si application promoted LAI by 71.28% compared with the dry cultivation (Figure 1E).

At the physiological level, silicon application performed better than no silicon application (Figures 1F–H). The H_2O_2 and O_2^- content and the SOD, POD, and CAT activities were affected under dry cultivation compared with flooding. The

TABLE 1 Effects of silicon on the leaf photosynthetic parameters of rice under flooding and dry cultivation.

Treatment	Pn (μmol CO_2 m^{-2} s^{-1})	Gs (mol H_2O m^{-2} s^{-1})	Ci (μmol CO_2 mol^{-1} air)	Tr (mmol H_2O m^{-2} s^{-1})	WUE (mmol CO_2 mol^{-1} H_2O)	AMC
W	17.13 ± 0.43^{b}	0.31 ± 0.03^{a}	237.77 ± 6.81^{c}	5.46 ± 0.34^{a}	3.14 ± 0.18^{c}	0.07 ± 0.00^{b}
WS	18.85 ± 1.25^{a}	0.32 ± 0.02^{a}	221.87 ± 4.42^{c}	5.24 ± 0.31^{a}	3.60 ± 0.19^{a}	0.08 ± 0.01^{a}
D	11.54 ± 0.67^{d}	0.24 ± 0.01^{b}	278.62 ± 3.96^{a}	3.80 ± 0.03^{b}	3.04 ± 0.20^{c}	0.04 ± 0.00^{d}
DS	13.38 ± 0.23^{c}	0.25 ± 0.00^{b}	258.61 ± 1.73^{b}	4.97 ± 0.14^{a}	3.37 ± 0.12^{b}	0.05 ± 0.00^{c}

Pn, net photosynthesis rate; Gs, stomatal conductivity; Ci, intercellular CO_2 concentration; Tr, transpiration rate; WUE, water-use efficiency; AMC, apparent mesophyll conductance. Different lowercase letters indicate significant differences at $P < 0.05$.

reactive oxygen species (ROS) such as O_2^- and H_2O_2 decreased under Si treatment (Figures 1F,G). The enzyme activities slightly increased, with differences in the extent of the increase. Silicon application increased the SOD, POD, and CAT activities (Figure 1H), which indicates that silicon application help rice to cope with oxidative stress. Furthermore, Si application increased the root length ($P < 0.05$) of rice compared with no Si treatment under both conditions, a similar trend was observed for root volume and numbers (Figures 1I–K). Under dry farming, the root branch density was significantly reduced; however, Si treatment increased the tissue density. These observations indicate that the root growth parameters restricted under dry farming are retained by Si treatment. In addition, Si application improved the root/shoot ratio (R/S) of rice (Figure 1L), with an obvious effect under dry cultivation.

Sugar is a source of energy and an important osmotic regulator. In this study, Si application increased the sugar content under flooding and dry farming conditions (Figures 1M–O). The soluble sugar, sucrose, and fructose content increased by 4.39, 21.57, and 10.10%, respectively in leaves and 15.63, 45.88%, and 60.36, respectively in roots after Si application compared with no Si in dry cultivation. These observations indicate a more significant effect of Si on the sugar content in the roots of rice under dry cultivation.

Influence of silicon on photosynthetic capacity of rice under dry cultivation

Furthermore, compared with the rice under flooding cultivation, the net photosynthetic rate of dry farming rice from 17.13 μmol m^{-2} s^{-1} decreased to 11.54 μmol m^{-2} s^{-1}. The stomatal conductivity (Gs) showed a decreasing trend after drought cultivation. The decrease of photosynthetic rate may be due to the increase of stomatal limitation. However, Si application increased the net photosynthetic rate of rice under dry cultivation (Table 1). Compared with flooding cultivation, leaf intercellular CO_2 concentration (Ci) showed an increase of 17.18% after dry cultivation, but Ci decreased after Si application, indicating that Si can increase the carbon assimilation capacity of photosynthesis. The present study also found that net photosynthesis rate (Pn) was significantly and positively correlated with AMC (Pn/Ci), suggesting that AMC is more useful in rice research. In addition, Si application increased transpiration rate (Tr) of rice under dry cultivation, while it reduced the water-use efficiency (WUE) (Pn/Tr) of the leaves. The WUE of plants increased significantly and reached significant levels after Si application under both flooding and drought conditions. These observations indicate that appropriate Si levels can reduce the decline of WUE under drought cultivation, and a higher WUE can ensure better photosynthesis of rice leaves.

Transcriptomic responses in silicon-treated rice under dry cultivation show a unique pattern

Further, to dissect the differences in the transcripts of Si-treated rice under dry farming rice, an in-depth RNA-seq strategy was used to construct the global transcriptome profiles of the root and leaf tissues of dry farming rice grown with and without Si (X101SC21063706-Z01-J001-B1-16) (Supplementary Table 8). Samples were obtained at the 45 days after sowing under dry cultivation, these samples were used for the metabolome analysis also. The standards DESeq2 $p_{adj} \leq 0.05$ | log2FoldChange| ≥ 1.0 were used to recognize the DEGs in response to drought. Analysis of the transcriptome data identified 520 DEGs in the roots of rice with Si application compared to those without Si application; 329 genes were upregulated, and 191 were downregulated. Similarly, 1416 DEGs were identified in the leaves of rice with Si application compared to those without Si; 1024 genes were upregulated and 392 were downregulated (Figure 2A). The samples were clustered together based on genes that showed similar expression patterns, the RNA-seq data were subjected to hierarchical clustering. Heatmap illustrating the Si-treated rice differed significantly from the no Si-treated rice under dry cultivation at the transcription levels also both in the roots and in the leaves (Figure 2B).

To gain insight into the biological processes of Si in response to drought stress, we analyzed the enrichment of gene ontology (GO) terms for DEGs. GO analysis revealed the top 10 enrichment categories for biological processes, cellular components, and molecular functions. The DEGs in

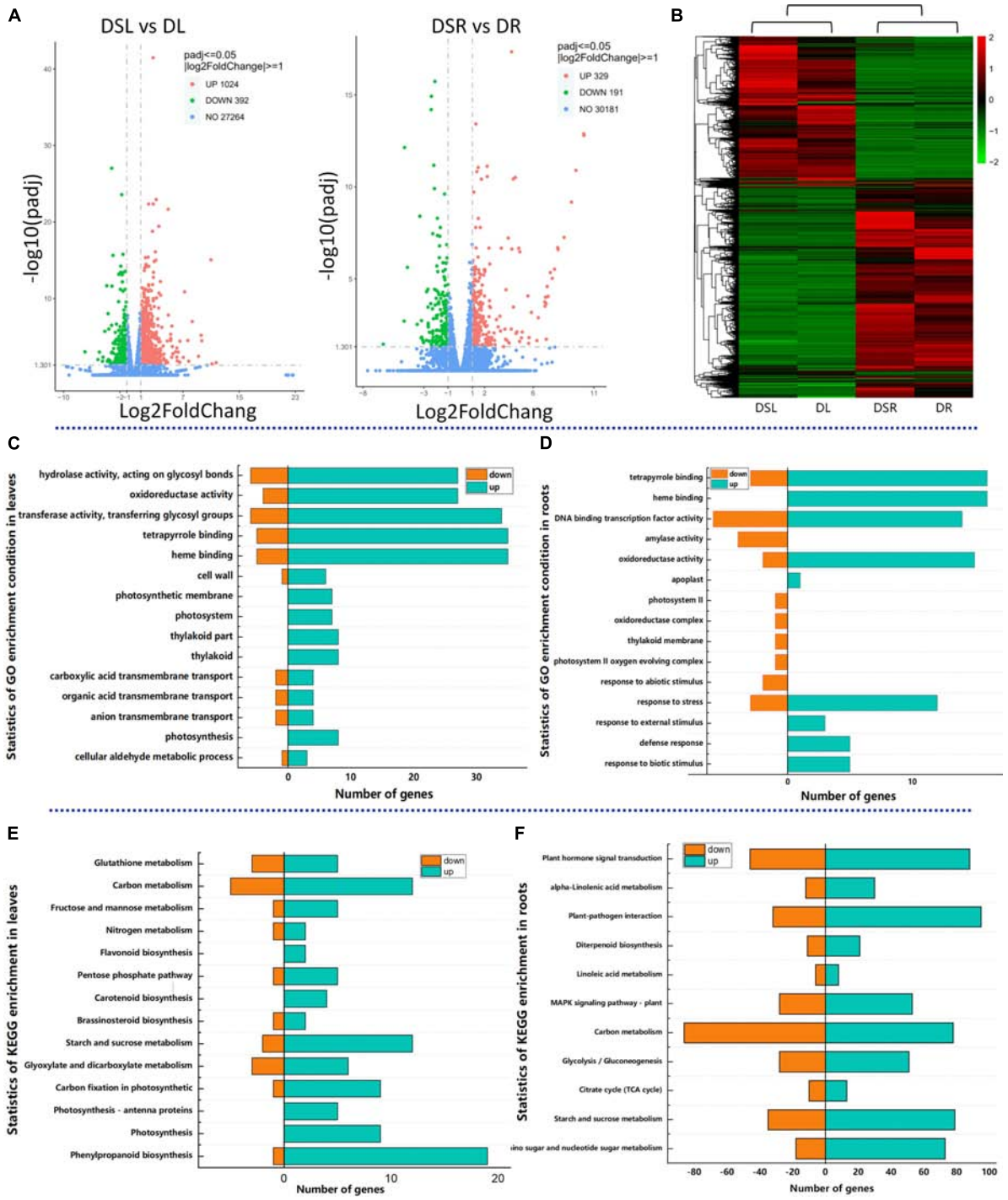


FIGURE 2
Analysis of effect of Si on the transcriptome of rice under dry cultivation. Volcano plots of differentially expressed genes (DEGs). DEGs in leaves (left) and roots (right). The horizontal coordinate shows the log2FoldChange value, and the vertical coordinate shows the −log10 p_{adj} or −log10 p-value. The blue dashed line indicates the threshold line for the differential gene screening criteria; Upregulated genes are in red, and downregulated genes are in blue **(A)**; Cluster dendrogram of differentially expressed genes in Si-treated and no Si-treated rice under dry cultivation **(B)**; GO enrichment with DEGs of leaves **(C)**; GO enrichment with DEGs of roots **(D)**; KEGG enrichment with DEGs of leaves **(E)**; KEGG enrichment with DEGs of roots **(F)**; The horizontal coordinate represents the ratio of the number of DEGs annotated in the GO/KEGG pathway, and the vertical coordinate represents the GO/KEGG pathway. DSL: Silicon-treated of rice under dry cultivation leaves; DL: Normal rice under dry cultivation leaves; DSR: Silicon-treated of rice under dry cultivation root; DR: Normal rice under dry cultivation roots.

the leaves and roots of dry farming rice treated with Si were enriched mainly in the biological process categories (Supplementary Table 1). We selected 15 GO enrichment processes for analysis. The significantly enriched GO terms of DEGs in DSL vs. DL were "oxidoreductase activity," "hydrolase activity," "tetrapyrrole binding," "photosynthesis" and anion "transmembrane transport" (Figure 2C). The GO terms of DEGs in DSR vs. DR were enriched in "DNA binding transcription factor activity," "amylase activity," and "defense response," except for "oxidoreductase activity" and "hydrolase activity" (Figure 2D).

Among the enriched GO terms, we observed that a large number of transcripts encoding transcription factors were differentially regulated after dry cultivation application of Si (570 transcription factors). The responsive transcription factors were grouped into several different families. These include WRKY, MYB, NAC, AP2 and bHLH, which play a key role in plant responses to abiotic stresses (Supplementary Table 2). In these families, the addition of Si, the larger part of these transcription factors in each cluster was upregulated.

The KEGG analysis revealed that most of the identified DEGs in the leaves were enriched in flavonoid biosynthesis, photosynthesis, carbon fixation in photosynthetic organisms and pentose phosphate pathway (Figure 2E), while in roots were enriched in amino sugar and nucleotide sugar metabolism, starch and sucrose metabolism, plant hormone signal transduction, and glutathione metabolism (Figure 2F). The results of GO and KEGG enrichment indicate that Si regulates various complex biological pathways of rice under dry cultivation.

Metabolomic adjustment of rice treated with silicon under dry cultivation conditions

Further, to assess the metabolic changes in rice under drought, a quasi-targeted metabolome analysis was performed. The unsupervised hierarchical cluster analysis revealed a clear separation of the metabolites of rice with and without Si treatment (Figure 3A). Meanwhile, the PCA explained 54.46% of the total variance (27.92 and 26.54% for PC1 and PC2, respectively) in leaves, and 53.6% of the total variance (32.28 and 21.32% for PC1 and PC2, respectively) in roots. The PCA showed precise separation on PC1 between treatments with and without Si. The biological replicates were distinguished by PC2 (Figures 3A,B). These results indicated that differences in the metabolic reactions between rice plants with and without Si treatment form the basis for Si to alleviate the damage of rice under dry cultivation.

A total of 1100 metabolites were detected in the leaves and root (Supplementary Table 3). These known metabolites in leaves belonged to 61 classes, with the majority belonging to amino acid and derivatives, benzene and substituted derivatives, coumarins and derivatives, flavonoids, phenylpropanoids, carbohydrates and its derivatives, and phytohormones. Similarly, 61 classes of metabolites were identified in the root, with the majority belonging to Alkaloids and Amino Acid and Derivatives, Carbohydrates and its Derivatives, Coumarins and derivatives, and Flavonoids and Phytohormones (Supplementary Table 3). Interestingly, the DAMs associated with Phytohormones and Carbohydrates and its derivatives were not differentially accumulated in DSL vs. DL. However, the DAMs related to Amino acid metabolism, Organic Acid and its derivatives, and flavonoid biosynthesis were all highly accumulated in DSL vs. DL and DSR vs. DR. The results suggest that Si induce changes in metabolites in rice under dry cultivation. Differentially accumulated metabolites (DAMs) with a FC $>$ 1.2, $P < 0.05$, and VIP $>$ 1 were screened. Then, to identify DAMs related to the process of Si alleviating drought stress in dry farming rice, the metabolites in leaves and roots were compared. Out of the total 1100 metabolites, 38 DAMs (23 upregulated and 15 downregulated) were identified from the DSL vs. DL comparison (Figure 3C); these metabolites belonged to 14 classes in leaves (Figure 3E; Supplementary Table 4). Meanwhile, 41 DAMs (31 upregulated and 10 downregulated) were identified from DSR vs. DR (Figure 3D; these belonged to 14 classes in roots (Figure 3F; Supplementary Table 4).

Further KEGG pathway analysis revealed that the differential metabolites were enriched in different pathways. Differential metabolites identified in the leaves between with and without Si treatments were involved in the secondary metabolome, carbon fixation in photosynthetic organisms, phenylalanine metabolism, flavonoid biosynthesis, carbon metabolism, and amino acid metabolism (Figure 3G; Supplementary Table 5). Differential metabolites identified in the roots between with and without Si treatments were involved in plant hormone signal transduction, purine metabolism, carbon metabolism, amino acid metabolism, and biosynthesis of secondary metabolites (Figure 3H; Supplementary Table 5).

Co-expression network analysis of differentially expressed genes and differentially accumulated metabolites in silicon-treated rice under dry cultivation

Gene-metabolite interaction networks are used to understand the functional relationships and identify novel regulatory pathways. Here, the differentially expressed genes and metabolites associated with photosynthetic carbon fixation and flavonoid biosynthesis were tested for Pearson correlation under Si treatment conditions (Pearson correlation coefficient >0.8 or <-0.8; P-value < 0.05;

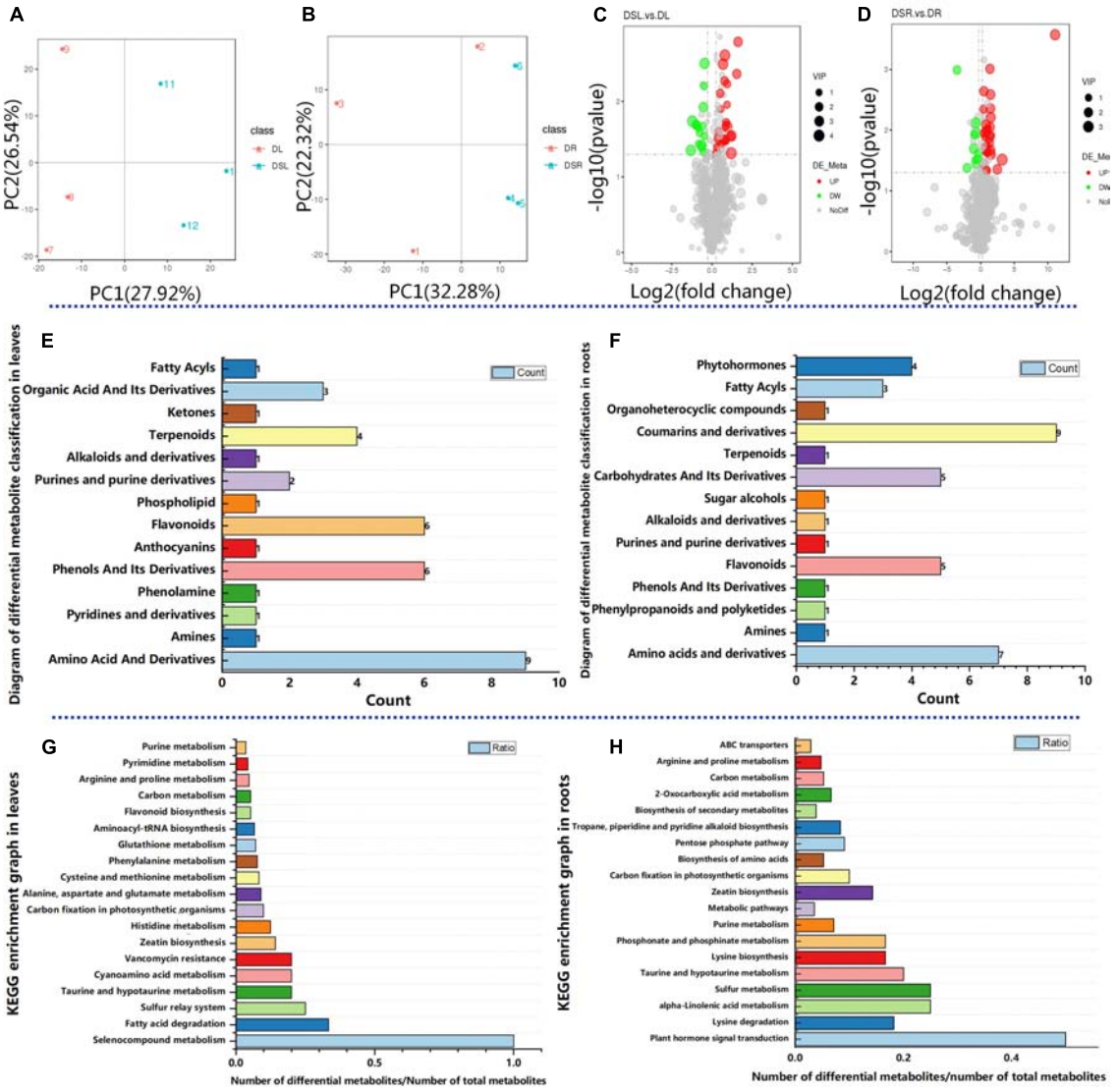


FIGURE 3
Effect of Si on quasi-targeted metabolomics in rice under dry cultivation. Principal component analysis (PCA) of metabolites in leaves **(A)** and roots **(B)**. The *X*-axis represents the first principal component (PC1), and the *Y*-axis represents the second principal component (PC2). Volcano plots for differentially accumulated metabolites (DAMs) from the leaves with and without Si treatment **(C)** and the roots with and without Si treatment **(D)**. Diagram of differential metabolite classification, with the horizontal coordinate showing the number of differential metabolites in the corresponding metabolic pathway and the vertical coordinate showing the corresponding metabolome classification in leaves **(E)** and roots **(F)**. Top KEGG enrichment results. The horizontal coordinate shows the number of differential metabolites in the corresponding metabolic pathway/the number of total metabolites identified in the pathway; the larger the value, the higher the enrichment of differential metabolites in the pathway in leaves **(G)** and roots **(H)**.

Figure 4; Supplementary Table 6). A significant positive correlation was observed between the genes related to photosystem II reaction center protein, photosystem I reaction center subunit, chlorophyll a-b binding protein, ribose-5-phosphate isomerase, fructose-bisphosphatase, and ribulose bisphosphate carboxylase and metabolites, such as erythrose 4-phosphate, fructose, galactose, and sedoheptulose anhydride in DSL vs. DL. In DSL and DL, a different pattern of regulation was observed compared to the photosynthesis-related DEGs and DAMs, providing additional evidence that the efficiency of photosynthesis differed between the treatments.

To further analyze the impact of Si on the genes and metabolites related to secondary metabolism in rice under dry cultivation, the interaction of DEGs and DAMs related to flavonoid biosynthesis was analyzed. For flavonoid biosynthesis, Pearson correlation analysis was performed for four DEGs and four DAMs related to flavonoids biosynthesis in leaves (Figure 4;

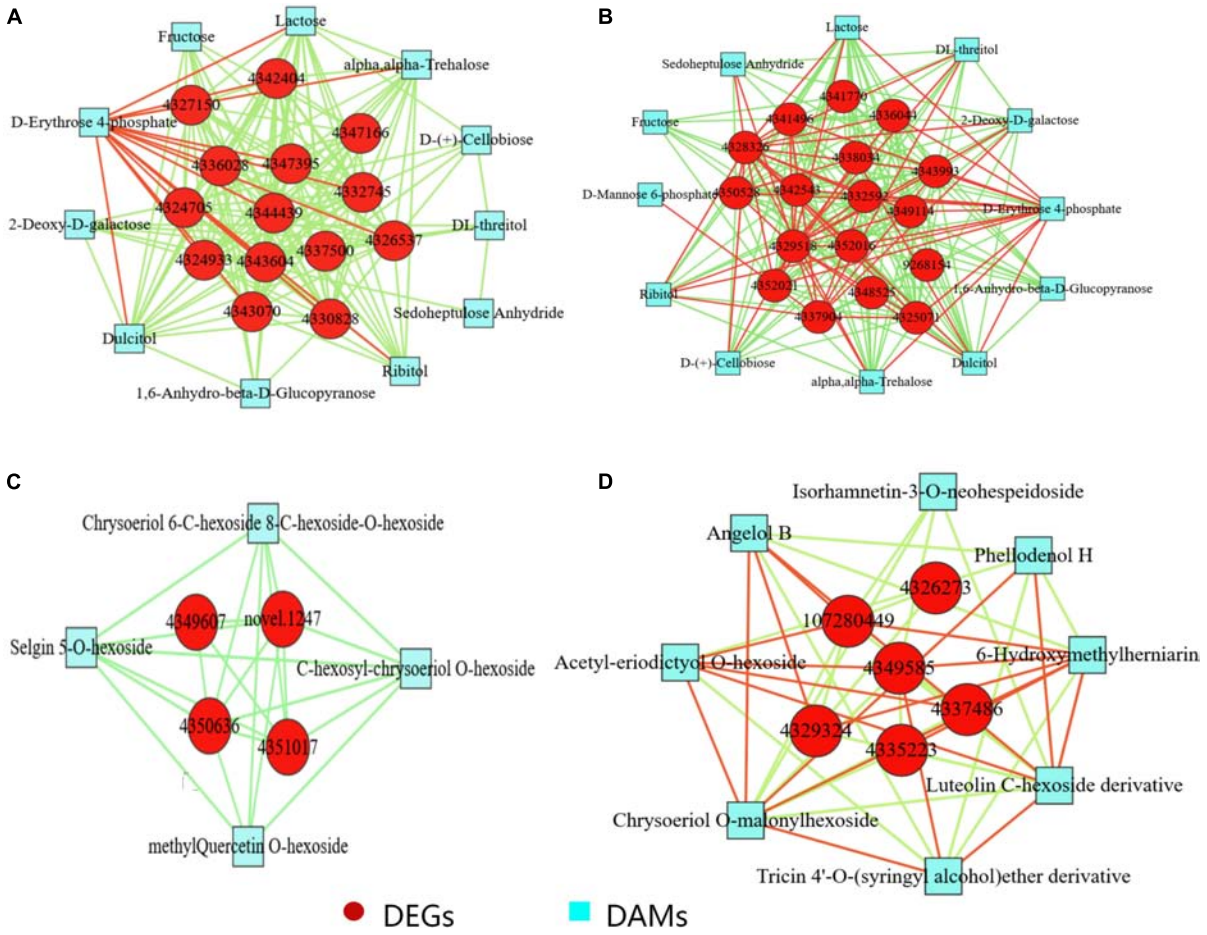


FIGURE 4
Co-expression analysis of DEGs and DAMs based on Pearson correlation coefficient. Interaction network of DEGs and DAMs involved in **(A)** photosynthesis in DSL vs. DL, 4326537, 4324933, 4337500, 4332745, 4327150, photosystem II gene; 4344439 ferredoxin gene; 4342404, 4347395, 4343070, 4330828, 4347166, photosystem I genes; 4343604, 4336028, 4324705, chlorophyll a-b binding protein. **(B)** Carbon metabolism in DSL vs. DL, 4329518, acetyl-coenzyme A synthetase; 4343993, malate dehydrogenase chloroplastic; 4325071, 4341770, fructose-bisphosphatase; 4341496, fructose-bisphosphate aldolase; 4350528, 6-phosphogluconate dehydrogenase; 4352021, 4328326, 4352016, ribulose bisphosphate carboxylase; 4342543, ribose-5-phosphate isomerase 4332592, acetate/butyrate–CoA ligase 4337904, acyl-coenzyme A oxidase; 4336044, glyceraldehyde-3-phosphate dehydrogenase; 9268154, malate synthase; 4349114, glycine cleavage system; 4348525, alanine aminotransferase 2; 4338034, 6-phosphofructokinase. **(C)** Flavonoid biosynthesis in DSL vs. DL, 4350636, novel.1247, chalcone synthase 1; 4349607, 4351017, chalcone–flavanone isomerase 3. **(D)** Flavonoid biosynthesis in DSR vs. DR. 4335223, cinnamyl alcohol dehydrogenase 6; 4349585, 4337486, cationic peroxidase; 4329324, cytochrome P450 CYP73A100; 107280449, 4326273, peroxidase. Red circles indicate differential genes, and blue squares indicate differential metabolites; Edges colored in "red" and "green" represent positive and negative correlations, respectively, based on Pearson correlation coefficient >0.8 and <−0.8, respectively.

Supplementary Table 6). The DEGs showed strong positive correlation (R^2 > 0.8 or <−0.8 and P-value < 0.05) with metabolites in leaves (Supplementary Table 6). For example, a significant positive correlation between the genes such as chalcone synthase 1 and chalcone–flavanone isomerase 3 and the metabolites such as chrysoeriol 6-C-hexoside 8-C-hexoside-O-hexoside, selgin 5-O-hexoside, C-hexosyl-chrysoeriol O-hexoside, and methyl quercetin O-hexoside in leaves. In roots, six DEGs related to flavonoids biosynthesis, cinnamyl alcohol dehydrogenase 6, and cytochrome P450 CYP73A100 were found to be upregulated in DSR. Moreover, the luteolin C-hexoside derivative, chrysoeriol O-malonylhexoside, acetyl-eriodictyol O-hexoside, and few coumarins and the downstream metabolites related to flavonoids biosynthesis were found to be accumulated in DSR.

Quantitative real-time PCR validation of differentially expressed genes in silicon-treated rice under dry cultivation

Finally, to validate our RNA-Seq data, quantitative RT-PCR (qRT-PCR) was performed on 16 DEGs (Figure 5;

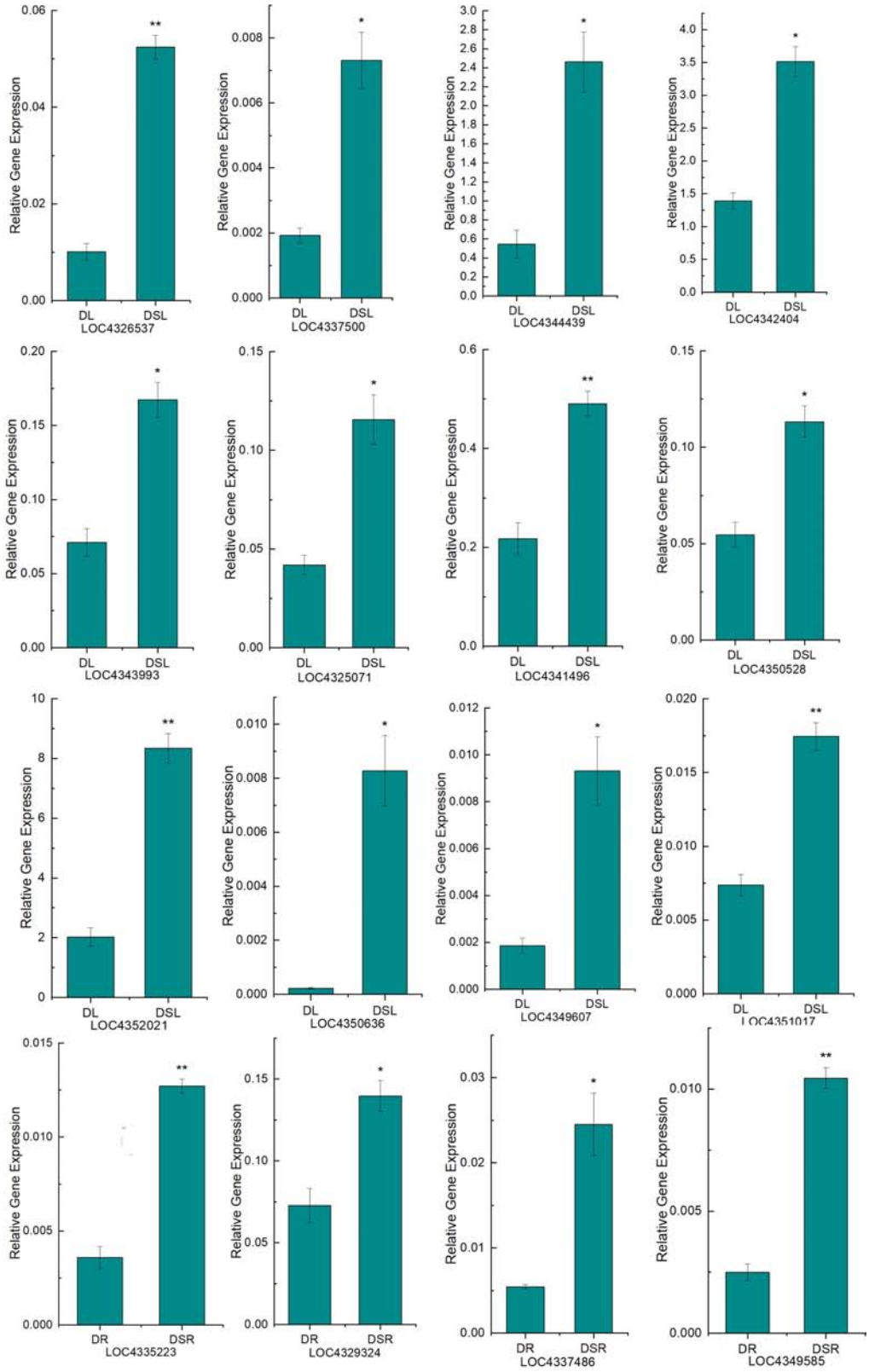


FIGURE 5
Quantitative real-time PCR (qRT-PCR) analysis of DEGs. The *X*-axis represents the treatment, and the *Y*-axis represents the relative expression of genes. DSL: Silicon-treated of rice under dry cultivation leaves; DL: Normal rice under dry cultivation leaves; DSR: Silicon-treated of rice under dry cultivation root; DR: Normal rice under dry cultivation roots. $^{*}P < 0.05$, $^{**}P < 0.01$.

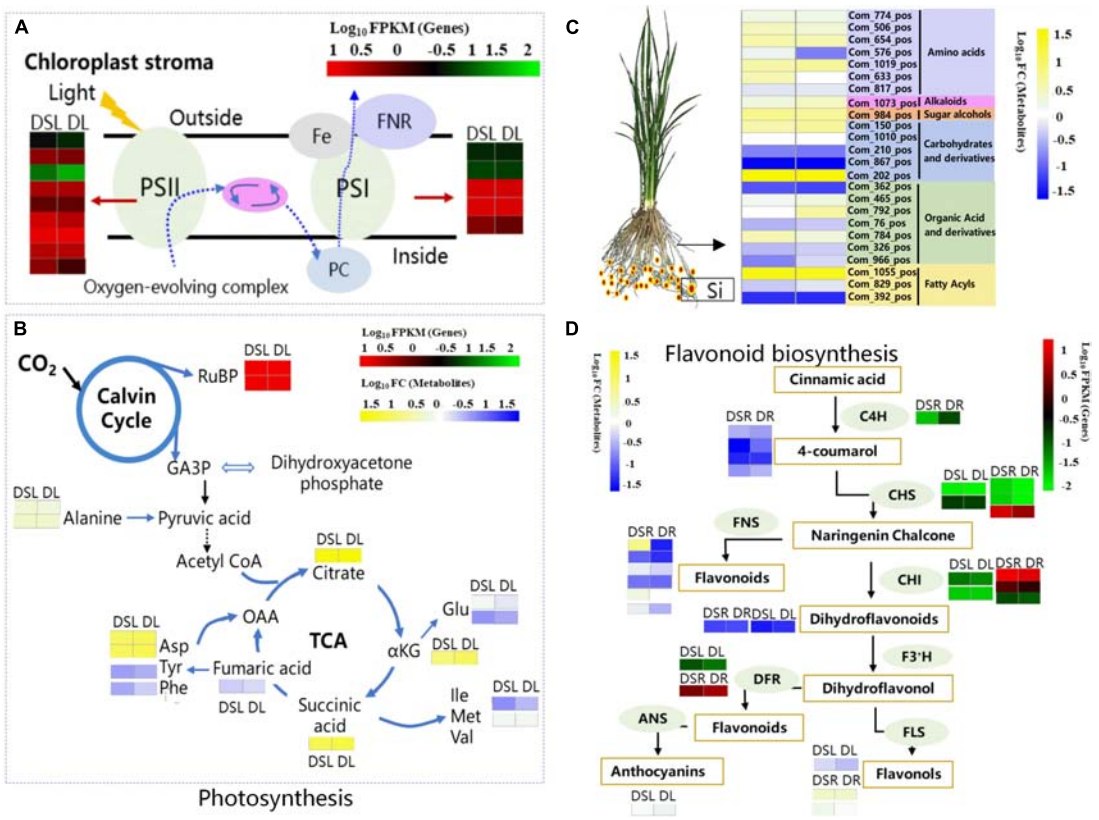


FIGURE 6
Summary model of metabolic processes regulated by Si on rice under dry cultivation. **(A)** Effect of Si on light reaction of rice leaves under dry cultivation. The DEGs in leaves and roots by the shade of red to green according to the color scale. **(B)** Effect of Si on the Calvin cycle of rice leaves under dry cultivation. The DEGs by the shade of red to green according to the color scale. The DAMs by the shade of yellow to blue according to the color scale. **(C)** Osmoregulation based on differential metabolites in roots. The DAMs by the shade of yellow to blue according to the color scale. **(D)** Flavonoid biosynthesis. The DEGs by the shade of red to green according to the color scale. The DAMs by the shade of yellow to blue according to the color scale in leaves and roots. C4H, cinnamic acid 4-hydroxylase; CHS, chalcone synthase; CHI, chalcone isomerase; F3′H, flavonoid 3′-hydroxylase; DFR, dihydroflavonol 4-reductase; ANS, leucoanthocyanidin dioxygenase; FLS, flavonol synthase.

Supplementary Table 7) related to photosynthetic metabolism and flavonoid biosynthesis. These genes showed similar expression patterns in RNA-seq (FPKM) and qRT-PCR analyses, verifying the reproducibility and credibility of RNA-seq data.

Discussion

Positive role of silicon in rice under dry cultivation production

Dry cultivation of rice is a cropping pattern different from transplanted rice and helps save water and improve labor efficiency (Jiang et al., 2021). Rice under dry cultivation changes the living environment and is susceptible to biotic and abiotic stresses. Therefore, overcoming these limitations, improve rice adaptability under dry cultivation conditions and improving yields has been a major research topic. Silicon (Si) has been shown to play an important role in enhancing plant resistance to environmental stresses and improving plant growth and development (Ma et al., 2007; Ma and Yamaji, 2008). Usually, the Si could strengthen the membranes of plant cells by depositing around the cell walls and changing their permeability to various stresses such as salt and drought (Zhang et al., 2017). Chen et al. (2011) demonstrated that Si application to rice under drought stress increased total root length, root surface area, and biomass production. Nolla et al. (2012) and Ibrahim et al. (2018) reported that the application of Si to rice under drought stress increased plant height, biomass, and grain yield. The present study's observations are consistent with most of these earlier results. Here, the application of Si had a significant effect on rice under dry cultivation; the root length, root volume and numbers were higher in the drought and flooding treatments with Si application than in the non-Si treatment. Additionally, applying Si in dry farming improved the yield (Su et al., 2022). The transcriptome and metabolome sequencing was performed to elucidate the mechanisms of Si regulation of adaptation in

rice under dry cultivation. Under dry cultivation, Si treatment resulted in 520 DEGs in the root, including 329 upregulated and 191 downregulated ones, and 1416 DEGs in leaves, including 1024 upregulated and 392 downregulated ones. Moreover, 38 DAMs (23 upregulated and 15 downregulated) were identified from the DSL vs. DL comparison and 41 DAMs (31 upregulated and 10 downregulated) from the DSR vs. DR comparison. These observations indicate that Si could regulate the gene expression and metabolite accumulation of rice under dry cultivation. The effect of Si on the transcriptome and metabolome also has been investigated in several studies, such as under non-stress conditions, the effect of Si was minimal, a result confirmed in wheat and soybean (Watanabe et al., 2004; Rasoolizadeh et al., 2018). In contrast, the transcriptome recovered to control levels after adding Si under biotic and abiotic stress conditions (Zhu et al., 2019; Jonas et al., 2015). Supplementation of Si also affects gene expression levels. For example, Si alleviates stressful conditions in rice by regulating Cd transporter expression levels (Ma et al., 2015), downregulating jasmonic acid (JA) biosynthesis (Kim et al., 2014), downregulating OsZIP1 gene expression (Huang and Ma, 2020).

Silicon improved the photosynthesis and carbon assimilation in rice under dry cultivation

Photosynthesis is one of the major metabolic pathways affected after silicon application; it is also the key physiological phenomena affected by drought stress (Farooq et al., 2009). During drought, the stomata close, reducing the availability of CO_2 and making plants more susceptible to damage (Lawlor and Cornic, 2002). A similar phenomenon was observed under heat stress, which reduced the activity of photosystem II (Camejo et al., 2005) and impaired the regenerative capacity of RuBP (Wise et al., 2004). Ma X. et al. (2016) found that chloroplast genes showed similar expression patterns, providing evidence for different photosynthetic efficiencies in the two rice cultivars (Ma X. et al., 2016). Li et al. (2020) screened the transcriptomic data corresponding to photosynthesis pathway and found that the drought-responsive DEGs related to photosynthesis included those encoding PS II, PS I, and chlorophyll a/b-binding proteins. Meanwhile, nine PSII genes and eight PSI genes were downregulated under drought stress in rose leaves (Li et al., 2020). In this study, three chlorophyll a/b-binding protein genes, five PSII genes, five PSI genes, one ferredoxin gene, and two RuBP carboxylase gene were upregulated in rice under dry cultivation after Si treatment in DSL, while they were downregulated in DL (**Figures 6A,B**). Additionally, Si application increased the photosynthetic efficiency and enhanced the net photosynthetic capacity of rice under dry conditions (**Table 1**), this observation is consistent with the higher relative photosynthesis rate measured in DSL than DL. All these results showed that photosynthesis increased or remained good in the Si treatment, which reasonably explains why Si produced relatively high yields in the dry cultivation.

Effect of silicon on osmoregulation in rice under dry cultivation

Osmoregulation is an important mechanism that allows plants to adapt to stress. Plants can survive longer and maintain metabolic processes in dry soil if osmoregulation occurs. Many substances, including inorganic cations and anions, organic acids, carbohydrates, and amino acids, contribute to osmoregulation (Sanders and Arndt, 2012). Ma X. et al. (2016) found 10 differential metabolites that significantly correlated with osmolality in drought-tolerant cultivar; osmotic adjustment improved drought tolerance in rice (Ma X. et al., 2016). In this study, 24 DAMs involved in amino acids and derivatives, carbohydrates and derivatives, organic acid, and fatty acyl were detected in DSR vs. DR (**Figure 6C**). In addition, the soluble sugar content of rice roots increased after Si application under dry cultivation (**Figure 1**). Soluble sugars play an important role in the osmoregulation of plants. In rice, Si maintains normal physiological and biochemical metabolism under dry conditions by regulating soluble sugars to increase the concentration of cytosol and reduce their osmotic potential. These results suggest that Si help maintain water uptake and cell turgor by accumulating large quantities of osmolytes, consequently maintaining the growth of rice under dry cultivation.

Silicon improved the flavonoids biosynthesis in rice under dry cultivation

Flavonoids are a group of polyphenol compounds with antioxidant activities. Researchers have suggested that the accumulation of such substances could be a key step in regulating plant tolerance to different environmental stresses (Wang P. Q. et al., 2018; Chen et al., 2019). Gai et al. (2020) showed that exogenous ABA significantly affects the expression of genes involved in flavonoid biosynthesis; it also increased the content of flavonoids, anthocyanins, flavonols, and isoflavones and improved drought tolerance of tea (Gai et al., 2020). Raza et al. (2021) identified many DAMs closely associated with DEGs in various cold-tolerant oilseed rape varieties based on a combined transcriptome and metabolome analysis (Raza et al., 2021). Sun et al. (2021), based on transcriptome and metabolome analyses, revealed that DEGs were induced in both high and low phosphorus conditions in apple leaves and roots, and metabolome analysis revealed that the levels of amino acids and their derivatives, organic acids, and flavonoids were higher in roots under low P stress than in those under controlled growth conditions (Sun et al., 2021).

Research has revealed that C4H, the second enzyme of the plant phenylpropanoid pathway, is involved in the drought defense of cucumber (Bellés et al., 2008) and the CHS from Abelmoschus esculentus regulated flavonoid accumulation and abiotic stress tolerance in transgenic Arabidopsis (Wang F. B. et al., 2018). A previous study also showed that the accumulation of quercetin and kaempferol under water deficit improved the drought tolerance of white clover (Lee et al., 2007). The main physiological functions of quercetin, kaempferol, luteolin C-hexoside derivative, and myricetin in plants were scavenging ROS and detoxifying free radicals (Yamasaki et al., 1997; Tattini et al., 2005; Iracema et al., 2007). Si application also upregulated the expression level of genes involved in flavonoid biosynthesis under drought stress (Ma D. Y. et al., 2014, 2016) thus protecting plants from drought affect. The present study found that C4H, CHS, CHI, DFR, and FLS genes were upregulated in DSL or DSR (**Figure 6D**). Meanwhile, three DAMs closely associated with differentially expressed genes (DEGs) were identified in DSL, and 13 DAMs, such as methyl quercetin, luteolin, angelol, and phellodenol, closely associated with DEGs in DSR. The accumulation of these flavonoids and derivatives is important during an environmental stress response. Flavonoids have been reported to play a role in the maintenance of ROS homeostasis (Chen et al., 2019; Mavrič Čermelj et al., 2021) also. In the present study, higher ROS levels (H_2O_2 and O_2^- activity) were also detected in rice under dry cultivation compared with flooding treatment (**Figure 1**). Meanwhile, Si supplementation increased flavonoid-related gene expression and metabolite accumulation and reduced H_2O_2 and O_2^- content in leaves. Moreover, to combat ROS attacks, plants recruit an impressive array of non-enzymatic and enzymatic antioxidants whose function is to maintain an adequate balance of ROS. Studies have shown that the application of Si can regulate ROS production during stress (Zhang et al., 2006) and increase these enzymatic activities in plants exposed to abiotic and biotic stresses (Liang et al., 2007). Ma D. Y. et al. (2016) found that Si application enhanced the expression of antioxidant enzyme coding genes in plants during drought stress which in turn help to reduce accumulation of H_2O_2 (Ma D. Y. et al., 2016). Silicon has significantly reduced O_2^- and H_2O_2 (**Figures 1E,F**) by increasing SOD, POD, and CAT activities (**Figure 1G**) under both dry and flooding treatment. MDA and electrical conductivity serve as indicators of the extent of oxidative damage in stressed plants (Munns and Tester, 2008). Here, Si significantly reduced MDA content and electrical conductivity. As mentioned previously, ROS accumulation under dehydration decreases photosynthetic capacity (Chaves et al., 2009; Saibo et al., 2009). Si treatment improved ROS scavenging capacity, increased photosynthetic efficiency, and enhanced net photosynthetic capacity under dry conditions (**Table 1**). Therefore, we hypothesized that Si could regulate the adaptation of rice under dry cultivation by regulating the expression of flavonoid-related genes and accumulation of metabolites in the above-ground and below-ground parts to improve ROS scavenging ability, enhance membrane stability, and promote photosynthetic capacity and osmoregulation levels.

Conclusion

The existing literature, reports of the benefits of silicon have proliferated of rice under flooded cultivation. Most of these studies typically focused on the impact of Si on drought, heat, cold, salt stress and metal toxicity and pathogens for recent reviews. However the role of Si in rice under dry cultivation has been little reported. The present study via physiological response combined with transcriptional and metabolic analyses found a positive influence of Si on aboveground and belowground parts rice under dry cultivation. Silicon is actively involved in physiological processes under dry cultivation and significantly improved photosynthetic performance and antioxidant enzyme activity and subsequently reduced lipid peroxidation of plant. Combined transcriptome and metabolome analyses revealed that Si upregulating flavonoid biosynthetic pathways in leaves and roots as well as osmoregulation in roots. These changes improved root parameters, nutrient uptake and transport, promoted root growth; while DEGs associated with photosynthesis were upregulated after Si treatment, enhancing photosynthesis and leading to increased organic matter production. Overall, these results emphasize that Si promotes the growth of rice under dry cultivation by coordinating the physiological metabolic processes of above- and belowground parts to enhance adaptation to stressful environments, and these findings also suggest that Si application is a feasible strategy to response to stress and will also promote further extension and application of rice under dry cultivation.

Data availability statement

The datasets presented in this study can be found in online repositories. The names of the repository/repositories and accession number(s) can be found below: NCBI - PRJNA847389.

Author contributions

X-SW and Z-HWu designed and supervised the project. HJ and X-SW analyzed the transcriptome metabolome data and wrote the manuscript. ZS, Q-WS, and Z-HWe participated in the determination of physiological indexes. W-CL and Z-XJ participated in the material preparation. PT, XY, Z-HWa, and M-YY revised the manuscript. Z-HWa analyzed the

transcriptomic and metabolomic data. All authors discussed the results and commented on the manuscript.

Funding

This study was supported by the following funding sources: Jilin Science and Technology Development Plan Project (20210509013RQ, 20190301061NY, 20210101045JC, and 20200403016SF).

Acknowledgments

We thank to researcher Shoujun Nie of Suihua Branch of Heilongjiang Provincial Academy of Agricultural Sciences for providing experimental materials.

Conflict of interest

The authors declare that the research was conducted in the absence of any commercial or financial relationships that could be construed as a potential conflict of interest.

Publisher's note

All claims expressed in this article are solely those of the authors and do not necessarily represent those of their affiliated organizations, or those of the publisher, the editors and the reviewers. Any product that may be evaluated in this article, or claim that may be made by its manufacturer, is not guaranteed or endorsed by the publisher.

Supplementary material

The Supplementary Material for this article can be found online at: https://www.frontiersin.org/articles/10.3389/fpls.2022.967537/full#supplementary-material

SUPPLEMENTARY TABLE 1
Gene ontology (GO) enrichment with DEGs of leaves and root in detail.

SUPPLEMENTARY TABLE 2
Details of leaf and root transcription factors in GO enrichment.

SUPPLEMENTARY TABLE 3
A total of 1100 metabolites were detected in the leaves and root, respectively.

SUPPLEMENTARY TABLE 4
All differential metabolites detected in leaves and roots.

SUPPLEMENTARY TABLE 5
Top KEGG enrichment results in leaves and roots in detail.

SUPPLEMENTARY TABLE 6
Co-expression analysis of DEGs and DAMs based on Pearson correlation coefficient associated with photosynthetic carbon fixation and flavonoid biosynthesis.

SUPPLEMENTARY TABLE 7
Primers used for quantitative RT-PCR analysis.

SUPPLEMENTARY TABLE 8
Original sequence read item.

References

Adekoya, M. A., Liu, Z., Vered, E., Zhou, L. G., Kong, D. Y., Qin, J. Y., et al. (2014). Agronomic and ecological evaluation on growing water-saving and drought-resistant rice (*Oryza sativa* L.) through drip irrigation. *J. Agric. Sci.* 6, 110–119. doi: 10.5539/jas.v6n5p110

Bellés, J. M., López-Gresa, M. P., Fayos, J., Pallás, V., Rodrigo, I., and Conejero, V. (2008). Induction of cinnamate 4-hydroxylase and phenylpropanoids in virus-infected cucumber and melon plants. *Plant Sci.* 174, 524–533. doi: 10.1016/j.plantsci.2008.02.008

Brennan, T., and Frenkel, C. (1977). Involvement of hydrogen peroxide in the regulation of senescence in pear. *Plant Physiol.* 59, 411–416. doi: 10.1104/PP.59.3.411

Camejo, D., Rodriguez, P., Morales, M. A., Dell'amico, J. M., Torrecillas, A., and Alarcon, J. J. (2005). High temperature effects on photosynthetic activity of two tomato cultivars with different heat susceptibility. *Plant Physiol.* 162, 281–289. doi: 10.1016/j.jplph.2004.07.014

Chain, F., Côté-Beaulieu, C., Belzile, F., Menzies, J. G., and Bélanger, R. R. (2009). A comprehensive transcriptomic analysis of the effect of silicon on wheat plants under control and pathogen stress conditions. *Mol. Plant Microbe Interact.* 22, 1323–1330. doi: 10.1094/MPMI-22-11-1323

Chaves, M. M., Flexas, J., and Pinheiro, C. (2009). Photosynthesis under drought and salt stress: regulation mechanisms from whole plant to cell. *Ann. Bot.* 103, 551–560. doi: 10.1093/aob/mcn125

Chen, S., Wu, F. Y., Li, Y. T., Qian, Y. L., Pan, X. H., Li, F. X., et al. (2019). NtMYB4 and NtCHS1 are critical factors in the regulation of flavonoid biosynthesis and are involved in salinity responsiveness. *Front. Plant Sci.* 10:178. doi: 10.3389/fpls.2019.00178

Chen, W., Yao, X. Q., Cai, K. Z., and Chen, J. N. (2011). Silicon alleviates drought stress of rice plants by improving plant water status, photosynthesis and mineral nutrient absorption. *Biol. Trace Elem. Res.* 142, 67–76. doi: 10.1007/s12011-010-8742-x

Clarke, J. M., and Mccaig, T. N. (1982). Evaluation of techniques for screening for drought resistance in wheat. *Crop Sci.* 22, 503–506. doi: 10.2135/cropsci1982.0011183X002200030015x

Coskun, D., Deshmukh, R., Sonah, H., Menzies, J. G., Reynolds, O., Ma, J., et al. (2019). The controversies of silicon's role in plant biology. *New Phytol.* 221, 67–85. doi: 10.1111/nph.15343

Farooq, M., Wahid, A., Basra, S. M. A., and Din, I. U. (2009). Improving water relations and gas exchange with brassinosteroids in rice under drought stress. *Agron. Crop Sci.* 195, 262–269. doi: 10.1111/j.1439-037X.2009.00368.x

Gai, Z. S., Wang, Y., Ding, Y. Q., Qian, W. J., Qiu, C., Xie, H., et al. (2020). Exogenous abscisic acid induces the lipid and flavonoid metabolism of tea plants under drought stress. *Sci. Rep.* 10:12275. doi: 10.1038/s41598-020-69080-1

Garg, A. K., Kim, J. K., Owens, T. G., Ranwala, A. P., Choi, Y. D., Kochian, L. V., et al. (2003). Trehalose accumulation in rice plants confers high tolerance levels to different abiotic stresses. *Proc. Natl. Acad. Sci. U.S.A.* 99, 15898–15903. doi: 10.1073/pnas.252637799

Gong, J. L., Xing, Z. P., Ya-Jie, H. U., Zhang, H. C., Dai, Q. G., Huo, Z. Y., et al. (2014). Difference of root morphological and several physiological characteristics

between indica and japonica super rice varieties. *Acta Agron. Sin.* 40, 1066–1080. doi: 10.3724/SP.J.1006.2014.01066

Guo, R., Shi, L. X., Jiao, Y., Li, M. X., Zhong, X. L., Gu, F. X., et al. (2018). Metabolic responses to drought stress in the tissues of drought-tolerant and drought-sensitive wheat genotype seedlings. *AoB Plants* 10:ply016. doi: 10.1093/aobpla/ply016

Gupta, A., Rico-Medina, A., and Caño-Delgado, A. I. (2020). The physiology of plant responses to drought. *Science* 368, 266–269. doi: 10.1126/science.aaz7614

Haddad, C., Trouverie, J., Arkoun, M., Yvin, J. C., Caïus, J., Brunaud, V., et al. (2019). Silicon supply affects the root transcriptome of *Brassica napus* L. *Planta* 249, 1645–1651. doi: 10.1007/s00425-019-03120-7

Holz, S., Kube, M., Bartoszewski, G., Huettel, B., and Büttner, C. (2015). Initial studies on cucumber transcriptome analysis under silicon treatment. *Silicon* 11, 2365–2369. doi: 10.1007/s12633-015-9335-2

Hu, H. H., and Xiong, L. Z. (2014). Genetic engineering and breeding of drought-resistant crops. *Annu. Rev. Plant Biol.* 65, 715–741. doi: 10.1146/annurev-arplant-050213-040000

Huang, S., and Ma, J. (2020). Silicon suppresses zinc uptake through down-regulating zinc transporter gene in rice. *Physiol. Plant.* 170, 580–591. doi: 10.1111/ppl.13196

Huang, S., Yamaji, N., Sakurai, G., Mitani-Ueno, N., Konishi, N., and Ma, J. (2022). A pericycle-localized silicon transporter for efficient xylem loading in rice. *New Phytol.* 234, 197–208. doi: 10.1111/NPH.17959

Ibrahim, M. A., Merwad, A. R. M., and Elnaka, E. A. (2018). Rice (*Oryza sativa* L.) tolerance to drought can be improved by silicon application. *Commun. Soil Sci. Plant Anal.* 49, 945–957. doi: 10.1080/00103624.2018.1448856

Iracema, B., Maria, A. A., Pedro, R., Victor, D. F., Pedro, M. F., Nuno, M., et al. (2007). Quercetin increases oxidative stress resistance and longevity in *Saccharomyces cerevisiae*. *J. Agric. Food Chem.* 55, 2446–2451. doi: 10.1021/JF063302E

Jiang, H., Thobakgale, T., Li, Y. Z., Liu, L. W., Su, Q. W., Cang, B. F., et al. (2021). Construction of dominant rice population under dry cultivation by seeding rate and nitrogen rate interaction. *Sci. Rep.* 11:7189. doi: 10.1038/s41598-021-86707-z

Jonas, V. B., Kathy, S., Ingvar, B., Shoshi, K., Takayuki, A., Monica, F., et al. (2015). Primary metabolism plays a central role in moulding silicon-inducible brown spot resistance in rice. *Mol. Plant Pathol.* 16, 811–824. doi: 10.1111/mpp.12236

Kim, Y., Khan, A., Waqas, M., Jeong, H., Kim, D., Shin, J., et al. (2014). Regulation of jasmonic acid biosynthesis by silicon application during physical injury to *Oryza sativa* L. *J. Plant Res.* 127, 525–532. doi: 10.1007/s10265-014-0641-3

Lawlor, D. W., and Cornic, G. (2002). Photosynthetic carbon assimilation and associated metabolism in relation to water deficits in higher plants. *Plant Cell Environ.* 25, 275–294. doi: 10.1046/j.0016-8025.2001.00814.x

Lee, B. R., Kim, K. Y., Jung, W. J., Avice, J. C., Ourry, A., and Kim, T. H. (2007). Peroxidases and lignification in relation to the intensity of water-deficit stress in white clover (*Trifolium repens* L.). *J. Exp. Bot.* 58, 1271–1279. doi: 10.1093/jxb/erl280

Li, W., Fu, L. F., Geng, Z. W., Zhao, X. J., Liu, Q. H., and Jiang, X. Q. (2020). Physiological characteristic changes and full-length transcriptome of rose (*Rosa chinensis*) roots and leaves in response to drought stress. *Plant Cell Physiol.* 61, 2153–2166. doi: 10.1093/pcp/pcaa137

Liang, Y. C., Sun, W. C., Zhu, Y. G., and Peter, C. (2007). Mechanisms of silicon-mediated alleviation of abiotic stresses in higher plants: a review. *Environ. Pollut.* 147, 422–428. doi: 10.1016/j.envpol.2006.06.008

Ling, F. L., Su, Q. W., Jiang, H., Cui, J. J., He, X., Wu, Z. H., et al. (2020). Effects of strigolactone on photosynthetic and physiological characteristics in salt-stressed rice seedlings. *Sci. Rep.* 10:6183. doi: 10.1038/s41598-020-63352-6

Livak, K. J., and Schmittgen, T. D. (2001). Analysis of relative gene expression data using real-time quantitative PCR and the 2(-Delta Delta C(T)) method. *Methods* 25, 402–408. doi: 10.1006/meth.2001.1262

Luo, L. (2010). Breeding for water-saving and drought-resistance rice (WDR) in China. *J. Exp. Bot.* 61, 3509–3517. doi: 10.1093/jxb/erq185

Luyckx, M., Hausman, J. F., Lutts, S., and Guerriero, G. (2017). Silicon and plants: current knowledge and technological perspectives. *Front. Plant Sci.* 8:411. doi: 10.3389/fpls.2017.00411

Ma, D. Y., Sun, D. X., Wang, C. Y., Li, Y. G., and Guo, T. C. (2014). Expression of flavonoid biosynthesis genes and accumulation of flavonoid in wheat leaves in response to drought stress. *Plant Physiol. Biochem.* 80, 60–66. doi: 10.1016/j.plaphy.2014.03.024

Ma, D. Y., Sun, D. X., Wang, C. Y., Qin, H. X., Ding, H. N., Li, Y., et al. (2016). Silicon application alleviates drought stress in wheat through transcriptional regulation of multiple antioxidant defense pathways. *J. Plant Growth Regul.* 35, 1–10. doi: 10.1007/s00344-015-9500-2

Ma, J., Cai, H. M., He, C. W., Zhang, W. J., and Wang, L. J. (2015). A hemicellulose-bound form of silicon inhibits cadmium ion uptake in rice (*Oryza sativa*) cells. *New Phytol.* 206, 1063–1107. doi: 10.1111/nph.13276

Ma, J., Chen, T., Lin, J., Fu, W., Feng, B., Li, G., et al. (2021). Functions of nitrogen, phosphorus and potassium in energy status and their influences on rice growth and development. *Rice Sci.* 29, 166–178. doi: 10.1016/j.rsci.2022.01.005

Ma, J. F. (2004). Role of silicon in enhancing the resistance of plants to biotic and abiotic stresses. *Soil Sci. Plant Nutr.* 50, 11–18. doi: 10.1080/00380768.2004.10408447

Ma, J. F., and Yamaji, N. (2006). Silicon uptake and accumulation in higher plants. *Trends Plant Sci.* 11, 392–397. doi: 10.1016/j.tplants.2006.06.007

Ma, J. F., and Yamaji, N. (2008). Functions and transport of silicon in plants. *Cell. Mol. Life Sci.* 65, 3049–3057. doi: 10.1007/s00018-008-7580-x

Ma, J. F., Yamaji, N., Mitani, N., Tamai, K., Konishi, S., Fujiwara, T., et al. (2007). An efflux transporter of silicon in rice. *Nature* 448, 209–212. doi: 10.1038/nature05964

Ma, X., Xia, H., Liu, Y., Wei, H., Zheng, X., Song, C., et al. (2016). Transcriptomic and metabolomic studies disclose key metabolism pathways contributing to well-maintained photosynthesis under the drought and the consequent drought-tolerance in rice. *Front. Plant Sci.* 7:1886. doi: 10.3389/fpls.2016.01886

Mauad, M., Costa, C., Nascente, A. S., Filho, H. G., and Lima, G. (2016). Effects of silicon and drought stress on biochemical characteristics of leaves of upland rice cultivars1. *Rev. Cienc. Agron.* 47, 532–539. doi: 10.5935/1806-6690.20160064

Mavrič Čermelj, A., Golob, A., VogelMikuš, K., and Germ, M. (2021). Silicon mitigates negative impacts of drought and UV-B radiation in plants. *Plants* 11:91. doi: 10.3390/PLANTS11010091

Mumtaz, M. Z., Saqib, M., Abbas, G., and Ul-Qamar, Z. (2020). Drought stress impairs grain yield and quality of different rice genotypes under field conditions by impaired photosynthetic attributes and K nutrition. *Rice Sci.* 27, 5–9. doi: 10.1016/j.rsci.2019.12.001

Munns, R., and Tester, M. (2008). Mechanisms of salinity tolerance. *Annu. Rev. Plant Biol.* 59, 651–681. doi: 10.1146/annurev.arplant.59.032607.092911

Nolla, A., Faria, R. J., Korndorfer, G. H., and Silva, T. R. B. (2012). Effect of silicon on drought tolerance of upland rice. *J. Food Agric. Environ.* 10, 269–272. doi: 10.1016/j.jcs.2011.10.005

Ranjan, A., Sinha, R., Bala, M., Pareek, A., Singla-Pareek, S. L., and Singh, A. K. (2021). Silicon-mediated abiotic and biotic stress mitigation in plants: underlying mechanisms and potential for stress resilient agriculture. *Plant Physiol. Biochem.* 163, 15–25. doi: 10.1016/J.PLAPHY.2021.03.044

Rasoolizadeh, A., Labbé, C., Sonah, H., Deshmukh, R. K., Belzile, F., Menzies, J. G., et al. (2018). Silicon protects soybean plants against *Phytophthora sojae* by interfering with effector-receptor expression. *BMC Plant Biol.* 18:97. doi: 10.1186/s12870-018-1312-7

Raza, A., Su, W., Hussain, M. A., Mehmood, S. S., Zhang, X., Cheng, Y., et al. (2021). Integrated analysis of metabolome and transcriptome reveals insights for cold tolerance in rapeseed (*Brassica napus* L.). *Front. Plant Sci.* 12:721681. doi: 10.3389/FPLS.2021.721681

Réthoré, E., Ali, N., Yvin, J. C., and Hosseini, S. A. (2020). Silicon regulates source to sink metabolic homeostasis and promotes growth of rice plants under sulfur deficiency. *Int. J. Mol. Sci.* 21:3677. doi: 10.3390/ijms21103677

Sadeghi, F., Samsampou, R. D., Seyahooei, M. A., Bagheri, A., and Soltani, J. (2020). Fungal endophytes alleviate drought-induced oxidative stress in mandarin (*Citrus reticulata* L.): toward regulating the ascorbate–glutathione cycle. *Sci. Hortic.* 261:108991. doi: 10.1016/j.scienta.2019.108991

Saibo, N., Tiago, L., and Margarida, O. M. (2009). Transcription factors and regulation of photosynthetic and related metabolism under environmental stresses. *Ann. Bot.* 103, 609–623. doi: 10.1093/aob/mcn227

Sairam, R. K., and Srivastava, G. C. (2002). Changes in antioxidant activity in sub-cellular fractions of tolerant and susceptible wheat genotypes in response to long term salt stress. *Plant Sci.* 162, 897–904. doi: 10.1016/S0168-9452(02)00037-7

Sanders, G. J., and Arndt, S. K. (2012). "Osmotic adjustment under drought conditions," in *Plant Responses to Drought Stress*, Vol. 8, ed. R. Aroca (Berlin: Springer), 199–229. doi: 10.1007/978-3-642-32653-0_8

Siriwach, R., Matsuda, F., Yano, K., and Hira, I. M. Y. (2020). Drought stress responses in context-specific genome-scale metabolic models of *Arabidopsis thaliana*. *Metabolites* 10:159. doi: 10.3390/metabo10040159

Su, Q. W., Cang, B. F., Bai, C. Y., Li, Y. Z., Song, Z., Li, J. C., et al. (2022). Effect of silicon application rate on yield and dry matter accumulation of rice under dry cultivation. *Chin. J. Rice Sci.* 36, 87–95. doi: 10.16819/j.1001-7216.2022.201208

Sun, T. T., Zhang, J. K., Zhang, Q., Li, X. L., Li, M. J., Yang, Y. Z., et al. (2021). Transcriptome and metabolome analyses revealed the response mechanism of apple to different phosphorus stresses. *Plant Physiol. Biochem.* 167, 639–650. doi: 10.1016/J.PLAPHY.2021.08.040

Tattini, M., Guidi, L., Morassi-Bonzi, L., Pinelli, P., Remorini, D., Degl'Innocenti, E., et al. (2005). On the role of flavonoids in the integrated mechanisms of response of Ligustrum vulgare and *Phillyrea latifolia* to high solar radiation. *New Phytol.* 167, 457–470. doi: 10.1111/j.1469-8137.2005.01442.x

Thorne, S., Stirnberg, P., Hartley, S., and Maathuis, F. (2022). The ability of silicon fertilisation to alleviate salinity stress in rice is critically dependent on cultivar. *Rice* 15:8. doi: 10.1186/S12284-022-00555-7

Valliyodan, B., and Nguyen, H. T. (2006). Understanding regulatory networks and engineering for enhanced drought tolerance in plants. *Curr. Opin. Plant Biol.* 9, 189–195. doi: 10.1016/j.pbi.2006.01.019

Wang, F. B., Ren, G., Li, F. S., Qi, S. T., Xu, Y., Wang, B. W., et al. (2018). A chalcone synthase gene AeCHS from *Abelmoschus esculentus* regulates flavonoid accumulation and abiotic stress tolerance in transgenic *Arabidopsis*. *Acta Physiol. Plant.* 40:97. doi: 10.1007/s11738-018-2680-1

Wang, P. Q., Zhang, L. J., Jiang, X. L., Dai, X. L., Xu, L. J., Li, T., et al. (2018). Evolutionary and functional characterization of leucoanthocyanidin reductases from *Camellia sinensis*. *Planta* 247, 139–154. doi: 10.1007/s00425-017-2771-z

Watanabe, S., Shimoid, E., Ohkamab, N., Hayashid, H., Yoneyamad, T., Yazakie, Y., et al. (2004). Identification of several rice genes regulated by Si nutrition. *Soil Sci. Plant Nutr.* 50, 1273–1276. doi: 10.1080/00380768.2004.10408603

Weller, S., Janz, B., Jörg, L., Kraus, D., Racela, H. S., Wassmann, R., et al. (2016). Greenhouse gas emissions and global warming potential of traditional and diversified tropical rice rotation systems. *Glob. Change Biol.* 22, 432–448. doi: 10.1111/gcb.13099

Wise, R. R., Olson, A. J., Schrader, S. M., and Sharkey, T. D. (2004). Electron transport is the functional limitation of photosynthesis in field-grown Pima cotton plants at high temperature. *Plant Cell Environ.* 27, 717–724. doi: 10.1111/j.1365-3040.2004.01171.x

Wu, L. L., Yu, Y. J., Tian, C., Zhang, L., Huang, J., Zhu, L. F., et al. (2022). Effects of different nitrogen application regimes on translocation of rice photosynthetic products and nitrogen under alternate wetting and drying irrigation. *Chin. J. Rice Sci.* 36, 295–307. doi: 10.16819/j.1001-7216.2022.210507

Xia, H., Huang, W. X., Xiong, J., Tao, T., Zheng, X. G., Wei, H. B., et al. (2016). Adaptive epigenetic differentiation between upland and lowland rice ecotypes revealed by methylation-sensitive amplified polymorphism. *PLoS One* 11:e0157810. doi: 10.1371/journal.pone.0157810

Xia, H., Zheng, X. G., Chen, L., Gao, H., Yang, H., Long, P., et al. (2014). Genetic differentiation revealed by selective loci of drought-responding EST-SSRs between upland and lowland rice in China. *PLoS One* 9:e106352. doi: 10.1371/journal.pone.0106352

Yamasaki, H., Sakihama, Y., and Ikehara, N. (1997). Flavonoid-peroxidase reaction as a detoxification mechanism of plant cells against H202. *Plant Physiol.* 115, 1405–1412. doi: 10.1104/pp.115.4.1397

Yin, L. N., Wang, S. W., Tanaka, K., Fujihara, S., Itai, A., Den, X. P., et al. (2016). Silicon-mediated changes in polyamines participate in silicon-induced salt tolerance in *Sorghum bicolor* L. *Plant Cell Environ.* 39, 245–258. doi: 10.1111/pce.12521

Yoo, Y. H., Kim, M., Chandran, A. K. N., Hong, W., Ahn, H. R., Lee, G. T., et al. (2019). Genome-wide transcriptome analysis of rice seedlings after seed dressing with *Paenibacillus yonginensis* DCY84T and silicon. *Int J Mol Sci.* 20:5883. doi: 10.3390/ijms20235883

Zhang, J. H., Liu, Y. P., Pan, Q. H., Zhan, J. C., Wang, X. Q., and Huang, W. D. (2006). Changes in membrane-associated H^+-ATPase activities and amounts in young grape plants during the cross adaptation to temperature stresses. *Plant Sci.* 170, 768–777. doi: 10.1016/j.plantsci.2005.11.009

Zhang, W. J., Xie, Z. C., Wang, L. H., Li, M., Lang, D. Y., and Zhang, X. H. (2017). Silicon alleviates salt and drought stress of *Glycyrrhiza uralensis* seedling by altering antioxidant metabolism and osmotic adjustment. *J. Plant Res.* 130, 611–624. doi: 10.1007/s10265-017-0927-3

Zheng, X. D., Li, Y. Q., Xi, X. L., Ma, C. Q., Sun, Z. J., Yang, X. Q., et al. (2020). Exogenous *Strigolactones alleviate* KCl stress by regulating photosynthesis, ROS migration and ion transport in *Malus hupehensis* Rehd. *Plant Physiol. Biochem.* 159, 113–122. doi: 10.1016/J.PLAPHY.2020.12.015

Zhu, Y. X., and Gong, H. J. (2013). Beneficial effects of silicon on salt and drought tolerance in plants. *Agron. Sustain. Dev.* 34, 455–472. doi: 10.1007/s13593-013-0194-1

Zhu, Y. X., Yin, J. L., Liang, Y. F., Liu, J. Q., Jia, J. H., Huo, H. Q., et al. (2019). Transcriptomic dynamics provide an insight into the mechanism for silicon-mediated alleviation of salt stress in cucumber plants. *Ecotoxicol. Environ. Saf.* 174, 245–254. doi: 10.1016/j.ecoenv.2019.02.075

frontiers | Frontiers in Plant Science

ORIGINAL RESEARCH
published: 04 August 2022
doi: 10.3389/fpls.2022.950064

Genome-Wide Identification and Functional Analysis of Polyamine Oxidase Genes in Maize Reveal Essential Roles in Abiotic Stress Tolerance

*Yan Xi†, Wenjing Hu†, Yue Zhou, Xiang Liu and Yexiong Qian**

Anhui Provincial Key Laboratory of Conservation and Exploitation of Important Biological Resources, College of Life Sciences, Anhui Normal University, Wuhu, China

OPEN ACCESS

Edited by:
Ji-Hong Liu,
Huazhong Agricultural University, China

Reviewed by:
Chenliang Yu,
Zhejiang Agriculture and Forestry University, China
Photini V. Mylona,
Hellenic Agricultural Organization (HAO), Greece

***Correspondence:**
Yexiong Qian
qyx2011@ahnu.edu.cn

†These authors have contributed equally to this work

Specialty section:
This article was submitted to Plant Abiotic Stress, a section of the journal Frontiers in Plant Science

Received: *22 May 2022*
Accepted: *21 June 2022*
Published: *04 August 2022*

Citation:
Xi Y, Hu W, Zhou Y, Liu X and Qian Y (2022) Genome-Wide Identification and Functional Analysis of Polyamine Oxidase Genes in Maize Reveal Essential Roles in Abiotic Stress Tolerance. Front. Plant Sci. 13:950064. doi: 10.3389/fpls.2022.950064

Polyamines (PAs) play a critical role in growth and developmental processes and stress responses in plants. Polyamine oxidase (PAO) is a flavin adenine dinucleotide (FAD)-dependent enzyme that plays a major role in PA catabolism. Here, for the first time, *PAO* genes in maize were screened for the whole genome-wide and nine *ZmPAO* genes were identified in this study, named as *ZmPAO1-9*. Based on structural characteristics and a comparison of phylogenetic relationships of *PAO* gene families from seven representative species, all nine PAO proteins in maize were categorized into three distinct subfamilies. Further, chromosome location and schematic structure revealed an unevenly distribution on chromosomes and evolutionarily conserved structure features of *ZmPAO* genes in maize, respectively. Furthermore, transcriptome analysis demonstrated that *ZmPAO* genes showed differential expression patterns at diverse developmental stages of maize, suggesting that these genes may play functional developmental roles in multiple tissues. Further, through qRT-PCR validation, these genes were confirmed to be responsive to heat, drought and salinity stress treatments in three various tissues, indicating their potential roles in abiotic stress responses. Eventually, to verify the biological function of *ZmPAO* genes, the transgenic *Arabidopsis* plants overexpressing *ZmPAO6* gene were constructed as a typical representative to explore functional roles in plants. The results demonstrated that overexpression of *ZmPAO6* can confer enhanced heat tolerance through mediating polyamine catabolism in transgenic *Arabidopsis*, which might result in reduced H_2O_2 and MDA accumulation and alleviated chlorophyll degradation under heat stress treatment, indicating that *ZmPAO6* may play a crucial role in enhancing heat tolerance of transgenic *Arabidopsis* through the involvement in various physiological processes. Further, the expression analysis of related genes of antioxidant enzymes including glutathione peroxidase (GPX) and ascorbate peroxidase (APX) demonstrated that *ZmPAO6* can enhance heat resistance in transgenic *Arabidopsis* through modulating heat-induced H_2O_2 accumulation in polyamine catabolism. Taken together, our results are the first to report the *ZmPAO6*

gene response to heat stress in plants and will serve to present an important theoretical basis for further unraveling the function and regulatory mechanism of *ZmPAO* genes in growth, development and adaptation to abiotic stresses in maize.

Keywords: polyamine oxidases, polyamines, *Zea mays* L., stress response, functional analysis

INTRODUCTION

Polyamines (PAs), largely including spermidine (Spd), spermine (Spm), and putrescine (Put), are small molecular aliphatic amine (Knott et al., 2007; Hussain et al., 2011). PAs have been detected and studied in many actively growing tissues and play crucial roles in nitrogen metabolism (Moschou et al., 2012), dark-induced senescence (Sobieszczuk-Nowicka et al., 2015), flowering (Ahmed et al., 2017), fruit ripening (Handa and Mattoo, 2010; Fortes and Agudelo-Romero, 2018), chloroplast chemical penetration (Ioannidis et al., 2016), callus growth (Liu and Moriguchi, 2007), regulation of protein synthesis (Igarashi and Kashiwagi, 2000), signal molecules (Pál et al., 2019) and especially in the oxidative balance of cells in plants (Murray Stewart et al., 2018). Moreover, increasing studies have elucidated that PAs are involved extensively in various abiotic and biotic stress responses (Alcázar et al., 2006; Kusano et al., 2008; Moschou et al., 2008b; Toumi et al., 2010; Tiburcio et al., 2014; Liu et al., 2015; Corpas et al., 2019). For instance, under salt stress, the application of spermine reduced the harmful effects on the growth and gas exchange of *Tropaeolum majus*, increased the activities of CAT and POD under severe salt stress, and the activities of POD and APX under moderate salt stress (da Silva et al., 2022). Foliar application of putrescine on cucumber alleviated the decrease of stomatal aperture and photosynthesis caused by salt stress treatment, and promoted the growth of cucumber (Ma et al., 2022). Moreover, exogenous putrescine significantly improved ROS scavenging ability and promoted the metabolism of endogenous PAs so as to provide better drought resistance for Cabernet Sauvignon (Zhao et al., 2021). Treatment of seeds of mung bean with PAs can enhance the drought resistance of mung bean plants by accumulating osmoprotectants, improving water status and chlorophyll value, and reducing oxidative damage (Sadeghipour, 2019). Therefore, PAs play a crucial role in maintaining normal growth and development and resisting adverse environmental stresses in plants.

The levels of cellular endogenous PAs largely depend on the dynamic balance of biosynthesis and catabolism of PAs. Polyamine biosynthesis has been thoroughly studied in animals and plants. Generally, the biosynthesis of PAs begins with the synthesis of putrescine. L-ornithine is used for precursor to synthesize Put in animals, whereas L-ornithine and L-arginine serve as precursors to generate Put in plants (Wu et al., 2005; Pegg and Casero, 2011). In plants, arginine decarboxylase (ADC) and ornithine decarboxylase (ODC) are required for catalyzing the synthesis of Put, respectively. Then, Put can be converted into Spd *via* Spd synthase (SPDS). Finally, Spd can be further converted into Spm under the catalysis of Spm synthase (SPMS; Moschou et al., 2008a). In contrast to the anabolism of PAs, the catabolism of PAs in plants is mainly dependent on the catalyzation from two major categories of amine oxidases: diamine oxidases (DAOs) containing divalent Cu^{2+}, also known as copper amine oxidases (CuAOs), and flavin-containing polyamine oxidases (PAOs; Pegg and Casero, 2011; Planas-Portell et al., 2013). As far as subcellular localization is concerned, some CuAO and PAO proteins are localized in peroxisomes (Wang et al., 2019). These proteins contain a C-terminal peroxisomal targeting type I (PTS1), a tripeptide consisting of the consensus sequence (S/A/C)(K/R/H)(L/M; Hao et al., 2018). For example, two CuAO (AtCuAO2 and AtCuA03) and three PAO (AtPAO2-AtPAO4) from *Arabidopsis* (Fincato et al., 2011; Planas-Portell et al., 2013), two PAO (CsPAO2 and CsPAO3) from sweet orange (Wang and Liu, 2015), four PAO (SLPAO2-SLPAO 5) from tomato (Hao et al., 2018), and three PAO (OsPAO3-OsPAO5) from rice (Ono et al., 2012) all carry a putative type-I peroxisomal targeting signal in their C-termini. The function of CuAOs is to catalyze the oxidation of Put and cadaverine (Cad) to 4-aminobutyraldehyde, H_2O_2 and ammonia (Moschou et al., 2012). In contrast, according to functional differentiation in PAOs involved in polyamine catabolism, PAOs are mainly categorized into two groups in plants. The PAOs of the first group in plants are required for participating in PA terminal catabolism and perform the oxidation and decomposition of Spd and Spm to produce H_2O_2, 1, 3-diaminopropane (DAP), and 4-aminobutanal (Spd catabolism) or N-(3-aminopropyl)-4-aminobutanal (Spm catabolism; Angelini et al., 2010; Moschou et al., 2012; Mo et al., 2015), whereas the PAOs in the second group resembles the mammalian Spm oxidases (SMOs), which are mainly involved in back-conversion reactions of PAs by catalyzing Spm to Spd and Spd to Put, in a reverse reaction of PA synthesis and with concomitant production of 3-aminopropanal and H_2O_2 (Angelini et al., 2010; Moschou et al., 2012).

In plants, genes encoding PAOs have been identified and characterized in several species including *Arabidopsis* (Fincato et al., 2011), rice (Sagor et al., 2017), sweet orange (Wang and Liu, 2015), tomato (Hao et al., 2018), and tea plant (Li et al., 2020). Most of the identified PAO genes in plants are largely involved in PA back-conversion pathway. For example, five *PAO* genes (*AtPAO1-AtPAO5*) in *Arabidopsis* have been revealed to encode PAO proteins (Fincato et al., 2011), all of which are involved in catalyzing PA back-conversion reactions (Tavladoraki et al., 2006; Kamada-Nobusada et al., 2008). Also, a total of seven *PAO* genes (*OsPAO1-OsPAO7*) have been identified in rice. Among them, there are four *OsPAO* genes (*OsPAO1*, *OsPAO3-OsPAO5*) encoding PAO proteins that are involved in the back-conversion reactions of PAs (Ono et al., 2012). Moreover, there are six *PAO genes* (*CsPAO1-CsPAO6*) identified to encode their proteins in sweet orange. Among them, the *CsPAO3* gene has been implicated in participating in the back-conversion reactions of PAs (Wang and Liu, 2015, 2016).

The catabolism of PA generally results in the accumulation of H_2O_2 (Liu et al., 2015). H_2O_2 can be regarded as a crucial

signal molecule at low levels, whereas at high levels it is a toxic compound that causes damage to plant cells (Quan et al., 2008). Therefore, the ratio of PA catabolism to biosynthesis has been considered to be a vital factor in inducing tolerance responses or plant cell death under biotic and abiotic stresses (Moschou et al., 2008a). This suggests that H_2O_2 produced by PA catabolism may play a crucial role in maintaining ROS homeostasis, which is closely related to the stress response of plants. For example, the overexpressing of *MdSPDS1* in sweet orange enhanced the activity of PAOs to catalyze polyamine catabolism and thereby result in the accumulation of H_2O_2, which likely triggered the hypersensitivity or activation of defense-related genes and eventually significantly reduced the sensitivity of transgenic plants to canker disease (Fu et al., 2011). Under salt stress, the contents of the apoplastic Spm and Spd in maize increased significantly and then the oxidation of free apoplast polyamine catalyzed by polyamine oxidase promoted maize leaf elongation (Rodríguez et al., 2009). In addition, Spd could outflow into the apoplast, and then Spd was decomposed by PAOs to produce H_2O_2, which led to stress tolerance response or induction of programmed cell death (PCD) under salt stress in tobacco (Moschou et al., 2008a). Similarly, the ABA signaling pathway integrated PAs and PAOs to regulate the H_2O_2 accumulation, which can also cause further stress response or PCD in grape (Toumi et al., 2010). Moreover, H_2O_2 produced by Spd oxidation that was catalyzed by PAOs as a signal molecule could trigger the opening of hyperpolarized Ca^{2+} channels to result in Ca^{2+} influx, and thereby regulate the growth of pollen tubes in *Arabidopsis* (Wu et al., 2010). Therefore, H_2O_2 produced by PAOs catalyzing the catabolism of PAs may play a vital role in growth, development and response to abiotic stresses in plants *via* modulating the dynamic balance of H_2O_2.

Maize (*Zea mays L.*), as one of the most important crop species in the world, has become one of the important model monocot species for functional genomics analysis. It has been of great significance to the study of molecular biology in plants. Meanwhile, maize is a vital part of the food system (Palacios-Rojas et al., 2020). However, biotic and abiotic stresses have significant adverse effects on maize yield and quality. Since PAOs play a vital role in responding to various stress treatments, the study of the roles of PAOs may provide a new way to enhance the stress resistance in plants. However, little is known about identification and functional analysis of polyamine oxidase gene family in maize up to now. In this study, the relevant information on *ZmPAO* genes for the whole genome-wide and the role of *ZmPAO6* under heat stress treatment were further clarified. Taken together, this study may contribute to an in-depth comprehension of the evolution of *PAO* gene family in maize and their crucial roles in abiotic stress resistance.

MATERIALS AND METHODS

Identification of *PAO* Family Genes From Maize

To obtain all putative *PAO* family genes in maize, taking the reported *PAO* gene sequences of *Arabidopsis*, rice, and maize as queries, the programs were used to search the maize genome databases, including the Maize Genome Browser (http://www.maizesequence.org), Phytozome (https://phytozome-next.jgi.doe.gov/), Maize Genetics and Genomics Database (MaizeGDB, http://www.maizegdb.org/), and NCBI (http://www.ncbi.nlm.nih.gov; Zhang et al., 2022). The information about the coding sequence length, amino acid length, and chromosomal localization of each gene was also obtained from NCBI. Furthermore, the molecular weight and theoretical isoelectric point (PI) value of the ZmPAO proteins were reckoned within the online Expasy Bioinformatics Resource Portal (http://web.expasy.org/compute_pi/).

Sequence Alignment and Phylogenetic Analysis

To determine the phylogenetic relationships of the PAO proteins, full-length amino acid sequences of PAO proteins identified in maize, rice, *Arabidopsis*, barley, tomato, sweet orange, and cotton were aligned by the Clustal W program using their default settings. The information of *PAO* genes in these plants were listed in **Supplementary Table S1**. Based on the aligned protein sequences, the phylogenetic tree was constructed through the neighbor-joining (NJ) method and examined by bootstrap analyses (1,000 replicates) with MEGA 7.0 (Kumar et al., 2016). Furthermore, the amino acid sequences of PAO proteins in maize were aligned using DNAMAN 7.0 software for multiple protein sequences alignment.

Analysis of Gene Structure and Conserved Motif of Maize PAO Proteins

The conserved motifs in the full-length amino acid sequences of ZmPAO proteins were identified by the motif analysis tool MEME Suite version 4.0.0 (MEME; http://alternate.meme-suite.org/tools/meme; Bailey et al., 2009). The parameters were set as the following: (1) the maximum number of patterns was set to identify ten motifs; (2) the optimal width of the motif was set between 10 and 50; (3) the rest were executed according to the default parameters (Hu et al., 2021). Furthermore, to analyze the exon and intron structures of *PAO* genes, the structures of *PAO* genes were analyzed by the Gene Structure Display Server database (GSDS, http://gsds.cbi.pku.edu.cn/; Hu et al., 2015).

Chromosomal Localization and Prediction of cis-Acting Elements in Maize *PAO* Genes

The chromosomal location image of *ZmPAO* genes was accomplished by MapInspect (https://mapinspect.software.informer.com/) based on the information from the Maize Genetics and Genomics Database (http://www.maizegdb.org/). To analyze the cis-regulatory elements of the *ZmPAO* genes in response to abiotic stresses, the promoter sequence in the upstream 2,000 bp of each *ZmPAO* gene start codon was submitted to the PlantCare database (http://bioinformatics.psb.ugent.be/webtools/plantcare/html) to predict stress response and hormone-related cis-acting elements (Chang et al., 2008).

Expression Profile Analysis of Maize *PAO* Genes in Different Tissues

To explore the spatiotemporal expression patterns of *ZmPAO* genes, the tissue-specific expression patterns of *ZmPAO* genes were analyzed using the genome-wide gene expression atlas of maize inbred line B73 that was reported previously (Sekhon et al., 2011). Microarray analysis was completed to determine the expression patterns of ten representative tissues (seed, root, seedling, stem, shoot tip, silks, leaf, tassel, husk, and endosperm). The signal values for maize *PAO* genes in the ten tissues were list in **Supplementary Table S2**. The Normalized expression values of the ten tissues were averaged. The gene expression levels were presented as log2 values which were used to generate the heat map of the expressions of *ZmPAO* genes using HEML1.0.3.3 (HeatMap Illustrator, http://ccd.biocuckoo.org/).

Maize Growth Conditions and Abiotic Stress Treatment

The maize B73 inbred seedlings were grown at 28°C with long-day conditions of 15 h of light and 9 h of dark and an environmental humidity of 60%. After 3 weeks, the seedlings were subjected to heat (42°C), drought, and salt treatments (200 mM NaCl) for 1, 2, 4, and 8 h, respectively. Notably, to impose the drought stress, the roots of the seedlings were pulled out from the soil at 28°C. Three biological replicates were performed for each sample. All collected samples were rapidly frozen in liquid nitrogen and stored at –80°C until RNA extraction.

Generation of *ZmPAO6* Transgenic *Arabidopsis* Plants

To create *ZmPAO6* overexpression constructs, the coding sequence of *ZmPAO6* was PCR-amplified, with maize B73 cDNA used the templates to clone with high-fidelity polymerase (Trans Start® Fast Pfu DNA Polymerase). The PCR product was purified and cloned into the PHB vector with the EasyGeno Assembly Cloning kit (TIANGEN, China). The vectors were transformed into *Agrobacterium* strain for transformation into *Arabidopsis* by the floral dip method. Seeds of the T_0 and T_1 generations were selected on 1/2 MS plates supplemented with hygromycin (30 μg/ml) and confirmed by PCR with primers (Hyg-F: GGTCGCGGAGGCTATGGATGC; Hyg-R: GCTTCTGC GGGCGATTTGTGT). All genes or clones were confirmed by sequencing.

Heat Tolerance Assay of Transgenic *Arabidopsis*

To evaluate the tolerance for heat stress, the seeds of WT and transgenic *Arabidopsis* homozygous T_3 lines were grown at 22°C under long-day conditions of 16 h of light and 8 h of dark and an environmental humidity of 60% for 7 days. The three-week-old seedlings were exposed to heat stress (42°C) in the incubator for 36 h. Phenotypic records and physiological parameters analysis were completed at the designed processing time.

RNA Extraction and Quantitative Real-Time PCR Analysis

According to the manufacturer's instruction, total RNA was extracted from the collected samples using Trizol RNA isolation (United States of America). For quantitative real-time PCR, cDNA from three distinct biological samples was used for analysis. The PCR condition was performed as follows: pre-denaturation for 15 min at 95°C, 40 cycles at 95°C for 10 s, 55°C for 30 s, and 72°C for 30 s. The gene expression levels were calculated using the $2^{-\Delta\Delta Ct}$ method (Rao et al., 2013). Each experiment was conducted in the form of at least three technologies and biological replication. All the primers in this study were listed in **Supplementary Table S3**.

Physiological Parameter Determination

3, 3′-Diaminobenzidine (DAB) was used to dye the leaves to observe the accumulation of H_2O_2. The contents of H_2O_2 and MDA were measured using the H_2O_2 assay kit (A064-1-1) and MDA assay kit (A003-1-1; Nanjing Jiancheng, Nanjing, China). Moreover, the contents of chlorophyll and polyamines were detected by the spectrophotometer and high-performance liquid chromatography, respectively. The experiment was repeated three times at least.

RESULTS

Identification and Analysis of *PAO* Genes in Maize

In this study, a total of nine *ZmPAO* genes (namely *ZmPAO1*-*ZmPAO9*) were identified. The related information of *ZmPAO* genes was shown in **Table 1**, including the chromosome location, the length of coding sequences and corresponding information about the nine proteins. The length of CDS sequences of these putative genes ranged from 504 bp (*ZmPAO7*) to 1,590 bp (*ZmPAO4*), and the amino acid sequences of these proteins ranged from 167 (*ZmPAO7*) residues to 529 (*ZmPAO4*) residues, respectively. The MWs of ZmPAO proteins varied from 19.0 kDa (ZmPAO7) to 57.9 kDa (ZmPAO1) and pIs from 5.21 (ZmPAO3) to 9.89 (ZmPAO7).

Phylogenetic Analysis and Sequence Alignment of ZmPAO Proteins

To identify the candidate PAO proteins in maize, the sequences of PAO proteins from several various species including maize, *Arabidopsis*, rice, barley, tomato, sweet orange and cotton were collected to construct a phylogenetic tree by MEGA 7.0 (**Figure 1**). The phylogenetic tree revealed that these proteins can be categorized into four groups (I–IV). However, the ZmPAO proteins in maize were only clustered into three groups (I, II, and IV). The Group I was consisted of 22 PAO proteins, including six PAO proteins (ZmPAO3, ZmPAO4, ZmPAO6, ZmPAO7, ZmPAO8, and ZmPAO9). ZmPAO2 protein was clustered into the Group II, and the two remaining proteins including ZmPAO1 and ZmPAO5 were clustered into the Group IV. Multiple sequence alignment was performed using the amino acid sequences of ZmPAO proteins by DNAMAN software

TABLE 1 | Basic information on *PAO* gene family in maize.

Gene name	Accession number	Genome location coordinates (5′–3′)	CDS (bp)	Protein			Chr
				Length (a.a)	pI	Mol.Wt (Da)	
ZmPAO1	Zm00001d024281	63,380,946–63,385,024	1,503	500	5.71	56.37	10
ZmPAO2	Zm00001d043681	209,194,699–209,196,394	1,515	504	5.44	53.94	3
ZmPAO3	Zm00001d001883	2,622,145–2,625,689	1,473	490	5.21	53.36	2
ZmPAO4	Zm00001d026586	149,850,826–149,854,922	1,590	529	5.49	57.95	10
ZmPAO5	Zm00001d028172	24,937,595–24,942,561	1,113	370	5.25	42.56	1
ZmPAO6	Zm00001d026334	145,108,335–145,113,560	1,449	482	5.60	53.36	10
ZmPAO7	Zm00001d037642	139,488,328–139,491,146	504	167	9.89	19.04	6
ZmPAO8	Zm00001d036513	97,485,127–97,490,455	1,419	472	5.76	52.39	6
ZmPAO9	Zm00001d002266	9,429,838–9,434,928	1,452	483	5.83	53.58	2

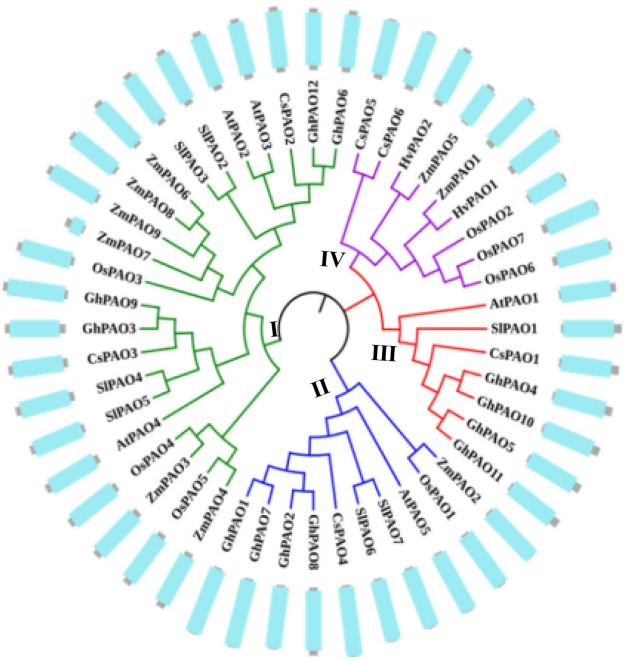


FIGURE 1 | Phylogenetic analysis among the polyamine oxidase (PAO) proteins from seven representative species. The accession numbers of the genes were listed in **Supplementary Table 1**. The colored branch of the tree indicated that the total PAO proteins were classed into four groups, and nine ZmPAO proteins were classed into three groups according to the amino acid sequence alignment by MEGA 7.0 software with the Neighbor-joining method. The conserved amine-oxidase domains of these proteins were exhibited in the outer ring. Gray represents the length of the amino acid sequence and blue represents the sequence of the conserved amine-oxidase domain.



FIGURE 2 | Alignment of the amino acid sequences of maize PAO proteins. Sequence alignment was performed by DNAMAN software. Identical and similar residues are shaded in black or pink and blue background, respectively. The peroxisomal targeting signal of ZmPAO3, ZmPAO4, ZmPAO6, and ZmPAO9 are indicated in the red box.

(**Figure 2**). The results demonstrated that ZmPAO4, ZmPAO6, and ZmPAO9 proteins contain SRL sequences. Moreover, ZmPAO3 protein contains CRT sequences, which share high homology with rice OsPAO4 protein. Thus, these results indicated that ZmPAO proteins in maize shared highly conserved homology with other plants in evolution.

Conserved Motifs of ZmPAO Proteins and Gene Structure of *ZmPAO* Genes

To further gain more insights into the evolutionarily conserved structure features of *PAO* gene family in maize, a total of ten conserved motifs in ZmPAO, OsPAO, and AtPAO proteins were identified by the MEME website (**Figure 3A**). In the Group I, all ZmPAO proteins contain the Motifs 1–9 except ZmPAO7 protein, which lacks the Motifs 2–8. All members of the Groups III and IV include the Motifs 3, 5, 8, 9, and

10. Meanwhile, to further perceive the structure of the *PAO* gene family in maize, the intron–exon structures of *ZmPAO* genes were analyzed by GSDS software (**Figure 3B**). *ZmPAO3*, *ZmPAO6*, and *ZmPAO9* genes all contain nine introns. Secondly, both *ZmPAO4* and *ZmPAO8* genes contain eight introns. Notably, there are some gene structures without introns in *ZmPAO2*, *OsPAO1*, and *AtPAO5* genes. In addition, *ZmPAO1*, *ZmPAO5*, and *ZmPAO7* genes contain 7, 5, and 3 introns, respectively. Overall, these results further demonstrated that the *PAO* gene family in maize exhibited highly conserved structure features during the evolution of plants.

Chromosomal Location and Gene Duplication of *PAO* Gene Family in Maize

To generate the chromosome location graphics of *ZmPAO* genes, the physical positions of *ZmPAO* genes were investigated by analyzing the genomic distribution of *ZmPAO* genes on chromosomes in maize. The results indicated that the *ZmPAO* genes were distributed unevenly across five of all the ten chromosomes in the maize genome (**Figure 4**). Among them, the Chromosome 10 contained the largest number of *ZmPAO* genes with three members (namely *ZmPAO1*, *ZmPAO4*, and *ZmPAO6*), whereas *ZmPAO5* and *ZmPAO1* were located on the Chromosomes 1 and 3, respectively. Moreover, *ZmPAO3* and *ZmPAO9* were distributed on the Chromosome 2. Similarly, *ZmPAO7* and *ZmPAO8* were distributed on the Chromosome 6. Moreover, gene duplication events were investigated to explore the evolutionary patterns of the *PAO* gene family in maize. Two *PAO* gene pairs (*ZmPAO3*/*ZmPAO4* and *ZmPAO6*/*ZmPAO9*) were revealed to be involved in maize segmental duplication for they were exhibited to have very high homology in the sequences by analyses of sequence alignment (**Figure 2**). This result indicated that gene duplication events might have occurred during their process of evolution.

The cis-Acting Regulatory Elements in the Promoter of Maize *PAO* Genes

To further explore the potential regulatory mechanisms of *ZmPAO* genes in response to abiotic stresses in maize, the promoter sequences were analyzed using the PLACE database to identify cis-regulatory elements in the promoter region. The results indicated that 11 types of stress- and hormone-related cis-acting regulatory elements were detected in the promoters of maize *PAO* genes: five hormone-related elements (ABRE, CGTCA-motif, TGACG-motif, GARE-motif, and P-box) and six stress-related elements (TC-rich repeats, MBS, LTR, ERE, WUN-motif, and W-box; **Figure 5**). It is worth noting that the ABRE (a cis-element involved in ABA responsiveness) were detected in the promoter regions of all the *ZmPAO* genes. Except for *ZmPAO3*, MeJA-responsive elements were discovered in the promoters of the other eight *ZmPAO* genes. In addition, ethylene-responsive element (ERE) was uncovered in the promoter regions of the *ZmPAO3* and *ZmPAO5* genes. Low temperature-responsive element (LTR) was predicted in the promoter regions of the *ZmPAO3*, *ZmPAO4*, *ZmPAO5*, and *ZmPAO6* genes, while WUN-motif (wound-responsive element) was discovered in the promoter region of the *ZmPAO7* gene. Meanwhile, the promoter regions of most *ZmPAO* genes contain the W-box element. TC-rich repeats as defense and stress-responsive elements were predicted to exist in the promoters

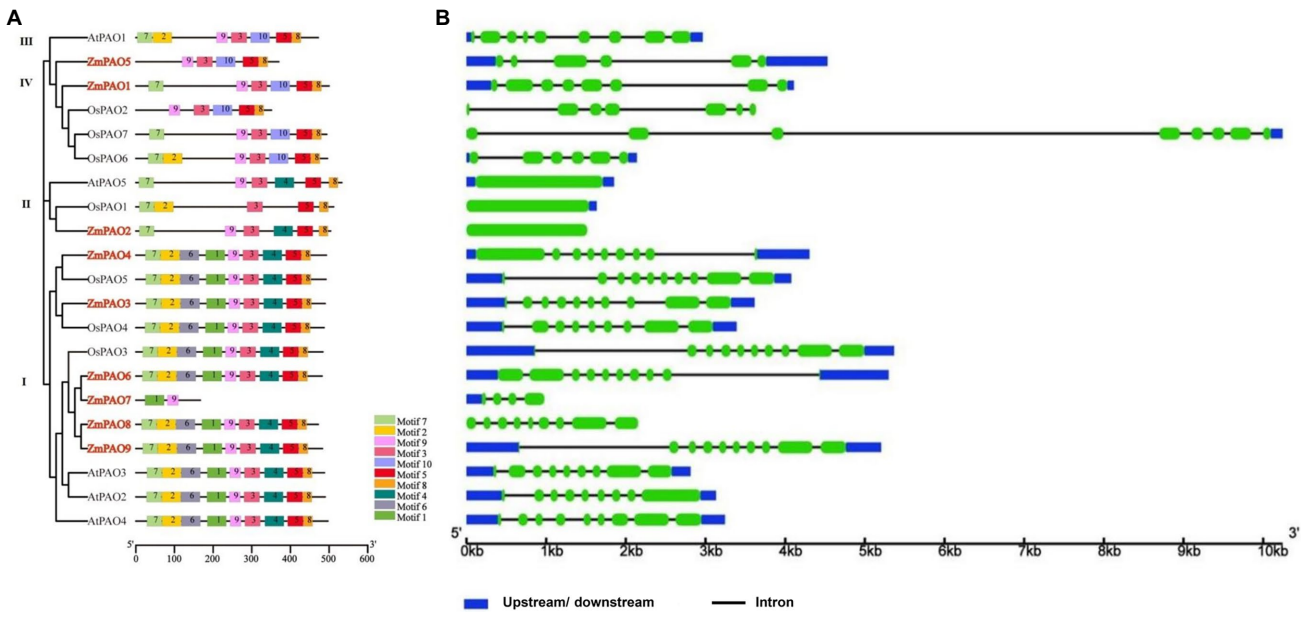


FIGURE 3 | Conserved motifs of PAO proteins and gene structure of *PAO* genes in maize, rice and *Arabidopsis*. **(A)** Distribution of all motifs in maize, rice and *Arabidopsis* were identified by MEME. Different motifs are indicated in various colored boxes. **(B)** Exon/intron structures of *PAO* genes in maize, rice and *Arabidopsis*. Exons are indicated with green boxes, and introns are shown as black lines. The upstream/downstream region of *PAO* genes are indicated in blue boxes. The length of each *PAO* gene inferred by the scale at the bottom.

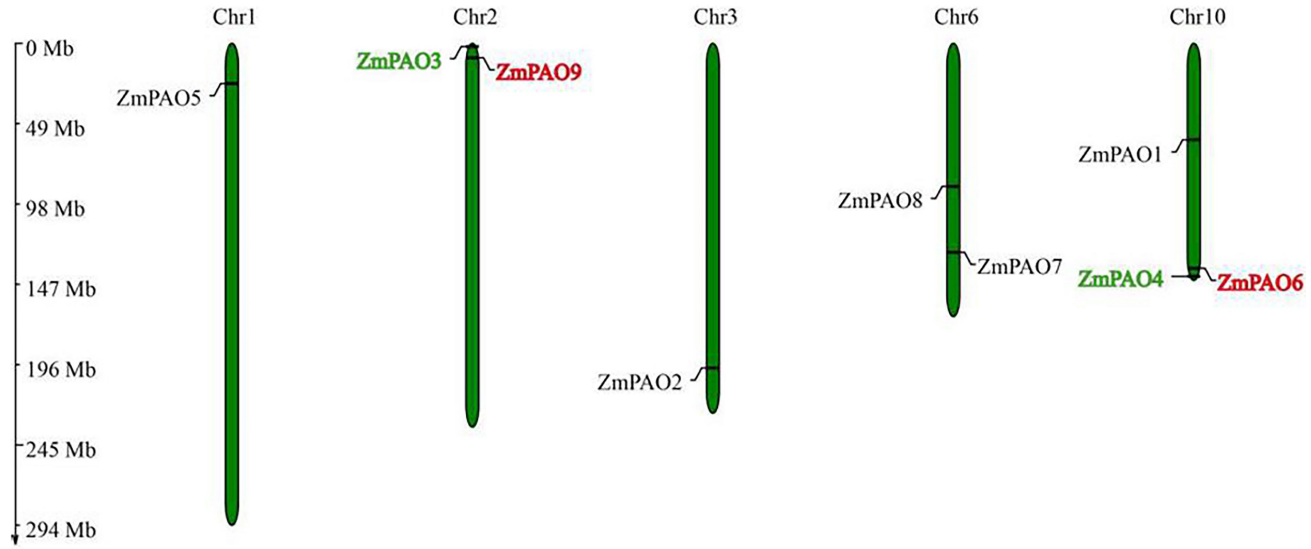


FIGURE 4 | Chromosomal location and gene duplication of the *PAO* gene family in maize. The gene names on each chromosome correspond to the approximate locations of each *ZmPAO* genes. Green and red gene names represent tandem duplicated gene pairs. The size of a chromosome is indicated by its relative length. The chromosome numbers are indicated at the top of each bar. The scale on the left is in megabases.

of the *ZmPAO2* and *ZmPAO8* genes. This result indicated that *ZmPAO* genes might be mainly involved in hormone regulation and adversity stress.

Analysis of Microarray Expression Profile of Maize *PAO* Genes

To further investigate the roles of maize *PAO* genes in plant growth and development, the expression profiles analysis was accomplished using the available transcriptomic data of maize B73 (Sekhon et al., 2011). The signal values for all these maize *PAO* genes are given in **Supplementary Table S2**. The expression heat map of all the *ZmPAO* genes from ten developmental stages was constructed using Helm software (**Figure 6**). The results revealed that all nine *ZmPAO* genes were expressed at varying levels in all tissues. Compared with the other *ZmPAO* genes examined, the transcripts of the *ZmPAO9* gene showed relatively high expression levels at all stages, while the transcripts of the *ZmPAO5* gene maintained low expression levels in all tissues. Interestingly, some tissue-specific genes were discovered, such as high expression levels of the *ZmPAO1* gene in seedlings and high expression levels of the *ZmPAO6* gene in roots and stems, suggesting that those genes may play a vital role in plant growth and development processes of specific tissues. In general, the expression patterns in the same paralogous gene pairs (*ZmPAO3*/*ZmPAO9*, *ZmPAO4*/*ZmPAO6*) were similar, indicating they might be formed by segmental duplication and retain their functions. It is noteworthy that the expression patterns of four *ZmPAO* genes (*ZmPAO2*, *ZmPAO5*, *ZmPAO8*, and *ZmPAO9*) in all tissues were relatively stable, implying that these genes might be involved in the basic metabolism. Furthermore, the hierarchically clustered heat map could be divided into two clusters. The first cluster included six members (*ZmPAO1*, *ZmPAO2*, *ZmPAO4*, *ZmPAO6*, *ZmPAO8*, and *ZmPAO9*), while the second cluster included three members (*ZmPAO3*, *ZmPAO5*, and *ZmPAO7*). Notably, the changing trend of gene expression levels of the members of the same cluster was similar in the ten tissues. Overall, the results demonstrated that these identified *ZmPAO* genes showed differential expression patterns at diverse developmental stages of maize, suggesting that these genes may function in multiple tissues.

Expression Profile Analyses of Maize *PAO* Genes Under Abiotic Stress Treatment

To survey if these predicted genes were expressed in maize and to further confirm their stress-responsiveness to abiotic stresses, the expression profiles of the nine *ZmPAO* genes in roots, stems, and leaves under heat, salt, and drought treatments were determined by qRT-PCR (**Figure 7**). The results indicated that the expression levels of the nine *ZmPAO* genes were different in three distinct tissues under varied abiotic stress conditions. The expression levels of most *ZmPAO* genes changed significantly before and after abiotic stress treatments, which indicated that these genes were responsive to these stress treatments and could be involved in distinct stress response pathways. Firstly, the detection of gene expression levels at different time points after heat stress revealed that most *ZmPAO* genes were sensitive to heat stress (**Figure 7A**). The gene expression levels of *ZmPAO3*, *ZmPAO4*, and *ZmPAO6* changed significantly in all tissues after heat stress, which indicated that they could be involved in heat stress. Notably, the expression of *ZmPAO1* was down-regulated at all time points in other tissues except that it was up-regulated at 8 h after heat stress in the roots. Moreover, most members exhibited low expression levels in the stems (**Figure 7B**). Secondly, under the treatment of 200 mM NaCl concentration, the expression level of *ZmPAO*

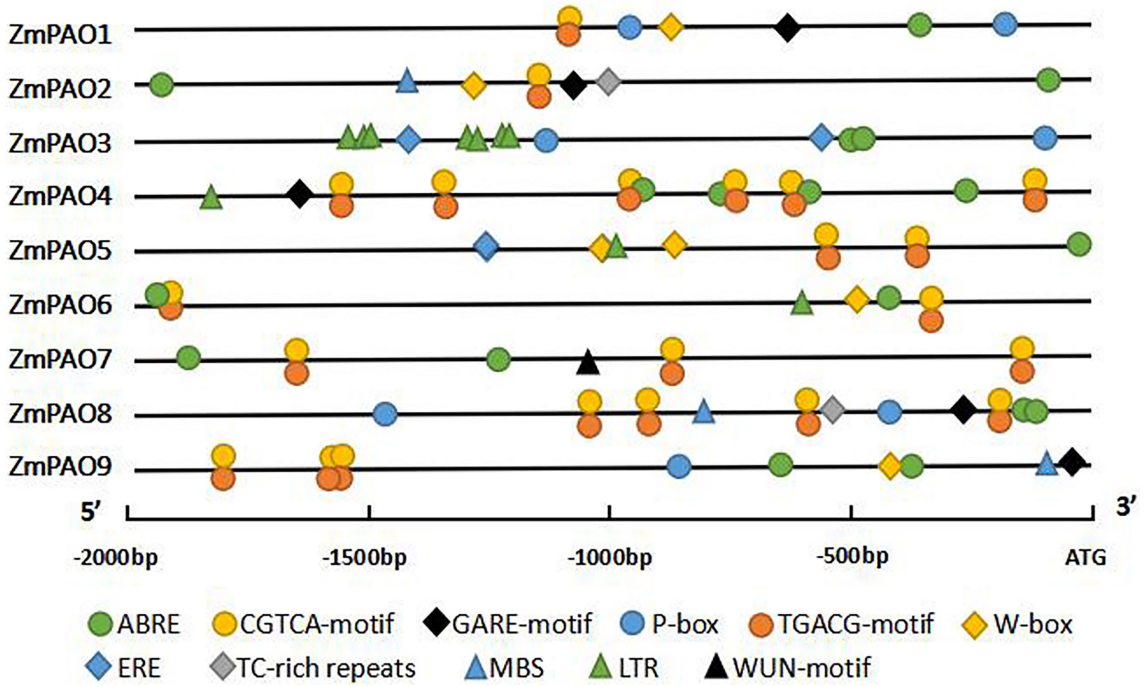


FIGURE 5 | Distribution of major stress-related cis-elements in the promoter sequences of the 9 *ZmPAO* genes. The putative core sequences of these cis-acting elements are represented by different symbols, as shown in the figure key at the bottom. The cis elements distributed on the sense chain and the reverse chain are above and below the black lines, respectively. The 2,000 bp sequences upstream of the initiation codon (ATG) of the PAO genes can be estimated using the scale per 500 bp at the bottom. ABRE, ABA responsive element; ERE, ethylene-responsive element; GARE-motif and P-box, gibberellin responsive element; CGTCA-motif and TGACG-motif, MeJA-responsive element; LTR, low temperature-responsive element; TC-rich repeats, defense and stress-responsive element; WUN-motif, wound-responsive element; MBS, MYB binding site. W-box, wound and pathogen responsive element.

gene changed significantly at different time points (**Figure 8**). In the leaves (**Figure 8A**), the expression levels of *ZmPAO2*, *ZmPAO3*, *ZmPAO4*, *ZmPAO7*, and *ZmPAO9* genes were significantly down-regulated at all time points. In the stems (**Figure 8B**), the expression levels of *ZmPAO1* and *ZmPAO5* genes under salt treatment were both down-regulated compared with the control group. In the roots (**Figure 8C**), the expression levels of 6 genes (*ZmPAO2-ZmPAO6* and *ZmPAO9*) were significantly up-regulated in the early stage of salt stress. Moreover, the expression level of *ZmPAO1* gene was inhibited during the whole salt stress period, and only the expression level of *ZmPAO6* gene was higher than the control group during the salt stress period. Finally, under drought treatment, the expression changes of *ZmPAO* genes at different times were analyzed (**Figure 9**). In the leaves (**Figure 9A**), the expression levels of *ZmPAO2*, *ZmPAO3*, *ZmPAO4*, *ZmPAO6*, *ZmPAO7*, and *ZmPAO9* genes decreased as a whole, among which the expression levels of *ZmPAO3* and *ZmPAO4* genes decreased the most. In the stems (**Figure 9B**), the expression levels of most *ZmPAO* genes were decreased under drought treatment compared with the control group. In the roots (**Figure 9C**), the expression levels of *ZmPAO3* and *ZmPAO8* genes were similar, which were slowly up-regulated at the beginning of drought treatment, reached the maximum at 2 h, and decreased at 4 h. Taken together, the results demonstrated that most of these predicted genes of the *PAO* gene family in maize were responsive to various abiotic stress treatments, suggesting their potential roles in abiotic stress responses.

Genetic Transformation and Overexpression Analysis of *ZmPAO6* Gene in *Arabidopsis*

The *ZmPAO6* clone map and the double enzyme (BamH I and Xba I) digestion map of the recombinant plasmid were shown in **Supplementary Figures 1A,B**, respectively. To investigate the role of *ZmPAO6* gene under heat stress, the recombinant vector with the *ZmPAO6* gene was transformed into the *Arabidopsis* line using *Agrobacterium*-mediated method by dipping the *Arabidopsis* floral to obtain the overexpressed *Arabidopsis* plants. Consequently, a total of 14 transgenic lines were generated in this study (**Supplementary Figure 2**). In addition, according to the analysis of the phylogenetic tree, the *ZmPAO6* gene is located in the Group I, and its orthologous genes in *Arabidopsis* (*AtPAO2* and *AtPAO3*) and rice (*OsPAO3*) are both confirmed to be located in peroxisomes and participate in the reverse conversion pathway of polyamine catabolism. Thus, the amino acid sequence of *ZmPAO6* gene and these three orthologous *PAO* genes were compared, and the results elaborated that the sequence homology of both *ZmPAO6* and *OsPAO3*, *AtPAO2*, or *AtPAO3* are 88.28, 69.29, and 68.28%, respectively (**Supplementary Figure 3**). Peroxisome targeting

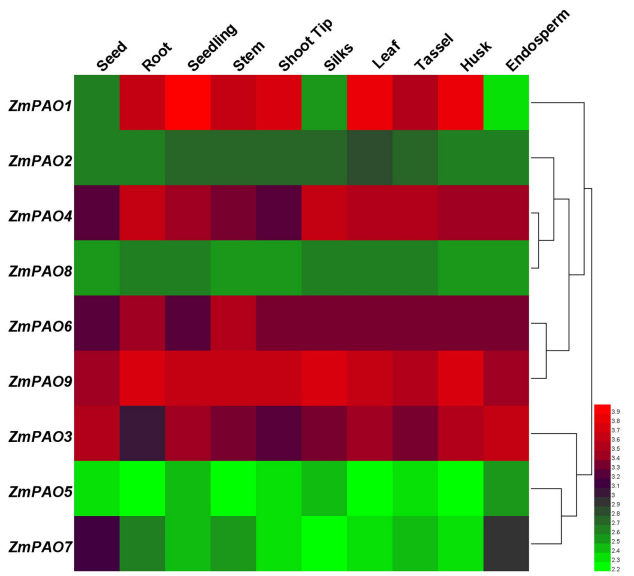


FIGURE 6 | Hierarchical clustering of expression profiles of *ZmPAO* gene family in ten tissues. Ten tissues from different developmental stages including seed, root, seedling, stem, shoot tip, silks, leaf, tassel, husk, and endosperm were investigated. The different tissues are marked at the top of each channel. Cluster dendrograms are displayed on the right. The color scale representing the value of the log 2 signal is shown on the right. Green represents low expression levels and red indicates high expression levels of the transcript abundance.

sequence (PSTI) SRL was also presented at the end of ZmPAO6 protein. The function of *ZmPAO6* gene may resemble the orthologous *OsPAO3* gene, which encompasses high homology, locates in subcellular peroxisome and participates in the reverse conversion pathway of decomposing PAs. Thus, this result indicated that the *ZmPAO6* gene may function in growth, development and adversity stress in maize.

Detection of Polyamine and Hydrogen Peroxide Contents in Transgenic Plants

To further confirm the function of *ZmPAO6* gene in transgenic *Arabidopsis*, two representative transgenic lines (#3 and #14) were selected and identified for further functional analysis (**Figure 10A**). According to the metabolic pathways and products of PAs, PAs can be decomposed by polyamine oxidase to produce H_2O_2 (Moschou et al., 2012). The leaves of the WT *Arabidopsis* and transgenic *Arabidopsis* lines were firstly stained by DAB, and the H_2O_2 content was detected as shown in **Figure 10B**. The leaves of transgenic lines # 3 and # 14 were stained in a darker color and larger area compared with the WT *Arabidopsis*, indicating that the content of $H_2O_2$was higher in transgenic plants, which may be due to the overexpression of *ZmPAO6* in *Arabidopsis* may promote the catabolism of PAs. Therefore, these results suggested that *ZmPAO6* gene may be involved in the catabolism of plant polyamines. To confirm the effect of overexpressed *ZmPAO6* gene on its polyamine catabolism in transgenic *Arabidopsis* plants, the content changes of PAs in the WT and transgenic lines with the overexpression of *ZmPAO6* gene were determined by high-performance liquid chromatography, respectively (**Figure 10C**). The contents of Put and Spd in the transgenic lines were higher than those of the WT *Arabidopsis*, especially the content of Spd. Meanwhile, compared with the WT *Arabidopsis*, the content of Spm in the transgenic lines were reduced and the line #14 had the lowest content of Spm. The results further revealed that the overexpressed *ZmPAO6* gene could be involved in decomposing Spm into Spd and further converting Spd into Put through catalyzing the back-conversion reactions in the catabolism of polyamines in the transgenic *Arabidopsis* plants. Therefore, these results suggested that the *ZmPAO6* gene may be implicated in promoting specific PA degradation mainly *via* participating in back-conversion reaction of PAs.

Overexpression of *ZmPAO6* Gene Enhances Heat Tolerance in Transgenic *Arabidopsis*

To detect the tolerance of transgenic *Arabidopsis* in response to heat stress, 3-week-old seedlings were chosen and treated for 36 h at 42°C. From the phenotypic observation, the leaves of WT *Arabidopsis* showed obvious withering and curling compared with those of the transgenic *Arabidopsis* lines (**Figures 11A,B**). However, the leaves of the line #14 were slightly curled, and the leaves of the line #3 were not significantly damaged. The results indicated that the damage of transgenic plants under heat stress was lower than that of the WT *Arabidopsis*. The expression level changes of *ZmPAO6* gene in the lines # 3 and # 14 before and after heat stress treatment were determined by qRT-PCR (**Figure 11C**). The results revealed that the expression levels of *ZmPAO6* gene in the lines # 3 and # 14 were up-regulated significantly after heat stress, indicating that the overexpression of *ZmPAO6* gene could enhance thermotolerance of transgenic *Arabidopsis* plants.

After heat stress treatment, the PA contents of the WT and transgenic plants were further determined (**Figures 11D–F**). Compared with the control, the Put content of transgenic plants decreased slightly or remained unchanged, while the Put content of WT plants increased, which were slightly higher than those of transgenic plants (**Figure 11D**). The Spm content of the WT and transgenic *Arabidopsis* increased, but the increasing of Spm content in WT *Arabidopsis* was higher than that in transgenic *Arabidopsis* plants (the lines # 3 and # 14; **Figure 11E**). In addition, the Spd content of all plants increased after heat treatment. Notably, the Spd content of the WT *Arabidopsis* were much lower than those of the transgenic plants (**Figure 11F**). This result further indicated that *ZmPAO6* gene is likely to mainly participate in back-conversion reaction of PAs. Furthermore, to explore molecular mechanism of heat tolerance of transgenic *Arabidopsis* in response to heat stress, the analyses of H_2O_2, MDA and chlorophyll contents were further determined according to the physiological methods (**Figures 11G–I**). The results demonstrated that the contents of H_2O_2 in the WT and transgenic plants increased under heat stress treatment compared with those under the control condition. However, the content of H_2O_2 in the WT *Arabidopsis* was obviously

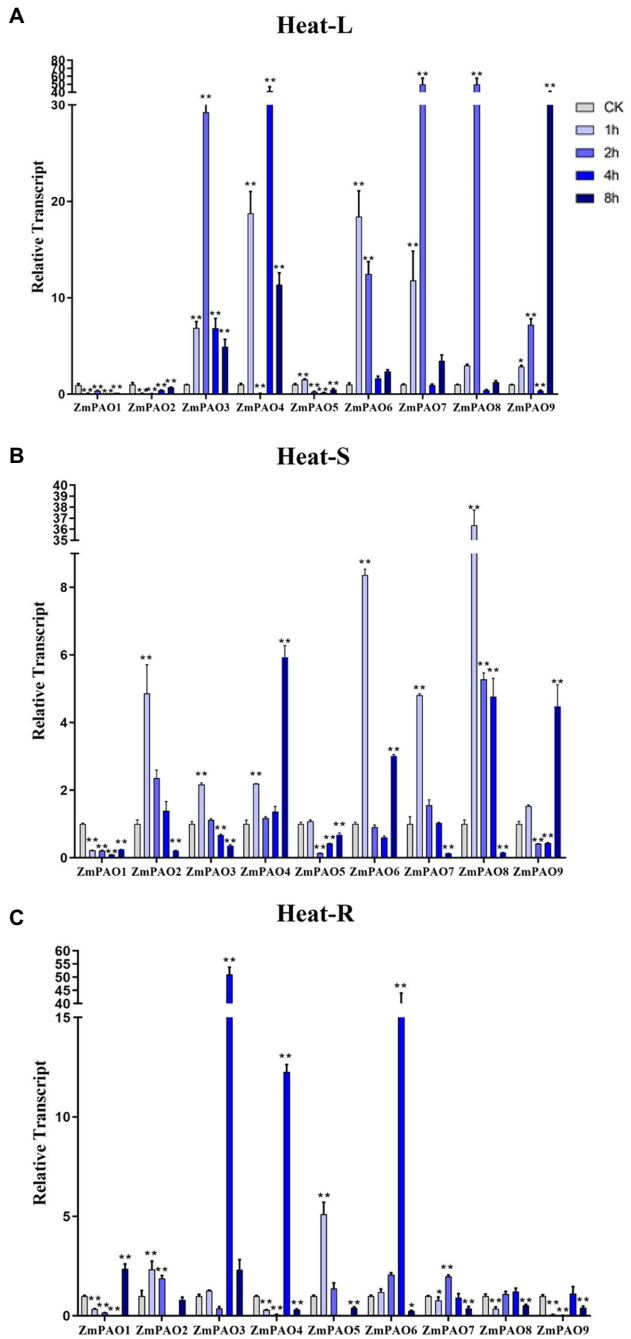


FIGURE 7 | Expression profiles of *ZmPAO* genes under heat stress treatment in different tissues. qRT-PCR data was normalized using *ZmActin* gene. **(A–C)** Expression profiles of *ZmPAO* genes under heat treatment (42°C) in leaves, stems, and roots, respectively. Error bars are caused by three biological replicates. Asterisks above the error bars represent statistical significance using one-way ANOVA and a Fisher's least significant difference (LSD). * Significantly different at $p < 0.05$; ** significantly different at $p < 0.01$.

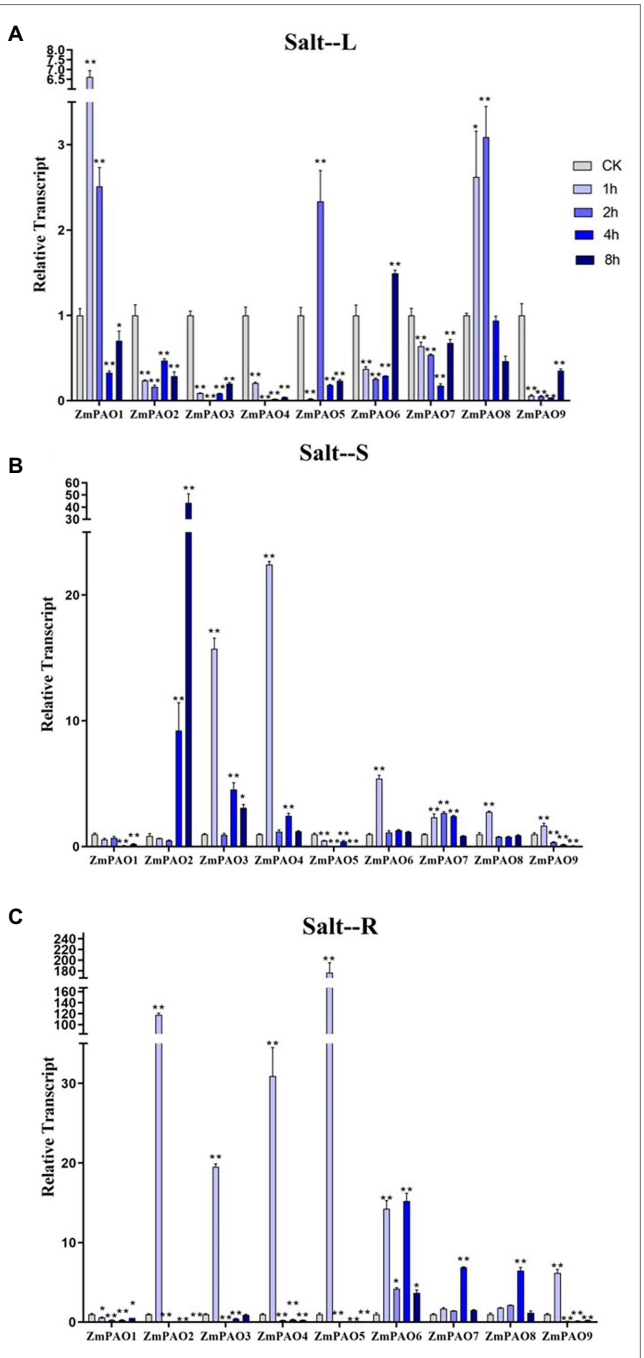


FIGURE 8 | Expression profiles of *ZmPAO* genes under salt stress treatment in different tissues. qRT-PCR data was normalized using *ZmActin* gene. **(A–C)** Expression profiles of *ZmPAO* genes under salt treatment with 200 mM NaCl in leaves, stems, and roots, respectively. Error bars are caused by three biological replicates. Asterisks above the error bars represent statistical significance using one-way ANOVA and a Fisher's LSD. * Significantly different at $p < 0.05$; ** significantly different at $p < 0.01$.

higher than those in the transgenic *Arabidopsis* lines. Therefore, the *ZmPAO6* gene could be involved in modulating heat-induced H_2O_2 accumulation through the catabolism pathways of polyamines in transgenic *Arabidopsis* plants to maintain the dynamic balance of H_2O_2 in the cell of plants and thereby enhancing thermotolerance of plants. In addition, the MDA contents both in WT *Arabidopsis* and in transgenic plants also increased after heat stress treatment, but the MDA content of

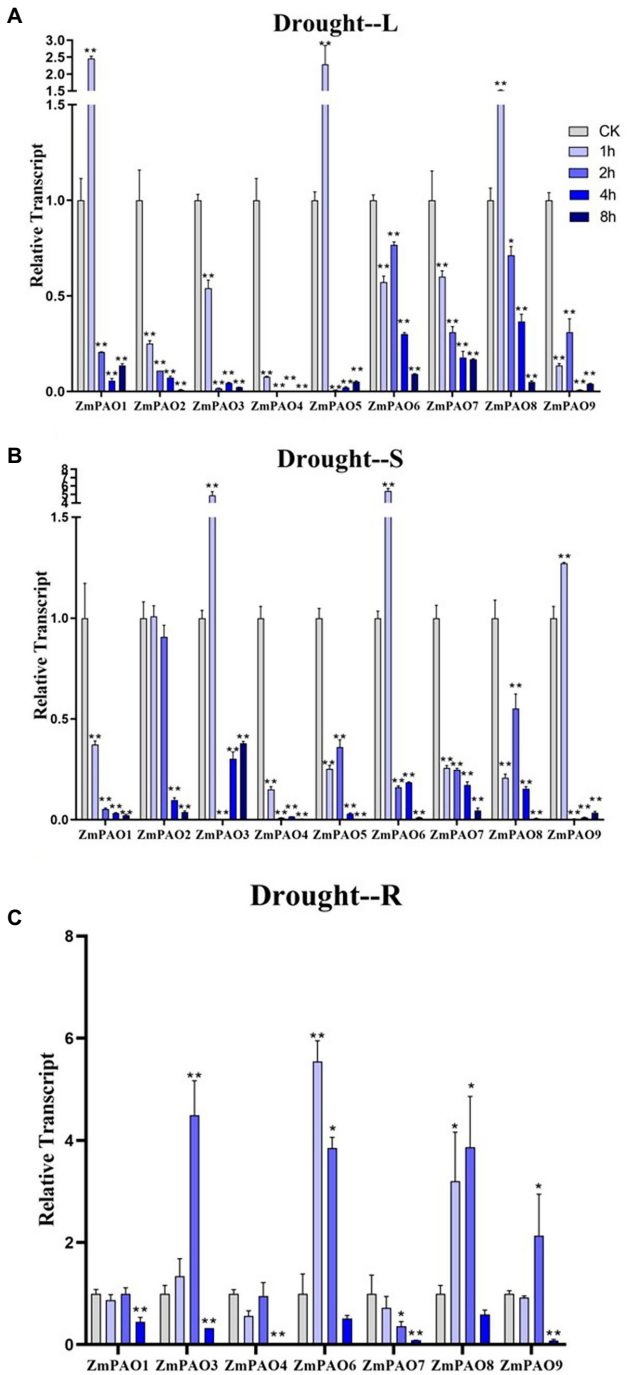


FIGURE 9 | Expression profiles of *ZmPAO* genes under drought stress treatment in different tissues. qRT-PCR data was normalized using *ZmActin* gene. **(A–C)** Expression profiles of *ZmPAO* genes under drought stress in leaves, stems, and roots, respectively. Error bars are caused by three biological replicates. Asterisks above the error bars represent statistical significance using one-way ANOVA and a Fisher's LSD. * Significantly different at $p < 0.05$; ** significantly different at $p < 0.01$.

WT *Arabidopsis* was higher than those of the transgenic *Arabidopsis* lines, indicating that the cells in the WT *Arabidopsis* were damaged more deeply than those in the transgenic *Arabidopsis* plants. Notably, the chlorophyll contents of the WT and transgenic *Arabidopsis* lines decreased after heat stress treatment. However, the chlorophyll contents of the transgenic *Arabidopsis* lines were higher than those of the WT *Arabidopsis*, suggesting that an enhanced heat resistance could occur in the transgenic *Arabidopsis* lines compared with in the WT *Arabidopsis*.

To further confirm the role of the *ZmPAO6* gene in regulating the dynamic balance of H_2O_2 in the transgenic *Arabidopsis* plants, the expression levels of some antioxidase genes (*AtGPX1-8* and *AtAPX1-8*) published in the previous studies after heat stress treatment were further determined in this study (**Figures 11J–M**). Under the control condition, the expression levels of most of *AtGPX* genes in the transgenic *Arabidopsis* plant (line #3) were higher than that of the WT *Arabidopsis*. However, under heat stress treatment, the expression levels of all *AtGPX* genes in the transgenic *Arabidopsis* plant (line #3) were significantly enhanced. Notably, the expression level of *AtGPX8* gene in the transgenic *Arabidopsis* plant was higher at more than 60 times than that in the WT Arabidopsis. Likewise, in the control group, the expression levels of only three genes (*AtAPX1*, *AtAPX3*, and *AtAPX4*) in the transgenic *Arabidopsis* plant were significantly higher than those in the WT *Arabidopsis*, while the expression levels of the other *AtAPX* genes in the transgenic *Arabidopsis* plant were the same as or lower than those in the WT *Arabidopsis*. However, after heat stress treatment, the expression levels of some genes such as *AtAPX3*, *AtAPX6*, and *AtAPX7* were significantly up-regulated in the transgenic *Arabidopsis* plant compared with those in the WT *Arabidopsis*, indicating that the expression levels of *AtAPX3*, *AtAPX6*, and *AtAPX7* genes can be induced intensively in the transgenic *Arabidopsis* plants in response to heat stress to further enhance the scavenging ability of hydrogen peroxide in cells of plants. Taken together, these results demonstrated that the *ZmPAO6* gene can enhance heat resistance in transgenic *Arabidopsis* through modulating heat-induced H_2O_2 accumulation in polyamine catabolism.

DISCUSSION

In plants, PAs play a vital role in regulating the growth and development and protecting the plants from adverse environment including biotic and abiotic stresses. However, the catabolism of PAs in maize is not well understood. The purpose of this study is to screen key *ZmPAO* genes that are more sensitive to abiotic stresses and to lay a foundation for further revealing the regulatory mechanism of *PAO* genes in maize. Meanwhile, the possible mechanism of *ZmPAO6* gene conferring the thermotolerance in the transgenic *Arabidopsis* plants in response to heat stress was also determined in this study.

Characterization of *PAO* Genes in Maize and Evolution of ZmPAO Proteins

An increasing number of studies have been devoted to elucidating the function of plant *PAO* genes in growth and stress responses. Until now, 5, 6, and 7 *PAO* genes have been identified in

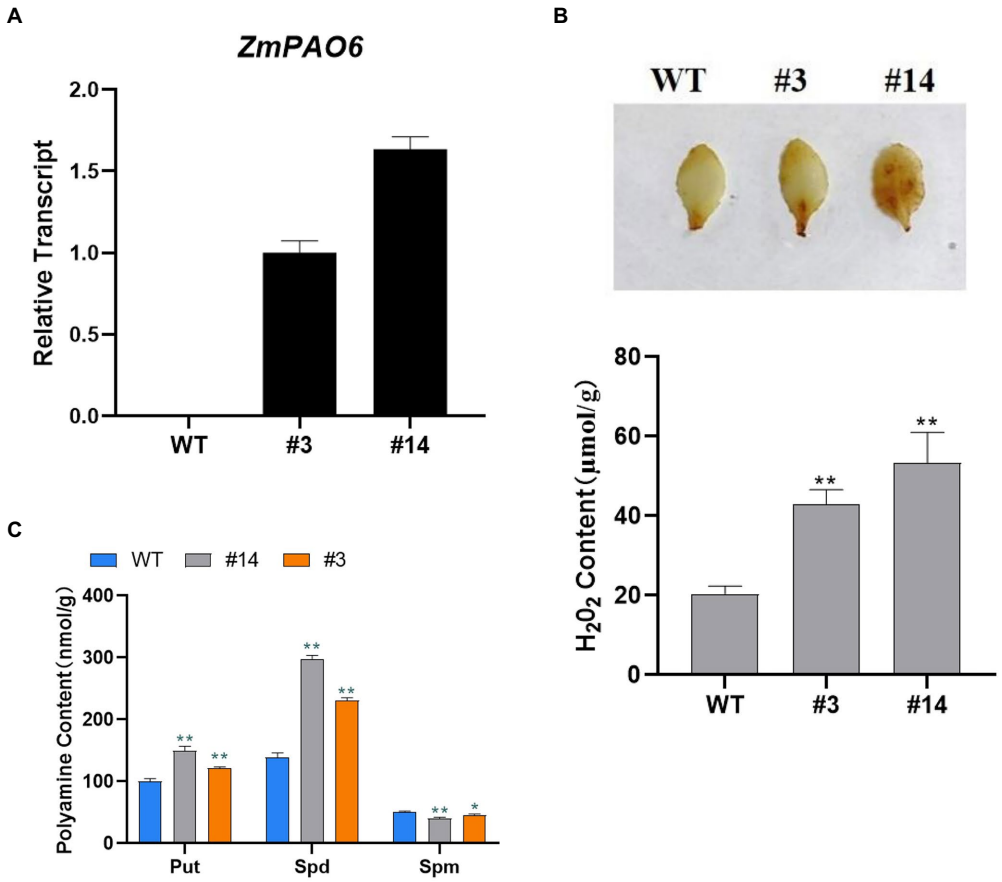


FIGURE 10 | Overexpression of *ZmPAO6* gene leads to changes in characteristics of transgenic *Arabidopsis*. **(A)** Molecular characterization of transgenic lines by qRT-PCR analysis. **(B)** H_2O_2 contents in WT and transgenic lines. **(C)** PAs contents in WT *Arabidopsis* and transgenic lines detected by HPLC. Error bars are caused by three biological replicates. Asterisks above the error bars represent statistical significance using one-way ANOVA and a Fisher's LSD. * Significantly different at $p < 0.05$; ** significantly different at $p < 0.01$.

Arabidopsis, sweet orange, and rice, respectively (Fincato et al., 2011; Ono et al., 2012; Wang and Liu, 2015). In this study, a total of nine *ZmPAO* genes were firstly identified from the latest maize B73 genome database. The number of *PAO* genes in maize was similar to that in rice. Phylogenetic analysis demonstrated that the plant *PAO* genes were generally classified into four clades, whereas the members of maize were mainly divided into the Groups I, II, and IV but not into the Group III. Notably, the *PAO* genes in maize were closer to that in rice in phylogenetic relationship compared with those in the other species, indicating that the evolution of the *PAO* genes may occur after divergence of monocots and dicots. Furthermore, it was revealed that the result of multiple sequence alignment was consistent with that of phylogenetic relationship analysis and that among the members of the same group of PAO proteins in these plants higher identities were shared for each other, indicating that the plant PAO proteins might be highly conversed in evolution. Interestingly, AtPAO2-4 and OsPAO3-5 were localized in peroxisomes based on possessing (S/A/C)(K/R/H)(L/M) in their C-termini (Fincato et al., 2011; Ono et al., 2012). In this study, presence of SRL sequence in the C-termini of maize ZmPAO4, ZmPAO6, and ZmPAO9 and presence of CRL sequence in the C-termini of maize ZmPAO3 suggest that in the Group I, all the PAO proteins from rice, Arabidopsis and maize carry peroxisome targeting signals at their C-termini. These data suggested that these ZmPAO proteins in the Group I may be localized in peroxisomes. Notably, the *ZmPAO2* gene had no introns in gene structure, suggesting that *ZmPAO2* likely has different functions than the other *ZmPAO* genes. In addition, the analysis of the conserved domain of ZmPAO proteins was performed to confirm that all nine ZmPAO proteins contained amine-oxidase domains, indicating that these proteins were highly conserved. The analysis of gene structures and conserved motifs of ZmPAO proteins demonstrated that the members in the same subfamily have similar structures and even the same or similar motifs. The analysis of gene duplication events of *ZmPAO* genes further elaborated that two pairs of genes (*ZmPAO3*/*ZmPAO4* and *ZmPAO6*/*ZmPAO9*) could be resulted from segmental duplication during their process of evolution, indicating that segmental duplication events might play a vital role in the evolution of *PAO* gene family in maize.

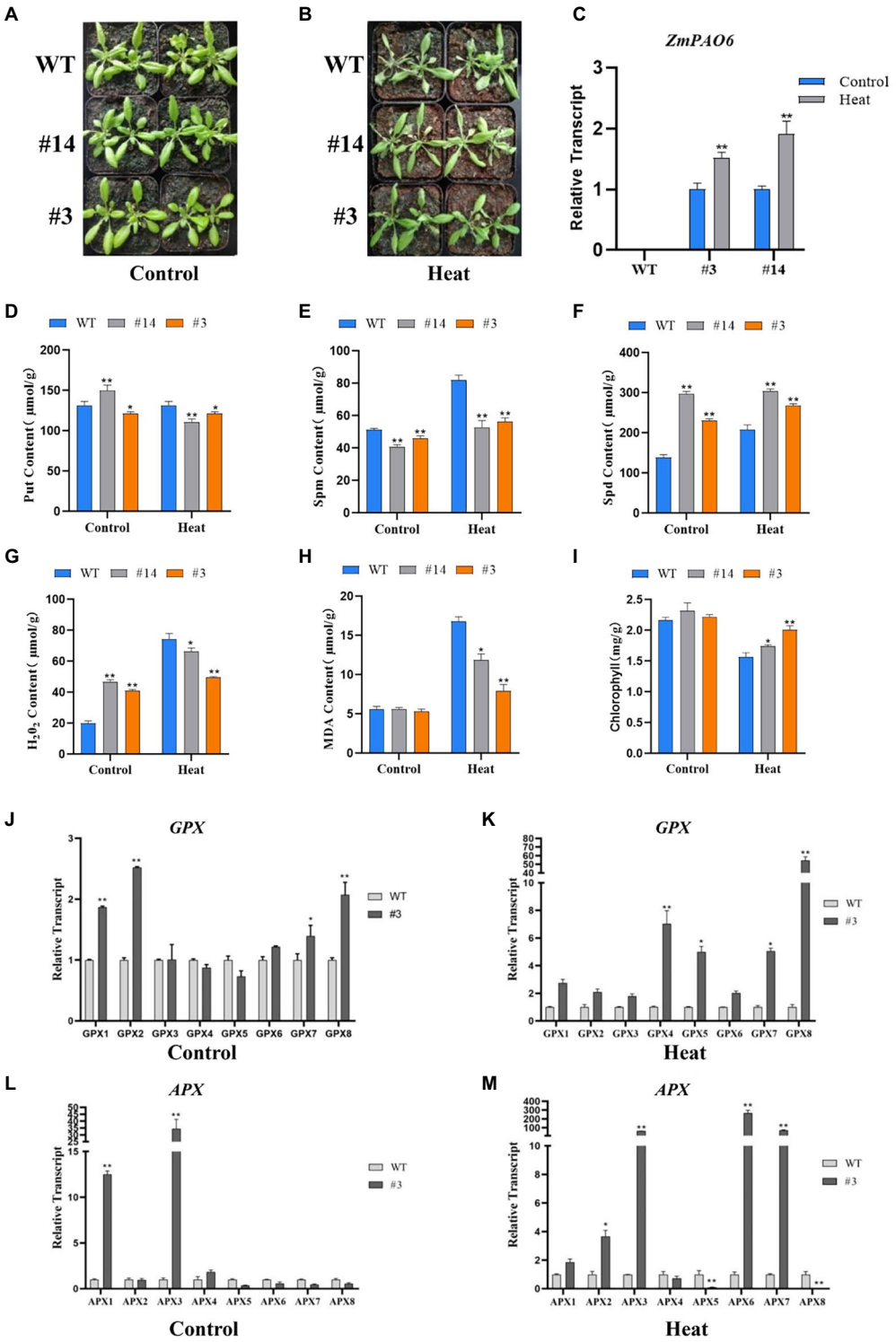


FIGURE 11 | Overexpression of *ZmPAO6* gene enhances heat tolerance in *Arabidopsis*. **(A,B)** The growth status of WT *Arabidopsis* and transgenic lines during heat stress treatment. **(C)** Expression profiles of *ZmPAO6* gene in WT *Arabidopsis* and the transgenic lines under control and heat stress treatment. **(D–F)** Analysis of Put, Spm and Spd contents in WT *Arabidopsis* and the transgenic lines under control and heat stress treatment. **(G–I)** The change of H_2O_2, MDA, and Chlorophyll contents in seedlings leaves. **(J–M)** The expression levels of *AtGPX1-8* and *AtAPX1-8* under control and heat stress treatment. Error bars are caused by three biological replicates. Asterisks above the error bars represent statistical significance using one-way ANOVA and a Fisher's LSD. * Significantly different at $p < 0.05$; ** significantly different at $p < 0.01$.

Expression Profiles Analysis of *ZmPAO* Genes in Response to Abiotic Stresses

The dynamic balance of intracellular polyamines was attributed to the regulation of PA biosynthesis and catabolism. Previous studies have shown that the dynamic balance of PAs could be challenged under adverse environmental conditions. For instance, the excessive accumulation of PAs caused by various abiotic stresses requires more PAO proteins to rebalance the dynamic balance of polyamines (Wang et al., 2011; Minocha et al., 2014). It was reported that a spaceflight induced wheat mutant, named salinity tolerance 1 (*st1*), is a salinity-tolerant line. In the salt-treated wheat mutant *st1*, genes encoding polyamine oxidase showed higher expression compared with the salt-treated WT, indicating that these genes may play a crucial role in salinity tolerance in *st1* mutant (Xiong et al., 2017). Moreover, previous studies have reported that polyamine oxidase encoding extracellular enzyme in rice may play a key role in the protection of plant cells (Sagor et al., 2021). Therefore, it is necessary to analyze the expression patterns of *ZmPAO* genes under various abiotic stresses. This study demonstrated that the expression levels of most *ZmPAO* genes were up-regulated under heat and salt treatments. In addition, except for the up-regulation of expression levels of *ZmPAO1*, *ZmPAO5*, and *ZmPAO8* genes in the early stage of stress, almost all *ZmPAO* genes in stems and leaves were down-regulated under drought treatment. These results suggested that maize *PAO* genes could be involved in various abiotic stress responses.

Ectopic Overexpression of *ZmPAO6* Enhances Heat Tolerance in Transgenic *Arabidopsis*

To adequately comprehend the role of *PAO* genes in plant development and abiotic stresses, it is crucial to conduct in-depth research by overexpressed transgenic plants, which will be helpful in further exploring the biochemical and physiological roles of these *PAO* genes in maize. PAOs have been proved to be the pivotal enzymes in regulating the levels of intracellular PAs, and the dynamic balance of PAs is essential for plant development (Handa and Mattoo, 2010; Tiburcio et al., 2014). The stress resistance of plants mainly depends on stress-responsive genes, and the overexpression of these genes could improve the adaptability of plants to various environmental stresses (Alcázar et al., 2006). According to the phylogenetic analysis and expression patterns of *ZmPAO* genes under various abiotic stresses in this study, the *ZmPAO6* gene was selected for performing the preliminary functional verification experiments under heat stress treatment to further reveal if this newly-identified gene could function in improving heat tolerance in transgenic *Arabidopsis* plants. Thus, the *ZmPAO6* gene was overexpressed in *Arabidopsis* by genetic transformation. Under control condition, overexpression of *ZmPAO6* resulted in an increased production of H_2O_2. Similarly, a previous study showed that overexpression of *AtPAO3* resulted to an increased production of H_2O_2 in *Arabidopsis* (Andronis et al., 2014). Moreover, ectopic overexpression of *AtPAO5* enhanced the conversion of lateral root primordia into shoots and influenced the PA homeostasis during this period, and resulted in elevated ROS level in the lateral root primordia of *Arabidopsis* (Kaszler et al., 2021). Therefore, overexpression of *ZmPAO6* in transgenic *Arabidopsis* may also share similar functional effects in this study. Moreover, high temperature is a vital environmental factor that affects plant growth and crop yield (Iba, 2002). In this study, compared with the WT *Arabidopsis*, the leaves of transgenic *Arabidopsis* plants maintained a better green and stretched state. After heat stress treatment, the phenotype and physiological indicators of the WT and transgenic *Arabidopsis* plants exhibited apparent different changes. Further studies demonstrated that the transgenic *Arabidopsis* plants had better growth vitality under heat stress treatment, indicating that the overexpression of *ZmPAO6* gene in the transgenic *Arabidopsis* conferred its tolerance to heat stress. The enhancement of adaptability of these transgenic plants in response to heat stress was required for the synchronous adaptation of external morphological and biochemical levels.

In previous studies, the plant protection depended on increased levels of H_2O_2 produced by Spm oxidation, implying that the catabolism of PAs mainly including Spm catalyzed by PAOs has been considered to be a crucial component of the plant defense response (Gonzalez et al., 2011). In this study, under normal and heat stress conditions, *Arabidopsis* plants overexpressing the *ZmPAO6* gene showed lower Spm contents compared with WT *Arabidopsis*, indicating that *ZmPAO6* may be involved in the back-conversion reactions of PAs, which is mainly involved in the oxidation of Spm to Spd. Accordingly, the Spd content of transgenic *Arabidopsis* was higher than those of WT *Arabidopsis*. Therefore, the results in this study suggested that plant-specific PA degradation (mainly Spm) may play a vital role in plant defense. Furthermore, MDA is used as a widely marker of lipid oxidation damage at the physiological level of plants, which reflects the level of membrane lipid peroxidation in plants to measure the degree of oxidative stress (Davey et al., 2005). In this study, less accumulation of MDA was detected in the *ZmPAO6*-overexpressed transgenic *Arabidopsis* lines compared with that in the WT *Arabidopsis*, which indicated that the overexpression of *ZmPAO6* gene could maintain the stability of lipid membrane structure under heat stress treatment.

In addition, the plants are likely to regulate stress resistance by complex signal regulatory pathways under various abiotic stresses. Among them, one of the consequences of abiotic stresses is to increase the concentration of intracellular ROS (Apel and Hirt, 2004). H_2O_2 was initially considered to be a toxic reactive oxygen species because of its damage to a variety of cell structures. In addition, H_2O_2 complements, cooperates or antagonizes many cellular regulatory circuits through positive interactions with other signals and plant hormones in growth, development and stress responses (Quan et al., 2008; Petrov and Van Breusegem, 2012). H_2O_2 is a vital molecule involved in signal transduction and plant defense responses, which is constantly generated from a variety of sources, including PA catabolism (Moschou et al., 2008a; Cheng et al., 2015; Jasso-Robles et al., 2020). Therefore, before the experiment, we hypothesized that the H_2O_2 content of transgenic *Arabidopsis* was higher than that of WT *Arabidopsis* under heat stress, and this could in turn affect the heat resistance of transgenic *Arabidopsis*. However, in this study,

contrary to our expectations, H_2O_2 contents in transgenic *Arabidopsis* lines were significantly lower than that in WT *Arabidopsis* under heat stress treatment. A previous study showed that ABA enhanced the accumulation of PA in grape and induced the PA oxidation pathway (Toumi et al., 2010). The accumulated PAs was mainly oxidized in the apoplast to produce H_2O_2 which integrated the signal pathway. The PAO generated apoplastic H_2O_2 resulting from osmotic stress acted as a secondary messenger in the signaling pathway and/or induces PCD in grape (Toumi et al., 2010). Under normal and stress conditions, maintaining the appropriate balance of PA catabolic pathways with the H_2O_2 dual action is helpful to clarify the adaptation mechanisms of plants (Yoda et al., 2009; Andronis et al., 2014). Therefore, we have reason to speculate that the overexpression of *ZmPAO6* gene may maintain the balance between PA catabolism and H_2O_2 in transgenic *Arabidopsis* under heat stress treatment. Taking together, although the H_2O_2 levels of WT and transgenic *Arabidopsis* plants increased significantly under heat stress treatment, the H_2O_2 contents in the transgenic plants were lower than those of the WT *Arabidopsis*, indicating that overexpression of *ZmPAO6* gene can result in the reduced accumulation of heat-induced H_2O_2 content, which suggested that maize PAO proteins might be crucial for modulating the dynamic balance of H_2O_2 in transgenic *Arabidopsis*.

To further explore the underlying molecular mechanism of H_2O_2 pathways involved in heat stress, the expression levels of glutathione peroxidase (*GPX*) and ascorbate peroxidase (*APX*) genes were investigated in this study, which belong to the main antioxidant enzymes for H_2O_2 scavenging and can catalyze the reduction of H_2O_2 to prevent the potential cell damage caused by H_2O_2 (Ozyigit et al., 2016). In this study, the expression levels of antioxidant enzyme genes (*AtGPX1-8* and *AtAPX1-8*) in the WT and transgenic *Arabidopsis* plants were determined under the control and heat stress treatment conditions, respectively. In this study, after heat stress treatment, the expression levels of most *AtGPX* and *AtAPX* genes in transgenic *Arabidopsis* plants were apparently greater than that of the WT *Arabidopsis*, especially the *AtGPX* genes. In addition, it has been revealed that the exogenous H_2O_2 increased the expression levels of *APX* genes in tomato seedlings under salinity-alkalinity stress (Xu et al., 2021). Therefore, the increased expression of most *AtAPX* and *AtGPX* genes in transgenic *Arabidopsis* lines may be resulted from the enhanced H_2O_2 contents exhibited in these lines. We speculate that the overexpressed *ZmPAO6* gene in transgenic *Arabidopsis* produced the corresponding polyamine oxidase to catalyze the decomposition of PA accumulated under heat stress treatment to produce H_2O_2. Moreover, compared with the WT *Arabidopsis*, the expression levels of antioxidant enzymes genes in transgenic plants were up-regulated. Studies have shown that all eight *APX* genes of *Arabidopsis* participated in the processes of growth and development and abiotic stress response (Li et al., 2019). Recent evidence suggested that GPXs can protect cells from stress-induced oxidative damages and function as a vital component of growth and development in plants (Bela et al., 2015). Moreover, the accumulation of ROS is regulated by a complex antioxidant scavenging system, including GRX, SOD, APX, etc., that function as antioxidants and allow the transmission of oxidative signals (Singh et al., 2022). Therefore, these data suggested that increased the activity of some key antioxidant enzymes and reduced heat-induced H_2O_2 accumulation, thus enhancing stress resistance of the transgenic plants. In this study, the H_2O_2 contents of transgenic *Arabidopsis* plants were lower than those of WT *Arabidopsis*, perhaps due to the increased activity of AtAPX and AtGPX enzymes, which is likely to scavenge excess H_2O_2. However, further studies are required for clarifying whether the increased expression levels of these antioxidant enzyme genes control the H_2O_2 content or whether the H_2O_2 content controls the induction of these genes or enzymes. Although it may be involved in some complicated metabolic processes, it is worth studying carefully to further understand the regulation of H_2O_2 homeostasis. In conclusion, alterations in PA catabolism affect the levels of H_2O_2 and the expression levels of *AtAPX* and *AtGPX* genes that enhance the antioxidant defense of the plants, suggesting a link between the *ZmPAO6* gene and other enzymes involved in H_2O_2 homeostasis in transgenic *Arabidopsis*, and indicating that this gene can enhance heat resistance in transgenic *Arabidopsis* through modulating heat-induced H_2O_2 accumulation in polyamine catabolism.

Furthermore, we proposed a model of the *ZmPAO6* gene involved in PA catabolism and H_2O_2 homeostasis in transgenic *Arabidopsis* (**Figure 12**). Under heat stress treatment, the expression level of *ZmPAO6* gene was up-regulated, and the corresponding activity of polyamine oxidase was also increased, which may promote the decomposition of PAs (mainly Spm) to produce H_2O_2. In addition, H_2O_2 may be used as a signal molecule to increase the expression levels of *AtAPX* and *AtGPX* genes to accelerate the degradation of H_2O_2. On the other hand, heat stress causes the accumulation of H_2O_2 in transgenic *Arabidopsis*, which may also act on related antioxidant enzyme genes. In addition, *Arabidopsis* plants overexpressing the *ZmPAO6* gene showed increased the expression levels of *AtAPX* and *AtGPX* genes, which represented an attempt to scavenge excess H_2O_2 generated from the oxidation of PAs catalyzed by potential ZmPAO6 protein. However, the exact mechanism is unknown for maintaining ROS homeostasis in regulating the heat stress response in transgenic *Arabidopsis*. Therefore, the positive regulatory mechanism of *ZmPAO6* gene in response to heat stress remains to be further elucidated in future.

CONCLUSION

In our study, a total of nine *PAO* genes were identified in maize, which were distributed on five chromosomes at different densities. These PAO proteins were mainly categorized into three distinct subfamilies based on the similarities of the amino acid sequences. The motif composition and exon/intron distribution were considerably conserved among the members of the same group or subgroup. The close phylogenetic relationship among PAO proteins of different species in the same subgroup provides insights into their putative functions. A comprehensive expression profile of all members of *PAO* gene family in maize suggests that

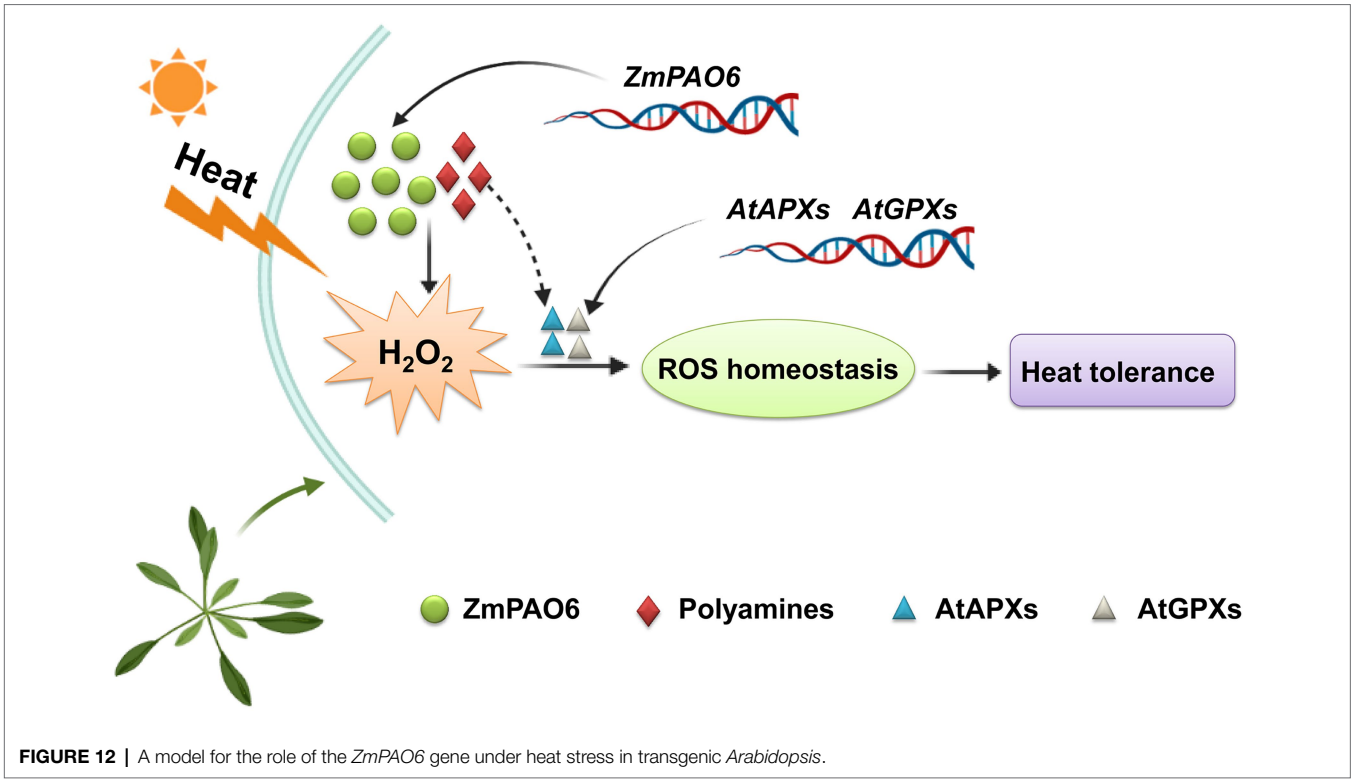


FIGURE 12 | A model for the role of the *ZmPAO6* gene under heat stress in transgenic *Arabidopsis*.

these genes play functional developmental roles in different tissues. Furthermore, the expression profiles of *ZmPAO* genes were up-regulated or down-regulated under three various abiotic stress treatments, indicating that these *PAO* genes may play a crucial role in resisting adverse environment of maize. Eventually, the functional analysis of the maize representative *ZmPAO6* gene in response to heat stress demonstrated that overexpression of *ZmPAO6* in transgenic *Arabidopsis* can confer enhanced heat tolerance through modulating heat-induced H_2O_2 accumulation in polyamine catabolism. Taken together, our results are the first to report the *ZmPAO6* gene response to heat stress in plants and will serve to present an important theoretical basis for further unraveling the function and regulatory mechanism of *ZmPAO* genes in growth, development and adaptation to abiotic stresses in maize.

DATA AVAILABILITY STATEMENT

The original contributions presented in the study are included in the article/**Supplementary Material**, further inquiries can be directed to the corresponding author.

ETHICS STATEMENT

These methods were carried out in accordance with relevant guidelines and regulations including the IUCN Policy Statement on Research Involving Species at Risk of Extinction and the Convention on the Trade in Endangered Species of Wild Fauna and Flora. We confirm that all experimental protocols were approved by Anhui Agriculture University and Anhui Normal University.

AUTHOR CONTRIBUTIONS

YQ, YX, WH, YZ, and XL designed the studies, carried out all the experimental analyses, and prepared all figures and tables. YX and WH drafted the manuscript. YQ assisted in explaining the results and revised the final manuscript. All authors contributed to the article and approved the submitted version.

FUNDING

This study was supported by grants from the National Natural Science Foundation of China (NSFC; grant no. 31571673) and the open fundings of National Engineering Laboratory of Crop Stress Resistance Breeding (grant no. KNZJ1023) and Anhui Provincial Key Laboratory of the Conservation and Exploitation of Biological Resources (grant no. Swzy202003) and Anhui Provincial Academic Funding Project for Top Talents in Disciplines (Majors; grant no. gxbjZD2021044). The funders had no role in the study design, collection, analysis, and interpretation of data, or in the writing of the report or decision to submit the article for publication.

ACKNOWLEDGMENTS

The authors are grateful to the editor and reviewers for critically evaluating the manuscript and providing constructive comments for its improvement.

SUPPLEMENTARY MATERIAL

The Supplementary Material for this article can be found online at: https://www.frontiersin.org/articles/10.3389/fpls.2022.950064/full#supplementary-material

REFERENCES

Ahmed, S., Ariyaratne, M., Patel, J., Howard, A. E., Kalinoski, A., Phuntumart, V., et al. (2017). Altered expression of polyamine transporters reveals a role for spermidine in the timing of flowering and other developmental response pathways. *Plant Sci.* 258, 146–155. doi: 10.1016/j.plantsci.2016.12.002

Alcázar, R., Marco, F., Cuevas, J. C., Patron, M., Ferrando, A., Carrasco, P., et al. (2006). Involvement of polyamines in plant response to abiotic stress. *Biotechnol. Lett.* 28, 1867–1876. doi: 10.1007/s10529-006-9179-3

Andronis, E. A., Moschou, P. N., Toumi, I., and Roubelakis-Angelakis, K. A. (2014). Peroxisomal polyamine oxidase and NADPH-oxidase cross-talk for ROS homeostasis which affects respiration rate in *Arabidopsis thaliana*. *Front. Plant Sci.* 5:132. doi: 10.3389/fpls.2014.00132

Angelini, R., Cona, A., Federico, R., Fincato, P., Tavladoraki, P., and Tisi, A. (2010). Plant amine oxidases "on the move": an update. *Plant Physiol. Biochem.* 48, 560–564. doi: 10.1016/j.plaphy.2010.02.001

Apel, K., and Hirt, H. (2004). Reactive oxygen species: metabolism, oxidative stress, and signal transduction. *Annu. Rev. Plant Biol.* 55, 373–399. doi: 10.1146/annurev.arplant.55.031903.141701

Bailey, T. L., Boden, M., Buske, F. A., Frith, M., Grant, C. E., Clementi, L., et al. (2009). MEME SUITE: tools for motif discovery and searching. *Nucleic Acids Res.* 37, W202–W208. doi: 10.1093/nar/gkp335

Bela, K., Horváth, E., Gallé, Á., Szabados, L., Tari, I., and Csiszár, J. (2015). Plant glutathione peroxidases: emerging role of the antioxidant enzymes in plant development and stress responses. *J. Plant Physiol.* 176, 192–201. doi: 10.1016/j.jplph.2014.12.014

Chang, W. C., Lee, T. Y., Huang, H. D., Huang, H. Y., and Pan, R. L. (2008). PlantPAN: Plant promoter analysis navigator, for identifying combinatorial cis-regulatory elements with distance constraint in plant gene groups. *BMC Genom.* 9:561. doi: 10.1186/1471-2164-9-561

Cheng, W. H., Wang, F. L., Cheng, X. Q., Zhu, Q. H., Sun, Y. Q., Zhu, H. G., et al. (2015). Polyamine and its metabolite H2O2 play a key role in the conversion of embryogenic callus into somatic embryos in upland cotton (*Gossypium hirsutum* L.). *Front. Plant Sci.* 6:1063. doi: 10.3389/fpls.2015.01063

Corpas, F. J., Del Río, L. A., and Palma, J. M. (2019). Plant peroxisomes at the crossroad of NO and H(2) O(2) metabolism. *J. Integr. Plant Biol.* 61, 803–816. doi: 10.1111/jipb.12772

da Silva, T. I., Dias, M. G., De Araújo, N. O., De Sousa Santos, M. N., Cruz, R. R. P., Dias, T. J., et al. (2022). Spermine reduces the harmful effects of salt stress in *Tropaeolum majus*. *Physiol. Mol. Biol. Plants* 28, 687–696. doi: 10.1007/s12298-022-01165-9

Davey, M. W., Stals, E., Panis, B., Keulemans, J., and Swennen, R. L. (2005). High-throughput determination of malondialdehyde in plant tissues. *Anal. Biochem.* 347, 201–207. doi: 10.1016/j.ab.2005.09.041

Fincato, P., Moschou, P. N., Spedaletti, V., Tavazza, R., Angelini, R., Federico, R., et al. (2011). Functional diversity inside the Arabidopsis polyamine oxidase gene family. *J. Exp. Bot.* 62, 1155–1168. doi: 10.1093/jxb/erq341

Fortes, A. M., and Agudelo-Romero, P. (2018). Polyamine metabolism in climacteric and non-climacteric fruit ripening. *Methods Mol. Biol.* 1694, 433–447. doi: 10.1007/978-1-4939-7398-9_36

Fu, X. Z., Chen, C. W., Wang, Y., Liu, J. H., and Moriguchi, T. (2011). Ectopic expression of MdSPDS1 in sweet orange (Citrus sinensis Osbeck) reduces canker susceptibility: involvement of H_2O_2 production and transcriptional alteration. *BMC Plant Biol.* 11:55. doi: 10.1186/1471-2229-11-55

Gonzalez, M. E., Marco, F., Minguet, E. G., Carrasco-Sorli, P., Blázquez, M. A., Carbonell, J., et al. (2011). Perturbation of spermine synthase gene expression and transcript profiling provide new insights on the role of the tetraamine spermine in Arabidopsis defense against Pseudomonas viridiflava. *Plant Physiol.* 156, 2266–2277. doi: 10.1104/pp.110.171413

Handa, A. K., and Mattoo, A. K. (2010). Differential and functional interactions emphasize the multiple roles of polyamines in plants. *Plant Physiol. Biochem.* 48, 540–546. doi: 10.1016/j.plaphy.2010.02.009

Hao, Y., Huang, B., Jia, D., Mann, T., Jiang, X., Qiu, Y., et al. (2018). Identification of seven polyamine oxidase genes in tomato (*Solanum lycopersicum* L.) and their expression profiles under physiological and various stress conditions. *J. Plant Physiol.* 228, 1–11. doi: 10.1016/j.jplph.2018.05.004

Hu, B., Jin, J., Guo, A. Y., Zhang, H., Luo, J., and Gao, G. (2015). GSDS 2.0: an upgraded gene feature visualization server. *Bioinformatics* 31, 1296–1297. doi: 10.1093/bioinformatics/btu817

Hu, W., Ren, Q., Chen, Y., Xu, G., and Qian, Y. (2021). Genome-wide identification and analysis of WRKY gene family in maize provide insights into regulatory network in response to abiotic stresses. *BMC Plant Biol.* 21:427. doi: 10.1186/s12870-021-03206-z

Hussain, S. S., Ali, M., Ahmad, M., and Siddique, K. H. (2011). Polyamines: natural and engineered abiotic and biotic stress tolerance in plants. *Biotechnol. Adv.* 29, 300–311. doi: 10.1016/j.biotechadv.2011.01.003

Iba, K. (2002). Acclimative response to temperature stress in higher plants: approaches of gene engineering for temperature tolerance. *Annu. Rev. Plant Biol.* 53, 225–245. doi: 10.1146/annurev.arplant.53.100201.160729

Igarashi, K., and Kashiwagi, K. (2000). Polyamines: mysterious modulators of cellular functions. *Biochem. Biophys. Res. Commun.* 271, 559–564. doi: 10.1006/bbrc.2000.2601

Ioannidis, N. E., Malliarakis, D., Torné, J. M., Santos, M., and Kotzabasis, K. (2016). The Over-expression of the plastidial transglutaminase from maize in Arabidopsis increases the activation threshold of photoprotection. *Front. Plant Sci.* 7:635. doi: 10.3389/fpls.2016.00635

Jasso-Robles, F. I., Gonzalez, M. E., Pieckenstain, F. L., Ramírez-García, J. M., Guerrero-González, M. L., Jiménez-Bremont, J. F., et al. (2020). Decrease of Arabidopsis PAO activity entails increased RBOH activity, ROS content and altered responses to Pseudomonas. *Plant Sci.* 292:110372. doi: 10.1016/j.plantsci.2019.110372

Kamada-Nobusada, T., Hayashi, M., Fukazawa, M., Sakakibara, H., and Nishimura, M. (2008). A putative peroxisomal polyamine oxidase, AtPAO4, is involved in polyamine catabolism in Arabidopsis thaliana. *Plant Cell Physiol.* 49, 1272–1282. doi: 10.1093/pcp/pcn114

Kaszler, N., Benkő, P., Bernula, D., Szepesi, Á., Fehér, A., and Gémes, K. (2021). Polyamine metabolism is involved in the direct regeneration of shoots from Arabidopsis lateral root primordia. *Plants (Basel)* 10:305. doi: 10.3390/plants10020305

Knott, J. M., Römer, P., and Sumper, M. (2007). Putative spermine synthases from *Thalassiosira pseudonana* and *Arabidopsis thaliana* synthesize thermospermine rather than spermine. *FEBS Lett.* 581, 3081–3086. doi: 10.1016/j.febslet.2007.05.074

Kumar, S., Stecher, G., and Tamura, K. (2016). MEGA7: Molecular Evolutionary Genetics Analysis Version 7.0 for Bigger Datasets. *Mol. Biol. Evol.* 33, 1870–1874. doi: 10.1093/molbev/msw054

Kusano, T., Berberich, T., Tateda, C., and Takahashi, Y. (2008). Polyamines: essential factors for growth and survival. *Planta* 228, 367–381. doi: 10.1007/s00425-008-0772-7

Li, Z. Q., Li, J. T., Bing, J., and Zhang, G. F. (2019). The role analysis of APX gene family in the growth and developmental processes and in response to abiotic stresses in *Arabidopsis thaliana*. *Yi Chuan* 41, 534–547. doi: 10.16288/j.yczz.19-026

Li, M., Lu, J., Tao, M., Li, M., Yang, H., Xia, E. H., et al. (2020). Genome-wide identification of seven polyamine oxidase genes in *Camellia sinensis* (L.) and their expression patterns under various abiotic stresses. *Front. Plant Sci.* 11:544933. doi: 10.3389/fpls.2020.544933

Liu, J. H., and Moriguchi, T. (2007). Changes in free polyamine titers and expression of polyamine biosynthetic genes during growth of peach in vitro callus. *Plant Cell Rep.* 26, 125–131. doi: 10.1007/s00299-006-0223-5

Liu, J. H., Wang, W., Wu, H., Gong, X., and Moriguchi, T. (2015). Polyamines function in stress tolerance: from synthesis to regulation. *Front. Plant Sci.* 6:827. doi: 10.3389/fpls.2015.00827

Ma, S., Zhou, X., Jahan, M. S., Guo, S., Tian, M., Zhou, R., et al. (2022). Putrescine regulates stomatal opening of cucumber leaves under salt stress via the H(2)O(2)-mediated signaling pathway. *Plant Physiol. Biochem.* 170, 87–97. doi: 10.1016/j.plaphy.2021.11.028

Minocha, R., Majumdar, R., and Minocha, S. C. (2014). Polyamines and abiotic stress in plants: a complex relationship. *Front. Plant Sci.* 5:175. doi: 10.3389/fpls.2014.00175

Mo, H., Wang, X., Zhang, Y., Zhang, G., Zhang, J., and Ma, Z. (2015). Cotton polyamine oxidase is required for spermine and camalexin signalling in the defence response to *Verticillium dahliae*. *Plant J.* 83, 962–975. doi: 10.1111/tpj.12941

Moschou, P. N., Paschalidis, K. A., Delis, I. D., Andriopoulou, A. H., Lagiotis, G. D., Yakoumakis, D. I., et al. (2008a). Spermidine exodus and oxidation in the apoplast induced by abiotic stress is responsible for H2O2 signatures that direct tolerance responses in tobacco. *Plant Cell* 20, 1708–1724. doi: 10.1105/tpc.108.059733

Moschou, P. N., Paschalidis, K. A., and Roubelakis-Angelakis, K. A. (2008b). Plant polyamine catabolism: The state of the art. *Plant Signal. Behav.* 3, 1061–1066. doi: 10.4161/psb.3.12.7172

Moschou, P. N., Wu, J., Cona, A., Tavladoraki, P., Angelini, R., and Roubelakis-Angelakis, K. A. (2012). The polyamines and their catabolic products are significant players in the turnover of nitrogenous molecules in plants. *J. Exp. Bot.* 63, 5003–5015. doi: 10.1093/jxb/ers202

Murray Stewart, T., Dunston, T. T., Woster, P. M., and Casero, R. A. Jr. (2018). Polyamine catabolism and oxidative damage. *J. Biol. Chem.* 293, 18736–18745. doi: 10.1074/jbc.TM118.003337

Ono, Y., Kim, D. W., Watanabe, K., Sasaki, A., Niitsu, M., Berberich, T., et al. (2012). Constitutively and highly expressed *Oryza sativa* polyamine oxidases localize in peroxisomes and catalyze polyamine back conversion. *Amino Acids* 42, 867–876. doi: 10.1007/s00726-011-1002-3

Ozyigit, I., Filiz, E., Vatansever, R., Kurtoglu, K. Y., Koc, I., Öztürk, M. X., et al. (2016). Identification and comparative analysis of H2O2-scavenging enzymes (ascorbate peroxidase and glutathione peroxidase) in selected plants employing bioinformatics approaches. *Front. Plant Sci.* 7:301. doi: 10.3389/fpls.2016.00301

Pál, M., Ivanovska, B., Oláh, T., Tajti, J., Hamow, K., Szalai, G., et al. (2019). Role of polyamines in plant growth regulation of Rht wheat mutants. *Plant Physiol. Biochem.* 137, 189–202. doi: 10.1016/j.plaphy.2019.02.013

Palacios-Rojas, N., Mcculley, L., Kaeppler, M., Titcomb, T. J., Gunaratna, N. S., Lopez-Ridaura, S., et al. (2020). Mining maize diversity and improving its nutritional aspects within agro-food systems. *Compr. Rev. Food Sci. Food Saf.* 19, 1809–1834. doi: 10.1111/1541-4337.12552

Pegg, A. E., and Casero, R. A. Jr. (2011). Current status of the polyamine research field. *Methods Mol. Biol.* 720, 3–35. doi: 10.1007/978-1-61779-034-8_1

Petrov, V. D., and Van Breusegem, F. (2012). Hydrogen peroxide-a central hub for information flow in plant cells. *AoB Plants* 2012:pls014. doi: 10.1093/aobpla/pls014

Planas-Portell, J., Gallart, M., Tiburcio, A. F., and Altabella, T. (2013). Copper-containing amine oxidases contribute to terminal polyamine oxidation in peroxisomes and apoplast of *Arabidopsis thaliana*. *BMC Plant Biol.* 13:109. doi: 10.1186/1471-2229-13-109

Quan, L. J., Zhang, B., Shi, W. W., and Li, H. Y. (2008). Hydrogen peroxide in plants: a versatile molecule of the reactive oxygen species network. *J. Integr. Plant Biol.* 50, 2–18. doi: 10.1111/j.1744-7909.2007.00599.x

Rao, X., Huang, X., Zhou, Z., and Lin, X. (2013). An improvement of the 2ˆ(−delta delta CT) method for quantitative real-time polymerase chain reaction data analysis. *Biostat. Bioinforma. Biomath.* 3, 71–85.

Rodríguez, A. A., Maiale, S. J., Menéndez, A. B., and Ruiz, O. A. (2009). Polyamine oxidase activity contributes to sustain maize leaf elongation under saline stress. *J. Exp. Bot.* 60, 4249–4262. doi: 10.1093/jxb/erp256

Sadeghipour, O. (2019). Polyamines protect mung bean [*Vigna radiata* (L.) Wilczek] plants against drought stress. *Biol. Futur.* 70, 71–78. doi: 10.1556/019.70.2019.09

Sagor, G. H. M., Inoue, M., Kusano, T., and Berberich, T. (2021). Expression profile of seven polyamine oxidase genes in rice (*Oryza sativa*) in response to abiotic stresses, phytohormones and polyamines. *Physiol. Mol. Biol. Plants* 27, 1353–1359. doi: 10.1007/s12298-021-01006-1

Sagor, G. H. M., Kusano, T., and Berberich, T. (2017). Identification of the actual coding region for polyamine oxidase 6 from rice (OsPAO6) and its partial characterization. *Plant Signal. Behav.* 12:e1359456. doi: 10.1080/15592324.2017.1359456

Sekhon, R. S., Lin, H., Childs, K. L., Hansey, C. N., Buell, C. R., De Leon, N., et al. (2011). Genome-wide atlas of transcription during maize development. *Plant J.* 66, 553–563. doi: 10.1111/j.1365-313X.2011.04527.x

Singh, A., Mehta, S., Yadav, S., Nagar, G., Ghosh, R., Roy, A., et al. (2022). How to cope with the challenges of environmental stresses in the era of global climate change: an update on ROS Stave off in plants. *Int. J. Mol. Sci.* 23:1995. doi: 10.3390/ijms23041995

Sobieszczuk-Nowicka, E., Kubala, S., Zmienko, A., Małecka, A., and Legocka, J. (2015). From accumulation to degradation: reprogramming polyamine metabolism facilitates dark-induced senescence in barley leaf cells. *Front. Plant Sci.* 6:1198. doi: 10.3389/fpls.2015.01198

Tavladoraki, P., Rossi, M. N., Saccuti, G., Perez-Amador, M. A., Polticelli, F., Angelini, R., et al. (2006). Heterologous expression and biochemical characterization of a polyamine oxidase from Arabidopsis involved in polyamine back conversion. *Plant Physiol.* 141, 1519–1532. doi: 10.1104/pp.106.080911

Tiburcio, A. F., Altabella, T., Bitrián, M., and Alcázar, R. (2014). The roles of polyamines during the lifespan of plants: from development to stress. *Planta* 240, 1–18. doi: 10.1007/s00425-014-2055-9

Toumi, I., Moschou, P. N., Paschalidis, K. A., Bouamama, B., Ben Salem-Fnayou, A., Ghorbel, A. W., et al. (2010). Abscisic acid signals reorientation of polyamine metabolism to orchestrate stress responses via the polyamine exodus pathway in grapevine. *J. Plant Physiol.* 167, 519–525. doi: 10.1016/j.jplph.2009.10.022

Wang, W., and Liu, J. H. (2015). Genome-wide identification and expression analysis of the polyamine oxidase gene family in sweet orange (*Citrus sinensis*). *Gene* 555, 421–429. doi: 10.1016/j.gene.2014.11.042

Wang, W., and Liu, J. H. (2016). CsPAO4 of *Citrus sinensis* functions in polyamine terminal catabolism and inhibits plant growth under salt stress. *Sci. Rep.* 6:31384. doi: 10.1038/srep31384

Wang, W., Paschalidis, K., Feng, J. C., Song, J., and Liu, J. H. (2019). Polyamine catabolism in plants: a universal process with diverse functions. *Front. Plant Sci.* 10:561. doi: 10.3389/fpls.2019.00561

Wang, J., Sun, P. P., Chen, C. L., Wang, Y., Fu, X. Z., and Liu, J. H. (2011). An arginine decarboxylase gene PtADC from *Poncirus trifoliata* confers abiotic stress tolerance and promotes primary root growth in Arabidopsis. *J. Exp. Bot.* 62, 2899–2914. doi: 10.1093/jxb/erq463

Wu, G., Bazer, F. W., Hu, J., Johnson, G. A., and Spencer, T. E. (2005). Polyamine synthesis from proline in the developing porcine placenta. *Biol. Reprod.* 72, 842–850. doi: 10.1095/biolreprod.104.036293

Wu, J., Shang, Z., Wu, J., Jiang, X., Moschou, P. N., Sun, W., et al. (2010). Spermidine oxidase-derived H_2O_2 regulates pollen plasma membrane hyperpolarization-activated Ca(2+) -permeable channels and pollen tube growth. *Plant J.* 63, 1042–1053. doi: 10.1111/j.1365-313X.2010.04301.x

Xiong, H., Guo, H., Xie, Y., Zhao, L., Gu, J., Zhao, S., et al. (2017). RNAseq analysis reveals pathways and candidate genes associated with salinity tolerance in a spaceflight-induced wheat mutant. *Sci. Rep.* 7:2731. doi: 10.1038/s41598-017-03024-0

Xu, J., Kang, Z., Zhu, K., Zhao, D., Yuan, Y., Yang, S., et al. (2021). RBOH1-dependent H(2)O(2) mediates spermine-induced antioxidant enzyme system to enhance tomato seedling tolerance to salinity-alkalinity stress. *Plant Physiol. Biochem.* 164, 237–246. doi: 10.1016/j.plaphy.2021.04.017

Yoda, H., Fujimura, K., Takahashi, H., Munemura, I., Uchimiya, H., and Sano, H. (2009). Polyamines as a common source of hydrogen peroxide in host- and nonhost hypersensitive response during pathogen infection. *Plant Mol. Biol.* 70, 103–112. doi: 10.1007/s11103-009-9459-0

Zhang, J., Liao, J., Ling, Q., Xi, Y., and Qian, Y. (2022). Genome-wide identification and expression profiling analysis of maize AP2/ERF superfamily genes reveal essential roles in abiotic stress tolerance. *BMC Genom.* 23:125. doi: 10.1186/s12864-022-08345-7

Zhao, J., Wang, X., Pan, X., Jiang, Q., and Xi, Z. (2021). Exogenous putrescine alleviates drought stress by altering reactive oxygen species scavenging and biosynthesis of polyamines in the seedlings of Cabernet Sauvignon. *Front. Plant Sci.* 12:767992. doi: 10.3389/fpls.2021.767992

Conflict of Interest: The authors declare that the research was conducted in the absence of any commercial or financial relationships that could be construed as a potential conflict of interest.

Publisher's Note: All claims expressed in this article are solely those of the authors and do not necessarily represent those of their affiliated organizations, or those of the publisher, the editors and the reviewers. Any product that may be evaluated in this article, or claim that may be made by its manufacturer, is not guaranteed or endorsed by the publisher.

Copyright © 2022 Xi, Hu, Zhou, Liu and Qian. This is an open-access article distributed under the terms of the Creative Commons Attribution License (CC BY). The use, distribution or reproduction in other forums is permitted, provided the original author(s) and the copyright owner(s) are credited and that the original publication in this journal is cited, in accordance with accepted academic practice. No use, distribution or reproduction is permitted which does not comply with these terms.

frontiers | Frontiers in Plant Science

TYPE Original Research
PUBLISHED 10 August 2022
DOI 10.3389/fpls.2022.968514

Check for updates

OPEN ACCESS

EDITED BY
Jiban Shrestha,
Nepal Agricultural Research Council, Nepal

REVIEWED BY
Muhammad Ahsan Farooq,
Zhejiang University,
China
Saad Farouk,
Mansoura University,
Egypt

*CORRESPONDENCE
Jihua Yu
yujihuagg@163.com

SPECIALTY SECTION
This article was submitted to Plant Abiotic Stress, a section of the journal Frontiers in Plant Science

RECEIVED 14 June 2022
ACCEPTED 25 July 2022
PUBLISHED 10 August 2022

CITATION
Lyu J, Jin N, Meng X, Jin L, Wang S, Xiao X, Liu Z, Tang Z and Yu J (2022) Exogenous silicon alleviates the adverse effects of cinnamic acid-induced autotoxicity stress on cucumber seedling growth. *Front. Plant Sci.* 13:968514. doi: 10.3389/fpls.2022.968514

COPYRIGHT
© 2022 Lyu, Jin, Meng, Jin, Wang, Xiao, Liu, Tang and Yu. This is an open-access article distributed under the terms of the Creative Commons Attribution License (CC BY). The use, distribution or reproduction in other forums is permitted, provided the original author(s) and the copyright owner(s) are credited and that the original publication in this journal is cited, in accordance with accepted academic practice. No use, distribution or reproduction is permitted which does not comply with these terms.

Exogenous silicon alleviates the adverse effects of cinnamic acid-induced autotoxicity stress on cucumber seedling growth

Jian Lyu[1,2], Ning Jin[1], Xin Meng[1], Li Jin[1], Shuya Wang[1], Xuemei Xiao[1], Zeci Liu[1], Zhongqi Tang[1] and Jihua Yu[1,2]*

[1]College of Horticulture, Gansu Agricultural University, Lanzhou, China, [2]State Key Laboratory of Arid Land Crop Science, Gansu Agricultural University, Lanzhou, China

Autotoxicity is a key factor that leads to obstacles in continuous cropping systems. Although Si is known to improve plant resistance to biotic and abiotic stresses, little is known about its role in regulating leaf water status, mineral nutrients, nitrogen metabolism, and root morphology of cucumber under autotoxicity stress. Here, we used cucumber seeds (*Cucumis sativus* L. cv. "Xinchun No. 4") to evaluate how exogenous Si (1mmolL^{-1}) affected the leaf water status, mineral nutrient uptake, N metabolism-related enzyme activities, root morphology, and shoot growth of cucumber seedlings under 0.8mmolL^{-1} CA-induced autotoxicity stress. We found that CA-induced autotoxicity significantly reduced the relative water content and water potential of leaves and increase their cell sap concentration. CA-induced stress also inhibited the absorption of major (N, P, K, Ca, Mg) and trace elements (Fe, Mn, Zn). However, exogenous Si significantly improved the leaf water status (relative water content and water potential) of cucumber leaves under CA-induced stress. Exogenous Si also promoted the absorption of mineral elements by seedlings under CA-induced stress and alleviated the CA-induced inhibition of N metabolism-related enzyme activities (including nitrate reductase, nitrite reductase, glutamine synthetase, glutamate synthase, glutamate dehydrogenase). Moreover, exogenous Si improved N uptake and utilization, promoted root morphogenesis, and increased the growth indexes of cucumber seedlings under CA-induced stress. Our findings have far-reaching implications for overcoming the obstacles to continuous cropping in cucumber cultivation.

KEYWORDS

silicon, cucumber, autotoxicity stress, mineral elements, nitrogen metabolism, root morphology

Introduction

Continuous cropping obstacle refers to the phenomenon where the successive plantation of the same crop on the same land leads to a decline in crop yield and quality. Continuous cropping obstacle is becoming increasingly severe in agricultural production worldwide, especially in facility cultivation. In particular, the continuous monoculture of

cucumber (*Cucumis sativus* L.)—a popular greenhouse vegetable—has caused increasingly prominent continuous cropping obstacles. This poses a major challenge to the sustainable development of cucumber facility agriculture (Xiao et al., 2019). The major reasons for continuous cropping obstacles are soil acidification, soil nutrient imbalance, autotoxicity, and microbial ecological imbalance (Bai et al., 2020; Zhang et al., 2020a). Of these, autotoxicity is a primary cause of continuous cropping obstacles and inhibits plant growth and development through the release of specific chemical substances into the surrounding environment. This mainly occurs through the volatilization and decomposition of plant leachates from the aerial parts, root exudates, and plant residues (Kato-Noguchi et al., 2018). In cucurbits—including cucumber (Xiao et al., 2020), watermelon (Ding et al., 2021), and melon (Zhang et al., 2021)—autotoxicity is caused by the excessive release of autotoxins secreted by the roots. Of these, cinnamic acid (CA) is the most important, and adversely affects plant growth and development through a range of physiological and biochemical changes (Yu and Matsui, 1994). However, current cultivation practices indicate that traditional methods to overcome continuous cropping obstacles are inefficient. For example, in melon cultivation, it usually takes 3–4 years of crop rotation to suppress continuous cropping obstacles caused by factors such as autotoxicity (Hu et al., 2017). However, this traditional practice of long-term crop rotation is increasingly unworkable under the existing cultivation model. Grafting is another agricultural measure that helps overcome obstacles to continuous cropping, but has been shown to adversely affect crop quality (Kyriacou et al., 2017; Miao et al., 2019). Hence, it is of utmost importance to find a new approach to effectively mitigate obstacles to the continuous cropping of cucumber, thus allowing the sustainable production of facility vegetables.

Si is the second most abundant element in Earth's crust after O_2, and is now considered a "quasi-essential" element (Al Murad et al., 2020). Si can be absorbed by plant roots in the form of soluble silicic acid at a pH of ≤9 (Abdelaal et al., 2020). The accumulation of Si in plants varies considerably depending on species and genotype. Most plants are non-silicon accumulators; Gramineae and Cyperaceae plants are usually high silicon accumulators; and Cucurbitaceae, Urticaceae, and Cruciferae plants are intermediate silicon accumulators (Mitani and Ma, 2005; Henriet et al., 2006). There is growing evidence that Si is a beneficial element for plants and that its accumulation positively contributes to plant growth and development under both abiotic and biotic stress conditions (Etesami and Jeong, 2018; Arif et al., 2021). Plants exposed to environmental stress respond by producing reactive oxygen species (ROS) that cause varying degrees of oxidative stress. Therefore, most research has focused on the mitigation of oxidative damage in plants through the Si-mediated modulation of antioxidant defense systems (both enzyme-enabled and non-enzyme-enabled components; Kim et al., 2017; Farouk and Al-Sanoussi, 2019). Si facilitates the alleviation of nutrient imbalance-induced stress, which in turn promotes plant growth, development, and yield (Fatemi et al., 2021). In a review, Souri et al. (2021) reported that Si effectively promoted plant seed germination, improved leaf water status and photosynthesis, and enhanced plant yield and quality. In a study on pepper plants, Jayawardana et al. (2014) showed that Si application improved branch and root morphology and improved pepper fruit quality by increasing mechanical strength, fruit hardness, and cuticle thickness.

Si is an environmentally friendly element due to its non-corrosive and non-polluting nature, and can applied to crops without the risk of harmful residues. Therefore, it is considered a high-quality fertilizer for the development of ecologically green agriculture (Etesami and Jeong, 2018). However, relatively few studies have reported the effects of Si on autotoxicity stress (an abiotic stress) in plants. Autotoxicity has been shown to significantly inhibit seed germination and subsequent seedling growth in melon. In particular, autotoxicity significantly reduced the photosynthetic pigment content, photosynthetic rate, transpiration rate, and water use efficiency of melon seedlings, which inhibited their growth (Zhang et al., 2021). Zhang et al. (2020b) demonstrated that appropriate concentrations of Si effectively alleviated autotoxicity stress in melon seeds, mainly by increasing starch degradation and the activities of enzymes such as amylase, superoxide dismutase, catalase, and peroxidase. In view of this, it is particularly important to explore the effects of Si on autotoxicity stress in cucumber. The effects of Si on ascorbate-glutathione metabolism and photosystem II responses in CA-treated cucumber seedlings have also been reported (Meng et al., 2021). However, no studies have reported the effects of Si on the water status, mineral nutrient uptake, N metabolism, and root morphology of cucumber seedlings under conditions of CA-induced autotoxicity stress. In this study, we evaluated the effects of Si on the above-mentioned indicators in cucumber seedlings under CA-induced autotoxicity stress. The results improve our understanding of Si alleviating physiological responses of cucumber seedlings under CA-induced autotoxicity stress and further reveal the mechanisms by which Si regulates CA resistance in cucumber plants. Our findings contribute to a new theoretical basis for overcoming barriers to continuous cropping in the facility-based cultivation of cucumber.

Materials and methods

Cultivation of the plant material

The cucumber seeds (*Cucumis sativus* L. cv. Xinchun No. 4) used in this study were purchased from the Gansu Academy of Agricultural Sciences, China. Neat and plump cucumber seeds were soaked for 8 h, sterilized for 15 min with 0.03% potassium permanganate solution, and placed in a Petri dish covered with two layers of filter paper (Wu et al., 2019). The culture dishes were placed in an artificial climate box (RDN-400E-4; Ningbo Dongnan Instrument Co. Ltd., Zhejiang, China) set to 28°C, and

the seeds were primed in the dark. Light culturing was performed when the germination rate exceeded 80%. After culturing for 5–6 days, cucumber seedlings with similar growth vigor were transplanted into a hydroponic box (4 plants/box), fixed with sponges, and further cultivated in an artificial climate box. During the cultivation period, the day and night temperatures were 28°C/18°C, the light intensity was 360 μmol·m^{-2}·s^{-1}, the photoperiod was 12 h, and the relative humidity was 75%. The nutrient solution used was Yamazaki's special nutrient formulation [3.5 mmol L^{-1} Ca $(NO_3)_2$·$4H_2O$, 6 mmol L^{-1} KNO_3, 1 mmol L^{-1} $NH_4H_2PO_4$, 2 mmol L^{-1} $MgSO_4$·$7H_2O$, 70 μmol L^{-1} $C_{10}H_{12}N_2O_8FeNa$·$3H_2O$, 10 μmol L^{-1} $MnSO_4$·$4H_2O$, and 50 μmol L^{-1} H_3BO_3] and was replaced every 2 days.

Experimental design

We divided cucumber seedlings with two leaves into four treatment groups as follows: (i) CK: normal nutrient solution; (ii) Si: normal nutrient solution with 1 mmol L^{-1} Si; (iii) CA: normal nutrient solution with 0.8 mmol L^{-1} CA; (V) CA + Si: normal nutrient solution with 0.8 mmol L^{-1} CA and 1 mmol L^{-1} Si. The CA concentration for medium stress (0.8 mmol L^{-1} CA) and the optimal Si concentration (1 mmol L^{-1} Si) for the alleviation CA-induced autotoxicity stress were selected based on our preliminary research (Meng et al., 2021). At 10 days after treatment, the cucumber seedlings were frozen with liquid nitrogen and stored at −80°C until further use. Each treatment was repeated thrice.

Growth indexes and measurement methods

Leaf moisture status

The relative water content (RWC) of leaves was determined according to Abdi et al. (2016) and calculated using the following formula:

$$\mathrm{RWC}\ (\%) = [(\mathrm{FW} - \mathrm{DW})/(\mathrm{TW} - \mathrm{DW})] \times 100$$

where FW is the fresh weight of the leaves (measured immediately after collection), TW is the leaf weight at full expansion (measured after floating the leaf in distilled water for 4 h at 25°C in the dark), and DW is the dry weight (measured after oven-drying the leaves at 70°C to constant weight). Each treatment included three biological replicates (Each replicate contains three leaves).

Leaf water potential was measured using a pressure chamber (Model 3,005; Soil Moisture Equipment Co. Ltd., Goleta, CA, United States; Bhusal et al., 2019), and the cell sap concentration of leaves was measured with an automatic refractometer (Jinan Haineng Instrument Co., Ltd.).

Mineral elements

The shoots and roots of cucumber plants were fixed at 105°C, dried at 80°C to constant weight, ground, sieved with a 0.25-mm sieve, and used for the measurement of mineral elements. Samples used for the measurement of total N, P, and K were digested by the H_2SO_4-H_2O_2 wet digestion method, and those used to measure total Ca, Mg, Cu, Fe, Mn, and Zn were dry-ashed in a muffle furnace. Total N was measured by the Kjeldahl method using a fully automatic Kjeldahl K1100F apparatus (Jinan Hanon Instruments Company, Jinan, China), and total P was measured using the Mo-Sb colorimetric method. Total K, Ca, Mg, Cu, Fe, Mn, and Zn were measured using a ZEEnit 700P atomic absorption spectrometer (Analytik Jena, Germany).

N metabolism-related enzyme activity

The activities of nitrate reductase (NR; EC 1.6.6.1), nitrite reductase (NiR; EC 1.7.1.15), glutamine synthase (GS; EC 6.3.1.2), glutamate synthase (GOGAT; EC 1.4.1.14), and glutamate dehydrogenase (GDH; EC 1.4.1.2) were measured using ELISA kits (Shanghai Yaji Biotechnology Co., Ltd.) according to the manufacturer's instructions. 1 g of chopped plant tissue was added to liquid nitrogen and ground into powder in a mortar. 9 ml of homogenate (0.01 mol/l PBS, pH: 7.2–7.4) was added, and the supernatant was collected after centrifugation. Then add the reagents in sequence according to the kit instructions. Finally, the absorbance at 450 nm was measured with HBS-1096A (DiTie, Nanjing, China) microplate reader. GDH enzyme activity was measured in mU·L^{-1}, and all other enzyme activities were measured in IU·L^{-1}.

Root morphology and growth indexes

The total root length, total root volume, total root surface area, number of root tips, number of branch roots, and leaf area were measured with a WinRHIZO System (WinRHIZO Pro LA2400; Regent Instruments Inc., Quebec, Canada). Plant height was measured with a ruler from the base of the plant to the stem tip, and the stem diameter was measured using vernier calipers. The shoots and roots of the cucumber plants were washed with ultrapure water, dried, and their fresh weights were recorded using an electronic balance. To measure the dry weight, the shoots and roots were oven-dried at 105°C for 15 min and then dried at 80°C to constant weight (Wu et al., 2019).

Statistical analysis

All tables and figures were created using Microsoft Excel 2010 (Microsoft Inc., Redmond, WA, United States). The data were analyzed by one-way analysis of variance (ANOVA) and significant differences were detected by Duncan's multiple range test ($p < 0.05$) using the SPSS software (IBM SPSS Statistics for Windows, version 22.0; IBM Corp., Armonk, NY, United States).

Results

Effect of exogenous Si on the leaf water status of cucumber seedlings under CA-induced autotoxicity stress

Treatment with CA significantly reduced the RWC of leaves by 11.48% compared with that of leaves in the CK treatment group (Figure 1A). However, there was no significant difference in RWC between the CA + Si and CK treatment groups. The leaf water potential was significantly lower in CA than in CK. Compared with the CA treatment, the CA + Si treatment alleviated the decline of leaf water potential in cucumber plants under autotoxicity stress. Moreover, the CA + Si treatment maintained the leaf water potential at a level that was not significantly different from that of plants in the CK treatment group (Figure 1B). The concentration of leaf cell sap was 19.32% higher in CA than in CK and 3.10% lower in CA + Si than in CA, although the difference between CA + Si and CA was not statistically significant (Figure 1A). There was no significant difference in RWC, leaf water potential, and leaf cell sap concentration between the Si and CK treatments (Figures 1A–C). These results indicated that CA-induced autotoxicity inhibited the absorption and utilization of water in leaves, reduced the leaf water potential, and increased the concentration of cell sap in leaves, which has adverse effects on their physiological and biochemical reactions. Moreover, the exogenous application of Si was beneficial for maintaining the normal water status of leaves under conditions of CA-induced stress.

Effect of exogenous Si on the mineral element composition of leaves and roots in cucumber seedlings under CA-induced autotoxicity stress

Major elements

CA-induced autotoxicity significantly affected the uptake of major elements (N, P, K, Ca, and Mg) by the leaves of cucumber seedlings (Figures 2A–E). Compared with the CK treatment, treatment with CA significantly reduced the N, P, and K contents of cucumber leaves by 7.81, 7.09, and 7.89%, respectively. However, treatment with CA + Si significantly increased the N and P contents of leaves by 34.99% and 7.63%, respectively, compared with those of leaves treated with *CA*. The K content of leaves in the CA + Si group increased by 2.77% compared with that of leaves in CA, but the difference was not significant. The N, P, and K contents of cucumber roots showed similar trends to those of leaves in each treatment group (Figures 2A–C). Compared with the CK treatment, treatment with CA significantly reduced the N and K

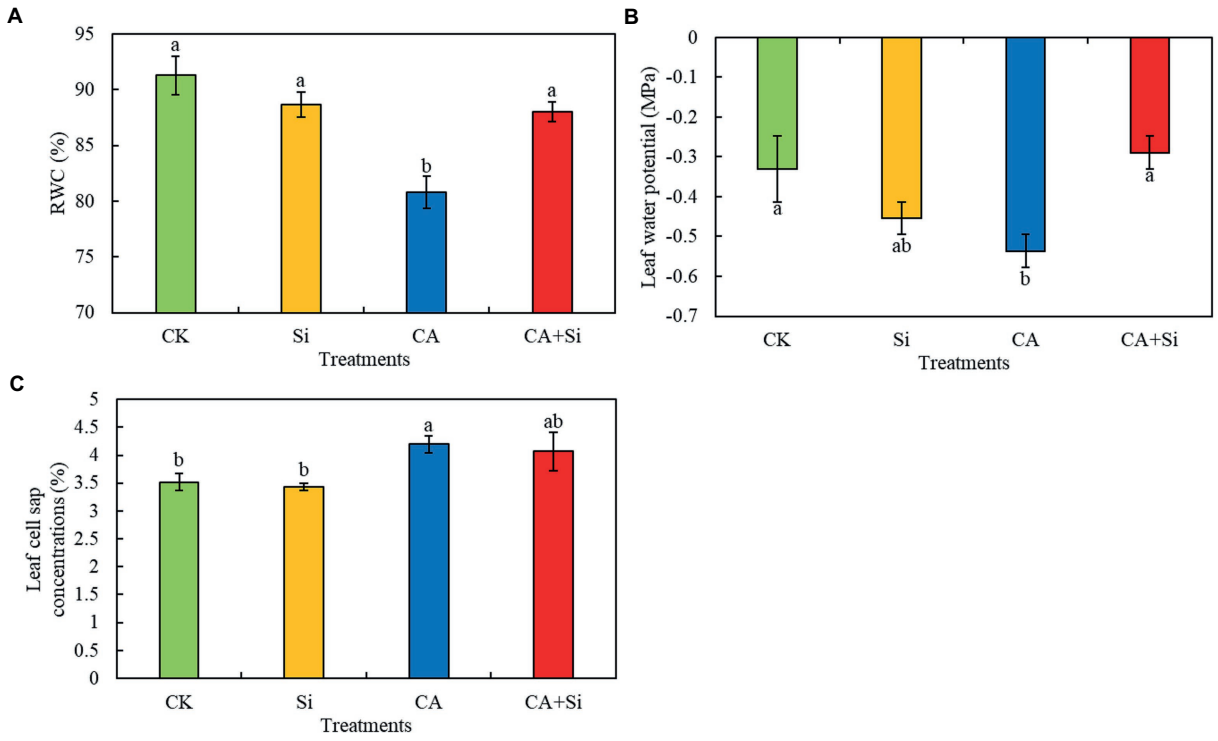


FIGURE 1
Effect of exogenous Si on the relative water content (RWC; **A**), water potential **(B)**, and cell sap concentration **(C)** of leaves in cucumber seedlings under cinnamic acid-induced autotoxicity stress. Vertical bars represent the mean±SE from three independent replicates (Each replicate contains three leaves). Different lowercase letters indicate significant differences according to Duncan's multiple range test ($p<0.05$).

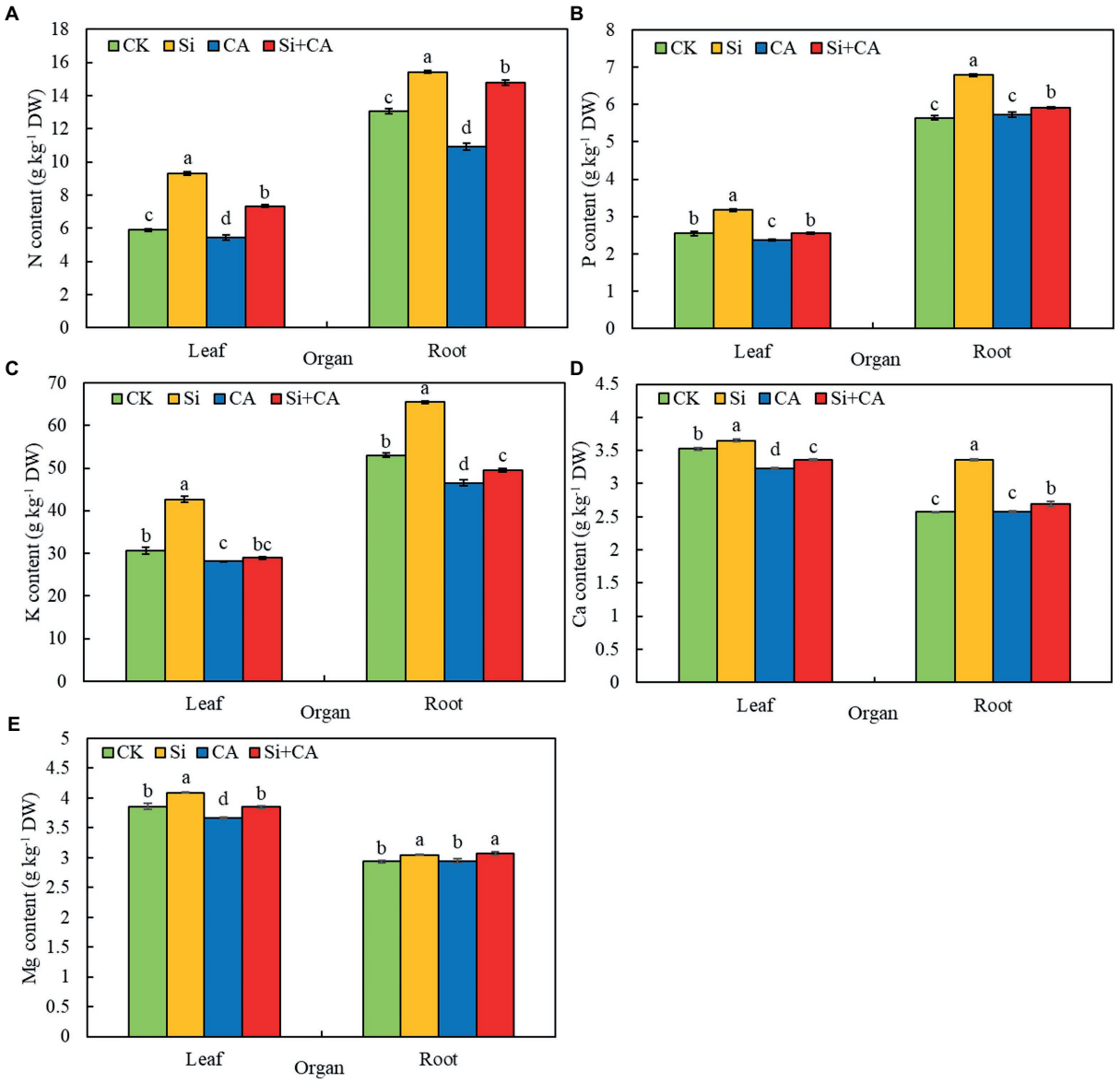


FIGURE 2
Effects of exogenous Si on the N **(A)**, P **(B)**, K **(C)**, Ca **(D)**, and Mg **(E)** contents of leaves and roots in cucumber seedlings under cinnamic acid-induced autotoxicity stress. The values (mean±SE) represent data from three replicates (n=3; each replicate contains three cucumber seedlings). Different lowercase letters indicate significant differences according to Duncan's multiple range test (p<0.05).

contents of roots by 16.51% and 12.23%, respectively. Compared with the CA treatment, CA + Si treatment significantly increased the N, P, and K contents of roots by 35.35%, 3.32%, and 6.24%, respectively. In addition, the N, P, and K contents of leaves and roots were significantly higher in the Si treatment group than in CK. Compared with the CK treatment, CA treatment significantly reduced the Ca and Mg contents of cucumber leaves by 8.24% and 4.92%, respectively. However, treatment with CA + Si significantly increased the Ca and Mg contents of leaves by 4.02% and 4.90%, respectively, compared with those of leaves in CA (Figures 2D,E). The Ca and Mg contents of CA-treated cucumber roots were not significantly different from those of leaves in CK (Figures 2D,E). Compared with the CA treatment, CA + Si treatment significantly increased the Ca and Mg contents of cucumber roots by 5.47% and 4.07%, respectively. Moreover, the Ca and Mg contents of leaves and roots were significantly higher in Si than in CK. These results indicated that exogenous Si promoted the absorption of major elements by the leaves and roots of cucumber seedlings, whether in normal conditions or under conditions of CA-induced autotoxicity.

Trace elements

The trends of change in trace element composition in each treatment group are shown in Figure 3. CA treatment seriously

affected the absorption of trace elements by cucumber leaves. Accordingly, the Fe, Mn, and Zn contents of cucumber leaves were significantly lower in CA than in CK, with a decrease of 14.22%, 32.48%, and 36.52%, respectively (Figures 3A–C). The Fe content of leaves was higher in CA + Si than in CA, but the difference was not significant. The Mn and Zn contents of leaves were significantly higher (by 15.41% and 53.72%, respectively), in CA + Si than in *CA*. The Fe, Mn, and Zn contents of leaves were not significantly different between the Si and CK groups. CA treatment significantly affected the uptake of Fe and Mn by cucumber roots (Figures 3A,B). Compared with the CK treatment, CA treatment significantly reduced the Fe and Mn levels of roots by 9.20% and 5.47%, respectively. The Fe content of roots was higher in CA + Si than in CA, but the difference was not significant. Compared with the CA treatment, CA + Si treatment significantly increased the Mn content roots by 9.65%. There were no significant differences in the Zn content of roots among the four treatments (Figure 3C). The Cu contents of leaves and roots were not significantly different among all four treatments (Figure 3D). These results indicated that exogenous Si alleviated some of the adverse effects of CA-induced autotoxicity stress on the absorption of trace elements by cucumber leaves and roots.

Effect of exogenous Si on the activities of N metabolism-related enzymes in the leaves and roots of cucumber seedlings under CA-induced autotoxicity stress

The activities of NR, NiR, GS, GOGAT, and GDH in cucumber leaves and roots showed similar trends across the four treatments (Figure 4). Compared with the CK treatment, CA treatment significantly reduced the NR activities of cucumber leaves and roots by 31.43% and 22.47%, respectively. Compared with the CA treatment, CA + Si treatment significantly increased the NR activities of leaves and roots by 52.84% and 20.78%, respectively (Figure 4A). Compared with the CK treatment, CA treatment reduced the NiR activities of cucumber leaves and roots by 10.91% and 14.34%, respectively; however, the differences were not significant. Compared with the CA treatment, CA + Si treatment significantly increased the NiR activities of leaves and roots by 55.27% and 26.11%, respectively (Figure 4B). The NR and NiR activities of leaves and roots were not significantly different between the CK and Si groups (Figures 4A,B).

CA-induced autotoxicity stress significantly inhibited the activities of GS and GOGAT in cucumber leaves and roots (Figures 4C,D). Compared with the CK treatment, CA treatment significantly reduced the GS activities of leaves and roots by

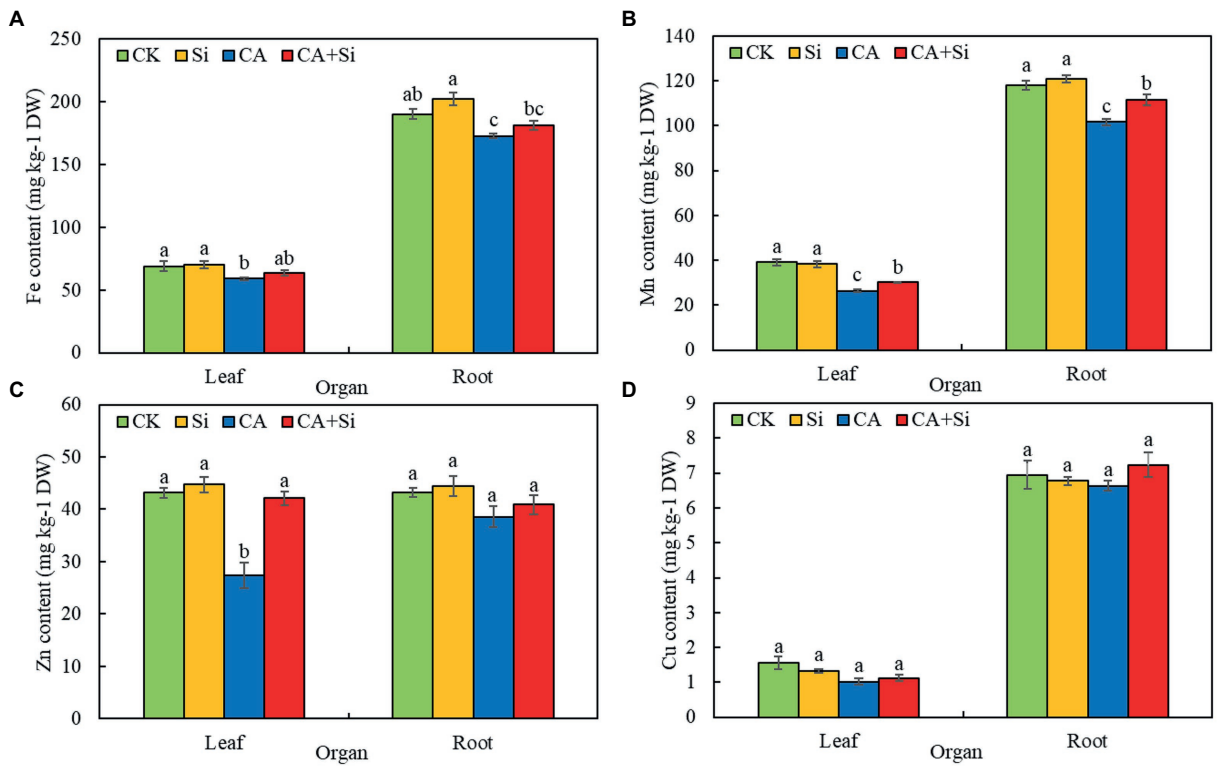


FIGURE 3
Effect of exogenous Si on the Fe **(A)**, Mn **(B)**, Zn **(C)**, and Cu **(D)** contents of leaves and roots in cucumber seedlings under cinnamic acid-induced autotoxicity stress. The values (mean±SE) represent data from three replicates (n=3; each replicate contains three cucumber seedlings). Different lowercase letters indicate significant differences according to Duncan's multiple range test (p<0.05).

25.28% and 28.71%, respectively (Figure 4C), and the GOGAT activities by 28.62% and 30.27%, respectively (Figure 4D). The exogenous addition of Si alleviated the CA-induced inhibition of GS and GOGAT activities in the leaves and roots of cucumber seedlings. Compared with the CA treatment, CA + Si treatment significantly increased the activities of GS (38.62% and 47.94%) and GOGAT (108.90 and 38.05%) in leaves and roots, respectively. The GS and GOGAT activities of cucumber leaves and roots were not significantly different between the Si and CK groups. Compared with the CK treatment, CA treatment significantly reduced the GDH activities of cucumber leaves and roots by 28.62% and 30.27%, respectively. Compared with the CA treatment, CA + Si treatment significantly increased the GDH activities of leaves and roots by 108.90% and 38.05%, respectively. The GDH activities of cucumber leaves and roots were not significantly different between the Si and CK groups (Figure 4E).

Effect of exogenous Si on the root morphology and growth indexes of cucumber seedlings under CA-induced autotoxicity stress

Root morphology

Compared with the CK treatment, CA treatment significantly reduced the total root length, average root diameter, total root

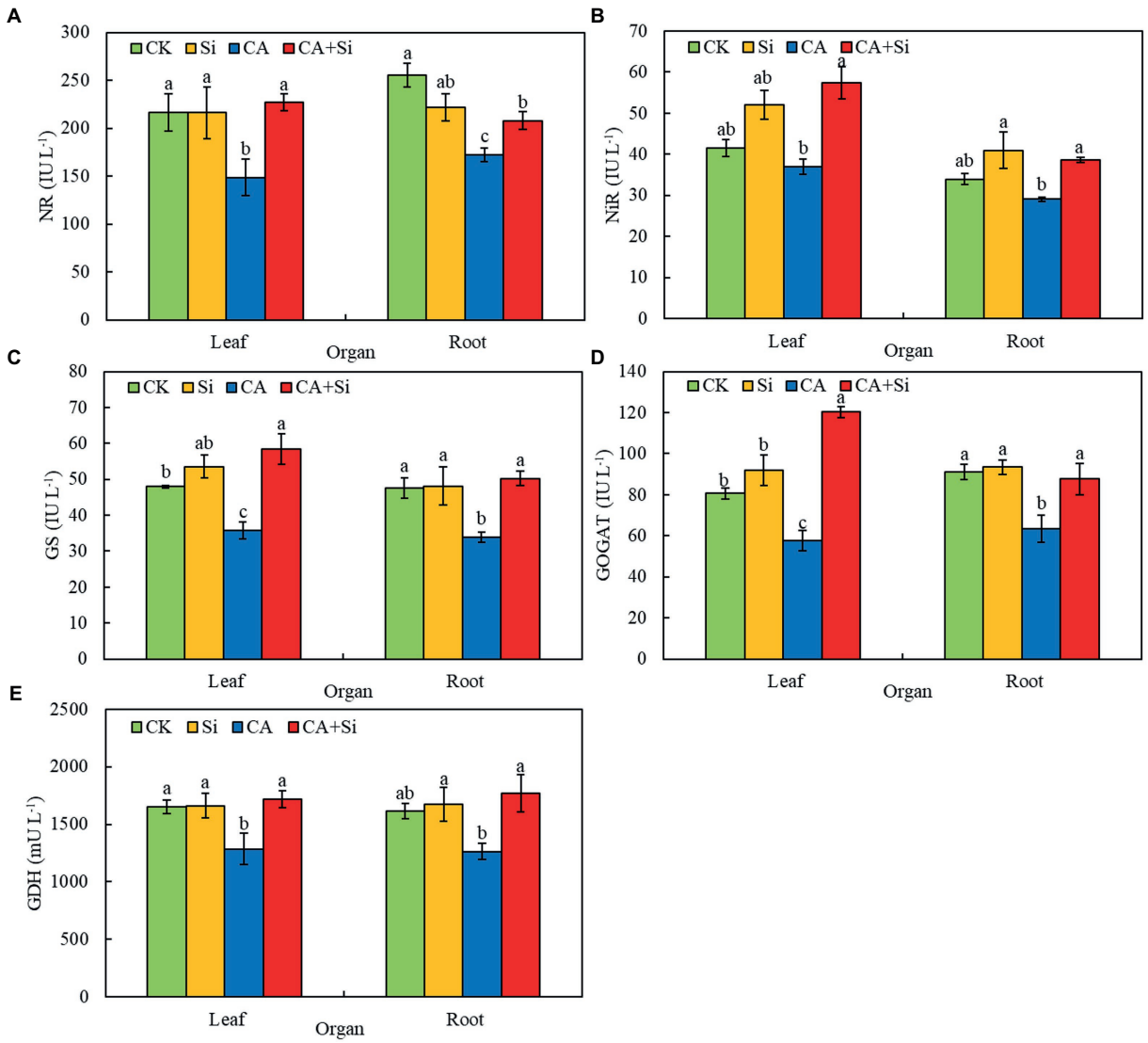


FIGURE 4
Effect of exogenous Si on the enzyme activities of nitrate reductase (NR; **A**), nitrite reductase (NiR; **B**), glutamine synthase (GS; **C**), glutamate synthase (GOGAT; **D**), and glutamate dehydrogenase (GDH; **E**) in the leaves and roots of cucumber seedlings under cinnamic acid-induced autotoxicity stress. Vertical bars represent the mean±SE from three independent replicates. Different lowercase letters indicate significant differences according to Duncan's multiple range test ($p<0.05$).

volume, total root surface area, and number of branch roots of cucumber seedlings by 33.34%, 25.53%, 50.00%, 45.53%, and 28.39%, respectively (Table 1). In contrast, CA + Si treatment significantly increased the total root length, average root diameter, total root volume, total root surface area, number of root tips, and number of branch roots of seedlings under CA-induced stress by 24.74%, 5.71%, 20.55%, 19.48%, 24.98%, and 15.67%, respectively. There was no significant difference in total root length, total root volume, total root surface area, number of root tips, and number of branch roots between the Si and CK groups. Similarly, CA-induced autotoxicity significantly inhibited root growth (Figure 5C), whereas exogenous addition of an appropriate concentration of Si promoted root morphogenesis (Figure 5D). The root morphology of the Si and CK groups was also similar in appearance (Figures 5A,B).

Growth indexes

CA-induced autotoxicity significantly reduced the plant height, stem diameter, and leaf area of cucumber seedlings compared with those of seedings in the CK group (Table 2). Furthermore, CA-induced autotoxicity also significantly reduced the fresh and dry weights of the shoots and roots of cucumber seedlings on the 10th day of treatment. However, compared with CA treatment, CA + Si treatment significantly increased the plant height, stem diameter, and leaf area of cucumber seedlings by 5.87%, 5.29%, and 25.69%, respectively. Compared with CA treatment, CA + Si treatment also significantly increased the fresh and dry weights of cucumber shoots (by 8.00% and 8.81%, respectively) and roots (by 18.21% and 20.04%, respectively). There were no significant differences in plant height, stem diameter, and leaf area between the Si and CK treatment groups. Si treatment significantly increased the fresh weight of shoots and the dry weight of roots, but had no significant effect on the fresh weight of roots and dry weight of shoots. These results indicated that Si treatment could promote the growth of cucumber seedlings to a certain extent even in normal conditions.

Discussion

Plant water status involves regulating the differences between water uptake through roots and leaf transpiration, and maintaining an adequate leaf water status is fundamental to the metabolic activities of plant tissues (Mali and Aery, 2008; Shi et al., 2016). The RWC, water potential, and cell sap concentration of plant leaves are known indicators of their water status. The cell sap concentration of leaves is characterized the consistency of the cell cytoplasm, and a high cell sap concentration is not conducive to the physiological and biochemical processes of cells (Munns et al., 2010). Ferulic acid, a CA derivative, has been reported to significantly inhibit water uptake by seedlings. Reduced water uptake leads to a reduction in leaf water potential and turgor pressure and inhibits seedling growth (Booker et al., 1992). In the present study, CA-induced autotoxicity stress significantly reduced the RWC and water potential of leaves in cucumber seedlings, resulting in an increase in leaf cell sap concentration. These results were consistent with previous findings. Previous studies have demonstrated that exogenous Si can increase leaf water potential and RWC under drought or salt stress in a variety of plants, including rice (Ming et al., 2012; Liu et al., 2019), wheat (Gong and Chen, 2012; Farouk and El-Metwally, 2019), and maize (Amin et al., 2014). In this study, the exogenous addition of Si increased the RWC and leaf water potential and reduced the leaf sap concentration of cucumber leaves. These results indicate that Si helps maintain the normal water status of leaf cells, which is beneficial for the various physiological and biochemical reactions that occur in plant cells. The elevated water potential of Si-treated leaves may be due to the deposition of a double-layered Si cuticle on the leaf epidermis, which reduces water loss from the leaf surface (Ahmed et al., 2014). This may also account for the elevated water potential of Si-treated leaves under CA-induced autotoxicity stress in the present study.

Under autotoxicity stress, plant roots are exposed to and absorb allelochemicals that can disrupt various physiological and biochemical processes, especially water and nutrient uptake (Talukder et al., 2019). Yu and Matsui (1997) reported that the isolates of cucumber root exudates significantly inhibited the uptake of Ca, K, Fe, and Mg by the cucumber root system. Similarly, in the present study, CA-induced autotoxicity stress inhibited the uptake of major (N, P, K, Ca, Mg) and trace elements (Cu, Fe, Mn, Zn) by the leaves and roots of cucumber seedlings to varying degrees. The substances involved in osmotic regulation in plants can be divided into two main categories: organic substances produced by the cells (such as soluble sugars, soluble proteins, and proline) and inorganic ions absorbed from the outside world (such as K, Ca, and Mg; Zhu and Gong, 2014). In addition, mineral elements are of major significance to dry matter

TABLE 1 Effect of exogenous Si on total root length, average root diameter, total root volume, total root surface area, number of root tip, and number of branch roots in cucumber seedlings under cinnamic acid (CA)-induced autotoxicity stress.

Treatment	Total root length ($cm \cdot plant^{-1}$)	Average root diameter ($mm \cdot plant^{-1}$)	Total root volume ($cm^3 \cdot plant^{-1}$)	Total root surface area ($cm^2 \cdot plant^{-1}$)	Number of root tips ($number \cdot plant^{-1}$)	Number of branch roots ($number \cdot plant^{-1}$)
CK	994.00 ± 29.02 a	0.47 ± 0.01 a	1.46 ± 0.05 a	140.79 ± 4.46 a	1108.33 ± 55.31 b	5420.92 ± 190.86 a
Si	984.82 ± 68.45 a	0.43 ± 0.01 b	1.37 ± 0.07 a	127.20 ± 8.10 a	1274.83 ± 114.35 ab	5577.58 ± 297.89 a
CA	662.60 ± 38.32 c	0.35 ± 0.00 c	0.73 ± 0.03 c	76.69 ± 4.16 c	1086.33 ± 61.94 b	3881.75 ± 220.86 b
CA + Si	826.50 ± 35.94 b	0.37 ± 0.01 c	0.88 ± 0.05 b	95.24 ± 5.01 b	1357.67 ± 80.55 a	4489.92 ± 270.54 b

Data indicate the mean ± SE ($n = 3$). Different lowercase letters in the same column indicate significant differences according to Duncan's multiple range test ($p < 0.05$). CK, control.

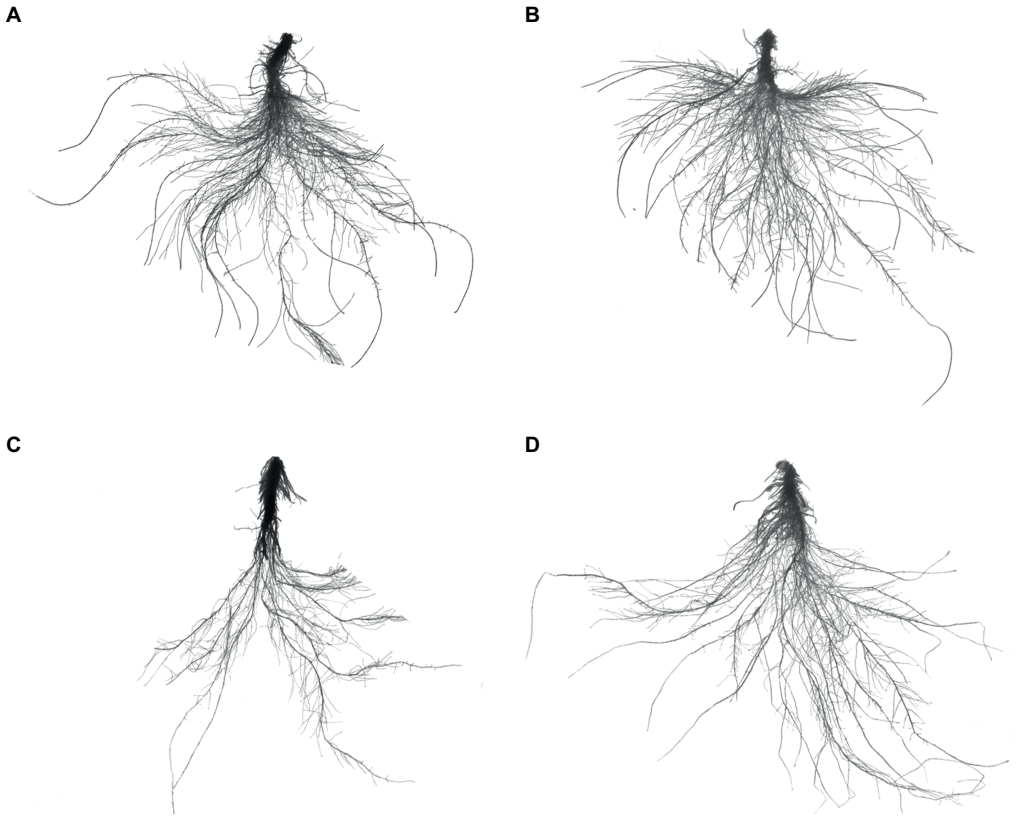


FIGURE 5
Effect of exogenous Si on the root morphology of cucumber seedlings under cinnamic acid (CA)-induced autotoxicity stress. **(A)** CK: normal nutrient solution; **(B)** 1mmolL^{-1} Si; **(C)** 0.8mmolL^{-1} CA; and **(D)** 0.8mmolL^{-1} CA+1mmolL^{-1} Si.

TABLE 2 Effect of exogenous Si on the plant height, stem diameter, leaf area, and biomass of cucumber seedlings under cinnamic acid (CA)-induced autotoxicity stress.

Treatment	Plant height (cm)	Stem diameter (mm)	Leaf area (cm^2)	Shoot		Root	
				Fresh weight (g)	Dry weight (g)	Fresh weight (g)	Dry weight (g)
CK	4.99 ± 0.09 a	4.31 ± 0.08 a	70.23 ± 1.95 a	5.35 ± 0.12 b	0.69 ± 0.01 a	1.12 ± 0.03 a	0.06 ± 0.003 b
Si	5.02 ± 0.10 a	4.34 ± 0.06 a	67.15 ± 2.60 a	5.91 ± 0.11 a	0.71 ± 0.01 a	1.12 ± 0.03 a	0.08 ± 0.002 a
CA	4.43 ± 0.07 c	3.97 ± 0.08 b	36.90 ± 1.59 c	4.30 ± 0.04 d	0.59 ± 0.00 c	0.84 ± 0.02 c	0.04 ± 0.001 d
CA + Si	4.69 ± 0.08 b	4.18 ± 0.06 a	46.38 ± 1.75 b	4.65 ± 0.05 c	0.64 ± 0.02 b	0.99 ± 0.01 b	0.05 ± 0.001 c

Data indicate the mean ± SE ($n = 3$). Different lowercase letters in the same column indicate significant differences according to Duncan's multiple range test ($p < 0.05$). CK, control.

accumulation and plant adaptability to adverse conditions. Si has been suggested to play crucial roles in balancing the uptake, transport, and distribution of minerals in plants under drought and salt stress (Rizwan et al., 2015). Numerous studies have indicated that Si treatment promotes the levels of nutrients—such as N (Detmann et al., 2012), P (Zhu and Gong, 2014), K (Farouk and Omar, 2020), Ca (Kaya et al., 2006), Mg (Gunes et al., 2008), Fe (Pavlovic et al., 2013), Zn (Pascual et al., 2016), Mn (Wang and Han, 2007) and Cu (Gunes et al., 2008)—in plant under stress conditions. Our findings are consistent with previous reports. Specifically, we show that under conditions of autotoxicity stress, the levels of major (N, P, K, Ca, Mg) and trace (Fe, Mn, Zn) elements are elevated to varying degrees in the leaves and roots of Si-treated cucumber seedlings. Some researchers have attributed the increased uptake of Ca and to the Si-mediated reduction in plasma membrane permeability and Si-induced increase in plasma membrane H^+-ATP activity (Liang, 1999; Kaya et al., 2006). These phenomena may also account for the increased Ca and K levels observed in this study. Our results suggest that promoting the uptake and accumulation of mineral elements may be an important nutritional basis for Si application to improve the resistance of cucumber seedlings to autotoxicity stress.

N is a key mineral element involved in plant growth and morphogenesis, and its effective utilization is crucial for plant growth, flowering, fruiting, photosynthesis, and the distribution of photosynthetic products (Prinsi et al., 2009; Nazir et al., 2016). Plants can absorb inorganic N from agroecosystems in various forms, including ammonium nitrogen (NH_4^+-N) and nitrate nitrogen (NO_3^-N; Carlisle et al., 2012). The most critical enzymes for N metabolism in plants include NR, NiR, GS, GOGAT, and GDH. Following its uptake by plants, NH_4^+-N can be directly used for amino acid synthesis. However, NO_3^--N can only be utilized by plants after it has been reduced to NH_4^+-N through a reaction catalyzed by NR and NiR (Horchani et al., 2010). NH_4^+ is rapidly assimilated into organic N *via* two highly regulated pathways: the GS/GOGAT pathway and the GDH pathway (Zhang et al., 2017). Typically, the GS/GOGAT pathway is the main pathway for NH_4^+ assimilation. When the GS/GOGAT pathway is inhibited by stress, the detoxification of NH_4^+ by GDH may play an important role (Shao et al., 2015). In addition, stress can severely inhibit N metabolism. Salt stress has been reported to reduce the N concentration of soybean roots and shoots, as well as the activities of GDH, GS, GOGAT, and NR (Farhangi-Abriz and Torabian, 2018). Singh et al. (2015) showed that drought stress reduced N uptake, the activities of GS and GOGAT, and the levels of N-containing compounds in the leaves of sunflower seedling. Consistent with this, our results show that CA-induced autotoxicity stress significantly reduced the activities of NR, NiR, GS, GOGAT, and GDH in cucumber seedlings. The application of exogenous Si can enhance the activity of NiR in pepper plants under drought stress (Pereira et al., 2013). Feng et al. (2010) also reported that Si treatment reduced the limiting effects of heavy metal stress on N metabolism-related enzymes (NR, GS, and GOGAT). In the present study, Si treatment increased the activities of NR, NiR, GS, GOGAT, and GDH in the leaves and roots of cucumber seedlings under autotoxicity stress. However, Si treatment alone had no significant effect on the activities of N metabolism-related enzymes in the leaves and roots of cucumber seedlings under normal conditions. This may be because the beneficial effects of Si on plants were more pronounced under adverse conditions than under normal conditions (Cooke and Leishman, 2016).

Plant roots are not only the first line of defense against autotoxicity, but are also the directly affected by it. Cheng et al. (2016) found that some plant responses to autotoxicity occurred only in the roots, and that the genes relevant to these responses were also expressed only in the roots. However, most studies on autotoxicity stress also focus on leaf photosynthetic parameters, ascorbate-glutathione metabolism, the activities of antioxidant enzymes, and other shoot parameters (Bu et al., 2018; Meng et al., 2021; Zhang et al., 2021). In the present study, CA stress changed the root morphology of cucumber seedlings, resulting in a significant adverse effect on morphological indicators such as total root length, average root diameter, total root volume, total root surface area, and number of branch roots. The inhibitory effects of CA stress on the root system of cucumber seedlings is evident in Figure 5C similar effect of autotoxicity stress has been reported in melons (Zhang et al., 2020b). The Si-induced changes in root morphology observed in this study may be due to increased root elongation as a result of cell wall elongation in the growing region, as reported in sorghum (Hattori et al., 2003). Si is considered a favorable element for plant growth and development, both in normal conditions and under conditions of environmental constraints (Ali et al., 2013). Si can effectively mitigate the effects of heavy metal toxicity in cotton by improving morphological traits such as leaf area, stem length, root length, and the biomasses of roots, shoots, and leaves. It also promotes nutrient uptake by regulating root morphology (Khaliq et al., 2016). In addition, Si has been shown to increase plant height, biomass, RWC, and leaf firmness, and reduce leaf cell death in coriander (Fatemi et al., 2020). Si supplementation not only improves root growth (including morphological traits such as root diameter, root surface area, root volume, total root length, and primary root length), but also the above-ground biomass of plants under abiotic stress (Hameed et al., 2013; Kim et al., 2014). Our findings are consistent with those reported in the above-mentioned studies. That is, the addition of exogenous Si ($1\,mmol\,L^{-1}$) effectively alleviated the inhibitory effects of CA-induced stress on cucumber seedlings by increasing the seedling height, stem thickness, leaf area, and shoot and root biomasses. Based on these findings, we hypothesize that Si-mediated changes in root morphology may be responsible for the increased leaf water status and mineral concentration of cucumber seedlings under CA-induced autotoxicity stress. Maintaining high levels of water status-related parameters in silica-treated plants can be achieved by improving root development to promote water uptake and by forming a silica-cornicle bilayer, a barrier against water loss, on the leaf epidermis (Farouk and Omar, 2020). The higher water status facilitates the enhancement of osmoregulation-maintained metabolic activity, which in turn effectively alleviates the drought and salt stress suffered by the plants (Farouk et al., 2020; Farouk and Omar, 2020). In the present study, in which Si effectively alleviated the adverse effects of CA-induced autotoxicity stress on seedlings, may also be similar to the above study, being that it facilitated the uptake of water and mineral elements through improved root morphology, maintaining a higher leaf water status and ionic homeostasis, and favoring various metabolic activities.

Conclusion

Our study revealed that CA-induced autotoxicity stress was detrimental to the maintenance of normal leaf water status in cucumber seedlings; inhibited the uptake of mineral nutrients and the normal functioning of nitrogen metabolism; and had adverse

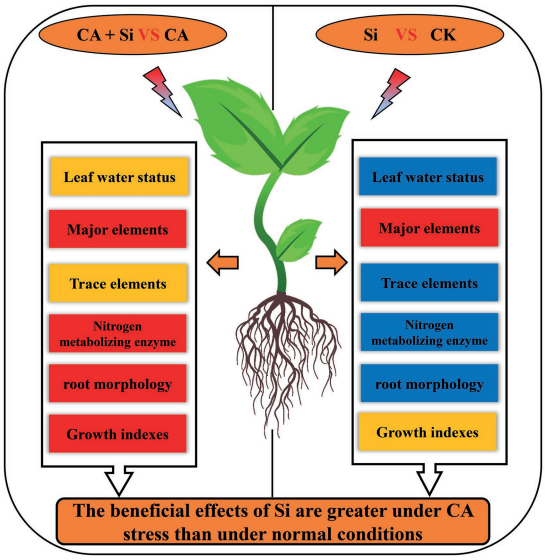


FIGURE 6
Effects of Si on the shoots and roots of cucumber seedlings under normal conditions and under cinnamic acid-induced autotoxicity stress. Red boxes represent a significant increase in all indicators, orange boxes represent significant increases in some indicators, and blue boxes represent no significant increase in any indicators.

effects on root morphology, thus suppressing shoot growth. The exogenous application of Si effectively improved the leaf water status, mineral nutrient uptake, activities of N metabolism-related enzymes, and root morphology of the seedlings, thus promoting shoot growth and development. The beneficial effects of Si on the activities of N metabolism-related enzymes in the leaves and roots of cucumber seedlings were greater under CA-induced autotoxicity stress than under normal conditions. As the root system is the first barrier against autotoxicity stress, we speculate that the Si-induced alterations in root morphology are the main reason for improved leaf water status and increased mineral uptake in cucumber seedlings. Our results clearly indicate that Si application at appropriate concentrations is an effective strategy for improving resistance to autotoxicity stress in cucumber seedlings. These findings provide new insights into overcoming CA-induced autotoxicity stress through the widespread use of Si in agricultural production (Figure 6).

Data availability statement

The original contributions presented in the study are included in the article/supplementary material, further inquiries can be directed to the corresponding author.

Author contributions

JL, NJ, and JY designed the study. JL, LJ, SW, and XM performed the work. JL was involved with writing the manuscript. JL, NJ, and XM analyzed the data. ZL, XX, ZT, JL, and JY revised the manuscript. All authors contributed to the article and approved the final version of this manuscript.

Funding

This research was funded by Fuxi Young Talents Fund of Gansu Agricultural University (GAUfx-04Y03); Gansu Top Leading Talent Plan (GSBJLJ-2021-14); Gansu People's Livelihood Science and Technology Project (20CX9NA099); Industrial support plan project of Gansu Provincial Department of Education (2021CYZC-45); and the Special Project of Central Government Guiding Local Science and Technology Development (ZCYD-2021-07).

Conflict of interest

The authors declare that the research was conducted in the absence of any commercial or financial relationships that could be construed as a potential conflict of interest.

Publisher's note

All claims expressed in this article are solely those of the authors and do not necessarily represent those of their affiliated organizations, or those of the publisher, the editors and the reviewers. Any product that may be evaluated in this article, or claim that may be made by its manufacturer, is not guaranteed or endorsed by the publisher.

References

Abdelaal, K. A., Mazrou, Y. S., and Hafez, Y. M. (2020). Silicon foliar application mitigates salt stress in sweet pepper plants by enhancing water status, photosynthesis, antioxidant enzyme activity and fruit yield. *Plan. Theory* 9:733. doi: 10.3390/plants9060733

Abdi, S., Abbaspur, N., Avestan, S., and Barker, A. (2016). Sana physiological responses of two grapevine (*Vitis vinifera* L.) cultivars to CycocelTM treatment during drought. *J. Hortic Sci. Biotech.* 91, 211–219. doi: 10.1080/14620316.2015.1123405

Ahmed, M., Asif, M., and Hassan, F.-U. (2014). Augmenting drought tolerance in sorghum by silicon nutrition. *Acta Physiol. Plant.* 36, 473–483. doi: 10.1007/s11738-013-1427-2

Al Murad, M., Khan, A. L., and Muneer, S. (2020). Silicon in horticultural crops: cross-talk, signaling, and tolerance mechanism under salinity stress. *Plan. Theory* 9:460. doi: 10.3390/plants9040460

Ali, S., Farooq, M. A., Yasmeen, T., Hussain, S., Arif, M. S., Abbas, F., et al. (2013). The influence of silicon on barley growth, photosynthesis and ultra-structure under chromium stress. *Ecotox. Environ. Safe.* 89, 66–72. doi: 10.1016/j.ecoenv.2012.11.015

Amin, M., Ahmad, R., Basra, S., and Murtaza, G. (2014). Silicon induced improvement in morpho-physiological traits of maize (*Zea mays* L.) under water deficit. *Pak. J. Agric. Sci.* 51, 187–196.

Arif, Y., Singh, P., Bajguz, A., Alam, P., and Hayat, S. (2021). Silicon mediated abiotic stress tolerance in plants using physio-biochemical, omic approach and cross-talk with phytohormones. *Plant Physiol. Biochem.* 166, 278–289. doi: 10.1016/j.plaphy.2021.06.002

Bai, X., Gao, J., Wang, S., Cai, H., Chen, Z., and Zhou, J. (2020). Excessive nutrient balance surpluses in newly built solar greenhouses over five years leads to high nutrient accumulations in soil. *Agric. Ecosyst. Environ.* 288:106717. doi: 10.1016/j.agee.2019.106717

Bhusal, N., Han, S.-G., and Yoon, T.-M. (2019). Impact of drought stress on photosynthetic response, leaf water potential, and stem sap flow in two cultivars of bi-leader apple trees (Malus× domestica Borkh.). *Sci. Hortic.* 246, 535–543. doi: 10.1016/j.scienta.2018.11.021

Booker, F. L., Blum, U., and Fiscus, E. L. (1992). Short-term effects of ferulic acid on ion uptake and water relations in cucumber seedlings. *J. Exp. Bot.* 43, 649–655. doi: 10.1093/jxb/43.5.649

Bu, R., Xiao, X., Liao, W., Hu, Y., Li, J., Lv, J., et al. (2018). Exogenous Si alleviation of autotoxicity in cucumber (*Cucumis sativus* L.) seed germination is correlated with changes in carbohydrate metabolism. *J. Plant Growth Regul.* 37, 784–793. doi: 10.1007/s00344-017-9773-8

Carlisle, E., Myers, S. S., Raboy, V., and Bloom, A. J. (2012). The effects of inorganic nitrogen form and CO2 concentration on wheat yield and nutrient accumulation and distribution. *Front. Plant Sci.* 3:195. doi: 10.3389/fpls.2012.00195

Cheng, F., Cheng, Z.-H., and Meng, H.-W. (2016). Transcriptomic insights into the allelopathic effects of the garlic allelochemical diallyl disulfide on tomato roots. *Sci. Rep.* 6, 1–14. doi: 10.1038/srep38902

Cooke, J., and Leishman, M. R. (2016). Consistent alleviation of abiotic stress with silicon addition: a meta-analysis. *Funct. Ecol.* 30, 1340–1357. doi: 10.1111/1365-2435.12713

Detmann, K. C., Araújo, W. L., Martins, S. C., Sanglard, L. M., Reis, J. V., Detmann, E., et al. (2012). Silicon nutrition increases grain yield, which, in turn, exerts a feed-forward stimulation of photosynthetic rates *via* enhanced mesophyll conductance and alters primary metabolism in rice. *New Phytol.* 196, 752–762. doi: 10.1111/j.1469-8137.2012.04299.x

Ding, S., Zhou, D., Wei, H., Wu, S., and Xie, B. (2021). Alleviating soil degradation caused by watermelon continuous cropping obstacle: application of urban waste compost. *Chemosphere* 262:128387. doi: 10.1016/j.chemosphere.2020.128387

Etesami, H., and Jeong, B. R. (2018). Silicon (Si): review and future prospects on the action mechanisms in alleviating biotic and abiotic stresses in plants. *Ecotox. Environ. Safe.* 147, 881–896. doi: 10.1016/j.ecoenv.2017.09.063

Farhangi-Abriz, S., and Torabian, S. (2018). Biochar improved nodulation and nitrogen metabolism of soybean under salt stress. *Symbiosis* 74, 215–223. doi: 10.1007/s13199-017-0509-0

Farouk, S., and Al-Sanoussi, A. (2019). The role of biostimulants in increasing barley plant growth and yield under newly cultivated sandy soil. *Cercetari Agronom. Moldova.* 52, 116–127. doi: 10.2478/cerce-2019-0012

Farouk, S., Elhindi, K. M., and Alotaibi, M. A. (2020). Silicon supplementation mitigates salinity stress on *Ocimum basilicum* L. *via* improving water balance, ion homeostasis, and antioxidant defense system. *Ecotox. Environ. Safe.* 206:111396. doi: 10.1016/j.ecoenv.2020.111396

Farouk, S., and El-Metwally, I. (2019). Synergistic responses of drip-irrigated wheat crop to chitosan and/or silicon under different irrigation regimes. *Agr. Water Manage.* 226:105807. doi: 10.1016/j.agwat.2019.105807

Farouk, S., and Omar, M. (2020). Sweet basil growth, physiological and ultrastructural modification, and oxidative defense system under water deficit and silicon forms treatment. *J. Plant Growth Regul.* 39, 1307–1331. doi: 10.1007/s00344-020-10071-x

Fatemi, H., Esmaiel Pour, B., and Rizwan, M. (2021). Foliar application of silicon nanoparticles affected the growth, vitamin C, flavonoid, and antioxidant enzyme activities of coriander (*Coriandrum sativum* L.) plants grown in lead (Pb)-spiked soil. *Environ. Sci. Pollut. R.* 28, 1417–1425. doi: 10.1007/s11356-020-10549-x

Fatemi, H., Pour, B. E., and Rizwan, M. (2020). Isolation and characterization of lead (Pb) resistant microbes and their combined use with silicon nanoparticles improved the growth, photosynthesis and antioxidant capacity of coriander (*Coriandrum sativum* L.) under Pb stress. *Environ. Pollut.* 266:114982. doi: 10.1016/j.envpol.2020.114982

Feng, J., Shi, Q., Wang, X., Wei, M., Yang, F., and Xu, H. (2010). Silicon supplementation ameliorated the inhibition of photosynthesis and nitrate metabolism by cadmium (cd) toxicity in *Cucumis sativus* L. *Sci. Hortic.* 123, 521–530. doi: 10.1016/j.scienta.2009.10.013

Gong, H., and Chen, K. (2012). The regulatory role of silicon on water relations, photosynthetic gas exchange, and carboxylation activities of wheat leaves in field drought conditions. *Acta Physiol. Plant.* 34, 1589–1594. doi: 10.1007/s11738-012-0954-6

Gunes, A., Kadioglu, Y. K., Pilbeam, D. J., Inal, A., Coban, S., and Aksu, A. (2008). Influence of silicon on sunflower cultivars under drought stress, II: essential and nonessential element uptake determined by polarized energy dispersive X-ray fluorescence. *Commun. Soil Sci. Plan.* 39, 1904–1927. doi: 10.1080/00103620802134719

Hameed, A., Sheikh, M. A., Jamil, A., and Basra, S. M. A. (2013). Seed priming with sodium silicate enhances seed germination and seedling growth in wheat (*Triticum aestivum* L.) under water deficit stress induced by polyethylene glycol. *Pak. J. Life Soc. Sci.* 11, 19–24.

Hattori, T., Inanaga, S., Tanimoto, E., Lux, A., Luxová, M., and Sugimoto, Y. (2003). Silicon-induced changes in viscoelastic properties of sorghum root cell walls. *Plant Cell Physiol.* 44, 743–749. doi: 10.1093/pcp/pcg090

Henriet, C., Draye, X., Oppitz, I., Swennen, R., and Delvaux, B. (2006). Effects, distribution and uptake of silicon in banana (Musa spp.) under controlled conditions. *Plant and Soil* 287, 359–374. doi: 10.1007/s11104-006-9085-4

Horchani, F., Hajri, R., and Aschi-Smiti, S. (2010). Effect of ammonium or nitrate nutrition on photosynthesis, growth, and nitrogen assimilation in tomato plants. *J. Plant Nutr. Soil Sci.* 173, 610–617. doi: 10.1002/jpln.201000055

Hu, W., Zhang, Y., Huang, B., and Teng, Y. (2017). Soil environmental quality in greenhouse vegetable production systems in eastern China: current status and management strategies. *Chemosphere* 170, 183–195. doi: 10.1016/j.chemosphere.2016.12.047

Jayawardana, H., Weerahewa, H., and Saparamadu, M. (2014). Effect of root or foliar application of soluble silicon on plant growth, fruit quality and anthracnose development of capsicum. *Trop. Agric.* 26, 74–81. doi: 10.4038/tar.v26i1.8073

Kato-Noguchi, H., Nakamura, K., and Okuda, N. (2018). Involvement of an autotoxic compound in asparagus decline. *J. Plant Physiol.* 224-225, 49–55. doi: 10.1016/j.jplph.2018.03.005

Kaya, C., Tuna, L., and Higgs, D. (2006). Effect of silicon on plant growth and mineral nutrition of maize grown under water-stress conditions. *J. Plant Nutr.* 29, 1469–1480. doi: 10.1080/01904160600837238

Khaliq, A., Ali, S., Hameed, A., Farooq, M. A., Farid, M., Shakoor, M. B., et al. (2016). Silicon alleviates nickel toxicity in cotton seedlings through enhancing growth, photosynthesis, and suppressing Ni uptake and oxidative stress. *Arch. Agron. Soil Sci.* 62, 633–647. doi: 10.1080/03650340.2015.1073263

Kim, Y.-H., Khan, A. L., Waqas, M., and Lee, I.-J. (2017). Silicon regulates antioxidant activities of crop plants under abiotic-induced oxidative stress: a review. *Front. Plant Sci.* 8:510. doi: 10.3389/fpls.2017.00510

Kim, Y. H., Khan, A. L., Waqas, M., Shim, J. K., Kim, D. H., Lee, K. Y., et al. (2014). Silicon application to rice root zone influenced the phytohormonal and antioxidant responses under salinity stress. *J. Plant Growth Regul.* 33, 137–149. doi: 10.1007/s00344-013-9356-2

Kyriacou, M. C., Rouphael, Y., Colla, G., Zrenner, R., and Schwarz, D. (2017). Vegetable grafting: The implications of a growing agronomic imperative for vegetable fruit quality and nutritive value. *Front. Plant Sci.* 8:741. doi: 10.3389/fpls.2017.00741

Liang, Y. (1999). Effects of silicon on enzyme activity and sodium, potassium and calcium concentration in barley under salt stress. *Plant and Soil* 209, 217–224. doi: 10.1023/A:1004526604913

Liu, B., Soundararajan, P., and Manivannan, A. (2019). Mechanisms of silicon-mediated amelioration of salt stress in plants. *Plan. Theory* 8:307. doi: 10.3390/plants8090307

Mali, M., and Aery, N. (2008). Influence of silicon on growth, relative water contents and uptake of silicon, calcium and potassium in wheat grown in nutrient solution. *J. Plant Nutr.* 31, 1867–1876. doi: 10.1080/01904160802402666

Meng, X., Luo, S., Dawuda, M. M., Gao, X., Wang, S., Xie, J., et al. (2021). Exogenous silicon enhances the systemic defense of cucumber leaves and roots against CA-induced autotoxicity stress by regulating the ascorbate-glutathione cycle and photosystem II. *Ecotox. Environ. Safe.* 227:112879. doi: 10.1016/j.ecoenv.2021.112879

Miao, L., Di, Q., Sun, T., Li, Y., Duan, Y., Wang, J., et al. (2019). Integrated metabolome and transcriptome analysis provide insights into the effects of grafting on fruit flavor of cucumber with different rootstocks. *Int. J. Mol. Sci.* 20:3592. doi: 10.3390/ijms20143592

Ming, D., Pei, Z., Naeem, M., Gong, H., and Zhou, W. (2012). Silicon alleviates PEG-induced water-deficit stress in upland rice seedlings by enhancing osmotic adjustment. *J. Agron. Crop Sci.* 198, 14–26. doi: 10.1111/j.1439-037x.2011.00486.x

Mitani, N., and Ma, J. F. (2005). Uptake system of silicon in different plant species. *J. Exp. Bot.* 56, 1255–1261. doi: 10.1093/jxb/eri121

Munns, R., James, R. A., Sirault, X. R., Furbank, R. T., and Jones, H. G. (2010). New phenotyping methods for screening wheat and barley for beneficial responses to water deficit. *J. Exp. Bot.* 61, 3499–3507. doi: 10.1093/jxb/erq199

Nazir, M., Pandey, R., Siddiqi, T. O., Ibrahim, M. M., Qureshi, M. I., Abraham, G., et al. (2016). Nitrogen-deficiency stress induces protein expression differentially in low-N tolerant and low-N sensitive maize genotypes. *Front. Plant Sci.* 7:298. doi: 10.3389/fpls.2016.00298

Pascual, M. B., Echevarria, V., Gonzalo, M. J., and Hernández-Apaolaza, L. (2016). Silicon addition to soybean (Glycine max L.) plants alleviate zinc deficiency. *Plant Physiol. Biochem.* 108, 132–138. doi: 10.1016/j.plaphy.2016.07.008

Pavlovic, J., Samardzic, J., Maksimović, V., Timotijevic, G., Stevic, N., Laursen, K. H., et al. (2013). Silicon alleviates iron deficiency in cucumber by promoting mobilization of iron in the root apoplast. *New Phytol.* 198, 1096–1107. doi: 10.1111/nph.12213

Pereira, T. S., Da Silva Lobato, A. K., Tan, D. K. Y., Da Costa, D. V., Uchoa, E. B., Nascimento, D., et al. (2013). Positive interference of silicon on water relations, nitrogen metabolism, and osmotic adjustment in two pepper ("*Capsicum annuum*") cultivars under water deficit. *Aust. J. Crop. Sci.* 7, 1064–1071. doi: 10.2991/icaicte.2013.146

Prinsi, B., Negri, A. S., Pesaresi, P., Cocucci, M., and Espen, L. (2009). Evaluation of protein pattern changes in roots and leaves of Zea mays plants in response to nitrate availability by two-dimensional gel electrophoresis analysis. *BMC Plant Biol.* 9, 1–17. doi: 10.1186/1471-2229-9-113

Rizwan, M., Ali, S., Ibrahim, M., Farid, M., Adrees, M., Bharwana, S. A., et al. (2015). Mechanisms of silicon-mediated alleviation of drought and salt stress in plants: a review. *Environ. Sci. Pollut. Res. Int.* 22, 15416–15431. doi: 10.1007/s11356-015-5305-x

Shao, Q., Shu, S., Du, J., Xing, W., Guo, S., and Sun, J. (2015). Effects of NaCl stress on nitrogen metabolism of cucumber seedlings. *Russ. J. Plant Physiol.* 62, 595–603. doi: 10.1134/S1021443715050155

Shi, Y., Zhang, Y., Han, W., Feng, R., Hu, Y., Guo, J., et al. (2016). Silicon enhances water stress tolerance by improving root hydraulic conductance in *Solanum lycopersicum* L. *Front. Plant Sci.* 7:196. doi: 10.3389/fpls.2016.00196

Singh, N. B., Singh, D., and Singh, A. (2015). Biological seed priming mitigates the effects of water stress in sunflower seedlings. *Physiol. Mol. Biol. Plants* 21, 207–214. doi: 10.1007/s12298-015-0291-5

Souri, Z., Khanna, K., Karimi, N., and Ahmad, P. (2021). Silicon and plants: current knowledge and future prospects. *J. Plant Growth Regul.* 40, 906–925. doi: 10.1007/s00344-020-10172-7

Talukder, M. R., Asaduzzaman, M., Tanaka, H., and Asao, T. (2019). Application of alternating current electro-degradation improves retarded growth and quality in lettuce under autotoxicity in successive cultivation. *Sci. Hortic.* 252, 324–331. doi: 10.1016/j.scienta.2019.04.001

Wang, X. S., and Han, J. G. (2007). Effects of NaCl and silicon on ion distribution in the roots, shoots and leaves of two alfalfa cultivars with different salt tolerance. *Soil Sci. Plant Nutr.* 53, 278–285. doi: 10.1111/j.1747-0765.2007.00135.x

Wu, Y., Hu, L., Liao, W., Dawuda, M. M., Lyu, J., Xie, J., et al. (2019). Foliar application of 5-aminolevulinic acid (ALA) alleviates NaCl stress in cucumber (*Cucumis sativus* L.) seedlings through the enhancement of ascorbate-glutathione cycle. *Sci. Hortic.* 257:108761. doi: 10.1016/j.scienta.2019.108761

Xiao, X., Cheng, Z., Lv, J., Xie, J., Ma, N., and Yu, J. (2019). A green garlic (*Allium sativum* L.) based intercropping system reduces the strain of continuous monocropping in cucumber (*Cucumis sativus* L.) by adjusting the micro-ecological environment of soil. *Peer J.* 7:e7267. doi: 10.7717/peerj.7267

Xiao, X., Lv, J., Xie, J., Feng, Z., Ma, N., Li, J., et al. (2020). Transcriptome analysis reveals the different response to toxic stress in rootstock grafted and non-grafted cucumber seedlings. *Int. J. Mol. Sci.* 21:774. doi: 10.3390/ijms21030774

Yu, J. Q., and Matsui, Y. (1994). Phytotoxic substances in root exudates of cucumber (*Cucumis sativus* L.). *J. Chem. Ecol.* 20, 21–31. doi: 10.1007/bf02065988

Yu, J. Q., and Matsui, Y. (1997). Effects of root exudates of cucumber (*Cucumis sativus*) and allelochemicals on ion uptake by cucumber seedlings. *J. Chem. Ecol.* 23, 817–827. doi: 10.1023/B:JOEC.0000006413.98507.55

Zhang, Z., Fan, J., Wu, J., Zhang, L., Wang, J., Zhang, B., et al. (2020b). Alleviating effect of silicon on melon seed germination under autotoxicity stress. *Ecotox. Environ. Safe.* 188:109901. doi: 10.1016/j.ecoenv.2019.109901

Zhang, R., Sun, Y., Liu, Z., Jin, W., and Sun, Y. (2017). Effects of melatonin on seedling growth, mineral nutrition, and nitrogen metabolism in cucumber under nitrate stress. *J. Pineal Res.* 62:e12403. doi: 10.1111/jpi.12403

Zhang, Z., Wu, J., Xi, Y., Zhang, L., Gao, Q., and Wang-Pruski, G. (2021). Effects of autotoxicity on seed germination, gas exchange attributes and chlorophyll fluorescence in melon seedlings. *J. Plant Growth Regul.* 41, 993–1003. doi: 10.1007/s00344-021-10355-w

Zhang, H., Zhang, Q., Song, J., Zhang, Z., Chen, S., Long, Z., et al. (2020a). Tracking resistomes, virulence genes, and bacterial pathogens in long-term manure-amended greenhouse soils. *J. Hazard. Mater.* 396:122618. doi: 10.1016/j.jhazmat.2020.122618

Zhu, Y., and Gong, H. (2014). Beneficial effects of silicon on salt and drought tolerance in plants. *Agron. Sustain. Dev.* 34, 455–472. doi: 10.1007/s13593-013-0194-1

frontiers | Frontiers in Plant Science

TYPE Original Research
PUBLISHED 11 August 2022
DOI 10.3389/fpls.2022.968496

Check for updates

OPEN ACCESS

EDITED BY
Ji-Hong Liu,
Huazhong Agricultural University, China

REVIEWED BY
Wei Zhang,
Nanjing Normal University,
China
Mohamed Lazali,
University of Khemis Miliana, Algeria

*CORRESPONDENCE
Chao Yan
yanchao504@neau.edu.cn
Chunmei Ma
chunmm@neau.edu.cn

SPECIALTY SECTION
This article was submitted to
Plant Abiotic Stress,
a section of the journal
Frontiers in Plant Science

RECEIVED 14 June 2022
ACCEPTED 25 July 2022
PUBLISHED 11 August 2022

CITATION
Lyu X, Sun C, Lin T, Wang X, Li S, Zhao S, Gong Z, Wei Z, Yan C and Ma C (2022) Systemic regulation of soybean nodulation and nitrogen fixation by nitrogen via isoflavones.
Front. Plant Sci. 13:968496.
doi: 10.3389/fpls.2022.968496

COPYRIGHT
© 2022 Lyu, Sun, Lin, Wang, Li, Zhao, Gong, Wei, Yan and Ma. This is an open-access article distributed under the terms of the Creative Commons Attribution License (CC BY). The use, distribution or reproduction in other forums is permitted, provided the original author(s) and the copyright owner(s) are credited and that the original publication in this journal is cited, in accordance with accepted academic practice. No use, distribution or reproduction is permitted which does not comply with these terms.

Systemic regulation of soybean nodulation and nitrogen fixation by nitrogen via isoflavones

Xiaochen Lyu[1], Chunyan Sun[1], Tao Lin[1], Xuelai Wang[1], Sha Li[1,2], Shuhong Zhao[1,3], Zhenping Gong[1], Ziwei Wei[4], Chao Yan[1]* and Chunmei Ma[1]*

[1]College of Agriculture, Northeast Agricultural University, Harbin, China, [2]College of Resources and Environment, Northeast Agricultural University, Harbin, China, [3]College of Engineering, Northeast Agricultural University, Harbin, China, [4]Harbin Agricultural Technology Extension Station, Harbin, China

Nitrogen (N) inhibits soybean (*Glycine max* L.) nodulation and N_2 fixation. Isoflavones secreted by soybean roots can stimulate signal transduction for symbiotic nodules, thus playing a key role in root nodule development and N_2 fixation. The relationship between the inhibition of soybean nodulation, N_2 fixation and isoflavones by N is still unclear. In this study, dual-root soybean plants were prepared by grafting, and N or isoflavones were supplied to unilateral roots. The number and dry weight of the soybean nodules, nitrogenase activity, isoflavone concentrations and relative changes in the level of expression of nodulation-related genes were measured to study the response relationship between the N systemic regulation the soybean nodule N_2 fixation and changes in the concentrations of isoflavones in its roots. The results showed that N supply to one side of the dual-root soybeans systematically affected the N_2 fixation of root nodules on both sides, and this effect began in the early stage of nodulation. Moreover, a unilateral supply of N systematically affected the concentrations of daidzein and genistein on both sides of the roots. The concentrations of isoflavones were consistent with the change trend of soybean root nodule and nodulation-related gene expression level. Treatment with unilateral N or isoflavones affected the soybean nodule N_2 fixation and its nodulation-related genes, which had the same response to the changes in concentrations of root isoflavones. N regulates soybean nodulation and N_2 fixation by systematically affecting the concentrations of isoflavones in the roots.

KEYWORDS

dual-root soybean, nitrogen, systemic regulation, isoflavones, nodulation

Introduction

A symbiotic relationship is established between soybean (*Glycine max* L.) and rhizobium to form root nodules, which can fix N from the air for their own growth (Mulder et al., 2005). When the soybean root is exposed to a high concentration of N, nodulation and N_2 fixation capacity will be inhibited; aging of the root nodules will be accelerated, and the N_2 fixation

efficiency will be reduced (Harper and Gibson, 1984; Carroll et al., 1985; Gibson and Harper, 1985; Streeter and Wong, 1988; Mizukoshi et al., 1995; Fujikake et al., 2003). Root hair deformation caused by the infection of leguminous crops by root nodulating bacteria is the most significant response during the early stage of nodulation (Zaat et al., 1987). *NFR1* and *NIN* are involved in the early nodulation processes, such as the identification of nodulation factors and infection line formation (Schauser et al., 1999; Indrasumunar et al., 2011). Abiotic stress suppresses the deformation of soybean root hairs while reducing the quantity of root nodules (Duzan et al., 2004). It has been demonstrated that a high concentration of N significantly reduces the rate of root hair deformation of Lotus japonicus and reduces the level of expression of *NIN*, while the level of expression in Lotus japonicus mutants resistant to high N remains at a high level (Barbulova et al., 2007). The overexpression of *GmNFR1* increased the number of nodules in soybean, and silencing *GmNFR1* inhibited the deformation of root hairs and the formation of infection threads in soybean (Indrasumunar et al., 2011). The early nodulin gene (Nguyen et al., 2019) is involved in the growth process of root nodules. After nitrate was applied to Medicago truncatula, the level of expression of the nodulin gene *ENOD93* was downregulated (Cabeza et al., 2014). Inoculating efficient rhizobia and treatment with 5 mM of nitrate increased the nodule number and dry weight of soybean, and the relative level of expression of *GmENOD40* also increased significantly (Nguyen et al., 2019). High amounts of N were supplied to the non-nodulation side of the unilateral nodulation dual-root soybean system, and the nodule number, dry weight and nitrogenase activity on the unsupplied nitrogen side were inhibited (Lyu et al., 2020; Lyu et al., 2022). Previous studies have suggested that the effect of N on N_2 fixation by root nodules not only causes local inhibition but also systemic regulation (Hinson, 1975; Tanaka et al., 1985; Silsbury et al., 1986; Arnone et al., 1994; Yashima et al., 2003, 2005).

As important signal molecules in root nodule symbiosis, flavonoids can stimulate the synthesis and secretion of nodulation factors by rhizobium, stimulate the symbiotic signal transduction for nodulation, participate in root nodule organogenesis and regulate the formation of root nodules (Redmond et al., 1986). It is very important for rhizobium to establish a symbiotic relationship with leguminous crops. Flavonoid synthesis genes are induced during the early stage of nodulation. It has been demonstrated that bradyrhizobium induces the expression of genes for key enzymes, such as phenylalanine ammonia lyase (*PAL*) and chalcone synthetase (*CHS*), that are involved in flavonoid synthesis in soybean roots (Estabrook and Sengupta-Gopalan, 1991). RNAi interference technology was used to interfere and silence the gene for the rate-limiting enzyme (*CHS*) of the flavonoid synthesis pathway in *Medicago truncatula*, the concentrations of root flavonoids decreased and inhibited the formation of root nodules, while the exogenous supply of naringenin and liquiritigenin, the precursors of flavonoids, restored the normal nodulation and root flavonoid content of *Medicago truncatula* (Wasson et al., 2006). Daidzein and genistein are the primary isoflavones in soybeans. Most of the isoflavones in root system secretions during the early growth stage of soybean are daidzein derivatives, and genistein can change the composition and molecular weight distribution of the extracellular polysaccharides produced by rhizobium and plays a key role in the generation of nodules and the adjustment of nodule ratio (Sugiyama et al., 2016). Isoflavone-sensitive rhizobium can still identify the soybean root and nodulate normally when there are low concentrations of daidzein and genistein in soybean roots (Subramanian et al., 2006). Supplying N directly to the root system significantly reduced the concentrations of daidzein and genistein in soybean roots (Cho and Harper, 1991; Sugiyama et al., 2016). N systematically regulates soybean nodule N_2 fixation whether isoflavones are involved merits further study.

In this study, we proposed the hypothesis that systemic effect of N on N_2 fixation in soybean nodules is regulated by isoflavones. Thus, the dual-root soybean materials were prepared by grafting, and N or isoflavones were supplied to unilateral roots. The nodule number, nodule dry weight, nitrogenase activity, root isoflavone concentrations and changes in the level of expression of nodulation-related genes were measured to study the response relationship between the N systemic regulation of the soybean nodule N_2 fixation and changes in the concentrations of isoflavones in its roots, so as to provide a basis and insights for the physiological regulatory mechanism of N_2 fixation by nodulation in soybean.

Materials and methods

The dual-root soybean material was prepared using the seedling grafting method of Xia et al. (2017), and a sand culture experiment was conducted. The soybean variety used was Heinong 40, and the N source tested was ammonium nitrate (NH_4NO_3). Two seedlings were grafted when the cotyledons of the soybean grew to 7–10 cm from the root tip. After 7 days of growth (cotyledon (VC) stage), the part above the grafted interface of downward notched seedlings was cut off, and two roots and one aboveground soybean seedling were prepared. They were then cultured and tested in the field. Supplementary material 1 shows the specific grafting method, preparation of nutrient solution and method of inoculating rhizobia.

Experimental treatments

Experiment 1

Dual-root soybean was treated in the VC stage, and both sides of the N0 treatment were supplied with N-free nutrient solution. The N100 treatment N-supply side (N+) was supplied with a 100 mg/l N concentration of nutrient solution, and the N-free side (N−) was supplied with N-free nutrient solution. Samples were taken on 1, 3, 7, and 21 days after treatment. After 1 and 3 days of treatment, the number of deformed root hairs was measured by sampling. The root system on both sides was washed with distilled water to remove the sand, and the root system was observed by optical microscopy. The degree of root hair deformation was determined by the number of deformations in every 60 root hairs in the microscope field of vision,

and each treatment was repeated six times. After 3 and 7 days of treatment, changes in the expression of genes in the roots were measured by sampling, and the expression of gene changes in the nodules was measured after 21 days of treatment. The root system on both sides was washed with distilled water, the nodules were then removed, and the roots were cut into pieces. The root and nodules were stored at −80°C to measure the level of gene expression, and each treatment was repeated three times. For RNA extraction and quantitative real-time reverse transcription-PCR (qRT-PCR) analysis, total RNA was extracted from root nodules using the TRIzol reagent (Servicebio, Wuhan, China), and cDNA was synthesized using a RevertAid reverse transcription kit (Servicebio, Wuhan, China). The primer sequences used for qRT-PCR amplification are shown in Supplementary material 2. Three biological replicates were performed. In this study, 18S rRNA was used as the reference to calculate the qRT-PCR data for genes as described by Carter and Tegeder (2016).

Experiment 2

The dual-root soybean was treated during the VC stage. The experiment was divided into two consecutive stages. The N_0 treatment supplied N-free nutrient solution on both sides of the two stages. The N_{100} treatment supplied a nutrient solution with an N concentration of 100 mg/l on the N+ side of the two stages, and the N-side was supplied with N-free nutrient solution. In $N_{100\text{-}0}$ treatment, the N+ side was supplied with nutrient solution with a concentration of 100 mg/l N in stage I and N-free nutrient solution in stage II. The N-side was supplied with N-free nutrient solution in two stages. There were two sampling times: (1) Stage I was treated for 21 days and stage II treatment was initiated at 22 days and ended at 42 days. Samples were taken on days 21 and 42, and the nodule number, nodule dry weight, and nitrogenase activity were determined (Lyu et al., 2019). Each treatment was repeated four times. (2) Stage I was treated for 7 days and stage II was started at 8 days and ended at 14 days. After 7 days of treatment, the soybean plants were completely pulled out. The roots were rinsed with distilled water and then transferred to a beaker that contained sterile deionized water, and the root exudates were collected for 48 h. The deionized water that contained the root exudates was passed through a 0.45 μm filter membrane, concentrated into a powder in a freeze-vacuum desiccator (Marin Christ, Osterode, Sachsen, Germany), and stored in a sterile desiccator for later use. Root samples were taken on days 7 and 14. The concentrations of daidzein and genistein in roots and root exudates were determined by high-pressure liquid chromatography (HPLC). Each treatment included four replicates.

Experiment 3

Isoflavones were unilaterally applied to a dual-root soybean during the VC stage. In the $I_{3.75}$ treatment, the treated side (T+) of the roots was supplied with nutrient solution that contained isoflavone, and the concentrations of daidzein and genistein were 3.75 mg/l. The untreated side (T-) of the roots was supplied with the nutrient solution without isoflavone. The treatment without isoflavone nutrient solution on both sides was used as a control, which was recorded as I_0. The N concentration of nutrient solution supplied on both sides of roots in two treatments was 25 mg/l. On day 7 of treatment, samples were taken to determine the concentrations of daidzein and genistein in roots and root exudates, and there were four replicates. On day 21 of treatment, samples were taken to determine the nodule number, nodule dry weight, and nitrogenase activity, and there were four replicates. The change in level of expression of genes in the roots was measured on days 3 and 7 of treatment, and the levels of expression of changes in the genes in nodules were measured 21 days after treatment. Each treatment was repeated four times. The specific sampling method and determination method were the same as those used in Experiments 1 and 2.

Data analysis

Data processing and statistical analysis were performed with Microsoft Excel 2016 (Redmond, WA, USA) and SPSS 21.0 (IBM, Inc., Armonk, NY, USA). All the data were tested for normality before a one-way analysis of variance (ANOVA) was conducted. The mean differences were compared using Duncan's multiple range test. Comparisons with $p < 0.05$ were considered significant.

Results

Nodulation and nitrogenase activity in dual-root soybeans

Figure 1 shows the difference in the number of deformed root hairs after N supply for 1 and 3 days. The number of deformed root hairs on the N+ side of N100 treatment for 1 day was 52.50% lower than that of the N0 treatment. The number of deformed root hairs on the N-side treated with N100 did not differ significantly from that treated with N0. The N supply treatment inhibited root hair deformation on both sides of the soybean for 3 days. The number of deformed root hairs on the N+ side of N100 treatment was 57.10% lower than that of the N0 treatment, and the number of deformed root hairs on the N-side of N100 treatment was 32.94% lower than that of the N0 treatment, indicating that N supply inhibited root hair deformation and thus affected nodulation. With the increase in time of N supplied, the degree of inhibition of root hair deformation on both sides of the dual-root soybean intensified, indicating that the N supply hindered the growth of root nodules on the direct contact side, while the growth of root nodules without contacting an N source also tended to be inhibited.

Table 1 shows the changes of nodules on the dual-root soybeans. After 21 days of N supply treatment, the nodule number and dry weight of the N-side in N_0 and N_{100} treatments were similar. Compared with the N_0 treatment, the nodule

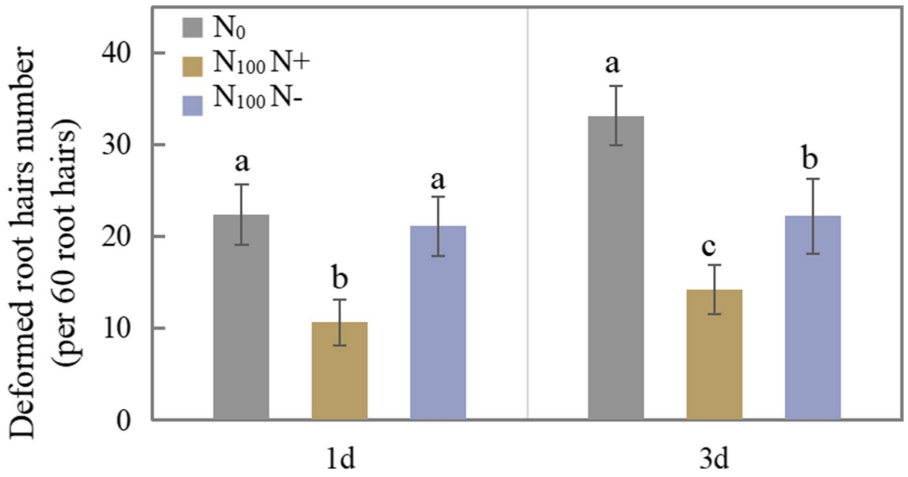


FIGURE 1
Number of deformed root hairs of dual-root soybeans, N_0 is N-free nutrient solution on both sides of dual-root soybeans, N_{100} N+ is N-supply side of dual-root soybeans treated with 100mg/l nutrient solution on unilateral side, N_{100} N-is N-free side of dual-root soybeans treated with 100mg/l nutrient solution on unilateral side, different lowercase letters above the bars indicate significant difference (p<0.05) by Duncan's multiple range test.

TABLE 1 Changes of dual-root soybean nodules.

	Treatments	21 days		42 days	
		N+	N−	N+	N−
Nodule number (per plant)	N_0	104.0 ± 9.71a	104.0 ± 9.71a	160.7 ± 8.72a	160.7 ± 8.72a
	N_{100}	64.3 ± 6.73b	91.3 ± 6.17a	118.4 ± 8.01c	142.1 ± 7.31b
	$N_{100\text{-}0}$			132.2 ± 6.14b	145.1 ± 5.14b
Nodule dry weight (g/plant)	N_0	0.19 ± 0.033a	0.19 ± 0.033a	0.49 ± 0.041a	0.49 ± 0.041a
	N_{100}	0.12 ± 0.019b	0.18 ± 0.061a	0.34 ± 0.022c	0.42 ± 0.062b
	$N_{100\text{-}0}$			0.42 ± 0.031b	0.43 ± 0.021b

N_0 is the N-free nutrient solution treatment on both sides of the dual-root soybeans, N_{100} is the N-supply concentration of 100 mg/l nutrient solution on the unilateral side of the dual-root soybeans, and $N_{100\text{-}0}$ is the N-supply concentration of 100 mg/l on the unilateral side of the dual-root soybeans and it was changed to N-free nutrient solution. N+ is the N-supply side, N-is the N-free side, the values in the table represent the mean ± standard error (n = 4), and different lowercase letters indicate significant difference (p < 0.05) by Duncan's multiple range test and longitudinal comparison.

number on the N+ side of N_{100} treatment decreased by 38.14%, and nodule dry weight decreased by 36.84%. After 42 days of N supply, the nodule number and dry weight of the N+ side were significantly different among the three treatments. Compared with the N_0 treatment, the nodule number decreased by 26.32 and 17.73% in the N_{100} and $N_{100\text{-}0}$ treatments, respectively, and nodule dry weight decreased by 30.61 and 14.29%, respectively. The N_{100} and $N_{100\text{-}0}$ treatments were close to the number and dry weight of the N-side nodules. In comparison with the N_0 treatment, nodule dry weight was reduced by 14.29 and 12.24%, and nodule number was reduced by 11.57 and 9.71%, respectively. This indicated that N supply hindered the growth of nodules on the direct contact side, and the growth of nodules without N was also inhibited. The removal of N from the N-supply roots restored the growth of nodules.

As shown in Table 2, changes in the specific nitrogenase activity (SNA) and acetylene reduction assay (ARA) of the dual-root soybean nodules were measured. After 21 days of unilateral N supply, the SNA and ARA of N+ side of N_{100} treatment were significantly lower than those of N_0 treatment, which decreased by 24.77 and 52.58%, respectively. There was no significant difference between N-side SNA and ARA of N_{100} and N_0 treatments. After 42 days of unilateral N supply, SNA and ARA of N+ side of each treatment were significantly different. Compared with N_0 treatment, SNA of N_{100} and $N_{100\text{-}0}$ treatments decreased by 38.71 and 14.31%, respectively, and that of ARA decreased by 57.45 and 26.54%, respectively. The N-side SNA and ARA of N_{100} and $N_{100\,0}$ treatments were very similar, and the SNA of the two treatments decreased by 21.17 and 14.92% compared with N_0 treatment, while the ARA decreased by 34.43 and 25.31% compared with N_0 treatment, respectively. This indicated that the N supply inhibited the nitrogenase activity of the nodules, and the nitrogenase activity was restored after N-free culture. Changes in the N-side were smaller than those in the N+ side.

10.3389/fpls.2022.968496

TABLE 2 Changes of nitrogenase activity in dual-root soybean nodules.

	Treatments	21 days		42 days	
		N+	N−	N+	N−
SNA (C_2H_4 μmol g^{-1}	N_0	22.4 ± 2.91a	22.4 ± 2.91a	49.6 ± 3.61a	49.6 ± 3.61a
nodule dry mass h^{-1})	N_{100}	16.8 ± 0.41b	21.2 ± 2.90a	30.4 ± 1.87c	39.1 ± 2.72b
	N_{100-0}			42.5 ± 1.87b	42.2 ± 1.65b
ARA (C_2H_4 μmol h^{-1}	N_0	4.2 ± 0.07a	4.2 ± 0.07a	24.3 ± 1.74a	24.3 ± 1.74a
$plant^{-1}$)	N_{100}	2.0 ± 0.22b	3.8 ± 0.04a	10.3 ± 0.98c	16.4 ± 1.47b
	N_{100-0}			17.8 ± 2.41b	18.1 ± 1.12b

N_0 is the N-free nutrient solution treatment on both sides of the dual-root soybeans, N_{100} is the N-supply concentration of 100 mg/l nutrient solution on the unilateral side of the dual-root soybeans, and N_{100-0} is the N-supply concentration of 100 mg/l on the unilateral side of the dual-root soybeans and it was changed to N-free nutrient solution. N+ is the N-supply side, N-is the N-free side, the values in the table represent the mean ± standard error ($n = 4$), and different lowercase letters indicate significant difference ($p < 0.05$) by Duncan's multiple range test and longitudinal comparison.

TABLE 3 Concentrations of daidzein and genistein in dual-root soybean roots (mg/g DW).

	Treatments	7 days		14 days	
		N+	N−	N+	N−
Daidzein	N_0	3.86 ± 0.031a	3.86 ± 0.035a	4.16 ± 0.034a	4.16 ± 0.035a
	N_{100}	2.78 ± 0.033b	3.32 ± 0.013b	3.17 ± 0.084c	3.38 ± 0.142b
	N_{100-0}			3.45 ± 0.075b	3.67 ± 0.051b
Genistein	N_0	0.197 ± 0.003a	0.197 ± 0.003a	0.291 ± 0.010a	0.291 ± 0.010a
	N_{100}	0.117 ± 0.027b	0.157 ± 0.006a	0.182 ± 0.003c	0.225 ± 0.002b
	N_{100-0}			0.210 ± 0.001b	0.234 ± 0.002b

N_0 is the N-free nutrient solution treatment on both sides of the dual-root soybeans, N_{100} is the N-supply concentration of 100 mg/l nutrient solution on the unilateral side of the dual-root soybeans, and N_{100-0} is the N-supply concentration of 100 mg/l on the unilateral side of the dual-root soybeans and it was changed to N-free nutrient solution. N+ is the N-supply side, N-is the N-free side, the values in the table represent the mean ± standard error ($n = 4$), and different lowercase letters indicate significant difference ($p < 0.05$) by Duncan's multiple range test and longitudinal comparison.

Isoflavones concentrations in dual-root soybean roots and root exudates

Table 3 shows the changes of daidzein and genistein concentrations in dual-root soybean roots. After 7 days of N supply, the daidzein concentration in N+ side roots of N_{100} treatment decreased by 27.95% and N-side by 13.90% compared with N_0 treatment. The genistein concentration in N+ side root of N_{100} treatment decreased by 40.61% compared with N_0 treatment, and genistein concentration in N-side decreased by 20.30%. After 7 days of unilateral N supply, the concentrations of daidzein and genistein in the root exudates of the N+ side in the N_{100} treatment were significantly lower than those in the N_0 treatment, while those in the N-side were also smaller than those in the N_0 treatment, but the difference was not significant (Supplementary Table S3). The changes of daidzein and genistein concentrations in root exudates of the dual-root soybeans were consistent with those in roots. After 14 days of nitrogen supply treatment, the daidzein concentrations in N+ side roots of each treatment were significantly different, and the daidzein concentrations in N_{100} and N_{100-0} treatments were 23.75 and 17.12% lower than those in N_0 treatment, respectively. The daidzein concentration in N-side roots of N_{100} and N_{100-0} treatments was also significantly lower than those of N_0 treatment, which decreased by 18.86 and 11.90%, respectively. The genistein concentration in N+ side of N_{100} and N_{100-0} treatment decreased by 37.46 and 27.84% compared with N_0 treatment. The genistein concentration in N-side of N_{100} and N_{100-0} treatments decreased by 22.68 and 19.59% compared with N_0 treatment. This indicated that a supply of N inhibited the concentrations of root daidzein and genistein on both sides of the dual-root soybean. In addition, the removal of N from the treatment that had been supplied with high N increased the concentrations of daidzein and genistein on both sides of the dual-root soybean, and the change was more significant on the N+ side.

Relative expression of nodulation-related genes in dual-root soybeans

As shown in Figure 2A, the relative expression of the *GmNFR1A*, *GmN1N1a* and *GmN1N2a* genes in the roots of N_{100} N+ side after 3 days of N supply was significantly downregulated compared with N_0 treatment, and the N_{100} N-side also showed a downward trend compared with N_0, but the reduction was smaller. Figure 2B shows that the expression levels of the three genes in the roots of the N+ side of N100 were significantly reduced, while the expression levels of the three genes in the roots of the N-side of

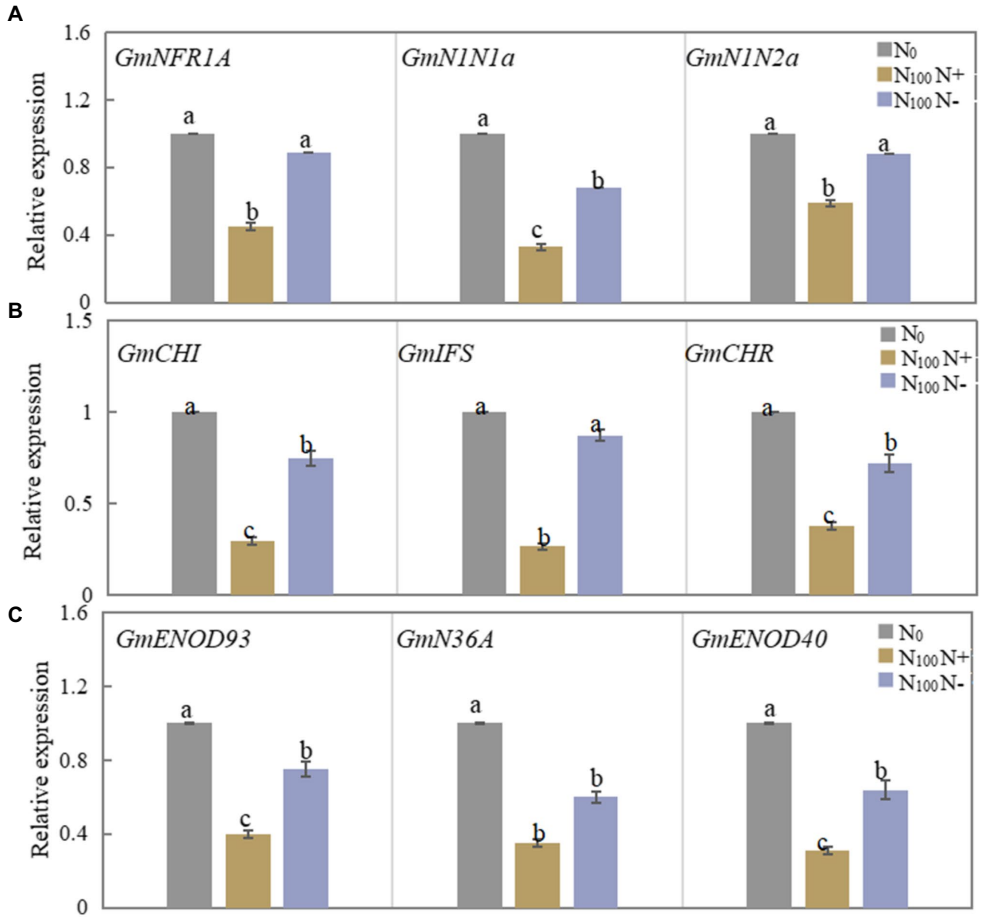


FIGURE 2
Changes of nodulation-related genes expression in roots and nodules of dual-root soybean, N_0 is N-free nutrient solution on both sides of dual-root soybeans, N_{100} N+ is N-supply side of dual-root soybeans treated with 100mg/l nutrient solution on unilateral side, N_{100} N-is N-free side of dual-root soybeans treated with 100mg/l nutrient solution on unilateral side, different lowercase letters above the bars indicate significant difference (p<0.05) by Duncan's multiple range test. **(A)** The expression level of the nodulation signal recognition gene on both sides of dual-root soybean after treatment for 3days. **(B)** The level of expression of the genes for roots isoflavone synthesis on both sides of the dual-root soybean after 7days of treatment. **(C)** The level of expression of the genes of early nodulin synthesis in root nodules after 21days of treatment.

N100 also showed a downward trend, but the reduction was smaller. As shown in Figure 2C, the three genes *GmENOD93*, *GmN36A* and *GmENOD40* all decreased in the nodules on both sides of the N_{100} treatment, while the range of change in the N-free side was smaller than that of the N-supply side. The results showed that the effect of N supply from one side of the dual-root soybean root system on root nodules on both sides of the roots started from the mutual recognition of early nodulation signals, and the regulation of nodulation process also involved changes in the synthesis of isoflavones in the roots.

Effects of unilateral supply of isoflavones on nitrogen fixation in soybean plants

Table 4 shows the changes in the number and dry weight of the dual-root soybean nodules after the unilateral application of isoflavones. The nodule number and dry weight of the T+ side in the $I_{3.75}$ treatment were significantly higher than those in the I_0 treatment, increasing by 29.20 and 7.78%, respectively. The nodule number and dry weight of the T-side in the $I_{3.75}$ treatment were significantly lower than those in the I_0 treatment. This showed that the mixed application of daidzein and genistein improved the

TABLE 4 Effects of unilateral application of isoflavones on double-rooted soybean nodules.

Treatments	Nodule number (per plant)		Nodule dry weight (g/plant)	
	T+	T−	T+	T−
I_0	113.0 ± 9.71b	113.0 ± 9.71a	0.18 ± 0.033b	0.18 ± 0.033a
$I_{3.75}$	146.0 ± 11.45a	98.6 ± 10.74b	0.23 ± 0.038a	0.12 ± 0.009b

I_0 is the nutrient solution without isoflavones supplied on both sides, and $I_{3.75}$ is the nutrient solution with daidzein and genistein applied unilateral side. Treated side denoted as T+, untreated side denoted as T−, the values in the table represent the mean ± standard error (n = 4), different lowercase letters indicate significant difference (p < 0.05) by Duncan's multiple range test and longitudinal comparison.

TABLE 5 Effects of unilateral application of isoflavones on nitrogenase activity.

Treatments	SNA(C_2H_4 μmol g^{-1} nodule dry mass h^{-1})		ARA(C_2H_4 μmol h^{-1} $plant^{-1}$)	
	T+	T−	T+	T−
I_0	24.5 ± 2.91a	24.5 ± 2.91a	4.4 ± 0.07b	4.4 ± 0.07a
$I_{3.75}$	23.3 ± 2.68a	21.5 ± 0.80a	5.3 ± 0.11a	2.5 ± 0.02b

I_0 is the nutrient solution without isoflavones supplied on both sides, and $I_{3.75}$ is the nutrient solution with daidzein and genistein applied unilateral side. Treated side denoted as T+, untreated side denoted as T−, the values in the table represent the mean ± standard error ($n = 4$), different lowercase letters indicate significant difference ($p < 0.05$) by Duncan's multiple range test and longitudinal comparison.

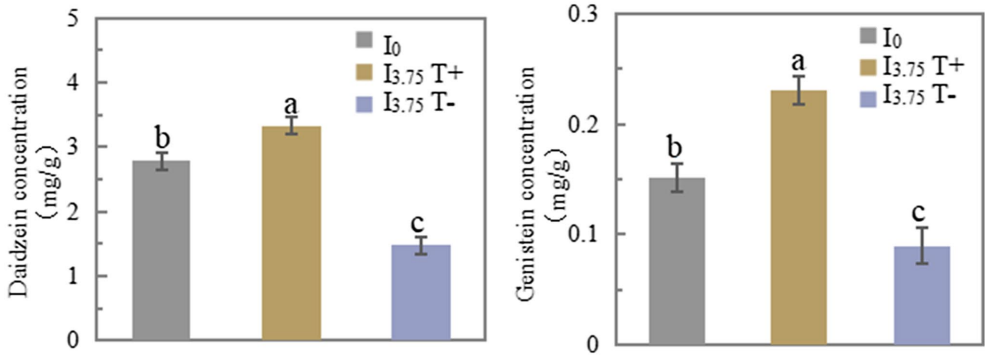


FIGURE 3
Changes in daidzein and genistein concentrations in roots after unilateral supply of isoflavones, different lowercase letters above the bars indicate significant difference ($p<0.05$) by Duncan's multiple range test. I_0 refers to conventional nutrient solution applied on both sides; $I_{3.75}$ T+ is the treatment side of unilateral application of nutrient solution containing daidzein and genistein, and $I_{3.75}$ T-is the untreated side of the unilateral application of nutrient solution that contained daidzein and genistein.

nodule number and dry weight on the contact side, but the nodule number and dry weight on the untouched side decreased.

As shown in Table 5, there were changes in the SNA and ARA of dual-root soybean after unilateral application of isoflavones. There was no significant difference in SNA on the T+ side of I_0 and $I_{3.75}$ treatments, while ARA on the T+ side of $I_{3.75}$ treatment was significantly higher than that of I_0 treatment. T-side SNA in $I_{3.75}$ and I_0 treatments had no significant difference, but the ARA of $I_{3.75}$ treatment in T-side was significantly lower than that in I_0 treatment. The mixed application of daidzein and genistein increased the activity of whole plant nitrogenase in nodules on the contact side, but it decreased on the untouched side. There was no significant change in nitrogenase activity per unit weight of nodules. The change of whole plant nitrogenase activity in nodules primarily originated from the change of nodule number and dry weight.

Effects of isoflavones unilateral supply on isoflavones concentration in soybean roots and root exudates

On 7 days after treatment, the daidzein and genistein concentrations in T+ side roots of the $I_{3.75}$ treatment were significantly higher than those of the I_0 treatment. The daidzein and genistein concentrations in T-side roots of $I_{3.75}$ treatment were significantly lower than those of I_0 treatment (Figure 3). The changes of daidzein and genistein concentrations in root exudates were consistent with those in roots (Supplementary Table S4). The mixed application of daidzein and genistein significantly increased the concentrations of daidzein and genistein on the contact side of roots and root exudates, while the concentrations of daidzein and genistein on the untouched side of the roots and root exudates decreased significantly, which was opposite to the trend on the contact side.

Effects of unilateral isoflavones supply on relative expression of nodulation-related genes

As shown in Figure 4A, the relative expressions of the three genes involved in the recognition of early nodulation signals increased significantly after the mixed administration of two isoflavones on the T+ side of $I_{3.75}$ treatment, while the expression levels of the three genes on the T-side significantly decreased. Figure 4B shows that the relative expression levels of the three genes involved in the synthesis of isoflavones on the T+ side increased, while the expression levels of the T-side genes decreased in $I_{3.75}$ treatment. As shown in Figure 4C, the expression of *GmENOD93* and *GmENOD40* on the T+ side of $I_{3.75}$ treatment was higher than

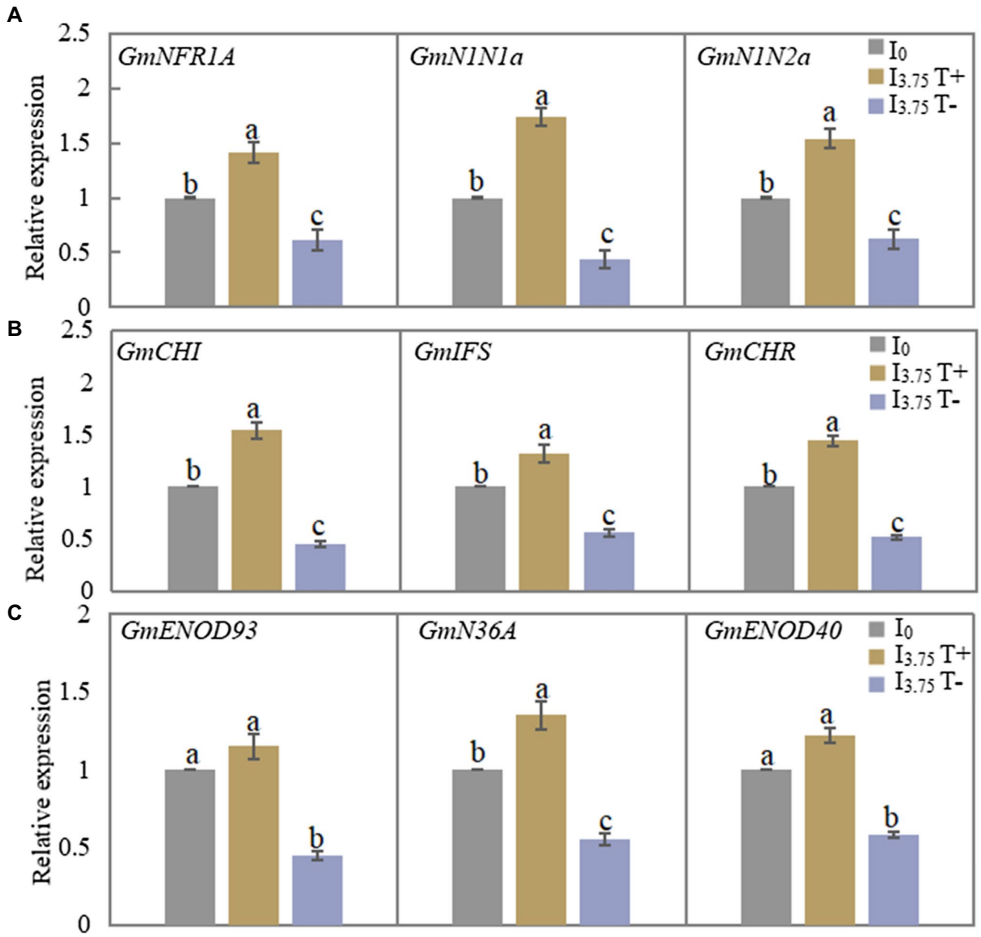


FIGURE 4
Changes of relative expression of nodulation-related genes in roots and nodules of dual-root soybean after unilateral supply of isoflavones, different lowercase letters above the bars indicate significant difference ($p<0.05$) by Duncan's multiple range test. I_0 refers to conventional nutrient solution applied on both sides; $I_{3.75}$ T+ is the treatment side of unilateral application of nutrient solution containing daidzein and genistein, and $I_{3.75}$ T-is the untreated side of the unilateral application of nutrient solution that contained daidzein and genistein. **(A)** The expression level of the nodulation signal recognition gene on both sides of dual-root soybean after treatment for 3days. **(B)** The level of expression of the genes for roots isoflavone synthesis on both sides of the dual-root soybean after 7days of treatment. **(C)** The level of expression of the genes of early nodulin synthesis in root nodules after 21days of treatment.

that of I_0 treatment, but the difference was not significant, while the relative expression of *GmN36A* gene is significantly higher than that of I_0 treatment, $I_{3.75}$ treatment T-side three genes relative expression was significantly decreased. Additionally, the unilateral application of isoflavones affected the signal recognition of nodules, isoflavone synthesis and the growth process of nodules.

Discussion

Systematic impacts of nitrogen on nitrogen fixation and nodulation in soybeans

The most significant characteristic of infection is the root hair deformation caused during the early stage of infection of the host by rhizobium (Zaat et al., 1987). *NFR1* and *NIN* are involved in signal recognition, infection thread formation and other processes during the early development of root nodules (Schauser et al., 1999; Indrasumunar et al., 2011). The mutation of *NFR1* can prevent early nodulation phenomena, such as root hairs deformation (Amor et al., 2003; Madsen et al., 2003; Radutoiu et al., 2003; Miwa et al., 2006). With the exacerbation of root hair deformation of soybean, the relative expression of *NIN* increased (Wang et al., 2019). A high concentration of N was found to significantly reduce the level of expression of the deformation rate of root hair and *NIN* in *Lotus japonicus* (Barbulova et al., 2007). After 3 days of unilateral N supply in this experiment, root hair deformation on both sides was inhibited. The levels of expression of root *GmNFR1A, GmN1N1a* and *GmN1N2a* decreased significantly on the N+ side and slightly on the

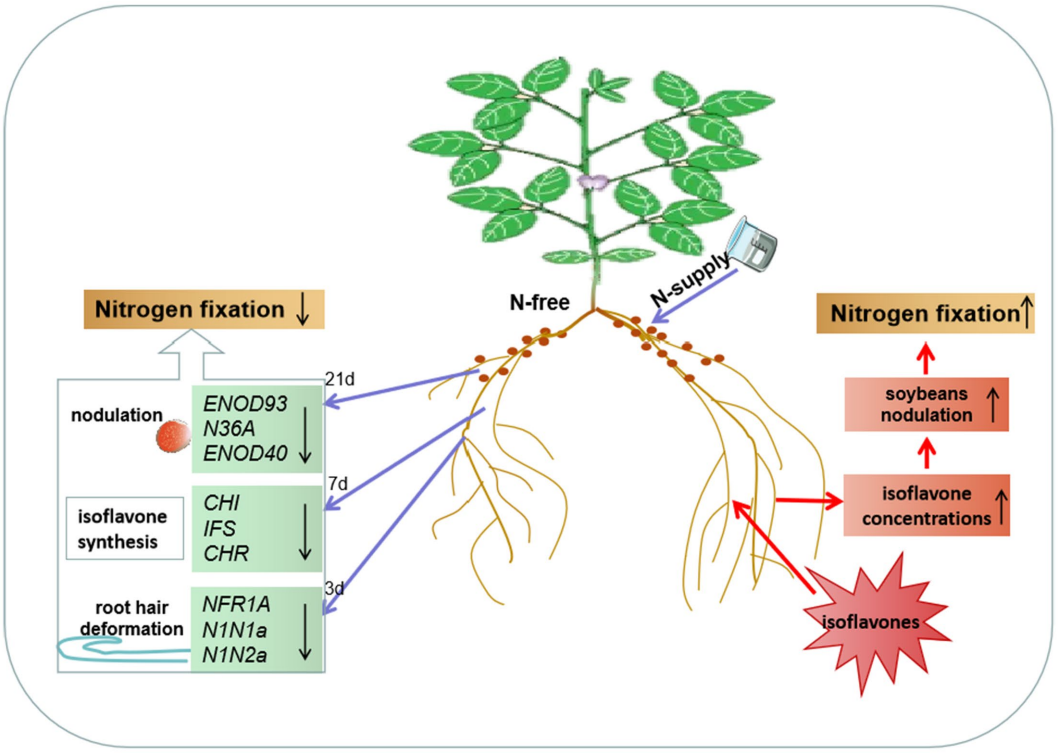


FIGURE 5
N systemically regulates soybean nodulation and N fixation through isoflavones. After unilateral N-supply, the expression of *NFR1A*, *N1N1a*, *N1N2a*, *CHI*, *IFS*, *CHR*, *ENOD93*, *N36A*, and *ENOD40* in the roots and nodules of the N-free side was downregulated, which at least partly explained root hair deformation, nodulation and isoflavone synthesis and secretion enhancement changes. Simultaneous, application of isoflavones promoted the isoflavones synthesis on the treated side and N_2 fixation in root nodules. Unilateral N or isoflavones supply, nodulation, nitrogen fixation and nodulation-related genes responded to the changes in root isoflavones concentrations in the same way.

N-side (Figure 5). The levels of expression of root hair deformation and early nodulation genes on both sides of soybean were inhibited by the unilateral N supply system, which was similar to the results of previous studies. In addition, the dual-root soybean study revealed that the systematic influence of N on soybean nodules appeared during the early stage of nodulation. Ma et al. (2019) and Zou et al., (2019) reported that the levels of expression of *GmNIN* and *GmNFR1* in soybean roots increased with the increase in N_2 fixation by nodulation in soybean roots. In this experiment, the nodule number, dry weight, SNA and ARA on both sides decreased after 21 days of unilateral N supply. After N removal, N_2 fixation on both sides of the soybean recovered. Previous studies have demonstrated that soybean that was supplied with high N on one side of the root inhibited the N_2 fixation on both sides of the root system (Xia et al., 2017; Lyu et al., 2019; Lyu et al., 2020; Li et al., 2021). *GmENOD93, GmN36A* and *GmENOD40* participate in nodulin synthesis and are closely related to the growth of root nodules (Nguyen et al., 2019; Wang et al., 2019). In this experiment, the relative levels of expression of *GmENOD93, GmN36A* and *GmENOD40* in both sides nodules decreased with the unilateral N supply, which is consistent with the trend of N_2 fixation by nodules (Figure 5). Unilateral N supply reduced the degree of root hair deformation on both sides, the ability to fix N by nodules and the level of expression of growth genes in early nodulation and nodules, indicating that the unilateral N supply systematically affected the N_2 fixation in soybean, this effect began during the early stage of nodulation.

Systematic impacts of nitrogen on the concentration of soybean isoflavones in the roots

Isoflavones secreted by soybean roots can activate the level of expression of nodulation factor nod genes of rhizobium, which play an important role in the development of nodules and their ability to fix N (Maj et al., 2010; Hassan and Mathesius, 2012). Genistein and daidzein are isoflavones that are the most prevalent in soybean (Peters et al., 1986; Kosslak et al., 1987; Smit et al., 1992; Sugiyama et al., 2007). The application of ammonium N, nitrate N and urea significantly reduced the daidzein and genistein concentrations in soybean roots, and the number of nodules decreased (Cho and Harper, 1991). Sugiyama et al. (2016)

reported that N supply significantly reduced the daidzein and genistein concentrations in soybean roots. Cho and Harper (1991) supplied N to the unilateral side of split-root soybeans, and nodule number and nitrogenase activity, as well as the daidzein and genistein concentrations in the roots, were lower on the N-supply side than on the N-free side. In this experiment, after the unilateral N supply of dual-root soybean for 7 days, the concentrations of daidzein and genistein in the roots and root exudates on the N-supply side were significantly reduced; the daidzein content on N-free side was significantly reduced, and the concentrations of genistein decreased slightly. After N removal treatment, the concentrations of daidzein and genistein in the roots on both sides of the dual-root soybean increased (Figure 5). The chalcone synthase gene (*GmCHS)* is involved in the synthesis of isoflavone basic skeleton; the isoflavone synthase gene (*GmIFS*) is involved in the synthesis of daidzein and genistein, and the chalcone reductase gene (*GmCHR)* is the key gene for daidzein synthesis (Sugiyama et al., 2016). After silencing the ability of soybean to synthesize key isoflavone genes, soybean inoculated with root nodulation bacteria failed to form root nodules (Subramanian et al., 2006; Wasson et al., 2006; Zhang et al., 2009). In this experiment, the isoflavones synthesized genes (*GmCHI, GmIFS* and *GmCHR*) level of expression on the N supply side roots decreased; the daidzein synthesis genes (*GmCHS* and *GmCHR*) level of expression on the N-free supply side roots decreased significantly, and the genistein synthesis gene (*GmIFS)* level of expression decreased slightly. The trend of changes in the three genes of the roots on both sides was consistent with that of the concentrations of root isoflavones, indicating that the reduction of root isoflavone concentrations caused by the N supply was related to their synthesis. In this experiment, the dual-root soybean unilateral N supply method was used to study the systematic regulation of isoflavone concentrations by N. The trend of changes in the concentrations of root and root exudates isoflavones on 7 days after treatment of the N supply was found to be consistent with that of the nodule numbers and nodulation-related genes after 21 days of treatment in soybeans, and the change in root system on both sides was synchronous. This suggested that soybean nodulation is systematically regulated by N, which is closely related to the early synthesis of isoflavones in the root. The unilateral N supply system inhibits isoflavone synthesis and secretion on both sides of the soybean roots, which affects the recognition process of rhizobium and the root system in the rhizosphere and thus affects soybean nodulation.

As the concentrations of genistein and daidzein in soybean roots decreased, the nodule number and weight decreased (Cho and Harper, 1993; Miransari and Smith, 2007). Rhizobium was used to inoculate the plants after genistein and daidzein culture to improve the dry weight and N_2 fixation capacity of soybean root nodules (Zhang and Smith, 1995; Miransari et al., 2009; Dolatabadian et al., 2012; Riviezzi et al., 2020). In this study, the mixed application of treatment with two isoflavones increased the concentrations of daidzein and genistein in roots on the T+ side, increased the level of expression of genes involved in isoflavone synthesis (*GmCHI*, *GmIFS* and *GmCHR*), and also increased nodule number and dry weight. It also increased the expression of genes involved in the early nodulation process (*GmNFR1A*, *GmN1N1a* and *GmN1N2a*) and nodule synthesis (*GmENOD93*, *GmN36A* and *GmENOD40*) in root nodules (Figure 5), indicating that the unilateral application of isoflavone not only promoted isoflavone synthesis in roots but also stimulated the expression of early nodulation genes and root nodule growth genes, so as to improve the effect of N_2 fixation by nodulation in soybean. In this study, under the conditions of unilateral N supply and unilateral external application of isoflavones, there was an identical response of N_2 fixation by nodulation in soybean and its nodulation-related genes to root isoflavone concentrations, which decreases with the decrease in the concentrations of root and root exudates isoflavones. It was demonstrated that N regulates N_2 fixation by nodulation in soybean through its systematic impacts on the concentrations of root isoflavones. However, the phenomenon of increased expression of early nodulation genes and root nodule growth genes depends on the exogenous application of isoflavones, the concentrations of root isoflavones or the synergistic effect of the two merits further research.

Conclusion

The systemic inhibitory effect of N on N_2 fixation in soybean nodules began at the early stage of nodulation and systematically inhibited the concentrations of isoflavones in soybean roots and root exudates. The changes in N_2 fixation by soybean nodules following treatment with a unilateral N supply or isoflavones were consistent with the changes of isoflavone concentrations in the roots and root exudates.

Data availability statement

The original contributions presented in the study are included in the article/Supplementary material; further inquiries can be directed to the corresponding authors.

Author contributions

XL and ZG: conceptualization, methodology, and writing—reviewing and editing. CS: data curation. TL and XW: funding acquisition. SL and ZW: investigation. XL and CY: resources. CM: software. XL: writing—original draft. All authors contributed to the article and approved the submitted version.

Funding

We are grateful for the support from the Project funded by China Postdoctoral Science Foundation (NO. 2022M710651).

Conflict of interest

The authors declare that the research was conducted in the absence of any commercial or financial relationships that could be construed as a potential conflict of interest.

Publisher's note

All claims expressed in this article are solely those of the authors and do not necessarily represent those of their affiliated organizations, or those of the publisher, the editors and the reviewers. Any product that may be evaluated in this article, or claim that may be made by its manufacturer, is not guaranteed or endorsed by the publisher.

Supplementary material

The Supplementary material for this article can be found online at: https://www.frontiersin.org/articles/10.3389/fpls.2022.968496/full#supplementary-material

References

Amor, B. B., Shaw, S. L., Oldroyd, G. E., Maillet, F., Penmetsa, R. V., Cook, D., et al. (2003). The NFP locus of Medicago truncatula controls an early step of nod factor signal transduction upstream of a rapid calcium flux and root hair deformation. *Plant J.* 34, 495–506. doi: 10.1046/j.1365-313X.2003.01743.x

Arnone, J. A., Kohls, S. J., and Baker, D. D. (1994). Nitrate effects on nodulation and nitrogenase activity of actinorhizal Casuarina studied in split-root systems. *Soil Biol. Biochem.* 26, 599–606. doi: 10.1016/0038-0717(94)90248-8

Barbulova, A., Rogato, A., D'Apuzzo, E., Omrane, S., and Chiurazzi, M. (2007). Differential effects of combined N sources on early steps of the nod factor–dependent transduction pathway in Lotus japonicus. *Mol. Plant-Microbe Interact.* 20, 994–1003. doi: 10.1094/mpmi-20-8-0994

Cabeza, R., Koester, B., Liese, R., Lingner, A., Baumgarten, V., Dirks, J., et al. (2014). An RNA sequencing transcriptome analysis reveals novel insights into molecular aspects of the nitrate impact on the nodule activity of Medicago truncatula. *Plant Physiol.* 164, 400–411. doi: 10.1104/pp.113.228312

Carroll, B. J., McNeil, D. L., and Gresshoff, P. M. (1985). Isolation and properties of soybean [*Glycine max* (*L.*) Merr.] mutants that nodulate in the presence of high nitrate concentrations. *Proc. Natl. Acad. Sci.* 82:4162–4166. doi: 10.1073/pnas.82.12.4162

Carter, A. M., and Tegeder, M. (2016). Increasing nitrogen fixation and seed development in soybean requires complex adjustments of nodule nitrogen metabolism and partitioning processes. *Curr. Biol.* 26, 2044–2051. doi: 10.1016/j.cub.2016.06.003

Cho, M. J., and Harper, J. E. (1991). Effect of localized nitrate application on isoflavonoid concentration and nodulation in split-root systems of wild-type and nodulation-mutant soybean plants. *Plant Physiol.* 95, 1106–1112. doi: 10.1104/pp.95.4.1106

Cho, M. J., and Harper, J. E. (1993). Effect of abscisic acid application on root isoflavonoid concentration and nodulation of wild-type and nodulation-mutant soybean plants. *Plant Soil* 153, 145–149. doi: 10.1007/BF00010552

Dolatabadian, A., Sanavy, S. A. M. M., Ghanati, F., and Gresshoff, P. M. (2012). Morphological and physiological response of soybean treated with the microsymbiont Bradyrhizobium japonicum pre-incubated with genistein. *S. Afr. J. Bot.* 79, 9–18. doi: 10.1016/j.sajb.2011.11.001

Duzan, H. M., Zhou, X., Souleimanov, A., and Smith, D. L. (2004). Perception of Bradyrhizobium japonicum nod factor by soybean [*Glycine max* (*L.*) Merr.] root hairs under abiotic stress conditions. *J. Exp. Bot.* 55, 2641–2646. doi: 10.1093/jxb/erh265

Estabrook, E., and Sengupta-Gopalan, C. (1991). Differential expression of phenylalanine ammonia-Lyase and Chalcone synthase during soybean nodule development. *Plant Cell* 3, 299–308. doi: 10.1105/tpc.3.3.299

Fujikake, H., Yamazaki, A., Ohtake, N., Sueyoshi, K., Matsuhashi, S., Ito, T., et al. (2003). Quick and reversible inhibition of soybean root nodule growth by nitrate involves a decrease in sucrose supply to nodules. *J. Exp. Bot.* 54, 1379–1388. doi: 10.1093/jxb/erg147

Gibson, A. H., and Harper, J. E. (1985). Nitrate effect on nodulation of soybean by Bradyrhizobium japonicum 1. *Crop Sci.* 25, 497–501. doi: 10.2135/cropsci1985.0011183X002500030015x

Harper, J. E., and Gibson, A. H. (1984). Differential nodulation tolerance to nitrate among legume species. *Crop Sci.* 24, 797–801. doi: 10.2135/cropsci1984.0011183X002400040040x

Hassan, S., and Mathesius, U. (2012). The role of flavonoids in root–rhizosphere signalling: opportunities and challenges for improving plant–microbe interactions. *J. Exp. Bot.* 63, 3429–3444. doi: 10.1093/jxb/err430

Hinson, K. (1975). Nodulation responses from nitrogen applied to soybean half-root Systems1. *Agron. J.* 67, 799–804. doi: 10.2134/agronj1975.00021962006700060018x

Indrasumunar, A., Searle, I., Lin, M. H., Kereszt, A., Men, A., Carroll, B. J., et al. (2011). Nodulation factor receptor kinase 1α controls nodule organ number in soybean (*Glycine max L.* Merr.). *Plant J.* 65, 39–50. doi: 10.1111/j.1365-313X.2010.04398.x

Kosslak, R. M., Bookland, R., Barkei, J., Paaren, H. E., and Appelbaum, E. R. (1987). Induction of Bradyrhizobium japonicum common nod genes by isoflavones isolated from Glycine max. *Proc. National Acad. Sci.* 84, 7428–7432. doi: 10.1073/pnas.84.21.7428

Li, S., Xiao, F., Yang, D., Lyu, X., Ma, C., Dong, S., et al. (2021). Nitrate transport and distribution in soybean plants with dual-root systems. *Front. Plant Sci.* 12:661054. doi: 10.3389/fpls.2021.661054

Lyu, X., Li, M., Li, X., Li, S., Yan, C., Ma, C., et al. (2020). Assessing the systematic effects of the concentration of nitrogen supplied to dual-root systems of soybean plants on nodulation and nitrogen fixation. *Agronomy* 10:763. doi: 10.3390/agronomy10060763

Lyu, X., Sun, C., Zhang, J., Wang, C., Zhao, S., Ma, C., et al. (2022). Integrated proteomics and metabolomics analysis of nitrogen system regulation on soybean plant nodulation and nitrogen fixation. *Int. J. Mol. Sci.* 23:2545. doi: 10.3390/ijms23052545

Lyu, X., Xia, X., Wang, C., Ma, C., Dong, S., and Gong, Z. (2019). Effects of changes in applied nitrogen concentrations on nodulation, nitrogen fixation and nitrogen accumulation during the soybean growth period. *Soil Sci. Plant Nutr.* 65, 479–489. doi: 10.1080/00380768.2019.1667213

Ma, W., Liu, W., Hou, W., Sun, S., Jiang, B., Han, T., et al. (2019). GmNMH7, a MADS-box transcription factor, inhibits root development and nodulation of soybean (*Glycine* max [*L.*] Merr.). *J. Integrative Agriculture* 18, 553–562. doi: 10.1016/S2095-3119(18)61992-6

Madsen, E. B., Madsen, L. H., Radutoiu, S., Olbryt, M., Rakwalska, M., Szczyglowski, K., et al. (2003). A receptor kinase gene of the LysM type is involved in legumeperception of rhizobial signals. *Nature* 425, 637–640. doi: 10.1038/nature02045

Maj, D., Wielbo, J., Marek-Kozaczuk, M., and Skorupska, A. (2010). Response to flavonoids as a factor influencing competitiveness and symbiotic activity of rhizobium leguminosarum. *Microbiol. Res.* 165, 50–60. doi: 10.1016/j.micres.2008.06.002

Miransari, M., Bahrami, H., Rejali, F., Malakouti, M. J. S., and Research, T. (2009). Effects of arbuscular mycorrhiza, soil sterilization, and soil compaction on wheat (Triticum aestivum L.) nutrients uptake. *Soil Tillage Res.* 104, 48–55. doi: 10.1016/j.still.2008.11.006

Miransari, M., and Smith, D. J. (2007). Overcoming the stressful effects of salinity and acidity on soybean nodulation and yields using signal molecule genistein under field conditions. *J. Plant Nutr.* 30, 1967–1992. doi: 10.1080/01904160701700384

Miwa, H., Sun, J., Oldroyd, G. E., and Allan Downie, J. (2006). Analysis of calcium spiking using a cameleon calcium sensor reveals that nodulation gene expression is regulated by calcium spike number and the developmental status of the cell. *Plant J.* 48, 883–894. doi: 10.1111/j.1365-313X.2006.02926.x

Mizukoshi, K., Nishiwaki, T., Ohtake, N., Minagawa, R., Ikarashi, T., and Ohyama, T. (1995). Nitrate transport pathway into soybean nodules traced by tungstate and $^{15}NO_3$. *Soil Sci. Plant Nutr.* 41, 75–88. doi: 10.1080/00380768.1995.10419560

Mulder, L., Hogg, B., Bersoult, A., and Cullimore, J. V. (2005). Integration of signalling pathways in the establishment of the legume-rhizobia symbiosis. *Physiol. Plant.* 123, 207–218. doi: 10.1111/j.1399-3054.2005.00448.x

Nguyen, H. P., Miwa, H., Obirih-Opareh, J., Suzaki, T., Yasuda, M., and Okazaki, S. (2019). Novel rhizobia exhibit superior nodulation and biological nitrogen fixation even under high nitrate concentrations. *FEMS Microbiol. Ecol.* 96:fiz184. doi: 10.1093/femsec/fiz184

Peters, N. K., Frost, J. W., and Long, S. R. (1986). A plant flavone, Luteolin, induces expression of rhizobium meliloti nodulation genes. *Science* 233, 977–980. doi: 10.1126/science.3738520

Radutoiu, S., Madsen, L. H., Madsen, E. B., Felle, H. H., Umehara, Y., Grønlund, M., et al. (2003). Plant recognition of symbiotic bacteria requires two LysM receptor-like kinases. *Nature* 425, 585–592. doi: 10.1038/nature02039

Redmond, J. W., Batley, M., Djordjevic, M. A., Innes, R. W., Kuempel, P. L., and Rolfe, B. G. (1986). Flavones induce expression of nodulation genes in rhizobium. *Nature* 323, 632–635. doi: 10.1038/323632a0

Riviezzi, B., Cagide, C., Pereira, A., Herrmann, C., Lombide, R., Lage, M., et al. (2020). Improved nodulation and seed yield of soybean (Glycine max) with a new isoflavone-based inoculant of Bradyrhizobium elkanii. *Rhizosphere* 15:100219. doi: 10.1016/j.rhisph.2020.100219

Schauser, L., Roussis, A., Stiller, J., and Stougaard, J. (1999). A plant regulator controlling development of symbiotic root nodules. *Nature* 402, 191–195. doi: 10.1038/46058

Silsbury, J. H., Catchpoole, D. W., and Wallace, W. (1986). Effects of nitrate and ammonium on Nitrogenase (C_2H_2 reduction) activity of swards of subterranean clover, Trifolium subterraneum L. *Funct. Plant Biol.* 13, 257–273. doi: 10.1071/PP9860257

Smit, G., Puvanesarajah, V., Carlson, R. W., Barbour, W. M., and Stacey, G. (1992). Bradyrhizobium japonicum nod D1 can be specifically induced by soybean flavonoids that do not induce the nod YABCSUIJ operon. *J. Biol. Chem.* 267, 310–318. doi: 10.1016/S0021-9258(18)48495-5

Streeter, J., and Wong, P. P. (1988). Inhibition of legume nodule formation and N_2 fixation by nitrate. *Crit. Rev. Plant Sci.* 7, 1–23. doi: 10.1080/07352688809382257

Subramanian, S., Stacey, G., and Yu, O. (2006). Endogenous isoflavones are essential for the establishment of symbiosis between soybean and Bradyrhizobium japonicum. *Plant J.* 48, 261–273. doi: 10.1111/j.1365-313X.2006.02874.x

Sugiyama, A., Shitan, N., and Yazaki, K. (2007). Involvement of a soybean ATP-binding cassette-type transporter in the secretion of Genistein, a signal flavonoid in legume-rhizobium Symbiosis. *Plant Physiol.* 144, 2000–2008. doi: 10.1104/pp.107.096727

Sugiyama, A., Yamazaki, Y., Yamashita, K., Takahashi, S., Nakayama, T., and Yazaki, K. (2016). Developmental and nutritional regulation of isoflavone secretion from soybean roots. *Biosci. Biotechnol. Biochem.* 80, 89–94. doi: 10.1080/09168451.2015.1062714

Tanaka, A., Fujlta, K., and Terasawa, H. (1985). Growth and Dinitrogen fixation, of soybean root system affected by partial exposure to nitrate. *Soil Sci. Plant Nutr.* 31, 637–645. doi: 10.1080/00380768.1985.10557471

Wang, Y., Yang, W., Zuo, Y., Zhu, L., Hastwell, A. H., Chen, L., et al. (2019). GmYUC2a mediates auxin biosynthesis during root development and nodulation in soybean. *J. Exp. Bot.* 70, 3165–3176. doi: 10.1093/jxb/erz144

Wasson, A. P., Pellerone, F. I., and Mathesius, U. (2006). Silencing the flavonoid pathway in Medicago truncatula inhibits root nodule formation and prevents Auxin transport regulation by rhizobia. *Plant Cell* 18, 1617–1629. doi: 10.1105/tpc.105.038232

Xia, X., Ma, C., Dong, S., Xu, Y., and Gong, Z. (2017). Effects of nitrogen concentrations on nodulation and nitrogenase activity in dual root systems of soybean plants. *Soil Sci. Plant Nutr.* 63, 470–482. doi: 10.1080/00380768.2017.1370960

Yashima, H., Fujikake, H., Sato, T., Ohtake, N., Sueyoshi, K., and Ohyama, T. (2003). Systemic and local effects of long-term application of nitrate on nodule growth and N_2 fixation in soybean (*Glycine max* [L.] Merr.). *Soil Sci. Plant Nutr.* 49, 825–834. doi: 10.1080/00380768.2003.10410344

Yashima, H., Fujikake, H., Yamazaki, A., Ito, S., Sato, T., Tewari, K., et al. (2005). Long-term effect of nitrate application from lower part of roots on nodulation and N2 fixation in upper part of roots of soybean (*Glycine max* (*L.*) Merr.) in two-layered pot experiment. *Soil Sci. Plant Nutr.* 51, 981–990. doi: 10.1111/j.1747-0765.2005.tb00137.x

Zaat, S. A., Brussel, A. A. v., Tak, T., Pees, E., and Lugtenberg, B. J. (1987). Flavonoids induce rhizobium leguminosarum to produce nod DABC gene-related factors that cause thick, short roots and root hair responses on common vetch. *J. Bacteriol.* 169, 3388–3391. doi: 10.1128/jb.169.7.3388-3391.1987

Zhang, F., and Smith, D. L. J. P. P. (1995). Preincubation of Bradyrhizobium japonicum with genistein accelerates nodule development of soybean at suboptimal root zone temperatures. *Plant Physiol.* 108, 961–968. doi: 10.1104/pp.108.3.929

Zhang, J., Subramanian, S., Stacey, G., and Yu, O. J. T. P. J. (2009). Flavones and flavonols play distinct critical roles during nodulation of Medicago truncatula by Sinorhizobium meliloti. *Plant J.* 57, 171–183. doi: 10.1111/j.1365-313X.2008.03676.x

Zou, H., Zhang, N.-N., Pan, Q., Zhang, J.-H., Chen, J., and Wei, G.-H. (2019). Hydrogen sulfide promotes nodulation and nitrogen fixation in soybean–rhizobia symbiotic system. *Mol. Plant-Microbe Interact.* 32, 972–985. doi: 10.1094/mpmi-01-19-0003-r

frontiers | Frontiers in Plant Science

TYPE Original Research
PUBLISHED 12 August 2022
DOI 10.3389/fpls.2022.968418

Check for updates

OPEN ACCESS

EDITED BY
Bhaskar Gupta,
Government General Degree College, Singur, India

REVIEWED BY
Yinbo Ma,
Yangzhou University, China
Grażyna Kłobus,
University of Wrocław, Poland

*CORRESPONDENCE
Huahua Wang
hhwang04@163.com

SPECIALTY SECTION
This article was submitted to Plant Abiotic Stress, a section of the journal Frontiers in Plant Science

RECEIVED 14 June 2022
ACCEPTED 27 July 2022
PUBLISHED 12 August 2022

CITATION
Huang J, Hai Z, Wang R, Yu Y, Chen X, Liang W and Wang H (2022) Genome-wide analysis of HSP20 gene family and expression patterns under heat stress in cucumber (*Cucumis sativus* L.). *Front. Plant Sci.* 13:968418. doi: 10.3389/fpls.2022.968418

COPYRIGHT
© 2022 Huang, Hai, Wang, Yu, Chen, Liang and Wang. This is an open-access article distributed under the terms of the Creative Commons Attribution License (CC BY). The use, distribution or reproduction in other forums is permitted, provided the original author(s) and the copyright owner(s) are credited and that the original publication in this journal is cited, in accordance with accepted academic practice. No use, distribution or reproduction is permitted which does not comply with these terms.

Genome-wide analysis of HSP20 gene family and expression patterns under heat stress in cucumber (*Cucumis sativus* L.)

Junjun Huang, Zhaoxin Hai, Ruoyi Wang, Yuanyuan Yu, Xin Chen, Weihong Liang and Huahua Wang*

College of Life Science, Henan Normal University, Xinxiang, China

Cucumber is an important vegetable in China, and its yield and cultivation area are among the largest in the world. Excessive temperatures lead to high-temperature disorder in cucumber. Heat shock protein 20 (HSP20), an essential protein in the process of plant growth and development, is a universal protective protein with stress resistance. HSP20 plays crucial roles in plants under stress. In this study, we characterized the *HSP20* gene family in cucumber by studying chromosome location, gene duplication, phylogenetic relationships, gene structure, conserved motifs, protein-protein interaction (PPI) network, and *cis*-regulatory elements. A total of 30 *CsHSP20* genes were identified, distributed across 6 chromosomes, and classified into 11 distinct subgroups based on conserved motif composition, gene structure analyses, and phylogenetic relationships. According to the synteny analysis, cucumber had a closer relationship with *Arabidopsis* and soybean than with rice and maize. Collinearity analysis revealed that gene duplication, including tandem and segmental duplication, occurred as a result of positive selection and purifying selection. Promoter analysis showed that the putative promoters of *CsHSP20* genes contained growth, stress, and hormone *cis*-elements, which were combined with protein-protein interaction networks to reveal their potential function mechanism. We further analyzed the gene expression of *CsHSP20* genes under high stress and found that the majority of the *CsHSP20* genes were upregulated, suggesting that these genes played a positive role in the heat stress-mediated pathway at the seedling stage. These results provide comprehensive information on the *CsHSP20* gene family in cucumber and lay a solid foundation for elucidating the biological functions of CsHSP20. This study also provides valuable information on the regulation mechanism of the *CsHSP20* gene family in the high-temperature resistance of cucumber.

KEYWORDS

cucumber, expression pattern, HSP20 gene family, heat stress, phylogenetic analysis

Introduction

Heat shock proteins (HSPs) are ancient, highly conserved intracellular molecular chaperones that widely exist in almost all organisms (Dattilo et al., 2015). When organisms are subjected to environmental stresses such as salinity, high temperature, heavy metals, and drought, HSPs can improve the adaptation of organisms to stress by stabilizing the cell structure, transporting and folding auxiliary proteins and maintaining cell function (Tyedmers et al., 2010; Yadav et al., 2021). Under normal conditions, the content of HSPs accounts for only 5% of the total protein, but when subjected to external stress, the content increases rapidly to up to 15% (Zhang et al., 2015; Ul Haq et al., 2019).

Heat shock proteins can be divided into HSP100, HSP90, HSP70, HSP60, and sHSP (small HSP) families on the basis of amino acid sequence homology and molecular weight (Wang et al., 2004; Waters, 2013). sHSP is a kind of protein with a molecular weight of about 20 kDa, so it is also called HSP20 (Wang et al., 2004). All members of the HSP20 family contain conserved a-crystallin domain (ACD), which is encoded by about 90 amino acids, including a number of β-strand structures, a conversed 80–100 amino acid sequence, and two conserved regions: CRI (N-terminal consensus region I) and CRII (C-terminal consensus region II) (Bondino et al., 2012; Lin et al., 2019).

HSP20 is abundant in plants and the most produced protein under heat stress. It has been proven to be involved in plant response to biotic and abiotic stresses (Peffer et al., 2019; Wu et al., 2019; Ding et al., 2020; He et al., 2021). In *Arabidopsis*, *HSP17.4* was highly expressed after infection by *Pseudomonas syringae* (Sewelam et al., 2019). Overexpression of *AtHSP20s* could improve the tolerance to salt, oxidation, penetration, and high temperature by enhancing the activity of antioxidant enzymes (Mu et al., 2013; Zhang et al., 2013; Sun et al., 2016; Yang et al., 2020). In rice, the *OsHSP18.0* gene could strengthen the resistance to bacterial stripe disease by participating in the basic defense response (Ju et al., 2017). *OsHSP17*-overexpressing transgenic rice exhibited heat tolerance and UV resistance (Murakami et al., 2004). In tomato, overexpression of *SlHSP17.7* could enhance the tolerance to cold stress by inducing intracellular sucrose and reducing the accumulation of reactive oxygen species (Zhang et al., 2020). Cui et al. (2021) found the HSP20 gene family of African bermudagrass were related to abiotic stresses, and the *CtHSP20-9* and *CtHSP20-10* seemed to be positively selected in response to extreme temperatures. Similarly, when *JrsHSP17.3* was expressed, it conferred the tolerance to abnormal temperature and salt stresses by producing less H2O2 and MDA and accumulating more antioxidant enzymes and proline content (Zhai et al., 2016). Under high-temperature treatment, most *HSP20* genes were highly induced in pepper (Guo et al., 2015). Moreover, transgenic plants (*MsHSP16.9* and *TaHSP23.9*) grew vigorously and exerted a protective effect on *Arabidopsis* in high-temperature environments (Yang et al., 2017; Wang et al., 2020). Overall, these results have shown that HSP20 plays important positive roles in improving plant immunity and abiotic stress. In particular, HSP20 plays vital roles in mediating temperature stress tolerance.

According to the analysis of subcellular localization, sequence homology and phylogenetic relationship, the HSP20 family can be divided into at least 17 subgroups. Among them, 12 subgroups (CII-CXII) are localized to the nucleus/cytoplasm, and 5 subgroups (MI, MII, P, ER, and Px) are localized to the mitochondria, mitochondria, plastids (Ps), endoplasmic reticulum (ER), and peroxisomes (Pos) (Scharf et al., 2001; Ma et al., 2006; Siddique et al., 2008). However, some *HSP20* genes have not been classified into known subgroups. These unclassified *HSP20* genes may replicate newly generated genes with unique functions in plants and may represent *HSP20* subgroups in the early stage of evolution. Plants have more HSP20s than other eukaryotes, and the number varies in different species (Sarkar et al., 2009). With the completion of whole genome sequencing of numerous plants, comprehensive identification and analysis of the *HSP20* gene family in different species have been carried out. For example, 42, 48, 48, 41, 44, and 41 *HSP20* gene family members have been identified in the genomes of tomato (*Solanum lycopersicum*), potato (*Solanum tuberosum*), grape (*Vitis vinifera*), apple (*Malus domestica* Borkh), watermelon (*Citrullus lanatus*), and African bermudagrass (*Cynodon transvaalensis* Burtt-Davy), which were divided into 13, 12, 11, 10, 18, and 12 subgroups, respectively (Yu et al., 2016; He et al., 2018; Zhao et al., 2018; Ji et al., 2019; Yao et al., 2020; Cui et al., 2021).

Cucumber is a temperature-bias, widely cultivated crop with good economic benefits and plays an important role in the global vegetable supply. In recent years, the annual average temperature has increased annually due to global warming. High-temperature stress has become an important factor that inhibits the growth and development of cucumber (Ahuja et al., 2010; Zhu et al., 2017). Therefore, studying the resistance mechanism and resistance-associated genes of cucumber is crucial. The completion of high-quality genome assembly at the chromosome level of cucumber provides a powerful basis for studying the mechanism of the cucumber defense system at the genome-wide level (Li et al., 2019). This study identified *HSP20* genes in cucumber, systematically analyzed the characteristics of family members, including physical and chemical properties, domain, gene structure, phylogeny, and *cis*-regulatory elements (CREs) of the promoter, and investigated the expression of *HSP20* under high-temperature stress. The findings are expected to provide a reference for revealing the role of HSP family members in cucumber development regulation and stress response and serve as molecular resources for further cultivating new varieties that are resistant to high temperatures.

Materials and methods

Identification of HSP20 family members in cucumber

The latest cucumber genomic data ("Chinese Long" v3) were retrieved.[1] The Hidden Markov Model (HMM) file of HSP20 was downloaded from Pfam,[2] the local database was established, and the cucumber ACD domain with PF00011 (*e* value $\leq 1e^{-20}$) was searched. The probable CsHSP20 members were submitted to Pfam and SMART[3] to further confirm the ACD domain. At the same time, the CsHSP20 protein sequences were submitted to https://web.expasy.org/protparam/ to determine the molecular weight. The CsHSP20s that lacked the ACD domain and had a molecular weight that exceeded 15∼42 KD were removed. The predicted CsHSP20s were named according to their molecular weight. Their physical and chemical properties were predicted using an online tool.[4] Subcellular localization prediction was performed using ProtComp 9.0.[5]

Phylogenetic analysis and classification of *CsHSP20* genes

The HSP20 protein sequences of rice and *Arabidopsis* were downloaded and combined with the identified CsHSP20 protein sequences for phylogenetic analysis. First, all of the protein sequences were aligned using MAFFT (version 7). Second, an un-rooted neighbor-joining (NJ) phylogenetic tree was constructed using MEGA-X with default parameters and a bootstrap test of 1000 times (Kumar et al., 2018). Lastly, the *CsHSP20* genes were classified into different subgroups on the basis of their subcellular localization predictions, classifications of HSP20s in other species, and topology of the phylogenetic tree.

Conserved motif and gene structure analysis of *CsHSP20* genes

The gene structures of the *CsHSP20* genes were identified with an online tool[6] (GSDS v2.0) (Hu et al., 2015). The conserved motifs of the CsHSP20s were identified using MEME Suite (version 5.4.1[7]). The maximum motif number was 10, and the default parameters were used for other parameters.

Chromosomal locations, gene duplications, and synteny analysis

All of the proposed *CsHSP20* genes were assigned to cucumber chromosomes on the basis of Cucumber (Chinese Long) v3 Genome and its annotation file. Gene duplication of *CsHSP20* and collinearity analysis was performed with TBtools (Chen et al., 2020a). DnaSP_v61203 was used to calculate *Ka* and *Ks*. The formula "$T = Ks/(2\lambda \times 10^{-6})$" ($\lambda = 6.5 \times 10^{-9}$) was used to calculate the occurrence time of each duplicated gene pair (Wang et al., 2015).

Analysis of *cis*-regulatory elements in *CsHsp20* genes' putative promoter regions

In order to study the potential regulatory mechanism of *CsHSP20* genes in abiotic stress response, 2 kb upstream sequences were downloaded from Cucurbit Genomic Database (see text footnote 1) and then submitted to PlantCARE[8] to identify the CREs (Lescot et al., 2002). At the same time, the heat-shock elements (HSEs) were searched using the motif-based sequence analysis tool MEME and *via* manual inspection.

Protein-protein interaction network

The sequences of CsHSP20 protein were submitted to STRING[9] (v11.5) to predict the relationships between CsHSP20 proteins and other related proteins (Szklarczyk et al., 2019). The organism was set to *Arabidopsis*, and the advanced settings remained in the default mode. The PPI networks were constructed and visualized with Cytoscape v3.9.0 (Shannon et al., 2003).

Plant materials and heat stress treatment

North China cucumber cultivar Jinchun No. 4 seeds were soaked in an incubator under room temperature for 2 days. The germinated seeds were then grown on a nursery tray under standard greenhouse conditions (light/dark cycle: 16/8 h at

1 http://www.cucurbitgenomics.org/
2 http://pfam.sanger.ac.uk
3 http://smart.embl-heidelberg.de/
4 https://web.expasy.org/protparam/
5 http://linux1.softberry.com/
6 http://gsds.gao-lab.org/index.php
7 http://meme-suite.org/tools/meme
8 http://bioinformatics.psb.ugent.be/webtools/plantcare/html/
9 https://cn.string-db.org/

28°C) for 2 weeks. The uniform seedlings were transferred to a growth chamber maintained at 45°C for heat stress. The first true leaf was collected at 0, 3, 6, and 12 h and used for quantitative real-time PCR (qRT-PCR) analysis to detect the expression of *CSHSP20* genes with *CsActin* as internal control. The cycling steps were 95°C for 5 min, followed by 40 cycles of 10 s at 95°C and 30 s at 60°C, and at the end, one cycle of 10 s at 95°C, 1 min at 65°C, and 15 s at 97°C. Each treatment was carried out in three independent replicates, and samples of five plants were collected in each replicate. The primers were listed in **Supplementary Table 1**.

Results

Genome-wide identification of HSP20 genes in cucumber

On the basis of the published cucumber (*Cucumis sativus* L. var. *sativus* cv. 9930) genome (Li et al., 2019), a total of 30 HSP20 genes were identified and confirmed with the ACD domain by using SMART, CDD, and Pfam (Letunic and Bork, 2018). Sequences with a molecular weight of more than 15–42 kDa were removed. The names of the CsHSP20s were determined according to their molecular weight (MW) (**Table 1**). Detailed information on the characteristics of the CsHSP20s is presented in **Table 1**. Overall, the identified cucumber CsHSP20 genes encoded protein with a size ranging within 130–356 amino acid residues. The theoretical isoelectric point (pI) and MW of the CsHSP20 proteins varied from 4.51 (CsHSP16.4) to 9.55 (CsHSP23.4) and from 15.03 kDa (CsHSP15.0) to 39.89 kDa (CsHSP39.8), respectively.

Chromosomal distribution and synteny analysis of CsHSP20s

The *CsHSP20* genes were found to be unevenly distributed across seven cucumber chromosomes (**Figure 1**). Chromosome 1 contained 6 *CsHSP20s*, chromosome 3 contained 7 *CsHSP20s*, and chromosome 5 contained 10 *CsHSP20s*. The four other chromosomes contained only four, two, one, and even no *CsHSP20* genes (Chr 2). Most of the *CsHSP20* genes were located at both ends of the chromosomes. This distribution was similar to that of gene density. The gene density at both ends of the chromosomes was large, but the density in the middle was small (**Figure 1**).

We analyzed the locations of CsHSP20 duplicates in the cucumber genome. Overall, 16 (53%) *CsHSP20* genes exhibited tandem or segmental duplication. As shown in **Figure 1**, we identified four pairs of segmental duplicates on chromosomes 1, 3, 5, and 6: CsHSP18.2/CsHSP20.3, CsHSP16.4/CsHSP25.0, CsHSP23.6/CsHSP25.0, and CsHSP25.0/CsHSP17.9. In addition, nine gene pairs (CsHSP16.4/CsHSP18.2, CsHSP18.2/CsHSP15.4, CsHSP39.8/CsHSP39.5, CsHSP23.8A/CsHSP23.8B, CsHSP23.6/CsHSP20.3, CsHSP25.0/CsHSP17.3, CsHSP17.3/CsHSP21.3, CsHSP23.4/CsHSP18.1, CsHSP18.1/CsHSP22.2B) seemed to occur through tandem duplication. We also determined the duplicate divergence times by calculating the *Ka*/*Ks* ratios. Tandem duplication event occurred in the past 50 MYA, whereas segmental duplicates occurred earlier, especially CsHSP23.6/CsHSP25.0 and CsHSP25.0/CsHSP17.9 from more ancient duplication events. All of the CsHSP20s paralogs, except for CsHSP23.6/CsHSP20.3, experienced purifying selection (*Ka*/*Ks* < 1) (**Table 2**).

Comparative syntenic maps of cucumber related to four representative species, namely, two dicots (*Arabidopsis thaliana* and *Glycine max*) and two monocots (*Oryza sativa* and *Zea mays*), were created to explore the phylogenetic mechanisms of CsHSP20 family (**Figure 2**). The results revealed that 3, 3, 7, and 21 HSP20 collinear gene pairs were identified in cucumber and rice, cucumber, and maize, cucumber and *Arabidopsis*, and cucumber and soybean, respectively (**Figure 2** and **Supplementary Table 2**). Half of the *CsHSP20s* had syntenic genes in at least one of the four species, and most of them had syntenic genes in only one species. The *Ka*/*Ks* values of all of the syntenic gene pairs were less than 1, indicating that they might have experienced purifying selection. Moreover, only one *CsHSP25.0* exhibited orthologous genes across in all of the four species (**Supplementary Table 2**). The remaining half of the *CsHSP20s* had no syntenic relationships with the four species, suggesting that they are conservative members of the CsHSP20 gene family.

Phylogenetic analysis of the *CsHSP20* gene family in cucumber

To thoroughly understand the evolutionary relationship of the HSP20 gene family, an unrooted neighbor-joining phylogenetic tree was established using MEGA X on the basis of the alignment of the amino acid sequences of HSP20 from cucumber, *Arabidopsis* (19 sequences), and rice (23 sequences) (**Figure 3**). The CsHSP20 proteins were divided into 11 subgroups, including 12 CI, 5 CVIII, 2 MI, 2 ER, 2 P, 2 PO and one each of CII, CV, CVI, CIV, MII based on previously reported results and phylogeny analysis (**Figure 3**; Ji et al., 2019; Yao et al., 2020). The clustering of the subfamilies in cucumber was basically consistent with the subcellular localization predicted by the online tool ProtComp 9.0 (**Table 1** and **Figure 3**). About half of the CsHSP20s were localized in the cytoplasm, which meant that they mainly played roles in the cytosol. CsHSP16.4 belonged to the CIV subgroup that exists only in dicot plants. The result is consistent with previous findings (Siddique et al., 2008; Zhao et al., 2018; Yao et al., 2020).

10.3389/fpls.2022.968418

TABLE 1 The basic information of CsHSP20 proteins identified in cucumber.

Named	Gene ID	Size (AA)	Strand	Location	Isoelectric point	Molecular weight (kDA)	Subcellular localization
CsHSP18.8	CsaV3_1G005060	168	+	3382876–3383465	9.46	18.82	Extracellular
CsHSP16.4	CsaV3_1G035810	148	–	21892088–21893838	4.51	16.49	Nuclear
CsHSP18.2	CsaV3_1G035820	160	–	21895476–21896585	6.13	18.21	Cytoplasmic
CsHSP15.4	CsaV3_1G035830	135	+	21898380–21898862	6.21	15.41	Cytoplasmic
CsHSP39.8	CsaV3_1G041750	356	–	26652841–26654260	9.21	39.89	Extracellular
CsHSP39.5	CsaV3_1G041760	355	–	26658938–26660854	9.45	39.57	Extracellular
CsHSP23.8A	CsaV3_3G002770	212	+	2251829–2254144	5.43	23.80	Chloroplast
CsHSP23.8B	CsaV3_3G002780	212	+	2255195–2257043	5.26	23.83	Chloroplast
CsHSP22.9	CsaV3_3G005420	200	+	4551319–4554535	4.86	22.98	Cytoplasmic
CsHSP29.9	CsaV3_3G006720	265	–	5920734–5922774	7.74	29.99	Endoplasmic reticulum
CsHSP16.3	CsaV3_3G027480	144	+	23792753–23793946	6.84	16.31	Cytoplasmic
CsHSP23.6	CsaV3_3G034390	200	+	29181040–29182090	8.34	23.67	Nuclear
CsHSP20.3	CsaV3_3G034400	172	+	29183236–29183754	9.01	20.33	Extracellular
CsHSP23.9	CsaV3_4G001560	210	+	880036–880668	5.49	23.99	Mitochondrial
CsHSP15.0	CsaV3_4G017440	130	–	10885738–10886969	8.6	15.03	Extracellular
CsHSP15.9	CsaV3_4G025700	143	–	15114379–15114810	6.76	15.91	Cytoplasmic
CsHSP36.1	CsaV3_4G035900	323	–	25245251–25248160	7.69	36.13	Cytoplasmic
CsHSP25.5	CsaV3_5G000040	229	+	35597–38762	9.12	25.51	Chloroplast
CsHSP25.0	CsaV3_5G008680	222	–	5339660–5344162	9.08	25.04	Cytoplasmic
CsHSP17.3	CsaV3_5G008690	152	+	5349881–5350786	9.27	17.38	Cytoplasmic
CsHSP21.3	CsaV3_5G008700	189	–	5360693–5363946	6.02	21.38	Cytoplasmic
CsHSP23.4	CsaV3_5G008750	202	–	5433169–5433777	9.55	23.42	Cytoplasmic
CsHSP18.1	CsaV3_5G008760	159	–	5435242–5437328	6.21	18.11	Nuclear
CsHSP22.2B	CsaV3_5G008770	191	+	5435387–5435962	6.47	22.29	Nuclear
CsHSP17.8	CsaV3_5G008780	156	+	5443251–5444088	5.97	17.83	Nuclear
CsHSP21.1	CsaV3_5G030610	183	+	25114220–25116088	4.93	21.11	Chloroplast
CsHSP38.0	CsaV3_5G035060	352	–	27756422–27758582	4.94	38.00	Extracellular
CsHSP17.9	CsaV3_6G001540	154	+	1008796–1012576	6.77	17.95	Cytoplasmic
CsHSP27.0	CsaV3_6G037900	246	+	21463616–21466526	7.6	27.06	Extracellular
CsHSP22.2A	CsaV3_7G008210	197	–	5140602–5141331	6.87	22.22	Cytoplasmic

Gene structure and conserved motifs analysis

GSDS v2.0 (Hu et al., 2015) analysis of the intron/exon structure of the *CsHSP20s* showed that almost all members of the *CsHSP20* genes contained only zero or one intron (13 with no intron, 15 with oner intron, one with two introns, and one with five introns) (**Figure 4B**). The different *CsHSP20* genes in each subgroup exhibited similar exon-intron structures, indicating their high conservatism and close evolutionary relationships (**Figures 4A,B**).

In order to better understand the CsHSP20s, the 30 sequences of CsHSP20s were imported to MEME software to predict the conserved motifs. The results showed that the length of motifs was between 15 and 50 aa (**Supplementary Table 3**) and the CsHSP20s in the same subgroup had similar motif compositions and order of arrangement (**Figure 4C**). Each CtHSP20 had motif 1. Motif 5 was found to be specific to subgroups CI and ER. Motif 7 was unique to subgroups CI and MI. Motifs 8 and 10 were found to be unique to subgroups CVIII and MI, respectively. Motif 9 was specific to subgroups CV and CVIII. Overall, the CsHSP20 proteins in the same subgroup had a similar domain composition and arrangement, which implies that they might have similar functions. Individual differences mean functional differences.

Protein–protein interaction network

To determine the interactions among the CsHSP20s and related proteins, a PPI network was constructed and visualized using the STRING database and Cytoscape software,

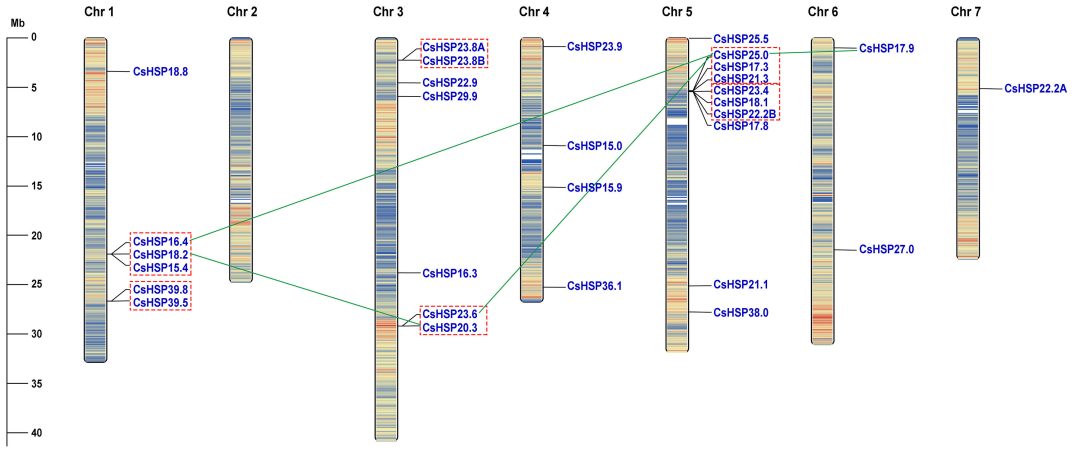


FIGURE 1
Chromosomal locations of *CsHSP20* genes. Tandem duplicated genes are indicated by red dashed box and segmental duplicated genes are connected by green line. Chromosome numbers are shown at the top of each bar. The scale presented on the left indicates chromosome sizes in mega bases (Mb).

TABLE 2 *Ka/Ks* calculation and divergent time of the duplicated cucumber *HSP20* gene pairs.

Duplicated gene pairs	Duplicated type	*Ka*	*Ks*	*Ka/Ks*	Purify selection	Time * (MYA)
CsHSP16.4/CsHSP18.2	Tandem	0.4865	2.9041	0.1675	Yes	221.35
CsHSP18.2/CsHSP15.4	Tandem	0.0586	0.2807	0.2088	Yes	21.39
CsHSP39.8/CsHSP39.5	Tandem	0.1454	0.2153	0.6753	Yes	16.41
CsHSP23.8A/CsHSP23.8B	Tandem	0.0472	0.2244	0.2103	Yes	17.1
CsHSP23.6/CsHSP20.3	Tandem	0.2937	0.2767	1.0614	Yes	21.09
CsHSP25.0/CsHSP17.3	Tandem	0.0841	0.6262	0.1343	Yes	47.73
CsHSP17.3/CsHSP21.3	Tandem	0.0699	0.4006	0.1745	Yes	30.53
CsHSP23.4/CsHSP18.1	Tandem	0.0681	0.4096	0.1663	Yes	31.22
CsHSP18.1/CsHSP22.2B	Tandem	0.2611	0.9184	0.2843	Yes	70
CsHSP18.2/CsHSP20.3	Segmental	0.6771	1.5501	0.4368	Yes	118.15
CsHSP16.4/CsHSP25.0	Segmental	0.5231	2.3015	0.2273	Yes	175.42
CsHSP23.6/CsHSP25.0	Segmental	0.6852	4.9858	0.1374	Yes	380.02
CsHSP25.0/CsHSP17.9	Segmental	0.1663	4.2341	0.0393	Yes	322.72

respectively (Shannon et al., 2003; Szklarczyk et al., 2019). In total, 26 proteins had *Arabidopsis* orthologs with identities from 33.7 to 78.1% (**Supplementary Table 4**). As shown in **Figure 5**, the PPI network consisted of 11 nodes and 43 edges, suggesting that the proteins were highly linked with other proteins and participated in some biological processes. For example, the interaction degree of HSP26.5, HSP21, and HSP23.6 was 10, and that of HSP18.2 was 4.

Promoter analysis of *CsHSP20s*

For the *CsHSP20* genes, a total of 469 CREs were predicted and classified into three main types: hormone-responsive (auxin, MeJA, GA, ABA, and SA), stress-responsive (anaerobic induction, defense and stress, low temperature, wound, and drought), and growth and biological process-responsive elements (circadian control, cell cycle, and light, etc.; **Figure 6** and **Supplementary Table 5**). The number of different CREs in each *CsHSP20* gene's promoter is shown in **Figures 6A,B**. Basically, each *CsHSP20* gene contained multiple CREs aside from *CsHSP17.3* and *CsHSP21.3*. The proportion of three types of CREs was almost the same (**Figure 6C**). As shown in **Figure 6D**, the *CsHSP20s* gene expression was mainly regulated by MeJA, followed by ABA, GA, SA, and IAA hormone. Notably, the CRE essential for anaerobic induction and the CRE involved in light responsiveness accounted for 60 and 76%, respectively (**Figures 6E,F**). HSP genes can usually be induced to express for the heat shock transcription factors (HSFs) binding HSEs. Eukaryotes have three types of HSEs:

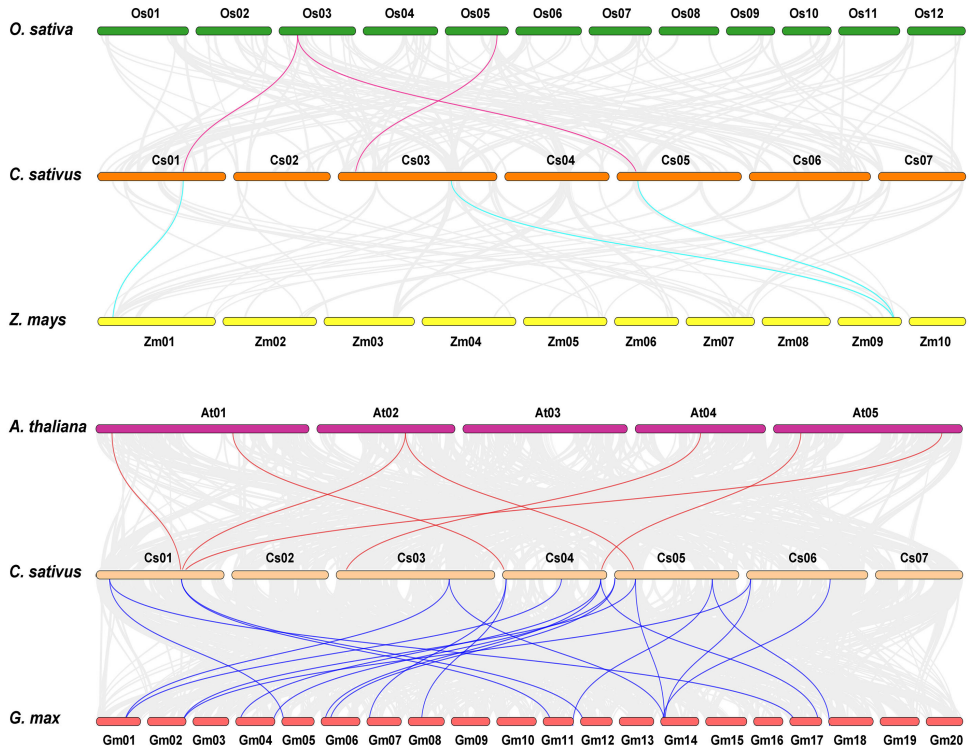


FIGURE 2
Synteny analysis of HSP20 gene family between *Cucumis sativus*, *Oryza sativa*, *Zea mays*, *Glycine max*, and *Arabidopsis thaliana*. The gray lines indicated collinear blocks within cucumber genome and other plant genomes, while the colored lines showed the syntenic HSP20 gene pairs.

perfect (P-type, nGAAnnTTCnnGAAn or TTCnnGAAnnTTC), gap [G-type, nTTCnnGAAn (5 bp) nGAAn], and step [S-type, nTTCn (5 bp) nTTCn (5 bp) nTTCn] (Mittal et al., 2011). From the manual inspection and the motif-based sequence analysis tool MEME, we found that only two HSEs, namely, P- and S-type HSEs, existed in CsHSP18.2 and CsHSP22.2B, respectively. Among all presumptive CREs, the different elements related to developmental processes accounted for the smallest proportion, that is, only 3.62% (**Figure 6F** and **Supplementary Table 5**). These results indicate that the ubiquitous CREs in *CsHSP20s*' promoters might function in gene expression regulation related to multiple stresses and in growth and development.

Expression profiling of *CsHSP20* genes under heat stress treatment

To explore the potential functions of *CsHSP20s* in response to heat stress, we performed a *CsHSP20s* expression analysis after heat treatment by qRT-PCR. We observed that except for *CsHSP29.9* and *CsHSP25.0*, all other genes were sensitive to heat stress and their relative expression level fluctuated during the 12 h treatments (**Figure 7**). The expression levels of most *CsHSP20* genes considerably increased and reached at a high level after short-term heat stress (45°C for 3 h); the expression levels were more than 20-fold, or even 10,000-fold higher than those under normal condition. The expression of minority *CsHSP20* genes increased gradually. *CsHSP18.8* was downregulated under heat stress, but the expression level of *CsHSP15.0* changed only slightly. The expression level of *CsHSP39.8* was not detected at 3 and 6 h, but it reached the highest value at 12 h. Overall, the vast majority of the *CsHSP20* genes responded to the heat stress treatment.

Discussion

HSP20, a class of molecular chaperones, is ubiquitous and the most abundant HSP family involved in abiotic stress in plants (Waters, 2013; Zhao et al., 2018). *HSP20* genes have been identified in dicot and monocot plants, such as potato (Zhao et al., 2018), apple (Yao et al., 2020), tomato (Yu et al., 2016), grape (Ji et al., 2019), watermelon (He et al., 2018), African bermudagrass (Cui et al., 2021), and red algae (Gao et al., 2022). However, the knowledge on *HSP20* genes in cucumber, an important vegetable crop, is limited. In this study, we identified 30 CsHSP20 family genes, more than in *Arabidopsis* (9), but fewer than in most

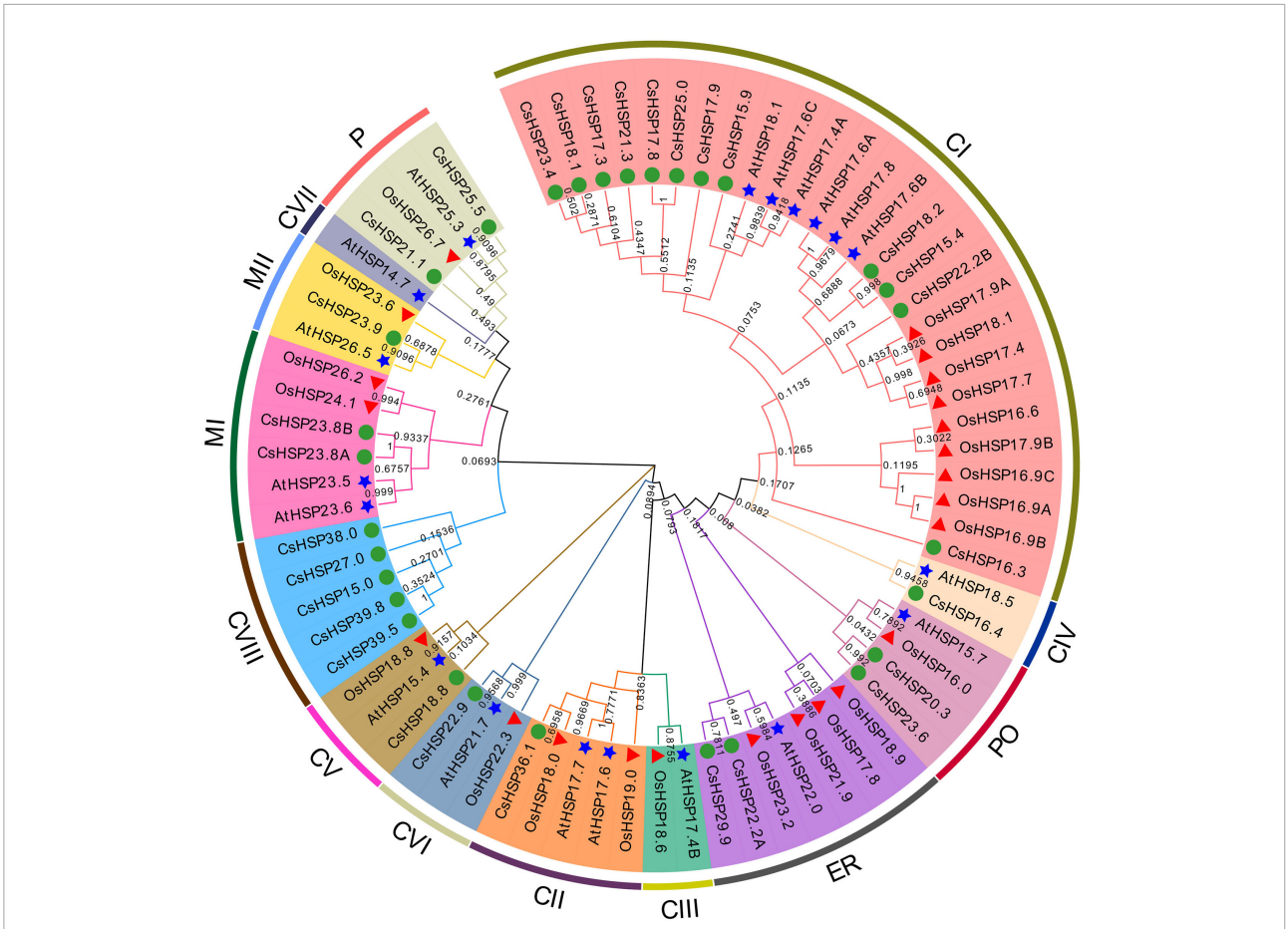


FIGURE 3
Phylogenetic tree of the total HSP20 proteins from cucumber, *Arabidopsis* (19 AtHSP20), and rice (23 OsHSP20). The NJ phylogenetic tree was constructed by MEGA-X with default parameters and bootstrap test of 1000 times. The arcs marked with distinct color represent different subgroups of HSP20 proteins. The green circle, red triangle, and blue star represent HSP20 from cucumber, rice, and *Arabidopsis*, respectively.

other species, such as apple (41) (Yao et al., 2020), African bermudagrass (41) (Cui et al., 2021), and grape (48) (Ji et al., 2019). The difference in the number of *HSP20* genes is probably due to the difference in genome size and gene replication in the process of plant evolution. The genome size of *Arabidopsis* is relatively small, with only 6 *HSP20* genes (Zhao et al., 2018).

Segmental duplication, tandem duplication, and whole-genome duplication events, especially the former two events, mainly contribute to the expansion of the gene family in plants (Cannon et al., 2004; Maere et al., 2005). We identified 13 gene pairs, including 4 segmental duplication and 9 tandem duplication gene pairs, constituted by 16 *CsHSP20s* (16/30, 53.3%) that were located on Chr 1, Chr 3, Chr 5, and Chr 6 (**Figure 1** and **Table 2**). This result meant that Chr 1, Chr 3, and Chr 5 had the most duplication events, which could partly explain the larger numbers of *HSP20* genes on Chr 1, Chr 3, and Chr 5. Meanwhile, the remaining chromosomes had no or only a few *HSP20* genes. The result also meant that tandem duplication contributed more to the expansion of CsHSP20 families than segmental duplication.

It had been reported the CCT (cucurbit-common tetraploidization, 90∼102 MYA) event plays a vital role in the establishment of all Cucurbitaceae plants (Wang et al., 2018). However, we found that segmental duplication occurred before the core-eudicot-common hexaploidization event (ECH, 115∼130 MYA), and tandem duplication occurred after the CCT event, indicating that the two events had no effect on the expansion of the *CsHSP20* gene family (**Table 2**). This result may explain why the CsHSP20 gene family is small. It also explains why many other cucumber gene families are quite small (Chen et al., 2020b; Cheng et al., 2020; Zhang et al., 2021). Half of the *CsHSP20* genes were conservative and did not have collinearity with the *HSP20* genes in the four tested species. However, the other half of the *CsHSP20* genes showed collinearity with the 2, 2, 5, and 18 *HSP20* genes in rice, maize, *Arabidopsis*, and soybean, respectively, which were orthologous genes (**Figure 2** and **Supplementary Table 2**). These results

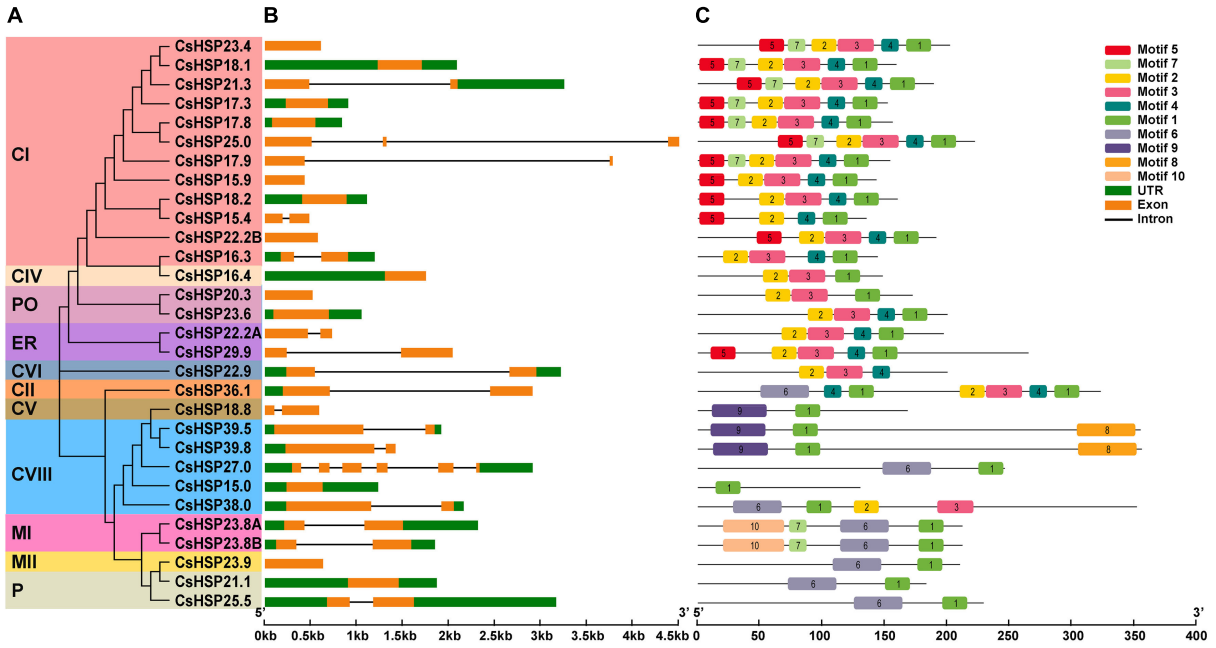


FIGURE 4
Gene structure and conserved protein motifs of HSP20 in cucumber. **(A)** The NJ phylogenetic tree of CsHSP20. The different colors represent the different subgroups. **(B)** Gene structure of *CsHSP20* genes. The untranslated regions, introns, and exons are indicated by green boxes, golden boxes, and solid gray lines, respectively. The scale at the bottom is in kp. **(C)** Conserved motifs in CsHSP20 proteins. Boxes of different colors represent different motifs. Details of each motif are shown in **Supplementary Table 2**.

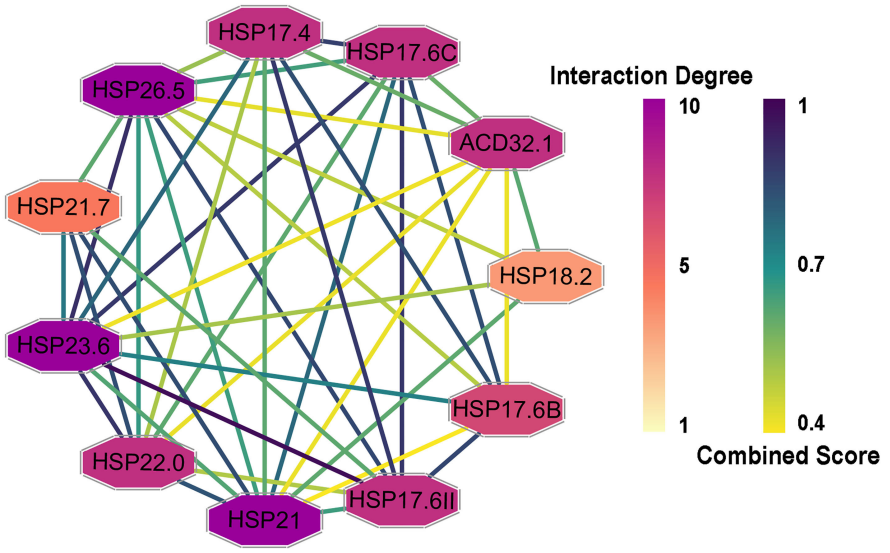


FIGURE 5
Protein-protein interaction (PPI) networks of CsHSP20s and their related proteins. The protein node color indicated the interaction degrees linked with each node, and the edge color represented the combined score, the darker the color, the greater the value.

suggest that the expansion of the *HSP20* gene family in each species was carried out in a specific way. The orthologous gene pairs provided effective information on the evolutionary relationships among species (Yu et al., 2014).

According to the phylogenetic relationships with *Arabidopsis* and rice, gene structures, and amino acid sequences, the 30 CsHSP20 proteins were similar to typical HSP20 family proteins in other species with classifications into 11 subgroups

10.3389/fpls.2022.968418

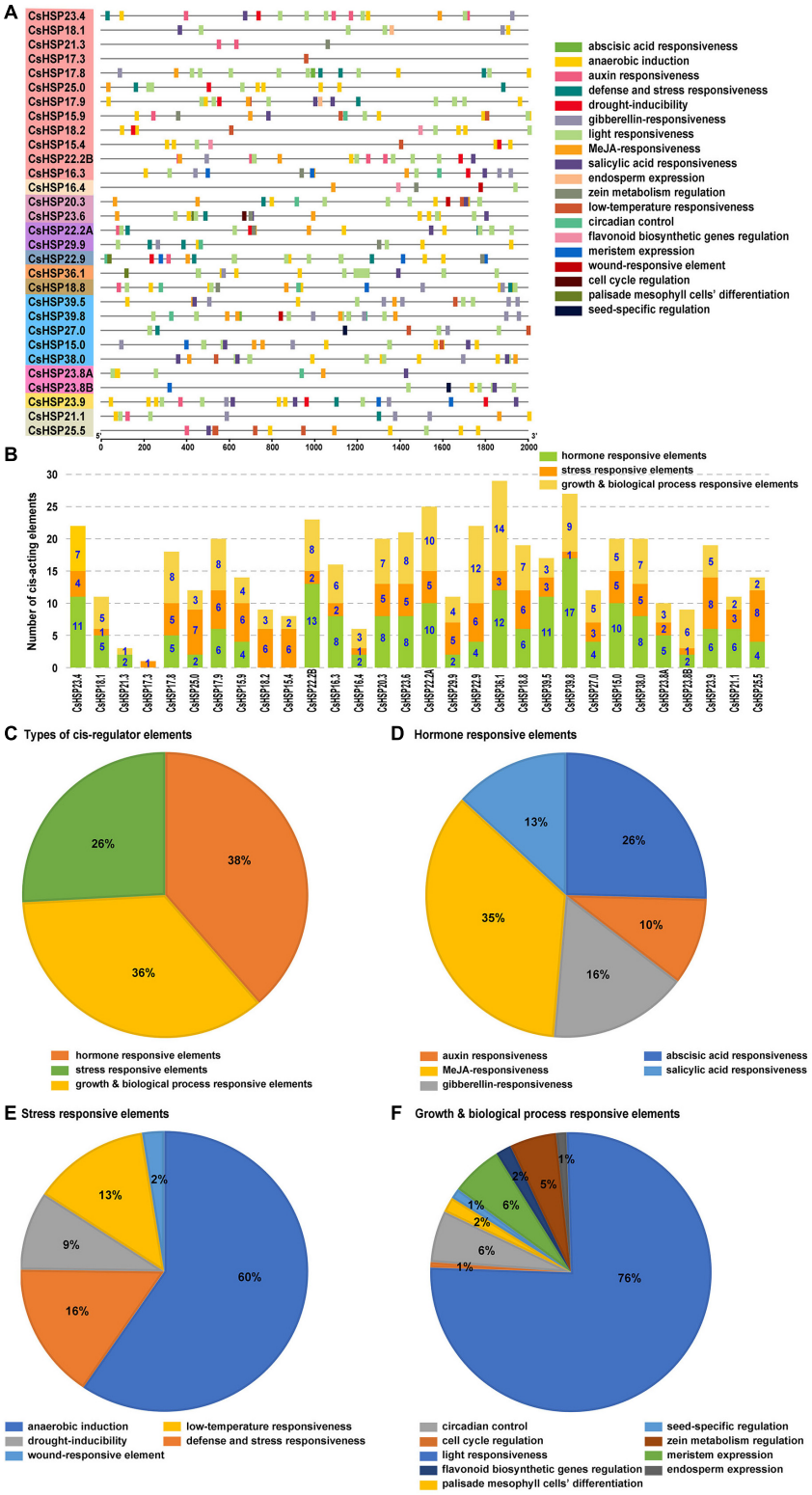


FIGURE 6

Statistical summary and distribution of *cis*-elements. **(A)** *Cis*-element distributions in the putative promoters of *CsHSP20s*. **(B)** The number of three kinds of *cis*-elements in the promoters of each *CsHSP20* gene. **(C)** The relative proportions of three kinds of *cis*-elements. **(D–F)** The detailed percentages of each type of *cis*-element.

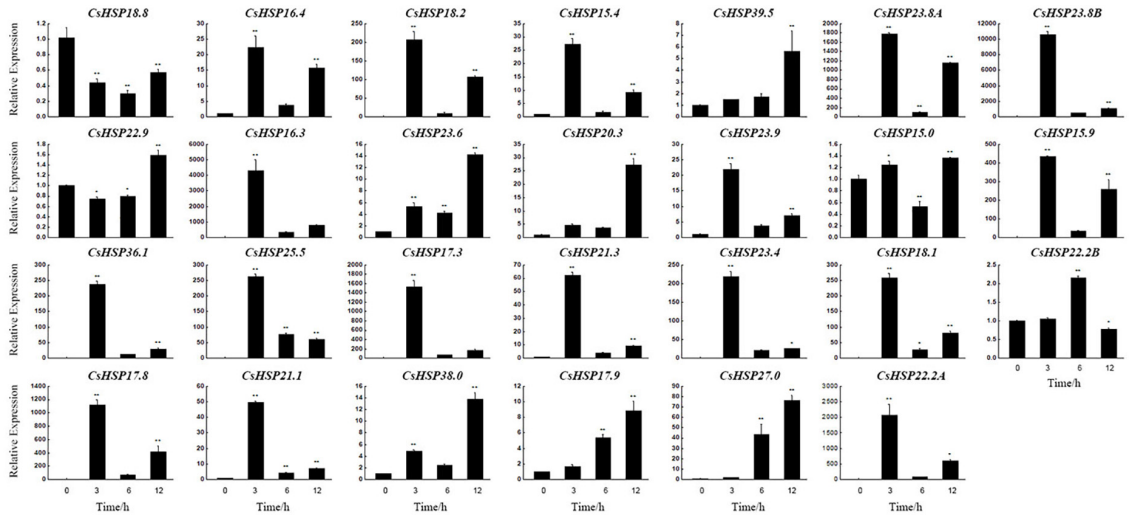


FIGURE 7
The relative expression levels of cucumber *HSP20* genes from qRT-PCR under heat stresses. The first true leaf of two-seedling exposed to 45°C for 0, 3, 6, and 12 h was used for analysis. All data shown are means SD of three biological replicates. The asterisks indicate the significant level (*$P < 0.05$, **$P < 0.01$) based on a Duncan's multiple range test.

(**Figures 3**, **4**), indicating a close relationship among them from different species (Ji et al., 2019; Yao et al., 2020). The biological function of *CsHSP20* genes can be predicted based on the function of similar genes in other species. Several subgroups in this study, including CIII, CX, CXI, CIX, and CVII, were not identified from the CsHSP20 genes of cucumber. The same happened in the other species, such as in rice where the HSP20 CVII and CIV subgroups were missing and in pepper where the HSP20 CIX, CV, CIV, CVIII, CXI, and CX subgroups were absent (Sarkar et al., 2009; Guo et al., 2015). This result indicates that gene loss and acquisition events are common in plant species. During evolution, the loss of *HSP20* gene may lead to the deletion of subpopulations.

Recent analysis results indicate that the average global temperature of the Earth is expected to increase by 1.5°C in the next two decades (Masson-Delmotte et al., 2021). Research shows that every 1°C increase in the annual average temperature will reduce the production of crops, such as rice, wheat, and corn by 3–8%. Therefore, studying the response mechanism of plants to high-temperature stress and improving the heat tolerance of crops are crucial in achieving world food security and human development. The Food and Agriculture Organization Corporate Statistical Database (FAOSTAT) shows that cucumber is widely cultivated in the world and its cultivated area is next only to that of tomato and onion (FAOSTAT, 2022). HSP20 plays a crucial role in extreme temperatures (Peffer et al., 2019; Wu et al., 2019; Cui et al., 2021; Li et al., 2021; Sun et al., 2022; Zhou et al., 2022). Therefore, it is very necessary to study the roles of *CsHSP20* genes under high temperature. According to the qRT-PCR conducted in this study, most of the *CsHSP20* genes responded rapidly to heat stress (**Figure 7**). This rapid response might be due to the compact gene structures with few introns (**Figure 4**). Studies have shown that a highly compact gene structure is conducive to achieve a fast and timely response from plants to diverse stresses (Ren et al., 2006). Moreover, genes with few or no introns were believed to have a high expression level in plants (Chung et al., 2006; Jeffares et al., 2008). These standpoints could be proven in other research. Although most of the *CsHSP20* genes in the current study showed a good response to heat stress, only two HSEs were present in their promoters, whereas many other elements were observed. Furthermore, a large proportion of the identified elements belonged to hormone and development related elements (**Figure 6** and **Supplementary Table 5**), indicating that CsHSP20s are involved in multiple or specific functions of growth and development. As we know, plant hormones are signal compounds that regulate the key aspects of plant growth, development, and environmental stress response. Among the nine common plant hormones in plants, five of them, including ABA, auxin, BR, GA, and MeJA, play significant roles in response to heat stress (Waadt et al., 2022). In response to heat stress, BES1, a key transcription factor in the BR signaling pathway, is activated and directly binds to HSEs, known binding sites of HSFs, to induce the expression of HSPs (Albertos et al., 2022). The sHSP22 heat shock protein can be induced by auxin (Li et al., 2018). These conditions mean that the expression of heat shock proteins is closely related to hormones. Thus, even though there are no heat-responsive *cis*-elements in the promoter of the CsHSP20s gene, their expression can still be induced. With regard to how *CsHSP20* genes participate in the response to high temperatures, further research is needed. Notably, the relative expression of

the *CsHSP20* genes (*CsHSP36.1*, *17.8*, *25.5*, *16.3*, *18.2*, *17.3*, *23.4*, *22.2A*, *18.1*, *23.8A*, *23.8B*, and *15.9*) increased hundreds or even thousands of times after 3 h of heat stress. The 12 *CsHSP20* genes may have been primarily involved in the biological pathway of heat stress and could be used as candidate genes for cucumber heat tolerance breeding. CsHSP20s not only contributed to the formation of biological heat tolerance, but also played important roles in the process of plant adaptation to the environment.

Conclusion

In this study, we identified 30 *CsHSP20* genes in cucumber and characterized their chromosomal location, physicochemical properties, synteny, homologous gene pairs, phylogenetic tree, gene structure, conserved domains, PPI network, and *cis*-elements. The expression of the *CsHSP20* genes under high temperatures was investigated through qRT-PCR, and the results showed that the majority of *CsHSP20* genes responded to the heat stress treatment. The rapid upregulation of *CsHSP20* genes expression at high temperatures indicates that *CsHSP20* genes play vital roles in the acquired thermotolerance of cucumber. This study can provide a comprehensive foundation for the *CsHSP20* gene family and can be helpful in screening candidate genes for breeding new cucumber varieties with heat stress tolerance.

Data availability statement

The datasets presented in this study can be found in online repositories. The names of the repository/repositories and accession number(s) can be found in the article/**Supplementary material**.

Author contributions

JH, WL, and HW designed the experiments and wrote the manuscript. ZH, RW, YY, and XC performed the experiments and contributed to data analysis. All authors read and approved the manuscript.

Funding

This work was financially supported by the National Natural Science Foundation of China (32071499, 31701508, and U1704121) and Program for Science and Technology Innovation Talents in Universities of Henan Province (20HASTIT038). These funding supported the study design, data collection and analysis, manuscript writing, and the open access payment.

Conflict of interest

The authors declare that the research was conducted in the absence of any commercial or financial relationships that could be construed as a potential conflict of interest.

Publisher's note

All claims expressed in this article are solely those of the authors and do not necessarily represent those of their affiliated organizations, or those of the publisher, the editors and the reviewers. Any product that may be evaluated in this article, or claim that may be made by its manufacturer, is not guaranteed or endorsed by the publisher.

Supplementary material

The Supplementary Material for this article can be found online at: https://www.frontiersin.org/articles/10.3389/fpls.2022.968418/full#supplementary-material

References

Ahuja, I., de Vos, R. C. H., Bones, A. M., and Hall, R. D. (2010). Plant molecular stress responses face climate change. *Trends Plant Sci.* 15, 664–674. doi: 10.1016/j.tplants.2010.08.002

Albertos, P., Dündar, G., Schenk, P., Carrera, S., Cavelius, P., Sieberer, T., et al. (2022). Transcription factor BES1 interacts with HSFA1 to promote heat stress resistance of plants. *EMBO J.* 41:e108664. doi: 10.15252/embj.2021108664

Bondino, H. G., Valle, E. M., and Ten Have, A. (2012). Evolution and functional diversification of the small heat shock protein/α-crystallin family in higher plants. *Planta* 235, 1299–1313. doi: 10.1007/s00425-011-1575-9

Cannon, S. B., Mitra, A., Baumgarten, A., Young, N. D., and May, G. (2004). The roles of segmental and tandem gene duplication in the evolution of large gene families in *Arabidopsis thaliana*. *BMC Plant Biol.* 4:10. doi: 10.1186/1471-2229-4-10

Chen, C., Chen, H., Zhang, Y., Thomas, H. R., Frank, M. H., He, Y., et al. (2020a). TBtools: An integrative toolkit developed for interactive analyses of big biological data. *Mol. Plant* 13, 1194–1202. doi: 10.1016/j.molp.2020.06.009

Chen, C., Chen, X., Han, J., Lu, W., and Ren, Z. (2020b). Genome-wide analysis of the WRKY gene family in the cucumber genome and transcriptome-wide identification of WRKY transcription factors that respond to biotic and abiotic stresses. *BMC Plant Biol.* 20:443. doi: 10.1186/s12870-020-02625-8

Cheng, C., Li, Q., Wang, X., Li, Y., Qian, C., Li, J., et al. (2020). Identification and expression analysis of the CsMYB gene family in root knot nematode-resistant

and susceptible cucumbers. *Front. Genet.* 11:550677. doi: 10.3389/fgene.2020.550677

Chung, B. Y., Simons, C., Firth, A. E., Brown, C. M., and Hellens, R. P. (2006). Effect of 5'UTR introns on gene expression in *Arabidopsis thaliana*. *BMC Genomics* 7:120. doi: 10.1186/1471-2164-7-120

Cui, F., Taier, G., Wang, X., and Wang, K. (2021). Genome-wide analysis of the HSP20 gene family and expression patterns of HSP20 genes in response to abiotic stresses in *Cynodon transvaalensis*. *Front. Genet.* 12:732812. doi: 10.3389/fgene.2021.732812

Dattilo, S., Mancuso, C., Koverech, G., Di Mauro, P., Ontario, M. L., Petralia, C. C., et al. (2015). Heat shock proteins and hormesis in the diagnosis and treatment of neurodegenerative diseases. *Immun. Ageing* 12:20. doi: 10.1186/s12979-015-0046-8

Ding, X., Guo, Q., Li, Q., Gai, J., and Yang, S. (2020). Comparative transcriptomics analysis and functional study reveal important role of high-temperature stress response gene GmHSFA2 during flower bud development of CMS-Based F1 in soybean. *Front. Plant Sci.* 11:600217. doi: 10.3389/fpls.2020.600217

FAOSTAT (2022). *Food and agriculture data*. Available online at: http://www.fao.org/faostat/en/#home (accessed June 13, 2022)

Gao, T., Mo, Z., Tang, L., Yu, X., Du, G., and Mao, Y. (2022). Heat shock protein 20 gene superfamilies in red algae: Evolutionary and functional diversities. *Front. Plant Sci.* 13:817852. doi: 10.3389/fpls.2022.817852

Guo, M., Liu, J. H., Lu, J. P., Zhai, Y. F., Wang, H., Gong, Z. H., et al. (2015). Genome-wide analysis of the CaHsp20 gene family in pepper: Comprehensive sequence and expression profile analysis under heat stress. *Front. Plant Sci.* 6:806. doi: 10.3389/fpls.2015.00806

He, Y., Fan, M., Sun, Y., and Li, L. (2018). Genome-wide analysis of watermelon HSP20s and their expression profiles and subcellular locations under stresses. *Int. J. Mol. Sci.* 20:12. doi: 10.3390/ijms20010012

He, Y., Yao, Y., Li, L., Li, Y., Gao, J., and Fan, M. (2021). A heat-shock 20 protein isolated from watermelon (ClHSP22.8) negatively regulates the response of Arabidopsis to salt stress via multiple signaling pathways. *PeerJ* 9:e10524. doi: 10.7717/peerj.10524

Hu, B., Jin, J., Guo, A. Y., Zhang, H., Luo, J., and Gao, G. (2015). GSDS 2.0: An upgraded gene feature visualization server. *Bioinformatics* 31, 1296–1297. doi: 10.1093/bioinformatics/btu817

Jeffares, D. C., Penkett, C. J., and Bähler, J. (2008). Rapidly regulated genes are intron poor. *Trends Genet.* 24, 375–378. doi: 10.1016/j.tig.2008.05.006

Ji, X. R., Yu, Y. H., Ni, P. Y., Zhang, G. H., and Guo, D. L. (2019). Genome-wide identification of small heat-shock protein (HSP20) gene family in grape and expression profile during berry development. *BMC Plant Biol.* 19:433. doi: 10.1186/s12870-019-2031-4

Ju, Y., Tian, H., Zhang, R., Zuo, L., Jin, G., Xu, Q., et al. (2017). Overexpression of OsHSP18.0-CI enhances resistance to bacterial leaf streak in rice. *Rice.* 10:12. doi: 10.1186/s12284-017-0153-6

Kumar, S., Stecher, G., Li, M., Knyaz, C., and Tamura, K. (2018). MEGA X: Molecular evolutionary genetics analysis across computing platforms. *Mol. Biol. Evol.* 35, 1547–1549. doi: 10.1093/molbev/msy096

Lescot, M., Déhais, P., Thijs, G., Marchal, K., Moreau, Y., Van de Peer, Y., et al. (2002). PlantCARE, a database of plant cisacting regulatory elements and a portal to tools for in silico analysis of promoter sequences. *Nucleic Acids Res.* 30, 325–327. doi: 10.1093/nar/30.1.325

Letunic, I., and Bork, P. (2018). 20 years of the SMART protein domain annotation resource. *Nucleic Acids Res.* 46, D493–D496. doi: 10.1093/nar/gkx922

Li, N., Jiang, M., Li, P., and Li, X. (2021). Identification, expression, and functional analysis of Hsf and Hsp20 gene families in *Brachypodium distachyon* under heat stress. *PeerJ* 9:e12267. doi: 10.7717/peerj.12267

Li, Q., Li, H., Huang, W., Xu, Y., Zhou, Q., Wang, S., et al. (2019). A chromosome-scale genome assembly of cucumber (*Cucumis sativus* L.). *Gigascience* 8:giz072. doi: 10.1093/gigascience/giz072

Li, Y., Li, Y., Liu, Y., Wu, Y., and Xie, Q. (2018). The sHSP22 heat shock protein requires the ABI1 protein phosphatase to modulate polar auxin transport and downstream responses. *Plant Physiol.* 176, 2406–2425. doi: 10.1104/pp.17.01206

Lin, Q., Xie, Y., Guan, W., Duan, Y., Wang, Z., and Sun, C. (2019). Combined transcriptomic and proteomic analysis of cold stress induced sugar accumulation and heat shock proteins expression during postharvest potato tuber storage. *Food Chem.* 297:124991. doi: 10.1016/j.foodchem.2019.124991

Ma, C., Haslbeck, M., Babujee, L., Jahn, O., and Reumann, S. (2006). Identification and characterization of a stress-inducible and a constitutive small heat-shock protein targeted to the matrix of plant peroxisomes. *Plant Physiol.* 141, 47–60. doi: 10.1104/pp.105.073841

Maere, S., De Bodt, S., Raes, J., Casneuf, T., Van Montagu, M., Kuiper, M., et al. (2005). Modeling gene and genome duplications in eukaryotes. *Proc. Natl. Acad. Sci. U.S.A.* 102, 5454–5459. doi: 10.1073/pnas.0501102102

Masson-Delmotte, V., Zhai, P., Pirani, A., Connors, S. L., Péan, C., Berger, S., et al. (2021). "Climate change 2021: The physical science basis," in *Contribution of working group I to the sixth assessment report of the IPCC*, eds V. Masson-Delmotte, P. Zhai, A. Pirani, S. L. Connors, C. Péan, S. Berger, et al. (Cambridge: Cambridge University Press).

Mittal, D., Enoki, Y., Lavania, D., Singh, A., Sakurai, H., and Grover, A. (2011). Binding affinities and interactions among different heat shock element types and heat shock factors in rice (*Oryza sativa* L.). *FEBS J.* 278, 3076–3085. doi: 10.1111/j.1742-4658.2011.08229.x

Mu, C., Zhang, S., Yu, G., Chen, N., Li, X., and Liu, H. (2013). Overexpression of small heat shock protein LimHSP16.45 in *Arabidopsis* enhances tolerance to abiotic stresses. *PLoS One* 8:e82264. doi: 10.1371/journal.pone.0082264

Murakami, T., Matsuba, S., Funatsuki, H., Kawaguchi, K., Saruyama, H., Tanida, M., et al. (2004). Over-expression of a small heat shock protein, sHSP17.7, confers both heat tolerance and UV-B resistance to rice plants. *Mol. Breed.* 13, 165–175. doi: 10.1016/j.gene.2004.03.022

Peffer, S., Gonçalves, D., and Morano, K. A. (2019). Regulation of the Hsf1-dependent transcriptome via conserved bipartite contacts with Hsp70 promotes survival in yeast. *J. Biol. Chem.* 294, 12191–12202. doi: 10.1074/jbc.RA119.008822

Ren, X. Y., Vorst, O., Fiers, M. W., Stiekema, W. J., and Nap, J. P. (2006). In plants, highly expressed genes are the least compact. *Trends Genet.* 22, 528–532. doi: 10.1016/j.tig.2006.08.008

Sarkar, N. K., Kim, Y. K., and Grover, A. (2009). Rice sHsp genes: Genomic organization and expression profiling under stress and development. *BMC Genomics.* 10:393. doi: 10.1186/1471-2164-10-393

Scharf, K. D., Siddique, M., and Vierling, E. (2001). The expanding family of *Arabidopsis thaliana* small heat stress proteins and a new family of proteins containing alpha-crystallin domains (Acd proteins). *Cell Stress Chaperones* 6, 225–237. tefoat>2.0.co;2 doi: 10.1379/1466-12682001006<0225:

Sewelam, N., Kazan, K., Hüdig, M., Maurino, V. G., and Schenk, P. M. (2019). The AtHSP17.4C1 gene expression is mediated by diverse signals that link biotic and abiotic stress factors with ROS and can be a useful molecular marker for oxidative stress. *Int. J. Mol. Sci.* 20:3201. doi: 10.3390/ijms20133201

Shannon, P., Markiel, A., Ozier, O., Baliga, N. S., Wang, J. T., Ramage, D., et al. (2003). Cytoscape: A software environment for integrated models of biomolecular interaction networks. *Genome Res.* 13, 2498–2504. doi: 10.1101/gr.1239303

Siddique, M., Gernhard, S., von Koskull-Döring, P., Vierling, E., and Scharf, K. D. (2008). The plant sHSP superfamily: Five new members in *Arabidopsis thaliana* with unexpected properties. *Cell Stress Chaperones* 13, 183–197. doi: 10.1007/s12192-008-0032-6

Sun, X., Sun, C., Li, Z., Hu, Q., Han, L., and Luo, H. (2016). AsHSP17, a creeping bentgrass small heat shock protein modulates plant photosynthesis and ABA-dependent and independent signalling to attenuate plant response to abiotic stress. *Plant Cell Environ.* 39, 1320–1337. doi: 10.1111/pce.12683

Sun, Y., Hu, D., Xue, P., and Wan, X. (2022). Identification of the DcHsp20 gene family in carnation (*Dianthus caryophyllus*) and functional characterization of DcHsp17.8 in heat tolerance. *Planta* 256:2. doi: 10.1007/s00425-022-03915-1

Szklarczyk, D., Gable, A. L., Lyon, D., Junge, A., Wyder, S., Huerta-Cepas, J., et al. (2019). STRING v11: Protein-protein association networks with increased coverage, supporting functional discovery in genome-wide experimental datasets. *Nucleic Acids Res.* 47, D607–D613. doi: 10.1093/nar/gky1131

Tyedmers, J., Mogk, A., and Bukau, B. (2010). Cellular strategies for controlling protein aggregation. *Nat. Rev. Mol. Cell Biol.* 11, 777–788. doi: 10.1038/nrm2993

Ul Haq, S., Khan, A., Ali, M., Khattak, A. M., Gai, W. X., Zhang, H. X., et al. (2019). Heat shock proteins: Dynamic biomolecules to counter plant biotic and abiotic stresses. *Int. J. Mol. Sci.* 20:5321. doi: 10.3390/ijms20215321

Waadt, R., Seller, C. A., Hsu, P. K., Takahashi, Y., Munemasa, S., and Schroeder, J. I. (2022). Plant hormone regulation of abiotic stress responses. *Nat. Rev. Mol. Cell Biol.* 23:516. doi: 10.1038/s41580-022-00479-6

Wang, J., Gao, X., Dong, J., Tian, X., Wang, J., Palta, J. A., et al. (2020). Over-expression of the heat-responsive wheat gene TaHSP23.9 in transgenic *Arabidopsis* conferred tolerance to heat and salt stress. *Front. Plant Sci.* 11:243. doi: 10.3389/fpls.2020.00243

Wang, J., Sun, P., Li, Y., Liu, Y., Yang, N., Yu, J., et al. (2018). An overlooked paleotetraploidization in cucurbitaceae. *Mol. Biol. Evol.* 35, 16–26. doi: 10.1093/molbev/msx242

Wang, W., Vinocur, B., Shoseyov, O., and Altman, A. (2004). Role of plant heat-shock proteins and molecular chaperones in the abiotic stress response. *Trends Plant Sci.* 9, 244–252. doi: 10.1016/j.tplants.2004.03.006

Wang, Y., Wang, Q., Zhao, Y., Han, G., and Zhu, S. (2015). Systematic analysis of maize class III peroxidase gene family reveals a conserved subfamily involved in abiotic stress response. *Gene* 566, 95–108. doi: 10.1016/j.gene.2015.04.041

Waters, E. R. (2013). The evolution, function, structure, and expression of the plant sHSPs. *J. Exp. Bot.* 64, 391–403. doi: 10.1093/jxb/ers355

Wu, D., Vonk, J. J., Salles, F., Vonk, D., Haslbeck, M., Melki, R., et al. (2019). The N terminus of the small heat shock protein HSPB7 drives its polyQ aggregation-suppressing activity. *J. Biol. Chem.* 294, 9985–9994. doi: 10.1074/jbc.RA118.007117

Yadav, R., Juneja, S., and Kumar, S. (2021). Cross priming with drought improves heat-tolerance in chickpea (*Cicer arietinum* L.) by stimulating small heat shock proteins and antioxidative defense. *Environ. Sustain.* 4, 171–182. doi: 10.1007/s42398-020-00156-4

Yang, M., Zhang, Y., Zhang, H., Wang, H., Wei, T., Che, S., et al. (2017). Identification of MsHsp20 gene family in Malus sieversii and functional characterization of MsHsp16.9 in heat tolerance. *Front. Plant Sci.* 8:1761. doi: 10.3389/fpls.2017.01761

Yang, R., Yu, G., Li, H., Li, X., and Mu, C. (2020). Overexpression of small heat shock protein LimHSP16.45 in *Arabidopsis* hsp17.6II mutant enhances tolerance to abiotic stresses. *Russ J. Plant. Physiol.* 67, 231–241. doi: 10.1134/S102144372002017X

Yao, F., Song, C., Wang, H., Song, S., Jiao, J., Wang, M., et al. (2020). Genome-wide characterization of the HSP20 gene family identifies potential members involved in temperature stress response in apple. *Front. Genet.* 11:609184. doi: 10.3389/fgene.2020.609184

Yu, J., Cheng, Y., Feng, K., Ruan, M., Ye, Q., Wang, R., et al. (2016). Genome-wide identification and expression profiling of tomato Hsp20 gene family in response to biotic and abiotic stresses. *Front. Plant Sci.* 7:1215. doi: 10.3389/fpls.2016.01215

Yu, J., Tehrim, S., Zhang, F., Tong, C., Huang, J., Cheng, X., et al. (2014). Genome-wide comparative analysis of NBS-encoding genes between *Brassica* species and *Arabidopsis thaliana*. *BMC Genomics* 15:3. doi: 10.1186/1471-2164-15-3

Zhai, M., Sun, Y., Jia, C., Peng, S., Liu, Z., and Yang, G. (2016). Over-expression of JrsHSP17.3 gene from *Juglans regia* confer the tolerance to abnormal temperature and NaCl stresses. *J. Plant Biol.* 59, 549–558. doi: 10.1007/s12374-015-0507-9

Zhang, K., Ezemaduka, A. N., Wang, Z., Hu, H., Shi, X., Liu, C., et al. (2015). A novel mechanism for small heat shock proteins to function as molecular chaperones. *Sci. Rep.* 5:8811. doi: 10.1038/srep08811

Zhang, K., He, S., Sui, Y., Gao, Q., Jia, S., Lu, X., et al. (2021). Genome-wide characterization of HSP90 gene family in cucumber and their potential roles in response to abiotic and biotic stresses. *Front. Genet.* 12:584886. doi: 10.3389/fgene.2021.584886

Zhang, L., Gao, Y., Pan, H., Hu, W., and Zhang, Q. (2013). Cloning and characterisation of a *Primula* heat shock protein gene, PfHSP17.1, which confers heat, salt and drought tolerance in transgenic *Arabidopsis thaliana*. *Acta. Physiol. Plant* 35, 3191–3200. doi: 10.1007/s11738-013-1354-2

Zhang, N., Zhao, H., Shi, J., Wu, Y., and Jiang, J. (2020). Functional characterization of class I SlHSP17.7 gene responsible for tomato cold-stress tolerance. *Plant Sci.* 298:110568. doi: 10.1016/j.plantsci.2020.110568

Zhao, P., Wang, D., Wang, R., Kong, N., Zhang, C., Yang, C., et al. (2018). Genome-wide analysis of the potato Hsp20 gene family: Identification, genomic organization and expression profiles in response to heat stress. *BMC Genomics* 19:61. doi: 10.1186/s12864-018-4443-1

Zhou, Y., Wang, Y., Xu, F., Song, C., Yang, X., Zhang, Z., et al. (2022). Small HSPs play an important role in crosstalk between HSF-HSP and ROS pathways in heat stress response through transcriptomic analysis in lilies (*Lilium longiflorum*). *BMC Plant Biol.* 22:202. doi: 10.1186/s12870-022-03587-9

Zhu, C. Z., Zhang, Z. X., Tan, G. Y., Gao, X., and He, D. G. (2017). Recent research advances in heat stress to vegetable crops. *Acta Agric. Jiangxi* 29, 53–57. doi: 10.19386/j.cnki.jxnyxb.2017.02.11

frontiers | Frontiers in Plant Science

TYPE Original Research
PUBLISHED 15 August 2022
DOI 10.3389/fpls.2022.941026

Check for updates

OPEN ACCESS

EDITED BY
Ji-Hong Liu,
Huazhong Agricultural University, China

REVIEWED BY
Massimo Galbiati,
National Research Council,
United States
Deguo Han,
Northeast Agricultural University,
China

*CORRESPONDENCE
Yongfeng Guo
guoyongfeng@caas.cn
Wei Li
liwei06@caas.cn

SPECIALTY SECTION
This article was submitted to
Plant Abiotic Stress,
a section of the journal
Frontiers in Plant Science

RECEIVED 11 May 2022
ACCEPTED 25 July 2022
PUBLISHED 15 August 2022

CITATION
Wen L, Liu T, Deng Z, Zhang Z, Wang Q, Wang W, Li W and Guo Y (2022) Characterization of NAC transcription factor NtNAC028 as a regulator of leaf senescence and stress responses. *Front. Plant Sci.* 13:941026. doi: 10.3389/fpls.2022.941026

COPYRIGHT
© 2022 Wen, Liu, Deng, Zhang, Wang, Wang, Li and Guo. This is an open-access article distributed under the terms of the Creative Commons Attribution License (CC BY). The use, distribution or reproduction in other forums is permitted, provided the original author(s) and the copyright owner(s) are credited and that the original publication in this journal is cited, in accordance with accepted academic practice. No use, distribution or reproduction is permitted which does not comply with these terms.

Characterization of NAC transcription factor NtNAC028 as a regulator of leaf senescence and stress responses

Lichao Wen, Tao Liu, Zhichao Deng, Zenglin Zhang, Qi Wang, Weifeng Wang, Wei Li* and Yongfeng Guo*

Tobacco Research Institute, Chinese Academy of Agricultural Sciences, Qingdao, Shandong, China

NAC proteins constitute one of the largest transcription factor families and are involved in regulation of plant development and stress responses. Our previous transcriptome analyses of tobacco revealed a significant increase in the expression of *NtNAC028* during leaf yellowing. In this study, we found that *NtNAC028* was rapidly upregulated in response to high salinity, dehydration, and abscisic acid (ABA) stresses, suggesting a vital role of this gene in abiotic stress response. *NtNAC028* loss-of-function tobacco plants generated *via* CRISPR-Cas9 showed delayed leaf senescence and increased tolerance to drought and salt stresses. Meanwhile *NtNAC028* overexpression led to precocious leaf senescence and hypersensitivity to abiotic stresses in *Arabidopsis*, indicating that *NtNAC028* functions as a positive regulator of natural leaf senescence and a negative regulator of stress tolerance. Furthermore, *NtNAC028*-overexpressing *Arabidopsis* plants showed lower antioxidant enzyme activities, higher reactive oxygen species (ROS), and H_2O_2 accumulation under high salinity, resulted in more severe oxidative damage after salt stress treatments. On the other hand, *NtNAC028* mutation in tobacco resulted in upregulated expression of ROS-scavenging and abiotic stress-related genes, higher antioxidant enzyme activities, and enhanced tolerance against abiotic stresses, suggesting that *NtNAC028* might act as a vital regulator for plant stress response likely by mediating ROS scavenging ability. Collectively, our results indicated that the *NtNAC028* plays a key regulatory role in leaf senescence and response to multiple abiotic stresses.

KEYWORDS

tobacco, *NtNAC028*, abiotic stress, leaf senescence, ROS, *Arabidopsis thaliana*

Introduction

Plants are sessile organisms that must withstand and cope with environmental pressures, including biotic and abiotic stresses. Adverse changes in environmental conditions usually cause loss of crop yield, even the death of plant tissues (Liliane and Charles, 2020). Abiotic stresses, including drought and salinity, pose threats to food security worldwide by causing significant loss of crop production (Moghaddam et al., 2021). These stresses often lead to excessive accumulation of reactive oxygen species (ROS), which disrupts cellular redox

homeostasis and causes oxidative damage of plant cells (Suzuki et al., 2012). In order to survive adverse environments, plants have developed a series of biochemical and physiological strategies during evolution (Haak et al., 2017). Gene regulation at the transcriptional level is the most critical and effective way for plants' adaptation to stresses and DNA-binding transcription factors (TFs) play a vital role in this process (Lata et al., 2011; Le Hénanff et al., 2013). To date, extensive studies have revealed a wide range of TFs including MYB, bZIP, WRKY, and NAC (NAM, ATAF1/2, and CUC2) that are involved in regulation of abiotic stress response (Guo and Gan, 2012; Pascual et al., 2018; Zhang et al., 2018).

NAC (NAM, ATAF1/2, and CUC2) proteins are one of the largest families of plant-specific TFs, most of which harbor a highly conserved DNA-binding domain at the N-terminal region and a variable transcriptional regulation C-terminal domain (Diao et al., 2020). NAC TFs have been implicated in multiple aspects of plant development. For example, CUP-SHAPED COTYLEDON1 (CUC1) and NAC WITH TRANSMEMBRANE MOTIF1 (NTM1) are involved in shoot and lateral root development. NAC SECONDARY WALL THICKENING PROMOTING FACTOR1 (NST1) and VASCULAR-RELATED NAC DOMAIN6 (VND6) are master regulators of secondary cell wall formation, ORESARA9 (ORE9) and NAC-LIKE, ACTIVATED BY AP3/PI (AtNAP) play important role in regulating leaf senescence (Takada et al., 2001; Guo and Gan, 2006; Kim et al., 2006; Zhong et al., 2010; Breeze et al., 2011; Diao et al., 2020; Liu et al., 2022). Besides, NAC proteins have also been reported to be implicated in different abiotic stress response (Nakashima et al., 2012). A number of NAC proteins involved in regulating stress response have been characterized and manipulated to develop crop varieties with enhanced stress tolerance. In *Arabidopsis*, expression of *ANAC019*, *ANAC072/RD26*, *ANAC053/NTL4*, or *ANAC055* could improve salt and drought tolerance of transgenic plants (Tran et al., 2004; Lee et al., 2014). *anac096* mutant is drought stress sensitive, indicating that ANAC096 functions as a positive regulator in dehydration stress response (Xu et al., 2013). Besides, ANAC016 could also positively regulate drought stress tolerance through suppressing *AREB1* expression (Sakuraba et al., 2015). In contrast, *ORE1* knockout mutants are more tolerant to salt stress, while overexpression lines show an opposite phenotype, suggesting that ORE1/ANAC092 functions as a negative regulator in salt stress response (Balazadeh et al., 2010). In rice, overexpression of *OsNAC5*, *OsNAC6/SNAC2*, *OsNAC45*, *OsNAC52*, or *OsNAC066* significantly enhanced the tolerance to drought and salt stresses in transgenic rice (Nakashima et al., 2007; Sperotto et al., 2009; Gao et al., 2010; Yuan et al., 2019; Zhang et al., 2020). For wheat, *TaNAC2*, *TaNAC67*, and *TaNAC29* have been reported to participate in abiotic stress responses. Overexpression of these genes in Arabidopsis and wheat improved plants' tolerance to low temperature, high salinity, and drought by activating stress-responsive genes (Mao et al., 2012, 2014, 2016; Huang et al., 2015). Similarly, overexpression of several maize NACs, including *ZmSNAC1*, *ZmNAC33*, *ZmNAC49*, and *ZmNAC55*, could confer tolerance to drought stress in transgenic plants (Lu et al., 2012; Mao et al., 2016; Liu et al., 2019; Xiang et al., 2021). Interestingly, many stress-related genes might also be involved in plant senescence process. For instance, OsNAC2, known to negatively regulate many abiotic stresses tolerances, can also promote rice leaf senescence *via* ABA biosynthesis (Shen et al., 2017). TaNAC29 has been reported to play crucial roles in senescence and abiotic stress response (Huang et al., 2015; Xu et al., 2015). It has been hypothesized that some of these genes integrate the different signaling pathways and play important roles in the crosstalk between stress responses and age-dependent senescence (He et al., 2005; Guo and Gan, 2006).

Compared with *Arabidopsis thaliana*, *Oryza sativa*, and other plant species, few studies have been conducted on the functional characteristics of tobacco *NAC* genes. *NtNAC-R1* has been reported to be involved in nicotine synthesis and lateral root development (Fu et al., 2013). Besides, overexpression of *NtNAC2* or *NtNAC053* could improve drought and/or salt stress tolerance in tobacco plants (Xu et al., 2018; Li et al., 2022). Our previous study has shown that overexpression of *NtNAC080* promotes leaf senescence in *Arabidopsis*, suggesting that it acts as a positive regulator of natural leaf senescence in tobacco (Li et al., 2018). A recent study has indicated that NaNAC29 may participate in the defense responses to *Alternaria alternata* and promote leaf senescence in *Nicotiana attenuata* (Ma et al., 2020). To our knowledge, no further studies have been conducted on stress-related *NAC* genes in tobacco.

We previously identified a NAC TF, NtNAC028 (accession number XM_016636746), as a senescence upregulated gene. In this work, we found that *NtNAC028* was also dramatically induced by high salinity, dehydration, and ABA treatments, suggesting that this gene might have multiple functions in different biological processes. Then we performed a detailed functional characterization of *NtNAC028* in abiotic stress responses using transgenic tobacco and *Arabidopsis*. Phenotypic analysis showed that NtNAC028 played a negative role in response to drought and salt stress. Further study revealed that the enhanced tolerance of *ntnac028* tobacco mutant obtained *via* CRISPR-Cas9 strategy was potentially achieved by activation of antioxidant enzymes in ROS scavenging and upregulation of stress-responsive genes. In addition to being involved in abiotic stress responses, NtNAC028 could also positively regulate leaf senescence in tobacco. Our findings demonstrated the role of NtNAC028 in leaf senescence, drought and salt stress responses and revealed the likely molecular mechanisms underlying abiotic stress response in tobacco.

Materials and methods

Plant growth conditions and stress treatments

Common tobacco (*Nicotiana tabacum* L. Cv. K326) seeds were sterilized by 70% ethanol for 1 min and 15% w/v H_2O_2 for

12 min, then rinsed in sterile water 4–5 times. The seeds were germinated and the plants were grown on Murashige and Skoog (MS) medium in a plant growth chamber (Conviron, Canada) at 25°C under long-day conditions (16 h light/8 dark). Then 4-week-old seedlings were removed from MS plates and treated in MS solution in 250 ml beakers with or without 200 mM NaCl, 150 μM abscisic acid (ABA), 150 μM salicylic acid (SA), or 150 μM jasmonic acid (JA) for 0–36 h. For drought treatments, 4-week-old seedlings were removed from MS medium, placed on Whatman No.5 filter paper, and dehydrated at room temperature for 0, 1, 3, 6, and 12 h. Whole plants were harvested, immediately frozen in liquid nitrogen, and stored at-80°C before further use. Three biological replicates were applied for each treatment.

Arabidopsis (Col-0) plants were grown on soil or on plates in a growth chamber at 22°C with hours a 16-h-light/8-h-dark cycle. For growth on plates, seeds were surface sterilized with 70% ethanol for 5 min, washed 4–5 times with sterile water, and then stored in the dark at 4°C for 3 days before the plates were transferred to growth chamber.

RNA isolation and quantitative real-time PCR analysis

Total RNA was extracted using the Ultrapure RNA kit (CW biotech, Beijing, China), and first-strand cDNAs were synthesized using the HiScript III All-in-one RT SuperMix (Vazyme, NanJing, China). Then the cDNA samples were used for qRT-PCR analysis, which was performed on a Light Cycler96 real-time PCR system (Roche, Germany). *NtActin* and *AtActin* were used as internal reference genes in tobacco and *Arabidopsis*, respectively. Three technical replicates were used for all reactions and three biological replicates were performed for each experiment. The relative expression values were calculated using the $2^{-\triangle\triangle Ct}$ method (Rao et al., 2013). The relevant primers are listed in Supplementary Table 1.

Generation of transgenic *Arabidopsis* plants

The full-length *NtNAC028* cDNA was amplified by PCR using primes (*NtNAC028*-35 s-F: 5′-CACTGT TGATACATATGGTT GGGAAAAATTGCTCCGAG-3′; *NtNAC028*-35 s-R: 5′-TGTTG ATTCAGAATTCTCACTGGA ACTGAAAGGCTGGAT-3′) and cloned into linearized *pRI101-AN* vector (digested with *NdeI* and *EcoRI*) using the Infusion kit (Clontech, Bejing, China). The recombinant vector was transferred into *Agrobacterium tumefaciens* GV3101 and then transformed into *Arabidopsis thaliana* (Col-0) *via* the floral dip method (Clough and Bent, 1998). The transgenic plants were selected on 1/2 MS medium supplemented with 50 mg/ml kanamycin and confirmed by qRT-PCR. Homozygous T_3 lines were used for senescence and stress response assays.

Generation of *NtNAC028* knockout tobacco *via* CRISPR-Cas9 genome editing

For CRISPR-Cas9 vector construction, an online software[1] was used to design the guide RNA (gRNA) targeting the *NtNAC028* coding region. The forward and reverse primers were annealed to form DNA double-strands and inserted into the *pORE-Cas9* vector (Gao et al., 2015). The recombinant vector was introduced into *Agrobacterium tumefaciens* LBA4404 and transformed into common tobacco (K326) by *Agrobacterium*-mediated transformation (Horsch et al., 1989). The transgenic plants were screened by kanamycin (50 mg/ml) resistance and used for extraction of genomic DNA. For each transgenic plant, the region of the gRNA targeting site was amplified by PCR using primers (*NtNAC028*-TS-F: 5′-ATGGTTGGGAAAAATTGCT-3′; *NtNAC028*-TS-R: 5′-GATTGCTTTATCTGTGCCTGT-3′) and cloned into the *pEASY-blunt* Zero vector (Transgene, China). DNAs from single colonies were used for sequencing to detect the mutation type. T_1 plants, derived from self-pollinated T_0 mutant lines, were sequenced again to confirm mutations. The homozygous mutants were further analyzed.

Measurements of chlorophyll content and Fv/Fm

The extraction and quantification of chlorophyll were performed as previously described (He and Gan, 2002). Briefly, 200 mg of fresh leaves was extracted with 5 ml of anhydrous ethanol in dark until the chlorophyll was completely dissolved. The supernatant was measured at 665 and 649 nm for absorbance. For determination of Fv/Fm, after 30 min of dark treatment, the leaves of individual plant were determined using a IMAGING-PAM M-series Chlorophyll Fluorescence System (LI-6400-40 LCF, Walz, Effeltrich, Germany). Chlorophyll contents and Fv/Fm were calculated and mean values from three biological replicates were obtained.

Dark/NaCl-induced senescence

Leaf disks from 60-day-old plants of the *ntnac028* mutant and WT were placed onto moistened filter paper inside Petri dishes, and kept in dark for 7 days. Three independent biological replicates of this experiment were carried out. For NaCl-induced senescence assay, leaf disks from 35-day-old plants were placed in dishes with 0 or 200 mM NaCl, and kept in light for 7 days. Similarly, the leaves of 4-week-old plants from *NtNAC028*-OE *Arabidopsis* lines and WT (Col-0) plants were placed in dishes with 0 or 200 mM NaCl, and kept in light for 3 days. Three independent biological replicates of this experiment were carried out.

1 http://www.multicrispr.net/index.html

Drought and salt stress tolerance assays in planta

For the drought tolerance assays, WT (Col-0) and *NtNAC028*-OE *Arabidopsis* lines were soil-grown for 4 weeks under well-watered conditions, then stressed by withholding water for 8 days. After that, the plants were re-watered and survival rate of each group of plants was calculated after 3 days. Similarly, 5-week-old plants of the *ntnac028* mutant and WT (K326) were subject to dehydration by halting water for 12 days, and then re-watered for 2 days. After that, the survival rates of tobacco seedlings were calculated. The water loss rate was measured by calculating the weight change of detached leaves of different genotypes after dehydration for 2 h at room temperature.

For salt stress treatment, the surface-sterilized tobacco seeds grown on MS medium were placed vertically in a growth chamber for 2 weeks and transferred to MS medium supplemented with 0, 50, 100, 150, or 200 mM NaCl, respectively. The plants were then grown for 2 weeks before measuring the length of primary roots. Similarly, 4-day-old seedlings of different *Arabidopsis* lines were transferred into 1/2 MS medium supplemented with 100 or 150 mM NaCl, respectively. After 1 week, the length of the primary roots was measured.

For germination assay, surface-sterilized seeds of *NtNAC028*-OE and WT were sown on 1/2 MS medium supplemented with different concentrations of NaCl (0, 100, and 150 mM) or ABA (0.5 μM), and kept at 4°C for 3 days in the dark before being transferred to a growth chamber under normal growth conditions. After 1 week, the germination rates of each group were calculated based on the presence of open cotyledons. All the experiments were performed with three independent biological replicates.

Measurements of MDA and antioxidant enzyme activities

The content of malondialdehyde (MDA) was determined as previously described (Draper et al., 1993). POD, SOD, and CAT enzymatic activities were measured using the detection kits provided by Beijing Solarbio Science & Technology Co., Ltd.

Determination of H_2O_2 accumulation

For NBT staining, the salt-treated leaves from *NtNAC028*-OE lines and WT were soaked in NBT staining buffer (10 mM potassium phosphate buffer, pH 7.2) for 12 h. After that, leaf chlorophyll was removed by a mixed solution (glycerol/acetic acid/ethanol, 1:1:3) and then stored in a solution consisting of ethanol/glycerol (4:1). The hydrogen peroxide content was determined using a hydrogen peroxide assay kit (Solarbio, China) according to the manufacturer's instruction.

Results

NtNAC028 expression is upregulated by multiple stresses

Our previous work showed that the expression of *NtNAC028* increased significantly during tobacco leaf senescence, especially at the early stage of senescence (Li et al., 2018). In this study, qRT-PCR was performed to measure the expression of *NtNAC028* in tobacco. Among the tested tissues, the transcript level of *NtNAC028* was the highest in the senescent leaves and very low in young leaves and stems (Figure 1A). In addition, *NtNAC028* showed high expression in roots, suggesting that *NtNAC028* might have multiple biological functions. To understand whether *NtNAC028* is also involved in abiotic stress response, we examined the expression patterns of *NtNAC028* under salt and drought stress treatments. As shown in Figures 1B,C, the transcript level of *NtNAC028* was induced significantly during the whole course (1–24 h) of these treatments. Meanwhile, the expression patterns of *NtNAC028* after exogenous plant hormone treatment were analyzed. The expression of *NtNAC028* increased continuously and rapidly after ABA treatments. However, no significant increase in *NtNAC028* expression was observed after treatments with SA or JA (Figures 1D–F).

NtNAC028 positively regulates leaf senescence

To understand the role of *NtNAC028* in regulating tobacco leaf senescence, we generated a *NtNAC028* loss-of-function line using the CRISPR-Cas9 system. A gRNA targeting the NAC domain of *NtNAC028* was designed and used for *Agrobacterium*-mediated transformation of tobacco plants. T_0 transgenic plants were obtained after kanamycin selection and sequenced to identify mutations. Then homozygous mutant plants were obtained from T_1 generation for further phenotypic analysis (Figure 2A). Here, the *ntnac028* mutant had a 1 bp insertion at the 3′ end of the gRNA sequence which introduced a stop codon after position P14 and led to a truncation of the DNA-binding NAC domain and loss of the transcriptional regulation domain at the C-terminus (Figure 2A). Compared with WT (K326), the *ntnac028* mutant plants showed a delayed leaf senescence phenotype. The chlorophyll content of middle leaves from the *ntnac028* mutant were higher than that in WT (Figures 2B,C). qRT-PCR showed that the transcript level of *NtNAC028* in the mutant was significantly lower than WT (Figure 2D), possibly due to decreased stability of the truncated coding region. Furthermore, the transcript levels of senescence-related genes were determined by qRT-PCR. Compared to WT, the expression level of *CYSTEINE PROTEINASE 1* (*NtCP1*, *SENESCENCE-ASSOCIATED GENE 12/SAG12* homolog in tobacco) was lower and the *RIBULOSE BISPHOSPHATE CARBOXYLASE SMALL CHAIN* (*NtRBCS*) was higher in the *ntnac028* mutant (Figures 2E,F). Likewise, we investigated the phenotype of the *ntnac028* mutant leaves under dark treatments

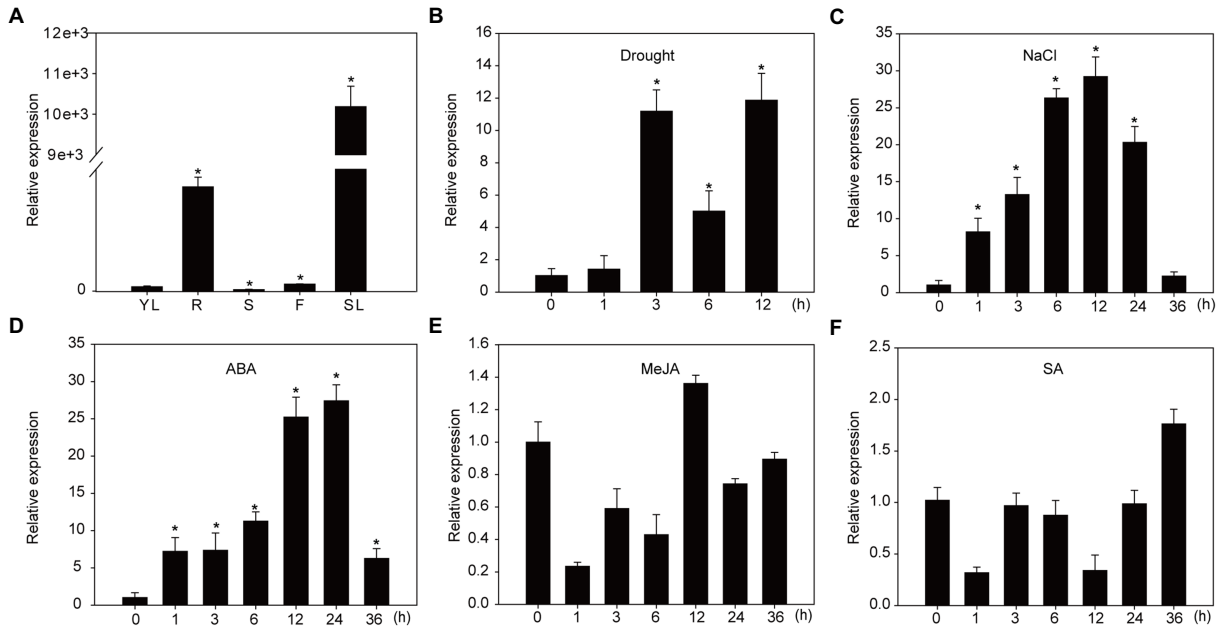


FIGURE 1
Expression profiling of *NtNAC028*. **(A)** The expression pattern of *NtNAC028* in various organs of tobacco plants (K326). YL, young leaf; R, root; S, stem; F, flower; SL, senescence leaf. **(B,C)** *NtNAC028* expression in response to different stress conditions. **(D–F)** The expression pattern of *NtNAC028* under exogenous phytohormone treatments. ABA, abscisic acid; JA, jasmonic acid; and SA, salicylic acid. The bars are SD of three biological replicates. Asterisks indicate significant difference by Student's *t*-test (*$p<0.05$).

(Figure 2G). Detached leaves of WT and *ntnac028* plants were covered with aluminum foil for 7 days. Leaves of the *ntnac028* mutant showed a delayed senescence phenotype compared with those from WT. Consistent with this finding, the leaves of *ntnac028* mutant had higher chlorophyll content compared with WT (Figure 2H). These data suggested that *NtNAC028* could act as a positive regulator in tobacco leaf senescence.

To further evaluate the role of *NtNAC028* in regulating leaf senescence, we generated transgenic *Arabidopsis* plants overexpressing *NtNAC028*. 45 days after sowing, the overexpression transgenic plants, with expression of *NtNAC028* confirmed by qRT-PCR, showed precocious leaf senescence (Supplementary Figures S1A,B). The chlorophyll contents and maximum quantum efficiency of PSII (Fv/Fm) of *NtNAC028*-OE plants (the fifth leaves) were lower than that of WT (Supplementary Figures S1C,D). Moreover, the premature senescence phenotype was also supported by the higher expression of *AtSAG12* (a senescence marker gene) in the fifth leaves of the two *NtNAC028* OE lines (Supplementary Figure S1E). These results also indicated that *NtNAC028* could positively regulate leaf senescence.

CRISPR/Cas9-mediated knockout of *NtNAC028* enhances abiotic stress tolerance in tobacco

In order to examine the biological role of NtNAC028 in response to drought stress, 5-week-old *ntnac028* and WT tobacco plants were subject to drought stress treatments. As shown in Figure 3A, the *ntnac028* plants displayed higher drought tolerance. Around 7 days after water withdraw, when most leaves of the WT plants were wilted, only a small portion of the *ntnac028* leaves started wilting. Most of the WT plants became desiccated 12 days after drought treatment and died after re-watering, with a survival rate of 6.9%. The *ntnac028* plants on the other hand, behaved much better at the end of the treatment with a survival rate of 96% after re-watering (Figures 3A,B). Detached leaves of the *ntnac028* mutant and WT (K326) were subject to dehydration stress for 2 h and water loss rate was calculated at each time point. During the first 30 min of dehydration stress, there was no significant difference in relative water content between *ntnac028* and WT plants. However, the relative water content of *ntnac028* plants was significantly higher than that of WT after 1 h of dehydration stress. After 2 h dehydration stress, the water content of WT was less than 42%, while it was still more than 55% in the *ntnac028* mutant (Figure 3C). This result was consistent with the enhanced drought tolerance in the *ntnac028* mutant. Besides, we also analyzed the root length of *ntnac028* and WT seedlings grown under treatments with different concentrations of NaCl. There was no significant difference in root length between *ntnac028* plants and WT under normal conditions. However, in the presence of various concentrations of NaCl, the *ntnac028* plants were more tolerant than WT. The root length of the *ntnac028* plants was dramatically longer than that of WT (Figures 3D,E). For the germination assay, there was no significant difference between *ntnac028* and WT plants in the absence of NaCl. However, the germination rates of

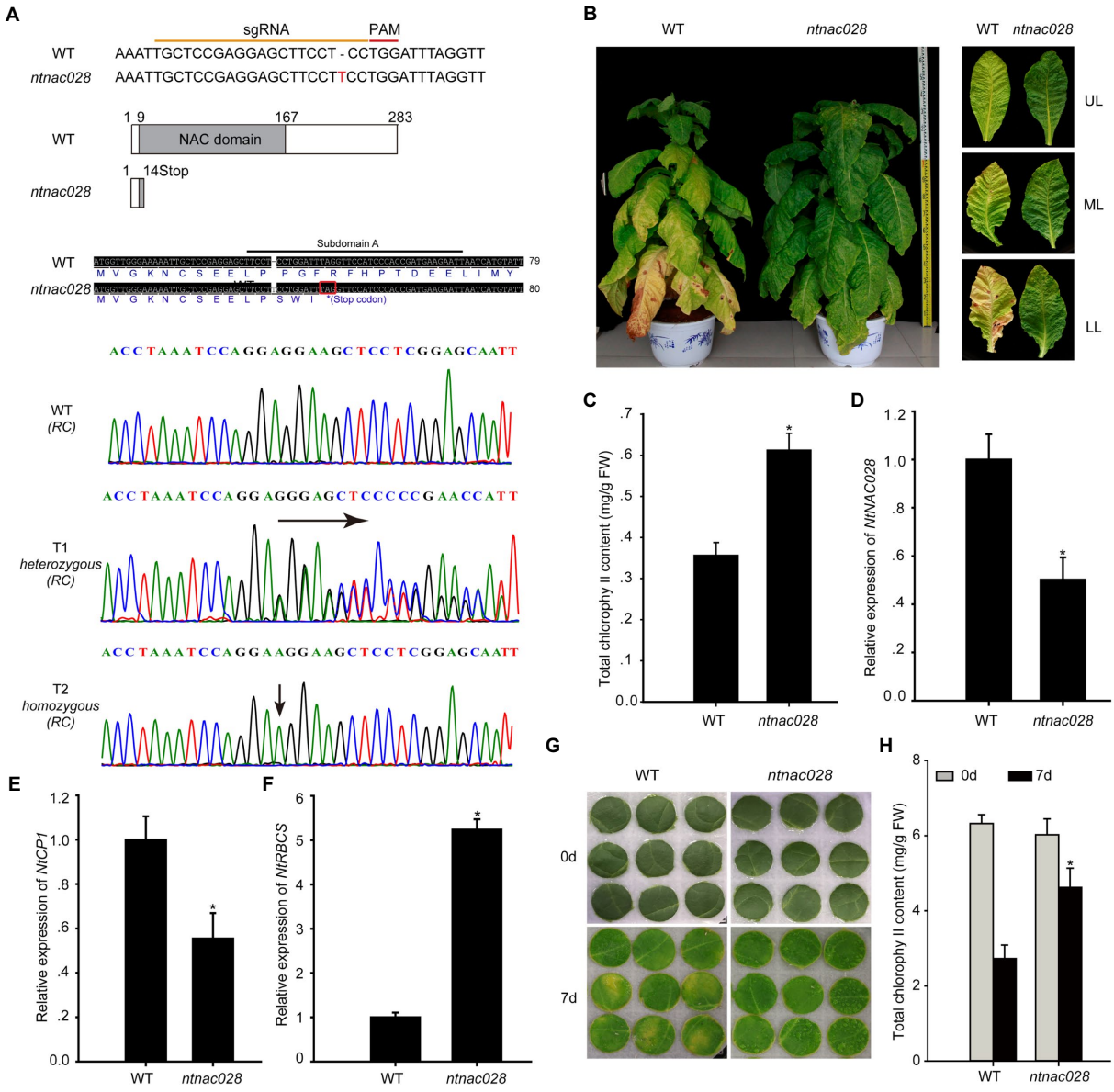


FIGURE 2
NtNAC028 positively regulates leaf senescence. **(A)** Construction of the *NtNAC028* CRISPR-Cas9 vector. Sanger sequencing results showed an insert of 1bp in the genomic DNA of *ntnac028*, compared to the WT. Red line represents the PAM sequence. **(B)** Leaf senescence phenotypes of *ntnac028*. **(C)** Chlorophyll content of middle leaves in age-matched wild-type (K326) and *ntnac028* plants. UL (upper leaf), ML (middle leaf), and LL (low leaf). **(D–F)** Expression of *NtNAC028, NtCP1, and NtRBCS* in middle leaves of WT and *ntnac028*. **(G)** Phenotypes of detached leaves under dark conditions. **(H)** Chlorophyll content of detached leaves in WT and *ntnac028* under darkness for 7days. The bars are SD of three biological replicates. Asterisks indicate statistically significant difference from WT (*p<0.05).

ntnac028 seeds treated with 50 or 100 mM NaCl were significantly higher than that of WT plants, indicating that the seeds of *ntnac028* mutant were insensitive to NaCl during the germination stage (Supplementary Figures S2A,B). Furthermore, detached leaves from 5-week-old plants of *ntnac028* and WT were treated with 200 mM NaCl for 7 days. The leaves of WT senesced early with lower levels of chlorophyll content than *ntnac028* leaves under NaCl stress conditions (Figures 3F,G). Taken together, these results indicated that the knockout of *NtNAC028* led to elevated abiotic stress tolerance in tobacco.

Overexpression of *NtNAC028* confers hypersensitivity to abiotic stress in transgenic *Arabidopsis*

To evaluate the effect of *NtNAC028* overexpression on drought stress tolerance, soil-grown *Arabidopsis* plants were subject to drought stress by withholding water. After the dehydration stress for 8 days, *NtNAC028*-OE6 and *NtNAC028*-OE17 plants exhibited severe leaf wilting phenotypes due to water deficiency, while no evident wilting symptom was observed for WT plants (Figure 4A).

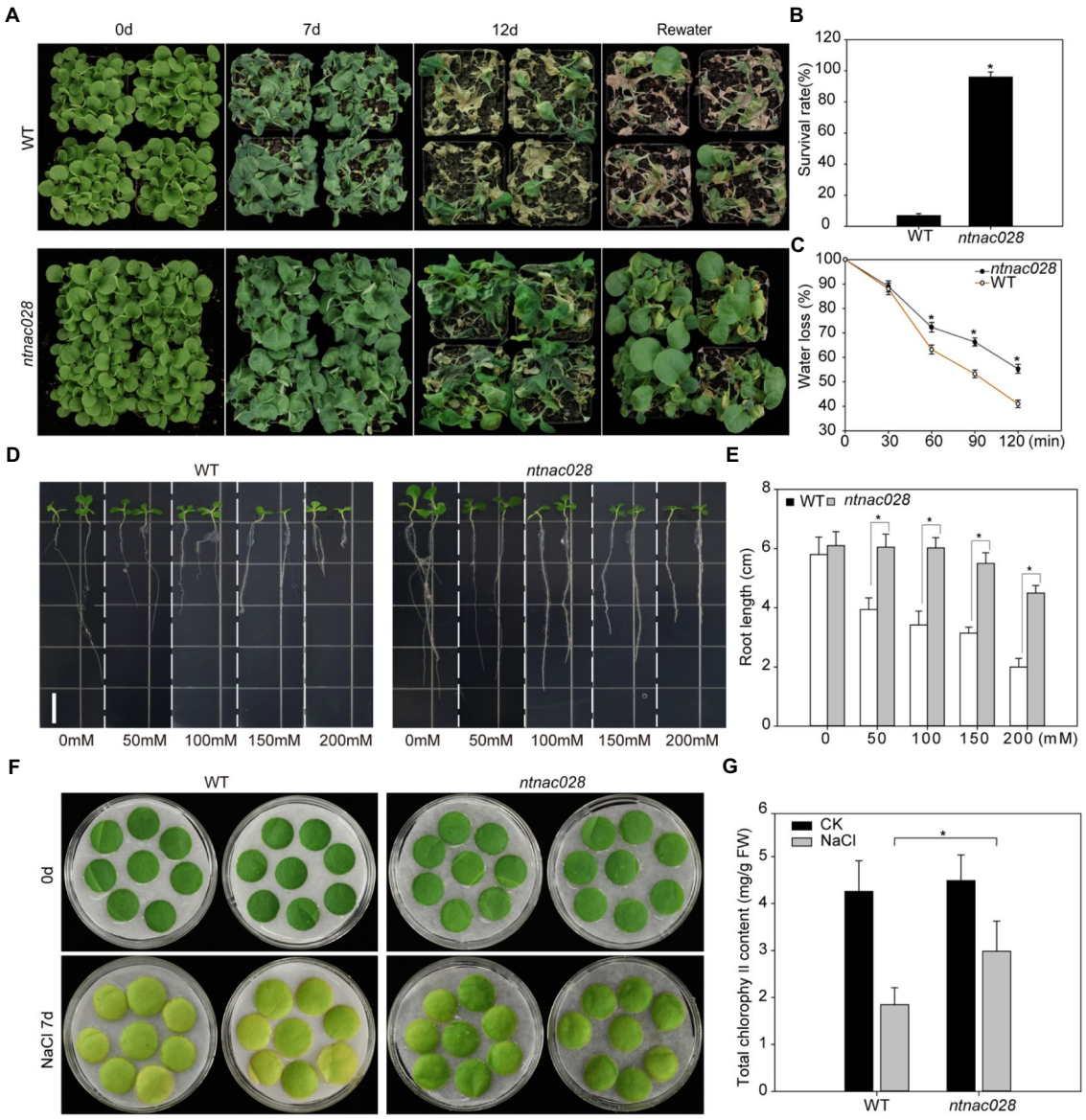


FIGURE 3
CRISPR/Cas9-mediated knockout of *NtNAC028* enhances abiotic stress tolerance in tobacco. **(A)** Phenotypes of tobacco plants treated with drought stress for 12days and recovered with water for 2days. **(B)** Phenotypes of *ntnac028* and wild-type tobacco under drought stress. **(C)** Water loss rates of detached leaves from WT and *ntnac028*. Water loss was determined as the percentage of initial fresh weight. Values are means from 10 plants for each of three independent experiments. **(D,E)** Root length of WT and *ntnac028* under control and NaCl treatments. Seedlings were vertically cultivated on MS plates containing 0, 50, 100, 150, or 200mM NaCl. Images were taken after 5days. Bars=1cm. Data were calculated using 20 seedlings for each genotype. The bars are SDs of three biological replicates. Asterisks indicate statistically significant difference from WT (*p <0.05). **(F,G)** The phenotypes and chlorophyll content of detached leaves from WT and *ntnac028* under NaCl treatment for 7days.

After re-watering for 3 days, less than 35% of the overexpression plants survived; whereas, the survival rates of WT plants were close to 100% (Figure 4B). Moreover, *NtNAC028*-OE lines lost more water than the WT plants at all time points in the water loss assay of detached leaves (Figure 4C). These results indicated that overexpression of *NtNAC028* reduced drought tolerance in *Arabidopsis*.

Meanwhile, *NtNAC028*-OE plants were examined for tolerance to salt stress. As shown in Figures 4D,E, no obvious difference in germination rate was observed without NaCl treatment. However, germination rates of *NtNAC028*-OE lines were significantly lower than that of WT in the presence of 100 or 150 mM NaCl. This result indicated that NaCl stress could severely inhibited seed germination of *NtNAC028* overexpression lines compared to WT. Meanwhile, the germination assay was carried out to assess the ABA sensitivity of *NtNAC028*-OE lines. Interestingly, the *NtNAC028*-OE lines had significantly lower germination rates than WT under ABA treatments

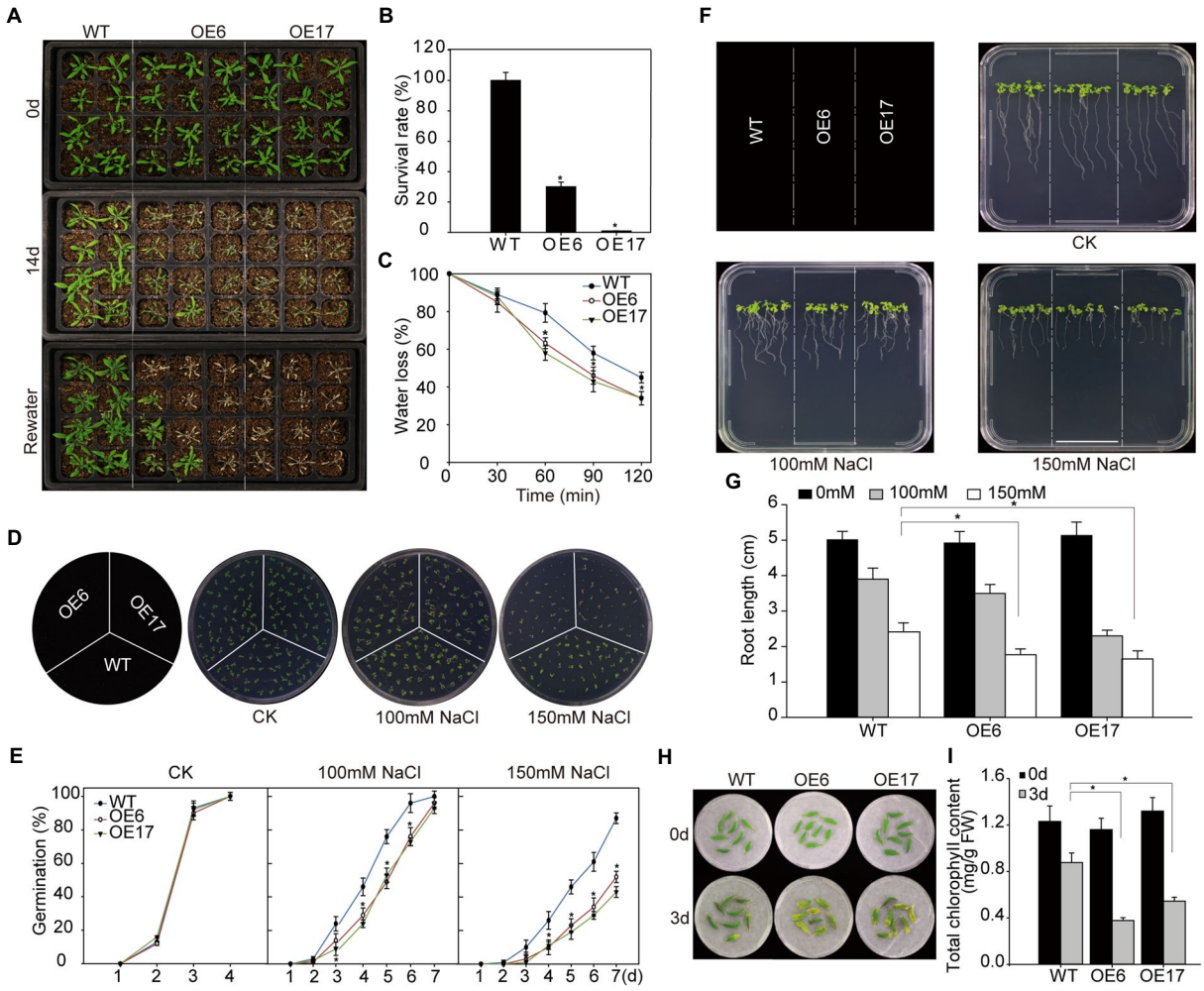


FIGURE 4
Overexpression of *NtNAC028* confers hypersensitivity to abiotic stress in transgenic *Arabidopsis*. **(A)** Phenotypes of *NtNAC028* overexpression lines (OE6 and OE17) and WT under drought stress treatments. Four-week-old *NtNAC028* overexpression lines and WT were withheld from watering for 14days, followed by re-watering and recovery for 3days. **(B)** Survival rates of *NtNAC028* overexpression lines and WT after drought stress. **(C)** Water loss rates of detached leaves from *NtNAC028* overexpression lines and WT. **(D,E)** Germination of WT and *NtNAC028* overexpression lines with different concentrations of NaCl as indicated. Representative images were taken after 7days. **(F,G)** Root length of *NtNAC028* overexpression lines and WT seedlings under NaCl treatments. Seedlings were vertically grown for 7days on 1/2 MS plates containing 0, 100, or 150mM NaCl. **(H,I)** The phenotypes and chlorophyll content of detached leaves from WT and NtNAC028 overexpression lines under NaCl treatments for 3days. The bars are standard deviations (SD) of three biological replicates. Asterisks indicate statistically significant difference from WT (*p<0.05).

(Supplementary Figures S3A,B), suggesting that *NtNAC028*-OE seeds were more sensitive to ABA during germination. Besides, the sensitivity to salt in *NtNAC028* overexpression lines was further assayed at the post-germination stage. Similarly, no significant difference in root length between *NtNAC028*-OE lines and WT was observed under the control conditions. In the presence of 100 or 150 mM NaCl, the roots of the *NtNAC028*-OE lines were significantly shorter than that of WT plants (Figures 4F,G). Furthermore, detached leaves from 4-week-old plants of *NtNAC028*-OE and WT were treated with 200 mM NaCl for 3 days. The leaves of *NtNAC028*-OE senesced early with lower levels of chlorophyll content than WT leaves under NaCl stress conditions (Figures 4H,I). Overall, these results suggested that overexpression of *NtNAC028* reduced salt tolerance in *Arabidopsis*.

NtNAC028 overexpression increases ROS accumulation and regulates expression of stress-responsive genes under abiotic stress treatments

Drought or salt stress often leads to oxidative stress which involves excessive ROS generation in plant cells (Choudhury et al., 2017). To explore whether the reduced tolerance to drought and salt in *NtNAC028*-OE lines is associated with the

alteration of ROS levels, we used NBT staining to visualize the levels of superoxide radical ($O^{\cdot 2-}$) in leaves. Without NaCl treatment, the color of NBT staining in leaves showed no significant difference between *NtNAC028*-OE and WT plants. When stressed by 200 mM NaCl, the *NtNAC028*-OE lines accumulated significantly more $O^{\cdot 2-}$, as densely stained with dark blue color in the leaves of *NtNAC028*-OE lines compared to WT (Figure 5A). Besides, we measured the endogenous H_2O_2 levels of plants with different genotypes. In the presence of NaCl stress, *NtNAC028*-OE plants accumulated significantly more H_2O_2 than that of WT (Figure 5B). These results indicated that *NtNAC028* overexpression could enhance ROS production in transgenic *Arabidopsis* under salt stress treatments.

Furtherly, we analyzed the activities of SOD, POD, and CAT, which are main enzymes responsible for scavenging ROS. No obvious difference was observed in the ROS scavenging activities under non-stress conditions. After salt and drought treatments, SOD, POD, and CAT activities of *NtNAC028*-OE lines and WT were all significantly increased. However, the increase in enzymatic activities of the *NtNAC028*-OE lines was significantly less than that of WT (Figures 5C–H). Furthermore, the expression levels of ROS-scavenging-related genes (SOD, POD, and CAT) in *NtNAC028*-OE lines were also lower than that of WT plants after salt and drought treatments (Supplementary Figures S4A–F). The expression patterns of stress-responsive genes including *AtRD29A, AtDREB1B, AtRD26, and AtNCED3-2* were analyzed in *NtNAC028*-OE lines and WT plants before and after drought/salt treatments (Supplementary Figures S5A–H). Under no-stressed conditions, no significant difference in the transcript levels of these stress-related genes was observed between *NtNAC028*-OE and WT plants. However, the expression levels of these gene were significantly lower in *NtNAC028*-OE lines than in WT under drought or salt treatments. These results suggested that *NtNAC028*-OE could reduce the expression levels of ROS scavenging-related and stress-responsive genes upon abiotic stresses.

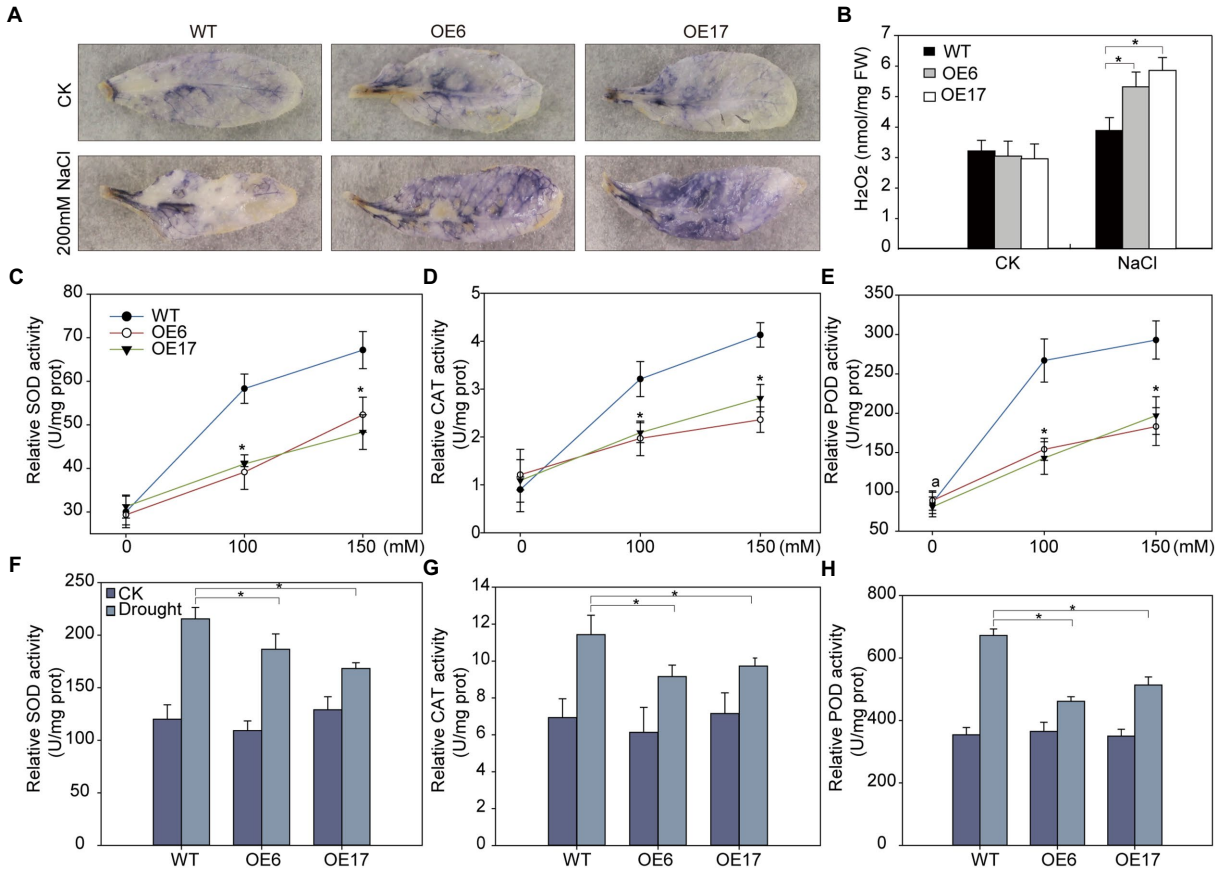


FIGURE 5
NtNAC028 promotes reactive oxygen species (ROS) accumulation under NaCl treatments. **(A)** NBT staining. The middle leaves of 4-week-old *NtNAC028* overexpression lines and WT with or without NaCl treatments were used for NBT staining. **(B)** Measurement of accumulation of H_2O_2 in detached leaves of plants with different genotypes. **(C–H)** POD, SOD, and CAT activities of *NtNAC028* overexpression lines and WT after salt and drought stress treatments. The bars are standard deviations (SD) of three biological replicates. Asterisks indicate statistically significant difference from WT (*p<0.05).

NtNAC028 mutation enhances the antioxidant activity of tobacco under abiotic stresses

To ascertain whether the enhanced stress tolerance of *ntnac028* plants was associated with the alteration of ROS scavenging capability, we examined the activities of SOD, POD, and CAT of *ntnac028* and WT plants under normal or stressed conditions. No significant difference was observed in activities of the antioxidant enzymes under non-stress conditions. However, the activities of SOD, POD, and CAT were more dramatically increased in *ntnac028* plants than that in WT after drought or salt stress treatments (Figures 6A–C,E). Consistently, MDA content of *ntnac028* plants was significantly lower than that in WT following drought/salt stress treatments (Figures 6D,H). These results indicated that NtNAC028 mutation could enhance stress tolerance possibly through enhancing the activities of antioxidant enzymes.

NtNAC028 regulates the expression of scavenging-related and stress-responsive genes in tobacco under abiotic stresses

To understand the mechanism of NtNAC028's regulation of abiotic stress response, the expression patterns of stress-responsive genes, including *NtRD29A*, *NtDREB1B*, *NtRD26*, and *NtNCED3-2* were analyzed in *ntnac028* and WT plants before and after drought/salt treatments (Figures 7A–H). Under no-stressed conditions, no significant difference in the transcript levels of these stress-related genes was observed between *ntnac028* and WT plants. However, the expression levels of these genes were significantly higher in *ntnac028* than in WT plants under drought or salt treatments. Furthermore, salt and drought treatments strongly induced the expression of ROS-scavenging-related genes (SOD, POD, and CAT) in *ntnac028* compared with WT (Supplementary Figures S6A–F). These results suggested that *NtNAC028* knockout could enhance the expression levels of ROS scavenging-related and stress-responsive genes upon abiotic stresses.

Discussion

The NAC superfamily is one of the largest transcription factor families in plants, which plays important regulatory roles in plant development and stress response (Forlani et al., 2021). Previously, we identified a total of 154 NAC genes (*NtNACs*) in tobacco and demonstrated that NtNAC080 was a positive regulator of leaf senescence (Li et al., 2018). However, the functions of most of the remaining NtNACs remain unclear. In this study, we carried out a detailed functional characterization of NtNAC028, which belongs to the same phylogenetic subgroup as NtNAC080. The results demonstrated that NtNAC028 could also positively regulate leaf senescence, sharing a redundant role with NtNAC080. In addition, the *NtNAC028* transcript was found to be upregulated rapidly and significantly under drought, salinity, and exogenous ABA treatments, suggesting it may be involved in abiotic stress response. Previous studies have revealed that some members of the NAC TFs are involved in senescence and also play vital roles in stress response (Guo and Gan, 2012; Zhang and Gan, 2012). For instance, overexpression of *TaNAC29* from wheat can enhance salt and drought tolerance in transgenic *Arabidopsis*, which exhibits a delayed senescence phenotype (Huang et al., 2015). It

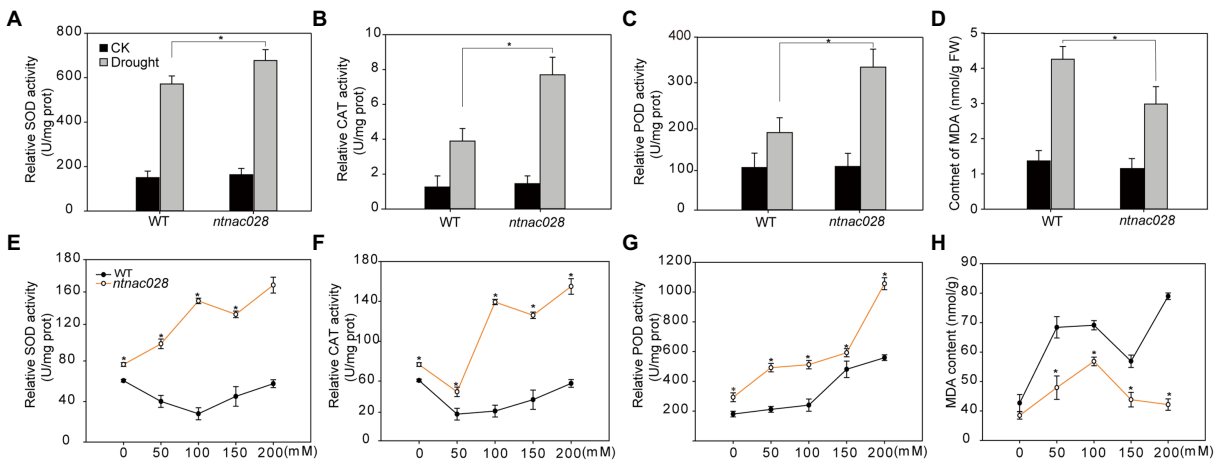


FIGURE 6
NtNAC028 mutation enhances the antioxidant activity of tobacco under abiotic stresses. **(A–C)** POD, SOD, and CAT activities of WT and *ntnac028* plants with or without drought stress treatments. **(E–G)** POD, SOD, and CAT activities of WT and *ntnac028* plants under various concentrations of NaCl. **(D,H)** MDA contents of WT and *ntnac028* plants under drought and salt treatments. The bars are standard deviations (SD) of three biological replicates. Asterisks indicate statistically significant difference from WT (*p<0.05).

10.3389/fpls.2022.941026

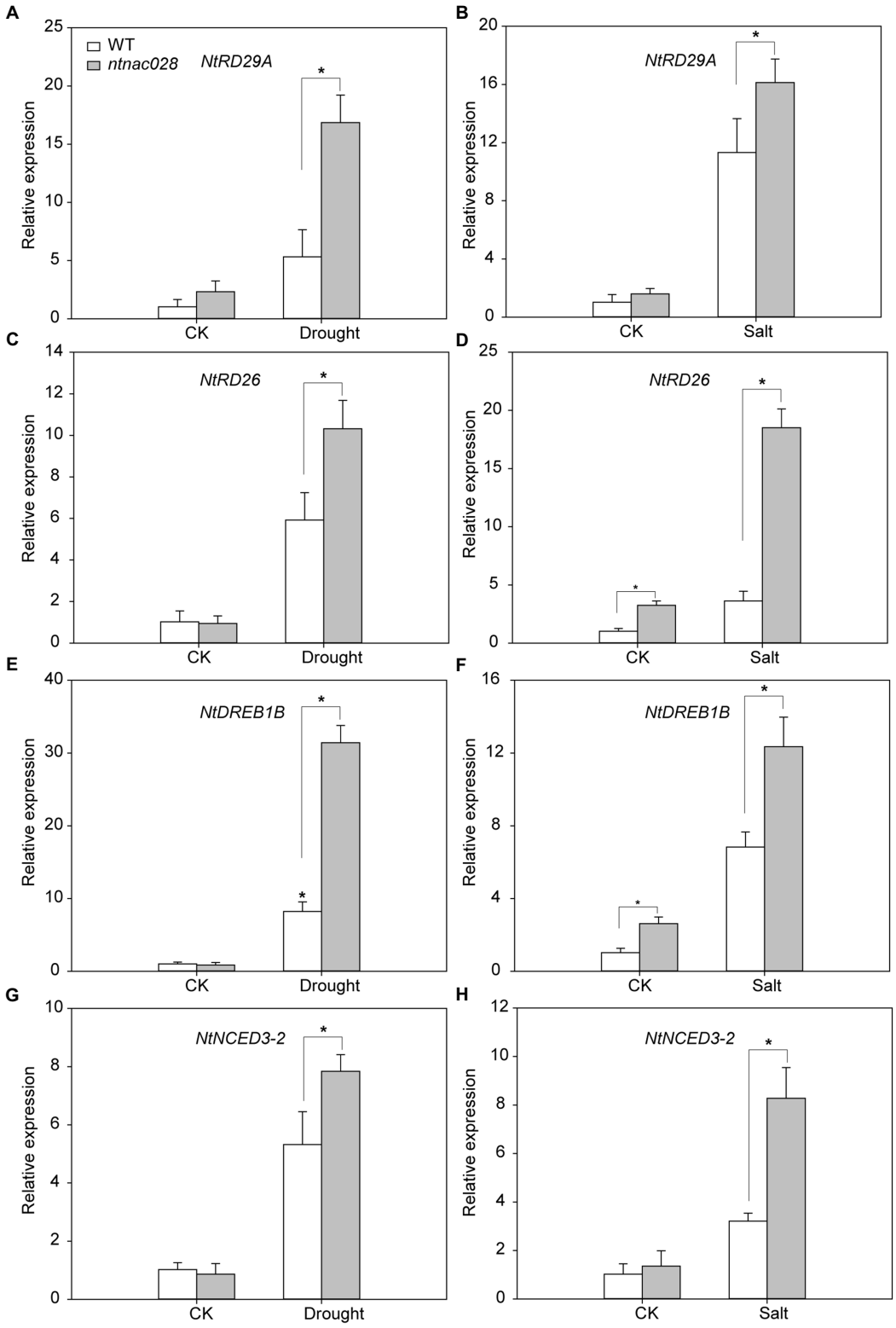


FIGURE 7
Expression patterns of stress-responsive genes in WT and *ntnac028* plants under salt and drought treatments. Relative transcript levels of four stress-responsive genes (RD29A, RD26, DREB1B, and NCED3-2) in WT and *ntnac028* plants before and after drought **(A,C,E,G)** and salt **(B,D,F,H)** treatments. The bars are standard deviations (SD) of three biological replicates. Asterisks indicate statistically significant difference from WT (*p<0.05).

was also showed that AtNAP negatively regulates tolerance to osmotic stress, while positively regulates leaf and fruit senescence (Guo and Gan, 2006; Xiaohong Kousup Sup, 2012). Interestingly, OsNAP, a rice homologue of AtNAP, functions as a positive regulator of leaf senescence and abiotic stress responses (high salinity and drought; Liang et al., 2014). In addition to having the similar function as positive regulators of leaf senescence, NAP homologues in different plant species seem to have more diversified functions in stress responses. In this study, several lines of evidence indicated that *NtNAC028* plays an important role in response to drought and high salinity. As expected, the promoter sequence of *NtNAC028* (about 3 kb upstream of the transcription start site) contains multiple cis-related elements of plant stress response, including seven ABA-responsive elements (ABREs) and three stress-related elements (TC-rich repeats: defense and stress responsiveness; LTR: low-temperature responsiveness; Supplementary Table 2). These results indicated that *NtNAC028* might have broad functions in abiotic response.

NAC TFs are known to be involved in environmental stresses, which in turn improve the ability of plants in tolerating these stresses (Nakashima et al., 2012). Previous studies have showed that abiotic stresses could induce premature leaf senescence, which accelerates dry matter accumulation in grains and plays a positive role in plant environmental adaptability (Sade et al., 2018). While the mutants with delayed leaf senescence often showed higher tolerance to stress treatments (Kang et al., 2019; Guo et al., 2021). Here, *ntnac028* tobacco mutant generated by CRISPR/Cas9 showed a lower rate of water loss and enhanced salt and drought stress tolerance, while *NtNAC028*-OE *Arabidopsis* lines were more sensitive to these stress than WT. In addition, seed germination rates of *NtNAC028*-OE lines were much lower than that of WT under NaCl treatments. These results suggested that NtNAC028 might negatively regulate salt and drought stress responses. It is known that the responsiveness of plants to abiotic stresses was mediated by ABA-dependent and ABA-independent pathways. In the ntnac028 mutant, the ABA-dependent pathway genes *NtRD26, NtRD29A, and NtNCED3-2*, as well as the ABA-independent gene *NtDREB1B*, were expressed at a higher level under stress conditions. It has been reported that these genes are involved in the mediation of oxidative or osmotic damages induced by stresses (Wei et al., 2016; Huang et al., 2018; Jiang et al., 2019; Orbović et al., 2021). For example, RD26 acts as a transcriptional activator of ABA-inducible gene expression in plants under various abiotic stress conditions (Fujita et al., 2004). DREB1B is a member of the AP2/ERF family, which can activate a subset of downstream stress-responsive genes and plays an essential role in drought stress response (Wei et al., 2016). Thus, increased expression of these genes could help *ntnac028* mutant plants in tolerating abiotic stresses. As being reported in our previous study, NtNAC028 is a homolog of AtNAP (Li et al., 2018). AtNAP has been documented to negatively regulate salt stress tolerance *via* repression of ABA-dependent stress-responsive genes (Seok et al., 2017), suggesting that NtNAC028 might perform similar regulatory function in abiotic stress response in tobacco.

It is well known that abiotic stresses could cause excessive accumulation of reactive oxygen species (ROS) in plants, which could lead to damage of cellular biomolecules, including proteins, lipids, and DNA (Parida and Das, 2005). In addition, the senescence process can also induce ROS generation, and the increase in ROS levels triggers and accelerates senescence (Maggiorani et al., 2017). Therefore, ROS may serve as a key signal in both senescence and stress responses. Besides, antioxidant enzymes, such as POD, SOD, and CAT are the enzymes responsible for scavenging ROS in plants (Gill and Tuteja, 2010; Miller et al., 2010). The genes encoding antioxidant enzymes are often upregulated to protect tissues under stresses (Jin et al., 2017). In the present study, *NtNAC028*-OE lines accumulated significantly higher levels of H_2O_2 than WT plants under salt stress conditions. The activities of POD, CAT, and SOD in *NtNAC028*-OE lines were also significantly lower than those of WT (Figure 5), indicating that the higher accumulation of ROS in *NtNAC028*-OE plants under stress conditions was due to their inability to remove ROS in time. In contrast, the transcript levels and activities of POD, SOD, and CAT in the *ntnac028* mutant were significantly higher than that in WT (K326; Figures 6, 7). Consistently, MDA content of *ntnac028* mutant plants was significantly lower than that of WT under stress conditions, indicating that the *ntnac028* mutant plants produced less ROS. Thus, it is possible that a more efficient ROS scavenging system in the *ntnac028* mutant is important for its abiotic stress tolerance.

Conclusion

In summary, we functionally characterized a tobacco NAC gene, *NtNAC028*, which was strongly induced by senescence and various abiotic stresses. *NtNAC028* mutation induced by CRISPR/Cas9 led to delayed senescence and enhanced tolerance to drought and salinity in tobacco, while *NtNAC028* overexpression transgenic *Arabidopsis* exhibited early senescence and hypersensitivity to high salinity and drought, indicating that NtNAC028 culd function as a negative regulator of leaf senescence and abiotic stress response in plants. Furthermore, our results revealed that the enhanced stress tolerance of the *ntnac028* mutant might be due to enhanced scavenging capacity of ROS and increased expression of stress-responsive genes.

Data availability statement

The original contributions presented in the study are included in the article/Supplementary material, further inquiries can be directed to the corresponding authors.

Author contributions

YG and WL conceived the research. WL and LW generated the transgenic materials and performed all experiments, and

drafted the manuscript. TL, ZD, and QW assisted in data collection and analysis. ZZ and WW designed the Crispr-Cas9 experiment and generated the constructs. All authors contributed to the article and approved the submitted version.

Funding

This work was financially supported by National Natural Science Foundation of China (No. 31970204), the Agricultural Science and Technology Innovation Program (ASTIP-TRIC02) and Funds for Special Projects of the Central Government in Guidance of Local Science and Technology Development (21-1-1-1-zyyd-nsh).

Conflict of interest

The authors declare that the research was conducted in the absence of any commercial or financial relationships that could be construed as a potential conflict of interest.

Publisher's note

All claims expressed in this article are solely those of the authors and do not necessarily represent those of their affiliated organizations, or those of the publisher, the editors and the reviewers. Any product that may be evaluated in this article, or claim that may be made by its manufacturer, is not guaranteed or endorsed by the publisher.

Supplementary material

The Supplementary Material for this article can be found online at: https://www.frontiersin.org/articles/10.3389/fpls.2022.941026/full#supplementary-material

SUPPLEMENTARY FIGURE S1
Overexpression of NtNAC028 in *Arabidopsis* plants causes precocious senescence.

SUPPLEMENTARY FIGURE S2
Seed germination under salt treatments.

SUPPLEMENTARY FIGURE S3
Seed germination under ABA treatments.

SUPPLEMENTARY FIGURE S4
Expression patterns of reactive oxidation species scavenging-related genes in WT and NtNAC028-OE plants in response to salt and drought treatments.

SUPPLEMENTARY FIGURE S5
Expression patterns of stress responsive genes in WT and NtNAC028-OE plants under salt and drought treatments.

SUPPLEMENTARY FIGURE S6
Expression patterns of ROS scavenging-related genes in WT and ntnac028 plants in response to salt and drought treatments.

References

Balazadeh, S., Siddiqui, H., Allu, A. D., Matallana Ramirez, L. P., Caldana, C., Mehrnia, M., et al. (2010). A gene regulatory network controlled by the NAC transcription factor ANAC092/AtNAC2/ORE1 during salt-promoted senescence. *Plant J.* 62, 250–264. doi: 10.1111/j.1365-313X.2010.04151.x

Breeze, E., Elizabeth, H., Stuart, M., Linda, H., Richard, H., and Claire, H. (2011). High-resolution temporal profiling of transcripts during Arabidopsis leaf senescence reveals a distinct chronology of processes and regulation. *Plant Cell* 23, 873–894. doi: 10.1105/tpc.111.083345

Choudhury, F. K., Rivero, R. M., Blumwald, E., and Mittler, R. (2017). Reactive oxygen species, abiotic stress and stress combination. *Plant J.* 90, 856–867. doi: 10.1111/tpj.13299

Clough, S. J., and Bent, A. F. (1998). Floral dip: a simplified method for agrobacterium-mediated transformation of Arabidopsis thaliana. *Plant J.* 16, 735–743. doi: 10.1046/j.1365-313x.1998.00343.x

Diao, P., Chen, C., Zhang, Y., Meng, Q., Lv, W., and Ma, N. (2020). The role of NAC transcription factor in plant cold response. *Plant Signal. Behav.* 15:1785668. doi: 10.1080/15592324.2020.1785668

Draper, H. H., Squires, E. J., Mahmoodi, H., Wu, J., Agarwal, S., and Hadley, M. (1993). A comparative evaluation of thiobarbituric acid methods for the determination of malondialdehyde in biological materials. *Free Radic. Biol. Med.* 15, 353–363. doi: 10.1016/0891-5849(93)90035-s

Forlani, S., Mizzotti, C., and Masiero, S. (2021). The NAC side of the fruit: tuning of fruit development and maturation. *BMC Plant Biol.* 21, 238–214. doi: 10.1186/s12870-021-03029-y

Fu, Y., Guo, H., Cheng, Z., Wang, R., Li, G., Huo, G., et al. (2013). NtNAC-R1, a novel NAC transcription factor gene in tobacco roots, responds to mechanical damage of shoot meristem. *Plant Physiol. Biochem.* 69, 74–81. doi: 10.1016/j.plaphy.2013.05.004

Fujita, M., Fujita, Y., Maruyama, K., Seki, M., Hiratsu, K., Ohme Takagi, M., et al. (2004). A dehydration-induced NAC protein, RD26, is involved in a novel ABA-dependent stress-signaling pathway. *Plant J.* 39, 863–876. doi: 10.1111/j.1365-313X.2004.02171.x

Gao, J., Wang, G., Ma, S., Xie, X., Wu, X., Zhang, X., et al. (2015). CRISPR/Cas9-mediated targeted mutagenesis in Nicotiana tabacum. *Plant Mol. Biol.* 87, 99–110. doi: 10.1007/s11103-014-0263-0

Gao, F., Xiong, A., Peng, R., Jin, X., Xu, J., Zhu, B., et al. (2010). OsNAC52, a rice NAC transcription factor, potentially responds to ABA and confers drought tolerance in transgenic plants. *Plant Cell Tissue Organ Cult.* 100, 255–262. doi: 10.1007/s11240-009-9640-9

Gill, S. S., and Tuteja, N. (2010). Reactive oxygen species and antioxidant machinery in abiotic stress tolerance in crop plants. *Plant Physiol. Biochem.* 48, 909–930. doi: 10.1016/j.plaphy.2010.08.016

Guo, Y., and Gan, S. (2006). AtNAP, a NAC family transcription factor, has an important role in leaf senescence. *Plant J.* 46, 601–612. doi: 10.1111/j.1365-313X.2006.02723.x

Guo, Y., and Gan, S. S. (2012). Convergence and divergence in gene expression profiles induced by leaf senescence and 27 senescence-promoting hormonal, pathological and environmental stress treatments. *Plant Cell Environ.* 35, 644–655. doi: 10.1111/j.1365-3040.2011.02442.x

Guo, Y., Ren, G., Zhang, K., Li, Z., Miao, Y., and Guo, H. (2021). Leaf senescence: progression, regulation, and application. *Mol. Hortic.* 1, 1–25. doi: 10.1186/s43897-021-00006-9

Haak, D. C., Fukao, T., Grene, R., Hua, Z., Ivanov, R., Perrella, G., et al. (2017). Multilevel regulation of abiotic stress responses in plants. *Front. Plant Sci.* 8:1564. doi: 10.3389/fpls.2017.01564

He, Y., and Gan, S. (2002). A gene encoding an acyl hydrolase is involved in leaf senescence in Arabidopsis. *Plant Cell* 14, 805–815. doi: 10.1105/tpc.010422

He, X. J., Mu, R. L., Cao, W. H., Zhang, Z. G., Zhang, J. S., and Chen, S. Y. (2005). AtNAC2, a transcription factor downstream of ethylene and auxin signaling pathways, is involved in salt stress response and lateral root development. *Plant J.* 44, 903–916. doi: 10.1111/j.1365-313X.2005.02575.x

Horsch, R. B., Fry, J., Hoffmann, N., Neidermeyer, J., Rogers, S. G., and Fraley, R. T. (1989). Leaf disc transformation. *Plant Molecular Biology Manual* 7, 63–71. doi: 10.1007/978-94-009-0951-9_5

Huang, Y., Guo, Y., Liu, Y., Zhang, F., Wang, Z., Wang, H., et al. (2018). 9-cis-epoxycarotenoid dioxygenase 3 regulates plant growth and enhances multi-abiotic stress tolerance in rice. *Front. Plant Sci.* 9:162. doi: 10.3389/fpls.2018.00162

Huang, Q., Wang, Y., Li, B., Chang, J., Chen, M., Li, K., et al. (2015). TaNAC29, a NAC transcription factor from wheat, enhances salt and drought tolerance in transgenic Arabidopsis. *BMC Plant Biol.* 15, 268–215. doi: 10.1186/s12870-015-0644-9

Jiang, H., Tang, B., Xie, Z., Nolan, T., Ye, H., Song, G. Y., et al. (2019). GSK 3-like kinase BIN 2 phosphorylates RD 26 to potentiate drought signaling in Arabidopsis. *Plant J.* 100, 923–937. doi: 10.1111/tpj.14484

Jin, C., Li, K., Xu, X., Zhang, H., Chen, H., Chen, Y., et al. (2017). A novel NAC transcription factor, PbeNAC1, of Pyrus betulifolia confers cold and drought tolerance via interacting with PbeDREBs and activating the expression of stress-responsive genes. *Front. Plant Sci.* 8:1049. doi: 10.3389/fpls.2017.01049

Kang, K., Shim, Y., Gi, E., An, G., and Paek, N.-C. (2019). Mutation of ONAC096 enhances grain yield by increasing panicle number and delaying leaf senescence during grain filling in rice. *Int. J. Mol. Sci.* 20:5241. doi: 10.3390/ijms20205241

Kim, Y., Sang-Gyu, K., Jung-Eun, P., Hye-Young, P., Mi-Hye, L., and Nam-Hai, C. (2006). A membrane-bound NAC transcription factor regulates cell division in Arabidopsis. *Plant Cell* 18, 3132–3144. doi: 10.1105/tpc.106.043018

Lata, C., Yadav, A., and Prasad, M. (2011). Role of plant transcription factors in abiotic stress tolerance. *Abiotic Stress Response in Plants* 10, 269–296. doi: 10.5772/23172

Le Hénanff, G., Profizi, C., Courteaux, B., Rabenoelina, F., Gérard, C., Clément, C., et al. (2013). Grapevine NAC1 transcription factor as a convergent node in developmental processes, abiotic stresses, and necrotrophic/biotrophic pathogen tolerance. *J. Exp. Bot.* 64, 4877–4893. doi: 10.1093/jxb/ert277

Lee, S., Lee, H., Huh, S. U., Paek, K., Ha, J., and Park, C. M. (2014). The Arabidopsis NAC transcription factor NTL4 participates in a positive feedback loop that induces programmed cell death under heat stress conditions. *Plant Sci.* 227, 76–83. doi: 10.1016/j.plantsci.2014.07.003

Li, W., Li, X., Chao, J., Zhang, Z., Wang, W., and Guo, Y. (2018). NAC family transcription factors in tobacco and their potential role in regulating leaf senescence. *Front. Plant Sci.* 9:1900. doi: 10.3389/fpls.2018.01900

Li, X., Wang, Q., Guo, C., Sun, J., Li, Z., Wang, Y., et al. (2022). NtNAC053, a novel NAC transcription factor, confers drought and salt tolerances in tobacco. *Front. Plant Sci.* 13:817106. doi: 10.3389/fpls.2022.817106

Liang, C., Wang, Y., Zhu, Y., Tang, J., Hu, B., Liu, L., et al. (2014). OsNAP connects abscisic acid and leaf senescence by fine-tuning abscisic acid biosynthesis and directly targeting senescence-associated genes in rice. *Proc. Natl. Acad. Sci.* 111, 10013–10018. doi: 10.1073/pnas.1321568111

Liliane, T. N., and Charles, M. S. (2020). *Factors Affecting Yield of Crops. Agronomy-Climate Change & Food Security*. London, UK: IntechOpen, 9.

Liu, G., Li, H., Grieson, D., and Fu, D. (2022). NAC transcription factor family regulation of fruit ripening and quality: a review. *Cell* 11:525. doi: 10.3390/cells11030525

Liu, W., Zhao, B., Chao, Q., Wang, B., Zhang, Q., Zhang, C., et al. (2019). Function analysis of ZmNAC33, a positive regulator in drought stress response in Arabidopsis. *Plant Physiol. Biochem.* 145, 174–183. doi: 10.1016/j.plaphy.2019.10.038

Lu, M., Ying, S., Zhang, D., Shi, Y., Song, Y., Wang, T., et al. (2012). A maize stress-responsive NAC transcription factor, ZmSNAC1, confers enhanced tolerance to dehydration in transgenic Arabidopsis. *Plant Cell Rep.* 31, 1701–1711. doi: 10.1007/s00299-012-1284-2

Ma, L., Li, R., Ma, L., Song, N., Xu, Z., and Wu, J. (2020). Involvement of NAC transcription factor NaNAC29 in Alternaria alternata resistance and leaf senescence in *Nicotiana attenuata*. *Plant Divers.* 43, 502–509. doi: 10.1016/j.pld.2020.11.003

Maggiorani, D., Manzella, N., Edmondson, D. E., Mattevi, A., Parini, A., Binda, C., et al. (2017). Monoamine oxidases, oxidative stress, and altered mitochondrial dynamics in cardiac ageing. *Oxidative Med. Cell. Longev.* 2017, 1–8. doi: 10.1155/2017/3017947

Mao, X., Chen, S., Li, A., Zhai, C., and Jing, R. (2014). Novel NAC transcription factor TaNAC67 confers enhanced multi-abiotic stress tolerances in Arabidopsis. *PLoS One* 9:e84359. doi: 10.1371/journal.pone.0084359

Mao, H., Yu, L., Han, R., Li, Z., and Liu, H. (2016). ZmNAC55, a maize stress-responsive NAC transcription factor, confers drought resistance in transgenic Arabidopsis. *Plant Physiol. Biochem.* 105, 55–66. doi: 10.1016/j.plaphy.2016.04.018

Mao, X., Zhang, H., Qian, X., Li, A., Zhao, G., and Jing, R. (2012). TaNAC2, a NAC-type wheat transcription factor conferring enhanced multiple abiotic stress tolerances in Arabidopsis. *J. Exp. Bot.* 63, 2933–2946. doi: 10.1093/jxb/err462

Miller, G., Suzuki, N., Ciftci Yilmaz, S., and Mittler, R. (2010). Reactive oxygen species homeostasis and signalling during drought and salinity stresses. *Plant Cell Environ.* 33, 453–467. doi: 10.1111/j.1365-3040.2009.02041.x

Moghaddam, M. S. H., Safaie, N., Soltani, J., and Hagh-Doust, N. (2021). Desert-adapted fungal endophytes induce salinity and drought stress resistance in model crops. *Plant Physiol. Biochem.* 160, 225–238. doi: 10.1016/j.plaphy.2021.01.022

Nakashima, K., Takasaki, H., Mizoi, J., Shinozaki, K., and Yamaguchi-Shinozaki, K. (2012). NAC transcription factors in plant abiotic stress responses. *BBA Gene Regulat. Mechan.* 1819, 97–103. doi: 10.1016/j.bbagrm.2011.10.005

Nakashima, K., Tran, L. S. P., Van Nguyen, D., Fujita, M., Maruyama, K., Todaka, D., et al. (2007). Functional analysis of a NAC-type transcription factor OsNAC6 involved in abiotic and biotic stress-responsive gene expression in rice. *Plant J.* 51, 617–630. doi: 10.1111/j.1365-313X.2007.03168.x

Orbović, V., Ravanfar, S. A., Acanda, Y., Narvaez, J., Merritt, B. A., Levy, A., et al. (2021). Stress-inducible Arabidopsis thaliana RD29A promoter constitutively drives Citrus sinensis APETALA1 and LEAFY expression and precocious flowering in transgenic citrus spp. *Transgenic Res.* 30, 687–699. doi: 10.1007/s11248-021-00260-z

Parida, A. K., and Das, A. B. (2005). Salt tolerance and salinity effects on plants: a review. *Ecotoxicol. Environ. Saf.* 60, 324–349. doi: 10.1016/j.ecoenv.2004.06.010

Pascual, M., Torre, F. D. L., Cañas, R. A., Cánovas, F. M., and Ávila, C. (2018). NAC transcription factors in woody plants. *Progress in Botany* 80, 195–222. doi: 10.1007/124_2018_19

Rao, X., Huang, X., Zhou, Z., and Xin, L. (2013). An improvement of the 2(−delta delta CT) method for quantitative real-time polymerase chain reaction data analysis. *Biostat. Bioinform. Biomath.* 3, 71–85.

Sade, N., del Mar Rubio-Wilhelmi, M., Umnajkitikorn, K., and Blumwald, E. (2018). Stress-induced senescence and plant tolerance to abiotic stress. *J. Exp. Bot.* 69, 845–853. doi: 10.1093/jxb/erx235

Sakuraba, Y., Kim, Y., Han, S., Lee, B., and Paek, N. (2015). The Arabidopsis transcription factor NAC016 promotes drought stress responses by repressing AREB1 transcription through a trifurcate feed-forward regulatory loop involving NAP. *Plant Cell* 27, 1771–1787. doi: 10.1105/tpc.15.00222

Seok, H., Woo, D., Nguyen, L. V., Tran, H. T., Tarte, V. N., Mehdi, S. M. M., et al. (2017). Arabidopsis AtNAP functions as a negative regulator via repression of AREB1 in salt stress response. *Planta* 245, 329–341. doi: 10.1007/s00425-016-2609-0

Shen, J., Lv, B., Luo, L., He, J., Mao, C., Xi, D., et al. (2017). The NAC-type transcription factor OsNAC2 regulates ABA-dependent genes and abiotic stress tolerance in rice. *Sci. Rep.* 7, 1–16. doi: 10.1038/srep40641

Sperotto, R. A., Ricachenevsky, F. K., Duarte, G. L., Boff, T., Lopes, K. L., Sperb, E. R., et al. (2009). Identification of up-regulated genes in flag leaves during rice grain filling and characterization of OsNAC5, a new ABA-dependent transcription factor. *Planta* 230, 985–1002. doi: 10.1007/s00425-009-1000-9

Suzuki, N., Koussevitzky, S., Mittler, R., and Miller, G. (2012). ROS and redox signalling in the response of plants to abiotic stress. *Plant Cell Environ.* 35, 259–270. doi: 10.1111/j.1365-3040.2011.02336.x

Takada, S., Ken-ichiro, H., Tetsuya, I., and Masao, T. (2001). The CUP-SHAPED COTYLEDON1 gene of Arabidopsis regulates shoot apical meristem formation. *Development* 128, 1127–1135. doi: 10.1242/dev.128.7.1127

Tran, L. P., Nakashima, K., Sakuma, Y., Simpson, S. D., Fujita, Y., Maruyama, K., et al. (2004). Isolation and functional analysis of Arabidopsis stress-inducible NAC transcription factors that bind to a drought-responsive cis-element in the early responsive to dehydration stress 1 promoter. *Plant Cell* 16, 2481–2498. doi: 10.1105/tpc.104.022699

Wei, T., Deng, K., Gao, Y., Liu, Y., Yang, M., Zhang, L., et al. (2016). Arabidopsis DREB1B in transgenic salvia miltiorrhiza increased tolerance to drought stress without stunting growth. *Plant Physiol. Biochem.* 104, 17–28. doi: 10.1016/j.plaphy.2016.03.003

Xiang, Y., Sun, X., Bian, X., Wei, T., Han, T., Yan, J., et al. (2021). The transcription factor ZmNAC49 reduces stomatal density and improves drought tolerance in maize. *J. Exp. Bot.* 72, 1399–1410. doi: 10.1093/jxb/eraa507

Xiaohong Kousup Sup, S. S. C. B. (2012). Arabidopsis AtNAP regulates fruit senescence. *J. Exp. Bot.* 63, 6139–6147. doi: 10.1093/jxb/ers266

Xu, Z., Kim, S. Y., Hyeon, D. Y., Kim, D. H., Dong, T., Park, Y., et al. (2013). The Arabidopsis NAC transcription factor ANAC096 cooperates with bZIP-type transcription factors in dehydration and osmotic stress responses. *Plant Cell* 25, 4708–4724. doi: 10.1105/tpc.113.119099

Xu, Z., Wang, C., Xue, F., Zhang, H., and Ji, W. (2015). Wheat NAC transcription factor TaNAC29 is involved in response to salt stress. *Plant Physiol. Biochem.* 96, 356–363. doi: 10.1016/j.plaphy.2015.08.013

Xu, X., Yao, X., Lu, L., and Zhao, D. (2018). Overexpression of the transcription factor NtNAC2 confers drought tolerance in tobacco. *Plant Mol. Biol. Report.* 36, 543–552. doi: 10.1371/journal.pone.0137098

Yuan, X., Wang, H., Cai, J., Bi, Y., Li, D., and Song, F. (2019). Rice NAC transcription factor ONAC066 functions as a positive regulator of drought and oxidative stress response. *BMC Plant Biol.* 19, 278–219. doi: 10.1186/s12870-019-1883-y

Zhang, K., and Gan, S. (2012). An abscisic acid-AtNAP transcription factor-SAG113 protein phosphatase 2C regulatory chain for controlling dehydration in senescing *Arabidopsis* leaves. *Plant Physiol.* 158, 961–969. doi: 10.1104/pp.111.190876

Zhang, Y., Li, D., Wang, Y., Zhou, R., Wang, L., Zhang, Y., et al. (2018). Genome-wide identification and comprehensive analysis of the NAC transcription factor family in *Sesamum indicum*. *PLoS One* 13:e0199262. doi: 10.1371/journal.pone.0199262

Zhang, X., Long, Y., Huang, J., and Xia, J. (2020). OsNAC45 is involved in ABA response and salt tolerance in rice. *Rice* 13, 79–13. doi: 10.1186/s12284-020-00440-1

Zhong, R., Chanhui, L., and Zheng, H. (2010). Global analysis of direct targets of secondary wall NAC master switches in Arabidopsis. *Mol. Plant* 3, 1087–1103. doi: 10.1093/mp/ssq062

frontiers | Frontiers in Plant Science

TYPE Original Research
PUBLISHED 19 August 2022
DOI 10.3389/fpls.2022.988505

Check for updates

OPEN ACCESS

EDITED BY
Jiban Shrestha,
Nepal Agricultural Research Council, Nepal

REVIEWED BY
Linhui Yu,
Northwest A&F University, China
Parviz Heidari,
Shahrood University of Technology, Iran

*CORRESPONDENCE
Guixiang Tang
tanggx@zju.edu.cn

SPECIALTY SECTION
This article was submitted to Plant Abiotic Stress, a section of the journal Frontiers in Plant Science

RECEIVED 07 July 2022
ACCEPTED 01 August 2022
PUBLISHED 19 August 2022

CITATION
Zhong X, Hong W, Shu Y, Li J, Liu L, Chen X, Islam F, Zhou W and Tang G (2022) CRISPR/Cas9 mediated gene-editing of *GmHdz4* transcription factor enhances drought tolerance in soybean (*Glycine max* [L.] Merr.).
Front. Plant Sci. 13:988505.
doi: 10.3389/fpls.2022.988505

COPYRIGHT
© 2022 Zhong, Hong, Shu, Li, Liu, Chen, Islam, Zhou and Tang. This is an open-access article distributed under the terms of the Creative Commons Attribution License (CC BY). The use, distribution or reproduction in other forums is permitted, provided the original author(s) and the copyright owner(s) are credited and that the original publication in this journal is cited, in accordance with accepted academic practice. No use, distribution or reproduction is permitted which does not comply with these terms.

CRISPR/Cas9 mediated gene-editing of *GmHdz4* transcription factor enhances drought tolerance in soybean (*Glycine max* [L.] Merr.)

Xuanbo Zhong[1], Wei Hong[1], Yue Shu[1,2], Jianfei Li[1,2], Lulu Liu[1], Xiaoyang Chen[3], Faisal Islam[1], Weijun Zhou[1] and Guixiang Tang[1,2]*

[1]Zhejiang Provincial Key Laboratory of Crop Germplasm, Institute of Crop Science, Zhejiang University, Hangzhou, Zhejiang, China, [2]Hainan Institute of Zhejiang University, Sanya, Hainan, China, [3]Seed Management Station of Zhejiang Province, Hangzhou, Zhejiang, China

The HD-Zip transcription factors play a crucial role in plant development, secondary metabolism, and abiotic stress responses, but little is known about HD-Zip I genes in soybean. Here, a homeodomain-leucine zipper gene designated *GmHdz4* was isolated. Chimeric soybean plants, *GmHdz4* overexpressing (*GmHdz4-oe*), and gene-editing *via* CRISPR/Cas9 (*gmhdz4*) in hairy roots, were generated to examine the *GmHdz4* gene response to polyethylene glycol (PEG)-simulated drought stress. Bioinformatic analysis showed *GmHdz4* belonged to clade δ, and was closely related to other drought tolerance-related HD-Zip I family genes such as *AtHB12*, *Oshox12*, and *Gshdz4*. The *GmHdz4* was located in the plant nucleus and showed transcriptional activation activity by yeast hybrid assay. Quantitative real-time PCR analysis revealed that *GmHdz4* expression varied in tissues and was induced by PEG-simulated drought stress. The *gmhdz4* showed promoted growth of aboveground parts, and its root system architecture, including the total root length, the root superficial area, and the number of root tips were significantly higher than those of *GmHdz4-oe* even the non-transgenic line (NT) on root tips number. The better maintenance of turgor pressure by osmolyte accumulation, and the higher activity of antioxidant enzymes to scavenge reactive oxygen species, ultimately suppressed the accumulation of hydrogen peroxide (H_2O_2), superoxide anion (O^{2-}), and malondialdehyde (MDA), conferring higher drought tolerance in *gmhdz4* compared with both *GmHdz4-oe* and NT. Together, our results provide new insights for future research on the mechanisms by which *GmHdz4* gene-editing *via* CRISPR/Cas9 system could promote drought stress and provide a potential target for molecular breeding in soybean.

KEYWORDS

***Glycine max*, HD-ZIP, *GmHdz4*, drought stress, root system architecture**

Introduction

Soybean (*Glycine max* [L.] Merr.) is an important oilseed crop, used as both food and feed due to its high protein content. China is a traditional soybean-producing country, and the people have long consumed soybeans and processed soybean products. However, a 100 million tons of soybeans need to be imported each year to meet domestic soybean consumption (Sun, 2020), accounting for about 60% of the global soybean trade volume, and external dependence is as high as 80% (Niu et al., 2021). In addition, due to the increase in extreme weather events, the impact of abiotic stresses such as drought, salinity, and high temperature on crop yields and economic losses has increased (Lesk et al., 2016). Soybean is sensitive to water shortage compared with many other crops, requiring about 450–700 mm of water throughout the growth period (Dogan et al., 2007). Especially at podding and filling stages, drought stress can seriously restrict soybean yield, resulting in a loss of about 40% of yield. During the soybean growth period, most areas of China experience different degrees of drought (You et al., 2021). Drought in Northeast China begins in mid-March, and develops into severe and extreme drought conditions from late April to May, which is the growing season for soybean. In addition to water-saving irrigation and raising irrigation efficiency, an effective way to improve soybean yield in water deficit areas is to identify the mechanism of drought tolerance and explore key genes to breed drought-tolerant soybean germplasm.

Homeodomain-leucine zipper (HD-Zip) protein is a class of transcription factor specific to higher plants (Schena and Davis, 1992). Its conserved domain is composed of a homeodomain (HD) and a closely linked leucine zipper (LZ). The HD-Zip proteins can be divided into four subfamilies: I, II, III, and IV. Studies on *Arabidopsis thaliana* (Peterson et al., 2013), rice (*Oryza sativa*) (Zhang et al., 2012), and sesame (*Sesamum indicum*) (Wei et al., 2019) have shown that HD-Zip I is mainly responsible for the regulation of plant growth and development, morphogenesis, and abiotic stress responses (Harris et al., 2011; Gong et al., 2019). For example, genes *AtHB6* and *AtHB7* were strongly induced under drought stress or exogenous abscisic acid (ABA) treatment and stomata were subsequently closed to adapt to these stresses (Perotti et al., 2017). Genes *AtHB7* and *AtHB12* acted as negative feedback regulation factors in the ABA signaling pathway, which influenced lateral root development under water-deficient conditions (Himmelbach et al., 2002; Romani et al., 2016). Expression of *MeHDZ14* was also upregulated under drought and exogenous ABA stress in cassava leaves and roots (Yu et al., 2017). Agalou et al. (2008) found that the expression of *Oshox22* was induced by polyethylene glycol (PEG)-simulated drought but that of *Oshox4*, which was specifically expressed in vascular bundles, was inhibited. In addition, *Oshox4* overexpression led to accelerated gibberellin (GA) metabolism, shortened internode, and prolonged the vegetative growth period in rice. This suggested that *Oshox4* was involved in the negative regulation of GA under drought stress (Zhou et al., 2015b). Overexpression of the *Helianthus annuus* HD-Zip homolog *HaHB4* in wheat increased the number of spikelets, tillers, and fertile florets, and improved grain yield under drought stress (González et al., 2019). Overexpression of *HaHB4* also improved drought tolerance in soybean by increasing xylem area and heat shock protein expression (Ribichich et al., 2020). The mechanisms of drought tolerance were found to be independent of traditional candidate genes such as *RD19* and *DREB1a* (Liu et al., 1998).

There are 36 members of the HD-Zip I transcription factor family in soybean (Chen et al., 2014), among which *GmHB13* was especially induced by water deficit in a drought-tolerant variety (EMBRAPA 48), while expression of *GmHB6* was inhibited in a drought-sensitive variety BR16 (Belamkar et al., 2014). Limited HD-Zip I genes were identified in previous studies. Gene *Gshdz4* (accession number: KHN 42008.1) was reported to participate in drought and salt tolerance regulation (Cao et al., 2017), while *GmHdz4* (Glyma11g06940) was a homologous gene of *Gshdz4* which had a 98.0% amino acid sequence similarity. Therefore, we speculate that *GmHdz4* may also be involved in drought stress response in soybean. The aims of this study were to (1) clone the coding sequence (CDS) of *GmHdz4*, analyze its phylogenetic relationship and the spatio-temporal expression pattern in response to drought stress, (2) analyze the subcellular localization and transcription activity of *GmHdz4*, (3) construct overexpression and CRISPR/cas9 vectors of *GmHdz4* to generate overexpression and knockout chimeric lines to study the function of *GmHdz4*, and (4) reveal the physiological and biochemical mechanisms of drought stress in overexpressing and gene-edited plants. These results may lay a theoretical foundation for further drought-tolerant soybean germplasm innovation.

Materials and methods

Plant materials and growth conditions

Soybean (*Glycine max* [L.] Merr.) cv. Tianlong No. 1 was used as the transgenic receptor in this experiment. The wild type and transgenic chimeric plants were grown in a temperature/light-controlled greenhouse at Zhejiang University, Zijingang Campus. All plants were grown under short-day conditions (light/dark of 10/14 h at 26/22°C). The roots, stems, unifoliolate leaves, flowers, and tender pods were taken at V1, R1, and R3 stages, for analysis of tissue-specific expression of *GmHdz4*. The PEG-simulated drought stress was imposed as follows: soybean seeds were germinated in a moist sand bed for 3 weeks. Uniform seedlings were selected and grown using half-strength Hoagland (Xu et al., 2017) solution with 15% PEG6000 (osmotic potential, $\Psi_\pi = -0.32$ MPa, pH 5.8) to simulate drought stress. The drought-stressed roots were sampled at 0, 3, 6, and 12 h; 1, 2, and 4 days to measure the relative expression of *GmHdz4*. Three biological replicates were used for each analysis. All samples were immediately frozen in liquid nitrogen and stored at −80°C for further analysis.

Sequence alignment and phylogenetic analysis

The sequences of HD-Zip I family members from *Arabidopsis*, rice, maize, tomato, sunflower, wild soybean, and soybean were screened using BLAST in Phytozome.[1] Multiple amino acid sequences were aligned using ClustalX 2.0 (Thompson et al., 1994) with default parameters. The phylogenetic tree was produced using MEGA 5.0 software (Tamura et al., 2011) with the neighbor-joining (NJ) method, and the bootstrap value was 1,000 times for each node to test branch reliability.

Total RNA extraction and cDNA synthesis

The CDS and genome sequence of *GmHdz4* (Glyma11g06940) were obtained and aligned from NCBI,[2] TAIR,[3] and Phytozome databases. Total RNA was extracted according to the modified Trizol method (Bekesiova et al., 1999), and RNA integrity was verified by 2% agarose gel electrophoresis. First-strand cDNA was synthesized using a reverse transcription kit (Vazyme, Nanjing, China). Three independent biological replicates were used for RNA extraction and subsequent cDNA synthesis. The CDS of *GmHdz4* was amplified by gene-specific primers GmHdz4_CDS_F (5′-ATGAATCATCGACCACCTTTCC-3′) and GmHdz4_CDS_R (5′-CAGATTAATCCATTCCATGCCG-3′) using Taq Master Mix (Vazyme, Nanjing, China). The target PCR products were cut and recycled with a gel extraction kit (Sangon Biotech, Shanghai, China) after separation by 2% agarose gel electrophoresis. The product was cloned into pUCI-T vector (Sangon Biotech, Shanghai, China) then transformed to *Escherichia coli* DH5α competent cells by the freeze–thaw method (Knopf, 1976). The selected single colonies were sequenced and stored at −20°C for subsequent experiments.

Real-time fluorescent quantitative PCR (qRT-PCR) analysis

The qRT-PCR was performed using ChamQ SYBR qPCR Master Mix (Vazyme, Nanjing, China), according to the manufacturer's instruction. Specific primers designed for *GmHdz4* were GmHdz4Q_F (5′-GACCACCTTTCCAAGACCACA-3′) and GmHdz4Q_R (5′-AGCTCCATTGCCAGCCTATC-3′). The normalizing reference gene was *Actine11* (Xue et al., 2012). Abnormal CT values ($>0.2+CT_{median}$) were eliminated, and relative expression levels were calculated according to the $2^{-\Delta\Delta CT}$ method (Livak and Schmittgen, 2001). All samples were selected randomly under the same greenhouse conditions. Three technical replicates for each biological replicate were used in qRT-PCR analysis.

Plasmid construction

For overexpression plant transformation, the full-length CDS of *GmHdz4* isolated from soybean root tissue was amplified by PCR using premiers: GmHdz4-plus-F (5′-CAGTGAATT CCTGGACGTCCGTACGTTCGA-3′) and GmHdz4-plus-R (5′-CGATGAATTCCGGCGCAAAAATCACCAGTC-3′). The amplification products were inserted into the pTF102 vector *EcoRI* site to generate pTF102–*GmHdz4* vector, containing a *bar* gene under the control of the CaMV35S promoter for the herbicide-based plant selection (Supplementary Figure S2A). For gene-editing plant transformation, the target sequence of *GmHdz4* (Supplementary Figure S2C) was predicted by CRISPR-P[4] (Lei et al., 2014) and the sgRNA sequence was 5′-GTCCGAAAGAAAGGATAGGC-3′. Specific designed oligo probes were 5′-GGGTTGGTCCGAAAGAAAGGATAGGC-3′ and 5′-AAACGTCCGAAAGAAAGGATAGGCCA-3′. The amplified dimer was inserted into the pBGK041 vector according to the manufacturer's instructions to generate gene-editing pBGK041–*GmHdz4* vector. The pBGK041 vector (Biogle, Jiangsu) contained Cas9 cassettes, driven by S35, and the inserted sgRNA was driven by GmU6 promoters (Supplementary Figure S2D). The plasmids of pTF102–*GmHdz4* recombinant vector and pBGK041–*GmHdz4* gene-editing vector were transformed into *Agrobacterium rhizogenes* K599 by the freeze–thaw method (Knopf, 1976), respectively.

Subcellular localization and transcriptional activation analysis

For subcellular localization, the recombinant vector pCAMBIA1302–*GmHdz4* expressing the *GmHdz4*–GFP fusion protein and the positive marker vector pBWD-NLSmKAT expressing a nuclear-localized red fluorescent protein (Zoonbio, Nanjing, China) were transferred into *Agrobacterium tumefaciens* GV3101 by electroporation, respectively. After incubating at 30°C for 12 h, single colonies were picked out and cultured at 170 rpm/min for 1 h. A needle-free syringe was used to inject the resuspended bacterial solution under the epidermis of *Nicotiana tabacum* leaves, and this was marked. The *GmHdz4*–GFP fusion protein was examined 2 days after culture under weak light using a confocal laser scanning microscope (FV1000; Olympus, Japan). This experiment was repeated three times independently.

For transcriptional activation analysis, the experiment was based on the GAL4 yeast two-hybrid (Y2H) system (Chien et al., 1991), and the *GmHdz4* gene was introduced into pGBKT7 vector. Plasmids pGBKT7-Lam and pGADT7-T were co-transformed

1 http://www.phytozome.net/index.php/
2 http://www.ncbi.nlm.nih.gov/
3 http://www.arabidopsis.org/
4 http://cbi.hzau.edu.cn/crispr/

into Y2HGold yeast as a negative control, and plasmids pGBKT7-53 and pGADT7-T were used as a positive control. Transcription activation activity was analyzed following the user manual of Takara Bio USA, Inc.

Hairy roots system generation and identification

Healthy and vigorous seeds of Tianlong No. 1 were selected, sterilized by chlorine gas, and germinated in sterile vermiculite for 5 days. After the hypocotyl grew about 2–3 cm length, 200 μl resuspended *A. rhizogenes* solution (OD600 ≈ 0.6) carrying recombinant plasmid was injected into each hypocotyl about 2 mm below the cotyledon node according to Kereszt et al. (2007). The *A. rhizogenes* without the target gene was used as a control. The photoperiod was controlled for 6 h of light and18 h of dark, temperature was maintained at 28°C, and relative humidity was about 70%. The hypocotyl and primary roots were excised when enough hairy roots were induced 1 week after injection. The chimeric seedlings were transplanted into half-strength Hoagland nutrient solution. The chimeric seedlings containing pTF102–*GmHdz4* and pBGK041–*GmHdz4* vectors were labeled *GmHdz4-oe* and *gmhdz4*, respectively, and seedlings without the target gene plasmids were labeled non-transgenic (NT).

The hairy roots of *GmHdz4-oe* chimeric seedlings were verified by PCR amplification using specific primers GmHdz4_CDS, which were mentioned above. The hairy roots of *gmhdz4* chimeric seedlings were verified by PCR using *Cas9* gene specific primers (5′-ACAAGGTGAGCGTTGTTTAT-3′ and 5′-CATGATGGTGGTATGTTTCG-3′). And the target site on the *GmHdz4* CDS of each *gmhdz4* hairy root was sequenced. The hairy roots from the independent chimera seedling line were collected and mixed to detect the expression of target sequence on *GmHdz4* CDS. Three independent transgenic lines as biological replicates were performed.

Identification of *GmHdz4* function by PEG-simulated drought stress

The positive overexpressed and gene-editing chimeric soybean seedlings were transplanted into half-strength Hoagland solution containing 15% PEG6000 (pH 5.8) for drought stress treatment. The phenotypic traits and physiological indexes were determined at 0, 6, and 12 h; 1, 2, 4, and 8 days after PEG treatment. Fresh root samples were immediately frozen in liquid nitrogen and stored at −80°C for further experiments. The following experiments had three biological replicates at least.

Biomass determination

After 8 days of PEG treatment, the fresh shoots and roots were dried for 3 h at 105°C and then for another 24 h at 80 ± 1.5°C to obtain a constant dry weight for the measurement for dry biomass. The ratios of root mass to shoot mass were then calculated.

Root system architecture analysis

The chimeric seedlings were cleaned in nutrient solution 8 days after PEG treatment. The hairy roots were scanned by Epson Perfection V850 Pro. The root system architecture was analyzed using WinRHIZO software (Win et al., 2016).

Hairy root activity determination

The root activity of each sample was measured by improved 2,3,5-triphenyl tetrazolium chloride (TTC) method (Higa et al., 2010). A microplate reader was used to detect the OD value of formazan at a wavelength of 485 nm. The TTC-reducing activity was converted to represent the root activity.

Osmoprotectant estimation

The content of free proline was determined according to Bates et al. (1973) and of soluble sugar according to Bailey (1958). The absorbance was measured using a microplate reader (Synergy™, BioTek).

Determination of hydrogen peroxide (H_2O_2), superoxide anion radical (O^{2-}), and malondialdehyde (MDA) contents and antioxidant enzyme activities

The H_2O_2 and O^{2-} contents in hairy roots were measured according to Alexieva et al. (2001) using reactive oxygen species (ROS) content reagent kits (Solarbio, Beijing). The enzyme activities of superoxide dismutase (SOD, EC1.15.1.1), peroxidase (POD, EC 1.11.1.7), and catalase (CAT, EC 1.11.1.6) were measured by NBT illumination, guaiacol reaction, and oxidation–reduction methods, respectively (Wang et al., 2021). The MDA was measured according to Heath and Packer (1968) and Tang et al. (2013).

Statistical analysis

All data are presented as the mean values with the standard deviation of three replications in figures. Statistical analysis was performed using EXCEL 2019 (Microsoft Inc., Redmond, WA, United States) and SPSS 20 (SPSS Inc., Chicago, IL, United States). Significant differences were determined using one-way ANOVA and Duncan's multiple range tests. The differences between treatments were considered significant at $p < 0.05$. Prism7 (GraphPad Inc., San Diego, CA, United States) was used to visualize the data.

Results

GmHdz4 cloning and phylogenetic analysis

The CDS sequence of *GmHdz4* (Glyma11g06940) was amplified by high-fidelity PCR using cDNA from total RNA of soybean cultivar Tianlong No. 1 as a template. The PCR product was cloned into pUCI-T vector to obtain pUCI–*GmHd4* (Supplementary Figure S1) and sequenced. The sequencing result was completely consistent with the NCBI database. Gene *GmHdz4* contained a 648-bp open reading frame encoding a protein of 215 amino acids; the molecular weight of GmHdz4 protein was 25.11 kDa, and the isoelectric point was 6.48. Sequence analyses revealed that most of the GmHdz4 amino acid sequence formed hydrophilic regions except for the aa10–24, aa64–72, and aa88–102, and nine out of 12 sites that may undergo phosphorylation modification were located in these regions. The results of multiple sequence alignment showed that GmHdz4 had a highly conserved HD compared with other HD-Zip I transcription factors, which was related with drought stress in *Arabidopsis*, rice, maize, tomato, wild soybean, and sunflower. The LZ domain was also relatively conserved, with only individual leucine sites mutated to threonine or valine (Figure 1A). The 3D model of GmHdz4 protein predicted by SWISS MODEL Workspace showed that the HD domain folded into three α-helices. This spatial conformation provided the conditions to recognize and bind the promoter elements of the target genes, and is consistent with the typical structural features of HD-Zip I transcription factors.

Phylogenetic analysis was performed among HD-Zip I subfamily members in *Arabidopsis*, rice, maize, tomato, wild soybean, and soybean. The clades in the tree were labeled according to previous studies in *Arabidopsis* and rice. The HD-Zip I subfamily members were clustered into eight subclasses: α, β1, ζ, γ, ε, β2, δ, and φ (Figure 1B). The distribution showed an obvious species preference. Six species contained HD-Zip I protein clades α, β1, β2, γ, and δ while only dicotyledons such as *Arabidopsis*, tomato, and soybean included clades ζ, ε, and φ. The results suggested that the main characteristics of this HD-Zip I subfamily were generated before the dicot–monocot split and differentiated continually after the split. Gene *GmHdz4* was located in clade δ, and was closely related to drought stress-related HD-Zip I genes such as *AtHB12*, *Oshox12*, and *Gshdz4*.

GmHdz4 spatio-temporal and tissue-specific expression

The relative expressions of *GmHdz4* in roots, stems, leaves, flowers, and pods significantly differed with the main expression in flowers and roots (Figure 2A). Expression of *GmHdz4* in roots was about 60-fold higher than that in leaves, and 1.3-fold higher than that in flowers. The relative expression of *GmHdz4* in roots showed a stepwise significant decrease within 12 h after 15% PEG6000 ($\Psi_\pi = -0.32$ MPa) simulated drought stress (Figure 2B). The relative expression of *GmHdz4* was reduced by 47.0% at 6 h after drought stress, and dropped to about 18% by 12 h after drought stress. Later, *GmHdz4* expression decreased slightly and basically remained at 16% before treatment. The results suggested that *GmHdz4* expression was inhibited by drought in soybean roots.

GmHdz4 subcellular localization and transcriptional activity

Gene *GmHdz4* might target the nucleus according to its amino acid sequence, which contained an NLS sequence at the region of aa35–60. The fluorescence signal of *GmHdz4* was only detected in the nucleus when tobacco cells were injected with a 35 s::*GmHdz4*–m*GFP* fusion construct and the NLS Red Marker (Figure 3B). However, the GFP signal was found throughout the cell using 35 s::mGFP as a control (Figure 3A).

The pGBKT7–*Gmhdz4* recombination vector was delivered into yeast strain Y2HGold to identify the transcriptional activation activity of *Gmhdz4* (Figure 4A). The interaction between pGBKT7-Lam and pGADT7-T was the negative control, while the interaction between pGBKT7-p53 and pGADT7-T was the positive control. Yeast cells carrying the pGBKT7 empty plasmid and the negative control could not grow on SD/Trp-/His−/Ade- medium (Figure 4B); however, yeast cells carrying pGBKT7–*GmHdz4* and the positive control grew well. This showed that the fusion expression of GmHdz4 and GAL4 DNA-binding domain could activate reporter genes *ADE2* and *HIS3*. Meanwhile, pGBKT7–*GmHdz4* also showed high galactosidase activity in the *LacZ* assay. The results indicated that *GmHdz4* regulated transcription activities in the nucleus, consistent with two basic characteristics of transcription factors.

The *gmhdz4* mutant were more tolerant to drought stress

The *A. rhizogenes*-mediated transformation system was used to generate *GmHdz4* overexpression and gene-editing chimeric soybean in order to explore *GmHdz4* function. The fragments of *GmHdz4* CDS with correct size could be amplified from most hairy roots of the three random selected *GmHdz4*-oe independent lines (Supplementary Figure S2B), that meant most individual hairy roots of *GmHdz4*-oe lines were successfully transformed. Similarly, majority hairy roots of *gmhdz4* lines have *Cas9* gene sequence (Supplementary Figure S2E), and there were three mutation types including a single base deletion on the 256 bp site, a single base insertion between the 256 bp site and the 257 bp site, and a four bases deletion of 254 bp to 257 bp (Supplementary Figure S2F). However, the target site of some transformed hairy roots were not edited successfully. In

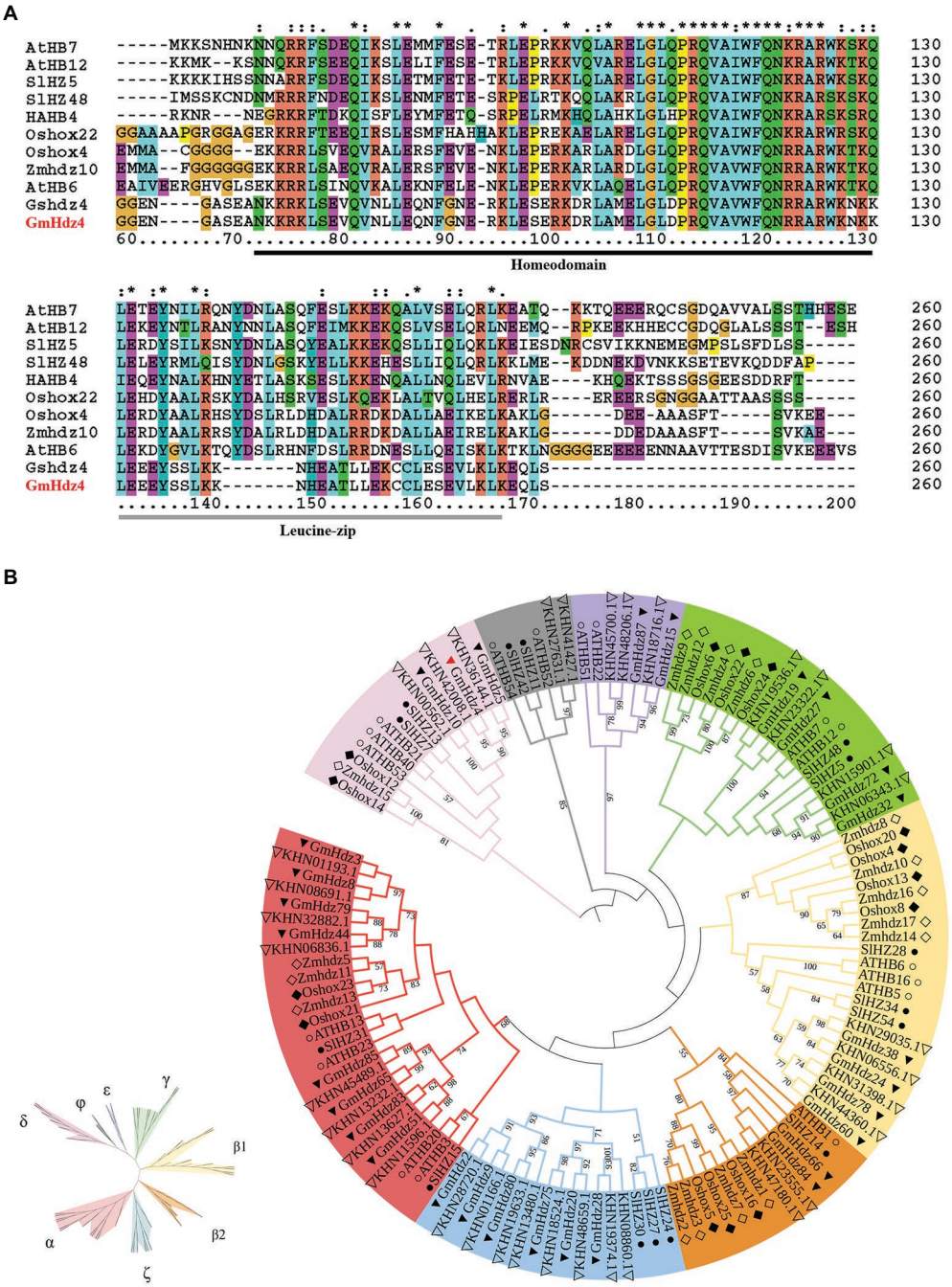


FIGURE 1
Sequence alignment and phylogenetic analysis. **(A)** Multiple sequence alignment for GmHdz4 and other drought stress-related HD-Zip I proteins. HD and LZ domains are underlined by black and gray, respectively. The corresponding IDs of Oshox22, Oshox4, AtHB7, AtHB12, AtHB6, Gshdz4, GmHdz4, HAHB4, Zmhdz10, SlHZ48, and SlHZ5, are Q7XUJ5.2, Q6K498.1, P46897.2, Q9M276.1, P46668.1, AOG74801, Glyma11g06940, XP_022022563, AFT92045, XP_004245456, and XP_004230017, respectively. **(B)** Phylogenetic analysis of HD-Zip I transcription factors from *Arabidopsis*, rice, maize, tomato, soybean, and wild soybean. The phylogenetic tree was built using NJ method in MEGA. Bootstrap support is indicated on the branches. Genes from each of the species are marked with different symbols: *Arabidopsis* (○), rice (■), maize (□), soybean (▼), wild soybean (▽), and tomato (●).

addition, the relative expression of *GmHdz4* in *GmHdz4*-oe hairy roots was 5.1–8.8-fold higher than that for NT, whereas *GmHdz4* expression in *gmhdz4* hairy roots was 2.7–5.3-fold lower than that of NT (Supplementary Figure S2G).

The phenotypes obviously differed among NT, *GmHdz4-oe*, and *gmhdz4* at 8 days after 15% PEG6000 simulated drought stress. The leaves were green and vigorous in NT (Figure 5A1) and *gmhdz4* (Figure 5B1) before PEG treatment, and hairy roots

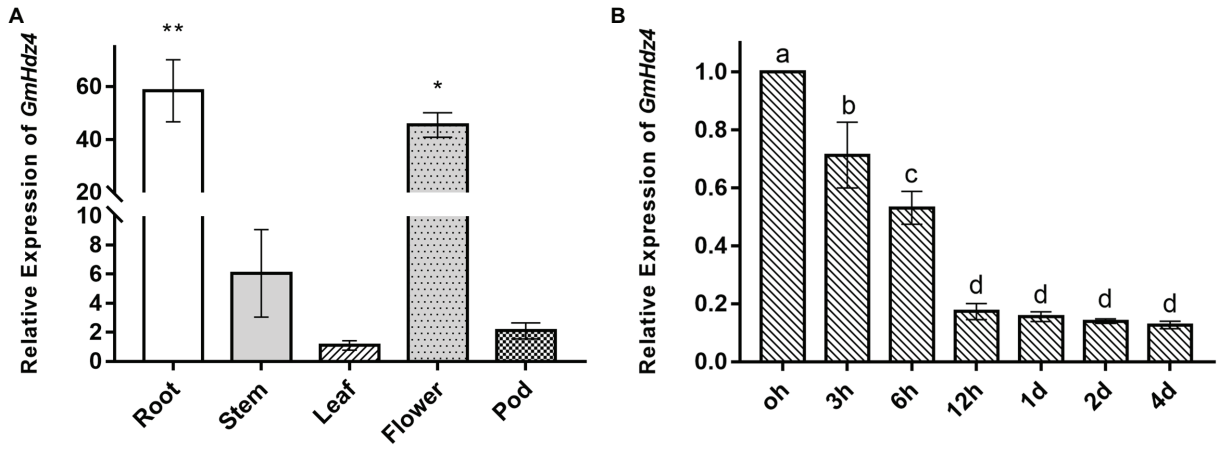


FIGURE 2
Tissue-specific and spatio-temporal expression of *GmHdz4*. Expression pattern of *GmHdz4* in various tissues in soybean **(A)** and PEG-induced expression pattern of *GmHdz4* in root **(B)**. Significant differences are indicated by * and ** for $p<0.05$ and $p<0.01$, respectively, according to Duncan's test in panel **A**; values with different letters (a–d) significantly differ at $p<0.05$ according to Duncan's test in panel **B**.

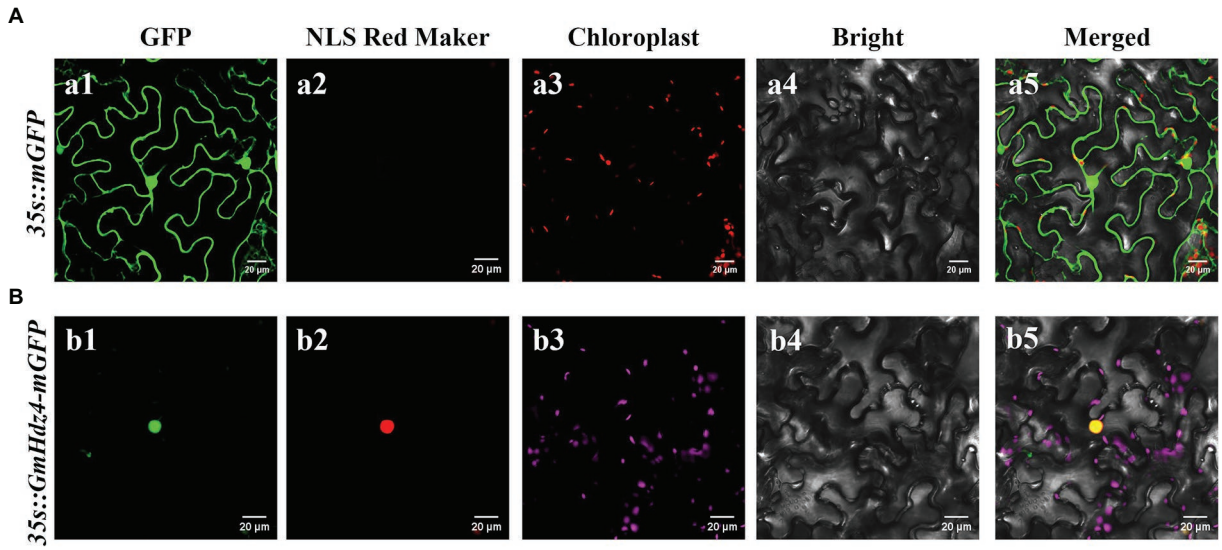


FIGURE 3
Subcellular localization analysis of *GmHdz4*. The fusion plasmid (35S::GmHdz4–GFP), the negative control plasmid (35S::mGFP), and pBWD-NLSmKAT expressing an NLS Red Marker protein were transiently transformed into tobacco epidermal cells. Images were taken in the dark field for green fluorescence (a1, b1), red fluorescence (a2, b2), and chloroplast fluorescence (a3, b3), while the outline of cells (a4, b4) and merged image (a5, b5) were photographed in a bright field. Microscopy detections of 35S::mGFP were displayed in penal **(A)**, and the detections of 35S::GmHdz4–mGFP were displayed in penal **(B)**. Bars represent 20μm.

developed normally (Figures 5A2,B2). However, leaves in *GmHdz4-oe* (Figures 5C1,C2) were etiolated and short, and hairy roots were stunted. Eight days after PEG treatment, most leaves in *GmHdz4-oe* were wilted and yellow, and the first trifoliolate leaf was dried and shed (Figures 5F1,F2). The dry weight of aboveground parts showed no significant difference between *gmhdz4* and NT after PEG treatment, while that of *GmHdz4-oe* was relatively low (Figure 6A). Eight days after PEG treatment, *gmhdz4* had the greatest root dry weight among the three chimeric lines with an average of 2.52 g/plant, which increased 411.2% before treatment. Emphatically, root dry weight in *GmHdz4-oe* was clearly the lowest, with less than one-half of that of *gmhdz4* and NT. Additionally, the root–shoot ratio in descending order was *gmhdz4*, NT, and *GmHdz4-oe* (Figure 6B).

The hairy root system in *GmHdz4-oe* was much weaker than that of NT (Figures 5D1,D2), while the root system in *gmhdz4* developed well (Figures 5E1,E2). Analysis of root system architecture showed that the total root length (Figure 5G),

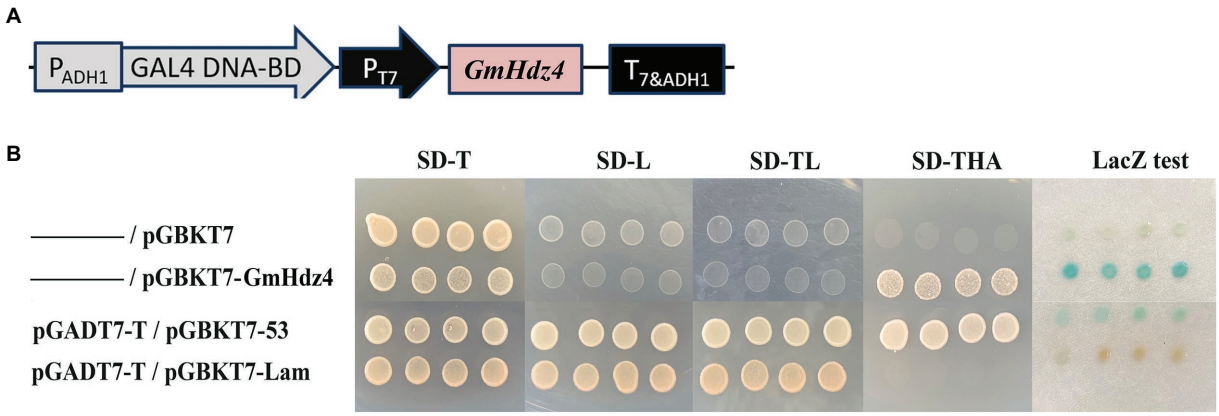


FIGURE 4
Transcription activity analysis of *GmHdz4*. **(A)** The construct of pGBKT7–GmHdz4; **(B)** ADE2 and HIS3 reporter assay, and galactosidase (LacZ) assay. pGADT7-T/pGBKT7-53 and pGADT7-T/pGBKT7-Lam vector groups were used as positive and negative controls, respectively.

superficial area (Figure 5H), and tip number (Figure 5J) in *gmhdz4* were significantly higher than that of *GmHdz4-oe,* but not average diameter (Figure 5I) after PEG treatment. The total root length in *gmhdz4* increased from 240 cm (before PEG treatment) to 2,100 cm (after PEG treatment), an increase of 775%, which was 5.8 times that of NT. The root surface area in *gmhdz4* also increased from 55.97 to 302.33 cm^2 and the number of root tips in *gmhdz4* increased from about 900 to 2,300, with a significantly higher increase than that of NT and *GmHdz4*-oe. These results suggested that gene editing of *GmHdz4* promoted the root morphogenesis under PEG treatment and enhanced drought tolerance in soybeans.

Accumulation of osmoprotectants, and hairy root activity enhanced in *gmhdz4* mutant

There was no significant difference in soluble sugar and free-proline contents among hairy roots of *GmHdz4-oe*, *gmhdz4*, and NT lines before PEG treatment (Figure 7). With the prolongation of PEG-simulated drought stress, the soluble sugar and free-proline contents increased gradually among the three different lines (Figures 7A,B). However, the osmoprotectants in *gmhdz4* increased significantly more than in *GmHdz4-oe* and NT. Eight days after PEG treatment, the soluble sugar content in *gmhdz4* was 1.76 and 1.84 times higher than that of NT and *GmHdz4-oe*, respectively (Figure 7A); correspondingly, the proline content was 1.48 and 1.63 times higher (Figure 7B). This suggested that *gmhdz4* obtained stronger osmotic accumulation ability under drought stress. Additionally, the root activity of *gmhdz4* and NT showed no significant difference, while that of *GmHdz4-oe* significantly decreased after PEG treatment. The results suggested that gene editing of *GmHdz4* maintained a high osmotic potential in hairy roots to ensure lower cellular water potential under drought stress, so that roots of *gmhdz4* maintained normal physiological activity to cope with drought stress.

The *gmhdz4* mutant promotes ROS scavenging capacity under drought stress

Accumulation of ROS increased gradually with continuing PEG treatment in soybean hairy roots. There was no significant difference in H_2O_2 contents in the hairy roots of NT and *gmhdz4* in the first 3 days after PEG treatment. However, the O^{2-} content in *GmHdz4-oe* was significantly higher than that of NT and *gmhdz4*. Subsequently, H_2O_2 accumulated rapidly in *GmHdz4-oe* chimeric lines (Figure 8A). The differences in O^{2-} contents between *GmHdz4-oe* and the other two lines reached a maximum of about 2.1 times at 4 days after PEG treatment (Figure 8B). Eight days after PEG treatment, H_2O_2 content in *gmhdz4* was only 12.0 μmol/g and was the lowest, compared with *GmHdz4-oe* and NT. Correspondingly, the MDA content was also significantly lower in *gmhdz4* chimeric lines (Figure 8C).

The antioxidase activities of hairy roots after PEG treatment are shown in Figures 8D–F. The CAT and SOD enzyme activities initially increased and then declined within 8 days after PEG treatment (Figures 8D,E). The CAT activity in *gmhdz4* and NT reached a maximum at 6 and 3 h after PEG treatment, respectively. The CAT activity in *gmhdz4* was higher than that of NT, while *GmHdz4-oe* maintained the lowest CAT activity during the PEG treatment (Figure 8D). The SOD activity in NT and *gmhdz4* was significantly higher than that of *GmHdz4-oe* from 6 h to 4 days after PEG treatment, with a peak at 12 h (Figure 8E). In addition, POD activity increased with extension of PEG treatment. The POD activity in *gmhdz4* was significantly higher than that of NT and *GmHdz4-oe* from 1 days after PEG treatment, and POD activity in NT was also higher than that of *GmHdz4-oe* during 4–8 days after PEG treatment (Figure 8F). The results suggested that

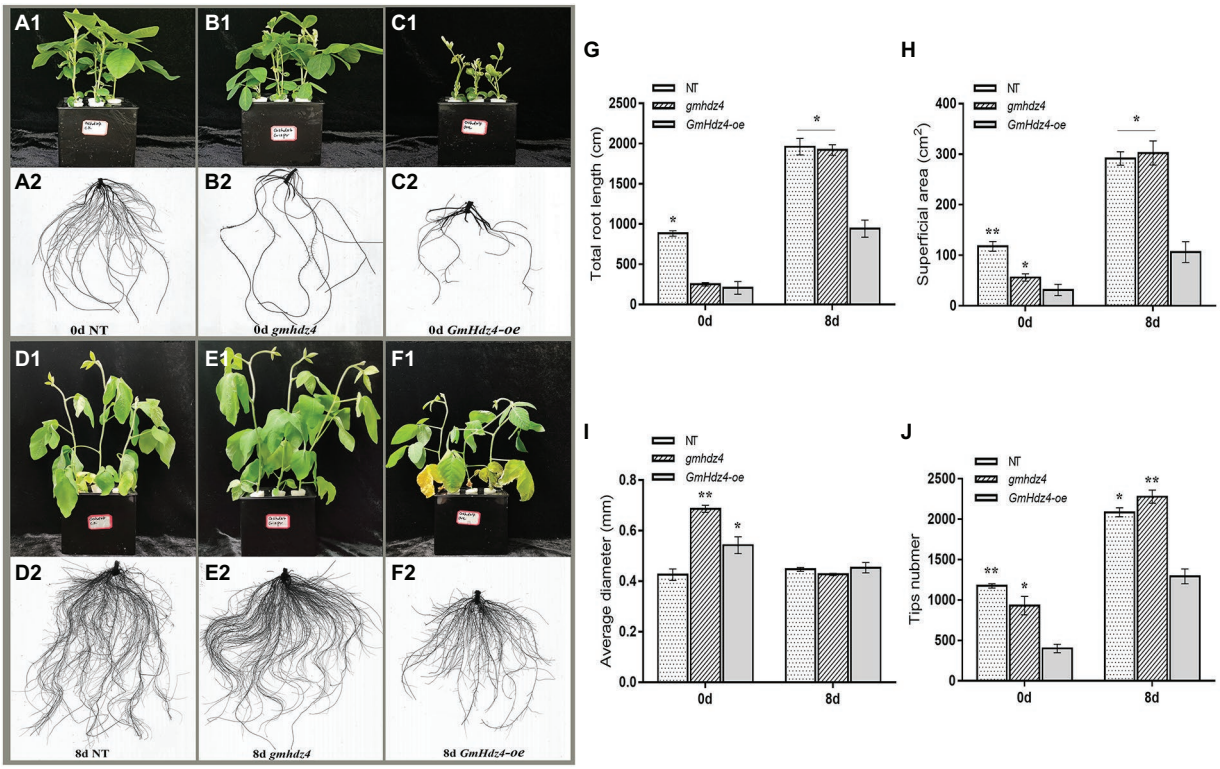


FIGURE 5
The phenotype and root system architecture among NT, *gmhdz4* chimeric lines, and *GmHdz4-oe* chimeric lines. Phenotypic comparison of transgenic hairy roots chimera and NT soybeans before and after PEG treatment **(A1–F2)**. The root system architecture analysis of total root length **(G)**, superficial area **(H)**, average diameter **(I)**, and tip numbers **(J)**. NT, non-transgenic soybeans; *gmhdz4*, gene-editing chimeric line; *GmHdz4-oe*, overexpression *GmHdz4* chimeric line. At least three biological replicates were performed, and the data before (0d) and after (8days) treatment were statistically analyzed, respectively. Significant differences are indicated by * and ** for $p<0.05$ and $p<0.01$, respectively, according to Duncan's test.

gmhdz4 created by CRISPR/Cas9 could stimulate the activities of antioxidases in soybean hairy roots under drought stress, and was beneficial to maintain the redox balance of the membrane system.

Discussion

The regulation of abiotic stress response by transcription factors is a hot topic in plant research. Most of the reported transcription factors associated with drought resistance in soybean are concentrated in the MYB, WRKY, bZIP, bHLH, and NAC families, accounting for about 63% of the total (Chai et al., 2015; Khan et al., 2018). In recent years, studies on *Arabidopsis*, rice, maize, and tomato showed that a plant-specific transcription factor, HD-Zip, was also involved in the response to abiotic stress. It was documented that 75% of HD-Zip genes in sesame were associated with drought and salt stress (Wei et al., 2019), but few studies in soybean were reported. In the present study, a novel HD-Zip I subfamily gene, *GmHdz4*, was cloned from the cDNA library of soybean cultivar Tianlong No. 1. It encodes a typical HD-Zip I protein which contains a conserved HD and a closely linked LZ domain (Ariel et al., 2007). The subcellular localization (Figure 3) and yeast hybridization assay (Figure 4) showed that *GmHdz4* had the function of nuclear localization and transcription activation. Phylogenetic analysis (Figure 1B) showed that *GmHdz4* was clustered in clade δ with other drought-tolerant HD-Zip I genes such as *AtHB7*, *SlHZ48*, and *SlHZ5* (Jiang, 2017). Compared with rice, maize, and other gramineous crops, soybean HD-Zip I members were more numerous and most of them had paralogous genes. Our study confirmed that soybean underwent two duplication events and genome expansion in a species-specific manner after mono–dicot differentiation (Kong et al., 2007; Jin et al., 2017). This approach is one of the main evolutionary mechanisms for generating new genes that help plants adapt to environmental stresses such as drought (Skirycz and Inze, 2010).

We found that *GmHdz4* was expressed in various organs in soybean, and notably its expression level was significantly higher in roots and flowers (Figure 2A). Whereas, Belamkar et al. (2014) found that *GmHdz4* homologs, *GmHdz5* and *GmHdz10*, were only expressed in flowers. Transcriptome studies showed that *GmHdz38* was highly expressed in the whole plant; *GmHdz24*, *GmHdz60*, and *GmHdz84* were mainly expressed in roots and flowers; and *GmHdz66* was only expressed in roots (Libault et al.,

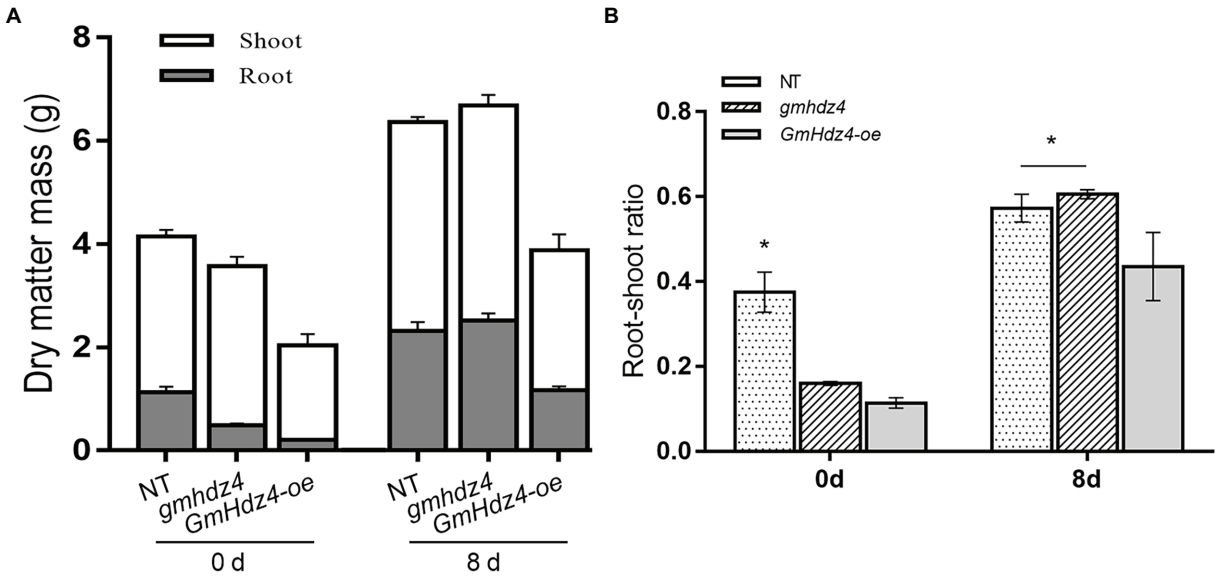


FIGURE 6
The dry matter mass **(A)** and root–shoot ratio **(B)** of each line before and after PEG treatment. Significant differences are indicated by * for $p<0.05$, according to Duncan's test.

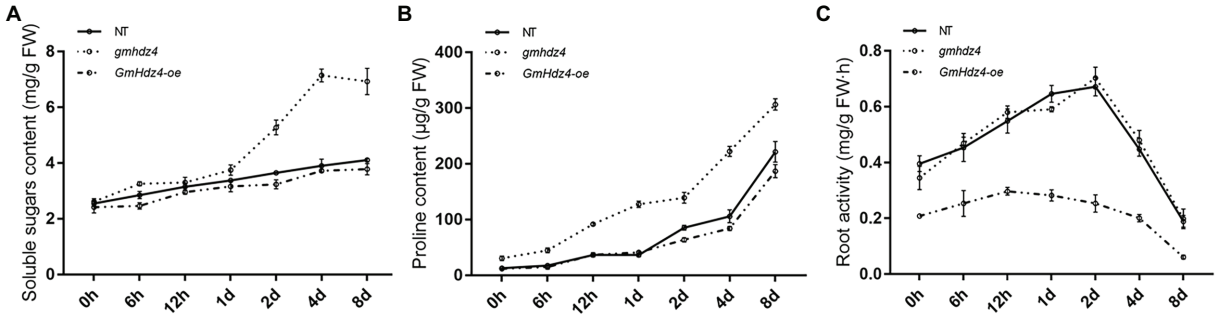


FIGURE 7
Soluble sugar content **(A)**, proline content **(B)**, and root activity **(C)** after PEG treatment. The straight line, dotted line, and dash-dotted line represent non-transgenic soybeans (NT), *gmhdz4* chimeric line, and *GmHdz4-oe* line, respectively.

2010a, 2010b; Belamkar et al., 2014). The complexity role of expression in the HD-Zip I family determines their diversity of gene functions. Expressions of *GmHdz19* and *GmHdz27* increased under drought stress, while those of *GmHdz24*, *GmHdz84*, and *GmHdz66* were significantly downregulated (Chen et al., 2014). Overexpression of *Zmhdz10* improved drought and salt tolerance in transgenic maize by regulating the ABA signaling pathway (Zhao et al., 2014). Furthermore, expression levels of *ATHB7* and *ATHB12* in *Arabidopsis* seedlings were upregulated 12–25 times after hydropenia or exogenous ABA treatment (Söderman et al., 1996; Lee et al., 2001; Valdes et al., 2012). Expressions of *ATHB40*, *ATHB21*, and *ATHB53*, which are orthologs of *GmHdz4*, were also upregulated by at least twice (Henriksson et al., 2005). We found that *GmHdz4* expression decreased by about 82% at 12 h after PEG-simulated drought stress (Figure 2B), with a similar response pattern to root-specifically expressed gene *GmHdz66* (Chen et al., 2014). The root system is the most important organ of plants in response to drought signals. Expression of *GmHdz4* was suppressed in roots by drought, suggesting that this transcription factor gene may function in soybean roots in response to drought stress.

The plant root system architecture is plastic and dynamic. Plants make their root systems stronger and more developed in order to absorb water. The more lateral roots formed and the wider they are distributed, the more drought resistant is the plant (Battisti and Sentelhas, 2017). In general, the root system is the first organ to sense changes in soil water content, when plants suffer water deficit and produce a large number of root signals for

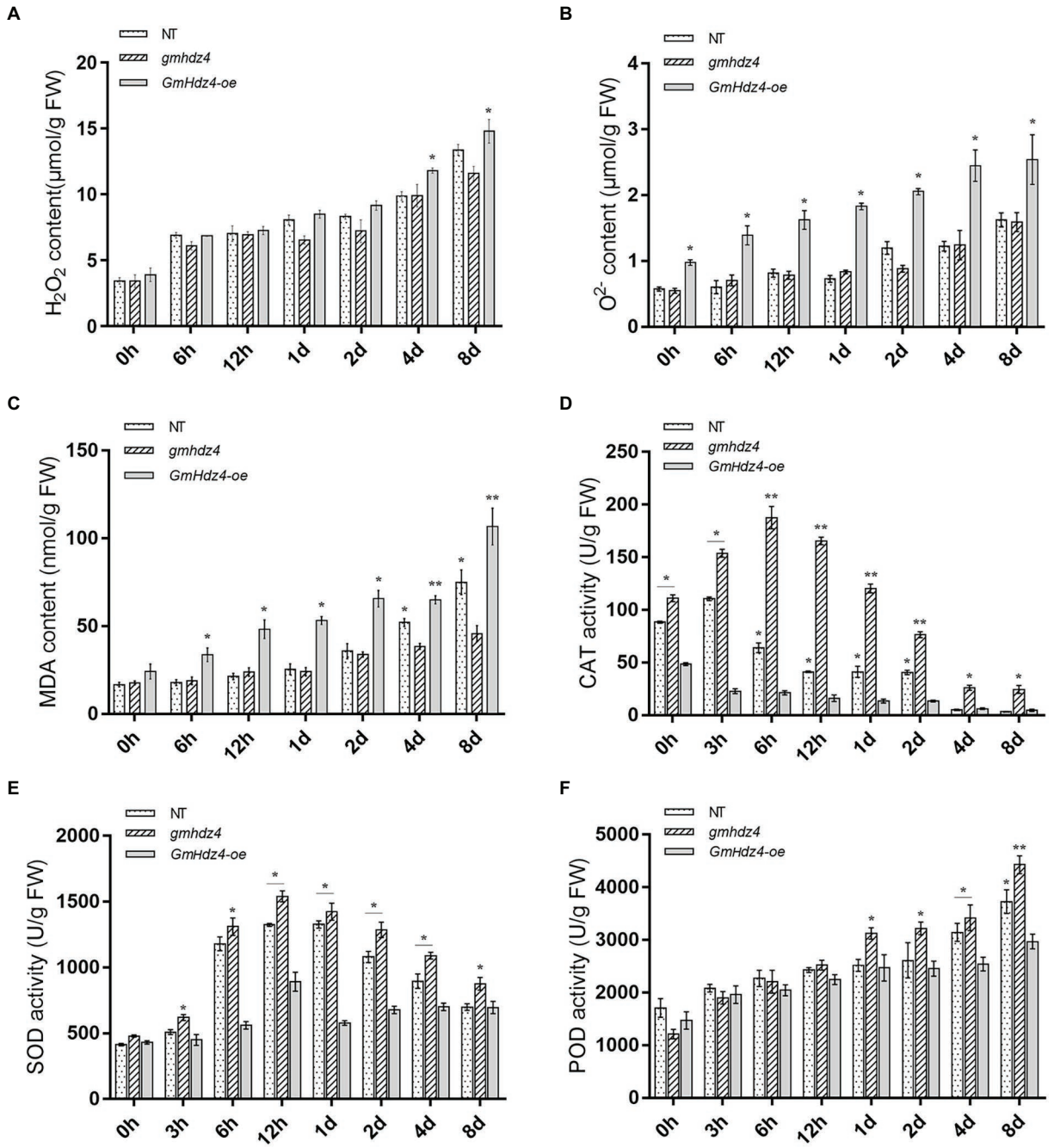


FIGURE 8
Knockout of *GmHdz4* promotes ROS scavenging in response to drought stress. Contents of H_2O_2 **(A)**, O^{2-} **(B)**, and malondialdehyde (MDA) **(C)**, and activities of catalase (CAT) **(D)**, superoxide dismutase (SOD) **(E)**, and peroxidase (POD) **(F)** were tested to assess the antioxidation systems under drought stress. Significant differences are indicated by * and ** for $p<0.05$ and $p<0.01$, respectively, according to Duncan's test.

transport to the aboveground parts. Thus, plants can promote root growth and development by regulating the distribution of assimilated substance to avoid hydropenia in the early stage of drought stress (Gilbert et al., 2011; Hu and Xiong, 2014). However, severe drought can inhibit growth of the root system and affect the formation of final yield (Huang et al., 2014; Ye et al., 2018). In our study, *gmhdz4* chimeric plants generated by CRISPR/Cas9 promoted hairy root growth to some extent, while overexpression of *GmHdz4* chimeric plants inhibited the development of hairy roots under drought stress (Figures 5A1–F2). The root system architecture results suggested that *GmHdz4* negatively regulated the development of lateral roots, since the root surface area and root tip numbers of *gmhdz4* increased significantly (Figures 5G–J).

Among the HD-Zip I subfamily in *Arabidopsis*, only *AtHB7* and *AtHB12* were found to be related to lateral root development under water deficit conditions, and played a negative feedback regulation role in the ABA pathway (Romani et al., 2016). The roots of the *athb7/athb12* double mutant were shorter than the wild type (Ré et al., 2014). The *AtHB53* gene, a *GmHdz4* homolog expressed in the root apical meristem, was induced by hyperthermia and osmotic stress, and played an important role in auxin/cytokinin signaling pathways in roots (Son et al., 2005). A recent study by Perotti et al. (2021) showed that most of the HD-Zip members related to root development belonged to subfamilies III and IV. Gene *AtHDG11* was involved in the auxin signaling pathway, which regulated drought resistance, and root biomass increased significantly in overexpressing plants. Expression of *IAA28* in mutant *hdg11* was downregulated and exhibited a drought-sensitive root phenotype (Rogg et al., 2001; Nakamura et al., 2006). In addition, *AtHB10* acted downstream of MYBs and was a negative regulator of root hair formation (Wang et al., 2010). Smetana et al. (2019) found downregulated expression of *AtHB8*, *AtHB9*, and *AtHB15* after drought stress, and their functions for differentiation and recognition of xylem were observed in the apical mature zone of roots. Gene *MtHB1* was strongly expressed in root tips and regulated lateral root formation (Ariel et al., 2010). Wild soybean *GsHdz4* was highly similar to *GmHdz4*, and regulated alkaline and osmotic stresses through different pathways. This positively regulated HCO_3^--stress tolerance, but sensitivity to osmotic stress was aggravated (Cao et al., 2017). This is consistent with the root phenotype of the soybean line overexpressing *GmHdz4* in the present study. Overexpression of *GmHdz4* affected aboveground growth and biomass accumulation by suppressing differentiation and elongation of lateral roots (Figure 6), resulting in plants with diminished drought tolerance. However, the molecular basis of *GmHdz4* regulating root morphology needs further study.

In addition to affecting root system architecture, the physiological mechanism of *GmHdz4* reducing the drought tolerance of soybean was further explored. Overexpression of *GmHdz4* resulted in decreased osmotic regulation capacity, accumulation of proline and soluble sugar were blocked (Figures 7A,B), and oxidative damage in hairy roots was aggravated under drought stress (Figures 8A–C). Conversely, gene-editing *GmHdz4* alleviated these damages to some extent. Free proline and soluble sugars are the most common osmoregulation substances in plants (Liu and Zhu, 1997). The content of free proline in plants is very low under normal circumstances, but it accumulates rapidly under abiotic stress such as drought and is positively correlated with plant tolerance to stress (Gilmour et al., 2000; Du et al., 2020). Varieties with stronger osmotic regulation ability had less yield reduction under drought stress (Blum, 2017). The soybean osmotic regulation inhibited by *GmHdz4* was similar to that by *MtHB2*, which reduced proline synthesis and accumulation by inducing expression of a proline dehydrogenase gene *ProDH*, which led to adverse effects on drought tolerance (Song et al., 2012). In addition, proline acts as a molecular chaperone to stabilize protein structure and reduce oxidative damage to cells (Székely et al., 2008). This oxidative damage is a complication of plants suffering from drought stress, which is manifest in significant accumulation of ROS and plasma membrane oxidative damage marker, MDA (Mittler, 2002; Verslues et al., 2007; Sun et al., 2018). We found that the activities of antioxidases (e.g., CAT, SOD, and POD) in *gmhdz4* increased rapidly and rhythmically under drought stress (Figures 8D–F). It is crucial to reduce the content of H_2O_2 and O^{2-} and relieve the oxidative senescence of roots. In contrast, these antioxidases in hairy roots overexpressing *GmHdz4* were relatively sluggish in response to drought, and the ROS could not be scavenged promptly, leading to continuous accumulation of the end-product of membrane lipid oxidation. Stability of plasma membrane and maintenance of redox balance is critical to plant drought resistance. Transgenic tomato plants created by *SlHB2-RNAi* had significantly higher expression levels of *CAT1* and *APX1* than NT plants, and showed less membrane damage (Hu et al., 2017). This indicated that *SlHB2* played a negative regulatory role in response to drought and high salt stress. Our findings in this experiment were consistent with those of Hu et al. (2017). However, in plants with high expression of HD-Zip genes such as *ATHB12*-like, *Zmhdz10*, *EsHdzip1*, and *MdHB-7*, the root system was more developed and activity of antioxidant enzymes significantly higher compared to the wild type under drought or salt stress (Zhao et al., 2014, 2020; Zhou et al., 2015a; Wu et al., 2016). This also illustrates the complexity of HD-Zip transcription factors in regulating plant response to drought.

Soybean HD-Zip transcription factor *GmHdz4* was isolated and identified for the first time in this study. The *A. rhizogenes* transient transformation system was used to preliminarily verify *GmHdz4* function. The gene negatively regulated drought tolerance in soybean hairy roots by inhibiting lateral root differentiation and weakening osmotic regulation ability and ROS scavenging ability. Our study provides some theoretical basis for further studies on HD-Zip I genes involved in soybean drought tolerance, and indicates the feasibility of breeding new germplasm for drought-tolerant soybean by gene editing. Due to the complex and variable regulation of transcription factors on abiotic stress, the signaling pathway of *GmHdz4* involved in drought response and the specific regulatory mechanism related to root development need to be studied in the future.

Data availability statement

The datasets presented in this study can be found in online repositories. The names of the repository/repositories and accession number(s) can be found in the article/Supplementary material.

Author contributions

XZ and GT proposed cloning of and investigating *GmHdz4* gene function under drought conditions. XZ cloned this gene, implemented the molecular and hydroponic work, analyzed the data, and wrote the manuscript. GT, FI, and WZ contributed substantially to the manuscript writing and revisions. WH, YS, JL, and LL participated in the phenotyping identification and root scanning. XC provided plant materials and contributed to paper revisions. All authors contributed to the article and approved the submitted version.

Funding

This work was supported by the Key Research Foundation of Science and Technology Department of Zhejiang Province (2021C02064-5-5), Hainan Provincial Joint Project of Sanya Yazhou Bay Science and Technology City (320LH033), Key R&D Projects of Zhejiang Province (2021C02057), and Collaborative Innovation Center for Modern Crop Production co-sponsored by Province and Ministry (CIC-MCP).

Acknowledgments

We thank International Science Editing (http://www.internationalscienceediting.com) for editing this manuscript.

Conflict of interest

The authors declare that the research was conducted in the absence of any commercial or financial relationships that could be construed as a potential conflict of interest.

Publisher's note

All claims expressed in this article are solely those of the authors and do not necessarily represent those of their affiliated organizations, or those of the publisher, the editors and the reviewers. Any product that may be evaluated in this article, or claim that may be made by its manufacturer, is not guaranteed or endorsed by the publisher.

Supplementary material

The Supplementary material for this article can be found online at: https://www.frontiersin.org/articles/10.3389/fpls.2022.988505/full#supplementary-material

SUPPLEMENTARY FIGURE S1
PCR amplification of *GmHdz4* M: DNA DL2000 marker; –, negative control; 1 and 2 represent amplification products using soybean total DNA and pUCI-GmHd4 as templates, respectively.

SUPPLEMENTARY FIGURE S2
Overexpression and targeted modification of the *GmHdz4* gene in the soybean hairy roots. **(A)** Schematic diagram of the pTF102–*GmHdz4* vector. The *GmHdz4* gene and *bar* gene were driven by the CaMV 35S promoter. **(B)** The *GmHdz4*-oe hairy root lines were identified by PCR amplification of the *GmHdz4* CDS. The length of the PCR product was 648 bp. **(C)** Schematic illustration of the sgRNA target sequence in the *GmHdz4* gene. The black rectangles represent exons, the black line represents the introns, and the red vertical bars represent the locations of the target sequence. **(D)** Schematic diagram of the pBGK041–*GmHdz4* vector. The Cas9 expression cassette was driven by the CaMV 35S promoter, and the sgRNA cassette was driven by the GmU6 promoter. **(E)** The *gmhdz4* hairy root lines were identified by PCR amplification of *Cas9* gene. The length of the PCR product was 502 bp. **(F)** Mutations induced by sgRNA in *GmHdz4*. The green letter represents the nucleotide insertion and the green dashes represent the deletions, and the labels on the left (*gmhdz4* L1–R1~ *gmhdz4* L3-R8) corresponds to each individual hairy root in panel **E**. M represents the DNA marker DL2000. Each individual hairy root on the chimera *GmHdz4-oe* Line 1~3 and *gmhdz4* Line 1~3 were examined. -, non-transgenic plant; +, positive control. **(G)** Relative expression of *GmHdz4* among transformed *GmHdz4-oe* chimeric lines, *gmhdz4* chimeric lines, and NT hairy roots. Significant differences are indicated by * and ** for $p<0.05$ and $p<0.01$, respectively, according to Duncan's test.

References

Agalou, A., Purwantomo, S., Overnas, E., Johannesson, H., Zhu, X., Estiati, A., et al. (2008). A genome-wide survey of HD-zip genes in rice and analysis of drought-responsive family members. *Plant Mol. Biol.* 66, 87–103. doi: 10.1007/s11103-007-9255-7

Alexieva, V., Sergiev, I., Mapelli, S., and Karanov, E. (2001). The effect of drought and ultraviolet radiation on growth and stress markers in pea and wheat. *Plant Cell Envi.* 24, 1337–1344. doi: 10.1046/j.1365-3040.2001.00778.x

Ariel, F. D., Diet, A., Crespi, M., and Chan, R. L. (2010). The LOB-like transcription factor MtLBD1 controls *Medicago truncatula* root architecture under salt stress. *Plant Signal. Behav.* 5, 1666–1668. doi: 10.4161/psb.5.12.14020

Ariel, F. D., Manavella, P. A., Dezar, C. A., and Chan, R. L. (2007). The true story of the HD-zip family. *Trends Plant Sci.* 12, 419–426. doi: 10.1016/j.tplants.2007.08.003

Bailey, R. W. (1958). The reaction of pentoses with anthrone. *Biochem. J.* 68, 669–672. doi: 10.1042/bj0680669

Bates, L. S., Waldren, R. P., and Teare, I. D. (1973). Rapid determination of free proline for water-stress studies. *Plant Soil* 39, 205–207. doi: 10.1007/BF00018060

Battisti, R., and Sentelhas, P. C. (2017). Improvement of soybean resilience to drought through deep root system in Brazil. *Agron. J.* 109, 1612–1622. doi: 10.2134/agronj2017.01.0023

Bekesiova, I., Nap, J. P., and Mlynarova, L. (1999). Isolation of high quality DNA and RNA from leaves of the carnivorous plant Drosera rotundifolia. *Plant Mol. Biol. Rep.* 17, 269–277. doi: 10.1023/A:1007627509824

Belamkar, V., Weeks, N. T., Bharti, A. K., Farmer, A. D., Graham, M. A., and Cannon, S. B. (2014). Comprehensive characterization and RNA-Seq profiling of the HD-zip transcription factor family in soybean (*Glycine max*) during dehydration and salt stress. *BMC Genom.* 15:950. doi: 10.1186/1471-2164-15-950

Blum, A. (2017). Osmotic adjustment is a prime drought stress adaptive engine in support of plant production. *Plant Cell Envi.* 40, 4–10. doi: 10.1111/pce.12800

Cao, L., Yu, Y., Ding, X., Zhu, D., Yang, F., Liu, B., et al. (2017). The *Glycine soja* NAC transcription factor GsNAC019 mediates the regulation of plant alkaline tolerance and ABA sensitivity. *Plant Mol. Biol.* 95, 253–268. doi: 10.1007/s11103-017-0643-3

Chai, C., Wang, Y., Joshi, T., Valliyodan, B., Prince, S., Michel, L., et al. (2015). Soybean transcription factor ORFeome associated with drought resistance: a valuable resource to accelerate research on abiotic stress resistance. *BMC Genom.* 16:6. doi: 10.1186/s12864-015-1743-6

Chen, X., Chen, Z., Zhao, H., Zhao, Y., Cheng, B., and Xiang, Y. (2014). Genome-wide analysis of soybean HD-zip gene family and expression profiling under salinity and drought treatments. *PLoS ONE* 9:e87156. doi: 10.1371/journal.pone.0087156

Chien, C. T., Bartel, P. L., Sternglanz, R., and Fields, S. (1991). The 2-hybrid system - A method to identify and clone genes for proteins that interact with a protein of interest. *Proc. Natl. Acad. Sci. USA* 88, 9578–9582. doi: 10.1073/pnas.88.21.9578

Dogan, E., Kirnak, H., and Copur, O. (2007). Deficit irrigations during soybean reproductive stages and CROPGRO-soybean simulations under semi-arid climatic conditions. *Field Crops Res.* 103:9. doi: 10.1016/j.fcr.2007.05.009

Du, Y., Zhao, Q., Chen, L., Yao, X., Zhang, W., Zhang, B., et al. (2020). Effect of drought stress on sugar metabolism in leaves and roots of soybean seedlings. *Plant Physiol. Biochem.* 146, 1–12. doi: 10.1016/j.plaphy.2019.11.003

Gilbert, M. E., Zwieniecki, M. A., and Holbrook, N. M. (2011). Independent variation in photosynthetic capacity and stomatal conductance leads to differences in intrinsic water use efficiency in 11 soybean genotypes before and during mild drought. *J. Exp. Bot.* 62, 2875–2887. doi: 10.1093/jxb/erq461

Gilmour, S. J., Sebolt, A. M., Salazar, M. P., Everard, J. D., and Thomashow, M. F. (2000). Overexpression of the *Arabidopsis* CBF3 transcriptional activator mimics multiple biochemical changes associated with cold acclimation. *Plant Physiol.* 124, 1854–1865. doi: 10.1104/pp.124.4.1854

Gong, S., Ding, Y., Hu, S., Ding, L., Chen, Z., and Zhu, C. (2019). The role of HD-zip class I transcription factors in plant response to abiotic stresses. *Physiol. Plantarum* 167, 516–525. doi: 10.1111/ppl.12965

González, F. G., Capella, M., Ribichich, K. F., Curín, F., Giacomelli, J. I., Ayala, F., et al. (2019). Field-grown transgenic wheat expressing the sunflower gene *HaHB4* significantly outyields the wild type. *J. Exp. Bot.* 70, 1669–1681. doi: 10.1093/jxb/erz037

Harris, J. C., Hrmova, M., Lopato, S., and Langridge, P. (2011). Modulation of plant growth by HD-zip class I and II transcription factors in response to environmental stimuli. *New Phytol.* 190, 823–837. doi: 10.1111/j.1469-8137.2011.03733.x

Heath, R. L., and Packer, L. (1968). Photoperoxidation in isolated chloroplasts. I. Kinetics and stoichiometry of fatty acid peroxidation. *Arch. Biochem. Biophys.* 125, 189–198. doi: 10.1016/0003-9861(68)90654-1

Henriksson, E., Olsson, A. S., Johannesson, H., Johansson, H., Hanson, J., Engstrom, P., et al. (2005). Homeodomain leucine zipper class I genes in *Arabidopsis*: expression patterns and phylogenetic relationships. *Plant Physiol.* 139, 509–518. doi: 10.1104/pp.105.063461

Higa, A., Mori, Y., and Kitamura, Y. (2010). Iron deficiency induces changes in riboflavin secretion and the mitochondrial electron transport chain in hairy roots of *Hyoscyamus albus*. *J. Plant Physiol.* 167, 870–878. doi: 10.1016/j.jplph.2010.01.011

Himmelbach, A., Hoffmann, T., Leube, M., Hohener, B., and Grill, E. (2002). Homeodomain protein ATHB6 is a target of the protein phosphatase ABI1 and regulates hormone responses in *Arabidopsis*. *EMBO J.* 21, 3029–3038. doi: 10.1093/emboj/cdf316

Hu, J., Chen, G., Yin, W., Cui, B., Yu, X., Lu, Y., et al. (2017). Silencing of SlHB2 improves drought, salt stress tolerance, and induces stress-related gene expression in tomato. *J. Plant Growth Regulation* 36, 578–589. doi: 10.1007/s00344-017-9664-z

Hu, H., and Xiong, L. (2014). Genetic engineering and breeding of drought-resistant crops. *Annu. Rev. Plant Biol.* 65, 715–741. doi: 10.1146/annurev-arplant-050213-040000

Huang, X., Chaparro, J. M., Reardon, K. F., Zhang, R., Shen, Q., and Vivanco, J. M. (2014). Rhizosphere interactions: root exudates, microbes, and microbial communities. *Botany* 92:75. doi: 10.1139/cjb-2013-0225

Jiang, X. (2017). Bioinformatics Analysis of HD-Zip Gene Family and Identification of HD-Zip I Genes Related to Stress Resistance in Tomato (in Chinese). *Northeast Agricultural University*.

Jin, J., Tian, F., Yang, D., Meng, Y., Kong, L., Luo, J., et al. (2017). PlantTFDB 4.0: toward a central hub for transcription factors and regulatory interactions in plants. *Nucleic Acids Res.* 45, D1040–D1045. doi: 10.1093/nar/gkw982

Kereszt, A., Li, D., Indrasumunar, A., Nguyen, C. D., Nontachaiyapoom, S., Kinkema, M., et al. (2007). *Agrobacterium rhizogenes*-mediated transformation of soybean to study root biology. *Nat. Protocols* 2, 948–952. doi: 10.1038/nprot.2007.141

Khan, S. A., Li, M. Z., Wang, S. M., and Yin, H. J. (2018). Revisiting the role of plant transcription factors in the Battle against abiotic stress. *International Journal of Molecular Sciences* 19, 1634–1662. doi: 10.3390/ijms19061634

Knopf, U. C. (1976). Studies on the bacteriophage PS8 of agrobacterium tumefaciens (smith and Townsend) conn: physico-chemical properties of its DNA. *Microbios* 17, 231–237.

Kong, H., Landherr, L. L., Frohlich, M. W., Leebens-Mack, J., Ma, H., and DePamphilis, C. W. (2007). Patterns of gene duplication in the plant *SKP1* gene family in angiosperms: evidence for multiple mechanisms of rapid gene birth. *Plant J.* 50, 873–885. doi: 10.1111/j.1365-313X.2007.03097.x

Lee, Y. H., Oh, H. S., Cheon, C. I., Hwang, I. T., Kim, Y. J., and Chun, J. Y. (2001). Structure and expression of the *Arabidopsis thaliana* homeobox gene Athb-12. *Biochem. Biophys. Res. Commun.* 284, 133–141. doi: 10.1006/bbrc.2001.4904

Lei, Y., Lu, L., Liu, H. Y., Li, S., Xing, F., and Chen, L. L. (2014). CRISPR-P: a web tool for synthetic single-guide RNA design of CRISPR-system in plants. *Mol. Plant* 7, 1494–1496. doi: 10.1093/mp/ssu044

Lesk, C., Rowhani, P., and Ramankutty, N. (2016). Influence of extreme weather disasters on global crop production. *Nature* 529, 84–87. doi: 10.1038/nature16467

Libault, M., Farmer, A., Brechenmacher, L., Drnevich, J., Langley, R. J., Bilgin, D. D., et al. (2010a). Complete transcriptome of the soybean root hair cell, a single-cell model, and its alteration in response to *Bradyrhizobium japonicum* infection. *Plant Physiol.* 152, 541–552. doi: 10.1104/pp.109.148379

Libault, M., Farmer, A., Joshi, T., Takahashi, K., Langley, R. J., Franklin, L. D., et al. (2010b). An integrated transcriptome atlas of the crop model *Glycine max*, and its use in comparative analyses in plants. *Plant J.* 63, 86–99. doi: 10.1111/j.1365-313X.2010.04222.x

Liu, Q., Kasuga, M., Sakuma, Y., Abe, H., Miura, S., Yamaguchi-Shinozaki, K., et al. (1998). Two transcription factors, DREB1 and DREB2, with an EREBP/AP2 DNA binding domain separate two cellular signal transduction pathways in drought- and low-temperature-responsive gene expression, respectively, in *Arabidopsis*. *Plant Cell* 10, 1391–1406. doi: 10.1105/tpc.10.8.1391

Liu, J. P., and Zhu, J. K. (1997). Proline accumulation and salt-stress-induced gene expression in a salt-hypersensitive mutant of *Arabidopsis*. *Plant Physiol.* 114, 591–596. doi: 10.1104/pp.114.2.591

Livak, K. J., and Schmittgen, T. D. (2001). Analysis of relative gene expression data using real-time quantitative PCR and the 2(T)(-Delta Delta C) method. *Methods* 25, 402–408. doi: 10.1006/meth.2001.1262

Mittler, R. (2002). Oxidative stress, antioxidants and stress tolerance. *Trends in Plant Science* 7, 405–410. doi: 10.1016/s1360-1385(02)02312-9

Nakamura, M., Katsumata, H., Abe, M., Yabe, N., Komeda, Y., Yamamoto, K. T., et al. (2006). Characterization of the class IV homeodomain-Leucine zipper gene family in *Arabidopsis*. *Plant Physiol.* 141, 1363–1375. doi: 10.1104/pp.106.077388

Niu, Y., Xie, G., Xiao, Y., Liu, J., Wang, Y., Luo, Q., et al. (2021). Spatiotemporal patterns and determinants of grain self-sufficiency in China. *Foods* 10:747. doi: 10.3390/foods10040747

Perotti, M. F., Arce, A. L., and Chan, R. L. (2021). The underground life of homeodomain-leucine zipper transcription factors. *J. Exp. Bot.* 72, 4005–4021. doi: 10.1093/jxb/erab112

Perotti, M. F., Ribone, P. A., and Chan, R. L. (2017). Plant transcription factors from the homeodomain-leucine zipper family I. role in development and stress responses. *IUBMB Life* 69, 280–289. doi: 10.1002/iub.1619

Peterson, K. M., Shyu, C., Burr, C. A., Horst, R. J., Kanaoka, M. M., Omae, M., et al. (2013). *Arabidopsis* homeodomain-leucine zipper IV proteins promote stomatal development and ectopically induce stomata beyond the epidermis. *Development* 140, 1924–1935. doi: 10.1242/dev.090209

Ré, D. A., Capella, M., Bonaventure, G., and Chan, R. L. (2014). *Arabidopsis AtHB7* and *AtHB12* evolved divergently to fine tune processes associated with growth and responses to water stress. *BMC Plant Biol.* 14:150. doi: 10.1186/1471-2229-14-150

Ribichich, K. F., Chiozza, M., Ávalos-Britez, S., Cabello, J. V., Arce, A. L., Watson, G., et al. (2020). Successful field performance in dry-warm environments of soybean expressing the sunflower transcription factor HaHB4. *J. Exp. Bot.* 71, 3142–3156. doi: 10.1101/2019.12.21.885798

Rogg, L. E., Lasswell, J., and Bartel, B. (2001). A gain-of-function mutation in *IAA28* suppresses lateral root development. *Plant Cell* 13, 465–480. doi: 10.1105/tpc.13.3.465

Romani, F., Ribone, P. A., Capella, M., Miguel, V. N., and Chan, R. L. (2016). A matter of quantity: common features in the drought response of transgenic plants overexpressing HD-zip I transcription factors. *Plant Sci.* 251, 139–154. doi: 10.1016/j.plantsci.2016.03.004

Schena, M., and Davis, R. W. (1992). HD-zip proteins: members of an *Arabidopsis* homeodomain protein superfamily. *Proc. Natl. Acad. Sci. USA* 89, 3894–3898. doi: 10.1073/pnas.89.9.3894

Skirycz, A., and Inze, D. (2010). More from less: plant growth under limited water. *Curr. Opin. Biotechnol.* 21, 197–203. doi: 10.1016/j.copbio.2010.03.002

Smetana, O., Makila, R., Lyu, M., Amiryousefi, A., Sanchez, R. F., Wu, M. F., et al. (2019). High levels of auxin signalling define the stem-cell organizer of the vascular cambium. *Nature* 565, 485–489. doi: 10.1038/s41586-018-0837-0

Söderman, E., Mattsson, J., and Engstrom, P. (1996). The *Arabidopsis* homeobox gene *ATHB-7* is induced by water deficit and by abscisic acid. *Plant J.* 10, 375–381. doi: 10.1046/j.1365-313x.1996.10020375.x

Son, O., Cho, H. Y., Kim, M. R., Lee, H., Lee, M. S., Song, E., et al. (2005). Induction of a homeodomain-leucine zipper gene by auxin is inhibited by cytokinin in *Arabidopsis* roots. *Biochem. Biophys. Res. Commun.* 326, 203–209. doi: 10.1016/j.bbrc.2004.11.014

Song, S., Chen, Y., Zhao, M., and Zhang, W. (2012). A novel *Medicago truncatula* HD-zip gene, MtHB2, is involved in abiotic stress responses. *Envi. Exp. Bot.* 80, 1–9. doi: 10.1016/j.envexpbot.2012.02.001

Sun, L. (2020). Analysis on the strategy of developing soybean science and technology and revitalizing soybean industry under the background of new era of China. *Soybean Science & Technology* 4, 20–31.

Sun, X., Wang, P., Jia, X., Huo, L., Che, R., and Ma, F. (2018). Improvement of drought tolerance by overexpressing MdATG18a is mediated by modified antioxidant system and activated autophagy in transgenic apple. *Plant Biotechnol. J.* 16, 545–557. doi: 10.1111/pbi.12794

Székely, G., Abraham, E., Cseplo, A., Rigo, G., Zsigmond, L., Csiszar, J., et al. (2008). Duplicated *P5CS* genes of *Arabidopsis* play distinct roles in stress regulation and developmental control of proline biosynthesis. *Plant J.* 53, 11–28. doi: 10.1111/j.1365-313X.2007.03318.x

Tamura, K., Peterson, D., Peterson, N., Stecher, G., Nei, M., and Kumar, S. (2011). MEGA5: molecular evolutionary genetics analysis using maximum likelihood, evolutionary distance, and maximum parsimony methods. *Mol. Biol. Evol.* 28, 2731–2739. doi: 10.1093/molbev/msr121

Tang, L., Cai, H., Ji, W., Luo, X., Wang, Z., Wu, J., et al. (2013). Overexpression of GsZFP1 enhances salt and drought tolerance in transgenic alfalfa (Medicago sativa L.). *Plant Physiology and Biochemistry* 71, 22–30. doi: 10.1016/j.plaphy.2013.06.024

Thompson, J. D., Higgins, D. G., and Gibson, T. J. (1994). CLUSTAL W: improving the sensitivity of progressive multiple sequence alignment through sequence weighting, position-specific gap penalties and weight matrix choice. *Nucleic Acids Res.* 22, 4673–4680. doi: 10.1093/nar/22.22.4673

Valdes, A. E., Overnas, E., Johansson, H., Rada-Iglesias, A., and Engstrom, P. (2012). The homeodomain-leucine zipper (HD-zip) class I transcription factors ATHB7 and ATHB12 modulate abscisic acid signalling by regulating protein phosphatase 2C and abscisic acid receptor gene activities. *Plant Mol. Biol.* 80, 405–418. doi: 10.1007/s11103-012-9956-4

Verslues, P. E., Batelli, G., Grillo, S., Agius, F., Mm, Y., Zhu, J., et al. (2007). Interaction of SOS2 with nucleoside diphosphate kinase 2 and catalases reveals a point of connection between salt stress and H2O2 signaling in *Arabidopsis thaliana*. *Mol. Cell. Biol.* 27, 7771–7780. doi: 10.1128/MCB.00429-07

Wang, S., Barron, C., Schiefelbein, J., and Chen, J. G. (2010). Distinct relationships between GLABRA2 and single-repeat R3 MYB transcription factors in the regulation of trichome and root hair patterning in *Arabidopsis*. *New Phytol.* 185, 387–400. doi: 10.1111/j.1469-8137.2009.03067.x

Wang, R., Zhang, Y., Wang, C., Wang, Y. C., and Wang, L. Q. (2021). ThNAC12 from Tamarix hispida directly regulates ThPIP2;5 to enhance salt tolerance by modulating reactive oxygen species. *Plant Physiol. Biochem.* 163, 27–35. doi: 10.1016/j.plaphy.2021.03.042

Wei, M., Liu, A., Zhang, Y., Zhou, Y., Li, D., Dossa, K., et al. (2019). Genome-wide characterization and expression analysis of the HD-zip gene family in response to drought and salinity stresses in sesame. *BMC Genom.* 20:748. doi: 10.1186/s12864-019-6091-5

Win, K. T., Oo, A. Z., Ookawa, T., Kanekatsu, M., and Hirasawa, T. (2016). Changes in hydraulic conductance cause the difference in growth response to short-term salt stress between salt-tolerant and -sensitive black gram (*Vigna mungo*) varieties. *J. Plant Physiol.* 193, 71–78. doi: 10.1016/j.jplph.2016.02.013

Wu, L., Yao, L., Ma, R., Zhu, X., Yang, J., Zhang, N., et al. (2016). Cloning and functional identification of the ATHB12 gene of HD-zip I family in potato (*Solanum tuberosum* L.). *Acta Agron. Sin.* 42, 1112–1121. doi: 10.3724/SP.J.1006.2016.01112

Xu, L., Islam, F., Ali, B., Pei, Z., Li, J., Ghani, M. A., et al. (2017). Silicon and water-deficit stress differentially modulate physiology and ultrastructure in wheat (*Triticum aestivum* L.). *3 Biotech* 7:273. doi: 10.1007/s13205-017-0904-5

Xue, Z., Zhang, X., Lei, C., Chen, X., and Fu, Y. (2012). Molecular cloning and functional analysis of one ZEITLUPE homolog *GmZTL3* in soybean. *Mol. Biol. Rep.* 39, 1411–1418. doi: 10.1007/s11033-011-0875-2

Ye, H., Roorkiwal, M., Valliyodan, B., Zhou, L., Chen, P., Varshney, R. K., et al. (2018). Genetic diversity of root system architecture in response to drought stress in grain legumes. *J. Exp. Bot.* 69, 3267–3277. doi: 10.1093/jxb/ery082

You, N., Dong, J., Huang, J., Du, G., Zhang, G., He, Y., et al. (2021). The 10-m crop type maps in Northeast China during 2017–2019. *Sci. Data* 8:9. doi: 10.1038/s41597-021-00827-9

Yu, X., Ruan, M., Wang, B., Yang, Y., Wang, S., and PENG, M. (2017). Cloning and analysis of the transcription factor gene *MeHDZ14* in cassava. *Acta Agron. Sin.* 43, 1181–1189. doi: 10.3724/SP.J.1006.2017.01181

Zhang, S., Haider, I., Kohlen, W., Jiang, L., Bouwmeester, H., Meijer, A. H., et al. (2012). Function of the HD-zip I gene *Oshox22* in ABA-mediated drought and salt tolerances in rice. *Plant Mol. Biol.* 80, 571–585. doi: 10.1007/s11103-012-9967-1

Zhao, S., Gao, H., Jia, X., Wang, H., Ke, M., and Ma, F. (2020). The HD-zip I transcription factor MdHB-7 regulates drought tolerance in transgenic apple (*Malus domestica*). *Environ. Exp. Bot.* 180:46. doi: 10.1016/j.envexpbot.2020.104246

Zhao, Y., Ma, Q., Jin, X., Peng, X., Liu, J., Deng, L., et al. (2014). A novel maize homeodomain-leucine zipper (HD-zip) I gene, *Zmhdz10*, positively regulates drought and salt tolerance in both rice and *Arabidopsis*. *Plant Cell Physiol.* 55, 1142–1156. doi: 10.1093/pcp/pcu054

Zhou, W., Malabanan, P. B., and Abrigo, E. (2015b). *OsHox4* regulates GA signaling by interacting with *DELLA*-like genes and GA oxidase genes in rice. *Euphytica* 201, 97–107. doi: 10.1007/s10681-014-1191-4

Zhou, C., Zhu, L., Ma, Z., and Wang, J. (2015a). A homolog of class IV HD-zip transcription factors, EsHdzip1, confers drought resistance in tobacco via enhanced the capacity of water conserving and absorbing. *Acta Physiol. Plant.* 37, 124–137. doi: 10.1007/s11738-015-1863-2

frontiers | Frontiers in Plant Science

TYPE Original Research
PUBLISHED 06 September 2022
DOI 10.3389/fpls.2022.968714

Check for updates

OPEN ACCESS

EDITED BY
Ji-Hong Liu,
Huazhong Agricultural University, China

REVIEWED BY
Kenji Miura,
University of Tsukuba,
Japan
Jun You,
Oil Crops Research Institute (CAAS), China

*CORRESPONDENCE
Anzhi Wei
weianzhi@nwafu.edu.cn

SPECIALTY SECTION
This article was submitted to Plant Abiotic Stress, a section of the journal Frontiers in Plant Science

RECEIVED 14 June 2022
ACCEPTED 12 August 2022
PUBLISHED 06 September 2022

CITATION
Hu H, He B, Ma L, Chen X, Han P, Luo Y, Liu Y, Fei X and Wei A (2022) Physiological and transcriptome analyses reveal the photosynthetic response to drought stress in drought-sensitive (Fengjiao) and drought-tolerant (Hanjiao) *Zanthoxylum bungeanum* cultivars. *Front. Plant Sci.* 13:968714. doi: 10.3389/fpls.2022.968714

COPYRIGHT
© 2022 Hu, He, Ma, Chen, Han, Luo, Liu, Fei and Wei. This is an open-access article distributed under the terms of the Creative Commons Attribution License (CC BY). The use, distribution or reproduction in other forums is permitted, provided the original author(s) and the copyright owner(s) are credited and that the original publication in this journal is cited, in accordance with accepted academic practice. No use, distribution or reproduction is permitted which does not comply with these terms.

Physiological and transcriptome analyses reveal the photosynthetic response to drought stress in drought-sensitive (Fengjiao) and drought-tolerant (Hanjiao) *Zanthoxylum bungeanum* cultivars

Haichao Hu[1,2], Beibei He[3], Lei Ma[1,2], Xin Chen[1,2], Peilin Han[1,2], Yingli Luo[1,2], Yonghong Liu[1,2], Xitong Fei[1,2] and Anzhi Wei[1,2]*

[1]College of Forestry, Northwest Agriculture and Forestry University, Xianyang, Shaanxi, China, [2]Research Centre for Engineering and Technology of Zanthoxylum State Forestry Administration, Xianyang, Shaanxi, China, [3]College of Horticulture, Northwest Agriculture and Forestry University, Xianyang, Shaanxi, China

As an important economical plant, *Zanthoxylum bungeanum* is widely cultivated in arid and semi-arid areas. The studies associated with photosynthesis under drought stress were widely carried out, but not yet in *Z. bungeanum*. Here, the photosynthesis of two *Z. bungeanum* cultivars (FJ, *Z. bungeanum* cv. "Fengjiao"; HJ, *Z. bungeanum* cv. "Hanjiao") was analyzed under drought stress using physiological indicators and transcriptome data. Drought decreased stomatal aperture and stomatal conductance (Gsw), reduced transpiration rate (E) and sub-stomatal CO_2 concentration (Ci), and lowered chlorophyll and carotenoid content, which reduced the net photosynthetic rate (Pn) of *Z. bungeanum*. The higher photosynthetic rate in HJ stemmed from its higher chlorophyll content, larger stomatal aperture and Gsw, and higher Ci. Weighted gene co-expression network analysis (WGCNA) identified several ABA signal transduction genes (*PYL4*, *PYL9*, and *PYR1*), LCH-encoding genes (*LHCB4.3*), and chlorophyll metabolism genes (*CRD1*, *PORA*, and *CHLH*). Additionally, seven transcription factor genes were identified as important factors regulating photosynthesis under drought conditions. In general, a photosynthetic response model under drought stress was built firstly in *Z. bungeanum*, and the key genes involved in photosynthesis under drought stress were identified. Therefore, the results in our research provide important information for photosynthesis under drought and provided key clues for future molecular breeding in *Z. bungeanum*.

KEYWORDS

***Zanthoxylum bungeanum*, photosynthetic rate, drought stress, transcriptome, WGCNA, transcription factor**

Introduction

Drought stress is one of the most important environment factors, which severe affected the growth and development of plants (Fathi and Barari, 2016). With the global warming in recent years, water shortage has become a large challenge for sustainable agriculture and attracted wide attentions from researchers (Dai, 2013). Plants have evolved various acclimation responses to harsh environments (Zhang et al., 2022). In response to drought stress, acclimations of plant mainly include lateral root growth, stomatal closure and leaf rolling (Basu et al., 2016). However, the acclimation generally comes at the cost of plant growth and development, and lead to weakness of many metabolic processes.

Photosynthesis is the most important metabolic process for carbon assimilation in plants and the fixed biochemical energy in photosynthesis was used to support nearly all life on Earth (Evans, 2013). Photosynthesis is divided into two stages: light reactions taking place in thylakoids and dark reactions occurring in chloroplast stroma (Kaiser et al., 2015). There are four photosynthetic protein complexes located in thylakoid membranes: photosystem I (PSI), photosystem II (PSII), the cytochrome b6f complex (Cytb6f), and adenosine triphosphate (ATP) synthase (van Bezouwen et al., 2017). PSI and PSII, which comprise core complexes and peripheral antenna systems, function in light capture and subsequent photochemical reactions (Huang et al., 2021). Light-harvesting chlorophyll-binding I (LHCI) and light-harvesting chlorophyll-binding II (LHCII) serve as light-absorbing antenna systems in PSI and PSII, respectively. The pigments in LHCI and LHCII are mainly chlorophyll *a* and chlorophyll *b*, respectively (Rochaix, 2013). The light energy is absorbed by LHCs and subsequently transferred to the photosynthesis reaction center (Huang et al., 2021). Photosynthesis is highly sensitive to water deficit, which is generally weakened under drought stress (Ma et al., 2016; Zhang et al., 2021). As known, stomata are highly sensitive to drought stress (Zhang et al., 2021). Given that stomata are channels for gas exchange in photosynthesis, closure or partial closure of stomata by drought stress largely reduced intercellular carbon dioxide (CO_2) concentration and sequenced inhibited photosynthesis. On the other hand, drought stress stimulated the accumulation of reactive oxygen species (ROS; Zhang et al., 2022). The excessive ROS destroyed pigments in photosystem and induced membrane peroxide, further inhibiting the photosystem II (PSII) activity (Gururani et al., 2015). Generally, drought-tolerant plants have higher water usage efficiency and a superior ROS-scavenging ability (Ma et al., 2016). Therefore, drought-tolerant plants typically have higher photosynthetic efficiency under drought conditions. Given that maintaining normal rates of photosynthesis under drought stress is important for ensuring high crop quality and yield (Lima-Melo et al., 2021), a large scale of researches have been carried out to explore the photosynthetic metabolism under drought stress. For instance, Ma et al. reported that the chlorophyll content in alfalfa declines significantly under drought stress (Ma et al., 2021). Zhang et al. explored the effects of drought on photosynthesis by measuring photosynthetic parameters and conducting transcriptome analysis in *Atractylodes lancea* (Zhang et al., 2021). Daszkowska-Golec et al. analyzed the physiological and genetic basis of photosynthesis in barley under drought stress (Daszkowska-Golec et al., 2019). Hong et al. found that chloroplast protein, PsbP domain protein 5 (PPD5), plays an important role in *Arabidopsis* under drought stress (Hong et al., 2020). D'Alessandro et al. revealed an important role of β-carotene oxidation in PSII in mediating stress tolerance, including drought tolerance (D'Alessandro and Havaux, 2019).

Zanthoxylum belongs to the family Rutaceae and is widely distributed in Asia countries, including China, Korea, Japan and India. Over 250 species to date have been identified in *Zanthoxylum* genus across the world, of which the most well-known species are *Zanthoxylum bungeanum* (Red Huajiao) and *Zanthoxylum armatum* (Green Huajiao; Wang et al., 2022). The pericarp of *Z. bungeanum* is an essential culinary spice and condiment in Chinese cuisine, including the well-known Sichuan hot pot (Okagu et al., 2021a). Additionally, *Z. bungeanum* pericarp is a kind of traditional Chinese medicine, with numerous biological functions in anti-inflammatory, analgesic, antimicrobial, and antiviral activities (Okagu et al., 2021b; Wang et al., 2022). *Zanthoxylum bungeanum* plant has evolved a large scale of prickles, which are distributed in the stems, branches, as well as leaves (Zhang et al., 2017). Like other prickle plants, *Z. bungeanum* plant exhibits a strong acclimation response to drought environment. Due to their economic value and drought tolerance, *Z. bungeanum* plants are widely grown in arid and semi-arid areas. In recent years, increasing researches have focused on *Z. bungeanum*, including the chemical component of *Z. bungeanum* pericarp (Fei et al., 2021), the disease control of *Z. bungeanum* plant (Li et al., 2021b) and *Z. bungeanum* genome sequencing for evolutionary relationship (Feng et al., 2020). In addition, the response mechanism of prickly ash plants underlying chilling injury has been preliminarily explored (Tian et al., 2021). However, response mechanism of photosynthesis under drought stress of *Z. bungeanum* remains unexplored and is urgent to reveal.

Here, we investigated the influence of drought stress on photosynthetic parameters, stomatal status and chlorophyll content of two different *Z. bungeanum* cultivars with diverse drought tolerance under progressive drought stress. Meanwhile, we explored the underlying mechanisms of photosynthesis variation through transcriptome analysis. Furthermore, we screened many structural genes and transcription factors (TFs) closely associated with the photosynthesis of *Z. bungeanum* plants through weighted gene co-expression network analysis (WGCNA). Therefore, our study provides important information for molecular breeding of *Z. bungeanum* plants.

Materials and methods

Plant material and sample

The mature seeds of a drought-sensitive cultivar (FJ, *Z. bungeanum* cv. "Fengjiao") and a drought-tolerant cultivar (HJ, *Z. bungeanum* cv. "Hanjiao") were harvested in the Fengxian Prickly Ash Experimental Station of Northwest A&F University in Shannxi Province, China (33°59′6.55″N, 106°39′29.38″E). The *Z. bungeanum* seeds were cleaned, air-dried, and sown in a cultivar soil mixture consisting of perlite, vermiculite, and chernozem in a research greenhouse of Northwest A&F University in Yangling, Shannxi Province, China. One week after germination, healthy seedlings were transplanted to cultivar pots for cultivation at 25°C ± 2°C and soil moisture of 85% ± 1%. After 3 months, 54 *Z. bungeanum* healthy seedlings of the same size of each cultivar were subjected to drought treatment (i.e., these plants were not provided water) for 15 days. On 0, 3, 6, 9, 12, and 15 days after the start of the drought treatment, leaf samples of *Z. bungeanum* seedlings were obtained, dipped into liquid nitrogen, and stored in a −80°C freezer. There were three biological replicates for each sample and three seedlings for each biological replicate.

Photosynthetic indicators

The net photosynthetic rate (Pn), transpiration rate (E), stomatal conductance (Gsw), and intercellular CO_2 concentration (Ci) of *Z. bungeanum* seedlings were measured using an LI-6800 photosynthesis measurement system (LI-COR, Lincoln, NE, United States) between 8:30 and 11:30 AM at 0, 3, 6, 9, 12, and 15 days of drought treatment. All measurements were performed on the third fully expanded mature leaves from the top of *Z. bungeanum* seedlings, and a total of nine seedlings were analyzed per cultivar.

Stomatal morphology

The third fully expanded leaves from the top of the seedlings were used for observations of stomatal morphology. Transparent acrylic nail polish was applied to the lower epidermis of *Z. bungeanum* leaves following the methods described in a previous study (Sun et al., 2020). When the nail polish was dried, it was gently peeled off with tweezers, placed on a glass slide, and covered with a cover slip. A fluorescence microscope (BX63, Olympus, Japan) was then used to take photographs of the slide at a 10 × 40 magnification. There were three epidermis samples per plant, and there were two fields of view of each epidermis sample. Stomatal density was calculated as the number of pores per unit area. Five stomata were randomly selected from each field of view for length and width measurements in ImageJ version 1.48 (National Institutes of Health, Bethesda, MD, United States). The stomatal aperture was indicated by the width of the stomata (Supplementary Figure 1).

Measurements of photosynthetic pigments from fresh leaves

Extractions and measurements of chlorophyll and carotenoids were performed following a previously described method (Xue et al., 2020) with some modifications. Briefly, 0.05 g of fresh leaves were ground into powder with liquid nitrogen and fully mixed with 8 ml of 80% acetone. After samples were on ice for 20 min, the homogenate was filtered through filter paper. The absorbance of the supernatants was measured at 652.4, 665.2, and 470 nm using a microplate reader (Infinite M200pro, Tecan, Switzerland). The content of photosynthetic pigments was calculated using the following equations:

$$\text{Chlorophyll } a = 16.72\ A665.2 - 9.16\ A652.4$$

$$\text{Chlorophyll } b = 34.09\ A652.4 - 15.28\ A665.2$$

$$\text{Total chlorophyll} = \text{chlorophyll } a + \text{chlorophyll } b$$

$$\text{Carotenoid} = (1{,}000\ A470 - 1.63\ \text{chlorophyll } a - 104.96\ \text{chlorophyll } b)/221.$$

RNA extraction and sequencing

The leaf samples of two *Z. bungeanum* cultivars obtained on 0 (D1), 6 (D2), 9 (D3), and 15 days (D4) were used for RNA extraction and sequencing. We extracted the total RNA from the *Z. bungeanum* leaves using the Tiangen RNA Pure kit for plants (Tiangen, Beijing, China). The purity and integrity of extracted RNA were determined on an Agilent 2,100 Bioanalyzer (Agilent Technologies, Inc., Santa Clara, CA, United States). RNA with an OD260/280 value between 1.8 and 2.2 and OD260/230 value over 2.0 was used for the construction of cDNA libraries with the NEBNext Ultra RNA Library Prep Kit for Illumina (New England Biolabs, Ipswich, United States). The resulting libraries were sequenced using the Illumina HiSeq 2,500 platform (Illumina, Inc., San Diego, United States).

RNA sequencing reads were aligned to the reference *Z. bungeanum* genome using HISAT2 (Kim et al., 2015). FPKM (Fragments Per Kilobase of transcript per Million fragments mapped) was calculated using StringTie (Pertea et al., 2015). Genes with fold change (FC) ≥ 2 and false discovery rate (FDR) < 0.01 were defined as differentially expressed genes (DEGs). The functions of genes were determined using the Gene Ontology (GO), Kyoto Encyclopedia of Genes and Genomes (KEGG), Clusters of Orthologous Groups of proteins (KOG/COG), Protein family (Pfam), Swiss-Prot (a manually annotated and reviewed protein sequence database), NCBI non-redundant

protein sequence (Nr), and NCBI non-redundant nucleotide sequence (Nt) database.

Weighted gene co-expression network analysis

Weighted gene co-expression network analysis (WGCNA) was carried out on the DEGs using R (version: 1.70–3) with default parameters (Langfelder and Horvath, 2008). The photosynthetic indicators were input as the trait file. The top 150 core genes in the green, purple and cyan modules were used to construct the co-expression network and visualized using Cytoscape 3.9.1 (Java 11.0.6).

Phylogenetic analysis and *cis*-element analysis of seven TF genes

The phylogenetic tree was built based on the amino acid sequences of seven TFs using the neighbor-joining (NJ) method in MEGA 7.0. The upstream 2,000-bp (bp) sequences of the start codon were extracted from the 13 TF genes using TBtools, which were then submitted to the PlantCARE database (http://bioinformatics.psb.ugent.be/webtools/plantcare/html/, accessed on 25 May 2022). The file generated from PlantCARE was used to characterize the *cis*-element distribution using TBtools (Chen et al., 2020).

Quantitative real-time PCR analysis

A Tiangen RNA Pure kit for plants (Tiangen, Beijing, China) was used to extract the total RNA in *Z. bungeanum* leaves. A NanoDrop 2000 spectrophotometer (Thermo Scientific, Wilmington, DE, United States) was used to analyze the quality of the total RNA; RNA with an OD260/280 value between 1.8 and 2.2 and OD260/230 value over 2.0 was reverse-transcribed into first-strand cDNA using the PrimeScript RT Reagent Kit with gDNA Eraser (Takara Biotechnology Inc., Dalian, China). qRT-PCR was carried out in a volume of 10 μl using the SYBR® Green Premix *Pro Taq* HS qPCR Kit (Accurate Biotechnology Co., Ltd., Hunan, China) on a CFX96 Real-Time System (Bio-Rad Laboratories, Inc., Hercules, United States). The quantitative primers in qRT-PCR were designed using Primer Premier 6.0 (PREMIER Biosoft, CA, United States; Supplementary Table 1). *ZbUBA* and *ZbUBQ* were used as reference genes (Fei et al., 2018), and relative expression levels were calculated using the $2^{-\Delta\Delta CT}$ method (Schmittgen and Livak, 2008).

Statistical analysis

The experimental data included three biological replicates, and significant differences were analyzed using one-way ANOVA, followed by Duncan's multiple-range test ($p < 0.05$), in SPSS 23.0 software (SPSS Inc., Chicago, IL, United States). Line charts and column charts were made using OriginPro 2021 (Originlab, Northampton, MA, United States). The inter-group correlation analysis was conducted, and the results were visualized using OriginPro 2021 (Originlab, Northampton, MA, United States). Venn diagrams and volcano diagrams were made using the BMKCloud platform.[1]

Results

Morphological traits and stomatal characteristic of *Zanthoxylum bungeanum* leaves under drought stress

The morphological traits of two *Z. bungeanum* cultivars under progressive drought stress are displayed in Figure 1A. The *Z. bungeanum* seedlings changed slightly before 6 days in both FJ and HJ. In FJ, the drought-sensitive cultivar, the leaves began to roll in at 9 days and such case became worse over time. However, the leaves roll in slightly at 12 and at 15 days in HJ, the drought-tolerant cultivar. Notably, the changes of morphological traits were much slighter in HJ than in FJ at each timepoint.

Stomata are an important kind of channel for gas exchange and an important basis for photosynthesis. Here, morphological characteristic of the stomata of *Z. bungeanum* leaves were observed under progressive drought stress using a fluorescence microscope (Figure 1B). The result showed that the stomatal morphology was significantly changed by drought stress. The stomatal aperture decreased with drought stress in both *Z. bungeanum* cultivars, with largest value in 0d (FJ, 6.41 μm; HJ, 5.39 μm) and smallest at 15 days (FJ, 0.72 μm; HJ, 1.22 μm; Figure 1C). The stomatal aperture was higher before 6 days and lower after 9 days in FJ than in HJ. The stomatal density increased steadily and was largest at 15 days (136.17/cm^2) in FJ (Figure 1D). However, in HJ, stomatal density reached a peak value at 6 days (117.64/cm^2) and then decreased until 12 days. Overall, drought stress decreased the stomatal aperture and increased the stomatal intensity in *Z. bungeanum* leaves.

Photosynthetic parameters of *Zanthoxylum bungeanum* leaves under drought stress

To explore the influence of drought stress on photosynthesis in *Z. bungeanum* plants, photosynthetic parameters, including the net photosynthetic rate (Pn), stomatal conductance (Gsw), sub-stomatal CO_2 concentration (Ci) and transpiration rate (E), were measured using a Li 6,800 photosynthesis measurement system (Figure 2). The Pn reached a peak value in both cultivars

1 https://www.biocloud.net

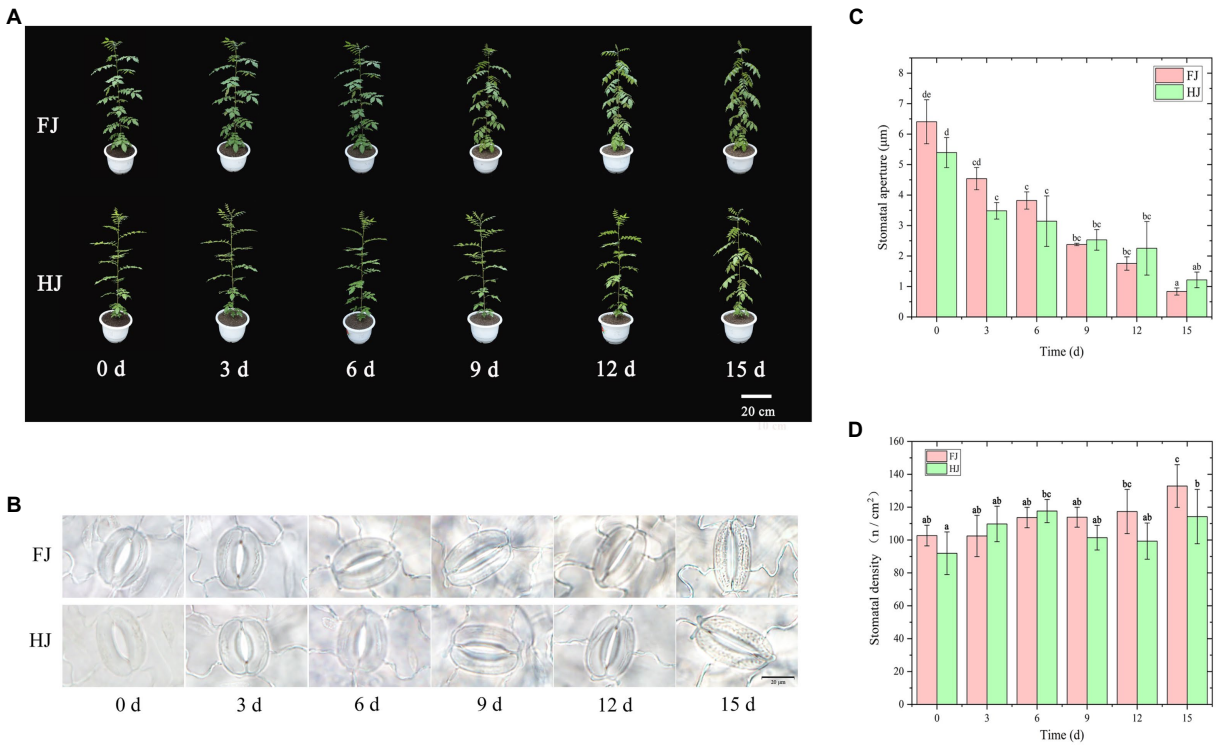


FIGURE 1
Morphological traits and stomatal characteristic of *Zanthoxylum bungeanum* leaves under drought stress. **(A)** Morphological traits of *Z. bungeanum* seedlings under progressive drought stress. **(B)** Images of the stomata and guard cells of *Z. bungeanum* leaves taken with a fluorescence microscope. **(C)** Stomatal aperture. **(D)** Stomatal density. All data are mean±standard error of three replicates. Values with different letters indicate significant differences at $p<0.05$ between FJ and HJ based on one-way ANOVA.

at 6 days (FJ, 8.48 μmol m^{-2} s^{-1}; HJ, 7.36 μmol m^{-2} s^{-1}) and then decreased steadily (Figure 2A). The stimulation of photosynthesis may be used to mitigate light damage caused by drought in the early stage. At 6 days, Pn was significantly higher in FJ than in HJ ($p<0.05$), but after that it was lower in FJ than in HJ, extremely for 12 and 15days ($p<0.05$), indicating that drought made more pronounced influence on FJ than on HJ in late stage of drought treatment. Similarly, Ci increased dramatically when suffering the drought stress and peaked at 6 days in FJ (277.01 μmol mol^{-1}) and in HJ (255.09 μmol mol^{-1}; Figure 2C). At days 12 and 15, the Ci was significantly lower in FJ than in HJ ($p<0.05$). The Gsw and E decreased significantly at the start of the drought stress and varied slightly after 6 days (Figures 2B,D). Taken together, drought stress negatively affected the photosynthetic efficiency in both cultivars, especially after 6 days of drought treatment.

The contents of chlorophyll and carotenoid in *Zanthoxylum bungeanum* leaves under drought stress

Given the key role of chlorophyll and carotenoid in plant photosynthesis system, we monitored their content variations under progressive drought conditions. The content of chlorophyll *a*, chlorophyll *b*, total chlorophyll and carotenoid decreased under drought stress in both cultivars (Figure 3). The content of chlorophyll *a* varied slightly before 6 days and decreased dramatically after 6 days in both FJ and HJ (Figure 3A). The content of chlorophyll *a* was higher in HJ than in FJ after 9 days ($p<0.05$). The content of chlorophyll *b* decreased dramatically after 3 days in FJ and after 6 days in HJ (Figure 3B). The content of chlorophyll *b* was significantly lower in FJ than in HJ on 12 and 15 days ($p<0.05$). In terms of the content of total chlorophyll, it was higher in HJ than in FJ on days 9, 12, and 15 ($p<0.05$; Figure 3C). Carotenoid content varied slightly in FJ before 6 days and decreased significantly after that (Figure 3D). Compared to that in FJ, the carotenoid content in HJ was significantly higher on 12 days ($p<0.05$). In general, drought stress decreased the contents of chlorophyll *a*, chlorophyll *b*, total chlorophyll and carotenoid in *Z. bungeanum* plants and these contents in HJ were relatively higher than in FJ in the late drought stage.

Correlation analysis of photosynthesis indicators

To clear the relationship among these photosynthesis indicators, intragroup correlation analysis was performed (Figure 4). Stomatal aperture was positively correlated with chlorophyll *b* ($R=0.78$,

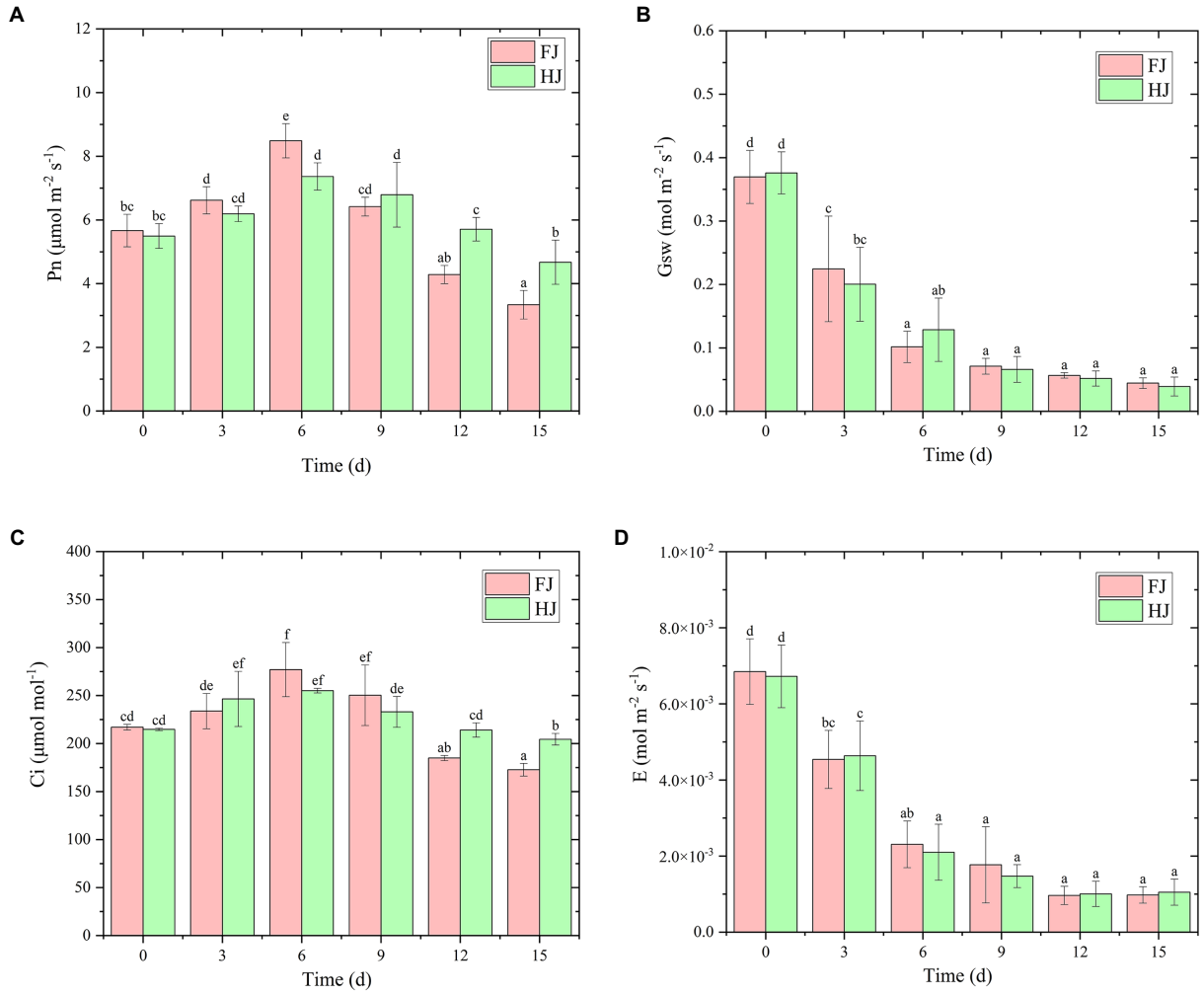


FIGURE 2
Photosynthetic parameters of two *Zanthoxylum bungeanum* cultivars under drought stress. **(A)** Net photosynthetic rate (Pn). **(B)** Stomatal conductance (Gsw). **(C)** Sub-stomatal CO_2 concentration (Ci). **(D)** Transpiration rate (E). All data are mean±standard error of three replicates. Values with different letters indicate significant differences at $p<0.05$ between FJ and HJ based on one-way ANOVA.

$p<0.05$), total chlorophyll ($R=0.75$, $p<0.05$), Gsw ($R=0.90$, $p<0.05$), and E ($R=0.88$, $p<0.05$). Stomatal density was negatively correlated with chlorophyll *a* ($R=-0.74$, $p<0.05$), total chlorophyll ($R=-0.74$, $p<0.05$) and carotenoid ($R=-0.76$, $p<0.05$). In terms of chlorophyll *a*, chlorophyll *b*, total chlorophyll and carotenoid, they were positively correlated with each other, indicating they functioned synergistically in photosystem. Besides, Pn was positively related to Ci ($R=0.96$, $p<0.05$), which reflects the fact that intercellular CO_2 is the raw material of photosynthesis. Gsw was highly positively related to E ($R=0.99$, $p<0.05$), in line with that stomata status is extremely important for plant transpiration.

Differentially expressed genes in FJ and HJ under drought stress

To explore the molecular mechanisms underlying the photosynthesis changes under drought, transcriptome sequencing was performed at four drought stages: D1 (0 days), D2 (6 days), D3 (9 days), and D4 (15 days), respectively. A total of 169.59 Gb clean data were obtained, with more than 5.82 Gb clean data in each sample.

The differentially expressed genes (DEGs) in different comparisons were shown in Venn diagrams (Figure 5). In FJ, there were 2,882 upregulated genes and 2,935 downregulated genes in F1 vs. F2, 800 upregulated genes and 817 downregulated genes in F2 vs. F3, and 1,221 upregulated genes and 3,459 downregulated genes in F3 vs. F4 (Figures 5A,D). In HJ, there were 2,282 upregulated genes and 2,047 downregulated genes in H1 vs. H2, 534 upregulated genes and 1,505 downregulated genes in H2 vs. H3, and 1,838 upregulated genes and 3,783 downregulated genes in H3 vs. H4 (Figures 5B,E). There was a greater number of upregulated genes in FJ than in HJ in D2 and D3, indicating more stable homeostasis in HJ in the early stage. Besides, the DEGs between FJ and HJ in each time were also analyzed (Figures 5C,F). There were 2,282 upregulated genes and 2,047 downregulated genes in F1 vs. H1, 534

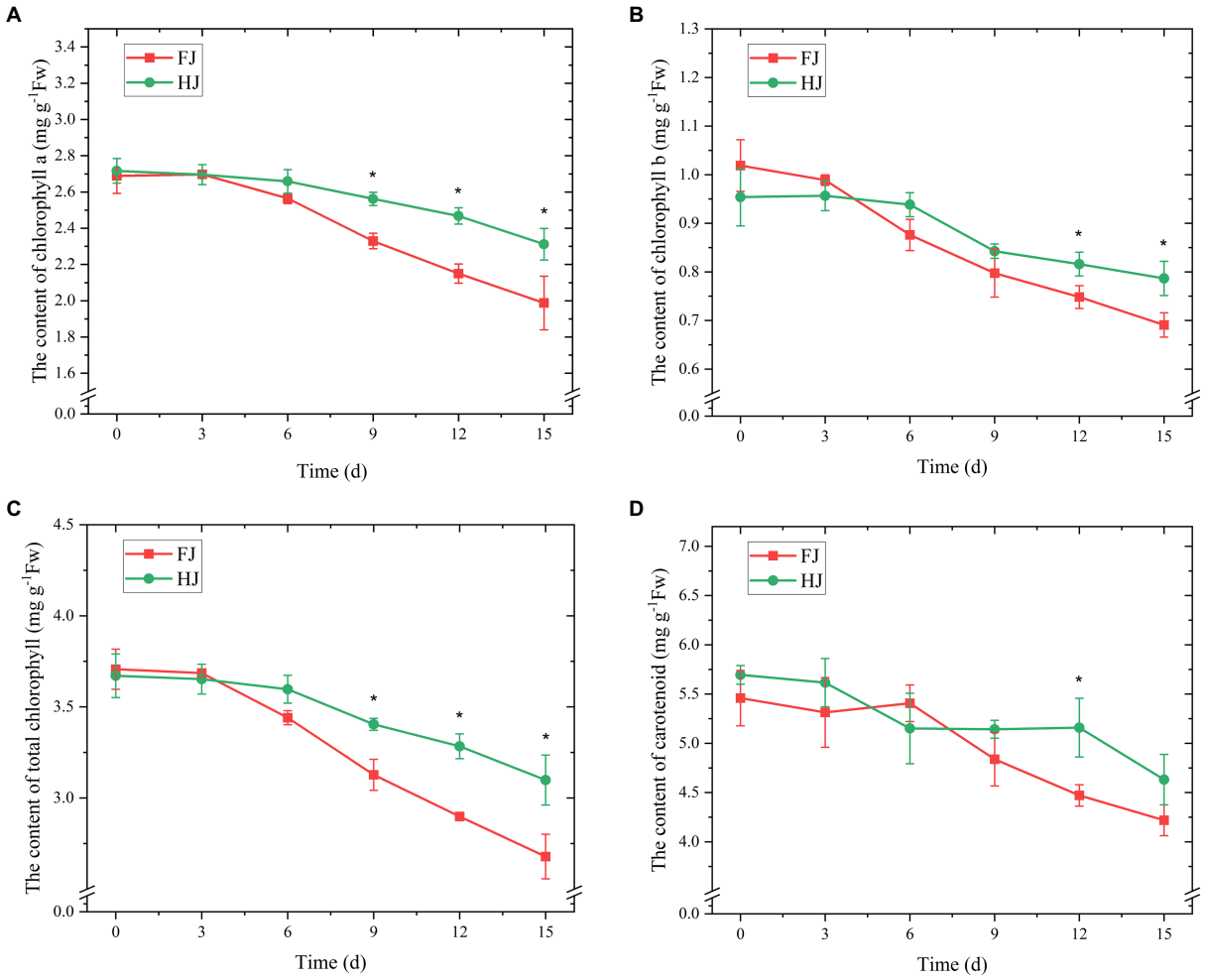


FIGURE 3
The content of chlorophyll *a* **(A)**, chlorophyll *b* **(B)**, total chlorophyll **(C)**, and carotenoids **(D)** of *Zanthoxylum bungeanum* leaves under drought stress. All data are mean±standard error of three replicates. Values with asterisks indicate significant differences at $p<0.05$ between FJ and HJ based on one-way ANOVA.

upregulated genes and 1,505 downregulated genes in F2 vs. H2, 1,838 upregulated genes and 3,783 downregulated genes in F3 vs. H3, and 534 upregulated genes and 1,505 downregulated genes in F4 vs. H4.The overlap of DEGs across all stages can provide insight into the response mechanism of plants to drought stress. The overlap analysis revealed that there were 39 upregulated genes and seven downregulated genes over the four stages in FJ and eight upregulated genes and 62 downregulated genes over the four stages in HJ.

To further explore the function of the DEGs, GO and KEGG enrichment analysis were performed (Figure 6). The upregulated genes were mainly enriched on hormone signaling transportation in both FJ and HJ, such as plant hormone signal transduction (ko04075) and MAPK signaling pathway—plant (ko04016), and metabolism of metabolites, including alanine, aspartate and glutamate metabolism (ko00250), and galactose metabolism (ko00052; Figures 6A,B). Interestingly, two photosynthesis related pathways, named photosynthesis (ko00195) and photosynthesis—antenna proteins (ko00196), were significantly enriched by downregulated genes in both FJ and HJ (Figures 6D,E). Between FJ and HJ, the DEGs with upregulation in HJ were mainly enriched in flavonoid biosynthesis (ko00941), brassinosteroid biosynthesis (ko00905), phenylpropanoid biosynthesis (ko00940) and MAPK signaling pathway—plant (ko04016; Figure 6C). The DEGs with downregulation in HJ were significantly enriched in biosynthesis of amino acids (ko01230), biosynthesis of unsaturated fatty acids (ko01040), starch and sucrose metabolism (ko00500), and glutathione metabolism (ko00480; Figure 6F). The results suggested drought response metabolism may diverse between two *Z. bungeanum* cultivars. Furthermore, DEGs upregulated in F3 vs. H3 significantly enriched in anthocyanin biosynthesis (ko00942), sulfur metabolism (ko00920), phenylpropanoid biosynthesis (ko00940) and flavonoid biosynthesis (ko00941; Supplementary Figure 2A). DEGs upregulated in F4 vs. H4

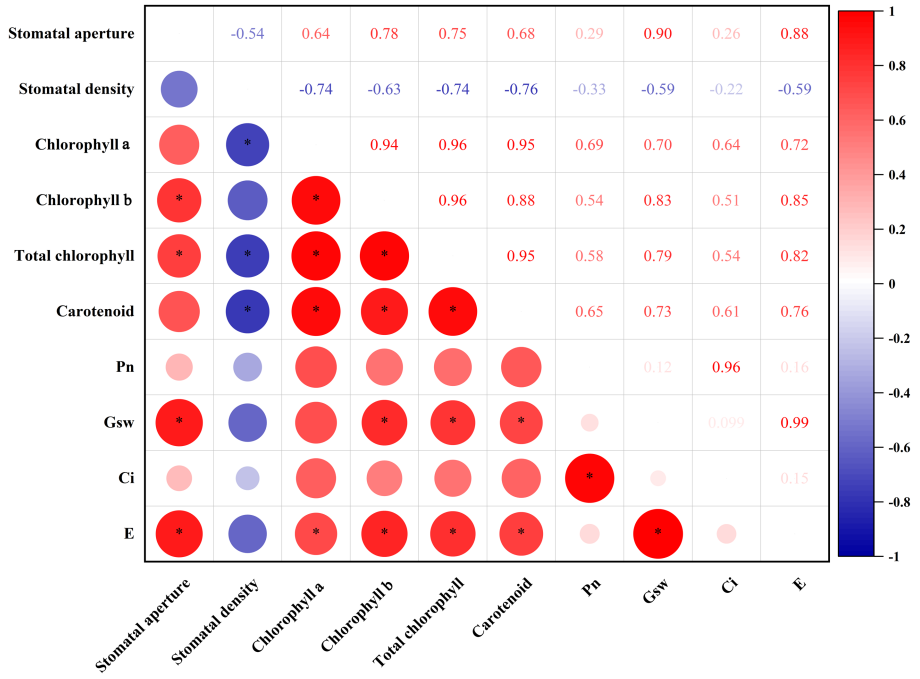


FIGURE 4
Intragroup correlation analysis of photosynthesis-related indicators. The size of the circles in the lower triangles indicates the strength of the correlation. Red indicates positive correlations; blue indicates negative correlations. Significant correlations (p<0.05) are indicated by asterisks. The numbers in the upper triangles indicate the correlation coefficients between two indicators. Pn, net photosynthetic rate; Gsw, stomatal conductance; Ci, sub-stomatal CO_2 concentration; and E, transpiration rate.

significantly enriched in phenylpropanoid biosynthesis (ko00940), biosynthesis of various secondary metabolites—part 2 (ko00998), phenylalanine metabolism (ko00360), MAPK signaling pathway—plant (ko04016), brassinosteroid biosynthesis (ko00905) and tyrosine metabolism (ko00350; Supplementary Figure 2B). These results suggested that the enhanced MAPK signal transduction, the activated synthesis of brassinosteroid, and the flavonoids metabolism may be responsible for the enhanced drought tolerance of HJ in the late stage of drought.

Furthermore, GO analysis was carried out on these downregulated DEGs in FJ and HJ under drought stress and the upregulated DEGs in FJ vs. HJ (Figures 6G–I). In FJ, seven of the top 20 GO terms were associated with photosynthesis, including photosynthesis (GO:0015979), photosystem (GO:0009521), photosystem I (GO:0009522), photosynthetic membrane (GO:0034357), chlorophyll binding (GO:0016168), photosynthesis, light harvesting (GO:0009765) and photosynthesis, light reaction (GO:0019684; Figure 6G; Supplementary Table 2). There were eight GO terms included in the top 20 GO terms in HJ, consisting of the seven aforementioned GO terms in FJ and photosynthesis, light harvesting in photosystem I (GO:0009768; Figure 6H; Supplementary Table 3). The results indicated that the weakened photosynthesis rate by drought stress may be resulted from the downregulation of photosynthesis related genes. Most of the top 20 GO terms in FJ and HJ belong to cellular component, indicating drought stress greatly influenced the cellular component in *Z. bungeanum* seedlings. Differently, most of the top 20 GO terms in FJ vs. HJ belong to molecular function (Figure 6I; Supplementary Table 4).

Weighted gene co-expression network analysis of DEGs under drought stress

WGCNA was performed based on the DEGs and physiological indicators (Figure 7). Totally, 11 modules with high gene co-expression were generated (Figure 7A). The correlation analysis among 11 modules was visualized using a heatmap (Supplementary Figure 3). There were positive correlations among the green-yellow, magenta, light-cyan, purple, green and tan modules ($R > 0.55$, $p < 0.01$).

Among these 11 modules, four contained more than 1,000 DEGs, and they were purple module (1,012 DEGs), black module (1,128 DEGs), blue module (1,137 DEGs) and turquoise module (1,488 DEGs), respectively (Figure 7B). Four modules (green-yellow, light-cyan, purple, and green) were positively correlated with most of the indicators and their expression patterns are displayed in Figure 7C ($R > 0.55$, $p < 0.005$). Among them, the purple module had a higher correlated coincidence with most indicators. Additionally, the green module was mostly positively related to Pn ($R = 0.63$, $p = 0.001$) and Ci ($R = 0.58$, $p = 0.003$). Besides, the gene expression level in cyan module increased under

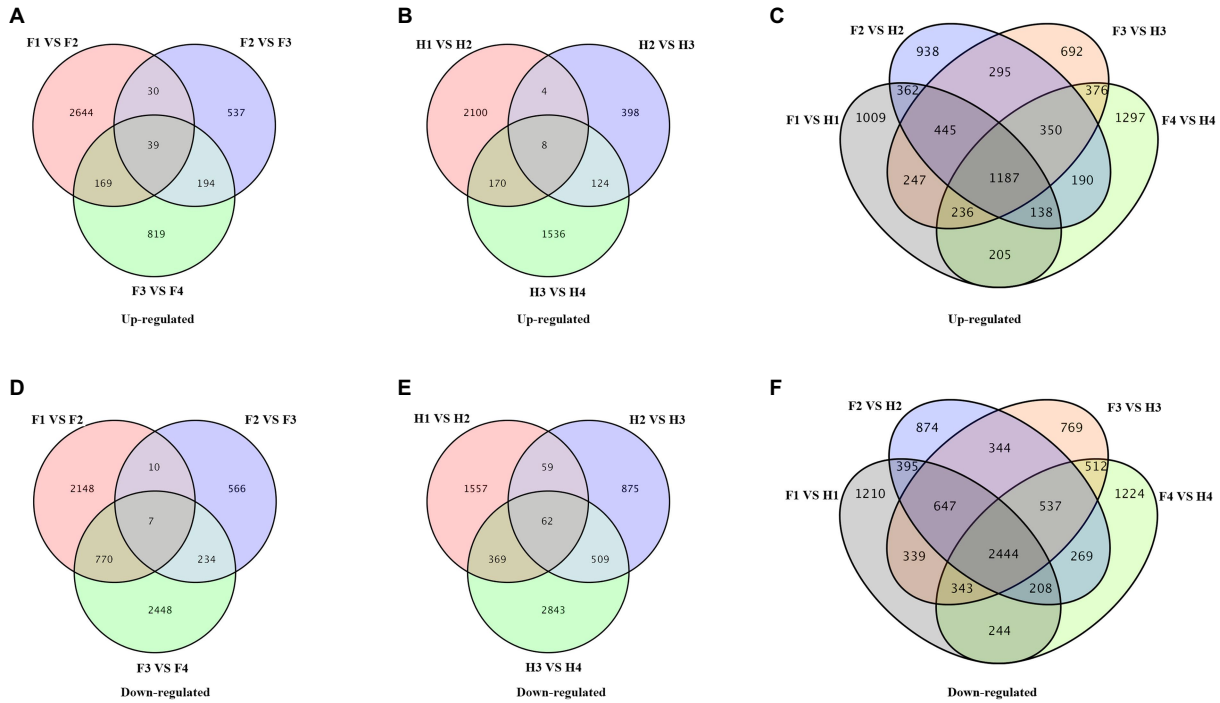


FIGURE 5
Venn diagrams of differentially expressed genes (DEGs) in different comparisons. **(A–C)** Venn diagrams of upregulated genes. **(D–F)** Venn diagrams of downregulated genes. F1, F2, F3, and F4 indicate FJ samples in 0, 6, 9, and 15 days under drought stress; H1, H2, H3, and H4 indicate HJ samples in 0, 6, 9, and 15 days under drought stress.

progressive drought and was higher in HJ than in FJ. Taken together, the green, purple and cyan modules were selected for further study.

The closure of stomata is one of the most important epigenetic changes in response to adverse environment, which is regulated by ABA. Interestingly, several genes encoding ABA signaling were included in purple module, including two *PYL4* (*EVM0086678*, *EVM0056698*), one *PYL9* (*EVM0004250*) and one *PYR1* (*EVM0057346*), and the expression level of these four genes decreased with drought treatment, which was consistent with most photosynthesis indicators (Supplementary Table 5).

Co-expression network of DEGs in green, purple, and cyan modules

The co-expression networks were constructed using the top 150 core genes in green, purple, and cyan modules (Figures 8A–C). In the green module, four genes (*LHCB4.3*, *LHCA4*, *LHCB4.2*, and *CAB-151*) were enriched in photosynthesis—antenna proteins (ko00196), and one gene (*psbW*) was enriched in photosynthesis (ko00195; Supplementary Figure 4A; Supplementary Table 6). In purple module, one gene (*CAB8*) was enriched in photosynthesis—antenna proteins (ko00196), six genes (three *PSAN*s, two *PSAF*s, and one *PSBQ2*) were enriched in photosynthesis (ko00195), and six genes (three *CHLH*s, *CRD1*, *HEMA1*, and *PORA*) were enriched in porphyrin and chlorophyll metabolism (ko00860; Supplementary Figure 4B; Supplementary Table 7). The expression pattern of these 19 photosynthesis related genes was analyzed (Supplementary Figure 5). The expression level of all these genes decreased with drought and six of them showed higher expression level in HJ than in FJ under drought stress, including *PSAN* (*EVM0004914*), *LHCB4.3* (*EVM0014783*), *CHLH*s (*EVM0019653*, *EVM0057103*), *PORA* (*EVM0025664*), and *CRD1* (*EVM0071735*). Therefore, these six photosynthesis related genes may be helpful to maintain higher photosynthesis in *Z. bungeanum* seedlings.

In cyan module, the biosynthesis and metabolism of metabolites were significantly enriched, including flavonoids, terpenoids, amino acids, fatty acids, etc. (Supplementary Figure 4C; Supplementary Table 8). Notably, these metabolites are closely related to enhancing the drought resistance of plants. TFs play important roles in regulating the gene expressions in various life processes. A total of seven TF genes were identified, including 3 *WRKY*s (*WRKY6*, *WRKY33*, *WRKY48*), 2 *BZIP*s (*BZIP23*, *GBF4*), *C2H2* (*IDD1*), and *GRAS* (*SCL14*; Supplementary Table 9). The phylogenetic analysis and *cis*-acting element analysis of these seven TFs were performed (Figure 8D). The phylogenetic analysis showed that the TFs belonging to the same family clustered together, indicating they were similar in sequence structure and molecular function. The

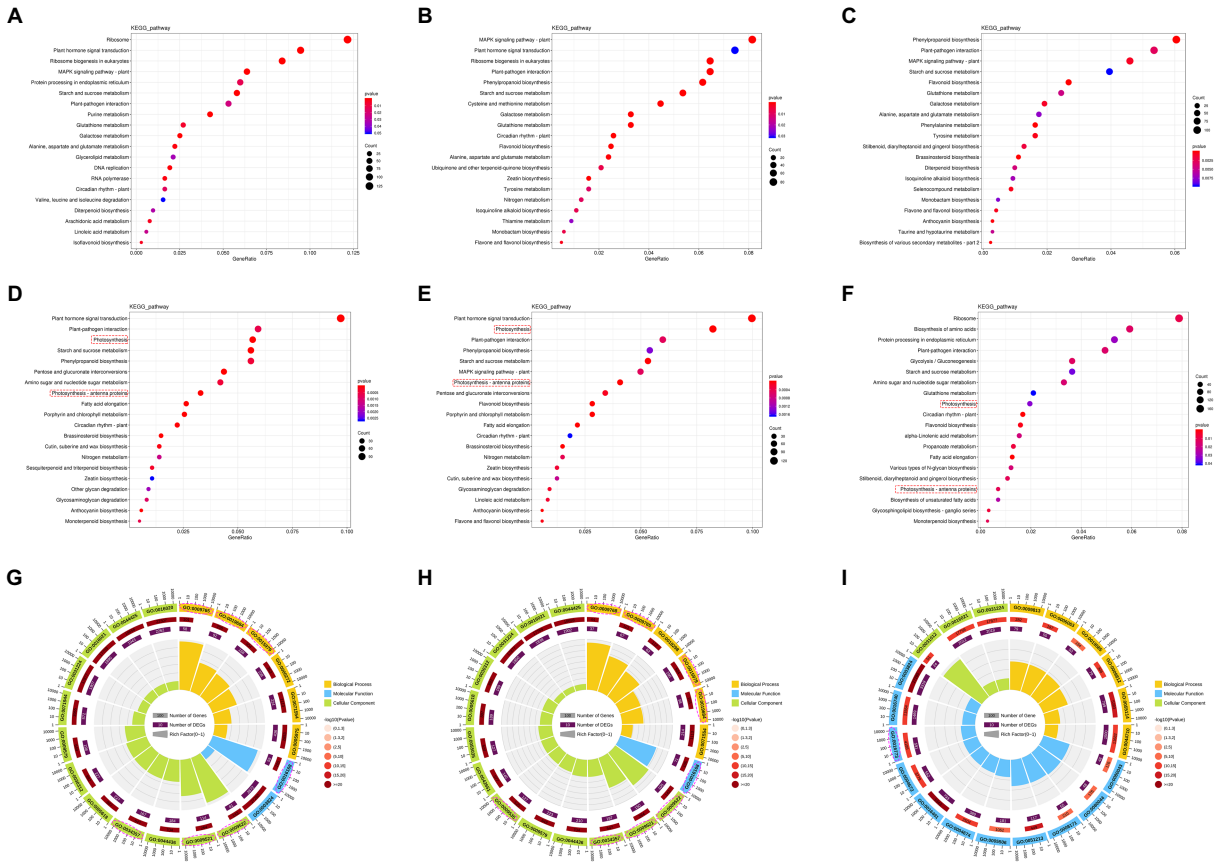


FIGURE 6
KEGG and GO enrichment analysis of DEGs in FJ and HJ. **(A)** Bubble diagram of the top 20 KEGG pathways of the upregulated genes in FJ. Bubble size indicates the number of DEGs enriched in KEGG pathways; bubble color indicates *p*-values. **(B)** Bubble diagram of the top 20 KEGG pathways of upregulated genes in FJ. **(C)** Bubble diagram of the top 20 KEGG pathways of upregulated genes in FJ vs. HJ. **(D)** Bubble diagram of the top 20 KEGG pathways of downregulated genes in FJ. **(E)** Bubble diagram of the top 20 KEGG pathways of downregulated genes in HJ. **(F)** Bubble diagram of the top 20 KEGG pathways of downregulated genes in FJ vs. HJ. **(G)** GO enrichment circle diagram of downregulated genes in FJ. The outer ring indicates the top 20 GO terms; the middle ring indicates the numbers of all genes in the GO terms and *p*-values for gene enrichment for the specified GO terms; and the inner ring indicates the numbers of DEGs. The ladder column in the center indicates the Rich factor of DEGs for each GO term. **(H)** GO enrichment circle diagram of downregulated genes in HJ. **(I)** GO enrichment circle diagram of downregulated genes in FJ vs. HJ. The pink dotted box and circle indicate the photosynthetic KEGG pathway and GO terms, respectively.

cis-acting elements were divided into 11 categories, including light responsiveness, drought responsiveness, low-temperature responsiveness and plant hormone responsiveness. The elements enriched in light responsiveness and drought responsiveness were widely existed in the promoters of the seven TFs, implying the important functions of these TFs in *Z. bungeanum* plant photosynthesis under drought stress (Figure 8E). In order to analyze the expression pattern of these seven TF genes, qRT-PCR was performed for two *Z. bungeanum* cultivar leaves under drought conditions. As shown in Figure 9, the relative expression level of these seven TF genes increased steadily and reach the peak value at D4 in both FJ and HJ. Besides, the relative expression level was higher in HJ than in FJ, especially in D3 and D4. The relative expression level in qRT-PCR was consistent to FPKM in RNA-seq, which validated the reliability of our transcriptome data.

Discussion

Drought negatively affects crop quality and yield, and photosynthesis is an essential metabolic process for carbon assimilation in plants. Therefore, the studies of the effects of drought on photosynthesis have been widely studied in many crops, such as melon (Chevilly et al., 2021), apple (Tan et al., 2017), rice (Todaka et al., 2017), and barley (Daszkowska-Golec et al., 2019). However, in *Z. bungeanum*, the effects of drought on photosynthesis and the underlying molecular mechanism remain unexplored. Here, we monitored photosynthesis indicators in two *Z. bungeanum* cultivars (FJ and HJ) under drought stress and explored the molecular mechanism of photosynthesis changes combining transcriptome data.

Photosynthesis is a complex metabolic process that is affected by multiple factors such as water, CO_2 concentration, and light

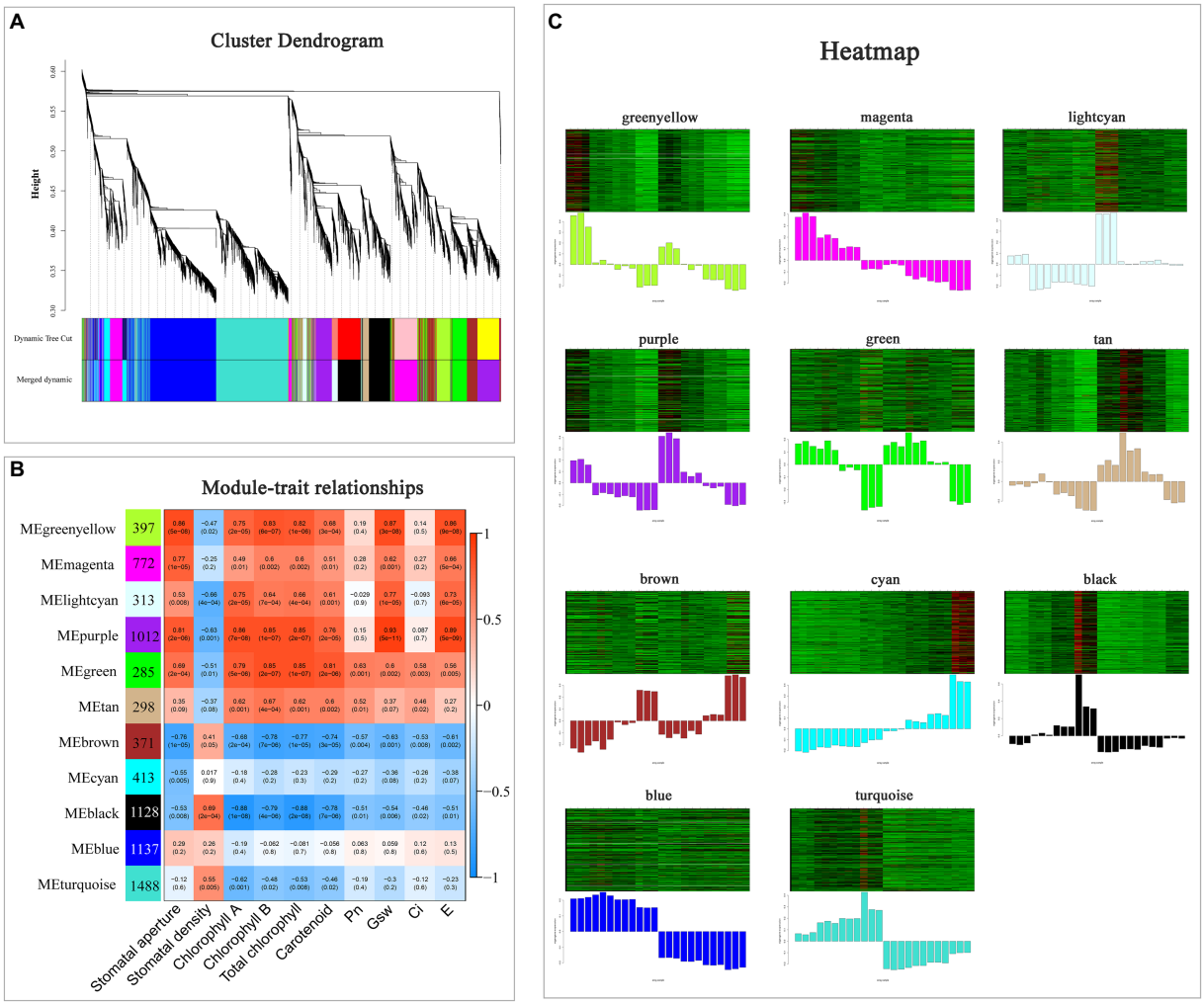


FIGURE 7
Weighted gene co-expression network analysis of DEGs under drought stress. **(A)** Cluster dendrogram of all DEGs. **(B)** Module–trait relationship heatmap of 11 modules and 10 physiological indicators. **(C)** Gene expression heatmaps of 11 modules. The column diagrams below show variation in the genes in specific modules.

(Evans, 2013). The physiological state of plants is also an important limiting factor for photosynthesis. Given that biochemical reactions *in vivo* are catalyzed by enzymes, activities of photosynthesis related enzymes, such as ribulose-1,5-bisphosphate carboxylase/oxygenase, could affect the rate of photosynthesis (Reddy et al., 2004). Besides, photosynthesis is often used as an important evaluation index for the healthy state of plants under abiotic stress conditions. When faced with environmental stress, photosynthesis usually declines sharply and this leads to the inhibition of plant growth and development, which results in a decline in crop quality and yield (Bhagat et al., 2014). In *Z. bungeanum*, the photosynthetic rate increased before 6 d and then decreased dramatically, and a similar pattern was observed for Ci. The initial increase in photosynthesis might stem from the stimulatory effect of abiotic stress. Besides, there was a positive correlation relationship between Pn and Ci ($R = 0.71$, $p < 0.05$). The aforementioned results were in accordance with that the CO_2 concentration is a key limitation factor to photosynthesis (Wang et al., 2015). Generally speaking, stress-tolerance can protect plants from the disturbance of surrounding environmental stress to a certain extent, which help maintain better quality and higher yield (Sun et al., 2013; Ma et al., 2016; Li et al., 2019). Consistently, we found that drought-tolerant *Z. bungeanum* cultivar HJ exhibited a higher photosynthesis in the late drought period than FJ. Given that sugars play a part in osmotic protection (Sánchez et al., 1998), maintaining higher photosynthesis in turn enhances plant resistance by the provision of more soluble sugars.

Stomata are composed of two guard cells and facilitate gas exchange; they thus play important metabolic roles in processes such as photosynthesis, transpiration, and respiration (Lawson, 2009). Stomatal activity is easily affected by water deficit stress, which could affect the CO_2 absorption and further influenced the photosynthesis (Osakabe et al., 2014). When suffered water stress, ion- and water-transport systems across membranes regulate the turgor pressure in

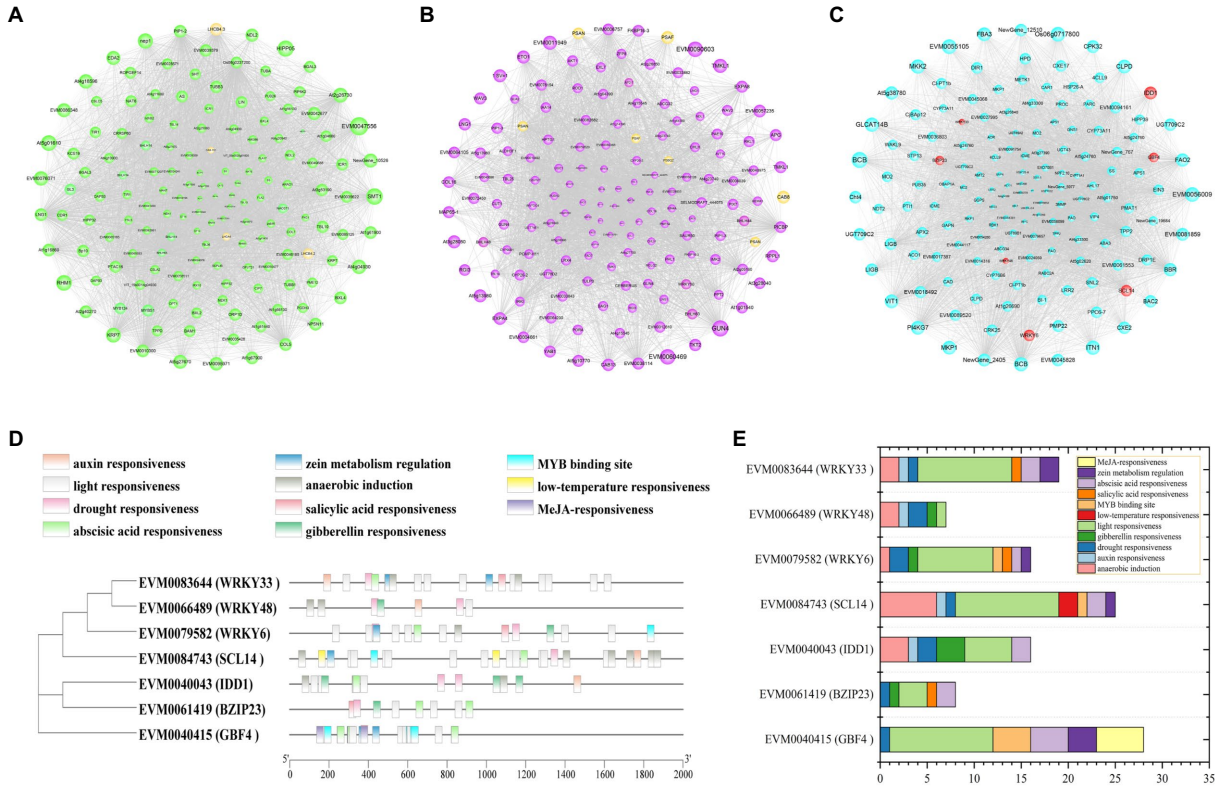


FIGURE 8
Co-expression network analysis of DEGs. **(A)** Co-expression network of 150 core DEGs in the green module. **(B)** Co-expression network of 150 core DEGs in the purple module. **(C)** Co-expression network of 150 core DEGs in the cyan module. The yellow bubbles show the genes enriched in photosynthetic related pathway. The red bubbles indicate the transcription factor genes. Bubble size indicates the connectivity degree. **(D)** *cis*-element locations in the promoters of seven TF genes identified in co-expression network in cyan module. **(E)** Statistics of *cis*-elements in each TF gene.

guard cells and induce stomatal closure (Osakabe et al., 2014). Endogenous ABA produced under drought stress also regulates the stomatal closure by a signal transduction network (Desikan et al., 2004). Morphological observations of stomata displayed that the stomatal aperture of *Z. bungeanum* leaves was significantly decreased after drought stress, which was beneficial to reduce water loss and improve drought tolerance. The promoted stomatal closure was consistent with the research in rice seedlings under drought (Todaka et al., 2017). Notably, the enhanced drought tolerance generally comes at the cost of photosynthesis. The stomatal aperture in HJ was larger than in FJ in the late drought period, which was favorable for maintaining a relatively high photosynthetic efficiency in the HJ. Besides, E was positively correlated with stomatal conductance ($R=0.99$, $p<0.05$) and stomatal aperture ($R=0.88$, $p<0.05$), supporting that the transpiration rate is directly affected by the stomata (Outlaw and De Vlieghere-He, 2001).

In the photosynthesis process, light energy is captured by LHC proteins and transferred into Calvin-Benson cycle for carbon reduction (Rochaix and Bassi, 2019). In photosynthetic electron transport reactions, the electrons are derived from water and then transferred from PSII to PSI. Thus, the weakened transpiration in *Z. bungeanum* played a negative role in photosynthesis. Chlorophyll *a* and chlorophyll *b* are the major pigments in PSI and PSII, which are responsible for the light energy capture in LHC. Besides, carotenoids play a pivotal role in photoprotection (Bassi and Caffarri, 2000). In this study, the contents of chlorophyll *a*, chlorophyll *b* and carotenoids were decreased in *Z. bungeanum* leaves under drought stress, which caused the decreased photosynthesis rate (Liang et al., 2018; Gao et al., 2020). However, the chlorophyll *a* and chlorophyll *b* contents were higher in HJ than in FJ after 12 days, which may be responsible for the higher photosynthesis in HJ in the late drought stage. Porphyrin and chlorophyll metabolism plays various important physiological roles in plant (Ma et al., 2021). In our study, KEGG analysis revealed that many DEGs were enriched in porphyrin and chlorophyll metabolism, indicated that there was a complex regulation underlying the chlorophyll concentration variation. Additionally, DEGs analysis in F3 vs. H3 and F4 vs. H4 suggested that MAPK signal transduction, the synthesis of brassinosteroid, and the flavonoids metabolism were stronger in HJ than in FJ. As reported, MAPK signal transduction cascades play a crucial role in the response to various abiotic stresses (He et al., 2020). Brassinosteroids widely take part in abiotic stress responses such as drought, salinity, high temperature, low temperature and heavy

metal stresses (Li et al., 2021c). As a kind of reductant, flavonoids could contribute to the mitigation of oxidative and enhanced drought tolerance (Nakabayashi et al., 2014; Li et al., 2021a). Taken together, these enhanced pathways may contribute to the higher drought tolerance in HJ.

WGCNA is a powerful tool that has been widely applied into physiological mechanism studies (Yu et al., 2020; Fei et al., 2021). To screen the important genes in photosynthesis, WGCNA was used combining DEGs and physiological indicators in photosynthesis in *Z. bungeanum*. The DEGs in two modules (purple and green) were positively correlated with most photosynthesis indicators. ABA is an important hormone involved in the response to drought stress, and ABA transduction signals play an important role in the activation of TFs and the regulation of the expression of downstream genes (Tuteja, 2007). At the same time, the status of stomata is sensitively regulated by ABA. In the purple module, several genes related to ABA metabolism were identified, including *PYL4* (*EVM0086678*, *EVM0056698*), *PYL9* (*EVM0004250*) and *PYR1* (*EVM0057346*). The dominant ABA-signaling inhibitor (FBPase::abi1-1) promotes biomass accumulation and elevated crop yields in transgenic *Arabidopsis* under drought stress (Negin et al., 2019). Therefore, these genes are thought to be the candidate genes for improving the photosynthesis in *Z. bungeanum* plant. In the co-expression network of the green module, the LHC-encoding gene, *LHCB4.3* (*EVM0014783*), was identified. Given the important role of LHC in light energy capture, the downregulated expression of *LHCB4.3* may decrease light utilization efficiency. In previous studies, inhibition of LCH protein synthesis has been shown to induce photoinhibition in PSII, which in turn caused more ROS accumulation (Pastenes et al., 2005; Guidi et al., 2019). Therefore, *LHCB4.3* was of great significance for the maintenance of photosynthesis and drought resistance in *Z. bungeanum*. In the co-expression network of the purple module, four genes, including *CRD1* (*EVM0071735*), *PORA* (*EVM0025664*) and two *CHLHs* (*EVM0019653*, *EVM0057103*), were selected, and they were enriched in the chlorophyll metabolic pathway, indicating that these four genes may be related to the change of chlorophyll content. However, in-depth research needs to be carried out to prove their function.

TFs are important proteins involved in the regulation of plant growth and development, as well as the response to abiotic stress (Lindemose et al., 2013). Many TFs have been shown to play key roles in the regulation of drought stress and photosynthesis, such as MYB, bZIP and DREB families (Saibo et al., 2009). In cyan module, a total of seven TF genes were identified, including 3

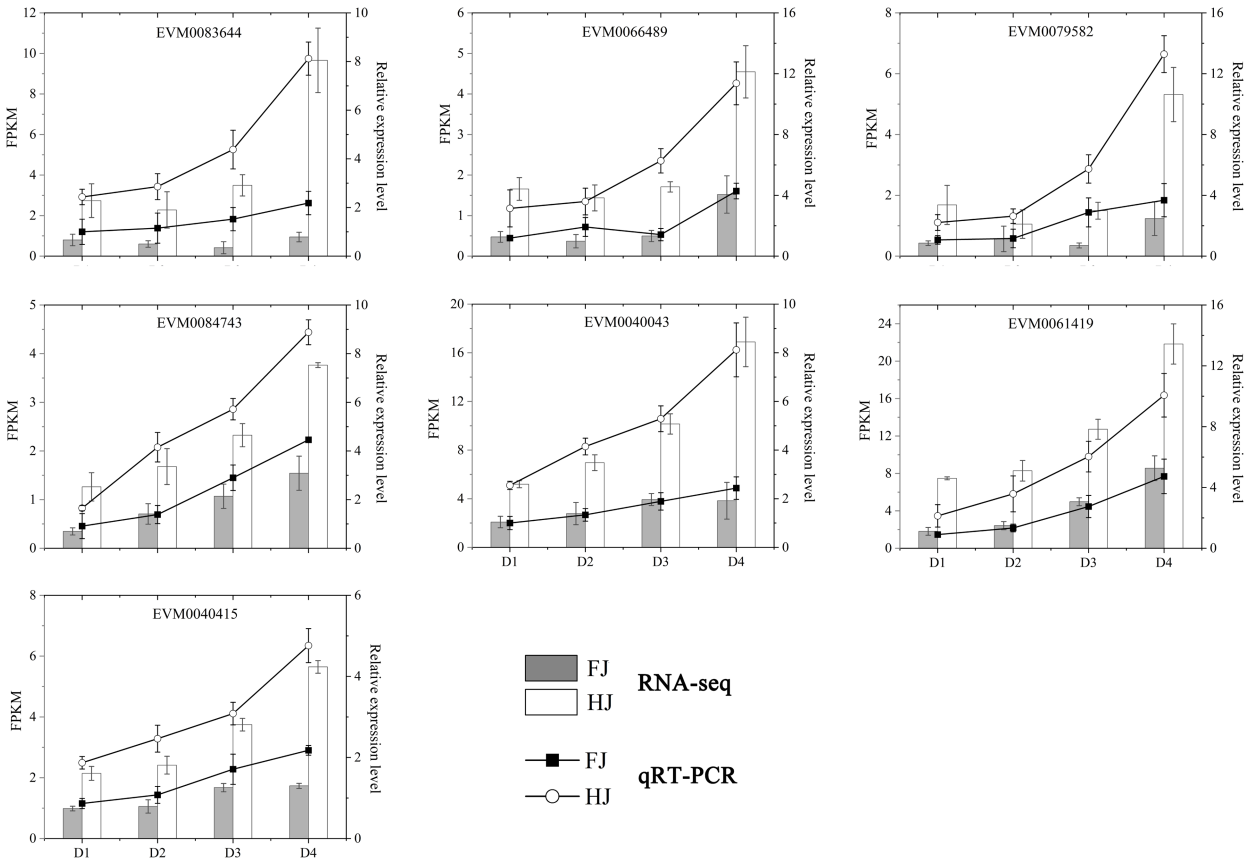


FIGURE 9
qRT-PCR validation of seven TF genes in co-expression networks. The column chart shows the FPKM values in RNA-seq data. The line diagram represents the relative expression level in qRT-PCR. D1, D2, D3, and D4 indicate 0, 6, 9, and 15 days under drought stress, respectively.

*WRKY*s (*WRKY6*, *WRKY33*, *WRKY48*), 2 *BZIP*s (*BZIP23*, *GBF4*), *C2H2* (*IDD1*) and *GRAS* (*SCL14*) and their expression levels increased under drought stress with higher expression level in HJ than in FJ. *Cis*-acting element analysis of these TFs revealed that a large number of light-responsive and drought-responsive binding sites were distributed in the upstream sequences. In addition, there were also some ABA-responsive binding sites in most TF gene promoters. Together, these results indicated that seven TFs play important roles in the regulation of photosynthesis under drought conditions. Previous research showed that overexpression of the TF encoding gene, *AP37*, elevated the grain yield under drought conditions with enhancing photosynthesis efficiency (Oh et al., 2009). Heterogeneous expression of maize TF *mEmBP-1* enlarged the photosynthesis, biomass, and yield in rice (Perveen et al., 2020). Overexpression of *VuNAC1* and *VuNAC2* promoted growth and stress tolerance by boosting photosynthetic activity in *Arabidopsis* (Srivastava et al., 2022). Therefore, we suspect that these TF genes are of great significance for improving yield of *Z. bungeanum* in the future.

In general, drought caused a decrease in photosynthesis in *Z. bungeanum* leaves through a stomatal-dependent pathway and a stomatal-independent pathway, which is displayed in Figure 10.

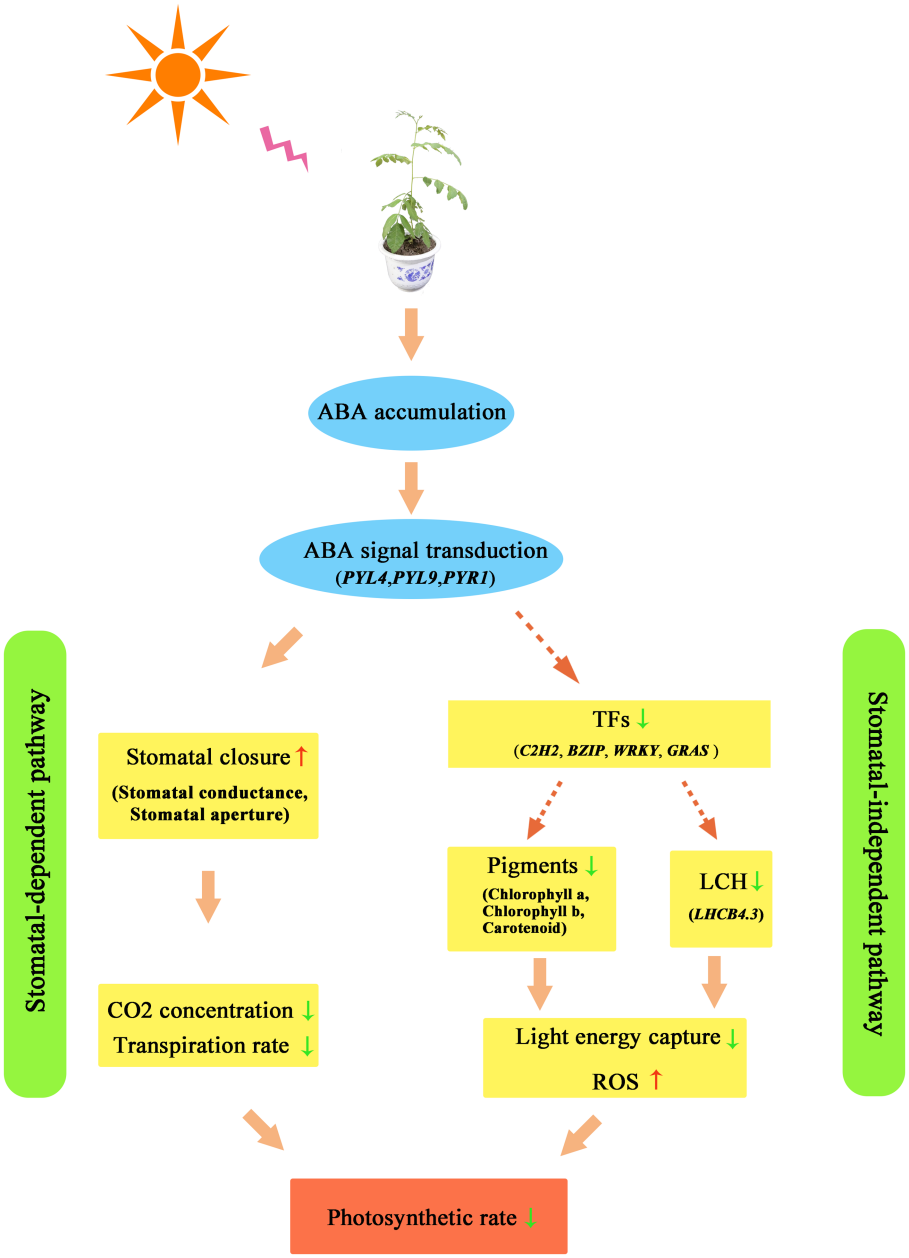


FIGURE 10
The photosynthesis response model in *Zanthoxylum bungeanum* under drought stress. TF, transcription factor; ROS, reactive oxygen species.

In the stomatal-dependent pathway, drought-induced ABA accumulation and activated ABA signaling, which resulted in stomatal closure. Then stomatal closure decreased Ci and inhibited E. In a stomatal-independent pathway, drought-induced ABA signaling is transmitted to TF proteins. The TFs affected the light energy capture and transformation efficiency by regulating the expression of genes related to chlorophyll metabolism and LCH protein-encoding genes. The above two pathways jointly led to the decrease in the photosynthetic rate of *Z. bungeanum* under drought conditions.

Conclusion

In this study, the physiological indicators and molecular mechanisms of photosynthesis under drought stress were explored in two *Z. bungeanum* cultivars with diverse drought-tolerance. Drought resulted in a decrease in photosynthesis due to a decrease in stomatal aperture and Gsw, a descend in Ci and E, and a degradation of chlorophyll and carotenoid. However, in the late drought period, there was a higher photosynthetic rate in HJ, possibly due to higher chlorophyll content, larger stomatal aperture and higher Ci. Through WGCNA analysis, we identified genes involved in ABA signal transduction, LCH-encoding genes, and chlorophyll metabolism genes. In addition, we identified seven TF genes that may be important for regulating photosynthesis under drought conditions. Taken together, our study proposed a model of the photosynthetic in *Z. bungeanum* under drought stress, and the key genes we identified provide important clues for future molecular breeding.

Data availability statement

The data presented in the study are deposited in the NCBI repository, accession number PRJNA784034.

Author contributions

HH and AW designed the experiments. HH wrote the manuscript. HH, BH, LM, and XC supervised the research. XF and YLi revised the manuscript. HH, BH, YLu, and PH performed the experiments and data analysis. All authors contributed to the article and approved the submitted version.

Funding

This study was financially supported by the Technology Innovation Guidance Special Foundation of Shaanxi Province (2020QFY07-01).

Acknowledgments

The authors would like to thank Juan Xie from College of Horticulture in Northwest A&F University for her help in our experiment.

Conflict of interest

The authors declare that the research was conducted in the absence of any commercial or financial relationships that could be construed as a potential conflict of interest.

Publisher's note

All claims expressed in this article are solely those of the authors and do not necessarily represent those of their affiliated organizations, or those of the publisher, the editors and the reviewers. Any product that may be evaluated in this article, or claim that may be made by its manufacturer, is not guaranteed or endorsed by the publisher.

Supplementary material

The Supplementary material for this article can be found online at: https://www.frontiersin.org/articles/10.3389/fpls.2022.968714/full#supplementary-material

References

Bassi, R., and Caffarri, S. (2000). Lhc proteins and the regulation of photosynthetic light harvesting function by xanthophylls. *Photosynth. Res.* 64:256. doi: 10.1023/a:1006409506272

Basu, S., Ramegowda, V., Kumar, A., and Pereira, A. (2016). Plant adaptation to drought stress. *F1000Res* 5:1554. doi: 10.12688/f1000research.7678.1

Bhagat, K. P., Kumar, R. A., Ratnakumar, P., Kumar, S., Bal, S. K., and Agrawal, P. K. (2014). "Photosynthesis and associated aspects Under abiotic stresses environment," in *Approaches to Plant Stress and Their Management*. eds. R. K. Gaur and P. Sharma (New Delhi: Springer India), 191–205.

Chen, C., Chen, H., Zhang, Y., Thomas, H., Frank, M., He, Y., et al. (2020). TBtools: an integrative toolkit developed for interactive analyses of big biological data. *Mol. Plant* 13, 1194–1202. doi: 10.1016/j.molp.2020.06.009

Chevilly, S., Dolz-Edo, L., Martínez-Sánchez, G., Morcillo, L., Vilagrosa, A., López-Nicolás, J. M., et al. (2021). Distinctive traits for drought and salt stress tolerance in melon (Cucumis melo L.). front. *Plant Sci.* 12:777060. doi: 10.3389/fpls.2021.777060

Dai, A. (2013). Increasing drought under global warming in observations and models. *Nat. Clim. Chang.* 3, 52–58. doi: 10.1038/nclimate1633

D'Alessandro, S., and Havaux, M. (2019). Sensing β-carotene oxidation in photosystem II to master plant stress tolerance. *New Phytol.* 223, 1776–1783. doi: 10.1111/nph.15924

Daszkowska-Golec, A., Collin, A., Sitko, K., Janiak, A., Kalaji, H. M., and Szarejko, I. (2019). Genetic and physiological dissection of photosynthesis in barley exposed to drought stress. *Int. J. Mol. Sci.* 20:6341. doi: 10.3390/ijms20246341

Desikan, R., Cheung, M. K., Bright, J., Henson, D., Hancock, J. T., and Neill, S. J. (2004). ABA, hydrogen peroxide and nitric oxide signalling in stomatal guard cells. *J. Exp. Bot.* 55, 205–212. doi: 10.1093/jxb/erh033

Evans, J. R. (2013). Improving photosynthesis. *Plant Physiol.* 162, 1780–1793. doi: 10.1104/pp.113.219006

Fathi, A., and Barari, D. (2016). Effect of drought stress and its mechanism in plants. *Int. J. Life Sci.* 10:1. doi: 10.3126/ijls.v10i1.14509

Fei, X., Qi, Y., Lei, Y., Wang, S., Hu, H., and Wei, A. (2021). Transcriptome and Metabolome dynamics explain aroma differences between green and red prickly ash fruit. *Foods* 10:391. doi: 10.3390/foods10020391

Fei, X., Shi, Q., Yang, T., Fei, Z., and Wei, A. (2018). Expression stabilities of ten candidate reference genes for RT-qPCR in *Zanthoxylum bungeanum* maxim. *Molecules* 23:802. doi: 10.3390/molecules23040802

Feng, S., Liu, Z., Hu, Y., Tian, J., Yang, T., and Wei, A. (2020). Genomic analysis reveals the genetic diversity, population structure, evolutionary history and relationships of Chinese pepper. *Hortic. Res.* 7:158. doi: 10.1038/s41438-020-00376-z

Gao, T., Zhang, Z., Liu, X., Wu, Q., Chen, Q., Liu, Q., et al. (2020). Physiological and transcriptome analyses of the effects of exogenous dopamine on drought tolerance in apple. *Plant Physiol. Biochem.* 148, 260–272. doi: 10.1016/j.plaphy.2020.01.022

Guidi, L., Lo Piccolo, E., and Landi, M. (2019). Chlorophyll fluorescence, Photoinhibition and abiotic stress: does it make Any difference the fact to be a C3 or C4 species? *Front. Plant Sci.* 10:174. doi: 10.3389/fpls.2019.00174

Gururani, M. A., Venkatesh, J., and Tran, L. S. P. (2015). Regulation of photosynthesis during abiotic stress-induced Photoinhibition. *Mol. Plant* 8, 1304–1320. doi: 10.1016/j.molp.2015.05.005

He, X., Wang, C., Wang, H., Li, L., and Wang, C. (2020). The function of MAPK cascades in response to various stresses in horticultural plants. *Front. Plant Sci.* 11:952. doi: 10.3389/fpls.2020.00952

Hong, Y., Wang, Z., Liu, X., Yao, J., Kong, X., Shi, H., et al. (2020). Two chloroplast proteins negatively regulate plant drought resistance Through separate pathways. *Plant Physiol.* 182, 1007–1021. doi: 10.1104/pp.19.01106

Huang, Z., Shen, L., Wang, W., Mao, Z., Yi, X., Kuang, T., et al. (2021). Structure of photosystem I-LHCI-LHCII from the green alga Chlamydomonas reinhardtii in state 2. *Nat. Commun.* 12:1100. doi: 10.1038/s41467-021-21362-6

Kaiser, E., Morales, A., Harbinson, J., Kromdijk, J., Heuvelink, E., and Marcelis, L. F. (2015). Dynamic photosynthesis in different environmental conditions. *J. Exp. Bot.* 66, 2415–2426. doi: 10.1093/jxb/eru406

Kim, D., Langmead, B., and Salzberg, S. L. (2015). HISAT: a fast spliced aligner with low memory requirements. *Nat. Methods* 12, 357–360. doi: 10.1038/nmeth.3317

Langfelder, P., and Horvath, S. (2008). WGCNA: an R package for weighted correlation network analysis. *BMC Bioinformatics* 9:559. doi: 10.1186/1471-2105-9-559

Lawson, T. (2009). Guard cell photosynthesis and stomatal function. *New Phytol.* 181, 13–34. doi: 10.1111/j.1469-8137.2008.02685.x

Li, B., Fan, R., Sun, G., Sun, T., Fan, Y., Bai, S., et al. (2021a). Flavonoids improve drought tolerance of maize seedlings by regulating the homeostasis of reactive oxygen species. *Plant and Soil* 461, 389–405. doi: 10.1007/s11104-020-04814-8

Li, P., Ruan, Z., Fei, Z., Yan, J., and Tang, G. (2021b). Integrated Transcriptome and Metabolome analysis revealed That flavonoid biosynthesis may dominate the resistance of *Zanthoxylum bungeanum* against stem canker. *J. Agric. Food Chem.* 69, 6360–6378. doi: 10.1021/acs.jafc.1c00357

Li, S. Y., Wang, W. B., Yao, X. D., Wang, C. L., Cao, Y. Q., Zhang, L. J., et al. (2019). Photosynthesis in reciprocal grafts of drought-tolerant and drought-sensitive cultivars of soybean under water stress. *Photosynthetica* 57, 942–949. doi: 10.32615/ps.2019.109

Li, S., Zheng, H., Lin, L., Wang, F., and Sui, N. (2021c). Roles of brassinosteroids in plant growth and abiotic stress response. *Plant Growth Regul.* 93, 29–38. doi: 10.1007/s10725-020-00672-7

Liang, B., Ma, C., Zhang, Z., Wei, Z., Gao, T., Zhao, Q., et al. (2018). Long-term exogenous application of melatonin improves nutrient uptake fluxes in apple plants under moderate drought stress. *Environ. Exp. Bot.* 155, 650–661. doi: 10.1016/j.envexpbot.2018.08.016

Lima-Melo, Y., Kılıç, M., Aro, E. M., and Gollan, P. J. (2021). Photosystem I inhibition, protection and Signalling: Knowns and unknowns. *Front. Plant Sci.* 12:791124. doi: 10.3389/fpls.2021.791124

Lindemose, S., O'Shea, C., Jensen, M. K., and Skriver, K. (2013). Structure, function and networks of transcription factors involved in abiotic stress responses. *Int. J. Mol. Sci.* 14, 5842–5878. doi: 10.3390/ijms14035842

Ma, X., Xia, H., Liu, Y., Wei, H., Zheng, X., Song, C., et al. (2016). Transcriptomic and Metabolomic studies disclose key metabolism pathways contributing to well-maintained photosynthesis under the drought and the consequent drought-tolerance in Rice. *Front. Plant Sci.* 7:1886. doi: 10.3389/fpls.2016.01886

Ma, Q., Xu, X., Xie, Y., Huang, T., Wang, W., Zhao, L., et al. (2021). Comparative metabolomic analysis of the metabolism pathways under drought stress in alfalfa leaves. *Environ. Exp. Bot.* 183:104329. doi: 10.1016/j.envexpbot.2020.104329

Nakabayashi, R., Mori, T., and Saito, K. (2014). Alternation of flavonoid accumulation under drought stress in Arabidopsis thaliana. *Plant Signal. Behav.* 9:e29518. doi: 10.4161/psb.29518

Negin, B., Yaaran, A., Kelly, G., Zait, Y., and Moshelion, M. (2019). Mesophyll Abscisic acid restrains early growth and flowering But does not directly suppress photosynthesis. *Plant Physiol.* 180, 910–925. doi: 10.1104/pp.18.01334

Oh, S.-J., Kim, Y. S., Kwon, C.-W., Park, H. K., Jeong, J. S., and Kim, J.-K. (2009). Overexpression of the transcription factor AP37 in Rice improves grain yield under drought conditions. *Plant Physiol.* 150, 1368–1379. doi: 10.1104/pp.109.137554

Okagu, I. U., Ndefo, J. C., Aham, E. C., and Udenigwe, C. C. (2021a). Zanthoxylum species: A comprehensive review of traditional uses, Phytochemistry, pharmacological and Nutraceutical applications. *Molecules* 26:4023. doi: 10.3390/molecules26134023

Okagu, I. U., Ndefo, J. C., Aham, E. C., and Udenigwe, C. C. (2021b). Zanthoxylum species: A review of traditional uses, Phytochemistry and pharmacology in relation to cancer, infectious diseases and sickle cell anemia. *Front. Pharmacol.* 12:713090. doi: 10.3389/fphar.2021.713090

Osakabe, Y., Osakabe, K., Shinozaki, K., and Tran, L.-S. P. (2014). Response of plants to water stress. *Front. Plant Sci.* 5:86. doi: 10.3389/fpls.2014.00086

Outlaw, W. H., and De Vlieghere-He, X. (2001). Transpiration rate. An important factor controlling the sucrose content of the guard cell apoplast of broad bean. *Plant Physiol.* 126, 1716–1724. doi: 10.1104/pp.126.4.1716

Pastenes, C., Pimentel, P., and Lillo, J. (2005). Leaf movements and photoinhibition in relation to water stress in field-grown beans. *J. Exp. Bot.* 56, 425–433. doi: 10.1093/jxb/eri061

Pertea, M., Pertea, G. M., Antonescu, C. M., Chang, T.-C., Mendell, J. T., and Salzberg, S. L. (2015). String tie enables improved reconstruction of a transcriptome from RNA-seq reads. *Nat. Biotechnol.* 33, 290–295. doi: 10.1038/nbt.3122

Perveen, S., Qu, M., Chen, F., Essemine, J., Khan, N., Lyu, M.-J. A., et al. (2020). Overexpression of maize transcription factor mEmBP-1 increases photosynthesis, biomass, and yield in rice. *J. Exp. Bot.* 71, 4944–4957. doi: 10.1093/jxb/eraa248

Reddy, A. R., Chaitanya, K. V., and Vivekanandan, M. (2004). Drought-induced responses of photosynthesis and antioxidant metabolism in higher plants. *J. Plant Physiol.* 161, 1189–1202. doi: 10.1016/j.jplph.2004.01.013

Rochaix, J.-D. (2013). Fine-tuning photosynthesis. *Science* 342, 50–51. doi: 10.1126/science.1244943

Rochaix, J.-D., and Bassi, R. (2019). LHC-like proteins involved in stress responses and biogenesis/repair of the photosynthetic apparatus. *Biochem. J.* 476, 581–593. doi: 10.1042/BCJ20180718

Saibo, N. J. M., Lourenço, T., and Oliveira, M. M. (2009). Transcription factors and regulation of photosynthetic and related metabolism under environmental stresses. *Ann. Bot.* 103, 609–623. doi: 10.1093/aob/mcn227

Sánchez, F. J., Manzanares, M. A., de Andres, E. F., Tenorio, J. L., and Ayerbe, L. (1998). Turgor maintenance, osmotic adjustment and soluble sugar and proline accumulation in 49 pea cultivars in response to water stress. *Field Crop Res* 59, 225–235. doi: 10.1016/S0378-4290(98)00125-7

Schmittgen, T. D., and Livak, K. J. (2008). Analyzing real-time PCR data by the comparative CT method. *Nat. Protoc.* 3, 1101–1108. doi: 10.1038/nprot.2008.73

Srivastava, R., Kobayashi, Y., Koyama, H., and Sahoo, L. (2022). Overexpression of cowpea NAC transcription factors promoted growth and stress tolerance by boosting photosynthetic activity in Arabidopsis. *Plant Sci.* 319:111251. doi: 10.1016/j.plantsci.2022.111251

Sun, J., Gu, J., Zeng, J., Han, S., Song, A., Chen, F., et al. (2013). Changes in leaf morphology, antioxidant activity and photosynthesis capacity in two different drought-tolerant cultivars of chrysanthemum during and after water stress. *Sci. Hortic.* 161, 249–258. doi: 10.1016/j.scienta.2013.07.015

Sun, M., Peng, F., Xiao, Y., Yu, W., Zhang, Y., and Gao, H. (2020). Exogenous phosphatidylcholine treatment alleviates drought stress and maintains the integrity of root cell membranes in peach. *Sci. Hortic.* 259:108821. doi: 10.1016/j.scienta.2019.108821

Tan, Y., Li, M., Yang, Y., Sun, X., Wang, N., Liang, B., et al. (2017). Overexpression of MpCYS4, A Phytocystatin Gene from Malus prunifolia (Willd.) Borkh., enhances Stomatal closure to confer drought tolerance in transgenic Arabidopsis and apple. Front. *Plant Sci.* 8:33. doi: 10.3389/fpls.2017.00033

Tian, J., Ma, Y., Tian, L., Huang, C., Chen, M., and Wei, A. (2021). Comparative physiology and transcriptome response patterns in cold-tolerant and cold-sensitive varieties of *Zanthoxylum bungeanum* maxim. *Ind. Crop Prod.* 167:113562. doi: 10.1016/j.indcrop.2021.113562

Todaka, D., Zhao, Y., Yoshida, T., Kudo, M., Kidokoro, S., Mizoi, J., et al. (2017). Temporal and spatial changes in gene expression, metabolite accumulation and phytohormone content in rice seedlings grown under drought stress conditions. *Plant J.* 90, 61–78. doi: 10.1111/tpj.13468

Tuteja, N. (2007). Abscisic acid and abiotic stress signaling. *Plant Signal. Behav.* 2, 135–138. doi: 10.4161/psb.2.3.4156

van Bezouwen, L. S., Caffarri, S., Kale, R. S., Kouřil, R., Thunnissen, A.-M. W. H., Oostergetel, G. T., et al. (2017). Subunit and chlorophyll organization of the plant photosystem II supercomplex. *Nat. Plants* 3:17080. doi: 10.1038/nplants.2017.80

Wang, C., Han, F., Chen, X., Zhao, A., and Wang, D. (2022). Time-series based metabolomics reveals the characteristics of the color-related metabolites during the different coloration stages of *Zanthoxylum bungeanum* peel. *Food Res. Int.* 155:111077. doi: 10.1016/j.foodres.2022.111077

Wang, Y., Stessman, D. J., and Spalding, M. H. (2015). The CO2 concentrating mechanism and photosynthetic carbon assimilation in limiting CO2: how Chlamydomonas works against the gradient. *Plant J.* 82, 429–448. doi: 10.1111/tpj.12829

Xue, Q., Fan, H., Yao, F., Cao, X., Liu, M., Sun, J., et al. (2020). Transcriptomics and targeted metabolomics profilings for elucidation of pigmentation in Lonicera japonica flowers at different developmental stages. *Ind. Crop Prod.* 145:111981. doi: 10.1016/j.indcrop.2019.111981

Yu, B., Liu, J., Wu, D., Liu, Y., Cen, W., Wang, S., et al. (2020). Weighted gene coexpression network analysis-based identification of key modules and hub genes associated with drought sensitivity in rice. *BMC Plant Biol.* 20:478. doi: 10.1186/s12870-020-02705-9

Zhang, A., Liu, M., Gu, W., Chen, Z., Gu, Y., Pei, L., et al. (2021). Effect of drought on photosynthesis, total antioxidant capacity, bioactive component accumulation, and the transcriptome of Atractylodes lancea. *BMC Plant Biol.* 21:293. doi: 10.1186/s12870-021-03048-9

Zhang, M., Wang, J., Zhu, L., Li, T., Jiang, W., Zhou, J., et al. (2017). *Zanthoxylum bungeanum* maxim. (Rutaceae): A systematic review of its traditional uses, botany, Phytochemistry, pharmacology, pharmacokinetics, and toxicology. *Int. J. Mol. Sci.* 18:2172. doi: 10.3390/ijms18102172

Zhang, H., Zhu, J., Gong, Z., and Zhu, J. K. (2022). Abiotic stress responses in plants. *Nat. Rev. Genet.* 23, 104–119. doi: 10.1038/s41576-021-00413-0

frontiers | Frontiers in Plant Science

TYPE Original Research
PUBLISHED 07 September 2022
DOI 10.3389/fpls.2022.990575

Check for updates

OPEN ACCESS

EDITED BY
Ji-Hong Liu,
Huazhong Agricultural University, China

REVIEWED BY
Zhaoxia Li,
Shandong University,
China
Sang-Kyu Lee,
Gyeongsang National University,
South Korea

*CORRESPONDENCE
Suiwen Hou
housw@lzu.edu.cn

SPECIALTY SECTION
This article was submitted to Plant Abiotic Stress, a section of the journal Frontiers in Plant Science

RECEIVED 10 July 2022
ACCEPTED 11 August 2022
PUBLISHED 07 September 2022

CITATION
Jadoon S, Qin Q, Shi W, Longfeng Y and Hou S (2022) Rice protein phosphatase 1 regulatory subunits OsINH2 and OsINH3 participate actively in growth and adaptive responses under abscisic acid. *Front. Plant Sci.* 13:990575. doi: 10.3389/fpls.2022.990575

COPYRIGHT
© 2022 Jadoon, Qin, Shi, Longfeng and Hou. This is an open-access article distributed under the terms of the Creative Commons Attribution License (CC BY). The use, distribution or reproduction in other forums is permitted, provided the original author(s) and the copyright owner(s) are credited and that the original publication in this journal is cited, in accordance with accepted academic practice. No use, distribution or reproduction is permitted which does not comply with these terms.

Rice protein phosphatase 1 regulatory subunits OsINH2 and OsINH3 participate actively in growth and adaptive responses under abscisic acid

Sawaira Jadoon, Qianqian Qin, Weiqiang Shi, Yan Longfeng and Suiwen Hou*

Ministry of Education Key Laboratory of Cell Activities and Stress Adaptations, School of Life Sciences, Lanzhou University, Lanzhou, China

Rice (*Oryza sativa* L.), a worldwide staple food crop, is affected by various environmental stressors that ultimately reduce yield. However, diversified physiological and molecular responses enable it to cope with adverse factors. It includes the integration of numerous signaling in which protein phosphatase 1 (PP1) plays a pivotal role. Research on PP1 has been mostly limited to the PP1 catalytic subunit in numerous cellular progressions. Therefore, we focused on the role of PP1 regulatory subunits (PP1r), *OsINH2* and *OsINH3*, homologs of *AtINH2* and *AtINH3* in Arabidopsis, in rice growth and stress adaptations. Our observations revealed that these are ubiquitously expressed regulatory subunits that interacted and colocalized with their counter partners, type 1 protein phosphatase (OsTOPPs) but could not change their subcellular localization. The mutation in *OsINH2* and *OsINH3* reduced pollen viability, thereby affected rice fertility. They were involved in abscisic acid (ABA)-mediated inhibition of seed germination, perhaps by interacting with osmotic stress/ABA-activated protein kinases (OsSAPKs). Meanwhile, they positively participated in osmotic adjustment by proline biosynthesis, detoxifying reactive oxygen species (ROS) through peroxidases (POD), reducing malondialdehyde formation (MDA), and regulating stress-responsive genes. Moreover, their co-interaction proposed they might mediate cellular processes together or by co-regulation; however, the special behavior of two different PP1r is needed to explore. In a nutshell, this research enlightened the involvement of *OsINH2* and *OsINH3* in the reproductive growth of rice and adaptive strategies under stress. Hence, their genetic interaction with ABA components and deep mechanisms underlying osmotic regulation and ROS adjustment would explain their role in complex signaling. This research offers the basis for introducing stress-resistant crops.

KEYWORDS

PP1, OsINH2, OsINH3, rice growth, ABA, ROS

Introduction

Rice (*Oryza sativa* L.) is a globally important cash crop, feeding half of the world's population and serving 80% sources of calories (Agarwal et al., 2016). However, multiple detrimental factors influence rice crops together and lead to remarkable production loss (Dolferus, 2014; Reddy et al., 2017). Up to 70% yield loss occurs due to various stressors which affect rice growth, seed development, and potential survival (Akram et al., 2019). Despite the deleterious effect of environmental factors, plants can survive by evolving numerous cellular and molecular mechanisms.

Complex pathways are involved in the perception and transduction of stress signals, among which key events are phosphorylation and dephosphorylation. In protein phosphorylation, kinase proteins play an active role, while the reverse reaction is catalyzed by protein phosphatases (You et al., 2014). Reversible protein phosphorylation is pivotal for the posttranslational regulation of cellular and developmental processes (Luan, 2003). In dephosphorylation, one potential player is protein phosphatase 1 (PP1). It belongs to the Ser/Thr phosphoprotein phosphatase family (Shi, 2009) and is strongly conserved among eukaryotes (Cohen, 2002). PP1 comprises a catalytic subunit (PP1c) and varied regulatory subunits (PP1r) that bind to specific targets, recruit PP1c, and define its catalytic activity and location in the cell (Bollen, 2001). The PP1r possesses an active site, consisting of a hydrophobic sequence (RVXF motif) for substrate recruitment and cellular targeting (Verbinnen et al., 2017). The PP1c is an approximately 37-kD protein (Lee et al., 1999) that has been studied in plants extensively, whereas, the identification and functioning of PP1r in plants, especially in crops, are neglected.

In mammals, about 140 PP1 regulatory subunits have been found with diverse functions (Hendrickx et al., 2009). These proteins exist as inhibitor proteins and were originally identified as heat-stable proteins (Brandt et al., 1975). The earliest discovered inhibitor proteins are Inhibitor-1(I-1, also named INH1; Connor et al., 1998), DARPP-32 (Svenningsson et al., 2004), Inhibitor-2 (INH2; Bollen and Stalmans, 1992), and Inhibitor-3 (INH3; Zhang et al., 1998). The INH2, identified from rabbit skeletal muscle, is a highly conserved protein that can inhibit phosphatase activity (Leach et al., 2003). The biochemical and sequence analysis reveals it contains four potential fragments including PXTP, [SG] ILK, RVXF, and αhelical (Hurley et al., 2007). Although it was identified 30 years ago, to date its role in plants is poorly understood. It has been reported in Arabidopsis as an inhibitor of Type One Protein Phosphatase's (TOPP) catalytic activity (Templeton et al., 2011) and also as a negative regulator of abscisic acid (ABA) signaling by interacting with TOPPs and sucrose non-fermenting 1-related protein kinases 2 (SnRK2.6; Hou et al., 2016). Likewise, the contribution of INH3, a small nuclear protein of 126 amino acids, was just reported in embryo development and inhibition of PP1c catalytic activity (Takemiya et al., 2009). Recently, our lab identified another PP1 regulatory subunit, Protein Phosphatase 1 Regulatory Subunit 3 (PP1R3) in Arabidopsis, which regulates ABA signaling as a holoenzyme with TOPPs (Zhang et al., 2020). Besides, another putative regulatory subunit of PP1, PP1 Regulatory Subunit 2-like Protein 1 (PRSL1) has also been studied as a positive modulator of stomatal opening and blue light signaling in *Vicia faba* (Takemiya et al., 2006; Shimazaki et al., 2007). However, the role of PP1r in crops, particularly in reproductive growth, osmotic adjustment and homeostasis of reactive oxygen species (ROS) are still unknown. Therefore, we decided to explore the roles of PP1r, OsINH2, and OsINH3 in rice growth and responses to ABA.

Plants have evolved multiple mechanisms and signaling routes for their better survival. The participation of PP1c has been explored in various signaling, such as TOPP4 regulating DELLA-mediated gibberellic acid (GA) signaling, pavement cell morphogenesis by Pin-formed 1 (PIN1), and light morphogenesis by modulating Phytochrome Interacting Factor5 (PIF5; Qin et al., 2014; Guo et al., 2015; Yue et al., 2015). Moreover, TOPPs were studied as holoenzymes with Pi0431 in the promotion of late blight disease (Boevink et al., 2016). TOPPs also contribute to plant immunity by interacting with suppressors of topp4-1 (SUT1; Yan et al., 2019; Liu et al., 2020) and reduce water soaking and disease susceptibility *via* ABA (Hu et al., 2022). By contrast, the study on plant's PP1r in signaling pathways is limited, thus we paid attention to the activity of OsINH2 and OsINH3 in the ABA signaling cascade.

The ABA, a foremost important stress hormone, regulates various aspects of plant growth under unfavorable conditions and enables it to survive potentially. It activates one of the signaling components, SnRK2s, which further phosphorylate downstream substrates, induce expression of ABA-responsive genes and stimulate other responses (Fujii and Zhu, 2009). In rice, 10 members of the SnRK2s have been identified termed as osmotic stress/ABA-activated protein kinases (SAPK1-10), which are involved in numerous growth responses (Umezawa et al., 2013). For instance, SAPK6 shows ABA insensitivity in tobacco during seed germination and root elongation (Chae et al., 2007) while SAPK2 is resistant to ABA in rice (Lou et al., 2017). The SAPK1 and SAPK2 participate in seed germination and seedling growth under NaCl (Lou et al., 2018); similarly, SAPK4 confers salt resistance in rice (Diédhiou et al., 2008). While the SAPK9 positively regulates the ABA-mediated signaling pathway in rice under drought (Dey et al., 2016). Whereas, SAPK10 stimulates jasmonic acid (JA) biosynthesis in the presence of ABA and inhibits seed germination (Wang et al., 2020).

Besides growth, ABA also regulates ROS, which act downstream of the ABA signaling pathway (Postiglione and Muday, 2020). The ROS generation is definite in higher plants during normal metabolism. However, ROS imbalance by various stressors can disrupt the normal functioning of a cell by damaging proteins, nucleic acid, and lipids (Mittler, 2006). Therefore, plants adopt integrated strategies including physiological changes, osmotic adjustment, ionic homeostasis, solute production, and activation of an antioxidant defense system, in which ABA plays a key role (Wei et al., 2015; Guajardo et al., 2016) For instance,

upon ROS accumulation, plants stimulate enzymatic protection strategies including APX ascorbate peroxidase (APX), catalase (CAT), glutathione reductase (GR), super oxidase dismutase (SOD), and peroxidase dismutase (POD) production (Lin and Pu, 2010; Luo et al., 2010; Zhang et al., 2013). As well as, non-enzymatic antioxidants, such as ascorbate (AsA) and glutathione (GSH), also adjust ROS imbalance (Noctor and Foyer, 1998). Previous studies reported that ABA application induces enzymatic and non-enzymatic antioxidants in maize (Jiang and Zhang, 2001). Besides, activation of stress-responsive genes and proline biosynthesis are also adaptive strategies of the plant under unfavorable conditions. The stress-responsive genes regulate the expression of other genes that encode important enzymes and metabolic proteins, while proline participates in osmotic adjustment, and protects proteins, enzymes, and membranes (Anwar Hossain et al., 2014). However, to date, the involvement of PP1r in above-mentioned responses has not been focused.

In summary, this article has described the contribution of OsINH2 and OsINH3, the homolog of Arabidopsis INH2 and INH3, in rice growth and adaptive responses under ABA. As regulatory subunits, they can interact with OsTOPPs and colocalize with them, but could not change their subcellular localization. Our findings revealed that *OsINH2* and *OsINH3* participate in the reproductive growth of rice, regulate ABA-mediated inhibition of seed germination, and contribute to ROS homeostasis. Our study would offer significant grounds for introducing stress-resistant crops.

Materials and methods

Plant materials and growth conditions

In this study, we used CRISPR/Cas9 generated knockout lines of *OsINH2* and *OsINH3* in wild type, Zhonghua-11 (ZH11) background. Homozygous mutant lines were screened by PCR-sequencing analysis and HYG-resistance by using genomic primers (Supplementary Table 1). While for *OsINH2* and *OsINH3* overexpression lines, their CDS was cloned into pOx vector driven by maize ubiquitin gene promoter and then transferred into ZH11. Plants were grown in a greenhouse with a 12 h light (28–30°C)/12 h dark (20–22°C) cycle with 60% humidity.

Growth observation and pollen morphology

All genotypes were keenly observed from seed germination up to harvesting. Reproductive traits such as pollen morphology and fertility were noticed after the heading stage. The pollen grains were observed microscopically after staining with Potassium Iodide (KI). Usually, after KI staining, the normal (viable) round pollen of rice turns dark blue, while non-viable or poorly developed pollen is often deformed, and becomes brown. We prepared KI solution by dissolving 2 g potassium in 5–10 ml ddH_2O, and then added 1 g Iodine and made the final volume up to 300 ml. To stain pollen grains, we selected fully developed flowers whose anthers were enclosed in florets and burst an anther on a slide in a drop of ddH_2O, then added 1–2 drops of KI solution and observed under a light microscope. The active and inactive pollen were counted per 100 pollen grains. The seeds were counted per tiller to analyze the fertility of all genotypes.

Seed germination assay

Seed germination assay was performed as previously reported (Lin et al., 2015) with a few modifications. The seeds of ZH11, *OsINH2,* and *OsINH3* lines were surface sterilized with 70% ethanol for 1 min and immersed in 50% NaOCl for 10 min, and then washed with sterilized water at least five times. Finally rinsed seeds were planted on half MS media without ABA (as mock) and MS supplemented with 5 µm ABA (as treatment). Then plates were placed in a growth chamber having conditions according to Liao et al. (2016). The germination rate was recorded every day for up to 7 days (until ZH11 seeds reached to maximum germination rate), and the relative germination was recorded at 4 days after germination (DAG). The ABA sensitivity of seeds was analyzed by one-way ANOVA.

Post germination growth assay and stress treatment

For post-germination, seeds germinated on half MS and 1 week old seedlings were transferred into nutrient solution as mentioned previously (Wang et al., 2014a). The transcript level of various genes including *OsINH2*, *OsINH3*, *OsNAC1*, *OsLEA3*, *OsLIP19*, *and OsP5CS1*, was measured at the three-leaf stage. Moreover, to check ROS and antioxidant enzymes, we followed the method described by You et al. (2014). Three leaf staged seedlings were sprayed with 100 µM ABA. After completion of the experiment duration, leaves were sampled, immediately frozen in liquid nitrogen, and stored at −80°C for further experiments.

Histochemical detection of GUS activity and subcellular localization

β-Glucuronidase (GUS) staining was described previously (Qin et al., 2014). The promoter sequences of *OsINH2* and *OsINH3* (3.3 and 3 kb), respectively, were inserted into the pCAMBIA1301 GUS plasmid. After transformation to ZH11, different tissues of GUS transgenic plants (*ProOsINH2: GUS*/ZH11 *and ProOsINH2: GUS*/ZH11) were stained by using GUS working solution for one night at 37°C. Then decolorize with 70% ethanol and imaged using a LEICA (M205A) stereomicroscope. In addition, for cellular localization, YFP-OsINH2 and

YFP-OsINH3 were applied to tobacco leaves and fluorescence signals were observed by using a laser microscope (Zeiss).

Quantitative RT-PCR analysis

To detect the expression profile of required genes in respective plant materials, we extracted total mRNA and converted it into cDNA according to Wang et al. (2014b). The cDNA was amplified by using specific qRT-PCR primers (Supplementary Table 2). For detection of transcriptional changes under NaCl and ABA stress, three leaf stage rice seedlings were used after treatment for a specific duration. The enzyme, SYBRPremix Ex Taq (Takara Bio) was used for amplification in ABI StepOnePlus™ Real-Time PCR Systems (Thermo Fisher Scientific). The *Ubiquitin 10* (*UBQ10*) was used as a reference gene.

Plasmids construction and plant transformation

To construct overexpression lines, the full-length CDS sequence of OsINH2 and OsINH3 was amplified by using primers having a specific enzyme sequence (Kpn1 linked to forward primers and BamH1 with reverse primers). Amplified fragments were inserted into the pOx plasmid by the enzyme digestion method, and the final plasmids were transferred into ZH11. Besides the overexpression vector, we constructed *ProOsINH2: GUS* and *ProINH3: GUS* plasmids by fusing (3.3 and 3 kb) promoter regions of *OsINH2* and *OsINH3,* respectively, with pCAMBIA1301 plasmid. Moreover, we generated plasmids for the Yeast-two-hybridization (Y2H) system. The CDS of OsINH2 and OsINH3 was linked to the Gal4-activation domain (prey protein, pGADT7), while OsTOPPs and OsSAPKs full-length coding sequences were fused to the Gal4 DNA binding domain (bait protein, pGBKT7) by the infusion method. Furthermore, plasmids for biomolecular fluorescence complementation (BiFC) assay were constructed by the GATEWAY system. The CDS of OsINH2 and OsINH3 was linked to YFP (to check cellular localization), while OsTOPPs were fused with RFP (to observe colocalization with regulatory proteins). Additionally, OsINH2 and OsINH3 were fused with the C-terminal half of yellow fluorescent protein (YFP^c), and OsTOPPs and OsSAPKs joined with the N-terminal of YFP (YFP^n). In the end, all plasmids were injected *Nicotiana benthamiana* through *agrobacterium* and fluorescence signals were observed through the confocal microscope.

Yeast-two-hybridization assay

The Y2H analysis was carried out according to Zhang et al. (2020). The yeast containing OsINH2-AD, OsINH3-AD, OsTOPPs-BD, and OsSAPK4-BD plasmids was spread onto DDO (SD/−Leu/−Trp) media plates and incubated at 28°C for 3–4 days. After completion of the incubation period, a single clone for every sample was inoculated on QDO (SD/−Leu/−Trp/-His/−Ade/+ X-a-Gal agar) plates and incubated for 3–7 days. Next, colony morphology was observed.

Bimolecular fluorescence complementation assay

For the biomolecular fluorescence complementation (BiFC) assay, we followed methods described by Hu et al. (2018). The OsINH2-YFP^c and OsINH3-YFPc were co-infiltrated with TOPPs-YFP^n and SAPKs-YFP^n. Moreover, for confirmation of OsINH2 interaction with OsINH3, the OsINH3-YFP^c and OsINH3-YFP^n were co-expressed in *Nicotiana benthamiana via Agrobacterium*. The fluorescence signals were observed by confocal laser microscope after 3 days of sample injection into leaves.

Measurement of stress-associated indicators

To determine ROS in all genotypes under normal conditions and after ABA treatment, leaves were stained with nitroblue tetrazolium (NBT) by using the reported method (He et al., 2012). Furthermore, oxidative damage was assessed by quantifying MDA content according to the instruction of the commercial kit (Solarbio, Cat No: BC0020). The free proline content was estimated according to Lou et al. (2017). L-Proline was used to calculate the standard concentration of proline and absorbance was measured at a wavelength of 530 nm by using a spectrophotometer. Besides, the enzymatic activities including POD, SOD, and CAT were estimated by using commercial kits (Solarbio Cat No: BC0090, BC0170, and BC0200), respectively, and followed the instructions of the above-mentioned kits.

Accession numbers

The accession numbers for *OsINH2*, *OsINH3*, *OsTOPPs,* and *OsSAPKs* are enlisted (Supplementary Table 3).

Results

Identification of *OsINH2* and *OsINH3* in rice

The conservative nature of PP1 among eukaryotes is well known. The inhibitor proteins, INH2 and INH3, have already been reported in mammals, yeast, and Arabidopsis. However, in rice (*Oryza sativa*), the activity of these proteins is still elusive. By keeping in view, the conservation of *INH2* and *INH3* in Plantae,

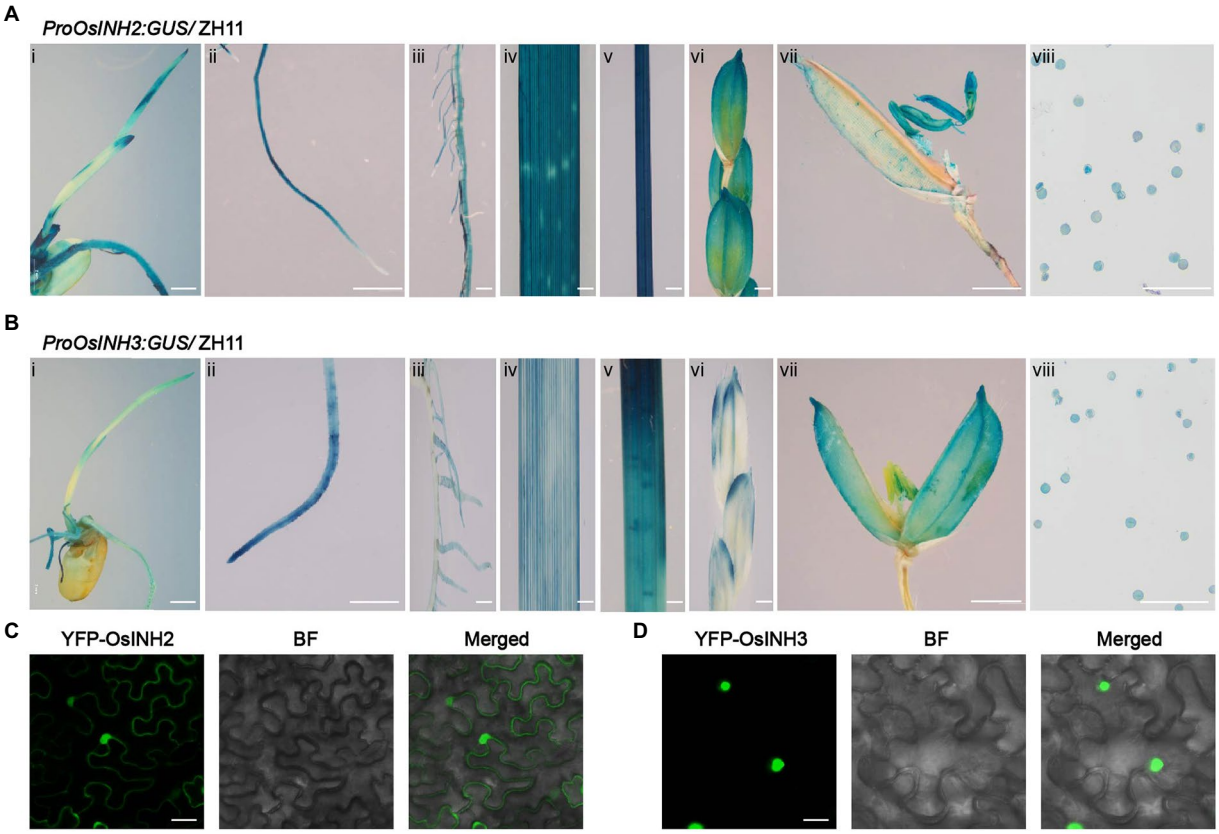


FIGURE 1
Tissue-specific expression of *OsINH2* and *OsINH3* and their protein subcellular localization. **(A)** Expression patterns of *OsINH2*. **(i)** A 4-day-old seedling, **(ii)** Primary root, **(iii)** Crown roots, **(iv)** Leaf, **(v)** Stem, **(vi)** Florets, **(vii)** Flower, and **(viii)** Pollen grains. **(B)** Expression patterns of *OsINH3*. **(i)** A 4-day-old seedling, **(ii)** Primary root, **(iii)** Crown roots, **(iv)** Leaf, **(v)** Stem, **(vi)** Florets, **(vii)** Flower, and **(viii)** Pollen grains. Scale bars, **(Ai)** and **(Bi)**=2mm, **(Aii–vii)** and **(Bii–vii)**=20mm, **(Aviii)** and **(Bviii)**=30μm. **(C,D)** Subcellular localization of OsINH2 and OsINH3. YFP-OsINH2 and YFP-OsINH3 were injected in *N.benthamiana* leaves. BF, bright field. Scale bars, 25μm.

we searched their homologs in rice. By blasting the protein sequence of Arabidopsis INH2 and INH3 in the database, National Center for Biotechnology Information (NCBI), we found one OsINH2 protein comprised of 165 amino acids while OsINH3 has two homologs of 13 kDa. The conservation pattern of these inhibitor proteins is alike across Plantae as they also possess RVXF motif like inhibitor proteins in Arabidopsis (Takemiya et al., 2009; Templeton et al., 2011). So, we compared an amino acid sequence of INH2 and INH3 in Arabidopsis and rice (Supplementary Figure 1) and predicted they are likely to have evolutionarily conserved functions in these two species. Therefore, we investigated their roles in rice growth and response to ABA.

Expression characterization of *OsINH2* and *OsINH3* and their protein subcellular localization

To study expression features, the *proOsINH2: GUS/* ZH11 *and proOsINH3: GUS/*ZH11 transgenic plants were used. Histochemical analysis disclosed that both *OsINH2* and *OsINH3* showed ubiquitous expression in rice. The promoter of *OsINH2* and *OsINH3* was highly activated at the germination and post-germination stages as high *GUS* activity was noticed in young seedlings, primary root, crown roots, leaf, and shoot (Figures 1A,B). While, at the reproductive stage, their expression was detected in panicle, anthers, and pollen grains (Figures 1A,B). In addition, consistent with *GUS* activity, the qRT-PCR analysis also showed a noticeable expression of *OsINH2* and *OsINH3* in various tissues (Supplementary Figure 2). Moreover, by focusing on that protein's functions depend on their localization inside the cell, we studied their subcellular localization. *Agrobacterium* carrying YFP-OsINH2 and YFP-OsINH3 was infiltrated into *Nicotiana benthamiana*. The transient expression analysis declared that the YFP-OsINH2 was localized both in the nucleus and cytoplasm while YFP-OsINH3 fluorescence signals were observed mainly in the nucleus (Figures 1C,D). These results suggest that inhibitor proteins may play redundant functions in rice.

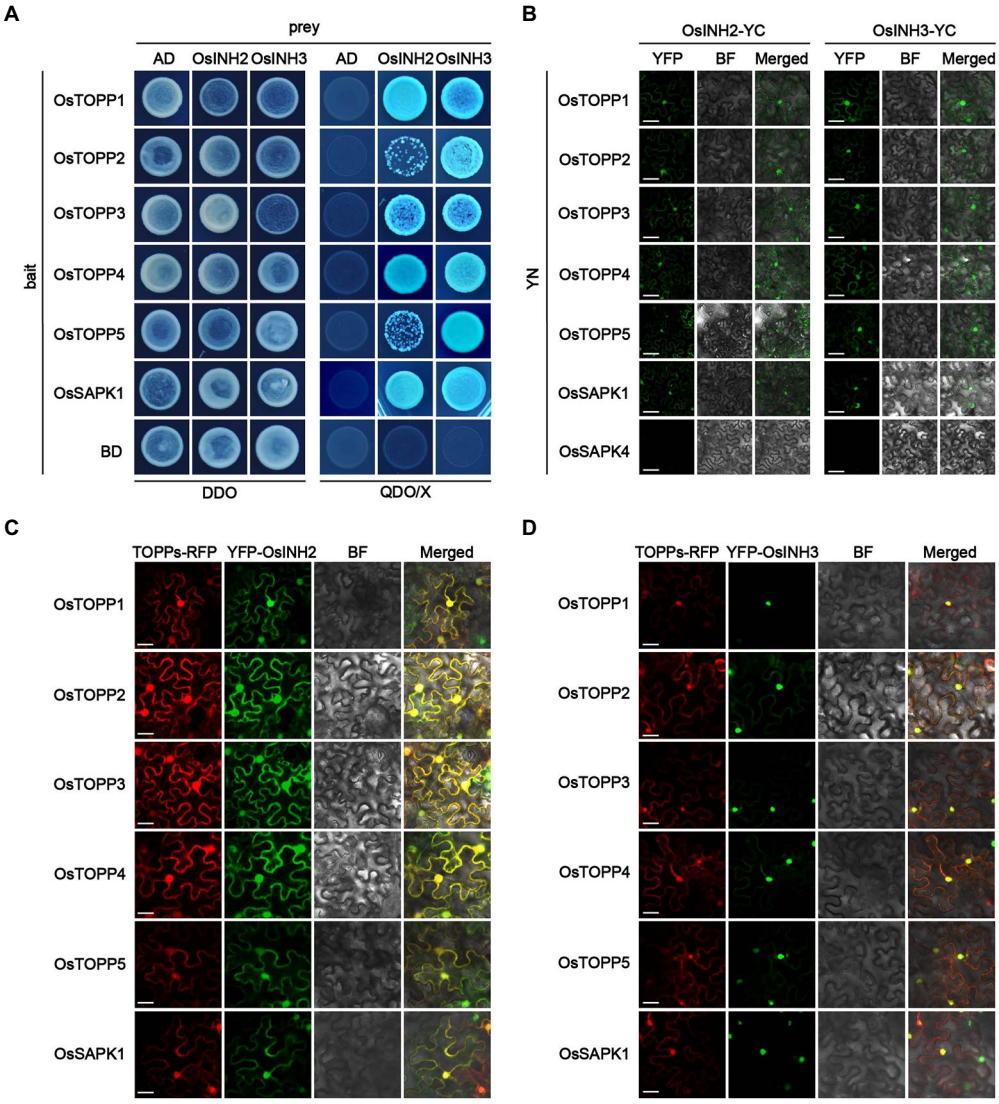


FIGURE 2
OsINH2 and OsINH3 interacted and colocalized with OsTOPPs. **(A)** Showing the interaction of OsINH2 and OsINH3 with OsTOPPs in the Yeast-two-hybridization (Y2H) system. OsINH2-AD and OsSAPK1-BD or OsINH3-AD and OsSAPK1-BD were used as a positive control. OsINH2 and OsINH3 fused with empty AD and OsTOPPs fused with empty BD were used as negative control. DDO, SD/−Leu/−Trp; QDO/X, SD/−Leu/−Trp/-His/−Ade supplemented with X-α-Gal. **(B)** Biomolecular fluorescence complementation (BiFC) assay representing the interaction of OsINH2 and OsINH3 with OsTOPPs. OsINH2-YC and OsTOPPs-YN or OsINH3-YC and OsTOPPs-YN were co-expressed in *Nicotiana benthamiana* leaves. OsINH2-YC and OsSAPK1-YN or OsINH3-YC and OsSAPK1-YN were used as positive control. OsINH2-YC and OsSAPK4-YN or OsINH3-YC and OsSAPK4-YN were used as negative control. Scale bars, 30μm. **(C,D)** Transient expression analysis illustrated OsINH2 and OsINH3 colocalized with OsTOPPs *in vivo*. OsTOPPs-RFP and YFP-OsINH2 or OsTOPPs-RFP and YFP-OsINH3 were co-infiltrated in *N. benthamiana* leaves. OsSAPK1-RFP and YFP-OsINH2 or OsSAPK1-RFP and YFP-OsINH3 were used as control. BF, bright field. Scale bars, 25μm.

OsINH2 and OsINH3 interacted and colocalized with OsTOPPs

As the PP1r could bind to the PP1c and regulates numerous physiological and cellular processes, we confirmed the binding ability of OsINH2 and OsINH3 with OsTOPPs by the Y2H system. As expected, OsINH2 and OsINH3, fused with the Gal4 activation domain (AD) interacted with OsTOPPs linked to the Gal4 DNA binding domain (BD; Figure 2A). To further validate PP1r-PP1c interaction in planta, we performed a BiFC assay in *N.benthamiana* leaves. Co-expression of OsINH2-YFP^{c} and OsINH3-YFP^{c} with OsTOPPs-YFP^{n} showed fluorescence signals in the nucleus and cytoplasm (Figure 2B). By knowing that majority of binding proteins interact with PP1 through the RVXF motif (Moorhead et al., 2007), we constructed OsINH2$^{V6A/W8A}$-AD and OsINH3$^{V50A/W52A}$-AD and checked their interaction with OsTOPPs. The Y2H and BiFC results demonstrated that mutant OsINH2 and OsINH3 also interacted with OsTOPPs (Supplementary Figure 3).

Moreover, from the interaction of PP1r-PP1c, we predicted their colocalization *in vivo*. Co-expression of YFP-OsINH2 or YFP-OsINH3 with OsTOPPs-RFP in *N.benthamiana* leaves indicated OsINH2 colocalized with OsTOPPs in the entire cell (Figure 2C), while OsINH3 colocalization with OsTOPPs was observed mainly in the nucleus (Figure 2D). However, both regulatory proteins have not changed OsTOPP's localization. Overall, these results suggest that OsINH2 may bind with OsTOPPs in the nucleus and cytoplasm, but OsINH3 bind with OsTOPPs only in the nucleus to play function. Therefore, we predicted that OsINH2 and OsINH3 could play role in growth and stress responses by interacting with OsTOPPs.

OsINH2 and OsINH3 were involved in the reproductive growth of rice

To study the involvement of *OsINH2 and OsINH3* in rice growth, we observed the growth of CRISPR/Cas9-mediated knockout mutants *osinh2 #6*, *osinh2 #11*, *osinh3 #4*, and *osinh3 #9*, and overexpression lines *OsINH2-OE #1*, *OsINH2-OE #3*, *OsINH3-OE #1*, and *OsINH3-OE #4* in the greenhouse (Supplementary Figure 4). The phenotypic observation revealed that the seedling growth of *OsINH2* and *OsINH3* lines was similar to their corresponding wild type (ZH11) (Supplementary Figure 4). However, at the reproductive stage, *OsINH2* and *OsINH3* knockout lines were less fertile, while overexpression lines showed the same fertility as ZH11 (Figures 3A,E). The number of seeds reduced significantly in *osinh2 #6*, *osinh2 #11*, *osinh3 #4*, and *osinh3 #9* lines. Whereas, in overexpression lines, the number of seeds was not markedly different from ZH11 (Figures 3B,F). Therefore, it was exciting to find out whether the *OsINH2* and *OsINH3* affect the rice yield by affecting pollen grains. Surprisingly, the anthers in knockout lines of *OsINH2* and *OsINH3* were dried, orange brown (Supplementary Figure 4), and possessed less active pollen grains in comparison with ZH11 (Figures 3C,G). The percentage of active pollen was significantly lower in knockout lines of OsINH2 and OsINH3, while the overexpression lines possessed the same pollen viability as the ZH11 (Figures 3D,H). Thus, it indicates that *OsINH2* and *OsINH3* might play a crucial role in the pollen development of rice.

OsINH2 and *OsINH3* participated in ABA stress response

Abscisic acid biosynthesis under various stress conditions, the role of phosphoproteins in complex signaling networks (Yin et al., 2018), and the negative regulation of ABA signaling by the INH2-TOPPs complex (Hou et al., 2016), incited us to study the involvement of *OsINH2* and *OsINH3* in rice under exogenous ABA. To clarify their role under stress conditions, firstly we checked their expression profiles precisely under ABA and NaCl stress. The *GUS* activity at the germination stage demonstrated that both ABA and NaCl applications reduced the expression of *OsINH2* and *OsINH3* (Figure 4A). Similarly, the qRT-PCR analysis also confirmed that the transcription levels of *OsINH2* and *OsINH3* were remarkably downregulated under ABA and NaCl (Figures 4B,C), which proposed that these proteins may play a fundamental role in ABA and NaCl signaling transduction. Thus, we observed their involvement in rice growth under ABA. The seed germination of *OsINH2* and *OsINH3* knockout and overexpression lines was the same as ZH11 in normal conditions. However, under ABA treatment, knockout lines showed ABA-mediated repression of seed germination (Figures 5A,F). The *osinh2 #6*, *osinh2 #11*, *osinh3 #4*, and *osinh3 #9* lines showed a remarkable reduction in seed germination percentage (Figures 5B,C,G,H). Moreover, besides seed germination, ABA also retarded seedling growth of *osinh2* and *osinh3* lines as their root and shoot growth reduced markedly in comparison with ZH11 (Figures 5D,E,I,J). Although seed germination and seedling growth of *OsINH2* and *OsINH3* overexpression lines were similar to ZH11, they showed resistance to ABA stress as compared to their respective knockout lines (Figure 5). In addition, the relative germination percentage at 4 DAG demonstrated that it was remarkably reduced in all the knockout lines, while overexpression lines possessed the same relative germination as ZH11 (Supplementary Figure 7). Therefore, our results endorse that *OsINH2* and *OsINH3* participate in ABA-mediated inhibition of seed germination and seedling growth of rice.

OsINH2 and OsINH3 interacted with OsSAPKs

Previously, it is determined that mammal's inhibitor-2 recruits various substrates (Brautigan, 2013), and the AtINH2-SnRKs complex negatively regulates ABA signaling in Arabidopsis (Hou et al., 2016). Thus, we hypothesized that in rice OsINH2 and OsINH3 may mediate cellular responses under ABA by targeting kinases (OsSAPKs). As anticipated, in the Y2H system, OsINH2 and OsINH3 linked to the Gal4 activation domain interacted with some of the OsSAPKs fused to the DNA-Gal4 binding domain. Similar to their alike responses in growth and ABA stress, their substrate recruitment was also alike, as both regulatory proteins showed interaction with the same OsSAPKs including OsSAPK1, OsSAPK2, OsSAPK3, OsSAPK8, and OsSAPK9 (Figure 6A). We then further verified their interaction *in vivo* by BiFC assay. As expected, co-expression of OsINH2-YFP^{c}, and OsSAPK-YFP^{n} showed strong fluorescence signals in the nucleus and weak signals were reported in the cytoplasm. However, OsINH3-YFP^{c} interacted with OsSAPKs-YFP^{n} mainly in the nucleus (Figure 6B). Taken together, our findings suggest that OsINH2 and OsINH3 might involve in ABA signaling transduction through OsSAPKs.

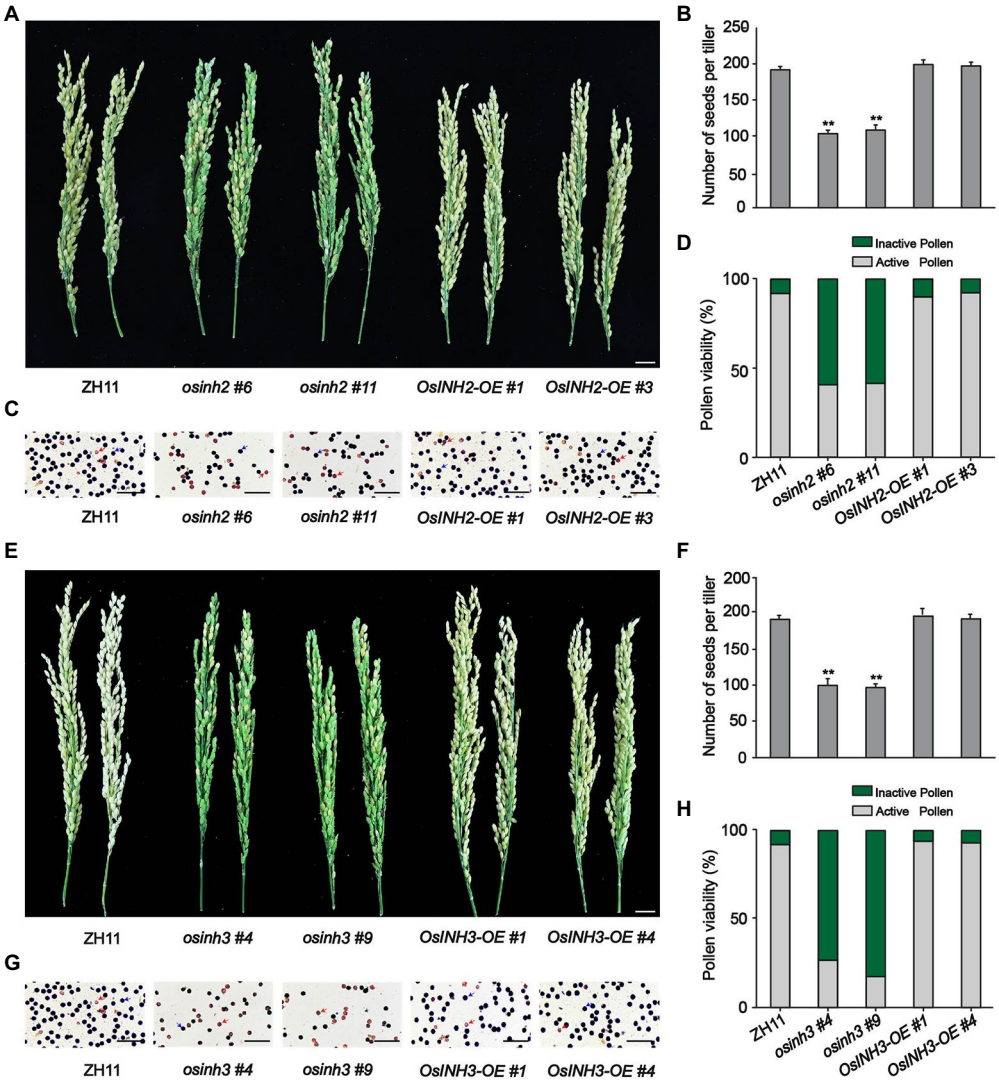


FIGURE 3
Performance of *OsINH2* and *OsINH3* in rice growth. **(A)** Phenotypes of the spikelet fertility in ZH11 and *OsINH2* genotypes. Scale bar, 2cm. **(B)** Illustrating the number of seeds in ZH11 and *OsINH2* lines. **(C)** Morphological observation of the pollen grains in ZH11 and *OsINH2* lines. Scale bars, 30μm. **(D)** Indicating percentage of active and inactive pollen in ZH11 and *OsINH2* genotypes. **(E)** Phenotypes of the spikelet fertility in ZH11 and *OsINH3* genotypes. Scale bar, 2cm. **(F)** Showing the number of seeds in ZH11 and *OsINH3* genotypes. **(G)** Morphological observation of the pollen grains in ZH11 and *OsINH3* lines. Scale bars, 30μm. **(H)** Representing the percentage of active and inactive pollen in ZH1 and *OsINH3* genotypes. After KI staining, the normal (viable) round pollen of rice turned dark blue, while non-viable or poorly developed pollen became brown. In **(C,G)**, blue arrows represent active pollen grains (dark blue) and red arrows represent inactive pollen grains (brown). In **(B,F)**, graph bars represent mean data. Error bars indicate ±SE with biological triplicates (n=25), asterisks specify the significant difference between the ZH11 and transgenic lines as determined by Student's t-test analysis, *$p < 0.05$; **$p < 0.01$. In **(D,H)** for pollen activity, n=6.

OsINH2 and *OsINH3* played positive role in osmotic adjustment

Recently Chen et al. (2022) reported that ABA induces ROS which represses seed germination and induces osmotic stress. Thus, we observed ROS accumulation in all genotypes under normal conditions and ABA. The detached leaves were subjected to nitroblue tetrazolium (NBT) staining overnight, and after decolorization with 75% ethanol, observed under a light microscope. We found that leaves of all the knockout lines were stained darker, in contrast, leaves from overexpression lines were less dark than ZH11 (Figure 7A). This prompted us to determine the contribution of *OsINH2* and *OsINH3* in osmotic adjustment *via* osmolyte production. The proline, a compatible osmolyte serves as a stress indicator influencing adaptive responses, by stabilizing subcellular structures and facilitating cell recovery after stress damage (Zhang et al., 2011). As a result, under ABA, knockout lines of both *OsINH2* and *OsINH3* accumulated remarkably less free proline content, while in overexpression lines it enhanced significantly over ZH11 (Figures 7B,C). Moreover, the

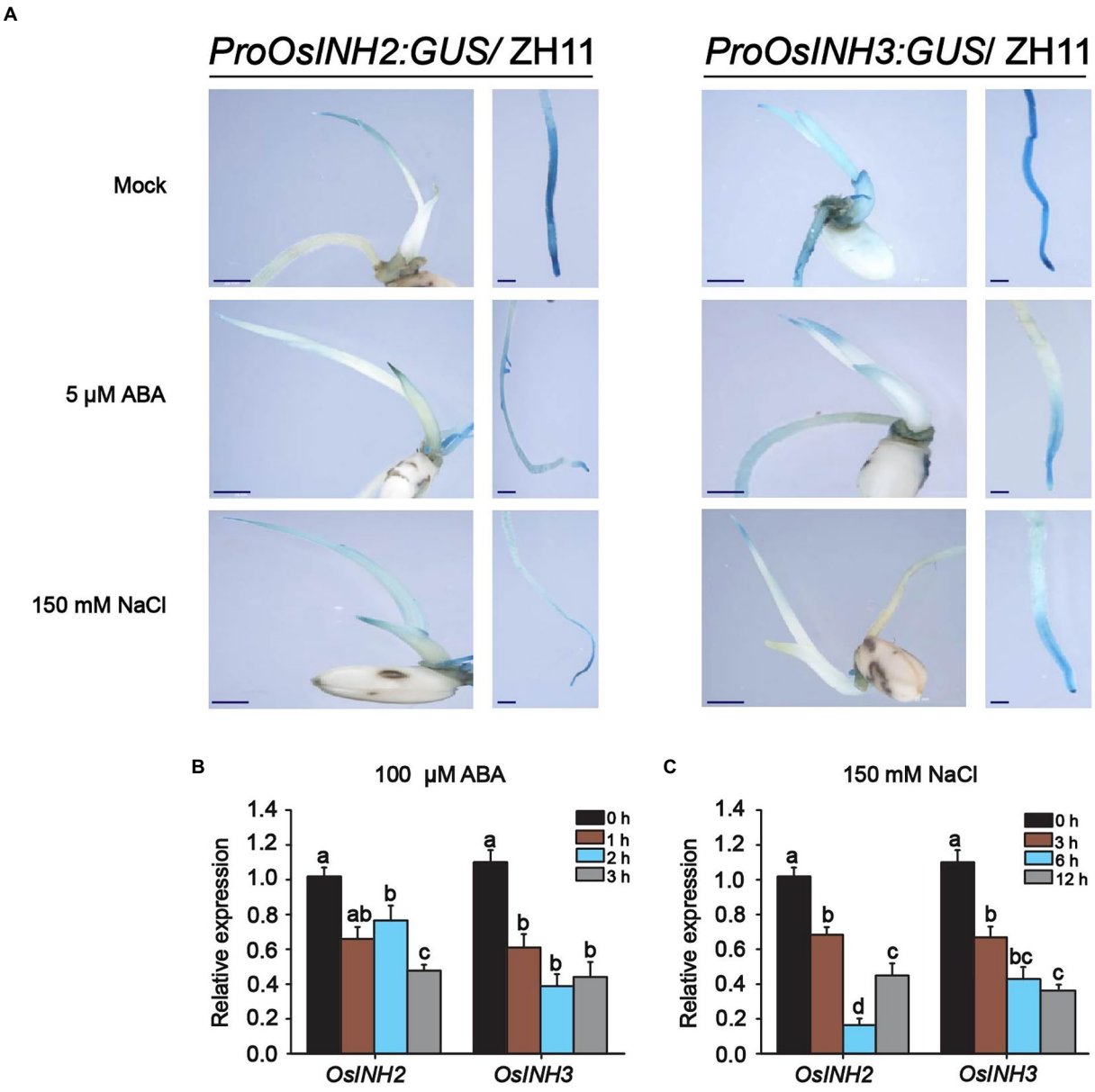


FIGURE 4
Expression patterns of *OsINH2* and OsINH3 under ABA and NaCl. **(A)** GUS activity of *OsINH2* and *OsINH3* were observed by GUS staining at the germination stage. Seeds were germinated on ½ MS media without and with 150mM NaCl and 5μM ABA. Scale bars, 20mm. **(B,C)** Expression levels of *OsINH2* and *OsINH3* under 100μM ABA and 150mM NaCl stress. Seeds were germinated on ½ MS media and one-week-old seedlings were transferred to the nutrient solution. At the three-leaf stage, leaves were sprayed with 100μM ABA for expression levels under ABA and sampled at 0, 1, 2, and 3h. For expression under NaCl treatment, seedlings were transferred to nutrient solution supplemented with 150mM NaCl and leaves were sampled at 0, 3, 6, and 12h. Total RNA was extracted from leaves. Graph bars represent mean data. Error bars show ±SE with biological triplicates. The *UBQ10* was used as a reference gene. Different letters on the graph bars indicate statistical significant differences analyzed by one-way ANOVA at $p < 0.05$.

expression level of the proline biosynthesis gene, delta-1-pyrroline-5-carboxylate synthase 1-like (*OsP5CS1*), significantly decreased in *osinh2* and *osinh3* lines, whereas overexpression lines showed a noticeable induction of *OsP5CS1* after ABA treatment (Figures 7D,E), which confirmed our above-mentioned results. These findings recommend that *OsINH2* and *OsINH3* might protect rice by balancing osmotic status, thereby minimizing ROS imbalance.

OsINH2 and *OsINH3* were involved in ROS detoxification

It is reported that ABA induces ROS accumulation and causes oxidative stress in leaves which led to membrane damage (Hu et al., 2006). Thus, we predicted, along with ROS production, ABA also enhances the formation of malondialdehyde (MDA) content. Predictably, the MDA

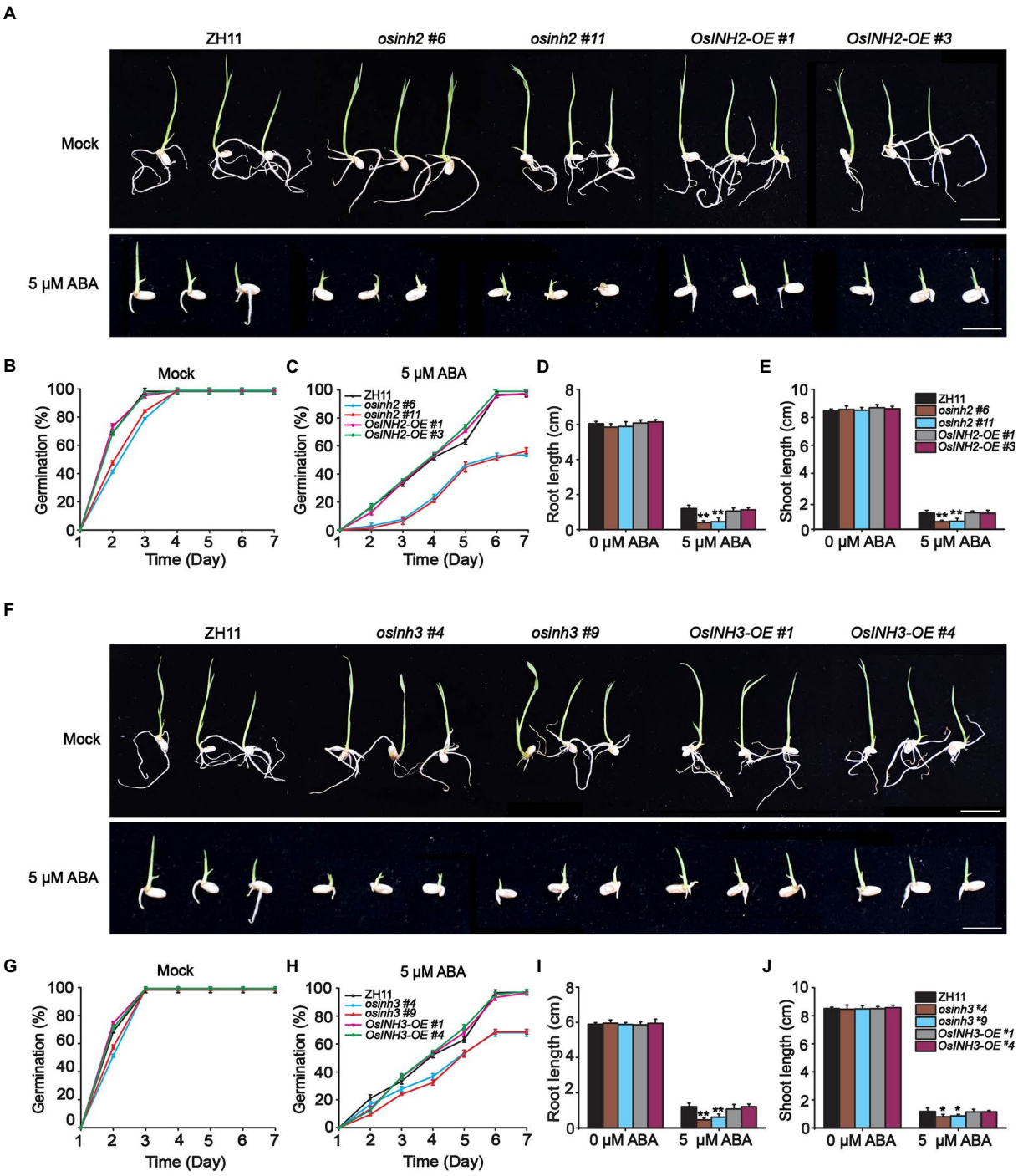


FIGURE 5
osinh2 and *osinh3* mutants were sensitive to ABA. **(A)** Phenotypes of *OsINH2* knockout and overexpression lines at germination stage grown in media without and with ABA. Scale bars, 2cm. **(B,C)** Graphical illustration of *OsINH2* seed germination (%) under mock and ABA treatment. **(D,E)** Indicating root and shoot length of *OsINH2* seedlings. **(F)** Phenotypes of *OsINH3* genotypes at germination stage in media without and with ABA. Scale bars, 2cm. **(G,H)** Graphical illustration of *OsINH3* seed germination (%) under mock and ABA treatment. **(I,J)** Represents root and shoot length of *OsINH3* seedlings. Seeds were germinated on ½ MS media supplemented with 0 and 5μM ABA. Germination (%) was recorded for up to 7days. In **(B,C,G,H)** graph lines represent mean data. Error bars in **(B–J)** show ±SE with biological triplicates (n=20). Seed germination (%) was analyzed by one-way ANOVA, followed by the Tukey's test and significance was calculated at $p < 0.05$. Root and shoot length were analyzed by student's t-test. Asterisks in **(D,E,I,J)** specify the significant difference between the ZH11 and transgenic lines, $*p < 0.05$; $**p < 0.01$.

formation increased greatly in knockout lines among which *osinh2 #6*, and *osinh3 #9* showed significant MDA induction after ABA treatment. Whereas, overexpression lines showed reduction in MDA content, remarkably in *INH2-OE #1*, as compared to control (Figures 8A,B). These results proposed that under ABA stress *OsINH2* and *OsINH3* could protect

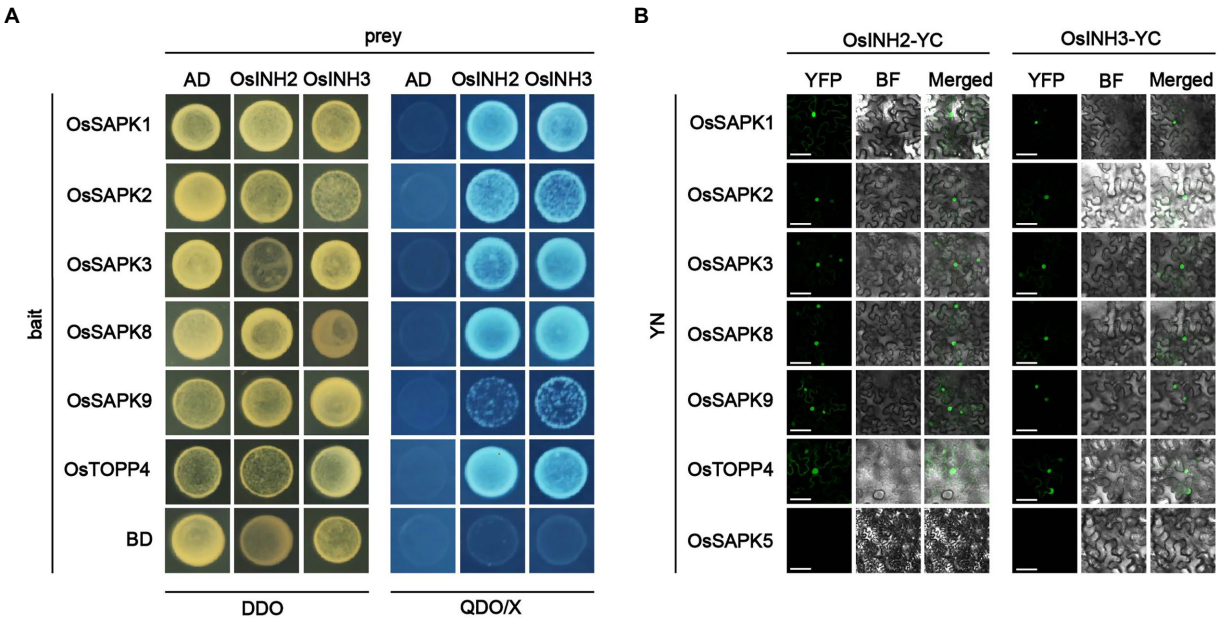


FIGURE 6
OsINH2 and OsINH3 interacted with OsSAPKs. **(A)** Y2H represents the interaction of OsINH2 and OsINH3 with OsSAPKs. OsINH2-AD and OsTOPP4-BD or OsINH3-AD and OsSAPK4-BD were used as positive control. OsINH2 and OsINH3 fused with empty AD and OsSAPKs fused with empty BD were used as negative control. DDO, SD/−Leu/−Trp; QDO/X, SD/−Leu/−Trp/-His/−Ade supplemented with X-α-Gal. **(B)** BiFC assay shows OsINH2-YC and OsINH3-YC interacted with OsSAPKs. OsINH2-YC and OsSAPKs-YN or OsINH3-YC and OsSAPKs-YN were co-expressed in *Nicotiana benthamiana* leaves. OsINH2-YC and OsTOPP4-YN or OsINH3-YC and OsTOPP4-YN were used as positive control. OsINH2-YC and OsSAPK5-YN or OsINH3-YC and OsSAPK5-YN were used as negative control. BF, bright field. Scale bars, 50μm.

against membrane damage by lowering lipid peroxidation formation.

Upon ROS imbalance and MDA formation, plants evolve numerous antioxidative enzymes to scavenge ROS (Blokhina and Fagerstedt, 2010). We speculated that *OsINH2* and *OsINH3* involve in tolerance mechanisms by antioxidant enzyme production. We analyzed the production of POD, CAT, and SOD in rice leaves before and after ABA treatment. Expectedly, POD was highly active to lower the ROS. The POD activity was noticeable in *OsINH2* knockout and overexpressing plants after ABA treatment. It was lower in *osinh2 #6* and *osinh2 #11* and higher in *INH2-OE #1* and *INH2-OE #3* than ZH11 (Figure 8C). While, in knockout and overexpression genotypes of *OsINH3*, except *osinh3 #9*, the POD activity was not significantly varied over ZH11 (Figure 8D). However, in all plants, neither CAT nor SOD was active under ABA. This suggests that *OsINH2* and *OsINH3* could regulate POD more actively than CAT and SOD and maintain ROS homeostasis.

Besides, we measured various stress-responsive genes which could either regulate the formation of protective contents or directly target other genes to confer tolerance against stressful conditions. The expression profile of well-known stress-responsive genes including *OsP5CS1*, NAC-domain containing protein 1(*NAC1*), late embryogenesis abundant 3 (*OsLEA3*), and ocs element-binding factor (*OsLIP9*) was assessed in respective plant materials. Presumably, in response to ABA, all knockout lines showed significant downregulation of *OsP5CS1*, *OsLEA3*, and *OsLIP9* gene expression in comparison with control (Figures 8E–H). However, the *OsNAC1* transcription was also reduced but not significantly (Supplementary Figure 8). In contrast, ABA induced the transcriptomic profile of these genes in overexpression genotypes (Figures 7E–H). These findings propose that *OsINH2* and *OsINH3* might contribute to ROS fine-tuning by stimulating antioxidant enzyme production and triggering stress-responsive genes that could play role in stress adaptation directly or indirectly.

OsINH2–OsINH3 formed complex

As we reported in the above-mentioned results, the characterization, growth, and adaptive responses of *OsINH2* and *OsINH3* were alike. So, we hypothesized that OsINH2 and OsINH3 form complex and regulate different functions in the plants. We co-expressed OsINH2-YFP^{c} with OsINH3-YFP^{n} in *N.benthamiana* leaves. Surprisingly, strong fluorescence signals were observed in the nucleus (Figure 9A), which revealed that these two regulatory proteins in rice form a big complex and contribute decisively to rice growth. Moreover, YFP-OsINH2 colocalized with OsINH3-RFP in tobacco leaves and their subcellular localization remained unchanged (Figure 9B). Our findings elucidate that the OsINH2-OsINH3 complex may recruit other substrates and supervise various activities in the plants collectively or in co-regulation.

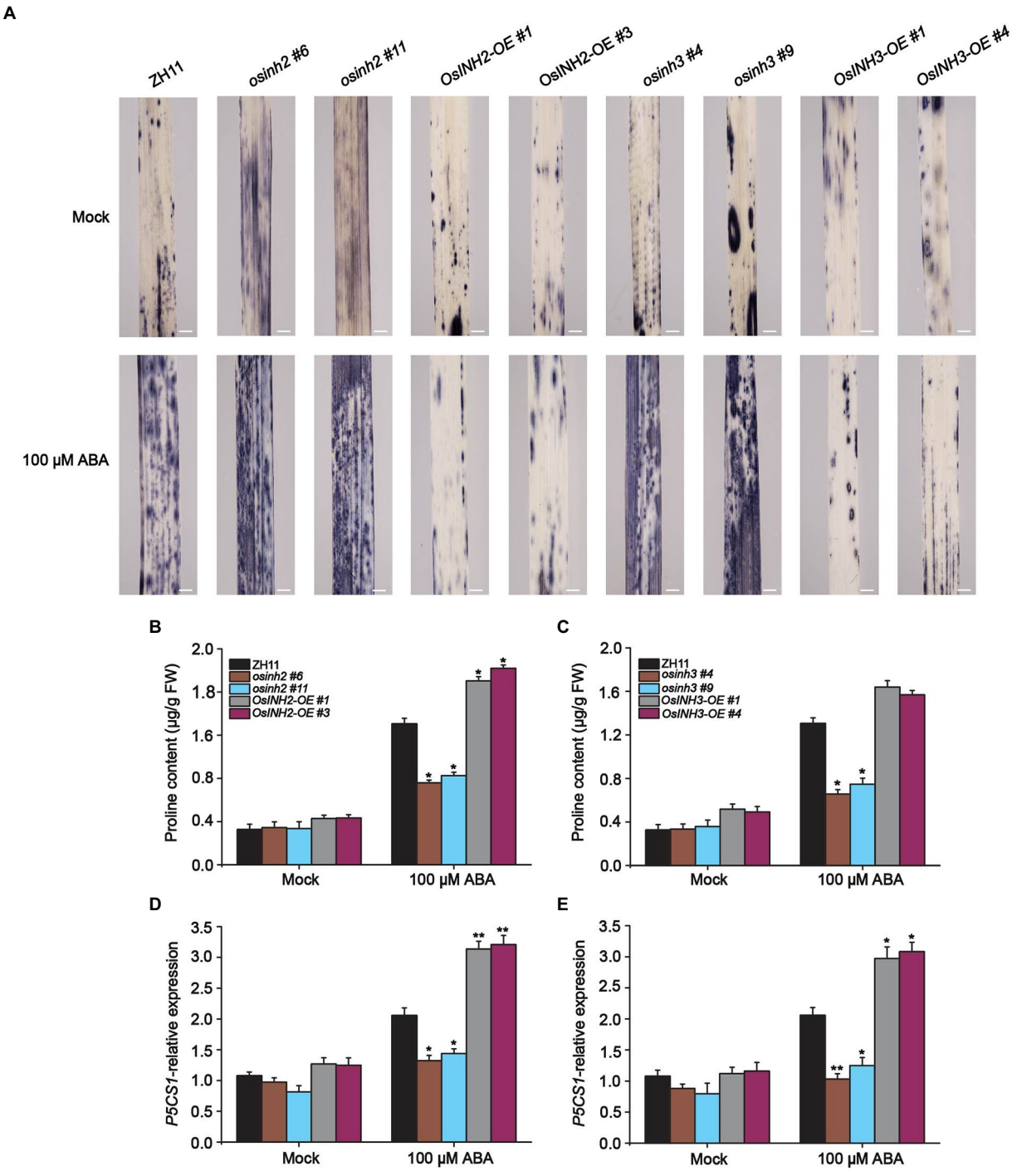


FIGURE 7
OsINH2 and *OsINH3* positively regulated osmotic adjustment. **(A)** ROS accumulation in *OsINH2* and *OsINH3* genotypes. Seeds were germinated on ½ MS media. One-week-old seedlings were transferred to the nutrient solution and sprayed at the three-leaf stage with 100μM ABA. Leaves samples were incubated at 37°C in NBT solution overnight and ROS were observed after decolorization with 75% ethanol. Scale bars, 10mm. The experiment was repeated three times with the same results. **(B,C)** Proline content in *OsINH2* and *OsINH3* lines. **(D,E)** Expression profile of *OsP5CS1* in *OsINH2* and *OsINH3* lines. Growth conditions and ABA application were similar as described in **(A)**. Proline content was assessed in leaves. In **(B–E)** graph bars represent mean data. Error bars show ±SE, with three biological repeats ($n=5$ for proline content, $n=3$ for *OsP5CS1* expression level). For all experiments, samples were collected before and after ABA treatment. Asterisks indicate a statistically significant difference between the ZH11 and transgenic lines was analyzed by Student's *t*-test, $*p < 0.05$; $**p < 0.01$.

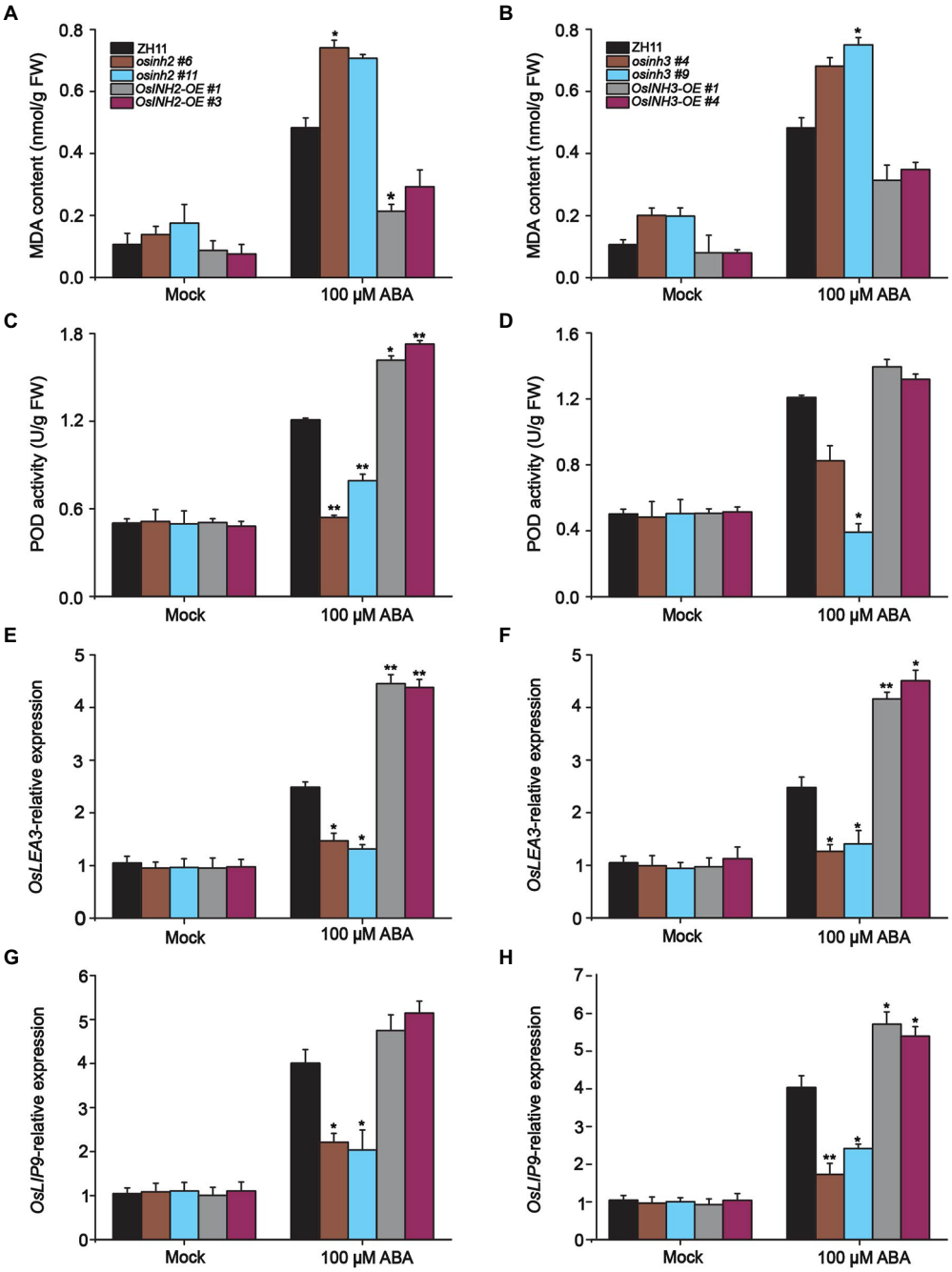


FIGURE 8
Participation of *OsINH2* and *OsINH3* in ROS detoxification. **(A,B)** MDA content in *OsINH2* and *OsINH3* lines. **(C,D)** POD activity in *OsINH2* and *OsINH3* genotypes. Seeds were germinated on ½ MS media. One-week-old seedlings were transferred to nutrient solution and at the three-leaf stage sprayed with 100μM ABA. MDA content and POD activity were detected from leaves. **(E–H)** Expression profile of *OsLEA3* and *OsLIP19* in *OsINH2* and *OsINH3* lines. Growth conditions and ABA application were the same as mentioned above. Graph bars indicate mean data. Error bars show ±SE with three biological repeats (n=5 for MDA and POD activity, for *OsLEA3* and *OsLIP19* expression levels, n=3). Asterisks represent a statistically significant difference between the ZH11 and transgenic lines was analyzed by Student's t-test, $*p < 0.05$; $**p < 0.01$.

Discussion

Protein phosphatases are strongly conserved enzymes that encode large gene families with versatile cellular progressions. To date, research on PP1 has mostly focused on the role of TOPPs (PP1c) in plants. However, the PP1r especially in crop growth and stress responses has not gained much attention. Thus, little knowledge of PP1r has attracted our attention to explore the contribution of *OsINH2* and *OsINH3* in rice. The expression features and localization demonstrated that these inhibitor

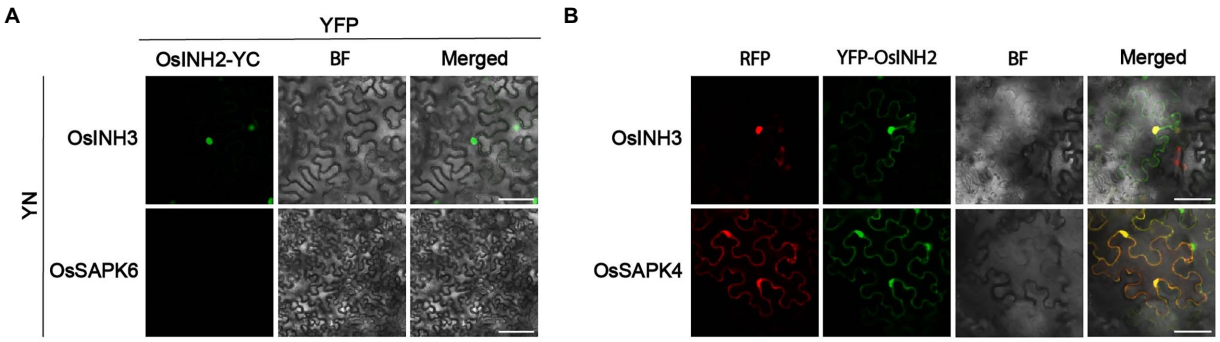


FIGURE 9
OsINH2 and OsINH3 interacted with each other. **(A)** BiFC assay showing the interaction of OsINH2 with OsINH3 *in vivo*. OsINH2-YC and INH3-YN were co-expressed in *N. benthamiana* leaves. Scale bars, 50μm. OsINH2-YC and OsSAPK6-YN were used as negative control. **(B)** Transient expression assay shows YFP-OsINH2 colocalized with OsINH3-RFP. YFP-OsINH2 and OsSAPK4-RFP were used as positive control. All samples were injected into *Nicotiana benthamiana* leaves Scale bars, 25μm.

proteins may supervise cellular processes all over the plant and at various locations in the cell, which explain their functional redundancy. Moreover, the interaction of OsINH2 and OsINH3 with OsTOPPs confirmed they recruit OsTOPPs. However, the OsTOPPs interaction with OsINH2$^{V6A/W8A}$ and OsINH3$^{V50A/W52A}$, having mutation in RVXF motif has revealed that rather than RVXF, there might be other potential motifs *via* which rice PP1r interacts with their complementary subunits and substrates. For instance, Templeton et al. (2011) reported two other conserved motifs in Inhibitor-2 (I-2), the PXTP, and HYNE. Further, OsINH2 and OsINH3 colocalization with OsTOPPs ensured they are counter partners of PP1c in rice and might define their activities without changing their location in the cell. In contrast, in Arabidopsis, INH3-W43A diminished the TOPP's nuclear localization and PRSL1 targeted PP1c to the cytoplasm (Takemiya et al., 2009, 2013). The co-localization of OsINH2 with OsTOPPs was similar to the colocalization of PP1R3 with TOPP4 (Zhang et al., 2020).

Growth observation revealed that *OsINH2* and *OsINH3* were involved in the reproductive growth of rice, as a mutation in *OsINH2* and *OsINH3* affected rice fertility. Therefore, the pollen inactivity of the knockout lines explains that reduced pollen grains viability may lead to fewer seeds. Moreover, after ABA application, premature spikelet abortion and a remarkable decrease in the number of seeds (Oliver et al., 2007) provide a clue that *OsINH2* and *OsINH3* might be involved in fertility by interrupting ABA signaling. Furthermore, the Low Seed Setting Rate 1 (*OsLSSR1*), which regulates the seed setting rate in rice (Xiang et al., 2019) might be affected in knockout lines as a result seed number became decreased. Besides, embryogenesis regulation by *AtINH3* (Takemiya et al., 2009) and short fluorescence and less fertility of Arabidopsis *topp4-1* double mutant (Qin et al., 2014) also confirmed that PP1 regulates yield-related traits. Additionally, the expression of *OsINH2* and *OsINH3* in the panicles and flowers further supported our notion that the regulatory proteins may contribute to the reproductive growth of rice. Besides, we found all the five isoforms of OsTOPP single knockout mutants have not shown obvious phenotype at the reproductive stage, which might be due to their functional redundancy. However, the *ostopp1-2* double mutant showed the same fertility phenotype as *osinh2* and *osinh3* lines (data not published). Moreover, the role of SAPK10 in rice flowering (Liu et al., 2019) and SAPK2 in rice yield under reproductive stage drought stress (Lou et al., 2020) demonstrated that OsSAPKs might contribute to rice reproductive growth along with OsINH2 and OsINH3, which could be explained clearly by observing their cross material. While the similar response of overexpression lines to ZH11 demonstrated that *OsINH2* and *OsINH3* active involvement in growth may depend on their specific expression level and interaction with other yield regulating genes, which could suppress their activity.

Given that OsINH2 and OsINH3 interacted with OsTOPPs, we investigated whether, like TOPPs, they also contribute to stress signaling. The disruption of *OsINH2* and *OsINH3* under ABA treatment has delayed the seed germination and impaired seedling growth in knockout lines in comparison with ZH11. These results indicated that mutation of *OsINH2* and *OsINH3* causes inhibition of rice growth under ABA which suggests their involvement in growth responses might be *via* ABA-dependent complex signaling. However, the response of overexpression lines explains that too high or too low expression of *OsINH2* and *OsINH3* may affect their performance in some growth responses. Our results are consistent with the involvement of *PP1R3* in stress responses, as Zhang et al. (2020) reported a mutation in *PP1R3* not only results in decreased seed germination and cotyledon greening but also retards seedling growth under ABA. Moreover, under exogenous brassinosteroid (BR), longer roots of *TdPP1* overexpressing transgenic lines (Bradai et al., 2021) confirmed the participation of PP1 under hormonal stress in crops. Similarly, NaCl tolerance of *OsPP1a* overexpression genotypes (Liao et al., 2016) highlighted that PP1 could also rescue plants under abiotic stresses. Besides, their interaction with the ABA signaling components (OsSAPKs) stated that they might mediate cellular

responses under stress by ABA-dependent pathways, similar to the mechanism in Arabidopsis. Based on previous findings that Os*SAPK1* and Os*SAPK2* positively regulate salt tolerance in rice (Lou et al., 2018), we suggested that *OsINH2* and *OsINH3* may play their potential role in stress adaptations by targeting OsSAPKs.

Recently, Chen et al. (2022) have reported that ROS generation by ABA causes inhibition of seed germination, which recommended that mutation in OsINH2 and OsINH3 may inhibit seed germination through ROS, thus we investigated ROS accumulation. ROS is a secondary messenger which mediates different responses in the cell being disrupted by various stressors. In the present research, under ABA more ROS accumulation in knockout lines, while less ROS in overexpression lines illustrated that *OsINH2* and *OsINH3* could play a positive role in osmotic adjustment and overcome ROS toxicity. Similarly, Shi et al. (2012) reported oxidative damage in rice under ABA stress. Further, Liu et al. (2020) studied ROS burst is enhanced in the *topp4-1* mutant in Arabidopsis, which signified the contribution of PP1 in ROS signaling. Therefore, to deal with osmotic stress, plants have evolved the production of compatible solute (proline) and antioxidant defense systems (Goggin and Colmer, 2007; Li and Wang, 2013). The proline adjusts osmotic disturbance, scavenge ROS and stabilizes proteins and cell membrane (Székely et al., 2008; Bailey-Serres et al., 2012), while the antioxidant defense mechanisms enhance plant tolerance by ROS detoxification (Zaefyzadeh et al., 2009). In the current research, regulation of the proline content and proline biosynthesis gene (*OsP5CS1*) in all genotypes, clarified that *OsINH2* and *OsINH3* might adjust osmotic disruption *via* osmotically active metabolites. Likewise, Cao et al. (2020) and Li et al. (2021), reported different stressors including salinity, drought, ABA and osmotic disruption affect proline biosynthesis in various rice genotypes. In addition, MDA quantification verified more ROS generation induces MDA formation in knockout lines while less MDA content in overexpression lines referred that probably *OsINH2* and *OsINH3* protect rice *via* decreasing MDA content. Similarly, Liao et al. (2016) investigated lower MDA content in OsPP1a transgenic lines under salt stress and Djanaguiraman et al. (2010) also described excessive ROS generation results in increased MDA content. To sum up, OsINH2 and OsINH3 might rescue rice against membrane damage *via* proline production and MDA reduction. However, exploration of other possible pathways could deeply explain the role of *OsINH2* and *OsINH3* in ROS balancing and membrane protection.

Besides, an antioxidant enzyme, POD activity was noticeable in all genotypes in response to ABA which evidenced that, upon ROS imbalance, *OsINH2* and *OsINH3* might activate POD to disintegrate excessive H_2O_2 into water and molecular oxygen, and assist rice to adapt ABA elevation. The research findings that more nitric oxide (NO) generation enhance transcription and activities of antioxidative enzymes against ABA (Zhang et al., 2007) also supported our results. Likewise, Shu et al. (2016) stated exogenous ABA induces POD activity in pumpkins. Similarly, Ding et al. (2010) and Wang et al. (2013) verified that excessive ABA

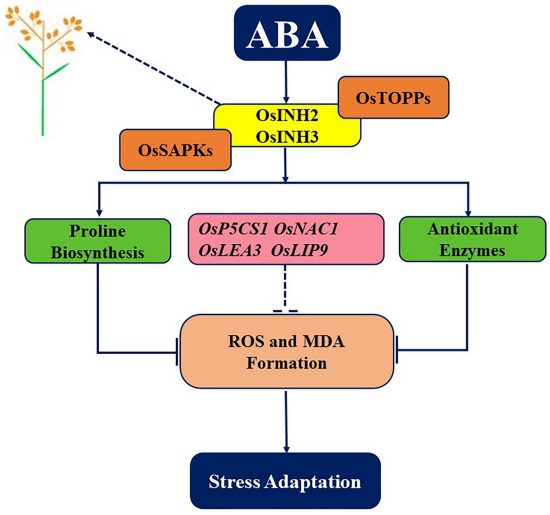


FIGURE 10
A graphical abstract depicting the role of *OsINH2* and *OsINH3* in rice. As regulatory subunits of PP1, OsINH2, and OsINH3 interact with OsTOPPs as well as with ABA signaling components (OsSAPKs). On one hand, they regulate the number of seeds in rice, and on other hand as a complex, they might regulate ABA-mediated repression of seed germination and maintain ROS levels by regulating antioxidants, osmolytes, and stress-responsive genes. Thereby, participating in the reproductive growth of rice and adaptative strategies under stress.

stimulates enzymatic as well as non-enzymatic protective strategies in different cold tolerant rice genotypes and common reed plants. Moreover, under ABA stress, *OsINH2* and *OsINH3* regulated the expression level of stress-responsive genes, such as *OsLEA3*, *OsLIP9,* and *OsNAC1* genes, which described that *OsINH2* and *OsINH3* might regulate adaptive strategies by peroxidases and coordinating with different stress-responsive genes which could activate various protective strategies. Finally, OsINH2 interaction and colocalization with OsINH3 pointed out that their similar behavior might be due to their co-regulation. Therefore, it is needed to underpin why these two inhibitor proteins, with different origins, sequences, and motifs, behave similarly and their contribution to different pathways.

To conclude, our study provides key insights into the contribution of OsINH2 and OsINH3 to rice growth and positive responses under ABA. Current findings illustrate that OsINH2 and OsINH3 are ubiquitous complementary partners of OsTOPPs, which participate in reproductive growth and the ABA signaling cascade by interacting with OsSAPKs. They release ABA-mediated repression of seed germination and fine-tuned the adaptive strategy of rice under ABA stress by detoxifying ROS, promoting proline biosynthesis, inhibiting MDA formation, and regulating stress-responsive genes (Figure 10). However, *OsINH2* and *OsINH3* functioning may depend on their specific transcription level in different responses. In Arabidopsis, tissue-specific expression of INH2 and INH3, participation of INH3 in embryogenesis, and negative regulation of ABA signaling by INH2-TOPP-SnRKs

complex (Takemiya et al., 2009; Hou et al., 2016), are the same as in rice. Our findings showed the involvement of ubiquitously expressed OsINH3 in rice reproductive growth, OsINH2 in rice seed germination under ABA, and interaction with ABA signaling components (SAPKs). This revealed that to some extent these two inhibitor proteins possessed functional conservation and similar expression features in rice and Arabidopsis. However, there is no knowledge about the contribution of INH2 to fertility and ROS adjustment in Arabidopsis. As well as the activity of AtINH3 under ABA *via* SAPKs is still elusive. Thus, the participation of INH2 in Arabidopsis reproductive growth, INH3 in ABA responses, and their involvement in ROS regulation could deeply explain the functional conservation of inhibitor proteins in Arabidopsis and crops. Our research explored for the first time the role of PP1r in crops and would contribute to introducing stress-resistant crops. However, further investigations are required to underpin underlying mechanisms widely.

Data availability statement

The original contributions presented in the study are included in the article/Supplementary material, further inquiries can be directed to the corresponding author.

Author contributions

SJ, QQ, and SH have designed the experiments. SJ has conducted the experimental work and data analyses and wrote the manuscript. SH and QQ have revised the manuscript. WS helped in plasmids construction. YL revised the manuscript and ensured equipment availability used in this research. All authors contributed to the article and approved the submitted version.

Funding

We are grateful to National Natural Science Foundation of China, General Project, 31870251 and 32170340, the Fundamental Research Funds for the Central Universities (lzujbky-2021-45), Xinyu Wang for providing Y2H-related vectors, Quansheng Qiu for the pUBC-RFP-Dest vector, and the core faculty of School of Life Sciences, Lanzhou University.

Conflict of interest

The authors declare that the research was conducted in the absence of any commercial or financial relationships that could be construed as a potential conflict of interest.

Publisher's note

All claims expressed in this article are solely those of the authors and do not necessarily represent those of their affiliated organizations, or those of the publisher, the editors and the reviewers. Any product that may be evaluated in this article, or claim that may be made by its manufacturer, is not guaranteed or endorsed by the publisher.

Supplementary material

The Supplementary material for this article can be found online at: https://www.frontiersin.org/articles/10.3389/fpls.2022.990575/full#supplementary-material

SUPPLEMENTARY FIGURE 1
Multiple sequence alignment INH2 and INH3 in rice and Arabidopsis. The sequences were aligned by using the ClustalW program. Asterisks represent an identical amino acid sequence. Dashes indicate gaps to allow for the optimal alignment of sequences. Redline indicates the RVXF motif (conserved region) among these proteins.

SUPPLEMENTARY FIGURE 2
Tissue-specific expression of *OsINH2* and *OsINH3*. Seeds were germinated on ½ MS media for a week and then one-week-old seedlings were transferred into a nutrient solution. Total RNA was extracted at 3 leaf stage from roots, leaves, and stems, while from florets and flowers after flowering. The expression level is indicated as a relative value, and expression in root was defined as 1.0. The graph bars represent mean data. The *UBQ10* was used as a reference gene. Error bars indicate ± SE. The expression level was analyzed by student's *t* test at $p < 0.05$.

SUPPLEMENTARY FIGURE 3
OsINH2$^{V6A/W8A}$ and OsINH3$^{V50A/W52A}$ interacted with OsTOPPs. **(A)** Y2H shows the interaction of OsINH2$^{V6A/W8A}$ and OsINH3$^{V50A/W52A}$ with OsTOPPs. OsINH2$^{V6A/W8A}$ -AD with OsSAPK1-BD or OsINH3$^{V50A/W52A}$ -AD with OsSAPK1-BD were used as positive control. OsINH2$^{V6A/W8A}$ and OsINH3$^{V50A/W52A}$ fused with empty AD and OsTOPPs fused with empty BD were used as negative control. DDO, SD/-Leu/-Trp; QDO/X, SD/-Leu/-Trp/-His/-Ade supplemented with X-α-Gal. **(B)** BiFC assay represents the interaction of OsINH2$^{V6A/W8A}$ and OsINH3$^{V50A/W52A}$ with OsTOPPs *in vivo*. OsINH2$^{V6A/W8A}$ -YC and OsINH3$^{V50A/W52A}$ -YC were co-expressed with OsTOPPs-YN in *N. benthamiana* leaves. OsINH2$^{V6A/W8A}$ -YC and OsSAPK1 or OsINH3$^{V50A/W52A}$ -YC and OsSAPK1-YN were used as positive control. OsINH2$^{V6A/W8A}$ -YC and OsSAPK5 or OsINH3$^{V50A/W52A}$ -YC and OsSAPK5-YN were used as negative control.

SUPPLEMENTARY FIGURE 4
Identification of *OsINH2* and *OsINH3* genotypes. **(A,B)** Sequencing analysis of CRISPR/ Cas9-mediated *OsINH2* and *OsINH3* knockout lines. Red lines represent the insertion or deletion of nucleotides in homozygous mutants. **(C,D)** Relative expression of *OsINH2* and *OsINH3* in overexpression lines. Seeds were germinated on ½ MS media for a week and then seedlings were transferred to the nutrient solution. Total RNA was extracted from leaves at the three-leaf stage. Graph bars represent mean data. Error bars indicate ±SE with three biological repeats. The *UBQ10* was used as a reference gene The expression levels were analyzed by student's *t*-test. Asterisks specify the significant difference between the ZH11 and overexpression lines, $*p < 0.05$; $**p < 0.01$.

SUPPLEMENTARY FIGURE 5
Growth of *OsINH2* and *OsINH3* lines at the seedling stage. **(A,B)** Growth of *OsINH2* and *OsINH3* knockout and overexpression lines. Seedlings were grown on ½ MS media for 14th days and photographed. Scale bars, 2 cm.

SUPPLEMENTARY FIGURE 6
Microscopic observation of flowers and anthers of *OsINH2* and *OsINH3* genotypes. **(A)** Flower phenotype of *OsINH2* lines. **(B)** Stained anthers of *OsINH2* genotypes. **(C)** Flower phenotype of *OsINH3* lines. **(D)** Stained

anthers of *OsINH3* genotypes. Flowers enclosed in bracts were selected for microscopic observation. Anthers were stained by 1–2 drops of potassium iodide solution (KI). In **(B,D)** anthers represent dark blue (active) enclosed pollens, scale bars, 20mm.

SUPPLEMENTARY FIGURE 7

Relative germination percentage of *OsINH2* and *OsINH3*. **(A,B)** Relative germination percentage of *OsINH2* and *OsINH3* lines. Seeds were germinated on ½ MS media with and without ABA. The germination (%) was recorded on the 4th day. The experiment was repeated three times with similar results.

SUPPLEMENTARY FIGURE 8

Relative expression of *OsNAC1* in *OsINH2* and *OsINH3* lines under ABA treatment. **(A,B)** Expression profile of *OsNAC1* in *OsINH2* and *OsINH3* transgenic materials. Seeds were germinated on ½ MS media and one-week-old seedlings were transferred to nutrient solution and sprayed with 100 μM ABA at the three-leaf stage. Total RNA was extracted from leaves. Graph bars represent mean data. Error bars show ± SE in three repeats. The *UBQ10* was used as a reference gene. The expression level was analyzed by student's *t*-test at $p < 0.05$.

References

Agarwal, P., Parida, S. K., Raghuvanshi, S., Kapoor, S., Khurana, P., Khurana, J. P., et al. (2016). Rice improvement Through genome-based functional analysis and molecular breeding in India. *Rice* 9:1. doi: 10.1186/s12284-015-0073-2

Akram, R., Fahad, S., Masood, N., Rasool, A., Ijaz, M., Ihsan, M. Z., et al. (2019). "Chapter 4- plant growth and morphological changes in rice under abiotic stress," in *Advances in Rice Research for Abiotic Stress Tolerance*. eds. M. Hasanuzzaman, M. Fujita, K. Nahar and J. K. Biswas (Sawston, Cambridge: Woodhead Publishing).

Anwar Hossain, M., Hoque, M. A., Burritt, D. J., and Fujita, M. (2014). "Chapter 16- Proline protects plants against abiotic oxidative stress: biochemical and molecular mechanisms," in *Oxidative Damage to Plants*. ed. P. Ahmad (San Diego: Academic Press).

Bailey-Serres, J., Fukao, T., Gibbs, D. J., Holdsworth, M. J., Lee, S. C., Licausi, F., et al. (2012). Making sense of low oxygen sensing. *Trends Plant Sci.* 17, 129–138. doi: 10.1016/j.tplants.2011.12.004

Blokhina, O., and Fagerstedt, K. V. (2010). Reactive oxygen species and nitric oxide in plant mitochondria: origin and redundant regulatory systems. *Physiol. Plant.* 138, 447–462. doi: 10.1111/j.1399-3054.2009.01340.x

Boevink, P. C., Wang, X., Mclellan, H., He, Q., Naqvi, S., Armstrong, M. R., et al. (2016). A Phytophthora infestans RXLR effector targets plant PP1c isoforms that promote late blight disease. *Nat. Commun.* 7:10311. doi: 10.1038/ncomms10311

Bollen, M. (2001). Combinatorial control of protein phosphatase-1. *Trends Biochem. Sci.* 26, 426–431. doi: 10.1016/S0968-0004(01)01836-9

Bollen, M., and Stalmans, W. (1992). The structure, role, and regulation of type 1 protein phosphatases. *Crit. Rev. Biochem. Mol. Biol.* 27, 227–281. doi: 10.3109/10409239209082564

Bradai, M., Amorim-Silva, V., Belgaroui, N., Esteban Del Valle, A., Chabouté, M. E., Schmit, A. C., et al. (2021). Wheat type one protein phosphatase participates in the Brassinosteroid control of root growth via activation of BES1. *Int. J. Mol. Sci.* 22:10424. doi: 10.3390/ijms221910424

Brandt, H., Capulong, Z., and Lee, E. (1975). Purification and properties of rabbit liver phosphorylase phosphatase. *J. Biol. Chem.* 250, 8038–8044. doi: 10.1016/S0021-9258(19)40812-0

Brautigan, D. L. (2013). Protein Ser/Thr phosphatases—the ugly ducklings of cell signalling. *FEBS J.* 280, 324–325. doi: 10.1111/j.1742-4658.2012.08609.x

Chae, M. J., Lee, J. S., Nam, M. H., Cho, K., Hong, J. Y., Yi, S. A., et al. (2007). A rice dehydration-inducible SNF1-related protein kinase 2 phosphorylates an abscisic acid responsive element-binding factor and associates with ABA signaling. *Plant Mol. Biol.* 63, 151–169. doi: 10.1007/s11103-006-9079-x

Cao, X., Wu, L., Wu, M., Zhu, C., Jin, Q., and Zhang, J. (2020). Abscisic acid mediated proline biosynthesis and antioxidant ability in roots of two different rice genotypes under hypoxic stress. *BMC Plant Biol.* 20:198.

Chen, Q. B., Wang, W. J., Zhang, Y., Zhan, Q. D., Liu, K., Botella, J. R., et al. (2022). Abscisic acid-induced cytoplasmic translocation of constitutive photomorphogenic 1 enhances reactive oxygen species accumulation through the HY5-ABI5 pathway to modulate seed germination. *Plant Cell Environ.* 45, 1474–1489.

Cohen, P. T. (2002). Protein phosphatase 1—targeted in many directions. *J. Cell Sci.* 115, 241–256. doi: 10.1242/jcs.115.2.241

Connor, J. H., Quan, H., Oliver, C., and Shenolikar, S. (1998). Inhibitor-1, a regulator of protein phosphatase 1 function. *Methods Mol. Biol.* 93, 41–58.

Dey, A., Samanta, M. K., Gayen, S., and Maiti, M. K. (2016). The sucrose non-fermenting 1-related kinase 2 gene SAPK9 improves drought tolerance and grain yield in rice by modulating cellular osmotic potential, stomatal closure and stress-responsive gene expression. *BMC Plant Biol.* 16:158. doi: 10.1186/s12870-016-0845-x

Diédhiou, C. J., Popova, O. V., Dietz, K.-J., and Golldack, D. (2008). The SNF1-type serine-threonine protein kinase SAPK4 regulates stress-responsive gene expression in rice. *BMC Plant Biol.* 8:49. doi: 10.1186/1471-2229-8-49

Ding, W., Song, L., Wang, X., and Bi, Y. (2010). Effect of abscisic acid on heat stress tolerance in the calli from two ecotypes of Phragmites communis. *Biol. Plant.* 54, 607–613.

Djanaguiraman, M., Prasad, P. V. V., and Seppanen, M. (2010). Selenium protects sorghum leaves from oxidative damage under high temperature stress by enhancing antioxidant defense system. *Plant Physiol. Biochem.* 48, 999–1007.

Dolferus, R. (2014). To grow or not to grow: a stressful decision for plants. *Plant Sci.* 229, 247–261. doi: 10.1016/j.plantsci.2014.10.002

Fujii, H., and Zhu, J. K. (2009). Arabidopsis mutant deficient in 3 abscisic acid-activated protein kinases reveals critical roles in growth, reproduction, and stress. *Proc. Natl. Acad. Sci. U. S. A.* 106, 8380–8385. doi: 10.1073/pnas.0903144106

Goggin, D. E., and Colmer, T. D. (2007). Wheat genotypes show contrasting abilities to recover from anoxia in spite of similar anoxic carbohydrate metabolism. *J. Plant Physiol.* 164, 1605–1611. doi: 10.1016/j.jplph.2007.01.007

Guajardo, E., Correa, J. A., and Contreras-Porcia, L. (2016). Role of abscisic acid (ABA) in activating antioxidant tolerance responses to desiccation stress in intertidal seaweed species. *Planta* 243, 767–781. doi: 10.1007/s00425-015-2438-6

Guo, X., Qin, Q., Yan, J., Niu, Y., Huang, B., Guan, L., et al. (2015). TYPE-ONE PROTEIN PHOSPHATASE4 regulates pavement cell interdigitation by modulating PIN-FORMED1 polarity and trafficking in Arabidopsis. *Plant Physiol.* 167, 1058–1075. doi: 10.1104/pp.114.249904

He, J., Duan, Y., Hua, D., Fan, G., Wang, L., Liu, Y., et al. (2012). DEXH box RNA helicase-mediated mitochondrial reactive oxygen species production in Arabidopsis mediates crosstalk between abscisic acid and auxin signaling. *Plant Cell* 24, 1815–1833. doi: 10.1105/tpc.112.098707

Hendrickx, A., Beullens, M., Ceulemans, H., Den Abt, T., Van Eynde, A., Nicolaescu, E., et al. (2009). Docking motif-guided mapping of the interactome of protein phosphatase-1. *Chemist. Amp. Biol.* 16, 365–371. doi: 10.1016/j.chembiol.2009.02.012

Hou, Y.-J., Zhu, Y., Wang, P., Zhao, Y., Xie, S., Batelli, G., et al. (2016). Type one protein phosphatase 1 and its regulatory protein inhibitor 2 negatively regulate ABA signaling. *PLoS Genet.* 12, e1005835. doi: 10.1371/journal.pgen.1005835

Hu, Y., Ding, Y., Cai, B., Qin, X., Wu, J., Yuan, M., et al. (2022). Bacterial effectors manipulate plant abscisic acid signaling for creation of an aqueous apoplast. *Cell Host Microbe* 30, 518–529.e6. doi: 10.1016/j.chom.2022.02.002

Hu, X., Zhang, A., Zhang, J., and Jiang, M. (2006). Abscisic acid is a key inducer of hydrogen peroxide production in leaves of maize plants exposed to water stress. *Plant Cell Physiol.* 47, 1484–1495. doi: 10.1093/pcp/pcl014

Hu, C., Zhu, Y., Cui, Y., Cheng, K., Liang, W., Wei, Z., et al. (2018). A group of receptor kinases are essential for CLAVATA signalling to maintain stem cell homeostasis. *Nat. Plants* 4, 205–211. doi: 10.1038/s41477-018-0123-z

Hurley, T. D., Yang, J., Zhang, L., Goodwin, K. D., Zou, Q., Cortese, M., et al. (2007). Structural basis for regulation of protein phosphatase 1 by inhibitor-2. *J. Biol. Chem.* 282, 28874–28883. doi: 10.1074/jbc.M703472200

Jiang, M., and Zhang, J. (2001). Effect of abscisic acid on active oxygen species, antioxidative defence system and oxidative damage in leaves of maize seedlings. *Plant Cell Physiol.* 42, 1265–1273. doi: 10.1093/pcp/pce162

Leach, C., Shenolikar, S., and Brautigan, D. L. (2003). Phosphorylation of phosphatase inhibitor-2 at centrosomes during mitosis. *J. Biol. Chem.* 278, 26015–26020. doi: 10.1074/jbc.M300782200

Lee, E. Y., Zhang, L., Zhao, S., Wei, Q., Zhang, J., Qi, Z. Q., et al. (1999). Phosphorylase phosphatase: new horizons for an old enzyme. *Front. Biosci.* 4, D270–D285.

Li, Y., and Wang, X. (2013). Root-induced changes in radial oxygen loss, rhizosphere oxygen profile, and nitrification of two rice cultivars in Chinese red soil regions. *Plant Soil* 365, 115–126. doi: 10.1007/s11104-012-1378-1

Li, X., Yu, B., Wu, Q., Min, Q., Zeng, R., and Xie, Z. (2021). OsMADS23 phosphorylated by SAPK9 confers drought and salt tolerance by regulating ABA biosynthesis in rice. *PLoS Genet.* 17:e1009699.

Liao, Y.-D., Lin, K.-H., Chen, C.-C., and Chiang, C.-M. (2016). Oryza sativa protein phosphatase 1a (OsPP1a) involved in salt stress tolerance in transgenic rice. *Mol. Breed.* 36:22. doi: 10.1007/s11032-016-0446-2

Lin, K. H., and Pu, S. F. (2010). Tissue-and genotype-specific ascorbate peroxidase expression in sweet potato in response to salt stress. *Biol. Plant.* 54, 664–670. doi: 10.1007/s10535-010-0118-8

Lin, Q., Wu, F., Sheng, P., Zhang, Z., Zhang, X., Guo, X., et al. (2015). The SnRK2-APC/C(TE) regulatory module mediates the antagonistic action of gibberellic acid and abscisic acid pathways. *Nat. Commun.* 6:7981. doi: 10.1038/ncomms8981

Liu, X., Li, Z., Hou, Y., Wang, Y., Wang, H., Tong, X., et al. (2019). Protein interactomic analysis of SAPKs and ABA-inducible bZIPs revealed key roles of SAPK10 in rice flowering. *Int. J. Mol. Sci.* 20, 1–9.

Liu, Y., Yan, J., Qin, Q., Zhang, J., Chen, Y., Zhao, L., et al. (2020). Type one protein phosphatases (TOPPs) contribute to the plant defense response in Arabidopsis. *J. Integr. Plant Biol.* 62, 360–377. doi: 10.1111/jipb.12845

Lou, D., Chen, Z., Yu, D., and Yang, X. (2020). SAPK2 contributes to rice yield by modulating nitrogen metabolic processes under reproductive stage drought stress. *Rice* 13:35. doi: 10.1186/s12284-020-00395-3

Lou, D., Wang, H., Liang, G., and Yu, D. (2017). OsSAPK2 confers abscisic acid sensitivity and tolerance to drought stress in rice. *Front. Plant Sci.* 8:993. doi: 10.3389/fpls.2017.00993

Lou, D., Wang, H., and Yu, D. (2018). The sucrose non-fermenting-1-related protein kinases SAPK1 and SAPK2 function collaboratively as positive regulators of salt stress tolerance in rice. *BMC Plant Biol.* 18, 203. doi: 10.1186/s12870-018-1408-0

Luan, S. (2003). Protein phosphatases in plants. *Annu. Rev. Plant Biol.* 54, 63–92. doi: 10.1146/annurev.arplant.54.031902.134743

Luo, M., Liu, J., Lee, R. D., Scully, B. T., and Guo, B. (2010). Monitoring the expression of maize genes in developing kernels under drought stress using oligo-microarray. *J. Integr. Plant Biol.* 52, 1059–1074. doi: 10.1111/j.1744-7909.2010.01000.x

Mittler, R. (2006). Abiotic stress, the field environment and stress combination. *Trends Plant Sci.* 11, 15–19. doi: 10.1016/j.tplants.2005.11.002

Moorhead, G., Trinkle-Mulcahy, L., and Ulke-Lemee, A. (2007). Moorhead GBG, Trinkle-Mulcahy L, Ulke-Lemee A. emerging roles of nuclear protein phosphatases. *Nat. Rev. Mol. Cell Biol.* 8, 234–244. doi: 10.1038/nrm2126

Noctor, G., and Foyer, C. H. (1998). Ascorbate and glutathione: keeping active oxygen Under control. *Annu. Rev. Plant Physiol. Plant Mol. Biol.* 49, 249–279. doi: 10.1146/annurev.arplant.49.1.249

Oliver, S., Zhao, X., Dennis, E., and Dolferus, R. (2007). *The Molecular Basis of Cold-Induced Pollen Sterility in Rice*. Springer, Dordrecht, Netherland.

Postiglione, A. E., and Muday, G. K. (2020). The role of ROS homeostasis in ABA-induced guard cell signaling. *Front. Plant Sci.* 11:968. doi: 10.3389/fpls.2020.00968

Qin, Q., Wang, W., Guo, X., Yue, J., Huang, Y., Xu, X., et al. (2014). Arabidopsis DELLA protein degradation is controlled by a type-one protein phosphatase, TOPP4. *PLoS Genet.* 10:e1004464. doi: 10.1371/journal.pgen.1004464

Reddy, I. N. B. L., Kim, B.-K., Yoon, I.-S., Kim, K.-H., and Kwon, T.-R. (2017). Salt tolerance in rice: focus on mechanisms and approaches. *Rice Sci.* 24, 123–144. doi: 10.1016/j.rsci.2016.09.004

Shi, Y. (2009). Serine/threonine phosphatases: mechanism through structure. *Cell* 139, 468–484. doi: 10.1016/j.cell.2009.10.006

Shi, B., Ni, L., Zhang, A., Cao, J., Zhang, H., Qin, T., et al. (2012). OsDMI3 is a novel component of abscisic acid signaling in the induction of antioxidant defense in leaves of rice. *Mol. Plant.* 5, 1359–74.

Shimazaki, K.-I., Doi, M., Assmann, S., and Kinoshita, T. (2007). Light regulation of stomatal movement. *Annu. Rev. Plant Biol.* 58, 219–247. doi: 10.1146/annurev.arplant.57.032905.105434

Shu, S., Gao, P., Li, L., Yuan, Y., Sun, J., and Guo, S. (2016). Abscisic acid-induced H_2O_2 accumulation enhances antioxidant capacity in pumpkin-grafted cucumber leaves under $Ca(NO_3)_2$ stress. *Front. Plant Sci.* 7.

Svenningsson, P., Nishi, A., Fisone, G., Girault, J. A., Nairn, A. C., and Greengard, P. (2004). DARPP-32: an integrator of neurotransmission. *Annu. Rev. Pharmacol. Toxicol.* 44, 269–296. doi: 10.1146/annurev.pharmtox.44.101802.121415

Székely, G., Abrahám, E., Cséplo, A., Rigó, G., Zsigmond, L., Csiszár, J., et al. (2008). Duplicated P5CS genes of Arabidopsis play distinct roles in stress regulation and developmental control of proline biosynthesis. *Plant J.* 53, 11–28. doi: 10.1111/j.1365-313X.2007.03318.x

Takemiya, A., Ariyoshi, C., and Shimazaki, K.-I. (2009). Identification and functional characterization of Inhibitor-3, a regulatory subunit of protein phosphatase 1 in plants. *Plant Physiol.* 150, 144–156. doi: 10.1104/pp.109.135335

Takemiya, A., Kinoshita, T., Asanuma, M., and Shimazaki, K. (2006). Protein phosphatase 1 positively regulates stomatal opening in response to blue light in *Vicia faba*. *Proc. Natl. Acad. Sci. U. S. A.* 103, 13549–13554. doi: 10.1073/pnas.0602503103

Takemiya, A., Yamauchi, S., Yano, T., Ariyoshi, C., and Shimazaki, K. (2013). Identification of a regulatory subunit of protein phosphatase 1 which mediates blue light signaling for stomatal opening. *Plant Cell Physiol.* 54, 24–35.

Templeton, G., Nimick, M., Morrice, N., Campbell, D., Goudreault, M., Gingras, A.-C., et al. (2011). Identification and characterization of AtI-2, an Arabidopsis homologue of an ancient protein phosphatase 1 (PP1) regulatory subunit. *Biochem. J.* 435, 73–83. doi: 10.1042/BJ20101035

Umezawa, T., Sugiyama, N., Takahashi, F., Anderson, J. C., Ishihama, Y., Peck, S. C., et al. (2013). Genetics and phosphoproteomics reveal a protein phosphorylation network in the abscisic acid signaling pathway in *Arabidopsis thaliana*. *Sci. Signal.* 6:rs8. doi: 10.1126/scisignal.2003509

Verbinnen, I., Ferreira, M., and Bollen, M. (2017). Biogenesis and activity regulation of protein phosphatase 1. *Biochem. Soc. Trans.* 45, 89–99. doi: 10.1042/BST20160154

Wang, W., Bai, M.-Y., and Wang, Z.-Y. (2014a). The brassinosteroid signaling network—a paradigm of signal integration. *Curr. Opin. Plant Biol.* 21, 147–153. doi: 10.1016/j.pbi.2014.07.012

Wang, Y., Hou, Y., Qiu, J., Wang, H., Wang, S., Tang, L., et al. (2020). Abscisic acid promotes jasmonic acid biosynthesis via a 'SAPK10-bZIP72-AOC' pathway to synergistically inhibit seed germination in rice (*Oryza sativa*). *New Phytol.* 228, 1336–1353. doi: 10.1111/nph.16774

Wang, G. J., Miao, W., Wang, J. Y., Ma, D. R., Li, J. Q., and Chen, W. F. (2013). Effects of exogenous abscisic acid on antioxidant system in weedy and cultivated rice with different chilling sensitivity under chilling stress. *J. Agron. Crop. Sci.* 199, 200–208.

Wang, W., Zhang, J., Qin, Q., Yue, J., Huang, B., Xu, X., et al. (2014b). The six conserved serine/threonine sites of REPRESSOR OF ga1-3 protein are important for its functionality and stability in gibberellin signaling in Arabidopsis. *Planta* 240, 763–779. doi: 10.1007/s00425-014-2113-3

Wei, L. X., Lv, B. S., Wang, M. M., Ma, H. Y., Yang, H. Y., Liu, X. L., et al. (2015). Priming effect of abscisic acid on alkaline stress tolerance in rice (*Oryza sativa* L.) seedlings. *Plant Physiol. Biochem.* 90, 50–57. doi: 10.1016/j.plaphy.2015.03.002

Xiang, X., Zhang, P., Yu, P., Zhang, Y., Yang, Z., Sun, L., et al. (2019). LSSR1 facilitates seed setting rate by promoting fertilization in rice. *Rice* 12, 31. doi: 10.1186/s12284-019-0280-3

Yan, J., Liu, Y., Huang, X., Li, L., Hu, Z., Zhang, J., et al. (2019). An unreported NB-LRR protein SUT1 is required for the autoimmune response mediated by type one protein phosphatase 4 mutation (topp4-1) in Arabidopsis. *Plant J.* 100, 357–373. doi: 10.1111/tpj.14447

Yin, X., Wang, X., and Komatsu, S. (2018). Phosphoproteomics: protein phosphorylation in regulation of seed germination and plant growth. *Curr. Protein Pept. Sci.* 19, 401–412. doi: 10.2174/1389203718666170209151048

You, J., Zong, W., Hu, H., Li, X., Xiao, J., and Xiong, L. (2014). A STRESS-RESPONSIVE NAC1-regulated protein phosphatase gene rice protein phosphatase18 modulates drought and oxidative stress tolerance through abscisic acid-independent reactive oxygen species scavenging in rice. *Plant Physiol.* 166, 2100–2114. doi: 10.1104/pp.114.251116

Yue, J., Qin, Q., Meng, S., Jin, H., Gou, X., Li, J., et al. (2015). TOPP4 regulates the stability of Phytochrome interacting factor 5 during Photomorphogenesis in Arabidopsis. *Plant Physiol.* 170, 1381–1397. doi: 10.1104/pp.15.01729

Zaefyzadeh, M., Quliyev, R. A., Babayeva, S., and Abbasov, M. (2009). The effect of the interaction between genotypes and drought stress on the superoxide dismutase and chlorophyll content in durum wheat landraces. *Turk. J. Biol.* 33, 1–7.

Zhang, A., Jiang, M., Zhang, J., Ding, H., Xu, S., Hu, X., et al. (2007). Nitric oxide induced by hydrogen peroxide mediates abscisic acid-induced activation of the mitogen-activated protein kinase cascade involved in antioxidant defense in maize leaves. *New Phytol.* 175, 36–50. doi: 10.1111/j.1469-8137.2007.02071.x

Zhang, J., Qin, Q., Nan, X., Guo, Z., Liu, Y., Jadoon, S., et al. (2020). Role of protein phosphatase1 regulatory subunit3 in mediating the abscisic acid response. *Plant Physiol.* 184, 1317–1332. doi: 10.1104/pp.20.01018

Zhang, Z., Zhang, Q., Wu, J., Zheng, X., Zheng, S., Sun, X., et al. (2013). Gene knockout study reveals that cytosolic ascorbate peroxidase 2(OsAPX2) plays a critical role in growth and reproduction in rice under drought, salt and cold stresses. *PLoS One* 8:e57472. doi: 10.1371/journal.pone.0057472

Zhang, A., Zhang, J., Zhang, J., Ye, N., Zhang, H., Tan, M., et al. (2011). Nitric oxide mediates brassinosteroid-induced ABA biosynthesis involved in oxidative stress tolerance in maize leaves. *Plant Cell Physiol.* 52, 181–192. doi: 10.1093/pcp/pcq187

Zhang, J., Zhang, L., Zhao, S., and Lee, E. Y. (1998). Identification and characterization of the human HCG V gene product as a novel inhibitor of protein phosphatase-1. *Biochemistry* 37, 16728–16734. doi: 10.1021/bi981169g

frontiers | Frontiers in Plant Science

TYPE Original Research
PUBLISHED 07 September 2022
DOI 10.3389/fpls.2022.952595

Check for updates

OPEN ACCESS

EDITED BY
Ji-Hong Liu,
Huazhong Agricultural University, China

REVIEWED BY
Tushar Suhas Khare,
Savitribai Phule Pune University, India
Weiqiang Li,
RIKEN, Japan
Xiuqin Zhao,
Chinese Academy of Agricultural Sciences (CAAS), China

*CORRESPONDENCE
Hongkai Zhou
zhouhk@gdou.edu.cn
Jianghuan Xu
xujianghuan@163.com

SPECIALTY SECTION
This article was submitted to Plant Abiotic Stress, a section of the journal Frontiers in Plant Science

RECEIVED 25 May 2022
ACCEPTED 09 August 2022
PUBLISHED 07 September 2022

CITATION
Yang S, Liu M, Chu N, Chen G, Wang P, Mo J, Guo H, Xu J and Zhou H (2022) Combined transcriptome and metabolome reveal glutathione metabolism plays a critical role in resistance to salinity in rice landraces HD961.
Front. Plant Sci. 13:952595.
doi: 10.3389/fpls.2022.952595

COPYRIGHT
© 2022 Yang, Liu, Chu, Chen, Wang, Mo, Guo, Xu and Zhou. This is an open-access article distributed under the terms of the Creative Commons Attribution License (CC BY). The use, distribution or reproduction in other forums is permitted, provided the original author(s) and the copyright owner(s) are credited and that the original publication in this journal is cited, in accordance with accepted academic practice. No use, distribution or reproduction is permitted which does not comply with these terms.

Combined transcriptome and metabolome reveal glutathione metabolism plays a critical role in resistance to salinity in rice landraces HD961

Shan Yang[1], Mengshuang Liu[1], Na Chu[2], Guanxiu Chen[1], Panpan Wang[1], Junjie Mo[1], Haifeng Guo[1], Jianghuan Xu[1]* and Hongkai Zhou[1]*

[1]College of Coastal Agricultural Sciences, South China Branch of National Saline-Alkali Tolerant Rice Technology Innovation Center, Guangdong Ocean University, Zhanjiang, China, [2]National Engineering Research Center for Sugarcane, Fujian Agriculture and Forestry University, Fuzhou, China

Rice (*Oryza sativa*) is one of the most important food crops around the world, which is sensitive to salt stress, especially in the seedling and booting stage. HD961 is a salt-tolerant rice landrace that grows along coastal beaches and has disease and insect pest resistance, salt tolerance, and vigorous growth characteristics. We performed a combined transcriptome and metabolome analysis to clarify salinity resistance mechanisms in cultivar HD961, which has adapted to salinity soil at the early seedling stage. The results showed that the growth and antioxidant capacity of HD961 were stronger than 9311 under salt stress (SS). Transcriptomic analysis showed that a total of 6,145, 3,309, 1,819, and 1,296 differentially expressed genes (DEGs) were identified in the groups of TH60 (control group vs. 60 mM group of HD961 for transcriptome), TH120 (control group vs. 120 mM group of HD961 for transcriptome), T60 (control group vs. 60 mM group of 9311 for transcriptome), and T120 (control group vs. 120 mM group of 9311 for transcriptome), respectively. Starch and sucrose metabolism and phenylpropanoid biosynthesis were shared in the four treatment groups based on a KEGG enrichment analysis of DEGs. In addition, alpha-linolenic acid metabolism, plant hormone signal transduction, plant-pathogen interaction, and fatty acid elongation were specific and significantly different in HD961. A total of 92, 158, 151, and 179 significantly regulated metabolites (SRMs) responded to SS in MH60 (control group vs. 60 mM group of HD961 for metabolome), MH120 (control group vs. 120 mM group of HD961 for metabolome), M60 (control group vs. 60 mM group of 9311 for metabolome), and M120 (control group vs. 120 mM group of 9311 for metabolome), respectively. The KEGG analysis showed that eight common metabolic pathways were identified in the four treatment groups, of which biosynthesis of amino acids was the most significant. Three specific metabolic pathways were identified in the HD961, including glutathione

10.3389/fpls.2022.952595

metabolism, ascorbate and aldarate metabolism, and pantothenate and CoA biosynthesis. Integrative analysis between the transcriptome and metabolome showed that glutathione metabolism was specific and significantly affected under SS in HD961. A total of seven SRMs and 48 DEGs and four SRMs and 15 DEGs were identified in the glutathione metabolism pathway in HD961 and 9311, respectively. The Pearson correlation analysis showed a significant correlation between reduced glutathione and 16 genes (12 upregulated and four downregulated genes), suggesting these genes could be candidates as salt-tolerance regulation genes. Collectively, our data show that glutathione metabolism plays a critical role in response to SS in rice. Moreover, the stronger regulative ability of related common genes and metabolites might contribute to salt resistance in HD961.

KEYWORDS

***Oryza sativa*, salt stress, glutathione, transcriptome, metabolome**

Introduction

As the human population continues to grow, the demand for cereals is increasing (Tilman et al., 2011). While breeders are trying to improve rice yield, the area of soil salinization is constantly expanding, seriously restricting the improvement in rice yield. Thus, collecting salt-tolerant rice germplasm and cultivating salt-tolerant rice varieties is particularly important. The HD961 variant, commonly known as "seawater rice," is salt-tolerant landrace rice that grows along coastal beaches or low-lying saline fields often flooded with seawater in Zhanjiang, China. It has the characteristics of diseases and insect pest resistance, salt tolerance, and vigorous growth. Therefore, exploring the mechanisms of salt tolerance in HD961 will aid in developing new salt-tolerant varieties.

Water stress, ion toxicity, nutritional disorders, oxidative stress, changes in metabolic processes, and membrane disorganization are induced in plants under salt stress (SS) (Demidchik et al., 2010; Flowers and Colmer, 2015). These effects result in plant growth inhibition, developmental changes, metabolic adaptations, and death (Liang et al., 2018). Therefore, plants have evolved various mechanisms to develop salt tolerance, including osmotic adjustment, signal transduction, ion sequestration or exclusion, molecular regulation, and adaptive responses (van Zelm et al., 2020). Many osmoprotectants, such as proline, glycine, betaine, and soluble sugar, are induced by SS and consequently increase rapidly (Kishor et al., 1995; Garg et al., 2002; Taji et al., 2002). The rapid development of gene sequencing technologies in recent years has led to the identification of differentially expressed genes (DEGs) in response to SS based on transcriptome analysis (Fu et al., 2019; Jahan et al., 2021). Many genes, including transcription factors (TFs), osmoprotectant genes, and ion transporter/channel genes, have subsequently been cloned in rice for functional analysis, including *OsMYB2*, *OsbZIP71*, *OsCMO*, and *OsHKT1;5* (Luo et al., 2012; Yang et al., 2012; Liu et al., 2014; Kobayashi et al., 2017). The mechanisms of plant salt tolerance involve complex regulatory networks; therefore, it is necessary to understand the relationship between genes and downstream metabolites.

Metabolomics has been widely used to study complex metabolites under biotic and abiotic stress in plants, providing insight into extensive metabolic data and daedal metabolic pathways. Metabolomics can be divided into non-targeted and targeted metabolomics (Saito and Matsuda, 2010; Luo et al., 2018; Ribbenstedt et al., 2018). Widely targeted metabolomics represents the next generation of metabolome technology, which combines the broad spectrum of non-targeted metabolome detection with the accuracy of targeted metabolome detection. It mainly collects data through multiple reaction monitoring technologies and establishes a metabolite database to achieve an accurate qualitative and quantitative analysis of metabolites (Luo et al., 2018). Li et al. (2021) found that flavonoid biosynthesis may represent the main resistance mechanism for *Zanthoxylum bungeanum* against stem canker based on combined transcriptome and metabolome analyses. Moreover, the metabolites of *Jerusalem artichoke* involved in glycolysis, phenolic metabolism, tricarboxylic cycle, glutamate-mediated proline biosynthesis, urea cycle, amino acid metabolism, unsaturated fatty acid biosynthesis, and the met salvage pathway respond to drought stress (Zhao et al., 2021). Nine salt-tolerance biomarkers were identified by comparing metabolome data of two cultivars of hulless barley. The ABA signaling pathway was shown to be essential during the SS response (Wang et al., 2019b). A comparison of different metabolites in cultivar FL478 (salt-tolerance) and cultivar IR64

(salt-sensitive) at the seedling stage under SS found that sugars and amino acids were more obviously increased in FL478 than IR64, but organic acids of FL478 were clearly decreased compared to IR64 (Zhao et al., 2014). The metabolism of amino acids, sugars, linoleic acid, and wax biosynthesis was highly correlated with melatonin-mediated SS responses in rice (Xie et al., 2020). Therefore, widely targeted metabolomics is a mature detection technology that can be applied in this study.

In this study, RNA sequencing and widely targeted metabolomics were performed for rice cultivars HD961 (salt-tolerant) and 9311 (salt-sensitive) at the three-leaf stage with different concentrations of NaCl stress treatment (0, 60, and 120 mM) for 0 and 7 days, respectively. We compared and analyzed the transcriptome and metabolome between HD961 and 9311 in response to SS at the seedling stage. Here, we explored gene-gene, metabolome-metabolome, and gene-metabolome regulatory network relationships in the SS response in rice. Based on these data, the molecular regulation mechanism of salt tolerance was elucidated in the new salt-tolerant rice cultivar HD961. Related regulatory genes and metabolites in the metabolic pathway were found to improve the salt tolerance of rice. Our findings enrich the molecular regulation theory of salt tolerance in rice and provide a theoretical basis for salt tolerance rice breeding.

Materials and methods

Plant materials and cultivation

The Indica rice cultivars HD961 (salt-tolerant, red rice) and 9311 (salt-sensitive and white rice) were used in this study. Plump seeds were picked from the seeds of HD961 and 9311, which were surface-sterilized with 30% (v/v) H_2O_2 for 30 min, rinsed thoroughly with ddH_2O and sown in a plastic tray (41.5 cm × 30.5 cm × 2 cm) covered with a layer of absorbent filter paper. The trays were then placed in the dark incubator at 28°C for 5 days, and the filter paper was kept moist with ddH_2O. Seedlings with consistent growth vigor were transferred to a 96-well black hydroponic box filled with Yoshida nutrient solution of rice (Coolaber, Beijing, China) and cultivated in an artificial climate chamber with 65% relative humidity under an 18 h/6 h light/dark (light intensity ∼ 16,000 LUX) cycle at 26°C. The nutrient solution was renewed every 3 days.

Salt stress treatment

The SS experiment used three NaCl concentrations: 0 mM (control group), 60 mM, and 120 mM, respectively. When the rice seedlings were at the stage of three leaves, plants with the same growth vigor were selected as experimental materials for a 7 days SS treatment. After the SS treatment, a phenotypic measurement was performed. The aerial part of the rice seedlings (a mix of stems and leaves) was collected for relevant omics and physiological analyses. All samples (18 samples) were frozen in liquid nitrogen and transferred to −80°C for storage. Three biological replicates were performed for each sample in this study.

Measurement of phenotypic and physiologically related parameters

The phenotypic measurements included plant height, total root length, dry weight of the aerial part for each plant, and dry weight of the root system for each plant. Plant height was measured for 20 plants of each cultivar using a ruler. The 20 plants were cut into aerial and root sections. The root systems of the 20 plants were scanned using a root scanner (Microtek Scanmaker i800 Plus, China), and the root length was analyzed using the bundled software from the root scanner. After root system scanning, the aerial and root sections of 20 plants were put into two envelopes and incubated at 105°C for 30 min, followed by 85°C until they achieved a stable weight. Free proline and soluble sugar concentrations were determined using the acid ninhydrin reagent and anthrone methods, respectively (Moustakas et al., 2011). The H_2O_2 content and superoxide dismutase (SOD) activity were determined using Dongsansuk's method (Dongsansuk et al., 2021).

RNA sequencing and transcriptomics analysis

The total RNA from 18 samples was extracted using TRIzol reagent (Invitrogen, Carlsbad, CA, United States) according to the standard protocol. The cDNA library was then constructed and sequenced on an Illumina HiSeq X-ten platform at Wuhan Metware Biotechnology Co., Ltd. (Wuhan, China), and the length of the generated reads was 150 bp paired-end (PE 150). To obtain clear reads, the low-quality reads, adapter sequences, and sequences with more than 10% poly-N in the raw reads were filtered using fastp 0.21.0 (Chen et al., 2018). The Q20, Q30, and GC content of each sample were calculated. Clear reads from each sample were mapped to the Nipponbare (*Oryza sativa* ssp. indica, ASM465v1[1]) reference genome using HISAT2 (Kim et al., 2015). Raw counts of genes were performed using feature counts (Liao et al., 2014). The differentially expressed genes (DEGs) between two samples were identified using DESeq2 with the parameters of $|\log_2\text{fold change}| \geq 1$ and false discovery rate (FDR) < 0.05 (Love et al., 2014). The functions of DEGs were annotated using the KEGG and

1 http://plants.ensembl.org/Oryza_indica/Info/Index

GO databases, whereby the KEGG pathway analysis of DEGs was performed using BLAST software (Camacho et al., 2009). KEGG enrichment was analyzed using KOBAS 2.0 software with a p-value < 0.05 (Mao et al., 2005; Xie et al., 2011), and the GO analysis of DEGs was carried out using the R package cluster Profiler (Yu et al., 2012). The transcription factors (TFs) were predicted using iTAK software (Zheng et al., 2016) with the PlnTFDB (Pérez-Rodríguez et al., 2010) and PlantTFDB (Jin et al., 2014) databases among the DEGs. Moreover, the samples were named as TR_HD961_0 (control group of HD961 for transcriptome), TR_HD961_60 (60 mM group of HD961 for transcriptome), TR_HD961_120 (120 mM group of HD961 for transcriptome), TR_9311_0 (control group of 9311 for transcriptome), TR_9311_60 (60 mM group of 9311 for transcriptome), and TR_9311_120 (120 mM group of 9311 for transcriptome). TH60, TH120, T60, and T120 were denoted as groups TR_HD961_0 vs. TR_HD961_60, TR_HD961_0 vs. TR_HD961_120, TR_9311_0 vs. TR_9311_60, and TR_9311_0 vs. TR_9311_120, respectively.

Real-time quantitative PCR

To confirm the accuracy of RNA-Seq, 12 candidate DEGs were verified by RT-qPCR. Based on the coding gene sequences, the primers of RT-qPCR were designed using primer premier 6.0 software, and β-actin was selected as the internal control gene (Kim et al., 2003) (**Supplementary Table 1**). The SYBR® Green Premix Pro Taq HS qPCR Kit (Accurate Biological Engineering LTD, Hunan, China) was used for the RT-qPCR assay. A 20 μl of reaction solution contained 10 μl 2 × SYBR Green Pro Taq HS Premix, 0.5 μl of primer F (10 μM), 0.5 μl of primer R (10 μM), 1 μl of cDNA, and 8 μl of nuclease-free water. The qPCR reactions involved denaturation at 95°C for 30 s, followed by 40 cycles of 5 s at 95°C and 30 s at 60°C. The RT-qPCR assays were carried out using the Bio-Rad CFX Connect Real-time System. The qPCR data were analyzed using the $2^{-\Delta\Delta Ct}$ quantitative method to determine differences in gene expression (Livak and Schmittgen, 2001). This study used three independent biological replicates and three technological replicates for each sample.

Sample preparation and extraction for widely targeted metabolomics

The sample preparation, extraction, identification, and quantification of the widely targeted metabolome was performed by Wuhan Metware Biotechnology Co., Ltd.[2]. Three biological replicates were performed in this study. The samples were named as follows: ME_HD961_0 (control group of HD961 for metabolome), ME_HD961_60 (60 mM group of HD961 for metabolome), ME_HD961_120 (120 mM group of HD961 for metabolome), ME_9311_0 (control group of 9311 for metabolome), ME_9311_60 (60 mM group of 9311 for metabolome), and ME_9311_120 (120 mM group of 9311 for metabolome). MH60, MH120, M60, and M120 were denoted as groups ME_HD961_0 vs. ME_HD961_60, ME_HD961_0 vs. ME_HD961_120, ME_9311_0 vs. ME_9311_60, and ME_9311_0 vs. ME_9311_120, respectively.

Biological samples were freeze-dried using a vacuum freeze dryer (Scientz-100F). The freeze-dried samples were crushed using a mixer mill (MM 400, Retsch) with a zirconia bead for 1.5 min at 30 Hz. Next, 100 mg of lyophilized powder was dissolved with 1.2 ml 70% methanol solution, vortexed for 30 s every 30 min for a total of six times, and then placed at 4°C overnight. Following centrifugation at 12,000 rpm for 10 min, the extracts were filtered (SCAA-104, 0.22 μm pore size; ANPEL, Shanghai, China) before UPLC-MS/MS analysis.

UPLC conditions

The sample extracts were analyzed using a UPLC-ESI-MS/MS system (UPLC, SHIMADZU Nexera X2; MS, Applied Biosystems 4500 Q TRAP). The analytical conditions were as follows: UPLC: column, Agilent SB-C18 (1.8 μm, 2.1 mm × 100 mm); the mobile phase consisted of solvent A, pure water with 0.1% formic acid, and solvent B, acetonitrile with 0.1% formic acid. Sample measurements were performed with a gradient program that employed starting conditions of 95% A and 5% B. Within 9 min, a linear gradient was programmed to 5% A and 95% B, and a composition of 5% A and 95% B was maintained for 1 min. Subsequently, a composition of 95% A and 5.0% B was adjusted within 1.10 min and maintained for 2.9 min. The flow velocity was set at 0.35 ml per minute, the column oven was set to 40°C, and the injection volume was set to 4 μl. The effluent was alternatively connected to an ESI-triple quadrupole-linear ion trap (QTRAP)-MS.

ESI-Q TRAP-MS/MS

The LIT and triple quadrupole (QQQ) scans were acquired on a triple quadrupole-linear ion trap mass spectrometer (Q TRAP), the AB4500 Q TRAP UPLC/MS/MS System, equipped with an ESI Turbo Ion-Spray interface that was operated in positive and negative ion mode and controlled by Analyst 1.6.3 software (AB Sciex). The ESI source operation parameters were as follows: an ion source, turbo spray; source temperature, 550°C; ion spray voltage (IS), 5,500 V (positive ion mode)/−4,500 V (negative ion mode); ion source gas I (GSI), gas II (GSII), and curtain gas (CUR) were set at 50, 60, and 25 psi, respectively; and the collision-activated dissociation

2 www.metware.cn

(CAD) was set at high. Instrument tuning and mass calibration were performed with 10 and 100 μM polypropylene glycol solutions in QQQ and LIT modes, respectively. QQQ scans were acquired as MRM experiments with collision gas (nitrogen) set to medium. DP and CE for individual MRM transitions were conducted with further DP and CE optimization. A specific set of MRM transitions were monitored for each period according to the metabolites eluted within this period.

Data analysis of metabolomics

The hierarchical cluster analysis (HCA) results of samples and metabolites were presented as heatmaps with dendrograms, while Pearson correlation coefficients (PCC) between samples were calculated by the cor function in R and presented as only heatmaps. Both HCA and PCC were carried out by the R package pheatmap. For HCA, normalized signal intensities of metabolites (unit variance scaling) were visualized as color spectra. Principal component analysis (PCA) was performed using the statistics function prcomp within R[3]. The data were unit variance scaled before PCA.

Significantly regulated metabolites (SRMs) between groups were determined by VIP $\geq$ 1 and absolute Log_2FC (fold change) $\geq$ 1. VIP values were extracted from the OPLS-DA results, which also contained score plots and permutation plots, and were generated using the R package MetaboAnalystR. The data were log-transformed (log_2) and mean centered before OPLS-DA. To avoid overfitting, a permutation test (200 permutations) was performed.

Identified metabolites were annotated using the KEGG compound database[4], and annotated metabolites were then mapped to the KEGG pathway database[5]. The pathways with SRMs mapped were then fed into the metabolite set enrichment analysis (MSEA), and their significance was determined using the hypergeometric test's *p*-values.

Statistical analysis

Duncan's multiple comparison method was conducted using Statistical Product and Service Solutions software (IBM SPSS 19.0) to assess the differences in phenotypic and physiological indices at three different levels of salinity. Statistical significance was set at $p < 0.05$. The bar diagram was drawn using Microsoft Office Excel 2016. The Pearson correlation analysis and gene-metabolite correlation network diagram between DEGs and SRMs in the glutathione pathway of HD961 were conducted using a tool of advanced correlation network graph in the Metware cloud platform (the threshold for association analysis > 0.8, $p < 0.05$[6]).

Results

Analysis of morphological response to salt stress

The HD961 cultivar showed better plant height, total root length, dry weight of the aerial part, and dry weight of roots than the cultivar 9311 after 7 days of SS treatment (**Supplementary Figure 1**). The plant height and root length of HD961 and 9311 decreased as the NaCl concentration increased (**Supplementary Figures 1A,B**). Compared with 0 mM NaCl, the dry weight of the aerial part and roots were slightly increased at 60 mM and 120 mM in HD961, but decreased for 9311 (**Supplementary Figures 1C,D**). In addition, the biomass of HD961 was significantly greater than 9311 after 7 days of SS treatment (**Supplementary Figure 2**). Therefore, the performance of HD961 was better than 9311 under NaCl stress.

Analysis of the physiological response to salt stress

The content of H_2O_2, proline, soluble sugar, and SOD activity were significantly increased in HD961 and 9311 cultivars under NaCl stress, except for the soluble sugar content of 9311 (**Figure 1**). The H_2O_2 content of HD961 was less than 9311, but the proline content, soluble sugar content, and SOD activity of HD961 were greater than those of 9311 under SS (**Figure 1**). Therefore, HD961 has a stronger osmotic adjustment ability and antioxidant capability than 9311 when the plants are under SS.

Transcriptome analysis

To investigate the transcriptome response to SS in rice, 18 cDNA libraries were sequenced using Illumina platforms. After quality control, there were 44,784,392 to 60,082,654 clean reads in HD961 and 44,686,470 to 56,907,604 clean reads in 9311 (**Supplementary Table 2**). The Q20 and Q30 of all libraries were more than 97.77 and 94.00%, respectively (**Supplementary Table 2**). Twelve genes were chosen for qRT-PCR to validate the RNA-seq data, including *LOC_Os01g19330*, *LOC_Os01g46760*, *LOC_Os01g51690*, *LOC_Os01g68460*, *LOC_Os03g44270*, *LOC_Os04g33920*, *LOC_Os05g04870*, *LOC_Os06g02040*, *LOC_Os06g09688*, *LOC_Os07g19320*, *LOC_Os08g36310,* and *LOC_Os10g08474*. The results showed

3 www.r-project.org

4 http://www.kegg.jp/kegg/compound/

5 http://www.kegg.jp/kegg/pathway.html

6 https://cloud.metware.cn/

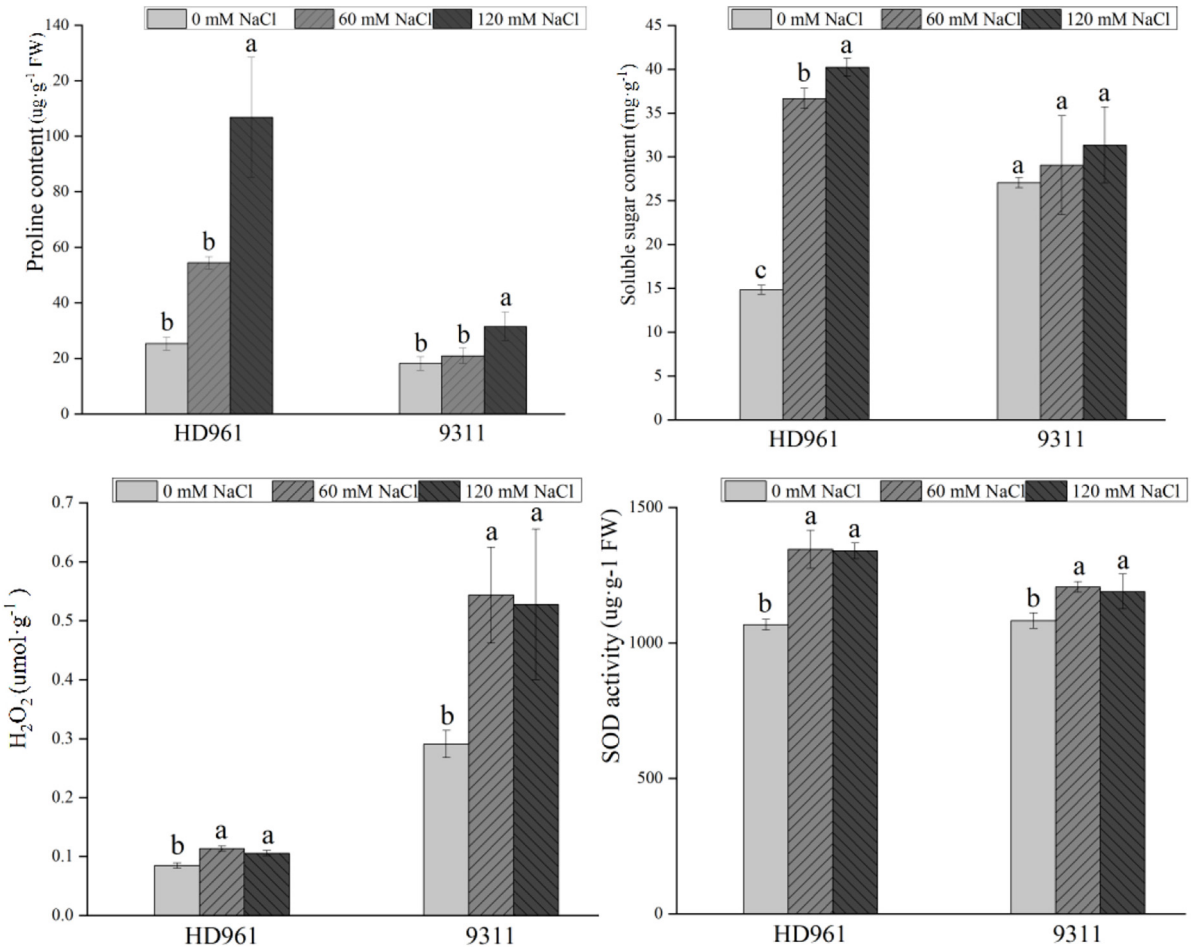


FIGURE 1
Physiologic parameters of HD961 and 9311 after 7-day salt stress treatment. The values of the error bars are plus and minus standard deviation values. The different letters denote that it is at the significance level among different concentrations of the same cultivar, $p < 0.05$.

that the expression profiles of these genes were consistent with those results of RNA-seq, suggesting that the RNA-seq data were accurate and reliable (**Supplementary Figure 3**).

A total of 6,145, 3,309, 1,819, and 1,296 DEGs were identified in the TH60, TH120, T60, and T120 groups, respectively, of which 1,867 common DEGs were expressed in both TH60 and TH120, and 490 common DEGs were expressed in T60 and T120 (**Figure 2A**). In addition, 2,784 and 520 common DEGs were expressed in two cultivars at 60 and 120 mM, respectively (**Figure 2A**). The 3,231, 2,093, 883, and 616 DEGs were expressed exclusively in groups T60, TH60, TH120, and T120 (**Figure 2A**). These results showed that the number of DEGs in HD961 was greater than in 9311. Compared with the 120 mM treatment group, the DEGs were more responsive at 60 mM in both cultivars. There were 3,795 up-DEGs and 2,350 down-DEGs, as well as 1,090 up-DEGs and 2,219 down-DEGs in TH60 and TH120, respectively. In addition, there were 627 up-DEGs and 669 down-DEGs, as well as 1,278 up-DEGs and 541 down-DEGs in T60 and T120, respectively (**Figure 2B**). A heatmap for all DEGs under different concentrations of SS was generated after RNA-seq analysis. It showed that the gene expression patterns of the two cultivars were clearly different under SS (**Supplementary Figure 4**). The DEGs of HD961 exhibited clearer differences under the tested NaCl concentrations than 9311.

The KEGG pathway enrichment analysis of DEGs showed that 134, 121, 100, and 108 KEGG pathways were enriched in the TH60, TH120, T60, and T120 groups, respectively (**Supplementary Tables 3–6**). Moreover, 21, 19, 8, and 19 KEGG pathways were significantly enriched in the TH60, TH120, T60, and T120 groups, respectively (**Figure 3**). The Top 5 KEGG pathways of TH60 were increased considerably by 404, 211, 89, 187, and 12 DEGs. They included plant-pathogen interaction, plant hormone signal transduction, starch and sucrose metabolism, MAPK signaling pathway-plant, and photosynthesis-antenna proteins, respectively (**Figure 3** and

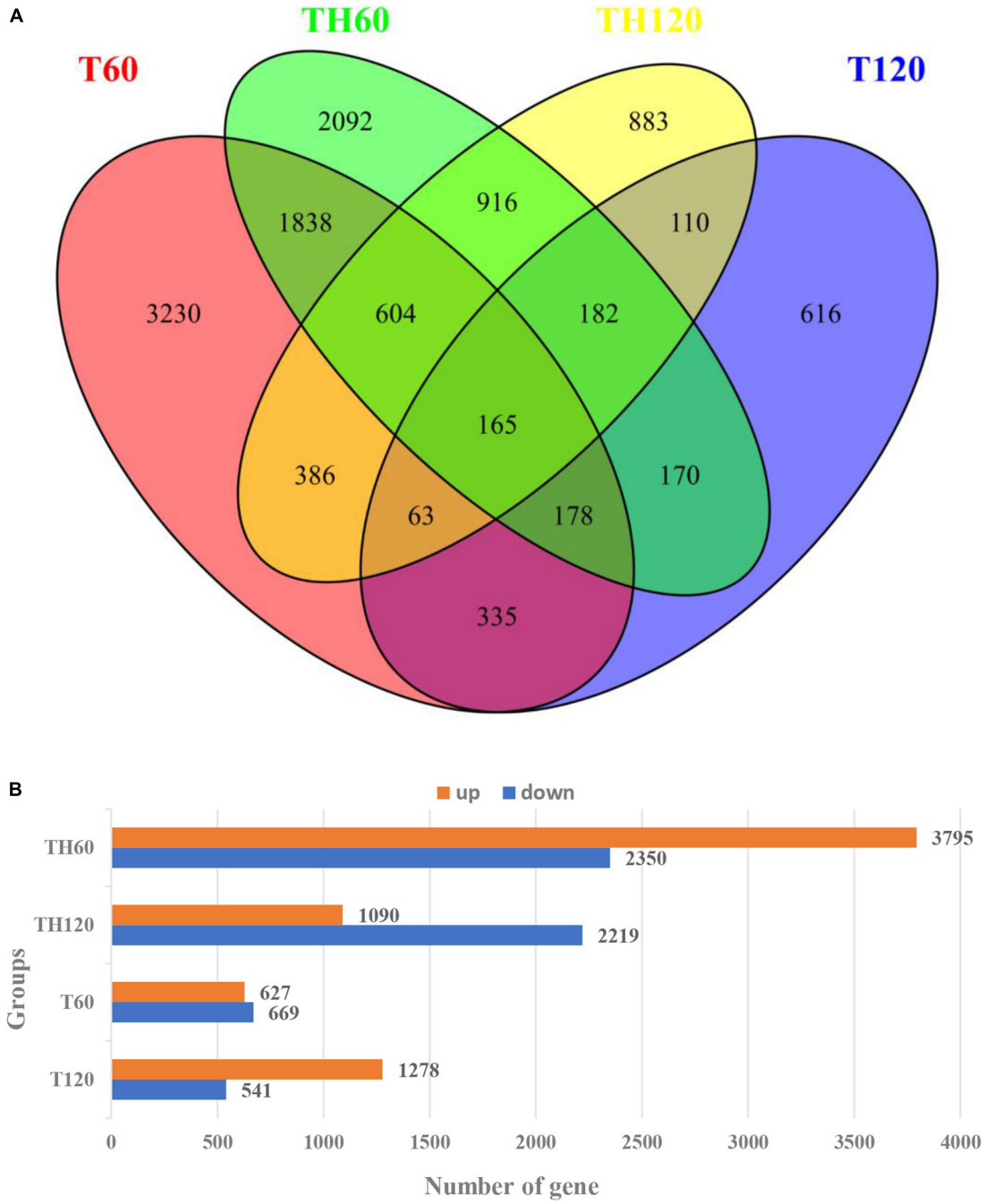


FIGURE 2
All differentially expressed genes (DEGs) at 60 mM and 120 mM NaCl treatment. **(A)** The DEGs Venn diagram of HD961and 9311. **(B)** The up and downregulated DEGs of HD961 and 9311.

Supplementary Table 3). In addition, 66, 216, 117, 101, and 27 DEGs were significantly enriched for the top 5 KEGG pathways in TH120, namely phenylpropanoid biosynthesis, plant–pathogen interaction, plant hormone signal transduction, MAPK signaling pathway-plant, and glutathione metabolism, respectively (Figure 3 and Supplementary Table 4). For the T60 group, 24, 10, 9, 19, and 14 DEGs were significantly enriched for the top 5 KEGG pathways: phenylpropanoid biosynthesis, DNA replication, cutin, suberine, and wax biosynthesis, starch, and sucrose metabolism, and amino sugar and nucleotide sugar metabolism, respectively (Figure 4 and Supplementary Table 5). 10, 29, 14, 13, and 11 DEGs

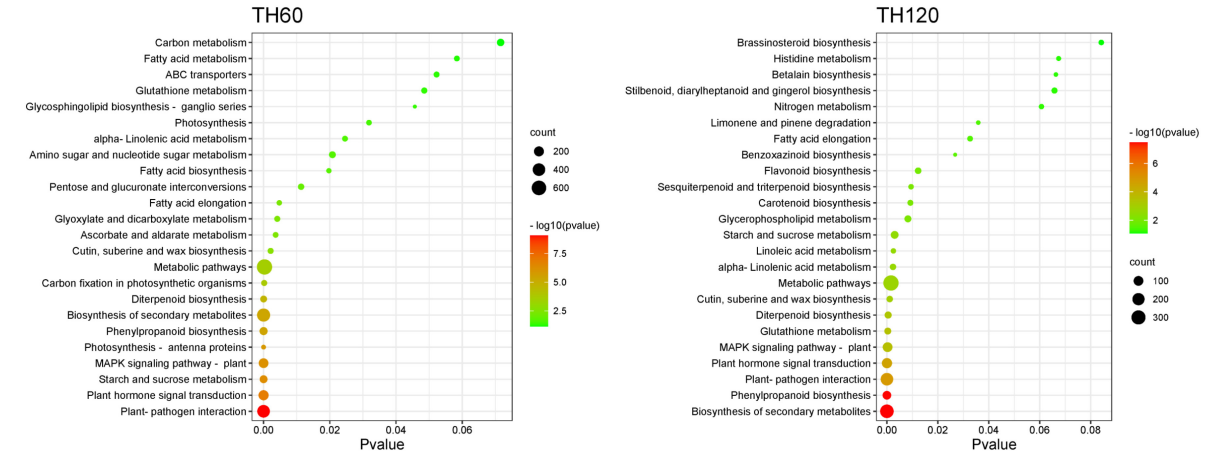


FIGURE 3
Top 24 pathways of KEGG enrichment of DEGs in HD961.

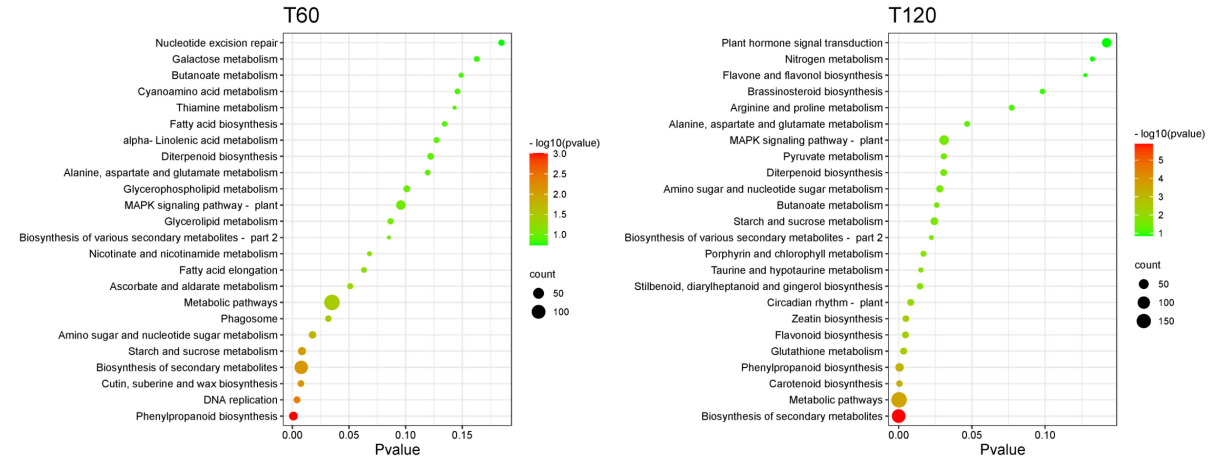


FIGURE 4
Top 24 pathways of KEGG enrichment of DEGs in 9311.

were significantly enriched to carotenoid biosynthesis, phenylpropanoid biosynthesis, glutathione metabolism, flavonoid biosynthesis, and zeatin biosynthesis in the T120, respectively (Figure 4 and Supplementary Table 6). Moreover, two KEGG pathways were shared and significantly different in four groups (TH60, TH120, T60, and T120; $p < 0.05$), including starch and sucrose metabolism (89, 44, 19, and 21 DEGs) and phenylpropanoid biosynthesis (96, 66, 24, and 29 DEGs), respectively (Figures 3, 4 and Supplementary Figure 5). Alpha-linolenic acid metabolism (51 and 19 DEGs), plant hormone signal transduction (211 and 117 DEGs), plant-pathogen interaction (404 and 216 DEGs), and fatty acid elongation (20 and 11 DEGs) were specific KEGG pathways in both TH60 and TH120 (Figure 3 and Supplementary Figure 5). In the MAPK signaling pathway–plant (187, 101, and 44 DEGs), glutathione metabolism (33, 27, and 14 DEGs) and diterpenoid biosynthesis (52, 30, and 13 DEGs) were shared between the TH60, TH120, and T120 groups (Figures 3, 4 and Supplementary Figure 5).

Metabolome analysis

The metabolites of HD961 and 9311 were analyzed to investigate the variation of the metabolomic profiles in response to SS using LC-MS/MS. A total of 92 (80 upregulated and 12 downregulated), 158 (120 upregulated and 38 downregulated), 151 (137 upregulated and 14 downregulated), and 179 (146 upregulated and 33 downregulated) SRMs accumulated in the MH60, MH120, M60, and M120 groups, respectively (Supplementary Figure 6). The 75 common SRMs accumulated in both MH60 and MH120, and the 134 common SRMs accumulated in both M60 and M120 (Figure 5A). The 69 and

97 common SRMs accumulated in two cultivars at 60 mM and 120 mM, respectively (Figure 5A). In addition, 13, 6, 48, and 30 SRMs were exclusively accumulated in the M60, MH60, MH120, and M120 groups (Figure 5A). These results show that as NaCl concentration increased, the number of SRMs also increased. Most of the SRMs were upregulated when the plants were subjected to SS. The PCA based on three QC samples (mix) and 18 test samples showed that 18 samples could separate clearly in the first two principal components, accounting for 61.2% of the total variability (Figure 5B). PCA1 and PCA2 accounted for 38.5% and 22.7% of the variability, respectively (Figure 5B). A heatmap of all metabolites showed significant differences in metabolites in HD961 and 9311 cultivars under NaCl stress (Supplementary Figure 7). These SRMs were classified into nine groups, of which the amino acids and derivatives (20%), organic acids (15.5%), lipids (14.8%), and alkaloids (12.3%) contained the majority of the upregulated SRMs. The flavonoids (25.7%), organic acids (24.5%), and lipids (12.8%) accounted for the largest proportion of downregulated SRMs (Figure 6 and Supplementary Figure 7). Therefore, amino acids and derivatives were the predominant upregulated SRMs, and the flavonoids and organic acids were the main downregulated SRMs in rice under NaCl stress.

KEGG pathway enrichment analysis of SRMs showed that the top 20 KEGG pathways were similar in both HD961 and 9311 cultivars (Figures 7, 8). The most significant enrichments in MH60, MH120, M60, and M120 groups were biosynthesis of amino acids, ABC transporters, biosynthesis of amino acids, and biosynthesis of amino acids, respectively (Figures 7, 8 and Supplementary Tables 9–12). Therefore, the biosynthesis of amino acids was the most important metabolic pathway under NaCl stress in both cultivars. For example, L-cysteine and L-lysine-butanoic acid were the top two upregulated SRMs in the biosynthesis of amino acids (Supplementary Tables 8, 9). L-isoleucine, L-ornithine, L-valine, and L-proline were also upregulated SRMs. To visually describe the relationship among the top 20 KEGG enrichment pathways of the four groups, we created a Venn diagram (Supplementary Figure 8). The results showed that eight common metabolic pathways were identified in the four groups: biosynthesis of amino acids, glucosinolate biosynthesis, aminoacyl-tRNA biosynthesis, penicillin, and cephalosporin biosynthesis, cyanoamino acid metabolism, valine, leucine and isoleucine degradation, lysine degradation, and valine, leucine, and isoleucine biosynthesis (Supplementary Figure 8 and Supplementary Table 13). Of these common metabolic pathways, the cyanoamino acid metabolism, penicillin, and cephalosporin biosynthesis, aminoacyl-tRNA biosynthesis, and valine, leucine, and isoleucine degradation reached a statistically significant enrichment level in the four groups ($p < 0.05$) (Figures 7, 8). There were three specific metabolic pathways in the HD961 cultivar (glutathione metabolism, ascorbate and aldarate metabolism, and pantothenate and CoA biosynthesis) (Supplementary Figure 8 and Supplementary Table 13), of which glutathione metabolism was significantly enriched ($p < 0.05$). Therefore, glutathione metabolism should be explored in rice grown under SS.

Integrative analysis between the transcriptome and metabolome

To understand the relationship between DEGs and SRMs, we conducted an integrative analysis between the transcriptome and metabolome. Glutathione metabolism was the only shared and significantly enriched pathway in the TH60, MH60, TH120, and MH120 groups (Supplementary Tables 14, 15). However, no shared and significantly enriched pathways were observed in both T60, M60, T120, and M120 groups (Supplementary Tables 16, 17). Therefore, the specific glutathione metabolism represented a significantly affected metabolic pathway in the cultivar HD961 undergoing SS. In this pathway, seven SRMs and 48 DEGs were identified in the HD961, and four SRMs and 15 DEGs were identified in the 9311 undergoing SS (Figure 9). Compared with 9311, the HD961 cultivar had a stronger response to SS, and its regulation was more complex. Reduced glutathione (GSH), spermidine, and dehydroascorbic acid were specific SRMs in HD961 (Figure 9A). Moreover, L-ornithine (upregulated), cadaverine (downregulated), L-ascorbic acid (downregulated), and L-cysteine (upregulated) were the same SRMs in both cultivars, of which L-cysteine was the most active substance in response to SS (Figure 9A). GSH and dehydroascorbic acid decreased, while spermidine increased as NaCl concentration increased (Figure 9A). With regard to DEGs, most of the DEGs were glutathione *S*-transferase (GST), of which the 'tau' class GST (U represents tau) was the most active, followed by the 'phi' class GST (F represents phi) (Figures 9B,C). Therefore, the *GSTs* were clearly induced by NaCl stress. In HD961, the expression of ascorbate peroxidase 3 (*APX3*, *LOC_Os04g14680*), gamma-glutamyl transpeptidase (*GGT*, *LOC_Os02g26700*), and glutathione reductase (*GSR*, *LOC_Os10g28000*) were increased under SS. The expression of *APX6* (*LOC_Os08g41090*), *APX8* (*LOC_Os02g34810*), glutathione peroxidase (*GPX*, *LOC_Os06g08670*), and glutathione synthase (*GSS*, *LOC_Os12g16200*) first increased and then decreased as the concentration of NaCl increased. To explore the relationship between these SRMs and DEGs in glutathione metabolism, we conducted the Pearson correlation analysis. The results showed that 34 DEGs strongly correlated with 7 SRMs ($R^2 > 0.8$ and $P < 0.05$) under NaCl stress (Figure 10). There was a significant correlation between the expression of genes (*LOC_Os10g38630*, *GSTU2*) and metabolite abundance (MA10039492, dehydroascorbic acid; pme0195, L-cysteine; mws0018, spermine; pme2527, L-ornithine; pme1841, cadaverine). Moreover, there were significant correlations

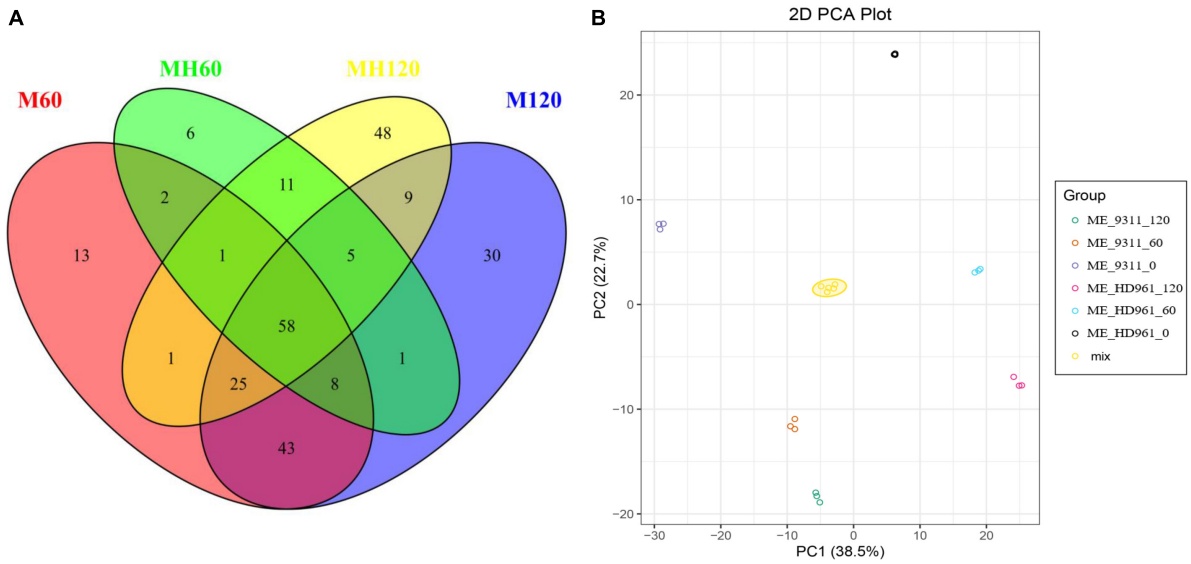


FIGURE 5
All SRMs at 60 mM and 120 mM NaCl treatment. **(A)** The SRMs Venn diagram of HD961and 9311. **(B)** PCA of metabolic data from different treatments in HD961 and 9311.

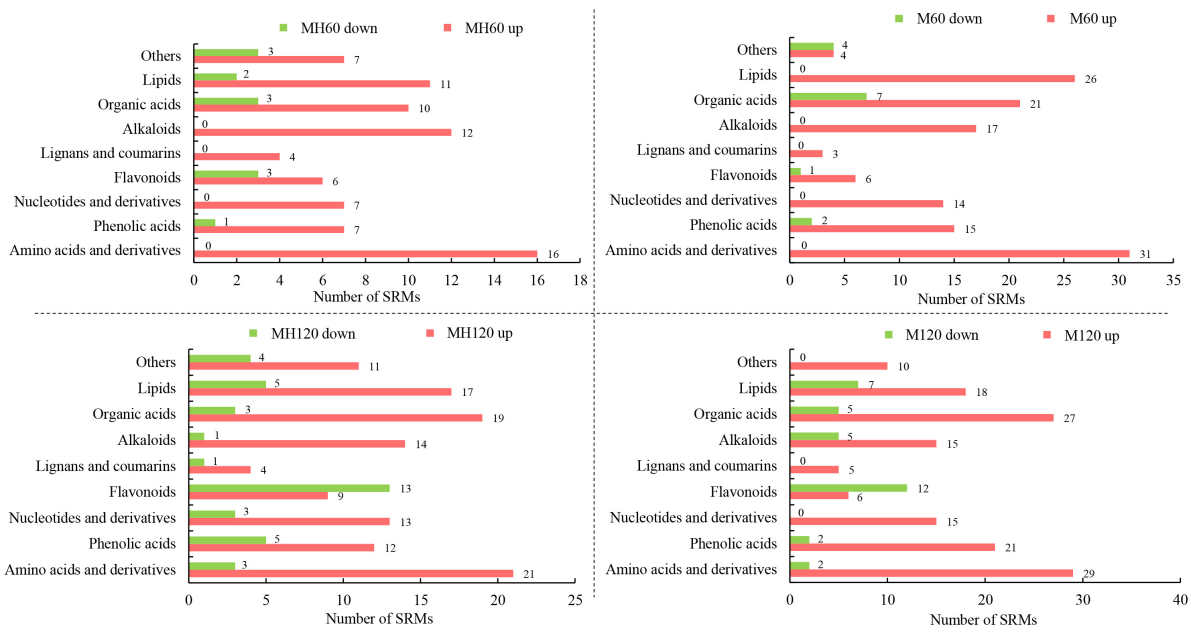


FIGURE 6
Significantly regulated metabolite (SRM) classification of HD961 and 9311.

between GSH and 16 genes (12 upregulated genes and four downregulated genes). For example, the correlation between the genes of *LOC_Os10g38340*, *LOC_Os09g37120*, *LOC_Os10g38160,* and *LOC_Os01g72130*. Further, the metabolite of GSH was extremely significant, with correlation coefficients of 0.993, 0.992, 0.963, and 0.939, respectively (Figure 10). Nevertheless, the correlation coefficient between GSH and the genes of *LOC_Os04g51300*, *LOC_Os03g17480*, *LOC_Os02g34810,* and *LOC_Os12g16200* were −0.934, −0.855, −0.837, and −0.836, respectively (Figure 10). Taken together, the correlation analysis revealed that specific genes were highly correlated with glutathione metabolites, indicating that these synthesis genes play a vital role in the synthesis of GSH under SS.

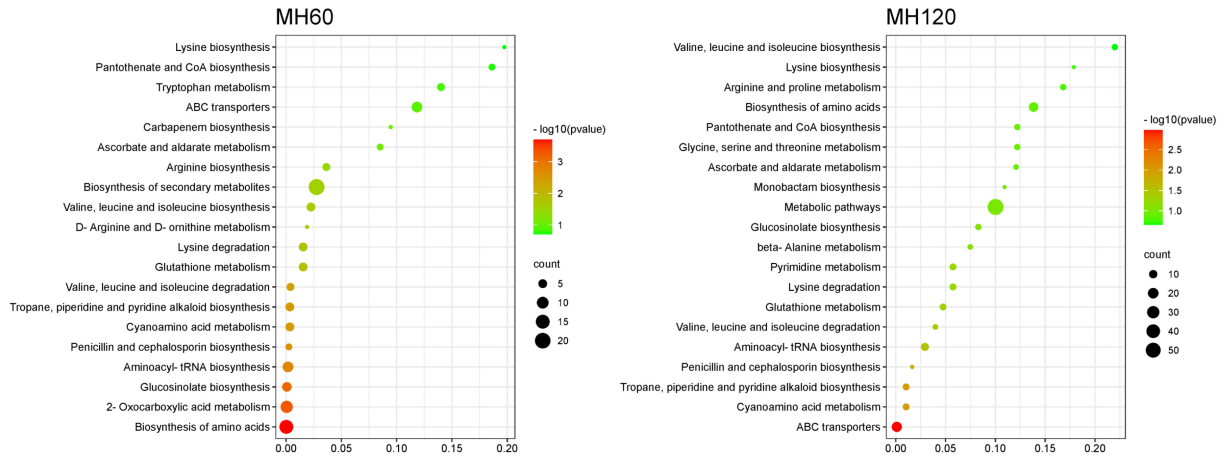


FIGURE 7
Top 20 pathways of KEGG enrichment of SRMs in HD961.

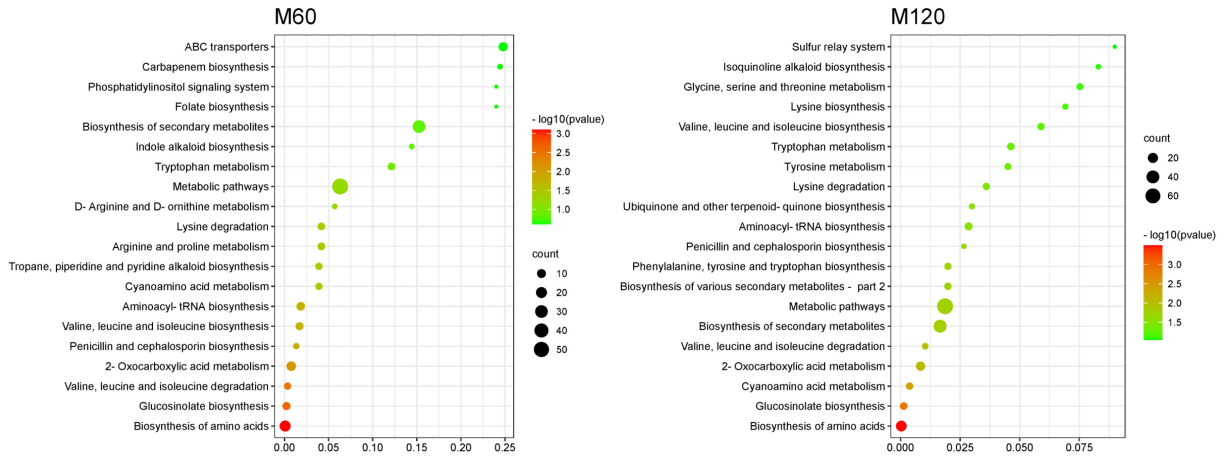


FIGURE 8
Top 20 pathways of KEGG enrichment of SRMs in 9311.

Discussion

Soil salinity is a global problem that affects seed germination, crop growth, and production (Yang and Guo, 2018). It is becoming a serious problem worldwide due to excessive use of fertilizers, inappropriate crop irrigation, excessive plowing, and seawater intrusion in the coastal area (Kamran et al., 2020). Rice is an important cereal crop that feeds more than 50% of the world's population but is sensitive to SS (Hussain et al., 2018). Fertile land is shrinking, the population is growing, and food shortages are becoming more prevalent. Therefore, there is a growing demand for salt-tolerant rice varieties. Understanding the growth, physiology, gene expression, and metabolic accumulation under SS is essential for developing salt-tolerant rice varieties.

The growth and development of plants are negatively affected by SS, resulting in several specific responses, including leaf rolling, reduced biomass, shorter plant height, and lower yields (Machado and Serralheiro, 2017; Razzaq et al., 2020). In this study, the plant height and root length of HD961 and 9311 cultivars were both decreased with an increasing concentration of NaCl. Therefore, the growth of HD961 and 9311 was restrained under SS. It is worth noting that the salt-tolerant cultivar HD961 exhibited greater biomass than the weak salt-tolerant cultivar 9311. With regard to physiology, several adaptive responses could occur in response to SS, including osmotic adjustment, regulation of ionic balance, nutritional balance, and reactive oxygen species (ROS) scavenging (Liu et al., 2022). In this study, the proline content, soluble sugar content, CAT activity, and SOD activity of HD961

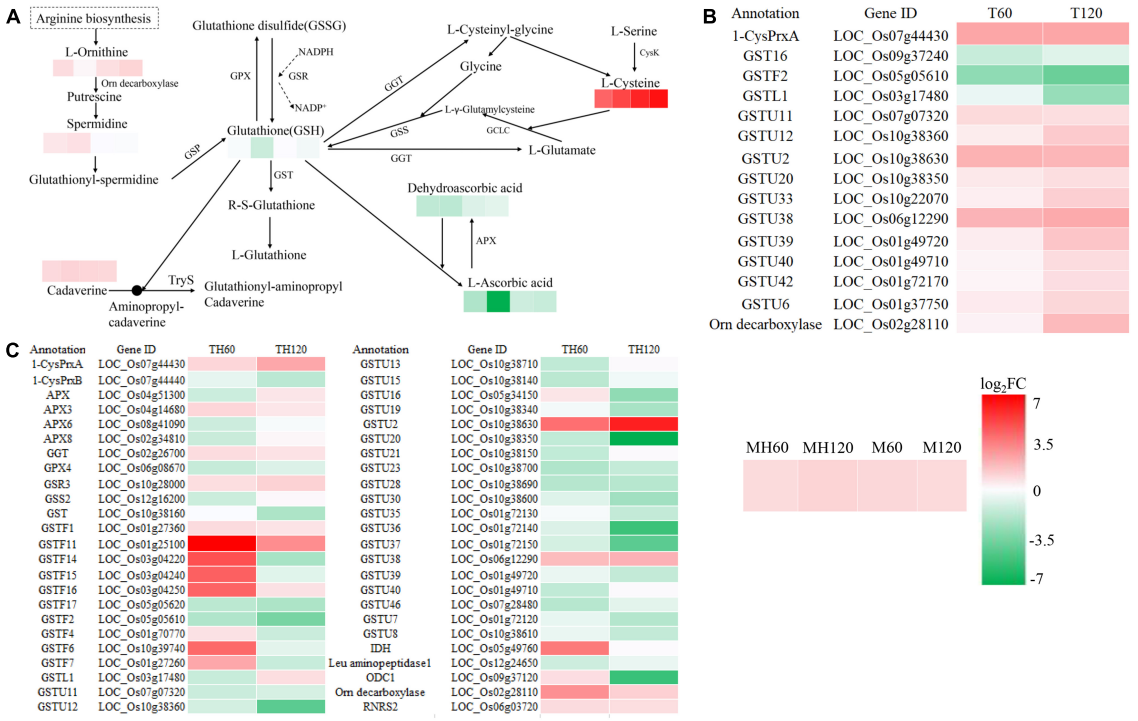


FIGURE 9
Analysis of DEGs and SRMs in the glutathione metabolic pathway. **(A)** The enriched SRMs of MH60, MH120, M60, and M120 in the glutathione metabolic pathway. Spermidine, GSH, and dehydroascorbic acid were not SRMs in the M60 and M120. **(B)** The enriched DEGs of T60 and T120 in the glutathione metabolic pathway. **(C)** The enriched DEGs of TH60 and TH120 in the glutathione metabolic pathway. $|\log_2 FC|$ denotes $|\log_2$fold change$|$.

were greater than 9311 under SS, and the O^{2-} and H_2O_2 concentrations of HD961 were less than 9311 under SS. Similar results have been shown in previous studies, including the upregulation of proline content, soluble sugar content, CAT activity, and SOD activity under SS (Liang et al., 2018; Nounjan and Theerakulpisut, 2021). Lee et al. (2013) found that the tolerance to SS in Pokkali is derived largely from constitutively maintained antioxidant enzymatic activities and induction of the antioxidant enzyme system. As a result, HD961 has a stronger ROS scavenging system than 9311, resulting in stronger salt resistance.

The gene expression of rice can be inducted by a diverse range of abiotic stresses, including SS (van Zelm et al., 2020; Liu et al., 2022). Our study performed an RNA-seq-based comparative transcriptome analysis to assess gene expression changes in rice in response to SS. A total of 6,145, 3,309, 1,819, and 1,296 DEGs were identified in the TH60, TH120, T60, and T120 groups, respectively, suggesting that more defense-responsive genes are activated in the salt-tolerant cultivar HD961 relative to the cultivar 9311. KEGG analysis showed that the majority of DEGs in rice that responded to SS included starch and sucrose metabolism as well as phenylpropanoid biosynthesis in both cultivars. These defense-responsive pathways were also previously reported as responses to SS in rice, further suggesting that these responses are largely conserved in rice exposed to SS (Wang et al., 2018; Kong et al., 2021). In addition to the pathways listed above, the majority of DEGs in the salt-tolerant cultivar HD961 that responded to SS through transcriptional activation is involved in pathways such as alpha-linolenic acid metabolism, plant hormone signal transduction, plant-pathogen interaction, fatty acid elongation, MAPK signaling pathway–plant, glutathione metabolism, and diterpenoid biosynthesis. Of these pathways, plant hormone signal transduction, MAPK signaling pathway–plant, and glutathione metabolism have been a focus of research on rice undergoing abiotic stress (Kong et al., 2019; Hao et al., 2022).

Several metabolites are changed in plants at different growth stages or when plants are exposed to biotic and abiotic stress, representing the end synthetic products of cells. Liu et al. (2020) postulated that anthocyanins, flavonols, and flavones directly affect the color formation of pepper fruit anthocyanins due to an abundance of flavonols and flavones compared to other varieties. Moreover, the coloration of the red pear fruit results from the induction of ethylene biosynthesis by jasmonate, which decreases anthocyanin production, thus increasing the availability of the precursors for flavone/isoflavone biosynthesis and enhancing the deep yellow fruit coloration (Ni et al., 2020).

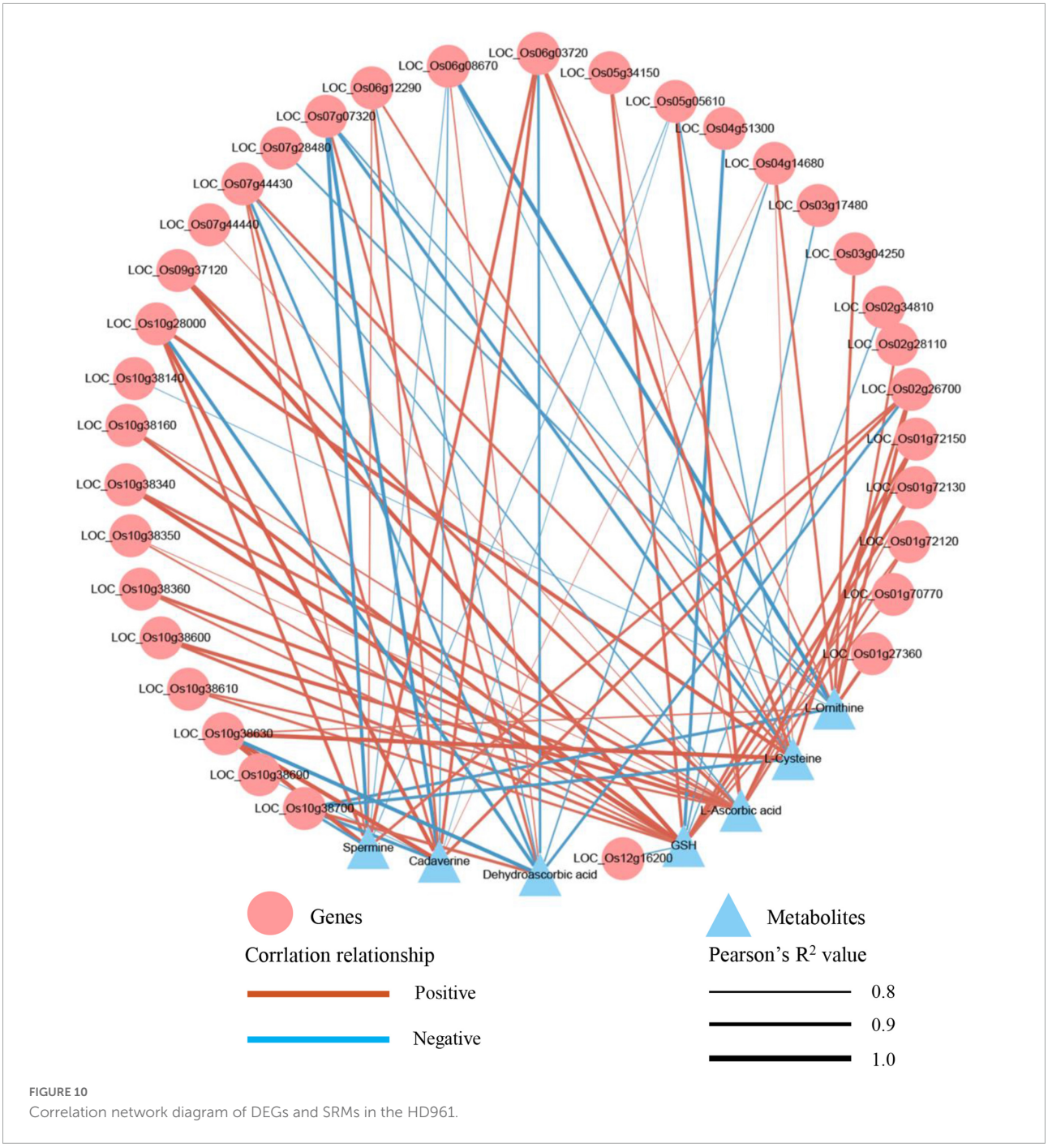


FIGURE 10
Correlation network diagram of DEGs and SRMs in the HD961.

The abundance of metabolites is most closely related to phenotypes and directly affects plant phenotypes (Fiehn, 2002). In our study, the results suggested that the higher concentration of NaCl (from 0 to 120 mM) resulted in more SRMs. Moreover, rice can synthesize more metabolites to resist damage under salt stress, and we found that most of the metabolites were upregulated. These upregulated SRMs consisted of amino acids and derivatives (20%), organic acids (15.5%), lipids (14.8%), and alkaloids (12.3%), while the downregulated SRMs consisted of flavonoids (25.7%), organic acids (24.5%), and lipids (12.8%). Therefore, amino acids and derivatives were the main upregulated SRMs, whereas flavonoids and organic acids were the main downregulated SRMs in rice under SS. Previous results have shown that sugars and amino acids increased significantly in the leaves and roots of both rice genotypes (FL478 and IR64). In contrast, organic acids increased in roots and decreased in leaves (Zhao et al., 2014). Gupta and De (2017) found that the conserved primary metabolites (sugars, polyols, amino

acids, organic acids, and certain purine derivatives) responded differently to NaCl stress in four rice varieties. The SRMs we observed in our study were similar to those previously shown, indicating that the metabolites responding to SS were conserved in rice. Moreover, KEGG pathway enrichment analysis of SRMs showed that the biosynthesis of amino acids was the most significant enrichment in both cultivars under SS among the top 20 KEGG enrichment pathways. Amino acids are the basic substances for synthesizing various metabolites and proteins in plants. Batista-Silva et al. (2019) found a tight relationship between amino acid metabolism and stress responses. We discovered that L-cysteine, L-lysine-butanoic acid, L-valine, L-lysine, and L-proline were all upregulated in these cultivars in response to SS. Previous studies have also shown that proline is a compatible osmolyte during the SS response, alanine and glutamine act as nitrogen stores, and leucine, valine, isoleucine, and lysine are involved with ATP production and detoxification (Hildebrandt, 2018; Liang et al., 2018; Batista-Silva et al., 2019).

This study identified specific metabolic pathways in the HD961 cultivar in response to SS, including glutathione metabolism, ascorbate and aldarate metabolism, and pantothenate and CoA biosynthesis. However, glutathione metabolism was the only pathway that exhibited significant enrichment. Furthermore, the results of the integrative analysis between the transcriptome and metabolome showed that glutathione metabolism was specific and significantly affected in the HD961 cultivar undergoing SS. GSH plays a vital role in plants and regulates various metabolic functions, including antioxidant defense, xenobiotic detoxification, reserving cysteine, maintaining redox balance, immunity modulation, fibrogenesis, cell cycle regulation, and apoptosis (Hasanuzzaman et al., 2017, 2019). Therefore, the glutathione pathway has been a key focus of research on plants undergoing abiotic stress (Khunpon et al., 2018; Wang et al., 2019a, 2021). Yang et al. (2020) found that the concentration of GSH and GSSG (oxidized glutathione) decreased during seed germination and young seedling growth stages in plants undergoing SS from day zero to four, and the DEGs mainly contained 2 GPX, 3 APX, 1 GSS, and 39 GST. We obtained similar results in this study, whereby GSH decreased in the two cultivars when the concentration of NaCl increased, indicating that a high salt concentration induces rice to produce more peroxides. There were 33 GST DEGs and 13 GST DEGs in the HD961 and 9311 cultivars, respectively, showing that HD961 had a better response to SS than 9311. Moreover, the GSH concentration was positively correlated with *LOC_Os10g38340* (*GSTU19*), *LOC_Os09g37120* (*Ornithine decarboxylase*, *ODC1*), *LOC_Os10g38160* (*GST*), and *LOC_Os01g72130* (*GSTU35*), and negatively correlated with *LOC_Os04g51300* (*APX*), *LOC_Os03g17480* (*GSTL1*), *LOC_Os02g34810* (*APX8*), and *LOC_Os12g16200* (*GSS2*) in HD961, suggesting that these DEGs were candidate salt-tolerance regulation genes. The functions of *OsAPX2* (Zhang et al., 2013), *OsAPX8* (Hong et al., 2007), *OsGSTL2* (Kumar et al., 2013), *OsGR2* (Kaminaka et al., 1998), *OsGR3* (Wu et al., 2015), and *OsGRX1* (Lima-Melo et al., 2016) have been previously identified; the results suggest that these genes are positively or negatively regulated in rice in response to SS. Taken together, the identification of these filtered candidate salt-tolerance regulation genes in this study warrants additional studies to verify their genetic function in the future.

Rice is most sensitive to SS at the seedling and reproductive stages (Ganie et al., 2019). We can improve the salt tolerance of rice in these two stages through water and fertilizer management. Based on the above results, amino acid metabolism and glutathione metabolism actively respond to salt stress during the rice seedling stage. Thus, exogenous application of amino acids on rice leaves is an approach that can enhance the salt tolerance of rice seedlings or appropriate application of nitrogen fertilizer, which has certain reference significance for rice planting and management on saline-alkali land.

Conclusion

This study found that the growth potential and antioxidant ability of the HD961 cultivar were stronger than those of the cultivar 9311 under SS. Numerous genes and metabolites related to SS were identified through transcriptome and metabolome analysis. Many of the genes and metabolites were common between both cultivars, but HD961 had a higher accumulation and regulation ability, suggesting that this might be the primary driver for salt resistance in HD961. The glutathione metabolism pathway was significantly enriched in HD961 but absent in 9311, and there were more DEGs and SRMs in HD961 than in 9311. These results indicate that glutathione metabolism plays an important role in response to SS and provide a better understanding of the rice regulatory network involved in responding to NaCl.

Data availability statement

The datasets can be found in an online database. The raw sequence data of RNA-sequencing has been deposited in the NCBI database under Bioproject number: PRJNA842927. The metabolite data reported in this article have been deposited in the OMIX, China National Center for Bioinformation/Beijing Institute of Genomics, Chinese Academy of Sciences (https://ngdc.cncb.ac.cn/omix; accession no. OMIX001300).

Author contributions

PW, SY, JX, and HZ contributed to the conception and design of the study. ML, NC, and GC organized the database.

HG and JM performed the statistical analysis. SY and ML wrote the first draft of the manuscript. JX, NC, GC, and HZ wrote sections of the manuscript. All authors contributed to manuscript revision, read, and approved the submitted version.

Funding

This work was funded by the research and development plan in key areas of Guangdong Province (2020B020219004) and supported by the provincial major scientific research project of Guangdong Provincial Universities (2017KZDXM044) and the science and technology special fund of Zhanjiang (2020A06013). This project was also supported by the doctoral start-up fund of Guangdong Ocean University (060302052011), the provincial construction project of agricultural science and technology innovation and extension system of Guangdong (2020KJ264), and the innovation and entrepreneurship team nurture of pilotage project of Zhanjiang (2020LHJH01). These funding institutions did not play a role in study design, data collection or analysis, or manuscript writing.

Acknowledgments

We thank Wuhan Metware Biotechnology Co., Ltd. for providing the data analysis tools for this study. We greatly appreciate Bioscience Editing Solutions for critically reading this paper and providing helpful suggestions.

Conflict of interest

The authors declare that the research was conducted in the absence of any commercial or financial relationships that could be construed as a potential conflict of interest.

Publisher's note

All claims expressed in this article are solely those of the authors and do not necessarily represent those of their affiliated organizations, or those of the publisher, the editors and the reviewers. Any product that may be evaluated in this article, or claim that may be made by its manufacturer, is not guaranteed or endorsed by the publisher.

Supplementary material

The Supplementary Material for this article can be found online at: https://www.frontiersin.org/articles/10.3389/fpls.2022.952595/full#supplementary-material

References

Batista-Silva, W., Heinemann, B., Rugen, N., Nunes-Nesi, A., Araújo, W. L., Braun, H. P., et al. (2019). The role of amino acid metabolism during abiotic stress release. *Plant Cell Environ.* 42, 1630–1644. doi: 10.1111/pce.13518

Camacho, C., Coulouris, G., Avagyan, V., Ma, N., Papadopoulos, J., Bealer, K., et al. (2009). BLAST+: architecture and applications. *BMC Bioinform.* 10:421. doi: 10.1186/1471-2105-10-421

Chen, S., Zhou, Y., Chen, Y., and Gu, J. (2018). fastp: an ultra-fast all-in-one FASTQ preprocessor. *Bioinformatics* 34, i884–i890. doi: 10.1093/bioinformatics/bty560

Demidchik, V., Cuin, T. A., Svistunenko, D., Smith, S. J., Miller, A. J., Shabala, S., et al. (2010). Arabidopsis root K+-efflux conductance activated by hydroxyl radicals: single-channel properties, genetic basis and involvement in stress-induced cell death. *J. Cell Sci.* 123, 1468–1479. doi: 10.1242/jcs.064352

Dongsansuk, A., Paethaisong, W., and Theerakulpisut, P. (2021). Membrane stability and antioxidant enzyme activity of rice seedlings in response to short-term high temperature treatments. *Chilean J. Agricultural Res.* 81, 607–617. doi: 10.4067/S0718-58392021000400607

Fiehn, O. (2002). Metabolomics–the link between genotypes and phenotypes. *Plant Mol. Biol.* 48, 155–171. doi: 10.1023/A:1013713905833

Flowers, T. J., and Colmer, T. D. (2015). Plant salt tolerance: adaptations in halophytes. *Ann. Bot.* 115, 327–331. doi: 10.1093/aob/mcu267

Fu, L., Shen, Q., Kuang, L., Wu, D., and Zhang, G. (2019). Transcriptomic and alternative splicing analyses reveal mechanisms of the difference in salt tolerance between barley and rice. *Environ. Exp. Bot.* 166:103810. doi: 10.1016/j.envexpbot.2019.103810

Ganie, S. A., Molla, K. A., Henry, R. J., Bhat, K. V., and Mondal, T. K. (2019). Advances in understanding salt tolerance in rice. *Theor. Appl. Genet.* 132, 851–870. doi: 10.1007/s00122-019-03301-8

Garg, A. K., Kim, J. K., Owens, T. G., Ranwala, A. P., Choi, Y. D., Kochian, L. V., et al. (2002). Trehalose accumulation in rice plants confers high tolerance levels to different abiotic stresses. *Proc. Natl. Acad. Sci. U S A.* 99, 15898–15903. doi: 10.1073/pnas.252637799

Gupta, P., and De, B. (2017). Metabolomics analysis of rice responses to salinity stress revealed elevation of serotonin, and gentisic acid levels in leaves of tolerant varieties. *Plant Signal. Behav.* 12:e1335845. doi: 10.1080/15592324.2017.1335845

Hao, Z., Ma, S., Liang, L., Feng, T., Xiong, M., Lian, S., et al. (2022). Candidate genes and pathways in rice co-responding to drought and salt identified by gcHap network. *Int. J. Mol. Sci.* 23:4016. doi: 10.3390/ijms23074016

Hasanuzzaman, M., Bhuyan, M., Anee, T. I., Parvin, K., Nahar, K., Mahmud, J. A., et al. (2019). Regulation of ascorbate-glutathione pathway in mitigating oxidative damage in plants under abiotic stress. *Antioxidants* 8:384. doi: 10.3390/antiox8090384

Hasanuzzaman, M., Nahar, K., Hossain, M. S., Mahmud, J. A., Rahman, A., Inafuku, M., et al. (2017). Coordinated actions of glyoxalase and antioxidant defense systems in conferring abiotic stress tolerance in plants. *Int. J. Mol. Sci.* 18:200. doi: 10.3390/ijms18010200

Hildebrandt, T. M. (2018). Synthesis versus degradation: directions of amino acid metabolism during *Arabidopsis* abiotic stress response. *Plant Mol. Biol.* 98, 121–135. doi: 10.1007/s11103-018-0767-0

Hong, C.-Y., Hsu, Y. T., Tsai, Y.-C., and Kao, C. H. (2007). Expression of ASCORBATE PEROXIDASE 8 in roots of rice (*Oryza sativa* L.) seedlings in response to NaCl. *J. Exp. Botany* 58, 3273–3283. doi: 10.1093/jxb/erm174

Hussain, M., Ahmad, S., Hussain, S., Lal, R., Ul-Allah, S., and Nawaz, A. (2018). "Chapter six - rice in saline soils: physiology, biochemistry, genetics, and management," in *Advances in Agronomy*, ed. D. L. Sparks (Cambridge, MA: Academic Press), 231–287. doi: 10.1016/bs.agron.2017.11.002

Jahan, N., Lv, Y., Song, M., Zhang, Y., Shang, L., Lu, Y., et al. (2021). Transcriptomic analysis of short-term salt-stress response in mega hybrid rice seedlings. *Agronomy* 11:1328. doi: 10.3390/agronomy11071328

Jin, J., Zhang, H., Kong, L., Gao, G., and Luo, J. (2014). PlantTFDB 3.0: a portal for the functional and evolutionary study of plant transcription factors. *Nucleic Acids Res.* 42, D1182–D1187. doi: 10.1093/nar/gkt1016

Kaminaka, H., Morita, S., Nakajima, M., Masumura, T., and Tanaka, K. (1998). Gene cloning and expression of cytosolic glutathione reductase in rice (*Oryza Sativa* L.). *Plant Cell Physiol.* 39, 1269–1280. doi: 10.1093/oxfordjournals.pcp.a029330

Kamran, M., Parveen, A., Ahmar, S., Malik, Z., Hussain, S., Chattha, M. S., et al. (2020). An overview of hazardous impacts of soil salinity in crops, tolerance mechanisms, and amelioration through selenium supplementation. *Int. J. Mol. Sci.* 21:148. doi: 10.3390/ijms21010148

Khunpon, B., Cha-Um, S., Faiyue, B., Uthaibutra, J., and Saengnil, K. (2018). Paclobutrazol mitigates salt stress in indica rice seedlings by enhancing glutathione metabolism and glyoxalase system. *Biologia* 73, 1267–1276. doi: 10.2478/s11756-018-0132-4

Kim, B. R., Nam, H. Y., Kim, S. U., Kim, S. I., and Chang, Y. J. (2003). Normalization of reverse transcription quantitative-PCR with housekeeping genes in rice. *Biotechnol. Lett.* 25, 1869–1872. doi: 10.1023/A:1026298032009

Kim, D., Langmead, B., and Salzberg, S. L. (2015). HISAT: a fast spliced aligner with low memory requirements. *Nat. Methods* 12, 357–360. doi: 10.1038/nmeth.3317

Kishor, P., Hong, Z., Miao, G. H., Hu, C., and Verma, D. (1995). Overexpression of [delta]-Pyrroline-5-Carboxylate synthetase increases proline production and confers osmotolerance in transgenic plants. *Plant Physiol.* 108, 1387–1394. doi: 10.1104/pp.108.4.1387

Kobayashi, N. I., Yamaji, N., Yamamoto, H., Okubo, K., Ueno, H., Costa, A., et al. (2017). OsHKT1;5 mediates Na(+) exclusion in the vasculature to protect leaf blades and reproductive tissues from salt toxicity in rice. *Plant J.* 91, 657–670. doi: 10.1111/tpj.13595

Kong, W., Sun, T., Zhang, C., Deng, X., and Li, Y. (2021). Comparative transcriptome analysis reveals the mechanisms underlying differences in salt tolerance between indica and japonica rice at seedling stage. *Front. Plant Sci.* 12:725436. doi: 10.3389/fpls.2021.725436

Kong, W., Zhong, H., Gong, Z., Fang, X., Sun, T., Deng, X., et al. (2019). Meta-analysis of salt stress transcriptome responses in different rice genotypes at the seedling stage. *Plants* 8:64. doi: 10.3390/plants8030064

Kumar, S., Asif, M. H., Chakrabarty, D., Tripathi, R. D., Dubey, R. S., and Trivedi, P. K. (2013). Differential expression of rice lambda class GST gene family members during plant growth, development, and in response to stress conditions. *Plant Mol. Biol. Rep.* 31, 569–580. doi: 10.1007/s11105-012-0524-5

Lee, M. H., Cho, E. J., Wi, S. G., Bae, H., Kim, J. E., Cho, J. Y., et al. (2013). Divergences in morphological changes and antioxidant responses in salt-tolerant and salt-sensitive rice seedlings after salt stress. *Plant Physiol. Biochem.* 70, 325–335. doi: 10.1016/j.plaphy.2013.05.047

Li, P., Ruan, Z., Fei, Z., Yan, J., and Tang, G. (2021). Integrated transcriptome and metabolome analysis revealed that flavonoid biosynthesis may dominate the resistance of zanthoxylum bungeanum against stem canker. *J. Agric. Food Chem.* 69, 6360–6378. doi: 10.1021/acs.jafc.1c00357

Liang, W., Ma, X., Wan, P., and Liu, L. (2018). Plant salt-tolerance mechanism: a review. *Biochem. Biophys. Res. Commun.* 495, 286–291. doi: 10.1016/j.bbrc.2017.11.043

Liao, Y., Smyth, G. K., and Shi, W. (2014). featureCounts: an efficient general purpose program for assigning sequence reads to genomic features. *Bioinformatics* 30, 923–930. doi: 10.1093/bioinformatics/btt656

Lima-Melo, Y., Carvalho, F. E. L., Martins, M. O., Passaia, G., Sousa, R. H. V., Neto, M. C. L., et al. (2016). Mitochondrial GPX1 silencing triggers differential photosynthesis impairment in response to salinity in rice plants. *J. Int. Plant Biol.* 58, 737–748. doi: 10.1111/jipb.12464

Liu, C., Mao, B., Ou, S., Wang, W., Liu, L., Wu, Y., et al. (2014). OsbZIP71, a bZIP transcription factor, confers salinity and drought tolerance in rice. *Plant Mol. Biol.* 84, 19–36. doi: 10.1007/s11103-013-0115-3

Liu, C., Mao, B., Yuan, D., Chu, C., and Duan, M. (2022). Salt tolerance in rice: physiological responses and molecular mechanisms. *Crop J.* 10, 13–25. doi: 10.1016/j.cj.2021.02.010

Liu, Y., Lv, J., Liu, Z., Wang, J., Yang, B., Chen, W., et al. (2020). Integrative analysis of metabolome and transcriptome reveals the mechanism of color formation in pepper fruit (*Capsicum annuum* L.). *Food Chem.* 306:125629. doi: 10.1016/j.foodchem.2019.125629

Livak, K. J., and Schmittgen, T. D. (2001). Analysis of relative gene expression data using real-time quantitative PCR and the 2(-Delta Delta C(T)) Method. *Methods* 25, 402–408. doi: 10.1006/meth.2001.1262

Love, M. I., Huber, W., and Anders, S. (2014). Moderated estimation of fold change and dispersion for RNA-seq data with DESeq2. *Genome Biol.* 15:550. doi: 10.1186/s13059-014-0550-8

Luo, D., Niu, X., Yu, J., Yan, J., Gou, X., Lu, B. R., et al. (2012). Rice choline monooxygenase (OsCMO) protein functions in enhancing glycine betaine biosynthesis in transgenic tobacco but does not accumulate in rice (*Oryza sativa* L. ssp. japonica). *Plant Cell Rep.* 31, 1625–1635. doi: 10.1007/s00299-012-1276-2

Luo, P., Yin, P., Hua, R., Tan, Y., Li, Z., Qiu, G., et al. (2018). A Large-scale, multicenter serum metabolite biomarker identification study for the early detection of hepatocellular carcinoma. *Hepatology* 67, 662–675. doi: 10.1002/hep.29561

Machado, R. M. A., and Serralheiro, R. P. (2017). Soil salinity: effect on vegetable crop growth. management practices to prevent and mitigate soil salinization. *Horticulturae* 3:30. doi: 10.3390/horticulturae3020030

Mao, X., Cai, T., Olyarchuk, J. G., and Wei, L. (2005). Automated genome annotation and pathway identification using the KEGG Orthology (KO) as a controlled vocabulary. *Bioinformatics* 21, 3787–3793. doi: 10.1093/bioinformatics/bti430

Moustakas, M., Sperdouli, I., Kouna, T., Antonopoulou, C. I., and Therios, I. (2011). Exogenous proline induces soluble sugar accumulation and alleviates drought stress effects on photosystem II functioning of *Arabidopsis thaliana* leaves. *Plant Growth Regulation* 65, 315–325. doi: 10.1007/s10725-011-9604-z

Ni, J., Zhao, Y., Tao, R., Yin, L., Gao, L., Strid, Å, et al. (2020). Ethylene mediates the branching of the jasmonate-induced flavonoid biosynthesis pathway by suppressing anthocyanin biosynthesis in red Chinese pear fruits. *Plant Biotechnol. J.* 18, 1223–1240. doi: 10.1111/pbi.13287

Nounjan, N., and Theerakulpisut, P. (2021). Physiological evaluation for salt tolerance in green and purple leaf color rice cultivars at seedling stage. *Physiol. Mol. Biol. Plants* 27, 2819–2832. doi: 10.1007/s12298-021-01114-y

Pérez-Rodríguez, P., Riaño-Pachón, D. M., Corrêa, L. G., Rensing, S. A., Kersten, B., and Mueller-Roeber, B. (2010). PlnTFDB: updated content and new features of the plant transcription factor database. *Nucleic Acids Res.* 38, D822–D827. doi: 10.1093/nar/gkp805

Razzaq, A., Ali, A., Safdar, L. B., Zafar, M. M., Rui, Y., Shakeel, A., et al. (2020). Salt stress induces physiochemical alterations in rice grain composition and quality. *J. Food Sci.* 85, 14–20. doi: 10.1111/1750-3841.14983

Ribbenstedt, A., Ziarrusta, H., and Benskin, J. P. (2018). Development, characterization and comparisons of targeted and non-targeted metabolomics methods. *PLoS One* 13:e0207082. doi: 10.1371/journal.pone.0207082

Saito, K., and Matsuda, F. (2010). Metabolomics for functional genomics, systems biology, and biotechnology. *Annu. Rev. Plant Biol.* 61, 463–489. doi: 10.1146/annurev.arplant.043008.092035

Taji, T., Ohsumi, C., Iuchi, S., Seki, M., Kasuga, M., Kobayashi, M., et al. (2002). Important roles of drought- and cold-inducible genes for galactinol synthase in stress tolerance in *Arabidopsis thaliana*. *Plant J.* 29, 417–426. doi: 10.1046/j.0960-7412.2001.01227.x

Tilman, D., Balzer, C., Hill, J., and Befort, B. L. (2011). Global food demand and the sustainable intensification of agriculture. *Proc. Natl. Acad. Sci. U S A.* 108, 20260–20264. doi: 10.1073/pnas.1116437108

van Zelm, E., Zhang, Y., and Testerink, C. (2020). Salt tolerance mechanisms of plants. *Annu. Rev. Plant Biol.* 71, 403–433. doi: 10.1146/annurev-arplant-050718-100005

Wang, J., Lv, J., Liu, Z., Liu, Y., Song, J., Ma, Y., et al. (2019a). Integration of transcriptomics and metabolomics for pepper (*Capsicum annuum* L.) in response to heat stress. *Int. J. Mol. Sci.* 20:5042. doi: 10.3390/ijms20205042

Wang, Y., Zeng, X., Xu, Q., Mei, X., Yuan, H., Jiabu, D., et al. (2019b). Metabolite profiling in two contrasting *Tibetan hulless* barley cultivars revealed the core salt-responsive metabolome and key salt-tolerance biomarkers. *AoB Plants* 11:lz021. doi: 10.1093/aobpla/plz021

Wang, J., Zhu, J., Zhang, Y., Fan, F., Li, W., Wang, F., et al. (2018). Comparative transcriptome analysis reveals molecular response to salinity stress of salt-tolerant and sensitive genotypes of indica rice at seedling stage. *Sci. Rep.* 8:2085. doi: 10.1038/s41598-018-19984-w

Wang, K., Yu, H., Ye, D., Wang, Y., Zhang, X., Huang, H., et al. (2021). The critical role of the shoot base in inhibiting cadmium transport from root to shoot in a cadmium-safe rice line (*Oryza sativa* L.). *Sci. Total Environ.* 765:142710. doi: 10.1016/j.scitotenv.2020.142710

Wu, T.-M., Lin, W.-R., Kao, C. H., and Hong, C.-Y. (2015). Gene knockout of glutathione reductase 3 results in increased sensitivity to salt stress in rice. *Plant Mol. Biol.* 87, 555–564. doi: 10.1007/s11103-015-0290-5

Xie, C., Mao, X., Huang, J., Ding, Y., Wu, J., Dong, S., et al. (2011). KOBAS 2.0: a web server for annotation and identification of enriched pathways and diseases. *Nucleic Acids Res.* 39, W316–W322. doi: 10.1093/nar/gkr483

Xie, Z., Wang, J., Wang, W., Wang, Y., Xu, J., Li, Z., et al. (2020). Integrated analysis of the transcriptome and metabolome revealed the molecular mechanisms underlying the enhanced salt tolerance of rice due to the application of exogenous melatonin. *Front. Plant Sci.* 11:618680. doi: 10.3389/fpls.2020.618680

Yang, A., Dai, X., and Zhang, W. H. (2012). A R2R3-type MYB gene, OsMYB2, is involved in salt, cold, and dehydration tolerance in rice. *J. Exp. Bot.* 63, 2541–2556. doi: 10.1093/jxb/err431

Yang, J., Su, L., Li, D., Luo, L., Sun, K., Yang, M., et al. (2020). Dynamic transcriptome and metabolome analyses of two types of rice during the seed germination and young seedling growth stages. *BMC Genomics* 21:603. doi: 10.1186/s12864-020-07024-9

Yang, Y., and Guo, Y. (2018). Elucidating the molecular mechanisms mediating plant salt-stress responses. *New Phytol.* 217, 523–539. doi: 10.1111/nph.14920

Yu, G., Wang, L. G., Han, Y., and He, Q. Y. (2012). clusterProfiler: an R package for comparing biological themes among gene clusters. *OMICS* 16, 284–287. doi: 10.1089/omi.2011.0118

Zhang, Z., Zhang, Q., Wu, J., Zheng, X., Zheng, S., Sun, X., et al. (2013). Gene knockout study reveals that cytosolic ascorbate peroxidase 2(OsAPX2) plays a critical role in growth and reproduction in rice under drought, salt and cold stresses. *PLoS One* 8:e57472. doi: 10.1371/journal.pone.0057472

Zhao, M., Ren, Y., Wei, W., Yang, J., Zhong, Q., and Li, Z. (2021). Metabolite analysis of jerusalem artichoke (*Helianthus tuberosus* L.) seedlings in response to polyethylene glycol-simulated drought stress. *Int. J. Mol. Sci.* 22:3294. doi: 10.3390/ijms22073294

Zhao, X., Wang, W., Zhang, F., Deng, J., Li, Z., and Fu, B. (2014). Comparative metabolite profiling of two rice genotypes with contrasting salt stress tolerance at the seedling stage. *PLoS One* 9:e108020. doi: 10.1371/journal.pone.0108020

Zheng, Y., Jiao, C., Sun, H., Rosli, H. G., Pombo, M. A., Zhang, P., et al. (2016). iTAK: a program for genome-wide prediction and classification of plant transcription factors, transcriptional regulators, and protein kinases. *Mol. Plant* 9, 1667–1670. doi: 10.1016/j.molp.2016.09.014

frontiers | Frontiers in Plant Science

TYPE Review
PUBLISHED 14 September 2022
DOI 10.3389/fpls.2022.972856

Check for updates

OPEN ACCESS

EDITED BY
Mirza Hasanuzzaman,
Sher-e-Bangla Agricultural University, Bangladesh

REVIEWED BY
Wen-Cheng Liu,
Henan University, China
Seyed Morteza Zahedi,
University of Maragheh, Iran

*CORRESPONDENCE
Yerramilli Vimala
yvimala17@gmail.com
Kadambot H. M. Siddique
kadambot.siddique@uwa.edu.au

†These authors have contributed equally to this work

SPECIALTY SECTION
This article was submitted to Plant Abiotic Stress, a section of the journal Frontiers in Plant Science

RECEIVED 19 June 2022
ACCEPTED 17 August 2022
PUBLISHED 14 September 2022

CITATION
Kumar S, Shah SH, Vimala Y, Jatav HS, Ahmad P, Chen Y and Siddique KHM (2022) Abscisic acid: Metabolism, transport, crosstalk with other plant growth regulators, and its role in heavy metal stress mitigation. *Front. Plant Sci.* 13:972856. doi: 10.3389/fpls.2022.972856

COPYRIGHT
© 2022 Kumar, Shah, Vimala, Jatav, Ahmad, Chen and Siddique. This is an open-access article distributed under the terms of the Creative Commons Attribution License (CC BY). The use, distribution or reproduction in other forums is permitted, provided the original author(s) and the copyright owner(s) are credited and that the original publication in this journal is cited, in accordance with accepted academic practice. No use, distribution or reproduction is permitted which does not comply with these terms.

Abscisic acid: Metabolism, transport, crosstalk with other plant growth regulators, and its role in heavy metal stress mitigation

Sandeep Kumar[1†], Sajad Hussain Shah[1†], Yerramilli Vimala[1*], Hanuman Singh Jatav[2], Parvaiz Ahmad[3], Yinglong Chen[4] and Kadambot H. M. Siddique[4*]

[1]Plant Physiology and Tissue Culture Laboratory, Department of Botany, Chaudhary Charan Singh University, Meerut, India, [2]Soil Science and Agricultural Chemistry, Sri Karan Narendra Agriculture University Jobner, Jaipur, India, [3]Department of Botany, GDC Pulwama, Jammu and Kashmir, India, [4]The UWA Institute of Agriculture and School of Agriculture and Environment, The University of Western Australia, Perth, WA, Australia

Heavy metal (HM) stress is threatening agricultural crops, ecological systems, and human health worldwide. HM toxicity adversely affects plant growth, physiological processes, and crop productivity by disturbing cellular ionic balance, metabolic balance, cell membrane integrity, and protein and enzyme activities. Plants under HM stress intrinsically develop mechanisms to counter the adversities of HM but not prevent them. However, the exogenous application of abscisic acid (ABA) is a strategy for boosting the tolerance capacity of plants against HM toxicity by improving osmolyte accumulation and antioxidant machinery. ABA is an essential plant growth regulator that modulates various plant growth and metabolic processes, including seed development and germination, vegetative growth, stomatal regulation, flowering, and leaf senescence under diverse environmental conditions. This review summarizes ABA biosynthesis, signaling, transport, and catabolism in plant tissues and the adverse effects of HM stress on crop plants. Moreover, we describe the role of ABA in mitigating HM stress and elucidating the interplay of ABA with other plant growth regulators.

KEYWORDS

abscisic acid, heavy metal, growth, physiological processes, antioxidant, productivity

Introduction

Plants encounter a plethora of environmental stresses classified as biotic or abiotic stresses. Among abiotic stresses, heavy metal (HM) stress is a severe ecological restraint with detrimental effects on plant growth, metabolic processes, and crop productivity (Ghori et al., 2019). Agrarian soils in different parts of the world are slightly/moderately

contaminated with HM, which is concerning due to their harmful effect on human health, ecosystem function, and global economic growth (Shahid et al., 2015). HM toxicity hampers normal plant functioning by producing excessive reactive oxygen species (ROS), repressing respiration, photosynthesis, and vascular and enzymatic activities, and disrupting ion homeostasis (He et al., 2021). Plants have complex inherent biological mechanisms to counter the adversities of HM but fail to mitigate them at toxic levels (Chandrakar et al., 2020). However, plant growth regulators (PGRs) play a crucial role in strengthening the tolerance mechanisms of plants against HM stress (Hasanuzzaman et al., 2018; Singh et al., 2020). PGRs are small chemical messengers that control various phenological characteristics, physio-biochemical, and developmental aspects in plants in a concentration of the molecular inducer-dependent and plant development stage-dependent manner (Vimala, 1985). The major PGR classes include abscisic acid (ABA), auxins, brassinosteroid (BR), cytokinins (CK), ethylene (ET), gibberellic acid (GA_3), jasmonic acid (JA), salicylic acid (SA), nitric oxide (NO), and polyamines (PAs). The roles of PGRs in enhancing endurance against abiotic stresses, including HM, are well established (Saini et al., 2021; Shah et al., 2021, 2022; Kumar et al., 2022). This review focuses on the role of ABA in mitigating HM stress at the metabolic, transport, and crosstalk with other PGRs levels.

Abscisic acid is a small sesquiterpene molecule with many crucial functions in plant phenological and developmental processes, including seed dormancy and development, vegetative growth, flowering, stomatal movement, lipid and storage protein synthesis, and leaf senescence (Chen et al., 2020). Under HM stress, ABA modulates various physiological, biochemical, and molecular processes in plants (Vishwakarma et al., 2017). Exogenous ABA application can enhance plant tolerance to toxic metal stress. For example, 10 and 20 μM foliar ABA spray alleviated cadmium (Cd) inhibitory effects in *Lactuca sativa* L. by increasing its growth, chlorophyll content, photosynthetic efficiency, catalase activity, and proline and protein contents (Tang et al., 2020). Deng et al. (2021) reported that 5 μM ABA application mitigated the Cd-induced damage in roots of *Malus hupehensis* (Pamp.) by decreasing cell death and hydrogen peroxide and malondialdehyde contents. Further, 10 μM foliar ABA treatment ameliorated Cd toxicity in *Vigna radiata* L. by increasing chlorophyll content, osmolyte concentration, and antioxidant defense machinery (Leng et al., 2021).

It is well-accepted that ABA plays a vital role in improving morphological features, developmental aspects, and yield and quality parameters, and ameliorating the adversities of HM stress in crop plants. This review characterizes ABA biosynthesis, signaling, transport, and catabolism in plants and summarizes the impact of HM stress on crop growth, photosynthesis, and yield. Toxic metal and metalloids evolved with the evolution of green plants, accumulating in edible parts. Hence, plants evolved mechanisms to uptake, exclude, and mitigate the impact of unrequired or toxic metals. ABA is one such PGR evolved to mitigate HM stress.

Abscisic acid biosynthesis

Abscisic acid is a 15-carbon terpenoid molecule identified in the 1960s and recognized as a growth-inhibiting compound (abscisin II) associated with bud dormancy in maple and fruit abscission in cotton (Schwartz and Zeevaart, 2010). Later work revealed that ABA plays an important role in several developmental and physio-biochemical processes and regulates abiotic stress responses in plants (Sah et al., 2016). ABA is synthesized in all cells with chloroplasts or amyloplasts and found in major organs and tissues (Taiz et al., 2015). ABA biosynthesis starts in the chloroplast and ends in the cytoplasm (Seo and Koshiba, 2002). The isopentenyl diphosphate (IPP) is formed in plastids from pyruvic acid and glyceraldehyde 3-phosphate (**Figure 1**) and converted into geranylgeranyl diphosphate (GGPP) through the methylerythritol 4-phosphate (MEP) pathway. GGPP then forms phytoene (C_{40}), which is converted into lycopene and β-carotene, and finally zeaxanthin. The conversion of zeaxanthin to all-*trans*-violaxanthin (C_{40}) is mediated by the enzyme zeaxanthin epoxidase (ZEP). The all-*trans*-violaxanthin (C_{40}) is then modified into 9-*cis*-neoxanthin (C_{40}) and divided into xanthoxin (C_{15}) and a C_{25} metabolite by 9-*cis*-epoxycarotenoid dioxygenase enzyme (NCED). This reaction is a rate-limiting step, and NCED is a crucial enzyme in ABA biosynthesis. Xanthoxin is transferred to the cytoplasm, where it is transformed into ABA-aldehyde by an enzyme that belongs to a short-chain dehydrogenase/reductase family. ABA-aldehyde is then converted into ABA with the reaction catalyzed by ABA-aldehyde oxidase (AAO) (Milborrow, 2001; Xiong and Zhu, 2003; Nambara and Marion-Poll, 2005; Mehrotra et al., 2014; Cardoso et al., 2020). Various enzymes, encoded by different genes, are involved in ABA biosynthesis. For instance, Arabidopsis aldehyde oxidases genes *(AAO3)* encode the AAO enzyme (Seo et al., 2000). The *ABA2* gene encodes the ZEP enzyme to enhance its activity. Increased upregulation of *ABA2* mRNA in genetically altered plants had a positive role in delaying germination and increasing ABA levels in mature seeds of transgenic plants (Frey et al., 1999). In *Arabidopsis thaliana* L., ABA biosynthesis is controlled by a small family of five *NCED* genes (*AtNCED2, 3, 5, 6,* and *9*) located in plastids. Moreover, there is a differential contribution of *NCEDs* to ABA synthesis during *Arabidopsis thaliana* L. growth and development; for instance, *NCED2* and *3* have high expression levels in roots and leaves but low expression levels for seed development, and *NCED5, 6* and 9 have increased expression levels during later maturation stages. Further, NCED expression is controlled by the transcription factor *MYB96,* with an essential role in seed dormancy (Tan et al., 2003; Lee et al., 2015;

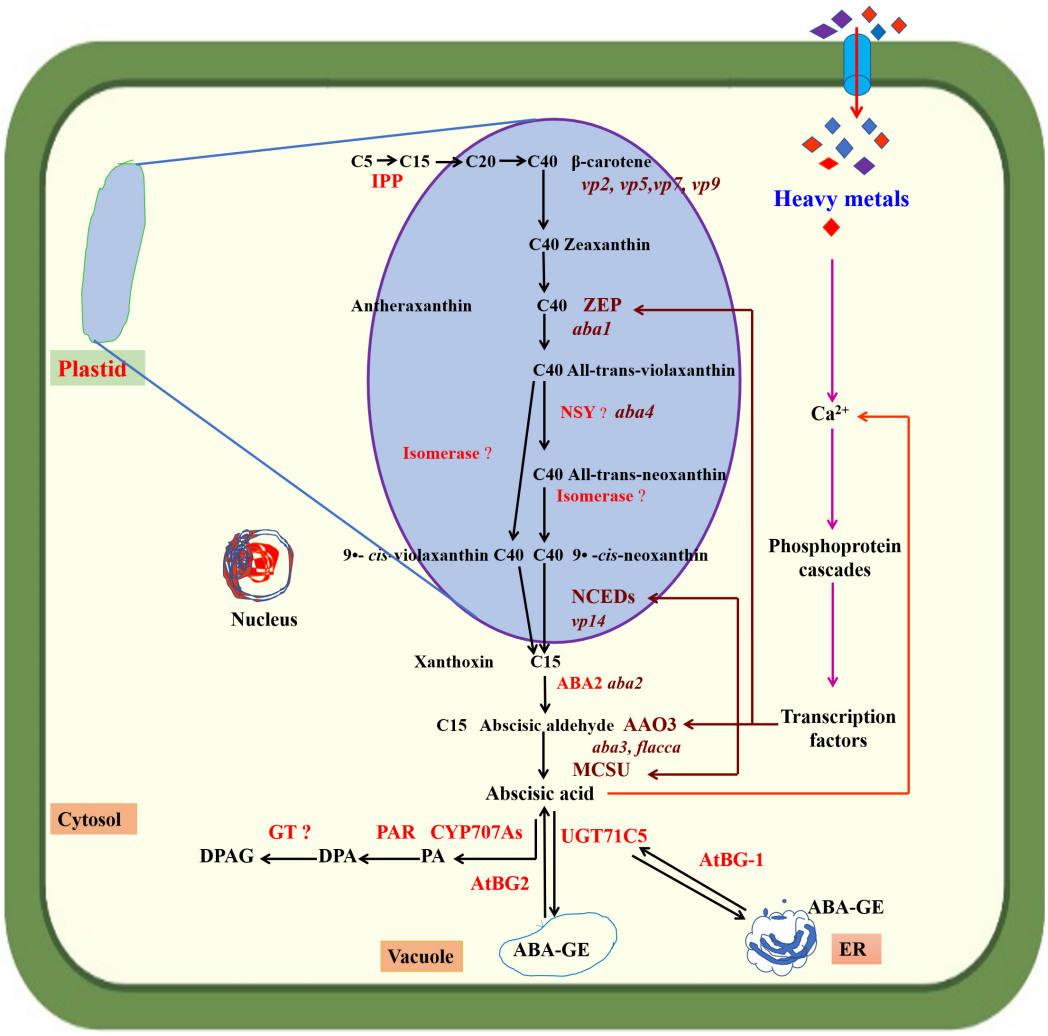


FIGURE 1
Abscisic acid (ABA) biosynthesis in plant cells. Endoplasmic reticulum (ER). The precursor of ABA in plants is (C40) β-carotene. Isopentenyl pyrophosphate (IPP) converts C5 to C15 and continues to C40. β-carotene converts C40 to xanthoxin (C15) in plastids and cytosol. Zeaxanthin epoxidase (ZEP), neoxanthin synthase (NYS), 9-*cis*-epoxycarotenoid dioxygenase (NCEDs), phasic acid (PA), dihydrophaseic acid (DPA), PA reductase (PAR), DPA-4-β-D-glucoside (DPAG), UDP-glucosyltransferase (UGT) encoded by (UGT71C5), cytochrome P450 monooxygenase (P450) encoded by (CYP707As), glycosyltransferase (GT), β-glucosidase encoded by (AtBG1 and AtBG2), ABA-glucose ester (ABA-GE), abscisic aldehyde oxidase (AAO3), and MCSU, molybdenum cofactor sulfurase.

Ma et al., 2018). *ATAF1* (*Arabidopsis thaliana* activating factor 1) is a transcription factor that regulates *Arabidopsis thaliana* L. development and environmental stress responses. *ATAF1* promotes *NCED3* expression that controls ABA biosynthesis (Jensen et al., 2013). HM stress affects plant ABA biosynthesis and varies between species and the type and level of HM stress. HM affect ABA biosynthesis at lower concentrations but inhibit it at higher levels. Copper (Cu) suppressed the transcription of ABA biosynthetic genes (*StABA1* and *StNCED1*, *AAO3*) in *Solanum tuberosum* L., decreasing ABA content (Liu et al., 2020). Cu stress significantly increased ABA contents in roots, shoots, and leaves of *Helianthus annuus* L. seedlings (Zengin and Kirbag, 2007). Hou et al. (2010) reported that aluminum (Al) enhanced endogenous ABA production in roots and leaves of *Glycine max*. L. Exposure to cadmium (Cd) stress significantly increased leaf ABA concentration in *Phaseolus vulgaris* L. but inhibited ABA accumulation in dry excised leaves (Poschenrieder et al., 1989). Cd stress increased endogenous ABA levels in the roots of a non-hyperaccumulating ecotype of *Sedum alfredii* due to upregulated expression of ABA biosynthesis genes (*SaABA2*, *SaNCED*) (Tao et al., 2019). Further, Cd stress increased ABA content more in roots than old leaves of *Boehmeria nivea* L., with the lowest levels in new leaves. Long-time treatment of high Cd concentrations decreased endogenous ABA biosynthesis (Chen et al., 2021). HM compete with other metal ions and depolarize membrane-inducing Ca^{2+}

efflux from organelles, initiating a Ca^{2+} signaling cascade of events that trigger the upregulation of ZEP, NCED, and MCSU genes (Ahmad et al., 2010).

Abscisic acid transport

Abscisic acid is produced primarily in vascular tissue with its transportation among cells, tissues, and organs essential for regulating plant physio-biochemical processes under varying environmental responses (Kuromori et al., 2010; Saradadevi et al., 2016). ABA exists in anionic (ABA^-) and protonated (ABAH) forms in plants. It is a weak acid, diffusing the bio-membrane passively when in protonated form (Ng et al., 2014; Chen et al., 2020). However, active ABA translocation across the plasma membrane can be mediated by transporters, including ATP-binding cassette (ABC) transporter proteins, nitrate or di/tri-peptide transporters [NRT1/PTR family proteins (NPF)], multidrug and toxic compound extrusion (MATE)-type/DTX transporters, and AWPM-19 family proteins (OsPM1). These transporters were first identified in *Oryza sativa* L. (Kanno et al., 2012; Zhang et al., 2014; Merilo et al., 2015). In eukaryotes, ABC transporters are categorized into sub-families from ABCA to ABCH. About 129 ABC transporters of ABA have been identified in *Arabidopsis thaliana* L. (Kang et al., 2010). Many ABCG members are suggested to play a role in ABA transportation. The AtABCG25 transporter, located in the plasma membrane of root vascular bundles and close to leaf vascular veins, exports ABA from vascular tissue to different plant parts (Kuromori et al., 2010; Andolfo et al., 2015). The AtABCG40 transporter mediates ABA import into plant cells, and its loss of function in guard cells delays stomatal closure by limiting ABA uptake (Kang et al., 2010). The AtABCG22 transporter may participate in stomatal regulation by promoting ABA uptake (Kuromori et al., 2011). AtABCG25 and AtABCG31 regulate ABA export from the endosperm to multiple sites in plants, whereas AtABCG30 and AtABCG40 import ABA into the embryo, controlling seed germination (Kang et al., 2015). AtDTX50 (DTX/MATE-type transporter) is localized in vascular tissue and guard cells, participating in ABA efflux in *Arabidopsis thaliana* L. and exogenous application of ABA upregulated *AtDTX50* gene expression (Zhang et al., 2014). Recently, Shimizu et al. (2021) detected two Arabidopsis NPF4.6 and NPF5.1 transporters in vascular tissues, guard cells, and leaf cell tissues that act as ABA importers to regulate stomatal movement by controlling ABA uptake. Studies have suggested that lower levels of HM contamination trigger ABA to increase inside plant cells, which is continuously transported throughout the plant, regulating plant defensive responses. However, under extreme HM stress, ABA synthesis and transport decreases due to blockages in the vascular transportation route. Under such conditions, exogenous supply of ABA can alleviate these perturbations.

Abscisic acid catabolism

Catabolism and biosynthesis rates determine ABA hormone levels and are essential for modulating plant growth and metabolic processes in response to varying environmental cues (Kitahata et al., 2005). Endogenous ABA levels change with varying ecological conditions. Under favorable environmental conditions, ABA is metabolized into an inactive form through hydroxylation and conjugation pathways (Ng et al., 2014). In the hydroxylation pathway, ABA is hydroxylated by the oxidation of its three methyl groups in the ring structure (C-7′, C-8′, and C-9′). C-8′ is the major catabolic route, in which 8′-hydroxy-ABA is unstable and spontaneously converted into phaseic acid (PA) and dihydro-phaseic acid (DPA), catalyzed by cytochrome P450 type enzyme (CYP707A), an important enzyme in ABA metabolism (Saito et al., 2004; Baron et al., 2012; Rodriguez, 2016; Seo and Marion-Poll, 2019). *CYP707A* gene expression in guard cells and vascular tissue controls ABA metabolism and function under diverse conditions (Okamoto et al., 2009). During seed development and germination, members of the *CYP707A* gene family (*CYP707A1* to *CYP707A4*) help decrease endogenous ABA levels (Zheng et al., 2018). The inactivation of ABA is also mediated by the conjugation of ABA with glucose to form ABA glucose ester (ABA-GE) catalyzed by uridine diphosphate glycosyltransferases (UGTs). ABA-GE (inactive ABA product) is formed in the cytoplasm and stored in the vacuoles (Priest et al., 2006; Zhu et al., 2011; Chen et al., 2020). However, under abiotic stress, ABA-GE is converted back into free ABA through enzyme-catalyzed hydrolysis regulated by beta-glycosidase homolog 1 and 2 (BG1 and BG2) enzymes (Xu et al., 2012). Therefore, ABA catabolism significantly controls ABA levels under normal and adverse conditions. In summary, HM toxicity decreases endogenous ABA levels by inhibiting the expression of genes involved in ABA biosynthesis and thus halting the ABA-mediated physiological effect.

Abscisic acid signaling

Understanding the mechanism of action of ABA is essential for plants to enhance their biological functions under unfavorable climatic conditions (Ali et al., 2020). Three main components are involved in ABA signaling: pyrabactin resistance (PYR)/pyrabactin resistance-like (PYL)/regulatory component of ABA receptor (RCAR), protein phosphatase 2C (PP2C; negative regulators), and sucrose non-fermenting (SNF1) related protein kinase 2 (SnRK2; positive regulators) (Ye et al., 2017). When ABA is present, PYR/PYL/RCAR-PP2C starts forming a complex structure that inhibits the negative effect of PP2C and further activators SnRK2 function for the phosphorylation of downstream proteins, including transcription factors to promote ABA-responsive gene expression (Yoshida et al., 2014). **Figure 2** is a diagrammatic

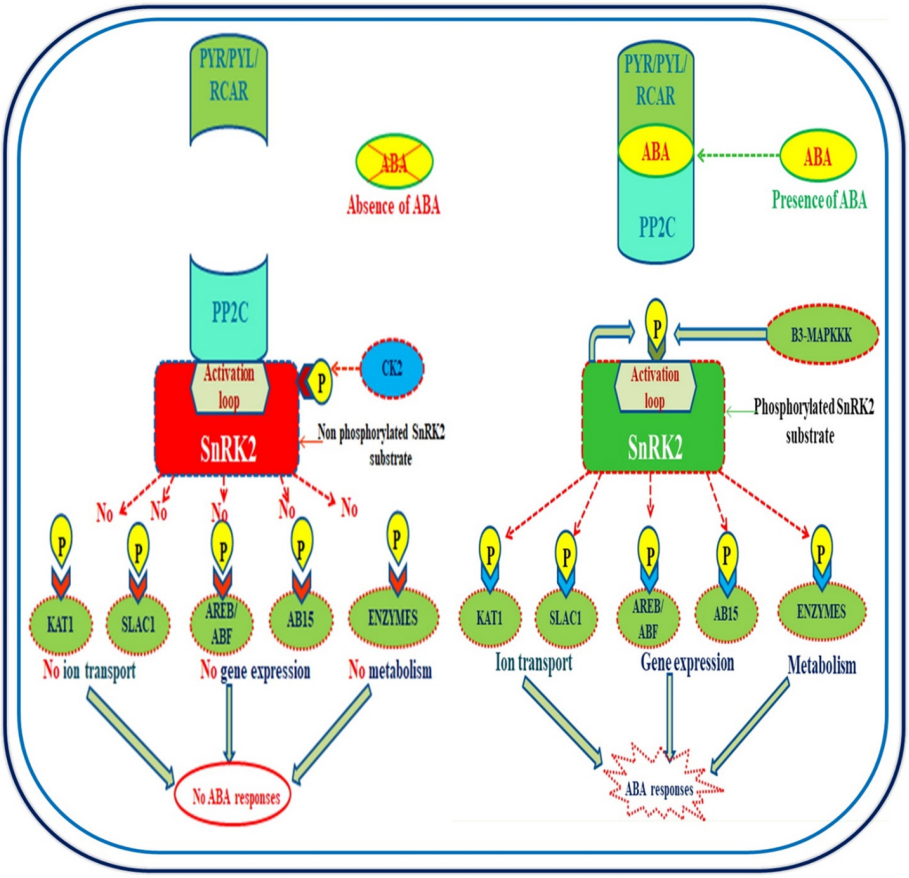


FIGURE 2
Schematic representation of the mechanism of action of abscisic acid (ABA). The core component of ABA signaling includes pyrabactin resistance 1 (PYR1)/PYR-Like (PYL), regulatory component of ABA receptors (RCARs), clade a protein phosphatases PP2C, ABA insensitive 1/2 ABI 1/2, hypersensitive to ABA1/2, HBA1/2, and sucrose non-fermenting-1-related protein kinase 2 family members (SnRK2s).

representation of the mechanism of action of ABA. In addition, HM contamination decreases endogenous ABA content and thus stopped ABA modulated processes due to the non-availability of ABA in cells.

Impact of heavy metal stress on plants

Heavy metals are naturally occurring elements with high atomic weight and density, including some micro-nutrients crucial for plant growth and development. However, excess HM concentrations adversely affect plant growth and survival. The main HM-comprising metals and metalloids, such as cadmium (Cd), lead (Pb), arsenic (As), mercury (Hg), silver (Ag), aluminum (Al), and chromium (Cr), do not play vital roles in plant growth and development but their toxic levels disturb plant development and metabolism (Gill, 2014; Keyster et al., 2020). HM are released and accumulated in soils from natural sources and anthropogenic activities, including industrialization, smelting, extensive mining, fertilizer application, polluted water irrigation, fossil fuel combustion, and vehicle emitted gases and pollutants (Khan et al., 2017; Lajayer et al., 2019). Elevated HM levels increase ROS generation, causing metabolic imbalance, disturbing ion homeostasis, disorganizing the antioxidant defense system, disrupting protein structure, pigment synthesis, enzyme activities and membrane integrity, increasing lipid peroxidation, and thus decreasing plant growth and productivity (Emamverdian et al., 2015; Jalmi et al., 2018). HM stress adversely affects crop growth, physiological processes, and production (**Table 1**).

Growth

Various studies have reported that HM contamination hinders crop plant growth features by altering root and shoot length morphology and anatomy and reducing plant biomass.

TABLE 1 Toxic effects of heavy metal (HM) stress on plant growth, physiology, and yield parameters.

Plant species	HM	HM dose	Impacts on plant	References
Cicer arietinum L.	Cd	23 mg kg^{-1} soil	Reduced plant biomass, nodule number, chlorophyll content, root and shoot N content, seed yield and grain yield	Wani et al. (2007)
Zea mays L.	Hg+Cr+Cd	151.9, 39.24, and 7.3 mg kg^{-1} soil	Decreased plant growth, N content, and seed protein content	Ghani (2010)
Sorghum bicolor L.	Cd	100 mg kg^{-1} soil	Minimized plant height and chlorophyll synthesis and increased lipid peroxidation	Da-lin et al. (2011)
Glycine max L.	Cd	100 mg kg^{-1} soil	Reduced photosynthetic efficiency, stomatal conductance, nitrate reductase activity and leghemoglobin content	Sunita et al. (2015)
Eruca sativa L.	Cd and Pb	200 mg and 1,500 mg kg^{-1} soil	Decreased stem diameter, leaf number and biomass and root fresh and dry weights	Yildirim et al. (2019)
Morus alba L.	Cd and Pb	100 and 200 μM L^{-1} nutrient solution	Decreased chlorophyll content, carbon fixation, rate and stomatal movement	Huihui et al. (2020)
Sassafras tzumu L.	Cd	100 mg kg^{-1} soil	Reduced plant height, biomass, chlorophyll content and photosynthetic rate	Zhao et al. (2021)
Vigna radiata L.	Cd	30 mg kg^{-1} soil	Decreased chlorophyll content, gas exchange parameters, soluble proteins, and free amino acids content	Aqeel et al. (2021)
Citrus aurantinum L.	Cu and Pb	800 μM (nutrient solution)	Decreased plant height, chlorophyll pigment, photosynthetic rate, antioxidant activity, mineral nutrient absorption and water balance	Giannakoula et al. (2021)

For instance, 900 μM Cd and 1500 μM Pb reduced root and shoot lengths of *Brassica juncea* L. seedlings (John et al., 2009). In another *Brassica juncea* L. study, Cr, Pb, Cd, and Hg application at 100, 200, 10, and 50 mg kg^{-1} soil, respectively, decreased root and stem dry weights (Sheetal et al., 2016). Two *Zea mays* L. genotypes with contrasting root systems exhibited differential growth responses to moderate Cd stress (20 mg kg^{-1} soil) with less growth reduction in small-rooted genotypes than large-rooted genotypes (An et al., 2022a,b).

Physio-biochemical processes

Heavy metal stress severely impacts physiological processes, including the electron transport system, enzymatic activities, nutrient uptake, photosynthetic pigments, and the photosystem. Moreover, high HM levels induce toxic ROS production, causing cellular damage by inactivating proteins and enzymes, increasing lipid peroxidation, damaging nucleic acids, and disrupting ion homeostasis and metabolic balance, leading to plant death (Goyal et al., 2020). In addition, HM decrease photosynthetic pigment content, negatively affect photosystems I and II, reduce transpiration rate, stomatal conductance, and water use efficiency, and disturb plant water relations and cellular nutrient balance (Małkowski et al., 2019). Studies have suggested that soil contaminated with HM alters overall plant physiology. For instance, a pre-sowing seed treatment with 100 μM Cd decreased the protein content in roots and peroxide activity in leaves of *Cicer arietinum* L. (Bavi et al., 2011). *Brassica juncea* L. grown in soil contaminated with Cr, Pb, Cd, and Hg at 100, 200, 10, and 50 mg kg^{-1} soil, respectively, had reduced photosynthetic rates and chlorophyll a and b contents (Sheetal et al., 2016). Soil-applied Pb (400, 800, and 1200 ppm) reduced photosynthetic pigments, antioxidant enzyme activities, increased hydrogen peroxide content, and lipid peroxidation and affected protein and proline content in *Oryza sativa* L. (Ashraf et al., 2017). *Tamarix usneoides* L. seedlings treated with 18 mg Cd kg^{-1} Cd had decreased chlorophyll contents and photosynthetic rates (Mayonde et al., 2021).

Yield

Heavy metal toxicity induces deleterious effects on various physiological and biochemical processes, decreasing crop productivity (Shahid et al., 2015). Soil-applied As (30 mg kg^{-1}) significantly decreased the number of panicles and filled grains per pot and total grain yield in *Oryza sativa* L. (Rahman et al., 2007). Soil incubated with 150 mg kg^{-1} Cr (VI) markedly decreased the yield of *Hordeum vulgare* L., but significantly increased the yield and ammonia nitrogen content of *Zea mays* L. (Wyszkowski and Radziemska, 2010). Arduini et al. (2014) reported that soil supplemented with 4.5 mg kg^{-1} Cd reduced plant height, biomass, and vegetative growth but increased dry matter and grain Cd accumulation in *Triticum durum*. Further, soil-applied Pb (400, 800, and 1,200 ppm) decreased tiller number per pot, grain number per panicle, 1000-grain weight, and grain yield in *Oryza sativa* L. Arduini et al. (2014). In another study, soil application of 100 mg kg^{-1} Cd significantly decreased pod number per plant, seed number per pod, seed weight, and seed yield in *Brassica juncea* L. (Irfan et al., 2015). Moderate Cd stress significantly reduced the grain yield of *Zea mays* L., especially under low nitrogen supply (An et al., 2022b). These studies suggest that HM stress impedes growth, physiological processes, and yield attributes, decreasing overall crop production.

Role of abscisic acid in mitigating HM toxicity

Abscisic acid is a prominent stress hormone that regulates numerous physiological processes and helps plants cope with the adverse impacts of HM stress (Shen et al., 2017). ABA regulates toxic metal translocation from roots to shoots. It closes stomata and reduces the transpiration rate, limiting the long-distance transfer of HM (Saradadevi et al., 2017; Hu et al., 2020). ABA enhances plant biomass, physiological processes, antioxidant defense system, and osmolyte accumulation, reducing the effects of HM stress. The activation of genes involved in ABA production increases endogenous ABA concentration in some plant species under Cd stress, including *Oryza sativa* L., *Solanum tuberosum* L., *Brassica napus* L., *Triticum aestivum* L., and others (Hsu and Kao, 2003; Stroiński et al., 2013; Shen et al., 2017; Hu et al., 2020). Exogenous ABA supply decreased transpiration rate and Cd concentration and increased Cd tolerance in *Oryza sativa* L. seedlings (Hsu and Kao, 2003). Further, exogenous ABA supplementation reduced the deleterious effects of Cd stress in *Brassica napus* L. by decreasing internal Cd accumulation and malondialdehyde content and enhancing fresh weight (Meng et al., 2009). According to Stroiński et al. (2013), *Solanum tuberosum* L. seedlings treated with 0.1 mM ABA increased StPCS1 content, the expression of genes coding 9-*cis*-epoxycarotenoid dioxygenase 1 and basic leucine zipper, phytochelatins synthase activity in roots, and the endogenous ABA level. In *Arabidopsis thaliana* L., Fan et al. (2014) and Pan et al. (2020) revealed that ABA reduced Cd absorption by inhibiting the process of iron-regulated transporter 1 (IRT1) and relieving Cd-induced toxicity. In *Populus euphratica* L. cells, ABA alleviated 100 μM Cd stress by improving antioxidant enzyme activity that scavenged H_2O_2 to prevent Cd from entering H_2O_2-induced Ca^{2+}-permeable channels (Han et al., 2016). ABA application at 20 μM L^{-1} improved Cd extraction and phytoremediation activity in *Solanum photeinocarpum* L. (Wang et al., 2016). The *JrVHAG1*gene functions as a Cd stress response regulator in the ABA signaling pathway and transcription regulation network of *MYB* in plants (Xu et al., 2018). *Vitis vinifera* L. seedlings treated with 10 μM ABA reduced Zn stress by decreasing Zn uptake and accumulation in roots and promoting the expression of the *ZIP* gene and detoxification-related genes in leaves and roots (Song et al., 2019). ABA-treated *Populus alba* L. seedlings had less Pb

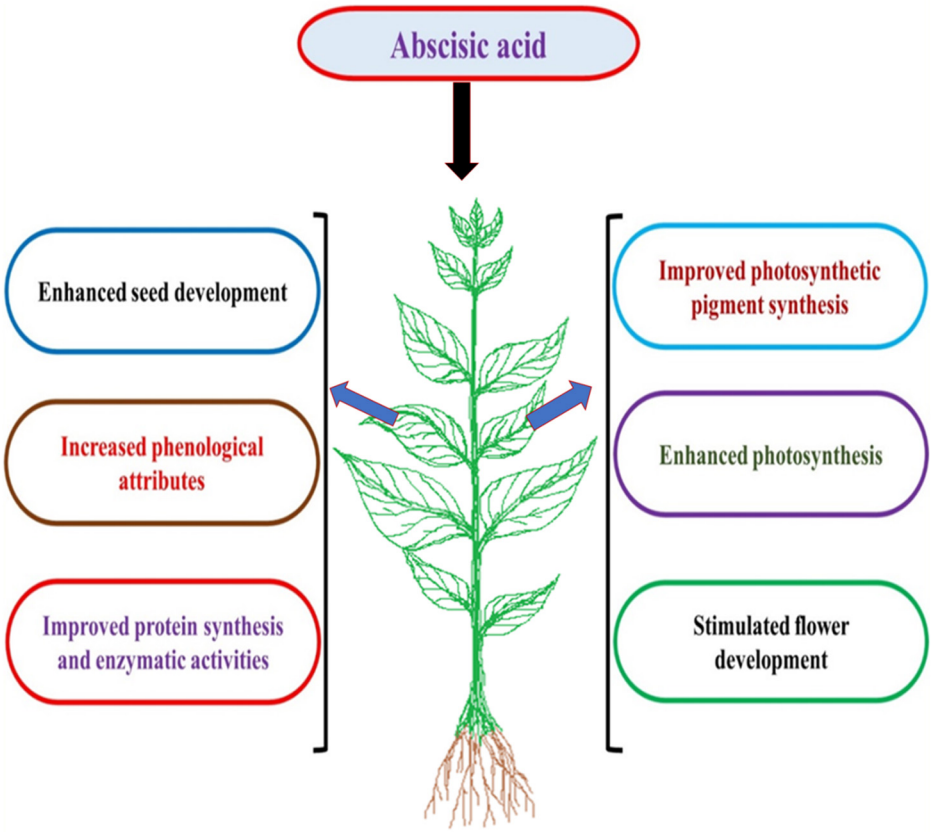


FIGURE 3
The effect of exogenous application of abscisic acid (ABA) on plant growth and physiological processes.

toxicity and increased expression of some genes involved in Pb transport and detoxification, including *NRAMP1.4, ABCG40, PCS1.1, FRD3.1,* and *ABCC1.1* (Shi et al., 2019). In *Lactuca sativa* L. seedlings, exogenously applied ABA decreased Cd absorption and relieved Cd toxicity (Dawuda et al., 2020). In *Sedum alfredii* L. seedlings, exogenously applied ABA (0.2 mg L^{-1}) alleviated Cd stress by increasing endogenous ABA content through enhanced ABA synthetase activity. It also promoted the expression of *HsfA4c* in roots and *NAS* and *HMA4* in shoots to improve Cd resistance (Lu et al., 2020). Exogenous ABA application minimized the damage of excess Zn by increasing endogenous ABA concentration, proline accumulation, and ascorbate peroxidase (APX) activity and inhibiting lipoxygenase (LOX) activity (Li and Song, 2020). ABA could also be involved in upregulating the *APX* gene and proline synthesis genes and downregulating the *LOX* gene in Arabidopsis thaliana L. (Li and Song, 2020). Exogenous ABA application at 40 and 60 μM L^{-1} ameliorated Cd and Pb toxic effects by improving total chlorophyll content and antioxidant capacity in Sedum alfredii L. and *Hylotelephium spectabile* L. (Cheng et al., 2022). Seed priming with ABA also reduced HM toxicity in plants by increasing glutathione content, non-protein thiol and cysteine, and phytochelatins synthesis (Saha et al., 2021). ABA reduced Zn stress damage by enhancing proline content and antioxidant enzyme activities in *Robinia pseudoacacia* L. (Lou et al., 2021). ABA also regulated Cd hyperaccumulation in Sedum alfredii by lowering aquaporin expression in roots, the number of xylem vessels in stems, and stomatal size and density in leaves (Tao et al., 2021). Chen et al. (2022) suggested that exogenously applied ABA improved the phytoremediation efficiency of Sedum alfredii grown in Cd, Pb, and Zn contaminated soil. **Figure 3** illustrates the role of exogenously applied ABA in plants. **Figure 4** and **Table 2** overview HM sequestration in plant cells mediated by ABA.

Crosstalk of abscisic acid with other plant growth regulators

Abscisic acid and auxin regulate several facets of plant growth and metabolism, mainly in a contrary manner (Sun and Li, 2014). For example, for seed germination and root growth, ABA-induced expression of Auxin Response Factor 2 (ARF2) and *arf2* mutants enhanced ABA sensitivity in Arabidopsis thaliana L. (Wang et al., 2011). ABA reduced cell division and altered auxin distribution more in *arf2* mutants than wild species. Exogenous ABA application to the *arf2* mutant reduced root length (Wang et al., 2011, 2013). ABA can also restrict primary root development by controlling cell proliferation in root tips (Wang et al., 2011). ABA slows seedling growth by increasing auxin signaling (Rock and Sun, 2005). The gene expression network containing the transcription factor ABA insensitive three regulates seed dormancy mediated by ABA and auxin *(ABI3).* Auxin controls *ABI3* gene expression during seed germination by selecting auxin response factors 10 and 16 (Wang et al., 2011; Liu et al., 2013). Auxin is required for seed dormancy while ABA suppresses seed germination, indicating that auxin and ABA have an interacting role in seed dormancy. Auxin acts in two directions in ABA modulated processes by (1) activating the ABA response and (2) improving biological ABA synthesis. However, endogenous and exogenous indoleacetic acid (IAA) inhibited seed germination in radical protrusions experiments, showing that ABA and auxin work together to prevent seed germination (Liu et al., 2013; Matilla, 2020). In the absence of ABA, an equal amount of IAA did not limit seed germination, suggesting that inhibition of seed germination mediated through auxin depends on ABA. In addition, basipetal transport of auxin increased with osmotically induced ABA by increasing AUX1 (Auxin Influx Transporter) and PIN2 (Auxin Efflux Transporter) (Xu et al., 2013; Wu et al., 2020). As a result, auxin and ABA communicate *via* the auxin response pathway to control plant growth and development.

Many aspects of plant development, such as seed dormancy and maturation, main root growth, and flowering are controlled by the antagonistic interactions of ABA and gibberellins (GA). ABA inhibits seed germination by promoting seed dormancy, whereas GA stimulates seed germination and promotes seedling growth (Yuan et al., 2011). Sustaining germination and dormancy requires balancing ABA and GA production and catabolism (White et al., 2000; Bicalho et al., 2015). In *Arabidopsis thaliana* L., exogenous ABA supply decreased primary root development, whereas GA promoted root growth (Ubeda-Tomás et al., 2008; Zhang et al., 2010; Shu et al., 2018). Similarly, ABA and brassinosteroids (BR) coordinate antagonistically to modulate plant physiological functions. It is well-known that ABA inhibits seed germination while BR promotes seed germination (Saini et al., 2015). Further, ABA has a regulatory effect on BR signaling. ABA components like AB11 and ABA12 interplay with BR signaling components such as BIN2 and BR11 receptors (Yang et al., 2016). The interaction of ABA and GA3 hormones with Pb and Zn may increase total phenolic content; however, their interaction with Cd prevents an increase in phenolic compounds (Ahmad et al., 2015). ABA is also involved in the interaction between BR and CKs, as it suppresses BR synthesis during metal toxicity (Zhang S. et al., 2009). However, the molecular interactions between ABA and GA and ABA and BR for regulating plant physiological processes need further investigation.

Abscisic acid and cytokinin interact to regulate the stress response. The enzyme cytokinin oxidase encoded by the multigenic family cytokinin oxidase (*CKX*) has several members responsible for cytokinin breakdown (Avalbaev et al., 2012; Sirko et al., 2021). For instance, ABA decreased the expression of *CKX* genes in *Arabidopsis thaliana* L. Under stress conditions, cytokinin receptor kinases (AHK2 and AHK3) negatively controlled ABA and the expression of genes responsible for osmotic stress, while mutants with cytokinin deficiency had increased survival rates (Werner et al., 2006; Tran et al., 2007).

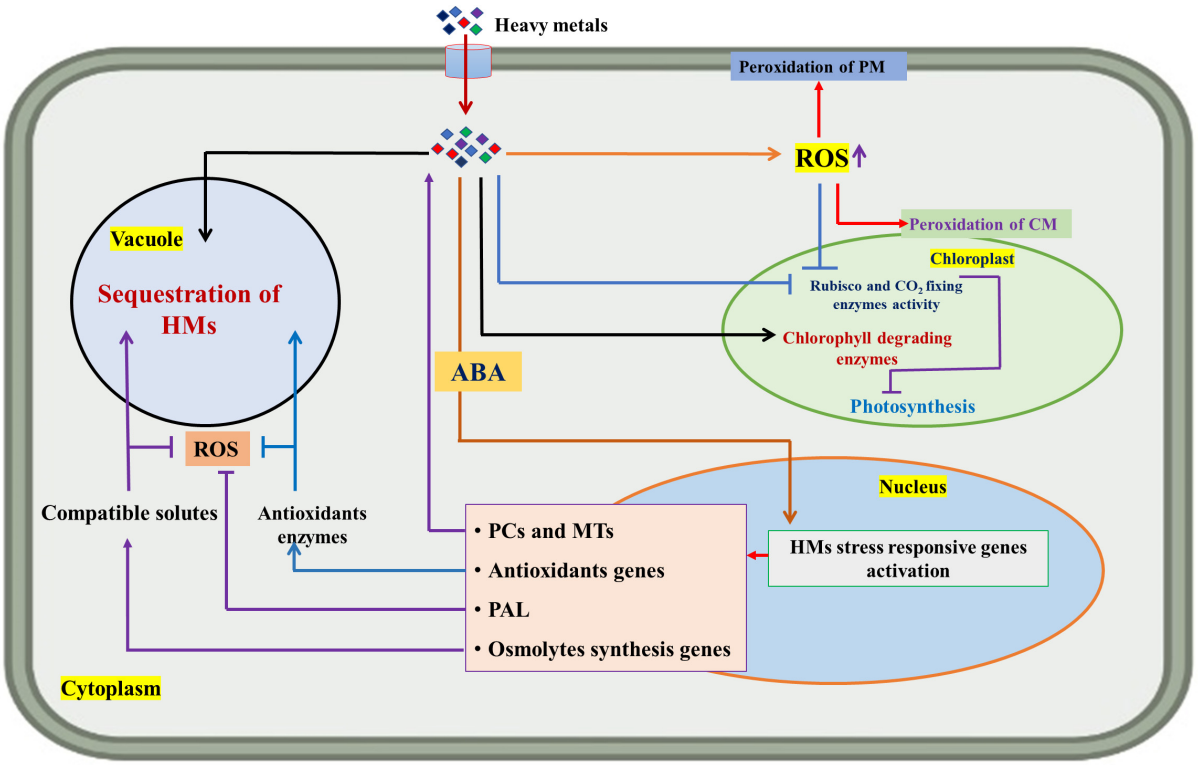


FIGURE 4
Diagram showing the sequestration mechanism of heavy metals (HMs) in plant cells and the role of abscisic acid (ABA) in mitigating HM stress. ROS (reactive oxygen species), PM (plasma membrane), CM (chloroplast membrane), PCs (phytochelatins), MTs (metallothioneins), and PAL (phenylalanine ammonia-lyase).

Abscisic acid and ethylene work together to control stomatal closure, with ABA controlling the increase in ethylene concentration in leaves (Chen et al., 2013), while ethylene blocks the ABA signaling pathway and leads to slow stomatal closure (Harrison, 2012; Arc et al., 2013). ABA inhibits the expression of the ethylene biosynthesis gene (*ACS5*) that encodes an enzyme for determining the rate-limiting step of ethylene biosynthesis. ABA also positively controls ethylene response factor 11 (ERF11) behavior through the long hypocotyl5 (HY5) replication factor, an important molecular contact between ABA and ethylene synthesis that represses *ACS5* gene expression. The regulation of *YF-AtERF11* expression is crucial for ABA-controlled ethylene biosynthesis (Li et al., 2011; Corbineau et al., 2014). Exogenous SA mitigated Cd stress in *Triticum aestivum* L. by increasing GSH content, resulting in metal detoxification and scavenging ROS induced by HM-triggered ethylene production. SA supplementation increased ABA levels in wheat seedlings under Cd stress, which was attributed to *de novo* ABA biosynthesis. Further, endogenous ABA-controlled SA-mediated changes in the concentration of dehydrin proteins under HM stress demonstrated the protective mechanism of SA in *Triticum aestivum* L. (Kovács et al., 2014; Shakirova et al., 2016).

A complex interaction between ABA and the jasmonate (JA) signaling pathway controls plant protection and gene expression. Exogenous ABA application reduces JA-induced transcription of defense genes. In contrast, mutations in the ABA synthesis genes *aba1* and *aba2* caused the overexpression of JA-responsive genes (Anderson et al., 2004). Several components of ABA and the JA-ethylene signaling pathway interact antagonistically to control the expression of several stress-responsive genes in response to abiotic and biotic stressors (Anderson et al., 2004; Proietti et al., 2018). Most JA signaling pathway components in *Arabidopsis thaliana* L. are regulated by the transcription factor MYC2. Furthermore, overexpression of the *MYC2* gene in genetically engineered plants has been linked to increased ABA sensitivity and activation of numerous ABA-induced genes. In contrast, *Myc2* mutants with *Ds* mutations are less susceptible to ABA and have lower gene expression (Chen et al., 2011). As a result, MYC2 in *Arabidopsis thaliana* L. is an integrative hub for controlling JA and ABA signals (Sun and Li, 2014).

Abscisic acid and nitric oxide (NO) may interact to regulate plant growth and physiological processes, including seed germination, root growth, stomatal movement, and antioxidant enzyme activities (Hancock et al., 2011; Prakash et al., 2019).

TABLE 2 Alleviation of heavy metal (HM) toxicity in plants by abscisic acid (ABA).

Plant species	Type of HM stress and concentration	Growth conditions	ABA dose	Plant response	References
Brassica napus L.	Cd (100 μM)	Hydroponic	10 μM	Enhanced plant biomass and decreased Cd accumulation and malondialdehyde content	Meng et al. (2009)
Populus euphratica L.	Cd (100 μM)	Culture medium	5 μM	Improved cell survival and proliferation and antioxidant enzyme activities	Han et al. (2016)
Brassica campestris L.	Cd (100 μM L^{-1})	Hydroponic	5 μM	Increased soluble protein and chlorophyll content, antioxidant defense system, and Cd in plant roots	Shen et al. (2017)
Populus alba L.	Pb (3 mM)	Soil	10 μM	Improved root biomass, photosynthetic rate and ascorbate and glutathione contents	Shi et al. (2019)
Lactuca sativa L.	Cd (10 μM L^{-1})	Soil	5 μM	Enhanced plant biomass, stomatal conductance, internal CO_2 concentration, antioxidant enzyme activity, proline content and soluble protein content.	Tang et al. (2020)
Arabidopsis thaliana L.	Zn (200 mg L^{-1})	Culture medium	15 μM	Increased proline accumulation, antioxidant enzyme activities, and endogenous ABA level	Li and Song (2020)
Vigna radiata L.	Cd (100 μM)	Seed tray	10 μM	Affected plant tolerance by stimulating antioxidant enzyme activity and inhibiting lipid peroxidation	Leng et al. (2021)
Oryza sativa L.	As (50 μM)	Culture medium	10 μM	Increased osmolyte concentrations, glutathione content, non-protein thiol, phytochelatins and glutathione reductase activity	Saha et al. (2021)
Solanum lycopersicum L.	Co (400 μM L^{-1})	Hydroponic	10 μM	Improved proline content and antioxidant enzyme activities, reduced Co translocation from roots to shoots	Kamran et al. (2021)
Perilla frutescens L.	Cd (10 mg kg^{-1})	Soil	5 μM	Enhanced plant biomass, photosynthetic pigments and antioxidant activities.	Shu et al. (2021)

Increasing ABA levels in tobacco by increasing the expression of the 9-*cis*-epoxycarotenoid dioxygenase gene (*SgNCED1*) increased H_2O_2 and NO levels in mesophyll and guard cells, increasing the replication and activity of many antioxidant enzymes (Zhang Y. et al., 2009). The breakdown of seed dormancy in *Arabidopsis thaliana* L. caused rapid ABA depletion due to rapid NO accumulation, with the opposite effect during seed germination (Liu et al., 2009; Signorelli and Considine, 2018). Moreover, in guard cells, ABA-induced endogenous H_2O_2 production increased NO production to control stomatal movement (Bright et al., 2006; Saradadevi et al., 2014). Furthermore, exogenous NO application alleviated the inhibitory effect of ABA on leaf senescence in *Oryza sativa* L. (Hung and Kao, 2003). ABA and NO modulate metabolic plant functions in response to environmental stress by improving osmolyte synthesis and the antioxidant defense system (Iqbal et al., 2021, 2022). During HM stress, NO may interact with ABA to weaken HM stress. NO reduced the As-induced upregulation of ABA content in *Vicia faba* L., reducing As toxicity (Mohamed et al., 2016). Sadeghipour (2017) revealed that exogenous application of NO to *Vigna unguiculata* L. reduced ABA content under Pb stress, enhancing Pb tolerance. Wu et al. (2018) reported that molybdenum (Mo) induced ABA synthesis in *Triticum aestivum* L. by upregulating aldehyde oxidase activity. The NO acting downstream of ABA was involved in oxidative stress induced by Mo, implying an intermediate linkage in the relationship between ABA and NO.

As a result, ABA is a crucial plant growth regulator that coordinates with other phytohormones to control plant growth and development under adverse environmental conditions. Further research is needed on the molecular mechanisms behind complex signaling networks of ABA and other hormones.

Conclusion

Heavy metal toxicity is a severe environmental restraint that hampers plant growth and productivity of food crops. PGRs are small signaling molecules that regulate many physiological and molecular processes in plants. Exogenous application of PGRs is an efficient approach to ameliorating the deleterious effects of HM and improving plant morphological characteristics, physio-biochemical processes, and production. As a vital PGR, ABA controls many developmental and metabolic functions of plants. This review revealed that exogenous ABA application alleviates the toxic effects of HM in plants by improving osmolyte synthesis, antioxidant machinery, phytochelatins synthesis, and enzymatic activities. It is also well-known that ABA has a significant role in providing abiotic stress tolerance in plants and improving plant growth and production. ABA application through the soil, foliar spray, seed priming, and culture media

positively enhances crop productivity and thus could be used to improve the growth and yield of economically important crops. ABA plays a crucial role in mitigating HM stress by strengthening the tolerance mechanism of plants. The available literature on the role of ABA in HM stress mitigation offers a brief insight into morphological and physio-biochemical functioning and modulation in plants under HM stress. Thus, more research is needed to explore the molecular mechanisms of HM sequestration regulated through ABA to (1) enhance our understanding of ABA homeostasis during the plant life cycle, (2) identify crosstalk mechanisms between ABA and other PGRs under HM and other abiotic stresses and (3) explore the dynamic role of ABA in crop plants using novel genomic, molecular, and proteomic approaches.

Author contributions

SK and SHS wrote and drafted the review article. YV, HSJ, PA, YC, and KHMS revised and edited the manuscript. All authors contributed to the article and approved the submitted version.

Conflict of interest

The authors declare that the research was conducted in the absence of any commercial or financial relationships that could be construed as a potential conflict of interest.

Publisher's note

All claims expressed in this article are solely those of the authors and do not necessarily represent those of their affiliated organizations, or those of the publisher, the editors and the reviewers. Any product that may be evaluated in this article, or claim that may be made by its manufacturer, is not guaranteed or endorsed by the publisher.

References

Aqeel, M., Khali, N., Tufail, A., Ahmad, R. Z., Akhter, M. S., Luqman, M., et al. (2021). Elucidating the distinct interactive impact of cadmium and nickel on growth, photosynthesis, metal-homeostasis, and yield responses of mung bean (*Vigna radiata* L.) varieties. *Environ. Sci. and Pollut. Res.* 28, 27376–27390. doi: 10.1007/s11356-021-12579-5

Ahmad, A., Hadi, F., and Ali, N. (2015). Effective phytoextraction of cadmium (Cd) with increasing concentration of total phenolics and free proline in *Cannabis sativa* (L) plant under various treatments of fertilizers, plant growth regulators and sodium salt. *Int. J. Phytoremediation* 17, 56–65. doi: 10.1080/15226514.2.13.828018

Ahmad, P., Jaleel, C. A., Salem, M. A., Nabi, G., and Sharma, S. (2010). Roles of enzymatic and nonenzymatic antioxidants in plants during abiotic stress. *Crit. Rev. Biotechnol.* 30, 161–175. doi: 10.3109/07388550903524243

Ali, A., Pardo, J. M., and Yun, D. J. (2020). Desensitization of ABA-signaling: The swing from activation to degradation. *Front. Plant Sci* 11:379. doi: 10.3389/fpls.2020.00379

An, T., Gao, Y., Kuang, Q., Wu, Y., uz Zaman, Q., Zhang, Y., et al. (2022a). Effect of silicon on morpho-physiological attributes, yield and cadmium accumulation in two maize genotypes with contrasting root system size and health risk assessment. *Plant Soil* 1–18. doi: 10.1007/s11104-022-05384-7

An, T., Wu, Y., Xu, B., Zhang, S., Deng, X., Zhang, Y., et al. (2022b). Nitrogen supply improved plant growth and Cd translocation in maize at the silking and physiological maturity under moderate Cd stress. *Ecotoxicol Environ. Saf.* 230:113137. doi: 10.1016/j.ecoenv.2021.113137

Anderson, J. P., Badruzsaufari, E., Schenk, P. M., Manners, J. M., Desmond, O. J., Ehlert, C., et al. (2004). Antagonistic interaction between abscisic acid and jasmonate-ethylene signaling pathways modulates defense gene expression and disease resistance in *Arabidopsis*. *Plant Cell.* 16, 3460–3479. doi: 10.1105/tpc.104.025833

Andolfo, G., Ruocco, M., Di Donato, A., Frusciante, L., Lorito, M., Scala, F., et al. (2015). Genetic variability and evolutionary diversification of membrane ABC transporters in plants. *BMC Plant Biol.* 15:1–15. doi: 10.1186/s12870-014-0323-2

Arc, E., Sechet, J., Corbineau, F., Rajjou, L., and Marion-Poll, A. (2013). ABA crosstalk with ethylene and nitric oxide in seed dormancy and germination. *Front. Plant Sci.* 4:63. doi: 10.3389/fpls.2013.00063

Arduini, I., Masoni, A., Mariotti, M., Pampana, S., and Ercoli, L. (2014). Cadmium uptake and translocation in durum wheat varieties differing in grain-Cd accumulation. *Plant Soil Environ.* 60, 43–49. doi: 10.17221/416/2013-pse

Ashraf, U., Kanu, A. S., Deng, Q., Mo, Z., Pan, S., Tian, H., et al. (2017). Lead (Pb) toxicity; physio-biochemical mechanisms, grain yield, quality, and Pb distribution proportions in scented rice. *Front. Plant Sci.* 8:259. doi: 10.3389/fpls.2017.00259

Avalbaev, A. M., Somov, K. A., Yuldashev, R. A., and Shakirova, F. M. (2012). Cytokinin oxidase is key enzyme of cytokinin degradation. *Biochemistry (Moscow).* 77, 1354–1361. doi: 10.1134/s0006297912120024

Baron, K. N., Schroeder, D. F., and Stasolla, C. (2012). Transcriptional response of abscisic acid (ABA) metabolism and transport to cold and heat stress applied at the reproductive stage of development in *Arabidopsis thaliana*. *Plant Sci.* 188, 48–59. doi: 10.1016/j.plantsci.2012.03.001

Bavi, K., Kholdebarin, B., and Moradshahi, A. (2011). Effect of cadmium on growth, protein content and peroxidase activity in pea plants. *Pak. J. Bot.* 43, 1467–1470.

Bicalho, E. M., Pintó-Marijuan, M., Morales, M., Müller, M., Munné-Bosch, S., and Garcia, Q. S. (2015). Control of macaw palm seed germination by the gibberellin/abscisic acid balance. *Plant Biol.* 17, 990–996. doi: 10.1111/plb.12332

Bright, J., Desikan, R., Hancock, J. T., Weir, I. S., and Neill, S. J. (2006). ABA-induced NO generation and stomatal closure in *Arabidopsis* are dependent on H2O2 synthesis. *Plant J.* 45, 113–122. doi: 10.1111/j.1365-313x.2005.02615.x

Cardoso, A. A., Gori, A., Da-Silva, C. J., and Brunetti, C. (2020). Abscisic acid biosynthesis and signaling in plants: Key targets to improve water use efficiency and drought tolerance. *Applied Sci.* 10:6322. doi: 10.3390/app10186322

Chandrakar, V., Yadu, B., Xalxo, R., Kumar, M., and Keshavkant, S. (2020). "Mechanisms of plant adaptation and tolerance to metal/metalloid toxicity," in *Plant ecophysiology and adaptation under climate change: Mechanisms and perspectives II*, (Singapore: Springer), 107–135. doi: 10.1007/978-981-15-2172-0_6

Chen, K., Chen, P., Qiu, X., Chen, J., Gao, G., Wang, X., et al. (2021). Regulating role of abscisic acid on cadmium enrichment in ramie (*Boehmeria nivea* L.). *Sci. Rep.* 11, 1–10. doi: 10.1038/s41598-021-00322-6

Chen, L. I. N., Dodd, I. C., Davies, W. J., and Wilkinson, S. (2013). Ethylene limits abscisic acid-or soil drying-induced stomatal closure in aged wheat leaves. *Plant Cell Environ.* 36, 1850–1859. doi: 10.1111/pce.12094

Chen, Q., Sun, J., Zhai, Q., Zhou, W., Qi, L., Xu, L., et al. (2011). The basic helix-loop-helix transcription factor MYC2 directly represses PLETHORA expression

during jasmonate-mediated modulation of the root stem cell niche in *Arabidopsis*. *Plant Cell.* 23, 3335–3352. doi: 10.1105/tpc.111.089870

Chen, T. T., Liu, F. F., Xiao, D. W., Jiang, X. Y., Li, P., Zhao, S. M., et al. (2020). The *Arabidopsis* UDP-glycosyltransferase75B1, conjugates abscisic acid and affects plant response to abiotic stresses. *Plant Mol. Biol.* 102, 389–401. doi: 10.1007/s11103-019-00953-4

Chen, Z., Liu, Q., Chen, S., Zhang, S., Wang, M., Munir, M. A. M., et al. (2022). Roles of exogenous plant growth regulators on phytoextraction of Cd/Pb/Zn by *Sedum alfredii* Hance in contaminated soils. *Environ. Pollut.* 293:118510. doi: 10.1016/j.envpol.2021.118510

Cheng, L., Pu, L., Li, A., Zhu, X., Zhao, P., Xu, X., et al. (2022). Implication of exogenous abscisic acid (ABA) application on phytoremediation: Plants grown in co-contaminated soil. *Environ. Sci. Pollut. Res.* 29, 8684–8693. doi: 10.1007/s11356-021-16241-y

Corbineau, F., Xia, Q., Bailly, C., and El-Maarouf-Bouteau, H. (2014). Ethylene, a key factor in the regulation of seed dormancy. *Front. Plant Sci.* 5:539. doi: 10.3389/fpls.2014.00539

Da-lin, L., Kai-qi, H., Jing-jing, M., Wei-wei, Q., Xiu-ping, W., and Shu-pan, Z. (2011). Effects of cadmium on the growth and physiological characteristics of sorghum plants. *Afr. J. Biotechnol.* 10, 15770–15776. doi: 10.5897/AJB11.848

Dawuda, M. M., Liao, W., Hu, L., Yu, J., Xie, J., Calderón-Urrea, A., et al. (2020). Foliar application of abscisic acid mitigates cadmium stress and increases food safety of cadmium-sensitive lettuce (*Lactuca sativa* L.) genotype. *Peer. J.* 8:e9270. doi: 10.7717/peerj.9270

Deng, B., Zhang, W., and Yang, H. (2021). Abscisic acid decreases cell death in *Malus hupehensis* Rehd. Under Cd stress by reducing root Cd 2+ influx and leaf transpiration. *J. Plant Growth Regul.* 40, 1–8. doi: 10.1007/s00344-021-10327-0

Emamverdian, A., Ding, Y., Mokhberdoran, F., and Xie, Y. (2015). Heavy metal stress and some mechanisms of plant defense response. *Sci. World J.* 2015:756120. doi: 10.1155/2015/756120

Fan, S. K., Fang, X. Z., Guan, M. Y., Ye, Y. Q., Lin, X. Y., Du, S. T., et al. (2014). Exogenous abscisic acid application decreases cadmium accumulation in *Arabidopsis* plants, which is associated with the inhibition of IRT1-mediated cadmium uptake. *Front. Plant Sci.* 5:721. doi: 10.3389/fpls.2014.00721

Frey, A., Audran, C., Marin, E., Sotta, B., and Marion-Poll, A. (1999). Engineering seed dormancy by the modification of zeaxanthin epoxidase gene expression. *Plant Mol. Biol.* 39, 1267–1274. doi: 10.1023/A:100614502563

Ghani, A. (2010). Toxic effects of heavy metals on plant growth and metal accumulation in maize (*Zea mays* L.). *Iran. J. Toxicol.* 325–334.

Ghori, N. H., Ghori, T., Hayat, M. Q., Imadi, S. R., Gul, A., Altay, V., et al. (2019). Heavy metal stress and responses in plants. *Int. J. Environ. Sci. Technol.* 16, 1807–1828. doi: 10.1007/s13762-019-02215-8

Giannakoula, A., Therios, I., and Chatzissavvidis, C. (2021). Effect of lead and copper on photosynthetic apparatus in citrus (*Citrus aurantium* L.) plants. The role of antioxidants in oxidative damage as a response to heavy metal stress. *Plants* 10:155. doi: 10.3390/plants10010155

Gill, M. (2014). Heavy metal stress in plants: A review. *Int. J. Adv. Res* 2, 1043–1055.

Goyal, D., Yadav, A., Prasad, M., Singh, T. B., Shrivastav, P., Ali, A., et al. (2020). "Effect of heavy metals on plant growth: An overview," in *Contaminants in agriculture*, (Cham: Springer), 79–101. doi: 10.1007/978-3-030-41552-5_4

Han, Y., Wang, S., Zhao, N., Deng, S., Zhao, C., Li, N., et al. (2016). Exogenous abscisic acid alleviates cadmium toxicity by restricting Cd 2+ influx in *Populus euphratica* cells. *J. Plant Growth Regul.* 35, 827–837. doi: 10.1007/s00344-016-9585-2

Hancock, J. T., Neill, S. J., and Wilson, I. D. (2011). Nitric oxide and ABA in the control of plant function. *Plant Sci.* 181, 555–559. doi: 10.1016/j.plantsci.2011.03.017

Harrison, M. A. (2012). "Cross-talk between phytohormone signaling pathways under both optimal and stressful environmental conditions," in *Phytohormones and abiotic stress tolerance in plants*, (Berlin: Springer), 49–76.

Hasanuzzaman, M., Bhuyan, M. H. M., Nahar, K., Hossain, M., Mahmud, J. A., Hossen, M., et al. (2018). Potassium: A vital regulator of plant responses and tolerance to abiotic stresses. *Agronomy.* 8:31. doi: 10.3390/agronomy8030031

He, G., Tian, W., Qin, L., Meng, L., Wu, D., Huang, Y., et al. (2021). Identification of novel heavy metal detoxification proteins in *Solanum tuberosum*: Insights to improve food security protection from metal ion stress. *Sci. Total Environ.* 779:146197. doi: 10.1016/j.scitotenv.2021.146197

Hou, N., You, J., Pang, J., Xu, M., Chen, G., and Yang, Z. (2010). The accumulation and transport of abscisic acid insoybean (*Glycine max* L.) under aluminum stress. *Plant Soil* 330, 127–137. doi: 10.1007/s11104-009-0184-x

Hsu, Y. T., and Kao, C. H. (2003). Role of abscisic acid in cadmium tolerance of rice (*Oryza sativa* L.) seedlings. *Plant Cell Environ.* 26, 867–874. doi: 10.1046/j.1365-3040.2003.01018.x

Hu, B., Den, F., Chen, G., Chen, X., Gao, W., Long, L., et al. (2020). Evolution of abscisic acid signaling for stress responses to toxic metals and metalloids. *Front. Plant Sci.* 11:909. doi: 10.3389/fpls.2020.00909

Huihui, Z., Xin, L., Zisong, X., Yue, W., Zhiyuan, T., Meijun, A., et al. (2020). Toxic effects of heavy metals Pb and Cd on mulberry (*Morus alba* L.) seedling leaves: Photosynthetic function and reactive oxygen species (ROS) metabolism responses. *Ecotoxicol. Environ. Saf.* 195:110469. doi: 10.1016/j.ecoenv.2020.110469

Hung, K. T., and Kao, C. H. (2003). Nitric oxide counteracts the senescence of rice leaves induced by abscisic acid. *J. Plant Physiol.* 160, 871–879. doi: 10.1078/0176-1617-01118

Iqbal, N., Sehar, Z., Fatma, M., Umar, S., Sofo, A., and Khan, N. A. (2022). Nitric oxide and abscisic acid mediate heat stress tolerance through regulation of osmolytes and antioxidants to protect photosynthesis and growth in wheat plants. *Antioxidants* 11:372. doi: 10.3390/antiox11020372

Iqbal, N., Umar, S., Khan, N. A., and Corpas, F. J. (2021). Crosstalk between abscisic acid and nitric oxide under heat stress: Exploring new vantage points. *Plant Cell Rep.* 40, 1429–1450. doi: 10.1007/s00299-021-02695-4

Irfan, M., Hasan, S. A., Hayat, S., and Ahmad, A. (2015). Photosynthetic variation and yield attributes of two mustard varieties against cadmium phytotoxicity. *Cogent Food Agric.* 1:1106186. doi: 10.1080/23311932.2015.1106186

Jalmi, S. K., Bhagat, P. K., Verma, D., Noryang, S., Tayyeba, S., Singh, K., et al. (2018). Traversing the links between heavy metal stress and plant signaling. *Front. Plant Sci.* 9:12. doi: 10.3389/fpls.2018.00012

Jensen, M. K., Lindemose, S., De Mas, F., Reimer, J. J., Nielsen, M., Perera, V., et al. (2013). ATAF1 transcription factor directly regulates abscisic acid biosynthetic gene NCED3 in *Arabidopsis thaliana*. *FEBS Open Bio.* 3, 321–327. doi: 10.1016/j.fob.2013.07.006

John, R., Ahmad, P., Gadgil, K., and Sharma, S. (2009). Heavy metal toxicity: Effect on plant growth, biochemical parameters and metal accumulation by *Brassica juncea* L. *Int. J. Plant Prod.* 3, 1735–8043.

Kamran, M., Danish, M., Saleem, M. H., Malik, Z., Parveen, A., Abbasi, G. H., et al. (2021). Application of abscisic acid and 6-benzylaminopurine modulated morpho-physiological and antioxidative defense responses of tomato (*Solanum lycopersicum* L.) by minimizing cobalt uptake. *Chemosphere* 263:128169. doi: 10.1016/j.chemosphere.2020.128169

Kang, J., Hwang, J. U., Lee, M., Kim, Y. Y., Assmann, S. M., Martinoia, E., et al. (2010). PDR-type ABC transporter mediates cellular uptake of the phytohormone abscisic acid. *Proc. Natl. Acad. Sci* 107, 2355–2360. doi: 10.1073/pnas.0909222107

Kang, J., Yim, S., Choi, H., Kim, A., Lee, K. P., Lopez-Molin, L., et al. (2015). Abscisic acid transporters cooperate to control seed germination. *Nat. Commun.* 6, 1–10. doi: 10.1038/ncomms9113

Kanno, Y., Hanada, A., Chiba, Y., Ichikawa, T., Nakazawa, M., Matsui, M., et al. (2012). Identification of an abscisic acid transporter by functional screening using the receptor complex as a sensor. *Proc. Natl. Acad. Sci.* 109, 9653–9658. doi: 10.1073/pnas.1203567109

Keyster, M., Niekerk, L. A., Basson, G., Carelse, M., Bakare, O., Ludidi, N., et al. (2020). Decoding heavy metal stress signalling in plants: Towards improved food security and safety. *Plants.* 9:1781. doi: 10.3390/plants9121781

Khan, M. A., Khan, S., Khan, A., and Alam, M. (2017). Soil contamination with cadmium, consequences and remediation using organic amendments. *Sci. Total Environ.* 601, 1591–1605. doi: 10.1016/j.scitotenv.2017.06.030

Kitahata, N., Saito, S., Miyazawa, Y., Umezawa, T., Shimada, Y., Min, Y. K., et al. (2005). Chemical regulation of abscisic acid catabolism in plants by cytochrome P450 inhibitors. *Bioorg. Med. Chem.* 13, 4491–4498. doi: 10.1016/j.bmc.2005.04.036

Kovács, V., Gondor, O. K., Szalai, G., Darkó, É, Majláth, I., Janda, T., et al. (2014). Synthesis and role of salicylic acid in wheat varieties with different levels of cadmium tolerance. *J. Hazard. Mater.* 280, 12–19. doi: 10.1016/j.jhazmat.2014.07.048

Kumar, S., Ahanger, M. A., Alshaya, H., Jan, B. L., and Yerramilli, V. (2022). Salicylic acid mitigates salt induced toxicity through the modifications of biochemical attributes and some key antioxidants in Capsicum annuum. *Saudi J. Biol. Sci.* 29, 1337–1347. doi: 10.1016/j.sjbs.2022.01.028

Kuromori, T., Miyaji, T., Yabuuchi, H., Shimizu, H., Sugimoto, E., Kamiya, A., et al. (2010). ABC transporter AtABCG25 is involved in abscisic acid transport and responses. *Proc. Natl. Acad. Sci. U.S.A.* 107, 2361–2366. doi: 10.1073/pnas.0912516107

Kuromori, T., Sugimoto, E., and Shinozaki, K. (2011). *Arabidopsis* mutants of AtABCG22, an ABC transporter gene, increase water transpiration and drought susceptibility. *Plant J.* 67, 885–894. doi: 10.1111/j.1365-313x.2011.04641.x

Lajayer, B. A., Moghadam, N. K., Maghsoodi, M. R., Ghorbanpour, M., and Kariman, K. (2019). Phytoextraction of heavy metals from contaminated soil, water and atmosphere using ornamental plants: Mechanisms and efficiency improvement strategies. *Environ. Sci. Pollut. Res.* 26, 8468–8484. doi: 10.1007/s11356-019-04241-y

Lee, H. G., Lee, K., and Seo, P. (2015). The *Arabidopsis* MYB96 transcription factor plays a role in seed dormancy. *Plant Mol. Biol.* 87, 371–381. doi: 10.1007/s11103-015-0283-4

Leng, Y., Li, Y., Ma, Y. H., He, L. F., and Li, S. W. (2021). Abscisic acid modulates differential physiological and biochemical responses of roots, stems, and leaves in mung bean seedlings to cadmium stress. *Environ. Sci. Pollut. Res.* 28, 6030–6043. doi: 10.1007/s11356-020-10843-8

Li, X. S., and Song, L. L. (2020). The role of ABA in the responses of wild-type and abscisic acid mutants of *Arabidopsis thaliana* to excess zinc. *Acta Physiol. Plant.* 42, 1–8. doi: 10.1007/s11738-020-03067-3

Li, Z., Zhang, L., Yu, Y., Quan, R., Zhang, Z., Zhang, H., et al. (2011). The ethylene response factor AtERF11 that is transcriptionally modulated by the bZIP transcription factor HY5 is a crucial repressor for ethylene biosynthesis in *Arabidopsis*. *The Plant J.* 68, 88–99. doi: 10.1111/j.1365-313x.2011.04670.x

Liu, H. F., Xue, X. J., Yu, Y., Xu, M. M., Lu, C. C., Meng, X. L., et al. (2020). Copper ions suppress abscisic acid biosynthesis to enhance defence against *Phytophthora infestans* in potato. *Mol. Plant Pathol.* 21, 636–651. doi: 10.1111/mpp.12919

Liu, X., Zhang, H., Zhao, Y., Feng, Z., Li, Q., Yan, H. Q., et al. (2013). Auxin controls seed dormancy through stimulation of abscisic acid signaling by inducing ARF-mediated ABI3 activation in *Arabidopsis*. *Proc. Natl Acad. Sci. U.S.A.* 110, 15485–15490. doi: 10.1073/pnas.1304651110

Liu, Y., Shi, L., Ye, N., Liu, R., Jia, W., and Zhang, J. (2009). Nitric oxide-induced rapid decrease of abscisic acid concentration is required in breaking seed dormancy in *Arabidopsis*. *New Phytologist.* 183, 1030–1042. doi: 10.1111/j.1469-8137.2009.02899.x

Lou, X., Zhang, X., Zhang, Y., and Tang, M. (2021). The synergy of arbuscular mycorrhizal fungi and exogenous abscisic acid benefits *Robinia pseudoacacia* L. growth through altering the distribution of Zn and endogenous abscisic acid. *J. Fungi.* 7:671. doi: 10.3390/jof7080671

Lu, Q., Chen, S., Li, Y., Zheng, F., He, B., and Gu, M. (2020). Exogenous abscisic acid (ABA) promotes cadmium (Cd) accumulation in *Sedum alfredii* hance by regulating the expression of Cd stress response genes. *Environ. Sci. Pollut. Res.* 27, 8719–8731. doi: 10.1007/s11356-019-07512-w

Ma, Y., Cao, J., He, J., Chen, Q., Li, X., and Yang, Y. (2018). Molecular mechanism for the regulation of ABA homeostasis during plant development and stress responses. *Int. J. Mol. Sci.* 19:3643. doi: 10.3390/ijms19113643

Małkowski, E., Sitko, K., Zieleźnik-Rusinowska, P., Gieroń, Ż, and Szopiński, M. (2019). *Heavy metal toxicity: Physiological implications of metal toxicity in plants. In Plant metallomics and functional omics*. Cham: Springer, 253–301. doi: 10.1007/978-3-030-19103-010

Matilla, A. J. (2020). Auxin: Hormonal signal required for seed development and dormancy. *Plants.* 9:705. doi: 10.3390/plants9060705

Mayonde, S., Cron, G. V., Glennon, K. L., and Byrne, M. J. (2021). Effects of cadmium toxicity on the physiology and growth of a halophytic plant, *Tamarix usneoides* (E. Mey. ex Bunge). *Int. J. Phytoremediation* 23, 130–138. doi: 10.1080/15226514.2020.1801573

Mehrotra, R., Bhalothia, P., Bansal, P., Basantani, M. K., Bharti, V., and Mehrotra, S. (2014). Abscisic acid and abiotic stress tolerance–Different tiers of regulation. *J. Plant Physiol.* 171, 486–496. doi: 10.1016/j.jplph.2013.12.007

Meng, H., Hua, S., Shamsi, I. H., Jilani, G., Li, Y., and Jiang, L. (2009). Cadmium-induced stress on the seed germination and seedling growth of *Brassica napus* L., and its alleviation through exogenous plant growth regulators. *Plant Growth Regul.* 58, 47–59. doi: 10.1007/s10725-008-9351-y

Merilo, E., Jalakas, P., Laanemets, K., Mohammadi, O., Hõrak, H., Kollist, H., et al. (2015). Abscisic acid transport and homeostasis in the context of stomatal regulation. *Mol. Plant.* 8, 1321–1333. doi: 10.1016/j.molp.2015.06.006

Milborrow, B. V. (2001). The pathway of biosynthesis of abscisic acid in vascular plants: A review of the present state of knowledge of ABA biosynthesis. *J. Exp. Bot* 52, 1145–1164. doi: 10.1093/jexbot/52.359.1145

Mohamed, H. I., Latif, H. H., and Hanafy, R. S. (2016). Influence of nitric oxide application on some biochemical aspects, endogenous hormones, minerals and phenolic compounds of *Vicia faba* plant grown under arsenic stress. *Gesunde Pflanzen* 68, 99–107. doi: 10.1007/s10343-016-0363-7

Nambara, E., and Marion-Poll, A. (2005). Abscisic acid biosynthesis and catabolism. *Annu. Rev. Plant Biol.* 56, 165–185. doi: 10.1146/annurev.arplant.56.0326040144046

Ng, L. M., Melcher, K., The, B. T., and Xu, H. E. (2014). Abscisic acid perception and signaling: Structural mechanisms and applications. *Acta Pharmacol. Sin.* 35, 567–584. doi: 10.1038/aps.2014.5

Okamoto, M., Tanaka, Y., Abrams, S. R., Kamiya, Y., Seki, M., and Nambara, E. (2009). High humidity induces abscisic acid 8′-hydroxylase in stomata and vasculature to regulate local and systemic abscisic acid responses in *Arabidopsis*. *Plant Physiol.* 149, 825–834. doi: 10.1104/pp.108.130823

Pan, W., You, Y., Shentu, J. L., Weng, Y. N., Wang, S. T., Xu, Q. R., et al. (2020). Abscisic acid (ABA)-importing transporter 1 (AIT1) contributes to the inhibition of Cd accumulation *via* exogenous ABA application in *Arabidopsis*. *J. Hazard Mater* 391:122189. doi: 10.1016/j.jhazmat.2020.122189

Poschenrieder, C., Gunse, B., and Barcelo, J. (1989). Influence of cadmium on water relations, stomatal resistance, and abscisic acid content in expanding bean leaves. *Plant Physiol.* 90, 1365–1371. doi: 10.1104/pp.90.4.1365

Prakash, V., Singh, V. P., Tripathi, D. K., Sharma, S., and Corpas, F. J. (2019). Crosstalk between nitric oxide (NO) and abscisic acid (ABA) signalling molecules in higher plants. *Environ. Exp. Bot.* 161, 41–49. doi: 10.1016/j.envexpbot.2018.10.033

Priest, D. M., Ambrose, S. J., Vaistij, F. E., Elias, L., Higgins, G. S., Ross, A. R., et al. (2006). Use of the glucosyltransferase UGT71B6 to disturb abscisic acid homeostasis in *Arabidopsis thaliana*. *The Plant J.* 46, 492–502. doi: 10.1111/j.1365-313X.2006.02701.x

Proietti, S., Caarl, L., Coolen, S., Van Pelt, J. A., Van Wees, S. C., and Pieterse, C. M. (2018). Genome-wide association study reveals novel players in defense hormone crosstalk in *Arabidopsis*. *Plant Cell Environ.* 41, 2342–2356. doi: 10.1111/pce.13357

Rahman, M. A., Hasegawa, H., Rahman, M. M., Islam, M. N., Miah, M. M., and Tasmen, A. (2007). Effect of arsenic on photosynthesis, growth and yield of five widely cultivated rice (*Oryza sativa* L.) varieties in Bangladesh. *Chemosphere* 67, 1072–1079. doi: 10.1016/j.chemosphere.2006.11.061

Rock, C. D., and Sun, X. (2005). Crosstalk between ABA and auxin signaling pathways in roots of *Arabidopsis thaliana* (L.) Heynh. *Planta* 222, 98–106. doi: 10.1007/s00425-005-1521-9

Rodriguez, P. L. (2016). Abscisic acid catabolism generates phaseic acid, a molecule able to activate a subset of ABA receptors. *Mol. Plant.* 9, 1448–1450. doi: 10.1016/j.molp.2016.09.009

Sadeghipour, O. (2017). Nitric oxide increases Pb tolerance by lowering Pb uptake and translocation as well as phytohormonal changes in cowpea (*Vigna unguiculata* (L.) Walp.). *Sains Malaysiana* 46, 189–195. doi: 10.17576/jms-2017-4602-02

Sah, S. K., Reddy, K. R., and Li, J. (2016). Abscisic acid and abiotic stress tolerance in crop plants. *Front. Plant Sci.* 7:571. doi: 10.3389/fpls.2016.00571

Saha, I., Hasanuzzaman, M., and Adak, M. K. (2021). Abscisic acid priming regulates arsenite toxicity in two contrasting rice (*Oryza sativa* L.) genotypes through differential functioning of sub1A quantitative trait loci. *Environ. Pollut.* 287:117586. doi: 10.1016/j.envpol.2021.117586

Saini, S., Kaur, N., and Pati, P. K. (2021). Phytohormones: Key players in the modulation of heavy metal stress tolerance in plants. *Ecotoxicol. Environ. Saf.* 223:112578. doi: 10.1016/j.ecoenv.2021.112578

Saini, S., Sharma, I., and Pati, P. K. (2015). Versatile roles of brassinosteroid in plants in the context of its homeostasis, signaling and crosstalks. *Front. Plant Sci.* 6:950. doi: 10.3389/fpls.2015.00950

Saito, S., Hirai, N., Matsumoto, C., Ohigashi, H., Ohta, D., Sakata, K., et al. (2004). Arabidopsis CYP707A s encode (+)-abscisic acid 8′-hydroxylase, a key enzyme in the oxidative catabolism of abscisic acid. *Plant Physiol.* 134, 1439–1449. doi: 10.1104/pp.103.037614

Saradadevi, R., Bramley, H., Palta, J. A., and Siddique, K. H. M. (2016). Stomatal behaviour under terminal drought affects post-anthesis water use in wheat. *Funct. Plant Biol.* 44, 279–289. doi: 10.1071/FP16078

Saradadevi, R., Bramley, H., Siddique, K. H. M., Edwards, E., and Palta, J. A. (2014). Reprint of "Contrasting stomatal regulation and leaf ABA concentrations in wheat genotypes when split root systems were exposed to terminal drought". *Field Crops Res.* 165, 5–14. doi: 10.1016/j.fcr.2014.02.004

Saradadevi, R., Palta, J. A., and Siddique, K. H. M. (2017). ABA-mediated stomatal response in regulating water use during the development of terminal drought in wheat. *Front. Plant Sci.* 8:1251. doi: 10.3389/fpls.2017.01251

Schwartz, S. H., and Zeevaart, J. A. (2010). *Abscisic acid biosynthesis and metabolism. In Plant hormones*. Dordrecht: Springer, 137–155.

Seo, M., and Koshiba, T. (2002). Complex regulation of ABA biosynthesis in plants. *Trends Plant Sci.* 7, 41–48. doi: 10.1016/s1360-1385(01)02187-2

Seo, M., and Marion-Poll, A. (2019). "Abscisic acid metabolism and transport," in *Advances in Botanical Research*, Vol. 92, (Cambridge, MA: Academic Press), doi: 10.1046/j.1365-313x.2000.00812.x

Seo, M., Peeters, A. J., Koiwai, H., Oritani, T., Marion-Poll, A., Zeevaart, J. A., et al. (2000). The *Arabidopsis* aldehyde oxidase 3 (AAO3) gene product catalyzes the final step in abscisic acid biosynthesis in leaves. *Proc. Natl. Acad. Sci. U.S.A.* 97, 12908–12913. doi: 10.1073/pnas.22042697

Shah, S. H., Islam, S., and Mohammad, F. (2022). Sulphur as a dynamic mineral element for plants: A review. *J. Soil Sci. Plant Nutr.* 22, 1–26. doi: 10.1007/s42729-022-00798-9

Shah, S. H., Islam, S., Parrey, Z. A., and Mohammad, F. (2021). Role of exogenously applied plant growth regulators in growth and development of edible oilseed crops under variable environmental conditions: A review. *J. Soil Sci. Plant Nutr.* 21, 1–25. doi: 10.1007/s42729-021-00606-w

Shahid, M., Khalid, S., Abbas, G., Shahid, N., Nadeem, M., Sabir, M., et al. (2015). *Heavy metal stress and crop productivity. In crop production and global environmental issues*. Cham: Springer, 1–25. doi: 10.1007/978-3-319-23162-4_1

Shakirova, F. M., Allagulova, C. R., Maslennikova, D. R., Klyuchnikova, E. O., Avalbaev, A. M., and Bezrukova, M. V. (2016). Salicylic acid-induced protection against cadmium toxicity in wheat plants. *Environ. Exp. Bot.* 122, 19–28. doi: 10.1016/j.envexpbot.2015.08.002

Sheetal, K. R., Singh, S. D., Anand, A., and Prasad, S. (2016). Heavy metal accumulation and effects on growth, biomass and physiological processes in mustard. *Indian J. Plant Physiol.* 21, 219–223. doi: 10.1007/s40502-016-0221-8

Shen, G., Niu, J., and Deng, Z. (2017). Abscisic acid treatment alleviates cadmium toxicity in purple flowering stalk (*Brassica campestris* L. ssp. *chinensis* var. *purpurea* Hort.) seedlings. *Plant Physiol. Biochem.* 118, 471–478. doi: 10.1016/j.plaphy.2017.07.018

Shi, W. G., Liu, W., Yu, W., Zhang, Y., Ding, S., Li, H., et al. (2019). Abscisic acid enhances lead translocation from the roots to the leaves and alleviates its toxicity in *Populus× canescens*. *J. Hazard. Mater.* 362, 275–285. doi: 10.1016/j.jhazmat.2018.09.024

Shimizu, T., Kanno, Y., Suzuki, H., Watanabe, S., and Seo, M. (2021). Arabidopsis NPF4. 6 and NPF5. 1 control leaf stomatal aperture by regulating abscisic acid transport. *Genes* 12:885. doi: 10.3390/genes12060885

Shu, J., He, Q., Zheng, H., Liao, M. A., Kuang, N., and Huang, Z. (2021). Abscisic acid improves the ability of accumulator plant *Perilla frutescens* to perform phytoremediation in cadmium-contaminated soils. *Int. J. Environ. Anal. Chem* 18, 1–10. doi: 10.1080/03067319.2021.1890058

Shu, K., Zhou, W., Chen, F., Luo, X., and Yang, W. (2018). Abscisic acid and gibberellins antagonistically mediate plant development and abiotic stress responses. *Front. Plant Sci.* 9:416. doi: 10.3389/fpls.2018.00416

Signorelli, S., and Considine, M. J. (2018). Nitric oxide enables germination by a four-pronged attack on ABA-induced seed dormancy. *Front. Plant Sci.* 9:296. doi: 10.3389/fpls.2018.00296

Singh, A. D., Sharma, P., Kohli, S. K., Kumar, P., Singh, R., Arora, P., et al. (2020). "Role of plant growth regulators (PGRs) in mitigation of heavy metal phytotoxicity in plants," in *Cellular and molecular phytotoxicity of heavy metals*, (Cham: Springer), 263–304. doi: 10.1007/978-3-030-45975-8_14

Sirko, A., Wawrzyńska, A., Brzywczy, J., and Sieńko, M. (2021). Control of ABA signaling and crosstalk with other hormones by the selective degradation of pathway components. *Int. J. Mol. Sci.* 22:4638. doi: 10.3390/ijms22094638

Song, C., Yan, Y., Rosado, A., Zhang, Z., and Castellarin, S. D. (2019). ABA alleviates uptake and accumulation of zinc in grapevine (*Vitis vinifera* L.) by inducing expression of ZIP and detoxification-related genes. *Front. Plant Sci* 10:872. doi: 10.3389/fpls.2019.00872

Stroiński, A., Giżewska, K., and Zielezińska, M. (2013). Abscisic acid is required in transduction of cadmium signal to potato roots. *Biol. Plant.* 57, 121–127. doi: 10.1007/s10535-012-0135-x

Sun, J., and Li, C. (2014). "Cross talk of signaling pathways between ABA and other phytohormones," in *Abscisic acid: Metabolism, transport and signaling*, (Dordrecht: Springer), 243–253.

Sunita, K., Lokesh, B., Anita, D., Swarna, S., and Suneja, A. (2015). Effect of cadmium on growth, nitrogen metabolism, photosynthesis and yield of soybean. *Int. J. Trop. Agric.* 33, 993–1001.

Taiz, L., Zeiger, E., Møller, I. M., and Murphy, A. (2015). *Plant physiology and development*, No. Ed. 6 Edn. Sunderland: Sinauer Associates Incorporated.

Tan, B. C., Joseph, L. M., Deng, W. T., Liu, L., Li, Q. B., Cline, K., et al. (2003). Molecular characterization of the *Arabidopsis* 9-cis epoxy carotenoid dioxygenase gene family. *Plant J.* 35, 44–56. doi: 10.1046/j.1365-313X.2003.01786.x

Tang, Y., Wang, L., Xie, Y., Yu, X., Li, H., Lin, L., et al. (2020). Effects of exogenous abscisic acid on the growth and cadmium accumulation of lettuce under cadmium-stress conditions. *Int. J. Environ. Anal. Chem.* 100, 720–731. doi: 10.1080/03067319.2019.1639686

Tao, Q., Jupa, R., Dong, Q., Yang, X., Liu, Y., Li, B., et al. (2021). Abscisic acid-mediated modifications in water transport continuum are involved in cadmium hyperaccumulation in *Sedum alfredii*. *Chemosphere.* 268:129339. doi: 10.1016/j.chemosphere.2020.129339

Tao, Q., Jupa, R., Liu, Y., Luo, J., Li, J., Kováč, J., et al. (2019). Abscisic acid-mediated modifications of radial apoplastic transport pathway play a key role in cadmium uptake in hyperaccumulator *Sedum alfredii*. *Plant Cell Environ.* 42, 1425–1440. doi: 10.1111/pce.13506

Tran, L. S. P., Urao, T., Qin, F., Maruyama, K., Kakimoto, T., Shinozaki, K., et al. (2007). Functional analysis of AHK1/ATHK1 and cytokinin receptor histidine kinases in response to abscisic acid, drought, and salt stress in *Arabidopsis*. *Proc. Natl. Acad. Sci. U.S.A.* 104, 20623–20628. doi: 10.1073/pnas.0706547105

Ubeda-Tomás, S., Swarup, R., Coates, J., Swarup, K., Laplaze, L., Beemster, G. T., et al. (2008). Root growth in *Arabidopsis* requires gibberellin/DELLA signalling in the endodermis. *Nat. Cell Biol.* 10, 625–628. doi: 10.1038/ncb1726

Vimala, Y. (1985). Change in the activity of certain enzyme during natural and induced loss of seed viability. *J. Indian Bot. Soc.* 63, 61b–68b.

Vishwakarma, K., Upadhyay, N., Kumar, N., Yadav, G., Singh, J., Mishra, R. K., et al. (2017). Abscisic acid signaling and abiotic stress tolerance in plants: A review on current knowledge and future prospects. *Front. Plant Sci.* 8:161. doi: 10.3389/fpls.2017.00161

Wang, J., Lin, L., Luo, L., Liao, M. A., Lv, X., Wang, Z., et al. (2016). The effects of abscisic acid (ABA) addition on cadmium accumulation of two ecotypes of *Solanum photeinocarpum*. *Environ. Monit. Assess.* 188, 1–8. doi: 10.1007/s10661-016-5194-6

Wang, L., Hua, D., He, J., Duan, Y., Chen, Z., Hong, X., et al. (2011). Auxin Response Factor2 (ARF2) and its regulated homeodomain gene HB33 mediate abscisic acid response in *Arabidopsis*. *PLoS Genet.* 7:e1002172. doi: 10.1371/journal.pgen.1002172

Wang, Y., Li, L., Ye, T., Lu, Y., Chen, X., and Wu, Y. (2013). The inhibitory effect of ABA on floral transition is mediated by ABI5 in *Arabidopsis*. *J. Exp. Bot.* 64, 675–684. doi: 10.1093/jxb/ers361

Wani, P. A., Khan, M. S., and Zaidi, A. (2007). Impact of heavy metal toxicity on plant growth, symbiosis, seed yield and nitrogen and metal uptake in chickpea. *Aust. J. Exp. Agric.* 47, 712–720. doi: 10.1071/EA05369

Werner, T., Köllmer, I., Bartrina, I., Holst, and Schmülling, T. (2006). New insights into the biology of cytokinin degradation. *Plant Biol.* 8, 371–381. doi: 10.1055/s-2006-923928

White, C. N., Proebsting, W. M., Hedden, P., and Rivin, C. J. (2000). Gibberellins and seed development in maize. I. Evidence that gibberellin/abscisic acid balance governs germination versus maturation pathways. *Plant Physiol.* 122, 1081–1088. doi: 10.1104/pp.122.4.1081

Wu, M., Wu, J., and Gan, Y. (2020). The new insight of auxin functions: Transition from seed dormancy to germination and floral opening in plants. *Plant Growth Regul.* 91, 169–174. doi: 10.1007/s10725-020-00608-1

Wu, S., Hu, C., Tan, Q., Zhao, X., Xu, S., Xia, Y., et al. (2018). Nitric oxide acts downstream of abscisic acid in molybdenum-induced oxidative tolerance in wheat. *Plant Cell Rep.* 37, 599–610. doi: 10.1007/s00299-018-2254-0

Wyszkowski, M., and Radziemska, M. (2010). Effects of chromium (III and VI) on spring barley and maize biomass yield and content of nitrogenous compounds. *J Toxicol Environ Health.* 73, 1274–1282. doi: 10.1080/15287394.2010.492016

Xiong, L., and Zhu, J. K. (2003). Regulation of abscisic acid biosynthesis. *Plant Physiol.* 133, 29–36. doi: 10.1104/pp.103.025395

Xu, W., Jia, L., Shi, W., Liang, J., Zhou, F., Li, Q., et al. (2013). Abscisic acid accumulation modulates auxin transport in the root tip to enhance proton secretion for maintaining root growth under moderate water stress. *New Phytol.* 197, 139–150. doi: 10.1111/nph.12004

Xu, Z. Y., Lee, K. H., Dong, T., Jeong, J. C., Jin, J. B., Kanno, Y., et al. (2012). A vacuolar β-glucosidase homolog that possesses glucose-conjugated abscisic acid hydrolyzing activity plays an important role in osmotic stress responses in *Arabidopsis*. *Plant Cell* 24, 2184–2199. doi: 10.1105/tpc.112.095935

Xu, Z., Ge, Y., Zhang, W., Zhao, Y., and Yang, G. (2018). The walnut JrVHAG1 gene is involved in cadmium stress response through ABA-signal pathway and MYB transcription regulation. *BMC Plant Biol.* 18:1–13. doi: 10.1186/s12870-018-1231-7

Yang, X., Bai, Y., Shang, J., Xin, R., and Tang, W. (2016). The antagonistic regulation of abscisic acid-inhibited root growth by brassinosteroids is partially mediated *via* direct suppression of abscisic acid insensitive 5 expression by brassinazole resistant 1. *Plant Cell Environ.* 39, 1994–2003. doi: 10.1111/pce.12763

Ye, Y., Zhou, L., Liu, X., Liu, H., Li, D., Cao, M., et al. (2017). A novel chemical inhibitor of ABA signaling targets all ABA receptors. *Plant Physiol.* 173, 2356–2369. doi: 10.1104/pp.16.01862

Yildirim, E., Ekinci, M., Turan, M., Güleray, A., Selda, ÖR. S., Dursun, A., et al. (2019). Impact of cadmium and lead heavy metal stress on plant growth and physiology of rocket (*Eruca sativa* L.). *Kahramanmaraş Sütçü Ýmam Üniversitesi Tarım ve Doğa Dergisi* 22, 843–850. doi: 10.18016/ksutarimdoga.vi.548626

Yoshida, T., Mogami, J., and Yamaguchi-Shinozaki, K. (2014). ABA-dependent and ABA-independent signaling in response to osmotic stress in plants. *Curr. Opin. Plant Biol.* 21, 133–139. doi: 10.1016/j.pbi.2014.07.009

Yuan, K., Rashotte, A. M., and Wysocka-Diller, J. W. (2011). ABA and GA signaling pathways interact and regulate seed germination and seedling development under salt stress. *Acta Physiol. Plant.* 33, 261–271. doi: 10.1007/s11738-010-0542-6

Zengin, F. K., and Kirbag, S. (2007). Effects of copper on chlorophyll, proline, protein and abscisic acid level of sunflower (*Helianthus annuus* L.) seedlings. *J Environ. Biol.* 28:561.

Zhang, H., Han, W., De Smet, I., Talboys, P., Loya, R., Hassan, A., et al. (2010). ABA promotes quiescence of the quiescent center and suppresses stem cell differentiation in the *Arabidopsis* primary root meristem. *Plant J.* 64, 764–774. doi: 10.1111/j.1365-313X.2010.04367.x

Zhang, H., Zhu, H., Pan, Y., Yu, Y., Luan, S., and Li, L. (2014). A DTX/MATE-type transporter facilitates abscisic acid efflux and modulates ABA sensitivity and drought tolerance in *Arabidopsis*. *Mol. Plant.* 7, 1522–1532. doi: 10.1093/mp/ssu063

Zhang, S., Cai, Z., and Wang, X. (2009). The primary signaling outputs of brassinosteroids are regulated by abscisic acid signaling. *Proc. Natl. Acad. Sci. U.S.A.* 106, 4543–4548. doi: 10.1073/pnas.0900349106

Zhang, Y., Tan, J., Guo, Z., Lu, S., He, S., Shu, W., et al. (2009). Increased abscisic acid levels in transgenic tobacco over-expressing 9 cis-epoxycarotenoid dioxygenase influence H2O2 and NO production and antioxidant defenses. *Plant Cell Environ.* 32, 509–519. doi: 10.1111/j.1365-3040.2009.01945.x

Zhao, H., Guan, J., Liang, Q., Zhang, X., Hu, H., and Zhang, J. (2021). Effects of cadmium stress on growth and physiological characteristics of sassafras seedlings. *Sci. Rep.* 11, 1–11. doi: 10.1038/s41598-021-89322-0

Zheng, C., Acheampong, A. K., Shi, Z., Mugzech, A., Halaly-Basha, T., Shaya, F., et al. (2018). Abscisic acid catabolism enhances dormancy release of grapevine buds. *Plant Cell Environ.* 41, 2490–2503. doi: 10.1111/pce.13371

Zhu, G., Liu, Y., Ye, N., Liu, R., and Zhang, J. (2011). Involvement of the abscisic acid catabolic gene CYP707A2 in the glucose-induced delay in seed germination and post-germination growth of *Arabidopsis*. *Physiol. Plant* 143, 375–384. doi: 10.1111/j.1399-3054.2011.01510.x

frontiers | Frontiers in Plant Science

TYPE Original Research
PUBLISHED 21 September 2022
DOI 10.3389/fpls.2022.946475

Check for updates

OPEN ACCESS

EDITED BY
Bhaskar Gupta,
Government General Degree College, Singur, India

REVIEWED BY
Juan F. Jimenez,
Instituto Potosino de Investigación Científica y Tecnológica (IPICYT), Mexico
Bing Zhang,
Yangzhou University, China

*CORRESPONDENCE
Feng Liu
liufengrich@126.com
Xiongze Dai
xiongzedai@126.com

SPECIALTY SECTION
This article was submitted to Plant Abiotic Stress, a section of the journal Frontiers in Plant Science

RECEIVED 17 May 2022
ACCEPTED 08 August 2022
PUBLISHED 21 September 2022

CITATION
Tang B, Li X, Zhang X, Yin Q, Xie L, Zou X, Liu F and Dai X (2022) Transcriptome data reveal gene clusters and key genes in pepper response to heat shock.
Front. Plant Sci. 13:946475.
doi: 10.3389/fpls.2022.946475

COPYRIGHT
© 2022 Tang, Li, Zhang, Yin, Xie, Zou, Liu and Dai. This is an open-access article distributed under the terms of the Creative Commons Attribution License (CC BY). The use, distribution or reproduction in other forums is permitted, provided the original author(s) and the copyright owner(s) are credited and that the original publication in this journal is cited, in accordance with accepted academic practice. No use, distribution or reproduction is permitted which does not comply with these terms.

Transcriptome data reveal gene clusters and key genes in pepper response to heat shock

Bingqian Tang[1,2,3,4], Xiumin Li[2], Xinhao Zhang[1], Qinbiao Yin[1], LingLing Xie[4], Xuexiao Zou[1,2,3,4], Feng Liu[1,2,3,4]* and Xiongze Dai[1,3,4]*

[1]College of Horticulture, Hunan Agricultural University, Changsha, China, [2]Longping Branch, Graduate School of Hunan University, Changsha, China, [3]ERC for Germplasm Innovation and New Variety, Breeding of Horticultural Crops, Changsha, China, [4]Key Laboratory for Vegetable Biology of Hunan Province, Changsha, China

Climate change and global warming pose a great threat to plant growth and development as well as crop productivity. To better study the genome-wide gene expression under heat, we performed a time-course (0.5 to 24 h) transcriptome analysis in the leaf and root of 40-day-old pepper plants under 40°C as well as in control plants. Clustering analysis (K-means) showed that the expression of 29,249 genes can be grouped into 12 clusters with distinct expression dynamics under stress. Gene ontology (GO) enrichment analysis and transcription factor (TF) identification were performed on the clusters with certain expression patterns. Comparative analysis between the heat-treated and control plants also identified differentially expressed genes (DEGs), which showed the largest degree of change at 24 h. Interestingly, more DEGs were identified in the root than in the leaf. Moreover, we analyzed the gene expression of 25 heat shock factor genes (HSFs) in pepper after heat stress, identified five of these HSFs that responded to heat stress, and characterized the role of these genes in heat-tolerant (17CL30) and heat-susceptible (05S180) pepper lines. The findings of this study improve our understanding of the genome-wide heat stress response in pepper.

KEYWORDS

pepper, heat stress, gene expression, heat shock factors (HSFs), clustering analysis

Abbreviations: HSFs, heat shock factors; HS, heat stress; h, hours; CaHSFs, capsicum annuum heat shock factors; DEGs, differentially expressed genes; HSPs, heat shock proteins; HSR, heat shock response; GO, gene ontology; BP, biological process; MF, molecular function; KEGG, Kyoto encyclopedia of genes and genomes; FC, fold change; FDR, false discovery rate; FPKM, fragments per kilobase million; HPT, hours post-treatment; TPM, transcripts per million; HCL, hierarchical clustering; PCA, principal component analysis; TFs, transcription factors; ER, endoplasmic reticulum.

Introduction

Global climate change makes extreme weather more frequent, presenting ever-increasing environmental stress on plants. Such stress dysregulates the normal growth and development in plants and is a major threatening factor for food safety (Fedoroff et al., 2010; Zhu, 2016; Jagadish et al., 2021). Among them, high-temperature stress is a significant challenge facing plants because an increase of 10–15°C in temperature would threaten the survival of plants (Lipiec et al., 2013). Indeed, heat stress has a significant negative impact on the growth and productivity of plants by inhibiting multiple biological processes such as photosynthesis, absorption of minerals, pollination, and seed germination of seeds (Nayyar et al., 2013; Bahuguna et al., 2016; Ali et al., 2019). To have a better understanding of how plant adapts to heat stress (HS), and to facilitate the process of breeding for heat tolerance, it is important to investigate the molecular mechanisms underlying the phenotypic changes when the plant was under HS treatment. The mechanism of plant sensing and subsequently responding to HS, and the complex transcriptional regulatory network involved in the sense and response processes have been widely studied (Ohama et al., 2017; Zhang et al., 2022). Recently, studies in rice have revealed for the first time that complex quantitative trait loci controlled HS resistance. Following *TT1* (Li et al., 2015) and *TT2* (Kan et al., 2022), a new rice HS resistance locus *TT3* was identified and the two constituent genes, *TT3.1* and *TT3.2*, were isolated and cloned. The ubiquitin ligase activity of TT3.1 induces the degradation of TT3.2, a chloroplast precursor protein that triggers chloroplast damage in the context of heat stress. Thus, these two genes interact antagonistically to enhance HS tolerance in rice (Zhang et al., 2022).

Plants have evolved a series of adaptive mechanisms to cope with long-term heat stress (Baurle, 2016). Heat stress activates heat shock factors (HSFs), and HSFs play critical roles in regulating the expression of heat-responsive genes (Tong et al., 2022), which further induce the expression of heat shock proteins (HSPs) to mediate the heat shock response (HSR) (Hu et al., 2009). Previous studies had shown that HSFs are the core components for effective protection against heat (Xue et al., 2014), but through gene transcription while HSPs are responsible for protein folding, assembly, translocation, and degradation (Molinier et al., 2006). As the terminal components of signal transduction, HSFs mediate the gene expression networks to various abiotic stresses (Nover et al., 2001; Scharf et al., 2012; Guo et al., 2016). Some studies in wheat have shown that Hsf may have the function of regulating wheat to cope with multiple stresses (Duan et al., 2019). Recent studies have shown that the wheat *TaHsfA2-13* plays an important role in responding to a variety of abiotic stresses and phytohormones (Meng et al., 2022). Related studies on the identification of *HsfA2* in tomato and pepper (Guo et al., 2014a, 2015; Fragkostefanakis et al., 2016). In addition, genes such as *CaHSP70-1* (Guo et al., 2014b), *CaHSP25.9* (Feng et al., 2019), and *CaHSP22.0* (Sun et al., 2019) were identified in pepper, which have positive regulatory effects on improving the high-temperature resistance of pepper.

Capsicum annuum L. is native to the tropical regions of Central and South America with an optimum growth temperature of 18 to 30°C (Olatunji and Afolayan, 2018). However, it is not heat-resistant as exposure to high temperature (above 32°C), leading to multiple heat stress symptoms such as abortion of the pollen, decrease in the number of flower and fruit, and reduction in pepper yield. Therefore, global warming and high temperature in summer could be detrimental to pepper yield and quality (Lee et al., 2018). It is critical to understand the molecular mechanisms underlying heat responses for selective breeding of heat-tolerant plants. To this end, a previous study assessed heat tolerance in pepper germplasms and identified a heat-tolerant variety (17CL30) and a heat-susceptible variety (05S180) (Wang et al., 2019). Furthermore, the authors profiled the metabolome and transcriptome of 17CL30 and 05S180 under normal conditions and high-temperature stress and identified HSR as an important heat-resistant mechanism. This study highlighted the importance of omics in understanding the molecular mechanisms of heat responses. In addition, it also provided a rich data source to mine key genes regulating homeostasis under heat. However, the previous study is limited in that single time point of leaf samples in heat-resistant and heat-susceptible varieties were used. Thus, it is necessary to profile the time-course gene expression of multiple tissues in normal pepper plants.

In this study, 40-day-old hydroponic pepper plants were subjected to 40°C heat. A time-course comparative transcriptomics analysis was performed using both leaf and root samples (Liu et al., 2017). Thus, a gene regulatory network under heat stress in pepper was constructed. Both time-dependent and tissue-dependent differentially expressed genes (DEGs) under heat stress were identified. Gene ontology (GO) analysis and Kyoto Encyclopedia of Genes and Genomes (KEGG) pathway enrichment analysis of these DEGs revealed important mechanisms underlying the heat response in pepper. Using K-means clustering, pepper genes expressed in response to HS on the genome-wide level were grouped into clusters based on similar biological functions or similar regulation. This facilitated the identification of co-functional genes, including transcription factors, which are downstream elements of signal transduction and play an indispensable role in the regulation of plant genes in response to abiotic stresses. We analyzed the transcription factors included in clusters 2 and 6, which were more clearly responsive to HS. In addition, we identified *CaTT3.1*, the ortholog of the rice HS-responsive gene *TT3.1* (Zhang et al., 2022), from cluster 2 and found that the expression of this gene was significantly upregulated after pepper was exposed to HS for 6 h. In addition, the expression profiles of HSF genes and their responses to heat in pepper were further determined.

Materials and methods

Plant materials and data sources

Total RNA from different pepper tissues was prepared as described previously (Liu et al., 2017). An elite breeding line of *C. annuum*, the inbred line "6421" (hereafter referred to as line 6421), was selected from a pepper landrace (long and red in phenotype) widely grown on the west side of Xiang Jiang River, Hunan Province, China.

The seedlings were grown at 25/18°C day/night temperature, and with a 16/8 light/dark cycle, relative humidity of 60–70%, and light intensity of 6000 Lux. For heat treatment, the seedlings were transferred into a growth chamber of 42°C, and the illumination, photoperiod, and relative humidity were kept the same as plants without the heat treatment. Leaf and root tissues were collected from both treated and control plants at 0.5, 1, 3, 6, 12, and 24 h post-treatment (HPT). Considering the effect of the circadian clock on plant gene expression, samples were collected at 8:30, 9:00, 11:00, 14:00, and 20:00 on the first day and 8:00 on the next day. A total of 24 samples (six time points for two types of tissue: leaf and root) were collected. Each sample had three biological repeats, and each repeat consisted of leaf or root tissues from five randomly selected seedlings. For each sample, averaged data from the three biological repeats were shown.

Measurements of the conductivity and the contents of chlorophylls, reactive oxygen species, and proline

The contents of chlorophylls, reactive oxygen species (ROS), and proline and the conductivity were measured in the leaf samples at 0, 6, 12, and 24 HPT. The contents of proline, ROS, and chlorophylls were measured by the methods described in Bates et al. (1973), Zhang et al. (2008), and Kim and Xue (2020), respectively. For the conductivity measurement, air in the intercellular space of pepper leaves was extracted using a vacuum dryer and an aspirator, and then, the leaves were hydrated by soaking in water. The conductivity of the solution was measured with a conductivity meter. All the above-mentioned measurements were conducted with three biological repeats for each sample.

Differential gene expression analysis

Quality control of the dataset was performed using fastp (Chen et al., 2018) and FastQC v0.11.7 (Andrews, 2017). Next, the data were aligned to the reference genome of pepper (Zunla genome) (Qin et al., 2014). Mapping was performed using HISAT 2.2.1 with default parameters (10 mismatches/read; nine multi-mapping locations/read) (Kim et al., 2015). The abundance of a transcript was measured as the mean normalized count of reads mapping onto the transcript (Love et al., 2014). The genome index was generated using the gene annotation file (gff file).

Differential gene expression analysis was carried out using DESeq2 v1.20.0, an R-based package available from Bioconductor (Love et al., 2014). The abundance of transcripts was used to identify DEGs between two conditions. The ratio of mean normalized counts between two conditions was log-transformed [log fold change, or log2(FC)]. Up- or downregulated DEGs were defined using the following criteria: $|\log2(FC)| \geq 2$ and adjusted p-value < 0.01. A statistical test was performed using the negative binomial Wald test followed by a Benjamini-Hochberg correction to obtain the adjusted p-value or false discovery rate (FDR). Venn diagrams were created as described (Lin et al., 2016). Heatmaps were generated using Python (seaborn heatmap). Summary statistics on the sequencing data are provided in **Supplementary Table 1**. DEGs identified in the leaf and root at each time point are available in **Supplementary Table 6**.

Clustering and gene enrichment analyses

Clustering analysis was performed on 12 control and 12 heat-treated samples using the k-means method in Python (**Supplementary Table 2**; Gasch and Eisen, 2002). For each gene, the normalized expression was calculated by dividing the expression levels from all samples with its maximum observed transcripts per million (TPM). Hierarchical clustering (HCL) and principal component analysis (PCA) were performed using the kernel PCA method in Python with default settings. Identified clusters responsive to heat stress were further subjected to gene enrichment with GOATOOLS (Klopfenstein et al., 2018) and a Python package for GO analysis. Statistically significant GO terms were defined using FDR < 0.05. The KEGG pathway analysis was performed by KofamKOALA (Aramaki et al., 2020), and enrichment analysis was carried out using R package clusterProfiler (Yu et al., 2012).

Identification of heat shock factor genes

The HSF domain was used for searching homologous genes in the tomato and pepper genomes. In total, 26 and 25 HSF genes were identified in tomato and pepper, respectively. For the identification of transcription factors (TFs), the iTAK database and associated rules were used[1] (Zheng et al., 2016). Final

1 http://itak.feilab.net/cgi-bin/itak/index.cgi

validation of potential HSFs was performed by comparing the list to that in the PlantTFcat (Dai et al., 2013) and PlnTFDB (Perez-Rodriguez et al., 2010).

Phylogenetic and homologous alignment analysis

The proteome databases for Lycopersicon esculentum (ITAG3.2) and C. annuum L. (Zunla) were downloaded from NCBI.[2] Protein sequences from the primary transcripts were used for the construction of orthogroups between the two species using OrthoMCL.[3] Multiple sequence alignment of Capsicum and Arabidopsis genes was conducted using MUSCLE (Multiple Protein Sequence Alignment) under Linux. Phylogenetic trees were constructed using Tree Best software with the contiguous algorithm (Edgar, 2004) and illustrated using the online tool iTOL (Interactive Tree Of Life)[4] (Letunic and Bork, 2016).

The gene *CaTT3.1*, orthologous to the rice gene *TT3.1*, was identified by homologous alignment of protein sequences of the two genes, followed by comparing their motifs predicted by MEME (Buske et al., 2010).[5]

cDNA generation and quantitative/real-time PCR analysis

The total RNA was isolated from the leaf of capsicum "6421" using RNAiso Plus reagent (TaKaRa) at 0, 6, 12, and 24 h after 42°C heat stress and treated with RNase-free DNase I (Promega) and HiScript II 1st Strand cDNA Synthesis kit (Vazyme). qPCR was performed using LightCycler 96 (Roche) with the SYBR Green Premix Ex Taq^{TM} II quantitative PCR system (TaKaRa, Dalian, China). The primers of *CaUBI3* and ten genes are listed in **Supplementary Table 12**. The ΔCT method was used to calculate the relative expression levels of these genes (Tang et al., 2021) based on the following equation: ΔCT = [Gene expression–mean (*CaUBI3* expression)]/3.

Results

Transcriptomics analysis of pepper plants under heat stress

To study heat stress responses in pepper at the transcript level, a time-course transcriptome analysis of both leaf and root tissues in pepper plants was performed and the normalized gene expression profiles were shown (**Figure 1A**). Sample data including all biological replicates are recorded in **Supplementary Table 1**. As expected, the overall expression showed a tissue-dependent pattern, as revealed by both Pearson's correlation analysis (**Figure 1A**) and PCA (principal components analysis) (**Figure 1B**). Interestingly, samples with shorter exposure to heat (0.5 to 3 h) were clustered together with the control, while samples under longer exposure (6 to 24 h) clustered together, indicating significant changes in gene expression after 6 h of treatment. By contrast, transcriptomics reprogramming was observed as early as 1 h after treatment, indicating a faster response in roots compared to that in leaves following heat treatment. Moreover, a drastic change in gene expression was observed even at 24 HPT. Thus, these data suggest heat significantly induces transcriptomics reprogramming in both leaves and roots with different levels of dynamics.

We conducted phenotypic examination and measurement of physiological parameters, including level of conductivity and contents of chlorophylls, ROS, and proline in the seedlings of the pepper line 6421 after heat treatment at 42°C for 0, 6, 12, and 24 h (**Figure 2**). No macroscopic wilting was found on pepper leaves at all the investigated time points (**Figure 2A**). In contrast, the measured physiological parameters were significantly changed after HS, compared to the 0-h control. At 24 HPT, the content of chlorophyll A in leaves decreased significantly, albeit chlorophyll B and total chlorophyll did not change (**Figure 2B**). Both the ROS content and the conductivity level increased significantly at 24 HPT ($P < 0.01$) (**Figure 2C,D**). Proline content started to increase significantly at 6 HPT ($P < 0.05$) and the increasing continued at 12 ($P < 0.001$) and 24 HPT ($P < 0.01$) (**Figure 2E**).

Tissue-dependent clustering analysis reveals distinct gene expression patterns under heat

Based on the expression of 29,249 genes, the k-means clustering algorithm was used to further understand the dynamic patterns of gene expression modulation under heat, which revealed 12 distinctive clusters (**Figure 3** and **Supplementary Table 2**). Among them, the solid lines (HS-treated leaf or root) of clusters 2, 6, 7, 10, and 12 were higher than the corresponding dotted lines, indicating that these clusters contained genes upregulated by HS at the investigated time points. On the contrary, in clusters 1, 3, 5, 8, and 9, the solid line was lower than the dashed line, indicating that these clusters contain genes downregulated by HS at the investigated time points. For example, 1,881 genes in cluster 2 showed much higher expression levels in roots at 6 and 24 HPT compared to those in control. A similar trend was found for cluster 6 genes

2 https://www.ncbi.nlm.nih.gov/
3 https://orthomcl.org/orthomcl/
4 https://itol.embl.de/
5 https://meme-suite.org/meme/tools/meme

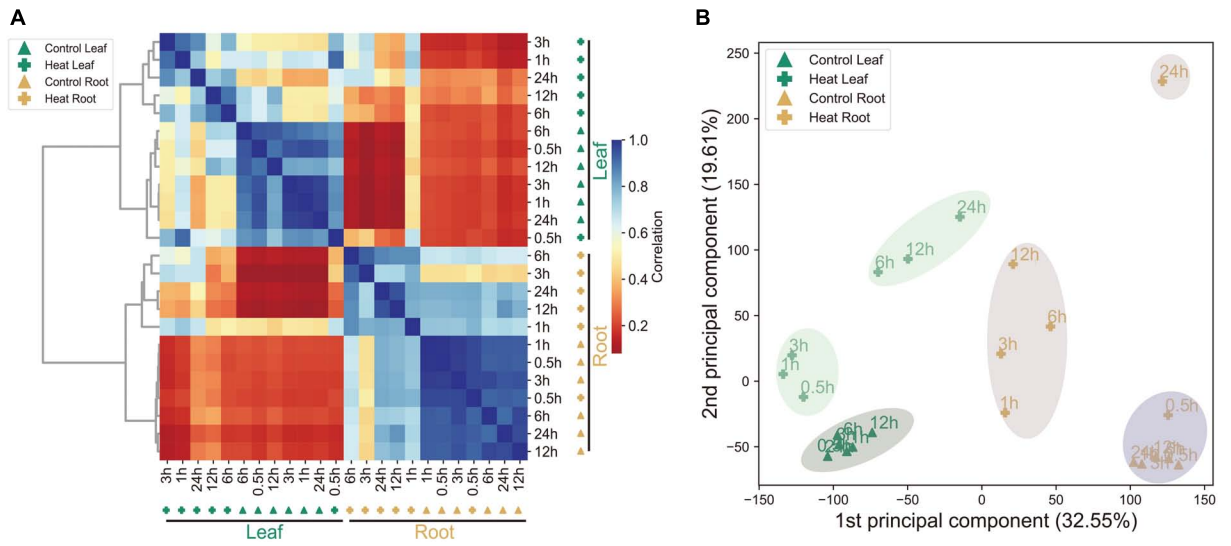


FIGURE 1
Summary of the transcriptomics data. **(A)** Hierarchical clustering analysis of 35,336 genes from 24 samples. Color scale represents Pearson's correlation coefficient (0–1). **(B)** PCA of the leaf and root transcriptomes from the control and heat-treated samples.

in the leaf. On the contrary, genes in clusters 3 and 9 (leaf) and cluster 8 (both leaf and root) showed reduced expression following heat treatment. Thus, our dataset provides rich information on the heat-inducible gene expression dynamics, which can be used to understand the molecular mechanisms by which pepper responds to heat.

According to the clustering situation in Figure 3, we further performed gene enrichment analysis on the genes in clusters 2 and 6 and found that the GO terms in cluster 2 (Figure 4A) were mainly enriched in ethylene binding, ethylene receptor activity, alkene binding, molecular transducer activity, ligase activity, and signaling receptor activity; and the GO terms in cluster 6 are mainly in response to toxic substance and herbicide, oxidoreductase activity (Figure 4B). In both clusters 2 and 6, the expression level in roots and leaves 6 h after heat stress was higher than that in untreated ones, among which cluster 2 was increased in both leaves and roots, while cluster 6 was only increased in leaves, so these two genes in each cluster have different expression patterns. Finally, 114 and 84 transcription factors were identified in cluster 2 (1881 genes) and cluster 6 (1688 genes), respectively, and their distributions are shown in Figure 4C (Cluster 2) and Figure 4D (Cluster 6). The most identified transcription factor family was the MYB family, with 16 and 10 MYB family members identified, respectively. A recent study suggested that the rice gene *TT3.1* might be a potential thermosensor (Zhang et al., 2022). In this study, comparing the protein sequences of *TT3.1* and its pepper ortholog *CaTT3.1* identified five large segments of motif conservation (Motif 1-5 in Figure 4E). *CaTT3.1* was clustered in the Cluster 2, in which all genes were significantly upregulated in roots and leaves at 6 HPT and thereafter. These results suggested that *CaTT3.1* is related to the HS response and may be functional in pepper as the counterpart of *TT3.1* in rice. However, study on functional verification of *CaTT3.1* is yet to be conducted.

Identification of differentially expressed genes under heat stress

Next, we identified DEGs under heat stress (24 h at 42°C) by a comparative analysis, which revealed 7,318 DEGs in the leaf (3,490 and 3,828 for up- and downregulated, respectively) and 7,271 DEGs in the root (3,791 and 3,480 for up- and downregulated, respectively). While a small fraction of genes showed opposite trends in regulation at different time points after treatment (73 in the leaf and 150 in the root), the majority of DEGs showed the same trend across the time course. Collectively, 9,981 DEGs were identified from either tissue type, constituting ~34.1% of all expressed genes in the dataset. The comparative analysis also revealed several trends in transcriptional reprogramming under heat in pepper plants. First, the largest degree of gene expression changes in both leaves and roots occurred at 24 HPT (1,834 and 2,577 up- and downregulated DEGs, respectively, in the leaf; and 2,389 and 2,911 up- and downregulated DEGs, respectively, in the root, Figure 5). The distribution of upregulated and downregulated DEGs identified in the leaves and roots in each cluster is shown in Table 1, and the results of the distribution corresponding to the trend map are shown in Figure 3. The observation that the number of DEGs increase as the treatment time increases indicates a time-dependent traditional reprogramming. In

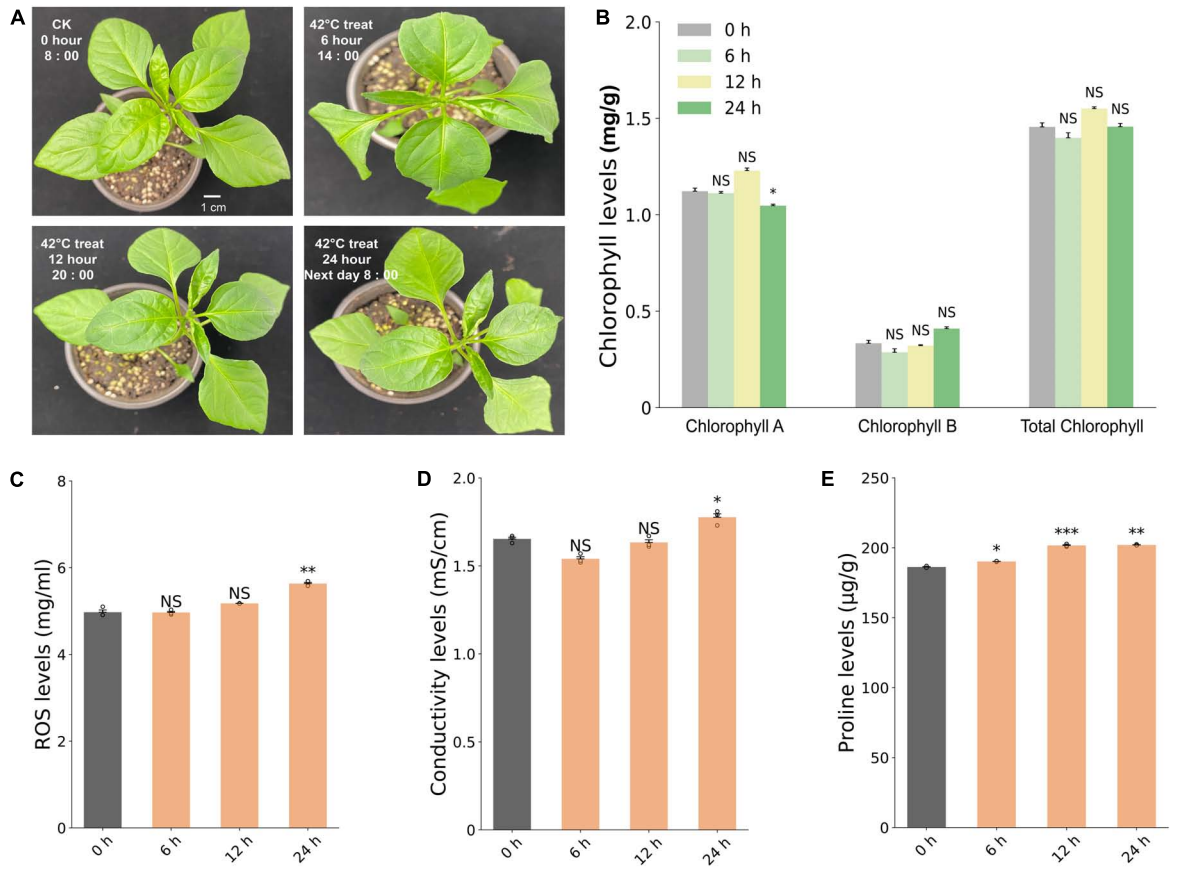


FIGURE 2
Phenotypic and physiological responses of pepper line 6421 under 42°C heat stress. **(A)** Seedlings of control (0 h) and heat (6, 12, and 24 h at 42°C) treatments. Changes in the content of chlorophyll including chlorophyll A, chlorophyll B, and total chlorophylls **(B)**, the content of ROS **(C)**, conductivity **(D)**, and the content of proline **(E)**. Student's *t*-test was conducted to compare each heat treatment time point with the 0-h control treatment. Stars indicate significance with one, two, and three stars representing significance at $*P < 0.05$, $**P < 0.01$, and $***P < 0.001$, respectively. NS: no significant difference. Error bar represents the standard deviation of each mean ($n = 3$).

addition, most DEGs at 24 HPT were time-dependent as they were uniquely differential-expressed at this time point (750 and 946 up- and downregulated DEGs, respectively, in the leaf; and 1,432 and 1,447 up- and downregulated DEGs, respectively, in the root). More DEGs in the root compared to the leaf at 24 HPT also indicate that the root responds more strongly to heat stress.

Heat shock factor enrichment analysis

Gene ontology analysis was performed to functionally annotate the DEGs in the leaf (Figures 6A,B) and root (Figures 6A,B) and the overlapping patterns (Figure 6C). In the leaf, upregulated DEGs were involved in cellular responses to various stimuli including heat and ethylene binding (Figure 6A), while downregulated DEGs were overrepresented in metabolic processes such as polysaccharide metabolic process, cell wall organization or biogenesis, regulation of cell cycle, and photosynthesis I/II. This is in line with the fact that high temperature activates a subset of genes in the leaf to regulate heat stress response and inhibits general metabolism by downregulating metabolism-regulated genes (Saibo et al., 2009). Since there were more DEGs identified in roots than in leaves, there were more GO terms identified in the root. Upregulated DEGs in the root were enriched in cellular components related to photosynthesis (chloroplast, membrane, photosystem I/II, thylakoid lumen, plastid thylakoid, and chloroplast thylakoid; Figure 7A). Downregulated DEGs were enriched in biological processes, such as "hydrogen peroxide catabolic process," "reactive oxygen species metabolic process," "phenylpropanoid metabolic process," "polysaccharide metabolic process," and "secondary metabolic process" (Figure 7B).

To further explore on which pathways the up- and downregulated DEGs identified were mainly enriched, we compared the upregulated DEGs (Figures 8A,B) and the upregulated DEGs KEGG pathway analysis was performed on downregulated DEGs (Figures 8C,D), and we found that the number of pathways enriched in downregulated DEGs

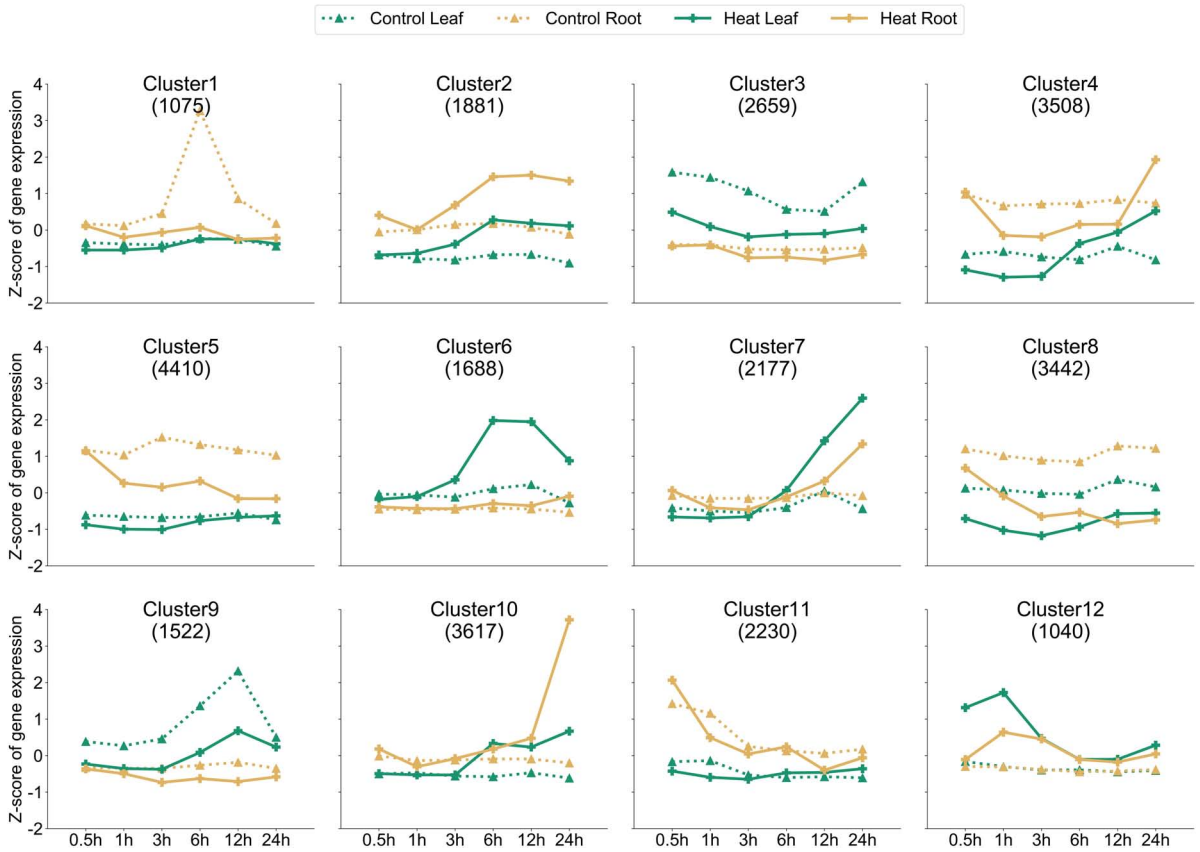


FIGURE 3
Dynamic gene expression. Twelve clusters (by k-means clustering) with different numbers of genes (shown under the cluster identification) are shown. The *x*-axis depicts six time points, and the *y*-axis depicts the standardized Z-score per gene. Dotted and solids lines (green for the leaf and orange for the root) denote the control and treated samples, respectively.

(**Figures 8C,D**) was much higher than that in upregulated DEGs (**Figures 8A,B**). The upregulated DEGs in leaves are enriched in the "MAPK signaling pathway," which has been shown in previous studies to be closely related to plant response to stress (Jagodzik et al., 2018). The downregulated DEGs in leaves were enriched in some key metabolic pathways, such as "phenylpropanoid biosynthesis," "starch and sucrose metabolism," "amino sugar and nucleotide sugar metabolism," "glyoxylate and dicarboxylate metabolism," and "flavonoid biosynthesis." The specific pathways enriched in root DEGs were "flavonoid biosynthesis" and "brassinosteroid biosynthesis" and other important metabolite pathways.

Phylogeny of the heat shock factor gene family and expression of capsicum annuum heat shock factors

Heat shock factors play a key role in plant heat stress (Scharf et al., 2012) and have also been identified at the genome-wide level in pepper (Guo et al., 2015) and tomato (Yang et al., 2016), but seldom systematically the study of HSFs genes in pepper after heat stress. Our datasets can comprehensively analyze the expression of CaHsfs in pepper of 42°C heat stress at six time points. A phylogenetic tree was constructed to understand the evolutionary relationship among these genes, which were grouped into eight subfamilies (**Figure 9A**). Interestingly, the expression levels of six CaHSFs (*CaHSF3*, *CaHSF8*, *CaHSF10*, and *CaHSF24* in the leaf; *CaHSF11* and *CaHSF18* in both tissues) were significantly higher in the heat-treated samples compared to control, indicating that heat may activate the expression of these HSFs in pepper (**Figure 9B** and **Supplementary Table 11**).

To validate these findings, we further analyzed data from a previous study in which the expression of HSFs was assessed in a heat-resistant variety (17CL30; RCK and RT for control and heat treatment, respectively) and a heat-susceptible variety (05S180; SCK and ST for control and heat treatment, respectively) (Wang et al., 2019). In both varieties, three HSFs (*CaHSF4*, *CaHSF9*, and *CaHSF22*) showed higher levels of expression at 28 h of heat treatment at 40°C compared to those in control (**Figure 10A**), indicating that they could play a role in heat tolerance. By

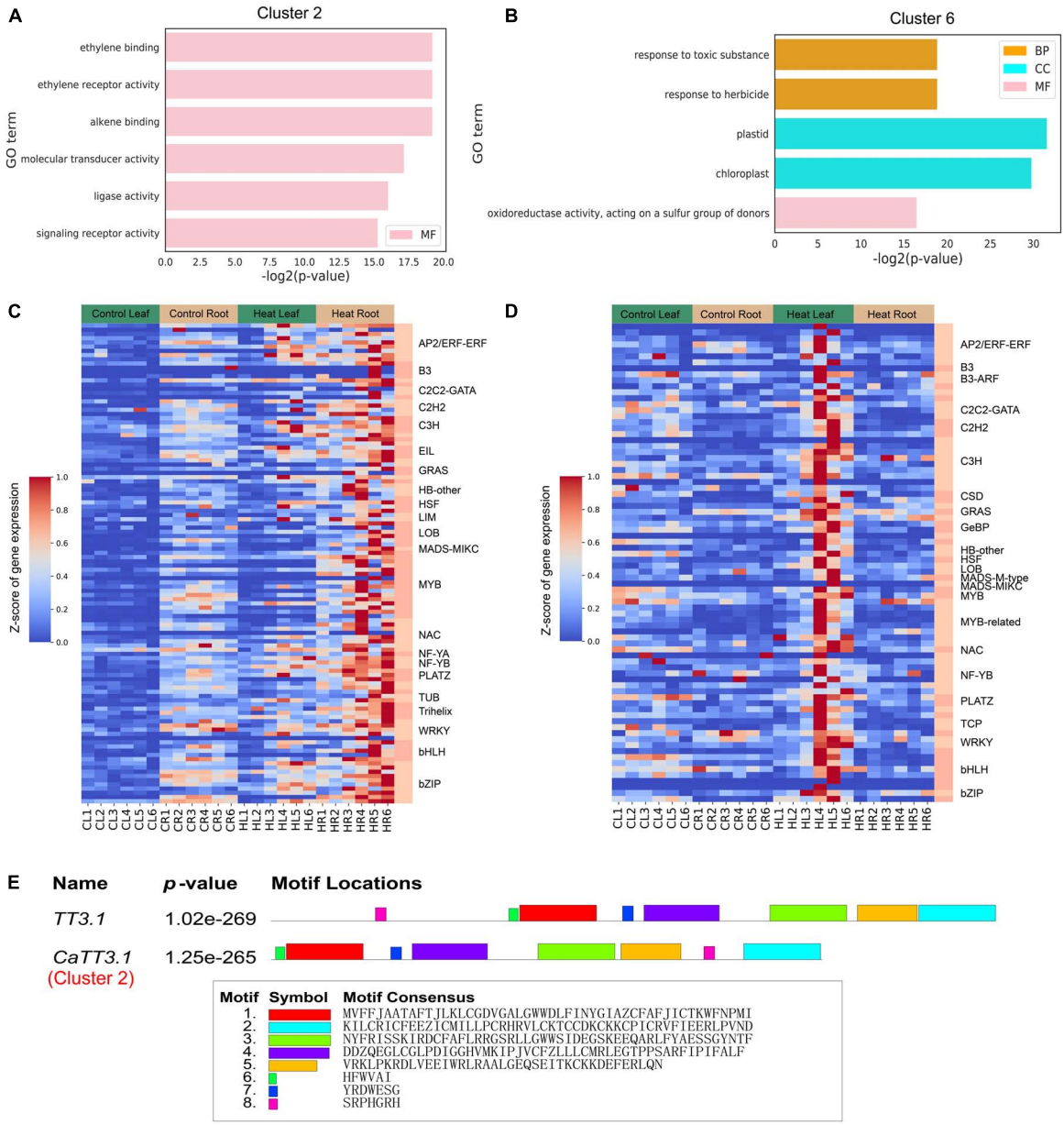


FIGURE 4
Gene ontology (GO) and heat-responsive transcriptional modulators of Cluster 2 and 6. **(A,B)** GO enrichment results in cluster 2(A) and cluster 6(B). GO terms with FDR < 0.01 are shown. CC, cellular component; MF, molecular function; BP, biological process. The full lists of DEGs and GO terms can be found in **Supplementary Tables 3, 4**. **(C,D)** Distribution and expression of transcription factors identified in cluster 2(C) and cluster 6(D). **(E)** Alignment of *TT3.1* and *CaTT3.1* protein sequences. The conserved motifs are highlighted and listed.

contrast, *CaHSF3* and *CaHSF11* showed opposite expression trends following heat treatment (**Figure 10B**). To verify the accuracy of the RNA-Seq data and the reproducibility of gene expression patterns, the five CaHSFs (**Figures 10A,B**) and five randomly selected DEGs from the GO term of "response to heat" (**Figure 6A**) were analyzed by qRT-PCR, with *CaUBI3* as the housekeeping gene control. The results indicated that the gene expression profiles produced by RNA-Seq and qRT-PCR were in good agreement, with Pearson's correlation coefficient in the range of 0.62–0.98 among the ten genes. These results confirmed that RNA-Seq in this study produced reliable data on the pepper gene expression profiling.

Discussion

Understanding the dynamic processes of gene regulation at the genome-wide level when plant is under HS, and

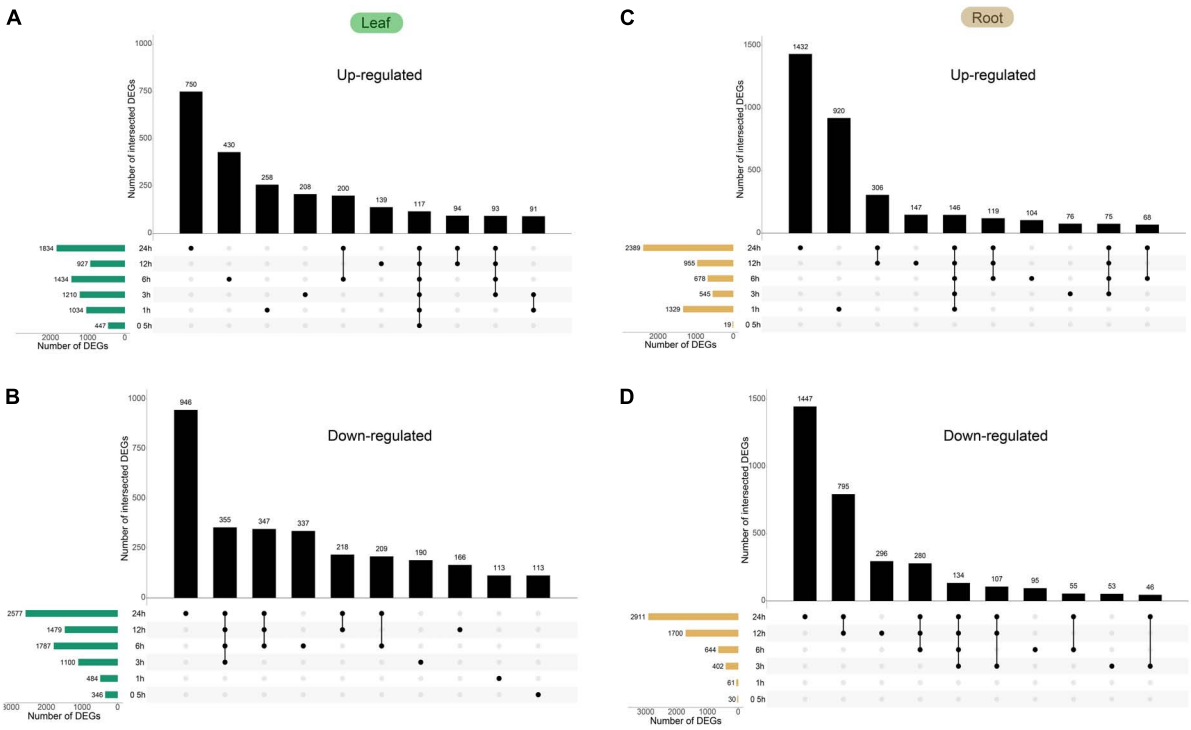


FIGURE 5
Time-course transcriptomics analysis of Capsicum annuum L. under heat. Plants were subjected to 42°C treatment for the indicated time. The total numbers of significant genes at each time point are shown on the left. **(A)** Upregulated genes in the leaf. **(B)** Downregulated genes in the leaf. **(C)** Upregulated genes in the root. **(D)** Downregulated genes in the root. All the DEGs in roots and leaves are shown in **Supplementary Table 5**.

TABLE 1 Distribution of DEGs among different clusters.

	Cluster												
	1	2	3	4	5	6	7	8	9	10	11	12	
Genes	1075	1881	2659	3508	4410	1688	2177	3442	1522	3617	2230	1040	Number
Leaf Up-regulated DEGs	89	517	8	230	164	355	418	2	21	1101	179	406	3490
Leaf Down-regulated DEGs	112	11	1006	88	674	20	21	1351	327	18	191	19	3838
Root Up-regulated DEGs	6	386	679	36	5	345	277	1	124	1493	95	344	3791
Root Down-regulated DEGs	241	3	535	14	980	32	8	1213	241	2	192	19	3480

identification of key candidate genes that may play important roles in such processes have been the core areas of research. In this study, we performed RNA-seq analysis in both the leaf and root of pepper plants under heat stress at six time points (0.5 to 24 h) and found 12 gene clusters based on the expression profile (**Figure 3**). In addition, to eliminate the differences in gene expression due to the factors related to circadian clock [i.e., genes may express differentially in day and night (Yu, 2018; Creux and Harmer, 2019)], a set of plants without heat treatment was prepared, from which samples were collected as control at each time point. Furthermore, we selected clusters 2 and 6 from these 12 clusters and performed GO analysis on the genes in these clusters, respectively, and found that they were involved in ethylene binding, molecular transducer activity, ligase activity, signaling receptor activity, response to toxic substances, and oxidoreductase activity, showed obvious enrichment in these GO terms (**Figures 4A,B**), and a total of 198 transcription factors were identified from these two clusters, of which MYB type transcription factors were the most, with 25, while six HSF transcription factors were also identified. The expression patterns of the transcription factors identified in these two clusters are consistent with the dynamic expression of clusters 2 and 6 in **Figure 3**, and the response to heat stress is obvious.

Comparative analysis also revealed that the most drastic gene expression changes occurred at 24 HPT following heat stress in both tissues, although the response in root was earlier

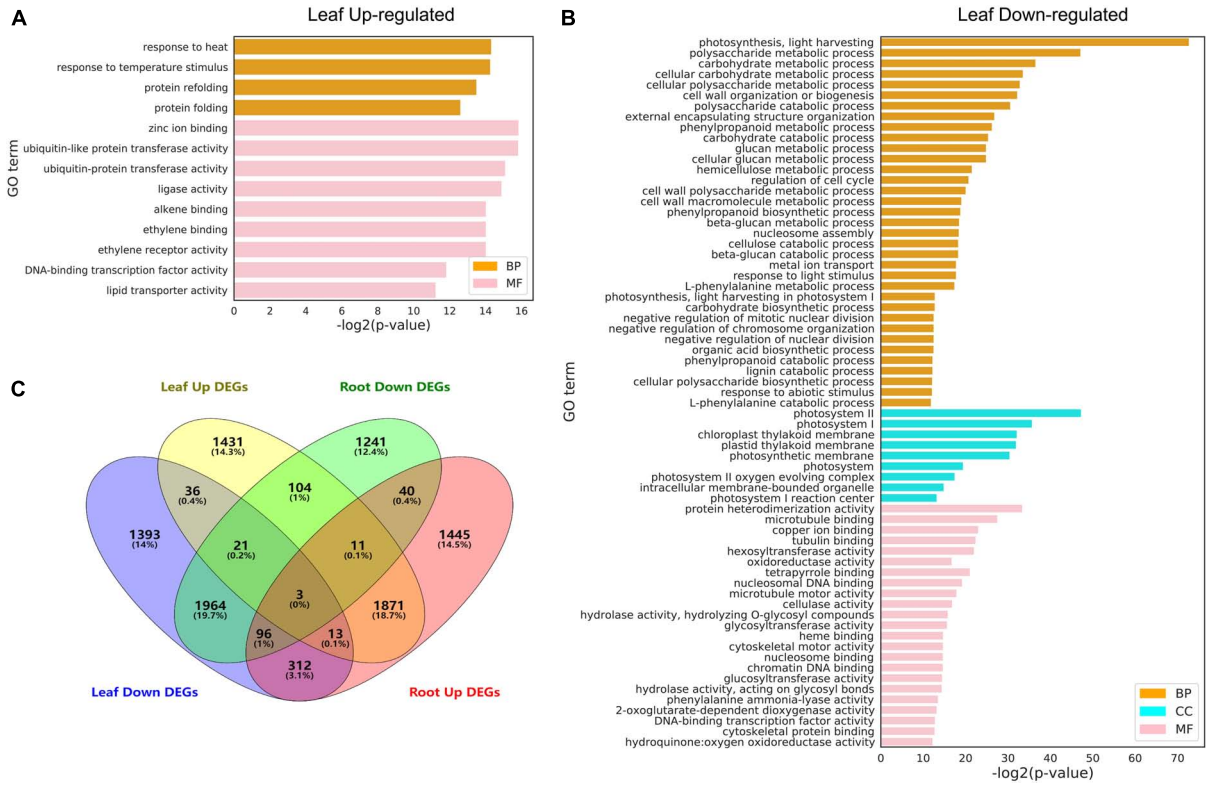


FIGURE 6
Gene ontology (GO) analysis of differentially expressed genes (DEGs) under heat stress. **(A)** Upregulated DEGs in the leaf. **(B)** Downregulated DEGs in the leaf. **(C)** Venn diagrams showing DEGs in the leaf and root. GO terms with FDR < 0.01 are shown. The full lists of DEGs and GO terms can be found in **Supplementary Tables 6, 7**.

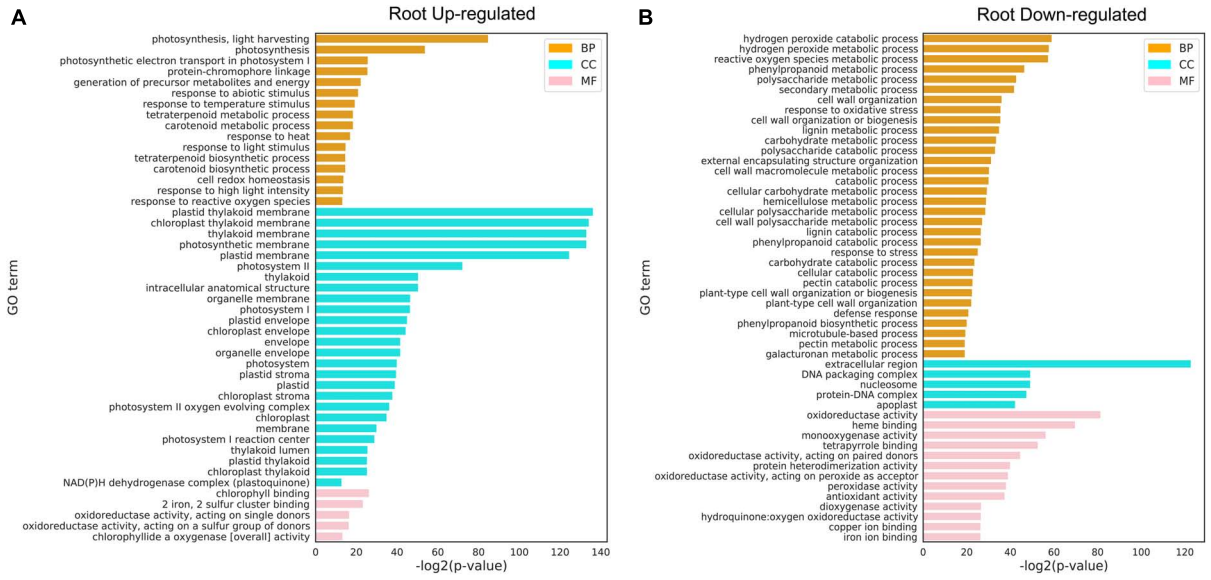


FIGURE 7
Gene Q20 ontology (GO) analysis of differentially expressed genes (DEGs) under heat stress. **(A)** Upregulated DEGs in the root. **(B)** Downregulated DEGs in the root. GO terms with FDR < 0.01 are shown. CC: cellular component; MF: molecular function; BP: biological process. The full lists of DEGs and GO terms can be found in **Supplementary Tables 8, 9**.

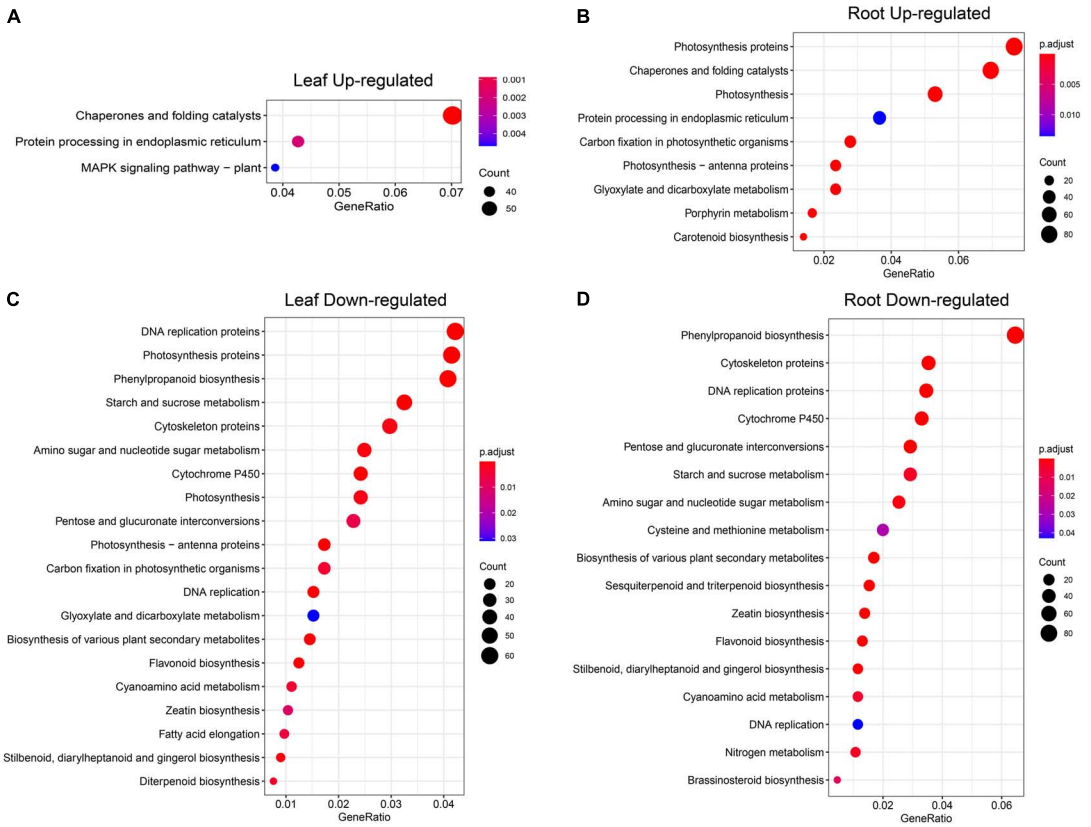


FIGURE 8
KEGG pathway analysis of DEGs under heat stress. **(A)** Upregulated DEGs in the leaf. **(B)** Upregulated DEGs in the root. **(C)** Downregulated DEGs in the leaf. **(D)** Downregulated DEGs in the root. The full lists of pathway result in **Supplementary Table 10**.

in time and stronger in magnitude (**Figure 5**). Thus, our data provide important insights for follow-up mechanistic studies to understand the signal transduction events during stress responses in pepper.

Time-course transcriptome analysis also grouped these genes into 12 clusters, in which the expression of each gene was clearly presented (**Supplementary Table 2**), and is divided them into different clusters by the difference in the dynamic expression pattern of each gene, which can more clearly show how many different dynamic expression conditions are presented in leaf and root at the whole gene level in pepper under heat stress. Furthermore, through the GO enrichment analysis of cluster 2 and cluster 6, which obviously responded to heat stress, it was found that 1,881 genes in cluster 2 were mainly enriched in terms of molecular function type (**Figure 4A**) and were mainly enriched in "ethylene binding" and "ethylene receptor activity," the expression of genes with cluster 2 expression pattern began to increase 3 h after heat stress in pepper, reached a peak at 6 h, and maintained higher levels of gene expression than control tissues, while ethylene is an important plant hormone that regulates multiple developmental and physiological processes throughout the life cycle of plants (Wang et al., 2006), while genes within cluster 2 may be effects on ethylene binding and signaling following heat stress, and transcription factors identified in cluster 2 (**Figure 4C**) may be involved in these functions. Interestingly, an ortholog of the potential rice thermoreceptor *TT3.1* (Zhang et al., 2022) was found in the cluster 2. This gene was named *CaTT3.1*, and its protein sequence is highly conserved with that of *TT3.1* (**Figure 4E**). At 3 HPT, *CaTT3.1* was significantly upregulated. It is speculated that *CaTT3.1*, as its counterpart in rice, carries the function of high-temperature sensing in peppers, which may be important for subsequent initiation of heat resistance responses and alleviation of heat damage. Clusters 2 and 6 may contain other genes related to high-temperature response. However, since the gene clusters we have constructed predicted gene functions based on gene expression trends rather than functional studies, the real functions of these genes are yet to be further experimentally confirmed.

Furthermore, GO analysis revealed that DEGs are enriched in heat response and other fundamental biological processes such as photosynthesis, redox regulation, and sugar metabolism. Further KEGG pathway analysis was performed on the upregulated and downregulated DEGs identified in **Figure 5**

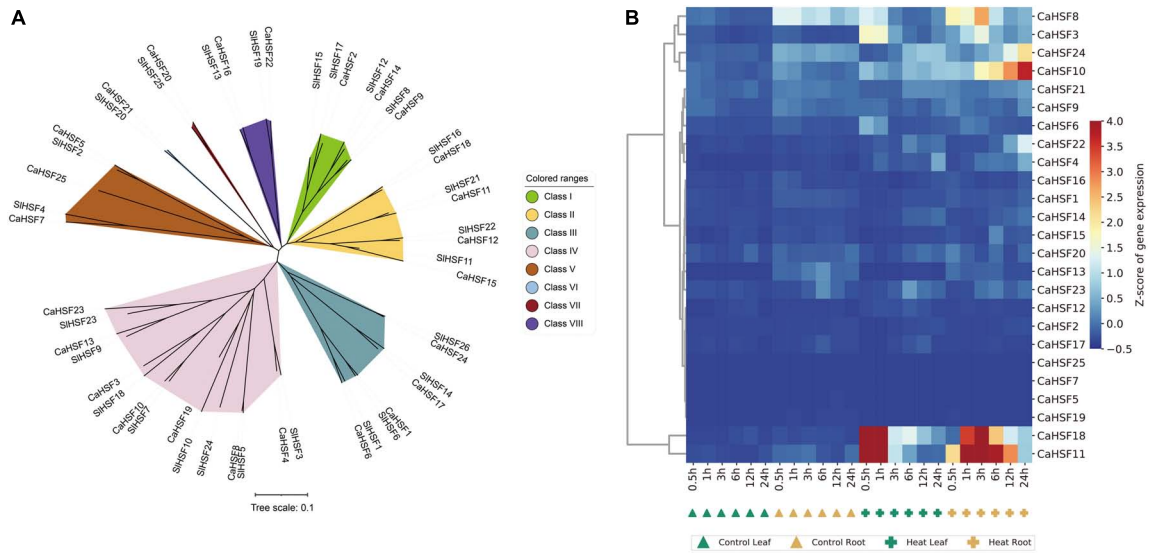


FIGURE 9
Phylogeny and gene expression of HSFs. **(A)** Phylogenetic analysis of tomato and pepper HSF proteins shows that they can be grouped into eight classes. **(B)** Heatmap showing the temporospatial expression of CaHSFs.

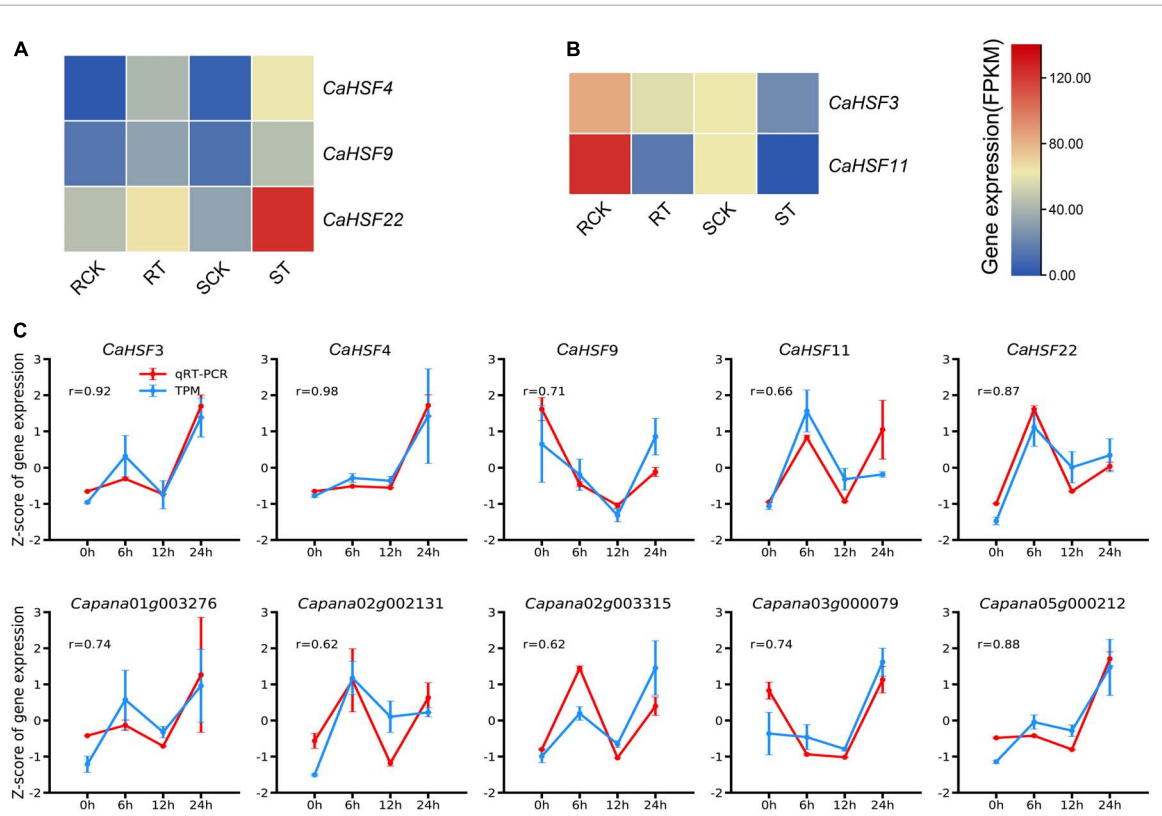


FIGURE 10
Expression of selected key genes in different pepper varieties. **(A,B)** Expression of *CaHSFs* in heat-tolerant variety 17CL30 and heat-susceptible variety 05S180 after treated at 40°C for 28 h. RCK: control 17CL30; RT: treated 17CL30; SCK: control 05S180; ST: treated 05S180. **(C)** RNA-Seq and qRT-PCR data of the expression profiles of ten selected genes in pepper line 6421 leaves after treated at 42°C for 0, 6, 12, and 24 h. Error bars represent the standard deviation ($n = 3$). r = Pearson's(r) correlation coefficient to describe the correlation between normalized expression values measured by RNA-Seq and qRT-PCR (normalized relative to *CaUBI3*).

in leaf and root (six time points), and it was found that the upregulated genes were enriched with unique "MAPK signaling pathway," "chaperones and folding catalysts," "protein processing in endoplasmic reticulum," "porphyrin metabolism," and "carotenoid biosynthesis," these results indicate that the expression of these genes is upregulated after heat stress treatment, which may make these pathways active in pepper, thereby responding to heat stress excited. Among them, studies have shown that mitogen-activated protein kinase (MAPK) modules play critical roles in the transduction of environmental and developmental signals (Jagodzik et al., 2018). A lot of studies in plants have described the role of endoplasmic reticulum (ER) stress signaling and UPR in regulation of HSFs and HSPs (Hayashi et al., 2012; Mittler et al., 2012; Sandhu et al., 2021). We found that upregulated DEGs in leaf and root (**Figures 8A,B**) were all enriched in the pathway "Protein processing in endoplasmic reticulum," which suggests that the expression of genes related to protein processing in the endoplasmic reticulum is significantly upregulated when pepper is subjected to heat stress, which may be involved in the process of pepper's response to heat stress. Furthermore, leaf genes clustered in the GO term "photosynthesis, light harvesting" were downregulated (**Figure 6A**). In contrast, root genes clustered in the term were upregulated (**Figure 7A**). These results indicated that photosynthesis genes in leaves and roots were regulated by HS differently. Understanding the effects of HS on the fate and functionality of chloroplast is particularly important because photosynthesis is usually inhibited by HS before other cellular functions are influenced (Zhang et al., 2010; Ning et al., 2021). Thus, our dataset provided a rich source for follow-up studies on gene regulatory networks under heat in plants.

Interactions between HSFs and HSPs play a key role in regulating adaptation to heat in plants (Driedonks et al., 2015). As the HSR is highly conserved (Richter et al., 2010; Meyer and Baker, 2011; Mittler et al., 2012), HSFs had been identified and analyzed in many plants (Guo et al., 2016). Here, we identified CaHSFs in the Zunla_1 genome (Qin et al., 2014). We found that the expression of multiple CaHSFs (*CaHSF3*, *CaHSF8*, *CaHSF10*, *CaHSF11*, *CaHSF18*, and *CaHSF21*) was inducible by heat in pepper plants. The heat responsiveness of HSF genes was further supported by a previous study, in which the expression of these genes can be either activated (*CaHSF4*, *CaHSF9*, and *CaHSF22*) or suppressed (*CaHSF3* and *CaHSF11*) by heat (**Figure 10**; Nover et al., 2001). The discrepancy of regulation in *CaHSF3* and *CaHSF11* could be attributed to differences in the genetic background of varieties used in these studies, as an elite breeding line of C. annuum (Line, 6421) was used here and 17CL30 and 05S180 (heat-tolerant and heat-susceptible, respectively) were used in the previous study. Nevertheless, the role of HSFs in heat stress and other abiotic stress had been established in other plants including tomato (Scharf et al., 1998; Wang et al., 2015; Fragkostefanakis et al., 2016). Thus, our finding on the potential role CaHSFs in mediating heat stress in pepper deserves further investigation.

Conclusion

In summary, we constructed a gene expression network in seedlings of the pepper line 6421 in response to HS and identified genes specifically upregulated in leaves and roots based on K-means analysis of gene expression at the genome-wide level. It is worth emphasizing that the *CaTT3.1* gene, the ortholog of *TT3.1* identified in rice, was captured in Cluster 2, in which all genes showed a significant increase in expression 6 h after heat treatment. In addition to *CaTT3.1*, we also found five CaHSFs whose expression was significantly upregulated after heat treatment. Our study provided important data for better understanding the effect of HS on pepper at a genome-wide level and identified candidate genes that can be potentially used as reference for the subsequent molecular improvement of heat-resistant traits in pepper or other crops.

Data availability statement

The original contributions presented in this study are publicly available. This data can be found here: https://ngdc.cncb.ac.cn/, CRA006985.

Author contributions

LX, XL, XZ, and QY: experiment. BT: data curation. FL, XD, and XZ: funding acquisition. BT: visualization. BT: writing—original draft. BT and FL: writing—review and editing. All authors contributed to the article and approved the submitted version.

Funding

This work was supported by the Laboratory of Lingnan Modern Agriculture Project (NT2021004), Special Funds for Construction of Innovative Provinces in Hunan Province (2021NK1006), and Joint Funds of the National Natural Science Foundation of China (Grant No. U21A20230).

Acknowledgments

We would like to thank TopEdit (www.topeditsci.com) for its linguistic assistance during the preparation of this manuscript.

Conflict of interest

The authors declare that the research was conducted in the absence of any commercial or financial relationships that could be construed as a potential conflict of interest.

Publisher's note

All claims expressed in this article are solely those of the authors and do not necessarily represent those of their affiliated organizations, or those of the publisher, the editors and the reviewers. Any product that may be evaluated in this article, or claim that may be made by its manufacturer, is not guaranteed or endorsed by the publisher.

Supplementary material

The Supplementary Material for this article can be found online at: https://www.frontiersin.org/articles/10.3389/fpls.2022.946475/full#supplementary-material

References

Ali, S., Rizwan, M., Arif, M. S., Ahmad, R., Hasanuzzaman, M., Ali, B., et al. (2019). Approaches in enhancing thermotolerance in plants: an updated review. *J. Plant Growth Regul.* 39, 456–480. doi: 10.1007/s00344-019-09994-x

Andrews, S. (2017). *FastQC: A Quality Control Tool for High Throughput Sequence Data. 2010*. Available online at: https://www.bioinformatics.babraham.ac.uk/projects/fastqc/ (accessed February 21, 2020).

Aramaki, T., Blanc-Mathieu, R., Endo, H., Ohkubo, K., Kanehisa, M., Goto, S., et al. (2020). KofamKOALA: KEGG ortholog assignment based on profile HMM and adaptive score threshold. *Bioinformatics* 36, 2251–2252. doi: 10.1093/bioinformatics/btz859

Bahuguna, R. N., Solis, C. A., Shi, W., and Jagadish, K. S. (2016). Post-flowering night respiration and altered sink activity account for high night temperature-induced grain yield and quality loss in rice (*Oryza sativa* L.). *Physiol. Plant* 159, 59–73. doi: 10.1111/ppl.12485

Bates, L. S., Waldren, R. P., and Teare, I. D. (1973). Rapid determination of free proline for water-stress studies. *Plant Soil* 39, 205–207. doi: 10.1007/BF00018060

Baurle, I. (2016). Plant heat adaptation: priming in response to heat stress. *F1000Res.* 5:F1000FacultyRev–694. doi: 10.12688/f1000research.7526.1

Buske, F. A., Boden, M., Bauer, D. C., and Bailey, T. L. (2010). Assigning roles to DNA regulatory motifs using comparative genomics. *Bioinformatics* 26, 860–866. doi: 10.1093/bioinformatics/btq049

Chen, S., Zhou, Y., Chen, Y., and Gu, J. (2018). fastp: an ultra-fast all-in-one FASTQ preprocessor. *Bioinformatics* 34, i884–i890. doi: 10.1093/bioinformatics/bty560

Creux, N., and Harmer, S. (2019). Circadian rhythms in plants. *Cold Spring Harb. Perspect. Biol.* 11:a034611. doi: 10.1101/cshperspect.a034611

Dai, X., Sinharoy, S., Udvardi, M., and Zhao, P. X. (2013). PlantTFcat: an online plant transcription factor and transcriptional regulator categorization and analysis tool. *BMC Bioinform.* 14:321. doi: 10.1186/1471-2105-14-321

Driedonks, N., Xu, J., Peters, J. L., Park, S., and Rieu, I. (2015). Multi-level interactions between heat shock factors, heat shock proteins, and the redox system regulate acclimation to heat. *Front. Plant Sci.* 6:999. doi: 10.3389/fpls.2015.00999

Duan, S., Liu, B., Zhang, Y., Li, G., and Guo, X. (2019). Genome-wide identification and abiotic stress-responsive pattern of heat shock transcription factor family in *Triticum aestivum* L. *BMC Genomics* 20:257. doi: 10.1186/s12864-019-5617-1

Edgar, R. C. (2004). MUSCLE: multiple sequence alignment with high accuracy and high throughput. *Nucleic Acids Res.* 32, 1792–1797. doi: 10.1093/nar/gkh340

Fedoroff, N. V., Battisti, D. S., Beachy, R. N., Cooper, P. J., Fischhoff, D. A., Hodges, C. N., et al. (2010). Radically rethinking agriculture for the 21st century. *Science* 327, 833–834. doi: 10.1126/science.1186834

Feng, X. H., Zhang, H. X., Ali, M., Gai, W. X., Cheng, G. X., Yu, Q. H., et al. (2019). A small heat shock protein CaHsp25.9 positively regulates heat, salt, and drought stress tolerance in pepper (*Capsicum annuum* L.). *Plant Physiol. Biochem.* 142, 151–162. doi: 10.1016/j.plaphy.2019.07.001

Fragkostefanakis, S., Mesihovic, A., Simm, S., Paupiere, M. J., Hu, Y., Paul, P., et al. (2016). HsfA2 controls the activity of developmentally and stress-regulated heat stress protection mechanisms in tomato male reproductive tissues. *Plant Physiol.* 170, 2461–2477. doi: 10.1104/pp.15.01913

Gasch, A. P., and Eisen, M. B. (2002). Exploring the conditional coregulation of yeast gene expression through fuzzy k-means clustering. *Genome Biol.* 3, 1–22. doi: 10.1186/gb-2002-3-11-research0059

Guo, M., Liu, J. H., Ma, X., Luo, D. X., Gong, Z. H., and Lu, M. H. (2016). The plant heat stress transcription factors (HSFs): structure, regulation, and function in response to abiotic stresses. *Front. Plant Sci.* 7:114. doi: 10.3389/fpls.2016.00114

Guo, M., Lu, J. P., Zhai, Y. F., Chai, W. G., Gong, Z. H., and Lu, M. H. (2015). Genome-wide analysis, expression profile of heat shock factor gene family (CaHsfs) and characterisation of CaHsfA2 in pepper (*Capsicum annuum* L.). *BMC Plant Biol.* 15:151. doi: 10.1186/s12870-015-0512-7

Guo, M., Yin, Y. X., Ji, J. J., Ma, B. P., Lu, M. H., and Gong, Z. H. (2014a). Cloning and expression analysis of heat-shock transcription factor gene CaHsfA2 from pepper (*Capsicum annuum* L.). *Genet. Mol. Res.* 13, 1865–1875. doi: 10.4238/2014.March.17.14

Guo, M., Zhai, Y. F., Lu, J. P., Chai, L., Chai, W. G., Gong, Z. H., et al. (2014b). Characterization of CaHsp70-1, a pepper heat-shock protein gene in response to heat stress and some regulation exogenous substances in *Capsicum annuum* L. *Int. J. Mol. Sci.* 15, 19741–19759. doi: 10.3390/ijms151119741

Hayashi, S., Wakasa, Y., Takahashi, H., Kawakatsu, T., and Takaiwa, F. (2012). Signal transduction by IRE1-mediated splicing of bZIP50 and other stress sensors in the endoplasmic reticulum stress response of rice. *Plant J.* 69, 946–956. doi: 10.1111/j.1365-313X.2011.04844.x

Hu, W., Hu, G., and Han, B. (2009). Genome-wide survey and expression profiling of heat shock proteins and heat shock factors revealed overlapped and stress specific response under abiotic stresses in rice. *Plant Sci.* 176, 583–590. doi: 10.1016/j.plantsci.2009.01.016

Jagadish, S. V. K., Way, D. A., and Sharkey, T. D. (2021). Plant heat stress: concepts directing future research. *Plant Cell Environ.* 44, 1992–2005. doi: 10.1111/pce.14050

Jagodzik, P., Tajdel-Zielinska, M., Ciesla, A., Marczak, M., and Ludwikow, A. (2018). Mitogen-activated protein kinase cascades in plant hormone signaling. *Front. Plant Sci.* 9:1387. doi: 10.3389/fpls.2018.01387

Kan, Y., Mu, X. R., Zhang, H., Gao, J., Shan, J. X., Ye, W. W., et al. (2022). TT2 controls rice thermotolerance through SCT1-dependent alteration of wax biosynthesis. *Nat. Plants* 8, 53–67. doi: 10.1038/s41477-021-01039-0

Kim, H., and Xue, X. (2020). Detection of total reactive oxygen species in adherent cells by 2',7'-dichlorodihydrofluorescein diacetate staining. *J. Vis. Exp.* 23. doi: 10.3791/60682

Kim, D., Langmead, B., and Salzberg, S. L. (2015). HISAT: a fast spliced aligner with low memory requirements. *Nat. Methods* 12, 357–360. doi: 10.1038/nmeth.3317

Klopfenstein, D. V., Zhang, L., Pedersen, B. S., Ramirez, F., Warwick Vesztrocy, A., Naldi, A., et al. (2018). GOATOOLS: a python library for gene ontology analyses. *Sci. Rep.* 8:10872. doi: 10.1038/s41598-018-28948-z

Lee, S. G., Kim, S. K., Lee, H. J., Lee, H. S., and Lee, J. H. (2018). Impact of moderate and extreme climate change scenarios on growth, morphological features, photosynthesis, and fruit production of hot pepper. *Ecol. Evol.* 8, 197–206. doi: 10.1002/ece3.3647

Letunic, I., and Bork, P. (2016). Interactive tree of life (iTOL) v3: an online tool for the display and annotation of phylogenetic and other trees. *Nucleic Acids Res.* 44, W242–W245. doi: 10.1093/nar/gkw290

Li, X. M., Chao, D. Y., Wu, Y., Huang, X., Chen, K., Cui, L. G., et al. (2015). Natural alleles of a proteasome alpha2 subunit gene contribute to thermotolerance and adaptation of African rice. *Nat. Genet.* 47, 827–833. doi: 10.1038/ng.3305

Lin, G., Chai, J., Yuan, S., Mai, C., Cai, L., Murphy, R. W., et al. (2016). VennPainter: a tool for the comparison and identification of candidate genes based on venn diagrams. *PLoS One* 11:e0154315. doi: 10.1371/journal.pone.0154315

Lipiec, J., Doussan, C., Nosalewicz, A., and Kondracka, K. (2013). Effect of drought and heat stresses on plant growth and yield: a review. *Int. Agrophys.* 27, 463–477. doi: 10.2478/intag-2013-0017

Liu, F., Yu, H., Deng, Y., Zheng, J., Liu, M., Ou, L., et al. (2017). PepperHub, an informatics hub for the chili pepper research community. *Mol. Plant* 10, 1129–1132. doi: 10.1016/j.molp.2017.03.005

Love, M. I., Huber, W., and Anders, S. (2014). Moderated estimation of fold change and dispersion for RNA-seq data with DESeq2. *Genome Biol.* 15:550. doi: 10.1186/s13059-014-0550-8

Meng, X., Zhao, B., Li, M., Liu, R., Ren, Q., Li, G., et al. (2022). Characteristics and regulating roles of wheat TaHsfA2-13 in abiotic stresses. *Front. Plant Sci.* 13:922561. doi: 10.3389/fpls.2022.92256

Meyer, A. S., and Baker, T. A. (2011). Proteolysis in the *Escherichia coli* heat shock response: a player at many levels. *Curr. Opin. Microbiol.* 14, 194–199. doi: 10.1016/j.mib.2011.02.001

Mittler, R., Finka, A., and Goloubinoff, P. (2012). How do plants feel the heat? *Trends Biochem. Sci.* 37, 118–125. doi: 10.1016/j.tibs.2011.11.007

Molinier, J., Ries, G., Zipfel, C., and Hohn, B. (2006). Transgeneration memory of stress in plants. *Nature* 442, 1046–1049. doi: 10.1038/nature05022

Nayyar, H., Kaur, R., Kaur, S., and Singh, R. (2013). γ-Aminobutyric acid (GABA) imparts partial protection from heat stress injury to rice seedlings by improving leaf turgor and upregulating osmoprotectants and antioxidants. *J. Plant Growth Regul.* 33, 408–419. doi: 10.1038/srep43609

Ning, G., Yan, X., Chen, H., Dong, R., Zhang, W., Ruan, Y., et al. (2021). Genetic manipulation of Soc1-like genes promotes photosynthesis in flowers and leaves and enhances plant tolerance to high temperature. *Plant Biotechnol. J.* 19, 8–10. doi: 10.1111/pbi.13432

Nover, L., Bharti, K., Döring, P., Mishra, S. K., Ganguli, A., and Scharf, K.-D. (2001). *Arabidopsis* and the heat stress transcription factor world: how many heat stress transcription factors do we need? *Cell Stress Chaperones* 6, 177–189. doi: 10.1379/1466-1268(2001)006<0177:aathst>2.0.co;2

Ohama, N., Sato, H., Shinozaki, K., and Yamaguchi-Shinozaki, K. (2017). Transcriptional regulatory network of plant heat stress response. *Trends Plant Sci.* 22, 53–65. doi: 10.1016/j.tplants.2016.08.015

Olatunji, T. L., and Afolayan, A. J. (2018). The suitability of chili pepper (*Capsicum annuum* L.) for alleviating human micronutrient dietary deficiencies: a review. *Food Sci. Nutr.* 6, 2239–2251. doi: 10.1002/fsn3.790

Perez-Rodriguez, P., Riano-Pachon, D. M., Correa, L. G., Rensing, S. A., Kersten, B., and Mueller-Roeber, B. (2010). PlnTFDB: updated content and new features of the plant transcription factor database. *Nucleic Acids Res.* 38, D822–D827. doi: 10.1093/nar/gkp805

Qin, C., Yu, C., Shen, Y., Fang, X., Chen, L., Min, J., et al. (2014). Whole-genome sequencing of cultivated and wild peppers provides insights into *Capsicum* domestication and specialization. *Proc. Natl. Acad. Sci. U.S.A.* 111, 5135–5140. doi: 10.1073/pnas.1400975111

Richter, K., Haslbeck, M., and Buchner, J. (2010). The heat shock response: life on the verge of death. *Mol. Cell* 40, 253–266. doi: 10.1016/j.molcel.2010.10.006

Saibo, N. J., Lourenco, T., and Oliveira, M. M. (2009). Transcription factors and regulation of photosynthetic and related metabolism under environmental stresses. *Ann. Bot.* 103, 609–623. doi: 10.1093/aob/mcn227

Sandhu, J., Irvin, L., Liu, K., Staswick, P., Zhang, C., and Walia, H. (2021). Endoplasmic reticulum stress pathway mediates the early heat stress response of developing rice seeds. *Plant Cell Environ.* 44, 2604–2624. doi: 10.1111/pce.14103

Scharf, K. D., Berberich, T., Ebersberger, I., and Nover, L. (2012). The plant heat stress transcription factor (Hsf) family: structure, function and evolution. *Biochim. Biophys. Acta* 1819, 104–119. doi: 10.1016/j.bbagrm.2011.10.002

Scharf, K.D, Heider, H., Höhfeld, I., Lyck, R., Schmidt, E., and Nover, L. (1998). The tomato Hsf system: HsfA2 needs interaction with HsfA1 for efficient nuclear import and may be localized in cytoplasmic heat stress granules. *Mol. Cell. Biol.* 18, 2240-2251. doi: 10.1128/MCB.18.4.2240

Sun, J.-T., Cheng, G.-X., Huang, L.-J., Liu, S., Ali, M., Khan, A., et al. (2019). Modified expression of a heat shock protein gene, CaHSP22.0, results in high sensitivity to heat and salt stress in pepper (*Capsicum annuum* L.). *Sci. Hortic.* 249, 364–373. doi: 10.1016/j.scienta.2019.02.008

Tang, B., Xie, L., Li, X., Yang, H., Liu, Y., Cheng, X., et al. (2021). Novel structural annotation and functional expression analysis of GTP_EFTU conserved genes in pepper based on the PacBio sequencing data. *Hortic. Plant J.* 7, 443–456. doi: 10.1016/j.hpj.2020.09.007

Tong, J., Ren, Z., Sun, L., Zhou, S., Yuan, W., Hui, Y., et al. (2022). ALBA proteins confer thermotolerance through stabilizing HSF messenger RNAs in cytoplasmic granules. *Nat. Plants* 8, 778–791. doi: 10.1038/s41477-022-01175-1

Wang, J., Lv, J., Liu, Z., Liu, Y., Song, J., Ma, Y., et al. (2019). Integration of transcriptomics and metabolomics for pepper (*Capsicum annuum* L.) in response to heat stress. *Int. J. Mol. Sci.* 20:5042. doi: 10.3390/ijms20205042

Wang, Y., Cai, S., Yin, L., Shi, K., Xia, X., Zhou, Y., et al. (2015). Tomato HsfA1a plays a critical role in plant drought tolerance by activating *ATG* genes and inducing autophagy. *Autophagy* 11, 2033–2047. doi: 10.1080/15548627.2015.1098798

Wang, W., Esch, J. J., Shiu, S. H., Agula, H., Binder, B. M., Chang, C., et al. (2006). Identification of important regions for ethylene binding and signaling in the transmembrane domain of the ETR1 ethylene receptor of *Arabidopsis*. *Plant Cell* 18, 3429–3442. doi: 10.1105/tpc.106.044537

Xue, G. P., Sadat, S., Drenth, J., and Mcintyre, C. L. (2014). The heat shock factor family from *Triticum aestivum* in response to heat and other major abiotic stresses and their role in regulation of heat shock protein genes. *J. Exp. Bot.* 65, 539–557. doi: 10.1093/jxb/ert399

Yang, X., Zhu, W., Zhang, H., Liu, N., and Tian, S. (2016). Heat shock factors in tomatoes: genome-wide identification, phylogenetic analysis and expression profiling under development and heat stress. *PeerJ* 4:e1961. doi: 10.7717/peerj.1961

Yu, G., Wang, L. G., Han, Y., and He, Q. Y. (2012). clusterProfiler: an R package for comparing biological themes among gene clusters. *OMICS* 16, 284–287. doi: 10.1089/omi.2011.0118

Yu, Q. (2018). Biological clock: the oscillator of gene expression. *Sci. China Life Sci.* 61, 128–130. doi: 10.1007/s11427-017-9239-6

Zhang, H. Q., Wang, Y. X., Guo, C. F., Tang, M. X., Liu, S. H., Deng, A., et al. (2022). A genetic module at one locus in rice protects to enhance thermotolerance. *Science* 376, 1293–1300. doi: 10.1126/science.abo5721

Zhang, R., Wise, R. R., Struck, K. R., and Sharkey, T. D. (2010). Moderate heat stress of *Arabidopsis* thaliana leaves causes chloroplast swelling and plastoglob. *Photosynth Res.* 105, 123–134. doi: 10.1007/s11120-010-9572-6

Zhang, X., Wollenweber, B., Jiang, D., Liu, F., and Zhao, J. (2008). Water deficits and heat shock effects on photosynthesis of a transgenic *Arabidopsis thaliana* constitutively expressing ABP9, a bZIP transcription factor. *J. Exp. Bot.* 59, 839–848. doi: 10.1093/jxb/erm364

Zheng, Y., Jiao, C., Sun, H., Rosli, H. G., Pombo, M. A., Zhang, P., et al. (2016). iTAK: a program for genome-wide prediction and classification of plant transcription factors, transcriptional regulators, and protein kinases. *Mol. Plant* 9, 1667–1670. doi: 10.1016/j.molp.2016.09.014

Zhu, J. K. (2016). Abiotic stress signaling and responses in plants. *Cell* 167, 313–324. doi: 10.1016/j.cell.2016.08.029

frontiers | Frontiers in Plant Science

TYPE Original Research
PUBLISHED 29 September 2022
DOI 10.3389/fpls.2022.932667

Check for updates

OPEN ACCESS

EDITED BY
Ji-Hong Liu,
Huazhong Agricultural University, China

REVIEWED BY
Zongliang Xia,
Henan Agricultural University, China
Zhulong Chan,
Huazhong Agricultural University, China

*CORRESPONDENCE
Shuyan Guan
guanshuyan@jlau.edu.cn
Yiyong Ma
m18404319202_1@126.com

SPECIALTY SECTION
This article was submitted to Plant Abiotic Stress, a section of the journal Frontiers in Plant Science

RECEIVED 30 April 2022
ACCEPTED 02 September 2022
PUBLISHED 29 September 2022

CITATION
Jiao P, Ma R, Wang C, Chen N, Liu S, Qu J, Guan S and Ma Y (2022) Integration of mRNA and microRNA analysis reveals the molecular mechanisms underlying drought stress tolerance in maize (*Zea mays* L.). *Front. Plant Sci.* 13:932667. doi: 10.3389/fpls.2022.932667

COPYRIGHT
© 2022 Jiao, Ma, Wang, Chen, Liu, Qu, Guan and Ma. This is an open-access article distributed under the terms of the Creative Commons Attribution License (CC BY). The use, distribution or reproduction in other forums is permitted, provided the original author (s) and the copyright owner(s) are credited and that the original publication in this journal is cited, in accordance with accepted academic practice. No use, distribution or reproduction is permitted which does not comply with these terms.

Integration of mRNA and microRNA analysis reveals the molecular mechanisms underlying drought stress tolerance in maize (*Zea mays* L.)

Peng Jiao[1,2], Ruiqi Ma[3], Chunlai Wang[1,2], Nannan Chen[1,2], Siyan Liu[2], Jing Qu[2], Shuyan Guan[2]* and Yiyong Ma[2]*

[1]College of Life Sciences, Jilin Agricultural University, Changchun, China, [2]Joint International Research Laboratory of Modern Agricultural Technology, Ministry of Education, Jilin Agricultural University, Changchun, China, [3]College of Plant Science, Jilin University, Changchun, China

Drought is among the most serious environmental issue globally, and seriously affects the development, growth, and yield of crops. Maize (*Zea mays* L.), an important crop and industrial raw material, is planted on a large scale worldwide and drought can lead to large-scale reductions in maize corn production; however, few studies have focused on the maize root system mechanisms underlying drought resistance. In this study, miRNA–mRNA analysis was performed to deeply analyze the molecular mechanisms involved in drought response in the maize root system under drought stress. Furthermore, preliminary investigation of the biological function of miR408a in the maize root system was also conducted. The morphological, physiological, and transcriptomic changes in the maize variety "M8186" at the seedling stage under 12% PEG 6000 drought treatment (0, 7, and 24 h) were analyzed. With prolonged drought stress, seedlings gradually withered, the root system grew significantly, and abscisic acid, brassinolide, lignin, glutathione, and trehalose content in the root system gradually increased. Furthermore, peroxidase activity increased, while gibberellic acid and jasmonic acid gradually decreased. Moreover, 32 differentially expressed miRNAs (DEMIRs), namely, 25 known miRNAs and 7 new miRNAs, and 3,765 differentially expressed mRNAs (DEMRs), were identified in maize root under drought stress by miRNA-seq and mRNA-seq analysis, respectively. Through combined miRNA–mRNA analysis, 16 miRNA–target gene pairs, comprising 9 DEMIRs and 15 DEMRs, were obtained. In addition, four metabolic pathways, namely, "plant hormone signal transduction", "phenylpropane biosynthesis", "glutathione metabolism", and "starch and sucrose metabolism", were predicted to have important roles in the response of the maize root system to drought. MiRNA and mRNA expression results were verified by real-time quantitative PCR. Finally, miR408a was selected for functional analysis and demonstrated to be a negative regulator of drought response, mainly through regulation of reactive oxygen species accumulation in the maize root system. This study helps to elaborate the regulatory response mechanisms of the maize root system under drought stress and predicts the biological functions of candidate miRNAs and mRNAs, providing strategies for

subsequent mining for, and biological breeding to select for, drought-responsive genes in the maize root system.

KEYWORDS

drought stress, maize, microRNA, mRNA, miR408a

Introduction

Maize is the largest food crop worldwide (Koester et al., 2021); therefore, ensuring stable maize production is of considerable significance to the sustainable development of agricultural output. As a stress-sensitive plant, maize is susceptible to interference and damage from stress conditions. With the development of modern industries, environmental challenges, such as reduction of arable land, deterioration of soil quality, shortage of freshwater resources, global warming, and frequent natural disasters, have become increasingly serious. Maize yields are limited by various abiotic stressors, including drought stress, which is an important limiting factor for crop yield that seriously threatens the sustainable development of global agriculture. Therefore, research on drought resistance of maize is essential.

Drought stress-induced signals undergo a series of transmission processes to finally regulate the expression of specific genes, leading to drought resistance at the tissue, cell, and physiological/biochemical levels in plants. The products encoded by these specific genes can generally be divided into two categories. First, functional proteins, such as osmolytes, various proteases, aquaporins, molecular chaperones, and LEA protein enzymes, related to active oxygen scavenging, among others, are directly involved in various biochemical environmental stress response resistance processes, resulting in drought tolerance effects (Battaglia et al., 2008; Ramanjulu and Bartels, 2022). Second, regulatory proteins act upstream of genes encoding functional proteins and mediate related signaling, for example, transcription factors and various kinases involved in signaling cascades (Tõldsepp et al., 2018; Su et al., 2019). At the molecular level, plant drought stress transcriptional regulatory networks comprise two different regulatory pathways: abscisic acid (ABA)-dependent and ABA-independent (Bulgakov et al., 2019).

Recently, increasing studies have shown that numerous miRNAs are involved in plant stress response processes; miRNAs are non-coding single-stranded RNA molecules of 16–29 nucleotides, encoded by endogenous genes, which have characteristic hairpin structures, and function at the post-transcriptional level. Degradation of target mRNA or translation inhibition by miRNAs to regulate gene expression is crucial for control of gene expression in eukaryotic cells (Cui et al., 2017; Pegler et al., 2019). Many plant miRNA genes map to intergenic or intronic genome regions (Voinnet, 2009), and some form clusters, which can be co-transcribed to form a common primary miRNA (pri-miRNA). miRNA was first discovered in nematodes (Lee et al., 1993). Subsequently, numerous miRNAs were also predicted in rice (Jian et al., 2010), Arabidopsis (Sunkar and Zhu, 2004), maize (Kaur et al., 2020), and other plants, and many have been successfully experimentally verified (Fang et al., 2014; Luan et al., 2015; Kravchik et al., 2019).

Many studies have shown that miRNAs regulate plant growth and development not only under normal conditions but also under abiotic stress conditions such as drought (Arshad et al., 2017; Zhang et al., 2018), saline-alkali (Zhai et al., 2014; Zhang et al., 2020), and low temperature (Yang et al., 2016; Zhou and Tang, 2019). Plants are also regulated to enhance tolerance to stress. Under stress, inducing or inhibiting the expression of the specific genes at the post-transcriptional level caused by different miRNA expression levels leads to the accumulation of individual substances or changes in metabolic pathways. It ultimately helps the plant make adaptive adjustments to improve plant stress resistance.

To date, numerous small-molecule RNAs have been identified in multiple organisms using various technologies, and this process has been accelerated by the emergence of high-throughput small-molecule sequencing methods and bioinformatics technologies. Although regulation of target gene expression generates robust regulatory networks, understanding this represents only an initial research step. Such networks ensure the operation of various physiological processes, and miRNAs are essential regulators of plant drought response (Akdogan et al., 2016). The first miRNAs identified as related to drought in rice were those of the miR169 family, which includes 17 members with 9 different mature sequences. miR169 is more sensitive to drought stress in roots than in buds (Zhao and Srivastava, 2007). Furthermore, miR169a and miR169c of Arabidopsis and miR169 of tomato are inhibited by drought (Ni et al., 2013). In transgenic tomatoes that overexpress miR169c, target gene expression is downregulated, and transgenic plants have lower transpiration rates and reduced stomatal openness relative to wild-type (WT) controls; hence, the reasons

underlying miR169c involvement in tomato drought stress responses have been determined (Zhang et al., 2011). MiR408 family is a well-recognized class of conserved miRNAs in plants, which mainly responds to adversity stress. Under drought stress, the expression of miR408 in alfalfa, barley, chickpea, and poplar also increases, while the expression of miR408 in rice and Arabidopsis is inhibited by drought stress (Ma et al., 2015; Hang et al., 2021). Zhang et al. (2017) found that miRNA408-mediated target genes can affect copper ion homeostasis in chloroplast, which, in turn, results in enhancement of stress resistance, photosynthetic rate, and yield of rice; Ma et al. (2015) proved that miR408 in Arabidopsis can mediate target genes to improve stress resistance and oxidative stress response in plants under the effects of low temperature, drought, oxidation, and osmotic pressure. Therefore, miRNAs are important in the response of plants to drought stress.

In this study, we used 12% PEG 6000 to conduct experiments simulating hydroponic drought treatment using three-leaf stage maize plants of the inbred line "H8186", with a treatment duration of 0, 7, and 24 h. Observation of the maize root system phenotype before and after drought treatment was conducted and physiological indices were measured. To investigate the molecular mechanism involved in drought stress responses, nine small RNA (sRNA) sequencing libraries and nine mRNA libraries were constructed, with three biological replicates each, and miRNA-seq and mRNA-seq data were generated and analyzed. Our findings contribute to understanding of post-transcriptional regulation of the maize root system under drought stress, and provide insight into drought tolerance in the grass family. Furthermore, high-throughput sequencing and bioinformatic analyses were adopted to identify candidate miRNAs and mRNAs involved in maize root responses to drought stress, providing new strategies for creation of novel drought-tolerant maize germplasm and cultivation of innovative varieties.

Materials and methods

Plant materials and experimental design

The plant material used in this experiment was the maize (Zea Mays L.) inbred line, M8186. All plant materials were preserved by Jilin Agricultural University Jilin Key Laboratory of Crop Molecular Breeding. Maize was grown in the greenhouse of the experimental base of Jilin Agricultural University at 27°C ± 2°C, with a 14-h light/10-h dark cycle. Three-leaf stage maize plants were randomly divided into drought (7 and 24 h) and control groups. Drought stress was simulated by watering plants with 12% PEG 6000; plants in the control group were watered as usual throughout the experiment. Morphological observation of maize plants was performed and experimental samples were collected before (0 h) and after (7 and 24 h) drought stress. Collected maize root system samples were frozen in liquid nitrogen for 30 min, then quickly transferred to an ultra-low-temperature refrigerator at −80°C. Three biological replicates were used for each time point.

Maize inbred lines used for genetic transformation included the drought-tolerant inbred line, GSH9901, which was obtained by Prof. Guan Shuyan's research group at the Joint International Research Laboratory of Modern Agricultural Technology (43° 47′ 56′ N, 125° 24′ 2′ E), Ministry of Education, after many years of field screening at multiple locations. The materials used were high-generation stable maize inbred lines, which grew in a greenhouse in well-mixed soil (1:1 ratio, forest soil:vermiculite) at 28°C/26°C, with a 12-h light/12-h dark cycle. To analyze changes in physiological indices and expression levels of ROS-related marker genes under drought, 12% (w/v) polyethylene glycol 6000 (PEG 6000) was used to simulate drought by treating the following groups of three-leaf stage maize plants: GSH9901 (WT control), miR408a-OE (maize lines generated using a T-DNA insertion system to overexpress miR408a: miR408a-OE#3 and miR408a-OE#9), and miR408a-KO (knockout maize mutants generated using the CRISPR/Cas9 system: miR408a-KO#2 and miR408a-KO#7). Plants were grown in soil under the conditions described above. All experiments were repeated three times, and >10 plants were used for each measurement.

Measurement of physiological indices

Physiological indices were measured using frozen maize root samples. High-performance liquid chromatography was applied to determine jasmonic acid (JA), ABA, gibberellic acid (GA3), and brassinolide (BR) content in the maize root system (Pan et al., 2010). Peroxidase activity was measured using the guaiacol method (Jiao et al., 2022b), and lignin content was determined in strict accordance with the operation process specified for testing kits from Suzhou Michy Biomedical Technology Co., Ltd. Reduced glutathione (GSH) and trehalose content were determined by UV spectrophotometry (Yang et al., 2021a; Kang et al., 2021).

sRNA isolation, library construction, and high-throughput sequencing

Root samples of maize were collected at 0, 7, and 24 h under drought treatment, respectively. Three biological replicates were prepared for each sample, and each biological replicate was collected from eight plants. Samples were quickly frozen in liquid nitrogen, and total RNA was extracted and then sequenced. Three groups of RNA samples were prepared (WT: roots with watering, DSSD: roots with drought stress 7 h, and DSFD: roots with drought stress 24 h), each group had three biological replicates, and each group of samples was mixed and combined with RNA. Therefore, a total of

nine samples were used to build an sRNA library. The construction of the sRNA library and high-throughput sequencing was completed by Shanghai Majorbio Bio-pharm Technology Co, Ltd. MiRNA and mRNA data were uploaded to the National Center for Biotechnology Information (PRJNA796152 and PRJNA793522) on 31 December 2021.

Identification of known and novel miRNAs

To identify known and novel miRNAs, bowtie software was used to align mapped sRNAs with a specified range of sequences in miRBase. Then, miRNA sequences were compared with the Rfam database, and rRNA, tRNA, snRNA, and snoRNA sequences were removed. MISA software was used to remove repeat sequences. PlantNATsDB analysis was used to remove sequences from the plant NAT-siRNATAS database, and UEA sRNA tools software was used to remove plant ta-siRNA sequences. After removal of interfering sRNA sequences, the unique hairpin structures of miRNA precursors were used to predict new miRNAs from remaining sRNAs.

Identification of known and novel mRNAs

After acquisition of read count data of genes/transcripts, the differential expression analysis of genes/transcripts between samples was performed for multi-sample (≥2) projects to identify the differentially expressed genes/transcripts between samples and in turn investigate the function of differentially expressed genes/transcripts. In this module, DESeq2 software was used to conduct statistical analysis of differentially expressed genes/transcripts, and the detailed table of differentially expressed genes/transcripts (expression of differentially expressed genes/transcripts in a single comparison group) and the statistical table of differentially expressed genes/transcripts (expression of differentially expressed genes/transcripts in multiple comparison groups) were included.

Prediction of miRNA targets and association analysis

The psRobot (http://omicslab.genetics.ac.cn/psRobot/index.php) software was used to predict the target genes of mature miRNAs. psRobot is a plant sRNA analysis tool and is divided into an online version and a local version. The local version has the function of reference sequence alignment, prediction of precursor and mature miRNAs, prediction of sRNA target genes, and degradation group analysis. Mature miRNA sequences were responsive to drought, identified in maize roots, and were used as custom miRNA sequences. The parameters for target prediction were set by default. The miRNAs and their target genes were counted, and a miRNA–mRNA network was constructed by Cytoscape.

Functional analysis of differentially expressed genes

Based on the principle of hypergeometric distribution, functional analysis of all genes with significantly altered expression in response to drought stress was conducted using the GO (http://www.geneontology.or) and Kyoto Encyclopedia of Genes and Genomes (KEGG; http://www.genome.jp/kegg/) databases. GO and KEGG enrichment analyses were performed using the OmicShare tool, a free online platform for data analysis (https://www.omicshare.com/tools).

Expression validation of miRNA and their targets

Chen et al. (2005) developed a stem-loop primer real-time PCR method that could detect the expression level of mature miRNA. This method was the first to design a specific stem-loop RT primer for mature miRNA. The primer had a stem-loop structure, and about six bases at its 3' end were reversely complementary to the 3' end of miRNA, thereby specifically reverse transcription of miRNA. Then, miRNA was amplified by specific forward primers and universal reverse primers. The transcription of miRNA was reversed using the Taq Man micro RNA Reverse Transcription Kit. Then, two-step PCR was used to perform PCR amplification. The procedures were denaturation at 95°C for 30 s, denaturation at 95°C for 5 s, and extension at 60°C for 31 s, a total of 40 cycles. Three biological and three experimental replicates were performed for each sample.

Primer 5.0 software was used to design primers for miRNA target gene quantitative PCR. The main design principles were as follows: (1) The amplified length of the fragment was generally between 100 and 200 bp. (2) The primer did not contain a secondary structure, and the primers were between the primers. Dimers could not be formed. (3) The primer length was generally about 19–25 nt, and G or C should be avoided at the 3' end. (4) The Tm value of the primer was generally about 60°C, and the GC content was about 40%–60%. All primers were synthesized by Kumei Biotechnology Co., Ltd. of Jilin Province. Target genes were reverse transcribed using the First-Strand c DNA Synthesis Kit. The PCR reaction was performed as follows: pre-denaturation at 94°C for 10 min, 94°C for 15 s, and 60°C for 1 min, for a total of 40 cycles. After the reaction, the dissolution curve was analyzed using the 2–ΔΔCT [ΔCT = CTtarget gene – CTinternal reference gene. ΔΔCT = ΔCTtreated – ΔCTcontrol]

method (Livak and Schmittgen, 2001). Three biological experiment replicates were set up per gene. Details regarding the primers used for this assay are listed in Supplementary Table S3.

β-Glucuronidase assay

β-Glucuronidase (GUS) histochemical staining of root systems from the miR408a transgenic maize inbred line, GSH9901, was performed; root systems from three-leaf stage plants were stained under vacuum in staining solution containing X-gluc (50×) and GUS staining PBS buffer. The specific steps for determining GUS activity were as described previously (Jiao et al., 2022a).

Nitrotetrazolium blue chloride staining and oxidative stress analyses

Drought simulation experiments were carried out using three-leaf stage miR408a OE, miR408a KO, and WT plants, by treatment with 12% PEG 6000. Seedling leaves (the middle part of the second leaf in the three-leaf stage) were stained using nitrotetrazolium blue chloride (NBT), and the accumulation of superoxide anion (O_2^-) was quantitatively detected. Superoxide dismutase (SOD), catalase (CAT), and ascorbic acid peroxidase (APX) activities were determined by spectrophotometry. Malondialdehyde (MDA) content, proline content, relative water content, hydrogen peroxide concentration, and O_2^- content were determined following the criteria described by Jiao et al. (2022a).

Statistical analysis

All of the data were tested by analysis of variance using SPSS 19.0 software. The data are the mean ± standard deviation (SD) of three biological replicates. The significance was analyzed in the Student's t-tests. The * and ** represent $p < 0.05$ and $p < 0.01$, respectively. The figures were prepared with GraphPad Prism 8.0.

Results

Effects of PEG-induced water stress on the morphological and biological characteristics of maize

The morphology of maize seedlings changed with increased duration of drought stress exposure. Compared with seedlings before drought stress, those exposed to drought stress for 7 h began to wither slightly, and the root length grew. Furthermore, after 24-h drought stress, seedlings had withered significantly and their root systems grew significantly. With prolonged drought stress, hormone levels, lignin content, and peroxidase activity in the root system were significantly affected; ABA, BRs, lignin, GSH, and trehalose content increased gradually, while peroxidase activity increased sharply, and GA3 and JA content decreased gradually (Figure 1).

miRNA and mRNA sequencing data quality assessment

To elucidate the molecular mechanisms underlying maize root system responses to drought stress, nine root samples, including three biological replicates from control and drought stress-exposed plants, were additionally selected and subjected to mRNA and sRNA library sequencing using the Illumina HiSeq™ 2500 platform. Approximately 12.979–17.682 × 106 clean reads and 358.219–476.732 × 106 clean bases were obtained by miRNA sequencing, and useful reads (9.600–13.970 × 106) were screened according to sRNA length 18–32 nt. CG content ranged from 51.15% to 52.64%. Numbers of known and new miRNAs identified in each sample are presented in Table 1.

A total of 64.42 GB clean data were obtained by mRNA sequencing, representing > 6.57 GB per sample and 82.90–95.64 million clean reads for each of the four samples. Q30 base call rates were all > 93.63%. Hisat2 was used to map clean reads to the maize reference genome, with proportions of clean reads that could be mapped to the genome ranging from 88.47% to 89.77%. Uniquely mapped clean reads (85.07%–86.68%) were applied for subsequent analyses (Table 2).

Analysis of differentially expressed miRNAs and differentially expressed mRNAs

Numbers of both differentially expressed miRNAs (DEMIRs) and differentially expressed mRNAs (DEMRs) gradually increased with prolonged drought stress (Figures 2A, B). A total of 32 DEMIRS were identified, comprising 22% and 78% that were up- and downregulated, respectively. Furthermore, 3,765 DEMRs were identified, of which 49% and 51% were up- and downregulated, respectively (Figures 2C, D). A cluster heatmap of all miRNAs and mRNAs illustrated the significant differences in miRNA and mRNA expression levels in response to drought stress (Figures 2E, F).

10.3389/fpls.2022.932667

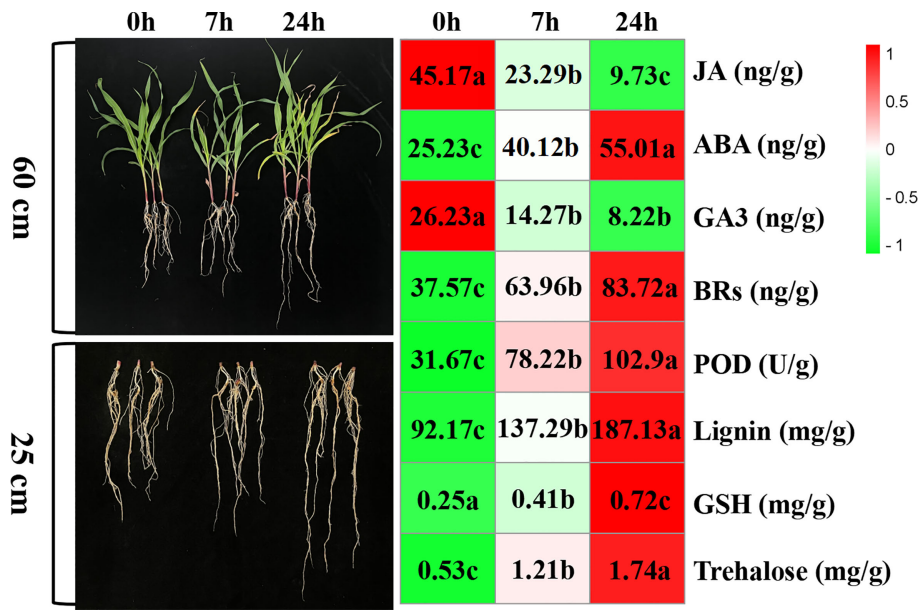


FIGURE 1
The morphology and physiochemical changes of maize variety "M8186" under drought stress. Values followed by different lowercase letters represent $p \leq 0.05$.

Functional analysis of DEMRs

To investigate the expression pattern of the 3,765 DEMRs under drought stress, their fragments per kilobase of transcript per million mapped reads (FPKM) values in roots were normalized, then analyzed using Short Time-series Expression Miner (STEM). Sixteen model profiles were constructed, eight of which were significant. Gene expression profiles are illustrated in Figure 3A; areas with colored backgrounds indicate significant differences, and genes of the same type are clustered. Profile 12 was significantly enriched in roots, with the smallest p-value; therefore, our subsequent research work may focus on genes in profile 12.

To further study the function of DEMRs in maize root, we annotated them into three categories (biological process, cellular component, and molecular function) using the GO database. Under drought stress, WT_vs_DSSD root DEMRs were mainly enriched in biological processes, including response to oxygen-containing compound (GO:1901700), response to lipid (GO:0033993), response to abscisic acid (GO:0009737), and response to alcohol (GO:0097305); cellular components comprising plasma membrane part (GO:0044459), intrinsic component of plasma membrane (GO:0031226), plant-type cell wall (GO:0009505), and integral component of plasma membrane (GO:0005887); and molecular functions, including receptor serine/threonine kinase binding (GO:0033612), monovalent inorganic cation transmembrane transporter activity (GO:0015077), potassium ion transmembrane transporter activity (GO:0015079), and microtubule binding (GO:0008017). Comparison of the WT_vs_DSFD groups under stress indicated that root biological processes were mainly enriched for transmembrane transport (GO:0055085), response to high light intensity (GO:0009644), response to hydrogen peroxide (GO:0042542), and ion transport (GO:0006811); cellular components were enriched for intrinsic component of plasma membrane (GO:0031226), integral component of plasma membrane (GO:0005887), plasma membrane part (GO:0044459), and intrinsic component of membrane (GO:0031224), while enriched molecular functions included transmembrane transporter activity (GO:0022857), transporter activity (GO:0005215), inorganic

TABLE 1 Summary of miRNA sequencing datasets.

Sample	Clean reads (×106)	Clean bases (×106)	GC content (%)	Useful reads (18 nt–32 nt) (×106)	Known miRNA	Novel miRNA
WT	17.682	476.732	51.15	13.970	240	449
DSSD	15.499	431.279	52.64	11.525	231	188
DSFD	12.979	358.219	52.19	9.600	229	175

TABLE 2 Summary of mRNA sequencing datasets.

Sample	Clean reads (×106)	Clean bases (×109)	Q30 (%)	Total mapped	Uniquely mapped
WT	47.253	7.05	94.35	88.47%	85.07%
DSSD	47.237	7.04	94.08	89.60%	86.68%
DSFD	49.672	7.39	94.46	89.77%	86.68%

molecular entity transmembrane transporter activity (GO:0015318), and carbohydrate transmembrane transporter activity (GO:0015144) (Figures 3B, C).

To further explore the similarities and differences in DEMR functional enrichment, KEGG enrichment analysis was performed for the 3,765 DEMRs and 20 pathways. The results showed that drought stress-altered DEMRs in the WT_vs_DSSD and WT_vs_DSFD groups were concentrated in pathways including phenylpropanoid biosynthesis (ko00940), plant hormone signal transduction (ko04075), starch and sucrose metabolism (ko00500), and glutathione metabolism (ko00480) (Figures 3D, E). The remaining eight pathways were enriched for DEMRs, but not for comparisons of both the WT_vs_DSSD and WT_vs_DSFD groups.

Analysis of co-expression networks and qRT-PCR validation of relationships between DEMIRs and DEMRs

To explore the regulatory relationship between miRNAs and mRNAs under drought stress, we constructed a molecular regulatory network diagram of DEMIRs and DEMRs (Figure 4), which showed that 9 DEMIRs negatively regulated the expression of 15 DEMRs. The reliability of the transcriptome data was verified by qRT-PCR analysis. Based on those with high FPKM and multiple changes, the expression patterns of 9 DEMIRs and 15 DEMRs closely related to drought stress response were verified at 0, 7, and 24 h. The results showed that the expression patterns determined by qRT-PCR and RNA-seq were consistent, confirming the accuracy of the RNA-seq data (Figure 5).

Analysis of key pathways in maize responses to drought stress

Based on biological characteristics and gene functions, we identified four pathways important for the maize root system response to drought stress (Figure 6, Supplementary Table S1), including: "plant hormone signal transduction", "phenylpropanoid biosynthesis", "glutathione metabolism", and "starch and sucrose metabolism". Molecules involved in "hormone signal transduction"

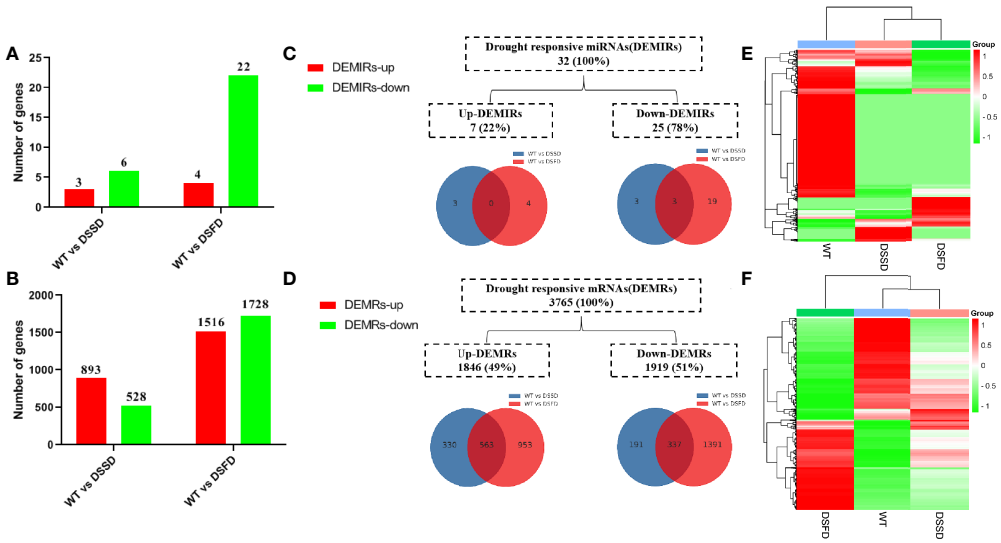


FIGURE 2
The expression profile of drought stress-regulated DEMIRs and DEMRs in maize roots. **(A, B)** Column diagram representing the numbers of DEMIRs and DEMRs. **(C, D)** Venn diagrams representing the numbers of DEMIRs and DEMRs, and the overlaps of sets obtained across two comparisons. **(E, F)** Heat map of all miRNAs and all mRNAs expression profiles before and after drought stress.

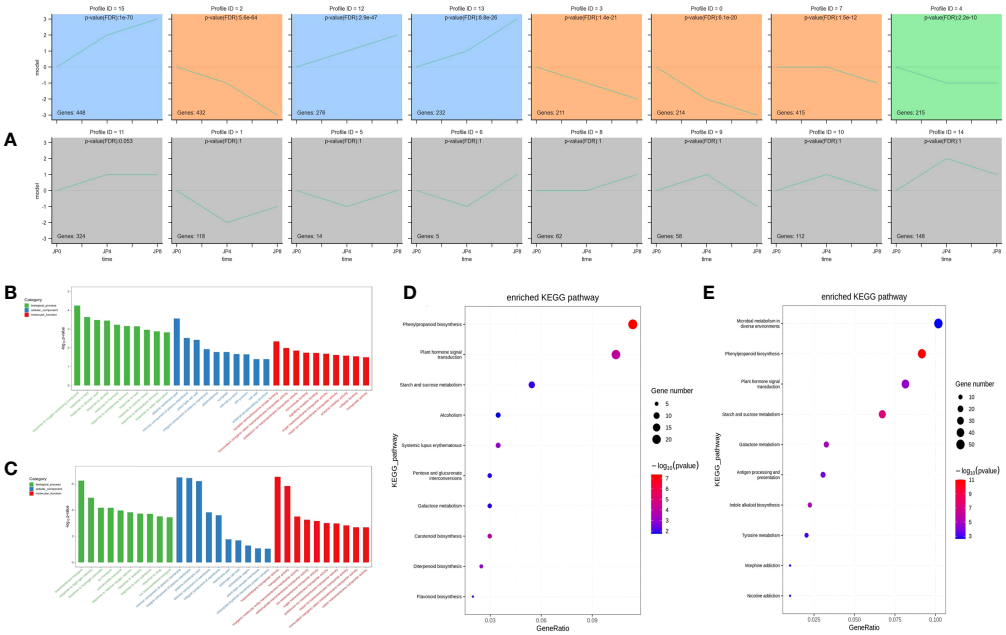


FIGURE 3
GO and KEGG enrichment analysis across three time points during drought stress of maize plant roots. **(A)** Twenty representative profiles of different expression trends. The colored background parts showed significance, and the genes of the same type were gathered in the same cluster. **(B, C)** The most significantly enriched GO terms of DEMRs from the two comparison groups. **(D, E)** The most significantly enriched KEGG pathway of DEMRs from the two comparison groups.

pathways, including ABA receptors, PYR/PYL (Zm00001d012475 and Zm00001d010445); positive regulator phosphokinase, SnRK2 (Zm00001d042695, Zm00001d013736, Zm00001d029975, and Zm00001d033339); and the downstream regulator of ABA signaling, ABF (Zm00001d012296, Zm00001d044940, Zm00001d020711, Zm00001d042721, Zm00001d050018, Zm00001d031790, and Zm00001d018178), were all upregulated in the maize root system after drought stress, which would be expected to enhance ABA signal transduction. Both the jasmonate amino acid conjugating enzyme, JAR1 (Zm00001d008957), and the JA signaling hub protein, JAZ (Zm00001d024455), were downregulated in response to drought, which would be predicted to attenuate JA signal transduction. BIN2 (Zm00001d053548), a negative regulator of the BR signaling pathway, is a type of protein kinase whose expression is downregulated under drought stress and negatively correlated with BR content. The DELLA protein is a negative regulator of the gibberellin signal transduction pathway, and a nuclear protein involved in growth inhibition. DELLA protein (Zm00001d044065) expression was upregulated 0–7 h after drought stress, and negatively correlated with GA3 content. In the starch and sucrose metabolic pathways, expression of the sucrose phosphate synthase (SPS) (Zm00001d012036, Zm00001d042353, Zm00001d048979, and Zm00001d050125) and sucrose phosphate phosphatase (Zm00001d010523) genes was upregulated following drought stress. Expression of genes related to trehalose 6-phosphate phosphatase (TPP) (Zm00001d006913) and α-glucosidase (Zm00001d036608) was also upregulated, and trehalose content was positively correlated with expression of these mRNAs. In the "glutathione metabolism" pathway, mRNA expression levels of glutamate decarboxylase (GAD) (Zm00001d031749 and Zm00001d033805), alanine aminotransferase (POP2) (Zm00001d049380, Zm00001d015444, and Zm00001d037507), and succinic semialdehyde dehydrogenase (SSADH) (Zm00001d015406) were all upregulated after drought stress. In the "phenylalanine biosynthesis" pathway, the expression levels of genes related to phenylalanine ammonia lyase (PAL) (Zm00001d051163), cinnamyl alcohol dehydrogenase (CAD) (Zm00001d015618), and peroxidase (Zm00001d048413, Zm00001d038599, Zm00001d009140, and Zm00001d014606) were all upregulated in the maize root system following drought stress.

Drought stress reduces the accumulation of ZmmiR408a, which negatively regulates drought tolerance in maize

Our analysis of miR408a expression, based on stem-loop RT-qPCR, demonstrated that ZmmiR408a was significantly downregulated in roots in response to drought treatment (Figure 7A); therefore, we conducted GUS-staining of pmiR408a: GUS. Levels of the miR408a-driven GUS gene were significantly

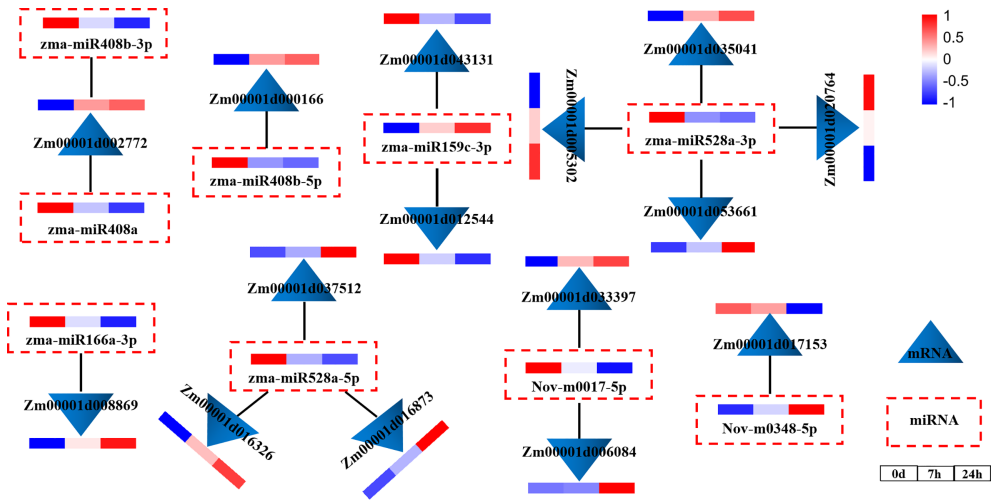


FIGURE 4
miRNA and mRNA co-expression network diagram. Network analysis was performed using the Cytoscape network platform.

reduced in the root system on increasing duration of exposure to 12% PEG6000-induced drought (Figure 7B). We further confirmed the consistency of ZmmiR408a expression patterns in the inbred line, GSH9901, under drought stress conditions.

To investigate the role of ZmmiR408a in drought responses, two independent ZmmiR408a gene-edited plant lines, miR408a KO2 and miR408a KO7, and two independent ZmmiR408a overexpressing plant lines, miR408a OE3 and miR408a OE9, were generated. Fluorescence quantitative PCR showed that miR408a expression was significantly decreased in miR408a KO plants, while it was significantly increased in miR408a OE plants (Figure 7C). Under normal conditions, there was no significant difference in seed germination between transgenic and WT strains; however, very interestingly, the seed germination ability of the miR408a KO strain was significantly improved compared with that of the WT and miR408a OE strains under treatment with 12% PEG 6000 stress for 5 days (Figures 7D, E). Furthermore, after 15 days of drought stress, leaf wilting degree (Figure 7F), plant survival rate (Figure 7G), dry weight (Figure 7H), and root length (Figure 7I) were superior in the miR408a KO strain than those of WT and miR408a OE strains. In maize fields under drought conditions, the height of transgenic strains did not differ significantly from that of WT plants (Figure 7J), while seed setting rate (Figure 7K), yield (Figure 7L), and seed vigor (Figure 7M) were significantly better in the miR408a KO strain than those of the WT and miR408a OE strains. Physiological analysis showed that, under drought treatment, the MDA content of the miR408a KO strain was lower than that of WT and miR408a OE strains (Figure 7N), while the proline content was higher (Figure 7O). In conclusion, these results show that ZmmiR408a is a negative regulator of drought tolerance.

ZmmiR408a regulates drought tolerance by modulating ROS accumulation in maize

To investigate whether ZmmiR408a can regulate ROS accumulation, we conducted NBT staining to evaluate O_2^- levels. Notably, under drought treatment, NBT staining intensity in the leaves of the miR408a-KO strain was significantly lower than that in the WT and miR408a-OE strains (Figure 8A). Furthermore, the accumulation and production of H_2O_2 and O_2^- in leaves from WT, miR408a-KO, and miR408a-OE maize seedlings were compared. Under normal growth conditions, there was no significant difference in H_2O_2 and O_2^- contents between the transgenic and WT strains; however, following 15 days of drought treatment using 12% PEG 6000, H_2O_2 and O_2^- contents in the leaves of the miR408a-KO strain were significantly lower than those in WT and miR408a-OE strain leaves (Figures 8B, C). Jiao et al. (2022a) found that antioxidant enzymes can effectively scavenge high concentrations of ROS. Therefore, SOD, CAT, peroxidase, and APX activities in WT and transgenic plant leaves were quantitatively analyzed. Under normal conditions, no significant difference in antioxidant enzyme activity was detected between WT, miR408a-KO, and miR408a-OE strains; however, under drought treatment, the miR408a-KO strain had the highest enzyme activity in its leaves (Figures 8D–G). Expression levels of ROS homeostasis-related genes (ZmSOD1, ZmCAT3, ZmPOD45, and ZmAPX2) were detected by real-time fluorescence quantitative PCR. Under normal conditions, there was minimal difference between levels in WT, miR408a-KO, and miR408a-OE strains. By contrast, ROS scavenging-related genes were all upregulated in WT, miR408a-KO, and miR408a-OE

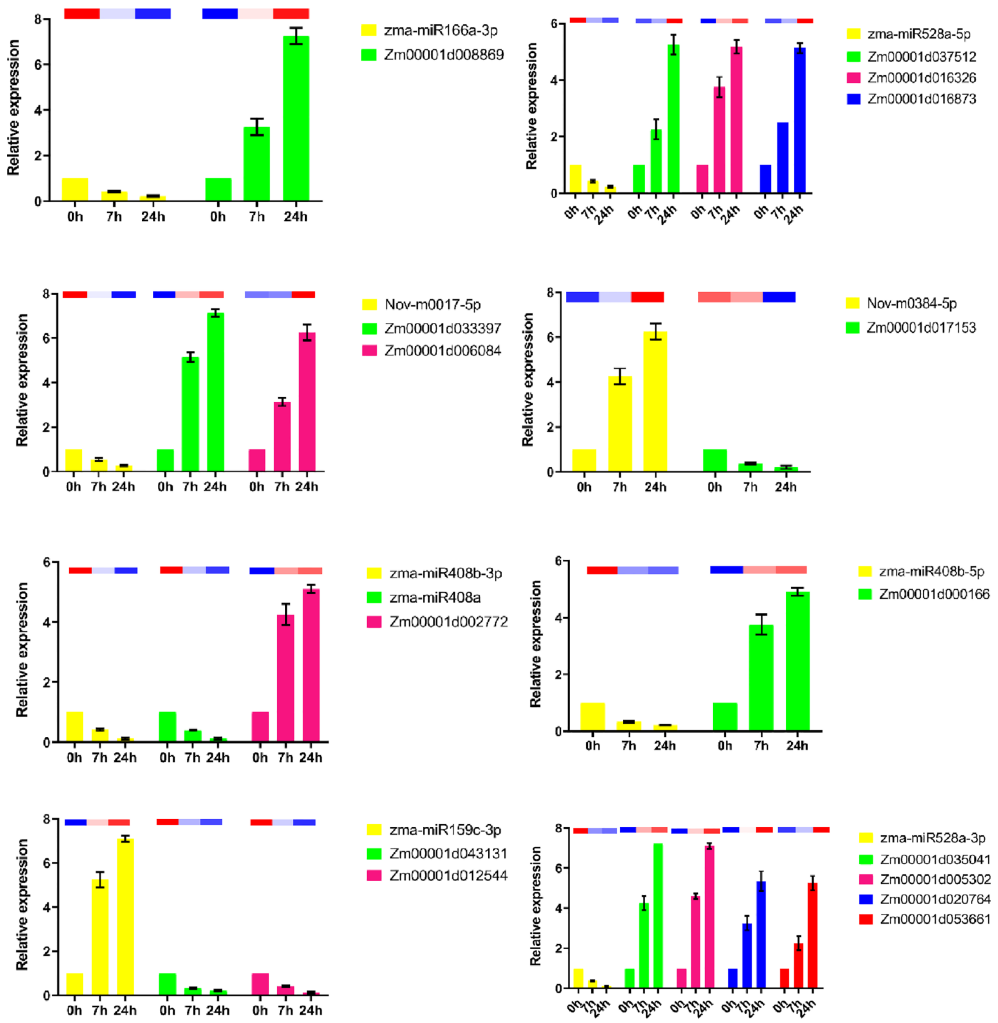


FIGURE 5
qRT-PCR analysis of DEMIs and DEMs in maize roots under drought stress. The $2^{-\Delta\Delta Ct}$ was used to calculate the fold change of expression in qRT-PCR analysis, with U6 and Actin as reference for miRNA and target genes, respectively. All experiments were repeated three times, and the expression data were log2 transformed before analysis. The error line is the standard error. The column charts represent qPCR data and heatmaps represent RNA-Seq data.

plants under drought stress, and those in miR408a-KO plants were consistently higher than corresponding levels in WT and miR408a-OE plants (Figures 8H–K). These results show that effective knockout of miR408a genes can improve SOD, APX, and CAT enzyme activities, as well as ROS-related gene expression, under drought conditions, thereby reducing ROS accumulation.

Discussion

Drought stress severely restricts the growth and development of corn plants in the field and is among abiotic stress factors important for yield loss (Guo et al., 2021). When grown under drought conditions, the roots of most plants change significantly (Chen et al., 2020); therefore, topics related to the response of the maize root system to drought resistance have become the focus of intense research. In this study, the morphological and physiological differences of maize seedlings under drought stress were investigated and a series of DEMIRs and DEMRs in the maize seedling root system in response to drought were identified. Furthermore, an miRNA–mRNA network was constructed and four key pathways were explored. Based on our findings, we also investigated the biological function of miR408a in the maize root system, providing a new strategy for further exploration of the mechanisms underlying maize root system responses to drought stress.

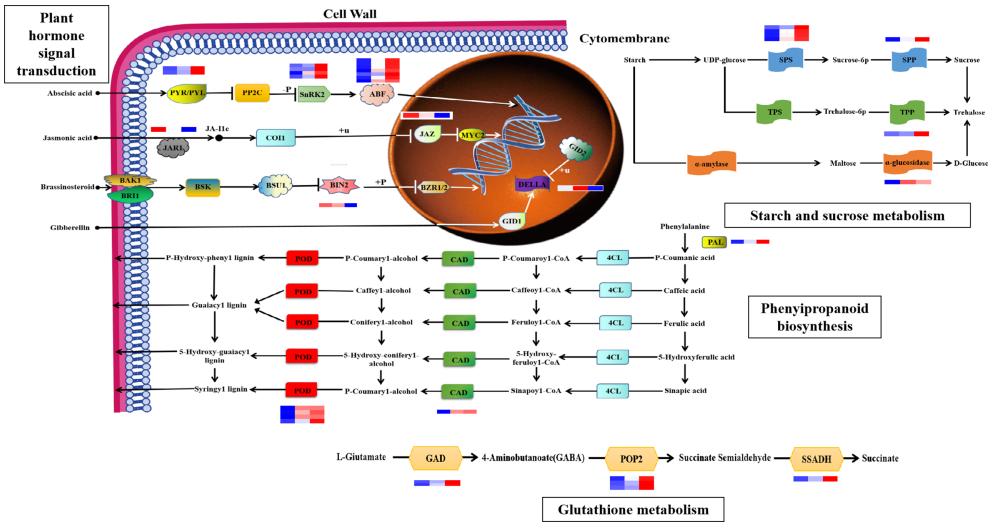


FIGURE 6
The key pathways of the drought stress response in maize. These pathways were "plant hormone signal transduction", "phenylpropanoid biosynthesis", "starch and sucrose metabolism", and "glutathione metabolism".

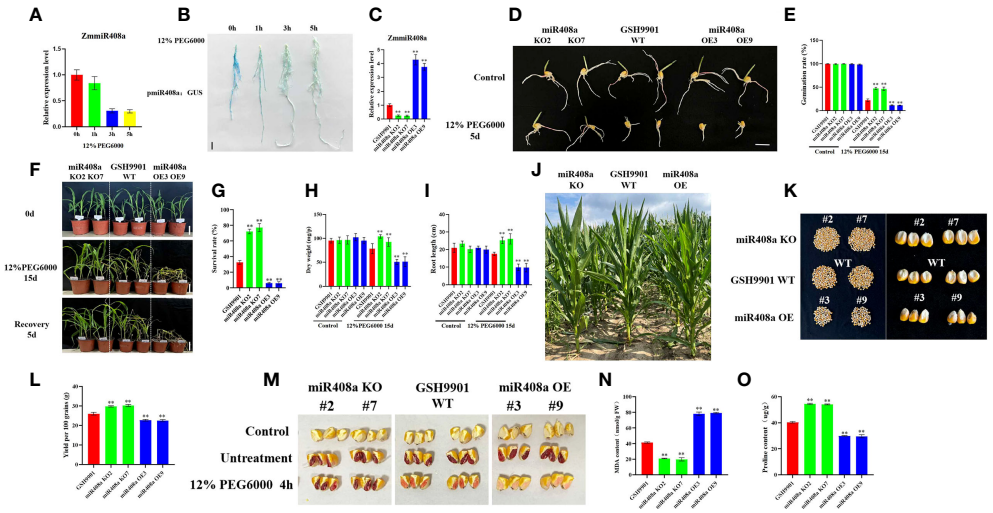


FIGURE 7
Analysis of phenotype and physiological and biochemical indexes of ZmmiR408a transgenic plants under drought stress. **(A)** Expression pattern analysis of ZmmiR408a in roots upon drought treatment. **(B)** Histochemical analysis of ZmmiR408a promoter: GUS transgenic maize roots were done under 0-h, 1-h, 3-h, and 5-h drought treatment. **(C)** Real-time quantitative PCR analysis of the expression level of ZmmiR408a gene in miR408a-OE and miR408a-KO plants. **(D, E)** Seed germination phenotypes of transgenic lines and wild-type plants under non-treatment and 12% PEG6000 treatment for 5 days. The scale bar represents 2 cm. **(F, G)** Analysis of wilting degree and recovery ability of transgenic lines and wild-type plants under drought treatment for 15 days and recovery for 5 days. All the plants were grown in a greenhouse at 25 ± 2°C under a 16-h light/8-h dark photoperiod. **(H)** Dry weight of wild-type, miR408a-KO, and miR408a-OE seedlings under normal and drought stress conditions. **(I)** Root length of wild-type, miR408a-KO, and miR408a-OE plants recorded after 15 days of non-treatment and drought treatment. **(J)** Phenotypes of plant height of wild-type, miR408a-KO and miR408a-OE plants under drought treatment in the field. **(K, L)** Grain phenotype and 100-seed weight analysis of wild-type, miR408a-KO, and miR408a-OE plants under drought treatment. **(M)** Seed vigor of wild-type, miR408a-KO and miR408a-OE plants under 12% PEG6000 treatment. A total of 0.4% TTC solution was used for staining observation of seed vigor. Control: maize kernels boiled in boiling water for 2 h; Untreatment: maize kernels without drought treatment. **(N, O)** Malondialdehyde (MDA) content and Proline (Pro) content in leaves of wild-type, miR408a-KO, and miR408a-OE plants under drought treatment. Data were expressed as the mean of triplicate values and error represented the SD, $p < 0.05$ (*) and $p < 0.01$ (**).

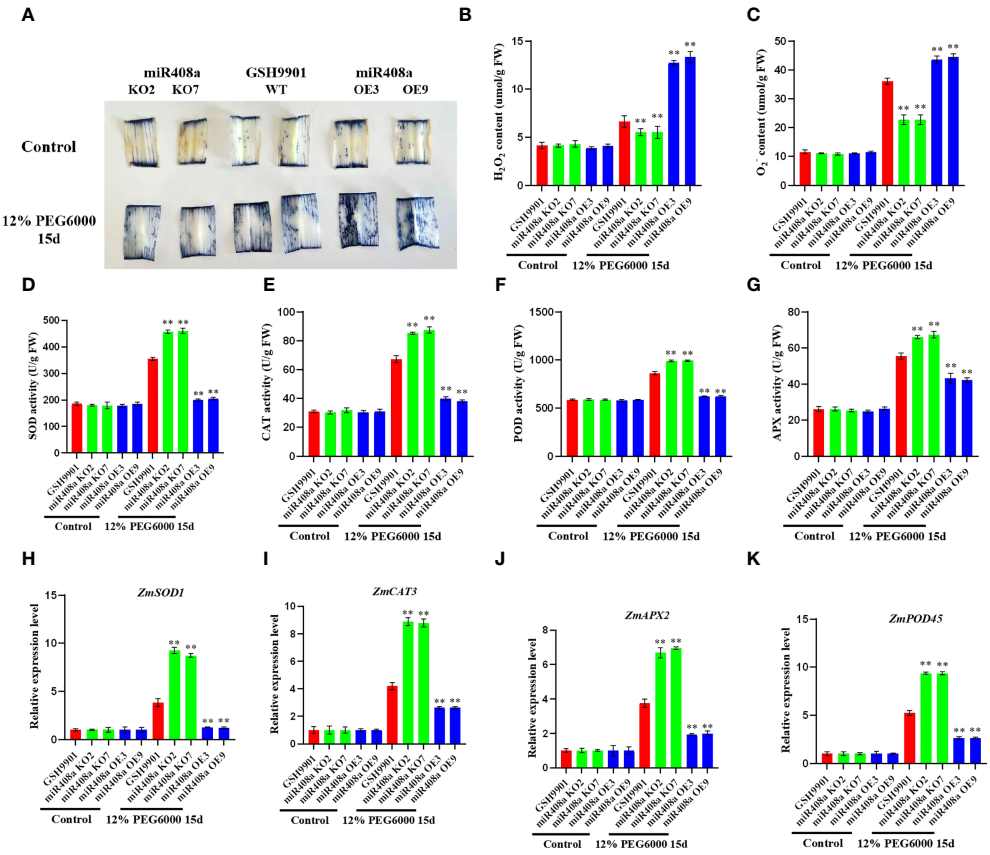


FIGURE 8
ZmmiR408a reduced drought tolerance by regulating ROS accumulation in maize. **(A)** Nitrotetrazolium Blue chloride (NBT) staining of wildtype, miR408a-KO, and miR408a-OE plants were conducted drought treatment for 15 days, which was used to monitor the ROS production in drought-treated leaves. **(B, C)** Hydrogen peroxide (H_2O_2) content and Superoxide radical (O_2^-) content in leaves. **(D–G)** Analysis of catalase (CAT), superoxide dismutase (SOD), peroxidase (POD), and ascorbate peroxidase (APX) activity in drought-treated leaves. **(H–K)** Analysis on expression patterns of ROS-related Marker genes in drought treated leaves. The expression level was normalized to that of Maize Actin. Data were expressed as the mean of triplicate values and error represented the SD, $p < 0.05$ (*) and $p < 0.01$ (**).

MiRNA sequencing analysis and drought stress response

Abiotic stress generates marked molecular responses that influence the healthy growth and development of plants. In recent years, the molecular mechanisms underlying plant responses to abiotic stress have attracted extensive attention (Alcázar et al., 2006; Shi and Chan, 2014; Luan et al., 2015; Ansari and Ahmad, 2019; Zhou et al., 2021). To investigate the molecular mechanisms involved in maize seedling root system responses to drought stress, we performed sRNA sequencing analysis. Data analysis identified 32 DEMIRs from 9 libraries, of which 25 known miRNAs were from 9 miRNA families (Table S2). Among these miRNA families, miR159, miR393, miR169, miR390, miR528, miR397, miR398, and miR166 have been shown to have roles in drought stress responses of other plants (Jagadeeswaran et al., 2009; Hamza et al., 2016; Lu et al., 2018; Zhang et al., 2018; López-Galiano et al., 2019; Yuan et al., 2019; Li et al., 2021a; Chen et al., 2021). Nevertheless, there are few relevant studies into the regulation of root drought resistance by the miR408 family. Zhang et al. (2017) found that miRNA408 in rice can affect the homeostasis of copper ions in chloroplasts by mediating target genes, resulting in enhanced stress resistance, enhanced photosynthetic rate, and yield. Ma et al. (2015) found that under the effects of low temperature, drought, oxidation, and osmotic pressure, miR408 in Arabidopsis thaliana mediated the target gene CSD1 to improve plant stress resistance and oxidative stress response. Therefore, we preliminarily conducted verification of the biological function of maize root system miR408a in response to drought stress. In addition, we predicted numerous new miRNAs, seven of which were DEMIRs (Supplementary Table S2), and a future study of their

biological functions in plant abiotic stress will be of considerable interest.

mRNA sequencing analysis and drought stress response

Transcriptome sequencing analysis of the maize root system under drought stress identified 1,846 upregulated and 1,919 downregulated DEGs. Based on sequencing data and KEGG enrichment analysis, the 3,765 DEGs were found to be mainly enriched in four pathways: "plant hormone signal transduction", "phenylpropane biosynthesis", "glutathione metabolism", and "starch and sucrose metabolism". This result was consistent with those of the current study, because differences in relevant biological data suggested that these four pathways may be involved in responses to drought stress. Kumar et al. (2020) found that DEGs related to plant hormone signal transduction are regulated under drought stress in mung beans, while Yu et al. (2020) found that DEGs related to phenylpropanoid biosynthesis have important regulatory roles under drought stress in foxtail millet. Furthermore, Song et al. (2021) found that japonica and indica rice exhibit strongly DEGs related to the glutathione metabolic pathway under water shortage conditions, while Qian et al. (2021) found that the expression of DEGs related to starch and sucrose metabolic pathways was increased under drought conditions, indicating their importance in stress tolerance. These findings, together with those of this study, confirm that "plant hormone signal transduction", "phenylpropane biosynthesis", "glutathione metabolism", and "starch and sucrose metabolism" are important pathways in maize responses to drought stress, which further supports the findings of the current study.

MiRNA–mRNA regulatory network plays a key role in plant responses to abiotic stresses

Kang et al. (2021) and Yang et al. (2021a) demonstrated that combined analysis of miRNA–mRNA can reveal relevant regulatory mechanisms with important roles in plant responses to abiotic stress. Here, we conducted combined analysis of miRNAs and mRNAs related to maize root system drought stress responses, detected correlations between a series of DEMIRs and DEMRs, and constructed a regulatory network map. Many studies have reported miRNA target genes related to plant hormone signal transduction (Li et al., 2019; Cui et al., 2020; Singh et al., 2021; Lei et al., 2021; Yang et al., 2021b). Most interestingly, we also found that numerous target genes regulated by miRNAs were also enriched in the three pathways: "phenylpropane biosynthesis", "glutathione metabolism", and "starch and sucrose metabolism". Discovery of these target genes lays a theoretical foundation for follow-up research into the biological functions of miRNAs regulated in the maize root system under drought stress.

Plant hormone signal transduction pathway is a crucial process in regulating environmental stress responses

Blázquez et al. (2020) proposed that, with developments in high-throughput sequencing and new gene manipulation techniques, various plant hormones with important roles in regulating environmental stress responses will be identified. As an important plant hormone, ABA functions in response to abiotic stressors (such as drought, saline, alkali, and cold), as well as in plant growth and development. Since abiotic stress affects crop yield, study of ABA signaling in plants can effectively improve crop quality. Overexpression of the ABA receptors, PYR/PYL, can effectively inhibit protein phosphatase 2C (PP2C) and release SnRK2 protein kinases during ABA signal transduction, and further activate ABF transcription factor-mediated regulation of downstream target genes. Here, we found that the PYR/PYL-PP2Cs-SnRK2s regulatory module was activated, and that related protein-coding genes were upregulated, thus triggering ABA signaling. Based on analysis of physiological indices, we confirmed that increased ABA content in the maize root system was positively correlated with expression of PYR/PYL, SnRK2s, and ABF-related genes.

JA molecules are a ubiquitous class of adipose hormones that regulate plant growth and development, as well as stress responses. Li et al. (2021b) found that the COI1–JAZ complex is a JA pathway receptor, which mediates JAZ degradation and thereby influences JA pathway transcription factors to regulate downstream target gene expression. In this study, we found that the jasmonate amino acid conjugating enzyme, JAR1, and the JA signaling hub protein, JAZ, were downregulated and, in turn, attenuated JA signal transduction, which was positively correlated with physiological changes in JA content.

BRs are a class of hormones with crucial roles in plant growth and development. Jiang et al. (2019) found that the negative regulator of BRs signaling, BIN2, can promote the upregulation of RD26 genes to improve plant drought resistance. Lin et al. (2013) found that miR395a regulated root growth and stress tolerance of Arabidopsis seedlings by inhibiting GUN5 expression and its downstream signal transduction under brassinolide treatment. Here, we found that BIN2 was significantly downregulated in response to increased drought duration, and negatively correlated with physiological alterations in BR content.

GA3 is a growth-regulating hormone involved in stress responses. Zheng et al. (2020) confirmed that miR396b targets SmGRFs, SmHDT1, and SmMYB37/4 to mediate the phytohormone, especially gibberellin signaling pathways and consequentially resulted in the phenotype variation of miR396b-OE hairy roots. Furthermore, miR396b could be activated by methyl jasmonate, abscisic acid, gibberellin, salt, and drought stresses. In this study, we found that decreased GA3 content with increased drought duration could affect the expression of DELLA genes.

Together, these findings show that plant hormones have important regulatory roles in responses to abiotic stress, that regulation of multiple hormones is a likely focus of intense plant research, and that the ABA, JA, BRS, and GA3 signaling pathways may be involved in maize root system-mediated drought tolerance.

Phenylpropanoid biosynthesis pathway affects plant resistance to stress

The phenylpropanoid biosynthesis pathway can affect stress responses, as well as plant growth and development. Dong and Lin (2021) found that the plant phenylpropane metabolic pathway, particularly lignin synthesis, has important regulatory functions in plant responses to biotic and abiotic stressors. The initial reaction of phenylpropane metabolism involves PAL, while CAD genes are important for lignin biosynthesis. Sun et al. (2020) found that overexpression of the cotton Gh4CL7 gene in Arabidopsis can increase the expression of the lignin synthesis gene PAL, thereby improving drought resistance. Liu et al. (2020) found that overexpression of CmCAD2 and CmCAD3 genes could improve drought tolerance through recovering lignin synthesis and root development in Arabidopsis. Here, we conducted deep analysis of the reasons underlying significant upregulation of PAL genes with increased drought duration, which in turn leads to significant elevation of CAD gene expression and activation of the phenylpropane biosynthesis pathway. Peroxidase genes function in the final pathway of "phenylpropane biosynthesis". Here, we demonstrated that CAD genes were activated with increased drought duration, followed by activation of peroxidase genes, leading to lignin accumulation and improved maize drought resistance, suggesting that lignin synthesis in the root system is an important feature of maize responses to drought stress.

Glutathione metabolic pathway plays an important resistance system in plant signal transduction and stress responses

Glutathione metabolism is important for plant responses to biotic and abiotic stress. Nerva et al. (2022) showed that expression of glutathione-S-transferase can effectively improve grape drought tolerance, and activate the expression of antioxidants and ABA-related transcripts. Priya et al. (2019) found that GABA genes can increase the activity of respiratory-related enzymes under heat stress in mung beans, thus protecting plant growth and development. Jin et al. (2019) found that exogenous application of GABA genes can effectively improve muskmelon tolerance to hypoxic stress and avoid photooxidative plant damage. Here, we showed that GAD gene expression was upregulated in the maize root system with increased drought duration, which, in turn, promoted the GABA gene expression. Furthermore, mRNA levels of four POP2-related genes were significantly increased, which promoted SSADH gene expression, and finally activated the glutathione metabolic pathway.

Starch and sucrose metabolic pathways are vital mechanisms in regulating the physiological mechanisms of plant abiotic stress

Starch and sucrose metabolism are important mechanisms in regulation of plant responses to drought stress. Wang et al. (2020) found that expression of key genes related to starch and sucrose metabolism is induced under long-term drought stress in tobacco. Moenga et al. (2020) conducted transcriptome analysis of wild and cultivated chickpeas under drought stress and found that some transcripts involved in starch and sucrose transport were activated. SPS is the key rate-limiting enzyme in sucrose anabolism, and Li et al. (2011) found that overexpression of the TPP gene in rice can effectively improve drought resistance. Furthermore, Nuccio et al. (2015) found that overexpression of TPP genes can promote trehalose metabolism to generate sucrose and improve potato drought tolerance in the greenhouse. In this study, we showed that SPS and TPP genes were significantly upregulated with increased drought duration, consistent with the results of the published studies mentioned above. Gupta et al. (2020) found that drought signaling can affect the generation of metabolites, such as trehalose and proline, stimulate the antioxidant system to maintain redox homeostasis, and prevent cell damage and disruption of cell membrane integrity, through oxide enzyme activity. Here, we found that TPP was a key enzyme in trehalose synthesis and that trehalose content increased rapidly in the maize root system with increased duration of drought. Therefore, upregulation of trehalose biosynthesis and trehalose accumulation may have protective and regulatory effects on the maize root system under drought stress.

Conclusions

Drought stress has significant effects on maize plant performance. ABA, BRs, GSH, lignin, and trehalose content, as well as peroxidase activity, increased, while GA and JA content decreased with increased drought stress duration. A total of 32 DEMIRs and 3,765 DEMRs were identified, and 16 miRNA–target gene pairs, composed of 9 DEMIRs and 15 DEMRs, were obtained by miRNA–mRNA combined analysis. Four important metabolic pathways, "plant hormone signal transduction", "phenylpropane biosynthesis", "glutathione metabolism", and "starch and sucrose metabolism", were analyzed. Additionally, we demonstrate that miR408a is a negative regulator of drought response in the maize root system, primarily through regulation of ROS accumulation.

Data availability statement

The datasets presented in this study can be found in online repositories. The data presented in the study are deposited in the NCBI repository, accession number PRJNA796152 and PRJNA793522.

Author contributions

SG and YM conceived research plans and designed experiments. PJ, CW, and NC conducted experiments. PJ and RM wrote the draft. SL and JQ analyzed the data. PJ, SG, and YM reviewed and edited this article and provided helpful comments and discussions. All authors read and approved the final manuscript.

Funding

This work was supported by Jilin Province Science and Technology Development Plan Project (20200402023NC and 20210302003NC). Furthermore, the funding body has no role in designing the study, collection and interpretation of data, or writing the manuscript.

Conflict of interest

The authors declare that the research was conducted in the absence of any commercial or financial relationships that could be construed as a potential conflict of interest.

Publisher's note

All claims expressed in this article are solely those of the authors and do not necessarily represent those of their affiliated organizations, or those of the publisher, the editors and the reviewers. Any product that may be evaluated in this article, or claim that may be made by its manufacturer, is not guaranteed or endorsed by the publisher.

Supplementary material

The Supplementary Material for this article can be found online at: https://www.frontiersin.org/articles/10.3389/fpls.2022.932667/full#supplementary-material

References

Akdogan, G., Tufekci, E. D., Uranbey, S., and Unver, T. (2016). miRNA-based drought regulation in wheat. *Funct. Integr. Genomics* 16 (3), 221–233. doi: 10.1007/s10142-015-0452-1

Alcázar, R., Marco, F., Cuevas, J. C., Patron, M., Ferrando, A., Carrasco, P., et al. (2006). Involvement of polyamines in plant response to abiotic stress. *Biotechnol. Lett.* 28 (23), 1867–1876. doi: 10.1007/s10529-006-9179-3

Ansari, F. A., and Ahmad, I. (2019). Isolation, functional characterization and efficacy of biofilm-forming rhizobacteria under abiotic stress conditions. *Antonie van Leeuwenhoek* 112 (12), 1827–1839. doi: 10.1007/s10482-019-01306-3

Arshad, M., Feyissa, B. A., Amyot, L., Aung, B., and Hannoufa, A. (2017). MicroRNA156 improves drought stress tolerance in alfalfa (Medicago sativa) by silencing SPL13. *Plant Sci.: Int. J. Exp. Plant Biol.* 258, 122–136. doi: 10.1016/j.plantsci.2017.01.018

Battaglia, M., Olvera-Carrillo, Y., Garciarrubio, A., Campos, F., and Covarrubias, A. A. (2008). The enigmatic LEA proteins and other hydrophilins. *Plant Physiol.* 148 (1), 6–24. doi: 10.1104/pp.108.120725

Blázquez, M. A., Nelson, D. C., and Weijers, D. (2020). Evolution of plant hormone response pathways. *Annu. Rev. Plant Biol.* 71, 327–353. doi: 10.1146/annurev-arplant-050718-100309

Bulgakov, V. P., Wu, H. C., and Jinn, T. L. (2019). Coordination of ABA and chaperone signaling in plant stress responses. *Trends Plant Sci.* 24 (7), 636–651. doi: 10.1016/j.tplants.2019.04.004

Chen, C., Ridzon, D. A., Broomer, A. J., Zhou, Z., Lee, D. H., Nguyen, J. T., et al. (2005). Real-time quantification of microRNAs by stem-loop RT-PCR. *Nucleic Acids Res.* 33 (20), e179. doi: 10.1093/nar/gni178

Chen, S., Yi, L., Korpelainen, H., Yu, F., and Liu, M. (2020). Roots play a key role in drought-tolerance of poplars as suggested by reciprocal grafting between male and female clones. *Plant Physiol. biochemistry: PPB* 153, 81–91. doi: 10.1016/j.plaphy.2020.05.014

Chen, J., Zhong, Y., and Qi, X. (2021). LncRNA TCONS_00021861 is functionally associated with drought tolerance in rice (Oryza sativa l.) *via* competing endogenous RNA regulation. *BMC Plant Biol.* 21 (1), 410. doi: 10.1186/s12870-021-03195-z

Cui, J., You, C., and Chen, X. (2017). The evolution of microRNAs in plants. *Curr. Opin. Plant Biol.* 35, 61–67. doi: 10.1016/j.pbi.2016.11.006

Cui, G., Zhao, M., Zhang, S., Wang, Z., Meng, M., Sun, F., et al. (2020). MicroRNA and regulation of auxin and cytokinin signalling during post-mowing regeneration of winter wheat (Triticum aestivum l.). *Plant Physiol. Biochem.* 155, 769–779. doi: 10.1016/j.plaphy.2020.08.032

Dong, N. Q., and Lin, H. X. (2021). Contribution of phenylpropanoid metabolism to plant development and plant-environment interactions. *J. Integr. Plant Biol.* 63 (1), 180–209. doi: 10.1111/jipb.13054

Fang, Y., Xie, K., and Xiong, L. (2014). Conserved miR164-targeted NAC genes negatively regulate drought resistance in rice. *J. Exp. Bot.* 65 (8), 2119–2135. doi: 10.1093/jxb/eru072

Guo, Q., Li, X., Niu, L., Jameson, P. E., and Zhou, W. (2021). Transcription-associated metabolomic adjustments in maize occur during combined drought and cold stress. *Plant Physiol.* 186 (1), 677–695. doi: 10.1093/plphys/kiab050

Gupta, A., Rico-Medina, A., and Caño-Delgado, A. I. (2020). The physiology of plant responses to drought. *Sci. (New York N.Y.)* 368 (6488), 266–269. doi: 10.1126/science.aaz7614

Hamza, N. B., Sharma, N., Tripathi, A., and Sanan-Mishra, N. (2016). MicroRNA expression profiles in response to drought stress in sorghum bicolor. *Gene Expression patterns: GEP* 20 (2), 88–98. doi: 10.1016/j.gep.2016.01.001

Hang, N., Shi, T., Liu, Y., Ye, W., Taier, G., Sun, Y., et al. (2021). Overexpression of os-microRNA408 enhances drought tolerance in perennial ryegrass. *Physiologia plantarum* 172 (2), 733–747. doi: 10.1111/ppl.13276

Jagadeeswaran, G., Saini, A., and Sunkar, R. (2009). Biotic and abiotic stress down-regulate miR398 expression in arabidopsis. *Planta* 229 (4), 1009–1014. doi: 10.1007/s00425-009-0889-3

Jiang, H., Tang, B., Xie, Z., Nolan, T., Ye, H., Song, G. Y., et al. (2019). GSK3-like kinase BIN2 phosphorylates RD26 to potentiate drought signaling in arabidopsis. *Plant journal: Cell Mol. Biol.* 100 (5), 923–937. doi: 10.1111/tpj.14484

Jian, X., Zhang, L., Li, G., Zhang, L., Wang, X., Cao, X., et al. (2010). Identification of novel stress-regulated microRNAs from. *Genomics* 95 (1), 47–55. doi: 10.1016/j.ygeno.2009.08.017

Jiao, P., Jiang, Z., Wei, X., Liu, S., Qu, J., Guan, S., et al. (2022a). Overexpression of the homeobox-leucine zipper protein ATHB-6 improves the drought tolerance of maize (Zea mays l.). *Plant science: an Int. J. Exp. Plant Biol.* 316, 111159. doi: 10.1016/j.plantsci.2021.111159

Jiao, P., Jin, S., Chen, N., Wang, C., Liu, S., Qu, J., et al. (2022b). Improvement of cold tolerance in maize (Zea mays l.) using agrobacterium-mediated transformation of ZmSAMDC gene. *GM Crops Food* 13 (1), 131–141. doi: 10.1080/21645698.2022.2097831

Jin, X., Liu, T., Xu, J., Gao, Z., and Hu, X. (2019). Exogenous GABA enhances muskmelon tolerance to salinity-alkalinity stress by regulating redox balance and chlorophyll biosynthesis. *BMC Plant Biol.* 19 (1), 48. doi: 10.1186/s12870-019-1660-y

Kang, Y., Yang, X., Liu, Y., Shi, M., Zhang, W., Fan, Y., et al. (2021). Integration of mRNA and miRNA analysis reveals the molecular mechanism of potato (Solanum tuberosum l.) response to alkali stress. *Int. J. Biol. macromolecules* 182, 938–949. doi: 10.1016/j.ijbiomac.2021.04.094

Kaur, K., Duhan, N., Singh, J., Kaur, G., and Vikal, Y. (2020). Computational identification of maize miRNA and their gene targets involved in biotic and abiotic stresses. *J. Biosci.* 45, 132. doi: 10.1007/s12038-020-00106-6

Koester, R. P., Pignon, C. P., Kesler, D. C., Willison, R. S., Kang, M., Shen, Y., et al. (2021). Transgenic insertion of the cyanobacterial membrane protein ictB increases grain yield in zea mays through increased photosynthesis and carbohydrate production. *PloS One* 16 (2), e0246359. doi: 10.1371/journal.pone.0246359

Kravchik, M., Stav, R., Belausov, E., and Arazi, T. (2019). Functional characterization of microRNA171 family in tomato. *Plants (Basel Switzerland)* 8 (1), 10. doi: 10.3390/plants8010010

Kumar, S., Ayachit, G., and Sahoo, L. (2020). Screening of mungbean for drought tolerance and transcriptome profiling between drought-tolerant and susceptible genotype in response to drought stress. *Plant Physiol. biochemistry: PPB* 157, 229–238. doi: 10.1016/j.plaphy.2020.10.021

Lee, R. C., Feinbaum, R. L., and Ambros, V. (1993). The c. elegans heterochronic gene lin-4 encodes small RNAs with antisense complementarity to lin-14. *Cell* 75 (5), 843–854. doi: 10.1016/0092-8674(93)90529-y

Lei, P., Qi, N., Zhou, Y., Wang, Y., Zhu, X., Xuan, Y., et al. (2021). Soybean miR159-GmMYB33 regulatory network involved in gibberellin-modulated resistance to heterodera glycines. *Int. J. Mol. Sci.* 22 (23), 13172. doi: 10.3390/ijms222313172

Li, J., Duan, Y., Sun, N., Wang, L., Feng, S., Fang, Y., et al. (2021a). The miR169n-NF-YA8 regulation module involved in drought resistance in brassica napus l. *Plant science: an Int. J. Exp. Plant Biol.* 313, 111062. doi: 10.1016/j.plantsci.2021.111062

Li, K., Liu, Z., Xing, L., Wei, Y., Mao, J., Meng, Y., et al. (2019). miRNAs associated with auxin signaling, stress response, and cellular activities mediate adventitious root formation in apple rootstocks. *Plant Physiol. Biochem.* 139, 66–81. doi: 10.1016/j.plaphy.2019.03.006

Li, Z., Luo, X., Ou, Y., Jiao, H., Peng, L., Fu, X., et al. (2021b). Jasmonate-zim domain proteins engage polycomb chromatin modifiers to modulate jasmonate signaling in arabidopsis. *Mol. Plant* 14 (5), 732–747. doi: 10.1016/j.molp.2021.03.001

Livak, K. J., and Schmittgen, T. D. (2001). Analysis of relative gene expression data using real-time quantitative PCR and the 2(-delta C(T)) method. *Methods (San Diego Calif.)* 25 (4), 402–408. doi: 10.1006/meth.2001.1262

Li, H. W., Zang, B. S., Deng, X. W., and Wang, X. P. (2011). Overexpression of the trehalose-6-phosphate synthase gene OsTPS1 enhances abiotic stress tolerance in rice. *Planta* 234 (5), 1007–1018. doi: 10.1007/s00425-011-1458-0

Lin, L. L., Wu, C. C., Huang, H. C., Chen, H. J., Hsieh, H. L., and Juan, H. F. (2013). Identification of microRNA 395a in 24- epibrassinolide-regulated root growth of Arabidopsis thaliana using microRNA arrays. *Int. J. Mol. Sci.* 14 (7), 14270–14286. doi: 10.3390/ijms140714270

Liu, W., Jiang, Y., Wang, C., Zhao, L., Jin, Y., Xing, Q., et al. (2020). Lignin synthesized by CmCAD2 and CmCAD3 in oriental melon (Cucumis melo L.) seedlings contributes to drought tolerance. *Plant. Mol. Biol.* 103 (6), 689–704. doi: 10.1007/s11103-020-01018-7

López-Galiano, M. J., García-Robles, I., González-Hernández, A. I., Camañes, G., Vicedo, B., Real, M. D., et al. (2019). Expression of miR159 is altered in tomato plants undergoing drought stress. *Plants (Basel Switzerland)* 8 (7), 201. doi: 10.3390/plants8070201

Luan, M., Xu, M., Lu, Y., Zhang, L., Fan, Y., and Wang, L. (2015). Expression of zma-miR169 miRNAs and their target ZmNF-YA genes in response to abiotic stress in maize leaves. *Gene* 555 (2), 178–185. doi: 10.1016/j.gene.2014.11.001

Lu, Y., Feng, Z., Liu, X., Bian, L., Xie, H., Zhang, C., et al. (2018). MiR393 and miR390 synergistically regulate lateral root growth in rice under different conditions. *BMC Plant Biol.* 18 (1), 261. doi: 10.1186/s12870-018-1488-x

Ma, C., Burd, S., and Lers, A. (2015). miR408 is involved in abiotic stress responses in arabidopsis. *Plant journal: Cell Mol. Biol.* 84 (1), 169–187. doi: 10.1111/tpj.12999

Moenga, S. M., Gai, Y., Carrasquilla-Garcia, N., Perilla-Henao, L. M., and Cook, D. R. (2020). Gene co-expression analysis reveals transcriptome divergence between wild and cultivated chickpea under drought stress. *Plant journal: Cell Mol. Biol.* 104 (5), 1195–1214. doi: 10.1111/tpj.14988

Nerva, L., Guaschino, M., Pagliarani, C., De Rosso, M., Lovisolo, C., and Chitarra, W. (2022). Spray-induced gene silencing targeting a glutathione s-transferase gene improves resilience to drought in grapevine. *Plant Cell Environ.* 45 (2), 347–361. doi: 10.1111/pce.14228

Ni, Z., Hu, Z., Jiang, Q., and Zhang, H. (2013). GmNFYA3, a target gene of miR169, is a positive regulator of plant tolerance to drought stress. *Plant Mol. Biol.* 82 (1-2), 113–129. doi: 10.1007/s11103-013-0040-5

Nuccio, M. L., Wu, J., Mowers, R., Zhou, H. P., Meghji, M., Primavesi, L. F., et al. (2015). Expression of trehalose-6-phosphate phosphatase in maize ears improves yield in well-watered and drought conditions. *Nat. Biotechnol.* 33 (8), 862–869. doi: 10.1038/nbt.3277

Pan, X., Welti, R., and Wang, X. (2010). Quantitative analysis of major plant hormones in crude plant extracts by high-performance liquid chromatography-mass spectrometry. *Nat. Protoc.* 5 (6), 986–992. doi: 10.1038/nprot.2010.37

Pegler, J. L., Oultram, J., Grof, C., and Eamens, A. L. (2019). Profiling the abiotic stress responsive microRNA landscape of *Arabidopsis thaliana*. *Plants (Basel Switzerland)* 8 (3), 58. doi: 10.3390/plants8030058

Priya, M., Sharma, L., Kaur, R., Bindumadhava, H., Nair, R. M., Siddique, K., et al. (2019). GABA (γ-aminobutyric acid), as a thermo-protectant, to improve the reproductive function of heat-stressed mungbean plants. *Sci. Rep.* 9 (1), 7788. doi: 10.1038/s41598-019-44163-w

Qian, H., Xu, Z., Cong, K., Zhu, X., Zhang, L., Wang, J., et al. (2021). Transcriptomic responses to drought stress in polygonatum kingianum tuber. *BMC Plant Biol.* 21 (1), 537. doi: 10.1186/s12870-021-03297-8

Ramanjulu, S., and Bartels, D. (2002). Drought- and desiccation-induced modulation of gene expression in plants. *Plant Cell Environ.* 25 (2), 141–151. doi: 10.1046/j.0016-8025.2001.00764.x

Shi, H., and Chan, Z. (2014). Improvement of plant abiotic stress tolerance through modulation of the polyamine pathway. *J. Integr. Plant Biol.* 56 (2), 114–121. doi: 10.1111/jipb.12128

Singh, P., Dutta, P., and Chakrabarty, D. (2021). miRNAs play critical roles in response to abiotic stress by modulating cross-talk of phytohormone signaling. *Plant Cell Rep.* 40 (9), 1617–1630. doi: 10.1007/s00299-021-02736-y

Song, T., Das, D., Ye, N. H., Wang, G. Q., Zhu, F. Y., Chen, M. X., et al. (2021). Comparative transcriptome analysis of coleorhiza development in japonica and indica rice. *BMC Plant Biol.* 21 (1), 514. doi: 10.1186/s12870-021-03276-z

Su, F., Li, Y., Liu, S., Liu, Z., and Xu, H. L. (2019). Application of xerophytophysiology and signal transduction in plant production: partial root-zone drying in potato crops. *Potato Res.* 63 (4), 41–56. doi: 10.1007/s11540-019-09427-y

Sunkar, R., and Zhu, J. K. (2004). Novel and stress-regulated microRNAs and other small RNAs from arabidopsis. *Plant Cell* 16 (8), 2001–2019. doi: 10.1105/tpc.104.022830

Sun, S. C., Xiong, X. P., Zhang, X. L., Feng, H. J., Zhu, Q. H., Sun, J., et al. (2020). Characterization of the Gh4CL gene family reveals a role of Gh4CL7 in drought tolerance. *BMC Plant Biol.* 20 (1), 125. doi: 10.1186/s12870-020-2329-2

Tõldsepp, K., Zhang, J., Takahashi, Y., Sindarovska, Y., Hõrak, H., Ceciliato, P., et al. (2018). Mitogen-activated protein kinases MPK4 and MPK12 are key components mediating CO2 -induced stomatal movements. *Plant journal: Cell Mol. Biol.* 96 (5), 1018–1035. doi: 10.1111/tpj.14087

Voinnet, O. (2009). Origin, biogenesis, and activity of plant microRNAs. *Cell* 136 (4), 669–687. doi: 10.1016/j.cell.2009.01.046

Wang, J., Zhang, S., Fu, Y., He, T., and Wang, X. (2020). Analysis of dynamic global transcriptional atlas reveals common regulatory networks of hormones and photosynthesis across *Nicotiana* varieties in response to long-term drought. *Front. Plant Sci.* 11. doi: 10.3389/fpls.2020.00672

Yang, X., Kang, Y., Liu, Y., Shi, M., Zhang, W., Fan, Y., et al. (2021a). Integrated analysis of miRNA-mRNA regulatory networks of potato (Solanum tuberosum l.) in response to cadmium stress. *Ecotoxicology Environ. Saf.* 224, 112682. doi: 10.1016/j.ecoenv.2021.112682

Yang, Y., Zhang, X., Chen, Y., Guo, J., Ling, H., Gao, S., et al. (2016). Selection of reference genes for normalization of MicroRNA expression by RT-qPCR in sugarcane buds under cold stress. *Front. Plant Sci.* 7, 86. doi: 10.3389/fpls.2016.00086

Yang, J., Zhang, N., Zhang, J., Jin, X., Zhu, X., Ma, R., et al. (2021b). Knockdown of MicroRNA160a/b by STTM leads to root architecture changes *via* auxin signaling in solanum tuberosum. *Plant Physiol. Biochem.* 166, 939–949. doi: 10.1016/j.plaphy.2021.06.051

Yuan, W., Suo, J., Shi, B., Zhou, C., Bai, B., Bian, H., et al. (2019). The barley miR393 has multiple roles in regulation of seedling growth, stomatal density, and drought stress tolerance. . *Plant Physiol. biochemistry: PPB* 142, 303–311. doi: 10.1016/j.plaphy.2019.07.021

Yu, A., Zhao, J., Wang, Z., Cheng, K., Zhang, P., Tian, G., et al. (2020). Transcriptome and metabolite analysis reveal the drought tolerance of foxtail millet significantly correlated with phenylpropanoids-related pathways during germination process under PEG stress. *BMC Plant Biol.* 20 (1), 274. doi: 10.1186/s12870-020-02483-4

Zhai, J., Dong, Y., Sun, Y., Wang, Q., Wang, N., Wang, F., et al. (2014). Discovery and analysis of microRNAs in leymus chinensis under saline-alkali and drought stress using high-throughput sequencing. *PloS One* 9 (11), e105417. doi: 10.1371/journal.pone.0105417

Zhang, H., Liu, X., Yang, X., Wu, H., Zhu, J., and Zhang, H. (2020). miRNA-mRNA integrated analysis reveals roles for miRNAs in a typical halophyte, *Reaumuria soongorica*, during seed germination under salt stress. *Plants (Basel Switzerland)* 9 (3), 351. doi: 10.3390/plants9030351

Zhang, J. P., Yu, Y., Feng, Y. Z., Zhou, Y. F., Zhang, F., Yang, Y. W., et al. (2017). MiR408 regulates grain yield and photosynthesis *via* a phytocyanin protein. *Plant Physiol.* 175 (3), 1175–1185. doi: 10.1104/pp.17.01169

Zhang, J., Zhang, H., Srivastava, A. K., Pan, Y., Bai, J., Fang, J., et al. (2018). Knockdown of rice MicroRNA166 confers drought resistance by causing leaf rolling and altering stem xylem development. *Plant Physiol.* 176 (3), 2082–2094. doi: 10.1104/pp.17.01432

Zhang, X., Zou, Z., Gong, P., Zhang, J., Ziaf, K., Li, H., et al. (2011). Over-expression of microRNA169 confers enhanced drought tolerance to tomato. *Biotechnol. Lett.* 33 (2), 403–409. doi: 10.1007/s10529-010-0436-0

Zhao, Y., and Srivastava, D. (2007). A developmental view of microRNA function. *Trends Biochem. Sci.* 32 (4), 189–197. doi: 10.1016/j.tibs.2007.02.006

Zheng, X., Li, H., Chen, M., Zhang, J., Tan, R., Zhao, S., et al. (2020). Smi-miR396b targeted SmGRFs, SmHDT1, and SmMYB37/4 synergistically regulates cell growth and active ingredient accumulation in salvia miltiorrhiza hairy roots. *Plant Cell Rep.* 39 (10), 1263–1283. doi: 10.1007/s00299-020-02562-8

Zhou, X., Joshi, S., Khare, T., Patil, S., Shang, J., and Kumar, V. (2021). Nitric oxide, crosstalk with stress regulators and plant abiotic stress tolerance. *Plant Cell Rep.* 40 (8), 1395–1414.

Zhou, M., and Tang, W. (2019). MicroRNA156 amplifies transcription factor-associated cold stress tolerance in plant cells. *Mol. Genet. genomics: MGG* 294 (2), 379–393. doi: 10.1007/s00438-018-1516-4

frontiers | Frontiers in Plant Science

TYPE Original Research
PUBLISHED 03 October 2022
DOI 10.3389/fpls.2022.985088

Check for updates

OPEN ACCESS

EDITED BY
Jiban Shrestha,
Nepal Agricultural Research Council, Nepal

REVIEWED BY
Mateja Germ,
University of Ljubljana, Slovenia
Panfeng Yao,
Gansu Agricultural University, China

*CORRESPONDENCE
Hong-You Li
lihongyouluod@163.com

†These authors have contributed equally to this work

SPECIALTY SECTION
This article was submitted to Plant Abiotic Stress, a section of the journal Frontiers in Plant Science

RECEIVED 03 July 2022
ACCEPTED 13 September 2022
PUBLISHED 03 October 2022

CITATION
Meng H-L, Sun P-Y, Wang J-R, Sun X-Q, Zheng C-Z, Fan T, Chen Q-F and Li H-Y (2022) Comparative physiological, transcriptomic, and WGCNA analyses reveal the key genes and regulatory pathways associated with drought tolerance in Tartary buckwheat. *Front. Plant Sci.* 13:985088. doi: 10.3389/fpls.2022.985088

COPYRIGHT
© 2022 Meng, Sun, Wang, Sun, Zheng, Fan, Chen and Li. This is an open-access article distributed under the terms of the Creative Commons Attribution License (CC BY). The use, distribution or reproduction in other forums is permitted, provided the original author(s) and the copyright owner(s) are credited and that the original publication in this journal is cited, in accordance with accepted academic practice. No use, distribution or reproduction is permitted which does not comply with these terms.

Comparative physiological, transcriptomic, and WGCNA analyses reveal the key genes and regulatory pathways associated with drought tolerance in Tartary buckwheat

Heng-Ling Meng[2†], Pei-Yuan Sun[1,3†], Jia-Rui Wang[1,3†], Xiao-Qian Sun[1], Chuan-Zhi Zheng[2], Ting Fan[2], Qing-Fu Chen[1] and Hong-You Li[1,4*]

[1]Research Center of Buckwheat Industry Technology, Guizhou Normal University, Guiyang, China, [2]Key Laboratory of High-Quality Crops Cultivation and Safety Control of Yunnan Province, Honghe University, Honghe, China, [3]College of Life Science, Guizhou Normal University, Guiyang, China, [4]Key Laboratory of Plant Resources Conservation and Germplasm Innovation in Mountainous Region of Ministry of Education, Guizhou University, Guiyang, China

Drought stress is one of the major abiotic stress factors that affect plant growth and crop productivity. Tartary buckwheat is a nutritionally balanced and flavonoid-rich pseudocereal crop and also has strong adaptability to different adverse environments including drought. However, little is known about its drought tolerance mechanism. In this study, we performed comparative physiological and transcriptomic analyses of two contrasting drought-resistant Tartary buckwheat genotypes under nature drought treatment in the reproductive stage. Under drought stress, the drought-tolerant genotype XZSN had significantly higher contents of relative water, proline, and soluble sugar, as well as lower relative electrolyte leakage in the leaves than the drought-susceptible LK3. A total of 5,058 (2,165 upregulated and 2,893 downregulated) and 5,182 (2,358 upregulated and 2,824 downregulated) potential drought-responsive genes were identified in XZSN and LK3 by transcriptome sequencing analysis, respectively. Among the potential drought-responsive genes of XZSN, 1,206 and 1,274 genes were identified to be potential positive and negative contributors for XZSN having higher drought resistance ability than LK3. Furthermore, 851 out of 1,206 positive drought-resistant genes were further identified to be the core drought-resistant genes of XZSN based on WGCNA analysis, and most of them were induced earlier and quicker by drought stress than those in LK3. Functional annotation of the 851 core drought-resistant genes found that a large number of stress-responsive genes were involved in TFs, abscisic acid (ABA) biosynthesis, signal transduction and response, non-ABA signal molecule biosynthesis, water holding, oxygen species scavenging, osmotic adjustment, cell damage prevention, and so on. Transcriptional regulatory network analyses identified the potential regulators

of these drought-resistant functional genes and found that the HD-ZIP and MYB TFs might be the key downstream TFs of drought resistance in Tartary buckwheat. Taken together, these results indicated that the XZSN genotype was more drought-tolerant than the LK3 genotype as evidenced by triggering the rapid and dramatic transcriptional reprogramming of drought-resistant genes to reduce water loss, prevent cell damage, and so on. This research expands our current understanding of the drought tolerance mechanisms of Tartary buckwheat and provides important information for its further drought resistance research and variety breeding.

KEYWORDS

Tartary buckwheat, drought stress, transcriptome, transcription factor, transcriptional regulatory network, WGCNA

Introduction

Drought/water deficit is one of the most significant environmental stresses, and it restricts plant growth, development, and reproduction as well as threatens worldwide agricultural production and food safety (Thirumalaikumar et al., 2018; Waititu et al., 2021; Wang et al., 2021; Ksouri et al., 2016; Tang et al., 2022; Zhao et al., 2022). It has been shown that drought stress in the reproductive stage will cause an average crop yield reduction of more than 50% (Hu and Xiong, 2014). In addition, 64% of the worldwide land area is affected by drought stress, and the area still continues to increase due to the current ongoing climate changes (Lesk et al., 2016; Omprakash et al., 2017; Waititu et al., 2021). Consequently, dissecting the drought resistance mechanisms in plants or crops and developing drought-resistant crop varieties are the most promising solutions to maintain crop yields under drought conditions and alleviate future threats to food security (Shaar-Moshe et al., 2015; Waititu et al., 2021).

In order to cope with and adapt to drought stress, plants have evolved various drought resistance mechanisms at multiple levels such as molecular, physiological, cellular, and morphological levels (Shaar-Moshe et al., 2015; Zhu, 2016; Wang et al., 2018a). These mechanisms include promoting the formation of deeper roots to increase water uptake, closing the stomata or thickening the leaf cuticle to prevent water loss, and shortening the life cycle through accelerating flowering (Zhu, 2016; Wang et al., 2018a). At the molecular level, plants have developed abscisic acid (ABA)-dependent and ABA-independent pathways to regulate drought resistance (Shinozaki and Yamaguchi-Shinozaki, 2007; Roychoudhury et al., 2013). Among the two regulatory pathways, the ABA-dependent pathway is the major and conserved molecule signal pathway for plant drought resistance (Saradadevi et al., 2017). The ABA content increases rapidly under drought stress by quickly inducing the expression of ABA synthesis genes. As a signal molecule, the accumulated ABA is recognized by the ABA receptor PYR/PYL/RCAR and subsequently initiates the corresponding signal transduction pathways mediated by phosphatases and protein kinases, which further activate or suppress the downstream target transcription factors (TFs) such as AREB/ABF, AP2/ERF, MYB, NAC, HD-ZF, HD-ZIP, bHLH, C2H2-ZF, B3, WRKY, and NF-Y TFs (Fujita et al., 2011; You et al., 2019; Waititu et al., 2021). These TFs further activate the expression of a large number of downstream stress-response genes, leading to a series of physiological, metabolic, cellular, and morphological responses, so as to enhance the drought resistance of plants. These responses include scavenging reactive oxygen species (ROS) through enzymatic and non-enzymatic components; increasing water uptake through the generation of deeper roots; reducing the water loss of leaves through the regulation of stomatal closure or leaf cuticular wax biosynthesis; increasing the accumulation of osmoprotectants such as amino acids, glycine betaine, polyamine, and sugars to perform osmotic adjustments; enhancing the accumulation of protective proteins such as late embryogenesis abundance (LEA) to prevent cell damage; and so on (Nadeem et al., 2019; Waititu et al., 2021). In the ABA-independent pathway, the major regulators are the CBF/DREB TFs, which belong to the ERF/AP2 family. CBF/DREB TFs activate the expression of a series of downstream non-ABA response stress-responsive genes through binding to the conserved DRE (dehydration-responsive element)/CRT (C-RepeaT) DNA-binding motif in the promoter of their target genes and enhance plant drought resistance (Shinozaki and Yamaguchi-Shinozaki, 2007; Roychoudhury et al., 2013; Fu et al., 2016; Huang et al., 2021). In addition, some non-ABA response NAC and bZIP TFs also play crucial roles in plant drought resistance, which have parallel functions with CBF/DREB TFs (Shinozaki and Yamaguchi-Shinozaki, 2007; Roychoudhury et al., 2013; Fu et al., 2016;

Huang et al., 2021). Although the drought resistance mechanisms among different plants are conserved to a certain degree, the drought resistance ability of specific plants strongly depends on the genotype. Under drought stress, the gene responses between drought-tolerant and sensitive genotypes are largely different, and there also exist genotypic-specific responses (Dal Santo et al., 2016; Rocheta et al., 2016; Pieczynski et al., 2018; Sprenger et al., 2018; You et al., 2019; Tarun et al., 2020; Waititu et al., 2021). Therefore, it is of great significance to analyze the transcriptome differences between plant drought-tolerant and drought-sensitive genotypes under drought and uncover the excellent drought resistance genes from the drought-tolerant genotypes for developing drought-resistant crop varieties through gene manipulation.

Tartary buckwheat (*Fagopyrum tataricum* Gaertn.) is a vital medicinal and edible minor grain crop which belongs to the eudicot Polygonaceae family (Li et al., 2019a; Li et al., 2022). It mainly grows in the mountainous areas of western China and the Himalayas and several other regions including Europe and North America (Zhang et al., 2017). China is the largest producing and consuming country of Tartary buckwheat in the world (Zhang et al., 2021a). Tartary buckwheat plays important roles in food security, economic development, and people's health in China, especially in the western mountainous areas (Li et al., 2022). However, the frequent drought events, which occurred recently in the mountainous areas of western China, especially in autumn, have seriously affected Tartary buckwheat production and threatened the food security in these areas. Thus, it is urgent to explore the wide-transcriptome response of Tartary buckwheat to drought stress and uncover the excellent drought-resistant genes, which will help us breed drought-resistant Tartary buckwheat varieties through molecular manipulation. To date, only one study has investigated the transcriptome response of one Tartary buckwheat genotype to drought stress, which was simulated by 20% polyethylene glycol (PEG-6000) (Huang et al., 2021). Recently, several studies have suggested that the drought resistance of Tartary buckwheat was strongly dependent on genotype (Lu et al., 2017; Lu et al., 2018; Wan et al., 2021). Furthermore, drought stress induced by PEG treatment could not be completely equal to the field soil drought stress. Consequently, it will be more meaningful to compare and analyze the transcriptome difference between Tartary buckwheat drought-tolerant and drought-sensitive genotypes under field soil drought stress, which will help us identify the excellent drought-resistant genes in the drought-tolerant genotype.

To the best of our knowledge, there is no information available about the comparative transcriptome analysis of drought-tolerant and drought-sensitive genotypes of Tartary buckwheat under field soil drought stress. In addition, drought stress, which happened in the reproductive stage, has the most negative effect on crop production. Therefore, in the present study, we performed comparative physiological and transcriptome analyses of drought-tolerant (XZSN) and drought-sensitive (LK3) genotypes under field soil drought stress in the reproductive stage. The aims of this study were to gain insights into the differences in the physiological and molecular mechanisms between drought-tolerant and drought-sensitive genotypes to cope with field soil drought stress and to identify the potentially excellent drought-resistant genes in the drought-tolerant genotypes. Our results provide bases for a better understanding of the genotype-dependent drought resistance response of Tartary buckwheat and potential candidate genes for further Tartary buckwheat drought resistance studies.

Materials and methods

Plant materials and stress treatment

The drought-tolerant (XZSN) and drought-sensitive (LK3) genotypes of Tartary buckwheat were used in this study. Seeds of the two genotypes were obtained from the Research Center of Buckwheat Industry Technology of Guizhou Normal University (Guiyang, Guizhou, China). Plants were sown in plastic pots (20-cm depth and 25-cm diameter) containing field soil mixed with an appropriate amount of compound fertilizer. The drought treatment was performed when plants were at the reproductive stage. Before the drought treatment, the plants of XZSN and LK3 were first poured with sufficient water and then subjected to natural drought stress conditions by withholding water for 3, 5, and 7 days. In addition, the 2-day rewatering treatment was also carried out at 8 days of drought treatment. Leaf samples were harvested between 9:30 and 10:00 a.m. from four different plants for each genotype at 0 (before stress), 3, 5, and 7 days and 2 days after rewatering, respectively. All samples from each time point were collected with three biological replicates. For each plant, the fourth, fifth, and sixth leaves from the plant top were collected. For transcriptome analysis, the leaf samples were immediately frozen in liquid nitrogen and stored at −80°C. For the determination of physiological indices, the harvested leaf samples were put on ice and were promptly used to investigate the relative physiological indices.

Phenotypic and physiological characterizations

The plant phenotype of each genotype was recorded by photographing at each time point. For the determination of physiological indices, the relative water content (RWC) and relative electrolyte leakage (REL) were performed as described in Waititu et al. (2021). The proline content (PC) and soluble

sugar content (SSC) were determined according to Dien et al. (2019).

Total RNA extraction, library construction, and sequencing

Total RNA extraction from each leaf sample was performed using the RNAprep Pure Plant Plus Kit (Tiangen, Beijing, China). The concentration, quality, and integrity of the total RNA were monitored using the NanoDrop spectrophotometer 2000 (NanoDrop, Wilmington, DE, USA) and 1.2% agarose gel electrophoresis. Then, the mRNA from total RNA was purified using the Dynabeads mRNA Purification Kit (Invitrogen, Carlsbad, CA, USA). Purified mRNA was further fragmented as 200–300 bp by divalent cations under elevated temperature in an Illumina proprietary fragmentation buffer and reverse-transcribed into first-strand cDNAs with random hexamer primers and SuperScript™ II (Invitrogen, Carlsbad, CA, USA). Subsequently, the double-stranded cDNAs were synthesized using the NEBNext Ultra RNA Library Prep Kit (NEB, MA, USA). The synthesized double-stranded cDNAs were purified, adenylated at the 3' ends, and ligated to adaptors. The obtained double-stranded cDNAs with adaptors were further enriched by PCR to construct the final sequencing cDNA library. The established cDNA library was sequenced on NovaSeq 6000 platform (Illumina) by Personal Biotechnology Co., Ltd. (Shanghai, China).

RNA-seq data analysis

The raw data were obtained and the sequence quality was assessed by using FastQC. The adaptor sequences, primers, and low-quality reads were filtered out using Cutadapt (v1.15) software to get the clean reads. After filtering, the clean reads were mapped to the reference genome (http://www.mbkbase.org/Pinku1/) (Zhang et al., 2017) using HISAT2 v2.0.5 (Kim et al., 2013). The aligned reads were assembled into transcripts, and the assembled transcripts from all samples were merged using Cufflinks (Waititu et al., 2021). The obtained unique transcripts were assigned to the annotated reference genes by aligning. The gene expression values were calculated using HTSeq-count (v.0.9.1) (Anders et al., 2015) and normalized to fragments per kilobase of transcript per million fragments mapped (FPKM). Differentially expressed genes (DEGs) were identified by using the software tximport and DESeq2 (Wang et al., 2009). For the identification of DEGs, the $|\log2(\text{fold change})|$ of ≥ 1 and the adjusted p-value ≤ 0.05 were applied.

Gene ontology and the kyoto encyclopedia of genes and genomes pathway enrichment analysis of DEGs

The gene ontology (GO) enrichment analysis of DEGs was performed by using the software GOseq R package. GO terms with a p-value ≤ 0.05 were defined as significantly enriched GO terms and further divided into the categories of biological process (BP), molecular function (MF), and cellular component (CC). For the Kyoto Encyclopedia of Genes and Genomes (KEGG) pathway enrichment analysis, the DEGs were first mapped to the KEGG pathway term in the KEGG database (Kanehisa et al., 2008). Then, KOBAS 3.0 (Xie et al., 2011) was used to obtain the KEGG enrichment results. KEGG pathway terms with a p-value ≤ 0.05 were assigned as significantly enriched KEGG pathways.

Weighted gene co-expression network analysis and gene network visualization

The potential drought-resistant genes of the drought-tolerant genotype (XZSN) were used to perform weighted gene co-expression network analysis (WGCNA) to identify the core drought-resistant genes especially TFs based on the previous description (Langfelder and Horvath, 2008). Then, the transcriptional regulatory network among these core drought-resistant TFs and downstream drought-resistant genes was conducted as previously described (Wang et al., 2022). In brief, the position frequency matrices (PFMs) of TFs were downloaded from the PlantTFDB database (Tian et al., 2020); then, the FIMO in the MEME database was used to predict the cis-motif information in the promoter region of these candidate genes (2,000 bp upstream of the initiation codon) under the condition $p < 1e{-}5$ (Grant et al., 2011); finally, the transcriptional regulatory network was constructed by integrating the availability of cis-element binding sites present in the promoter regions of candidate genes and the Pearson correlation coefficient ($r > 0.8$) between these candidate genes and TFs. The network was visualized by Cytoscape (v3.9.1) (Kohl et al., 2011).

Quantitative real-time polymerase chain reaction analysis

Ten candidate core drought-resistant genes were randomly selected to verify the reliability of the RNA-seq data by quantitative real-time polymerase chain reaction (qRT-PCR). The Tartary buckwheat helicase gene (*HLK/FtPinG0000667700.01*) was used as the internal reference to normalize the expression

data. All primer sequences are listed in Supplementary Table S1. qRT-PCR was performed as previously described (Li et al., 2021a).

Statistical analysis

The SPSS software (version 20.0) was used to perform the statistical analysis by one-way analysis of variance (ANOVA) and *t*-test. A *p*-value <0.05 was considered a statistically significant difference.

Results

Morphological and physiological differences of XZSN and LK3 plants in response to drought stress

The morphological and physiological differences of XZSN and LK3 plants were investigated at 0, 3, 5, and 7 days under withholding water treatment. As shown in Figure 1, there was no visible phenotypic difference observed between the two genotypes at 0 and 3 days of treatment. However, the phenotypes between the two genotypes showed visible differences at 5 days of treatment (Figure 1). The leaves of the LK3 plants were rolled and wilted to some degree, while this finding was not observed in the XZSN plants. The rolling and wilting of the leaves of LK3 became more serious at 7 days of treatment. In comparison, the leaves of the XZSN seedlings only displayed slight wilting although some old leaves were dried (Figure 1). Consistent with the phenotypic results, no significant difference was observed in the physiological characterizations including RWC, SSC, and REL between LK3 and XZSN at 0 and 3 days of treatment (Figure 2). However, the XZSN had significantly higher RWC, PC, and SSC and lower REL than LK3 at 5 and 7 days of treatment (Figure 2).

Transcriptome analysis of XZSN and LK3 plants in response to drought stress

To gain insights into the molecular mechanisms involved in the drought stress resistance of XZSN, we performed RNA-seq for the collected leaf samples of XZSN and LK3 at 0, 3, 5, and 7 days of drought treatment as well as 2 days of rehydration. In total, 30 samples were subjected to RNA-seq, resulting in a total of 13.40 billion raw reads (Supplementary Table S2). After removing the adaptor sequences and low-quality sequences, a total of 12.18 billion clean reads were obtained with the samples ranging from 36.42 to 45.61 million. The Q30 base percentage changed from 90.83% to 93.91%, and the GC content varied from 45.47% to 48.81%. Among all the samples, 92.20% to 96.01% of the clean reads were mapped to the reference genome.



FIGURE 1
Phenotypic response of the drought-tolerant genotype XZSN and the drought-susceptible genotype LK3. Days 0, 3, 5, and 7 represent natural drought stress conditions by withholding water for 0, 3, 5, and 7 days after pouring sufficient water, respectively.

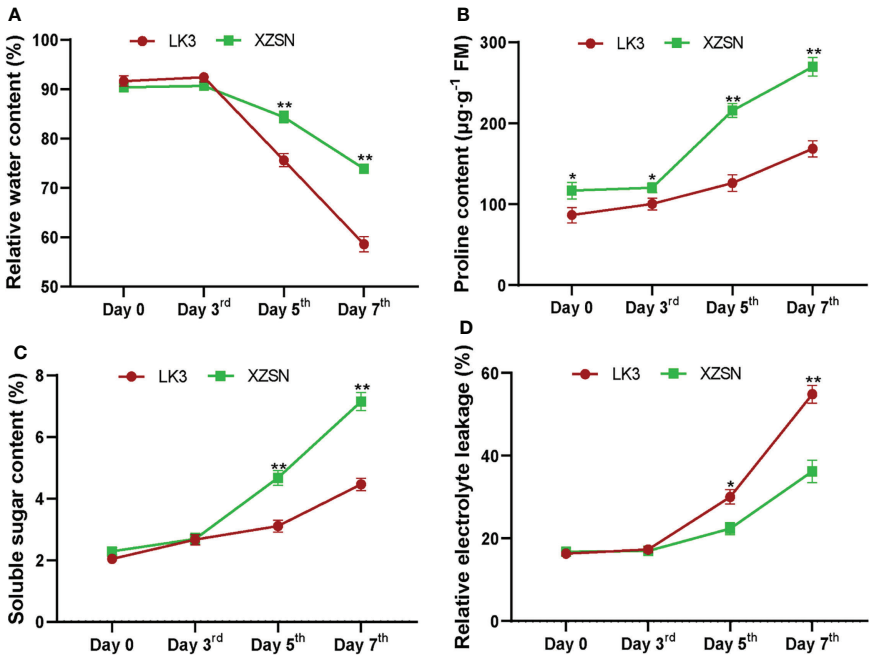


FIGURE 2
Physiological response of the drought-tolerant genotype XZSN and the drought-susceptible genotype LK3. **(A)** Relative water content (%), **(B)** proline content (μg·g^{-1} FM), **(C)** soluble sugar content (%), and **(D)** relative electrolyte leakage (%). Days 0, 3, 5, and 7 represent natural drought stress conditions by withholding water for 0, 3, 5, and 7 days after pouring sufficient water, respectively. Bars with one (*) and two (**) stars are significantly different at p <0.05 and p <0.01.

The Pearson correlation coefficient (PCC) among the biological replicates was over 0.93 for each sample except LK0_1 and XZ0_1, which were deleted from further analysis (Supplementary Figure S1). All the results indicated that the RNA-seq was of high quality.

The normalized expression level (FPKM) of each gene was obtained, and the genes with average FPKM ≥1 at least in one tissue sample were considered to be expressed. In total, 18,258 expressed genes, including 17,846 in XZSN and 17,790 in LK3, were identified (Supplementary Figure S2A). The number of expressed genes ranged from 15,821 (LKRW) to 16,577 (LK3) for LK3 and 15,743 (XZ5) to 16,629 (XZ3) for XZSN (Supplementary Figure S2A), respectively. Among these genes, about 8.22%–9.50%, 9.36%–12.01%, 41.71%–44.30%, and 34.94%–39.58% of the genes displayed very high (FPKM ≥ 100), high (50 ≤ FPKM < 100), moderate (10 ≤ FPKM < 50), and low (1 ≤ FPKM < 10) expression (Supplementary Figure S2B), respectively. Interestingly, the LK7 and LKRW samples had the largest and lowest number of genes which displayed very high and high expression, respectively. Overall, these analyses showed that we obtained sufficient coverage of the transcriptome of the drought treatment leaves of these two contrasting Tartary buckwheat genotypes and could be used for further analysis and identification of drought-resistant genes.

Transcriptome comparison of XZSN and LK3 revealed the vital time point for drought response difference

To investigate the relationships of leaf transcriptome response to drought stress between XZSN and LK3, hierarchical cluster analysis (HCA) and principal component analysis (PCA) were carried out based on the average FPKM values of the 18,258 expressed genes (Figure 3). HCA showed that the samples of the two genotypes at the same treatment time points exhibited higher correlation and clustered except at drought treatment for 5 and 7 days (Figure 3A). The PCA analysis displayed LK0 and XZ0, LK3 and XZ3, and LKRW and XZRW being grouped together, while clear separations were observed between LK5 and XZ5 as well as between LK7 and XZ7 (Figure 3B). In addition, LK0, LK3, XZ0, and XZ3 were closely clustered together. These indicated that a higher similarity in transcriptional programs and obvious transcriptional differences between the two genotypes existed at drought treatment for 0 and 3 days and at drought treatment for 5 and 7 days, respectively. Furthermore, these also suggested that both genotypes might be subjected to drought stress at drought treatment for 5 and 7 days, and the 5-day drought treatment might be the vital time point to determine the drought resistance difference between the two genotypes at the molecular level.

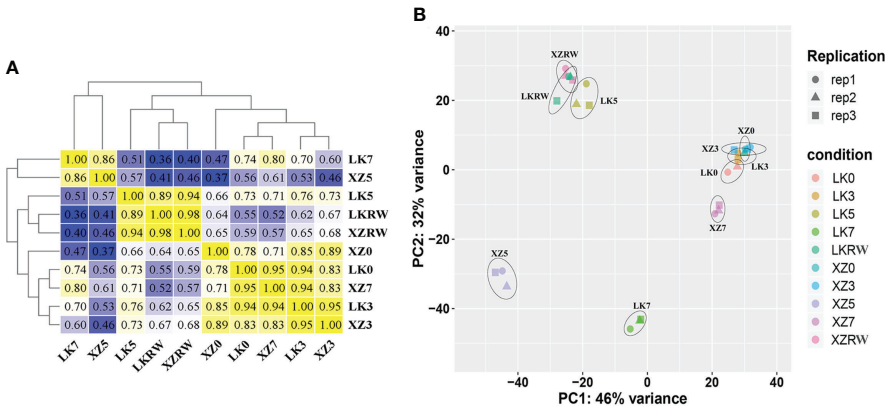


FIGURE 3
Pearson correlation **(A)** and principal component analyses **(B)** of RNA-seq data from five time points of drought treatment in XZSN and LK3. LK0, LK3, LK5, LK7, and LKRW represent genotype LK3 being subjected to natural drought stress conditions by withholding water for 0, 3, 5, and 7 days and rewatering treatment for 2 days, respectively. XZ0, XZ3, XZ5, XZ7, and XZRW represent genotype XZSN being subjected to natural drought stress conditions by withholding water for 0, 3, 5, and 7 days and rewatering treatment for 2 days, respectively.

To further ascertain that 5 and 7 days of drought treatment as well as the drought treatment for 5 days were the critical time points for the drought transcriptional response difference of the two genotypes subjected to drought stress, the expression levels of *RD22*, *RAB18B*, *APX2*, and *DREB2B*, which are well-known genes of drought response in different plants, were analyzed based on the RNA-seq data. As shown in Figure 4, the expression of the four genes was not induced both in XZSN and LK3 at drought treatment for 3 days; however, their expression significantly increased at drought treatment for 5 and 7 days. Interestingly, obviously higher expression levels of the four genes were observed in XZSN than in LK3 at drought treatment for 5 days, although there was no significant expression difference at drought treatment for 0 and 3 days. These indicated that both XZSN and LK3 were really subjected to drought stress at drought treatment for 5 and 7 days and the drought treatment for 5 days was the real key time point that led to the drought resistance difference between the two genotypes at the molecular level.

Identification of drought-responsive genes in XZSN and LK3

The physiological and transcriptome data showed that both XZSN and LK3 were subjected to drought stress at drought treatment for 5 and 7 days. Consequently, genes with a significant expression change (|log2(fold change)| of ≥1 and adjusted p-value ≤ 0.05) were considered as the drought-responsive genes when they underwent drought treatment for 5 and 7 days compared with genes under drought treatment for 0 and 3 days. As a result, a total of 4,631 (2,015 upregulated and 2,616 downregulated) and 1,360 (410 upregulated and 950

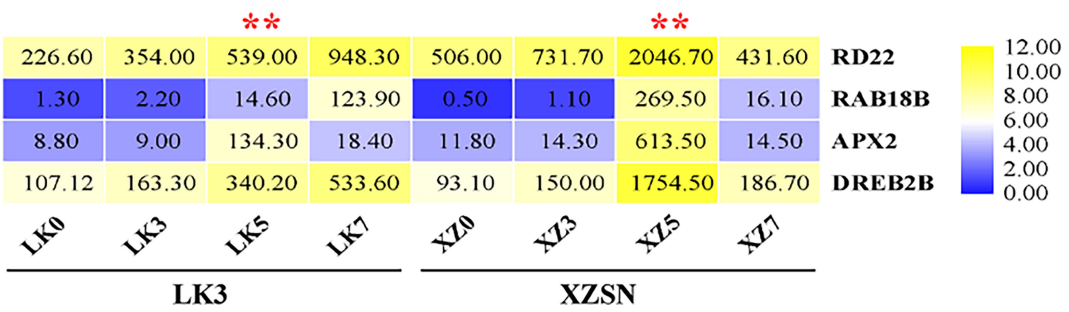


FIGURE 4
FPKM value of four drought-responsive marker genes in LK3 and XZSN at different treatment points. ** represents the time point of response to drought stress.

downregulated) genes were identified to be potential drought-responsive genes in XZSN at drought treatment for 5 and 7 days (Figures 5A, B), respectively. Similarly, a total of 2,672 (1,356 upregulated and 1,316 downregulated) and 3,086 (1,224 upregulated and 1,862 downregulated) genes were found to have positive and negative responses to drought stress in LK3 at drought treatment for 5 and 7 days (Figures 5C, D), respectively. XZSN had more and less drought-responsive genes than LK3 at drought treatment for 5 and 7 days, respectively. In addition, among these potential drought-responsive genes, only 1,306 drought-induced and 1,741 drought-repressed genes overlapped in XZSN and LK3.

Identification and functional annotation of differentially expressed drought-responsive genes between XZSN and LK3

To gain insights into the potential molecular mechanism of XZSN having a stronger drought resistance ability than LK3 and identify drought-resistant genes in XZSN, the DEGs between ZXSN and LK3 were investigated at drought treatment for 5 and 7 days, respectively. In addition, the DEGs between ZXSN and LK3, which were also the potential drought-responsive genes in XZSN, were considered as the drought-resistant genes that contributed to the higher drought resistance ability of ZXSN. In total, 2,371 (1,168 upregulated and 1,203 downregulated) and 117 (45 upregulated and 72 downregulated) potential drought-responsive genes in XZSN displayed significantly higher and lower expression in XZSN than LK3 at drought treatment for 5 and 7 days, respectively. These genes were identified to be the potential contributors for ZXSN having higher drought resistance ability than LK3. Interestingly, over half of these genes with higher or lower expression in ZXSN than in LK3 at drought treatment for 5 days were obviously upregulated or downregulated in LK3 only at drought treatment for 7 days (Figure 6), respectively.

GO enrichment analysis of these upregulated drought-responsive genes of LK3 vs. XZSN obtained 229 significantly enriched GO terms ($p < 0.05$), which could be divided into three functional categories: biological processes (187), cell components (14), and molecular functions (28) (Supplementary Table S3). The top 20 GO terms of each functional category are shown in Figure 7A. Notably, in the category of biological processes, a large number of genes were enriched in response to stress (abiotic stimulus, water deprivation, heat, cold, osmotic stress, salt stress, oxidative stress, reactive oxygen species, alcohol, hydrogen peroxide, cadmium, and so on), hormone (abscisic acid and gibberellin), carbohydrate and sucrose metabolism (phenylpropanoid metabolic process, glutamine family amino acid metabolic process, inositol phosphate metabolic process, organic acid metabolic process, hexose metabolic process, fatty acid metabolic process, lipid metabolic process, flavonoid metabolic process, and so on), and so on (Figure 7A; Supplementary Table S3). In contrast, a total of 159 significantly enriched GO terms, consisting of 99 biological

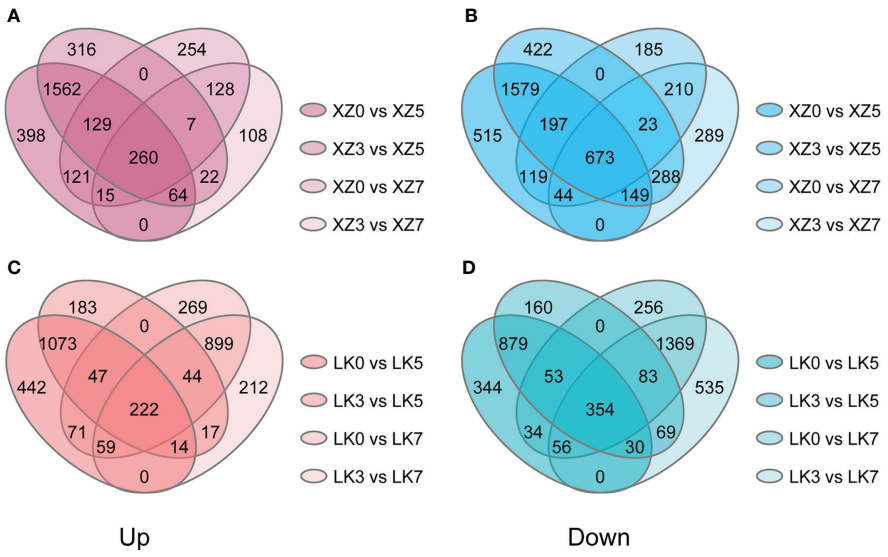


FIGURE 5
Drought-responsive genes in XZSN and LK3. **(A)** Upregulated drought-responsive genes in XZSN, **(B)** downregulated drought-responsive genes in XZSN, **(C)** upregulated drought-responsive genes in LK3, and **(D)** downregulated drought-responsive genes in LK3.

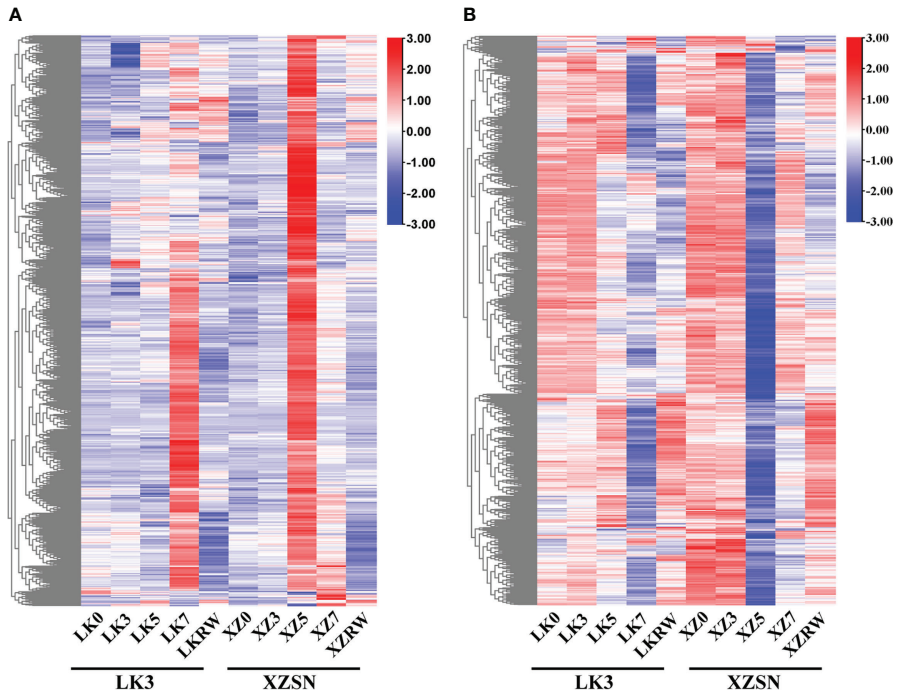


FIGURE 6
Heatmap of differentially expressed drought-responsive genes between XZSN and LK3. **(A)** Heatmap of upregulated drought-responsive genes in LK3 vs. XZSN. **(B)** Heatmap of downregulated drought-responsive genes in LK3 vs. XZSN.

process terms, 27 cell component terms, and 33 molecular function terms, were identified for these downregulated drought-responsive genes of LK3 vs. XZSN (Figure 7B; Supplementary Table S3). In the category of biological processes, these enriched GO terms were primarily involved in cell wall biogenesis, cell wall organization or biogenesis, response to auxin, cellular response to abiotic stimulus, and cellular response to an environmental stimulus (Figure 7B; Supplementary Table S3). The KEGG pathway enrichment analysis found that the up- and downregulated drought-responsive genes were significantly enriched to 27 and 34 pathways ($p < 0.05$) of LK3 vs. XZSN, respectively (Figures 7C, D; Supplementary Table S4). For the upregulated drought-responsive genes, the enriched pathways were primarily involved in chaperones and folding catalysts, lipid biosynthesis and metabolism, wax biosynthesis, phenylpropanoid and flavonoid biosynthesis, amino acid biosynthesis and metabolism, starch and sucrose metabolism, fatty acid biosynthesis and degradation, carotenoid biosynthesis, and so on. In contrast, photosynthesis, energy metabolism, steroid biosynthesis, glyoxylate and dicarboxylate metabolism, and plant hormone signal transduction pathways were significantly enriched in the downregulated drought-responsive genes of LK3 vs. XZSN (Figures 7C, D; Supplementary Table S4).

Identification and functional annotation of positive core drought-resistant genes in XZSN

To identify the positive core drought-resistant genes in XZSN, we selected the 1,206 upregulated differentially expressed drought-responsive genes in LK5_vs_XZ5 (1,168) and LK7_vs_XZ7 (45) to further perform the WGCNA analysis. As a result, 851 out of the 1,206 genes were assigned to four modules (blue, brown, turquoise, and yellow) (Figure 8). The blue, brown, turquoise, and yellow modules contain 220, 182, 301, and 148 genes, respectively. The genes in the blue, brown, and yellow modules were highly expressed both in ZX5 and LK7, but their expression levels were higher (brown and yellow) and lower (blue) in XZ5 than in LK7, respectively. In contrast, genes from the turquoise module showed a specific high expression in ZX5 (Figure 8). Because drought treatment for 5 days was the real key time point to determine the drought resistance difference between XZSN and LK3, the 851 genes were considered as the core drought-resistant genes in XZSN and further used to perform functional annotation.

TFs

A total of 67 TFs were identified among the 851 positive core drought-resistant genes in XZSN, consisting of 26, 12, 21, and 8

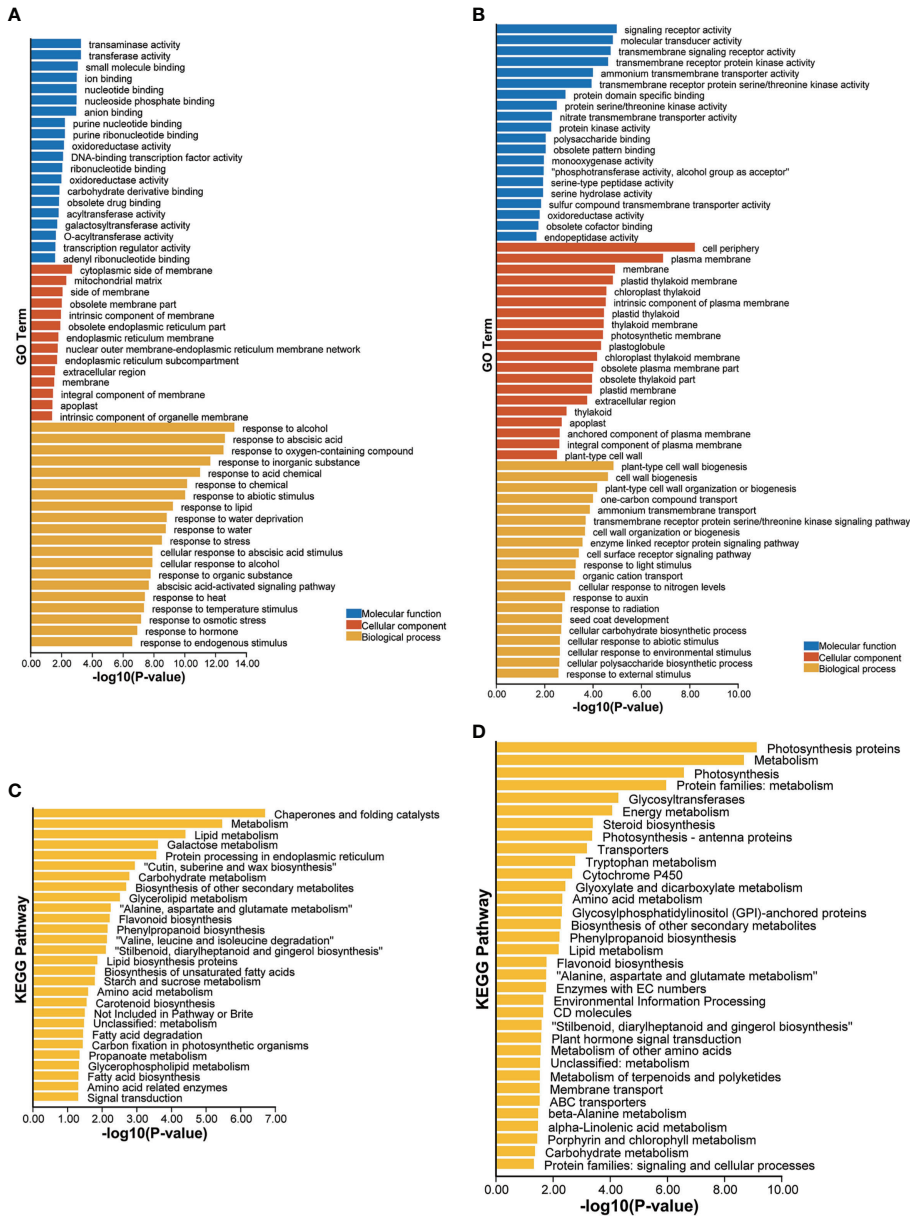


FIGURE 7
Gene ontology (GO) and Kyoto Encyclopedia of Genes and Genomes **(KEGG)** enrichment analysis of differentially expressed drought-responsive genes between XZSN and LK3. **(A)** GO enrichment of upregulated drought-responsive genes in LK3 vs. XZSN. **(B)** GO enrichment of downregulated drought-responsive genes in LK3 vs. XZSN. **(C)** KEGG enrichment of upregulated drought-responsive genes in LK3 vs. XZSN. **(D)** KEGG enrichment of downregulated drought-responsive genes in LK3 vs. XZSN.

from the blue, brown, turquoise, and yellow modules (Supplementary Table S5), respectively. The 67 TFs could be classified into 21 families (TFs from the same family were named based on their number), and the top 5 largest TF families were NAC (12), MYB (7), HD-ZIP (7), bZIP (6), and WRKY (5) (Supplementary Table S5). Among these TFs, two bZIP TF genes (*FtPinG0003196200.01*/*FtbZIP5* and *FtPinG0002143600.01*/*FtbZIP83*), which are homologous to *AtABF2*, have been demonstrated to play a positive regulatory role in drought resistance of transgenic *Arabidopsis* (Li et al., 2019b; Li et al., 2020). Four NAC TF genes (*FtPinG0002561000.01*, *FtPinG0005791100.01*, *FtPinG0006087500.01*, and *FtPinG0005167000.01*) are homologous to *ANAC019*, *ANAC72*/*RD26*, *NAC029*, and *ANAC2*, which are necessary for drought resistance in *Arabidopsis* (Fujita et al., 2011), respectively. In addition, some *Arabidopsis thaliana*

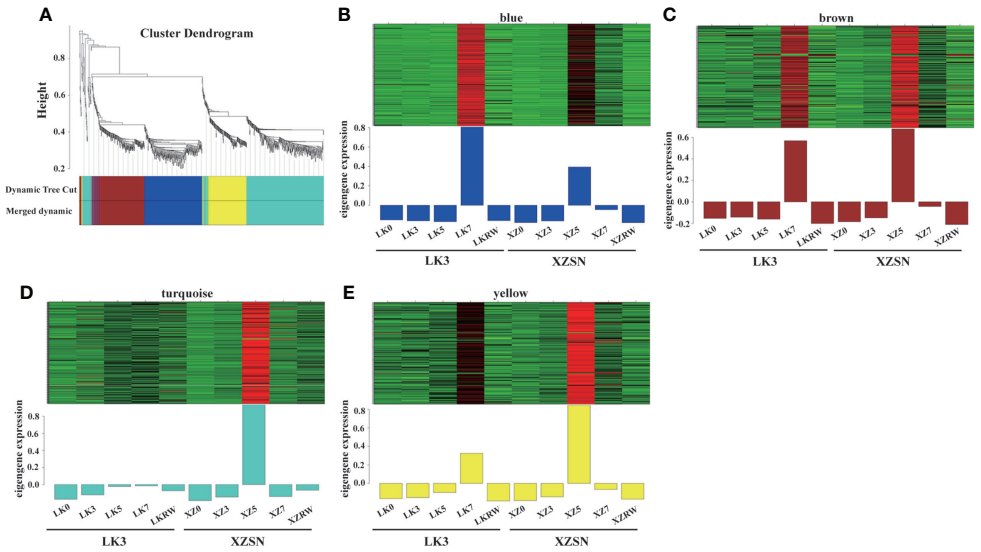


FIGURE 8
Co-expression network of the 1,206 potentially positive drought-resistant genes in XZSN. **(A)** Hierarchical clustering tree (dendrogram) of all genes. **(B)** Blue module, **(C)** brown module, **(D)** turquoise module, and **(E)** yellow module.

homologous genes of the rest of the 61 TFs were involved in biotic and abiotic stress response or resistance, although there was no report about their drought resistance (Supplementary Table S5). Notably, among the 67 TFs, only 15 were induced in LK3 at drought treatment for 5 days, but 44 out of the remaining 52 TFs were upregulated in LK3 at drought treatment for 7 days (Supplementary Table S5). Furthermore, 8 TFs were specifically induced by drought stress in XZSN (Supplementary Table S5).

To further gain insights into the transcriptional regulatory relationship among these TFs, we constructed their potential regulatory network based on the expression correlations ($r > 0.8$) and the potential binding sites of these TF promoters (Figure 9). The regulatory network consists of 62 TFs. In this regulatory network, 11 potential target genes (*bHLH-2*, *GRAS*, *MYB-7*, *NAC-2*, *NAC-3*, *NAC-8*, *NAC-10*, *NAC-11*, *NAC-12*, *NF-YA-1*, and *WRKY-1*) of the homologous genes (*bZIP-2* and *bZIP-3*) of *AtABFs* were found. Notably, among the 11 potential target genes, the *Arabidopsis* homologous genes of *NAC-3*, *NAC-8*, and *NAC-10* were the direct target genes of *AtABFs* in drought resistance (Hickman et al., 2013). In addition, *bHLH-2*, *C3H-1*, *ERF-1*, *GRAS*, *HSF-2*, *MYB-3*, *MYB-5*, *NAC-2*, *NAC-6*, and *WRKY-1* had the largest number of potential upstream regulatory TFs (Figure 9).

Genes involved in ABA biosynthesis, signal transduction, and response

Among the 851 positive core drought-resistant genes in XZSN, 3 ABA biosynthesis genes (1 *ZEP*/*ABA1* and 2 *NCED3*) and 8 ABA signal transduction genes (1 *PYL*/*PYR*, 4 *PP2C*, 1 *SnRK2.6*/*OST1*, and 2 *AREB*/*ABF*) were found (Supplementary Table S6). In addition, according to the GO and *Arabidopsis* homologous annotation, 91 out of the 851 core drought-resistant genes in XZSN were identified to be ABA-responsive genes (Supplementary Table S6). Among the 91 ABA-responsive genes, 23 belonged to TFs including 1 bHLH, 1 bZIP, 1 ERF, 2 HSF, 2 G2-like, 4 HD-ZIP, 4 MYB, 5 NAC, 2 NF-YA, and 1 WRKY. The potential transcriptional regulatory network among these ABA-responsive TFs is shown in Figure 10A. The regulatory network consisted of 21 TFs, and *NAC-2* had the largest number of putative upstream regulators. For the rest of the 68 ABA-responsive genes, most of them were further identified to be stress-responsive genes, which were primarily involved in drought, salt, cold, heat, and oxidative stress responses (Supplementary Table S6). Notably, 2 ABA biosynthesis genes (1 *ZEP*/*ABA1* and 1 *NCED3*) were not induced in LK3 at drought treatment for 5 days (Supplementary Table S6). Coincidentally, 5 ABA signal transduction genes (3 *PP2C*, 1 *SnRK2.6*/*OST1*, and 1 *AREB*/*ABF*) and 63 ABA-responsive genes were also not induced in LK3 at drought treatment for 5 days (Supplementary Table S6). However, all identified ABA biosynthesis and ABA signal transduction genes as well as most ABA-responsive genes were obviously upregulated in LK3 at drought treatment for 7 days (Supplementary Table S6).

To further identify the potential TFs that regulated the ABA biosynthesis, the expression correlations ($r > 0.8$) among 67 potential drought-resistant TFs and 3 ABA biosynthesis genes as well as the potential binding sites of the 3 ABA biosynthesis gene

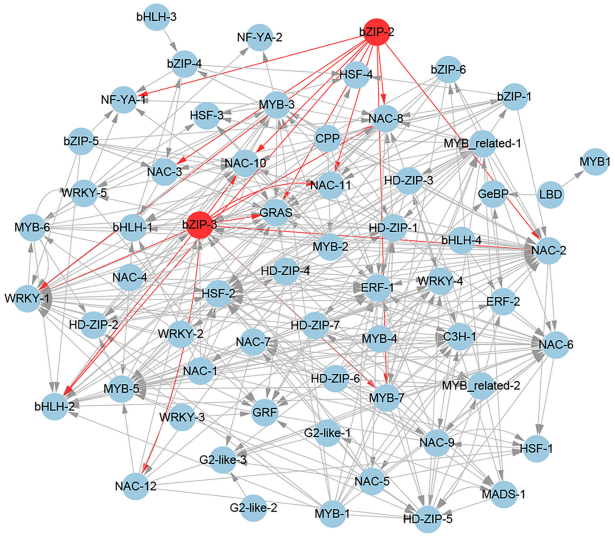


FIGURE 9
The regulatory network of potential drought-resistant TFs in XZSN. TFs (bZIP-2 and bZIP-3), labeled by a red circle, represents the homologs of key TFs (ABFs) of the abscisic acid (ABA) signal pathway in *Arabidopsis*.

promoters were analyzed. A total of 17 (1 ERF, 5 HD-ZIP, 1 MADS, 7 NAC, and 3 WRKY), 14 (1 ERF, 2 G2-like, 5 HD-ZIP, 1 LBD, 1 MYB-related, and 4 MYB), and 20 (2 bHLH, 2bZIP, 1 MADS, 2 MYB-related, 5 MYB, and 8 NAC) TFs were identified to be the putative regulators of the ABA biosynthesis genes *ZEP*, *NCED3-1*, and *NCED3-1* (Figure 10B), respectively. Among these TFs, 3 (HD-ZIP-3, HD-ZIP-6, and HD-ZIP-7), 3 (NAC-1, NAC-2, and NAC-3), and 4 (MYB-4, MYB-5, MYB-7, and MYB-related-2) TFs were found as the common regulators of *ZEP* and *NCED3-1*, *ZEP* and *NCED3-2*, and *NCED3-1* and *NCED3-2*, respectively. Notably, among these TFs, 18 were also ABA-responsive TFs (Supplementary Table S6).

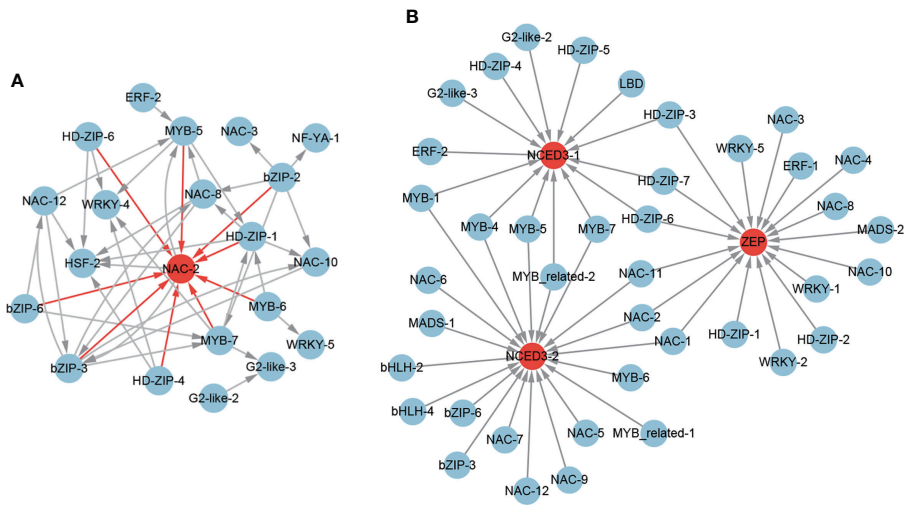


FIGURE 10
The regulatory network of ABA-responsive TFs **(A)** and ABA biosynthesis genes **(B)** from the core drought-resistant genes in XZSN.

Genes involved in non-ABA signal molecules

Among the 851 positive core drought-resistant genes in XZSN, we found 3 non-ABA signal molecules biosynthesis genes, namely, 1 carbon monoxide (CO) biosynthesis gene (*HO1*, heme oxygenase), 1 hydrogen sulfide (H_2S) biosynthesis gene (*OAS-TL*, cytosolic O-acetylserine(thiol)lyase), and 1 melatonin biosynthesis gene (*COMT1*, caffeic acid/5-hydroxyferulic acid O-methyltransferase) (Supplementary Table S7). Notably, the *HO1* and *OAS-TL*, involved in CO and H_2S biosynthesis, were specifically induced in XZSN at drought treatment for 5 days. In contrast, the melatonin biosynthesis gene *COMT1* was upregulated in LK3 at drought treatment for 7 days, although it was not induced in LK3 at drought treatment for 5 days (Supplementary Table S7).

Genes involved in stomatal closure and cuticular wax biosynthesis

A total of 7 ABA-dependent stomatal closure genes were found among the 851 positive core drought-resistant genes in XZSN (Supplementary Table S8), consisting of 2 ABA transporter genes which are homologous to *AtABCG22* and *OsABCG5* with the function of transporting ABA into the leaf guard cell to regulate stomatal closure (Kuromori et al., 2011; Matsuda et al., 2016), 1 NADPH/respiratory burst oxidase gene (*RBOHF*), 1 anion transporter gene (*ALMT12*), 2 nucleocytoplasmic lectin genes (*EULS3*), and 1 receptor-like cytoplasmic kinase gene (*CDL1*). Furthermore, 1 ABA-independent stomatal closure gene (hexokinase, *HXK1*) was also identified (Supplementary Table S8). Among these 8 stomatal closure genes, only 1 was induced by drought treatment for 5 days in LK3, but 5 of them were upregulated in LK3 under drought treatment for 7 days (Supplementary Table S8). For cuticular wax biosynthesis, a total of 10 homologous genes involved in cuticular wax biosynthesis were identified in the 851 positive core drought-resistant genes in XZSN (Supplementary Table S8). These genes included 1 long-chain acyl-CoA synthetase (*LACS1*), 2 β-ketoacyl-coenzyme A synthases (*KCS1* and *KCS6*), 1 β-hydroxyacylcoenzyme A dehydratase (*HCD*/*PAS2*), 2 BAHD acyltransferase (*CER1*), 2 sterol desaturase (*CER3*/*WAX2*), 1 alcohol-forming fatty acyl-CoA reductase (*CER4*/*FAR3*), and 1 wax ester synthase and diacylglycerol acyltransferase (*WSD1*) (Supplementary Table S8). In addition, 2 homologs to GPI-anchored lipid transfer protein (2 *LTPG2*) were also identified, involved in cuticular wax transport. Notably, among the 10 cuticular wax biosynthesis and 2 wax transport genes, only 1 was upregulated in LK3 at drought treatment for 5 days, but 11 genes were induced in LK3 at drought treatment for 7 days (Supplementary Table S8).

To further identify the potential regulator of these stomatal closure and wax biosynthesis and transport genes, the putative regulatory network was constructed (Figure 11). A total of 41 and 47 TFs were identified to be the potential regulators of the stomatal closure and wax biosynthesis and transport genes (Figures 11A, B), respectively. Among the TFs, some were

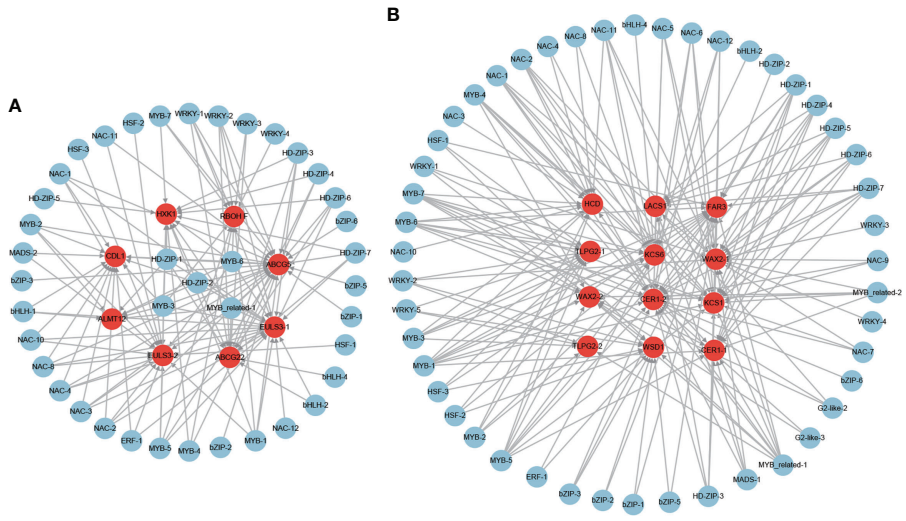


FIGURE 11
The regulatory network of stomatal closure **(A)** and cuticular wax biosynthesis and transport **(B)** genes from the core drought-resistant genes in XZSN.

predicted as the regulators of both stomatal closure and wax biosynthesis genes. Furthermore, some played the putative regulatory role in multiple stomatal closure or wax biosynthesis and transport genes. For example, MYB-3, MYB-6, MYB_related-1, HD-ZIP-1, and HD-ZIP-2 were the potential regulators of 7, 7, 6, 6, and 6 stomatal closure genes (Figure 11A), respectively. MYB-1, MYB-5, MYB-6, and MYB-7 were the putative regulators of 8, 8, 7, and 7 wax biosynthesis and transport genes (Figure 11B), respectively. Notably, MYB-6, which is the ABA-responsive TF, was predicted as the regulator of 7 stomatal closure and 7 wax biosynthesis and transport genes.

Genes involved in reactive oxygen species scavenging

A total of 6 genes involved in enzymatic antioxidants from the 851 positive core drought-resistant genes in XZSN were identified, including 1 ascorbate peroxidase (*APX*), 2 peroxidase (*PRXs*), and 3 glutathione S-transferase (*GSTFs*) (Supplementary Table S9). In addition, 2 (*PGM2* and *MIOX1*) and 2 (*CHI* and *F3H*) genes, involved in the biosynthesis of the non-enzymatic antioxidant ascorbic acid and flavonoids, were also identified (Supplementary Table S9), respectively. Only 3 out of the 10 genes were induced in LK3 at drought treatment for 5 days. Furthermore, 4 genes, which were not induced in LK3 at drought treatment for 5 days, were upregulated in LK3 at drought treatment for 7 days (Supplementary Table S9). The putative regulators of *APX*, *GSTFs*, *PGM2*, *MIOX1*, *CHI*, and *F3H* were identified as well as the potential regulatory network as shown in Figure 12.

Genes involved in osmotic adjustment

A total of 12 amino acid biosynthesis genes were identified among the 851 positive core drought-resistant genes in XZSN. These genes encoded the key enzymes involved in glutamine (1 glutamine synthetase), glutamate (1 glutamate synthase), aspartate (2 aspartate aminotransferase), glycine (2 alanine-glyoxylate aminotransferase), cysteine (1 O-acetylserine(thiol) lyase), methionine (1 cystathionine β-lyase), and proline (1 ornithine delta-aminotransferase and 1 pyrroline-5-carboxylate synthetase) biosynthesis, as well as in valine, leucine, and isoleucine (1 branched-chain amino acid transaminase) biosynthesis. One gene encoding the rate-limiting enzyme (arginine decarboxylase, *ADC1*) of polyamine biosynthesis was also found (Supplementary Table S10). In addition, 9 genes involved in soluble sugar biosynthesis were identified, which contained 2, 5, and 2 for sucrose biosynthesis, raffinose biosynthesis, and starch degradation (Supplementary Table S10), respectively. Among these identified genes, most of the genes involved in amino acid biosynthesis and starch degradation were not induced in LK3 at drought treatment for 5 days, but most of them were upregulated at drought treatment for 7 days. In contrast, genes involved in polyamine and raffinose biosynthesis were induced in LK3 at both drought treatments for 5 and 7 days (Supplementary Table S10). The putative regulatory network of amino acid, polyamine, sucrose, and raffinose biosynthesis genes was constructed and shown in Figure 13. A total of 49, 6, and 44 TFs were predicted as the potential regulators of amino acid, polyamine, and sucrose and raffinose biosynthesis genes, respectively. Among these TFs, some played potential regulatory roles in two or more osmotic adjustment solutes (Figure 13). Notably, among these TFs, MYB-3, MYB-6,

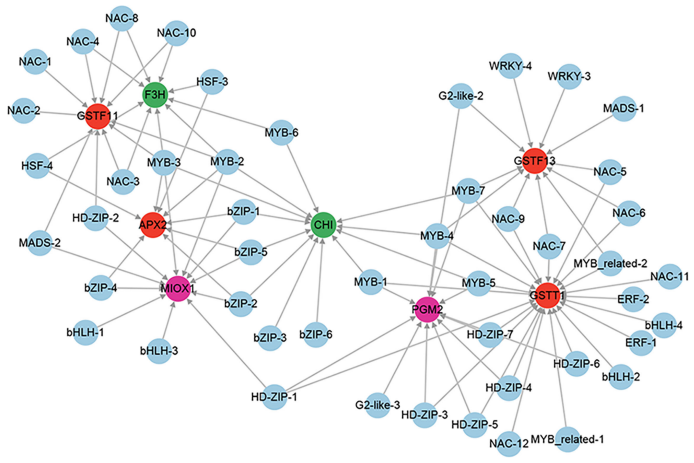


FIGURE 12
The regulatory network of ROS scavenging genes from the core drought-resistant genes in XZSN. Genes labeled by a red circle encode the enzymatic antioxidants. Genes labeled by green and magenta circles represent the genes involved in non-enzymatic antioxidant biosynthesis.

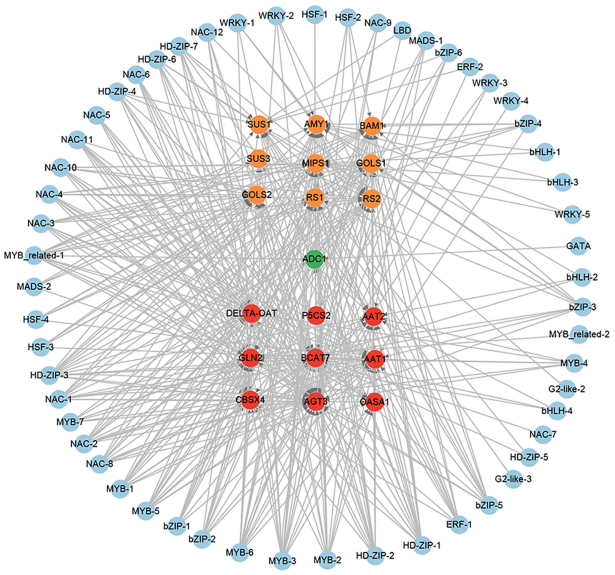


FIGURE 13
The regulatory network of osmotic adjustment genes from the core drought-resistant genes in XZSN. Genes labeled by yellow, green, and red circles represent the soluble sugar, amino acid, and polyamine biosynthesis genes, respectively.

HD-ZIP-1, HD-ZIP-2, HD-ZIP-3, MYB-2, MYB_related-1, and NAC-1 were predicted as the regulators of 17, 16, 16, 16, 14, 13, and 12 out of the 21 osmotic adjustment genes, respectively.

Genes involved in cell damage prevention

A total of 3 late embryogenesis abundant (*LEA*) and 5 heat shock protein (*HSP*) genes were identified among the 851 positive core drought-resistant genes in XZSN (Supplementary Table S11), which play crucial roles in preventing cell damage under different abiotic stresses (Priya et al., 2019; Shi et al., 2020). Half of these genes were not upregulated in LK3 at drought treatment for 5 days, while 2 of them were induced in LK3 at drought treatment for 7 days. In addition, 2 *HSP* genes were specifically induced in XZSN at drought treatment for 5 days (Supplementary Table S11).

Identification of the key downstream TFs involved in drought resistance in tartary buckwheat

To identify the key downstream TFs involved in drought resistance in Tartary buckwheat, we performed an integrated analysis of the above identified TFs, which were putative as the regulators of the expression of 20 water holding (8 stomatal closure and 12 cuticular wax biosynthesis and transport), 7 reactive oxygen species scavenging, and 18 osmotic adjustment (8 amino acid, 1 polyamine, and 9 soluble sugar biosynthesis) genes. As a result, 3 HD-ZIPs (HD-ZIP-1, HD-ZIP-2, and HD-ZIP-3), 1 MYB-related (MYB-related-1), and 5 MYBs (MYB-1, MYB-2, MYB-3, MYB-5, and MYB-6) were found as the putative regulators of 31, 25, 26, 28, 27, 26, 34, 27, and 32 out of the 45 drought-resistant functional genes (Figure 14). This indicated that HD-ZIP and MYB TFs might be the key downstream TFs of drought resistance in Tartary buckwheat.

Confirmation of the core droughtresistant genes by qRT-PCR

To confirm the reliability of these identified core drought-resistant genes from XZSN, 10 TFs from the 851 core drought-resistant genes were selected to perform the qRT-PCR analysis in the leaf samples of XZSN and LK3 with treatment by naturally withholding water for 0, 3, 5, and 7 days and rewatering for 2 days. As shown in Figure 15, a highly significant correlation ($R \geq 0.77$) was observed between qRT-PCR (log2 fold change) and RNA-seq (log2 fold change) data, thus verifying the authenticity of the identified core drought-resistant genes from XZSN in this study.

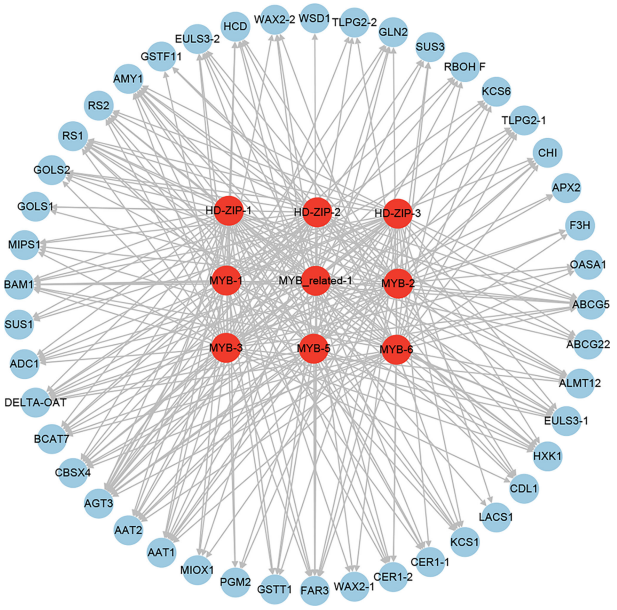


FIGURE 14
The regulatory network of the key downstream TFs involved in drought resistance in Tartary buckwheat.

Discussion

Morphological and physiological responses to drought

In many plants, the morphological and physiological indices highlight that the tolerant and susceptible genotypes respond differently to drought stress (Dossa et al., 2017; Wang et al., 2018b; Kumar et al., 2019; Harb et al., 2020; Ma et al., 2021; Wan et al., 2021; Waititu et al., 2021; Zhao et al., 2021; Zhang et al., 2021a). For example, the RWC of the leaf of the tolerant genotype was higher and the wilting was slower compared with the susceptible genotype. In addition, the accumulations of some protective substances such as proline, polyamine, soluble sugar, soluble protein, and so on were faster and higher in the tolerant genotype than in the susceptible genotype. In contrast, the malondialdehyde (MAD) content and REL, which indirectly reflect the degree of cell damage, were lower in the tolerant genotype than in the susceptible genotype. Consistent with these observations in other plants, our study found that the leaves of the Tartary buckwheat drought-susceptible genotype LK3 rolled and wilted quicker and more serious than the drought-tolerant genotype XZSN under drought stress (Figure 1). Physiological characterization

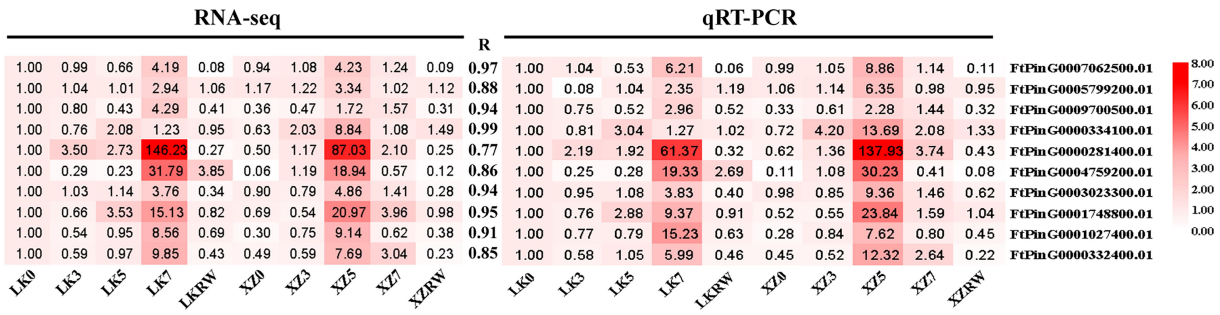


FIGURE 15
Correlation analysis between RNA-seq and qRT-PCR methods. The expression fold change of genes is used to construct the heatmaps. The LK0 is used as a control. The left heatmap represents the RNA-seq, and the right heatmap represents qRT-PCR.

analyses showed that the RWC, PC, and SSC in the drought-tolerant genotype XZSN were significantly higher than in the drought-susceptible genotype LK3, while the REL showed the opposite result (Figure 2). These indicated that the XZSN genotype was more effective in resisting drought stress than the LK3 genotype by reducing the leaf water loss, more quickly accumulating protective substances, and reducing cell membrane damage.

Transcriptional differences between drought-tolerant and drought-susceptible genotypes of tartary buckwheat for drought stress response

Integrating the physiological characterizations and the expression of the drought-responsive marker genes, our results showed that both the drought-tolerant (XZSN) and the drought-susceptible (LK3) genotypes were subjected to drought stress at nature drought treatment for 5 and 7 days. The analysis of the drought stress-responsive genes in XZSN and LK3 found that the XZSN had more drought stress-responsive genes than LK3 in the early stage (drought treatment for 5 days) of drought stress. However, in the later stage (drought treatment for 7 days) of drought stress, the situation was just the opposite. In addition, only about half of these drought stress-responsive genes overlapped between XZSN and LK3. These indicated that XZSN and LK3 had the same and different transcriptional responses for drought stress and the transcriptional differences of the early stage of drought stress might be the key reason for leading to the drought resistance ability difference between them.

Rapid and dramatic transcriptional reprogramming of drought-resistant genes occurs in the drought-tolerant genotype

A total of 1,206 and 1,274 genes were identified to be the potential positive (upregulated in LK3 vs. XZSN) and negative (downregulated in LK3 vs XZSN) contributors for XZSN having higher drought resistance ability than LK3, respectively. GO enrichment analysis showed that a large number of upregulated genes in LK3 vs. XZSN were enriched in response to stress (including water deprivation, heat, cold, osmotic stress, salt stress, oxidative stress, hydrogen peroxide, cadmium, and so on), hormone (abscisic acid and gibberellin), carbohydrate, sucrose, metabolism, and so on (Figure 7A; Supplementary Table S3). In contrast, the downregulated genes in LK3 vs. XZSN were primarily enriched in response to auxin, cellular response to abiotic stimulus, and cellular response to an environmental stimulus (Figure 7B; Supplementary Table S3). These indicated that the identified genes could be the candidate genes for XZSN having higher drought resistance ability than LK3. In some plants, it was shown that the rapid and dramatic transcriptional reprogramming of the stress tolerance genotype contributes to higher stress resistance than the susceptible genotype (Dossa et al., 2017; Simopoulos et al., 2020; Waititu et al., 2021; Yang et al., 2021). Interestingly, among these identified genes, over 90% of the genes were identified at drought treatment for 5 days, and over half of them in LK3 were not induced or inhibited at drought treatment for 5 days but were obviously upregulated or downregulated at drought treatment for 7 days (Figure 6). Therefore, our results also indicated that the quick and strongly active transcriptional reprogramming of the drought-resistant genes in XZSN under drought stress could be the major reason for its higher drought resistance ability than LK3.

Core drought-resistant genes and the potential transcriptional regulatory network in XZSN

The positive regulation of gene expression plays the most important role in plant drought resistance (Hu and Xiong, 2014). Based on the WGCNA analysis of 1,206 positive contributors for XZSN having higher drought resistance ability than LK3, we identified 851 genes to be the core drought-resistant genes in XZSN. According to their homologous function, we classified these core drought-resistant genes and explored their potential transcriptional regulatory network.

TFs

TFs are the master regulators of plant drought resistance. Many TFs such as AREB/ABF, AP2/ERF, MYB, NAC, HD-ZF, HD-ZIP, bHLH, C2H2-ZF, B3, WRKY, and NF-Y TFs have been confirmed to play roles in drought resistance in different plant species (Fujita et al., 2011; You et al., 2019; Waititu et al., 2021). In our study, a total of 67 TFs from 21 families were identified in the 851 core drought-resistant genes in XZSN. Among the TF families, some new TF families such as C3H, G2-like, HSF, MYB-related, and MADS were found except for some known TF families involved in plant drought resistance. Notably, among these TFs, two bZIP TFs (FtPinG0003196200.01/FtbZIP5 and FtPinG0002143600.01/FtbZIP83) have been demonstrated to play a positive regulatory role in drought resistance in transgenic *Arabidopsis* (Li et al., 2019b; Li et al., 2020). Four NAC TFs are the homologs of *Arabidopsis* drought-resistant TFs (ANAC019, ANAC72/RD26, NAC029, and ANAC2, respectively) (Fujita et al., 2011). These indicated that these TFs have a conserved function in different plants to resist drought stress. In addition, we also found that the *Arabidopsis* homologs of some identified TFs in this study were involved in

biotic and abiotic stress resistance, although there was no report about their drought resistance based on the homologous function annotation. All these suggested that the TFs identified by us might be the master regulators of drought resistance in XZSN, and it was reliable to identify them as the drought-resistant candidate TFs. Notably, most of these TFs were earlier induced by drought stress in XZSN than in LK3. Furthermore, some TFs were specifically induced in XZSN. These indicated that the rapid, strong, and special activation of the expression of drought-resistant TFs in XZSN contributed to its higher drought resistance ability than LK3.

Based on the expression correlation and the potential binding sites of the 67 TFs promoters, we constructed the putative regulatory network of these TFs. In the regulatory network, we found that bZIP-2 and bZIP-3, which are the homologs of *Arabidopsis* AtABFs, had 11 potential target TF genes (*bHLH-2*, *GRAS*, *MYB-7*, *NAC-2*, *NAC-3*, *NAC-8*, *NAC-10*, *NAC-11*, *NAC-12*, *NF-YA-1*, and *WRKY-1*). Notably, among the 11 potential target TF genes, the *Arabidopsis* homologs (*ANAC072*/*RD26*, *ANAC019*, and *ANAC072*/*RD26*) of *NAC-3*, *NAC-8*, and *NAC-10* were the direct target genes of AtABFs in drought resistance (Hickman et al., 2013). In addition, the *Arabidopsis* homologs (*MYB32*, *ANAC2*, *NAC029*, and *ANAC2*) of *MYB-7*, *NAC-2*, *NAC-11*, and *NAC-12* were responsive to drought or salt stress (Supplementary Table S5). These suggested that we constructed the drought-resistant TF regulatory network to be credible to some extent, and the 8 TF genes except *NAC-3*, *NAC-8*, and *NAC-10* might be the direct target genes of bZIP-2 and bZIP-3 and played crucial regulatory roles in Tartary buckwheat drought resistance. In addition, we also found that *bHLH-2*, *C3H-1*, *ERF-1*, *GRAS*, *HSF-2*, *MYB-3*, *MYB-5*, *NAC-2*, *NAC-6*, and *WRKY-1* have the largest number of putative upstream regulatory TFs (Figure 9). This implied that these TFs might be the crucial downstream regulatory TFs that directly regulated the expression of the functional genes in drought resistance in Tartary buckwheat.

ABA signaling

In plants, the ABA content increases rapidly under drought stress and further activates the ABA-dependent drought resistance pathway, which is the major and conservative molecule signal pathway for plant drought resistance (Shinozaki and Yamaguchi-Shinozaki, 2007; Roychoudhury et al., 2013; Saradadevi et al., 2017). Among the 851 core drought-resistant genes in XZSN, 3 ABA biosynthesis genes (1 *ZEP*/*ABA1* and 2 *NCED3*) and 8 ABA signal transduction genes (1 *PYL*/*PYR*, *4 PP2C*, 1 *SnRK2.6*/*OST1*, and 2 *AREB*/*ABF*) were identified. In addition, 91 ABA-responsive genes were also identified based on *Arabidopsis* homologous annotation. The 91 ABA-responsive genes contained 23 TFs. Interestingly, the *MYB-7*, *NAC-2*, *NAC-12*, *NF-YA-1*, and *WRKY-1*, which were predicted as the target genes of the ABF TFs (key TFs of the ABA signal pathway) by us, were found in these 23 ABA-responsive TFs. This further confirmed that the method, integrating the expression correlation and the potential binding sites of the promoter analysis to identify the potential regulator of genes, was reliable. It is well known that ABA activates a large number of downstream stress-responsive gene expression to enhance the drought resistance of plants (Fujita et al., 2011; You et al., 2019; Waititu et al., 2021). Among the 91 ABA-responsive genes, we found that most of the non-TF ABA-responsive genes were the stress-responsive genes, primarily involved in drought, salt, cold, heat, and oxidative stress responses (Supplementary Table S6). These indicated that the ABA-dependent pathway played a vital role in the higher drought resistance ability of XZSN than that of LK3. Notably, among these ABA biosynthesis, signal transduction, and responsive genes, 2 ABA biosynthesis genes (1 *ZEP*/*ABA1* and 1 *NCED3*), 5 ABA signal transduction genes (3 *PP2C*, 1 *SnRK2.6*/*OST1* and 1 *AREB*/*ABF*), and 63 ABA-responsive genes were also not induced in LK3 at drought treatment for 5 days, but most of them were obviously upregulated in LK3 at drought treatment for 7 days. These suggested that the rapid and strong activation of the ABA-dependent pathway under drought stress led to XZSN having a higher drought resistance ability than LK3. Interestingly, by analyzing the potential transcriptional regulator of ABA biosynthesis genes, we found that many identified ABA-responsive TFs in our study were predicted to be the regulators of ABA biosynthesis genes. This indicated that there might be a feedback regulation between ABA biosynthesis and ABA-responsive TFs.

Non-ABA signaling

As signal molecules, CO, H_2S, NO, and melatonin play important roles in the resistance of abiotic stresses including drought stress (Wang and Liao, 2016; Fancy et al., 2017; Sun et al., 2021; Zhang et al., 2021b; Supriya et al., 2022). In our study, we identified 1 CO biosynthesis gene (*HO1*), 1 H_2S biosynthesis gene (*OAS-TL*), and 1 melatonin biosynthesis gene (*COMT1*) among the 851 core drought-resistant genes in XZSN and found that *HO1* and *OAS-TL* were specifically induced in XZSN at drought treatment for 5 days. These suggested that non-ABA signaling such as CO, H_2S, and melatonin participated in drought resistance in Tartary buckwheat, and the CO and H_2S signaling involved in drought resistance in Tartary buckwheat might be genotype-dependent.

Water holding

A large number of studies have demonstrated that the stomatal closure and the cuticular wax biosynthesis of the

leaves play the most crucial role in preventing leaf water loss under drought stress (Shepherd and Wynne Griffiths, 2006; Lee and Suh, 2015; Xue et al., 2017; Nadeem et al., 2019). Consistent with the physiological analysis result that the drought-tolerant genotype XZSN had significantly higher RWC than the drought-susceptible LK3, we identified 7 ABA-dependent and 1 ABA-independent stomatal closure genes in the 851 core drought-resistant genes in XZSN. The ABA-dependent stomatal closure genes included 2 ABA transporter genes which are homologs of *AtABCG22* and *OsABCG5* with the function of transporting ABA into the leaf guard cell to regulate stomatal closure (Kuromori et al., 2011; Matsuda et al., 2016), 1 NADPH/respiratory burst oxidase gene (*RBOHF*) which mediated ABA-dependent H_2O_2 production for stomatal closure (Postiglione and Muday, 2020), 1 anion transporter gene (*ALMT12*) (Meyer et al., 2010), 2 nucleocytoplasmic lectin genes (*EULS3*) (Van Hove et al., 2015), and 1 receptor-like cytoplasmic kinase gene (*CDL1*) (Kim et al., 2018). The ABA-independent stomatal closure genes consisted of 1 hexokinase gene (*HXK1*) (Lugassi et al., 2019). In addition, a total of 10 (*LACS1*, *KCS1*, *KCS6*, *HCD*, 2 *CER1*, 2 *WAX2*, *CER4*, and *WSD1*) and 2 (2 *LTPG2*) homologous genes of cuticular wax biosynthesis and transport were also identified in the 851 core drought-resistant genes (Lee and Suh, 2015). Notably, in LK3, most of the stomatal closure and cuticular wax biosynthesis genes were not induced by the early drought stress (drought treatment for 5 days), but they were significantly upregulated by the later drought stress (drought treatment for 7 days). All these indicated that both stomatal closure and cuticular wax biosynthesis participated in the prevention of Tartary buckwheat leaf water loss under drought stress, and the quick and strong induction of the stomatal closure and the cuticular wax biosynthesis in XZSN contributed to its higher leaf water holding and drought resistance ability than LK3. To date, little is known about the regulator of stomatal closure genes. In our study, we identified that MYB-3, MYB-6, MYB-related-1, HD-ZIP-1, and HD-ZIP-2 TFs might be the major regulators of stomatal closure of Tartary buckwheat under drought stress because they were the potential upstream regulators of most stomatal closure genes. In *Arabidopsis*, the MYB TFs were identified to be the major regulators of wax biosynthesis and transport (Lee and Suh, 2015). In our study, we found that 4 MYB TFs (MYB-1, MYB-5, MYB-6, and MYB-7) might be the major regulators of wax biosynthesis and transport of Tartary buckwheat under drought stress on account that they are the putative upstream regulators of 8, 8, 7, and 7 wax biosynthesis and transport genes. This suggested that MYB TFs have conserved roles in wax biosynthesis and transport in different plants. Notably, MYB-6, which is an ABA-responsive TF, was predicted to be the regulator of 7 stomatal closure and 7 wax biosynthesis and transport genes, implying that it might be the major regulator of the water retention genes under drought stress.

Reactive oxygen species scavenging

Enzymatic and non-enzymatic antioxidants are the major defensive mechanism of ROS in plants under drought stress (Nadeem et al., 2019). The enzymatic antioxidants include CAT, superoxide dismutase (SOD), ascorbate peroxide (APX), glutathione peroxidase (GPX), glutathione reductase (GR), dehydroascorbate reductase (DHAR), monodehydroascorbate reductase (MDHAR), and glutathione s-transferase (GSTFs), and the non-enzymatic antioxidants comprise glutathione, ascorbic acid, flavonoids, and so on (Nadeem et al., 2019). In our study, we identified 6 genes encoding the enzymatic antioxidants (1 APX, 2 PRXs, and 3 GSTFs) and 4 non-enzymatic antioxidants consisting of 2 ascorbic acid (*PGM2* and *MIOX1*) and 2 flavonoid (*CHI* and *F3H*) biosynthesis genes among the 851 core drought-resistant genes in XZSN. Among these identified ROS scavenging genes, most of them were not induced in LK3 at drought treatment for 5 days but were upregulated in LK3 at drought treatment for 7 days. This was consistent with the physiological analysis results that the drought-tolerant genotype XZSN had significantly lower MAD content and REL than the drought-susceptible LK3 and suggested that the quick, strong, and specific activation of the enzymatic and non-enzymatic ROS defensive mechanisms played an important role in the high drought resistance ability of XZSN.

Osmotic adjustment

Under drought stress, plants quickly synthesize a large number of osmotic adjustment solutes such as amino acid, polyamine, and soluble sugar to protect cells from osmotic damage (Zhu, 2016; Todaka et al., 2017). In our study, we identified many key genes that participated in the biosynthesis of amino acid, polyamine, and soluble sugar among the 851 core drought-resistant genes in XZSN (Supplementary Table S10). In amino acid biosynthesis, 2 proline-related genes were identified, which was consistent with the physiological results that XZSN had higher PC than LK3 under stress drought. Furthermore, 10 genes, involved in glutamine, glutamate, aspartate, glycine, cysteine, and methionine biosynthesis, as well as in valine, leucine, and isoleucine biosynthesis, also were identified. In rice, metabolome analysis reveals that the contents of many amino acids are significantly increased under drought stress (Todaka et al., 2017). All these suggested that most amino acids except proline might also play crucial roles in drought stress resistance. In *Arabidopsis*, the *ADC1* encodes the rate-limiting enzyme of PA biosynthesis and plays a crucial role in abiotic stress resistance (Soyka and Heyer, 1999; Capell et al., 2004). In our study, the homologs of *ADC1* were found among the 851 core drought-resistant genes in XZSN, which suggested that the PA might play an important role in drought stress resistance. For soluble sugar biosynthesis, we identified 2, 5, and 2 genes involved in sucrose biosynthesis, raffinose biosynthesis, and

starch degradation among the 851 core drought-resistant genes in XZSN. Notably, these raffinose biosynthesis genes were involved in almost all steps of the raffinose biosynthesis pathway. This indicated that raffinose might be the most important soluble sugar involved in drought stress resistance of Tartary buckwheat. Among these identified osmotic adjustments, most were not induced in LK3 at drought treatment for 5 days but were upregulated in LK3 at drought treatment for 7 days. These indicated that the quick accumulation of compatible solutes contributed to the higher drought resistance ability of XZSN than LK3. A transcriptional regulatory network analysis of these osmotic adjustment genes identified many TFs to be their potential upstream regulators. Among these TFs, the MYB-3, MYB-6, HD-ZIP-1, HD-ZIP-2, HD-ZIP-3, MYB-2, MYB_related-1, and NAC-1 were putative as the regulators of 17, 16, 16, 16, 14, 13, and 12 out of the 21 osmotic adjustment genes. These indicated that the 8 TFs might be the major regulators of the accumulation of osmotic adjustment solutes in Tartary buckwheat under drought stress.

Conclusion

In the present study, we carried out comparative physiological and transcriptomic analyses between the drought-tolerant and drought-sensitive genotypes at the reproductive stage under the field environment of drought stress to gain insight into the molecular mechanism of genotype-dependent drought resistance of Tartary buckwheat. We identified the key genes and regulatory pathways associated with drought tolerance in Tartary buckwheat. Our results showed that the quick, strong, and special transcriptional reprogramming of a large number of genes related to stress resistance in the drought-tolerant genotype in the early stage of drought stress contributed to its higher drought resistance, through decreasing leaf water loss, activating osmotic protection, ROS scavenging, enhancing cell damage protection mechanisms, and so on. These results enhanced our understanding of the physiological and molecular mechanisms of the genotype-dependent drought resistance of Tartary buckwheat and highlighted the possible candidate genes that might play important roles in the drought tolerance of Tartary buckwheat.

Data availability statement

The original contributions presented in the study are publicly available. This data can be found here: NCBI, PRJNA859365

Author contributions

H-YL designed the study, performed the data analysis, revised the original draft, and supervised the study. H-LM performed the experiments and wrote the original draft. P-YS and J-RW performed the experiments and data analysis. X-QS, C-ZZ, and TF participated in the experiments. Q-FC revised the original draft. All authors contributed to the article and approved the submitted version.

Funding

This work was supported by the Joint Fund of the National Natural Science Foundation of China and the Karst Science Research Center of Guizhou Province (U1812401), the Opening Foundation of the Key Laboratory of Plant Resources Conservation and Germplasm Innovation in Mountainous Region of the Ministry of Education (QianJiaoHeKYZi[2019] 035), the Science and Technology Foundation of Guizhou Province (QianKeHeJiChu-ZK[2021]ZhongDian035), the Science and Technology Foundation of Guizhou Province (QianKeHeJiChu[2019]1235), and the Earmarked Fund for China Agriculture Research System (CARS-07-A5).

Conflict of interest

The authors declare that the research was conducted in the absence of any commercial or financial relationships that could be construed as a potential conflict of interest.

Publisher's note

All claims expressed in this article are solely those of the authors and do not necessarily represent those of their affiliated organizations, or those of the publisher, the editors and the reviewers. Any product that may be evaluated in this article, or claim that may be made by its manufacturer, is not guaranteed or endorsed by the publisher.

Supplementary material

The Supplementary Material for this article can be found online at: https://www.frontiersin.org/articles/10.3389/fpls.2022.985088/full#supplementary-material

References

Anders, S., Pyl, P. T., and Huber, W. (2015). HTSeq-a Python framework to work with high-throughput sequencing data. *Bioinformatics* 31, 166–169. doi: 10.1093/bioinformatics/btu638

Capell, T., Bassie, L., and Christou, P. (2004). Modulation of the polyamine biosynthetic pathway in transgenic rice confers tolerance to drought stress. *Proc. Natl. Acad. Sci. U. S. A.* 101, 9909–9914. doi: 10.1073/pnas.0306974101

Dal Santo, S., Palliotti, A., Zenoni, S., Tornielli, G. B., Fasoli, M., Paci, P., et al. (2016). Distinct transcriptome responses to water limitation in isohydric and anisohydric grapevine cultivars. *BMC Genomics* 17, 815. doi: 10.1186/s12864-016-3136-x

Dien, D. C., Mochizuki, T., and Yamakawa, T. (2019). Effect of various drought stresses and subsequent recovery on proline, total soluble sugar and starch metabolisms in rice (*Oryza sativa* l.) varieties. *Plant Prod. Sci.* 22, 530–545. doi: 10.1080/1343943X.2019.1647787

Dossa, K., Li, D., Wang, L., Zheng, X., Liu, A., Yu, J., et al. (2017). Transcriptomic, biochemical and physio-anatomical investigations shed more light on responses to drought stress in two contrasting sesame genotypes. *Sci. Rep.* 7, 8755. doi: 10.1038/s41598-017-09397-6

Fancy, N. N., Bahlmann, A. K., and Loake, G. J. (2017). Nitric oxide function in plant abiotic stress. *Plant Cell Environ.* 40, 462–472. doi: 10.1111/pce.12707

Fu, L., Ding, Z., Han, B., Hu, W., Li, Y., and Zhang, J. (2016). Physiological investigation and transcriptome analysis of polyethylene glycol (PEG)-induced dehydration stress in *Cassava*. *Int. J. Mol. Sci.* 17, 283. doi: 10.3390/ijms17030283

Fujita, Y., Fujita, M., Shinozaki, K., and Yamaguchi-Shinozaki, K. (2011). ABA-mediated transcriptional regulation in response to osmotic stress in plants. *J. Plant Res.* 124, 509–425. doi: 10.1007/s10265-011-0412-3

Grant, C. E., Bailey, T. L., and Noble, W. S. (2011). FIMO: scanning for occurrences of a given motif. *Bioinformatics* 27, 1017–1018. doi: 10.1093/bioinformatics/btr064

Harb, A., Simpson, C., Guo, W., Govindan, G., Kakani, V. G., and Sunkar, R. (2020). The effect of drought on transcriptome and hormonal profiles in barley genotypes with contrasting drought tolerance. *Front. Plant Sci.* 11. doi: 10.3389/fpls.2020.618491

Hickman, R., Hill, C., Penfold, C. A., Breeze, E., Bowden, L., Moore, J. D., et al. (2013). A local regulatory network around three NAC transcription factors in stress responses and senescence in *Arabidopsis* leaves. *Plant J.* 75, 26–39. doi: 10.1111/tpj.12194

Huang, J., Chen, Q., Rong, Y., Tang, B., Zhu, L., Ren, R., et al. (2021). Transcriptome analysis revealed gene regulatory network involved in PEG-induced drought stress in tartary buckwheat (*Fagopyrum tararicum*). *Peer J.* 9, e11136. doi: 10.7717/peerj.11136

Hu, H., and Xiong, L. (2014). Genetic engineering and breeding of drought-resistant crops. *Annu. Rev. Plant Biol.* 65, 715–741. doi: 10.1146/annurev-arplant-050213-040000

Kanehisa, M., Araki, M., Goto, S., Hattori, M., Hirakawa, M., Itoh, M., et al. (2008). KEGG for linking genomes to life and the environment. *Nucleic. Acids Res.* 36, D480–D484. doi: 10.1093/nar/gkm882

Kim, D., Pertea, G., Trapnell, C., Pimentel, H., Kelley, R., and Salzberg, S. L. (2013). TopHat2: accurate alignment of transcriptomes in the presence of insertions, deletions and gene fusions. *Genome Biol.* 14, R36. doi: 10.1186/gb-2013-14-4-r36

Kim, T. W., Youn, J. H., Park, T. K., Kim, E. J., Park, C. H., Wang, Z. Y., et al. (2018). OST1 activation by the brassinosteroid-regulated kinase CDG1-LIKE1 in stomatal closure. *Plant Cell* 30, 1848–1863. doi: 10.1105/tpc.18.00239

Kohl, M., Wiese, S., and Warscheid, B. (2011). Cytoscape: software for visualization and analysis of biological networks. *Methods Mol. Biol.* 696, 291–303. doi: 10.1007/978-1-60761-987-1_18

Ksouri, N., Jiménez, S., Wells, C. E., Contreras-Moreira, B., and Gogorcena, Y. (2016). Transcriptional responses in root and leaf of *Prunus persica* under drought stress using RNA sequencing. front. *Plant Sci.* 7. doi: 10.3389/fpls.2016.01715

Kumar, M., Chauhan, A. S., Kumar, M., Yusuf, M. A., Sanyal, I., and Chauhan, P. S. (2019). Transcriptome sequencing of chickpea (*Cicer arietinum* l.) genotypes for identification of drought-responsive genes under drought stress condition. *Plant Mol. Biol. Rep.* 37, 186–203. doi: 10.1007/s11105-019-01147-4

Kuromori, T., Sugimoto, E., and Shinozaki, K. (2011). *Arabidopsis* mutants of *AtABCG22*, an ABC transporter gene, increase water transpiration and drought susceptibility. *Plant J.* 67, 885–894. doi: 10.1111/j.1365-313X.2011.04641.x

Langfelder, P., and Horvath, S. (2008). WGCNA: an r package for weighted correlation network analysis. *BMC Bioinf.* 9, 559. doi: 10.1186/1471-2105-9-559

Lee, S. B., and Suh, M. C. (2015). Advances in the understanding of cuticular waxes in *Arabidopsis thaliana* and crop species. *Plant Cell Rep.* 34, 557–572. doi: 10.1007/s00299-015-1772-2

Lesk, C., Rowhani, P., and Ramankutty, N. (2016). Influence of extreme weather disasters on global crop production. *Nature* 529, 84–87. doi: 10.1038/nature16467

Li, H., Lv, Q., Liu, A., Wang, J., Sun, X., Deng, J., et al. (2022). Comparative metabolomics study of tartary (*Fagopyrum tataricum* (L.) gaertn) and common (*Fagopyrum esculentum* moench) buckwheat seeds. *Food Chem.* 371, 131125. doi: 10.1016/j.foodchem.2021.131125

Li, H., Lv, Q., Ma, C., Qu, J., Cai, F., Deng, J., et al. (2019a). Metabolite profiling and transcriptome analyses provide insights into the flavonoid biosynthesis in the developing seed of tartary buckwheat (*Fagopyrum tataricum*). *J. Agric. Food Chem.* 67, 11262–11276. doi: 10.1021/acs.jafc.9b03135

Li, H., Meng, H., Sun, X., Deng, J., Shi, T., Zhu, L., et al. (2021a). Integrated microRNA and transcriptome profiling reveal key miRNA-mRNA interaction pairs associated with seed development in tartary buckwheat (*Fagopyrum tataricum*). *BMC Plant Biol.* 21, 132. doi: 10.1186/s12870-021-02914-w

Li, Q., Wu, Q., Wang, A., Lv, B., Dong, Q., Yao, Y., et al. (2019b). Tartary buckwheat transcription factor FtbZIP83 improves the drought/salt tolerance of *Arabidopsis via* an ABA-mediated pathway. *Plant Physiol. Biochem.* 144, 312–323. doi: 10.1016/j.plaphy.2019.10.003

Li, Q., Zhao, H., Wang, X., Kang, J., Lv, B., Dong, Q., et al. (2020). Tartary buckwheat transcription factor FtbZIP5, regulated by FtSnRK2.6, can improve salt/drought resistance in transgenic *Arabidopsis*. *Int. J. Mol. Sci.* 21, 1123. doi: 10.3390/ijms21031123

Lugassi, N., Yadav, B. S., Egbaria, A., Wolf, D., Kelly, G., Neuhaus, E., et al. (2019). Expression of *Arabidopsis* hexokinase in tobacco guard cells increases water-use efficiency and confers tolerance to drought and salt stress. *Plants (Basel)* 8, 613. doi: 10.3390/plants8120613

Lu, Z. J., Zhang, Y. Q., and Zhang, C. (2018). The seedling growth and root physiological traits of *Fagopyrum tataricum* cultivars under drought stress. *Acta Botanica Boreali-Occidentalia Sin.* 38, 0112–0120. doi: 10.7606/J.ISSN.1000-4025.2018.01.0112

Lu, Z. J., Zhang, Y. Q., Zhang, C., Liu, L. Q., and Yang, C. T. (2017). Comprehensive evaluation and indicators of the drought resistance of different genotypes of *Fagopyrum tataricum* at seedling stage. *Sci. Agricult. Sin.* 50, 3311–3322. doi: 10.3864/j.issn.0578-1752.2017.17.006

Matsuda, S., Takano, S., Sato, M., Furukawa, K., Nagasawa, H., Yoshikawa, S., et al. (2016). Rice stomatal closure requires guard cell plasma membrane ATP-binding cassette transporter RCN1/OsABCG5. *Mol. Plant* 9, 417–427. doi: 10.1016/j.molp.2015.12.007

Ma, Q., Xu, X., Wang, W., Zhao, L., Ma, D., and Xie, Y. (2021). Comparative analysis of alfalfa (*Medicago sativa* l.) seedling transcriptomes reveals genotype-specific drought tolerance mechanisms. *Plant Physiol. Biochem.* 166, 203–214. doi: 10.1016/j.plaphy.2021.05.008

Meyer, S., Mumm, P., Imes, D., Endler, A., Weder, B., Al-Rasheid, K. A., et al. (2010). AtALMT12 represents an r-type anion channel required for stomatal movement in *Arabidopsis* guard cells. *Plant J.* 63, 1054–1062. doi: 10.1111/j.1365-313X.2010.04302.x

Nadeem, M., Li, J., Yahya, M., Sher, A., Ma, C., Wang, X., et al. (2019). Research progress and perspective on drought stress in *Legumes*: a review. *Int. J. Mol. Sci.* 20, 2541. doi: 10.3390/ijms20102541

Omprakash, G., Bisen, P., Baghel, M., and Chourasia, K. N. (2017). Resistance/tolerance mechanism under water deficit (drought) condition in plants. *Int. J. Curr. Microbiol. App. Sci.* 6, 66–78. doi: 10.20546/ijcmas.2017.604.009

Pieczynski, M., Wyrzykowska, A., Milanowska, K., Boguszewska-Mankowska, D., Zagdanska, B., Karlowski, W., et al. (2018). Genome wide identification of genes involved in the potato response to drought indicates functional evolutionary conservation with *Arabidopsis* plants. *Plant Biotechnol. J.* 16, 603–614. doi: 10.1111/pbi.12800

Postiglione, A. E., and Muday, G. K. (2020). The role of ROS homeostasis in ABA-induced guard cell signaling. *Front. Plant Sci.* 11. doi: 10.3389/fpls.2020.00968

Priya, M., Dhanker, O. P., Siddique, K., HanumanthaRao, B., Nair, R. M., Pandey, S., et al. (2019). Drought and heat stress-related proteins: An update about their functional relevance in imparting stress tolerance in agricultural crops. *Theor. Appl. Genet.* 132, 1607–1638. doi: 10.1007/s00122-019-03331-2

Rocheta, M., Coito, J. L., Ramos, M. J., Carvalho, L., Becker, J. D., Carbonell-Bejerano, P., et al. (2016). Transcriptomic comparison between two *Vitis vinifera* l. varieties (*Trincadeira* and *Touriga nacional*) in abiotic stress conditions. *BMC Plant Biol.* 16, 224. doi: 10.1186/s12870-016-0911-4

Roychoudhury, A., Paul, S., and Basu, S. (2013). Cross-talk between abscisic acid-dependent and abscisic acid-independent pathways during abiotic stress. *Plant Cell Rep.* 32, 985–1006. doi: 10.1007/s00299-013-1414-5

Saradadevi, R., Palta, J. A., and Siddique, K. (2017). ABA-mediated stomatal response in regulating water use during the development of terminal drought in wheat. *Front. Plant Sci.* 8. doi: 10.3389/fpls.2017.01251

Shaar-Moshe, L., Hübner, S., and Peleg, Z. (2015). Identification of conserved drought-adaptive genes using a cross-species meta-analysis approach. *BMC Plant Biol.* 15, 111. doi: 10.1186/s12870-015-0493-6

Shepherd, T., and Wynne Griffiths, D. (2006). The effects of stress on plant cuticular waxes. *New Phytol.* 171, 469–499. doi: 10.1111/j.1469-8137.2006.01826.x

Shi, H., He, X., Zhao, Y., Lu, S., and Guo, Z. (2020). Constitutive expression of a group 3 LEA protein from *Medicago falcata* (*MfLEA3*) increases cold and drought tolerance in transgenic tobacco. *Plant Cell Rep.* 39, 851–860. doi: 10.1007/s00299-020-02534-y

Shinozaki, K., and Yamaguchi-Shinozaki, K. (2007). Gene networks involved in drought stress response and tolerance. *J. Exp. Bot.* 58, 221–227. doi: 10.1093/jxb/erl164

Simopoulos, C., MacLeod, M., Irani, S., Sung, W., Champigny, M. J., Summers, P. S., et al. (2020). Coding and long non-coding RNAs provide evidence of distinct transcriptional reprogramming for two ecotypes of the extremophile plant *Eutrema salsugineum* undergoing water deficit stress. *BMC Genomics* 21, 396. doi: 10.1186/s12864-020-06793-7

Soyka, S., and Heyer, A. G. (1999). *Arabidopsis* knockout mutation of ADC2 gene reveals inducibility by osmotic stress. *FEBS Lett.* 458, 219–223. doi: 10.1016/s0014-5793(99)01125-4

Sprenger, H., Erban, A., Seddig, S., Rudack, K., Thalhammer, A., Le, M. Q., et al. (2018). Metabolite and transcript markers for the prediction of potato drought tolerance. *Plant Biotechnol. J.* 16, 939–950. doi: 10.1111/pbi.12840

Sun, C., Liu, L., Wang, L., Li, B., Jin, C., and Lin, X. (2021). Melatonin: a master regulator of plant development and stress responses. *J. Integr. Plant Biol.* 63, 126–145. doi: 10.1111/jipb.12993

Supriya, L., Durgeshwar, P., Muthamilarasan, M., and Padmaja, G. (2022). Melatonin mediated differential regulation of drought tolerance in sensitive and tolerant varieties of upland cotton (*Gossypium hirsutum* l.). *Front. Plant Sci.* 13. doi: 10.3389/fpls.2022.821353

Tang, D., Quan, C., Lin, Y., Wei, K., Qin, S., Liang, Y., et al. (2022). Physio-morphological, biochemical and transcriptomic analyses provide insights into drought stress responses in *Mesona chinensis benth*. *Front. Plant Sci.* 13. doi: 10.3389/fpls.2022.809723

Tarun, J. A., Mauleon, R., Arbelaez, J. D., Catausan, S., Dixit, S., Kumar, A., et al. (2020). Comparative transcriptomics and co-expression networks reveal tissue- and genotype-specific responses of qDTYs to reproductive-stage drought stress in rice (*Oryza sativa* l.). *Genes* 11, 1124. doi: 10.3390/genes11101124

Thirumalaikumar, V. P., Devkar, V., Mehterov, N., Ali, S., Ozgur, R., Turkan, I., et al. (2018). NAC transcription factor JUNGBRUNNEN1 enhances drought tolerance in tomato. *Plant Biotechnol. J.* 6, 354–366. doi: 10.1111/pbi.12776

Tian, F., Yang, D. C., Meng, Y. Q., Jin, J., and Gao, G. (2020). PlantRegMap: charting functional regulatory maps in plants. *Nucleic. Acids Res.* 48, D1104–D1113. doi: 10.1093/nar/gkz1020

Todaka, D., Zhao, Y., Yoshida, T., Kudo, M., Kidokoro, S., Mizoi, J., et al. (2017). Temporal and spatial changes in gene expression, metabolite accumulation and phytohormone content in rice seedlings grown under drought stress conditions. *Plant J.* 90, 61–78. doi: 10.1111/tpj.13468

Van Hove, J., De Jaeger, G., De Winne, N., Guisez, Y., and Van Damme, E. J. (2015). The *Arabidopsis* lectin *EULS3* is involved in stomatal closure. *Plant Sci.* 238, 312–322. doi: 10.1016/j.plantsci.2015.07.005

Waititu, J. K., Zhang, X., Chen, T., Zhang, C., Zhao, Y., and Wang, H. (2021). Transcriptome analysis of tolerant and susceptible maize genotypes reveals novel insights about the molecular mechanisms underlying drought responses in leaves. *Int. J. Mol. Sci.* 22, 6980. doi: 10.3390/ijms22136980

Wang, L., Feng, Z., Wang, X., Wang, X., and Zhang, X. (2009). DEGseq: an r package for identifying differentially expressed genes from RNA-seq data. *Bioinformatics* 26, 136–138. doi: 10.1093/bioinformatics/btp612

Wang, M., Jiang, B., Peng, Q., Liu, W., He, X., Liang, Z., et al. (2018b). Transcriptome analyses in different cucumber cultivars provide novel insights into drought stress responses. *Int. J. Mol. Sci.* 19, 2067. doi: 10.3390/ijms19072067

Wang, M., and Liao, W. (2016). Carbon monoxide as a signaling molecule in plants. *Front. Plant Sci.* 7. doi: 10.3389/fpls.2016.00572

Wang, R., Shu, P., Zhang, C., Zhang, J., Chen, Y., Zhang, Y., et al. (2022). Integrative analyses of metabolome and genome-wide transcriptome reveal the regulatory network governing flavor formation in kiwifruit (*Actinidia chinensis*). *New Phytol.* 233, 373–389. doi: 10.1111/nph.17618

Wang, Z., Wang, F., Hong, Y., Yao, J., Ren, Z., Shi, H., et al. (2018a). The flowering repressor *SVP* confers drought resistance in *Arabidopsis* by regulating abscisic acid catabolism. *Mol. Plant* 11, 1184–1197. doi: 10.1016/j.molp.2018.06.009

Wang, X., Yang, X., Feng, Y., Dang, P., Wang, W., Graze, R., et al. (2021). Transcriptome profile reveals drought-induced genes preferentially expressed in response to water deficit in cultivated peanut (*Arachis hypogaea* l.). *Front. Plant Sci.* 12. doi: 10.3389/fpls.2021.645291

Wan, Y., Ouyang, J., Gong, X., Le, L., Wu, X., Wu, Q., et al. (2021). Water deficit and recovery-induced changes in growth, photosynthetic characteristics, antioxidant enzymes and yield of two tartary buckwheat genotypes. *Int. J. Agric. Biol.* 25, 483–491. doi: 10.17957/IJAB/15.1692

Xie, C., Mao, X., Huang, J., Ding, Y., Wu, J., Dong, S., et al. (2011). KOBAS 2.0: a web server for annotation and identification of enriched pathways and diseases. *Nucleic. Acids Res.* 39, W316–W322. doi: 10.1093/nar/gkr483

Xue, D., Zhang, X., Lu, X., Chen, G., and Chen, Z. H. (2017). Molecular and evolutionary mechanisms of cuticular wax for plant drought tolerance. *Front. Plant Sci.* 8. doi: 10.3389/fpls.2017.00621

Yang, D., Li, S., Xiao, Y., Lu, L., Zheng, Z., Tang, D., et al. (2021). Transcriptome analysis of rice response to blast fungus identified core genes involved in immunity. *Plant Cell Environ.* 44, 3103–3121. doi: 10.1111/pce.14098

You, J., Zhang, Y., Liu, A., Li, D., Wang, X., Dossa, K., et al. (2019). Transcriptomic and metabolomic profiling of drought-tolerant and susceptible sesame genotypes in response to drought stress. *BMC Plant Biol.* 19, 267. doi: 10.1186/s12870-019-1880-1

Zhang, K., He, M., Fan, Y., Zhao, H., Gao, B., Yang, K., et al. (2021a). Resequencing of global tartary buckwheat accessions reveals multiple domestication events and key loci associated with agronomic traits. *Genome Biol.* 22, 23. doi: 10.1186/s13059-020-02217-7

Zhang, L., Li, X., Ma, B., Gao, Q., Du, H., Han, Y., et al. (2017). The tartary buckwheat genome provides insights into rutin biosynthesis and abiotic stress tolerance. *Mol. Plant* 10, 1224–1237. doi: 10.1016/j.molp.2017.08.013

Zhang, J., Zhou, M., Zhou, H., Zhao, D., Gotor, C., Romero, L. C., et al. (2021b). Hydrogen sulfide, a signaling molecule in plant stress responses. *J. Integr. Plant Biol.* 63, 146–160. doi: 10.1111/jipb.13022

Zhao, N., Cui, S., Li, X., Liu, B., Deng, H., Liu, Y., et al. (2021). Transcriptome and co-expression network analyses reveal differential gene expression and pathways in response to severe drought stress in peanut (*Arachis hypogaea* l.). *Front. Genet.* 12. doi: 10.3389/fgene.2021.672884

Zhao, X., Huang, L. J., Sun, X. F., Zhao, L. L., and Wang, P. C. (2022). Transcriptomic and metabolomic analyses reveal key metabolites, pathways and candidate genes in *Sophora davidii* (Franch.) skeels seedlings under drought stress. *Front. Plant Sci.* 13. doi: 10.3389/fpls.2022.785702

Zhu, J. K. (2016). Abiotic stress signaling and responses in plants. *Cell* 167, 313–324. doi: 10.1016/j.cell.2016.08.029

frontiers | Frontiers in Plant Science

TYPE Original Research
PUBLISHED 13 October 2022
DOI 10.3389/fpls.2022.1020944

Check for updates

OPEN ACCESS

EDITED BY
Mirza Hasanuzzaman,
Sher-e-Bangla Agricultural University,
Bangladesh

REVIEWED BY
Michael Vincent Mickelbart,
Purdue University, United States
Brant McNeece,
PhD/Nutrien Ag Solutions,
United States

*CORRESPONDENCE
Hugh James Earl
hjearl@uoguelph.ca

SPECIALTY SECTION
This article was submitted to
Plant Abiotic Stress,
a section of the journal
Frontiers in Plant Science

RECEIVED 16 August 2022
ACCEPTED 29 September 2022
PUBLISHED 13 October 2022

CITATION
Gebre MG, Rajcan I and Earl HJ (2022)
Genetic variation for effects of drought
stress on yield formation traits among
commercial soybean [*Glycine max*
(L.) Merr.] cultivars adapted to
Ontario, Canada.
Front. Plant Sci. 13:1020944.
doi: 10.3389/fpls.2022.1020944

COPYRIGHT
© 2022 Gebre, Rajcan and Earl. This is
an open-access article distributed under
the terms of the Creative Commons
Attribution License (CC BY). The use,
distribution or reproduction in other
forums is permitted, provided the
original author(s) and the copyright
owner(s) are credited and that the
original publication in this journal is
cited, in accordance with accepted
academic practice. No use,
distribution or reproduction is
permitted which does not comply with
these terms.

Genetic variation for effects of drought stress on yield formation traits among commercial soybean [*Glycine max* (L.) Merr.] cultivars adapted to Ontario, Canada

Michael Gebretsadik Gebre, Istvan Rajcan and Hugh James Earl*

Department of Plant Agriculture, University of Guelph, Guelph, ON, Canada

Drought stress significantly limits soybean [*Glycine max* (L.) Merr.] yields in Ontario, Canada. Many studies of genetic variation for drought tolerance compare commercial lines with exotic, unadapted germplasm. We hypothesized that even current commercial cultivars adapted to Ontario would differ significantly for traits related to drought tolerance. In a greenhouse experiment, we grew fifteen soybean cultivars in field soil amended with sand in 1-m rooting columns, which allowed for simulation of field-like soil water profiles and rooting depths. Two watering treatments were imposed from the first flower until maturity by daily restoration of soil water to either 100% (control), or 50% (drought stress) of the maximum soil water holding capacity. Throughout the experiment, we measured volumetric soil water content at different depths in the soil profile, but found no evidence at any developmental stage that the cultivars differed for their ability to extract soil water from different depths. Drought stress reduced seed yield by 51% on average. Similar to the effects of drought in the field, pod number was the yield component most affected, with effects on seeds per pod and single-seed weight being comparatively minor. There were significant cultivar × treatment interactions for seed yield, pod number, shoot dry matter, and water use. We identified two drought-sensitive (*Saska* and *OAC Drayton*) and three drought-tolerant (*OAC Lakeview*, *OAC Champion*, and *PRO 2715R*) cultivars based on their ratios of seed yield under drought stress to seed yield under control conditions (seed yield ratio, SYR). Regression and principal component analyses revealed that drought-tolerant (high-SYR) cultivars were consistently those that maintained relatively high values for water use, biomass accumulation and pod number under drought stress; high water use efficiency under drought stress was also associated with a high SYR. One of the cultivars, *OAC Lakeview*, displayed a distinct mode of drought tolerance, maintaining a very high fraction of its control pod number under drought stress. This study helps define the physiological basis of soybean cultivar differences in drought tolerance, and

provides direction for soybean breeders to select traits that could improve yield under drought stress.

KEYWORDS

Drought stress, genetic variation, soil water deficits, soil water extraction, soybean, water use efficiency, yield components, seed yield ratio

Introduction

Soybean [*Glycine max* (L.) Merr.] is the most valuable oilseed crop grown in Ontario, Canada, where it is typically produced under rainfed conditions. Drought stress occurring during the critical stages of the crop's development can significantly reduce its yield potential (Hufstetler et al., 2007; Visser, 2014). Recent research demonstrates that drought stress constitutes a significant constraint to Ontario's soybean yield in most growing seasons. Reported yield losses attributed to drought stress in field experiments ranged from 8 to 24% and supplemental irrigation during the reproductive stage under field conditions was observed to significantly increase soybean yield, largely by increasing the number of pods per plant (Earl, 2012; Visser, 2014). The occurrence of transient soil water deficits in the region especially during drier years may lead to yield losses even exceeding 25% (H. J. Earl, unpublished data). Drought stress in Ontario soybean mainly occurs during the critical periods of pod-setting and seed-filling, typically from July to August when the crop's growth rate and daily water use are highest. Such yield-limiting soil water deficits frequently occur with no obvious outward signs of water stress such as leaf wilting, but result in fewer pods, reduced single-seed weight, and hastened crop maturity, which shortens the seed-filling period and finally reduces seed yield (Snyder et al., 1982; Brevedan and Egli, 2003; Visser, 2014; Giordani et al., 2019).

In this scenario of mild but cumulative soil water deficits in Ontario soybean production, targeted improvement for drought stress tolerance among adapted commercial cultivars is vital. Identification of physiological traits underlying tolerance to drought stress for specific regions would benefit from this effort. To do so, traits need to be measured accurately in controlled environments to pinpoint specific processes that may be missed in field trials. Previous studies suggest that there is a benefit to the adoption of controlled environment phenotyping methods that permit the use of mineral soils and produce field-like soil water profiles and root biomass distributions by depth (Gebre, 2020; Gebre and Earl, 2020; Gebre and Earl, 2021).

It has been reported that commercial soybean cultivars have a wide genetic variation for physiological traits related to drought stress tolerance such as (a) whole-plant water use efficiency (WUE), (b) regulation of whole-plant water use in response to soil water content, and (c) leaf epidermal conductance to water vapor when stomata are closed, also known as dark-adapted leaf conductance which predicts WUE of soybean (Walden-Coleman et al., 2013; Visser, 2014). The genetic variation in soybean for the critical soil water content at which water use begins to decline (Hufstetler et al., 2007) indicates that different genotypes make differing "decisions" about how to respond to reduced water availability. Moreover, genetic variation for WUE among Ontario soybean cultivars has been reported to significantly impact the cultivars' relative susceptibilities to yield loss under naturally-occurring drought stress conditions in the region (Visser, 2014).

Oya et al. (2004) reported a wide genetic variation for drought tolerance (~25 to 44%) among ten Brazilian soybean cultivars tested across two growing seasons. The authors concluded that higher drought tolerance in those soybean cultivars, which they defined to be higher yielding under drought stress, was correlated with maintaining a higher crop growth rate under drought stress conditions, especially during the early reproductive developmental stages. They also speculated that a higher vegetative growth together with the capacity to remobilize photo-assimilates from the vegetative organs (leaves, stems, and pericarps) to the reproductive sinks (e.g., seeds; supporting the seed growth rate) under drought stress could be considered as physiologically important traits contributing to soybean drought tolerance.

Drought stress affects soybean yield through a reduction of any of its yield components (pod number, seeds per pod, single-seed weight) (e.g., Gebre, 2020; Gebre and Earl, 2021). Moreover, yield loss in soybean can result from soil water deficits occurring at any time, though the magnitude of the yield reduction

Abbreviations: CV, coefficient of variation (%); DTM, days to maturity; HI, harvest index; PN, pod number (pods plant^{-1}); SN, seed number (seeds plant^{-1}); RDM, root dry matter (g plant^{-1}); R:S, root to shoot dry matter ratio; SDM, shoot dry matter (g plant^{-1}); SPP, seeds per pod; SW, single-seed weight (g seed^{-1}); SWHC, soil water holding capacity; SY, seed yield (g plant^{-1}); SYR, seed yield ratio (ratio of yield under drought conditions to yield under control conditions); TDM, total dry matter (g plant^{-1}); TDR, time-domain reflectometry; VSWC, volumetric soil water content (%); WU, water use (L plant^{-1}); WUE, water use efficiency (g L^{-1}).

depends on the stage of development, the timing of the stress, and the severity of the stress (Snyder et al., 1982). Brown et al. (1985) identified a soybean cultivar *'Sohoma'* that displayed a significantly lower reduction in its seed yield and yield components (100-seed weight and seed number) under soil water deficit conditions in the field, as compared to three other cultivars. In that work, the authors imposed the drought stress treatments at either the R2 (full flowering) or R4 (full pod) developmental stage; stress imposed at R2 resulted in a greater reduction (~31%) in seed yield than stress imposed at R4 (~21%).

Many studies of genetic variation for drought stress tolerance and related traits compare elite commercial lines with exotic, unadapted germplasm (e.g., Oya et al., 2004; Hufstetler et al., 2007; Walden-Coleman et al., 2013; He et al., 2016; He et al., 2017; Fried et al., 2019; Giordani et al., 2019). We hypothesized that even current commercial soybean cultivars grown in Ontario would differ significantly for their response to drought stress in terms of their growth, yield and yield components. The specific objectives of the present study were to: (1) assess the effect of drought stress on seed yield, yield components (pod number, seeds per pod, single-seed weight), biomass, and water use for fifteen commercial soybean cultivars adapted to Ontario; (2) evaluate the genetic variation for yield formation and related traits contributing to drought tolerance, and the relationships among these traits; and (3) identify drought-sensitive and drought-tolerant cultivars based on their ratio of seed yield under drought stress: seed yield under control conditions (SYR).

Materials and methods

Plant material and culture system

Plants were grown in the Crop Science Building's greenhouses at the University of Guelph (43.5314° N, -80.2244° W), Guelph, ON, Canada, in 2017 and 2018 using a culture system and drought stress simulation method developed and described in detail by Gebre and Earl (2020; 2021). Fifteen Ontario-adapted commercial soybean cultivars of similar maturity were selected based on days to maturity (DTM) ratings in the Ontario Oil and Protein Seed Crop Committee soybean cultivar trials brochure. These cultivars were from ten different public- and private-sector organizations: University of Guelph Ridgetown, Agriculture and Agri-Food Canada Ottawa, Mycogen, SeCan, Woodrill Farms, Prograin, La Coop Federee, Hendrick Seeds, Hensall District Coop, PRO Seeds, Bramhill Seeds, and Syngenta (Table 1; Figure 1).

The plants were grown in 1 m long 10 cm diameter PVC rooting columns (tubes) lined with polyethylene liners, and PVC end caps at the bottom, each with a drainage hole. The soil mixture was a blend of six parts by volume field soil, two parts granitic sand (B-sand; Hutcheson Sand and Gravel Ltd., Huntsville, ON, Canada), and one part peat-based potting mix (PGX; Premier Tech, Brantford, ON, Canada).

The field soil used, classified as a *London loam* (Grey-brown Podzolic loam till), was collected from the topsoil (upper 15 cm) at the Elora Research Station (Elora, ON, Canada; 44.6837° N, -80.4305° W) that had a prior history of soybean production. It was a silty loam (silt = 50%, sand = 31%, clay = 19%, mineral components by mass) texture that contained 4.2% organic matter, 23.5 ppm P, 61.5 ppm K, 280 ppm Mg, 2375 ppm Ca, 15 ppm Na, 14.4 meq per 100 g CEC, and had a pH of 7.4 according to a soil test performed by A&L Laboratories Inc., London, ON, Canada. During the process of potting, the tubes were filled in a systematic fashion of loading and packing until the soil reached approximately 1 cm below the top of the tube. The total weight of each tube with its soil was then recorded. A commercial 20-20-20 N-P-K plus micronutrients fertilizer (Master Plant Products Inc., Brampton, ON, Canada) at the rate of 0.8 g tube^{-1} dissolved in 500 mL of water was added at the top of the soil surface in each tube so that the first 0-30 cm of the soil profile could be thoroughly wetted with the fertilizer solution.

The experiment was repeated sequentially, with sowing dates of April 29, July 02, September 25, October 30, and December 27, 2017, for the five replications. Four seeds were sown per tube at 3 cm depth, and then thinned after emergence to one seedling per tube. Target greenhouse temperatures were 25°C during the day and 20°C during the night with an average relative humidity

TABLE 1 The 15 Ontario-adapted commercial soybean cultivars used in the greenhouse screening study.

Cultivar's name	Supplier	Days to maturity
5A090RR2	Mycogen	117
Absolute RR	SeCan	120
Blade RR	Woodrill	117
Bruce	Prograin	115
Dares	La Coop Federee	113
DH420	Hendrick Seeds	117
HDC 2701	Hensall District Coop	114
OAC Champion	PRO Seeds	115
OAC Drayton	Bramhill Seeds	116
OAC Lakeview	SeCan	112
OAC Purdy	SeCan	118
PRO 2715R	PRO Seeds	120
S08-C3	Syngenta	116
Saska	Prograin	116
Wildfire	Woodrill Farms	117
Mean		116
S.E.		0.5

Days to maturity data represent the mean of two years (2011 and 2013) measured in a field experiment under rainfed conditions (Visser, 2014).



FIGURE 1
A single replicate of the study. The 15 soybean cultivars were grown in a greenhouse in 1-m PVC rooting columns (tubes). Tubes are drilled on the sides to allow for time-domain reflectometry measurements of volumetric soil water content. Plastic liners allow for the removal of intact root systems. The photo was taken at the R1 developmental stage.

of 80%. The actual greenhouse daily minimum, maximum, and average temperatures from planting to physiological maturity (R7 developmental stage; developmental staging as per Fehr et al., 1971 and Purcell et al., 2014) for each replication are provided in Figure 2. Natural sunlight was supplemented with overhead high-pressure sodium and metal halide lamps to provide a supplementary 400 μmol m^{-2} s^{-1} photosynthetic photon flux density at the top of the canopy during the photoperiod, and to provide daylength extension to achieve 16 h of light and 8 h of dark.

Determining soil water holding capacity

To determine the soil water content and mass of dry soil in each tube, soil samples were taken during the potting process and dried in a forced-air drier at 80°C until a constant weight was attained. The maximum soil water holding capacity (SWHC) of the soil loaded in each tube was approximately 2.5 L (Gebre and Earl, 2020; Gebre and Earl, 2021). Thus, 24 h after wetting the first 0-30 cm of the soil profile with 500 mL of a fertilizer solution, about 3.5 L of water was added to exceed the maximum SWHC (against free drainage) of each tube. After another 24 h, the tubes were watered (~500 mL $tube^{-1}$) again to free drainage to ensure maximum SWHC was achieved. Elastic bands were used to close the plastic liners at the tops of the tubes to prevent surface evaporation. The tubes were allowed to drain until a constant weight was achieved (tube weight at maximum SWHC). The weights of the dry soil and the tubes were then subtracted from this weight to determine the soil water content at maximum SWHC. Then, the target weight for each tube was calculated as the tube + soil dry weight, plus the water weight at maximum SWHC measured for that tube multiplied by the target fraction of the maximum SWHC (either 100 or 50%, depending on the watering treatment).

Experimental design, treatments, and measurements

Each replicate of the experiment was arranged as a 15 × 2 split-plot design (15 × 2 = 30 tubes), with the 15 soybean cultivars as the main-plot factor and the two watering treatments (watered daily to either 100 or 50% of the maximum SWHC) as the sub-plot factor. The experiment consisted of five sequential replicates (replicated in time). The 30 experimental units (tubes) in each replicate were placed on a wooden stand (Figure 1), arranged in two rows of 15 tubes. Four tubes (two at each end) were used to grow border plants to minimize border effects.

Until the R1 (beginning flowering) developmental stage, all tubes were weighed and watered daily to their maximum SWHC. When more than 50% of the plants in a replicate had reached R1, watering treatments were imposed and lasted through the R8 (full maturity) developmental stage. During this period (R1 to R8 stages), tubes were returned to either 100% (control) or 50% (drought stress) of the maximum SWHC by daily weighing and watering. There was no leaching of water from the drainage holes in the bottoms of the tubes at any time during the experiment, so total plant water use (WU) per day was

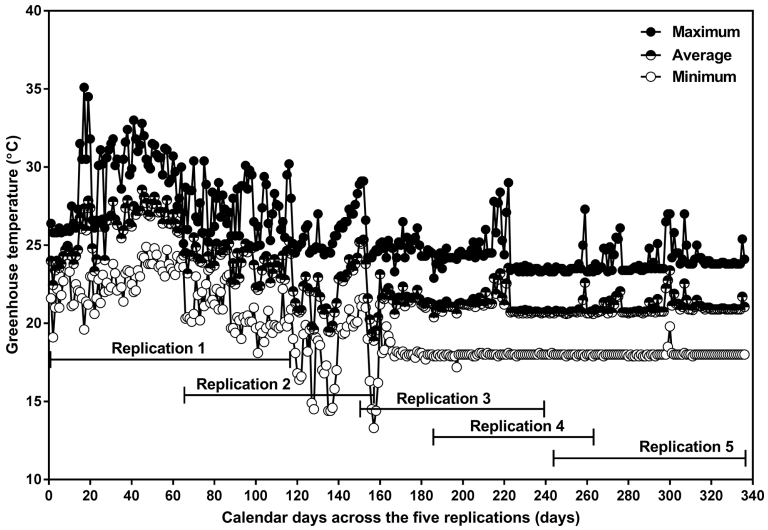


FIGURE 2
Daily minimum (open circle), average (half-closed circle), and maximum (closed circle) greenhouse air temperature as a function of calendar days from planting to physiological maturity in the 2017 summer and fall seasons, and the 2018 winter season. The experiment consisted of five sequential replicates. The planting dates for replications 1, 2, 3, 4, and 5 were April 29, July 2, September 25, October 30, and December 27 in 2017, respectively. The physiological maturity dates for replications 1, 2, and 3 were August 27 (122 days after planting; DAP), September 30 (90 DAP), December 22 (88 DAP) in 2017, and for replications 4, and 5 were January 15 (77 DAP) and March 29 (92 DAP) in 2018, respectively. Replication 1 was excluded from the data analysis due to extreme temperatures that occurred in the greenhouse.

calculated from the water additions at the top of the tubes. The whole-plant WU from planting to harvest was calculated as WU (g plant^{-1}) = [total amount of water added to each tube from planting to harvest + (starting weight – end weight of each tube at harvest) + whole-plant fresh biomass at harvest].

Time-domain reflectometry (TDR; Field Scout^{TM} TDR 100 Soil Moisture Meter, Spectrum Technologies, Inc., Aurora, IL, United States) millisecond readings were recorded once per week for the duration of the study, from the planting date until the R7 (physiological maturity) stage. The TDR measurements were performed at five equally spaced points (at 10, 30, 50, 70, and 90 cm below the soil surface) *via* pre-drilled TDR access holes in the sides of the tubes. The TDR measurements were always made just before daily watering (i.e., 24 h after the previous watering). The volumetric soil water content (VSWC; %) was calculated from the TDR millisecond readings using a calibration curve developed for the specific soil mix used in this experiment (Gebre and Earl, 2020).

Harvest and postharvest procedures

About 5 to 10 days after the full maturity date when 95% of the pods were brown (at the R8 developmental stage), all plants were cut at soil level and total aboveground plant fresh biomass was recorded. Immediately after harvest, the number of filled pods (pods with seeds) per plant (pod number; PN) was counted. All aboveground samples were then dried in a forced air drier at 80°C until a constant weight was attained. Then, the total aboveground (shoot) dry matter (SDM) per plant was determined, pods were threshed by hand, seed yield (SY, the weight of seeds per plant; g plant^{-1}) was recorded, and the total number of seeds per plant was counted. Seeds per pod (SPP) was then calculated as the number of seeds divided by PN. Individual seed weight (SW; g seed^{-1}) was calculated by dividing the SY by the seed number. Harvest index (HI), the fraction of SDM allocated to the seed, was calculated as the SY divided by the SDM for each plant. After harvesting the aboveground plant parts, the soil and the intact root systems within each rooting column were carefully removed by pulling out the plastic liner after laying the tube down on its side. The root samples were washed, placed into labelled paper bags, and then oven-dried in a forced air drier at 80°C until a constant weight was attained (typically 4 days) and then the final root dry matter (RDM) of each sample was recorded. Root-to-shoot ratio (R:S) was calculated as the ratio of RDM to SDM. Whole-plant water use efficiency (WUE; g L^{-1}) was calculated by dividing total plant dry matter (TDM; RDM + SDM) by total WU from planting to full maturity.

Statistical analyses

Analysis of variance was performed using the PROC GLIMMIX procedure of SAS Version 9.4 (SAS Institute Inc., Cary, NC, United States). A Type 1 error rate of 0.05 was used for all statistical tests. Since the dependent variables SY, PN, SPP, SW, SDM, RDM, R:S, TDM, HI, WU, WUE, and DTM were quantitative and continuous, a generalized linear mixed model (GLMM) was fitted with an identity link function and a Gaussian response distribution. The variances of the dependent variables were partitioned into the fixed effects of cultivar and watering treatments, and their interactions (cultivar × watering treatments), and the random effects of blocks, and block × cultivar interactions. We used the following statistical model:

$$Y_{ijk} = \mu + c_i + w_j + c_i w_j + B_k + c_i B_k + \epsilon_{ijk}$$

where Y_{ijk} denotes the value of the measured trait for the ith cultivar treatment (15 cultivars) of the jth watering treatment (control or drought stress) in the kth block, μ is the grand mean, c_i is the cultivar treatment effect (i.e., the main-plot factor), w_j is the watering treatment effect (i.e., the sub-plot factor), $c_i w_j$ is the interaction effect between cultivar and watering treatments, B_k is the effect of the kth block (treated as a random effect), $c_i B_k$ is the main-plot random error (treated as a random effect), and ϵ_{ijk} is the residual.

For each day on which VSWC was measured, the repeated measures analysis of variance of VSWC by depth was partitioned into the fixed effects of cultivars, watering treatments, and depth, and their interactions (cultivar × water, cultivar × depth, water × depth, and cultivar × water × depth), and the random effects of blocks, and block × cultivar interactions. The random interaction term *subject* × *depth* was included in the model where the *subjects* (tubes) were assumed independent (identity covariance structure) and for *depth* three possible types of covariance structures [*compound symmetric*, CS; autoregressive *order 1*, AR(1); and *heterogeneous autoregressive order 1*, ARH (1)] were compared. In each case, the most appropriate model was selected based on AICC and BIC fit statistics, no overdispersion based on the generalized Chi-square/df, and assessment of conditional studentized residual plots. Since the spacing interval between VSWC by depth measurements was equally spaced, the *Kenward-Roger* adjustment for bias correction for the denominator degrees of freedom was applied (Kenward and Roger, 1997).

F-tests and log-likelihood ratio tests were used to determine the significance of fixed and random effects, respectively. Least-square means comparisons were performed using a Protected Fisher's LSD test. The assumptions for the GLMM, in particular, random and normally distributed experimental errors and constant (homogeneous) error variance were tested by (1) plotting the studentized residuals against factor levels and predicted values; (2) generating a Q-Q plot and scatterplots of the residuals versus fitted values; and (3) performing a formal test of normality using a Shapiro-Wilk. Putative outliers, if any, were detected if the values of the studentized residuals were not within the range of -3.4 to 3.4 (Bowley, 2015).

Drought tolerance of each cultivar was quantified as the drought stress seed yield ratio (SYR), defined as the fraction of a cultivar's seed yield per plant under control conditions (100% SWHC) that was maintained under drought stress conditions (50% SWHC), i.e., SYR = SY per plant (drought stress)/SY per plant (control). The genetic variation for the various physiological traits was calculated using the cultivar least square means as the [(maximum value - minimum value)/ minimum value × 100]). The relationships among selected yield formation and related traits contributing to drought tolerance were investigated *via* correlation and regression analyses using the PROC CORR and PROC REG procedures in SAS Version 9.4 (SAS Institute Inc., Cary, NC, United States). The biplot display of principal component analysis (PCA) was also used to determine the relationship between multiple traits (drought stress to control ratio values) using the Multivariate procedure of PAST Software Version 3.25 (Hammer et al., 2001).

Results

Extreme temperatures occurred in the greenhouse during Replication 1 (Figure 2); data from this replicate were excluded, and so all analyses were based on the remaining four replicates.

Effects of drought stress on soybean yield, yield components, and related traits

Table 2 shows the main effects of drought stress treatment on soybean yield, yield components and other related traits. The drought stress treatment had a significant effect on every trait except HI. It reduced SY by 51% relative to the control ($p < 0.0001$), PN by 51% ($p < 0.0001$), SPP by 4% ($p < 0.01$), SDM by 51% ($p < 0.0001$), RDM by 36% ($p < 0.0001$), TDM by 48% ($p < 0.0001$), WU by 51% ($p < 0.0001$), and DTM by 4 days ($p < 0.0001$). The drought stress treatment increased single SW by 6% ($p < 0.0001$), R:S by 35% ($p < 0.0001$), and WUE by 6% ($p < 0.0001$), as compared to the control watering treatment (Table 2). Roots were extensively nodulated in both watering treatments.

TABLE 2 Effect of watering treatments [control (100% soil water holding capacity; SWHC), and drought stress (50% SWHC) on yield, yield components, and related traits.

Yield and related traits	Watering treatments					
	Control	Stress	Mean	Standard error	Difference (%)	*p* Water‡
Seed yield (g plant^{-1})	24.3	12.0	18.1	1.17	-51	**<0.0001**
Pods per plant	63.1	30.6	47.0	2.69	-51	**<0.0001**
Seeds per pod	2.26	2.16	2.21	0.062	-4	**0.0017**
Seed weight (g seed^{-1})	0.175	0.186	0.180	0.0073	6	**<0.0001**
Shoot dry wt. (g plant^{-1})	48.6	23.8	36.2	2.48	-51	**<0.0001**
Root dry wt. (g plant^{-1})	13.1	8.4	10.7	0.78	-36	**<0.0001**
Root: shoot (g g^{-1})	0.27	0.37	0.32	0.033	35	**<0.0001**
Total dry wt. (g plant^{-1})	61.7	32.2	47.0	2.81	-48	**<0.0001**
Water use (L plant^{-1})	32.2	15.6	24.0	0.88	-51	**<0.0001**
Total dry wt. WUE (g L^{-1})	1.92	2.04	1.98	0.072	6	**<0.0001**
Harvest index (g g^{-1})	0.50	0.50	0.50	0.013	0.3	0.7251
Days to maturity (days)	102	98	100	2.9	-4	**<0.0001**

Each value is the mean of four replications averaged across the 15 cultivars tested. The percent difference between treatments is calculated as (Control – Stress)/Control × 100.
‡Significant watering treatment effects ($p < 0.05$) are indicated in bold.

Effects of cultivar and drought stress on yield, yield components, and related traits

The cultivars differed significantly ($p < 0.001$) for every parameter measured. Table 3 shows the cultivar by treatment interaction means for those traits for which there was a significant cultivar × treatment interaction effect: SY, PN, SDM, and WU. Traits for which there were significant cultivar effects but no interaction (SPP, SW, RDM, TDM, R:S, WUE, HI, and DTM) are presented in Table 4. The overall coefficient of variation (CV) for SY was low (9%) while the other CVs ranged from 8 to 13%.

Although the cultivars did not statistically differ for their WU under drought stress, *PRO 2715R* had the highest WU, 16.9 L plant^{-1}, while *S08-C3* had the lowest WU, 14.7 L plant^{-1}, which nominally amounted to a genetic WU variation of 15% (calculated as the [(maximum - minimum value)/minimum value × 100]). The cultivars did statistically differ for their WU under control watering treatment conditions; *Saska* had the highest WU, 37.0 L plant^{-1}, while *OAC Lakeview* had the lowest WU, 28.5 L plant^{-1}, which amounted to a genetic WU variation of 30% (Table 3).

Although there were no significant cultivar × water interaction effects for WUE and HI, under drought stress, *5A090RR2* had the highest WUE, 2.37 g L^{-1}, while *Wildfire* had the lowest WUE, 1.83 g L^{-1}, which amounted to a genetic variation in WUE of about 30%. Under control watering treatment conditions, *OAC Drayton* had the highest WUE, 2.08 g L^{-1}, while *Saska* had the lowest WUE, 1.63 g L^{-1}, which amounted to a genetic variation of 27%. Moreover, under drought stress, *OAC Lakeview* had the highest HI, 0.58 g g^{-1}, while *PRO 2715R* had the lowest HI, 0.42 g g^{-1}, which amounted to a genetic variation in HI of about 37%. Under control watering treatment conditions, *OAC Lakeview* had the highest HI, 0.54 g g^{-1}, while *PRO 2715R* had the lowest HI, 0.41 g g^{-1}, which amounted to a genetic variation in HI of about 33% (Supplementary Table 1).

Using cultivar means averaged across watering treatments, genetic variation of 21% was recorded for SPP, 51% for SW, 93% for RDM, 34% for TDM, 92% for R:S, 33% for HI, 24% for WUE, and 14% for DTM (Table 4).

Effects of cultivar and drought stress on soil water extraction

Figure 3 shows the effects of watering treatment and soil depth on VSWC across different developmental stages. Once the watering treatments were imposed (after the R1 stage), there were clear differences in VSWC profiles between the control and drought stress watering treatments throughout the remainder of the experiment, with the control watering treatment having a significantly higher VSWC at every depth as compared to the drought stress watering treatment.

Consistent with the effect of cultivar on WU shown in Table 3, the cultivar main effects on VSWC (averaged across five measurement depths and two watering treatments) were significant ($p < 0.05$) at several developmental stages, (R1, R5 and R7; Supplementary Tables 2-5), but no significant cultivar × water interaction effects were detected. Also, there were no significant cultivar × depth, or cultivar × water × depth interaction effects on VSWC. That is, there was no evidence that the cultivars differed in their ability to extract soil water from different depths in the soil profile at any developmental stage.

TABLE 3 Cultivar and watering treatment interactive effects on seed yield (SY), pod number (PN), shoot dry matter (SDM), and water use (WU) for 15 soybean cultivars grown in a greenhouse in 1-m rooting columns under two watering treatments [control (100% soil water holding capacity; SWHC), and drought stress (50% SWHC)].

Yield and related traits	SY(g plant^{-1})		PN(pods plant^{-1})		SDM(g plant^{-1})		WU(L plant^{-1})	
Cultivar	**Stress**	**Control**	**Stress**	**Control**	**Stress**	**Control**	**Stress**	**Control**
5A090RR2	12.8	26.0	35.0	70.8	24.5	49.4	16.0	33.1
Absolute RR	12.5	26.1	31.8	68.3	23.5	50.0	15.2	31.3
Blade RR	11.8	24.8	32.5	75.8	22.9	46.6	15.5	31.4
Bruce	10.8	22.2	27.0	60.8	23.8	51.8	15.9	34.3
Dares	11.5	23.6	27.5	54.0	24.8	51.2	15.3	31.7
DH420	11.4	22.7	25.8	47.8	22.1	42.6	15.3	30.5
HDC 2701	10.8	23.4	21.5	51.8	21.4	48.3	15.0	30.7
OAC Champion	12.4	22.9	25.3	50.0	25.0	45.6	15.3	28.6
OAC Drayton	12.8	28.6	31.8	73.3	23.9	56.7	15.9	33.7
OAC Lakeview	14.7	24.5	37.8	58.0	25.5	45.4	15.8	28.5
OAC Purdy	12.0	25.4	30.5	66.5	24.3	48.6	16.1	34.2
PRO 2715R	12.3	22.1	37.3	77.0	28.9	54.8	16.9	33.7
S08-C3	11.4	24.0	35.5	64.8	22.0	45.0	14.7	30.8
Saska	11.9	27.0	35.5	76.8	22.8	51.0	15.4	37.0
Wildfire	10.7	20.9	24.3	50.8	21.7	42.4	16.2	33.7
S.E.	1.50		4.16		3.09		1.28	
CV (%)	9.45		13.25		9.71		8.28	
p Cultivar (C) ‡	**0.0024**		**<0.0001**		**0.0010**		**0.0004**	
p Water (W) ‡	**<0.0001**		**<0.0001**		**<0.0001**		**<0.0001**	
p C × W‡	**0.0212**		**0.0037**		**0.0317**		**0.0171**	

Each value is the mean of four plants, one from each of the four sequential replications. Data are presented only for those traits that showed a significant ($p < 0.05$) cultivar by water interaction effect.

‡Within a measured trait, significant cultivar, water, and cultivar by water interaction effects ($p < 0.05$) are indicated in bold.

Genetic variation for drought tolerance

Table 5 shows the effects of cultivar on the drought stress to control ratios of SY (i.e., SYR), PN, SPP, SW, SDM, and WU. The cultivars differed significantly ($p < 0.05$) for the drought stress to control ratios of SY, PN, SW, and WU, but not for the drought stress to control ratios of SPP and SDM. Among the 15 cultivars, two drought-sensitive cultivars (*Saska* and *OAC Drayton*; SYR of ~ 0.44 each) and three drought-tolerant cultivars [*OAC Lakeview* (SYR of ~ 0.60), *OAC Champion* (SYR of ~ 0.54), and *PRO 2715R* (SYR of ~ 0.55)] were identified. That is, the drought-tolerant cultivars had a significantly higher SYR (lower fractional yield loss under drought stress) than the drought-sensitive cultivars (higher yield loss) (Table 5). Averaged across the 15 cultivars, the average drought stress to control ratios for SY, PN, SDM, and WU were each 0.49 (about 51% loss in SY, PN, SDM, and WU due to drought stress). In contrast, the average drought stress to control ratios for SPP and SW were 0.96 and 1.06, respectively (Table 5).

To test if drought tolerance (high SYR) was associated with a smaller effect of drought stress on days to maturity, we regressed SYR on the drought stress to control ratio for DTM. However, there was no relationship between the two drought stress to control ratios (r = 0.17; $p \geq 0.05$; Supplementary Figure 1).

Relationships between yield and other traits

Figure 4 plots the mean SY under drought stress conditions against the mean SY under control conditions, for each cultivar, along with the best-fit regression line forced through the origin. Correlation analyses revealed that SYR was strongly associated with the drought:control ratios of PN (r = 0.72; $p < 0.01$), SDM (r = 0.87; $p < 0.0001$), WU (r = 0.81; $p < 0.001$) and TDM (r = 0.73; $p < 0.01$) (Figure 5). Moreover, there was a strong relationship between WU and TDM under drought stress (r = 0.68; $p < 0.01$); the drought stress to control ratio for WU also correlated with the ratio for TDM (r = 0.73; $p < 0.01$) (Supplementary Table 6) and the ratio for PN (r = 0.58; $p < 0.05$) (Supplementary Table 6).

High SDM-based WUE under drought stress was significantly associated with high SY under drought stress (r = 0.61; $p < 0.05$) and with high SYR (r = 0.54; $p < 0.05$) (Supplementary Table 6). However, under control conditions SDM-based WUE was not significantly associated with either SY

TABLE 4 Cultivar effects on seeds per pod (SPP; seeds pod^{-1}), single-seed weight (SW; g seed^{-1}), root dry matter (RDM; g plant^{-1}), total dry matter (TDM; g plant^{-1}), root-to-shoot ratio (R:S; g g^{-1}), harvest index (HI; g g^{-1}), whole-plant DM-based water use efficiency (WUE; g L^{-1}), and days to maturity (DTM; days) for 15 soybean cultivars grown in a greenhouse in 1-m rooting columns under two watering treatments [control (100% soil water holding capacity; SWHC), and drought stress (50% SWHC)].

Cultivar	SPP	SW	RDM	TDM	R:S	HI	WUE	DTM
5A090RR2	2.30	0.158	15.4	52.3	0.46	0.53	2.19	104
Absolute RR	2.24	0.175	10.8	47.5	0.31	0.53	2.04	103
Blade RR	2.35	0.146	14.0	48.8	0.43	0.52	2.08	106
Bruce	2.24	0.174	13.3	51.0	0.36	0.44	2.04	101
Dares	2.36	0.181	9.1	47.1	0.26	0.46	2.02	103
DH420	2.27	0.203	8.1	40.5	0.27	0.52	1.8	95
HDC 2701	2.16	0.220	9.9	44.7	0.33	0.50	1.95	96
OAC Champion	2.45	0.195	10.2	45.4	0.31	0.50	2.10	98
OAC Drayton	2.23	0.184	10.4	51.7	0.27	0.52	2.07	101
OAC Lakeview	2.09	0.195	9.1	44.5	0.27	0.56	2.02	99
OAC Purdy	2.05	0.191	10.3	46.7	0.30	0.51	1.89	94
PRO 2715R	2.07	0.149	12.6	54.4	0.33	0.42	2.19	107
S08-C3	2.02	0.173	9.5	43.0	0.29	0.53	1.88	98
Saska	2.21	0.158	8.0	44.9	0.24	0.53	1.76	99
Wildfire	2.08	0.205	10.5	42.5	0.34	0.50	1.73	103
Mean	2.21	0.180	10.7	47.0	0.32	0.50	1.98	100
S.E.	0.085	0.0094	1.19	3.45	0.040	0.017	0.096	3.2
p Cultivar[‡]	**0.0001**	**<0.0001**	**<0.0001**	**0.0010**	**<0.0001**	**<0.0001**	**<0.0001**	**<0.0001**
LSD $_{(0.05)}$	0.165	0.0105	2.62	5.17	0.077	0.023	0.156	2.9

Each value is the mean of eight plants, one from each of the two watering treatments in each of the four sequential replications. Data are presented only for those traits that did not show a significant cultivar by water interaction effect.
[‡]Within a measured trait (column), significant cultivar main effects ($p < 0.05$) are indicated in bold.

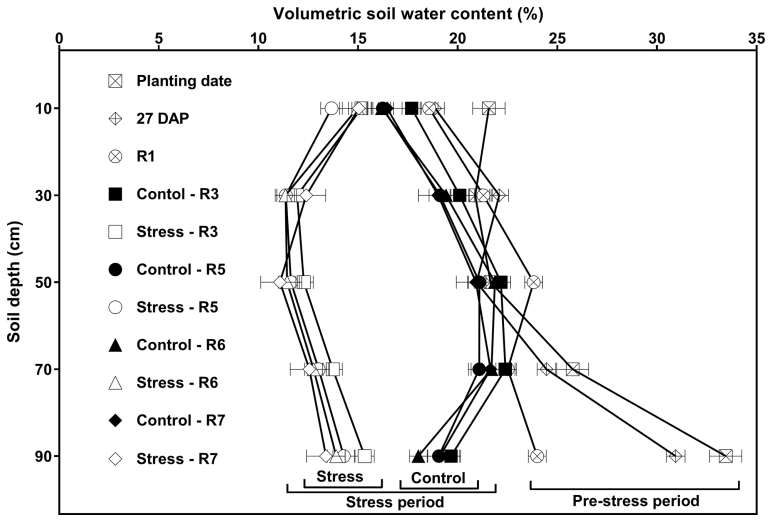


FIGURE 3
Effects of watering treatment and soil depth on volumetric soil water content (VSWC; %) at different developmental stages, averaged across 15 soybean cultivars and four replications. Watering treatments are watering daily to either 100% soil water holding capacity (SWHC; Control) or 50% SWHC (Stress). The stress treatment was imposed at the R1 developmental stage. The VSWC measurements were taken 24 h after the previous watering. Measurements were made during the pre-stress period [at planting date, 27 days after planting (DAP), and R1 stage; each value is the least squares mean of 120 data points] and stress period (at R3, R5, R6, and R7 stages; each value is the least squares mean of 60 data points). Error bars represent ± 1 S.E. and if not shown are smaller than the symbol.

(r = 0.29; $p \geq 0.05$) or SYR (r = 0.15; $p \geq 0.05$) (Supplementary Table 6). Furthermore, SDM under drought stress and the drought stress to control ratio of TDM were also predictive of SYR (r = 0.56; $p < 0.05$, and r = 0.73; $p < 0.01$, respectively) (Supplementary Table 6).

PCA of drought stress to control ratios of yield and related traits

Figure 6 shows the biplot display of the Principal Component Analysis (PCA) of the drought stress to control ratios for SY, PN, SPP, SW, SDM, and WU for the 15 cultivars. The first principal component accounted for 56% of the total variation and was strongly influenced by the stress to control ratios of WU, SY, SDM, and to some extent, PN. The second principal component explained about 24% of the total variability and was strongly associated with the ratios for SW and to some extent SPP. The PCA analysis revealed that SYR was strongly associated with the drought stress to control ratios for WU, SDM, and to a lesser extent with the PN ratio. Drought stress to control ratios of the other two yield components, SW and SPP, appeared to be quite independent of SYR (i.e., their vectors on the PCA were at nearly 90 degrees to the SYR vector). The PN vector was approximately opposite to the vectors for the other two yield components (SW and SPP), indicating that cultivars that had largest reductions in PN under drought stress tended to compensate with higher values of SW and/or SPP. As expected, the drought-tolerant cultivars (*OAC Lakeview*, *OAC Champion*, and *PRO 2715R*) had the longest SYR vectors, whereas the drought-sensitive cultivars (*Saska* and *OAC Drayton*) had the shortest ones, which were clustered on the opposite side to the drought-tolerant cultivars. Overall, the PCA indicates that the drought-tolerant cultivars were generally those that maintained high WU and SDM and, to a lesser extent, high PN, under drought stress conditions relative to control watering treatment conditions (Figure 6; Table 5). In contrast, the drought-sensitive cultivars were those that had lower drought stress to control ratio values for these traits (Figure 6; Table 5).

Discussion

The main purpose of this study was to test the hypothesis that commercial soybean cultivars adapted to Ontario differ in their tolerance to drought stress (defined as the ratio of their seed

TABLE 5 Drought stress to control ratio for seed yield (SY; g g^{-1}), pod number (PN; pods $pods^{-1}$), seeds per pod (SPP; seeds $seeds^{-1}$), single-seed weight (SW; g g^{-1}), shoot dry matter (SDM; g g^{-1}), and water use (WU; L L^{-1}) for 15 soybean cultivars grown in a greenhouse under two watering treatments [control (100% soil water holding capacity; SWHC), and drought stress (50% SWHC) conditions] in 1-m rooting columns.

	Ratio of drought stress to control plant					
Cultivar	**SY**	**PN**	**SPP**	**SW**	**SDM**	**WU**
5A090RR2	0.486	0.494	0.932	1.053	0.490	0.485
Absolute RR	0.472	0.465	0.965	1.059	0.466	0.487
Blade RR	0.474	0.427	0.992	1.101	0.493	0.499
Bruce	0.491	0.441	0.995	1.114	0.457	0.460
Dares	0.486	0.511	0.914	1.053	0.482	0.485
DH420	0.501	0.546	0.932	0.992	0.520	0.504
HDC 2701	0.461	0.418	0.963	1.143	0.439	0.494
OAC Champion	0.542^{+}	0.505	0.986	1.087	0.547	0.537
OAC Drayton	0.443^{-}	0.430	1.019	1.043	0.420	0.473
OAC Lakeview	0.601^{+}	0.649	0.881	1.055	0.559	0.555
OAC Purdy	0.471	0.463	0.900	1.151	0.499	0.469
PRO 2715R	0.551^{+}	0.494	0.996	1.134	0.521	0.502
S08-C3	0.471	0.555	0.871	0.978	0.489	0.480
Saska	0.437^{-}	0.461	0.955	0.998	0.444	0.416
Wildfire	0.515	0.496	1.048	1.012	0.523	0.485
Mean	0.493	0.490	0.957	1.065	0.490	0.489
S.E.	0.052	0.053	0.051	0.039	0.050	0.033
CV (%)	11.8	16.5	10.2	7.4	12.2	8.8
p Cultivar‡	**0.0219**	**0.0238**	0.3839	**0.0431**	0.0714	**0.0267**
LSD $_{(0.05)}$	0.083	0.115	0.139	0.113	0.085	0.062

$^{+}$Cultivars marked with "+" have a significantly higher seed yield ratio (SYR) ($p < 0.05$) than cultivars marked with "-", according to a protected Fisher's LSD test. ‡Significant cultivar effects ($p < 0.05$) are indicated in bold.
Data represent the least-squares mean values of four sequential replicates.

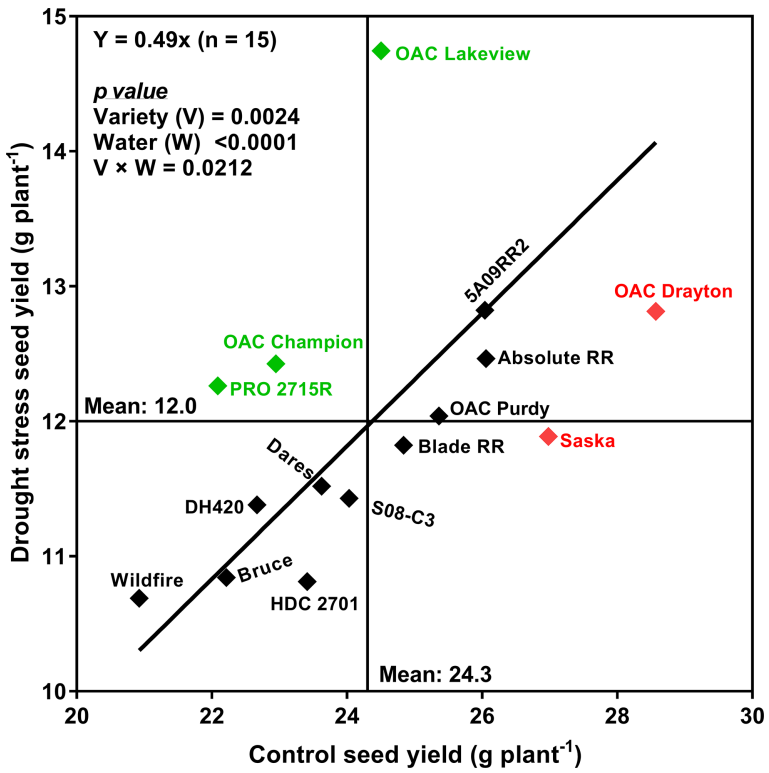


FIGURE 4
Relationship between seed yield under control (watered daily to 100% soil water holding capacity; SWHC) and drought stress (watered daily to 50% SWHC) conditions for the 15 soybean cultivars grown in a greenhouse in 1-m rooting columns in 2017 and 2018. The line is the best fit regression through the origin. Four sequential replicates were used.

yield under drought conditions compared to control conditions; SYR) and to characterize the physiological basis for any such differences in drought tolerance. Specifically, we wanted to see how a high SYR was related to drought effects on yield components (PN, SPP, and SW), plant WU and dry matter (DM) production.

While not producing symptoms of severe stress such as leaf wilting, which are also not common under Ontario field conditions, the drought stress treatment that was imposed through the entire reproductive period (R1 to R8 developmental stages) resulted in a significant reduction in SY as well as every other trait that we measured, except for SW and HI. When averaged across the cultivars, the drought stress treatment reduced final plant DM and total plant WU by about 50%. SY was also reduced by about 50%, and almost all of this reduction could be attributed to a single yield component – PN. SPP decreased significantly under drought stress, and SW increased significantly, but these changes were very small compared to the change in PN. Effects of drought on DTM were also statistically significant, but small. These findings are consistent with our previous study and further indicate that PN is the most important yield component driving SY response to drought stress in this culture system (Gebre, 2020; Gebre and Earl, 2021), which is also typically observed in the field. Other studies have also reported similar effects of drought stress on soybean SY (He et al., 2016; He et al., 2017; Giordani et al., 2019; Gebre and Earl, 2021), WU (Earl, 2002; He et al., 2016; He et al., 2017; Gebre and Earl, 2020; Gebre and Earl, 2021), TDM (Earl, 2002; He et al., 2016; Gebre and Earl, 2020; Gebre and Earl, 2021), PN (Snyder et al., 1982; He et al., 2017; Gebre and Earl, 2021), and DTM (Earl, 2012; Visser, 2014).

As expected, the drought stress treatment increased R:S and WUE. This indicates a greater proportion of DM allocation to the roots and a more efficient utilization of available water (i.e., more DM produced per unit of water used) under drought stress conditions. Similar increases in R:S and WUE under drought stress have been reported previously (e.g., Earl, 2002; Gebre and Earl, 2020; Gebre and Earl, 2021). In contrast, HI was not responsive to watering treatment as about 50% of the total SDM was allocated to the seed in both watering treatments. Contrary to our results, reduced HI under drought stress has been reported in soybean in some past research (e.g., Giordani et al., 2019; Oya et al., 2004). However, a significantly higher HI was reported in a single Ontario-adapted commercial soybean cultivar *OAC Bayfield* grown under drought stress (about 16%

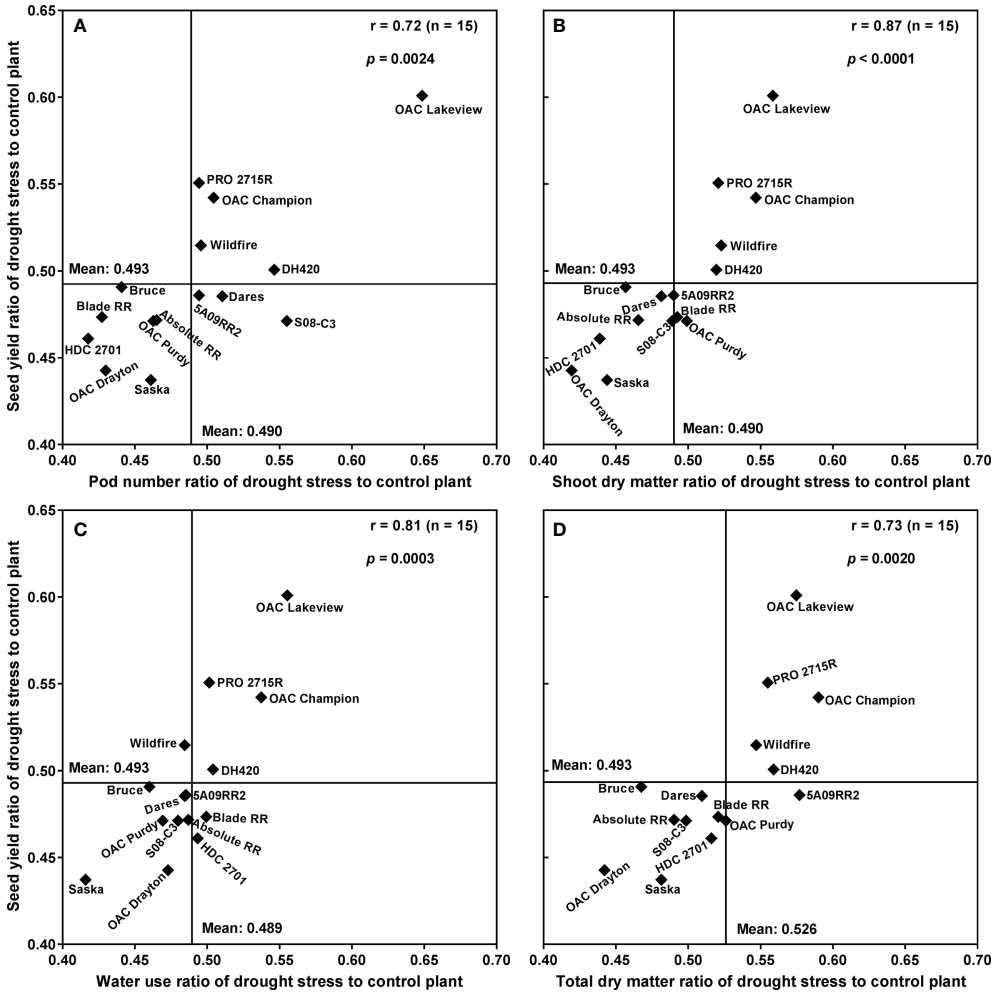


FIGURE 5
Relationships between the drought stress to control seed yield ratio and pod number ratio **(A)**, shoot dry matter ratio **(B)**, water use ratio **(C)**, and whole-plant dry matter ratio **(D)** for 15 soybean cultivars grown in a greenhouse in 1-m rooting columns in 2017 and 2018. Four sequential replicates were used.

higher than the control) in a previous study (Gebre and Earl, 2021), while He et al. (2016) reported no significant difference in HI between drought stress and control watering treatments for two old and two new soybean cultivars.

Overall, this experiment supports the following model of yield reduction due to drought stress: the drought stress treatment reduces whole-plant WU, which produces a nearly proportional decrease in whole-plant DM (since WUE increased only slightly) and in SY, with PN being the yield component most affected. This is consistent with the more general model that PN and thereby SN, primarily determines SY in soybean, with PN being strongly determined by plant growth rates during the "critical period" from about R2 to R5.5 (e.g., Vega et al., 2001). Also consistent with this model, cultivars that were able to use water to produce more yield did so by producing more TDM and more specifically SDM, not by allocating a larger fraction of that SDM to the seed.

There were significant cultivar × watering treatment interaction effects for SY, PN, SDM, and WU, indicating that the cultivars differed for their response to drought stress for those traits. The significant cultivar × treatment interaction effect for SY suggests that there is genetic variation for drought tolerance among these 15 cultivars. Similar to SY, the cultivars also differed for PN loss and SDM reduction under drought stress conditions. All four traits that showed significant cultivar × water interaction effects also showed a very uniform average 51% reduction due to drought stress, suggesting a quantitative, mechanistic relationship between them. Similar to our findings, He et al. (2017; 2019) reported significant genotype × treatment interaction effects in soybean for SY, PN, SDM, and WU, while Giordani et al. (2019) reported significant

genotype × treatment interaction effects for SY and PN but not for SDM (they did not measure WU in their work). Fried et al. (2019) also reported a significant genotype × watering treatment interaction effect for SY among 10 soybean genotypes at one of their experimental locations.

Similar genetic variation in susceptibility to yield loss under typical rainfed conditions in Ontario has been reported by Visser (2014). The author found that in a three-year field study, cultivars that increased their SDM the most under irrigation also showed the largest yield response to irrigation, while HI was quite stable across years, treatments, and cultivars. This finding is also in agreement with our results where HI was unaffected by drought stress, although in our experiment the cultivar main effect for HI was significant, indicating genetic variation for this trait.

Based on their SYR, two drought-sensitive cultivars (*Saska* and *OAC Drayton*) and three drought-tolerant cultivars (*OAC Lakeview*, *OAC Champion*, and *PRO 2715R*) were identified. We chose SYR *a priori* as an index of drought tolerance, but it must be recognized that SYR is increased when either the SY under drought stress is higher than expected, or the SY under control conditions is lower than expected. The latter case raises the possibility that cultivars identified as drought-sensitive according to SYR may just actually be unusually productive when water is plentiful. Indeed, both cultivars identified as being particularly drought-sensitive (*OAC Drayton* and *Saska*) had much higher than average yields under control conditions, while all three "drought-tolerant" cultivars had average (*OAC Lakeview*) or below average (*OAC Champion* and *PRO 2715R*) yields under control conditions. This may indicate that cultivars with high SYR are systematically those with poor yields under well-watered conditions, or it may just be a coincidence, unique to this particular set of cultivars. The latter possibility is unlikely given that cultivars such as *OAC Lakeview* and *OAC Champion* have been grown by Ontario farmers for close to two decades and still perform reasonably well for yield as compared to the more recent, modern ones. However, a broader selection of germplasm should be evaluated to determine if in fact high SYR is generally associated with average or low yield potential. Even if that is the case, a cultivar such as *OAC Lakeview* would still warrant further investigation, given that i) it produced the highest yield under drought stress while still producing average yield in the absence of drought stress, and ii) its mode of drought tolerance appeared to be unique, with PN being unusually insensitive to drought stress (stress:control PN ratio of 0.649, by far the highest of any of the cultivars tested (Table 5).

In the present study, SYR was positively and strongly associated with the stress:control ratios of both TDM and WU, consistent with our previous findings with soybean in this culture system that WU and TDM are closely tied (Gebre, 2020; Gebre and Earl, 2020; Gebre and Earl, 2021). This raises the prospect that soybean drought tolerance could be usefully assayed in real time and non-destructively by measuring WU alone. In other words, if biomass accumulation during some critical developmental period strongly predicts SY, and WU predicts biomass accumulation, then a non-destructive measure of the response of WU to stress during that period should be a useful measure of drought tolerance.

The PCA of the drought stress to control ratios for SY, PN, SPP, SW, SDM, and WU for the 15 cultivars further supported most of the above relationships. It confirmed that SYR was strongly associated with the drought stress to control ratios of WU, SDM, and to a lesser extent with PN ratio, further supporting the idea that increasing WU under drought stress significantly increased SY by increasing SDM and PN. In general, the drought-tolerant cultivars were those that

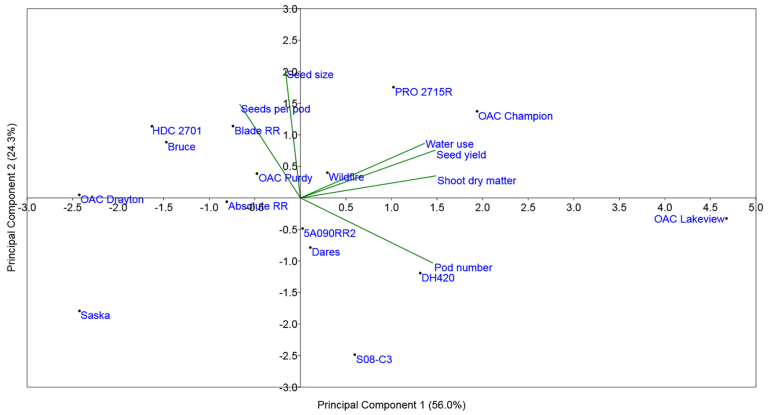


FIGURE 6
Principal Component Analysis (PCA) of seed yield, yield components, and related yield formation traits for the 15 commercial elite soybean cultivars adapted to Ontario grown in a greenhouse in 1-m rooting columns in 2017 and 2018. For all traits, the analysis was carried out using the ratio of the drought stress to the control ratio, determined from means across four replications.

continued to use water under drought stress conditions to produce a significantly higher DM accumulation and higher PN compared to the drought-sensitive cultivars. By contrast, the cultivars that slowed their WU (i.e., shut down to an extent) under drought stress suffered more in terms of the loss to SDM and SY.

The PCA also revealed the expected relationships between changes in the various yield components. Among them, PN was the primary driver and predictor of SY, as compared to SW and SPP, but there was also evidence of the expected compensation between yield components. For example, those cultivars that saw the largest reductions in PN under stress (lower PN ratio) tended to be those that had higher stress:control ratios for SW and especially SPP, as also observed by Visser (2014) in field trials. These slightly different modes of drought tolerance among cultivars are evident in the PCA, where for example, *OAC Champion* and *PRO 2715R* are more closely associated with the SW ratio vector, and *OAC Lakeview* with the PN ratio vector.

In the current study, the lack of significant cultivar × watering treatment interaction effect for DTM and the lack of association between SYR and the stress:control ratio for DTM indicate that cultivar differences in SY response to drought stress cannot be attributed to differences in the way drought stress affected maturity (i.e., by differentially shortening the seed-filling period).

The total genetic variation for WUE in this experiment was 24%. Hufstetler et al. (2007) also reported similar total genetic variation (~25%) for WUE among 23 soybean cultivars, breeding lines and plant introductions. We also found a significant positive association between WUE under stress (only) and SYR. In interpreting this result, it should be noted that WUE under stress is mathematically auto-correlated with the stress:control ratio for SDM (which itself is positively correlated with SYR); however, it is *negatively* auto-correlated with the stress:control ratio for WU, (which is also positively correlated with SYR). Hence, on balance, it appears that the correlation between WUE under stress and SYR is not simply a mathematical artefact. High WUE can arise from reduced transpiration (e.g., through reduced stomatal conductance, leading to soil water conservation) or from higher photosynthetic response to leaf internal CO_2 concentration (Earl, 2002). The design of the present experiment would have disadvantaged plants with the former strategy, since all transpired water was replaced on a daily basis regardless of the daily WU. This suggests that in this experiment it was the higher photosynthetic response to leaf internal CO_2 under drought stress that gave high-WUE cultivars a yield advantage. It is not clear how this would translate to a field environment where soil water conservation might also be advantageous.

In conclusion, drought stress significantly affected every trait we measured, except HI. There exists substantial genetic variation among Ontario-adapted commercial soybean cultivars for their response to drought stress, and there was a broad range of genetic variation for SYR among the cultivars tested. Based on their SYR, we identified two drought-sensitive cultivars (*Saska* and *OAC Drayton*) and three drought-tolerant cultivars (*OAC Lakeview*, *OAC Champion*, and *PRO 2715R*). Drought-tolerant cultivars were those that maintained higher WU, SDM, and PN under drought stress conditions. However, the different cultivars had slightly different modes of drought tolerance in terms of yield components (PN, SPP, or SW). Our study helps to define the physiological basis of soybean cultivar differences in drought tolerance, and provides direction for soybean breeders wishing to target specific traits that could improve soybean yield when soil water is limiting.

Data availability statement

The original contributions presented in the study are included in the article/Supplementary Material. Further inquiries can be directed to the corresponding author.

Author contributions

MG performed the experiment, data collection, statistical data analysis and presentation, and drafted the manuscript. MG and HE conceived the project and experimental design and collaborated on the data interpretation and manuscript revision. IR assisted with cultivar selection, project management and manuscript revision. All authors contributed to the article and approved the submitted version.

Funding

This research was funded by Grain Farmers of Ontario (Project number: GF2 0122) and the Natural Sciences and Engineering Research Council of Canada (Grant number: CRDPJ 513541 – 17).

Acknowledgments

Financial support from the Grain Farmers of Ontario (Project number: GF2 0122) and the Natural Sciences and Engineering Research Council of Canada (Grant number: CRDPJ 513541 – 17) is gratefully acknowledged. The authors are also grateful to Godfrey Chu (University of Guelph), Laxhman Ramsahoi (University of Guelph) and Austin Bruch (University of Guelph) for their technical assistance.

Conflict of interest

The authors declare that the research was conducted in the absence of any commercial or financial relationships that could be construed as a potential conflict of interest.

Publisher's note

All claims expressed in this article are solely those of the authors and do not necessarily represent those of their affiliated organizations, or those of the publisher, the editors and the reviewers. Any product that may be evaluated in this article, or claim that may be made by its manufacturer, is not guaranteed or endorsed by the publisher.

Supplementary material

The Supplementary Material for this article can be found online at: https://www.frontiersin.org/articles/10.3389/fpls.2022.1020944/full#supplementary-material

References

Bowley, S. R. (2015). *A hitchhiker's guide to statistics in biology: Generalized linear mixed model edition* (Kincardine, Ontario: Plants et al.).

Brevedan, R., and Egli, D. (2003). Short periods of water stress during seed filling, leaf senescence, and yield of soybean. *Crop Sci.* 43 (6), 2083–2088. doi: 10.2135/cropsci2003.2083

Brown, E., Caviness, C., and Brown, D. (1985). Response of selected soybean cultivars to soil moisture deficit 1. *Agron. J.* 77 (2), 274–278. doi: 10.2134/agronj1985.00021962007700020022x

Earl, H. J. (2002). Stomatal and non-stomatal restrictions to carbon assimilation in soybean (Glycine max) lines differing in water use efficiency. *Environ. Exp. Bot.* 48 (3), 237–246. doi: 10.1016/S0098-8472(02)00041-2

Earl, H. J. (2012). *Drought stress in Ontario soybean – what's really going on?* (Cincinnati, OH). [Paper presentation] 2012 ASA, CSSA, and SSSA Annual Meetings.

Fehr, W. R., Caviness, C. E., Burmood, D. T., and Pennington, J. S. (1971). Stage of development descriptions for soybeans, *Glycine max* (L.) merr. *Crop Sci.* 11 (6), 929–931. doi: 10.2135/cropsci1971.0011183X001100060051x

Fried, H. G., Narayanan, S., and Fallen, B. (2019). Evaluation of soybean [Glycine max (L.) merr.] genotypes for yield, water use efficiency, and root traits. *PloS One* 14 (2), e0212700. doi: 10.1371/journal.pone.0212700

Gebre, M. G. (2020). Genetic variation for physiological traits affecting drought tolerance among Ontario-adapted commercial soybean [Glycine max (L.) merr.] varieties grown in 1-m rooting columns. PhD thesis. University of Guelph. Guelph, Ontario, Canada.

Gebre, M. G., and Earl, H. J. (2020). Effects of growth medium and water stress on soybean [*Glycine max* (L.) merr.] growth, soil water extraction and rooting profiles by depth in 1-m rooting columns. *Front. Plant Sci.* 11 (487). doi: 10.3389/fpls.2020.00487

Gebre, M. G., and Earl, H. J. (2021). Soil water deficit and fertilizer placement effects on root biomass distribution, soil water extraction, water use, yield, and yield components of soybean [*Glycine max* (L.) merr.] grown in 1-m rooting columns. *Front. Plant Sci.* 12 (581127). doi: 10.3389/fpls.2021.581127

Giordani, W., Gonçalves, L. S. A., Moraes, L. A. C., Ferreira, L. C., Neumaier, N., Farias, J. R. B., et al. (2019). Identification of agronomical and morphological traits contributing to drought stress tolerance in soybean. *Aust. J. Crop Sci.* 13 (1), 35. doi: 10.21475/ajcs.19.13.01.p1109

Hammer, Ø., Harper, D. A., and Ryan, P. D. (2001). PAST: Paleontological statistics software package for education and data analysis. *Palaeontol. Electronica* 4 (1), 9.

He, J., Du, Y. L., Wang, T., Turner, N., Xi, Y., and Li, F. M. (2016). Old and new cultivars of soya bean (*Glycine max* l.) subjected to soil drying differ in abscisic acid accumulation, water relations characteristics and yield. *J. Agron. Crop Sci.* 202 (5), 372–383. doi: 10.1111/jac.12143

He, J., Jin, Y., Du, Y.-L., Wang, T., Turner, N. C., Yang, R.-P., et al. (2017). Genotypic variation in yield, yield components, root morphology and architecture, in soybean in relation to water and phosphorus supply. *Front. Plant Sci.* 8 (1499). doi: 10.3389/fpls.2017.01499

He, J., Jin, Y., Turner, N. C., Chen, Z., Liu, H.-Y., Wang, X.-L., et al. (2019). Phosphorus application increases root growth, improves daily water use during the reproductive stage, and increases grain yield in soybean subjected to water shortage. *Environ. Exp. Bot.* 166, 103816. doi: 10.1016/j.envexpbot.2019.103816

Hufstetler, E. V., Boerma, H. R., Carter, T. E., and Earl, H. J. (2007). Genotypic variation for three physiological traits affecting drought tolerance in soybean. *Crop Sci.* 47 (1), 25–35. doi: 10.2135/cropsci2006.04.0243

Kenward, M. G., and Roger, J. H. (1997). Small sample inference for fixed effects from restricted maximum likelihood. *Biometrics* 53 (3), 983–997. doi: 10.2307/2533558

Oya, T., Nepomuceno, A. L., Neumaier, N., Farias, J. R. B., Tobita, S., and Ito, O. (2004). Drought tolerance characteristics of Brazilian soybean cultivars. *Plant Product. Sci.* 7 (2), 129–137. doi: 10.1626/pps.7.129

Purcell, L. C., Salmeron, M., and Ashlock, L. (2014). "Soybean growth and development," in *Arkansas Soybean production handbook. MP197*, (University of Arkansas, Division of Agriculture Research and Extension)1–8.

Snyder, R. L., Carlson, R. E., and Shaw, R. H. (1982). Yield of indeterminate soybeans in response to multiple periods of soil-water stress during reproduction. *Agron. J.* 74, 855–859. doi: 10.2134/agronj1982.00021962007400050020x

Vega, C. R. C., Andrade, F. H., Sadras, V. O., Uhart, S. A., and Valentinuz, O. R. (2001). Seed number as a function of growth. a comparative study in soybean, sunflower and maize. *Crop Sci.* 41 (3), 748–754. doi: 10.2135/cropsci2001.413748x

Visser, B. (2014). *Impact of varietal differences in water use efficiency on soybean yield under water stress* (University of Guelph).

Walden-Coleman, A. E., Rajcan, I., and Earl, H. J. (2013). Dark-adapted leaf conductance, but not minimum leaf conductance, predicts water use efficiency of soybean (*Glycine max* l. merr.). *Can. J. Plant Sci.* 93 (1), 13–22. doi: 10.4141/cjps2012-178

frontiers | Frontiers in Plant Science

TYPE Review
PUBLISHED 20 October 2022
DOI 10.3389/fpls.2022.1002596

Check for updates

OPEN ACCESS

EDITED BY
Mirza Hasanuzzaman,
Sher-e-Bangla Agricultural University, Bangladesh

REVIEWED BY
Praveen Soni,
University of Rajasthan, India
Yinghua Pan,
Guangxi Academy of Agricultural Sciences, China

*CORRESPONDENCE
Mushtaq Ahmad
drmushtaqdarskuastk@rediffmail.com;
darmush4@unl.edu

SPECIALTY SECTION
This article was submitted to Plant Abiotic Stress, a section of the journal Frontiers in Plant Science

RECEIVED 25 July 2022
ACCEPTED 29 September 2022
PUBLISHED 20 October 2022

CITATION
Ahmad M (2022) Genomics and transcriptomics to protect rice (*Oryza sativa.* L.) from abiotic stressors: -pathways to achieving zero hunger. *Front. Plant Sci.* 13:1002596. doi: 10.3389/fpls.2022.1002596

COPYRIGHT
© 2022 Ahmad. This is an open-access article distributed under the terms of the Creative Commons Attribution License (CC BY). The use, distribution or reproduction in other forums is permitted, provided the original author(s) and the copyright owner(s) are credited and that the original publication in this journal is cited, in accordance with accepted academic practice. No use, distribution or reproduction is permitted which does not comply with these terms.

Genomics and transcriptomics to protect rice (*Oryza sativa.* L.) from abiotic stressors: -pathways to achieving zero hunger

Mushtaq Ahmad*

Visiting Scientist Plant Sciences, University of Nebraska, Lincoln, NE, United States

More over half of the world's population depends on rice as a major food crop. Rice (*Oryza sativa* L.) is vulnerable to abiotic challenges including drought, cold, and salinity since it grown in semi-aquatic, tropical, or subtropical settings. Abiotic stress resistance has bred into rice plants since the earliest rice cultivation techniques. Prior to the discovery of the genome, abiotic stress-related genes were identified using forward genetic methods, and abiotic stress-tolerant lines have developed using traditional breeding methods. Dynamic transcriptome expression represents the degree of gene expression in a specific cell, tissue, or organ of an individual organism at a specific point in its growth and development. Transcriptomics can reveal the expression at the entire genome level during stressful conditions from the entire transcriptional level, which can be helpful in understanding the intricate regulatory network relating to the stress tolerance and adaptability of plants. Rice (*Oryza sativa* L.) gene families found comparatively using the reference genome sequences of other plant species, allowing for genome-wide identification. Transcriptomics *via* gene expression profiling which have recently dominated by RNA-seq complements genomic techniques. The identification of numerous important qtl,s genes, promoter elements, transcription factors and miRNAs involved in rice response to abiotic stress was made possible by all of these genomic and transcriptomic techniques. The use of several genomes and transcriptome methodologies to comprehend rice (*Oryza sativa*, L.) ability to withstand abiotic stress have been discussed in this review

KEYWORDS

rice (*Oryza sativa*, L.), abiotic stress, adaptability, gene, genomics, transcriptomics

Introduction

Adversity is the general term for a variety of environmental challenges that plants frequently face in the natural world and which hinder their survival and development. Abiotic and biotic stresses are the two main types of stress experienced by plants. Physical or chemical factors such high temperatures, droughts, cold injuries; high salt contents, heavy metals, and mechanical damage are the main causes of abiotic stress (Figure 1). The main biological causes of biotic stress are fungi, bacteria, viruses, nematodes, and parasitic plants. Plants alter over time at the cellular, organ, physiological, biochemical, and molecular levels to cope with adversity, which has ultimately represented as morphological changes. Following treatment to rice with (200 mM NaCl, 14 days) crop showing salt stress, the chlorophyll a and b contents of rice (*Oryza sativa.* L.) leaves have found to reduced, with the chlorophyll b content of the leaves being more significantly affected (41%) than the chlorophyll a (33%) content. Leaves with low transpiration rates have frequently exposed to high temperatures because heat can cause leaves to heat up quickly (up to 15°C above air temperature). When Na^+ and Cl^-, as well as other cations, are present in the soil in various concentrations (1 to 150 mM for glycophytes; more for halophytes), the roots of plants undergo salt stress. Ion uptake have influenced by a plant's genotype, growth stage, temperature, relative humidity and light intensity. A surplus of salt in the rhizosphere slows plant growth, reduces yield, and can even kill plants (Hao et al., 2022). The plants benefit from this adaptation to take precautions because it lessens the harm caused by stress. Plant stress has become a significant factor limiting the growth of contemporary agriculture as result of the deterioration of the global environment and research into the plant stress responses mechanism has expanding as well. The chemical mechanism behind the extraordinarily complicated biological process of a plant's response to stress has not yet fully understood. The term "transcriptome" refers to the collection of all RNAs, including mRNA and noncoding RNA, produced by a particular cell or tissue in a certain functional state. Transcriptomics is the study of gene transcription (type, structure, and function) and regulatory mechanisms in cells at the systemic level. This includes investigating non-coding region function, transcript structure, gene transcription level and novel transcriptional regions.

Transcriptomics can be used to identify new genes involved in plant resistance, disclose the intricate regulatory network and expression at the whole genome level under stress, and quantitatively quantify changes in plant gene expression at a specific time point and in a certain condition. The purpose of this study was to review recent developments in rice genomics and transcriptomics studies of plant stress, introduce changes in differentially expressed genes (DEGs) in the metabolic pathways under plant stress Figure 2, and look ahead to future research

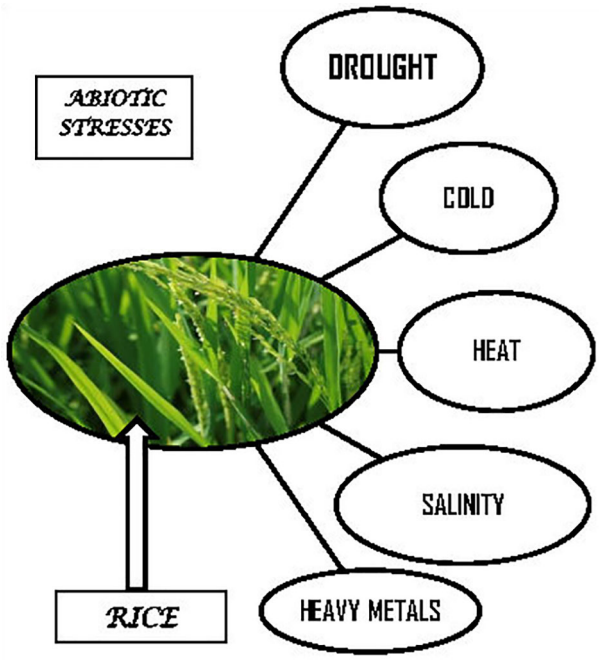


FIGURE 1
Common abiotic stresses effecting Rice crop.

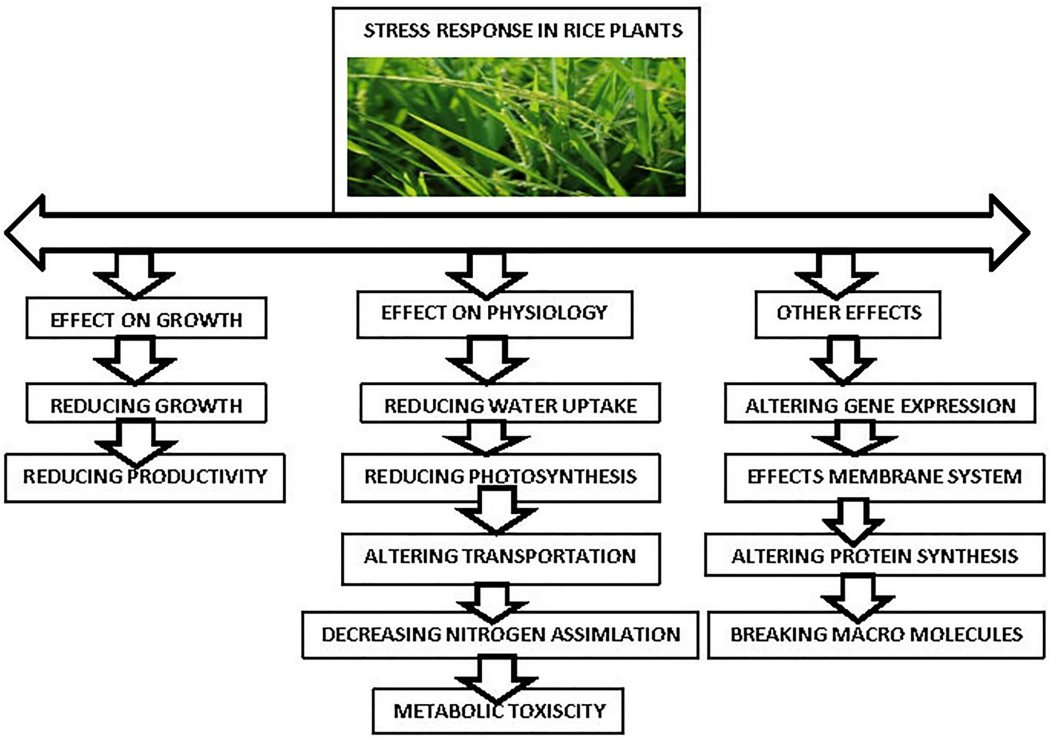


FIGURE 2
Stress response in Rice crop.

trends to provide a framework for additional plant stress research.

Most of the world's population relies on rice as a staple diet, making it a significant crop in terms of agriculture (Deepika and Singh, 2021). With a population of over eight billion people in this century, rice is essential for ensuring global food security (Sasaki and Ashikari, 2018). Similar to other crops, rice is susceptible to unfavorable environmental factors like biotic and abiotic stressors. Pathogens and herbivore assaults are examples of biotic stress, while heat, cold, drought, osmotic, salinity, and heavy metal toxicity are examples of abiotic stress (Grennan, 2006; Zhang et al., 2021). Salinity, temperature swings and drought are abiotic stresses that have an impact on plant production all over the world. This has an impact on productivity, which therefore has an impact on food security. As a result of anthropogenic climate change, which results in more frequent harsh weather, magnifies this adversity (Zhu, 2016). Due to its semi-aquatic and partly radiation environment during evolution, rice has developed a special pattern of abiotic stress susceptibility and tolerance. While other cereal crops may perish in damp environments, rice is tolerant of submersion. However, compared to other grains, rice is extremely sensitive to salinity, vulnerable to drought, and cold (Gregorio et al., 2013). Additionally, because it has grown mostly in tropical and subtropical regions, rice is very susceptible to the chilling stress. As a result, cold stress substantially hinders rice cultivation in temperate regions, especially during the reproductive period (Paul and Roychoudhury, 2019). As a result, rice grown at high latitudes and altitudes is of poor quality (Zhang et al., 2014). Heat stress during reproduction and grain development is particularly harmful to rice (Aghamolki et al., 2014). By the end of the twenty-first century, it has predicted that temperature stress will cause rice yields to drop to 41% (Aghamolki et al., 2014). Two crucial areas need to improve in order to handle these environmental issues: crop management tactics and the creation of elite cultivars. Elite cultivar development has always been accomplished through breeding (Lei et al., 2020). Since the creation of numerous sequencing and bioinformatics technologies, multi-omics methods have now used to create elite cultivars (Roychoudhury et al., 2011). Genomic, transcriptomic, proteomic, and metabolomics methods known as "multi-omics" aid in the discovery and functional analysis of genes, expression analyses, protein-protein interaction studies and the study of their regulatory networks (Rashid et al., 2014). This review goes into detail about the genomic and transcriptomic methods used to identify numerous genes and the regulatory networks that control how rice responds to abiotic stress. Based on the methodology and intended results, genomics has been widely categorized into

functional, structural, and comparative genomics (Akpinar et al., 2013). The three categories of genomics, their techniques, and their use in rice for abiotic stress tolerance will covered in this part. Figure 3 various genetic strategies for rice development is depicted.

Functional genomics

It has discovered that functional genomic investigations easily yield information useful for crop development. Characterizing how genes function and how they interact with other genes in regulatory networks is a component of functional genomics (Joshi et al., 2019). New genes and their functions has found thanks to recent developments in biotechnological methods. In functional genomics, techniques based on sequencing, hybridization and gene inactivation or editing are all employed (Joshi et al., 2019). Sequence-based techniques include EST (expressed sequence tags), SAGE (serial analysis of gene expression) and 50RACE (rapid amplification of cDNA ends). DNA microarray should have used. Since these methods work with RNA transcripts, they have covered under transcriptomics (Rashid et al., 2014). TILLING (Targeting Induced Local Lesions in Genomes) and T-DNA insertion mutation are the two basic methods based on gene inactivation (Ma et al., 2012). TILLING is a high-throughput method for locating single nucleotide changes brought about by chemically induced mutagenesis in a particular area of a gene of interest. TILLING populations can be used to test for phenotypic and genotypic differences in response to abiotic stressors (Casella et al., 2013). For the purpose of identifying natural polymorphisms, a new technique called EcoTILLING was created (Negrão et al., 2011). Targeted genes are rendered inactive when random T-DNA fragments are inserted into coding or non-coding regions. Targeting candidate genes in plants has shown to be a successful use of T-DNA transformation using Agrobacterium. In addition, gene inactivation and functional research can be done using RNAi technology (Pervaiz et al., 2022).

Genome editing techniques such as targeted mutation, INDEL, and genome-wide sequence changes can be used to characterize the function of plant genes (Rashid et al., 2014). Zinc finger nucleases (ZFNs), transcription activator-like effector nucleases (TALENs) and clustered regularly interspaced short palindromic repeat (CRISPR)-Cas9 (CRISPR associated nuclease 9) are the most frequently utilized genome editing tools (Stephen, 2019: Pervaiz et al., 2022).

ZFNs are nucleases made to cause double-strand breaks (DSB) at particular genomic loci, which results in targeted mutagenesis such as chromosomal deletions, transgene removal and targeted DNA integration (Ran et al., 2018). ZFNs are made up of a *FoKI* type IIS restriction endonuclease's non-specific

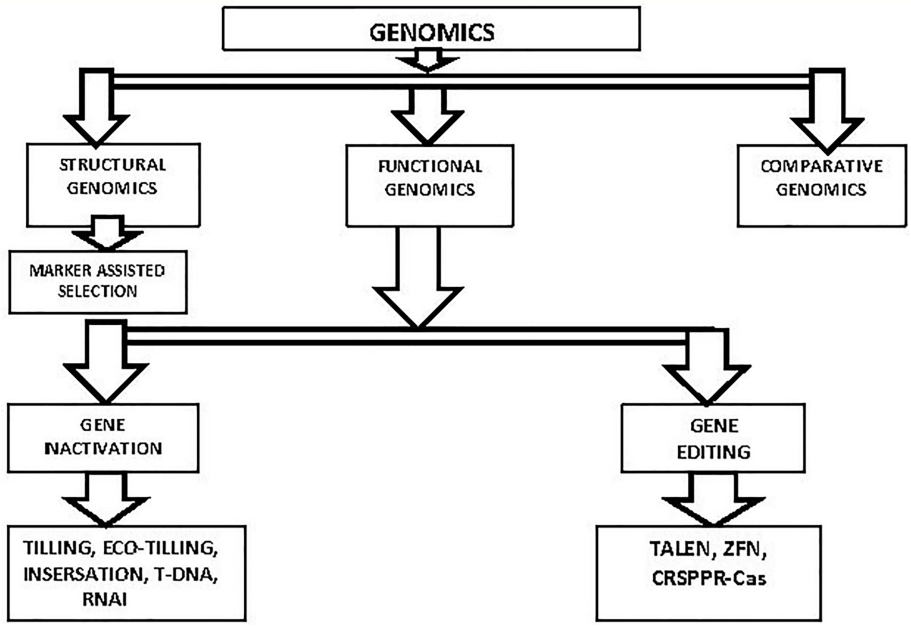


FIGURE 3
Genomic methods for Rice improvement are. Three main groups of genomic techniques are distinguished: (1) structural genomics, which involves general gene structure and aids in the creation of physical maps; (2) functional genomics, which uses approaches such as gene inactivation and gene editing to identify a gene's specific function; and (3) comparative genomics, which uses the reference genome sequence of a species to identify gene families in the species of interest.

cleavage domain coupled to specially made *Cys2-His2* zinc finger proteins and these enzymes produce a DSB. The DNA repair method used by plants is called error-prone non-homologous end joining (NHEJ) (Tsutsui et al., 2011). As an alternative to ZFNs, TALENs came into play; recombinant adeno-associated viruses have used by TALEN to produce specific double-strand breaks and very high success rate for TALEN (Bi and Yang, 2017). CRISPR-Cas9 is now the method of genome editing with the greatest adoption. CRISPRCas9 is an adaptive immune system that fights DNA viral infections in prokaryotes. CRISPR-Cas9, a component of the body's immune system, has modified to produce an effective genome editing technique. It is made of a synthetic short guide RNA and a Cas9 nuclease that can be modified (sgRNA). Target specificity has provided *via* sgRNA (Bi and Yang, 2017). Consequently, the CRISPR-Cas9 system is simpler to use than ZFNs or TALENs and permits the simultaneous targeting of numerous genes (Zhang et al., 2021).

The effect of RNAi-mediated down-regulation of RACK1, a highly conserved scaffold protein with multiple roles, including plant growth and development was reported by (Li et al., 2009) comparing the transgenic rice to non-transgenic rice plants revealed lower RACK1 expression and resistance to drought stress. The study also showed that transgenic rice (*Oryza sativa.* L.) plants had much higher superoxide dismutase activity than non-transgenic rice (*Oryza sativa*. L.) plants, but membrane peroxidation and malondialdehyde (MDA) generation were significantly reduced (Pervaiz et al., 2022). This implied that rice redox system-related resistance to drought stress negatively regulated by *RACK1*. When the floral meristem specific cytokinin oxidase (*OsCKX2*), gene was silenced in rice using the siRNA method, salt-stress tolerant rice transgenic plants were created without any yield loss (Joshi et al., 2018). Two rice PCS homolog genes, *OsPCS1* and *OsPCS2* have silenced by RNA interference (RNAi) in a recent study, revealing their functions in arsenic tolerance as well (Yamazaki et al., 2018). Transgenic rice with *OsMATE2* from the rice *MATE* family transporter gene was less likely to accumulate harmful arsenic levels (36.9–47.8%) (Das et al., 2018). Summary of abiotic stress-responsive genes in rice identified using genomic approaches Table 1

Structural genomics

Functional genomics focuses on the gene, whereas physical genome structure is the emphasis of Structural genomics. The ability to manipulate genes and DNA strands can benefit from understanding the structure of a single genome (Rashid et al., 2014). In structural genomics, high-resolution genetic and physical maps are created. An important method in structural genomics for crop development is molecular mapping and genome sequencing (Chaudhary et al., 2019). Molecular markers are helpful in describing the genetic variety in the germplasm since they has based on the polymorphism seen in any particular DNA (Nogoy et al., 2016). Gene mapping, quantitative trait loci (QTL), germplasm evaluation, and marker-assisted breeding are all common uses of DNA markers in plant breeding (MAB). With the recent advent of genotyping technique based on single nucleotide, polymorphisms have advanced.

Comparative genomics

The comparative genomics method compares two or more genomes to find out how similar and dissimilar they are, Model plant gene annotations can be applied to freshly sequenced crop species for which functional research has not yet been conducted. For comparative genomics, information on the orthologs that developed from a common ancestor is necessary because these carry out the same function in all species that descended from that ancestor (Wei et al., 2002). In order to find stress-related genes and compare the expression profiles of species, comparative genomics can also use to evaluate the expression profiles of less studied plants under various conditions. The development of phylogenetic trees and multiple sequence alignment are two examples of computational techniques that have used for both intraspecific and interspecific sequence comparisons (Haubold and Wiehe, 2004).

Functional analysis using gene inactivation and gene editing

Though many polygenes are involved in the regulation of several abiotic stress-related characteristics, these traits are undetectable in single-locus GWAS models. Later on, salt-tolerant loci in rice during the seed germination stage have discovered using multi-locus GWAS techniques. There have found to be 371 QTNs in relation to salt tolerance. In addition, 66 genes have found nearby the 56 QTNs based on functional annotation (Lei et al., 2020). The multi-locus GWAS is therefore highly helpful for identifying salt tolerance genes in rice to identify novel salinity-related candidate genes, characterize the genes and conduct functional investigation *via* overexpression, a number of biotechnological methods have been devised (Lei et al., 2020). The development of next-generation sequencing (NGS) has made it possible to identify thousands of SNPs through genome re-sequencing and the comparison of different genotypes (Lei et al., 2020). Incorporating insertion site-based polymorphisms into molecular markers is a new trend (ISBPs). The polymorphism produced by the insertion regions in the repeat junctions have utilized in this (Nogoy et al., 2016). Chemically altered lines with SNPs in membrane transport genes and variations in how they react to salt stress were found

TABLE 1 Summary of abiotic stress-responsive genes in rice identified using genomic approaches.

S. No.	Genes	Function	Associated stress response	Method of validation	References
1	*VP14*	Carotenoid dioxygenase	Drought stress	ECOTILLING	Wang et al. (2004)
2	*OsTP1*	Trehalose-6- phosphate synthase	Drought stress	T-DNA insertional mutation	Kim et al. (2005)
3	*Os05g30750*	Anthranilate phosphoribosyl	Chilling stress	TILLING	Cho et al. (2012)
	Os12g39210	Transferase			
	Os07g36630	Cyclin			
	Os01g61160	CSLF8- cellulose synthase-like family			
	Laccase precursor protein				
4	*OsPIN5*	Auxin transporter	Cold stress	CRISPR-Cas9 mutagenesis	Zeng et al. (2020)
5	*OsAKT1*	Ion transporters	Salt tress	TILLING	Hwang et al. (2016)
	OsHKT6				
	OsNSCC2				
	OsHAK11				
	OsSOS1				
6	*SD1*	Plant height	Drought stress	TILLING	Casella et al. (2013)
	Hd1	Flowering time			
	SNAC1	Drought tolerance			
	BADH2	Aroma			
7	*OsCPK17*	Stress signal transduction	Salt stress	ECOTILLING	Negrão et al. (2011))
8	*Os02g0528900*	ABC transporter	Heat stress	TILLING	Hwang et al. (2020))
9	*OsGSK1*	Glycogen synthase kinase	Cold and salt stress	T-DNA insertional mutation	Koh et al. (2007)
10	*OsRR22*	Transcription factor	Salinity stress	CRISPR-Cas9 mutagenesis	Zhang et al. (2019)
11	*OsHSP40*	Heat shock protein	Salt stress	T-DNA insertional mutation	Wang et al. (2019b))
12	*OsCYP19-4*	Cytochrome protein	Cold stress	T-DNA insertional mutation	Yoon et al. (2016))
13	*OsSAP1*	Stress- associated protein	Drought	T-DNA insertional mutation	Giri et al. (2011)
14	*OsRLCK253*	Receptor-like cytoplasmic kinase			
15	*OsLEA3-2*	Late embryogenesis abundant proteins	Salt and drought stress	T-DNA insertional mutation	Duan and Cai (2012))
16	*OsDST*	Drought and salt tolerance	Osmotic and salt stress	CRISPR-Cas9 mutagenesis	Santosh Kumar et al. (2020))
17	*OsMIR528*	MiRNA	Salt stress	CRISPR-Cas9 mutagenesis	Zhou et al. (2017)
18	*OsTEF1*	Transcription elongation factor	Drought	T-DNA insertional mutation	Paul et al. (2012)
19	*OsABF2*	ABA- responsive element-binding factor 2	Drought, salinity, and oxidative stress	T-DNA insertional mutation	Hossain et al. (2010)

using the TILLING technique. 41 mutant lines with SNPs in the nine target membrane transporters were found among 2961 M2 mutant lines. One study indicated that, 9 out of these genes have exon regions with changed sequences of them, seven could withstand salt stress. Additionally, five mutant lines with SNPs in the exon region of the genes *OsAKT1, OsHKT6, OsNSCC2, OsHAK1* and *OsSOS1* each exhibited different levels of gene expression. These mutations can use to create salt-tolerant lines of plants (Hwang et al., 2020). Similar to this, the Donganbyeo rice cultivar's TLLING mutant population has screened. These cold-tolerant lines and wild-type plants underwent comparative transcriptome investigations, which revealed that monosaccharide catabolic pathways have related to the resistance to chilling stress. This demonstrates the energy needed for rice to adjust to cold temperatures (Cho et al., 2012). Chalkiness in the grain is a result of high-temperature

stress during grain filling, which slows down endosperm production. A multi-omics analysis revealed that α-amylases were upregulated while starch production enzymes have down regulated. According to some research, TILLING mutants of the α-amylases genes may reduce the chalkiness in grains grown under heat stress, obviating the requirement for transgenic lines (Mitsui et al., 2016). Four target genes from TILLING M2 populations of ethyl methane Sulfonate (EMS)-mutagenized lines were validated *(SD1*, *HD1, SNAC1* and *BADH2* involved in determining plant height, flowering time, drought tolerance, and aroma respectively). Since the drop in height shortens the development cycle and triggers drought escape, the two distinct mutations in the *SD1* gene that generated the 21 percent height reduction may aid in drought resistance (Casella et al., 2013). Six abiotic stress treatments have used to analyze the M7 TILLING population made from gamma ray-induced mutations, and a genome-wide association study have used to perform principal component analysis (GWAS). There are two heat-tolerant SNPs at the *Os02g0528900* locus. Future mutational breeding may benefit from these SNPs (Hwang et al., 2020). Eco-TILLING, a strategy that targets genes involved in salt stress signal transduction (*OsCPK17)* or tolerance mechanisms (*SalT)* discovered 15 and 23 SNPs or indels, respectively, among 375 accessions of cultivated rice. According to Negro et al. (2011), it has discovered that these allelic variations are located in the 30-untranslated region (*30-UTR*), which has investigated for salt-tolerant breeding. It was discovered that the group A bZIP transcription factors are crucial for ABA signaling pathways (Banerjee and Roychoudhury, 2017). A homozygous T-DNA insertion mutant of *OsABF2* has created in order to comprehend its function in rice. The mutant was more vulnerable to abiotic stressors such drought, salt, and oxidative stress compared to wild type, and additionally, the mutant was having lower sensitivity for ABA. *OsABF2* was therefore determined to be a stress-responsive gene in rice (Hossain et al., 2010). *OsPP2CA* group members have discovered to be stress-responsive genes in rice. Lines that overexpressed *OsPP108* exhibited greater ABA insensitivity and greater tolerance to drought stress. Additionally, ABA-dependent and ABA-independent signaling pathways interacted in these lines for abiotic stress tolerance, as evidenced by expression profiling employing multiple stress marker genes (Singh et al., 2015).

A total of 11,688 differentially expressed genes (DEGs) were induced by drought and salt stress, including nine materials found in Plantsexpress (accessed on February 1, 2022 at http://plantomics.mind.meiji.ac.jp/OryzaExpress/). There were 6742 DEGs under drought stress, including 2930 up-regulated genes. Salt stress was associated with 7328 DEGs in total, including 3729 up-regulated genes. The heat map of all DEGs showed that some genes' levels of expression in the leaf or root reduced in comparison to the control during drought or salt stress. Rice has shown to have the abundant late embryogenesis protein *OsLEA3-2*. In comparison to the wild type, the *OsLEA3-2* rice overexpression line created utilizing a binary *pHB* vector performed better under salt stress and was able to resume development after 20 days of abiotic stress treatments (Duan and Cai, 2012). Different plants have discovered to have increased abiotic stress tolerance when exposed to stress-associated proteins (SAPs) that include A20/AN1 zinc finger domains. It was discovered that *OsSAP1* in rice (*Oryza sativa*. L.) interacts with *OsSAP11*, a closely related homolog, and *OsRLCK235*, rice receptor-like cytoplasmic kinase, *via* the A20 domain. Abiotic stress tolerance in rice has boosted by overexpressing *OsSAP11* and *OsRLCK253* (Giri et al., 2011). *CYP5*, an immunophilin protein, has identified to interact with members of ARF guanine nucleotide exchange factors and is required for localization of *PIN1* (auxin efflux carrier). *OsCYP19-4* has discovered to be highly increased in rice under cold stress and to be controlled by stress. Additionally, functional studies using rice that had this protein overexpressed shown that it improved rice grain output and increased resistance to cold stress (Yoon et al., 2016). There has not yet been a lot of genome editing in rice using TALEN and ZFN for abiotic stress tolerance. However, this decade has seen widespread usage of CRISPR-Cas9 for genome editing in rice. *OsMIR408* and *OsMIR528* lines were created using CRISPR-Cas9 knockout mutations of the miRNAs. These lines were salt-sensitive, and it was discovered that these genes were good salt stress regulators (Yan et al., 2011). Numerous salt-related genes has discovered in the last ten years. One of these, *OsRR22*, encodes a 696-amino acid transcription factor known as a B-type response regulator that participates in cytokine signaling. *OsRR22* gene mutation by CRISPR-Cas9 revealed improved salt tolerance. This demonstrates that an increase in salt tolerance is caused by the reduction of *OsRR22* function (Zhang et al., 2019). RNA-Seq analysis revealed that the expression of seven genes, including *LOC Os03g37290*, *LOC Os06g31800, LOC Os09g13440, LOC Os09g19229, LOC Os10g13430, LOC Os10g41040* and *LOC Os12g28177* had been considerably changed (Zhu et al., 2016) *via* controlling the transcription of the downstream genes involved in salt tolerance in plants. Sequence analysis showed that *Os07g0569700 (OsSAP16)* under drought stress had a 1 bp Indel difference between IR36 and Weiguo. The stress-associated protein *OsSAP16* is expressed more when there is a drought (Lei et al., 2020).

Additionally, *OsSAP16*, a candidate gene for *qRSL7*, which controls relative shoot development under salt stress, was found. Accelerator of internode elongation 1 (*ACE1*) and Decelerator of internode elongation 1 (*DEC1)* are two more genes that control stem elongation (Nagai et al., 2020). The *DEC1* gene produces a zinc finger transcription factor (TF) that prevents internode elongation, whereas the *ACE1* gene produces an undetermined function protein that is associated with internode elongation *via* gibberellic acids (GA). Both genes influence cell division induced by gibberellin in the stem node. The gene ACE1C9285 is

regulated by SUB1C, a gibberellin-activated transcription factor (TF) whose activity rises in response to submersion (Fukao and Bailey-Serres 2008). SUB1C expression levels seem to be low in cultivars that possess the *SUB1A-1* regulator gene, which is a homolog of SUB1C. Briefly put, rice (*Oryza sativa*. L.) cultivars that express the gene *SUB1A-1* have altered GAs responsiveness, which causes them to use carbon pools for leaf elongation and impede plant growth in general. This adaptability enables them to withstand large floods (Fukao et al., 2006; Xu et al., 2006). However, transcriptome analysis is employed to examine the alterations at the transcript level under diverse environmental or biological contexts (Thompson and Goggin 2006; Stephen, 2019; Pervaiz et al., 2022). Plant annexins are calcium-dependent, multigene families of phospholipid-binding proteins. The OsAnn3 CRISPR-Cas9 knockout mutation demonstrated a cold tolerance phenotype in comparison to the wild type (Shen et al., 2017). One gene discovered through mutation experiments was the drought and salt tolerance (DST) gene, which has shown to be undesired and is present in the genome due to linkage. The DST gene underwent loss-of-function mutation and a 366 bp deletion because of CRISPR-Cas9 genome editing. This mutant line demonstrated better leaf water retention under dehydration stress. These are only a few instances of how functional genomic approaches have applied to analyses rice (*Oryza sativa.* L.) gene expression under abiotic stress. However, many more have been finished throughout time (Yang et al., 2022). The establishment of transgenic or targeted mutant lines for abiotic stress tolerance would be made easier with the use of all this knowledge.

Molecular mapping and marker-assisted breeding for abiotic stress tolerance

Traditional breeding methods that involve molecular markers are helpful for creating elite lines. The discovery of genotypes with significant structural variation in the genome and the correlation of this variation with stress conditions has made possible through mapping studies. These differences help confirm the target genes for the abiotic stress response (Rashid et al., 2014). Numerous QTLs connected to stress has found. The advancement of accurate NGS technology, DNA polymorphism detection methods, and map-based cloning aid in the identification of more QTLs and the creation of marker sets (Nogoy et al., 2016), 235 accessions of the temperate japonica rice were tested for salinity tolerance, 30,000 SNP markers had already been applied to these accessions. 27 QTLs had been found because of the GWAS analysis. These QTL locations has compared with 300 genes already known to be involved in rice salt tolerance. Numerous QTLs has discovered in close proximity to genes that are involved in calcium signaling and kinases, demonstrating the significance of calcium signaling in the response to salt stress (Frouin et al., 2018). Four potential areas for thousand-grain weight (TGW) under alkali stress have found using bulked segregant analysis-NGS (BSA-Seq). On Chr.2, which had 18 predictive genes, *QTL-qATGW2-2* was located inside a 116 kb region between two molecular markers, *RM13592* and Indel3. Os02g39884 was identified by BSA sequencing as the potential gene for the alkali-tolerance gene locus in rice known as *QTL-qATGW2-2* (Sun et al., 2021). Muthu et al. (2020) goal was to pyramid QTLs in improved white ponni (IWP) for increasing the plant's capacity to withstand the three stresses of submersion, salinity, and drought. Drought (qDTY1.1; qDTY2.1), salinity (Saltol), and submergence (Sub1) were the QTLs used (Muthu et al., 2020). Numerous molecular markers, or QTLs, haas been established over the past ten years, and these might be used to find rice (*Oryza sativa.* L.) accessions with desired traits and speed up breeding for the creation of new hybrid lines with a variety of abiotic stress tolerance.

Gene families involved in abiotic stress response

Genome-Wide Analysis Genome-wide gene family analysis and identification are often carried out using sequence homology of known genes found in a novel crop genome. This results in almost all of the members of that specific gene family being identified. Additional expression analysis aids in the discovery of a powerful gene family member participating in a certain function and aids in the discovery of pseudogenes (Haubold and Wiehe, 2004). Numerous gene families has found in the rice genome using this method. Pentatricopeptide repeat proteins (*PPRs*) are motifs made up of 35 amino acids that have the ability to bind RNA strands after transcription and take part in RNA processing. 491 *PPR* genes discovered in rice (*Oryza sativa.* L.) by genome-wide research, of which *246 PPR* genes belong to subclass P and 245 genes to subclass *PLS*, 7 of these PPR genes were strongly activated under salinity and drought, according to expression analyses, which revealed that numerous PPR genes were induced under biotic and abiotic conditions (Chen et al., 2018). A comparative investigation of 11 rice (*Oryza sativa.* L.) species has conducted to examine the evolutionary and conservation pattern of dehydrin in rice (*Oryza sativa.* L.). Three DHNs were determined to be highly conserved out of the *65 DHNs* that were detected. Dehydrin gene conservation and patterns of domestication and diversification were studied for their association. This demonstrated that while domesticated species like *Oryza nivara* and *Oryza sativa* spp. indica display a conserved evolutionary pattern, wild species like *Oryza rufipogon* and *Oryza sativa* ssp. japonica follow an adaptive evolutionary pattern (beneficial genes getting selected against

deleterious alleles) suggesting diversification (Verma et al., 2017). *DUF221* domain-containing genes (DDP genes) are known to play significant roles in stress responses, hormone signaling pathways, and plant growth. Comparative genomics has revealed that both farmed and wild rice (*Oryza sativa*. L.) contains at least nine DDP gene members. *OsDDP6* was upregulated at all stages of development in FL478, salt-tolerant rice genotype despite several expression investigations demonstrating that they are upregulated by salt stress (Ganie et al., 2017).

A key secondary messenger, Ca2+, participates in several signaling pathways that activated by stress. Rice has a diverse set of Ca2+ transport genes that has found using genomic techniques. Utilizing microarray and qRT-PCR techniques, their expression pattern was investigated during several vegetative and reproductive developmental phases, including seedling, mature leaf, panicle, and seed developments (Singh et al., 2014). By taking part in the ribosome biogenesis process, ribosomal proteins (RPs) contribute to translation. It has previously discovered that both biotic and abiotic stress responses include the ribosomal protein large subunit (RPL). 56 ribosomal protein small subunits were found in the rice genome, according to genome-wide investigations (RPS). It has discovered that all 56 *RPS*, evenly distributed among the 12 chromosomes. *RPS* genes have found to implicate in both biotic and abiotic stress responses, according to expression analyses. Under the majority of the abiotic stressors, RPS4, 13a, 18a, and 4a have demonstrated to have greater transcript levels (Saha et al., 2017). It has discovered that proteins from the Dirigent (DIR) and DIR-like family are involved in lignification. 49 DIR or DIR-like genes were found in rice as a consequence of the genome-wide study Of 49, 23 DIR or DIR-like genes are discovered to be involved in the response to abiotic stress (Liao et al., 2017). Phospholipase A (Singh et al., 2012a), MADS-box family (Arora et al., 2007), phytocyanin (Ma et al., 2011), BURP (Ding et al., 2009), armadillo (Sharma et al., 2014) and arabinogalactan (Ma and Zhao, 2010) are examples of other gene families that include members, Nuclear factor Y (Yang et al., 2017); ABA repressor (ABR1) (Mishra et al., 2013);

transcription factors; *NAC*, *ZF-HD*, *WRKY*, *EREBP* and *bHLH* (Muthuramalingam et al., 2018); phospholipase C (Singh et al., 2013); autophagy-associated genes (*ATG*); Transcriptional regulation of gene expression is a component of a plant's response to stress, and it is dependent on a number of transcription factors and how they interact with the promoter region of the genes. Finding stress-inducible promoter regions is crucial (Roychoudhury et al., 2008). This knowledge may help with the deployment of transgenes with certain stress-inducible promoters (Cohen et al., 2017). Three stress-responsive genes *OsABA2*, which codes for zeaxanthin epoxidase, rab16A, which codes for dehydrin, and HP1, which codes for an unidentified protein—had their promoter elements chosen by Rai et al. (2009), inserted into the rice plant system coupled to the gusA reporter, and it was discovered that the *OsABA2* promoter was the most efficient one. Because it demonstrated that a transgene expressed weakly constitutively under normal circumstances and strongly under abiotic stress (Rai et al., 2009). Cis-acting promoter elements involved in the expression of genes that respond to cold and dehydration have thoroughly studied in Arabidopsis. The same has not done with rice (*Oryza sativa*. L.), though; three different rice species' transcription patterns for cold and dehydration were created in order to achieve the same goal. Additionally, all three species shared similar responsive genes. The conserved regions in these genes' promoters that have induced by cold and dehydration revealed that they contain the abscisic acid-responsive element (ABRE) and were the most responsive to dehydration in all three species. Additionally, the sequences *CGTACG* and *GTAGTA*, has found to be novel cold-inducible rice promoters (Maruyama et al., 2012). Aluminum detoxification in rice mediated by a transcription factor known as *ART1* (AL RESISTANCE TRANSCRIPTION FACTOR1). The 31 downtown genes have controlled by ART1, a zinc finger transcription factor of the C2H2 type. These genes' promoter regions were examined, and it was discovered that *GGN(T/g/a/C)V(C/A/g)S(C/G)* functions as a cis-acting element to cause an aluminium poisoning response (Tsutsui et al., 2011). In rice and Arabidopsis, the distribution and spatial patterns of 2 cis-regulatory elements, *ABRE* and *CE3* has investigated. In contrast to *CE3*, it has discovered that ABRE is equally common in both rice and Arabidopsis (Roychoudhury et al., 2008). The *ABRE* element has organized as an *ABRE-ABRE* pair and creates complexes that respond to ABA. *ABRE* and *CE3* were also present in numerous additional unique combinations in rice gene promoters (Gómez-Porras et al., 2007). Using comparative genomic techniques, numerous more gene families have described at the genome-wide level in rice in addition to these genes and promoter sequences. All of this knowledge will be useful for future functional and structural genomic approaches to the development of novel kinds.

Transcriptomics methods for rice abiotic stress tolerance

The collection of all RNAs produced by the cell or tissue in a specific functional state is known as the transcriptome. While the name "transcriptomics" refers to the study of the type, structure, function, and regulation of gene transcription, this covers both coding and non-coding RNA (Nejat et al., 2018). Transcriptomics can be used to quantitatively analyze the variations in plant gene expression at a particular time point and state during stressful conditions; this aids in understanding the regulatory network and expression at the whole genome level and identifies new genes related to stress tolerance and adaptability (Wang et al., 2020). Since the advancement of transcript sequencing and analysis

technology, transcriptomics has reached its pinnacle. Only single transcripts or small groups of transcripts may be studied at a particular time using traditional transcriptomic methods like northern blotting and RT-PCR (Roychoudhury and Banerjee, 2015; Lowe et al., 2017). Transcript profiling underwent a revolution when microarrays entered clinical use in the middle of the 1990s. This enables the simultaneous investigation of thousands of genes on a massive scale (Wang et al., 2020). Later, the real-time RT-PCR or qRT-PCR technology developed into a very sensitive approach for the detection of transcripts with low abundance. It has been frequently utilised for relative quantification of many gene expressions or absolute quantification of a certain gene (Nejat et al., 2018). For the second time recently, NGS has essentially changed gene expression profiling. High-throughput sequencing enhanced our understanding of epigenetics and gene regulation networks. The discovery and quantification of known unique and less common transcripts, including coding and non-coding RNA, are made possible by NGS-based RNA sequencing (RNA-Seq) (Lowe et al., 2017).

Technologies in transcriptomics

Individual transcripts at random called ESTs are sequenced from cDNA libraries. One-time, low-throughput Sanger sequencing of ESTs was once thought to be a highly effective way to determine an organism's gene composition without sequencing its complete genome (Nejat et al., 2018). Serial analysis of gene expression, a type of sequencing-based gene expression study that followed ESTs, has developed in 1995 (SAGE). This comprises concatenated random transcript segments that have undergone sanger sequencing. By comparing the transcripts with recognized genes, the quantification has completed. Digital gene expression analysis, a SAGE version utilizing high-throughput sequencing methods, was also briefly used (Lowe et al., 2017). Modern methods like RNA-Seq and microarrays have surpassed these ones (Wang et al., 2020). Figure 4 depicts the process of transcriptomic methods for the identification of genes. EST can be used to determine which genes an organism expresses at a certain moment. EST can be used to determine which genes an organism expresses at a certain moment. A cloned cDNA is sequenced once to produce an EST. The first step in EST production is the extraction of mRNA from an entire organism or a selected set of tissues (Lowe et al., 2017). Libraries of cDNA are produced by reverse transcription of mRNAs. Random colonies are put through a single sequencing procedure with universal primers. Following sequencing, the raw sequence reads are processed using bioinformatics techniques to get rid of contaminated vector sequences and low-quality sequences. Following that, the generated sequences are added to the dbEST database (Parkinson and Blaxter, 2009; Meng et al., 2010). In addition to supporting complete genome sequencing and gene discovery, EST has its applications.

ESTs are unaffected by probe selection and hybridization intensity, unlike microarray. However, according to Parkinson

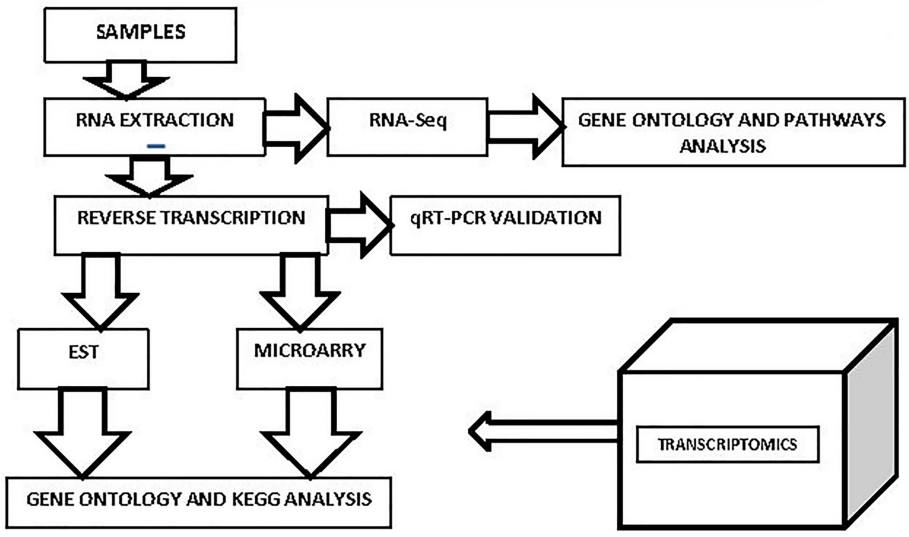


FIGURE 4
Workflow for transcriptomic techniques for crop improvement Transcriptomics entails the extraction of an organism's total RNA at a specific time point and under a specific environmental situation, which is then processed differently for expression analysis. Reverse transcriptase is used to create cDNAs for EST and microarray research, and cDNA libraries are then created. For the purpose of creating ESTs and microarray probes for expression profiling, this might be sequenced. If not, the total RNA could be normalised and sequenced in order to identify all the genes with differential expression. qRT-PCR offers additional validation. KEGG analysis and gene ontology aid in the functional connection of discovered genes.

and Blaxter (2009), ESTs can offer sequence data for creating new microarray platforms. The "probes" that make up microarrays are small nucleotide oligomers that are bonded in an arrayed pattern on a solid substrate. The determination of transcript abundance of the transcripts is used for the expression analysis. It happens when the fluorescently tagged transcript has hybridized to these probes. Each probe locus' fluorescence intensity on the array corresponds to the amount of transcripts for that probe sequence (Lowe et al., 2017). High-throughput sequencing and computational techniques have coupled in RNA-Seq to determine the number of transcripts in an RNA pool. Depending on the sequencing technique used, the nucleotide sequences produced can range in length from about 100 bp to more. A reference genome or another transcript is used to align the RNA transcripts. RNA-Seq is helpful in identifying genes within a genome or determining which genes are active at a specific period, and it may precisely determine the relative gene expression level (Fujii et al., 2011; Garg and Jaiswal, 2016; Nejat et al., 2018).

EST and microarrays for rice abiotic stress-related gene identification

Gorantla et al. (2007) discovered genes linked to rice (*Oryza sativa*. L.) sensitivity to water stress. The discovery of 5815 rice ESTs was made possible through the analysis of 7794 cDNA sequences. In the public databases of rice farmed under normal conditions, 334 of these revealed no sequence homology with any rice ESTs or full-length cDNAs; this suggests that these transcripts have enriched during drought stress. A study of these ESTs revealed that 1677 of them contained unique sequences. This sequence has contrasted with abiotic stress-induced sequences from Arabidopsis, barley, maize, and rice expression profiling. 589 potential stress sensitive genes were discovered as a result of this analysis. These have once more compared to the expression profile of the panicle library during drought stress, and these revealed 125 genes out of 589 has expressed in both the panicle and leaf tissues under drought. These 125 genes' gene ontologies revealed that the majority of them have connected to cellular metabolism, signal transduction, and transcriptional control (Zhou et al., 2008; Gorantla et al., 2007). Similar to this, numerous distinct gene families in charge of abiotic stress in rice have been discovered over time utilising ESTs and microarray approaches. Here, a handful of them are covered. It was discovered that rice (*Oryza sativa*. L.) ability to withstand biotic, abiotic, and arsenate stress depends on glutathione S-transferases (GSTs). GSTs were found to play overlapping and distinct roles in rice during different developmental stages and to mediate cross-talk across multiple stress and hormone response pathways, according to transcript profiling utilizing microarray and ESTs (Jain et al., 2010; Sato et al., 2013). Plants respond to heat stress by producing heat shock proteins, which has then activated by heat shock factors (HSFs). According to Andrási et al., 2021, there are three classifications of plant *HSFs*: A, B, and C. Eight *OsHSTs* are increased during seed development and six HSFs are upregulated during abiotic stress in both the root and shoot, according to expression profiling research using ESTs, microarrays, and qRT-PCR. Stress from cold and dryness results in an up regulation of OsHSFA2a and OsHSFA3. When OsHSFB4a's expression was profiled using FL-cDNA/ESTs and qRT-PCR, it exhibited either no change or a very little change (Chauhan et al., 2011). Low molecular weight, cysteine-rich metal-binding proteins have known as metallothioneins (MT). The rice genome sequence's bioinformatics analysis identified 13 genes and 15 protein products (Banerjee and Roychoudhury, 2021). The cysteine amino acid has preserved in the *OsMT1e-P* protein and it was discovered that this contributed to salinity stress. *OsMT1e-P* was abundant throughout seedling and reproductive phases, which are stress-sensitive stages, according to the EST database and publically available microarray data (Gautam et al., 2012). In dicot model plants Arabidopsis thaliana, half-size adenosine triphosphate-binding cassette transporter subgroup G (ABCG) genes were discovered to play a function in abiotic stress, however, this was not confirmed for rice (*Oryza sativa*. L.). Using *FL-cDNA* and EST databases, 30 half-size *ABCGs* in rice were discovered, and their preliminary proof of gene expression under abiotic stress was established. The expression of *OsABCG2*, 6, 10, 24, and 29 has not shown to exist. Under semi-quantitative RT-PCR, the expressions for *OsABCG6* and *OsABCG10* have not found. It was inferred from this that these two genes are psuedogenes (Matsuda et al., 2012). Being a model plant and significant agricultural crop, rice is a C3 plant and hence a prospective candidate for genetic engineering of the C4 pathway. It is already known that C3 plants contain the genes necessary to make C4 enzymes. Through sequence homology, 15 genes from the rice C4 gene families have discovered in the rice genome using the maize C4 gene sequence as a query (Hamada et al., 2017; Jiang et al., 2019; Muthusamy et al., 2019). All of the identified genes had at least one EST or FL-cDNA, according to the results of the expression study utilizing the EST and FL-cDNA databases. Osnadp-me2 and Osnadp-me3 have found to be elevated under salt and drought stress employing microarray datasets for abiotic stress and heavy metal-regulated expression analyses. During salt, drought, and anoxic environments, *Osppdk1* was increased (Muthusamy et al., 2019). The protein breakdown process and the ubiquitination of proteins are both mediated by the ubiquitin-conjugating enzyme E2s (UBCs) in rice (*Oryza sativa*. L.), 39 UBC genes were discovered. EST, microarray and qRT-PCR-based *OsUBC* gene expression profiling revealed that many of these genes had widespread and tissue-specific expression patterns. Furthermore, it has discovered that 14 *OsUBCs* showed differential expression in treatments with salt or drought conditions (Singh et al., 2012b; Zhiguo et al., 2015). A microarray-based analysis of rice seedlings' salt-induced genes

revealed 1834 genes to be elevated by salt stress. One of these revealed a 23.3-fold induction in an EST. Database searches revealed that this EST encodes a type 2C protein phosphatase that was previously unidentified called *Oryza\sativa* salt-induced *PP2C* protein 1 (*OsSIPP2C1*) (Li et al., 2013). Cold induced *MYB1* is a potential MYB transcription factor that was discovered through analysis of the cold-induced transcriptome (*CMYB1*). The expression of *CMYB1* rose more than 100-fold during cold stress, according to qRT-PCR analysis. Additionally, it was discovered that *CMYB1* contributes to circadian rhythm (Duan et al., 2014). It has established that the protein MDCP, which contains the Meprin and TRAF homology (MATH) domain, participates in the response to biotic stress. *OsM4* and *OsMB11* are engaged drought and salinity stress out of the 11 MDCP in rice according to expression analysis utilizing qRT-PCR and microarray (Kushwaha et al., 2016). Similar to this, several genes in rice that respond to abiotic stress have been discovered using EST and microarray techniques. EST libraries have uploaded to the internet for public use in the future. Two sizable EST databases, dbEST and UniGene, both from NCBI, provide EST information from a range of organisms (Singh et al., 2019). There are also numerous EST databases dedicated to rice (*Oryza sativa*. L.) viz, OryGenesDB (Droc et al., 2006), rice Genome Knowledgebase (RGKbase) and the rice Genome Annotation Project (Tanaka et al., 2008: Wang et al., 2013). The rice Expression Profile Database rice (*Oryza sativa*. L.) (XPro) is a collection of gene expression profiles obtained using microarray analysis, and it may contain data from all growth stages, tissues, and stressors (Sato et al., 2013). Rice Oligonucleotide Array Database (ROAD) (Cao et al., 2012), Rice ArrayNet (Lee et al., 2009), Rice MetaSys (Sandhu et al., 2017) and Oryza Express are more rice microarray databases (Hamada et al., 2011; Bandurska, 2022).

Rice RNA-seq for abiotic stress-related gene identification

Expression analysis utilizing RNA-Seq has reached its pinnacle in the last 5–10 years. The few abiotic stress-responsive genes discovered by RNA-Seq are listed in Table 2. Two inbred indica lines, Apo, a moderately drought-sensitive line, and IR64, a drought-sensitive line, were analysed using RNA-Seq to reveal that IR64 underwent transcriptional alterations linked to signal transduction, protein binding, and receptor function (Ereful et al., 2020). Genes connected to an oxygen-binding function and the peroxisome pathway has higher expression levels. The scientists concluded that drought-tolerant cultivars use energy-efficient routes as a reaction to drought while drought-sensitive lines use energy-consuming pathways, failing to live as tolerant plants (Ereful et al., 2020). In order to reduce stress during germination and ingestation, seeds turn on a number of genes. In initial imbibition of rice seed germination, genes related to the cell wall, abiotic stress, and antioxidant-related DEGs were associated with stress response, according to RNA-Seq analysis between 8 h of imbibed seeds and dry seeds of rice (Zhao et al., 2020). Pectin esterase and polygalacturonase were major genes connected to cell walls, while receptor kinase and pectin esterase were prominent genes associated to signaling. Significant abiotic stress-related genes included those with the cup in domain protein, methyl transferases, SPX domain, GSTs, and peroxidase. At that moment, qRT-PCR analysis revealed GST to have the maximum activity. GSTs may stop the early imbibition stage's burst of H2O2 buildup, which is a factor in the subsequent successful seed germination (Zhao et al., 2020). To deal with the water shortage and to assure a sustainable production in the future, rice needs to be adapted to the aerobic condition. When comparing cultivars that were aerobically adapted (drought tolerant) and those that were anaerobically adapted (drought intolerant), RNA-Seq analysis of the root and shoot revealed that the number of differentially expressed transcripts was higher in the root than it was in the shoot in both aerobic and anaerobic conditions (Phule et al., 2019). Additionally, it was revealed that anaerobic cultivars lacked the high expression of MADS transcription factors and transporters involved in sugar (*SWEET3A*) and nutrient uptake. This implies that these genes are crucial for the ability to withstand drought (Phule et al., 2019). 56 differentially expressed genes were discovered in growing seeds during combined heat and drought stress using RNA-Seq analysis of Aus, drought, and heat-tolerant cultivars. *B12288*, one of the significantly induced genes, has *RAB21* as its annotation. Different *O. sativa* subspecies and various wild species of *Oryza* include homologs of this gene. It is a member of the LEA protein family known as dehydrin (Roychoudhury et al., 2007). Other rice cultivars also included the *RAB21* gene. Despite the small sequence variations, the functions were different (Jing et al., 2020; Schaarschmidt et al., 2020). It is yet unknown how dehydrin causes plants to respond positively to stress control. Recent research has revealed that in Arabidopsis, a change of four amino acids in the LEA protein increased membrane stability under cold stress. (Shankar et al., 2016). Therefore, it was determined that even little changes in the amino acid sequence of RAB21 from various species of rice have a big functional impact (Schaarschmidt et al., 2020). Using RNA-Seq for comparative study, it has discovered that members of the NAC and DBP transcription factors have differentially regulated under salt and dehydration stress in the drought- and salt-tolerant cultivars N22 and Pokkali, respectively (Shankar et al., 2016; Yuan et al., 2021). While transcripts involved in wax and terpenoid metabolism were upregulated in Pokkali, transcripts encoding thioredoxin and those related in phenylpropanoid metabolism were upregulated

TABLE 2 Summary of abiotic stress-responsive genes in rice identified using transcriptomic approaches.

S. No.	Genes	Function	Associated stress response	Method of validation	References
1	*OsMT1e-P*	Metallothioneins	Drought and salinity stress	Microarray	Gautam et al. (2012)
2	*OsUBCs*	Ubiquitin- conjugating enzymes	Salt and drought stress	EST, Microarray	Zhiguo et al. (2015)
3	*OsHsfA3* *OsHsfA7* *OsHsfA9* *OsHsfA1*	Heat shock factor	Heat stress	EST, Microarray	Chauhan et al. (2011)
4	*Os01g47050, Os01g59690, Os02g15950, Os02g51350, Os04g33820, Os05g43490, Os06g39370, Os07g09710, Os10g30280*	F-box proteins	Osmotic stress	EST, Microarray	Jain et al. (2007)
5	*OsABCG26* *OsABCG27*	Half-ABC proteins	Cold stress Salt stress	EST	Matsuda et al. (2012)
6	*OsDhn1*	Dehydrins	Drought stress	EST	Lee et al. (2005)
7	*Os02g47744, Os12g41920 Os06g19980*	MYB transcription factors	Drought stress	EST, Microarray	Katiyar et al. (2012)
8	*OsZFP177, OsZFP181, OsZFP176* *OsZFP173* *OsZFP181* *OsZFP176* *OsZFP157*	A20/AN1-type zinc finger protein	Drought, cold, and osmotic stress	EST, Microarray	Huang et al. (2008)
9	*OsDHOD1*	Dihydroorotate dehydrogenase	Salt, drought	EST, Microarray	Liu et al. (2009)
10	*OsSAP16*	Stress- associated protein	Drought stress	RNA-Seq	Lei et al. (2020)
11	*OsHPPD* *OsyTMT* *OsHPT* *OsMPBQ MT2*	Vitamin E biosynthetic enzymes	Dehydration, cold, and salt stress	EST, Microarray	Chaudhary and Khurana (2009)
12	*Osnadp-me2* *Osnadp-me3*	C4 photosynthetic enzymes	Salt and drought stress	EST, Microarray	Muthusamy et al. (2019)
13	*OsSIPP2C1*	Protein phosphatase 2C	Salt and drought stress	EST, Microarray	Li et al. (2013)
14	*OsFKBP20* *OsSce1*	SUMO- conjugating enzyme and peptidyl prolyl cis-trans isomerase	Heat stress	EST	Zhang et al. (2018)
15	*OsGLYI6, OsGLYI11*	Glyoxalase enzymes	Drought stress	EST, Microarray	Mustafiz et al. (2011)
16	*OsM4* *OsMB11*	Meprin and TRAF homology (MATH) domain- containing protein	Salinity and drought	Microarray	Kushwaha et al. (2016)
17	*OsPP2C* *OsPP2A*	Protein phosphatase	Salt, cold, and drought	Microarray and Q-PCR	Singh et al. (2010)
18	*OsMADS4, OsMADS5, OsMADS6, OsMADS7, OsMADS15*	Transcription factors	Aerobic adaptation	RNA-Seq	Phule et al. (2019)
19	*OsSWEET3A*	Sugar transporters	Aerobic adaptation	RNA-Seq	Phule et al. (2019)
20	*OsLEA3*	Late embryogenesis abundant proteins	Drought stress	RNA-Seq	Mangrauthia et al. (2016)
	OsDREB1A	Dehydration- responsive element binding			
	OsRAB16B	Responsive to ABA			
22	*OsPRX* *OsKET*	Peroxidase precursor 3-Ketoacyl-CoA synthase	Cold stress	RNA-Seq	Dametto et al. (2015)

(Continued)

TABLE 2 Continued

S. No.	Genes	Function	Associated stress response	Method of validation	References
	OsAQU	Aquaporin protein			
	OsCSLE1	Cellulose synthase-like family E			
	OsCDKB2;1	Cyclin- dependent kinase B2-1			
21	*OsSulfT2.1*, *OsPotT2*	Sulfate transporter Potassium transporter	Fluoride susceptibility	RNA-Seq	Banerjee et al. (2020)
22	*OsMYB-R1*	Transcription factor	Drought stress	RNA-Seq	Tiwari et al. (2020)
23	*OsPhyB*	Phytochrome B	Drought stress	RNA-Seq	Yoo et al. (2017)
24	*OsSweet11*	Sugar transporter	Fluoride tolerance	RNA-Seq	Banerjee et al. (2020)

in N22. This demonstrates how rice plants respond to varying levels of abiotic stress through a variety of transcription factors and metabolic pathways.

Two rice cultivars, IR36 (salt-sensitive) and Weiguo (salt tolerant), were used for QTL discovery. This resulted in the identification of *qRSL7*, which have related to relative shoot length (RSL) and situated on chromosome 7 (Li et al., 2018; Mao et al., 2019; Lei et al., 2020). After 36 hours of salt exposure at the budburst stage, RNA sequencing for IR36 and Weiguo identified five differentially upregulated genes in this potential area. *Os0790569700* (*OsSAP16*) a stress-associated protein increased during drought stress, was discovered to have a 1 bp indel difference using qRT-PCR investigation and further deep RNA-Seq (Lei et al., 2020). Using RNA-Seq, it was possible to pinpoint the photosynthesis-related chloroplast genes that were differentially expressed in response to salt, iron, and cold stress. Cold has the most differentially expressed genes (DEGs) related to light and chloroplast responses out of all the genes expressed in each condition (do Amaral et al., 2016; Sunkar and Zhu, 2019). Cold sensitive and cold-tolerant varieties' comparative transcriptome investigations using RNA-Seq revealed 13,930 and 10,599 DEGs, respectively. Functional classification of these DEGs\s showed that in cold-tolerant variety lipid-binding activity, catalytic and hydrolase activities, photosynthesis, energy and carbohydrate metabolism were enhanced during cold stress, while in susceptible variety absence of photosynthesis related genes, storage products like starch and fatty acids were noticed (Pradhan et al., 2019). These two investigations imply that genes involved in photosynthetic processes play a direct role in the response to cold stress.

Small RNA molecules known as microRNAs (miRNAs) perform crucial regulatory roles in plant development and stress responses (Barrera-figueroa et al., 2012; Sato et al., 2013). The list of rice miRNAs and siRNAs that provide tolerance to diverse abiotic stimuli is summarized in Table 3. Four small RNA libraries from the inflorescence of rice plants grown under control conditions and under abiotic stress, conditions like drought, cold, and salt stress were subjected to RNA sequencing using Illumina deep sequencing. This led to the identification of 227 miRNAs belonging to 127 families. These

TABLE 3 Examples of miRNAs identified in Rice (Oryza Sativa) under drought, cold and salinity stress.

Stress Condition	Inducible Genes	Responsive miRNAs	Functions	References
Drought stress	*SalT (LOC_Os01g24710)* *TIR1* *OsLEA3(LOC_Os05g46480)*	miR393 miR402	Salt/cold tolerance	Zhao et al., 2007; Sunkar and Zhu, 2004; Wang and Long, 2010; Raffaele et al., 2007
cold stress	*OsWRKY71 (LOC_Os02g08440)* *OsMAPK2 (LOC_Os03g17700)* *Os05g47550, Os03g42280* *Os01g73250, Os12g16350* *Os03g19380*	miR319, miR389, miR393, miR1320, miR1435 miR1884b, CHY1 CP12-2	Drought/salt tolerance Cold tolerance Pathogen immunity response	Sunkar and Zhu, 2004; Raffaele et al., 2007; Rabbani et al., 2003
Salinity stress	*SalT (LOC_Os01g24710)* *OsLEA3 (LOC_Os05g46480)*	miR156, miR158, miR159, miR397, miR398, miR482.2, miR530a, miR1445	Drought tolerance Pathogen immune response Heat stress tolerance	Cui et al., 2015; Rabbani et al., 2003; Arenas-Huertero et al., 2009

miRNAs' expression levels has compared, and the results showed that 18, 15, and 10 miRNAs, respectively, were involved in the responses of rice to drought, cold, and salt stress (Barrera-figueroa et al., 2012). Singh and Prasad (2021) reviewed the part played by small interfering RNAs (siRNAs) in the epigenetic modifications of the chromatin region mediated by siRNA-dependent DNA methylation (RdDM) pathways. Plants create dsRNAs that drive DNA methyl transferases to homologous loci for cytosine methylation and engage Pol IV and RNA-dependent RNA polymerase 2 (RDR2) to carry out this task (Matzke and Mosher, 2014). One-third of the methylation loci in Arabidopsis has methylated by this route (Singh and Prasad, 2021). *RDR6-dependent*, *PolII-DCL3-dependent*, *RDR6-DCL3-dependent* and dicer-independent RdDM pathways, as well as other non-canonical RdDM pathways, are known in plants (Liu and He, 2020). When exposed to stress again over the course of succeeding generations, epigenetic markers like DNA methylation serve as stress memories (Wang et al., 2020; Singh et al., 2021; Yuan et al., 2021).

During times of temperature stress and at particular stages of plant growth, the RdDM pathway also controls the methylation of transposons and chromatin condensation (Papareddy et al., 2020; Pervaiz et al., 2022). Using RNAi transgenics raises certain biosafety issues because chromatin alteration and transcriptional gene silencing have the potential to cause hereditary modifications that have negative repercussions. Crops cultivated with an appropriate RNAi technique and an assessment of the danger to food safety, however, will help allay biosafety worries. Despite several limitations, sRNAs have a huge promise for improving crops. Key to creating abiotic stress tolerance in crop plants lies in the more recent discoveries of sRNAs and their targets. For the up- and down-regulation of sRNAs, one method is the over-expression and short tandem target mimicry (STTM). Li et al. (2020) created transgenic maize plants for the knockdown of miR166 using STTM technology, and these transgenic plants have demonstrated abiotic stress tolerance. By genetically altering plants to express dsRNA, RNAi has successfully used to improve crop tolerance to a variety of abiotic stresses. The use of artificial miRNAs (amiRNAs) and ta-siRNAs (ata-siRNAs) in the deregulation of target genes is a further intriguing strategy (Cisneros and Carbonell, 2020). Primarily, pre-miRNA or pri-miRNA expression in expression vectors is required to achieve miRNA over-expression. Clustered regularly interspaced short palindromic repeats (CRISPR) and the CRISPR associated protein (Cas), a recent technological advance, have enormous potential for crop development and can be effectively used for editing MIR genes for phenotypic modification. One aspect of miRNAs is that their potential applications as short peptides known as micro peptides (miPEPs), which are translated from pri-miRNA sequences, have not yet been fully investigated (Iborra et al., 2001; Prasad et al., 2020). Thus, in order to close the gap between the growing population and food insecurity, scientists are looking into a variety of technologies with broader applications and acceptance. Compared to traditional target discovery techniques, degradation genome sequencing in conjunction with small RNA sequencing has significant advantages. Cleavage-specific information has provided by degradome sequencing in addition to high-throughput identification of the thousands of targets that miRNAs have cut. Plant stress research using degradome analysis has been successful in both biotic and abiotic environments (Yang et al., 2022; Pervaiz et al., 2022). Using panicles on the day of full emergence, small RNA sequencing has done to identify the miRNAs and understand how they have regulated in Swarnaprabha (SP) rice to tolerate prolonged shade (Tanaka et al., 2019; Yang et al., 2022). Degradome sequencing has applied to the same samples to identify degraded targets. The expression levels of the cleaved targets have examined using microarray and qRT-PCR. Another goal of this work was to identify the SP shade-tolerant phenotypic responses that have controlled by miR-mediated PTGS pathways. Yang et al., 2022 studied that the expression of 191 lncRNAs, 2115 mRNAs, and 32 miRNAs (microRNAs) altered in rice during drought stress. They are essential elements of pathways for protein synthesis, chlorophyll synthesis, hormone signal transduction, and other processes, according to a functional analysis of the data.

The results of (Yang et al., 2022) provide a theoretical framework for additional investigation into the potential function of lncRNA in plant drought resistance as well as new genetic resources for rice breeding to generate drought-resistant crops. MiRNAs are essential for regulating gene expression in plants at various stages of development. For instance, 178 miRNA families have 959 founding members in the rice plant *Oryza sativa* (Pervaiz et al., 2022).

Using high-throughput sequencing (HTS) microarray techniques, gene expression profiling under environmental stresses has carried out (Pervaiz et al., 2022). Zinc finger to cold and drought, *AP2* family to cold and drought, MYB to dehydration, NAC and *bHLH* to drought, ABA and salinity, and *bZIP* to dehydration are some of the members of stress-regulated gene families that have found in crop plants (Wang et al., 2021; Pervaiz et al., 2022). In order to comprehend the role of microRNA, an oligonucleotide microarray has used to regulate the expression profile of rice microRNA against drought stress. Drought was found to be a factor in the development of mir169g along with the mir169 family however, the presence of mir169g was more prominent in roots than in shoots (Tiwari and Rajam, 2022). Therefore, sRNA treatments have the potential to improve crop cultivars' agronomic features and increase food safety. Understanding the mechanism of post-transcriptional gene regulation in managing plant stress response is made possible by the interaction between miRNAs and their targets (Stephen, 2019; Pervaiz et al., 2022; Yang et al., 2022). RNA-Seq analysis following NaF treatment revealed up regulation of 1303 transcripts and down regulation of 93 transcripts this Increased

fluoride levels suppress ABA signaling and biosynthetic pathways, according to expression analysis (Banerjee et al., 2020). However, signaling *via* ABA-independent transcription factors and the gibberellic acid pathway have both activated? When DEGs from the IR-64 and fluoride-tolerant varieties were compared, Khitish found that the fluoride sensitive variety had increased levels of autophagy (Banerjee et al., 2020). Further expression analysis showed that fluoride tolerance was associated with high expression of Sweet11 while fluoride susceptibility was associated with high expression of genes responsible for amino acid transport, monosaccharide transport, and nutrient transport (Banerjee et al., 2020). Root transcriptome analysis of the rice (*Oryza sativa*. L.) after Cd and As treatment revealed that the genes shared by Cd and As stress were involved in signal transduction, trans membrane transport, redox control, stress response, transcriptional regulation and the biosynthesis and metabolism of macromolecules and Sulphur compounds (Zheng et al., 2017; Huang et al., 2019).

Tools and databases for geneticists and breeders of rice using the genome

Numerous databases have built in order to better organize and make use of the extensive genomic data produced by rice genome studies. Comprehensive databases include a variety of data formats for many different species including rice (*Oryza sativa*. L.), The National Center for Biotechnology's GenBank database Information (NCBI) is a well-known comprehensive database that offers a sizable collection of biological data and information (https://www.ncbi.nlm.nih.gov/); Ensembl Plant incorporates tools for viewing, mining, and analyzing plant genomes data (https://plants.ensembl.org/); China National Center for Bioinformation's NGDC- GWH (https://bigd.big.ac.cn/gwh/) is a public repository that holds genome-scale data for a variety of species; rich plant genomics resources may be found at Phytozome (https://phytozome-next.jgi.doe.gov/) and comparative plant resources can be found at Gramene (http://www.gramene.org). A resource for extensive access to details about genome sequencing initiatives is the Genome OnLine Database (GOLD) (https://gold.jgi.doe.gov/). With an emphasis on rice genomic resources including genome sequences, genome annotations and genome variants, several databases are specifically for the grain (Table 4). Two well-known databases that offer genome annotation resources for the first rice reference genome Nipponbare are the Rice Annotation Project Database (RAP-DB) and rice Genome Annotation Project (MSU-RGAP) database (Sasaki et al., 2008; Sakai et al., 2013). RAP-genomic DB's annotations have been updated often. Song et al. created the rice Information Gateway (RIGW) database, which houses multi-omics data covering genomics, transcriptomics, and protein-protein interactions, based on the Indian reference genomes *ZS97* and *MH63* Kawahara et al. (2013). The Molecular Breeding Knowledgebase (MBKBASE) unifies rice germplasm data, population sequencing data, phenotypic data and several other genomics data sets based on Nipponbare and a high-quality indica reference genome, Song et al. (2018). Rice Genome Hub and Information Commons for rice (IC4R) Peng et al. (2018) offer a comprehensive resource for combining multiomics data for rice (*Oryza sativa*. L.) to enable effective epigenomic studies in rice Zhang et al. (2020) created the species-specific epigenomic database eRice (an Epigenomic & Genomic Annotation Database for rice (*Oryza sativa*. L.). Two databases that offer information and resources for rice pan-genome study are rice Pan-genome Browser (RPAN) and rice PanGenome Sun et al. (2017). Oryza Genome is a database of wild Oryza species' genome diversity that houses genomic materials for the genus Oryza. Twelve rice relatives from the Poaceae family have housed in the Rice Relatives Genomic Data Base (RRGD) Mao et al. (2020). Other databases concentrating on rice genomic variation, gene expression, gene function, and mutations. Rice Functional Genomics & Breeding (RFGB), rice SNP-Seek Database, and rice Variation Map (RiceVar-Map) all give information regarding genomic variation in addition to phenotype, rice cultivars, and functional annotation of variation (Zhao et al., 2015). SnpReady provides Haplotype map (hapmap) SNPs and haplotype information for rice for rice (SR4R) and HapRice, (Yonemaru et al., 2014). Resources for rice transposable elements can be found in the databases rice Transposons Insertion Polymorphism Database (RTRIP) and rice TE Database (RiTE DB) Copetti et al. (2015).

The rice, Functionally Related Gene Expression Network Database (RiceFREND), Rice Expression Profile Database (RiceXPro) and Rice Expression Database (Sato et al., 2013 and Xia et al., 2017) provide Gene expression profiles and co-expressed genes. Data-bases describing rice mutants and mutations include the Rice Mutant Database (RMD), KitaakeX Mutant Database (KitBase), and The PGSB *Oryza sativa* database (MOsDB) Li et al. (2017). eRice offers tools for analysing DNA methylation and a 6 mA AI predictor, while Rice (*Oryza sativa*. L.)VarMap offers tools for analyzing haplotype networks. There are websites other than these databases where you can find web tools made exclusively for research on rice. In addition to a variety of published genomic prediction techniques, Rice Galaxy offers tools for developing SNP tests, assessing GWAS research, population diversity, and diagnosing rice bacterial pathogens Liu et al. (2015). Rice Diversity offers GWAS viewer, Rice Sub-population Viewer, and Seed Photo Library Viewer among other features. Yao et al. (2018) created the comprehensive database fun rice Genes, which contains about 2800 functionally defined rice genes, by fusing publicly accessible data and analyzing papers describing rice functional genomic investigations. A handy, integrated toolkit for accelerating all experimental designs for CRISPR/Cas9/Cpf1-based genome editing and analyzing the

TABLE 4 List of resources for genomic and transcriptome databases of rice is.

Database	Full name	Country	Keywords	Tools	Website	Last update	References
Genome/pan-genomes							
RAP-DB	The Rice Annotation Project Database	Japan	Nipponbare; IRGSP-1.0 reference genome; Genome annotation	Tools including keyword search, Blast, ID converter and batch retriever	https://rapdb.dna.affrc.go.jp/	Sep. 2020	Sakai et al. (2013)
MSU-RGAP	Rice Genome Annotation Project	USA	Nipponbare; MSUv7 reference genome; Genome annotation	Rice gene expression, rice gene expression (gene expression plots, gene correlation search within a module or experiment), genome nomenclature, genome facts	http://rice(Oryzasativa.L.).plantbiology.msu.edu/	Feb. 2013	Kawahara et al. (2013)
RIGW	Rice Information Gateway	China	ZS97 reference genome; MH63 reference genome; Omics data; Interaction Data	Orthologous, KEGG/GO enrichment, CRISPR-design etc	http://rice(Oryzasativa.L.).hzau.edu.cn/rice(Oryzasativa.L.)_rs3/	Apr. 2018	Song et al. (2018)
MBKBASE	Molecular Breeding Knowledgebase	China	R498 reference genome; Germplasm information; Population data; Phenotypic data	CustomGT, WebArray, etc	http://www.mbkbase.org/rice (Oryzasativa.L.)	Oct. 2020	Peng et al. (2018)
IC4R	Information Commons for Rice	China	Genome sequences; Genome annotation	HK-TS Gene Finder	http://ic4r.org/	May 2018	Sang et al. (2020)
Rice Genome Hub	–	France	Genomics and genetics Data	Tools to browse, visualize and search among all data sets available	https://rice(Oryzasativa.L.)-genome-hub.southgreen.fr/	Jan. 2019	Agret et al. (2020)
ERice (Oryza sativa. L.)	Epigenomic & Genomic Annotation Database for Rice	China	Reference genome 93-11; DNA methylation; N6-methyldeoxyadenosine (6 mA)	Tools for DNA Methylation analysis and 6 mA AI predictor	http://www.elabcaas.cn/rice (Oryzasativa.L.)/index.html	Jan. 2020	Zhang et al. (2020)
RPAN	Rice Pan-genome Browser	China	Pan-genome browser; 3KRGP		http://cgm.sjtu.edu.cn/3krice (Oryzasativa.L.)db/	Feb. 2018	Sun et al. (2017)
Rice (Oryza sativa. L.) PanGenome		China	Pan-genome; Genome assembly; Genomic variation		http://db.ncgr.ac.cn/Rice (Oryzasativa.L.)PanGenome/	Feb. 2018	Zhao et al. (2018)
OryzaGenome		Japan	Genomic variation; Genus Oryza		http://viewer.shigen.info/oryzagenome2detail/index.xhtml	Oct. 2018	Ohyanagi et al. (2016)
Rice (Oryza sativa. L.) RelativesGD	Rice Relatives Genomic Database	China	Rice relatives; Genome assembly; Genes	Tools for phylogenetic tree build	http://ibi.zju.edu.cn/rice (Oryzasativa.L.)relativesgd/	Apr. 2020	Mao et al. (2020)
Genomic variation							
Rice (Oryza sativa. L.) VarMap	Rice Variation Map	China	Genomic variation; Cultivar information	Tools for primer design, haplotype network analysis etc	http://rice(Oryzasativa.L.)varmap.ncpgr.cn/v2/	Jun. 2018	Zhao et al. (2015)
Rice SNP-Seek Database		Philippines	Genomic variation; Variety information	Tools for browse 3KRG project related Dat	https://snp-seek.irri.org/	Mar. 2020	Mansueto et al. (2017)

(Continued)

TABLE 4 Continued

Database	Full name	Country	Keywords	Tools	Website	Last update	References
RFGB	Rice Functional Genomics & Breeding	China	Genomic variation; Phenotype information; Germplasm information	3K Grouping (group samples based on population structure of 3K rice (*Oryza sativa*. L.) genome)	http://www.rmbreeding.cn/	Jul. 2019	Wang et al. (2020)
SR4R	SnpReady for Rice	China	Genomic variation based on 4 reference panels; Hapmap SNPs	Tools for basic genotype processing, population diversity analysis and rice (*Oryza sativa*. L.) varieties classification and identification	http://sr4r.ic4r.org/	Jun. 2019	Yan et al. (2020)
HapRice		Japan	SNP; Haplotype	Web tools for finding polymorphic SNPs between any two rice accessions and for primer design to develop cleaved amplified polymorphic sequence markers	http://qtaro.abr.affrc.go.jp/index.html	Aug. 2013	Yonemaru et al. (2014)
RTRIP	Rice Transposons Insertion Polymorphism Database	China	TE polymorphisms; Variety information		http://ibi.zju.edu.cn/Rtrip/index.html	Nov. 2019	Liu et al. (2020)
RiTE DB	Rice TE Database	USA	Repeat sequences; TE		https://www.genome.arizona.edu/cgi-bin/rite/index.cgi	Aug. 2015	Copetti et al. (2015)
Gene expression							
Rice FREND	Rice (Oryza sativa. L.) Functionally	Japan	Gene coexpression; Microarray data		https://rice(Oryzasativa.L.)frend.dna.affrc.go.jp/	Sep. 2012	Sato et al. (2013)
Rice XPro	Rice Expression Profile Database	Japan	Gene expression profiles; Microarray data	Exp_blast, ExProFlip	https://rice(Oryzasativa.L.)xpro.dna.affrc.go.jp/		Sato et al. (2013)
RED	Rice Expression Database	China	Gene expression profiles; RNA-Seq	Co-expression and JBrowse	http://expression.ic4r.org/	Aug. 2016	Xia et al. (2017)
Mutants and mutation							
RMD	Rice Mutant Database	China	Information of 129,000 rice T-DNA insertion lines; Comprehensive information about mutant phenotypes	Tools for identification of novel genes, regulatory elements etc	http://rmd.ncpgr.cn/	Mar. 2012	Zhang et al (2006)
KitBase	KitaakeX Mutant Database	USA	Fast-neutron-induced mutant population; KitaakeX	Tools including JBrowse, Search and Blast	https://kitbase.ucdavis.edu/home		Li et al. (2017)
MOsDB	The PGSB Oryza sativa Database	Germany	Genomes; Genes; Mutant Information; Expression Profiles	Genome view, Comparative map Viewer	http://pgsb.helmholtz-muenchen.de/plant/rice(Oryzasativa.L.)/index.jsp		Karlowski et al. (2003)
Bioinformatics tools							

(Continued)

TABLE 4 Continued

Database	Full name	Country	Keywords	Tools	Website	Last update	References
Rice Galaxy		Philippines		Tools for designing SNP assays, analyzing GWAS, population diversity, rice (*Oryza sativa*. L.)-bacterial pathogen diagnostics, and a suite of published genomic prediction methods	https://galaxy.irri.org/		Juanillas et al. (2019)
Rice Diversity		USA		GWAS Viewer, Genome Browser, Rice (*Oryza sativa*. L.) Sub-population Viewer, Seed Photo Library Viewer, etc	http://rice(Oryzasativa.L.)diversity.org/	Sep. 2017	
FunRice (Oryza sativa. L.)Genes	Functionally Rice Genes	China		An advanced search tool that provides data associated with functionally characterized rice genes such as genes, gene families, keywords, and literature.	https://funrice(Oryzasativa.L.)genes.github.io/		Yao et al. (2018)
DSDecodeM		China		A web tool for rapid decoding of multiple superimposed sequencing chromatograms	http://skl.scau.edu.cn/dsdecode/		Liu et al. (2015)
CRISPR-GE	CRISPR-Genome Editing	China		A toolkit for CRISPR-based genome editing	http://skl.scau.edu.cn/home/		Xie et al. (2017); Liu et al. (2019)
Hi-TOM	High-throughput Tracking Of Mutations	China		An online tool to track the mutations with precise percentage for multiple samples and multiple target sites	http://www.hi-tom.net/hi-tom/		
MMEJ-KO		China		Tool for automatically designing paired guide-RNAs for MMEJ-mediated fragment deletion using CRISPR/Cas genome editing.	http://skl.scau.edu.cn/mmejko/		Xie et al. (2020)
CAFRI-Rice (Oryza sativa. L.)	CRISPR Applicable Functional Redundancy Inspector	The Republic of Korea		CRISPR applicable functional redundancy inspector to accelerate functional genomics in rice (*Oryza sativa*. L.)	http://cafri-rice(Oryzasativa.L.).khu.ac.kr/	Dec. 2019	Hong et al., (2020)

resulting mutations in rice and other plants, CRISPR-GE was created by Xie et al, and includes DSDecodeM and MMEJ-KO Xie et al. (2017) and Liu et al. (2019). Using the web Programme (Hi-TOM), it is possible to calculate the precise percentages of gene editing mutations for numerous samples and target sites Xie et al. (2020). CRISPR applicable functional redundancy inspector (CAFRI-Rice) is another gene-editing tool that may be used to locate suitable target genes for editing in order to prevent functional redundancy (Hong et al., 2020)

Over the past year, a number of databases including mRNA sequences acquired from rice have created; a list of sequenced genomes of rice and its relatives summarized in (Table 5). A comprehensive mRNA-Seq database for rice called TENOR (Transcriptome ENcyclopedia of rice along with novel genes

TABLE 5 List of sequenced genomes of rice and its relatives.

Species	Genome type	Genome size (Estimated/assembly)	Predicted gene	Accession	Refrences
O. sativa (japonica group*)*	AA (2*n* = 24)	420 Mb/390 Mb	*35 825*	Nipponbare	Kawahara et al., 2013
O. sativa (indica group*)*	AA (2*n* = 24)	−−/396 Mb	*38 729*	R498	Du et al., 2017; Stein et al., 2018
O. rufipogon	AA (2*n* = 24)	−−/338 Mb	*37 071*	W1943	
O. nivara	AA (2*n* = 24)	−−/338 Mb	*36 313*	IRGC100897	Stein et al., 2018
O. glaberrima	AA (2*n* = 24)	−−/316 Mb	*33 164*	CG14	Wang et al., 2014
O. barthii	AA (2*n* = 24)	−−/308 Mb	*34 575*	IRGC105608	Stein et al., 2018
O. glumaepatula	AA (2*n* = 24)	−−/373 Mb	*38 149*	GEN1233_2	Stein et al., 2018
O. meridionalis	AA (2*n* = 24)	−−/336 Mb	*34 897*	W2112	Stein et al., 2018
O. puntaca	BB (2*n* = 24)	−−/394 Mb	*31 762*	IRGC105690	Stein et al., 2018
O. brachyantha	FF (2*n* = 24)	297 Mb/261 Mb	*32 037*	IRGC101232	Chen et al., 2013
Leersia perrieri	−−/(2*n* = 24)	−−/267 Mb	*29 078*	IRGC105164	Stein et al., 2018
Zizania latifolia	−−/(2*n* = 34)	594 Mb/604 Mb	*43 703*	HSD2	Guo et al., 2015

discovered from mRNA-Seq data, expression profiles, co-expressed genes, and cis-regulatory elements, mRNA sequences from diverse abiotic and hormone treatments are provided. This database is accessible to the public (Kawahara et al., 2016). An integrated gene expression database for rice (Rice Expression Database) (RED) was developed from RNA-Seq data. RED integrates Gene expression patterns from all growth phases and diverse abiotic stressors (Xia et al., 2017). The Rice Environment Coexpression Network (RECoN) is used to analyses abiotic stress responses at the systems level. The novel differential expression profile is helpful in locating groups of tightly co-expressed genes that are functionally characterized and uncharacterized during abiotic stress (Krishnan et al., 2017). Wang et al., to find circular RNA that is responsible for stress circumstances, created CropCircDB, a comprehensive circular RNA resource for crops in response to abiotic stress, in 2019; CropCircDB have developed primarily for rice and maize. Future addition of additional crops is the goal of this database (Wang et al., 2019a; Wang et al., 2019b).

The term "single-cell sequencing technologies" refers to the sequencing of a single cell's genome and/or transcriptome in order to obtain genomic, transcriptomic, or other multi-omics information with the goal of learning about the differences between different cell populations and the relationships between them throughout time (Tang et al., 2019). The data produced by sequencing could be extremely heterogeneous, making bioinformatics analysis difficult, depending on the tissues used. Recent research on the biology of rice has used single-cell sequencing. Han et al. studied the allelic expression patterns in the mesophyll cells of the 93-11 and Nipponbare inbred lines, as well as of their F1 reciprocal hybrids, in 2017 using a bioinformatics technique based on single-cell RNA-seq data from rice (Han et al., 2017). A common RNA-seq variant analysis workflow has used to find SNPs between indica and japonica rice using RNA-seq data from rice mesophyll cells. A bioinformatics approach has built to categorize genes into biallelic, monoallelic and silent genes by combining the information from SNPs and SNP-covering reads. An excellent opportunity to look into the causes and prevalence of monoallelic gene expression in plant cells have provided by the development of a single-cell RNA-seq bioinformatics analysis procedure in this study. To compare three-dimensional (3D) chromatin organization and dynamics before and after rice fertilization, Zhou et al. created a high-resolution *in situ* Hi-C approach and examined individual nuclei isolated from rice eggs, sperms, unicellular zygotes, and shoot mesophyll cells in a different study based on single-cell sequencing and Hi-C (Zhou et al., 2019). Their findings offered a spatial chromatin basis for zygotic genome activation and epigenetic control in rice as well as distinct 3D genome characteristics of rice gametes and the unicellular zygote. Recently, the cell biology of rice plants growing in varied environments has studied using single-cell sequencing. (Wang et al., 2020) used a bioinformatics pipeline based on single-cell RNA sequencing to identify the main cell types and recreate their developmental trajectories. According to their research, abiotic stressors have an impact on cell-type-specific gene expression as well as the physical dimensions of cells and the makeup of cell populations.

Conclusion

The world's main crop is rice (*Oryza sativa.* L.). Production of rice is impacted by agricultural difficulties like biotic and abiotic stressors. In order to combat these pressures and the growing global population, rice productivity must increase. Rice productivity has negatively affected by abiotic factors such as drought, cold, salt, and heavy metal stress. Two main tactics have used to combat the detrimental impact of these undesirable effects: (2) crop breeding, and (1) crop management techniques. Multi-omics methods like genomics, transcriptomics, proteomics and metabolomics are currently supporting crop-

breeding technologies for the discovery of new genes, protein regulatory networks and functional study of existing genes. Among these omics methods, genomics and transcriptomics greatly contribute by identifying genes that are responsive to abiotic stress, creation of numerous markers and QTLs for marker-assisted breeding using genome-wide analyses of different rice accessions. New genes, transcription factors, and non-coding RNAs implicated in the response to abiotic stress has found by combining transcriptome analysis with next-generation sequencing (NGS). In the past few decades, numerous genes in rice has discovered, and numerous elite cultivars have been created in rice using gene pyramiding, transgenic technology and gene editing., however functional genes must be investigated. The study of numerous orphan crops, halophytes, thermophytes, and other plants living in extreme environments can help identify new target genes in rice that respond to abiotic stress, Less undesirable genes would result from successful breeding, and during natural selection, many undesirable traits are passed on to future generations along with desirable ones. These genes must be located and their structural makeup examined in order to eliminate. Integrated omics techniques could be used to apply all of these.

Prospective

Genomics and transcriptome technology can quickly identify the necessary defense factors against stress and reveal the connections between metabolic pathways, signal transduction, and defense response, which are crucial for enhancing plant stress resistance and comprehending the mechanism underlying plant stress resistance. Plants to respond to stress use sophisticated metabolic networks and a wide variety of intricate cellular, molecular and physiological processes. The understanding of plant antistress is still limited, and more research is required to determine the synergistic effect of these pathways or other associations. Although several genes related to the antistress metabolic pathway in plants have cloned and their molecular mechanisms have been gradually been elucidated, the understanding of plant antistress is still limited. There may be a cross-interaction when plants are able to withstand different pressures in the natural environment. It is important to comprehend the distinct and shared signaling and metabolic pathways that have found in plants. The research of plant resistance genes centers on the signal transduction and metabolic pathways that are unique to and shared by different plant species. We must employ a range of techniques in this study process to fully and to completely depict the molecular mechanism of plant resistance.

Author contributions

The author contributed to the planning the work, to the writing of the manuscript, and to designing the figure.

Acknowledgment

It is acknowledged that the Emirates Professor P. Stephen Baenziger, Department of genetics and Plant Breeding University of Nebraska Lincoln-USA provided valuable guidance and suggestions during manuscript writing and IT department university of Nebraska USA are grateful for making e-resources available to author

Conflict of interest

The author declares that the research was conducted in the absence of any commercial or financial relationships that could be construed as a potential conflict of interest.

Publisher's note

All claims expressed in this article are solely those of the authors and do not necessarily represent those of their affiliated organizations, or those of the publisher, the editors and the reviewers. Any product that may be evaluated in this article, or claim that may be made by its manufacturer, is not guaranteed or endorsed by the publisher.

References

Aghamolki, M. T. K., Yusop, M. K., Oad, F. C., Zakikhani, H., Jaafar, H. Z., Kharidah, S., et al. (2014). Heat stress effects on yield parameters of selected rice cultivars at reproductive growth stages. *J. Food Agric. Environ.* 12, 741–746.

Agret, C., Gottin, C., Dereeper, A., Tranchant-dubreuil, C., Chateau, A., Sarah, G., et al. (2020). "*South green resources to manage rice big genomics data*," In : Abstracts workshops of the PAG XXVIII. (San Diego : PAG Résumé) 302. . Available at: https://plan.core-apps.com/pag_2020/abstract/aee41b47-958f-4594-8538-47be97ffeeeb

Akpinar, B. A., Lucas, S. J., and Budak, H. (2013). Genomics approaches for crop improvement against abiotic stress. *Sci. World J.* 2013, 361921. doi: 10.1155/2013/361921

Andrási, N., Pettkó-Szandtner, A., and Szabados, L. (2021). Diversity of plant heat shock factors: regulation, interactions, and functions. *J. Exp. Bot.* 72, 1558–1575. doi: 10.1093/jxb/eraa576

Arenas-Huertero, C., Pérez, B., Rabanal, F., Blanco-Melo, D., de la Rosa, C., Estrada-Navarrete, G., et al. (2009). Conserved and novel miRNAs in the legume phaseolus vulgaris in response to stress. *Plant Mol. Biol.* 70, 385–401. doi: 10.1007/s11103-009-9480-3

Arora, R., Agarwal, P., Ray, S., Singh, A. K., Singh, V. P., Tyagi, A. K., et al. (2007). MADS-box gene family in rice (Oryza sativa. l.).genome-wide identification, organization and expression profiling during repro- ductive development and stress. *BMC Genomics* 8, 242. doi: 10.1186/1471-2164-8-242

Bandurska, H.Drought Stress Responses (2022). Coping strategy and resistance. *Plants* 11, 922. doi: 10.3390/plants11070922

Banerjee, A., and Roychoudhury, A. (2017). Abscisic-acid-dependent basic leucine zipper (bZIP) tran- scription factors in plant abiotic stress. *Protoplasma* 254 (1), 3–16. doi: 10.1007/s00709-015-0920-4

Banerjee, A., and Roychoudhury, A. (2021). "Metallothionein-assisted phytoremediation of inorganic pollutants," in *Handbook of bioremediation*. Eds. M. Hasanuzzaman and M. N. V. Prasad (London: Academic Press), 81–90.

Banerjee, A., Singh, A., and Roychoudhury, A. (2020). *De novo* RNA-seq analysis in sensitive rice cultivar and comparative transcript profiling in contrasting genotypes reveal genetic biomarkers for fluoride-stress response. *Environ. Pollut.* 267, 115378. doi: 10.1016/j.envpol.2020.115378

Barrera-figueroa, B. E., Gao, L., Wu, Z., Zhou, X., Zhu, J., Jin, H., et al. (2012). High throughput sequencing reveals novel and abiotic stress-regulated microRNAs in the inflorescences of rice. *BMC Plant Biol.* 12, 1–11. doi: 10.1186/1471-2229-12-132

Bi, H., and Yang, B. (2017). Gene editing with TALEN and CRISPR/Cas in rice (Oryza sativa. l.). *Prog. Mol. Biol. Transl. Sci.* 149, 81. doi: 10.1016/bs.pmbts.2017.04.006

Cao, P., Jung, K. H., Choi, D., Hwang, D., Zhu, J., and Ronald, P. C. (2012). The rice oligonucleotide array database: an atlas of rice gene expression. *Rice* 5, 1–9. doi: 10.1186/1939-8433-5-17

Casella, L., Greco, R., Bruschi, G., Wozniak, B., Dreni, L., Kater, M., et al. (2013). TILLING in European rice. *hunting mutations Crop Improvement Crop Sci.* 53, 2550–2562. doi: 10.2135/cropsci2012.12.0693

Chaudhary, J., Khatri, P., Singla, P., Kumawat, S., Kumari, A., Vinaykumar, R., et al. (2019). Advances in omics approaches for abiotic stress tolerance in tomato. *Biology* 8, 1–19. doi: 10.3390/biology8040090

Chaudhary, N., and Khurana, P. (2009). Vitamin e biosynthesis genes in rice (*Oryza sativa*. l.) molecular characterization, expression profiling and comparative phylogenetic analysis. *Plant Sci.* 177, 479–491. doi: 10.1016/j.plantsci.2009.07.014

Chauhan, H., Khurana, N., Agarwal, P., and Khurana, P. (2011). Heat shock factors in rice (*Oryza sativa* l.): genome-wide expression analysis during reproductive development and abiotic stress. *Mol. Gen. Genomics* 286, 171–187. doi: 10.1007/s00438-011-0638-8

Chen, J., Huang, Q., and Gao, D. (2013). Whole-genome sequencing of *Oryza brachyantha* reveals mechanisms underlying oryza genome evolution. *Nat. Commun.* 4, 1595. doi: 10.1038/ncomms2596

Chen, G., Zou, Y., Hu, J., and Ding, Y. (2018). Genome-wide analysis of the rice PPR gene family and their expression profiles under different stress treatments. *BMC Genomics* 19, 1–14. doi: 10.1186/s12864-018-5088-9

Cho, H. Y., Hwang, S. G., Kim, D. S., and Jang, C. S. (2012). Genome-wide transcriptome analysis of rice genes responsive to chilling stress. *Can. J. Plant Sci.* 92, 447–460. doi: 10.4141/cjps2011-165

Cisneros, A. E., and Carbonell, A. (2020). Artificial small RNA-based silencing tools for antiviral resistance in plants. *Plants* 9, 669. doi: 10.3390/plants9060669

Cohen, S. P., Liu, H., Argueso, C. T., Pereira, A., Cruz, C. V., Verdier, V., et al. (2017). RNA-Seq analysis reveals insight into enhanced rice Xa7-mediated bacterial blight resistance at high temperature. *PloS One* 12, 1–19. doi: 10.1371/journal.pone.0187625

Copetti, D., Zhang, J., El Baidouri, M., Gao, D., Wang, J., Barghini, E., et al. (2015). RiTE database: a resource database for genus-wide rice genomics and evolutionary biology. *BMC Genomics*, 16–538. doi: 10.1186/s12864-015-1762-3

Cui, H., Zhai, J., and Ma, C. (2015). miRLocator: Machine learning-based prediction of mature microRNAs within plant pre-miRNA sequences. *PloS One* 10, e0142753. doi: 10.1371/journal.pone.0142753

Dametto, A., Sperotto, R. A., Adamski, J. M., Blasi, ÉAR, Cargnelutti, D., de Oliveira, L. F. V., et al. (2015). Cold tolerance in rice germinating seeds revealed by deep RNAseq analysis of contrasting indica genotypes. *Plant Sci.* 238, 1–12. doi: 10.1016/j.plantsci.2015.05.009

Das, N., Bhattacharya, S., Bhattacharyya, S., and Maiti, M. K. (2018). Expression of rice MATE family transporter OsMATE2 modulates arsenic accumulation in tobacco and rice (Oryza sativa. l.). *Plant Mol. Biol.* 98, 101–120. doi: 10.1007/s11103-018-0766-1

Deepika,, and Singh, A. (2021). Expression dynamics indicate the role of jasmonic acid biosynthesis pathway in regulating macronutrient (N, p and k+) deficiency tolerance in rice (Oryza sativa l.). *Plant Cell Rep.* 40, 1495–1512. doi: 10.1007/s00299-021-02721-5

Ding, X., Hou, X., Xie, K., and Xiong, L. (2009). Genome-wide identification of BURP domain-containing genes in rice reveals a gene family with diverse structures and responses to abiotic stresses. *Planta.* 230, 149–163 doi: 10.1007/s00425-009-0929-z

do Amaral, M. N., Arge, L. W. P., Benitez, L. C., Danielowski, R., da Silveira Silveira, S. F., da Rosa Farias, D., et al. (2016). Differential expression of photosynthesis-related genes and quantification of gas exchange in rice plants under abiotic stress. *Acta Physiol. Plant* 38, 153. doi: 10.1007/s11738-016-2176-9

Droc, G., Ruiz, M., Larmande, P., Pereira, A., Piffanelli, P., Morel, J. B., et al. (2006). OryGenesDB: a database for rice reverse genetics. *Nucleic Acids Res.* 34, 736–740. doi: 10.1093/nar/gkj012

Duan, J., and Cai, W. (2012). OsLEA3-2, an abiotic stress induced gene of rice plays a key role in salt and drought tolerance. *PLoS One* 7, e45117. doi: 10.1371/journal.pone.0045117

Duan, M., Huang, P., Yuan, X., Chen, H., Huang, J., and Zhang, H. (2014). CMYB1 encoding a MYB transcriptional activator is involved in abiotic stress and circadian rhythm in rice. *Sci. World J.* 2014, 178038. doi: 10.1155/2014/178038

Du, H., Yu, Y., and Ma, Y. (2017). Sequencing and *de novo* assembly of a near complete indica rice genome. *Nat. Commun.* 8, 15324. doi: 10.1038/ncomms15324

Ereful, N. C., Liu, L. Y., Greenland, A., Powell, W., Mackay, I., and Leung, H. (2020). RNA-Seq reveals differentially expressed genes between two indica inbred rice genotypes associated with drought-yield QTLs. *Agronomy* 10, 621. doi: 10.3390/agronomy10050621

Frouin, J., Languillaume, A., Mas, J., Mieulet, D., Boisnard, A., Labeyrie, A., et al. (2018). Tolerance to mild salinity stress in japonica rice a genome-wide association mapping study highlights calcium signaling and metabolism genes. *PloS One* 13, 1–27. doi: 10.1371/journal.pone.0190964

Fukao, T., and Serres, B. B. (2008). Submergence tolerance confer ed by Sub1A is mediated by SLR1 and SLRL1 restriction of gibberellin responses in rice. *Proc Natl Acad Sci U S A*. 105 (43), 16814–9. doi: 10.1073/pnas.0807821105

Fukao, T., Xu, K., Ronald, P. C., and Bailey-Serres, J.. (2006). A variable cluster of ethylene response factor-like genes regulates metabolic and developmental acclimation responses to submergence in rice. *Plant Cell* 18 (8), 2021–2034. doi: 10.1105/tpc.106.043000.

Fujii, T., Yokoyama, K., Tsuchida, H., Sano, K., Mochizuki, T., Oki, N., et al. (2011). OryzaExpress: an integrated database of gene expression networks and omics annotations in rice. *Plant Cell Physiol.* 52, 220–229. doi: 10.1093/pcp/pcq195

Ganie, S. A., Pani, D. R., and Mondal, T. K. (2017). Genome-wide analysis of DUF221 domain-containing gene family in oryza species and identification of its salinity stress-responsive members in rice (*Oryza sativa*.L.). *PloS One* 12, 1–27. doi: 10.1371/journal.pone.0182469

Garg, P., and Jaiswal, P. (2016). Databases and bioinformatics tools for rice research, *Curr. Plant Biol.* 7–8, 39–52. doi: 10.1016/j.cpb.2016.12.006

Gautam, K., Kushwaha Hemant, R., Vaishali, P.-S., Sumita, K., Rohit, J., Ratna, K., et al. (2012). Clustered metallothionein genes are co-regulated in rice and ectopic expression of OsMT1e-p confers multiple abiotic stress tolerance in tobacco *via* ROS scavenging. *BMC Plant Biol.* 12, 107. doi: 10.1186/1471-2229-12-107

Giri, J., Vij, S., Dansana, P. K., and Tyagi, A. K. (2011). Rice A20/AN1 zinc-finger containing stress-associated proteins (SAP1/11) and a receptor-like cytoplasmic kinase (*OsRLCK253*) interact *via* A20 zinc- finger and confer abiotic stress tolerance in transgenic arabidopsis plants. *New Phytol.* 191, 721–732. doi: 10.1111/j.1469-8137.2011.03740.x

Gómez-Porras, J. L., Riaño-Pachón, D., Dreyer, I., Mayer, J. E., and Mueller-Roeber, B. (2007). Genome-wide analysis of ABA-responsive elements ABRE and CE3 reveals divergent patterns in arabidopsis and rice. *BMC Genomics* 8, 1–13.

Gorantla, M., Babu, P. R., Reddy Lachagari, V. B., Reddy, A. M. M., Wusirika, R., Bennetzen, J. L., et al. (2007). Identification of stress-responsive genes in an indica rice (Oryza sativa l.) using ESTs generated from drought-stressed seedlings. *J. Exp. Bot.* 58, 253–265. doi: 10.1093/jxb/erl213

Gregorio, G. B., Islam, M. R., Vergara, G. V., and Thirumeni, S. (2013). Recent advances in rice science to design salinity and other abiotic stress tolerant rice varieties. *Sabrao J. Breed Genet.* 45, 31–41.

Grennan, A. K. (2006). Abiotic stress in rice (*Oryza sativa*. l.). an "omic" approach. *Plant Physiol.* 140, 1139–1141. doi: 10.1104/pp.104.900188

Guo, L., Qiu, J., and Han, Z. (2015). A host plant genome (Ziza- nia latifolia) after a century-long endophyte infection. *Plant J.* 83, 600–609. doi: 10.1111/tpj.12912

Hamada, H, Linghu, Q, and Nagira, Y. (2017). An in planta biolistic method for stable wheat transformation. *Sci Rep* 7(1), 11443. doi: 10.1038/s41598-017-11936-0

Han, Y., Chu, X., Yu, H., Ma, Y.-K., Wang, X.-J., Qian, W., and Jiao, Y. (2017). Single-cell transcriptome analysis reveals widespread monoallelic gene expression in individual rice mesophyll cells, sci. *Bull* 62, 1304–1314.

Hao, Z., Ma, S., Liang, L., Feng, T., Xiong, M., Lian, S., et al. (2022). Candidate genes and pathways in rice Co-responding to drought and salt identified by gcHap network. *Int. J. Mol. Sci.* 23, 4016. doi: 10.3390/ijms23074016

Haubold, B., and Wiehe, T. (2004). Comparative genomics: methods and applications. *Naturwissenschaften* 91, 405–421. doi: 10.1007/s00114-004-0542-8

Hong, W. J., Kim, Y. J., Kim, E. J., Kumar Nalini Chandran, A., Moon, S., Gho, Y. S., et al. (2020). CAFRI-rice (*Oryza sativa.* L.).CRISPR applicable functional redundancy inspector to accelerate functional genomics in rice. *Plant J.* 104, 532–545. doi: 10.1111/tpj.14926

Hossain, M. A., Cho J, I. I., Han, M., Ahn, C. H., Jeon, J. S., An, G., et al. (2010). The ABRE-binding bZIP transcription factor OsABF2 is a positive regulator of abiotic stress and ABA signaling in rice. *J. Plant Physiol.* 167, 1512–1520. doi: 10.1016/j.jplph.2010.05.008

Huang, Y., Chen, H., Reinfelder, J. R., Liang, X., Sun, C., Liu, C., et al. (2019). A transcriptomic (RNA-seq) analysis of genes responsive to both cadmium and arsenic stress in rice root. *Sci. Total Environ.* 666, 445–460. doi: 10.1016/j.scitotenv.2019.02.281

Huang, J., Wang, M. M., Jiang, Y., Bao, Y. M., Huang, X., Sun, H., et al. (2008). Expression analysis of rice A20/AN1-type zinc finger genes and characterization of ZFP177 that contributes to temperature stress tolerance. *Gene* 420, 135–144. doi: 10.1016/j.gene.2008.05.019

Hwang, J. E., Jang, D. S., Lee, K. J., Ahn, J. W., Kim, S. H., Kang, S. Y., et al. (2016). Identification of gamma ray irradiation-induced mutations in membrane transport genes in a rice population by TILLING. *Genes Genet. Syst.* 91 (5), 245–256. doi: 10.1266/ggs.15-00052

Hwang, S. G., Lee, S. C., Lee, J., Lee, J. W., Kim, J. H., Choi, S. Y., et al. (2020). Resequencing of a core rice mutant population induced by gamma-ray irradiation and its application in a genome-wide association study. *J. Plant Biol.* 63, 463–472. doi: 10.1007/s12374-020-09266-2

Iborra, F. J., Jackson, D. A., and Cook, P. R. (2001). Coupled transcription and translation within nuclei of mammalian cells. *Science* 293, 1139–1142. doi: 10.1126/science.1061216

Jain, M., Ghanashyam, C., and Bhattacharjee, A. (2010). Comprehensive expression analysis suggests overlapping and specific roles of rice glutathione s-transferase genes during development and stress responses. *BMC Genomics* 11, 1–17. doi: 10.1186/1471-2164-11-73

Jain, M., Nijhawan, A., Arora, R., Agarwal, P., Ray, S., Sharma, P., et al. (2007). F-box proteins in rice. genome-wide analysis, classification, temporal and spatial gene expression during panicle and seed development, and regulation by light and abiotic stress. *Plant Physiol.* 143, 1467–1483. doi: 10.1104/pp.106.091900

Jiang, D., Zhou, L., Chen, W., Ye, N., Xia, J., and Zhuang, C. (2019). Overexpression of a microRNA-targeted NAC transcription factor improves drought and salt tolerance in rice *via* ABA-mediated pathways. *Rice* 12 (1), 76. doi: 10.1186/s12284-019-0334-6

Jing, X. Q., Shalmani, A., Zhou, M. R., Shi, P. T., Muhammad, I., Shi, Y., et al. (2020). Genome-wide identification of malectin/malectin-like domain containing protein family genes in rice and their expression regulation under various hormones, abiotic stresses, and heavy metal treatments. *J. Plant Growth Regul.* 39, 492–506. doi: 10.1007/s00344-019-09997-8

Joshi, R., Gupta, B. K., Pareek, A., Singh, M. B., and Singla-Pareek, S. L. (2019). *Functional genomics approach towards dissecting out abiotic stress tolerance trait in plants* (Cham: Springer International Publishing).

Joshi, R., Sahoo, K. K., Tripathi, A. K., Kumar, R., Gupta, B. K., Pareek, A., et al. (2018). Knockdown of an inflorescence meristem-specific cytokinin oxidase–OsCKX2 in rice reduces yield penalty under salinity stress condition. *Plant Cell Environ.* 41, 936–946. doi: 10.1111/pce.12947

Juanillas, V., Dereeper, A., Beaume, N., Droc, G., Dizon, J., Mendoza, J. R., et al. (2019). Rice galaxy: an open resource for plant science. *GigaScience* 8(5), 1–14. doi: 10.1093/gigascience/giz028

Karlowski, W. M., Schoof, H., Janakiraman, V., Stuempflen, V., and Mayer, K. F. X. (2003). MOsDB: an integrated information resource for rice genomics. *Nucleic Acids Res.* 31, 190–192. doi: 10.1093/nar/gkg073

Katiyar, A., Smita, S., Lenka, S. K., Rajwanshi, R., Chinnusamy, V., and Bansal, K. C. (2012). Genome-wide classification and expression analysis of MYB transcription factor families in rice and arabidopsis. *BMC Genomics* 13, 544. doi: 10.1186/1471-2164-13-544

Kawahara, Y., de la Bastide, M., Hamilton, J. P., et al. (2013). Improvement of the *Oryza sativa* nipponbare reference genome using next generation sequence and optical map data. *Rice* 6(1), 4. doi: 10.1186/1939-8433-6-4

Kawahara, Y., de la Bastide, M., Hamilton, J. P., Kanamori, H., McCombie, W. R., Ouyang, S., et al. (2013). Improvement of the oryza sativa nipponbare reference genome using next generation sequence and optical map data. *Rice (Oryza sativa. L.)*, 6–4. doi: 10.1186/1939-8433-6-4

Kawahara, Y., Oono, Y., Wakimoto, H., Ogata, J., Kanamori, H., Sasaki, H., et al. (2016). TENOR: database for comprehensive mRNA-seq experiments in rice (*Oryza sativa.* l.). *Plant Cell Physiol.* 57, e7. doi: 10.1093/pcp/pcv179

Kim, S. J., Jeong, D. H., An, G., and Kim, S. R. (2005). Characterization of a drought-responsive gene, OsTPS1, identified by the T-DNA gene-trap system in rice (*Oryza sativa.* l.). *J. Plant Biol.* 48, 371–379. doi: 10.1007/BF03030578

Koh, S., Lee, S. C., Kim, M. K., Koh, J. H., Lee, S., An, G., et al. (2007). T-DNA Tagged knockout mutation of rice OsGSK1, an orthologue of arabidopsis BIN2, with enhanced tolerance to various abiotic stresses. *Plant Mol. Biol.* 65, 453–466. doi: 10.1007/s11103-007-9213-4

Krishnan, A., Gupta, C., Ambavaram, M. M. R., and Pereira, A. (2017). RECoN: rice environment coexpression network for systems level analysis of abiotic-stress response. *Front. Plant Sci.* 8, 1–15. doi: 10.3389/fpls.2017.01640

Kushwaha, H. R., Joshi, R., Pareek, A., and Singla-Pareek, S. L. (2016). MATH-domain family shows response toward abiotic stress in arabidopsis and rice (*Oryza sativa.* l.). *Front. Plant Sci.* 7, 1–19.

Lee, T. H., Kim, Y. K., Pham, T. T. M., Song, S. I., Kim, J. K., Kang, K. Y., et al. (2009). Rice (*Oryza sativa.* l.) ArrayNet: a database for correlating gene expression from transcriptome profiling, and its application to the analysis of coexpressed genes in rice (Oryza sativa. l.). *Plant Physiol.* 151, 16–33. doi: 10.1104/pp.109.139030

Lee, S. C., Lee, M. Y., Kim, S. J., Jun, S. H., An, G., and Kim, S. R. (2005). Characterization of an abiotic stress- inducible dehydrin gene, OsDhn1, in rice (Oryza sativa l.). *Mol. Cell* 19, 212–218.

Lei, L., Zheng, H., Bi, Y., Yang, L., Liu, H., Wang, J., et al. (2020). Identification of a major QTL and candidate gene analysis of salt tolerance at the bud burst stage in rice (Oryza sativa l.) using QTL-seq and RNA-seq. *Rice* 13, 1–14. doi: 10.1186/s12284-020-00416-1

Liao, Y., Liu, S., Jiang, Y., Hu, C., Zhang, X., Cao, X., et al. (2017). Genome- wide analysis and environmental response profiling of dirigent family genes in rice (*Oryza sativa*). *Genes Genom* 39, 47–62. doi: 10.1007/s13258-016-0474-7

Li, D. H., Hui, L. I. U., Yang, Y. L., Zhen, P. P., and Liang, J. S. (2009). Down-regulated expression of RACK1 gene by RNA interference enhances drought tolerance in rice (*Oryza sativa.* l.). *Rice Sci.* 16, 14–20. doi: 10.1016/S1672-6308(08)60051-7

Li, G., Jain, R., Chern, M., Pham, N. T., Martin, J. A., Wei, T., et al. (2017). The sequences of 1504 mutants in the model rice variety kitaake facilitate rapid functional genomic studies. *Plant Cell* 29, 1218–1231. doi: 10.1105/tpc.17.00154

Li, Y. S., Sun, H., Wang, Z. F., Duan, M., Huang, S. D., Yang, J., et al. (2013). A novel nuclear protein phosphatase 2C negatively regulated by ABL1 is involved in abiotic stress and panicle development in rice (*Oryza sativa.* l.). *Mol. Biotechnol.* 54, 703–710. doi: 10.1007/s12033-012-9614-8

Liu, J., and He, Z. (2020). Small DNA methylation, big player in plant abiotic stress responses and memory. *Front. Plant Sci.* 11, e595603. doi: 10.3389/fpls.2020.595603

Liu, W. Y., Wang, M. M., Huang, J., Tang, H. J., Lan, H. X., and Zhang, H. S. (2009). The OsDHODH1 gene is involved in salt and drought tolerance in rice (Oryza sativa. *L.). J. Integr. Plant Biol.* 51, 825–833. doi: 10.1111/j.1744-7909.2009.00853.x

Liu, Q., Wang, C., Jiao, X., Zhang, H., Song, L., Li, Y., et al. (2019). Hi-TOM: a platform for high-throughput tracking of mutations induced by CRISPR/Cas systems, sci. *China Life Sci.* 62, 1–7. doi: 10.1007/s11427-018-9402-9

Liu, Z., Wang, T., Wang, L., Zhao, H., Yue, E., Yan, Y., et al. (2020). RTRIP: a comprehensive profile of transposon insertion polymorphisms in rice (*Oryza sativa.* l.). *Plant Biotechnol. J.* 18, 12.

Liu, W., Xie, X., Ma, X., Li, J., Chen, J., and Liu, Y. G. (2015). DSDecode: a web-based tool for decoding of sequencing chromatograms for genotyping of targeted mutations, mol. *Plant* 8, 1431–1433. doi: 10.1016/j.molp

Li, Y., Xiao, J., Chen, L., Huang, X., Cheng, Z., Han, B., et al. (2018). Rice functional genomics research: past decade and future. *Mol. Plant* 11, 359–380. doi: 10.1016/j.molp.2018.01.007

Li, N., Yang, T., Guo, Z., Wang, Q., Chai, M., Wu, M., et al. (2020). Maize microRNA166 inactivation confers plant development and abiotic stress resistance. *Int. J. Mol. Sci.* 21 (24), 9506. doi: 10.3390/ijms21249506

Lowe, R., Shirley, N., Bleackley, M., Dolan, S., and Shafee, T. (2017). Transcriptomics technologies. *PloS Comput. Biol.* 13, 1–23. doi: 10.1371/journal.pcbi.1005457

Mangrauthia, S. K., Agarwal, S., Sailaja, B., Sarla, N., and Voleti, S. R. (2016). Transcriptome analysis of oryza sativa (rice (Oryza sativa. l.)) seed germination at high temperature shows dynamics of genome expression associated with hormones signalling and abiotic stress pathways. *Trop. Plant Biol.* 9, 215–228. doi: 10.1007/s12042-016-9170-7

Mansueto, L., Fuentes, R. R., Borja, F. N., Detras, J., Abriol-Santos, J. M., Chebotarov, D., et al. (2017). Rice SNP-seek database update: new SNPs, InDels, and queries. *Nucleic Acids Res.* 45, D1075–D1081. doi: 10.1093/nar/gkw1135

Mao, L., Chen, M., Chu, Q., Jia, L., Sultana, M. H., Wu, D., et al. (2019). Rice (Oryza sativa. L.)RelativesGD: a genomic database of rice relatives for rice research. *Database*, 2019, 1–8. doi: 10.1093/database/baz110baz110

Ma, Y., Qin, F., and Tran, L. S. P. (2012). Contribution of genomics to gene discovery in plant abiotic stress responses. *Mol. Plant* 5, 1176–1178. doi: 10.1093/mp/sss085

Maruyama, K., Todaka, D., Mizoi, J., Yoshida, T., Kidokoro, S., Matsukura, S., et al. (2012). Identification of cis-acting promoter elements in cold-and dehydration-induced transcrip- tional pathways in arabidopsis, rice (Oryza sativa. *L.) soybean. DNA Res.* 19, 37–49. doi: 10.1093/dnares/dsr040

Matsuda, S., Funabiki, A., Furukawa, K., Komori, N., Koike, M., Tokuji, Y., et al. (2012). Genome-wide analysis and expression profiling of half-size ABC protein subgroup G in rice in response to abiotic stress and phytohormone treatments. *Mol. Gen. Genomics* 287, 819–835. doi: 10.1007/s00438-012-0719-3

Matzke, M. A., and Mosher, R. A. (2014). RNA-Directed DNA methylation: an epigenetic pathway of increasing complexity. *Nat. Rev. Genet.* 15, 394–408. doi: 10.1038/nrg3683

Ma, H., and Zhao, J. (2010). Genome-wide identification, classification, and expression analysis of the arabinogalactan protein gene family in rice (Oryza sativa l.). *J. Exp. Bot.* 61, 2647–2668. doi: 10.1093/jxb/erq104

Ma, H., Zhao, H., Liu, Z., and Zhao, J. (2011). The phytocyanin gene family in rice (Oryza sativa l.): genome-wide identification, classification and transcriptional analysis. *PloS One* 6, e25184. doi: 10.1371/journal.pone.0025184

Meng, Y., Ma, X., Chen, D., Wu, P., and Chen, M. (2010). MicroRNA-mediated signaling involved in plant root development. *Biochem. Biophys. Res. Commun.* 393, 345–349. doi: 10.1016/j.bbrc.2010.01.129

Mishra, M., Kanwar, P., Singh, A., Pandey, A., Kapoor, S., and Pandey, G. K. (2013). Plant omics: genome-wide analysis of ABA repressor1 (ABR1) related genes in rice during abiotic stress and development. *Omics J. Integr. Biol.* 17 (8), 439–450. doi: 10.1089/omi.2012.0074

Mitsui, T., Yamakawa, H., and Kobata, T. (2016). Molecular physiological aspects of chalking mechanism in rice grains under high-temperature stress. *Plant Prod. Sci.* 19, 22–29. doi: 10.1080/1343943X.2015.1128112

Mustafiz, A., Singh, A.K., Pareek, A., SK, S., and Singla-Pareek, S. L. (2011). Genome-wide analysis of rice and arabidopsis identifies two glyoxalase genes that are highly expressed in abiotic stresses. *Funct. Integr. Genom* 11, 293–305. doi: 10.1007/s10142-010-0203-2

Muthu, V., Abbai, R., Nallathambi, J., Rahman, H., Ramasamy, S., Kambale, R., et al. (2020). Pyramiding QTLs controlling tolerance against drought, salinity, and submergence in rice through marker assisted breeding. *PloS One* 15, 1–18. doi: 10.1371/journal.pone.0227421

Muthuramalingam, P., Krishnan, S. R., Saravanan, K., Mareeswaran, N., Kumar, R., and Ramesh, M. (2018). Genome-wide identification of major transcription factor superfamilies in rice identifies key candidates involved in abiotic stress dynamism. *J. Plant Biochem. Biotechnol.* 27, 300–317. doi: 10.1007/s13562-018-0440-3

Muthusamy, S. K., Lenka, S. K., Katiyar, A., Chinnusamy, V., Singh, A. K., and Bansal, K. C. (2019). Genome-wide identification and analysis of biotic and abiotic stress regulation of c 4 photosynthetic pathway genes in rice (*Oryza sativa.* l.). *Appl. Biochem. Biotechnol.* 187, 221–238. doi: 10.1007/s12010-018-2809-0

Nagai, K., Mori, Y., Ishikawa, S., Furuta, T., Gamuyao, R., Niimi, Y., et al (2020). Antagonistic regulation of the gibberellic acid response during stem growth inrice. *Nature* 584, 109–114. doi: 10.1038/s41586-020-2501-8

Negrão, S., Almadanim, C., Pires, I., McNally, K. L., and Oliveira, M. M. (2011). Use of EcoTILLING to identify natural allelic variants of rice candidate genes involved in salinity tolerance. *Plant Genet. Resour.* 9, 300–304. doi: 10.1017/S1479262111000566

Nejat, N., Ramalingam, A., and Mantri, N. (2018). Advances in transcriptomics of plants. *Adv. Biochem. Eng. Biotechnol.* 164, 161–185. doi: 10.1007/10_2017_52

Nogoy, F. M., Song, J.-Y., Ouk, S., Rahimi, S., Kwon, S. W., Kang, K.-K., et al. (2016). Current applicable DNA markers for marker assisted breeding in abiotic and biotic stress tolerance in rice (*Oryza sativa l.*). *Plant Breed Biotechnol.* 4, 271–284. doi: 10.9787/PBB.2016.4.3.271

Ohyanagi, H., Ebata, T., Huang, X., Gong, H., Fujita, M., Mochizuki, T., Kurata, N., et al. (2016). Oryza genome: genome diversity database of wild oryza species. *Plant Cell Physiol.*, 57(1), e1(1–7). doi: 10.1093/pcp/pcv171

Papareddy, R. K., Pa´ldi, K., Paulraj, S., Kao, P., Lutzmayer, S., and Nodine, M. D. (2020). Chromatin regulates expression of small RNAs to help maintain transposon methylome homeostasis in arabidopsis. *Genome Biol.* 21, 251. doi: 10.1186/s13059-020-02163-4

Parkinson, J., and Blaxter, M. (2009). Expressed sequence tags: an overview. *Expressed sequence tags (ESTs)* pp, 1–12. doi: 10.1007/978-1-60327-136-3_1

Paul, P., Awasthi, A., Rai, A. K., Gupta, S. K., Prasad, R., Sharma, T. R., et al. (2012). Reduced tillering in basmati rice T-DNA insertional mutant OsTEF1 associates with differential expres- sion of stress related genes and transcription factors. *Funct. Integr. Genom* 12, 291–304. doi: 10.1007/s10142-012-0264-5

Paul, S., and Roychoudhury, A. (2019). Comparative analysis of the expression of candidate genes governing salt tolerance and yield attributes in two contrasting rice genotypes, encountering salt stress during grain development. *J. Plant Growth Regul.* 38, 539–556. doi: 10.1007/s00344-018-9869-9

Peng, H., Wang, K., Chen, Z., Cao, Y., Gao, Q., Li, Y., Liang, C., et al. (2018). MBKbase for rice, an integrated omics knowledgebase for molecular breeding in rice (*Oryza sativa.* l.). *Nucleic Acids Res. 48 Genet.* 50, 278–284. doi: 10.1093/nar/gkz921

Pervaiz, T., Amjid, M. W., El-kereamy, A., Niu, S.-H., and Wu, H. X. (2022). MicroRNA and cDNA-microarray as potential targets against abiotic stress response in plants: Advances and prospects. *Agronomy* 12(1), 2–22. doi: 10.3390/agronomy12010011.

Phule, A. S., Barbadikar, K. M., Maganti, S. M., Seguttuvel, P., Subrahmanyam, D., Babu, M. B. B. P., et al. (2019). RNA-Seq reveals the involvement of key genes for aerobic adaptation in rice (*Oryza sativa.* l.). *Sci Rep* 9, 1–10 doi: 10.1038/s41598-019-41703-2

Pradhan, S. K., Pandit, E., Nayak, D. K., Behera, L., and Mohapatra, T. (2019). Genes, pathways and transcrip- tion factors involved in seedling stage chilling stress tolerance in indica rice through RNA-seq analysis. *BMC Plant Biol.* 19 (1), 352 doi: 10.1186/s12870-019-1922-8.

Prasad, A., Sharma, N., and Prasad, M. (2020). Noncoding but CODING: PrimiRNA into the action. *Trends Plant Sci.* 26, 204–206. doi: 10.1016/j.tplants.2020.12.004

Rabbani, M. A., Maruyama, K., Abe, H., Khan, M. A., Katsura, K., Ito, Y., et al. (2003). Monitoring expression profiles of rice genes under cold, drought, and high-salinity stresses and abscisic acid application using cDNA microarray and RNA gel-blot analyses. *Plant Physiol.* 133, 1755–1767. doi: 10.1104/pp.103.025742

Raffaele, S., Mongrand, S., Gamas, P., Niebel, A., and Ott, T. (2007). Genome-wide annotation of remorins, a plant-specific protein family: Evolutionary and functional perspectives. *Plant Physiol.* 145, 593–600. doi: 10.1104/pp.107.108639

Rai, M., He, C., and Wu, R. (2009). Comparative functional analysis of three abiotic stress-inducible promoters in transgenic rice (Oryza sativa. l.). *Transgenic Res.* 18, 787–799. doi: 10.1007/s11248-009-9263-2

Ran, Y., Patron, N., Kay, P., Wong, D., Buchanan, M., Cao, Y. Y., et al. (2018). Zinc finger nuclease-mediated precision genome editing of an endogenous gene in hexaploid bread wheat (Triticum aestivum) using a DNA repair template. *Plant Biotechnol. J.* 16, 2088–2101. doi: 10.1111/pbi.12941

Rashid, B., Husnain, T., and Riazuddin, S. (2014). "Genomic approaches and abiotic stress tolerance in plants," in *Emerging technologies and management of crop stress tolerance: volume 1: biological techniques* (London: Academic Press).

Roychoudhury, A., and Banerjee, A. (2015). Transcriptome analysis of abiotic stress response in plants. *Transcriptomics*, 3 (2), e115 doi: 10.4172/2329-8936.1000e115

Roychoudhury, A., Datta, K., and Datta, S. K. (2011). "Abiotic stress in plants: from genomics to metabolomics," in *Omics and plant abiotic stress tolerance*. Eds. N. Tuteja, S. S. Gill and R. Tuteja (Al Sharjah: Bentham Science Publishers), 91–120.

Roychoudhury, A., Gupta, B., and Sengupta, D. N. (2008). Trans-acting factor designated OSBZ8 interacts with both typical abscisic acid responsive elements as well as abscisic acid responsive element- like sequences in the vegetative tissues of indica rice cultivars. *Plant Cell Rep.* 27 (4), 779–794. doi: 10.1007/s00299-007-0498-1

Roychoudhury, A., Roy, C., and Sengupta, D. N. (2007). Transgenic tobacco plants overexpressing the heterologous lea gene Rab16A from rice during high salt and water deficit display enhanced tolerance to salinity stress. *Plant Cell Rep.* 26 (10), 1839–1859. doi: 10.1007/s00299-007-0371-2

Saha, A., Das, S., Moin, M., Dutta, M., Bakshi, A., Madhav, M. S., et al. (2017). Genome-wide identification and comprehensive expression profiling of ribosomal protein small subunit (RPS) genes and their comparative analysis with the large subunit (RPL) genes in rice. *Front. Plant Sci.* 8, 1–21. doi: 10.3389/fpls.2017.01553

Sakai, H., Lee, S. S., Tanaka, T., Numa, H., Kim, J., Kawahara, Y., et al. (2013). Rice annotation project database (RAP-DB): an integrative and interactive database for rice genomics. *Plant Cell Physiol.*, 54 (2), e6. doi: 10.1093/pcp/pcs183

Sandhu, M., Sureshkumar, V., Prakash, C., Dixit, R., Solanke, A. U., Sharma, T. R., et al. (2017). Rice (*Oryza sativa.* L.)MetaSys for salt and drought stress responsive genes in rice (*Oryza sativa.* l.).a web interface for crop improvement. *BMC Bioinf.* 18, 1–11. doi: 10.1186/s12859-017-1846-y

Sang, J., Zou, D., Wang, Z., Wang, F., Zhang, Y., Xia, L., et al. (2020).), IC4R-2.0: rice (*Oryza sativa.* l.) genome reannotation using massive RNA-seq data. *Genom. Proteom. Bioinform.* 18, 161–172. doi: 10.1016/j.gpb.2018.12.011

Santosh Kumar, V. V., Verma, R. K., Yadav, S. K., Yadav, P., Watts, A., Rao, M. V., et al. (2020). CRISPR-Cas9 mediated genome editing of drought and salt tolerance (OsDST) gene in indica mega rice cultivar MTU1010. *Physiol. Mol. Biol. Plants* 26, 1099–1110. doi: 10.1007/s12298-020-00819-w

Sasaki, T., Aono, R., Fujii, Y., Habara, T., Harada, E., Kanno, M., et al. (2008). The rice annotation project database (RAP-DB): 2008 update. *Nucleic Acids Res.* 36, 1028–1033.

Sasaki, T., and Ashikari, M.(2018). Rice genomics, genetics and breeding. (Singapore: Springer), 191–206. doi: 10.1007/978-981-10-7461-5

Sato, Y., Namiki, N., Takehisa, H., Kamatsuki, K., Minami, H., Ikawa, H., et al. (2013). Rice (*Oryza sativa*. L.)FREND: a platform for retrieving coexpressed gene networks in rice (*Oryza sativa*. l.). *Nucleic Acids Res.* 41, 1214–1221. doi: 10.1093/nar/gks1122

Sato, Y., Takehisa, H., Kamatsuki, K., Minami, H., Namiki, N., Ikawa, H., et al. (2013). Rice (Oryza sativa. L.)XPro version 3.0: expanding the informatics resource for rice transcriptome. *Nucleic Acids Res.* 41, 1206–1213. doi: 10.1093/nar/gks1125

Sato, Y., Takehisa, H., Kamatsuki, K., Minami, H., Namiki, N., Ikawa, H., et al. (2013b). Rice (*Oryza sativa*. L.)XPro version 3.0: expanding the informatics resource for rice transcriptome. *Nucleic Acids Res.* 41, 1206–1213. doi: 10.1093/nar/gks1125

Schaarschmidt, S., Fischer, A., Lawas, L. M. F., Alam, R., Septiningsih, E. M., Bailey-Serres, J., et al. (2020). Utilizing pacbio iso-seq for novel transcript and gene discovery of abiotic stress responses in oryza sativa l. *Int. J. Mol. Sci.* 21, 1–26. doi: 10.3390/ijms21218148

Shankar, R., Bhattacharjee, A., and Jain, M. (2016). Transcriptome analysisin different rice cultivars provides novel insights into desiccation and salinity stress responses. *Sci. Rep.* 6, 1–15. doi: 10.1038/srep23719

Sharma, M., Singh, A., Shankar, A., Pandey, A., Baranwal, V., Kapoor, S., et al. (2014). Comprehensive expression analysis of rice armadillo gene family during abiotic stress and development. *DNA Res.* 21, 267–283. doi: 10.1093/dnares/dst056

Shen, C., Que, Z., Xia, Y., Tang, N., Li, D., He, R., et al. (2017). Knock out of the annexin gene OsAnn3 *via* CRISPR/Cas9-mediated genome editing decreased cold tolerance in rice (*Oryza sativa*. l.). *J. Plant Biol.* 60, 539–547. doi: 10.1007/s12374-016-0400-1

Singh, A., Baranwal, V., Shankar, A., Kanwar, P., Ranjan, R., Yadav, S., et al. (2012a). Rice phospholipase a superfamily: organization, phylogenetic and expression analysis during abiotic stresses and development. *PloS One* 7, e30947. doi: 10.1371/journal.pone.0030947

Singh, A., Giri, J., Kapoor, S., Tyagi, A. K., and Pandey, G. K. (2010). Protein phosphatase complement in rice (Oryza sativa. l.).genome-wide identification and transcriptional analysis under abiotic stress conditions and reproductive development. . *BMC Genomics* 11, 435. doi: 10.1186/1471-2164-11-435

Singh, A., Jha, S. K., Bagri, J., and Pandey, G. K. (2015). ABA inducible rice protein phosphatase 2C confers ABA insensitivity and abiotic stress tolerance in arabidopsis. *PLoS One* 10, 1–24. doi: 10.1371/journal.pone.0125168

Singh, A., Kanwar, P., Pandey, A., Tyagi, A. K., Sopory, S. K., Kapoor, S., et al. (2013). Comprehen- sive genomic analysis and expression profiling of phospholipase c gene family during abiotic stresses and development in rice (Oryza sativa. l.). *PloS One* 8 (4), 1–14. doi: 10.1371/journal.pone.0062494

Singh, A., Kanwar, P., Yadav, A. K., Mishra, M., Jha, S. K., Baranwal, V., et al. (2014). Genome-wide expressional and functional analysis of calcium transport elements during abiotic stress and development in rice (*Oryza sativa*. l.). *FEBS J.* 281, 894–915. doi: 10.1111/febs.12656

Singh, A., Pandey, A., Baranwal, V., Kapoor, S., and Pandey, G. K. (2012b). Comprehensive expression analysis of rice phospholipase d gene family during abiotic stresses and development. *Plant Signal Behav.* 7, 847–855. doi: 10.4161/psb.20385

Singh, R. K., and Prasad, M. (2021). Delineating the epigenetic regulation of heat and drought response in plants. *Crit. Rev. Biotechnol.*, 1, 14. doi: 10.1080/07388551.2021.1946004

Singh, R. K., Prasad, A., Maurya, J., and Prasad, M. (2021). Regulation of small RNA-mediated high temperature stress responses in crop plants. *Plant Cell Rep.* 41 (3), 765–773. doi: 10.1007/s00299-021-02745-x.

Singh, R. B., Singh, B., and Singh, R. K. (2019). Development of potential dbEST-derived microsatellite markers for genetic evaluation of sugarcane and related cereal grasses. *Ind. Crops Prod.* 128, 38–47. doi: 10.1016/j.indcrop.2018.10.071

Song, J. M., Lei, Y., Shu, C. C., Ding, Y., Xing, F., Liu, H., et al. (2018). Rice information GateWay: a comprehensive bioinformatics platform for indica rice genomes. *Mol. Plant* (11), 505–507. doi: 10.1016/j.molp.2017.10.003

Stein, J. C., Yu, Y., and Copetti, D. (2018). Genomes of 13 domes- ticated and wild rice relatives highlight genetic conservation, turnover and innovation across the genus oryza. *Nat. Genet.* 50, 285–296. doi: 10.1038/s41588-018-0040-0

Stephen, P. (2019). Abiotic and biotic stresses induce a core transcriptome response in rice (Oryza sativa. l.). *Sci. Rep.* 9, 6273. doi: 10.1038/s41598-019-42731-8

Sun, C., Hu, Z., Zheng, T., Lu, K., Zhao, Y., Wang, W., et al. (2017). RPAN: rice pan-genome browser for ~3000 rice genomes. *Nucleic Acids Res.* 45, 597–605. doi: 10.1093/nar/gkw958

Sunkar, R., and Zhu, J. K. (2004). Novel and stress-regulated microRNAs and other small RNAs from arabidopsis. *Plant Cell* 16, 2001–2019. doi: 10.1105/tpc.104.022830

Sunkar, R., and Zhu, J.-K. (2019). Novel and stress-regulated microRNAs and other small RNAs from arabidopsis. *Plant Cell* 16, 2001–2019. doi: 10.1105/tpc.104.022830

Sun, J., Wang, J., Guo, W., Yin, T., Zhang, S., Wang, L., et al. (2021). Identification of alkali- tolerant candidate genes using the NGS assisted BSA strategy in rice (Oryza sativa. *L.). Mol. Breed* 41, 1–14.

Tanaka, Y., and Sasaki, N. (2008). Biosynthesis of plant pigments: anthocyanins, betalains and carotenoids. *THE PLANT* 54 (4), 733–749

Tang, X., Huang, Y., Lei, J., Luo, H., and Zhu, X. (2019). The single-cell sequencing: new developments and medical applications. *Cell Biosci.* 9, 53. doi: 10.1186/s13578-019-0314-y

Thompson, G.A, and Goggin, F.L. (2006). Transcriptomics and functional genomics of plant defence induction by phloem-feeding insects. *J Exp Bot*, 57 (4), 755–766. doi: 10.1093/jxb/erj135

Tiwari, P., Indoliya, Y., Chauhan, A. S., Pande, V., and Chakrabarty, D. (2020). Over-expression of rice R1-type MYB transcription factor confers different abiotic stress tolerance in transgenic arabidopsis. *Ecotoxicol. Environ. Saf.* 206, 111361. doi: 10.1016/j.ecoenv.2020.111361

Tiwari, R., and Rajam, R. (2022). RNA-And miRNA-interference to enhance abiotic stress tolerance in plants. *J. Plant Biochem. Biotechnol.* 3 (2), e115. doi: 10.1007/s13562-022-00770-9

Tsutsui, T., Yamaji, N., and Ma, J. F. (2011). Identification of a cis-acting element of ART1, a C2H2-type zinc-finger transcription factor for aluminum tolerance in rice (*Oryza sativa*. l.). *Plant Physiol.* 156, 925–931. doi: 10.1104/pp.111.175802

Verma, G., Dhar, Y. V., Srivastava, D., Kidwai, M., Chauhan, P. S., Bag, S. K., et al. (2017). Genome-wide analysis of rice dehydrin gene family: its evolutionary conservedness and expression pattern in response to PEG induced dehydration stress. *PloS One* 12, 1–22. doi: 10.1371/journal.pone.0176399

Wang, X., Li, N., Li, W., Gao, X., Cha, M., Qin, L., et al. (2020). Advances in transcriptomics in the response to stress in plants. *Glob Med. Genet.* 07 (02), 030–034. doi: 10.1055/s-0040-1714414

Wang, Y., and Long, L.-H. (2010). Identification and isolation of the coldresistance related miRNAs in pisum sativum Linn. *J. Liaoning Norm. Univ.* 2, 027.

Wang, H. H., Naredo, M. E., Wu, J. L., Till, B. J., Greene, E. A., Henikoff, S., et al. (2004). "EcoTILLING candidate genes for drought tolerance in rice (Oryza sativa. l.)," in *Resilient crops for water limited environments: proceedings of a workshop held at cuernavaca Mexico* (Mexico: CIMMYT), 75–76.

Wang, K., Wang, C., Guo, B., Song, K., Shi, C., Jiang, X., et al. (2019a). CropCircDB: a comprehensive circular RNA resource for crops in response to abiotic stress. *Database* 2019, 1–7. doi: 10.1093/database/baz053

Wang, D., Xia, Y., Li, X., Hou, L., and Yu, J. (2013). The rice genome knowledgebase (RGKbase): an annotation database for rice comparative genomics and evolutionary biology. *Nucleic Acids Res.* 41, 1199–1205. doi: 10.1093/nar/gks1225

Wang, Y. Q. H., Chu, X., Li, K., and Qian, W. (2021).). single-cell transcriptome atlas of the leaf and root of rice seedlings. *J. Genet. Genomics* 48 (2021), 881–898. doi: 10.1016/j.jgg.2021.06.001

Wang, M., Yu, Y., and Haberer, G. (2014). The genome sequence of African rice (Oryza glaberrima) and evidence for independent domestication. *Nat. Genet.* 46, 982–988. doi: 10.1038/ng.3044

Wang, C. C., Yu, H., Huang, J., Wang, W., Faruquee, M., Zhang, F., et al. (2020). Towards a deeper haplotype mining of complex traits in rice with RFGB v2.0. *Plant Biotechnol. J.* 18, 14–16. doi: 10.1111/pbi.13215

Wang, X., Zhang, H., Shao, L. Y., Yan, X., Peng, H., Ouyang, J. X., et al. (2019b). Expression and function analysis of a rice OsHSP40 gene under salt stress. *Genes Genom* 41, 175–182. doi: 10.1007/s13258-018-0749-2

Wei, L., Liu, Y., Dubchak, I., Shon, J., and Park, J. (2002). Comparative genomics approaches to study organism similarities and differences. *J. BioMed. Inform* 35, 142–150. doi: 10.1016/S1532-0464(02)00506-3

Xia, K., Liu, T., Ouyang, J., Wang, R., Fan, T., and Zhang, M. (2011). Genome-wide identification, classifica- tion, and expression analysis of autophagy-associated gene homologues in rice (*Oryza sativa* l.). *DNA Res.* 18, 363–377. doi: 10.1093/dnares/dsr024

Xia, L., Zou, D., Sang, J., Xu, X., Yin, H., Li, M., et al. (2017). Rice expression database (RED): an integrated RNA-seq-derived gene expression database for rice (*Oryza sativa*. l. *.) J. Genet. Genomics* 44, 235–241. doi: 10.1016/j.jgg.2017.05.003

Xie, X., Liu, W., Dong, G., Zhu, Q., and Liu, Y. G. (2020). MMEJ-KO: a web tool for designing paired CRISPR guide RNAs for microhomology-mediated end joining fragment deletion, *Sci. China Life Sci* 2020. doi: 10.1007/s11427-020-1797-3

Xie, X., Ma, X., Zhu, Q., Zeng, D., Li, G., and Liu, Y. G. (2017). CRISPR-GE: a convenient software toolkit for CRISPR-based genome editing. *Mol. Plant* 10, 1246–1249. doi: 10.1016/j.molp.2017.06.004

Xu, K., Xu, X., Fukao, T., Canlas, P., Maghirang-Rodriguez, R., Heuer, S., et al. (2006). Sub1A is an ethylene-response-factor-like gene that confers submergence tolerance to rice. *Nature*. 442 (7103), 705–708. doi: 10.1038/nature04920

Yamazaki, S., Ueda, Y., Mukai, A., Ochiai, K., and Matoh, T. (2018). Rice phytochelatin synthases os PCS 1 and os PCS 2 make different contributions to cadmium and arsenic tolerance. *Plant Direct* 2, e00034. doi: 10.1002/pld3.34

Yang, X., Liu, C., Niu, X., Wang, L., Li, L., Yuan, Q., and Pei, X. (2022). Research on lncRNA related to drought resistance of shanlan upland rice yang. *BMC Genomics* 1-15. doi: 10.1186/s12864-022-08546-0

Yang, W., Lu, Z., Xiong, Y., and Yao, J. (2017). Genome-wide identification and co-expression network analysis of the OsNF-y gene family in rice (Oryza sativa. l.). *Crop J.* 5, 21–31. doi: 10.1016/j.cj.2016.06.014

Yan, Y., Zhang, Y., Yang, K., Sun, Z., Fu, Y., Chen, X., et al. (2011). Small RNAs from MITE-derived stem-loop precursors regulate abscisic acid signaling and abiotic stress responses in rice (Oryza sativa. l.). *Plant J.* 65, 820–828. doi: 10.1111/j.1365-313X.2010.04467.x

Yan, J., Zou, D., Li, C., Zhang, Z., Song, S., and Wang, X. (2020). SnpReady for rice (SR4R) database. *bioRxiv*. doi: 10.1101/2020.01.11.902999

Yao, W., Li, G., Yu, Y., and Ouyang, Y. (2018). funRice (Oryza sativa. L.)Genes dataset for comprehensive understanding and application of rice functional genes. *GigaScience* 7(1), gix119. doi: 10.1093/gigascience/gix119

Yonemaru, J. I., Ebana, K., and Yano, M. (2014). HapRice (Oryza sativa. l.), an SNP haplotype database and a web tool for rice (Oryza sativa. l.). *Plant Cell Physiol.* 55, 1–12. doi: 10.1093/pcp/pct188

Yoo, Y. H., Nalini Chandran, A. K., Park, J. C., Gho, Y. S., Lee, S. W., An, G., et al. (2017). OsPhyB- mediating novel regulatory pathway for drought tolerance in rice root identified by a global RNA-seq transcriptome analysis of rice genes in response to water deficiencies. *Front. Plant Sci.* 8, 580. doi: 10.3389/fpls.2017.00580

Yoon, D. H., Lee, S. S., Park, H. J., Lyu J, I. I., Chong, W. S., Liu, J. R., et al. (2016). Overexpression of OsCYP19-4 increases tolerance to cold stress and enhances grain yield in rice (Oryza sativa). *J. Exp. Bot.* 67, 69–82. doi: 10.1093/jxb/erv421

Yuan, Z., Long, W., Hu, H., Liang, T., Luo, X., Hu, Z., et al. (2021). Genome-wide identification and expansion patterns of sultr gene family in gramineae crops and their expression profiles under abiotic stress in oryza sativa. *Genes (Basel)* 12, 634. doi: 10.3390/genes12050634

Zeng, Y., Wen, J., Zhao, W., Wang, Q., and Huang, W. (2020). Rational improvement of rice yield and cold tolerance by editing the three genes OsPIN5b, GS3, and OsMYB30 with the CRISPR–Cas9 system. *Front. Plant Sci.* 10, 1–13. doi: 10.3389/fpls.2019.01663

Zhang, Q., Chen, Q., Wang, S., Hong, Y., and Wang, Z. (2014). Rice and cold stress: methods for its evaluation and summary of cold tolerance-related quantitative trait loci. *Rice* 7, 1–12. doi: 10.1186/s12284-014-0024-3

Zhang, A., Liu, Y., Wang, F., Li, T., Chen, Z., Kong, D., et al. (2019). Enhanced rice salinity tolerance *via* CRISPR/Cas9-targeted mutagenesis of the OsRR22 gene. *Mol. Breed* 39, 47. doi: 10.1007/s11032-019-0954-y

Zhang, J., Li, C., Wu, C., Xiong, L., Chen, G., Zhang, Q., et al. (2006). RMD: a rice mutant database for functional analysis of the rice genome. *Nucleic Acids Res.* 34, 745–748. doi: 10.1093/nar/gkj016

Zhang, P., Wang, Y., Chachar, S., Tian, J., and Gu, X. (2020). eRice (*Oryza sativa.* l.).a refined epigenomic platform for japonica and indica rice. *Plant Biotechnol. J.* 18, 1642–1644. doi: 10.1111/pbi.13329

Zhang, S., Wang, S., Lv, J., Liu, Z., Wang, Y., Ma, N., et al. (2018). SUMO E3 ligase SlSIZ1 facilitates heat tolerance in tomato. *Plant Cell Physiol.* 59, 58–71. doi: 10.1093/pcp/pcx160

Zhang, D., Zhang, Z., Unver, T., and Zhang, B. (2021). CRISPR/Cas: a powerful tool for gene function study and crop improvement. *J. Adv. Res.* 29, 207–221. doi: 10.1016/j.jare.2020.10.003

Zhao, Q., Feng, Q., Lu, H., Li, Y., Wang, A., Tian, Q., et al. (2018). Pan-genome analysis highlights the extent of genomic variation in cultivated and wild rice (*Oryza sativa.* l.). *Nat. Genet.* 50, 278–284. doi: 10.1038/s41588-018-0041-z

Zhao, J., He, Y., Li, X., Weng, X., Feng, D., Ying, J., et al. (2020). An integrated RNA-seq and physiological study reveals gene responses involving in the initial imbibition of seed germination in rice (*Oryza sativa.* l.). *Plant Growth Regul.* 90, 249–263. doi: 10.1007/s10725-019-00567-2

Zhao, B., Liang, R., Ge, L., Li, W., Xiao, H., Lin, H., et al. (2007). Identification of drought-induced microRNAs in rice (*Oryza sativa.* l.). *Biochem. Biophys. Res. Commun.* 354, 585–590. doi: 10.1016/j.bbrc.2007.01.022

Zhao, H., Yao, W., Ouyang, Y., Yang, W., Wang, G., Lian, X., et al. (2015). Rice (Oryza sativa. L.)VarMap: a comprehensive database of rice genomic variations. *Nucleic Acids Res.* 43, D1018–D1022. doi: 10.1093/nar/gku894.

Zheng, G. X., Terry, J. M., Belgrader, P., Ryvkin, P., Bent, Z. W., Wilson, R., et al. (2017). Massively parallel digital transcriptional profiling of single cells. *Nat. Commun.* 8, 14049. doi: 10.1038/ncomms14049

Zhiguo, E., Yuping, Z., Tingting, L., Lei, W., and Heming, Z. (2015). Characterization of the ubiquitin- conjugating enzyme gene family in rice and evaluation of expression profiles under abiotic stresses and hormone treatments. *PloS One* 10, 1–24. doi: 10.1371/journal.pone.0122621

Zhou, J., Deng, K., Cheng, Y., Zhong, Z., Tian, L., Tang, X., et al. (2017). CRISPR-cas9 based genome editing reveals new insights into microRNA function and regulation in rice (Oryza sativa. l.). *Front. Plant Sci.* 8, 1–12. doi: 10.3389/fpls.2017.01598

Zhou, X., Jeker, L. T., Fife, B. T., Zhu, S., Anderson, M. S., McManus, M. T., et al. (2008). Selective miRNA disruption in T reg cells leads to uncontrolled autoimmunity. *J. Exp. Med.* 2008, 205, 1983–1991. doi: 10.1084/jem.20080707

Zhou, S., Jiang, W., Zhao, Y., and Zhou, D.-X. (2019).) single-cell three-dimensional genome structures of rice gametes and unicellular zygotes. *Nat. Plants* 5, 795–800. doi: 10.1038/s41477-019-0471-3

Zhu, J. K. (2016). Abiotic stress signaling and responses in plants. *Cell* 167 (2), 313–324. doi: 10.1016/j.cell.2016.08.029

frontiers | Frontiers in Plant Science

TYPE Original Research
PUBLISHED 10 November 2022
DOI 10.3389/fpls.2022.1030763

Check for updates

OPEN ACCESS

EDITED BY
Mirza Hasanuzzaman,
Sher-e-Bangla Agricultural University, Bangladesh

REVIEWED BY
Sawsen Ayadi,
National Agricultural Institute of Tunisia, Tunisia
Muhammad Rizwan,
Nuclear Institute of Agriculture, Pakistan

*CORRESPONDENCE
Aiwang Duan
duanaiwang@aliyun.com;
skun5@qq.com

†These authors have contributed equally to this work and share first authorship

SPECIALTY SECTION
This article was submitted to Plant Abiotic Stress, a section of the journal Frontiers in Plant Science

RECEIVED 29 August 2022
ACCEPTED 24 October 2022
PUBLISHED 10 November 2022

CITATION
Sheng K, Xu L, Wang M, Lei H and Duan A (2022) The end-use quality of wheat can be enhanced by optimal water management without incurring yield loss. *Front. Plant Sci.* 13:1030763. doi: 10.3389/fpls.2022.1030763

COPYRIGHT
© 2022 Sheng, Xu, Wang, Lei and Duan. This is an open-access article distributed under the terms of the Creative Commons Attribution License (CC BY). The use, distribution or reproduction in other forums is permitted, provided the original author(s) and the copyright owner(s) are credited and that the original publication in this journal is cited, in accordance with accepted academic practice. No use, distribution or reproduction is permitted which does not comply with these terms.

The end-use quality of wheat can be enhanced by optimal water management without incurring yield loss

Kun Sheng[1†], Lina Xu[2†], Mingxia Wang[1], Heng Lei[1] and Aiwang Duan[3*]

[1]School of Hydraulic Engineering, Yellow River Conservancy Technical Institute, Kaifeng, China, [2]College of Life Science and Technology, Henan Institute of Science and Technology, Xinxiang, China, [3]Farmland Irrigation Research Institute, Chinese Academy of Agricultural Sciences, Xinxiang, China

In China, water-saving irrigation is playing important roles in ensuring food security, and improving wheat quality. A barrel experiment was conducted with three winter wheat (Triticum aestivum L.) genotypes and two irrigation pattens to examine the effects of regulated deficit irrigation (RDI) on wheat grain yield, water-use efficiency (WUE), and grain quality. In order to accurately control the soil water content, wheat was planted in the iron barrels set under a rainproof shelter, and the soil water content in the iron barrel was controlled by gravity method. The mechanisms whereby water management influences the end-use functional properties of wheat grain were also investigated. The results revealed that RDI improved the end-use functional properties of wheat and WUE, without significant yield loss (less than 3%). Moderate water deficit (60% to 65% field capacity) before jointing and during the late grain-filling stage combined with a slight water deficit (65% to 70% field capacity) from jointing to booting increased grain quality and WUE. The observed non-significant reduction in wheat yield associated with RDI may be attributed to higher rate of photosynthesis during the early stage of grain development and higher rate of transfer of carbohydrates from vegetative organs to grains during the later stage. By triggering an earlier rapid transfer of nitrogen deposited in vegetative organs, RDI enhances grain nitrogen content, which in turn could enhance dough elasticity, given the positive correlation between grain nitrogen content and dough midline peak value. Our results also indicate that the effects of RDI on grain quality are genotype dependent. Therefore, the grain end-use quality of some specific wheat genotypes may be enhanced without incurring yield loss by an optimal water management.

KEYWORDS

wheat quality, water deficit, regulated deficit irrigation, grain growth, grain nitrogen content

1 Introduction

It will be necessary for increasing continually food supplies to meet the demands of the growing world population in the future, and ensuring food security has accordingly become a primary focus of human society. In turn, food security is dependent on dependable supply of water resources (Kang et al., 2017), which is negatively affected by changes in agricultural water supply associated with the changing climate. It has been estimated that food production should increase at least 30% in order to meet the nutritional demands of the growing population in China. However, the average water resource amount per capita in China is less than one-third of the world average value, which shows that ensuring agricultural water supply in China is extremely important for food security.

In China, wheat is one of the most important cultivated food crops, with an annual production of more than 134 million tons (FAO, 2020), ranking third after corn and rice in terms of productivity. Wheat is primarily planted in northern China, in which only 19% of the country's total water resources is distributed. Moreover, duo to the main precipitation period generally does not coincide with the peak water demand stages in wheat production, the wheat yield and quality are often affected significantly by drought in the main production regions (Zaveri and Lobell, 2019). Irrigation plays prominent roles in ensuring stable yield and high grain quality in wheat production in China. Therefore, to ensure synchronously water and food security in China, it is essential to understand the response mechanisms of wheat yield and quality to farmland water management patterns.

Regulated deficit irrigation (RDI), a water-saving irrigation method widely adopted in China, can be employed to reduce water consumption without causing a significant wheat yield lose. Under RDI, a limited water deficit is imposed during a given specific growth stage to control the redundant growth of vegetative organs, thereby promoting the distribution of photosynthates to reproductive organs, which is benefit for increasing economic yield and conserving water consumption. The successful application of RDI is dependent closely on understanding of the effects of soil moisture management on wheat yield and quality, as well as the associated physiological mechanisms. Meng et al. (2016) have previously suggested that a slight or moderate water deficit prior to the stem elongation stage, or a slight water deficit at the grain-filling stage, promotes high yield and water conservation in winter wheat. Yan et al. (2019) found that a mild water deficit could enhance grain filling rate and productivity of winter wheat. Furthermore, it has previously been established that to obtain high wheat grain yields, priority should be placed on ensuring irrigation during the jointing and filling periods (Mu et al., 2021a). A slight or moderate water deficit has been demonstrated to increase yield by inhibiting vegetative growth, increasing the harvest index (HI), and promoting growth compensation after the water stress was relieved in the next growth stage.

Numerous studies have been conducted to examine the effects of optimal water management (i.e., RDI) during entire growth season on grain protein content in wheat, and it has been established that generally, there is a negative linear correlation between grain protein content and grain yield. However, few studies have sought to evaluate the effects of RDI on the end-use functional properties of wheat.

The end-use functional properties of wheat, which determine the type and quality of the associated food products, are mainly determined by the content and characteristics of grain protein and starch in wheat grain. For example, protein characteristics, including content, composition, and polymerization, play important roles in determining bread and hard-bite noodle quality (Hou et al., 2013), whereas the swelling and pasting properties of starch are important determinants of soft noodle quality (e.g., udon). Furthermore, it has been demonstrated that protein content is positively correlated with bread volume (Dowell et al., 2008; Hu et al., 2021), but negatively correlated with noodle surface smoothness and visual brightness are protein content (Ohm et al., 2008). In addition, the proportion of low molecular weight glutenins/gliadins has shown a positively correlated with the hardness, gumminess, and chewiness of cooked Chinese hard-bite white-salted noodles (Hou et al., 2013), whereas wheat starches that confer high peak viscosity, high swelling potential, low pasting temperature, and high breakdown have been established to be associated closely with the superior quality of Japanese white-salted noodles (Noda et al., 2001).

Drought stress has significant effects on the parameters of Mixograph and GI. For example, the mixing characteristics associated with dough strength (e.g., midline peak value) have been shown to be increased, whereas the midline right slope is not significantly influenced by drought stress at the soft dough stage (Labuschagne and Moloi, 2015). Furthermore, irrigation regime plays an important role in determining the end-use quality of a given wheat genotype, and GI appears to be predominantly reduced under an abundant moisture regime (Gil et al., 2011). Flagella et al. (2010) demonstrated that terminal water stress during grain filling consistently enhances gluten strength, as indicated by GI. Li et al. (2013) detected a significant increase in gluten strength, although no significant increase in the midline peak time. However, there are few studies for examining the influence of RDI on mixograph parameters and the GI, and little knowledge on the mechanisms whereby water management modifies the end-use functional properties of wheat.

Grain protein concentration (GPC), proportional composition of protein, and protein polymerization are influenced to varying degrees by the characteristics of grain dry matter and nitrogen (N) accumulation. GPC, expressed as the ratio of protein weight to dry matter weight, is determined by the characteristics of both grain filling and grain N accumulation. In this regard, given that grain protein content is diluted by non-nitrogenous compounds as grain

yield increases, yield is negatively correlated with protein concentration (Moral et al., 2007; Graziano et al., 2019; Tatar et al., 2020; Santis et al., 2021). However, the relationship between grain yield and GPC changes in response to different water treatments (Meng et al., 2016). Given the allometric scaling relationships between protein fraction composition and total quantity of N per grain (Plessis et al., 2013; Ferrise et al., 2015), the proportional composition of protein is primarily dependent on the total quantity of N per grain (Triboï et al., 2003). As total protein content increased, the ratio of low molecular weight to high molecular weight glutenins decreased consistently under water deficit occurred throughout the growing season (Flagella et al., 2010; Giuliani et al., 2015). Moreover, given that the glutenin polymer backbone is composed of high molecular weight glutenins, the content of these glutenins affects gluten strength. Accordingly, understanding the influences of water deficit at different wheat growing stages on the characteristics of grain dry matter and N accumulation are essential for gaining an insight on the physiological mechanisms whereby RDI affects GPC, composition, and protein polymerization.

Grain dry matter and N accumulation are also influenced by sucrose and N concentration in plants. The characteristics of grain dry matter accumulation is predominantly associated with starch, which accounts for more than 80% of the total grain dry matter (Evers et al., 1999). During grain filling in wheat, photoassimilates in leaves and carbohydrates in vegetative organs are transported to grains in the form of sucrose, providing a source of carbon for starch accumulation in the grains (Dong and Beckles, 2019; Zhang et al., 2021), with the translocation of assimilate from source to sink influencing the accumulation of grain dry matter (Ma et al., 1996). In this context, it has previously been established that a mild desiccation of soil enhances whole-plant senescence, thereby promoting a more rapid and efficient remobilization of carbon from vegetative tissues to grains, and accelerating the rate of grain-filling (Yang and Zhang, 2006). Moreover, the source of N incorporated into filling grains is assumed to be derived from the N remobilized from leaves (Kong et al., 2016). The accumulation of grain N occurs almost simultaneously with the decrease of leaf N content. It has also been reported that water deficit enhances N remobilization efficiency in wheat (Li et al., 2021). Consequently, a better understanding of the effects of water deficit on the changes in sucrose and N concentrations in different organs is important for clarifying the physiological mechanism whereby RDI influences grain filling and N accumulation characteristics.

In this study, we investigated the effects of RDI on wheat grain yield, water-use efficiency (WUE), and the grain quality traits e.g. GPC, GI, midline peak time (MPT), midline peak value (MPV), and right of midline peak slope (MRS), to demonstrate that optimal water management can enhance grain quality and WUE in the absence of any apparent reduction in grain yield. In addition, we also examined the mechanisms whereby water management influences the end-use functional properties of wheat. The main hypotheses in present study are as follows: (a) grain quality and WUE may be improved by optimal water management without apparent yield loss, (b) moderate water stress may increase deposit of carbohydrates and nitrogen in grain, and (c) grain nitrogen content may enhance grain end-use quality.

2 Material and methods

2.1 Experimental site

The experiment was carried out during the 2017–2018 growing season at the experimental station of the Farmland Irrigation Research Institute, Chinese Academy of Agricultural Sciences (35°19′N, 113°53′E), located in Xinxiang City, Henan Province, P. R. China. In order to accurately control soil water content (SWC), wheat was planted in the iron barrels under the rainproof shelter. The SWC in the iron barrel was controlled by gravity method, and irrigation was applied appropriately to regulate the SWC went to upper limit when the SWC was below lower limit.

The iron barrel comprised an inner and outer layer, and the inner layer was closely nested in the outer layer (Figure 1). During the experiment, the outer barrel was buried 25 cm below ground level to maintain the temperature of soil within the barrel close to that of the surrounding soil. The inner barrel (30 cm diameter × 30 cm depth), which could be readily weighed, contained 20.5 kg (dry weight) of sandy loam soil. The SWC in the inner barrel was obtained by determining the gross weight of the inner barrel and plant fresh weight. SWC in the inner barrel = water weight in the inner barrel/dry soil weight in the inner barrel; water weight in the inner barrel = (inner barrel weight + wet soil weight in the inner barrel + plant fresh weight) – (inner barrel weight + dry soil weight in the inner barrel); inner barrel weight was 1.5 kg. Prior to water treatment, assuming that the fresh weight of plants in each water treatment was the same, we determined the fresh weight values of plants by measuring 10 plants from each variety. Following the water treatment, five plants were sampled for each water treatment and weighed at each growth stage. SWC was measured at weekly intervals prior to the jointing stage, at 3-day intervals from jointing to anthesis, and daily during the grain-filling stage.

2.2 Experimental site

Two water treatments were utilized in this experiment, and the lower limit of SWC for water treatment is shown in Figure 2

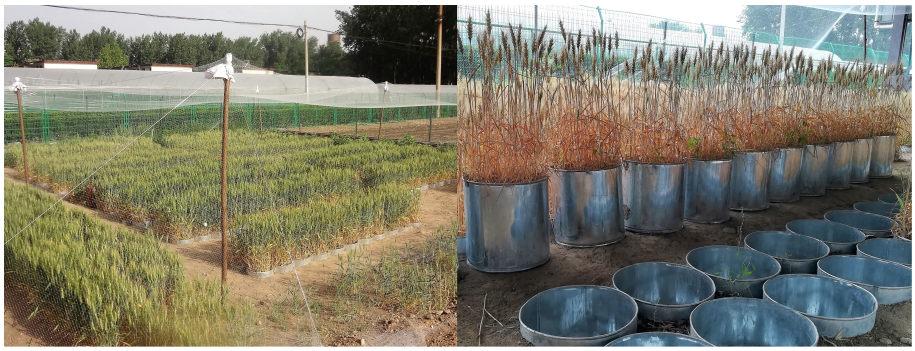


FIGURE 1
Photos of the experiment at ripening.

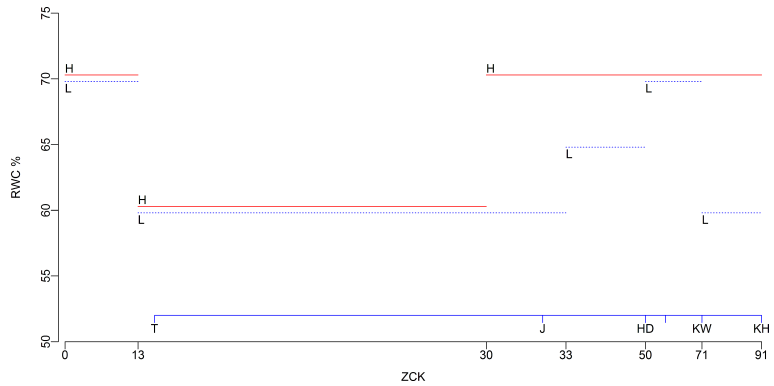


FIGURE 2
The lower limit of soil water content for water treatments. Red and blue lines indicate high-and low-water treatments, respectively. RWC, relative soil water content, percentage of field water capacity; H, high-water treatments; L, low-water treatments; ZCK, Zadoks-Chang-Konzak wheat developmental scale; T, tillering; J, jointing; HD, heading; KW, watery-ripe kernel; KH, hard kernel.

(Meng et al., 2016; Mu et al., 2021a). For high-water treatments (H, red lines), SWCs were no less than 70% of the field capacity (FC) from the sowing period to the seedling period (Zadoks-Chang-Konzak wheat developmental scale, ZCK 13), 60% to 65% FC from tillering (ZCK 21) to the erect leaf sheath stage (ZCK 30), and 70% to 75% FC from jointing (ZCK 31) to the hard kernel stage (ZCK 92). For low-water treatments (L, blue lines), SWCs were no less than 70% FC from sowing to the seedling period (ZCK 13), 60% to 65% FC from tillering (ZCK 21) to the visible third node stage (ZCK 33), 65% to 70% FC from the visible fourth node (ZCK 34) to booting (ZCK 49) stages, 70% to 75% FC from the heading (ZCK 50) to watery-ripe kernel (ZCK 72) stages, and 60% to 65% FC from the early milky-ripe (ZCK 73) to hard kernel (ZCK 92) stages.

For the purposes of the present study, we used three wheat genotypes, Xinmai-26 (XM26), Xinmai-49 (XM49), and Zhoumai-18 (ZM18), whose MPTs were 12, 8, and 4 min, respectively. These genotypes can thus be considered to be representative of very strong gluten, strong, and medium-strong cultivars, respectively. Among these, XM26 whose high molecular weight glutenin subunits were 1, 7 + 8, and 5 + 10, and ZM18 whose yield stability outperform other cultivars are widely cultivated in the Huang-Huai-Hai Plain of China. Whereas, XM49 is a new breeding line with a higher thousand-grain weights (TGW).

The treatments were set up using a split-plot design, with three replicates. The barrels were grouped into three blocks, each distributed in two plots, with each plot being subdivided into three subplots, each containing three barrels. Water treatments were randomly assigned to the plots within each block and genotypes were randomly assigned to the subplots within each plot.

2.3 Experimental procedure

Fertilizers (1.7 g N, 1.13 g P_2O_5, and 0.56 g K_2O) were applied to each barrel. Half of the N was applied prior to sowing, with the remainder being applied at the jointing stage. Wheat seeds were sown on October 18, 2017, and plants were harvested on May 21, 2018. In each barrel, we sowed 36 seeds at a depth of 3 cm, which were thinned to 12 seedlings per barrel at the three-leaf stage.

At 3- to 5-day intervals post anthesis, three spikes bearing flag leaves were cut from the plants, from which the grains were harvested by hand and dried with the leaves at 80°C for 24 h. The mean dry weight of a single kernel was determined after weighing all kernels (approximately 100 kernels). Following these weight determinations, the dried grains, flag leaves, and rachises were ground to determine the sucrose and nitrogen contents.

In each sub-plot, one barrel of plants without destructive sampling was reserved for harvesting, with all plants in each of the barrels being harvested for grain yield determination. After weighing, the grains were ground for quality determination. For each barrel, we counted the number of spikes, and obtained measurements for total biomass (BM), HI, number of grains per spike (NGS), number of spikelets per spike (NSS), and number of infertile spikelets per spike (NIS) from 10 plants. TGWs were estimated from the measurements of three 200-grain samples.

Wheat evapotranspiration (ET) was determined using a soil water balance equation:

$$ET = I + P + \Delta S + \Delta WS + \Delta WV \quad \text{Eq. [1]}$$

Where I is the total irrigation amount (mm), P precipitation (mm), ΔS change of soil water storage (mm), ΔWS water exchange with outside through surface ways, and ΔWV water exchange with outside through vertical ways in a barrel during the whole wheat growing season. For the given situation in this experiment, the P, ΔWS, ΔWV may be considered as zero, and then the Eq. [1] may be simplified as follows:

$$ET = I + \Delta S \quad \text{Eq. [2]}$$

The WUE was calculated with following formula:

$$WUE = GY/ET \quad \text{Eq. [3]}$$

Where GY is the grain yield.

GPC was determined using the micro-Kjeldahl method according to the AACC Method 46-11A. GN (mg/grain) = GPC × grain weight, and sucrose content was measured using resorcinol. GI values were determined based on the ICC standard No. 158 using a Perten Glutomatic 2200 Instrument (Perten, Sweden). Flour mixing characteristics were evaluated using a 10 g Mixograph (National Mfg. Div., TMCO, Lincoln, NE, USA) with an absorption of 0.625 mL/g (Peterson and Graybosch, 1992), according to the approved AACC Method 54-40A, 2002. MPT, MPV, and MRS were analyzed based on the correlations between the mixograph and baking parameters (Wikstrom and Bohlin, 1996; Chung et al., 2001; Neacşu et al., 2009).

2.4 Statistical analyses

Data analysis and plotting were performed by using R 4.1.3 software (R Foundation for Statistical Computing, Vienna, Austria) and RStudio 2022.02.1 + 461 integrated development environment. Data were analyzed using an analysis of variance (ANOVA), with means being compared using a least significant difference (LSD) test at the 5% level of significance. Pearson correlation coefficients among yield, ET, and quality traits were calculated using the software package "psych", correlation diagnosis was performed using the package "corrgram", and dynamic curves of sucrose and nitrogen concentration were plotted using the package "ggplot2" with the "loess" method.

The grain weight data were fitted using a re-parameterized Richards growth model, with the statistical expectation of the Richards model being expressed using Eq. [4] (Richards, 1959).

$$Q(t) = K \cdot (1 - a \cdot e^{-bt})^{\frac{1}{1-c}} \quad \text{Eq. [4]}$$

Where Q is the quantity of grain weight; t is the number of days after anthesis (DAA); K is the final value of Q approached as $t \to \infty$; and a, b, and c are coefficients determined by regression. The parameter c controls the inflection values. The maximum rate of accumulation (R) was defined as the derivative of the point of inflection, and the duration of grain filling (t95) was defined as the duration, from anthesis, in which 95% of K is accumulated (Ferrise et al., 2015).

$$R = K \cdot b \cdot c^{\frac{c}{1-c}} \quad \text{Eq. [5]}$$

$$t95 = -\frac{1}{b}\ln\left[\frac{1 - 0.95^{(1-c)}}{a}\right] \quad \text{Eq. [6]}$$

Substituting Eq. [5]and Eq. [6] into Eq. [4] yields the re-parameterized Richards growth model shown in Eq. [7]:

$$Q(t) = K \cdot \left\{1 + [0.95^{(1-c)} - 1] \cdot e^{\left[\frac{R\cdot(t95-t)}{K\cdot c^{\frac{c}{1-c}}}\right]}\right\}^{\frac{1}{1-c}} \quad \text{Eq. [7]}$$

When c = 2, Eq. [7] becomes a three-parameter logistic model (Triboï et al., 2003). The nonlinear effect models for grain weight were fitted using the "nlst" function of the R/nlme package (Pinheiro and Bates, 2000). Within-barrel heteroscedasticity was modeled using a power-variance function, and alternative models were evaluated using the likelihood ratio test, log-likelihood, Akaike information criterion (AIC), Bayesian information criterion (BIC), and residual variance (Razali et al., 2015). Smaller AIC, BIC, and

residual variance values indicate a better fit of the model to the experimental data (Aggrey, 2009). Finally, the parameter c in Eq. [7] was treated as a purely fixed effect and assigned a value of 2.4.

3 Results

3.1 Grain yield, water-use efficiency, and harvest index of winter wheat

3.1.1 Grain yield and yield components

The grain yield and yield components of wheat exposed to the different irrigation treatments are shown in Table 1. The genotype (G) and genotype-by-water interaction (G×W) were found to have significant effects on grain yield, whereas the effects of water (W) on grain yield did not reach the significant level ($P > 0.05$). Relative to the value obtained in response to the H, the reduction in grain yield under L was 2.96% (1.4g). Compared with H treatment, there were significant reductions of 7.57% and 7.47% in the number of spikes per barrel (NSB) and NGS, respectively, in the L treatment. Although NIS was not significantly affected by the irrigation regime, a 6.43% reduction of NSS was recorded under L treatment, compared with that under H treatment. In addition, the TGW was found to be significantly influenced by water treatment levels, with an increase of 3.14% under L treatment.

3.1.2 Evapotranspiration and water-use efficiency

The values of ET and WUE in response to the different treatments are summarized in Table 1. WUE was significantly affected by W and G, although the effect of G×W on WUE was not statistically significant ($p > 0.05$). Wheat subjected to L treatment was found to have a 11.6% higher mean WUE than that under H regime. Comparing the mean ET values obtained from H treatment, a significant ET reduction of 12.78% was recorded under L treatment. Conversely, we detected no significant differences among the wheat genotypes with respect to ET ($p > 0.05$), whereas a significant reduction in WUE was recorded in the XM49 genotype.

3.1.3 Aboveground biomass and harvest index

The BM and HI values recorded in response to the different treatments (showed in Table 1) clearly indicated that HI was significantly increased from 41.6% to 44.0% ($p< 0.01$) under L treatment, although G and G×W appeared to have no significant effects on HI. The BM of wheat subjected to L treatment was found to be significantly lower (by 7.98%, $p< 0.01$) than that under H treatment. Moreover, BM was significantly influenced by both G and G×W.

3.2 Grain quality parameters of winter wheat

Mean values of several grain quality parameters for three wheat genotypes grown under the two irrigation regimes and their ANOVA results are presented in Table 2. These values indicate that whereas L treatment significantly increased GN and GI, it significantly decreased GPC. Low-water regime result in a significant increase in MPV and MRS. Contrastingly, the effects of W on the MPT were not statistically significant ($p > 0.05$). All quality parameters were, however, significantly affected by G, with both GI and MRS of XM26 were the highest among the three genotypes examined in this study.

3.3 Relationships between quality parameters, yield, yield components, and evapotranspiration

The observed values from all 18 samples were used to examine correlations among yield, yield components, ET, and quality traits, and the results were presented in Table 3 and

TABLE 1 Grain yield, yield components, water-use efficiency and harvest index of winter wheat genotypes under the different levels of irrigation.

	GY	ET	WUE	BM	HI	NSB	TGW	NGS	NSS	NIS
Water(W)	ns	**	**	**	**	**	**	*	**	ns
H	47.2	35.92a	1.3183b	113.14a	41.64b	42.67a	45.19b	30.489a	18.133a	3.322
L	45.8	31.33b	1.472a	104.11b	44.0a	39.44b	46.61a	28.211b	16.967b	3.167
Genotype(G)	**	ns	**	*	ns	ns	**	*	ns	ns
XM26	49.84a	33.59	1.492a	113.55a	44	42.33	42.46c	30a	17.317	2.85
XM49	39.69b	34.86	1.1443b	94.5b	42.02	40.67	49.88a	27.983b	17.367	3.8
ZM18	49.97a	32.42	1.5491a	117.83a	42.44	40.17	45.38b	30.067a	17.967	3.083
W*G	*	ns	ns	*	ns	**	**	ns	ns	ns

Level of significance: * $p \leq 0.05$; ** $p \leq 0.01$; ns: not significant. Means denoted by the same letter are not statistically different, as assessed using the LSD test at $p \leq 0.05$. H and L indicate high-and low-water treatments, respectively. GY, grain yield (g/barrel); ET, evapotranspiration (L/barrel); WUE, water-use efficiency (kg/m^3); BM, aboveground biomass (g/barrel); HI, harvest index (%); NSB, number of spikes per barrel; TGW, thousand-grain weight (g); NGS, number of grains per spike; NSS, number of spikelets per spike; NIS, number of infertile spikelets per spike.

TABLE 2 Grain quality parameters of different winter wheat genotypes under the different irrigation treatments and results of the analysis of variance.

	GPC	GN	GI	MPT	MPV	MRS
Water(W)	**	**	**	ns	**	*
H	15.40a	1.253b	73.48b	7.924	50.73b	-4.883b
L	15.29b	1.293a	76.21a	8.361	55.65a	-4.021a
Genotype(G)	**	**	**	**	**	**
XM26	15.73a	1.182c	92.17a	11.78a	50.44b	-1.112a
XM49	15.52b	1.392a	76.43b	7.828b	58.35a	-3.915b
ZM18	14.79c	1.244b	55.93c	4.823c	50.77b	-8.330c
W*G	ns	**	**	*	ns	ns

Level of significance: * $p \leq 0.05$; ** $p \leq 0.01$; ns: not significant. Means denoted by the same letter are not statistically different, as assessed using the LSD test at $p \leq 0.05$. H and L indicate high- and low-water treatments, respectively. GPC, grain protein concentration (%); GN, grain nitrogen content (mg/grain); GI, gluten index (%); MPT, midline peak time (min); MPV, midline peak value (% torque); MRS, right of midline peak slope (% torque/min).

TABLE 3 Pearson's correlation coefficients (above the diagonal) and probability values (below the diagonal) between the quality parameters, yield, yield components, and evapotranspiration of different wheat genotypes subjected to different irrigation regimes.

	GPC	GN	GI	MPT	MPV	MRS	GY	ET	TGW	NGB
GPC	1	-0.004	0.924	0.865	0.165	0.920	-0.245	0.305	-0.113	0.163
GN	0.986	1	-0.189	-0.336	0.842	-0.121	-0.830	0.039	0.977	-0.584
GI	<0.001	0.453	1	0.972	0.050	0.986	-0.078	0.093	-0.278	0.117
MPT	<0.001	0.173	<0.001	1	-0.080	0.954	0.063	0.079	-0.413	0.201
MPV	0.514	<0.001	0.843	0.754	1	0.139	-0.723	-0.158	0.819	-0.696
MRS	<0.001	0.633	<0.001	<0.001	0.583	1	-0.170	0.030	-0.217	0.023
GY	0.327	<0.001	0.757	0.805	0.001	0.501	1	0.184	-0.793	0.603
ET	0.218	0.879	0.713	0.757	0.530	0.906	0.464	1	-0.012	0.643
TGW	0.656	<0.001	0.265	0.088	<0.001	0.387	<0.001	0.961	1	-0.580
NGB	0.517	0.011	0.644	0.424	0.001	0.928	0.008	0.004	0.012	1

GPC, grain protein concentration (%); GN, grain nitrogen content (mg/grain); GI, gluten index (%); MPT, midline peak time (min); MPV, midline peak value (% torque); MRS, right of midline peak slope (% torque/minute); GY, grain yield (g/barrel); ET, evapotranspiration (L/barrel); TGW, thousand-grain weight (g); NGB, number of grains per barrel.

Figure 3. The data indicated that yield correlated negatively with TGW ($r = -0.793$, $p < 0.01$), although positively correlated with the number of grains per barrel (NGB; $r = 0.603$, $p < 0.01$). NGB was significantly positively correlated with ET ($r = 0.643$, $p < 0.01$). In addition, a significant negative correlation ($r = -0.58$, $p < 0.05$) between TGW and NGB was also recorded.

Correlations between MPT and GPC, between GI and GPC, and between MRS and GPC were significantly positive ($p < 0.01$), whereas MPT, GI, and MRS were slightly and non-significantly correlated with yield. Significant relationships were observed between GN and either MPV or TGW, with correlation coefficients of 0.842 ($p < 0.001$) and 0.977 ($p < 0.001$), respectively. Moreover, we detected a significant reduction in GN coinciding with an increase in NGB ($r = -0.584$, $p < 0.05$), whereas GN appeared to be not correlated with GPC.

3.4 Grain growth pattern

3.4.1 Grain weight dynamic curves and parameters of grain filling

The pattern of grain growth was suitable to be characterized by a sigmoidal curve (Figure 4). The correlation coefficient between the actual and fitted grain weights determined using Eq. [7] was 0.9953 ($p < 0.01$), which indicated that Eq. [7] provides a good estimate of the grain growth patterns observed in this study. Specifically, the differences in grain weight between the wheat subjected to L and H treatments were small during the early grain-filling period (prior to 9 DAA), and these differences gradually increased with further grain development. Moreover, a similar mode of grain growth among the three examined wheat genotypes was identified.

The parameters of grain filling under the different treatments are shown in Figure 5. Fitted values of final grain

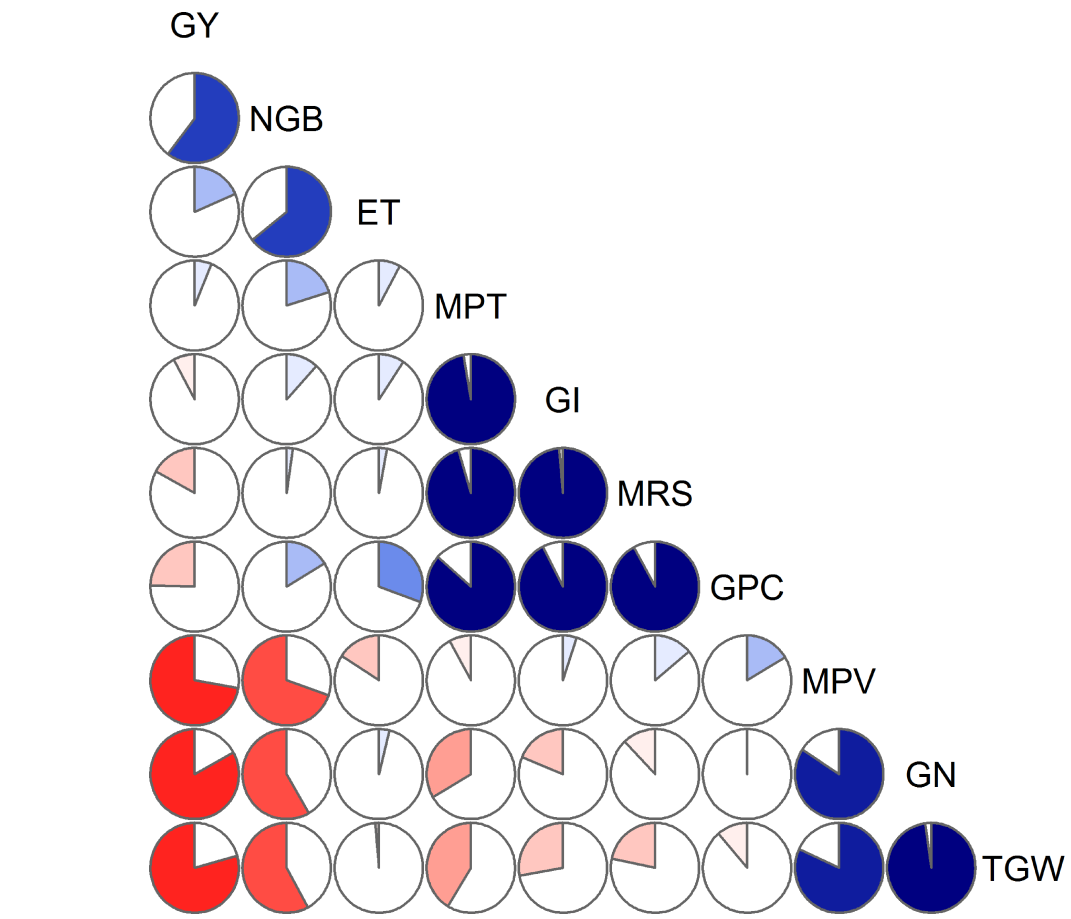


FIGURE 3
Correlation diagnosis of grain yield, evapotranspiration, and quality parameters. Blue color represents a positive correlation between the two variables that meet at that cell. Conversely, red color represents a negative correlation. The darker and more saturated the color, the greater is the magnitude of the correlation. GY, grain yield (g/barrel); NGB, number of grains per barrel; ET, evapotranspiration (L/barrel); MPT, midline peak time (minute); GI, gluten index (%); MRS, right of midline peak slope (% torque/minute); GPC, grain protein concentration (%); MPV, midline peak value (% torque); GN, grain nitrogen content (mg/grain); TGW, thousand-grain weight (g).

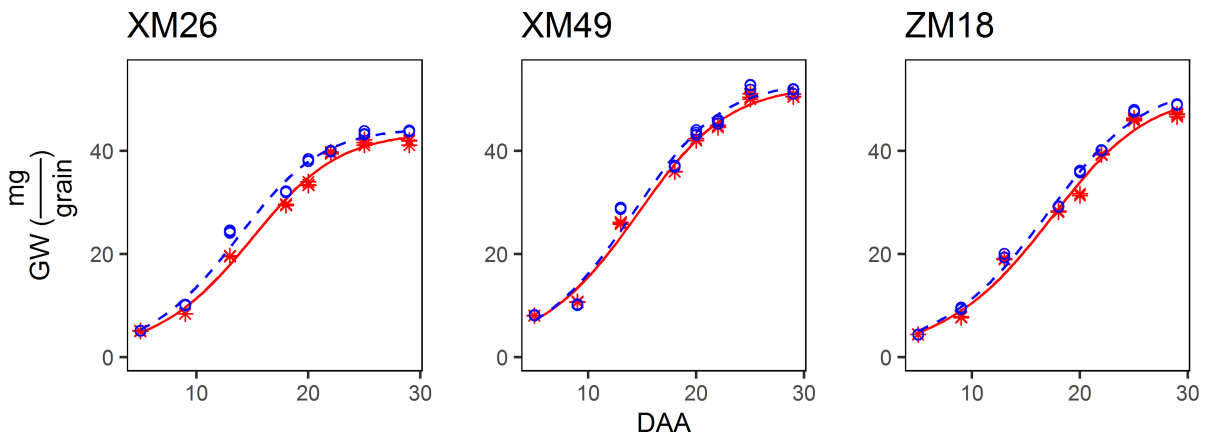


FIGURE 4
Dynamics of the grain weight (GW) of different genotypes of winter wheat under different levels of irrigation. Red lines indicate high-water treatment, blue lines indicate low-water treatment, red stars represent high-water treatment observations, and blue circles represent low-water treatment observations. DAA, days after anthesis; XM26, Xinmai-26; XM49, Xinmai-49; ZM18, Zhoumai-18.

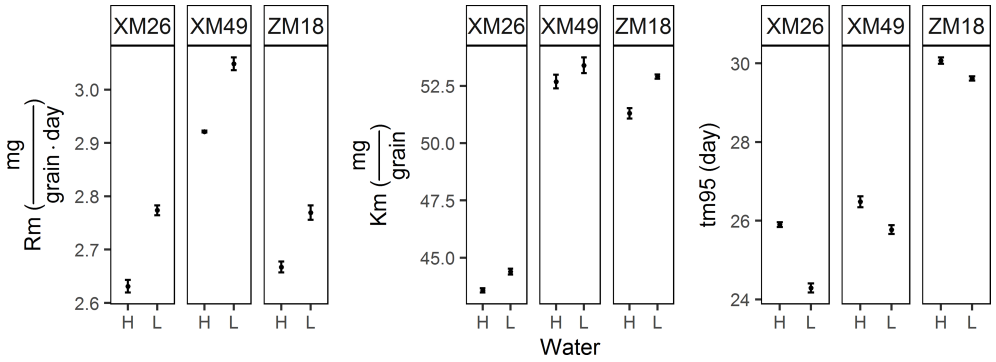


FIGURE 5
Parameters of the grain filling of different winter wheat genotypes under different irrigation levels. Error bars indicate the confidence interval of the mean. Rm, maximum rate of grain filling; Km, final grain weight; tm95, duration of grain filling. XM26, Xinmai-26; XM49, Xinmai-49; ZM18, Zhoumai-18; H, high-water treatment; L, low-water treatment.

weight (Km) for L were higher than those for H. Increases of 1.86%, 1.37%, and 3.14%, were obtained for genotypes XM26, XM49, and ZM18, respectively. When comparing the means obtained in the two irrigation regimes, we also observed an increase in maximum rate of grain filling (Rm) in response to the L treatment, with increases of 5.32%, 4.45%, and 3.75% recorded for XM26, XM49, and ZM18 respectively. We also detected reductions in the duration of grain filling (tm95) of grain filling in response to the L treatment, with reductions of 6.22%, 2.68% and 0.53% being recorded for XM26, XM49 and ZM18, respectively.

3.4.2 Grain nitrogen weight dynamic curves and grain nitrogen accumulation parameters

Patterns of grain N accumulation can be described as sigmoidal curves (Figure 6). In present study, the correlation coefficient between actual grain N weight and the grain N weight fitted from Eq. [7] was 0.9930 ($p< 0.01$), which indicated the dependability of Eq. [7] in describing the grain N weight dynamics observed in this study. Moreover, we also found that the observed pattern of grain N accumulation was similar to that of the grain growth. The differences between the GN values recorded under L and H treatments were generally small during the early grain-filling period (prior to 9 DAA). Overall, among the three wheat genotypes examined, the GN values obtained in L treatment were higher than those in H treatment.

The grain N accumulation parameters recorded in different treatments are presented in Figure 7. Relative to the H treatment, the fitted values of the final GN (Kn) under L treatment increased by 1.01%, 1.05%, and 0.17% for XM26, XM49, and ZM18, respectively. Similarly, maximum rate of grain nitrogen accumulation (Rn) increased by 1.55%, 2.45% and 0.59% for the three genotypes of XM26, XM49, and ZM18, respectively. In contrast, duration of grain nitrogen accumulation (tn95)

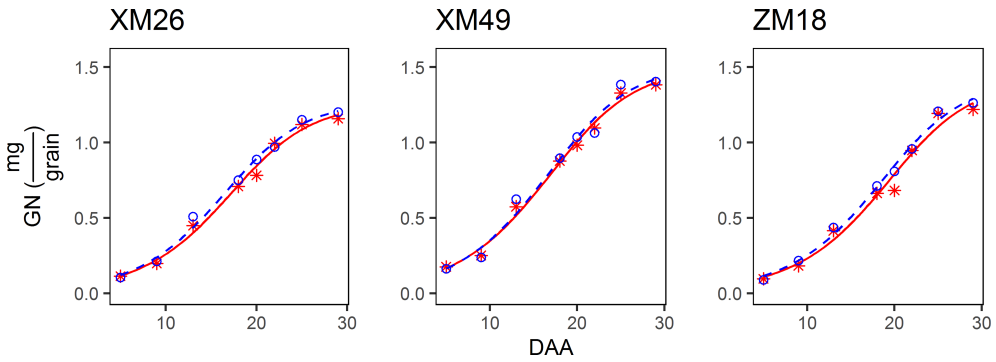


FIGURE 6
Dynamics of grain nitrogen content (GN) of different winter wheat genotypes under different irrigation levels. Red lines indicate high-water treatment, blue lines indicate low-water treatment, red stars represent high-water treatment observations, and blue circles represent low-water treatment observations. DAA, days after anthesis; XM26, Xinmai-26; XM49, Xinmai-49; ZM18, Zhoumai-18.

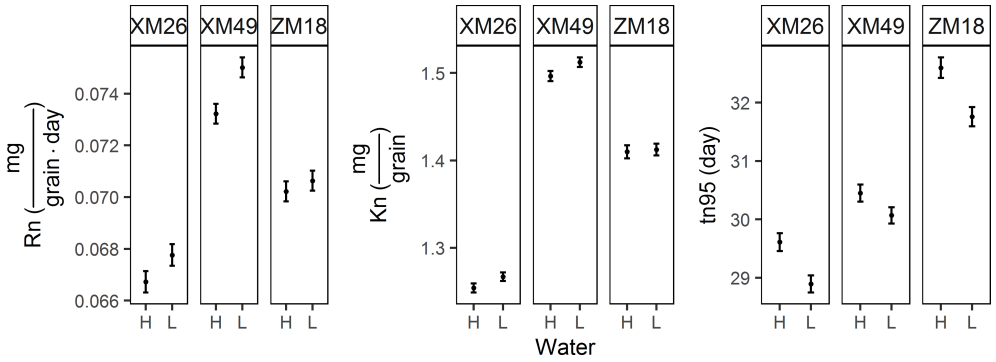


FIGURE 7
Parameters of grain nitrogen accumulation of different winter wheat genotypes subjected to different irrigation treatments. Error bars indicate the confidence interval of themean. Rn, maximum rate of grain nitrogen accumulation; Kn, final grain nitrogen weight; tn95, duration of grain nitrogen accumulation. XM26, Xinmai-26; XM49, Xinmai-49; ZM18, Zhoumai-18; H, high-water treatment; L, low-water treatment.

decreased by 2.42%, 1.26%, and 2.58% under L treatment for XM26, XM49, and ZM18, respectively.

3.5 Dynamics of sucrose and nitrogen concentration

3.5.1 Dynamics of grain nitrogen concentration

Figure 8 shows the dynamics of grain N concentration (GNC). It was observed that GNC was characterized with a gradual increase and a significant fluctuation.

Moreover, with the exception of 18 DAA, the GNCs under L treatment were invariably lower than those under H treatment. During the early grain-filling period (prior to 13 DAA), we detected a great difference between the GNCs recorded in wheat under the L and H treatments. However, during the late grain-filling stage (after 18 DAA), there was a more rapid increase of GNC under L treatment, which narrowed notably the difference between the GNC values from the two different irrigation treatments consequently.

3.5.2 Dynamics of leaf and rachis nitrogen concentrations

Both leaf and rachis nitrogen concentrations (LNC and RNC, respectively) can be characterized by gradual reductions during grain development (Figure 9). In most cases, the LNC

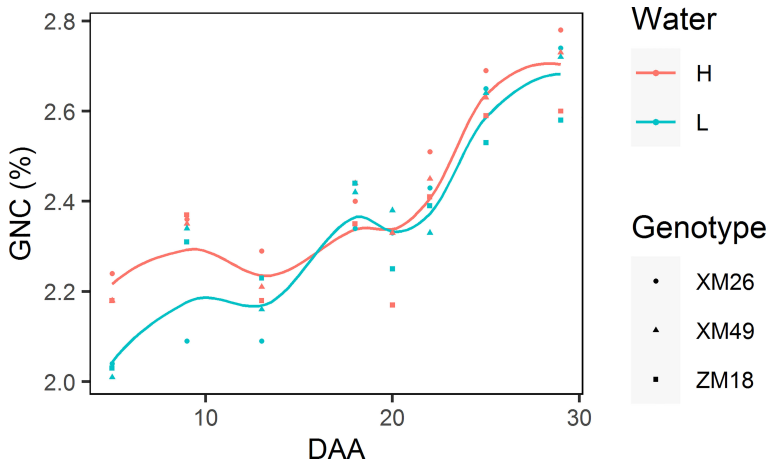


FIGURE 8
Dynamics of grain nitrogen concentration (GNC) of different winter wheat genotypes subjected to two different irrigation treatments. Lines represent values fitted using the "loess" method and the points denote observations. DAA, days after anthesis; H, high-water treatment; L, low-water treatment; XM26, Xinmai-26; XM49, Xinmai-49; ZM18, Zhoumai-18.

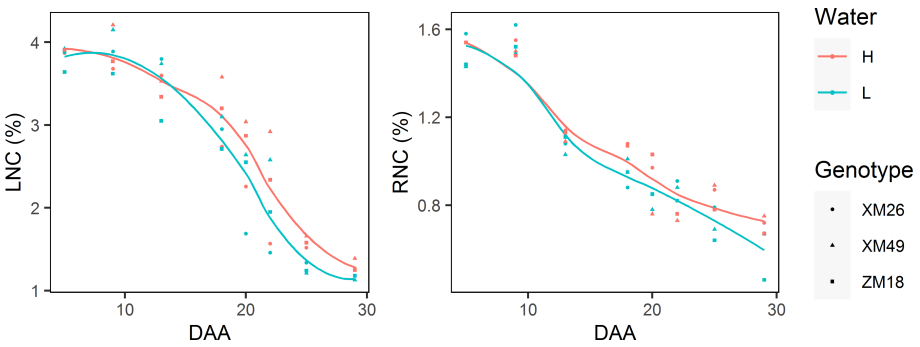


FIGURE 9
The dynamics of leaf nitrogen concentration (LNC) and rachis nitrogen concentration (RNC) of different winter wheat genotypes grown under different levels of irrigation. Lines represent values fitted using the "loess" method and the points denote observations. DAA, days after anthesis; H, high-water treatment; L, low-water treatment; XM26, Xinmai-26; XM49, Xinmai-49; ZM18, Zhoumai-18.

and RNC of wheat subjected to L treatment were lower than those under H treatment, which became particularly apparent after 18 DAA duo to the rapid LNC and RNC reductions under L treatment.

3.5.3 Dynamics of leaf and rachis sucrose concentrations

As shown in Figure 10, the leaf and rachis sucrose concentrations (LSC and RSC, respectively) of the three wheat genotypes reduced gradually during grain development stage. During the early stages of grain filling (prior to 18 DAA), the LSC under L treatment was higher than that under H treatment. After 18 DAA, however, a rapid decrease of LSC was record, with the rate of reduction being more pronounced under L treatment. Consequently, the LSC value measured at 20 DAA under L treatment was lower than that under H treatment. Under H treatment, RSC declined rapidly at 23 DAA, which was later than the decline observed in response to the L treatment (20 DAA). Meanwhile, after 23 DAA the RSC of wheat subjected to L treatment was lower than that of H treatment plants.

4 Discussion

4.1 Effects of drought stress on the yield and the mechanisms whereby water management alters wheat yield

Studies that have examined the effects of drought stress on wheat yield have tended to obtain inconsistent results, and Farooq et al. (2017) suspect that these discrepancies could reflect differences in the times at which stress occurred and/or differences in the durations and intensities of the stress experienced. For example, Mu et al. (2021a) found that short-term drought after the jointing period reduced the yield of wheat by 2.03% - 64.39% compared with that of wheat receiving an

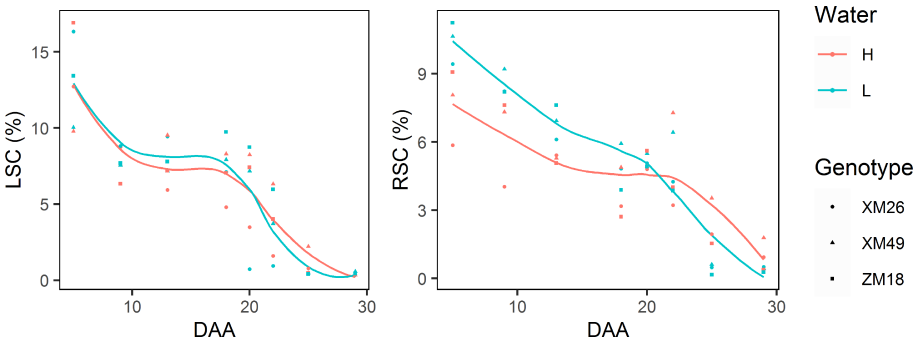


FIGURE 10
The dynamics of leaf sucrose concentration (LSC) and rachis sucrose concentration (RSC) in different winter wheat genotypes under different levels of irrigation. Lines represent values fitted using the "loess" method and points denote observations. DAA, days after anthesis; H, high-water treatment; L, low-water treatment; XM26, Xinmai-26; XM49, Xinmai-49; ZM18, Zhoumai-18.

adequate supply of water. Similarly, Santis et al. (2021) found that drought stress could lead to poor grain sets and yields, and Li et al. (2021) recorded low yields in plants subjected to low-level irrigation. However, it has previously been reported that a slight or moderate water deficit prior to the stem elongation stage and slight water deficit during the grain-filling stage did not significantly reduce grain yield, which lead to a significant water conservation (Meng et al., 2016). Slight and moderate water deficits can be defined as 60% to 65% and 50% to 55% of FC, respectively. Results obtained in previous studies by Yan et al. (2019; 2020) revealed that a mild water deficit can cause a slight, although non-significant, reduction (2.58%) in the yield of winter wheat, which is consistent with our findings in the present study. We established that low-water treatment non-significantly reduced the yield of wheat by less than 3%.

The number of grains per m^2 has been identified as the main determinant of grain yield in wheat (Beral et al., 2020). In the present study, we found that yield reductions were associated with declines in the NGB. Our findings tend to indicate that drought stress experienced during the jointing stage reduces the survival rates of tillers and harvestable spikes. Although drought stress during the booting stage inhibited spikelet development and reduced the number of spikelets, we established that the effects on the NIS were non-significant. These findings are consistent with those presented by Tatar et al. (2020), who observed drought-induced reductions in spike and spikelet numbers during the stem elongation stage. The lower NGS in wheat exposed to the low-water treatment can be assumed to reflect insufficient spikelet development. However, an increase in TGW under low-water conditions was found to have a compensatory effect on grain yield, thereby reducing yield loss.

This increase in TGW in response to low-water treatment provides an evidence of compensatory effects among the yield components and, more importantly, an increase in dry matter remobilization efficiency. In this regard, the findings of some studies (Beral et al., 2020; Sanchez-Bragado et al., 2020) have indicated that the TGW is negatively correlated with grain number. Wu et al. (2020) also found that irrigation at the jointing stage increased spike number, kernels per spike, and grain yield, but reduced grain weight. Consistently, we detected a significant negative relationship between TGW and the NGB ($r = -0.58$, $p < 0.05$) in the present study. A slight water deficit applied at the jointing stage can inhibit the growth of ineffective tillers and improve the harvest index. It has been widely reported that dry matter remobilization efficiency and the harvest index can been enhanced by drought stress (Tatar et al., 2020; Moradi et al., 2022). One benefit of soil drying at the later grain-filling stage is enhancing plant senescence, and thereby promoting a more rapid and efficient remobilization of pre-stored carbon from vegetative tissues to developing grains (Yang et al., 2000). In the present study, we detected a significant increase of harvest index from 41.6% to 44.0% in response to low-water treatment, although there was a 7.98% reduction in BM.

The variation in TGW was confirmed by the fitted value of the re-parameterized Richards growth model. Richards and Logistic sigmoidal curves are commonly utilized to model organism and kernel growth (Raobert et al., 1999; Zahedi and Jenner, 2003; Yang et al., 2004; Tjørve and Tjørve, 2010; C. E. Timothy Paine et al., 2012; Wu et al., 2018). The Richards equation is a generalized form of the logistic function that has considerable flexibility when analyzing responses under stress conditions (Richards, 1959; Tjørve and Tjørve, 2010). With the inclusion of the tm95 and Rm of grain filling, the re-parameterized Richards growth model is more convenient when used to fit the grain filling process. In previous studies, it has been revealed that "controlled soil drying" at the later stage of grain filling can significantly increase the rate of grain filling and grain weight (Yang and Zhang, 2005). Although severe post-anthesis water deficit can reduce the duration and rate of dry mass accumulation and grain weight (Triboï et al., 2003; Ercoli et al., 2008; Yang et al., 2016), grain filling can be significantly promoted by a moderate post-anthesis water deficit (Zhang et al., 2012; Yang et al., 2016). In the present study, we found that Rm increased significantly in response to low-water treatment in all three wheat genotypes, which may be a good evidence in support of the opinion that Rm is responsible for increases in grain weight.

The rate of grain filling appears to reflect the rate of biochemical reactions involved in the synthesis of starch deposited in the grains (Jenner et al., 1991). In this regard, our examination of sucrose concentrations in wheat subjected to high- and low-water treatments tended to indicate that lower soil moisture promotes the accumulation of starch in grains. The concentration of sucrose in leaves reflects the progress of photosynthesis and the rachis has been identified as providing a temporary store of carbohydrates assimilated *via* leaf photosynthesis. On the commencement of grain filling, the leaves begin to senesce and sucrose stored in leaves and rachis is transferred to the grain. Consequently, gradual reductions in the concentrations of leaf and rachis sucrose are detected concomitant with the progression of grain filling. In the present study, we found that during the early stage of grain filling, the concentrations of sucrose in the leaves of wheat subjected to the low-water treatment were higher than those in the leaves of wheat receiving a higher level of irrigation, although the rate of decline was higher during the late stage of grain filling. During leaf senescence, carbohydrates deposited in the leaves are transferred to the grain, and the more rapid the reduction in sucrose concentration, the faster is the transfer of carbohydrate. Compared to wheat plants under high-water treatment, the rapid decline in rachis sucrose concentration was detected at an earlier stage of grain development in wheat subjected to low-water treatment. It has been previously reported that drought stress increases the remobilization of carbon reserves from vegetative tissues to grains (Farooq et al., 2017), but the duration of grain filling decreases with an increase in water

deficit. The grain-filling rate has been found to increase in response to a mild water deficit (Yan et al., 2019). The aforementioned observations thus indicate that a higher rate of photosynthesis during the early stage of grain filling and a higher rate of carbohydrate transfer from vegetative organs to grains during the later stage are the main factors associated with an increase in grain filling rate and grain weight in wheat subjected to low-level irrigation.

4.2 Effects of drought stress on the end-use functional properties of wheat

During the growth period, drought stress affects the concentration of grain proteins, and variations in the concentration of these proteins is typically dependent on the intensity of the stress experienced (Ozturk et al., 2021). However, the relationship between stress intensity and protein concentration is non-linear, with drought stress experienced during the growth period generally promoting an increase in GPC (Barutçular et al., 2016; Rakszegi et al., 2019; Tatar et al., 2020; Kamara et al., 2022). Moreover, there is a negative association between GPC and total irrigation amount (Moradi et al., 2022). Wu et al. (2020) also found that the concentration of grain protein was significantly increased by a water deficit during the grain-filling stage. However, the effects of drought at the grain-filling stage were found to differ according to stress intensity, with a slight water deficit significantly reducing GPC, whereas severe water deficit has been found to increase the concentration of grain proteins during the grain-filling stage (Meng et al., 2016). Furthermore, the findings of some studies have indicated that the concentration of grain proteins initially increases and subsequently declines in response to an increase in drought stress degree (Silva et al., 2020; Yan et al., 2020). In the present study, we detected reductions in protein concentrations in the grains of wheat subjected to the low-water treatment, which is consistent with the findings of Meng et al. (2016), but contrasts with observations of Silva et al. (2020); Tatar et al. (2020), and Yan et al. (2020). We suspect that these discrepant findings could reflect differences in the respective intensities of the applied stresses.

The GI, an indicator of gluten strength, is predominantly determined by genotype (Vida et al., 2014; Sekularac et al., 2018; Kun et al., 2020), although can also be significantly influenced by irrigation, precipitation, and soil moisture content (Gil et al., 2011; Oikonomou et al., 2015). Generally, drought stress is associated with an increase in the GI. For example, Ames et al. (2003) have found that the GI appeared to be slightly but significantly higher under dry conditions than under irrigated conditions for all genotypes used in their study. Moreover, Flagella et al. (2010) established that drought stress occurred in the late grain-filling stage increases gluten strength, and Li et al. (2013) also found that gluten strength is higher under drought stress conditions. Consistently, the findings of some studies have revealed that gluten strength is higher in severe drought environments compared with full irrigation (Hernandez-Espinosa et al., 2018). In the present study, we recorded an increase in the GI of wheat subjected to the low-water treatment, which contrasts with the findings of Yang et al. (2018), who revealed that the GI was not significantly affected by drought stress, although the highest GI value was recorded in plants subjected to mild drought stress. This discrepancy could be attributed to differences in the intensities of the drought stress applied and/or the genotypes of wheat examined in previous studies. Whereas a negative correlation between GPC and the GI has been detected in some previous studies (Ames et al., 2003; Yang et al., 2018), Kun et al. (2020) observed a slightly positive, albeit statistically non-significant, relationship between GPC and the GI. In the present study, however, we found GI values to be significantly positively correlated with GPCs. We suspect that the differences in the finding of these studies could be associated with differences in the genotypes of wheat assessed. The three genotypes examined in the present study were selected according to dough strength, and the sample space was insufficiently large. In contrast, previous studies have typically examined a more extensive range of genotypes, for which protein concentrations varied considerably.

Dough elasticity exhibited as a rubber can be significantly increased by light or moderate drought stress. In previous studies, the MPT (Li et al., 2013; Hernandez-Espinosa et al., 2018; Yang et al., 2018), MPV (Labuschagne and Moloi, 2015; Yang et al., 2018) and midline peak integral (Labuschagne and Moloi, 2015; Hernandez-Espinosa et al., 2018) have been shown to increase in response drought stress. MRS (negative value), which is negatively correlated with midline peak integral, is used as an indicator of the degree of dough softening. Our findings with respect to dough elasticity are generally in accordance with those reported previously, although we detected a slight, albeit non-significant, increase in MPT, which can be attributed to differences in the degree of applied stress. In general, strong gluten dough is associated with a high MPT and low absolute values of MRS (Mao et al., 2013), and in the present study, we found that the MPT and MRS (negative values) also exhibited significant positive relationships with GPC.

4.3 Possible causes for the higher grain quality under low-water treatment

GN is a reliable indicator of dough elasticity and can be used to determine the proportional composition of grain proteins (Martre et al., 2003; Ferrise et al., 2015; Mefleh et al., 2020; Snowdon et al., 2021). Consequently, changing GN will inevitably modify the proportional composition of grain proteins, which is determined by the "allometric scaling" relationships among the protein compositions. The ratio of the

grain protein composition (i.e., gliadin to glutenin) determines the balance between dough viscosity and elasticity. In the current study, we found that MPV was positively correlated with GN ($r = 0.842$, $p < 0.001$), although showed a non-significant correlation with GPC ($r = 0.165$, $p = 0.514$). Moreover, we detected no evident correlation between GN and GPC levels, which is conceivably attributable to a synchronous increase in GN and TGW, and the change in the ratio of these two parameters became smaller. When comparing only the means of the water treatments, we established that the low-water treatment promoted simultaneous increases in GN, GI, MPV, and MRS (negative values). Accordingly, it can be speculated that drought stress enhances gluten strength and dough elasticity *via* its effect on increasing GN. In this context, studies on the molecular weight distribution of grain proteins are required to confirm the relationship between GN and protein polymerization. Some studies have shown that grain N accumulation is source-regulated (Martre et al., 2003; Zhao et al., 2021), and GN has been observed to increase significantly in response to a reduction in grain number per m^2. The results obtained in the present study revealed that GN is negatively correlated with NGB, which is consistent with the findings of previous studies.

An increase in the amount of GN is assumed to be associated with an increase in grain Rn promoted by low-water treatment. In turn, an increase in Rn indicates that the nitrogen supplied to the grains is sufficient. The findings of previous studies have revealed that mild water deficits promote N availability and uptake (Széles et al., 2012; Yan et al., 2020), whereas irrigation at the anthesis and grain-filling stages has been found to cause reductions in the N harvest index (Moradi et al., 2022). GN is primarily determined by the N stored in the leaves at anthesis (Zheng et al., 2020), and during the grain-filling stage, proteins deposited in the leaves are broken down into free amino acids that are remobilized to the grain *via* rachis (Zhao et al., 2015; Hecke et al., 2020). In response to water deficit, the leaves of wheat plants at the late grain-filling stage undergo premature senescence, with concomitant rapid reductions in the concentration of leaf and rachis N. The process of leaf senescence, reductions in the sucrose and N concentration in leaves, and increases in GNC occur synchronously, and Gomez-Sanchez et al. (2019) have established that a delay in leaf senescence in barley resulted in lower amounts of seed N due to a reduction in leaf N remobilization. In the present study, we found that the low-water treatment triggered an earlier rapid transfer of N deposited in vegetative organs. At the late grain-filling stage, we observed that the decline in the N content of leaves in response to low-water treatment occurred at an earlier time point than the reduction in sucrose content. Given that GNC (Figure 7) is affected by the amount of grain starch, it tends to be characterized by considerable fluctuations, and accordingly, would be unsuitable as a predictor of grain quality.

4.4 Effects of drought stress on grain yield and quality are also genotype-dependent

Genetic variations in the responsiveness of wheat genotypes to drought stress have previously been reported (Farooq et al., 2014; Yang et al., 2016; Moradi et al., 2022), and it has been established that drought-resistant genotypes can maintain appropriate functionality in a severely dehydrated state by producing a well-developed root system, initiating osmotic adjustment, and remobilizing water-soluble stem carbohydrates. In this regard, it has been proven that the effects of drought stress on TGW vary according to genotype (Yang et al., 2016; Silva et al., 2020; Rezzouk et al., 2022), and Silva et al. (2020) have similarly established that the effects of water deficit on protein content in grains are genotype dependent. In the present study, we found that the wheat genotype ZM18 was characterized by the smallest reduction in duration (tm95), and the most pronounced increase in grain weight (Km), which thereby indicates that ZM18 has a higher adaptability to drought stress than the other two assessed wheat genotypes. However, we also established that ZM18 was characterized by the smallest increase in Kn (GN fitted value) and Rn, thus indicating that it would be difficult to improve grain N accumulation in this genotype. Strong gluten genotypes are characterized large increases in Kn and Rn in response to water deficit, which indicates that grain N accumulation could be readily enhanced in these genotypes. These findings thus confirmed that the effects of drought stress on grain yield and quality are genotype dependent, and accordingly, further studies are required that seek to identify the effects of drought-by-genotype interactions on grain yield and quality in wheat using a more extensive selection of genotypes.

4.5 Relationships between grain yield, quality, and WUE

In this study, we detected no significant relationship between wheat yield and ET. However, we observed a significant enhancement of WUE in response to low-water treatment, which is consistent with the findings of Mu et al. (2021b). The findings of some previous studies have revealed that yield and grain weight are negatively correlated with GPCs (Souza et al., 2004; Nehe et al., 2020; Ali and Akmal, 2022). Although in the present study, we also detected negative correlations between yield and grain weight and GPC, the associations were comparatively slight and non-significant, which is consistent with the findings of Li et al. (2013). In contrast, however, Yan et al. (2020) have previously reported a positive relationship between grain yield and GNC. These discrepancies in the findings of different studies are assumed to be attributable to differences in the intensities of the

applied stress and assessed genotypes. Furthermore, given that the correlation coefficients obtained for the associations between wheat yield and the parameters GI, MPT, and MRS were not statistically significant, it is conceivable that the negative relationship between yield and grain quality could be altered, and that by optimizing water management and variety selection, we can achieve high yield, high quality, and water-saving wheat production targets.

Our findings in this study indicate that the end-use functional properties of wheat are influenced by water management, and that RDI may be used to enhance wheat quality and WUE without incurring yield loss. A moderate water deficit (60% to 65% FC) applied prior to the jointing stage and at the late grain-filling stage, combined with a slight water deficit (65% to 70% FC) from jointing to booting was found to increase grain quality and WUE. The non-significant reduction of less than 3% in the yield of wheat subjected to RDI can be attributed to a higher photosynthetic rate during the early stage of grain filling and a higher rate of carbohydrate transfer from vegetative organs to grains during the later stage under low-water treatment. We speculate that RDI might contribute to enhancing grain quality *via* an increase in GN, whereby RDI triggers an earlier rapid transfer of N deposited in vegetative organs, resulting in a synchronous reduction in the N concentration in leaves and an increase in GNC. Furthermore, our observations of a positive correlation between MPV and GN, indicate that by increasing GN, it would be possible to enhance dough elasticity. Given that the effects of RDI on grain quality were genotype dependent, further studies on the interactive effects of genotypes and water management are required.

Data availability statement

The raw data supporting the conclusions of this article will be made available by the authors, without undue reservation.

Author contributions

DA and SK conceived and designed the experiments. SK conducted field experiments. SK and XL (physiological parameters) conducted laboratory analyses and wrote the manuscript. WM and LH analyzed the data and revised manuscript. All authors contributed to the article and approved the submitted version.

Funding

This study was financed by the Ministry of education of the PRC (grant number ZH2021040101), the Ministry of Science and Technology of PRC (grant number 2018YFD0300703) and China Agriculture Research System project (grant number CARS-3).

Conflict of interest

The authors declare that the research was conducted in the absence of any commercial or financial relationships that could be construed as a potential conflict of interest.

Publisher's note

All claims expressed in this article are solely those of the authors and do not necessarily represent those of their affiliated organizations, or those of the publisher, the editors and the reviewers. Any product that may be evaluated in this article, or claim that may be made by its manufacturer, is not guaranteed or endorsed by the publisher.

References

Aggrey, S. E. (2009). Logistic nonlinear mixed effects model for estimating growth parameters. *Poultry Sci.* 88, 276–280. doi: 10.3382/ps.2008-00317

Ali, N., and Akmal, M. (2022). Wheat growth, yield, and quality under water deficit and reduced nitrogen supply. a review. *Gesunde Pflanzen.* 2022, 1–13. doi: 10.1007/s10343-021-00615-w

Ames, N. P., Clarke, J. M., Marchylo, B. A., Dexter, J. E., Schlichting, L. M., and Woods, S. M. (2003). The effect of extra-strong gluten on quality parameters in durum wheat. *Can. J. Plant Sci.* 83, 525–532. doi: 10.4141/P02-072

Barutçular, C., Yıldırım, M., Koc, M., Dizlek, H., Akinci, C., El Sabagh, A., et al. (2016). Quality traits performance of bread wheat genotypes under drought and heat stress conditions. *Fresenius Environ. Bulletin.* 25, 6159–6165.

Beral, A., Rincent, R., Gouis, J., Girousse, C., and Allard, V. (2020). Wheat individual grain-size variance originates from crop development and from specific genetic determinism. *PloS One* 15, e0230689. doi: 10.1371/journal.pone.0230689

Chung, O. K., Ohm, J. B., Caley, M. S., and Seabourn, B. W. (2001). Prediction of baking characteristics of hard winter wheat flours using computer-analyzed mixograph parameters. *Cereal Chem.* 78, 493–497. doi: 10.1094/CCHEM.2001.78.4.493

Dong, S., and Beckles, D. (2019). Dynamic changes in the starch-sugar interconversion within plant source and sink tissues promote a better abiotic stress response. *J. Plant Physiol.* 234-235, 80–93. doi: 10.1016/j.jplph.2019.01.007

Dowell, F., Maghirang, E., Pierce, R., Lookhart, G., Bean, S., Xie, F., et al. (2008). Relationship of bread quality to kernel, flour, and dough properties. *Cereal Chem.* 85, 82–91. doi: 10.1094/CCHEM-85-1-0082

Ercoli, L., Lulli, L., Mariotti, M., Masoni, A., and Arduini, I. (2008). Post-anthesis dry matter and nitrogen dynamics in durum wheat as affected by nitrogen supply and soil water availability. *Eur. J. Agron.* 28, 138–147. doi: 10.1016/j.eja.2007.06.002

Evers, A. D., O'Brien, L., and Blakeney, A. B. (1999). Cereal structure and composition. *Aust. J. Agric. Res.* 50, 629–650. doi: 10.1071/AR98158

FAO (2020) *E. coli.* Available at: http://www.fao.org/faostat/zh/#rankings/commodities_by_country (Accessed August 29, 2022).

Farooq, M., Gogoi, N., Barthakur, S., Baroowa, B., Bharadwaj, N., Alghamdi, S. S., et al. (2017). Drought stress in grain legumes during reproduction and grain filling. *J. Agron. Crop Sci.* 203, 81–102. doi: 10.1111/jac.12169

Farooq, M., Hussain, M., and Siddique, K. H. M. (2014). Drought stress in wheat during flowering and grain-filling periods. *Crit. Rev. Plant Sci.* 33, 331–349. doi: 10.1080/07352689.2014.875291

Ferrise, R., Bindi, M., and Martre, P. (2015). Grain filling duration and glutenin polymerization under variable nitrogen supply and environmental conditions for durum wheat. *Field Crops Res.* 171, 23–31. doi: 10.1016/j.fcr.2014.10.016

Flagella, Z., Giuliani, M. M., Giuzio, L., Volpi, C., and Masci, S. (2010). Influence of water deficit on durum wheat storage protein composition and technological quality. *Eur. J. Agron.* 33, 197–207. doi: 10.1016/j.eja.2010.05.006

Gil, D. H., Bonfil, D. J., and Svoray, T. (2011). Multi scale analysis of the factors influencing wheat quality as determined by gluten index. *Field Crops Res.* 123, 1–9. doi: 10.1016/j.fcr.2011.04.001

Giuliani, M. M., Palermo, C., De Santis, M. A., Mentana, A., Pompa, M., Giuzio, L., et al. (2015). Differential expression of durum wheat gluten proteome under water stress during grain filling. *J. Agric. Food Chem.* 63, 6501. doi: 10.1021/acs.jafc.5b01635

Gomez-Sanchez, A., Gonzalez-Melendi, P., Santamaria, M. E., Arbona, V., Lopez-Gonzalvez, A., Garcia, A., et al. (2019). Repression of drought-induced cysteine-protease genes alters barley leaf structure and responses to abiotic and biotic stresses. *J. Exp. Bot.* 70, 2143–2155. doi: 10.1093/jxb/ery410

Graziano, S., Marando, S., Prandi, B., Boukid, F., Marmiroli, N., Francia, E., et al. (2019). Technological quality and nutritional value of two durum wheat varieties depend on both genetic and environmental factors. *J. Agric. Food Chem.* 67, 2384–2395. doi: 10.1021/acs.jafc.8b06621

Hecke, J., Cour, R., Jørgensen, H., and Schjoerring, J. (2020). Residual nitrogen pools in mature winter wheat straw as affected by nitrogen application. *Plant Soil.* 453, 561–575. doi: 10.1007/s11104-020-04600-6

Hernandez-Espinosa, N., Mondal, S., Autrique, E., Gonzalez-Santoyo, H., Crossa, J., Huerta-Espino, J., et al. (2018). Milling, processing and end-use quality traits of CIMMYT spring bread wheat germplasm under drought and heat stress. *Field Crops Res.* 215, 104–112. doi: 10.1016/j.fcr.2017.10.003

Hou, G. G., Saini, R., and Ng, P. K. W. (2013). Relationship between physicochemical properties of wheat flour, wheat protein composition, and textural properties of cooked Chinese white salted noodles. *Cereal Chem.* 90, 419–429. doi: 10.1094/CCHEM-10-12-0137-R

Hu, X., Cheng, L., Yan, H., Li, Z., Li, C., and Gu, Z. (2021). An extensive review: How starch and gluten impact dough machinability and resultant bread qualities. *Crit. Rev. Food Sci. Nutr.* 2021, 1–12. doi: 10.1080/10408398.2021.1969535

Jenner, C., Ugalde, T., and Aspinall, D. (1991). The physiology of starch and protein deposition in the endosperm of wheat. *Funct. Plant Biol.* 18, 211–226. doi: 10.1071/PP9910211

Kamara, M. M., Rehan, M., Mohamed, A., Mantawy, R., Kheir, A., Abd El-Moneim, D., et al. (2022). Genetic potential and inheritance patterns of physiological, agronomic and quality traits in bread wheat under normal and water deficit conditions. *Plants* 11, 952. doi: 10.3390/plants11070952

Kang, S., Hao, X., Du, T., Tong, L., Su, X., Lu, H., et al. (2017). Improving agricultural water productivity to ensure food security in China under changing environment: From research to practice. *Agric. Water Manag.* 179, 5–17. doi: 10.1016/j.agwat.2016.05.007

Kong, L., Xie, Y., Hu, L., Feng, B., and Li, S. (2016). Remobilization of vegetative nitrogen to developing grain in wheat (Triticum aestivum l.). *Field Crops Res.* 196, 134–144. doi: 10.1016/j.fcr.2016.06.015

Kun, S., Lijuan, Y., Xiaohang, L., Yang, G., Zhikai, J., and Duan, A. (2020). Grain quality variations from year to year among the Chinese genotypes. *Cereal Res. Commun.* 48, 499–505. doi: 10.1007/s42976-020-00060-x

Labuschagne, M. T., and Moloi, M. J. (2015). The influence of abiotic stress conditions on dough mixing characteristics of two hard red spring wheat cultivars. *J. Cereal Sci.* 63, 134–139. doi: 10.1016/j.jcs.2015.03.007

Li, Y., Wu, Y., Hernandez-Espinosa, N., and Peña, R. J. (2013). The influence of drought and heat stress on the expression of end-use quality parameters of common wheat. *J. Cereal Sci.* 57, 73–78. doi: 10.1016/j.jcs.2012.09.014

Li, W., Zhou, X., Yu, K., Zhang, Z., Liu, Y., Hu, N., et al. (2021). Spectroscopic estimation of n concentration in wheat organs for assessing n remobilization under different irrigation regimes. *Front. Plant Sci.* 12. doi: 10.3389/fpls.2021.657578

Ma, Y.-Z., MacKown, C., and Sanford, D. (1996). Kernel growth of *in vitro* cultured wheat spikes of cultivars with divergent source-sink limitations. *Plant Sci.* 119, 135–148. doi: 10.1016/0168-9452(96)04456-1

Mao, X., Li, Y., Zhao, S., Zhang, J., Lei, Q., Meng, D., et al. (2013). The interactive effects of transgenically overexpressed 1Ax1 with various HMW-GS combinations on dough quality by introgression of exogenous subunits into an elite Chinese wheat variety. *PloS One* 8, e78451. doi: 10.1371/journal.pone.0078451

Martre, P., Porter, J. R., Jamieson, P. D., and Triboï, E. (2003). Modeling grain nitrogen accumulation and protein composition to understand the Sink/Source regulations of nitrogen remobilization for wheat. *Plant Physiol.* 133, 1959–1967. doi: 10.1104/pp.103.030585

Mefleh, M., Motzo, R., Samson, M.-F., Morel, M.-H., and Giunta, F. (2020). N partitioning between gluten fractions in a set of Italian durum wheat cultivars: Role of the grain n content. *Food* 9, 1684. doi: 10.3390/foods9111684

Meng, Z. J., Duan, A. W., Dassanayake, K. B., Chen, D. L., Gao, Y., Wang, X. S., et al. (2016). Effects of regulated deficit irrigation on grain yield and quality traits in winter wheat. *Trans. ASABE.* 59, 897–907. doi: 10.13031/trans.59.11400

Moradi, L., Siosemardeh, A., Sohrabi, Y., Bahramnejad, B., and Hosseinpanahi, F. (2022). Dry matter remobilization and associated traits, grain yield stability, n utilization, and grain protein concentration in wheat cultivars under supplemental irrigation. *Agric. Water Manag.* 263, 107449. doi: 10.1016/j.agwat.2021.107449

Moral, L. F. G., Del, Yahia, R., Martos, V., and Royo., C. (2007). Environmentally induced changes in amino acid composition in the grain of durum wheat grown under different water and temperature regimes in a Mediterranean environment. *J. Agric. Food Chem.* 55, 8144–8151. doi: 10.1021/jf063094q

Mu, Q., Cai, H., Sun, S., Wen, S., Jiatun, X., Dong, M., et al. (2021a). The physiological response of winter wheat under short-term drought conditions and the sensitivity of different indices to soil water changes. *Agric. Water Manag.* 243, 106475. doi: 10.1016/j.agwat.2020.106475

Mu, Q., Dong, M., Jiatun, X., Cao, Y., Ding, Y., Sun, S., et al (2021b). Photosynthesis of winter wheat effectively reflected multiple physiological responses under short-term drought-rewatering conditions. *J. Sci. Food Agric.* 102:2472–2483. doi: 10.1002/jsfa.11587

Neacşu, A., Stanciu, G., and Săulescu, N. (2009). Most suitable mixing parameters for use in breeding breadwheat for processing quality. *Cereal Res. Commun.* 37, 83–92. doi: 10.1556/CRC.37.2009.1.10

Nehe, A., Misra, S., Murchie, E. H., Chinnathambi, K., Tyagi, B., and Foulkes, M. (2020). Nitrogen partitioning and remobilization in relation to leaf senescence, grain yield and protein concentration in Indian wheat cultivars. *Field Crops Res.* 251, 107778. doi: 10.1016/j.fcr.2020.107778

Noda, T., Tohnooka, T., Taya, S., and Suda, I. (2001). Relationship between physicochemical properties of starches and white salted noodle quality in Japanese wheat flours. *Cereal Chem.* 78, 395–399. doi: 10.1094/CCHEM.2001.78.4.395

Ohm, J. B., Ross, A. S., Peterson, C. J., and Ong, Y. L. (2008). Relationships of high molecular weight glutenin subunit composition and molecular weight distribution of wheat flour protein with water absorption and color characteristics of noodle dough. *Cereal Chem.* 85, 123–131. doi: 10.1094/CCHEM-85-2-0123

Oikonomou, N. A., Bakalis, S., Rahman, M. S., and Krokida, M. K. (2015). Gluten index for wheat products: Main variables in affecting the value and nonlinear regression model. *Int. J. Food Properties.* 18, 1–11. doi: 10.1080/10942912.2013.772198

Ozturk, A., Aydin, M., and Karaoğlu, M. (2021). The effects of drought after anthesis on the grain quality of bread wheat depend on drought severity and drought resistance of the variety. *Cereal Res. Commun.* 50, 105–116. doi: 10.1007/s42976-021-00155-z

Peterson, C. J., and Graybosch, R. A. (1992). Genotype and environment effects on quality characteristics of hard red winter wheat. *Crop Sci.* 32, 98–103. doi: 10.2135/cropsci1992.0011183X003200010022x

Pinheiro, J. C., and Bates, D. M. (2000). *Mixed-effects models in s and s-plus* (New York: Springer-Verlag).

Plessis, A., Ravel, C., Bordes, J., Balfourier, F., and Martre, P. (2013). Association study of wheat grain protein composition reveals that gliadin and glutenin composition are trans-regulated by different chromosome regions. *J. Exp. Bot.* 64, 3627–3644. doi: 10.1093/jxb/ert188

Rakszegi, M., Darkó, É., Lovegrove, A., Istvan, M., Láng, L., Bedő, Z., et al. (2019). Drought stress affects the protein and dietary fiber content of wholemeal wheat flour in wheat/Aegilops addition lines. *PloS One* 14, e0211892. doi: 10.1371/journal.pone.0211892

Raobert, N., Huet, S., Hennequet, C., and Bouvier, A. (1999). Methodology for choosing a model for wheat kernel growth. *Agronomie* 19, 405–417. doi: 10.1051/agro:19990507

Razali, W. W., Razak, T. A., Azani, A. M., and Kamziah, A. (2015). Mixed-effects models for predicting early height growth of forest trees planted in Sarawak, Malaysia. *J. Trop. For. Sci.* 27, 267–276.

Rezzouk, F., Gracia Romero, A., Kefauver, S., Nieto-Taladriz, M., Serret, M., and Araus, J. (2022). Durum wheat ideotypes in Mediterranean environments differing in water and temperature conditions. *Agric. Water Manag.* 259, 107257. doi: 10.1016/j.agwat.2021.107257

Richards, F. J. (1959). A flexible growth function for empirical use. *J. Exp. Bot.* 10, 290–300. doi: 10.1093/jxb/10.2.290

Sanchez-Bragado, R., Kim, J. W., Rivera-Amado, A., Molero, G., Araus, J., Savin, R., et al. (2020). Are awns truly relevant for wheat yields? a study of performance of awned/awnless isogenic lines and their response to source–sink manipulations. *Field Crops Res.* 254, 107827. doi: 10.1016/j.fcr.2020.107827

Santis, M., Soccio, M., Laus, M., and Flagella, Z. (2021). Influence of drought and salt stress on durum wheat grain quality and composition: A review. *Plants* 10, 2599. doi: 10.3390/plants10122599

Sekularac, A., Torbica, A., Zivancev, D., Tomić, J., and Knezevic, D. (2018). The influence of wheat genotype and environmental factors on gluten index and the possibility of its use as bread quality predictor. *Genetika* 50, 85–93. doi: 10.2298/GENSR1801085S

Silva, A., Ramos, M. L. G., Júnior, W. Q. R., Alencar, E., Silva, P., Lima, C., et al. (2020). Water stress alters physical and chemical quality in grains of common bean, triticale and wheat. *Agric. Water Manag.* 231, 1–10. doi: 10.1016/j.agwat.2020.106023

Snowdon, R. J., Wittkop, B., Chen, T.-W., and Stahl, A. (2021). Crop adaptation to climate change as a consequence of long-term breeding. *Theor. Appl. Genet.* 134, 1613–1623. doi: 10.1007/s00122-020-03729-3

Souza, E. J., Martin, J. M., Guttieri, M. J., O'Brien, K. M., Habernicht, D. K., Lanning, S. P., et al. (2004). Influence of genotype, environment, and nitrogen management on spring wheat quality. *Crop Sci.* 44, 425–432. doi: 10.2135/cropsci2004.0425

Széles, A., Megyes, A., and Nagy, J. (2012). Irrigation and nitrogen effects on the leaf chlorophyll content and grain yield of maize in different crop years. *Agric. Water Manag.* 107, 133–144. doi: 10.1016/j.agwat.2012.02.001

Tatar, O., Çakaloğulları, U., Aykut Tonk, F., Istipliler, D., and Karakoç, R. (2020). Effect of drought stress on yield and quality traits of common wheat dring grain filling stage. *Turkish J. Field Crops.* 25, 236–244. doi: 10.17557/tjfc.834392

Timothy Paine, C. E., Marthews, T. R., Vogt, D. R., Purves, D., Rees, M., Hector, A., et al. (2012). How to fit nonlinear plant growth models and calculate growth rates: an update for ecologists. *Methods Ecol. Evol.* 2012, 245–256. doi: 10.1111/j.2041-210X.2011.00155.x

Tjørve, E., and Tjørve, K. M. C. (2010). A unified approach to the richards-model family for use in growth analyses: Why we need only two model forms. *J. Theor. Biol.* 267, 417–425. doi: 10.1016/j.jtbi.2010.09.008

Triboï, E., Martre, P., and Triboïblondel, A. M. (2003). Environmentally-induced changes in protein composition in developing grains of wheat are related to changes in total protein content. *J. Exp. Bot.* 54, 1731–1742. doi: 10.1093/jxb/erg183

Vida, G., Szunics, L., Veisz, O., Bedő, Z., Láng, L., Árendás, T., et al. (2014). Effect of genotypic, meteorological and agronomic factors on the gluten index of winter durum wheat. *Euphytica* 197, 61–71. doi: 10.1007/s10681-013-1052-6

Wikstrom, K., and Bohlin, L. (1996). Multivariate analysis as a tool to predict bread volume from mixogram parameters. *Cereal Chem.* 73, 686–690.

Wu, B., Shang, Y., Wang, S., Hu, X., Zhang, R., Zhang, B., et al. (2020). Response of nitrogen redistribution to irrigation at jointing in winter wheat. *Agron. J.* 113, 381–396. doi: 10.1002/agj2.20458

Wu, X., Tang, Y., Li, C., and Wu, C. (2018). Characterization of the rate and duration of grain filling in wheat in southwestern china. *Plant Production Sci.* 21, 1–12. doi: 10.1080/1343943X.2018.1518722

Yang, L., Liang, H., Lv, X., Liu, D., Wen, X., and Liao, Y. (2016). Effect of polyamines on the grain filling of wheat under drought stress. *Plant Physiol. Biochem.* 100, 113–129. doi: 10.1016/j.plaphy.2016.01.003

Yang, R., Liang, X., Torrion, J., Walsh, O., O'Brien, K., and Liu, Q. (2018). The influence of water and nitrogen availability on the expression of end-use quality parameters of spring wheat. *Agronomy* 8, 257. doi: 10.3390/agronomy8110257

Yang, J., and Zhang, J. (2006). Grain filling of cereals under soil drying. *New Phytol.* 169, 38–38. doi: 10.1111/j.1469-8137.2005.01597.x

Yang, J. C., Zhang, J. H., Huang, Z. L., Zhu, Q. S., and Wang, L. (2000). Remobilization of carbon reserves is improved by controlled soil-drying during grain filling of wheat. *Crop Sci.* 40, 1645–1655. doi: 10.2135/cropsci2000.4061645x

Yang, J., Zhang, J., Wang, Z., Xu, G., and Zhu, Q. (2004). Activities of key enzymes in sucrose-to-starch conversion in wheat grains subjected to water deficit during grain filling. *Plant Physiol.* 135, 1621–1629. doi: 10.1104/pp.104.041038

Yan, S., Wu, Y., Fan, J., Zhang, F., Qiang, S., Zheng, J., et al. (2019). Effects of water and fertilizer management on grain filling characteristics, grain weight and productivity of drip-fertigated winter wheat. *Agric. Water Manag.* 213, 983–995. doi: 10.1016/j.agwat.2018.12.019

Yan, S., Wu, Y., Fan, J., Zhang, F., Zheng, J., Qiang, S., et al. (2020). Dynamic change and accumulation of grain macronutrient (N, p and K) concentrations in winter wheat under different drip fertigation regimes. *Field Crops Res.* 250, 107767. doi: 10.1016/j.fcr.2020.107767

Zahedi, M., and Jenner, C. F. (2003). Analysis of effects in wheat of high temperature on grain filling attributes estimated from mathematical models of grain filling. *J. Agric. Sci.* 14, 203–212. doi: 10.1017/S0021859603003411

Zaveri, E., and Lobell, D. (2019). The role of irrigation in changing wheat yields and heat sensitivity in India. *Nat. Commun.* 10, 1–7. doi: 10.1038/s41467-019-12183-9

Zhang, Y., Du, W., Zhang, Y., Wang, Z., Li, H., Xia, H., et al. (2021). Metabolic analysis reveals temporal changes in C/N metabolites and senescence of flag leaf in wheat during grain filling. *Acta Physiologiae Plantarum.* 43, 104. doi: 10.1007/s11738-021-03272-8

Zhang, H., Li, H., Yuan, L., Wang, Z., Yang, J., and Zhang, J. (2012). Post-anthesis alternate wetting and moderate soil drying enhances activities of key enzymes in sucrose-to-starch conversion in inferior spikelets of rice. *J. Exp. Bot.* 63, 215–227. doi: 10.1093/jxb/err263

Zhao, B., Ata-Ul-Karim, S., Lemaire, G., Duan, A., Liu, Z., Guo, Y., et al. (2021). Exploring the nitrogen source-sink ratio to quantify ear nitrogen accumulation in maize and wheat using critical nitrogen dilution curve. *Field Crops Res.* 274, 108332. doi: 10.1016/j.fcr.2021.108332

Zhao, Y., Xi, M., Zhang, X., Lin, Z., Ding, C.-Q., Tang, S., et al. (2015). Nitrogen effect on amino acid composition in leaf and grain of japonica rice during grain filling stage. *J. Cereal Sci.* 64, 29–33. doi: 10.1016/j.jcs.2015.03.011

Zheng, X., Yu, Z., Zhang, Y., and Shi, Y. (2020). Nitrogen supply modulates nitrogen remobilization and nitrogen use of wheat under supplemental irrigation in the north China plain. *Sci. Rep.* 10, 3305. doi: 10.1038/s41598-020-59877-5

frontiers | Frontiers in Plant Science

TYPE Original Research
PUBLISHED 15 November 2022
DOI 10.3389/fpls.2022.1051935

Check for updates

OPEN ACCESS

EDITED BY
Mirza Hasanuzzaman,
Sher-e-Bangla Agricultural University, Bangladesh

REVIEWED BY
Puja Khare,
Council of Scientific and Industrial Research (CSIR), India
Ewa Joanna Hanus-Fajerska,
University of Agriculture in Krakow, Poland

*CORRESPONDENCE
Jing Cui
cuijing530@163.com

SPECIALTY SECTION
This article was submitted to Plant Abiotic Stress, a section of the journal Frontiers in Plant Science

RECEIVED 23 September 2022
ACCEPTED 28 October 2022
PUBLISHED 15 November 2022

CITATION
Zhu Y, Lv X, Li T, Zhong M, Song J, Wang H and Cui J (2022) Cotton straw biochar and compound *Bacillus* biofertilizer reduce Cd stress on cotton root growth by regulating root exudates and antioxidant enzymes system.
Front. Plant Sci. 13:1051935.
doi: 10.3389/fpls.2022.1051935

COPYRIGHT
© 2022 Zhu, Lv, Li, Zhong, Song, Wang and Cui. This is an open-access article distributed under the terms of the Creative Commons Attribution License (CC BY). The use, distribution or reproduction in other forums is permitted, provided the original author(s) and the copyright owner(s) are credited and that the original publication in this journal is cited, in accordance with accepted academic practice. No use, distribution or reproduction is permitted which does not comply with these terms.

Cotton straw biochar and compound *Bacillus* biofertilizer reduce Cd stress on cotton root growth by regulating root exudates and antioxidant enzymes system

Yongqi Zhu, Xin Lv, Tiansheng Li, Mingtao Zhong, Jianghui Song, Haijiang Wang and Jing Cui*

College of Agriculture, Shihezi University, Shihezi, Xinjiang, China

Introduction: Cotton straw biochar (biochar) and compound *Bacillus* biofertilizer (biofertilizer) have attracted wide attentions in the remediation of heavy metal-contaminated soils in recent years. However, few studies have explored the metabolomics of lateral roots of Cd-stressed cotton to determine the mechanism of biochar and biofertilizer alleviating Cd stress.

Methods: In this pot experiment, biochar and biofertilizer were applied to the soils with different Cd contamination levels (1, 2, and 4 mg kg^{-1}). Then, the responses of cotton root morphology, vitality, Cd content, and antioxidant enzyme activities were analyzed, and the mechanism of biochar and biofertilizer alleviating Cd stress was determined by metabolomic analysis.

Results: The results showed that exogenous Cd addition decreased the SOD and POD activities in cotton taproot and lateral root. Besides, with the increase of soil Cd content, the maximum Cd content in taproot (0.0250 mg kg^{-1}) and lateral root (0.0288 mg kg^{-1}) increased by 89.11% and 33.95%, respectively compared with those in the control ($p< 0.05$). After the application of biochar and biofertilizer, the SOD and POD activities in cotton taproot and lateral root increased. The Cd content of cotton taproot in biochar and biofertilizer treatments decreased by 16.36% and 19.73%, respectively, and that of lateral root decreased by 13.99% and 16.68%, respectively. The metabolomic analysis results showed that the application of biochar and biofertilizer could improve the resistance of cotton root to Cd stress through regulating the pathways of ABC transporters and phenylalanine metabolism.

Discussion: Therefore, the application of biochar and biofertilizer could improve cotton resistance to Cd stress by increasing antioxidant enzyme activities, regulating root metabolites (phenols and amino acids), and reducing Cd content, thus promoting cotton root growth.

KEYWORDS

antioxidant enzyme activities, cadmium stress, metabolites, metabolomics, root exudates

Introduction

Heavy metals, especially Cd, can interfere with plant physiological processes by stimulating H_2O_2 generation and inhibit plant growth (Lai et al., 2020). Previous studies have shown that soil Cd pollution in farmlands is closely related to the excessive application of chemical fertilizers and pesticides and wastewater irrigation (Hong et al., 2020). Cd in soil is easily absorbed by plant roots and transmitted upward to other tissues. High content of Cd can inhibit plant seed germination and root growth, and lead to leaf withering, lipid peroxidation, and reduced enzyme activity (Rizwan et al., 2016; Berthet et al., 2018). Cd enriched in crops, ultimately, may result in the decline of yield and quality, and endanger human health through the food chain.

Plant root, the organ for fixation, absorption, and metabolism of exogenous elements, plays an important role in the physical, chemical, and biological processes that occur in the rhizosphere. Besides, it also actively responds to soil environment changes (Kopittke and Wang, 2017). Song et al. (2017) reported that the absorption of Cd by plant roots led to an increase in malondialdehyde (MDA) content and a decrease in antioxidant enzyme activity in plant roots through increasing the synthesis of protein and damaging nucleic acid and lipid cell membrane. Arif et al. (2019) found that major organic compounds involved in the chelation of metal ions, such as phytochelatins (PCs), metallothioneins (MTs), organic acids, amino acids, and cell wall proteins/pectins/polyphenols, could reduce the concentrations of metal ions, thereby reducing heavy metal-induced phytotoxicity. In addition, heavy metals can induce plant roots to produce secondary metabolites. Some studies have shown that the contents of alanine, proline, serine, putrescine, and phytohormones (campesterol, β-sitosterol, isoflavones, and α- tocopherol) increase significantly under Cd stress (Arif et al., 2019; Zhou et al., 2019).

Biochar, a carbon-rich organic material, can stimulate the growth of plant roots. Previous studies have shown that the application of biochar could increase the biomass, length, tip number, and density of plant roots, and reduce the available Cd in soil by 97.31% (Yang et al., 2016; Farrar et al., 2021). Biofertilizer, containing living cells or latent cells (Nascimento et al., 2020), could transform bioavailable heavy metals in the soil into unavailable states through microbial adsorption and fixation. For example, Iftikhar et al. (2019) reported that after the application of biofertilizer, the available Cd content in soil decreased by 75.59% compared with that in the control. Zhu et al. (2022) reported that the Cd content in cotton roots and leaves decreased significantly after biofertilizer application.

According to the statistics of the International Cotton Advisory Committee (ICAC), China's cotton output in 2020 was 5.9237 million tons, accounting for 23.43% of global cotton output. Xinjiang is the main cotton producing area of China. At present, the contents of Pb, Zn, Cd, and Cu are very high in cotton fields in Northern Xinjiang, China, and the Cd content exceeds the soil background value in 20.38% of the farmland soils. Chen et al. (2019) reported that the soil Cd, Hg, Cr, and Ni contents in Minfeng County, Xinjiang, China were 1.147, 1.124, 1.116, and 1.041 times of the background values of the soil in Xinjiang, respectively. Therefore, the ecological risk of soil heavy metal pollution is very high in Xinjiang, China (Liu et al., 2020).

Many studies have used biochar and biofertilizer as modifiers in the remediation of heavy metal-contaminated soils, and explored changes in soil physical and chemical properties and heavy metal bioavailability (Sun et al., 2017; Elsayed et al., 2020). However, there are few studies on the effects of biochar and biofertilizer on the morphological and physiological characteristics of cotton roots as well as cotton root-secreted metabolites under Cd stress. Therefore, in this study, the effects of exogenous Cd, biochar, and biofertilizer on the morphology, vitality, and antioxidant enzyme activities of cotton roots were determined, and the mechanism of biochar and biofertilizer alleviating Cd stress was explored by metabolomics analysis. We hypothesized that: (1) the application of biochar and biofertilizer might reduce the absorption of Cd in soil by cotton roots, and (2) biochar and biofertilizer might alleviate Cd stress by regulating the secretion of metabolites by cotton roots. This study will provide guidance for the remediation of Cd-contaminated soils in arid regions.

Materials and methods

Experimental site

The pot experiment was conducted at the Experimental Station of Shihezi University in Xinjiang, China (44°18′42.37″ N, 86°03′20.72″E). This region has a temperate continental climate, with an annual average temperature of 7.5 ~ 8.2°C, sunshine duration of 2318 ~ 2732 h, frost free period of 147 ~ 191 d, annual rainfall of 180 ~ 270 mm, and annual evaporation of 1000 ~ 1500 mm. The main crops were cotton, wheat, corn, and sugar beet.

Preparation of experimental materials

Soil was collected from a cotton field continuously cropped for 25 years in the study area. The texture was clay loam. The physical and chemical properties are shown in Table 1. Then, exogenous $CdCl_2{\cdot}2.5\ H_2O$ (2.44 g, analytical purity) was dissolved in distilled water, shaken well, and diluted into 1,000 mL to obtain 1.2 $g{\cdot}L^{-1}$ of Cd^{2+} solution. After that, 10 mL, 20 mL,

TABLE 1 Physicochemical properties of modifiers and soil.

Property	Cotton-straw biochar	Compound *Bacillus* biofertilizer	Soil
pH	9.50	7.8	7.76
Total nitrogen ($g \cdot kg^{-1}$)	0.89	91	0.46
Total P ($g \cdot kg^{-1}$)	2.54	62.2	0.82
Organic matter ($g \cdot kg^{-1}$)	625	422	14.73
Total K ($g \cdot kg^{-1}$)	8.62	86.1	246.83
Total Cd ($mg \cdot kg^{-1}$)	0.002	0.0001	0.25
Available Cd	–	–	0.121
Total salinity ($g \cdot kg^{-1}$)	–	–	3.36
Carboxyl ($mmol \cdot g^{-1}$)	0.20	–	–
Lactone ($mmol \cdot g^{-1}$)	0.25	–	–
Phenolic hydroxyl ($mmol \cdot g^{-1}$)	0.21	–	–
The Colony-Forming Units	–	>20 billion$\cdot g^{-1}$	–

and 40 mL of the solution were separately mixed with 12 kg collected soil to prepare the test soils with different Cd contents (0.25 (H0), 1 (H1), 2 (H2), and 4 (H3) mg kg^{-1}). The H1, H2 and H3 levels are 3, 6, and 11 times the global average soil Cd content (Adriano, 2001; Rawlins et al., 2012). The prepared soils were used for the experiment after 60 days.

The biochar (B) was prepared by using cotton straw according to the method of Lehmann et al. (2011). Biochar was air-dried and passed through a 5 mm sieve before the determination of pH, organic matter, total nitrogen, total phosphorus, total potassium, and total Cd (Sun et al., 2007) (Table 2). Biofertilizer (J) was purchased from the Lvlong Biotechnology Co., Ltd, Shandong, China. The number of viable bacteria in J was greater than 20 billion$\cdot g^{-1}$, the dominant bacterial species was *Bacillus*, the proportion of miscellaneous bacteria was less than 0.4%, the water content was less than 10%, the pH was 7.8, the total Cd content was 0.0001 mg$\cdot L^{-1}$, the total nitrogen content was 900 mg$\cdot L^{-1}$, and the organic carbon content was 3791 mg$\cdot L^{-1}$ (Zhu et al., 2022).

Experimental design

This experiment was conducted from 2019 to 2020. There were twelve treatments totally (Table 1), and each treatment had five replicates. In April 25, 2019, 3% B (360 g/pot, w/w) and 1.5% J (180 g/pot, w/w) were mixed with the prepared Cd-contaminated soils respectively (Kim et al., 2015; Zhu et al., 2022). Then, the soils were transferred into pots with a height of 40 cm and a diameter of 25 cm. After one week, deionized water was used for irrigation to maintain soil water content at 60% of the field capacity. After 60 days, B and J were applied to the soils according to the experimental design, and compound fertilizer (555 kg hm^{-2}; N-P_2O_2-K_2O, 17-17-17), potassium polyacrylate (4.8 kg hm^{-2}), and 50% of nitrogen fertilizer (urea, 345 kg hm^{-2}) were also applied. On May 2, 2019, ten cotton seeds (variety Xinluzao 53) were sown in each pot. During the whole growth period, the soil water content was maintained at 60% of the field capacity. The rest nitrogen fertilizer was applied after planting. Cotton plants were harvested on October 1, 2019, and the soils in the pots were put outdoors for winter.

TABLE 2 Experimental design.

Treatments	Cd ($mg \cdot kg^{-1}$)	Biochar (%)	Biofertilizer (%)
H0T (Control)	0.25	0	0
H0B	0.25	3%	0
H0J	0.25	0	1.5%
H1T	1	0	0
H1B	1	3%	0
H1J	1	0	1.5%
H2T	2	0	0
H2B	2	3%	0
H2J	2	0	1.5%
H3T	4	0	0
H3B	4	3%	0
H3J	4	0	1.5%

T, no modifiers; B, 3% biochar was applied; J, 1.5% biofertilizer was applied; H0, no Cd; H1, 1 mg$\cdot kg^{-1}$ of Cd was applied; H2, 2 mg$\cdot kg^{-1}$ of Cd was applied; H3, 4 mg$\cdot kg^{-1}$ of Cd was applied.

In 2020, cotton planting and the application of fertilizers, B, J, and field managements were consistent with those in 2019, but Cd was no more applied. All cotton root were sampled after 120 d cultivation (on September 10, 2020). Then, the roots were washed with water after removing impurities, put into ice bags, and brought back to the lab. Twelve taproot samples and twelve lateral root samples were obtained from each treatment. The total biomass of each root (RB) was weighed and recorded. After that, half of the taproot and one third of the lateral root were used for the determination of antioxidant enzyme activity and root vitality. The other half of the taproot and one third of the lateral root was first dried in an oven at 105°C for 2 h and then dried to constant weight at 85°C for the determination of Cd content. The remaining lateral roots were reserved at -80°C for metabolomics analysis. Following formulas were used for calculating root length density (RD, $cm \cdot cm^{-3}$), root tissue mass density (RTD, $mg \cdot cm^{-3}$), and specific root length (SRL, $m \bullet g^{-1}$) (Birouste et al., 2014).

$$RD = \frac{\text{Root length}}{\text{Soil sample volume}} \quad (1)$$

$$RTD = \frac{\text{Root dry mass}}{\text{Root volume}} \quad (2)$$

$$SRL = \frac{\text{Root length}}{\text{Root dry mass}} \quad (3)$$

Determination methods

Accurately weighed 0.5 g dried root (taproot and lateral root) was digested with the mixture of nitric acid and perchloric acid (2:1, v/v) (Yang et al., 2016), and then the Hitachi Z2000 graphite atomic absorption spectrophotometer (Z2000, Hitachi, Tokyo, Japan) was used to determine the Cd content.

The standard curve of graphite atomic absorption spectrometry: Accurately absorb cadmium standard solution (Meryer (Shanghai) Chemical Technology Co., Ltd. Shanghai) (100 μg L^{-1}) 0, 0.5, 1.0, 1.5, 2.0, 3.0 mL in 100 mL volumetric flask, the standard series solutions containing 0, 0.50, 1.0, 1.5, 2.0 and 3.0 μg L^{-1} cadmium were obtained by constant volume of 2% HNO_3 to the scale. The calibration curves were linear in the range of 0~3.0μg/L for cadmium, R^2 = 0.9997, the determination of metals with limits of detection 0.23μg/L. The precision of the procedures was also calculated as 7.6%, the recovery percentages varied between 105% and 109%.

The activity of antioxidant enzymes in roots was determined by spectrophotometry. Superoxide dismutase (SOD) activity was determined using the method of Paoletti et al. (1986) based on NBT photochemical reduction. The catalase (CAT) and peroxidase (POD) activities were determined by using the method of Cakmak and Marschner (1992). The content of malondialdehyde (MDA) was determined by the content of thiobarbituric acid reactive substances (TBARS) according to the method of Bharwana et al. (2014). Electrolyte leakage rate (REC) was determined by the method of Bharwana et al. (2014).

The root vitality was determined by triphenyltetrazole chloride (TTC) method (Liu et al., 2008). Root samples were washed with distilled water and dried with thin paper. Then, root sample (0.5 g) was completely immersed in a solution composed of 5 mL of 0.4% TTC and 5 mL of phosphate buffer (0.06 mol·L^{-1}, pH: 7.0), and placed in the dark at 37°C for 3 h. After that, 2 mL of 1 mol·L^{-1} sulfuric acid was added to stop the chemical reaction. The roots were removed, and the residue was homogenized in a mortar containing 4 mL of ethyl acetate. The red extract was transferred to test tube, and 10 mL of ethyl acetate was added, followed by spectrophotometric measurement at 485 nm. The amount of tetrazolium reduced in the standard reaction was quantified with absorbance to calculate the root vitality.

Metabolonomic analysis

The test results showed the vitality and Cd content of cotton lateral roots were higher than those of taproot. Therefore, the metabonomics of cotton lateral roots was determined in this study.

The H0T, H4T, H4B, and H4J treatments were selected for metabolomic analysis. Small molecular metabolites including polar and non-polar metabolites were extracted from 1.0 g of soil using a mixture of methanol and H_2O (v/v=3:1) and then a mixture of ethyl acetate and H_2O (v/v=1:1). After that, all metabolites were dissolved in 30 μL of methoxylamine hydrochloride (20 m·mL^{-1} in pyridine) before an incubation at 80 °C for 30 min and an incubation with 40 μL of BSTFA (Bis (trimethylsilyl)trifluoroacetamide) reagent (1% TMCS (Trimethylchlorosilane), v/v) at 70 °C for 1.5 h. After cooling to room temperature, 5 μL of FAMEs (dissolved in chloroform) were added to the quality control sample. The composition and content of soil metabolites were analyzed in a gas chromatograph (GC) system (Agilent 7890, Santa Clara, USA) equipped with a DB-5 mass spectrometer (MS) capillary column (inner diameter: 30 m × 250 μm, film thickness: 0.25 μm) (J&W Scientific, Folsom, CA, USA) and linked with a Pegasus high-throughput time-of-flight mass spectrometer (Pegasus® HT TOF-MS, LECO, MI, USA). Helium, as carrier gas, was accessed at a constant flow rate of 1.0 mL·min^{-1}. Full-scan mode with a range of 50-500 m/z and a rate of 20 spectra·s^{-1} were used for MS data acquisition. Finally, following the Metabolomics Standards Initiative (MSI) convention, the

extraction, alignment, identification, and integration of peaks were implemented on the LECO-Fiehn Rtx5 database (Zhu et al., 2022). The comparative analyses included H3T vs CK, H3J vs H3T, and H3B vs H3T.

Data analysis

Significance of the differences in root biomass, specific root volume/area/weight, root vitality, root Cd, and antioxidant enzyme activities was determined using Duncan test at $p< 0.05$ (SPSS version 20.0 software, Inc., Chicago, IL, USA). All charts (bar chart, OPLS-DA chart, boxplot, metabolite expression chart, heatmap, and Venn diagram) were drawn using Origin 8.0 (Origin Lab, Massachusetts, USA). Image layout was completed using Adobe Illustrator CS6 (Adobe Systems Incorporated, USA).

Results

Root structure

Exogenous Cd addition reduced cotton RB and RTD, but had no obvious effect on RD and SRL. Cotton RB and RTD in the H3T treatment decreased by 10.46% and 21.81% ($p< 0.05$), respectively compared with those in the H0T treatment. The application of B and J increased cotton RB, RD, SRL, and RTD. Cotton RB, RD, SRL, and RTD in the H3B treatment increased by 5.23%, 15.25%, 14.29%, and 11.83% ($p< 0.05$), respectively compared with those in the H3T treatment, and RB, RD, SRL, and RTD in the H3J treatment increased by 9.25%, 16.39%, 15.69%, and 13.24% ($p< 0.05$), respectively compared with those in the H3T treatment. The results of regression analysis showed that Cd and modifier application had effects on cotton RB ($p< 0.05$), RD ($p< 0.01$), SRL ($p< 0.01$), and RTD ($p< 0.01$) (Table 3).

Vitality of cotton taproot and lateral root

The vitality of cotton taproot and lateral root were affected by exogenous Cd to varying degrees (Figure 1). The vitality of cotton taproot and lateral root in the H1T, H2T, and H3T treatments decreased compared with those in the H0T treatment ($p< 0.05$). With the increase of Cd content, the vitality of cotton taproot and lateral root showed a downward trend, and were the lowest in the H3T treatment (92.06 and 63.38 $\mu g \cdot g^{-1} \cdot h^{-1}$, respectively). However, the application of B and J increased the vitality of cotton taproot and lateral root ($p< 0.05$). The vitality of cotton taproot in the H3B and H3J treatments increased by 21.20% and 21.25% ($p< 0.05$), respectively, and that of lateral root increased by 60.01% and 74.63% ($p< 0.05$), respectively, compared with those in the H3T treatment.

TABLE 3 Cotton root structure in different treatments.

Treatments	RB (g)	RD ($cm \cdot cm^{-3}$)	SRL ($m \bullet g^{-1}$)	RTD ($mg \cdot cm^{-3}$)
H0T	0.985±0.0493 bcd	124.699±6.235 cd	119.030±5.951 b	0.454±0.0227 d
H0B	1.012±0.0506 b	154.946±7.747 b	135.342±6.767 a	0.724±0.0362 b
H0J	1.094±0.0547 a	161.549±8.077 a	142.358±7.118 a	0.854±0.0427 a
H1T	0.934±0.0467 bcde	151.457±5.773 def	120.252±6.013 b	0.403±0.0201 e
H1B	0.967±0.0484 bcd	134.569±6.728 c	133.855±6.693 a	0.523±0.0262 c
H1J	1.001±0.0501 b	148.255±7.413 b	138.545±6.927 a	0.683±0.0342 b
H2T	0.902±0.0453 def	108.646±5.432 f	119.236±5.962 b	0.395±0.0198 e
H2B	0.905±0.0541 cdef	120.546±6.027 de	130.455±6.523 ab	0.487±0.0243 cd
H2J	0.992±0.0496 bc	121.456±6.072 de	140.745±7.037 a	0.499±0.0250 cd
H3T	0.822±0.0411 f	95.646±4.782 g	119.655±5.983 b	0.355±0.0177 e
H3B	0.865±0.0433 ef	110.235±5.512 ef	136.754±6.838 a	0.397±0.0199 e
H3J	0.898±0.0449 def	111.326±5.566 ef	138.425±6.921 a	0.402±0.0201 e
Regression Tests (significance)				
H	**	**	**	**
B	*	**	**	**
J	*	**	**	**
H*BJ	**	**	**	**

T, no modifiers; B, 3% biochar was applied; J, 1.5 % biofertilizer was applied; H0, no Cd; H1, 1 $mg \cdot kg^{-1}$ of Cd was applied; H2, 2 $mg \cdot kg^{-1}$ of Cd was applied; H3, 4 $mg \cdot kg^{-1}$ of Cd was applied. RB, root biomass; RD, root length density ($cm \cdot cm^{-3}$); RTD, root tissue mass density ($mg \cdot cm^{-3}$); SRL, specific root length ($m \bullet g^{-1}$). Different lowercase letters in the same column indicate significant differences. **, $p< 0.01$; *, $0.01< p< 0.05$; ns, $p \geq 0.05$. The same below.

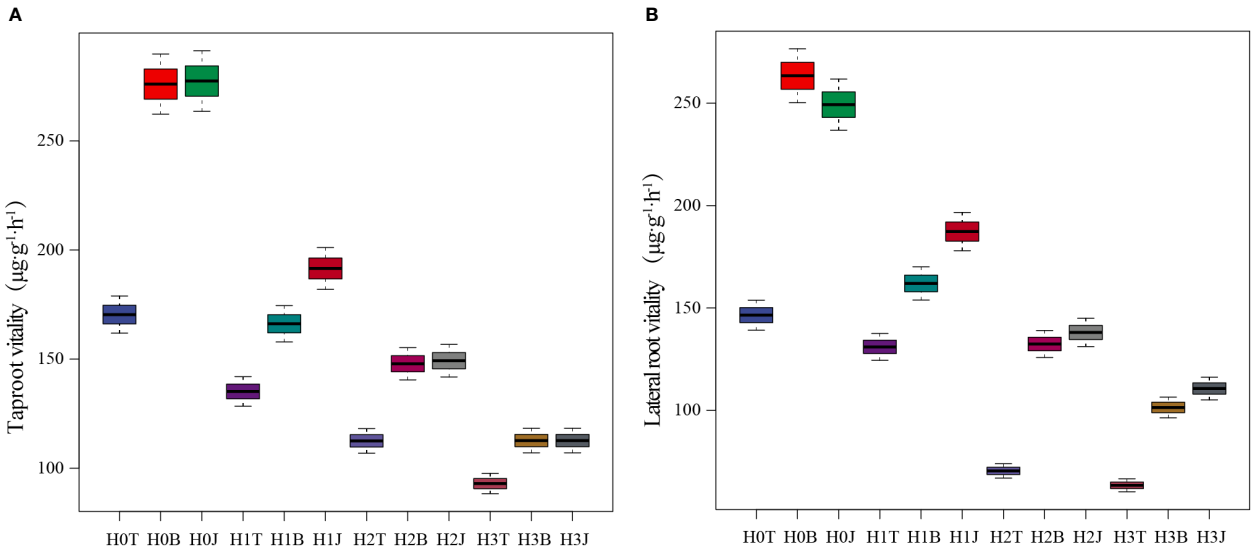


FIGURE 1
Effect of biochar and biofertilizer applications on the vitality of cotton taproot **(A)** and lateral root **(B)**. Notes: T, no modifiers; B, 3% biochar was applied; J, 1.5 % biofertilizer was applied; H0, no Cd; H1, 1 mg·kg-1 of Cd was applied; H2, 2 mg·kg-1 of Cd was applied; H3, 4 mg·kg-1 of Cd was applied. The same below.

Oxidative stress response of cotton taproot and lateral root

In this study, exogenous Cd addition reduced the SOD activity and CAT activity of cotton taproot and lateral root. With the increase of Cd content, the SOD and CAT activities of cotton root showed a decreasing trend. The SOD activity of cotton taproot and lateral root in the H3T treatment decreased by 7.17% and 5.89% ($p > 0.05$), respectively, while the CAT activity decreased by 27.45% and 34.63%, respectively ($p< 0.05$) compared with those in the H0T treatment. The MDA content and REC increased with the increase of Cd content ($p< 0.05$), reaching the maximum in H3T treatment. The highest MDA content of cotton taproot and lateral root were 11.39 and 14.98 μmol·mg^{-1} (protein), respectively, and the highest REC were 16.67% and 15.03%, respectively (Figure 2).

The application of B and J increased the activities of SOD and CAT in taproot and lateral root. The activities of SOD and CAT of taproot in the H3B treatment increased by 3.07% ($p > 0.05$) and 45.95% ($p< 0.05$), respectively, and those of lateral root increased by 6.37% ($p > 0.05$) and 88.24% ($p< 0.05$), respectively compared with those in the H3T treatment. The activities of SOD and CAT of taproot in the H3J treatment increased by 3.072% ($p > 0.05$) and 64.86% ($p< 0.05$), respectively, and those of lateral root increased by 8.724% ($p > 0.05$) and 111.7% ($p< 0.05$), respectively compared with those in the H3T treatment (Figure 2). The MDA content of taproot and lateral root in the H3B treatment decreased by 41.12% and 18.02%, respectively ($p< 0.05$), and the REC of taproot and lateral root decreased by 13.32% and 16.11%, respectively ($p< 0.05$), compared with those in the H3T treatment. The MDA content of taproot and lateral root in the H3J treatment decreased by 42.32% and 33.58%, respectively ($p< 0.05$), and the REC of taproot and lateral root decreased by 16.68% and 16.91%, respectively ($p< 0.05$), compared with those in the H3T treatment. There was no difference in the MDA content and REC between other treatments ($p > 0.05$) (Figure 3).

Changes in Cd content in taproot and lateral root of cotton after biochar and biofertilizer applications

Modifiers and exogenous Cd had obvious influences on the enrichment of Cd in cotton roots (Figure 1). The Cd contents of cotton taproot and lateral root in the H1T, H2T, and H3T treatments increased compared with those in the H0T treatment ($p< 0.05$). The Cd content of cotton taproot (0.0250 mg kg^{-1}) and lateral root (0.0288 mg kg^{-1}) in the H3T treatment were the highest, increasing by 89.11% and 33.95%, respectively ($p< 0.05$) compared with those in the H0T treatment. The application of B and J significantly reduced the accumulation of Cd in cotton roots ($p< 0.05$). The taproot Cd content in the H3B and H3J treatments reduced by 13.32% and 19.47%, respectively, and the lateral root Cd content reduced by 14.24% and 20.49%, respectively, compared with those in the H3T treatment ($p< 0.05$).

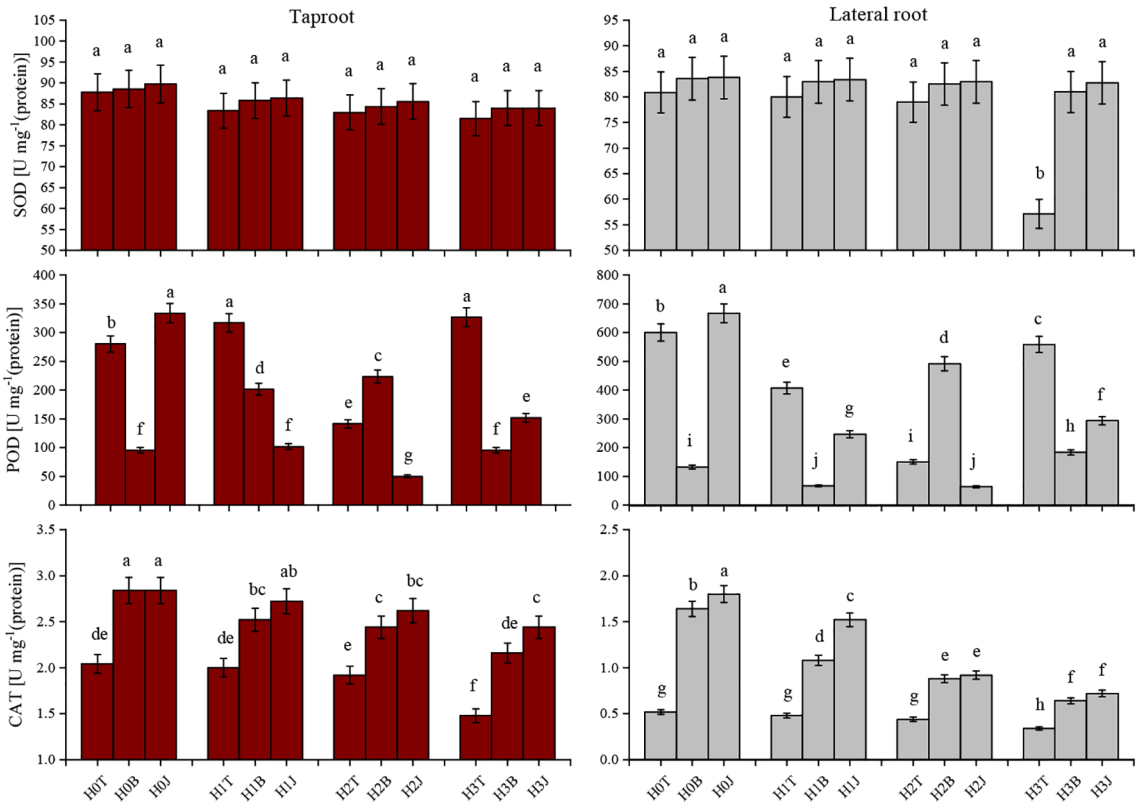


FIGURE 2
Effect of biochar and biofertilizer applications on cotton root antioxidant defense system. Values are means ± SE (n=5). Different lowercase letters indicate significant differences at P < 0.05 (the Duncan test).

Metabolic profiling of lateral roots exposed to biochar, biofertilizer, and Cd

As shown in Figure 4, there were statistically significant differences between the treatments, and all samples were within the 95% confidence interval. Figure 4A shows the cation grouping information in the measured samples, and Figure 4B shows anions. The samples in the H3B and H3J treatments showed obvious differences.

Metabolic pathway and expression pattern analysis of DEMs

The main DEMs in cotton lateral root in the treatments were selected through pairwise comparison (Figure S1). The network of main DEMs (Figure 5) showed that in ABC transporters, L-aspartic acid, Uridine, and Guanosine were the main DEMs, and their relative abundance were up-regulated after Cd addition. In Phenylalaninc metabolism, the relative abundance of the main DEMs N-acetylphenylalanine, N-acetyl-d-phenylalanine, and Dihydro-3-coumaric acid in the H3B treatment were up-regulated compared with those in the H0T treatment. In Ubiquinone and other terpenoid quinone biosynthesis, the relative abundance of 4-hydroxyphenylpyruvic acid, P-salicylie acid, and Gamma tocotrienol in the H3B treatment and that of Gamma tocotrienolu in the H3J treatment were up-regulated compared with those in the H0T treatment. The Cd addition reduced the relative abundance of Gossypol (Figure S2).

Interaction network between the primary metabolism and environment factors

The main DEMs in cotton lateral root were screened (e.g: PE (15:0/16:1(9z), dodecylbenzenesulfonic acid, and some organic acids) (Figure S2) to construct the heatmap of cotton root morphology, physiological indexes, and metabolites (Figure 6). It was found that root Cd content, MDA content, RTD, RB, RD, and root activity were negatively correlated with the relative abundance of (3.4.5.6-ethoxyoxan-2-y)methyl 4-hydroxybenzoate, Mahaleboside, and 2-[(sulfoxy)methyl]butanoic acid ($p< 0.01$), and positively correlated with the relative abundance of

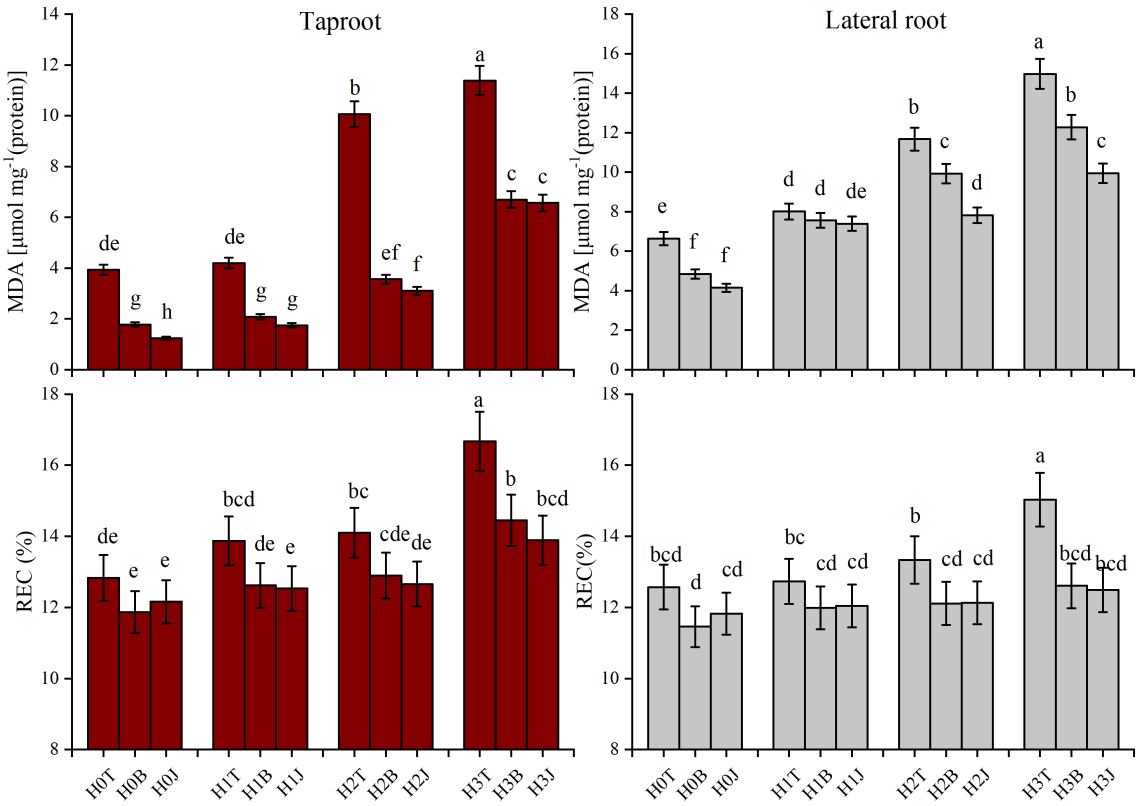


FIGURE 3
Effect of biochar and biofertilizer applications on cotton root malondialdehyde (MDA) and electrolyte leakage rate (REC). Values are means ± SE (n=5). Different lowercase letters indicate significant differences at P < 0.05 (the Duncan test).

Dehydromodesmone, Pteroside D, and 2,2-Bis-(4-hydroxyphenyl)-1-propanol ($p< 0.01$).

SOD and CAT activities of cotton lateral root were negatively correlated with the relative abundance of Tiglylcarmitine, PA(18:3(6Z,9Z,12Z)0:0), LPC(18:2), N-(1-deoxy-1-fluorosyl)threonine, PE(16:0/0:0), 1-(6Z.9Z.12Z-octadecarieny)-glycoro-3-phosphate, 6”-malonylapin, Muramic acid, Glaucarubin, and Epicatechin ($p< 0.01$), and positively correlated with (1S.2S.4R)-p-menth-8-ene-1.2.10-riol 2-glucoside, 4-(3-pyridyl)-3-butenolc acid, and Caryophyllene epoxy ($p< 0.01$). REC was negatively correlated with 3-Hydroxychavicol 1-thamnosyl-(1->6)-glucoside, 5-methylcytidine, 6-gingerdiol 4-0-beta-d-glucopyranoside, Corchoionoside B, lcariside B8, (4R,5S,7R.11)-11,12-Dihydroxy-1(10)-spirovetiven-2-one 12-glucoside, Citronellyl beta-sophoroside, and Cycasin ($p< 0.01$), and positively correlated with 2,3-dinor-8-IS0-PGF2a, PE(15:0/16:1(9Z), and FA(18:2(OH3). POD activity was negatively correlated with Cassiaside B, Endoiten o-glucuronide, Gluconolactone, Hydroxyprolyl-asparagine, and Oxynarcotine ($p< 0.01$).

The different responses of cotton lateral root metabolites to the treatments led to differences in the physiological and growth characteristics of cotton lateral roots and the interactions between metabolites. Therefore, the interactions of root growth characteristics, Cd content, physiological characteristics, and metabolites in different treatments were analyzed by using the co-occurrence network (Figure 7). In H0T treatment, the main metabolites were L-isolecine, L-valine, L-argininc, Lasparagine, and Shikimic acid (Figure 7A). In the H3T treatment, exogenous Cd addition increased Cd content in cotton roots and decreased SOD and CAT activities and root vitality. Besides, it also increased the relative abundance of key metabolites including L-glutamate, L-histidine, L-arginine, and 4,hydroxyphenylpyruvic acid (Figure 7B). In the H3B treatment, B application increased cotton root vitality, REC, and the relative abundance of 4-Hydrophenylpyruvic acid and Oxoglutaric acid (Figure 7C). In the H3J treatment, J application reduced cotton root Cd content, MDA content, and the relative abundance of Shikimic acid (Figure 7D).

Discussion

Taproot and lateral roots are the main parts enriched by Cd in cotton plants (Nan et al., 2020). The development of lateral roots has a great influence on plants. Massive lateral roots can

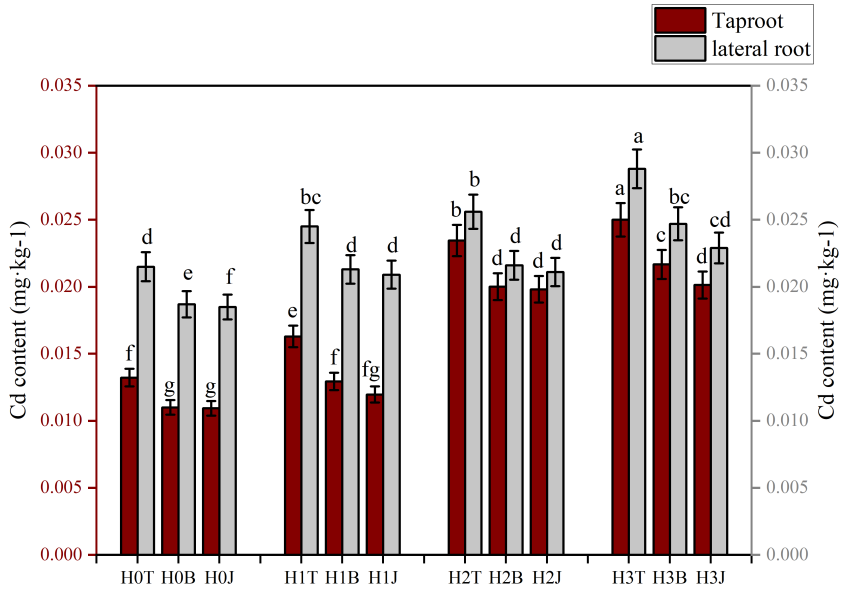


FIGURE 4
Effect of biochar and biofertilizer applications on cotton root Cd content. T, no modifiers; B, 3% biochar was applied; J, 1.5 % biofertilizer was applied; H0, no Cd; H1, 1 mg·kg-1 of Cd was applied; H2, 2 mg·kg-1 of Cd was applied; H3, 4 mg·kg-1 of Cd was applied. Values are means ± SE (n=5). Different lowercase letters indicate significant differences at P < 0.05 (the Duncan test).

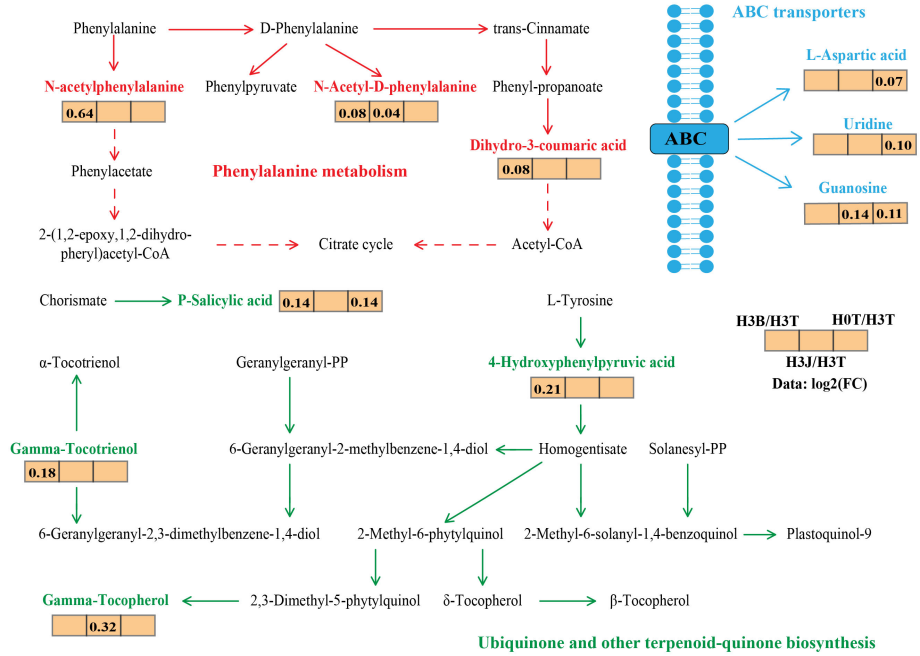


FIGURE 5
PLS-DA analysis of untargeted metabolomics data of cotton lateral root in the Cd, biochar, and biofertilizer treatments (left, cation) (right, anion). Ellipses represent the 95% confidence interval.

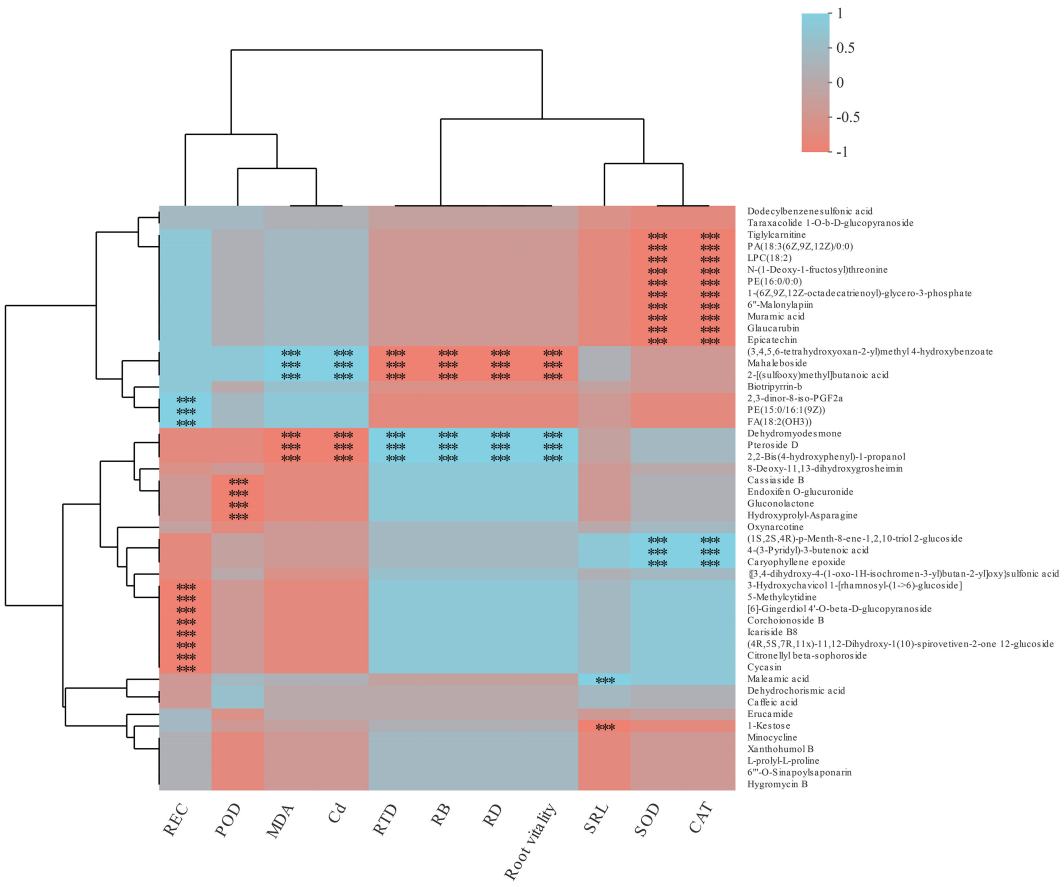


FIGURE 6
Primary metabolic flux map labeled with the differentially expressed metabolites of cotton lateral root. The data represents the ratio of the average expression of metabolites in the two groups of samples (Log2FC), with positive value indicating up-regulation and negative value indicating down-regulation. Solid arrows indicate direct action and dashed arrows indicate indirect action. Red represents Phenylalaninc metabolism; Green represents Ubiquinone and other terpenoid-quinone biosynthesis; Blue represents ABC transporters.

increase the plants' uptake of nutrients, water, and metal ions (Wang et al., 2020). In this study, exogenous Cd addition reduced cotton RB, RTD, and root vitality, but had no obvious effect on RD and SRL (Table 3). This is different from the research results of Ng et al. (2019). This difference is mainly caused by the differences in the root growth characteristics of different plants and the sensitivity to different metal elements (Ng et al., 2020). In addition, in this study, the application of 4 mg kg^{-1} Cd decreased the vitality of cotton taproot and lateral root by 45.45% and 56.73%, respectively compared with the control (Figure 1). This indicates that exogenous Cd addition could inhibit the growth and development of cotton root system (Lambrechts et al., 2014).

The application of B and J increased RB, SRL, RD, and root vitality, and reduced the content of bioavailable Cd in soil, thus inhibiting the absorption of Cd by plants and alleviating Cd stress (Liu et al., 2008; Jha et al., 2020). Shah and Nahakpam (2012) showed that the POD and CAT activities of rice root increased under Cd stress. This is contrary to the results of the present study (Figure 3). It may be caused by differences in the scavenging of reactive oxygen species, the reduction of lipid membrane peroxidation, and the adaptability to adverse environments in different crops (Sun et al., 2017; Elsayed et al., 2020). Bashir et al. (2020) showed that the application of B and J increased the activities of POD and SOD in wheat roots in Zn-contaminated soil. This is consistent with the results of this study. The application of B and J increased the activities of POD and CAT in cotton root (Figure 2), and reduced MDA content and REC (Figure 3). This may be due to that B and J could reduce the accumulation of Cd in cotton root by adsorbing and fixing Cd (Ogunkunle et al., 2018).

In this study, after 1, 2, 4 mg kg^{-1} of Cd were applied, the Cd content in cotton taproot and lateral root increased by 89.11% and 33.95% on average (Figure 8) compared with those in the control, and the Cd content of cotton lateral root was higher than that of taproot. This may be due to that the increase of

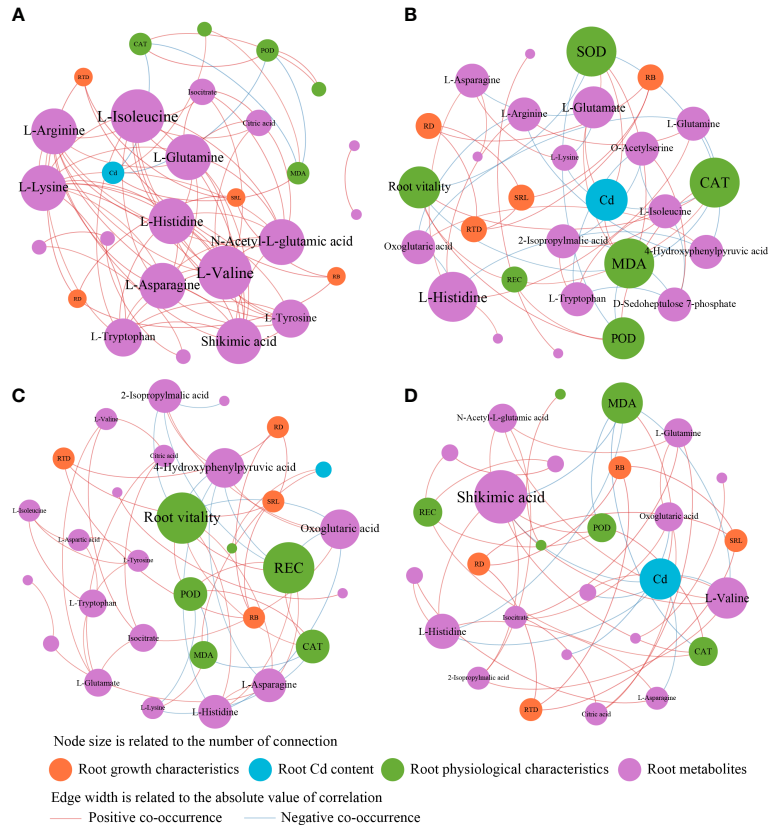


FIGURE 7
Heatmap of the correlation between metabolites and environmental factors in each treatment. REC, electrolyte leakage rate; MDA, malondialdehyde; POD, peroxidase; SOD, superoxide dismutasee; CAT, catalas; RTD, root tissue mass density; RB, root biomass; RD, specific root length density; SRL, specific root length; Cd, root Cd content.

cotton lateral roots not only increases the absorption of water and nutrients, but also increases the absorption of metal ions (Wang et al., 2020). Besides, it was also found that after the application of B and J, the Cd content of cotton roots decreased by 13.31%-26.63% and 13.02%-20.49%, respectively compared with that of the control. This may be due to that (1) B and J are rich in carboxyl groups and minerals, which can improve soil fertility and structure and fix toxic elements, thereby reducing the uptake of toxic elements by plants (Elsayed et al., 2020; Jha et al., 2020); Besides, B and J can also promote plant growth and development. (2) The application of B and J can increase soil microbial diversity to produce more organic acids and enhance the adsorption and fixation of toxic elements by soil microorganisms (Zhang et al., 2020). (3) The application of B and J can stimulate plant roots to produce more exudates, increasing the release of toxic elements (Cheng et al., 2018; Vinci et al., 2018).

Under heavy metal stresses, amino acids and their derivatives secreted by plants play important roles in resisting the toxicity of metal ions (Anjum et al., 2015; Olmo et al., 2016). Studies have shown that increases in the contents of alanine, proline, serine and putrescine in plant root exudates can alleviate the Cd stress on plants (Wang et al., 2015). In this study, when 4 mg kg^{-1} of Cd was applied, the relative abundance of DEMs including L-aspartic acid, Uridine, and Guanosine were up-regulated (Figure 6, Figure S3). Wang et al. (2015) and Yang and Shen (2020) showed that when the Cd content was 1 mg kg^{-1}, the secretion of amino acids and organic acids by the roots of *Typha latifolia* L. significantly increased, but the content of organic acids decreased significantly with the increase of Cd concentration. However, in this study, the relative abundance of L-aspartic acid increased after exogenous Cd addition. This may be related to the amount of exogenous Cd. Different Cd contents have different toxicity to plants and microorganisms, resulting in different antitoxicity of plants. In addition, the species difference between *Typha latifolia* L. and cotton and different planting environments may also lead to difference in plant root exudates (Yang and Shen, 2020).

Studies have also shown that differences in heavy metals and cultivation conditions have significant impacts on the composition of plant metabolites (Fu et al., 2017). That is, plants can regulate

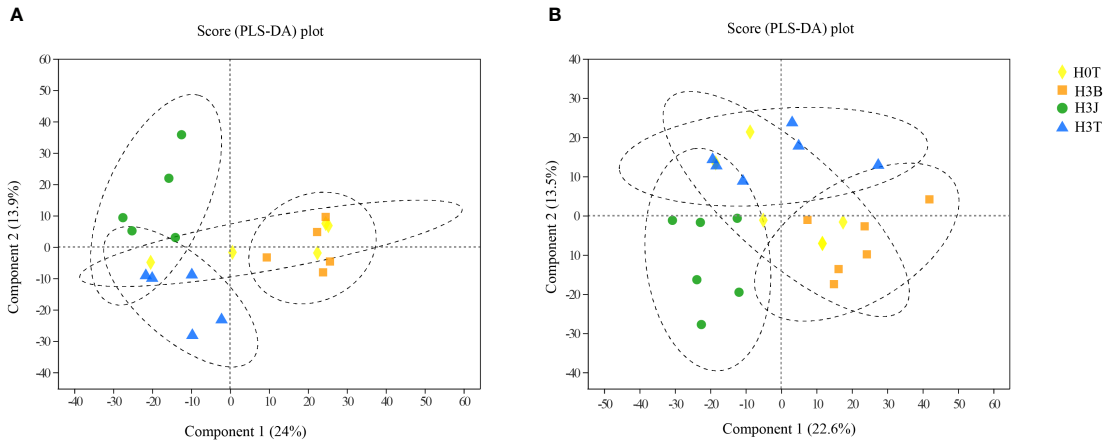


FIGURE 8
Co-occurrence analysis of root growth characteristics, root Cd content, root physiological characteristics, and root metabolites in response to different treatments. (a) H0T treatment, (b) H3T treatment, (c) H3B treatment, (d) H3J treatment.

their metabolic intensity to improve their adaptability to the polluted environment (Yang and Shen, 2020). In this study, cotton root exudates were rich in organic acids and amino acids (Figures S2-4). This indicates that under Cd stress, cotton mainly secretes organic acids and amino acids to resist Cd stress, which is consistent with the results of Fan et al. (2016) and Arif et al. (2019). In this study, there was a negative correlation between root Cd content and Pteroside D abundance ($p< 0.01$) (Figure 6). Pteroside D is a kind of carbohydrates. Heavy metals have a great impact on the synthesis of carbohydrates in plants. Excessive accumulation of heavy metals may inhibit the synthesis of carbohydrates by breaking the photosynthetic electron transport chain and producing ROS, thus affecting the photosynthesis and nutrient absorption of plants (Khan et al., 2015). It was also found that root Cd content was closely related to amino acids (Figures 7A, D). This indicates that amino acids play important roles in the resistance to Cd stress. After B and J were applied, the relative abundance of N-acetylphenylalanine, N-acetyl-D-phenylalanine, and Gamma-tocotrienol increased (Figure 5), and the activities of root antioxidant enzymes were closely related to root exudates (Figures 7B, C). This indicates that phenolic substances and phenylalanine secreted by cotton roots play important roles in antioxidation and the resistance to Cd stress (Kováčik and Bačkor, 2007). However, An et al. (2022) found that after applying polymer modifier to Cd-contaminated soil, cotton leaves mainly secreted jasmonic acid, stearic acid, and other organic acids to resist Cd stress, and no amino acids were found. This difference may be caused by the type or amount of modifiers applied.

Epicatechin and coumaric acid are closely related to the biosynthesis pathway of flavonoids and phenolic acids, which can enhance the free radical scavenging ability and the oxidative stress response of plants (Banik and Bhattacharjee, 2020). In this study, SOD and CAT activities of cotton root were negatively correlated with the relative abundance of Muramic acid, Glaucarubin, and Epicatechin ($p< 0.01$) (Figure 6), and positively correlated with the relative abundance of L-glutamate, L-asparagine, and 4-hydroxyphenylpyruvic acid (Figures 7C, D). This indicates that the application of B and J could improve the resistance to Cd stress through improving the antioxidant defense system and increasing the secretion of amino acids by cotton root. In this study, the relative abundance of Mahaleboside and 2-[(sulfooxy)methyl] butanoic acid were positively correlated with RD, root biomass, and RTD ($p< 0.01$) (Figure 6). Mahaleboside is a kind of phylpropanoids and polyketides, which plays an important role in the metabolic pathway of plant defense system and nutritional synthesis. It can enhance cotton resistance to abiotic stress and promote cotton growth and development (Wu et al., 2016; Li et al., 2018). Cotton root vitality and root growth indicators were positively correlated with Pteroside D ($p< 0.01$) (Figure 6). Pteroside D is a kind of carbohydrates. Root growth and development consume a large amount of carbohydrates produced by energy metabolism (Singh et al., 2015; Sun et al., 2017). Therefore, B and J application could regulate the growth indicators (RTD, SRL, and RD) and metabolites (organic acids and amino acid compounds) of Cd-stressed cotton root to reduce the absorption of Cd by cotton taproot and lateral roots (Figures 7B, C), thus reducing the Cd stress on cotton growth.

Conclusion

Exogenous Cd application inhibited the growth and development of cotton roots (RB, RTD, and root vitality), and reduced the antioxidant enzyme activities. However, applications of cotton straw-derived biochar and compound *Bacillus* biofertilizer promoted root growth and root vitality, and increased the SOD and

CAT activities of Cd-stressed cotton root. Besides, cotton straw-derived biochar and compound *Bacillus* biofertilizer mainly regulate the relative abundance of cotton root metabolites including phenolic substances and amino acids to reduce the absorption of Cd by cotton roots, thus improving cotton resistance to Cd stress.

Data availability statement

The original contributions presented in the study are included in the article/Supplementary Material, further inquiries can be directed to the corresponding author.

Author contributions

YZ and JC conceived and designed the experiments. HW and JS conducted laboratory analyses. YZ and MZ analyzed the data and wrote results. YZ, XL, and TL wrote the manuscript (Introduction and Discussion). All authors provided editorial advice and revised manuscript.

Funding

This work was supported by the National Natural Science Foundation of China (Grant No. 42161042), the Corps Science and Technology Project (Grant No.2020AB018), and the Shihezi University Project (Grant No. RCZX201425 and RCZK20208).

Conflict of interest

The authors declare that the research was conducted in the absence of any commercial or financial relationships that could be construed as a potential conflict of interest.

Publisher's note

All claims expressed in this article are solely those of the authors and do not necessarily represent those of their affiliated organizations, or those of the publisher, the editors and the reviewers. Any product that may be evaluated in this article, or claim that may be made by its manufacturer, is not guaranteed or endorsed by the publisher.

Supplementary material

The Supplementary Material for this article can be found online at: https://www.frontiersin.org/articles/10.3389/fpls.2022.1051935/full#supplementary-material

References

Adriano, D. C. (2001). *Trace elements in terrestrial environments: biogeochemistry, bioavailability and risks of metals. 2nd ed* (New York: Springer).

An, M. J., Hong, D. S., Chang, D. D., Zhang, C. Y., Fan, H., and Wang, K. Y. (2022). Polymer amendment regulates cadmium migration in cadmium contaminated cotton field: Insights from genetic adaptation and phenotypic plasticity. *Sci. Total. Environ.* 807 (3), 151075. doi: 10.1016/j.scitotenv.2021.151075

Anjum, N. A., Hasanuzzaman, M., Hossain, M. A., Thangavel, P., Roychoudhury, A., Gill, S. S., et al. (2015). Jacks of metal/metalloid chelation trade in plants-an overview. *Front. Plant Sci.* 6. doi: 10.3389/fpls.2015.00192

Arif, N., Sharma, N. C., Yadav, V., Ramawat, N., Dubey., N. K., Tripathi, D. K., et al. (2019). Understanding heavy metal stress in a rice crop: Toxicity, tolerance mechanisms, and amelioration strategies. *J. Plant Biol.* 62, 239–253. doi: 10.1007/s12374-019-0112-4

Banik, N., and Bhattacharjee, S. (2020). Complementation of ROS scavenging secondary metabolites with enzymatic antioxidant defense system augments redox-regulation property under salinity stress in rice. *Physiol. Mol. Biol. Plants* 26, 1623–1633. doi: 10.1007/s12298-020-00844-9

Bashir, A., Rizwan., M., Ali, S., Adrees, M., Rehman, M. Z., and Qayyum, M. F. (2020). Effect of composted organic amendments and zinc oxide nanoparticles on growth and cadmium accumulation by wheat; a life cycle study. *Environ. Sci. pollut. Res.* 27, 23926–23936. doi: 10.1007/s11356-020-08739-8

Berthet, S., Villiers, F., Alban, C., Serre, N. B. C., Martin-Laffon, J., Figuet, S., et al. (2018). *Arabidopsis thaliana* plants challenged with uranium reveal new insights into iron and phosphate homeostasis. *New Phytol.* 217, 657–670. doi: 10.1111/nph.14865

Bharwana, S., Ali, S., Farooq, M., Ali, B., Iqbal, N., Abbas, F., et al. (2014). Hydrogen sulfide ameliorates lead-induced morphological, photosynthetic, oxidative damages and biochemical changes in cotton. *Environ. Sci. pollut. Res.* 21, 717–731. doi: 10.1007/s11356-013-1920-6

Birouste, M., Zamora-Ledezma, E., and Bossard, C. (2014). Measurement of fine root tissue density: a comparison of three methods reveals the potential of root dry matter content. *Plant Soil* 374, 299–313. doi: 10.1007/s11104-013-1874-y

Cakmak, I., and Marschner, H. (1992). Magnesium deficiency and high light intensity enhance activities of superoxide dismutase, ascorbate peroxidase, and glutathione reductase in bean leaves. *Plant Physiol.* 98 (4), 1222–1227. doi: 10.1104/pp.98.4.1222

Cheng, N., Peng, Y., Kong, Y., Li, J. J., and Sun, C. X. (2018). Combined effects of biochar addition and nitrogen fertilizer reduction on the rhizosphere metabolomics of maize (*Zea mays* l.) seedlings. *Plant Soil.* 433, 19–35. doi: 10.1007/s11104-018-3811-6

Chen, J., Lu, J., Ning, J., Yan, Y. J., Li, S. M., and Zhou, L. (2019). Pollution characteristics, sources, and risk assessment of heavy metals and perfluorinated compounds in PM2.5 in the major industrial city of northern xinjiang, China. *Air. Qual. Atmos. Health* 12, 909–918. doi: 10.1007/s11869-019-00706-8

Elsayed, S. I. M., Glala, A. A., Abdalla, A. M., El-Sayed, A. E. G. A., and Darwish, M. A. (2020). Effect of biofertilizer and organic fertilization on growth, nutrient contents and fresh yield of dill (*Anethum graveolens*). *Bull. Natl. Res. Cent.* 44, 122. doi: 10.1186/s42269-020-00375-z

Fan, X., Wen, X., Huang, F., Cai, Y. X., and Cai, K. Z. (2016). Effects of silicon on morphology, ultrastructure and exudates of rice root under heavy metal stress. *Acta Physiol. Plant* 38, 197. doi: 10.1007/s11738-016-2221-8

Farrar, M. B., Wallace, H, M., Xu, C. Y., Joseph, S., Dunn, P. K., Nguyen, T. T. N., et al. (2021). Biochar co-applied with organic amendments increased soil-plant potassium and root biomass but not crop yield. *J. Soils Sediments* 21, 784–798. doi: 10.1007/s11368-020-02846-2

Fu, H., Yu, H., Li, T., and Zhang, X. (2017). Influence of cadmium stress on root exudates of high cadmium accumulating rice line (*Oryza sativa* l.). *Ecotoxicol. Environ. Saf.* 150, 168–175. doi: 10.1016/j.ecoenv.2017.12.014

Hong, Y. K., Kim, J. W., Lee, S. P., Yang, J. E., and Kim, S. C. (2020). Heavy metal remediation in soil with chemical amendments and its impact on activity of antioxidant enzymes in lettuce (*Lactuca sativa*) and soil enzymes. *Appl. Biol. Chem.* 63, 42. doi: 10.1186/s13765-020-00526-w

Iftikhar, S., Saleem, M., Ahmad, K. S., and Jaffri, S. B. (2019). Synergistic mycoflora–natural farming mediated biofertilization and heavy metals decontamination of lithospheric compartment in a sustainable mode *via helianthus annuus*. *Int. J. Environ. Sci. Technol.* 16, 6735–6752. doi: 10.1007/s13762-018-02180-8

Jha, P. N., Gomaa, A. B., Yanni, Y. G., El-Saadany, A. Y., Stedtfeld, T. M., Stedtfeld, R. D., et al. (2020). Alterations in the endophyte-enriched root-associated microbiome of rice receiving growth-promoting treatments of urea fertilizer and rhizobium biofertilizer. *Microb. Ecol.* 79, 367–382. doi: 10.1007/s00248-019-01406-7

Khan, A., Khan, S., Khan, M. A., Qamar, Z., and Waqas, M. (2015). The uptake and bioaccumulation of heavy metals by food plants, their effects on plants nutrients, and associated health risk: A review. *Environ. Sci. pollut. Res.* 22, 13772–13799. doi: 10.1007/s11356-015-4881-0

Kim, H. S., Kim, K. R., and Kim, H. J. (2015). Effect of biochar on heavy metal immobilization and uptake by lettuce (*Lactuca sativa l.*) in agricultural soil. *Environ. Earth Sci.* 74 (2), 1249–1259. doi: 10.1016/j.jenvman.2018.11.013

Kopittke, P. M., and Wang, P. (2017). Kinetics of metal toxicity in plant roots and its effects on root morphology. *Plant Soil* 419, 269–279. doi: 10.1007/s11104-017-3342-6

Kováčik, J., and Bačkor, M. (2007). Phenylalanine ammonia-lyase and phenolic compounds in chamomile tolerance to cadmium and copper excess. *Water Air Soil pollut.* 185, 185–193. doi: 10.1007/s11270-007-9441-x

Lai, J. L., Zhang, X. D., and Xiao, H. J. (2020). Absorption and interaction mechanisms of uranium & cadmium in purple sweet potato (*Ipomoea batatas* l.). *J. Hazard. Mater.* 400, 123264. doi: 10.1016/j.jhazmat.2020.123264

Lambrechts, T., Lequeue, G., Lobet, G., Lobet, G., Godin, B., Bielders, C. L., et al. (2014). Comparative analysis of cd and zn impacts on root distribution and morphology of *Lolium perenne* and *Trifolium repens*: implications for phytostabilization. *Plant Soil.* 376, 229–244. doi: 10.1007/s11104-013-1975-7

Lehmann, J., Rillig, M. C., Thies, J., Masiello, C. A., Hockaday, W. C., and Crowley, D. (2011). Biochar effects on soil biota-a review. *Soil Biol. Biochem.* 43 (9), 1812–1836. doi: 10.1016/j.envpol.2013.07.025

Li, L., Aslam, M., Rabbi, F., Vanderwel, M. C., Ashton, N. W., and Suh, D. (2018). PpORS, an ancient type III polyketide synthase, is required for integrity of leaf cuticle and resistance to dehydration in the moss, *Physcomitrella patens*. *Planta* 247, 527–541. doi: 10.1016/j.envpol.2013.07.025

Liu, Y., Fu, B., Liu, C., Shen, Y., and Lan, Z. (2020). Temporal variation and distribution of size fractionated: platinum group elements and heavy metals in total suspended particulate. *Meteorol. Atmos. Phys.* 132, 483–488. doi: 10.1007/s00703-019-00705-5

Liu, R. X., Zhou, Z. G., Guo, W. Q., Chen, B. L., and Oosterhuis, D. M. (2008). Effects of n fertilization on root development and activity of water-stressed cotton (*Gossypium hirsutum* l.) plants. *Agr. Water Manage.* 95, 1261–1270. doi: 10.1016/j.agwat.2008.05.002

Nan, G. J., Meng, X. X., Song, N., Liu, Z. Z., Liu, Y., Li, Y. Z., et al. (2020). Uptake and distribution characteristic and health risk assessment of heavy metal(loid)s in *Platycodon grandiflorum* (Jacq.) A.DC. with growth from a medicinal herb garden of xi'an, China. *Biol. Trace Elem. Res.* 153, 2770–2778. doi: 10.1007/s12011-020-02364-9

Nascimento, A., Maciel, A. M., Silva, J. B. G., Mendonça, H. V., Paula, V. R., and Otenio, M. H. (2020). Biofertilizer application on corn (*Zea mays*) increases the productivity and quality of the crop without causing environmental damage. *Water Air Soil pollut.* 231, 414. doi: 10.1007/s10661-019-7573-2

Ng, C. C., Boyce, A. N., Abas, M. R., Mahmood, N. Z., and Han, F. X. (2019). Phytoassessment of vetiver grass enhanced with EDTA soil amendment grown in single and mixed heavy metal-contaminated soil. *Environ. Monit. Assess.* 191, 434. doi: 10.1007/s10661-019-7573-2

Ng, C. C., Boyce, A. N., Abas, M. R., Mahmood, N. Z., and Han, F. X. (2020). Evaluation of vetiver grass uptake efficiency in single and mixed heavy metal contaminated soil. *Environ. Process.* 7, 207–226. doi: 10.1007/s40710-019-00418-2

Ogunkunle, C. O., Varun, M., Ogundele, I. G., Olorunmaiye, K. S., and Paul, M. S. (2018). Citrus epicarp-derived biochar reduced cd uptake and ameliorates oxidative stress in young *Abelmoschus esculentus* (L.) moench (okra) under low cd stress. *Bull. Environ. Contam. Toxicol.* 100, 827–833. doi: 10.1007/s00128-018-2339-z

Olmo, M., Villar, R., Salazar, P., and Manuel, O. (2016). Changes in soil nutrient availability explain biochar's impact on wheat root development. *Plant Soil* 399, 333–343. doi: 10.1007/s11104-015-2700-5

Paoletti, F., Aldinucci, D., Mocali, A., and Caparrini, A. (1986). A sensitive spectrophotometric method for the determination of superoxide dismutase activity in tissue extracts. *Anal. Biochem.* 154 (2), 536–541. doi: 10.1016/0003-2697(86)90026-6

Rawlins, B. G., McGrath, S. P., Scheib, A. J., Breward, N., Cave, M., Lister, T. R., et al. (2012). *The advanced soil geochemical atlas of England and wales British geological survey* (Keyworth, Nottingham, U.K.: British Geological Survey, Environmental Science Centre).

Rizwan, M., Ali, S., Adrees, M., Rizvi, H., Zia-ur-Rehman, M., Hannan, F., et al. (2016). Cadmium stress in rice: toxic effects, tolerance mechan-isms, and management: a critical review. *Environ. Sci. pollut. Res.* 23, 17859–17879. doi: 10.1007/s11356-016-6436-4

Shah, K., and Nahakpam, S. (2012). Heat exposure alters the expression of SOD, POD, APX and CAT isozymes and mitigates low cadmium toxicity in seedlings of sensitive and tolerant rice cultivars. *Plant Physiol. Biochem.* 57, 106–113. doi: 10.1016/j.plaphy.2012.05.007

Singh, J., Sabir, F., Sangwan, R. S., Narnoliya, L. K., Saxena, S., and Sangwan, N. S. (2015). Enhanced secondary metabolite production and pathway gene expression by leaf explants-induced direct root morphotypes are regulated by combination of growth regulators and culture conditions in *Centella asiatica* (L.) urban. *Plant Growth Regul.* 75, 55–66. doi: 10.1007/s10725-014-9931-y

Song, J., Feng, S. J., Chen, J., Zhao, W. T., and Yang, Z. M. (2017). A cadmium stress-responsive gene *AtFC1* confers plant tolerance to cadmium toxicity. *BMC Plant Biol.* 17, 187. doi: 10.1186/s12870-017-1141-0

Sun, C. X., Chen, X., Cao, M. M., Li, M. Q., and Zhang, Y. L. (2017). Growth and metabolic responses of maize roots to straw biochar application at different rates. *Plant Soil* 416, 487–502. doi: 10.1007/s11104-017-3229-6

Sun, C. X., Chen, L. J., Wu, Z. J., Zhou, L. K., and Shimizu, H. (2007). Soil persistence of *Bacillus thuringiensis* (Bt) toxin from transgenic bt cotton tissues and its effect on soil enzyme activities. *Biol. Fertil. Soils* 43, 617–620. doi: 10.1007/s00374-006-0158-6

Vinci, G., Cozzolino, V., Mazzei, P., Monda, H., Savy, D., Drosos, M., et al. (2018). Effects of *Bacillus amyloliquefaciens* and different phosphorus sources on maize plants as revealed by NMR and GC-MS based metabolomics. *Plant Soil.* 429, 437–450. doi: 10.1007/s11104-018-3701-y

Wang, Y. Q., Liu, J. G., Zhao, G. Y., Geng, Z., Qi, H., Dou, H. K., et al. (2020). Dynamic transcriptome and co-expression network analysis of the cotton (*Gossypium hirsutum* l.) root response to salinity stress at the seedling stage. *Acta Physiol. Plant* 42, 143. doi: 10.1007/s11738-020-03117-w

Wang, Y., Xu, L., Shen, H., Wang, J., Liu, W., Zhu, X., et al. (2015). Metabolomic analysis with GC-MS to reveal potential metabolites and biological pathways involved in Pb & cd stress response of radish roots. *Sci. Rep.* 5, 18296. doi: 10.1038/srep18296

Wu, C. S., Zhu, H., Van, W. G. P., and Choi, Y. H. (2016). Metabolomics-guided analysis of isocoumarin production by *Streptomyces* species MBT76 and biotransformation of flavonoids and phenylpropanoids. *Metabolomics* 12, 90. doi: 10.1007/s11356-019-07262-9

Yang, X., Liu, J., McGrouther, K., Huang, H., Lu, K., Guo, X., et al. (2016). Effect of biochar on the extractability of heavy metals (Cd, Cu, Pb, and zn) and enzyme activity in soil. *Environ. Sci. pollut. Res.* 23, 974–984. doi: 10.1007/s11356-015-4233-0

Yang, Y., and Shen, Q. (2020). Phytoremediation of cadmium-contaminated wetland soil with *Typha latifolia* l. and the underlying mechanisms involved in the heavy-metal uptake and removal. *Environ. Sci. pollut. Res.* 27, 4905–4916. doi: 10.1007/s11356-019-07256-7

Zhang, Y., Zhao, C., Chen, G., Zhou, J. L., Chen, Z., Li, Z. X., et al. (2020). Response of soil microbial communities to additions of straw biochar, iron oxide, and iron oxide-modified straw biochar in an arsenic-contaminated soil. *Environ. Sci. pollut. Res.* 27, 23761–23768. doi: 10.1007/s11356-020-08829-7

Zhou, M. X., Renard, M. E., Quinet, M., and Lutts, S. (2019). Effect of NaCl on proline and glycinebetaine metabolism in *Kosteletzkya pentacarpos* exposed to cd and zn toxicities. *Plant Soil.* 441, 525–542. doi: 10.1007/s11104-019-04143-5

Zhu, Y. Q., Zhong, M. T., Li, W. D., Qiu, Y., Wang, H. J., and Lv, X. (2022). Cotton straw biochar and bacillus compound biofertilizer decreased cd migration in alkaline soil: Insights from relationship between soil key metabolites and key bacteria. *Ecotox. Environ. Safe.* 232, 113293. doi: 10.1016/j.ecoenv.2022.113293

Appendix A. Supplementary material

All data generated or analyzed during this study are available from the corresponding author on reasonable request.

frontiers | Frontiers in Plant Science

TYPE Original Research
PUBLISHED 17 November 2022
DOI 10.3389/fpls.2022.1056193

Check for updates

OPEN ACCESS

EDITED BY
Bhaskar Gupta,
Government General Degree College,
Singur, India

REVIEWED BY
Zhipeng Liu,
Lanzhou University, China
Xuebin Zhang,
Henan University, China

*CORRESPONDENCE
Yong Li
xmliyong@sdau.edu.cn
Zhenlin Wang
zlwang@sdau.edu.cn

†These authors have contributed equally to this work

SPECIALTY SECTION
This article was submitted to Plant Abiotic Stress, a section of the journal Frontiers in Plant Science

RECEIVED 28 September 2022
ACCEPTED 02 November 2022
PUBLISHED 17 November 2022

CITATION
Luo Y, Chang Y, Li C, Wang Y, Cui H, Jin M, Wang Z and Li Y (2022) Shading decreases lodging resistance of wheat under different planting densities by altering lignin monomer composition of stems.
Front. Plant Sci. 13:1056193.
doi: 10.3389/fpls.2022.1056193

COPYRIGHT
© 2022 Luo, Chang, Li, Wang, Cui, Jin, Wang and Li. This is an open-access article distributed under the terms of the Creative Commons Attribution License (CC BY). The use, distribution or reproduction in other forums is permitted, provided the original author(s) and the copyright owner(s) are credited and that the original publication in this journal is cited, in accordance with accepted academic practice. No use, distribution or reproduction is permitted which does not comply with these terms.

Shading decreases lodging resistance of wheat under different planting densities by altering lignin monomer composition of stems

Yongli Luo†, Yonglan Chang†, Chunhui Li, Yuanyuan Wang, Haixing Cui, Min Jin, Zhenlin Wang* and Yong Li*

State Key Laboratory of Crop Biology, College of Agronomy, Shandong Agricultural University, Tai'an, Shandong, China

To clarify the influences of shading stress and planting density on the lignin monomer composition of wheat stems and their relationship with lodging resistance, Lodging resistant variety Shannong 23 (SN23) and lodging sensitive variety Shannong 16 (SN16) were grown during 2018–2019 and 2019–2020 growing seasons. The planting densities were 150×10^4 plants ha^{-1} (D1), 225×10^4 plants ha^{-1} (D2) and 300×10^4 plants ha^{-1} (D3). At the jointing stage, an artificial shading shed was used to simulate shading stress. Then the effects of shading on stem morphological characteristics, lignin monomer composition and lodging resistance of wheat under different planting densities were studied. Results indicate that shading at the jointing stage increased the length of basal internodes and the plant height and moved the height of center of gravity (CG) upward. Moreover, the stem diameter and the wall thickness decreased by 0.10–0.53 mm and 0.18–0.40 mm, respectively. The stem filling degree was reduced accordingly. As indicated by the correlation analysis and the stepwise regression analysis, shading-induced lodging mainly resulted from changes in the stem morphological characteristics and lignin accumulation. The influential magnitude of these factors was ordered as follows: stem filling degree, wall thickness, lignin content, contents and proportions of monomers S and H, and length of the second internode. The expression abundance of *TaPAL*, *TaCOMT*, *TaCCR*, and *TaCAD* declined in response to shading stress and high planting density. As a result, the distribution ratios of photosynthetic carbon sources to lignin monomers S, G and H were changed. The lignin content of stems on the day 42 after the jointing stage decreased by 18.48%. The monomer S content decreased, while the content and proportion of monomer H increased, thus weakening the breaking strength of wheat stems.

KEYWORDS

wheat, shading, stem, lignin, lodging

1 Introduction

Wheat is the main grain crop in China. To ensure China's food security, it is crucial to consistently raise the yield of wheat produced per unit of land area. In recent years, with the impact of global climate change, wheat has frequently encountered rainy and sunless weather during its growing season, indicating decreased solar radiation (Yang et al., 2022). According to reports, the total sunshine hours in the Huang-Huai-Hai wheat region of China have decreased by 3.74–9.22 hours annually on average. Furthermore, sunshine hours have reduced by 2.98–3.67 hours annually on average during the winter wheat growing season (Cai and Jiang, 2011). Low light stress dramatically affects the lodging resistance of wheat stems by reducing stem filling degree (Hussain et al., 2019). Increasing plant density to enhance spikes per unit area is the main cultivation measure to further improve the wheat yield. However, among the dense planting population, the light environment becomes worse, including the weakened light intensity and the reduced ratio of red light to far red light, and so on. As a result, shading avoidance response arises, such as increased stem elongation and decreased stem diameter (Pantazopoulou et al., 2021), resulting in the poor quality of stems and a high risk of lodging. Stem lodging has become a significant barrier to the improvement of yield and quality in wheat. Consequently, studying the mechanism of low light stress on stem lodging of wheat with different population structures has crucial theoretical and productive significance.

Stem lodging is the permanent displacement of stems in the vertical direction (Dixon et al., 2020). Lignin is an important raw material for secondary wall thickening. In the lignification of plant cell walls, lignin is synthesized in the cytoplasm and transported to the polysaccharide framework of the cell walls for polymerization and deposition. In this way, the hardness of the tissue can be enhanced and the support and pressure resistance of cells can be increased (Alejandro et al., 2010; Miao and Liu, 2010). Lignin is strongly related to the lodging resistance of crop stems (Hussain et al., 2020). The lignin content accounts for 10%–20% of gramineous crops (Ragauskas et al., 2014). Increasing lignin content results in higher mechanical strength of crop stems, while decreasing lignin content causes a higher lodging risk (Wang et al., 2015; Chen et al., 2018). Rice dwarf mutant pex that has high expression of lignin synthesis pathway genes and high lignin content in the stem owns strong lodging resistance (Ke et al., 2019).

Lignin is mainly polymerized by three monomers, syringyl lignin (S), guaiacyl lignin (G) and p-hydroxyphenyl lignin (H). When the total lignin content maintains constant, changes in lignin monomer composition have no significant effect on the morphology and development of plants (Vanholme et al., 2012). However, the contents and proportions of lignin monomers are closely related to the lodging resistance of plants (Li et al., 2017). The high monomer G content improves the lodging resistance of rice stems (Li et al., 2015). The S/G ratio is negatively correlated with lodging resistance (Wei et al., 2017). Zheng et al. (2017a) discovered that the decreased monomer S content, the decreased S/G ratio, and the increased monomer H content are the key causes for decreasing the breaking strength under high nitrogen fertilizer and high density. It was also found that monomer S can help improve the breaking strength of wheat stems, the dominant structural units. However, the high proportion of monomer H is not conducive to the breaking strength of wheat stems (Luo et al., 2019). Paeonia lactiflora mutants overexpressing *HCT* have higher breaking strength due to their increased lignin content and contents of monomers G and S (Zhao et al., 2021). To summarize, the findings on the relationship between lignin monomers composition and lodging resistance of crop stems are inconsistent, so the relationship needs to be further clarified. Therefore, it is necessary to further study the changes in lignin monomers composition in wheat stems in response to low light stress and its relationship with lodging resistance.

Plants synthesize lignin through a series of biochemical reactions, which require many enzymes (Figure S1). Phenylalanine ammonia lyase (PAL), cinnamate 4-hydroxylase (C4H), p-coumaroyl shikimate 3'-hydroxylase (C3'H), p-hydroxycinnamoyl CoA:shikimate/quinate hydroxycinnamoyltransfera (HCT), and 4-hydroxycinnamate:CoA ligase (4CL) are the key enzymes of carbon flow distribution in the lignin synthesis pathway. Downregulation of these genes can decrease the lignin content, change the lignin monomer composition, and thus weaken the rigidity of stems (Xu et al., 2011; Sykes et al., 2015; Liu et al., 2019; Fang et al., 2020). Ferulate/coniferaldehyde 5-hydroxylase (F5H), caffeate/5-hydroxyferulate 3-O-methyltransferase (COMT) and caffeoyl-CoA 3-O-methyltransferase (CCoAOMT) are the key enzymes in the formation of lignin monomers. Downregulation of these genes has no significant effect on total lignin content,but can change the composition of lignin monomers and thus decrease the breaking strength of stems (Wagner et al., 2011). Peroxidase (POD) and laccase (LAC) are key enzymes in the lignification process at later stages (Ruben et al., 2010; Fetherolf et al., 2020).

Lignin is a photosensitive phenolic compound. Changes in the light environment directly affect the lignin synthesis pathway. Due to shading stress, the expression abundance of *PAL*, *4CL*, *F5H*, and *LAC* dropped, reducing the lignin content in the tea plant (Teng et al., 2021). Low light stress reduced the expression of *C3'H*, *CCR*, *CCoAOMT*, and *POD* and decreased the activities of POD, CAD, 4CL and PAL, finally reducing the lignin content in soybean stems (Liu et al., 2018; Hussain et al., 2021). However, it is unclear about the mechanisms of lignin monomers composition in response to low light stress in wheat under different planting densities. Thus it is urgent to ascertain this mechanism in the study of lodging resistance and yield increase cultivation of wheat.

In summary, the effects of low light stress on lignin metabolism, and lignin monomers composition, as well as

their relationships with lodging resistance are required to be further studied. Hence, in this experiment, low light stress at the jointing stage was simulated using artificial shading targeting two wheat varieties with significantly different lodging resistance in different planting densities. Ultimately, this study aims to explore a cultivation regulation way for increasing lodging resistance under the conditions of overcast rain and scant sunshine and guide for the breeding of wheat varieties with lodging resistance and shade tolerance.

2 Materials and methods

2.1 Experimental site

A field experiment was conducted at the agricultural experiment station of Shandong Agricultural University in Tai'an City, Shandong Province (36°9'N, 117°9'E; altitude 128 m) during the two wheat growing seasons of 2018–2019 and 2019–2020. This region where the experimental site is located has a warm temperate semi-humid continental monsoon climate. During the wheat growing season, it has solar radiation of 3141.33 MJ m^{-2}, an average temperature of 8.92°C, and precipitation of 193.06 mm. The soil of the experimental site is sandy loam, on which corn was planted. All the corn stalks were returned to the field after harvest. Before sowing, the soil at a depth of 0–20 cm had organic matter content of 12.81 **g** kg^{-1}, total nitrogen was 1.08 **g** kg^{-1}, alkali hydrolyzable nitrogen of 87.3 **g** kg^{-1}, available phosphorus of 31.21 **g** kg^{-1}, and available potassium of 91.83 **g** kg^{-1}.

2.2 Experimental design

Two winter wheat varieties with significantly different lodging resistance, lodging sensitive variety Shannong 16 (SN16) and lodging resistant variety Shannong 23 (SN23), were planted in the main area. The sub area was shading treatment, with natural light (S0) as the control, including shading from the jointing stage to the heading stage (S1) and shading from the jointing stage to the maturity stage (S2). Three planting densities were set in the sub-sub area, which were 150 × 10^4 plants ha^{-1} (D1), 225 × 10^4 plants ha^{-1} (D2) and 300 × 10^4 plants ha^{-1} (D3). The specific treatment methods were as follows: at the jointing stage (when the first basal internode of wheat elongates to 1.5–2 cm), a removable shading shed was built using a self-made scaffold and a black nylon net with light transmittance of 50% for shading treatment. The photosynthetic effective radiation (PAR) intensity at 1 m above ground from the jointing stage (April 5, 2020) to the maturity stage (June 9, 2020) of wheat under normal light and shading treatment was shown in Figure S2. Shading stress treatment significantly reduced the PAR intensity in the upper part of wheat canopy. In order to ensure the normal ventilation conditions, the height of the shed top was 2 m from the ground. Each process was repeated three times, and the area of each plot was 3 m × 3 m = 9 m^2. Artificial furrow was used for planting and seedlings were fixated at the three leaf stage. The nitrogen fertilizer used was urea (46% N), with a total application amount of 240 kg ha^{-1}. Specifically, 50% was used as base fertilizer, and the remaining 50% was used as topdressing at the jointing stage. Total application amounts of potassium chloride (60% K_2O) and calcium superphosphate (12% P_2O_5) were 120 kg ha^{-1} and 150 kg ha^{-1}, respectively. Both phosphorus and potassium fertilizers were applied as base fertilizers at one time. Other field management was the same as that of general high-yield fields. The sowing dates during wheat growing seasons were October 8, 2018 and October 12, 2019 and the corresponding and harvest dates were June 6, 2019 and June 9, 2020.

2.3 Determination items and methods

2.3.1 Determination of light interception of wheat canopy

The SunScan (Delta, UK) canopy analyzer was adopted. At the anthesis stage (GS65), sunny and cloudless weather was chosen. From 10:00 to 13:00, the PAR in the upper part of the wheat canopy (10 cm above the spike) = and the PAR at the bottom (TPAR) in the lower part of the wheat canopy (10 cm from the ground) were measured. The canopy PAR interception rate (CaR) was calculated as follows: CaR(%) = (PAR-TPAR)/PAR × 100%.

2.3.2 Determination of morphological characteristics and filling degree of wheat stems

At anthesis stage (GS65), milk stage (GS75) and dough stage (GS85) (Zadoks et al., 1974), the morphological indexes including plant height, internode length, height of center of gravity, stem diameter and wall thickness were measured.

Wheat stems filling degree was measured from the second basal internode with a length of 2 cm. At this time, it was recorded as day 0, and samples were taken every 7 days. Samples were oven-dried at 105°C for 30 min and then oven-dried at 50°C to constant weight. The dry weight per unit length was used to define the filling degree.

2.3.3 Determination of breaking strength of wheat stems

At anthesis stage (GS65), milk stage (GS75), and dough stage (GS85), ten uniform stems were selected for each treatment, with their second basal internodes were cut. Then the YYD-1 strength tester (Zhejiang Top Instrument Co., Ltd.) was used to measure the breaking strength of stems according to previous studies (Peng et al., 2014).

2.3.4 Determination of lignin content in wheat stems

The sampling method was the same as 3.3.2. Ten uniform stems were selected for each treatment. The second basal internodes were cut and quickly frozen in liquid nitrogen and then stored in a -80°C refrigerator for determination of lignin content according to previous studies (Zheng et al., 2017a). The lignin content was expressed by the absorbance value at 280 nm per milliliter of fresh sample per unit mass.

2.3.5 Determination of lignin monomers in wheat stems

The sampling method was the same as 3.3.2. Twenty uniform stems were selected for each treatment. Samples were oven-dried at 105°C for 30 **min** and then oven-dried at 50°C to constant weight. Lignin monomers were determined by alkaline nitrobenzene oxidation method (Zheng et al., 2017b). The qualitative and quantitative analysis of lignin monomers in wheat stems was carried out by ultra high performance liquid chromatography coupled with triple quadrupole mass spectrometry. The steps were as follows: 1.0 **g** of sample was weighed. Add 30 mL of NaCl, absolute ethanol solution, 95% ethanol, acetone, chromatographic chloroform/chromatographic methanol to remove the pigment, protein, lipid and other components in the sample. The sediment was put into the oven for drying at 50°C and then was accurately weighed. 0.02 **g** sediment was put into the digestion tube. 3 mL of 2 M NaOH and 0.5 ml of nitrobenzene was added into the tube for microwave digest at 170°C for 1 h. Then ethyl acetate was added for extraction after digestion. 7 ml of ethyl acetate phase was evaporated with a vacuum centrifuge concentrator (Thermo Fisher), 6 mL of 50% acetonitrile water was added for redissolution. Finally, the redissolved solution was filter through 0.22 μm organic system filter membrane for concentration determination.

2.3.6 Determination of gene expression of key enzymes in the lignin synthesis pathway of wheat stems

Samples were taken on day 0 when the second basal internode of wheat had an approximate length of 2 cm. After that, samples were taken every 7 days until the end of the dough stage (GS85). Five uniform stems were selected for each treatment. The second basal internodes were cut and ground into powder in liquid nitrogen. Ribonucleic acid (RNA) was extracted using the plant sample RNA extraction kit manufactured by Tiangen Biotechnology (Beijing, China; Cat. No. DP432), according to manufacturer instructions. The PrimeScript™ RT reagent Kit (TaKaRa Bio, No. RR047B) with g-deoxyribonucleic acid (gDNA) eraser was used for cDNA reverse transcription. The target gene and internal control of each sample were subject to quantitative real-time PCR (qRT-PCR), and each sample was tested in three replicates. The relative expression levels were analyzed using the comparative $2^{-\triangle\triangle CT}$ method. The primer sequences for *TaPAL*, *TaCCR*, *TaCAD*, *TaCOMT* and *TaActin* are listed in Table S1.

2.4 Statistical analysis

The obtained experimental data were statistically analyzed using Excel 2007 and DPS 7.05. Differences between mean values were determined using the least significant difference (LSD) test at $P < 0.05$ and $P < 0.01$. All figures were drawn using the Sigmaplot 10.0.

3. Results and analysis

3.1 Effects of shading on PAR interception rate of wheat under different planting densities

It was demonstrated that SN16 had a higher PAR interception rate than SN23 (Figure S3). Under the same planting density, shading reduced the PAR interception rate of wheatin the order of S0 > S1 > S2. Under the same shading treatment, the trend was D3 > D2 > D1.

3.2 Effects of shading on the plant height, internode configuration and CG height of wheat under different planting densities

The plant height, internode length and CG height (at the milk stage) of two wheat varieties are shown in Figure 1A. Compared with lodging sensitive wheat SN16, lodging resistant wheat SN23 had low values in plant height, the length of the 1st-4th basal internodes, and the CG height but higher values in the length of the 5th basal internode and spike length. With an increase in the planting density, the internode length, spike length, plant height, and CG height of two wheat varieties increased. When planting density was increased by 75×10^4 plants ha^{-1}, the plant height and CG height increased by 1.82 cm and 1.11 cm, respectively under shading from the jointing stage to the heading stage (S1), and increased by 1.57 cm and 0.86 cm, respectively under shading from the jointing stage to the maturity stage (S2).

Shading had significant effects on plant height, internode configuration and CG height of two wheat varieties. Under the same planting density, shading significantly increased plant height, CG height, length of the 2nd-5th internodes (especially the 4th internode), and spike length. Moreover, with the extension

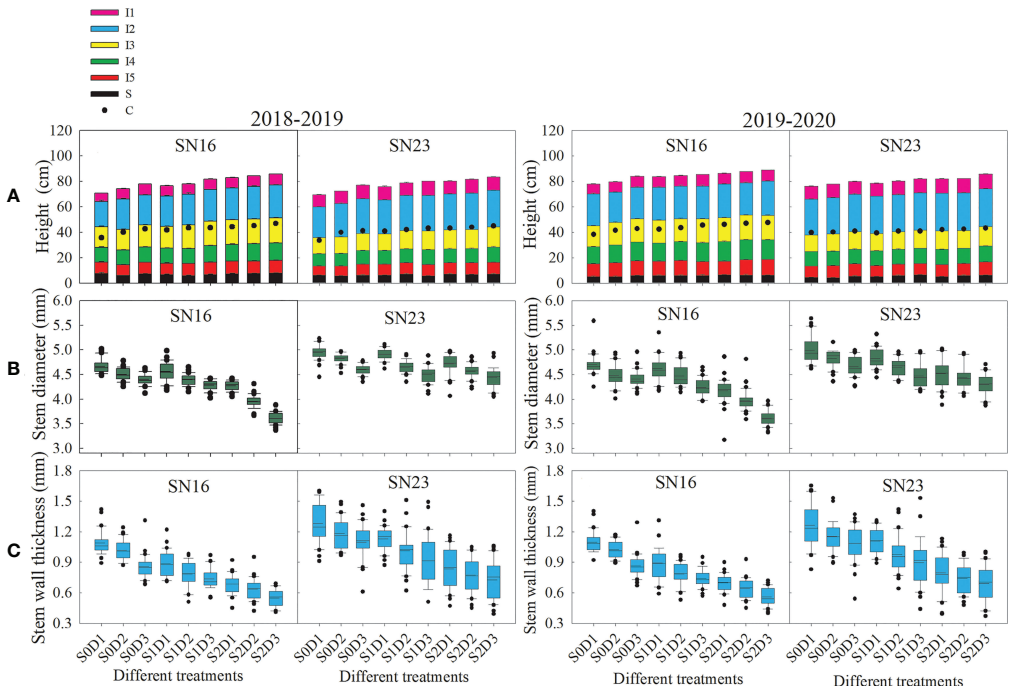


FIGURE 1
Effects of shading on morphological indexes stem of wheat under different planting densities. **(A)** Plant height, configuration of internnodes, and center of gravity of wheat at milk stage. Error bars represent the standard deviation of the mean (n = 10). **(B, C)** Stem diameter and wall thickness of the second basal internode. Solid lines and dotted line indicate medians and means, respectively. Box boundaries indicate upper and lower quartiles, whisker caps and points indicate internal limiting and outliers (n = 30).

of shading time, these indices significantly increased. As for the two wheat varieties in 2018–2019 wheat growing seasons, samples under treatments S1D1 and S2D1 had the average plant height increased by 8.88% and 19.35% and the average CG height increased by 16.17% and 26.01%, compared with those under treatment S0D1. Additionally, samples under S1D2 and S2D2 treatments had the average plant height increased by 7.17% and 13.23% and the average CG height increased by 6.74% and 11.22%, compared with those under treatment S0D2. Samples under treatments S1D3 and S2D3 had the average plant height increased by 4.51% and 9.20% and the average CG height increased by 3.55% and 9.37%, compared with those under treatment S0D3. The results suggested that the changing range of shading stress affecting the plant height and CG height of two wheat varieties decreased with increased density, which might be due to shade avoidance response (Figure 1A).

3.3 Effects of shading on the stem diameter and wall thickness of wheat under different planting densities

The stem diameter and wall thickness of the second basal internode were measured at the anthesis, milk, and dough stages. The results show that lodging resistant variety SN23 had much larger values than the lodging sensitive variety SN16 (Figures 1B, C). With increasing planting density, the stem diameter and wall thickness of the second basal internode of wheat decreased significantly. When planting density was increased by 75×10^4 plants ha^{-1}, samples under S0, S1, and S2 treatments had the average stem diameter decreased by 0.15 mm, 0.18 mm and 0.21 mm, and the average wall thickness reduced by 0.10 mm, 0.09 mm and 0.06 mm, respectively, under S0, S1, and S2 treatments.

Taken 2018–2019 wheat season as an example, compared with those under S0D1 treatment, the stem diameter of two wheat varieties was increased by 0.10 mm and 0.41 mm on average, and thickness increased by 0.18 mm and 0.43 mm on average, respectively, under S1D1 and S2D1 treatments. Additionally, compared with those under S0D2 treatment, the stem diameter of two wheat varieties was increased by 0.12 mm and 0.42 mm on average, and thickness increased by 0.20 mm and 0.40 mm on average, respectively, under S1D2 and S2D2 treatments. Compared with those under S0D3 treatment, the stem diameter of two wheat varieties was increased by 0.15 mm and 0.53 mm on average, and thickness increased by 0.16 mm and 0.35 mm on average, respectively, under S1D3 and S2D3 treatments (Figures 1B, C).

3.4 Effects of shading on the filling degree of the second basal internode in wheat under different planting densities

With the progress of growth, the filling degree of wheat stems first increased, then decreased, and finally peaked on day 28 after the formation of the second basal internode (Figure 2). Lodging resistant wheat SN23 had a significantly higher filling degree than lodging sensitive wheat SN16 in the second basal internode. Shading and planting density had significant negative effects on the stem filling degree of two wheat varieties. With increasing planting density, the second basal internode filling degree of wheat was decreased significantly.

When planting density was increased by 75×10^4 plants ha^{-1}, the average stem filling degree of samples under S0, S1, and S2 treatments was decreased by 1.93 mg cm^{-1}, 1.33 mg cm^{-1}, and 1.44 mg cm^{-1}, respectively. As for the two wheat varieties in 2018-2019 wheat season, samples under treatments S1D1 and S2D1 had the average stem filling degree increased by 4.02 mg cm^{-1} and 6.89 mg cm^{-1}, compared with those under treatment S0D1. Additionally, samples under S1D2 and S2D2 treatments had the average stem filling degree increased by 3.16 mg cm^{-1} and 6.17 mg cm^{-1}, compared with those under treatment S0D2. Samples under treatments S1D3 and S2D3 had the average stem filling degree increased by 2.82 mg cm^{-1} and 5.91 mg cm^{-1}, compared with those under treatment S0D3 (Figure 2).

3.5 Effects of shading on the breaking strength of wheat stems under different planting densities

In field production, the lodging of wheat stems usually occurs in the middle and late stages. Therefore, the breaking strength of the second basal internode was measured at the anthesis stage (GS65), milk stage (GS75) and dough stage (GS85) of wheat in 2018–2019 and 2019–2020. The results show that the lodging sensitive variety SN16 had significantly weak breaking strength than lodging resistant variety SN23 (Figure 3). With the process of growth, the second basal internode of the two wheat varieties had gradually decreased breaking strength, shown as GS65 > GS75 > GS85. The breaking strength of the second basal internode of two wheat varieties was decreased with increased planting density at different stages, shown as D1 > D2 > D3. Shading treatment significantly reduced the breaking strength of stems, and with the extension of shading time, the declined range of stem breaking strength was increased. As for the two wheat varieties in 2018–2019 wheat season,

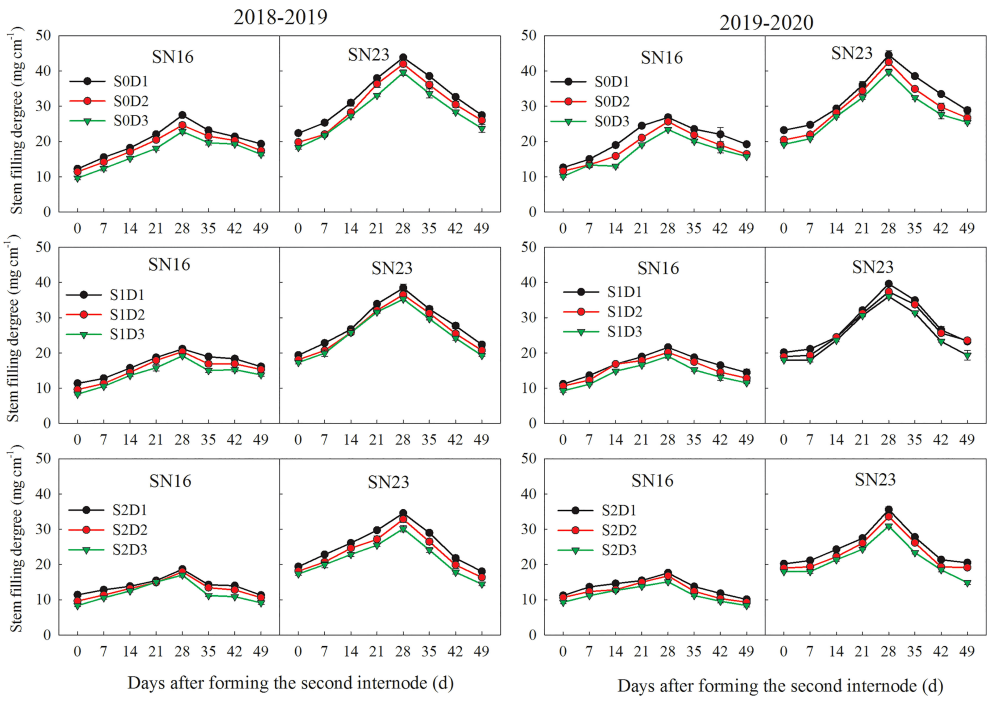


FIGURE 2
Effects of shading on filling degree of the second basal internode of wheat under different planting densities. Error bars represent the standard deviation of the mean (n = 10).

10.3389/fpls.2022.1056193

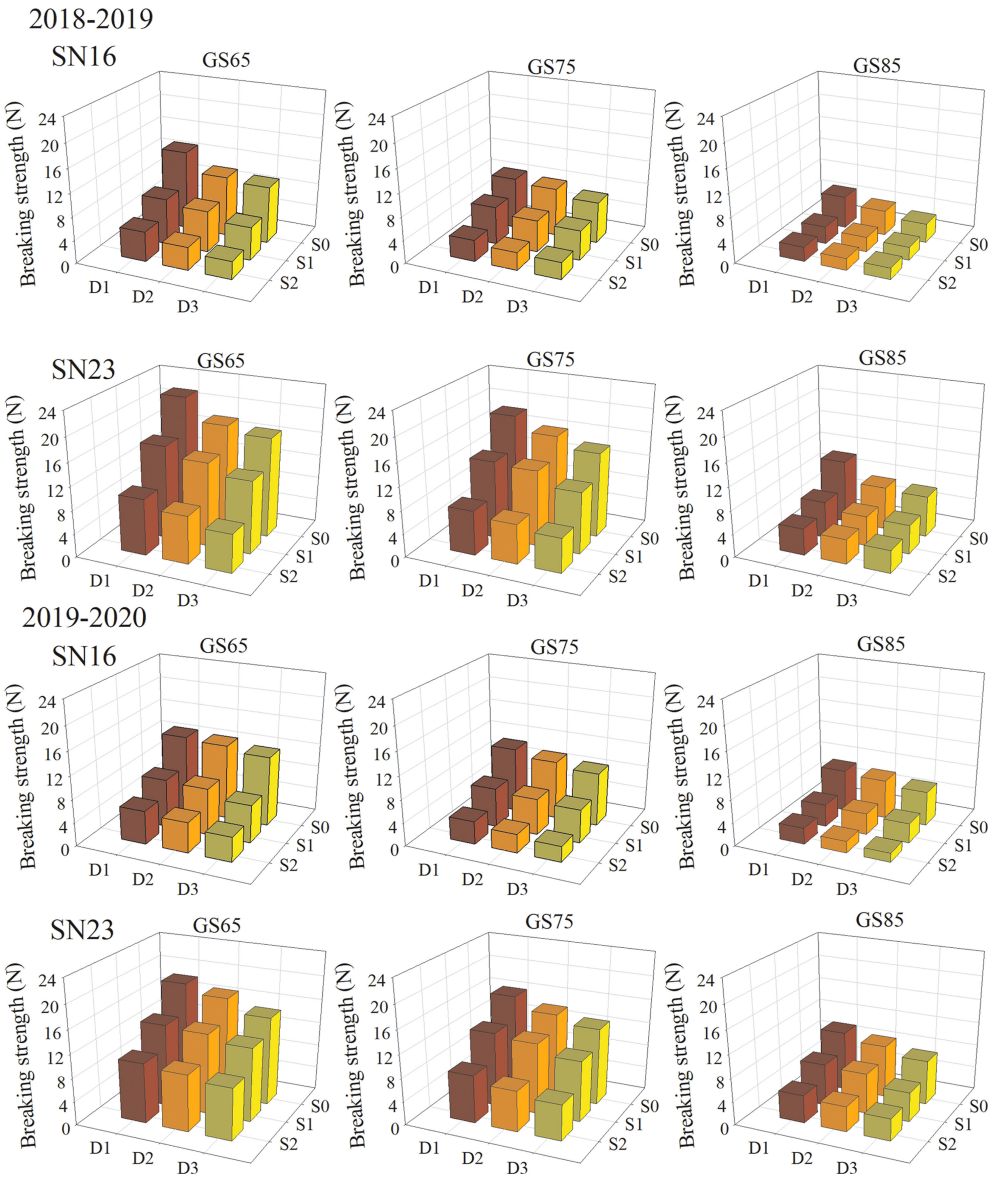


FIGURE 3
Effects of shading on breaking strength in different winter wheat populations at anthesis stage.

samples under treatments S1D1 and S2D1 had the average breaking strength increased by 34.47% and 58.49%, compared with those under treatment S0D1. Additionally, samples under S1D2 and S2D2 treatments had the average breaking strength increased by 28.21% and 57.16%, compared with those under treatment S0D2. Samples under treatments S1D3 and S2D3 had the average breaking strength increased by 31.26% and 58.84%, compared with those under treatment S0D3 (Figure 3). Taken 2018–2019 wheat season as an example, compared with that under S0D1 treatment, breaking strength of two wheat varieties was increased by 34.47%, and 58.49% on average, respectively, under S1D1 and S2D1 treatments. Additionally, compared with that under S0D2 treatment, breaking strength of two wheat varieties was increased by 28.21%, and 57.16% on average, respectively, under S1D2 and S2D2 treatments. Compared with that under S0D3 treatment, breaking strength of two wheat varieties was increased by 31.26%, and 58.84% on average, respectively, under S1D3 and S2D3 treatments.

3.6 Effects of shading on the lignin content of wheat stems under different planting densities

Lignin accumulation in wheat stems gradually increased with the process of growth (Figure 4). The accumulation rate of lignin was faster from 0 to 28 days, while the rate tended to be relatively flat from 28 to 42 days. Compared with that of lodging sensitive wheat SN16, lignin accumulation of lodging resistant wheat SN23 was higher. Lignin accumulation of wheat stems was decreased significantly with increasing planting density. Taken 2018–2019 wheat season as an example, when planting density was increased by 75 × 10^4 plants ha^{-1}, lignin accumulation decreased by 10.14%, 11.01%, and 12.67% on average, respectively, under S0, S1, and S2 treatments. This indicates that lignin accumulation of wheat stems was more sensitive to increasing planting density under shading treatment.

Under the same planting density condition, shading significantly reduced the lignin accumulation of wheat stems, and with the extension of shading time, the decreased range became larger. As for the two wheat varieties in 2018–2019 wheat season, samples under treatments S1D1 and S2D1 had average lignin accumulation decreased by 13.56% and 27.07%, compared with those under treatment S0D1. Additionally, samples under S1D2 and S2D2 treatments had average lignin accumulation increased by 14.23% and 29.01%, compared with those under treatment S0D2. Samples under treatments S1D3 and S2D3 had average lignin accumulation increased by 14.53%, and 29.17%, compared with those under treatment S0D3.

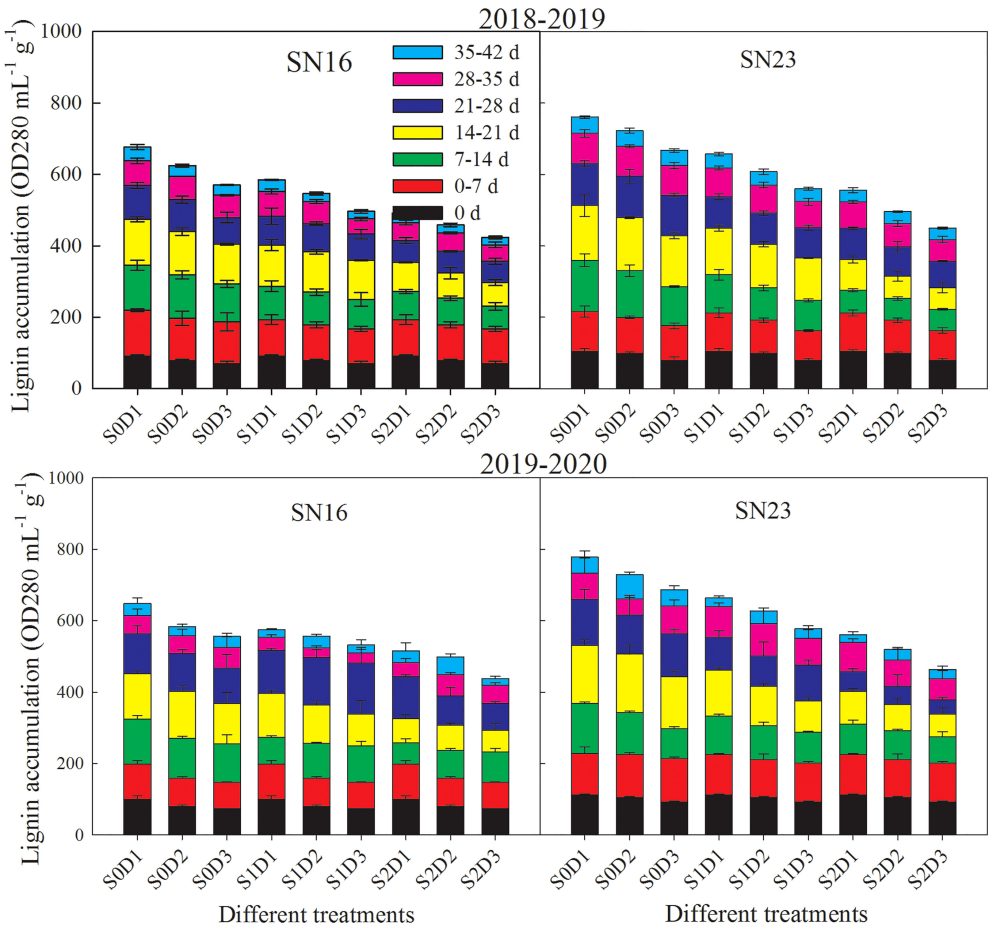


FIGURE 4
Effects of shading on the content of lignin in wheat stems under different planting densities. Error bars represent the standard deviation of the mean (n = 3).

10.3389/fpls.2022.1056193

3.7 Effects of shading on the content and proportion of lignin monomers in wheat stems under different planting densities

As shown in Figure 5, with the advance of growth process, the content of three lignin monomers and the proportion of S monomer increased, the proportion of H monomer decreased, but the proportion of G monomer varied with different varieties and treatments. Compared with those of lodging sensitive wheat variety SN16, lodging resistant wheat variety SN23 had higher content of S, G, and H monomers, higher proportion of S and G monomers, but a lower proportion of H monomer.

With increasing planting density, the content of S and G monomers in wheat stems decreased, and the content and proportion of H monomer increased. Nevertheless, the proportion of S and G monomers varied with different wheat varieties and treatments. Taken 2018–2019 wheat season as an



FIGURE 5
Effects of shading on the lignin monomers content **(A)** and the proportion of lignin monomers **(B)** in wheat stems under different planting densities. Error bars represent the standard deviation of the mean (n = 3).

example, when the planting density was increased by 75 × 10^4 plants ha^{-1}, the content of S and G monomers was decreased by 58.02 μg g^{-1}, and 50.92 μg g^{-1}, while, the content and proportion of H monomer was enhanced by 12.26 μg g^{-1}, and 13.29%.

Under the same planting density, shading reduced the content and proportion of S and G monomers in wheat stems, and increased those of H monomer. Taken 2018–2019 wheat season as an example, under shading treatment from jointing stage to heading stage (S1), the content and proportion of S monomer were decreased by 245.68 μg g^{-1}, and 2.20%, respectively, the content and proportion of G monomer were decreased by 221.58 μg g^{-1}, and 2.37%, but those of H monomer were increased by 36.67 μg g^{-1}, and 4.57%. Under low density (D1), shading treatment reduced the proportion of S and G monomers and increased the proportion of H monomer, both of which were greater than those under high density (D2, and D3).

3.8 Effects of shading on the expression abundance of lignin monomers synthesis genes in wheat stems under different planting densities

The relative expression of *TaPAL* and *TaCAD* decreased with the progress of growth (Figures 6A, D), By contrast the relative expression of *TaCOMT*, and *TaCCR* first increased, then decreased, and finally peaked on day 7 and day 14, respectively (Figures 6B, C).

Compared with that under treatment S0D1, the relative expression of *TaPAL*, *TaCOMT*, *TaCCR*, and *TaCAD* was decreased on average by 22.24%, 25.09%, 21.80% and 30.44%, respectively, under S1D1 treatment, while 28.31%, 32.58%, 36.28% and 43.86%, under S2D1 treatment. Compared with that under S0D2 treatment, the relative expression of *TaPAL*, *TaCOMT*, *TaCCR*, and *TaCAD* was decreased on average by 19.06%, 29.07%, 4.51% and 32.42%, respectively, under S1D2 treatment, while 26.38%, 37.70%, 38.11% and 45.18%, under S2D2 treatment. Compared with that under S0D3 treatment, the relative expression of *TaPAL*, *TaCOMT*, *TaCCR*, and *TaCAD* was decreased on average by 20.26%, 29.31%, 26.89% and 34.56%, respectively, under S1D3 treatment, while 28.55%, 38.42%, 40.12% and 47.94%, under S2D3 treatment.

The above results show that shading and density significantly influenced the relative expression of genes, indicating that the relative expression was decreased with increased planting density under the same shading treatment. Under the same planting density, shading significantly reduced the relative expression of genes, and with the extension of shading time, the reduction range was increased. Moreover, lodging resistant wheat SN23 had higher relative expression of these genes than the lodging sensitive wheat SN16.

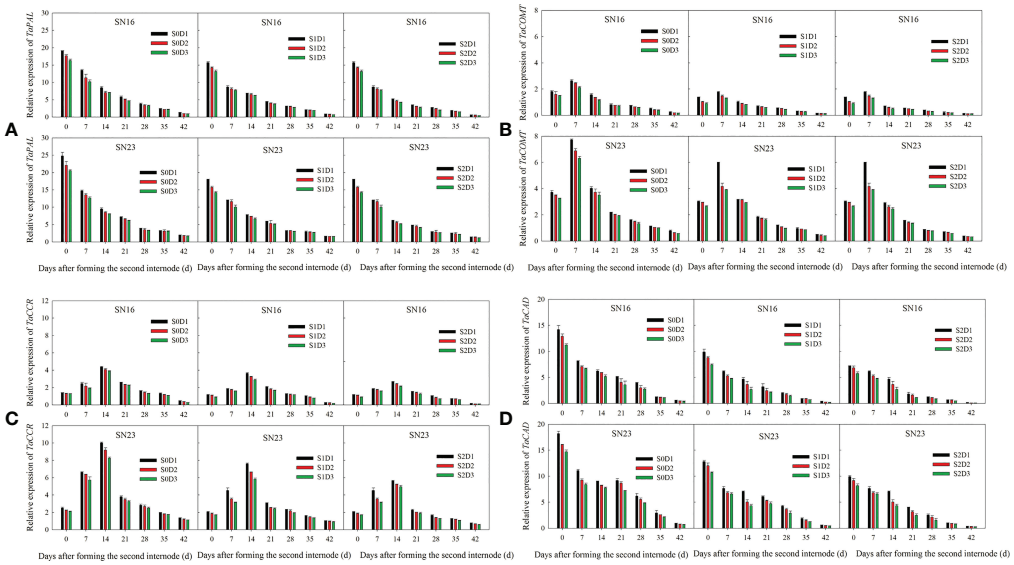


FIGURE 6
Effects of shading on the expression of lignin biosynthetic genes in wheat stems under different planting densities in 2018-2019. Error bars represent the standard deviation of the mean (n = 3). **(A)** Phenylalanine ammonialyases gene (*PAL*). **(B)** Caffeic acid O-methyl transferase gene (*COMT*). **(C)** Cinnamoyl CoA reductase gene (*CCR*). **(D)** Cinnamyl alcohol dehydrogenase gene (*CAD*).

3.9 The relationship between breaking strength and morphological indices, lignin monomers composition of wheat stems

Correlation analysis shows that the breaking strength of wheat stems was significantly positively correlated with stem diameter, wall thickness, filling degree, lignin content, the contents and proportions of monomers S and G ($P < 0.01$), and negatively correlated with length of the basal second internode, height of center of gravity, H monomer content and proportion ($P < 0.01$) (Figure S4).

To further analyze the primary and secondary effects of stem morphological indices and lignin monomers composition on the breaking strength of stems under shading treatment, this study analyzed the relationship between the breaking strength and the stem diameter, wall thickness, filling degree, the length of the second basal internode, CG height, lignin content, the contents of monomers S, G, and H, and the proportions of monomers S, G, and H (recorded as X1, X2, X3, X4, X5, X6, X7, X8, X9, X10, X11, and X12, respectively) through a stepwise regression analysis (Table 1). When $P < 0.05$, the independent variable entered the stepwise regression equation. Conversely, when $P > 0.05$, the independent variable did not enter the regression equation. According to this principle, X2, X3, X4, X6, X7, X9, and X12 entered the equation, and the partial correlation coefficients of the seven variables were in the order of X3 (0.734) > X2 (0.656) > X9 (-0.580) > X6 (-0.422) > X7 (0.407) > X4 (0.284) > X12 (-0.203). This result indicates that stem filling degree, wall thickness, H monomer content, lignin content, S monomer content, length of the basal second basal internode, and H monomer proportion are the main factors affecting the breaking strength of stems in wheat in response to shading stress. Others are the secondary factors.

3.10 Variance analysis of the morphological indices, lignin monomers composition and bending resistance of wheat stems

It was indicated that year had no significant effects on the breaking strength, stem diameter, wall thickness, filling degree, CG height and S monomer content of stems, but had significant effects on the length of the second basal internode, the content and proportion of G and H monomers (Table 2). Variety, shading and planting density had significant effects on the breaking strength, morphological indices and lignin monomers composition of wheat stems. Shading and planting density interacted significantly on the wall thickness and the proportion of lignin monomers of wheat stems ($P < 0.01$).

4 Discussion

4.1 Effects of shading on the breaking strength and morphological characteristics in wheat stems under different planting densities

Shading and density significantly influenced the interception rate of PAR of two wheat varieties, shown as S0 > S1 > S2 and D3 > D2 > D1 (Figure S3). Moreover, the breaking strength was markedly affected by planting density and shading (Table 1). The breaking strength of the second basal internode in two wheat varieties was decreased with increased planting density at different stages. The breaking strength in wheat stems showed a larger decline range. At high density of 300×10^4 plants ha^{-1}, shading at the jointing stage reduced the stem breaking strength of two wheat varieties more significantly than that at low density (150×10^4 plants ha^{-1}), and medium density (225×10^4 plants ha^{-1}). The results indicated that the breaking strength of wheat stems was more sensitive to shading stress under high density. The formation of breaking strength is mainly affected by morphological characteristics and structural component content of crop stems (Zhang R. et al., 2020; Guo et al., 2021).

The morphological characteristics (plant height, CG height, internode length, stem diameter, wall thickness, filling degree, etc.) of crop stems are influenced by shading stress and planting density. As the density increased, the plant height of maize first increased and then decreased. The length of basal internodes (especially the third basal internodes) significantly increased. Conversely, the stem diameter, cell wall thickness mechanical

TABLE 1 Stepwise regression analysis between wheat stem morphological indices, lignin monomers composition and breaking strength.

Indices	Stepwise regression equation	Variables	Partial correlation coefficient	P value
Morphological characteristics	Y=-13.35+10.63X2+0.31X3+0.51X4	Wall thickness (X2)	0.6557	0.0001
		Filling degree (X3)	0.7335	0.0001
		Second internode length (X4)	0.2843	0.0031
Lignin and monomers composition	Y=33.58-0.03X6+0.01X7-0.07X9-0.22X12	Lignin content (X6)	-0.4227	0.0001
		S monomer content (X7)	0.4069	0.0001
		H monomer content (X9)	-0.5804	0.0001
		H monomer proportion (X12)	-0.2028	0.0380

TABLE 2 Analysis of variance of the effects of year (Y), cultivar (C), shading (N) and density (D) on breaking strength, morphological characteristics, and lignin monomers composition of stems in wheat at milk stage.

Source of variation	BS	SD	WT	SFD	LSI	HCG	LC	S content	G content	H content	S proportion	G proportion	H proportion
Year (Y)	ns	ns	ns	ns	**	ns	**	ns	*	**	**	**	**
Cultivar (C)	**	**	**	**	**	**	**	**	**	**	**	**	**
Shading (S)	**	**	**	**	**	**	**	**	**	**	**	**	**
Density (D)	**	**	**	**	**	**	**	**	**	**	**	**	**
C×S×	**	**	ns	**	ns	**	**	**	**	ns	**	**	**
C×D×	*	ns	ns	ns	ns	ns	*	ns	ns	ns	**	**	**
S×D×	ns	**	ns	ns	ns	**	ns	ns	ns	ns	**	**	**
C×S×D×	ns	**	ns	ns	ns	ns	ns	ns	ns	ns	**	**	**

BS, breaking strength; SD, Stem diameter; WT, Wall thickness; SFD, Stem filling degree; LSI, Length of the second internode; HCG, Height of center of gravity; LC, Lignin content. ns, *and ** represent no significant, significant at 0.05 and 0.01 levels, respectively.

tissue, mechanical cell layer, and cortex decreased. As a result, the lodging rate of maize gradually increased (Sher et al., 2018). Moreover, the plant height, and the CG height of wheat increased. The filling degree of stems were decreased, resulting in the decline of stem breaking strength. Consistent with that, our research showed that with the increase of planting density, the internode length, spike length, and the plant height were increased and the CG height moved up (Figure 1A). When the planting density was increased by 75×10^4 plants ha^{-1}, the plant height and the CG height increased by 1.82 cm and 1.11 cm, respectively under shading treatment from the jointing stage to the heading stage, with 1.57 cm and 0.86 cm, respectively, to offset the negative effects partially of shading stress (Lyu et al., 2021).

It was found that shading treatment from the jointing stage to the heading stage decreased the plant height of rice, but had no significant difference from the normal light treatment. Besides, the lengths of the first and second basal internodes increased in response to shading treatment. The spike length, the lengths of the first and the second internodes from the spike, the stem diameter and wall thickness of the second basal internode showed the opposite regularity (Zhang, W. J. et al., 2020). Wu et al. (2017) reported that the plant height and CG height increased in response to shading stress, however, the stem diameter and wall thickness were reduced. The results of this study showed that shading stress at the jointing stage significantly increased the lengths of the second to the fifth basal internodes (especially the fourth internode), and the spike length, resulting in higher plant height, and CG height of wheat (Figure 1A). However, the stem diameter and wall thickness of the second internode were reduced due to shading stress (Figures 1B, C). With the extension of shading time, the above indicators increased or decreased much more. Liu et al. (2018) found that shading significantly increased plant height, but decreased stem diameter, which leading to higher lodging risk of soybean. However, previous researches demonstrated that the effects of shading stress on soybean varied with different cultivars (Yao et al., 2017). The above results showed that shading had different effects on plant height, CG height and internode length, mainly due to different shading periods and crop types (Figure 1A), but had the same effects on crop stem diameter and wall thickness (Figures 1B, C). According to comprehensive correlation analysis (Figure S4) and stepwise regression analysis (Table 1), the filling degree, wall thickness and length of the second basal internode are the main factors affecting the breaking strength of wheat stems in response to shading stress, and others are secondary factors.

At planting density of 150×10^4 plants ha^{-1}, shading from the jointing to the heading stages increased the plant height and CG height of two wheat varieties by 8.88%, and 16.17% on average. At planting density of 225×10^4 plants ha^{-1}, these were 7.17%, and 6.74%. Besides, when planting density was 300×10^4 plants ha^{-1}, these were 4.51%, and 3.55% (Figure 1A). These results indicated that under the condition of high density, the increase in plant height and CG height (Figure 1A) of wheat were lower than those at low and medium density. This may be because of shade avoidance of wheat under population densification. By extension, shading signals are perceived by the phytochrome photoreceptors, phytochrome B (phyB) and phyA, which play antagonistic roles in stem elongation. Lowering the R:FR to shading stress deactivates phyB, resulting in the internode elongation promotion. By contrast, when the planting density is high, R:FR is very low under shading conditions. Thus, phyA accumulates and is strongly

activated under very low R:FR to prevent excessive internode elongation of wheat (Molina-Contreras et al., 2019; Paulišić et al., 2021). Therefore, shading promoted the elongation of wheat internodes, and its elongation decreased with an increase in the planting density.

4.2 Effects of shading on the lignin metabolism in wheat stems under different planting densities

Welton (1928) first proposed that lodging was caused by the lack of lignin in wheat stems. Lignin could support and prevent the stems from lodging. It was also exhibited that the content of lignin in pex1 semi dwarf mutant was increased, and the lodging resistance of rice was enhanced. The breaking strength of wheat stems is determined by the vascular system and mechanical tissues, and lignin provides rigidity for stems (Khobra et al., 2019). The rigidity strength of stems is mainly composed by two parts: ① oxidative covalent crosslinking strength of lignin polymer chains and cell wall polysaccharides; ② filling degree of lignin polymer chains in vascular units such as cellulose macrofibrils and hemicellulose (Ragauskas et al., 2014; Anderson et al., 2015; Balakshin et al., 2020). Lignin plays a decisive role as a "binder" in the formation of breaking and pressure strength of stems. It can be seen that the synthesis and accumulation of lignin is the basis for determining the rigid breaking resistance of stems. This study indicated that the lignin content of the second basal internode in wheat increased gradually after the jointing stage. The accumulation rate of lignin became faster from 0 to 28 days after the jointing stage. Lignin was also enhanced from 28 to 42 days after the jointing stage, but the rate tended to be stable (Figure 4). Shading apparently reduced lignin accumulation, and with the extension of shading time, lignin accumulation in wheat stems was significantly decreased. At the planting density of 150×10^4 plants ha^{-1}, S1 and S2 treatments decreased the lignin accumulation by 13.56%, and 27.07%, respectively at 42 days after jointing. At the planting density of 225×10^4 plants ha^{-1}, S1 and S2 treatments decreased the lignin accumulation by 14.23%, and 29.01%, respectively. Moreover, at the planting density of 300×10^4 plants ha^{-1}, S1 and S2 treatments decreased the lignin accumulation by 14.53%, and 29.17%, respectively. It was indicated that lignin accumulation in wheat stems was more sensitive to shading under high density conditions.

TaPAL, *TaCOMT*, *TaCCR*, and *TaCAD* are key enzyme genes of carbon flow distribution in wheat lignin synthesis pathway. Their expression abundance significantly influenced the synthesis and accumulation of lignin (Ma, 2007; Ma, 2010; Levy et al., 2018). The results of this study showed that the relative expression of these genes of lodging resistant wheat SN23 was significantly higher than that of lodging sensitive wheat SN16 (Figure 6), and the stem lignin content of SN23 was higher than that of SN16 (Figures 4, 5), indicating that SN23 showed a comparatively greater lodging resistance in response to shade stress and high planting density. Shading and planting density significantly affected the expression of key enzyme genes in the lignin synthesis pathway of wheat stems. With the increasing planting density, the expression of *TaPAL*, *TaCOMT*, *TaCCR* and *TaCAD* in wheat stems was decreased. Moreover, it was also reduced in response to shading stress, which was consistent with the change of lignin accumulation and breaking strength of stems. At high density, the reduction range of the expression of *TaPAL*, *TaCOMT*, *TaCCR* and *TaCAD* in wheat stems suffered from shading stress was larger than that at low density and medium density. The results suggested that the expression of those genes was much more sensitive to shading stress at high density, which was related to lignin accumulation and breaking strength of stems.

TaPAL is the key enzyme in the carbon flow distribution in the lignin pathway, and its downregulation mainly decreases the G monomer (Feduraev et al., 2021). TaCOMT is the key enzyme in the formation of G monomer switched into S monomer and free radicals from carbon sources, while its downregulation reduces the proportion of S and H monomers, but increases the proportion of G monomer (Wang et al., 2018). TaCCR and TaCAD are enzymes that catalyze the last two steps of lignin monomers synthesis, respectively (Ma, 2007; Ma, 2010). When CCR was downregulated, there was a slight decrease in lignin content, but significant changes in lignin composition. The ratio of H monomer was dramatically reduced and the S/G ratio was slightly enhanced (Tamasloukht et al., 2011). Downregulation of *CAD* would result in lower content of S monomer, higher content of G and H monomers and lower S/G ratio (Trabucco et al., 2013). The results of this study showed that shading decreased PAR interception rate of two wheat varieties, reduced the content and proportion of S and G monomers, but increased the content and proportion of H monomer, which was due to a combination of factors, including downregulation of *TaPAL*, *TaCOMT*, *TaCCR*, and *TaCAD* genes under shading stress. Under the condition of shading from jointing stage to heading stage, the content and proportion of S monomer were reduced by 245.68 μg g^{-1} and 2.20%, while those of G monomer were decreased by 221.58 μg g^{-1} and 2.37%, respectively. By contrary, the content and proportion of H monomer were enhanced by 36.67 μg g^{-1} and 4.57%, respectively. Moreover, under the condition of shading from jointing stage to maturity stage, the content and proportion of S monomer were reduced by 375.96

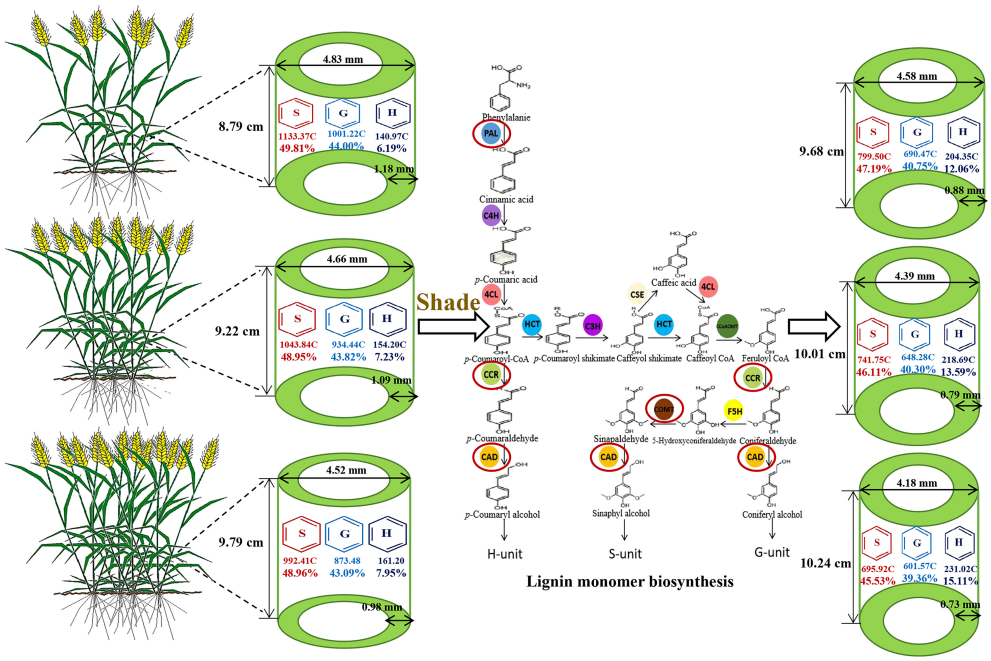


FIGURE 7
Pattern graph of shading affecting stem morphological characteristics and lignin metabolism of wheat under different planting densities. S, syringyl; G, guaiacyl; H, *p*-hydroxyphenyl; C, concentration unit (μg g^{-1}). PAL, phenylalanine ammonia-lyase; C4H, cinnamate 4-hydroxylase; 4CL, 4-hydroxycinnamate:CoA ligase; HCT, *p*-hydroxycinnamoyl-CoA shikimate/quinate hydroxycinnamoyl transferase; C3H, coumarate 3-hydroxylase; CSE, caffeoyl shikimate esterase; CCoAOMT, caffeoyl CoA o-methyl transferase; F5H, ferulate/coniferaldehyde 5-hydroxylase; CCR, cinnamoyl CoA reductase; CAD, cinnamyl alcohol dehydrogenase.

μg g^{-1} and 4.55%, while those of G monomer were decreased by 357.64 μg g^{-1} and 6.07%, respectively. The content and proportion of H monomer were enhanced by 95.12 μg g^{-1} and 10.63%, respectively. These results indicated that the changed range of lignin monomers in wheat stems was increased with the extension of shading time (Figure 5). According to comprehensive correlation analysis (Figure S4) and stepwise regression analysis (Table 1), the content and proportion of H monomer, lignin content and S monomer content in wheat stems are the main factors influencing the breaking strength of wheat stems. Among these factors, the content and proportion of H monomer were negative factors, whereas lignin content and S monomer content were positive factors. The above results demonstrated that under the condition of shading at jointing stage, the expression of *TaPAL*, *TaCOMT*, *TaCCR*, and *TaCAD* in wheat stems decreased (Figure 6), thereby, the lignin accumulation and monomers composition of wheat stems were changed. Lignin content and S monomer at 42 days after jointing were decreased by 18.48%, and 296.49 μg g^{-1}, respectively. The content and proportion of H monomer were enhanced by 69.82 μg g^{-1} and 8.37%, respectively (Figure 5).

5 Conclusions

The decreased filling degree, wall thickness, lignin content, and S monomer content in wheat stems, the increased content and proportion of H monomer, and the increased length of the second basal internode play pivotal roles in decreasing the breaking strength of wheat stems in response to shading stress. Under shading stress and high density, the limited photosynthetic carbon source flowing to the lignin synthesis pathway hinders the expression of *TaPAL*, *TaCOMT*, *TaCCR* and *TaCAD*. As a result, the lignin synthesis and its distribution proportion in S, G, and H monomers were altered. The lignin accumulation and the S monomer content decreased. Additionally, the content and proportion of H monomer were increased, which led to low breaking strength (Figure 7).

Data availability statement

The original contributions presented in the study are included in the article/Supplementary Material. Further inquiries can be directed to the corresponding authors.

Author contributions

YLu and YC: Software, Methodology, Investigation, Data Curation, Writing – Original Draft. CL: Methodology, Validation, Data curation. YW, HC and MJ: Methodology, Data curation. ZW and YLi: Conceptualization, Funding acquisition, Writing – review and editing, Validation, Supervision. All authors contributed to the article and approved the submitted version.

Funding

The work was supported by the National Natural Science Foundation of China (NO. 32101834, 32172117), the Natural Science Foundation of Shandong Province (NO. ZR2020QC106), Post-doctoral Science Foundation of China (2022M711968), the Shandong Mount Tai Program for Industrial Leading Talents (NO. LJNY2015001), the National Key Research and Development Program of China (NO. 2017YFD0301001, 2016YFD0300403).

Conflict of interest

The authors declare that the research was conducted in the absence of any commercial or financial relationships that could be construed as a potential conflict of interest.

Publisher's note

All claims expressed in this article are solely those of the authors and do not necessarily represent those of their affiliated organizations, or those of the publisher, the editors and the reviewers. Any product that may be evaluated in this article, or claim that may be made by its manufacturer, is not guaranteed or endorsed by the publisher.

Supplementary material

The Supplementary Material for this article can be found online at: https://www.frontiersin.org/articles/10.3389/fpls.2022.1056193/full#supplementary-material

References

Alejandro, S., Lee, Y., Tohge, T., Sudre, D., Osorio, S., Park, J., et al. (2010). AtABCG29 is a monolignol transporter involved in lignin biosynthesis. *Curr. Biol.* 22, 1207–1212. doi: 10.1016/j.cub.2012.04.064

Anderson, N. A., Tobimatsu, Y., Ciesielski, P. N., Ximenes, E., and Ralph, J. (2015). Manipulation of guaiacyl and syring monomer biosynthesis in an arabidopsis cinnamyl alcohol dehydrogenase mutant results in atypical lignin biosynthesis and modifed cell wall structure. *Plant Cell* 27, 2195–2209. doi: 10.1105/tpc.15.00373

Balakshin, M., Capanema, E. A., Zhu, X., Sulaeva, I., Potthast, A., Rosenau, T., et al. (2020). Spruce milled wood lignin: linear, branched or cross-linked? *Green Chem.* 22 (13), 3985–4001. doi: 10.1039/D0GC00926A

Cai, J., and Jiang, D. (2011). The effect of climate change on winter wheat production in China. *J. Agro-Environ. Sci.* 30 (9), 1726–1733. doi: 10.1016/S1671-2927(11)60313-1

Chen, X., Wang, J., Wang, Z., Li, W., Wang, C., Yan, S., et al. (2018). Optimized nitrogen fertilizer application mode increased culms lignin accumulation and lodging resistance in culms of winter wheat. *Field Crops Res.* 228, 31–38. doi: 10.1016/j.fcr.2018.08.019

Dixon, L. E., Pasquariello, M., and Boden, S. A. (2020). TEOSINTE BRANCHED1 regulates height and stem internode length in bread wheat. *J. Exp. Bot.* 71, 4742–4750. doi: 10.1093/jxb/eraa252

Fang, L., Xu, X., Li, J., Zheng, F., Li, M., Yan, J., et al. (2020). Transcriptome analysis provides insights into the non-methylated lignin synthesis in paphiopedilum armeniacum seed. *BMC Genom.* 21, 524. doi: 10.21203/rs.2.13152/v3

Feduraev, P., Riabova, A., Skrypnik, L., Pungin, A., Tokupova, E., Maslennikov, P., et al. (2021). Assessment of the role of PAL in lignin accumulation in wheat (*Triticum aestivum* l.) at the early stage of ontogenesis. *Int. J. Mol. Sci.* 22, 9848. doi: 10.3390/ijms22189848

Fetherolf, M. M., Levy-Booth, D. J., Navas, L. E., Liu, J., Grigg, J. C., Wilson, A., et al. (2020). Characterization of alkylguaiacol-degrading cytochromes P450 for the biocatalytic valorization of lignin. *PNAS* 117, 25771–25778. doi: 10.1073/pnas.1916349117

Guo, Z., Liu, X., Zhang, B., Yuan, X., Xing, Y., Liu, H., et al. (2021). Genetic analyses of lodging resistance and yield provide insights into post-Green-Revolution breeding in rice. *Plant Biotechnol. J.* 19, 814–829. doi: 10.1111/pbi.13509

Hussain, S., Iqbal, N., Rahman, T., Liu, T., Brestic, M., Safdar, M. E., et al. (2019). Shade effect on carbohydrates dynamics and stem strength of soybean genotypes. *Environ. Exp. Bot.* 162, 374–382. doi: 10.1016/j.envexpbot.2019.03.011

Hussain, S., Li, S., Mumtaz, M., Shafiq, I., Iqbal, N., Brestic, M., et al. (2021). Foliar application of silicon improves stem strength under low light stress by regulating lignin biosynthesis genes in soybean (*Glycine max* (L.) merr.). *J. Hazard. Mater.* 401, 123256. doi: 10.1016/j.jhazmat.2020.123256

Hussain, S., Liu, T., Iqbal, N., Brestic, M., Pang, T., Mumtaz, M., et al. (2020). Effects of lignin, cellulose, hemicellulose, sucrose and monosaccharaides carbohydrates on soybean physical stem strength and yield in intercropping. *Photochem. Photobiol. Sci.* 19, 462–472. doi: 10.1039/C9PP00369J

Ke, S., Luan, X., Liang, J., Hung, Y. H., Hsieh, T. F., and Zhang, X. Q. (2019). Rice OsPEX1, an extensin-like protein, affects lignin biosynthesis and plant growth. *Plant Mol. Biol.* 100, 151–161. doi: 10.1007/s11103-019-00849-3

Khobra, R., Sareen, S., Meena, B. K., Arvind Kumar, A., Tiwari, V., and Singh, G. P. (2019). Exploring the traits for lodging tolerance in wheat genotypes: a review. *Physiol. Mol. Biol. Plants.* 25, 589–600. doi: 10.1007/s12298-018-0629-x

Levy, H. L., Sarkissian, C. N., and Scriver, C. R. (2018). Phenylalanine ammonia lyase (PAL): From discovery to enzyme substitution therapy for phenylketonuria. *Mol. Genet. Metab.* 124, 223–229. doi: 10.1016/j.ymgme.2018.06.002

Liu, W. G., Ren, M. L., Liu, T., Du, Y. L., Zhou, T., Liu, X. M., et al. (2018). Effect of shade stress on lignin biosynthesis in soybean stems. *J. Integr. Agric.* 17 (7), 1594–1604. doi: 10.1016/S2095-3119(17)61807-0

Liu, X. T., Wang, J., Hou, X. F., Li, Q., Jia, D. H., Gu, Y. G., et al. (2019). Progress of functions of lignin and relevant genes in plant lodging resistance. *Mol. Plant Breed* 17, 655–662. doi: 10.13271/j.mpb.017.000655

Li, F., Xie, G., Huang, J., Zhang, R., Li, Y., Zhang, M., et al. (2017). *OsCESA9* conserved-site mutation leads to largely enhanced plant lodging resistance and biomass enzymatic saccharification by reducing cellulose DP and crystallinity in rice. *Plant Biotechnol. J.* 15, 1093–1104. doi: 10.1111/pbi.12700

Li, F. C., Zhang, M. L., Guo, K., Hu, Z., Zhang, R., Feng, Y. Q., et al. (2015). High-level hemicellulosic arabinose predominately affects lignocellulose crystallinity for genetically enhancing both plant lodging resistance and biomass enzymatic digestibility in rice mutants. *Plant Biotechnol. J.* 13, 514–525. doi: 10.1111/pbi.12276

Luo, Y. L., Ni, J., Pang, D. W., Jin, M., Chen, J., Kong, X., et al. (2019). Regulation of lignin composition by nitrogen rate and density and its relationship with stem

mechanical strength of wheat. *Field Crops Res.* 241, 107572. doi: 10.1016/j.fcr.2019.107572

Lyu, X., Cheng, Q., Qin, C., Li, Y., Xu, X., Ji, R., et al. (2021). GmCRY1s modulate gibberellin metabolism to regulate soybean shade avoidance in response to reduced blue light. *Mol. Plant* 14 (2), 298–314. doi: 10.1016/j.molp.2020.11.016

Ma, Q. H. (2007). Characterization of a cinnamoyl-CoA reductase that is associated with stem development in wheat. *J. Exp. Bot.* 58, 2011–2021. doi: 10.1093/jxb/erm064

Ma, Q. H. (2010). Functional analysis of a cinnamyl alcohol dehydrogenase involved in lignin biosynthesis in wheat. *J. Exp. Bot.* 61, 2735–2744. doi: 10.1093/jxb/erm064

Miao, Y. C., and Liu, C. J. (2010). ATP-binding cassette-like transporters are involved in the transport of lignin precursors across plasma and vacuolar membranes. *PNAS* 107, 22728–22733. doi: 10.1073/pnas.1007747108

Molina-Contreras, M. J., Paulišić, S., Then, C., Moreno-Romero, J., Pastor-Andreu, P., Morelli, L., et al. (2019). Photoreceptor activity contributes to contrasting responses to shade in cardamine and arabidopsis seedlings. *Plant Cell* 31, 2649–2663. doi: 10.1105/tpc.19.00275

Pantazopoulou, C. K., Bongers, F. J., and Pierik, R. (2021). Reducing shade avoidance can improve arabidopsis canopy performance against competitors. *Plant Cell Environ.* 44, 1130–1141. doi: 10.1101/792283

Paulišić, S., Qin, W., Verasztó, H. A., Then, C., Alary, B., Nogue, F., et al. (2021). Adjustment of the PIF7-HFR1 transcriptional module activity controls plant shade adaptation. *EMBO J.* 40, e104273. doi: 10.15252/embj.2019104273

Peng, D. L., Chen, X. G., Yin, Y. P., Lu, K. L., Yang, W. B., Tang, Y. H., et al. (2014). Lodging resistance of winter wheat (*Triticum aestivum* l.): Lignin accumulation and its related enzymes activities due to the application of paclobutrazol or gibberellin acid. *Field Crops Res.* 157, 1–7. doi: 10.1016/j.fcr.2013.11.015

Ragauskas, A. J., Beckham, G. T., Biddy, M. J., Chandra, R., Chen, F., Davis, M. F., et al. (2014). Lignin valorization: improving lignin processing in the biorefinery. *Science* 344, 1246843. doi: 10.1126/science.1246843

Ruben, V., Brecht, D., Kris, M., John, R., and Wout, B. (2010). Lignin biosynthesis and structure. *Plant Physiol.* 153, 895–905. doi: 10.1104/pp.110.155119

Sher, A., Khan, A., Ashraf, U., Liu, H. H., and Li, J. C. (2018). Characterization of the effect of increased plant density on canopy morphology and stalk lodging risk. *Front. Plant Sci.* 9. doi: 10.3389/fpls.2018.01047

Sykes, R. W., Gjersing, E. L., Foutz, K., Rottmann, W. H., Kuhn, S. A., Foster, C. E., et al. (2015). Down-regulation of p-coumaroyl quinate/shikimate 3'-hydroxylase (C3'H) and cinnamate 4-hydroxylase (C4H) genes in the lignin biosynthetic pathway of *Eucalyptus urophylla*×*E. grandis* leads to improved sugar release. *Biotechnol. Biofuels.* 8, 128. doi: 10.1186/s13068-015-0316-x

Tamasloukht, B., Lam, M. S. J. W.Q., Martinez, Y., Tozo, K., Barbier, O., Jourda, C., et al. (2011). Characterization of a cinnamoyl-CoA reductase 1 (CCR1) mutant in maize: effects on lignification, fibre development, and global gene expression. *J. Exp. Bot.* 62, 3837–3848. doi: 10.1093/jxb/err077

Teng, R. M., Wang, Y. X., Li, H., Lin, S. J., Liu, H., and Zhuang, J. (2021). Effects of shading on lignin biosynthesis in the leaf of tea plant (*Camellia sinensis* (L.) o. kuntze). *Mol. Genet. Genomics* 296, 165–177. doi: 10.1007/s00438-020-01737-y

Trabucco, G. M., Matos, D. A., Scott, J., Lee, S. J., Saathoff, A. J., Priest, H. D., et al. (2013). Functional characterization of cinnamyl alcohol dehydrogenase and caffeic acid O-methyltransferase in *Brachypodium distachyon*. *BMC Biotechnol.* 13, 61. doi: 10.1186/1472-6750-13-61

Vanholme, R., Morreel, K., Darrah, C., Oyarce, P., Grabber, J. H., Ralph, J., et al. (2012). Metabolic engineering of novel lignin in biomass crops. *New Phytol.* 196, 978–1000. doi: 10.1111/nph.12028

Wagner, A., Tobimatsu, Y., Phillips, L., Flint, H., Torr, K., Donaldson, L., et al. (2011). CCoAOMT suppression modifies lignin composition in *Pinus radiata*. *Plant J.* 67, 119–129. doi: 10.1111/j.1365-313X.2011.04580.x

Wang, C., Hu, D., Liu, X., She, H., Ruan, R., Yang, H., et al. (2015). Effects of uniconazole on the lignin metabolism and lodging resistance of culm in common buckwheat (*Fagopyrum esculentum* m.). *Field Crops Res.* 180, 46–53. doi: 10.1016/j.fcr.2015.05.009

Wang, M., Zhu, X., Wang, K., Lu, C., Luo, M., Shan, T., et al. (2018). A wheat cafeic acid 3-o-methyltransferase TaCOMT-3D positively contributes to both resistance to sharp eyespot disease and stem mechanical strength. *Sci. Rep.* 8, 6543. doi: 10.1038/s41598-018-24884-0

Wei, L., Jian, H., Lu, K., Yin, N., Wang, J., Duan, X., et al. (2017). Genetic and transcriptomic analyses of lignin- and lodging-related traits in *Brassica napus*. *Theor. Appl. Genet.* 130, 1961–1973. doi: 10.1007/s00122-017-2937-x

Welton, F. A. (1928). Lodging in oats and wheat. *Botanical Gazatte.* 85, 121–151.

Wu, L. M., Zhang, W. J., Ding, Y., Zhang, J., Cambula, E. D., Weng, F., et al. (2017). Shading contributes to the reduction of stem mechanical strength by decreasing cell wall synthesis in japonica rice (*Oryza sativa* l.). *Front. Plant Sci.* 8. doi: 10.3389/fpls.2017.00881

Xu, B., Escamilla-Treviño, L. L., Sathitsuksanoh, N., Shen, Z., Shen, H., Zhang, Y. H. P., et al. (2011). Silencing of 4-coumarate:coenzyme a ligase in switchgrass leads to reduced lignin content and improved fermentable sugar yields for biofuel production. *New Phytol.* 192, 611–625. doi: 10.2307/41320544

Yang, H., Li, Y. P., Li, D. X., Liu, L. T., Qiao, Y. Z., Sun, H. Y., et al. (2022). Wheat escapes low light stress by altering pollination types. *Front. Plant Sci.* 13. doi: 10.3389/fpls.2022.924565

Yao, X., Li, C., Li, S., Qian Zhu, Q., Zhang, F., Wang, H., et al. (2017). Effect of shade on leaf photosynthetic capacity, light-intercepting, electron transfer and energy distribution of soybeans. *Plant Growth Regul.* 83, 409–416. doi: 10.1007/s10725-017-0307-y

Zadoks, J. C., Chang, T. T., and Konzak, C. F. (1974). A decimal code for the growth stages of cereals. *Weed. Res.* 14, 415–421. doi: 10.1111/j.1365-3180.1974.tb01084.x

Zhang, W. J., Duan, X. J., Yao, X., Liu, Q. M., Xiao, R. P., Zhang, X. W., et al. (2020). Effects of shading on stem morphological characteristics and lodging resistance of heavy panicle hybrid rice. *Chin. Rice* 26, 9–13. doi: 10.3969/j.issn.1006-8082.2020.02.003

Zhang, R., Jia, Z., Ma, X., Ma, H., and Zhao, Y. (2020). Characterising the morphological characters and carbohydrate metabolism of oat culms and their association with lodging resistance. *Plant Biol.* 22, 267–276. doi: 10.1111/plb.13058

Zhao, D., Xu, C., Luan, Y., Shi, W., Tang, Y., and Jun Tao, J. (2021). Silicon enhances stem strength by promoting lignin accumulation in herbaceous peony (*Paeonia lactiflora* pall.). *Int. J. Biol. Macromol.* 190, 769–779. doi: 10.1016/j.ijbiomac.2021.09.016

Zheng, M. J., Chen, J., Shi, Y. H., Li, Y. X., Yin, Y. P., Yang, D. Q., et al. (2017a). Manipulation of lignin metabolism by plant densities and its relationship with lodging resistance in wheat. *Sci. Rep.* 7, 41805. doi: 10.1038/srep41805

Zheng, M. J., Gu, S. B., Chen, J., Luo, Y. L., Li, W. Q., Ni, J., et al. (2017b). Development and validation of a sensitive UPLC-MS/MS instrumentation and alkaline nitrobenzene oxidation method for the determination of lignin monomer in wheat straw. *J. Chromatogr. B.* 1055, 178–184. doi: 10.1016/j.jchromb.2017.04.034

frontiers | Frontiers in Plant Science

TYPE Original Research
PUBLISHED 17 November 2022
DOI 10.3389/fpls.2022.1006806

Check for updates

OPEN ACCESS

EDITED BY
Jiban Shrestha,
Nepal Agricultural Research Council, Nepal

REVIEWED BY
Qibin Ma,
South China Agricultural University, China
Ewa Hanus-Fajerska,
University of Agriculture in Krakow, Poland

*CORRESPONDENCE
Lianxuan Shi
lianxuanshi@nenu.edu.cn

SPECIALTY SECTION
This article was submitted to Plant Abiotic Stress, a section of the journal Frontiers in Plant Science

RECEIVED 29 July 2022
ACCEPTED 28 October 2022
PUBLISHED 17 November 2022

CITATION
Li M, Zhou J, Lang X, Han D, Hu Y, Ding Y, Wang G, Guo J and Shi L (2022) Integrating transcriptomic and metabolomic analysis in roots of wild soybean seedlings in response to low-phosphorus stress.
Front. Plant Sci. 13:1006806.
doi: 10.3389/fpls.2022.1006806

COPYRIGHT
© 2022 Li, Zhou, Lang, Han, Hu, Ding, Wang, Guo and Shi. This is an open-access article distributed under the terms of the Creative Commons Attribution License (CC BY). The use, distribution or reproduction in other forums is permitted, provided the original author(s) and the copyright owner(s) are credited and that the original publication in this journal is cited, in accordance with accepted academic practice. No use, distribution or reproduction is permitted which does not comply with these terms.

Integrating transcriptomic and metabolomic analysis in roots of wild soybean seedlings in response to low-phosphorus stress

Mingxia Li[1], Ji Zhou[2], Xianyu Lang[1], Defu Han[1], Yongjun Hu[1], Yinan Ding[1], Guangye Wang[1], Jixun Guo[3] and Lianxuan Shi[3]*

[1]School of Life Sciences, Changchun Normal University, Changchun, China, [2]Land Consolidation and Rehabilitation Centre, The Ministry of Land and Resources, Beijing, China, [3]Institute of Grassland Science, Northeast Normal University, Key Laboratory of Vegetation Ecology, Ministry of Education, Changchun, China

Introduction: Plants undergo divergent adaptations to form different ecotypes when exposed to different habitats. Ecotypes with ecological adaptation advantages are excellent germplasm resources for crop improvement

Methods: his study comprehensively compared the differences in morphology and physiological mechanisms in the roots of two different ecotypes of wild soybean (Glycine soja) seedlings under artificially simulated low-phosphorus (LP) stress.

Result: The seedlings of barren-tolerant wild soybean (GS2) suffered less damage than common wild soybean (GS1). GS2 absorbed more phosphorus (P) by increasing root length. In-depth integrated analyses of transcriptomics and metabolomics revealed the formation process of the ecological adaptability of the two different ecotypes wild soybean from the perspective of gene expression and metabolic changes. This study revealed the adaptation process of GS2 from the perspective of the adaptation of structural and molecular metabolism, mainly including: (1) Enhancing the metabolism of phenolic compounds, lignin, and organic acid metabolism could activate unavailable soil P; (2) Up-regulating genes encoding pectinesterase and phospholipase C (PLC) specifically could promote the reuse of structural P; (3) Some factors could reduce the oxidative damage to the membranes caused by LP stress, such as accumulating the metabolites putrescine and ascorbate significantly, up-regulating the genes encoding SQD2 (the key enzyme of sulfolipid substitution of phospholipids) substantially and enhancing the synthesis of secondary antioxidant metabolite anthocyanins and the AsA-GSH cycle; (4) enhancing the uptake of soil P by upregulating inorganic

phosphate transporter, acid phosphatase ACP1, and purple acid phosphatase genes; (5) HSFA6b and MYB61 are the key TFs to resist LP stress.

Discussion: In general, GS2 could resist LP stress by activating unavailable soil P, reusing plant structural P, rebuilding membrane lipids, and enhancing the antioxidant membrane protection system. Our study provides a new perspective for the study of divergent adaptation of plants.

KEYWORDS

adaptations, metabolomics, phosphorus deficiency, transcriptomics, wild soybean

1 Introduction

Phosphorus (P) is one of the important mineral nutrients for plant growth and development (Gamuyao et al., 2012). Due to the adsorption of metal cations and the activities of microorganisms, the effective P concentration that can be absorbed by plants from the soil is only 0.1–10 μmol·L^{-1}. The solubility of phosphate in soil is very low and its diffusion rate is very slow, making it difficult for plants to use (Lambers et al, 2006; Shen et al., 2018), which often does not ensure plant productivity, resulting in plants in a state of low-phosphorus (LP) stress (Huang et al., 2008). In this case, supplementing basic knowledge of the effects of poor soil on plant genetics and physiological metabolism helps in understanding how plants have evolved by adapting to their habitat (Dool et al., 2022).

Soybean (*Glycine max*) has the highest protein content among existing crops, and is also the oil crop ranking first in oil production in the world. In addition to being an important component of soybean plants, P is also involved in enzymatic, metabolism, nodule nitrogen fixation, and other physiological and biochemical processes. In soybean production, P deficiency is more harmful than other stresses, so it is very important to improve soybean's tolerance to LP stress and P absorption efficiency (Zhang et al., 2014). After a long period of natural selection, wild soybean (*Glycine soja*) has evolved many excellent traits and has a strong ability to tolerate barrenness, such as low nitrogen and salt stress (Li et al., 2018). As a relative of soybean, wild soybean is an important natural wild plant resource to breed soybeans tolerant to LP stress. Thus, clarifying the processes of gene expression and physiological and metabolic adaptations that occurred during the differentiation into different ecotypes of wild soybean for habitat adaptation can inform breeding programs and germplasm conservation strategies.

Under extreme P deficiency, plants adjust morphological structure, physiological metabolism, and break down structural P (e.g., membrane lipids and cell walls) to release organic P for reuse to maintain plant survival (Yang et al., 2016; Wei et al., 2020). The P in plants is mainly obtained from the soil P pool through the roots. In response to LP, root length increases as do the density of lateral roots and root hairs (Li et al., 2015). Increasing the accumulation of organic acids in roots and the secretion of organic acid anions and releasing soluble phosphates in the soil is an effective way for plants to adapt to P deficiency, and has been reported in white lupin (*Lupinus albus*), oats, alfalfa pigeon peas, common bean, rice, maize, barley, canola and radish (Lin et al., 2011; Chen and Liao, 2016; Zou et al., 2018). The accumulation of secondary antioxidants is of great significance for scavenging reactive oxygen species (ROS) and protecting membrane structure under P deficiency, which has been confirmed in wheat, sorghum, and switchgrass (Ding et al., 2021; Kumar et al., 2021). When P is insufficient, to ensure the normal function of cells, the enzyme SQD2 can make up for the lack of phospholipids and maintain the integrity of membrane structure (Yang et al., 2003; Mo et al., 2019). Based on previous studies, clarifying the mechanism of resistance of the wild soybean root system to P deficiency in soil is of great significance to improve the LP tolerance of cultivated soybean. This provides new ideas and methods for research on the adjustment of physiological metabolism and adaptive evolution of plants in adapting to different environments.

Our goal here is to clarify the reasons for evolutionary adaptability differences in different wild soybean ecotypes

Abbreviations: GS2, barren-tolerant wild soybean; GS1, common wild soybean; PLC, phospholipase C; SQD2, the key enzyme of sulfolipid substitution of phospholipids; P, Phosphorus; LP, low- phosphorus; ROS, reactive oxygen species; CAD, cinnamyl-alcohol dehydrogenase; GSH-GSSH, glutathione-glutathione disulfide; gpx, glutathione peroxidase; AsA, ascorbate; DFR, flavanone 4-reductase; F3H, naringenin 3-dioxygenase; CHS, chalcone synthase; TF, Transcription factor; PC1, the first principal component; PC2, The second principal component; SQDG, sulfoquinovosyl diacylglycerol; CYP73A, cinnamate hydroxylase; CK, control; DEGs, differentially expressed genes; GC/MS, gas chromatograph-mass spectrometer; PCA, principal component analysis; OPLS-DA, orthogonal partial least-squares discrimination analysis; PLS-DA, partial least squares discriminant analysis.

under natural conditions, to evaluate the hypothesis that the resistance of barren-tolerant wild soybean to LP stress depends on increasing root length, decomposing structural phosphorus, improving organic acid metabolism, and enhancing antioxidant system. This study compared differences in morphological structure, physiology metabolism, and gene expression in two ecotypes of wild soybean seedlings under artificially simulated LP stress by in-depth integrated analyses of transcriptomics and metabolomics. The objectives were to (1) identify differentially expressed genes (DEGs) in barren-tolerant wild soybean under LP stress, particularly associated with activating unavailable soil P, reusing plant structural P, rebuilding membrane lipids, and enhancing the antioxidant membrane protection system. (2) determine metabolites changes and key metabolic pathways caused by gene expression changes under LP stress. (3) reveal the key metabolic pathways, key genes and key metabolites of adaptation of barren-tolerant wild soybean to LP stress. This study could provide an important reference value for research on the adaptive evolution of plants and provides quantitative system parameters for resource evaluation.

2 Materials and methods

2.1 Plant materials, growth conditions, and plant harvest

Barren-tolerant wild soybean was obtained from 20 wild soybean varieties sampled on-site from saline-alkaline barren grassland in Tongyu County, Baicheng City, western Jilin Province. Tongyu is a county with an average annual precipitation of 350 mm, the soil feature of which is barren and saline alkali sandy soil. The best barren-tolerant wild soybeans were screened and identified from these varieties through a P-deficiency experiment. Meanwhile, common types of wild soybean were selected from those grown in nutrient-rich soils in Huinan County, Tonghua City, Southeast Jilin Province. Huinan is a county with an average annual precipitation of 737.4 mm, the soil feature of which is black humus and fertile. The ecological environment of Tongyu is more barren than Huinan. The resulting experimental materials were common wild soybean ("Huinan 06116", GS1) and barren-tolerant wild soybean ("Tongyu 06311", GS2). Seeds were uniformly sown in a mud film in a 14-cm diameter flowerpot and covered with clean sand, and then watered until germination. After germination, seedlings were irrigated with 1× Hoagland nutrient solution (with KH_2PO_4 concentration of 2000 μM). When the seedlings had their third compound leaves, the two ecotypes of wild soybean were randomly divided into control (CK) and LP stress groups, with 12 pots in each group. The CK group continued to be irrigated with 1× Hoagland nutrient solution, and the LP stress group was irrigated with 1× Hoagland nutrient solution containing 2.5 μM KH_2PO_4; the insufficient potassium in the LP stress group was supplemented with the same concentration of KCl. After 10 days of treatment, four pots were randomly selected from each group to harvest the seedling roots for transcriptomic analysis. After 14 days of treatment, four pots were randomly selected from each group to harvest the seedlings to determine growth parameters and ion contents. After 14 days of treatment, the remaining four pots from each group were used to harvest the seedling roots for metabonomic analysis. The experimental materials were cultivated in the outdoor test field of Northeast Normal University (Changchun City, Jilin Province, China). The average temperature during day and night was 26 ± 2°C and 18.5 ± 1.5°C, respectively; the relative humidity was 60.5%.

2.2 Measurement of growth parameters

The plant height, root length, and underground fresh and dry weights of seedlings of both wild soybean ecotypes were measured (Li et al., 2018). All measurements were repeated four times with four biological replicates per sample. The data obtained were analyzed using SAS 9.2 (NCSU, NC, USA).

2.3 Measurement of P contents

After collecting fresh samples of plant roots and drying them, 50 mg of each dry sample was placed in deionized water, boiled and soaked overnight, and centrifuged at 3000 × g for 15 min. The supernatant was collected then add deionized water to boil and centrifuge twice without overnight, and the supernatant was collected. The volume of the three supernatants was adjusted to 10 mL, and used to determine the P contents using inductively coupled plasma mass spectrometry (ICP-MS, iCAP RQ, Germany) (Zhu et al., 2021). Data of P content are presented as the mean ± standard deviation of three biological replicates. The data obtained were analyzed using SAS 9.2 (NCSU, NC, USA).

2.4 Transcriptomics analysis

2.4.1 RNA extraction, library preparation, and Illumina sequencing

The total RNA of samples was extracted by Trizol method. The RNA concentration was measured using a NanoDrop 2000 (Thermo Scientific Inc., DE, USA). The RNA integrity was assessed using an RNA Nano 6000 Assay Kit on an Agilent Bioanalyzer 2100 system (Agilent Technologies, CA, USA). Sequencing libraries were generated using NEBNext®Ultra™ RNA Library Prep Kit for Illumina® (NEB, USA), and index codes were added to assign sequences to each sample. Clustering of the index-coded samples was performed on a cBot Cluster

Generation System using TruSeq PE Cluster Kit v3-cBot-HS (Illumina, NEB, USA) according to the manufacturer's instructions. After cluster generation, the library preparations were sequenced on an Illumina HiSeq platform. After the original number, a series of processing and analyses was performed to obtain clean reads, which were then mapped to the reference Williams 82 genome sequence based on good comparison efficiency.

2.4.2 Data processing, screening, and functional analysis of differential genes

The DESeq R package (1.10.1) was used to analyze the expression in genes of the CK and LP stress groups of both experimental materials. Each experimental material was screened for differentially expressed genes (DEGs) using FDR < 0.05 and $|\log_2 FC| \geq 1$.

FPKM = cDNA fragments/mapped fragments (millions) × transcript length (kb) (Florea et al., 2013).

The FC in $\log_2 FC$ is fold change, which represents the ratio of expression between the samples of the LP and CK groups. Gene function was annotated based on the GO (Gene Ontology) database. The GO enrichment analysis of the DEGs was implemented using the GOseq R package based on a Wallenius non-central hyper-geometric distribution (Young et al., 2010). The DEGs related to metabolism were identified based on the Kyoto Encyclopedia of Genes and Genomes (KEGG) (http://www.genome.jp/keg).

2.4.3 Quantitative real-time PCR validation

To ensure reliability of transcriptome analysis data, 10 DEGs randomly selected from both ecotypes of wild soybean separately were detected by real-time fluorescence quantitative PCR (qRT-PCR) to verify the data. Primer Premier 6 software (Premier Biosoft International, Palo Alto, CA, USA) was used to design primers. TBtools software (http://www.tbtools.com) was used to assess the specificity of primers, and the primer sequences of these genes are listed in Supplementary material Table S1 (Schmittgen and Livak, 2008).

2.5 Metabolome analyses

2.5.1 Root metabolite extraction and GC/MS untargeted metabolic profiling

Of frozen plant root samples, 100 ± 5 mg was transferred into a 2-mL centrifuge tube, extracted with 0.3 mL methanol and 0.1 mL chloroform, and 60 µL was added to ribitol-containing water as an internal standard. The pellet was ground in a 70-Hz grinding system (Jinxin Biotechnology Co., Ltd., Shanghai, China) for 5 min, then incubated at 70°C for 10 min, and centrifuged at 12,000 × g or 10 min at 4°C. Of the supernatant, 0.35 mL was placed in a 2-mL glass tube, dried in a vacuum at 30°C for 2 h, dissolved in 80 µL of methoxyamine hydrochloride (20 mg/mL pyridine solution), then placed in a vacuum concentrator and dried, and then placed in an oven (MKX-J1-10, Qingdao Microwave Technology Co., Ltd., Qingdao, China) at 37°C for 2 h. The sample was further derivatized with N,O-bis (trimethylsilyl)-trifluoroacetamide containing 1% trimethylchlorosilane (100 µL) at 70°C for 1 h. Then the derived sample was cooled to room temperature. The samples were used for gas chromatograph-mass spectrometer (GC/MS) analysis using a one-dimensional Agilent 7890 GC system coupled with a Pegasus HT time-of-flight MS. There were four biological replicates for each experimental material and each treatment.

2.5.2 Metabolomics data analysis

The raw data were preprocessed with ChromaTOF software (version 2.12, 2.22, 3.34; LECO, St. Joseph, MI, USA). The LECO-Fiehn Rtx5 database was used for metabolite identification by matching the mass spectrum and retention index. Then, metabolite data were normalized according to Li et al. (2017) and imported into the SIMCA-P 13.0 software package (Umetrics, Umea, Sweden) for further data analysis, including principal component analysis (PCA), orthogonal partial least-squares discrimination analysis (OPLS-DA) and partial least squares discriminant analysis (PLS-DA). Finally, based on changes in metabolite concentration compared to the corresponding control, Student's t-test ($p < 0.05$), VIP > 1, and similarity value > 700 were used to screen differential metabolites. Then, KEGG was used to analyze metabolites and construct metabolic pathways, and the MetaboAnalyst website (http://http://www.metaboanalyst.ca) was used to analyze the pathways (Xia et al., 2012).

2.5.3 Integrated transcriptomics and metabolomics analysis

Pearson's correlation coefficients among the DEGs and differential metabolites were calculated using MetaboAnalyst 3.0 (www.metaboanalyst.ca). The integration network was analyzed using Cytoscape (version 3.8.2).

3 Results

3.1 Changes in plant morphology and P content

The plant height, root length, underground fresh weight and underground dry weight of the two ecotypes of wild soybean seedlings changed significantly under LP stress. Compared with CK, the roots of both ecotypes became sparse and lateral roots were significantly reduced (Figure 1A). Under LP stress, plant height, underground fresh weight, and underground dry weight in GS1

10.3389/fpls.2022.1006806

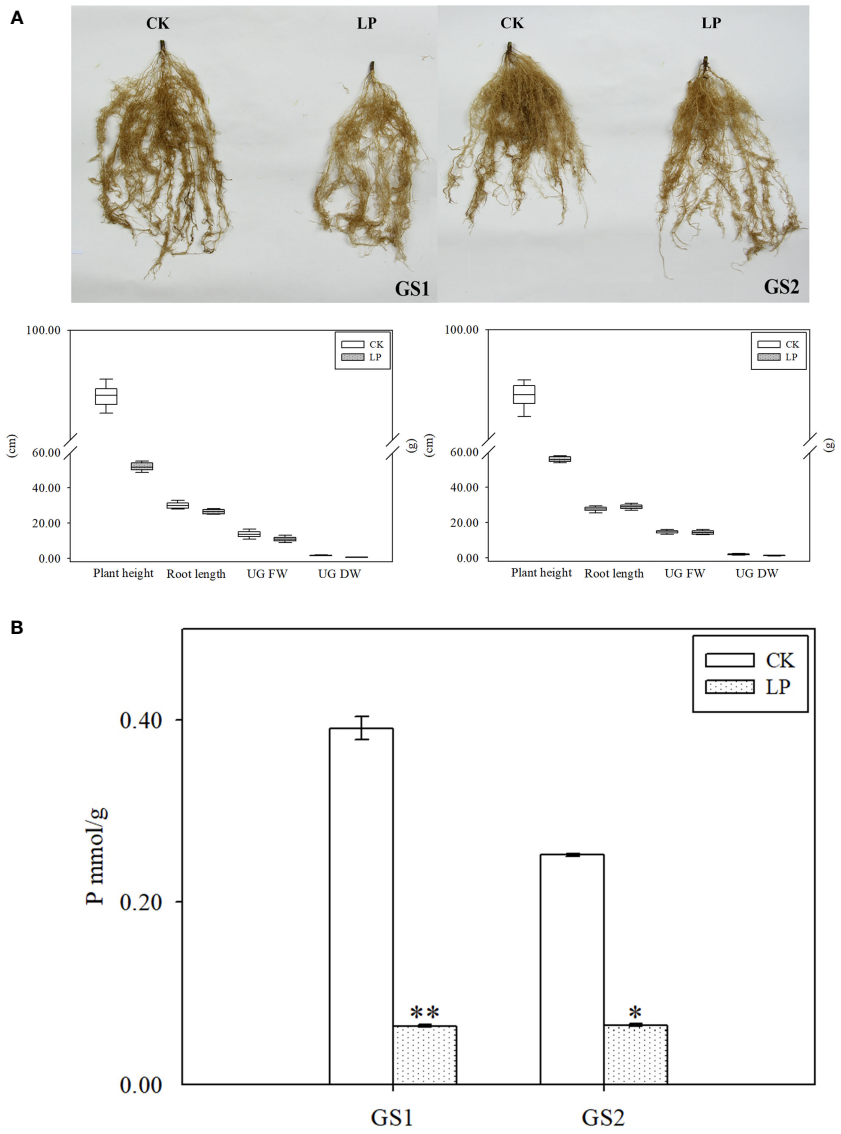


FIGURE 1
(A) Root phenotypes and **(B)** phosphorus content of roots of two ecotypes of wild soybean seedlings under control and low-phosphorus stress. GS1, common wild soybean; GS2, barren-tolerant wild soybean; CK, control group; LP, low-phosphorus stress group. * Significant at $P < 0.05$, ** significant at $P < 0.01$.

TABLE 1 Effects of LP stress on growth parameters of two ecotypes of wild soybean seedlings.

	GS1		GS2		FD	
	CK	LP	CK	LP	GS1	GS2
Plant height (cm)	91	52	91	56	-0.81*	-0.70*
Root length (cm)	30	27.2	27.7	28.93	-0.14	0.06*
Underground fresh weight (g)	13.7	11	14.8	14.3	-0.32	-0.05
Underground dry weight (g)	1.73	0.7	2	1.27	-1.31**	-0.66

GS1, common wild soybean; GS2, barren-tolerant wild soybean; CK, control group; LP, low-phosphorus stress group. * Significant at $P < 0.05$, ** significant at $P < 0.01$. FD, fold changes that the change of growth parameters is represented by $\log_2^{(LP/CK)}$.

decreased by 0.81-fold ($p < 0.05$) and 0.32- and 1.31-fold ($p < 0.01$), respectively, and correspondingly in GS2 decreased by 0.70-fold ($p < 0.05$) and 0.05- and 0.66-fold ($p < 0.05$). The change of plant root length was opposite in the two ecotypes: root length decreased by 0.14-fold in GS1, but increased significantly by 0.06-fold in GS2 (Table 1). The changes of morphology showed significantly greater growth inhibition for GS1 than GS2 under LP stress. In addition, the P content in the seedling roots of common and barren-tolerant wild soybean under LP stress decreased significantly by 2.61-fold ($p < 0.01$) and 1.95-fold ($p < 0.05$), respectively (Figure 1B). The decline degree of P in GS1 was significantly higher than that in GS2.

3.2 Changes in transcription level

Transcriptomics sequencing produced a total of 88.67 Gb of clean data, and the clean data of each sample reached 6.68 Gb with the quality score 30 (Q30) base percentage being 93.96% and above. The comparison efficiency of the clean reads of each sample and the reference genome was within 89.01–93.48% (Supplementary material Table S2). Ten DEGs were randomly selected from the two ecotypes of wild soybean to perform qRT-PCR separately. The results were very similar to the transcriptome sequencing data, and so verified their accuracy (Supplementary material Figure S1).

Compared with CK, there were 340 DEGs in GS1 seedling roots (139 significantly up-regulated and 201 significantly down-regulated), 2948 DEGs in GS2 seedling roots (1688 significantly up-regulated and 1260 significantly down-regulated) under LP stress, and there were 108 common DEGs in roots of both ecotypes (Supplementary material Figure S2). There were many more DEGs in GS2 than GS1 seedling roots, showing that GS2 could more actively respond to and resist LP stress. The GO annotation analysis of DEGs showed that 145 and 1624 DEGs in biological processes were annotated to 86 and 399 items, respectively; 16 and 1285 DEGs in cell components were annotated to 16 and 40 items, respectively; and 75 and 1036 DEGs in molecular function were annotated to 51 and 206 entries in GS1 and GS2 seedling roots, respectively (items p value < 0.05) (Supplementary Material Figure S3). Further analysis of the DEGs in biological processes in GS1 roots showed that these were significantly mainly distributed in cellular response to phosphate starvation (GO:0016036, 11 DEGs), ion transport (GO:0006811, eight DEGs), coumarin biosynthetic process (GO:0009805, seven DEGs), phosphate ion transport (GO:0006817, six DEGs), and positive regulation of cellular response to phosphate starvation (GO:0080040, three DEGs) (Figure 2A; Supplementary Material Table S3). Further analysis of DEGs in biological processes in GS2 roots showed that the significant distribution was divided into two major parts: mineral nutrition and metabolic activities. Among them, mineral nutrients included cellular response to phosphate starvation (GO:0016036, 44 DEGs), ion transport (GO:0006811, 35 DEGs), cellular cation homeostasis (GO:0030003, 32 DEGs), phosphate ion transport (GO:0006817, 10 DEGs), cellular copper ion homeostasis (GO:0006878, nine DEGs), and metabolic activities, including flavonoid biosynthetic process (GO:0009813, 59 DEGs), positive regulation of flavonoid biosynthetic process (GO:0009963, 27 DEGs), anthocyanin-containing compound biosynthetic process (GO:0009718, 26 DEGs), secondary metabolic process (GO:0019748, 25 DEGs), response to ROS (GO:0000302, 17 DEGs), carboxylic acid metabolic process (GO:0019752, 16 DEGs), phenylpropanoid metabolic process (GO:0009698, 15 DEGs), and pectin catabolic process (GO:0045490, 13 DEGs) (Figure 2B, Supplementary Material Table S3). Thus, GS2 was more active than GS1 in response to LP stress at the level of mineral nutrition and metabolism. The

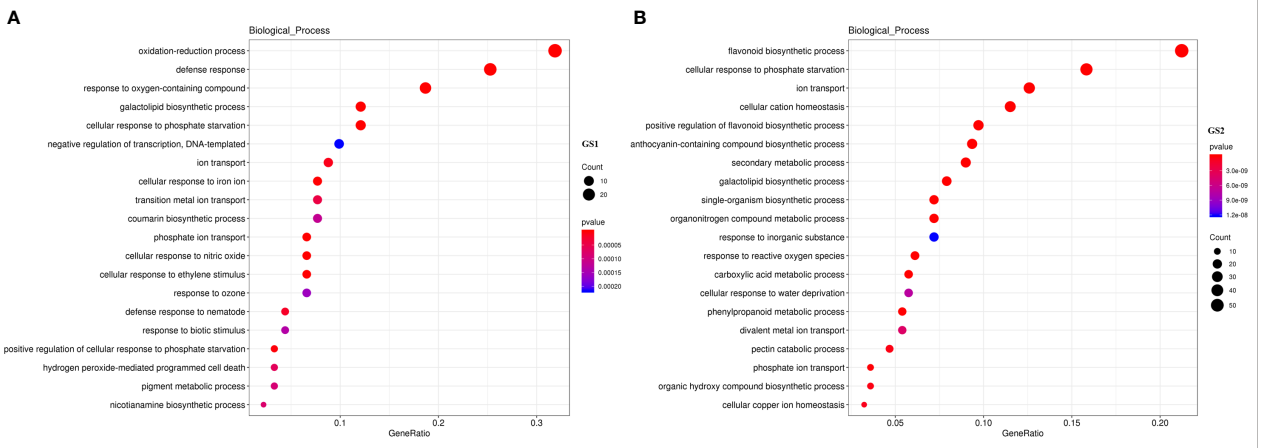


FIGURE 2
GO enriched biological process annotation of DEGs in **(A)** common and **(B)** barren-tolerant wild soybean. GS1, common wild soybean; GS2, barren-tolerant wild soybean.

TABLE 2 The expression of typical LP stress induced genes of DEGs in roots of two ecotypes wild soybean seedlings under LP.

	Name	ID	FPKM		FC	Description
			CK	LP		
GS1	PHT1-3	Glyma.10G006700.Wm82.a2.v1	22.65	55.64	1.19	Inorganic phosphate transporter 1-3
	PAP36	Glyma.12G007500.Wm82.a2.v1	2.55	4.29	0.64	purple acid phosphatase 36
	LOC100782755	Glyma.10G071000.Wm82.a2.v1	2.98	11.61	1.23	purple acid phosphatase 22
GS2	PHT1-2	Glyma.03G162800.Wm82.a2.v1	12.25	34.56	1.53	inorganic phosphate transporter 1-2
	PHT1-3	Glyma.10G006700.Wm82.a2.v1	18.19	91.31	2.31	Inorganic phosphate transporter 1-3
	ACP1	Glyma.08G195100.Wm82.a2.v1	0.58	4.1	2.82	acid phosphatase ACP1
	PAP36	Glyma.12G007500.Wm82.a2.v1	1.14	4.53	1.87	purple acid phosphatase 36
	PAP14	Glyma.09G229200.Wm82.a2.v1	0.6	2.27	1.67	purple acid phosphatase
	LOC100782755	Glyma.10G071000.Wm82.a2.v1	1.18	5.58	1.8	purple acid phosphatase 22

DEGs related to the acquisition of P and transportation of phosphate, including PHT1, ACP and PAP were significantly up-regulated in GS2 (Table 2). Among them, the DEGs Glyma.03G162800.Wm82.a2.v1, which is responsible for encoding inorganic phosphate transporter 1-2 (PHT1-2) and Glyma.10G006700.Wm82.a2.v1, which is responsible for encoding inorganic phosphate transporter 1-3 (PHT1-3), were significantly up-regulated by 1.53- and 2.31-fold in GS2. The acid phosphatase ACP1 (ACP1) gene Glyma.08G195100.Wm82.a2.v1 was significantly up-regulated by 2.82-fold in GS2 seedling roots. Furthermore, the purple acid phosphatase genes, Glyma.12G007500.Wm82.a2.v1 (PAP36), Glyma.09G229200.Wm82.a2.v1 (PAP14), and Glyma.10G071000.Wm82.a2.v1 (LOC100782755) were significantly upregulated by 1.87-, 1.67- and 1.80-fold in GS2 seedling roots (Supplementary material Table S4).

The KEGG enrichment analysis for 2948 DEGs showed that 591 DEGs were enriched in 111 pathways, among which the top 20 metabolic pathways with $p < 0.05$ are shown in Supplementary material Figure S4. Mapping the annotated DEGs to the KEGG database showed that four, two, one, one, and four transcripts were significantly enriched in phenylpropanoid biosynthesis (Ko00940), pentose phosphate pathway (Ko00030), glutathione metabolism (Ko00480), glycerolipid metabolism (Ko00561), and pentose and glucuronate interconversions (ko00040), respectively, in GS1 roots (Table 3, Supplementary material Figure S4.). Mapping the annotated DEGs to the KEGG database showed that 31, 13, 4, 6, 3, 4, 2, 1, and 10 transcripts were significantly enriched in phenylpropanoid biosynthesis (ko00940); flavonoid biosynthesis (ko00941); phenylalanine, tyrosine, and tryptophan biosynthesis (ko00400); pentose phosphate pathway (ko00030); glycine, serine, and threonine metabolism (ko00260); glutathione metabolism (ko00480); glycerolipid metabolism (ko00561); pentose and glucuronate interconversions (ko00040); and glycerophospholipid metabolism (ko00564), respectively, in

TABLE 3 KEGG pathway of DEGs in roots of common wild soybean seedlings under LP.

KO	KO ID	ID	FPKM		FC	Enzyme
			CK	LP		
Phenylpropanoid biosynthesis	ko00940	Glyma.03G208200.Wm82.a2.v1	18.17	44.04	1.28	cinnamyl-alcohol dehydrogenase (CAD)
		Glyma.09G277900.Wm82.a2.v1	3.26	7.95	1.02	
		Glyma.10G022500.Wm82.a2.v1	12.92	29.93	1.04	peroxidase
		Glyma.18G055400.Wm82.a2.v1	4.14	17.55	1.62	
		Glyma.18G055500.Wm82.a2.v1	6.37	28.96	1.25	
Pentose phosphate pathway	ko00030	Glyma.11G111400.Wm82.a2.v1	1.10	–	-2.65	6-phosphofructokinase (PFK)
		Glyma.02G202500.Wm82.a2.v1	4.66	1.49	-1.36	triosephosphate dehydrogenase (gapN)
Glutathione metabolism	ko00480	Glyma.11G024000.Wm82.a2.v1	5.16	1.82	-1.10	glutathione peroxidase (gpx)
Glycerollipid metabolism	ko00561	Glyma.03G078300.Wm82.a2.v1	1.52	3.73	1.10	sulfoquinovosyltransferase (SQD2)
Pentose and glucuronate interconversions	ko00040	Glyma.04G119100.Wm82.a2.v1	1.21	3.48	1.16	pectinesterase
		Glyma.06G314100.Wm82.a2.v1	0.34	1.40	1.16	
		Glyma.06G319100.Wm82.a2.v1	0.95	2.99	1.31	
		Glyma.19G212400.Wm82.a2.v1	0.66	2.93	1.39	

10.3389/fpls.2022.1006806

TABLE 4 KEGG pathway of DEGs in roots of barren-tolerant wild soybean seedlings under LP.

KEGG_map	ko_ID	ID	FPKM		FC	Enzyme
			CK	LP		
Phenylpropanoid biosynthesis	ko00940	Glyma.08G145900.Wm82.a2.v1	4.42	11.24	1.30	cinnamyl-alcohol dehydrogenase (CAD)
		Glyma.14G221200.Wm82.a2.v1	105.85	247.13	1.11	
		Glyma.02G008900.Wm82.a2.v1	0.58	2.59	1.75	peroxidase
		Glyma.02G052700.Wm82.a2.v1	15.09	36.00	1.24	
		Glyma.02G151700.Wm82.a2.v1	2.36	10.08	1.92	
		Glyma.02G233900.Wm82.a2.v1	3.57	15.98	1.95	
		Glyma.02G234000.Wm82.a2.v1	4.05	19.59	2.13	
		Glyma.02G234200.Wm82.a2.v1	8.94	55.05	2.47	
		Glyma.03G038100.Wm82.a2.v1	0.49	1.66	1.30	
		Glyma.03G039800.Wm82.a2.v1	2.36	11.75	1.92	
		Glyma.03G208200.Wm82.a2.v1	8.58	39.84	2.14	
		Glyma.05G103600.Wm82.a2.v1	111.04	302.51	1.44	
		Glyma.06G302600.Wm82.a2.v1	41.15	228.92	2.44	
		Glyma.06G302700.Wm82.a2.v1	2.88	17.52	1.81	
		Glyma.08G162700.Wm82.a2.v1	0.64	3.27	1.59	
		Glyma.09G022500.Wm82.a2.v1	64.71	194.37	1.43	
		Glyma.09G022800.Wm82.a2.v1	75.04	201.51	1.33	
		Glyma.09G023000.Wm82.a2.v1	144.66	313.17	1.05	
		Glyma.09G057100.Wm82.a2.v1	2.31	5.18	1.09	
		Glyma.09G284400.Wm82.a2.v1	1.61	4.62	1.32	
		Glyma.09G284700.Wm82.a2.v1	15.75	35.92	1.10	
		Glyma.10G022500.Wm82.a2.v1	5.44	21.92	1.90	
		Glyma.10G222400.Wm82.a2.v1	30.65	143.38	2.08	
		Glyma.11G161600.Wm82.a2.v1	1.67	8.56	2.00	
		Glyma.12G101200.Wm82.a2.v1	27.27	96.36	1.79	
		Glyma.13G172300.Wm82.a2.v1	0.86	1.84	1.01	
		Glyma.13G346100.Wm82.a2.v1	7.30	26.51	1.52	
		Glyma.14G201700.Wm82.a2.v1	57.16	162.20	1.46	
		Glyma.14G221400.Wm82.a2.v1	2.93	10.01	1.58	
		Glyma.15G028200.Wm82.a2.v1	2.28	10.72	1.94	
		Glyma.20G114200.Wm82.a2.v1	6.87	17.09	1.09	cinnamate hydroxylase (CYP73A)
Flavonoid biosynthesis	ko00941	Glyma.02G158700.Wm82.a2.v1	75.53	199.02	1.37	flavanone 4-reductase (DFR)
		Glyma.02G048400.Wm82.a2.v1	2.14	17.74	2.58	flavanone synthase I (F3H)
		Glyma.02G048600.Wm82.a2.v1	1.39	13.81	1.60	
		Glyma.01G091400.Wm82.a2.v1	1.45	6.66	1.74	chalcone synthetase (CHS)
		Glyma.01G228700.Wm82.a2.v1	505.56	1132.52	1.13	
		Glyma.02G130400.Wm82.a2.v1	5.49	21.24	1.61	
		Glyma.05G153200.Wm82.a2.v1	5.21	11.98	1.12	
		Glyma.08G109200.Wm82.a2.v1	6.75	16.75	1.20	
		Glyma.08G109400.Wm82.a2.v1	14.54	40.21	1.19	
		Glyma.08G110500.Wm82.a2.v1	25.83	63.77	1.06	
		Glyma.08G110700.Wm82.a2.v1	17.41	60.64	1.48	
		Glyma.08G110900.Wm82.a2.v1	12.40	37.26	1.49	
		Glyma.11G011500.Wm82.a2.v1	283.06	640.68	1.10	
Phenylalanine, tyrosine and tryptophan biosynthesis	ko00400	Glyma.01G131100.Wm82.a2.v1	1.41	4.82	1.36	aspartate-prephenate aminotransferase (PAT)
		Glyma.11G238300.Wm82.a2.v1	0.84	3.97	2.00	
		Glyma.06G235500.Wm82.a2.v1	0.58	2.27	1.62	tyrosine transaminase (TAT)

(Continued)

10.3389/fpls.2022.1006806

TABLE 4 Continued

KEGG_map	ko_ID	ID	FPKM		FC	Enzyme
			CK	LP		
		Glyma.19G239800.Wm82.a2.v1	0.67	2.46	1.54	shikimate dehydrogenase (DHQ-SDH)
Pentose phosphate pathway	ko00030	Glyma.05G056400.Wm82.a2.v1	8.75	21.46	1.28	transaldolase (talA)
		Glyma.08G199800.Wm82.a2.v1	3.02	1.14	-1.20	6-phosphofructokinase (PFK)
		Glyma.10G194300.Wm82.a2.v1	7.69	2.79	-1.68	
		Glyma.10G293500.Wm82.a2.v1	0.25	0.85	1.49	transketolase (tktA)
		Glyma.02G202500.Wm82.a2.v1	6.09	1.71	-1.73	triosephosphate dehydrogenase (gapN)
		Glyma.08G182300.Wm82.a2.v1	4.52	12.86	1.41	fructose-bisphosphatase (FBP)
Glycine, serine and threonine metabolism	ko00260	Glyma.04G104500.Wm82.a2.v1	5.10	11.39	1.18	phosphoglyceromutase (PGAM)
		Glyma.06G105600.Wm82.a2.v1	0.91	3.03	1.30	
		Glyma.04G254300.Wm82.a2.v1	2.60	1.19	-1.01	glycine hydroxymethyltransferase (glyA)
Glutathione metabolism	ko00480	Glyma.04G020200.Wm82.a2.v1	20.13	83.51	1.71	ornithine decarboxylase (ODC1)
		Glyma.06G020300.Wm82.a2.v1	1.01	14.05	1.71	
		Glyma.14G177200.Wm82.a2.v1	0.48	2.06	1.21	L-ascorbate peroxidase
		Glyma.02G149100.Wm82.a2.v1	1.24	3.66	1.10	glutathione peroxidase (gpx)
Glycerollipid metabolism	ko00561	Glyma.03G078300.Wm82.a2.v1	1.61	6.08	1.71	sulfoquinovosyltransferase (SQD2)
		Glyma.15G034100.Wm82.a2.v1	0.32	1.37	1.41	lysophosphatidic acid-acyltransferase (AGPAT3_4)
Pentose and glucuronate interconversions	ko00040	Glyma.03G215900.Wm82.a2.v1	0.34	3.30	1.94	pectinesterase
		Glyma.03G216000.Wm82.a2.v1	9.99	39.58	1.75	
		Glyma.04G119100.Wm82.a2.v1	0.22	1.29	1.98	
		Glyma.05G236800.Wm82.a2.v1	0.21	0.56	1.27	
		Glyma.06G314100.Wm82.a2.v1	0.29	1.11	1.31	
		Glyma.06G319100.Wm82.a2.v1	0.12	0.81	2.18	
		Glyma.09G232100.Wm82.a2.v1	2.15	4.88	1.14	
		Glyma.12G004400.Wm82.a2.v1	1.03	3.61	1.44	
		Glyma.19G212500.Wm82.a2.v1	0.43	1.52	1.41	
		Glyma.19G231400.Wm82.a2.v1	0.13	1.75	2.58	
Glycerophospholipid metabolism	ko00564	Glyma.03G092800.Wm82.a2.v1	3.88	13.60	1.72	phospholipase C (PLC)

GS2 roots (Table 4; Supplementary Material Figure S4.). Related to lignin synthesis enzyme cinnamyl-alcohol dehydrogenase (CAD), the DEGs Glyma.03G208200.Wm82.a2.v1 and Glyma.09G277900.Wm82.a2.v1 were up-regulated 1.28- and 1.02-fold in GS1 roots, respectively, and Glyma.08G145900.Wm82.a2.v1 and Glyma.14G221200.Wm82.a2.v1 were up-regulated 1.30- and 1.11-fold in GS2 roots, respectively. There were three and 28 DEGs related to the lignin synthesis enzyme peroxidase significantly up-regulated in GS1 and GS2 roots, respectively, with significantly greater up-regulation in GS2 than GS1 roots. Related to glutathione-glutathione disulfide (GSH-GSSH) metabolism, the glutathione peroxidase (gpx) gene Glyma.11G024000.Wm82.a2.v1 was significantly down-regulated 1.10-fold in GS1 roots, but Glyma.02G149100.Wm82.a2.v1 in GS2 roots was up-regulated 1.10-fold. In addition, related to ascorbate (AsA)–GSH cycle ornithine decarboxylase, DEGs Glyma.04G020200.Wm82.a2.v1 and Glyma.06G020300.Wm82.a2.v1 were up-regulated 1.71- and 1.71-fold, respectively, and L-ascorbate peroxidase gene Glyma.14G177200.Wm82.a2.v1 was up-regulated 1.21-fold in GS2 roots, but there was no change in GS1. Related to the enzyme SQD2 that promotes the substitution of sulfolipids for phospholipids, gene Glyma.03G078300.Wm82.a2.v1 was up-regulated 1.10-fold in GS1 roots and Glyma.03G078300.Wm82.a2.v1 was up-regulated 1.71-fold in GS2 roots, showing that GS2 had a stronger sulfolipid–phospholipid substitution effect. There were three and 10 DEGs, related to pectin esterase that catalyzes the reaction of cell-wall pectin, significantly up-regulated in GS1 and GS2 roots, respectively, with significantly greater up-regulation in GS2 than in GS1. In addition, DEGs related to anthocyanin synthesis, flavanone 4-reductase (DFR), naringenin 3-dioxygenase (F3H), and chalcone synthase (CHS) in ko00941 were significantly up-regulated in GS2 roots.

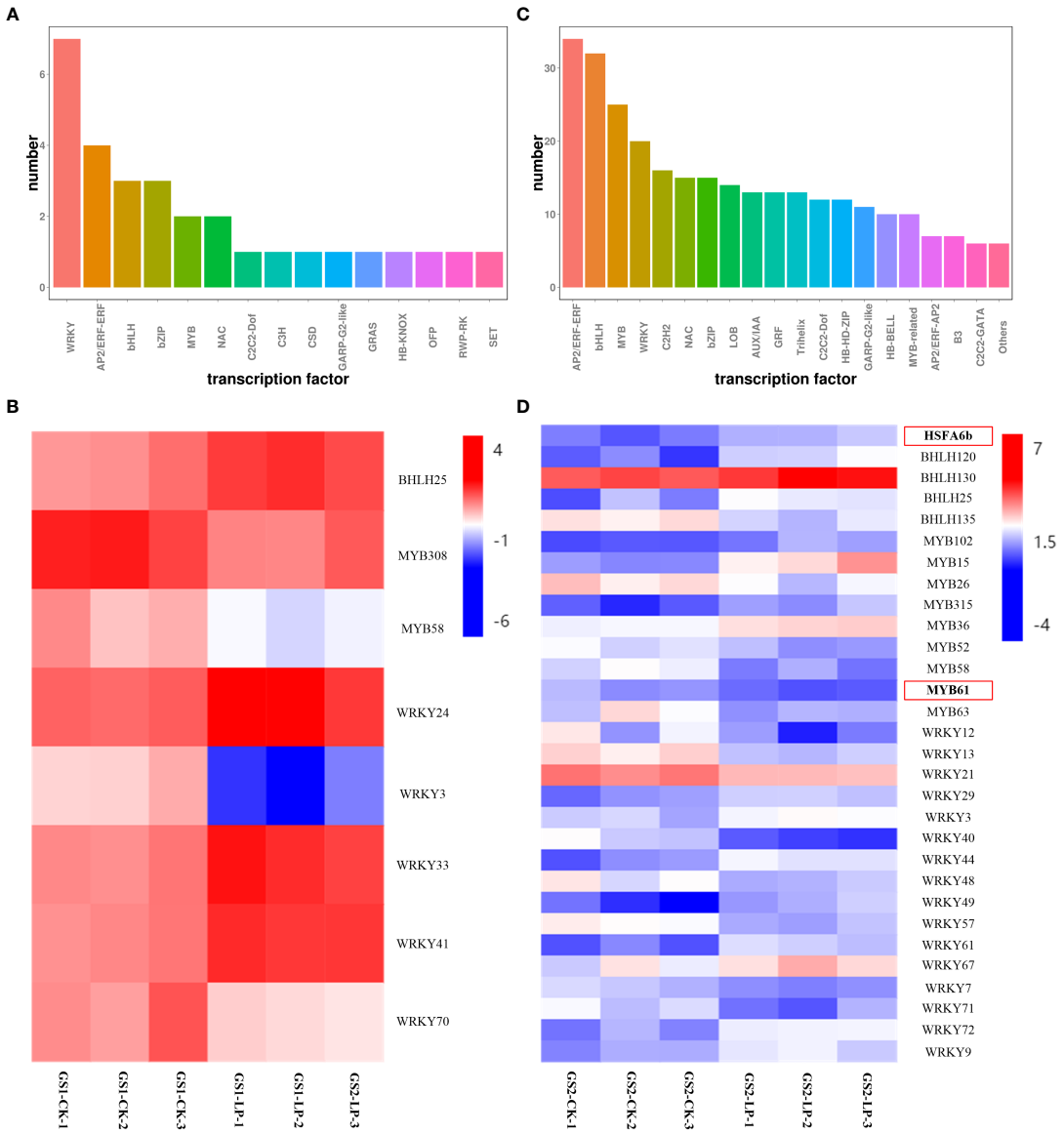


FIGURE 3
Differentially expressed transcription factor in roots of two ecotypes of wild soybean seedlings under control and low-phosphorus conditions. GS1, common wild soybean; GS2, barren-tolerant wild soybean; CK, control group; LP, low-phosphorus stress group. **(A)** Number of differentially expressed transcription factor in common wild soybean; **(B)** Regulation of the transcription factors in common wild soybean; **(C)** Number of differentially expressed transcription factor in barren-tolerant wild soybean; **(D)** Regulation of the transcription factors in barren-tolerant wild soybean. The expression levels represented as fold change; red indicates up-regulation; blue indicates down-regulation.

Transcription factor (TF) enrichment analysis showed that 30 DEGs were enriched in 15 TF families in GS1 roots, and 345 DEGs were enriched in 20 TF families in GS2 roots under LP stress (Figure 3; Supplementary Material Table S5). There were 1, 2, and 5 DEGs in the BHLH, MYB, and WRKY families in GS1 roots, respectively, and correspondingly 4, 9, and 16 DEGs in GS2 roots (Figure 3C). The *bHLH25*, *WRKY24*, *WRKY33* and *WRKY41* genes were specifically up-regulated 1.12-, 1.27-, 1.46- and 1.28-fold respectively; but *MYB308*, *MYB58*, *WRKY3*, *WRKY70* down-regulated 1.1-, 1.21-, 2.26- and 1.43-fold respectively in GS1 seedling roots. Genes *HSFA6b*, *BHLH120*, *BHLH130*, *BHLH25*, *MYB102*, *MYB15*, *MYB315*, *MYB36*, *WRKY29*, *WRKY3*, *WRKY44*, *WRKY49*, *WRKY61*, *WRKY67*, *WRKY72* and *WRKY9* were specifically up-regulated 1.29-, 1.82-, 1.17-, 1.39-, 1.21-, 2.8-, 1.4-, 1.05-, 1.09-, 1.07-, 1.7-, 1.5-, 1.75-, 1.03-, 1.7- and 1.12-fold respectively; but *BHLH35*, *MYB26*, *MYB52*, *MYB58*, *MYB61*, *MYB63*, *WRKY12*, *WRKY13*, *WRKY21*, *WRKY40*, *WRKY48*, *WRKY57*, *WRKY7* and *WRKY71* down-regulated 1.26-, 1.05-, 1.08-, 1.43-, 1.07-, 1.37-, 1.46-, 1.77-, 1.2-, 2.4-, 1.16-, 1.53-, 1.04- and 1.29-fold respectively in GS2 seedling roots. The expression of

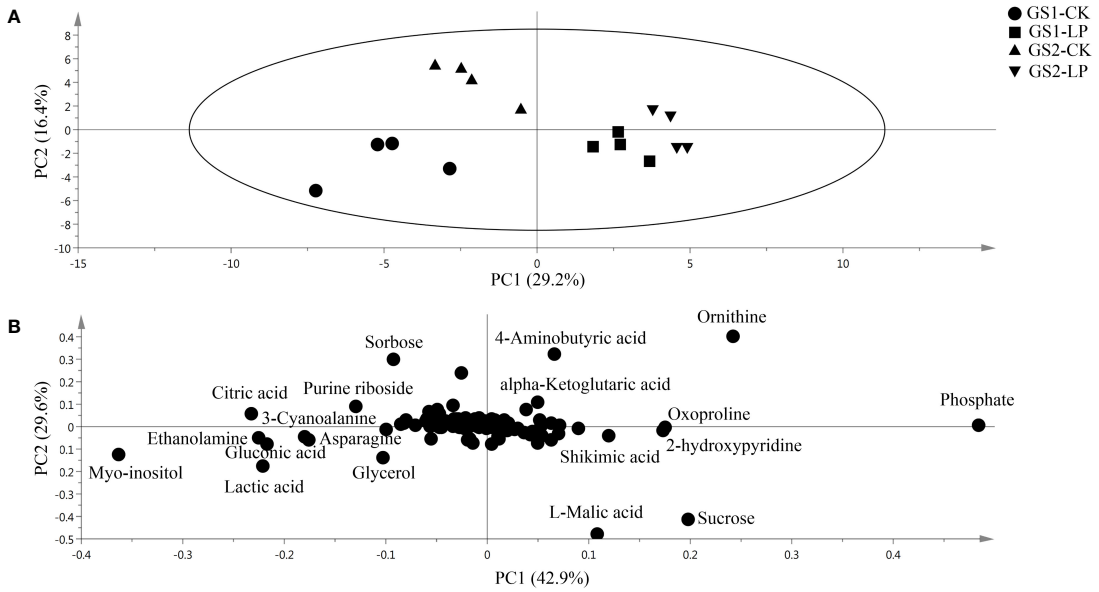


FIGURE 4
(A) Principal component analysis and **(B)** loading plots of metabolites in roots of two ecotypes of wild soybean seedlings under control and low-phosphorus conditions. PC1 and PC2 are the first and second principal components, respectively. GS1, common wild soybean; GS2, barren-tolerant wild soybean; CK, control group; LP, low-phosphorus stress group.

HSFA6b family gene Glyma.10G244000.Wm82.a2.v1 and the *MYB61* family gene Glyma.19G222200.Wm82.a2.v1 were significantly changed in GS2 seedling roots, but not detected in GS1 roots (Figure 3D; Supplementary Material Table S5).

3.3 Changes in metabolic levels

Based on GC-MS, we conducted metabonomics studies on the seedling roots of two wild soybean ecotypes under LP stress (Supplementary Material Figure S5). Metabolomics PCA showed that the first principal component (PC1) explained 29.2% of the variation (Figure 4A), showing significant differences in the metabolomics for GS1 and GS2 roots in CK and LP stress. The second principal component (PC2) explained 16.4% of the variation (Figure 4A), among which the difference in metabonomics between CK and LP stress of GS1 roots was greater than that in GS2. The PLS-DA showed that the main contributors to PC1 were myo-inositol, ethanolamine, gluconic acid, citric acid, 3-cyanoalanine, lactic acid, ornithine, oxoproline, shikimic acid and phosphate; and the main contributors to PC2 were ornithine, L-malic acid, sucrose and 4-aminobutyric acid (Figure 4B; Supplementary material Table S6). There were 50 different metabolites screened according to $p < 0.05$, similarity ≥ 600, and VIP > 1 from the measured metabolites: 12 amino acid metabolites, 12 sugar alcohol metabolites, 18 organic acid metabolites, and eight secondary metabolites.

The responses of metabolites in the two ecotypes to LP stress significantly differed (Table 5; Figure 5). Lignin and the anthocyanin synthesis key metabolite, phenylalanine, increased 1.76-fold in GS2 ($p < 0.01$), but with no significant difference in GS1 roots ($p > 0.05$). Naringin related to anthocyanin synthesis decreased 0.17-fold in GS1 roots, but increased 0.66-fold in GS2 ($p < 0.05$). Related to the GSH-GSSG and AsA–GSH cycles, with functions of scavenging ROS metabolites, proline, serine, glutamic acid, putrescine, and ascorbate increased 0.08-, 0.24-, 0.75-, 1.88-, and 1.06-fold, respectively, in GS2 roots ($p < 0.05$), but there was no significant change in GS1 ($p > 0.05$). Under LP stress, sugar alcohol metabolites accumulated in roots of both ecotypes. Raffinose and cellobiose significantly increased by 1.39- and 0.74-fold (both $p < 0.05$) in GS1 roots, respectively, and significantly by 1.80- and 0.88-fold (both $p < 0.01$) in GS2. The sugar alcohol metabolism under LP stress was more enhanced in GS2 roots than GS1 compared with CK. Under LP stress, the response of organic acid metabolites in GS1 and GS2 roots was very different. Citric acid significantly increased by 0.70-fold ($p < 0.01$) and succinic, L-malic, and oxalacetic acids increased by 0.07-, 0.46-, and 1.63-fold (all $p < 0.05$), in GS2 roots under LP stress. Aconitic, succinic, fumaric, and L-malic acids significantly decreased by 3.74-, 0.27-, 0.48-, and 0.44-fold in GS1 roots, respectively (all $p < 0.05$), and α-ketoglutaric acid significantly decreased by 2.42-fold ($p < 0.01$). This showed that the TCA cycle was enhanced in GS2 roots and inhibited in those of GS1. Glycerol, involved in sulfoquinovosyl diacylglycerol (SQDG) synthesis significantly increased by 0.45-fold ($p < 0.05$) and 0.57-fold ($p < 0.01$) in GS1 and GS2 roots, respectively.

10.3389/fpls.2022.1006806

TABLE 5 Changes of metabolite contents of two ecotypes wild soybean seedling roots under LP.

Metabolite name		Relative concentration				FD	
		GS1		GS2			
		CK	LP	CK	LP	GS1	GS2
	Oxoproline	18.82	8.78	15.98	10.34	-1.10**	-0.63*
	Proline	1.33	1.52	1.6	1.69	0.19	0.08*
	Glycine	1.3	2.67	1.89	2.12	1.04*	0.17*
	Serine	4.71	6.36	6.49	7.65	0.43	0.24*
	Glutamic acid	0.15	0.14	0.14	0.23	-0.13	0.75*
Amino acid metabolites	Ornithine	0.49	0.36	0.74	0.5	-0.44	-0.57*
	Phenylalanine	0.35	0.88	0.31	1.04	1.32	1.76**
	Citrulline	2.15	1.4	1.71	1.28	-0.62*	-0.42*
	Asparagine	1.14	12.55	1.21	9.08	3.46*	2.91*
	Leucine	0.38	0.22	0.84	4.22	-0.81*	2.33*
	Isoleucine	1.77	2.9	2.3	3.42	0.71*	0.57*
	L-Allothreonine	8.27	10.21	8.65	11.15	0.30*	0.37*
Sugar alcohol metabolites	Sorbose	37.35	36.65	51.33	68.03	-0.03	0.41*
	Glucose	1.79	2.45	3.53	4.19	0.45	0.25*
	Fructose	25.16	21.39	34.02	41.12	-0.23	0.27*
	Ribose	2.68	5.75	4.43	5.33	1.10*	0.27
	Raffinose	0.86	2.25	0.99	3.46	1.39*	1.80**
Organic acid metabolites	Lyxose	0.62	0.79	0.76	1.19	0.35*	0.66*
	Cellobiose	3.36	5.63	4.22	7.75	0.74*	0.88**
	Galactose	0.09	0.24	0.16	0.28	1.42*	0.78*
	Mannose	0.09	0.17	0.15	0.2	0.99*	0.45*
	Galactinol	1.12	3.3	0.83	3.91	1.56**	2.24**
	Fucose	0.14	0.17	0.19	0.24	0.30*	0.34*
	Glycerol	11.39	15.52	8.09	12.01	0.45*	0.57**
	Glucose-6-phosphate	1.5	0.13	1.31	0.21	-3.56**	-2.62*
	Glucose-1-phosphate	5.7	6.06	5.93	6.26	0.09	0.08*
	Pyruvate	0.53	0.84	0.73	0.81	0.65*	0.16
	Citric acid	44.64	57.14	44.6	72.38	0.36	0.70**
	Aconitic acid	0.34	0.03	0.01	0.03	-3.74*	-2.02
	α-Ketoglutaric acid	0.14	0.03	0.09	0.04	-2.42**	-1.28
	Succinic acid	16.38	13.59	13.19	13.85	-0.27*	0.07*
	Fumaric acid	5.05	3.63	3.97	3.46	-0.48*	-0.2
	L-Malic acid	126.78	93.23	59.91	82.13	-0.44**	0.46*
	Oxalacetic acid	0.18	0.36	0.14	0.44	1.01*	1.63*
	5-Aminovaleric acid	2.85	4.36	2.98	5.67	0.61*	0.93**
	Maleamate	0.02	0.03	0.01	0.11	0.61	4.04*
	Galactonic acid	0.29	0.69	0.52	1.04	1.26**	1.00**
	Threonic acid	0.7	1.37	0.75	2.29	0.96**	1.62*
	Malonic acid	3.35	2.26	2.44	2.53	-0.57*	0.05
	Glutaric acid	0.87	0.56	0	0.08	-0.63	11.63**
	Linoleic acid	0.27	0.47	0.23	0.59	0.79	1.39*
	D-Glyceric acid	0.15	0.36	0.19	0.3	1.28*	0.69**
	Putrescine	0.62	0.76	0.36	1.32	0.29	1.88*
	Ascorbate	0.04	0.06	0.03	0.07	0.52	1.06*
	Shikimic acid	0.48	0.45	0.63	0.55	-0.10*	-0.2

(Continued)

TABLE 5 Continued

Metabolite name		Relative concentration				FD	
		GS1		GS2			
		CK	LP	CK	LP	GS1	GS2
Secondary metabolites	Quinic acid	0.04	0.03	0.03	0.03	-0.83*	0.23*
	Cinnamic acid	1.82	1.03	2.11	1.22	-0.82*	-0.80*
	Naringin	0.03	0.02	0.27	0.42	-0.17*	0.66*
	Ferulic acid	0.17	0.1	0.18	0.11	-0.73*	-0.69
	Caffeic acid	0.04	0.02	0.05	0.02	-1.30*	-1.12

Relative concentration values were presented as the mean of four biological replicates. Relative concentration values were increased 1000 times. The * and ** indicate significant (P<0.05) and highly significant difference (P<0.01), respectively. FD, fold changes that the change of growth parameters is represented by $\log_2^{(LP/CK)}$.

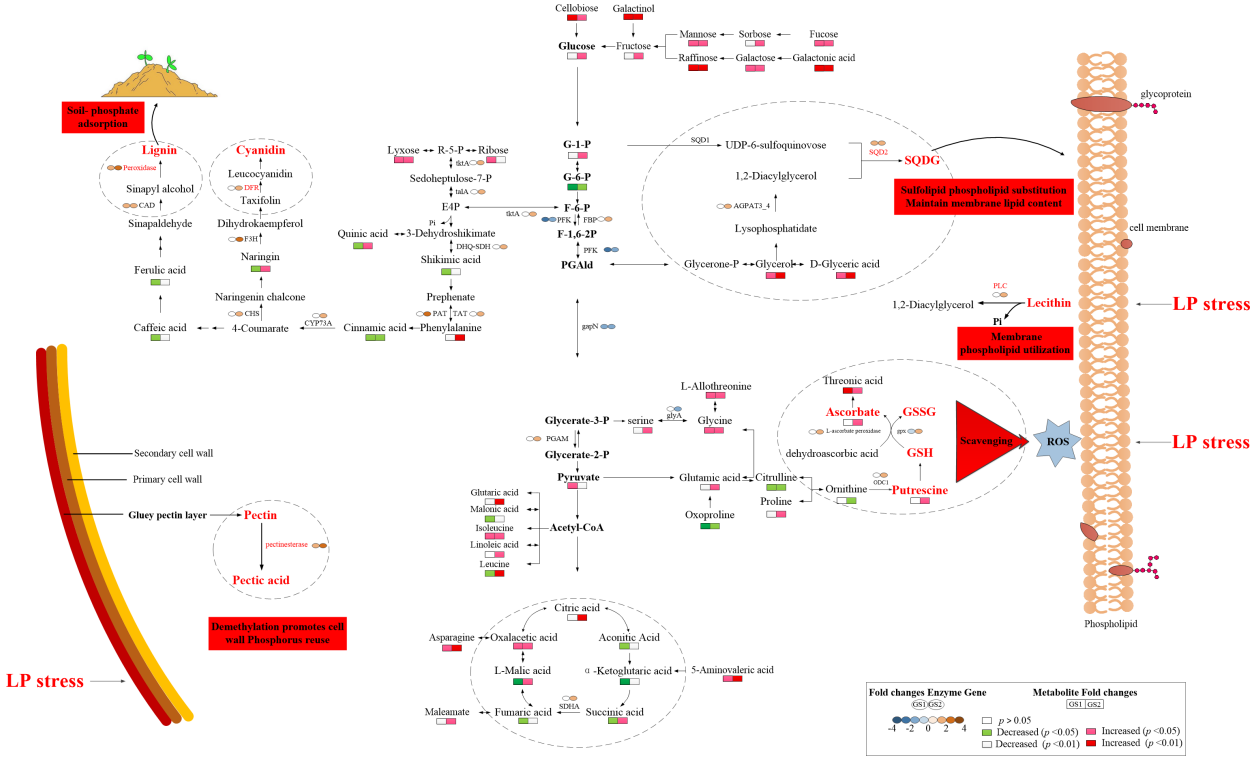


FIGURE 5
Key mechanisms of resistance to phosphorus deficiency in wild soybean. GS1, common wild soybean; GS2, barren-tolerant wild soybean; AGPAT3_4, lysophosphatidic acid acyltransferase; CAD, cinnamyl-alcohol dehydrogenase; CHS, chalcone synthase; CYP73A, trans-cinnamate 4-monooxygenase; DFR, bifunctional dihydroflavonol 4-reductase/flavanone 4-reductase; DHQ-SDH, 3-dehydroquinate dehydratase/shikimate dehydrogenase; F3H, naringenin 3-dioxygenase; FBP, fructose-1,6-bisphosphatase; gapN, glyceraldehyde-3-phosphate dehydrogenase ($NADP^+$); glyA, glycine hydroxymethyltransferase; gpx, glutathione peroxidase; GSH, glutathione; GSSG, glutathione disulfide; ODC1, ornithine decarboxylase; PAT, aspartate-prephenate aminotransferase; PFK, 6-phosphofructokinase; PGAM, 2,3-bisphosphoglycerate-dependent phosphoglycerate mutase; PLC, phospholipase C; SDHA, succinic dehydrogenase, SQD2, sulfoquinovosyltransferase; talA, transaldolase; TAT, tyrosine aminotransferase; tktA, transketolase.

3.4 Integrated analysis of transcriptome and metabolomics in barren-tolerant wild soybean

In order to determine the key regulatory network mechanism of GS2 tolerance to LP stress, we mapped 50 different metabolites and 2948 DEGs to the KEGG database, and performed Pearson correlation analysis in GS2 seedling roots under LP stress (Supplementary Material Table S7). The correlation interaction networks in GS2 roots showed that 76 transcripts had high correlation coefficients with 22 metabolites (Figure 6; Supplementary Material Table S7). The networks showed that the transcripts and metabolites were in four groups (A-D).

Group A was closely related to secondary metabolism and included phenylpropanoid biosynthesis (Ko00940); flavonoid biosynthesis (Ko00941); phenylalanine, tyrosine, and tryptophan biosynthesis (Ko00040); and pentose phosphate pathway (Ko00030) related transcripts and metabolites. Among them, phenylalanine and ferulic, caffeic, and cinnamic acids were significantly related to the DEGs of CAD, peroxidase, and cinnamate hydroxylase (CYP73A), which are involved in lignin synthesis. The flavonoid metabolites naringin, quinic acid, and shikimic acid were significantly related to the DEGs of DFR, F3H, and CHS, which are the key enzymes for anthocyanin synthesis of secondary antioxidants. Group B included glycine, serine, and threonine metabolism (Ko00260) and glutathione metabolism (Ko00480) which can remove ROS and protect the stability of cell membranes. Putrescine and ascorbic acid were significantly related to the DEGs of L-ascorbate peroxidase and gpx in the AsA–GSH cycle. Group C was related to membrane lipid remodeling and membrane phospholipid breakdown, including glycerolipid metabolism (Ko00561) and glycerophospholipid metabolism (Ko00564). The metabolites glycerol and D-glyceric acid were significantly related to the gene encoding SQD2, a key enzyme in SQDG synthesis. The Pearson's correlation coefficient between glucose-6-phosphate and the gene encoding PLC was −0.85306. Group D was related to the hydrolysis of pectin in the pectin layer of the cell wall that includes pentose and glucuronate interconversions (Ko00040), in which glycerol, pyruvate, and α-ketoglutarate were significantly negatively correlated with genes encoding pectinesterase, the key enzyme for pectin hydrolysis, with Pearson's correlation coefficients between −0.35914 and −0.8638 (Ko00040) (Figure 6).

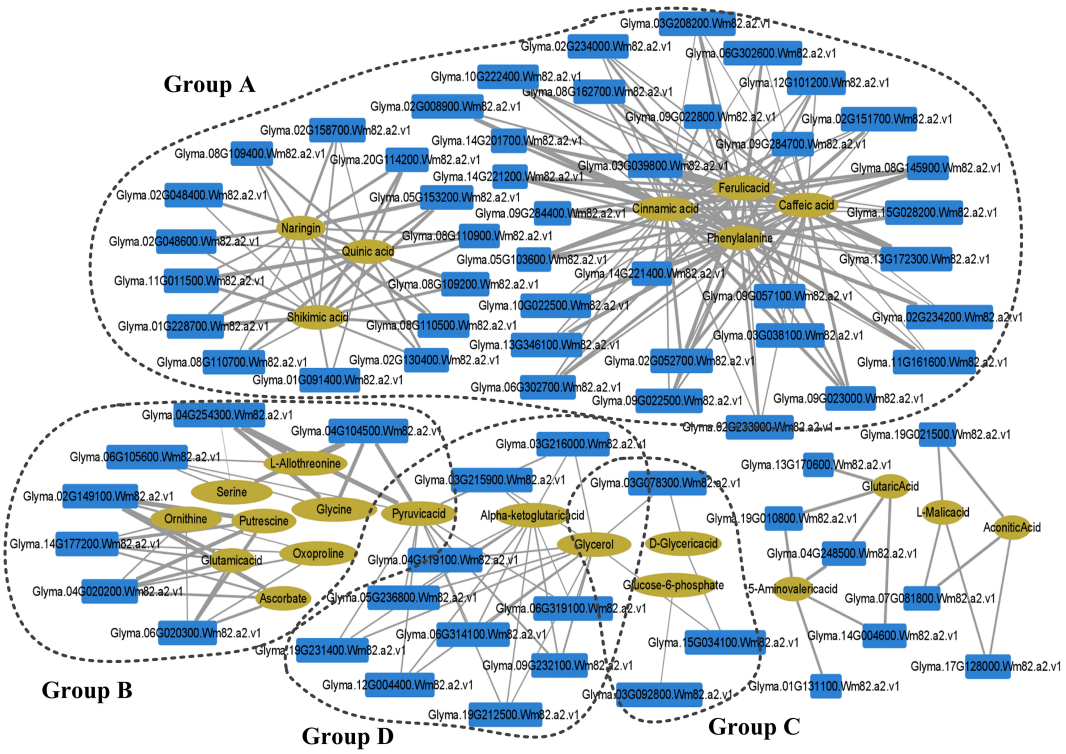


FIGURE 6
Integration network of metabolites and genes in barren-tolerant wild soybean seedling roots under phosphorus deficiency. The thicker the edge, the stronger the correlation. The size of a node is proportional to the correlation between nodes. Group A, closely related to secondary metabolism; Group B, related to remove ROS and protect the stability of cell membranes; Group C, related to membrane lipid remodeling and membrane phospholipid breakdown.

4 Discussion

The adaptation of plants to their environment is due to the variation of certain physiological and biochemical functions in the plant. These variations are due to mutations in the genetic material that cause differences within the one species, forming different ecotypes adapt to different environments (Ellis et al., 2021; Postolache et al., 2021). Therefore, the causes of variation from multiple perspectives, such as morphological structure, physiology, metabolism, and molecules, can better reveal the mechanisms of ecological adaptation formation during plant evolution.

The smaller inhibition of growth and the smaller decrease of P content in GS2 roots with LP compared to GS1 suggests that GS2 is more tolerant to soil P deficiency and has more free-P. In general, LP-resistant ecotypes of plants can enhance external P uptake and adjust internal P reuse to better adapt to P deficient environments by modulating morphological structures, as well as genetic and metabolic changes. Studies have confirmed that plants can expand the contact area with soil P through increasing the number and length of root hairs and lateral roots, increasing the root-to-shoot ratio, and the production of cluster roots, thereby increasing the plant's absorption of P (Watanabe et al., 2006; Niu et al., 2012; Yuan et al., 2016). In this study, the growth of GS1 plants was inhibited by P deficiency, and both plant height and root length decreased. The plant height of GS2 was reduced, but root length significantly increased, showing that in order to resist LP stress, GS2 plants distributed a larger proportion of material and energy to root growth, which greatly increased the root–soil contact area and so enhanced P absorption. Enhanced expression of the genes encoding PHT1 could promote P transport in plants, so as to maintain P homeostasis, and better respond to P deficiency (Fan et al., 2013; Song et al., 2014). Zhang et al., 2014 The purple acid phosphatase in plants is induced by P deficiency and could hydrolyze and release P from organophosphorus substrates for plant uptake and reuse. Low-P tolerant plants could significantly induce the purple acid phosphatase gene expression under P deficiency, so as to synthesize more purple phosphatase to promote P uptake and reuse, thus maintaining stable P content and better responding to low-P stress (Li et al., 2012). At the same time, the lignin in plant roots can significantly reduce the soil's ability to adsorb and fix P, and increase availability of P in the soil (Zhang, 2006). The key enzyme of lignin synthesis, peroxidase, and CAD-related DEGs were up-regulated, phenylalanine significantly accumulated, phenol metabolism was enhanced, and more P could be obtained in GS2 under LP stress. Transcriptomics GO annotation of DEGs also confirmed the significant enrichment of the flavonoid biosynthetic process (GO:0009813) and positive regulation of the flavonoid biosynthetic process (GO:0009963). Most of the insoluble inorganic P in the soil is bound by Al^{3+}, Fe^{3+}, and Ca^{2+} to form insoluble compounds; however, the P can be replaced by organic acid anions secreted by roots, releasing more available P for plants to use (Shane and Lambers, 2006). Significant accumulation of organic acids and rhizosphere secretion of organic acids have been detected in the roots of different species grown under low-P stress positive correlations were found (Haichar et al., 2014). Thus plants can resist low-P stress by increasing the content of organic acids in roots and then secreting more organic acids to the outside to increase the content of available P in plants (Lipton et al., 1987). The contents of citric and L-malic acids increased significantly, indicating that GS2 could effectively regulate the accumulation of organic acids in roots under low-P stress, which is beneficial to its secretion of organic acids to activate unavailable P in soil to resist low-P stress. Transcriptomic GO annotation of DEGs also confirmed the significant enrichment in carboxylic acid metabolic process (GO:0019752). *Lupinus albus* and *Vicia faba* can secrete large amounts of organic acids to enhance the efficiency of P acquisition under LP stress (Shen et al., 2018). Organic acid metabolism was significantly enhanced in GS2, showing that this was an important mechanism of GS2 to deal with LP stress. However, the metabolism of organic acids in GS1 changed irregularly under the influence of LP stress.

In addition to enhancing absorption of P, improving the utilization efficiency of P and structural P reuse in plant cells, such as hydrolyzing non-organic P in senescent tissues and being used by new tissues, is an important mechanism for plants to tolerate P deficiency in soil (Gong et al., 2011). Pectinesterase can maintain the degree of pectin methyl esterification of the cell wall at a low level, thereby promoting the release of cell wall P to increase the soluble P content in the body for reuse in other parts (Micheli, 2001; Zhu et al., 2012). Under LP stress, DEGs were significantly enriched in the pectin catabolic process (GO:0045490), and the pectinesterase-related DEGs in the two ecotypes of wild soybean were up-regulated, and the greater changes in GS2 indicated that GS2 could better actively regulate the reuse of endogenous P in the cell wall and resist soil P deficiency. Membrane phospholipids absorb one-third of the P in plant cells, when phosphate is insufficient, and PLC can hydrolyze phospholipids and promote the mobilization of organic phosphate in membrane phospholipids for other physiological metabolic activities (Tjellström et al., 2010). At the same time, PLC is also an important regulatory enzyme in the process of abiotic stress response (Peters et al., 2014). The PLC-related DEGs were up-regulated, showing that active regulation of membrane lipid metabolism is one key mechanism for GS2 to respond to LP stress, while this phenomenon does not exist in GS1. Accompanied by changes in membrane lipid metabolism, it is necessary to improve the structural stability of membrane lipids in cells to resist LP stress. Under P-limited conditions, the content of phosphatidylglycerol (PG) in *Arabidopsis* membrane lipids decreased, and the content of sulfur-containing glycolipid SQDG increased, replacing PG with SQDG to maintain stable membrane lipid content and

membrane lipid structure. Consistent with previous studies, the accumulations of D-glyceric acid and glycerol were significantly related to the up-regulated gene for SQDG, showing that SQDG activity was enhanced, maintaining the structural integrity of the biofilm system under LP stress in GS2. This revealed that the key mechanism to resisting LP stress was the decomposition and reuse of structural P, at the same time maintaining the stable structure and function of the cell membrane in GS2. In addition, enhanced sugar metabolism in plants facilitates the reduction of phosphorylation of metabolites to P-free sugars for efficient P use. Metabolomics research found that, under LP stress, the content of UDP-glucose in *Arabidopsis* leaves and di- and tri-saccharides in maize shoots accumulated and so enhanced the ability of plants to resist soil P deficiency (Ciereszko and Kleczkowski, 2006; Ganie et al., 2015). In this study, the disaccharides raffinose and cellobiose showed extremely significant accumulation, the sugar alcohol metabolism of GS2 was enhanced and its ability to withstand soil P deficiency was improved, consistent with previous studies. Sugar alcohol metabolism was enhanced in GS1, but the increase was not as great as GS2. In addition, citric and L-malic acids are important metabolites in the TCA cycle, and oxalacetic and succinic acids also accumulated significantly, showing that the TCA cycle was enhanced to provide energy for plant metabolic activities in GS2 under LP stress.

Under P deficiency, plants will produce ROS to initiate membrane lipid peroxidation, leading to membrane damage and destruction. One plant phenotype in response to soil P deficiency is the accumulation of anthocyanins in tissues, which can scavenge free radicals under adverse conditions and increase plant tolerance to P deficiency (Liang and He, 2018; He et al., 2020). Transcriptomics and metabolomics correlation analysis showed that genes related to DFR, a key enzyme for anthocyanin synthesis, were significantly up-regulated, and naringin accumulated significantly in GS2. The GSH is an important antioxidant and free radical scavenger. Under the catalysis of gpx, toxic peroxides are reduced to non-toxic compounds, and at the same time, GSH becomes GSSG. In the AsA–GSH cycle, AsA significantly accumulated, gpx-related DEGs were significantly up-regulated, and enhancement of the AsA–GSH cycle could effectively remove free radicals produced by LP stress and inhibit stress-induced oxidative damage in GS2. The AsA–GSH cycle also had a similar response when *Cunninghamia lanceolata* and *Oryza sativa* were subjected to soil P deficiency (Luo et al., 2018).

In the signal transduction system of plants, TFs play an important role in response to adverse environments. It has been reported that TFs of the BHLH, MYB, and WRKY families are closely related to the regulation of gene expression under P deficiency (Liang et al., 2013; Fan et al., 2014). In this study, two ecotypes of wild soybean were enriched in the WRKY, BHLH, and MYB families under LP stress, especially GS2. It is noteworthy that the HSFA6b gene was significantly up-regulated, and the MYB61 gene was significantly down-regulated in GS2 seedling roots. Previous studies have shown that HSFA6b and MYB61 play an important role in LP stress in Arabidopsis thaliana (Liang et al., 2005; Romano et al., 2012; Huang et al., 2016). Previous studies have shown that the MYB61 gene is essential for lignin biosynthesis (Rahmawati et al., 2022). The key enzyme of lignin synthesis, peroxidase, and CAD-related DEGs were up-regulated, further demonstrating that the ability of MYB61 to improve the ability of GS2 to resist low phosphorus stress may be related to the promotion of lignin synthesis.

5 Conclusions

Due to variation in the environment, the adaptation of plants to the environment is in a constant process of regulation. This coordination between different ecotypes of plants and environments can be achieved by plants changing their morphological structure, physiology, and molecular metabolism. In this study, through morphological and integrated analysis of transcriptomics and metabolomics of the roots of two ecotypes of wild soybean seedlings, on the one hand, GS2 enhanced soil P uptake by increasing root length, promoting the synthesis and secretion of lignin and organic acids and upregulating inorganic phosphate transporter (PHT1-2 and PHT1-3), acid phosphatase ACP1, and purple acid phosphatase genes (PAP36, PAP14 and LOC100782755) promote P uptake and transport to maintain stable P content in plants, and thus better adapt to low-P stress. On the other hand, GS2 increased pectin esterase and PLC activities to promote the reuse of structural P in the cell wall and membrane lipids, respectively, to maintain the P source required for normal cellular activities. In addition, GS2 generated SQDG to replace PG and maintain the stability of biofilm structure, and enhanced the synthesis of secondary antioxidant metabolite anthocyanins and the AsA–GSH cycle to reduce the oxidative damage to the membranes caused by P deficiency in soil. It was also found that HSFA6b and MYB61 were key TFs for barren-tolerant wild soybean to resist LP stress. Our study provides new perspectives for the divergence evolution of plants and provides quantitative system parameters for resource evaluation.

Data availability statement

The original contributions presented in the study are publicly available. This data can be found here: NCBI, PRJNA865466.

Author contributions

ML and LS designed the study and methodology. JZ, XL, DH, YH, YD and GW performed the analyses and discussed the results. ML wrote the manuscript draft. JG and LS performed writing-review, editing and supervision. All authors contributed to the article and approved the submitted version.

Funding

This work was supported by the National Natural Science Foundation of China (No. 32072012), Natural Science Foundation of Jilin Province, China (No. 20200201134JC), and Natural Science Foundation of Jilin Province, China (No. 20220508057RC).

Acknowledgments

We thank International Science Editing (http://www.internationalscienceediting.com) for editing this manuscript.

Conflict of interest

The authors declare that the research was conducted in the absence of any commercial or financial relationships that could be construed as a potential conflict of interest.

Publisher's note

All claims expressed in this article are solely those of the authors and do not necessarily represent those of their affiliated organizations, or those of the publisher, the editors and the reviewers. Any product that may be evaluated in this article, or claim that may be made by its manufacturer, is not guaranteed or endorsed by the publisher.

Supplementary material

The Supplementary Material for this article can be found online at: https://www.frontiersin.org/articles/10.3389/fpls.2022.1006806/full#supplementary-material

References

Chen, Z. C., and Liao, H. (2016). Organic acid anions: An effective defensive weapon for plants against aluminum toxicity and phosphorus deficiency in acidic soils. *J. Genet. Genomics* 43, 631–638. doi: 10.1016/j.jgg.2016.11.003

Ciereszko, I., and Kleczkowski, L. A. (2006). Phosphate deficiency-dependent upregulation of UDP-glucose pyrophosphorylase genes is insensitive to ABA and ethylene status in arabidopsis leaves. *Acta Physiol. Plant* 28, 387–393. doi: 10.1007/BF02706620

Ding, N., Huertas, R., Torres-Jerez, I., Liu, W., Watson, B., Scheible, W. R., et al. (2021). Transcriptional, metabolic, physiological and developmental responses of switchgrass to phosphorus limitation. *Plant Cell Environ.* 44, 186–202. doi: 10.1111/pce.13872

Dool, S. E., Picker, M. D., and Eberhard, M. J. B. (2022). Limited dispersal and local adaptation promote allopatric speciation in a biodiversity hotspot. *Mol. Ecol.* 31, 279–295. doi: 10.1111/mec.16219

Ellis, T. J., Postma, F. M., Oakley, C. G., and Ågren, J. (2021). Life-history trade-offs and the genetic basis of fitness in *Arabidopsis thaliana*. *Mol. Ecol.* 30, 2846–2858. doi: 10.1111/mec.15941

Fan, F. H., Cui, B. W., Zhang, T., Qiao, G., Ding, G. J., and Wen, X. P. (2014). The temporal transcriptomic response of pinus massoniana seedlings to phosphorus deficiency. *PloS One* 9, 1–11. doi: 10.1371/journal.pone.0105068

Fan, C. M., Wang, X., Hu, R. B., Wang, Y. H., Xiao, C. W., Jiang, Y., et al. (2013). The pattern of phosphate transporter 1 genes evolutionary divergence in *Glycine max* l. *BMC Plant Biol.* 13, 48. doi: 10.1186/1471-2229-13-48

Florea, L., Song, L., and Salzberg, S. L. (2013). Thousands of exon skipping events differentiate among splicing patterns in sixteen human tissues. *F1000Res* 2, 188. doi: 10.12688/f1000research.2-188.v1

Gamuyao, R., Chin, J. H., Pariasca-Tanaka, J., Pesaresi, P., Catausan, S., Dalid, C., et al. (2012). The protein kinase Pstol1 from traditional rice confers tolerance of phosphorus deficiency. *Nature* 488, 535–539. doi: 10.1038/nature11346

Ganie, A. H., Ahmad, A., Pandey, R., Aref, I. M., Yousuf, P. Y., Ahmad, S., et al. (2015). Metabolite profiling of low-p tolerant and low-p sensitive maize genotypes under phosphorus starvation and restoration conditions. *PloS One* 10, 1–25. doi: 10.1371/journal.pone.0129520

Gong, Y. M., Guo, Z. H., He, L. Y., and Li, J. S. (2011). Identification of maize genotypes with high tolerance or sensitivity to phosphorus deficiency. *J. Plant Nutr.* 34, 1290–1302. doi: 10.1080/01904167.2011.580816

Haichar, F. Z., Santaella, C., Heulin, T., and Achouak, W. (2014). Root exudates mediated interactions belowground. *Soil Biol. Biochem.* 77, 69–80. doi: 10.1016/j.soilbio.2014.06.017

He, Y. Q., Zhang, X. Y., Li, L. Y., Sun, Z. T., Li, J. M., Chen, X. Y., et al. (2020). SPX4 interacts with both PHR1 and PAP1 to regulate critical steps in phosphorus-status-dependent anthocyanin biosynthesis. *New Phytol.* 230, 205–217. doi: 10.1111/nph.17139

Huang, Y. C., Niu, C. Y., Yang, C. R., and Jinn, T. L. (2016). The heat-stress factor hsfa6b connects aba signaling and aba-mediated heat responses. *Plant Physiol.* 172, 00860.2016. doi: 10.1104/pp.16.00860

Huang, C. Y., Roessner, U., Eickmeier, I., Genc, Y., Callahan, D., Shirley, N., et al. (2008). Metabolite profiling reveals distinct changes in carbon and nitrogen metabolism in phosphate-deficient barley plants (*Hordeum vulgare* l.). *Plant Cell Physiol.* 49, 691–703. doi: 10.1093/pcp/pcn044

Kumar, S., Arora, P., Chugh, C., Seem, K., Kumar, S., Vinod, K. K., et al. (2021). Characterization of contrasting rice (*Oryza sativa* l.) genotypes reveals the pi-efficient schema for phosphate starvation tolerance. *BMC Plant Biol.* 21, 1–26. doi: 10.1186/s12870-021-03015-4

Lambers, H., Shane, M. W., Cramer, M. D., Pearse, S. J., and Veneklaas, E. J. (2006). Root structure and functioning for efficient acquisition of phosphorus: matching morphological and physiological traits. *Ann. Botany* 98, 693–713. doi: 10.1093/aob/mcl114

Liang, Y. K., Dubos, C., Dodd, I. C., Holroyd, G. H., and Campbell, M. M. (2005). Atmyb61, an r2r3-myb transcription factor controlling stomatal aperture in arabidopsis thaliana. *Curr. Biol.* 15, 1201–1206. doi: 10.1016/j.cub.2005.06.041

Liang, J., and He, J. X. (2018). Protective role of anthocyanins in plants under low nitrogen stress. *Biochem. Bioph Res. Co* 498, 946–953. doi: 10.1016/j.bbrc.2018.03.087

Liang, C. Y., Pineros, M. A., Tian, J., Yao, Z. F., Sun, L. L., Liu, J. P., et al. (2013). Low pH, aluminum, and phosphorus coordinately regulate malate exudation

through GmALMT1 to improve soybean adaptation to acid soils. *Plant Physiol.* 161, 1347–1361. doi: 10.1104/pp.112.208934

Li, C. C., Gui, S. H., Yang, T., Walk, T., Wang, X. T., and Liao, H. (2012). Identification of soybean purple acid phosphatase genes and their expression responses to phosphorus availability and symbiosis. *Ann. Bot-London* 109, 275–285. doi: 10.1093/aob/mcr246

Li, M. X., Guo, R., Jiao, Y., Jin, X. F., Zhang, H. Y., and Shi, L. X. (2017). Comparison of salt tolerance in soja based on metabolomics of seedling roots. *Front. Plant Sci.* 8. doi: 10.3389/fpls.2017.01101

Li, G. H., Li, H., Leffelaar, P. A., Shen, J. B., and Zhang, F. S. (2015). Dynamics of phosphorus fractions in the rhizosphere of fababean (*Vicia faba* l.) and maize (*Zea mays* l.) grown in calcareous and acid soils. *Crop Pasture Sci.* 66, 1151–1160. doi: 10.1071/cp14370

Lin, Z. H., Chen, R. B., and Chen, C. S. (2011). Research progress on physiological adaptability of plants to nitrogen deficiency. *Hubei Agric. Sci.* 23, 4761–4764. doi: 10.14088/j.cnki.issn0439-8114.2011.23.003

Lipton, D. S., Blanchar, R. W., and Blevins, D. G. (1987). Citrate, malate, and succinate concentration in exudates from p-sufficient and p-stressed *Medicago sativa* l. seedlings. *Plant Physiol.* 85, 315–317. doi: 10.1104/pp.85.2.315

Li, M. X., Xu, J. S., Wang, X. X., Fu, H., Zhao, M. L., Wang, H., et al. (2018). Photosynthetic characteristics and metabolic analyses of two soybean genotypes revealed adaptive strategies to low-nitrogen stress. *J. Plant Physiol.* 229, 132–141. doi: 10.1016/j.jplph.2018.07.009

Luo, H. Y., Shi, L. S., Wang, F. L., Chen, X. X., Cao, G. Q., Lin, S. Z., et al. (2018). Effects of low phosphorus and aluminum toxicity coupled stress on ascorbate-glutathione cycle in leaves of *Cunninghamia lanceolata*. *Chin. J. Trop. Crop* 39, 873–880. doi: 10.3969/j.issn.1000-2561.2018.05.007

Micheli, F. (2001). Pectin methylesterases: cell wall enzymes with important roles in plant physiology. *Trends Plant Sci.* 6, 414–419. doi: 10.1016/s1360-1385(01)02045-3

Mo, X., Zhang, M., Liang, C., Cai, L., and Tian, J. (2019). Integration of metabolome and transcriptome analyses highlights soybean roots responding to phosphorus deficiency by modulating phosphorylated metabolite processes. *Plant Physiol. Bioch.* 139, 697–706. doi: 10.1016/j.plaphy.2019.04.033

Niu, Y. F., Chai, R. S., Jin, G. L., Wang, H., Tang, C. X., and Zhang, Y. S. (2012). Responses of root architecture development to low phosphorus availability: a review. *Ann. Bot.* 112, 391–408. doi: 10.1093/aob/mcs285

Peters, C., Kim, S. C., Devaiah, S., Li, M. Y., and Wang, X. M. (2014). Non-specific phospholipase C5 and diacylglycerol promote lateral root development under mild salt stress in arabidopsis. *Plant Cell Environ.* 37, 2002–2013. doi: 10.1111/pce.12334

Postolache, D., Oddou-Muratorio, S., Vajana, E., Bagnoli, F., Hampe, A., Provost, G. L., et al. (2021). Genetic signatures of divergent selection in European beech (*Fagus sylvatica* l.) are associated with the variation in temperature and precipitation across its distribution range. *Mol. Ecol.* 30, 5029–5047. doi: 10.1111/mec.16115

Rahmawati, S., Pantouw, C. F., Estiati, A., Satrio, B., Widyajayantie, D., Astuti, D., et al. (2022). Agrobacterium-mediated transformation of two rice varieties with Atmyb61 gene for lignin content manipulation toward biomass refinery. *IOP Conf. Ser: Earth Environ. Sci.* 1018, 012002. doi: 10.1088/1755-1315/1018/1/012002

Romano, J. M., Dubos, C., Prouse, M. B., Wilkins, O., Hong, H., Poole, M., et al. (2012). Atmyb61, an r2r3-myb transcription factor, functions as a pleiotropic regulator *via* a small gene network. *New Phytol.* 195, 774–786. doi: 10.1111/j.1469-8137.2012.04201.x

Schmittgen, T. D., and Livak, K. J. (2008). Analyzing real-time PCR data by the comparative CT method. *Nat. Protoc.* 3, 1101–1108. doi: 10.1038/nprot.2008.73

Shane, M. W., and Lambers, H. (2006). Cluster roots: a curiosity in context. *Plant Soil* 274, 101–125. doi: 10.1007/1-4020-4099-7_5

Shen, Q., Wen, Z. H., Dong, Y., Li, H. G., Miao, Y. X., and Shen, J. B. (2018). The responses of root morphology and phosphorus-mobilizing exudations in wheat to increasing shoot phosphorus concentration. *AoB Plants* 10, 1–11. doi: 10.1093/aobpla/ply054

Song, H. N., Yin, Z. T., Chao, M. N., Ning, L. H., Zhang, D., and Yu, D. Y. (2014). Functional properties and expression quantitative trait loci for phosphate transporter GmPT1 in soybean. *Plant Cell Environ.* 37, 462–472. doi: 10.1111/pce.12170

Tjellström, H., Hellgren, L. I., Wieslander, Å., and Sandelius, A. S. (2010). Lipid asymmetry in plant plasma membranes: phosphate deficiency-induced phospholipid replacement is restricted to the cytosolic leaflet. *FASEB J.* 24, 1128–1138. doi: 10.1096/fj.09-139410

Watanabe, T., Osaki, M., Yano, H., and Rao, I. M. (2006). Internal mechanisms of plant adaptation to aluminum toxicity and phosphorus starvation in three tropical forages. *J. Plant Nutr.* 29, 1243–1255. doi: 10.1080/01904160600767484

Wei, B., Hou, K., Zhang, H. H., Wang, X. Y., and Wu, W. (2020). Integrating transcriptomics and metabolomics to studies key metabolism, pathways and candidate genes associated with drought-tolerance in *Carthamus tinctorius* l. under drought stress. *Ind. Crop Prod.* 151, 1–15. doi: 10.1016/j.indcrop.2020.112465

Xia, J., Mandal, R., Sinelnikov, I. V., Broadhurst, D., and Wishart, D. S. (2012). MetaboAnalyst 2.0-a comprehensive server for metabolomic data analysis. *Nucleic Acids Res.* 40, 127–133. doi: 10.1093/nar/gks374

Yang, W., Hou, H. T., Feng, F. Y., Xu, Y. N., Li, L. B., and Kuang, T. Y. (2003). The biosynthesis and function of sulfoquinovosyl diacylglycerol. *Chin. Bull. Botany* 20, 103–104. doi: 10.3969/j.issn.1674-3466.2003.01.015

Yang, L., Tang, H., Li, H., Zhang, F., Zed, R., Whalley, W. R., et al. (2016). Major crop species show differential balance between root morphological and physiological responses to variable phosphorus supply. *Front. Plant Sci.* 7. doi: 10.3389/fpls.2016.01939

Young, M. D., Wakefield, M. J., Smyth, G. K., and Oshlack, A. (2010). Gene ontology analysis for RNA-seq: accounting for selection bias. *Genome Biol.* 11, 1–12. doi: 10.1186/gb-2010-11-2-r14

Yuan, H. M., Blackwell, M., Mcgrath, S., George, T. S., Granger, S. H., Hawkins, J. M. B., et al. (2016). Morphological responses of wheat (*Triticum aestivum* l.) roots to phosphorus supply in two contrasting soils. *J. Agr Sci.* 154, 98–108. doi: 10.1017/S0021859615000702

Zhang, Q. D. (2006). Effects of lignin on soil phosphate adsorption. *J. Agro-Environ Sci.* 25, 152–155. doi: 10.1111/j.1744-7917.2006.00098.x

Zhang, D., Song, H. N., Cheng, H., Hao, D. R., Wang, H., Kan, G., et al. (2014). The acid phosphatase-encoding gene GmACP1 contributes to soybean tolerance to low-phosphorus stress. *PloS Genet.* 10, 1–16. doi: 10.1371/journal.pgen.1004061

Zhu, X. F., Lei, G. J., Jiang, T., Liu, Y., Li, G. X., and Zheng, S. G. (2012). Cell wall polysaccharides are involved in p-deficiency-induced cd exclusion in *Arabidopsis thaliana*. *Planta* 236, 989–997. doi: 10.1007/s00425-012-1652-8

Zhu, L. L., Xu, J., Dou, P. Y., Dou, D. Q., and Huang, L. Q. (2021). The rhizosphere soil factors on the quality of wild-cultivated herb and its origin traceability as well as distinguishing from garden-cultivated herb: Mountainous forest cultivated ginseng for example. *Ind. Crop Prod.* 172, 114078. doi: 10.1016/j.indcrop.2021.114078

Zou, X. H., Dan, W., Wu, P. F., Zhang, Y., Hu, Y. N., Chen, S. T., et al. (2018). Strategies of organic acid production and exudation in response to low-phosphorus stress in Chinese fir genotypes differing in phosphorus-use efficiencies. *Trees* 32, 897–912. doi: 10.1007/s00468-018-1683-2

frontiers | Frontiers in Plant Science

TYPE Original Research
PUBLISHED 24 November 2022
DOI 10.3389/fpls.2022.1032646

Check for updates

OPEN ACCESS

EDITED BY
Mirza Hasanuzzaman,
Sher-e-Bangla Agricultural University, Bangladesh

REVIEWED BY
Xin Li,
Tea Research Institute, Chinese Academy of Agricultural Sciences, China
Izhar Ali,
Guangxi University, China

*CORRESPONDENCE
Caihong Wang
chwang@qau.edu.cn

†These authors have contributed equally to this work

SPECIALTY SECTION
This article was submitted to Plant Abiotic Stress, a section of the journal Frontiers in Plant Science

RECEIVED 31 August 2022
ACCEPTED 09 November 2022
PUBLISHED 24 November 2022

CITATION
Sun Z, Zou Y, Xie C, Han L, Zheng X, Tian Y, Ma C, Liu X and Wang C (2022) Brassinolide improves the tolerance of *Malus hupehensis* to alkaline stress. *Front. Plant Sci.* 13:1032646. doi: 10.3389/fpls.2022.1032646

COPYRIGHT
© 2022 Sun, Zou, Xie, Han, Zheng, Tian, Ma, Liu and Wang. This is an open-access article distributed under the terms of the Creative Commons Attribution License (CC BY). The use, distribution or reproduction in other forums is permitted, provided the original author(s) and the copyright owner(s) are credited and that the original publication in this journal is cited, in accordance with accepted academic practice. No use, distribution or reproduction is permitted which does not comply with these terms.

Brassinolide improves the tolerance of *Malus hupehensis* to alkaline stress

Zhijuan Sun[1†], Yawen Zou[2,3†], Cheng Xie[2,3], Lei Han[2,3], Xiaodong Zheng[2,3], Yike Tian[2,3], Changqing Ma[2,3], Xiaoli Liu[2,3] and Caihong Wang[2,3*]

[1]College of Life Science, Qingdao Agricultural University, Qingdao, China, [2]College of Horticulture, Qingdao Agricultural University, Qingdao, China, [3]Qingdao Key Laboratory of Genetic Improvement and Breeding in Horticulture Plants, Qingdao, China

Malus hupehensis is one of the most widely used apple rootstocks in china but is severely damaged by alkaline soil. Alkaline stress can cause more serious harmful effects on apple plants than salt stress because it also induces high pH stress except for ion toxicity, osmotic stress, and oxidative damage. Brassinolide (BL) plays important roles in plant responses to salt stress. However, its role and function mechanism in apple plants in response to alkaline stress has never been reported. This study showed that applying exogenous 0.2 mg/L BL significantly enhanced the resistance of *M. hupehensis* seedlings to alkaline stress. The main functional mechanisms were also explored. First, exogenous BL could decrease the rhizosphere pH and promote Ca^{2+} and Mg^{2+} absorption by regulating malic acid and citric acid contents and increasing H^+ excretion. Second, exogenous BL could alleviate ion toxicity caused by alkaline stress through enhancing Na^+ efflux and inhibiting K^+ expel and vacuole compartmentalization. Last, exogenous BL could balance osmotic stress by accumulating proline and reduce oxidative damage through increasing the activities of antioxidant enzymes and antioxidants contents. This study provides an important theoretical basis for further analyzing the mechanism of exogenous BL in improving alkaline tolerance of apple plants.

KEYWORDS

brassinolide, *Malus hupehensis*, alkaline stress, rhizosphere pH, oxidative damage

Introduction

Soil salinization seriously restricts the sustainable development of agricultural production around the world (Hu et al., 2016; Liang et al., 2017; Christian et al., 2018). About 20% of the global arable land is affected by salinization, which will continue to expand with global warming and excessive application of pesticides and fertilizers (Xia

et al., 2019; Negi et al., 2021). Apple (*Malus domestica* Borkh.) is one of the most valuable horticultural fruit crops and widely cultivated in the world (Ma et al., 2019). However, large areas of salinization soil exist in main apple producing areas, resulting in yellow leaves and weakening the growth of the fruit trees, which seriously affect the production and quality of apples (An et al., 2018; Su et al., 2020). Therefore, improving the tolerance of fruit trees to saline-alkali stress is of great significance for effectively utilizing saline-alkali land and giving full play to its economic and ecological effect.

Saline-alkali stress in natural environment is usually accompanied by neutral salt stress (caused by NaCl) and alkaline stress (caused by $NaHCO_3$ and Na_2CO_3) (Liu et al., 2015). Plants have different response mechanisms to neutral salt stress and alkaline stress (Sharma et al., 2016), and the latter causes a more complex and significant damage to plants than the former (Wang T. et al., 2015; Gong et al., 2017). Under alkaline stress, in addition to osmotic stress and ion poisoning, the roots of the fruit trees suffer from damage caused by high pH stress, thereby reducing the absorption of trace elements (such as Ca^{2+}, Mg^{2+}, Fe^{2+} and Mn^{2+}). This phenomenon causes the symptoms of element deficiency, disturbs the acid-base balance, and affects the quality of the fruit (Fan et al., 2021). Moreover, osmotic stress caused by alkaline stress could harm the photosynthetic system of plants, which usually affects the photosynthetic rate and fluorescence parameters of chlorophyll. Besides the direct damage to plants, alkaline stress could trigger oxidative damage indirectly, which result in the excessive accumulation of reactive oxygen species (ROS), leading to the destruction of plant cell membranes, impairment of vital biological processes, and acceleration of plant death. A number of previous studies focused on physiological and biochemical responses of plants to neutral salt stress. Nevertheless, the resistance mechanism to alkaline stress remains unclear in fruit trees.

In long-term struggle with alkaline stress, plants have evolved their own physiological and molecular mechanisms to adapt this situation (Mao et al., 2017; Hu et al., 2018; Chen et al., 2019). Plants can regulate the ion balance by expelling Na^+ and absorbing K^+ to maintain the cytoplasmic Na^+/K^+. Antioxidant enzymes, including superoxide dismutase (SOD), peroxidase (POD), catalase (CAT) and peroxidase (APX), in plants' defense systems can remove ROS to reduce oxidative damage (Tofighi et al., 2017; Wu et al., 2017). Meanwhile, ascorbic acid (AsA) and glutathione (GSH) are important non-enzymatic antioxidants, which play a crucial role in quenching the ROS and protecting plants from damaging effects of highly oxidizing ROS (Wang et al., 2019; Li et al., 2022). In addition, plants can regulate osmotic potential and ion balance by increasing the concentrations of osmolytes (e.g., proline, glycine, betaine, soluble sugar, and soluble protein). Under high pH stress, plants regulate the rhizosphere pH primarily by regulating the proton pump (H^+-ATP enzyme) activity and the secretion of organic acids (Zhan et al., 2019).

Plant hormones play an important role in plant growth and development and response to environmental stress (Ryu and Cho, 2015). Exogenous application of plant growth regulators is one of the effective ways to improve the salt and alkali resistance of crops (Shahzad et al., 2018; Su et al., 2020). Multiple plant hormones, such as abscisic acid, melatonin, and jasmonic acid, play key roles in plants' response to salt stress (Zhu, 2016; Wu et al., 2019; Zhao et al., 2021). Brassinosteroids (BRs) are sterol hormones that regulate vegetative growth and reproductive growth in plants (Xiong et al., 2022). Exogenous analog brassinolide (BL) is recognized as a highly efficient, universal, and non-toxic regulator of plant growth, which can significantly increase the plant photosynthesis efficiency and promote nutrient growth at low concentrations (Dong et al., 2017; Nawaz et al., 2017; Tofighi et al., 2017). Exogenous application of BL can also improve the cold resistance, drought resistance, and salt resistance of crops (Sharma et al., 2013; Jia et al., 2021). BL promotes nutrient absorption and metabolism in plant growth by reducing the accumulation of toxic ions and oxidative damage, and plays a positive role in abiotic stress tolerance (Li et al., 2015). For instance, exogenous BL application improved the drought tolerance through modulation of enzymatic antioxidants and leaf gas exchange in maize (Li et al., 2020). In cucumber plants, exogenous BL application alleviated $Ca(NO_3)_2$ stress by regulating mineral nutrients uptake and distribution (Yuan et al., 2015). However, the effect of BL on apple plants growth and the underlying mechanism under alkaline stress remains unclear.

To investigate the role and mechanism of BL on *Malus hupehensis* seedlings under alkaline stress, our study analyzed the its function from four aspects: rhizosphere pH balance, ion homeostasis, osmotic regulation, and antioxidant system. Moreover, the expression of alkaline-responding genes was detected under alkaline stress and exogenous BL treatment by qPCR. This study provides an important theoretical basis for further analyzing the mechanism of exogenous BL in improving alkaline tolerance of apple plants by focusing on roots.

Materials and methods

Plant materials and growth conditions

Seeds of *M. hupehensis* after cold stratification were sown in a 50-hole tray containing seedling substrate [nutrient soil (65% fertile garden soil, 10% fine sand, 25% burning soil, and 0.4% calcium magnesium phosphate fertilizer) and vermiculite with the ratio of 1:1]. They were cultivated in a greenhouse under the controlled condition of photoperiod (16/8 h day/night), light intensity (100 $\mu mol \cdot m^{-2} \cdot s^{-1}$), humidity (60%-65%), and temperature (25°C). When the apple seedlings developed to six leaves, they were transplanted into plastic pots (one seedling per pot) with dimensions of 7 cm × 7 cm × 10 cm (length, width and

height) and watered with Hoagland's nutrient solution (pH = 5.9) every 3 days. After 7 days, seedlings with similar growth status were selected for alkaline stress and exogenous BL treatment.

Alkaline stress and exogenous BL treatment

A total of 120 apple seedlings were randomly divided into three groups. The control group was irrigated with Hoagland's nutrient solution (group I). The alkaline treatment group (group II) was irrigated with Hoagland's nutrient solution containing 80 mM Na_2CO_3:$NaHCO_3$ = 1:1 (pH = 8.3) every 3 days. In group III, except for the same alkaline treatment [Hoagland's nutrient solution containing 80 mM Na_2CO_3:$NaHCO_3$ = 1:1 (pH = 8.3)] with group II, the apple seedlings were also irrigated and sprayed with 0.2 mg/L BL (Solarbio, Beijing, China) every 3 days. After 15 days of alkaline stress and BL treatment, the phenotype of the apple seedlings was recorded. Wilting rate, plant height, fresh weight (FW), dry weight (DW), chlorophyll content, and photosynthetic rate were measured as described by Zheng et al. (2021). Total root length and fibrous root number were analyzed by root scanner (Epson, Beijing, China). Each experiment was independently repeated three times.

Roots pH staining and determination of organic acid contents

Rhizosphere pH staining was conducted according to Zhao Q. et al. (2016). The roots of apple seedlings under alkaline stress and exogenous BL treatment were placed in culture medium containing 0.01% bromocresol purple (Solarbio, Beijing, China), 0.2 mM $CaSO_4$, and 0.7% agar (pH = 6.5) for 24 h. Bromocresol purple was used as an acid-base indicator, and its pH change range was 5.2 (yellow)-6.8 (purple). Acidification was indicated by yellow colour around the apple roots. The color presents the accurate pH value.

A total of 0.5 g of roots from each treatment were used to detect the contents of organic acids, including malic acid and citric acid, as described by Li T. et al. (2021). Each experiment was independently repeated three times.

Determination of ROS Level, antioxidant enzyme activities and antioxidants contents

Fifteen apple seedlings were randomly selected from each group for ROS detection. The ROS level in the roots and H_2O_2 and $O_2\cdot^-$ staining in leaves were detected as described by Zheng et al. (2017). The content of malondialdehyde (MDA) was determined by thiobarbituric acid (TBA) as described by Alam et al. (2019).

Each 0.1 g of apple seedling roots or leaves were separately weighed to detect antioxidant enzyme activities and antioxidants contents. The apple seedlings roots were ground into homogenates on ice and then centrifuged at 12 000 rpm for 10 min at 4°C. For the assay of activity of SOD, the reaction mixture comprising enzyme extract (100 μL), phosphate buffer (100 mM, pH 7.4), riboflavin (50 μM), EDTA (1.0 mM), methionine (10 mM), and NBT (75 μM) was kept for 15 min under fluorescent light. The optical density (OD) was noted at 560 nm (Alam et al., 2019). POD activity was estimated using the guaiacol colorimetric at 470 nm for 1 min, as described by Zheng et al. (2017). The activity of CAT was detected by detecting the reduction of H_2O_2 at 510 nm for 5 min by the method of Alam et al. (2019). APX activity was assayed following a reduction in absorbance of the mixture containing hydrogen peroxide and ascorbic acid at 290 nm for 3 min as described by Alam et al. (2019).

Each 0.1 g of apple seedling roots were ground into homogenates in liquid nitrogen and then centrifuged at 12 000 rpm for 10 min at 4°C. GSSG, GSH, AsA, and DHA contents were measured using visible photometry as described previously (Li et al., 2018; Song et al., 2018; Ji et al., 2019). Each experiment was independently repeated three times.

Determination of electrolyte leakage and osmolyte content

Ten seedlings were randomly selected from each group after treatment for 15 days to detect electrolyte leakage as described previously (Ahmad et al., 2016). Firstly, the electrical conductivity (ECa) of the 10 leaf disks submerged was measured. Secondly, the leaf disks were put in test tubes and incubated at 55°C for 25 min, and the electrical conductivity (ECb) was measured. Finally, the test tubes were boiled at 100°C for 10 min, and the electrical conductivity (ECc) was determined. Electrolyte leakage was calculated using the following formula: electrolyte leakage (%) = (ECb − ECa)/ECc × 100. Both the biological and technical duplications of each experiment were repeated three times.

0.5 g of roots from each group were used to detect osmolytes including proline and soluble sugar. The roots were ground in 5 mL of pre-cooled extracted buffer and centrifuged (12,000 rpm) at 4°C for 10 min. The supernatant was used for proline and soluble sugar content assays as described by Li T. et al. (2021). Each experiment was independently repeated three times.

Quantification of mineral elements

Fifteen apple seedlings were randomly selected from each group and cleaned with distilled water after 15 days of treatment. The samples were dehydrated at 105°C for 30 min and then baked in an oven at 80°C for 72 h. A total of 0.5 g of the dried roots were

ground into powder and mixed with 10 mL of HNO_3 and 2 mL of $HClO_4$ to digestion. The solution was added with deionized water and diluted to 25 mL. The contents of Na^+, K^+, Ca^{2+}, Fe^{2+}, Mg^{2+}, and other mineral ions were determined by inductively coupled plasma atomic emission spectrometry (PerkinElmer, Waltham, USA), as described by Li T. et al. (2021). Each experiment was independently repeated three times.

RNA extraction and quantitative real-time PCR analysis

After alkaline stress and exogenous BL treatments, the total RNA of different groups was extracted using the RNAprep pure Plant Plus Kit (Tiangen, Beijing, China). Inverse transcription and qPCR assay were conducted as described by Zheng et al. (2021). *MhActin* (accession number: MDP0000774288) was used as internal control. Primer sequences for qPCR were designed according to the coding sequence of *MhAHAs*, *MhNHXs*, *MhBZRs*, *MhMATE1*, *MhALMT1*, *MhSOS1*, *MhCHX15*, and *MhSKOR* by using Primer 5 software and checked using BLAST search in the apple genomic database. The primer sequences are shown in Table S1. Each experiment was independently repeated three times.

Experimental design and statistical analysis

All experiments were repeated three times. Data were analyzed by ANOVA followed by Fisher's least-significance difference or Student's *t*-test analysis. Statistically significant differences were indicated by P-value < 0.05. Statistical computations were conducted using SPSS (IBM, Armonk, USA).

Results

Effects of exogenous BL on the aboveground phenotype of apple seedlings under alkaline stress

As shown in Figure 1A, the apple seedlings were wilted and seriously damaged by alkaline stress, and the wilting rate was as high as 75%. After application of 0.2 mg/L BL for 15 days, the growth vigor of exogenous BL-treated seedlings was better than that of the alkaline-stressed seedlings. The wilting rate also decreased to 19% (Figure 1A, B). In addition, the plant height, fresh weight, and dry weight were detected. The plant height under alkaline stress was only 6.4 cm, which was 4.2 cm shorter than that of the control, while it only reduced by 3.2 cm after application of exogenous BL (Figure 1C). After 15 days of alkaline stress, the fresh weight and dry weight were significantly lower than those in the control group. However, after 15 days of treatment with exogenous BL, the fresh weight and dry weight increased by 54.5% and 47.2%, respectively, compared with those under alkaline stress (Figure 1D, E). These results indicated that alkaline stress seriously inhibited the aboveground part growth of the apple seedlings, and the treatment of exogenous BL significantly alleviated this damage.

Effects of exogenous BL on chlorophyll content and photosynthetic rate under alkaline stress

Alkaline stress caused plant wilting, and exogenous BL alleviated the chlorosis of the apple seedlings under alkaline stress. Chlorophyll content and photosynthetic rate were measured to explore the physiological mechanism. As shown in Figure 2A, the chlorophyll content in the apple seedlings under alkaline stress was only 21.1 SPAD, which reduced a third compared with that in the control group (32.4 SPAD). When exogenous BL was applied, the chlorophyll content significantly increased to 27.7 SPAD. The variation in photosynthetic rate was similar to that in chlorophyll content. The photosynthetic rate was significantly inhibited under alkaline stress but increased after application of exogenous BL. Under alkaline stress, the photosynthetic rate decreased significantly but recovered when exogenous BL was applied (Figure 2B). These results suggested that exogenous BL protected the chlorophyll level and photosynthetic system from alkaline stress.

Effects of exogenous BL on the underground phenotype of apple seedlings under alkaline stress

For the underground part, the root growth of the apple seedlings was seriously inhibited under alkaline stress, but the inhibitory effect was alleviated after application of exogenous BL (Figure 3A). The root length of the apple seedlings was only 5.69 cm under alkaline stress, which was 10.30 cm shorter than that of the control group, but it increased significantly to 8.37 cm after exogenous BL was applied (Figure 3B). Similar to root length, the fibrous root number under alkaline stress was decreased significantly compared with the control group and increased by about threefold after exogenous application of BL (Figure 3C). The above results indicated that exogenous BL treatment significantly alleviated the root damage caused by alkaline stress.

Effects of exogenous BL on rhizosphere pH and organic acid contents under alkaline stress

Alkaline stress would cause high pH stress to the roots. A medium containing the pH indicator bromocresol purple could

10.3389/fpls.2022.1032646

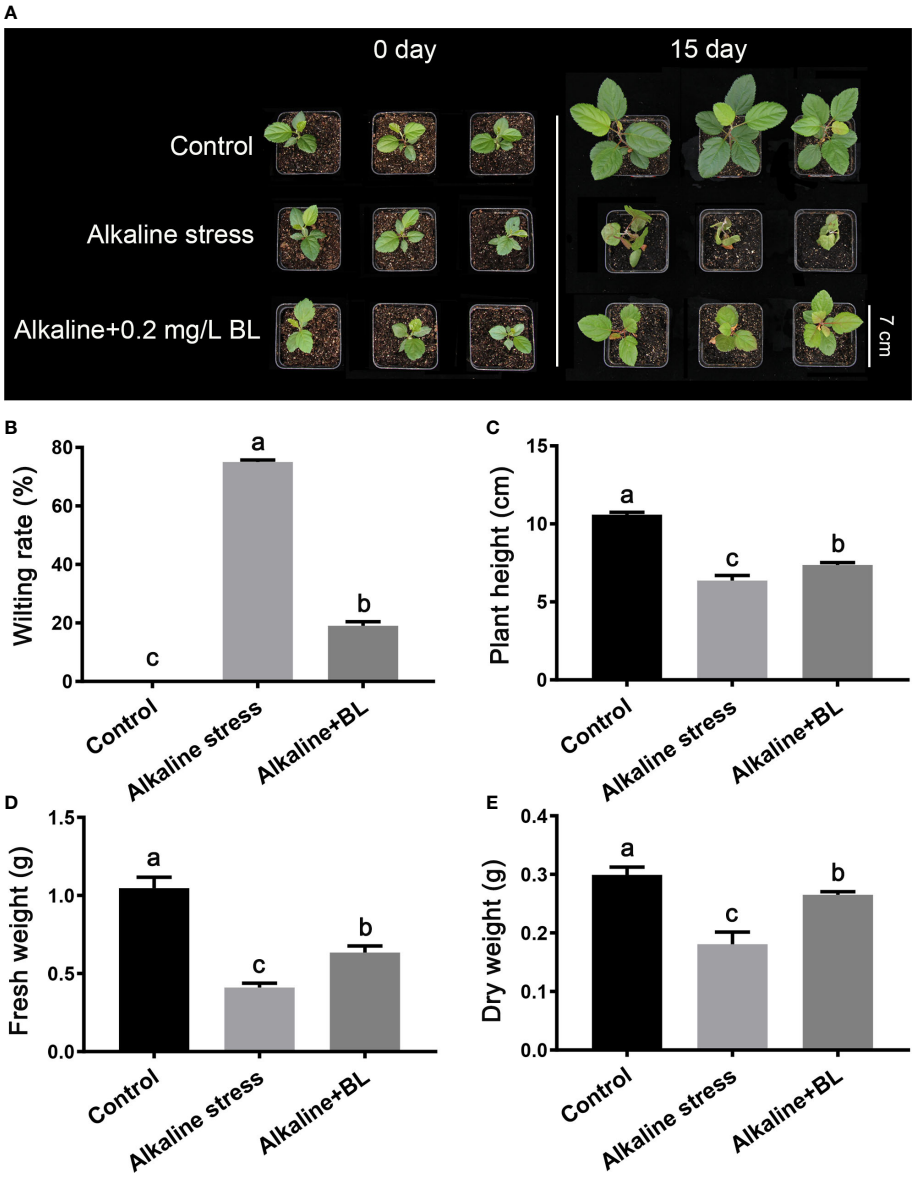


FIGURE 1
The aboveground phenotypes of *M. hupehensis* seedlings treated with alkaline stress and 0.2 mg/L BL. **(A)** The phenotypes of *M. hupehensis* seedlings treated with alkaline stress and BL at day 0 and day 15. The scale bar represents 7.0 cm. Effects of exogenous BL on wilting rate **(B)**, plant height **(C)**, fresh weight **(D)**, and dry weight **(E)** of the seedlings after alkaline stress for 15 days. Data represent the mean ± SD of triplicate experiments. Different lowercase letters indicate significant differences according to Fisher's least significant difference ($P < 0.05$).

be effective in reflecting rhizosphere pH. As shown in Figure 4A, the surrounding of the roots turned purple under alkaline stress, but it returned yellow after application of exogenous BL, meanwhile, the control roots showed yellow color. Moreover, the contents of malic acid and citric acid under alkaline stress increased significantly, but decreased respectively after application of exogenous BL (Figure 4B, C). These results demonstrated that exogenous BL alleviated the high pH stress caused by alkaline stress by regulating organic acid contents.

Effects of exogenous BL on the oxidative damage under alkaline stress

The fluorescence staining results revealed that alkaline stress significantly elevated the ROS levels in the roots of apple seedlings, but the levels were significantly decreased when exogenous BL was applied (Figure 5A). Consistently, the MDA contents in the roots and leaves under alkaline stress were more than twice that in the control group, but significantly decreased

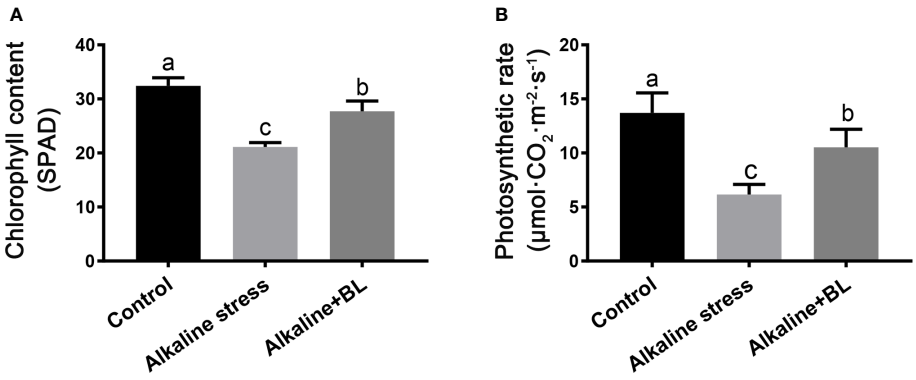


FIGURE 2
Effects of exogenous BL treatment on chlorophyll content **(A)**, photosynthesis rate **(B)** of *M. hupehensis* seedlings under alkaline stress. The data represent the mean ± SD of three biological replicates. Different lowercase letters indicate significant differences according to Fisher's least significant difference ($P < 0.05$).

after the application of exogenous BL (Figure 5B). The activities of SOD, POD, CAT and APX in roots were detected. As shown in Figure 5C, the SOD activity in roots had no significant change under alkaline stress and exogenous BL treatment. In contrast to SOD, the POD, CAT and APX activities in roots showed a significant decline under alkaline stress, nevertheless, enhanced after exogenous application of BL. The POD, CAT and APX activities under alkaline stress were significantly lower than

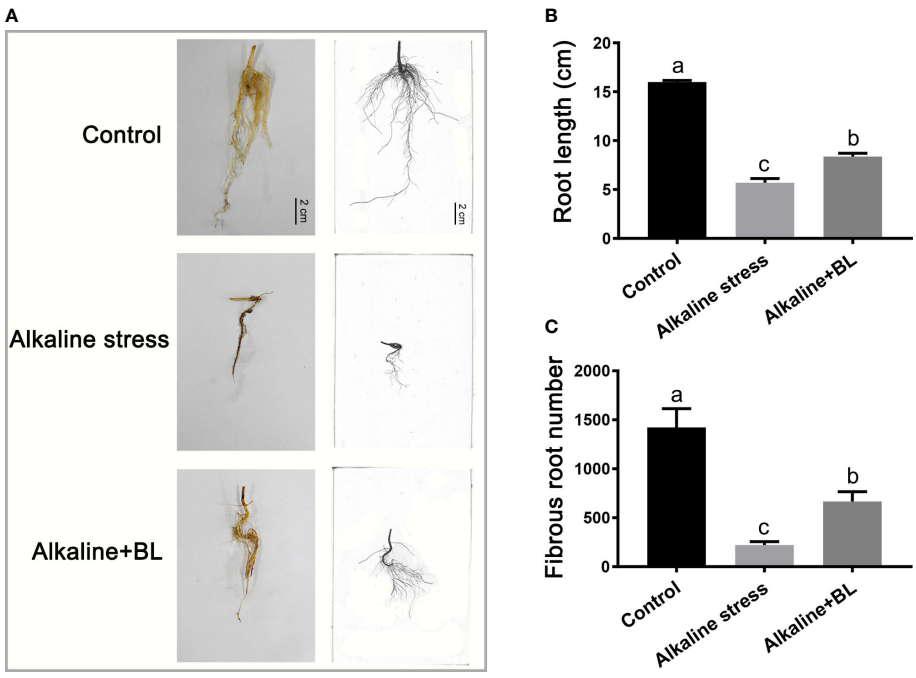


FIGURE 3
The underground phenotypes of *M. hupehensis* seedlings treated with alkaline stress and exogenous BL. **(A)** The roots phenotypes of the seedlings treated with alkaline stress and BL at day 15. The scale bar represents 2.0 cm. Effects of exogenous BL on root length **(B)** and fibrous root number **(C)** of the seedlings after alkaline stress for 15 days. The data represent the mean ± SD of three biological replicates. Different lowercase letters indicate significant differences according to Fisher's least significant difference ($P < 0.05$).

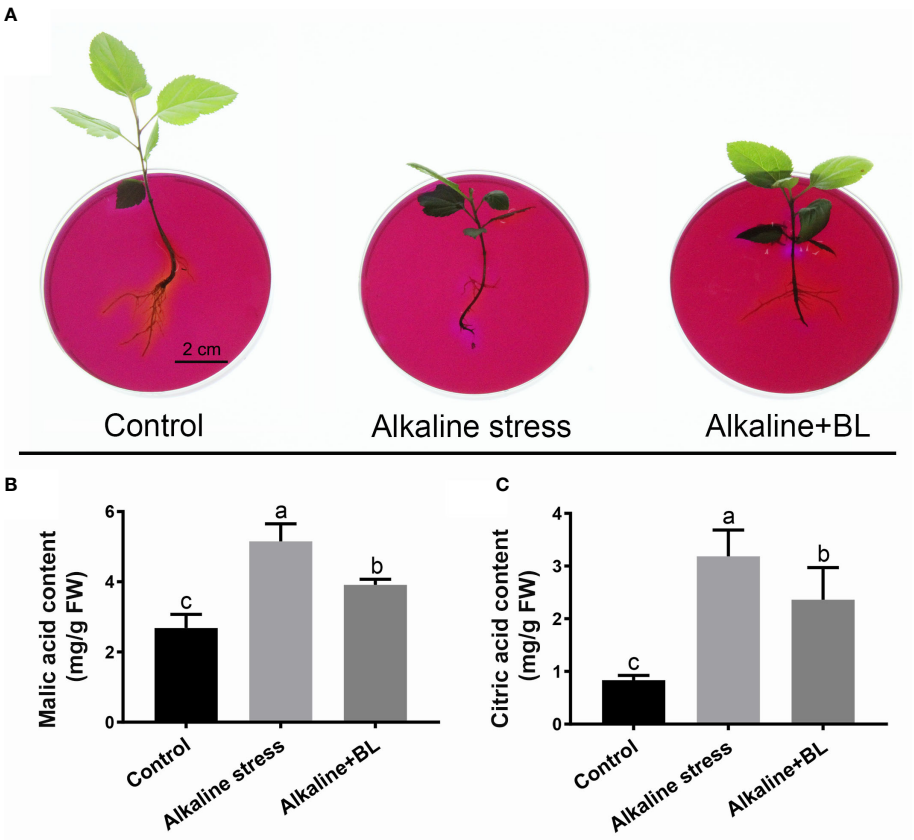


FIGURE 4
Effects of exogenous BL on rhizosphere pH and organic acid contents of *M. hupehensis* under alkaline stress. **(A)** Effects of alkaline stress and exogenous BL on rhizosphere pH of the seedlings by bromocresol violet staining. The scale bar represents 2.0 cm. Effects of alkaline stress and exogenous BL on malic acid content **(B)** and citric acid content **(C)** of the seedlings at day 15. The data represent the mean ± SD of three biological replicates. Different lowercase letters indicate significant differences according to Fisher's least significant difference ($P < 0.05$).

those in the control group, but increased significantly when exogenous BL was applied (Figures 5D–F). Moreover, the ratios of GSH/GSSG and AsA/DHA showed a significant decline under alkaline stress, but increased evidently after application of exogenous BL (Figures 5G, H).

Furthermore, the above indicators of oxidative damage were also determined on leaves. The leaves exhibited a notably increased H_2O_2 level relative to the WT control under alkaline stress, but a decreasing trend after application of exogenous BL. However, the level of $O_2 \cdot^-$ in leaves had no significant change under alkaline stress and exogenous BL treatment (Figure S1A). The activities of SOD, POD and CAT in leaves were also detected. Similar to the roots, the SOD activity in leaves had no significant change under alkaline stress and exogenous BL treatment. In contrast to SOD, the POD and CAT activities in leaves were also decreased significantly under alkaline stress, but increased when exogenous BL was applied (Figure S1B-D). The above results suggested that exogenous BL could alleviate oxidative damage by improving the activities of the antioxidant enzymes (POD, CAT, and APX) and increasing the ratios of GSH/GSSG and AsA/DHA in the non-enzymatic antioxidant protection system of apples.

Effects of exogenous BL on the electrolyte leakage and osmolytes of apple seedling roots under alkaline stress

As shown in Figure 6A, after alkaline stress, the electrolyte leakage increased significantly from 19% to 42% compared with that in the control group but decreased to as low as 32% when exogenous BL was applied. In addition, we measured the contents of osmolytes including proline and soluble sugar. Both of them were significantly induced by alkaline stress. However, the proline content was significantly increased, while the soluble sugar content had no remarkable change when exogenous BL was applied compared with that under alkaline stress group (Figure 6B, C). These results indicated that

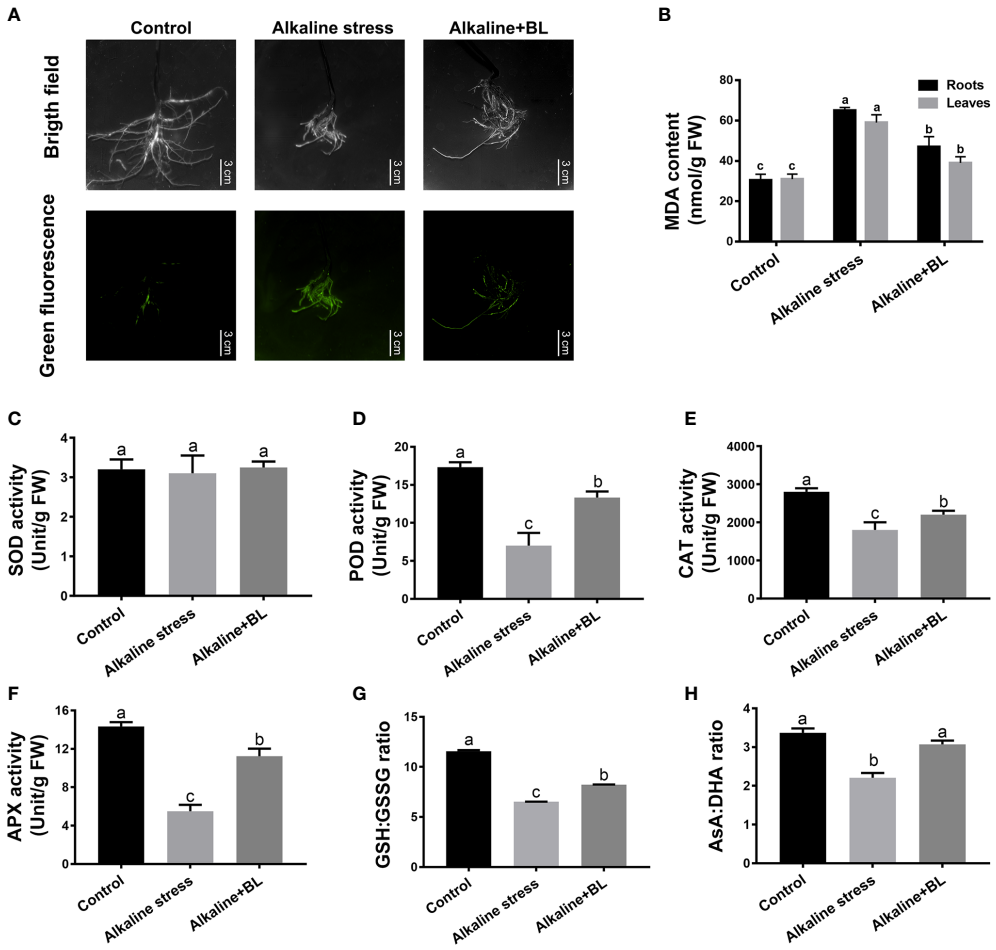


FIGURE 5
Effects of exogenous BL on the oxidative damage, antioxidant enzyme activities and antioxidants contents of *M. hupehensis* seedlings roots under alkaline stress. **(A)** Effects of alkaline stress and exogenous BL on the ROS level in roots. The scale bar represents 3.0 cm. Effects of exogenous BL treatment on MDA content **(B)**, SOD activity **(C)**, POD activity **(D)**, CAT activity **(E)**, APX activity **(F)**, GSH : GSSG ratio **(G)** and AsA : DHA ratio **(H)** under alkaline stress. The data represent the mean ± SD of three biological replicates. Different lowercase letters indicate significant differences according to Fisher's least significant difference ($P < 0.05$).

exogenous BL balanced the osmotic stress by accumulating proline.

Effects of exogenous BL on the mineral elements of apple seedling roots under alkaline stress

The mineral elements including micronutrients and macronutrients of apple seedlings were measured. The content of Na^+ was significantly under alkaline stress but decreased when exogenous BL was applied (Figure 7A). In contrast to Na^+, the content of K^+ was sharply decreased under alkaline stress but increased when exogenous BL was applied (Figure 7B). The Na^+/K^+ ratio is an important indicator of plant tolerance to alkaline stress and was also detected. As shown in Figure 7C, the Na^+/K^+ ratio was significantly increased under alkaline stress compared with that in the control group but decreased to extremely after application of exogenous BL. The variation tendency of Ca^{2+}, Fe^{2+}, and Mg^{2+} was similar to that of K^+ (Figure 7D-F).

Effects of exogenous BL on the expression levels of alkaline-related genes in roots under alkaline stress

As shown in Figure 8, the expression levels of 12 candidate genes, which were screened from RNA-Seq data (NCBI number: PRJNA588566) under alkaline stress, were detected under

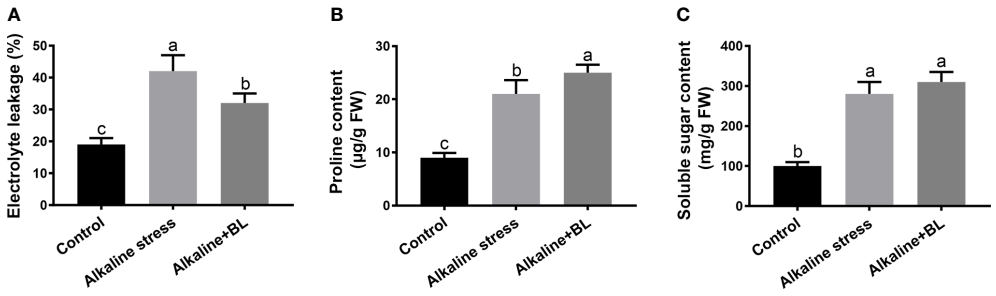


FIGURE 6
Effects of exogenous BL treatment on electrolyte leakage **(A)**, proline content **(B)**, and soluble protein content **(C)** under alkaline stress. The data represent the mean ± SD of three biological replicates. Different lowercase letters indicate significant differences according to Fisher's least significant difference ($P < 0.05$).

alkaline and exogenous BL treatment. These genes were divided into five categories. First, the three H^+ transporter genes, namely, *MhAHA1*, *MhAHA2*, and *MhAHA9* had significantly decreased expression level under alkaline stress but significantly increased expression level when exogenous BL was applied. Second, the expression of organic acid transport genes, including *MhMATE1* and *MhALMT1*, were significantly decreased by alkaline stress and increased under exogenous BL treatment in the roots. Third, for Na^+ transporter genes including *MhSOS1* and *MhCHX15*, the expression of *MhCHX15* showed a decreasing tendency under alkaline stress and exogenous BL treatment; however, the expression of *MhSOS1* was significantly increased after the application of exogenous BL. Fourth, for K^+ transporter genes, a decreasing tendency variation was observed for *MhSKOR* under alkaline stress and exogenous BL treatment. *MhNHX1* and *MhNHX4* had significantly increased expression under alkaline stress but had significantly decreased expression when exogenous BL was applied. Finally, the expression of two selected transcription factors, namely, *MhBZR3* and *MhBZR5*, significantly changed under alkaline and exogenous BL treatment. For both of them, the expression level was increased significantly under alkaline

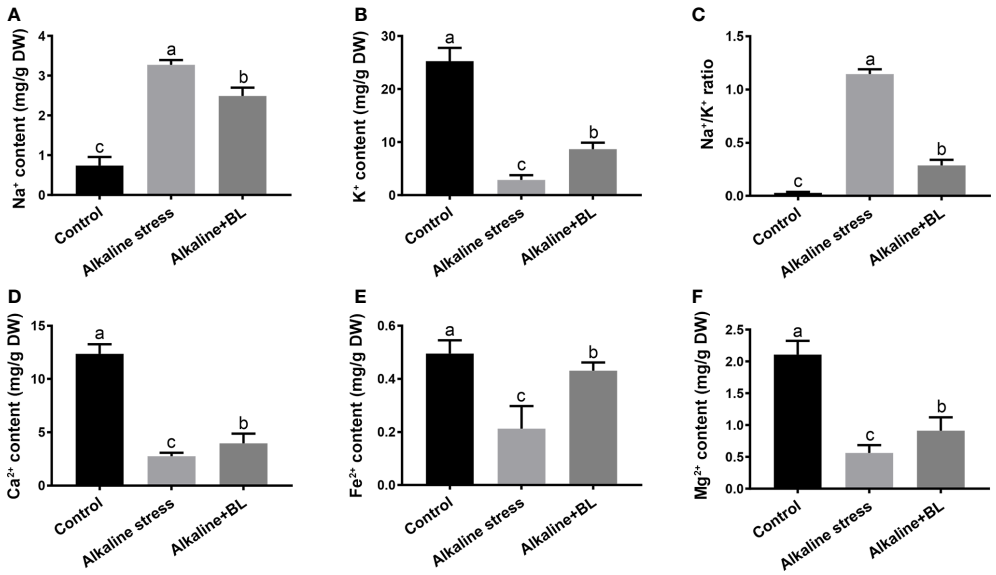


FIGURE 7
Effects of exogenous BL treatment on Na^+ content **(A)**, K^+ content **(B)**, and Na^+/K^+ ratio **(C)**, Ca^{2+} content **(D)**, Fe^{2+} content **(E)** and Mg^{2+} content **(F)** under alkaline stress. The data represent the mean ± SD of three biological replicates. Different lowercase letters indicate significant differences according to Fisher's least significant difference ($P < 0.05$).

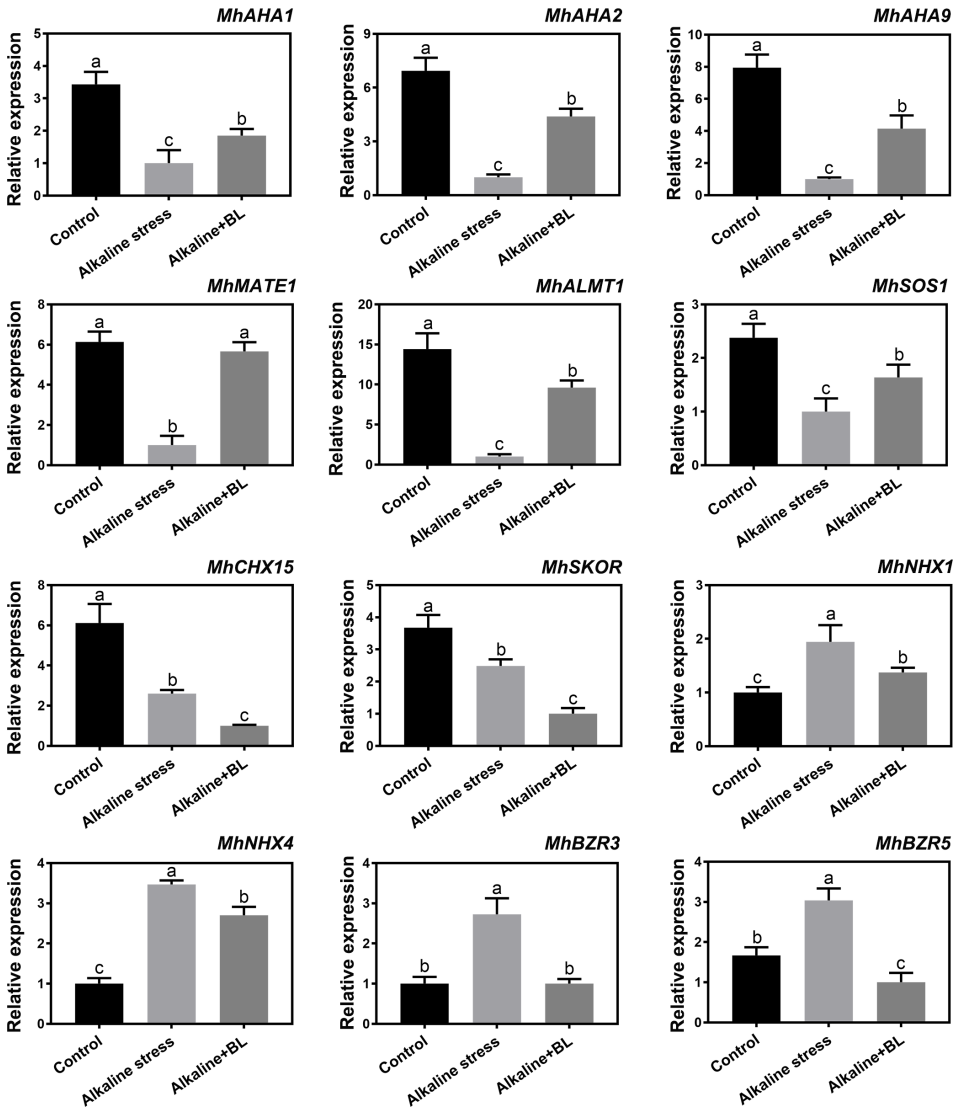


FIGURE 8
The expression of the 12 candidate genes (*MhAHA1*, *MhAHA2*, *MhAHA9*, *MhMATE1*, *MhALMT1*, *MhSOS1*, *MhCHX15*, *MhSKOR*, *MhNHX1*, *MhNHX4*, *MhBZR3* and *MhBZR5*) in roots under alkaline stress and exogenous BL treatment for 15 days. The data represent the mean ± SD of biological replicates. Different lowercase letters indicate significant differences according to Fisher's least significant difference ($P < 0.05$).

stress, while decreased dramatically when exogenous BL was applied. These results suggested that exogenous BL responded to alkaline stress by regulating the expression of alkaline-related genes and *MhBZRs*.

Discussion

Soil salinization seriously restricts the development of the global fruit industry (Hu et al., 2016). *M. hupehensis* is one of the most popular rootstocks in apple cultivation, but it is severely affected by saline-alkali stress (Su et al., 2020). Saline-alkali stress includes salt stress and alkaline stress. Alkaline stress causes more serious damage to plants than salt stress because it also induces high pH stress except for ion toxicity, osmotic stress, and oxidative damage (Yang and Guo, 2018; Fan et al., 2021). Nevertheless, most studies focus on the mechanism of plants in response to salt stress and on how to alleviate salt stress damage, ignoring the occurrence of salt stress is usually accompanied by alkaline stress in soil (Liang et al., 2017; Christian et al., 2018). Therefore, this study mainly focuses on the response of apple seedlings to alkaline stress.

Exogenous application of plant growth regulators is one of the effective methods to alleviate abiotic stress for hormones play

important roles in plant growth and development and environmental stress response (Dong et al., 2017; Wu et al., 2017). Our previous study reported that exogenous BL could alleviate the salt stress of apple rootstock by regulating the transcription of NHX-type Na^+ (K^+)/H^+ antiporters (Su et al., 2020). In the present study, we mainly focused on the root phenotype under alkaline stress. The roots were seriously damaged by alkaline stress with significantly short root length and less fibrous root number. Exogenous BL reduced the damage and partly recovered the root phenotype (Figure 3). Yang and Guo (2018) reported that the main damage to roots under alkaline stress was caused by high pH stress, which affected the roots absorption of nutrient elements and led to a series of symptoms related to nutrient deficiency. Ca is an important secondary messenger, maintaining its concentration in the cytoplasm can contribute to the regulation of plant signaling-transduction pathways under alkaline stress (Ding et al., 2010). Mg also has numerous positive effects on plant development (Zirek and Uzal, 2020). Fe is involved in chlorophyll synthesis and essential for maintaining the structure and function of chloroplasts (Casiraghi et al., 2020). Our results showed that the Ca^{2+}, Fe^{2+} and Mg^{2+} contents were significantly decreased under alkaline stress, but increased when exogenous BL was applied (Figure 7). Hence, exogenous BL could promote Ca^{2+}, Fe^{2+} and Mg^{2+} absorption, and the increase of the Fe^{2+} content would be the cause of the protection of chlorophyll and photosynthesis under alkaline stress (Figure 2). Previous study also reported that the application of BL promoted Ca^{2+} and Mg^{2+} absorption in soybean plants under normal conditions (Alam et al., 2019). The precipitation of nutrient elements could be attributed mainly to increased rhizosphere pH under alkaline stress (Veremeichik et al., 2021). Our staining results showed that the rhizosphere pH of apple roots significantly increased under alkaline stress but decreased after the application of exogenous BL (Figure 4A). However, the rhizosphere pH value under normal conditions was not affected by exogenous BL in cucumber (Wang et al., 2012). Our results suggested that the influence of exogenous BL to rhizosphere pH existed in the presence of alkaline stress. Root exudation of organic acids and H^+-ATPase are the main responses of plants to high pH stress (Ghassemi-Golezani and Abdoli, 2021). On the one hand, we found that exogenous BL could significantly induce the expression of *MhALMT1* and *MhMATE1*, which are important genes involved in the transport of malic acid and citric acid. Moreover, the contents of malic acid and citric acid significantly decreased in the roots after exogenous BL was applied (Figure 4 and Figure 8). These results indicated that exogenous BL could enhance the excretion of malic acid and citric acid outside of the roots in response to high pH stress. On the other hand, the H^+-ATP enzyme in the plasma membrane acidified the pH environment in the roots through the external pump of H^+ and improved the plants' response to high pH stress (Sukhov et al., 2016; Zhao S. et al. (2016)). In this study, qPCR results also showed that exogenous BL could significantly induce the expression of *MhAHAs* (*MhAHA1*, *MhAHA2*, and *MhAHA9*), which encode the synthesis of H^+-ATP enzyme (Figure 8). Taken together, our results indicated that exogenous BL could decrease the rhizosphere pH and promote Ca^{2+} and Mg^{2+} absorption by regulating malic acid and citric acid contents and increasing H^+ excretion under alkaline stress.

Alkaline stress caused substantial accumulation of ROS in plants, resulting in oxidative damage (Sharma et al., 2016). Previous studies reported that salt stress could increase the contents of $O_2\cdot^-$ and H_2O_2, whereas exogenous BL could alleviate this damage in leaves (Su et al., 2020). The present study focused on roots and found that the ROS level and MDA contents were significantly increased by alkaline stress and then decreased after the application of exogenous BL in the roots (Figure 5). SOD, POD and CAT are three major antioxidant enzymes (Tan et al., 2012; Abdelaal et al., 2018). They increased the resistance of sorghum roots to oxidative damage caused by heavy metal stress (Yilmaz et al., 2017). SOD is responsible for $O_2\cdot^-$ clearance, while POD and CAT are responsible for H_2O_2 clearance in plant antioxidant systems. In this study, the results demonstrated that exogenous BL induced the activities of POD and CAT, but exerted no significant activity change in SOD to mitigate ROS in the roots (Figure 5). In addition, the $O_2\cdot^-$ level had no significant change, but suffered severe H_2O_2 damage in leaves under alkaline stress. When exogenous BL was applied, the H_2O_2 content was substantially decreased (Figure S1A). Moreover, the POD and CAT activities were significantly repressed under alkaline stress but increased in leaves after BL was applied, while the SOD activity had no significantly change both in leaves and roots. Therefore, we speculated that exogenous BL could eliminate H_2O_2 through increasing the activities of POD and CAT, with no remarkably effect on SOD activity and $O_2\cdot^-$ scavenging both in leaves and roots. The AsA-GSH cycle is an important non-enzymatic antioxidant protection system in plants, and its function on ROS scavenging is mainly through the combination of the antioxidants AsA, GSH and the key enzyme APX (Wang et al., 2019; Li et al., 2022). For normal cell functioning, exogenous BL supplementation is useful in maintaining the GSH/GSSG and AsA/DHA ratios (Batth et al., 2017; Alam et al., 2019). In this study, the change of APX activity was similar with POD and CAT, which was decreased under alkaline stress, but increased under exogenous BL treatment. The ratios of GSH/GSSG and AsA/DHA showed a significant decline under salt stress; nevertheless, application of exogenous BL improved productions of GSH and AsA, which transformed more GSSG and DHA to its reduced form and generate a reduced redox homeostatic environment (Figure 5 and Figure S2). Taken together, our study concluded that exogenous BL has the potential to improving the activities of the antioxidant enzymes and modulate the AsA-GSH cycle to a redox state that plays a fundamental role in alkaline stress tolerance of apple plants.

Osmotic stress is a direct damage to plants caused by alkaline stress (Wu et al., 2017). Our results showed that electrolyte leakage was induced significantly under alkaline stress but decreased after exogenous BL treatment (Figure 6). Previous studies reported that the accumulation of substances such as proline and soluble sugars is a common defense mechanism of plants under osmotic stress (Liang et al., 2017; Zhang et al., 2017). Our data indicated that exogenous BL could protect apple seedlings from osmotic stress by accumulating proline (Figure 6).

Another major damage caused by alkaline stress is ion toxicity because large amounts of Na^+ entering cells can lead to cation imbalance (Lv et al., 2013). Regulating Na^+/K^+ in the cytoplasm is one of the core mechanisms of plants in response to saline-alkali stress (Wang X. et al., 2015; Azhar et al., 2017). In the present study, the Na^+/K^+ ratio increased significantly under alkaline stress; after exogenous BL treatment, the K^+ content increased and the Na^+ content was inhibited (Figure 7). The SOS pathway is one of the classical responses of plants to alkaline stress, and SOS1 in the plasma membrane alleviates the harmful effects of alkaline stress by discharging Na^+ from the cells (Fan et al., 2019; Gupta et al., 2021). Our results indicated that the expression of *MhSOS1* was significantly induced after exogenous BL application, resulting in reduced Na^+ content (Figure 7 and Figure 8). In the regulation of K^+, the SKOR family in the plasma membrane functions in the efflux of potassium ions outside the cells (Zheng et al., 2020). NHX1-4 in tonoplast is responsible for K^+ compartmentalization between the cytosol and the vacuole (Barragan et al., 2012; Li Y. et al. (2021); Solis et al., 2022). Exogenous BL treatment significantly decreased the levels of *MhSKOR*, *MhNHX1*, and *MhNHX4* (Figure 8). Hence, exogenous BL could inhibit K^+ expel and compartmentalization, resulting in more K^+ concentration in the cytoplasm to maintain relatively stable Na^+/K^+ ratio. In a word, the ion toxicity caused by alkaline stress could be alleviated by exogenous BL through enhancing Na^+ efflux and inhibiting K^+ expel and vacuole compartmentalization.

The expression of *MhBZRs*, as the key transcription factor in the BR signaling pathway, was also detected in the current study. The results indicated that the expression levels of *MhBZR3* and *MhBZR5* were significantly induced by alkaline stress and inhibited after exogenous BL was applied (Figure 8). This variation tendency was similar to that of K^+ transport genes (*MhNHX1* and *MhNHX4*) and opposite to that of *MhAHAs*, *MhSOS1*, *MhMATE1*, and *MhALMT1*. BR regulates a variety of biological processes mainly through the key transcription factors (BZRs) in its signal transduction pathway, while the *BZR* family transcription factors can directly regulate gene expression to participate in biological reactions (Sun et al., 2022). Recently, it was found that MaBZR1, MaBZR2, and MaBZR3 could bind specifically to the promoters of ethylene biosynthesis-related genes, thus reducing ethylene synthesis, and then inhibit the ripening of banana fruit (Guo et al., 2019). In maize, *ZmBZR* genes responds positively to salt stress but negatively to high temperature stress (Manoli et al., 2018). Therefore, *BZRs* expression patterns differed among different species or within the same species under different stresses. Previous studies showed that MhBZR1 and MhBZR2 can bind to the promoter of *MhSOS1* or *MhNHX4-1* and inhibit their transcription, respectively (Sze and Chanroj, 2018; Fan et al., 2019; Su et al., 2020). Future research will focus on the regulatory relationship between BR-signaling transduction pathway genes and alkaline-related genes.

Conclusion

Our study explored that exogenous BL could effectively improve the tolerance of apple plants on alkaline stress. Exogenous BL could decrease the rhizosphere pH by regulating malic acid and citric acid contents and increasing H^+ excretion, reduce oxidative damage through increasing the activities of antioxidant enzymes and the antioxidants contents, regulate osmotic balance by accumulating proline, and alleviate ion toxicity through enhancing Na^+ efflux and inhibiting K^+ expel and vacuole compartmentalization. Overall, the application of exogenous BL mitigated the alkaline toxicity in apple plants and thus it can be applied to other plants as well. Such a sustainable approach can be used to achieve enhanced fruit production under saline-alkali soils.

Data availability statement

The raw data supporting the conclusions of this article will be made available by the authors, without undue reservation.

Author contributions

XZ and CW planned and designed the research. ZS, YZ, CX, LH, XZ, YT, CM, XL, and CW performed experiments, XZ, YT, CM, XL, and CW performed experiments, conducted fieldwork, analyzed data etc. XZ, YZ, ZS, and CW wrote the manuscript. All authors contributed to the article and approved the submitted version.

Funding

This work was supported by the National Natural Science Foundation of China (32172542, 32102351), Breeding Plan of Shandong Provincial Qingchuang Research Team (2019), Funds for Modern Agricultural Industry Technology System in Shandong Province, China (SDAIT-06-06).

Conflict of interest

The authors declare that the research was conducted in the absence of any commercial or financial relationships that could be construed as a potential conflict of interest.

Publisher's note

All claims expressed in this article are solely those of the authors and do not necessarily represent those of their affiliated organizations, or those of the publisher, the editors and the reviewers. Any product that may be evaluated in this article, or claim that may be made by its manufacturer, is not guaranteed or endorsed by the publisher.

Supplementary material

The Supplementary Material for this article can be found online at: https://www.frontiersin.org/articles/10.3389/fpls.2022.1032646/full#supplementary-material

References

Abdelaal, K., Hafez, Y. M., El-Afry, M. M., Tantawy, D. S., and Alshaal, T. (2018). Effect of some osmoregulators on photosynthesis, lipid peroxidation, antioxidative capacity and productivity of barley (Hordeum vulgare l.) under water deficit stress. *Environ. Sci. pollut. Res. Int.* 25, 30199–30211. doi: 10.1007/s11356-018-3023-x

Ahmad, P., Abdel Latef, A. A., Hashem, A., Abd Allah, E. F., Gucel, S., and Tran, L. (2016). Nitric oxide mitigates salt stress by regulating levels of osmolytes antioxidant enzymes in chickpea. *Plant Sci.* 7. doi: 10.3389/fpls.2016.00347

Alam, P., Albalawi, T. H., Altalayan, F. H., Bakht, M. A., Ahanger, M. A., Raja, V., et al. (2019). 24-epibrassinolide (EBR) confers tolerance against NaCl stress in soybean plants by up-regulating antioxidant system, ascorbate-glutathione cycle, and glyoxalase system. *Biomolecules* 9 (11), 640. doi: 10.3390/biom9110640

An, J. P., Yao, J. F., Xu, R. R., You, C. X., Wang, X. F., and Hao, Y. J. (2018). An apple NAC transcription factor enhances salt stress tolerance by modulating the ethylene response. *Physiol. Plant.* 164, 279–289. doi: 10.1111/ppl.12724

Azhar, N., Su, N., Shabala, L., and Shabala, S. (2017). Exogenously applied 24-epibrassinolide (EBL) ameliorates detrimental effects of salinity by reducing k+ efflux *via* depolarization-activated k+ channels. *Plant Cell Physiol.* 58 (4), 802–810. doi: 10.1093/pcp/pcx026

Barragan, V., Leidi, E. O., Andres, Z., Rubio, L., Luca, A. D., Fernandez, J. A., et al. (2012). Ion exchangers NHX1 and NHX2 mediate active potassium uptake into vacuoles to regulate cell turgor and stomatal function in arabidopsis. *Plant Cell.* 24 (3), 1127–1142. doi: 10.1105/tpc.111.095273

Batth, R., Singh, K., Kumari, S., and Mustafiz, A. (2017). Transcript profiling reveals the presence of abiotic stress and developmental stage specific ascorbate oxidase genes in plants. *Front. Plant Sci.* 8. doi: 10.3389/fpls.2017.00198

Casiraghi, F. M., Landi, M., Donnini, S., Borlotti, A., and Vigani, G. (2020). Modulation of photorespiration and nitrogen recycling in fe-deficient cucumber leaves. *Plant Physiol. Biochem.* 154, 142–150. doi: 10.1016/j.plaphy.2020.05.032

Chen, Z., Zhao, P., Miao, Z., Qi, G., Wang, Z., Yuan, Y., et al. (2019). SULTR3s function in chloroplast sulfate uptake and affect ABA biosynthesis and the stress response. *Plant Physiol.* 180, 593–604. doi: 10.1104/pp.18.01439

Christian, Z., Christoph-Martin, G., and Karl-Josef, D. (2018). Salinity and crop yield. *Plant Biol.* 21, 31–38. doi: 10.1111/plb.12884

Ding, F., Chen, M., Sui, N., and Wang, B. (2010). Ca2+ signifificantly enhanced development and salt-secretion rate of salt glands of limonium bicolor under NaCl treatment. *S. Afr. J. Bot.* 76, 95–101. doi: 10.1016/j.sajb.2009.09.001

Dong, Y., Wang, W., Hu, G., Chen, W., Zhuge, Y., Wang, Z., et al. (2017). Role of exogenous 24-epibrassinolide in enhancing the salt tolerance of wheat seedlings. *J. Soil Sci. Plant Nutt.* 17 (3), 554–569. doi: 10.4067/S0718-95162017000300001

Fan, Y., Lu, X., Chen, X., Wang, J., Wang, D., Wang, S., et al, et al. (2021). Cotton transcriptome analysis reveals novel biological pathways that eliminate reactive oxygen species (ROS) under sodium bicarbonate (NaHCO3) alkaline stress. *Genomics* 113, 1157–1169. doi: 10.1016/j.ygeno.2021.02.022

Fan, Y., Yin, X., Xie, Q., Xia, Y., Wang, Z., Song, J., et al. (2019). Co-Expression of SpSOS1 and SpAHA1 in transgenic arabidopsis plants improves salinity tolerance. *BMC. Plant Biol.* 19, 1–13. doi: 10.1186/s12870-019-1680-7

Ghassemi-Golezani, K., and Abdoli, S. (2021). Improving ATPase and PPase activities, nutrient uptake and growth of salt stressed ajowan plants by salicylic acid and iron-oxide nanoparticles. *Plant Cell Rep.* 40 (1), 1–15. doi: 10.1007/s00299-020-02652-7

Gong, X., Shi, S., Dou, F., Song, Y., and Ma, F. (2017). Exogenous melatonin alleviates alkaline stress in malus hupehensis rehd. by regulating the biosynthesis of polyamines. *Molecules* 22 (9), 1542. doi: 10.3390/molecules22091542

Guo, Y. F., Shan, W., Liang, S. M., Wu, C. J., Wei, W., Chen, J. Y., et al. (2019). MaBZR1/2 act as transcriptional repressors of ethylene biosynthetic genes in banana fruit. *Physiol. Plant.* 165 (3), 555–568. doi: 10.1111/ppl.12750

Gupta, B. K., Sahoo, K. K., Anwar, K., Nongpiur, R. C., Deshmukh, R., Pareek, A., et al. (2021). Silicon nutrition stimulates salt-overly sensitive (SOS) pathway to enhance salinity stress tolerance and yield in rice. *Plant Physiol. Biochem.* 166, 593–604. doi: 10.1016/j.plaphy.2021.06.010

Hu, Y., Xia, S., Su, Y., Wang, H., Luo, W., Su, S., et al. (2016). Brassinolide increases potato root growth *in vitro* in a dose-dependent way and alleviates salinity stress. *Biomed. Res. Int.* 2016, 8231873. doi: 10.1155/2016/8231873

Hu, L., Zhou, K., Li, Y., Chen, X., Liu, B., Li, C., et al. (2018). Exogenous myoinositol alleviates salinity-induced stress in malus hupehensis rehd. plant physiol. *Biochem* 133, 116–126. doi: 10.1016/j.plaphy.2018.10.037

Jia, C., Zhao, S., Bao, T., Zhao, P., Peng, K., Guo, Q., et al. (2021). Tomato BZR/BES transcription factor SIBZR1 positively regulates BR signaling and salt stress tolerance in tomato and arabidopsis. *Plant Sci.* 302, 110719. doi: 10.1016/j.plantsci.2020.110719

Ji, Y., Zhang, P., Xing, Y., Jia, L., Zhang, Y., Jia, T., et al. (2019). Effect of 1α, 25-dihydroxyvitamin D3 on the osteogenic differentiation of human periodontal ligament stem cells and the underlying regulatory mechanism. *Int. J. Mol. Med.* 43 (1), 167–176. doi: 10.3892/ijmm.2018.3947

Liang, W., Ma, X., Wan, P., and Liu, L. (2017). Plant salt-tolerance mechanism: A review. *Biochem. Bioph. Res. Co.* 495, 286–291. doi: 10.1016/j.bbrc.2017.11.043

Li, B., Fu, Y., Li, X., Yin, H., and Xi, Z. (2022). Brassinosteroids alleviate cadmium phytotoxicity by minimizing oxidative stress in grape seedlings: Toward regulating the ascorbate-glutathione cycle. *Sci. Hortic.* 299, 111002. doi: 10.1016/j.scienta.2022.111002

Li, T., Li, Y., Sun, Z., Xi, X., Sha, G., Ma, C., et al. (2021). Resveratrol alleviates the KCl salinity stress of malus hupehensis rhed. *Front. Plant Sci.* 12. doi: 10.3389/fpls.2021.650485

Liu, N., Jin, Z., Wang, S., Gong, B., Wen, D., Wang, X., et al. (2015). Sodic alkaline stress mitigation with exogenous melatonin involves reactive oxygen metabolism and ion homeostasis in tomato. *Sci. Hortic.* 181, 18–25. doi: 10.1016/j.scienta.2014.10.049

Li, H., Wang, L., and Luo, Y. (2018). Composition analysis by UPLC-PDA-ESI (–)-HRMS and antioxidant activity using saccharomyces cerevisiae model of herbal teas and green teas from hainan. *Molecules* 23 (10), 2550. doi: 10.3390/molecules23102550

Li, Y., Wu, Y., Liao, W., Hu, L., Dawuda, M. M., Jin, X., et al. (2020). Nitric oxide is involved in the brassinolide-induced adventitious root development in cucumber. *BMC Plant Biol.* 20 (1), 1–12. doi: 10.1186/s12870-020-2320-y

Li, J., Yang, P., Xie, J., and Yu, J. (2015). Effects of 24-epibrassinolide on growth and antioxidant enzymes system in pepper roots under chilling stress. J. *Nucl. Agric. Sci.* 29, 1001–1008. doi: 10.11869/j.issn.100-8551.2015.05.1001

Li, Y., Zheng, X., Tian, Y., Ma, C., and Wang, C. (2021). Comparative transcriptome analysis of NaCl and KCl stress response in malus hupehensis rehd. provide insight into the regulation involved in na+ and k+ homeostasis. *Plant Physiol. Biochem.* 164 (2), 101–114. doi: 10.1016/j.plaphy.2021.04.022

Lv, B., Li, X., Ma, H., Sun, Y., Wei, L., Jiang, C., et al. (2013). Differences in growth and physiology of rice in response to different saline-alkaline stress factors. *Agron. J.* 105 (4), 1119–1128. doi: 10.2134/agronj2013.0017

Ma, C., Liang, B., Chang, B., Yan, J., Liu, L., Wang, Y., et al. (2019). Transcriptome profiling of anthocyanin biosynthesis in the peel of 'Granny smith' apples (Malus domestica) after bag removal. *BMC Genomics* 20, 1–18. doi: 10.1186/s12864-019-5730-1

Manoli, A., Trevisan, S., Quaggiotti, S., and Varotto, S. (2018). Identification and characterization of the BZR transcription factor family and its expression in response to abiotic stresses in zea mays l. *Plant Growth Regul.* 84 (3), 423–436. doi: 10.1007/s10725-017-0350-8

Mao, K., Dong, Q., Li, C., Liu, C., and Ma, F. (2017). Genome wide identification and characterization of apple bHLH transcription factors and expression analysis in response to drought and salt stress. *Front. Plant Sci.* 8. doi: 10.3389/fpls.2017.00480

Nawaz, F., Naeem, M., Zulfiqar, B., Akram, A., Ashraf, M. Y., Raheel, M., et al. (2017). Understanding brassinosteroid-regulated mechanisms to improve stress tolerance in plants: a critical review. *Environ. Sci. Pollut. R.* 24 (19), 15959–15975. doi: 10.1007/s11356-017-9163-6

Negi, P., Mishra, S., Ganapathi, T. R., and Srivastava, A. K. (2021). Regulatory short RNAs: A decade's tale for manipulating salt tolerance in plants. *Physiol. Plant.* 173, 1535–1555. doi: 10.1111/ppl.13492

Ryu, H., and Cho, Y. G. (2015). Plant hormones in salt stress tolerance. *J. Integr. Plant Biol.* 58, 147–155. doi: 10.1007/s12374-015-0103-z

Shahzad, B., Tanveer, M., Che, Z., Rehman, A., Cheema, S. A., Sharma, A., et al. (2018). Role of 24-epibrassinolide (EBL) in mediating heavy metal and pesticide induced oxidative stress in plants: A review. *Ecotox. Environ. Safe.* 147, 935–944. doi: 10.1016/j.ecoenv.2017.09.066

Sharma, I., Bhardwaj, R., and Pati, P. K. (2013). Stress modulation response of 24-epibrassinolide against imidacloprid in an elite indica rice variety pusa basmati-1. *Pestic. Biochem. Phys.* 105 (2), 144–153. doi: 10.1016/j.pestbp.2013.01.004

Sharma, P., Kumar, A., and Bhardwaj, R. (2016). Plant steroidal hormone epibrassinolide regulate-heavy metal stress tolerance in oryza sativa l. by modulating antioxidant defense expression. *Environ. Exp. Bot.* 122, 1–9. doi: 10.1016/j.envexpbot.2015.08.005

Solis, C. A., Yong, M. T., Zhou, M., Venkataraman, G., Shabala, L., Holford, P., et al. (2022). Evolutionary significance of NHX family and NHX1 in salinity stress adaptation in the genus oryza. int. *J. Mol. Sci.* 23 (4), 2092. doi: 10.3390/ijms23042092

Song, M., Chen, F. F., Li, Y. H., Zhang, L., Wang, F., Qin, R. R., et al. (2018). Trimetazidine restores the positive adaptation to exercise training by mitigating statin-induced skeletal muscle injury. *J. Cachexia. Sarcopeni.* 9 (1), 106–118. doi: 10.1002/jcsm.12250

Sukhov, V., Surova, L., Morozova, E., Sherstneva, O., and Vodeneev, V. (2016). Changes in h+-ATP synthase activity, proton electrochemical gradient, and pH in pea chloroplast can be connected with variation potential. *Front. Plant Sci.* 7. doi: 10.3389/fpls.2016.01092

Sun, Z., Guo, D., Lv, Z., Bian, C., Ma, C., Liu, X., et al. (2022). Brassinolide alleviates fe deficiency-induced stress by regulating the fe absorption mechanism in malus hupehensis rehd. *Plant Cell Rep.* 41 (9), 1863–1874. doi: 10.1007/s00299-022-02897-4

Su, Q., Zheng, X., Tian, Y., and Wang, C. (2020). Exogenous brassinolide alleviates salt stress in malus hupehensis rehd. by regulating the transcription of NHX-type na+ (K+)/H+ antiporters. *Front. Plant Sci.* 11. doi: 10.3389/fpls.2020.00038

Sze, H., and Chanroj, S. (2018). pH and ion homeostasis on plant endomembrane dynamics: insights from structural models and mutants of K+/H + antiporters. *Plant Physiol.* 177, 875–895. doi: 10.1104/pp.18.00142

Tan, D., Hardeland, R., Manchester, L. C., Korkmaz, A., Ma, S., Rosales, S. C., et al. (2012). Functional roles of melatonin in plants, and perspectives in nutritional and agricultural science. *J. Exp. Bot.* 63, 577–597. doi: 10.1093/jxb/err256

Tofighi, C., Khavari-Nejad, R. A., Najafi, F., Razavi, K., and Rejali, F. (2017). Responses of wheat plants to interactions of 24-epibrassinolide and glomus mosseae in saline condition. *Physiol. Mol. Biol. Pla.* 23 (3), 557–564. doi: 10.1007/s12298-017-0439-6

Veremeichik, G. N., Shkryl, Y. N., Silantieva, S. A., Gorpenchenko, T. Y., Brodovskaya, E. V., Yatsunskaya, M. S., et al. (2021). Managing activity and Ca2 + dependence through mutation in the junction of the AtCPK1 coordinates the salt tolerance in transgenic tobacco plants. *Plant Physiol. Biochem.* 165, 104–113. doi: 10.1016/j.plaphy.2021.05.026

Wang, X., Geng, S., Ma, Y., Shi, D., Yang, C., and Wang, H. (2015). Growth, photosynthesis, solute accumulation, and ion balance of tomato plant under sodium-or potassium-salt stress and alkali stress. *Agron. J.* 65 (2), 927–928. doi: 10.2134/agronj14.0344

Wang, B., Li, Y., and Zhang, W. H. (2012). Brassinosteroids are involved in response of cucumber (Cucumis sativus) to iron deficiency. *Ann. Bot.* 110 (3), 681–688. doi: 10.1093/aob/mcs126

Wang, T., Tohge, T., Ivakov, A., Mueller-Roeber, B., Fernie, A. R., Mutwil, M., et al. (2015a). Salt-related MYB1 coordinates abscisic acid biosynthesis and signaling during salt stress in arabidopsis. *Plant Physiol.* 169, 1027–1041. doi: 10.1104/pp.15.00962

Wang, F., Zhang, X., Yang, Q., and Zhao, Q. (2019). Exogenous melatonin delays postharvest fruit senescence and maintains the quality of sweet cherries. *Food Chem.* 301, 125311. doi: 10.1016/j.foodchem.2019.125311

Wu, J., Cao, J., Su, M., Feng, G., Xu, Y., and Yi, H. (2019). Genomewide comprehensive analysis of transcriptomes and small RNAs offers insights into the molecular mechanism of alkaline stress tolerance in a citrus rootstock. *Hortic. Res.* 6, 33–51. doi: 10.1038/s41438-018-0116-0

Wu, W., Zhang, Q., Ervin, E., Yang, Z., and Zhang, X. (2017). Physiological mechanism of enhancing salt stress tolerance of perennial ryegrass by 24-epibrassinolide. *Front. Plant Sci.* 8. doi: 10.3389/fpls.2017.01017

Xia, L., Marquès-Bueno, M., Bruce, C. G., and Karnik, R. (2019). Unusual roles of secretory SNARE SYP132 in plasma membrane h+-ATPase traffic and vegetative plant growth. *Plant Physiol.* 180, 837–858. doi: 10.1111/ppl.13492

Xiong, M., Yu, J., Wang, J., Gao, Q., Huang, L., Chen, C., et al. (2022). Brassinosteroids regulate rice seed germination through the BZR1-RAmy3D transcriptional module. *Plant Physiol.* 189 (1), 402–418. doi: 10.1093/plphys/kiac043

Yang, Y., and Guo, Y. (2018). Elucidating the molecular mechanisms mediating plant salt-stress responses. *New Phytol.* 217, 523–539. doi: 10.1111/nph.14920

Yilmaz, S. H., Kaplan, M., Yilmaz, R., and Temizgul, S. (2017). Antioxidant enzyme response of sorghum plant upon exposure to aluminum, chromium and lead heavy metals. *Turk. J. Biochem.* 42 (4), 503–512. doi: 10.1515/tjb-2016-0112

Yuan, L., Zhu, S., Shu, S., Sun, J., and Guo, S. (2015). Regulation of 2, 4-epibrassinolide on mineral nutrient uptake and ion distribution in Ca(NO3)2 stressed cucumber plants. *J. Plant Physiol.* 188, 29–36. doi: 10.1016/j.jplph.2015.06.010

Zhang, H., Liu, X., Zhang, R., Yuan, H., Wang, M., Yang, H., et al. (2017). Root damage under alkaline stress is associated with reactive oxygen species accumulation in rice (Oryza sativa l.). *Front. Plant Sci.* 8. doi: 10.3389/fpls.2017.01580

Zhan, H., Nie, X., Zhang, T., Li, S., Wang, X., Du, X., et al. (2019). Melatonin: a small molecule but important for salt stress tolerance in plants. *Int. J. Mol. Sci.* 20 (3), 709. doi: 10.3390/ijms20030709

Zhao, C., Jiang, W., Omar, Z., Liu, X., Tang, K., Nie, W., et al. (2021). The LRXs-RALFs-FER module controls plant growth and salt stress responses by modulating multiple plant hormones. *Natl. Sci. Rev.* 8 (01), 40–55. doi: 10.1093/nsr/nwaa149

Zhao, Q., Ren, Y., Wang, Q., Yao, Y., You, C., and Hao, Y. (2016). Overexpression of MdbHLH104 gene enhances the tolerance to iron deficiency in apple. *Plant Biotechnol. J.* 14, 1633–1645. doi: 10.1111/pbi.12526

Zhao, S., Zhang, M., Ma, T., and Wang, Y. (2016). Phosphorylation of ARF2 relieves its repression of transcription of the k+ transporter gene HAK5 in response to low potassium stress. *Plant Cell.* 28, 3005–3019. doi: 10.1105/tpc.16.00684

Zheng, X., Chen, H., Su, Q., Wang, C., Sha, G., Ma, C., et al. (2021). Resveratrol improves the iron deficiency adaptation of malus baccata seedlings by regulating iron absorption. *BMC Plant Biol.* 21, 433. doi: 10.21203/rs.3.rs-168975/v1

Zheng, X., Li, Y., Xi, X., Ma, C., Sun, Z., Yang, X., et al. (2020). Exogenous strigolactones alleviate KCl stress by regulating photosynthesis, ROS migration and ion transport in malus hupehensis rehd. *Plant Physiol. Biochem.* 159, 113–122. doi: 10.1016/j.plaphy.2020.12.015

Zheng, X., Zhou, J., Tan, D., Wang, N., Wang, L., Shan, D., et al. (2017). Melatonin improves waterlogging tolerance of malus baccata (Linn.) borkh. seedlings by maintaining aerobic respiration, photosynthesis and ROS migration. *Front. Plant Sci.* 8. doi: 10.3389/fpls.2017.00483

Zhu, J. K. (2016). Abiotic stress signaling and responses in plants. *Cell* 167, 313–324. doi: 10.1016/j.cell.2016.08.029

Zirek, N. S., and Uzal, O. (2020). The developmental and metabolic effects of different magnesium dozes in pepper plants under salt stress. *No. Bot. Horti. Agrobo.* 48 (2), 967–977. doi: 10.15835/nbha48211943

frontiers | Frontiers in Plant Science

TYPE Original Research
PUBLISHED 28 November 2022
DOI 10.3389/fpls.2022.1049954

Check for updates

OPEN ACCESS

EDITED BY
Ji-Hong Liu,
Huazhong Agricultural University,
China

REVIEWED BY
Xiaochuang Cao,
China National Rice Research Institute,
Chinese Academy of Agricultural Sciences, China
Krishan K. Verma,
Guangxi Academy of Agricultural Sciences, China

*CORRESPONDENCE
Xiu Zhang
zhangxiu101@aliyun.com

SPECIALTY SECTION
This article was submitted to Plant Abiotic Stress, a section of the journal Frontiers in Plant Science

RECEIVED 21 September 2022
ACCEPTED 07 November 2022
PUBLISHED 28 November 2022

CITATION
Ji H, Yang G, Zhang X, Zhong Q, Qi Y, Wu K and Shen T (2022) Regulation of salt tolerance in the roots of *Zea mays* by L-histidine through transcriptome analysis.
Front. Plant Sci. 13:1049954.
doi: 10.3389/fpls.2022.1049954

COPYRIGHT
© 2022 Ji, Yang, Zhang, Zhong, Qi, Wu and Shen. This is an open-access article distributed under the terms of the Creative Commons Attribution License (CC BY). The use, distribution or reproduction in other forums is permitted, provided the original author(s) and the copyright owner(s) are credited and that the original publication in this journal is cited, in accordance with accepted academic practice. No use, distribution or reproduction is permitted which does not comply with these terms.

Regulation of salt tolerance in the roots of *Zea mays* by L-histidine through transcriptome analysis

Hongfei Ji, Guoping Yang, Xiu Zhang*, Qiumei Zhong, Yuxi Qi, Kaihua Wu and Tingting Shen

Ningxia Key Laboratory for the Development and Application of Microbial Resources in Extreme Environments, College of Biological Science and Engineering, North Minzu University, Yinchuan, China

Soil salinization is an important worldwide environmental problem and the main reason to reduce agricultural productivity. Recent findings suggested that histidine is a crucial residue that influences the ROS reduction and improves the plants' tolerance to salt stress. Herein, we conducted experiments to understand the underlying regulatory effects of histidine on maize root system under salt stress (100 mM NaCl solution system). Several antioxidant enzymes were determined. The related expressed genes (DEGs) with its pathways were observed by Transcriptome technologies. The results of the present study confirmed that histidine can ameliorate the adverse effects of salt stress on maize root growth. When the maize roots exposed to 100 mM NaCl were treated with histidine, the accumulation of superoxide anion radicals, hydrogen peroxide, and malondialdehyde, and the content of nitrate nitrogen and ammonium nitrogen were significantly reduced; while the activities of superoxide dismutase, peroxidase, catalase, nitrate reductase, glutamine synthetase, and glutamate synthase were significantly increased. Transcriptome analysis revealed that a total of 454 (65 up-regulated and 389 down-regulated) and 348 (293 up-regulated and 55 down-regulated) DEGs were observed when the roots under salt stress were treated with histidine for 12 h and 24 h, respectively. The pathways analysis of those DEGs showed that a small number of down-regulated genes were enriched in phytohormone signaling and phenylpropanoid biosynthesis at 12 h after histidine treatment, and the DEGs involved in the phytohormone signaling, glycolysis, and nitrogen metabolism were significantly enriched at 24 h after treatment. These results of gene expression and enzyme activities suggested that histidine can improve the salt tolerance of maize roots by enriching some DEGs involved in plant hormone signal transduction, glycolysis, and nitrogen metabolism pathways.

KEYWORDS

***Zea mays*, enzymatic activity, transcriptomic, L-histidine, salt stress**

Introduction

Soil salinization is one of the most well-known threats to the development of global agriculture. The Food and Agriculture Organization of the United Nations estimates that salt has affected more than 6% of the land area (Ilangumaran and Smith, 2017), and about 20% of the world's irrigated land is impacted by salt, with a direct economic loss of $12 billion per year (Tang et al., 2014). The monitoring of soil salinity and land cover revealed that Asia is one of the continents most affected by salt, especially the northwest of China (Hassani et al., 2020). The total area of saline soil in China is about 3.6×10^7 ha, accounting for 4.88% of the country's total available land base. The excessive accumulation of water-soluble salts in soil, such as K^+, Mg^{2+}, Ca^{2+} , Cl^-, SO_4^{2-}, CO_3^{2-}, HCO_3^-, Na^+ plasma, etc., can damage the soil structure, produce toxic effects on plants, hinder the growth of crops, cause the decline of soil fertility, and seriously reduce the productivity of the land (Parida and Das, 2005).

Salinization of soil results from a combination of evaporation, salt precipitation and dissolution, salt transport, and ion exchange. Excessive soluble salt in the soil can lead to plant salt stress, one of the most detrimental environmental stresses, osmotic stress, ionic toxicity, and oxidative stress (Bojórquez-Quintal et al., 2014; Tanveer and Shabala, 2018). High salt stress can increase the levels of the reactive oxygen species (ROS) and result in oxidative stress, which in turn affects the plants both at cellular and metabolic levels (Duan et al., 2015).

ROS play important roles in maintaining normal plant growth and improving their tolerance to environmental stresses. It has been implicated as second messengers in plant hormone responses and function as important signaling molecules that regulate normal plant growth and response hormones to stresses, such as salt stress (Yu et al., 2020). At high levels, active oxygen species can lead to impaired physiological function through cellular damage and oxidization of DNA, protein, and lipid membrane of plant cells. For example, the accumulation of Ca^{2+} can activate the ROS signals and change their phospholipid components, induce plant hormone signal transmission, and regulate cytoskeleton dynamics and cell wall structure, which will slow down the plant root growth and increase the metabolites (Bybordi, 2010; Zhao et al., 2021).

Nitrogen is an essential element in plant growth. Plant absorbs nitrate from soil and transforms it into amino acids through a series of assimilation processes such as nitrogen metabolism. These processes are affected by abiotic stress, especially salt stress. The change of enzyme activity in nitrogen metabolism depends on the species of plants and the sensitivity of plants to salt stress (Gouia et al., 1994; Li et al., 2019; Yin et al., 2020). In addition, salt stress also affects sugar metabolism, changes sugar levels, such as sucrose and fructose, and causes changes in enzyme activity in glycolysis (Shumilina et al., 2009). The hormones in plant play an important role in mediating salt stress signals and controlling the balance between growth and salt stress response. Plants will regulate growth and development through hormone signal transduction and improve the adaptability to salt stress (Yu et al., 2020).

Root is the first organ to undergo salinity stress and plays an important role in salt sensing. Root system can dynamically adjust its development and performance in response to biotic and abiotic stresses, including modulation of root growing, branching, forking, and redirecting. These responses can be manifested differentially at the cellular, tissue, or organ levels. To fully capture the responses of root system to salt stress, it is critical to explore the key genes and associated functions for development of salt tolerance in crops.

L-histidine is one of the standard amino acids in proteins and critical for plant growth and development. Histidine kinases (HK) play important roles in the regulation of plant development in response to hormones, as well as environmental stimuli (Nongpiur et al., 2012). The study of the interaction between histidine and membranes and macromolecules confirmed that histidine plays a unique role in enabling protein/peptide-membrane interactions that occur in marine or other high-salt environments (Xian et al., 2022). Previous studies also showed that histidine takes an important role in regulating the biosynthesis of other amino acids, the chelation transport of metal ions, and the development and growth of plant embryos in different plants, including rice (*Arabidopsis)* and maize (*Zea mays)* (Radwanski and Last, 1995; Kramer et al., 1996; Noutoshi et al., 2005; Stepansky and Leustek, 2006; Irtelli et al., 2009). However, the genetic effects of salinity on maize's root development at the gene level remain unclear and the genetic machinery underlying maize root responses to salt stress remains uncharacterized.

Maize is the most widely planted grain in the world and ranked second in the important crops of China, which accounts for 29.5% of total grain production (Medeiros et al., 2021). Soil salinization is one of the major abiotic stresses negatively impacting growth, development, yield, and seed quality of maize production. The critical challenge for enhancing the quality and productivity of maize is how to improve its tolerance or to incorporate resistance to different stresses, including salt stress.

In the present study, maize seeds were grown in lab. After gemination, we treated the seedling roots with salt stress and histidine for different time periods to 1) compare the natural traits and morphological variations of seedling roots among the control and treatment samples, 2) evaluate the antioxidant roles and activities of histidine in antioxidant enzymes and nitrogen metabolism in the seedling roots under salt stress, 3) identify differentially expressed genes under control, salt stress, and histidine treatment conditions by RNA-seq analysis, and 4) investigate the effects of histidine on the potential pathways responsible for differences in root salt stress responses by gene co-expression network and pathway analyses. Our study will provide accurate quantitative analysis of an effective treatment of soil salinization and scientific guidance for the future formulation of salinization control in crops.

Materials and methods

Plant materials and treatments

All plant materials used in the experiments were from the maize variety "ningdan 33". All experiments were conducted at the Ningxia Key Laboratory for the Development and Application of Microbial Resources in Extreme Environments, North Minzu University, China. The seeds from the variety were disinfected with 0.1% $HgCl_2$ and inoculated in 0.8% agar medium (containing hoagland nutrient solution) supplemented with sterile water and 0.1 μM histidine for 12 h at 4°C. The samples were retained in a box with the relative humidity at 75% and the temperature at 28°C. When seed roots grew up to 3 cm, all samples were randomly divided into 4 groups, including (i) the non-stress control (CK0) treated with hoagland nutrient solution, (ii) the non-stress treatment group (T0) treated with 0.1 μM histidine+hoagland nutrient solution, (iii) the salt stress control (CK1) treated with100 mM NaCl +hoagland nutrient solution, and (iv) the salt stress treatment group (T1) treated with 0.1 μM histidine+100 mM NaCl +hoagland nutrient solution. Each group has 15 hydroponic plastic bottles of 4 seeds and 450g sterilized small stones each. The incubator was set with the relative humidity 75% and conditions of 13,000 LX at 28°C for 4 h, 11,000 LX at 25°C for 4 h, 9,000 LX at 20°C for 3 h, 6,000 LX at 20°C for 2 h, 9,000 LX, at 25°C for 3 h and dark at 18°C for 8 h.

Our previous experiment confirmed the alleviating effect of the histidine at 100 μM, 10 μM, 1 μM, 0.1 μM, 0.01 μM, 0.001 μM on the NaCl induced damage to the root, with the treatment of 0.1 μM of histidine resulted in the most substantial resistance in the maize seedling roots (Figure S1). After treatment for 12 h and 24 h, 12 young roots were randomly selected and divided into three sub-groups at each time point. All samples were snap-frozen with liquid nitrogen and stored at -80°C. RNA was extracted from each sample for transcriptomic analysis. After 7 days treatment, the root tips were stained with DAB and NBT. After 14 days treatment, the total root length, root projected area, root volume, root surface area, numbers of root tips, and forks from each treatment were measured with an Analyzer (GXY-A, Sichuan, China), and the activities of root related enzymes were simultaneously measured.

Nitroblue tetrazolium and diaminobenzidine staining of root tips

The DBA reaction was conducted in the dark at 28 °C for 6 h following the method of Li et al. (2013). The root tips of each treatment group were collected and plated into the culture plate with 1mg ml^{-1} DAB reaction solution (pH 5.5, 50 mM Tris HCl). The samples were then transferred to 90% (v/v) ethanol for decolorization in a 70 °C water bath and stored in 50% glycerol. The highly localized accumulation of H_2O_2 was observed as dark brown at X100 magnification. The NBT staining was based on the method of Khokon et al. (2011). The root tips of each treatment were placed into the culture plate with adding 0.5 mg ml^{-1} NBT reaction solution (pH 7.8, 50 mm PBS). The culture plates were kept in dark at 28°C for 4 h, and then transferred to a 70°C water bath containing 90% (v/v) ethanol for decolorization and stored in 50% glycerol. The localization of O_2^- was observed as blue at X100 magnification.

Measurement of $O_2^{\cdot-}$and H_2O_2 content

The contents of O_2^- and H_2O_2 of the samples were determined following the method of Jambunathan (2010). One gram of the frozen root tissue of each sample mixed with 5mL of 50 mM PBS (pH 7.8) was grinded and homogenized by centrifugation. One mL of extraction solution of each sample was mixed with 0.5 mL PBS and 10 mM hydroxylamine hydrochloride, and then reacted at 25°C for 30 min. After added 1 mL of 17 mM p-Aminobenzene Sulfonic Acid and α-Naphthylamine, the mixture was incubated at 25°C for 15 min. The absorbance value was measured at 530 nm and the content of O_2^- was calculated based on the standard curve.

The extraction solution for determining the contents of H_2O_2 was processed by using acetone grinding and homogenization by centrifuging. One mL of the extraction solution was mixed with 0.1 mL of 5% titanium sulfate (v/v) and 0.2 mL of strong aqua ammonia and precipitated. After discarded the supernatant, 5 mL of 2 M sulphuric acid was added in the mixture, and the absorbance value was read at 415 nm and the H_2O_2 content was determined with the standard curve.

Measurement of the contents of ammonium nitrogen and nitrate nitrogen

The method of Cataldo et al. (1975) was referred for determining the content of nitrate nitrogen (NO_3^-) in plants. One gram of the frozen root tissue of each sample was extracted in a distilled boiling water bath for 30 min. After cooled, the extraction solution was diluted with distilled water to 25 mL. Then 0.1 ml of the diluted extraction solution was mixed with 0.4 mL salicylic acid ($H_2SO_4^-$ [1:5 (v/v)]) for 20 min. After addition of 9.5 mL of 2 M NaOH, the absorbance value of the solution was read at 410 nm and the NO_3^- content was calculated with the standard curve.

The content of ammonium nitrogen (NH_4^+) was determined by a ninhydrin colorimetry. Half of a gram of the frozen root tissue of each sample was mixed with 1.7 M acetic acid and diluted with distilled water to 100 mL. Two mL of the diluted extraction solution was mixed with 3 mL of 54 mM acidic ninhydrin acetic acid buffer (pH 5.4) and 0.1 mL of 60 mM

ascorbic acid, and incubated in a boiling water bath for 15 min. After cooled, absolute ethanol was added to 10 mL. The absorbance was read at 580nm and the NH_4^+ content was estimated through the standard curve.

Assay of the enzyme activities

The activities of glutamate synthase (GOGAT), glutamine synthetase (GS), glutamate dehydrogenase (GDH), and nitrate reductase (NR) were evaluated based on the methods of Lin and Kao (1996) and Gangwar et al. (2011). The root tissue and extraction solution of the transcriptomic analysis were homogenized in ice bath in the ratio of 1:5. After centrifugated at 4°C with 150,00×g for 20 min, the supernatant of the homogenized solution was collected as the crude solution for measuring the enzyme activities.

The GS crude enzyme solution was extracted with 50 mM Tris-HCl buffer (pH 8.0, 2 mM $MgCl_2$, 2 mM DTT, 0.4 M sucrose). The mixture of 0.7 mL of the crude enzyme solution with 1.6 mL of 0.1 M Tris-HCl buffer (pH 7.5, 2 mM $MgCl_2$, 20 mM sodium glutamate, 20 mM cysteine, 2 mM EGTA, 80 mM hydroxylamine hydrochloride) and 0.7 mL of 40 mM ATP was incubated at 37°C for 30 min. After addition of 1 mL of color developing agent (0.2 M TCA, 0.35 M $FeCl_3$, 0.6 M HCl), the absorbance was measured at 540 nm.

The crude enzyme solution of GOGAT was extracted with 10 mM Tris-HCl buffer (pH 7.5, containing 1 mM $MgCl_2$, 1 mM EDTA, 1 mM DTT). A total of 0.5 mL of crude enzyme solution was mixed with 0.05 mL of 0.1 M α-Ketoglutarate, 0.1 mL of 10 mM KCl, 0.2 mL of 3 mM NADH and 1.75 mL of buffer. After added 0.4 mL of 20 mM glutamine, the absorbance changes for 3 min were immediately recorded at 340 nm. The crude enzyme solution of GDH was extracted with 0.2 M Tris-HCl buffer (pH 8.0). One mL of the crude enzyme solution was thoroughly mixed with 0.3 mL of 0.1 M α-Ketoglutarate, 0.3 mL of 1 M NH_4Cl, 0.2 mL of 3 mM NADH and 1.2 mL of buffer. The decrease of absorbance was recorded for 3 min at 340 nm. The crude enzyme solution for NR was extracted with 25 mM phosphate buffer (pH 8.7, 10 mM cysteine, 1.3 mM EDTA). 1.5 mL of the crude enzyme solution was mixed with 1.2 mL of 0.1 M KNO_3 phosphoric acid buffer (pH 7.5) and 0.5 mL of 3 mM NADH and incubated in a water bath at 25°C for 1 h in dark. After added 1 mL of 1% sulphonamide solution (v/v) and 1 mL of 0.02% naphthalene ethylenediamine hydrochloride solution (v/v), the mixed reaction was kept in dark for 15 min. The absorbance was read at 540nm and the NO_2^- was calculated according to the standard curve.

The activities of superoxide dismutase (SOD), peroxidase (POD) and catalase (CAT) were estimated following the methods of Decleire et al. 2012 and Maehly and Chance, 1954. The root tissues of each sample were mixed with 50 mM of PBS (pH 7.8) at a ratio of 1:10 on ice bath and centrifugated at 15000×g for 20 min at 4°C. After mixed 0.1 mL of SOD crude enzyme solution with 0.3 mL of 0.13 M methionine, 0.75 mM nitrogen blue tetrazole, 0.1 mM EDTA-Na_2, 20 μM riboflavin and 1.7 mL PBS, the mixture solution was incubated at 4000 LX for 20 min. The absorbance was measured at 560 nm. The POD activity was evaluated by mixing 0.1 mL crude enzyme solution with 2.9 mL of 0.5% guaiacol (containing a small amount of H_2O_2). The increase of absorbance was recorded for 3 min at 470 nm. The mixture of 0.1 mL of the crude enzyme solution and 0.4 mL of 0.1 M H_2O_2 and 2.5 mL of PBS was used to measure the absorbance of CAT at 240 nm and record the changes of absorbance in 3 minutes

Measurement of the malondialdehyde content

The content of malondialdehyde (MDA) was determined by the thiobarbituric acid method (TBA) (Li et al., 2013). The mixture of 1 g of the frozen root tissue and 10 mL of TCA was grinded for homogenization by centrifugation. Then 2 mL of the extraction solution was mixed with 0.6% TBA (v/v) and incubated in a boiling water bath for 15 min. The absorbance values were read at 532, 600, and 450 nm.

RNA extraction, cDNA library preparation, and sequencing

Total RNA was extracted from the root tissues by using the Plant RNA Purification Reagent (Invitrogen, USA) following the manufacturer's instructions. The potential contaminating genomic DNA was removed from RNA preparation with the DNase I kit (TaKara Bio, Japan). RNA integrity was checked by 1% agarose gel electrophoresis. Total RNA concentration was determined using a 2100 Bioanalyser (Agilent Technologies, USA) and RNA quality was assessed using the ND-2000 NanoDrop (NanoDrop Technologies, USA).

RNA-seq libraries were constructed using the TruSeq™ RNA sample preparation kit from Illumina (San Diego, USA). 1,000 ng of total RNA was used to isolate mRNA using a polyA selection method by oligo(dT) beads. The extracted mRNA was fragmented in the first-strand synthesis buffer by heating at 94°C, followed by first-strand cDNA synthesis using reverse transcriptase and random primers. Synthesis of double-stranded cDNA was performed using the 2nd strand master mix provided using a SuperScript double-stranded cDNA synthesis kit (Invitrogen, USA). Resulting double-stranded cDNA was end-repaired, dA-tailing and ligated with NEBNext adaptors. Libraries were fragmented as 300 bp on 2% Low Range Ultra Agarose. Finally, libraries were enriched by 15 cycles of amplification. After quantified by TBS380, paired-end RNA-seq libraries were sequenced with the Illumina HiSeq xten/NovaSeq 6000 sequencer (2 ×150bp read length). The data

presented in the study are deposited in the NCBI repository, accession number PRJNA874354

Bioinformatics and RNA-seq analysis

The transcriptomic analysis was based on the genome of *Zea mays* (GCF_902167145.1, https://www.ncbi.nlm.nih.gov/genome/?term=Zea_mays) from the NCBI database. The acquired paired-end reads were trimmed and quality controlled by SeqPrep (https://github.com/jstjohn/SeqPrep) and Sickle with default parameters. The clean reads in each sample were independently mapped to the reference genome with the orientation mode of the HISAT2 package (Kim et al., 2015). The mapped reads of each sample were further assembled by using the reference-based approach of the StringTie package (Pertea et al., 2015).

The differential expression of genes between the control and treatment groups were calculated based on the transcripts per million reads (TPM) by using the DESeq2 (Love et al., 2014). Genes with $|\log_2^{\text{fold change}}| \geq 1$ and *p-adjust* < 0.05 were considered to be significantly different. For functional enrichment analysis, significantly up- and down-regulated genes (Benjamini-Hochberg with an FDR ≤ 0.05) were selected for GO and KEGG metabolic pathways analysis by using the Goatools (https://github.com/tanghaibao/Goatools)and KOBAS (http://kobas.cbi.pku.edu.cn/home.do) (Xie et al., 2011). The outputs were generated by AI and the GraphPad Prism (v 8.0) and the significant differences were evaluated by the IBM SPSS Statistics (v 25) package.

qRT-PCR Assays

cDNAs were synthesized from the purified 100 ng total RNA using a PrimeScript™ RT Reagent Kit and gDNA Eraser (TaKaRa, China). The quantitative real-time polymerase chain reaction (qRT-PCR) analysis was conducted with a TB Green *Premix Ex Taq*™ II Kit (Takara, China). The reaction mixture contained 12.5 µL TB Green Premix Ex Taq, 1 µL forward and reverse primers respectively, 1 µL cDNA and 9.5 µL ddH_2O. The qPCR thermal cycling was as follows: 95 °C for 30 s followed by 40 cycles of 95 °C for 5 s, 55 °C for 30 s and 72 °C for 30 s. Each reaction was repeated three times. In every qPCR run, *ZmGAPDH* was used as an internal control to minimize systematic variations in the amount of cDNA template. The primers used for qRT-PCR were listed in Table S1.

Results

Effect of histidine on root morphology under salt stress

Our results confirmed that when the root was under salt stress, the total length of root (all fibrous roots) was significantly increased by adding histidine, the average length increased from 1690 cm to 2621 cm and the root projected area and surface area enlarged by 45.8% and 45.31%, respectively. In addition, the numbers of the root furcation and root tips were significantly increased by 63.2% and 30.12%, respectively (Figure 1C).

Effect of histidine on the ROS accumulation under salt stress

The level of ROS is related to the adaptation of plants to salt stress. After salt stress treatment, the O_2^- level of root was significantly increased. When the roots were further treated with histidine, the ROS levels were significantly increased, while the accumulative levels of O_2^- and H_2O_2 were significantly reduced (Figure 2A). The DAB and NBT staining results revealed that the root tips showed dark brown and deep blue patches with the salt stress treatment, but the patch colors became light after the histidine treatment (Figure 1B). Antioxidant enzymes are very important in the process of salt tolerance of plants, and they are often used as indicators to evaluate plant salt tolerance. The analysis of enzyme activities showed that, after the treatment of histidine, the activities of SOD, POD and CAT in the root tissues were significantly increased by 21.92%, 12.84% and 59%, respectively (Figure 2A), which were significantly higher than those with the salt stress treatment. In addition, the content of MDA was significantly reduced after the histidine treatment.

Effects of histidine on the nitrogen use efficiency in maize with salt stress treatment

When the roots were treated with the salt stress, the contents of nitrate and ammonium nitrogen were significantly accumulated; while the activities of NR, GS, and GOGAT were significantly decreased (Figure 2B). However, after the histidine treatment, compared to the control group (CK1), the contents of nitrate nitrogen and ammonium nitrogen in roots were significantly decreased by 69.54% and 34.48%, respectively, while the activities of NR, GS, and GOGAT were increased significantly, by 53.2%, 9.26% and 176.52%, respectively.

Expression profiles of transcripts

A total of 1,253,271,938 raw paired-end reads were obtained from the Illumina sequencing platform. After quality control, 1,239,263,410 clean paired-end reads with 53.86 - 54.74% of GC content were used in transcriptomic analysis. All samples were independently aligned with the reference genome using HISAT2. About 87.98% - 89.75% of the reads were mapped to the maize

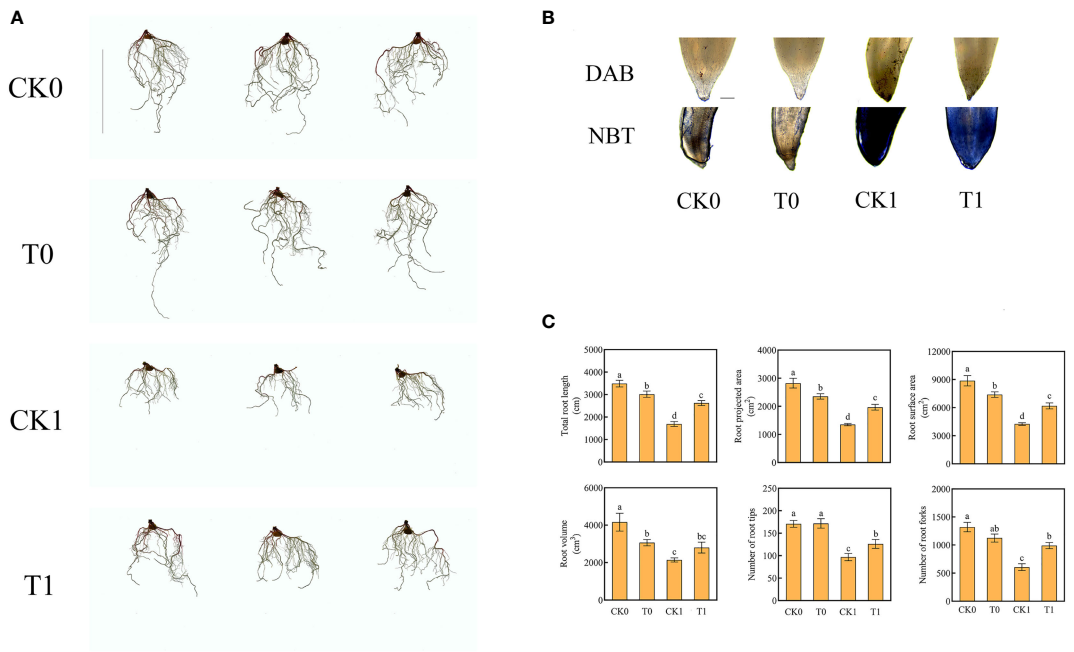


FIGURE 1
Root morphology (Ruler represents 20cm) **(A)**, root tips with DAB and NBT staining (Ruler represents 200 μm) **(B)**, total root length, root projected area, root surface area, root volume, number of root tips, number of root forks **(C)** in the four different treatments. Data were presented as the mean ± SEM for six biological replicate samples. Bars labeled with different letters indicated significant difference between treatments.

genome and 85.29% - 86.96% of reads uniquely mapped to the reference sequences (Table S2).

Based on the reference genome, the mapped reads in each sample were processed using the StringTie package and the assembled contigs were compared with the original genomic annotation information for novel transcripts and genes. A total of 52,229 transcripts with >1,800 bp and 4,432 transcripts with ≤ 200 bp were derived. The search against the known transcripts of the genome identified 28,976 potential novel transcripts, 5,977 of which may produce new genes (Figure S2).

The principal component analysis (PCA) revealed that the CK0 and T0 samples at 12 h and 24 h showed no difference along PCI (39.80% and 24.36%) and PCII (8.82% and 15.94%). The CK1 and T1 treatment samples were not significantly different along PCI, but they could be separated as two different groups along the PCII at 12h and 24h (Figure 3A). The unique and shared genes across all samples were identified by the Venn diagram analysis (Figure 3B). At 12 h and 24 h after treatment, 400, 281, 304, 393 and 330, 357, 321, and 270 uniquely expressed genes were found in the CK0, T0, CK1 and T1 samples, and 22,349 and 22,739 co-expressed genes of those samples, respectively. In the RNA-seq analysis by DESeq2, genes with p-adjust < 0.05, $|\log_2^{\text{fold change}}| \geq 1$ were defined as DEGs in our analysis. A total of 671 (up 251, down 420), 454 (up 65, down 389), 43 (up 39, down 4) and 348 (up 293, down 55) DEGs were found in the analysis of the CK0_12 vs T0_12, CK1_12 vs T1_12, CK0_24 vs T0_24 and CK1_24 vs T1_24, respectively (Figure 3C). The details of the DEGs were presented in Table S3.

Functional annotation of genes

All genes obtained from the transcriptomic assembly were searched against six major databases for gene functional annotation. In a total of 47,042 (94.47%) annotated genes, 36,571, 18,364, 42,430, 46,966, 32,196, 27,808 genes were annotated by the GO, KEGG, COG, NR, Swiss prot and Pfam databases, respectively, accounting for 77.74%, 39.04%, 90.20%, 99.84%, 68.44% and 59.11% of the total annotated genes (Table S4). The gene function predictions based on the COG database suggested that a total of 42,430 genes were annotated into 23 annotated categories, including the largest group (n = 26,306, 62%) of unknown, followed by the posttranslational modification, protein turnover, chapters (n = 3,145, 7.41%) and the transcription (n = 2,749, 6.48%) categories. Only 7 and 5 genes were assigned to the nuclear structure and cell motility categories, accounting for 0.016% and 0.012%, respectively (Figure 4A).

The GO functional annotations of DEGs assigned to the biological process, cellular component and molecular function categories were presented in Table S5 and Figure 4B. In all comparisons, most of DEGs were assigned to the cellular process

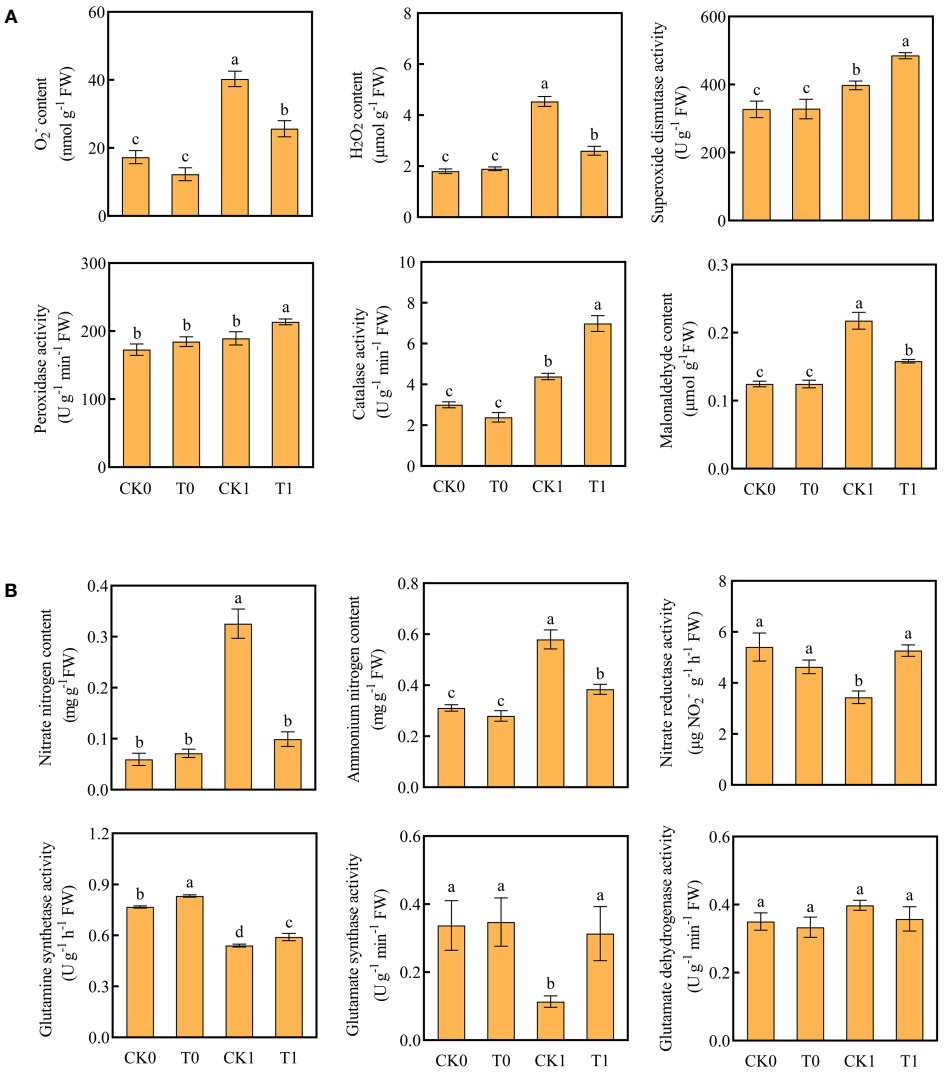


FIGURE 2
Contents of O_2^-, H_2O_2, MDA, antioxidant enzyme activities **(A)** and contents of ammonium nitrogen, nitrate nitrogen, nitrogen metabolizing enzyme activity **(B)** in the four treatments. Data are presented as the mean ± SEM for six biological replicate samples and each sample included 3 plants. Bars labeled with different letters for significant difference between treatments.

of the biological process, the cell part in cellular component, and the binding and/or catalytic activity in molecular function.

Functional pathway enrichment analysis

The GO enrichment analysis found that the DEGs in the comparisons of the CK0_12 vs T0_12 (569 genes), CK1_12 vs T1_12 (385 genes), CK0_24 vs T0_24 (59) and CK1_24 vs T1_24 (278 genes) were enriched in 252, 146, 133, and 280 pathways, respectively (Table S6). With the p-adjust <0.05 as the significance threshold, about 22, 16, 12, and 32 GO pathways were significantly enriched in those analysis. Most of DEGs in the 12 h and 24 h groups with histidine treatment alone were related to the plasma membrane (GO:0005886) and response to hydrogen peroxide (GO:0042542). Under salt stress, most of DEGs in 12 h and 24 h histidine treatment groups were associated with the reactive oxygen species metabolic process (GO: 0072593) and response to wounding (GO: 0009611) (Figure 5)

The KEGG enrichment analysis on DEGs showed that 266, 178, 20 and 120 DEGs in the analysis of CK0_12 vs T0_12, CK1_12 vs T1_12, CK0_24 vs T0_24 and CK1_24 vs T1_24 were enriched to 76, 61, 17 and 44 pathways, respectively (Table S7 and Figure 6). With the *p*-adjust < 0.05 as a cutoff, 4 enriched KEGG pathways in the analysis of CK0_12 vs T0_12 were related to the environmental information processing and

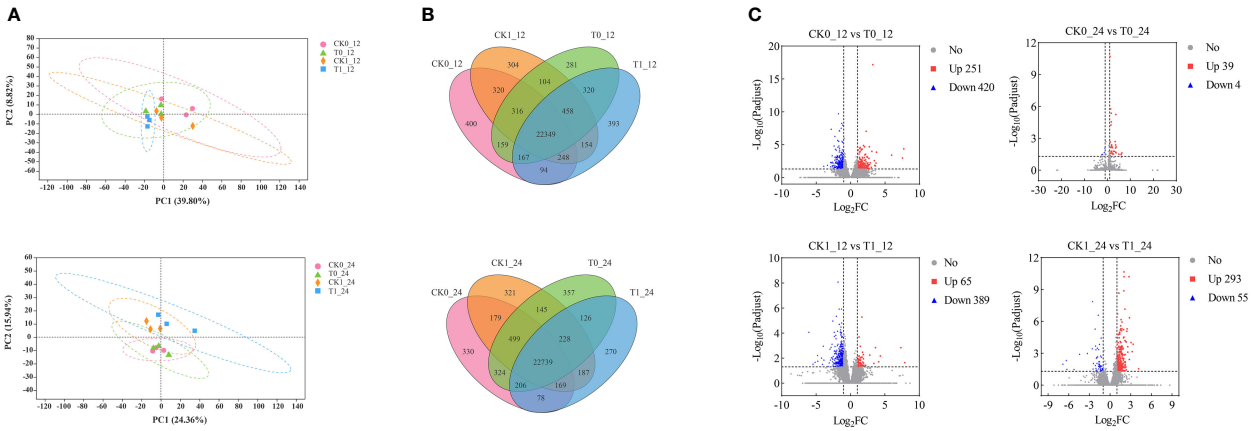


FIGURE 3
Identification and analysis of DEGs in the *Zea mays* root samples of CK0, T0, CK1, and T1. **(A)** PCA analysis of 4 treatment groups. **(B)** The Venn diagram for common and/or unique DEGs among those groups using. **(C)** Differentially expressed genes between groups.

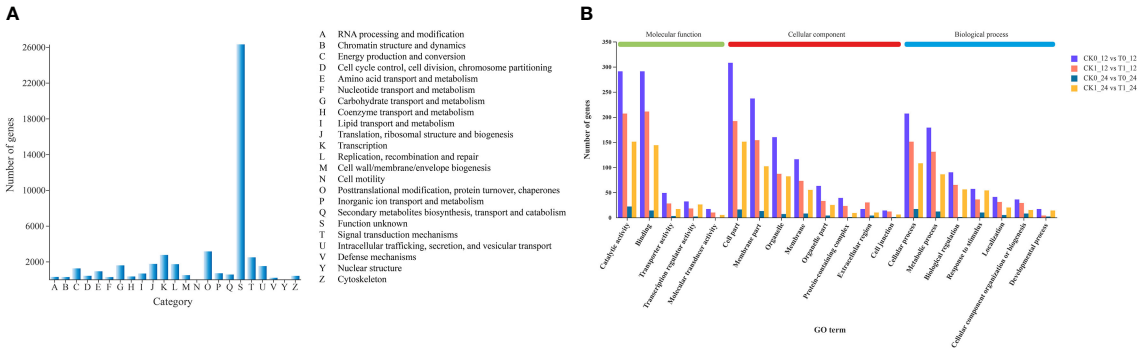


FIGURE 4
Cluster of Orthologous Groups (COG) function categories of unigenes **(A)** and the Gene Ontology (GO) classification of DEGs **(B)** in *Zea mays*.

starch and sucrose metabolism, plant hormone signal transduction, inoleic acid metabolism, and phenylpropanoid biosynthesis. The significantly enriched KEGG pathways in the analysis of CK0_24 vs T0_24 were related to genetic information processing and metabolism, including cutin, suberine and wax biosynthesis, protein processing in endoplasmic reticulum, flavonoid biosynthesis. Without salt stress, the DEGs in the 12 h treatment group were mainly associated with the carbohydrate metabolism, signal transmission, lipid metabolism, biosynthesis of other secondary metals. While in the 24 h groups, the DEGs were involved in lipid metabolism, biosynthesis of other secondary metals, as well as folding, sorting, and degradation. For the samples with salt stress treatment, the KEGG pathways enriched by DEGs were all associated with environmental information processing and metabolism. In the analysis of CK1_12 vs T1_12, the DEGs only in phenylpropanoid biosynthesis and plant hormone signaling transduction were significantly enriched. In the comparison of CK1_24 vs T1_24, 6 pathways related to environmental information processing and metabolism were significantly enriched, including plant hormone signal transduction, glycolysis/gluconegenesis, nitrogen metabolism, pentose phosohate pathway, fructose and mannose metabolism and linoleic acid metabolism (Figure 6). The RT-qPCR analysis of 10 DEGs from the enriched KEGG pathways also confirmed the consistency of the results between RNA-seq and RT-qPCR analysis (Figure 7).

Integrated pathway analysis of histidine on regulating salt tolerance in maize roots

Figure 8 listed the DEGs of the samples in CK1 and T1 groups that are related to the plant hormone signal transduction.

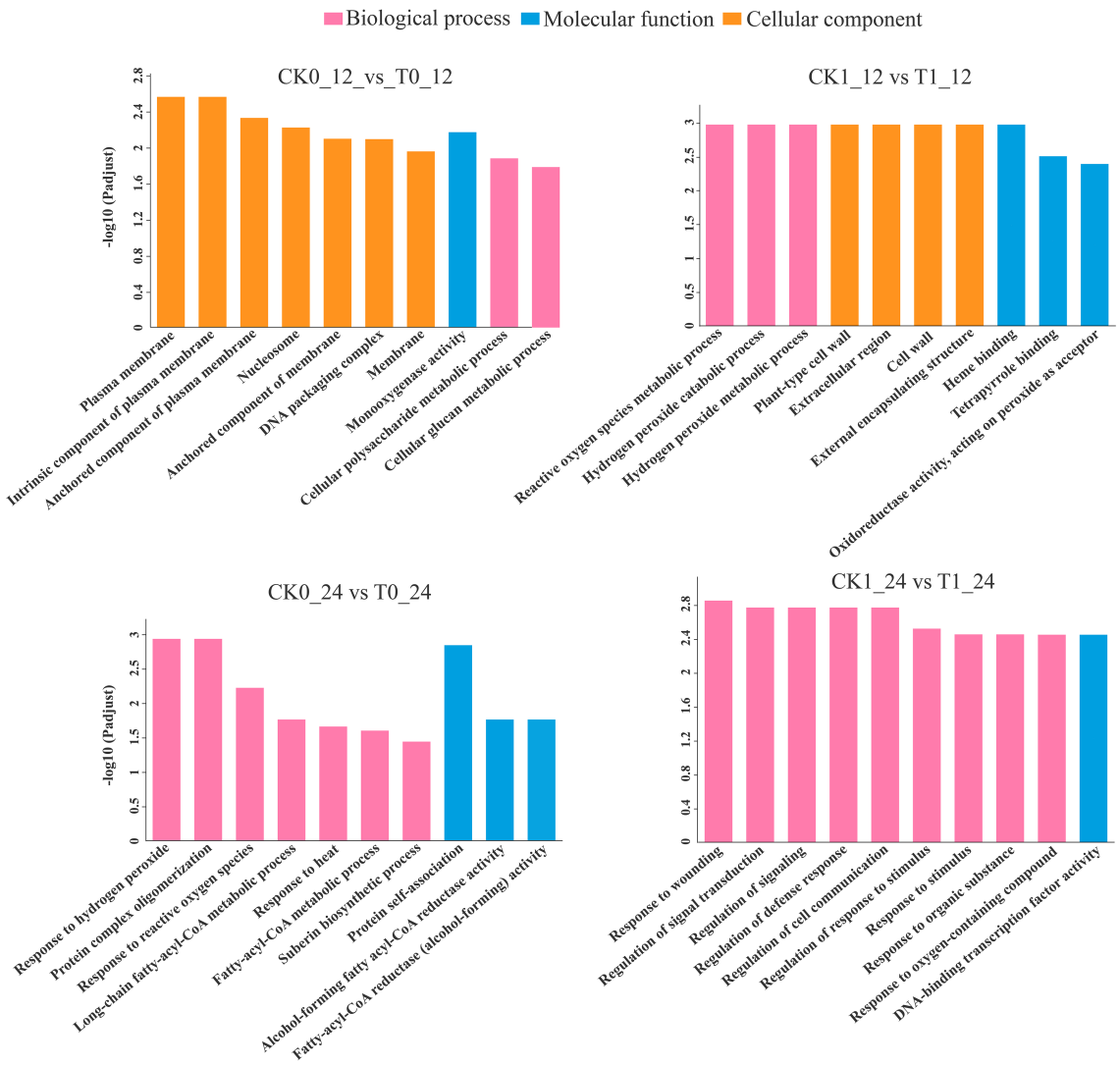


FIGURE 5
GO enrichment analysis of DEGs. *p*-adjust < 0.05 was considered to be significantly different.

After 12 h of histidine treatment, all DEGs in T1 were downregulated, including Auxin early response genes (AUX/IAA), auxin response factor (ARF), small auxin upregulated RNA(SAUR), gretchen hagen3 (GH3), Abscisic acid receptor (PYL), Jasmonic acid inhibitor (JAZ). However, after 24 h of histidine treatment, some DEGs were up-regulated and some down-regulated. Thirteen up-regulated genes were involved GH3, cytokinin receptor (AHK2/3/4), DELLA, phytochrome interaction factors 4 (PIF4), ABA response element (ABRE), ABRE binding protein (AREB/ABF), and JAZ. Five down-regulated genes were involved GH3, SAUR, and TCH4.

A total of 39 DEGs were identified that are associated with the phenylpropanoid biosynthesis, glycolysis and nitrogen metabolism were identified in CKI and T1 groups. In the 24 h treatment group, 11 and 5 up-regulated genes were significantly enriched in glycolysis and nitrogen metabolism, respectively. In glycolysis, these up-regulated genes were related to 6-phosphofructokinase (pfkA), pyrophosphate fructose 6-phosphate 1-phosphotransferase (PFP), triose phosphate isomerase (TPI), glyceraldehyde-3-phosphate dehydrogenase (gapN), pyruvate kinase (PK), pyruvate decarboxylase (PDC), alcohol dehydrogenase (ADH1), and acetyl-coenzyme A synthetase (ACSS1/2). In nitrogen metabolism, these up-regulated genes were related to nitrate reductase [NADH] (NR), glutamine synthetase (glnA), and glutamate synthase [NADH](GLT1). In the 12 h treatment group, 1 and 3 down-regulated genes were enriched in glycolysis and nitrogen metabolism, respectively, whichis related to pfkA and carbonic

10.3389/fpls.2022.1049954

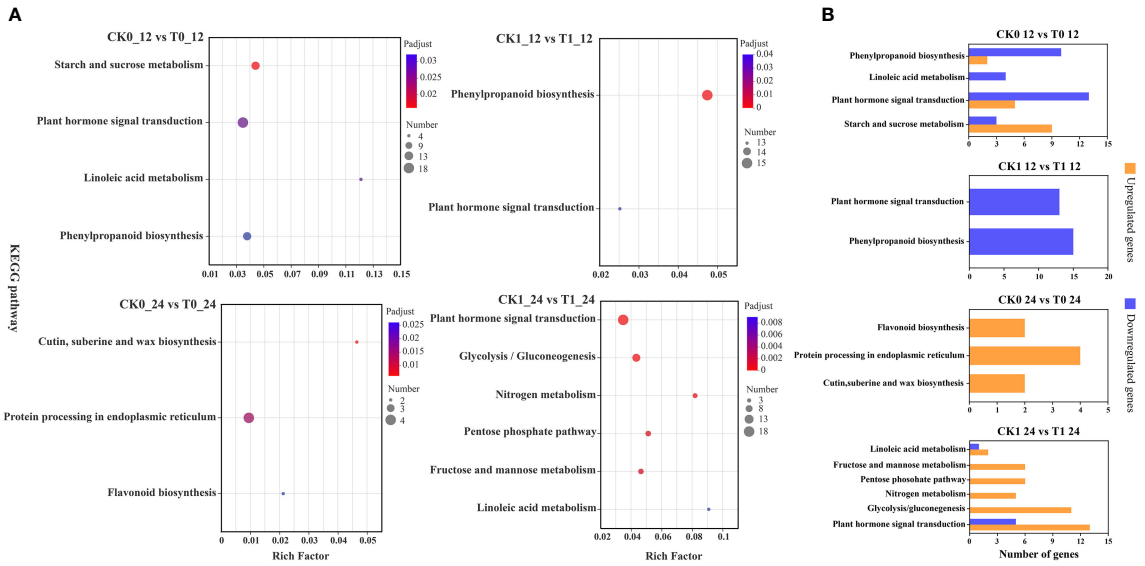


FIGURE 6
KEGG enrichment analysis of DEGs **(A)**, up- and down-regulated DEGs in KEGG pathways **(B)**. *p*-adjust < 0.05 was considered to be significantly different.

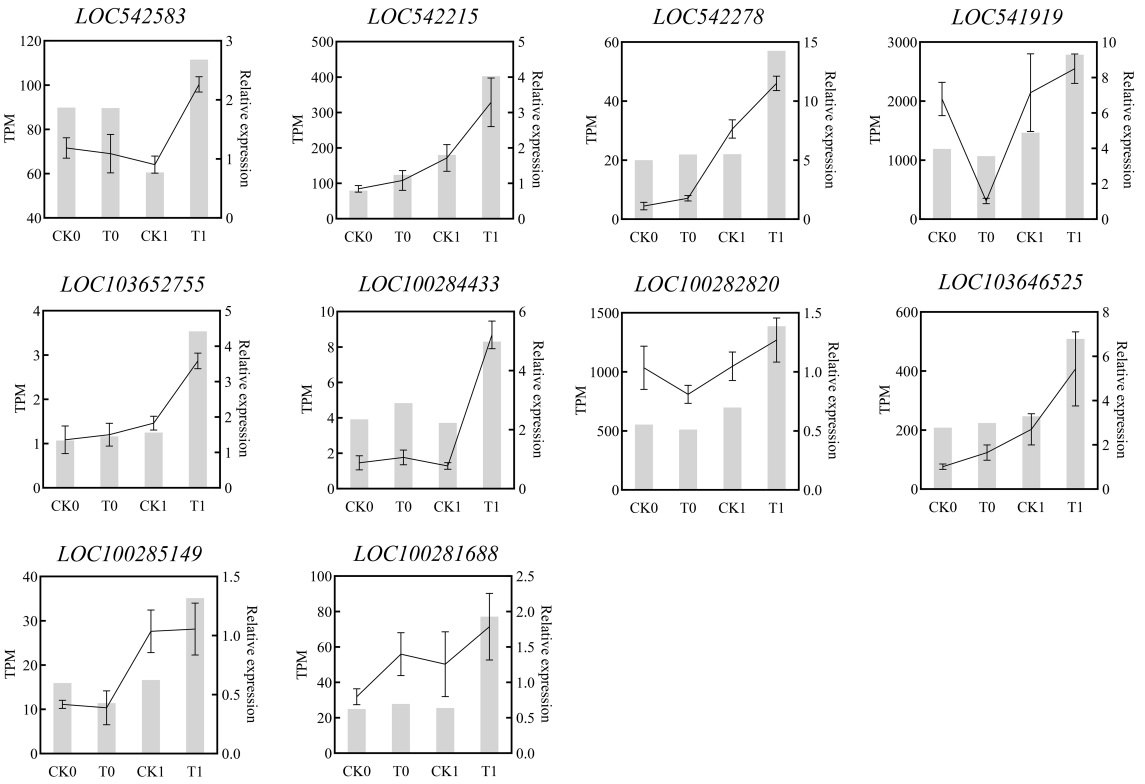


FIGURE 7
Quantitative real-time PCR (RT-qPCR) validation of the selected DEGsfrom RNA-seq analysis.The relative expression amount obtained by RT-PCR was expressed by broken lines. RT-qPCR data showed the mean values from three replicates, and the error bars represented the SEM of the means, while the corresponding expression data for RNA-seq were presented in the grey histogram.

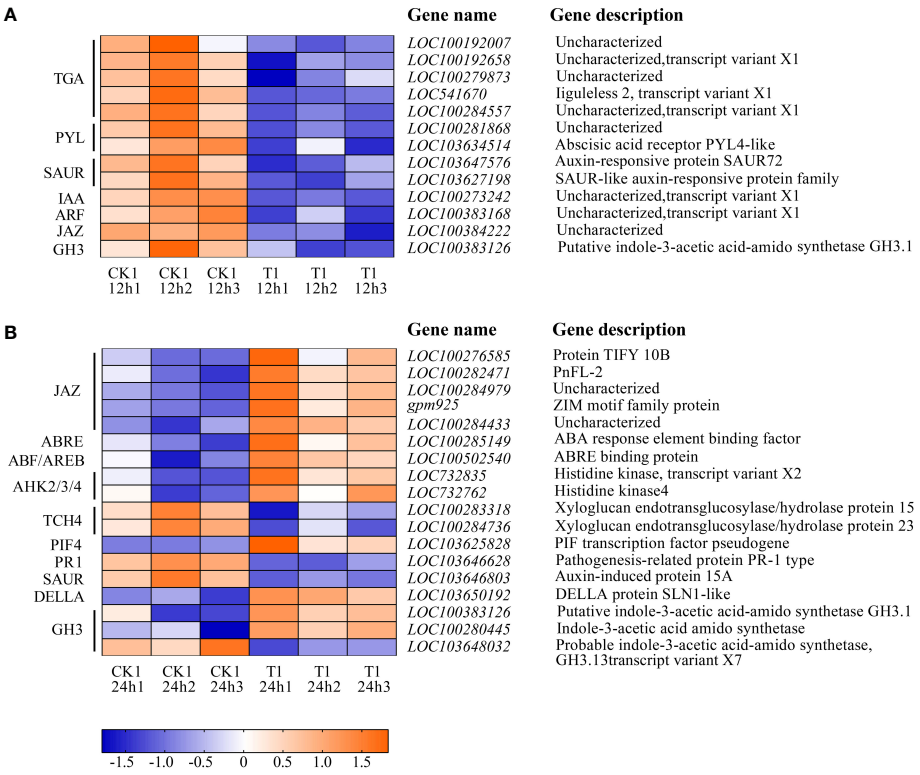


FIGURE 8
Heatmap of the DEGs involved in plant hormone signal transduction between CK1 and T1. **(A)** Treatment for 12 h. **(B)** Treatment for 24 h. The color in the figure indicates the expression magnitude of the gene after normalization treatment in each sample. Orange means upregulated expression of genes, and blue means downregulated expression of genes. The number in each sample name represents the sample order.

anhydrase (cynT) in glycolysis and nitrogen metabolism. In the 12 h treatment group, 15 down-regulated genes were significantly enriched in the phenylpropanoid biosynthesis, phenylalanine ammonia lyase (PAL), cinnamoyl-CoA reductase (CCR), cinnamyl alcohol dehydrogenase (CAD), and peroxidase (E1.11.1.7) (Figure 9).

Discussion

The interaction between plant and environment is a constant and essential activity throughout the plant life cycle, which influences plant growth, development, and survival. In arid and semi-arid regions, soil salinization is an important worldwide environmental problem. As one of the most important crops and the main material for bioethanol production in China, maize crops are extremely sensitive to drought and salt stresses, which significantly affect plant growth and development. The results of the present study showed that histidine can protect the maize root system from salt stress and enhance the abiotic stress tolerance of maize. When applied exogenously to maize exposed to salt stress, histidine not only resulted in increased growth and other physiological characteristics of roots, but also overcame the environmental salt stress by activating the antioxidant enzyme activities and regulating nitrogen metabolism and plant hormone signal transduction pathways.

Roots are highly sensitive to changes in their surrounding environment and the responses to stresses such as salinity and drought are very dynamic and complex in nature (Duan et al., 2015). Studies have shown that the addition of amino acids from hydrolyzed meat meal will induce structural changes in maize roots (Ertani et al., 2010; Colla et al. (2015). Our results confirmed that salt stress caused damage to maize roots and reduced the root area, number of lateral roots, and root length. However, after histidine was applied, the root length, root projected area, root surface area, root volume, and numbers of root tips, and furcation were significantly increased (Figure 1).

Plants antioxidant system plays an important role in resisting environmental stresses. Salinity exposure causes enhanced energy consumption and often enhanced respiration which are directly linked to the enhanced production of ROS (Tiwari et al., 2002). Acting as signaling molecules including hydroxyl radicals (OH), hydrogen peroxide (H_2O_2), and

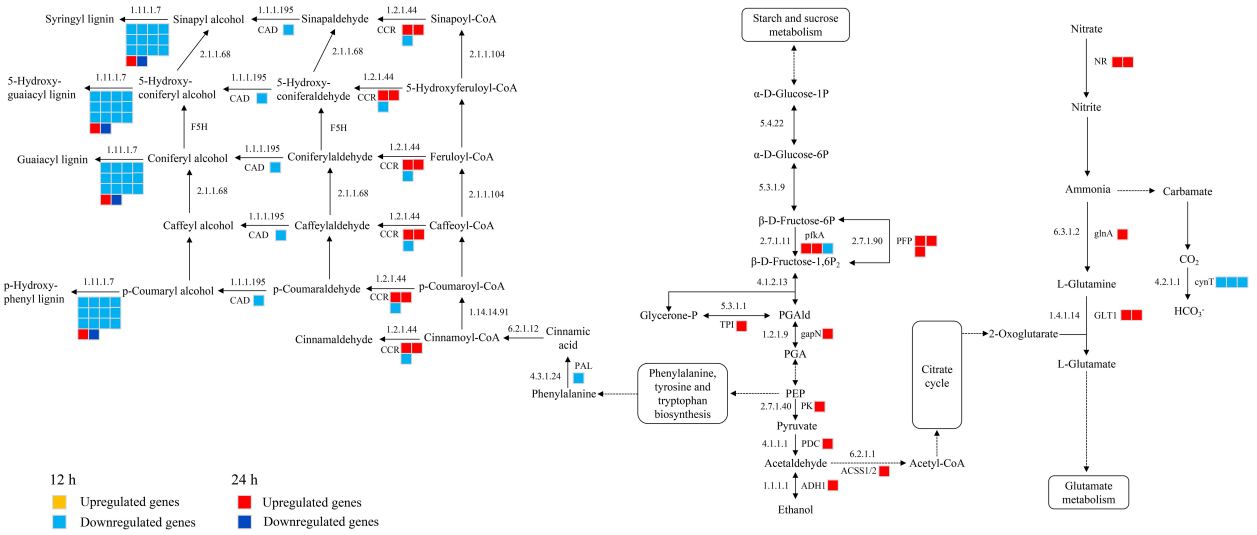


FIGURE 9
Glycolysis, nitrogen metabolism, phenylpropanoid biosynthetic metabolic pathways in histidine treatment atb12 h and 24 h under salt stress. Abbreviations are as follows: NR, nitrate reductase [NADH]; glnA, glutamine synthetase; GLT1, glutamate synthase [NADH]; cynT, carbonic anhydrase; pfkA, 6-phosphofructokinase; PFP, pyrophosphate fructose 6-phosphate 1-phosphotransferase; TPI, triose phosphate isomerase; gapN, glyceraldehyde-3-phosphate dehydrogenase; PK, pyruvate kinase; PDC, pyruvate decarboxylase; ADH1, alcohol dehydrogenase; ACSS1/2, acetyl-coenzyme A synthetase; PAL, phenylalanine ammonia lyase; CCR, cinnamoyl-CoA reductase; CAD, cinnamyl alcohol dehydrogenase; E1.11.1.7, lignin peroxidase.

superoxide anion (O_2^-), ROS can trigger signal transduction pathways in response to salt stress (Jiang et al., 2012). Previous studies suggested that plant roots could absorb amino acids, which in turn as bio-stimulants could improve the ability of plants to resist salt stress (Watson and Fowden, 1975; Colla et al., 2014). For example, proline can remove free radicals in plants, significantly increase the activity of antioxidant enzymes, and reduce the content of MDA (Ashraf and Foolad, 2007; Satoh et al., 2002; Rady et al., 2019). Exogenous ornithine and glutamate and γ-aminobutyric acid can increase the activities of CAT, SOD, POD, and reduce the Na^+/K^+ ratio and content of H_2O_2 and MDA under salt stress (Chang et al., 2010; Da Rocha et al., 2012; Kaspal et al., 2021; Ahmadi et al., 2021). Our experiments revealed that the histidine treatment significantly increased the resistance enzyme activities of SOD, CAT, and POD in maize roots and decreased the accumulation of $O_2^{\cdot-}$, H_2O_2, and MDA (Figures 1A and 2A). In the antioxidant enzymatic system of plants, SOD forms the first line of defense against oxidative stress POD is to oxidize phenolic compounds (Hasanuzzaman et al., 2020), and CAT can rapidly decompose H_2O_2 to produce H_2O and O_2 (Hao et al., 2021). The increased CAT activity and the reduced H_2O_2 content in the maize roots demonstrated that histidine can mitigate oxidative damage and improve the tolerance of maize to salt stress.

Plants can adapt to salinity stress through flexible regulation of hormone levels and/or signaling. Accumulating evidence indicates that plant hormones, besides controlling plant growth and development under normal conditions, also mediate various environmental stresses (e.g., salt stress) and thus regulate plant growth adaptation. It has been proved that amino acids are closely associated with plant hormones. For example, auxins are a group of plant hormones that affect plant growth and development. The exogenous L-glutamate acid can affect the auxin level of the root tips in *Arabidopsis thaliana* and L-tryptophan can improve growth and photosynthetic capacity as the precursor of auxin synthesis (Müller et al., 1998; Walch-Liu 2006). Our results revealed that, after 24 h of the histidine treatment, the DEGs involved in 5 plant hormone signal transduction pathways were significantly up-regulated, including the growth promoting hormones in auxin (IAA), cytokinin (CTK), and gibberellin (GA) and the stress response hormones in abscisic acid (ABA), and jasmonic acid (JA) signal transduction pathways (Figure 8).

The plant hormone auxin controls growth and developmental responses throughout the life of a plant. The auxin early response gene Gretchen Hagen3 (*GH3*) plays dual roles in plant development and responses to biotic or abiotic stress. GH3 genes participates in auxin homeostasis by catalyzing auxin coupling and binding of free IAA with amino acids (Jain et al., 2006). GH3 can regulate the activity of indole-3-acetic acid amido synthetase, indole-3-acetic acid amido synthetase produces IAA conjugates containing various amino acids, which changes the sensitivity of seedlings to auxin. The

results of this study also confirmed that histidine can induce GH3 (*LOC100280445*; *LOC100383126*) expression, which involved in IAA synthesis and regulate the content of free IAA in maize roots (Feng et al., 2015) to improve the tolerance of maize to environmental stress.

CTK is another major phytohormone that not only regulate the plant growth/development but also play an important role during stress and in the nutrient metabolic pathway of crop plants. Research showed that the decrease of CTK level will improve the survival ability of plants under salt stress (Nishiyama et al., 2011; Pizarro et al., 2021). After 24 h of the histidine treatment, genes associated with CTK signaling pathway were up-regulated, including genes in AHK2/3/4 (*LOC732762*; *LOC732835*). AHKs act as receptors during cytokinin signaling and play a significant role in providing cytokinin function during plant development (Cucinotta et al., 2020). AHKs also can regulate histidine kinase activity, and sense CTK signal and mediate the function of CTK. Previous research reported that drought, cold and salt stress can induce the expression of AHK3 and the survival rate of *ahk* mutant increased under salt stress and drought (Tran et al., 2007; Kumar and Verslues, 2015). The up-regulated DEGs related to CTK signal transduction may be closely linked to the histidine treatment, which participated in signal transduction through AHK and act as signal molecules to interact with specific receptors on the cell membrane, causing changes in plant morphology, physiology and biochemistry as other amino acids reported by Ryan and Pearce (2001).

GA is a plant hormone and controls major aspects of plant growth such as germination, elongation growth, flower development, and flowering time. DELLA proteins are negative regulators of GA signaling that act immediately downstream of the GA receptor. When the maize roots were treated with histidine, the genes related to DELLA (*LOC103650192*) and PIF4 (*LOC103625828*) in the GA signal transduction pathway were up-regulated. In the absence of GA, DELLA will block the binding of PIF3 and PIF4 to DNA, thus inhibiting the growth of hypocotyl. In the presence of GA, it will form a GA-GID1-DELLA complex, leading to the ubiquitination and degradation of DELLA, causing PIF expression and promoting hypocotyl elongation (Li et al., 2016). This suggested that DELLA proteins promote the expression of downstream negative components of GA signaling and provide a direct feedback mechanism for regulating GA homeostasis.

ABA is an important phytohormone regulating plant growth, development, stress responses to abiotic stress, and control of seed dormancy and germination. Plants will produce ABA under high salt stress, and ABA will improve the stress resistance of plants (Nakashima and Yamaguchi-Shinozaki, 2013). In the present study ABRE (*LOC100285149*) and AREB/ABF (*LOC100502540*) were up-regulated under the histidine treatment. ABA activates the expression of many genes through the ABRE in promoter region. AREB/ABF regulates the transcription of downstream target genes mediated by ABRE (Zhu, 2002). The AREB/ABF overexpressing in maize root suggested that the addition of histidine can improve the stress resistance by regulating the expression of genes related to the stress response hormones. Several other studies also reported that *AREB/ABF*-overexpressing plants showed ABA hypersensitivity and enhanced tolerance to abiotic stresses, such as freezing, drought and salt stress in *Arabidopsis* (Fujita et al., 2005; Fujita et al., 2013).

JA is a stress-related hormone and plays a crucial role in a variety of plant development and defense mechanisms. The JA signaling pathway is involved in the response and adaptation process of plants to abiotic stresses, including cold, drought, and salinity. JAZ proteins play pervasive roles in the response to biotic stress and development of plants. Jasmonate can promote the binding of JAZ proteins with SCF^{COI1} ubiquitin ligase, cause JAZ degradation, release MYC2 transcription factors, and cause jasmonic acid dependent gene expression. The up-regulated JAZ (*LOC100284433; LOC100282471*; *LOC100282471*; *LOC100276585*; *gpm925*) at 24 h after histidine treatment in T1 group indicated that the expression of JAZ genes play an important role in plant hormone signal transduction and defense response against salt stress.

In fact, JAZ protein is a key hub of crosstalk between JA and other hormone signaling pathways (such as auxin, gibberellin, and salicylic acid) (Kazan and Manners, 2012). JAZ can promote the transcription of GA response genes and bind with DELLA to interfere with the interaction between DELLA and PIF transcription factors and offset the growth inhibition produced by DELLA (Staswick, 2008). Studies have shown that amino acids can trigger related processes of plant hormones and induce the biosynthesis genes of jasmonic acid, abscisic acid, salicylic acid (Colla et al., 2014). Based on our results we speculate that histidine may act as a signal molecule to regulate genes involved in the plant hormone signal transduction pathways by mediating plant hormone levels.

The nitrogen sources of plants include organic nitrogen (e.g., amino acids) and inorganic nitrogen (e.g., nitrate nitrogen and ammonium nitrogen). Amino acids can be directly used for protein and other nitrogen-containing compounds synthesis (Rentsch et al., 2007) and transported through the vascular system for plant metabolism and development. They worked as the signal role in the process of nitrogen acquisition by roots to stimulate nitrogen metabolism and assimilation (Tegeder, 2012; Calvo et al., 2014). Assimilation of nitrate and ammonium are vital procedures for plant development and growth. The main enzymes involved in assimilation include NR, NIR, GS, GOGAT, and GDH. Our study demonstrated that the histidine treatment can enhance the activities of NR, GS, and GOGAT (Figure 2B). The mechanism of histidine involved in nitrogen metabolism in maize roots under salt stress may be like that of the above amino acids.

Most nitrogen sources in soil are in the form of NO_3^-. The primary sources of nitrogen for plants are nitrate (NO_3^-) and ammonium (NH_4^+). Nitrate is the form of nitrogen most used by plants for growth and development; while $NH4^+$ is a critical intermediate in the metabolism of plants (Glass et al., 2002). As an inducible enzyme, nitrate reductase (NR)together with nitrite reductase (NIR) can reduce NO_3^- to NH_4^+ (Privalle et al., 1989; Chen et al., 2017). Although excess $NH4^+$ can result in root and shoot growth inhibition such as biomass reduction, oxidative stress with overproduction of reactive oxygen species (ROS), plants can eliminate or reduce the toxicity of NH_4^+ by either directly reacting with 2-oxoglutarate to produce glutamate or combining glutamate to generate glutamine under the catalysis of GS and then reacting with 2-oxoglutarate under the action of GOGAT to produce glutamine (Liu and von Wirén, 2017). Our study showed that the activities of NR, GOGAT, and GS in roots were still at high levels after 14 days of histidine treatment, implying that histidine can regulate the activity of NR, GS, and GOGAT and improve the utilization and transformation efficiency of nitrogen and glutamate anabolism in maze root system under salt stress.

Amino acids can promote nitrogen reduction and assimilation and increase the activity of NAD dependent NR, GS, GOGAT, and GDH in maize roots, as well as the expression of genes encoding nitrogen metabolism enzymes (Schiavon et al., 2008; Ertani et al., 2010; Colla et al, 2015). Phenylpropanoids are also key mediators of plants resistance towards a number of biotic and abiotic stresses. Phenylpropanoid metabolism in plants mainly includes phenylalanine metabolism and the synthesis of secondary metabolites such as lignin and flavonoids. After 24 h of the histidine treatment, the genes associated with NR (*LOC100383210*; *LOC542278*), glnA (*LOC542215*), and GLT1 (*LOC103636185*; *LOC103652755*) were significantly expressed (Figure 9), which regulated the activity of NADH-NR and NADH-GOGAT. Also, the histidine treatment induced the enrichment of CCR (*LOC103634692*; *LOC103634692*) and E1.11.1.7 (*LOC103638313*) in phenylpropane biosynthesis pathway (Figure 9), which enhance the defense response of plants (Schiavon et al., 2010), especially E1.11.1.7 (*LOC103638313*) which plays a role in the antioxidant system. These results confirmed that histidine can play a regulatory role on the stress resistance ability and growth and development of maize by modulating genes related to nitrogen metabolism. Although the gene expression in phenylpropane biosynthesis pathway was down-regulated at 12 h after the histidine treatment, the genes associated with the above pathways were up-regulated at 24 hours, which might imply that the lignin synthesis in maize root under salt stress was not dominant in the early phase of histidine treatment.

In plant, glycolysis is a common process to provide energy for aerobic and anaerobic respiration by decomposing sugars. When plants were exposed to high salinity, glycolysis and amino acid synthesis in leaves of wheat were enhanced and the levels of some amino acids and sugars increased, including proline, lysine, sucrose, and etc. (Guo et al., 2015). Other studies suggested that the intermediates in the glycolysis process and free amino acids can affect the metabolism of plants by stimulating the glycolysis process and the activities of glucose phosphate isomerase and pyruvate kinase ((Fernie et al., 2004; Sukumar et al., 2017; Palumbo et al., 2018). The present study revealed that when the roots under salt stress were treated with histidine, some genes associated with glycolysis were significantly enriched, which induced the high expression levels of pfkA (*LOC100192478*; *LOC100281688*), PFP (LOC103652493; LOC101027252; LOC103632535), TPI (LOC100282142), gapN (*LOC100282142*), PK (*LOC100282142*), PDC (*LOC541919*), ADH1 (*LOC542364*), and ACSS1/2 (*LOC103646525*) (Figure 9). The protein hydrolysate with amino acids can change the gene expression levels in the glycolysis, tricarboxylic acid cycle and pentose phosphate pathways of maize roots (Ebinezer et al., 2020). Our findings indicated that the histidine treatment dramatically increased the glycolysis process of maize root and enhanced the salt tolerance of roots mainly through increasing glycolysis and energy consumption. This suggested that the modulation of energy metabolism is essential for a response to salinity to balance the production of ROS with the requirements for defense.

Conclusion

In summary, histidine has been implicated in the mechanism regulating salt tolerance in plants. The results of the present study confirmed that histidine can ameliorate the adverse effects of salt stress on maize root growth. When the roots were treated with histidine for 12 h or 24 h, the activity of SOD, POD, and CAT were significantly increased, alleviating the accumulation of ROS and improving the salt tolerance of maize roots. Also, the histidine treatment enhanced the activities of NR, GS, and GOGAT and promoted the nitrogen utilization, glutamate anabolism and other amino acid anabolism in maze by expressing the genes related to nitrogen metabolism. Interestingly, transcriptomic analysis revealed that the number of upregulated DEGs and enriched pathways of the roots under salt stress were increased after 24 h of histidine treatment. KEGG enrichment analysis found that these DEGs that involved in glycolysis and plant hormone signal transduction pathways were significantly up-regulated, including the growth promoting (IAA), (CTK), and (GA) and the stress response hormones in (ABA), and (JA) signal transduction pathways. Based on the above results, we speculate that histidine may act as a signal molecule to regulate genes involved in the plant hormone synthesis, signal transduction, stress perception and metabolite production for alleviation of salt stress in the maize root system.

Data availability statement

The data presented in the study are deposited in the NCBI repository, accession number PRJNA874354.

Author contributions

GY and XZ designed the experiments and edited the manuscript. HJ conducted the experiments. QZ, YQ, KW and TS analyzed the data. HJ wrote the paper and prepared the manuscript. All authors contributed to the paper and approved the submitted version.

Funding

This research was supported by the National Natural Science Foundation of China (32060424) and Talent Project of the National Ethnic Affairs Commission of China (2016).

Conflict of interest

The authors declare that the research was conducted in the absence of any commercial or financial relationships that could be construed as a potential conflict of interest.

Publisher's note

All claims expressed in this article are solely those of the authors and do not necessarily represent those of their affiliated organizations, or those of the publisher, the editors and the reviewers. Any product that may be evaluated in this article, or claim that may be made by its manufacturer, is not guaranteed or endorsed by the publisher.

Supplementary material

The Supplementary Material for this article can be found online at: https://www.frontiersin.org/articles/10.3389/fpls.2022.1049954/full#supplementary-material

References

Ahmadi, F., Nazari, F., Ghaderi, N., and Teixeira da Silva, J. A. (2021). Assessment of morpho-physiological and biochemical responses of perennial ryegrass to gamma-aminobutyric acid (GABA) application under salinity stress using multivariate analyses techniques. *J. Plant Growth Regul.* 12, 1–15. doi: 10.1007/s00344-021-10538-5

Ashraf, M., and Foolad, M. R. (2007). Roles of glycine betaine and proline in improving plant abiotic stress resistance. *Environ. Exp. Bot.* 59 (2), 206–216. doi: 10.1016/j.envexpbot.2005.12.006

Bojórquez-Quintal, E., Velarde-Buendía, A., Ku-González, A., Carillo-Pech, M., Ortega-Camacho, D., Echevarría-Machado, I., et al. (2014). Mechanisms of salt tolerance in habanero pepper plants (Capsicum chinense jacq.): proline accumulation, ions dynamics and sodium root-shoot partition and compartmentation. *Front. Plant Sci.* 5. doi: 10.3389/fpls.2014.00605

Bybordi, A. (2010). The influence of salt stress on seed germination, growth and yield of canola cultivars. *Ecotoxicol. Environ. Saf.* 38 (1), 128–133. doi: 10.1111/j.1756-1051.2010.00941.x

Calvo, P., Nelson, L., and Kloepper, J. W. (2014). Agricultural uses of plant biostimulants. *Plant Soil.* 383 (1), 3–41. doi: 10.1007/s11104-014-2131-8

Cataldo, D. A., Maroon, M., Schrader, L. E., and Youngs, V. L. (1975). Rapid colorimetric determination of nitrate in plant-tissue by nitration of salicylic-acid. commun. *Soil Sci. Plant Anal.* 6 (1), 71–80. doi: 10.1080/00103627509366547

Chang, C. S., Wang, B. L., Shi, L., Li, Y. Y., Duo, L., and Zhang, W. H. (2010). Alleviation of salt stress-induced inhibition of seed germination in cucumber (Cucumis sativus l.) by ethylene and glutamate. *J. Plant Physiol.* 167 (14), 1152–1156. doi: 10.1016/j.jplph.2010.03.018

Chen, J. N., Nolan, T. M., Ye, H. X., Zhang, M. C., Tong, H. N., and Xin, P. Y. (2017). Arabidopsis WRKY46, WRKY54, and WRKY70 transcription factors are involved in brassinosteroid-regulated plant growth and drought responses. *Plant Cell.* 29 (6), 1425–1439. doi: 10.1105/tpc.17.00364

Colla, G., Nardi, S., Cardarelli, M., Ertani, A., Lucini, L., Canaguier, R., et al. (2015). Protein hydrolysates as biostimulants in horticulture. *Sci. Hortic.* 196, 28–38. doi: 10.1016/j.scienta.2015.08.037

Colla, G., Rouphael, Y., Canaguier, R., Svecova, E., and Cardarelli, M. (2014). Biostimulant action of a plant-derived protein hydrolysate produced through enzymatic hydrolysis. *Front. Plant Sci.* 5. doi: 10.3389/fpls.2014.00448

Cucinotta, M., Di Marzo, M., Guazzotti, A., de Folter, S., Kater, M. M., and Colombo, L. (2020). Gynoecium size and ovule number are interconnected traits that impact seed yield. *J. Exp. Bot.* 71 (9), 2479–2489. doi: 10.1093/jxb/eraa050

Da Rocha, I. M., Vitorello, V. A., Silva, J. S., Ferreira-Silva, S. L., Viégas, R. A., Silva, E. N., et al. (2012). Exogenous ornithine is an effective precursor and the δ-ornithine amino transferase pathway contributes to proline accumulation under high n recycling in salt-stressed cashew leaves. *J. Plant Physiol.* 169 (1), 41–49. doi: 10.1016/j.jplph.2011.08.001

Decleire, M., Cat, D. W., Temmerman, D. L., and Baeten, H. (2012). Changes of peroxidase, catalase, and superoxide dismutase activities in ozone-fumigated spinach leaves. *J. Plant Physiol.* 116 (2), 147–152. doi: 10.1016/S0176-1617(84)80071-1

Duan, L., Sebastian, J., and Dinneny, J. R. (2015). Salt-stress regulation of root system growth and architecture in arabidopsis seedlings. *Methods Mol. Biol.* 1242, 105–122. doi: 10.1007/978-1-4939-1902-4_10

Ebinezer, L. B., Franchin, C., Trentin, A. R., Carletti, P., Trevisan, S., Agrawal, G. K., et al. (2020). Quantitative proteomics of maize roots treated with a protein hydrolysate: a comparative study with transcriptomics highlights the molecular mechanisms responsive to biostimulants. *J. Agric. Food Chem.* 68 (28), 7541–7553. doi: 10.1021/acs.jafc.0c01593

Ertani, A., Cavani, L., Pizzeghello, D., Brandellero, E., Altissimo, A., Ciavatta, C., et al. (2010). Biostimulant activity of two protein hydrolyzates in the growth and nitrogen metabolism of maize seedlings. *J. Plant Nutr. Soil Sci.* 172 (2), 237–244. doi: 10.1002/jpln.200800174

Feng, S. G., Yue, R. Q., Tao, S., Yang, Y. J., Zhang, L., Xu, M. F., et al. (2015). Genome-wide identification, expression analysis of auxin-responsive GH3 family genes in maize (Zea mays l.) under abiotic stresses. *J. Integr. Plant Biol.* 57 (9), 783–795. doi: 10.1111/jipb.12327

Fernie, A. R., Carrari, F., and Sweetlove, L. J. (2004). Respiratory metabolism: glycolysis, the TCA cycle and mitochondrial electron transport. *Curr. Opin. Plant Biol.* 7 (3), 254–261. doi: 10.1016/j.pbi.2004.03.007

Fujita, Y., Fujita, M., Satoh, R., Maruyama, K., Parvez, M. M., Seki, M., et al. (2005). AREB1 is a transcription activator of novel ABRE-dependent ABA signaling that enhances drought stress tolerance in arabidopsis. *Plant Cell* 17, 3470–3488. doi: 10.1105/TPC.105.035659

Fujita, Y., Yoshida, T., and Yamaguchi-Shinozaki, K. (2013). Pivotal role of the AREB/ABF-SnRK2 pathway in ABRE-mediated transcription in response to osmotic stress in plants. *Physiol. Plant* 147 (1), 15–27. doi: 10.1111/j.1399-3054.2012.01635.x

Gangwar, S., Singh, V. P., Garg, S. K., Prasad, S. M., and Maurya, J. N. (2011). Kinetin supplementation modifies chromium (VI) induced alterations in growth

and ammonium assimilation in pea seedlings. *Biol. Trace Elem. Res.* 144 (1-3), 1327–1343. doi: 10.1007/s12011-011-9157-z

Glass, A. D. M., Britto, D. T., Kaiser, B. N., Kinghorn, J. R., Kronzucker, H. J., and Kumar, A. (2002). The regulation of nitrate and ammonium transport systems in plants. *J. Exper. Bot.* 370, 855–864. doi: 10.1093/JEXBOT/53.370.855

Gouia, H., Ghorbal, M. H., and Touraine, B. (1994). Effects of NaCl on flows of n and mineral ions and on NO3- reduction rate within whole plants of salt-sensitive bean and salt-tolerant cotton. *Plant Physiol.* 105 (4), 1409–1418. doi: 10.1104/pp.105.4.1409

Guo, R., Yang, Z. Z., Li, F., Yan, C. R., Zhong, X. L., Liu, Q., et al. (2015). Comparative metabolic responses and adaptive strategies of wheat (Triticum aestivum) to salt and alkali stress. *BMC Plant Bio.* 15, 170. doi: 10.1186/s12870-015-0546-x

Hao, S. H., Wang, Y. R., Yan, Y. X., Liu, Y. H., Wang, J. Y., and Chen, S. (2021). A review on plant responses to salt stress and their mechanisms of salt resistance. *Horticulturae* 7, 132. doi: 10.3390/horticulturae7060132

Hasanuzzaman, M., Bhuyan, M. H. M. B., Parvin, K., Bhuiyan, T. F., Anee, T. I., Nahar, K., et al. (2020). Regulation of ROS metabolism in plants under environmental stress: a review of recent experimental evidence. *Int. J. Mol. Sci.* 21 (22), 8695. doi: 10.3390/ijms21228695

Hassani, A., Azapagic, A., and Shokri, N. (2020). Predicting long-term dynamics of soil salinity and sodicity on a global scale. *Proc. Natl. Acad. Sci. U.S.A.* 117 (52), 33017–33027. doi: 10.1073/pnas.2013771117

Ilangumaran, G., and Smith, D. L. (2017). Plant growth promoting rhizobacteria in amelioration of salinity stress: a systems biology perspective. *Front. Plant Sci.* 8. doi: 10.3389/fpls.2017.01768

Irtelli, B., Petrucci, W. A., and Navari-Izzo, F. (2009). Nicotianamine and histidine/proline are, respectively, the most important copper chelators in xylem sap of brassica carinata under conditions of copper deficiency and excess. *J. Exp. Bot.* 60 (1), 269–277. doi: 10.1093/jxb/ern286

Jain, M., Kaur, N., Tyagi, A. K., and Khurana, J. P. (2006). The auxin-responsive GH3 gene family in rice (Oryza sativa). *Funct. Integr. Genomics* 6 (1), 36–46. doi: 10.1007/s10142-005-0142-5

Jambunathan, N. (2010). Determination and detection of reactive oxygen species (ROS), lipid peroxidation, and electrolyte leakage in plants. *Methods Mol. Biol.* 639, 292–298. doi: 10.1007/978-1-60761-702-0_18

Jiang, C. F., Belfield, E. J., Mithani, A., Visscher, A., Ragoussis, J., Mott, R., et al. (2012). ROS-mediated vascular homeostatic control of root-to-shoot soil Na delivery in arabidopsis. *EMBO J.* 31 (22), 4359–4370. doi: 10.1038/emboj.2012.273

Kaspal, M., Kanapaddalagamage, M. H., and Ramesh, S. A. (2021). Emerging roles of γ aminobutyric acid (GABA) gated channels in plant stress tolerance. *Plants (Basel).* 10 (10), 2178. doi: 10.3390/plants10102178

Kazan, K., and Manners, J. M. (2012). JAZ repressors and the orchestration of phytohormone crosstalk. *Trends Plant Sci.* 17 (1), 22–31. doi: 10.1016/j.tplants.2011.10.006

Khokon, A. R., Okuma, E., Hossain, M. A., Munemasa, S., Uraji, M., Nakamura, Y., et al. (2011). Involvement of extracellular oxidative burst in salicylic acid-induced stomatal closure in arabidopsis. *Plant Cell Environ.* 34 (3), 434–443. doi: 10.1111/j.1365-3040.2010.02253.x

Kim, D., Langmead, B., and Salzberg, S. L. (2015). HISAT: a fast spliced aligner with low memory requirements. *Nat. Methods* 12 (4), 357–360. doi: 10.1038/nmeth.3317

Kramer, U., Charnock, J. M., Baker, A. J. M., Smith, J. A. C., and Cotterhowells, J. D. (1996). Free histidine as a metal chelator in plants that accumulate nickel. *Nature.* 379 (6566), 635–638. doi: 10.1038/379635a0

Kumar, M. N., and Verslues, P. E. (2015). Stress physiology functions of the arabidopsis histidine kinase cytokinin receptors. *Physiol. Plant* 154 (3), 369–380. doi: 10.1111/ppl.12290

Li, S. H., Li, Y. M., He, X. R., Li, Q. M., Liu, B. B., Ai, X. Z., et al. (2019). Response of water balance and nitrogen assimilation in cucumber seedlings to CO2 enrichment and salt stress. *Plant Physiol. Biochem.* 139, 256–263. doi: 10.1016/j.plaphy.2019.03.028

Lin, C. C., and Kao, C. H. (1996). Disturbed ammonium assimilation is associated with growth inhibition of roots in rice seedlings caused by NaCl. *Plant Growth Regul.* 18 (3), 233–238. doi: 10.1007/BF00024387

Liu, Y., and von Wirén, N. (2017). Ammonium as a signal for physiological and morphological responses in plants. *J. Exp. Bot.* 68 (10), 2581–2592. doi: 10.1093/jxb/erx086

Li, H., Wang, X. M., Chen, L., Ahammed, G. J., Xia, X. J., Shi, K., et al. (2013). Growth temperature-induced changes in biomass accumulation, photosynthesis and glutathione redox homeostasis as influenced by hydrogen peroxide in cucumber. *Plant Physiol. Biochem.* 71, 1–10. doi: 10.1016/j.plaphy.2013.06.018

Li, K. L., Yu, R. B., Fan, L. M., Wei, N., Chen, H., and Deng, X. W. (2016). DELLA-mediated PIF degradation contributes to coordination of light and gibberellin signalling in arabidopsis. *Nat. Commun.* 7, 11868. doi: 10.1038/ncomms11868

Love, M. I., Huber, W., and Anders, S. (2014). Moderated estimation of fold change and dispersion for RNA-seq data with DESeq2. *Genome Biol.* 15 (12), 550. doi: 10.1186/s13059-014-0550-8

Maehly, A. C., and Chance, B. (1954). The assay of catalases and peroxidases. *Methods Biochem. Anal.* 1, 357–424. doi: 10.1002/9780470110171.ch14

Medeiros, D. B., Brotman, Y., and Fernie, A. R. (2021). The utility of metabolomics as a tool to inform maize biology. *Plant Commun.* 2 (4), 100187. doi: 10.1016/j.xplc.2021.100187

Müller, A., Hillebrand, H., and Weiler, E. W. (1998). Indole-3-acetic acid is synthesized from l-tryptophan in roots of arabidopsis thaliana. *Planta.* 206 (3), 362–369. doi: 10.1007/s004250050411

Nakashima, K., and Yamaguchi-Shinozaki, K. (2013). ABA signaling in stress-response and seed development. *Plant Cell Rep.* 32 (7), 959–970. doi: 10.1007/s00299-013-1418-1

Nishiyama, R., Watanabe, Y., Fujita, Y., Le, D. T., Kojima, M., Werner, T., et al. (2011). Analysis of cytokinin mutants and regulation of cytokinin metabolic genes reveals important regulatory roles of cytokinins in drought, salt and abscisic acid responses, and abscisic acid biosynthesis. *Plant Cell.* 23 (6), 2169–2183. doi: 10.1105/tpc.111.087395

Nongpiur, R., Soni, P., Karan, R., Singla-Pareek, S. L., and Pareek, A. (2012). Histidine kinases in plants: cross talk between hormone and stress responses. *Plant Signal. Behav.* 7, 1230–1237. doi: 10.4161/psb.21516

Noutoshi, Y., Ito, T., and Shinozaki, K. (2005). ALBINO AND PALE GREEN 10 encodes BBMII isomerase involved in histidine biosynthesis in arabidopsis thaliana. *Plant Cell Physiol.* 46 (7), 1165–1172. doi: 10.1093/pcp/pci119

Palumbo, G., Schiavon, M., Nardi, S., Ertani, A., Celano, G., Colombo, C. M., et al. (2018). Biostimulant potential of humic acids extracted from an amendment obtained *via* combination of olive mill wastewaters (OMW) and a pre-treated organic material derived from municipal solid waste (MSW). *Front. Plant Sci.* 9. doi: 10.3389/fpls.2018.01028

Parida, A. K., and Das, A. B. (2005). Salt tolerance and salinity effects on plants: a review. *Ecotoxicol. Environ. Saf.* 60 (3), 324–349. doi: 10.1016/j.ecoenv.2004.06.010

Pertea, M., Pertea, G. M., Antonescu, C. M., Chang, T. C., Mendell, J. T., and Salzberg, S. L. (2015). StringTie enables improved reconstruction of a transcriptome from RNA-seq reads. *Nat. Biotechnol.* 33 (3), 290–295. doi: 10.1038/nbt.3122

Pizarro, L., Munoz, D., Marash, I., Gupta, R., Anand, G., Leibman-Markus, M., et al. (2021). Cytokinin modulates cellular trafficking and the cytoskeleton, enhancing defense responses. *Cells.* 10 (7), 1634. doi: 10.3390/cells10071634

Privalle, L. S., Lahners, K. N., Mullins, M. A., and Rothstein, S. (1989). Nitrate effects on nitrate reductase activity and nitrite reductase mRNA levels in maize suspension cultures. *Plant Physiol.* 90 (3), 962–967. doi: 10.1104/pp.90.3.962

Radwanski, E. R., and Last, R. L. (1995). Tryptophan biosynthesis and metabolism: biochemical and molecular genetics. *Plant Cell.* 7 (7), 921–934. doi: 10.1105/tpc.7.7.921

Rady, M. M., Elrys, A. S., Abo El-Maati, M. F., and Desoky, E. M. (2019). Interplaying roles of silicon and proline effectively improve salt and cadmium stress tolerance in phaseolus vulgaris plant. *Plant Physiol. Biochem.* 139, 558–568. doi: 10.1016/j.plaphy.2019.04.025

Rentsch, D., Schmidt, S., and Tegeder, M. (2007). Transporters for uptake and allocation of organic nitrogen compounds in plants. *FEBS Lett.* 581 (12), 2281–2289. doi: 10.1016/j.febslet.2007.04.013

Ryan, C. A., and Pearce, G. (2001). Polypeptide hormones. *Plant Physiol.* 125 (1), 65–68. doi: 10.1104/pp.125.1.65

Satoh, R., Nakashima, K., Seki, M., Shinozaki, K., and Yamaguchi-Shinozaki, K. (2002). ACTCAT, a novel cis-acting element for proline- and hypoosmolarity-responsive expression of the ProDH gene encoding proline dehydrogenase in arabidopsis. *Plant Physiol.* 130 (2), 709–719. doi: 10.1104/pp.009993

Schiavon, M., Ertani, A., and Nardi, S. (2008). Effects of an alfalfa protein hydrolysate on the gene expression and activity of enzymes of the tricarboxylic acid (TCA) cycle and nitrogen metabolism in zea mays l. *J. Agric. Food Chem.* 56 (24), 11800–11808. doi: 10.1021/jf802362g

Schiavon, M., Pizzeghello, D., Muscolo, A., Vaccaro, S., Francioso, O., and Nardi, S. (2010). High molecular size humic substances enhance phenylpropanoid metabolism in maize (Zea mays l.). *J. Chem. Ecol.* 36 (6), 662–669. doi: 10.1007/s10886-010-9790-6

Shumilina, J., Kusnetsova, A., Tsarev, A., Janse van Rensburg, H. C., Medvedev, S., Demidchik, V., et al. (2009). Glycation of plant proteins: regulatory roles and interplay with sugar signalling? *Int. J. Mol. Sci.* 20 (9), 2366. doi: 10.3390/ijms20092366

Staswick, P. E. (2008). JAZing up jasmonate signaling. *Trends Plant Sci.* 13 (2), 66–71. doi: 10.1016/j.tplants.2007.11.011

Stepansky, A., and Leustek, T. (2006). Histidine biosynthesis in plants. *Amino Acids* 30 (2), 127–142. doi: 10.1007/s00726-005-0247-0

Sukumar, G., Divya, L. D., Mithula, S., Chandra, S. R., and Lakshmi, P. M. (2017). Biostimulant activity of plant protein hydrolysate on the growth of beta vulgaris subs. vulgaris (linn.). *Int. J. Pharm. Bio Sci.* 8 (4), 173–178. doi: 10.22376/ijpbs.2017.8.4.b173-178

Tang, X. L., Mu, X. M., Shao, H. B., Wang, H. Y., and Brestic, M. (2014). Global plant-responding mechanisms to salt stress: physiological and molecular levels and implications in biotechnology. *Crit. Rev. Biotechnol.* 35 (4), 425–437. doi: 10.3109/07388551.2014.889080

Tanveer, M., and Shabala, S. (2018). Targeting redox regulatory mechanisms for salinity stress tolerance in crops. *Salinity Responses Tolerance Plants* 1 (8), 213–234. doi: 10.1007/978-3-319-75671-4_8

Tegeder, M. (2012). Transporters for amino acids in plant cells: some functions and many unknowns. *Curr. Opin. Plant Biol.* 15 (3), 315–321. doi: 10.1016/j.pbi.2012.02.001

Tiwari, B., Belenghi, B., and Levine, A. (2002). Oxidative stress increased respiration and generation of reactive oxygen species, resulting in ATP depletion, opening of mitochondrial permeability transition, and programmed cell death. *Plant Physiol.* 128, 1271–1281. doi: 10.1104/pp.010999

Tran, L. S., Urao, T., Qin, F., Maruyama, K., Kakimoto, T., Shinozaki, K., et al. (2007). Functional analysis of AHK1/ATHK1 and cytokinin receptor histidine kinases in response to abscisic acid, drought, and salt stress in arabidopsis. *Proc. Natl. Acad. Sci. U.S.A.* 104 (51), 20623–20628. doi: 10.1073/pnas.0706547105

Walch-Liu, P., Liu, L. H., Remans, T., Tester, M., and Forde, B. G. (2006). Evidence that l-glutamate can act as an exogenous signal to modulate root growth and branching in arabidopsis thaliana. *Plant Cell Physiol.* 47 (8), 1045–1057. doi: 10.1093/pcp/pcj075

Watson, R., and Fowden, L. (1975). The uptake of phenylalanine and tyrosine by seedling root tips. *Phytochemistry.* 14, 1181–1186. doi: 10.1016/S0031-9422(00)98591-1

Xian, W. J., Hennefarth, M. R., Lee, M. W., Do, T., Lee, E. Y., Alexandrova, A. N., et al. (2022). Histidine-mediated ion specific effects enable salt tolerance of a pore-forming marine antimicrobial peptide. *Angew Chem. Int. Ed. Engl.* 61 (25), e202108501. doi: 10.1002/anie.202108501

Xie, C., Mao, X. Z., Huang, J. J., Ding, Y., Wu, J. M., Dong, S., et al. (2011). KOBAS 2.0: a web server for annotation and identification of enriched pathways and diseases. *Nucleic Acids Res.* 39, W316–W322. doi: 10.1093/nar/gkr483

Yin, F. M., Liu, X. N., Cao, B. L., and Xu, K. (2020). Low pH altered salt stress in antioxidant metabolism and nitrogen assimilation in ginger (Zingiber officinale) seedlings. *Physiol. Plant* 168 (3), 648–659. doi: 10.1111/ppl.13011

Yu, Z. P., Duan, X. B., Luo, L., Dai, S. J., Ding, Z. J., and Xia, G. G. (2020). How plant hormones mediate salt stress responses. *Trends Plant Sci.* 25 (11), 1117–1130. doi: 10.1016/j.tplants.2020.06.008

Zhao, S. S., Zhang, Q. K., Liu, M. Y., Zhou, H. P., Ma, C. L., and Wang, P. P. (2021). Regulation of plant responses to salt stress. *Int. J. Mol. Sci.* 22 (9), 4609. doi: 10.3390/ijms22094609

Zhu, J. K. (2002). Salt and drought stress signal transduction in plants. *Annu. Rev. Plant Biol.* 53, 247–273. doi: 10.1146/annurev.arplant.53.091401.143329

frontiers | Frontiers in Plant Science

TYPE Original Research
PUBLISHED 02 December 2022
DOI 10.3389/fpls.2022.1027662

Check for updates

OPEN ACCESS

EDITED BY
Mirza Hasanuzzaman,
Sher-e-Bangla Agricultural University, Bangladesh

REVIEWED BY
Anis Ali Shah,
University of Education Lahore, Pakistan
Muhammad Ahsan Altaf,
Hainan University, China

*CORRESPONDENCE
Sudhir Kumar
sudhirnp2@gmail.com

SPECIALTY SECTION
This article was submitted to Plant Abiotic Stress, a section of the journal Frontiers in Plant Science

RECEIVED 25 August 2022
ACCEPTED 09 November 2022
PUBLISHED 02 December 2022

CITATION
Karwa S, Taunk J, Maurya S, Das A, Krishna GK, Arya SS, Kumar A, Kumar S, Kumar P, Chinnusamy V and Pal M (2022) Spermidine exogenous application mollifies reproductive stage heat stress ramifications in rice. *Front. Plant Sci.* 13:1027662. doi: 10.3389/fpls.2022.1027662

COPYRIGHT
© 2022 Karwa, Taunk, Maurya, Das, Krishna, Arya, Kumar, Kumar, Kumar, Chinnusamy and Pal. This is an open-access article distributed under the terms of the Creative Commons Attribution License (CC BY). The use, distribution or reproduction in other forums is permitted, provided the original author(s) and the copyright owner(s) are credited and that the original publication in this journal is cited, in accordance with accepted academic practice. No use, distribution or reproduction is permitted which does not comply with these terms.

Spermidine exogenous application mollifies reproductive stage heat stress ramifications in rice

Sourabh Karwa[1,2], Jyoti Taunk[1,3], Sadhana Maurya[1], Adhip Das[1], G. K. Krishna[1,4], Sunder Singh Arya[2], Awadhesh Kumar[5], Sudhir Kumar[1]*, Pramod Kumar[1], Viswanathan Chinnusamy[1] and Madan Pal[1]

[1]Division of Plant Physiology, ICAR-Indian Agricultural Research Institute, New Delhi, India, [2]Department of Botany, Maharshi Dayanand University, Rohtak, Haryana, India, [3]Department of Biotechnology, University Centre for Research and Development (UCRD), Chandigarh University, Mohali, Punjab, India, [4]Department of Plant Physiology, College of Agriculture, Kerala Agricultural University, Thrissur, India, [5]Crop Physiology and Biotechnology Division, Indian Council of Agricultural Research-National Rice Research Institute (ICAR-NRRI), Cuttack, Odisha, India

Introduction: Rice productivity is severely hampered by heat stress (HS) which induces oxidative stress in this crop. This oxidative stress can be alleviated using various exogenous chemicals, including spermidine (Spd). Therefore, the present study was carried out to characterize HS components and to elucidate the role of exogenous Spd application in rice at the flowering stage.

Methods: Two contrasting rice genotypes, i.e. Nagina22 (N22) and Pusa Basmati-1121 (PB-1121) were placed in temperature tunnels and exposed to HS (38–43°C) with and without Spd (1.5 mM) foliar application during the heading stage till the end of the anthesis stage.

Result: Heat stress induced the production of H_2O_2 and thiobarbituric acid reactive substances, which resulted in lower photosynthesis, spikelet sterility, and reduced grain yield. Interestingly, foliar application of Spd induced antioxidant enzyme activities and thus increased total antioxidant capacity resulting in higher photosynthesis, spikelet fertility, and improved grain yield under HS in both genotypes. Under HS with Spd, higher sugar content was recorded as compared to HS alone, which maintained the osmotic equilibrium in leaf and spikelets. Spd application initiated *in vivo* polyamine biosynthesis, which increased endogenous polyamine levels.

Discussion: This study corroborates that the exogenous application of Spd is promising in induction of antioxidant defence and ameliorating HS tolerance in rice *via* improved photosynthesis and transpiration. Thereby, the study

proposes the potential application of Spd to reduce HS in rice under current global warming scenario.

KEYWORDS

Antioxidant enzymes, flowering, heat stress, polyamine, rice, spermidine, spikelet fertility

Introduction

Rice is the most important staple food crop cultivated over 167.13 mha across the globe (http://www.fao.org/faostat/en/#compare, accessed on 20th January 2021), feeding over 3.5 billion people (FAO, 2014). Rice production is facing an unprecedented challenge with increasing global mean temperature and diminishing freshwater resources. The climate change scenario predicted a rise in temperature by 1.6-4.4°C by 2100 and a more frequent occurrence of heat episodes during the sensitive growth stages such as flowering in case of rice (Teixeira et al., 2013; IPCC, 2021). At this stage, heat stress (HS) could result in anther dehiscence, poor pollen germination, ultimately reducing spikelet fertility and grain yield (Hu et al., 2021). Under HS, the plant follows various tolerance and avoidance mechanisms to cope with the HS conditions (Hasanuzzaman et al., 2013), including high transpirational cooling (Karwa et al., 2020).

Heat stress induces oxidative stress at the tissue level by overproducing reactive oxygen species (ROS), damaging protein function and membrane integrity (Zhao et al., 2018). In addition, gas exchange, membrane permeability, sugar and starch accumulation are also vulnerable to HS at the flowering stage in rice and other crops (Paupière et al., 2014). Under stress conditions (HS), the plant responds *via* an orchestrated and complex network of different plant regulators that plays a vital role in acquiring tolerance (Garay-Arroyo et al., 2012). Growth regulators or stress hormones such as salicylic acid, proline, betaine and brassinosteroids can ameliorate the negative effect of oxidative stress by fortifying antioxidant defence machinery (Ghosh et al., 2022; Hossain et al., 2022; Raza et al., 2022). Recently, a new class of small and low molecular weight aliphatic amines, i.e. polyamines, have been suggested to improve plant tolerance towards various abiotic stresses such as drought, salinity and heavy metals (Capell et al., 2004; Zhao et al., 2004; Handa and Mattoo, 2010; Do et al., 2014; Soudek et al., 2016). There are three common and naturally occurring polyamines, namely putrescine (Put), spermidine (Spd) and spermine (Spm). Spd has been documented to directly act as a stress protecting compound (Chen et al., 2021) and is involved in various stress signal transduction pathways (Kasukabe et al., 2004). The potential of Spd to improve plant tolerance towards various abiotic stresses like drought (Kubiś, 2001; Kubiś, 2003), salinity (Roy et al., 2005; ElSayed et al., 2018), heat (Tian et al., 2009) and submergence (Liu et al., 2015) is well documented. Spd application on rice seedlings under HS has reduced H_2O_2, proline and malondialdehyde (MDA) contents (Mostofa et al., 2014). Spd alleviated drought stress in maize seedlings by protecting the photosynthetic apparatus, which improved their photosynthetic performance (Li et al., 2018). However, the effect of Spd in ameliorating HS has not been investigated in rice, particularly at the flowering stage. Therefore, the present study was aimed to analyse the impact of HS on rice growth and yield metrics; and to authenticate the hypothesis that exogenous Spd application induces HS tolerance in rice at the reproductive stage.

Materials and methods

Plant material and growth conditions

Effects of HS on physio-biochemical traits and mitigation response of Spd against HS were studied in two rice genotypes *viz.* Nagina22 (N22) (03911) and Pusa Basmati-1121 (PB-1121) (Table 1). The experiments were conducted in the Pot culture facility, Division of Plant Physiology, Indian Council of

TABLE 1 Rice genotypes tested under this study.

Genotype	Origin	Species	Stress tolerance	Reference(s)
Nagina22 (N22) (03911)	India	*Oryza sativa* aus	Heat tolerant	Prasad et al. (2006); Jagadish et al. (2008); Jagadish et al. (2010), Selote and Khanna-Chopra (2004)
Pusa Basmati-1121 (PB-1121)	India	*Oryza sativa* indica	Heat sensitive	Singh et al. (2018)

Agricultural Research (ICAR)-Indian Agricultural Research Institute (IARI), New Delhi, during *Kharif*, 2016. Plants were raised in pots (14 cm diameter and 12 cm height) by transplanting 21 days old rice seedlings from the nursery. Each pot was filled with 20 kg of clay-loam soil supplemented with farmyard manure (800 g pot^{-1}). The N: P: K fertilizer was provided as $(NH_4)_2SO_4$ (0.375 g kg^{-1}), SSP (0.075 g kg^{-1}) and KCl (0.075 g kg^{-1}), respectively, in split doses. Another dose of N (0.125 g kg^{-1} soil) was top-dressed 25–30 d. Fifteen biological replicates were followed in all the experiments. All pots were arranged randomly as per the layout obtained through Statistical Tool for Agricultural Research (STAR; Version: 2.0.1) and placed at the Net house facility. Plants were kept under flooded conditions (water 3-5 cm above the soil surface) till their physiological maturity. Heat stress treatment was commenced at the heading stage by shifting the pots in a temperature tunnel, with an average temperature of ~5°C more than the ambient temperature and was kept for at least ten days, covering flowering and post-flowering representative genotypes. Sampling was done on the main tiller, tagged before stress treatments. No significant insects or pests were observed during the experiment. For the present study, three sets of treatments were designed as (1) C: Ambient temperature (Control); (2) HS: Heat stress (elevated temperature) and (3) HS+Spd: Heat stress (elevated temperature) with Spd (1.5mM) application.

Heat stress treatment in the high-temperature tunnel

The plants were grown in ambient conditions until booting and were shifted to high temperature tunnel (HTT) at the heading stage. The design and control system of the temperature tunnel was followed as described by Sinclair et al. (1995). The air temperature and relative humidity (RH) were recorded on a real-time basis at every 30 min interval by MINCER (Micrometeorological Instrument for the Near-Canopy Environment of Rice) as per Fukuoka et al. (2012). MINCER was installed at the centre of the HTT, and sensor height was kept at the height of the rice canopy. For comparison, data represented in the figures includes the HS period (heading to 100% flowering) for both ambient net house and HTT. The ambient and HTT was recorded diurnally and expressed as the mean day (0700–1800 h)/night (1800–0700 h) temperature for both the experiments.

Growth environments in ambient and HTT

The mean maximum temperature (T_{max}) was 34.3°C (SD ± 1.68), and mean minimum temperature (T_{min}) was 22.6°C (SD ± 0.78) in ambient conditions, while in HTT, T_{max} was 39.2°C (SD ± 2.78), and T_{min} was 26.3°C (SD ± 1.03) (Supplementary Figures 1A, B). There was an increment of 4.8°C during day and 3.7°C at night over ambient conditions in HTT. In the present study, both the genotypes differed in the onset of flowering, first observed in N22, followed by PB-1121.

Exogenous Spd application

Spd (Himedia, India) stock solution (1.5 mM) was prepared in distilled water containing 0.01% (v/v) Tween-20 as surfactant to enhance foliar adhesion. For foliar application, 20–25 ml of solution per plant was sprayed during 1700 to 1900 h before HS.

Sampling

The flag leaf and spikelets were used as samples for evaluating all the biochemical parameters, and the evaluations were performed at 100% flowering of the respective genotype. Only the tagged panicles were harvested to avoid sampling error. The samples were flash-frozen in liquid nitrogen and stored at -80°C until further analysis.

Evaluation of spikelet fertility and yield-associated traits

Data on spikelet fertility, grain weight $plant^{-1}$ and 1000 grain weight were recorded according to Prasad et al. (2006). At physiological maturity, panicle and biomass were separately harvested and packed into separate envelopes. Panicle was sun dried for 3-4 days or till the constant weight was achieved. Then grains were threshed from the panicles and weight was measured using analytical balance (model: BSA124S-CW, Sartorius AG, Germany) which was expressed as grain weight $plant^{-1}$. From the harvested panicles, five random panicles per plants were selected and counting of filled and unfilled grains per panicle was performed manually. The ratio of filled grains with total number of spikelet per panicle was expressed in percentage. The 1000 grain weight of seeds was counted manually from final thrashed grains and weight was calculated using analytical balance.

Physiological parameters

Measurement of relative water content and membrane stability index

To derive RWC, the fresh weight (FW) of the flag leaf was recorded, then it was hydrated overnight to take the turgid weight (TW) and oven-dried for two days for dry weight (DW)

analysis. RWC was calculated according to Barrs and Weatherley (1962).

Fresh leaf samples were cut into pieces of equal sizes and transferred to test tubes containing distilled water to obtain MSI. The samples were incubated in the water bath at 45°C for 60 min. After cooling, the conductivity (C1) of the solution was measured. Samples were further kept at 100°C for 10 min, and then conductivity was again measured after cooling. After that, MSI was calculated according to Sairam et al. (2002).

Measurement of net photosynthesis rate and associated gas exchange parameters

Gas exchange parameters such as net photosynthesis rate (P_N; $\mu molCO_2\ m^{-2}s^{-1}$), stomatal conductance (gS; $molH_2Om^{-2}s^{-1}$) and transpiration rate (E; $mmolH_2Om^{-2}s^{-1}$) were measured using the LI-COR portable photosynthesis system (LI-6400 model, LI-COR, Lincoln, NE). The gas exchange measurements were recorded from the flag leaf between 0830 and 1130 hours. The CO_2 concentration of the reference air entering the leaf chamber (3 x 2 cm; Model 6400–02B; LI-COR Inc. USA) was adjusted with a CO_2 mixer control unit, keeping it at 400 µmol mol^{-1} with a constant flow rate of 500 µmol s^{-1}. Measurements were recorded with a Photosynthetic photon flux density (PPFD) at 1200 mmol $m^{-2}s^{-1}$ supplied with red LEDs (LI-6400–02; LI-COR Inc.). Chamber block temperature was set as per ambient conditions, and the RH was kept close to 60% (Bahuguna et al., 2018).

Biochemical parameters

Measurement of sugar and starch content

Sugar and starch contents were measured in flag leaf and spikelets spectrophotometrically, as described by McCready et al. (1950). In brief, samples were grounded in pestle motar using liquid nitrogen. Sample (0.1g) was then mixed with 80% ethanol (V/V) and centrifuged. The extract was collected and sugar analysis was performed using anthrone reagent. Remaning pellet was dried after sugar anlaysis and perchloric acid was added for starch extraction from the sample. Again it was centrifuged and further analyzed using anthrone reagent. Quantitative estimation of these samples was performed using UV-visible spectrophotometer at an absorbance of 630 nm (Model: Specord Bio. 200, AnalytikJena, Germany).

Measurement of hydrogen peroxide and thiobarbituric acid reactive substances

The H_2O_2 and TBARS contents were calculated in both flag leaves and spikelets. H_2O_2 content ($\mu molg^{-1}FW$) was measured spectrophotometrically as described by Alexieva et al. (2001). The concentration of H_2O_2 was calculated from the standard curve plotted against Hydrogen peroxide solution (Merck, Germany). TBARS content ($\mu molg^{-1}FW$) was measured spectrophotometrically as described by Larkindale and Knight (2002) and calculated using an extinction coefficient of 155 mM cm^{-1}.

Measurement of total antioxidant capacity

TAC was measured by Ferric reducing antioxidant power (FRAP) assay as per Benzie and Strain (1999) and expressed as the ferric-reducing ability of mmol L^{-1} $FeSO_4$. In brief, sample was grounded using liquid nitrogen in pestle and mortar. Grounded sample was aliquoted with 70% ethanol (v/v). After centrifugation, supernatant was collected and further analyzed using FRAP reagent (3 ml) in dark. It was then incubated in water bath for 10 min at 37^0C and absorbance was recorded at 593 nm using UV-visible spectrophotometer (Model: Specord Bio. 200, AnalytikJena, Germany).

Measurement of antioxidant enzyme activity

Total soluble protein extraction

Total protein was extracted from flag leaf and spikelets to estimate antioxidant enzyme activities. The samples were homogenized and transferred to microcentrifuge tubes containing ice-cold potassium phosphate buffer (0.1 M, pH=7.0) and 0.1 mM disodium ethylene diamine tetra acetate dehydrate (Na-EDTA). In case of protein extraction for estimation of ascorbate peroxidase activity, Na-EDTA was replaced by 10 mM ascorbate in the buffer. The homogenate was then centrifuged at 18,400 g for 20 min at 4°C, and the supernatant was used as crude enzyme extract. Protein content was estimated following the Bradford method (Bradford, 1976).

Antioxidant enzyme assays

Superoxide dismutase (SOD; EC 1.15.1.1) activity was assayed by monitoring the inhibition of photochemical reduction of nitro blue tetrazolium (NBT) following the method of Jiang and Zhang (2002). It was expressed as one unit of SOD activity mg^{-1} protein. Catalase (CAT; EC 1.11.1.6) activity was assayed by measuring the disappearance of H_2O_2 at 240 nm (extinction coefficient = 39.4 $mM^{-1}cm^{-1}$) and was expressed as µmol of H_2O_2 consumed mg^{-1} protein min^{-1} (Jiang and Zhang, 2002). Ascorbate peroxidase (APX; EC 1.11.1.11) activity was determined by decrement in absorbance at 290 nm, as described by Sharma and Dubey (2004). The enzyme was quantified using the extinction coefficient of 2.8 $mM^{-1}cm^{-1}$ and expressed as µmol ascorbate mg^{-1} protein min^{-1}. Guaiacol

peroxidase (GPX; EC 1.11.1.7) activity was determined as described by de Azevedo Neto et al. (2006). Enzyme activity was quantified using molar extinction coefficient (26.6 $mM^{-1}cm^{-1}$) to calculate the formation of tetraguaiacol and was expressed as µmol H_2O_2 mg^{-1} protein min^{-1}.

Estimation of endogenous free-polyamines

The extraction and estimation of free polyamines (Put, Spd and Spm) were performed following the perchloric acid method given by Flores and Galston (1982). Derivatization of free polyamines was done by alkali (NaOH) treatment followed by benzoylation. The reaction was terminated using saturated NaCl. Cold diethyl ether (2 mL) was used for extracting polyamines from benzyl polyamine. The ether phase was collected and evaporated to dryness and re-dissolved in 100 µL High-Performance Liquid Chromatography (HPLC) grade methanol (Merck, Germany). HPLC analysis was performed using the reverse-phase (C18) column (Agilent) on Agilent 1100. Benzoylated polyamine sample (20 µL) was injected by an autosampler with a flow rate of 1 mL/min of mobile phase (acetonitrile: water; 52:48 v/v) (Merck, Germany). The area and data retrieval calculations were performed using CHEM STATION for LC system Rev B.040.3 (16) software. The concentrations of individual polyamines were calculated from the standard curve plotted against HPLC grade standards of Put, Spd and Spm (Sigma chemicals, USA) and expressed as nmol g^{-1} FW (Supplementary Figure 2).

Statistical analysis

Data were analyzed by two-way Analysis of variance (ANOVA) in a completely randomized design using Statistical Package for the Social Sciences (SPSS) 13.0 (LEAD Technologies Inc.) to compare the differences between cultivars, treatments and their interaction. *Post-hoc* test (Tukey's) was performed to retrieve the difference between treatments and genotypes at least significant (LSD) of 5% and 1%.

Results

Effect of Spd on yield-related parameters under HS

The reduction was recorded in spikelet fertility, grain yield $plant^{-1}$ and 1000 grain weight under HS. Spikelet fertility and grain yield $plant^{-1}$ showed significant genotype (G) x treatment (T) interaction (P<0.05-0.001) under HS at the flowering stage (Table 2). Heat stress significantly reduced spikelet fertility in both the genotypes, as 23.5% and 6.5% reduction was recorded in PB-1121 and N22, respectively with respect to the control. Application of Spd significantly decreased yield penalty under HS. Compared to HS alone (without any exogenous application of polyamine), Spd application under HS significantly improved spikelet fertility by 9.5% and 2.0% in PB-1121 and N22, respectively. Under HS, maximum reduction of 67.3% grain yield $plant^{-1}$ was recorded in case of PB-1121, and minimum reduction (8.1%) was recorded in case of N22 (Table 2). Under HS, a significant reduction in 1000 grain weight was recorded in PB-1121 (28.8%) while a lower reduction was observed in N22 (8.1%) as compared to the ambient conditions. In addition, 1000 grain weight showed significant (P<0.001) treatment interaction (Table 2). Spd application under HS resulted in comparatively lesser reductions of 1000 grain weight which was estimated to be 11% and 6.5% in PB-1121 and N22 genotypes, respectively.

Effect of Spd on net photosynthesis rate and associated gas exchange parameters

P_N varied significantly in G and T (P<0.001) (Figure 1A; Supplementary Table 1). Within the genotypes, P_N reduced on

TABLE 2 Yield components (spikelet fertility, grain yield $plant^{-1}$ and 1000 grain weight) of rice genotypes under heat stress.

Genotype	Treatment	Spd application	Grain yield $plant^{-1}$ (g)	Spikelet fertility (%)	1000 grain weight (g)
N22	Ambient	-Spd	51.2 ± 3.66	93.7 ± 1.26	20.70 ± 0.12
	HS	-Spd	47.1 ± 4.92	87.6 ± 1.48	19.02 ± 0.59
		+Spd	48.8 ± 4.43	89.3 ± 0.97	20.27 ± 0.37
PB-1121	Ambient	-Spd	55.8 ± 4.19	89.8 ± 0.59	22.97 ± 0.92
	HS	-Spd	18.2 ± 2.01	68.7 ± 2.56	16.37 ± 0.37
		+Spd	29.0 ± 5.83	75.2 ± 3.99	17.72 ± 0.09
Lsd<0.05		G	7.71***	2.32***	0.89*
		T	8.95***	2.81***	1.09***
		G X T	12.66**	3.98**	1.504***

Each point represents the mean of five replicates with their ± SE. Least significant difference (Lsd) P<0.05, 0.01 and 0.001 were denoted by *, **, and*** respectively. G, Genotypes; T, Treatment; HS, Heat stress; SE, Standard error; Spd, Spermidine.

10.3389/fpls.2022.1027662

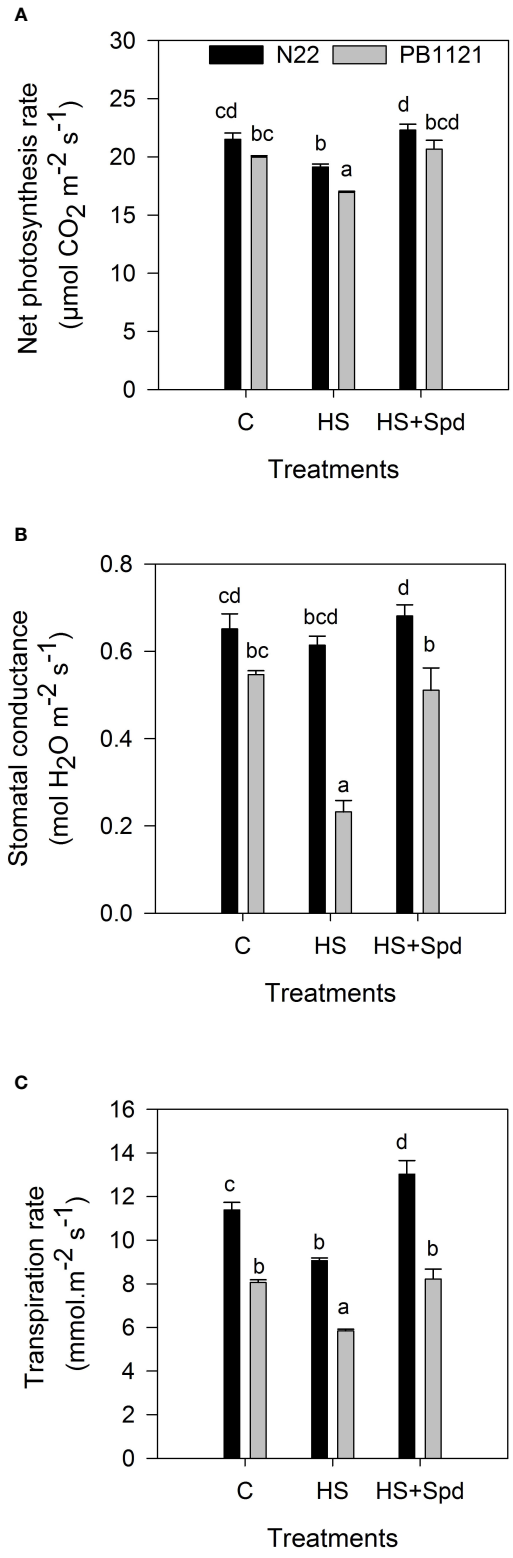


FIGURE 1
Net Photosynthesis rate **(A)**, Stomatal conductance **(B)** and Transpiration rate **(C)** under different treatments in the contrasting rice genotypes (N22 and PB-1121). Bars indicate mean ± SE. Comparison of means was obtained from Tukey's honestly significant difference test where means with the same letter are not significantly different at 5%. C, Control; HS, Heat stress; Spd, Spermidine. Least significant difference values at 5% for comparison are given in Supplementary Table 1.

the 7th day of HS in the range 11–15% with respect to the C (Figure 1A). There was a significant reduction in P_N by 15.1% in PB-1121 and by 11.1% in N22 under HS with respect to the ambient. Spd application significantly recovered the P_N in tested genotypes. When compared with HS, the maximum rescue of P_N was recorded in N22 (16.5%) followed by PB-1121 (21.9%) under HS+Spd. The *gS* showed significant variation within G x T interaction (P<0.001) (Figure 1B; Supplementary Table 1). Compared to the ambient, HS showed reductions in the range of 5.0-57%, with a minimum reduction in N22 and a maximum in PB-1121. Spd application significantly improved *gS* by 10.9% and 119.9% in N22 and PB-1121, respectively, compared to HS. A similar trend was recorded in E, with significant G x T interaction on the 7th day of HS (Figure 1C; Supplementary Table 1). HS+Spd significantly increased E in both the tested genotypes. When compared with HS, a higher increase in E was recorded in N22 (43%) and lower in PB-1121 (41%).

Effect of Spd on RWC and MSI

RWC showed significant variation between genotypes (G) and treatment (T) (P<0.001) (Table 3). Within the two genotypes, RWC reduction was recorded in the range of 18–30% under HS with respect to the ambient. Spd application significantly increased water retention efficiency under HS+Spd (9-19%) over corresponding HS treated plants on the 7th day of heat exposure. Compared to HS alone, RWC increased by 19.0% in PB-1121 and 9.2% in N22 after Spd application under HS. MSI also showed a significant G and T (P<0.001) response (Table 3). Across the genotypes, reduction in MSI was recorded in a range of 16.0–24.0% under HS. Spd application significantly improved membrane stability by 6.0% and 5.0% in PB-1121 and N22, respectively.

Effect of Spd on H_2O_2 and TBARS

To understand the impact of heat stress on flag leaf and spikelets and the protective role of Spd, H_2O_2 and TBARS were measured at the flowering stage. H_2O_2 accumulation showed significant G x T interaction (P<0.001) in flag leaf and spikelet (Table 3) with higher accumulation in former. The flag leaf of PB-1121 showed H_2O_2 accumulation of 15.2 μmol g^{-1} FW, while in case of spikelet, 11.7 μmol g^{-1} FW was observed under HS on the 7th day of heat exposure. When compared with HS alone, Spd application reduced H_2O_2 production in both the genotypes. Higher H_2O_2 accumulation was recorded in flag leaf and spikelets of PB-1121 (13.7 and 10.8 μmol g^{-1}FW, respectively) under HS+Spd as compared to N22 (12.4 and 10.5 μmol g^{-1}FW, respectively). TBARS, which was calculated in terms of MDA accumulation, showed significant G x T interaction (P<0.001) in flag leaf and spikelet (Table 3). TBARS accumulated maximally in both flag leaf and spikelets with 44.3% and 118.7%, respectively, in PB-1121 under HS compared to ambient. Compared with HS, Spd application reduced MDA accumulation in N22 (10.0% and 0.6%) and PB-1121 (13% and 26%) in flag leaf and spikelets, respectively.

Effect of Spd on sugar and starch content

Total soluble sugar content in flag leaf and spikelets showed significant variation (P<0.01-0.001) among genotypes and treatment (Figure 2) after exposure to HS. On the 7th day of HS, significant sugar reduction was recorded in flag leaf (13% and 34%) and spikelets (10% and 57%) of N22 and PB-1121, respectively with respect to the control. Heat stress with Spd foliar application enhanced sugar accumulation in N22 (4% and

TABLE 3 Stress responses RWC, MSI, H_2O_2 accumulation, TBARS and TAC) in rice genotypes (N22 and PB-1121) under heat stress in flag leaf and spikelets.

Genotypes	Treatment	Spd applications	RWC (%)	MSI (%)	H_2O_2 (μmol g^{-1} FW)		TBARS (μmol g^{-1} FW)		TAC (mM g^{-1} FW)	
			Flag leaf	Flag leaf	Flag leaf	Spikelets	Flag leaf	Spikelets	Flag leaf	Spikelets
N22	Ambient	-Spd	88.3 ± 1.32	88.3 ± 1.24	11.5 ± 0.06	10.4 ± 0.01	20.4 ± 0.43	10.2 ± 0.56	56.5 ± 4.54	23.8 ± 3.39
	HS	-Spd	72.1 ± 0.85	74.1 ± 2.13	12.6 ± 0.14	10.5 ± 0.01	22.1 ± 1.18	11.0 ± 0.62	57.3 ± 1.79	23.1 ± 0.88
		+Spd	78.7 ± 1.03	77.7 ± 2.50	12.4 ± 0.04	10.5 ± 0.01	19.7 ± 0.54	10.9 ± 0.45	60.1 ± 1.83	33.0 ± 2.09
PB-1121	Ambient	-Spd	87.2 ± 0.91	81.9 ± 2.76	12.9 ± 0.19	10.5 ± 0.03	28.1 ± 2.05	31.0 ± 1.40	50.5 ± 2.08	13.6 ± 0.95
	HS	-Spd	61.8 ± 1.28	61.8 ± 1.58	15.2 ± 0.15	11.7 ± 0.02	40.6 ± 0.97	67.8 ± 2.29	53.3 ± 2.24	11.1 ± 0.25
		+Spd	73.1 ± 1.07	65.3 ± 1.45	13.7 ± 0.34	10.8 ± 0.12	35.2 ± 2.72	50.2 ± 2.83	64.8 ± 0.41	19.4 ± 0.84
Lsd<0.05		G	1.94***	3.60***	0.32***	0.09***	2.75***	2.91***	ns	3.10***
		T	2.37***	4.40***	0.39***	0.11***	3.37**	3.57***	5.38*	3.80***
		G X T	3.36**	ns	0.55**	0.16***	4.77*	5.50***	ns	ns

Each point represents the mean of five replicates with their SE. Least significant difference (Lsd) P<0.05, 0.01 and 0.001 were denoted by *, **, and *** respectively, and ns denotes non-significant; FW, Fresh weight; G, Genotypes; T, treatment; GxT, Interaction between genotype and treatment; HS, Heat stress; RWC, Relative water content; MSI, Membrane stability index; TBARS, lipid peroxidation; H_2O_2, reactive oxygen spices; TAC, Total antioxidant capacity; SE, Standard error; Spd, Spermidine.

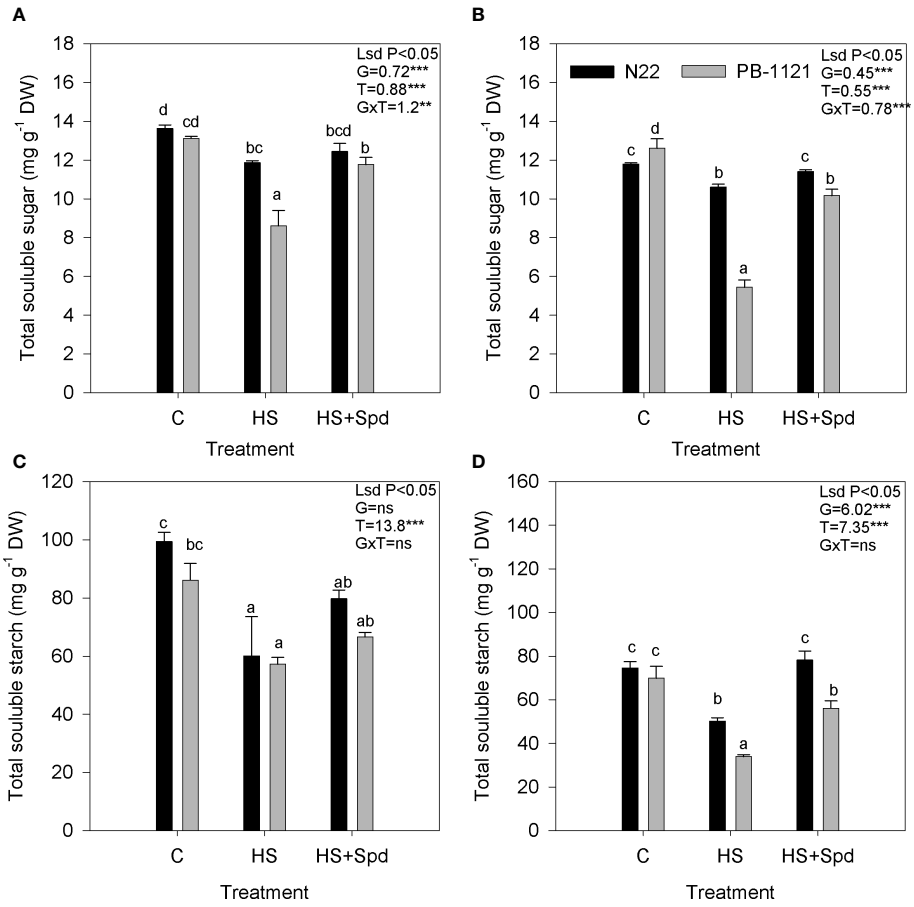


FIGURE 2
Effect of heat stress on sugar and starch contents under different treatments in rice flag leaf **(A, C)** and spikelets **(B, D)**, respectively. Each point represents mean of five replicates. C, Control; DW, Dry weight; HS, Heat stress; Spd, Spermidine. Significance level: **P < 0.01; ***P < 0.001; ns, nonsignificant.

8%) and PB-1121 (36% and 86%) in flag leaf and spikelets, respectively with respect to HS. Similarly, starch content showed significant variation (P<0.05-0.001) among the genotypes and under treatment. On the 7th day of HS, a significant reduction of starch content was recorded in flag leaf (39% and 34%) and spikelet (32.6% and 51.5%) of N22 and PB-1121, respectively with respect to the control. When Spd application under HS was compared with HS alone, it was found that starch content was increased in both the genotypes in case of both flag leaf and spikelets. In case of spikelets higher increase in starch content was noticed in N22 (55%) as compared to PB-1121 (23%).

Effect of Spd on total antioxidant capacity and enzymes activity

To underline the decrease in the accumulation of H_2O_2 and MDA contents, we also analyzed TAC and corresponding enzymes' activities. TAC showed significant interaction in T of flag leaf (P<0.05), whereas G and T interation was presented in spikelets (P<0.001) of rice genotypes (Table 3). In flag leaf, maximum TAC was recorded in N22, while HS+Spd showed significant enhancement in TAC in PB-1121 (64.8 mMg^{-1}FW). A similar trend was observed in spikelets of both the genotypes. A significant rise in TAC was recorded under HS+Spd treatment in both N22 (33.0 mM g^{-1}FW) and PB-1121 (19.4 mM g^{-1}FW).

Heat stress significantly induced activities of antioxidant enzymes *viz*. SOD, CAT, APX and GPX. SOD activity recorded significant variability in G and T in flag leaf (P<0.001-0.01), while in spikelet, significant G x T interactions were present (P<0.01) (Figure 3; Supplementary Table 2). In flag leaf, SOD activity was recorded in a range of 0.21-0.30 units mg^{-1}protein. Under HS, its maximum activity was recorded in N22 (0.28 units mg^{-1}protein) followed by PB-1121 (0.23 units mg^{-1}protein). Spd application under HS significantly induced SOD

10.3389/fpls.2022.1027662

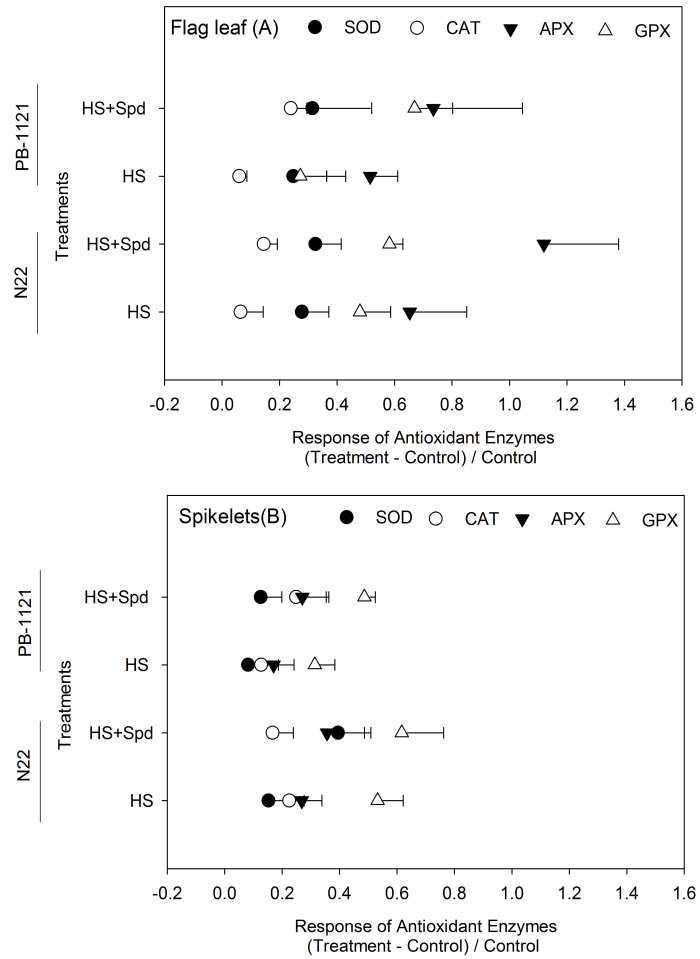


FIGURE 3
Response of antioxidant enzymes in contrasting rice genotypes (N22 and PB-1121) under different treatments in flag leaf **(A)** and spikelets **(B)**. Each point represents mean of five replicates. APX, Ascorbate peroxidase; CAT, Catalase; GPX, Guaiacol peroxidase; HS, Heat stress; Spd, Spermidine; SOD, Superoxide dismutase. SOD was expressed as units µmol; CAT and GPX was expressed as µmol of H_2O_2 consumption min–1 mg–1 protein and for APX, µmol ascorbate oxidized (APX) min^{-1} mg^{-1} protein, respectively. Least significant difference values at 5% for comparison are given in Supplementary Table 2.

activity in N22 (0.30 units mg^{-1}protein) as well as PB-1121 (0.27 units mg^{-1}protein). In spikelets, SOD activity was recorded in a range of 0.34-0.50 units mg^{-1}protein. A similar trend was recorded in spikelets as well. CAT activity showed a significant difference among G and T in flag leaf (P<0.001-0.01) (Figure 3; Supplementary Table 2), whereas non-significant interaction was recorded in spikelets. Induction in CAT activity was recorded by Spd application in HS as shown in N22 (0.054 µmol H_2O_2 $min^{-1}g^{-1}$ protein) and PB-1121 (0.038 µmol H_2O_2 $min^{-1}g^{-1}$ protein) in flag leaf, whereas the marginal increase was recorded in spikelets of PB-1121.

APX activity showed a significant difference for G x T interaction among flag leaf (P<0.05), whereas in case of spikelets it was G and T interaction (P<0.001) (Figure 3; Supplementary Table 2). In flag leaf, APX activity was recorded in the range of 0.28-0.99 µmol ascorbate $min^{-1}g^{-1}$protein, whereas in spikelets, it ranged from 0.56 to 1.00 µmol ascorbate $min^{-1}g^{-1}$protein. Under HS, its maximum activity was induced in N22 (0.77 µmol ascorbate $min^{-1}g^{-1}$protein) followed by PB-1121 (0.42 µmol ascorbate $min^{-1}g^{-1}$protein). After Spd application under HS, significant APX activity was induced in N22 (0.99 µmol ascorbate $min^{-1}g^{-1}$protein) followed by PB-1121 (0.47 µmol ascorbate $min^{-1}g^{-1}$protein). A similar trend was recorded in spikelets where APX was recorded in the range of 0.56-1.0 µmol ascorbate $min^{-1}g^{-1}$protein. GPX activity was significant for G x T interaction in both flag leaf and spikelets (P<0.001) (Figure 3; Supplementary Table 2). In flag leaf, its activity ranged from 0.51–1.3 units, whereas in spikelet, the values ranged between 0.78-1.70 units. Higher GPX activity was recorded under HS

10.3389/fpls.2022.1027662

+Spd in N22 (1.6 µmol H_2O_2 $min^{-1}g^{-1}$ protein). In general, Spd application significantly improved GPX activity in the flag leaf of PB-1121 among the genotypes and within treatments. In spikelets, its activity varied significantly in the range of 0.78–1.70 µmol H_2O_2 $min^{-1}g^{-1}$ protein with the highest activity in N22 (1.70 units).

Effect of Spd on endogenous free-polyamines

Endogenous Put, Spd and Spm contents (units; nmoles g^{-1}FW) showed significant variation among G and T in both flag leaf and spikelets (P<0.001-0.01) (Figure 4). Across the

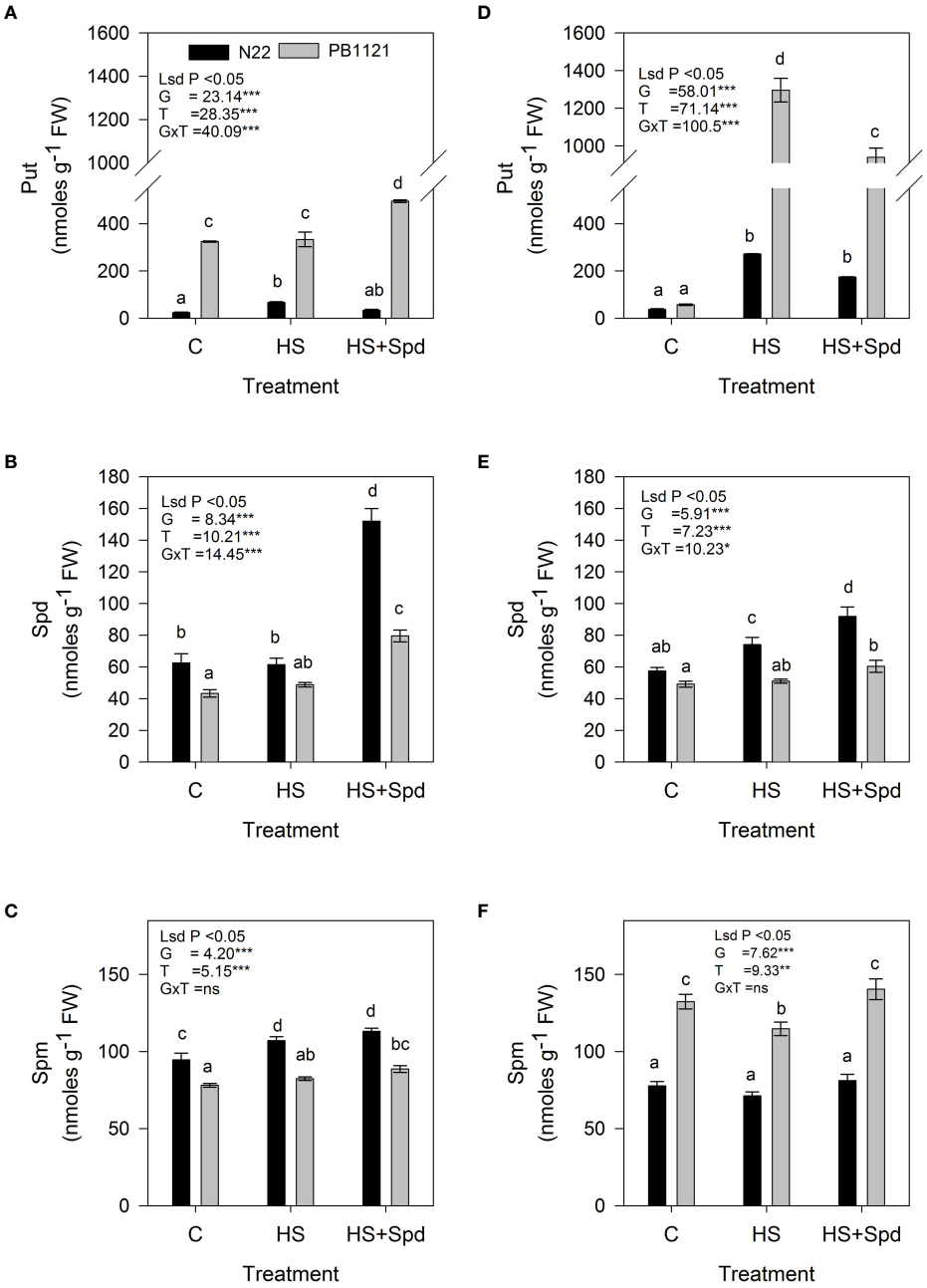


FIGURE 4
Effect of treatments on the endogenous content of polyamines in flag leaf **(A–C)** and spikelet **(D–F)** of rice genotypes. Bars indicate mean ± SE. Comparison of means was obtained from Tukey's honestly significant difference test and means with the same letter are not significantly different at 5%. Fw, Fresh weight; Put, Putrescine; Spd, Spermidine; Spm, Spermine; LSD, least significant difference; G, Genotypes; T, treatment; GxT, Interaction between genotype and treatment. Significance level: *P < 0.05; **P < 0.01; ***P < 0.001; ns, nonsignificant.

genotypes, endogenous Put levels in flag leaf varied significantly in the range of 23–495 nmoles g^{-1}FW on the 7th day of the treatment (Figure 4A). A significantly higher endogenous Put level under HS was recorded in Pusa-1121 (333 nmoles g^{-1}FW), while it was comparatively lower in N22 (67 nmoles g^{-1}FW). Compared to HS alone, Spd foliar application under HS significantly increased Put contents of PB-1121 by 48.6% while lowering its content in N22 by 50%. In spikelets significant increase in Put contents was recorded in both N22 and PB-1121 (271.8 and 1296 units, respectively) under HS. Spd application under HS significantly decreased Put contents in spikelets of both N22 and PB-1121 (35.9% and 27.0%, respectively) (Figure 4D).

Among the genotypes, endogenous Spd level in flag leaf varied significantly in the range of 43–151 nmoles g^{-1}FW (Figure 4B) on the 7th day of treatment. A significantly higher endogenous level of Spd under HS was recorded in N22 (61.4 nmoles g^{1}FW), while it was lower in PB-1121 (48.7 nmoles g^{-1}FW). When compared to HS alone, Spd foliar application under HS significantly increased Spd contents of PB-1121 by 63.1%, while in N22, it increased by 147.1% in flag leaf. A similar trend was observed in spikelets, where a significant increase in Spd content was recorded in N22 (74 unit), which was lower in PB-1121 (51 unit) under HS. Exogenous application of Spd under HS significantly increased endogenous Spd content in spikelets of both N22 and PB-1121 (24.1% and 18%, respectively) (Figure 4E). Among the genotypes, endogenous Spm level in flag leaf varied significantly in the range of 78–113 nmoles g^{-1}FW (Figure 4C) on the 7th day of treatment. A significantly higher endogenous level of Spm under HS was recorded in both N22 (107 nmoles g^{-1}FW) and PB-1121 (82.4 nmoles g^{-1}FW). When compared with HS alone, Spd foliar application in HS significantly increased Spm content of PB-1121 by 7.6%, while in case of N22, it showed a non-significant increase under HS. A similar trend was observed in spikelets, where a significant increase in Spm content was observed in PB-1121 (114.74 units) which was lower in N22 (77.8 units) under HS. Spd application under HS significantly increased Spm content in spikelets of both N22 and PB-1121 (4.37 and 22.4%, respectively) with respect HS (Figure 4F).

Discussion

Heat stress (HS), particularly at the flowering stage, has detrimental effects on rice grain yield and quality (Barnabás, et al., 2008; Lyman et al., 2013; Jagadish et al., 2015; Jagadish, 2020). Predication suggested that short spells of heat spikes at the flowering stage have critical effects on rice (Krishnan et al., 2011). Therefore, increasing stress tolerance in rice at the most sensitive stage, i.e. flowering, is an ideal strategy to develop future climate-resilient varieties (Horie et al., 1996). Heat stress tolerance is majorly contributed by the robust antioxidant mechanism in crops like rice (Bahuguna et al., 2015), chickpea (Kumar et al., 2013) and many other crops (Hasanuzzaman et al., 2020). This mechanism has contributed towards high spikelet fertility and reproductive success under HS in rice (Bahuguna et al., 2015; Karwa et al., 2020).

It is documented that polyamines act as an essential regulatory component in response to various abiotic stresses in rice (Yang et al., 2007; Do et al., 2014; Karwa et al., 2020). Some reports of Spd for alleviating stress were presented under drought (Farooq et al., 2009) and heat (Mostofa et al., 2014) stresses. However, no studies are presented at the flowering stage. Therefore, this study was planned to address the vital gap, i.e. which polyamine regulates the defence mechanism under HS and how it helps maintain spikelet fertility and grain yield components under HS.

Heat stress at the flowering stage showed adverse effects on spikelet fertility and grain yield in PB-1121. However, in the case of N22, lower reduction was recorded (Table 2), illustrating HS resilience in the latter genotype. Qi and Wu (2022) has suggested that spikelet fertility in rice plants under HS is primarily attributed to poor pollination manifesting. It has also been suggested that under HS, pollen viability and pollen dehiscence are severely affected, which would ultimately result in a decline in spikelet fertility when exposed during the flowering stage (Jagadish et al., 2010; Bahuguna et al., 2015; Karwa et al., 2020). Another reason was reported by Zhang et al. (2018) who explained that cross talk among auxins and ROS occur during HS, which inhibits pollen tube elongation in pistil. This decline in spikelet fertility results in grain yield reduction under HS. We recorded grain yield per plant reduction of 67% in PB-1121, while only 8% reduction was observed in N22 under HS. Spd is associated with pollen maturation and pollen tube growth in plants (Falasca et al., 2010; Aloisi et al., 2016). In our study, Spd application showed an alleviated effect of HS as its exogenous application improved spikelet fertility and grain yield per plant in both the genotypes (Figure 5).

Gaseous exchange traits *viz.* photosynthesis rate (i.e. CO_2 uptake) and transpiration rate (i.e. H_2O loss) are regulated through the stomatal behaviour of the plants. Stomatal pore opening and closing maintain the tissue temperature and movement of metabolites or signalling compounds in plants (Brownlee, 2001; Lake et al., 2001). Limitations in gas exchange can limit plant growth and development in various stresses (Wahid et al., 2007). In our study, it was observed that HS caused a higher decrease in P_N in PB-1121 than N22 (Figure 1A). Degradation of chlorophyll and impartment of PSII system are the major factors for reduction in P_N under HS (Efeuglee and Terzider, 2009). Therefore, these systems must have been severely impacted in case of PB-1121 as compared to N22 under HS. Polyamines regulate the voltage-dependent inward K^+ channel in the plasma membrane of the guard cells and modulate stomatal aperture. All polyamines including Spd strongly induces closure of stomata under stress condition (Liu

10.3389/fpls.2022.1027662

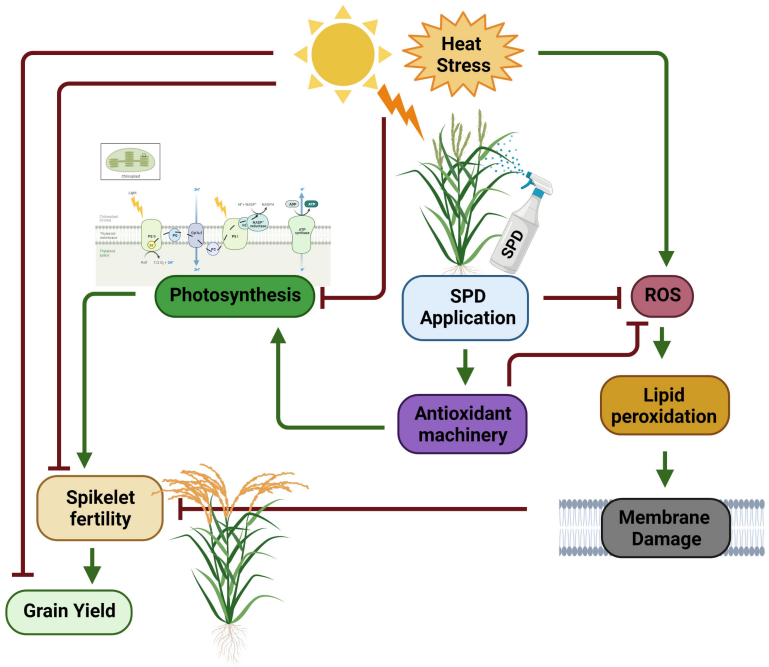


FIGURE 5
Exogenous Spermidine mediated response under heat stress in rice. Heat stress negatively imapcts photosynthesis, spikelet fertility and consequently grain yield in rice. Heat sress causes oxidative stress by producing ROS which leads to lipid peroxidation and thereby cell membrane damage. Damaged cell membrane often reduces spikelet fertility. Foliar application of Spd under heat stress induces antioxidant machinery (ROS scavenging mechanism) in rice plants which increases total antioxidant capacity resulting in higher photosynthesis, spikelet fertility and improved grain yield under HS. SPD, spermidine; ROS, Reactive oxygen species. This figure is created by Biorender.com.

et al., 2000). Polyamine especially Spm and Spd induces secondary messenger in guard cell viz. NO causing stomatal closure. This increase in NO have a direct relation with H_2O_2 content (Gayatri et al., 2013). Recently, Spd application showed higher chlorophyll accumulation and relieved stomatal damage under HS that was maintaining P_N under stress conditions (Yang et al., 2022). Our results are consistent with these findings as P_N was directly linked with *gS* and E under HS, and a decrease in both the traits was recorded in PB-1121.

In contrast, higher E was recorded in N22, which maintained canopy temperature under HS (Figures 1B, C). The reduction in *gS* was due to the loss of leaf water potential under HS. We also annotated it in RWC under HS, which suggest that water content was reduced and membrane stability was also affected under HS (Table 3). Spd application under HS has improved water content, membrane stability, increased chlorophyll content and delayed leaf senescence in bentgrass (Li et al., 2015). In this study, we also observed similar trends with Spd application under HS where RWC and MSI were improved in PB-1121 followed by N22 with respect to HS. Torabian et al. (2018) have reported that exogenous Spd application alleviates water stress through protection of photosynthetic pigments, increase of proline and carotenoid contents and reduction of malondialdehyde content.

Sugar and starch are the essential components for regulating plant metabolism under HS. The role of sugar in osmotic adjustment in case of rice and other crops has previously been discussed in many reports (Morsy et al., 2007). There are various studies with divergent points of view that sugar is either accumulated (Lu et al., 2009) or decreased (Liu et al., 2008; Liao et al., 2013) under HS. Our results suggest that under HS, total sugar and starch contents were reduced in flag leaf and spikelets. This can be explained by the fact that the source to sink relationship from flag leaf to spikelet is impaired under HS. Because of this, sugar transportation and its conversion to starch is also hindered (Kim et al., 2011; Ahmed et al., 2015). Present study suggest that, Spd application enhanced sugar accumulation and also supports the conversion of sugar into starch *via* regulating activity of soluble starch synthase, sucrose synthase and ADP glucose pyrophosphorylase (Wang et al., 2012; Fu et al., 2019). Fu et al. (2019) have reported that exogenous Spd application in rice upregulated the expression of starch synthetases genes which led to the increased accumulation of amylose in rice grains. This might be one of

the reasons for significant variation of 1000 grain weight under HS with and without Spd application. Now, since N22 has more effective HS mitigation process/adaptive mechanism as compared to PB-1121, so in case of spikelets, these enzymes were more effectively operative under N22 as compared to PB-1121, when Spd was applied under HS, consequently resulting in higher increase in starch content in N22 as compared to PB-1121.

Like various other abiotic stresses, HS inhibits metabolic pathways, resulting in ROS production at the tissue level (Asada, 2006). ROS accumulation further induces membrane lipid damage in the form of increased MDA content. To counter ROS induced membrane damage, robust antioxidant machinery is required in plants (Gill and Tuteja, 2010). Conversely, the accumulation of ROS is also essential for stress signalling in plants; but beyond the optimal range, it damages metabolic processes in plants (Gupta et al., 2016). Our study indicates that H_2O_2 and MDA accumulated more in both flag leaf and spikelets of PB-1121 under HS than N22 (Table 3). These results are consistent with previous studies, which suggested that under HS, ROS and MDA accumulates in rice (Bahuguna et al., 2015; Karwa et al., 2020). Also, to metabolize these ROS radicals in cells, scavenging mechanisms in both enzymatic and non-enzymatic systems were reported in this crop (Basu et al., 2017; Szymańska et al., 2017). Various reports suggest that exogenous polyamines induce scavenging enzymes under stress conditions (Minocha et al., 2014, Liu et al., 2015); however, the nature of their interaction is a topic of debate (Groppa et al., 2001; Groppa et al., 2007). In our study, we recorded higher activities of APX and GPX under HS (Figure 3). Under HS, it was reported that downregulation of salicylic acid-binding protein (CAT) favours a rise in APX and GPX activities (Conrath et al., 1995; Dat et al., 1998). Upregulation of APX and GPX enzymes triggers a compensating mechanism to maintain H_2O_2 levels (Apel and Hirt, 2004; Sofo et al., 2015). In the present study, we observed that Spd application under HS significantly induced APX in flag leaf while in spikelets, GPX was induced under HS+Spd.

It was inferred that free polyamines (Put, Spd and Spm) levels behave genotype-dependently under various environmental conditions (Yang et al., 2007; Do et al., 2013; Pál et al., 2015). Endogenous polyamines serve as membrane surface stabilizers and increases the P_N of plants by increasing photochemical efficiency of PSII (Shu et al., 2012). Further, it has been reported that exogenous application of polyamines might result in more substrate for proline biosynthesis specially under stress conditions (Farooq et al., 2009; Shi and Chan, 2014; Pál et al., 2018). Osmolytes like proline helps in osmotic adjustments, increases cell protoplasm concentration to maintain normal membrane function under heat and drought stresses. Exogenous Spd application has improved drought tolerance in bentgrass, maize and white clover by regulating endogenous polyamine metabolism (Li et al., 2015; Li et al., 2018; Li et al., 2016). Raziq et al. (2022) has found that exogenous Spd application has increased the biosynthesis of endogenous Spd and Spm from Put.

In the present study, HS increased Put content more in spikelets than flag leaf of PB-1121 (Figures 4A, D). These results are consistent with reports under heat (Mostafa et al., 2014) and drought stresses in rice (Mostafa et al., 2014). These results are collinear with the rise in endogenous Put accumulation, where a higher accumulation was observed in sensitive genotype—Pusa-1121. In this study, foliar application of Spd also alleviated Put content in spikelets and flag leaf of both the genotypes, where the most prominent rise was recorded in PB-1121. Put is biosynthesized from arginine *via* ADC or from ornithine *via* ODC. Qin et al. (2019) proposed that exogenous Spd augmented the content of Put as former increased *ADC1* and *ODC1* expression in case of *Malus domestica*.

Foliar application led to significant change in endogenous Spd content across the stress treatments in both the tissues, with the highest increase in N22 spikelets (Figures 4B, E). N22 consistently recorded higher Spd, while PB-1121 recorded lowest Spd across the treatments. Saha and Giri (2017) suggested that the increase in level of Spd was because of higher induction of *OsSPDS* in tolerant as compared to sensitive genotype. This can be the possible reason for rise in Spd content under HS. Exogenous Spd treatment has been reported to improve endogenous content together with imparting tolerance towards HS in rice (Mostafa et al., 2014) and towards drought stress in *Rosa damascena* (Hassan et al., 2018). We also observed a similar response in rice genotypes under HS.

It has been noted that another polyamine, Spm, was also elevated in the flag leaf of N22 and spikelets of PB-1121 under HS. Spd application resulted in increase in Spm endogenous content in PB-1121, whereas it was unchanged in N22. Elevated levels of both Spd and Spm has been reported to contribute towards plant stress tolerance under HS and other abiotic stresses (Liu et al., 2004; Do et al., 2014; Ikbal et al., 2014). For example, in case of oats, HS induced lipid peroxidation and membrane destabilization, but increased levels of Spd and Spm reversed this action by interaction with macromolecules (Tiburcio et al., 1994). In the present study, a marked decrease in Put accumulation was concomitant with an increase in endogenous levels of both Spd and Spm in N22. This accumulation pattern of the three polycations was previously reported in various crops under drought (Hassan et al., 2018) and salinity (Duan et al., 2008) stresses. Xu and Wu (2009) suggested that higher levels of Spd and Spm with respect to Put contributed towards water stress tolerance in pine. We found endogenous Put accumulation in the sensitive genotype, PB-1121. This might be due to lesser conversion of Put into Spd and Spm in the sensitive genotype. Bouchereau et al. (1999) proposed that a higher accumulation of Put indicates stress sensitivity of any organism. This is in agreement with the findings of Liu et al.

(2004), where drought-tolerant wheat genotypes exhibited higher levels of Spd, whereas sensitive genotypes had more Put.

Conclusion

The present study confirms that HS elevates oxidative stress in rice by increasing H_2O_2 and TBARS, decreasing photosynthesis, spikelet fertility and grain yield. Robust antioxidant machinery in tolerant genotype, N22 allowed minimum damage across the stress conditions. However, antioxidant defence in sensitive genotype was not at par to combat stress without applying Spd. Our study found that foliar application of Spd significantly induced ROS scavenging mechanism that resulted in increased photosynthesis, spikelet fertility, and grain yield under HS. This study highlights the probable association of Spd in HS tolerance in rice at the flowering stage *via* regulating robust antioxidant machinery, photosynthesis and spikelet fertility. There might be two possibilities for induction of antioxidant enzymes, either they bind with the polyamines and restore their functional stability and integrity, or catabolism of polyamine produces H_2O_2 byproduct, which acts as a signalling molecule and regulates series of signal transduction steps which activates antioxidant defence system to counter stress responses. Major research direction in the future should be to study the regulatory mechanism of Spd at molecular level and to study its role in stress signalling pathways. Development of overexpression lines or mutant lines of Spd synthase might help to elucidate the precise role of Spd to act as stress signal regulator or stress protecting compound under HS in rice. Also, future analyses focusing on manipulation of Spd metabolism and its environmental impact when applied exogenously are important to cope with the problem of climate change and for sustainable agricultural practices.

Data availability statement

The original contributions presented in the study are included in the article/Supplementary Material. Further inquiries can be directed to the corresponding author.

Author contributions

The authors have made the following declaration about their contributions. Conceived and designed the experiments: MP, SKU, SSA and SK. Performed the experiments: SK, JT, SM, AD and GKK. Analyzed and interpreted the data: SK and SKU. Performed statistical analysis: SK, SKU and AK. Drafted the manuscript: MP, SK, JT, SSA, SKU and VC. Edited and finalized the manuscript: MP, VC, JT, SKU and SK. All authors contributed to the article and approved the submitted version.

Funding

Authors acknowledge the financial grant received from the Indian Council of Agricultural Research (ICAR), New Delhi, India, through National Innovations on Climate Resilient Agriculture (NICRA) Grant No.12-115 and ACRIP Project.

Conflict of interest

The authors declare that they have no known competing financial interests or personal relationships that could have appeared to influence the work reported in this paper.

Publisher's note

All claims expressed in this article are solely those of the authors and do not necessarily represent those of their affiliated organizations, or those of the publisher, the editors and the reviewers. Any product that may be evaluated in this article, or claim that may be made by its manufacturer, is not guaranteed or endorsed by the publisher.

Supplementary material

The Supplementary Material for this article can be found online at: https://www.frontiersin.org/articles/10.3389/fpls.2022.1027662/full#supplementary-material

SUPPLEMENTARY TABLE 1
ANOVA for leaf gas exchange parameters of rice cultivars, N22 and PB-1121. Values presented are least significant difference (LSD) for each trait where *, **, *** indicate the significant difference and ns indicates non-significant difference; LSD with P< 0.05, 0.01 and 0.001 respectively. P_n, Net photosynthetic rate; gS, stomatal conductance; E, transpiration rate; G, Genotype; T, Treatment; GxT, Interaction between genotype and treatment.

SUPPLEMENTARY TABLE 2
ANOVA for antioxidant enzymes of rice cultivars, N22 and PB-1121. Values presented are least significant difference (LSD) for each trait where *, **, *** indicate the significant difference and ns indicates non-significant difference; LSD with P < 0.05, 0.01 and 0.001 respectively. SOD, Superoxide dismutase; CAT, Catalase; APX, Ascorbate peroxidase; GPX, Guaiacol peroxidise; G, Genotype; T, Treatment; GxT, Interaction between genotype and treatment.

References

Ahmed, N., Tetlow, I. J., Nawaz, S., Iqbal, A., Mubin, M., Nawaz ul Rehman, M. S., et al. (2015). Effect of high temperature on grain filling period, yield, amylose content and activity of starch biosynthesis enzymes in endosperm of basmati rice. *J. Sci. Food Agric.* 95 (11), 2237–2243. doi: 10.1002/jsfa.6941

Alexieva, V., Sergiev, I., Mapelli, S., and Karanov, E. (2001). The effect of drought and ultraviolet radiation on growth and stress markers in pea and wheat. *Plant Cell Environ.* 24 (12), 1337–1344. doi: 10.1046/j.1365-3040.2001.00778.x

Aloisi, I., Cai, G., Serafini-Fracassini, D., and Del Duca, S. (2016). Polyamines in pollen: from microsporogenesis to fertilization. *Front. Plant Sci.* 7, 155. doi: 10.3389/fpls.2016.00155

Apel, K., and Hirt, H. (2004). Reactive oxygen species: metabolism, oxidative stress, and signal transduction. *Annu. Rev. Plant Biol.* 55, 373–399. doi: 10.1146/annurev.arplant.55.031903.141701

Asada, K. (2006). Production and scavenging of reactive oxygen species in chloroplasts and their functions. *Plant Physiol.* 141 (2), 391–396. doi: 10.1104/pp.106.082040

Bahuguna, R. N., Jha, J., Pal, M., Shah, D., Lawas, L. M., Khetarpal, S., et al. (2015). Physiological and biochemical characterization of NERICA-L-44: a novel source of heat tolerance at the vegetative and reproductive stages in rice. *Physiologia plantarum* 154 (4), 543–559. doi: 10.1111/ppl.12299

Bahuguna, R. N., Tamilselvan, A., Muthurajan, R., Solis, C. A., and Jagadish, S. V. K. (2018). Mild preflowering drought priming improves stress defences, assimilation and sink strength in rice under severe terminal drought. *Funct. Plant Biol.* 45 (8), 827–839. doi: 10.1071/FP17248

Barnabás, B., Jäger, K., and Fehér, A. (2008). The effect of drought and heat stress on reproductive processes in cereals. *Plant Cell Environ.* 31 (1), 11–38.

Barrs, H. D., and Weatherley, P. E. (1962). A re-examination of the relative turgidity technique for estimating water deficits in leaves. *Aust. J. Biol. Sci.* 15 (3), 413–428. doi: 10.1071/BI9620413

Basu, S., Giri, R. K., Benazir, I., Kumar, S., Rajwanshi, R., Dwivedi, S. K., et al. (2017). Comprehensive physiological analyses and reactive oxygen species profiling in drought tolerant rice genotypes under salinity stress. *Physiol. Mol. Biol. Plants* 23 (4), 837–850. doi: 10.1007/s12298-017-0477-0

Benzie, I. F., and Strain, J. J. (1999). "Ferric reducing/antioxidant power assay: direct measure of total antioxidant activity of biological fluids and modified version for simultaneous measurement of total antioxidant power and ascorbic acid concentration," in *Methods in enzymology* (Academic press), vol. 299, 15–27. doi: 10.1016/s0076-6879(99)99005-5

Bouchereau, A., Aziz, A., Larher, F., and Martin-Tanguy, J. (1999). Polyamines and environmental challenges: recent development. *Plant Sci.* 140 (2), 103–125. doi: 10.1016/S0168-9452(98)00218-0

Bradford, M. M. (1976). A rapid and sensitive method for the quantitation of microgram quantities of protein utilizing the principle of protein-dye binding. *Analytical Biochem.* 72 (1-2), 248–254. doi: 10.1016/0003-2697(76)90527-3

Brownlee, C. (2001). The long and the short of stomatal density signals. *Trends Plant Sci.* 6 (10), 441–442. doi: 10.1016/S1360-1385(01)02095-7

Capell, T., Bassie, L., and Christou, P. (2004). Modulation of the polyamine biosynthetic pathway in transgenic rice confers tolerance to drought stress. *Proc. Natl. Acad. Sci.* 101 (26), 9909–9914. doi: 10.1073/pnas.0306974101

Chen, M., Fu, Y., Mou, Q., An, J., Zhu, X., Ahmed, T., et al. (2021). Spermidine induces expression of stress associated proteins (SAPs) genes and protects rice seed from heat stress-induced damage during grain-filling. *Antioxidants* 10 (10), 1544. doi: 10.3390/antiox10101544

Conrath, U., Chen, Z., Ricigliano, J. R., and Klessig, D. F. (1995). Two inducers of plant defense responses, 2, 6-dichloroisonicotinec acid and salicylic acid, inhibit catalase activity in tobacco. *Proc. Natl. Acad. Sci.* 92 (16), 7143–7147. doi: 10.1073/pnas.92.16.7143

Dat, J. F., Lopez-Delgado, H., Foyer, C. H., and Scott, I. M. (1998). Parallel changes in H2O2 and catalase during thermotolerance induced by salicylic acid or heat acclimation in mustard seedlings. *Plant Physiol.* 116 (4), 1351–1357. doi: 10.1104/pp.116.4.1351

de Azevedo Neto, A. D., Prisco, J. T., Enéas-Filho, J., de Abreu, C. E. B., and Gomes-Filho, E. (2006). Effect of salt stress on antioxidative enzymes and lipid peroxidation in leaves and roots of salt-tolerant and salt-sensitive maize genotypes. *Environ. Exp. Bot.* 56 (1), 87–94. doi: 10.1016/j.envexpbot.2005.01.008

Do, P. T., Degenkolbe, T., Erban, A., Heyer, A. G., Kopka, J., Köhl, K. I., et al. (2013). Dissecting rice polyamine metabolism under controlled long-term drought stress. *PLoS One* 8 (4), e60325. doi: 10.1371/journal.pone.0060325

Do, P. T., Drechsel, O., Heyer, A. G., Hincha, D. K., and Zuther, E. (2014). Changes in free polyamine levels, expression of polyamine biosynthesis genes, and performance of rice cultivars under salt stress: a comparison with responses to drought. *Front. Plant Sci.* 5, 182. doi: 10.3389/fpls.2014.00182

Duan, J., Li, J., Guo, S., and Kang, Y. (2008). Exogenous spermidine affects polyamine metabolism in salinity-stressed cucumis sativus roots and enhances short-term salinity tolerance. *J. Plant Physiol.* 165 (15), 1620–1635. doi: 10.1016/j.jplph.2007.11.006

Efeoglu, B., and Terzioglu, S. (2009). Photosynthetic responses of two wheat varieties to high temperature. *Eurasian J. Biosci.* 3, 97–106. doi: 10.5053/ejobios.2009.3.0.13

ElSayed, A. I., Rafudeen, M. S., El-Hamahmy, M. A., Odero, D. C., and Hossain, M. S. (2018). Enhancing antioxidant systems by exogenous spermine and spermidine in wheat (Triticum aestivum) seedlings exposed to salt stress. *Funct. Plant Biol.* 45 (7), 745–759. doi: 10.1071/FP17127

Falasca, G., Franceschetti, M., Bagni, N., Altamura, M. M., and Biasi, R. (2010). Polyamine biosynthesis and control of the development of functional pollen in kiwifruit. *Plant Physiol. Biochem.* 48 (7), 565–573. doi: 10.1016/j.plaphy.2010.02.013

FAO (2014) *(Food and agriculture organization)*. Available at: http://www.fao.org/faostat/en/?#home.

Farooq, M., Wahid, A., and Lee, D. J. (2009). Exogenously applied polyamines increase drought tolerance of rice by improving leaf water status, photosynthesis and membrane properties. *Acta Physiologiae Plantarum* 31 (5), 937–945. doi: 10.1007/s11738-009-0307-2

Flores, H. E., and Galston, A. W. (1982). Analysis of polyamines in higher plants by high performance liquid chromatography. *Plant Physiol.* 69 (3), 701–706. doi: 10.1104/pp.69.3.701

Fu, Y., Gu, Q., Dong, Q., Zhang, Z., Lin, C., Hu, W., et al. (2019). Spermidine enhances heat tolerance of rice seeds by modulating endogenous starch and polyamine metabolism. *Molecules* 24 (7), 1395. doi: 10.3390/molecules24071395

Fukuoka, M., Yoshimoto, M., and Hasegawa, T. (2012). MINCER: A novel instrument for monitoring the micrometeorology of rice canopies. *J. Agric. Meteorol.*, 68(2), pp.135-147. doi: 10.2480/agrmet.68.2.1

Garay-Arroyo, A., de la Paz Sánchez, M., García-Ponce, B., Azpeitia, E., and Álvarez-Buylla, E. R. (2012). Hormone symphony during root growth and development. *Dev. dynamics* 241 (12), 1867–1885. doi: 10.1002/dvdy.23878

Gayatri, G., Agurla, S., and Raghavendra, A. S. (2013). Nitric oxide in guard cells as an important secondary messenger during stomatal closure. *Front. Plant Sci.* 4, 425. doi: 10.3389/fpls.2013.00425

Ghosh, U. K., Islam, M. N., Siddiqui, M. N., Cao, X., and Khan, M. A. R. (2022). Proline, a multifaceted signalling molecule in plant responses to abiotic stress: understanding the physiological mechanisms. *Plant Biol.* 24 (2), 227–239. doi: 10.1111/plb.13363

Gill, S. S., and Tuteja, N. (2010). Reactive oxygen species and antioxidant machinery in abiotic stress tolerance in crop plants. *Plant Physiol. Biochem.* 48 (12), 909–930. doi: 10.1016/j.plaphy.2010.08.016

Groppa, M. D., Ianuzzo, M. P., Tomaro, M. L., and Benavides, M. P. (2007). Polyamine metabolism in sunflower plants under long-term cadmium or copper stress. *Amino Acids* 32 (2), 265–275. doi: 10.1007/s00726-006-0343-9

Groppa, M. D., Tomaro, M. L., and Benavides, M. P. (2001). Polyamines as protectors against cadmium or copper-induced oxidative damage in sunflower leaf discs. *Plant Sci.* 161 (3), 481–488. doi: 10.1016/S0168-9452(01)00432-0

D. K. Gupta, J. M. Palma and F. J. Corpas (Eds.) (2016). *Redox state as a central regulator of plant-cell stress responses* (Germany: Springer International Publishing), 386.

Handa, A. K., and Mattoo, A. K. (2010). Differential and functional interactions emphasize the multiple roles of polyamines in plants. *Plant Physiol. Biochem.* 48 (7), 540–546. doi: 10.1016/j.plaphy.2010.02.009

Hasanuzzaman, M., Bhuyan, M. H. M., Zulfiqar, F., Raza, A., Mohsin, S. M., Mahmud, J. A., et al. (2020). Reactive oxygen species and antioxidant defense in plants under abiotic stress: Revisiting the crucial role of a universal defense regulator. *Antioxidants* 9 (8), 681. doi: 10.3390/antiox9080681

Hasanuzzaman, M., Nahar, K., Alam, M., Roychowdhury, R., and Fujita, M. (2013). Physiological, biochemical, and molecular mechanisms of heat stress tolerance in plants. *Int. J. Mol. Sci.* 14 (5), 9643–9684. doi: 10.3390/ijms14059643

Hassan, F. A. S., Ali, E. F., and Alamer, K. H. (2018). Exogenous application of polyamines alleviates water stress-induced oxidative stress of Rosa damascena miller var. trigintipetala dieck. *South Afr. J. Bot.* 116, 96–102. doi: 10.1016/j.sajb.2018.02.399

Horie, T., Matsui, T., Nakagawa, H., and Omasa, K. (1996). "Effects of elevated CO 2 and global climate change on rice yield in Japan," in *Climate change and plants in East Asia* (Tokyo: Springer), 39–56.

Hossain, A., Pamanick, B., Venugopalan, V. K., Ibrahimova, U., Rahman, M. A., Siyal, A. L., et al. (2022). "Emerging roles of plant growth regulators for plants adaptation to abiotic stress–induced oxidative stress," in *Emerging plant growth regulators in agriculture* (Cambridge, MA, USA: Academic Press), 1–72.

Hu, Q., Wang, W., Lu, Q., Huang, J., Peng, S., and Cui, K. (2021). Abnormal anther development leads to lower spikelet fertility in rice (*Oryza sativa* l.) under high temperature during the panicle initiation stage. *BMC Plant Biol.* 21 (1), 1–17. doi: 10.1186/s12870-021-03209-w

Ikbal, F. E., Hernández, J. A., Barba-Espín, G., Koussa, T., Aziz, A., Faize, M., et al. (2014). Enhanced salt-induced antioxidative responses involve a contribution of polyamine biosynthesis in grapevine plants. *J. Plant Physiol.* 171 (10), 779–788. doi: 10.1016/j.jplph.2014.02.006

IPCC (2021). "Summary for policymakers," in *Climate change 2021: The physical science basis. contribution of working group I to the sixth assessment report of the intergovernmental panel on climate change*. Eds. V. Masson-Delmotte, P. Zhai, A. Pirani, S. L. Connors, C. Péan, S. Berger, N. Caud, Y. Chen, L. Goldfarb, M. I. Gomis, M. Huang, K. Leitzell, E. Lonnoy, J. B. R. Matthews, T. K. Maycock, T. Waterfield, O. Yelekçi, R. Yu and B. Zhou (Cambridge University Press). Available at: https://www.ipcc.ch/report/ar6/wg1/downloads/report/IPCC_AR6_WGI_SPM_final.pdf.

Jagadish, S. K. (2020). Heat stress during flowering in cereals–effects and adaptation strategies. *New Phytol.* 226 (6), 1567–1572. doi: 10.1111/nph.16429

Jagadish, S. V. K., Cairns, J., Lafitte, R., Wheeler, T. R., Price, A. H., and Craufurd, P. Q. (2010). Genetic analysis of heat tolerance at anthesis in rice. *Crop Sci.* 50 (5), 1633–1641. doi: 10.2135/cropsci2009.09.0516

Jagadish, S. V. K., Craufurd, P. Q., and Wheeler, T. R. (2008). Phenotyping parents of mapping populations of rice for heat tolerance during anthesis. *Crop Sci.* 48 (3), 1140–1146. doi: 10.2135/cropsci2007.10.0559

Jagadish, S. V. K., Murty, M. V. R., and Quick, W. P. (2015). Rice responses to rising temperatures–challenges, perspectives and future directions. *Plant Cell Environ.* 38 (9), 1686–1698. doi: 10.1111/pce.12430

Jiang, M., and Zhang, J. (2002). Water stress-induced abscisic acid accumulation triggers the increased generation of reactive oxygen species and up-regulates the activities of antioxidant enzymes in maize leaves. *J. Exp. Bot.* 53 (379), 2401–2410. doi: 10.1093/jxb/erf090

Karwa, S., Bahuguna, R. N., Chaturvedi, A. K., Maurya, S., Arya, S. S., Chinnusamy, V., et al. (2020). Phenotyping and characterization of heat stress tolerance at reproductive stage in rice (Oryza sativa l.). *Acta Physiologiae Plantarum* 42 (2), 1–16. doi: 10.1007/s11738-020-3016-5

Kasukabe, Y., He, L., Nada, K., Misawa, S., Ihara, I., and Tachibana, S. (2004). Overexpression of spermidine synthase enhances tolerance to multiple environmental stresses and up-regulates the expression of various stress-regulated genes in transgenic arabidopsis thaliana. *Plant Cell Physiol.* 45 (6), 712–722. doi: 10.1093/pcp/pch083

Kim, J., Shon, J., Lee, C. K., Yang, W., Yoon, Y., Yang, W. H., et al. (2011). Relationship between grain filling duration and leaf senescence of temperate rice under high temperature. *Field Crops Res.* 122 (3), 207–213. doi: 10.1016/j.fcr.2011.03.014

Krishnan, P., Ramakrishnan, B., Reddy, K. R., and Reddy, V. R. (2011). High-temperature effects on rice growth, yield, and grain quality. *Adv. Agron.* 111, 87–206. doi: 10.1016/B978-0-12-387689-8.00004-7

Kubiś, J. (2001). Polyamines and" scavenging system": influence of exogenous spermidine on catalase and guaiacol peroxidase activities, and free polyamine level in barley leaves under water deficit. *Acta Physiol Plant* 25 (4), 335–341. doi: 10.1007/s11738-001-0041-x

Kubiś, J. (2003). Polyamines and" scavenging system": influence of exogenous spermidine on catalase and guaiacol peroxidase activities, and free polyamine level in barley leaves under water deficit. *Acta Physiologiae Plantarum* 25 (4), 337–343. doi: 10.1007/s11738-003-0014-3

Kumar, S., Thakur, P., Kaushal, N., Malik, J. A., Gaur, P., and Nayyar, H. (2013). Effect of varying high temperatures during reproductive growth on reproductive function, oxidative stress and seed yield in chickpea genotypes differing in heat sensitivity. *Arch. Agron. Soil Sci.* 59 (6), 823–843. doi: 10.1080/03650340.2012.683424

Lake, J. A., Quick, W. P., Beerling, D. J., and Woodward, F. I. (2001). Signals from mature to new leaves. *Nature* 411 (6834), 154–154. doi: 10.1038/35075660

Larkindale, J., and Knight, M. R. (2002). Protection against heat stress-induced oxidative damage in arabidopsis involves calcium, abscisic acid, ethylene, and salicylic acid. *Plant Physiol.* 128 (2), 682–695. doi: 10.1104/pp.010320

Liao, J., Xiao, X., Song, Y., et al (2013). Effects of high temperature on grain-filling of rice caryopsis and physiological and biochemical characteristic of flag leave at early milky stage. *Plant Physiology Journal* 49 (2), 175–180.

Li, L., Gu, W., Li, C., Li, W., Li, C., Li, J., et al. (2018). Exogenous spermidine improves drought tolerance in maize by enhancing the antioxidant defence system and regulating endogenous polyamine metabolism. *Crop Pasture Sci.* 69 (11), 1076–1091. doi: 10.1071/CP18271

Liu, H. P., Dong, B. H., Zhang, Y. Y., Liu, Z. P., and Liu, Y. L. (2004). Relationship between osmotic stress and the levels of free, conjugated and bound polyamines in leaves of wheat seedlings. *Plant Sci.* 166 (5), 1261–1267. doi: 10.1016/j.plantsci.2003.12.039

Liu, K., Fu, H., Bei, Q., and Luan, S. (2000). Inward potassium channel in guard cells as a target for polyamine regulation of stomatal movements. *Plant Physiol.* 124 (3), 1315–1326. doi: 10.1104/pp.124.3.1315

Liu, Y., Teng, Z., Wang, S., and He, G. (2008). Effects of high temperature stress on soluble sugar and membrane protective enzyme in rice. *J. Southwest Univ. (Natural Science Edition)* 30 (2), 59–63.

Liu, J. H., Wang, W., Wu, H., Gong, X., and Moriguchi, T. (2015). Polyamines function in stress tolerance: from synthesis to regulation. *Front. Plant Sci.* 6, 827. doi: 10.3389/fpls.2015.00827

Li, Z., Zhou, H., Peng, Y., Zhang, X., Ma, X., Huang, L., et al. (2015). Exogenously applied spermidine improves drought tolerance in creeping bentgrass associated with changes in antioxidant defense, endogenous polyamines and phytohormones. *Plant Growth Regul.* 76 (1), 71–82. doi: 10.1007/s10725-014-9978-9

Li, Z., Zhang, Y., Zhang, X., Peng, Y., Merewitz, E., Ma, X., et al (2016). he alterations of endogenous polyamines and phytohormones induced by exogenous application of spermidine regulate antioxidant metabolism, metallothionein and relevant genes conferring drought tolerance in white clover. *Environmental and Experimental Botany* 124, 22–38.

Lu, J., Zhang, R., Zong, X., Wang, S., and He, G. (2009). Effect of salicylic acid on heat resistance of rice seedling under heat stress. *Chin. J. Eco-Agricult.* 17 (6), 1168–1171. doi: 10.3724/SP.J.1011.2009.01168

Lyman, N. B., Jagadish, K. S., Nalley, L. L., Dixon, B. L., and Siebenmorgen, T. (2013). Neglecting rice milling yield and quality underestimates economic losses from high-temperature stress. *PloS One* 8 (8), e72157. doi: 10.1371/journal.pone.0072157

McCready, R. M., Guggolz, J., Silviera, V., and Owens, H. S. (1950). Determination of starch and amylose in vegetables. *Analytical Chem.* 22 (9), 1156–1158. doi: 10.1021/ac60045a016

Minocha, R, Majumdar, R, and Minocha, SC (2014). Polyamines and abiotic stress in plants: A complex relationship. *Front. Plant Sci.* 5 (9), 175. doi: 10.3389/fpls.2014.00175

Morsy, M. R., Jouve, L., Hausman, J. F., Hoffmann, L., and Stewart, J. M. (2007). Alteration of oxidative and carbohydrate metabolism under abiotic stress in two rice (Oryza sativa l.) genotypes contrasting in chilling tolerance. *Jouranl Plant Physiol.* 164, 157–167. doi: 10.1016/j.jplph.2005.12.004

Mostofa, M. G., Yoshida, N., and Fujita, M. (2014). Spermidine pretreatment enhances heat tolerance in rice seedlings through modulating antioxidative and glyoxalase systems. *Plant Growth Regul.* 73 (1), 31–44. doi: 10.1007/s10725-013-9865-9

Pál, M., Szalai, G., and Janda, T. (2015). Speculation: polyamines are important in abiotic stress signaling. *Plant Sci.* 237, 16–23. doi: 10.1016/j.plantsci.2015.05.003

Pál, M., Tajti, J., Szalai, G., Peeva, V., Végh, B., and Janda, T. (2018). Interaction of polyamines, abscisic acid and proline under osmotic stress in the leaves of wheat plants. *Sci. Rep.* 8 (1), 1–12. doi: 10.1038/s41598-018-31297-6

Paupière, M. J., Van Heusden, A. W., and Bovy, A. G. (2014). The metabolic basis of pollen thermo-tolerance: perspectives for breeding. *Metabolites* 4 (4), 889–920. doi: 10.3390/metabo4040889

Prasad, P. V. V., Boote, K. J., Allen, Jr. L.H., Sheehy, J. E., and Thomas, J. M. G. (2006). Species, ecotype and cultivar differences in spikelet fertility and harvest index of rice in response to high temperature stress. *Field Crops Res.* 95 (2-3), 398–411. doi: 10.1016/j.fcr.2005.04.008

Qin, L., Zhang, X., Yan, J., Fan, L., Rong, C., Mo, C., et al. (2019). Effect of exogenous spermidine on floral induction, endogenous polyamine and hormone production, and expression of related genes in 'Fuji'apple (Malus domesticaBorkh.). *Sci. Rep.* 9 (1), 1–11. doi: 10.1038/s41598-019-49280-0

Qi, B., and Wu, C. (2022). Potential roles of stigma exsertion on spikelet fertility in rice (*Oryza sativa* l.) under heat stress. *Front. Plant Sci.* 3346. doi: 10.3389/fpls.2022.983070

Raza, A., Salehi, H., Rahman, M. A., Zahid, Z., Madadkar Haghjou, M., Najafi-Kakavand, S., et al. (2022). Plant hormones and neurotransmitter interactions mediate antioxidant defenses under induced oxidative stress in plants. *Front. Plant Sci.* 13. doi: 10.3389/fpls.2022.961872

Raziq, A., Din, A. M. U., Anwar, S., Wang, Y., Jahan, M. S., He, M., et al. (2022). Exogenous spermidine modulates polyamine metabolism and improves stress responsive mechanisms to protect tomato seedlings against salt stress. *Plant Physiol. Biochem.* 187, 1–10. doi: 10.1016/j.plaphy.2022.07.005

Roy, P., Niyogi, K., Sengupta, D. N., and Ghosh, B. (2005). Spermidine treatment to rice seedlings recovers salinity stress-induced damage of plasma membrane and PM-bound h+-ATPase in salt-tolerant and salt-sensitive rice cultivars. *Plant Sci.* 168 (3), 583–591. doi: 10.1016/j.plantsci.2004.08.014

Saha, J., and Giri, K. (2017). Molecular phylogenomic study and the role of exogenous spermidine in the metabolic adjustment of endogenous polyamine in two rice cultivars under salt stress. *Gene* 609, 88–103. doi: 10.1016/j.gene.2017.02.001

Sairam, R. K., Rao, K. V., and Srivastava, G. C. (2002). Differential response of wheat genotypes to long term salinity stress in relation to oxidative stress, antioxidant activity and osmolyte concentration. *Plant Sci.* 163 (5), 1037–1046. doi: 10.1016/S0168-9452(02)00278-9

Selote, D. S., and Khanna-Chopra, R. (2004). Drought-induced spikelet sterility is associated with an inefficient antioxidant defence in rice panicles. *Physiologia Plantarum* 121 (3), 462–471. doi: 10.1111/j.1399-3054.2004.00341.x

Sharma, P., and Dubey, R. S. (2004). Ascorbate peroxidase from rice seedlings: properties of enzyme isoforms, effects of stresses and protective roles of osmolytes. *Plant Sci.* 167 (3), 541–550. doi: 10.1016/j.plantsci.2004.04.028

Shi, H., and Chan, Z. (2014). Improvement of plant abiotic stress tolerance through modulation of the polyamine pathway. *J. Integr. Plant Biol.* 56 (2), 114–121. doi: 10.1111/jipb.12128

Shu, S., Yuan, L. Y., Guo, S. R., Sun, J., and Liu, C. J. (2012). Effects of exogenous spermidine on photosynthesis, xanthophyll cycle and endogenous polyamines in cucumber seedlings exposed to salinity. *Afr. J. Biotechnol.* 11 (22), 6064–6074. doi: 10.5897/AJB11.1354

Sinclair, T. R., Allen, L. H., and Drake, G. M. (1995). Temperature gradient chambers for research on global environment change: II. design for plot studies. *BIOTRONICS* (24), 99–108. Available at: https://catalog.lib.kyushu-u.ac.jp/opac_detail_md/?lang=0&amode=MD100000&bibid=8213.

Singh, V., Singh, A. K., Mohapatra, T., and Ellur, R. K. (2018). Pusa basmati 1121–a rice variety with exceptional kernel elongation and volume expansion after cooking. *Rice* 11 (1), 1–10. doi: 10.1186/s12284-018-0213-6

Sofo, A., Scopa, A., Nuzzaci, M., and Vitti, A. (2015). Ascorbate peroxidase and catalase activities and their genetic regulation in plants subjected to drought and salinity stresses. *Int. J. Mol. Sci.* 16 (6), 13561–13578. doi: 10.3390/ijms160613561

Soudek, P., Ursu, M., Petrová, Š., and Vaněk, T. (2016). Improving crop tolerance to heavy metal stress by polyamine application. *Food Chem.* 213, 223–229. doi: 10.1016/j.foodchem.2016.06.087

Szymańska, R., Ślesak, I., Orzechowska, A., and Kruk, J. (2017). Physiological and biochemical responses to high light and temperature stress in plants. *Environ. Exp. Bot.* 139, 165–177. doi: 10.1016/j.envexpbot.2017.05.002

Teixeira, E. I., Fischer, G., Van Velthuizen, H., Walter, C., and Ewert, F. (2013). Global hot-spots of heat stress on agricultural crops due to climate change. *Agric. For. Meteorol.* 170, 206–215. doi: 10.1016/j.agrformet.2011.09.002

Tian, J., Guo, S. R., Liu, X. E., Zhang, R. H., and Cheng, Y. J. (2009). Effects of exogenous spermidine pretreatment on antioxidant system in cucumber seedling leaves under high temperature stress. *Acta Botanica Boreali-Occidentalia Sin.* 11, 020.

Tiburcio, A. F., Besford, R. T., Capell, T., Borrell, A., Testillano, P. S., and Risueño, M. C. (1994). Mechanisms of polyamine action during senescence responses induced by osmotic stress. *J. Exp. Bot.* 45 (12), 1789–1800. doi: 10.1093/jxb/45.12.1789

Torabian, S., Shakiba, M. R., Nasab, D. M. A., and Toorchi, M. (2018). Leaf gas exchange and grain yield of common bean exposed to spermidine under water stress. *Photosynthetica* 56 (4), 1387–1397. doi: 10.1007/s11099-018-0834-4

Wahid, A., Gelani, S., Ashraf, M., and Foolad, M. R. (2007). Heat tolerance in plants: an overview. *Environ. Exp. Bot.* 61 (3), 199–223. doi: 10.1016/j.envexpbot.2007.05.011

Xu, C., and Wu, X. (2009). Impact of DArg on drought resistance and endogenous polyamines in mycorrhizal pinus massoniana. *J. Nanjing Forestry Univ.* 52 (04), 19. Available at: http://njlydxxb.periodicals.net.cn/default.html.

Yang, X., Han, Y., Hao, J., Qin, X., Liu, C., and Fan, S. (2022). Exogenous spermidine enhances the photosynthesis and ultrastructure of lettuce seedlings under high-temperature stress. *Scientia Hortic.* 291, 110570. doi: 10.1016/j.scienta.2021.110570

Yang, J., Zhang, J., Liu, K., Wang, Z., and Liu, L. (2007). Involvement of polyamines in the drought resistance of rice. *J. Exp. Bot.* 58 (6), 1545–1555. doi: 10.1093/jxb/erm032

Zhang, C., Li, G., Chen, T., Feng, B., Fu, W., Yan, J., et al. (2018). Heat stress induces spikelet sterility in rice at anthesis through inhibition of pollen tube elongation interfering with auxin homeostasis in pollinated pistils. *Rice* 11 (1), 1–12. doi: 10.1186/s12284-018-0206-5

Zhao, W., Sun, G., and Li, S. (2004). Polyamines and plant stress resistance. *J. South. Agric.* 35, 443–447. doi: 10.3969/j.issn.2095-1191.2004.06.003

Zhao, Q., Zhou, L., Liu, J., Cao, Z., Du, X., Huang, F., et al. (2018). Involvement of CAT in the detoxification of HT-induced ROS burst in rice anther and its relation to pollen fertility. *Plant Cell Rep.* 37 (5), 741–757. doi: 10.1007/s00299-018-2264-y

frontiers | Frontiers in Plant Science

TYPE Original Research
PUBLISHED 08 December 2022
DOI 10.3389/fpls.2022.1049323

Check for updates

OPEN ACCESS

EDITED BY
Mirza Hasanuzzaman,
Sher-e-Bangla Agricultural University,
Bangladesh

REVIEWED BY
Guray Akdogan,
Ankara University, Turkey
Marzena Małgorzata Kurowska,
University of Silesia in Katowice,
Poland

*CORRESPONDENCE
Manuela Nagel
Nagel@ipk-gatersleben.de

†These authors share last authorship

SPECIALTY SECTION
This article was submitted to
Plant Abiotic Stress,
a section of the journal
Frontiers in Plant Science

RECEIVED 20 September 2022
ACCEPTED 10 November 2022
PUBLISHED 08 December 2022

CITATION
Nagel M, Arc E, Rajjou L, Cueff G,
Bailly M, Clément G,
Sanchez-Vicente I, Bailly C, Seal CE,
Roach T, Rolletschek H, Lorenzo O,
Börner A and Kranner I (2022) Impacts
of drought and elevated temperature
on the seeds of malting barley.
Front. Plant Sci. 13:1049323.
doi: 10.3389/fpls.2022.1049323

COPYRIGHT
© 2022 Nagel, Arc, Rajjou, Cueff, Bailly,
Clément, Sanchez-Vicente, Bailly, Seal,
Roach, Rolletschek, Lorenzo, Börner
and Kranner. This is an open-access
article distributed under the terms of
the Creative Commons Attribution
License (CC BY). The use, distribution
or reproduction in other forums is
permitted, provided the original
author(s) and the copyright owner(s)
are credited and that the original
publication in this journal is cited, in
accordance with accepted academic
practice. No use, distribution or
reproduction is permitted which does
not comply with these terms.

Impacts of drought and elevated temperature on the seeds of malting barley

Manuela Nagel [1*], Erwann Arc [2], Loïc Rajjou [3], Gwendal Cueff [3], Marlene Bailly [3], Gilles Clément [3], Inmaculada Sanchez-Vicente [4], Christophe Bailly [5], Charlotte E. Seal [6], Thomas Roach [2], Hardy Rolletschek [1], Oscar Lorenzo [4], Andreas Börner [1†] and Ilse Kranner [2†]

[1]Genebank Department, Leibniz Institute of Plant Genetics and Crop Plant Research (IPK), Gatersleben, Seeland, Germany, [2]Department of Botany and Center for Molecular Biosciences Innsbruck (CMBI), University of Innsbruck, Innsbruck, Austria, [3]Université Paris-Saclay, INRAE, AgroParisTech, Institut Jean-Pierre Bourgin (IJPB), Versailles, France, [4]Department of Botany and Plant Physiology, Instituto de Investigación en Agrobiotecnología (CIALE), Facultad de Biología, Universidad de Salamanca, Salamanca, Spain, [5]Unité Mixte de Recherche (UMR) 7622 Biologie du Développement, Institut de Biologie Paris Seine (IBPS), Sorbonne Université, CNRS, Paris, France, [6]Royal Botanic Gardens, Kew, Wakehurst, Ardingly, Haywards Heath, West Sussex, Haywards Heath, United Kingdom

High seed quality is key to agricultural production, which is increasingly affected by climate change. We studied the effects of drought and elevated temperature during seed production on key seed quality traits of two genotypes of malting barley (*Hordeum sativum* L.). Plants of a "Hana-type" landrace (B1) were taller, flowered earlier and produced heavier, larger and more vigorous seeds that resisted ageing longer compared to a semi-dwarf breeding line (B2). Accordingly, a NAC domain-containing transcription factor (TF) associated with rapid response to environmental stimuli, and the TF ABI5, a key regulator of seed dormancy and vigour, were more abundant in B1 seeds. Drought significantly reduced seed yield in both genotypes, and elevated temperature reduced seed size. Genotype B2 showed partial thermodormancy that was alleviated by drought and elevated temperature. Metabolite profiling revealed clear differences between the embryos of B1 and B2. Drought, but not elevated temperature, affected the metabolism of amino acids, organic acids, osmolytes and nitrogen assimilation, in the seeds of both genotypes. Our study may support future breeding efforts to produce new lodging and drought resistant malting barleys without trade-offs that can occur in semi-dwarf varieties such as lower stress resistance and higher dormancy.

KEYWORDS

barley, climate change, dwarfing genes, drought, metabolite, temperature, seed viability and seedling growth, ABI5 (ABA insensitive 5) and ANAC089

Introduction

Barley (*Hordeum vulgare* L.) is among the four most important crops globally (http://faostat.fao.org) and its caryopses, henceforth termed seeds, are used for staple food, for animal feed and in the brewing industry. Malting barley varieties must meet specific quality criteria, especially low lodging potential and high tolerance against diseases, high and stable seed yield, a seed size > 2.5 mm and for malting, the seed protein content should not exceed 12% (Federal Variety Office, 2021) as higher proteins contents interfere with the malting process (Jaeger et al., 2021). Significant breeding success with malting barleys was achieved around 1900 when Austrian breeders, including Tschermak-Seysenegg, used spring barleys from the Hana region of the Czech Republic (then Central Moravia) for hybridization. Due to their high malting quality, 'Hana'-type barleys dominated markets until the 1940s (Grausgruber et al., 2002). Later, i.e. during the Green Revolution, 'Hana'-type barleys were largely replaced by semi-dwarf varieties that were less susceptible to lodging. Notably, up to a 4.7 fold increase in seed yield could be achieved using dwarf and semi-dwarf varieties (Jing and Wanxia, 2003), resulting in improved harvest index, and it was easier to control nitrogen supply to achieve optimal seed nitrogen contents (Laidig et al., 2017), whereas old landraces with longer stems are prone to lodging as they produce heavier spikes when receiving more nitrogen (Grausgruber et al., 2002). The shorter plant height of semi-dwarfs is due to short culm mutation alleles related to changes in the metabolism and signal transduction of gibberellins (Gao and Chu, 2020) or brassinosteroids (Dockter et al., 2014). Most modern barley varieties carry a mutation at the *semi-dwarf* (*sdw*) gene, such as the *Sdw1/Denso* gene (Kuczyńska et al., 2013; Dockter and Hansson, 2015), an orthologue of the rice Green Revolution gene *SD1* encoding gibberellin 20-oxidase *HvGA20ox2*, a 2-oxoglutarate-dependent dioxygenase involved in the last steps of GA synthesis (Xu et al., 2017). Modifications of biosynthesis and signal transduction pathways of these hormones were the basis for plant breeding progress, and thus for improved seed and malt quality of spring barley (Dockter et al., 2014; Dockter and Hansson, 2015).

A deterioration of agro-climatic conditions affecting cereal productivity is forecast for many areas globally (Zhao et al., 2017; Ortiz-Bobea et al., 2021). In Europe, more erratic precipitation and shortening of the active growing season between cold winters and hot summers (Trnka et al., 2014) have been shown to negatively affect spring barley yield (Gammans et al., 2017; Jacott and Boden, 2020) and malt quality (Howard et al., 1996). Specifically, drought during seed production increases barley seed protein contents and thus, impairs malt quality (Jaeger et al., 2021). Furthermore, in warmer and drier regions, undesirable higher protein contents with the associated lower malt extract were observed after nitrogen application (Eagles et al., 1995). However, for a comprehensive understanding of the effects of climate change on plant productivity, the effects of the environment on plant and seed physiology must be appreciated. Moreover, focus must not only be placed on the nutritional quality and industrially desirable traits of barley seeds, such as malt quality, but also on key seed quality traits that are the basis for crop production, such as seed germination, vigour, viability and dormancy. Seed germination, the first critical step in the life cycle of most crop plants, can be defined as the process by which a quiescent seed develops into a seedling, starting with water uptake and ending with the protrusion of the radicle (the embryonic root) through the surrounding covers in conjunction with cell division in the radicle (Bewley, 1997; Nonogaki, 2014). Seed vigour, often best observed under stress conditions, can be defined as the sum total of those properties, including germination speed, that determine seed performance during germination and seedling emergence (Finch-Savage and Bassel, 2015). Viability is the capability of a seed to germinate, and dormancy is the inability of a seed to germinate under favourable conditions before certain environmental cues, such as low temperatures for an extended time, have been received (Hampton and TeKrony, 1995; Graeber et al., 2012). Lack of dormancy may result in pre-harvest sprouting, i.e. germination on the mother plant, which is an undesirable agronomic trait that compromises yield, nutritional and processing quality, and in barley, renders seeds unsuitable for malting (Rodriguez et al., 2015). The depth of seed dormancy is determined during seed maturation on the mother plant, subject to environmental and parental control, through genetic and hormonal regulation (Penfield and MacGregor, 2017; Iwasaki et al., 2022).

Here, we report on the response of two malting barleys, the Austrian landrace HOR 2110 (B1), in the 'Hana' progeny, and a semi-dwarf breeding line HOR 4710 (B2) used in Northern Germany. These two genotypes were part of the "EcoSeed" mapping panel, which revealed that plant height, dormancy, number of seeds per spike and days to anthesis are heritable phenotypic traits (Nagel et al., 2019). We hypothesised that drought and elevated temperature during seed production differentially affect seed quality traits such as seed vigour, germination, dormancy and reserve deposition in the two genotypes. To assess seed stress level, responses of malondialdehyde (MDA), a marker of oxidative stress (Kranner et al., 2010), and two transcription factors (TFs), ABI5 and ANAC089, with prominent roles in the regulation of seed germination were studied. The TF ABI5, a member of the basic leucine zipper (bZIP) family, represents a hub in the abscisic acid (ABA) signalling network (Sanchez-Vicente et al., 2019) during seed germination and post-germinative developmental checkpoints (Finkelstein and Lynch, 2000; Lopez-Molina et al., 2001). In barley seeds, the ABI5 protein is expressed in the aleurone cells (Casaretto and Ho, 2003).

Moreover, ABI5 is involved in the perception of various developmental cues and in stress response (Jakoby et al., 2002) and transgenic cotton expressing *AtABI5* showed enhanced resistance to drought stress (Mittal et al., 2014). ABI5 protein accumulation is triggered by ABA-induced phosphorylation resulting in the stabilization of the protein (Lopez-Molina et al., 2001). Furthermore, *S*-nitrosylation of ABI5 by nitric oxide (NO) leads to its proteolysis, thereby alleviating the repression of seed germination by ABI5 (Albertos et al., 2021). Nitric oxide affects seed physiology by counteracting ABA signalling and dormancy maintenance, thereby promoting germination (Arc et al., 2013; Nagel et al., 2019) and in Arabidopsis, NO levels can be regulated by the extranuclear-localized NAC-domain TF, ANAC089 (Albertos et al., 2021). Members of the NAC gene family have been suggested to play important roles in the regulation of the transcriptional reprogramming associated with plant stress response (Singh et al., 2021; Alshareef et al., 2022). For example, in rice NAC domain-containing proteins can interact with phytohormones and regulate plant response to different stress factors, i.e. by modulating ABA signalling (Hong et al., 2016). ANAC089 can bind the specific *cis*-regulatory CGTnAG motif that is overrepresented in the promoters of downregulated ABA-responsive genes and of upregulated redox-related homeostasis genes, and Arabidopsis seeds of the *gap1* mutant with a gain-of-function mutation in *ANAC089* showed increased tolerance against abiotic stress factors (Albertos et al., 2021). Changes in the abundance of the TFs ABI5, ANAC089 and of the stress marker, MDA, were assessed in combination with in-depth plant and seed phenotyping in the two barley genotypes, and metabolism of the embryo was evaluated by GC-MS-based metabolite profiling.

Materials and methods

Plant material, growth conditions and phenotyping

Caryopses (in which seed and fruit coats are fused), hereafter termed "seeds" for simplicity, of two barley genotypes (*Hordeum vulgare* L. convar. *distichon* (L.) Alef. var. *nutans* (Rode) Alef.), the Austrian landrace HOR 2110 (https://doi.org/10.25642/IPK/GBIS/18216 termed "B1") and the breeding line HOR 4710 (https://doi.org/10.25642/IPK/GBIS/94164 termed "B2") originally received from the VEG Saatzucht Boldebuck/Güstrow, were taken after 40 years of long-term storage at 0°C at the Federal *ex situ* Genebank for agricultural and horticultural plants of Germany (IPK Gatersleben). Seeds were multiplied in 2012 and the progeny was used for experiments in 2014. Of each genotype, 336 seedlings were grown in a greenhouse in pots (30 x 30 x 15 cm, 4 plants per pot) at a 23/15°C day/night cycle until anthesis. After half of the spikes had flowered, plants were kept for another seven days under the same conditions, and then randomly selected and subjected either to "control" conditions (C, 22/18°C and regular watering) or "elevated temperature" (ET, 28/25°C and regular watering), or "drought" (D, 22/18°C and 15% field capacity). After harvest, seeds were cleaned, dried at 20°C and 20% relative humidity (RH) for eight weeks (for after-ripening), and then stored at -18°C. The agronomic traits days to anthesis, days to maturity, number of spikes on the tillers and of seeds harvested, plant height, spike length, thousand seed weight (TSW) and seed grades (<2.2 mm, >2.2 mm, >2.5 mm and >2.8 mm) were evaluated.

Seed phenotyping: Germination, vigour test, stratification and controlled deterioration

Three replicates of 40 seeds were placed on moistened filter paper and germinated at 5, 10, 20 or 25°C under 150 µmol m^{-2} s^{-1} for 8 h light/16 h dark cycle. Total germination (TG) was scored daily and considered completed when the radicle had protruded by more than 2 mm. Root and shoot lengths of seedlings were recorded for untreated (non-stratified) seed lots. After 14 days, seeds were categorised for vigour testing into normal seedlings (NS), abnormal seedlings (damaged, deformed, or decayed with no potential to develop into a normal plant), and non-germinating seeds according to ISTA (2014). For germination in the presence of ABA, seed germination and germination speed was tested according to Collin et al. (2020). For this, 35 seeds were placed in a Petri dish containing two layers of filter papers wetted with 12 mL distilled water (control) or ABA solution (75 and 300 µM). After a four-day stratification treatment at 4°C, seeds were germinated in a growth chamber at 22°C under an 8 h light/16 h dark cycle, and germination was scored daily. Total germination, the percentage of NS, the time to reach 10% and 50% of maximum TG (T_{10}, T_{50}), and the area under the germination progress curve ("area under curve"; AUC) after 100 h were calculated using the curve-fitting module of the Germinator software (Joosen et al., 2010). Cold stratification was conducted at 10°C for 7 days before transfer to 20°C for another week. For controlled deterioration, seeds were equilibrated at 24°C and 75% RH above NaCl for 10 days, and then subjected to 40°C for up to 9 weeks, during which time they lost viability, assessed by their failure to germinate.

Determination of seed reserves

Seed protein, lipid and starch contents were extracted from freeze-dried and finely ground seed material. Total nitrogen content was measured by elemental analysis using a Vario EL3 (Elementaranalysesysteme GmbH) and multiplied by a known conversion factor, 5.7, for wheat grains (Sosulski and Imafidon, 1990), to estimate the total protein content. Total lipid content

was analysed using nuclear magnetic resonance spectroscopy (NMR; MQ-60, Bruker GmbH) according to the manufacturer's instructions. Starch was determined using near infrared (NIR) spectroscopy (MPA, Multi Purpose Analyzer, Bruker GmbH), applying multivariate calibration algorithms (software OPUS, Bruker GmbH) and the reference material library B-FING-S (Bruker GmbH).

Assessment of malon dialdehyde and transcription factors

Malondialdehyde was determined as described in Bailly and Kranner (2011). Seeds were ground using a chilled mortar and pestle with 5 mL of thiobarbituric acid:trichloroacetic acid solution of 0.5% (w/v):20% (w/v), the homogenate was heated to 95°C and kept for 30 min in a water bath and then quickly cooled on ice. After centrifugation of the homogenate at 16,000×*g* for 30 min, 2 mL of the supernatant was used for MDA determination. Equivalents of MDA were calculated from the difference in absorbance at 532 and 600 nm using an extinction coefficient of 155 mM^{-1} cm^{-1}.

For the assessment of ABI5 and NAC-domain-containing TFs, total proteins were extracted from dry seeds or after imbibition in sterile distilled water for 12 h in the dark. Seeds were ground using mortar and pestle and homogenized in extraction buffer (100 mM Tris-HCl, 150 mM NaCl, 0.25% NP-40; v/v) containing 1 mM PMSF and 1 x cOmplete® EDTA-free protease inhibitors (Sigma) followed by centrifugation for 10 min at 15,800 g at 4°C. Final protein concentration was determined by the Bio-Rad Protein Assay (Bio-Rad) based on the Bradford method (Bradford, 1976). In total, 45 µg of total protein per well were loaded in SDS-acrylamide/bisacrylamide gel electrophoresis using Tris-glycine-SDS buffer. Proteins were electrophoretically transferred to a 0.2 µM polyvinylidene difluoride (PVDF) membrane (Bio-Rad) using the Trans-Blot Turbo (Bio-Rad). Membranes were blocked in Tris-buffered saline-0.1% Tween 20 containing 5% blocking agent and probed with antibodies diluted in blocking buffer with 1% blocking agent. Anti-ANAC089 purified rabbit immunoglobulin (Biomedal, 1:10,000), a polyclonal antibody binding to the Arabidopsis ANAC089 (Albertos et al., 2021), and anti-ABI5 purified rabbit immunoglobulin (Biomedal, 1:10,000) (Albertos et al., 2015), anti-Actin (Sigma, 1:10,000) and ECL-peroxidase-labelled anti-rabbit (Amersham, 1:10,000) and anti-mouse (Amersham, 1:10,000) antibodies were used in the western blot analyses. Proteins were detected using ECL Advance Western Blotting Detection Kit (Amersham) by their chemiluminescence using a ChemiDoc MP Imaging System (Bio-Rad).

Metabolite profiling

For metabolite profiling, three replicates of 20 mg of barley embryos manually dissected from dry mature seeds were ground with mortar and pestle in liquid nitrogen and stored at -80°C. Each sample was placed in a 2 mL Safe-Lock Eppendorf tube (Eppendorf AG). The ground, frozen samples were re-suspended in 1 mL of ice-cold (-20°C) water:acetonitrile: isopropanol (2:3:3 v/v/v) containing 4 mg L^{-1} ribitol as an internal standard and extracted for 10 min at 4°C by shaking (1,400 rpm) with an Eppendorf Thermomixer (Eppendorf AG). Insoluble material was removed by centrifugation at 20,000 g for 5 min. 25 µL were collected and dried for 150 min in a SpeedVac (Savant SPD131DDA, Thermo Fisher Scientifi) and stored at -80°C. Seed samples were removed from the freezer and allowed to equilibrate with ambient temperature for 15 min before opening and drying in a SpeedVac for 1 hour before adding 10 µL of 20 g L^{-1} methoxyamine in pyridine to the samples, the blanks or the standard solutions of amino acids and sugars. After 90 min of continuous shaking in an Eppendorf Thermomixer at 28°C, 90 µL of N-methyl-N-trimethylsilyl-trifluoroacetamide (MSTFA) were added and the reaction continued for 30 min at 37°C. After cooling, 50 µL were transferred to an autosampler vial. Two hours after derivatization, 1 µL of sample was injected in splitless mode into an Agilent 7890A gas chromatograph coupled to an Agilent 5975C mass spectrometer and separated on a Rxi-5SilMS column (Restek, 30 m with 10 m Integra-Guard column). The liner (Restek # 20994) was changed before each series of analysis and 10 cm of column were cut. Oven temperature ramp was 70°C for 7 min, then 10°C min^{-1} to 325°C for 4 min for a total run time of 36.5 min. Helium flow was 1.5231 mL min^{-1}, injector temperature 250°C, transfer line temperature 290°C, ion source temperature 250°C and quadrupole temperature was 150°C. Samples and blanks were analysed in a randomized manner. Amino acid standards were injected at the beginning and end of each sample batch for monitoring of the derivatization stability. An alkane mix (C10, C12, C15, C19, C22, C28, C32, C36) was injected in the middle of the queue for external calibration of retention indices. Five scans per second were acquired. Raw Agilent data files were converted to NetCDF format and analysed with AMDIS (http://chemdata.nist.gov/mass-spc/amdis/), and metabolites identified according to their retention indices and mass spectra. Peak areas were then analysed using the QuanLynx software (Waters Corporation, Milfords, MA, USA) after conversion of the NetCDF file to MassLynx (Waters) format. Two analytical replicates of each biological replicate (n=3) were analysed. The data is available as part of the Metabolomics Workbench repository (Project: R001453; datatrack_id:3436, study_id: ST002272; (Sud et al., 2016) under http://dx.doi.org/10.21228/M8X13R.

10.3389/fpls.2022.1049323

Statistics

Data for plant and seed phenotyping and for seed reserves were tested for normality using the Shapiro-Wilk test. If no normal distribution was found, the Kruskal Wallis one-way analysis of variance of ranks was used. Then, data were tested for significance (P<0.05) by the Tukey or Dunn's *post-hoc* test, as appropriate. For the metabolite profiling data, raw values were transformed *via* log1p transformation (formula = ln(value + 1)) and imputation of missing values was performed using the R package 'missForest' (Stekhoven and Bühlmann, 2011). Metabolites displaying more than 20% of missing values were not considered for the statistical analysis. To test for significances in the metabolite data set, two-way ANOVA and Benjamini and Hochberg false discovery rate (FDR) adjustment were used at P<0.05. Multivariate statistical analysis was performed using Principal Component Analysis (PCA) to assess differences between metabolites profiles for the six groups (2 genotypes x 3 growth conditions).

Results

Effects of the maternal environment on plant and seed phenotype

Controls. The barley genotype B1 developed significantly taller plants (Figure 1A) that flowered earlier (Figure S1A) and had longer spikes (Figure S1D) producing heavier (Figure 1B) and larger seeds (Figure S1F) than B2. When germinated without stratification, TG and % NS of B2 seeds were lower than in B1 seeds (Figure 1C; Figure S2A) and this difference became significant when viewed through T_{50} (Figure 1D), revealing that B1 seeds germinated faster and produced longer shoots (Figure S2B). Differences in TG, % NS and T_{50} were mitigated when seeds were stratified prior to germination at 20°C (Figures 1C, D; Figure S2A). The significantly lower TG of B2 seeds when germinated at 25°C, but only to a small degree at 5 or 10°C (Figure 1E), confirmed that B2 seeds exhibited a more pronounced thermodormancy, which was broken by the stratification treatment (Figure 1D). When seeds were germinated in the presence of ABA, TG of seeds of both genotypes dropped significantly with increasing ABA concentration, with a 40% decrease in response to 300 µM ABA (Figure S2E). At this concentration, T_{50} of B1 was significantly delayed compared to B2 (Figure S2E). In response to artificial ageing by CD, used as a vigour parameter, seeds of both genotypes lost TG after 9 weeks of CD (Figure S2C, D). However, B1 seeds resisted the ageing treatment longer than B2 seeds, as shown by significantly compromised TG after 3 and 5 weeks of CD for B2 and B1 seeds, respectively (Figure S2C, D).

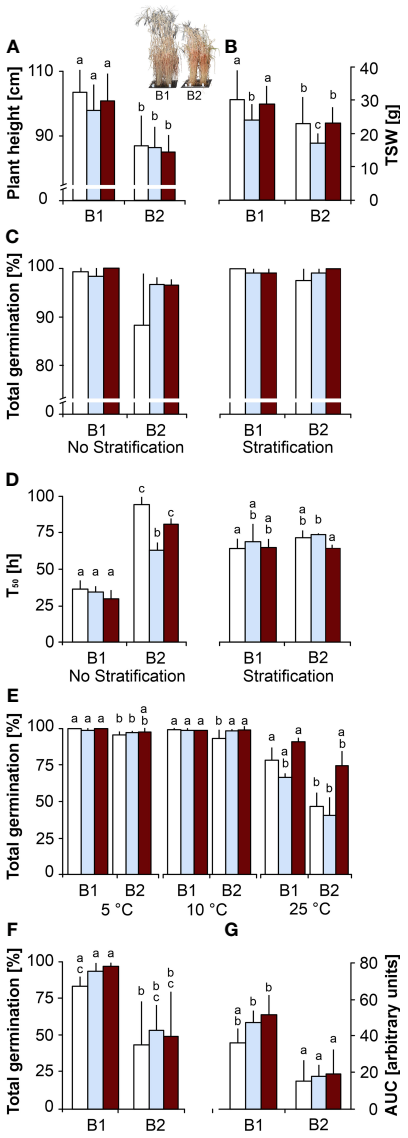


FIGURE 1
Effects of the maternal environment on plant and seed phenotype. Plants of genotypes B1 and B2 were grown in a greenhouse set to a 23/15°C day/night cycle until anthesis and then subjected to control conditions (22/18°C and regular watering; white bars), drought stress (22/18°C and 15% field capacity; blue bars) or elevated temperature (28/25°C and regular watering; red bars). Seeds were germinated at 20°C under an 8 h light/16 h dark cycle. The effects of the maternal environment are shown for **(A)** plant length (the inset shows a typical picture of the B1 and B2 plant phenotypes), **(B)** thousand seed weight (TSW), **(C, D)** total germination and time to reach 50% total germination (T_{50}), respectively, with and without breaking of dormancy after stratification by exposing imbibed seeds to 10°C for 7 days, **(E)** total germination at 5, 10 and 25°C, **(F, G)** total germination and time to reach 10% total germination (T_{10}), respectively, after 4 weeks of controlled deterioration at 75% RH and 40°C. Bars labelled with the same or no letters do not differ significantly at P<0.05; bars show mean ± SD of n = 112 plants in **(A, B)** and n = 3 x 40 seeds each in **(C-F)**.

Germination speed, expressed as AUC, was halved after 4 weeks of CD (Figure 1G).

Drought. Compared to controls, plants exposed to drought upon anthesis had significantly reduced spike numbers (Figure S1C), and their seeds needed less time to mature (Figure S1B), were lighter (Figure 1B) and smaller (Figure S1F) in both genotypes. Drought in the maternal environment did not affect TG in genotype B1, but the thermodormancy observed in B2 control seeds was reduced when seeds were produced under drought, which showed higher TG (Figure 1C) and faster germination at 20°C without stratification (Figure 1D; $P<0.05$). The effects of increasing ABA concentration on TG and T50 were less pronounced in seeds produced under drought in both genotypes, although B1 seeds took more time to germinate than B2 seeds (Figures S2E, F). In both genotypes, seeds produced under drought tended to resist CD slightly better than control seeds, but this effect was not significant at $P<0.05$ (Figures 1F, G; Figures S2C, D).

Elevated temperature. Compared to controls, plants grown under elevated temperature had significantly reduced spike numbers and seeds needed less time to mature in genotype B1 only (Figures S1B, C); TSW was not affected in either genotype (Figure 1B). The thermodormancy observed in B2 control seeds was reduced in seeds produced under elevated temperature (Figures 1C-E), which tended to resist CD slightly better than control seeds (not significant at $P<0.05$; Figures S2C, D). Compared to control seeds, seeds produced under elevated temperature and germinated in the presence of ABA had higher TG and germinated faster (lower T50), especially at 75 mM ABA (Figure S2E, F).

In summary, plants of genotype B1 were higher, flowered earlier and produced heavier, larger and more vigorous seeds without thermodormancy that germinated better in response to ABA and resisted ageing longer than those of genotype B2. Drought during seed development significantly reduced seed weight and size, and therefore total seed yield, in both genotypes, and elevated temperature reduced seed size, but not TSW significantly. Drought and elevated temperature in the maternal environment reduced thermodormancy and affected germination in response to ABA in genotype B2. Seeds produced under drought and elevated temperature in the maternal environment tended to resist CD slightly better than control seeds.

In addition, we show a re-analysed subset of phenotyping data for the B1 and the B2 genotypes grown in four different years in the field (Nagel et al., 2019; Tarawneh et al., 2020), showing that some traits of B2, such as shorter plant height (Figure S3D) and dormancy (Figure S3H-J) were also expressed in the field, but other traits were improved compared to the plants grown in the greenhouse in B2 (Figure 1, Figure S1); for example, genotype B2 and genotype B1 had the same or better performance in the field regarding TSW (Figure S3F) and harvest index (Figure S3G), respectively.

Effects of the maternal environment on seed reserves, malon dialdehyde and transcription factors

Starch, protein, oil and MDA contents. Seeds of genotype B2 had significantly higher protein contents than B1 seeds, but comparable oil and starch contents. B1 seeds produced under drought had lower starch contents than seeds produced under elevated temperature, and compared to controls, B1 seeds had higher protein levels when produced under drought (Figure 2). Seed MDA levels were significantly higher in B2 seeds, and were not affected by the maternal environment in either genotype (Figure 3A).

ABI5 and NAC domain-containing protein. Dry seeds of both genotypes showed comparable ABI5 levels under control conditions (Figures 3B, C). In dry B1 seeds produced under drought (Figure 3B) and elevated temperature (Figure 3C), ABI5 levels appeared to be higher compared to control seeds. In imbibed seeds of both genotypes, a second ABI5 band with a slightly higher molecular weight was detected and up-accumulated as compared to dry seeds. Moreover, ABI5 levels were higher in B1 seeds produced under drought and under elevated temperature compared to B2 seeds, consistent with the higher tolerance to the CD treatment (Figures 1F, G, S2C, D). A NAC domain-containing protein with a similar size to ANAC089 (>37 kDa) was more abundant under all conditions in B1 compared to B2 (Figures 3B, C), consistent with its ability to produce more and heavier seeds even under adverse conditions compared to genotype B2 (Figure 1B; Figure S1F).

Effects of the maternal environment on seed metabolite profiles

Principal component analysis of all metabolites across three maternal environments in genotypes B1 and B2. In total, 173 compounds were detected and quantified (97 identified and 76 unknown molecules, Table S1A) in embryos isolated from dry barley seeds. After filtering for missing values, 140 metabolites (90 identified and 50 unknown metabolites, Table S1B) were considered for statistical evaluation. Visualization of the metabolite profiles by PCA revealed differences between the two genotypes along principal component (PC) 1, accounting for 33.2% of variance. In both genotypes, PC 2 clearly separated the metabolite profiles of embryos from seeds produced under drought, but not elevated temperature (Figure 4A). Separate PCA for each genotype (Figures 4B, C) confirmed that the effect of drought in the maternal environment on the metabolism of the embryo was more pronounced than that of elevated temperature.

Comparison between the two genotypes B1 and B2. Comparison between the embryos dissected from dry seeds of

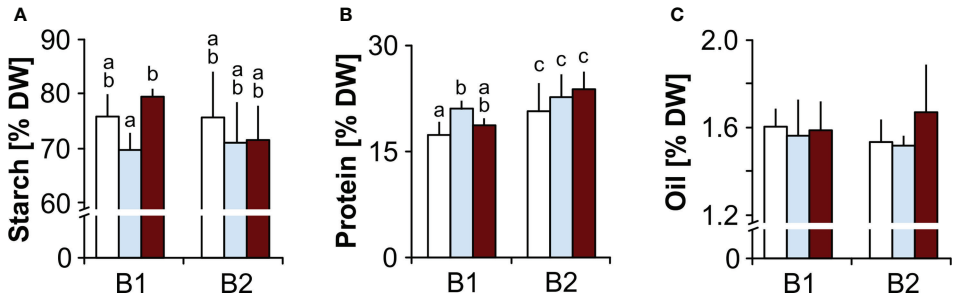


FIGURE 2
Effects of the maternal environment on seed reserves. Plants of genotypes B1 and B2 were grown in a greenhouse set to a 23/15°C day/night cycle until anthesis and then subjected to control conditions (22/18°C and regular watering; white bars), drought stress (22/18°C and 15% field capacity; blue bars) or elevated temperature (28/25°C and regular watering; red bars). The effects of the maternal environment on **(A)** starch, **(B)** protein and **(C)** seed oil contents are shown. Within each genotype, bars labelled with the same or no small letters do not differ significantly at $P<0.05$; bars show mean ± SD of n = 3 x 40 seeds.

the two genotypes revealed differential accumulation of 38 metabolites (Figure 5). In embryos of B2 seeds, the contents of most amino acids, organic acids, sugars, sugar alcohols and glycerol phosphates, were higher compared to B1 embryos in all three maternal environments. Specifically, under control conditions, B2 had higher levels of glutamine, histidine, proline, threonine, nicotinic acid, allantoin, arabitol, erythritol, threitol, sn-glycerol-2-phosphate and sn-glycerol-3-phosphate, mannose and ribose, whereas campesterol, erythronic acid and myo-inositol were significantly lower than in embryos of B1 seeds.

Comparison between control conditions and drought or elevated temperature. The accumulation of 18 metabolites was differentially influenced by the maternal environment, especially by drought, leading to the up-accumulation of 8 amino acids, 9 organic acids and down-accumulation of γ-tocopherol, sorbitol, uridine and xylitol (Figure 6). No significant differences were found in embryos dissected from dry seeds produced under elevated temperature. In summary, drought, but not elevated temperature, upon seed maturation clearly affected the embryo metabolome, especially in B2.

Discussion

We investigated if stress factors predicted to increase due to climate change, namely drought and elevated temperature, during seed production affect seed metabolism and seed quality traits in two genetically distinct genotypes of two-row spring barley, the Hana-type landrace B1 and the semi-dwarf B2. Plants of genotype B2 were significantly shorter, expressed more dormancy and had less vigorous seeds that deteriorated faster upon CD, and clear constitutive differences between genotypes in seed metabolism were identified

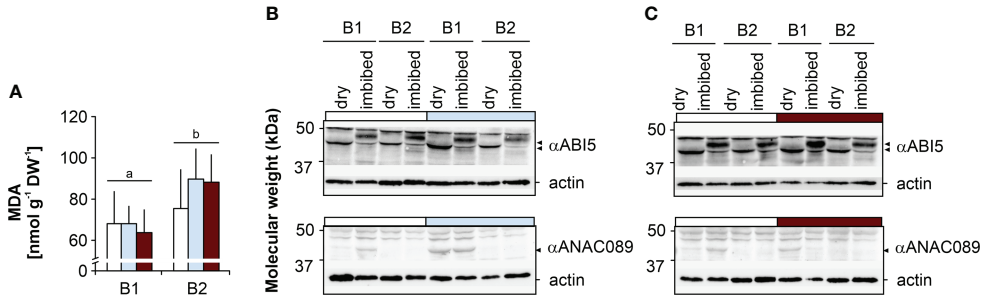


FIGURE 3
Effects of the maternal environment on malon dealdehyde (MDA) and the ABI5 and ANAC089-like transcription factors. Plants of genotypes B1 and B2 were grown in a greenhouse set to a 23/15°C day/night cycle until anthesis and then subjected to control conditions (22/18°C and regular watering; white bars), drought stress (22/18°C and 15% field capacity; blue bars) or elevated temperature (28/25°C and regular watering; red bars). The effects of the maternal environment are shown for **(A)** MDA (bars labelled with the same or no letters do not differ significantly at $P<0.05$; bars show mean ± SD of n = 3 x 40 seeds) and **(B)** the abundance of two transcription factors, ABI5 and ANAC089-like, in dry seeds and germinating seeds 12 h after the onset of imbibition after drought and **(C)** elevated temperatures.

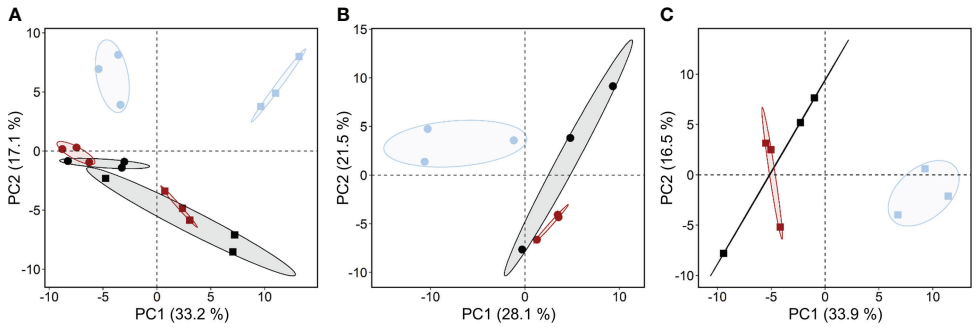


FIGURE 4
Effects of the maternal environment on metabolite profiles. Principal component (PC) analysis of all metabolites detected in embryos of barley seeds produced under different maternal environments. Plants of genotypes B1 (circles) and B2 (squares) were grown in a greenhouse set to a 23/15°C day/night cycle until anthesis and then subjected to control conditions (22/18°C and regular watering; black symbols), drought stress (22/18°C and 15% field capacity; blue symbols) or elevated temperature (28/25°C and regular watering; red symbols). The effects of the maternal environment on the metabolite profiles are shown for **(A)** both genotypes; **(B)** genotype B1 and **(C)** genotype B2.

(Figures 1, 5). Semi-dwarf varieties carry mutation alleles related to changes in the metabolism and signal transduction of gibberellins or brassinosteroids (Dockter et al., 2014), and these phytohormones also affect seed traits. In seeds of the "EcoSeed" mapping panel, which included genotypes B1 and B2, the gibberellin 20-oxidases *HvGA20ox1* and *HvGA20ox3*, involved in the last steps of GA synthesis, were associated with pre-harvest sprouting and dormancy release (Nagel et al., 2019; Figures S3H-J). In addition, the genes *CONSTITUTIVE PHOTOMORPHOGENIC DWARF* (*HvCPD*), and *DIMINUTO* (*HvDIM*), both involved in brassinosteroid biosynthesis, and *HvBRI1*, which encodes a

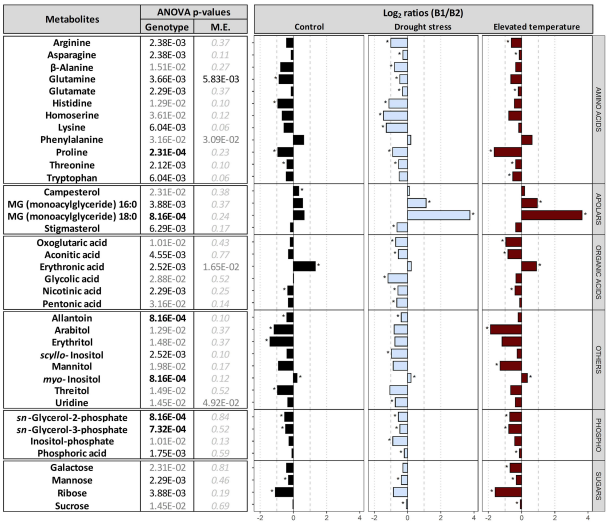


FIGURE 5
Differences in metabolites between genotypes. Plants of genotypes B1 and B2 were grown in a greenhouse set to a 23/15°C day/night cycle until anthesis and then subjected to control conditions (22/18°C and regular watering; black), drought stress (22/18°C and 15% field capacity; blue) or elevated temperature (28/25°C and regular watering; red). Metabolites differentially accumulated between the embryos of the two genotypes, across all maternal environments, were selected based on their two-way ANOVA p-value after false discovery rate (FDR) correction [left panel; bold black, black and grey numbers indicate significant differences at P<0.001, P<0.01 and P<0.05, respectively; light grey italic letters: not significant; interactive effects of genotypes x maternal environments (M.E.) were not significant]. The right panel shows $\log_2$ ratios for metabolites differentially accumulated between the two genotypes. Asterisks indicate significant differences between the two genotypes under a given M.E.

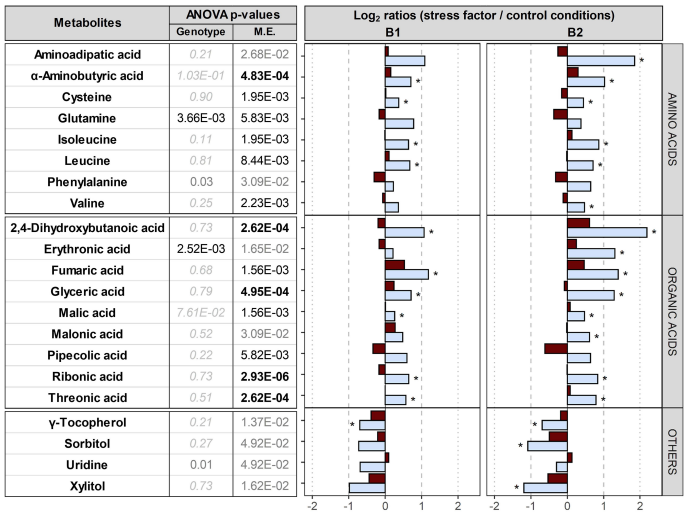


FIGURE 6
Impact of the maternal environment on metabolites. Plants of genotypes B1 and B2 were grown in a greenhouse set to a 23/15°C day/night cycle until anthesis and then subjected to control conditions (22/18°C and regular watering; black), drought stress (22/18°C and 15% field capacity; blue) or elevated temperature (28/25°C and regular watering; red). Metabolites differentially accumulated in embryos produced under the three maternal environments were selected based on their two-way ANOVA p-value after false discovery rate (FDR) correction [left panel; bold black, black and grey numbers indicate significant differences at P<0.001, P<0.01 and P<0.05, respectively; light grey italic letters: not significant; interactive effects of genotypes x maternal environments (M.E.) were not significant]. The right panel shows $\log_2$ ratios for metabolites differentially accumulated under drought or elevated temperature compared to control conditions. Asterisks indicate significant differences between drought or elevated temperature in the M.E. compared to control conditions.

brassinosteroid receptor (Dockter et al., 2014), were also associated with dormancy (Nagel et al., 2019), and can also affect plant height (Dockter et al., 2014) and seed germination (Vriet et al., 2012). Plants with mutations in brassinosteroid synthesis or signalling pathways were also more susceptible to temperature stress, whereby hormonal interactions depended on genetic background and stress factor applied (Gruszka et al., 2016; Sadura et al., 2019). Taken together, the above studies provide evidence that traits selected for spring barley breeding involved modifications to the metabolism and/or signalling of gibberellins and brassinosteroids, which likely contributed to the differences between B1 and B2 in plant height and seed dormancy. However, germplasm selection for plant height can also introduce unwanted pleiotropic effects, such as late heading, low TKW, reduced seed size and yield and traits undesirable for brewing (Thomas et al., 1991). In field experiments, the B2 genotype did not show such compromised plant performance (Nagel et al., 2019; Tarawneh et al., 2020). However, later anthesis, lower TSW, reduced seed size and higher seed MDA levels in the B2 genotype were observed when plants were grown in the greenhouse (Figures 1, 3; Figure S1), suggesting a lower tolerance to growth under sub-optimal environmental conditions, a trade-off sometimes found in semi-dwarfs (Thomas et al., 1991), i.e. genotype B2 appears to be more susceptible to stress than genotype B1.

Furthermore, the clear accumulation of a NAC domain-containing protein in dry and imbibed seeds of B1, but not B2, suggests that ABA metabolism and signalling are also differentially regulated in the two genotypes. NAC TFs have been reported to be involved in plant stress response generally, and in barley are implicated in the molecular crosstalk between ABA and jasmonic acid. Thus, the NAC gene family appears to be involved in regulatory pathways affecting agronomic traits (Christiansen et al., 2011). Genotype B1 accumulated more of a NAC-like orthologue, in agreement with the better resistance of B1 seeds to ageing, drought and elevated temperature (Figures 1D, F, G). As a polyclonal antibody against ANAC089 was used (Albertos et al., 2021), other NAC-like orthologues could have been detected, pointing at a similar NAC involved in stress responses of barley. On the other hand, seeds of the two genotypes had similar ABI5 levels under control conditions, but differed in dormancy status. The transcription factor ABI5, a key repressor of seed germination, regulates the expression of seed-specific genes (Finkelstein and Lynch, 2000) and is important for post-germination development (Lopez-Molina et al., 2001). The higher amount of ABI5 in response to drought and elevated temperature in the seeds of genotype B1, which have higher vigour and tolerate CD better, during imbibition also supports the view that B1 is more stress tolerant. Furthermore, ABI5 levels can remain unchanged while ABI5 function is altered. Besides NO-mediated

degradation of ABI5 (Albertos et al., 2015), NO can reversibly modify thiol groups of specific cysteine residues (Stamler et al., 2001), affecting ABI5 redox state. B1 seeds with higher NO levels under field conditions compared to B2 were non-dormant (Figure S3), consistent with the previously reported correlation between NO release and lack of dormancy in barley (Nagel et al., 2019). Hence, subtle differences in the intricate network comprising hormonal interaction, *S*-nitrosylation and redox-regulation may account for differences in NO and ABA metabolism and signalling between the two genotypes, which may contribute to the different expression of dormancy and stress response in the two genotypes.

Metabolite profiles reveal constitutive differences between the two genotypes

Metabolite profiling revealed clear differences between the embryos of the two genotypes, irrespective of the maternal environment under which the seeds were produced (Figure 5). The significantly higher abundance of 11 amino acids in B2 (Figure 5) is consistent with higher protein levels found in B2 seeds (Figure 2B). Higher levels of glutamine and amino acids synthesized from it, including arginine and proline (Forde and Lea, 2007), all of which were significantly enhanced in B2, support the synthesis of hordeins, which make up 30-50% of the barley proteins (Howard et al., 1996). This also agrees with the finding that levels of glutamic acid and proline were associated with high protein contents in barley seeds (Smith, 1972). Furthermore, accumulation of osmolytes and compatible solutes such as proline in response to various stress factors has been associated with antioxidative defence, signalling and chelation of metals (Hayat et al., 2012) and in spring barley, a protective role for proline in response to water shortage during spike formation was suggested to support seed development (Frimpong et al., 2021). Other compatible solutes, including sugar alcohols, such as arabitol, erythritol, mannitol and threitol, were also more abundant in B2 than in B1, regardless of the maternal environment, and indicative of an elevated stress response of the B2 genotype compared to B1.

In Arabidopsis, histidine was shown to promote oil deposition by activating genes of ABA biosynthesis (Ma and Wang, 2016). Therefore, histidine accumulation in B2 (Figure 5) leading to higher ABA contents would be consistent with the higher dormancy levels in B2 seeds (Figures 1C, D). Although the total lipid contents in seeds did not differ between the two genotypes (Figure 2), the differential accumulation of two monoacylglycerols and glycerol phosphates in isolated embryos (Figure 5) could also point at differences in lipid metabolism, possibly linked to lipid composition or distribution between endosperm and embryo. Furthermore, an accumulation of glycerol-2-P and glycerol-3-P has been associated with lower seed germinability after storage (Wiebach et al., 2020), in agreement with the lowered resistance to CD and increased level of MDA of B2 seeds.

Campesterol, a key precursor of brassinolide (Grove et al., 1979), was up-accumulated in embryos of the B1 genotype (Figure 5). Brassinosteroids promote germination by activating GA and inactivating ABA signalling (Kim et al., 2019), and a role for brassinolide in promoting plant growth and stress resistance through down-regulation of ABA signalling has been suggested (Bajguz and Hayat, 2009). Although an elevated level of a phytohormone precursor alone does not allow one to draw conclusions on signalling, the higher levels of campesterol in B1 embryos are at least consistent with the lack of dormancy in B1 seeds and their enhanced resistance to CD. Furthermore, *myo*-inositol was also significantly up-accumulated in B1 seeds, and this could be related to ABI5, which down-regulates PHOSPHATE1 (PHO1) gene expression associated with phosphate homeostasis and phosphorus mobilization from phytic acid (Wild et al., 2016; Huang et al., 2017), and variations in the *myo-inositol monophosphatase (CaIMP)* gene was associated with increased seed size in chickpea (Dwivedi et al., 2017). Therefore, ABI5 may control the phytate pool *via PHO1* and modulate *myo*-inositol metabolism, supporting increased seed size and lower stress levels in genotype B1. In summary, differences in the metabolite profiles in the embryos of the two genotypes produced in different maternal environments reflect clear genetic differentiation, also accounting for some of their individual traits.

Effects of drought and elevated temperature in the maternal environment on metabolites

When elevated temperature was applied during seed filling, TSW, a key yield parameter, was unaffected in both genotypes. Genotype B1 matured earlier and produced less spikes, and B1 seeds had less thermodormancy, but these effects were not reflected in the metabolites assessed in this study, none of which were significantly changed in seeds produced under elevated temperature compared to controls (Figure 6). However, B1 seeds produced under drought or elevated temperature had higher ABI5 levels, especially upon imbibition. In barley, *HvABI5* is involved in the ABA-dependent regulation and fine-tuning of plant response to drought stress, associated with better membrane protection, higher flavonoid contents, and faster stomatal closure (Collin et al., 2020). In Arabidopsis, ABI5 binds to the promoter regions of LEA genes, such as *AtEm1* and *AtEm6*, delaying LEA protein accumulation in ABI5 mutants (Carles et al., 2002). Mutants deficient in AtEm6 fail to develop normal seeds due to a lower capacity to buffer water loss, resulting in premature dehydration in the seed filling phase (Manfre et al., 2005). Following this line of reasoning, higher ABI5 levels in B1 seeds could have led to a

better water buffering capacity, supporting the development of more vigorous seeds compared to those of the B2 genotype.

In contrast to elevated temperature, drought applied during seed filling clearly affected seed metabolites in the embryos of both genotypes, and the effects of drought were very similar in both genotypes, irrespective of their distinct genetic backgrounds. Drought during seed filling resulted in lower TSW in both genotypes compared to controls (Figure 1), and alleviated pre-harvest sprouting and dormancy in B2 seeds under field conditions (Figures S3H–J), in agreement with previous reports (Gualano and Benech-Arnold, 2009). Hong et al. (2020) also reported that drought applied in the seed filling phase reduces seed weight and alters ABA signalling, and suggested a key role for reactive oxygen species (ROS) and flavonoids in drought response of barley by comparing a drought-tolerant Tibetan crop wild relative, *H. spontaneum*, to a drought-sensitive *H. vulgare* genotype.

Drought during seed production led to up-accumulation of amines and amino acids (Figure 6); 2-aminobutyric acid, cysteine, isoleucine and leucin were up-accumulated in both genotypes and also aminoadipic acid and valine in B2, together with elevated seed protein contents (significant for B1). Branched-chain amino acids, i.e. leucin, valine and isoleucine (Galili et al., 2016), contribute to target of rapamycin (TOR) activation and signalling, an evolutionarily conserved hub of nutrient sensing and metabolic signalling. Of the two distinct multiprotein complexes of TOR, TORC1 is highly conserved in all eukaryotes, and is implicated in protein synthesis and cell proliferation (Cao et al., 2019). In maize and barley, drought enhances the expression of genes involved in N uptake and assimilation in roots, promoting amino acid accumulation (Chloupek et al., 2010; Wang et al., 2017). In addition, a key step in sulphur assimilation is the incorporation of sulphur taken up by plant roots into cysteine, which is a precursor for all other organic sulphur-containing molecules, including methionine and the antioxidant glutathione, and can be further catabolized to pyruvate (Hell et al., 2002). Therefore, the observed up-accumulation of amino acids (Figure 6) supports previous findings that drought during seed filling enhances nitrogen and sulphur assimilation, and/or deposition of these two elements into seeds relative to carbon.

Furthermore, organic acids and osmolytes such as erythronic, threonic, fumaric, glyceric, pipecolic and ribonic acids were up-accumulated in seeds produced under drought in both genotypes (Figure 6). Plant response to water deficit includes metabolic adjustment involving organic acids and osmolytes in all organs, e.g. in grape leaves or wheat seeds (Hochberg et al., 2013; Mahmood et al., 2020); glyceric acid was up-accumulated in wheat roots after drought exposure and may support water and nutrient uptake (Kang et al., 2019); pipecolic acid, a product of lysine catabolism, was also suggested to be involved in osmo-regulation in oilseed rape (Moulin et al., 2006). Erythronic and threonic acids were positively correlated with drought-induced yield reduction and were suggested to be markers of yield stability (Lawas et al., 2019). By contrast, sorbitol, xylitol and the lipophilic antioxidant γ-tocopherol, a member of the tocochromanols (the vitamin E family) found at high concentrations in barley embryo and scutellum (Falk et al., 2004; Abbasi et al., 2007), were down-accumulated in embryos of both genotypes in response to drought during seed production (Figure 6). γ-tocopherol has been suggested to effectively mediate osmoprotection by preventing oxidative damage to polyunsaturated fatty acids (Sattler et al., 2004; Abbasi et al., 2007), and the down-accumulation in barley embryos of both genotypes may indicate a relatively higher consumption for this antioxidant under drought. In summary, modifications to the accumulation of osmolytes, organic acids and γ-tocopherol in the embryos of both genotypes appears to reflect general metabolic re-arrangements in response to drought independent of genotype.

Summary and conclusions

Traits selected for spring barley breeding, which led to the replacement of barley landraces, such as the Hana-type landrace B1, by semi-dwarf varieties such as genotype B2, involved modifications to phytohormone metabolism and/or signalling, including gibberellins, brassinosteroids and ABA. We do not intend to draw general conclusions about the metabolism of landraces *versus* semi-dwarfs, but our study points out that the particular semi-dwarf genotype B2, used here, also has trade-offs such as lower stress resistance, higher dormancy and higher seed nitrogen contents, compensated for by enhanced lodging resistance. Metabolite profiling revealed clear heritable differences between the two genotypes, irrespective of the maternal environment under which the seeds were produced, reflecting clear genetic differentiation. By contrast, drought affected seed metabolites in the embryos of both genotypes in a rather similar way, independent of genotype, with modifications to the metabolism of osmolytes, organic acids and γ-tocopherol, and enhanced nitrogen and sulphur assimilation. Our study may support future breeding efforts to produce new lodging and drought resistant malting barleys, by targeting re-introduction of some of the beneficial traits of old landraces such as lower dormancy and a generally higher stress resistance.

Data availability statement

The original contributions presented in the study are included in the article/supplementary files. The GC-MS based metabolite profiling dataset was submitted to the Metabolomics

Workbench repository (https://www.metabolomicsworkbench.org, datatrack_id:3436, study_id:ST002272). The DOI for this project (PR001453) is: http://dx.doi.org/10.21228/M8X13R. Further inquiries can be directed to the corresponding author.

Author contributions

MN, LR, GCl, GCu, and MB conducted the main experiments together with CS, IS-V, and HR. MN, IK, EA, LR, GCl, GCu, CB, CS, TR, IS-V, HR, and OL analysed the data. MN and IK wrote the paper with inputs from all other authors. All authors contributed to the article and approved the submitted version.

Funding

We gratefully acknowledge financial support by the European Union, FP7 grant 311840 "Impacts of Environmental Conditions on SEED quality" (EcoSeed). The Royal Botanic Gardens, Kew, receives grant-in-aid from the Department of Environment, Food and Rural Affairs, UK. I.S.-V. and O.L. were funded by PID2020-119731RB-I00 from the Spanish Ministry of Science and Innovation, SA137P20 from the Regional Government of Castile and Leon and "Escalera de Excelencia" CLU-2018-04 co-funded by the FEDER Operative Program of the Regional Government of Castile and Leon 2014–2020 Spain. This work has benefited from the support of IJPB's Plant Observatory technological platforms, which is supported by Saclay Plant Sciences-SPS (ANR-17-EUR-0007). Costs for open access publishing were partially funded by the Deutsche Forschungsgemeinschaft (DFG, German Research Foundation, grant 491250510).

Acknowledgments

The EcoSeed project was conceived by IK together with AB, CB, LR, OL, Hugh W Pritchard, Bill Finch-Savage, Wim Soppe, Anja Liszkay, and Christine Foyer, and coordinated by IK assisted by EA. We thank Sibylle Pistrick, Gabrielle Matzig and IPK gardeners for supporting seed production and germination experiments, and Edwige Declercq for measuring MDA.

Conflict of interest

The authors declare that the research was conducted in the absence of any commercial or financial relationships that could be construed as a potential conflict of interest.

Publisher's note

All claims expressed in this article are solely those of the authors and do not necessarily represent those of their affiliated organizations, or those of the publisher, the editors and the reviewers. Any product that may be evaluated in this article, or claim that may be made by its manufacturer, is not guaranteed or endorsed by the publisher.

Supplementary material

The Supplementary Material for this article can be found online at: https://www.frontiersin.org/articles/10.3389/fpls.2022.1049323/full#supplementary-material

References

Abbasi, A.-R., Hajirezaei, M., Hofius, D., Sonnewald, U., and Voll, L. M. (2007). Specific roles of α- and γ-tocopherol in abiotic stress responses of transgenic tobacco. *Plant Physiol.* 143, 1720–1738. doi: 10.1104/pp.106.094771

Albertos, P., Romero-Puertas, M. C., Tatematsu, K., Mateos, I., Sánchez-Vicente, I., Nambara, E., et al. (2015). S-nitrosylation triggers ABI5 degradation to promote seed germination and seedling growth. *Nat. Commun.* 6, 8669. doi: 10.1038/ncomms9669

Albertos, P., Tatematsu, K., Mateos, I., Sánchez-Vicente, I., Fernández-Arbaizar, A., Nakabayashi, K., et al. (2021). Redox feedback regulation of ANAC089 signaling alters seed germination and stress response. *Cell Rep.* 35, 109263. doi: 10.1016/j.celrep.2021.109263

Alshareef, N. O., Otterbach, S. L., Allu, A. D., Woo, Y. H., De Werk, T., Kamranfar, I., et al. (2022). NAC transcription factors ATAF1 and ANAC055 affect the heat stress response in arabidopsis. *Sci. Rep.* 12, 11264. doi: 10.1038/s41598-022-14429-x

Arc, E., Galland, M., Godin, B., Cueff, G., and Rajjou, L. (2013). Nitric oxide implication in the control of seed dormancy and germination. *Front. Plant Sci.* 4. doi: 10.3389/fpls.2013.00346

Bailly, C., and Kranner, I. (2011). "Analyses of reactive oxygen species and antioxidants in relation to seed longevity and germination," in *Seed dormancy: Methods and protocols, methods in molecular biology, 2011/09/08 ed.* Ed. A. R. Kermode (Totowa, New Jersey, Humana Press), 343–367. Available at: http://www.ncbi.nlm.nih.gov/pubmed/21898265.

Bajguz, A., and Hayat, S. (2009). Effects of brassinosteroids on the plant responses to environmental stresses. *Plant Physiol. Biochem.* 47, 1–8. doi: 10.1016/j.plaphy.2008.10.002

Bewley, J. D. (1997). Seed germination and dormancy. *Plant Cell* 9, 1055–1066. doi: 10.1105/tpc.9.7.1055

Bradford, M. M. (1976). A rapid and sensitive method for the quantitation of microgram quantities of protein utilizing the principle of protein-dye binding. *Anal. Biochem.* 72, 248–254. doi: 10.1016/0003-2697(76)90527-3

Cao, P., Kim, S.-J., Xing, A., Schenck, C. A., Liu, L., Jiang, N., et al. (2019). Homeostasis of branched-chain amino acids is critical for the activity of TOR signaling in Arabidopsis. *eLife* 8, e50747. doi: 10.7554/eLife.50747

Carles, C., Bies-Etheve, N., Aspart, L., Léon-Kloosterziel, K. M., Koornneef, M., Echeverria, M., et al. (2002). Regulation of *Arabidopsis thaliana em* genes: Role of ABI5. *Plant J.* 30, 373–383. doi: 10.1046/j.1365-313X.2002.01295.x

Casaretto, J., and Ho, T.-H. D. (2003). The transcription factors HvABI5 and HvVP1 are required for the abscisic acid induction of gene expression in barley aleurone cells. *Plant Cell* 15, 271–284. doi: 10.1105/tpc.007096

Chloupek, O., Dostál, V., Středa, T., Psota, V., and Dvořáčková, O. (2010). Drought tolerance of barley varieties in relation to their root system size. *Plant Breed.* 129, 630–636. doi: 10.1111/j.1439-0523.2010.01801.x

Christiansen, M. W., Holm, P. B., and Gregersen, P. L. (2011). Characterization of barley (*Hordeum vulgare* L.) NAC transcription factors suggests conserved functions compared to both monocots and dicots. *BMC Res. Notes* 4, 302. doi: 10.1186/1756-0500-4-302

Collin, A., Daszkowska-Golec, A., Kurowska, M., and Szarejko, I. (2020). Barley ABI5 (Abscisic acid INSENSITIVE 5) is involved in abscisic acid-dependent drought response. *Front. Plant Sci.* 11. doi: 10.3389/fpls.2020.01138

Dockter, C., Gruszka, D., Braumann, I., Druka, A., Druka, I., Franckowiak, J., et al. (2014). Induced variations in brassinosteroid genes define barley height and sturdiness, and expand the green revolution genetic toolkit. *Plant Physiol.* 166, 1912–1927. doi: 10.1104/pp.114.250738

Dockter, C., and Hansson, M. (2015). Improving barley culm robustness for secured crop yield in a changing climate. *J. Exp. Bot.* 66, 3499–3509. doi: 10.1093/jxb/eru521

Dwivedi, V., Parida, S. K., and Chattopadhyay, D. (2017). A repeat length variation in myo-inositol monophosphatase gene contributes to seed size trait in chickpea. *Sci. Rep.* 7, 4764–4764. doi: 10.1038/s41598-017-05332-x

Eagles, H., Bedggood, A., Panozzo, J., and Martin, P. (1995). Cultivar and environmental effects on malting quality in barley. *Aust. J. Agric. Res.* 46, 831–844. doi: 10.1071/AR9950831

Falk, J., Krahnstover, A., van der Kooij, T. A. W., Schlensog, M., and Krupinska, K. (2004). Tocopherol and tocotrienol accumulation during development of caryopses from barley (*Hordeum vulgare* l.). *Phytochemistry* 65, 2977–2985. doi: 10.1016/j.phytochem.2004.08.047

Federal Variety Office (2021). *Beschreibende Sortenliste - Getreide, Mais Öl- und Faserpflanzen, Leguminosen, Rüben, Zwischenfrüchte 2021 (Descriptive list of varieties - cereals, maize, oil and fibre plants, legumes, beet, intercrops 2021)* (Bundessortenamt Hanover, Germany: Bundessortenamt).

Finch-Savage, W. E., and Bassel, G. W. (2015). Seed vigour and crop establishment: Extending performance beyond adaptation. *J. Exp. Bot.* 67, 567–591. doi: 10.1093/jxb/erv490

Finkelstein, R. R., and Lynch, T. J. (2000). The Arabidopsis abscisic acid response gene *ABI5* encodes a basic leucine zipper transcription factor. *Plant Cell* 12, 599–609. doi: 10.1105/tpc.12.4.599

Forde, B. G., and Lea, P. J. (2007). Glutamate in plants: Metabolism, regulation, and signalling. *J. Exp. Bot.* 58, 2339–2358. doi: 10.1093/jxb/erm121

Frimpong, F., Windt, C. W., Van Dusschoten, D., Naz, A. A., Frei, M., and Fiorani, F. (2021). A wild allele of pyrroline-5-carboxylate synthase1 leads to proline accumulation in spikes and leaves of barley contributing to improved performance under reduced water availability. *Front. Plant Sci.* 12. doi: 10.3389/fpls.2021.633448

Galili, G., Amir, R., and Fernie, A. R. (2016). The regulation of essential amino acid synthesis and accumulation in plants. *Annu. Rev. Plant Biol.* 67, 153–178. doi: 10.1146/annurev-arplant-043015-112213

Gammans, M., Mérel, P., and Ortiz-Bobea, A. (2017). Negative impacts of climate change on cereal yields: Statistical evidence from France. *Environ. Res. Lett.* 12, 054007. doi: 10.1088/1748-9326/aa6b0c

Gao, S., and Chu, C. (2020). Gibberellin metabolism and signaling: Targets for improving agronomic performance of crops. *Plant Cell Physiol.* 61, 1902–1911. doi: 10.1093/pcp/pcaa104

Graeber, K., Nakabayashi, K., Miatton, E., Leubner-Metzger, G., and Soppe, W. J. J. (2012). Molecular mechanisms of seed dormancy. *Plant Cell Environ.* 35, 1769–1786. doi: 10.1111/j.1365-3040.2012.02542.x

Grausgruber, H., Bointner, H., Tumpold, R., Ruckenbauer, P., and Fischbeck, G. (2002). Genetic improvement of agronomic and qualitative traits of spring barley. *Plant Breed.* 121, 411–416. doi: 10.1046/j.1439-0523.2002.756385.x

Grove, M. D., Spencer, G. F., Rohwedder, W. K., Mandava, N., Worley, J. F., Warthen, J. D., et al. (1979). Brassinolide, a plant growth-promoting steroid isolated from *Brassica napus* pollen. *Nature* 281, 216–217. doi: 10.1038/281216a0

Gruszka, D., Janeczko, A., Dziurka, M., Pociecha, E., Oklestkova, J., and Szarejko, I. (2016). Barley brassinosteroid mutants provide an insight into phytohormonal homeostasis in plant reaction to drought stress. *Front. Plant Sci.* 7. doi: 10.3389/fpls.2016.01824

Gualano, N. A., and Benech-Arnold, R. L. (2009). The effect of water and nitrogen availability during grain filling on the timing of dormancy release in malting barley crops. *Euphytica* 168, 291–301. doi: 10.1007/s10681-009-9948-x

Hampton, J. G., and TeKrony, D. M. (1995). *Handbook of vigour test methods* (Zürich: International Seed Testing Association).

Hayat, S., Hayat, Q., Alyemeni, M. N., Wani, A. S., Pichtel, J., and Ahmad, A. (2012). Role of proline under changing environments: A review. *Plant Signaling Behav.* 7, 1456–1466. doi: 10.4161/psb.21949

Hell, R., Jost, R., Berkowitz, O., and Wirtz, M. (2002). Molecular and biochemical analysis of the enzymes of cysteine biosynthesis in the plant *Arabidopsis thaliana*. *Amino Acids* 22, 245–257. doi: 10.1007/s007260200012

Hochberg, U., Degu, A., Toubiana, D., Gendler, T., Nikoloski, Z., Rachmilevitch, S., et al. (2013). Metabolite profiling and network analysis reveal coordinated changes in grapevine water stress response. *BMC Plant Biol.* 13, 184. doi: 10.1186/1471-2229-13-184

Hong, Y., Ni, S.-J., and Zhang, G.-P. (2020). Transcriptome and metabolome analysis reveals regulatory networks and key genes controlling barley malting quality in responses to drought stress. *Plant Physiol. Biochem.* 152, 1–11. doi: 10.1016/j.plaphy.2020.04.029

Hong, Y., Zhang, H., Huang, L., Li, D., and Song, F. (2016). Overexpression of a stress-responsive NAC transcription factor gene *ONAC022* improves drought and salt tolerance in rice. *Front. Plant Sci.* 7. doi: 10.3389/fpls.2016.00004

Howard, K. A., Gayler, K. R., Eagles, H. A., and Halloran, G. M. (1996). The relationship between d hordein and malting quality in barley. *J. Cereal Sci.* 24, 47–53. doi: 10.1006/jcrs.1996.0036

Huang, Y., Sun, M.-M., Ye, Q., Wu, X.-Q., Wu, W.-H., and Chen, Y.-F. (2017). Abscisic acid modulates seed germination *via* ABA INSENSITIVE5-mediated PHOSPHATE1. *Plant Physiol.* 175, 1661–1668. doi: 10.1104/pp.17.00164

ISTA (2014). *International rules for seed testing* (Bassersdorf, Switzerland: International Seed Testing Association).

Iwasaki, M., Penfield, S., and Lopez-Molina, L. (2022). Parental and environmental control of seed dormancy in *Arabidopsis thaliana*. *Annu. Rev. Plant Biol.* 73, 355–378. doi: 10.1146/annurev-arplant-102820-090750

Jacott, C. N., and Boden, S. A. (2020). Feeling the heat: Developmental and molecular responses of wheat and barley to high ambient temperatures. *J. Exp. Bot.* 71, 5740–5751. doi: 10.1093/jxb/eraa326

Jaeger, A., Zannini, E., Sahin, A. W., and Arendt, E. K. (2021). Barley protein properties, extraction and applications, with a focus on brewers' spent grain protein. *Foods* 10, 1389. doi: 10.3390/foods10061389

Jakoby, M., Weisshaar, B., Dröge-Laser, W., Vicente-Carbajosa, J., Tiedemann, J., Kroj, T., et al. (2002). bZIP transcription factors in Arabidopsis. *Trends Plant Sci.* 7, 106–111. doi: 10.1016/S1360-1385(01)02223-3

Jing, Z., and Wanxia, Z. (2003). Tracing sources of dwarfing genes in barley breeding in China. *Euphytica* 131, 285–293. doi: 10.1023/A:1024032732443

Joosen, R. V. L., Kodde, J., Willems, L. A. J., Ligterink, W., van der Plas, L. H. W., and Hilhorst, H. W. M. (2010). GERMINATOR: A software package for high-throughput scoring and curve fitting of arabidopsis seed germination. *Plant J.* 62, 148–159. doi: 10.1111/j.1365-313X.2009.04116.x

Kang, Z., Babar, M. A., Khan, N., Guo, J., Khan, J., Islam, S., et al. (2019). Comparative metabolomic profiling in the roots and leaves in contrasting genotypes reveals complex mechanisms involved in post-anthesis drought tolerance in wheat. *PloS One* 14, e0213502. doi: 10.1371/journal.pone.0213502

Kim, S. Y., Warpeha, K. M., and Huber, S. C. (2019). The brassinosteroid receptor kinase, BRI1, plays a role in seed germination and the release of dormancy by cold stratification. *J. Plant Physiol.* 241, 153031. doi: 10.1016/j.jplph.2019.153031

Kranner, I., Minibayeva, F. V., Beckett, R. P., and Seal, C. E. (2010). What is stress? Concepts, definitions and applications in seed science. *New Phytol.* 188, 655–673. doi: 10.1111/j.1469-8137.2010.03461.x

Kuczyńska, A., Surma, M., Adamski, T., Mikołajczak, K., Krystkowiak, K., and Ogrodowicz, P. (2013). Effects of the semi-dwarfing *sdw1/denso* gene in barley. *J. Appl. Genet.* 54, 381–390. doi: 10.1007/s13353-013-0165-x

Laidig, F., Piepho, H.-P., Rentel, D., Drobek, T., and Meyer, U. (2017). Breeding progress, genotypic and environmental variation and correlation of quality traits in malting barley in German official variety trials between 1983 and 2015. *Theor. Appl. Genet.* 130, 2411–2429. doi: 10.1007/s00122-017-2967-4

Lawas, L. M. F., Erban, A., Kopka, J., Jagadish, S. V. K., Zuther, E., and Hincha, D. K. (2019). Metabolic responses of rice source and sink organs during recovery from combined drought and heat stress in the field. *GigaScience* 8, giz102. doi: 10.1093/gigascience/giz102

Lopez-Molina, L., Mongrand, S., and Chua, N.-H. (2001). A postgermination developmental arrest checkpoint is mediated by abscisic acid and requires the ABI5 transcription factor in arabidopsis. *Proc. Natl. Acad. Sci.* 98, 4782–4787. doi: 10.1073/pnas.081594298

Mahmood, T., Abdullah, M., Ahmar, S., Yasir, M., Iqbal, M. S., Yasir, M., et al. (2020). Incredible role of osmotic adjustment in grain yield sustainability under water scarcity conditions in wheat (*Triticum aestivum* L.). *Plants* 9, 1208. doi: 10.3390/plants9091208

Manfre, A. J., Lanni, L. M., and Marcotte, W. R.Jr. (2005). The Arabidopsis group 1 LATE EMBRYOGENESIS ABUNDANT protein ATEM6 is required for normal seed development. *Plant Physiol.* 140, 140–149. doi: 10.1104/pp.105.072967

Ma, H., and Wang, S. (2016). Histidine regulates seed oil deposition through abscisic acid biosynthesis and β-oxidation. *Plant Physiol.* 172, 848–857. doi: 10.1104/pp.16.00950

Mittal, A., Gampala, S. S. L., Ritchie, G. L., Payton, P., Burke, J. J., and Rock, C. D. (2014). Related to ABA-Insensitive3(ABI3)/Viviparous1 and AtABI5 transcription factor coexpression in cotton enhances drought stress adaptation. *Plant Biotechnol. J.* 12, 578–589. doi: 10.1111/pbi.12162

Moulin, M., Deleu, C., Larher, F., and Bouchereau, A. (2006). The lysine-ketoglutarate reductase–saccharopine dehydrogenase is involved in the osmo-induced synthesis of pipecolic acid in rapeseed leaf tissues. *Plant Physiol. Biochem.* 44, 474–482. doi: 10.1016/j.plaphy.2006.08.005

Nagel, M., Alqudah, A. M., Bailly, M., Rajjou, L., Pistrick, S., Matzig, G., et al. (2019). Novel loci and a role for nitric oxide for seed dormancy and pre-harvest sprouting in barley. *Plant Cell Environ.* 42, 1318–1327. doi: 10.1111/pce.13483

Nonogaki, H. (2014). Seed dormancy and germination - emerging mechanisms and new hypotheses. *Front. Plant Sci.* 5. doi: 10.3389/fpls.2014.00233

Ortiz-Bobea, A., Ault, T. R., Carrillo, C. M., Chambers, R. G., and Lobell, D. B. (2021). Anthropogenic climate change has slowed global agricultural productivity growth. *Nat. Climate Change* 11, 306–312. doi: 10.1038/s41558-021-01000-1

Penfield, S., and MacGregor, D. R. (2017). Effects of environmental variation during seed production on seed dormancy and germination. *J. Exp. Bot.* 68, 819–825. doi: 10.1093/jxb/erw436

Rodriguez, M. V., Barrero, J. M., Corbineau, F., Gubler, F., and Benech-Arnold, R. L. (2015). Dormancy in cereals (not too much, not so little): About the mechanisms behind this trait. *Seed Sci. Res.* 25, 99–119. doi: 10.1017/S0960258515000021

Sadura, I., Pociecha, E., Dziurka, M., Oklestkova, J., Novak, O., Gruszka, D., et al. (2019). Mutations in the HvDWARF, HvCPD and HvBRI1 genes-involved in brassinosteroid biosynthesis/signalling: Altered photosynthetic efficiency, hormonal homeostasis and tolerance to high/low temperatures in barley. *J. Plant Growth Regul.* 38, 1062–1081. doi: 10.1007/s00344-019-09914-z

Sanchez-Vicente, I., Albertos, P., and Lorenzo, O. (2019). Protein shuttle between nucleus and cytoplasm: New paradigms in the ABI5-dependent ABA responses. *Mol. Plant* 12, 1425–1427. doi: 10.1016/j.molp.2019.09.005

Sattler, S. E., Gilliland, L. U., Magallanes-Lundback, M., Pollard, M., and Dellapenna, D. (2004). Vitamin E is essential for seed longevity, and for preventing lipid peroxidation during germination. *Plant Cell* 16, 1419–1432. doi: 10.1105/Tpc.021360

Singh, S., Koyama, H., Bhati, K. K., and Alok, A. (2021). The biotechnological importance of the plant-specific NAC transcription factor family in crop improvement. *J. Plant Res.* 134, 475–495. doi: 10.1007/s10265-021-01270-y

Smith, D. B. (1972). The amino acid composition of barley grain protein during development and germination. *J. Agric. Sci.* 78, 265–273. doi: 10.1017/S0021859600069100

Sosulski, F. W., and Imafidon, G. I. (1990). Amino acid composition and nitrogen-to-protein conversion factors for animal and plant foods. *J. Agric. Food Chem.* 38, 1351–1356. doi: 10.1021/jf00096a011

Stamler, J. S., Lamas, S., and Fang, F. C. (2001). Nitrosylation: The prototypic redox-based signaling mechanism. *Cell* 106, 675–683. doi: 10.1016/S0092-8674(01)00495-0

Stekhoven, D.J., and Bühlmann, P. (2011). MissForest—non-parametric missing value imputation for mixed-type data. *Bioinformatics* 28, 112-118. doi: 10.1093/bioinformatics/btr597

Sud, M., Fahy, E., Cotter, D., Azam, K., Vadivelu, I., Burant, C., et al. (2016). Metabolomics workbench: An international repository for metabolomics data and metadata, metabolite standards, protocols, tutorials and training, and analysis tools. *Nucleic Acids Res.* 44, D463–D470. doi: 10.1093/nar/gkv1042

Tarawneh, R. A., Alqudah, A. M., Nagel, M., and Börner, A. (2020). Genome-wide association mapping reveals putative candidate genes for drought tolerance in barley. *Environ. Exp. Bot.* 180, 104237. doi: 10.1016/j.envexpbot.2020.104237

Thomas, W. T. B., Powell, W., and Swanston, J. S. (1991). The effects of major genes on quantitatively varying characters in barley. 4. the *GPert* and *denso* loci and quality characters. *Heredity* 66, 381–389. doi: 10.1038/hdy.1991.48

Trnka, M., Rotter, R. P., Ruiz-Ramos, M., Kersebaum, K. C., Olesen, J. E., Zalud, Z., et al. (2014). Adverse weather conditions for European wheat production will become more frequent with climate change. *Nat. Climate Change* 4, 637–643. doi: 10.1038/Nclimate2242

Vriet, C., Russinova, E., and Reuzeau, C. (2012). Boosting crop yields with plant steroids. *Plant Cell* 24, 842–857. doi: 10.1105/tpc.111.094912

Wang, H., Yang, Z., Yu, Y., Chen, S., He, Z., Wang, Y., et al. (2017). Drought enhances nitrogen uptake and assimilation in maize roots. *Agron. J.* 109, 39–46. doi: 10.2134/agronj2016.01.0030

Wiebach, J., Nagel, M., Borner, A., Altmann, T., and Riewe, D. (2020). Age-dependent loss of seed viability is associated with increased lipid oxidation and hydrolysis. *Plant Cell Environ.* 43, 303–314. doi: 10.1111/pce.13651

Wild, R., Gerasimaite, R., Jung, J.-Y., Truffault, V., Pavlovic, I., Schmidt, A., et al. (2016). Control of eukaryotic phosphate homeostasis by inositol polyphosphate sensor domains. *Science* 352, 986–990. doi: 10.1126/science.aad9858

Xu, Y., Jia, Q., Zhou, G., Zhang, X.-Q., Angessa, T., Broughton, S., et al. (2017). Characterization of the *sdw1* semi-dwarf gene in barley. *BMC Plant Biol.* 17, 11. doi: 10.1186/s12870-016-0964-4

Zhao, C., Liu, B., Piao, S., Wang, X., Lobell, D. B., Huang, Y., et al. (2017). Temperature increase reduces global yields of major crops in four independent estimates. *Proc. Natl. Acad. Sci.* 114, 9326–9331. doi: 10.1073/pnas.1701762114

frontiers | Frontiers in Plant Science

TYPE Review
PUBLISHED 12 December 2022
DOI 10.3389/fpls.2022.1022167

Check for updates

OPEN ACCESS

EDITED BY
Jiban Shrestha,
Nepal Agricultural Research Council, Nepal

REVIEWED BY
Zhou Li,
Sichuan Agricultural University, China
Bin Wang,
Shaoguan University, China

*CORRESPONDENCE
Amit Kumar Goswami
amit.tkg@gmail.com
Suneha Goswami
suneha08@gmail.com
Kirti Bardhan
kirtivardhan@nau.in

†These authors have contributed equally to this work

SPECIALTY SECTION
This article was submitted to Plant Abiotic Stress, a section of the journal Frontiers in Plant Science

RECEIVED 18 August 2022
ACCEPTED 16 November 2022
PUBLISHED 12 December 2022

CITATION
Goswami AK, Maurya NK, Goswami S, Bardhan K, Singh SK, Prakash J, Pradhan S, Kumar A, Chinnusamy V, Kumar P, Sharma RM, Sharma S, Bisht DS and Kumar C (2022) Physio-biochemical and molecular stress regulators and their crosstalk for low-temperature stress responses in fruit crops: A review. *Front. Plant Sci.* 13:1022167. doi: 10.3389/fpls.2022.1022167

COPYRIGHT
© 2022 Goswami, Maurya, Goswami, Bardhan, Singh, Prakash, Pradhan, Kumar, Chinnusamy, Kumar, Sharma, Sharma, Bisht and Kumar. This is an open-access article distributed under the terms of the Creative Commons Attribution License (CC BY). The use, distribution or reproduction in other forums is permitted, provided the original author(s) and the copyright owner(s) are credited and that the original publication in this journal is cited, in accordance with accepted academic practice. No use, distribution or reproduction is permitted which does not comply with these terms.

Physio-biochemical and molecular stress regulators and their crosstalk for low-temperature stress responses in fruit crops: A review

Amit Kumar Goswami[1*†], Naveen Kumar Maurya[1†], Suneha Goswami[2*], Kirti Bardhan[3*], Sanjay Kumar Singh[1], Jai Prakash[1], Satyabrata Pradhan[1], Amarjeet Kumar[4], Viswanathan Chinnusamy[5], Prabhat Kumar[6], Radha Mohan Sharma[1], Stuti Sharma[7], Deepak Singh Bisht[8] and Chavlesh Kumar[1]

[1]Division of Fruits and Horticultural Technology, ICAR-Indian Agricultural Research Institute, New Delhi, India, [2]Division of Biochemistry, ICAR-Indian Agricultural Research Institute, New Delhi, India, [3]Department of Basic Sciences and Humanities, Navsari Agricultural University, Navsari, India, [4]Multi Testing Technology Centre and Vocational Training Centre, Selesih, Central Agricultural University, Imphal, India, [5]Division of Plant Physiology, ICAR-Indian Agricultural Research Institute, New Delhi, India, [6]Department of Agriculture and Farmers Welfare, Ministry of Agriculture & Farmers Welfare, Govt. of India, Krishi Bhavan, New Delhi, India, [7]Department of Plant Breeding and Genetics, Jawaharlal Nehru Krishi Vishwavidyalaya, Jabalpur, Madhya Pradesh, India, [8]ICAR-National Institute for Plant Biotechnology, New Delhi, India

Low-temperature stress (LTS) drastically affects vegetative and reproductive growth in fruit crops leading to a gross reduction in the yield and loss in product quality. Among the fruit crops, temperate fruits, during the period of evolution, have developed the mechanism of tolerance, i.e., adaptive capability to chilling and freezing when exposed to LTS. However, tropical and sub-tropical fruit crops are most vulnerable to LTS. As a result, fruit crops respond to LTS by inducing the expression of LTS related genes, which is for climatic acclimatization. The activation of the stress-responsive gene leads to changes in physiological and biochemical mechanisms such as photosynthesis, chlorophyll biosynthesis, respiration, membrane composition changes, alteration in protein synthesis, increased antioxidant activity, altered levels of metabolites, and signaling pathways that enhance their tolerance/resistance and alleviate the damage caused due to LTS and chilling injury. The gene induction mechanism has been investigated extensively in the model crop Arabidopsis and several winter kinds of cereal. The ICE1 (inducer of C-repeat binding factor expression 1) and the CBF (C-repeat binding factor) transcriptional cascade are involved in transcriptional control. The functions of various CBFs and aquaporin genes were well studied in crop plants and their role in multiple stresses including cold stresses is deciphered. In addition, tissue nutrients and plant growth regulators like ABA, ethylene, jasmonic acid etc., also play a significant role in alleviating the LTS and chilling injury in fruit crops.

10.3389/fpls.2022.1022167

However, these physiological, biochemical and molecular understanding of LTS tolerance/resistance are restricted to few of the temperate and tropical fruit crops. Therefore, a better understanding of cold tolerance's underlying physio-biochemical and molecular components in fruit crops is required under open and simulated LTS. The understanding of LTS tolerance/resistance mechanism will lay the foundation for tailoring the novel fruit genotypes for successful crop production under erratic weather conditions.

KEYWORDS

cold tolerance, transcriptome, aquaporins, membrane injury, phytohormone, CBFs

Introduction

Plants are sessile and experience several abiotic stresses episode in their life due to harsh climatic conditions. These circumstances triggered several molecular changes in the plants, which led to a variety of responses of physiology and biochemistry of the plant cells, which determine the fitness of the plant in the environment. Temperature is one of the decisive and essential abiotic factors regulating plant's ontogeny. The process for how Plants sense temperature is elusive. However, several candidate thermos-sensors proteins are known that respond to the membrane changes and other cellular changes triggered by low temperature, leading to downstream events of change in the pattern of gene expressions and plant's responses (Ding and Yang, 2022). Low temperature (LT) influences plant growth and development by causing various morpho-physiological and biochemical changes (Nishiyama, 1976; Medina et al., 2011) (Figure 1). LT has an impact on many processes, including, photosynthesis, cell division, membrane stability, absorption and transport of water and nutrients, yield, and ultimately species survival. Plants experience low temperature stress (LTS) in two ways: (i) Chilling stress: when plants are exposed to LT below 10–15°C for a certain period, causing injury without formation of ice crystals within the plant

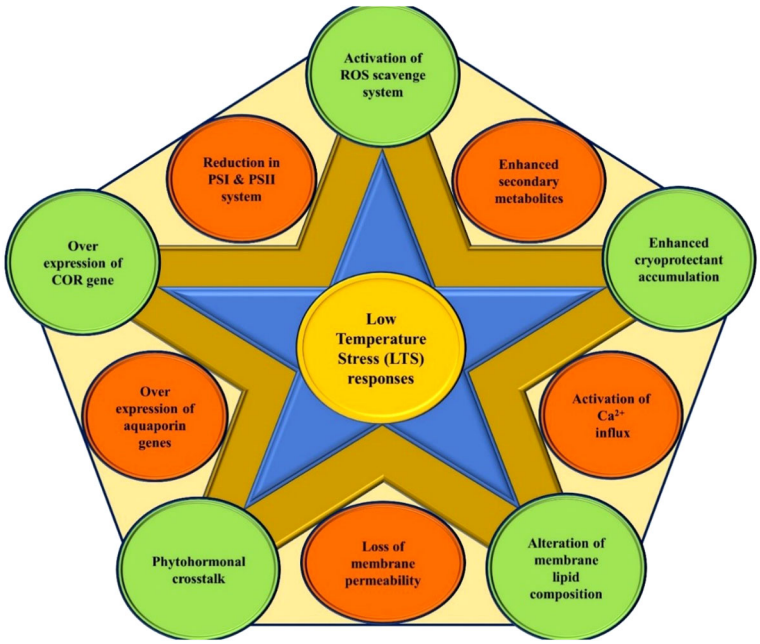


FIGURE 1
Low-temperature stress responses in plant system.

cells; (ii) Freezing stress: when plants are exposed to sub-zero °C low temperatures, inducing ice crystallization of cellular content, resulting in cell dehydration and freezing injury (Beck et al., 2007; Zhu et al., 2007). Two processes lead to freezing injury: (i) vitrification, which results from the fast freezing of cellular substance, and (ii) supercooling, which results in the formation of ice crystals from intra or extracellular content. An overview of the optimum temperature range for vegetative and reproductive growth for some tropical and subtropical fruit species is given in Table 1. Eco-physiological and biophysical studies on tropical and subtropical fruit species are crucial for understanding how LTS affects fruit crops and how it might be managed. (Barlow et al., 1974). Tropical and subtropical fruit species exhibit distinct damaging symptoms when exposed to LT below 10–15°C for a certain period, resulting in drastic yield reduction or even death over prolonged exposure (Chen and Patterson, 1985; Herner, 1990; Alonso et al., 1997). The ability to withstand mild non-freezing temperature stress has evolved over thousands of years in temperate fruits such as apple, pear, peach, plum, strawberry, *etc*. The coping mechanism used by temperate fruits to adjust to cold conditions comprises alterations in a number of physio-morphological and biochemical parameters as well as the expression of stress-associated genes (Medina et al., 2011).

Temperate fruit crops undergo dormancy during the winter to avoid the detrimental consequences of LTS. Different physio-biochemical changes are brought on by LTS exposure in tolerant and sensitive genotypes. The extent of changes decides the genotype's tolerance and ability to acclimate to the cold stress (Barlow et al., 1974; Martin and Douglas, 1979). The aim of this review is to understand physio-morphological, biochemical, and molecular processes connected to LTS in fruit crops as well as the role of phytohormones and other signaling molecules in reducing low-temperature damage. A better understanding of the physiological mechanisms underlying LTS tolerance in fruit crops will relate to improved crop damage management and breeding strategies to combat LTS.

Physiological responses

LTS significantly affects the vegetative and reproductive growth of tropical and subtropical fruits (Alonso et al., 1997), thereby supressing their yield. For instance, if the temperature falls <4°C in the winter for over three hours, the papaya plants may die due to the leakage of white (oozing out milky) latex from the stem of frost-damaged plants (Ram, 2005). Frost or unexpected temperature fluctuations during late winter cause severe damage to fruit crop foliage, crown, flowers, and fruits resulting in a limited yield of low-quality papaya fruit, which ripens unevenly (Singh et al., 2010). Moreover, under chilling temperatures and humid conditions, a hermaphrodite flower of papaya may revert to femaleness (carpelloidy of stamens), resulting in deformed fruits (Awada, 1958; Storey, 1969; Ram, 2005; Lin et al., 2016). In coffee plants, temperatures <16°C suppress vegetative growth, limiting net photosynthesis, resulting in irregular maturity and poor yields (Bauer et al., 1985). However, the reduction in vegetative growth was not due to the decrease in leaf water potential but it was attributed to more prolonged exposure to LT (<16°C exposure) (Barros et al., 1997). However, during LTS acclimation, relative water content (RWC) of the leaves in guava was associated with decrease in vegetative growth. The non-acclimated guava leaves had three to four time's higher anthocyanin accumulation than the latter cold-acclimated guava leaves (Hao et al., 2009). Similarly, Pradhan et al. (2017) reported that under the LT regimes,

TABLE 1 Optimum temperature ranges for the growth of some tropical and subtropical fruit species.

Sl. No.	Fruit crop	Optimum temperature (°C)	Reference (s)
01	Grapevine *(Vitis vinifera)*	10-35°C	White et al. (2006)
02	Banana *(Musa* spp.*)*	20-35°C	Viktorova (1983)
03	Guava *(Psidium guajava)*	23-28°C	Verheij and Coronel (1992)
04	Mango *(Mangifera indica)*	24-27°C	Davanport (2009)
05	Logan *(Dimocarpus longan)*	20-25°C	Verheij and Coronel (1992)
06	Rambutan (*Nephelium lappaceum*)	25-32°C	Verheij and Coronel (1992)
07	Jackfruit *(Artocarpus heterophyllus)*	16-28°C	Haq (2006)
08	Litchi (*Litchi chinensis)*	25-35°C	Tindall (1994)
09	Durian *(Durio zibethinus)*	24-30°C	Verheij and Coronel (1992)
10	Langsat (*Lansium domesticum* L.)	25-35°C	UDPSM (2002)
11	Pomelo (*Citrus maxima* L.)	23-30°C	Verheij and Coronel (1992)
12	Cashew nut *(Anacardium occidentale)*	20-35°C	Joubert and Thomas (1965)
13	Coconut *(Cocos nucifera)*	20-32°C	Louis and Annappan (1980)
14	Mangosteen (*Garcinia mangostana* L.)	25-35°C	Osman and Milan (2006)
15	Citrus (*Citrus* spp.)	23-27°C	Verheij and Coronel (1992)

RWC and fresh leaf weight in papaya decreased, while dry leaf weight reflected the opposite trend. Pradhan et al. (2018) found that the percent change in plant height in control papaya plants was more substantial than its LT-treated counterpart. The decrease in plant growth was due to the reduced photosynthetic rate under LT. In addition, chilling stress in plant roots can alter their metabolic heat rates as detected by micro calorimetry (Criddle et al., 1988), cause cortical destruction and reduce root elongation (Harrington and Kihara, 1960).

Cellular changes

Several studies have found that cell membrane networks are the primary sites of freezing injury in plants (Levitt, 1980; Steponkus, 1984), and that freeze-induced membrane damage is caused primarily by the acute dehydration caused by freezing (Steponkus, 1984; Steponkus, 1993). The extracellular fluids of the apoplastic space contain a lower solute concentration than the intracellular fluid and thus have a higher freezing point; therefore, ice formation is initiated first in the apoplastic space (Jan and Andrabi, 2009). Since ice has a lower water potential than liquid, extracellular ice has a lower water potential than inside the cell, resulting in dehydration. LTS causes some cellular function abnormalities, and membrane damage and the LTS injury is evaluated through electrolyte leakage, changes in membrane lipid composition, and malondialdehyde (MDA) production. Cell dehydration leads to lipid peroxidation and an increase in MDA content, as well as damage to cell membrane fluidity, thus disrupting membrane selectivity, resulting in the permeability of unwanted nutrient elements and ions, leading to ion leakage and disrupting cellular ionic homeostasis (Mahajan and Tuteja, 2005; Yadav, 2010; Shin et al., 2018). The membrane stability index (MSI) of papaya genotypes exposed to LT regimes decreased (Pradhan et al., 2019) while the membrane injury index (MII) increased (Pradhan et al., 2017). Cold stress reduced the MSI gradually, indicating a loss of cell membrane integrity. Campos et al. (2003) reported that electrolyte leakage and lipid degradation influence cold sensitivity in *Coffea* sp. leaves.

Numerous studies have noted that chilling stress significantly reduces the photosynthetic efficiency of sensitive plants (Yang et al., 2005; Fariduddin et al., 2011). The disruption of the thylakoid ETS pathway and carbon reduction cycle significantly altered photosynthesis under LTS. Furthermore, stomatal control of CO_2 supply may be primarily responsible for decreasing the net photosynthetic rate (Allen and Ort, 2001). Limiting stomatal conductance may be attributed to loss of turgor of guard cells due to LTS induced dehydration. The ultrastructure of chloroplasts has changed after a prolonged cooling period, and thus ability to intercept light energy may be lost (Yang et al., 2005). Potassium (K) and calcium (Ca) were two essential nutrients in improving plant chilling tolerance. Several studies have revealed that electrolyte leakage is primarily related to K^+ efflux from plant cells, mediated by plasma membrane cation conductance. When K+ levels are low, photo-oxidative damage caused by chilling or frost is worsened. This makes plant growth and yield decrease.

High cellular potassium levels can protect against oxidative damage caused by cooling or frost (Waraich et al., 2012). Furthermore, several studies have shown that applying a higher concentration of K+ could reduce LTS-induced damage in crops such as potatoes (Grewal and Singh, 1980), carnations (Kafkafi, 1990), and vegetable seedlings (Hakerlerler et al., 1997). Pradhan et al. (2018) also reported a high level of K^+ content with a decline in stomatal conductance and transpiration rate, which would help to maintain plant water status. Recently, Maurya et al. (2020) also noted an increase in leaf K^+ content in papaya seedlings grown under LTS. Similarly, Ca also influences both development and responses to environmental challenges like cold stress by regulating various physiological processes in plants at the tissue, cellular, and molecular levels (Waraich et al., 2011). Plant genotypes that are LTS tolerant can maintain their high leaf water potential by closing their stomata and limiting water loss during transpiration (Wilkinson et al., 2001). However, Yadav (2010) reported that dehydration occurs under exposure to LTS due to low water uptake due to stomata closure.

Furthermore, Ca also modulates the stress responses during cold injury, healing, and adaptation to cold stress (Palta, 1990). LTS activates Ca^{2+}channels, resulting in the accumulation of Ca^{2+} in the cytosol and the induction of phospholipid signaling. The vacuole is the intracellular source of Ca^{2+}, and which triggers stomatal closure with increasing Ca^{2+} levels in the cell, a distinguishing feature of plants grown at or exposed to LTS. According to some studies, Ca^{2+} (released from internal guard cell stores or the apoplast) regulates ABA-induced stomatal closure (Wilkinson et al., 2001). Ca^{2+} is required for LTS recovery because it activates the plasma membrane enzyme ATPase, which is needed to pump nutrients lost during the cell injury back into the cell (Palta, 1990). Calcium also acts as calmodulin under LTS conditions, regulating plant metabolic activity and promoting plant development (Waraich et al., 2012). Compared with different *Carica papaya* genotypes, Pradhan et al. (2018) found the highest Ca^{2+}accumulation in the leaf and roots of a cold-tolerant wild relative of papaya, *V. cundinamarcensis.*

Chlorophyll

The most critical component of the photosystem is chlorophyll. LTS represses chlorophyll bio-synthesis and accumulation in actively growing leaves (Glaszmann et al., 1990). For example, the chlorophyll content of papaya seedlings at a 20°/10°C (day/night) temperature regime was

8.16% lower than the control plants at 28°/18°C (day/night). Cold-tolerant genotypes may accumulate higher chlorophyll content under LTS than cold-sensitive lines (Pradhan et al., 2019). An alternative measure for determining the freezing tolerance and accessing freezing damage and cold acclimation responses of leaves is chlorophyll fluorescence (Ehlert and Hincha, 2008). The chlorophyll fluorescence technique has been employed in various other crops to assess the extent of photodamage at LT, including *Arabidopsis* (Ehlert and Hincha, 2008), soybean (Tambussi et al., 2004), maize (Aroca et al., 2001), *etc*. Regardless of the plant species investigated, Maxwell and Johnson (2000) found that the value of chlorophyll fluorescence (*Fv*/*Fm*) in healthy leaves was close to 0.80. The lower value of chlorophyll fluorescence (*Fv*/*Fm*) indicates photoinhibition of PS II reaction canters, disrupted due to LTS. Smillie (1979) observed that the quantum efficiency (QE) of the PS II center (*Fv*/*Fm*) in papaya was 0.42 in the winter season, having a temperature range of 6°/17°C (min./max.) and 0.72 in the summer, in a temperature range of 18°/26°C (min./max.), indicating that LT likely lowered the PSII activity. Perturbance of photosynthetic machinery in Strawberry, also reflected by chlorophyll fluorescence ((*Fv*/*Fm*) and LTS significantly reduced the chlorophyll fluorescence (*Fv*/*Fm*) value (Zareei et al., 2021). Pradhan et al. (2019) also found reduction in *Fv*/*Fm* during LTS. The treated plants expressed a significantly lower *Fv*/*Fm* value than the control. The lowest observed values were 0.438 and 0.584 in the temperature regime of 20°/10°C (day/night), followed by 22°/12°C (day/night), respectively. In contrast, the control plants (28°/18°C day/night) exhibited the highest (0.736) value of *Fv*/*Fm*. Classified mango cultivars based on LTS and *Fv*/*Fm* responses. An *Fv*/*Fm* ratio of less than 0.5 is denoted as chilling sensitive, while those with an *Fv*/*Fm* value greater than 0.6 are considered as chilling tolerant cultivars.

Photosynthesis

With the lowering of temperature, the rate of metabolic processes slows steadily and eventually stops under extreme stress (Taiz and Zeiger, 2002). LT affects different dimensions of photosynthesis in fruit crops. Cellular photosynthesis under LTS is substantially inhibited or reduced due to the disruption of all major components, including the thylakoid electron transport system and carbon reduction cycle. After a long cooling period, the chloroplast ultrastructure has altered, and the capacity to efficiently trap light energy may be lost by the thylakoids membranes (Yang et al., 2005). LTS thermodynamically reduces enzymatic activities, such as Calvin cycle enzymes and ROS (Reactive Oxygen Species) scavenging enzyme activities. LT causes a photostatic imbalance in thylakoid membranes, leading to an over-reduction of the electron transport chain and ROS generation at PSII and PSI (Soitamo et al., 2008; Ruelland et al., 2009; Yun et al., 2010). Papaya plants exposed to an LT regime of 20°/10°C (day/night) exhibited a 57.96% reduction in the photosynthesis rate compared to the control plants. This reduction was genotype-dependent and decided their degree of tolerance. The chilling susceptible Red Lady papaya had a drastic reduction (82.10%) compared to the other genotypes (Pradhan et al., 2018). Similarly, Grau and Halloy (1997) also reported a 15% reduction in the photosynthesis rate of papaya plants exposed to the LT regime (15°/5°C; day/night; 4 days) as compared to the control (25°/15°C; day/night). LTS also contributes to ROS generation by reducing the leaf gas exchange in fruit crops due to decreased stomatal conductance. The genotypes that can withstand LTS can keep their leaf water potential high by closing their stomata and avoiding water loss through transpiration. (Wilkinson et al., 2001). In mango, reported that LTS was attributed to a rise in stomatal resistance of net CO_2 assimilation rate and a decrease in Rubisco activity, chlorophyll concentrations, *etc*., with increased activity of the chlorophyll-degrading enzyme chlorophyllase. Similarly, among various papaya genotypes, the cold-tolerant wild relative *V. cundinamarcensis* exhibited a lower transpiration rate than other susceptible genotypes (Pradhan et al., 2018). Grau and Halloy (1997) also reported that the reduction in stomatal conductance under cold stress was up to 25-30% compared to the control in papaya.

Biochemical responses

The biochemistry of various cellular components and reactions changed during LTS to help the plant acclimatize to the cold. LTS induced changes range from changes in membrane lipids composition to cellular metabolites, disruption in the equilibrium of gel to liquid-crystalline phase, synthesis of diverse cryoprotective molecules *viz.* soluble sugars (raffinose, saccharose, stachyose, trehalose), sugar alcohols (inositol, ribitol, sorbitol) and low-molecular-weight nitrogenous compounds (glycine betaine, proline) (Janska et al., 2009).

Cell membrane

Phospholipids are the fundamental components of the plasma membrane, and their composition and properties give membrane fluidity and selectivity. The cell membrane is the first place affected by LTS damage, which results in alterations in the plasma membrane's lipid composition. Compared to non-acclimated plants, the amount of unsaturated fatty acids in the cellular membranes of acclimated plants increases, minimizing injury caused by threshold temperature (Theocharis et al., 2012). These modifications protect the plasma membrane and chloroplast envelope from LTS injury (Matteucci et al., 2011). However, in susceptible genotypes, the proportion of saturated

fatty acids in the phosphatidyl glycerol (PG) backbone of the chloroplast membrane was higher under the LTS. (Yokoi et al., 1998).

The ROS produced under LTS due to photostatic imbalance induced lipid peroxidation in the cell, damaging the cell membrane's structural and dynamic features, and hence responsible for the non-functionality of the membrane by modifying the fluidity, ion leakage, and producing malondialdehyde (MDA). For example, lipid order in a phospholipid bilayer of a cell membrane diminishes when lipid peroxidation products are added. Pore formation might occur if all phospholipids are oxidized. Reactive species such as reactive oxygen and nitrogen species (RONS) will be able to cause oxidative damage to intracellular macromolecules like DNA and proteins, too (Alonso et al., 1997; Van der Paal et al., 2016). Coffee seedlings, while exposed for six days at the different treatments of temperatures (10°, 15°, 20°, and 25°C), a higher amount of MDA is generated under low temperatures (10°C), leading to higher electrolyte leakage from the root tip. Under completely controlled conditions. Pradhan et al. (2019) evaluate the effects of five LT regimes on five *Carica papaya* genotypes and one distantly related cold-tolerant plant, *V. cundinamarcensis*, They observed lower MDA content in the cold-tolerant papaya genotype and *V. cundinamarcensis* than in the other *C. papaya* genotypes. The higher rate of oxidation of membrane lipids in susceptible genotypes was linked to a higher amount of MDA, which caused damage to the membrane.

LTS related proteins

LTS affects a variety of metabolites and metabolic processes, including lipoproteins. Cryoprotection, which is the change of lipid biosynthetic enzymes during LTS (Miura and Furumoto, 2013), keeps the plasma membrane, chloroplastic envelope, and other cellular membranes safe and stable. Plant cells synthesize the specific proteins under the LTS, primarily hydrophilic in nature. Cold-regulated proteins (CORs), Low-Temperature Induced (LTI), Late Embryogenesis Abundant (LEA), Responsive to Abscisic acid (RAB), Early Responsive to Dehydration (ERD), Cold Induced (KIN), heat-shock proteins (HSPs), *etc*. are examples of such protein families. Dehydrins are the most common LEA proteins during cold acclimation and stabilize cell membranes against FI (Bies-Etheve et al., 2008; Sun et al., 2013). Hao et al. (2009) performed the leaf protein analyses after cold acclimation in guava and observed the accumulation of dehydrin protein in FI tolerant guava variety (Lucknow-49). Several freeze-induced membrane injuries have been associated with ice nucleation in the apoplast initiated by freezing. It has also been reported that denaturation of proteins occurs in plants under LT, potentially resulting in cellular damage (Guy et al., 1985). For instance, Pradhan et al. (2017) noted a 35.51% higher total soluble protein content in the cold-treated papaya leaves than in the non-treated plants. The cold-tolerant wild relative, *V. cundinamarcensis*, reported the highest increase (79.06%), while the lowest was in the cold susceptible variety, Pusa Nanha (8.78%).

Antioxidant

Low temperature induced membrane injuries also accelerate generation of reactive oxygen species (ROS), and enhanced antioxidants activities plays key role in cold acclimation. (Arora, 2018). Antioxidant enzymes influence plant abiotic stress tolerance as they play a crucial role in balancing the ROS concentration within the cell. The antioxidant defense system of plants is comprised of non-enzymatic antioxidants such as glutathione, vitamin C (ascorbic acid), phenolic compounds, flavonoids, carotenoids, α-tocopherol, the osmolyte proline, and antioxidant enzymes such as CAT (catalase), PPO (polyphenol-oxidase), SOD (superoxide dismutase), POD (peroxidase), GR (glutathione reductase), DHAR (dehydro ascorbate reductase), MDHAR (monodehydro ascorbate reductase), and APOX (ascorbate peroxidase) (Cao et al., 2009; Kumar and Yadav, 2009; Zhang et al., 2009 and Ding and Wang, 2018). Geng et al. (2019) reported that overexpression of antioxidant enzymes such as CAT, POX, and SOD under cold stress dramatically lowers the ROS levels in *Citrus grandis*. Lee and Lee (2000) also reported increasing antioxidant enzyme activity in cucumbers under chilling stress. The LT induces CAT and SOD, which act as antioxidant system and are integral parts of the plant's defensive responses under LTS (Figure 2). It is evident that *V. cundinamarcensis*, a cold-tolerant wild relative of papaya, also expressed higher SOD, GPX, APX, and GR (Pradhan et al., 2017). However, SOD and APX activities increased in cultivated papaya regardless of genotype under LT conditions (Maurya et al., 2020). In strawberries, the increased levels of H_2O_2 and MDA are associated with decreased activity of SOD, POD, and CAT under LTS (Xu et al., 2020).

Non enzymatic antioxidants also play a crucial role in ROS balancing during abiotic stresses, including LTS (Ahmad et al., 2010). For instance, higher lycopene containing peels of grapes show better ROS scavenging, and higher chilling tolerance, without significant effect of enzymatic antioxidants activities (Lado et al., 2016). Though, Rooy et al. (2017) also observed cold tolerance of grapevines was associated with both, carotenoids as well as enzymatic antioxidants activities. In cold sensitive, mandarin, chilling injury was associated with low carotenoid content (Rey et al., 2020). However, effective antioxidant defense against ROS, is dependent upon the coordinate action of enzymatic and non-enzymatic antioxidants (Kerchev and Van Breusegem, 2022). For instance, activities of GR, DHAR, MDHAR and APX regulate glutathione-ascorbic acid (GSH/AA) cycle (Foyer and Noctor, 2011) and thus exogenous application of compounds which boosts the plants

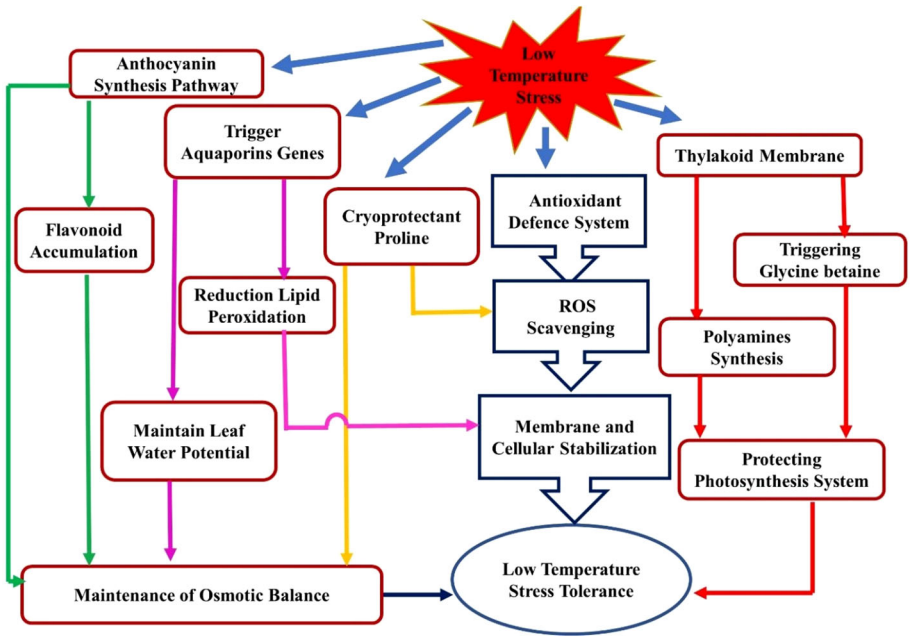


FIGURE 2
Systematic representation of stress responses and stress regulator crosstalk for low-temperature tolerance in plants.

antioxidants defense, ameliorate the chilling injury in fruits (Zhang et al., 2021).

Cryoprotectant

Accumulation of compatible osmolytes or osmoprotectants in the cytoplasm is a typical response under various abiotic stresses, where dehydration is involved, including LTS. For instance, plants exposed to chilling stress accumulated more fructans and had better freezing tolerance (Livingston et al., 2009). They safeguard the structure of proteins and enzymes; help to maintain the osmotic gradient between the cell's surroundings and the cytoplasm (Kempf and Bremer, 1998; Fedotova, 2019). Under cold stress, the organic osmolytes like sugars, proline, glycine betaine, amino acids, *etc*., change the cell's osmotic potential. This change narrows the water potential gradient between the apoplastic region of ice generation and the cytoplasm. As a result, the pace at which water moves away from the cell slows down, and the cell membrane becomes more stable, making it more resistant to LTS stress (Elbein et al., 2003). The role of osmoprotectants in ameliorating LTS is well known in fruit crops. Red Delicious apple's cortical tissues and buds' cold hardiness were associated with the concentration of total sugars, sorbitol, and RFO (raffinose family oligosaccharides) (Stushnoff et al., 1993). Another compatible solute, trehalose (α-D-glucopyranosyl-1, 1-α-D- glucopyranoside), a non-reducing disaccharide, is found in many organisms, including bacteria, fungi, insects, and plants. One of the crucial functions of trehalose is to maintain biological membranes and proteins through H-bonding during dehydration due to FI (Donnamaria et al., 1994; Goddijn and Van Dun, 1999; Elbein et al., 2003). Plants exposed to chilling stress accumulated more fructans and had better freezing tolerance (Livingston et al., 2009).

Proline, a type of amino acid, is found abundantly in higher plants and is known to accumulate in considerable amounts in response to environmental challenges (Hayat et al., 2012; Jogawat, 2019). Proline helps maintain osmotic balance and helps in scavenging free radicals (Figure 2) and their crosstalk. It also serves to preserve the integrity of subcellular structures (e.g., membranes and proteins), limits electrolyte leakage, and buffers cellular redox potential during stress by bringing ROS concentrations into normal ranges (Ozturk and Demir, 2002; Hsu et al., 2003; Kishor et al., 2005). There is a significant correlation between cold stress tolerance and increased proline content in various plants (Swaaij et al., 1985; Dorffling et al., 1990; Kaplan et al., 2007). Kushad and Yelenosky (1987) observed the effect of proline and polyamines in LTS tolerance in three citrus genotypes: sour orange (SO), *Citrus aurantium* L., 'Valencia' (VAL), *Citrus sinensis* (L.) Osbeck, and rough lemon (RL), *Citrus jambhiri* Lush. After three weeks of exposure to cold hardening (temperature range: 15.6°/4.4°C day/night) and non-hardening (temperature range: 32.2°/21.1°C day/night), Sour orange had the highest proline content (7.9mg/g dry weight), whereas the lowest content (4.2 and 3.9mg/g dry weight) was found in VAL and RL, respectively. According to the authors,

there is a direct association between higher spermidine (Spd) content and citrus cold hardiness. Pradhan et al. (2019) also found a significant proline accumulation in papaya genotypes as temperatures decrease.

Strawberry (*Fragaria* x *ananassa* Duch.) crown sugar content was also positively correlated with cold tolerance (Paquin et al., 1989). The amount of sucrose decreased, and total sugar content in the crowns of Bounty and Redcoat cultivars increased during cold hardening and peaking in January, coinciding with maximum hardiness. The high glucose levels, fructose, raffinose, and stachyose content are attributed to cold hardiness in Chardonnay and Riesling grape (*Vitis vinifera*) buds and cortical tissues (Hamman et al., 1996). An endophytic gram-negative bacteria (*Burkholderia phytofirmans)* altered carbohydrate metabolism in the grapevine (*V. vinifera*) and helped to acclimatize to LTS (Fernandez et al., 2012). Most sugars, such as mannose, glucose, fructose, sucrose, galactinol, raffinose, and maltose, were higher when grapevine was treated with *B. phytofirmans* under LTS. Yooyongwech et al. (2009) found that the high-chill peach cv. Kansuke Hakuto had a higher total soluble sugar content in the bud cushion sample during December and January (temperature about 2°C), but the low-chill peach cv. Coral had a lower total soluble sugar content. Pradhan et al. (2019) found that cold (20°/10°C; day/night) exposed papaya plants had 117.10 percent higher total soluble sugars than control plants. Polyamines, such as putrescine (Put), spermidine spermidine: (Spd), and spermine (Spm), play a significant role in the green mango (*Mangifera indica* L. 'Kensington Pride') LT tolerance during storage (Nair and Singh, 2004). Similarly, membrane integrity and fluidity were protected from LTS, in pomegranates due to higher polyamine levels during storage (Mirdehghan et al., 2007). In addition, experimental evidence suggests that polyamines also play a role in protecting photosynthetic function (Figure 2). Polyamines interact with proteins present in the thylakoid membranes, particularly the light-harvesting complex II (LHCII) and the PSII, through hydrogen bonding and stabilize the tertiary structure of proteins under stress (Kotzabasis et al., 1993; Hamdani et al., 2011). Glycine betaine is an ammonium molecule synthesized in chloroplasts that accumulates under stress conditions, including high salt levels and cold temperatures (Sakamoto and Murata, 2002). In four weeks of cold-acclimation treatment of strawberry (*Fragaria* x *ananassa* Duch.), LTS tolerance was raised from -5.8° to -17°C with a two-fold increase in endogenous glycine betaine levels in the leaves (Rajashekar et al., 1999). Exogenous glycine betaine (2 mM) to unhardened plants boosted cold leaf tolerance nearly two-fold within 72 h. Furthermore, it promoted whole-plant freezing survival and regeneration. Sirooeinejad et al. (2020) investigated the level of freezing tolerance of four pomegranate (*Punica granatum* L.) varieties, including 'Alak Torsh' (AT), 'Tabestaneh Torsh' (TT), 'Poostsefid Torsh' (PT), and 'Poostsyah Shirin' (PS), and its association with several physiological events and antioxidant response during cold acclimation and de-acclimation. The lethal temperature (LT_{50}) of pomegranate shoots was positively associated with MDA, starch, and antioxidant enzyme activity but negatively related to total phenolic content, proline, and soluble carbohydrates. Similarly, Pradhan et al. (2019) also noted a significant positive correlation of LT exposed papaya plantlet survival (%) with relative water content (RWC), membrane stability index (MSI), and chlorophyll fluorescence, while noting a significant negative association with MDA, proline, and sugar contents.

Aquaporins

Aquaporins are membrane-bound water channels that facilitate water flow with small solutes across the membrane (Moshelion et al., 2015). Plant aquaporins are present in the plasma membrane and other cellular membranes like the tonoplast, endoplasmic reticulum, plastids, and membrane compartments that interact with symbiotic organisms in some species (Baiges et al., 2002; Maurel et al., 2015). Aquaporins are classified into four clades: AQP1, AQP2, AQP3, and AQP4, of a broad superfamily of major intrinsic proteins (MIPs). Various reports show that aquaporins play a significant role in imparting abiotic stress tolerance, including LTS tolerance (Yooyongwech et al., 2009; Lee et al., 2012; Li et al., 2015; Wei et al., 2019) in various crops. Several reports have suggested that aquaporins play a significant role in the cold tolerance of temperate fruits during winter dormancy. Yooyongwech et al. (2009) reported that gamma tonoplast intrinsic protein (*Pp-γTIP1*) and plasma membrane intrinsic protein (*Pp-PIP1)* play essential roles in intra- and intercellular membrane transport, enhancing cold resistance in the bud cushions of high-chill peach cultivars.

Among the tropical fruits, the role of aquaporins was studied in cold tolerance in bananas. According to Sreedharan et al. (2013), transgenic banana plants that overexpressed a natural plasma membrane aquaporin (*MusaPIP1;2*) showed remarkable tolerance to cold stress. In addition, transgenic lines showed lower MDA accumulation, higher proline content, RWC, and increased photosynthetic efficiency (*Fv*/*Fm*) than controls under exposure to cold stress. Moreover, these transgenic plants exhibited lower damage to the cell membrane and chloroplastic membrane under LTS. Cold-tolerance of banana Dajiao, also associated with aquaporins *viz*. MaPIP1;1, MaPIP1;2, MaPIP2;4, MaPIP2;6, MaTIP1;3, and membrane bounds Peroxidase 52 and Peroxidase P7. These proteins are the vital cellular adaptations that led to a reduction in lipid peroxidation and maintained leaf cell water potential (WP) (Figure 2) (He et al., 2018). Xu et al. (2020) reported that the overexpression of *MaPIP2-7*, an aquaporin gene in bananas, improved tolerance to various stresses, including cold, salt, and drought. When compared to wild-type (WT) banana plants

under stress, *MaPIP2-7* transgenic plants had reduced levels of MDA and ion leakage (IL) but higher levels of chlorophyll content, proline, soluble sugar, and abscisic acid (ABA). Furthermore, Xu et al. (2021) determined the function of the aquaporin gene MaPIP1;1 and confirmed that overexpression led to multiple stress tolerance in bananas, including drought and cold. Recently, Lopez-Zaplana et al. (2022) elucidated that aquaporins (*PIP2;1*, *PIP2;5* and *PIP2;6*) decreases with the magnitude of different abiotic stresses in melon.

Signaling and molecular responses

Phytohormones

Plant growth-regulating hormones such as abscisic acid (ABA), ethylene, jasmonic acid, and salicylic acid (SA) play a significant role during abiotic stresses, including cold, salinity, drought, light, and heavy metal stresses and they acts as links between stress regulator and responses at cellular, tissue and organ level to external stimuli (Rachappanavar et al., 2022). When *Vitis vinifera* cv. 'Pinot Gris' was sprayed with ABA @ 400 mg L^{-1} between veraison and three weeks post veraison, it efficiently accelerated and induced deeper dormancy and increased bud frost tolerance without influencing vine size, yield, or fruit quality (Li et al., 2015). Postharvest foliar treatments of ABA @ 5000 ppm to Merlot grapevines promoted leaf abscission and boosted autumn bud cold tolerance. However, ABA at a lower concentration of 1000 ppm encourages a delay in bud break in the spring season. It has been noted that after ABA treatments, fruit yield and elemental composition were less affected (Bowen et al., 2016). Foliar application of ABA (500 mg· L^{-1}) increased freeze tolerance in grapefruit trees (Wang et al., 2020). In grapevine, ethylene is released under low-temperature stress, which induces the expression of ethylene-responsive factor (*VaERF057*) and enhances cold tolerance (Sun et al., 2016). Ethylene plays a crucial role in preventing chilling injury in nectarines (Zhou et al., 2001). In *Arabidopsis*, cold stress reduces the amount of active gibberellin (GA) content and the accumulation of DELLAs, which are negative regulators of GA (Achard et al., 2006; Achard et al., 2016). SA treatment (2 mM) is highly effective in reducing the chilling injury effects, electrolyte leakage, and ascorbic acid loss in the husk of pomegranates (Sayyari et al., 2009). Furthermore, SA treatment alleviates chilling injury in 'Qingnai' plum fruit during postharvest storage (Luo et al., 2011). Exogenous application of methyl jasmonate (MeJA) (10^{-4} M) reduced the chilling injury index and ion leakage in Tommy Atkins mangos during storage at 7°C (Gonzalez-Aguilar et al., 2000). Application of MeJA vapor for 20 h at 20°C to 'Kent' mango fruits has enhanced the shelf-life under cold storage with a lower chilling injury score (Gonzalez-Aguilar et al., 2001). Similar reports are also available for guava (Gonzalez-Aguilar et al., 2004), loquat (Cao et al., 2009), and pomegranate (Sayyari et al., 2011).

Molecular responses

The response of a plant to LTS is to limit or eliminate the negative consequences of LT. It leads to biochemical and physiological changes in the plant cells, like membrane rigidification, lowering of enzyme kinetics, ROS generation, metabolic disequilibrium, etc. Plant species' responses to cold stress vary, and the expression of several stress-associated genes are redirected to alter their metabolism accordingly (Chinnusamy et al., 2010; Guo et al., 2018). Plants can activate a cascade of processes that produce changes in gene expression (Zuther et al., 2019) and, as a result, promote biochemical and physiological adaptations that improve their resistance to low non-freezing temperatures. This process is known as cold acclimatization. Plants follow the adaptive mechanism against cold stress by changing the proteins at the translational level, the composition of the cell membrane, and triggering the ROS scavenging system. In addition, gene expression plays a crucial role in these adaptive mechanisms. The molecular mechanisms of cold stress tolerance and freezing tolerance have been studied in detail in *Arabidopsis* and winter cereals. It has been shown that temperate crops mainly acquire adaptive tolerance, whereas tropical and subtropical crops are vulnerable to cold stress (Chinnusamy et al., 2010). Many cold-regulated (*COR*) genes require specific signal transduction pathway activation for acclimatization under LTS (Thomashow, 1998) such as membrane linked receptor proteins, and the most extensively studied pathway: *ICE-CBF-COR* pathway (Zinta et al., 2022). (Figure 3).

The list of various gene families/gene(s) responsible for LTS tolerance in different fruit crops is listed in Table 2. The *COR* genes in *Arabidopsis* plants are regulated by CRT/DRE binding factors (*CBF*) at the transcription level to enhance the freezing tolerance (Jaglo-Ottosen et al., 1998; Gilmour et al., 2000). CBF related genes, namely, C*BF1*, *CBF2*, and *CBF3*, are rapidly and transiently expressed in response to LT (Gilmour et al., 1998). In the transgenic *Arabidopsis* plants, susceptible to cold stress, it has been found that ectopic synthesis of CBF proteins leads to constitutive expression of COR genes, resulting in enhanced freezing tolerance (Jaglo-Ottosen et al., 1998; Gilmour et al., 2000). The inducer of C-repeat binding factor (*CBF*) expression 1 (*ICE1*), part of the *CBF* transcriptional cascade, regulates transcription (Zhu et al., 2007). In addition, the activation of transcriptional cascades involving *CBF* is mediated by Ca^{2+} signaling (Figure 3). Under cold stress, the function of *ICE1* is to induce the constitutive expression of *CBF*s (Chinnusamy et al., 2007). PIF4 (Phytochrome Interacting Factor 4) and PIF7 (Phytochrome Interacting Factor 7) negatively regulate CBFs during the long day. On the other hand, when days are

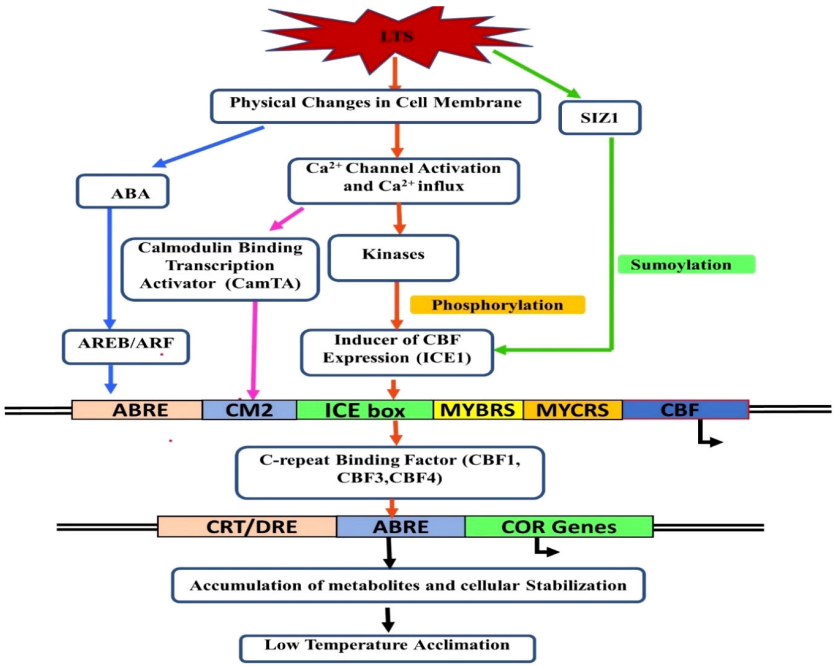


FIGURE 3
Signaling network for low-temperature stress acclimation in plants.

short, PIF4 and PIF7 are turned off, which makes plants more resistant to freezing. However, the actual mechanisms of photoperiod-induced repression of *CBFs*, *PIF4* and *PIF7*, are still not very evident; therefore, it may not be the sole mechanism engaged in acclimation processes (Fennell, 2014).

Despite this, the *CBF/DREB1* dependent low-temperature signaling network is the most crucial regulatory system (Chinnusamy et al., 2007). Maurya et al. (2020) investigated the similarity of the putative amino acid sequence of *CBF1* of *Carica papaya* through a BLAST search. They reported higher similarities with *Quercus suber* (53%), *Malus domestica* (50%), *Durio zibethinus* (49%), *Theobroma cacao* (49%), *Ziziphus jujube* (48%) and *Rosa chinensis* (48%) (Table 3). Furthermore, the phylogenetic tree revealed the evolutionary link between the *CBFs* of different plants (Figure 3). The phylogenetic tree of *CBFs* was classified into three major groups, and *C. papaya CBF1/DREB* belonged to group-II, as presented in Figure 4. The comparison of amino acid sequence and multiple sequence alignment of *Carica papaya's CBF1/DREB* protein and other plant species was shown in Figure 5. Dhekney et al. (2007) found cold-inducible regions and *CBF* sequences in *C. papaya* and *Vasconcellea* and reported sequence homology with *the Arabidopsis* genome. Recently, Maurya et al. (2020) studied the comparative expression profile of *CBF1* and *CBF2* gene transcripts under LTS and observed that the *CBF1* expression profiles was up-regulated while *CBF2* was down-regulated in six *C. papaya* genotypes (Red Lady, Pusa Nanha, P-7-2, P-7-9, P-7-14, and *V. cundinamarcensis*). In addition, they noted that *V. cundinamarcensis* had the highest expression profile of *CBF1*, followed by P-7-9, whereas the lowest level was found in Red Lady. On the other hand, the *CBF2* expression profile followed the opposite pattern. According to Zhu et al. (2007), high-temperature stress (HTS) had minimal influence on the *CpCBF2* expression profile, whereas LT inhibited it. The induction of *CBF1/DREB1B* and *CBF3/DREB1A* is simultaneous and before *CBF2/DREB1C* under cold stress (Medina et al., 2011). Fursova et al. (2009) found that overexpression of *ICE2* increased the expression profile of *CBF1/DREB1B* and improved freezing tolerance in *Arabidopsis*. Takuhara et al. (2011) found that the grapevine cold-induced transcription factors (*VvCBF2*, *VvCBF4*, *VvCBFL*, *VvZFPL*) also enhance LT tolerance in transgenic Arabidopsis plants. Transgenic strawberry leaves over expressing wheat acidic dehydrin gene (*Wcor410a*) improved their cold tolerance when exposed to 5°C (Houde et al., 2004). In addition, Hara et al. (2004) reported that a dehydrin gene, *i.e.,CuCOR19*, from *Citrus unshiu*, can operate as a hydroxyl radical scavenger under LT and found more tolerance to freezing when over expressed in *Nicotiana tabacum* (Hara et al., 2003). Apart from this, they also reported a negative association between the accumulation of *CuCOR19* and electrolyte ion leakage. The approximate size of peach's dehydrin gene (*ppdhn1*) is 50 kDa, which encodes PCA60 protein, consisting of 472 amino acids. In the deciduous genotype, the protein accumulates earlier and is retained at

TABLE 2 Various gene (s) responsible for LTS tolerance in different fruit crops.

Sl. No.	Fruit crop	Gene (s)	Reference (s)
01	Grapevine (*Vitis vinifera*)	*VvCBF1, VvCBF2, VvCBF3, and VvCBF4*	Xiao et al. (2008)
02	Apple (*Malus x domestica*)	*MdCBF1, MdCBF2, MdCBF3, MdCBF4 and MdCBF5*	Feng et al. (2012)
03	Almond (*Prunus dulcis*)	*PdCBF1 and PdCBF2*	Barros et al. (2012)
04	Strawberry (*Fragaria* × *ananassa*)	*FaCBF1*	Owens et al. (2002)
05	Crab apple (*Malus baccata*)	*DREB1/CBF(Mb-DREB1)*	Yang et al. (2011)
06	Sour cherry (*Prunus cerasus*)	*PcCBF1*	Owens et al. (2002)
07	Sweet cherry (*Prunus avium*)	*PaCBF*	Kitashiba et al. (2004)
08	Blueberry (*Vaccinium corymbosum*)	*BB-CBF*	Polashock et al. (2010)
09	*Vitis riparia*	*VrCBF4 and VrCBF1a*	Xiao et al. (2008)
10	*Poncirus trifoliata*	*COR11, COR19*	Thomashow (2010)
11	Peach (*Prunus persica*)	*ppdhn1*	Artlip et al. (1997)
12	*Citrus unshiu*	*Cu-COR19*	Hara et al. (2004)
13	Banana *(Musa* spp.*)*	*MusaDHN-1*	Upendra et al. (2011)
14	Apple (*M. domestica*)	Dehydrin (*MdDHN*)	Liang et al. (2012)
15	Grape (*V. vinifera*)	Dehydrin (*DHN*)	Yang et al. (2012).
16	Banana *(Musa* spp.*)*	MaCslD4, MaCslA4/12, MaCslE2	Yuan et al. (2021)

TABLE 3 Percent identity matrix of Carica papaya CBF1/DREB with other plants CBF/DREB factors (Table adapted from Maurya et al., 2020).

CBF1/DREB *Carica papaya*	100.00															
DREB 1B *Juglans regia*	47.55	100.00														
DREB 1F *Quercus suber*	53.16	59.67	100.00													
DREB 1F *Durio zibethinus*	49.48	59.69	55.00	100.00												
DREB 1F *Gossypium arboretum*	46.45	60.10	61.83	67.51	100.00											
DREB 1B *Ziziphus jujube*	48.80	59.02	61.58	66.50	82.27	100.00										
DREB 1B *Theobroma cacao*	49.50	47.06	53.63	50.00	45.59	43.78	100.00									
DREB 1B *Cinnamomum micranthum*	45.93	47.37	51.89	49.48	46.95	46.67	66.82	100.00								
DREB 1B *Ricinus communis*	45.58	51.44	54.79	52.82	48.61	48.84	52.68	51.42	100.00							
CBF6 *Populus trichocarpa*	47.09	51.00	52.91	51.05	53.02	53.70	44.72	43.27	50.00	100.00						
CBF like *Vitis riaparia*	45.60	51.91	58.60	51.18	56.52	54.89	43.24	45.79	50.54	53.59	100.00					
CBF/DREB *Rosa chinensis*	48.24	47.03	55.37	52.94	54.95	56.28	48.06	45.02	47.29	57.00	55.32	100.00				
A)2/ERF *Artemisia annua*	46.94	53.54	54.70	58.51	57.58	56.63	46.67	46.73	52.76	56.10	62.36	56.37	100.00			
CRT binding factor 3 *Solanum tuberosum*	46.63	55.88	54.59	52.36	56.87	56.87	44.66	45.50	49.53	53.49	62.23	53.85	62.44	100.00		
AP2/ERF *Trema orientale*	46.12	55.88	62.78	56.08	58.17	59.71	45.15	44.08	52.86	57.77	58.42	55.98	61.93	61.86	100.00	
DREB 1D *Malus domestica*	50.54	55.88	61.18	57.14	59.36	63.04	47.85	45.79	52.38	58.20	58.38	62.77	59.79	61.78	71.05	100.00

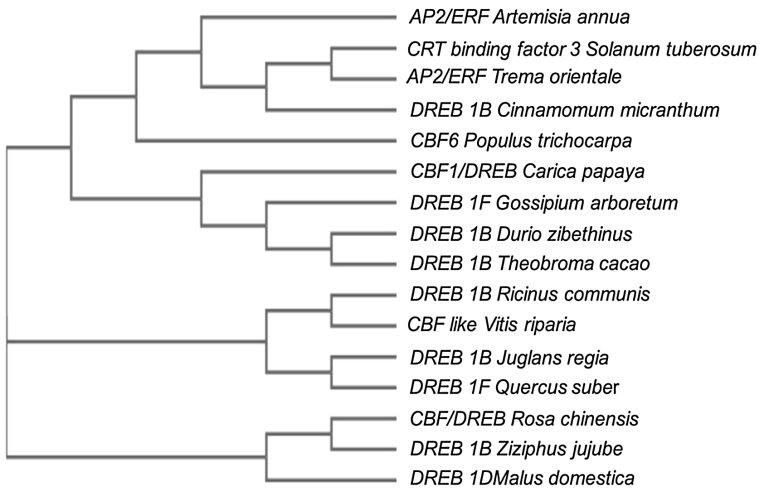


FIGURE 4
Phylogenetic tree of *CBFs* from different plants. *Carica papaya CBF1* (XP_021908755.1), *Juglans regia DREB 1B* Like (XP_018812676.1), *Quercus suber DREB 1 F* Like (XP_023913339.1), *Durio zibethinus DREB 1B* Like (XP_022744533.1), *Gossypium arboretum DREB 1F* Like (XP_017622119.1), *Ziziphus jujube DREB 1B* Like (XP_015901948.1), *Theobroma cacao DREB 1B* Like (EOY08142.1), *Cinnamomum micranthus DREB 1B* Like (RWR82367.1), *Ricinus communis DREB 1B* Like (EEF33807.1), *Populus trichocarpa* C-repeat binding factor 6 (ABO48367.1), *Vitis riparia CBF*-Like transcription factor (ARD27023.1), *Rosa chinensis* putative *CBF*/*DREB* transcription factor (ABQ53132.1), *Artemisia annua AP2*/*ERF* domain-containing protein (PWA50609), *Solanum tuberosum* CRT binding factor 3 (ACB45095.1), *Trema arientale AP2*/*ERF* domain-containing protein (PON57830.1), *Malus domestica DREB 1D* (XP_028948628.1) (FIGURE adapted from Maurya et al., 2020).

higher levels for a longer time than in the evergreen genotype, indicating that it plays a role in cold tolerance (Artlip et al., 1997). Furthermore, the PCA60 protein acts as an anti-freeze protein that modifies ice crystal growth in the cell and is present in the cytosol and nucleus but absent in the vacuole when investigated under the light electron microscope (Wisniewski et al., 1999). LT tolerance is increased when MpRCI, a cold-tolerance-related plasma membrane protein gene of the 'Dajiao banana cultivar, is overexpressed in transgenic tobacco. (Feng et al., 2009).

Overexpression of the *MbDREB1* transcription factor improved cold tolerance and other abiotic stresses in apples (Yang et al., 2011). Additionally, *Prunus persica CBF1* gene overexpression significantly enhanced freezing tolerance in transgenic apples (Wisniewski et al., 2011). Feng et al. (2012) studied the adaptive responses to cold tolerance in apples and discovered that the transcription factor MdCIbHLH1 plays an important role in the LTS.

Bananas are highly susceptible to chilling stress (Chen et al., 2020). Recently, Meng et al. (2020) reported that the accumulation of fasciclin-like arabinogalactan protein (*FLA*) in banana under low temperatures could improve chilling tolerance by facilitating cold signal pathways, which increases the biosynthesis of plant cell wall components. The results provided background information on *MaFLAs* and suggested their involvement in plant chilling tolerance and their potential as candidate genes to be targeted when breeding for cold tolerance. Yuan et al. (2021) reported that the *Csl* (*Cellulose synthase-like*) gene family imparts tolerance against LT in bananas by synthesizing a special kind of hemicellulose, an essential component of the cell wall, and strengthening the stiffness of the cell wall. The expression of genes *MaCslD4* (*Musa acuminate Cellulose synthase-like gene*), *MaCslA4/12*, and *MaCslE2* (member of *the Csl* gene family) were found to be significantly higher in the tolerant variety than in the susceptible banana variety under LTS (Yuan et al., 2021).

The commercially important diversity of citrus is available for cultivation. However, it has been observed that most cold-acclimated citrus cultivars can only sustain temperature variations of -4° to -10°C. However, *Poncirus trifoliata*, a citrus relative, is a genetic resource for cold-hardiness that can survive at temperatures as low as -26°C (Yelenosky, 1985). Zhang et al. (2005) studied the gene expression profile of *P. trifoliata* by mRNA DDRT-PCR (differential display-reverse transcription) and quantitative relative-RT-PCR in a cold acclimation temperature regime. The up-regulated genes showed high similarities at the amino acid level with genes with known functions like water channel protein, betaine or proline transporter, early light-induced protein, nitrate transporter, aldo-ketoreductase, tetratricopeptide-repeat protein, F-box protein, ribosomal (r) protein L15. These cold-acclimation up-regulated genes of *P. trifoliata* are also regulated by osmotic and photo-oxidative signals in other plants.

Anthocyanins, a water-soluble pigment available across the plant kingdom, have a significant role in mitigating cold stress by increasing their content in the cell and maintaining the osmotic

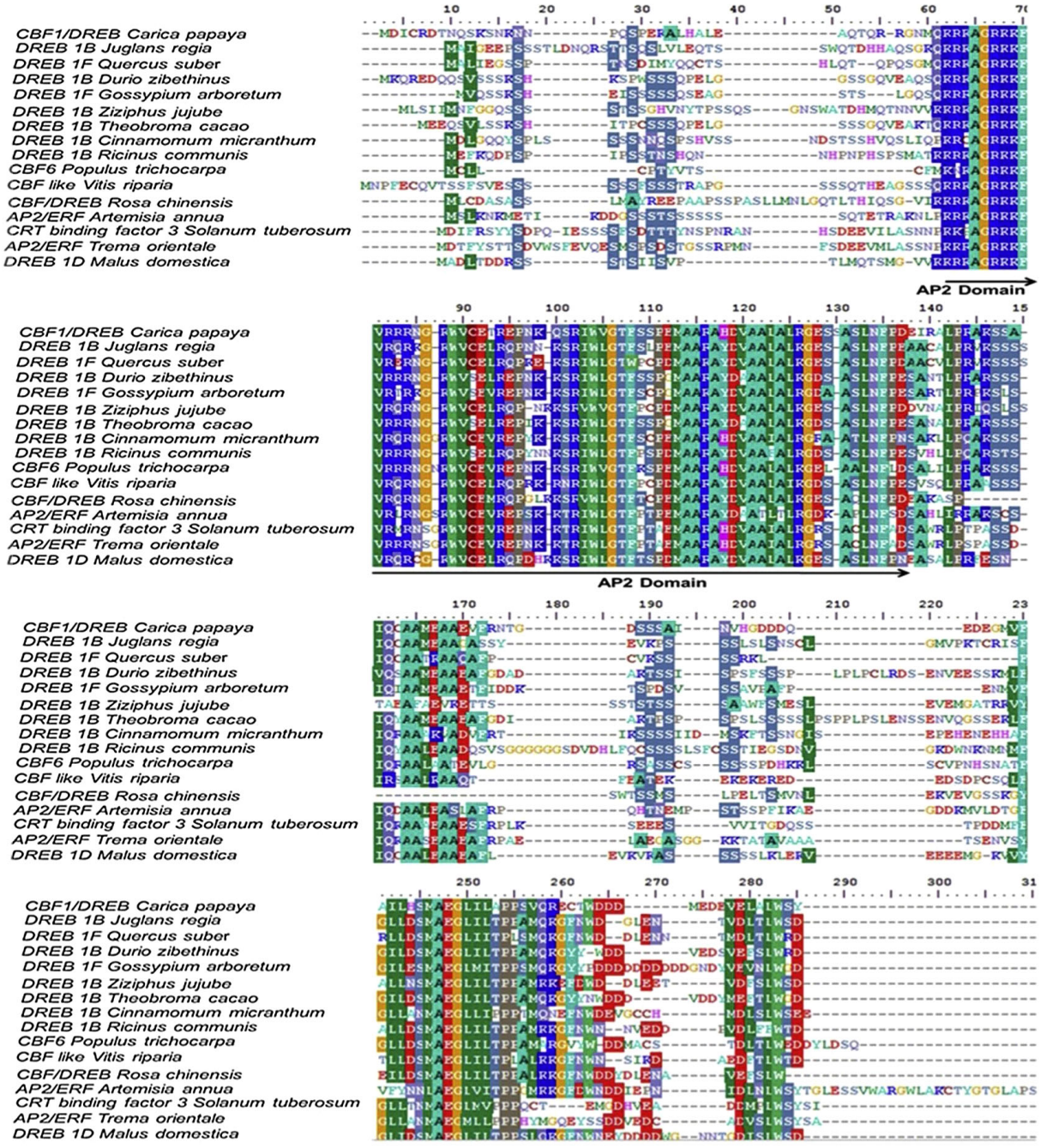


FIGURE 5
Alignment of the predicted amino acid sequences of the *Carica papaya CBF1/DREB* from with another plant *CBFs/DERB*. All the designated sequences showed conserved domain of AP2, the characteristics of c-repeat binding factors. (FIGURE adapted from Maurya et al., 2020).

balance to improve the chilling tolerance (Chalker-Scott, 1999; Hao et al., 2009). Lo Piero et al. (2005) reported an accumulation of anthocyanin in red-orange juice vesicles under LTS. The biosynthesis pathway of anthocyanin is complex and involves several structural genes: *PAL* (phenylalanine ammonia-lyase), *CHS* (chalcone synthase), *DFR* (dihydro flavonol 4-reductase), and *UFGT* (UDP-glucose flavonoid glucosyltransferase), which are strongly triggered during LTS.

According to Crifo et al. (2011), cold stress causes transcriptome changes in blood oranges that trigger enhancement of flavonoid biosynthesis, including the metabolic pathways of anthocyanin biosynthesis. Similarly, in red-skinned

grapes, cold stress promoted anthocyanin biosynthesis but did not increase the accumulation of endogenous levels of abscisic acid (Gao-Takai et al., 2019). Using an RNA-seq study of leaves from the 'Gala' apple variety after exposure to LT (16°C), Song et al. (2019) identified additional regulatory genes ROS1 in apple (*M. domestica*) that may be involved in controlling LT-induced anthocyanin production.

Conclusion

LTS unfavorably affects the fruit crop's overall growth and development because it affects almost all aspects of cellular activity and, ultimately the quality production of the crop. However, according to the current review, the method of comprehending low-temperature damage have been adequately tried by researchers on many field crops, while very limited studies have been conducted on fruit crops. These include primarily temperate fruit crops and some tropical crops like bananas. Therefore, new avenues like the role and use of aquaporin genes to alleviate the LTS need to be explored in tropical and sub-tropical fruit crops. Furthermore, under open and simulated low-temperature conditions, more detailed research is required to elucidate the underlying physio-biochemical and molecular mechanisms for LTS tolerance and resistance in fruit crops. These strategies will immensely help in genetic improvement and standardizing cultural practices for successful cultivation of the fruit crops, particularly in the erratic weather conditions of sub-tropical and tropical regions.

Author contributions

AKG, NKM, SG, and KB conceived the idea of the review and prepared the initial outline, and wrote the first draft. AKG and NKM had major and equal contributions to the overall preparation of the manuscript. SKS, JP, SP, AKG, VC, PK, SP, DB, and CK gathered the literature and contributed to writing the different sections. SKS, SG, KB, and RMS provided technical guidance and editing support. All authors have read and approved the manuscript.

Acknowledgments

The authors would like to acknowledge the ICAR-Indian Agricultural Research Institute, New Delhi, Navsari Agricultural University, Navsari, Gujarat, Central Agricultural University, Imphal, Ministry of Agriculture & Farmers Welfare, Govt. of India, Krishi Bhavan, New Delhi, Jawaharlal Nehru Krishi Vishwavidyalaya, Jabalpur, Madhya Pradesh and ICAR-National Institute for Plant Biotechnology, New Delhi.

Conflict of interest

The authors declare that the research was conducted in the absence of any commercial or financial relationships that could be construed as a potential conflict of interest.

Publisher's note

All claims expressed in this article are solely those of the authors and do not necessarily represent those of their affiliated organizations, or those of the publisher, the editors and the reviewers. Any product that may be evaluated in this article, or claim that may be made by its manufacturer, is not guaranteed or endorsed by the publisher.

References

Achard, P., Cheng, H., De Grauwe, L., Decat, J., Schoutteten, H., Moritz, T., and Harberd, N. P. (2006). Integration of plant responses to environmentally activated phytohormonal signals. *Science* 311(5757), 91–94.

Achard, P., Gong, F., Cheminant, S., Alioua, M., Hedden, P., and Genschik, P. (2016). The cold-inducible CBF1 factor–dependent signaling pathway modulates the accumulation of the growth-repressing DELLA proteins *via* its effect on gibberellin metabolism. *Plant Cell* 20, 2117–2129. doi: 10.1105/tpc.108.058941

Ahmad, P., Jaleel, C. A., Salem, M. A., Nabi, G., and Sharma, S. (2010). Roles of enzymatic and nonenzymatic antioxidants in plants during abiotic stress. *Crit. Rev. Biotechnol.* 30 (3), 161–175. doi: 10.3109/07388550903524243

Allen, D. J., and Ort, D. R. (2001). Impacts of chilling temperatures on photosynthesis in warm-climate plants. *Trends Plant Sci.* 6, 36–42. doi: 10.1016/S1360-1385(00)01808-2

Alonso, A., Queiroz, C. S., and Magalhaes, A. C. (1997). Chilling stress leads to increased cell membrane rigidity in roots of coffee (Coffea arabica l.) seedlings. *Biochim. Biophys. Acta* 1323, 75–84. doi: 10.1016/S0005-2736(96)00177-0

Aroca, R., Irigoyen, J. J., and Sanchez-Diaz, M. (2001). Photosynthetic characteristics and protective mechanisms against oxidative stress during chilling and subsequent recovery in two maize varieties differing in chilling sensitivity. *Plant Sci.* 161, 719–726. doi: 10.1016/S0168-9452(01)00460-5

Arora, R. (2018). Mechanism of freeze-thaw injury and recovery: a cool retrospective and warming up to new ideas. *Plant Sci.* 270, 301–313. doi: 10.1016/j.plantsci.2018.03.002

Artlip, T. S., Callahan, A. M., Bassett, C. L., and Wisniewski, M. E. (1997). Seasonal expression of a dehydrin gene in sibling deciduous and evergreen genotypes of peach (Prunus persica [L.] batsch). *Plant Mol. Biol.* 33, 61–70. doi: 10.1023/A:1005787909506

Awada, M. (1958). "Relationships of minimum temperature and growth rate with sex expression of papaya plants (Carica papaya l.)," in *Hawaii Agricultural experiment station technical bulletin*, vol. 38. (Honolulu: University of Hawaii).

Baiges, I., Schaffner, A. R., Affenzeller, M. J., and Mas, A. (2002). Plant aquaporins. *Physiol. Plant* 115, 175–182. doi: 10.1034/j.1399-3054.2002.1150201.x

Barlow, K. K., Lee, J. W., Vesk, M., RL, B., AR, F., and MM, C. (1974). "Mechanisms of regulation of plant growth," in *The royal society of new Zealand*, R. L. Bieleski, A. R. Ferguson and M. M. Cresswell Eds. (Wellington: Royal Society of New Zealand) 793–797.

Barros, R. S., da Se Mota, J. W., Da Matta, F. M., and Maestri, M. (1997). Decline of vegetative growth in coffea arabica l. @ in relation to leaf temperature, water potential and stomatal conductance. *Field Crops Res.* 54, 65–72. doi: 10.1016/S0378-4290(97)00045-2

Barros, P. M., Gonçalves, N., Saibo, N. J., and Oliveira, M. M. (2012). Cold acclimation and floral development in almond bud break: insights into the regulatory pathways. *J. Exp. Bot.* 63, 4585–4596. doi: 10.1093/xb/ers144

Bauer, H., Wierer, R., Hatheway, W. H., and Larcher, W. (1985). Photosynthesis of coffea arabica after chilling. *Physiol. Plant* 64, 449–454. doi: 10.1111/j.1399-3054.1985.tb08521.x

Beck, E. H., Fettig, S., Knake, C., Hartig, K., and Bhattarai, T. (2007). Specific and unspecific responses of plants to cold and drought stress. *J. Biosci.* 32, 501–510. doi: 10.1007/s12038-007-0049-5

Bies-Etheve, N., Gaubier-Comella, P., Debures, A., Lasserre, E., Jobet, E., Raynal, M., et al. (2008). Inventory, evolution and expression profiling diversity of the LEA (late embryogenesis abundant) protein gene family in arabidopsis thaliana. *Plant Mol. Biol.* 67, 107–124. doi: 10.1007/s11103-008-9304-x

Bowen, P., Shellie, K. C., Mills, L., Willwerth, J., Bogdanoff, C., and Keller, M. (2016). Abscisic acid form, concentration, and application timing influence phenology and bud cold hardiness in merlot grapevines. *Can. J. Plant Sci.* 96, 347–359. doi: 10.1139/cips-2015-0257

Campos, P. S., Quartin, V., Ramalho, J. C., and Nunes, M. ,. A. (2003). Electrolyte leakage and lipid degradation account for cold sensitivity in leaves of coffea sp. *plants. J. Plant Physiol.* 160, 283–292. doi: 10.1078/0176-1617-00833

Cao, S., Zheng, Y., Wang, K., Jin, P., and Rui, H. (2009). Methyl jasmonate reduces chilling injury and enhances antioxidant enzyme activity in postharvest loquat fruit. *Food Chem.* 115, 1458–1463. doi: 10.1016/j.foodchem.2009.01.082

Chalker-Scott, L. (1999). Environmental significance of anthocyanins in plant stress responses. *Photochem. Photobiol.* 70, 1–9. doi: 10.1111/j.1751-1097.1999.tb01944.x

Chen, Y. Z., and Patterson, B. D. (1985). Ethylene and 1-aminocyclopropane-1-carboxylic acid as indicators of chilling sensitivity in various plant species. *Funct. Plant Biol.* 12, 377–385. doi: 10.1071/PP9850377

Chen, L., Zhao, X., Wu, J. E., He, Y., and Yang, H. (2020). Metabolic analysis of salicylic acid-induced chilling tolerance of banana using NMR. *Food Res. Int.* 128, 108796. doi: 10.1016/j.foodres.2019.108796

Chinnusamy, V., Zhu, J. K., and Sunkar, R. (2010). Gene regulation during cold stress acclimation in plants. *Meth. Mol. Biol.* 639, 39–55. doi: 10.1007/978-1-60761-702-0_3

Chinnusamy, V., Zhu, J., and Zhu, J. K. (2007). Cold stress regulation of gene expression in plants. *Trends Plant Sci.* 12, 444–451. doi: 10.1016/j.tplants.2007.07.002

Criddle, R. S., Breidenbach, R. W., Lewis, E. A., Eatough, D. J., and Hansen, L. D. (1988). Effects of temperature and oxygen depletion on metabolic rates of tomato and carrot cell cultures and cuttings measured by calorimetry. *Plant Cell Environ.* 11, 695–701. doi: 10.1111/j.1365-3040.1988.tb01152.x

Crifo, T., Puglisi, I., Petrone, G., Recupero, G. R., and Piero, A. R. L. (2011). Expression analysis in response to low temperature stress in blood oranges, implication of the flavonoid biosynthetic pathway. *Gene* 476, 1–9. doi: 10.1016/j.gene.2011.02.005

Davanport, T. L. (2009). "Reproductive physiology," in *The mango, 2nd edn. botany, production and uses*. Ed. R. E. Litz (London: CABI).

Dhekney, S. A., Litz, R. E., Moraga, D., and Yadav, A. (2007). Is it possible to induce cold tolerance in papaya through genetic transformation? *Acta Hortic.*, vol. 738, 159–164. doi: 10.17660/ActaHortic.2007.738.13

Ding, F., and Wang, R. (2018). Amelioration of postharvest chilling stress by trehalose in pepper. *Scientia Hortic.* 232, 52–56. doi: 10.1016/j.scienta.2017.12.053

Ding, Y., and Yang, S. (2022). Surviving and thriving: How plants perceive and respond to temperature stress. *Dev. Cell* 57, 947–958. doi: 10.1016/j.devcel.2022.03.010

Donnamaria, M. C., Howard, E. I., and Grigera, J. R. (1994). Interaction of water with α, α-trehalose in solution, molecular dynamics simulation approach. *J. Chem. Soc. Faraday Trans.* 90, 2731–2735. doi: 10.1039/FT9949002731

Dorffling, K., Schulenburg, S., Lesselich, G., and Dorffling, H. (1990). Abscisic acid and proline levels in cold hardened winter wheat leaves in relation to variety-specific differences in freezing resistance. *J. Agron. Crop Sci.* 165, 230–239. doi: 10.1111/j.1439-037x.1990.tb00857.x

Ehlert, B., and Hincha, D. K. (2008). Chlorophyll fluorescence imaging accurately quantifies freezing damage and cold acclimation responses in arabidopsis leaves. *Plant Meth.* 4, 1–7. doi: 10.1186/1746-4811-4-12

Elbein, A. D., Pan, Y. T., Pastuszak, I., and Carroll, D. (2003). New insights on trehalose: a multifunctional molecule. *Glycob.* 13, 17–27. doi: 10.1093/glycob/cwg047

Fariduddin, Q., Yusuf, M., Chalkoo, S., Hayat, S., and Ahmad, A. (2011). 28-homobrassinolide improves growth and photosynthesis in cucumis sativus l. through an enhanced antioxidant system in the presence of chilling stress. *Photosynthetica* 49, 55–64. doi: 10.1007/s11099-011-0022-2

Fedotova, M. V. (2019). Compatible osmolytes-bioprotectants: is there a common link between their hydration and their protective action under abiotic stresses? *J. Mol. Liq.* 292, 111339. doi: 10.1016/j.molliq.2019.1111339

Feng, D. R., Liu, B., Li, W. Y., He, Y. M., Qi, K. B., Wang, H. B., et al. (2009). Over-expression of a cold-induced plasma membrane protein gene (MpRCI) from plantain enhances low temperature-resistance in transgenic tobacco. *Environ. Exp. Bot.* 65, 395–402. doi: 10.1016/j.envexpbot.2008.12.009

Feng, X. M., Zhao, Q., Zhao, L. L., Qiao, Y., Xie, X. B., Li, H. F., et al. (2012). The cold-induced basic helix-loop-helix transcription factor gene MdCIbHLH1 encodes an ICE-like protein in apple. *BMC Plant Biol.* 12, 1–14. doi: 10.1186/1471-2229-12-22

Fennell, A. (2014). Genomics and functional genomics of winter low temperature tolerance in temperate fruit crops. *Crit. Rev. Plant Sci.* 33, 125–140. doi: 10.1080/07352689.2014.870410

Fernandez, O., Theocharis, A., Bordiec, S., Feil, R., Jacquens, L., Clement, C., et al. (2012). Burkholderia phytofirmans PsJN acclimates grapevine to cold by modulating carbohydrate metabolism. *Mol. Plant Microbe Interact.* 25, 496–504. doi: 10.1094/MPMI-09-11-0245

Foyer, C. H., and Noctor, G. (2011). Ascorbate and glutathione: the heart of the redox hub. *Plant Physiol.* 155 (1), 2–18. doi: 10.1104/pp.110.167569

Fursova, O. V., Pogorelko, G. V., and Tarasov, V. A. (2009). Identification of ICE2, a gene involved in cold acclimation which determines freezing tolerance in arabidopsis thaliana. *Gene* 429, 98–103. doi: 10.1016/j.gene.2008.10.016

Gao-Takai, M., Katayama-Ikegami, A., Matsuda, K., Shindo, H., Uemae, S., and Oyaizu, M. (2019). A low temperature promotes anthocyanin biosynthesis but does not accelerate endogenous abscisic acid accumulation in red-skinned grapes. *Plant Sci.* 283, 165–176. doi: 10.1016/j.plantsci.2019.01.015

Geng, J., Wei, T., Wang, Y., Huang, X., and Liu, J. H. (2019). Overexpression of PtrbHLH, a basic helix-loop-helix transcription factor from poncirus trifoliata, confers enhanced cold tolerance in pummelo (Citrus grandis) by modulation of H2O2 level *via* regulating a CAT gene. *Tree Physiol.* 39, 2045–2054. doi: 10.1093/treephys/tpz081

Gilmour, S. J., Zarka, D. G., Stockinger,E. J., Salazar, M. P., Houghton, J. M., and Thomashow, M. F. (1998). Low temperature regulation of the Arabidopsis CBF family of AP2 transcriptional activators as an early step in cold - induced COR gene expression. *Plant Journal* 16, 433–442. doi: 10.1046/j.1365-313x.1998.00310.x

Gilmour, S. J., Sebolt, A. M., Salazar, M. P., Everard, J. D., and Thomashow, M. F. (2000). Overexpression of the arabidopsis CBF3 transcriptional activator mimics multiple biochemical changes associated with cold acclimation. *Plant Physiol.* 124, 1854–1865. doi: 10.1104/pp.124.4.1854

Glaszmann, J. C., Kaw, R. N., and Khush, G. S. (1990). Genetic divergence among cold tolerant rices (Oryza sativa l.). *Euphytica* 45, 95–104. doi: 10.1007/BF00033276

Goddijn, O. J., and Van Dun, K. (1999). Trehalose metabolism in plants. *Trends Plant Sci.* 4, 315–319. doi: 10.1016/S1360-1385(99)01446-6

Gonzalez-Aguilar, G. A., Buta, J. G., and Wang, C. Y. (2001). Methyl jasmonate reduces chilling injury symptoms and enhances colour development of 'Kent' mangoes. *J. Sci. Food Agric.* 81, 1244–1249. doi: 10.1002/jsfa.933

Gonzalez-Aguilar, G. A., Fortiz, J., Cruz, R., Baez, R., and Wang, C. Y. (2000). Methyl jasmonate reduces chilling injury and maintains postharvest quality of mango fruit. *J. Agric. Food Chem.* 48, 515–519. doi: 10.1021/jf9902806

Gonzalez-Aguilar, G. A., Tiznado-Hernandez, M. E., Zavaleta-Gatica, R., and Martınez-Tellez, M. A. (2004). Methyl jasmonate treatments reduce chilling injury and activate the defense response of guava fruits. *Biochem. Biophys. Res. Commun.* 313, 694–701. doi: 10.1016/j.bbrc.2003.11.165

Grau, A., and Halloy, S. (1997). Effect of chilling on CO2 gas-exchange in carica papaya l. and carica quercifolia (A. st. hil.) solms. *J. Plant Physiol.* 150, 475–480. doi: 10.1016/S0176-1617(97)80101-0

Grewal, J. S., and Singh, S. N. (1980). Effect of potassium nutrition on frost damage and yield of potato plants on alluvial soils of the punjab (India). *Plant Soil* 57, 105–110. doi: 10.1007/Bf02139646

Guo, X., Liu, D., and Chong, K. (2018). Cold signaling in plants: Insights into mechanisms and regulation. *J. Integr. Plant Biol.* 60 (9), 745–756. doi: 10.1111/jipb.12706

Guy, C. L., Niemi, K. J., and Brambl, R. (1985). Altered gene expression during cold acclimation of spinach. *Proc. Natl. Acad. Sci.* 82, 3673–3677. doi: 10.1073/pnas.82.11.3673

Hakerlerler, H., Oktay, M., Eryuce, N., and Yagmur, B. (1997). "Effect of potassium sources on the chilling tolerance of some vegetable seedlings grown in hotbeds," in *Food*

security in the WANA region, the essential need for balanced fertilization. Ed. A. E. Johnston (Switzerland: International Potash Institute), 317–327.

Hamdani, S., Yaakoubi, H., and Carpentier, R. (2011). Polyamines interaction with thylakoid proteins during stress. *J. Photochem. Photobiol.* 104, 314–319. doi: 10.1016/j.jphotobiol.2011.02.007

Hamman, R. A., Dami, I. E., Walsh, T. M., and Stushnoff, C. (1996). Seasonal carbohydrate changes and cold hardiness of Chardonnay and Riesling grapevines. *Am. J. Enol. Vitic.* 47, 31–36.

Hao, W., Arora, R., Yadav, A. K., and Joshee, N. (2009). Freezing tolerance and cold acclimation in guava (Psidium guajava l.). *Hort Sci.* 44, 1258–1266. doi: 10.21273/HORTSCI.44.5.1258

Haq, N. (2006). "Jackfruit (Artocarpus heterophyllus)," in *Tropical fruit trees, Southampton centre for underutilised crops*. Eds. J. T. Williams, R. W. Smith and Z. Dunsiger (Southampton, UK: University of Southampton).

Hara, M., Fujinaga, M., and Kuboi, T. (2004). Radical scavenging activity and oxidative modification of citrus dehydrin. *Plant Physiol. Biochem.* 42, 657–662. doi: 10.1016/j.plaphy.2004.06.004

Hara, M., Terashima, S., Fukaya, T., and Kuboi, T. (2003). Enhancement of cold tolerance and inhibition of lipid peroxidation by citrus dehydrin in transgenic tobacco. *Planta* 217, 290–298. doi: 10.1007/s00425-003-0986-7

Harrington, J. F., and Kihara, G. M. (1960). Chilling injury of germinating muskmelon and pepper seed. *Proc. Am. Soc Hortic. Sci.* 75, 485–489.

Hasanuzzaman, M., Nahar, K., and Fujita, M. (2013). "Extreme temperatures, oxidative stress and antioxidant defense in plants," in *Abiotic stress-plant responses and applications in agriculture*, vol. 13 . Eds. K. Vahdati and C. Leslie (Rijeka: InTech), 169–205.

Hayat, S., Hayat, Q., Alyemeni, M. N., Wani, A. S., Pichtel, J., and Ahmad, A. (2012). Role of proline under changing environments: a review. *Plant Signal. Behav.* 7, 1456–1466. doi: 10.4161/psb.21949

He, W. D., Gao, J., Dou, T. X., Shao, X. H., Bi, F. C., Sheng, O., et al. (2018). Early cold-induced peroxidases and aquaporins are associated with high cold tolerance in dajiao (Musa spp. 'Dajiao'). *Front. Plant Sci.* 9. doi: 10.3389/fpls.2018.00282

Herner, R. C. (1990). *Chilling injury of horticultural crops*. Ed. C. V. Wang (Boca Raton, FL., USA: CRC Press), 51–69.

Houde, M., Dallaire, S., N'Dong, D., and Sarhan, F. (2004). Overexpression of the acidic dehydrins WCOR410 improves freezing tolerance in transgenic strawberry leaves. *Plant Biotechnol. J.* 2, 381–387. doi: 10.1111/j.1467-7652.2004.00082.x

Hsu, S. Y., Hsu, Y. T., and Kao, C. H. (2003). The effect of polyethylene glycol on proline accumulation in rice leaves. *Biol. Plant* 46, 73–78. doi: 10.1023/A:1022362117395

Jaglo-Ottosen, K. R., Gilmour, S. J., Zarka, D. G., Schabenberger, O., and Thomashow, M. F. (1998). Arabidopsis CBF1 overexpression induces COR genes and enhances freezing tolerance. *Science* 280, 104–106. doi: 10.1126/science.280.5360.104

Jan, N., and Andrabi, K. I. (2009). Cold resistance in plants: A mystery unresolved. *Electronic J. Biotechnol.* 12, 14–15. doi: 10.4067/S0717-34582009000300014

Janska, A., Mars, P., Zelenkova, S., and Ovesna, J. (2009). Cold stress and acclimation-what is important for metabolic adjustment? *Plant Biol.* 12, 395–405. doi: 10.1111/j.1438-8677.2009.00299.x

Jogawat, A. (2019). "Osmolytes and their role in abiotic stress tolerance in plants," in *Molecular plant abiotic stress: Biology and biotechnology*. Eds. A. Roychoudhury and D. Tripathi (Hoboken, NJ, USA: John Wiley and Sons Ltd), 91–104. doi: 10.1002/9781119463665.ch5

Joubert, A. S., and Thomas, D. D. S. (1965). The cashew nut. *Farming south Africa* 40, 6–7.

Kafkafi, U. (1990). "Impact of potassium in relieving plants from climatic and soil-induced stresses," in *Food security in the WANA region, the essential need for balanced fertilization*. Ed. A. E. Johnston (Basel: International Potash Institute), 317–327.

Kaplan, F., Kopka, J., Sung, D. Y., Zhao, W., Popp, M., Porat, R., et al. (2007). Transcript and metabolite profiling during cold acclimation of arabidopsis reveals an intricate relationship of cold-regulated gene expression with modifications in metabolite content. *Plant J.* 50, 967–981. doi: 10.1111/j.1365-313X.2007.03100.x

Kempf, B., and Bremer, E. (1998). Stress responses of bacillus subtilis to high osmolarity environments, uptake and synthesis of osmoprotectants. *J. Biosci.* 23, 447–455. doi: 10.1007/BF02936138

Kerchev, P. I., and Van Breusegem, F. (2022). Improving oxidative stress resilience in plants. *Plant J.* 109 (2), 359–372. doi: 10.1111/tpj.15493

Kishor, P. K., Sangam, S., Amrutha, R. N., Laxmi, P. S., Naidu, K. R., Rao, K. S., et al. (2005). Regulation of proline biosynthesis, degradation, uptake and transport in higher plants, its implications in plant growth and abiotic stress tolerance. *Curr. Sci.* 88, 424–438.

Kitashiba, H., Ishizaka, T., Isuzugawa, K., Nishimura, K., and Suzuki, T. (2004). Expression of a sweet cherry DREB1/CBF ortholog in arabidopsis confers salt and freezing tolerance. *J. Plant Physiol.* 161, 1171–1176. doi: 10.1016/j.jplph.2004.04.008

Kotzabasis, K., Christakishampsas, M. D., and Roubelakisangelakis, K. A. (1993). A narrow-bore HPLC method for the identification and quantitation of free, conjugated, and bound polyamines. *Anal. Biochem.* 214, 484–489. doi: 10.1006/abio.1993.1526

Kumar, V., and Yadav, S. K. (2009). Proline and betaine provide protection to antioxidant and methylglyoxal detoxification systems during cold stress in camellia sinensis (L.) o. kuntze. *Acta Physiol. Plant* 31, 261–269. doi: 10.1007/s11738-008-0227-6

Kushad, M. M., and Yelenosky, G. (1987). Evaluation of polyamine and proline levels during low temperature acclimation of citrus. *Plant Physiol.* 84, 692–695. doi: 10.1104/pp.84.3.692

Lado, J., Rodrigo, M. J., López-Climent, M., Gómez-Cadenas, A., and Zacarías, L. (2016). Implication of the antioxidant system in chilling injury tolerance in the red peel of grapefruit. *Postharvest Biol. Technol.* 111, 214–223. doi: 10.1016/j.postharvbio.2015.09.01

Lee, S. H., Chung, G. C., Jang, J. Y., Ahn, S. J., and Zwiazek, J. J. (2012). Overexpression of PIP2; 5 aquaporin alleviates effects of low root temperature on cell hydraulic conductivity and growth in arabidopsis. *Plant Physiol.* 159, 479–488. doi: 10.1104/pp.112.194506

Lee, D. H., and Lee, C. B. (2000). Chilling stress-induced changes of antioxidant enzymes in the leaves of cucumber, in gel enzyme activity assays. *Plant Sci.* 159, 75–85. doi: 10.1016/S0168-9452(00)00326-5

Levitt, J. (1980). *Responses of plant to environmental stress chilling, freezing, and high temperature stresses, second ed* Vol. 1 (New York: Academic Press), 23–64.

Li, J., Ban, L., Wen, H., Wang, Z., Dzyubenko, N., Chapurin, V., et al. (2015). An aquaporin protein is associated with drought stress tolerance. *Biochem. Biophys. Res. Commun.* 459, 208–213. doi: 10.1016/j.bbrc.2015.02.052

Li, S., and Dami, I. E. (2016). Responses of vitis vinifera 'Pinot gris' grapevines to exogenous abscisic acid (aba), i. yield, fruit quality, dormancy, and freezing tolerance. *J. Plant Growth Reg.* 35, 245–255. doi: 10.1007/s00344-015-9529-2

Liang, D., Xia, H., Wu, S., and Ma, F. (2011). Genome-wide identification and expression profiling of dehydrin gene family in Malus domestica. *Mol. Biol. Rep.* 59, 10759–10768. doi: 10.1007/s11033-012-1968-2

Lin, H., Liao, Z., Zhang, L., and Yu, Q. (2016). Transcriptome analysis of the male-to-hermaphrodite sex reversal induced by low temperature in papaya. *Tree Genet. Genomes* 12, 94. doi: 10.1007/s11295-016-1055-2

Livingston, D. P., Hincha, D. K., and Heyer, A. G. (2009). Fructan and its relationship to abiotic stress tolerance in plants. *Cell. Mol. Life Sci.* 66, 2007–2023. doi: 10.1007/s00018-009-0002-x

Lopez-Zaplana, A., Martinez-Garcia, N., Carvajal,M., and Barzana, G. (2022). Relationships between aquaporins gene expression and nutrient concentrations in melon plants (Cucumis melo l.) during typical abiotic stresses. *Environ. Exp. Bot.* 195, 104759. doi: 10.1016/j.envexpbot.2021.104759

Lo Piero, A. R., Puglisi, I., Rapisarda, P., and Petrone, G. (2005). Anthocyanins accumulation and related gene expression in red orange fruit induced by low temperature storage. *J. Agric. Food Chem.* 53, 9083–9088. doi: 10.1021/jf051609s

Louis, H., and Annappan, R. S. (1980). Environmental effects on yield of coconut palm. *Indian Coconut J.* 12, 1–4.

Luo, Z., Chen, C., and Xie, J. (2011). Effect of salicylic acid treatment on alleviating postharvest chilling injury of 'Qingnai'plum fruit. *Postharvest Biol. Technol.* 62, 115–120. doi: 10.1016/j.postharvbio.2011.05.012

Maestri, M., and Barros, R. S. (1977). "Coffee," in *Ecophysiology of tropical crops*. Eds. P. T. de Alvim and T. T. Kozlowski (New York: Academic Press), 249–278.

Mahajan, S., and Tuteja, N. (2005). Cold, salinity and drought stresses: An overview. *Arch. Biochem. Biophys.* 444, 139–158. doi: 10.1016/j.abb.2005.10.018

Martin, L. J., and Douglas, G. (1979). "Proceedings of an international seminar on low temperature stress in crop plants held at the East-West center," in *Low temperature stress in crop plants: the role of the membrane* (Honolulu, Hawaii: Academic Press rapid manuscript reproduction (USA).

Matteucci, M., D'angeli, S., Errico, S., Lamanna, R., Perrotta, G., and Altamura, M. M. (2011). Cold affects the transcription of fatty acid desaturases and oil quality in the fruit of olea europaea l. genotypes with different cold hardiness. *J. Exp. Bot.* 62, 3403–3420. doi: 10.1093/jxb/err013

Maurel, C., Boursiac, Y., Luu, D. T., Santoni, V., Shahzad, Z., and Verdoucq, L. (2015). Aquaporins in plants. *Physiol. Rev.* 95, 1321–1358. doi: 10.1152/physrev.00008.2015

Maurya, N. K., Goswami, A. K., Singh, S. K., Prakash, J., Goswami, S., Chinnusamy, V., et al. (2020). Studies on expression of CBF1 and CBF2 genes and antioxidant enzyme activities in papaya genotypes exposed to low temperature stress. *Sci. Hortic.* 261, 108914. doi: 10.1016/j.scienta.2019.108914

Maurya, N. K., Goswami, A. K., Singh, S. K., Prakash, J., Goswami, S., Chinnusamy, V., et al. (2020). Low temperature stress induced changes in the

seedling growth and nutrient content of papaya genotypes. *Indian J. Hortic.* 77, 80–87. doi: 10.5958/0974-0112.2020.00006.7

Maxwell, K., and Johnson, G. N. (2000). Chlorophyll fluorescence- a practical guide. *J. Exp. Bot.* 51, 659–668. doi: 10.1093/jexbot/51.345.659

Medina, J., Catala, R., and Salinas, J. (2011). The CBFs: three arabidopsis transcription factors to cold acclimate. *Plant Sci.* 180, 3–11. doi: 10.1016/j.plantsci.2010.06.019

Meng, J., Hu, B., Yi, G., Li, X., Chen, H., Wang, Y., et al. (2020). Genome-wide analyses of banana fasciclin-like AGP genes and their differential expression under low-temperature stress in chilling sensitive and tolerant cultivars. *Plant Cell Rep.* 39, 693–708. doi: 10.1007/s00299-020-02524-0

Mirdehghan, S. H., Rahemi, M., Martinez-Romero, D., Guillen, F., Valverde, J. M., Zapata, P. J., et al. (2007). Reduction of pomegranate chilling injury during storage after heat treatment, role of polyamines. *Postharvest Biol. Technol.* 44, 19–25. doi: 10.1016/j.postharvbio.2006.11.001

Miura, K., and Furumoto, T. (2013). Cold signaling and cold response in plants. *Int. J. Mol. Sci.* 14, 5312–5337. doi: 10.3390/ijms14035312

Moshelion, M., Halperin, O., Wallach, R., Oren, R. A. M., and Way, D. A. (2015). Role of aquaporins in determining transpiration and photosynthesis in water-stressed plants, crop water-use efficiency, growth and yield. *Plant Cell Environ.* 38, 1785–1793. doi: 10.1111/pce.12410

Nair, S., and Singh, Z. (2004). Chilling injury in mango fruit in relation to biosynthesis of free polyamines. *J. Hortic. Sci. Biotechnol.* 79, 515–522. doi: 10.1080/14620316.2004.11511798

Nishiyama, I. (1976). Male Sterility caused by cooling treatment at the young microspore stage in rice plants. *Proc. Crop Sci. Soc* 45, 254–262. doi: 10.1626/jcs.45.254

Osman, M. B., and Milan, A. R. (2006). *Mangosteen- Garcinia Mangostana; Southampton Centre for Underutilised Crops* (Southampton, UK: University of Southampton) 2006.

Owens, C. L., Thomashow, M. F., Hancock, J. F., and Iezzoni, A. F. (2002). CBF1 orthologs in sour cherry and strawberry and the heterologous expression of CBF1 in strawberry. *J. Amer. Soc Hortic. Sci.* 127, 489–494. doi: 10.21273/JASHS.127.4.489

Ozturk, L., and Demir, Y. (2002). *In Vivo Vitro protective role proline. Plant Growth Regul.* 38, 259–264. doi: 10.1023/A:1021579713832

Palta, J. P. (1990). Stress interactions at the cellular and membrane levels. *Hort Sci.* 25, 1377–1381. doi: 10.21273/HORTSCI.25.11.1377

Paquin, R., Bolduc, R., Zizka, J., Pelletier, G., and Lechasseur, P. (1989). Tolerance au gel et teneur en sucres et en proline du collet du fraisier (Fragaria ananassa duch.) durant l'hiver. *Can. J. Plant Sci.* 69, 945–954. doi: 10.4141/cjps89-11

Polashock, J. J., Arora, R., Peng, Y., Dhananjay, N., and Rowland, L. J. (2010). Functional identification of a blueberry CBF/DREB-like element associated with cold acclimation and freezing tolerance. *J. Am. Soc Hortic. Sci.* 135, 40–48. doi: 10.21273/JASHS.135.1.40

Pradhan, S., Goswami, A. K., Singh, S. K., Prakash, J., Goswami, S., Chinnusamy, V., et al. (2017). Physiological and biochemical alterations due to low temperature stress in papaya genotypes. *Indian J. Hortic.* 74, 491–497. doi: 10.5958/0974-0112.2017.00096.2

Pradhan, S., Goswami, A. K., Singh, S. K., Prakash, J., Goswami, S., Chinnusamy, V., et al. (2019). Low temperature stress induced physiological and biochemical alterations in papaya genotypes. *S. Afr. J. Bot.* 123, 133–141. doi: 10.1016/j.sajb.2019.02.004

Pradhan, S., Goswami, A. K., Singh, S. K., Prakash, J., Goswami, S., Viswanathan, C., et al. (2018). Growth, nutrient acquisition and physiological responses of papaya (Carica papaya) plants to controlled low temperature stress. *Indian J. Agric. Sci.* 88, 726–732.

Rachappanavar, V., Padiyal, A., Sharma, J. K., and Gupta, S. K. (2022). Plant hormone-mediated stress regulation responses in fruit crops- a review. *Sci. Hortic.*, 304, 1000302. doi: 10.1016/j.scienta.2022.11130

Rajashekar, C. B., Zhou, H., Marcum, K. B., and Prakash, O. (1999). Glycine betaine accumulation and induction of cold tolerance in strawberry (Fragaria X ananassa duch.) plants. *Plant Sci.* 148, 175–183. doi: 10.1016/S0168-9452(99)00136-3

Ram, M. (2005). *Papaya* (New Delhi: Indian Council of Agricultural Research), 78.

Rey, F., Zacarias, L., and Rodrigo, M. J. (2020). Carotenoids, vitamin c, and antioxidant capacity in the peel of mandarin fruit in relation to the susceptibility to chilling injury during postharvest cold storage. *Antioxidants.* 9 (12), 1296. doi: 10.3390/antiox9121296

Rooy, S. S.B., Salekdeh, G. H., Ghabooli, M., Gholami, M., and Karimi, R. (2017). Cold-induced physiological and biochemical responses of three grapevine cultivars differing in cold tolerance. *Acta Physiol. Plant* 39, 1–13. doi: 10.1007/s11738-017-2561-z

Ruelland, E., Vaultier, M. N., Zachowski, A., and Hurry, V. (2009). Cold signalling and cold acclimation in plants. *Adv. Bot. Res.* 49, 35–150. doi: 10.1016/S0065-2296(08)00602-2

Sakamoto, A., and Murata, N. (2002). The role of glycine betaine in the protection of plants from stress, clues from transgenic plants. *Plant Cell Environ.* 25, 163–171. doi: 10.1046/j.0016-8025.2001.00790.x

Sayyari, M., Babalar, M., Kalantari, S., Martinez-Romero, D., Guillen, F., Serrano, M., et al. (2011). Vapour treatments with methyl salicylate or methyl jasmonate alleviated chilling injury and enhanced antioxidant potential during postharvest storage of pomegranates. *Food Chem.* 124, 964–970. doi: 10.1016/j.foodchem.2010.07.036

Sayyari, M., Babalar, M., Kalantari, S., Serrano, M., and Valero, D. (2009). Effect of salicylic acid treatment on reducing chilling injury in stored pomegranates. *Postharvest Biol. Technol.* 53, 152–154. doi: 10.1016/j.postharvbio.2009.03.005

Shin, H., Min, K., and Arora, R. (2018). Exogenous salicylic acid improves freezing tolerance of spinach (Spinacia oleracea l.) leaves. *Cryobiology* 81, 192–200. doi: 10.1016/j.cryobiol.2017.10.006

Singh, A., Deka, B. C., Prakash, J., Patel, R. K., and Ojah, H. (2010). Problems and prospects of papaya cultivation in northeastern states of India in *Acta Hortic.* vol. 851, 61–66. doi: 10.17660/ActaHortic.2010.851.6

Sirooeinejad, B., Zamani, Z., and Fatahi, M. R. (2020). Study of physiological and biochemical responses to freezing stress in pomegranate (Punica granatum l.) trees during acclimation and deaclimation cycle. *J. Hortic. Sci. Biotechnol.* 95, 341–355. doi: 10.1080/14620316.2019.1674699

Smillie, R. M. (1979). "The useful chloroplast, a new approach for investigating chilling stress in plants," in *Low temperature stress in crop plants* (New York: Academic Press), 187–202.

Soitamo, A. J., Piippo, M., Allahverdiyeva, Y., Battchikova, N., and Aro, E. M. (2008). Light has a specific role in modulating arabidopsis gene expression at low temperature. *BMC Plant Biol.* 8, 1–13. doi: 10.1186/1471-2229-8-13

Song, T., Li, K., Wu, T., Wang, Y., Zhang, X., Xu, X., et al. (2019). Identification of new regulators through transcriptome analysis that regulate anthocyanin biosynthesis in apple leaves at low temperatures. *PloS One* 14, e0210672. doi: 10.1371/journal.pone.0210672

Sreedharan, S., Shekhawat, U. K., and Ganapathi, T. R. (2013). Transgenic banana plants over expressing a native plasma membrane aquaporin MusaPIP1; 2 display high tolerance levels to different abiotic stresses. *Plant Biotechnol. J.* 11, 942–952. doi: 10.1111/pbi.12086

Steponkus, P. L. (1984). Role of the plasma membrane in freezing injury and cold acclimation. *Annu. Rev. Plant Physiol.* 35, 543–584. doi: 10.1146/annurev.pp.35.060184.002551

Steponkus, P. L. (1993). A contrast of the cryostability of the plasma membrane of winter rye and spring oat. *Adv. Low-Temperature Biol.* 2, 211–312.

Storey, W. B. (1969). Pistillate papaya flower: a morphological anomaly. *Science* 163, 401–405. doi: 10.1126/science.163.3865.401

Stushnoff, C., Remmele, R. L.Jr., Essensee, V., and McNeil, M. (1993). "Low temperature induced biochemical mechanisms, implications for cold acclimation and de-acclimation," in *Interacting stresses on plants in a changing climate* (Berlin, Heidelberg: Springer), 647–657. doi: 10.1007/978-3-642-78533-7_42

Sun, X., Rikkerink, E. H., Jones, W. T., and Uversky, V. N. (2013). Multifarious roles of intrinsic disorder in proteins illustrate its broad impact on plant biology. *Plant Cell* 25, 38–55. doi: 10.1105/tpc.112.106062

Sun, X., Zhao, T., Gan, S., Ren, X., Fang, L., Karungo, S. K., et al. (2016). Ethylene positively regulates cold tolerance in grapevine by modulating the expression of ETHYLENE RESPONSE FACTOR 057. *Scient. Rep.* 6, 1–14. doi: 10.1038/srep24066

Swaaij, A. V., Jacobsen, E., and Feenstra, W. J. (1985). Effect of cold hardening, wilting and exogenously applied proline on leaf proline content and frost tolerance of several genotypes of solanum. *Physiol. Plant* 64, 230–236. doi: 10.1111/j.1399-3054.1985.tb02341.x

Taiz, L., and Zeiger, E. (2002). *Plant physiology, second edition* (Sunderland, Massachusetts: Sinauer Associates Publishers), 607.

Takuhara, Y., Kobayashi, M., and Suzuki, S. (2011). Low-temperature-induced transcription factors in grapevine enhance cold tolerance in transgenic arabidopsis plants. *J. Plant Physiol.* 168, 967–975. doi: 10.1016/j.jplph.2010.11.008

Tambussi, E. A., Bartoli, C. G., Guiamet, J. J., Beltrano, J., and Araus, J. L. (2004). Oxidative stress and photodamage at low temperatures in soybean (Glycine max l. merr.) leaves. *Plant Sci.* 167, 19–26. doi: 10.1016/j.plantsci.2004.02.018

Theocharis, A., Clement, C., and Barka, E. A. (2012). Physiological and molecular changes in plants grown at low temperatures. *Planta* 235, 1091–1105. doi: 10.1007/s00425-012-1641-y

Thomashow, M. F. (1998). Role of cold-responsive genes in plant freezing tolerance. *Plant Physiol.* 118, 1–8. doi: 10.1104/pp.118.1.1

Thomashow, M. F. (2010). Molecular basis of plant cold acclimation: insights gained from studying the CBF cold response pathway. *Plant Physiol.* 154, 571–577. doi: 10.1104/pp.110.161794

Tindall, H. D. (1994). *Rambutan cultivation* (Rome: Food and Agriculture Organization of the United Nations. FAO), 978–9-25103-325-8.

UDPSM (2002). "Plant propagation and planting in uplands," in *Training manual for municipal extension staff* (Davao, Philippines: Upland Development Programin Southern Mindanao).

Upendra, K., Shekhawat, S., Srinivas, L., and Ganapathi, T. R. (2011). Musa DHN-1, a novel multiple stress-inducible SK sub 3-type dehydrin gene, contributes affirmatively to drought-and salt-stress tolerance in banana. *Planta* 234, 915. doi: 10.1007/s00425-011-1455-3

Van der Paal, J., Neyts, E. C., Verlackt, C., and Bogaerts, A. (2016). Effect of lipid peroxidation on membrane permeability of cancer and normal cells subjected to oxidative stress. *Chem. Sci.* 7, 489–498. doi: 10.1039/C5SC02311D

Verheij, E. W. M., and Coronel, R. E. (1992). "Edible fruits and nuts," in *Plant resources of south-East Asia*, vol. 2. (Bogor: Prosea Foundation), 128–131.

Viktorova, M. K. (1983). *Plant growing in the tropics and subtropics* (Moscow: Mir Publisher), 214–218.

Wang, H., Blakeslee, J. J., Jones, M. L., Chapin, L. J., and Dami, I. E. (2018). Exogenous abscisic acid enhances physiological, metabolic, and transcriptional cold acclimation responses in greenhouse-grown grapevines. *Plant Sci.* 293, 110437. doi: 10.1016/j.plantsci.2020.110437

Waraich, E. A., Ahmad, R., Ashraf, M. Y., and Saifullah Ahmad, M. (2011). Improving agricultural water use efficiency by nutrient management in crop plants. *Acta Agric. Scand. B Soil Plant Sci.* 61, 291–304. doi: 10.1080/09064710.2010.491954

Waraich, E. A., Ahmad, R., Halim, A., and Aziz, T. (2012). Alleviation of temperature stress by nutrient management in crop plants, a review. *J. Soil Sci. Plant Nutt.* 12, 221–244. doi: 10.4067/S0718-95162012000200003

Wei, Q., Ma, Q., Ma, Z., Zhou, G., Feng, F., Le, S., et al. (2019). Genome-wide identification and characterization of sweet orange (Citrus sinensis) aquaporin genes and their expression in two citrus cultivars differing in drought tolerance. *Tree Genet. Genomes* 15, 17. doi: 10.1007/s11295-019-1321-1

White, M. A., Diffenbaugh, N. S., Jones, G. V., Pal, J. S., and Giorgi, F. (2006). Extreme heat reduces and shifts united states premium wine production in the 21st century. *Proc. Natl. Acad. Sci.* 103, 11217–11222. doi: 10.1073/pnas.060323010

Wilkinson, S., Clephan, A. L., and Davies, W. J. (2001). Rapid low temperature-induced stomatal closure occurs in cold-tolerant cammelina communis leaves but not in cold-sensitive tobacco leaves, *via* a mechanism that involves apoplastic calcium but not abscisic acid. *Plant Physiol.* 126, 1566–1578. doi: 10.1104/pp.126.4.1566

Wisniewski, M., Norelli, J., Bassett, C., Artlip, T., and Macarisin, D. (2011). Ectopic expression of a novel peach (Prunus persica) CBF transcription factor in apple (Malus × domestica) results in short-day induced dormancy and increased cold hardiness. *Planta* 233, 971–983. doi: 10.1007/s00425-011-1358-3

Wisniewski, M., Webb, R., Balsamo, R., Close, T. J., Yu, X. M., and Griffith, M.. (1999). Purification, immunolocalization, cryoprotective, and anti-freeze activity of PCA60, a dehydrin from peach (Prunus persica). *Physiol. Plant* 105, 600–608. doi: 10.1034/j.1399-3054.1999.105402.x

Xiao, H., Tattersall, E. A., Siddiqua, M. K., Cramer, G. R., and Nassuth, A. (2008). CBF4 is a unique member of the CBF transcription factor family of vitis vinifera and vitis riparia. *Plant Cell Environ.* 31, 1–10. doi: 10.1111/j.1365-3040.2007.01741.x

Xu, Y., Hu, W., Liu, J., Song, S., Hou, X., Jia, C., et al. (2020). An aquaporin gene MaPIP2-7 is involved in tolerance to drought, cold and salt stresses in transgenic banana (Musa acuminata l.). *Plant Physiol. Biochem.* 147, 66–76. doi: 10.1016/j.plaphy.2019.12.011

Xu, Y., Liu, J., Jia, C., Hu, W., Song, S., Xu, B., et al. (2021). Overexpression of a banana aquaporin gene MaPIP1; 1 enhances tolerance to multiple abiotic stresses in transgenic banana and analysis of its interacting transcription factors. *Front. Plant Sci.* 12. doi: 10.3389/fpls.2021.699230

Xu, C., Wang, M. T., Yang, Z. Q., and Zheng, Q. T. (2020). Low temperature and low irradiation induced irreversible damage of strawberry seedlings. *Photosynthetica* 58, 156–164. doi: 10.32615/ps.2020.001

Yadav, S. K. (2010). Cold stress tolerance mechanisms in plants. A review. *Agron. Sustain. Dev.* 30, 515–527. doi: 10.1051/agro/2009050

Yang, M. T., Chen, S. L., Lin, C. Y., and Chen, Y. M. (2005). Chilling stress suppresses chloroplast development and nuclear gene expression in leaves of mung bean seedlings. *Planta* 221, 374–385. doi: 10.1007/s00425-004-1451-y

Yang, W., Liu, X. D., Chi, X. J., Wu, C. A., Li, Y. Z., Song, L. L., et al. (2011). Dwarf apple MbDREB1 enhances plant tolerance to low temperature, drought, and salt stress *via* both ABA-dependent and ABA-independent pathways. *Planta* 233, 219–229. doi: 10.1007/s00425-010-1279-6

Yang, Y., He, M., Zhu, Z., Li, S., Xu, Y., Zhang, C., et al. (2012). Identification of the dehydrin gene family from grapevine species and analysis of their responsiveness to various forms of abiotic and biotic stress. *BMC Plant Biol.* 12, 1–17. doi: 10.1186/1471-2229-12-140

Yelenosky, G. (1985). Cold hardiness in citrus. *Hortic. Rev.* 7, 201–238. doi: 10.1002/9781118060735.ch5

Yokoi, S., Higashi, S. I., Kishitani, S., Murata, N., and Toriyama, K. (1998). Introduction of the cDNA for shape arabidopsis glycerol-3-phosphate acyltransferase (GPAT) confers unsaturation of fatty acids and chilling tolerance of photosynthesis on rice. *Mol. Breed.* 4, 269–275. doi: 10.1023/A:1009671231614

Yooyongwech, S., Sugaya, S., Sekozawa, Y., and Gemma, H. (2009). Differential adaptation of high-and low-chill dormant peaches in winter through aquaporin gene expression and soluble sugar content. *Plant Cell Rep.* 28, 1709. doi: 10.1007/s00299-009-0770-7

Yuan, W., Liu, J., Takac, T., Chen, H., Li, X., Meng, J., et al. (2021). Genome-wide identification of banana csl gene family and their different responses to low temperature between chilling-sensitive and tolerant cultivars. *Plants* 10, 122. doi: 10.3390/plants10010122

Yun, K. Y., Park, M. R., Mohanty, B., Herath, V., Xu, F., Mauleon, R., et al. (2010). Transcriptional regulatory network triggered by oxidative signals configures the early response mechanisms of japonica rice to chilling stress. *BMC Plant Biol.* 10, 16. doi: 10.1186/1471-2229-10-16

Zareei, E., Karami, F., Gholami, M., Ershadi, A., Avestan, S., Aryal, R., et al. (2021). Physiological and biochemical responses of strawberry crown and leaf tissues to freezing stress. *BMC Plant Biol.* 21, 1–17. doi: 10.1186/s12870-021-03300-2

Zhang, W., Jiang, H., Cao, J., and Jiang, W. (2021). Advances in biochemical mechanisms and control technologies to treat chilling injury in postharvest fruits and vegetables. *Trends Food Sci. Technol.* 113, 355–365. doi: 10.1016/j.tifs.2021.05.009

Zhang, C. K., Lang, P., Dane, F., Ebel, R. C., Singh, N. K., Locy, R. D., et al. (2005). Cold acclimation induced genes of trifoliate orange (Poncirus trifoliata). *Plant Cell Rep.* 23, 764–769. doi: 10.1007/s00299-004-0883-y

Zhang, Y., Tang, H. R., Luo, Y., and Hou, Y. X. (2009). Responses of antioxidant enzymes and compounds in strawberry (Fragaria × ananassa 'Toyonaka') to cold stress. *New Z. J. Crop Hortic. Sci.* 37, 383–390. doi: 10.1080/01140671.2009.9687594

Zhou, H. W., Dong, L., Ben-Arie, R., and Lurie, S. (2001). The role of ethylene in the prevention of chilling injury in nectarines. *J. Plant Physiol.* 158, 55–61. doi: 10.1078/0176-1617-00126

Zhu, J., Dong, C. H., and Zhu, J. K. (2007). Interplay between cold-responsive gene regulation, metabolism and RNA processing during plant cold acclimation. *Curr. Opin. Plant Biol.* 10, 290–295. doi: 10.1016/j.pbi.2007.04.010

Zinta, G., Singh, R. K., and Kumar, R. (2022). Cold adaptation strategies in plants-an emerging role of epigenetics and antifreeze proteins to engineer cold resilient plants. *Front. Genet.* 13. doi: 10.3389/fgene.2022.909007

Zuther, E., Schaarschmidt, S., Fischer, A., Erban, A., Pagter, M., Mubeen, U., et al. (2019). Molecular signatures associated with increased freezing tolerance due to low temperature memory in arabidopsis. *Plant Cell Environm.* 42, 854–873. doi: 10.1111/pce.13502

frontiers | Frontiers in Plant Science

TYPE Original Research
PUBLISHED 04 January 2023
DOI 10.3389/fpls.2022.1023571

Check for updates

OPEN ACCESS

EDITED BY
Jiban Shrestha,
Nepal Agricultural Research Council, Nepal

REVIEWED BY
Bin Xu,
Nanjing Agricultural University, China
Wangfeng Zhang,
Shihezi University, China

*CORRESPONDENCE
Berkley James Walker
berkley@msu.edu

SPECIALTY SECTION
This article was submitted to Plant Abiotic Stress, a section of the journal Frontiers in Plant Science

RECEIVED 19 August 2022
ACCEPTED 07 December 2022
PUBLISHED 04 January 2023

CITATION
Tejera-Nieves M, Abraha M, Chen J, Hamilton SK, Robertson GP and Walker BJ (2023) Seasonal decline in leaf photosynthesis in perennial switchgrass explained by sink limitations and water deficit. *Front. Plant Sci.* 13:1023571. doi: 10.3389/fpls.2022.1023571

COPYRIGHT
© 2023 Tejera-Nieves, Abraha, Chen, Hamilton, Robertson and Walker. This is an open-access article distributed under the terms of the Creative Commons Attribution License (CC BY). The use, distribution or reproduction in other forums is permitted, provided the original author(s) and the copyright owner(s) are credited and that the original publication in this journal is cited, in accordance with accepted academic practice. No use, distribution or reproduction is permitted which does not comply with these terms.

Seasonal decline in leaf photosynthesis in perennial switchgrass explained by sink limitations and water deficit

Mauricio Tejera-Nieves[1,2], Michael Abraha[2,3,4], Jiquan Chen[2,4,5], Stephen K. Hamilton[2,3,6], G. Philip Robertson[2,3,7] and Berkley James Walker[1,2,8]*

[1]MSU-DOE Plant Research Laboratory, Michigan State University, East Lansing, MI, United States, [2]Great Lakes Bioenergy Research Center, Michigan State University, East Lansing, MI, United States, [3]W. K. Kellogg Biological Station, Michigan State University, Hickory Corners, MI, United States, [4]Center for Global Change and Earth Observations, Michigan State University, East Lansing, MI, United States, [5]Department of Geography, Environment, and Spatial Sciences, Michigan State University, East Lansing, MI, United States, [6]Department of Integrative Biology, Michigan State University, East Lansing, MI, United States, [7]Department of Plant, Soil, and Microbial Sciences, Michigan State University, East Lansing, MI, United States, [8]Department of Plant Biology, Michigan State University, East Lansing, MI, United States

Leaf photosynthesis of perennial grasses usually decreases markedly from early to late summer, even when the canopy remains green and environmental conditions are favorable for photosynthesis. Understanding the physiological basis of this photosynthetic decline reveals the potential for yield improvement. We tested the association of seasonal photosynthetic decline in switchgrass (*Panicum virgatum* L.) with water availability by comparing plants experiencing ambient rainfall with plants in a rainfall exclusion experiment in Michigan, USA. For switchgrass exposed to ambient rainfall, daily net CO_2 assimilation (A'_{net}) declined from 0.9 mol CO_2 m^{-2} day^{-1} in early summer to 0.43 mol CO_2 m^{-2} day^{-1} in late summer (53% reduction; P<0.0001). Under rainfall exclusion shelters, soil water content was 73% lower and A'_{net} was 12% and 26% lower in July and September, respectively, compared to those of the rainfed plants. Despite these differences, the seasonal photosynthetic decline was similar in the season-long rainfall exclusion compared to the rainfed plants; A'_{net} in switchgrass under the shelters declined from 0.85 mol CO_2 m^{-2} day^{-1} in early summer to 0.39 mol CO_2 m^{-2} day^{-1} (54% reduction; P<0.0001) in late summer. These results suggest that while water deficit limited A'_{net} late in the season, abundant late-season rainfalls were not enough to restore A'_{net} in the rainfed plants to early-summer values suggesting water deficit was not the sole driver of the decline. Alongside change in photosynthesis, starch in the rhizomes increased 4-fold (P<0.0001) and stabilized when leaf photosynthesis reached constant low values. Additionally, water limitation under shelters had no negative effects on the timing of rhizome starch accumulation, and rhizome starch content increased ~ 6-fold. These results showed that rhizomes also affect leaf photosynthesis during the growing season. Towards the end of the growing season, when vegetative growth is completed and rhizome reserves are filled,

diminishing rhizome sink activity likely explained the observed photosynthetic declines in plants under both ambient and reduced water availability.

KEYWORDS

photosyhthesis, storage carbohydrates, sink limitation, perennial grass, drought, circadian, source- sink- relationships, C4 photosynthesis

Introduction

Leaf photosynthesis of perennial grasses follows a clear seasonal dynamic – peaking with vegetative growth in summer and declining towards late summer several weeks before the end of the growing season while leaves are still green. This dynamic occurs in many genera of grasses including the bioenergy crops *Panicum*, *Miscanthus*, and *Saccharum* spp., and even in some evergreen and deciduous trees (Eggemeyer et al., 2006; Kosugi and Matsuo, 2006; Inman-Bamber et al., 2011; De Souza et al., 2013; Boersma et al., 2015; Gao et al., 2015; Yan et al., 2015; De Souza et al., 2018; Endres et al., 2019; Rusinowski et al., 2019; Stavridou et al., 2020). This seasonal decline in photosynthesis could be partially adaptative as it is associated with the remobilization of nutrients from leaves to belowground perennating organs, which allows the plant to recycle nutrients that otherwise would be lost to leaf drop (Yang et al., 2009; Yang et al., 2016; Yang and Udvardi, 2018; Massey et al., 2020). Beyond this putative adaptive role in nutrient retranslocation, additional physiological and environmental drivers of this decrease in photosynthesis are unknown but could have large effects on end-of-season biomass and long-term yield dynamics.

Perennial grasses notably increase in size during the growing season, with larger plants being progressively more susceptible to water limitation as a larger transpiring leaf area increases total water demand and increasingly depletes available soil water (Liu et al., 2016; Mocko and Jones, 2021; Wang et al., 2021). Therefore, the observed photosynthetic decline could be a consequence of water limitation as plants become larger and soil water becomes less available later in the growing season. Alternatively, the larger size could also lead to a nitrogen (N) limitation (Leroy et al., 2022), however, this decline was not affected by N availability across a wide range of N fertilization rates (Tejera et al., 2022).

Among perennial grasses, switchgrass (*Panicum virgatum* L.) is a leading candidate for cellulosic bioenergy feedstock in the United States (Parrish and Fike, 2005). Evidence increasingly supports switchgrass as a drought tolerant species, based on its leaf photosynthesis and plant growth resiliency in the face of water limitation (Barney et al., 2009; Lovell et al., 2016; Taylor et al., 2016; Hawkes and Kiniry, 2018; Chen et al., 2020). This suggests that water limitation may not drive the photosynthesis decline observed late in the growing season. However, previous water limitation studies mainly focused on the initial photosynthetic response to drought (Lovell et al., 2016; Taylor et al., 2016; Chen et al., 2020), and the response through the entire growing season is not as well resolved. Measuring drought effects on photosynthesis over the growing season is costly as it requires large rainfall-exclusion shelters in field experiments. Additionally, these experiments usually rely on natural precipitation events as control treatments, reducing the power of the experiment to detect water-deficit effects during dry periods. Despite these drawbacks, rainfall-exclusion experiments can be more realistic than controlled irrigation studies performed in greenhouses because field experiments include other environmental factors (Lovell et al., 2016).

Switchgrass leaf photosynthesis response to water limitation is mainly studied at peak light availability (Lovell et al., 2016; Taylor et al., 2016; Chen et al., 2020). While measurements at peak solar irradiance are useful to characterize photosynthesis when heat stress is maximal, they do not capture diurnal changes in light and water availability. These point measurements thus fail to incorporate the midday or early afternoon periods of photosynthesis depression observed in other perennials (Gao et al., 2015; Bucci et al., 2019), and overlook changes in the source-sink dynamic during the day.

The late-season photosynthesis decline could also be driven by co-occurring physiological changes. Specifically, physiological signals like carbohydrate buildup and sink strength are known to limit development and leaf photosynthesis in certain perennial grasses (McCormick et al., 2009; Van Heerden et al., 2010; De Souza et al., 2018; Ruiz-Vera et al., 2021; Tejera et al., 2021; Tejera et al., 2022) . For example, when the photoassimilate source-sink balance was perturbed by shading some leaves of sugarcane plants, photosynthesis in the unshaded leaves increased by 32%, indicating source-sink coordination at the level of the entire plant to match supply (source) with demand (sinks) (McCormick et al., 2006). Similarly, when sink strength was reduced by cold-girdling leaves or by placing leaves in sucrose solution, photosynthesis decreased by 30 – 45%, probably inhibited by foliar sucrose and hexose concentrations that increased 2 – 3 fold (McCormick et al., 2008). These studies reveal the short-term effects of source/sink relationships on photosynthetic rates in perennial systems but fail to explain

seasonal dynamics and environmental limitations. The late-season decrease in photosynthesis could be caused by sink limitations in carbohydrate storage organs (Van Heerden et al., 2010; De Souza et al., 2018). As the season progresses, major sink organs and processes (i.e., growth, storage refill, reproduction) cease activity and limit their carbohydrate consumption, which would then lead to a lower demand for photosynthate and ultimately reducing leaf photosynthesis (Tejera et al., 2022).

Water limitation also imposes restrictions on carbon sink organs and processes that may interact with carbohydrate buildup and photosynthesis limitations (Lemoine et al., 2013; Rodrigues et al., 2019). On the one hand, water limitation causes a decrease in photosynthesis which in turn may lead to depletion of carbohydrate in belowground storage organs (Barney et al., 2009; Lovell et al., 2016; Taylor et al., 2016; Hawkes and Kiniry, 2018; Ivanov et al., 2019; Chen et al., 2020). After water stress is ameliorated, rhizomes would then resume carbohydrate accumulation, allowing photosynthesis to persist for longer in the season. On the other hand, water limitation also reduces above- and below-ground growth (Barney et al., 2009; Mann et al., 2013; Hui et al., 2018), which could cause additional sink limitations. In this case, the carbohydrate buildup in the rhizomes would diminish earlier in the season, with corresponding declines in switchgrass photosynthesis.

To resolve these interacting and potentially conflicting effects of source-sink relations and water deficit on the seasonal changes of photosynthesis, we studied the seasonal dynamics of photosynthesis in switchgrass, representing a fast-growing perennial grass, under rainfed and experimentally induced water limitation treatments. Specifically, we asked: 1) Does switchgrass photosynthesis correlate with rhizome sink strength on a seasonal basis under conditions of ambient rainfall and soil water availability? and 2) Does experimentally imposed season-long water limitation affect seasonal patterns of photosynthesis and sink strength, and particularly does it accelerate the onset of the observed late-season photosynthesis decline? To address these questions, we measured switchgrass source activity (i.e., diurnal course of photosynthesis) and sink strengths of carbohydrates in source (leaves) and sink (rhizome) organs in mature switchgrass stands across an entire growing season. The expected seasonal decrease in leaf photosynthesis, found in both plot and field-scale switchgrass stands, co-occurred with peak carbohydrate concentrations in both leaves and rhizomes. Water limitation reduced switchgrass leaf photosynthesis in July and September but, abundant late-season rainfalls were not enough to restore A'_{net} in the rainfed plants to early-summer values. Additionally, water limitations had no effects on rhizome starch dynamics and starch in the rhizomes increased ~ 6-fold. These results suggest that while water deficit limited A'_{net} in the late season, late-season precipitations did not restore A'_{net} to early-summer values suggesting that other limitations were also in place. Towards the end of the growing season, when vegetative growth is completed and rhizome reserves are filled, the insufficient sink activity presents a strong limitation, leading to the observed photosynthetic decline.

Materials and methods

Experimental design

Water limitation was imposed by placing rainfall exclusion shelters over switchgrass plots that are part of the Biofuel Cropping System Experiment (BCSE) of the Great Lakes Bioenergy Research Center (GLBRC), located at the Kellogg Biological Station (KBS) Long-term Ecological Research site in Hickory Corners, Michigan, USA (42.394290 N, -85.374126 W). For our experiment, we used four replicate switchgrass plots. Switchgrass (cv. Cave-in-rock) was planted in June 2008 at a seeding rate of 7.71 kg ha^{-1} and row spacing of 0.2 m and received 56 kg N ha^{-1} yr^{-1} after its initial establishment year (Sanford et al., 2016). The switchgrass was re-seeded in 2009 due to intense storms in mid-summer 2008 that redistributed un-germinated seeds. Each plot was 30 x 40 m and had a rainfall exclusion shelter that measured 4.2 x 5.5 m and 2.6 m tall located at least 1 m inside the plot. Corrugated roofing panels (Greca Lexan; Amerilux, De Pere, WI, USA) allowed ~90% light transmittance (385-700 nm). In 2020, the year of sampling, rainfall exclusion shelters were in place from May 27 – September 10. In 2019 rainfall exclusion shelters had been in place over the same footprints from May 24 – June 22 and September 9 – October 11, and in 2018 from June 13 – October 24. Soil volumetric water content (VWC) sensors (CS655; Campbell Scientific Inc. CSI, Logan, UT, USA) were installed in two plots horizontally at 0.10 m and 0.25 m depth under the rainfall exclusion shelter, and in the open field within 4m radius of the shelter.

Data and sample collection

We sampled the experiment five times during the 2020 growing season (19 June, 1 July, 28 July 6 August, and 3 September) to cover the entire switchgrass growth cycle. For the first two sampling dates switchgrass stands were in vegetative stages, for the third and fourth dates the stands were in reproductive stages, and for the last date the stands were >75% senesced. On each sampling date, we sampled plants outside the rainfall exclusion shelter (Rainfed treatment) and under the shelters (Rainfall exclusion shelter treatment) from each plot. Rainfall exclusion shelter samples were taken from a sampling area of 1 m^2. Rainfed samples were collected from two sampling areas separated 4 m from each other. A 1-m^2 end-of-season biomass sample was collected on November 3, 2020, from the

center portion of each shelter, as well as from the rainfed sampling locations. Samples were dried at 60°C until constant moisture and weighed to estimate the dry biomass.

On each sampling date, we conducted a diurnal sampling of photosynthetic rate, leaf water potential (LWP), and carbohydrate content in source (leaves) and sink (rhizome) organs. The first and last timepoints of the diurnal samplings were collected before sunrise and after sunset. Three timepoints were collected during the day: at mid-morning (9:00 – 10:00 h), noon (13:00 – 14:00 h) and mid-afternoon (17:00 – 18:00 h). We sampled rhizomes before sunrise, around solar noon, and after sunset. Leaf net CO_2 assimilation rate (A_{net}) and stomatal conductance to water (g_{sw}) were measured in the middle portion of the youngest fully expanded leaf using an open gas exchange system (Li-6800; LI-COR Biosciences, Lincoln, NE, USA) equipped with an integrated modulated chlorophyll fluorometer and a light source. Air temperature, photosynthetic photon flux density (PPDF), and relative humidity (RH) inside the leaf chamber were set to mimic ambient conditions at each sampling time The Li-6800 controls the leaf environment using internal LED lighting, Peltier heating/cooling units and controlling incoming CO_2 and H_2O content using a series of chemical scrubbing columns. The CO_2 concentration was maintained at 400 µmol mol^{-1}. The diurnal sum of A_{net} (A'_{net}) was calculated using the area under the curve (AUC), with sunrise and sunset as the limits of integration. Non-photochemical quenching and dark-adapted Photosystem II (PSII) maximum quantum yield (F_v/F_m) values were measured using chlorophyll fluorescence from dark-adapted leaves at the pre-dawn sampling.

PSII quantum efficiency ($\phi PSII$) was calculated as:

$$\phi PSII = \frac{F'_m - F_s}{F'_m}$$

where F_s is the steady-state fluorescence, and F'_m is the maximum fluorescence after a saturating light flash.

At each sampling in each plot, we evaluated two leaf samples for a total of 16 samples per sampling, 80 per sampling date, and 400 for the entire experiment. The same leaf was first measured with the Li-6800, then placed in a pressure chamber (model 1505D; PMS Instruments, Albany, OR, USA) equipped with a grass compression gland to measure its leaf water potential (LWP), and then flash-frozen in liquid nitrogen (N) within 5 min of harvest. A small rhizome sample (~3 g) was harvested from the same stem that bore the leaf and immediately frozen in liquid N. In all samplings, rhizomes were clearly distinguished from stems and newly formed tillers (Figure S1). All samples were kept in liquid N until the next day and then stored at -80°C until further processing.

Sample processing

Leaf samples were ground to a fine powder with a mortar and pestle. Rhizome samples were ground with a spice mixer (Cuisinart; SG-10). All samples stayed frozen during grinding and were then freeze-dried for at least 48 hours in a lyophilizer. Diurnal concentrations of starch, sucrose and free glucose were measured in leaves ($[starch]_{leaf}$, $[suc]_{leaf}$, $[glu]_{leaf}$, respectively) and rhizomes ($[starch]_{rhi}$, $[suc]_{rhi}$, $[glu]_{rhi}$) for the five sampling dates. Diurnal accumulation rates of these carbohydrates were estimated as the slope of the linear regression of predawn and daylight values over time. All assays were performed at the Biomass Analytics Facility at Michigan State University following procedures described in Santoro et al. (2010) and Sekhon et al. (2016). In brief, glucose content was assayed using the glucose oxidase/peroxidase (GOPOD) method (K-GLUC, Megazyme, Ireland). To determine sucrose and starch concentrations, samples were first treated with a combination of alkaline buffer and high heat to degrade all pre-existing free glucose. Then samples were treated with invertase (Sigma-Aldrich, St. Louis, MO), or amyloglucosidase (K-TSTA, Megazyme, Ireland) and 5 µL α-amylase (K-TSTA, Megazyme) for sucrose and starch extraction, respectively. The rest of the processing was identical to that used for glucose.

Canopy-level gross CO_2 assimilation

Gross primary production (GPP), defined here as canopy-level gross CO_2 assimilation (canopy A_{gross}), was estimated from eddy covariance tower net ecosystem CO_2 exchange (NEE) observations in an 18-ha switchgrass stand of the same age with similar soil type and management at the Lux Arbor reserve (42.476100N, -85.446945W), 11 km from the experimental site (Abraha et al., 2018). NEE was measured at 10 Hz using an LI-7500 open-path infrared gas analyzer (LI-COR Biosciences) and a CSAT3 three-dimensional sonic anemometer (Campbell Scientific Inc.). The raw data were processed to compute 30-min NEEs. The 30-min NEEs were gap-filled and partitioned into ecosystem respiration (R_{eco}) and GPP using the nighttime partitioning method in REddyProc package (Reichstein et al., 2005; Wutzler et al., 2018). The method assumes NEE is equal to R_{eco}, and GPP is zero during the night. R_{eco} is then estimated – for both day and nighttime – from air temperature and nighttime R_{eco} relationship, and GPP is computed as a residual of the estimated R_{eco} and NEE (Abraha et al., 2018). Air temperature, incident solar radiation and vapor pressure deficit were also measured at the site.

Data analysis

We used R software (R Core Team, 2017) for all analyses and plots. All models had the same random structure. We used lmer () in the lme4 package (Bates et al., 2015) to fit the mixed models, Anova() in the car package (Fox and Weisberg, 2011) for analysis of deviance using type II Wald chi-square test, and emmeans() in the emmeans package (Lenth et al., 2018) for mean and slope comparisons.

Results

Leaf photosynthesis decreased by ~50% in the latter half of the growing season.

Leaf photosynthesis decreased by ~50% in the latter half of the growing season. Under ambient rainfall, switchgrass photosynthesis during the growing season markedly decreased by late July, prior to visible canopy senescence. Specifically, A'_{net} decreased from 0.84 – 0.96 mol CO_2 m^{-2} day^{-1} in early summer (19 June and 1 July) to 0.30 – 0.50 mol CO_2 m^{-2} day^{-1} in late summer (28 July, 6 August and 3 September; Figures 1, 2). This ~53% reduction in A'_{net} from early to late summer (P< 0.001) was contributed from the consistently low A_{net} values throughout the day (Figure 2; P< 0.001). Changes in A_{net} or A'_{net} were not explained by increases in leaf respiration because nocturnal respiration rates changed little during the season, with no significant differences found between early and late summer (Figure 2A; P = 0.90). Corresponding with changes in A_{net} , $\phi PSII$ and the electron transport rate (ETR) had similar seasonal pattern, with mid-morning, noon and mid-afternoon $\phi PSII$ at 29 – 45% lower in late-summer (Figure 3; P< 0.001).

Canopy-level CO_2 gross assimilation decreased by ~34% from June to September

Canopy photosynthesis under ambient rainfall as measured by eddy covariance at the Lux Arbor switchgrass stand peaked in July and steadily decreased during the second half of the growing season (Figure 4). Specifically, Canopy A_{gross} decreased by ~34%, from ~1.24 mol CO_2 m^{-2} day^{-1} in early-summer (June 19 – July 1) to ~0.82 mol CO_2 m^{-2} day^{-1} in late-summer (July 28 – September 3; Figure S2). Canopy A_{gross} and leaf A_{net} were highly correlated both as individual measurements and daily accumulation (P<0.0001; Figure S3), indicating that the observed decline at the leaf level in the upper canopy was not compensated by a larger canopy leaf area in late summer. Comparison of canopy A_{gross} with climatic variables shows that the beginning of the canopy A_{gross} decline occurred almost six weeks sooner than the seasonal declines in air temperature or incident radiation (Figure S4).

Leaf carbohydrates had strong diurnal dynamics, while rhizome carbohydrate followed strong seasonal dynamics

Under ambient rainfall, leaf carbohydrates had no clear seasonal dynamics but did show clear diurnal dynamics

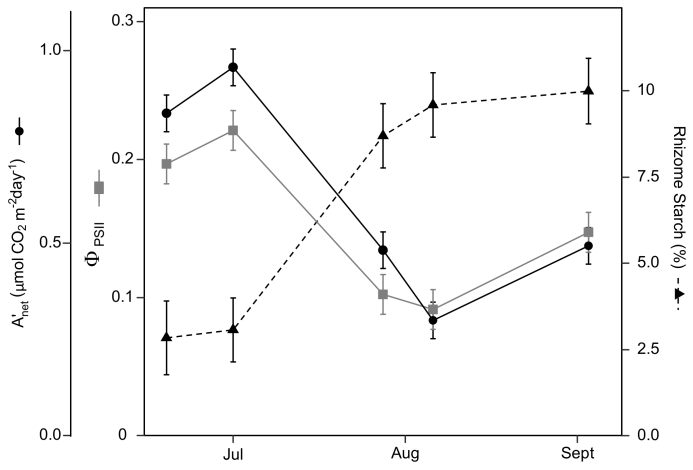


FIGURE 1
Switchgrass daily net CO_2 assimilation (A'_{net}), efficiency of photosystem II ($_{PSII}$), and rhizome starch content during 2020. As the season progressed A'_{net} and $_{PSII}$ decreased by ~50%, while rhizome starch increased 4-fold. During the first two sampling dates, switchgrass was in vegetative stages, the next two was in reproductive stages and in the last measurement switchgrass was 70% senesced. Error bars represent plus/minus one standard error of the mean (n = 4).

10.3389/fpls.2022.1023571

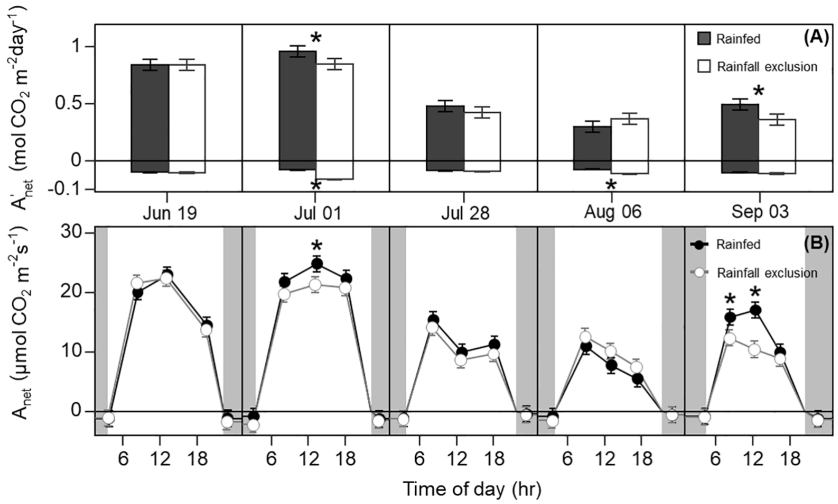


FIGURE 2
Switchgrass daily net CO_2 assimilation (A'_{net}; A) integrated over each sampling date, and net CO_2 assimilation rate (A_{net}; B) at each timepoint during the day, for plants grown under (white fill, grey line) and outside (black fill, black line) rainfall exclusion shelters. Negative values indicate dark respiration during the night period **(A)**, and dark respiration at predawn and post-dusk timepoints **(B)**. Asterisks indicate a significant difference between treatments ($P < 0.05$). Data are mean ± S.E. (n = 4).

(Figure S5). Leaf glucose and sucrose followed the diurnal pattern of photosynthesis, being lower in morning and afternoon samplings, and higher at noon. Leaf starch, in contrast, tended to accumulate during the day; its accumulation rate was ~7-fold higher than the other carbohydrates when expressed on a glucose-equivalent basis (Figure S5; Table S1). September 4 showed the largest fluctuation in rhizome starch in the ambient treatment. It is unclear if this midday decrease in rhizome starch is of physiological meaning or a product of sample variability. Overall, rhizome carbohydrate concentrations remained constant during the day and changed over the course of the

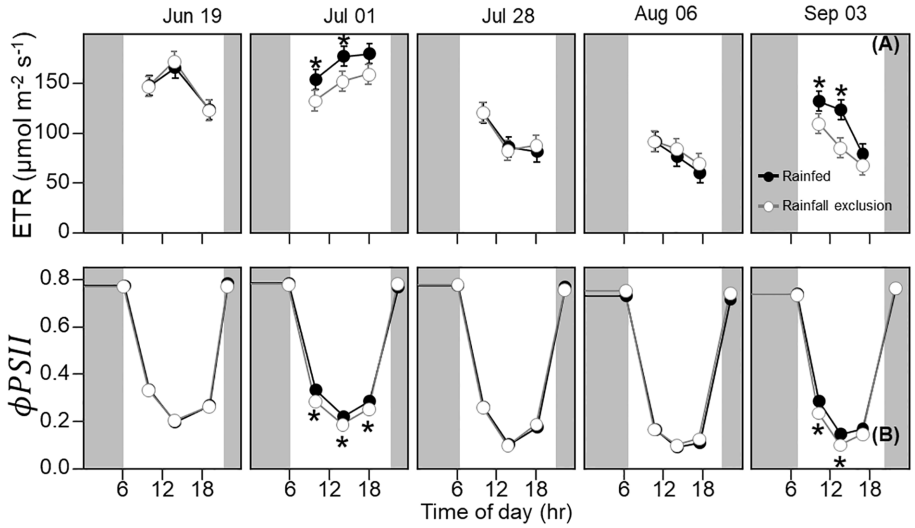


FIGURE 3
Switchgrass electron transport rate (*ETR* ; **(A)** and photosystem II quantum efficiency (*ϕPSII* ; **(B)** at each timepoint during the day, over the course of the growing season, for plants grown under (white fill, grey line) and outside (black fill, black line) rainfall exclusion shelters. Asterisks indicate a significant difference between treatments ($P < 0.05$). Data are mean ± S.E. (n = 4).

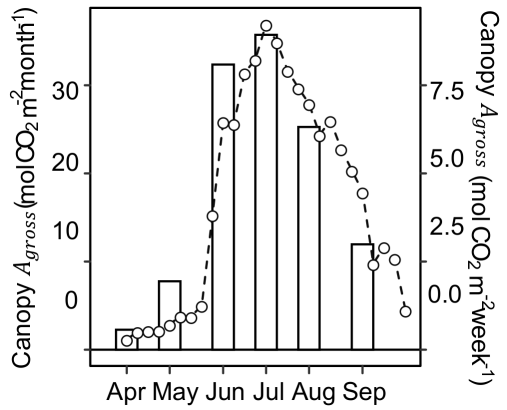


FIGURE 4
Monthly (bars) and weekly (lines and open circles) canopy gross CO_2 assimilation (Canopy A_{gross}) during the 2020 growing season. Canopy A_{gross} was computed from net ecosystem CO_2 exchange (NEE) observations using eddy covariance method conducted at a switchgrass field of the same age as the experimental site but located 11 km away.

season (Figure 5). Glucose and sucrose concentrations decreased from late July onward, while the starch concentration showed a corresponding increase (Figure 5 and Table 1S). Rhizome glucose decreased from 3.1% in early summer to 1.5% in late summer (52% decrease; P< 0.0001; Figure 5), while rhizome sucrose decreased from 2.2% to 1.6% (28% decrease; P = 0.022; Figure 5). Starch increased from 2.6% in early summer to 9.9% in late summer (3.94-fold increase; P< 0.0001; Figure 5).

End-of-season biomass was 33% lower, and soil water content was ~27% lower under the rainfall exclusion shelters

The 2020 growing season witnessed several large rain events (Table 1; Figure S6A). Rainfall exclusion shelters successfully blocked rainfall and imposed water limitation for the switchgrass plots. Soil VWC was consistently lower under the rainfall exclusion shelters at the 10-cm and 25-cm depths (Table 1; Figure S6B). After each rain event, soil VWC under the shelters was at least 2-fold, and on average 3.7-fold, lower than outside the rainfall exclusion shelters. End-of-season aboveground biomass of the switchgrass was 4.67 ± 0.52 kg m^{-2} outside the rainfall exclusion shelters and 2.95 ± 0.52 kg m^{-2} under the rainfall exclusion shelters (~37% decrease; P = 0.059).

Imposed water-deficit conditions decreased leaf photosynthesis, $\phi PSII$, and leaf water potential

The imposed season-long water deficit reduced leaf photosynthesis during the growing season. Plants under the shelters showed 12% and 26% lower A'_{net} on July 1 (P = 0.059) and September 3, respectively, compared to outside of the shelters (P = 0.030; Figure 2). These differences were mainly driven by reductions in A_{net} at noon, which decreased by 14% and 38% on July 1 (P = 0.023) and September 3, respectively (P< 0.0001; Figure 2). In addition, A_{net} under the shelters was 22% lower in the mid-morning on September 3 (P = 0.023). Similarly,

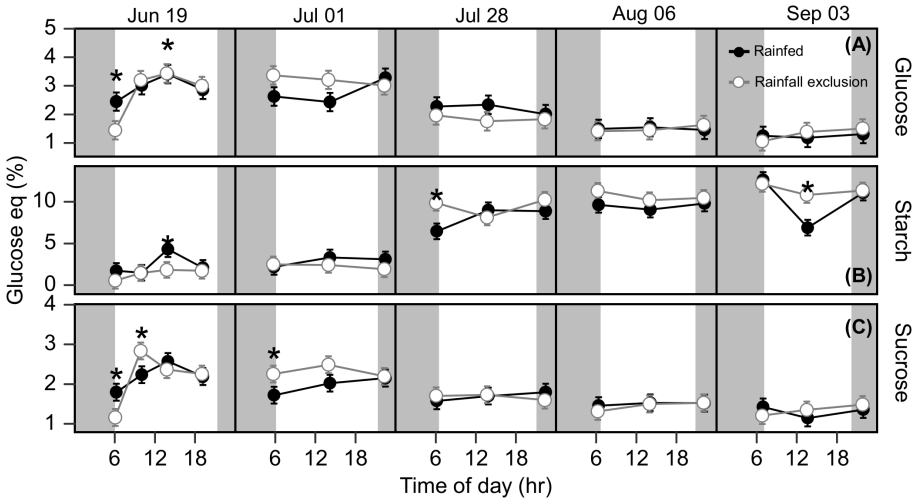


FIGURE 5
Rhizome free glucose **(A)**, starch **(B)** and sucrose **(C)** at each timepoint during the day, over the course of the growing season, for plants grown inside (white fill, grey line) and outside (black fill, black line) rainfall exclusion shelters. Asterisks indicate a significant difference between treatments (P< 0.05). Data are mean ± S.E. (n = 4).

TABLE 1 Total monthly precipitation (mm) and soil volumetric water content (VWC; m3/m3) in 2020 at the rainfall exclusion shelters Biofuel Cropping System Experiment (42.394290, -85.374126) and historic record (2009-2018) between shelter deployment (May 27th) and last sampling date (Sept 3rd).

		Precipitation (mm)			soil VWC (m^3/m^3)	
Month	Days	2020	2009-2018		2020	2009-2018
May	5	8	20		0.35	0.33
Jun	30	86	78		0.25	0.33
Jul	31	50	82		0.22	0.3
Aug	31	114	86		0.25	0.31
Sep	5	30	9		0.28	0.32
Total		288	275	Average	0.27	0.32

The 2020 data were collected from Soil VWC measured at 0.25 m depth in 2020 and at 0.30 m depth for 2009-2018 period. Total precipitation and average soil VWC for the entire period of study is also presented.

plants under the shelters had reduced $\phi PSII$ on the same dates and timepoints of the day; $\phi PSII$ was on average ~5% lower under the shelters on July 1 (P = 0.013) and September 3 (P< 0.0049; Figure 3).

Water-deficit effects on LWP were consistent over the season, and we found significant effects for at least one sampling timepoint in 4 out of the 5 sampling dates (Figure 6A). Plants under the rainfall exclusion shelters had 12 – 37% lower LWP than rainfed plants. These differences only corresponded with significant effects on A_{net} and A'_{net} on September 3 after a large precipitation event. No water-deficit effects were found on stomatal conductance (g_{sw}) during the day or across the growing season (P > 0.1; Figure 6B).

Imposed water-deficit conditions had only marginal effects on leaf glucose accumulation, and no effects on rhizome carbohydrates

Rhizome carbohydrates were not affected significantly by the imposed water-deficit conditions in most comparisons (Figure 5). Leaves had on average 12 – 22% higher mean sucrose and starch concentrations outside the shelters, but the differences were not significant ($P_{glucose}$ = 0.13; $P_{sucrose}$ = 0.17; P_{starch} = 0.015; Figure S5). In late summer, plants outside the shelters had higher leaf glucose and starch accumulation rates

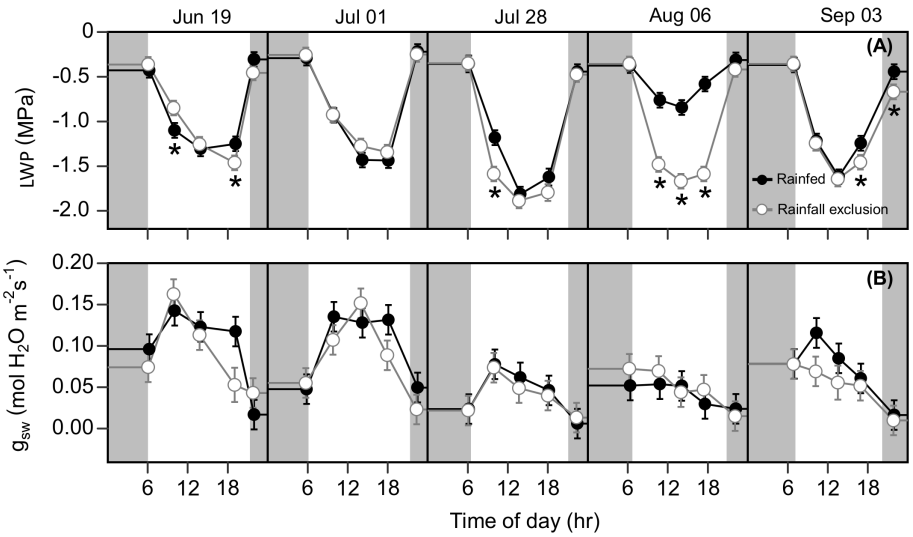


FIGURE 6
Switchgrass leaf water potential (*LWP* ; **(A)** and stomatal conductance to water (g_{sw} ; **(B)** at each timepoint during the day, over the course of the growing season, for plants grown under (white fill, grey line) and outside (black fill, black line) rainfall exclusion shelters. Asterisks indicate a significant difference between treatments (P< 0.05). Data are mean ± S.E. (n = 4).

than under the shelters (Table S1). Sucrose accumulation rates in the leaf were positive in plants outside the shelters until July 28 and then became almost null until the end of the experiment (Table S1). In turn, sucrose accumulation in plants under the shelters followed the opposite pattern, i.e., positive only after July 28 (Table S1).

Discussion

Switchgrass carbon source-sink balances markedly changed during the growing season. In early summer under ambient rainfall, source indicators (i.e., leaf photosynthesis: A_{net} , A'_{net}, $\phi PSII$, ETR; Figures 1, 2, 4) were at their seasonal maximum, and sink indicators (i.e., leaf and rhizome carbohydrate concentrations) were at their seasonal minimum (Figures 1, 5). As the season progressed, switchgrass plants transitioned to lower photosynthetic activity (A_{net} and A'_{net} decreased by ~ 50%) and higher sink activities (4-fold increase in rhizome starch; Figure 5). This seasonal decline in photosynthetic rates was also observed at the canopy level based on eddy covariance estimates of canopy A_{gross} (Figure 4) at a companion site. Exclusion of rainfall by shelters across the entire growing season showed that water limitation did not alter these dynamics; the photosynthetic decline and carbohydrate accumulation showed similar onsets and magnitudes to the rainfed plants (Figures 2, 3, 5; Figure S4). While late-season rainfalls increased switchgrass photosynthesis, they did not restore A'_{net} to early-summer values, which supports the hypothesis that decreasing rhizome sink demand drives the seasonal photosynthetic decrease more than does decreasing water availability.

Sink limitations

The late summer photosynthetic decline may be driven by sink limitations triggered by rhizome carbohydrate buildup. As perennial grass biomass allocation to flowers and seeds is minimal (Boe, 2007; Giannoulis et al., 2016), mature stands may lack major sinks for photosynthates once vegetative growth has ceased (Tejera et al., 2021; Tejera et al., 2022) and rhizome carbohydrate accumulation is complete. Rhizome carbohydrate concentrations and leaf photosynthesis were inversely correlated, and as rhizome starch reached maximum accumulation in mid-summer, leaf photosynthesis declined to low rates (Figures 1, 5). Similar seasonal patterns have been reported in other perennial grasses. In sugarcane (*Saccharum* sp.), sucrose (the carbohydrate storage molecule for that species) increased 5-fold in the main sink organ during summer while A_{net} decreased by >50% (De Souza et al., 2018), and in *Miscanthus* × *giganteus* starch content in the leaf increased by 8-fold by the end of the growing season while A_{net} decreased ~50% (De Souza et al., 2013). The findings of our study on switchgrass support the sink limitation hypothesis and resolve the interacting and potentially conflicting effects of source-sink relations and water deficit on seasonal changes of photosynthesis. Our results showed that water deficit conditions later in the season had insignificant effects on the photosynthetic decline.

The decrease in leaf photosynthesis was accompanied by a decrease in $\phi PSII$ (Figures 1, 3), suggesting that autumnal senescence was ongoing. Autumnal senescence is characterized by a decrease in chlorophyll content and an up-regulation of genes associated with protein degradation (Palmer et al., 2015; Palmer et al., 2019). During this process, light-harvesting pigments of the photosynthetic system are degraded (Moy et al., 2015), leading to N retranslocation from aboveground to belowground organs (Yang et al., 2009; Yang et al., 2016; Yang and Udvardi, 2018; Massey et al., 2020), and a concomitant decrease in photosynthetic capacity (Tang et al., 2005; Galvagno et al., 2013; Donnelly et al., 2020). Therefore, the decline in leaf photosynthesis may not be driven solely by sink limitations but also a decrease in photochemical efficiency of photosynthesis resulting from senescence. Note that sink limitations and senescence are not mutually exclusive mechanisms but rather could be a coherent response triggered by the environment or carbohydrate buildup and sink limitations. Sugar and/or starch accumulation is known to trigger leaf senescence in maize, trees, and other species, but this has not been tested in perennial grasses (Noodén et al., 1997; Wingler and Roitsch, 2008; Holland et al., 2016).

Water-deficit

Experimentally imposed water stress affected switchgrass photosynthesis both in early and late summer. If water availability had been the sole driver of the late-season photosynthesis decline, switchgrass plants outside the shelters, where soil water was replenished after precipitation events, would have shown different seasonal dynamics (e.g., later onset of the decline or no decline). In our experiment, we found that late-season rainfall increased switchgrass photosynthesis, but the magnitude of the effect was not enough to compensate for the seasonal decline. In comparison, the imposed water limitation had marginal effects on rhizome carbohydrate accumulation; concentrations from plants under and outside the rainfall exclusion shelters were almost identical (Figure 5). Leaf carbohydrates were less resilient to water deficit; during the growing season switchgrass leaves under the shelters had 12 – 22% lower sucrose and starch content (Figure S5). Carbohydrate accumulation rate, as a direct proxy for sink activity, was also higher under the shelters than outside the shelter in early-summer (Table S1). These differences in leaf starch corresponded with some differences in A'_{net}. Our

interpretation is that plants under the shelter with lower A_{net} had less carbon available for sucrose and starch synthesis, leading to lower sucrose and starch in the leaf (Figure S5). With lower carbohydrate concentrations in the leaf, switchgrass growing under the shelters would need to adjust carbohydrate mobilization and degradation through the night to avoid carbon starvation at the end of the night (Smith and Stitt, 2007). This reduction in carbohydrate mobilization and degradation at night may drive the lower nocturnal respiration rates observed on July 1 and August 6.

Water deficit effects on switchgrass are mainly studied using leaf photosynthesis and physiological responses, while effects on sink activities are not as well understood. Few studies reporting changes in leaf carbohydrate under drought conditions in switchgrass suggest that the response may be specific to the particular storage carbohydrate. Key carbohydrates such as trehalose, fructose (Liu et al., 2015), and proline (Kim et al., 2016; Hoover et al., 2018) seem to be more readily affected, while other soluble sugars such as glucose or sucrose as well as starch remain relatively constant (Hoover et al., 2018). Our work is distinct from earlier water deficit studies because we present diurnal and seasonal leaf carbohydrate measurements. We found that the small effects of water deficit on diurnal dynamics of leaf carbohydrates did not show a clear relationship with the seasonal course. Our results suggest that starch, in addition to accumulating in the rhizomes during the growing season, acts as a transitory carbohydrate storage molecule in switchgrass leaves, accumulating during the day and presumably being consumed overnight.

Switchgrass resilience to drought

Switchgrass photosynthesis was resistant to water limitation. Even when soil VWC dropped by ~4-fold under the shelters, A'_{net} and A_{net} decreased by up to ~26%. Other studies have found a stronger negative leaf photosynthesis response to water deficit (Barney et al., 2009; Lovell et al., 2016; Taylor et al., 2016; Hawkes and Kiniry, 2018; Chen et al., 2020), including across 49 switchgrass genotypes in which A_{net} decreased by 40 – 80% under drought stress (Liu et al., 2015). This discrepancy may be because the control treatment in our field experiment (i.e., plants outside the shelter) experienced ambient environmental conditions, while other studies used irrigated plants as the control. While the latter is useful to characterize the response, our approach is more consistent with the natural environment and allows a better characterization of the seasonal dynamics.

In light of our results, it may seem counterintuitive that, at the whole-plant level, end-of-season aboveground biomass was reduced by 33% by the shelters. The switchgrass strategy to cope with water deficit stress may rely on whole-plant responses, such as modifying the number of tillers and/or leaves per tiller, producing smaller and thinner stands under the shelter while maintaining leaves that had similar photosynthetic performance to leaves outside the shelters. Alternatively, differences in end-of-season biomass could be driven by switchgrass stands with similar tiller density and leaf area, but small (and often insignificant) differences in leaf photosynthesis accumulate over the growing season yielding larger differences in end-of-season biomass.

The presence of late-season decline in photosynthesis as an improvement strategy for switchgrass and other perennials

The switchgrass photosynthetic decline over the growing season, which we observed in both plot and field-scale switchgrass stands, reveals a potential for yield improvement. Using simple linear interpolation between sampling dates, the upper canopy of switchgrass assimilated ~45 mol CO_2 m^{-2} during the growing season. If leaf photosynthesis had remained constant at early summer levels during the 6 weeks when the environment was still favorable, switchgrass would have assimilated an additional 52% carbon. Scaling leaf-level photosynthesis to end-of-season biomass is beyond the scope of this study, but assuming end-of-season biomass is proportional to the accumulated CO_2 during the study period, this forgone 52% of CO_2 assimilation could potentially lead to an extra ~1.2 Mg ha^{-1} of end-of-season aboveground biomass. While these calculations oversimplify the relationship between gross carbon fixation and biomass production, the physiological understanding of this decline could elucidate ways to maintain higher photosynthetic rates for longer in the season and thereby increase biomass yields. This late-season decline in photosynthesis is commonly observed in many perennial grasses, and therefore improvement strategies could have a broader impact on cropping systems that include perennial grasses and possibly trees (Kosugi and Matsuo, 2006; Boersma et al., 2015; De Souza et al., 2018; Kar et al., 2020; Stavridou et al., 2020).

Conclusions

Switchgrass leaf photosynthesis decreased by ~50% during the latter half of the growing season. This seasonal photosynthetic decline appears to be common across several perennial grasses, but the underlying mechanisms and the potential implications for management are not well understood. Our results suggest that this decline is not entirely driven by water limitation since leaf photosynthesis outside the rainfall exclusion shelters remained at low values even after heavy rain events in late-summer and early spring. Eddy covariance data shows that the decline also occurred at the whole-field scale and represents a physiological response that occurs even when environmental conditions remain favorable

for photosynthesis. We suggest sink limitation as an important driving mechanism of the photosynthetic decline, as rhizome starch reached peak concentrations around the same time that leaf photosynthesis fell to lower rates. If sink limitation were the leading cause of the seasonal photosynthesis decline, then strategies to alleviate sink limitation could be included in switchgrass breeding programs with the goal of increasing yields.

Data availability statement

The raw data supporting the conclusions of this article will be made available by the authors, without undue reservation.

Author contributions

All authors contributed ideas; MT-N collected and analyzed field data and led the writing of the manuscript. MA and JC maintained eddy covariance towers, and collected and curated the data. SH and GR contributed to conception and design of the experiment. BW oversaw and provided substantial contributions to the project. All authors contributed to the article and approved the submitted version.

Funding

This work was supported by the Great Lakes Bioenergy Research Center, U.S. Department of Energy, Office of Science, Office of Biological and Environmental Research under Award Number DE-SC0018409, by the National Science Foundation Long-term Ecological Research Program (DEB 1832042) at the Kellogg Biological Station, and by Michigan State University AgBioResearch.

Acknowledgments

We thank Kevin Kahmark for constructing and maintaining the rainfall exclusion shelters, and Joe Simmons and Stacey VanderWulp for site management.

Conflict of interest

The authors declare that the research was conducted in the absence of any commercial or financial relationships that could be construed as a potential conflict of interest.

Publisher's note

All claims expressed in this article are solely those of the authors and do not necessarily represent those of their affiliated organizations, or those of the publisher, the editors and the reviewers. Any product that may be evaluated in this article, or claim that may be made by its manufacturer, is not guaranteed or endorsed by the publisher.

Supplementary material

The Supplementary Material for this article can be found online at: https://www.frontiersin.org/articles/10.3389/fpls.2022.1023571/full#supplementary-material

References

Abraha, M., Hamilton, S. K., Chen, J., and Robertson, G. P. (2018). Ecosystem carbon exchange on conversion of conservation reserve program grasslands to annual and perennial cropping systems. *Agric. For. Meteorology.* 253–254, 151–160. doi: 10.1016/J.AGRFORMET.2018.02.016

Barney, J. N., Mann, J. J., Kyser, G. B., Blumwald, E., Van Deynze, A., and DiTomaso, J. M. (2009). Tolerance of switchgrass to extreme soil moisture stress: Ecological implications. *Plant Sci.* 177 (6), 724–732. doi: 10.1016/j.plantsci.2009.09.003

Bates, D., Mächler, M., Bolker, B., and Walker, S. (2015). Fitting linear mixed-effects models using lme4. *J. Stat. Softw.* 67 (1), 1–48. doi: 10.18637/jss.v067.i01

Boe, A. (2007). Variation between two switchgrass cultivars for components of vegetative and seed biomass. *Crop Science.* 47 (2), 636–640. doi: 10.2135/CROPSCI2006.04.0260

Boersma, N. N., Dohleman, F. G., Miguez, F. E., and Heaton, E. A. (2015). Autumnal leaf senescence in *Miscanthus* × *giganteus* and leaf [N] differ by stand age. *J Experimental Botany* 66, 14, 4395–4401. doi: 10.1093/jxb/erv129

Bucci, S. J., Carbonell Silletta, L. M., Garré, A., Cavallaro, A., Efron, S. T., Arias, N. S., et al. (2019). Functional relationships between hydraulic traits and the timing of diurnal depression of photosynthesis. *Plant Cell Environment. John Wiley Sons Ltd* 42 (5), 1603–1614. doi: 10.1111/pce.13512

Chen, P., Chen, J., Sun, M., Yan, H., Feng, G., Wu, B., et al. (2020). Comparative transcriptome study of switchgrass (*Panicum virgatum* l.) homologous autopolyploid and its parental amphidiploid responding to consistent drought stress. *Biotechnol. Biofuels. BioMed. Cent.* 13 (1), 1–18. doi: 10.1186/s13068-020-01810-z

Core Team, R. (2017) (Vienna). Available at: https://www.r-project.org/.

De Souza, A. P., Arundale, R. A., Dohleman, F. G., Long, S. P., and Buckeridge, M. S. (2013). Will the exceptional productivity of *Miscanthus* x *giganteus* increase further under rising atmospheric CO_2? *Agric. For. Meteorology.* 171–172, 82–92. doi: 10.1016/j.agrformet.2012.11.006

De Souza, A. P., Grandis, A., Arenque-Musa, B. C., and Buckeridge, M. S.. (2018). Diurnal variation in gas exchange and nonstructural carbohydrates throughout sugarcane development. *Funct. Plant Biol.* 45 (8), 865–876. doi: 10.1071/FP17268

Donnelly, A., Yu, R., Rehberg, C., Meyer, G., and Young, E. B. (2020). Leaf chlorophyll estimates of temperate deciduous shrubs during autumn senescence using a SPAD-502 meter and calibration with extracted chlorophyll. *Ann. For. Sci.* 77 (2), 30. doi: 10.1007/s13595-020-00940-6

Eggemeyer, K. D., Awada, T., Wedin, D. A., Harvey, F. E., and Zhou, X. (2006). Ecophysiology of two native invasive woody species and two dominant warm-

season grasses in the semiarid grasslands of the Nebraska sandhills. *Int. J. Plant Sci.* 167 (5), 991–999. doi: 10.1086/505797

Endres, L., dos Santos, C. M., Silva, J. V., Barbosa de, G. V. S., Silva, A. L. J., Froehlich, A., et al. (2019). Inter-relationship between photosynthetic efficiency, Δ13C, antioxidant activity and sugarcane yield under drought stress in field conditions. *J. Agron. Crop Sci.* 205 (5), 433–446. doi: 10.1111/jac.12336

Fox, J., and Weisberg, S. (2011). Available at: http://socserv.socsci.mcmaster.ca/jfox/Books/Companion.

Galvagno, M., Rossini, M., Migliavacca, M., Cremonese, E., Colombo, R., and Morra di Cella, U. (2013). Seasonal course of photosynthetic efficiency in *Larix decidua* mill. in response to temperature and change in pigment composition during senescence. *Int. J. Biometeorology* 57 (6), 871–880. doi: 10.1007/s00484-012-0614-y

Gao, Z. J., Xu, B. C., Wang, J., Huo, L. J., and Li, S.. (2015). Diurnal and seasonal variations in photosynthetic characteristics of switchgrass in semiarid region on the loess plateau of China. *Photosynthetica* 53 (4), 489–498. doi: 10.1007/s11099-015-0108-3

Giannoulis, K. D., Karyotis, T., Sakellariou-Makrantonaki, M., Bastiaans, L., Struik, P. C., and Danalatos, N. G. (2016). Switchgrass biomass partitioning and growth characteristics under different management practices. *NJAS - Wageningen J. Life Sci. Taylor Francis* 78, 61–67. doi: 10.1016/j.njas.2016.03.011

Hawkes, C., and Kiniry, J. (2018). Legacies in switchgrass resistance to and recovery from drought suggest that good years can sustain plants through bad years. *Bioenergy Res. Bioenergy Res.* 11 (1), 86–94. doi: 10.1007/s12155-017-9879-7

Holland, V., Koller, S., Lukas, S., and Brüggemann, W. (2016). Drought- and frost-induced accumulation of soluble carbohydrates during accelerated senescence in quercus pubescens. *Trees* 30 (1), 215–226. doi: 10.1007/s00468-015-1290-4

Hoover, A., Emerson, R., Ray, A., Stevens, D., Morgan, S., Cortez, M., et al. (2018). Impact of drought on chemical composition and sugar yields from dilute-acid pretreatment and enzymatic hydrolysis of miscanthus, a tall fescue mixture, and switchgrass. *Front. Energy Res.* 6, 54. doi: 10.3389/fenrg.2018.00054

Hui, D., et al. (2018). Effects of precipitation changes on switchgrass photosynthesis, growth, and biomass: A mesocosm experiment. *PloS One* 13 (2), 1–18. doi: 10.1371/journal.pone.0192555

Inman-Bamber, N. G., Jackson, P. A., and Hewitt, M. (2011). Sucrose accumulation in sugarcane stalks does not limit photosynthesis and biomass production. *Crop Pasture Sci.* 62 (10), 848–858. doi: 10.1071/CP11128

Ivanov, Y. V., Kartashov, A. V., Zlobin, I. E., Sarvin, B., Stavrianidi, A. N., Kuznetsov, V. V., et al. (2019). Water deficit-dependent changes in non-structural carbohydrate profiles, growth and mortality of pine and spruce seedlings in hydroculture. *Environ. Exp. Bot.* 157, 151–160. doi: 10.1016/j.envexpbot.2018.10.016

Kar, S., Weng, T. Y., Nakashima, T., Villanueva-Morales, A., Stewart, J. R., Sacks, E. J., et al. (2020). Field performance of *Saccharum* × *Miscanthus* intergeneric hybrids (Miscanes) under cool climatic conditions of northern Japan. *Bioenergy Res.* 13 (1), 132–146. doi: 10.1007/s12155-019-10066-x

Kim, J., Liu, Y., Zhang, X., Zhao, B., and Childs, K. L. (2016). Analysis of salt-induced physiological and proline changes in 46 switchgrass (*Panicum virgatum*) lines indicates multiple response modes. *Plant Physiol. Biochem.* 105, 203–212. doi: 10.1016/j.plaphy.2016.04.020

Kosugi, Y., and Matsuo, N. (2006). Seasonal fluctuations and temperature dependence of leaf gas exchange parameters of co-occurring evergreen and deciduous trees in a temperate broad-leaved forest. *Tree Physiol.* 26 (9), 1173–1184. doi: 10.1093/treephys/26.9.1173

Lemoine, R., La Camera, S., Atanassova, R., Dédaldéchamp, F., Allario, T., Pourtau, N., et al. (2013). Source-to-sink transport of sugar and regulation by environmental factors. *Front. Plant Sci.* 4. doi: 10.3389/fpls.2013.00272

Lenth, R., et al. (2018). Available at: https://cran.r-project.org/package=emmeans.

Leroy, J., Ferchaud, F., Giauffret, C., Mary, B., Fingar, L., Mignot, E., et al. (2022). Miscanthus sinensis is as efficient as *Miscanthus* × *giganteus* for nitrogen recycling in spite of smaller nitrogen fluxes. *Bioenergy Res.* 15 (2), 686–702. doi: 10.1007/s12155-022-10408-2

Liu, Y., Zhang, X., Tran, H., Shan, L., Kim, J., Childs, K., et al. (2015). Assessment of drought tolerance of 49 switchgrass (*Panicum virgatum*) genotypes using physiological and morphological parameters. *Biotechnol. Biofuels. BioMed. Cent.* 8 (1), 1–18. doi: 10.1186/s13068-015-0342-8

Liu, J. C., Temme, A. A., Cornwell, W. K., van Logtestijn, R. S. P., Aerts, R., and Cornelissen, J. H. C. (2016). Does plant size affect growth responses to water availability at glacial, modern and future CO_2 concentrations? *Ecol. Res.* 31 (2), 213–227. doi: 10.1007/s11284-015-1330-y

Lovell, J. T., Shakirov, E. V., Schwartz, S., Lowry, D. B., Aspinwall, M. J., Taylor, S. H., et al. (2016). Promises and challenges of eco-physiological genomics in the field: Tests of drought responses in switchgrass. *Plant Physiol.* 172 (2), 734–748. doi: 10.1104/pp.16.00545

Mann, J. J., Barney, J. N., Kyser, G. B., and DiTomaso, J. M. (2013). Root system dynamics of *Miscanthus* × *giganteus* and *Panicum virgatum* in response to rainfed and irrigated conditions in California. *Bioenergy Res.* 6 (2), 678–687. doi: 10.1007/s12155-012-9287-y

Massey, J., Antonangelo, J., and Zhang, H. (2020). Nutrient dynamics in switchgrass as a function of time. *Agronomy* 10 (7), 940. doi: 10.3390/AGRONOMY10070940

McCormick, A. J., Cramer, M. D., and Watt, D. A. (2006). Sink strength regulates photosynthesis in sugarcane. *New Phytol.* 171 (4), 759–770. doi: 10.1111/j.1469-8137.2006.01785.x

McCormick, A. J., Cramer, M. D., and Watt, D. A. (2008). Regulation of photosynthesis by sugars in sugarcane leaves. *J. Plant Physiol. Urban Fischer* 165 (17), 1817–1829. doi: 10.1016/J.JPLPH.2008.01.008

McCormick, A. J., Watt, D. A., and Cramer, M. D. (2009). Supply and demand: Sink regulation of sugar accumulation in sugarcane. *J. Exp. Bot.* 60 (2), 357–364. doi: 10.1093/jxb/ern310

Mocko, K., and Jones, C. S. (2021).) do seedlings of larger geophytic species outperform smaller ones when challenged by drought? *Am. J. Bot.* 108 (2), 320–333. doi: 10.1002/ajb2.1612

Moy, A., Le, S., and Verhoeven, A. (2015). Different strategies for photoprotection during autumn senescence in maple and oak. *Physiologia Plantarum* 155 (2), 205–216. doi: 10.1111/ppl.12331

Noodén, L. D., Guiamét, J. J., and John, I. (1997). Senescence mechanisms. *Physiologia Plantarum*. 101 (4), 746–753. doi: 10.1111/J.1399-3054.1997.TB01059.X

Palmer, N. A., Donze-Reiner, T., Horvath, D., Heng-Moss, T., Waters, B., Tobias, C., et al. (2015). Switchgrass (*Panicum virgatum* l) flag leaf transcriptomes reveal molecular signatures of leaf development, senescence, and mineral dynamics. *Funct. Integr. Genomics* 15 (1), 1–16. doi: 10.1007/s10142-014-0393-0

Palmer, N. A., Chowda-Reddy, R. V., Muhle, A. A., Tatineni, S., Yuen, G., Edmé, S. J., et al. (2019). Transcriptome divergence during leaf development in two contrasting switchgrass (*Panicum virgatum* l.) cultivars. *PloS One* 14 (9):e0218352. doi: 10.1371/journal.pone.0222080

Parrish, D. J., and Fike, J. H. (2005). The biology and agronomy of switchgrass for biofuels. *Crit. Rev. Plant Sci.* 24, 423–459. doi: 10.1080/07352680500316433

Reichstein, M., Falge, E., Baldocchi, D., Papale, D., Aubinet, M., Berbigier, P., et al. (2005). On the separation of net ecosystem exchange into assimilation and ecosystem respiration: review and improved algorithm. *Global Change Biol. John Wiley Sons Ltd* 11 (9), 1424–1439. doi: 10.1111/J.1365-2486.2005.001002.X

Rodrigues, J., Inzé, D., Nelissen, H., and Saibo, N. J. M. (2019). Source–sink regulation in crops under water deficit. *Trends Plant Sci.* 24 (7), 652–663. doi: 10.1016/j.tplants.2019.04.005

Ruiz-Vera, U. M., De Souza, A. P., Ament, M. R., Gleadow, R. M., and Ort, D. R.. (2021). High sink strength prevents photosynthetic down-regulation in cassava grown at elevated CO_2 concentration. *J. Exp. Bot.* 72 (2), 542–560. doi: 10.1093/jxb/eraa459

Rusinowski, S., Krzyżak, J., Clifton-Brown, J., Jensen, E., Mos, M., Webster, R., et al. (2019). New miscanthus hybrids cultivated at a polish metal-contaminated site demonstrate high stomatal regulation and reduced shoot Pb and cd concentrations. *Environ. pollut.* 252, 1377–1387. doi: 10.1016/j.envpol.2019.06.062

Sanford, G. R., Oates, L. G., Jasrotia, P., Thelen, K. D., Robertson, G. P., Jackson, R. D., et al. (2016). Comparative productivity of alternative cellulosic bioenergy cropping systems in the north central USA. *Agriculture Ecosyst. Environment. Elsevier* 216, 344–355. doi: 10.1016/j.agee.2015.10.018

Santoro, N., Cantu, S. L., Tornqvist, C.-E., Falbel, T. G., Bolivar, J. L., Patterson, S. E., et al. (2010). A high-throughput platform for screening milligram quantities of plant biomass for lignocellulose digestibility. *Bioenergy Res.* 3, 93–102. doi: 10.1007/S12155-009-9074-6

Sekhon, R. S., Breitzman, M. W., Silva, R. R., Santoro, N., Rooney, W. L., De Leon, N., et al. (2016). Stover composition in maize and sorghum reveals remarkable genetic variation and plasticity for carbohydrate accumulation. *Front. Plant Sci.* 7, 822. doi: 10.3389/FPLS.2016.00822

Smith, A. M., and Stitt, M. (2007). Coordination of carbon supply and plant growth. *Plant Cell Environ.* 30 (9), 1126–1149. doi: 10.1111/j.1365-3040.2007.01708.x

Stavridou, E., Webster, R. J., and Robson, P. R. H. (2020). The effects of moderate and severe salinity on composition and physiology in the biomass crop *Miscanthus* × *giganteus*. *Plants* 9 (10), 1–27. doi: 10.3390/plants9101266

Tang, Y., Wen, X., and Lu, C. (2005). Differential changes in degradation of chlorophyll-protein complexes of photosystem I and photosystem II during flag leaf senescence of ric. *Plant Physiol. Biochem.* 43 (2), 193–201. doi: 10.1016/j.plaphy.2004.12.009

Taylor, S. H., Lowry, D. B., Aspinwall, M. J., Bonnette, J. E., Fay, P. A., Juenger, T. E., et al. (2016). QTL and drought effects on leaf physiology in lowland *Panicum virgatum*. *Bioenergy Res.* 9 (4), 1241–1259. doi: 10.1007/s12155-016-9768-5

Tejera, M., Boersma, N. N., Archontoulis, S. V, Miguez, F. E., VanLoocke, A., and Heaton, E. A. (2022). Photosynthetic decline in aging perennial grass is not fully explained by leaf nitroge. *J. Exp. Bot* 73 (22), 7582–7595. doi: 10.1093/jxb/erac382

Tejera, M. D., Miguez, F. E., and Heaton, E. A. (2021). The older plant gets the sun: Age-related changes in *Miscanthus* × *giganteus* phenology. *GCB Bioenergy* 13 (1), 4–20. doi: 10.1111/gcbb.12745

Van Heerden, P. D. R., Donaldson, R. A., Watt, D. A., and Singels, A. (2010). Biomass accumulation in sugarcane: Unravelling the factors underpinning reduced growth phenomena. *J. Exp. Bot.* 61 (11), 2877–2887. doi: 10.1093/jxb/erq144

Wang, N., Li, Q., Liu, X., Yi, S., Zhao, M., Sun, X., et al. (2021). Plant size plays an important role in plant responses to low water availability and defoliation in two woody leguminosae species. *Front. Plant Sci.* 12, 1–14. doi: 10.3389/fpls.2021.643143

Wingler, A., and Roitsch, T. (2008). Metabolic regulation of leaf senescence: interactions of sugar signalling with biotic and abiotic stress responses. *Plant Biol.* 10, 50–62. doi: 10.1111/j.1438-8677.2008.00086.x

Wutzler, T., Lucas-Moffat, A., Migliavacca, M., Knauer, J., Sickel, K., Šigut, L., et al. (2018). Basic and extensible post-processing of eddy covariance flux data with REddyProc. *Biogeosciences.* 15 (16), 5015–5030. doi: 10.5194/BG-15-5015-2018

Yan, J., Zhu, C., Liu, W., Luo, F., Mi, J., Ren, Y., et al. (2015). High photosynthetic rate and water use efficiency of *Miscanthus lutarioriparius* characterize an energy crop in the semiarid temperate region. *GCB Bioenergy* 7 (2), 207–218. doi: 10.1111/gcbb.12118

Yang, J., Worley, E., Wang, M., Lahner, B., Salt, D. E., and Saha, M.. (2009). Natural variation for nutrient use and remobilization efficiencies in switchgrass. *Bioenergy Res.* 2, 4. doi: 10.1007/S12155-009-9055-9

Yang, J., Preiser, A. L., Li, Z., Weise, S. E., Sharkey, T. D, et al. (2016). Triose phosphate use limitation of photosynthesis: short-term and long-term effects. *Planta* 243, 687–698. doi: 10.1007/s00425-015-2436-8

Yang, J., and Udvardi, M. (2018). Senescence and nitrogen use efficiency in perennial grasses for forage and biofuel production. *J. Exp. Botany.* 69 (4), 855–865. doi: 10.1093/JXB/ERX241

frontiers | Frontiers in Plant Science

TYPE Original Research
PUBLISHED 18 January 2023
DOI 10.3389/fpls.2022.1067076

Check for updates

OPEN ACCESS

EDITED BY
Bhaskar Gupta,
Government General Degree College, Singur, India

REVIEWED BY
Uday Chand Jha,
Indian Institute of Pulses Research (ICAR), India
Alok Ranjan,
Indian Institute of Agricultural Biotechnology (ICAR), India

*CORRESPONDENCE
Wenli Zhang
wzhang25@njau.edu.cn
Xuejiao Cheng
xuejiaocheng@njau.edu.cn
Zexue He
hezexue@stu.njau.edu.cn
Risheng Hu
495298768@qq.com

†These authors have contributed equally to this work

SPECIALTY SECTION
This article was submitted to Plant Abiotic Stress, a section of the journal Frontiers in Plant Science

RECEIVED 11 October 2022
ACCEPTED 30 November 2022
PUBLISHED 18 January 2023

CITATION
Hu Z, He Z, Li Y, Wang Q, Yi P, Yang J, Yang C, Borovskii G, Cheng X, Hu R and Zhang W (2023) Transcriptomic and metabolic regulatory network characterization of drought responses in tobacco.
Front. Plant Sci. 13:1067076.
doi: 10.3389/fpls.2022.1067076

COPYRIGHT
© 2023 Hu, He, Li, Wang, Yi, Yang, Yang, Borovskii, Cheng, Hu and Zhang. This is an open-access article distributed under the terms of the Creative Commons Attribution License (CC BY). The use, distribution or reproduction in other forums is permitted, provided the original author(s) and the copyright owner(s) are credited and that the original publication in this journal is cited, in accordance with accepted academic practice. No use, distribution or reproduction is permitted which does not comply with these terms.

Transcriptomic and metabolic regulatory network characterization of drought responses in tobacco

Zhengrong Hu[1†], Zexue He[2*†], Yangyang Li[1†], Qing Wang[2], Pengfei Yi[3], Jiashuo Yang[1], Chenkai Yang[4], Gennadii Borovskii[5], Xuejiao Cheng[2*], Risheng Hu[1*] and Wenli Zhang[2*]

[1]Hunan Tobacco Research Institute, Changsha, Hunan, China, [2]State Key Laboratory for Crop Genetics and Germplasm Enhancement, Jiangsu Collaborative Innovation Center for Modern Crop Production (JCIC-MCP), Collaborative Innovation Center for Modern Crop Production Co-Sponsored by Province and Ministry (CIC-MCP), Nanjing Agricultural University, Nanjing, Jiangsu, China, [3]Hu'nan Tobacco Company Changde Company, Changde, Hunan, China, [4]College of Agronomy, Hunan Agricultural University, Changsha, Hunan, China, [5]Siberian Institute of Plant Physiology and Biochemistry Siberian Branch of Russian Academy of Sciences (SB RAS) Irkutsk, Lermontova, Russia

Drought stress usually causes huge economic losses for tobacco industries. Drought stress exhibits multifaceted impacts on tobacco systems through inducing changes at different levels, such as physiological and chemical changes, changes of gene transcription and metabolic changes. Understanding how plants respond and adapt to drought stress helps generate engineered plants with enhanced drought resistance. In this study, we conducted multiple time point-related physiological, biochemical,transcriptomic and metabolic assays using K326 and its derived mutant 28 (M28) with contrasting drought tolerance. Through integrative analyses of transcriptome and metabolome,we observed dramatic changes of gene expression and metabolic profiles between M28 and K326 before and after drought treatment. we found that some of DEGs function as key enzymes responsible for ABA biosynthesis and metabolic pathway, thereby mitigating impairment of drought stress through ABA signaling dependent pathways. Four DEGs were involved in nitrogen metabolism, leading to synthesis of glutamate (Glu) starting from NO–3 /NO–2 that serves as an indicator for stress responses. Importantly, through regulatory network analyses, we detected several drought induced TFs that regulate expression of genes responsible for ABA biosynthesis through network, indicating direct and indirect involvement of TFs in drought responses in tobacco. Thus, our study sheds some mechanistic insights into how plant responding to drought stress through transcriptomic and metabolic changes in tobacco. It also provides some key TF or non-TF gene candidates for engineering manipulation for breeding new tobacco varieties with enhanced drought tolerance.

KEYWORDS

drought stress, transcriptome, metabolome, regulatory network, *Nicotiana tabacum* L.

Introduction

Drought stress is one of key restricting environmental factors that adversely affect plant growth and development. In particular, it dramatically reduces global crop productivity in arid and semi-arid regions, depending on its severity and duration (Kumar et al., 2018). It attracts more attention worldwide with the increasing severity of global warming. Drought stress exhibits multifaceted impacts on plant systems through inducing changes at different levels, such as physiological and chemical changes, changes of gene transcription and epigenetic changes (Chang et al., 2020; Li et al., 2021; Hura et al., 2022). For instance, it causes small plant architectures or plant death (Liu et al., 2017; Romdhane et al., 2020) and reactive oxygen species (ROS) related cell or membrane damage (Cruz de Carvalho, 2008; Abid et al., 2018; Couchoud et al., 2019); decreases transpiration through reducing stomatal conductance or stomatal closure (Li et al., 2017), and photosynthetic performance (Cornic, 2000); alters water use efficiency (WUE) (Karaba et al., 2007; Liu et al., 2017), phytohormone levels and distributions (Gupta et al., 2017; Tiwari et al., 2017; Pavlovic et al., 2018), changes of antioxidant or other enzyme activities (Abid et al., 2018; Laxa et al., 2019); alters transcription of transcription factors (TFs), non-TF genes, or non-coding RNAs (ncRNAs) (Sakuma et al., 2006; Harb et al., 2010; Guo et al., 2013; Huang et al., 2018; Yuan et al., 2018; Li et al., 2019b; Roca Paixao et al., 2019; Tang et al., 2019; Wang et al., 2020; Weidong et al., 2020). Moreover, it has been documented that drought stress can affect accumulation of different osmolytes or metabolites such as glycinebetaine, organic acids, polyols, polyamines, proline (Capell et al., 2004; Quan et al., 2004; Zhang et al., 2017; Abid et al., 2018; Michaletti et al., 2018; Pal et al., 2018). Thus, plants usually experience multiple changes on exposure to drought stress, including morphological, cellular, physiological, biochemical, transcriptional, epigenetic and metabolic alterations (Farooq et al., 2009; Xu et al., 2010; Fathi and Barari, 2016; Joshi et al., 2016; Hussain et al., 2018; Kapoor et al., 2020).

Understanding how plants respond and adapt to drought stress helps to generate bioengineered plants with enhanced drought resistance, which is an urgent need for crops, as the global warming has become the subject of debate worldwide. Transcriptional changes are one of the underlying molecular mechanisms responsible for the subsequent physiological, biochemical and metabolic alterations under the drought conditions. Therefore, transcriptional analyses of key TFs and non-TF genes involved in drought responses have been extensively explored in multiple plant species, including rice (Degenkolbe et al., 2009; Moumeni et al., 2015; Chung et al., 2016), maize (Cao et al., 2018; Zenda et al., 2019), wheat (Aprile et al., 2009; Liu et al., 2018), peal millet (Shivhare et al., 2020), sorghum (Varoquaux et al., 2019), *Brassica rapa* (Greenham et al., 2017), tomato (Gong et al., 2010), tea (Parmar et al., 2019), and tobacco (Rabara et al., 2015; Yin et al., 2015; Yang et al., 2017). In general, global transcriptional landscapes across various species provide an overview regarding how drought-inducible genes are involved in drought responses or adaptation in plants, thereby facilitating identification of key genes for further validation or applications.

In addition to be as an economic commercial non-food crop worldwide (Hu et al., 2006), tobacco (*Nicotiana tabacum* L.) is also a popular model plant for functional genomic studies (Elleuch et al., 2001; Rushton et al., 2008). Unfortunately, tobacco production in arid and semi-arid regions worldwide occasionally suffers from drought stress (Yang et al., 2017), inevitably leading to huge economic losses for tobacco growers and industries. Breeding and cultivation of bioengineered tobacco varieties with enhanced drought resistance will be a feasible way to avoid economic loss for tobacco production. Currently, mechanisms related to drought resistance in tobacco have been investigated at transcriptional, biochemical and metabolic levels (Rizhsky et al., 2002; Rabara et al., 2015; Rabara et al., 2017; Su et al., 2017; Yang et al., 2017; Chen et al., 2019), providing some valuable information to guide tobacco breeding. However, comprehensive transcriptional and metabolic network analyses of wild type tobacco and its derived mutant with contrasting drought responses are still not well studied.

In this study, we conducted transcriptional and metabolic analyses using K326 and its derived mutant 28 (M28) with contrasting drought tolerance. Through integration of RNA-seq with metabolic data, and construction of gene regulatory networks, we revealed that some key genes directly or indirectly regulate differential gene expression or accumulation of metabolites potentially involved in drought responses.

Materials and methods

Plant growth and drought treatment

Seeds of K326 and its derived EMS mutant, M28 with enhanced drought resistance, were sterilized and pretreated at 4°C for 2 days. The pretreated seeds were put into pots with nutrient soil for germination. The germinated seedlings with fully expanded cotyledons were transferred into small pots. Each pot contained the exactly same amount (120g) of nutrient soil, 10 seedlings per pot for each replicate, total three replicates for K326 or M28. All pots were randomly put into the incubator to grow under 22 ± 1°C,16h/8h light-dark cycle and 70% humidity. At the fully expanded five-leaf stage, each pot with 3 similar-sized seedlings was fully watered, and then all pots with K326 or M28 were randomly divided into 3 parts for drought treatment, natural drought (ND) treatment and 200 mM mannitol for simulated drought (SD) treatment. According to visible phenotypic changes (4h/24h for SD and 7D/14D for ND), we decided to collect the third leaf of each plant from the top to the bottom at 7 and 14 days after ND, or at 1h and 4h post SD for the downstream physiological and biochemical assays. Considering that

drought induced transcriptional changes occur prior to occurrence of phenotypic changes, we decided to collect leaves with ND and SD and the corresponding CK at 0, 1, 2, 4 and 8h, respectively, for the downstream RNA-seq and metabolome analyses.

Physiological and biochemical assays

Leaf water content assay: The collected leaves from drought treatment and CK were measured with a balance for fresh weight (FW) followed by merging the leaves into ddH2O for 6-8h for maximizing turgidity. Completely turgid leaves were measured with a balance for saturated fresh weight (SFW) followed by oven-dried at 80 °C for 24 h for measuring dry weight (DW). Relative leaf water content (RWC) and water saturation deficit (WSD) were calculated according to the formulas:

$$RWC = (FW - DW)/(SFW - DW);\ WSD = (SFW - FW)/(SFW - DW)$$

Relative conductivity: The leaves were submerged into 10 ml ddH_2O in the centrifuge tube, and constantly shaking at RT for 24 h. The first conductivity (A) was measured followed by heating to 95 °C for 15 min, after cooling down to RT, the second conductivity (B) was measured. The relative conductivity was calculated as A/B*100%.

Net photosynthetic rate, Stomatal conductance and Transpiration rate: Those three parameters were measured and recorded by using portable photosynthesis system (LI-6400XT, LI-COR, Inc., Lincoln, NE, USA), which was conducted from 9:30 AM to 11:00 AM at 26°C and photosynthetic photon flux as 600 $\mu mol \cdot m^{-2} \cdot s^{-1}$.

Enzyme activity assays: Firstly, 0.2 g of fully expanded functional leaves were weighed and ground into powder using liquid nitrogen. 4 mL of pre-cooled 150 mmol/L phosphate buffer solution (pH 7.0) was added to mix well, and the homogenate was transferred into a 15 mL centrifuge tube. After centrifugation at 12,000 rpm at 4 °C for 20 min, the supernatant was collected and used as the crude enzyme solution. MDA content and POD activity were determined according to the method described in Hu (Hu et al., 2016). SOD activity and H_2O_2 content were measured using SOD assay kit (A001-3-2, Nanjing Jiancheng Bioengineering Institute, China) and Hydrogen Peroxide assay kit (A064-1-1, Nanjing Jiancheng Bioengineering Institute, China) respectively, according to the manufacturer's instructions.

Virus-induced Gene silencing of the target genes

For construction of the recombinant of pTRV2: NCED1, a fragment of about 300 bp of NCED1 was cloned and inserted into the restriction site of rDNA11 of pTRV2. pTRV2: PP2C-37L and pTRV2: P450 84A1L were constructed by using the same method. pTRV1 and the three vectors containing the target gene sequences were then transformed into a bacteria A. tumefaciens strain GV3101, respectively.

Tumefaciens positive clones were selected for culture in 500 µL LB liquid medium (containing 50 µg/ml kana and 25 µg/ml rifampicin) with constant shaking at 200 rpm, at 28°C overnight. They were further cultured with 50 mL the same LB medium with constant shaking at 28°C for 16-24 h with OD600 reaching about 0.6-0.8. The thalli were collected by centrifugation (4,000 rpm for 20 min) and treated with infection buffer (10 mM MES; 10 mm MgCl2; 200 µm AS), adjusted to OD600 between 1.0-1.5. The Agrobacterium solution with equal concentration of pTRV1 and pTRV2 (pTRV2: NCED1, pTRV2: PP2C-37L, pTRV2: P450 84A1L) were mixed and left at room temperature for 3 h. A syringe without a needle was used to inject 400-600 µL of the prepared infection solution into the back of the leaf from 25-day-old tobacco (*Nicotiana benthamiana*) for infection. After 24-hour dark acclimation, inoculated tobacco plants were transferred to normal culture conditions (25°C, 240 µmol m-2s-1wih 16 h/8 h light/dark cycle) for 14 days. They were then subjected to drought stress treatment for 14 days, after which it was rehydrated. The leaf samples were collected at 7 days of drought stress for RNA extraction.

RNA extraction and reverse transcription were performed using the kits (Norvezan RC401, Norvezan R312-01) according to the instructions. qRT-PCR was conducted by using fluorescent intercalating dye PowerUp™ SYBR™ Green Master Mix (Thermo Fisher Scientific, 100029284) with the QuantStudio™ 3 Real-Time PCR Instrument (Applied Biosystems, USA). The gene-specific primers are listed in Supplementary Table S10. The 18S rDNA was used as the internal standard gene. Each sample was biologically triplicated.

RNA-seq and data analyses

Total RNA was extracted using collected leaves with ND and SD at 0, 1, 2, 4 and 8h. After completely removal of genomic DNA contamination, mRNA was enriched for RNA-seq library preparation following the kit instruction.

For RNA-seq analyses, the quality of raw reads was processed using FastQC (Kroll et al., 2014). Adapter contamination and poor-quality bases were removed using Trimmomatic (version 0.39) (Bolger et al., 2014). Hisat2 (version 2.1.0) (Kim et al., 2015) was used to align clean reads to the tobacco reference genome. FeatureCounts (version 1.6.4) (Yan et al., 2014) was used for counting number of reads and FPKM (Fragments Per Kilobase of exon model per Million mapped fragments) values, representing gene expression levels. DESeq2 R package (version 1.30.1) (Varet et al., 2016) was used for identification of differentially expressed genes (DEGs)

between M28 and K326. DGEs were determined with a cutoff as padj<0.01 and $|\log_2^{FoldChange}|>1$.

Gene Ontology and KEGG analyses

Gene Ontology (GO) and KEGG analyses of DEGs were analyzed using AgriGO (Tian et al., 2017) and KOBAS (version3.0) (Bu et al., 2021), respectively.

UPLC-MS/MS metabolite measurements and data analyses

The freeze-dried samples were crushed using a mixer mill (MM 400, Retsch) with a zirconia bead for 1.5 min at 30 Hz. 100 mg of lyophilized powder per sample was dissolved using 1.2 ml of 70% methanol solution, vortexed 30 seconds every 30 minutes for 6 times in total. The homogenized samples were placed in a refrigerator at 4°C overnight. After centrifugation at 12,000rpm for 10 min, the extracts were filtrated using millipore filter (0.22 μm pore size). The filtrates were analyzed using an UPLC-ESI-MS/MS system. The analytical conditions were conducted as follows: UPLC: column, Agilent SB-C18 (1.8 μm, 2.1 mm*100 mm), the mobile phase consisting of solvent A (pure water with 0.1% formic acid) and solvent B (acetonitrile with 0.1% formic acid). Sample measurements were performed with a gradient program as below: the starting conditions as 95% A, 5% B, then a programmed linear gradient as 5% A, 95% B within 9 min, and a composition of 5% A, 95% B kept for 1 min; a composition of 95% A, 5.0% B subsequently adjusted within 1.10 min and kept for 2.9 min; the flow velocity set as 0.35ml per minute; the column oven set to 40°C. The injection volume was 4 μl. The effluent was alternatively connected to an ESI-triple quadrupole-linear ion trap (QTRAP)-MS. LIT and triple quadrupole (QQQ) scans were acquired on a triple quadrupole-linear ion trap mass spectrometer (Q TRAP), AB4500 Q TRAP UPLC/MS/MS System, equipped with an ESI Turbo Ion-Spray interface, which was operated in positive and negative ion mode and controlled by Analyst 1.6.3 software (AB Sciex). The ESI source operation parameters were as follows: ion source, turbo spray; source temperature 550°C; ion spray voltage (IS) 5500 V (positive ion mode)/-4500 V (negative ion mode); ion source gas I (GSI), gas II (GSII) and curtain gas (CUR) were set at 50, 60, and 25.0 psi, respectively; the collision-activated dissociation (CAD) was high. Instrument tuning and mass calibration were performed with 10 and 100 μmol/L polypropylene glycol solutions in QQQ and LIT modes, respectively. QQQ scans were acquired as MRM experiments with collision nitrogen gas set to medium. DP and CE for individual MRM transitions were done with further DP and CE optimization. A specific set of MRM transitions were monitored for each period according to the metabolites eluted within this period

Drought induced differential metabolic changes in M28 or K326 or between M28 and K326 were analyzed using MetaboAnalyst5.0 (Pang et al., 2021). PCA and orthogonal partial least squares discrimination analysis (OPLS-DA) were performed for unsupervised multivariate statistical analyses and supervised analyses, respectively, and to identify important variables with discriminative power. VIP is the weighted sum of the squares of the OPLS-DA analyses, indicating the importance of a variable to the entire model. The significantly differential metabolites were determined based on the combinations of a statistically significant threshold of a VIP > 1.0, a Student's t-test $p < 0.05$ and $|\log_2^{FoldChange}| > 1$.

Co-expression network analyses

The FPKM matrix of gene expression was used as input data for filtering the genes with low variations of expression levels among 30 samples according to the median absolute deviation (MAD) value > 0.5 for each gene. The remaining 14,445 genes were used to construct the weighted gene co-expression network using the R package WGCNA (v1.69) (Langfelder and Horvath, 2008). The best-weighted coefficient ($\beta = 14$) was determined by using the function pickSoftThreshold in the R package. The default parameters were used to construct the scale-free network. The module Hub genes were identified using the threshold as $|kME| > 0.8$.

Construction of predicted TF regulatory networks

TF centered regulatory networks were predicted using all sample gene expression matrix exprMatr as input argument, which was conducted using the R package GENIE3 (v1.12.0) (Huynh-Thu and Geurts, 2018). The predicted TF regulatory networks were constructed using the three TFs in the blue co-expressed module. The DGEs within the predicted TF regulatory networks were used as potential regulatory genes, which were extracted according to the calculated "weight" values (≥ 0, a measure of the regulatory confidence level as defined by GENIE3). All TF-centered regulatory networks are visualized using Cytoscape (v3.7.2) software.

Results

Differential morphological, physiological and biochemical changes between K326 and M28 during drought stress

Through EMS (Ethylmethanesulfonate) treatment following by subsequent screening, we obtained one mutant, named as

M28, with increased tolerance to drought stress as compared to the wild type K326. To assess drought responses between K326 and M28, we grew them in the growth chamber, three plants per pot, for two weeks followed by progressive natural drought (ND) stress without watering. As shown in Supplementary Figure S1, leaves of both plants became markedly wilt started at 14D post ND. For instance, M28 had more green leaves than K326 at 31 D post ND. At 3D post re-watering, three M28 and one K326 plants were recovered, respectively, indicating that M28 is more drought resistance than K326. We also applied 200 mM mannitol to simulate the drought conditions (simulated drought stress, SD). As illustrated in Supplementary Figure S2, K326 had visible droop leaves starting at 4h post SD, and the number of droop leaves increased with a longer duration, like from 8h to 48h post SD, by contrast, there were almost no visible morphological changes in leaves of M28 with SD at all time points.

We then measured the physiological and biochemical changes between K326 and M28 at different time points after exposure to ND or SD. As compared to K326 under ND or SD treatment, M28 exhibited slightly decreased SOD activity, but markedly increased POD activity (Figures 1A–D). As expected, H_2O_2 accumulation at 14 D post ND, and 4h/24h post SD was less in M28 than in K326 (Figures 1E, F). As compared to K326, M28 had less content of malondialdehyde (MDA) at 7D/14D post ND and 24h post SD, but higher MDA content at 4h post SD (Figures 1G, H). Moreover, higher relative leaf water content at 14 D post ND, higher water saturation deficit (WSD) before and after ND, higher net photosynthetic rate at 7D/14D post ND were detected in M28 than in K326 (Figures 2A–C). In addition, less relative conductivity, stomatal conductance and transpiration rate at 7D/14D post ND were detected in M28 as compared to K326 (Figures 2D–F). These result indicated that drought stress caused less damage in M28 than in K326.

Taken together, all above analyses show that differential morphological, physiological and biochemical changes occur between K326 and M28 during drought stress, confirming that M28 is more resistant to drought stress than K326.

Differential gene expression in response to drought treatment between K326 and M28

To assess if genes are differentially expressed between K326 and M28 during drought stress, we conducted RNA-seq using K326 and M28 under drought treatment at multiple time points (0, 1, 2, 4 and 8 h), and obtained well-correlated biological triplicates for each time point (Supplementary Figure S3). After identifying time-point-related differentially expressed genes (DEGs, padj < 0.01 & $|\log_2^{\text{FoldChange}}| > 1$) in K326/M28 or between K326 and M28 before and post drought treatment (Supplementary Table S1), we found that 700/782 genes were down- and up-regulated, respectively, in M28 relative to K326 before drought treatment. These DEGs are most likely caused by EMS-induced genomic sequence variations between two samples. For post drought treatment at the time point for each sample or between samples as indicated (Supplementary Table S1), we found that the highest number of DEGs occurred at 8 h post drought treatment, indicative of time point-dependent gene expression changes in response to drought treatment.

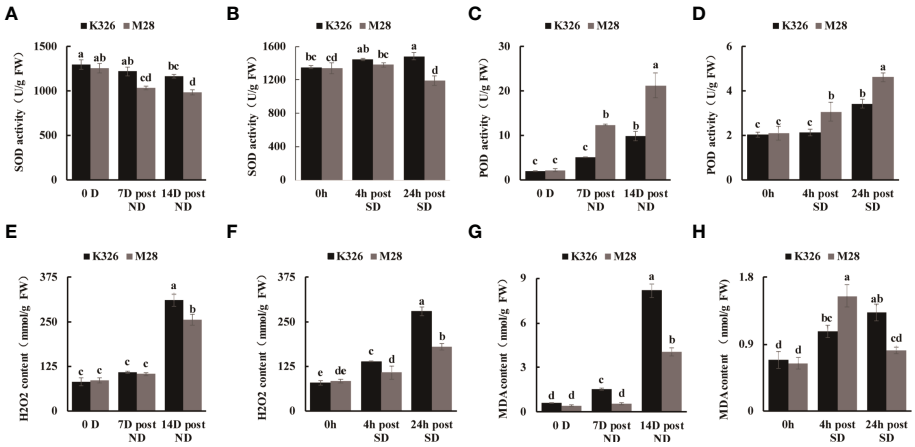


FIGURE 1
Biochemical comparisons between tobacco K326 and M28 at different time points after exposing to ND and SD, respectively. **(A, B)** SOD activity at 0 D,7 D,14 D post ND, and 0h,4h,24h between tobacco K326 and M28. **(C, D)** POD activity at 0 D,7 D,14 D post ND, and 0h,4h,24h between tobacco K326 and M28. **(E, F)** H2O2 content at 0 D,7 D,14 D post ND, and 0h,4h,24h between tobacco K326 and M28. **(G, H)** MDA content at 0 D,7 D,14 D post ND, and 0h,4h,24h between tobacco K326 and M28. Different letters represent significant differences (P< 0.05, one-way ANOVA).The difference is not significant if there is a letter with the same marker, and significant if there is a letter with a different marker.

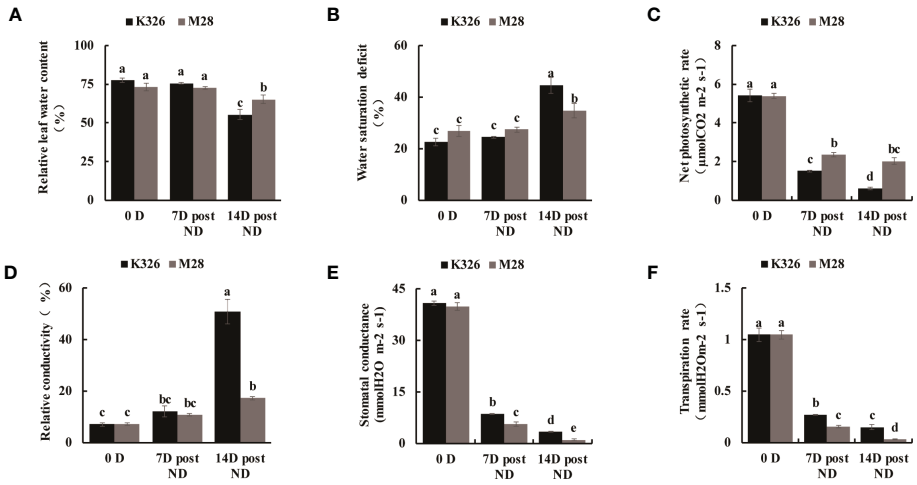


FIGURE 2
Physiological comparisons between tobacco K326 and M28 at different time points after exposing to ND. **(A, B)** Relative leaf water content at 0 D,7 D,14 D post ND, and 0h,4h,24h between tobacco K326 and M28. **(C)** Net photosynthetic rate at 0 D,7 D,14 D post ND between tobacco K326 and M28. **(D)** Relative conductivity at 0 D,7 D,14 D post ND between tobacco K326 and M28. **(E)** Stomatal conductance at 0 D,7 D,14 D post ND between tobacco K326 and M28. **(F)** Transpiration rate at 0 D,7 D,14 D post ND between tobacco K326 and M28.Different letters represent significant differences (P< 0.05, one-way ANOVA).The difference is not significant if there is a letter with the same marker, and significant if there is a letter with a different marker.

After pair-wise comparisons of DEGs between K326 and M28 at each individual time point, we found that 133 down-regulated genes and 150 up-regulated genes were shared for all time points (Figures 3A, B). Besides, we observed that some genes exhibited time-point-dependent expression (Figures 3A, B). For instance, 246/300 and 81/123 genes were down/up-regulated at 0 and 8 h, respectively. Among 1,327 up-regulated and 1,249 down-regulated genes occurred in M28 relative to K326, we found that 545 and 549 genes corresponding to the drought-induced up- and down-regulation, respectively, in M28, by contrast, 482 up-regulated and 454 down-regulated genes were possibly caused by genomic sequence variations in combination with drought treatment

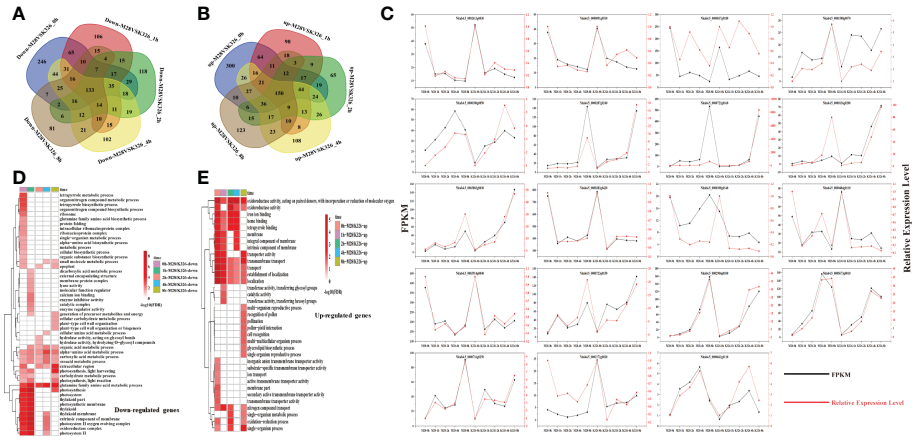


FIGURE 3
Characterization of differentially expressed genes before and after drought treatment in M28 or K326. **(A)** Pairwise comparisons of down-regulated genes at the same time point between M28 and K326 after drought treatment. **(B)** Pairwise comparisons of up-regulated genes at the same time point between M28 and K326 after drought treatment. **(C)** 19 DEGs were randomly selected for RT-qPCR assay. The red line represents the relative expression, and the black line represents the FPKM values. **(D)** GO term enrichment analyses of down-regulated genes at the same time point between M28 and K326 after drought treatment. **(E)** GO term enrichment analyses of up-regulated genes at the same time point between M28 and K326 after drought treatment.

(Supplementary Figure S4). We randomly chose 19 DEGs for RT-qPCR assay, and observed a similar expression trend as RNA-seq data (Figure 3C), confirming the reliability of DEGs identified by analyzing RNA-seq data.

To examine if these DEGs have any specific biological functions facilitating drought tolerance, we conducted GO terms enrichment assays. We found that 133 common down-regulated genes were overrepresented in metabolic processes such as oxoacid and organic acids (Supplementary Figure S5); distinct GO terms occurred in time-point-related DEGs (Figures 3D, E). For example, down-regulated genes at 1 h post drought treatment were more enriched in dicarboxylic acid metabolic processes, regulator activities and calcium ion binding; by contrast, up-regulated genes at 8 h post drought treatment were more enriched in reproductive events, such as pollination, pollen-pistil interaction, recognition of pollen and single/multi-organism reproductive processes.

Similarly, we conducted pair-wise comparisons and GO terms enrichment of time-point-related DEGs in M28 or K326 (Supplementary Figures S6A, B). We found that differential GO terms mainly occurred in up-regulated genes between M28 and K326 (Supplementary Figure S6C). As illustrated in Figure 3D, up-regulated genes in M28 had more enriched terms in response to heat or temperature stimulus, by contrast, up-regulated genes in K326 were more enriched in GO terms associated with the regulation of cellular and biological processes, gene transcription and regulation of RNA biosynthetic or metabolic processes.

Collectively, these results indicate that drought induced DEGs between M28 and K326 had distinct GO terms, which may partially explain differential drought responses between two materials.

Differential metabolic changes in response to drought treatment between M28 and K326

To determine if drought treatment causes differential accumulation of metabolites between M28 and K326, we generated time-point-related metabolomics data *via* LC-MS in M28 and K326 before and after drought treatment. Principal component analysis (PCA) showed a clear separation between M28 and K326. We noticed that, after drought treatment, M28 mainly exhibited the first principal component (PC1) changes, whereas K326 mainly exhibited the second principal component (PC2) changes (Supplementary Figure S7), indicating dramatic changes of metabolic profiles between M28 and K326 before and after drought treatment.

We then identified drought induced metabolites (DiffExp, a variable importance in projection (VIP) score >1, an FC > 1.5 or <0.66 and $p < 0.05$) in M28 or K326, and between M28 and K326 using orthogonal partial least squares discriminant analysis (OPLS-DA) (Supplementary Table S2). As shown in Figure 4A, the highest number (69) of up-regulated DiffExp metabolites was observed at 2 h post drought treatment in K326, and the highest number (51) of down-regulated DiffExp metabolites was observed at 2 h post drought treatment between K326 and M28. To assess if

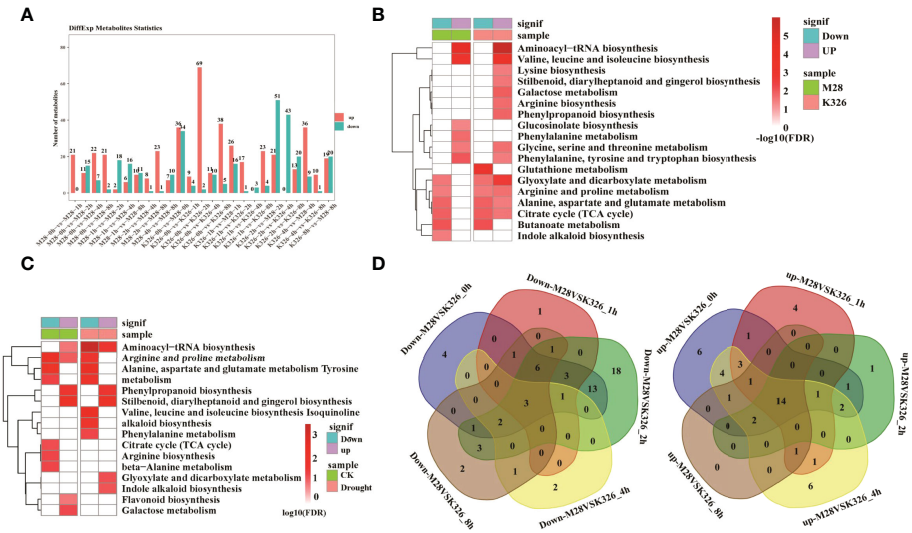


FIGURE 4
Differential metabolic changes in response to drought treatment between M28 and K326. **(A)** Histogram showing the number of differential metabolic changes in response to time-point-related drought-induced in M28 or K326 or between M28 and K326. **(B)** KEGG pathway enrichment analyses of up- and down-regulated metabolites in K326 or M28 under drought treatment. **(C)** KEGG pathway enrichment analyses of metabolites that were up- or down-regulated before (CK) or under drought treatment. **(D)** Pairwise comparisons of down- (left) and up-regulated (right) metabolites at the same time point between M28 and K326 after drought treatment.

DiffExp metabolites are involved in any metabolic pathways, we conducted KEGG pathway analyses using DiffExp metabolites between K326 and M28 (Figure 4B). In addition to some metabolic pathways related to up or down-regulated DiffExp metabolites shared between K326 and M28, distinct metabolic pathways occurred between K326 and M28. For example, down-regulated DiffExp metabolites were more enriched in indole alkaloid biosynthesis in M28, whereas were more enriched in glutathione metabolism in K326; up-regulated DiffExp metabolites were overrepresented in glucosinolate biosynthesis and phenylalanine metabolism in M28, whereas were more enriched in lysine/arginine/gingerol/phenylpropanoid biosynthesis, galactose metabolism in K326.

We also conducted KEGG pathway analyses using DiffExp metabolites before and after drought treatment, including 8/13 up-regulated and 4/28 down-regulated metabolites corresponding to CK and post drought treatment, respectively (Supplementary Figure S8). Differential enrichment of metabolic pathways was observed between CK- and drought-related DiffExp metabolites (Figure 4C). For instance, drought-related up-regulated metabolites were overrepresented in glyoxylate and dicarboxylate metabolism and indole alkaloid biosynthesis; by contrast, CK-related up-regulated metabolites were overrepresented in galactose metabolism and flavonoid biosynthesis. After pairwise comparisons, we found that there were 3 down-regulated and 14 up-regulated metabolites present at all time points in M28 post drought treatment (Figure 4D). According to KEGG pathway analyses, we found that 2 down-regulated metabolites (spermidine and putrescine) were involved in arginine/proline/glutathione metabolisms (Supplementary Figure S9); 3 up-regulated metabolites (gluconic acid, 5-O-p-coumaroylquinic acid and chlorogenic acid) were involved in pentose phosphate pathway and stilbenoid diarylheptanoid and gingerol biosynthesis (Supplementary Figure S10).

Furthermore, we conducted KEGG enrichment analysis using all differentially expressed metabolites significantly changed post drought treatment. We observed and 29 significantly enriched KEGG pathways (Supplementary Figure S11), including Nitrogen_/Alanine_/Arginine_/Pyruvate_metabolism pathways (Supplementary Figure S12) involved in drought stress (Winter and Holtum, 2015; Shen et al., 2017; Cui et al., 2019; Parthasarathy et al., 2019).

Collectively, these results indicate that drought induced DiffExp metabolites between M28 and K326 had distinct GO terms, possibly leading to differential drought responses between two materials.

Integrated analyses of transcriptome and metabolome related to drought stress

To investigate if DEGs directly result in DiffExp metabolites during drought treatment, we first conducted KEGG pathway analyses using drought inducible DEGs between M28 and K326. We observed differential KEGG pathways occurred in down- and up-regulated genes between M28 and K326 before and after drought treatment (Figure 5A). For example, before drought treatment, down-regulated genes were mainly enriched in pathways associated with biosynthesis of secondary metabolites and ubiquinone, ribosome and porphyrin and chlorophyll metabolism; by contrast, up-regulated genes were overrepresented in pathways related to phenylalanine/tyrosine metabolism, ABC transporters and carotenoid biosynthesis. Particularly, we observed that down-regulated genes (Supplementary Table S3) were involved in plant hormone signal transduction such as auxin-responsive or induced proteins and ethylene-response factors, while up-regulated genes (Supplementary Table S4) were involved in carotenoid biosynthesis such as abscisic acid 8'-hydroxylase and 9-cis-epoxycarotenoid dioxygenase NCED1 for biosynthesis of ABA (Song et al., 2021). After drought treatment, down-regulated genes were mainly enriched in pathways associated with photosynthesis, carbon fixation, glutathione/alpha-linolenic acid/galactose/arginine and proline metabolism, biosynthesis of unsaturated fatty acids and amino acids; by contrast, up-regulated genes were overrepresented in pathways related to glucerolipid/C5-branched dibasic acid metabolism, and flavonoid/phenylpropanoid/brassinosteroid/zeatin biosynthesis.

Similarly, we conducted KEGG pathway analyses using drought inducible DEGs in M28 or K326 (Figure 5B). We observed differences in up- and down-regulated genes in M28 or K326. We found that distinct pathways occurred in up- and down-regulated genes between M28 and K326. For example, compared with genes in K326, down-regulated genes in M28 were more enriched in amino sugar and nucleotide sugar metabolism; up-regulated genes in M28 were more enriched in glutathione/alpha-linolenic acid/beta-alanine metabolism, up-regulated genes in K326 were more enriched in carotenoid biosynthesis. In particular, we found that up-regulated genes in K326 (Supplementary Table S5) were involved in carotenoid biosynthesis, down-regulated genes in M28 and DEGs in K326 (Supplementary Table S6) were involved in MAPK signaling pathway like PP2C and plant hormone signal transduction. These results indicated that more enriched KEGG pathways may facilitate more drought tolerance in M28 than K326. To further confirm involvement of genes *NCED1*, *PP2C-37L* and *P450 84A1L* in drought responses, we conducted VIGS-mediated knock-down of each individual genes in combination with drought treatment. We found that the sensitivity of each VIGS line to drought treatment was directly associated with the expression level of the corresponding gene (Figure 5C), indicative of positive roles of each gene in drought responses in tobacco.

After associating DEGs- and DiffExp metabolites-related KEGG pathways, we detected 16 pathways shared between DEGs and DiffExp metabolites (Supplementary Table S7), such as phenylalanine, galactose and glutathione metabolisms.

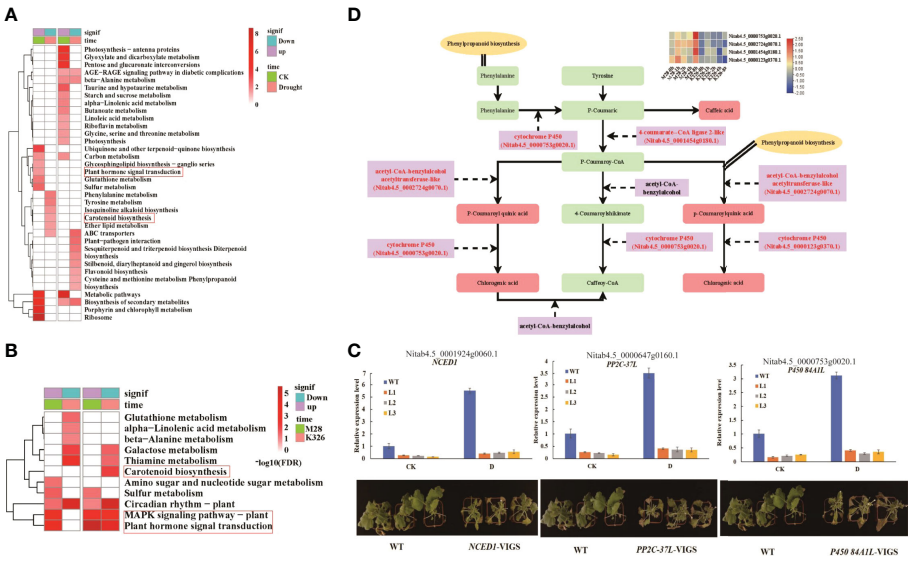


FIGURE 5
Integrated analyses of transcriptome and metabolome. **(A)** KEGG pathway enrichment analyses of genes that were up- or down-regulated before (CK) or under drought treatment. **(B)** KEGG pathway enrichment analyses of up- and down-regulated genes in K326 or M28 under drought treatment. **(C)** Relative expression levels (up) and phenotypes (down) of VIGS-mediated knock-down of gene *NCED1, PP2C-37L* and *P450 84A1L* before or post drought treatment. **(D)** Overview of DEGs and metabolites involved in "Phenylpropanoid biosynthesis" and "Flavonoid biosynthesis". The red representing differentially expressed genes and differential metabolites that are significantly enriched in the pathways of Phenylpropanoid biosynthesis terms and Flavonoid biosynthesis pathway. Four differentially expressed genes with relative expression levels (FPKM value) in the M28 and K326 are shown in the heatmap.

We noticed that DEGs were markedly enriched in "phenylpropanoid biosynthesis" terms and "flavonoid biosynthesis" pathways. We then combined our RNA-seq and metabolomics data to construct a gene-metabolite network (Figure 5D). We observed that cytochrome P450 gene (*Nitab4.5_0000753g0020.1*) was involved in several key steps for phenylpropanoid biosynthesis such as cinnamic acid to p-coumaric acid, and p-coumaroyl quinic acid to chlorogenic acid, indicating that this gene plays important roles in controlling phenylpropanoid biosynthesis in tobacco.

In addition, we found that L-Valine (C00183) was involved in Acetoacetyl coenzyme A biosynthesis, which is the key component in terpenoid pathways for synthesis of ABA (Boba et al., 2020) (Figure 6A); S-Malate(C00149), citric acid (C00158) and 2-Oxoglutarate (C00026) were involved in Citrate-cycle (TCA-cycle) (Figure 6B), leading to production of Acetoacetyl coenzyme A for ABA synthesis. Among DEGs, we found that NCEDs is the key enzyme catalyzing Zeaxanthin to form Xanthoxin during ABA synthesis pathway, and *Nitab4.5_0000287g0290.1* and *Nitab4.5_0000986g0020.1* are key enzymes catalyzing ABA to form 8'-hydroxy-ABA during ABA metabolic pathway (Figure 6C). Besides, we found that four DEGs, such as *Nitab4.5_0002255g0010.1*, *Nitab4.5_0001650g0160.1* (*glutamine synthetase*), *Nitab4.5_0000777g0010.1* (*glutamine synthetase*) and *glutamate synthase* (*GOGAT*), were involved in nitrogen metabolism, leading to synthesis of glutamate (Glu) starting from NO_3^-/NO_2^- (Supplementary Figure S13). Glutamate has been reported to involve in plant growth and development, and stress response and adaptation in plants (Qiu et al., 2019). We validated expression of *Nitab4.5_0001454g0180.1* and *Nitab4.5_0000123g0370.1* by using RT-qPCR assay, which were identified from metabolic pathways linked with RNA-seq. Both genes were more expressed at 1 h, 2 h and 4 h but less at 8 h in M28 as compared to K326 post drought stress (Supplementary Figure S14).

Collectively, all above analyses indicate that a subset of drought induced DEGs function in drought response through the regulation of DiffExp metabolite synthesis in tobacco.

Co-expression network in relation to drought responses

To interrogate if functions of transcription factors (TFs) in drought responses are mediated by their interactive genes, we performed Weighted Gene Co-Expression Network Analysis (WGCNA) with 2,568 DEGs. We obtained 13 modules containing co-expression genes according to the WGCNA package function (Supplementary Figure S15). We found that blue/brown and MEtan models displaying a high correlation with up- and down-regulated genes, respectively, in M28 at 8h post drought treatment (Figures 7A, B; Supplementary Figure S16A).

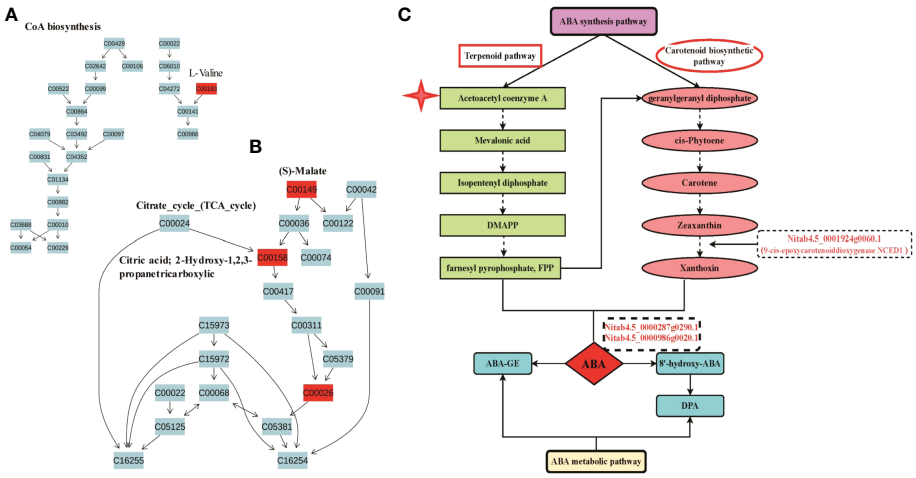


FIGURE 6
Involvement of Abscisic acid in drought responses in tobacco. **(A)** Overview of the KEGG pathway of CoA biosynthesis. The red indicating significantly up-regulated metabolites between M28 and K326 after drought treatment. **(B)** Overview of the KEGG pathway of Citrate cycle (TCA cycle). The red indicating significantly up-regulated metabolites between M28 and K326 after drought treatment. **(C)** Involvement of DEGs in combination with metabolites in synthesis and decomposition pathways of Abscisic acid in tobacco.

There were 26 up-regulated and 24 down-regulated genes in brown and Tan modules, respectively (Supplementary Table S8). Blue module contained 15 up-regulated genes and 3 TFs (*Nitab4.5_0000175g0070*, *bHLH*; *Nitab4.5_0000540g0010*, *C3H*; *Nitab4.5_0000082g0020*, *CCAAT*) (Supplementary Table S9). We then constructed TF-centered co-expression networks for those 3 modules (Figures 7C, D; Supplementary Figure S16). In blue module, we observed interactions between *bHLH* and some of up-regulated genes (Figure 7D). To confirm this possibility, we conducted *de novo* motif identification using promoter regions of

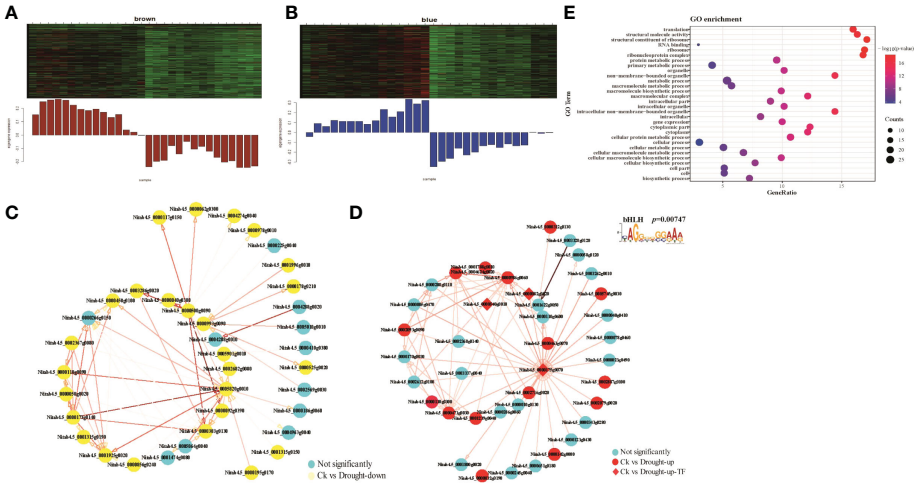


FIGURE 7
WGCNA analyses. **(A)** Module gene expression pattern in the brown module, red representing up-regulated genes, the green representing down-regulated genes. **(B)** The correlation network of genes in the brown module. A gene network is constructed by WGCNA, in which each node represents a gene, and the connecting line between genes represents the co-expression correlation, the blue representing not significant genes and the yellow representing down-regulated genes between M28 and K326 before and after drought treatment. The genes with weights >0.1 are visualized by Cytoscape. **(C)** The correlation network of genes in the blue module. **(D)** The correlation network of genes in the blue module. The red representing up-regulated genes and the blue representing not significant genes. The diamond representing the TF in the co-expression network. **(E)** GO term enrichment analyses of down-regulated genes in the brown module.

all up-regulated genes in blue module. We indeed detected a typical CAGGGGGGAAA motif for the potential binding of bHLH, which is similar to CACGTG motif associated with bHLH69 identified through DAP-seq data in *Arabidopsis* (O'Malley et al., 2016).

To examine if genes in each module mentioned above have any biological implications, we conducted GO term enrichment assays. We found that genes in blue module were significantly enriched in functions associated with protein translation-related functions, structural molecule activity, gene expression and cytoplasm (Figure 7E). By contrast, no significant GO terms were detected for genes in brown and tan modules. To interrogate how *bHLH* is involved in drought responses in M28, we constructed *bHLH*-related regulatory network and found that *bHLH* can directly interact with *CCAAT* TF, and may indirectly interact with C3H (Figure 8A). We further found that CCAAT and C3H TFs can interact with 10 and 25 up-regulated genes in M28 during drought treatment. After performing GO enrichment analyses, we found that C3H-regulated genes were mainly involved in nucleoside-triphosphatase activity, pyrophosphatase/hydrolase activity, acting on acid anhydrides, in phosphorus-containing anhydrides; by contrast, CCAAT regulated genes exhibited functions highly enriched in methyltransferase activity, nucleotide binding and stress responses (Figure 8B). Thus, these analyses provided evidence showing direct and indirect involvement of *bHLH* TF in drought responses in tobacco.

Collectively, all above analyses indicate that, in addition to direct functions of a subset of TFs in drought stress, they can be indirectly involved in drought responses through the regulatory networks in tobacco.

Discussion

To acclimate various severe stress factors for normal development or survival, sessile plants have to adjust multifaceted changes, including physiological, biochemical and metabolic changes, reprogramming of gene expression and DNA methylation, chromatin modification and ncRNA-related epigenetic changes as well (Covarrubias and Reyes, 2010; Kim et al., 2010; Ramakrishna and Ravishankar, 2011; Krasensky and Jonak, 2012; Kumar, 2014; Kim et al., 2015; Janiak et al., 2016; Takahashi et al., 2018; Liu and He, 2020; Bhadouriya et al., 2021; Hussain et al., 2021; Kumar et al., 2021). In this study, we explored possible mechanisms underlying contrasting drought responses between K326 and its derived mutant M28, including physiological and biochemical, transcriptional and metabolic levels.

Resistance of M28 to drought can be achieved at physiological and biochemical levels. M28 exhibited less H2O2 and MDA accumulation and higher POD activities as compared to K326 post drought treatment, particularly for a long duration of ND (14D) or SD (24h). Moreover, M28 had higher photosynthetic rate, less stomatal conductance and transpiration rate. These changes lead to less membrane damage and water loss and higher capacity for producing energy through photosynthesis, facilitating M28 to adapt to drought stress through alleviating drought related damage. Similar findings have been reported in tobacco or other plant species in response to drought or other stress factors such as salt, cold and heat (Su et al., 2017; Jamshidi Goharrizi et al., 2020; Mude et al., 2020).

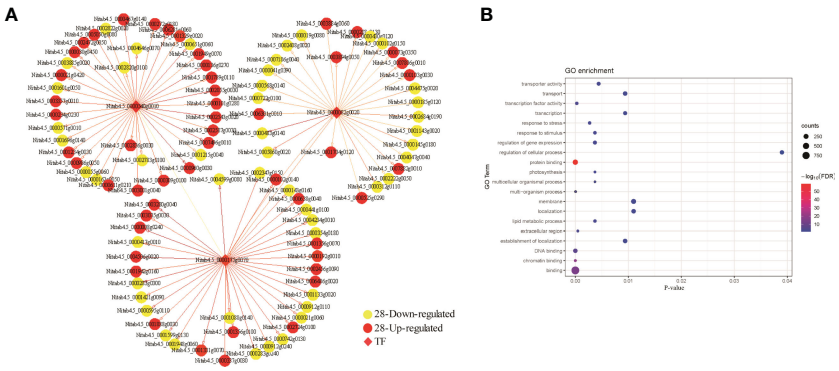


FIGURE 8
Prediction of TF regulatory networks using the co-expression correlation network of three TFs in the blue module. **(A)** The correlation network of genes related to regulation of the three TFs. The red representing up-regulated genes and the yellow representing down-regulated genes between M28 and K326 before and after drought treatment. The direction of the arrow indicates the regulatory relationship. The genes with weights > 0.1 are visualized by Cytoscape. **(B)** GO term enrichment analyses of down- and up-regulated genes related to regulation of the three TFs.

At the transcription levels, down-regulated genes in M28 were mainly involved in some fundamental biological processes, including cellular and biological processes, gene transcription and the regulation of RNA biosynthetic or metabolic processes, therefore plants with the down-regulation of these genes can save more energy to cope with drought stress for better survival; while up-regulated genes in M28 had functions overrepresented in heat or temperature stimuli (Figure 3D) or reproductive events, such as pollination, pollen-pistil interaction, recognition of pollen and single/multi-organism reproductive processes (Figures 3D, E). Those up-regulated genes either help the plants alleviate impairment of drought stress or promote transition from the vegetative stage to the reproductive stage, leading to rapidly complete the whole lifecycle and produce seeds, and facilitating better development and survival of plants under drought conditions. For instance, *NtEXGT* gene, encoding xyloglucan endotransglucosylases/hydrolases (XTHs) in *Nicotiana tabacum* L., has been reported to be involved in abiotic stress response through ABA-dependent signaling pathway (Kuluev et al., 2017). It was slightly induced by drought stress in *Nicotiana tabacum* L. (Kuluev et al., 2017), by contrast, we found that it was down-regulated in K326 but almost no changes in M28 in different time points after drought treatment. The contrasting change in expression of this gene is possibly caused by variations in cis-regulatory elements.

Furthermore, metabolic analyses provided evidence showing that enhanced resistance of M28 to drought stress was ABA signaling pathway-dependent. We detected that Diffexp metabolites were involved in valine biosynthesis, citrate cycle (TCA cycle), carotenoid biosynthesis KEGG pathway (Figures 4C, B). Those secondary metabolites are necessary for ABA biosynthesis (Xie et al., 2022) (Figure 6). The plant hormone abscisic acid (ABA) is the key active regulator functioning in plant stress response and tolerance through the regulation of stress-responsive genes or stomatal movement and modulating ROS homeostasis (Smyk-Randall and Brown, 1987; Fujita et al., 2011; Nakashima and Yamaguchi-Shinozaki, 2013; Dong et al., 2021). Transcriptome and metabolome integrative analyses linked DEGs with the Diffexp metabolites. For instance, drought induced NCEDs, the key enzyme catalyzing Zeaxanthin to form Xanthoxin during ABA synthesis pathway, and *Nitab4.5_0000287g0290.1* and *Nitab4.5_0000986g0020.1*, key enzymes catalyzing ABA to form 8'-hydroxy-ABA during ABA metabolic pathway, mitigated impairment of drought stress through affecting ABA biosynthesis and metabolic pathway (Figure 6C). In addition, Nitrogen_/Alanine_/Arginine_/Pyruvate_metabolism pathways involved in drought responses were more enriched in M28 than K326. Pyruvate has been found to promote stomatal closure through inducing ROS production in response to drought stress, thus regulating stomatal motility to reduce transpiration rate and avoid water loss (Shen et al., 2017). Alanine accumulation acts as a generic stress response molecule to help mitigate multiple stress factor induce damages including drought, thereby facilitating plants to survive during stress responses (Parthasarathy et al., 2019). Arginine serves as precursor for nitric oxide (NO) and polyamines, thereby involving in biotic and abiotic responses in plants (Winter et al., 2015).

TFs are key regulators, acting individually or through regulatory networks, responsible for adaptive responses to abiotic stresses (Golldack et al., 2014; Manna et al., 2021). *MYB* TFs, which can be induced by drought stress, play vital roles in plants responding to drought stress, including maintaining cellular or organ structures and functions, adjusting stomatal movement and the regulation of secondary metabolisms (Dubos et al., 2010; Shin et al., 2011; Li et al., 2019a). *TabHLH1* was found to function in drought and salt stress through regulating expression of genes involving in ABA signaling pathway (Yang et al., 2016). Overexpression of *TaSNAC8-6A*, a drought responsive gene, and *TaABL1* can facilitate drought tolerance in transgenic *Arabidopsis* or wheat (Xu et al., 2014; Mao et al., 2020). Involvement of overexpressed *GhWRKY17* in enhancing drought tolerance is mediated by ABA signaling pathway and control of reactive oxygen species (ROS) generation in transgenic *Nicotiana benthamiana* (Yan et al., 2014). Through regulatory network analyses, we found that drought induced TFs (*Nitab4.5_0000175g007*, *bHLH*; *Nitab4.5_0000540g0010*, *C3H*; *Nitab4.5_0000082g0020*, *CCAAT*) can regulate expression of genes responsible for ABA biosynthesis (Figure 7D), thereby involving in drought responses in tobacco. It has been reported that *bHLH* is involved in stress-response and iron homeostasis in different plants (Wang et al., 2015; Qiu et al., 2016; Khan et al., 2018; Wang et al., 2018; Kobayashi et al., 2019).

Conclusion

Our study provides evidence showing that drought tolerance of M28 can be achieved at multiple levels. At biochemical and physiological levels, it elevates POD activity, net photosynthesis rate along with reducing H2O2 and MDA accumulation, decrease of relative conductivity, stomatal conductance and transpiration rate; at transcriptional and metabolic levels, it exhibits differential gene expression and metabolite changes directly and indirectly involved in drought responses, thereby facilitating plants to adapt to drought stress.

Data availability statement

The datasets presented in this study can be found in online repositories. The names of the repository/repositories and accession number(s) can be found in the article/Supplementary Material.

Author contributions

WZ and RH conceived the study. ZHe analyzed the data. YL, PY, CY, RH, ZHu and JY performed the experiments. XC and QW assisted data analyses. BG edited the manuscript. ZHe and WZ wrote the manuscript with contribution from all authors. All authors contributed to the article and approved the submitted version.

Funding

This work was supported by grants from the National Natural Science Foundation of China (32070561); The Natural Science Foundation of Jiangsu Province (BK20210383); The Key Science and Technology Program of Hunan Provincial Tobacco Corporation (17-18Aa05, HN2021KJ04 and HN2021KJ02).

Acknowledgments

We thank the Bioinformatic Center in Nanjing Agricultural University for providing facilities to assist sequencing data analyses.

Conflict of interest

Author PY was employed by company Hu'nan Tobacco Company Changde Company, Changde, Hunan, China.

The remaining authors declare that the research was conducted in the absence of any commercial or financial relationships that could be construed as a potential conflict of interest.

Publisher's note

All claims expressed in this article are solely those of the authors and do not necessarily represent those of their affiliated organizations, or those of the publisher, the editors and the reviewers. Any product that may be evaluated in this article, or claim that may be made by its manufacturer, is not guaranteed or endorsed by the publisher.

Supplementary material

The Supplementary Material for this article can be found online at: https://www.frontiersin.org/articles/10.3389/fpls.2022.1067076/full#supplementary-material

SUPPLEMENTARY TABLE S3
Down-regulated gene list after drought.

SUPPLEMENTARY TABLE S4
Up-regulated gene list after drought.

SUPPLEMENTARY TABLE S5
Down-regulated gene list in K326 after drought.

SUPPLEMENTARY TABLE S6
Down-regulated gene list in M28 after drought.

SUPPLEMENTARY TABLE S7
Pathways shared between DEGs and DiffExp metabolites.

References

Abid, M., Ali, S., Qi, L. K., Zahoor, R., Tian, Z., Jiang, D., et al. (2018). Physiological and biochemical changes during drought and recovery periods at tillering and jointing stages in wheat (Triticum aestivum l.). *Sci. Rep.* 8 (1), 1–15. doi: 10.1038/s41598-018-21441-7

Aprile, A., Mastrangelo, A. M., De Leonardis, A. M., Galiba, G., Roncaglia, E., Ferrari, F., et al. (2009). Transcriptional profiling in response to terminal drought stress reveals differential responses along the wheat genome. *BMC Genomics* 10 (1), 1–18. doi: 10.1186/1471-2164-10-279

Bhadouriya, S. L., Mehrotra, S., Basantani, M. K., Loake, G. J., and Mehrotra, R. (2021). Role of chromatin architecture in plant stress responses: An update. *Front. Plant Sci.* 11. doi: 10.3389/fpls.2020.603380

Boba, A., Kostyn, K., Kozak, B., Wojtasik, W., Preisner, M., Prescha, A., et al. (2020). Fusarium oxysporum infection activates the plastidial branch of the terpenoid biosynthesis pathway in flax, leading to increased ABA synthesis. *Planta* 251 (2), 1–14. doi: 10.1007/s00425-020-03339-9

Bolger, A. M., Lohse, M., and Usadel, B. (2014). Trimmomatic: A flexible trimmer for Illumina sequence data. *Bioinformatics* 30, 2114–20. doi: 10.1093/bioinformatics/btu170

Bu, D., Luo, H., Huo, P., et al. (2021). KOBAS-i: Intelligent prioritization and exploratory visualization of biological functions for gene enrichment analysis. *Nucleic Acids Res.* 49(W1), W317–W325. doi: 10.1093/nar/gkab447

Cao, L., Lu, X., Zhang, P., Ku, L., Wang, G., Yuan, Z., et al. (2018). Regulatory networks of gene expression in maize (Zea mays) under drought stress and re-watering. *bioRxiv* 2018, 361964. doi: 10.1007/s00438-021-01820-y

Capell, T., Bassie, L., and Christou, P. (2004). Modulation of the polyamine biosynthetic pathway in transgenic rice confers tolerance to drought stress. *Proc. Natl. Acad. Sci. United States America* 101 (26), 9909–9914. doi: 10.1073/pnas.0306974101

Chang, Y. N., Zhu, C., Jiang, J., Zhang, H., Zhu, J. K., and Duan, C. G. (2020). Epigenetic regulation in plant abiotic stress responses. *J. Integr. Plant Biol.* 62 (5), 563–580. doi: 10.1111/jipb.12901

Chen, Z., Xu, J., Wang, F., Wang, L., and Xu, Z. (2019). Morpho-physiological and proteomic responses to water stress in two contrasting tobacco varieties. *Sci. Rep.* 9 (1), 1–15. doi: 10.1038/s41598-019-54995-1

Chung, P. J., Jung, H., Jeong, D. H., Ha, S. H., Choi, Y. D., and Kim, J. K. (2016). Transcriptome profiling of drought responsive noncoding RNAs and their target genes in rice. *BMC Genomics* 17 (1), 1–12. doi: 10.1186/s12864-016-2997-3

Cornic, G. (2000). Drought stress inhibits photosynthesis by decreasing stomatal aperture - Not by affecting ATP synthesis. *Trends Plant Sci.* 5 (5), 187–188. doi: 10.1016/S1360-1385(00)01625-3

Couchoud, M., Der, C., Girodet, S., Vernoud, V., Prudent, M., and Leborgne-Castel, N. (2019). Drought stress stimulates endocytosis and modifies membrane lipid order of rhizodermal cells of medicago truncatula in a genotype-dependent manner. *BMC Plant Biol.* 19 (1), 1–14. doi: 10.1186/s12870-019-1814-y

Covarrubias, A. A., and Reyes, J. L. (2010). Post-transcriptional gene regulation of salinity and drought responses by plant microRNAs. *Plant Cell Environ.* 33 (4), 481–489. doi: 10.1111/j.1365-3040.2009.02048.x

Cruz de Carvalho, M. H. (2008). Drought stress and reactive oxygen species: Production, scavenging and signaling. *Plant Signaling Behav.* 3 (3), 156–165. doi: 10.4161/psb.3.3.5536

Cui, G., Zhang, Y., Zhang, W., Lang, D., Zhang, X., Li, Z., et al. (2019). Response of carbon and nitrogen metabolism and secondary metabolites to drought stress and salt stress in plants. *J. Plant Biol.* 62 (6), 387–399. doi: 10.1007/s12374-019-0257-1

Degenkolbe, T., Do, P. T., Zuther, E., Repsilber, D., Walther, D., Hincha, D. K., et al. (2009). Expression profiling of rice cultivars differing in their tolerance to long-term drought stress. *Plant Mol. Biol.* 69 (1-2), 133–153. doi: 10.1007/s11103-008-9412-7

Dong, T., Yin, X., Wang, H., Lu, P., Liu, X., Gong, C., et al. (2021). ABA-INDUCED expression 1 is involved in ABA-inhibited primary root elongation *via* modulating ROS homeostasis in arabidopsis. *Plant Sci.* 304, 110821. doi: 10.1016/j.plantsci.2021.110821

Dubos, C., Stracke, R., Grotewold, E., Weisshaar, B., Martin, C., and Lepiniec, L. (2010). MYB transcription factors in arabidopsis. *Trends Plant Sci.* 15 (10), 573–581. doi: 10.1016/j.tplants.2010.06.005

Elleuch, H., Belbahri, L., Boetti, H., David, H., Thomassetb, B., and David, A. (2001). Rice salT promoter is activated in papaver somniferum and nicotiana tabacum transgenic cells in the absence of exogenous ABA. *Enzyme Microbial. Technol.* 28 (1), 106–113. doi: 10.1016/s0141-0229(00)00286-6

Farooq, M., Wahid, A., Kobayashi, N., Fujita, D., and Basra, S. M. A. (2009). Plant drought stress: Effects, mechanisms and management. *Agron. Sustain. Dev.* 29 (1), 185–212. doi: 10.1051/AGRO:2008021

Fathi, A., and Barari, D. (2016). Effect of drought stress and its mechanism in plants. *Int. J. Life Sci.* 10 (1), 1–6. doi: 10.1016/j.plaphy.2013.08.005

Fujita, Y., Fujita, M., Shinozaki, K., and Yamaguchi-Shinozaki, K. (2011). ABA-mediated transcriptional regulation in response to osmotic stress in plants. *J. Plant Res.* 124 (4), 509–525. doi: 10.1007/s10265-011-0412-3

Golldack, D., Li, C., Mohan, H., and Probst, N. (2014). Tolerance to drought and salt stress in plants: Unraveling the signaling networks. *Front. Plant Sci.* 5. doi: 10.3389/fpls.2014.00151

Gong, P., Zhang, J., Li, H., Yang, C., Zhang, C., Zhang, X., et al. (2010). Transcriptional profiles of drought-responsive genes in modulating transcription signal transduction, and biochemical pathways in tomato. *J. Exp. Bot.* 61 (13), 3563–3575. doi: 10.1093/jxb/erq167

Greenham, K., Guadagno, C. R., Gehan, M. A., Mockler, T. C., Weinig, C., Ewers, B. E., et al. (2017). Temporal network analysis identifies early physiological and transcriptomic indicators of mild drought in brassica rapa. *eLife* 6, e29655. doi: 10.7554/eLife.29655

Guo, C., Ge, X., and Ma, H. (2013). The rice OsDIL gene plays a role in drought tolerance at vegetative and reproductive stages. *Plant Mol. Biol.* 82 (3), 239–253. doi: 10.1007/s11103-013-0057-9

Gupta, A., Hisano, H., Hojo, Y., Matsuura, T., Ikeda, Y., Mori, I. C., et al. (2017). Global profiling of phytohormone dynamics during combined drought and pathogen stress in arabidopsis thaliana reveals ABA and JA as major regulators. *Sci. Rep.* 7 (1), 1–13. doi: 10.1038/s41598-017-03907-2

Harb, A., Krishnan, A., Ambavaram, M. M., and Pereira, A. (2010). Molecular and physiological analysis of drought stress in arabidopsis reveals early responses leading to acclimation in plant growth. *Plant Physiol.* 154 (3), 1254–1271. doi: 10.1104/pp.110.161752

Huang, L., Wang, Y., Wang, W., Zhao, X., Qin, Q., Sun, F., et al. (2018). Characterization of transcription factor gene OsDRAP1 conferring drought tolerance in rice. *Front. Plant Sci.* 9. doi: 10.3389/fpls.2018.00094

Hu, Z., Fan, J., Xie, Y., Amombo, E., Liu, A., Gitau, M. M., et al. (2016). Comparative photosynthetic and metabolic analyses reveal mechanism of improved cold stress tolerance in bermudagrass by exogenous melatonin. *Plant Physiol. Biochem.* 100, 94–104. doi: 10.1016/j.plaphy.2016.01.008

Hu, T. W., Mao, Z., Ong, M., Tong, E., Tao, M., Jiang, H., et al. (2006). China At the crossroads: The economics of tobacco and health. *Tobacco control* 15 Suppl 1, i37–i41. doi: 10.1136/tc.2005.014621

Hura, T., Hura, K., and Ostrowska, A. (2022). Drought-stress induced physiological and molecular changes in plants. *Int. J. Mol. Sci.* 23 (9), 4698. doi: 10.3390/ijms23094698

Hussain, Q., Asim, M., Zhang, R., Khan, R., Farooq, S., and Wu, J. (2021). Transcription factors interact with ABA through gene expression and signaling pathways to mitigate drought and salinity stress. *Biomolecules* 11 (8), 1159. doi: 10.3390/biom11081159

Hussain, H. A., Hussain, S., Khaliq, A., Ashraf, U., Anjum, S. A., Men, S., et al. (2018). Chilling and drought stresses in crop plants: Implications, cross talk, and potential management opportunities. *Front. Plant Sci.* 9. doi: 10.3389/fpls.2018.00393

Huynh-Thu, V. A., and Geurts, P. (2018). dynGENIE3: dynamical GENIE3 for the inference of gene networks from time series expression data. *Scientific reports* 8 (1), 1–12. doi: 10.1038/s41598-018-21715-0.

Jamshidi Goharrizi, K., Amirmahani, F., and Salehi, F. (2020). Assessment of changes in physiological and biochemical traits in four pistachio rootstocks under drought, salinity and drought + salinity stresses. *Physiol. plant.* 168 (4), 973–989. doi: 10.1111/ppl.13042

Janiak, A., Kwasniewski, M., and Szarejko, I. (2016). Gene expression regulation in roots under drought. *J. Exp. Bot.* 67 (4), 1003–1014. doi: 10.1093/jxb/erv512

Joshi, R., Wani, S. H., Singh, B., Bohra, A., Dar, Z. A., Lone, A. A., et al. (2016). Transcription factors and plants response to drought stress: Current understanding and future directions. *Front. Plant Sci.* 7. doi: 10.3389/fpls.2016.01029

Kapoor, D., Bhardwaj, S., Landi, M., Sharma, A., Ramakrishnan, M., and Sharma, A. (2020). The impact of drought in plant metabolism: How to exploit tolerance mechanisms to increase crop production. *Appl. Sci.* 10 (16), 5692. doi: 10.1111/pce.12417

Karaba, A., Dixit, S., Greco, R., Aharoni, A., Trijatmiko, K. R., Marsch-Martinez, N., et al. (2007). Improvement of water use efficiency in rice by expression of HARDY, an arabidopsis drought and salt tolerance gene. *Proc. Natl. Acad. Sci. U. S. A.* 104 (39), 15270–15275. doi: 10.1073/pnas.0707294104

Khan, S. A., Li, M. Z., Wang, S. M., and Yin, H. J. (2018). Revisiting the role of plant transcription factors in the battle against abiotic stress. *Int. J. Mol. Sci.* 19 (6), 1634. doi: 10.3390/ijms19061634

Kim, J. M., Sasaki, T., Ueda, M., Sako, K., and Seki, M. (2015). Chromatin changes in response to drought, salinity, heat, and cold stresses in plants. *Front. Plant Sci.* 6. doi: 10.3389/fpls.2015.00114

Kim, J. M., To, T. K., Nishioka, T., and Seki, M. (2010). Chromatin regulation functions in plant abiotic stress responses. *Plant Cell Environ.* 33 (4), 604–611. doi: 10.1111/j.1365-3040.2009.02076.x

Kobayashi, T., Ozu, A., Kobayashi, S., An, G., Jeon, J. S., and Nishizawa, N. K. (2019). OsbHLH058 and OsbHLH059 transcription factors positively regulate iron deficiency responses in rice. *Plant Mol. Biol.* 101 (4-5), 471–486. doi: 10.1007/s11103-019-00917-8

Krasensky, J., and Jonak, C. (2012). Drought, salt, and temperature stress-induced metabolic rearrangements and regulatory networks. *J. Exp. Bot.* 63 (4), 1593–1608. doi: 10.1093/jxb/err460

Kroll, K. W., Mokaram, N. E., and Pelletier, A. R.. (2014). Quality Control for RNA-Seq (QuaCRS): An Integrated Quality Control Pipeline. *Cancer Inform* 13, 7–14. doi: 10.4137/CIN.S14022

Kuluev, B., Mikhaylova, E., Berezhneva, Z., Nikonorov, Y., Postrigan, B., Kudoyarova, G., et al. (2017). Expression profiles and hormonal regulation of tobacco NtEXGT gene and its involvement in abiotic stress response. *Plant Physiol. Biochem. PPB* 111, 203–215. doi: 10.1016/j.plaphy.2016.12.005

Kumar, R. (2014). Role of microRNAs in biotic and abiotic stress responses in crop plants. *Appl. Biochem. Biotechnol.* 174 (1), 93–115. doi: 10.1007/s12010-014-0914-2

Kumar, M., Kumar Patel, M., Kumar, N., Bajpai, A. B., and Siddique, K. H. M. (2021). Metabolomics and molecular approaches reveal drought stress tolerance in plants. *Int. J. Mol. Sci.* 22 (17), 9108. doi: 10.3390/ijms22179108

Kumar, M., Yusuf, M. A., Nigam, M., and Kumar, M. (2018). An update on genetic modification of chickpea for increased yield and stress tolerance. *Mol. Biotechnol.* 60 (8), 651–663. doi: 10.1007/s12033-018-0096-1

Langfelder, P., and Horvath, S. (2008). WGCNA: An R package for weighted correlation network analysis. *BMC bioinformatics*, 9(1), 1–13. doi: 10.1186/1471-2105-9-559.

Laxa, M., Liebthal, M., Telman, W., Chibani, K., and Dietz, K. J. (2019). The role of the plant antioxidant system in drought tolerance. *Antioxidants* 8 (4), 94. doi: 10.3390/antiox8040094

Li, J., Han, G., Sun, C., and Sui, N. (2019a). Research advances of MYB transcription factors in plant stress resistance and breeding. *Plant Signaling Behav.* 14 (8), 1613131. doi: 10.1080/15592324.2019.1613131

Li, S., He, X., Gao, Y., Zhou, C., Chiang, V. L., and Li, W. (2021). Histone acetylation changes in plant response to drought stress. *Genes* 12 (9), 1409. doi: 10.3390/genes12091409

Li, S., Lin, Y. J., Wang, P., Zhang, B., Li, M., Chen, S., et al. (2019b). The AREB1 transcription factor influences histone acetylation to regulate drought responses and tolerance in populus trichocarpa. *Plant Cell* 31 (3), 663–686. doi: 10.1105/tpc.18.00437

Li, J., Li, Y., Yin, Z., Jiang, J., Zhang, M., Guo, X., et al. (2017). OsASR5 enhances drought tolerance through a stomatal closure pathway associated with ABA and H2 O2 signalling in rice. *Plant Biotechnol. J.* 15 (2), 183–196. doi: 10.1111/pbi.12601

Liu, J., and He, Z. (2020). Small DNA methylation, big player in plant abiotic stress responses and memory. *Front. Plant Sci.* 11. doi: 10.3389/fpls.2020.595603

Liu, Y., Li, P., Xu, G. C., Xiao, L., Ren, Z. P., and Li, Z. B. (2017). Growth, morphological, and physiological responses to drought stress in bothriochloa ischaemum. *Front. Plant Sci.* 8. doi: 10.3389/fpls.2017.00230

Liu, Z., Qin, J., Tian, X., Xu, S., Wang, Y., Li, H., et al. (2018). Global profiling of alternative splicing landscape responsive to drought, heat and their combination in wheat (Triticum aestivum l.). *Plant Biotechnol. J.* 16 (3), 714–726. doi: 10.1111/pbi.12822

Manna, M., Thakur, T., Chirom, O., Mandlik, R., Deshmukh, R., and Salvi, P. (2021). Transcription factors as key molecular target to strengthen the drought stress tolerance in plants. *Physiol. plant.* 172 (2), 847–868. doi: 10.1111/ppl.13268

Mao, H., Li, S., Wang, Z., Cheng, X., Li, F., Mei, F., et al. (2020). Regulatory changes in TaSNAC8-6A are associated with drought tolerance in wheat seedlings. *Plant Biotechnol. J.* 18 (4), 1078–1092. doi: 10.1111/pbi.13277

Michaletti, A., Naghavi, M. R., Toorchi, M., Zolla, L., and Rinalducci, S. (2018). Metabolomics and proteomics reveal drought-stress responses of leaf tissues from spring-wheat. *Sci. Rep.* 8 (1), 5710. doi: 10.1038/s41598-018-24012-y

Moumeni, A., Satoh, K., Venuprasad, R., Serraj, R., Kumar, A., Leung, H., et al. (2015). Transcriptional profiling of the leaves of near-isogenic rice lines with contrasting drought tolerance at the reproductive stage in response to water deficit. *BMC Genomics* 16 (1), 1–20. doi: 10.1186/s12864-015-2335-1

Mude, L. N., Mondam, M., Gujjula, V., Jinka, S., Pinjari, O. B., Yellodu Adi Reddy, N., et al. (2020). Morpho-physiological and biochemical changes in finger millet [Eleusine coracana (L.) gaertn.] under drought stress. *Physiol. Mol. Biol. Plants* 26 (11), 2151–2171. doi: 10.1007/s12298-020-00909-9

Nakashima, K., and Yamaguchi-Shinozaki, K. (2013). ABA signaling in stress-response and seed development. *Plant Cell Rep.* 32 (7), 959–970. doi: 10.1007/s00299-013-1418-1

O'Malley, R. C., Huang, S. C., Song, L., Lewsey, M. G., Bartlett, A., Nery, J. R., et al. (2016). Cistrome and epicistrome features shape the regulatory DNA landscape. *Cell* 165 (5), 1280–1292. doi: 10.1016/j.cell.2016.08.063

Pal, M., Tajti, J., Szalai, G., Peeva, V., Vegh, B., and Janda, T. (2018). Interaction of polyamines, abscisic acid and proline under osmotic stress in the leaves of wheat plants. *Sci. Rep.* 8 (1), 1–12. doi: 10.1038/s41598-018-31297-6

Pang, Z., Chong, J., Zhou, G., David, M., Le, C., Michel, B., et al. (2021). MetaboAnalyst 5.0: Narrowing the gap between raw spectra and functional insights. *Nucleic acids research* 49(W1), W388–96. doi: 10.1093/nar/gkab382.

Parmar, R., Seth, R., Singh, P., Singh, G., Kumar, S., and Sharma, R. K. (2019). Transcriptional profiling of contrasting genotypes revealed key candidates and nucleotide variations for drought dissection in camellia sinensis (L.) o. kuntze. *Sci. Rep.* 9 (1), 1–12. doi: 10.1038/s41598-019-43925-w

Parthasarathy, A., Savka, M. A., and Hudson, A. O. (2019). The synthesis and role of beta-alanine in plants. *Front. Plant Sci.* 10. doi: 10.3389/fpls.2019.00921

Pavlovic, I., Petrik, I., Tarkowska, D., Lepedus, H., Vujcic Bok, V., Radic Brkanac, S., et al. (2018). Correlations between phytohormones and drought tolerance in selected brassica crops: Chinese cabbage, white cabbage and kale. *Int. J. Mol. Sci.* 19 (10), 2866. doi: 10.3390/ijms19102866

Qiu, X. M., Sun, Y. Y., Ye, X. Y., and Li, Z. G. (2019). Signaling role of glutamate in plants. *Front. Plant Sci.* 10. doi: 10.3389/fpls.2019.01743

Qiu, Z., Wang, X., Gao, J., Guo, Y., Huang, Z., and Du, Y. (2016). The tomato hoffman's anthocyaninless gene encodes a bHLH transcription factor involved in anthocyanin biosynthesis that is developmentally regulated and induced by low temperatures. *PloS One* 11 (3), e0151067. doi: 10.1371/journal.pone.0151067

Quan, R., Shang, M., Zhang, H., Zhao, Y., and Zhang, J. (2004). Engineering of enhanced glycine betaine synthesis improves drought tolerance in maize. *Plant Biotechnol. J.* 2 (6), 477–486. doi: 10.1111/j.1467-7652.2004.00093.x

Rabara, R. C., Tripathi, P., Reese, R. N., Rushton, D. L., Alexander, D., Timko, M. P., et al. (2015). Tobacco drought stress responses reveal new targets for solanaceae crop improvement. *BMC Genomics* 16 (1), 1–23. doi: 10.1186/s12864-015-1575-4

Rabara, R. C., Tripathi, P., and Rushton, P. J. (2017). Comparative metabolome profile between tobacco and soybean grown under water-stressed conditions. *BioMed. Res. Int.* 2017, 3065251. doi: 10.1155/2017/3065251

Ramakrishna, A., and Ravishankar, G. A. (2011). Influence of abiotic stress signals on secondary metabolites in plants. *Plant Signaling Behav.* 6 (11), 1720–1731. doi: 10.4161/psb.6.11.17613

Rizhsky, L., Liang, H., and Mittler, R. (2002). The combined effect of drought stress and heat shock on gene expression in tobacco. *Plant Physiol.* 130 (3), 1143–1151. doi: 10.1104/pp.006858

Roca Paixao, J. F., Gillet, F. X., Ribeiro, T. P., Bournaud, C., Lourenco-Tessutti, I. T., Noriega, D. D., et al. (2019). Improved drought stress tolerance in arabidopsis by CRISPR/dCas9 fusion with a histone AcetylTransferase. *Sci. Rep.* 9 (1), 1–9. doi: 10.1038/s41598-019-44571-y

Romdhane, L., Radhouane, L., Farooq, M., Dal Cortivo, C., Panozzo, A., and Vamerali, T. (2020). Morphological and biochemical changes in maize under drought and salinity stresses in a semi-arid environment. *Plant Biosyst.* 154 (3), 396–404. doi: 10.1080/11263504.2019.1635221

Rushton, P. J., Bokowiec, M. T., Han, S., Zhang, H., Brannock, J. F., Chen, X., et al. (2008). Tobacco transcription factors: Novel insights into transcriptional regulation in the solanaceae. *Plant Physiol.* 147 (1), 280–295. doi: 10.1104/pp.107.114041

Sakuma, Y., Maruyama, K., Osakabe, Y., Qin, F., Seki, M., Shinozaki, K., et al. (2006). Functional analysis of an arabidopsis transcription factor, DREB2A, involved in drought-responsive gene expression. *Plant Cell* 18 (5), 1292–1309. doi: 10.1105/tpc.105.035881

Shen, J. L., Li, C. L., Wang, M., He, L. L., Lin, M. Y., Chen, D. H., et al. (2017). Mitochondrial pyruvate carrier 1 mediates abscisic acid-regulated stomatal closure and the drought response by affecting cellular pyruvate content in arabidopsis thaliana. *BMC Plant Biol.* 17 (1), 217. doi: 10.1186/s12870-017-1175-3

Shin, D., Moon, S. J., Han, S., Kim, B. G., Park, S. R., Lee, S. K., et al. (2011). Expression of StMYB1R-1, a novel potato single MYB-like domain transcription factor, increases drought tolerance. *Plant Physiol.* 155 (1), 421–432. doi: 10.1104/pp.110.163634

Shivhare, R., Asif, M. H., and Lata, C. (2020). Comparative transcriptome analysis reveals the genes and pathways involved in terminal drought tolerance in pearl millet. *Plant Mol. Biol.* 103 (6), 639–652. doi: 10.1007/s11103-020-01015-w

Smyk-Randall, E. M., and Brown, O. R. (1987). A reverse-phase high-performance liquid chromatography assay for dihydroxy-acid dehydratase. *Anal. Biochem.* 164 (2), 434–438. doi: 10.1016/0003-2697(87)90516-1

Song, J., Shang, L., Wang, X., Xing, Y., Xu, W., Zhang, Y., et al. (2021). MAPK11 regulates seed germination and ABA signaling in tomato by phosphorylating SnRKs. *J. Exp. Bot.* 72 (5), 1677–1690. doi: 10.1093/jxb/eraa564

Su, X., Wei, F., Huo, Y., and Xia, Z. (2017). Comparative physiological and molecular analyses of two contrasting flue-cured tobacco genotypes under progressive drought stress. *Front. Plant Sci.* 8. doi: 10.3389/fpls.2017.00827

Takahashi, F., Kuromori, T., Sato, H., and Shinozaki, K. (2018). Regulatory gene networks in drought stress responses and resistance in plants. *Adv. Exp. Med. Biol.* 1081, 189–214. doi: 10.1007/978-981-13-1244-1_11

Tang, Y., Bao, X., Zhi, Y., Wu, Q., Guo, Y., Yin, X., et al. (2019). Overexpression of a MYB family gene, OsMYB6, increases drought and salinity stress tolerance in transgenic rice. *Front. Plant Sci.* 10. doi: 10.3389/fpls.2019.00168

Tian, T., Liu, Y., Yan, H., et al. (2017). AgriGO v2. 0: aA GO analysis toolkit for the agricultural community, 2017 update. *Nucleic Acids Research* 45 (W1), W122–W129. doi: 10.1093/nar/gkx382.

Tiwari, S., Lata, C., Chauhan, P. S., Prasad, V., and Prasad, M. (2017). A functional genomic perspective on drought signalling and its crosstalk with phytohormone-mediated signalling pathways in plants. *Curr. Genomics* 18 (6), 469–482. doi: 10.2174/1389202918666170605083319

Varoquaux, N., Cole, B., Gao, C., Pierroz, G., Baker, C. R., Patel, D., et al. (2019). Transcriptomic analysis of field-droughted sorghum from seedling to maturity reveals biotic and metabolic responses. *Proc. Natl. Acad. Sci. United States America* 116 (52), 27124–27132. doi: 10.1073/pnas.1907500116

Varet, H., Brillet-Gueguen, L., Coppee, J. Y., and Dillies, M. A. (2016). SARTools: A DESeq2- and EdgeR-Based R Pipeline for Comprehensive Differential Analysis of RNA-Seq Data. *PLoS One* 11, e0157022 . doi: 10.1371/journal.pone.0157022.

Wang, J., Hu, Z., Zhao, T., Yang, Y., Chen, T., Yang, M., et al. (2015). Genome-wide analysis of bHLH transcription factor and involvement in the infection by yellow leaf curl virus in tomato (Solanum lycopersicum). *BMC Genomics* 16 (1), 1–14. doi: 10.1186/s12864-015-1249-2

Wang, L., Lee, M., Ye, B., and Yue, G. H. (2020). Genes, pathways and networks responding to drought stress in oil palm roots. *Sci. Rep.* 10 (1), 21303. doi: 10.1038/s41598-020-78297-z

Wang, P., Wang, H., Wang, Y., Ren, F., and Liu, W. (2018). Analysis of bHLH genes from foxtail millet (Setaria italica) and their potential relevance to drought stress. *PloS One* 13 (11), e0207344. doi: 10.1371/journal.pone.0207344

Weidong, Q., Hongping, C., Zuozhen, Y., Biaolin, H., Xiangdong, L., Bing, A., et al. (2020). Systematic characterization of long non-coding RNAs and their responses to drought stress in dongxiang wild rice. *Rice Sci.* 27 (1), 21–31. doi: 10.1016/j.rsci.2019.12.003

Winter, K., and Holtum, J. A.M. (2015). Cryptic crassulacean acid metabolism (CAM) in Jatropha curcas. *Functional Plant Biology*, 42(8), 711–717. doi: 10.1071/FP15021.

Xie, H., Bai, G., and Lu, P. (2022). Exogenous citric acid enhances drought tolerance in tobacco (Nicotiana tabacum). *Plant Biol.* 24 (2), 333–343. doi: 10.1111/plb.13371

Xu, D. B., Gao, S. Q., Ma, Y. Z., Xu, Z. S., Zhao, C. P., Tang, Y. M., et al. (2014). ABI-like transcription factor gene TaABL1 from wheat improves multiple abiotic stress tolerances in transgenic plants. *Funct. Integr. Genomics* 14 (4), 717–730. doi: 10.1007/s10142-014-0394-z

Xu, Z., Zhou, G., and Shimizu, H. (2010). Plant responses to drought and rewatering. *Plant Signaling Behav.* 5 (6), 649–654. doi: 10.4161/psb.5.6.11398

Yang, T., Yao, S., Hao, L., Zhao, Y., Lu, W., and Xiao, K. (2016). Wheat bHLH-type transcription factor gene TabHLH1 is crucial in mediating osmotic stresses tolerance through modulating largely the ABA-associated pathway. *Plant Cell Rep.* 35 (11), 2309–2323. doi: 10.1007/s00299-016-2036-5

Yang, H., Zhao, L., Zhao, S., Wang, J., and Shi, H. (2017). Biochemical and transcriptomic analyses of drought stress responses of LY1306 tobacco strain. *Sci. Rep.* 7 (1), 1–10. doi: 10.1038/s41598-017-17045-2

Yan, H., Jia, H., Chen, X., Hao, L., An, H., and Guo, X. (2014). The cotton WRKY transcription factor GhWRKY17 functions in drought and salt stress in transgenic nicotiana benthamiana through ABA signaling and the modulation of reactive oxygen species production. *Plant Cell Physiol.* 55 (12), 2060–2076. doi: 10.1093/pcp/pcu133

Yin, F., Qin, C., Gao, J., Liu, M., Luo, X., Zhang, W., et al. (2015). Genome-wide identification and analysis of drought-responsive genes and microRNAs in tobacco. *Int. J. Mol. Sci.* 16 (3), 5714–5740. doi: 10.3390/ijms16035714

Yuan, J., Li, J., Yang, Y., Tan, C., Zhu, Y., Hu, L., et al. (2018). Stress-responsive regulation of long non-coding RNA polyadenylation in oryza sativa. *Plant J. Cell Mol. Biol.* 93 (5), 814–827. doi: 10.1111/tpj.13804

Zenda, T., Liu, S., Wang, X., Liu, G., Jin, H., Dong, A., et al. (2019). Key maize drought-responsive genes and pathways revealed by comparative transcriptome and physiological analyses of contrasting inbred lines. *Int. J. Mol. Sci.* 20 (6), 1268. doi: 10.3390/ijms20061268

Zhang, M., Wang, L.-F., Zhang, K., Liu, F.-Z., and Wan, Y.-S. (2017). Drought-induced responses of organic osmolytes and proline metabolism during pre-flowering stage in leaves of peanut (Arachis hypogaea l.). *J. Integr. Agric.* 16 (10), 2197–2205. doi: 10.1016/S2095-3119(16)61515-0

frontiers | Frontiers in Plant Science

TYPE Original Research
PUBLISHED 24 January 2023
DOI 10.3389/fpls.2023.1065334

Check for updates

OPEN ACCESS

EDITED BY
Bhaskar Gupta,
Government General Degree College, Singur, India

REVIEWED BY
Sarika Jaiswal,
Indian Agricultural Statistics Research Institute, India
Xiangjin Wei,
State Key Laboratory of Rice Biology and Chinese National Center for Rice Improvement, China National Rice Research Institute, Chinese Academy of Agricultural Sciences (CAAS), China

*CORRESPONDENCE
Longzhi Han
hanlongzhi@caas.cn

SPECIALTY SECTION
This article was submitted to Plant Abiotic Stress, a section of the journal Frontiers in Plant Science

RECEIVED 09 October 2022
ACCEPTED 04 January 2023
PUBLISHED 24 January 2023

CITATION
Geng L, Zhang W, Zou T, Du Q, Ma X, Cui D, Han B, Zhang Q and Han L (2023) Integrating linkage mapping and comparative transcriptome analysis for discovering candidate genes associated with salt tolerance in rice. *Front. Plant Sci.* 14:1065334. doi: 10.3389/fpls.2023.1065334

COPYRIGHT
© 2023 Geng, Zhang, Zou, Du, Ma, Cui, Han, Zhang and Han. This is an open-access article distributed under the terms of the Creative Commons Attribution License (CC BY). The use, distribution or reproduction in other forums is permitted, provided the original author(s) and the copyright owner(s) are credited and that the original publication in this journal is cited, in accordance with accepted academic practice. No use, distribution or reproduction is permitted which does not comply with these terms.

Integrating linkage mapping and comparative transcriptome analysis for discovering candidate genes associated with salt tolerance in rice

Leiyue Geng[1,2,3], Wei Zhang[2,3], Tuo Zou[2,3], Qi Du[2,3], Xiaoding Ma[1], Di Cui[1], Bing Han[1], Qixing Zhang[2,3] and Longzhi Han[1]*

[1]Institute of Crop Sciences, Chinese Academy of Agricultural Sciences, Beijing, China, [2]Institute of Coastal Agriculture, Hebei Academy of Agriculture and Forestry Sciences, Tangshan, China, [3]Tangshan Key Laboratory of Rice Breeding, Tangshan, China

Salinity is one of the most widespread abiotic stresses affecting rice productivity worldwide. Understanding the genetic basis of salt tolerance is key for breeding salt-tolerant rice varieties. Numerous QTLs have been identified to help dissect rice salt-tolerance genetic mechanisms, yet only rare genes located in significant QTLs have been thoroughly studied or fine-mapped. Here, a combination of linkage mapping and transcriptome profiling analysis was used to identify salt tolerance-related functional candidate genes underlying stable QTLs. A recombinant inbred line (RIL) population derived from a cross between Jileng 1 (salt-sensitive) and Milyang 23 (salt-tolerant) was constructed. Subsequently, a high-density genetic map was constructed by using 2921 recombination bin markers developed from whole genome resequencing. A total of twelve QTLs controlling the standard evaluation score under salt stress were identified by linkage analysis and distributed on chromosomes 2, 3, 4, 6, 8 and 11. Notably, five QTL intervals were detected as environmentally stable QTLs in this study, and their functions were verified by comparative transcriptome analysis. By comparing the transcriptome profiles of the two parents and two bulks, we found 551 salt stress-specific differentially expressed genes. Among them, fifteen DEGs located in stable QTL intervals were considered promising candidate genes for salt tolerance. According to gene annotations, the gene *OsRCI2-8*(*Os06g0184800*) was the most promising, as it is known to be associated with salt stress, and its differential expression between the tolerant and sensitive RIL bulks highlights its important role in salt stress response pathways. Our findings provide five stable salt tolerance-related QTLs and one promising candidate gene, which will facilitate breeding for improved salt tolerance in rice varieties and promote the exploration of salt stress tolerance mechanisms in rice.

KEYWORDS

rice, salt stress, linkage mapping, RNA-Seq, candidate gene

Abbreviations: W2SES, Standard evaluating score with two and four weeks after salt treatment; W4SES, Standard evaluating score with two and four weeks after salt treatmen; RIL, Recombinant Inbred Lines; LG , Linkage Group; Chr, Chromosome; LOD, Logarithm of the odds; PVE, Phenotypic variation explained; QTL, Quantitative trait locus; SNP, Single nucleotide polymorphisms; DEG, Differentially expressed genes.

1 Introduction

Rice (*Oryza sativa* L.) is a premier staple food for more than half of the world's population, and soil salinity is a major abiotic stress hindering rice production because it reduces rice yield and limits agricultural land utilization (Munns and Tester, 2008). Rice is usually considered a salt-sensitive crop, and the normal growth of conventional cultivars is seriously affected when the soil salinity exceeds 6 dS/m (Kumar et al., 2013). Therefore, more salt tolerant cultivars are required. Genetic improvement is an economical and effective way to improve salt tolerance in rice (Qin et al., 2020). Salt tolerance in rice is a quantitative trait controlled by multiple genes with a complex genetic mechanism, and it is difficult to improve salt tolerance using traditional breeding methods (Liu et al., 2022). Modern molecular breeding strategies such as marker assisted-selection (MAS), transgene and gene editing can accelerate the process of selecting for salt-tolerant varieties and improve breeding efficiency (Chen et al., 2021). However, it is necessary to identify quantitative trait loci (QTLs) or clone the key genes controlling salt tolerance (Ganie et al., 2021).

Linkage mapping is a classical strategy that is powerful enough to dissect complex quantitative traits (Xu et al., 2017). Over the past two decades, remarkable efforts have been made to identify salt tolerance-related QTLs in rice (Jing and Zhang, 2017). Based on information from the Gramene database (https://archive.gramene.org/qtl/) and supplementary literature (Jing and Zhang, 2017), more than one thousand salt tolerance-related QTLs have been discovered and are evenly distributed on all 12 rice chromosomes. The dissection of the genetic basis of tolerance to salinity has provided useful information for understanding the possible mechanism of salt tolerance (Ganie et al., 2019).

Although salt-tolerant QTLs are numerous, only rare QTLs showing significant effects have been thoroughly studied or map-based cloned. For example, *qSKC-1* and *qSNC-7* are involved in regulating K^+/Na^+ homeostasis under salt stress and explain 48.5% and 40.1%, respectively, of the total phenotypic variance (Lin et al., 2004). Isolation of the *qSKC-1* gene by map-based cloning revealed that it encodes a member of the HKT-type transporter family (Ren et al., 2005). Subsequently, *DST*, which encodes a zinc-finger transcription factor that negatively regulates salt tolerance and controls stomatal closure by directly modulating genes related to H_2O_2 homeostasis, was isolated by mutant and map-based cloning (Huang et al., 2009b). *HST*, which encodes a B-type response regulator and negatively regulates salt tolerance, was cloned by MutMap (Takagi et al., 2015). *qSE3*, which encodes a K^+ transporter gene, *OsHAK21*, promotes seed germination and seedling establishment under salinity stress in rice (He et al., 2019). Compared to the number of mapped QTLs, the number of cloned genes is very small. There is a large gap between discovering salt-tolerant QTLs and effectively exploring functional salt-tolerant genes.

In our opinion, there are at least three reasons for this gap: (1) some QTLs, which were only identified in a single study with a minor LOD and contribution rate, may not be completely reliable and should be further validated. (2) The majority of reported QTLs are minor QTLs and may not be stably detected across multiple environments. It was difficult to identify functional genes by traditional map-based cloning. (3) Most of the reported QTLs have been identified based on low-density markers, such as SSRs and RFLPs, with large confidence intervals containing too many genes. These markers are not able to provide precise and complete information about the numbers and locations of the QTLs controlling salt tolerance. It is imperative to identify reliable major QTLs by combining ultra-high-density genetic maps and precise phenotypic data across multiple environments.

In the current paper, we utilized an ultra-high-density genetic map that could rapidly anchor major genes to improve the precision of QTL positioning and narrow the range of candidate genes. Moreover, we evaluated the salt tolerance of RILs across two environments and three years to obtain convincing results. As a result, we have attained a few stable and major QTL intervals controlling salt tolerance. However, the linkage mapping strategy does not usually provide an accurate way to distinguish candidate genes underlying the QTLs without further fine-mapping (Bohra et al., 2020). Positional cloning of QTLs may be an effective approach for the identification of genes underlying target QTLs, but this is still a laborious, time-consuming task (Takeda and Matsuoka, 2008). An alternative method is to screen target QTL intervals for physically proximate genes with annotations or gene ontologies reflecting the trait of interest. However, hundreds of candidate genes usually reside in target QTLs, and it is still very difficult to predict which of these genes is actually responsible for the functional polymorphism leading to trait differences.

RNA-Seq, which uses next-generation sequencing technology to profile transcriptomes and detect differentially expressed genes (DEGs), has been employed to characterize the responses of various plant species to environmental stresses (Urano et al., 2010). RNA-Seq analysis has shown high resolution, sensitivity, and reproducibility (Ozsolak and Milos, 2011). Recently, a strategy integrating linkage mapping and RNA-Seq was developed that can mutually verify functional chromosome regions or genes and can accurately identify the potential candidate genes residing in target QTLs. Through a platform combining QTL mapping and RNA-Seq analysis, four candidate genes were colocalized with QTLs for salt tolerance (Wang et al., 2017). In that paper, six candidate genes related to anaerobic germination tolerance in rice were revealed by combining QTL mapping and RNA-Seq (Yang et al., 2019). Kong et al. (2021) integrated GWAS, QTL, mapping and RNA-Seq to identify candidate genes for seed vigor in rice (*Oryza sativa* L.) and successfully predicted seven promising candidates associated with seed vigor. The combined use of linkage mapping with transcriptome profiling represents a practical solution to further refine the mapping resolution and identify potential candidate genes.

The identification of genes for quantitative traits is difficult when using any single approach due to the complex inheritance patterns of the traits and limited resolving power of the individual techniques. The aim of the present study was to identify promising candidate genes for salt tolerance in rice by combining genetic mapping and transcriptome profiling of bulked RILs with extreme phenotypes.

2 Materials and methods

2.1 Plant materials

An RIL population containing 253 lines was developed by crossing the salt-tolerant japonica cultivated variety Jileng 1 (P1) as the donor and the salt-sensitive indica cultivated variety Milyang 23 (P2) as the receptor using the single seed descent (SSD) method (Figure S1). The F_2 generation from Jileng 1×Milyang 23 was subjected to more than ten rounds of self-pollination to generate the RIL population.

Twenty of the most tolerant (T) and most sensitive (S) RILs of the Jileng 1×Milyang23 mapping population were identified based on the consistency and performance of SES across three years (2017, 2018 and 2019) to create the two bulks. Two bulks along with the parents were planted under salt stress and normal conditions and prepared for RNA-Seq analysis. The parents under salt stress and normal conditions were named SalP1, SalP2, NorP1, and NorP2, respectively. Similarly, the bulks under salt stress and normal conditions were named SalT, SalS, NorT and NorS, respectively.

2.2 Phenotyping for SES under saline

2.2.1 Experimental design

Phenotyping for SES was performed on stabilized F10 plants of 253 RILs along with two parents and five control varieties. During the middle of June to late July from 2017 to 2019, each independent trial was carried out under two environments (greenhouse and paddy field, Figure S2) on the salt identification base of HAAFS, Tangshan, China (39° 20'N, 118° 17'E), respectively. The seedlings were arranged by an α-lattice design (Table S2) and transplanted into two environments (greenhouse and paddy field) at the 3-leaf stage, with 2 to 4 independent replicates.

2.2.2 Field management and salt treatment

In the greenhouse, the transplantation area was 15 ×10 cm, with 10 holes in each plot in a single row and a single seedling in each hole. In the field, the transplantation area was 25×13 cm, with 30 holes in each plot in 6 rows and a single seedling in each hole. All seedlings were planted on the same day in conventionally tilled plots. Field management practices were performed according to the most followed agricultural practices of local farmers. The nitrogen (N), phosphorus (P), and potassium (K) fertilizers, in the form of urea, single superphosphate, and murate of potash, were applied at rates of 120, 60, and 60 kg/ha, respectively.

The salt stress condition consisted of applying underground brine to the established seedings starting at 7 days after transplanting, and the conductivity of the irrigated water layer was adjusted to 10 ds/m. The normal condition consisted of applying fresh water with a conductivity less than 1 ds/m. Five samples were collected every day to measure the conductivity of the irrigated water layer. If the conductivity of the irrigated water layer increased or decreased due to water evaporation or rainfall, fresh water or underground brine was adjusted.

2.2.3 Phenotypic evaluation

Salt injury symptoms, such as leaf drying and burning, stunted plant growth, reduced tillering, and leaf tip drying and withering, were perceptible in the stressed environments. The overall phenotypic performance of the population under salt stress was reflected by visual SES scores. After two and four weeks of salt stress, plants were scored following the standard protocol of IRRI with some modifications (Gregorio et al., 1997). W2SES and W4SES corresponded to standard evaluation score of two and four weeks after salt treatment, respectively. The SES of RILs under field conditions were assigned to five grades, 1, 3, 5, 7, and 9, corresponding to extremely tolerant, tolerant, moderately tolerant, moderately sensitive, and sensitive, respectively (Figure S3). The SES of RILs in the greenhouse was scored as 10 contiguous plants per line and calculated by the modified standard evaluation score in the plot as follows (Geng et al., 2020):

$$\mathrm{SES} = \sum(\text{number of salt-injured plants at all levels ñ salt evaluation score})/\text{total number of plants under investigation}$$

2.3 DNA and RNA extraction, genotyping by sequencing, and SNP identification

2.3.1 DNA extraction, sequencing and SNP calling

DNA was extracted from the two parents and 253 RILs at the F10 generation using the CTAB method and quantified using both a NanoDrop 2000c Spectrophotometer and 1% agarose gel electrophoresis. Sequencing was performed on the Illumina HiSeq2500 platform to generate 150 bp paired-end reads (Novogene Bioinformatics Technology Co., Ltd, China). In this study, Jileng 1 and Milyang 23 were sequenced to ~40× coverage, while RILs were sequenced to ~5× coverage. The primary sequencing datasets generated during the current study are available in the Genome Sequence Archive, https://ngdc.cncb.ac.cn/gsa (accession no. CRA008901).

Filtering of the low-quality data was performed to produce better-quality mapping. The clean data were then aligned to the Nipponbare reference genome (Os-Nipponbare-Reference-IRGSP-1.0, http://plants.ensembl.org/Oryza_sativa) (Kawahara et al., 2013) using BWA software (Li et al., 2009). The calculations of the sequencing coverage and depth were performed using Samtools (Li and Durbin, 2009). Then, the Genome Analysis Toolkit (GATK) (Mckenna et al., 2010) was used to detect the SNPs with default parameters. High-quality SNPs with a minimum sequencing depth of 3 for each RIL and a quality score of 30 were selected for further analysis.

2.3.2 RNA extraction, transcriptome profiling and qRT–PCR

Under both salt stress and normal conditions, after approximately 14 days of treatment, leaf samples of the parents and each line within the tolerant and sensitive bulks were collected and immediately stored in liquid nitrogen for RNA extraction. Total RNA was extracted using a Sigma Spectrum Plant Total RNA Kit (Sigma–Aldrich, St. Louis, MO, USA). RNA samples were reverse-transcribed to cDNA using the High-Capacity cDNA Archive Kit (Applied Biosystems, Foster City, California, USA). Sequencing libraries were constructed by

using the Illumina TruSeq Stranded RNA Kit (Illumina, San Diego, CA, USA) following the manufacturer's recommendations. The quality and quantity of the libraries were assessed with an Agilent 2100 Bioanalyzer and an ABI StepOnePlus Real-Time PCR System, respectively. Purified cDNA (20 ng/μl) from each line within the bulks was combined in equal amounts to prepare tolerant and sensitive bulk libraries. The cDNA libraries of 8 samples were sequenced on an Illumina HiSeq2500 platform strictly in accordance with standard procedures by Novogene Bioinformatics Technology Co., Ltd, China. The primary sequencing datasets generated during the current study are available Genome Sequence Archive, https://ngdc.cncb.ac.cn/gsa (accession no. CRA008748).

A total of fifteen genes from the list of possible candidate genes were selected (Table S6) for validation by quantitative real-time PCR (qRT–PCR) of leaf tissue. The gene sequences of the fifteen genes were downloaded from the Ensembl Plants database, and exonic sequences were used to design primers with Primer3 software (http://plants.ensembl.org/Oryza_sativa/). qRT–PCR with three independent biological replicates was performed using a LightCycler® 96 Real-Time PCR System (Roche Life Science, Germany) and SYBR Premix without ROX based on the manufacturer's protocol. The actin gene of rice (*Os03g0836000*) was employed as a suitable internal control gene. Transcript levels of nominated genes from three biological replicates were computed as $2^{-\Delta\Delta Ct.}$

2.3.3 Sequence analysis of candidate gene(Os06g0184800)

To characterize the sequence variation of candidate gene (*Os06g0184800*) in RILs, a re-sequencing data analysis was performed with the gene body and the 2 kb promoter of *Os06g0184800*. PCR-based sequencing was also conducted to confirm and estimate these markers between Jileng1 and Milyang23 (Primers list on file S1). Sequence alignments of candidate genes were performed with DNAman (https://dnaman.software.informer.com/).

2.4 Statistics and analysis

2.4.1 Genetic mapping and bin map construction

To reduce the false positive SNP genotypes in the population, consecutive SNPs were joined into one bin using a sliding window approach, and the genotype of each bin was determined based on the ratio between SNPs from the two parents (Huang et al., 2009a). The genetic linkage map was constructed based on bin markers using JoinMap4 software (Ooijen et al., 2006). In each linkage group, the maximum likelihood method was used to determine the final marker order according to the optimal AIC value, and the Kosambi mapping function was used to convert the recombination rate into genetic distance.

2.4.2 Statistical analysis of SES

As the standard evaluating score data were collected from two environments and three years, best linear unbiased predictors (BLUP) were used for the overall linkage analysis by the Lme4 package in the R program. The linear model for BLUP was $Y_{ijk}=L_k+E_i+R\ I_{ij}+(L\times E)_{ik}+e_{ijk}$, where Y_{ijk} is the observed phenotype for the k^{th} line in the j^{th} replicate of the i^{th} environment; L_k is the random effect of the k^{th} line; E_i is the random effect of the i_{th} year $I(E)_{ij}$ is the random effect of the j^{th} replicate in the i^{th} year; $(L\times E)_{ik}$ is the random interaction effect of the i^{th} year and the k^{th} line; and e_{ijk} is the error. The heritability estimates were calculated using variance components obtained by the BLUP linear model, according to the formula (Nyquist and Baker, 1991): $H^2(\%) = \sigma_g^2/(\sigma_g^2+ \sigma_{ge}^2/n + \sigma_e^2/nr) \times 100\%$, where σ_g^2 is the genotypic variance, σ_{ge}^2 is the variance for interactions of genotype with environment, σ_e^2 is the error variance, n is the number of environments, and r is the number of replications. The estimated values were used as the phenotype of subsequent QTL mapping. Pearson correlation coefficients between environments and years were calculated using the PROC CORR procedure in SAS 9.4 (SAS Institute Inc, 2015) based on the BLUPs of the traits across environments.

2.4.3 QTL mapping

The multi-interval mapping function (MQM) was employed to detect QTLs for standard evaluation scores based on their BLUP value using MapQTL6.0 (Van Ooijen, 2010). Locations, contribution rates and additive effects were estimated based on BLUP values of W2SES and W4SES. The LOD threshold was determined by applying 1000 permutation tests with 5% probability. The physical confidence interval of the QTL corresponded to a 2-LOD decrease from the peak LOD value, and the QTLs with overlapping candidate intervals were merged. To ascertain the stability of QTLs, we carried out QTL mapping analysis under both greenhouse and field environments. QTLs detected under all three conditions (greenhouse, field and BLUP) were considered to be stable QTLs and were used to carry out subsequent candidate gene prediction. Genes located in stable QTL intervals were annotated and analyzed based on the Rice Annotation Project (RAP) (http://rapdb.dna.affrc.go.jp) and Ensembl (http://plants.ensembl.org/Oryza_sativa) databases.

2.4.4 Transcriptome profiling by RNA-Seq

Gene expression profiles associated with salt stress were analyzed by performing a large-scale inspection of differentially expressed genes (DEGs). The raw RNA-Seq data of eight samples (SalP1, SalP2, NorP1, NorP2, SalT, SalS, NorT and NorS) were processed. Raw data was filtered by fastp (Chen and Gu, 2018). The clean data was mapped to the Nipponbare genome (Os-Nipponbare-Reference-IRGSP 1.0, http://plants.ensembl.org/Oryza_sativa/), and read counts were generated using HISAT (Kim et al., 2015) with default parameters. Read counts were normalized by edgeR with TMM method (Robinson et al., 2010). Normalized read counts were used as input data for differential expression analysis in the tolerant vs. susceptible plants. Differentially expressed genes (DEGs) between Jileng1 versus Milyang 23 and tolerant versus sensitive bulks under salt stress and normal conditions were identified. The DEGs of SalT vs. SalS, NorT vs. NorS, SalP1 vs. SalP2 and NorP1 vs. NorP2 were discriminated with |log2 fold change|≥1 and a false discovery rate (FDR) ≤ 0.05.

Subsequently, a more meaningful comparison for identifying the DEGs responding to salt stress would be to examine the DEGs between (SalP1 vs. SalP2) vs. (NorP1 vs. NorP2) and (SalT vs. SalS) vs. (NorT vs. NorS). Both constitutive and stress-induced gene expression could be important for identifying salt tolerance-related DEGs. Unshared DEGs between (SalP1 vs. SalP2) and (NorP1 vs.

NorP2) were both regarded as target DEGs responding to salt stress in the parents. Therefore, there were six classes of unshared DEGs that were considered: genes that were upregulIted (i, "SalOnly_up") or downregulated (ii, "SalOnly_down") only in the salt stress condition and unchanged in the normal condition; genes that were upregulated (iii, "NorOnly_up") or downregulated (iv, "NorOnly_down") only in normal conditions and unchanged in salt stress conditions; and DEGs that were detected under both salt stress and normal conditions but showed a difference in LFC (△LFC = LFC of the salt stress condition —LFC of the normal condition), (v, "△LFC > 1") or (vi, △LFC<-1). The types i, iv and v were regarded as upregulated DEGs specifically related to salt stress, and the types ii, iii and vi were considered downregulated DEGs specifically related to salt stress (Buti et al., 2019).

Finally, such a large number of the DEGs could not be complete responsible for the variation of salt stress, as the inevitable RNA-Seq detection errors. Hence, a similar analysis process with (SalR vs. SalS) vs. (NorR vs. NorS) was also taken to explore target DEGs related to salt stress as the background noise of differential expression. Those specifically induced target DEGs were compared between (SalT vs. SalS) vs. (NorT vs. NorS) and (SalP2 vs. P1) vs. (NorP2 vs. P1), and the shared target DEGs were subjected to enrichment analyses and overlaid with stable QTL confidence intervals according to sequence and QTL location information.

3 Results

3.1 Construction of the Bin map and assessment of quality and accuracy

For proper identification of SNPs between the two parents that could be used as molecular markers, deep resequencing was performed for Jileng 1 and Milyang 23. The effective sequencing depths of Jileng 1 and Milyang 23 reached 39.2-fold and 43.8-fold, respectively. Construction of the genetic linkage map for the RILs was carried out by resequencing the 253 RILs, resulting in approximately 16,694,396 to 41,400,184, reads per line with a mean value of 24,061,543. The overall effective depth of coverage of these RILs ranged from 6.19-fold to 14.68-fold, with an average depth of 8.94-fold. The overall effective coverage (1X) of these RILs ranged from 87.49% to 98.59%, with an average coverage of 93.58%.

A total of 1,860,935 high-quality, biallelic, homozygous SNP markers were detected between 'Jileng 1' and 'Milyang 23' and used to construct a bin map (Table 1; Supplementary Table S1). Using the sliding window approach (Huang et al., 2009a), a total of 3,061 bin markers were created, and the average physical interval of the adjacent bins was 121.94 kb. Each chromosome contained 255 bins on average, among which the maximum number of bins was 366 on chromosome 1, and the minimum number of bins was 181 on chromosome 9 (Table 1).

Bins instead of individual SNPs were used as markers to increase mapping efficiency. Finally, a high-density linkage map containing 2921 bin markers was constructed, and the total length of the genetic map was 1408.03 cM. The largest chromosome 1 had a genetic distance of 165.63 cM, and the smallest chromosome 10 had a genetic distance of 78.82 cM. All bin markers were evenly distributed across 12 chromosomes, and the average genetic distance was 0.48 cM; only one marker interval, located on chromosome 12, was larger than 5 cM Figure 1), and the calculation accuracy of the genetic recombination rate was high, which met the requirements of QTL mapping.

To evaluate the power and accuracy of this genetic map for detecting loci related to a highly heritable trait, plant height, heading date and grain width were subjected to QTL analysis in this RIL population. The QTL *qPH1-1*, whose peak encompassed the cloned gene *SD1 (Os01g0883800)* (Spielmeyer et al., 2002), was detected on chromosome 1 at position 38.41 Mb with a high LOD value of 15.16

TABLE 1 Characteristics of the high-density genetic map based on bin markers.

Chromosome	Bin number	Bin average length(kb)	LG Length(cM)	Average gap(cM)	Max gap(cM)
1	349(366) [a]	118.23	165.63	0.47	2.36
2	297(304)	118.21	129.4	0.44	1.76
3	286(290)	125.56	157.38	0.55	3.02
4	260(275)	129.10	123.2	0.47	2.59
5	202(213)	140.65	116.44	0.58	2.79
6	246(261)	119.73	125.74	0.51	4.97
7	240(255)	116.46	96.62	0.40	2.91
8	230(250)	113.77	123.04	0.53	3.7
9	168(181)	127.14	79.51	0.47	4.81
10	206(215)	107.94	78.82	0.38	1.74
11	239(252)	115.16	108.19	0.45	2.66
12	198(199)	138.35	104.08	0.53	5.66
Genome	2921(3061)	121.94	1408.03	0.48	5.66

[a] The number in bracket represents bin markers located on Chromosome, and the number out of bracket represents bin markers was included in the linkage group building.

(Figure 2). In addition to the *SD1* gene, QTLs detected for heading date (*qHD7-1*) (GHD7, *Os07g0261200*) (Xue et al., 2008) and grain width (*qGW5-1*) (GW5, *Os05g0187500*) (Weng et al., 2008) also verified the accuracy. Here, we detected *qHD7-1* as a major QTL (LOD=13.2) on chromosome 7 (9.22 Mb) controlling heading date and explaining 21.4% of the phenotypic variation. This QTL encompassed the cloned gene *GHD7(Os07g0261200)*. *qGW5-1* (LOD=13.76), which was located on chromosome 5 (5.43 Mb), controlled grain width, and explained 23.1% of the phenotypic variation, encompassed the cloned gene GW5 (*Os05g0187500*). Thus, mapping of the *SD1*, *GHD7* and *GW5* genes using our bin map demonstrates the accuracy of this map and shows that QTL mapping with an ultra-high-density bin map will appropriately identify genetic loci.

3.2 Assessing SES among the parents and RILs

Parent Jileng 1 is a salt-sensitive cultivar with a high SES (W2SES=4.5, W4SES=6.3). In contrast, the parent Milyang 23 is a salt-tolerant cultivar with a relatively low SES (W2SES=2.9, W4SES=3.7) throughout both investigation time points. The two parents showed significant difference in salt tolerance (Table 2).

The SES of the population in each year and environment was analyzed and displayed a continuous distribution (Figure 3), indicating that the SES trait was controlled by multiple genes and had a quantitative inheritance pattern. We conducted ANOVA for SES across environments and years and calculated the effects of genotype (G), environment (E), and genotype-environment interactions (G×E) on the traits (Table 2). These traits showed high broad-sense heritability, ranging from 65.7% to 86.2%, suggesting a major role of genetic factors in the expression of these traits as well as a considerable proportion of environmental variation.

To elucidate the repeatability of SES across populations, correlation coefficients (r) between years and environments were calculated. The results showed that the correlation coefficient of W2SES and W4SES between the field and greenhouse reached 0.69 and 0.78, respectively, which was extremely significant. From 2017 to 2019, the correlation coefficients of the SES between populations after two weeks of salt treatment ranged from 0.46 to 0.6 in different years, reaching extremely significant levels. The correlation coefficients of the SES between populations after 4 weeks of salt treatment ranged from 0.55 to 0.66 in different years, also reaching extremely significant levels. The results of the correlation analysis showed that the salt tolerance of the population was highly correlated in different environments, and the repeatability of the experiment was good (Figure 4).

The salt tolerance of the RILs across different environments was evaluated (Figure 5). The mean SES at two weeks was 4.3, with a range of 2.7-6.0 and a coefficient of variation of 15.1%. The mean SES at 4 weeks reached 5.1, with a range of 2.8-7.1 and a coefficient of variation of 16.8%. The range of the variation in both W2SES and W4SES was large, showing transgressive segregation. The skewness and kurtosis of SES were between -1 and 1, presenting a normal distribution. The generalized heritability of W2SES and W4SES reached 69.5% and 75.5%, respectively. This result indicated that the salt tolerance of the population is greatly affected by genetic factors. The best linear unbiased predictions of W2SES and W4SES were used for the subsequent QTL mapping.

3.3 QTL analysis

Using the high-density bin genetic map and BLUP analysis, twelve QTLs for two traits (W2SES and W4SES) across two environments were identified and explained 6.0–17.4% of the phenotypic variance (Figure 6; Table 3). All of the QTLs related to salt stress showed an additive effect contributed by Jileng 1.

After two weeks of salt treatment, four QTLs related to SES were identified. These QTLs were located on chromosome 2 (*qW2SES2.1*), chromosome 6 (*qW2SES6.1*) and chromosome 11 (*qW2SES11.1*,

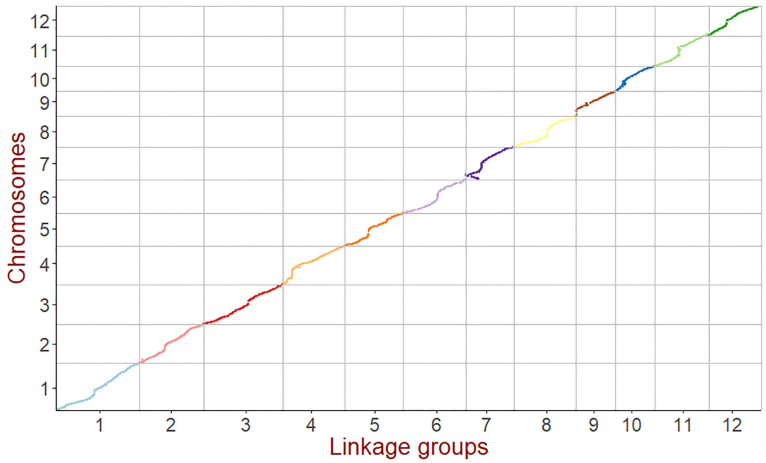


FIGURE 1
Collinearity analysis of the genetic map and genome. The x-axis is the genetic distance of each linkage group. The y-axis is the physical length of each chromosome, with the collinearity of genomic markers and genetic maps represented in the scatter plot. Different colors represent different chromosomes or linkage groups.

10.3389/fpls.2023.1065334

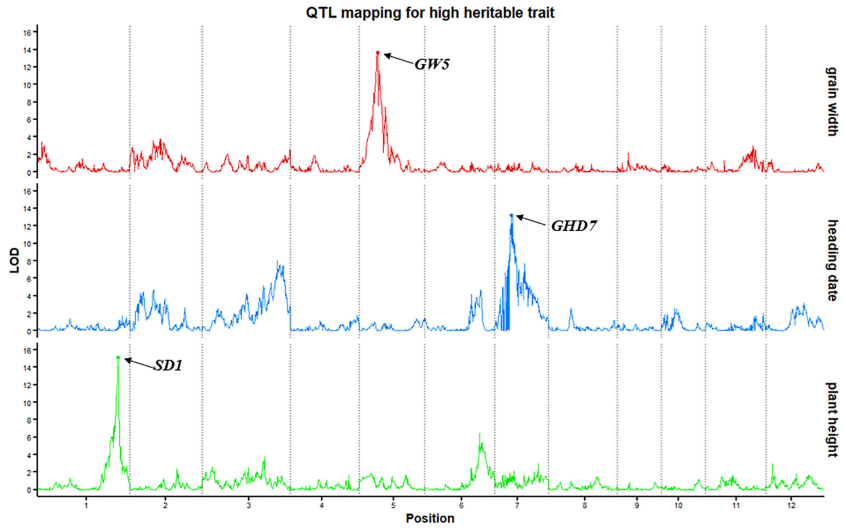


FIGURE 2
QTL mapping for highly heritable traits (plant height, heading date and grain width). The x-axis scales genetic distance on chromosomes, while the y-axis represents the LOD scores of each trait.

TABLE 2 SES of salt tolerance in parents and RILs.

Trait	Parent		Mean ± SD	Range	CV(%)	Skew	Kurt.	H_g^2(%)
	Jileng 1	Milyang 23						
W2SES	4.5 ± 1.0	2.9 ± 0.6	4.3 ± 0.7	2.7-6.0	15.1	0.00	-0.36	69.5
W4SES	6.3 ± 0.8	3.7 ± 0.3	5.1 ± 0.9	2.8-7.1	16.8	-0.11	-0.13	75.5

qW2SES11.2), and all of them explained at least 10% of the variation. Among them, the QTL *qW2SES11.1*, whose contribution reached 15.8%, was identified as the major QTL for W2SES. After four weeks of salt treatment, eight QTLs related to SES were identified, and they were distributed on chromosomes 2, 3, 4, 6, 8 and 11 respectively. The variance explained by *qW4SES2.1*, *qW4SES6.1*, *qW4SES11.1* and *qW4SES11.2* was more than 10%, and those QTLs identified for W2SES in the meanwhile. Among them, the QTL *qW4SES6.1*, whose contribution reached 17.4%, was identified as the major QTL for W4SES.

To ascertain the stability of the detected QTLs, linkage analysis was individually applied to the W2SES and W4SES values for RILs under field and greenhouse environments. Five physical regions located on chromosomes 2, 6, 8 and 11 were repeatedly detected across the field, greenhouse and BLUP and could be considered environmentally stable QTLs (Table 4). Significantly, three stable

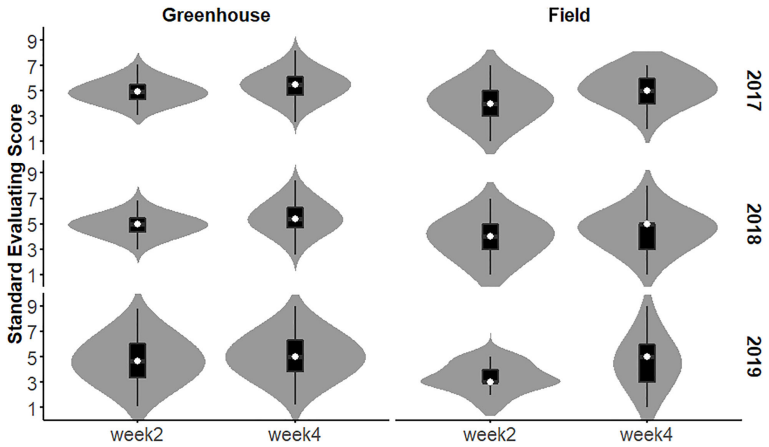


FIGURE 3
Distribution of RIL SES under greenhouse and field conditions from 2017 to 2019.

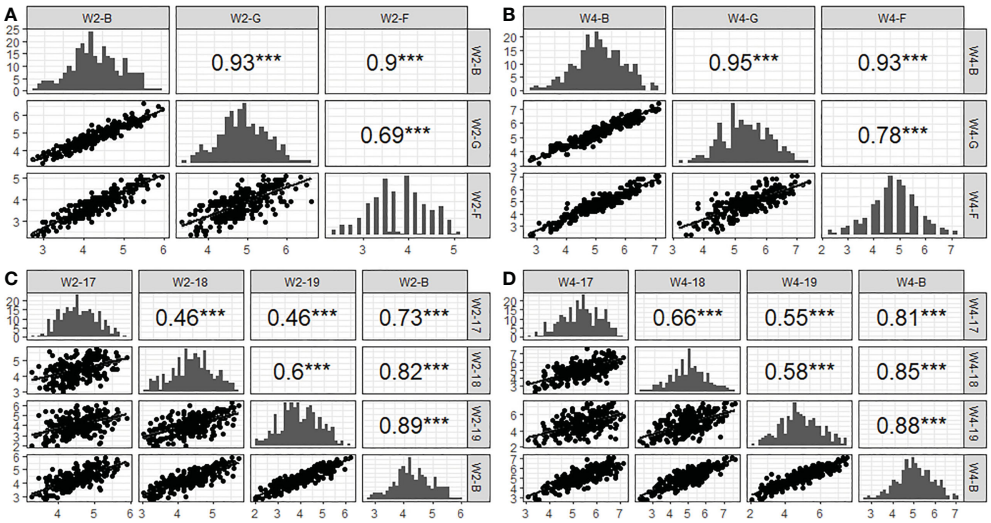


FIGURE 4
Correlation and distribution of SES from 2017 to 2019 acorss three conditions (greenhouse, field and BLUP). **(A)**: W2-B, W2-G and W2-F represent two week' s SES of BLUP, greenhouse and field, respectively. **(B)**: W4-B, W4-G and W4-F representfour week's SES of BLUP, greenhouse and field, respectively. **(C)**: W2-17, W2-18 and W2-19 represent two week's SES of 2017, 2018 and 2019, respectively. **(D)**: W4-17, W4-18 and W4-19 represent four week's SES of 2017, 2018 and 2019, respectively. *** indicated the level of significance reached 0.001.

QTLs that were located on chromosome 2: 20.92 Mb-23.44 Mb, chromosome 6: 4.13 Mb-4.85 Mb, and chromosome 11: 6.65 Mb-8.34 Mb were detected across all environments and evaluation time. Thus, given their value and reliability, these QTLs should be strongly considered for exploring candidate genes.

3.4 Gene expression profile and comparative transcriptome analysis

To complement the QTL mapping and help identify salt stress-responsive genes, the extent of transcriptomic differences in response to salt stresses between the two parents of the RILs was determined by RNA-Seq. As shown in Table 5, under salt stress, compared to Jileng 1, 2081 upregulated and 3002 downregulated DEGs were identified in Milyang 23. Even without salt stress, there were 1603 constitutively overexpressed and 2934 constitutively underexpressed DEGs between the two parents. To remove the background noise caused by constitutive variation between the parents, those DEGs detected under normal conditions were taken as the baseline control. By comparing and removing these baseline DEGs, we retained 1484 SalOnly_up, 1840 SalOnly_down, 1006 NorOnly_up, 1772 NorOnly_down, 265 "△LFC>1", and 498 "△LFC<-1" DEGs that were specific to salt stress. The types SalOnly_up, NorOnly_down and △LFC>1 were regarded as upregulated DEGs specifically related to salt stress, and the types SalOnly_down, NorOnly_up and △LFC<-1 were considered downregulated DEGs specifically related to salt stress. As a result, there were a total of 6,865 salt stress-specific DEGs, with 3,521 upregulated and 3344 downregulated DEGs.

Not all of the DEGs are likely to be responsible for the variation in salt stress, as detection errors are inevitable. Therefore, the difference in the transcriptomic profiles between salt-tolerant and salt-sensitive

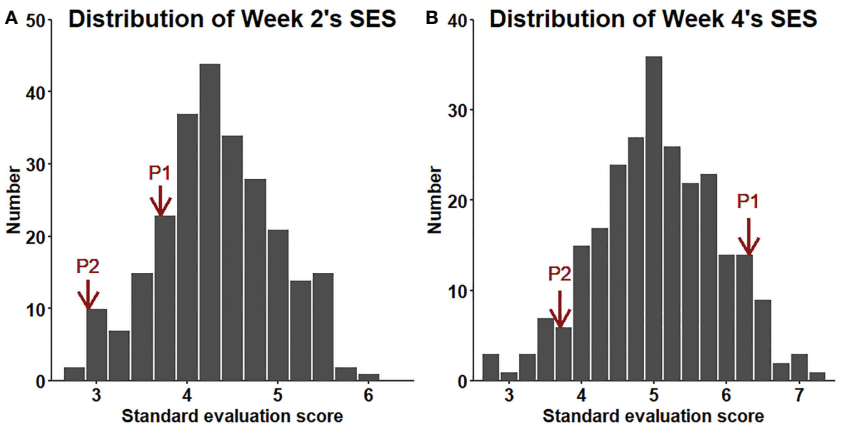


FIGURE 5
(A): Distribution of the SES (BLUP) values of the RILs after two weeks of salt treatment. **(B)**: Distribution of the SES (BLUP) values of the RILs after four weeks of salt treatment.

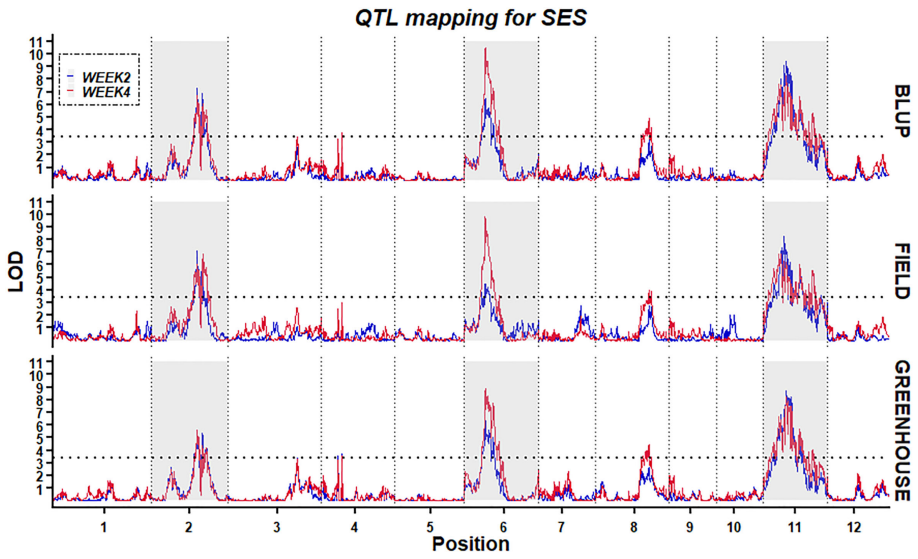


FIGURE 6
Stability of QTL mapping. The x-axis scales genetic distance on chromosomes, while the y-axis represents the LOD scores of W2SES and W4SES.

bulks were analyzed. As a result (Table 5), 1,482 upregulated and 2,135 downregulated salt stress-specific DEGs were detected between the bulks. The identified salt stress-specific DEGs between the parents and bulks were combined to decrease the background noise, and the number of salt stress-specific DEGs was drastically reduced to only 551. Those overlapping DEGs were taken as potential candidates for salt tolerance genes.

3.5 Colocalization of differentially expressed genes in QTL regions

Subsequently, those salt stress-specific DEGs were overlaid on the stable QTL confidence intervals to reduce the number of candidate genes. A total of 551 salt stress-specific DEGs were compared with the candidate genes residing in the stable QTLs. Markers flanking the stable QTLs were used to anchor them to the Japonica Nipponbare reference genome (IRGSP-1.0), and 989 annotated genes were obtained from five stable QTLs. Based on the combined, fifteen highly promising candidate genes were identified. The functional annotations of those candidates are listed in Table 6. Of these candidates, two were located on chromosome 2: 20.92 Mb-23.44 Mb, two were located on chromosome 6: 4.13 Mb-4.85 Mb, nine were located on chromosome 8: 19.81Mb-24.23 Mb, two were located on chromosome 11: 6.65 Mb-8.34 Mb and no candidates located on chromosome 11: 23.65 Mb-25.43 Mb.

To confirm the accuracy and reproducibility of the Illumina RNA-Seq results, those promising genes were compared for their

TABLE 3 QTL mapping of BLUP values of W2SES and W4SES.

Trait	QTL	Chromosome	LOD	Genetic Interval(cM)	Physical Interval(Mb)	PVE(%)	Additive
W2SES (4*)	*qW2SES2.1*	2	7.32	75.68-79.81	21.94-23.11	12.5	0.24
	qW2SES6.1	6	6.46	34.05-44.79	4.13-5.61	11.1	0.22
	qW2SES11.1	**11**	**9.43**	**36.63-40.57**	**6.65-7.63**	**15.8**	**0.26**
	qW2SES11.2	11	5.97	57.42-67.57	18.62-20.74	10.3	0.22
W4SES (8)	*qW4SES2.1*	2	6.68	71.95-79.81	21.15-23.11	11.5	0.29
	qW4SES3.1	3	3.42	112.66-118.05	27.64-28.64	6.0	0.21
	qW4SES4.1	4	3.77	34.42-34.81	15.81-18.24	6.6	0.23
	qW4SES6.1	**6**	**10.5**	**34.33-37.32**	**4.13-4.84**	**17.4**	**0.36**
	qW4SES8.1	8	4.87	77.19-94.96	20.54-24.05	8.5	0.25
	qW4SES11.1	11	8.24	37.06-40.57	6.83-7.63	13.9	0.32
	qW4SES11.2	11	9.43	58.29-66.15	18.70-20.45	11.3	0.29
	qW4SES11.3	11	5.97	81.94-88.01	24.25-25.43	9.2	0.26

* The number in brackets represents QTL detected for corresponding trait, and the bold represents main effect QTL whose contribution reached more than 15%.

TABLE 4 Comparing QTL confidence interval among greenhouse, field and BULP.

Chr.	Genetic Interval (cM)	Physical Interval(Mb)	Greenhouse		Field		BLUP	
			W2SES	W4SES	W2SES	W4SES	W2SES	W4SES
2	70.60-80.44	20.92-23.44	√	√	√	√	√	√
6	31.63-45.10	4.13-4.85	√	√	√	√	√	√
8	75.65-96.15	19.81-24.23		√		√		√
11	36.36-42.05	6.65-8.34	√	√	√	√	√	√
11	80.03-88.01	23.65-25.43		√		√		√

TABLE 5 Number of genes which were differentially regulated between susceptible or tolerant genotypes in response to satt stress, according to their classification in the six classes.

Regulated to Salt-stress	DEGs Type	P1 versus P2	Sensitive versus tolerant Bulk	Common
Up	SalOnly_up(i)	1484	1040	248
	NorOnly_down(iv)	1772	449	
	△LFC>1(v)	265	8	
Down	SalOnly_down(ii)	1840	1666	303
	NorOnly_up(iii)	1006	438	
	△LFC<-1(vi)	498	17	
Total		6865	3618	551

TABLE 6 The promising genes associated with salt tolerance.

GeneID	Position	QTL	Gene name/function
Os02g0568600	chr02: 21625022.21625725	*qW2SES2.1/ qW4SES2.1*	Zinc finger protein, putative, expressed.
Os02g0570400	chr02: 21765011.21773418	*qW2SES2.1/ qW4SES2.1*	*OsDTC1*, Similar to Ent-kaurene synthase 1A.
Os06g0184800	chr06: 4264424.4265115	*qW2SES6.1/ qW4SES6.1*	*OsRCI2-8*, similar to Low-temperature induced protein lt101.1(Blt101.1).
Os06g0184900	chr06: 4269116.4270614	*qW2SES6.1/qW4SES6.1*	*OsHCT3*, Hydroxycinnamoyl transferase 3, Transferase family protein.
Os08g0414700	chr08: 19830425.19836080	*qW4SES8.1*	Similar to Trehalose-6-phosphate synthase (Fragment).
Os08g0417000	chr08: 19950692.19952388	*qW4SES8.1*	Oxidoreductase, 2OG-FeII oxygenase domain containing protein, putative, expressed
Os08g0417100	chr08: 19954825.19956227	*qW4SES8.1*	Oxidoreductase, 2OG-FeII oxygenase domain containing protein, putative, expressed
Os08g0434300	chr08: 21054660.21056008	*qW4SES8.1*	lactate/malate dehydrogenase, putative, expressed
Os08g0440800	chr08: 21445787.21450773	*qW4SES8.1*	*OsALDH11A3*, Glyceraldehyde-3-phosphate dehydrogenase.
Os08g0450700	chr08: 22003703.22006379	*qW4SES8.1*	Chaperonin Cpn60/TCP-1 family protein.
Os08g0458200	chr08: 22462399.22464860	*qW4SES8.1*	Oxidative Stress 3-like 6, Similar to MTD1
Os08g0474866	chr08: 23403049.23404168	*qW4SES8.1*	Similar to gibberellin receptor GID1L2
Os08g0480000	chr08: 23712632.23717520	*qW4SES8.1*	Multi antimicrobial extrusion protein. MatE family protein
Os11g0234200	chr11: 7125124.7128857	*qW2SES11.1/qW4SES11.1*	Zinc finger RING/FYVE/PHD-type domain containing protein, putative, expressed
Os11g0235700	chr11: 7221675.7228567	*qW2SES11.1/qW4SES11.1*	Similar to *FHY1*

Both those located in stable QTL regions and those detected by comparative transcriptome analysis were assumed to be promising candidate genes in this study.

expression level differences between Jileng 1 and Milyang 23 by quantitative real-time PCR (qRT–PCR) analysis under normal and salt stress conditions. The validation results for the fifteen genes are shown in Figure 7. The gene expression trend was basically consistent with the RNA-Seq analysis, supporting the reliability of the data from RNA sequencing. Functional annotation of the genes in stable QTL regions helped to reveal the biological functions of those genes. The functional annotation and gene expression data suggested that *Os06g0184800* might be the most a plausible candidate for *qW2SES6.1*/*qW4SES6.1*, but genetic modification complementation or gene editing verification is needed. *Os06g0184800* are highly promising functional candidate genes for salt tolerance.

The SNPs located on the gene body and the 2 kb promoter of Os06g0184800 were screened out and fifity-four SNPs were found in this region and five SNPs were verified by PCR-based sequencing between Jileng1 and Milyang23, which four SNPs located on promoter and one SNP located on the gene body (Table S10). In the gene body, the SNP (Chr6: 4264591, C to T), was detected on the 3' UTR region with C to A transition. In the promoter, the four SNPs were respectively detected on position -279 (Chr6: 4265394, C to T), -526 (Chr6: 4,265,630, insert A), -585 (Chr6:4265699, G to A), -766 (Chr6: 4,265,880, T to C) from transcription start site (ATG) of *Os06g0184800* (Figure S4). Based on the significance test on haplotype of those markers, except Chr6: 4265630 with too much missing from resequence, Chr6:4265699 and Chr6: 4265880 shown extremely significant difference bewteen their haplotype, and Chr6: 4265394 and Chr6: 4265630 didn't show difference (Figure 8).

4 Discussion

4.1 High-density bin genetic mapping assisted in precise QTL exploration

Linkage analysis is an efficient approach to understanding the genetic basis of quantitative traits in crops (Bohra et al., 2020). Genetic map was fundamental to precise linkage analysis (Xie et al., 2010). Parental genetic diversity and marker density are the major factors affecting the efficiency and accuracy of QTL mapping. Previously, the insufficiency of molecular markers were major limitation in discovering QTLs in rice (Bohar et al., 2020). Many QTL studies have been performed using sparse genetic maps

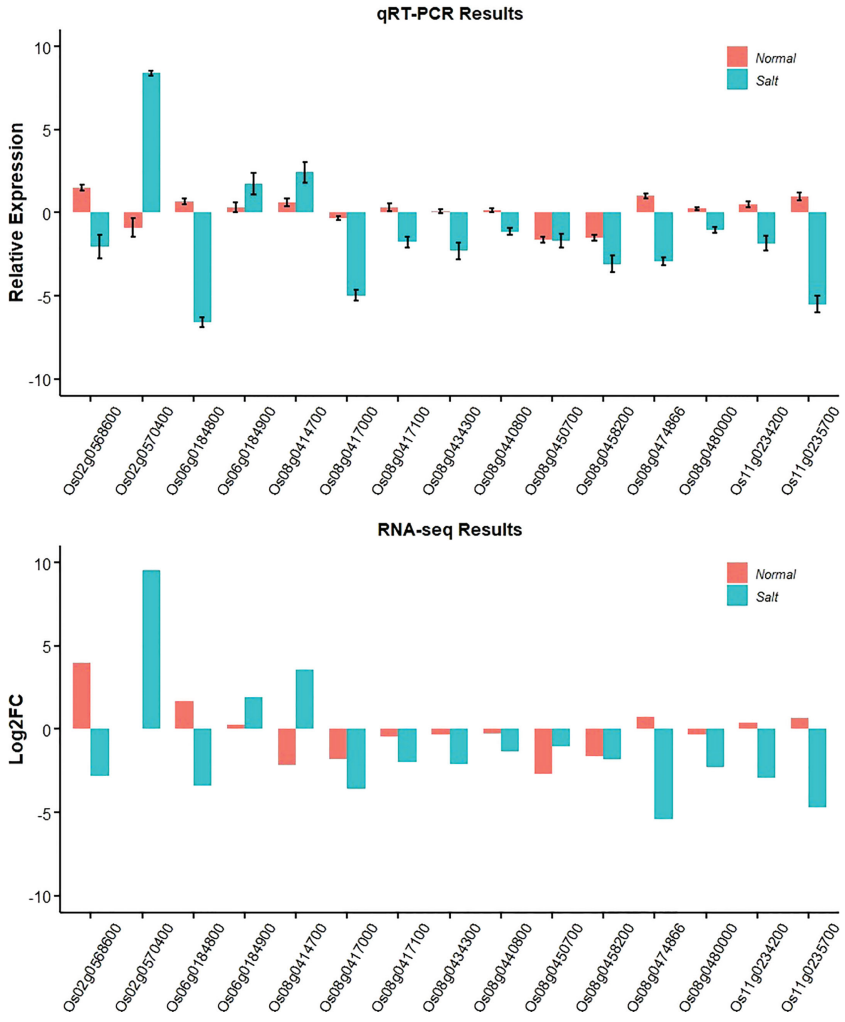


FIGURE 7
Gene expression changes under salt stress and normal conditions based on qRT-PCR and RNA-Seq.

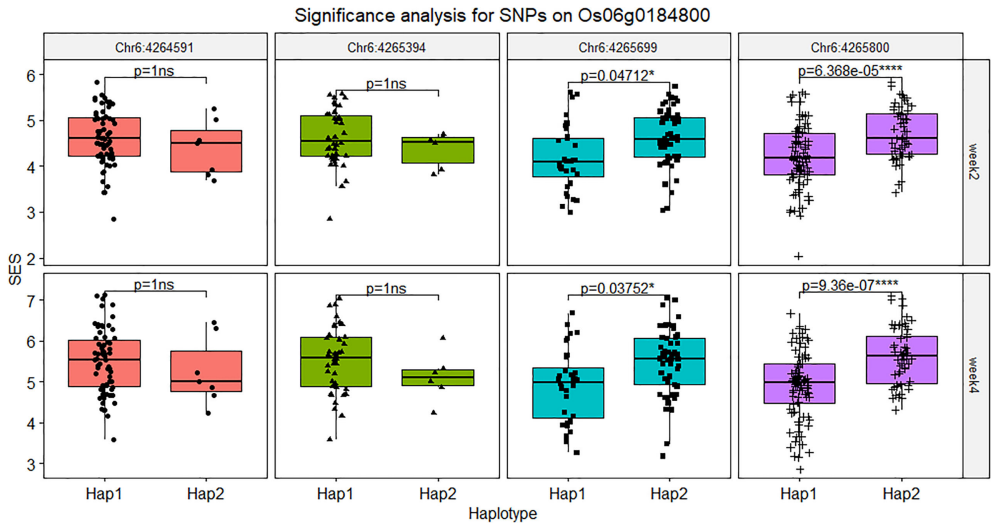


FIGURE 8
Significance analysis for SNPs on *Os06g0184800*. The symbol "ns" indicated not reach significant difference, * indicated the level of significance reached 0.05, **** indicated the level of significance reached 0.0001.

constructed using RFLP and SSR markers, resulting in large intermarker intervals (Lander and Botstein, 1989; Lin et al., 1998; Koyama et al., 2001; Chai et al., 2014).

Generally, increasing marker density is an effective means of improving QTL mapping resolution (Bevan et al., 2017). The rapid development of high-throughput next-generation sequencing genotyping platforms has provided the extensive capacity to develop comprehensive polymorphic markers , including SNPs and InDels.The use of whole genome resequencing and the construction of bin maps has been shown to improve efficiency of QTL mapping and accelerate genes discovery in rice (Huang et al., 2009a; Xie et al., 2010). In the current study, 2921 bin markers developed from 1,860,935 high-quality, biallelic, homozygous SNPs were used to construct a high-density genetic map covering 1,408.03 cM, with an average interval of 0.48 cM between adjacent bin markers (Table 1), which significantly increased the QTL mapping resolution compared with traditional markers. Compared to the average interval of 9.00 cM between adjacent markers in the previous SSR/InDel/single SNP map also derived from Jileng 1×Milyang 23 (Zhang et al., 2021), the marker density of this genetic map was observably increased (7.83 markers/Mb vs 0.78 markers/Mb), and the confidence interval of QTLs was significantly reduced.

The quality and accuracy of this genetic map was assessed by identifying known genes underlying QTL mapping from other studies. The precision and accuracy of linkage analysis were significantly improved based on the high-density bin genetic map, and was sufficient to accurately map *SD1* (Spielmeyer et al., 2002), *GHD7* (Xue et al., 2008), and *GW5* (Weng et al., 2008), which control plant height, heading date and grain width, respectively (Figure 1). For example, basing on this study's high-density genetic map of Jileng1×Milyang23 RILs, *qPH1-1*, which controls plant height, was located on the interval Chr01:38,008,469bp - 38,642,574bp (634.11 kb) and explained 24.1% of the phenotypic variance, including the famous green revolution gene *SD1*. Taking the previous linkage analysis with the same RILs for comparison, a major QTL for plant height had been located in the interval Chr01:34, 949, 898 bp-36, 728, 487 bp (1.78 Mb) and explained 10.30–17.99% of the phenotypic variance (Tang, 2019). This QTL interval of current study narrowed significantly compared to previous studies and it was in more close proximity to functional gene *SD1*.

Combining this genetic map and precise phenotype, this population is competent for identifying major QTL and functional gene.

Gene prediction, however, depended also on the high accuracy and collinearity of the region of interest between genetic map and reference genome. In current study, a high collinearity between genetic map and Nipponbare reference genome (IRGSP-1.0) (Figure 1) indicated that this map was suitable for subsequent gene discovery.

4.2 Environmentally stable and major QTLs for salt tolerance

Salt tolerance is quantitative trait controlled by multiple genes with a complex genetic mechanism (Horie et al., 2012). To date, the rapid development of next-generation sequencing has accelerated QTL mapping and gene discovery in crops, and more than one thousand rice salt-tolerance QTLs have been identified (http://gramene.org/ ; Jing and Zhang, 2017). Despite many attempts using different strategies to discover functional genes controlling salt tolerance in rice, the achievements thus far have been quite modest. Only rare genes with significant effects have been thoroughly studied and cloned (Ganie et al., 2021). The inefficient exploration of salt stress-related genes is partial due to that those QTLs were mainly detected by low-density markers with large confidence intervals that contained too many genes and lacked reliability and stability. In the current study, an ultra-high-density genetic map which could rapidly anchor major genes was utilized to improve the precision of QTL positioning and narrow the range of candidate genes. Moreover, the

SES values of populations across two environments and three years were evaluated to assure the accuracy of the phenotype. Through the above process, five stable QTLs were discovered.

Among the five stable QTLs, two major QTLs (*qW2SES11.1* and *qW4SES6.1* explained more than 15% phenotypic variance) were worth to lucubrate.

4.3 Validation of QTLs across mapping populations

Validation of QTLs in different genetic backgrounds/environments is required before they can be used in marker-assisted selection or gene cloning to rule out statistical errors (Price, 2006). Among the QTLs identified in this study, four stable QTLs partially or completely overlapped with the chromosomal regions carrying loci detected by previous studies.

The QTL *qSSR2.3*, published by Xu et al. (2020), controlling seedling survival under salt stress, was colocated on a region of chromosome 2 (71.95 cM-79.81 cM, 21.15 Mb-23.11 Mb) that contained *qW2SES2.1* and *qW4SES2.1*. Chai et al. (2014) discovered two QTLs (*qGW6.2* and *qGYP6.2*) affecting 1000 grain weight and yield per plant under salt stress, and these QTLs overlapped with a region on chromosome 6 (34.05 cM-44.79 cM, 4.13 Mb) containing *qW2SES6.1* and *qW4SES6.1*. On chromosome 11 (36.63 cM – 40.57 cM, 6.65 Mb-7.63 Mb), Chai et al. (2014) also identified two QTLs (*qSF11.5* and *qGYP11.7*) affecting seed setting rate and yield per plant under salt stress, and Puram et al. (2017) located two QTLs (*qSHL11.1* and *qRHL11.1*) for bud length and root length under salt stress. On chromosome 11 (57.42 cM -67.57 cM, 24.25-25.43 Mb), Xu et al. (2020) found a QTL for seedling survival time under salt stress (*qSSD11.1*), and Shen et al. (2009) found a QTL for chlorophyll fluorescence under salt stress (*qSFM-11*). The mutual comparative result reflect the accuracy of this study, as well as indicated that those QTL regions are also consistent across more than one genetic background. Thus, it was reasonably surmise the existence of salt tolerance-related genes in those intervals. These results not only strengthen the findings of previous studies but also reflect the complexity of salt tolerance in accelerating the breeding programs for enhanced salt-tolerance among rice cultivars.

There are many similarities in the genetic mechanisms controlling plant resistance to various abiotic stresses. Drought- and cold tolerance-related genes in rice can also play an important role in salt tolerance, which was further confirmed by the results of the current study. Han et al. (2007) identified QTLs affecting cold tolerance at the seedling stage (*qCSH2*, Chr2:21.66 Mb-26.76 Mb), employing the $F_{2:3}$ population constructed by the same parents of this RIL population. Hemamalini et al. (2000) located a QTL controlling root density under drought stress (*qRTT2-1*, Chr2:20.72 Mb-25.43 Mb) that partially overlapped with the QTL interval we identified on chromosome 2 (71.95 cM-79.81 cM, 21.15 Mb-23.11 Mb). Li et al. (2005) found a QTL (*qRRSD6b*, Chr6:4.84 Mb-5.43 Mb) that controlled the ratio of root dry weight to root fresh weight under drought stress, and Dai et al. (2004) found a QTL (*qRCT6b*, Chr6:4.93 Mb-5.43 Mb) that affected the cold tolerance of rice at the reproductive stage; both of which partially overlapped with the QTL interval of chromosome 6 (34.05 cM-44.79 cM, 4.13 Mb-5.61 Mb) identified from the current study. Toojinda et al. (2003) mapped SSR markers affecting rice flooding tolerance (RM206, 24.32 Mb) to a QTL interval on chromosome 11 (81.94 cM-88.01 cM, 24.25 Mb-25.43 Mb). The results of this study further verified that within these QTL confidence intervals, pleiotropic genes may affect multiple abiotic stresses.

4.4 Gene expression profile and identification of candidate genes associated with salt stress

The advantageous feature of our study was the integration of high-density QTL mapping and bulked segregant RNA-Seq analysis. High marker density is preferable for improving the resolution in QTL position and assisting in determining functional causative variations in genes (Liu et al., 2014). However, there were still 989 annotated genes underlying the five stable QTLs, making it difficult to pinpoint the genes responsible for the functional differences in salt tolerance. Obtaining gene expression information by combining bulked segregant analysis and RNA-Seq is an effective strategy for filtering out background noise and can reduce the number of DEGs (Zou et al., 2016). Transcriptome profiling of bulked RILs normalized the irrelevant DEGs between the tolerant and sensitive parents while retaining the DEGs relevant for salt tolerance or sensitivity. In current study, the transcriptome profiles of two parents and two bulks under two conditions were depicted by RNA-Seq. Through the comparative analysis, a total of 551 salt stress-specific DEGs were obtained. However, there were still too many DEGs to initiate any downstream validation studies. Integrating of high-density QTL mapping and bulked segregant RNA-Seq analysis, the number of overlaped candidate genes was dramatically reduced, and only fifteen candidate genes were obtained.

Among the fifteen highly promising candidate genes, *Os06g0184800* and *Os06g0184900* located on *qW4SES6.1*, *Os11g0234200* and *Os11g0235700* located on *qW2SES11.1* respectively, which explained more than 15% phenotypic variance and play a more important role on salt tolerance, might be the most plausible prospect for target genes. Among them, *Os06g0184800* encodes small hydrophobic polypeptides, *Os06g0184900* encodes hydroxycinnamoyl transferases (Fang et al., 2022), *Os11g0234200* encodes FYVE/PHD-type domain containing protein (Wywial and Singh, 2010), and *Os11g0235700* is similar to far-red elongated hypocoty 1 (Chen et al., 2012).

Basing on those annotation, *Os06g0184800* is highly promising and worthy of further study to determine its role in the response to salt stress. *Os06g0184800*, also called *OsRCI2-8*, which belongs to the RCI2 family, is also known as plasma membrane protein 3 (PMP3). As reported previously, this gene family encodes small hydrophobic polypeptides in maintenance of ion homeostasis, and it is responsible for salt, drought, cold, and abscisic acid (Medina et al., 2007). The homologous gene of *Os06g0184800* has been described both in many cereal crops (rice, arabidopsis maize, wheat, barley) (Mitsuya et al., 2006; Nylander et al., 2001; Mustafa et al., 2005; Fu et al., 2012) and many halophytes (sheep grass, alkali grass, plaintan)

(Zhang et al., 2008), and had been verified to regulates cellular Na^+ and K^+ accumulation, promote seed germination and lateral root growth under abiotic stress. It is reasonable to speculated that *Os06g0184800* was the target gene for *qW2SES6.1/qW4SES6.1*, which was supported by DEGs and previous studies.

Basing on the gene expression analysis of RNA-seq and qRT-PCR, *Os06g0184800* shown significant downward adjustment under salt stress with Milyang23 vs Jileng1. So it is inferred this lower expression level may be associated with salt stress. From the subsequent haplotype analysis, two SNPs (Chr6:4265699 and Chr6:4265880) located on pro moter region of *Os06g0184800* showed significant difference in different haplotypes, which were also confirmed by the database ricevarmap2 (http://ricevarmap.ncpgr.cn/). Those SNPs might be suitable for the development of functional markers for salt tolerance in rice to facilitate marker-assisted breeding.

In summary, the integration of QTL mapping, RNA-Seq analysis, and gene annotation provided credible candidate genes for the identified QTLs, constitutes an effective strategy for identifying promising candidate genes involved in salt tolerance for QTL mapping, which was very important for subsequent gene function verification. The function of promising candidate genes will be validated by genetic modification complementation or gene editing verification.

5 Conclusion

Using the whole genome resequencing approach, a genetic linkage map with an average distance of 0.48 cM between adjacent markers was constructed based on an RIL population in rice. Comparative analysis of QTLs and fine mapping suggest the high efficiency and accuracy of this genetic map. Global mapping of QTLs affecting salt tolerance was performed, and a total of twelve loci were detected across three conditions. Including the three loci that overlapped with previous reports, a total of five were defined as stable loci. The stable QTLs were highlighted and analyzed. The results of the transcriptome analysis revealed a gene expression profile responsible for responding to salt stress, and several important differentially expressed genes were colocalized in the salt stress-related QTL regions on chromosomes 2, 6, 8 and 11. Critical loci were investigated and identified as candidate genes; these were considered suitable for functional validation and breeding utilization. This study will not only help to better understand the genes and mechanisms of salt tolerance in rice but also provide new insights that will assist in the development of breeding strategies for salt-tolerant rice.

Data availability statement

The data presented in the study are deposited in the National Genomics Data Center (NGDC), part of the China National Center for Bioinformation (CNCB), accession number CRA008901 and CRA008748.

Author contributions

LG and LH designed the project and LG performed all the experiments and wrote the manuscript. WZ, DC, XM, and BH assisted in conducting experiments and data analysis. QZ and LH provided the direction for the study and the correction of the manuscript. All authors contributed to the article and approved the submitted version.

Funding

This research was financially supported by the National Key Research and Development Program of China (2021YFD1200500, 2016YFD0100101), CAAS Science and Technology Innovation Program, Protective Program of Crop Germplasm of China (19200385-1), The third national survey and collection action on crop germplasm resource (19210859, 19210860), National Crop Germplasm Resources Center (NCGRC-2021-02), HAAFS Science and Technology Innovation Special Project (No. 2022KJCXZX-BHS-1) and Basic Research Funds of Hebei Academy of Agriculture and Forestry Sciences).

Conflict of interest

The authors declare that the research was conducted in the absence of any commercial or financial relationships that could be construed as a potential conflict of interest.

Publisher's note

All claims expressed in this article are solely those of the authors and do not necessarily represent those of their affiliated organizations, or those of the publisher, the editors and the reviewers. Any product that may be evaluated in this article, or claim that may be made by its manufacturer, is not guaranteed or endorsed by the publisher.

Supplementary material

The Supplementary Material for this article can be found online at: https://www.frontiersin.org/articles/10.3389/fpls.2023.1065334/full#supplementary-material

SUPPLEMENTARY TABLE 1
Plant height, heading date and grain width phenotypic variation of RIL.

SUPPLEMENTARY TABLE 2
The RILs arranged by an α-lattice design (Taking the trial in greenhouse of 2018 for example)

SUPPLEMENTARY TABLE 3
Phenotypic variation of parents and RILs.

SUPPLEMENTARY TABLE 4
Population sequencing and mapping

SUPPLEMENTARY TABLE 5
Overview of SNP number

SUPPLEMENTARY TABLE 6
Information of Bin marker.

SUPPLEMENTARY TABLE 7
Information of genetic map

SUPPLEMENTARY TABLE 8
Genes regulated to salt-stress by RNA-seq analysis

SUPPLEMENTARY TABLE 9
Primer of candidate genes for qRT-PCR

SUPPLEMENTARY TABLE 10
Haplotype of SNPs on *Os06g0184800* and respective SES.

SUPPLEMENTARY FIGURE 1
Performance of parents (Jileng 1 and Milyang 23) after salt treatment and control condition

SUPPLEMENTARY FIGURE 2
Performance of RILs under two environments (greenhouse and field)

SUPPLEMENTARY FIGURE 3
The evaluation criterion of SES.

SUPPLEMENTARY FIGURE 4
Alignment of reference, Jileng 1 and Milyang23 for *Os06g0184800*

References

Bevan, M. W., Uauy, C., Wulff, B. B., Zhou, J., Krasileva, K., and Clark, M. D. (2017). Genomic innovation for crop improvement. *Nature* 543, 346–354. doi: 10.1038/nature22011

Bohar, R., Chitkineni, A., and Varshney, R. K. (2020). Genetic molecular markers to accelerate genetic gains in crops. *Biotechniques* 69, 158–160. doi: 10.2144/btn-2020-0066

Bohra, A., Chand Jha, U., Godwin, I. D., and Kumar Varshney, R. (2020). Genomic interventions for sustainable agriculture. *Plant Biotechnol. J.* 18, 2388–2405. doi: 10.1111/pbi.13472

Buti, M., Baldoni, E., Formentin, E., Milc, J., Frugis, G., Lo Schiavo, F., et al. (2019). A meta-analysis of comparative transcriptomic data reveals a set of key genes involved in the tolerance to abiotic stresses in rice. *Int. J. Mol. Sci.* 20, 5662. doi: 10.3390/ijms20225662

Chai, L., Zhang, J., Pan, X.-B., Zhang, F., Zheng, T.-Q., Zhao, X.-Q., et al. (2014). Advanced backcross QTL analysis for the whole plant growth duration salt tolerance in rice (*Oryza sativa* l.). *J. Integr. Agric.* 13, 1609–1620. doi: 10.1016/S2095-3119(13)60575-4

Chen, Y. R., and Gu, J. (2018). Fastp: an ultra-fast all-in-one FASTQ preprocessor. *Bioinformatics* 34, 884–890. doi: 10.1093/bioinformatics/bty560

Chen, T., Shabala, S., Niu, Y., Chen, Z.-H., Shabala, L., Meinke, H., et al. (2021). Molecular mechanisms of salinity tolerance in rice. *Crop J.* 9, 506–520. doi: 10.1016/j.cj.2021.03.005

Chen, F., Shi, X. R., Chen, L., Dai, M. Q., Zhou, Z. Z., Shen, Y. P., et al. (2012). Phosphorylation of FAR-RED ELONGATED HYPOCOTYL1 is a key mechanism defining signaling dynamics of phytochrome a under red and far-red light in arabidopsis. *Plant Cell* 24 (5), 1907–1920. doi: 10.1105/tpc.112.097733

Dai, L., Lin, X., Ye, C.-R., Ise, K., Saito, K., Kato, A., et al. (2004). Identification of quantitative trait loci controlling cold tolerance at the reproductive stage in yunnan landrace of rice, kunmingxiaobaigu. *Breed Sci.* 54, 253–258. doi: 10.1270/jsbbs.54.253

Fang, H., Zhang, F., Zhang, C. Y., Wang, D., Shen, S. Q., He, F., et al. (2022). Function of hydroxycinnamoyl transferases for the biosynthesis of phenolamides in rice resistance to magnaporthe oryzae. *J. Genet. Genomics* 49 (8), 776–786. doi: 10.1016/j.jgg.2022.02.008

Fu, J., Zhang, D. F., Liu, Y. H., Ying, S., Shi, Y. S., Song, Y. C., et al. (2012). Isolation and characterization of maize PMP3 genes involved in salt stress tolerance. *PloS One* 7, e31101. doi: 10.1371/journal.pone.0031101

Ganie, S. A., Molla, K. A., Henry, R. J., Bhat, K. V., and Mondal, T. K. (2019). Advances in understanding salt tolerance in rice. *Theor. Appl. Genet.* 132, 851–870. doi: 10.1007/s00122-019-03301-8

Ganie, S. A., Wani, S. H., Henry, R., and Hensel, G. (2021). Improving rice salt tolerance by precision breeding in a new era. *Curr. Opin. Plant Biol.* 60, 101996. doi: 10.1016/j.pbi.2020.101996

Geng, L. Y., Zhang, W., Ma, X. D., Cui, D., Han, B., Zhang, Q. X., et al. (2020). Establishment of an updated assay for testing salt tolerance at the tillering stage of rice and germplasm screening. *J. Plant Genet. Resour.* 21 (3), 587–595. doi: 10.13430/j.cnki.jpgr.20191231005

Gregorio, G. B., Sendhira, D., and Mendoza, R. T. (1997). Screening rice for salinity tolerance. *IRRI Discuss Pap Ser.* 22, 1–30.

Han, L., Qiao, Y., Zhang, S., Zhang, Y., Cao, G., Kim, J., et al. (2007). Identification of quantitative trait loci for cold response of seedling vigor traits in rice. *J. Genet. Genomics* 34, 239–246. doi: 10.1016/S1673-8527(07)60025-3

Hemamalini, G. S., Shashidhar, H. E., and Hittalmani, S. (2000). Molecular marker assisted tagging of morphological and physiological traits under two contrasting moisture regimes at peak vegetative stage in rice (*Oryza sativa* l.). *Euphytica* 112, 69–78. doi: 10.1023/A:1003854224905

He, Y., Yang, B., He, Y., Zhan, C., Cheng, Y., Zhang, J., et al. (2019). A quantitative trait locus, qSE3, promotes seed germination and seedling establishment under salinity stress in rice. *Plant J.* 97, 1089–1104. doi: 10.1111/tpj.14181

Horie, T., Karahara, I., and Katsuhara, M. (2012). Salinity tolerance mechanisms in glycophytes: an overview with the central focus on rice plants. *Rice (N Y)* 5, 11. doi: 10.1186/1939-8433-5-11

Huang, X. Y., Chao, D. Y., Gao, J. P., Zhu, M. Z., Shi, M., and Lin, H. X. (2009b). A previously unknown zinc finger protein, DST, regulates drought and salt tolerance in rice *via* stomatal aperture control. *Genes Dev.* 23, 1805–1817. doi: 10.1101/gad.1812409

Huang, X., Feng, Q., Qian, Q., Zhao, Q., Wang, L., Wang, A., et al. (2009a). High-throughput genotyping by whole-genome resequencing. *Genome Res.* 19, 1068–1076. doi: 10.1101/gr.089516.108

Jing, W., and Zhang, W. (2017). Research progress on gene mapping and cloning for salt tolerance and variety improvement for salt tolerance by molecular marker-assisted selection in rice. *Chin. J. Rice Sci.* 31, 111–123. doi: 10.16819/j.1001-7216.2017.6083

Kawahara, Y., de la Bastide, M., Hamilton, J. P., Kanamori, H., McCombie, W. R., Ouyang, S., et al. (2013). Improvement of the *Oryza sativa* nipponbare reference genome using next generation sequence and optical map data. *Rice (N Y)* 6, 4. doi: 10.1186/1939-8433-6-4

Kim, D., Landmead, B., and Salzberg, S. L. (2015). HISAT: a fast spliced aligner with low memory requirements. *Nat. Methods* 12, 357–U121. doi: 10.1038/nmeth.3317

Kong, W., Zhang, C., Zhang, S., Qiang, Y., Zhang, Y., Zhong, H., et al. (2021). Uncovering the novel QTLs and candidate genes of salt tolerance in rice with linkage mapping, RTM-GWAS, and RNA-seq. *Rice* 14, 93. doi: 10.1186/s12284-021-00535-3

Koyama, M. L., Levesley, A., Koebner, R. M., Flowers, T. J., and Yeo, A. R. (2001). Quantitative trait loci for component physiological traits determining salt tolerance in rice. *Plant Physiol.* 125, 406–422. doi: 10.1104/pp.125.1.406

Kumar, K., Kumar, M., Kim, S. R., Ryu, H., and Cho, Y. G. (2013). Insights into genomics of salt stress response in rice. *Rice (N Y)* 6, 27–42. doi: 10.1186/1939-8433-6-27

Lander, E. S., and Botstein, D. (1989). Mapping mendelian factors underlying quantitative traits using RFLP linkage maps. *Genetics* 121, 185–199. doi: 10.1093/genetics/121.1.185

Li, H., and Durbin, R. (2009). Fast and accurate short read alignment with burrows-wheeler transform. *Bioinformatics* 25 (14), 1754–1760. doi: 10.1093/bioinformatics/btp324

Li, H., Handsaker, B., Wysoker, A., Fennell, T., Ruan, J., Homer, N., et al. (2009). The sequence alignment/map format and SAMtools. *Bioinformatics* 25, 2078–2079. doi: 10.1093/bioinformatics/btp352

Li, Z., Mu, P., Li, C., Zhang, H., Li, Z., Gao, Y., et al. (2005). QTL mapping of root traits in a doubled haploid population from a cross between upland and lowland japonica rice in three environments. *Theor. Appl. Genet.* 110, 1244–1252. doi: 10.1007/s00122-005-1958-z

Lin, H., Yanagihara, S., Zhuang, J., Senboku, T., Zheng, K., and Yashima, S. (1998). Identification of QTL for salt tolerance in rice *via* molecular markers. *Chin. J. Rice Sci.* 12, 72–78.

Lin, H. X., Zhu, M. Z., Yano, M., Gao, J. P., Liang, Z. W., Su, W. A., et al. (2004). QTLs for na+ and k+ uptake of the shoots and roots controlling rice salt tolerance. *Theor. Appl. Genet.* 108, 253–260. doi: 10.1007/s00122-003-1421-y

Liu, D., Ma, C., Hong, W., Huang, L., Liu, M., Liu, H., et al. (2014). Construction and analysis of high-density linkage map using high-throughput sequencing data. *PloS One* 9, e98855. doi: 10.1371/journal.pone.0098855

Liu, C., Mao, B., Yuan, D., Chu, C., and Duan, M. (2022). Salt tolerance in rice: physiological responses and molecular mechanisms. *Crop J.* 10, 13–25. doi: 10.1016/j.cj.2021.02.010

Mckenna, A., Hanna, M., Banks, E., Sivachenko, A., Cibulskis, K., Kernytsky, A., et al. (2010). The genome analysis toolkit: A MapReduce framework for analyzing next-generation DNA sequencing data. *Genome Res.* 20, 1297–1303. doi: 10.1101/gr.107524.110

Medina, J., Ballesteros, M. L., and Salinas, J. (2007). Phylogenetic and functional analysis of arabidopsis RCI2 genes. *J. Exp. Bot.* 58, 4333–4346. doi: 10.1093/jxb/erm285

Mitsuya, S., Taniguchi, M., Miyake, H., and Takabe, T. (2006). Overexpression of RCI2A decreases na+ uptake and mitigates salinity-induced damages in arabidopsis thaliana plants. *Physiol. Plantarum* 128, 95–102. doi: 10.1111/j.1399-3054.2006.00714.x

Munns, R., and Tester, M. (2008). Mechanisms of salinity tolerance. *Annu. Rev. Plant Biol.* 59, 651–681. doi: 10.1146/annurev.arplant.59.032607.092911

Mustafa, R. M., Abeer, M. A., James, G., Song, J. Y., and Benildo, G. R. (2005). The OsLti6 genes encoding low-molecular-weight membrane proteins are differentially expressed in rice cultivars with contrasting sensitivity to low temperature. *Gene* 344, 171–180. doi: 10.1016/j.gene.2004.09.033

Nylander, M., Heino, P., Helenius, E., Palva, T., Ronne, H., Palva, E. T., et al. (2001). The lowtemperature- and salt-induced RCI2A gene of arabidopsis complements the sodium sensitivity caused by a deletion of the homologous yeast gene SNA1. *Plant Mol. Biol.* 45, 341–352. doi: 10.1023/A:1006451914231

Nyquist, W. E., and Baker, R. J. (1991). Estimation of heritability and prediction of selection response in plant populations. *Crit. Rev. Plant Sci.* 10, 235–322. doi: 10.1080/07352689109382313

Ooijen, J. V., Ooijen, J. V., Verlaat, J. V., Ooijen, J., Tol, J. V., Dalen, J., et al. (2006). *JoinMap 4, software for the calculation of genetic linkage maps in experimental populations*. Ed. B. V. Kyazma (Wageningen, Netherlands).

Ozsolak, F., and Milos, P. M. (2011). RNA Sequencing: advances, challenges and opportunities. *Nat. Rev. Genet.* 12, 87–98. doi: 10.1038/nrg2934

Price, A. H. (2006). Believe it or not, QTLs are accurate! *Trends Plant Sci.* 11, 213–216. doi: 10.1016/j.tplants.2006.03.006

Puram, V. R. R., Ontoy, J., Linscombe, S., and Subudhi, P. K. (2017). Genetic dissection of seedling stage salinity tolerance in rice using introgression lines of a salt tolerant landrace nona bokra. *J. Hered* 108, 658–670. doi: 10.1093/jhered/esx067

Qin, H., Li, Y., and Huang, R. (2020). Advances and challenges in the breeding of salt-tolerant rice. *Int. J. Mol. Sci.* 21, 8385. doi: 10.3390/ijms21218385

Ren, Z. H., Gao, J. P., Li, L. G., Cai, X. L., Huang, W., Chao, D. Y., et al. (2005). A rice quantitative trait locus for salt tolerance encodes a sodium transporter. *Nat. Genet.* 37, 1141–1146. doi: 10.1038/ng1643

Robinson, M. D., McCarthy, D. J., and Smyth, G. K. (2010). edgeR: a bioconductor package for differential expression analysis of digital gene expression data. *Bioinformatics* 26, 139–140. doi: 10.1093/bioinformatics/btp616

SAS Institute Inc (2015). *SAS 9.4 intelligence platform: system administration guide* (Cary: SAS Institute Inc).

Shen, B., Jiang, J., Yu, W.-D., Fan, Y.-Y., and Zhuang, J.-Y. (2009). QTL analysis of chlorophyll fluorescence parametersin rice seedlings under salt stress. *China J. Rice Sci.* 23, 319–322.

Spielmeyer, W., Ellis, M. H., and Chandler, P. M. (2002). Semidwarf (sd-1), "green revolution" rice, contains a defective gibberellin 20-oxidase gene. *Proc. Natl. Acad. Sci. U.S.A.* 99, 9043–9048. doi: 10.1073/pnas.132266399

Takagi, H., Tamiru, M., Abe, A., Yoshida, K., Uemura, A., Yaegashi, H., et al. (2015). MutMap accelerates breeding of a salt-tolerant rice cultivar. *Nat. Biotechnol.* 33, 445–449. doi: 10.1038/nbt.3188

Takeda, S., and Matsuoka, M. (2008). Genetic approaches to crop improvement: responding to environmental and population changes. *Nat. Rev. Genet.* 9, 444–457. doi: 10.1038/nrg2342

Tang, J. H. (2019). Detection of cold tolerance QTLs of rice early seedling stage and booting flowering stage by using recombinant inbred lines. Chongqing.

Toojinda, T., Siangliw, M., Tragoonrung, S., and Vanavichit, A. (2003). Molecular genetics of submergence tolerance in rice: QTL analysis of key traits. *Ann. Bot.* 91, 243–253. doi: 10.1093/aob/mcf072

Urano, K., Kurihara, Y., Seki, M., and Shinozaki, K. (2010). 'Omics' analyses of regulatory networks in plant abiotic stress responses. *Curr. Opin. Plant Biol.* 13, 132–138. doi: 10.1016/j.pbi.2009.12.006

Van Ooijen, J. W. (2010). *MapQTL 6.0, software for mapping the quantitative trait loci in experimental populations* (Wageningen, Netherlands).

Wang, S., Cao, M., Ma, X., Chen, W., Zhao, J., Sun, C., et al. (2017). Integrated RNA sequencing and QTL mapping to identify candidate genes from *Oryza rufipogon* associated with salt tolerance at the seedling stage. *Front. Plant Sci.* 8, 1427. doi: 10.3389/fpls.2017.01427

Weng, J., Gu, S., Wan, X., Gao, H., Guo, T., Su, N., et al. (2008). Isolation and initial characterization of GW5, a major QTL associated with rice grain width and weight. *Cell Res.* 18, 1199–1209. doi: 10.1038/cr.2008.307

Wywial, E., and Singh, S. M. (2010). Identification and structural characterization of FYVE domain-containing proteins of *Arabidopsis thaliana*. *BMC Plant Biol.* 10, 157. doi: 10.1186/1471-2229-10-157

Xie, W., Feng, Q., Yu, H., Huang, X., Zhao, Q., Xing, Y., et al. (2010). Parent-independent genotyping for constructing an ultrahigh-density linkage map based on population sequencing. *Proc. Natl. Acad. Sci. U.S.A.* 107, 10578–10583. doi: 10.1073/pnas.1005931107

Xue, W., Xing, Y., Weng, X., Zhao, Y., Tang, W., Wang, L., et al. (2008). Natural variation in Ghd7 is an important regulator of heading date and yield potential in rice. *Nat. Genet.* 40, 761–767. doi: 10.1038/ng.143

Xu, Y., Li, P., Yang, Z., and Xu, C. (2017). Genetic mapping of quantitative trait loci in crops. *Crop J.* 5, 175–184. doi: 10.1016/j.cj.2016.06.003

Xu, R., Zhang, L.-Z., Xie, X.-Z., Wang, Y.-Y., Huang, J.-F., Zheng, X.-M., et al. (2020). QTL mapping revealed salt tolerance traits from o. rufipogon using chromosome segment substitution lines. *J. Plant Genet. Resour* 21, 442–451. doi: 10.13430/j.cnki.jpgr.20190627004

Yang, J., Sun, K., Li, D., Luo, L., Liu, Y., Huang, M., et al. (2019). Identification of stable QTLs and candidate genes involved in anaerobic germination tolerance in rice *via* high-density genetic mapping and RNA-seq. *BMC Genomics* 20, 355. doi: 10.1186/s12864-019-5741-y

Zhang, C. Q., Nishiuchi, S., Liu, S. K., and Takano, T. (2008). Characterization of two plasma membrane protein 3 genes (PutPMP3) from the alkali grass, puccinellia tenuiflora, and functional comparison of the rice homologues, OsLti6a/b from rice. *BMB Rep. BMB Rep.* 41, 448–454. doi: 10.5483/BMBRep.2008.41.6.448

Zhang, L. N., Tang, J. H., Cui, D., Tang, C. F., Ma, X. D., XX, A., et al. (2021). Identification of QTLs for cold tolerance at the booting and flowering stages in rice (Oryza sativa l.). *Euphytica* 217, 214. doi: 10.1007/s10681-021-02898-6

Zou, C., Wang, P. X., and Xu, Y. B. (2016). Bulked sample analysis in genetics, genomics and crop improvement. *Plant Biotechnol. J.* 14, 1941–1955. doi: 10.1111/pbi.12559

frontiers | Frontiers in Plant Science

TYPE Original Research
PUBLISHED 25 January 2023
DOI 10.3389/fpls.2023.1016993

Check for updates

OPEN ACCESS

EDITED BY
Mirza Hasanuzzaman,
Sher-e-Bangla Agricultural University, Bangladesh

REVIEWED BY
Kulasekaran Ramesh,
Indian Institute of Oilseeds Research (ICAR), India
Mohamed Anli,
Cadi Ayyad University, Morocco

*CORRESPONDENCE
Baisha Weng
wengbs@iwhr.com

SPECIALTY SECTION
This article was submitted to Plant Abiotic Stress, a section of the journal Frontiers in Plant Science

RECEIVED 11 August 2022
ACCEPTED 12 January 2023
PUBLISHED 25 January 2023

CITATION
Jing L, Weng B, Yan D, Zhang S, Bi W and Yan S (2023) The persistent impact of drought stress on the resilience of summer maize.
Front. Plant Sci. 14:1016993.
doi: 10.3389/fpls.2023.1016993

COPYRIGHT
© 2023 Jing, Weng, Yan, Zhang, Bi and Yan. This is an open-access article distributed under the terms of the Creative Commons Attribution License (CC BY). The use, distribution or reproduction in other forums is permitted, provided the original author(s) and the copyright owner(s) are credited and that the original publication in this journal is cited, in accordance with accepted academic practice. No use, distribution or reproduction is permitted which does not comply with these terms.

The persistent impact of drought stress on the resilience of summer maize

Lanshu Jing[1,2], Baisha Weng[1,3]*, Denghua Yan[1], Shanjun Zhang[1], Wuxia Bi[1] and Siying Yan[1]

[1]State Key Laboratory of Simulation and Regulation of Water Cycle in River Basin, China Institute of Water Resources and Hydropower Research, Beijing, China, [2]College of Hydrology and Water Resources, Hohai University, Nanjing, China, [3]Yinshanbeilu Grassland Eco-hydrology National Observation and Research Station, China Institute of Water Resources and Hydropower Research, Beijing, China

Crop resilience refers to the adaptive ability of crops to resist drought at a certain level. Currently, most of the research focuses on the changes in root or photosynthesis traits of crops after drought and rehydration. Still, the persistence effect (drought period (T2) - rehydration period (T3) - harvest period (T4)) of drought stress on crops and quantitative estimation of resilience is still unclear. Field experiments were conducted in this study to determine the persistence effects on above-ground and below-ground growth indicators of summer maize at different levels and durations of drought. Next, an evaluation method for integrated resilience of summer maize was proposed, and a quantitative assessment of integrated resilience was made by Principal Component Analysis (PCA) and resilience index calculation. The results showed that the resilience of summer maize decreased with increasing drought levels, which persisted until harvest. Although summer maize resilience was strong after rewatering under light drought (DR1), declined after sustained rewatering. At the same time, production had decreased. However, a specific drought duration could improve the resilience of summer maize under light drought conditions. In particular, leaf biomass and root growth in the 30-50 cm layer could be enhanced under long duration light drought (LDR1), thus improving summer maize resilience and yield. Thus, under water shortage conditions, a certain level and duration drought could improve the resilience and yield of summer maize, which would persist until harvest. Clarifying the persistent effects on the growth indicators of summer maize and quantitatively evaluating the resilience of summer maize could improve agricultural food production and water use efficiency.

KEYWORDS

drought degree, drought duration, root growth, summer maize growth, PCA analysis

1 Introduction

Under climate change, drought will become more frequent and severe in most parts of the world (Spinoni et al., 2020; Pokhrel et al., 2021; Li P, et al., 2022). As a kind of extreme weather phenomenon, drought is the main factor limiting agricultural production (Panda et al., 2021; Yao et al., 2022). Maize is one of the most significant food crops globally.

Meanwhile, maize yield was more sensitive to drought (Liu et al., 2022). For instance, drought caused maize biomass losses in the northeast and north China plain from 2000 to 2019 (Cai et al., 2020; Wan et al., 2022). In the summer maize planting-tasseling and tasseling-physiological maturity periods, drought showed an increasing trend in the most Huang-Huai-Hai Plain of China from 1961 to 2015 (Wu X, et al., 2021). Consequently, drought poses a serious threat to maize growth and production.

The level and duration of droughts are closely related to maize growth. At the young ear development of maize, the maize biomass decreased by 54.3% and 61.4% under light (soil moisture at 60 ± 5%) and moderate (soil moisture at 40 ± 5%) drought stress, respectively (Shao et al., 2021). And as the drought increased in severity, the maize biomass and yield decreased (Zhang et al., 2019; Li et al., 2020; Liu et al., 2022). And, severe drought stress (35% field water capacity) adversely affected growth and yield parameters at different maize growth stages and resulted in delayed maturation (Ge et al., 2011). In addition, prolonged drought resulted in a reduction of growth rate, lower biomass, and delayed flowering (Verbraeken et al., 2021). For instance, with increasing drought duration, the number of filled grains per maize plant declined (Shin et al., 2015). Meanwhile, prolonged drought could cause maize cell dysfunction by the accumulation of reactive oxygen species (Xiao et al., 2020).

However, some researches also showed that during rehydration after drought, maize could recover, which was closely related to the degree and duration of drought (Ge et al., 2011; Sun et al., 2016). For example, drought limited the photosynthetic of maize, after rehydration could restore most photosynthetic traits (Qi et al., 2021). But the longer the drought duration, the weaker the maize's photosynthetic capacity to recover (Jia et al., 2020). Although drought can affect the growth and development of maize, maize has resilience to resist drought. With different levels and durations of drought, maize resilience varies.

The resilience enables that crop could recover even exceed normal growth after rehydration at a certain level and duration drought (Müller et al., 2016; Qi et al., 2021). Originally, resilience refers to the ability of an ecological system to sustain relationships within an environmental system (Holling, 1973; Müller et al., 2016). Subsequently, some scholars proposed that resilience be incorporated into agroecosystems research, and believed that resilience could add tangible value to agroecosystems research (Peterson et al., 2018). Thus, some studies found crop diversity might contribute to increase crop resilience at a certain level drought (Elsalahy et al., 2020). Beyond that, coordinated changes in chlorophyll content, gas exchange, and fluorescence parameters possibly contributed to enhance maize resilience under drought conditions (Qi et al., 2021). Crop resilience is rapidly becoming a hot research issue. However, few studies have examined maize resilience under drought conditions based on maize growth indicators (Matsushita et al., 2016; El Chami et al., 2020).

Here, we conducted field experiments to quantitatively describe the persistent effects of drought on summer maize growth indexes and yield. Furthermore, we constructed the comprehensive resilience assessment method based on the growth indexes and quantitatively analyzed the resilience under different drought degrees and durations. This study aimed to test the following hypotheses: (i) Different degrees and durations of droughts can significantly reduce the resilience of summer maize. (ii) The drought impact on summer maize can last until the harvest period and then reduce the yield of summer maize. These results can contribute to better understanding the persistent impacts on summer maize resilience and serve as a scientific reference for drought risk responses in agriculture.

2 Materials and methods

2.1 Site description and drought evaluation

The experiment was conducted at Wudaogou experimental research station (33°09′N, 117°21′E) in Bengbu City, China. The area is a subtropical semi-humid warm temperate, continental monsoon climate. The main soil types are dark-hydromorphic clay loam and flavor-aquic soil, which account for 52.2% and 30.9% of the total area, respectively. The soil bulk density is 1.41 g/cm^3 (Bi et al., 2021). Precipitation is unevenly distributed throughout the year, and droughts and floods are frequent. It is the central disaster area of agricultural drought in the Huaihe River Basin (Liu et al., 2017; Chen et al., 2020; Wang et al., 2020).

The drought degree is determined by China's "Standards of Drought Situations" (SL424-2008). The calculation equation was as follows:

$$RSH = \frac{\theta}{F_c} \times 100\,\%$$

Where θ was the soil average weight moisture, which was calculated from the ratio of soil volumetric water content to soil bulk density in 10-20 cm layer. F_c was the field capacity (Bi et al., 2021).

The drought is divided into five levels. When RSH>60% means no drought; When RSH is within 50%-60%, indicating light drought; When RSH is within 40%-50%, indicating moderate drought; When RSH is within 30%-40%, indicating severe drought; When RSH< 30%, indicating extreme drought.

2.2 Experiment design

We explored the drought persistent impact on the resilience of summer maize during jointing, tasseling, and grain filling. We designed six drought scenarios, i.e., Light drought (DR1), Moderate drought (DR2), Short duration light drought (5 days, SDR1), Long duration light drought (7 days, LDR1), Short duration moderate drought (14 days, SDR2), and long duration moderate drought (24 days, LDR2). In addition, a control system (CK) was set for reference under no drought conditions. The specific process of the experiment is shown in Figure 1. In particular, before the start of the experiment, the initial conditions of each field were the same (seed type, fertilization amount, suitable soil water content). And the ventilated shed with an artificial rainfall device was used to block the entry of external precipitation. After the drought, the soil moisture would be restored to the suitable summer maize growth range through artificial rainfall.

All experiments were conducted during the growing season of summer maize from 18 June to 28 September 2020 and from 19 June

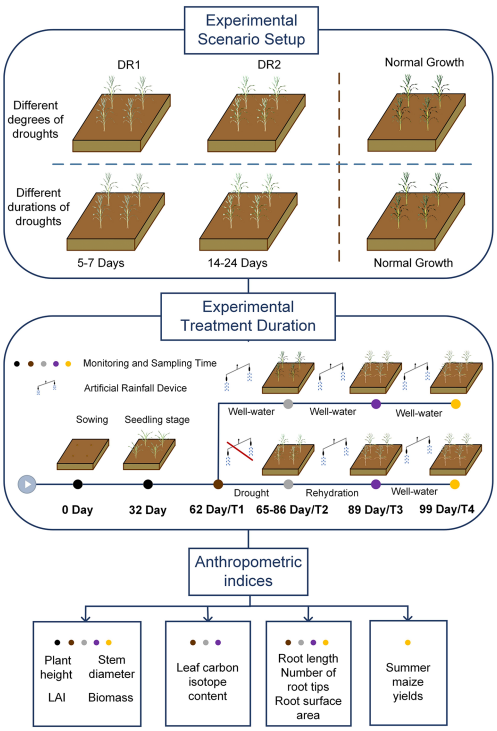


FIGURE 1
The specific process of the experiment. DR1, Light drought; DR2, Moderate drought; T1, before drought; T2, drought period; T3, rehydration period; T4, harvest period.

to 25 September 2021. Field planting was used at the experiment site. Due to the limitations of the site, each scenario included two fields (length×width=3.7 m×5.5 m). Figures 2A, B shows the specific layout details. Each area used aluminum-plastic composite panels with a depth of 1.2 m as baffles to prevent shallow water and groundwater. Apart from this, Denghai 618 was selected as the sowing variety of summer maize in the experiment, and the fertilizer was urea and compound fertilizer. The row spacing is 60 cm and the plant spacing is 25 cm, and about 135 plants were planted in each field.

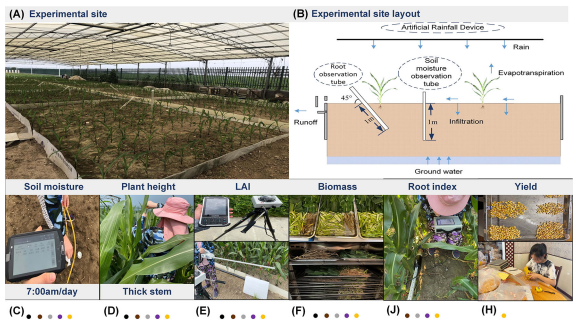


FIGURE 2
(A) experimental site and **(B)** experimental site layout and **(C)** soil moisture monitoring and **(D)** plant height and thick stem monitoring and **(E)** LAI monitoring and **(F)** biomass monitoring and **(J)** root monitoring and **(H)** yield monitoring.

2.3 Soil moisture measurement

Soil moisture was measured with an AIM-WiFi soil multiparameter monitoring system (Beijing Aozuo Ecology Instrumentation Ltd., Beijing, China), which used the Time Domain Reflectometry principle (Figure 2C). The rated accuracy was 1%. In this experiment, we collected four layers of soil moisture data (10 cm, 30 cm, 50 cm, and 70 cm) in each field from 7:00 am to 8:00 am (GMT + 8), and each layer was measured three times. This was one of the primary indicators to judge the levels of drought.

2.4 Growth index measurement

The growth indexes included plant height, thick stem, leaf area index (LAI), biomass, leaf carbon isotope content, root surface area, root length, number of root tips, and summer maize yield. Notably, plant height and thick stem were measured with a tape measure (Figure 2D), and each field selected three plants for measurement. LAI was measured with a Sun-scan system (Senpro Mechanical & Electrical Co., Ltd, Shanghai, China) (Figure 2E). To ensure the accuracy of the measurement results, each measurement time was selected from 9:00 am to 11:00 am (GMT + 8) in the morning. Biomass data (root, stem, leaf, fruit) were obtained by digging the whole summer maize, decomposing, drying, and weighing it (Figure 2F). The root growth indexes (the root surface area (RSA), root tip number (RNB), and root length (RLT)) were measured by the micro-root window technology of the AZR_100 root ecological monitoring system (Beijing Aozuo Ecology Instrumentation Ltd., Beijing, China) (Figure 2G). Each point measured 4 layers, 10 cm, 30 cm, 50 cm and 70 cm. The yield of summer maize was determined by the statistics of agronomic traits of mature maize ears in each field. (Figure 2H).

2.5 Calculation of comprehensive resilience index

Based on field experiments, we used the comprehensive resilience index to quantitatively analyze the persistence effects of different drought on the resilience of summer maize. To establish a comprehensive resilience index, we need to clarify the contribution rate of each growth index of summer maize under drought conditions. The purpose of principal component analysis (PCA) is to decrease the elements of the indicator dataset and to select new significant underlying factors (Banerjee et al., 2015; Otitoju et al., 2016). Therefore, we used the PCA method to select the central component (PC) and factor as the weight value of each main growth index.

In order to calculate the comprehensive resilience index, we also need to build a single factor resilience index, the specific formula is as follows (Orwin and Wardle, 2004; Elsalahy et al., 2020) (Eq (1)) :

$$R_I = \begin{cases} 1 - \frac{2|D_0|}{(|D_0|+|D_x|)}, D_x > 0 \\ 0 \qquad\qquad\quad , D_x < 0 \end{cases}$$

Where D_0 is the difference between the indexes of no drought-stressed summer maize and drought-stressed summer maize at

theend of drought; D_x is the difference between drought-stressed summer maize and drought-stressed summer maize after rehydration. If $D_x < 0$, it means that the summer maize failed to recover after rehydration ($R_l = 0$); While $D_x > 0$, the summer maize has resilience after rehydration. If $R_l < 0$, indicates that summer maize has not been able to recover fully, the greater the R_l, the stronger the resilience; If $R_l \geq 0$, indicates that summer maize has been able to recover fully, the greater the R_l, the stronger the resilience.

Further, according to the weight of each main growth index and single factor resilience, the comprehensive resilience index of summer maize is calculated. The formula is as follows: (Eq (2)):

$$R_{Tl} = \lambda_1 \times R_{l1} + \lambda_2 \times R_{l2} + \cdots + \lambda_k \times R_{lk}$$

Where $\lambda_1 \ldots \lambda_k$ are the weight of each main growth index (based on PCA calculation results); $R_{l1} \ldots R_{lk}$ are the resilience of main growth index.

2.6 Statistical analysis

The growth characteristics of summer maize under different drought conditions were analyzed by taking the difference between the drought-stressed and no drought-stressed summer maize indexes. The drought treatment group data minus the mean value of the control group data was used to represent the variation of each index. Difference data were shown in mean + standard deviation. The figures were drawn in Origin version 2021 (OriginLab Inc., Hampton, MA, USA).

3 Results

3.1 Effects of different drought degrees and durations on summer maize in the T2-T3 period

Figure 3A showed that the changes of various growth indexes of maize in the T2-T3 period. In the T2 period, the biomass of stem, leaf, and grain decreased by 3.317 g, 2.05 g, and 3.85 g under DR1, 9.017 g, 3.583 g, and 20.06 g under DR2 respectively. DR2 decreased more than DR1. However, the reduction of root biomass under DR2 was less than that under DR1, which was 3.31 g and 3.133 g, respectively. In addition, the plant height under DR1 was taller than the CK, which was 2.317 cm. thick stem, carbon stable isotope, and LAI under DR2 were higher than that under DR1. Plant height, stem, leaf, and grain biomass decreased with drought degree. Meanwhile, thick stem, root biomass, carbon stable isotopes, and LAI increased slightly with the increasing of drought degree. In the T3 period (Figure 3A), the plant height, thick stem, stem, leaf, grain, and root biomass of summer maize affected by DR2 were lower than those affected by DR1. Additionally, LAI was lower than CK under DR1, but higher than CK under DR2. The thick stem, stem, leaf, grain, and root biomass affected by DR1 could be recovered to normal growth state, however, plant height, carbon stable isotopes, and LAI could not be recovered. While root biomass and LAI could recover to normal growth from DR2, other growth indicators are not. It represented that the stronger the drought level, the stronger the effect on summer maize growth indicators.

Figure 4A showed that the changes of various root growth indexes of maize in the T2-T3 period. In the T2 period, the reduction of root growth indexes under DR1 were higher than that under DR2, but only the reduction of the RNB and RLT in the 50 cm layer was lower. RSA in the 10 cm layer and RSA, RNB, and RLT in the 30 cm layer under DR2 were better than the normal growth state. The RSA, RNB, and RLT in the 50cm and 70cm layer under DR2 were worse than the normal growth state. In the T3 period (Figure 4A), the reduction of RSA, RNB, and RLT in the 10 cm and 70 cm layers under DR2 were higher than that under DR1, but only the reduction of the RSA in the 10 cm layer was lower. The RSA, RNB, and RLT in the 30-50 cm layer under DR2 were higher than that under DR1. The root growth of 10 cm and 70 cm was damaged and could not be recovered to the normal growth state. The RSA, RNB, and RLT in the 30-50 cm layer could recover to the normal growth state under DR2.

Figure 3B showed that the changes of various growth indexes of maize under different drought duration in the T2-T3 period. In the T2 period, thick stem, plant height, root, leaf, stem, grain biomass under LDR1 were all higher than that under SDR1. Carbon stable isotopes and LAI under SDR1 were higher than that under LDR1. plant height, root, stem, leaf, grain biomass, and LAI under SDR2 were all higher than that under LDR2. The thick stem and carbon stable isotope under SDR2 were lower than that under LDR2. In the T3 (Figure 3B), thick stem, root, stem, leaf, grain biomass, carbon stable isotope, and LAI under SDR1 were all higher than that under LDR1. The plant height under SDR1 was lower than that under LDR1. The plant height, thick stem, root, stem, leaf, grain biomass, and LAI under SDR2 were all higher than that under LDR2. The carbon stable isotope under SDR2 was lower than that under LDR2. In addition, the plant height could not recover to the normal growth state, other growth indicators could recover under SDR1. The thick stem, plant height, root, and stem biomass could recover to the normal growth state, other growth indicators could not recover under LDR1. The thick stem, plant height, grain biomass, and LAI could not recover to the normal growth state, other growth indicators could recover under SDR2. The carbon stable isotope could recover to the normal growth state, other growth indicators could not recover under LDR2.

Figure 4B showed that the changes of various root growth indexes of maize under different drought duration in the T2-T3 period. In the T2 period, the RSA, RNB, and RLT in the 30 and 50 cm layers were all higher under LDR1 than that under SDR1. However, the RSA, RNB, and RLT in the 10cm and 70 cm layers were all lower under LDR1 than under SDR1, except for the RSA in the 10 cm layer. The RSA, RNB, and RLT in the 10 cm and 30 cm layers under SDR2 were also lower than that under LDR2. The RSA, RNB, and RLT in the 50cm and 70cm layers under LDR2 were lower than that under SDR2. In the T3 period, the RSA, RNB, and RLT in the 10, 30, and 50 cm layers under LDR1 were all higher than that under SDR1. But the RSA, RNB, and RLT in the 70 cm layer under LDR1 was lower than that under SDR1. It indicated that under light drought stress, the root growth in the 10, 30, and 50 cm layers increased with the drought duration. Besides, the RSA, RNB, and RLT in the 10 cm, 30 cm, and 70 cm layers under SDR2 were higher than that under LDR2, apart from the RLT in the 30 cm. But the RSA, RNB, and RLT in the 50 cm under SDR2 were lower than that under LDR2. It could be explained that

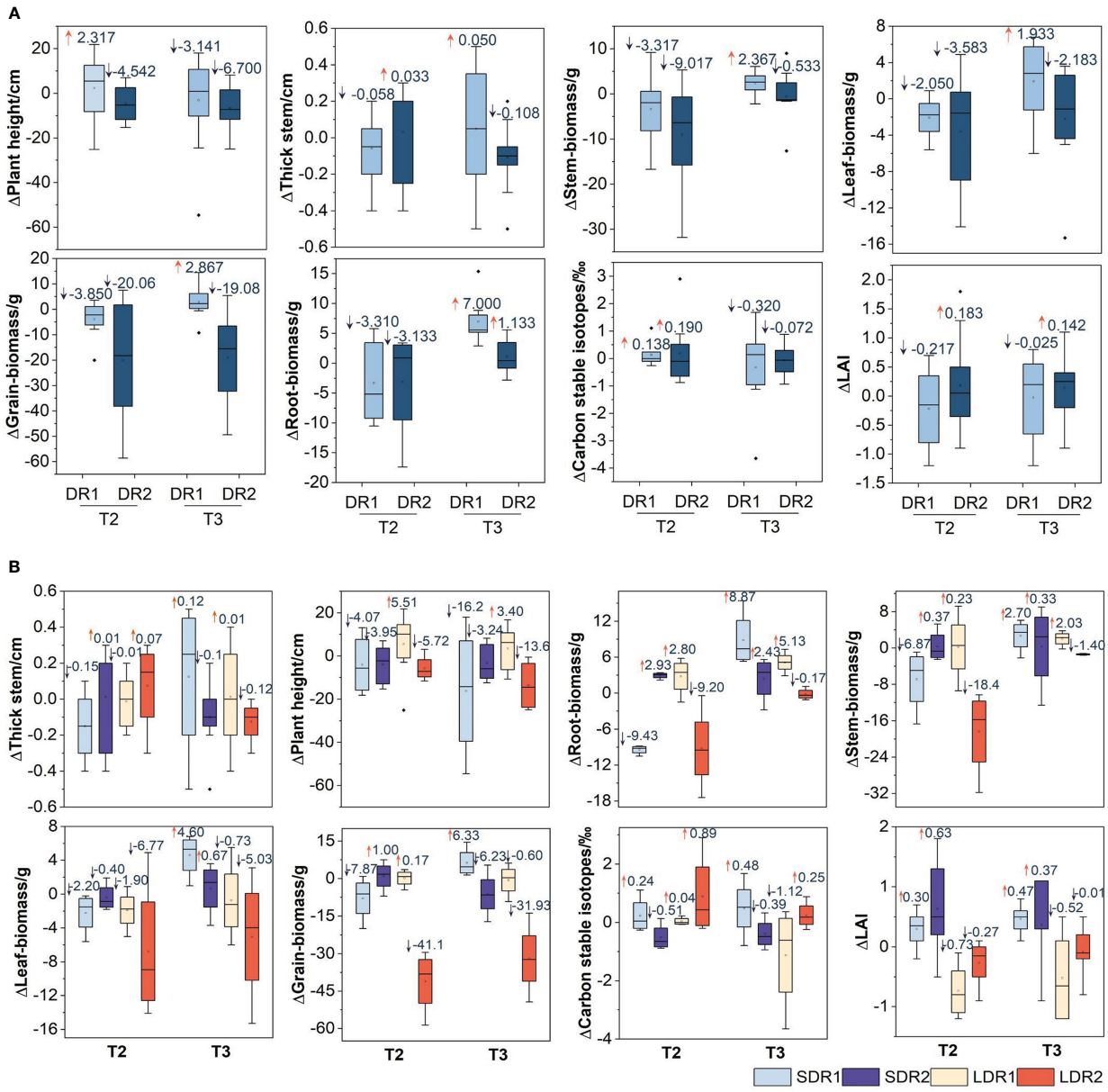


FIGURE 3
Effects of different **(A)** drought degree and **(B)** drought duration in the T2-T3 period on growth indexes of summer maize. in filling. SDR1, Short duration light drought (5 days); LDR1, Long duration light drought (7 days); SDR2, Short duration moderate drought (14 days); LDR2, Long-duration moderate drought (24 days).

under moderate drought stress, the root growth in the 10, 30, and 70 cm layers decreased with the drought duration.

3.2 Effects of different drought degrees and durations on summer maize in the T4 period (harvest period)

The change in each growth indexes in the T4 period could reflect the persistent effect of drought on the growth process of summer maize. Figure 5A showed that in the T4 period, root, stem, leaf biomass, and yield were lower than CK. Although the root, stem, leaf, and grain biomass affected by drought in the T3 period could recover to the normal growth state, but it could not last until harvest. Plant height and grain biomass under DR1 were higher than CK, 3.608 cm and 0.55 g, respectively. But, that under DR2 were lower than CK, 3.742 cm and 18.51 g, respectively. It points out that the recovery of summer maize could decreased with the drought degree. In addition, the yield of summer maize decreased with the increase in drought degree.

Figure 5B showed that leaf biomass and LAI under LDR1 were lower than CK, but other growth indexes were higher than CK. The thick stem and LAI under SDR1 were higher than CK, but other growth indexes were lower than CK. However, compared with the T3 period, under light drought stress, the recovery and yield of summer maize could increase with the increased drought duration. Thick stem, root, stem biomass, LAI, and yield were higher than the CK under SDR2. Among them, except for thick stem and LAI, the other indicators under LDR2 were lower than CK. Therefore, compared with the T3 period, under moderate

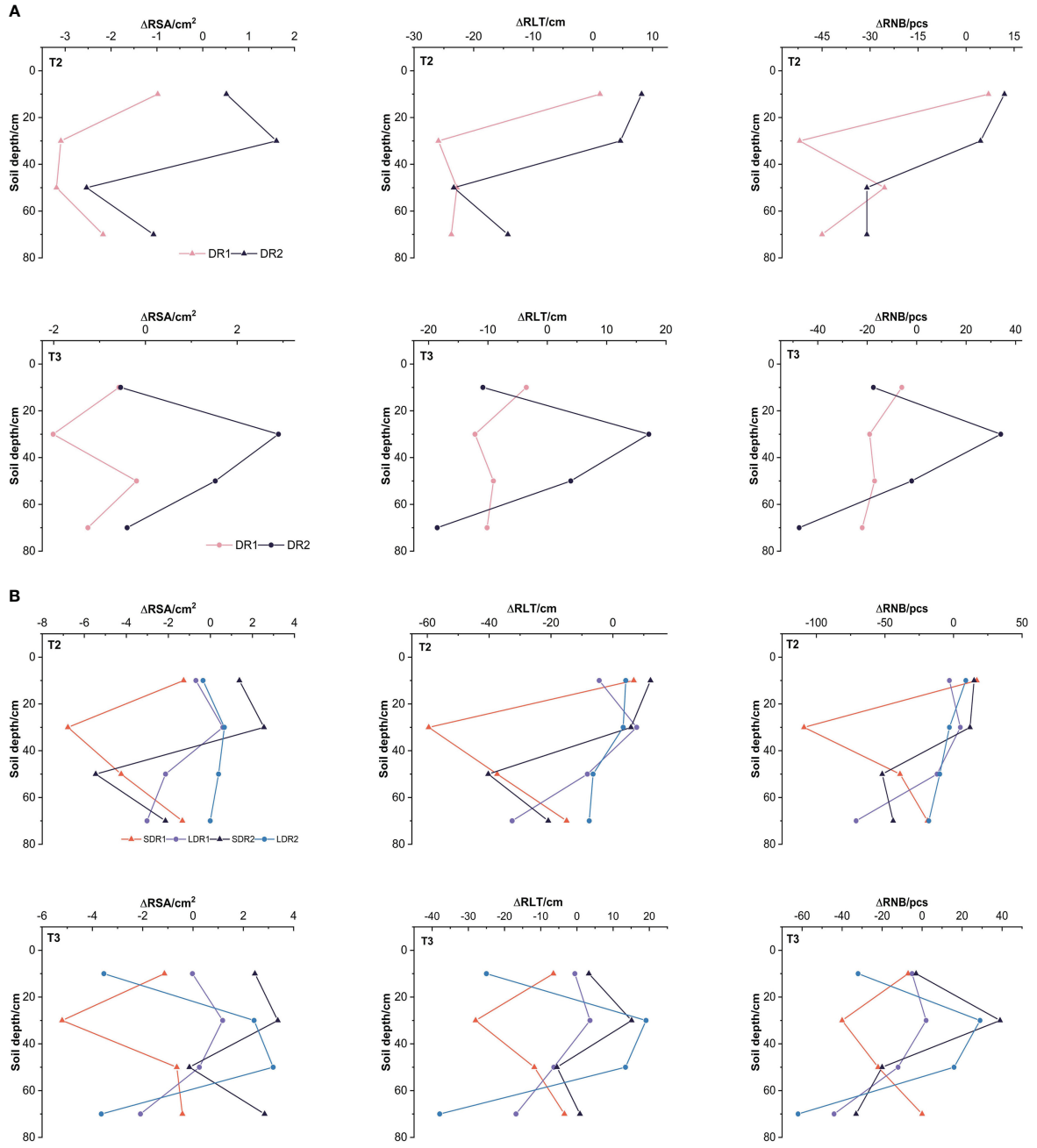


FIGURE 4
Effects of different **(A)** drought degree and **(B)** drought duration in the T2-T3 period on root growth indexes of summer maize. RSA, root surface area; RNB, root apex number; RLT, root length.

drought stress, the recovery and yield of summer maize could decrease with the increased drought duration.

Figure 6A showed that the RSA, RNB, and RLT in the 10 cm layer and the RSA in the 70 cm layer under DR2 were higher than CK, but other conditions were lower than CK. Only the RSA in the 30 cm layer under DR1 was higher than CK, and other root indexes were lower than CK. Furthermore, the RSA and RLT in the 30 and 50 cm layer under DR2 were reduced more than that under the DR1. Compared with the T3 period, it indicated that drought reduced the root growth ability of summer maize in 30 and 50 cm layer, which increased with increasing drought levels in the T4 period. Figure 6B showed that the RSA, RNB, and RLT in the 30 cm layers were all higher than CK under LDR1. However, the RSA, RNB, and RLT in each layer were all lower than CK. Except for the RLT in the 10 cm and the RSA in the 50 cm, other root indexes under LDR1 were all higher than SDR1. Compared with the T3 period, it indicated that a certain duration of light drought could promote root growth and this effect can last until harvest in the T4 period. Apart from that, the RNB and RLT in the 10 cm layer, the RNB in the 30 cm layers and the RSA, RNB, and RLT in the 70 cm layer under LDR2 were higher than CK. The RSA, RNB, and RLT in the 30 cm, 70 cm layers and the RNB in the 50 cm layer under LDR2 were higher than SDR2. However, the reduction of RNB and RLT in the 30 cm layer were more elevated under LDR2 than SDR2. Thus, in the T4 period, under moderate drought stress, longer

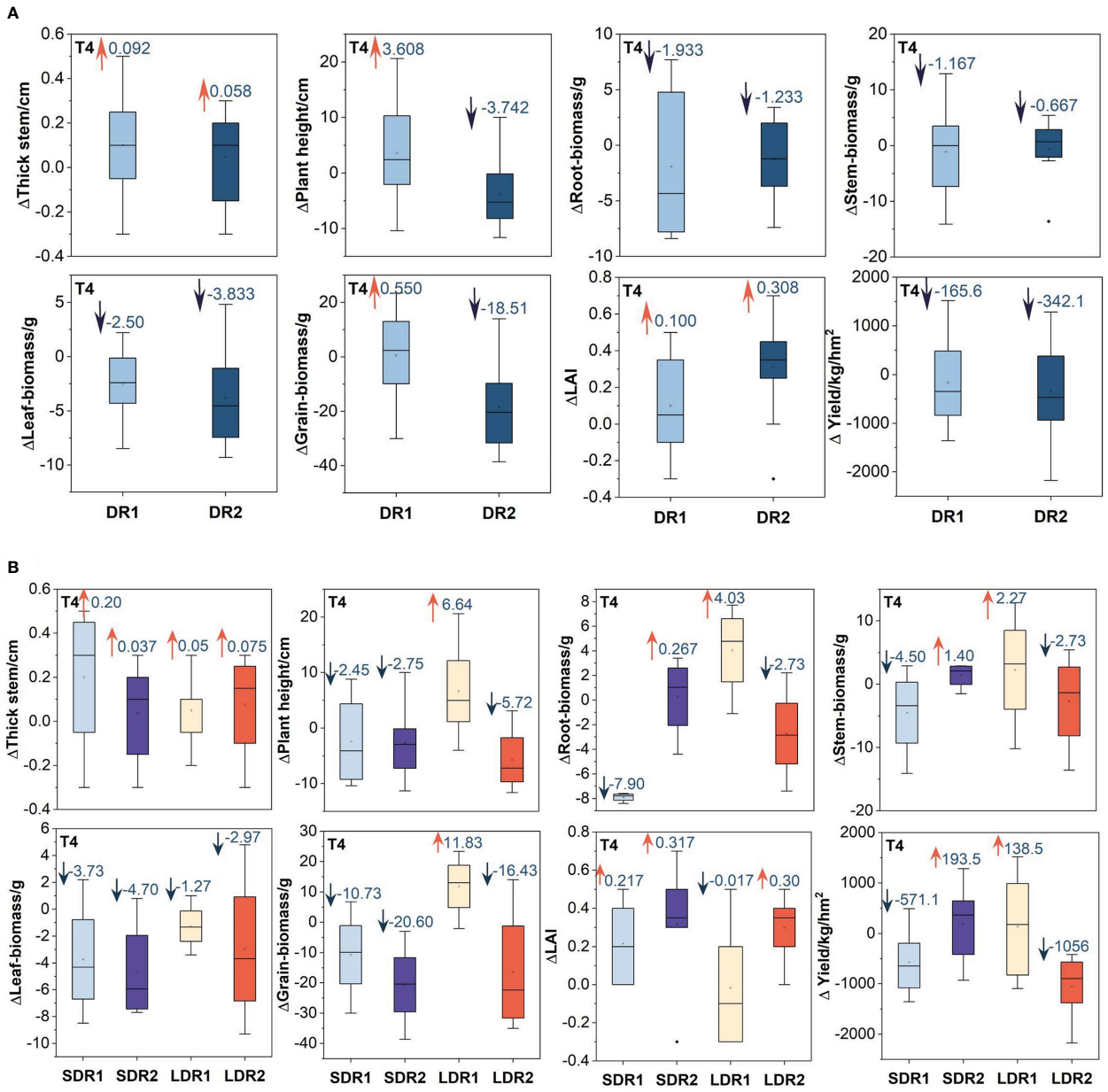


FIGURE 5
The persistent effects of different **(A)** drought degrees and **(B)** drought duration on growth indexes of summer maize in the T4 period.

duration of drought significantly reduced root growth in the 30 cm layer and inhibited summer maize recovery.

3.3 The persistence effects of different drought degrees and durations on the resilience of summer maize

The main factors influencing summer maize growth during T3 were analyzed by PCA. Figure 7A showed that the main factors affecting summer maize growth under different degrees of drought were leaf biomass, carbon stable isotopes, RLT in the 50 cm layer and RSA in the 50 cm layer. Figure 7B showed that the main factors affecting summer maize growth under different durations of light drought stress were RSA in the 10 and 50 cm layers, RNB in the 10 cm layer and RLT. Figure 7C showed that under moderate drought stress, the main factors affecting summer maize growth at different durations were RSA, RNB and RLT in the 10-70 cm layer.

In the T4 period, Figure 8A showed that the main factors affecting persistence of summer maize at different drought levels were stem thickness, RNB and RLT in the 30 cm layer and grain biomass. Figure 8B showed that the main factors affecting persistence of summer maize under light drought stress at different durations were stem biomass, RNB in the 10 cm layer and RNA B and RLT in the 70 cm layer. Figure 8C showed that the main factors affecting summer maize under moderate drought stress were grain biomass, yield and RSA, RNB and RLT.

Based on these results, the resilience of summer maize under different drought stresses was quantified. Figure 9 showed that drought-affected summer maize had two states of complete and

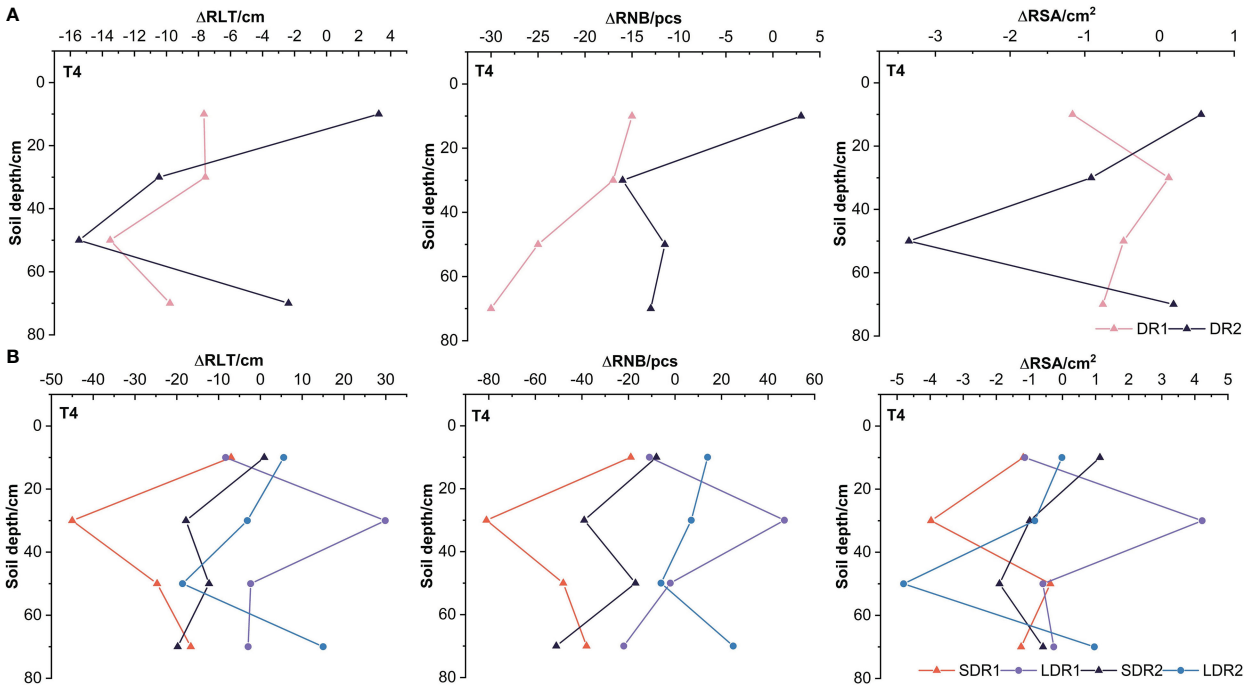


FIGURE 6
The persistent effects of different **(A)** drought degrees and **(B)** drought duration on root growth indexes of summer maize in the T4 period.

incomplete resilience after rehydration. Thus, the resilience under DR2 was weaker than DR1 during T3. Moreover, summer maize could not recover completely under DR2, but could recover completely under DR1. In the T4 period, summer maize could not recover completely under both DR1 and DR2. However, the resilience under DR2 was higher than that under DR1. This revealed that the stronger the drought stress, the weaker the resilience in the T3 period. Meanwhile, the effect of drought on summer maize growth could last until the T4 period, reducing the resilience of summer maize. In addition, summer maize could not fully recover under SDR1 and LDR1 during T3 period, and the resilience under SDR1 was higher than that under LDR1. However, in T4 period, summer maize resilience increased under both drought conditions. And summer maize could recover completely under LDR1. This demonstrated that the resilience of long-term light drought was higher than that of short-term light drought under light drought stress. In the T3 period, summer maize has stronger resilience under SDR2 than LDR2, and summer maize could recover completely under SDR2 but not under LDR2. This suggest that summer maize affected by drought stress needs a certain amount of time to recover and a certain level of drought stress can enhance the resilience of summer maize.

4 Discussion

4.1 The response and resilience mechanism of summer maize under different drought degrees

Drought is a key factor affecting summer maize growth (Webber et al., 2018; Pokhrel et al., 2021). Previous studies had shown that increased drought limited the total biomass of summer maize plants, particularly grain and leaf biomass (Lesk et al., 2016; Shao et al., 2021; Wu H, et al., 2021). Moreover, drought stress reduced leaf size, stem elongation, and root proliferation, disrupted plant water relationships, and reduced water use efficiency (Efeoğlu et al., 2009; Farooq et al., 2009; Zhang et al., 2015). These conclusions were similar to those obtained in the T2 period analysis in this study. Drought stress could promote lateral root development, and induce lateral roots to grow into the middle soil layer to absorb more water, thereby increasing root biomass (Hussain et al., 2020; Hazman & Kabil, 2022). Also, this study showed that RSA, RLT and RNB in the 30 cm layer increased with increasing drought. A strong root structure could enhance the drought tolerance of maize (Hussain et al., 2020). Summer maize roots are affected by drought stress and secreted ABA (abscisic acid) synthase, which transmit drought signals to the aboveground organs (Wang et al., 2018). After receiving the drought signal, the leaves control the stomatal conductance through osmoregulation and reduce the photosynthetic rate and sap flow rate, thus reducing the biomass of each organ (Cai et al., 2020). Drought stress can also significantly alter the metabolism of carbohydrates, sugars and their derivatives, thereby reducing pollen viability and inhibiting the development of the male and fruiting ears (Li H, et al., 2022). This is in general agreement with the findings of the present study. However, this study still found that carbon stable isotopes and LAI increased slightly with increasing drought. The increase in carbon stable isotopes was mainly due to changes in enzyme activity in the leaves, leading to assimilation of C^{13} (Zhang et al., 2015). These phenomena indicated that drought stress negatively affected the growth of summer maize, but summer maize could resist certain drought damage.

However, summer maize affected by drought stress could recover after rehydrated (Qi et al., 2021). Previous studies had shown that maize could recover biomass, most photosynthetic traits, and growth rate, but

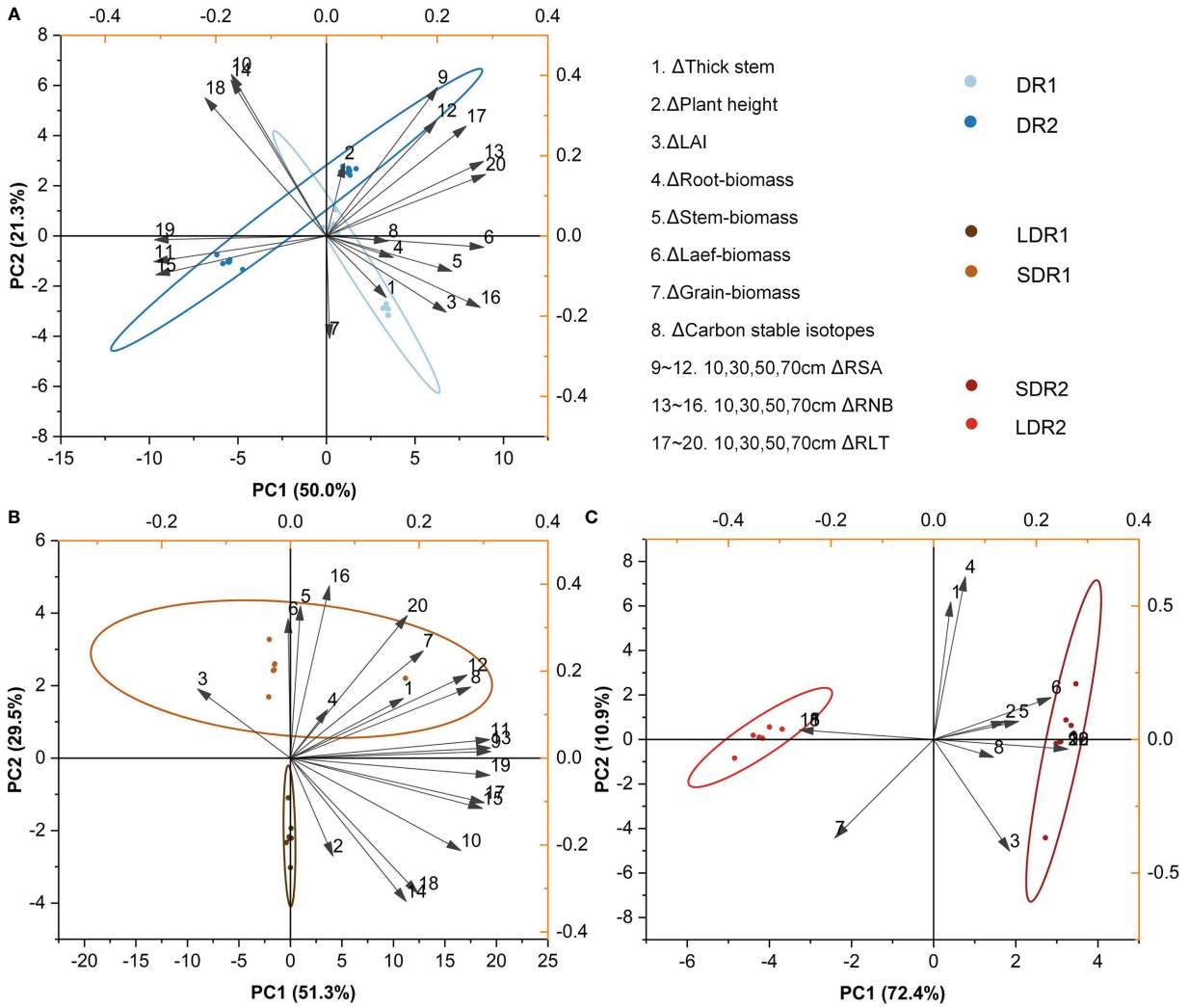


FIGURE 7
PCA analysis of the effects of different **(A)** drought degrees and **(B)** drought durations under light drought stress and **(C)** drought durations under moderate drought stress on various growth indexes of summer maize in the T3 period.

not the plant height and leaf area (Efeoğlu et al., 2009; Song et al., 2018). The above results were only consistent with the summer maize recovery of DR1 in this study. This ability of summer maize was known as resilience. The resilience of summer maize to drought may be due to root-induced cytokines, which promote the recovery of summer maize growth after rehydration (Qin & Wang, 2018). And the overexpression of ZmbZIP33 could also promote the accumulation of abscisic acid and improve the resilience of summer maize (Cao et al., 2021). In addition, this study also found that the resilience of RSA, RNB and RLT in the 30-50 cm layer showed an increasing trend with increasing drought level. It indicates that root growth in the 30-50 cm layer plays an important role in the resilience of summer maize. Moreover, root hydraulic conductance was closely related to stomatal conductance (Wang et al., 2017). Photosynthetic and transpiration rates recovered gradually after root growth was restored (Shao et al., 2021). Sap rate recovered, but decreased with increasing drought (Cai et al., 2020). Similar findings were found in the present study, with the exception of root biomass and LAI, which decreased in resilience as the degree of drought increased. In addition, maize is also able to return to normal levels at different rates through energy production, osmotic protection and signal regulation, but there are some differences between the metabolome and normal levels, e.g., the anthocyanin and proline content of leaves decreases with increasing drought levels after rehydration. In contrast, sucrose and glucose are overcompensated after rehydration (Efeoğlu et al., 2009). And with the increase in the degree of drought, the photosynthesis ability weakened, the leaves senesced, and the biomass accumulation and transport ability of maize weakened (Mansouri-Far et al., 2010; Zhang et al., 2019). Further explanation, the resilience of summer maize decreased with the increase of drought level.

4.2 The response and resilience mechanism of summer maize under different drought duration

Drought duration was another key factor affecting summer maize growth (Qi et al., 2021). As previous studies have revealed that the long duration of drought effects on the process of plant growth, leaf morphological characteristics and photosynthesis were severely remarked (Song et al., 2018; Jia et al., 2020). The prolonged

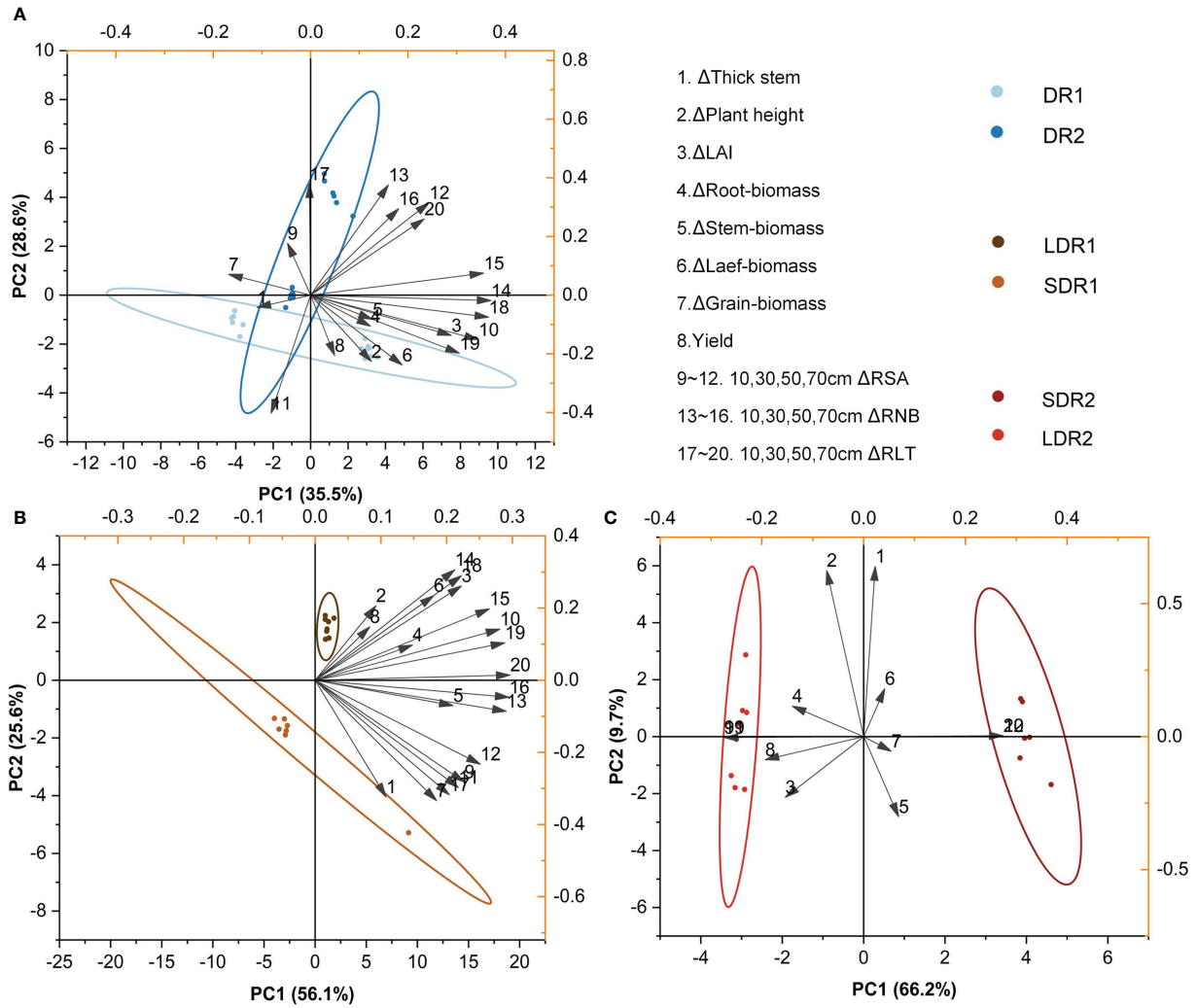


FIGURE 8
PCA analysis of the effects of different **(A)** drought degrees and **(B)** drought durations under light drought stress and **(C)** drought durations under moderate drought stress on various growth indexes of summer maize in the T4 period.

drought resulted in a reduction in growth rate of individual organs and an extension of growth duration of summer maize (Verbraeken et al., 2021). It was consistent with the results in this study, but the results obtained under light drought stress differently. This study found that longer duration of drought could promote the growth of summer maize under light drought stress. But carbon stable isotopes decreased with increasing drought duration. Longer duration of drought inhibited the growth of summer maize under moderate drought stress. The possible reason for this is that under mild drought, summer maize adapts to drought by changing enzyme activities in the root zone and leaves to improve water use efficiency (Hu et al., 2010). This revealed that the growth of the above-ground organs of summer maize is closely related to the root growth. Therefore, this study further analyzed the growth characteristics of the root system. Under light long-duration drought stress, summer maize improved its drought resistance by increasing and refining the root system in the 30-50 cm layer. As the drought level increased, the resistance of summer maize decreased. Under moderate short drought stress, summer maize improved resistance by increasing the root system in the 30 cm layer, whereas under moderate long-duration drought stress, summer maize improved resistance by increasing the root system in the 50 cm layer. But this ability was weaker than under moderate short-duration. This phenomenon may suggest that root growth in the 30-50 cm layer has a certain influence on the drought resistance of summer maize, but its ability is limited.

The recovery of summer maize affected by different drought durations after rewatering was different. This study found that under light and moderate drought stress, the recovery of summer maize growth was inhibited with the increase of drought duration. This result was consistent with some previous studies (Sun et al., 2016; Song et al., 2019; Jia et al., 2020). Ammonia-oxidizing bacterial strains in rhizosphere soil coexisted with maize and increased resilience by regulating soil nitrification and root-induced leaf cytokinin (Wang et al., 2022). The direct induction of cytokinin synthesis in maize roots by NO^3 released from the soil due to inter-root soil nitrification (Wang et al., 2021). Cytokinin transport to the leaves promotes recovery of summer maize (Wang et al., 2018). The root is the most direct organ that receives the stimulation. The root structure of summer maize in the 30-50 cm layer played an important role in

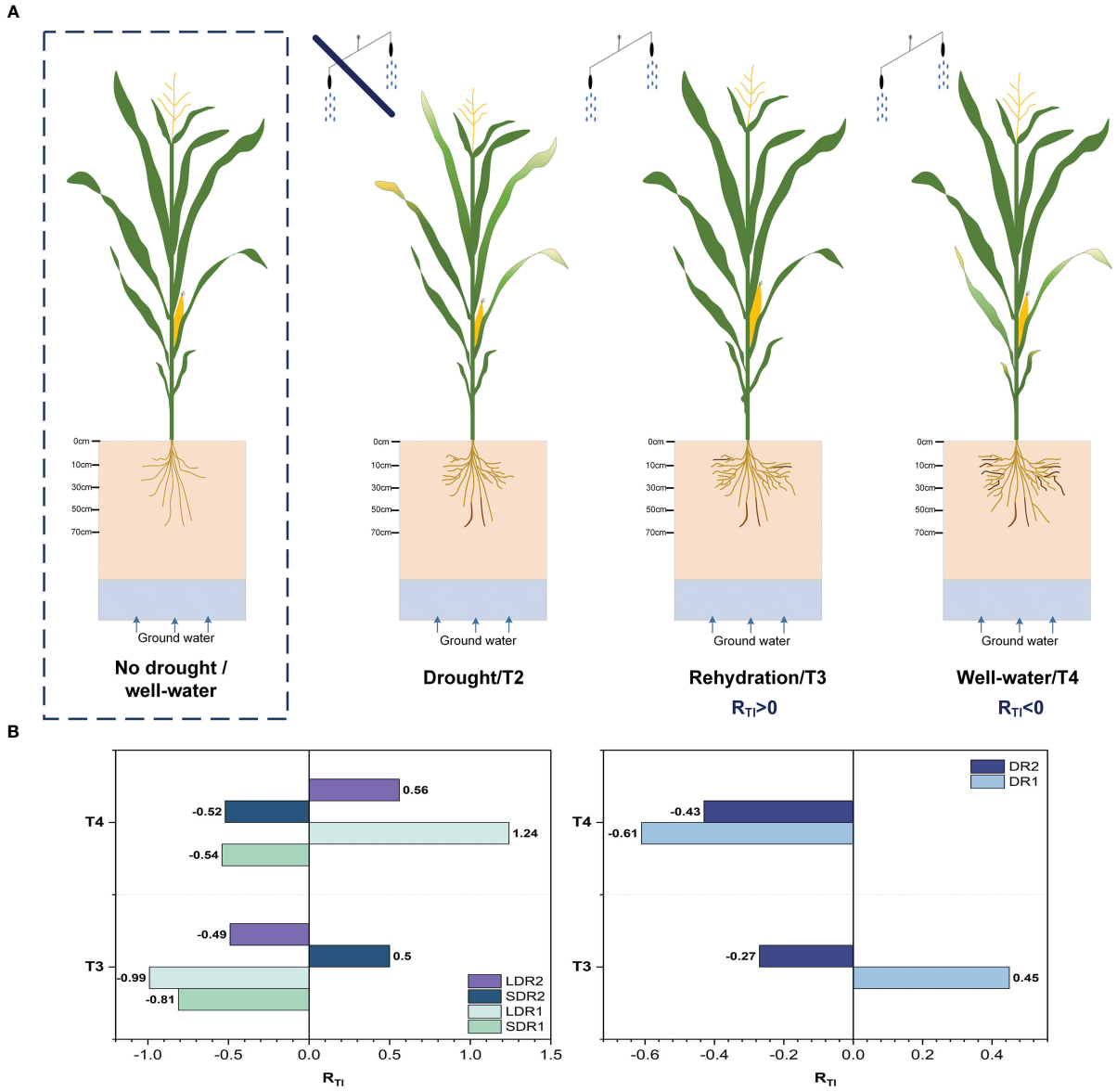


FIGURE 9
(A) Growth process and **(B)** resilience evaluation results of summer maize. (Darker color roots were dead roots, while lighter color roots were living roots.).

adapting to drought, while the root structure of summer maize in the layer of 10 cm could adapt to the influence of light drought, and the root structure of summer maize in the 70 cm layer was more seriously damaged during the drought and had weaker resilience.

4.3 The persistent effects of the resilience of summer maize under different degrees and durations of drought

Although many studies related to the effects of drought and rehydration conditions on physiological traits of summer maize, less attention paid to the effects of persistence on growth characteristics and yield of summer maize after rehydration at maturity (Sheoran et al., 2022). In this study, by analyzing the growth characteristics of summer maize during T4, we inferred that the effects of drought stress on summer maize continued until harvest, which was able to reduce the recovery capacity of summer maize and affect the yield. Also, the degree of root recovery of summer maize in the 30-50 cm layer decreased as the degree of drought increased. The root system is very closely related to summer maize resilience, indicating that summer maize does not sustain recovery. Furthermore, summer maize affected by severe drought, although it was able to recover to normal conditions after rehydration, continued rehydration still resulted in reduced growth status and lower yields.

It is worth noting that the effect of different drought durations on summer maize resilience during the T4 period was different. In this study, it was inferred that under light drought stress, a certain range of drought ephemeris and sustained rehydration increased the recovery and yield of summer maize, e.g., under LDR1. Although summer maize recovered to a lesser extent after rehydration, the resilience gradually increased. Yield was relatively higher after sustained

rehydration. Under moderate drought stress, yields decreased with increasing drought duration, and the degree of recovery was higher but still below normal growth. Previous studies have shown that under drought stress, maize yield showed a non-linear response to drought severity (Jin et al., 2020; Shao et al., 2021; Liu et al., 2022). Consistent with the results of this study, summer maize yield could be increased under SDR2 conditions. This may be related to the root system. The root system in the 30 cm layer was less redacted and improved the resilience of summer maize under SDR2. Under water deficit conditions, a range of drought duration and continuous rehydration were able to improve summer maize resilience and yield.

4.4 Quantitative evaluation of resilience of summer maize

Roots and leaves played a key role in the growth process of summer maize under drought stress. Similar conclusions were obtained by PCA analysis in this study. The main influencing factors of different levels and duration of drought on summer maize were leaf biomass and root growth index. This showed that the results obtained by PCA analysis in this study were more reasonable. Therefore, this study proposed a comprehensive calculation method for evaluating the resilience of summer maize. The results of the PCA analysis were combined to quantitatively evaluate the resilience of summer maize. The evaluation results verified the previous hypothesis. The stronger the degree of drought, the weaker the resilience of summer maize. Under DR1, resilience was able to exceed the normal growth state during T3 and decreased below normal growth during T4. This also indicated that drought was able to affect the harvest period of summer maize even with continued rehydration. Under a range of light drought duration, the resilience of summer maize was improved. Under LDR1, resilience was lower than normal growth during T3 and increased beyond normal growth during T4, with a relative increase in yield. This indicated that summer maize needed some time and rehydration to recover. Even though summer maize recovered less well after rehydration, continued rehydration increased resilience and yield. Under LDR2, summer maize suffered yield losses despite higher resilience. Therefore, evaluation of summer maize resilience cannot only analyze growth characteristics after rehydration, but still needs to be combined with growth characteristics and yield during the sustained rehydration period. In this study, the osmotic metabolic processes of summer maize were not analyzed due to experimental constraints and will be added in future studies.

5 Conclusion

Based on field trials, the persistence effects of different levels and durations of drought on growth indicators and yield of summer maize were quantified, and a comprehensive evaluation method for summer maize resilience was proposed under different drought conditions. The results showed that the resilience of summer maize decreased as the drought level increased, and this effect was able to last until the harvesting period. However, under DR1, summer maize recovery was stronger at T3, but weakened at T4, while all growth indicators and yield decreased. In this process, drought reduced summer maize leaf biomass and root growth capacity in the 30-50 cm layer. In addition, a range of duration under light drought stress was able to improve the resilience of summer maize. Under SDR1, summer maize had less resilience during T3, but continued rehydration was able to improve resilience and yield. Therefore, a certain degree and duration of drought can improve the resilience and yield of summer maize under water deficit conditions. This study provides support for agricultural drought risk response and efficient water use. In the future, physiological changes will further be analysed under different drought conditions. Combined with crop growth models still needed to quantify the relationship between crop water consumption and resilience.

Data availability statement

The raw data supporting the conclusions of this article will be made available by the authors, without undue reservation.

Ethics statement

Written informed consent was obtained from the individual(s) for the publication of any potentially identifiable images or data included in this article.

Author contributions

LJ and BW contributed to the conception and design of the study. DY confirmed and guided the study. LJ and SY carried out the experiments. LJ performed the statistical analysis and wrote the first draft of the manuscript. SZ, WB, and SY wrote sections of the manuscript. All authors contributed to the article and approved the submitted version.

Acknowledgments

This work was supported by the National Key R&D Program of China (No. 2022YFC3080300), the National Natural Science Foundation of China (No. 52022110 and No. 52209043), and the IWHR Research & Development Support Program (No. MK0145B022021). Many thanks to Wudaogou Experimentation Research Station for their full support and help during this study.

Conflict of interest

The authors declare that the research was conducted in the absence of any commercial or financial relationships that could be construed as a potential conflict of interest.

Publisher's note

All claims expressed in this article are solely those of the authors and do not necessarily represent those of their affiliated organizations, or those of the publisher, the editors and the reviewers. Any product that may be evaluated in this article, or claim that may be made by its manufacturer, is not guaranteed or endorsed by the publisher.

References

Banerjee, V., Krishnan, P., Das, B., Verma, A. P. S., and Varghese, E. (2015). Crop status index as an indicator of wheat crop growth condition under abiotic stress situations. *Field Crops Res.* 181, 16–31. doi: 10.1016/j.fcr.2015.06.009

Bi, W., Weng, B., Yan, D., Wang, H., Wang, M., Yan, S., et al. (2021). Responses of phosphate-solubilizing microorganisms mediated phosphorus cycling to drought-flood abrupt alternation in summer maize field soil. *Front. Microbiol.* 12. doi: 10.3389/fmicb.2021.768921

Cai, F., Zhang, Y., Mi, N., Ming, H., Zhang, S., Zhang, H., et al. (2020). Maize (Zea mays l.) physiological responses to drought and rewatering, and the associations with water stress degree. *Agric. Water Manage.* 24, 106379. doi: 10.1016/j.agwat.2020.106379

Cao, L., Lu, X., Wang, G., Zhang, Q., Zhang, X., Fan, Z., et al. (2021). Maize ZmbZIP33 is involved in drought resistance and recovery ability through an abscisic acid-dependent signaling pathway. *Front. Plant Sci.* 12. doi: 10.3389/fpls.2021.629903

Chen, M., Ning, S., Jin, J., Cui, Y., Wu, C., and Zhou, Y. (2020). Risk assessment of agricultural drought disaster on the huaibei plain of China based on the improved connection number and entropy information diffusion method. *Water* 12 (4), 1089. doi: 10.3390/w12041089

Efeoğlu, B., Ekmekçi, Y., and Çiçek, N. (2009). Physiological responses of three maize cultivars to drought stress and recovery. *South Afr. J. Bot.* 75 (1), 34–42. doi: 10.1016/j.sajb.2008.06.005

El Chami, D., Daccache, A., and El Moujabber, M. (2020). How can sustainable agriculture increase climate resilience? a systematic review. *Sustainability* 12 (8), 3119. doi: 10.3390/su12083119

Elsalahy, H. H., Bellingrath-Kimura, S. D., Roß, C.-L., Kautz, T., and Döring, T. F. (2020). Crop resilience to drought with and without response diversity. *Front. Plant Sci.* 11. doi: 10.3389/fpls.2020.00721

Farooq, M., Wahid, A., Kobayashi, N., Fujita, D., and Basra, S. M. A. (2009). Plant drought stress: Effects, mechanisms and management. *Agron. Sustain. Dev.* 29 (1), 185–212. doi: 10.1051/agro:2008021

Ge, T., Sui, F., Bai, L., Tong, C., and Sun, N. (2011). Effects of water stress on growth, biomass partitioning, and water-use efficiency in summer maize (Zea mays l.) throughout the growth cycle. *Acta Physiol. Plant.* 34 (3), 1043–1053. doi: 10.1007/s11738-011-0901-y

Hazman, M. Y., and Kabil, F. F. (2022). Maize root responses to drought stress depend on root class and axial position. *J. Plant Res.* 135 (1), 105–120. doi: 10.1007/s10265-021-01348-7

Holling, S. ,, C. (1973). Resilience and stability of ecological systems. *Annu. Rev. Ecol. Syst.* 4 (1), 1–23. doi: 10.1146/annurev.es.04.110173.000245

Hu, T., Yuan, L., Wang, J., Kang, S., and Li, F. (2010). Antioxidation responses of maize roots and leaves to partial root-zone irrigation. *Agric. Water Manage.* 98 (1), 164–171. doi: 10.1016/j.agwat.2010.06.019

Hussain, H. A., Men, S., Hussain, S., Zhang, Q., Ashraf, U., Anjum, S. A., et al. (2020). Maize tolerance against drought and chilling stresses varied with root morphology and antioxidative defense system. *Plants (Basel)* 9 (6), 720. doi: 10.3390/plants9060720

Jia, Y., Xiao, W., Ye, Y., Wang, X., Liu, X., Wang, G., et al. (2020). Response of photosynthetic performance to drought duration and re-watering in maize. *Agronomy* 10 (4), 533. doi: 10.3390/agronomy10040533

Jin, N., He, J., Fang, Q., Chen, C., Ren, Q., He, L., et al. (2020). The responses of maize yield and water use to growth stage-based irrigation on the loess plateau in China. *Int. J. Plant Prod.* 14 (4), 621–633. doi: 10.1007/s42106-020-00105-5

Lesk, C., Rowhani, P., and Ramankutty, N. (2016). Influence of extreme weather disasters on global crop production. *Nature* 529 (7584), 84–87. doi: 10.1038/nature16467

Li, H., Tiwari, M., Tang, Y., Wang, L., Yang, S., Long, H., et al. (2022). Metabolomic and transcriptomic analyses reveal that sucrose synthase regulates maize pollen viability under heat and drought stress. *Ecotoxicol. Environ. Saf.* 246, 114191. doi: 10.1016/j.ecoenv.2022.114191

Li, P., Huang, Q., Huang, S., Leng, G., Peng, J., Wang, H., et al. (2022). Various maize yield losses and their dynamics triggered by drought thresholds based on copula-Bayesian conditional probabilities. *Agric. Water Manage.* 261, 107391. doi: 10.1016/j.agwat.2021.107391

Li, Y., Wang, Z., Huo, Z., and chen, C. (2020). Experiments of water stress on Root/Shoot growth and yield of summer maize. *J. Appl. Meteorol. Sci.* 31 (01), 83–94. doi: 10.11898/1001-7313.20200108

Liu, S., Wang, H., Yan, D., Qin, T., Wang, Z., and Wang, F. (2017). Crop growth characteristics and waterlogging risk analysis of huaibei plain in anhui province, China. *J. Irrig. Drain. Eng.* 143. doi: 10.1061/(ASCE)IR.1943-4774.0001219

Liu, S., Xiao, L., Sun, J., Yang, P., Yang, X., and Wu, W. (2022). Probability of maize yield failure increases with drought occurrence but partially depends on local conditions in China. *Eur. J. Agron.* 139126552. doi: 10.1016/j.eja.2022.126552

Mansouri-Far, C., Modarres Sanavy, S. A. M., and Saberali, S. F. (2010). Maize yield response to deficit irrigation during low-sensitive growth stages and nitrogen rate under semi-arid climatic conditions. *Agric. Water Manage.* 97 (1), 12–22. doi: 10.1016/j.agwat.2009.08.003

Matsushita, K., Yamane, F., and Asano, K. (2016). Linkage between crop diversity and agro-ecosystem resilience: Nonmonotonic agricultural response under alternate regimes. *Ecol. Econ.* 126, 23–31. doi: 10.1016/j.ecolecon.2016.03.006

Müller, F., Bergmann, M., Dannowski, R., Dippner, J. W., Gnauck, A., Haase, P., et al. (2016). Assessing resilience in long-term ecological data sets. *Ecol. Indic.* 65, 10–43. doi: 10.1016/j.ecolind.2015.10.066

Orwin, K. H., and Wardle, D. A. (2004). New indices for quantifying the resistance and resilience of soil biota to exogenous disturbances. *Soil Biol. Biochem.* 36 (11), 1907–1912. doi: 10.1016/j.soilbio.2004.04.036

Otitoju, M. A., Enete, A. A., and Tejada Moral, M. (2016). Climate change adaptation: Uncovering constraints to the use of adaptation strategies among food crop farmers in south-west, Nigeria using principal component analysis (PCA). *Cogent Food Agric.* 2 (1), 1178692. doi: 10.1080/23311932.2016.1178692

Panda, D., Mishra, S. S., and Behera, P. K. (2021). Drought tolerance in rice: Focus on recent mechanisms and approaches. *Rice Sci.* 28 (2), 119–132. doi: 10.1016/j.rsci.2021.01.002

Peterson, C. A., Eviner, V. T., and Gaudin, A. C. M. (2018). Ways forward for resilience research in agroecosystems. *Agric. Syst.* 162, 19–27. doi: 10.1016/j.agsy.2018.01.011

Pokhrel, Y., Felfelani, F., Satoh, Y., Boulange, J., Burek, P., Gädeke, A., et al. (2021). Global terrestrial water storage and drought severity under climate change. *Nat. Climate Change* 11 (3), 226–233. doi: 10.1038/s41558-020-00972-w

Qi, M., Liu, X., Li, Y., Song, H., Yin, Z., Zhang, F., et al. (2021). Photosynthetic resistance and resilience under drought, flooding and rewatering in maize plants. *Photosynth. Res.* 148 (1-2), 1–15. doi: 10.1007/s11120-021-00825-3

Qin, R., and Wang, X. (2018). Effects of root depth on compensatory growth of corn seedlings during post-drought re-watering. *Chin. J. Ecol.* 37 (11), 3291–3297. doi: 10.13292/j.1000-4890.201811.030

Shao, R., Jia, S., Tang, Y., Zhang, J., Li, H., Li, L., et al. (2021). Soil water deficit suppresses development of maize ear by altering metabolism and photosynthesis. *Environ. Exp. Bot.* 192, 104651. doi: 10.1016/j.envexpbot.2021.104651

Sheoran, S., Kaur, Y., Kumar, S., Shukla, S., Rakshit, S., and Kumar, R. (2022). Recent advances for drought stress tolerance in maize (Zea mays l.): Present status and future prospects. *Front. Plant Sci.* 13. doi: 10.3389/fpls.2022.872566

Shin, S., Lee, J. S., Kim, S. G., Go, T.-H., Shon, J., Kang, S., et al. (2015). Yield of maize (Zea mays l.) logistically declined with increasing length of the consecutive visible wilting days during flowering. *J. Crop Sci. Biotechnol.* 18 (4), 237–248. doi: 10.1007/s12892-015-0112-y

Song, H., Li, Y., Zhou, L., Xu, Z., and Zhou, G. (2018). Maize leaf functional responses to drought episode and rewatering. *Agric. For. Meteorol.* 249, 57–70. doi: 10.1016/j.agrformet.2017.11.023

Song, L., Jin, J., and He, J. (2019). Effects of severe water stress on maize growth processes in the field. *Sustainability* 11 (18), 5086. doi: 10.3390/su11185086

Spinoni, J., Barbosa, P., Bucchignani, E., Cassano, J., Cavazos, T., Christensen, J. H., et al. (2020). Future global meteorological drought hot spots: A study based on CORDEX data. *J. Climate* 33 (9), 3635–3661. doi: 10.1175/jcli-d-19-0084.1

Sun, C., Gao, X., Chen, X., Fu, J., and Zhang, Y. (2016). Metabolic and growth responses of maize to successive drought and re-watering cycles. *Agric. Water Manage.* 172, 62–73. doi: 10.1016/j.agwat.2016.04.016

Verbraeken, L., Wuyts, N., Mertens, S., Cannoot, B., Maleux, K., Demuynck, K., et al. (2021). Drought affects the rate and duration of organ growth but not inter-organ growth coordination. *Plant Physiol.* 186 (2), 1336–1353. doi: 10.1093/plphys/kiab155

Wan, W., Liu, Z., Li, J., Xu, J., Wu, H., and Xu, Z. (2022). Spatiotemporal patterns of maize drought stress and their effects on biomass in the northeast and north China plain from 2000 to 2019. *Agric. For. Meteorol.* 315, 10882. doi: 10.1016/j.agrformet.2022.108821

Wang, C., Linderholm, H. W., Song, Y., Wang, F., Liu, Y., Tian, J., et al. (2020). Impacts of drought on maize and soybean production in northeast China during the past five decades. *Int. J. Environ. Res. Public Health* 17 (7), 947476. doi: 10.3390/ijerph17072459

Wang, N., Gao, J., and Zhang, S. (2017). Overcompensation or limitation to photosynthesis and root hydraulic conductance altered by rehydration in seedlings of sorghum and maize. *Crop J.* 5 (4), 337–344. doi: 10.1016/j.cj.2017.01.005

Wang, X.-L., Ma, K., Qi, L., Liu, Y.-H., Shi, J., Li, X.-L., et al. (2022). Effect of ammonia-oxidizing bacterial strain that survives drought stress on corn compensatory growth upon post-drought rewatering. *Front. Plant Sci.* 13. doi: 10.3389/fpls.2022.947476

Wang, X.-L., Qin, R.-R., Sun, R.-H., Wang, J.-J., Hou, X.-G., Qi, L., et al. (2018). No post-drought compensatory growth of corns with root cutting based on cytokinin induced by roots. *Agric. Water Manage.* 205, 9–20. doi: 10.1016/j.agwat.2018.04.035

Wang, X.-L., Sun, R.-H., Wu, D., Qi, L., Liu, Y.-H., Shi, J., et al. (2021). Increasing corn compensatory growth upon post-drought rewatering using ammonia-oxidising bacterial strain inoculation. *Agric. Water Manage.* 256, 107066. doi: 10.1016/j.agwat.2021.107066

Webber, H., Ewert, F., Olesen, J. E., Muller, C., Fronzek, S., Ruane, A. C., et al. (2018). Diverging importance of drought stress for maize and winter wheat in Europe. *Nat. Commun.* 9 (1), 4249. doi: 10.1038/s41467-018-06525-2

Wu, H., Su, X., Singh, V. P., Feng, K., and Niu, J. (2021). Agricultural drought prediction based on conditional distributions of vine copulas. *Water Resour. Res.* 57 (8). doi: 10.1029/2021wr029562

Wu, X., Wang, P., Ma, Y., Gong, Y., Wu, D., Yang, J., et al. (2021). Standardized relative humidity index can be used to identify agricultural drought for summer maize in the Huang-Huai-Hai plain, China. *Ecol. Indic.* 131, 108222. doi: 10.1016/j.ecolind.2021.108222

Xiao, G., Cai, H., Mu, Q., and Zhao, L. (2020). Physiological response mechanism of summer maize seedlings to drought-rehydration of different durations. *Agric. Res. Arid. Areas* 38 (05), 57–63. doi: 10.1016/j.agwat.2020.106379

Yao, N., Li, Y., Liu, Q., Zhang, S., Chen, X., Ji, Y., et al. (2022). Response of wheat and maize growth-yields to meteorological and agricultural droughts based on standardized precipitation evapotranspiration indexes and soil moisture deficit indexes. *Agric. Water Manage.* 266, 107566. doi: 10.1016/j.agwat.2022.107566

Zhang, C., Zhang, J., Zhang, H., Zhao, J., Wu, Q., Zhao, Z., et al. (2015). Mechanisms for the relationships between water-use efficiency and carbon isotope composition and specific leaf area of maize (Zea mays l.) under water stress. *Plant Growth Regul.* 77 (2), 233–243. doi: 10.1007/s10725-015-0056-8

Zhang, H., Han, M., Comas, L. H., DeJonge, K. C., Gleason, S. M., Trout, T. J., et al. (2019). Response of maize yield components to growth stage-based deficit irrigation. *Agron. J.* 111 (6), 3244–3252. doi: 10.2134/agronj2019.03.0214

frontiers | Frontiers in Plant Science

TYPE Original Research
PUBLISHED 31 January 2023
DOI 10.3389/fpls.2022.1031466

Check for updates

OPEN ACCESS

EDITED BY
Ji-Hong Liu,
Huazhong Agricultural University, China

REVIEWED BY
Lisa David,
North Carolina State University, United States
Quaid Hussain,
Shenzhen University, China

*CORRESPONDENCE
Honggang Sun
honggangsun@caf.ac.cn

SPECIALTY SECTION
This article was submitted to Plant Abiotic Stress, a section of the journal Frontiers in Plant Science

RECEIVED 30 August 2022
ACCEPTED 28 December 2022
PUBLISHED 31 January 2023

CITATION
Wu C, Wang Y and Sun H (2023) Targeted and untargeted metabolomics reveals deep analysis of drought stress responses in needles and roots of *Pinus taeda* seedlings. *Front. Plant Sci.* 13:1031466. doi: 10.3389/fpls.2022.1031466

COPYRIGHT
© 2023 Wu, Wang and Sun. This is an open-access article distributed under the terms of the Creative Commons Attribution License (CC BY). The use, distribution or reproduction in other forums is permitted, provided the original author(s) and the copyright owner(s) are credited and that the original publication in this journal is cited, in accordance with accepted academic practice. No use, distribution or reproduction is permitted which does not comply with these terms.

Targeted and untargeted metabolomics reveals deep analysis of drought stress responses in needles and roots of *Pinus taeda* seedlings

Chu Wu[1], Yun Wang[2] and Honggang Sun[3]*

[1]College of Horticulture & Gardening, Yangtze University, Jingzhou, Hubei, China, [2]College of Life Sciences, Yangtze University, Jingzhou, Hubei, China, [3]Institute of Subtropic Forestry, Chinese Academy of Forestry, Fuyang, Zhejiang, China

Drought stress is one of major environmental stresses affecting plant growth and yield. Although *Pinus taeda* trees are planted in rainy southern China, local drought sometime occurs and can last several months, further affecting their growth and resin production. In this study, *P. taeda* seedlings were treated with long-term drought (42 d), and then targeted and untargeted metabolomics analysis were carried out to evaluate drought tolerance of *P. taeda*. Targeted metabolomics analysis showed that levels of some sugars, phytohormones, and amino acids significantly increased in the roots and needles of water-stressed (WS) *P. taeda* seedlings, compared with well-watered (WW) pine seedlings. These metabolites included sucrose in pine roots, the phytohormones abscisic acid and sacylic acid in pine needles, the phytohormone gibberellin (GA4) and the two amino acids, glycine and asparagine, in WS pine roots. Compared with WW pine seedlings, the neurotransmitter acetylcholine significantly increased in needles of WS pine seedlings, but significantly reduced in their roots. The neurotransmitters L-glutamine and hydroxytyramine significantly increased in roots and needles of WS pine seedlings, respectively, compared with WW pine seedlings, but the neurotransmitter noradrenaline significantly reduced in needles of WS pine seedlings. Levels of some unsaturated fatty acids significantly reduced in roots or needles of WS pine seedlings, compared with WW pine seedlings, such as linoleic acid, oleic acid, myristelaidic acid, myristoleic acid in WS pine roots, and palmitelaidic acid, erucic acid, and alpha-linolenic acid in WS pine needles. However, three saturated fatty acids significantly increased in WS pine seedlings, i.e., dodecanoic acid in WS pine needles, tricosanoic acid and heptadecanoic acid in WS pine roots. Untargeted metabolomics analysis showed that levels of some metabolites increased in WS pine seedlings, especially sugars, long-chain lipids, flavonoids, and terpenoids. A few of specific metabolites increased greatly, such as androsin, piceatanol, and panaxatriol in roots and needles of WS pine seedlings. Comparing with WW pine seedlings, it was found that the most enriched pathways in WS pine needles included flavone and flavonol biosynthesis, ABC transporters, diterpenoid biosynthesis, plant hormone signal transduction, and flavonoid biosynthesis; in WS pine roots, the most enriched pathways included tryptophan metabolism, caffeine metabolism, sesquiterpenoid and triterpenoid biosynthesis, plant hormone signal transduction, biosynthesis of phenylalanine, tyrosine, and tryptophan. Under long-term drought stress, *P. taeda* seedlings showed their own

metabolomics characteristics, and some new metabolites and biosynthesis pathways were found, providing a guideline for breeding drought-tolerant cultivars of *P. taeda*.

KEYWORDS

drought tolerance, phytohormones, fatty acids, neurotransmitters, sugars, amino acids, organic acids, flavenoids and terpenoids

1 Introduction

Loblolly pine (*Pinus taeda* L.) has garnered great attention in China since its introduction to China, as is cultivated widely in southern China due to its rapid growth, high resin yield, and adaptability to warm and humid climatic conditions (Lilian et al., 2021; Zhang et al., 2021). In recent years, loblolly pine has been highly valued due to its economic and ecological benefits. China produced around 0.6 million tons of resin each year, accounting for about half of the worldwide turpentine trade (McConnell et al., 2021; Yi et al., 2021), most of which was harvested from loblolly pine. However, these benefits are affected by drought stress. Although plantations of loblolly pine distribute in rainy southern China, under the background of global climate change, drought stress often occurs in this region, affecting growth and development of loblolly pine trees and their resin prodcution. For example, severe drought occurred in autumn, winter, and spring in 2009/2010 and 2011/2012 in southwestern China, especially in Yunnan province (Sun et al., 2014). In March-June of 2018, severe drought occurred in Fujian province, located in southeastern China (He et al., 2022). Therefore, climatic change-induced drought is considered a serious threat to forest health due to reduction in water transport, stomatal conductance and net photosynthesis and, consequently, decrease in plant growth and biomass, as well as fire susceptibility and pathogen and insect attacks (Maggard et al., 2016; Brodribb et al., 2020; Liu et al., 2022).

In order to maintain good ecological safety and forest environment, research on drought tolerance of forest trees has been emphasized. Water availability in terrestrial ecosystems has also been identified as the most important single factor in predicting net primary productivity (Lorenz et al., 2006). During sylvicultural activity, drought stress is a major cause of mortality for both planted and naturally-regenerated pine seedlings, especially long-term severe drought (Burns and Honkala, 1990; Kolb and Robberecht, 1996; Mueller et al., 2005; Lorenz et al., 2006). Differentiation in drought tolerance of crop species has long been recognized to reflect their genetic basis (Thabet et al., 2018; Dossa et al., 2019; Mahmood et al., 2019), thus coniferous species also have their genetic basis for differentiation in drought tolerance. Because of this reason, recently substantial effort has been devoted to understanding genetic basis in differential drought tolerance of coniferous species and other forest trees using molecular and genomic tools (Haas et al., 2021; Xiao et al., 2021; Li M. et al., 2022). The loblolly pine genome has been completely sequenced (Neale et al., 2014; Zimin et al., 2014; Zimin et al., 2017). This advancement provided the prerequisite for better understanding the genetic basis of loblolly pine response to drought stress.

Although modern agriculture has considerably reduced the effects of drought on crop growth and yield due to extensive water administration systems, climatic change scenarios that present the possibility of greatly changed rainfall patterns, combined with a rising human population's demands on water resources, have emphasized the significance of studying plant responses to drought stress (Seleiman et al., 2021). Drought stress provokes a multitude of dramatic alterations in all plant organs at the morphological, biochemical, physiological, and molecular level (Hura et al., 2022), virtually disrupting the link between source and sink organs of plants (Michaletti et al., 2018). The responses of plants to environmental stresses are highly dynamic and complicated, with the goal of developing a new homeostasis under adverse growing conditions. Particularly, drought-responsive mechanisms contain regulation of gene expression (Janiak et al., 2016; Castroverde, 2019), kinase cascades of signaling (Razi and Muneer, 2021), hormone signaling (Jogawat et al., 2021), osmolyte biosynthesis (Ozturk et al., 2021), morphological and anatomical changes in roots and leaves (Jogawat et al., 2021), cell structure modulation (Jogawat et al., 2021), carbohydrate metabolism and allocation (Aaltonen et al., 2017; Kreuzwieser et al., 2021; Razi and Muneer, 2021), stability and activation of water channels (aquaporins) (Yepes-Molina et al., 2020; Chen Q et al., 2021; Patel and Mishra, 2021), fatty acid metabolism (Asakura et al., 2021; Chen et al., 2021), nitrogen assimilation (Das et al., 2017; Miranda-Apodaca et al., 2020), as well as amino acid metabolism (Batista-Silva et al., 2019; Diniz et al., 2020). However, little research was carried out about comprehensive analysis on molecular responses of these alternations to drought stress. Therefore, multiple -omics provide a whole access to understand the comprehensiveness.

Although proteins play important roles in plant responses to drought stress, some small secondary metabolites also shown important functions to enhance drought tolerance, such as the phytohormone ABA (Li et al., 2021; Mathan et al., 2021) and the neurotransmitter melatonin (Sharma and Zheng, 2019; Tiwari et al., 2021; Zeng et al., 2022). Therefore, accurate and simultaneous studies of transcriptomics, proteomics and metabolomics are needed to identify the biochemical and physiological responses of plants to drought stress. It is generally believed that high-performance "omics" approaches enable researchers to examine the biochemical, physiological, and molecular responses of plants under environmental stresses in a more comprehensive way. More specifically, the explanation of the composite regulatory system

triggered by plants under environmental stresses is enabled by the integration of such comprehensive techniques (Kosová et al., 2015; Jorge et al., 2016; Michaletti et al., 2018).

In current studies, transcriptomic, proteomic, and metabolomic approaches are mostly used to identify the response of model plants to drought stress (Chmielewska et al., 2016; Michaletti et al., 2018; Lima et al., 2019; Du et al., 2020; Guo et al., 2020; Zhou et al., 2022), but there is a lack of integrated research on metabolites involved in drought tolerance of forest trees. Therefore, the aim of this study was to measure changes in metabolite levels in the roots and needles of loblolly pine seedlings under long-term drought stress, and to identify major metabolic pathways in loblolly pine seedlings related to drought stress. This work lays the foundation for understanding the metabolic mechanisms of drought tolerance in loblolly pine trees, and provides a framework for metabolomics studies in coniferous species.

2 Materials and methods

2.1 Experimental materials

Seeds of loblolly pine (*Pinus taeda*) came from the Forest Farm of Maple Moutain in Jingdezhen, Jiangxi province, China. These seeds were sterilized using 75% ethanol for 10 min and rinsing 3 times in sterilized water, and then sown in sterilized sand in big plastic pots. After these seeds germinated, the pots were transferred to a growth chamber (16 h light/8 h dark, 350 $\mu mol \cdot m^{-2} \cdot s^{-1}$ PPFD, 80% RH, 25°C). When pine seedlings grew with 4 true needles, they were transplanted into plastic pots (20 cm in diameter and 30 cm in height) containing sterilized cultivation substance (peat:vermiculite = 50:50, pH~7.0), three pine seedlings per pot. These pots were then transferred into a greenhouse with natural sunlight and temperature. Water was provided according to the moisture of the cultivation substance in the pots. When these pine seedlings grew for 7 months, drought treatment was carried out: 30 pots were supplied with 100 ml of water every week, i.e., water-stressed (WS) pine seedlings, and 30 pots were supplied with enough water as control, i.e. well-watered (WW) pine seedlings. The drought treatment continued for 42 d. The pine seedlings were dug out and their roots and needles were rinsed with sterilized water and treated with liquid nitrogen and stored under -80°C for further analysis.

2.2 Methods of targeted metabolomic analysis

2.2.1 Amino acids analysis

Metabolite extraction was carried out according to methods introduced by Fuertig et al. (2016) and Virág et al. (2020). Samples were weighed accurately and encased in 2 ml Eppendorf tubes. 600 µL 10% formic acid/methanol-H_2O (1:1, V/V) and 2 steel beads were added to every tube. The tubes were mixed by well vortex for 30 s. Then samples were ground 90 s under 60 Hz, and then centrifuged for 5 min (12000 rpm under 4°C. 100 µL of the supernatant was added 900 µL of 10% formic acid/methanol-H_2O (1:1, V/V), and then mixed for 30 s. 100 µL of the diluent was taken out and added 100 ppb isotope internal standard solution. After mixing, the solution was treated with 0.22 µm filter membrane. The filtrate was added into detection bottle.

The LC/MS analysis methods were according to introduction by Liyanaarachchi et al. (2018) and Thiele et al. (2019). A liquid chromatograph (EXion LC, SCIEX) and ZORBAX Eclipse XDB-C18 chromatographic column (4.6 × 150 mm, Agilent company, USA) were used for amino acid analysis. 50 µL of sample solution was added, column temperature: 40°C, moving phase A-10% methanol with 0.1% formic acid; moving phase B-50% methanol with 0.1% formic acid. Gradient elution condition was listed below: 0~6.5 min, 10%~30% B; 6.5~7 min, 30~100% B; 7~18 min, 100% B; 18~18.5 min, 100~10% B; 18.5~21 min, 10% B, 0~8 min, flow speed: 0.3 mL/min; 8.5~21 min. Flow rate: 0.4 mL/min. A mass spectrometer (SCIEX 6500+) was used for the amino acid analysis. Analysis condition was listed below: electrospray ion source: negative and positive ion mode; temperature of ion source: 500°C; voltage of ion source: 5500 V; collision gas: 6 psi; curtain gas: 30 psi; atomization gas and auxiliary gas: 50 psi. Multiple reaction monitoring was used to scan metabolites.

2.2.2 Phytohormone analysis

About 0.1 mg sample was weighed and added 1 ml cool 50% ACN solution. The sample was treated using ultrasonic wave for 3 min under 4°C, and then extracted for 30 min under 4°C. The sample was centrifuged for 10 min (12000 rpm, 4°C). The supernatant was treated using RP-SPE column: 1 mL 100% MeOH and 1 mL de-ionized water was added. 50% ACN solution was used for balance. After sample was loaded, 1 mL 30% ACN was used to rinse column, the components were collected. The collected components were treated to dryness under nitrogen gas flow. 200 µL 30%ACN was added to the dry sample and make it dissolved. The sample was transferred to a sample bottle with insert. HPLC chromatograph (Vanquish, UPLC, Thermo, USA) was used. Column: Waters HSS T3 (50 × 2.1 mm, 1.8 µm). Moving phase **(A)** ultrapure water with 0.1% acetic acid; moving phase **(B)** acetonitrile with 0.1% acetic acid; flow rate: 0.3 ml/min; column temperature: 40°C; sample size: 2 µL; elution gradient: 0 min water/acetonitrile (90:10, V/V), 1 min water/acetonitrile (90:10, V/V), 7 min water/acetonitrile (90:10, V/V), 7.1 min water/acetonitrile (10:90, V/V), 9 min water/acetonitrile (10:90, V/V). A mass spectrometer (Q Exactive, Thermo, USA) was used. Spectrometer parameters were listed below: electrospray ionization source, sheath gas: 40 arb; auxiliary gas: 10 arb;electrospray voltage: -2800 V; temperature: 350°C; temperature of ion transmission pipe: 320°C; scanning mode: single ion detection; scanning way: negative ion.

2.2.3 Neurotransmitter analysis

About 50 mg samples were weighed and mixed with 30 µL 10% formic acid/methanol solution twice under 30 Hz 90 s and then were treated 30 min using ultrasonic wave. The samples were centrifuged for 10 min (13000 rpm, 4°C). The supernatant was taken out and then the centrifugation was repeated once. The supernatant was used for neurotransmitters with lower concentrations in samples. For determination of few neurotransmitters (such as GABA, Gln, Glu, Tyr, Trp), the supernatant was diluted 200 times. AB 4000 triple stage quadrupole mass spectrometry and Waters UPLC

liquidchromatograph were used for neurotransmitter analysis. Analysis condition of liquid chromatograph was listed below: ACQUITY UPLC® BEH C18 chromatographic column (2.1×100 mm, 1.7 μm, Waters company, USA); sample size: 5 μL; column temperature: 40°C; moving phase **(A)** 10% methanol with 0.1% formic acid; moving phase **(B)** 50% methanol with 0.1% formic acid. Gradient elution condition: 0~1 min, 20~100% B; 1~7 min, 100% B; 7~7.5 min, 100~20% B; 7.5~11 min, 20% B. Flux rate 0.4 mL/min. Analysis condition of mass spectrometer was listed below: electrospray ion source: negative and positive ion mode; temperature of ion source: 500°C; voltage of ion source: 5000 V; collision gas: 6 psi; curtain gas: 30 psi; atomization gas and auxiliary gas: 50 psi. Multiple reaction monitoring was used to scan metabolites.

2.2.4 Sugar analysis

About 100 mg sample was weighed and loaded in 2.0 mL tube. 700 μl of 80% ethanol was added and mixed for 2 h under 50°C. The sample was diluted with 700 μl H_2O and was centrifuged for 3 min (10000 rpm). The supernatant was transferred a new centrifuge tube. The supernatant was detected using Thermo ICS5000 ion chromatograph (Dionex, Thermo Scientific, Waltham, USA). An electrochemical detector was used for sugar determination. Ion chromatograph condition was listed below: liquid chromatograph column: CarboPac™ PA1(50 × 4.0mm); moving phase **(A)** H_2O; moving phase **(B)** 100 mM NaOH; sample size: 5 uL, flow rate: 0.5 ml/min, column temperature: 30°C; gradient elution: 0 min A phase/B phase (95:5, V/V), 9 min A phase/B phase (95:5, V/V), 20 min A phase/B phase (0: 100, V/V), 30 min A phase/B phase (0: 100, V/V), 30.1 min A phase/B phase (95:5, V/V), 40 min A phase/B phase (95:5, V/V), 60 min A phase/B phase (95:5, V/V).

2.2.5 Organic acid analysis

Metabolite extract was carried out according to the method introduced by Selli et al. (2018). Sample was weighed accurately and loaded in a 2 mL EP tube with a steel bean. 500 μL 30% methanol with 0.1% formic acid was added. The sample was ground using a high throughput tissue grinder (60 Hz) for 120 s and then centrifuged for 10 min (12000 rpm, 4°C). 20 μL of supernatant was added to 980 μL 30% methanol with 0.1% formic acid and then mixed for 30 s using a well vortex. The supernatant wad poured into the detective bottle.

Waters UPLC liquid chromatograph and AB4000 mass spectrometer (SCIEX) were used for analysis (Fiori et al., 2018; Pawlak et al., 2019). Chromatograph condition was listed below: chromatograph column: ACQUITY UPLC® BEH C18 column(2.1 × 100 mm, 1.7 μm, Waters company, USA); sample size: 5 μL; column temperature: 40°C; moving phase **(A)** water with 0.1% formic acid; moving phase **(B)** methanol with 0.1% formic acid; gradient elution condition: 0~3 min, 30% B; 3~5 min, 30~50% B; 5~7 min, 50~90% B; 7~9 min, 90% B; 9~13 min, 30% B. Flow rate: 0.4 mL/min. Analysis condition of mass spectrometer was listed below: electrospray ion source: negative ion mode, ion source temperature: 500°C; ion source voltage: -4500 V; collision gas: 6 psi; curtain gas: 30 psi; atomization gas and auxiliary gas: 50 psi. Multiple reaction monitoring was used to scan metabolites.

2.2.6 Fatty acid analysis

The samples (100 mg) were resuspended with liquid nitrogen, then were taken respectively and homogenized with 300 μL of isopropanol/acetonitrile (1:1) which contained mixed internal standards and centrifuged at 12,000 rpm for 10 min. The supernatant was diluted 20 times by Isopropanol/acetonitrile (1:1) which contained mixed internal standards and centrifuged at 12,000 rpm for 10 min. The supernatant was injected into the LC-MS/MS system for analysis. An ultra-high performance liquid chromatography coupled to tandem mass spectrometry (UHPLC-MS/MS) system (ExionLC™ AD UHPLC-QTRAP 6500+, AB SCIEX Corp., Boston, MA, USA) was used to quantify fatty acids in Novogene Co., Ltd. (Beijing, China). Separation was performed on a Waters ACQUITY UPLC BEH C18 column (2.1×100 mm, 1.7 μm) which was maintained at 50°C. The moving phase, consisting of 0.05% formic acid in water (solvent A) and isopropanol/acetonitrile (1:1) (solvent B), was delivered at a flow rate of 0.30 mL/min. The solvent gradient was set as follows: initial 30% B, 1 min; 30-65% B, 2 min; 65-100% B, 11 min; 100% B, 13.5 min; 100-30% B, 14 min; 30% B, 15 min. The mass spectrometer was operated in negative multiple reaction mode (MRM) mode. Parameters were as follows: ionspray voltage (-4500 V), curtain gas (35 psi), ion source temperature (550°C), ion source gas of 1 and 2 (60 psi). Standard curve and limit of quantification (LOQ): LC-MS was used to detect the concentration series of standard solution. The ratio of concentration of standard to internal standard as abscissa, and the ratio of peak area of standard to internal standard as ordinate to investigate the linearity of standard solution. The correlation coefficient (r) > 0.99 of each metabolite was the necessary condition. LOQ were determined by the method of signal-to-noise ratio (S/N), which is comparing the signal measured by the standard solution concentration with the blank matrix. Generally, when the S/N = 10:1, the corresponding concentration is the LOQ (Chinese Pharmacopoeia Commission, 2015; Chevolleau et al., 2018).

2.3 Methods of untargeted metabolomic analysis

2.3.1 Metabolite extraction

Tissues (100 mg) were individually grounded with liquid nitrogen and the homogenate was resuspended with prechilled 80% methanol by well vortex. The samples were incubated on ice for 5 min and then were centrifuged at 15,000 *g*, 4°C for 20 min. Some of supernatant was diluted to final concentration containing 53% methanol by LC-MS grade water. The samples were subsequently transferred to a fresh Eppendorf tube and then were centrifuged at 15000 g, 4°C for 20 min. Finally, the supernatant was injected into the LC-MS/MS system analysis (Want et al., 2013).

2.3.2 UHPLC-MS/MS analysis

UHPLC-MS/MS analyses were performed using a Vanquish UHPLC system (ThermoFisher, Germany) coupled with an Orbitrap Q ExactiveTM HF mass spectrometer (Thermo Fisher, Germany) in Novogene Co., Ltd. (Beijing, China). Samples were injected into a Hypesil Gold column (100×2.1 mm, 1.9 μm) using a 17-min linear gradient at a flow rate of 0.2 mL/min. The eluents for

the positive polarity mode were eluent A (0.1% FA in water) and eluent B (methanol). The eluents for the negative polarity mode were eluent A (5 mM ammonium acetate, pH 9.0) and eluent B (methanol). The solvent gradient was set as follows: 2% B, 1.5 min; 2-85% B, 3 min; 100% B, 10 min; 100-2% B, 10.1 min; 2% B, 12 min. Q ExactiveTM HF mass spectrometer was operated in positive/negative polarity mode with spray voltage of 3.5 kV, capillary temperature of 320°C, sheath gas flow rate of 35 psi and aux gas flow rate of 10 L/min, S-lens RF level of 60, aux gas heater temperature of 350°C.

2.3.3 Data processing and metabolite identification

The raw data files generated by UHPLC-MS/MS were processed using the Compound Discoverer 3.1 (CD3.1, ThermoFisher) to perform peak alignment, peak picking, and quantitation for each metabolite (Schymanski et al., 2014). The main parameters were set as follows: retention time tolerance, 0.2 minutes; actual mass tolerance, 5 ppm; signal intensity tolerance, 30%; signal/noise ratio, 3; and minimum intensity, *etc*. After that, peak intensities were normalized to the total spectral intensity. The normalized data was used to predict the molecular formula based on additive ions, molecular ion peaks and fragment ions. Then, peaks were matched with the mzCloud (https://www.mzcloud.org/), mzVault and MassList database to obtain the accurate qualitative and relative quantitative results. Statistical analyses were performed using the statistical software R (R version R-3.4.3), Python (Python 2.7.6 version) and CentOS (CentOS release 6.6), When data were not normally distributed, normal transformations were attempted using of area normalization method.

2.3.4 Data analysis

These metabolites were annotated using the KEGG database (https://www.genome.jp/kegg/pathway.html), HMDB database (https://hmdb.ca/metabolites) and LIPIDMaps database (http://www.lipidmaps.org/). Principal components analysis (PCA) and Partial Least Squares-Discriminant Analysis (PLS-DA) were performed at metaX (a flexible and comprehensive software for processing metabolomics data) (Wen et al., 2017). We applied univariate analysis (t-test) to calculate the statistical significance (*p*-value).The metabolites with VIP > 1 and *p*-value < 0.05 and fold change ≥ 2 or FC ≤ 0.5 were considered to be differential metabolites. Volcano plots were used to filter metabolites of interest which based on log2 (FoldChange) and -log10 (*p*-value) of metabolites by ggplot2 in R language. For clustering heat maps, the data were normalized using z-scores of the intensity areas of differential metabolites and were plotted by Pheatmap package in R language. The correlation between differential metabolites were analyzed by cor () in R language (method=pearson). Statistically significant of correlation between differential metabolites were calculated by cor.mtest() in R language. *p*-value < 0.05 was considered as statistical significance and correlation plots were plotted by corrplot package in R language. The functions of these metabolites and metabolic pathways were studied using the KEGG database. The metabolic pathways enrichment of differential metabolites was performed, when ratio were satisfied by x/n > y/N, metabolic pathway were considered as enrichment, when *p*-value of metabolic pathway < 0.05, metabolic pathway were considered as statistically significant enrichment. Data of targeted metabolomics were analyzed using SPSS software (17 v.), and the test level was set to $p = 0.05$. Multiple comparisons were carried out among the four sample groups, i.e., roots and needles of WW and WS pine seedlings.

3 Results

3.1 Targeted metabolics analysis

3.1.1 Changes in concentrations of sugars in *Pinus taeda* seedlings under drought stress

Under drought stress, great changes occurred in concentrations of sugars in needles and roots of *P. taeda* seedlings. Sucrose levels in needles of WS pine seedlings were significantly lower than those in needles of WW pine seedlings ($p < 0.05$, Figure 1A), but the status of sucrose levels in roots were just reversed, i.e., sucrose levels in roots of WS pine seedlings were significantly higher than those in roots of WW pine seedlings ($p < 0.05$, Figure 1A). Fructose concentrations in needles did not show significant changes between WW and WS pine seedlings ($p > 0.05$, Figure 1A), but fructose concentrations in roots of WS pine seedlings were significantly lower than those in roots of WW pine seedlings ($p < 0.05$, Figure 1A). Glucose concentrations in needles did not show significant difference between WS and WW pine seedlings ($p > 0.05$, Figure 1B), but glucose concentrations in roots of WS pine seedlings were significantly lower than those in roots of WW pine seedlings ($p < 0.05$, Figure 1B). Raffinose concentrations showed no differences among needles and roots of WW and WS pine seedlings ($p > 0.05$, Figure 1B). Fucose concentrations in needles of WS pine seedlings were significantly lower than those in needles of WW pine seedlings ($p < 0.05$, Figure 1C), but no difference between their roots (Figure 1C). Galactose was not detected in needles of WW and WS pine seedlings, and galactose levels in roots of WS pine seedlings were significantly lower than those in roots of WW pine seedlings ($p < 0.05$, Figure 1C).

3.1.2 Changes in concentrations of amino acids in *Pinus taeada* seedlings under drought stress

Great changes in concentrations of some amino acids occurred in needles and roots of *P. taeda* seedlings under drought stress. Pro levels in needles of WW and WS pine seedlings showed no statistical difference ($p > 0.05$, Figure 2A), and Pro levels were significantly higher in roots than those in needles of WS pine seedlings ($p < 0.05$, Figure 2A), but showed no statistical difference, compared with those in roots of WW pine seedlings ($p > 0.05$, Figure 2A). Gln levels in roots of WS pine seedlings were significantly higher than those in roots of WW pine seedlings ($p < 0.05$, Figure 2A). Concentrations of Asp and Arg showed no statistical differences among the needles and roots of WW and WS pine seedlings ($p > 0.05$, Figure 2B). Levels of Asn and Lys in needles of WW and WS pine seedlings showed no statistical difference, but levels of Asn and Lys in WS pine roots were significantly higher than those in WW pine roots ($p < 0.05$, Figure 2C). Orn and Trp levels in needles and roots of WW and WS pine seedlings showed no statistical differences ($p > 0.05$, Figure 2D).

10.3389/fpls.2022.1031466

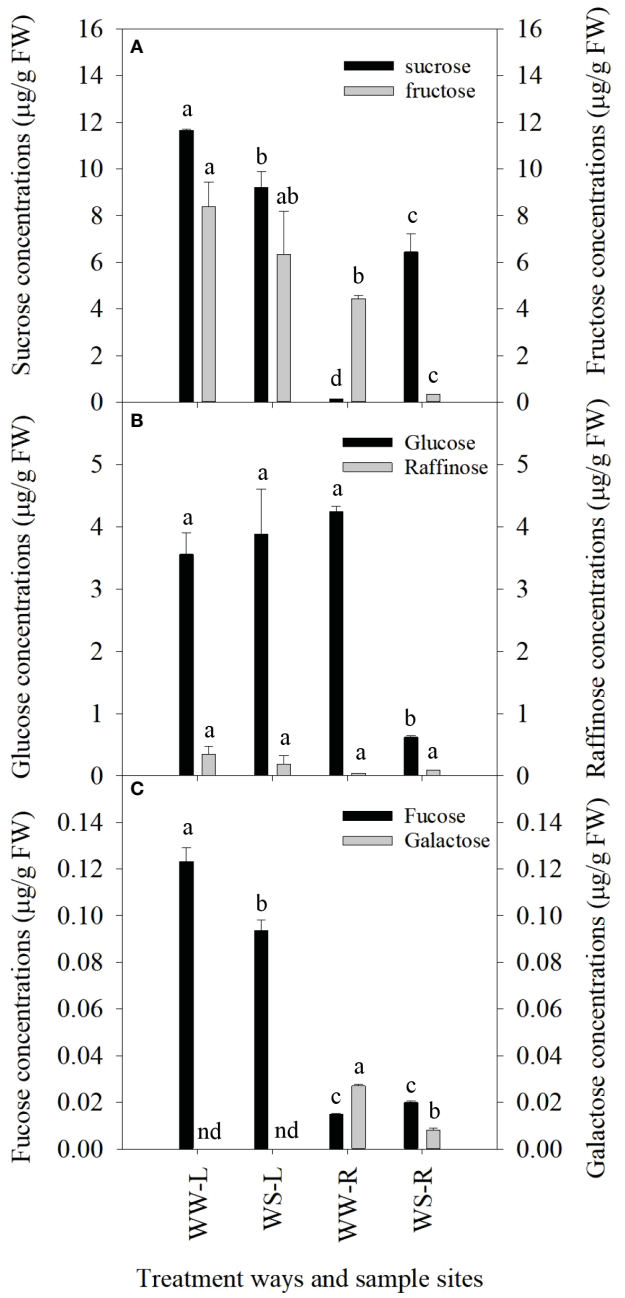


FIGURE 1
Concentrations of sugars in leaves (L) and roots (R) of *P. taeda* seedlings under well-watered (WW) and water-stressed (WS) conditions. **(A)** concentrations of sucrose and fructose; **(B)** concentrations of glucose and raffinose; **(C)** concentrations of fucose and galactose. nd=not determined in sample. For the same sugar, the different low case letters above the bars stand for the significant differences between them ($p < 0.05$).

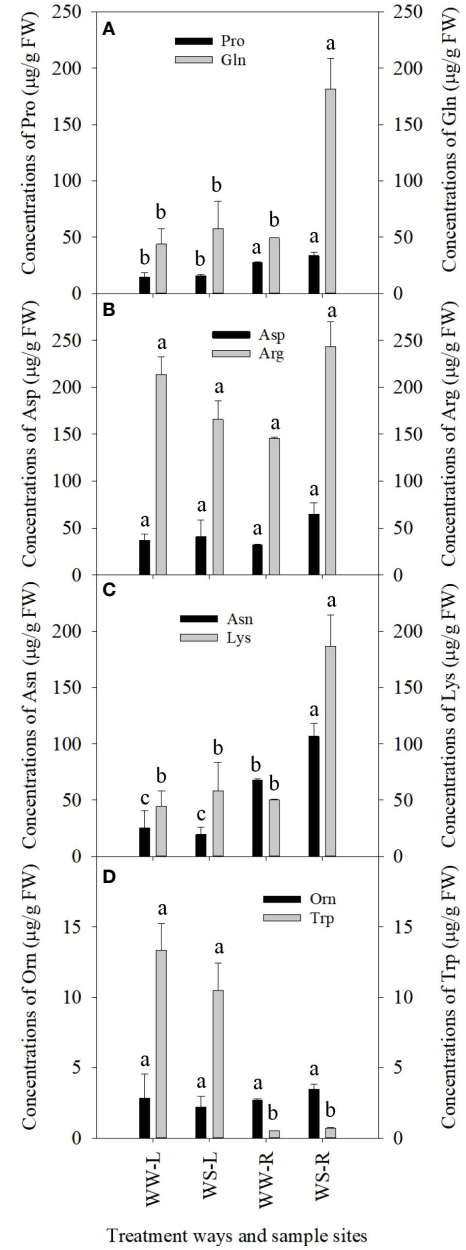


FIGURE 2
Concentrations of amino acids in needles (L) and roots (R) of *P. taeada* seedlings under well-watered (WW) and water-stressed (WS) conditions. **(A)** concentrations of the two amino acids, Pro and Gln, in needles and roots; **(B)** concentrations of the two amino acids, Asp and Arg, in needles and roots; **(C)** concentrations of the two amino acids, Asn and Lys, in needles and roots; **(D)** concentrations of the two amino acids, Orn and Trp, in needles and roots. For the same amino acid, the different low case letters above the bars stand for the significant differences between them ($p < 0.05$).

3.1.3 Changes in concentrations of organic acids in *Pinus taeda* seedlings under drought stress

Concentrations of 5-hydroxymethyl-2-furoic acid (HMFA) showed no statistical differences between needles and roots of WW and WS pine seedlings ($p > 0.05$, Figure 3A), but HMFA concentrations in roots of WS pine seedlings were significantly lower than those in their needles ($p < 0.05$, Figure 3A). Levels of tartaric acid showed no statistical differences among the needles and roots of WW and WS pine seedlings ($p > 0.05$, Figure 3A). The similar situation occurred in concentrations of malonic acid (MA) and pyroglutamic acid (PA) (Figure 3B). Concentrations of fumaric acid (FA) in needles or roots showed no statistical difference between WW and WS pine seedlings ($p > 0.05$, Figure 3C), but FA concentrations in roots of WW and WS pine seedlings were significantly higher than those in their needles, respectively ($p < 0.05$, Figure 3C). Concentrations of citric acid (CA) and lactic acid (LA) showed no

10.3389/fpls.2022.1031466

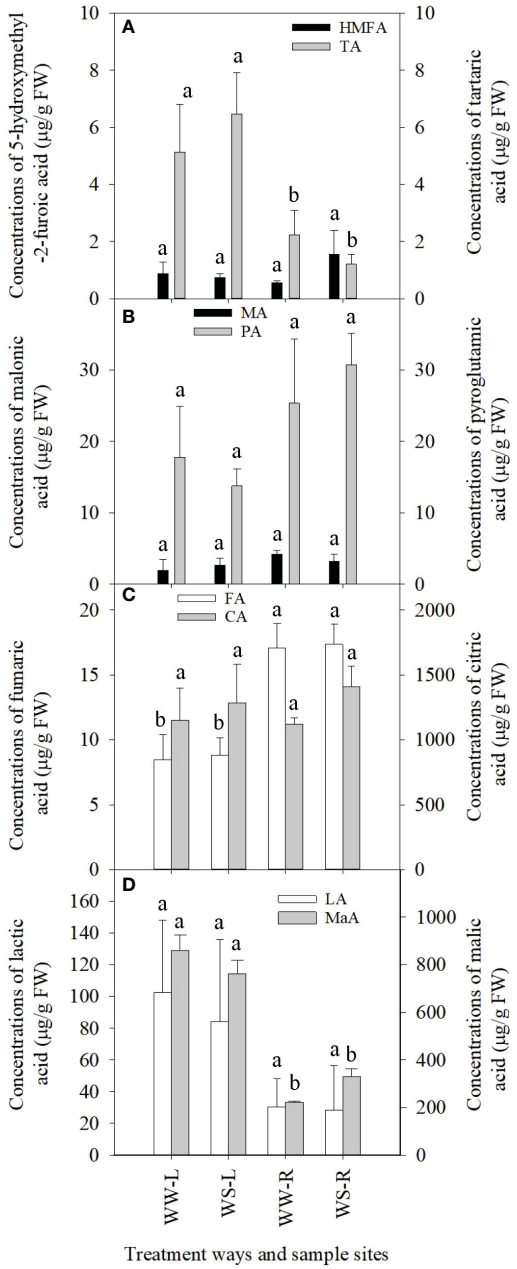


FIGURE 3
Concentrations of organic acids in needles (L) and roots (R) of *P. taeda* seedlings under well-watered (WW) and water-stressed (WS) conditions. **(A)** 5-hydroxymethyl-2-furoic acid (HMFA) and tartaric acid (TA); **(B)** malonic acid (MA) and pyroglutamic acid (PA); **(C)** fumaric acid (FA) and citric acid (CA); **(D)** lactic acid (LA) and malic acid (MaA). For the same organic acid, the different low case letters above the bars stand for the significant differences between them ($p < 0.05$).

statistical differences among the four samples (Figures 3C, D). Concentrations of malic acid (MaA) in roots of WW and WS pine seedlings were significantly lower than those in their needles, respectively ($p < 0.05$, Figure 3D), but no statistical differences in the two organic acids occurred in needles or roots between WW and WS pine seedlings (Figure 3D). In addition, concentrations of glucuronic acid and pyridoxine in needles and roots of pine seedlings under drought stress significantly reduced ($p < 0.05$, unshown data), compared with WW condition, respectively.

3.1.4 Changes in concentrations of phytohormones in *Pinus taeda* seedlings under drought stress

Phytohormones play important roles in plant response to drought stress, thus concentrations of some phytohormones were determined in needles and roots of WW and WS pine seedlings (Figure 4). IAA concentrations showed no statistical differences among all the four samples (Figure 4A). ABA concentrations in WS pine needles were significantly higher than those in WW pine needles ($p < 0.05$, Figure 4A), but ABA levels in roots showed no statistical difference between WW and WS pine seedlings (Figure 4A). Concentrations of

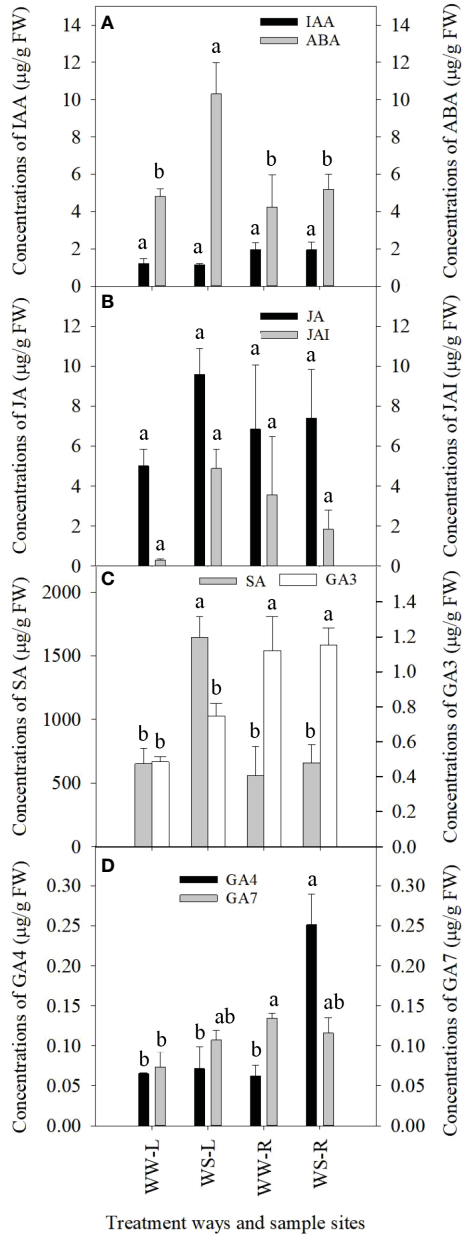


FIGURE 4
Concentrations of phytohormones in needles (L) and roots (R) of *P. taeda* seedlings under well-watered (WW) and water-stressed (WS) condition. **(A)** concentrations of IAA and ABA; **(B)** concentrations of JA and JAI; **(C)** concentrations of SA and GA3; **(D)** concentrations of GA4 and GA7. For the same phytohormone, the different low case letters above the bars stand for the significant differences between them ($p < 0.05$).

jasmonic acid (JA) and jasmonic acid-isoleucine (JAI) showed no statistical differences among needles and roots of WW and WS pine seedlings (Figure 4B). Salicylic acid (SA) concentrations in needles of WS pine seedlings were significantly higher than those in needles of WW pine seedlings ($p < 0.05$, Figure 4C), but no statistical difference in SA concentrations occurred in roots of WW and WS pine seedlings (Figure 4C). GA3 concentrations in roots were significantly higher than those in needles of WW and WS pine seedlings ($p < 0.05$, Figure 4C), but no statistical differences occurred in needles or roots between WW and WS pine seedlings (Figure 4C). No statistical differences occurred in GA4 concentrations in needles of WW and WS pine seedlings (Figure 4D), but GA4 concentrations in roots of WS pine seedlings were significantly higher than those in roots of WW pine seedlings ($p < 0.05$, Figure 4D). No statistical differences in GA7 concentrations occurred in needles or roots of WS pine seedlings, compared with those in WW pine seedlings, respectively (Figure 4D).

3.1.5 Changes in concentrations of neurotransmitters in *Pinus taeda* seedlings under drought stress

Plant neurotransmitters also play important roles in plant growth and development and responses to environmental stresses, especially drought stress. Concentrations of 4-aminobutyric acid in WS pine needles were lower than those in WW pine needles, but no statistical difference occurred ($p > 0.05$, Table 1), and the similar situation also occurred in roots of WW and WS pine seedlings (Table 1). No statistical differences in concentrations of histamine and tyramine occurred in needles and roots of WW and WS pine seedlings (Table 1). Concentrations of acetylcholine in WS pine needles were significantly higher than those in WW pine needles ($p < 0.05$, Table 1), but acetylcholine concentrations in roots of WS pine seedlings were significantly lower than those in WW pine seedlings ($p < 0.05$, Table 1). Concentrations of L-glutamine in needles of WW and WS pine seedlings showed no statistical difference (Table 1), but concentrations of L-glutamine in WS pine roots were significantly higher than those in WW pine roots ($p < 0.05$, Table 1). Levels of L-glutamic acid showed no statistical difference in needles or roots of WS pine seedlings, compared with those in needles or roots of WW pine seedlings, respectively (Table 1), but levels of L-glutamic acid in WS pine roots were significantly higher than those in their needles ($p < 0.05$, Table 1). Hydroxytyramine concentrations in WS pine needles were significantly higher than those in WW pine needles ($p < 0.05$, Table 1), but no statistical difference occurred in roots of WW and WS pine seedlings ($p > 0.05$, Table 1). No differences in L-histidine concentrations occurred in needles and roots of WW and WS pine seedlings (Table 1). Noradrenaline concentrations in WS pine needles were significantly lower than those in WW pine needles ($p < 0.05$, Table 1), but no statistical difference in noradrenaline concentrations occurred in roots of WW and WS pine seedlings (Table 1). Serotonin, adrenaline, xanthurenic acid, DL-kynurenine, and vanillymandelic acid were not

TABLE 1 Concentrations of neurotransmitters in leaves (L) and roots (R) of *P. taeda* seedlings under well-watered (WW) and water-stressed (WS) conditions.

Neurotransmitters determined	Treatment ways and sample sites (μg/g FW)			
	WW-L	WS-L	WW-R	WS-R
4-aminobutyric acid	37.4955 ± 7.3055ab	17.8785 ± 3.2485b	55.1240 ± 5.104941a	42.9950 ± 4.1090ab
histamine	0.0240 ± 0.0072a	0.0243 ± 0.0012a	0.02433 ± 0.0007a	0.0297 ± 0.0009a
tyramine	0.0087 ± 0.0063a	0.0547 ± 0.0403a	0.0600 ± 0.0006a	0.0600 ± 0.0084a
acetylcholine	0.0850 ± 0.0620c	0.2460 ± 0.02500b	0.4797 ± 0.0412a	0.3043 ± 0.0291b
L-glutamine	142.4405 ± 7.8965b	125.9545 ± 3.0665b	29.93833 ± 2.71357c	241.5407 ± 3.38523a
L-glutamic acid	137.6510 ± 4.6980b	173.6890 ± 3.8909b	283.4957 ± 5.1912a	346.5337 ± 9.5964a
hydroxytyramine	0.1400 ± 0.0433b	0.3477 ± 0.1092a	0.0777 ± 0.0009b	0.1227 ± 0.0150b
L-histidine	2.9977 ± 0.9932a	3.1627 ± 0.3392a	1.3850 ± 0.0276a	1.8730 ± 0.0653a
noradrenaline	22.6815 ± 0.2675a	12.0277 ± 3.3743b	4.8177 ± 0.1711c	4.6537 ± 0.3468c
serotonin	0.0150 ± 0.0093a	0.0197 ± 0.0030a	nd	nd
L-tyrosine	7.9373 ± 4.0388a	3.4217 ± 0.7135a	3.8870 ± 0.3950a	3.900 ± 0.3295a
Adrenaline	0.0434 ± 0.0099a	0.0380 ± 0.0041a	nd	nd
Kynurenic acid	0.0093 ± 0.0047a	0.0047 ± 0.0018ab	0.0003 ± 0.0000b	0.0007 ± 0.0003b
levodopa	0.0540 ± 0.0093b	0.0307 ± 0.0070b	0.4427 ± 0.0070a	0.4427 ± 0.0665a
L-tryptophan	43.9020 ± 12.1440a	47.0855 ± 18.5515a	3.66230.3897b	4.9403 ± 1.5273b
xanthurenic acid	70.2590 ± 6.3627a	75.07433 ± 9.2933a	nd	nd
DL-kynurenine	0.2263 ± 0.1204a	0.3233 ± 0.060a	nd	nd
vanillymandelic acid	1.7335 ± 0.4045a	2.5145 ± 0.7415a	nd	nd
melatonin	nd	nd	0.0137 ± 0.0003a	0.0140 ± 0.0010a

nd, not determined. Different lowercases for the same physiological parameters indicate significant differences.

determined in roots of WW and WS pine seedlings, and no statistical differences in their concentrations occurred between needles of WW and WS pine seedlings (Table 1). L-tyrosine concentrations show no statistical differences among needles and roots of WW and WS pine seedlings (Table 1). Concentration of kynurenic acid in needles or roots showed no statistical differences between WW and WS pine seedlings, respectively (Table 1). Concentrations of levodopa in roots were significantly higher than those in needles of WW and WS pine seedlings, respectively ($p < 0.05$, Table 1), but levodopa concentrations showed no statistical difference in needles or roots of WW and WS pine seedlings, respectively (Table 1). The situation about L-tryptophan concentrations was just opposite to that of levodopa (Table 1). Melatonin was not determined in needles of WW and WS pine seedlings, and melatonin concentrations showed no statistical difference between roots of WW and WS pine seedlings (Table 1).

3.1.6 Changes in concentrations of fatty acids in *Pinus taeda* seedlings under drought stress

Changes in compositions of fatty acids often occur due to environmental stresses. Concentrations of fatty acids in needles and roots of WW and WS pine seedlings were determined (Table 2). Few saturated and unsaturated fatty acids did not show significant level changes in needles or roots between WW and WS pine seedlings ($p > 0.05$, Table 2), such as hendecanoic acid (C11:0), tridecanoic acid (C13:0), myristelaidic acid (C14:1n-5), tetracosanoic acid (C24:0), linoelaidic acid (C18:2n-6,9). Levels of some unsaturated fatty acids significantly reduced in roots or needles of WS pine seedlings, compared with those in WW pine seedlings ($p < 0.05$, Table 2), such as elaidic acid (C18:1n-10), gamma-linolenic acid (C20:3n-6,9,12), *cis*-11-eicosenoic acid (C20:1n-9), alpha-linolenic acid (C18:3n-3,6,9), *cis*-11,14-eicosadienoic acid (C20:2n-6,9), erucic acid

TABLE 2 Changes in fatty acids in roots and needles of WW and WS pine seedlings.

Fatty acids detected	Treatment ways and sample sites (μg/g FW)			
	WW-L	WS-L	WW-R	WS-R
Hendecanoic acid	314.66 ± 120.49ab	487.81 ± 69.56a	89.21 ± 6.34b	27.89 ± 17.71b
Dodecanoic acid	2862.35 ± 183.88b	3837.71 ± 111.75a	3960.13 ± 97.47a	3859.43 ± 60.24a
Tridecanoic acid	524.52 ± 29.19a	551.34 ± 44.82a	318.28 ± 5.91b	338.59 ± 14.05b
Tetradecanoic acid	1962.58 ± 48.21a	1803.38 ± 31.30327b	1699.46 ± 59.54b	767.27 ± 30.57c
Myristoleic acid	27.86 ± 2.51ab	39.26 ± 14.42ab	45.87 ± 1.37a	10.29 ± 0.12b
Myristelaidic acid	100.24 ± 3.50a	123.84 ± 37.01a	154.60 ± 17.02a	98.75 ± 7.07a
Pentadecanoic acid	938.97 ± 37.37c	612.06 ± 5.15c	15424.23 ± 107.96a	11545.74 ± 361.47b
cis-10-Pentadecenoic acid	27.17 ± 2.04c	13.37 ± 1.62c	1173.61 ± 72.26a	887.98 ± 120.69b
trans-10-Pentadecenoic acid	15.12 ± 5.30c	21.36 ± 3.15c	175.14 ± 10.86a	64.00 ± 2.79b
Hexadecanoic acid	14205.14 ± 529.26c	18327.18 ± 306.24bc	29726.44 ± 2649.84a	21797.17 ± 1117.47b
Palmitoleic acid	431.00 ± 120.08c	428.45 ± 127.36c	15521.51 ± 459.59a	8191.67 ± 148.08b
Palmitelaidic acid	928.00 ± 18.47c	744.84 ± 54.80d	6070.39 ± 56.35a	3131.41 ± 66.63b
Heptadecanoic acid	866.68 ± 18.56b	652.10 ± 15.14c	792.21 ± 37.72b	998.02 ± 15.70a
cis-10-Heptadecenoic acid	1929.29 ± 77.51c	1272.01 ± 116.98c	11795.22 ± 498.14a	8556.85 ± 510.76b
trans-10-Heptadecenoic acid	346.01 ± 28.10c	122.04 ± 12.47c	11491.97 ± 510.88a	4306.78 ± 192.95b
Oleic acid	3550.43 ± 237.20c	4048.19 ± 107.72c	15939.42 ± 688.10a	13234.24 ± 172.57b
cis-Vaccenic acid	3111.10 ± 185.87c	3746.72 ± 125.58c	15153.28 ± 592.00a	11852.87 ± 235.33b
Elaidic acid	849.18 ± 32.06b	799.59 ± 59.60b	1772.57 ± 74.33a	785.60 ± 34.18b
Arachidic acid	1902.72 ± 95.66c	1787.19 ± 385.70c	12437.19 ± 1151.27a	9150.42 ± 197.86b
gamma-Linolenic acid	N.D.	431.46 ± 54.16c	2410.87 ± 110.79a	925.88 ± 50.61b
cis-11-Eicosenoic acid	1917.13 ± 20.71b	1646.72 ± 140.67b	2379.12 ± 137.52a	1195.31 ± 24.74c
alpha-Linolenic acid	38117.23 ± 948.47a	28789.38 ± 321.82b	7491.62 ± 354.52c	5149.44 ± 66.69d
Heneicosanoic acid	5022.86 ± 131.02bc	4347.61 ± 468.23c	7137.18 ± 109.31a	5928.13 ± 301.74b
cis-11,14-Eicosadienoic acid	3957.46 ± 101.05a	4392.56 ± 429.13a	1946.12 ± 53.10b	667.06 ± 27.65c
Docosanoic acid	4995.50 ± 396.54b	3608.82 ± 373.27c	14060.54 ± 271.14a	13229.26 ± 333.13b

(Continued)

TABLE 2 Continued

Fatty acids detected	Treatment ways and sample sites (μg/g FW)			
	WW-L	WS-L	WW-R	WS-R
Erucic acid	341.53 ± 46.53ab	131.92 ± 19.73c	444.36 ± 33.08a	313.39 ± 20.36b
Tricosanoic acid	1401.62 ± 43.30c	1623.82 ± 147.39c	2593.76 ± 190.17b	3172.68 ± 73.24a
cis-13,16-Docosadienoic acid	174.16 ± 0.70ab	123.89 ± 19.72bc	223.26 ± 36.79a	92.0345 ± 15.22c
trans-Vaccenic acid	802.89 ± 10.87b	734.71 ± 67.64b	1724.33 ± 76.83a	718.57 ± 43.27b
Linoleic acid	28668.41 ± 509.75c	29830.99 ± 882.18c	66436.76 ± 1231.70a	44188.78 ± 2038.21b
Linoelaidic acid	1124.83 ± 138.47b	1121.83 ± 343.89b	3080.31 ± 254.61a	2586.22 ± 99.378a
Tetracosanoic acid	10668.56 ± 439.94b	10589.24 ± 885.52b	44924.82 ± 442.74a	41705.67 ± 2744.47a
Nervonic acid	66.70 ± 2.03c	59.72 ± 6.20c	258.01 ± 28.39a	189.83 ± 4.38b

The results are shown as mean ± SD (n=3) (ng/g FW). For every fatty acid, data with the same lowercases are not significantly different ($p > 0.05$, LSD). In this table, N.D. represents not determined. WW-L and WW-R represent needles and roots of well-watered pine seedlings; WS-L and WS-R represent needles and roots of water-stress pine seedlings.

(C22:1n-9), *cis*-13,16-docosadienoic acid (C22:2n-6,9), *trans*-vaccenic acid (C18:1n-7), linoleic acid (C18:2n-6,9), nervonic acid (C24:1n-9), *cis*-vaccenic acid (C18:1n-7), oleic acid (C18:1n-9), *trans*-10-heptadecenoic acid (C17:1n-7), *cis*-10-heptadecenoic acid (C17:1n-7), palmitelaidic acid (C16:1n-7), palmitoleic acid (C16:1n-7), *trans*-10-pentadecenoic acid (C15:1n-5), *cis*-10-pentadecenoic acid (C15:1n-5), myristoleic acid (C14:1n-5) in roots; palmitelaidic acid (C16:1n-7), erucic acid (C22:1n-9), alpha-linolenic acid (C18:3n-3,6,9) in needles. Gamma-linolenic acid was not determined in WW pine needles, but in WS pine needles; and its levels in WS pine roots were significantly lower than those in WW pine roots (Table 2). Astonishingly, compared with WW pine seedlings, three saturated fatty acids significantly increased in WS pine seedlings, i.e., dodecanoic acid (C12:0) in needles, tricosanoic acid (C23:0) and heptadecanoic acid (C17:0) in roots ($p < 0.05$, Table 2).

3.2 Untargeted metabolome analysis

3.2.1 Quality control, screening and identification of differential compounds in different samples

As described in M & M, metabolites in all the four treatment groups were identified and characterized as many as possible, and then their relatively quantitative levels were analyzed (Table S1). Quality control (QC) of untargeted metabolomics analysis was evaluated. Before the subsequent analyses, all the data of differential metabolites were subjected to a data integrity check, and no missing values were detected. The distribution of metabolic profiles for the tested samples and QC samples in PCA is shown in Figure 5. All the tested samples and QC samples clustered together, suggesting that the method had good reproducibility overall.

PLS-DA and PCA were used to screen and identify differential metabolites (Figures 6, S1, S2). Results from PLS-DA and PCA showed that metabolite differentiation and variations between the four sample groups were satisfactory and identified metabolites were suitable. According to results from PLS-DA under positive mode, 281 and 255 metabolites were up- and down-regulated, respectively, comparing between needles and roots of WW pine seedlings (i.e., WW_L.vs.WW_R_pos); 38 and 63 metabolites were up- and down-regulated, respectively, comparing between the needles of WS and WW pine seedlings (i.e., WS_L.vs.WW_L_pos); 240 and 290 metabolites were up- and down-regulated, respectively, comparing needles and roots of WS pine seedlings (i.e., WS_L.vs.WS_R_pos); 103 and 74 metabolites were up- and down-regulated, respectively, comparing roots of WS and WW pine seedlings (i.e., WS_R.vs.WW_R_pos) (Table 3). Under negative ion mode, 27 and

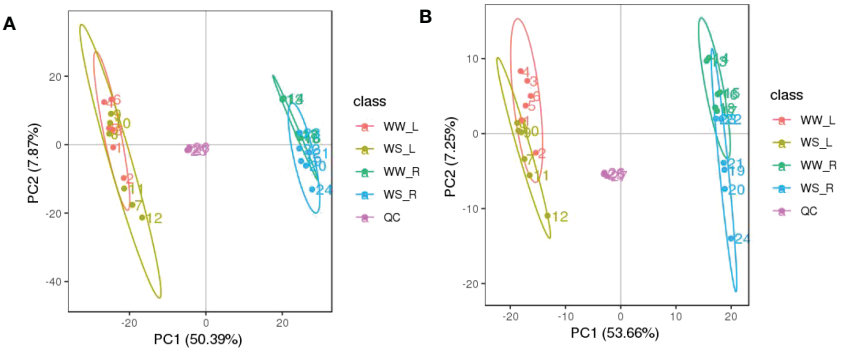


FIGURE 5
PCA score plots based on the UHPLC-Q-TOF/MS data of needles (L) and roots (R) of *P. taeda* seedlings under well-watered (WW) and water-stressed (WS) condition, based on positive **(A)** and negative **(B)** ion mode.

10.3389/fpls.2022.1031466

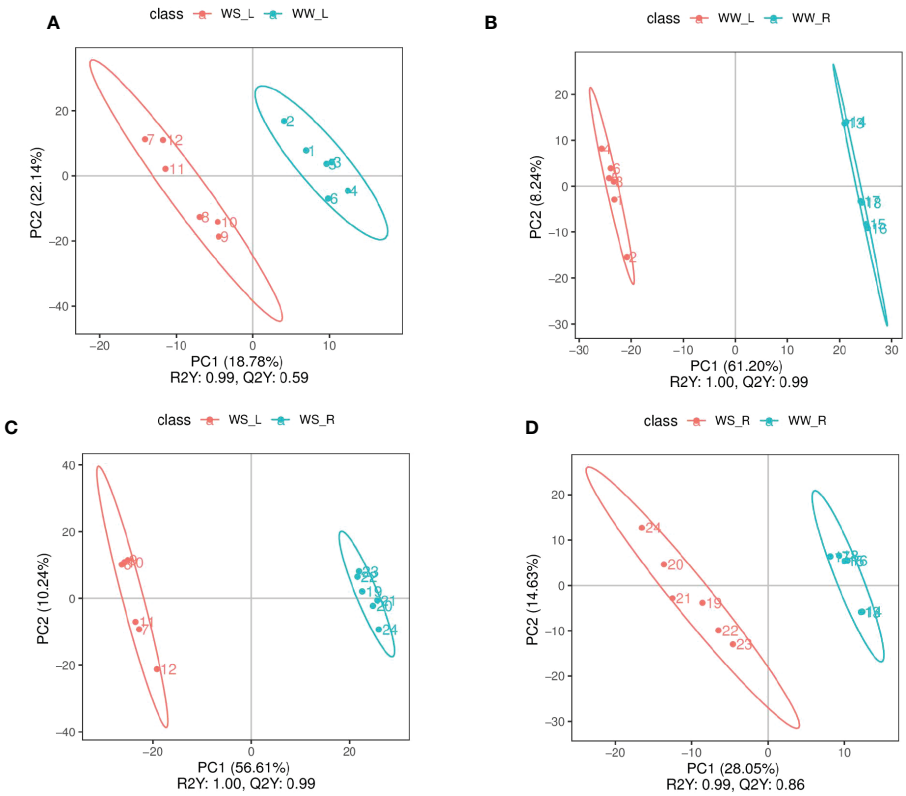


FIGURE 6
PLS-DA scores of experimental groups under positive ion mode. **(A)** needles (red) vs. roots (blue) of WW seedlings; **(B)** needles of WS (red) vs.WW (blue) pine seedlings; **(C)** needles (red) vs. roots (blue) of WS pine seedlings; **(D)** roots of WS (red) vs. WW (blue) pine seedlings. WW, well-watered; WS, water-stressed.

17 metabolites were up- and down-regulated, respectively, compared with the needles of WS and WW pine seedlings (i.e., WS_L.vs.WW_L_neg, Table 3); 49 and 28 metabolites were up- and down-regulated, respectively, comparing with the roots of WS and WW pine seedlings (i.e., WS_R.vs.WW_R_neg, Table 3). Thus, all together, 65 and 80 metabolites were up- and down-regulated in WS pine needles, respectively, comparing with those in the needles of WW pine seedlings; 152 and 102 metabolites were up- and down-regulated in WS pine roots, compared with those in the roots of WW pine seedlings. The differential metabolites were annotated and some metabolites showed great fold changes (Tables S2, S3).

3.2.2 Venn diagram analysis of differential metabolites

Venn diagrams showed that 61 and 125 unique differential metabolites occurred between needles and roots of WW pine seedlings under positive and negative ion mode, respectively; 44 and 86 unique differential metabolites occurred between needles and roots of WS pine seedlings under positive and negative ion mode, respectively. 22 and 62 unique differential metabolites occurred between roots of WS and WW pine seedlings under positive and negative ion mode, respectively; 12 and 26 unique differential metabolites occurred between needles of WS and WW pine

TABLE 3 Summary of selective results of differential metabolites.

Compared Samples[1]	Num. of Total Ident.[2]	Num. of Total Sig.[3]	Num. of Sig. UP[4]	Num. of Sig. Down[5]
WW_L. vs. WW_R_pos	1059	536	281	255
WS_L. vs. WW_L_pos	1059	101	38	63
WS_L vs. WS_R_pos	1059	530	240	290
WS_R. vs. WW _R_pos	1059	177	103	74
WW_L. vs. WW_R_neg	526	282	117	165
WS_L. vs. WW_L_neg	526	44	27	17
WS_L. vs. WS_R_neg	526	286	115	171
WS_R. vs.WW_R_neg	526	77	49	28

(1) WW-L and WW-R represent needles and roots of well-watered pine seedlings; WS-L and WS-R represent needles and roots of water-stress pine seedlings. (2) Total number of identified metabolites; (3) Total number of metabolites with significant differences; (4) Total number of metabolites significantly up-regulated; (5) Total number of metabolites significantly down-regulated.

seedlings under positive and negative ion mode, respectively (Figure 7; Table S4). The intersections of all the four sample groups were 6-shogaol and lupulin A under positive and negative ion mode, respectively (Table S4).

Considering totals of specific differential metabolites under positive and negative ion mode, Venn analysis showed that the greatest changes in the number of differential metabolites occurred between needles and roots of WW pine seedlings, in total,186 differential metabolites 125 and 61 unique differential metabolites under positive (Figure 7A) and negative (Figure 7B) ion mode, respectively. Figure 7 also showed that the least changes in the number of unique differential metabolites occurred between needles of WS and WW pine seedlings, in total, 38 unique differential metabolites, 22 and 16 metabolites under positive (Figure 7A) and negative (Figure 7B) ion mode. In addition, 130 unique differential metabolites occurred needles and roots of WS pine seedlings (86 and 44 metabolites under positive and negative ion mode, respectively) and 84 unique differential metabolites occurred between roots of WS and WW pine seedlings (62 and 22 metabolites under positive and negative ion mode, respectively) (Figure 7). Interestingly, 337 and 194 differential metabolites were overlapped between needles and roots of WW and WS pine seedlings under positive and negative ion mode, respectively (Figures 7A, B). The numbers of the overlapped differential metabolites were the greatest among all the sample groups under positive and negative ion mode, suggesting many metabolites did not show changes under drought stress. All the results suggest that many of the same differential metabolites take part in response to drought stress in needles and roots of *P. taeda* seedlings.

3.2.3 Hierarchical clustering analysis of total differential metabolites

In this study, many fatty acids and lipids were identified. Their nomenclatures and classification were carried out according to the LIPID MAPS Lipid Classification System (https://www.lipidmaps.org/). Hierarchical clustering analysis was carried out on all differential metabolites of the individual sample groups under positive ion mode (Figure 8) and negative ion mode (Figure S3). Under positive or negative ion mode, metabolites in needles and roots of WS pine seedlings showed great differences from those in needles and roots of WW pine seedlings, respectively (Figures 8, S3).

In detail, under positive ion mode, phosphatidylcholine (PC) (18:5e/2:0), PC (16:1e/2:0), lyso phosphoethanolamine (LPE) 15:1, LPE 16:1, LPE 17:1, monoacylglycerol (MAG) (18:1), LPE 18:2, MAG (18:2), digalactosylmonoacylglycerol (DGMG) (18:2), oleanic acid, oleanolic acid, 4-coumaric acid, botulin, quaillaic acid, betaine, and methyl jasmonate showed lower levels in needles of WW pine seedlings, but salicylic acid, PC (14:0e/2:0), PC (18:3e/2:0), histamine, muramic acid, and N-acetylglucosamine showed higher levels, compared to those in roots of WW pine seedlings (Figure S4A). Under negative ion mode, raffinose, sucrose, N-acetylvaline, lyso phosphatidylcholine (LPC) 18:2, phosphatidylethanol (PEtOH) (17:2/20:5), PEtOH (16:2/20:5), benzoic acid, jasmonic acid, quercetin, α,α-trehalose showed higher levels in needles of WW pine seedlings, but LPC 20:3, LPC 16:0, fumaric acid, and D-(-)-quinic acid show lower levels, compared to those in roots of WW pine seedlings (Figure S4B).

Under positive ion mode, compared with those in needles of WW pine seedlings, 6-shogaol, lyso phosphatidic acid (LPA) 16:0, phylloquinone, anisic aldehyde showed higher levels in needles of WS pine seedlings (Figure S4C), and under negative ion mode, abscisic acid, hirsuteine, asperulosid, topotecan showed higher levels in WS pine needles (Figure S4D). Under positive ion mode, LPE 17:1, LPE 18:2, betaine, melatonin, D-(+)-proline, L-glutamine, LPE 15:0, LPE15:1, LPE 16:1, LPE 18: 1, MAG (18:1), MAG (18:2), monogalactosylmonoacylglycerol (MGMG) (18:2), DGMG (18:2), PC (16:1e/2:0), PC (18:5e/2:0), LPC (1-acyl 16:0), oleanolic acid, oleanic acid, and indole-3-acetic acid show lower levels in the needles of WS pine seedlings, but muramic acid, DL-tryptophan, ferulic acid, histidine, coumalic acid, vitamin C, salicylic acid show higher levels in the needles of WS pine seedlings, compared to those in roots of WW pine seedlings (Figure S4E). Under negative ion mode, D-proline, PEtOH (18:2/20:5), N-acetylvaline, LPE 14:0, jasmonic acid, sucrose, PEtOH (16:2/20:5), PEtOH (17:2/20:5), fatty acyl esters of hydroxy tatty acid (FAHFA) (20:5/20:4), LPC 18:2, allantoin, L-phenylalanine, quercetin showed lower levels in needles of WS pine seedlings, but ascorbic acid, L-histidine, gluconic acid, MAG (18:3), sorbic acid, lupulin A, abscisic acid, DL-malic acid, and fumaric acid showed higher levels their needles, compared to those in their roots (Figure S4F).

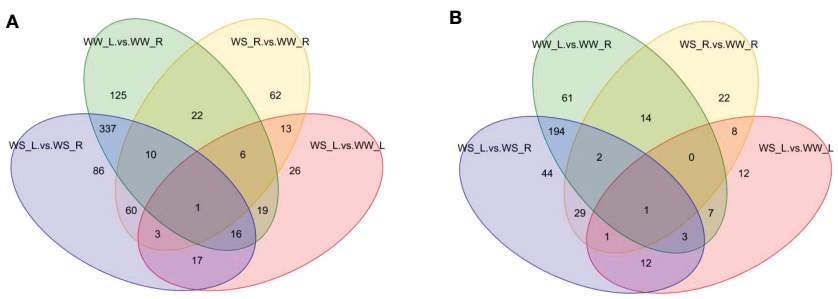


FIGURE 7
Venn diagram of differential metabolites under positive **(A)** and negative **(B)** ion modes. WW-L and WW-R represent needles and roots of well-watered pine seedlings, respectively; WS-L and WS-R represent needles and roots of water-stress pine seedlings, respectively.

10.3389/fpls.2022.1031466

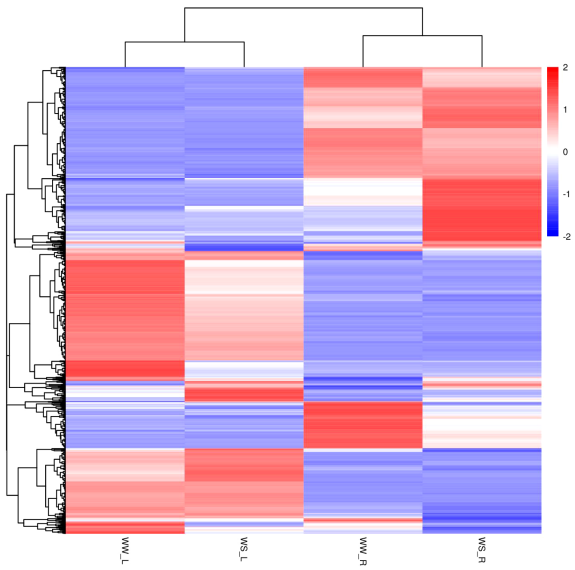


FIGURE 8
Hierarchical clustering analysis of all differential metabolites from the four groups of samples (positive ion mode). WW-L and WW-R represent needles and roots of well-watered pine seedlings, respectively; WS-L and WS-R represent needles and roots of water-stress pine seedlings, respectively.

Roots of WS pine seedlings showed different patterns of differential metabolites, compared with WW pine roots (Figures S4G, H). Under positive ion mode, compared to those in roots of WW pine seedlings, DL-tryptophan, melatonin, cinnamic acid, LPE 14:0, mevalonic acid, and indole-3-acrylic acid showed lower levels in roots of WS pine seedlings, but LPE 18:2, D-(+)-proline, gamma-glutamylglutamine, nicotinic acid, LPE 18:1, histamine, and palmitoleic acid showed higher levels in their roots (Figure S4G). Under negative ion mode, D-proline, D-(-)-fructose, LPC16:0, L-citrulline, resveratrol showed higher levels in WS pine roots, compared with those in WW pine roots (Figure S4H).

Under positive ion mode, compared with metabolites in needles of WW pine seedlings, some metabolites were significantly up- or down-regulated in needles of WS pine seedlings. The first five up-related metabolites were ingenol-3-angelate, α-aspartylphenylalanine, 3-methoxy prostaglandin F1α, 16,16-dimethyl prostaglandin A2, 7-(2-hydroxypropan-2-yl)-1,4a-dimethyl-decahydronaphthalen-1-ol (WS_L.vs.WW_L_pos_diff.anno in Table S2). The first five down-regulated metabolites were cepharanthine, oxymorphone, 4-methyl-5-oxo-2-pentyl-2,5-dihydrofuran-3-carboxylic acid, p-nitroaniline, glycyrrhizin (WS_L.vs.WW_L_pos_diff.anno in Table S2).

Under positive ion mode, compared with metabolites in roots of WW pine seedlings, some metabolites were significantly up- or down-regulated in roots of WS pine seedlings. The first five up-regulated metabolites were perillartine, 2-(2-oxo-2-{[2-(2-oxo-1-imidazolidinyl) ethyl]amino}ethoxy)acetic acid, 1-(3,4-dimethoxyphenyl)ethan-1-one oxime, tacrolimus, N-feruloylagmatine (WS_R.vs.WW_R_pos_diff.anno in Table S2). Astonishingly, perillartine was up-regulated up to 352 times in roots of WS pine seedlings, compared with that in roots of WW pine seedlings (WS_R.vs.WW_R_pos_diff.anno in Table S2). The first five down-regulated metabolites were dehydrotumulosic acid, tetrahydroxyxanthone, phylloquinone, solasonine, (20R)ginsenoside Rh2 (WS_R.vs.WW_R_pos_diff.anno in Table S2).

3.2.4 Correlation analysis of differential metabolites

Figure 9 and Table S4 showed the correlations between differential metabolites in different sample groups under positive ion mode. Comparing metabolites in needles and roots of WW pine seedlings (Figure 9A and WW_L.vs.WW_R_pos_corr in Table S5), it was found that γ-glutamylcysteine was in negative relation to some metabolites, such as glycyrrhetinic acid, betulin, solasonine, panaxatriol, LPE 15:1, LPE 17:1, and glabrolide. 3-((5-phenyloxazol-2-yl)amino)benzonitrile was also in negative relation to some metabolites, such as LPE 15: 1, LPE 17:1, botulin, and glabrolide. Interestingly, γ-glutamylcysteine and 3-((5-phenyloxazol-2-yl)amino) benzonitrile were in positive relation to each other. Drought stress induced great changes in metabolites in needles of WS and WW pine seedlings (Figure 9B and WS_L.vs.WW_L_pos_corr in Table S5). Urocanic acid was in positive relation to gamma-glutamylmethionine, polypodine B, and ethyl 5-methoxy-2-methyl-1-phenyl-1H-indole-3-carboxylate, but in negative relation to phylloquinone. Oxymorphone was in positive relation to N-p-coumaroylspermidine (Figure 9B and WS_L.vs.WW_L_pos_corr in Table S5). Comparing metabolites in needles and roots of WS pine seedlings, it was found that L-glutathine (reduced) was in negative relation to botulin, alisol B, and ginsenoside F1, but in positive relation to salicylic acid, coumalic acid, trifolin, and vitamin C (Figure 9C and WS_L.vs.WS_R_pos_corr in Table S5). Salicylic acid was in positive relation to coumalic acid, vitamin C, and trifolin, but in negative relation to piceatrannol, mulberroside A, panaxatriol, betullin, Ala-Ile, Alisol B (Figure 9C and WS_L.vs.WS_R_pos_corr in Table S5). Similarly, drought stress resulted in great changes in metabolites in roots of WS and WW pine seedlings (Figure 9D and WS_R.vs.WW_R_pos_corr in Table S5). Pantothenic acid was in negative relation to valylproline, curcumenol, alanyltyrosine, but in positive relation to bruceine D (Figure 9D, and WS_R.vs.WW_R_pos_corr in Table S5). Carbaprostacyclin was in positive relation to leonurine, L-glutamic acid, histamine, adenine, 5-methyluridine, alanyltrosine (Figure 9D). L-glutamic acid was in positive relation to leonurine, histamine, methyl dihydrojasmonate, but in negative relation to flavokawain A (Figure 9D and WS_R.vs.WW_R_pos_corr in Table S5).

Under negative ion mode, great changes occurred in metabolites in needles of WS and WW pine seedlings, (±)-abscisic acid was in positive relation to ganoderic acid C6, asperulosid, 11-deoxyl prostaglandin F2β, MAG (18:3), and topotecan, but in negative relation to neohesperidin (Figure S5B and WS_L.vs.WW_L_neg_corr in Table S6). Tracheloside was in positive relation to erythronolactone, lupulin A, and saikosaponin B2, but in negative relation to prostaglandin H2 (Figure S5B and WS_L.vs.WW_L_neg_corr in Table S6).

Under negative mode, comparing changes in metabolites in needles and roots of WS pine seedlings, it was found that ascorbic acid was in positive relation to sorbic acid, D-(-)-quinic acid, sinapaldehyde glucoside, tenuifoliside A, skimming, and gluconolactone, but in negative relation to 20(R)-ginsenoside Rh1, astringin, aloesin, perillic acid, sweroside, bufalin, jasmonic acid, and epimedin B (Figure S5C and WS_L.vs.WS_R_neg_corr in Table S6).

Comparing changes in metabolites in roots of WS and WW pine seedlings, it was found that D-(+)-maltose was in positive relation to cyaniding-3-*O*-glucoside, prostaglandin D3, and uridine 5'-dephosphogalactose, but in negative relation to sinapoyl *O*-hexoside

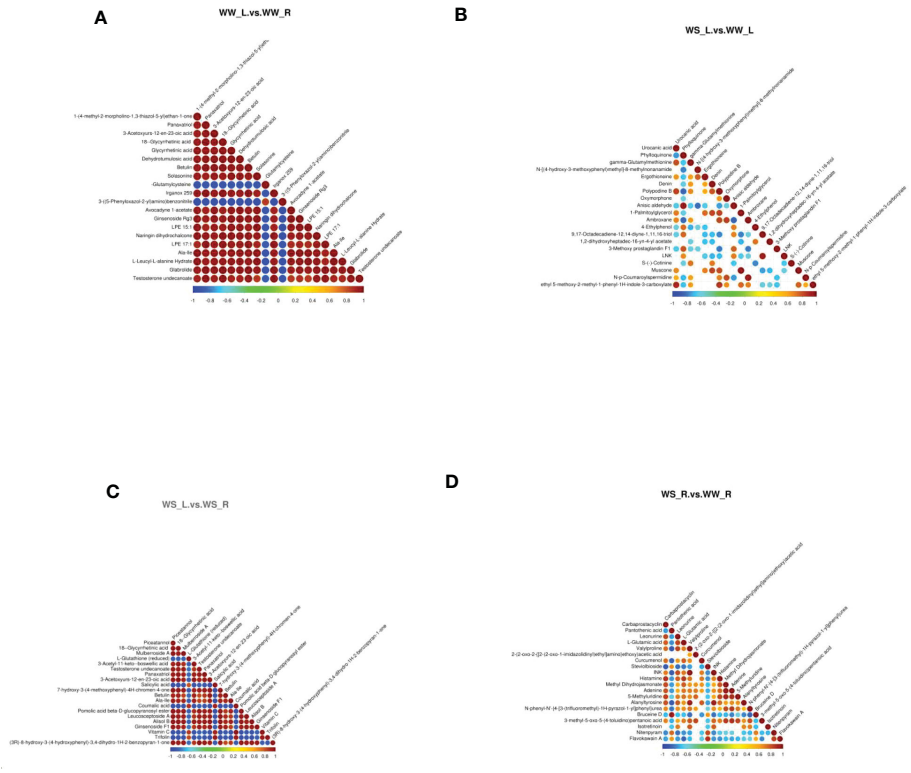


FIGURE 9
Correlation analysis of metabolites (positive ion mode) with *p* values of top 20 (beginning from the minimal *p* value). The highest correlation with correlation coefficient of 1 was represented in red; the lowest correlation with correlation coefficient of -1 was represented in blue. Colorless parts indicated *p* value > 0.05. **(A)** leaves vs. roots of WW seedlings; **(B)** leaves of WS vs. WW pine seedlings; **(C)** leaves vs. roots of WS pine seedlings; **(D)** roots of WS vs. WW pine seedlings. WW, well-watered; WS, water-stressed.

(Figure S5D and WS_R.vs.WW_R_neg_corr in Table S6). β-muricholic acid was in positive relation to schizandrol A, 16 α-hydroxyestrone (Figure S5D and WS_R.vs.WW_R_neg_corr in Table S6).

3.2.5 Z-score analysis

Under positive ion mode, Z-score analysis was carried out (Figure 10 and Table S7). Under WW condition, WW pine needles had higher levels of γ-glutamylcysteine, 3-((5-phenyloxazol-2-yl)amino)benzonitrile, octyl hydrogen phthalate, octyl hydrogen phthalate, coumalic acid, and vitamin C (Figure 10A and WW_L.vs.WW_R_pos_zscore in Table S7). Comparing metabolites in needles of WS and WW pine seedlings, it was found that some metabolites showed higher concentrations in needles of WS pine seedlings, such as phylloquinone, anisic aldehyde, 1,2-dihydroxyheptadec-16-yn-4-yl acetate (Figure 10B and WS_L.vs.WW_L_pos_zscore in Table S7). Few metabolites showed much higher levels in needles of WS pine seedlings than those in WS pine roots, such as L-glutathione (reduced), salicylic acid, coumalic acid, and vitamin C (Figure 10C and WS_L.vs.WS_R_pos_zscore in Table S7). Comparing metabolites in roots of WS and WW pine seedlings, it was found that L-glutamic acid, 2-(2-oxo-2-{[2-(2-oxo-1-imidazolidinyl) ethyl]amino}ethoxy)acetic acid, curcumenol showed higher levels in WS pine roots (Figure 10D and WW_R.vs.WW_R_pos_zscore in Table S7).

Z-scores under negative ion mode were shown in Figure S6 and Table S7. Few metabolites show much higher levels in needles of WW pine seedlings than those in in their roots, such as 2-hydroxymyristic acid, 3,4,5-trihydroxycyclohex-1-ene-1-carboxylic acid, kynurenic acid *O*-hexside, sorbic acid (Figure S6A and WW_L.vs.WW_R_neg_zscore in Table S7). Under negative ion mode, ganoderic acid C6, asperulosid, 11-deoxy prostaglandin F2β, MAG (18:3), hirsuteine, and (±)-abscisic acid showed higher concentrations in needles of WS pine seedlings than those in needles of WW pine seedlings (Figure S6B and WS_L.vs.WW_L_neg_zscore in Table S7). Under negative ion mode, 3,4,5-trihydroxycyclohex-1-ene-1-carboxylic acid, sorbic acid, D-(-)-quinic acid, tenuifoliside A, and abscorbic acid showed higher levels in WS pine needles, compared with their roots (Figure S6C and WS_L.vs.WS_R_neg_zscore in Table S7). Comparing metabolites in roots of WS and WW pine seedlings, it was found that ethyl 3-cyano-6-methyl-2-(phenylthio)isonicotinate, 1,3,5-trimethoxybenzene, ganoderic acid C6, L-citrulline, 16α-Hydroxyestrone, and 4-oxoproline showed higher concentrations in roots of WS pine seedlings (Figure S6D and WS_R.vs.WW_R_neg_zscore in Table S7).

3.2.6 KEGG enrichment analysis

The most enriched metabolite pathways under positive ion mode were shown in Figure 11 and Table S8. Comparing needles and roots of WW pine seedlings, the first five enriched pathways included flavone and flavonol biosynthesis, ABC transporters, plant hormone signal transduction, flavonoid biosynthesis, and pantothenate and CoA biosynthesis (Figure 11A and WW_L.vs.WW_R_pos_kegg_enrichment in Table S8). Comparing needles of WS and WW pine

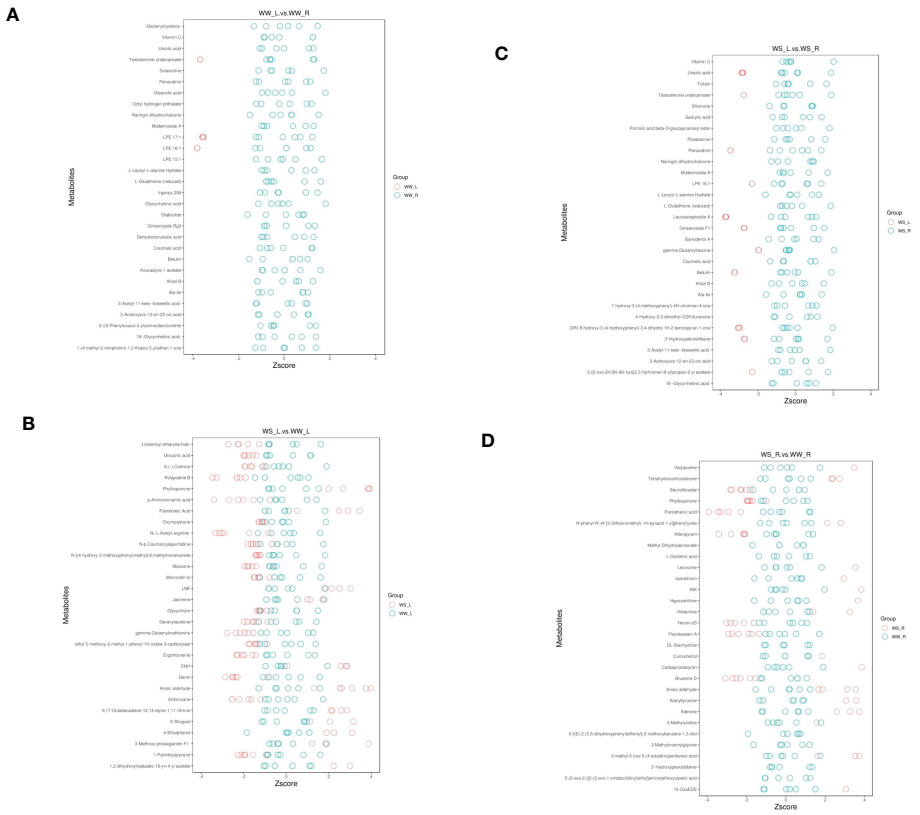


FIGURE 10
Z score analysis of the four sample groups under positive ion mode. **(A)** leaves vs. roots of WW seedlings; **(B)** leaves of WS vs. WW pine seedlings; **(C)** leaves vs. roots of WS pine seedlings; **(D)** roots of WS vs. WW pine seedlings. WW, well-watered; WS, water-stressed.

seedlings, the first five enriched pathways included histidine metabolism, folate biosynthesis, ubiquinone and other terpenoid-quinone biosyntehsis, vitamin B6 metabolism, and zeatin biosynthesis (Figure 11B and WS_L.vs.WW_L_pos_kegg_enrichment in Table S8). Comparing needles and roots of WS pine seedlings, the first five enriched pathways included tryptophan metabolism, caffeine metabolism, sesquiterpenoid and triterpenoid biosynthesis, plant hormone signal transduction, and phenylalanine, tyrosine and tryptophan biosynthesis (Figure 11C and WS_L.vs.WS_R_pos_kegg_enrichment in Table S8). Comparing roots of WS and WW pine seedlings, the first five enriched pathways included metabolic pathways, zeatin biosynthesis, pentose phosphate pathway, carbapenem biosynthesis, and benzoxazinoid biosynthesis (Figure 11D and WS_R.vs.WW_R_pos_kegg_enrichment in Table S8).

Under negative ion mode, the most enriched pathways were shown in Figure S7 and Table S9. Comparing needles and roots of WW pine seedlings, the first five enriched pathways included phenylalanine metabolism, butanoate metabolism, starch and sucrose metabolism, anino sugar and nucleotide sugar metabolism, and phyenylpropanoid biosynthesis (Figure S7A and WW_L.vs.WW_R_neg_kegg_enrichment in Table Table S9). Comparing needles of WS and WW pine seedlings, the first five enriched pathways included biosynthesis of unsaturated fatty acids, arachidonic acid metabolism, plant hormone signal transduction, carotenoid biosynthesis, and porphyrin and chlorophyll metabolism (Figure S7B and WS_L.vs.WW_L_neg_kegg_enrichment in Table S9). Comparing needles and roots of WS pine seedlings, the first three enriched pathways included phenylalanine metabolism, tyrosine metabolism, butanoate metabolism (Figure S7B and WS_L.vs.WS_R_neg_kegg_enrichment in Table S9). Comparing roots of WS and WW pine seedlings, the first five enriched pathways included arginine and proline metabolism, lysine degradation, tryptophan metabolism, biosynthesis of unsaturate fatty acids, biosyntehsis of amino acids (Figure S7B and WS_R.vs.WW_R_neg_kegg_enrichment in Table S9).

4 Discussion

4.1 Roles of phytohormomes in *P. taeda* under drought stress

Phytohormones regulate plant growth and response to abiotic/biotic stress, especially ABA under drought stress (Yu et al., 2019; Zhang et al., 2020; Wang et al., 2021b; Muhammad Aslam et al., 2022). Under long-term drought, ABA concentration significantly was higher in needles of WS pine seedlings than those in the other samples, but ABA levels did not show differences among roots of WS pine seedlings and needles and roots of WW pine seedlings (Figure 4A). Our untargeted metabolomics analysis also showed ABA level increased about 50% in needles of WS pine seedlings, but slightly increased in their roots (Table S10, negative ion mode). The results suggest that ABA played an important role in controlling water loss by transpiration. At present, it has been well known about

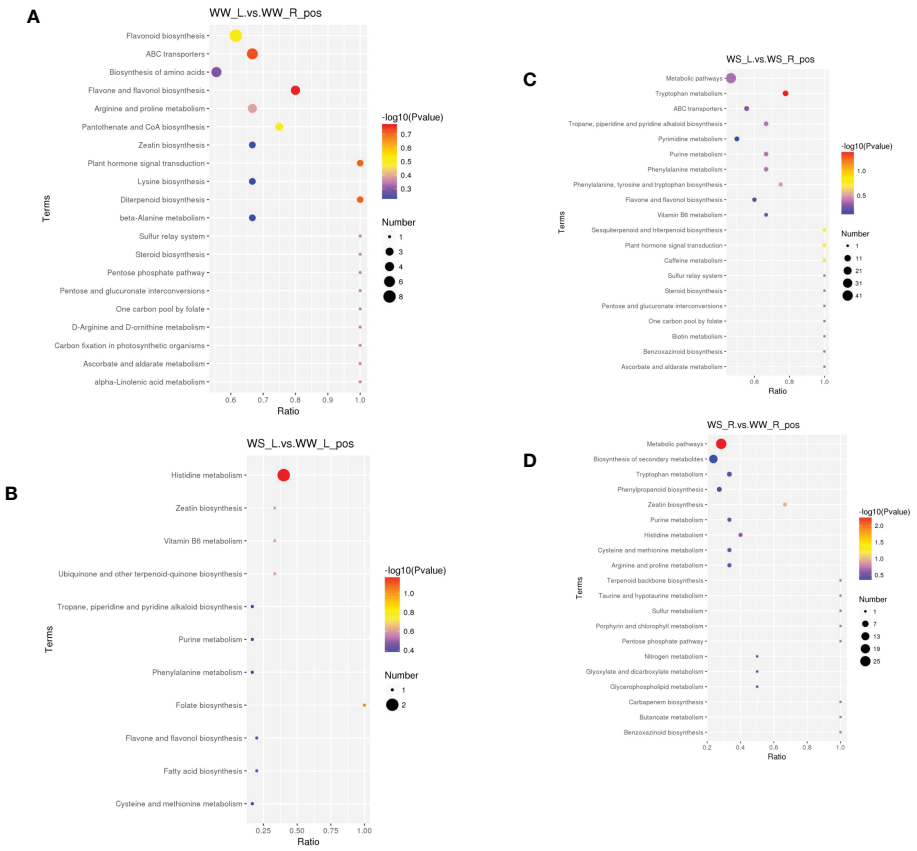


FIGURE 11
Metabolites enriched in KEGG pathways under positive ion mode (top 20 pathways). In the small figures, horizontal axis represented the ratio of number of differential metabolites to the total numbers of metabolites identified in a pathway. Greater the ratio was, higher the differential metabolites enriched in the pathway. Color of a circle represented *p* value in geometric test. The size of a circle represented the number of differential metabolites in the corresponding pathway. **(A)** needles vs. roots of WW seedlings; **(B)** needles of WS vs. WW pine seedlings; **(C)** needles vs. roots of WS pine seedlings; **(D)** roots of WS vs. WW pine seedlings. WW, well-watered; WS, water-stressed.

the mechanism that ABA regulates stomatal closure. The activation of a slow anion current in guard cells is a key event resulting in stomatal closure (Schroeder and Hagiwara, 1989; Pandey et al., 2007; Roelfsema et al., 2012; Saito and Uozumi, 2019). Environmental stresses induce increase in ABA biosynthesis and ABA leads to phosphoactivation of slow anion channel 1 (SLAC1), and SLAC1 reduces turgor pressure in guard cells and stomatal closure occurs (Brandt et al., 2012; Hedrich and Geiger, 2017). Recently, Deng et al. (2021) analyzed structure and activity of SLAC1 channels and confirmed that SLAC1 phosphorylaltion fine-tunes equilibrium between basal and activated SLAC1 trimers controlling the degree of stomatal opening. Similarly, salicylic acid (SA) concentration was significantly higher in WS pine needles than that in WW pine needles and showed no difference in roots of WW and WS pine seedlings (Figure 4C). Some experimental results showed that SA can induce stomatal closure (Manthe et al., 1992; Khokon et al., 2011; Poór and Tari, 2012). SA-induced stomatal closure is related to increased levels of reactive oxygen species (ROS) and nitric oxide (NO) (Poór and Tari, 2012). Previous research supported our results of targeted metabolomics analysis (Sharma et al., 2017; Khan et al., 2021; Ahmad et al., 2021). Ahmad et al. (2021) reported that exogenous SA induced drought tolerance in wheat (*Triticum aestivum*) grown under hydroponic culture and it was confirmed that plants increase SA accumulation after being exposed to drought stress (Okuma et al., 2014). Therefore, increased SA levels in needles of WS pine seedlings are helpful stomatal closure, further reducing water loss by transpiration under drought stress. During control over stomatal closure, SA interacts with ABA and shares components of ABA signaling pathway (Khokon et al., 2017; Bharath et al., 2021).

In contrast to the situations of ABA and SA mentioned above, GA4 concentration was significantly higher in roots of WS pine seedlings than that in roots of WW pine seedlings (Figure 4D). In grafted tomato plants, constitutive gibberellin response modulated root-to-shoot signaling under drought stress (Gaion et al., 2018). The results from Gaion et al. (2018) showed that the GA sensitivity of the rootstock modulated stomatal conductance and water use efficiency under drought stress, indicating that GA and ABA crosstalk in the adjustment of growth and water economy. Transcriptome survey and expression analysis revealed that pear mRNA expression of enzyme genes involved in gibberellin signaling was higher than that in control in response to long-term drought stress (Yang et al., 2021). However, gibberellins occur in many structures in plants, and they did not show consistent roles in plants under long-term drought stress, such as GA3 and GA4 (Figures 4C, D). GA3 levels increased in WS pine needles, compared with that in WW pine needles (Figure 4C), and untargeted metabolomics analysis showed that GA3 levels increased

in WS pine roots and needles (Table S2 and positive ion mode in Table S10). A report showed drought triggered reduction in RWC and chlorophyll concentrations, but these parameters recovered when droughty plants of sugarcane (*Saccharum* spp. hybrids) were exposed to GA3 (Tripathi et al., 2019). Therefore, increased GA3 levels in WS pine roots and needles could improve drought tolerance of *P. taeda* seedlings.

Drought stress provokes JA signaling and JA is involved in root development under drought stress by the antagonistic interaction with cytokinin (Jang et al., 2017; Jang and Choi, 2018; Ali and Baek, 2020). But in our research, JA and JAI did not show significant changes in roots and needles of WW and WS pine seedlings (Figure 4B), however, JA increased 91% in WS pine roots, compared with WW pine seedlings (Figure 4B). In addition, untargeted metabolomics analysis showed that levels of JA and methyl jasmonate (MJ) increased in roots and needles of WS pine seedlings, compared with WW pine seedlings (Table S2 and negative ion mode in Table S10). Previous research confirmed that water stress increases JA concentrations in leaves and roots of rice (*Oryza sativa*) plants (Kiribuchi et al., 2005). Thus increased JA levels in WS pine seedlings can promote drought tolerance of *P. taeda* seedlings (Wasternack and Song, 2017).

4.2 Roles of sugars and amino acids in *Pinus taeda* under drought stress

Sugars maintain energy activity in plant cells and show their roles as osmoregulators and membrane protectors (Sami et al., 2016), thus they often show great responses to environmental changes. In this study, glucose concentrations showed no statistical difference between needles of WW and WS pine seedlings, but glucose concentration significantly reduced in WS pine roots (Figure 1B). High glucose accumulation in WS pine needles (Figure 1B) is helpful for controlling water loss, because glucose can induces stomatal closure (Osakabe et al., 2013). Sucrose is a main sugar transported from source to sink organs in most plants, and carbon allocation between source and sink organs decides fate of sink organs. Untargeted metabolomics analysis showed that sucrose levels increased in roots and needles of WS pine seedlings, compared with those in roots and needles of WW pine seedlings, respectively (Table S10, negative ion mode). Sucrose concentrations in WS pine needles were significantly lower than those in WW pine seedlings, but significantly higher in roots of WS pine seedlings (Figure 1A). All the results suggest sucrose role in *P. taeda* seedlings under drought stress. The sucrose accumulation in roots under drought stress is helpful to increase root activity and ability to explore water source.

Compared with WW pine seedlings, raffinose level increased in roots of WS pine seedlings (Figure 1B), and untargeted metabolomics analysis showed that raffinose levels in roots and needles of WS pine seedlings also increased (Table S10, negative ion mode). Previous research showed that raffionose family oligosaccharides have important roles against abiotic stress (ElSayed et al., 2014; Mukherjee et al., 2019), thus increase in raffinose levels in roots and needles of WS pine seedlings is helpful for enhanced tolerance to drought stress.

Some experimental results showed that trehalose, acting as an osmoprotectant, plays an important role in plants under drought stress (Ilhan et al., 2015; Kosar et al., 2021; Mukarram et al., 2021; Zulfiqar et al., 2021). However, in our targeted metabolomics analysis, trehalose was not detected in roots and needles of WW and WS pine seedlings. This result suggests trehalose levels should be very low, as reported by Ingram & Bartels (1996). Our untargeted metabolomics analysis showed that trehalose levels increased in roots and needles of WS pine seedlings, compared with those in roots and needles of WW pine seedlings, respectively (Table S10, negative ion mode). The result is consistent with that reported by Mibei et al. (2018). Their metabolomics analysis showed that trehalose level increased in African eggplants (*Solanum aethiopicum*) under drought stress. Thus it might be speculated that trehalose played a role in pine seedlings under drought stress, just like its role in other plant species.

In roots and needles of WS pine seedlings, the enriched KEGG pathways were involved in biosynthesis and metabolism of secondary metabolites (Figures 11, S7; Tables S8, S9), suggesting that amiono acids played important roles in *P. taeda* seedlings under long-term drought stress. Some amino acids were studied well about their roles under drought stress. For example, proline acts as an osmoprotectant against drought stress in plants (Furlan et al., 2020; Adamipour et al., 2020; Mukarram et al., 2021). Proline levels increased in roots of WS pine seedlings, but not significantly, compared with that in roots of WW pine seedlings (Figure 2A). Similarly, untargeted metabolomics analysis showed increased proline level in roots of WS pine seedlings, compared with that in roots of WW pine seedlings (Tables S2, S10, negative ion mode). Results from Díaz et al. (2010) showed that deficiency in plastidic glutamine synthetase alters proline metabolism and transcriptomic response in *Lotus japonicas* under drought stress. Since glutamine synthetase is in charge of conversion of ammonium to glutamine, glutamine is related to proline metabolism, because deficiency in plastidic glutamine synthetase alters proline metabolism in Lotus japonicus under drought stress (Díaz et al., 2010) and glutamine synthetase in the phloem plays a major role in controlling proline production (Brugiere et al., 1999). Our results showed that glutamine levels significantly increased in roots of WS pine seedlings, compared with that in WW pine seedlings (Figure 2A), and untargeted metabolomics analysis also showed glutamine levels significantly increased in WS pine roots, compared with those in WW pine roots (Tables S2, S10, negative ion mode). Therefore, significant increase in glutamine levels in roots of WS pine seedlings is helpful for enhanced drought tolerance of *P. taeda* seedlings by regulating proline metabolism. In addition, proline derivative, DL-stachydrine (proline betaine, a quaternary ammonium derivative of proline that occurs widely in *Medicago* species), was up-regulated in WS pine roots (Table S2). Proline betaine accumulated in alfalfa (*Medicago sativa*) plants under salt stress (Trinchant et al., 2004), however, at present, no information has been known about the function of DL-stachydrine in plants under drought stress.

Previous research showed that arginine and aspartate play roles in plants under drought stress (Hasanuzzaman et al., 2018; You et al., 2019; Ali et al., 2021). In roots of WS pine seedlings, levels of arginine and aspartate increased, compared with those in roots of WW pine seedlings, respectively (Figure 2B), but untargeted metabolomics analysis showed that levels of L-aspartic acid in roots and needles of WS pine seedlings reduced, compared with those in WW pine seedlings, respectively (Table S10, positive ion mode). The

inconsistency might stem from sampling differentiation. Based on targeted analysis results, the two amino acids should possess the same roles in *P. taeda* seedlings under drought stress as they function in other plant species.

The saccharopine pathway (SACPATH) involves the conversion of lysine into α-aminoadipate by three enzymatic reactions catalyzed by the bifunctional enzyme lysine-ketoglutarate reductase/saccharopine dehydrogenase (LKR/SDH) and the enzyme α-aminoadipate semialdehyde dehydrogenase (AASADH) (Arruda and Barreto, 2020). Level of free lysine significantly increased in drought-tolerant and drought susceptible sesame (*Sesamum indicum*) under drought stress (You et al., 2019), suggesting role of lysine in plants under drought stress. Our results showed that lysine level significantly increased in roots of WS pine seedlings, compared with that in roots of WW pine seedlings (Figure 2C). The significant increase in lysine level in roots of WS pine seedlings resulted in significant reduction in L-saccharopine and significant increase in pipecolic acid (Tables S2, S10). Both saccharopine and pipecolic acid stem from lysine, but pipecolic acid is synthesized from saccharopine (Arruda and Barreto, 2020), thus it is reasonable to explain significant reduction in saccharopine level and increase in pipecolic acid level. Furthermore, our result is consistent with previous research which showed that saccharopine levels significantly reduced in drought-tolerant wheat (*Triticum aestivum*) genotypes HX10 under drought stress (Guo et al., 2020).

Asparagine is synthesized from glutamine by the reaction of aspargine synthetase (AS). The up-regulation of AS gene may contribute the higher leaf nitrogen remobilization in maize (*Zea mays* L.) when exposed to drought stress (Li et al., 2016). Our results showed that aspargine level significantly increased in WS pine roots, compared with that in WW pine roots (Figure 2C). The result is consistent with the previous one.

Targeted metabolomics analysis showed that levels of L-tyrosine reduced in WS pine roots (Table 1), and untargeted metabolomics analysis showed that tyrosine reduced in roots and needles of WS pine seedlings (Table S2 and positive ion mode in Table S10). However, previous research showed that tyrosine levels increased and suggested that tyrosine accumulation might play a positive role in response to drought stress (Liu et al., 2012; Khan et al., 2019; Tong et al., 2020). Thus, the function of tyrosine in plants under drought stress should be investigated in detail.

4.3 Roles of fatty acids and lipids in *Pinus taeda* under drought stress

Some lipids contain fatty acids. Fatty acids possess three main functions, i.e., membrane components, energy metabolism and store, and signaling. Some lipids with fatty acids are important components of biological membranes in plants. For example, phosphatidylcholine (PC) and phosphoethanolamine (PE) are the major glycerolipids of the cell membranes, and mitochondria membrane and endoplasmic reticulum membranes, and chloroplast membranes mainly contain monogalactosyldiacylglycerol (MGDG) and digalactosyldiacy lglycerol (DGDG) (Zhukov and Shumskaya, 2020). In higher plants, the most common unsaturated fatty acids (UFAs) are three 18-carbon species, namely, oleic (18:1), linoleic (18:2), and a-linolenic (18:3) acids, and these UFAs possess multiple functions in plants, especially under abiotic stress (He and Ding, 2020). Untargeted metabolomics analysis showed that the most enriched KEGG pathway was biosyntehsis of unsaturated fatty acids in needles of WS pine seedlings under negative ion mode (Figure S7 and WS_L.vs.WW_L _neg_kegg_enrichem in Table S9); under positive ion mode, fatty acid biosynthesis was one of the most enriched pathways in WS pine needles (Figure 11B and WS_L.vs.WW_L_pos_kegg_enrichment in Table S8), suggesting that great changes in fatty acids in WS pine needles. Targeted metabolomics analysis showed that levels of some fatty acids significantly reduced in roots and/or needles of WS pine seedlings, compared with WW pine seedlings (Table 2). The significant reduction in fatty acid levels might be based on the reason that plants reduce carbon fixation under drought stress, further affecting biosynthesis of fatty acids. However, three saturated fatty acids significantly increased in WS pine seedlings, i.e., dodecanoic acid in needles, and tricosanoic acid and heptadecanoic acid in roots (Table 2). At present, little has been known about their functions in plants under drought stress.

Untargeted metabolics analysis showed that LPA 14:00 and LPA 16:0 showed higher levels in needles of WS pine seedlings (Figures S4C, D), and that LPC16:0, LPE 18:2, LPE 18:1, and palmitoleic acid showed higher levels in their roots (Figures S4G, H), compared with those in WW pine roots and needles, respectively. Similarly, compared with those in needles of WS pine seedlings, some unsaturated lipids had higher levels in their roots, such as LPC15:1, LPE15:1, LPE16:1, LPE17:1, LPE 18:1, LPE18:2, MAG (18:1), MAG (18:2), MGMG (18:2), DGMG (18:2), PC (16:1e/2:0), PC (18:5e/2:0), PEtOH (18:2/20:5), PEtOH (16:2/20:5), PEtOH (17:2/20:5), FAHFA (20:5/20:4), LPC 18:2 (Figures S4E, F). Their increased levels improved membrane flexibility in roots and needles of *P. taeda* seedlings under drought stress. Previous studies supported our results (Gu et al., 2020). As mentioned above, in needles of WS pine seedlings, ABA levels significantly increased (Figure 4A) and (±)-ABA was in positive relation to MAG (18:3) (Figure S5B and WS_L.vs.WW_L_neg_corr in Table S6), suggesting that ABA accumulation might improve unsaturated lipid biosynthesis in WS pine needles and sustain membrane stability and flexibility under drought stress, because ABA improves biosynthesis of some fatty acids in plants (Norlina et al., 2020; Shi et al., 2021).

4.4 Roles of neurotransmitters in *Pinus taeda* under drought stress

Neurotransmitters play important roles in plant growth/development and responses to environmental stresses (Erland et al., 2018; Akula and Mukherjee, 2020; Qin et al., 2020; Sun et al., 2021). Among the neurotransmitters in plants, melatonin is up to now the most important one in response to drought stress. Melatonin enhances drought stress tolerance (Ahmad et al., 2019; Tiwari et al., 2021; Imran et al., 2021; Ren et al., 2021), and the regulatory mechanisms are involved in many aspects (Tiwari et al., 2021). In our research, melatonin was not determined in WS pine needles, and melatonin concentrations in roots showed no difference between WW and WS pine seedlings (Table 1). But untargeted metabolomics analysis showed that melatonin levels in WS pine roots and needles

significantly increased (Table S2 and positive ion mode in Table S10). The results might suggest that melatonin still play an important role in *P. taeda* seedlings under long-term drought stress.

At present, little knowledge was known about function of glutamine, acting as a neurotransmitter, in plants under drought stress. Under drought stress, glutamine synthetase (GS, EC 6.3.1.2) showed different activities in drought-sensitive (cv. IR-64) and drought-tolerant (cv. Khitish) rice (*Oryza sativa*) cultivars, and OsGS2 and OsGS1;1 may contribute to drought tolerance of drought-tolerant cultivar Khitish under drought stress (Singh and Ghosh, 2013). Another report showed GS expression was up-regulated in maize leaves under drought stress (Li et al., 2016). The overexpression of wheat (*Triticum aestivum*) cytosolic and plastic GS in tobacco enhanced drought tolerance of tobacco (*Nicotiana tabacum*) (Yu et al., 2020). All the results indicate that glutamine synthesized through GS activity possesses an important role in plants under drought stress. In the GS2 mutant (*Ljgln2-2*) of *Lotus japonicas* under drought stress, proline accumulation was substantially lower than that in WT plants (Díaz et al., 2010), suggesting GS2 was involved in proline biosynthesis, thus implying that glutamine might be related to proline biosynthesis. Since GS converts ammonium to glutamine, up-regulated GS expression means increase in glutamine biosynthesis. Therefore, glutamine might play a role in response to drought stress *via* proline metabolism. In our research, among the neurotransmitters detected, L-glutamine concentrations showed the greatest changes in roots, i.e., significant increase in roots of WS pine seedlings (Figure 2A; Table 1), and untargeted metabolomics analysis also showed that L-glutamine significantly increased in roots and needles of WS pine seedlings (Table S2 and positive ion mode in Table S10), compared with WW pine seedlings, suggesting that our result is consistent with the previous results mentioned above. Although proline concentrations in roots of WS pine seedlings did not show significant changes, compared with WW pine seedlings (Figure 2A), untargeted metabolomics analysis showed that proline levels significantly increased in WS pine roots, compared with that in WW pine roots, suggesting a close relationship between glutamine and proline accumulation.

Acetylcholine showed different concentration patterns in roots and needles of WW and WS pine seedlings, i.e., acetylcholine concentration was significantly higher in WS pine needles, but significantly lower in WS pine roots, compared with WW pine seedlings, respectively (Table 1). In addition, hyoscyamine and atropine, acting as antagonists of acetylcholine receptors, significantly increased in WS pine roots, compared with those in WW pine roots, and was not determined in needles of WW and WS pine seedlings (Table S2). A research report showed acetylcholine regulates stomatal movement *via* nicotinic acetylcholine receptors (Wang et al., 1998). Furthermore, acetylcholine acts as a long-distance signaling molecule (Lou, 1998; Jia and Zhang, 2008). Therefore, significant acetylcholine increase in needles and reduction in roots of WS pine seedlings might suggest that acetylcholine was delivered from roots to needles of WS pine seedlings under drought stress, acting as a long-distance signaling molecule, as mentioned above. Significant increase in atropine and hyoscyamine levels in WS pine roots might result in their binding to acetylcholine receptors prior to acetylcholine and make more acetylcholine transport to needles under drought stress. However, results from Wang et al. (1998) showed that acetylcholine induced stomatal opening. Our results showed that acetylcholine concentration increased about 3 times in WS pine needles, compared with that in WW pine needles (Table 1), therefore, we speculate that acetylcholine acts as a two-tier regulator, i.e., acetylcholine regulates stomatal opening under WW condition, and under WS condition acetylcholine is transported from roots to needles and accumulates to higher levels as to induce stomatal closure, just like 2,4-dichlorophenoxyacetic acid (2,4-D) acting as an herbicide when its level is higher and an auxin analog when its level is lower (Song, 2014; Agathokleous et al., 2019). Based on the fact that our result about acetylcholine levels is contrary to that of Wang et al. (1998), more research on functions of acetylcholine is needed, especially its regulating stomatal movement under drought stress.

Dopamine (3-hydroxytyramine) is an important neurotransmitter in animals, and show many roles in plant physiology. Exogenous dopamine improved the tolerance against several abiotic stresses, such as drought, salt, and nutrient stress (Liu et al., 2020). Pretreatment with 100 μM dopamine alleviated drought stress in apple (*Malus domestica*) seedlings, inhibited the degradation of photosynthetic pigments, and increased net photosynthetic rate under drought stress (Gao et al., 2020). Their results also showed that dopamine may improve apple drought tolerance by activating Ca^{2+} signaling pathways through increased expression of CNGC and CAM/CML family genes, and analysis of transcription factor expression suggested that dopamine affected drought tolerance mainly through the regulation of WRKY, ERF, and NAC transcription factors (Gao et al., 2020). Thus, our results, i.e., significant increase in hydroxytyramine level in WS pine needles (Table 1), suggest its role in *P. taeda* seedlings under long-term drought stress.

Little is known about the role of the neurotransmitter noradrenaline in plants. It was reported that heat-treated noradrenaline induced flowering in short-day *Lemna paucicostata* strains 441 and 6746 and long-day *Lemna gibba* strain G3 (Miyawaki et al., 2013). In our research, noradrenaline concentration significantly reduced in WS pine needles and had no difference in their roots, compared with WW pine seedlings (Table 1), suggesting noradrenaline might be related to controlling water loss under drought stress. If so, the relationship between ABA signaling and noradrenaline in plants under drought stress should be investigated.

Increased accumulation of γ-aminobutyric acid (GABA) during abiotic stresses is well documented, especially drought stress (Mekonnen et al., 2016; Li et al., 2018; Li et al., 2020), and exogenous application of GABA can mitigate drought stress (Abd El-Gawad et al., 2021; Abdel Razik et al., 2021), therefore, GABA acts as a key player in drought tolerance in plants (Hasan et al., 2021a). However, in our research, GABA significantly reduced in WS pine needles and reduced in WS pine roots, compared with those in WW pine seedlings, respectively (Table 1). The result is consistent with that reported by Khan et al. (2019). Their results showed that GABA levels decreased in both drought-tolerant and -sensitive lines of chickpea (*Cicer arietinum*) under drought stress. Based on our results and previous results, the neurotransmitter should be investigated in detail about its function in plants under drought stress.

4.5 Roles of organic acids in *Pinus taeda* under drought stress

Previous research showed that levels of some organic acids increased in plants under drought stress, such as alpha-phocaecholic acid, kynurenic acid, homovanillic acid, gallic acid, picolinic acid in drought-tolerant wheat genotype HX10 under drought stress (Guo et al., 2020). Our results also showed that few organic acids increased in response to long-term drought in *P. taeda* seedlings, such as 5-hydroxymethyl-2-furoic acid in needles, tartaric acid, malonic acid, citric acid, and malic acid in roots (Figure 3). Untargeted metabolomics analysis showed that gallic acid reduced in roots and needles of WS pine seedlings (Table S2 and positive ion mode in Table S10). The result is in contrast to that reported by Guo et al. (2020). They reported level of gallic acid increased more than 3 times in drought-tolerant wheat genotype HX10, compared with that in drought-sensitive wheat genotype YN211 when exposed to drought stress. Maybe increased gallic acid level is a rapid response to drought stress and its level reduces when exposed long-term drought stress. Our result also showed that syringic acid increased in WS pine roots (Table 9, positive ion mode). The result is also in contrast to that reported by Guo et al. (2020). They reported that syringic acid reduced in drought-tolerant wheat genotype HX10. Kynurenic acid significantly reduced in roots and needles of WS pine seedlings (Table S2). The result about kynurenic acid is also in contrast to that reported by Guo et al. (2020). We cannot explain the two differences. A report showed high level of ferulic acid in drought-resistant winter triticale (Triticosecale Wittmack) genotype Lamberto under drought stress (Hura et al., 2009) and its drought resistance was correlated with high free ferulic acid level in leaf tissues (Hura et al., 2007). Ferulic acid bound with carbohydrates of the cell-wall of Lamberto under drought stress and the markedly better parameters of chlorophyll fluorescence for this genotype under both treatments correlated strongly and positively with the high contents of cell-wall-bound ferulic acid (Hura et al., 2009). However, our untargeted metabolomics analysis showed that ferulic acid significantly reduced in roots and needles of WS pine seedlings (Table S2 and negative ion mode in Table S10). This suggests that ferulic acid had less function in *P. taeda* seedlings under long-term drought stress. In drought-tolerant leafy vegetable amaranth (*Amaranthus tricolor*) genotypes (VA16, VA14, VA11, and VA6), levels of ellagic acid showed significant changes among these genotypes (the highest level, 6.23 $\mu g \cdot g^{-1}$ FW, in VA16), but no situation was observed about ellagic acid levels in these amaranth genotypes under drought stress (Sarker and Oba, 2020). In this study, ellagic acid reduced in roots and needles of WS pine seedlings (Table S10, negative ion mode). Reduction in ellagic acid in roots and needles of WS pine seedlings suggests less importance of ellagic acid in *P. taeda* seedlings under long-term drought stress. Caffeic acid slightly reduced in needles of WS pine seedlings, and showed no change in their roots (Table S10, positive ion mode). Since caffeic acid is involved in melatonin biosynthesis and caffei acid *O*-methyltransferase gene confers melatoin-mediated drought tolerance (Chang et al., 2021; Li et al., 2022), function of caffei acid should be related to melatonin in plants under drought stress. *p*-coumaric acid ethyl ester increased in roots and needles of WS pine seedlings (Table S2 and positive ion mode in Table S10). At present, little is known about funtion of *p*-coumaric acid ethyl ester in plants under drought stress. Based on our results of organic acids mentioned above, it was known that these organic acids showed great differences in their levels in response to long-term drought stress in *P. taeda* seedlings, and exhibited response differences of these organic acids from other plant species. In general, little has been known about detailed functions of organic acids in plants under drought stress. Therefore, more research is needed in view of some contradictory results mentioned above.

4.6 Roles of flavonoids, terpenoids, and other small molecules in *Pinus taeda* under drought stress

Flavonoids possess many physiological functions in plants, especially under abiotic stress (Treutter, 2005; Falcone Ferreyra et al., 2012). Under drought stress, some genes involved in flavonoids biosynthesis were up-regulated in the leaves of hybrid poplar (*Populus tremula* × *Populus alba*), such as these genes encoding phenylalanine ammonia-lyase, 4-coumarate CoA ligase, chalcone synthase, flavonol synthase, flavanone 3-hydroxylase, dihydro flavonol-4-reductase, and anthocyanidin synthase (Ahmed et al., 2021). Levels of quercetin-3-*O*-rutinoside and dihydroxyflaone luteolin 7-*O*-glucoside increased in leaves of *Ligustrum vulgare* under drought stress, compared with well-watered plants (Tattini et al., 2004). In *Achillea pachycephala*, flavonoid biosynthesis responded to drought stress, including apigenin-7-O-glycoside, luteolin, apigenin and kaempferol (Gharibi et al., 2019). Our untargeted metabolomics identified some unique flavonoids in *P. taeda* seedlings under drought stress (Table S2, S3).

Rutin significantly reduced in roots and needles of WS pine seedlings, but quercetin significantly increased in their roots and needles, compared with WW pine seedlings, respectively (Table S10, negative ion mode). Two other flavonoids, isorhamnetin and myricetin, significantly reduced in roots and needles of WS pine seedlings, compared with WW pine seedlings (Table S2 and positive ion mode in Table S10). Our results about rutin and quercetin are consistent with that reported by Yang et al. (2020) and Su et al. (2020), but our result about isorhamnetin is in contrast to that in *Bupleurum chinense* reported by Yang et al. (2020). The contrary results might be related to plant species.

In addition, compared with WW pine seedlings, epigallocatechin increased in WS pine needles (Table S2); naringenin increased in roots and needles of WS pine seedlings (Table S10, positive ion mode); catechin levels did not show changes in roots and needles of WS pine seedlings (Table S10, negative ion mode); apigenin C-glucoside increased in WS pine roots (Table S2). However, drought stress resulted in down-regulation of proteins involved in flavonoids biosynthesis in tea (*Camellia sinensis*) seedlings, such as chalcone synthase, flavanone 3-hydroxylase, flavonol synthase (Gu et al., 2020). The down-regulation might be related to reduction in the biosynthesis of these flavonoids in tea seedlings under drought stress. In general, WS pine seedlings showed different patterns of flavonoids and their spatial distribution and increase or reduction in levels are related to response of *P. taeda* to long-term drought stress.

Previous research showed contradictory results about terpenoids response to drought stress. Some research showed that increased

levels of terpenoids in leaves to respond to drought stress (Sangwan et al., 2001; Delfine et al., 2005; Asensio et al., 2012; Yadav et al., 2014; Kleine and Müller, 2014). Similarly, previous research found that terpenoid levels in plant roots responded to drought stress in contradictory ways (Bezemer et al., 2004; Asensio et al., 2012; Kleine and Müller, 2014). Saikosaponins are oleanolic triterpenoid saponins. Yang et al. (2020) reported that drought stress induced biosynthesis of saikosaponins in roots of *Bupleurum chinense*. Our untargeted metabolomics analysis showed that saikosaponin B4 significantly increased in WS pine roots, but significantly reduced in WS pine needles (Table S2 and negative ion mode in Table S10), and that saikosaponin B2 and saikosaponin E significantly reduced in roots and needles of WS pine seedlings (Table S10, negative ion mode). These results suggest that saikosaponins showed differential spatial distribution in *P. taeda* and carried out different functions. Quillaic acids (quillaja saponins) are triterpenoid saponins comprising a hydrophobic quillaic acid backbone and hydrophilic sugar moieties. In roots and needles of WS pine seedlings, quillaic acids increased (Table S2 and positive ion mode in Table S10). At present, no report was described about its function in plants under drought stress. Hecogenin is a steroid saponin isolated from *Agave sisalana* and *Agave salmiana*. Hecogenin glycosides (HG 1-2) increased as the increase of PEG concentrations from 0 to 20% in *Agave salmiana* plants under *in vitro* water stress conditions with PEG8000 (Puente-Garza et al., 2017). But our results showed that hecogenin levels reduced in roots and needles of WS pine seedlings (Table S2 and positive ion mode in Table S10).

Reduced glutathione and ascorbate are two important antioxidants in plants and plants accumulate the two compounds under drought stress (Szarka et al., 2012; Liu et al., 2021). However, in our untargeted metabolomics analysis, reduced glutathione and ascorbate significantly reduced in roots and needles of WS pine seedlings (Table S2), and oxidized glutathione significantly increased in their roots and needles (Table S10, negative ion mode), suggesting that the conversion of oxidized glutathione to its reduced form was affected by long-term drought stress, i.e., activity of glutathione reductase reduced in P. taeda seedlings under long-term drought stress. Under long-term drought stress, their biosynthesis and conversion from their respective oxidized forms might be affected.

Betaine is an important osmoprotectant in plants under drought stress, just like proline (Mukarram et al., 2021). Betaine significantly increased in roots and needles of WS pine seedlings (Table S2and positive ion mode in Table S10). The significant increase in betaine levels is helpful for *P. taeda* seedlings under drought stress, because it can protect functional proteins, enzymes (e.g., Rubisco) and lipids of the photosynthetic apparatus, and maintain electron flow through the thylakoid membranes, and intracellular accumulation of betaine allows for water retention in the cell and prevents its dehydration (Hasan et al., 2021b; Mukarram et al., 2021). Three polyamines, i.e., diamine putrescine, triamine spermidine, and tetraamine spermine were often investigated in plants under drought stress, acting as osmoprotectants (Mukarram et al., 2021). However, in our untargeted metabolomics analysis, the three polyamines were not detected (Table S2 and Table S10). The result suggests the three polyamines showed less functions in *P. taeda* seedlings under long-term drought stress. Similarly, β-cyclocitral was not detected in roots and needles of WW and WS pine seedlings (Table S2 and Table S10), suggesting that the compound might be not synthesized in *P. taeda*, although the compound and its analogs showed its function in plants under drought stress (D'Alessandro et al., 2019; Havaux, 2020; Deshpande et al., 2021). β-cyclocitral function in plants under drought stress is independent of ABA (Deshpande et al., 2021), lack of β-cyclocitral in *P. taeda* implies that the tree species might not need the compound to protect itself and ABA might be more important than β-cyclocitral in *P. taeda* plants under drought stress.

Allantoin is one of the main compounds used to store and transport the nitrogen fixed in nodules, thereby it is involved in nitrogen use in legumes. Allantoin increased in roots and needles of WS pine seedlings and more allantoin was allocated in their roots, compared with WW pine seedlings (Table S10, negative ion mode). The result is consistent with previous research (Casartelli et al., 2019; Khan et al., 2019). Functions of allantoin in plants under drought stress are involved few aspects. (1) defense function: to reduce radical oxygen species accumulation and death of plant cells (Brychkova et al., 2008); (2) signaling function: to trigger stress responses by increasing ABA levels and expression of ABA-related genes (Watanabe et al., 2014; Takagi et al., 2016); (3) nutritional function: to circumvent allantoin degradation to ammonium as to prevent nitrogen losses (Casartelli et al., 2019). Therefore, increased levels of allantoin in WS pine seedlings can promote such three functions, further increasing drought tolerance of *P. taeda* seedlings.

4.7 Enriched metabolite pathways in *Pinus taeda* under drought stress

Under positive ion mode, comparing needles of WS and WW pine seedlings, the most enriched pathways included histidine metabolism, folate biosynthesis, ubiquinone and other terpenoid-quinone biosyntehsis, vitamin B6 metabolism, zeatin biosynthesis, fatty acid biosynthesis, flavone and flavonol biosynthesis (Figure 11B and WS_L.vs.WW_L_pos_kegg_enrichment in Table S8).

In the histidine metabolism pathway, urocanic acid and ergothioneine were enriched (WS_L.vs.WW_L_pos_kegg_enrichment in Table S8). Little has known about roles of urocanic acid in plants under environmental stresses. Recently, Xue et al. (2021) showed that urocanic acid was largely enriched in *Pinellia ternata* under shaded environment, which likely contributed to tuber quality and growth. Enrichment of urocanic acid in needles of WS pine seedlings might possess another function in plants under drought stress, i.e., acting as an antioxidant (Boo, 2020). Ergothioneine also act as an antioxidant (Kalaras et al., 2017). In folate biosynthesis pathway, sepiapterin was enriched, which acts as an antioxidant against reactive oxygen species (Ishii et al., 1999). Other enriched KEGG pathways were mainly involved in biosynthesis of fatty acids (palmitoleic acid), their functions were discussed as above. In flavone and flavonol biosynthesis pathways, syringetin was enriched and no information was known about its functions in plants under drought stress.

Comparing needles and roots of WS pine seedlings, the first five enriched pathways included tryptophan metabolism, caffeine metabolism, sesquiterpenoid and triterpenoid biosynthesis, plant hormone signal transduction, phenylalanine, tyrosine and tryptophan biosynthesis (Figure 11C and WS_L.vs.WW_

R_pos_kegg_enrichment in Table S8). In tryptophan metabolism, tryptophol, melatonin, 3-indoleacetonitrile, kynurenic acid, L-kynurenine, indole-3-acetic acid, and indole were enriched. Kynurenic acid is a metabolite of tryptophan and is an endogenous antagonist of the ionotropic glutamate receptors and the α7 nicotinic acetylcholine receptor as well as an agonist of the G-protein-coupled receptor GPR35 in plants (Turski et al., 2011). Just as mentioned above, glutamate and acetylcholine act as neurotransmitters. Enriched kynurenic acid in *P. taeda* seedlings under drought stress could affect the roles of glutamate and acetylcholine, further affecting drought tolerance of *P. taeda* seedlings. Kynurenine and kynurenic acid are neuroactive compounds in plants (Yılmaz and Gökmen, 2020), maybe they function just like melatonin in plants under drought stress. Their enrichment in WS pine needles might improve drought tolerance of *P. taeda*.

Comparing roots of WS and WW pine seedlings, the most enriched pathways included metabolic pathways, zeatin biosynthesis, pentose phosphate pathway, carbapenem biosynthesis, benzoxazinoid biosynthesis, taurine and hypotaurine metabolism, butanoate metabolism (Figure 11D and WS_R.vs.WW_R_pos_kegg_enrichment in Table S8). In the pathway of taurine and hypotaurine metabolism, carbapenem biosynthesis, butanoate metabolism, porphyrin and chlorophyll metabolism, glyoxylate and dicarboxylate metabolism, and nitrogen metabolism, L-glutamic acid was enriched (WS_R.vs.WW_R_pos_kegg_enrichment in Table S8). Thus glutamate showed important roles in *P. taeda* seedlings under drought stress. Furthermore, glutamate acts as a neurotransmitter in plants, its receptor GLR3.7 in Arabidopsis is involved in ABA response (Chen et al., 2021). Therefore, glutamate enrichment improved drought tolerance, performing together with ABA signaling in *P. taeda* under drought stress.

Under negative ion mode, some enriched KEGG pathways were analyzed. Comparing needles of WS and WW pine seedlings, the most enriched pathways included biosynthesis of unsaturated fatty acids, arachidonic acid metabolism, plant hormone signal transduction, carotenoid biosynthesis, porphyrin and chlorophyll metabolism, flavonoid biosynthesis (Figure S7B and WS_L.vs.WW_L_neg_kegg_enrichment in Table S9). In biosynthesis of unsaturated fatty acids, eicosapentaenoic acid was enriched in needles of WS pine seedlings. Eicosapentaenoic acid is a long-chain fatty acid (20:5), five unsaturated double bonds can better maintain membrane flexibility in plants under drought stress, furthermore maintaining cell function. In the pathways of plant hormone signal transduction and carotenoid biosynthesis, ABA was enriched in WS pine needles (Figure S7B and WS_L.vs.WW_L_neg_kegg_enrichment in Table S9). In flavonoid biosynthesis, neohesperidin was enriched in WS pine needles. Neohesperidin has free radical scavenging activity (Xu et al., 2012), thus its enrichment in WS pine needles improves scavenging of reactive oxygen species and maintain functions of macromolcules in plant cells under drought stress. In porphyrin and chlorophyll metabolism, bilirubin was enriched in WS pine needles. Bilirubin shows multiple physiological functions, such as antioxidant effects, generation of reactive oxygen species, and cell signaling (Vítek and Ostrow, 2009). Maybe it also showed these functions in plants under drought stress.

Comparing needles and roots of WS pine seedlings, the most enriched pathways included phenylalanine metabolism, tyrosine metabolism, butanoate metabolism (Figure S7B and WS_L.vs.WS_R_neg_kegg_enrichment in Table S9). In the three pathways, fumaric acid was the most enriched metabolite in needles of WS pine seedlings. But targeted metabolics analysis showed that level of fumaric acid was significantly lower in needles of WS pine seedlings than those in their roots (Figure 4C). Fumaric acid is a component of the tricarboxylic acid cycle and can be transformed to yield energy and carbon skeletons for other compounds. Previous research showed that fumaric acid levels increased with plant age and light intensity in Arabidopsis leaves and that higher levels were determined in Arabidopsis phloem, suggesting the possibility that fumaric acid may function in carbon transport (Chia et al., 2000). Under drought stress, the possibility might increase because levels of fumaric acid significantly increased in WS pine roots (Figure 3C).

Comparing roots of WS and WW pine seedlings, the most enriched pathways included arginine and proline metabolism, lysine degradation, tryptophan metabolism, biosynthesis of unsaturate fatty acids, biosyntehsis of amino acids (Figure S7B and WS_R.vs.WW_R_neg_kegg_enrichment in Table S9). In arginine and proline metabolism, D-proline and 4-oxoproline were enriched in WS pine roots. It is very clear about role of proline in plants under drought stress (as mentioned above), but little has been known about 4-oxoproline. In the five pathways, i.e., lysine biosynthesis and degradation, biosynthesis of amino acids, 2-oxocarboxylic acid metabolism, and tryptophan metabolism, 2-oxoadipic acid was enriched in WS pine roots (WS_R.vs.WW_R_neg_kegg_enrichment in Table S9). 2-oxoadipic acid is a key metabolite of tryptophan and lysine. Enrichment of 2-oxoadipic acid in WS pine roots suggested that the acid was strengthened in metabolism of tryptophan and lysine and biosynthesis of amino acids in plants under drought stress. In biosynthesis of amino acids, L-citrulline was enriched in WS pine roots. In few plant species, citrulline showed a significant amount in their phloem exudates (Joshi and Fernie, 2017). Previous research showed that the genes involved in the citrulline biosynthesis significantly enriched in plants under drought stress (Gong et al., 2010; Shaik and Ramakrishna, 2012; Liu et al., 2015; Garg et al., 2016; Borah et al., 2017), suggesting a universal role of citrulline as a compatible solute in response to drought stress.

Data availability statement

The original contributions presented in the study are included in the article/Supplementary materials. Further inquiries can be directed to the corresponding author.

Author contributions

CW planned the all experiments and wrote the rough draft of the article. YW and CW carried out targeted analyses. HS financially supported the research in part and reviewed and revised the rough draft of the article. All authors contributed to the article and approved the submitted version.

Funding

This work was supported by the National Natural Science Foundation of China (grant number: 31870378) and the General Program of the National Natural Science Foundation of China (31470635).

Acknowledgments

We thank Novogene Co. Ltd. for its technological support for metabolomics analysis.

Conflict of interest

The authors declare that the research was conducted in the absence of any commercial or financial relationships that could be construed as a potential conflict of interest.

Publisher's note

All claims expressed in this article are solely those of the authors and do not necessarily represent those of their affiliated organizations, or those of the publisher, the editors and the reviewers. Any product that may be evaluated in this article, or claim that may be made by its manufacturer, is not guaranteed or endorsed by the publisher.

Supplementary material

The Supplementary Material for this article can be found online at: https://www.frontiersin.org/articles/10.3389/fpls.2022.1031466/full#supplementary-material

SUPPLEMENTARY FIGURE 1
PLS-DA scores of experimental groups under negative ion mode. **(A)** needles (red) vs. roots (blue) of WW seedlings; **(B)** needles of WS (red) vs.WW (blue) pine seedlings; **(C)** needles (red) vs. roots (blue) of WS pine seedlings; **(D)** roots of WS (red) vs. WW (blue) pine seedlings. WW, well-watered; WS, water-stressed.

SUPPLEMENTARY FIGURE 2
PCA analysis under positive and negative ion mode. **(A–D)** positive ion mode. **(A)** needles (red) vs. roots (blue) of WW seedlings; **(B)** needles of WS (red) vs.WW (blue) pine seedlings; **(C)** needles (red) vs. roots (blue) of WS pine seedlings; **(D)** roots of WS (red) vs. WW (blue) pine seedlings. **(E–H)**: negative ion mode. **(E)** needles (red) vs. roots (blue) of WW seedlings; **(F)** needles of WS (red) vs.WW (blue) pine seedlings; **(G)** needles (red) vs. roots (blue) of WS pine seedlings; **(H)** roots of WS (red) vs. WW (blue) pine seedlings. WW, well-watered; WS, water-stressed.

SUPPLEMENTARY FIGURE 3
Hierarchical clustering analysis of all differential metabolites from the four groups of samples (negative ion mode). L and R indicated the leaves and roots of *P. taeda* seedlings under WW and WS conndition, respectively. WW, well-watered; WS, water-stressed.

SUPPLEMENTARY FIGURE 4
Heatmaps of differential metabolites. **(A, B)** needles vs. roots of WW seedlings, positive and negative ion mode, respectively; **(C, D)** needles of WS vs.WW pine seedlings, positive and negative ion mode, respectively; **(E, F)** needles vs. roots of WS pine seedlings, positive and negative ion mode, respectively; **(G, H)** roots of WS vs. WW pine seedlings, positive and negative ion mode, respectively.

SUPPLEMENTARY FIGURE 5
Correlation analysis of metabolites (negative ion mode) with *p* values of top 20 (beginning from the minimal p value). The highest correlation with correlation coefficient of 1 was represented in red; the lowest correlation with correlation coefficient of -1 was represented in blue. Colorless parts indicated *p* value > 0.05. A: WW_L vs. WW_R; B: WS_L vs. WW_L; B: WS_L vs. WS_R; D: WS_R vs. WW_R. L and R indicated the leaves and roots of *P. taeda* seedlings under WW and WS conndition, respectively. WW, well-watered; WS, water-stressed.

SUPPLEMENTARY FIGURE 6
Z score analysis of the four sample groups under negative ion mode. A: WW_L vs. WW_R; B: WS_L vs. WW_L; B: WS_L vs. WS_R; B: WS_R vs. WW_R. L and R indicated the leaves and roots of *P. taeda* seedlings under WW and WS conndition, respectively. WW, well-watered; WS, water-stressed.

SUPPLEMENTARY FIGURE 7
Metabolites enriched in KEGG pathways under positive ion mode (top 20 pathways). In the small figures, horizontal axis represented the ratio of number of differential metabolites to the total numbers of metabolites identified in a pathway. Greater the ratio was, higher the differential metabolites enriched in the pathway. Color of a circle represented *p* value in geometric test. The size of a circle represented the number of differential metabolites in the corresponding pathway. A: WW_L vs. WW_R; B: WS_L vs. WW_L; B: WS_L vs. WS_R; D: WS_R vs. WW_R. L and R indicated the leaves and roots of *P. taeda* seedlings under WW and WS conndition, respectively. WW, well-watered; WS, water-stressed.

SUPPLEMENTARY TABLE 1
Relatively quantitative levels of identified metabolites in all the samples.

SUPPLEMENTARY TABLE 2
Annotations of differential metabolites under positive ion mode.

SUPPLEMENTARY TABLE 3
Annotations of differential metabolites under negative ion mode.

SUPPLEMENTARY TABLE 4
Differential metabolite analysis–Venn analysis.

SUPPLEMENTARY TABLE 5
Correlation analysis of differential metabolites under positive ion mode.

SUPPLEMENTARY TABLE 6
Correlation analysis of differential metabolites under negative ion mode.

SUPPLEMENTARY TABLE 7
Z-score analysis of differential metabolites.

SUPPLEMENTARY TABLE 8
KEGG enrichment analysis of differential metabolites under positive ion mode.

SUPPLEMENTARY TABLE 9
KEGG enrichment analysis of differential metabolites under negative ion mode.

SUPPLEMENTARY TABLE 10
Heatmaps of differential metabolites.

References

Aaltonen, H., Lindén, A., Heinonsalo, J., Biasi, C., and Pumpanen, J. (2017). Effects of prolonged drought stress on scots pine seedling carbon allocation. *Tree Physiol.* 37, 418–427. doi: 10.1093/treephys/tpw119

Abd El-Gawad, H. G., Mukherjee, S., Farag, R., Abd Elbar, O. H., Hikal, M., Abou El-Yazied, A., et al. (2021). Exogenous γ-aminobutyric acid (GABA)-induced signaling events and field performance associated with mitigation of drought stress in *Phaseolus vulgaris* l. *Plant Signal Behav.* 16 (2), 1853384. doi: 10.1080/15592324.2020.1853384

Abdel Razik, E. S., Alharbi, B. M., Pirzadah, T. B., Alnusairi, G. S. H., Soliman, M. H., and Hakeem, K. R. (2021). γ-aminobutyric acid (GABA) mitigates drought and heat stress in sunflower (*Helianthus annuus* l.) by regulating its physiological, biochemical and molecular pathways. *Physiol. Plant* 172 (2), 505–527. doi: 10.1111/ppl.13216

Adamipour, N., Khosh-Khui, M., Salehi, H., Razi, H., Karami, A., and Moghadam, A. (2020). Metabolic and genes expression analyses involved in proline metabolism of two rose species under drought stress. *Plant Physiol. Biochem.* 155, 105–113. doi: 10.1016/j.plaphy.2020.07.02

Agathokleous, E., Feng, Z., and Calabrese, E. J. (2019). Systemic herbicide 2,4-dichlorophenoxyacetic acid is another hormetin: What does it mean for agriculture and the environment? *J. Agric. Food Chem.* 67 (35), 9695–9696. doi: 10.1021/acs.jafc.9b04757

Ahmad, A., Aslam, Z., Naz, M., Hussain, S., Javed, T., Aslam, S., et al. (2021). Exogenous salicylic acid-induced drought stress tolerance in wheat (*Triticum aestivum* l.) grown under hydroponic culture. *PloS One* 16 (12), e0260556. doi: 10.1371/journal.pone.0260556

Ahmad, S., Kamran, M., Ding, R., Meng, X., Wang, H., Ahmad, I., et al. (2019). Exogenous melatonin confers drought stress by promoting plant growth, photosynthetic capacity and antioxidant defense system of maize seedlings. *PeerJ* 7, e7793. doi: 10.7717/peerj.779

Ahmed, U., Rao, M. J., Qi, C., Xie, Q., Noushahi, H. A., Yaseen, M., et al. (2021). Expression profiling of flavonoid biosynthesis genes and secondary metabolites accumulation in *Populus* under drought stress. *Molecules* 26 (18), 5546. doi: 10.3390/molecules26185546

Akula, R., and Mukherjee, S. (2020). New insights on neurotransmitters signaling mechanisms in plants. *Plant Signal Behav.* 15 (6), 1737450. doi: 10.1080/15592324.2020.1737450

Ali, M. S., and Baek, K. H. (2020). Jasmonic acid signaling pathway in response to abiotic stresses in plants. *Int. J. Mol. Sci.* 21 (2), 621. doi: 10.3390/ijms21020621

Ali, Q., Mazhar, M. W., Ishtiaq, M., Hussain, A. I., Bhatti, K. H., Maqbool, M., et al. (2021). Efficacy of zn-aspartate in comparison with $ZnSO_4$ and l-aspartate in amelioration of drought stress in maize by modulating antioxidant defence; osmolyte accumulation and photosynthetic attributes. *PloS One* 16 (12), e0260662. doi: 10.1371/journal.pone.0260662

Arruda, P., and Barreto, P. (2020). Lysine catabolism through the saccharopine pathway: Enzymes and intermediates involved in plant responses to abiotic and biotic stress. *Front. Plant Sci.* 11. doi: 10.3389/fpls.2020.00587

Asakura, H., Yamakawa, T., Tamura, T., Ueda, R., Taira, S., Saito, Y., et al. (2021). Transcriptomic and metabolomic analyses provide insights into the upregulation of fatty acid and phospholipid metabolism in tomato fruit under drought stress. *J. Agric. Food Chem.* 69, 2894–2905. doi: 10.1021/acs.jafc.0c06168

Asensio, D., Rapparini, F., and Penuelas, J. (2012). AM fungi root colonization increases the production of essential isoprenoids vs. non-essential isoprenoids especially under drought stress conditions or after jasmonic acid application. *Phytochem* 77, 149–161. doi: 10.1016/j.phytochem.2011.12.012

Batista-Silva, W., Heinemann, B., Rugen, N., Nunes-Nesi, A., Araújo, W. L., Braun, H. P., et al. (2019). The role of amino acid metabolism during abiotic stress release. *Plant Cell Environ.* 42, 1630–1644. doi: 10.1111/pce.13518

Bezemer, T. M., Wagenaar, I. R., van Dam, N. M., van der Putten, W. H., and Wäckers, F. L. (2004). Above- and below-ground terpenoid aldehyde induction in cotton, gossypium herbaceum, following root and leaf injury. *J. Chem. Ecol.* 30 (1), 53–67. doi: 10.1023/b:joec.0000013182.50662.2a

Bharath, P., Gahir, S., and Raghavendra, A. S. (2021). Abscisic acid-induced stomatal closure: An important component of plant defense against abiotic and biotic stress. *Front. Plant Sci.* 12. doi: 10.3389/fpls.2021.615114

Boo, Y. C. (2020). Emerging strategies to protect the skin from ultraviolet rays using plant-derived materials. *Antiox. (Basel)* 9 (7), 637. doi: 10.3390/antiox9070637

Borah, P., Sharma, E., Kaur, A., Chandel, G., Mohapatra, T., Kapoor, S., et al. (2017). Analysis of drought-responsive signaling network in two contrasting rice cultivars using transcriptomebased approach. *Sci. Rep.* 7, 42131. doi: 10.1038/srep42131

Brandt, B., Brodsky, D. E., Xue, S., Negi, J., Iba, K., Kangasjärvi, J., et al. (2012). Reconstitution of abscisic acid activation of SLAC1 anion channel by CPK6 and OST1 kinases and branched ABI1 PP2C phosphatase action. *Proc. Natl. Acad. Sci. U.S.A.* 109 (26), 10593–10598. doi: 10.1073/pnas.1116590109

Brodribb, T. J., Powers, J., Cochard, H., and Choat, B. (2020). Hanging by a thread? forests and drought. *Science* 368, 261–266. doi: 10.1126/science.aat763

Brugiere, N., Dubois, F., Limami, A. M., Lelandais, M., Roux, Y., Sangwan, R. S., et al. (1999). Glutamine synthetase in the phloem plays a major role in controlling proline production. *Plant Cell* 11 (10), 1995–2012. doi: 10.1105/tpc.11.10.1995

Brychkova, G., Alikulov, Z., Fluhr, R., and Sagi, M. (2008). A critical role for ureides in dark and senescence-induced purine remobilization is unmasked in the Atxdh1 arabidopsis mutant. *Plant J.* 54 (3), 496–509. doi: 10.1111/j.1365-313X.2008.03440.x

Burns, R. M., and Honkala, B. H. (1990). "Silvics of north America," in *Agriculture handbook 654, 2nd edition*, vol. 1990. (Washington, DC: U.S: Department of Agriculture, Forest Service), 877.

Casartelli, A., Melino, V. J., Baumann, U., Riboni, M., Suchecki, R., Jayasinghe, N. S., et al. (2019). Opposite fates of the purine metabolite allantoin under water and nitrogen limitations in bread wheat. *Plant Mol. Biol.* 99 (4-5), 477–497. doi: 10.1007/s11103-019-00831-z

Castroverde, C. D. M. (2019). The AREB1-ADA2b-GCN5 complex regulates gene expression during drought stress. *Plant Cell* 31 (3), 559–560. doi: 10.1105/tpc.18.00940

Chang, J., Guo, Y., Yan, J., Zhang, Z., Yuan, L., Wei, C., et al. (2021). The role of watermelon caffeic acid O-methyltransferase (ClCOMT1) in melatonin biosynthesis and abiotic stress tolerance. *Hortic. Res.* 8 (1), 210. doi: 10.1038/s41438-021-00645-5

Chen, P. Y., Hsu, C. Y., Lee, C. E., and Chang, I. F. (2021). Arabidopsis glutamate receptor GLR3.7 is involved in abscisic acid response. *Plant Signal Behav.* 16 (12), 1997513. doi: 10.1080/15592324.2021.1997513

Chen, K., Huang, Y., Liu, C., Liang, Y., and Li, M. (2021). Transcriptome profile analysis of arabidopsis reveals the drought stress-induced long non-coding RNAs associated with photosynthesis, chlorophyll synthesis, fatty acid synthesis and degradation. *Front. Plant Sci.* 12. doi: 10.3389/fpls.2021.643182

Chen, Q., Liu, R., Wu, Y., Wei, S., Wang, Q., Zheng, Y., et al. (2021). ERAD-related E2 and E3 enzymes modulate the drought response by regulating the stability of PIP2 aquaporins. *Plant Cell* 33, 2883–2898. doi: 10.1093/plcell/koab141

Chevolleau, S., Noguer-Meireles, M. H., Jouanin, I., Naud, N., Pierre, F., Gueraud, F., et al. (2018). Development and validation of an ultra high performance liquid chromatography-electrospray tandem mass spectrometry method using selective derivatisation, for the quantification of two reactive aldehydes produced by lipid peroxidation, HNE (4-hydroxy-2(E)-nonenal) and HHE (4-hydroxy-2(E)-hexenal) in faecal water. *J Chromatogr B Analyt Technol Biomed Life Sci* 1083, 171-179. doi: 10.1016/j.jchromb.2018.03.002

Chia, D. W., Yoder, T. J., Reiter, W. D., and Gibson, S. I. (2000). Fumaric acid: an overlooked form of fixed carbon in arabidopsis and other plant species. *Planta* 211 (5), 743–751. doi: 10.1007/s004250000345

Chinese Pharmacopoeia Commission (2015). *The pharmacopoeia of the people's republic of china. part IV* (China Medical Science Press: Beijing), 56–73.

Chmielewska, K., Rodziewicz, P., Swarcewicz, B., Sawikowska, A., Krajewski, P., Marczak, Ł, et al. (2016). Analysis of drought-induced proteomic and metabolomic changes in barley (*Hordeumvulgare* l.) leaves and roots unravels some aspects of biochemical mechanisms involved in drought tolerance. *Front. Plant Sci.* 7. doi: 10.3389/fpls.2016.01108

D'Alessandro, S., Mizokami, Y., Légeret, B., and Havaux, M. (2019). The apocarotenoid β-cyclocitric acid elicits drought tolerance in plants. *iScience* 19, 461–473. doi: 10.1016/j.isci.2019.08.003

Das, A., Rushton, P. J., and Rohila, J. S. (2017). Metabolomic profiling of soybeans (*Glycine max* l.) reveals the importance of sugar and nitrogen metabolism under drought and heat stress. *Plants (Basel)* 6 (2), 21. doi: 10.3390/plants6020021

Delfine, S., Loreto, F., Pinelli, P., Tognetti, R., and Alvino, A. (2005). Isoprenoids content and photosynthetic limitations in rosemary and spearmint plants under water stress. *Agric. Ecosyst. Environ.* 106, 243–252. doi: 10.1016/j.agee.2004.10.012

Deng, Y. N., Kashtoh, H., Wang, Q., Zhen, G. X., Li, Q. Y., Tang, L. H., et al. (2021). Structure and activity of SLAC1 channels for stomatal signaling in leaves. *Proc. Natl. Acad. Sci. U.S.A.* 118 (18), e2015151118. doi: 10.1073/pnas.201515111

Deshpande, S., Manoharan, R., and Mitra, S. (2021). Exogenous β-cyclocitral treatment primes tomato plants against drought by inducing tolerance traits, independent of abscisic acid. *Plant Biol. (Stuttg)* 23 Suppl 1, 170–180. doi: 10.1111/plb.13210

Díaz, P., Betti, M., Sánchez, D. H., Udvardi, M. K., Monza, J., and Márquez, A. J. (2010). Deficiency in plastidic glutamine synthetase alters proline metabolism and transcriptomic response in *Lotus japonicus* under drought stress. *New Phytol.* 188 (4), 1001–1013. doi: 10.1111/j.1469-8137.2010.03440.x

Diniz, A. L., da Silva, D. I. R., Lembke, C. G., Costa, M. D. L., Ten-Caten, F., Li, F., et al. (2020). Amino acid and carbohydrate metabolism are coordinated to maintain energetic balance during drought in sugarcane. *Int. J. Mol. Sci.* 21 (23), 9124. doi: 10.3390/ijms21239124

Dossa, K., Li, D., Zhou, R., Yu, J., Wang, L., Zhang, Y., et al. (2019). The genetic basis of drought tolerance in the high oil crop *Sesamum indicum*. *Plant Biotechnol. J.* 17 (9), 1788–1803. doi: 10.1111/pbi.13100

Du, J., Shen, T., Xiong, Q., Zhu, C., Peng, X., He, X., et al. (2020). Combined proteomics, metabolomics and physiological analyses of rice growth and grain yield with heavy nitrogen application before and after drought. *BMC Plant Biol.* 20 (1), 556. doi: 10.1186/s12870-020-02772-y

ElSayed, A. I., Rafudeen, M. S., and Golldack, D. (2014). Physiological aspects of raffinose family oligosaccharides in plants: protection against abiotic stress. *Plant Biol. (Stuttg)* 16 (1), 1–8. doi: 10.1111/plb.12053

Erland, L. A. E., Shukla, M. R., Singh, A. S., Murch, S. J., and Saxena, P. K. (2018). Melatonin and serotonin: Mediators in the symphony of plant morphogenesis. *J. Pineal Res.* 64 (2), e12452. doi: 10.1111/jpi.12452

Falcone Ferreyra, M. L., Rius, S. P., and Casati, P. (2012). Flavonoids: biosynthesis, biological functions, and biotechnological applications. *Front. Plant Sci.* 3. doi: 10.3389/fpls.2012.00222

Fiori, J., Amadesi, E., Fanelli, F., Tropeano, C. V., Rugolo, M., and Gotti, R. (2018). Cellular and mitochondrial determination of low molecular mass organic acids by LC-MS/MS. *J. Pharm. BioMed. Anal.* 150, 33–38. doi: 10.1016/j.jpba.2017.11.071

Fuertig, R., Ceci, A., Camus, S. M., Bezard, E., Luippold, A. H., and Hengerer, B. (2016). LC-MS/MS-based quantification of kynurenine metabolites, tryptophan, monoamines and neopterin in plasma, cerebrospinal fluid and brain. *Bioanalysis* 8 (18), 1903–1917. doi: 10.4155/bio-2016-0111

Furlan, A. L., Bianucci, E., Giordano, W., Castro, S., and Becker, D. F. (2020). Proline metabolic dynamics and implications in drought tolerance of peanut plants. *Plant Physiol. Biochem.* 151, 566–578. doi: 10.1016/j.plaphy.2020.04.010

Gaion, L. A., Monteiro, C. C., Cruz, F. J. R., Rossatto, D. R., López-Díaz, I., Carrera, E., et al. (2018). Constitutive gibberellin response in grafted tomato modulates root-to-shoot signaling under drought stress. *J. Plant Physiol.* 221, 11–21. doi: 10.1016/j.jplph.2017.12.003

Gao, T., Zhang, Z., Liu, X., Wu, Q., Chen, Q., Liu, Q., et al. (2020). Physiological and transcriptome analyses of the effects of exogenous dopamine on drought tolerance in apple. *Plant Physiol. Biochem.* 148, 260–272. doi: 10.1016/j.plaphy.2020.01.02

Garg, R., Shankar, R., Thakkar, B., Kudapa, H., Krishnamurthy, L., Mantri, N., et al. (2016). Transcriptome analyses reveal genotype- and developmental stage-specifc molecular responses to drought and salinity stresses in chickpea. *Sci. Rep.* 6, 19228. doi: 10.1038/srep19228

Gharibi, S., Sayed Tabatabaei, B. E., Saeidi, G., Talebi, M., and Matkowski, A. (2019). The effect of drought stress on polyphenolic compounds and expression of flavonoid biosynthesis related genes in *Achillea pachycephala* rech. f. *Phytochem* 162, 90–98. doi: 10.1016/j.phytochem.2019.03.004

Gong, P., Zhang, J., Li, H., Yang, C., Zhang, C., Zhang, X., et al. (2010). Transcriptional profles of drought-responsive genes in modulating transcription signal transduction, and biochemical pathways in tomato. *J. Exp. Bot.* 61 (13), 3563–3575. doi: 10.1093/jxb/erq167

Guo, X., Xin, Z., Yang, T., Ma, X., Zhang, Y., Wang, Z., et al. (2020). Metabolomics response for drought stress tolerance in Chinese wheat genotypes (*Triticum aestivum*). *Plants (Basel)* 9 (4), 520. doi: 10.3390/plants9040520

Gu, H., Wang, Y., Xie, H., Qiu, C., Zhang, S., Xiao, J., et al. (2020). Drought stress triggers proteomic changes involving lignin, flavonoids and fatty acids in tea plants. *Sci. Rep.* 10 (1), 15504. doi: 10.1038/s41598-020-72596-1

Haas, J. C., Vergara, A., Serrano, A. R., Mishra, S., Hurry, V., and Street, N. R. (2021). Candidate regulators and target genes of drought stress in needles and roots of Norway spruce. *Tree Physiol.* 41 (7), 1230–1246. doi: 10.1093/treephys/tpaa178

Hasan, M. M., Alabdallah, N. M., Alharbi, B. M., Waseem, M., Yao, G., Liu, X. D., et al. (2021a). GABA: A key player in drought stress resistance in plants. *Int. J. Mol. Sci.* 22 (18), 10136. doi: 10.3390/ijms221810136

Hasan, M. M., Skalicky, M., Jahan, M. S., Hossain, M. N., Anwar, Z., Nie, Z. F., et al. (2021b). Spermine: its emerging role in regulating drought stress responses in plants. *Cells* 10 (2), 261. doi: 10.3390/cells10020261

Hasanuzzaman, M., Nahar, K., Rahman, A., Inafuku, M., Oku, H., and Fujita, M. (2018). Exogenous nitric oxide donor and arginine provide protection against short-term drought stress in wheat seedlings. *Physiol. Mol. Biol. Plants* 24 (6), 993–1004. doi: 10.1007/s12298-018-0531-6

Havaux, M. (2020). β-cyclocitral and derivatives: Emerging molecular signals serving multiple biological functions. *Plant Physiol. Biochem.* 155, 35–41. doi: 10.1016/j.plaphy.2020.07.032

He, M., and Ding, N. Z. (2020). Plant unsaturated fatty acids: Multiple roles in stress response. *Front. Plant Sci.* 11. doi: 10.3389/fpls.2020.562785

Hedrich, R., and Geiger, D. (2017). Biology of SLAC1-type anion channels - from nutrient uptake to stomatal closure. *New Phytol.* 216 (1), 46–61. doi: 10.1111/nph.14685

He, F., Lai, S., Chi, Y., Pan, H., Cao, R., and Bao, R. (2022). Variation characteristics of drought circulation in fujian province from march to June 2018. *J. Arid Meteorol.* 40, 22–29. doi: 10.11755/j.issn.1006-7639(2002)-01-0022

Hura, T., Grzesiak, S., Hura, K., Thiemt, E., Tokarz, K., and Wedzony, M. (2007). Physiological and biochemical tools useful in drought-tolerance detection in genotypes of winter triticale: accumulation of ferulic acid correlates with drought tolerance. *Ann. Bot.* 100, 767–775. doi: 10.1093/aob/mcm162

Hura, T., Hura, K., and Grzesiak, S. (2009). Possible contribution of cell-wall-bound ferulic acid in drought resistance and recovery in triticale seedlings. *J. Plant Physiol.* 166 (16), 1720–1733. doi: 10.1016/j.jplph.2009.04.01

Hura, T., Hura, K., and Ostrowska, A. (2022). Drought-stress induced physiological and molecular changes in plants. *Int. J. Mol. Sci.* 23 (9), 4698. doi: 10.3390/ijms23094698

Ilhan, S., Ozdemir, F., and Bor, M. (2015). Contribution of trehalose biosynthetic pathway to drought stress tolerance of *Capparis ovata* desf. *Plant Biol. (Stuttg)* 17 (2), 402–407. doi: 10.1111/plb.12227

Imran, M., Latif Khan, A., Shahzad, R., Aaqil Khan, M., Bilal, S., Khan, A., et al. (2021). Exogenous melatonin induces drought stress tolerance by promoting plant growth and antioxidant defence system of soybean plants. *AoB Plants* 13 (4), plab026. doi: 10.1093/aobpla/plab026

Ingram, J., and Bartels, D. (1996). The molecular basis of dehydration tolerance in plants. *Annu. Rev. Plant Physiol. Plant Mol. Biol.* 47, 377–403. doi: 10.1146/annurev.arplant.47.1.377

Ishii, M., Shimizu, S., Momose, K., and Yamamoto, T. (1999). SIN-1-induced cytotoxicity in cultured endothelial cells involves reactive oxygen species and nitric oxide: protective effect of sepiapterin. *J. Cardiovasc. Pharmacol.* 33 (2), 295–300. doi: 10.1097/00005344-199902000-00018

Jang, G., Chang, S. H., Um, T. Y., Lee, S., Kim, J.-K., and Do Choi, Y. (2017). Antagonistic interaction between jasmonic acid and cytokinin in xylem development. *Sci. Rep.* 7, 10212. doi: 10.1038/s41598-017-10634-1

Jang, G., and Choi, Y. D. (2018). Drought stress promotes xylem differentiation by modulating the interaction between cytokinin and jasmonic acid. *Plant Signal Behav.* 13 (3), e1451707. doi: 10.1080/15592324.2018.1451707

Janiak, A., Kwaśniewski, M., and Szarejko, I. (2016). Gene expression regulation in roots under drought. *J. Exp. Bot.* 67, 1003–1014. doi: 10.1093/jxb/erv512

Jia, W., and Zhang, J. (2008). Stomatal movements and long-distance signaling in plants. *Plant Signal Behav.* 3, 772–777. doi: 10.4161/psb.3.10.6294

Jogawat, A., Yadav, B., Chhaya,, Lakra, N., Singh, A. K., and Narayan, O. P. (2021). Crosstalk between phytohormones and secondary metabolites in the drought stress tolerance of crop plants: A review. *Physiol. Plant* 172 (2), 1106–1132. doi: 10.1111/ppl.13328

Jorge, T. F., Rodrigues, J. A., Caldana, C., Schmidt, R., van Dongen, J. T., Thomas-Oates, J., et al. (2016). Mass spectrometry-based plant metabolomics: Metabolite responses to abiotic stress. *Mass Spectrom Rev.* 35 (5), 620–649. doi: 10.1002/mas.21449

Joshi, V., and Fernie, A. R. (2017). Citrulline metabolism in plants. *Amino Acids* 49 (9), 1543–1559. doi: 10.1007/s00726-017-2468-4

Kalaras, M. D., Richie, J. P., Calcagnotto, A., and Beelman, R. B. (2017). Mushrooms: A rich source of the antioxidants ergothioneine and glutathione. *Food Chem.* 233, 429–433. doi: 10.1016/j.foodchem.2017.04.109

Khan, N., Bano, A., Rahman, M. A., Rathinasabapathi, B., and Babar, M. A. (2019). UPLC-HRMSbased untargeted metabolic profiling reveals changes in chickpea (*Cicer arietinum*) metabolome following long-term drought stress. *Plant Cell Environ.* 42, 115–132. doi: 10.1111/pce.13195

Khan, F. S., Gan, Z. M., Li, E. Q., Ren, M. K., Hu, C. G., and Zhang, J. Z. (2021). Transcriptomic and physiological analysis reveals interplay between salicylic acid and drought stress in citrus tree floral initiation. *Planta* 255 (1), 24. doi: 10.1007/s00425-021-03801-2

Khokon, A. R., Okuma, E., Hossain, M. A., Munemasa, S., Uraji, M., Nakamura, Y., et al. (2011). Involvement of extracellular oxidative burst in salicylic acid-induced stomatal closure in arabidopsis. *Plant Cell Environ.* 34 (3), 434–443. doi: 10.1111/j.1365-3040.2010.02253.x

Khokon, M. A. R., Salam, M. A., Jammes, F., Ye, W., Hossain, M. A., Okuma, E., et al. (2017). MPK9 and MPK12 function in SA-induced stomatal closure in *Arabidopsis thaliana*. *Biosci. Biotechnol. Biochem.* 81 (7), 1394–1400. doi: 10.1080/09168451.2017.1308244

Kiribuchi, K., Jikumaru, Y., Kaku, H., Minami, E., Hasegawa, M., Kodama, O., et al. (2005). Involvement of the absic hexix-loop-helix transcription factor RERJ1 in wounding and drought stress responses in rice plants. *Biosci. Biotechnol. Biochem.* 69 (5), 1042–1044. doi: 10.1271/bbb.69.1042

Kleine, S., and Müller, C. (2014). Drought stress and leaf herbivory affect root terpenoid concentrations and growth of *Tanacetum vulgare*. *Chem. Ecol.* 40 (10), 1115–1125. doi: 10.1007/s10886-014-0505-2

Kolb, P. F., and Robberecht, R. (1996). High temperature and drought stress effects on survival of *Pinus ponderosa* seedlings. *Tree Physiol.* 16 (8), 665–672. doi: 10.1093/treephys/16.8.665

Kosar, F., Akram, N. A., Ashraf, M., Ahmad, A., Alyemeni, M. N., and Ahmad, P. (2021). Impact of exogenously applied trehalose on leaf biochemistry, achene yield and oil composition of sunflower under drought stress. *Physiol. Plant* 172 (2), 317–333. doi: 10.1111/ppl.13155

Kosová, K., Vítámvás, P., Urban, M. O., Klíma, M., Roy, A., and Prášil, I. T. (2015). Biological networks underlying abiotic stress tolerance in temperate crops–a proteomic perspective. *Int. J. Mol. Sci.* 16 (9), 20913–20942. doi: 10.3390/ijms160920913

Kreuzwieser, J., Meischner, M., Grün, M., Yáñez-Serrano, A. M., Fasbender, L., and Werner, C. (2021). Drought affects carbon partitioning into volatile organic compound biosynthesis in scots pine needles. *New Phytol.* 232, 1930–1943. doi: 10.1111/nph.17736

Li, Z., Cheng, B., Peng, Y., and Zhang, Y. (2020). Adaptability to abiotic stress regulated by γ-aminobutyric acid in relation to alterations of endogenous polyamines and organic metabolites in creeping bentgrass. *Plant Physiol. Biochem.* 157, 185–194. doi: 10.1016/j.plaphy.2020.10.025

Li, M., Hou, L., Zhang, C., Yang, W., Liu, X., Zhao, H., et al. (2022). Genome-wide identification of direct targets of ZjVND7 reveals the putative roles of whole-genome duplication in sour jujube in regulating xylem vessel differentiation and drought tolerance. *Front. Plant Sci.* 13. doi: 10.3389/fpls.2022.829765

Lilian, P. M., Ross, W. W., Georgina, M. S., and Kitt, G. P. (2021). Breeding for climate change resilience: A case study of loblolly pine (*Pinu staeda* l.) in north America. *Front. Plant Sci.* 12. doi: 10.3389/fpls.2021.606908

Lima, L. L., Balbi, B. P., Mesquita, R. O., Silva, J., Coutinho, F. S., Carmo, F. M. S., et al. (2019). Proteomic and metabolomic analysis of a drought tolerant soybean cultivar from Brazilian savanna. *Crop Breed Genet. Genom* 1, e190022. doi: 10.20900/cbgg20190022

Li, Z., Peng, Y., and Huang, B. (2018). Alteration of transcripts of stress-protective genes and transcriptional factors by γ-aminobutyric acid (GABA) associated with improved heat and drought tolerance in creeping bentgrass (*Agrostis stolonifera*). *Int. J. Mol. Sci.* 19 (6), 1623. doi: 10.3390/ijms19061623

Li, Y., Sun, Y., Cui, H., Li, M., Yang, G., Wang, Z., et al. (2022). *Carex rigescens* caffeic acid *O*-methyltransferase gene CrCOMT confer melatonin-mediated drought tolerance in transgenic tobacco. *Front. Plant Sci.* 13. doi: 10.3389/fpls.2022.971431

Liu, L., Chen, X., Ciais, P., Yuan, W., Maignan, F., Wu, J., et al. (2022). Tropical tall forests are more sensitive and vulnerable to drought than short forests. *Glob Chang Biol.* 28 (4), 1583–1595. doi: 10.1111/gcb.16017

Liu, B., Fan, J., Zhang, Y., Mu, P., Wang, P., Su, J., et al. (2012). OsPFADSP1, a rice protein tyrosine phosphatase, negatively regulates drought stress responses in transgenic tobacco and rice plants. *Plant Cell Rep.* 31, 1021–1032. doi: 10.1007/s00299-011-1220-x

Liu, Q., Gao, T., Liu, W., Liu, Y., Zhao, Y., Liu, Y., et al. (2020). Functions of dopamine in plants: a review. *Plant Signal Behav.* 15 (12), 1827782. doi: 10.1080/15592324.2020.1827782

Liu, B., Jing, D., Liu, F., Ma, H., Liu, X., and Peng, L. (2021). *Serendipita indica* alleviates drought stress responses in walnut (*Juglans regia* l.) seedlings by stimulating osmotic adjustment and antioxidant defense system. *Appl. Microbiol. Biotechnol.* 105 (23), 8951–8968. doi: 10.1007/s00253-021-11653-9

Liu, H., Sultan, M. A. R. F., Liu, Xl, Zhang, J., Yu, F., and Zhao, H. (2015). Physiological and comparative proteomic analysis reveals different drought responses in roots and leaves of drought-tolerant wild wheat (*Triticum boeoticum*). *PloS One* 10 (4), e0121852. doi: 10.1371/journal.pone.0121852

Li, Y., Wang, M., Zhang, F., Xu, Y., Chen, X., Qin, X., et al. (2016). Effect of post-silking drought on nitrogen partitioning and gene expression patterns of glutamine synthetase and asparagine synthetase in two maize (*Zea mays* l.) varieties. *Plant Physiol. Biochem.* 102, 62–69. doi: 10.1016/j.plaphy.2016.02.002

Liyanaarachchi, G. V. V., Mahanama, K. R. R., Somasiri, H. P. P. S., and Punyasiri, P. A. N. (2018). Development and validation of a method for direct, underivatized analysis of free amino acids in rice using liquid chromatography-tandem mass spectrometry. *J. Chromatogr A* 1568, 131–139. doi: 10.1016/j.chroma.2018.07.035

Li, X., Yu, B., Wu, Q., Min, Q., Zeng, R., Xie, Z., et al. (2021). OsMADS23 phosphorylated by SAPK9 confers drought and salt tolerance by regulating ABA biosynthesis in rice. *PloS Genet.* 17 (8), e1009699. doi: 10.1371/journal.pgen.1009699

Lorenz, W. W., Sun, F., Liang, C., Kolychev, D., Wang, H., Zhao, X., et al. (2006). Water stress-responsive genes in loblolly pine (*Pinus taeda*) roots identified by analyses of expressed sequence tag libraries. *Tree Physiol.* 26, 1–16. doi: 10.1093/treephys/26.1.1

Lou, C. H. (1998). "Integrated action in plant irritability," in *Discoveries in plant biology*, vol. 2 . Eds. S. D. Kung and S. F. Yang (Singapore: World Scientific), 327–347. doi: 10.1142/9789812813046_0018

Maggard, A., Will, R., Wilson, D., and Meek, C. (2016). Response of mid-rotation loblolly pine (*Pinus taeda* l.) physiology and productivity to sustained, moderate drought on the western edge of the range. *Forests* 7 (9), 203. doi: 10.3390/f7090203

Mahmood, T., Khalid, S., Abdullah, M., Ahmed, Z., Shah, M. K. N., Ghafoor, A., et al. (2019). Insights into drought stress signaling in plants and the molecular genetic basis of cotton drought tolerance. *Cells* 9 (1), 105. doi: 10.3390/cells9010105

Manthe, B., Schulz, M., and Schnabl, H. (1992). Effects of salicylic acid on growth and stomatal movements of *Vicia faba* l.: Evidence for salicylic acid metabolization. *J. Chem. Ecol.* 18 (9), 1525–1539. doi: 10.1007/BF00993226

Mathan, J., Singh, A., and Ranjan, A. (2021). Sucrose transport in response to drought and salt stress involves ABA-mediated induction of OsSWEET13 and OsSWEET15 in rice. *Physiol. Plant* 171 (4), 620–637. doi: 10.1111/ppl.13210

McConnell, T. E., Silva, B. K. D., Sun, C. Y., and Tanger, S. M. (2021). Forest to mill timber price trends and volatility for Mississippi timber products. *For Prod J.* 71, 177–187. doi: 10.13073/FPJ-D-21-00010

Mekonnen, D. W., Flügge, U. I., and Ludewig, F. (2016). Gamma-aminobutyric acid depletion affects stomata closure and drought tolerance of *Arabidopsis thaliana*. *Plant Sci.* 245, 25–34. doi: 10.1016/j.plantsci.2016.01.005

Mibei, E. K., Owino, W. O., Ambuko, J., Giovannoni, J. J., and Onyango, A. N. (2018). Metabolomic analyses to evaluate the effect of drought stress on selected African eggplant accessions. *J. Sci. Food Agric.* 98, 205–216. doi: 10.1002/jsfa.8458

Michaletti, A., Naghavi, M. R., Toorchi, M., Zolla, L., and Rinalducci, S. (2018). Metabolomics and proteomics reveal drought-stress responses of leaf tissues from spring-wheat. *Sci. Rep.* 8, 5710. doi: 10.1038/s41598-018-24012-y

Miranda-Apodaca, J., Agirresarobe, A., Martínez-Goñi, X. S., Yoldi-Achalandabaso, A., and Pérez-López, U. (2020). N metabolism performance in *Chenopodium quinoa* subjected to drought or salt stress conditions. *Plant Physiol. Biochem.* 155, 725–734. doi: 10.1016/j.plaphy.2020.08.00

Miyawaki, T., Matsumoto, S., Takahashi, W., and Tanaka, O. (2013). Effect of heat-treated noradrenaline on flowering in lemna. *Biosci. Biotechnol. Biochem.* 77 (7), 1586–1588. doi: 10.1271/bbb.13013

Mueller, R. C., Scudder, C. M., Porter, M. E., Trotter, R. T., Gehring, C. A., and Whitham, T. G. (2005). Differential tree mortality in response to severe drought: evidence for long-term vegetation shifts. *J. Ecol.* 93, 1085–1093. doi: 10.1111/j.1365-2745.2005.01042.x

Muhammad Aslam, M., Waseem, M., Jakada, B. H., Okal, E. J., Lei, Z., Saqib, H. S. A., et al. (2022). Mechanisms of abscisic acid-mediated drought stress responses in plants. *Int. J. Mol. Sci.* 23 (3), 1084. doi: 10.3390/ijms23031084

Mukarram, M., Choudhary, S., Kurjak, D., Petek, A., and Khan, M. M. A. (2021). Drought: Sensing, signalling, effects and tolerance in higher plants. *Physiol. Plant* 172 (2), 1291–1300. doi: 10.1111/ppl.13423

Mukherjee, S., Sengupta, S., Mukherjee, A., Basak, P., and Majumder, A. L. (2019). Abiotic stress regulates expression of galactinol synthase genes post-transcriptionally through intron retention in rice. *Planta* 249 (3), 891–912. doi: 10.1007/s00425-018-3046-z

Neale, D. B., Wegrzyn, J. L., Stevens, K. A., Zimin, A. V., Puiu, D., Crepeau, M. W., et al. (2014). Decoding the massive genome of loblolly pine using haploid DNA and novel assembly strategies. *Genome Biol.* 15 (3), R59. doi: 10.1186/gb-2014-15-3-r59

Norlina, R., Norashikin, M. N., Loh, S. H., Aziz, A., and Cha, T. S. (2020). Exogenous abscisic acid supplementation at early stationary growth phase triggers changes in the regulation of fatty acid biosynthesis in *Chlorella vulgaris* UMT-M1. *Appl. Biochem. Biotechnol.* 191 (4), 1653–1669. doi: 10.1007/s12010-020-03312-y

Okuma, E., Nozawa, R., Murata, Y., and Miura, K. (2014). Accumulation of endogenous salicylic acid confers drought tolerance to arabidopsis. *Plant Signal Behav.* 9 (3), e28085. doi: 10.4161/psb.28085

Osakabe, Y., Shinozaki, Y., Shinozaki, K., and Tran, L. (2013). ABA control of plant macro element membrane transport systems in response to water deficit and high salinity. *New Physiol.* 202, 35–49. doi: 10.1111/nph.12613

Ozturk, M., Turkyilmaz Unal, B., García-Caparrós, P., Khursheed, A., Gul, A., and Hasanuzzaman, M. (2021). Osmoregulation and its actions during the drought stress in plants. *Physiol. Plant* 172 (2), 1321–1335. doi: 10.1111/ppl.13297

Pandey, S., Zhang, W., and Assmann, S. M. (2007). Roles of ion channels and transporters in guard cell signal transduction. *FEBS Lett.* 581, 2325–2336. doi: 10.1016/j.febslet.2007.04.008

Patel, J., and Mishra, A. (2021). Plant aquaporins alleviate drought tolerance in plants by modulating cellular biochemistry, root-architecture, and photosynthesis. *Physiol. Plant* 172, 1030–1044. doi: 10.1111/ppl.13324

Pawlak, M., Klupczynska, A., Kokot, Z. J., and Matysiak, J. (2019). Extending metabolomic studies of *Apis mellifera* venom: LC-MS-based targeted analysis of organic acids. *Toxins(Basel)* 12 (1), 14. doi: 10.3390/toxins12010014

Poór, P., and Tari, I. (2012). Regulation of stomatal movement and photosynthetic activity in guard cells of tomato abaxial epidermal peels by salicylic acid. *Funct. Plant Biol.* 39 (12), 1028–1037. doi: 10.1071/FP12187

Puente-Garza, C. A., Meza-Miranda, C., Ochoa-Martinez, D., and Garcia-Lara, S. (2017). Effect of *in vitro* drought stress on phenolic acids, flavonols, saponins, and antioxidant activity in *Agave salmiana*. *Plant Physiol. Biochem.* 115, 400–407. doi: 10.1016/j.plaphy.2017.04.012

Qin, C., Ahanger, M. A., Zhou, J., Ahmed, N., Wei, C., Yuan, S., et al. (2020). Beneficial role of acetylcholine in chlorophyll metabolism and photosynthetic gas exchange in *Nicotiana benthamiana* seedlings under salinity stress. *Plant Biol. (Stuttg)* 22 (3), 357–365. doi: 10.1111/plb.13079

Razi, K., and Muneer, S. (2021). Drought stress-induced physiological mechanisms, signaling pathways and molecular response of chloroplasts in common vegetable crops. *Crit. Rev. Biotechnol.* 41 (5), 669–691. doi: 10.1080/07388551.2021.1874280

Ren, J., Yang, X., Ma, C., Wang, Y., and Zhao, J. (2021). Melatonin enhances drought stress tolerance in maize through coordinated regulation of carbon and nitrogen assimilation. *Plant Physiol. Biochem.* 167, 958–969. doi: 10.1016/j.plaphy.2021.09.007

Roelfsema, M. R. G., Hedrich, R., and Geiger, D. (2012). Anion channels: Master switches of stress responses. *Trends Plant Sci.* 17, 221–229. doi: 10.1016/j.tplants.2012.01.009

Saito, S., and Uozumi, N. (2019). Guard cell membrane anion transport systems and their regulatory components: An elaborate mechanism controlling stress-induced stomatal closure. *Plants* 8 (1), 9. doi: 10.3390/plants8010009

Sami, F., Yusuf, M., Faizan, M., Faraz, A., and Hayat, S. (2016). Role of sugars under abiotic stress. *Plant Physiol. Biochem.* 109, 54–61. doi: 10.1016/j.plaphy.2016.09.005

Sangwan, N. S., Farooqi, A. H. A., Shabih, F., and Sangwan, R. S. (2001). Regulation of essential oil production in plants. *Plant Growth Regul.* 34, 3–21. doi: 10.1023/A:1013386921596

Sarker, U., and Oba, S. (2020). Phenolic profiles and antioxidant activities in selected drought-tolerant leafy vegetable amaranth. *Sci. Rep.* 10 (1), 18287. doi: 10.1038/s41598-020-71727-y

Schroeder, J. I., and Hagiwara, S. (1989). Cytosolic calcium regulates ion channels in the plasma membrane of *Vicia faba* guard cells. *Nature* 338, 427–430. doi: 10.1038/338427a0

Schymanski, E. L., Jeon, J., Gulde, R., Fenner, K., Ruff, M., Singer, H. P., et al. (2014). Identifying small molecules *via* high resolution mass spectrometry: communicating confidence. *Environ. Sci. Technol.* 48 (4), 2097–2098. doi: 10.1021/es5002105

Seleiman, M. F., Al-Suhaibani, N., Ali, N., Akmal, M., Alotaibi, M., Refay, Y., et al. (2021). Drought stress impacts on plants and different approaches to alleviate its adverse effects. *Plants (Basel)* 10 (2), 259. doi: 10.3390/plants10020259

Selli, S., Keebek, H., Kesen, S., and Sonmezdag, A. S. (2018). GC-MS olfactometric and LC-DAD-ESI-MS/MS characterization of key odorants and phenolic compounds in black dry-salted olives. *J. Sci. Food Agric.* 98 (11), 4104–4111. doi: 10.1002/jsfa.8927

Shaik, R., and Ramakrishna, W. (2012). Bioinformatic analysis of epigenetic and MicroRNA mediated regulation of drought responsive genes in rice. *PloS One* 7 (11), e49331. doi: 10.1371/journal.pone.0049331

Sharma, M., Gupta, S. K., Majumder, B., Maurya, V. K., Deeba, F., Alam, A., et al. (2017). Salicylic acid mediated growth, physiological and proteomic responses in two wheat varieties under drought stress. *J. Proteomics* 163, 28–51. doi: 10.1016/j.jprot.2017.05.011

Sharma, A., and Zheng, B. (2019). Melatonin mediated regulation of drought stress: physiological and molecular aspects. *Plants (Basel)* 8 (7), 190. doi: 10.3390/plants8070190

Shi, P., Hua, W., Htwe, Y. M., Zhang, D., Li, J., and Wang, Y. (2021). Abscisic acid improves linoleic acid accumulation possibly by promoting expression of EgFAD2 and other fatty acid biosynthesis genes in oil palm mesocarp. *Front. Plant Sci.* 12. doi: 10.3389/fpls.2021.748130

Singh, K. K., and Ghosh, S. (2013). Regulation of glutamine synthetase isoforms in two differentially drought-tolerant rice (*Oryza sativa* l.) cultivars under water deficit conditions. *Plant Cell Rep.* 32 (2), 183–193. doi: 10.1007/s00299-012-1353-6

Song, Y. (2014). Insight into the mode of action of 2,4-dichlorophenoxyacetic acid (2,4-d) as an herbicide. *J. Integr. Plant Biol.* 56 (2), 106–113. doi: 10.1111/jipb.12131

Sun, G., Li, Z., and Feng, J. (2014). Relationship between atmospheric low-frequency oscillation and two severe drought events in southwest China. *Plateau Meteorol* 33, 1562–1567. doi: 10.7522/j.issn.1000-0534.2013.00166

Sun, C., Liu, L., Wang, L., Li, B., Jin, C., and Lin, X. (2021). Melatonin: A master regulator of plant development and stress responses. *J. Integr. Plant Biol.* 63 (1), 126–145. doi: 10.1111/jipb.12993

Szarka, A., Tomasskovics, B., and Bánhegyi, G. (2012). The ascorbate-glutathione-α-tocopherol triad in abiotic stress response. *Int. J. Mol. Sci.* 13 (4), 4458–4483. doi: 10.3390/ijms13044458

Takagi, H., Ishiga, Y., Watanabe, S., Konishi, T., Egusa, M., Akiyoshi, N., et al. (2016). Allantoin, a stress-related purine metabolite, can activate jasmonate signaling in a MYC2-regulated and abscisic acid-dependent manner. *J. Exp. Bot.* 67, 2519–2532. doi: 10.1093/jxb/erw071

Tattini, M., Galardi, C., Pinelli, P., Massai, R., Remorini, D., and Agati, G. (2004). Differential accumulation of flavonoids and hydroxycinnamates in leaves of *Ligustrum vulgare* under excess light and drought stress. *New Phytol.* 163, 547–561. doi: 10.1111/j.1469-8137.2004.01126.x

Thabet, S. G., Moursi, Y. S., Karam, M. A., Graner, A., and Alqudah, A. M. (2018). Genetic basis of drought tolerance during seed germination in barley. *PloS One* 13 (11), e0206682. doi: 10.1371/journal.pone.0206682

Thiele, B., Hupert, M., Santiago-Schübel, B., Oldiges, M., and Hofmann, D. (2019). Direct analysis of underivatized amino acids in plant extracts by LC-MS/MS (improved method). *Methods Mol. Biol.* 2030, 403–414. doi: 10.1007/978-1-4939-9639-1_30

Tiwari, R. K., Lal, M. K., Kumar, R., Chourasia, K. N., Naga, K. C., Kumar, D., et al. (2021). Mechanistic insights on melatonin-mediated drought stress mitigation in plants. *Physiol. Plant* 172 (2), 1212–1226. doi: 10.1111/ppl.13307

Tong, R., Zhou, B., Cao, Y., Ge, X., and Jiang, L. (2020). Metabolic profiles of moso bamboo in response to drought stress in a field investigation. *Sci. Total Environ.* 720, 137722. doi: 10.1016/j.scitotenv.2020.137722

Treutter, D. (2005). Significance of flavonoids in plant resistance and enhancement of their biosynthesis. *Plant Biol. (Stuttg)* 7 (6), 581–591. doi: 10.1055/s-2005-873009

Trinchant, J. C., Boscari, A., Spennato, G., Van de Sype, G., and Le Rudulier, D. (2004). Proline betaine accumulation and metabolism in alfalfa plants under sodium chloride stress. exploring its compartmentalization in nodules. *Plant Physiol.* 135 (3), 1583–1594. doi: 10.1104/pp.103.037556

Tripathi, P., Chandra, A., and Prakash, J. (2019). Physio-biochemical assessment and expression analysis of genes associated with drought tolerance in sugarcane (*Saccharum* spp. hybrids) exposed to GA3 at grand growth stage. *Plant Biol. (Stuttg)* 21 (1), 45–53. doi: 10.1111/plb.12919

Turski, M. P., Turska, M., Zgrajka, W., Bartnik, M., Kocki, T., and Turski, W. A. (2011). Distribution, synthesis, and absorption of kynurenic acid in plants. *Planta Med.* 77 (8), 858–864. doi: 10.1055/s-0030-1250604

Virág, D., Király, M., Drahos, L., Édes, A. D., Gecse, K., Bagdy, G., et al. (2020). Development, validation and application of LCMS/MS method for quantification of amino acids, kynurenine and serotonin in human plasma. *J. Pharm. BioMed. Anal.* 180, 113018. doi: 10.1016/j.jpba.2019.113018

Vítek, L., and Ostrow, J. D. (2009). Bilirubin chemistry and metabolism; harmful and protective aspects. *Curr. Pharm. Des.* 15 (25), 2869–2883. doi: 10.2174/138161209789058237

Wang, J., Wang, L., Yan, Y., Zhang, S., Li, H., Gao, Z., et al. (2021b). GhWRKY21 regulates ABA-mediated drought tolerance by fine-tuning the expression of GhHAB in cotton. *Plant Cell Rep.* 40 (11), 2135–2150. doi: 10.1007/s00299-020-02590-4

Wang, H., Wang, X., Zhang, S., and Lou, C. (1998). Nicotinic acetylcholine receptor is involved in acetylcholine regulating stomatal movement. *Sci. China C Life Sci.* 41 (6), 650–656. doi: 10.1007/BF02882908

Want, E. J., Masson, P., Michopoulos, F., Wilson, I. D., Theodoridis, G., Plumb, R. S., et al. (2013). Global metabolic profiling of animal and human tissues *via* UPLC-MS. *Nat. Protoc.* 8 (1), 17–32. doi: 10.1038/nprot.2012.135

Wasternack, C., and Song, S. (2017). Jasmonates: biosynthesis, metabolism, and signaling by proteins activating and repressing transcription. *J. Exp. Bot.* 68 (6), 1303–1321. doi: 10.1093/jxb/erw443

Watanabe, S., Matsumoto, M., Hakomori, Y., Takagi, H., Shimada, H., and Sakamoto, A. (2014). The purine metabolite allantoin enhances abiotic stress tolerance through synergistic activation of abscisic acid metabolism. *Plant Cell Environ.* 37, 1022–1036. doi: 10.1111/pce.12218

Wen, B., Mei, Z., Zeng, C., and Liu, S. (2017). metaX: a flexible and comprehensive software for processing metabolomics data. *BMC Bioinf.* 18 (1), 183. doi: 10.1186/s12859-017-1579-y

Xiao, F., Zhao, Y., Wang, X. R., Liu, Q., and Ran, J. (2021). Transcriptome analysis of needle and root of pinus massoniana in response to continuous drought stress. *Plants (Basel)* 10 (4), 769. doi: 10.3390/plants10040769

Xue, T., Xiong, Y., Shi, J., Chao, Q., Zhu, Y., Duan, Y., et al. (2021). UHPLC-MS-based metabolomic approach for the quality evaluation of *Pinellia ternata* tubers grown in shaded environments. *J. Nat. Med.* 75 (4), 1050–1057. doi: 10.1007/s11418-021-01550-w

Xu, F., Zang, J., Chen, D., Zhang, T., Zhan, H., Lu, M., et al. (2012). Neohesperidin induces cellular apoptosis in human breast adenocarcinoma MDA-MB-231 cells *via* activating the bcl-2/Bax-mediated signaling pathway. *Nat. Prod Commun.* 7 (11), 1475–1478. doi: 10.1177/1934578X1200701116

Yadav, R. K., Sangwan, R. S., Sabir, F., Srivastava, A. K., and Sangwan, N. S. (2014). Effect of prolonged water stress on specialized secondary metabolites, peltate glandular trichomes, and pathway gene expression in *Artemisia annua L.* l. *Plant Physiol. Biochem.* 74, 70–83. doi: 10.1016/j.plaphy.2013.10.023

Yang, S., Bai, M., Hao, G., Zhang, X., Guo, H., and Fu, B. (2021). Transcriptome survey and expression analysis reveals the adaptive mechanism of 'Yulu xiang' pear in response to long-term drought stress. *PloS One* 16 (2), e0246070. doi: 10.1371/journal.pone.0246070

Yang, L. L., Yang, L., Yang, X., Zhang, T., Lan, Y. M., Zhao, Y., et al. (2020). Drought stress induces biosynthesis of flavonoids in leaves and saikosaponins in roots of *Bupleurum chinense* DC. *Phytochem* 177, 112434. doi: 10.1016/j.phytochem.2020.112434

Yepes-Molina, L., Bárzana, G., and Carvajal, M. (2020). Controversial regulation of gene expression and protein transduction of aquaporins under drought and salinity stress. *Plants (Basel)* 9 (12), 1662. doi: 10.3390/plants912166

Yi, M., Jia, T., Dong, L. M., Zhang, L., Leng, C. H., Liu, S. Y., et al. (2021). Resin yield in *Pinus elliottii* engelm. is related to the resin flow rate, resin components and resin duct characteristics at three locations in southern China. *Ind. Crops Prod* 160, 113–141. doi: 10.1016/j.indcrop.2020.113141

Yılmaz, C., and Gökmen, V. (2020). Neuroactive compounds in foods: Occurrence, mechanism and potential health effects. *Food Res. Int.* 128, 108744. doi: 10.1016/j.foodres.2019.108744

You, J., Zhang, Y., Liu, A., Li, D., Wang, X., Dossa, K., et al. (2019). Transcriptomic and metabolomic profiling of drought-tolerant and susceptible sesame genotypes in response to drought stress. *BMC Plant Biol.* 19 (1), 267. doi: 10.1186/s12870-019-1880-1

Yu, H., Zhang, Y., Zhang, Z., Zhang, J., Wei, Y., Jia, X., et al. (2020). Towards identification of molecular mechanism in which the overexpression of wheat cytosolic and plastid glutamine synthetases in tobacco enhanced drought tolerance. *Plant Physiol. Biochem.* 51, 608–620. doi: 10.1016/j.plaphy.2020.04.013

Yu, W., Zhao, R., Wang, L., Zhang, S., Li, R., Sheng, J., et al. (2019). ABA signaling rather than ABA metabolism is involved in trehalose-induced drought tolerance in tomato plants. *Planta* 250 (2), 643–655. doi: 10.1007/s00425-019-03195-2

Zeng, W., Mostafa, S., Lu, Z., and Jin, B. (2022). Melatonin-mediated abiotic stress tolerance in plants. *Front. Plant Sci.* 13. doi: 10.3389/fpls.2022.847175

Zhang, H., Liu, D., Yang, B., Liu, W. Z., Mu, B., Song, H., et al. (2020). Arabidopsis CPK6 positively regulates ABA signaling and drought tolerance through phosphorylating ABA-responsive element-binding factors. *J. Exp. Bot.* 71, 188–203. doi: 10.1093/jxb/erz432

Zhang, Y., Luan, Q., Jiang, J., and Li, Y. (2021). Prediction and utilization of malondialdehyde in exotic pine under drought stress using near-infrared spectroscopy. *Front. Plant Sci.* 12. doi: 10.3389/fpls.2021.735275

Zhou, Z., Tang, J., Cao, Q., Li, Z., and Ma, D. (2022). Differential response of physiology and metabolic response to drought stress in different sweet potato cultivars. *PloS One* 17 (3), e0264847. doi: 10.1371/journal.pone.0264847

Zhukov, A. V., and Shumskaya, M. (2020). Very-long-chain fatty acids (VLCFAs) in plant response to stress. *Funct. Plant Biol.* 47 (8), 695–703. doi: 10.1071/FP19100

Zimin, A., Stevens, K. A., Crepeau, M. W., Holtz-Morris, A., Koriabine, M., Marçais, G., et al. (2014). Sequencing and assembly of the 22-gb loblolly pine genome. *Genetics* 196 (3), 875–890. doi: 10.1534/genetics.113.159715

Zimin, A. V., Stevens, K. A., Crepeau, M. W., Puiu, D., Wegrzyn, J. L., Yorke, J. A., et al. (2017). An improved assembly of the loblolly pine mega-genome using long-read single-molecule sequencing. *Gigascience* 6 (1), 1–4. doi: 10.1093/gigascience/giw016

Zulfiqar, F., Chen, J., Finnegan, P. M., Younis, A., Nafees, M., Zorrig, W., et al. (2021). Application of trehalose and salicylic acid mitigates drought stress in sweet basil and improves plant growth. *Plants (Basel)* 10 (6), 1078. doi: 10.3390/plants10061078

frontiers | Frontiers in Plant Science

TYPE Original Research
PUBLISHED 14 February 2023
DOI 10.3389/fpls.2022.1034788

Check for updates

OPEN ACCESS

EDITED BY
Jiban Shrestha,
Nepal Agricultural Research Council, Nepal

REVIEWED BY
Mohamed Magdy F. Mansour,
Ain Sham University, Egypt
Klára Kosová,
Crop Research Institute (CRI), Czechia

*CORRESPONDENCE
Luisa Bascunan-Godoy
lubascun@udec.cl
Patricio A. Castro
pacastro@udec.cl

†These authors have contributed equally to this work

SPECIALTY SECTION
This article was submitted to Plant Abiotic Stress, a section of the journal Frontiers in Plant Science

RECEIVED 02 September 2022
ACCEPTED 14 December 2022
PUBLISHED 14 February 2023

CITATION
Cifuentes L, González M, Pinto-Irish K, Álvarez R, Coba de la Peña T, Ostria-Gallardo E, Franck N, Fischer S, Barros G, Castro C, Ortiz J, Sanhueza C, Del-Saz NF, Bascunan-Godoy L and Castro PA (2023) Metabolic imprint induced by seed halo-priming promotes a differential physiological performance in two contrasting quinoa ecotypes. *Front. Plant Sci.* 13:1034788. doi: 10.3389/fpls.2022.1034788

COPYRIGHT
© 2023 Cifuentes, González, Pinto-Irish, Álvarez, Coba de la Peña, Ostria-Gallardo, Franck, Fischer, Barros, Castro, Ortiz, Sanhueza, Del-Saz, Bascunan-Godoy and Castro. This is an open-access article distributed under the terms of the Creative Commons Attribution License (CC BY). The use, distribution or reproduction in other forums is permitted, provided the original author(s) and the copyright owner(s) are credited and that the original publication in this journal is cited, in accordance with accepted academic practice. No use, distribution or reproduction is permitted which does not comply with these terms.

Metabolic imprint induced by seed halo-priming promotes a differential physiological performance in two contrasting quinoa ecotypes

Leonardo Cifuentes[1†], Máximo González[2†], Katherine Pinto-Irish[2], Rodrigo Álvarez[2], Teodoro Coba de la Peña[2], Enrique Ostria-Gallardo[2], Nicolás Franck[3], Susana Fischer[4], Gabriel Barros[5], Catalina Castro[5], José Ortiz[5], Carolina Sanhueza[5], Néstor Fernández Del-Saz[5], Luisa Bascunan-Godoy[5*] and Patricio A. Castro[6*]

[1]Instituto Forestal (INFOR), Sede Diaguitas, La Serena, Chile, [2]Laboratorio de Fisiología Vegetal, Centro de Estudios Avanzados en Zonas Áridas (CEAZA), La Serena, Chile, [3]Centro de Estudios en Zonas Áridas (CEZA), Facultad de Ciencias Agronómicas, Universidad de Chile, Coquimbo, Chile, [4]Laboratorio de Fisiología Vegetal, Departamento de Producción vegetal Facultad de Agronomía, Universidad de Concepción, Concepción, Chile, [5]Laboratorio de Fisiología Vegetal, Departamento de Botánica, Facultad de Ciencias Naturales y Oceanográficas, Universidad de Concepción, Concepción, Chile, [6]Departamento de Fisiología, Facultad de Ciencias Biológicas, Universidad de Concepción, Concepción, Chile

"Memory imprint" refers to the process when prior exposure to stress prepares the plant for subsequent stress episodes. Seed priming is a strategy to change the performance of seedlings to cope with stress; however, mechanisms associated with the metabolic response are fragmentary. Salinity is one of the major abiotic stresses that affect crop production in arid and semiarid areas. *Chenopodium quinoa* Willd. (Amaranthaceae) is a promising crop to sustain food security and possesses a wide genetic diversity of salinity tolerance. To elucidate if the metabolic memory induced by seed halo-priming (HP) differs among contrasting saline tolerance plants, seeds of two ecotypes of Quinoa (Socaire from Atacama Salar, and BO78 from Chilean Coastal/lowlands) were treated with a saline solution and then germinated and grown under different saline conditions. The seed HP showed a more positive impact on the sensitive ecotype during germination and promoted changes in the metabolomic profile in both ecotypes, including a reduction in carbohydrates (starch) and organic acids (citric and succinic acid), and an increase in antioxidants (ascorbic acid and α-tocopherol) and related metabolites. These changes were linked to a further reduced level of oxidative markers (methionine sulfoxide and malondialdehyde), allowing improvements in the energy use in photosystem II under saline conditions in the salt-sensitive ecotype. In view of these results,

we conclude that seed HP prompts a "metabolic imprint" related to ROS scavenger at the thylakoid level, improving further the physiological performance of the most sensitive ecotype.

KEYWORDS

halophyte, preconditioning, salt-tolerant, photosynthetic performance, memory, metabolomic, *Chenopodium quinoa*

Introduction

Plants modulate their physiological responses in order to acclimate to stressful conditions in their local environment. Priming has emerged as a tool that may benefit plant physiology and metabolism under stress conditions (Ashraf and Foolad, 2005; Paparella et al., 2015). The term "stress imprint" can be defined as the priming or hardening process in which prior exposure to environmental stress increases plant resistance to future exposures (Bruce et al., 2007). Multiple examples of imprint have been observed in higher plant species in response to drought, salinity, and high and low temperatures, among others (Ashraf and Foolad, 2005; Paparella et al., 2015; Ibrahim, 2016). In seeds of several species, priming improves germination and uniform emergencies and improves seedling's vigor, establishment, and growth (Kaya et al., 2006; Dezfuli et al., 2008; Bakht et al., 2011; Manonmani et al., 2014; Raj and Raj, 2019). Mechanisms associated with priming may occur at different levels, including epigenetic (e.g., by DNA and histone modification), transcriptional (e.g., changes in the abundance of transcripts and transcription factors), protein level, and by modulating enzyme activities (Schwachtje et al., 2019). However, the priming-related changes in the metabolism remain largely unexplored, although it is highly compromised during stress (Schwachtje et al., 2019).

Salinity is one of the most brutal environmental factors limiting crop productivity (Shrivastava and Kumar, 2015), with germination being one of the most critical salt-sensitive periods (Jacobsen et al., 1999; Maleki et al., 2018). *Chenopodium quinoa* (Willd.) is an annual crop native from the Andean region and has been nominated as one of the crops that could contribute to global food security during the next century (FAO, 2011; Ruiz-Carrasco et al., 2011; Adolf et al., 2013). Even though quinoa is considered a facultative halophyte (Biondi et al., 2015), there is a great gradient in saline tolerance according to its origin (Delatorre-Herrera and Pinto, 2009; Razzaghi et al., 2011). Altiplano and Lowlands are two representative quinoa ecotypes with contrasting salinity resilience (Jacobsen and Stølen, 1993; Delatorre-Herrera and Pinto, 2009; Ruiz-Carrasco et al., 2011). Recent reports indicate that different seed priming treatments (chemical priming, osmopriming, saponins, etc.), including halo-priming (pretreatment with a low level of salt), improved germination under salt stress conditions in quinoa (Daur, 2018; Moreno et al., 2018) and mitigated the negative effects of salt stress on growing (Yang et al., 2018).

It is reported that quinoa plants reconfigure their metabolism under salt stress conditions. Comparative studies between tolerant and sensitive genotypes reveal enrichment of diverse pathways including photosynthesis-related, phenylpropanoid biosynthesis, tyrosine metabolism, and ROS scavenging pathways in tolerant salt-sensitive genotypes (Shi and Gu, 2020; Derbali et al., 2021). Interestingly, the stress memory is not the simple repetitious activation of the same strategies of the original stress (Liu H et al., 2022), and the metabolic pathways induced by seed HP in quinoa and their impact on plant performance are far from being clarified. Moreover, as has been demonstrated in rice, the extent of the effect of memory could be different between sensitive and tolerant genotypes (do Amaral et al., 2020).

In this work, we wonder: Which are the metabolic pathways induced by salinity? Could seed halo-priming be involved in the induction of a metabolic memory that can enhance salt tolerance during growing? What is the link of this metabolic imprint with plant physiological performance? Could this response be different depending on the saline tolerance of the ecotype? The identification of metabolic pathways involved in the imprint of stress memory may provide potential keys for global food production in a scenario of climatic change.

Materials and methods

Plant material

Seeds of two Chilean ecotypes of *C. quinoa* (Willd.) from contrasting agro-ecological origins were used in the experiments: the Socaire ecotype from the Chilean Altiplano (Socaire, 23° 35'31.58" S, 67°53'17.69" W) and the coastal BO78 ecotype (Temuco, 39°10' S, 72°68' W). Seeds were obtained from the National Seed Bank of Chile managed by the Genetic Resources

section of the National Institute of Agriculture Research (http://163.247.128.32/gringlobal/search.aspx, INIA-Intihuasi Vicuña, Chile).

Seed sensitivity test to salt

Considering that salinity tolerance in quinoa does not always correlate with geographic distribution, to reveal a differential saline tolerance on germination traits between Socaire and BO78 ecotypes, we evaluated the effect of different salt concentrations over seed germination. Seeds were incubated at 0, 200, 250, 300, 350, and 400 mM NaCl for 48 h at 24°C in the dark. Fifty seeds were used for each treatment, and experiments were performed in triplicate. The final germination percentage, mean germination time, and mean velocity germination were recorded every 4 h up to 48 h after seed imbibition following Scott et al. (1984) and Ranal and Santana (2006). Germination was considered complete when the radicle emerged from the seed.

Effect of saline shock on net photosynthesis in two contrasting ecotypes

In order to evaluate the performance of Socaire and BO78 ecotypes under salt stress during the vegetative stage, plants were exposed to a saline shock treatment under greenhouse conditions. Seeds of Socaire and BO78 were sown directly in 5 kg of dry soil, in 10-L pots (22 cm tall by 28 cm diameter), containing a mixture of sand and peat in a 2:1 ratio and fertilized with 4 g of 6 M Basacote Plus Compo Expert (16% N, 3.5% P, 10% K, 1.2% Mg, 5% S, and micronutrients). The environmental conditions were as follows: 1,200 µmol m^{-2} s^{-1} PAR at noon (natural light); maximum and minimum temperatures (daily ranges) of 23°C and 17°C, respectively; 12-h day length; and 80% relative humidity. Seedlings were irrigated with distilled water at field capacity, and the water content of each pot was monitored every 3 days by weight, and additional irrigation was applied for moisture fulfillment. At the stage of six pairs of true leaves (24 days after germination), seedlings (n = 12) were subjected to a saline shock by unique irrigation with 400 mM NaCl solution (~ the salinity of sea water, electrical conductivity of 40 dS/m; Adolf et al., 2013), while control plants were maintained irrigated with distilled water. After the application of the saline shock treatment, plants under control and salt stresses were irrigated every 2 days with distilled water. The effects of salinity stress and recovery were determined by evaluating changes in net photosynthetic rate (P_n) 10 days after the application of the salt treatment. Leaf photosynthetic rate (P_n) was measured in fully expanded leaves during mid-morning (between 11:00 a.m. and 13:00 p.m.) with a gas exchange system (Li-6400, Li-Cor Inc., Nebraska, USA) equipped with a light source (6200-02B LED, Li-Cor). Environmental conditions in the leaf chamber were as follows: photosynthetically active photon flux density = 1500 µmol photon m^{-2} s^{-1} and CO_2 concentration (Ca) = 400 µmol mol^{-1}. The experiment was performed in a completely randomized design. Plants from pots in border rows of the experimental design were discarded in order to avoid the border effect.

Effect of halo-priming on seed germination

In order to choose the conditions for halo-priming (HP), seeds of each ecotype were embedded at different times and NaCl concentrations in the dark at room temperature. Considering the improvement of BO78 germination, we selected for HP the solution of 68 mM NaCl by 12 h (Supplementary Figure S1). Then, for all experiments, seeds were embedded under those conditions and subsequently washed twice with distilled water and then surface-dried with adsorbent paper at room temperature for 12 h before establishing the germination assays. Unprimed (UP) seeds were not treated with the priming solution. Germination experiments were performed in a completely randomized design with three factors under study: Ecotypes (E), Priming (P), and Saline treatment (S). Haloprimed (HP) and unprimed (UP) seeds of both ecotypes were submitted to control (C, distilled water) or saline (S, 300 mM NaCl) treatment. This concentration reduced germination-related parameters in both ecotypes and has been widely used to compare salt tolerance among quinoa genotypes (Ruiz et al., 2017). Germination was carried out as previously described, and the germination parameters (final germination percentage, mean germination time, and mean velocity germination) were recorded after 48 h in both ecotypes to each treatment (Unprimed Control: UP-C; Haloprimed Control: HP-C; Unprimed Salt: UP-S; Haloprimed Salt: HP-S).

Effect of seed priming on seedling physiological performance under salt treatment

To study the establishment of juvenile plants in pots, UP and HP seeds of Socaire and BO78 were sown directly in soil (n = 12; 96 plants in total). Four seeds per treatment were sown in order to obtain one established seedling per pot. The environmental conditions of the greenhouse were as follows: 1,200 µmol m^{-2} s^{-1} PAR at noon (natural light); maximum and minimum temperatures (daily ranges) of 23°C and 17°C, respectively; 12-h day length; and 80% relative humidity. From seed imbibition to seedling growth, two irrigation treatments were applied: Control (C) by irrigation with distilled water and Saline (S) with increased soil salinization by weekly irrigation of 100 mM NaCl. Pots were irrigated to 90% of soil water-holding capacity

to minimize NaCl losses from soil. The experiment was run in a completely randomized design and supplementary plants were used in order to prevent the border effect.

At 24 days after germination (at the stage of six pairs of true leaves), parameters from chlorophyll *a* fluorescence were recorded. Plants were collected for biochemical analysis (n = 6) including determination of chlorophyll content, lipid peroxidation, starch, soluble sugars, proline, and metabolomic profile.

Chlorophyll *a* fluorescence

Chlorophyll *a* fluorescence parameters were obtained by an FMS 2 portable fluorometer (Hansatech Instruments, UK) as described by Bascuñán-Godoy et al. (2012); Bascuñán-Godoy et al. (2015). Fully expanded leaves of plants from each ecotype and treatment (n = 6) were dark-adapted at room temperature for 30 min prior to measurement. The intensity of actinic light for measurements was 1,200 mmol photons m^{-2} s^{-1}. The following parameters were recorded: maximum photochemical efficiency of photosystem II (Fv/Fm), effective quantum yield (ΦPSII), and thermal dissipation measured as non-photochemical quenching (NPQ) (Maxwell and Johnson, 2000).

Lipid peroxidation, total soluble sugars, starch, and proline content

Fully expanded leaves of plants from each ecotype and treatment (n = 6) were used for the spectrophotometric analysis of metabolites. Fresh leaf tissue (100 mg) was collected, flash-frozen in liquid nitrogen, and stored at −80°C to posterior analysis.

The lipid peroxidation in leaves was assayed using the thiobarbituric acid method according to Ortega-Villasante et al. (2005). This test determines malondialdehyde (MDA) as an end product of the thiobarbituric acid reaction. Total soluble sugars (TSS) and starch were determined according to McCready et al. (1950) and Rose et al. (1991), respectively. Chlorophyll extraction was performed according to Mackinney (1941), while its concentrations (*a* and *b*) were determined according to Lichtenthaler and Buschmann (2001). Proline (Pro) was determined at 520 nm using the rapid method developed by Bates et al. (1973).

Metabolome profiling

For metabolome profiling, leaves from plants subjected to different treatments were frozen and then freeze-dried. Metabolome profiling analysis was performed at the West Coast Metabolomics Center (UC Davis, Davis, CA, USA), according to the methodology described in Botanga et al. (2012). Raw data were normalized, filtered, and analyzed using the MetaboAnalyst 3.0 webserver (Xia et al., 2015).

Statistical analysis

A two-way analysis of variance (ANOVA) ($p < 0.05$) was conducted to determine the effects of Ecotypes (E, Socaire and BO78) and salinity (S, 0 to 400 mM) on germination parameters. Photosynthetic data were analyzed using repeated measures ANOVA ($p < 0.05$). A three-way ANOVA was conducted in order to determine the effects of Ecotypes (Socaire and BO78), Saline treatment (C or S), and Priming (UP or HP) on physiological parameters and metabolites. Tukey HSD test (level of significance $p < 0.05$) was used as a *post-hoc* test, in order to explore evidence of significant differences. All analyses were performed with the STATISTICA v7.0 software package (StatSoft Inc., Tulsa, OK, USA).

Heatmap plots (to visualize metabolites profiles) were performed using the heatmap R package. Data were scaled by *Z*-score to capture metabolites with similar behavior. Clustering of metabolites was performed using the default pheatmap Ward method. Metabolite pathway information was obtained from KEGG API (https://www.kegg.jp/kegg/rest/keggapi.html) using a Shell script. For metabolome profiling analysis, a principal component analysis (PCA) and hierarchical cluster analysis using Ward clustering algorithm and Euclidian distance were performed to identify relations among variables; normalized data corresponding to different treatments were analyzed by three-way ANOVA.

Statistical interpretations of data were based on the complex interactions that nest the simple effect and independent effects that are not included in an interaction.

Results

Effect of salinity on germination of two quinoa ecotypes

In order to verify a differential physiological salt tolerance between the two quinoa ecotypes from contrasting origins, a comparative analysis of germination capacity was performed (Figure 1). A statistically significant interaction between plant ecotype (E) and treatment (S) was observed in all the parameters related to germination studied ($p < 0.0001$). After 48 h from seed imbibition, the two ecotypes displayed similar final germination percentages in control and under 200 and 250 mM NaCl with values higher than 85% (Figure 1A). Germination values of Socaire were maintained close to 100% in the presence of up to 350 mM NaCl, and only a significant decrease was observed at 400 mM NaCl (70% of germination). Contrastingly, BO78 seeds displayed significant decreases in germination at 300 and 350

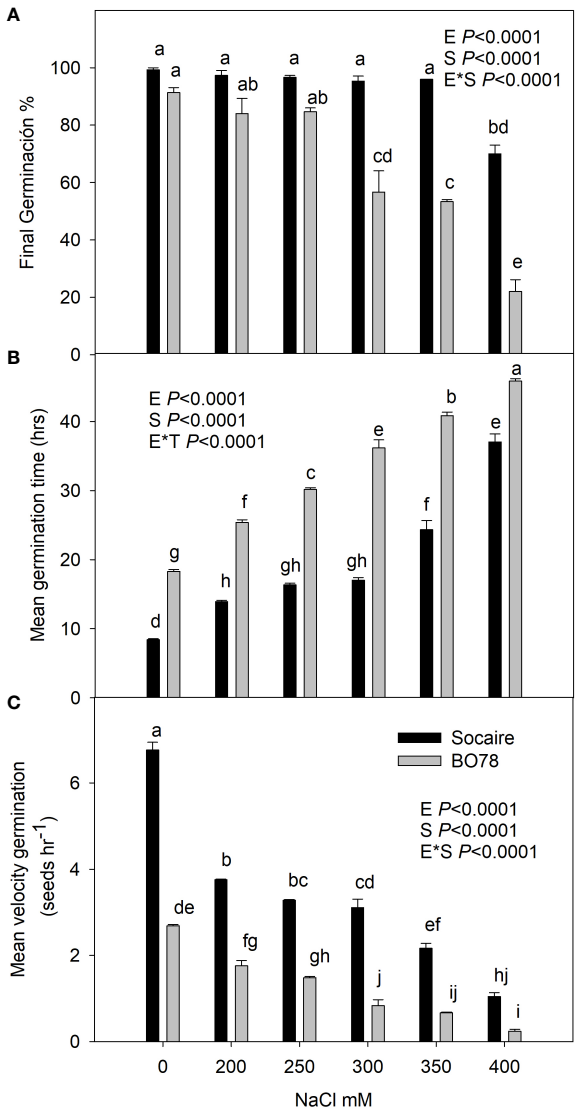


FIGURE 1
Salinity effect on germination percentage **(A)**, mean germination time **(B)**, and mean velocity germination **(C)** of Socaire and BO78 ecotypes of quinoa seeds. Seeds were germinated under 0, 200, 250, 300, 350, and 400 mM of NaCl. Error bars show mean ± SE (n = 12). Different letters indicate significant differences between ecotypes (E) and salinity treatments (T) using two-way ANOVA. Tukey HSD was used as a *post-hoc* test ($p < 0.05$).

mM NaCl (56% of GP), and at 400 mM of NaCl, only 22% of final germination was reached.

The study of mean germination time indicates that Socaire takes 10 h for germination (Figure 1B) while BO78 takes 20 h. Additionally, the mean velocity of germination indicates that Socaire germinates 2.5 times faster than BO78 under control conditions (Figure 1C). A significant increase in the time for germination and a decrease in velocity was observed in both ecotypes in the presence of NaCl from 200 to 400 mM. A stronger change in those parameter values was observed through all concentrations studied in BO78 than in Socaire (Figure 1B).

Effect of salinity shock on the photosynthetic performance of both quinoa ecotypes

Additionally, to test the effect of salinity on germination parameters, we compared the ability to recover the net photosynthetic rate (P_n) in seedlings submitted to salinity shock (400 mM NaCl). Similarly to germination parameters, we found the interaction E × S ($p < 0.0001$). Prior to the application of saline shock (control conditions, day 0), all the plant groups exhibited similar P_n values Figure 2 (Net Photosynthesis) Furthermore, a similar and significant decline of about 50% of P_n values was observed in both quinoa ecotypes after 3 days from the salinity shock (Figure 1). Interestingly, 10 days after the salinity shock treatment, it was observed that Socaire plants were able to recover P_n values similar to those observed in control plants, while BO78 plants were unable to recover P_n.

Effect of seed halo-priming on germination

Once the differential salinity tolerance of the ecotypes studied was verified, halo-priming (HP) studies were carried out. All the parameters related to germination were affected by HP (Figure 3), and the final germination percentage and mean velocity of germination were dependent on the interaction among E × S × P ($p < 0.005$).

The final germination percentage of the Socaire ecotype was not reduced by salinity, while in BO78, it decreased to 50% (UP-S treatment) (Figure 3A). Remarkably, seed HP reverted the effect of salinity in BO78, reaching 100% of germination.

Salinity treatment prolonged the mean germination time (Figure 3B), reducing the speed of germination in both ecotypes (Figure 3C). Seed HP significantly reduced germination time and increased the speed of germination under control conditions in Socaire and in both conditions (control and saline) in the most sensitive genotype.

Effect of seed halo-priming on "chlorophyll *a*" fluorescence parameters in juvenile plants of both ecotypes

Seedling of both *C. quinoa* ecotypes showed similar values of the maximal fluorescence of PSII (Fv/Fm) that were maintained at about 0.8 through the treatments Figure 4 (Chlorphyll fluorescence). The quantum yield of photosynthesis (ΦPSII)

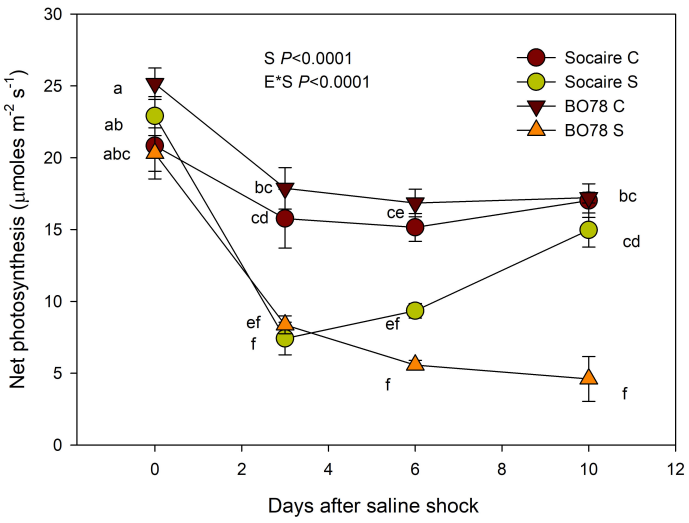


FIGURE 2
Salinity effect on net photosynthesis (Pn) of Socaire and BO78 ecotypes of quinoa. Plants grown under control conditions (C, 0 mM NaCl) were exposed to salinity shock (S, 400 mM NaCl) and recovered by 10 days. Error bars show mean ± SE (n = 12). Different letters indicate significant differences between ecotypes (E) and salinity treatments (T) using repeated measures ANOVA ($p < 0.05$).

was dependent on the interactions between E × P ($p < 0.001$) and S × P ($p < 0.001$) (Figure 4B). Ecotypes presented similar levels of ΦPSII at control conditions (UP-C), and salinity treatment negatively affected only BO78. Seed HP enhanced 30% ΦPSII value in this ecotype (BO78) under saline conditions (HP-S), while no effect was observed in Socaire.

NPQ was dependent on the interaction of E × S ($p < 0.001$) and E × P ($p < 0.001$). Saline treatment tended to increase NPQ in BO78 but not in Socaire (Figure 4C). Seed HP significantly reduced NPQ values in BO78 at both control and saline conditions (HP-C and HP-S), to similar levels to those observed in Socaire (Figure 4C). Interestingly, this decrease in NPQ values in BO78 HP-S plants (reduction of 40%) was concomitant with the enhanced ΦPSII values.

Effect of seed HP and salinity treatment on lipid peroxidation, carbohydrates, chlorophylls, and proline

The levels were calculated as the ratio of each value to the Control (UP-C) treatment (Figure 5). Original data of measurements and concentrations at the different conditions are summarized in Supplementary Table 1.

MDA (a product of membrane lipid peroxidation) level was dependent on the interaction of E × S × P ($p < 0.009$, Supplementary Table 1). MDA increased about two times in both ecotypes under saline treatments, reaching the highest value in BO78 UP-S. Seed HP reduced the content of MDA to similar levels to control conditions (UP-C) (Figure 5).

Total soluble sugar (TSS) amount was dependent on the interaction of E × S × P ($p < 0.005$, Supplementary Table 1). Salinity (UP-S treatment) induced a significant increase in the content of TSS in Socaire, which was not observed in BO78 (Figure 5). Halo-priming induced a significant decrease in TSS, which was most notorious in Socaire HP-S (Supplementary Table 1).

BO78 stored an 18% higher amount of starch than Socaire plants (Supplementary Table 1) and HP reduced the starch in both ecotypes in control and saline conditions ($p < 0.001$). No interaction among factors was observed for leaf starch amount.

Chlorophyll levels were dependent on the interaction E × P ($p = 0.01$). Both Chl *a* and *b* contents were significantly higher in BO78 than in Socaire, and tended to increase by HP effect but only in Socaire (Figure 5 and Supplementary Table 1).

Proline was dependent on the interaction of P × S ($p = 0.008$). A significant reduction in proline content was observed in Socaire and BO78 plants submitted to saline treatment because of the effect of HP (Figure 5).

Metabolome profiling

Metabolome profiling was performed to gain insight into the metabolic changes in Socaire and BO78 ecotypes upon seed halo-priming and subsequent growing at control or saline treatment. A total of 371 metabolites were detected, 161 of which were identified by assignment to a PubChem or KEGG code.

A PCA was applied to the different relative parameters to identify those that accounted for the major component of

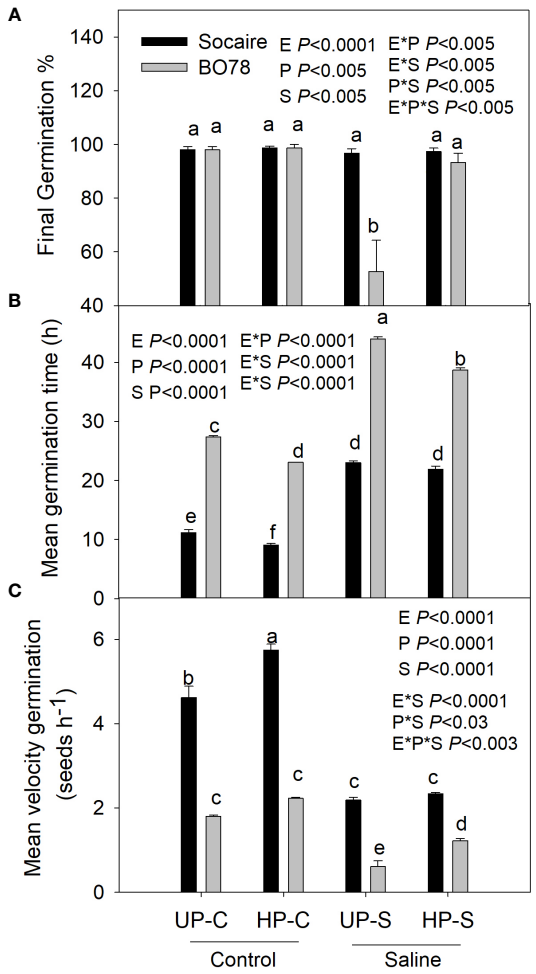


FIGURE 3
Salinity and priming effect on germination percentage **(A)**, mean germination time **(B)**, and mean velocity germination **(C)** of Socaire and BO78 ecotypes of quinoa seeds. Error bars show mean ± SE (n = 12). Different letters indicate significant differences between ecotypes (E, Socaire or BO78), priming (P, UP or HP), and treatment (T, C, or S) using three-way ANOVA. Tukey HSD was used as a post-hoc test ($p < 0.05$).

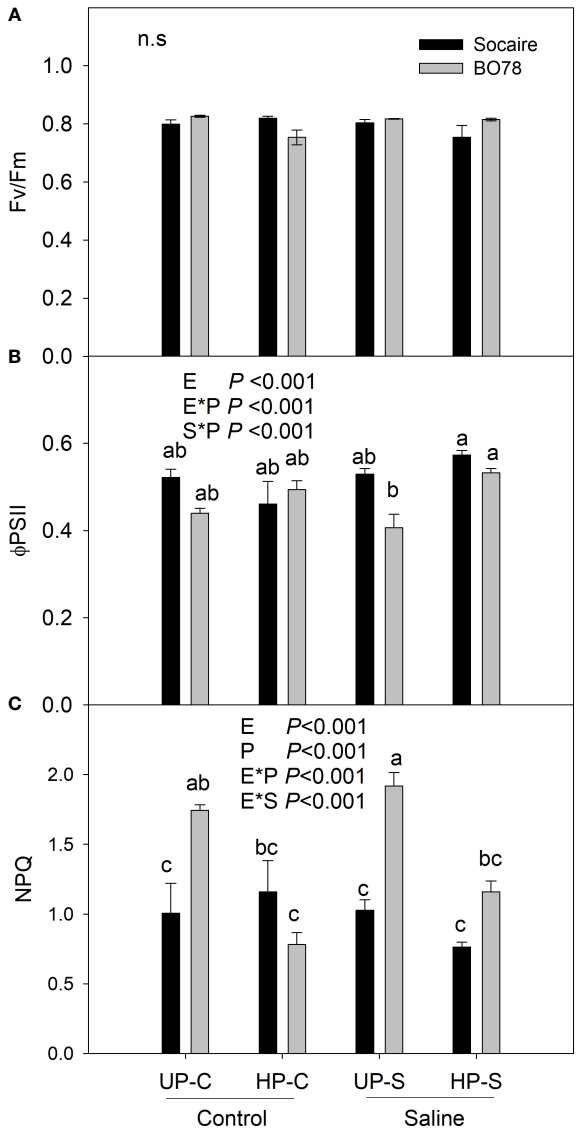


FIGURE 4
Salinity and priming effect on the chlorophyll *a* fluorescence parameters of Socaire and BO78 ecotypes. Haloprimed and unprimed seeds of both ecotypes were germinated and grown under control and salinity conditions. At 20 days after germination, chlorophyll a fluorescence parameters were registered: Fv/Fm, maximum efficiency of the PSII **(A)**, FPSII, effective quantum yield **(B)**, and NPQ, non-photochemical quenching **(C)**. Error bars show mean ± SE (n = 6). Letters indicate significant differences between ecotypes (E, Socaire or BO78), priming (P, UP or HP), and treatment (C or S) using threeway ANOVA. Tukey HSD was used as a post-hoc test ($p < 0.05$).

variability. The PCA revealed two components that accounted for 34.3% of the total variance. On one hand, PC1 (associated with ecotype) accounted for 20.5% of the variance, while the second component PC2 (associated with halo-priming and salt treatments) accounted for 13.8% of the total variance (Figure 6).

In addition, hierarchical cluster analysis of data showed that all biological replicates clustered into two clades, which matched with both quinoa ecotypes (Figure 6B). Clade I is composed of all Socaire replicates; no match between clades and treatments was observed (Figure 6B). Clade II is composed of replicates of the BO78 ecotype; interestingly, all replicates of BO78 priming plants and submitted to salinity conditions were grouped in a single cluster (Figure 6B).

According to the metabolomic analysis, 99 metabolites were differentially accumulated among ecotypes, salinity and halo-priming, or interactions. Of them, 42 metabolites were identified in PubChem or KEGG database and 57 were unknown. The identified metabolites belong to different pathways, including the Shikimic acid pathway, amino acids, TCA cycle, ornithine cycle,

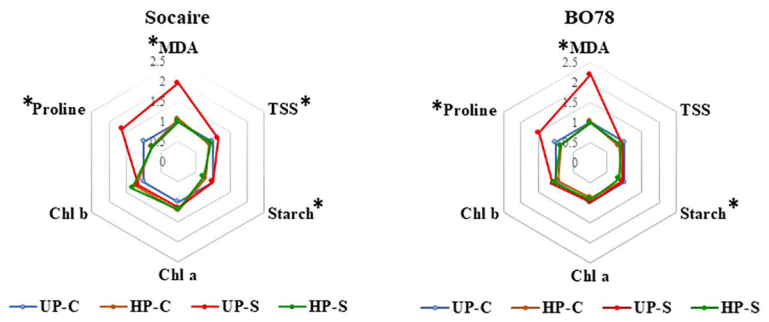


FIGURE 5
Salinity and priming effect on metabolites in Socaire and BO78 ecotypes of quinoa. Radar chart shows relative changes in lipid peroxidation (measured as MDA levels), total soluble sugars (TSS), starch, chlorophylls (Chl *a* and *b*), and proline. Relative changes were calculated as the ratio of the content of each metabolite to UP-C samples, for each ecotype. Asterisks indicate significant differences among treatments.

sugar metabolism, fatty acid metabolism, purine metabolism, and ascorbic acid pathway (detailed in Figure 6C). The *p*-values of the effect of the different factors on these 42 metabolites are included in Table 1. Significant changes in metabolites are highlighted in red and bold, while the independent effect factors (not included in any further interaction) were underlined. From the identified metabolites, it was observed that 30 displayed significant differences between ecotypes, 31 were modified in response to salinity, and 10 changed significantly by seed HP (Figure 6C and Table 1).

Interestingly, from these 30 metabolites that were displayed differentially between ecotypes, 21 were also affected by salinity treatment, namely, glucose, galactose, gluconic acid, lactic acid, fructose, raffinose, sucrose, tagatose, glyceric acid, pantothenic acid, threonic acid, shikimic acid, asparagine, phenylalanine, serine, threonine, tryptophan, tyrosine, ornithine, allantoic acid, and orotic acid. Additionally, seven metabolites were modulated by salinity but not for ecotype, namely, mannonic acid, aspartic acid, phenylethylamine, citrulline, urea, and phosphate (Table 1).

Significant E × S independent interactions were found for the following nine metabolites: raffinose, erythritol, methyl O-D-galactopyranoside, ascorbic acid, threonic acid, citric acid, succinic acid, 3,4-dihydroxycinnamic acid, and cis-caffeic acid.

Regarding seed HP, from the 10 that changed significantly, 7 had a significant independent effect, namely, ascorbic acid, threonic acid, alpha-tocopherol, citric acid, aspartic acid, tyrosine, and urea.

Significant E × P interactions were found for phenylalanine ($p \leq 0.01$) and serine ($p \leq 0.05$). Seed HP induced an increase of phenylalanine and serine in BO78, and a decrease of these amino acids in Socaire.

Significant S × P interaction was observed for succinic acid (that also presented S × E interactions), suggesting that the effect of HP on their level is dependent on the treatment but not on the ecotype.

Interactions among three factors (E × S × P) were found for dehydroascorbic acid (the oxidized form of ascorbic acid), isothreonic acid (product of catabolism of ascorbic acid), and methionine sulfoxide (product of methionine oxidation). HP reduces the level of methionine sulfoxide and isothreonic acid under saline conditions in both ecotypes, but at control conditions, the response level contrasted between ecotypes. Additionally, HP increased the level of dehydroascorbic acid under control and salinity in Socaire, but in BO7, this is observed only in saline conditions, reaching a considerably higher level than in the tolerant ecotype. In fact, dehydroascorbic acid and ascorbic acid were the most modified metabolites through the metabolomic profile.

Discussion

Here, we postulate that seed halo-priming induces a metabolic stress memory that is different from the programming induced by salinity and might be more important for the tolerance of the most sensitive ecotype.

In this study, ecotype was an important factor in explaining the variability of germination capacity under saline conditions (Figure 1), the ability to recover P_n after a shock of saline stress (Figure 2), and the extent of seed HP effect on germination (Figure 3) and during juvenile phase (Figure 4). In fact, their metabolites (Figure 5) and metabolomic profile showed a clear clade separation between ecotypes (Figure 6).

Considering the changing metabolites in the E × S interaction, we suggest that carbohydrates have a central role as a C source for interconnection routes. Salinity maintains TSS (Figure 5 and Supplementary Table 1) but reduces levels of those carbohydrates involved in the glycolysis pathway. In the case of Socaire, this could be related to the increasingly significant level of raffinose, erythritol, and ascorbic acid (Table 1 and Figure 6C). Raffinose and erythritol increase the osmotic

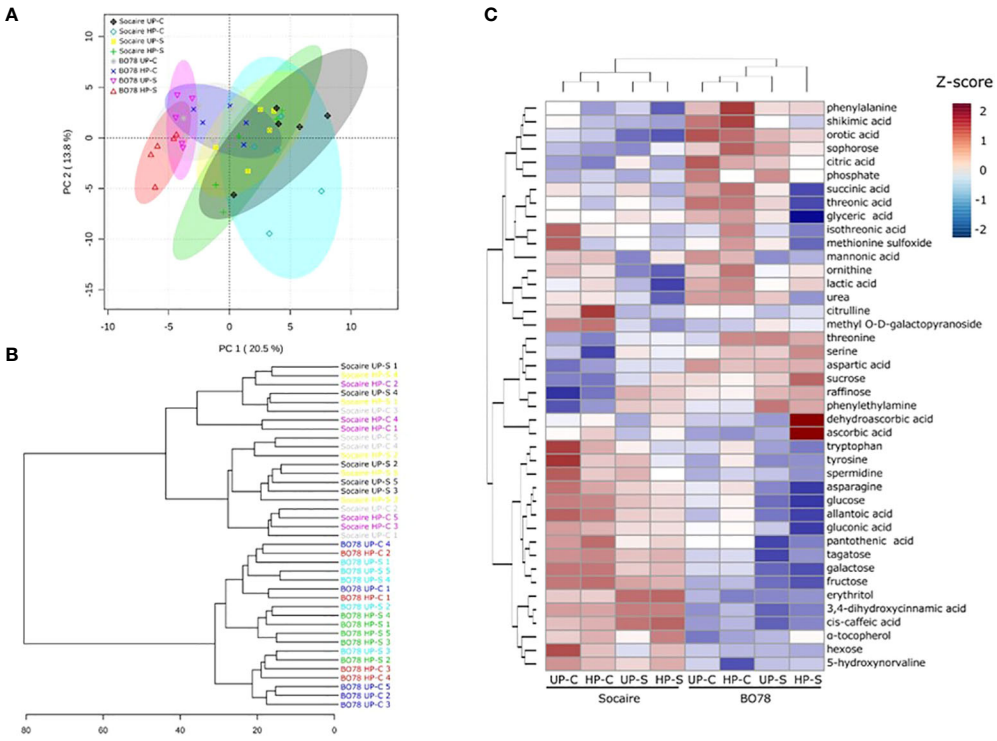


FIGURE 6
Principal component analysis (PCA) **(A)**, hierarchical clustering dendrogram **(B)**, and heatmap for metabolome profiling data **(C)**. The PCA, hierarchical clustering dendrogram, and clustered heatmap show the most changing metabolites (42 metabolites) under the different conditions (UP-C, HP-C, UP-S, and HP-S) in both ecotypes. Heatmap scale bar shows standardized metabolite values color-coded from low (blue) to high (red).

TABLE 1 *P*-values for the effects of Ecotype (E), Salt treatment (S), Priming (P), and their interactions, determined by three-way ANOVA analysis, on metabolites during the vegetative stage.

	Ecotype	Salt	Priming	E × S	E × P	P × S	E × S × P
Glucose	**0.00**	**0.00**	0.71	0.06	0.77	0.25	0.37
Galactose	**0.00**	**0.00**	0.98	0.29	0.68	0.92	0.63
Gluconic acid	**0.00**	**0.02**	0.31	0.31	0.51	0.34	0.22
Hexose	**0.00**	0.09	0.83	0.20	0.87	0.12	0.12
Lactic acid	**0.00**	**0.00**	0.84	0.31	0.34	0.23	0.19
Fructose	**0.00**	**0.00**	0.85	0.48	0.94	0.39	0.79
Raffinose	**0.00**	**0.00**	0.69	**0.00**	0.77	0.59	0.33
Sophorose	**0.00**	0.56	0.82	0.69	0.92	0.98	0.13
Sucrose	**0.00**	**0.00**	0.28	0.39	0.98	0.11	0.81
Tagatose	**0.00**	**0.00**	0.98	0.34	0.87	0.82	0.62
Erythritol	**0.00**	0.12	0.69	**0.04**	0.67	0.46	0.60
Methyl O-D-galactopyranoside	0.12	**0.05**	0.50	**0.00**	0.89	0.32	0.86
Glyceric acid	**0.01**	**0.02**	0.13	0.25	0.90	0.45	0.32

(Continued)

10.3389/fpls.2022.1034788

TABLE 1 Continued

	Ecotype	Salt	Priming	E × S	E × P	P × S	E × S × P
Pantothenic acid	**0.00**	**0.00**	0.24	0.27	0.95	0.75	0.58
Ascorbic acid	0.51	0.77	**0.04**	**0.01**	0.36	0.06	0.37
Dehydroascorbic acid	0.94	0.31	**0.00**	**0.00**	0.06	**0.01**	**0.03**
Isothreonic acid	0.17	**0.00**	0.34	0.99	0.06	0.18	**0.03**
Mannonic acid	0.77	**0.00**	0.28	0.25	0.26	0.14	0.58
Threonic acid	**0.05**	**0.00**	**0.01**	**0.00**	0.40	0.08	0.08
α-tocopherol	**0.00**	0.84	**0.01**	0.46	0.07	0.37	0.39
Citric acid	**0.00**	0.78	**0.03**	**0.01**	0.91	0.60	0.43
Succinic acid	0.35	**0.00**	**0.01**	**0.01**	0.71	**0.02**	0.12
3,4-Dihydroxycinnamic acid	**0.00**	0.68	0.44	**0.04**	0.32	0.93	0.82
cis-Caffeic acid	**0.00**	0.61	0.26	**0.00**	0.66	0.89	0.92
Shikimic acid	**0.00**	**0.00**	0.46	0.06	0.50	0.70	0.21
5-Hydroxynorvaline	**0.00**	0.50	0.17	0.80	0.70	0.37	0.86
Asparagine	**0.00**	**0.00**	0.47	0.13	0.62	0.36	0.15
Aspartic acid	0.31	**0.04**	**0.01**	0.74	0.58	0.94	0.56
Phenylalanine	**0.00**	**0.03**	0.54	0.56	**0.01**	0.29	0.41
Phenylethylamine	0.40	**0.00**	0.68	0.42	0.39	0.49	0.51
Serine	**0.00**	**0.02**	0.69	0.28	**0.04**	0.52	0.59
Threonine	**0.00**	**0.04**	0.52	0.83	0.27	0.31	0.09
Tryptophan	**0.00**	**0.00**	0.30	0.50	0.10	0.56	0.23
Tyrosine	**0.00**	**0.01**	**0.03**	0.98	0.05	0.68	0.08
Methionine sulfoxide	0.74	**0.00**	**0.01**	0.60	0.17	0.45	**0.00**
Citrulline	0.10	**0.00**	0.47	0.30	0.55	0.68	0.59
Ornithine	**0.01**	**0.00**	0.70	0.13	0.15	0.78	0.75
Spermidine	**0.00**	0.20	0.15	0.48	0.21	0.66	0.45
Urea	0.11	**0.00**	**0.02**	0.68	0.30	0.06	0.52
Allantoic acid	**0.00**	**0.00**	0.95	0.40	0.47	0.16	0.09
Orotic acid	**0.00**	**0.00**	0.27	0.80	0.89	0.97	0.99
Phosphate	0.06	**0.02**	0.07	0.26	0.26	0.46	0.14
Total significant	30	31	10	10	2	2	3
Total independent	22	25	7	9	2	1	3

Significant p-values are in bold and red. The underline shows the significant independent effect that is not included in a significant interaction and the more complex interaction that includes the effect of independent factors or more simple interactions (the posterior interpretation is only based on the complex interactions that nest the simple effect and the independent effect that are not included in an interaction).

potential of the cell, helping to maintain osmotic and redox balance in many species in response to salinity, even in halophytes (Zhang et al., 2018; Jiménez-Becker et al., 2019). Ascorbic acid participates in the stromal AsA-GSH cycle and water–water cycle. The water–water cycle is essential for suppressing the photoinhibition by scavenging of ROS generated in chloroplasts, and by the dissipation of energy as an alternative electron flux (Asada, 2000). On the other hand, BO78, but not Socaire, increases the level of methyl O-D-galactopyranoside, which could be related to limiting the

accumulation of methanol and the toxic formaldehyde production in the cytoplasm produced by saline conditions (Gout et al., 2000; Aubert et al., 2004). Alternatively to the role of producing other carbohydrates, the reduction of sugar levels could be related to feeding another important pathway: the shikimate pathway. This relates to the metabolism of carbohydrates with aromatic amino acid production (and their secondary metabolites). Shikimic acid content was higher in BO78 than in Socaire, but both ecotypes tended to decrease the aromatic amino acids (phenylalanine, tryptophan, and tyrosine) under salinity conditions (Table 1). Interestingly, an alkaloid derived from phenylalanine, phenylethylamine, increased in both ecotypes under salt stress. This biogenic amine is involved in the major pathway for the synthesis of 2-phenylethanol, an aromatic alcohol, playing a major role in plant defense against herbivores and pathogens (Günther et al., 2019). Also, it is suggested that it can be related to polyamine and ethylene accumulation under stress (Irsfeld et al., 2013). Other derivatives from the shikimic acid pathway affected by E × S interactions were 3,4-dihydroxycinnamic acid and cis-caffeic acid. These are important polyphenols with osmoregulatory and high antioxidant capacity (Nishizawa et al., 2008) and are candidates to be part of the salt tolerance mechanism of Socaire but not for BO78 (Figure 6 and Table 1). We suggest that the induction of raffinose, erythritol, ascorbic acid, 3,4-dihydroxycinnamic acid, and cis-caffeic acid could be key molecules that explain the lower level of lipid oxidation (measured as MDA) under saline conditions in Socaire compared to BO78 (Figure 4; Supplementary Table 1).

Citric and succinic acids are two main components of the TCA cycle that are maintained in the tolerant ecotype and decreased in the sensitive ecotype. It is known that the TCA cycle can influence the carbon balance and partition to growth, supplying electrons (succinate) to the ETC (electron transport chain in the mitochondria) and directly synthesizing compatible solutes such as sugars and amino acids and reactive oxygen species (ROS) detoxification (Che-Othman et al., 2017). The TCA network is flexible under salinity stress to enable to fulfill cellular energy demands, including the induction of the malate/pyruvate pathway (Kazachkova et al., 2013) and the γ-aminobutyric acid (GABA) shunt (Che-Othman et al., 2020).

The majority of the N-related metabolites changing were downregulated by salinity treatments, except by the following amino acids: proline, serine, threonine, and aspartic acid. Interestingly, the increased level of these amino acids was similarly reported for *Sargassum muticum* and *Jania rubens*, attributed to an osmopotential role (Abdel Latef et al., 2017). Here, we suggest that serine and aspartic acid can feed the TCA cycle through its conversion into pyruvate and oxaloacetate (or fumarate), respectively. Moreover, serine increase could be associated with photorespiratory reactions that can dissipate excess reducing equivalents and energy, providing an internal CO_2 pool and NADH used for respiration in the mitochondria (Busch, 2020). Additionally, proline was positively regulated under salt and is considered an important osmoregulator involved in the transport of NaCl into the bladder cells in quinoa salt-tolerant ecotypes (Böhm et al., 2018). Indeed, it has been pointed out as one major factor in the regulation of the expulsion of NaCl crystals in leaves of quinoa (Böhm et al., 2018).

It is noteworthy that while salinity affects C- and N-related metabolites, we found no interactions between E × S in N-content metabolites. In fact, salinity affects similarly N-related compounds independent of the constitutive tolerance level of the ecotypes. This response could be related to the great disruption that saline involves in the acquisition of macronutrients including N and P (Miranda-Apodaca et al., 2020; Bouras et al., 2022).

The metabolic basis of plant stress memory and how these affect the physiology of plants are still largely unknown. Moreno et al. (2018) reported that seed hydro-priming and osmo-priming enhanced germination-related traits of Titicaca cultivar, a hybrid variety of quinoa breeds from a Peruvian and a southern Chilean landrace. Our results indicate that, under saline conditions, seed HP affected the germination of the most saline-sensitive ecotype, BO78, allowing an increase in both the speed of germination and final germination percent (Figure 3). By contrast, seed HP did not affect the germination parameters of the Altiplano ecotype (Socaire) under saline conditions (Figure 3). Thus, we found that seed halo-priming had a differential effect on the germination traits of quinoa depending on the salt tolerance ecotype.

In juvenile plants, the level of the quantum yield of PSII (ΦPSII) in BO78 under saline conditions improved significantly by seed HP (Figure 4). This enhancement was concomitant with a reduction process that dissipates as heat the excess of absorbed energy in the PSII antenna (NPQ to antenna level). Our results suggest that seed HP modified the photochemistry of PSII in BO78 towards an increased capacity to use the light energy in the photochemical process, which eventually may improve its photosynthetic performance under salinity conditions. We suggest that the changes in ascorbic acid and α-tocopherol induced by seed HP can act synergistically to preserve plastid redox homeostasis and protect PSII, thus promoting the use of energy in the photochemical process (Szarka et al., 2012). The changes in the levels of dehydroascorbic acid, isothreonic acid, and threonic acid are in concordance with the promotion of ascorbic acid metabolism induced by seed HP. Regarding α-tocopherol, it is known that it can neutralize lipid peroxy-radicals, consequently blocking lipid peroxidation by quenching oxidative cations and then maintaining cell membrane stability (Chen et al., 2018). The increased level of α-tocopherol induced by HP could be related to the maintenance of the integrity and fluidity of photosynthesizing membranes, contributing to enhanced salt resistance.

We suggest that the increase in ascorbic acid and α-tocopherol by seed HP is sustained in the use of carbohydrates (starch decrease by HP). Recently, it has been reported that Tyr (modulated by P), a derivate of Phe, could be involved in the

biosynthesis of α-tocopherol (Tohge et al., 2013). The optimization of the shikimate pathway could be in the dismemberment TCA metabolite (citrate and succinic) with a decrement in amino acid production derivate from TCA (such as Asp), probably to avoid the depletion of carbohydrates under salinity stresses (Hill et al., 2013).

The increase in ascorbic acid and α-tocopherol induced by seed HP affected the redox status more in the sensitive ecotype than in the tolerant one. This is observed in lipid peroxidation (measured as MDA levels) and methionine sulfoxide (product of protein oxidation), which were further reduced in the sensitive ecotype during salinity. Considering that chloroplast is one of the most important sources of plant ROS, we postulate that enhancing ΦPSII and decreasing NPQ in the most sensitive ecotype could be the result of changes in oxidative status. A schematic representation of the effect of HP on metabolites and physiology is presented in Figure 7.

There is also emerging evidence that redox status, promoted by priming, can impact chromatin methylation and epigenetics (Locato et al., 2018). For instance, ascorbic acid may act as a cofactor for dioxygenases that modify chromatin and DNA (Reid et al., 2017). Contrastingly, succinate can inhibit the activity of chromatin-modifying enzymes. Thus, it seems that metabolic routes involving ascorbic acid and succinic acid could lead to a higher level of demethylation and changes in gene expression under saline conditions. The crossroads of the metabolism and the mechanisms controlling chromatin methylation and epigenetics need to be tested in plants with contrasting tolerance.

Conclusions

In summary, Altiplano ecotypes of quinoa could be more tolerant than the Lowland ecotype because of the constitutive high storage of osmolytes and antioxidants that are also induced by salinity. Our work supports the idea that salinity differentially compromises the C between ecotypes, while N metabolism was strongly affected in both. Contrastingly, seed HP finely orchestrated changes in relation to the antioxidant metabolism related to ascorbic acid and α-tocopherol, inducing a metabolic imprint that has effects during germination and plant growth. The differential signature of seed HP in ecotypes confers improved tolerance to salinity to the most sensitive ecotype, which is observed in the strengthening of PSII. Future investigations must study the reciprocal role of a metabolic imprint and the epigenetic response.

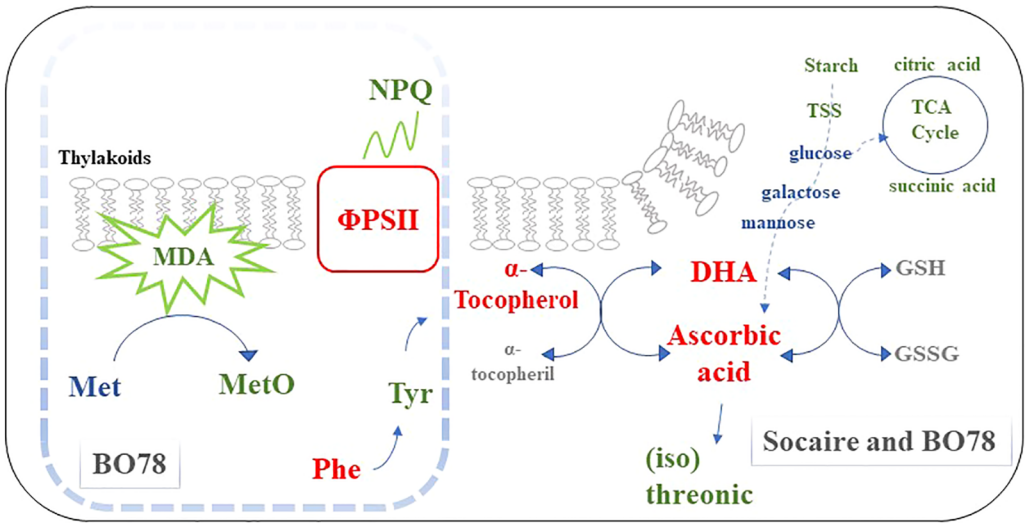


FIGURE 7
Simplified schematic of seed HP effect on physiological processes and metabolites in *C. quinoa* ecotypes. Seed HP (as a unique factor) induces a reduction of starch and citric acid, and, in interaction with salinity, reduced TSS and succinic acid; however, seed HP maintains glucose, galactose, and mannose, which are important substrates for ascorbic acid biosynthesis. Seed HP enhanced the level of ascorbic acid, dehydroascorbic (DHA), and α-tocopherol, which are involved in antioxidant cycles associated with stabilize membranes. Additionally, seed HP reduced levels of threonic and isothreonic acids, suggesting that ascorbic acid could be less degraded. It is suggested that the higher level of α-tocopherol contributes to this response. The enhanced aromatic amino acids pathways (Phe and Tyr) observed in BO78 have been pointed out as an alternative pathway to produce α-tocopherol. Finally, the level of oxidative markers (methionine sulfoxide and MDA) (that increases under saline conditions) was reduced by the effect of seed HP, and further reductions were observed in the most sensitive than in the tolerant ecotype. We suggest that these changes might increase the robustness of PSII through an increase of ΦPSII and a decrease of NPQ, which was observed in the most sensitive ecotype (BO78). Red, green, and blue colors represent an increase, reduction, or non-change in the physiological process or metabolite accumulation upon HP (compared to UP) or HP-S (compared to UP-S treatment), respectively. The gray color represents metabolites that were not present (or not identified) in the metabolome profiling. The processes and metabolites inside the square dotted line correspond to changes only in the BO78 ecotype.

Data availability statement

The datasets presented in this study can be found in online repositories. The names of the repository/repositories and accession number(s) can be found in the article/Supplementary Material.

Author contributions

LB-G, LC, NF, EO-G, SF, and PC designed the assays and led the writing of the manuscript. MG conducted metabolomics analysis. RÁ and KP grew both C. quinoa genotypes. CS, GB, JO, and CC performed the assays and measurements. LB-G, ND-S, and PC led the supported projects and edited the manuscript. All authors read, edited and approved the final version of the manuscript for publication.

Funding

This work was supported by ANID Fondecyt Regular N° 1211473. NFDS and CS thank to ANID Fondecyt 1191118.

Acknowledgments

We thank INIA-Intihuasi Chile National Seed Bank Repository for providing quinoa seeds.

Conflict of interest

The authors declare that the research was conducted in the absence of any commercial or financial relationships that could be construed as a potential conflict of interest.

Publisher's note

All claims expressed in this article are solely those of the authors and do not necessarily represent those of their affiliated organizations, or those of the publisher, the editors and the reviewers. Any product that may be evaluated in this article, or claim that may be made by its manufacturer, is not guaranteed or endorsed by the publisher.

Supplementary material

The Supplementary Material for this article can be found online at: https://www.frontiersin.org/articles/10.3389/fpls.2022.1034788/full#supplementary-material

SUPPLEMENTARY FIGURE 1
Effect of different seed priming treatments on germination percentage in BO78 ecotype of quinoa. Seeds were primed with various treatments and then germinated at 300 mM of NaCl (Details in Materials and Methods). Error bars show mean ± SE (n=50).

SUPPLEMENTARY TABLE 1
Effect of seed HP on metabolites and biomass under Control or Salinity conditions in two genotypes of *C. quinoa*. Different parameters were determined in four different individuals (n = 4). Fully expanded third leaves (from the top part of the plant) were used for measurements. Statistical differences were established ($P < 0.05$) using three-way ANOVA. The last rows of the table show the significance levels (P) of the factors (E, S and P) and interactions. Significant P-values are in bold and red. The underline shows the significant independent effect that are not included in a significant interaction, and the more complex interaction that includes the effect of independent factors or more simple interactions (The posterior interpretation is only based on the complex interactions that nests the simple effect, and independent effect that are not included in an interaction).

DATASET 1
The file shows the metabolome data obtained from the West Coast Metabolomics Center (UC Davis, Davis, CA, USA) using leaves of juvenile plants of two ecotypes of Quinoa subjected to seed priming (UP or HP) and grown under Control or saline stress conditions.

References

Abdel Latef, A. A. H., Srivastava, A. K., Saber, H., Alwaleed, E. A., and Tran, L.-S. P. (2017). *Sargassum muticum* and *Jania rubens* regulate amino acid metabolism to improve growth and alleviate salinity in chickpea. *Sci. Rep.* 7, 10537. doi: 10.1038/s41598-017-07692-w

Adolf, V. I., Jacobsen, S. E., and Shabala, S. (2013). Salt tolerance mechanisms in quinoa (*Chenopodium quinoa* willd.). *Environ. Exp. Bot.* 92, 43–54. doi: 10.1016/j.envexpbot.2012.07.004

Afzal, I., Rauf, S., Basra, S. M. A., and Murtaza, G. (2008). Halopriming improves vigor, metabolism of reserves and ionic contents in wheat seedlings under salt stress. *Plant Soil. Environ.* 54, 382–388. doi: 10.17221/408-PSE

Apel, K., and Hirt, H. (2004). Reactive oxygen species: Metabolism, oxidative stress, and signal transduction. *Annu. Rev. Plant Biol.* 55, 373–399. doi: 10.1146/annurev.arplant.55.031903.141701

Armbruster, U., Leonelli, L., Correa Galvis, V., Strand, D., Quinn, E. H., Jonikas, M. C., et al. (2016). Regulation and levels of the thylakoid K+/H+ antiporter KEA3 shape the dynamic response of photosynthesis in fluctuating light. *Plant Cell Physiol.* 7, 1557–1567. doi: 10.1093/pcp/pcw085

Asada, K. (2000). The water-water cycle as alternative photon and electron sinks. *Philos. Trans. R. Soc. Lond. B. Biol. Sci.* 355, 1419–1431. doi: 10.1098/rstb.2000.0703

Ashraf, M., and Foolad, M. R. (2005). Pre-sowing seed treatment–a shotgun approach to improve germination, plant growth, and crop yield under saline and non-saline conditions. *Adv. Agron.* 88, 223–271. doi: 10.1016/S0065-2113(05)88006-X

Aubert, S., Choler, P., Pratt, J., Douzet, R., Gout, E., and Bligny, R. (2004). Methyl-β-D-glucopyranoside in higher plants: Accumulation and intracellular localization in *Geum montanum* l. leaves and in model systems studied by ^{13}C nuclear magnetic resonance. *J. Exp. Bot.* 55(406), 2179–2189. doi: 10.1093/jxb/erh235

Bakht, J., Shafi, M., Jamal, Y., and Sher, H. (2011). Response of maize (*Zea mays* l.) to seed priming with NaCl and salinity stress. *Span. J. Agric. Res.* 9, 252–261. doi: 10.5424/sjar/20110901-113-10

Bascuñán-Godoy, L., Alcaíno, C., Carvajal, D. E., Sanhueza, C., Montecinos, S., and Maldonado, A. (2015). Ecophysiological responses to drought followed by re-watering of two native Chilean swamp forest plants: Myrceugenia exsucca (DC.) O. *Berg and Luma chequen (Molina) A. Gray.*

Bascuñán-Godoy, L., Reguera, M., Abdel-Tawab, Y. M., and Blumwald, E. (2016). Water deficit stress-induced changes in carbon and nitrogen partitioning in *Chenopodium quinoa* willd. *Planta* 243, 591–603. doi: 10.1007/s00425-015-2424-z

Bascuñán-Godoy, L., Sanhueza, C., Cuba, M., Zuñiga, G. E., Corcuera, L. J., and Bravo, L. A. (2012). Cold-acclimation limits low temperature induced photoinhibition by promoting a higher photochemical quantum yield and a more effective PSII restoration in darkness in the Antarctic rather than the Andean ecotype of *Colobanthus quitensis* kunt bartl (Caryophyllaceae). *BMC Plant Biol.* 12, 114. doi: 10.1186/1471-2229-12-114

Bates, L. S., Waldren, R. P., and Teare, I. D. (1973). Rapid determination of free proline for water-stress studies. *Plant Soil* 39, 205–207. doi: 10.1007/BF00018060

Ben, F. M., Zhani, K., Hannachi, C., Mehwachi, T., and Belanger, A. (2014). Effect of priming on growth, biochemical parameters and mineral composition of different cultivars of coriander (*Coriandrum sativum* l.) under salt stress. *J. Stress Physiol. Biochem.* 10, 84–109.

Biondi, S., Ruiz, K. B., Martinez, E. A., Zurita-Silva, A., Orsini, F., Antognoni, F., et al. (2015). *State of the art report on quinoa around the world in 2013*. Eds. D. Bazile, H. D. Bertero and C. Nieto (Santiago du Chili: FAO, CIRAD), 143–156.

Böhm, J., Messerer, M., Müller, H. M., Scholz-Starke, J., Gradogna, A., Scherzer, S., et al. (2018). Understanding the molecular basis of salt sequestration in epidermal bladder cells of *Chenopodium quinoa*. *Curr. Biol.* 8, 3075–3085.e7. doi: 10.1016/j.cub.2018.08.004

Bolton, M. D. (2009). Primary metabolism and plant defense–fuel for the fire. *Mol. Plant Microbe Interact.* 22, 487–497. doi: 10.1094/MPMI-22-5-0487

Botanga, C. J., Bethke, G., Chen, Z., Gallie, D. R., Fiehn, O., and Glazebrook, J. (2012). Metabolite profiling of arabidopsis inoculated with *Alternaria brassicicola* reveals that ascorbate reduces disease severity. *Mol. Plant Microbe In.* 25, 1628–1638. doi: 10.1094/MPMI-07-12-0179-R

Bouras, H., Choukr-Allah, R., Amouaouch, Y., Bouaziz, A., Devkota, K. P., El Mouttaqi, A., et al. (2022). How does quinoa (*Chenopodium quinoa* willd.) respond to phosphorus fertilization and irrigation water salinity? *Plants* 11, 216. doi: 10.3390/plants11020216

Bruce, T. J., Matthes, M. C., Napier, J. A., and Pickett, J. A. (2007). Stressful "memories" of plants: evidence and possible mechanisms. *Plant Sci.* 173, 603–608. doi: 10.1016/j.plantsci.2007.09.002

Busch, F. A. (2020). Photorespiration in the context of rubisco biochemistry, CO_2 diffusion and metabolism. *Plant J.* 101, 919–939. doi: 10.1111/tpj

Chen, X., Zhang, L., Miao, X., Hu, X., Nan, S., Wang, J., et al. (2018). Effect of salt stress on fatty acid and α-tocopherol metabolism in two desert shrub species. *Planta* 247, 499–511. doi: 10.1007/s00425-017-2803-8

Che-Othman, M. H., Jacoby, R. P., Millar, A. H., and Taylor, N. L. (2020). Wheat mitochondrial respiration shifts from the tricarboxylic acid cycle to the GABA shunt under salt stress. *New Phytol.* 225, 1166–1180. doi: 10.1111/nph.15713

Che-Othman, M. H., Millar, A. H., and Taylor, N. L. (2017). Connecting salt stress signaling pathways with salinity-induced changes in mitochondrial metabolic processes in C3 plants. *Plant Cell Environ.* 40, 2875–2905. doi: 10.1111/pce.13034

Daur, I. (2018). Effects of hydro and hormonal priming on quinoa (*Chenopodium quinoa* willd.) seed germination under salt and drought stress. *Pak. J. Bot.* 50, 1669–1673.

Delatorre-Herrera, J., and Pinto, M. (2009). Importance of ionic and osmotic components of salt stress on the germination of four quinua (*Chenopodium quinoa* willd.) selections. *Chil. J. Agr. Res.* 69, 477–485. doi: 10.4067/S0718-58392009000400001

Demidchik, V., Cuin, T. A., Svistunenko, D., Smith, S. J., Miller, A. J., Shabala, S., et al. (2010). Arabidopsis root k+-efflux conductance activated by hydroxyl radicals: single-channel properties, genetic basis and involvement in stress-induced cell death. *J. Cell Sci.* 123, 1468–1479. doi: 10.1242/jcs.064352

Demmig-Adams, B., and Adams, W. W. (1992). Photoprotection and other responses of plants to high light stress. *Annu. Rev. Plant Physiol. Plant Mol. Biol.* 43, 599–626. doi: 10.1146/annurev.pp.43.060192.003123

Derbali, W., Manaa, A., Spengler, B., Goussi, R., Abideen, Z., Ghezellou, P., et al. (2021). Comparative proteomic approach to study the salinity effect on the growth of two contrasting quinoa genotypes. *Plant Physiol. And Biochem.* 163, 215–229. doi: 10.1016/j.plaphy.2021.03.055

Dezfuli, P. M., Sharif-Zadeh, F., and Janmohammadi, M. (2008). Influence of priming techniques on seed germination behavior of maize inbred lines (*Zea mays* l.). *J. Agric. Biol. Sci.* 3, 22–25.

do Amaral, M. N., Auler, P. A., Rossatto, T., Barros, P. M., Oliveira, M. M., and Braga, E. J. B. (2020). Long-term somatic memory of salinity unveiled from physiological, biochemical and epigenetic responses in two contrasting rice genotypes. *Physiol. Plant* 170 (2), 248–268. doi: 10.1111/ppl.13149

FAO (2011) *The state of food insecurity in the world*. Available at: http://www.fao.org/docrep/014/i2330e/i2330e.pdf (Accessed 20 May 2020).

Fraire-Velázquez, S., and Balderas-Hernández, V. E. (2013). "Abiotic stress in plants and metabolic responses." in abiotic stress–plant responses and applications in agriculture. *InTech*. 25–48. doi: 10.5772/54859

Fuller, M. P., Hamza, J. H., Rihan, H. Z., and Al-Issawi, M. (2012). Germination of primed seed under NaCl stress in wheat. *ISRN Bot.*, 167801. doi: 10.5402/2012/167804

Ghiyasi, M., Seyahjani, A. A., Tajbakhsh, M., Amirnia, R., and Salehzadeh, H. (2008). Effect of osmopriming with polyethylene glycol, (8000) on germination and seedling growth of wheat (*Triticum aestivum* l.) seeds under salt stress. *Res. J. Biol. Sci.* 3, 1249–1251.

González, J. A., and Prado, F. E. (1992). Germination in relation to salinity and temperatura in *Chenopodium quinoa* (Willd.). *Agrochimica* 36, 101–107.

Gout, E., Aubert, S., Bligny, R., Rébeillé, F., Nonomura, A. R., Benson, A. A., et al. (2000). Metabolism of methanol in plant cells. carbon-13 nuclear magnetic resonance studies. *Plant Physiol.* 123, 287–296. doi: 10.1104/pp.123.1.287

Günther, J., Lackus, N. D., Schmidt, A., Huber, M., Stödtler, H. J., Reichelt, M., et al. (2019). Separate pathways contribute to the herbivore-induced formation of 2-phenylethanol in poplar. *Plant Physiol.* 180, 767–782. doi: 10.1104/pp.19.00059

Hernández, J. A., Ferrer, M. A., Jiménez, A., Barceló, A. R., and Sevilla, F. (2001). Antioxidant systems and O2.–/H2O2 production in the apoplast of pea leaves. its relation with salt-induced necrotic lesions in minor veins. *Plant Physiol.* 127, 817–831. doi: 10.1104/pp.010188

Hill, C. B., Jha, D., Bacic, A., Tester, M., and Roessner, U. (2013). Characterization of ion contents and metabolic responses to salt stress of different arabidopsis AtHKT1;1 genotypes and their parental strains. *Mol. Plant* 6, 350–368. doi: 10.1093/mp/sss125

Hirata, H., Ohnishi, T., and Watanabe, N. (2016). Biosynthesis of floral scent 2-phenylethanol in rose flowers. *Biosci. Biotech. Bioch.* 80, 1865–1873. doi: 10.1080/09168451.2016.1191333

Ibrahim, E. A. (2016). Seed priming to alleviate salinity stress in germinating seeds. *J. Plant Physiol.* 192, 38–46. doi: 10.1016/j.jplph.2015.12.011

Irsfeld, M., Spadafore, M., and Prüß, B. M. (2013). β-phenylethylamine, a small molecule with a large impact. *Webmedcentral* 4, 4409.

Jacobsen, S.-E., and Bach, A. P. (1998). The influence of temperature on seed germination rate in quinoa (*Chenopodium quinoa* willd.). *Seed Sci. Technol.* 26, 515–523.

Jacobsen, S.-E., and Stølen, O. (1993). Quinoa - morphology, phenology and prospects for its production as a new crop in Europe. *Eur. J. Agron.* 2, 19–29. doi: 10.1016/S1161-0301(14)80148-2

Jacobsen, S. E., Quispe, H., and Mujica, A. (1999). Quinoa: an alternative crop for saline soils in the Andes. Scientist and farmer-partners in research for the 21st century. *CIP Program Report* 2000, 403–408.

Jiménez-Becker, S., Ramírez, M., and Plaza, B. M. (2019). The influence of salinity on the vegetative growth, osmolytes and chloride concentration of four halophytic species. *J. Plant Nutr.* 42, 1838–1849. doi: 10.1080/01904167.2019.1648666

Kaya, M. D., Gamze, O., Atal, M., Yakup, M., and Ozer, K. (2006). Seed treatments to overcome salt and drought stress during germination in sunflower (*Helianthus annuus* l.). *Eur. J. Agron.* 24, 291–295. doi: 10.1016/j.eja.2005.08.001

Kazachkova, Y., Batushansky, A., Cisneros, A., Tel-Zur, N., Fait, A., and Barak, S. (2013). Growth platform-dependent and-independent phenotypic and metabolic responses of arabidopsis and its halophytic relative, eutrema salsugineum, to salt stress. *Plant Physiol.* 162, 1583–1598. doi: 10.1104/pp.113.217844

Krasensky, J., and Jonak, C. (2012). Drought, salt, and temperature stress-induced metabolic rearrangements and regulatory networks. *J. Exp. Bot.* 63, 1593–1608. doi: 10.1093/jxb/err460

Lichtenthaler, H. K., and Buschmann, C. (2001). Chlorophylls and carotenoids: Measurement and characterization by UV-VIS spectroscopy. *Curr. Protoc. Food Anal. Chem.* 1, F4.3.1–F4.3.8. doi: 10.1002/0471142913.faf0403s01

Liu, H., Able, A. J., and Able, J. A. (2022). Priming crops for the future: rewiring stress memory. *Trend. Plant Sci.* 27 (7): 699–716. doi: 10.1016/j.tplants.2021.11.015

Liu, X., Quan, W., and Bartels, D. (2022). Stress memory responses and seed priming correlate with drought tolerance in plants: An overview. *Planta* 255, 45. doi: 10.1007/s00425-022-03828-z

Locato, V., Cimini, S., and De Gara, L. (2018). ROS and redox balance as multifaceted players of cross-tolerance: Epigenetic and retrograde control of gene expression. *J. Exp. Bot.* 69, 3373–3391. doi: 10.1093/jxb/ery168

Mackinney, G. (1941). Absorption of light by chlorophyll solutions. *J. Biol. Chem.* 140, 315–322. doi: 10.1016/S0021-9258(18)51320-X

Maleki, P., Bahrami, H. A., Saadat, S., Sharifi, F., Dehghany, F., and Salehi, M. (2018). Salinity threshold value of quinoa (*Chenopodium quinoa* Willd.) at various growth stages and the appropriate irrigation method by saline water. *Commun. Soil Sci. Plan.* 49, 1815–1825. doi: 10.1080/00103624.2018.1474917

Mamedi, A., Sharifzadeh, F., Maali-Amiri, R., Divargar, F., and Rasoulnia, A. (2022). Seed osmopriming with Ca2+ and k+ improves salt tolerance in quinoa

seeds and seedlings by amplifying antioxidant defense and ameliorating the osmotic adjustment process. *Physiol. Mol. Biol. Plants.* 1, 251–274. doi: 10.1007/s12298-022-01125-3

Manonmani, V., Ameer Junaithal Begum, M., and Jayanthi, M. (2014). Halo priming of seeds. *Res. J. Seed Sci.* 7, 1–13. doi: 10.3923/rjss.2014.1.13

Maswada, H. F., and Abd El-Kader, N. I. K. (2016). Redox halopriming: a promising strategy for inducing salt tolerance in bread wheat. *J. Agron. Crop Sci.* 202, 37–50. doi: 10.1111/jac.12123

Maxwell, K., and Johnson, G. N. (2000). Chlorophyll fluorescence a practical guide. *J. Exp. Bot.* 51, 659–668. doi: 10.1093/jexbot/51.345.659

McCready, R. M., Guggolz, J., Silviera, V., and Owens, H. S. (1950). Determination of starch and amylose in vegetables. *Anal. Chem.* 22, 1156–1158. doi: 10.1021/ac60045a016

Miranda-Apodaca, J., Agirresarobe, A., Martínez-Goñi, X. S., Yoldi-Achalandabaso, A., and Pérez-López, U. (2020). N metabolism performance in *Chenopodium quinoa* subjected to drought or salt stress conditions. *Plant Physiol. Biochem.* 155, 725–734. doi: 10.1016/j.plaphy.2020.08.007

Moreno, C., Seal, C. E., and Papenbrock, J. (2018). Seed priming improves germination in saline conditions for *Chenopodium quinoa* and *Amaranthus caudatus*. *J. Agro. Crop Sci.* 204, 40–48. doi: 10.1111/jac.12242

Navarro, J. M., Botella, M. A., Cerdá, A., and Martinez, V. (2001). Phosphorus uptake and translocation in salt-stressed melon plants. *J. Plant Physiol.* 158, 375–381. doi: 10.1078/0176-1617-00147

Nishizawa, A., Yabuta, Y., and Shigeoka, S. (2008). Galactinol and raffinose constitute a novel function to protect plants from oxidative damage. *Plant Physiol.* 147, 1251–1263. doi: 10.1104/pp.108.122465

Ortega-Villasante, C., Rellán-Álvarez, R., Del Campo, F. F., Carpena-Ruiz, R. O., and Hernández, L. E. (2005). Cellular damage induced by cadmium and mercury in *Medicago sativa*. *J. Exp. Bot.* 56, 2239–2251. doi: 10.1093/jxb/eri223

Paparella, S., Araújo, S. S., Rossi, G., Wijayasinghe, M., Carbonera, D., and Balestrazzi, A. (2015). Seed priming: state of the art and new pespectives. *Plant Cell Rep.* 34, 1281–1293. doi: 10.1007/s00299-015-1784-y

Raj, A. B., and Raj, S. K. (2019). Seed priming: An approach towards agricultural sustainability. *J. Appl. Nat. Sci.* 11, 227–234. doi: 10.31018/jans.v11i1.2010

Ranal, M. A., and Santana, D. G. D. (2006). How and why to measure the germination process? *Braz. J. Bot.* 29, 1–11. doi: 10.1590/S0100-84042006000100002

Razzaghi, F., Ahmadi, S. H., Adolf, V. I., Jensen, C. R., Jacobsen, S. E., and Andersen, M. N. (2011). Water relations and transpiration of quinoa (*Chenopodium quinoa* willd.) under salinity and soil drying. *J. Agron. Crop Sci.* 197, 348–360. doi: 10.1111/j.1439-037X.2011.00473.x

Reid, M. A., Dai, Z., and Locasale, J. W. (2017). The impact of cellular metabolism on chromatin dynamics and epigenetics. *Nat. Cell Biol.* 19, 1298–1306. doi: 10.1038/ncb3629

Rose, R., Rose, C. L., Omi, S. K., Forry, K. R., Durall, D. M., and Bigg, W. L. (1991). Starch determination by perchloric acid vs enzymes: Evaluating the accuracy and precision of six colorimetric methods. *J. Agr. Food Chem.* 39, 2–11. doi: 10.1021/jf00001a001

Ruffino, A. M. C., Rosa, M., Hilal, M., González, J. A., and Prado, F. E. (2010). The role of cotyledon metabolism in the establishment of quinoa (*Chenopodium quinoa*) seedlings growing under salinity. *Plant Soil* 326, 213–224. doi: 10.1007/s11104-009-9999-8

Ruiz, K. B., Aloisi, I., Del Duca, S., Canelo, V., Torrigiani, P., Silva, H., et al. (2016). Salares versus coastal ecotypes of quinoa: Salinity responses in Chilean landraces from contrasting habitats. *Plant Physiol. Bioch.* 101, 1–13. doi: 10.1016/j.plaphy.2016.01.010

Ruiz-Carrasco, K., Antognoni, F., Coulibaly, A. K., Lizardi, S., Covarrubias, A., Martínez, E. A., et al. (2011). Variation in salinity tolerance of four lowland genotypes of quinoa (*Chenopodium quinoa* willd.) as assessed by growth, physiological traits, and sodium transporter gene expression. *Plant Physiol. Biol.* 49, 1333–1341. doi: 10.1016/j.plaphy.2011.08.005

Ruiz, K. B., Maldonado, J., Biondi, S., and Silva, H. (2019). RNA-Seq analysis of salt-stressed versus non salt-stressed transcriptomes of *Chenopodium quinoa* landrace R49. *Genes* 10, 1042. doi: 10.3390/genes10121042

Ruiz, K. B., Rapparini, F., Bertazza, G., Silva, H., Torrigiani, P., and Biondi, S. (2017). Comparing salt-induced responses at the transcript level in a salares and coastal-lowland landrace of quinoa (*Chenopodium quinoa* willd). *Environ. Exp. Bot.* 139, 127–142. doi: 10.1016/j.envexpbot.2017.05.003

Saddiq, M. S., Iqbal, S., Afzal, I., Ibrahim, A. M. H., Bakhtavar, M. A., Hafeez, M. B., et al. (2019). Mitigation of salinity stress in wheat (*Triticum aestivum* l.) seedlings through physiological seed enhancements. *J. Plant Nutr.* 42, 1192–1204. doi: 10.1080/01904167.2019.1609509

Sadiq, M., Akram, N. A., Ashraf, M., Al-Qurainy, F., and Ahmad, P. (2019). Alpha-Tocopherol-Induced regulation of growth and metabolism in plants under non-stress and stress conditions. *J. Plant Growth Regul.* 38, 1325–1340. doi: 10.1007/s00344-019-09936-7

Schwachtje, J., and Baldwin, I. T. (2008). Why does herbivore attack reconfigure primary metabolism? *Plant Physiol.* 146, 845–851. doi: 10.1104/pp.107.112490

Schwachtje, J., Whitcomb, S. J., Firmino, A. A. P., Zuther, E., Hincha, D. K., and Kopka, J. (2019). Induced, imprinted, and primed responses to changing environments: Does metabolism store and process information? *Front. Plant Sci.* 10. doi: 10.3389/fpls.2019.00106

Scott, S. J., Jones, R. A., and Williams, W. (1984). Review of data analysis methods for seed germination. *Crop Sci.* 24, 1192–1199. doi: 10.2135/cropsci1984.0011183X002400060043x

Shabala, S., Bose, J., and Hedrich, R. (2014). Salt bladders: Do they matter? *Trends Plant Sci.* 19, 687–691. doi: 10.1016/j.tplants.2014.09.001

Shi, P., and Gu, M. (2020). Transcriptome analysis and differential gene expression profiling of two contrasting quinoa genotypes in response to salt stress. *BMC Plant Biol.* 20, 568. doi: 10.1186/s12870-020-02753-1

Shrivastava, P., and Kumar, R. (2015). Soil salinity: A serious environmental issue and plant growth promoting bacteria as one of the tools for its alleviation. *Saudi J. Biol. Sci.* 22, 123–131. doi: 10.1016/j.sjbs.2014.12.001

Smirnoff, N. (1993). The role of active oxygen in the response of plants to water deficit and desiccation. *New Phytol.* 125, 27–58. doi: 10.1111/j.1469-8137.1993.tb03863.x

Stephan, A. B., Kunz, H. H., Yang, E., and Schroeder, J. I. (2016). Rapid hyperosmotic-induced Ca2+ responses in arabidopsis thaliana exhibit sensory potentiation and involvement of plastidial KEA transporters. *P. Natl. Acad. Sci. U.S.A.* 113, E5242–E5249. doi: 10.1073/pnas.1519555113

Szarka, A., Tomasskovics, B., and Bánhegyi, G. (2012). The ascorbate-glutathione-α-tocopherol triad in abiotic stress response. *Int. J. Mol. Sci.* 13, 4458–4483. doi: 10.3390/ijms13044458

Tahjib-Ul-Arif, M., Zahan, M. I., Karim, M. M., Imran, S., Hunter, C. T., Islam, M. S., et al. (2021). Citric acid-mediated abiotic stress tolerance in plants. *Int. J. Mol. Sci.* 22, 7235. doi: 10.3390/ijms22137235

Tieman, D., Taylor, M., Schauer, N., Fernie, A. R., Hanson, A. D., and Klee, H. J. (2006). Tomato aromatic amino acid decarboxylases participate in synthesis of the flavor volatiles 2-phenylethanol and 2-phenylacetaldehyde. *Proc. Natl. Acad. Sci. U. S. A.* 103, 8287–8292. doi: 10.1073/pnas.0602469103

Tohge, T., Watanabe, M., Hoefgen, R., and Fernie, A. R. (2013). Shikimate and phenylalanine biosynthesis in the green lineage. *Front. Plant Sci.* 4. doi: 10.3389/fpls.2013.00062

Tsujii, M., Kera, K., Hamamoto, S., Kuromori, T., Shikanai, T., and Uozumi, M. (2019). Evidence for potassium transport activity of arabidopsis KEA1-KEA6. *Sci. Rep.* 9, 10040. doi: 10.1038/s41598-019-46463-7

Xia, J., Sinelnikov, I. V., Han, B., and Wishart, D. S. (2015). MetaboAnalyst 3.0–making metabolomics more meaningful. *Nucleic Acids Res.* 43, W251–W257. doi: 10.1093/nar/gkv380

Yang, A., Akhtar, S. S., Iqbal, S., Qi, Z., Alandia, G., Saddiq, M. S., et al. (2018). Saponin seed priming improves salt tolerance in quinoa. *J. Agro. Crop Sci.* 20431–39. doi: 10.1111/jac.12229

Zhang, Q., Song, X., and Bartels, D. (2018). Sugar metabolism in the desiccation tolerant grass *Oropetium thomaeum* in response to environmental stresses. *Plant Sci.* 270, 30–36. doi: 10.1016/j.plantsci.2018.02.004

frontiers | Frontiers in Plant Science

TYPE Original Research
PUBLISHED 17 February 2023
DOI 10.3389/fpls.2023.1065604

Check for updates

OPEN ACCESS

EDITED BY
Ji-Hong Liu,
Huazhong Agricultural University, China

REVIEWED BY
Honghai Luo,
Shihezi University, China
Wenqing Zhao,
Nanjing Agricultural University, China
Ritesh Kumar,
Boyce Thompson Institute (BTI),
United States

†These authors have contributed equally to this work

*CORRESPONDENCE
Dong Jiang
jiangd@njau.edu.cn
Cunxiang Wu
wucunxiang@caas.cn

SPECIALTY SECTION
This article was submitted to Plant Abiotic Stress, a section of the journal Frontiers in Plant Science

RECEIVED 10 October 2022
ACCEPTED 01 February 2023
PUBLISHED 17 February 2023

CITATION
Yang L, Song W, Xu C, Sapey E, Jiang D and Wu C (2023) Effects of high night temperature on soybean yield and compositions.
Front. Plant Sci. 14:1065604.
doi: 10.3389/fpls.2023.1065604

COPYRIGHT
© 2023 Yang, Song, Xu, Sapey, Jiang and Wu. This is an open-access article distributed under the terms of the Creative Commons Attribution License (CC BY). The use, distribution or reproduction in other forums is permitted, provided the original author(s) and the copyright owner(s) are credited and that the original publication in this journal is cited, in accordance with accepted academic practice. No use, distribution or reproduction is permitted which does not comply with these terms.

Effects of high night temperature on soybean yield and compositions

Lin Yang[1,2†], Wenwen Song[2†], Cailong Xu[2], Enoch Sapey[2,3], Dong Jiang[1*] and Cunxiang Wu[2*]

[1]Key Laboratory of Crop Physiology and Ecology in Southern China, Ministry of Agriculture, Nanjing Agricultural University, Nanjing, China, [2]Ministry of Agriculture and Rural Affairs Key Laboratory of Soybean Biology (Beijing), Institute of Crop Sciences, Chinese Academy of Agricultural Sciences, Beijing, China, [3]Council for Scientific and Industrial Research (CSIR), Oil Palm Research Institute, Kade, Ghana

Introduction: Soybean is sensitive to light and temperature. Under the background of global asymmetric climate warming.

Methods: The increase of night temperature may have an important impact on soybean yield. In this study, three varieties with different level of protein were planted under 18°C and 28°C night temperatures for investigating the effects of high night temperatures on soybean yield formation and the dynamic changes of non-structural carbohydrates (NSC) during the seed filling period (R5-R7).

Results and discussion: The results indicated that high night temperatures resulted in smaller seed size, lower seed weight, and a reduced number of effective pods and seeds per plant, and thus, a significant reduction in yield per plant. Analysis of the seed composition variations showed carbohydrates were more substantially affected by high night temperature than protein and oil. We observed "carbon hunger" caused by high night temperature increased photosynthesis and sucrose accumulation in the leaves during the early stage of high night temperature treatment. With elongated treated time, the excessive carbon consumption led to the decrease of sucrose accumulation in soybean seeds. Transcriptome analysis of leaves after 7 days of treatment showed that the expression of most sucrose synthase and sucrose phosphatase genes decreased significantly under the high night temperature. Which could be another important reason for the decrease of sucrose. These findings provided a theoretical basis for enhancing the tolerance of soybean to high night temperature.

KEYWORDS

high night temperature, soybean, yield, carbohydrates, transcriptome

1 Introduction

Soybean (*Glycine max*) is one of the most important food crops. One of the major compositions in soybean seeds is protein, which is necessary for human nutrition; soy is also a valuable source of edible oil (Medic et al., 2014). During the developmental stage, soybeans are often at risk of high temperature stress. The Intergovernmental Panel on Climate Change (IPCC) reports that future climate change will expose crops to heightened average

temperatures and increase the frequency of short-term high temperatures (Solomon, 2008). High temperature causes significant agricultural losses, affects nutrient cycling in many crops, and leads to substantial yield decline (Asseng et al., 2014, Schauberger et al., 2017; Zhao et al., 2017). When soybeans suffer high temperatures during the seed filling stage, their yields are reduced and their seed compositions changed (Medic et al., 2014; Song et al., 2016; Nakagawa et al., 2020). For legumes such as faba beans, various genetic approaches have been used to breed for heat stress tolerance varieties (Lavania et al., 2015; Lavania et al., 2016). Global climate model projections indicate that nighttime warming rises more rapidly than daytime warming and is the primary driver of global warming (Davy et al., 2016), reducing diurnal temperature differences (Vose et al., 2005). A study by our research group found that the diurnal temperature difference had a greater effect on soybean protein and oil contents relative to the average daily temperature, suggesting that night temperature plays an important role in soybean protein and oil accumulation (Song et al., 2016). Therefore, studying the effects of nighttime warming on soybean growth and yield will provide a theoretical basis for developing future food security strategies in China.

Several studies have confirmed the effects of temperature on soybean seed growth in different developmental stages, duration of high temperature treatments, and intensities of temperatures (Gibson, 1992; Tacarindua et al., 2013; Nakagawa et al., 2020). The impact of high temperatures on soybean yield and quality has been studied using open-enclosure facilities, controlled artificial climate chambers, or crop models based on historical data (Gibson, 1992; Tacarindua et al., 2013; Nakagawa et al., 2020). A negative correlation between soybean yield and seasonal warming has been discovered (Kucharik and Serbin, 2008). For every 1°C increase, soybean yield decreases by an average of 17% (Lobell and Asner, 2003). The high temperature associated with damage to soybean growth and development took place in controlled chambers and greenhouses (Gibson, 1992; Tacarindua et al., 2013; Nakagawa et al., 2020). Some studies reported a decrease in yield at high temperatures in the soybean seed filling stage (Gibson and Mullen, 1996; Siebers et al., 2015). It was observed that high temperature stress experienced during mid-reproductive growth is more detrimental to seed yield and seed size than that experienced during early or late reproductive development stage (Puteh et al., 2013). Extreme heat or heat stress can cause irreversible damage to soybean growth and development, and can even cause death (Feng et al., 2020). The moderately high temperatures are more likely to lead to morphological, structural, physiological, and biochemical changes in the thermal adaptation to warming conditions (Puteh et al., 2013). It was found that moderate high night temperature of 29°C reduced photosynthetic rates and pollen germination, resulting in decreased pod numbers and seed weight (Djanaguiraman et al., 2013). However, the effect of high night temperature, seed's C and N accumulation, and corresponding underlying mechanisms in soybeans remains unclear.

It has been suggested that high night temperature stimulate carbohydrate usage (Loka and Oosterhuis, 2010). The yield decline is mainly due to a reduction in the biomass allocated to the coffers and a decrease in the content of dry matter and its synthetics. Losses caused by high night temperature are usually accompanied by a decline in biomass accumulation (Zhang et al., 2013; Jing et al., 2016). Daytime is a crucial period for photosynthesis in soybeans; at night, the plants turn into mere consumers of the bioproducts of photosynthesis, which accumulate during the day (Xu et al., 2021). Many studies have confirmed that respiration rates of many crops such as rice (Alvarado-Sanabria et al., 2017), wheat and barley (García et al., 2015), maize (Kucharik and Serbin, 2008), and cotton (Loka and Oosterhuis, 2010) increase at high night temperature. The same result was also reported for soybeans (Bunce, 2005; Djanaguiraman et al., 2013; Lin et al., 2021). As plants enhance nocturnal respiration (Rn), more photosynthetic bioproducts are consumed, thereby reducing the sugar reserves available for seed filling (Xu et al., 2021), night temperatures of 10°C above ambient lead to a 2.6-fold enhancement in rapid nocturnal respiration. However, the response diminishes after thermal acclimation and causes yield loss (Peraudeau et al., 2015). It was reported that the high night temperature resulted in the higher Rn and decline of the yield in soybean by 4.6% per °C (Lin et al., 2021). Another study found that various soybean varieties showed different level of tolerance to high temperature, only a few varieties showed decrease yield under high night temperature (Shu, 2021). One study has also observed that high night temperature causes many environmental variables and that respiration has no effect on yield or biomass (Frantz et al., 2004).

Non-structural carbohydrates in leaves, such as sucrose and starch, represent the state of photosynthesis in the leaf, provide whole-plant energy, and contribute to the accumulation of structural carbohydrates (Hussain et al., 2019; Stitt et al., 1987). Leaf senescence may affect crop yield in two different ways. On one hand, delayed leaf senescence can increase yield by prolonging photosynthesis and extending seed filling period; On the other hand, delayed leaf senescence may affect nutrient reuse to the sink organ, which may harm yield (Guo et al., 2021). Sucrose is the main source of carbon energy for developing seeds and sucrose transport is the central system of carbon resource allocation for the whole plant (Ruan, 2014; Petridis et al., 2020; Zhang et al., 2016). It has been reported that sucrose content decreases with the increase in temperature (Loka and Oosterhuis, 2010). Studies have shown proteomic changes in different tissues like leaves and anthers of plants at high temperatures, as well as differential expression of proteins related to various physiological processes, such as carbohydrate metabolism (Das et al., 2015; Kumar et al., 2022; Zhou et al., 2017). The balance between sucrose synthesis and catabolism in leaves is mediated by influencing the activity of sucrose synthase (SS) and sucrose phosphate synthase (SPS), two key enzymes that also control the biosynthesis of carbon into starch (Stitt and Zeeman, 2012) However, few researchers have studied the effect of night temperature on the biosynthesis of leaf sucrose.

Currently, RNA-seq technology is widely used in temperature regulation studies in plants (Gillman et al., 2019; Shu et al., 2020). RNA-Seq analysis of whole wheat kernels showed that high temperature induced down-regulation of genes involved in regulating pericarp cell wall expansion (Kino et al., 2020). This down-regulation coincided with a reduction in total grain water content and weight after the same treatment period, supporting the theory that high temperature may lead to a reduction in mature grain weight (Kino et al., 2020). Proteins like heat shock proteins also known to play a key role in leguminous plants like *Vicia faba* and

other plants under heat stress (Kumar et al., 2015; Kumar et al., 2016; Kumar et al., 2020; Tiwari et al., 2021).

The aims of the study were (i) to evaluate the effect of high night temperature during the seed filling stage on the yield and seed compositions, (ii) to discover the dynamic changes of photosynthetic physiological characteristics, dry matter accumulation and NSC linked to stress tolerance triggered by high night temperature, and (iii) to analyze the molecular basis of changes in the leaves, specifically sugar metabolism.

2 Materials and methods

2.1 Experimental site and materials

The experiment was conducted for two years (2020-2021) at the Photothermal Control Complex at Changping Experimental Station (Beijing, 40°18′ N,116°25′ E), Institute of Crop Sciences, Chinese Academy of Agricultural Sciences.

The high-protein variety Zhonghuang 39 (ZH39), medium-protein variety Zheng 1307 (Z1307), and low-protein variety Zhonghuang 76 (ZH76), which have the same growth period traits (belonging to MG III, with similar flowering time and growth period), were selected as experimental materials. All the materials were planted in pots with dimensions of 18.5 cm in height and 18 cm in diameter and filled with 10 kg of soil. Ten seeds were sown in each pot on June 24th, and the plants were thinned to five healthy and uniform plants in each pot after emergence. All the plants were grown to the beginning of seed stage (R5) under natural light and temperature conditions, and good agronomic practices were carried out. From the stage of R5 to R7 (physiological maturity), the materials were treated with different night temperature.

2.2 Experimental design and management

Four temperature-controlled chambers (6m×3m×2.5m) were used to study the impact of high night temperature. According to the average daily and nightly temperatures (28°C and 18°C) and the sunlight duration (12.5 h) during seed filling stage (September) in Beijing, all the plants were exposed to 18°C or 28°C night temperature with a natural day temperature and 12-h light (7 pm - 7 am) treatment. Each night temperature treatment corresponded to a chamber installed with two platform trailers, and the pots were placed on the trailers during the experimental period. During the day time, the trailers were pushed outside the chambers, and all the plants grew under the natural light and day temperature, and at night they were pushed into the chambers with different temperature treatment.

Temperature and humidity data were recorded every 30 min from the seed filling stage to the maturity stage using a temperature and humidity recorder (OM-EL-WIFI-TH, OMEGA Engineering, USA). The temperature changes during the treatment period (R5-R7) are shown in Figure S1. The average night temperature of 18 °C treatment during the period in 2020 was 18.06 °C, with a minimum of 17.36 °C and a maximum of 21.52 °C. The average temperature of the 28 °C treatment was 27.16 °C, with a minimum of 25.21 °C and a maximum of 28.79 °C. During the treatment period in 2021, the average temperature of the 18 °C treatment temperature was 18.29°C, with a minimum of 17.36°C and a maximum of 21.52°C. The average temperature of 28°C treatment was 27.53°C, with a minimum of 25.21°C and a maximum of 28.79°C. Any observed differences were acceptable for the single-night temperature control, and the differences between temperature treatments remained constant, making the two years of experimental condition control reliable.

2.3 Seed size

We randomly selected pods grown in similar positions for sampling and analysis. We peeled and photographed the seeds after they reached maturity. Vernier calipers were used as a scale, and LED light was used to remove the soybean seeds' shadows, in order to get as clear an image as possible. Each seed's basic dimensions and thickness were measured using a standard vernier caliper (Baek et al., 2020). Each measurement was repeated five times.

2.4 Dry matter, sucrose and starch content

Three plants were cut at the cotyledon scars so that aboveground parts could be extracted every 7 days at 9 am - 11 am. Different organs of the plants were separated and placed in an oven at 105°C for 30 minutes for dehydration, then dried at 70°C to constant mass, and weighed. Keming Sucrose Content Test Kit (ZHT-1-Y, Keming, China) and Keming Starch Content Test Kit (DF-1-Y, Keming, China) were used for sucrose and starch content determinations. Each sample was analyzed five times.

2.5 Net photosynthesis and SPAD

The net photosynthetic rate of leaves was measured at the same time using a Li-6400 portable photosynthesizer (LI-COR 6400, Lincoln, USA) with the following parameters set: light quantum flux at 1200 umol/(m^2·s), CO_2 concentration at 450 umol/m^2, flow rate at 500 umol/s, and temperature at 25°C. Ten plants were measured during each treatment. The leaf chlorophyll content, denoted by the SPAD value, was measured on a SPAD meter (Chlorophyll Meter Model SPAD-502, Konica Minolta Inc, Japan) every 7 days at 9-11 am after different night temperature treatments (Ergo et al., 2018).

2.6 Agronomic traits

Ten mature plants were taken to investigate yield-related agronomic traits (plant height, number of nodes, number of pods per plant, number of seeds per plant, and 100-seed weight) for each treatment. Protein and oil contents of seeds were determined using near-infrared spectroscopy NIR (MPA, Bruker Optics, Germany), and the sum of protein and oil content were calculated. Any remaining fractions (primarily carbohydrates) were labeled 'residual' (Tamagno et al., 2022).

2.7 RNA-seq (transcriptome) and data analysis

The middle leaves of the third ternately compound leaves from the top of ZH39 at 7 DAT (about 30 days after flowering and 77 days after planting) were collected and flash-frozen with liquid nitrogen, and stored at -80°C freezer for transcriptome analysis. For each treatment, three leaves were sampled and pooled as one biological replicate, and three biological replicates were used. According to the method described by Metware Biotechnology Co. Ltd. (Wuhan, China), total RNA was extracted using RNAprep Pure Plant Plus Kit (DP441, Tiangen, China) according to its protocol. Before library construction, the RNA quality was assessed using the NanoPhotometer spectrophotometer (IMPLEN, CA, USA), Qubit 2.0 Fluorometer (Life Technologies, CA, USA), and Agilent Bioanalyzer 2100 system (Agilent Technologies, CA, USA). Then cluster generation, the library preparations were sent to the llumina Novaseq6000 system for sequencing. Clean data (clean reads) were obtained by removing reads with adapter reads containing ploy-N and low quality reads from raw data. Gene expression levels were determined using the fragments per kilobase of transcript per million reads (FPKM) to compare among different samples. The thresholds for differentially expressed genes (DEGs) were defined by $p < 0.05$ and $\log_2$ fold ≥ 1 or ≤ -1.

The RNA-seq reads used for this study were deposited at the National Center for Biotechnology Information under project SUB12180172, and the accession number was SAMN31361599-31361604.

2.8 Data analysis

Data were entered using Excel 2019 software (Microsoft Corporation, USA) and plotted using Graphpad 8.0.2 (San Diego, USA) and Rstudio 4.20 (R team 2021, USA). Analysis of variance (ANOVA) was done using DPS 7.05 statistical software (Data Processing System, China). Duncan's multiple comparisons tested the significant differences between means ($P < 0.05$). Other statistical analyses were performed using SPSS 22.0 software (IBM, USA).

3 Results and analysis

3.1 Seed yield and yield components

High night temperature induced significantly ($P < 0.01$) lower yield in all the three varieties compared (Table 1) in 2020 and 2021. In 2020, the yield of ZH39 decreased the most by 33.69%, while the yield of ZH76 dropped the most by 45.45% in 2021. It was shown that the

TABLE 1 Effects of different high night temperature on yield and components of soybean.

Year	Cultivars	Treatment (°C)	Effective pods number per plant	Seed number per plant	100-seed weight (g)	Yield(g/plant)
2020	Z1307	18	26.67±0.33aA	62.00±1.73aA	16.31±0.06aA	8.41±0.21aA
		28	21.00±1.73bA	28.33±1.45bB	15.40±0.17bB	7.32±0.29bA
	ZH39	18	16.00±0.58aA	41.67±2.33aA	21.98±0.10aA	8.40±0.57aA
		28	10.33±1.86bA	32.67±0.88bA	19.04±0.13bB	5.57±0.35bA
	ZH76	18	22.00±1.53aA	47.33±5.24aA	18.86±0.16aA	7.97±0.35aA
		28	15.33±0.67bA	25.00±1.00bA	17.79±0.07bB	5.96±0.07bB
2021	Z1307	18	34.00±1.00aA	65.67±2.73aA	15.92±0.09aA	9.28±0.29aA
		28	21.33±0.33bB	31.33±4.81bB	13.45±0.07bB	6.12±0.28bB
	ZH39	18	20.33±0.88aA	42.67±2.19aA	22.24±0.11aA	8.09±0.03aA
		28	17.00±0.58bA	22.67±1.20bB	19.69±0.76bA	6.61±0.21bB
	ZH76	18	26.67±1.86aA	55.33±5.67aA	18.40±0.42aA	6.93±0.19aA
		28	20.67±0.33bA	18.00±0.58bB	15.14±0.53bB	3.78±0.28bB
F-value						
Year(Y)			53.21**	NS	18.02**	7.63**
Cultivar(C)			75.24**	18.55**	316.34**	31.38**
Treatment(T)			103.60**	225.18**	152.11**	183.77**
Y*C			NS	NS	11.95**	12.24**
Y*T			NS	6.52*	9.97**	NS
C*T			4.29*	11.61**	NS	NS
Y*C*T			4.81*	NS	4.78*	9.10**

*, ** represent the test significant at the 5% level (P < 0.05) and 1% level (P < 0.01), respectively; NS, test non-significant at the 5% level.

yield components of number of pods per plant, seed number per plant, 100-seed weight, and seed yield per plant completely dropped in various degree under high night temperature condition. The interaction between year and variety effected the 100-seed weight and yield significantly. The interaction between year and treatment showed significant differences in the number of seeds per plant. The interaction of variety and treatment showed significant differences in effective pod number per plant and highly significant differences in seed number per plant. The year, variety, and treatment interaction showed significant differences in effective pods per plant, 100-seed weight, and yield.

3.2 Seed compositions

The protein, oil, and residue contents in soybean seeds were affected in various degree by the high night temperature in three varieties (Figure 1). Under high night temperature, the protein content of ZH76 significantly increased in 2020 (3.69%) and 2021 (7.87%), as well as ZH39 (3.95%) in 2021. However, the protein content of Z1307 showed insignificant change under high night temperature condition in both growing seasons. The oil content of ZH76 significantly increased in 2020 (5.59%) and 2021 (2.31%), as well as Z1307 (6.21%) in 2021 under high night temperature. While, the oil content of ZH39 showed insignificant change in both two years. For the total protein plus oil, ZH76 and ZH39 showed a significant increase average by 5.07% and 3.72% in 2020 and 2021 under the high night temperature, while non-significant difference was found in Z1307 between the treatments. The residual content in ZH39 and ZH76 significant decreased by 5.69% and 6.97% on average under high night temperature condition, respectively. However, the residual content of Z1307 showed non-significant change under high night temperature in both two years.

3.3 Dry matter accumulation

The aboveground dry matter accumulation of the three varieties showed the same trend of increasing during the 14 DAT and then decreased (Figures 2A-C). The peak of aboveground dry matter accumulation appeared at 21 DAT for the 18°C night temperature treatment and 14 DAT for the 28°C night temperature (Figures 2D-F). The seed yield per plant of ZH39 was higher under high night temperature before 21 DAT at 28°C night temperature treatment, and it was lower after 21 DAT. For Z1307 and ZH76, the seed yield per plant was consistently lower at 28°C night temperature comparing with 18°C night temperature. No significant differences in the pod ratio were found among the treatments in the three varieties (Figures 2G-I).

3.4 Seed size

High night temperature had a detrimental effect on seed size in the three varieties (Figure 3 and Figure S2). Generally, the length, width and diameter of seeds showed a significant decrease under high night temperature in the two years (Table 2). Among the traits, the length of the seed was mostly affected. The length of Z1307 was reduced by 12.8% and 9.4% in 2020 and 2021, and it was reduced by 11.3% and 16.1% in ZH76. The seed of ZH39 also showed a slight decrease in the length. The seed-length-to-width ratio did not change significantly between the two treatments.

3.5 Photosynthetic characteristics

There was no change of the SPAD value in both varieties until 28 DAT in the three varieties, while it was obviously raised under 28°C night temperature treatment at 35 DAT, indicating that high night temperature induced slight green-stay of the leaves (Figures 4A-C). The high night

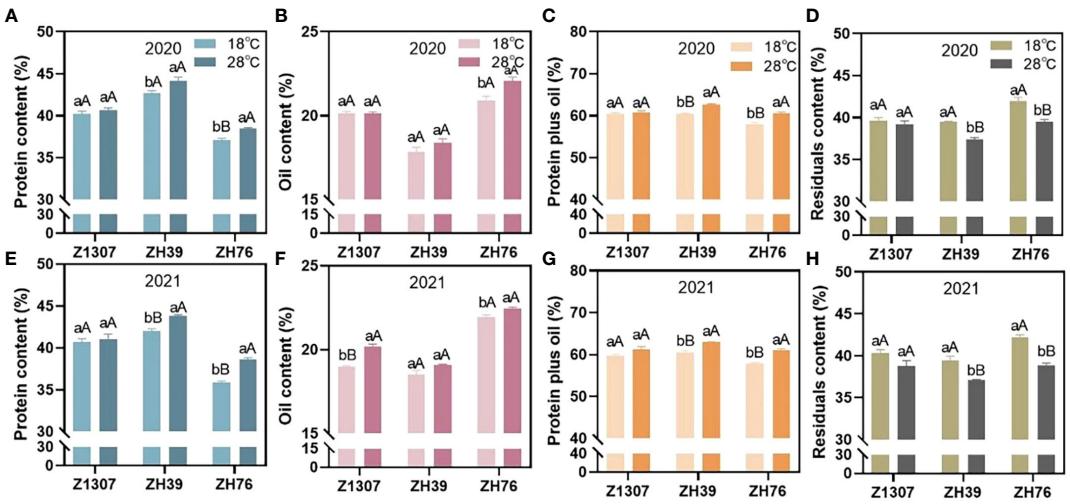


FIGURE 1
Effect of high night temperature on protein, oil, protein plus oil and residual contents in mature soybean seeds. The soybean seed protein (A-2020, E-2021), oil (B-2020, F-2021), protein plus oil content (C-2020, G-2021) and residual (D-2020, H-2021) contents of the three varieties Z1307, ZH39 and ZH76 under 18°C and 28°C night temperature during seed-filling stage were showed in the figure. The different letters indicate significant difference at 0.05 level (small letter) and 0.01 level (big letter).

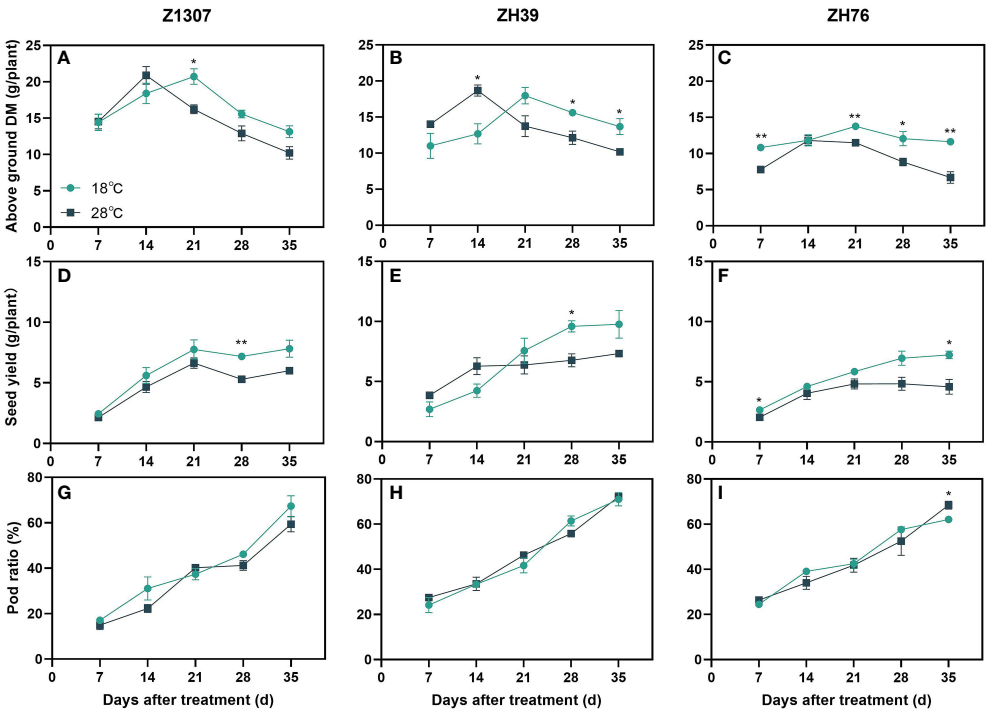


FIGURE 2
Effects of high night temperature on total dry matter(DM), seed yield and pod ratio. The light blue /dark blue line indicates the 18 ℃/28 ℃ treatment. DM means dry matter. The broken lines respect the dynamic changes of soybean above ground DM **(A-C)**, seed yield **(D-F)** and pod ratio **(G-I)** with the days of different high night temperature treatments for the three varieties of Z1307, ZH39 and ZH76. Values shown are means ± SE from three biological replicates. (*,$P < 0.05$; **, $P < 0.01$).

temperature significantly improved the net photosynthetic rate of leaves before 14 DAT (Figures 4D-F), while it was decreased gradually after 14 DAT in the three varieties. No significant difference in the net photosynthetic rate between the two treatments during 21 and 28 DAT in both varieties. In addition, no significant difference in net photosynthetic rate was found between the two treatments at 35 DAT in Z1307 and ZH39, while it was significantly increased in ZH76 at 35 DAT.

3.6 Sucrose and starch content

The dynamic change pattern of sucrose in stem and seed was similar under different night treatments for the three varieties, however, it was obviously different in leaf (Figure 5). The sucrose content in leaf was significantly higher before 14 DAT, while decreased rapidly during 14-21 DAT. The sucrose content in stem and seed of 28°C night temperature treatment was always lower than 18°C treatment. The three varieties showed the same trend, but the period of difference was not consistent.

Leaf starch content in the elevated night temperature treatment was significantly higher in ZH39 and ZH76 at 7 DAT, and it showed no difference in Z1307 (Figure 6). For the three varieties, leaf starch content changed non-significantly after 14 DAT. Under the 28°C night temperature, stem starch content peaked at 21 DAT and then decreased, with significant differences in Z1307 and ZH39 varieties and no difference in ZH76. High night temperature improved the starch accumulation in the seed, with significant differences in Z1307 and ZH39 at 21 DAT, highly significant differences in ZH39 and ZH76 at 28 DAT, and non-significant differences at maturity between treatments.

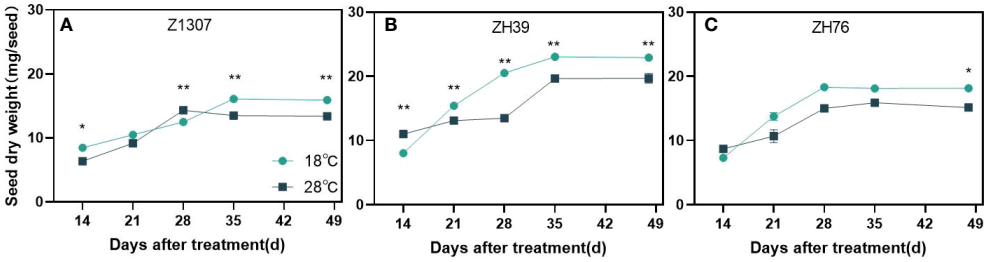


FIGURE 3
Dynamic changes of soybean seed weight under different night temperatures. The dark blue/black blue line indicates the 18 ℃/28 ℃ treatment. The broken lines respect the dynamic changes of soybean seed weight of the variety Z1307 **(A)**, ZH39 **(B)** and ZH76 **(C)** under different night temperatures. Values shown are means ± SE from three biological replicates. (*,$P < 0.05$;**, $P < 0.01$).

10.3389/fpls.2023.1065604

TABLE 2 Effects of different night temperature on seed size of soybean.

Year	Cultivars	Treatment(℃)	Seed length (mm)	Seed width (mm)	Seed diameter (mm)	Ratio of seed length to width
2020	Z1307	18	7.57±0.07aA	6.23±0.03aA	6.73±0.07aA	1.21±0.02aA
		28	6.60±0.00bB	5.63±0.07bB	6.07±0.03bB	1.17±0.01aA
	ZH39	18	7.83±0.03aA	6.50±0.06aA	6.93±0.18aA	1.21±0.01aA
		28	7.33±0.09bB	6.27±0.07aA	6.53±0.03aA	1.17±0.02aA
	ZH76	18	7.70±0.06aA	5.97±0.12aA	6.67±0.03aA	1.29±0.02aA
		28	6.83±0.07bB	5.58±0.02bA	6.37±0.09bA	1.22±0.01aA
2021	Z1307	18	7.23±0.13aA	6.40±0.09aA	6.73±0.02aA	1.13±0.03bA
		28	6.55±0.12bA	5.10±0.06bB	5.71±0.22bA	1.28±0.03aA
	ZH39	18	7.96±0.05aA	6.51±0.15aA	7.01±0.10aA	1.22±0.02aA
		28	7.57±0.07bB	5.95±0.08bA	6.70±0.02bA	1.27±0.02aA
	ZH76	18	8.27±0.10aA	5.56±0.08aA	6.89±0.06aA	1.49±0.04aA
		28	6.95±0.17bB	4.96±0.22aA	6.05±0.15bB	1.41±0.06aA
F-value						
Year(Y)			4.48*	23.29**	NS	26.17**
Cultivar(C)			60.77**	61.33**	21.78**	33.15**
Treatment(T)			229.04**	109.99**	94.67**	NS
Y*C			9.46**	3.87*	NS	9.52**
Y*T			NS	12.49**	4.82*	6.80*
C*T			13.02**	8.62**	5.46*	5.04*
Y*C*T			4.56*	NS	NS	NS

*, ** represent the test significant at the 5% level ($P < 0.05$) and 1% level ($P < 0.01$), respectively; NS, non-significant at the 5% level.

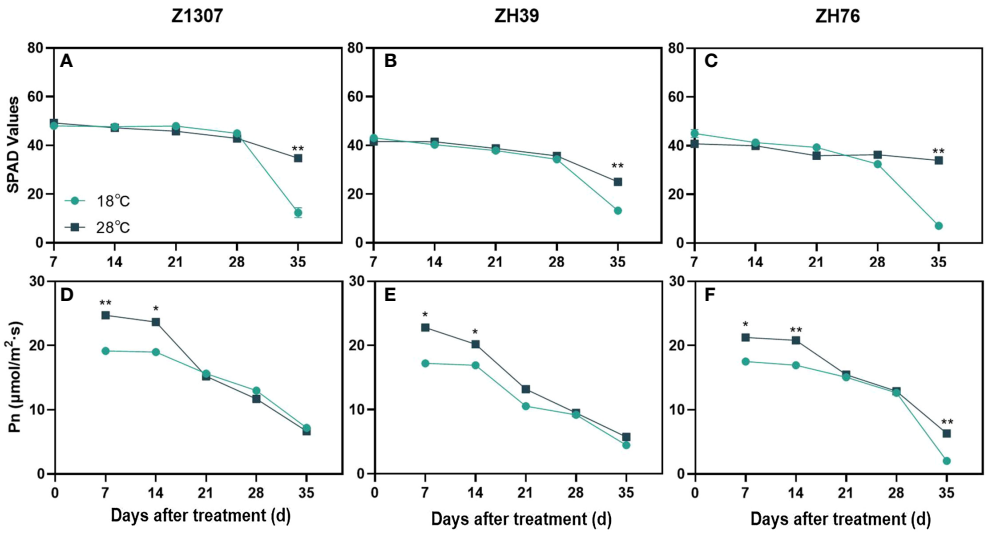


FIGURE 4
Effects of high night temperature on SPAD value and net photosynthetic rate of leaves under different night temperatures. The light blue/ black blue line indicates the 18 ℃/28 ℃ treatment. The broken lines respect the dynamic changes of the SPAD value **(A-C)** and photosynthetic rate **(D-F)** of soybean leaves with the days of different high night temperature treatments for the three varieties of Z1307, ZH39 and ZH76. Values shown are means ± SE from three biological replicates. (*, $P < 0.05$; **, $P < 0.01$).

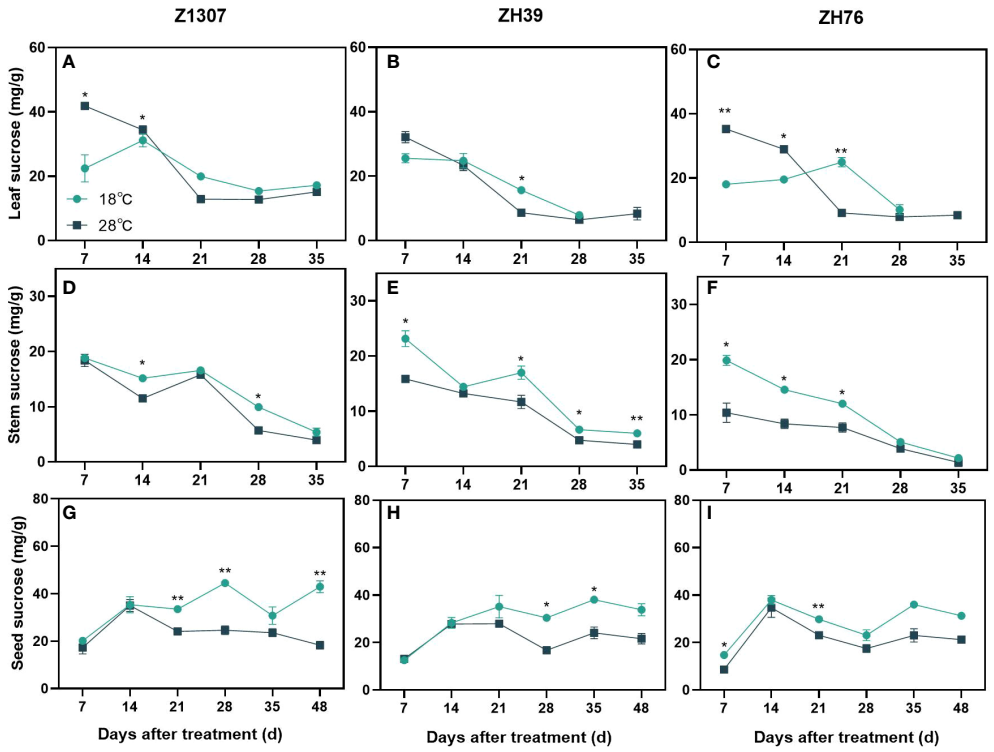


FIGURE 5
Effects of high night temperature on sucrose content in soybean leaf, stem and seed. The light blue/ black blue line indicates the 18 ℃/28 ℃ treatment. The broken lines respect the dynamic changes of the sucrose content of leaf **(A-C)**, stem **(D-F)** and seed **(G-I)** with the days of different high night temperature treatments for the three varieties of Z1307, ZH39 and ZH76. Values shown are means ± SE from three biological replicates. (*, $P < 0.05$; **, $P < 0.01$).

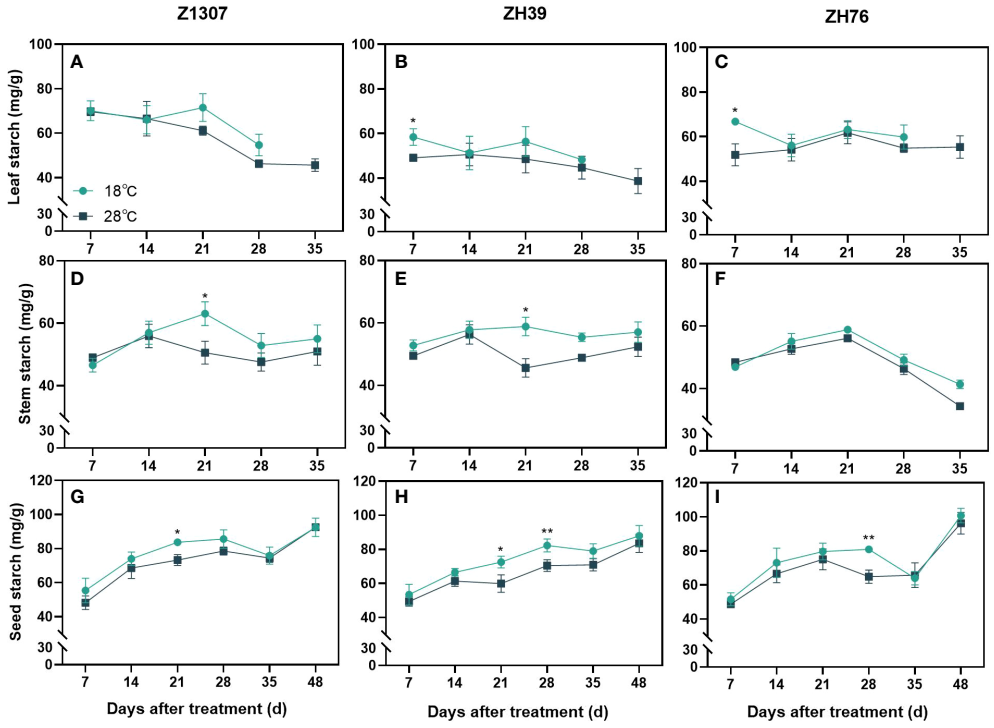


FIGURE 6
Effect of high night temperature on starch content in soybean leaf, stem and seed. The light blue/ black blue line indicates the 18 ℃/28 ℃ treatment. The broken lines respect the dynamic changes of the starch content of leaf **(A-C)**, stem **(D-F)** and seed **(G-I)** with the days of different high night temperature treatments for the three varieties of Z1307, ZH39 and ZH76. Values shown are means ± SE from three biological replicates. (*, $P < 0.05$; **, $P < 0.01$).

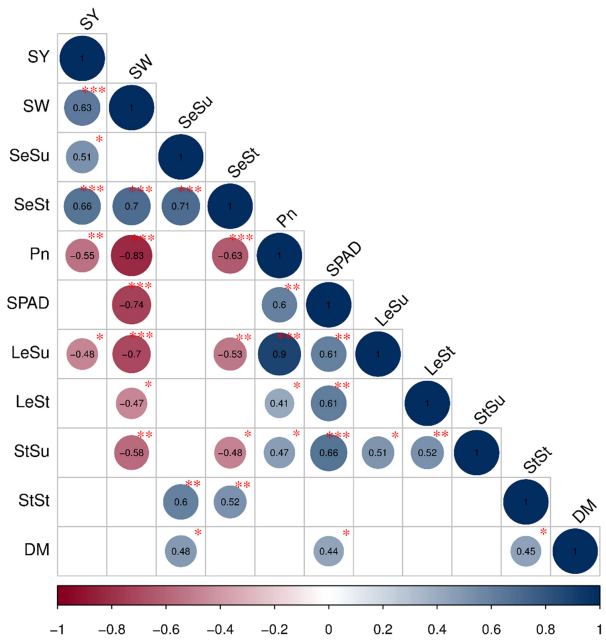


FIGURE 7
Pearson correlation analysis showing the relationships between growth factors and grain yield. The circle size shows the significant level and the circle color exhibited the positive or negative correlations. P-values less than 0.001, 0.01, 0.05 are indicated by the asterisks and dot symbols: '***', '**' and '*'.The abbreviations used in the figure are followed as: seed yield per plant (SY), seed weight (SW), seed sucrose content (SeSu), seed starch content (SeSt), photosynthetic rate (Pn), leaf sucrose content (LeSu), leaf starch content (LeSt), stem sucrose content (StSu), stem starch content (StSt), dry matter per plant (DM).

3.7 Relationships between dry matter accumulation and yield per plant

As shown in Figure 7, single plant yield was positively correlated with single seed weight ($P<0.001$), starch ($P<0.001$) and sucrose content in seeds ($P<0.05$) and negatively correlated with both the net photosynthetic rate ($P<0.01$) and sucrose content in leaf($P<0.05$). Single seed weight was positively correlated with starch content in seeds ($P<0.001$), and negatively correlated with the net photosynthetic rate in leaves ($P< 0.001$), the SPAD value ($P<0.001$), the sucrose content ($P<0.001$) and the starch content in leaves ($P<0.05$), and the sucrose content in stems ($P<0.01$).

3.8 Transcriptome analysis

A total of 1861 differentially expressed genes (DEGs) were identified between 18°C and 28°C treatment, 953 of which were down-regulated (Figure S3 and Table S1). GO and KEGG analysis indicated that these DEGs perform a wide range function, but the most of them are involved in carbohydrate metabolism, transmembrane transport, and ion channel-related processes, photosynthesis, amino acid metabolism, biosynthesis of other secondary metabolites and biological clock (Figure S4). This analysis suggests that DEGs are associated with energy expenditure, ion uptake, transport, stress tolerance, oxidative stress and scavenging under high night temperature.

High night temperature regulated the major differential pathways of carbohydrate metabolism in soybean leaves, including 11 DEGs for photosynthetic carbon fixation (7 up-regulated and 4 down-regulated), 30 DEGs for carbon metabolism (14 up-regulated and 16 down-regulated), 19 DEGs for glycolysis/gluconeogenesis (7 up-regulated and 12 down-regulated), 19 DEGs for pyruvate metabolism (9 up-regulated and 10 down-regulated), 29 DEGs for starch and sucrose metabolism (8 up-regulated and 21 down-regulated), 16 DEGs for amino and nucleotide sugar metabolism (5 up-regulated and 11 down-regulated), 5 DEGs for pentose phosphate pathway (1 up-regulated and 4 down-regulated), and 6 DEGs for fructose and mannose metabolism (3 up-regulated and 3 down-regulated).

It was found that among the DEGs for sucrose metabolism, 7 of 8 sucrose synthase genes and 2 Sucrose-phosphatase genes were down-regulated, including LOC100802045(Glyma.19G212800), LOC100788584 (Glyma.17G045800), LOC100788717

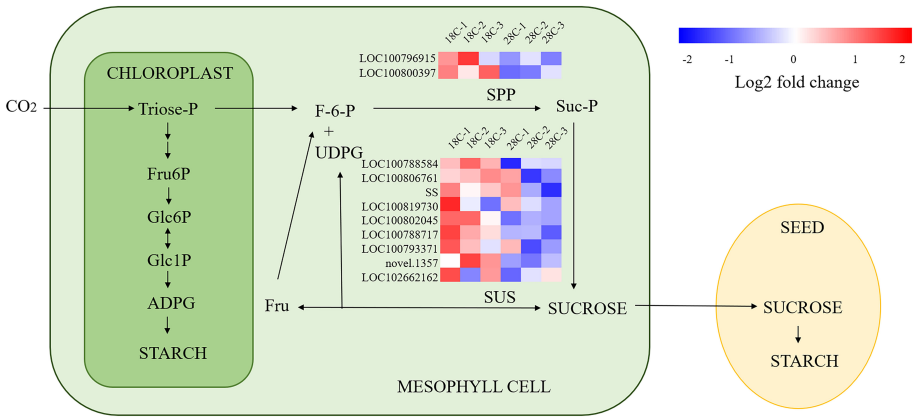


FIGURE 8
A simplified version of the starch and sucrose metabolic pathway. Heat map indicates the Differential Expression Genes (DEGs) associated to the starch and sucrose metabolic pathway. Red indicates up-regulated genes, and blue indicates down-regulated genes. The pathway is modified from a figure in ref (Fünfgeld et al., 2022).

(Glyma.15G151000), LOC102662162 (Glyma.03G048351v4), LOC100806761 (Glyma.09G073600), LOC100793371 (Glyma.03G216300), SS, LOC100819730 (Glyma.15G182600), LOC100800397 (Glyma.10G086600), LOC100796915 (Glyma.20G070500), implying the sucrose synthesis of leaves was regulated at the transcriptional level by high night temperature at 7 DAT (Figure 8). Among the photosynthetic carbon fixation-related genes, *RBCS2*, which catalyzes the reaction of fixing CO_2 in photosynthesis and is an important enzyme related to chloroplast function (Xing et al., 2022) is found up-regulated, which may be related to the rise of the photosynthesis at 7 DAT in this study.

4 Discussion

Soybean is sensitive to light and temperature. When subjected to photothermal change, it must constantly employ adaptive mechanisms to maintain homeostasis in photosynthesis, carbon fixation, and photosynthetic production (Pommerrenig et al., 2018). These adaptive mechanisms can both ensure the normal growth of the soybean but caused changes of biomass accumulation, individual development, material partitioning, and yield (Du et al., 2020). A systematic understanding of the relationship between elevated night temperatures and yield-related physiological indicators is beneficial for improving field cropping strategies and achieving improved soybean yield and quality.

The negative effect of high night temperature on soybean yield was reported in previous studies (Egli, 2010; Nakagawa et al., 2020), and it was consistent with the results of many other crops such as rice (Bahuguna et al., 2016, Welch et al., 2010), wheat (García et al., 2015; García et al., 2016), and cotton (Loka and Oosterhuis, 2010). It was found that high night temperature increased respiration-driven carbon losses and hindered the transport of photosynthetic assimilation products from source organs to reservoir, resulting in inadequate seed filling and ultimately a reduction in yield, which is consistent with the study of Tacarindua et al. (2013). The source-sink relationship during grain development was affected by temperature was also studied in many crops, such as rice (Arshad et al., 2017) and wheat (Hein et al., 2022). The negative correlation of soybean yield and quality under high night temperature reported in previous study (Choi et al., 2016) was confirmed in our study. It has also been reported that high temperature may affect seed weight by altering protein content (Nakagawa et al., 2020). A "concentration effect" resulted from a decline in the proportion of carbohydrate and seed size, caused the increase relative protein and oil content was also observed in our study. Furthermore, the protein and oil yield of individual soybean plants was found reduced under high night temperature, implying the high night temperature affects the accumulation of different components, but it had more effects on the carbohydrates than proteins and oils.

In this study, 28°C high night temperature treatment led to an increase in net photosynthetic rate in early 7 DAT functional leaves, contrary to the results of some studies of heat stress (Jumrani et al., 2016; Prasad et al., 2017; Ferguson et al., 2021), this may as a result of treatment carried out in the night and the 28°C night temperature was a mild heat stress for soybean (Hatfield et al., 2011). Some studies investigating the effects of night temperature concluded that there was no effect on net photosynthetic rate (Zhang et al., 2020), which was also different from our results. This may be due to the differences of treatment and crop species. Previous studies have reported that soybean leaves senesce later in controlled temperature treatments with 1-3°C higher environmental temperature (Tacarindua et al., 2013). This is consistent with the findings of our study and the stay-green of the leaf could be the reason for the decrease translocation of accumulated photosynthetic assimilation products in the leaves and the weakened efficiency of the photosynthetic product utilization.

Elevated levels of sucrose occurred early in this study, which may be related to the compensation for the carbon starvation caused by its accelerated degradation at night (Peraudeau et al., 2015; MacNeill et al., 2017). After a period of treatment, the sucrose content begins to remain relatively stable as it adapts to the change in temperature. The starch content in stems and leaves was found to be lower than the control under the high night temperature treatment after 21 DAT. The decrease in sucrose content in the seeds partly explains the decrease of the residue in seeds. Similarly, in rice, it was found that one of the causes for grain stunting under heat stress during reproductive growth was the restricted carbohydrate availability, and that heat stress reduced the movement of photosynthetic assimilation products into the seeds and inhibited the accumulation of starch in the seeds (Arshad et al., 2017).

The identified DEGs for photosynthetic and carbohydrate are associated with early increased sugar accumulation in the leaves treated under high night temperature treatment. Photosynthesis could be improved by the increased carbon fixation and sugar metabolism. Also, leaf senescence triggered by sugar accumulation leads to increase of nitrogen content (Wingler et al., 2006, Kaschuk et al., 2010). DEGs related to the transported nitrogenous compounds glutamine and glutamate were identified (Masclaux-Daubresse et al., 2010). Some amino acids or organic acids, such as proline and glutamate, are synthesized in large quantities when plants are subjected to heat stress (Vergara-Diaz et al., 2020; Wahid, 2006), and we also find the DEGs for these compounds. The transcriptome results reflect the response mechanism to high night temperature treatment conditions at the beginning of the seed filling stage. Some previous studies have suggested that changes in seed size and quality under heat treatment conditions could be associated with the expression of some heat-stimulated proteins (Kumar et al., 2015; Kumar et al., 2016; Kumar et al., 2020; Tiwari et al., 2021). Most HSP-related genes showed down-regulation in our study (Table S1), it could be explained by the mild stress caused by the moderate high night temperature we used.

This study expounds on the current understanding of the relationships between photosynthesis, plant development, carbon and nitrogen transport, and metabolism under high night temperature conditions. In addition to exploring response and tolerance mechanisms at the molecular level, we also need to optimize crop management strategies to improve soybean plants' resistance to nighttime warming. In the context of global warming, breeding soybean varieties with low respiration and high energy efficiency is one of the most important ways to effectively address the world food crisis.

5 Conclusion

This study indicated that high night temperature during the soybean seed filling period (R5-R7) reduced seed yield and changed the proportion of the seed compositions. The decline of carbohydrates in seeds was the primary reason for the reduction in yield. The dynamic changes of dry matter accumulations, non-structural carbohydrates, net photosynthetic rate and SPAD value, as well as the transcriptome analysis explained the adaptive mechanisms for soybean to high night temperature stress at physiological and molecular level. The study is of significance for improving soybean breeding and cultivation practice to fight the global warming.

Data availability statement

The original contributions presented in the study are publicly available. This data can be found here: NCBI, PRJNA892245 and SAMN31361599-31361604.

Author contributions

LY and WS conceived the initial research plan, conducted the experiments, and analyzed the data. CW supervised the research and provided the laboratory infrastructure and funding. LY prepared the graphs and wrote the article. CW, DJ, WS, CX, and ES critically reviewed and edited the manuscript. All authors contributed to the article and approved the submitted version.

Funding

This study was supported by the National Key R&D Program of China (2018YFD1000900), the China Agriculture Research System (CARS-04) and the Agriculture Science and Technology Innovation Program in CAAS.

Conflict of interest

The authors declare that the research was conducted in the absence of any commercial or financial relationships that could be construed as a potential conflict of interest.

The reviewer WZ declared a shared affiliation with the authors LY and DJ to the handling editor at the time of review.

Publisher's note

All claims expressed in this article are solely those of the authors and do not necessarily represent those of their affiliated organizations, or those of the publisher, the editors and the reviewers. Any product that may be evaluated in this article, or claim that may be made by its manufacturer, is not guaranteed or endorsed by the publisher.

Supplementary material

The Supplementary Material for this article can be found online at: https://www.frontiersin.org/articles/10.3389/fpls.2023.1065604/full#supplementary-material

References

Alvarado-Sanabria, O. H., Garces-Varon, G. A., and Restrepo-Diaz, H. (2017). The effects of night-time temperatures on physiological and biochemical traits in rice. *Notulae Botanicae Horti Agrobotanici Cluj Napoca* 45 (1), 157–163. doi: 10.15835/nbha45110627

Arshad, M. S., Farooq, M., Asch, F., Krishna, J. S. V., Prasad, P. V. V., and Siddique, K. H. M. (2017). Thermal stress impacts reproductive development and grain yield in rice. *Plant Physiol. Biochem.* 115, 57–72. doi: 10.1016/j.plaphy.2017.03.011

Asseng, S., Ewert, F., Martre, P., Rötter, R. P., Lobell, D. B., Cammarano, D., et al. (2014). Rising temperatures reduce global wheat production. *Nat. Climate Change* 5 (2), 143–147. doi: 10.1038/NCLIMATE2470

Baek, J., Lee, E., Kim, N., Kim, S. L., Choi, I., Ji, H., et al. (2020). High throughput phenotyping for various traits on soybean seeds using image analysis. *Sensors* 20 (1), 1–9. doi: 10.3390/s20010248

Bahuguna, R. N., Solis, C. A., Shi, W., and Jagadish, K. S. V. (2016). Post-flowering night respiration and altered sink activity account for high night temperature-induced grain yield and quality loss in rice (*Oryza sativa* l.). *Physiol. Plantarum* 159 (1), 59–73. doi: 10.1111/ppl.12485

Bunce, J. A. (2005). Response of respiration of soybean leaves grown at ambient and elevated carbon dioxide concentrations to day-to-day variation in light and temperature under field conditions. *Ann. Bot.* 95 (6), 1059–1066. doi: 10.1093/aob/mci117

Choi, D. H., Ban, H. Y., Seo, B. S., Lee, K. J., and Lee, B. W. (2016). Phenology and seed yield performance of determinate soybean cultivars grown at elevated temperatures in a temperate region. *PloS One* 11 (11), 1–18. doi: 10.1371/journal.pone.0165977

Das, S., Krishnan, P., Mishra, V., Kumar, R., Ramakrishnan, B., and Singh, N. K. (2015). Proteomic changes in rice leaves grown under open field high temperature stress conditions. *Mol. Biol. Rep.* 42 (11), 1545–1558. doi: 10.1007/s11033-015-3923-5

Davy, R., Esau, I., Chernokulsky, A., Outten, S., and Zilitinkevich, S. (2016). Diurnal asymmetry to the observed global warming. *Int. J. Climatol.* 37 (1), 79–93. doi: 10.1002/joc.4688

Djanaguiraman, M., Prasad, P. V. V., and Schapaugh, W. T. (2013). High day- or nighttime temperature alters leaf assimilation, reproductive success, and phosphatidic acid of pollen grain in soybean [*Glycine max* (L.) merr.]. *Crop Sci.* 53 (4), 1594–1604. doi: 10.2135/cropsci2012.07.0441

Du, Y., Zhao, Q., Chen, L., Yao, X., Zhang, H., Wu, J., et al. (2020). Effect of drought stress during soybean R2-R6 growth stages on sucrose metabolism in leaf and seed. *Int. J. Mol. Sci.* 21 (2), 1–19. doi: 10.3390/ijms21020618

Egli, D. B. (2010). Soybean reproductive sink size and short-term reductions in photosynthesis during flowering and pod set. *Crop Sci.* 50 (5), 1971–1977. doi: 10.2135/cropsci2009.09.0518

Ergo, V. V., Lascano, R., Vega, C. R. C., Parola, R., and Carrera, C. S. (2018). Heat and water stressed field-grown soybean: A multivariate study on the relationship between physiological-biochemical traits and yield. *Environ. Exp. Bot.* 148, 1–11. doi: 10.1016/j.envexpbot.2017.12.023

Feng, Z., Ding, C., Li, W., Wang, D., and Cui, D. (2020). Applications of metabolomics in the research of soybean plant under abiotic stress. *Food Chem.* 310, 125914. doi: 10.1016/j.foodchem.2019.125914

Ferguson, J. N., Tidy, A. C., Murchie, E. H., and Wilson, Z. A. (2021). The potential of resilient carbon dynamics for stabilizing crop reproductive development and productivity during heat stress. *Plant Cell Environ.* 44 (7), 2066–2089. doi: 10.1111/pce.14015

Frantz, J. M., Cometti, N. N., and Bugbee, B. (2004). Night temperature has a minimal effect on respiration and growth in rapidly growing plants. *Ann. Bot.* 94 (1), 155–166. doi: 10.1093/aob/mch122

Fünfgeld, M. M., Wang, W., Ishihara, H., Arrivault, S., Feil, R., Smith, A. M., et al. (2022). Sucrose synthases are not involved in starch synthesis in *Arabidopsis* leaves. *Nat. Plants* 8 (5), 574–582. doi: 10.1038/s41477-022-01140-y

García, G. A., Dreccer, M. F., Miralles, D. J., and Serrago, R. A. (2015). High night temperatures during grain number determination reduce wheat and barley grain yield: a field study. *Global Change Biol.* 21 (11), 4153–4164. doi: 10.1111/gcb.13009

García, G. A., Serrago, R. A., Dreccer, M. F., and Miralles, D. J. (2016). Post-anthesis warm nights reduce grain weight in field-grown wheat and barley. *Field Crops Res.* 195, 50–59. doi: 10.1016/j.fcr.2016.06.002

Gibson, L. (1992). *Day and night temperature effects on soybean (Glycine max merr.) seed yield, seed quality, and seed composition recommended citation. master* (Iowa State University).

Gibson, L. R., and Mullen, R. E. (1996). Influence of day and night temperature on soybean seed yield. *Crop Sci.* 36 (1), 98–104. doi: 10.2135/cropsci1996.0011183X003600010018x

Gillman, J. D., Biever, J. J., Ye, S., Spollen, W. G., Givan, S. A., Lyu, Z., et al. (2019). A seed germination transcriptomic study contrasting two soybean genotypes that differ in terms of their tolerance to the deleterious impacts of elevated temperatures during seed fill. *BMC Res. Notes* 12 (1), 1–8. doi: 10.1186/s13104-019-4559-7

Guo, Y., Ren, G., Zhang, K., Li, Z., Miao, Y., and Guo, H. (2021). Leaf senescence: progression, regulation, and application. *Mol. Horticult.* 1 (1), 1–25. doi: 10.1186/s43897-021-00006-9

Hatfield, J. L., Boote, K. J., Kimball, B. A., Ziska, L. H., Izaurralde, R. C., Ort, D., et al. (2011). Climate impacts on agriculture: implications for crop production. *Agron. J.* 103 (2), 351–370. doi: 10.2134/agronj2010.0303

Hein, N. T., Impa, S. M., Wagner, D., Bheemanahalli, R., Kumar, R., Tiwari, M., et al. (2022). Grain micronutrient composition and yield components in field-grown wheat are negatively impacted by high night-time temperature. *Cereal Chem.* 99 (3), 615–624. doi: 10.1002/cche.10523

Hussain, S., Iqbal, N., Rahman, T., Liu, T., Brestic, M., Safdar, M. E., et al. (2019). Shade effect on carbohydrates dynamics and stem strength of soybean genotypes. *Environ. Exp. Bot.* 162 (4), 374–382. doi: 10.1016/j.envexpbot.2019.03.011

Jing, P., Wang, D., Zhu, C., and Chen, J. (2016). Plant physiological, morphological and yield-related responses to night temperature changes across different species and plant functional types. *Front. Plant Sci.* 7, 1774. doi: 10.3389/fpls.2016.01774

Jumrani, K., Bhatia, V. S., and Pandey, G. P. (2016). Impact of elevated temperatures on specific leaf weight, stomatal density, photosynthesis and chlorophyll fluorescence in soybean. *Photosynth. Res.* 131 (3), 333–350. doi: 10.1007/s11120-016-0326-y

Kaschuk, G., Hungria, M., Leffelaar, P. A., Giller, K. E., and Kuyper, T. W. (2010). Differences in photosynthetic behaviour and leaf senescence of soybean (*Glycine max* [L.] Merrill) dependent on N_2 fixation or nitrate supply. *Plant Biol.* 12 (1), 60–69. doi: 10.1111/j.1438-8677.2009.00211.x

Kino, R. I., Pellny, T. K., Mitchell, R. A. K., Gonzalez-Uriarte, A., and Tosi, P. (2020). High post-anthesis temperature effects on bread wheat (Triticum aestivum L.) grain transcriptome during early grain-filling. *BMC Plant Biol.* 20 (1), 170. doi: 10.1186/s12870-020-02375-7

Kucharik, C. J., and Serbin, S. P. (2008). Impacts of recent climate change on Wisconsin corn and soybean yield trends. *Environ. Res. Lett.* 3 (3), 034003. doi: 10.1088/1748-9326/3/3/034003

Kumar, R., Bahuguna, R. N., Tiwari, M., Pal, M., Chinnusamy, V., Sreeman, S., et al. (2022). Walking through crossroads–rice responses to heat and biotic stress interactions. *Theor. Appl. Genet.* 135, 1–17. doi: 10.1007/s00122-022-04131-x

Kumar, R., Khungar, L., Shimphrui, R., Tiwari, L. D., Tripathi, G., Sarkar, N. K., et al. (2020). AtHsp101 research sets course of action for the genetic improvement of crops against heat stress. *J. Plant Biochem. Biotechnol. Lett.* 29 (4), 715–732. doi: 10.1007/s13562-020-00624-2

Kumar, R., Lavania, D., Singh, A. K., Negi, M., Siddiqui, M. H., Al-Whaibi, M. H., et al. (2015). Identification and characterization of a small heat shock protein 17.9-CII gene from faba bean (*Vicia faba* l.). *Acta Physiologiae Plantarum* 37 (9), 1–13. doi: 10.1007/s11738-015-1943-3

Kumar, R., Singh, A. K., Lavania, D., Siddiqui, M. H., Al-Whaibi, M. H., and Grover, A. (2016). Expression analysis of ClpB/Hsp100 gene in faba bean (*Vicia faba l.*) plants in response to heat stress. *Saudi J. Biol. Sci.* 23 (2), 243–247. doi: 10.1016/j.sjbs.2015.03.006

Lavania, D., Kumar, R., Goyal, I., Rana, S., and Grover, A. (2016). Genetic improvement of rice crop under high temperature stress: Bridging plant physiology with molecular biology. *Indian J. Plant Physiol.* 21 (4), 391–408. doi: 10.1007/s40502-016-0255-y

Lavania, D., Siddiqui, M. H., Al-Whaibi, M. H., Singh, A. K., Kumar, R., and Grover, A. (2015). Genetic approaches for breeding heat stress tolerance in faba bean (*Vicia faba* l.). *Acta Physiologiae Plantarum* 37 (1), 1–9. doi: 10.1007/s11738-014-1737-z

Lin, T., Okamoto, Y., Nagasaki, Y., and Shiraiwa, T. (2021). The influence of high night temperature on yield and physiological attributes of soybean cv. *Fukuyutaka Plant Product. Sci.* 24 (3), 267–278. doi: 10.1080/1343943X.2020.1842215

Lobell, D. B., and Asner, G. P. (2003). Climate and management contributions to recent trends in US agricultural yields. *Science* 299 (5609), 1032–1032. doi: 10.1126/science.1077838

Loka, D. A., and Oosterhuis, D. M. (2010). Effect of high night temperatures on cotton respiration, ATP levels and carbohydrate content. *Environ. Exp. Bot.* 68 (3), 258–263. doi: 10.1016/j.envexpbot.2010.01.006

MacNeill, G. J., Mehrpouyan, S., Minow, M. A. A., Patterson, J. A., Tetlow, I. J., and Emes, M. J. (2017). Starch as a source, starch as a sink: The bifunctional role of starch in carbon allocation. *J. Exp. Bot.* 68 (16), 4433–4453. doi: 10.1093/jxb/erx291

Masclaux-Daubresse, C., Daniel-Vedele, F., Dechorgnat, J., Chardon, F., Gaufichon, L., and Suzuki, A. (2010). Nitrogen uptake, assimilation and remobilization in plants: challenges for sustainable and productive agriculture. *Ann. Bot.* 105 (7), 1141–1157. doi: 10.1093/aob/mcq028

Medic, J., Atkinson, C., and Hurburgh, C. R. (2014). Current knowledge in soybean composition. *J. Am. Oil Chemists' Soc.* 91 (3), 363–384. doi: 10.1007/s11746-013-2407-9

Nakagawa, A. C. S., Ario, N., Tomita, Y., Tanaka, S., Murayama, N., Mizuta, C., et al. (2020). High temperature during soybean seed development differentially alters lipid and protein metabolism. *Plant Product. Sci.* 23 (4), 504–512. doi: 10.1080/1343943X.2020.1742581

Peraudeau, S., Lafarge, T., Roques, S., Quiñones, C. O., Clement-Vidal, A., Ouwerkerk, P. B. F., et al. (2015). Effect of carbohydrates and night temperature on night respiration in rice. *J. Exp. Bot.* 66 (13), 3931–3944. doi: 10.1093/jxb/erv193

Petridis, A., van der Kaay, J., Sungurtas, J., Verrall, S. R., McCallum, S., Graham, J., et al. (2020). Photosynthetic plasticity allows blueberry (*Vaccinium corymbosum* l.) plants to compensate for yield loss under conditions of high sink demand. *Environ. Exp. Bot.* 174, 104031. doi: 10.1016/j.envexpbot.2020.104031

Pommerrenig, B., Ludewig, F., Cvetkovic, J., Trentmann, O., Klemens, P. A. W., and Neuhaus, H. E. (2018). In concert: orchestrated changes in carbohydrate homeostasis are critical for plant abiotic stress tolerance. *Plant Cell Physiol.* 59 (7), 1290–1299. doi: 10.1093/pcp/pcy037

Prasad, P. V. V., Bheemanahalli, R., and Jagadish, S. V. K. (2017). Field crops and the fear of heat stress–opportunities, challenges and future directions. *Field Crops Res.* 200, 114–121. doi: 10.1016/j.fcr.2016.09.024

Puteh, A., Thuzar, M., Monjurul, M., Mondal, A., Abdullah, N., Ridzwan, M., et al. (2013). Soybean [*Glycine max* (L.) Merrill] seed yield response to high temperature stress during reproductive growth stages. *AJCS* 7 (10), 1472–1479. doi: 10.3316/informit.618691733672149

Ruan, Y. L. (2014). Sucrose metabolism: gateway to diverse carbon use and sugar signaling. *Annu. Rev. Plant Biol.* 65 (1), 33–67. doi: 10.1146/annurev-arplant-050213-040251

Schauberger, B., Archontoulis, S., Arneth, A., Balkovic, J., Ciais, P., Deryng, D., et al. (2017). Consistent negative response of US crops to high temperatures in observations and crop models. *Nat. Commun.* 8 (1), 1–9. doi: 10.1038/ncomms13931

Shu, T. (2021). *Soybean phenotypic variation under high night temperature stress master* (Auburn State University).

Shu, Y., Zhou, Y., Mu, K., Hu, H., Chen, M., He, Q., et al. (2020). A transcriptomic analysis reveals soybean seed pre-harvest deterioration resistance pathways under high temperature and humidity stress. *Genome* 63 (2), 115–124. doi: 10.1139/gen-2019-0094

Siebers, M. H., Yendrek, C. R., Drag, D., Locke, A. M., Rios Acosta, L., Leakey, A. D. B., et al. (2015). Heat waves imposed during early pod development in soybean (*Glycine max*) cause significant yield loss despite a rapid recovery from oxidative stress. *Global Change Biol.* 21 (8), 3114–3125. doi: 10.1111/gcb.12935

Solomon, S. (2008). *Climate change 2007: mitigation of climate change: contribution of working group III to the fourth assessment report of the intergovernmental panel on climate change* Vol. 45 (Choice Reviews Online). 45-500645-5006.

Song, W., Yang, R., Wu, T., Wu, C., Sun, S., Zhang, S., et al. (2016). Analyzing the effects of climate factors on soybean protein, oil contents, and composition by extensive and high-density sampling in china. *J. Agric. Food Chem.* 64 (20), 4121–4130. doi: 10.1021/acs.jafc.6b00008

Stitt, M., Huber, S., and Kerr, P. (1987). Control of photosynthetic sucrose formation. *photosynthesis* 10, 327–409. doi: 10.1016/B978-0-12-675410-0.50012-9

Stitt, M., and Zeeman, S. C. (2012). Starch turnover: pathways, regulation and role in growth. *Curr. Opin. Plant Biol.* 15 (3), 282–292. doi: 10.1016/j.pbi.2012.03.016

Tacarindua, C. R. P., Shiraiwa, T., Homma, K., Kumagai, E., and Sameshima, R. (2013). The effects of increased temperature on crop growth and yield of soybean grown in a temperature gradient chamber. *Field Crops Res.* 154, 74–81. doi: 10.1016/j.fcr.2013.07.021

Tamagno, S., Sadras, V. O., Aznar-Moreno, J. A., Durrett, T. P., and Ciampitti, I. A. (2022). Selection for yield shifted the proportion of oil and protein in favor of low-energy seed fractions in soybean. *Field Crops Res.* 279, 108446. doi: 10.1016/j.fcr.2022.108446

Tiwari, L. D., Kumar, R., Sharma, V., Sahu, A. K., Sahu, B., Naithani, S. C., et al. (2021). Stress and development phenotyping of Hsp101 and diverse other hsp mutants of *Arabidopsis thaliana*. *J. Plant Biochem. Biotechnol. Lett.* 30 (4), 889–905. doi: 10.1007/s13562-021-00706-9

Vergara-Diaz, O., Vatter, T., Vicente, R., Obata, T., Nieto-Taladriz, M. T., Aparicio, N., et al. (2020). Metabolome profiling supports the key role of the spike in wheat yield performance. *Cells* 9 (4), 1025. doi: 10.3390/cells9041025

Vose, R. S., Easterling, D. R., and Gleason, B. (2005). Maximum and minimum temperature trends for the globe: An update through 2004. *Geophys. Res. Lett.* 32 (23), 1–5. doi: 10.1029/2005GL024379

Wahid, A. (2006). Physiological implications of metabolite biosynthesis for net assimilation and heat-stress tolerance of sugarcane (*Saccharum officinarum*) sprouts. *J. Plant Res.* 120 (2), 219–228. doi: 10.1007/s10265-006-0040-5

Welch, J. R., Vincent, J. R., Auffhammer, M., Moya, P. F., Dobermann, A., and Dawe, D. (2010). Rice yields in tropical/subtropical Asia exhibit large but opposing sensitivities to minimum and maximum temperatures. *Proc. Natl. Acad. Sci.* 107 (33), 14562–14567. doi: 10.1073/pnas.1001222107

Wingler, A., Purdy, S., MacLean, J. A., and Pourtau, N. (2006). The role of sugars in integrating environmental signals during the regulation of leaf senescence. *J. Exp. Bot.* 57 (2), 391–399. doi: 10.1093/jxb/eri279

Xing, J., Pan, J., Yi, H., Lv, K., Gan, Q., Wang, M., et al. (2022). The plastid-encoded protein Orf2971 is required for protein translocation and chloroplast quality control. *Plant Cell* 34 (9), 3383–3399. doi: 10.1093/plcell/koac180

Xu, J., Misra, G., Sreenivasulu, N., and Henry, A. (2021). What happens at night? physiological mechanisms related to maintaining grain yield under high night temperature in rice. *Plant Cell Environ.* 44 (7), 2245–2261. doi: 10.1111/pce.14046

Zhang, Y., Tang, Q., Peng, S., Zou, Y., Chen, S., Shi, W., et al. (2013). Effects of high night temperature on yield and agronomic traits of irrigated rice under field

chamber system condition. *AJCS* 7 (1), 7–13. doi: 10.3316/informit.142507520197589

Zhang, Y., Wang, J. K., and Wang, Y. L. (2020). Response of rice starch synthesis to night temperature changes. *Chin. J. OF Rice Sci.* 34 (6), 525–538. doi: 10.16819/j.1001-7216.2020.0701

Zhang, L., Zhu, L., Yu, M., and Zhong, M. (2016). Warming decreases photosynthates and yield of soybean [*Glycine max* (L.) Merrill] in the north China plain. *Crop J.* 4 (2), 139–146. doi: 10.1016/j.cj.2015.12.003

Zhao, C., Liu, B., Piao, S., Wang, X., Lobell, D. B., Huang, Y., et al. (2017). Temperature increase reduces global yields of major crops in four independent estimates. *Proc. Natl. Acad. Sci.* 114 (35), 9326–9331. doi: 10.1073/pnas.1701762114

Zhou, R., Kjaer, K., Rosenqvist, E., Yu, X., Wu, Z., and Ottosen, C. O. (2017). Physiological response to heat stress during seedling and anthesis stage in tomato genotypes differing in heat tolerance. *J. Agron. Crop Sci.* 203, 68–80. doi: 10.1111/jac.12166

frontiers | Frontiers in Plant Science

TYPE Original Research
PUBLISHED 02 March 2023
DOI 10.3389/fpls.2023.1045112

Check for updates

OPEN ACCESS

EDITED BY
Jiban Shrestha,
Nepal Agricultural Research Council, Nepal

REVIEWED BY
Hongliang Zhu,
China Agricultural University, China
Huihui Zhang,
Northeast Forestry University, China

*CORRESPONDENCE
Yufeng Liu
yufengliu@syau.edu.cn
Tianlai Li
ltl@syau.edu.cn

SPECIALTY SECTION
This article was submitted to Plant Abiotic Stress, a section of the journal Frontiers in Plant Science

RECEIVED 15 September 2022
ACCEPTED 15 February 2023
PUBLISHED 02 March 2023

CITATION
Li Y, Liu Y, Gao Z, Wang F, Xu T, Qi M, Liu Y and Li T (2023) MicroRNA162 regulates stomatal conductance in response to low night temperature stress *via* abscisic acid signaling pathway in tomato. *Front. Plant Sci.* 14:1045112. doi: 10.3389/fpls.2023.1045112

COPYRIGHT
© 2023 Li, Liu, Gao, Wang, Xu, Qi, Liu and Li. This is an open-access article distributed under the terms of the Creative Commons Attribution License (CC BY). The use, distribution or reproduction in other forums is permitted, provided the original author(s) and the copyright owner(s) are credited and that the original publication in this journal is cited, in accordance with accepted academic practice. No use, distribution or reproduction is permitted which does not comply with these terms.

MicroRNA162 regulates stomatal conductance in response to low night temperature stress *via* abscisic acid signaling pathway in tomato

Yangyang Li[1,2,3], Yang Liu[1,4], Zhenhua Gao[1,2,3], Feng Wang[1,2,3], Tao Xu[1,2,3], Mingfang Qi[1,2,3], Yufeng Liu[1,2,3]* and Tianlai Li[1,2,3]*

[1]Department of Horticulture, Shenyang Agricultural University, Shenyang, China, [2]Key Laboratory of Protected Horticulture of Education Ministry and Liaoning Province, Shenyang, China, [3]Collaborative Innovation Center of Protected Vegetable Surrounds Bohai Gulf Region, Shenyang, China, [4]Tongliao Agricultural Technology Extension Center, Tongliao, China

MicroRNAs (miRNAs) mediate the degradation of target mRNA and inhibit mRNA translation to regulate gene expression at the transcriptional and post-transcriptional levels in response to environmental stress in plants. We characterized the post-transcriptional mechanism by deep sequencing small RNA (sRNA) to examine how miRNAs were involved in low night temperature (LNT) stress in tomato and whether the molecular mechanism depended on the abscisic acid (ABA) signaling pathway. We annotated conserved miRNAs and novel miRNAs with four sRNA libraries composed of wild-type (WT) tomato plants and ABA-deficient mutant (*sit*) plants under normal growth and LNT stress conditions. Reverse genetics analysis suggested that miR162 participated in LNT resistance and the ABA-dependent signaling pathway in tomato. miR162-overexpressing (pRI-miR162) and miR162-silenced (pRNAi-miR162) transgenic tomato plants were generated to evaluate miR162 functions in response to LNT stress. miR162 deficiency exhibited high photosynthetic capacity and regulated stomatal opening, suggesting negative regulation of miR162 in the ABA-dependent signaling pathway in response to LNT stress. As feedback regulation, miR162 positively regulated ABA to maintain homeostasis of tomato under diverse abiotic stresses. The mRNA of *DICER-LIKE1* (*DCL1*) was targeted by miR162, and miR162 inhibited DCL1 cleavage in LNT response, including the regulation of miRNA160/164/171a and their targets. The DCL1-deficient mutants (*dcl1*) with CRISPR/Cas9 prevented stomatal opening to influence photosynthesis in the ABA signaling pathway under LNT stress. Finally, we established the regulatory mechanism of ABA-miR162-DCL1, which systematically mediated cold tolerance in tomato. This study suggests that post-transcriptional modulators acted as systemic signal responders *via* the stress hormone signaling pathway, and the model at the post-transcriptional level presents a new direction for research in plant abiotic stress resistance.

KEYWORDS

microRNAs, ABA, stomata, resistance, cold stress, tomato

Introduction

MicroRNAs (miRNAs) are endogenous non-coding small RNAs (sRNAs) that participate in plant development, organ formation, signal transduction, and stress response (Cai et al., 2009). Although miRNAs do not directly encode proteins, their target genes are activated to promote functions (Jones-Rhoades et al., 2006). miRNAs modulate target genes at the transcriptional and post-transcriptional stages, like Dicer-like (DCL) cleavage functional processes. DCL plays an important role in RNA degradation and regulation of gene expression as a conserved double-stranded RNA specific endonuclease (Ketting et al., 2001). DCL1 mainly cleaves the miRNA precursor to form mature miRNA and participates in miRNA biosynthesis (Gasciolli et al., 2005; Margis et al., 2006; Kravchik et al., 2014b). A previous study showed that miR162 affects post-transcription by regulating DCL1, which is a target gene of miR162 in tomato (Kravchik et al., 2014b). Further, DCL1 is the major producer of miRNAs (Park et al., 2002). In *DCL1*-deficient mutants of tomato, the expression of three miRNAs (miR160, miR164, and miR171a) are decreased, and the expression of their targets are increased (Kravchik et al., 2014a), indicating the function of DCL1 cleavage in miRNA regulation. However, some researchers have developed a DCL1-independent model in miRNA generation and have revealed that the reduction in miR172 causes flowering delay in *dcl1-7* mutant of *Arabidopsis thaliana* (Tsuzuki et al., 2014). Whether the feedback regulation consisted of miRNAs and DCL1 cleavage is still unknown.

miRNAs are considered vital molecular tools for studying stress tolerance of plants (Noman et al., 2017), including low temperature (Chen et al., 2015a), drought (Zhou et al., 2016), and other abiotic stresses (Hackenberg et al., 2015). However, it is still limited and sometimes contradictory about the identity of miRNAs in tomato (Arazi and Khedia, 2022). There are three functional mechanisms of miRNAs in the responsive regulation of plants. The first function is targeting mRNAs by specific cleavage. For example, miR166 cleaves mRNA by the RNA-induced silencing complex (RISC) with the transcription factor (TF) basic region leucine zipper (bZIP) (Castanotto et al., 2009). The second function is inhibiting translation. miR172 is involved in flower development by repressing AP2 protein translation in Arabidopsis (Chen, 2004; Ricci et al., 2011). The third function of miRNA regulation is silencing of related genes. It is indicated that the chromosome structure was changed as genes silenced by miRNA regulated DNA methylation (Ricci et al., 2011). In recent years, more studies have been devoted to elucidating how miRNAs are involved in plant stress response. Under salt stress, miR162a biosynthesis is regulated by pri-miRNA polyadenylation in Arabidopsis (Jones, 2002). Further, miRNAs are involved in post-transcription to affect plant resistance (Sun et al., 2012) and regulate stomatal movement to mediate stress responses; for example, miR169c targets stochastic location model with risk pooling 1 (SlMRP1) to activate stomatal aperture in tomato response to drought stress (Zhang et al., 2011), and miR824 targets AGL16 to affect the development and movement of guard cells in Arabidopsis (Kutter et al., 2007). The finding suggests that sly-miR164a is required for normal fruit development and has negative regulations in tomato cold tolerance by promoting ethylene production (Dong et al., 2022). In addition to abiotic stress, the resistance of *Fusarium oxysporum* f. sp. lycopersici (race 2) has been enhanced in sly-miR482e-knocked down tomato plants (Gao et al., 2021). In protected cultivation during winter, crops such as tomato often experience low temperature stress that limits plant growth and development at night (Liu et al., 2012). However, studies of the association between low night temperature (LNT) stress and miRNA-modulated responses are limited.

Abscisic acid (ABA) is a phytohormone that efficiently responds to multiple abiotic stresses. The ABA-dependent signaling pathway is a common defense mechanism in plants (Roychoudhury et al., 2013). It is indicated that miRNAs such as miR167 and miR413 are regulated by ABA in previous studies (Liu et al., 2009). Meanwhile, miRNAs activated the ABA signaling pathway temporarily in osmotic stress (Jung and Kang, 2007). Both ABA content and sensitivity to salt stress are enhanced in miRNA mutants, and the expression levels of ABA response factors are increased with miRNA deficiency (Zhang et al., 2011). The miR166 targets participated in the ABA pathway as bZIP TFs (Baloglu et al., 2014). Auxin response factor 10 (ARF10) is sensitive to ABA, which was targeted by miR160 in tomato (Liu et al., 2007). Although miRNA plays regulatory roles in the ABA pathway, whether the regulation of defense miRNAs depends on ABA remains unclear. The presence of a feedback relationship between miRNAs and ABA in response to cold stress still needs further study in tomato. A promoter scan of DCL detected numerous *cis*-elements implicated in hormone responses, but it is not clear whether ABA-related TFs affect DCL and miRNA formation in stress resistance. Sucrose non-fermenting 1-related protein kinases 2 (SnRK2) was sensitive to ABA and affected miRNA production by acting on the DCL processing complex in Arabidopsis (Boudsocq et al., 2004; Yan et al., 2017). However, it is unknown whether ABA participates in DCL1 cleavageand directly affects the production of downstream miRNAs in plant response to stresses. The relationship between phytohormones and post-transcriptional regulatory mechanism of miRNAs has become the next research direction in plant stress resistance.

In the present study, we constructed sRNA libraries with four tomato groups, including wild-type (WT) tomato plants and ABA-deficient mutant (*sit*) plants under normal growth conditions and LNT stress. LNT-responsive miRNAs were identified by the ABA signaling pathway in tomato. Based on these results, miR162-overexpressing/-silenced transgenic lines (pRI-miR162/pRNAi-miR162) and DCL1-deficient mutants (*dcl1*) with CRISPR/Cas9 were generated to elucidate how the post-transcriptional process participates in cold tolerance in tomato. Furthermore, we provide a theoretical basis for artificial regulation in tomato cultivation under cold stress and provide ideas for research on miRNAs regulating targets to improve cold resistance in plants.

Materials and methods

Plant materials and growth conditions

Seeds of the ABA-deficient mutant sitiens (*sit*) and WT cultivar Rheinlands Ruhm (RR) of tomato (*Solanum lycopersicum* L.) plants were obtained from the Tomato Genetics Resource Center (TGRC; http://tgrc.ucdavis.edu). The *sit* mutant reduces a substantial proportion of ABA-aldehyde to alcohol and is deficient in functional enzymatic activity at the final step of ABA biosynthesis (Harrison et al., 2011). All experiments were completed in the artificial climate chamber. Seeds were germinated in plug trays with natural light and 60% humidity under normal temperature conditions (25°C, 12 h for day/15°C, 12 h for night). Seedlings with the fourth functional leaf fully expanded were transferred to 18 × 18 cm plots to use for experiments. Four sample groups with sixteen tomato seedlings per group were created, including WT tomato plants under normal conditions (WC), WT tomato plants under LNT stress condition (WL), *sit* tomato mutant under normal conditions (SC) and *sit* tomato mutant under LNT stress condition (SL). The LNT treatment condition was set to 12 h/12 h (day/night), which daytime is during 7:00-19:00 with 600 μmol m^{-2} s^{-1} light intensity, the temperature is 25°C, and the nighttime is during 19:00-7:00, the temperature is 6°C for 9 days. The treatment of control was set to 12 h/12 h and 25°C/15°C(day/night), other conditions are the same as LNT.Four biological replicates were used, according to four leaves in the same position of different tomato seedlings in each treatment.

sRNA isolation and identification

Tomato leaves of each group were collected from 0 to 9 treatment days.Total RNA was isolated from tomato leaves according to the manufacturer's instructions of the miRNA isolation Kit (TIANGEN, Beijing, China). Concentration of total RNA were determined by OD value. Purity of RNA was obtained by gel electrophoresis (2 μg).

Deep sequencing of sRNAs

An individual sRNA library was constructed for each sample group. 3'NEXTflex Adenylated Adapter 1 μL was added into 2 μg total RNA and placed in a PCR apparatus at 70°C for 2 min after centrifugation and incubated at 22°C for 2 h. Then, 1 μL primer was added for the reaction: 70°C, 5 min; 37°C, 30 min; 25°C, 15 min. Then, 4 μL 5'NEXTflex Adapter was added, and heated for 2 min at 70°C, and incubated at 20°C for 1 h. After reverse transcription of RNA and PCR amplification of cDNA, all samples were stored at −20°C. Reverse-transcription and PCR amplification was reacted with products after dephosphorylation and ligation with an adapter sequence (Xie et al., 2014). Sequencing was performed on the Illumina HiSeq^{TM} 2000 system at Biomarker Technologies (Beijing, China).

To obtain the clean reads, vector sequences and contaminants were removed from sequences. sRNA distribution and expression were analyzed by Bowtie. Both sRNA tags matching exons and introns of mRNAs or ncRNAs, including rRNA, tRNA, snRNA, snoRNA, and other ncRNAs were deposited into Rfam (Li et al., 2013). Filtered reads were compared with tomato miRNA sequences available from miRBase by a BLAST search (Kozomara and Griffiths-Jones, 2014). Mireap pipeline was used to identify precursor sequences of conserved and novel miRNAs (http://sourceforge.net/projects/mireap). Potential miRNA-target genes were annotated using ITAG2.3. MiRNAs obtained from different samples were compared pairwise to identity differences in expression using a $\log_2$-ratio scatter plot. Pathway classification was performed on the BMK cloud analysis platform.

Quantitative RT-PCR (qRT-PCR) analysis

qRT-PCR analysis was performed to determine the expression levels of several randomly selected conserved or novel miRNAs. Primers were coupled in 6 to 8-nts that complement corresponding miRNA at the 3' end of stem-loop structure, which were designed based on miRNA sequences (Table S4). U6 snRNA (X52315) of maize was used as an internal control. SYBR Premix Ex Taq^{TM} Kit was used for qRT-PCR. The 7500 RT-PCR System was performed with a reaction volume of 20 μL, containing 2.5 μL cDNA, 2.5 μL forward/reverse primers, 5 μL of ddH_2O, and 12.5 μL of 2 × SYBR Green PCR master mix (Applied Bio systems, CA, USA). The reaction mainly included three steps: pre-denaturation (95°C; 10 min), denaturation (95°C; 15 s) followed by 40 cycles, and annealing (60°C; 30 s). The relative miRNA quantities were calculated by Ct ($2^{-\Delta\Delta ct}$) method (Livak and Schmittgen, 2001).

Generation of miR162 and DCL1 transgenic tomato plants

To generate miR162-overexpressing and -silenced transgenic lines by using the tomato cultivar Ailsa Craig (AC), plasmids were extracted using a plasmid kit (TIANGEN, Beijing, China) and preserved in strains after extraction by the alkaline lysis method. Target fragments were recovered and purified with an agarose gel recovery kit (AXYGEN), and a carrier was recovered by double enzyme digestion. Top10 *Escherichia coli* competent cells were gently mixed with finishing products for culture. The miR162 precursor sequence has a typical hairpin structure, which can form an almost complete stem-loop structure. A recombinant plasmid was constructed by inserting miR162 into overexpressed and silenced pRI101-AN vectors, respectively. miR162 was inserted into pRI101-AN (SBS Genetech Co., Ltd, China), which plant expression binary vector by carrying a selectable marker gene NPT II (Figure 1A). Positive recombinant plasmids (pRI-miR162) were screened by PCR amplification using the corresponding primers (Table S4). The Sly-miR162 synthetic precursor was inserted into the prokaryotic expression pRI101-AN vector to construct the recombinant plasmid. The plasmid pRNAi-miR162

was transformed into LBA4404 by electroporation. Five miR162 overexpression and three miR162 silent single colonies were randomly selected for PCR and agarose gel electrophoresis. Primers for PCR identification were designed by kanamycin resistance marker gene NPTIII on pRI101-AN.

The recombinant plasmid was transformed into the *Agrobacterium tumefaciens* strain that was used to infect tomato leaves by electroporation. Eighty overexpression plants and 55 RNAi plants were generated by tissue culture, and these robust plants grew in the greenhouse.

Genomic DNA was extracted from tomato leaves of transformants using the Tissue DNA Kit (TIANGEN, Beijing, China) and was quantified based on spectrophotometric absorbance at 260/280 nm. For transgenic confirmation, isolated genomic DNA was used as templates to detect *NPT* II gene using PCR amplification (Table S4).

qRT-PCR analysis was performed to confirm silencing of miR162 using the SYBR Green Kit (TAKALA) in transgenic plants. RNA of tomato leaves was extracted by TRIzol. RNA reverse transcription was performed using the Reverse Transcription Kit (TAKALA).

DCL1-deficient mutants (*dcl1*) were generated with CRISPR/Cas9 technology using the tomato cultivar AC. The pYLCRISPR/Cas9 Pubi-H system manual was used to construct a CRISPR/Cas9-mediated knockout system (Ma et al., 2015). Briefly, Breaking-Cas web software was used to design the sgRNA target sequence (TACTCCACTACTACTTCTGA) within the coding region of the DCL1 (Solyc10g005130) gene. Because homozygous dcl1 is fatal (Castle et al., 1993), we obtained *dcl1-1-2/4/6/7/13/24* mutant tomatoes. Genomic DNA were extracted from tomato leaves to analyze DCL1 mutations with the Plant Genomic DNA Kit (TIANGEN, Beijing, China). DCL1 fragment was amplified using PCR, then sequencing results were compared to analyze the mutations. All primers used were listed in Table S4. The low temperature treatment method was the same as above.

ABA extraction and determination

Extraction of ABA was performed with the protocol described by Xu et al. (Xu et al., 2018). Leaves were carefully weighed (0.5 g of fresh material) and ground into a fine powder with liquid nitrogen. Powdered samples were suspended in 10 mL extraction solvent (80% methanol with 1 mmol/L^{-1} butylated hydroxytoluene) at −20°C and incubated overnight at 4°C. Extracts obtained were vortexed and centrifuged for 10 min at 8,000 rpm. The pellets were extracted one more time with 5 mL extraction solvent and incubated for 1 h and centrifuged again under the same conditions. All supernatants were pooled and dried under a nitrogen stream. Extracts were treated with 5 mL petroleum ether for 15 min until decolorized. The resulting extracts were dissolved in 500 µL mobile phase (methanol with 3% glacial acetic acid).

ABA content was determined using high-performance liquid chromatography procedure (Waters e2695, USA). Water phase passed through a C18 column (250 mm × 4.6 mm, 5 µm particle size). It was eluted equivalently in methanol 3% glacial acetic acid aqueous solution (volume ratio 45:55). UV detection was acquired using wavelength of 265 nm, flow rate was 0.7 mL/min, column temperature was 25°C, and injection volume was 5 µL.

Photosynthetic parameters and chlorophyll fluorescence

The photosynthetic parameters (*Pn:* photosynthetic rate, *Gs:* stomatal conductance, *Ci:* CO_2 concentration, and *Tr:* transpiration rate) were measured by the GFS-3000 gas analyzer with the DUAL-PAM-100 measurement system. Light intensity photon flux density (PFD) was 1000 µmol·m^{-2}·s^{-1} and the area of the standard measuring head used was 1.3 cm^2 with atmospheric CO_2 concentrations (approximately 500 ppm) and room temperature (Yang et al., 2020). Tomato plants were adapted in a dark environment for 30 min. Chlorophyll fluorescence of seedling was measured with the DUAL-PAM-100 measurement system (Heinz Walz, Effeltrich, Germany) at normal growth temperature. The intensity and duration of the light saturation pulse were 10,000 µmol photons·m^{-2}·s^{-1} and 300 ms in measurement of the maximum photochemical efficiency of photosystem II (Fv/Fm).

Stomatal aperture bioassays

Bioassays were performed on tomato plants at the six-week stage. The abaxial leaf epidermis was removed with tweezers and placed in Milli-Q water. Images of stomatal guard cells were captured using the Zeiss fluorescence inverted microscope (Axio Observer A1, Germany) and analyzed with the Zen 2012 software (Zeiss, Germany). A total of 200 stomata images of each treatment were composed of four biological replicates, and 50 stomata were randomly selected from each replicate for observation.

Statistical analyses

ANOVA (analysis of variance) with SPSS software v17.0 (SAS Institute, Cary, NC, USA) were used to do statistical analyzes, and the mean values were presented with standard deviation of four biological replicates, which compared by the to the one-way ANOVA comparison test at the probability level of $P < 0.05$ or 0.01. All graphs were created using Prism 8 software (GraphPad, CA, USA).

Results

sRNA profiles and identification of ABA-associated miRNAs under LNT stress

To identify which miRNAs responded to LNT stress and were involved in the ABA-dependent signaling pathway in tomato, four independent sRNA libraries were constructed for deep sequencing, including samples of WT tomato plants under normal conditions

(WC), WT tomato plants under LNT stress (WL), *sit* tomato mutants under normal conditions (SC), and *sit* tomato mutants under LNT stress (SL). The sRNA libraries yielded 32,338,934 raw reads on average (Table S1). miRNAs mainly gathered in 23-nt and 24-nt in response to LNT stress (Figure S1). After removing low-quality raw reads, contaminated adapter sequences, and poly A tail sequences, the related miRNAs were identified with 19,290,244 clean reads. These miRNA sequences were compared with the miRNA precursor and mature sequences that were known in miRbase 22.1 (Table S2). Except for known miRNAs, 299 new miRNAs were predicted with criteria that included the presence of the hairpin structure of miRNA precursors, reverse sequence of initial transcription of miRNAs, and Dicer enzyme of mature miRNAs. Secondary structures of new miRNAs were predicted by RNAFold (Figure S2). Among conserved miRNAs that were differentially expressed genes (DEGs) in the comparison of the four groups, twenty-one miRNAs were regulated by LNT stress (WL/WC), in which nineteen miRNAs were decreased and two miRNAs were increased. Among twenty DEGs, fourteen decreasing miRNAs and six increasing miRNAs were individually modulated by ABA under normal conditions (SC/WC). Eighteen DEGs were changed in the comparison of WT and *sit* mutants with sixteen increasing miRNAs and two decreasing miRNAs (SL/WL). Eleven DEGs were significantly changed in response to LNT stress and depended on the ABA signaling pathway, in which three miRNAs were decreased and eight miRNAs were increased (SL/SC) (Figure 2A). Venn diagram analysis demonstrated that four known miRNAs were ubiquitous in all groups, including *miR160a, miR162, miR1919b*, and *miR5300* (Figure 2B). The pattern cluster of twenty-nine DEGs showed which miRNAs have similar regulation and biological characteristics in each cluster. Upregulated miRNAs are represented with yellow squares, and downregulated miRNAs are represented with blue squares (Figure 2C). Gene ontology (GO) enrichment analysis of significantly changed miRNAs suggested that the LNT-related miRNAs were mostly associated with the cell and membrane cellular components. Furthermore, they participated in 16 biological processes in LNT resistance in tomato (Figure S3).

Among differentially expressed miRNAs, seven known miRNAs (*miR156, miR160, miR5300, miR166, miR1919, miR159*, and *miR162*) and two novel miRNAs (*novel-m0005-3p* and *novel-m0088-3p*) were quantified by real-time RT-PCR on the basis of the sRNA-seq results (Figure 3). *miR159* expression in *sit* mutants was significantly changed under LNT stress in the real-time RT-PCR results, but not in the sRNA-seq results. *miR162* was significantly decreased in WL than that in WC after LNT stress, which suggested that miR162 was a negative regulator in response to LNT stress. However, miR162 expression increased under LNT

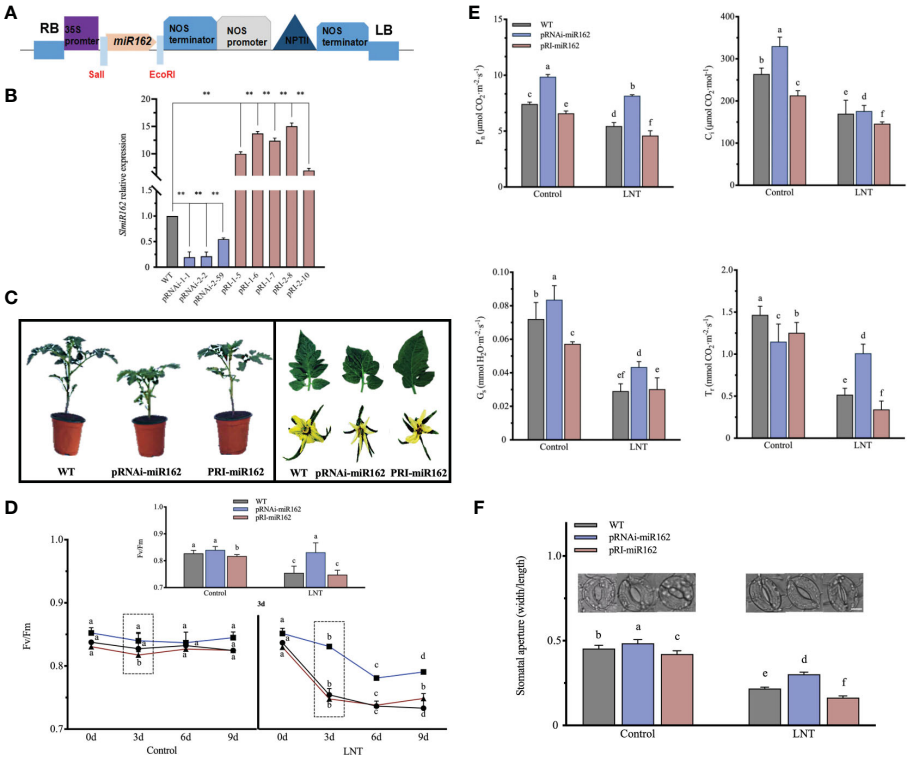


FIGURE 1
Photosynihetic effects of mR162 in response to LNT stress in tomato. **(A)** Diagram of miR162 recombinant plasmid. *NPTIII* is the marker gene with kanamycin resistance on pRI101-AN vector. **(B)** Quanitative realime PCR analysis of miR162 in WT and transgenic lines. Data are mean and standard error of four independent experiments (n = 4), **P < 0.01 according to the t-test. **(C)** Morphological characterization of miR162 transgenic tomato plants (6-week whole plants, leaves, and flowers). **(D)** Maximum photochemical eficiency of photosystem II (Fv/Fm) in miR162 transgenic lines during the nine-day LNT stress treatment. **(E)** Stomatal parameters of mIR162 transgenic lines under LNT stress: net photosynthetic rate (*Pn*); intercellular Co2 concentration (*Ci*); stomatal conductance (*Gs*): and transpiration rate (*Tr*). **(F)** Stomatal aperture and phenotype of miR162 transgenic tomato plants. Data are mean and standard error of four independent experiments (n = 4) with at least 50 individual stomata measured for each replicate. Scale bar = 5 mm. Control: 25°C/15°C, LNT stress: 25°C/15 (day/night temperature) Data are mean and standard error of four independent experiments (n = 4). Lowercase letters indicate significant differences at P< 0.05 according to Tukey's test.

10.3389/fpls.2023.1045112

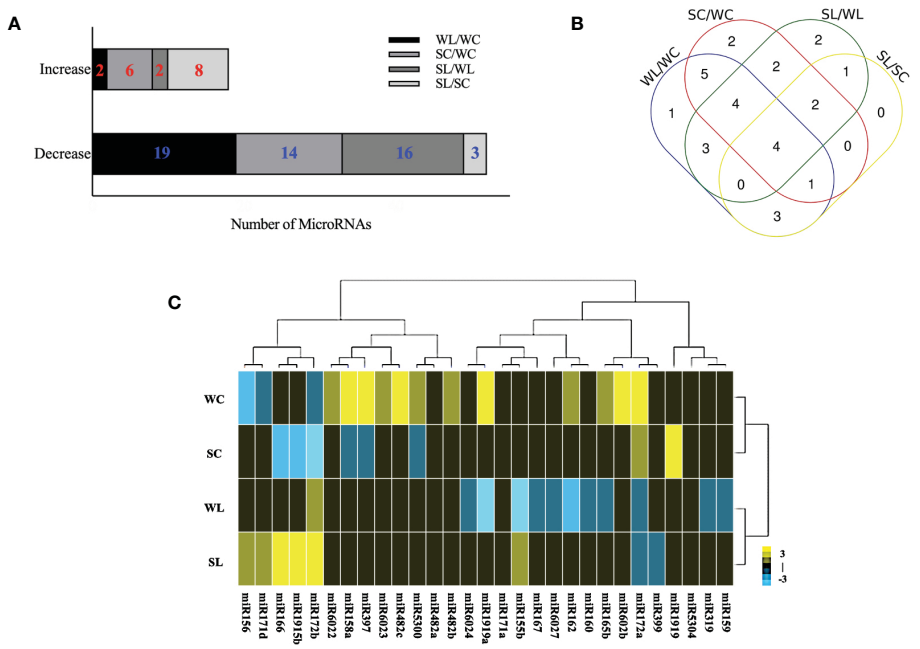


FIGURE 2
SRNA-seq profiing of differentially expressed mRNAS under LNT stress in tomato. **(A)** Diferential expression of conserved miRNAs in four libraries (WC, wild-type tomato plants under normal conditions; WL, wild-ype tomato plants under LNT stress; SC, *sit* tomato mutans under normal condilons; SL, *sit* tomato mutans under LNT stress). Data are means and standard error of four independent experiments (n = 4). Significant differences compared with each group was determined using $P < 0.05$. **(B)** Venn diagram of significantly different miRNAS in the four groups. **(C)** Clustering of diflferentially expressed miRNAs. Yellow indicates high expression, while blue indicates low expression. The consecutive fold change was set from -3 to 3.

stress in *sit* mutants, indicating that the function of miR162 was disturbed without ABA biosynthesis in LNT response (Figure 3B). Specifically, miR162 participated in LNT resistance negatively with the ABA-dependent signaling pathway in tomato. Notably, miR162 expression was downregulated in *sit* mutants under normal conditions (Figure 3B). Compared with miR162, the fold change of the other three miRNAs (miR160, miR1919 and miR5300) that also respond to LNT stress and ABA (Figure 2B) were significantly less than 51.21 times of miR162, and the miR162 expression trend of LNT response was opposite to that of WT in *sit*. It is interesting that ABA might regulated the miR162 mechanism in response to LNT stress in tomato.

miR162 regulates stomatal conductance in response to LNT stress

To examine the negative functions of miR162 in response to LNT stress, we obtained 55 RNAi and 80 overexpression transgenic tomato plants by ligating the *sly-miR162* precursor into the pRI101-AN vector (Figure 1A). According to the marker gene *NPTIII*, conferring kanamycin resistance, transgenic adult plants were confirmed by DNA and RNA analysis. Three RNAi and five overexpression tomato transgenic lines were identified. Compared with WT, miR162 expression in RNAi tomato plants (pRNAi-1-1, pRNAi-2-2, and pRNAi-2-59) was significantly downregulated by 5.1, 4.7, and 1.8-fold, respectively. miR162 expression in pRI-1-5, pRI-1-6, pRI-1-7, pRI-2-8, and pRI-2-10 was significantly higher than that in WT, upregulated by 10, 13.7, 12.4, 15.1, and 7-fold (Figure 1B). Morphological analysis of miR162 transgenic plants showed that plant growth and leaf morphology were affected by miR162 expression (Figure 1C). pRNAi-miR162 plants were stronger with thicker stem compared with the easily breakable tall and slender stem in WT plants. pRNAi-miR162 plants had lesser leaf margin serrations than WT plants. However, the changes in flower morphology and florescence were not significant between pRNAi-miR162 and WT plants. The plant growth and flower morphology in pRI-miR162 plants did not change significantly compared with WT plants. Green leaves are the main organs of plant photosynthesis. As changes of miR162 transgenic plants, we sought to elucidate the role of miR162 in the photosynthesis of tomato. The statistical analyzes is based on average data from three pRNAi and pRI transgenic lines in Figures 1, 4. The maximum photochemical efficiency of photosystem II (Fv/Fm) was elevated in pRNAi-miR162 under LNT stress, but it did not significantly change in pRI-miR162 compared with WT (Figure 1D). For nine days of LNT treatment, the most significant difference was observed on the third day among miR162 transgenic lines, which was further analyzed for photosynthetic performance. Under LNT stress, Fv/Fm was significantly reduced in pRI-miR162, even lower than that in WT. However, Fv/Fm was no significant change in comparison of control and LNT stress in pRNAi-miR162. The similar trends with Fv/Fm were shown in gas exchange parameters of tomato that pRNAi-miR162 had higher *Pn* than

10.3389/fpls.2023.1045112

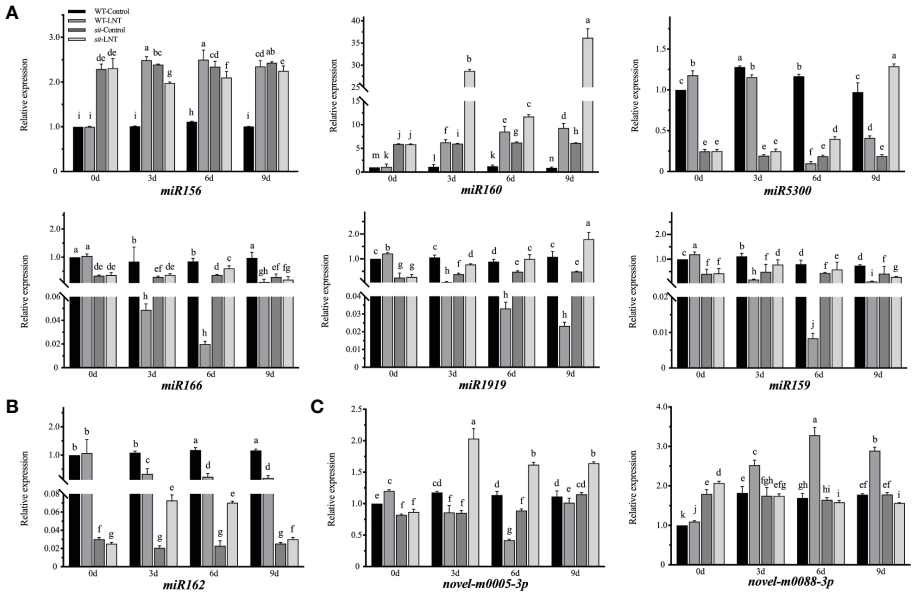


FIGURE 3
Mature miRNA changes in response to LNT stress with the ABA-dspendsnt signaling pathway in tomato. **(A)** Relative expression of known miRNAS (*miR156, miR160, miR5300, mIR166, mIR1919,* and *miR159*) in succession of LNT treatment. **(B)** Relative expression of *miR162* as the candidate miRNA. **(C)** Relative expression of new mIRNAS (*novel-m0005-3p* and *novel-m0082-3p*) in succession of LNT treatment. d, Days of LNT treatment (0, 3, 6, and 9 days). Control: 25 °C/15 °C, LNT stress: 25 °C/6 °C (daylight temperature). Data are means and standard error of four independent experiments (n = 4). Lowercase letters indicate significant differences at $P < 0.05$ according to Tukey's test.

WT under LNT stress (Figure 1E). Under LNT stress, both intercellular *Ci* and *Tr* increased in pRNAi-miR162 but were significantly decreased in pRI-miR162 compared with WT. The same trends between *Pn* and *Ci* indicated that stomatal restriction limited photosynthetic rate of miR162 transgenic lines in response to LNT stress. Specifically, stomata opened more in pRNAi-miR162 than in WT under LNT stress (Figure 1F), indicating a high *Gs* in pRNAi-miR162 (Figure 1E). Therefore, miR162 negatively modulated LNT tolerance in tomato by regulating stomatal conductance.

miR162 participated in the ABA signaling pathway to mediate LNT responses

Based on the four sRNA-seq libraries, ABA inhibited miR162 to regulate the LNT response in tomato. The feedback relationship was hypothesized between miR162 and ABA. To elucidate how miR162 regulates the ABA signaling pathway in response to LNT stress, the ABA content was elevated in miR162 transgenic lines (Figure 4A). Under LNT stress, ABA content was increased to mediate LNT resistance of tomato. However, it was inhibited in pRNAi-miR162, but was enhanced in pRI-miR162 compared with WT. miR162 might positively regulate ABA as feedback in response to LNT stress. The expression of ABA biosynthesis genes (*NCED1* and *ZEP1*) decreased in pRNAi-miR162 but increased in pRI-miR162 during LNT stress (Figure 4B). In contrast, both ABA catabolism genes (*CYP707A1* and *CYP707A2*) had significantly lower expression in pRI-miR162 but had higher expression in pRI-miR162 than in WT (Figure 4C). The increase in ABA biosynthesis and decrease in ABA catabolism resulted in ABA accumulation in pRI-miR162, indicating that miR162 regulated the ABA content of tomato plants and participated in the ABA signaling pathway in response to LNT stress. As regulators involved in the ABA response mechanism, the expression levels of *ABI3* and *AREB* were downregulated like the ABA content of pRNAi-miR162 but were upregulated in pRI-miR162 under LNT stress (Figure 4D). The feedback regulation of miR162 and the ABA signaling pathway might regulate ABA-depended LNT resistance to preserve plant defense in homeostasis of tomato. Indeed, further evidence has showed that miR162 regulated LNT resistance by the ABA signaling pathway. Both CBF1 and CBF2 can respond to LNT and ABA (Knight et al., 2004), and the expression levels of *CBF1/2* (examined by qRT-PCR) were higher in pRNAi-miR162 compared with WT and pRI-miR162 (Figure 4E). These results demonstrate that miR162 played a negative role in the ABA signaling pathway in response to LNT stress and provided feedback regulation of ABA content, maintaining homeostasis in response to diverse abiotic stresses.

miR162 modulates DCL1 cleavage in response to LNT stress at the post-transcriptional level

miRNAs mediated mRNA degradation of target genes and inhibited targeted mRNA translation to regulate gene expression

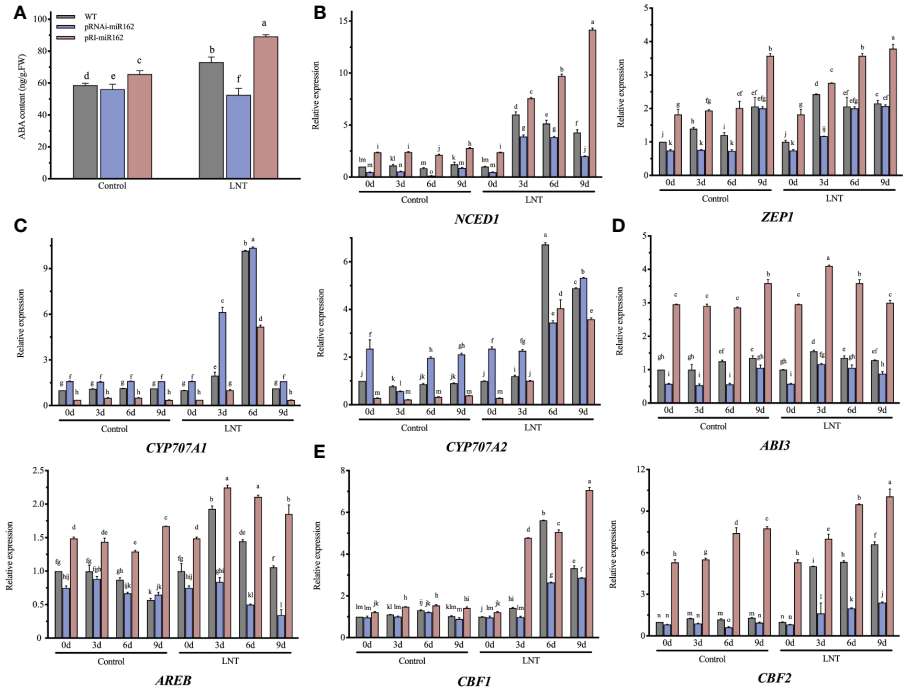


FIGURE 4
Effects of mIR162 on the ABA signaling pathway in response to LNT stress. **(A)** ABA content of miR162 transgenic lines under LNT stress. **(B)** Expression of ABA biosynthesis genes in miR162 transgenic lines during LNT stress. **(C)** Expression of ABA catabolism genes in mIR162 transgenic lines during LNT stress. **(D)** Expression of ABA responsive genes in miR162 transgenic lines during LNT stress. **(E)** Expression of ABA-related cold-induced genes in miR162 transgenic lines during LNT stress. **(D)** Days of LNT treatment (0, 3, 6, and 9 days). Control: 25°C/15°C, LNT stress: 25°C/6°C (day/night temperature). Data are mean standard error of four independent experiments (n = 4). Lowercase letters indicate significant ferences at $P< 0.05$ according to Tukey's test.

in response to environmental stress (Xie et al., 2015). The miR162 target sequence might be near the middle of DCL1 mRNA, which was subjected to negative feedback regulation by miR162 activity (Xie et al., 2003). To investigate whether miR162 regulated DCL1 in LNT resistance of tomato, SlDCL1 expression was evaluated by real-time PCR. It was upregulated in pRNAi-miR162 and downregulated in pRI-miR162, indicating negative regulation between miR162 and DCL1 (Figure 5A). DCL1, as the major producer of miRNAs, is involved in post-transcriptional regulation in response to a series of stresses (Park et al., 2002). We examined whether DCL1 cleavage was regulated by miR162. DCL1-cleavable miRNAs (miR160, miR164, and miR171a) (Kravchik et al., 2014b) were highly expressed in pRNAi-miR162 compared with WT (Figure 5B), and their corresponding target genes (ARF10, NAC, and GRAS) had opposite expression levels in pRNAi-miR162 (Figure 5C; Table S3). miR162 negatively modulated DCL1 cleavage, which inhibited the responses of SlARF10, SlNAC, and SlGRAS by increasing miR160, miR164, and miR171a at the post-transcriptional level.

Previous studies have suggested that miRNAs are strategically located in negative, positive, and double-negative feedback loops to mediate stress responses (Leung and Sharp, 2010). DCL1-deficient mutants (dcl1) were generated to examine the adaptive mechanisms of miR162-DCL1 post-transcription loops in LNT resistance. Homozygous mutation of DCL1 leads to embryo death in Arabidopsis (Castle et al., 1993), and the same embryo death phenomenon might exist in tomato because of a mutation in SlDCL1. The mutation of SlDCL1 was obtained by CRISPR/cas9. In dcl1 plants, the gene of a sister chromosome of SlDCL1 was edited (single base deletion and addition), which affected the mRNA encoding the protein. Monoclonal sequencing indicated that dcl1-1-4/6/7 belonged to the same tomato strain. In the coding region, loci 1 and 2 had another base addition that led to the partial or total loss of function of SlDCL1 (Figure 5D). Under LNT stress, stomatal apertures of dcl1 plants were significantly reduced compared with WT plants, which had a phenotype similar to pRI-miR162 (Figure 5E). Similarly, in the response mechanism of miR162, SlDCL1 was involved in the ABA signaling pathway and regulated ABA-dependent cold tolerance genes (CBF1, CBF2, and CBF3) that were upregulated in dcl1 plants under LNT stress (Figure 5F). The ABA signaling pathway and cold resistance of tomato might have been activated with DCL1 cleavage. Taken together, the post-transcriptional mechanism of miR162 in response to LNT stress was determined. With DCL1 regulating the processing of mature miR162, miR162 conversely inhibited DCL1 cleavage, which modulated miRNAs and miRNA targets to regulate resistant gene expression and cold tolerance by the ABA-dependent signaling pathway under LNT stress. Besides, the feedback regulation between the post-transcriptional process of miR162 and ABA maintained resistance to LNT stress in tomato plants (Figure 6).

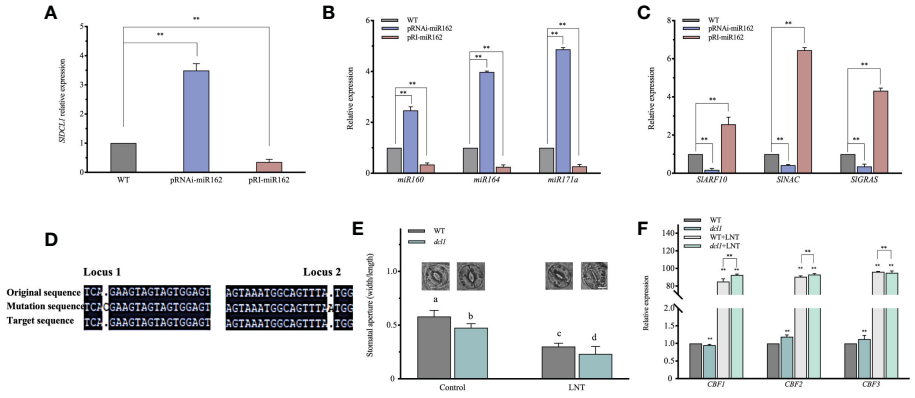


FIGURE 5
mIR162 regulated DCL1 cleavage and participated in the ABA signaling pathway in response to LNT stress. **(A)** DCL 1 expression in miR162 transgenic lines. **(B)** Expression analysis of DCL1-cleavable miRNAs (*miR160, miR164*, and *miR171a*) in miR162 transgenic lines. **(C)** Expression analysis of target genes (*ARF10, NAC*, and *GRAS*) of DCL1-cleavable miRNAS in miR162 transgenic lines. **(D)** Monoclonal sequencing of SIDCL1 mutant identification (*dcl1-1-4/6/7*). **(E)** Stomatal aperture and phenotype of *dcl* tomato plants under LNT stress. Data are mean and standard error of four independent experiments (n = 4) with at least 50 individual stomata measured for each replicate. Scale bar = 5 µm. **(F)** Expression analysis of ABA-dependent cold tolerance genes (*CBF1, CBF2*, and *GBF3*) in *dcl* tomato plants under LNT stress. Control: 25°C/15°C, LNT stress: 25°C/G°C (dayinight temperature). Data are mean and standard error of four independent experiments (n = 4). Lowercase letters indicat significant differences at P < 0.05 according fo Tukey's test. **P< 0.01 according o the test.

Discussion

miR162 plays a negative role in response to LNT stress

miRNAs are non-coding RNAs (ncRNAs) that respond to abiotic stress in plants. They act on target genes to regulate plant growth and development in stress resistance (Zhang, 2015). Cold stress not only affects the geographical distribution and planting season of crops but also destroys their normal activities causing plant damage (Chinnusamy et al., 2007). miRNAs are involved in cold resistance in plants and play key roles in response to cold stress (Zhang et al., 2009). Following high-throughput sequencing, 192 increased and 205 decreased miRNAs are identified in response to chilling stress in leaves of *S. habrochaites* seedlings (Cao et al., 2014). It is worth comparing that the role of miR167, miR169, miR172 and miR393 has been confirmed in tomato cold resistance, which are activated in the early time points of cold treatment (Koc et al., 2015). We verified 21 known miRNAs in response to LNT stress, a common stress of tomato during winter. Using miRNA microarrays and deep sequencing technologies (<xr rid="r70">Zhang et al., 2014</xr>), most miRNAs decreased under LNT stress (Figure 2A). The responsive miR162 inhibited cold tolerance *via* the ABA signaling pathway in tomato (Figure 3B). This result was consistent with relevant studies of miRNA in rice, in which 24 miRNAs responded to cold stress, including miR1425, which played a negative role in the improvement of cold tolerance in rice. In contrast, *miR393* expression continuously increased to cope with cold stress (Jeong and Green, 2012). Indeed, different miRNAs play different roles in response to cold stress. The expression of the *miR319* family positively correlated with cold tolerance in tomato (Chen et al., 2015b). Compared with WT tomato, *ShamiR319d* overexpression significantly enhanced stress resistance with weaker photoinhibition of PS II and higher scavenging activity of reactive oxygen species (Shi et al., 2019a). miR319 regulated TCP3/TCP29, which is involved in Ca^{2+} transduction and anthocyanin biosynthesis in response to cold stress. MBSI, a MYB binding site, was found in the promoter regions of miR319a and miR319b, indicating that miR319 targeted

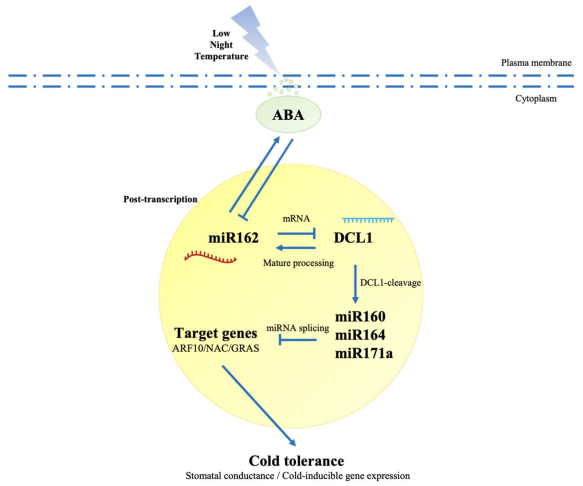


FIGURE 6
miR162-mediated DCL1 cleavage regulated cold tolerance with the ABA-dependent signaling patfway in tomato. Under LNT stress, ABA was activated to mediate multiple responses of tomato plants, including the negative regulation of miR162. Post-transcription was a crucial process in response to environmental stress. miR162 inhibited DCL1 cleavage by targeting the mRNA of DCL1. In DCL1 cleavage, DCL1 mediated miRNAs (miR160, mIR164, and miR171a) and their targets (ARF10, NAC, and GRAS) to regulate the expression of cold-inducible genes and stomatal movement under LNT stress. DCL1 is in the processing of mature miRNAs, including mIR162, which provides feedback to the ABA signaling pathway, so tomato plants resist LNT stress and maintain equlibrium. Sold lines represent regulatory links overserved in the network. Arrows indicate positive regulation, and blunt-ended bars indicate inhibition. A line does not necessarily represent unique or direct regulation by miR162 In the post-transcriptional process in cold stress response.

MYB65 and was involved in flavonoid biosynthesis regulation and mediated cold tolerance (Shi et al., 2019b). It is concluded that sly-miR166 acts as a cold-inducible switch that regulates SlHB15A levels in the ovule (Clepet et al., 2021). In our study, the photosynthetic efficiency was elevated by the stomatal opening with *SlmiR162* deficiency (pRNAi-miR162) that targeted DCL1 cleavage and DCL1-cleavable miRNAs (miR160, miR164, and miR171a) in response to LNT stress (Figures 1D, E; 5A–C). Besides cold stress, miRNAs respond to various stress treatments; for example, miR472b and miR530 play positive roles in poplar under hypoxia stress (Ren et al., 2012). *miR168*, *miR408*, and *miR396* expression decreased during drought (Zhou et al., 2010), but miR156 expression was induced by salt stress in Arabidopsis (Liu et al., 2008). The reason might be the different growth environments of different plants (Zhang et al., 2014). Even in the same plant species, differential gene expression might be due to individual selection of their WT relatives under same stress. Although several plant miRNAs have been identified by sequencing, their functions in stress response are little known. To investigate the biological functions of miRNAs and predict their corresponding target genes by proteome sequencing can provide a molecular basis for environmental stress resistance in crop breeding.

miR162 mediates DCL1 cleavage to regulate gene expression at the transcriptional and post-transcriptional levels

miRNA regulates gene expression by three mechanisms-RNA cleavage, translation inhibition, and transcriptional silencing. Most plant miRNAs are highly complementary to target mRNAs that encode TFs or other functional proteins. miRNAs are the main factors and hold an important position in the core of the regulatory network. For example, leaf development was affected by *miR319b* deficiency but recovered after *TCP3* inserted, indicating that miR319b regulates plant biological functions by targeting *TCP3* mRNA in Arabidopsis (Koyama et al., 2017). The encoded transcripts of *SlIPT2* and *SlIPT4* undergo sly-miR208-guided cleavage in the leaves of *35S::pre-miR208* plants, which revealed their targeting by this putative miRNA (Zhang et al., 2020). In addition, miRNA targets F-box proteins and ubiquitin-binding enzymes, which are related to proteasome degradation, to regulate protein stability. DCL1 is necessary for miRNA accumulation as an RNase endonuclease, which splices pri-miRNA to form mature miRNA. DCL1 mRNA is also subject to negative feedback regulation by miR162 activity (Xie et al., 2003). To characterize the negative relationship between miR162 and DCL1 in tomato, *SlDCL1* expression was evaluated in miR162 transgenic lines (Figure 5A). This feedback mechanism suggests that miRNA regulated its biogenesis and function in plants. Similarly, miR168 targets *AGO1* mRNA (Vaucheret et al., 2004) and miR403 targets *AGO2* mRNA (Allen et al., 2005), and these proteins contain a PAZ sRNA binding domain and a PIWI–RNase H-like domain, respectively. Proteins such as DCL1, AGO1, HEN1, and HYL are fundamental to miRNA effector pathways identified during genetic screening for developmental defects in pleiotropic phenotypes (Hunter et al., 2003). For example, the most severe mutations in the DCL1 mutant led to early embryonic arrest and pleiotropic defects, including abnormalities in flower organogenesis, leaf morphology, and axillary meristem initiation (Schauer et al., 2002). In the present study, a homozygous mutation in *SlDCL1* led to embryo death in tomato. Although these developmental defects might be caused by impaired miRNAs, the disruption of the other pathways also reflects the action of these functional genes in the generation and function of sRNA. However, the specific regulatory effect still needs further research in plants.

miRNAs do not function directly in response to stress but are indirectly involved in the complex gene networks and regulate key components (Winter and Diederichs, 2011). miR162 mediated DCL1 cleavage negatively by regulating DCL1-cleavable miRNAs (miR160, miR164, and miR171a) and their corresponding target genes (ARF10, NAC, and GRAS) at the post-transcriptional level (Figures 5B, C). Recent studies have suggested that the post-transcriptional modification of NAC domain TFs play a positive role in abiotic stress tolerance (Redillas et al., 2012). In Arabidopsis, miR156 targeted *SPL*, which increase and preserve defense against heat stress that recurs later (Stief et al., 2014). Because of high complementarity between miRNA and target mRNA (Kravchik et al., 2014a), miRNA-mediated cleavage has been the main action of miRNA regulation. Although miRNA-mediated cleavage has been applicable to many of these targets *in vivo*, both regulatory mechanisms of miRNAs responded to complex environmental stress at the transcriptional and post-transcriptional levels, and the biological significance of target genes regulated by miRNA still need to be explored.

miR162 participates in the ABA signaling pathway to activate LNT resistance in tomato

The initial increase in ABA is a crucial regulatory mechanism when plants experience cold stress (Knight et al., 2004). Previous studies have revealed that miRNAs can respond to ABA treatment (Sunkar and Zhu, 2004). Based on reverse genetics, miR162 was identified as a key response factor that played negative roles in the ABA-dependent resistance pathway under LNT stress (Figure 3B). miR162 transgenic lines were obtained to evaluate how miR162 mediates LNT response in combination with the ABA signaling pathway. miR162 deficiency inhibited biosynthesis and enhanced catabolism of ABA as a feedback regulation to maintain homeostasis under LNT stress (Figure 4). Correspondingly, the expression of ABA biosynthesis genes (*OsNCED1*/*OsNCED3*) were increased in miR164b-resistant OsNAC2 overexpression lines of rice (Redillas et al., 2012). The same conclusion in maize showed that miR168 and miR528 are inhibited by MAPK and peroxidase genes inducted in the ABA signaling pathway (Wei et al., 2009). Similarly, the expression of drought-suppressed *miR169* was inhibited by an ABA-dependent pathway (Li et al., 2008). Indeed, miRNAs participate in stress response by regulating their downstream targets in ABA response, auxin signaling pathway, osmotic protection, and antioxidant system (Xu et al., 2014). Consistent

with a study in *A. thaliana*, miR167a targets PpAPF8 and is involved in the auxin signaling pathway and regulates fruit development in peach (Kasschau et al., 2003). ARF10 can induce ABA accumulation by promoting ABA synthesis ABI5 gene expression in tomato (Liu et al., 2016). SlmiR160 might target SlARF10 to regulate stomatal closure, which reduces water loss and maintains water balance of leaves through the ABA signaling pathway. The association of miRNAs and ABA was demonstrated in tomato before; miR156 is an ABA-dependent regulator on the after-effect of drought on stomata (Visentin et al., 2020). Studies in the past decade have associated miRNAs with the development of guard cells and the regulation of stomatal movement, especially in stress conditions (Ding et al., 2013; Curaba et al., 2014). Under LNT stress, miR162 regulated stomatal closing to affect photosynthesis in tomato (Figures 3D–F). Similarly, miR169c reduces stomatal opening, thereby enhancing drought tolerance in tomato (Zhang et al., 2011). At the post-transcriptional level, miRNA promotes stomatal development by targeting AGO1 (Jover-Gil et al., 2012). *miR171c* overexpression was sensitive to ABA treatment and increased stomatal density, indicating that miR171c regulates stress gene expression and stomatal development by the ABA pathway (Yang et al., 2017). Taken together, these results suggest that miR162 regulated stomatal conductance and modulated ABA accumulation in LNT-responsive networks. Except for TFs and response behaviors, stress response genes are regulated by miRNAs in plants. The C-repeat binding factor (CBF) family not only responds to cold stress (Gilmour et al., 1998) but is also involved in the ABA signaling pathway (Knight et al., 2004). As we presented, *CBF1/CBF2* expression decreased in pRNAi-miR162, enabling the improvement of cold tolerance in tomato (Figure 4E). Indeed, ABA-dependent cold tolerance genes (*CBF1, CBF2*, and *CBF3*) were upregulated in *dcl1* plants (Figure 5F). The ABA signaling pathway and cold resistance of tomato might have been activated with DCL1 cleavage under LNT stress. On analysis of the *cis*-elements of the DCL promoter, all DCL family members had hormone response elements. For example, AtDCL1 silencing leads to the hypersensitivity of seeds to ABA during Arabidopsis seed germination. The expression of ABA-related and stress-induced genes increased in *dcl2* mutant and *dcl2/3/4* triple mutants, including ABF3, DREB1A, KIN2, and RAB18 (Zhang et al., 2008). Further analysis of miRNA biogenesis genes are indicated that not only ABA and salt sensitivity but also the expression level of ABA response factors (ABI3, ABI4, and ABI5) are enhanced in mutant plants (Song et al., 2013). It is not clear whether ABA-related TFs affect the formation of DCL and miRNA. The relationship between phytohormones and the synergistic regulation of miRNA biogenesis can be a research direction in the future.

Phytohormones are at the heart of regulatory networks that respond to environmental stressors (Peleg and Blumwald, 2011). Here, we proposed a model of post-transcription and ABA (Figure 6). These rapid processes are based on initial ABA response to cold stress and maintains the ABA signaling pathway to improve cold tolerance. Most miRNAs and their targeted TFs are highly evolutionarily conserved in plants (Axtell and Bartel, 2005). Therefore, plants may use regulatory mechanisms at the post-transcriptional level to quickly respond to stress conditions. miRNA-mediated gene targeting combined with phytohormones might be a mechanism common to all plant species in response to environmental stresses.

Conclusion

SlmiR162 was identified from known miRNAs that have differential expression in four sRNA libraries connected with LNT stress and the ABA signaling pathway. miR162 was involved in the LNT responsive pathway by indirectly regulating stomatal conductance and photosynthesis. A clear negative correlation was observed between miR162 and its target DCL1. Post-transcriptional interaction with the ABA signaling pathway occurred in the regulation of cold resistance. Confirmed with DCL1-deficient mutants, miRNA160/miRNA164/miRNA171a were reduced by miR162 with DCL1 cleavage. miR162 acted as a negative regulator and participated in the ABA signaling pathway of cold tolerance in tomato. The model of the association between ABA and post-transcriptional processes could be used to understand the complex mechanism of plant resistance that eventually impacts crop yield under abiotic stress.

Data availability statement

The data presented in the study are deposited in the Zenodo repository, accession number DOI: 10.5281/zenodo.7659370.

Author contributions

YYL performed the experiments, analyzed the data, and participated in the drafting. YL and ZG carried out the experiments. FW, XT, and MQ coordinated the study. YFL and TL designed the experiments, granted funds, and revised the manuscript. All authors contributed to the article and approved the submitted version.

Funding

This study was supported by the National Natural Science Foundation of China (Grant No. 31772356, 31301813), the Agriculture Research System of China (Grant No. CARS-23), joint fund for innovation enhancement of Liaoning Province (2021-NLTS-11-01), and the support program of young and middle-aged scientific and technological innovation talents of Shenyang Science and Technology Bureau (RC210293).

Conflict of interest

The authors declare that the research was conducted in the absence of any commercial or financial relationships that could be construed as a potential conflict of interest.

Publisher's note

All claims expressed in this article are solely those of the authors and do not necessarily represent those of their affiliated organizations, or those of the publisher, the editors and the reviewers. Any product that may be evaluated in this article, or claim that may be made by its manufacturer, is not guaranteed or endorsed by the publisher.

Supplementary material

The Supplementary Material for this article can be found online at: https://www.frontiersin.org/articles/10.3389/fpls.2023.1045112/full#supplementary-material

SUPPLEMENTARY FIGURE 1
Small RNA library sequencing fragment length.

SUPPLEMENTARY FIGURE 2
Prediction and secondary structure of new miRNAs.

SUPPLEMENTARY FIGURE 3
GO categories of differentially expressed miRNAs in the four groups.

SUPPLEMENTARY TABLE 1
Overview of the high-throughput sequenced sRNA libraries.

SUPPLEMENTARY TABLE 2
Comparison of miRbase.

SUPPLEMENTARY TABLE 3
Promoter cis-acting elements analysis of DCL1-cleaved miRNAs target genes.

SUPPLEMENTARY TABLE 4
All primers used for quantitative RT-PCR.

References

Allen, E., Xie, Z., Gustafson, A. M., and Carrington, J. C. (2005). microRNA-directed phasing during trans-acting siRNA biogenesis in plants. *Cell* 121, 207–221. doi: 10.1016/j.cell.2005.04.004

Arazi, T., and Khedia, J. (2022). Tomato MicroRNAs and their functions. *Int. J. Mol. Sci.* 23, 1–20. doi: 10.3390/ijms231911979

Axtell, M. J., and Bartel, D. P. (2005). Antiquity of microRNAs and their targets in land plants. *Plant Cell* 17, 1658–1673. doi: 10.1105/tpc.105.032185

Baloglu, M. C., Eldem, V., Hajyzadeh, M., and Unver, T. (2014). Genome-wide analysis of the bZIP transcription factors in cucumber. *PloS One* 9, e96014. doi: 10.1371/journal.pone.0096014

Boudsocq, M., Barbier-Brygoo, H., and Laurière, C. (2004). Identification of nine sucrose nonfermenting 1-related protein kinases 2 activated by hyperosmotic and saline stresses in arabidopsis thaliana. *J. Biol. Chem.* 279, 41758–41766. doi: 10.1074/jbc.M405259200

Cai, Y., Yu, X., Hu, S., and Yu, J. (2009). A brief review on the mechanisms of miRNA regulation. *Genom Proteomics Bioinform* 7, 147–154. doi: 10.1016/S1672-0229(08)60044-3

Cao, X., Wu, Z., Jiang, F., Zhou, R., and Yang, Z. (2014). Identification of chilling stress-responsive tomato microRNAs and their target genes by high-throughput sequencing and degradome analysis. *BMC Genomics* 15, 1–16. doi: 10.1186/1471-2164-15-1130

Castanotto, D., Lingeman, R., Riggs, A. D., and Rossi, J. J. (2009). CRM1 mediates nuclear-cytoplasmic shuttling of mature microRNAs. *Proc. Natl. Acad. Sci. U. S. A.* 106, 21655–21659. doi: 10.1073/pnas.0912384106

Castle, L. A., Errampalli, D., Atherton, T. L., Franzmann, L. H., Yoon, E. S., and Meinke, D. W. (1993). Genetic and molecular characterization of embryonic mutants identified following seed transformation in arabidopsis. *MGG Mol. Gen. Genet.* 241, 504–514. doi: 10.1007/BF00279892

Chen, X. (2004). A MicroRNA as a translational repressor of APETALA2 in arabidopsis flower development. *Science* 303, 2022–2025. doi: 10.1126/science.1088060

Chen, D., Chen, C., Baiyee, Z. M., Shao, Z., and Ciucci, F. (2015a). Nonstoichiometric oxides as low-cost and highly-efficient oxygen Reduction/Evolution catalysts for low-temperature electrochemical devices. *Chem. Rev.* 115, 9869–9921. doi: 10.1021/acs.chemrev.5b00073

Chen, H., Chen, X., Chen, D., Li, J., Zhang, Y., and Wang, A. (2015b). A comparison of the low temperature transcriptomes of two tomato genotypes that differ in freezing tolerance: Solanum lycopersicum and solanum habrochaites. *BMC Plant Biol.* 15, 1–16. doi: 10.1186/s12870-015-0521-6

Chinnusamy, V., Zhu, J., and Zhu, J. K. (2007). Cold stress regulation of gene expression in plants. *Trends Plant Sci.* 12, 444–451. doi: 10.1016/j.tplants.2007.07.002

Clepet, C., Devani, R. S., Boumlik, R., Hao, Y., Morin, H., Marcel, F., et al. (2021). The miR166–SlHB15A regulatory module controls ovule development and parthenocarpic fruit set under adverse temperatures in tomato. *Mol. Plant* 14, 1185–1198. doi: 10.1016/j.molp.2021.05.005

Curaba, J., Singh, M. B., and Bhalla, P. L. (2014). MiRNAs in the crosstalk between phytohormone signalling pathways. *J. Exp. Bot.* 65, 1425–1438. doi: 10.1093/jxb/eru002

Ding, Y., Tao, Y., and Zhu, C. (2013). Emerging roles of microRNAs in the mediation of drought stress response in plants. *J. Exp. Bot.* 64, 3077–3086. doi: 10.1093/jxb/ert164

Dong, Y., Tang, M., Huang, Z., Song, J., Xu, J., Ahammed, G. J., et al. (2022). The miR164a-NAM3 module confers cold tolerance by inducing ethylene production in tomato. *Plant J.* 111, 440–456. doi: 10.1111/tpj.15807

Gao, Y., Li, S. J., Zhang, S. W., Feng, T., Zhang, Z. Y., Luo, S. J., et al. (2021). SlymiR482e-3p mediates tomato wilt disease by modulating ethylene response pathway. *Plant Biotechnol. J.* 19, 17–19. doi: 10.1111/pbi.13439

Gasciolli, V., Mallory, A. C., Bartel, D. P., and Vaucheret, H. (2005). Partially redundant functions of arabidopsis DICER-like enzymes and a role for DCL4 in producing trans-acting siRNAs. *Curr. Biol.* 15, 1494–1500. doi: 10.1016/j.cub.2005.07.024

Gilmour, S. J., Zarka, D. G., Stockinger, E. J., Salazar, M. P., Houghton, J. M., and Thomashow, M. F. (1998). Low temperature regulation of the arabidopsis CBF family of AP2 transcriptional activators as an early step in cold-induced COR gene expression. *Plant J.* 16, 433–442. doi: 10.1046/j.1365-313X.1998.00310.x

Hackenberg, M., Gustafson, P., Langridge, P., and Shi, B. J. (2015). Differential expression of microRNAs and other small RNAs in barley between water and drought conditions. *Plant Biotechnol. J.* 13, 2–13. doi: 10.1111/pbi.12220

Harrison, E., Burbidge, A., Okyere, J. P., Thompson, A. J., and Taylor, I. B. (2011). Identification of the tomato ABA-deficient mutant sitiens as a member of the ABA-aldehyde oxidase gene family using genetic and genomic analysis. *Plant Growth Regul.* 64, 301–309. doi: 10.1007/s10725-010-9550-1

Hunter, C., Sun, H., and Poethig, R. S. (2003). The arabidopsis heterochronic gene ZIPPY is an ARGONAUTE family member. *Curr. Biol.* 13, 1734–1739. doi: 10.1016/j

Jeong, D. H., and Green, P. J. (2012). Methods for validation of miRNA sequence variants and the cleavage of their targets. *Methods* 58, 135–143. doi: 10.1016/j.ymeth.2012.08.005

Jones, L. (2002). Revealing micro-RNAs in plants. *Trends Plant Sci.* 7, 473–475. doi: 10.1016/S1360-1385(02)02361-0

Jones-Rhoades, M. W., Bartel, D. P., and Bartel, B. (2006). MicroRNAs and their regulatory roles in plants. *Annu. Rev. Plant Biol.* 57, 19–53. doi: 10.1146/annurev.arplant.57.032905.105218

Jover-Gil, S., Candela, H., Robles, P., Aguilera, V., Barrero, J. M., Micol, J. L., et al. (2012). The MicroRNA pathway genes AGO1, HEN1 and HYL1 participate in leaf proximal-distal, venation and stomatal patterning in arabidopsis. *Plant Cell Physiol.* 53, 1322–1333. doi: 10.1093/pcp/pcs077

Jung, H. J., and Kang, H. (2007). Expression and functional analyses of microRNA417 in arabidopsis thaliana under stress conditions. *Plant Physiol. Biochem.* 45, 805–811. doi: 10.1016/j.plaphy.2007.07.015

Kasschau, K. D., Xie, Z., Allen, E., Llave, C., Chapman, E. J., Krizan, K. A., et al. (2003). P1/HC-pro, a viral suppressor of RNA silencing, interferes with arabidopsis development and miRNA function. *Dev. Cell* 4, 205–217. doi: 10.1016/S1534-5807(03)00025-X

Ketting, R. F., Fischer, S. E. J., Bernstein, E., Sijen, T., Hannon, G. J., and Plasterk, R. H. A. (2001). Dicer functions in RNA interference and in synthesis of small RNA involved in developmental timing in c. elegans. *Genes Dev.* 15, 2654–2659. doi: 10.1101/gad.927801

Knight, H., Zarka, D. G., Okamoto, H., Thomashow, M. F., and Knight, M. R. (2004). Abscisic acid induces CBF gene transcription and subsequent induction of cold-

regulated genes *via* the CRT promoter element. *Plant Physiol.* 135, 1710–1717. doi: 10.1104/pp.104.043562

Koc, I., Filiz, E., and Tombuloglu, H. (2015). Assessment of miRNA expression profile and differential expression pattern of target genes in cold-tolerant and cold-sensitive tomato cultivars. *Biotechnol. Biotechnol. Equip.* 29, 851–860. doi: 10.1080/13102818.2015.1061447

Koyama, T., Sato, F., and Ohme-Takagi, M. (2017). Roles of miR319 and TCP transcription factors in leaf development. *Plant Physiol.* 175, 874–885. doi: 10.1104/pp.17.00732

Kozomara, A., and Griffiths-Jones, S. (2014). MiRBase: Annotating high confidence microRNAs using deep sequencing data. *Nucleic Acids Res.* 42, 68–73. doi: 10.1093/nar/gkt1181

Kravchik, M., Damodharan, S., Stav, R., and Arazi, T. (2014a). Generation and characterization of a tomato DCL3-silencing mutant. *Plant Sci.* 221–222, 81–89. doi: 10.1016/j.plantsci.2014.02.007

Kravchik, M., Sunkar, R., Damodharan, S., Stav, R., Zohar, M., Isaacson, T., et al. (2014b). Global and local perturbation of the tomato microRNA pathway by a trans -activated DICER-LIKE 1 mutant. *J. Exp. Bot.* 65, 725–739. doi: 10.1093/jxb/ert428

Kutter, C., Schöb, H., Stadler, M., Meins, F., and Si-Ammour, A. (2007). MicroRNA-mediated regulation of stomatal development in arabidopsis. *Plant Cell* 19, 2417–2429. doi: 10.1105/tpc.107.050377

Leung, A. K. L., and Sharp, P. A. (2010). MicroRNA functions in stress responses. *Mol. Cell* 40, 205–215. doi: 10.1016/j.molcel.2010.09.027

Li, H., Mao, W., Liu, W., Dai, H., Liu, Y., Ma, Y., et al. (2013). Deep sequencing discovery of novel and conserved microRNAs in wild type and a white-flesh mutant strawberry. *Planta* 238, 695–713. doi: 10.1007/s00425-013-1917-x

Li, W. X., Oono, Y., Zhu, J., He, X. J., Wu, J. M., Iida, K., et al. (2008). The arabidopsis NFYA5 transcription factor is regulated transcriptionally and posttranscriptionally to promote drought resistance. *Plant Cell* 20, 2238–2251. doi: 10.1105/tpc.108.059444

Liu, X., Dong, X., Liu, Z., Shi, Z., Jiang, Y., Qi, M., et al. (2016). Repression of ARF10 by microRNA160 plays an important role in the mediation of leaf water loss. *Plant Mol. Biol.* 92, 313–336. doi: 10.1007/s11103-016-0514-3

Liu, P. P., Montgomery, T. A., Fahlgren, N., Kasschau, K. D., Nonogaki, H., and Carrington, J. C. (2007). Repression of AUXIN RESPONSE FACTOR10 by microRNA160 is critical for seed germination and post-germination stages. *Plant J.* 52, 133–146. doi: 10.1111/j.1365-313X.2007.03218.x

Liu, Y. F., Qi, M. F., and Li, T. L. (2012). Photosynthesis, photoinhibition, and antioxidant system in tomato leaves stressed by low night temperature and their subsequent recovery. *Plant Sci.* 196, 8–17. doi: 10.1016/j.plantsci.2012.07.005

Liu, H. H., Tian, X., Li, Y. J., Wu, C. A., and Zheng, C. C. (2008). Microarray-based analysis of stress-regulated microRNAs in arabidopsis thaliana. *Rna* 14, 836–843. doi: 10.1261/rna.895308

Liu, Q., Zhang, Y. C., Wang, C. Y., Luo, Y. C., Huang, Q. J., Chen, S. Y., et al. (2009). Expression analysis of phytohormone-regulated microRNAs in rice, implying their regulation roles in plant hormone signaling. *FEBS Lett.* 583, 723–728. doi: 10.1016/j.febslet.2009.01.020

Livak, K. J., and Schmittgen, T. D. (2001). Analysis of relative gene expression data using real-time quantitative PCR and the 2-ΔΔCT method. *Methods* 25, 402–408. doi: 10.1006/meth.2001.1262

Ma, X., Zhang, Q., Zhu, Q., Liu, W., Chen, Y., Qiu, R., et al. (2015). A robust CRISPR/Cas9 system for convenient, high-efficiency multiplex genome editing in monocot and dicot plants. *Mol. Plant* 8, 1274–1284. doi: 10.1016/j.molp.2015.04.007

Margis, R., Fusaro, A. F., Smith, N. A., Curtin, S. J., Watson, J. M., Finnegan, E. J., et al. (2006). The evolution and diversification of dicers in plants. *FEBS Lett.* 580, 2442–2450. doi: 10.1016/j.febslet.2006.03.072

Noman, M. Z., Janji, B., Abdou, A., Hasmim, M., Terry, S., Tan, T. Z., et al. (2017). The immune checkpoint ligand PD-l1 is upregulated in EMT-activated human breast cancer cells by a mechanism involving ZEB-1 and miR-200. *Oncoimmunology* 6, 1–7. doi: 10.1080/2162402X.2016.1263412

Park, W., Li, J., Song, R., Messing, J., and Chen, X. (2002). CARPEL FACTORY, a dicer homolog, and HEN1, a novel protein, act in microRNA metabolism in arabidopsis thaliana. *Curr. Biol.* 12, 1484–1495. doi: 10.1016/S0960-9822(02)01017-5

Peleg, Z., and Blumwald, E. (2011). Hormone balance and abiotic stress tolerance in crop plants. *Curr. Opin. Plant Biol.* 14, 290–295. doi: 10.1016/j.pbi.2011.02.001

Redillas, M. C. F. R., Jeong, J. S., Kim, Y. S., Jung, H., Bang, S. W., Choi, Y. D., et al. (2012). The overexpression of OsNAC9 alters the root architecture of rice plants enhancing drought resistance and grain yield under field conditions. *Plant Biotechnol. J.* 10, 792–805. doi: 10.1111/j.1467-7652.2012.00697.x

Ren, Y., Chen, L., Zhang, Y., Kang, X., Zhang, Z., and Wang, Y. (2012). Identification of novel and conserved populus tomentosa microRNA as components of a response to water stress. *Funct. Integr. Genomics* 12, 327–339. doi: 10.1007/s10142-012-0271-6

Ricci, E. P., Limousin, T., Soto-Rifo, R., Allison, R., Pöyry, T., Decimo, D., et al. (2011). Activation of a microRNA response in trans reveals a new role for poly (A) in translational repression. *Nucleic Acids Res.* 39, 5215–5231. doi: 10.1093/nar/gkr086

Roychoudhury, A., Paul, S., and Basu, S. (2013). Cross-talk between abscisic acid-dependent and abscisic acid-independent pathways during abiotic stress. *Plant Cell Rep.* 32, 985–1006. doi: 10.1007/s00299-013-1414-5

Schauer, S. E., Jacobsen, S. E., Meinke, D. W., and Ray, A. (2002). DICER-LIKE1: Blind men and elephants in arabidopsis development. *Trends Plant Sci.* 7, 487–491. doi: 10.1016/S1360-1385(02)02355-5

Shi, X. P., Jiang, F. L., Wen, J. Q., Cui, S. Y., Zhou, Y. Z., and Wu, Z. (2019b). MicroRNA319 family members play an important role in solanum habrochaites and s. lycopersicum responses to chilling and heat stresses. *Biol. Plant* 63, 200–209. doi: 10.32615/bp.2019.023

Shi, X., Jiang, F., Wen, J., and Wu, Z. (2019a). Overexpression of solanum habrochaites microRNA319d (sha-miR319d) confers chilling and heat stress tolerance in tomato (S. lycopersicum). *BMC Plant Biol.* 19, 1–17. doi: 10.1186/s12870-019-1823-x

Song, J. B., Gao, S., Sun, D., Li, H., Shu, X. X., and Yang, Z. M. (2013). MiR394 and LCR are involved in arabidopsis salt and drought stress responses in an abscisic acid-dependent manner. *BMC Plant Biol.* 13 (1), 1–16. doi: 10.1186/1471-2229-13-210

Stief, A., Altmann, S., Hoffmann, K., Pant, B. D., Scheible, W. R., and Bäurle, I. (2014). Arabidopsis miR156 regulates tolerance to recurring environmental stress through SPL transcription factors. *Plant Cell* 26, 1792–1807. doi: 10.1105/tpc.114.123851

Sun, G., Stewart, C. N., Xiao, P., and Zhang, B. (2012). MicroRNA expression analysis in the cellulosic biofuel crop switchgrass (panicum virgatum) under abiotic stress. *PloS One* 7 (3), e32017. doi: 10.1371/journal.pone.0032017

Sunkar, R., and Zhu, J. K. (2004). Novel and stress-regulated microRNAs and other small RNAs from. *Arab. Plant Cell* 16, 2019. doi: 10.1105/tpc.104.022830.The

Tsuzuki, M., Takeda, A., and Watanabe, Y. (2014). Recovery of dicer-like 1-late flowering phenotype by miR172 expressed by the noncanonical DCL4-dependent biogenesis pathway. *Rna* 20, 1320–1327. doi: 10.1261/rna.044966.114

Vaucheret, H., Vazquez, F., Crété, P., and Bartel, D. P. (2004). The action of ARGONAUTE1 in the miRNA pathway and its regulation by the miRNA pathway are crucial for plant development. *Genes Dev.* 18, 1187–1197. doi: 10.1101/gad.1201404

Visentin, I., Pagliarani, C., Deva, E., Caracci, A., Turečková, V., Novák, O., et al. (2020). A novel strigolactone-miR156 module controls stomatal behaviour during drought recovery. *Plant Cell Environ.* 43, 1613–1624. doi: 10.1111/pce.13758

Wei, L., Zhang, D., Xiang, F., and Zhang, Z. (2009). Differentially expressed miRNAs potentially involved in the regulation of defense mechanism to drought stress in maize seedlings. *Int. J. Plant Sci.* 170, 979–989. doi: 10.1086/605122

Winter, J., and Diederichs, S. (2011). Argonaute proteins regulate microRNA stability: Increased microRNA abundance by argonaute proteins is due to microRNA stabilization. *RNA Biol.* 8, 1149–1157. doi: 10.4161/rna.8.6.17665

Xie, Z., Kasschau., K. D., and Carrington, J. C. (2003). Negative feedback regulation of dicer-Like1 in arabidopsis by microRNA-guided mRNA degradation. *Curr. Biol.* 13, 784–789. doi: 10.1016/S

Xie, F., Stewart, C. N., Taki, F. A., He, Q., Liu, H., and Zhang, B. (2014). High-throughput deep sequencing shows that microRNAs play important roles in switchgrass responses to drought and salinity stress. *Plant Biotechnol. J.* 12, 354–366. doi: 10.1111/pbi.12142

Xie, M., Zhang, S., and Yu, B. (2015). microRNA biogenesis, degradation and activity in plants. *Cell. Mol. Life Sci.* 72, 87–99. doi: 10.1007/s00018-014-1728-7

Xu, J., Yuan, Y., Xu, Y., Zhang, G., Guo, X., Wu, F., et al. (2014). Identification of candidate genes for drought tolerance by whole-genome resequencing in maize. *BMC Plant Biol.* 14, 1–15. doi: 10.1186/1471-2229-14-83

Xu, L., Yue, Q., Xiang, G., Bian, F., and Yao, Y. (2018). Melatonin promotes ripening of grape berry *via* increasing the levels of ABA, H2O2, and particularly ethylene. *Hortic. Res.* 5. doi: 10.1038/s41438-018-0045-y

Yan, J., Wang, P., Wang, B., Hsu, C. C., Tang, K., Zhang, H., et al. (2017). The SnRK2 kinases modulate miRNA accumulation in arabidopsis. *PloS Genet.* 13, 1–21. doi: 10.1371/journal.pgen.1006753

Yang, W., Fan, T., Hu, X., Cheng, T., and Zhang, M. (2017). Overexpressing osa-miR171c decreases salt stress tolerance in rice. *J. Plant Biol.* 60, 485–492. doi: 10.1007/s12374-017-0093-0

Yang, X., Li, Y., Chen, H., and Huang, J. (2020). Photosynthetic response mechanism of soil. *Plants* 9, 1–15. doi: 10.3390/plants9030363

Zhang, B. (2015). MicroRNA: A new target for improving plant tolerance to abiotic stress. *J. Exp. Bot.* 66, 1749–1761. doi: 10.1093/jxb/erv013

Zhang, J., Xu, Y., Huan, Q., and Chong, K. (2009). Deep sequencing of brachypodium small RNAs at the global genome level identifies microRNAs involved in cold stress response. *BMC Genomics* 10, 449. doi: 10.1186/1471-2164-10-449

Zhang, N., Yang, J., Wang, Z., Wen, Y., Wang, J., He, W., et al. (2014). Identification of novel and conserved microRNAs related to drought stress in potato by deep sequencing. *PloS One* 9 (4), e95489. doi: 10.1371/journal.pone.0095489

Zhang, Y., Yin, S., Tu, Y., Mei, H., and Yang, Y. (2020). A novel microRNA, SlymiR208, promotes leaf senescence *via* regulating cytokinin biosynthesis in tomato. *Physiol. Plant* 169, 143–155. doi: 10.1111/ppl.13068

Zhang, J. F., Yuan, L. J., Shao, Y., Du, W., Yan, D. W., and Lu, Y. T. (2008). The disturbance of small RNA pathways enhanced abscisic acid response and multiple stress responses in arabidopsis. *Plant Cell Environ.* 31, 562–574. doi: 10.1111/j.1365-3040.2008.01786.x

Zhang, X., Zou, Z., Gong, P., Zhang, J., Ziaf, K., Li, H., et al. (2011). Over-expression of microRNA169 confers enhanced drought tolerance to tomato. *Biotechnol. Lett.* 33, 403–409. doi: 10.1007/s10529-010-0436-0

Zhou, L., Liu, Y., Liu, Z., Kong, D., Duan, M., and Luo, L. (2010). Genome-wide identification and analysis of drought-responsive microRNAs in oryza sativa. *J. Exp. Bot.* 61, 4157–4168. doi: 10.1093/jxb/erq237

Zhou, R., Wang, Q., Jiang, F., Cao, X., Sun, M., Liu, M., et al. (2016). Identification of miRNAs and their targets in wild tomato at moderately and acutely elevated temperatures by high-throughput sequencing and degradome analysis. *Sci. Rep.* 6, 1–13. doi: 10.1038/srep33777

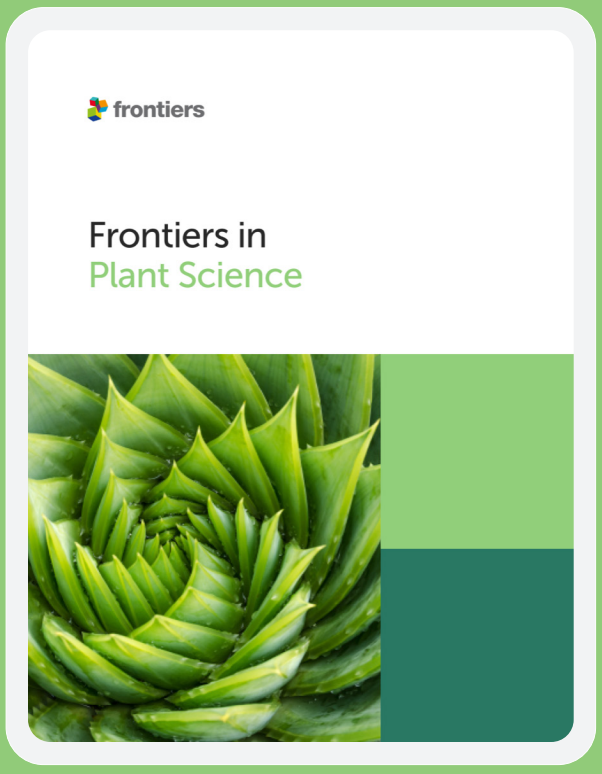
Frontiers in Plant Science

Cultivates the science of plant biology and its applications

The most cited plant science journal, which advances our understanding of plant biology for sustainable food security, functional ecosystems and human health.

Discover the latest Research Topics

See more →



Frontiers

Avenue du Tribunal-Fédéral 34
1005 Lausanne, Switzerland
frontiersin.org

Contact us

+41 (0)21 510 17 00
frontiersin.org/about/contact